ESB2019

30th ANNUAL CONFERENCE OF THE EUROPEAN SOCIETY FOR BIOMATERIALS

TOGETHER WITH THE 26TH ANNUAL CONFERENCE OF THE GERMAN SOCIETY FOR BIOMATERIALS (DGBM)

ABSTRACTS

9 – 13 SEPTEMBER 2019

DRESDEN, GERMANY

WWW.ESB2019.ORG

European Society for Biomaterials

Contents

Contents

Contents

Schedule Monday, 9 September, 2019

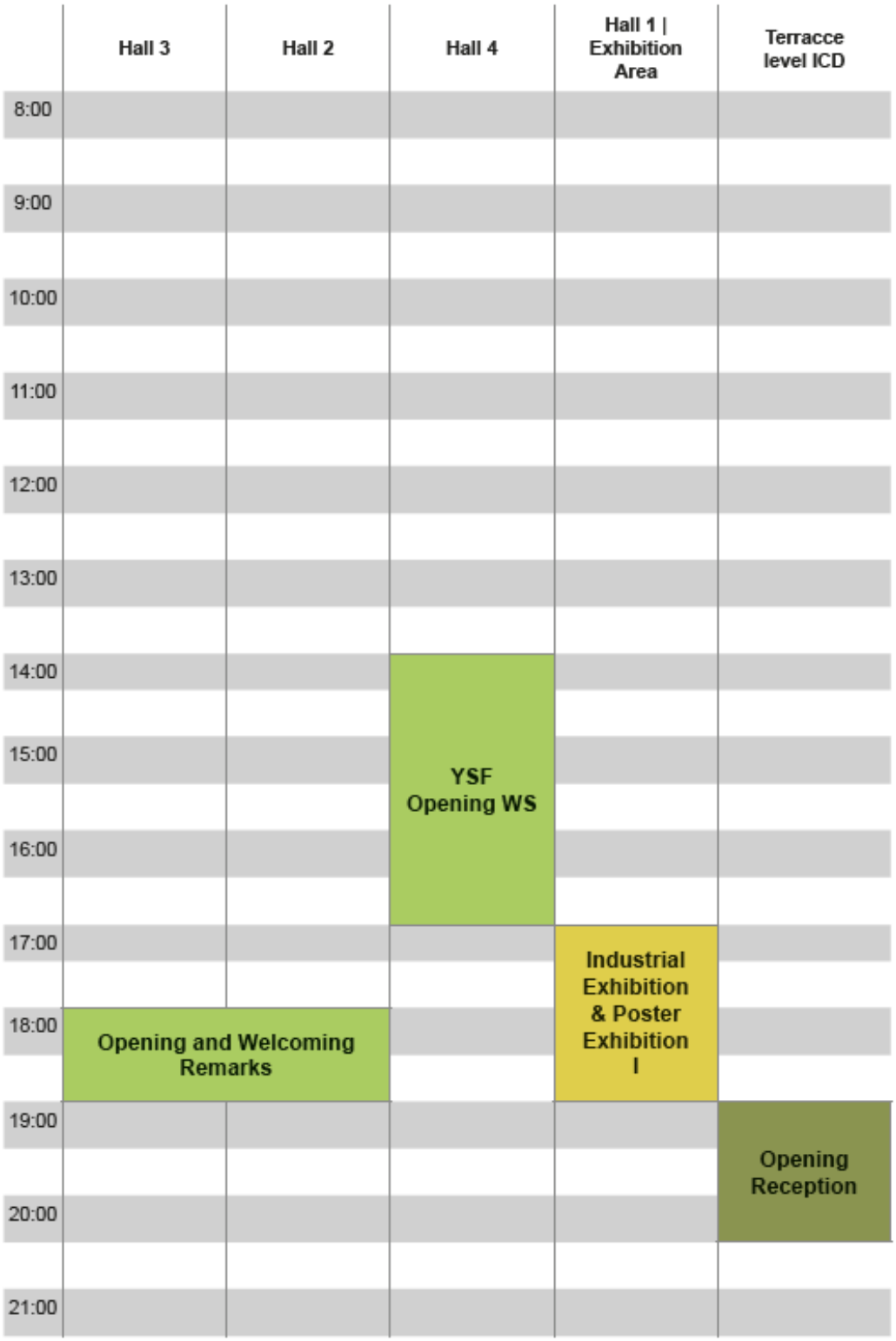

Schedule Tuesday, 10 September, 2019

	Hall 3	Hall 2	Hall 4	Hall 5	Conference room 4+5	Conference room 2+3	Hall 1 | Exhibition Area
8:00							
8:30	**PL1** Plenary Lecture 1						Industrial Exhibition & Poster Exhibition I
9:00	**IntAW** International Award						
9:30							
10:00	COFFEE BREAK						
10:30	**I-OS1** Bioinks for bioprinting	**I-OS2** Biomaterials for TE 1	**I-SY1** Bioactive glasses	**I-OS3** Composites & stimuli responsive 1	**I-OS4** Application-related aspects	**I-OS5** Soft tissues	
11:00							
11:30							
12:00	LUNCH BREAK						
12:30							
13:00	**II-OS6** Hydrogels for TE 1	**II-OS7** Biomaterials for TE 2	**II-SY2** Local antibiotics delivery with hydrogels in orthop. trauma	**II-OS8** Composites & stimuli responsive 2	**II-SY3** DGBM: Biomin. and calcification in reg. med.	**II-OS9** Strategies for Vascula-risation	
13:30							
14:00							
14:30	BREAK						
							PS1 Poster-session 1
15:00							
15:30							
16:00							
16:30	COFFEE BREAK						Industrial Exhibition & Poster Exhibition I
17:00	**III-SY4** Electro-hydro-dynamic AM technologies	**III-OS10** Polymeric biomaterials 1	**III-OS11** Biomaterials for bone regeneration	**III-SY5** Matrix engin.: skin and bone	**III-OS12** Cancer models	**YSF Grant Writing WS**	
17:30							
18:00							
	YSF GA YSF General Assembly						
18:30							
19:00							

8:30 a.m. – 9:15 a.m.

Hall 3 + Hall 2

PL1 | Plenary Lecture 1

PL1-01

The structural interplay between cells, organic matrix and mineral in collagenous tissues

Peter Fratzl[1], Zhaoyong Zou[1], Tengteng Tang[1], Elena Macias-Sánchez[1], Mahdi Ayoubi[1], Andreas Roschger[1], William J. Landis[2], Paul Roschger[3], Klaus Klaushofer[3], Wolfgang Wagermaier[1], Richard Weinkamer[1], Luca Bertinetti[1]

[1]Max Planck Institute of Colloids and Interfaces, Department of Biomaterials, Potsdam, DE; [2]University of California San Francisco, Department of Preventive and Restorative Dental Sciences, San Francisco, US; [3]Ludwig Boltzmann Institute of Osteology, Hanusch Hospital, Vienna, AT

Introduction

The deposition of new bone tissue during growth or remodeling is orchestrated in part by osteoblasts, some of which differentiate to osteocytes and form a network within the newly formed tissue. Osteocyte networks have a variety of functions mostly related to mineral homeostasis in the body [1]. They form complex three-dimensional networks where cells are connected through canalicular channels across the mineralized tissue. The arrangement of these channels is known to be strongly related to the microarchitecture of collagenous tissue, most notably the local fiber orientation and mineral density [2]. Consequently, woven and lamellar bone differ not only in their tissue structure but also in the architecture of their lacuno-canalicular network [3]. Previous *in-vitro* work using osteoblasts [4] and fibroblasts [5] suggests that mechanical interaction between cells, mediated by actin fibers, might control the orientation of collagen fibrils in the tissue extracellular matrix. While the structure of mineralized collagen fibrils has long been studied by transmission electron microscopy [6,7], surprisingly little is known about the three-dimensional arrangement of collagen fibrils and mineral with respect to the osteocyte network within a bone matrix undergoing mineralization. One of the reasons for such uncertainty is that this type of information requires both a high resolution in the nanometer range and a large field of view to visualize several cells with their processes.

Experimental Methods

We use focused ion-beam scanning electron microscopy combined with confocal microscopy and other methods to study the three-dimensional structural relationship between cells, organic matrix and mineral in mineralizing turkey leg tendon (TLT) as well as in human bone-forming sites.

Results and Discussion

When reconstructing the cellular and extracellular matrix organization within highly mineralized regions of TLT, tendon fibroblasts were found to generate a cell network connected by canaliculi with a diameter of ~100 nm that closely resembles the osteocyte network in bone. In regions of the TLT that just begin to mineralize, strings of separate mineral-rich globules were observed in channels between collagen fibrils and interpreted as vesicles containing mineralization precursors. Collagen fibrils situated in the neighborhood of these globules are seen to start intrafibrillar mineralization.

Globular mineral foci of a size smaller than about 200 nm were also seen in mineralizing osteoid of human bone. Using three-dimensional reconstruction and image analysis, the location of these mineral foci was analyzed with respect to the lacuno-canalicular network in mineralizing osteoid. The structure of this network was found sufficiently dense, so that any point within the osteoid was no further away than a few micrometers from the closest canaliculus.

Mineralization foci were found to appear preferentially at some distance from the canaliculi, typically about 400 nm away.

Conclusion

From these results we conclude that, in mineralizing collagenous tissue, the architecture of a dense network of cells not only generates the structure of the collagenous extracellular matrix but also seems to tightly control the patterns by which mineral is deposited. This conclusion will also be discussed in the context of *in-vivo* and *in-vitro* observations, that bone-forming cells deposit lamellar tissue in relation to pre-existing scaffold surfaces with potential consequences both for the design of porous tissue engineering scaffolds [8] and for understanding bone fragility [9].

References

[1] S. L. Dallas, M. Prideaux, L. F. Bonewald, “The Osteocyte: An Endocrine Cell … and More”, Endocr Rev. 2013; 34: 658–690.

[2] M. Kerschnitzki, P. Kollmannsberger, M. Burghammer, G. N. Duda, R. Weinkamer, W. Wagermaier, P. Fratzl, "Architecture of the osteocyte network correlates with bone material quality”, J. Bone Miner. Res. 2013; 28: 1837-1845.

[3] P. Kollmannsberger M. Kerschnitzki, F. Repp, W. Wagermaier, R. Weinkamer, P. Fratzl, "The small world of osteocytes: connectomics of the lacuno-canalicular network in bone”, New J. Phys. 2017; 19: 073019.

[4] C. M. Bidan et al. “Gradual conversion of cellular stress patterns into pre-stressed matrix architecture during in vitro tissue growth”, J. Roy. Soc. Interface 2016; 13: 20160136.

[5] P. Kollmannsberger et al. "Tensile forces drive a reversible fibroblast-to-myofibroblast transition during tissue growth in engineered clefts”, Science Advances 2018; 4: eaao4881.

[6] W.J. Landis, M.J. Song, A. Leith, L. McEwen, B.F. McEwen, “Mineral and organic matrix interaction in normally calcifying tendon visualized in three dimensions by high-voltage electron microscopic tomography and graphic image reconstruction”, J. Struct. Biol. 1993; 110:39-54.

[7] N. Reznikov, M. Bilton, L. Lari, M.M. Stevens, R. Kröger, “Fractal-like hierarchical organization of bone begins at the nanoscale”, Science 2018; 360: eaao2189.

[8] C.M. Bidan et al. “Geometry as a factor for tissue growth: towards shape optimization of tissue engineering scaffolds”, Adv. Healthc. Mater. 2013; 2:186-194.

[9] W. Wagermaier, K. Klaushofer, P. Fratzl, "Fragility of bone material controlled by internal interfaces”, Calcif. Tissue Int. 2015; 97: 201-212.

9:15 a.m. – 10:00 a.m.

Hall 3 + Hall 2

IntAW | International Award

IntAW

The unbearable lightness of being…a biomaterials scientist

Paul Ducheyne

University of Pennsylvania, Philadelphia, USA

How do we know we formulate the question right…

Could it be that the answer is to be found in the gradual evolution of biomaterials to include biological functionality? In fact, stent surfaces are modified to release Rapamycin; RGD and other peptides are immobilized on device surfaces to stimulate tissue formation. In my group we have focused on biological functionality of orthopaedic devices, and this from several perspectives. In situ biological functionalization can be invoked to explain the excellent tissue response of existing biomaterials, namely the class of bioactive ceramics. Taking a next step, biological functionality can also be achieved by modifying surfaces to be controlled release surfaces; sol gel processed nanoporous thin films lend themselves very well to this goal. But what is more, these controlled release materials can also be used stand-alone to achieve enhanced biological functionality and repair anywhere in tissue, not just at implant surfaces.

How do we know that our solutions are patient-centric, and therefore right?

The knowledge base regarding controlled release silica sol gels is extensive. These are room temperature processed, porous, resorbable materials with excellent biocompatibility. Many molecules including drugs, proteins and growth factors can be released from sol gels and the quantity and duration of the release can vary widely. Modifying processing parameters render these release properties exquisitely versatile. In addition, the simultaneous, controlled, local delivery of several molecules can be achieved. Thus, growth factors and adjuvant molecules can be released in tandem with antibiotics for achieving a tuned treatment regimen.

But the question still nags, how do we turn such fundamental advances in materials processing into real advances in medicine, and especially in orthopaedics, the medical discipline that was at the center of my group's studies. This question gave rise to a unique controlled release particle that adapts to the needs of surgery at the time of the surgery, a true patient centric solution.

10:30 a.m. – 12:00 p.m.

Hall 3

I-OS1 | Bioinks for bioprinting

I-OS1-KL01

Formulating Bioinks for Tissue Bioprinting

Y. Shrike Zhang

Harvard Medical School, Department of Medicine, Cambridge, USA

Over the last decade, three-dimensional (3D) bioprinting has offered great versatility to fabricate biomimetic volumetric tissues that are structurally and functionally relevant. It enables precise control over the composition, spatial distribution, and architecture of the bioprinted constructs, facilitating recapitulation of the delicate shapes and structures of targeted organs and tissues. In this talk, I will discuss our recent efforts on developing various cytocompatible and cell-instructive bioink formulations for the fabrication of engineered tissue constructs, using a series of established or customized bioprinting strategies.

Acknowledgement

This work was supported by the National Institutes of Health (CA201603, EB025270, EB026175, and EB028143) .

I-OS1-02

An injectable scaffold based on temperature responsive hydrogel and factors loaded nano-particles for potential application of vascularization in tissue engineering

Dan He, **Ansha Zhao**

Southwest Jiaotong University, Key Laboratory of Advanced Technologies of Materials, Ministry of Education,School of Materials Science and Engineering, Chengdu, CN

Introduction

Tissue engineering vascularization plays a key role in tissue repair and regeneration.[1] At the same time, Stem cells homing and vascular endothelial cells target migration, as well as their rapid proliferation *in situ* play important parts in the vascularization process.[2,3] Here, we developed an injectable system based on temperature responsive hydrogel and stromal derived factor-1 (SDF-1)/vascular endothelial growth factor (VEGF) separately-loaded nanoparticles to induce the target migration and rapid proliferation of the mesenchymal stem cells (MSCs) and endothelial cells (ECs) via SDF-1/VEGF selective release.

Experimental Methods

SDF-1 and VEGF release from the nano-composite system

C_5F_5@SDF-1 and C_2F_5@VEGF nano particles were distributed into the hydrogel to prepare the nano-composite system (the concentration of both SDF-1 and VEGF solution was 50 ng/ml, the samples were labeled as hydrogel@$NP_{VEGF\&SDF-1}$), and then were set onto the table concentrator at 37 ^oC for gelling. All the gelling hydrogels were immersed in Phosphate buffer solution (PBS, pH7.4) at 37 ^oC and the concentration of the released SDF-1 and VEGF from each hydrogel was detected via a typical ELISA assay at the 1st day, 3rd day, 5th day and 7th day, respectively. [4]

MSC homing and proliferation

The protocol of MSC homing was carried out using a Millipore transwell (aperture: 8.0 μm).Cells were fed with freshly prepared growth medium every 24 h. After culturing for 1 day and 3 days, the MSC-loaded hydrogels were stained with acridine orange (AO) solution (AO: DMEM/F12 = 1: 50) at 37 oC for 10 min and observed under a confocal laser scanning microscope (CLSM, Nikon C2 Plus, Japan) in Z-axis scanning mode to investigate the MSC proliferation, and a typical Cell Counting Kit-8 (CCK-8) assay was also applied for the quantitative characterization.[5]

Establishment of Chick embryo chorioallantoic membrane model

100 μl of hydrogel@$NP_{VEGF\&SDF-1}$, hydrogel@VEGF&SDF-1, hydrogel@NP_{SDF-1}, hydrogel@NP_{VEGF} and the single hydrogel control were placed on the large vascular branches of the CAM (each group has 5 parallel CAM, n=5) at 20 ^oC.After 3 days culture, 4% paraformaldehyde was added from the hole for a 15 min fixed step, and then the CAM covered by the hydrogels were cut off and rinsed in the PBS; the paraffin embedded sections were stained with HE to observe each hydrogel of blood vessel ingrowth. [6]

Results and Discussion

The hydrogels had a porous network structure with uniform pore sizes ranged from 30 μm to 50 μm.The C5f5 @ SDF-1 nanoparticles have positive charges and the c2f5 @ VEGF nanoparticles have negative charges. They interact with hydrogels through electrostatic interaction (chitosan hydrogels have positive charges), regulating the scaffolds

to release more SDF-1 and less VEGF. The MSC migration experiment proved that the SDF-1/VEGF selective released scaffold (hydrogel@NPVEGF&SDF-1) induced more MSC homing compared with the non-selective one (hydrogel@VEGF&SDF-1), while the cell proliferation and apoptosis investigation verified that the SDF-1/VEGF selective released scaffold (hydrogel@NPVEGF&SDF-1) also enhanced cell proliferation and led to less cell apoptosis compared to the non-selective scaffold (hydrogel@VEGF&SDF-1). In the typical CAM model, the SDF-1/VEGF selective released scaffold obviously possessed more areas of blood vessel ingrowth compared with the non-selective scaffold, which suggested better ability on vascularization.

Conclusion

In this contribution, we developed an injectable system composed of temperature responsive hydrogel and factors loaded nano-particles for potential application of vascularization in tissue engineering. This composite system can control the MSC chemokines (SDF-1) and cell growth factor (VEGF) selective release (more SDF-1 release and less VEGF release) via two different nanoparticles co-loading: the SDF-1 nanoparticles possessed positive charge and bigger scales (304 nm), while the VEGF nanoparticles possessed negative charge and smaller scales (154 nm); wherein smaller nanoscales and the loaded VEGF contributed to in situ cell growth, while the sustained SDF-1 release was conductive to the MSC homing. The CAM model further demonstrated that the composite system significantly improved angiogenesis of the hydrogels scaffold. We expect our research to facilitate the in situ vascularization during application of tissue/organ repair and/or regeneration. Future studies will focus on further fine-tuning the parameters of the functional nanoparticles, such as scales, degradability and/ or more factors, aiming at more rapid vascularization.

References

1. Caccavo D, Cascone S, Lamberti G, Barba A A. Hydrogels: Experimental Characterization and Mathematical Modelling of Their Mechanical and Diffusive Behaviour. *Chemical Society Reviews***2018;** *47 (7):* 2357-2373.
2. Laiva A L, Raftery R M, Keogh M B, O'Brien F J. Pro-angiogenic Impact of SDF-1α Gene-Activated Collagen-Based Scaffolds in Stem Cell Driven Angiogenesis. International Journal of Pharmaceutics **2018**; 544(2): 372-379.
3. Li J A, Zhang K, Xu Y, Chen J, Yang P, Zhao Y C, Zhao A S, Huang N. A novel co-culture models of human vascular endothelial cells and smooth muscle cells by hyaluronic acid micro-pattern on titanium surface. Journal of Biomedical Materials Research: Part A **2014**; 102A: 1950-1960.
4. Li J A, Qin W, Zhang K, Wu F, Yang P, He Z K, Zhao A S, Huang N. Controlling Mesenchymal Stem Cells Differentiate into Contractile Smooth Muscle Cells on a TiO_2 Micro/nano Interface: Towards Benign Pericytes Environment for Endothelialization. *Colloids and Surfaces B: Biointerfaces***2016;***145:* 410-419.
5. Zhang K, Shi Z Q, Zhou J K, Xing Q, Ma S S, Li Q H, Zhang Y T, Yao M H, Wang X F, Li Q, Li J A, Guan F X. Potential Application of an Injectable Hydrogel Scaffold Loaded with Mesenchymal Stem Cells for Treating Traumatic Brain Injury. *Journal of Materials Chemistry B***2018;***6:* 2982-2992.
6. Zou D, Luo X, Li J A, Wang S, Zhang K, Sun J Y, Yang P, Zheng Q J, Zhang C J. Investigating Blood Compatibility and Tissue Compatibility of a Biomimetic ECM layer on Cardiovascular Biomaterials. *Journal of Biomaterials and Tissue Engineering***2018;** *8(5):* 640-646.

Acknowledgement

This work was supported by the National Natural Science Foundation of China (NSFC 81771988), Key Project and Special Foundation of Research, Development and Promotion in Henan province (No. 182102310076), the Joint Fund for Fostering Talents of NCIR-MMT & HNKL-MMT (No. MMT2017-01), and Top Doctor Program of Zhengzhou University (No. 32210475).

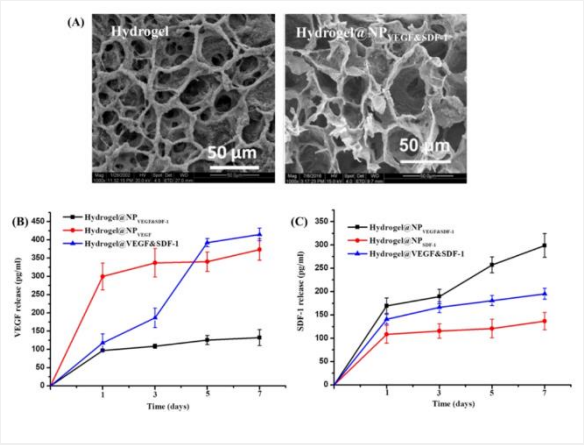

Figure1
Figure 1 (A) SEM images ; (B) VEGF release ; (C) SDF-1 release.

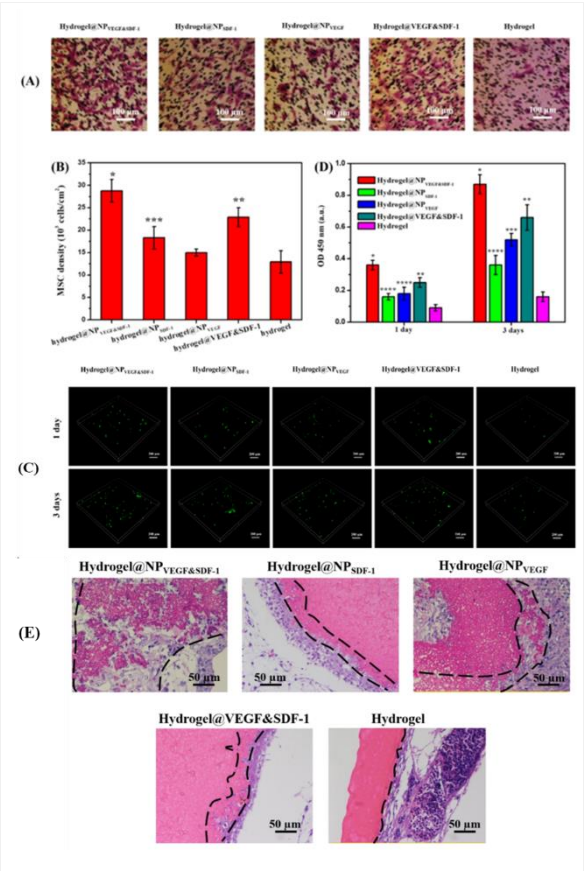

Figure2
Figure 2 (A) Crystal violet staining of MSC migrated to the under side of bottom membrane; (B) Amounts of migrated MSC; (C) CLSM images of MSC distributed in different hydrogels; (D) Proliferation of MSC by CCK-8 assay. (E) Histological analysis results.

I-OS1-03

Biomimetic 3D bioprinted periodontium modules for periodontal defect repair

Yue Ma[1,2,3], Bo Yang[1,2,3], Weidong Tian[1,2,3]

[1]Sichuan University/West China Hospital of Stomatology, Department of Oral and Maxillofacial Surgery, Chengdu, CN; [2]Sichuan University/West China Hospital of Stomatology, National Engineering Laboratory for Oral Regenerative Medicine, Chengdu, CN; [3]Sichuan University/West China Hospital of Stomatology, Department of Oral and Maxillofacial Surgery, Chengdu, CN

Introduction

The periodontal tissue defects caused by periodontitis occur as a common disease in clinical, not only affects the mastication and stable of the teeth, but also leads to a series of physiological and psychological problems. The periodontium exhibits a typical 'sandwich structure' that comprises the cementum, alveolar bone and periodontal ligament with fiber bundles in different directions. Current methods in periodontal regeneration lack appropriate biofabrication techniques to build such complex 3D micro-architectures essential for guiding cell growth while promoting hard and soft tissues maturation. Here, we report the use of a microscale continuous digital light projection (DLP)-based bioprinting method to create a complex periodontium structure for regenerative medicine applications in the periodontal defect in rodent and mammal animal models.

Experimental Methods

The matrix material used for bioprinting the scaffolds was made by mixing 10% (w/v) GelMA and 0.225% (w/v) LAP in α-MEM with 10% fetal bovine serum (FBS, HyClone, USA) solution. Human dental follicle cells (hDFCs) were encapsulated within the hydrogels. Digital model of the periodontium module was designed according to the computer, which were later imported into a digital micromirror device chip to control the UV light and project an optical pattern we designed. Cellar viability and distribution were examined *in vitro*. The periodontal defects were constructed in the jaw bone of Sprague-Dawley rats and Beagles. Orthotopic implantations were carried to further verify the regenerative potential.

Results and Discussion

The GelMA-based solution presented porous structures after curing via SEM (Figure 1A). A fiber-aligned structure was fabricated to mimic the natural periodontal fibers (Figure 1B). Whereafter, to improve the stability and mechanical properties, a micro-scale mesh and rod structure was constructed and there exists three-dimensional spaces between the two types of microstructures for stem cells to exchange of nutrition and metabolism (Figure 1C&D). *In vitro*, more than 90% cell viability of hDFCs encapsulated in the scaffolds was promised after 3-14 days cultured (Figure 1E&F). Fiber-like structure generated *in vitro*, about 300-400 μm in length, which was similar to natural human periodontal ligament (Figure 1 G-I). After 2 months *in situ* implantation in rodent animals, the 3×2×1 mm periodontal detects were almost completely restored that both hard and soft new-born tissues were found (Figure 2A). The alveolar bone was better restored compared to the control group according to the micro-CT (Figure 2B). And the regenerated cementu, presented at interface between the scaffolds and host tooth root. Notably, in comparision with the random control group, highly-aligned fibers regenerated while presenting a certain angle to the root of the tooth according to the H&E and Masson's trichrome staining (Figure 2 C&D), which is similar to the natural periodontal tissues. The immunofluorescence staining showed remarkable specificity about periodontium related proteins and extensively vascularized as shown in Figure 2E. Moreover, the imageology results showed good efficacy of 3D-bioprinted periodontium modules for repaired the detects of Beagles in 3 months.

Conclusion

DLP-based 3D bioprinting can constructed 3D biomimetic hydrogel cell-contained scaffolds tailored to the dimensions of human periodontium in 3-5 s and is scalable to human periodontal tissues sizes and lesion geometries. A new born 'sandwich structure', especially the highly-aligned periodontal fibers was found after implantation. Thus, the biomimetic 3D-bioprinted periodontium modules offer a means of inducing the periodontium regeneration through precision medicine, confirmed to be promising and reliable for periodontal tissue engineering regeneration.

Acknowledgement

This study was supported by the National Key Research and Development Program of China (Nos. 2017YFA0104800), National Natural Science Foundation of China (31600789) and Fundamental Research Funds for the Central Universities (2016SCU11051).

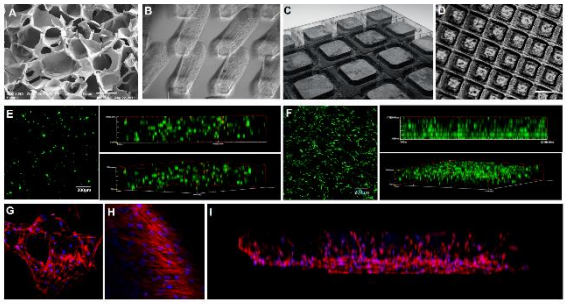

Construction of biomimetic 3D bioprinted periodontium modules
The fabrication of mimetic 3D bioprinted periodontium modules and cell-guiding properties (Figure 1).

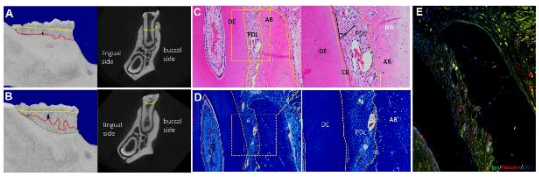

Regeneration of periodontium tissues
Both hard and soft new-born tissues were almost completely restored after 2 months *in situ* implantation in periodontal detects (Figure A). The alveolar bone was well restored and the regenerated cementum presented at interface between the scaffolds and host tooth root. Highly-aligned fibers regenerated while presenting a certain angle to the root of the tooth (C&D). The immunofluorescence staining showed remarkable specificity about periodontium related proteins and extensively vascularized (E).

I-OS1-04

Fabrication of high-resolution poly(trimethylene)-based scaffolds using 2-photon polymerization

Gregor Weisgrab[1,3], Olivier Guillaume[1,3], Zhengchao Guo[2], André Poot[2], Dirk Grijpma[2], **Aleksandr Ovsianikov**[1,3]

[1]Technical University Vienna, Institute of Materials Science and Technology, Vienna, AT; [2]University of Twente, Department of Biomaterials Science and Technology, Enschede, NL; [3]Austrian Cluster for Tissue Engineering, www.tissue-regeneration.at, Vienna, AT

Introduction

When aiming at recreating the architectural features of native tissues, the field of tissue engineering and regenerative medicine often relies on advanced technologies, such as additive manufacturing [1]. One of the main bottlenecks is the trade-off on the part of resolution when upscaling. Larger constructs lack the resolution, whereas highly intricate scaffolds lack the volume to fill a defect. As a proof-of-concept, we employed 2-photon polymerization (2PP) technique to fabricate a 3D scaffold based on methacrylated-poly(trimethylene) biomaterial (PTMC-MA). The resulting structures were composed of highly complex building blocks (buckyballs) that, when printed in clusters, move towards upscaled high-resolution 3D-printing. This study shows that 2-PP is a reliable and advantageous AM technique to produce 3D structures with an unprecedented degree of resolution promising great potential in the field of tissue engineering.

Experimental Methods

The three-armed macromer of PTMC was synthesized using ring-opening polymerization, followed by a treatment with methacrylic anhydride to obtain PTMC-MA with a molar mass of 4 kg/mol as reported here [2]. A resin based on PTMC-MA, dissolved in THF with 0.5 wt% of photo-initiator (M2CMK [3]), was cast and let to dry over night before 2-PP processing. First, a printability test was conducted to determine the optimal 2-PP laser parameters by screening intensities ranging from 150 to 300 mW. Then, a complex structure with intricate geometries was designed by clustering an array of 8x8x3 buckyballs, and printed at a laser intensity of 150 mW and a scanning speed of 1000 mm/sec. The produced structures were extracted with THF, isopropanol and ethanol 70% before being dried and then characterized using fluorescence imaging and scanning electron microscopy (SEM). Finally, *in vitro* cytocompatibility of the biomaterials was assessed by seeding the scaffolds with 50.000 GFP-labelled human-adipose derived stem cells (hASC). The scaffolds were imaged using fluorescence microscopy and SEM after one week of culture.

Results and Discussion

The printability test revealed that a laser power of 150 mW was required to obtain accurate structures without damaging the polymer. Above this intensity, the material burned and formed bubbles, preventing efficient polymerization. Brightfield-, fluorescence- and scanning electron microscopy confirmed the accuracy of the highly-detailed scaffolds (Figure 1), composed of a merged array of 8x8x3 buckyballs with an individual diameter of 300 µm and struts of approximately 20 µm in thickness.

The *in vitro* cytocompatibility test showed that the biomaterial allowed for rapid cell invasion, with hASC being able to proliferate not only on the surface of the printed scaffold, but also to colonize its porous core (Figure 2).

Conclusion

In this preliminary study, we demonstrated that 2-PP is a viable technique to produce scaffolds at an extremely high resolution. By adjusting the laser intensity and the writing speed, we successfully produced complex structures from PTMC-MA. The arrayed design was selected as a proof-of-concept for the printability of a larger, albeit still complex structure. This proof-of-concept allows the future fabrication of scaffolds that require complex designs to accurately mimic natural features of organs and tissues. Moreover, further fine-tuning of the printing parameters to achieve an even higher throughput will encourage the fabrication of even larger macroscaffolds while retaining high-resolution features.

References

[1] A. Ovsianikov et al., 3D printing and biofabrication. Tissue Engineering and Regeneration Series, Springer International Publishing (2018).

[2] O. Guillaume et al., Acta Biomaterialia (2017) 54, 386-98.

[3] R. Whitby et al., RSC Adv. (2017) 7, 13232-13239.

Acknowledgement

This work was financially supported by the European Research Council (Consolidator Grant 772464 A.O.)

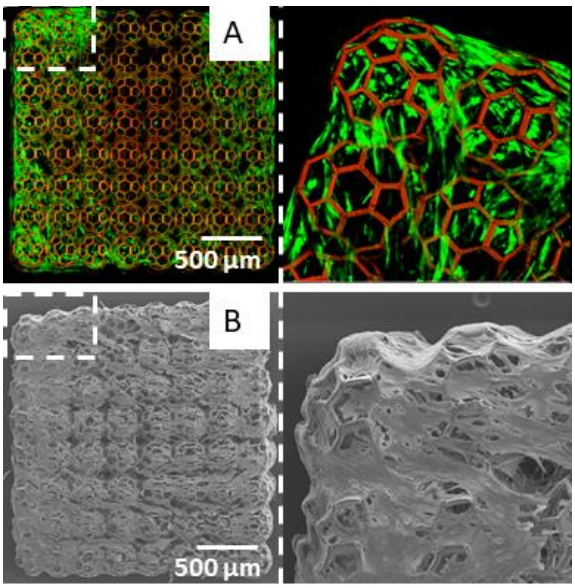

2-PP produced PTMC-based scaffolds allow for rapid-cell colonization

Microscopic (A, mag 25 and 100) and SEM (B, mag 30 and 150) observation of the cell-laden scaffolds after 7 days of culture. In A), the scaffold appears in red and GFP-hASC in green fluorescence.

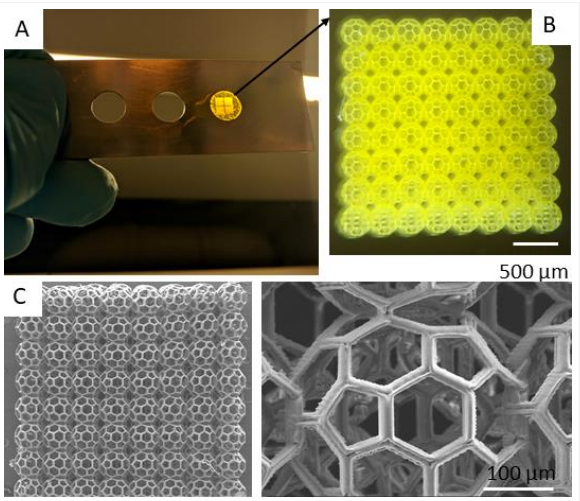

2-PP is a viable AM technique to produce high-resolution structures

Macroscopic (A and B) and SEM (C) observation of the 3D scaffolds produced using 2PP, based on multiple buckyballs. A) illustrates the sample-holder on which 4 scaffolds were printed.

I-OS1-05

The interplay between chondrocyte spheroids and mesenchymal stem cells boots cartilage regeneration within a 3D natural-based hydrogel

Annachiara Scalzone[1], Ana M. Ferreira-Duarte[1], Chiara Tonda-Turo[2], Gianluca Ciardelli[2], Kenneth Dalgarno[1], Piergiorgio Gentile[1], Annachiara Scalzone was supported by EPSRC (Ph.D. studentship,GRANT EP/R51309X/1).

[1]Newcastle University, School of Engineering, Newcastle upon Tyne, GB; [2]Politecnico di Torino, Dipartimento di Ingegneria Meccanica e Aerospaziale (DIMEAS), Turin, IT

Introduction

Articular cartilage (AC) tissue lacks the ability to self-repair and significant progress has been made in the field of Tissue Engineering over the last two decades demonstrating how combinations of biomaterials and cells can be used to engineer cartilage tissue *in vitro* [1][2]. In this work it was developed a direct contact co-culture between human TERT immortalised bone marrow stromal cells (Y201 MSCs) and human articular chondrocyte (hACH) spheroids for cartilage regeneration. As co-culture substrate, an innovative 3D thermo-sensitive chitosan (CH)-based hydrogel, ionically crosslinked with the addition of β–glycerophosphate (BGP) salt was proposed. This co-culture system aimed to facilitate cell-cell interactions through surface receptors and enhance the transduction of molecular signals boosting MSCs chondrogenic differentiation.

Purpose of the work

This work purpose was to manufacture and characterise the CH/BGP hydrogel as *in vitro* co-culture platform. Therefore the hydrogel was firstly **physico-chemically** characterised *(OBJ1)*, then embedded with Y201 MSCs to test its **cytocompatibility***(OBJ2)* and finally the hACHs/Y201 MSCs **co-culture technology was investigated** to analyse the faster *hyaline*-like cartilage tissue formation compared to hACHs mono-culture *(OBJ3)*.

Experimental Methods

CH (3.6%w/v) was dissolved in 5 ml of 0.2M HCl and BGP (1.1g in 2.2 ml of PBS) was added to obtain a 2.5% w/v solution for sol/gel transition at 37°C and pH 7.4. Hydrogels were physico-chemically (FTIR-ATR, XPS, gelation time, thermal-reversibility, swelling, nutrients diffusion), morphologically (ESEM) and mechanically (compression test, stress relaxation and rheology) characterised. The cytocompatibility of a Y201 MSC-laden hydrogel was assessed with a Live/Dead, PrestoBlue and immunostaining assays. Immunofluorescence analysis on the production of collagen type II and the expression of CD44, chondrogenic marker were carried out up to 28 days as well as a histological study on GAGs (AlcianBlue) and collagen (SiriusRed) production.

Results and Discussion

The CH/BGP sol/gel transition occurred at 31-33°C within 5±1 minutes as demonstrated by the tube-inverted test and the rheological analysis, with thermo-irreversible behaviour at room temperature and 4 °C. The hydrogel showed a hydrophilic nature, leading to a high capacity to hold water molecules and to offer a good nutrient transport matrix, as evaluated with glucose diffusion and release test. In fact the CH/BGP hydrogels showed an open porous and interconnected network **(Fig.1)**, fundamental for the integration within the surrounding tissue. Pores diameters were up to 30 µm, suitable for cells adhesion [4]. Nevertheless, this high porosity did not compromise the mechanical

properties and Young's modulus of ~ 40 kPa and equilibrium modulus of ~17kPa were calculated. Live/dead assay confirmed the viability of the encapsulated Y201 MSCs within the hydrogels at day 1 and 3. Immunostaining analysis showed the tendency of agglomerates formation after 3 days of culture and cells metabolic activity, assessed via Presto- Blue, resulted to be stable without statistically differences up to day 7. Finally, the influence of a hACHS spheroid, in close-contact with y201 MSCs-laden hydrogels, was successfully assessed by immunofluorescence and confirmed by histological analysis after 28 days **(Fig.2)**, with enhanced GAGs accumulation and collagen production, distributed uniformly throughout the sections of the co-culture samples compared with the hACHs mono-culture control.

Conclusion

The manufactured hydrogels presented fast sol/gel transition time allowing the easy MSCs encapsulation, while their intrinsic porous structure and high uptake capability were vital for cell maintenance. Finally, the proposed formulation offered a new and valuable platform for co-culturing MSCs and hACHs spheroids that supported enhanced chondrogenesis and cartilage production.

References

[1] Kelly et al. 2013 *J.Biomech* **46:**1184
[2] Zhou et al 2015 CarbohydrPolym **117**:524-36
[3] Bian et al 2011 TissueEng Part A **17**:1137-45
[4] Loh et al 2013 TissueEng Part B **19**:485-502

Acknowledgement

The authors thank Dr K White for TEM images (Electron Microscopy Research Services), L Boyd and X Xu for Ultramicrotome sectioning (Medical School), Dr I A Garcia for E-SEM Images (Herschel Building) and P Melo for SEM images (School of Engineering) for their support at Newcastle University.

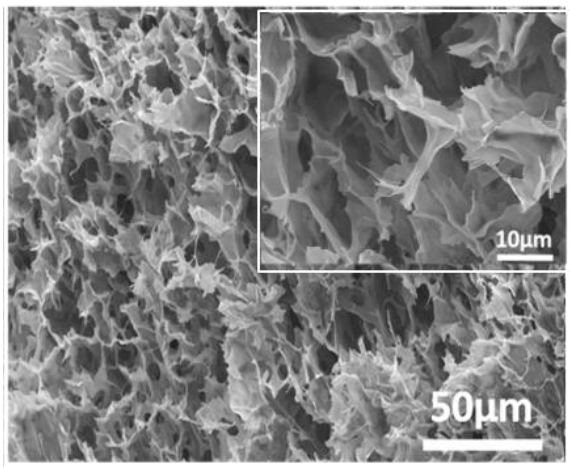

Figure 1
SEM image of the freeze-dried CH/BGP hydrogel.

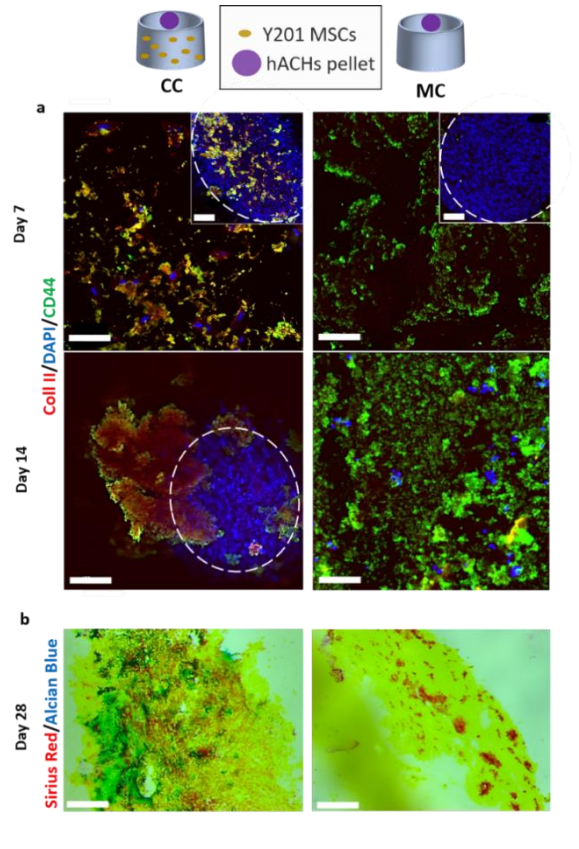

Figure 2
(a) Immunofluorescence staining at 7 (dashed line inserts represents spheroid area) and 14 days. Red staining for Col II, Blue for nuclei and Green for CD44 marker in co-culture (CC) (hACHs spheroid on MSCs-laden hydrogel) and mono-culture (MC) (hACHs spheroid on empty hydrogel). Bars=100µm. (b) Histological sections of the hydrogels after 28 culture days. GAGs were visualized by Alcian blue and Collagen by Sirius red staining respectively. Bars=200µm.

10:30 a.m. – 12:00 p.m.

Hall 2

I-OS2 | Biomaterials for tissue engineering applications 1

I-OS2-01

Structurally Graduated Collagen Scaffolds for the *ex vivo* generation of blood platelets

Jennifer H. Shepherd[1,2], Daniel Howard[3], Eleonora Vriend[1], Cedric Ghevaert[3], Serena M. Best[1], Ruth E. Cameron[1]

[1]University of Cambridge, Department of Materials Science and Metallurgy, Cambridge, GB; [2]University of Leicester, Department of Engineering, Leicester, GB; [3]University of Cambridge, Department of Haematology, Cambridge, GB

Introduction

Platelet transfusions are key in the treatment of a range of conditions including bone marrow failure, inherited platelet disorders and cancer. Unlike red blood cells there are considerable challenges to the supply of blood platelets and a real demand for the development of a system for the *ex vivo* generation of donor independent platelets. Whilst large quantities of megakaryocytes (MKs) can be generated from human pluripotent stem cells (hPSC)[1], 2D culture can limit the numbers of platelets harvested from these MKs. This work considers the development of a porous structurally graduated scaffold that can not only provide a structure to support the MKs in a bone marrow-like material but also offer sieving capacity and shear flow over the cells surface to enhance the platelet output. Whilst the scaffold has been combined with a bespoke bioreactor and highly efficient hPSC culture protocol[2] we concentrate here on the production and characterisation of the scaffolds and the role of micro-tomography (µCT) and micro-particle filtration in predicting cell distribution.

Experimental Methods

Scaffolds with a graduated pore structure were produced through a multi-stage lyophilisation process from insoluble type I collagen from bovine dermis (Collagen Solutions (UK)). Collagen was swollen in 0.05M acetic acid prior to blending to produce a 1wt% suspension. In preliminary lyophilisation studies a number of freezing temperatures and rates were considered and pore size and interconnectivity analysis carried out from µCT. Based upon this analysis, a two-stage freezing process was applied with the base layer frozen at -20°C before the application and freezing of a top layer at -40°C; scaffold structure was then defined through sublimation. EDC/NHS cross-linking was carried out at a concentration of 100% as defined previously [3], prior to a second lyophilisation step.

Two methods were considered as predictive tools for cell migration. µCT was carried out on 5mm diameter samples with a pixel size of 1.5 µm. Systematic volumes of interest were selected and a detailed 3D pore size analysis carried out in CTAn (Bruker Belgium). The shrink-wrap capabilities of CTAn were applied for a directional interconnectivity analysis as described elsewhere[2]. This allowed for calculation of the percentage of pore space theoretically accessible from the input surface for a sphere of given diameter. In addition the set-up within the bioreactor was replicated and filtration of 20 µm and 10 µm polystyrene microparticles (Sigma Aldrich) (approximately diameters of MKs and blood platelets respectively) carried out. Scaffolds after filtration were then imaged using µCT in order to analyse particle distribution.

Results and Discussion

In preliminary studies interconnectivity analysis suggested differential filtration capabilities of scaffolds produced with rapid freezing to -20 and -40°C. Application of the 2-stage process resulted in a well-integrated structure with ‘top’ regions demonstrating a significantly more open structure. This result was reinforced in the interconnectivity analysis

where the top region maintained high accessibility to a size of up to 50 µm diameter whilst the base region was only around 10% accessible to this largest theoretical sphere (*Figure 1*). However both structures were found to be highly accessible to particles of diameters similar to an MK (20-30 µm).

Micro-particle filtration experiments conversely suggested a high level of cell selection (*Figure 2*). Very few of the 20 µm particles were able to fully penetrate the scaffold structure, whilst approximately 60% of the 10 µm particles could be counted in the outlet flow. µCT of scaffolds after micro-particle filtration showed 20 µm particles to be well distributed through the scaffold structure – encouraging for MK distribution.

This theoretical analysis is a simplification. No account is taken of cell-substrate interactions, the ability of cells to change shape, the blocking of pathways by cells, generated extra-cellular matrix or high cell loiter times. However a similar analysis with platelets and megakaryocytes suggested micro-particle filtration to be a predictor of cell behaviour in the context discussed here.

Conclusion

A graded porous collagen material has been produced for *in vitro* platelet production and parent cell distribution and platelet release modelled using a simplified test system of sized beads and µCT simulation.

References

[1] MOREAU, T. et al. **Nature Communications**, (2016) v. 7, p. 11208, 2016.

[2] SHEPHERD, J. H., Howard D.H. et al. **Biomaterials,** (2018) v. 182, p. 135-144, 2018.

[3] DAVIDENKO, N. et al. **Acta Biomaterialia,** (2016) v. 25, p. 131-142, 2015.

Acknowledgement

The work was supported by the European Research Council [ERC Advanced Grant 320598 3D-E], EPSRC grant EP/N019938/1 and grants from the NHS Blood and Transplant, the Medical Research Council (MR/L022982/1) and the European Union (SilkFusion: AMD-767309-3).

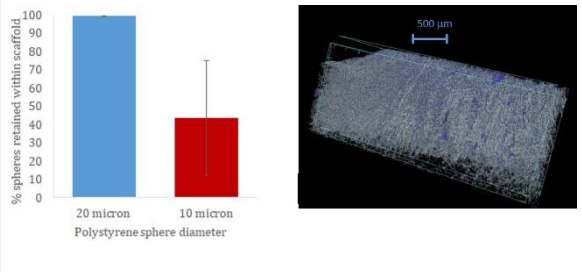

Figure 2: Micro-particle filtration
Figure 2: Micro-particle filtration experiments demonstrated a good degree of separation capability for MK and platelet analogues. MK sized particles were also observed to be uniformly distributed within the scaffold structure

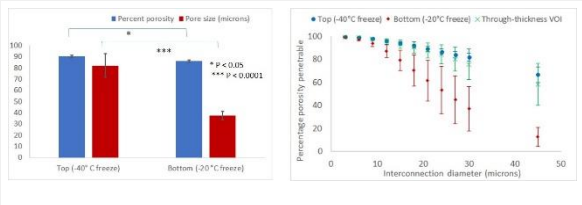

Figure 1: Porosity and Interconnectivity analysis
Figure 1: The more open and interconnected nature of the upper layer was demonstrated by pore size and interconnectivity analysis

I-OS2-02

Platelet Pro-angiogenic Factors or Hyaluronan Oligomers Promote Revascularization of Injectable Hydrogels Aiming Endodontic Regeneration

Pedro S. Babo[1,2], Cristiana R. Silva[1,2], Ana L. Silva[1,2], Rui M. A. Domingues[1,2,3], Rui L. Reis[1,2,3], Manuela E. Gomes[1,2,3]

[1]University of Minho, 3B's Research Group, I3Bs – Research Institute on Biomaterials, Biodegradables and Biomimetics, Barco - Guimarães, PT; [2]University of Minho, ICVS/3B's – PT Government Associate Laboratory, Braga/Guimarães, PT; [3]University of Minho, The Discoveries Centre for Regenerative and Precision Medicine, Barco - Guimarães, PT

Introduction

The revascularization of teeth subjected to endodontic treatment has been proposed as a mean to rescue teeth from mid-term pathology recurrence or extraction fate. Herein is explored the proangiogenic effect of platelet-origin mediators modulated release [1] or hyaluronan oligomers-coated [2] instructive cues in the vascularization of hydrogels aiming dentin-pulp complex regeneration.

Experimental Methods

Hyaluronic acid (HA) hydrogels incorporating PL were produced by mixing equal amounts of 2% aldehyde-modified HA solution containing aldehyde-functionalized cellulose nanocrystals (CNCs) with 2% hydrazide- functionalized HA dissolved in human platelet lysate (PL). The entrapment and release of PDGF and VEGF after incubation in culture medium or 2 U/mL hyaluronidase at 37ºC for up to 21 days was quantified by western blot and ELISA. The sprouting of human dental pulp cells (hDPCs) pellets or DPCs/HUVECs 1:1 pellets encapsulated in the HA hydrogels was followed during 3 days. The neovascularization promoted by the hydrogels was assessed in a chicken chorioallantoic membrane (CAM) assay.

Aldehyde-modified HA oligomers of low and high (6 kDa and 230 kDa; Lifecore) molecular weights were immobilized over methacrylated gelatin hydrogels (GelMA) surfaces, by Schiff's base reaction. The response of HUVECs to the HA oligomer coatings was analyzed in terms of viability, proliferation and network complexity.

Results and Discussion

Western blot analysis showed that the proangiogenic factors PDGF and VEGF remained stable inside the hydrogels up to 21 days in culture conditions. Their release was dependent on HA enzymatic degradation and the release kinetics was proportional with the amount of incorporated CNC ($p>0.05$). PL incorporation enhanced the sprouting of DPCs both in the single and co-cultures ($p>0.001$). Moreover, the combined effect of PL and DPCs encapsulation promoted the recruitment of CAM vasculature and the ingrowth of a vascularized pulp-like tissue into the hydrogels as soon as three days after implantation (Fig. 1). Moreover, the immobilization of low molecular weight HA oligomers over GelMA hydrogels has a significant effect on HUVECs. It enhanced the metabolic activity and promoted the organization into reticular structures of HUVECs seeded on its surface (Fig. 2). This could be further explored for the creation of instructive paths aiming the revascularization of hydrogels.

Conclusion

Overall, our findings show that both the incorporation of human-origin proangiogenic growth factors and the creation of instructive paths of HA oligomers within injectable hydrogels might promote the revascularization required for endodontic regeneration.

References

[1] Fortunato TM et al. Sci Rep. 2016;6(1):25326

[2] Slevin M et al. J Biol Chem. 2002;277(43):41046–59

Acknowledgement

Financial support from FCT (UTAP-ICDT/CTM-BIO/0023/2014; RMAD postdoc grant SFRH/BPD/112459/2015; P.S.B. postdoc grant from project PTDC/CTM-BIO/4706/2014-POCI-01-0145-FEDER 016716); and ERDF NORTE-01-0145-FEDER-000021. *Serviço de Imunohematologia*-CHSJ (Porto, Portugal) for the platelet concentrate batches.

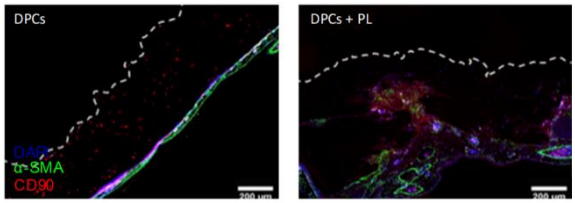

Fig 1. CAM response to HA hydrogels encapsulating DPCs or DPCs + PL

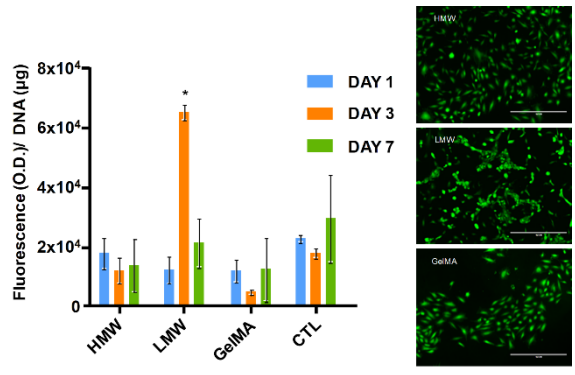

Fig 2. Response of HUVECs to HA oligomers-coated GelMA hydrogels
Metabolic activity per cell and Calcein/Propidium iodine stained HUVECs seeded over high (HMW) and low (LMW) molecular weight HA coated GelMA hydrogels after 7 days in culture (* $p<0.005$).

I-OS2-03

Eumelanin decorated polylactic acid electrospun substrates as new strategy for neurodegenerative diseases treatment

Ines Fasolino[1], Maria G. Raucci[1], Irene Bonadies[1], Alessandra Soriente[1], Alessandro Pezzella[2], Eva Carvalho[3], Ana P. Pêgo[3], Luigi Ambrosio[1]

[1]Institute of Polymers, Composites and Biomaterials, National Research Council (IPCB-CNR), Naples, IT; [2]Department of Chemical Sciences, University of Naples "Federico II", Naples, IT; [3]Instituto de Engenharia Biomédica (INEB) and i3S-Instituto de Investigação e Inovação em Saúde, Porto, PT

Introduction

The hallmark of neurodegenerative diseases is the loss of neuronal structure and function. Early stages of neural injury are characterized by a decreased neurotrasmission and an overexpression of inflammatory genes [1]. Current studies suggest natural and synthetic melanins show several biological and pharmacological properties, including photoprotective and immunological action. Specifically melanin antioxidant, anti-inflammatory, immunomodulatory, radioprotective benefits have only recently been recognized [2]. Here, the induction of neuroregenerative processes from 3D substrates based on eumelanin-coated PLA random and aligned microfibers were investigated.

Experimental Methods

3D electrospun substrates were prepared combining electrospinning, spin coating and solid-state polymerization processes [3]. 3D substrates characterization was performed by SEM analysis to study eumelanin coated microfiber orientation and integrity. In order to evaluate if the microfibers produce biological signals to direct the axonal growth cone to the distal stump, a pre-neuronal human derived cell line from neuroblastoma (SHSY5Y) was cultured onto the 3D electrospun substrates without the adding of any differentiating factor. Cell growth and differentiation on eumelanin microfibers were detected using Class-III β tubulin and GAP-43 expression, marker of differentiating neurons, by using confocal analysis. Additionally, to investigate microfibers antioxidant and antinflammatory potential, microglial cells that play a key role in neuronal homeostasis were seeded on the substrates. In detail, cell cultures based on microglial cells were stimulated with lipopolysaccharide (LPS), in order to reproduce an *in vitro* model of inflammation. The biological response in terms of antioxidant and antinflammatory activity [NF-kB and pro-inflammatory interleukins downregulation, nitrites and reactive oxygen species (ROS) inhibition, antinflammatory marker overexpression] was investigated. Furthermore, cell morphology by using SEM analysis and confocal analysis was assessed.

Results and Discussion

3D electrospun substrates represent a valid tool for reproducing more realistically 3D *in vivo* microenvironments thus promoting cell-cell interaction and biological response in terms of viability and differentiation [3]. Biological results showed that eumelanin microfibers support pre-neuronal cell survival, adhesion and the formation of neuritic processes (GAP-43 expression) over culture time. Recent findings indicate that neuromelanin may prevent CXCL10 expression through NF-κB inflammatory signaling inhibition [4]. Here, the results on neuroinflammatory response related to neural injury suggested that the microfibers inhibited nitrite production induced by LPS in microglia cells. Additionally, the microfibers were able also to decrease ROS levels and NF-κB expression thus confirming eumelanin antioxidant and antinflammatory properties. Furthermore, morphological studies (SEM and confocal microscopy) revealed that eumelanin microfibers were able to induce a good cellular spreading.

Conclusion

Our results show that eumelanin microfibers show promise as new therapeutic strategies for neurodegenerative diseases thanks to their ability to eliminate the need of differentiating factors in the media, in driving neuronal cell growth and maturation and through their capability to modulate neuroinflammation related to neurodegenerative disorders.

References

1. Huebner E. A., Strittmatter S.M. Results Probl Cell Differ. 48:339-51, 2009
2. ElObeid A.S. et al. Basic Clin Pharmacol Toxicol. 120:515-522. doi: 10.1111/bcpt.12748, 2017
3. Fasolino I. et al. ACS applied materials & interfaces 9:40070-76, 2017
4. Tousi N.S. et al. Neurosci Lett. 486:47-50, 2010

Acknowledgement

The study was supported by Progetto Premiale di Area Science Park “OPEN LAB - A System of Open Research Facilities”, Short Term Mobility (CNR) Program 2018 and project MECHANO (FCT, Portugal). The authors also thank Mrs. Cristina Del Barone of LAMEST laboratory for SEM investigations and Mrs Stefania Zeppetelli for supporting biological investigations.

I-OS2-04

Porous scaffolds with precise microarchitecture and spatiotemporal release properties prepared by a new bottom-up approach

Giuseppe Cesarelli[1,2], Aurelio Salerno[2], Paolo A. Netti[1,3]

[1]University of Naples, Department of Chemical, Materials and Production Engineering, Naples, IT; [2]Istituto Italiano di Tecnologia, Center for Advanced Biomaterials for Health Care - IIT@CRIB, Naples, IT; [3]University of Naples, Interdisciplinary Research Centre on Biomaterials, Naples, IT

Introduction

Bottom-up tissue engineering (TE) is one of the approaches that is catching on TE scientists' interest for the possibility to assembly multiple building blocks into highly complex architectures. An advantage of bottom-up TE is the opportunity to embed different biochemical cues within scaffolds while assembling modules. Accurate design of the entire 3D structure [1], biochemical cues localization [2] and temporal release kinetic [3] have been demonstrated to be an important feature for *in vitro* and *in vivo* scaffold-mediated tissue regeneration in many case studies. Nevertheless, there is still the need to provide a bottom-up approach enabling complex system design and fabrication considering those requisites all together.

In this context we show a new, bottom-up approach for fabricating 3D scaffolds with controlled microstructural properties, namely morphology, porosity, pore size distribution and mechanical properties, as well as spatiotemporal release capability of vascular endothelial growth factor (VEGF), for enhancing *in vitro* and *in vivo* vascularization.

Experimental Methods

Polymeric composite modules for drug release and polymeric layers suitable as structural elements were separately fabricated through different soft-lithography micromoulding processes. The processing steps to fabricate the different modules consisted in (1) mould CAD designing; (2) master fabrication by μ–milling machining; (3) polydimethylsiloxane (PDMS) replication of master features and (4) modules fabrication by soft lithography.

The structural layers were obtained from poly (ε-caprolactone) (PCL) discs (10 mm diameter and 0.6 mm thick) previously fabricated by compression moulding. The embossing process was carried out in a custom – made compression system into which neodymium magnets are placed in predefined positions to control compression force. The process was repeated until the complete removal of any residual layer, resulting in fully interconnected samples.

The drug releasing modules were designed to have an internal microparticles-sintered structure for VEGF loading and an external biodegradable shell made of gelatin that enables fast fluid penetration and promotes VEGF diffusion to the exterior. VEGF-loaded poly(lactic-co-glycolic acid) (PLGA) microparticles were fabricated by means of double water/oil/water emulsion and analysed to assess their morphology, size distribution, drug loading and release capability. Modules were assembled using an automatic micro-positioning apparatus that enabled drug releasing modules integration within well-defined PCL layers sites. Layers stacking and precise assembly enabled the achievement of the final scaffolds (Figure 1).

The as obtained scaffolds were characterized by scanning electron microscopy (SEM) and MicroCT techniques to assess their morphology, pore structure features and mechanical properties. VEGF release from scaffolds was determined by an enzyme-linked immunosorbent assay (ELISA). Scaffolds bioactivity was evaluated *in vitro* by endothelial cells adhesion and *in vivo* by means of rat subcutaneous implantation.

Results and Discussion

Melt moulding of PCL disks proved as an effective way to fabricate layers with desired geometrical and morphological features. In particular, the method was tested for the fabrication of 6.4 x 6.4 x 0.7 mm layers. Stereomicroscope and SEM characterization of such layers evidenced proper replica fidelity while MicroCT analysis demonstrated minor filling defects. Regarding VEGF delivery modules, the implemented approach enabled the achievement of excellent replica fidelity for the external shells (stereomicroscope and SEM) and their uniform filling with PLGA microparticles (mean particles diameter equal to 20 μm).

The ELISA assay indicated that VEGF encapsulation efficiency within microparticles was 40% and its release lasted more than 30 days. The automatic micro-positioning apparatus enabled the high–precision positioning of the drug delivery composite modules in the PCL layers avoiding microstructures modification (MicroCT image of Figure 1).

The as obtained scaffolds are biocompatible and promoted *in vitro* cell adhesion and blood vessels formation.

Conclusion

This paper presents a pilot study, based on bottom-up TE paradigm, that shows fabrication and integration of multiple building blocks with different functionalities to create a modular scaffold capable of VEGF spatiotemporal release. The originality of our solution lies in the fact that using the automatic micro-positioning apparatus it is possible to precise integrate at the microscale the two systems and achieve porous scaffolds with pre-defined microstructural properties and drug release behaviour to stimulate biological properties involved in the *in vitro* and *in vivo* new tissue genesis.

Acknowledgement

[1] Mata A et al (2009). Biomaterials (30).

[2] Akar B et al (2015). Biomaterials (72).

[3] Richardson TP et al (2001). Nature Biotechnology (19).

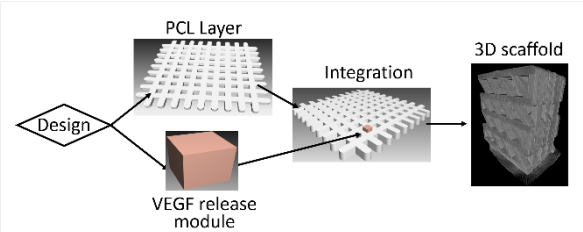

Figure 1: Bottom-up approach for 3D scaffolds preparation: process flowchart

I-OS2-05

3D nano fiber scaffolds for the generation of tissue models

Tobias Weigel[1], Tobias Schmitz[1], Kristina Andelovic[2], Maren Jannasch[1], Sebastian Schürlein[1], Jan Hansmann[1,3]

[1]University Hospital Würzburg, Tissue Engineering and Regenerative Medicine, Würzburg, DE; [2]University Hospital Würzburg, Experimental Biomedicine, Würzburg, DE; [3]Fraunhofer ISC, Translational Center Regenerative Therapies, Würzburg, DE

Introduction

Besides cellular components, the scaffold represents a main building block in the generation of tissue models. Often applied are animal derived materials like decellularized matrices[1] or hydrogels[2] with collagen as example. To replace these with synthetic materials nano fiber scaffolds are developed, which allow cell migration and proliferation in the complete scaffold as well as the biologization of this matrix by its own proteins and extracellular matrix. The combination of different cell types and a stepwise setup for the tissues allows the generation of several complex tissue models.

Experimental Methods

Materials for the development of 3D nano fiber scaffolds were polycaprolacton (PCL) as a degradable material, and polyamide 6 as a non-degradable material. The scaffolds were generated by electrospinning of the concerning polymer solutions (PCL: 12 %; PA6: 10 % in HFP) additional to strewing of NaCl particles during the spinning process to extent the fiber mesh and to introduce pores into the fiber fleece. Cell compatibility and migration into the scaffolds as well as the ECM formation was evaluated with several cell types like hdFs, SMCs and MSCs. Stacking of seeded scaffolds as well as the cell differentiation resulted in tissue models on a synthetic base.

Results and Discussion

The structural composition of the scaffolds was characterized by SEM and LSM. Thereby, the PCL scaffold showed with a fiber diameter of around 700 nm an increased size in mesh openings as the PA6 scaffold with a fiber diameter of around 400 nm. When seeding with fibroblasts, the more extended network of the PCL scaffold provided a faster cell migration as well as an increased ECM synthesis. On the other hand, the denser network of the PA6 scaffold formed a more tissue like morphology. The differentiation of MSCs to adipose cells in co-culture with fibroblasts and keratinocytes is able to form three-layered skin models, which were characterised by histology and imunhistology.
When combining the developed extended fiber meshes with standard spun dense membranes, barrier models like endothelium in co-culture with tissue cells are developed.
Concerning further applications, additional cell types and co-cultures are tested on the extended electrospun matrices to classify the application range of potential tissue models.

Conclusion

As a proof of concept, the generated tissue models showed the applicability of highly porous electrospun scaffolds for soft tissue engineering. Ongoing characterizations and scaffold modifications will classify the field of adaptable engineered tissues.

References

1. Porzionato A. et al., International Journal of Molecular Sciences, 19, 4117, 2018.
2. Xiong S. et al., Scientific Reports, 7:4288, 2017.

Acknowledgement

The work was funded by the German Federal Ministry of Education and Research; program NanoMatFutur; grant agreement number 13N12971 – ETface.

I-OS2-RF06

Electrospun biopolymeric patterned structures to support ovarian follicles growth: fabrication and characterization

Liliana Liverani[1], Nathalie Raffel[2], Amir Fattahi[2], Inge Hoffmann[2], Matthias W. Beckmann[2], Ralf Dittrich[2], Aldo R. Boccaccini[1]

[1]Institute of Biomaterials, Department of Materials Science and Engineering, University of Erlangen-Nuremberg, Erlangen, DE; [2]Department of Obstetrics and Gynecology, Erlangen University Hospital, Friedrich Alexander University of Erlangen–Nuremberg, Comprehensive Cancer Center ER-EMN, Erlangen, DE

Introduction

The application of tissue engineering in the field of reproductive organs repair is attracting the interest of the scientific community (1). Several biomaterials have been considered to mimic three-dimensional culture systems of ovarian follicles, but in most cases they were unsuitable to warrant follicles development (2). Recently, scaffold fabrication techniques, like 3D printing were applied for the development of constructs suitable to host follicles, leading to the birth of pups in mouse model (3). On this basis, the present work is based on the application of the electrospinning technique as convenient alternative to obtain patterned macroporous scaffolds able to mimic the morphology of native ovarian cortex and suitable for follicles adhesion and growth (4).

Experimental Methods

Neat poly(epsilon caprolactone) (PCL) and its blend with gelatin (type A) (PCL/gel) were used for the fabrication of electrospun scaffolds. Glacial acetic acid and formic acid were selected as benign solvents. The electrospinning process was performed by using a commercial device EC-CLI (IME Medical Electrospinning) with climate chamber in which temperature and relative humidity were set at 25°C and 25%, respectively. The optimized process parameters were: 15kV applied voltage, 11cm distance tip-collector, 23G needle diameter, while the solution flow rate was 0.4mL/h for neat PCL and 0.6 mL/h for the blend. SEM and FTIR analyses were performed on the obtained scaffolds. Porcine ovarian follicles were isolated enzymatically from ovarian tissue pieces (collected from slaughterhouse, registration number DE09562003821) and incubated for 10 days on the scaffolds. After incubation, follicle viability was evaluated via Live/Dead assay and follicle morphology was investigated by fluorescent f-actin staining and SEM analysis.

Results and Discussion

The scaffolds´ morphology and macroporous structure were assessed and macroporosity with an average pore size of 0.3 mm was obtained. After 10 days of culture, the number of viable follicles (= >99% granulosa cells alive) was 76.64% for PCL and 90.21% on the PCL/gel samples. Even if both PCL and PCL/gel electrospun scaffolds showed positive results in terms of reduced follicles loss during the seeding and follicles survival, PCL/gel mats led to better results in terms of preservation of follicles spheroidal shape and higher number of adhesion points with the electrospun mats.

Conclusion

In the emerging field of reproductive tissue regeneration, patterned fibrous scaffolds obtained by electrospinning of PCL/gel represent a promising technology which warrants further research.

References

1. Amorim CA. Special Issue Devoted to a New Field of Regenerative Medicine: Reproductive Tissue Engineering. Ann Biomed Eng [Internet]. Springer US; 2017 Jul 31 [cited 2018 Apr 6];45(7):1589–91. Available from: http://link.springer.com/10.1007/s10439-017-1862-0

2. Brito IR, Lima IM, Xu M, Shea LD. Three-dimensional systems for in vitro follicular culture : overview of alginate-based matrices. Reprod Fertil Dev. 2014;26(7):915–30.

3. Laronda MM, Rutz AL, Xiao S, Whelan KA, Duncan FE, Roth EW, et al. A bioprosthetic ovary created using 3D printed microporous scaffolds restores ovarian function in sterilized mice. Nat Commun [Internet]. Nature Publishing Group; 2017 May 16 [cited 2017 Oct 10];8:15261. Available from: http://www.nature.com/doifinder/10.1038/ncomms15261

4.Liverani L, Raffel N, Fattahi A, Preis A, Hoffmann I, Boccaccini AR, et al. Electrospun patterned porous scaffolds for the support of ovarian follicles growth: a feasibility study. Sci Rep. 2019;9:1150.

I-OS2-RF07

Fiber-based structures lead to superior mechanical properties in 3D hydrogel systems

Ronny Brünler, Dilbar Aibibu, Chokri Cherif

TU Dresden, Institute of Textile Machinery and High Performance Material Technology, Dresden, DE

Introduction

Hydrogels and Bioinks are promising substances for realizing three dimensional structures for tissue engineering or organ-on-a-chip systems [1]. They may contain living cells and thus have to be deposited at suitable temperatures and renouncing cell damaging cross-linking or hardening processes which occur e.g. in many 3D printing approaches [2]. The viscosity of such hydrogel or bioink systems has to be precisely adjusted to allow cell migration, growth and forming of networks and at the same time avoiding cell immobilization or gravity-driven cell sinking due to unfavorable ratios between the traction forces of the cells and the stability of the hydrogel system. The overall low viscosity and high water content of the (hydro)gel-based materials results in very low strength, dimensional stability and geometric integrity [3].

Fiber-reinforced composites (FRC) are well established in multiple applications for lightweight construction, mechanical and civil engineering, transport and many more [4]. The overall mechanical strength of FRCs may exceed the strength of the matrix material manifold. Since the native structure of the four most important tissue types (connective and supporting tissue, nerve, muscle and epithelial tissue), from which organs such as bones, blood vessels, muscles, tendons and ligaments are formed, consists of fibrous constructs and thus can be reproduced biomimetically with textile structures with particularly high precision [5]. Three-dimensional, complex geometries with interconnecting pore spaces can be created with the help of pre-considered fiber layouts [6–8]. Based on these findings, a novel approach for the combination of hydrogels as matrix system and fiber-based systems as reinforcement structure is presented.

Experimental Methods

Multiple materials such as the biocompatible thermoplastics PCL or PES and the biopolymers chitosan or silk fibroin were processed into fibers with different demand-oriented properties by using spinning plants for melt-spinning and solution spinning. The fibers with adjustable properties were subsequently manufactured into multiple three-dimensional structures by weaving, knitting, warp-knitting, braiding and fiber-based additive manufacturing processes.

The complex fiber-based constructs were infiltrated with polysaccharide hydrogels to serve as reinforcing systems for 3D-hydrogel systems and were extensively investigated with regard to their mechanical behavior.

Results and Discussion

Unique fiber-based structures with specifically adapted geometries, pore-sizes and morphologies were realized and infiltrated with hydrogels. The mechanical behavior was tested under static and cyclic compression and tensile loading.

In comparison to the hydrogels alone, the mechanical strength of the novel fiber reinforced 3D-hydrogel structures was increased manifold. Seeded cells align according to the fiber orientation within the structures that provide excellent overall conditions for cell adhesion and differentiation.

Conclusion

A broad range of biocompatible materials can be processed into fibers via melt spinning and solution spinning. Due to the extraordinary ratio between surface and volume fiber-based structures are predestined for use in medical products by providing large functional surfaces for cell adhesion and interaction on interfaces. The developed textile scaffolds and implants exhibit an excellent strength and offer large, interconnected pore spaces for cells to migrate into the structures and for nutrients to supply the cells or metabolic waste to be removed, respectively. The fibers serve as guidance structure for cells according to their growth direction and also take up the mechanical loads. The wide range of textile technologies allows realizing patient-specific, load-adapted scaffolds and implants for regenerative medicine, mimicking the natural tissue that is to be supported or replaced.

References

[1] Caló, E.; Khutoryanskiy, V. V.: Biomedical applications of hydrogels: A review of patents and commercial products. In: European Polymer Journal 65 (2015), pp 252–267

[2] Chimene, D.; Lennox, K. K.; Kaunas, R. R. et al: Advanced Bioinks for 3D Printing: A Materials Science Perspective. In: Annals of Biomedical Engineering 44 (2016) 6, pp 2090–2102

[3] Ahmed, E. M.: Hydrogel: Preparation, characterization, and applications: A review. In: Journal of Advanced Research 6 (2015) 2, pp 105–121

[4] Cherif, Ch.: Textile materials for lightweight constructions: Technologies - methods - materials - properties. Springer 2011

[5] Wintermantel, E.; Ha, Suk-Woo: Medizintechnik - Life Science Engineering. Springer, 2009

[6] Brünler, R.; Aibibu, D.; Wöltje, M. et al: In silico modeling of structural and porosity properties of additive manufactured implants for regenerative medicine. In: Materials Science and Engineering: C 76 (2017), pp 810–817

[7] Brünler, R.; Hild, M.; Aibibu, D.; Cherif, C.: Fiber-based hybrid structures as scaffolds and implants for regenerative medicine. In: Koncar, V.: Smart Textiles and their Applications. Elsevier, 2016, pp 241–256

[8] Aibibu, D.; Hild, M.; Wöltje, M.; Cherif, Ch.: Textile cell-free scaffolds for in situ tissue engineering applications. In: Journal of Materials Science: Materials in Medicine 27 (2016) 63

I-OS2-RF08

Effect of Conventional Self-Assembled Molecules with Different Functional Groups on Cardiac Differentiation of Induced Pluripotent Stem Cells

Ozgen Ozturk-Oncel[1], Carlos Heras-Bautista[2], Lokman Uzun[3], Deniz Hür[4], Kurt Pfannkuche[2], Bora Garipcan[1]

[1]Boğaziçi University, Biomedical Engineering, İstanbul, TR; [2]University of Cologne, Neurophysiology, Cologne, DE; [3]Hacettepe University, Biochemistry, Ankara, TR; [4]Eskisehir Technical University, Chemistry, Eskişehir, TR

Introduction

Surface chemical modification plays an important role in regulating cellular behavior, in vitro. Recent studies showed that functional groups on biomaterial surfaces regulate cellular adhesion, migration, proliferation and differentiation [1,2]. Self-assembled molecules (SAMs) form organized structures and with these molecules, desired surface properties can be easily generated.

In the present study, we aimed to prepare polydimethylsiloxane (PDMS) substrates in natural myocardium-like stiffness range [3] and investigate the effect of their surface modifications with SAMs, having two functional end groups (-CH_3 and –NH_2) and different wettability properties, on cardiac differentiation of murine induced pluripotent stem cells (mIPS, TαP4).

Experimental Methods

PDMS (Sylgard 184, DOWSIL) substrates were prepared with different ratios of silicone elastomer base and curing agent (10:1 – 70:1) and spin coated (Brewer Science, CEE 200X) on glass slides. Substrates were cured for a week at 60°C. Young's moduli of substrates were characterized with nanoindentation (Optics 11).

Next, hydroxyl groups were created on substrate surfaces by using oxygen plasma treatment (Nordson March Plasma Systems) for 1 min, followed by dipping into 1% concentrations of either 3-Aminopropoyl triethoxy silane (APTES, Sigma) for -NH_2 end groups or Trimethoxy (octadecyl) silane for –CH_3 end groups. Characterizations of these modified substrates were done by water contact angle measurements (WCA) and X-Ray ray photoelectron spectroscopy analysis (XPS, Thermo Scientific K-Alpha).

mIPS cells were cultured and differentiated into cardiomyoctes on native and SAMs modified PDMS substrates by using a previously published protocol [4]. Cell viability (3-[4,5-dimethylthiazol-2-yl]-2,5-diphenyltetrazolium bromide, MTT) and Western Blot (Bio-Rad) analysis were performed.

Results and Discussion

According to nanoindentation results with different silicone elastomer base crosslinker concentrations of PDMS, the ratio of 50:1 was found to be in natural myocardium-like stiffness range with a Young's modulus of 26.42 ± 6 kPa.

In low resolution XPS survey spectra of all unmodified and modified PDMS, four characteristic peaks were found as O1s, C1s, Si2s and Si2p at 533, 286, 155 and 104 eV, respectively. -CH_3 functionalization of PDMS substrates lead to a remarkable increase in the carbon peak, due to high carbon content of the molecule, whereas N1s peak appeared after modifications with APTES at 401 eV. WCA analysis showed hydrophobic nature of native and –CH_3 modified PDMS (104.1±5 and 112.7±5, respectively) and hydrophilic properties of –NH_2 modified PDMS (61.9±4).

MTT analysis of mIPS cells on these substrates showed no statistical difference between SAMs modified PDMS. Both modified substrates showed higher viability when compared to native PDMS ($p<0.05$). Western blot analysis results were given in Fig.1 on day 12 of differentiation. Similar to viability analysis, both functional end groups enhanced cardiac differentiation significantly, when compared to native PDMS. Cardiac marker Troponin-T (Sc-20025) expressions were higher in hydrophilic -NH_2 groups.

Conclusion

Conventional SAMs modified PDMS substrates in myocardium-like stiffness range were confirmed to be nontoxic to mIPS cells and also these modifications enhanced cardiac differentiation of mIPS cells on PDMS substrates.

References

1. Cao, B. *et al.* (2017) 'Effects of Functional Groups of Materials on Nonspecific Adhesion and Chondrogenic Induction of Mesenchymal Stem Cells on Free and Micropatterned Surfaces', *ACS Applied Materials & Interfaces*, 9(28), pp. 23574–23585.

2. Hasan, A. *et al*. (2018) 'Effect of Functional Groups of Self-Assembled Monolayers on Protein Adsorption and Initial Cell Adhesion', *ACS Biomaterials Science & Engineering*. American Chemical Society, 4(9), pp. 3224–3233.

3. Berry, M. F. *et al.* (2006) 'Mesenchymal stem cell injection after myocardial infarction improves myocardial compliance', *American Journal of Physiology-Heart and Circulatory Physiology*. American Physiological Society, 290(6), pp. H2196–H2203.

4. Heras-Bautista, C.O. *et al*. (2014) 'The influence of physiological matrix conditions on permanent culture of induced pluripotent stem cell-derived cardiomyocytes', *Biomaterials,*35, pp. 7374–7385.

Acknowledgement

This study was supported by TUBITAK (Project number: 113T026).

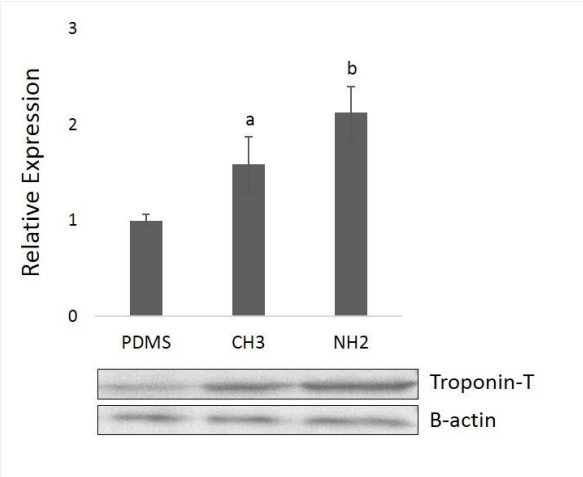

Western blot analysis results.
[a] p<0,05 significantly different from PDMS;
[b] p<0,01 significantly different from PDMS.

10:30 a.m. – 12:00 p.m.

Hall 4

I-SY1 | Bioactive glasses: from the laboratory to the clinic

Aldo R. Boccaccini (Erlangen, DE)
Delia Brauer (Jena, DE)

The biomaterial “bioactive glass” celebrates this year its first 50 years since its invention by Prof. Larry Hench in 1969. The special symposium at ESB 2019 is organized to highlight the current status in the broad field of bioactive glasses, both from the fundamental and application viewpoints. Indeed, over the last 50 years, bioactive glasses, originally intended for applications as bone substituting materials and small orthopedic implants, have expanded in their functionalities and applications. Novel chemical compositions and advanced processing techniques pave the way to a great variety of medical applications, including biomedical coatings, dental care, scaffolds for tissue engineering, advanced drug delivery devices, wound healing, soft tissue repair and cancer treatment. Various applications of bioactive glasses will be presented and discussed in this special symposium.

I-SY1-KL01

Bouncy Bioglass for Cartilage and Bone Regeneration

Julian R. Jones

Imperial College London, Department of Materials, London, GB

Introduction

Bioglass® has now been used in more than 1.5 million patients as a synthetic bone graft (e.g. NovaBone®, NovaBone Products LLC, FL). It has outperformed other bioactive ceramics in comparative in vivo studies and regulatory claims of “osteostimulaton” (NovaBone) and antimicrobial properties (BonAlive) show the acceptance that it is the ions that they release that provide added bioactivity. Bioglass’ potential for bone regeneration is limited because it is only available as a particulate or putty[1]. Only now are Bioglass scaffolds reaching clinical use (Bio2 Technologies), but they remain brittle. For bone regeneration, we need materials that can maintain the biological properties of Bioglass but can take cyclic loads and biodegrade at a controlled rate. No materials can currently regenerate articular cartilage.

Experimental Methods

We have developed sol-gel hybrids of covalently bonded co-networks of degradable polymers and bioactive silica. The hybrid acts as a single material with tailored mechanical properties and congruent degradation[2]. Sol-gel hybrids can be 3D extrusion printed to obtain porous scaffolds with regular and reproducible architecture that can be tuned in order to match the desired requirements. Herein, I will report on our covalently-linked silica/polycaprolactone (SiO_2/PCL) hybrid material for regeneration of articular cartilage focal defects. The device is composed of a 3D printed porous scaffold capped with a dense thin layer of the same material: while the scaffold is intended to be fixed into the defect and promote cartilage regeneration, the cap should have optimised tribological properties to ensure low friction in contact with the opposing cartilage.

Hybrid Challenges

The chemistry and processing is complex to create a successful bioactive hybrid. Challenges to overcome are: creating a porous structure while controlling degradation rate and mechanical properties. Critical to the success of the hybrids is achieving mechanical properties and controlled congruent degradation. This can only be achieved by synthesising hybrids that have covalent coupling between the co-networks.

Hybrids of Synthetic Polymers

SiO_2/PCL hybrids with glycidyloxypropyltrimethoxy-silane (GTPMS) as the coupling agent have unprecedented mechanical properties, including elastic recovery and the ability to bounce or be hit by a hammer. Scaffolds can be directly printed through extrusion printing (Fig. 1). Chondrocytes seeded on 3D printed scaffolds demonstrated chondrogenic differentiation and cartilaginous matrix formation in vitro, showing positive staining for Collagen Type II, indicative of articular cartilage. Bone marrow stem cells seeded in the scaffolds also differentiate and produce Type II collagen. In vivo subcutaneous implantation in mice showed minimal inflammatory response (similar to sham). Bespoke synthetic polymers can be synthesised with the coupling agents built in through controlled polymerisation, e.g. acrylate based polymers containing links of TMSPMA, spacer monomers and biodegradable linkers. Degree of branching and architecture (star v linear v branched) has a large effect on mechanical properties.

Conclusion

Hybrids have the potential to combine bioactivity of bioactive glasses with controlled degradation and mechanical properties. They have potential in bone and cartilage regeneration.

References

1. Jones J.R. Brauer D.S. Hupa L. Greenspan D.S. Int J Appl Glasses: 2016:7: 423-434.
2. Jones J.R., Acta Biomater. 9:4457-4486, 2013.
3. Tallia F. et al. Materials Horizons, 2018, 5, 849-860.
4. Chung J. et al. Acta Biomaterialia, 2017: 54: 411-418

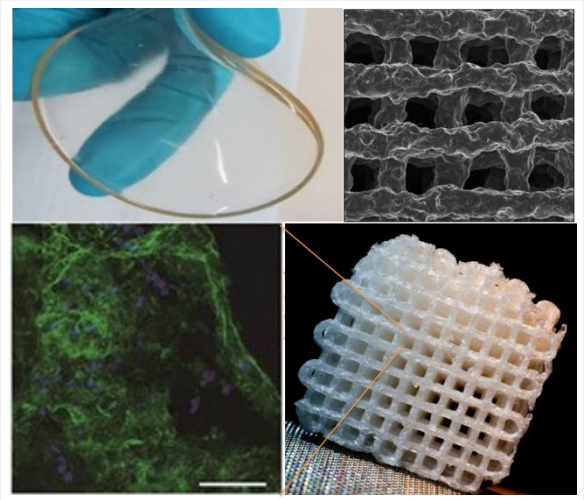

Bouncy bioglass can be printed and stimulate type II collagen production
Clockwise: Flexible silica/PCL hybrids; SEM & photo of a 3D printed hybrid; Col II matrix in a pore produced by chondrocytes

I-SY1-KL02

Bioactive glass: from the laboratory to the clinic

Nina Lindfors, Robert Björkenheim, Gustav Strömberg, Jukka Pajarinen, Elin Eriksson

Helsinki University, Helsinki University Hospital, Helsinki, FI

Introduction

Bioactive glasses (BAGs) are bone substitutes with proven osteoconductive, osteostimulative, angiogenetic and antibacterial properties. Implanted in the body a rapid exchange of Na^+ from the glass and H^+ and H_3O^- from the solution takes place, forming silanol groups and a SiO_2-layer at the glass surface. Migration of Ca^{2+} and PO_4^{3-} to the surface of the BAG results in a CaO-P_2O_5-rich layer on top of the silica-layer. Subsequent protein adsorption and chemical bonding of apatite crystallites around collagen fibrils finally then form a bond between the BAG and the surrounding bone.

Bone formation and fracture healing is a highly regulated process involving several factors e.g. the mechanical environment, inflammatory and osteogenic cells, vascular and inflammatory mediators and when needed an osteogenic scaffold.

Experimental Methods

Clinically e.g. BAG-S53P4 granules have been used in benign tumor surgery, head and neck- spine and neurosurgery and in the treatment of osteomyelitis. Osteomyelitis is an infectious process that leads to bone destruction. Surgical procedures are often performed in combination with systemic and local antibiotics using a two-stage procedure, in which autograft or synthetic bone is used for filling the bone defect. In a multinational study involving six countries and eleven centers, 116 patients with verified chronic osteomyelitis were treated using antibacterial BAG-S53P4 granules as part of the treatment. The success rate was 90%. The study showed that BAG-S53P4 granules could be used in a one-stage procedure with excellent results.

Results and Discussion

The iv-vivo behavior of BAGs is also dependent on the manufacturing process. By developing the sintering process of BAG-S53P4, new stable scaffolds have been manufactured and designed for a single-stage induced membrane technique. Expressions of BMP and VEGF induced by BAG-S53P4 and PLGA coating, as well as, new bone formation have been observed iv-vivo, implying promising preclinical results.

Conclusion

Preclinical and clinical results of BAG-S53P4 support the use of BAG-S53P4 as bone graft subsitute in the treatment of bone defects, as well as in the treatment of infected bone.

References

1. Hench LL. The story of Bioglass. J Mater Sci: Mater Med 2006;17:967–978.
2. Lindfors NC, Heikkilä J, Koski I, Mattila K, Aho J. Bioactive glass and autogenous bone as bone graft substitutes in benign bone tumors. J Biomed Mater Res 2008;90B:131-136.

3. Rantakokko J, Frantzen J, Heinänen J, Kajander S, Kotilainen E, Gullichsen E, Lindfors NC. Posterolateral spondylodesis using bioactive glass S53P4 and autogenous bone in instrumented unstable lumbar spine burst fracture – A prospective 10-year follow-up study. Scand J Surg 2012;101:66-71.
4. Frantzen J, Rantakokko J, Aro HT, Kajander S, Koski I, Gullichsen E, Kotilainen E, Lindfors NC. Instrumented spondylodesis in degenerative spondylolisthesis with bioactive glass and autologous bone – A prospective 11-year follow-up. J Spinal Disord Tech 2011;24:455-461.
5. Lindfors NC, Hyvönen P, Nyyssönen M, Kirjavainen M, Kankare J, Gullichsen E, Salo J. Bioactive glass S53P4 as bone graft substitute in treatment of osteomyelitis. Bone 2010;47:212-218.
6. Lindfors NC, Geurts J, Drago L, Arts JJ, Juutilainen V, Hyvönen P, Suda AJ, Aloj, D, Artiaco S, Alizadeh Ch, Brychcy A, Bialecki J, Romano` C. Bioactive glass S53P4 in the treatment of osteomyelitis – a multinational study. Adv Exp Med Biol 2017;971:81-92.
7. Björkenheim R, Strömberg G, Pajarinen J, Ainola M, Uppstu P, Hupa L, Böhling TO, Lindfors NC. Polymer coated bioactive glass S53P4 increases VEGF and TNF expression in an induced membrane model in vivo. J Mater Sci 2017;52:9055-9065.
8. Björkenheim R, Strömberg G, Ainola M, Uppstu P, Aalto-Setälä L, Hupa L, Pajarinen J, Lindfors NC. BMP expression and bone formation are induced by bioactive glass S53P4 scaffolds in vivo. J Biomed Mater Res Part B Appl B 2018;11:45

I-SY1-03

Development and characterization of B and Co ions co-doped 45S5 bioactive glass for possible use in angiogenesis

Si Chen[1], Martin Michálek[1], Dagmar Galusková[2], Monika Michálková[2], Peter Švančárek[2], Ali Talimian[2], Hana Kaňková[1], Jozef Kraxner[1], Liliana Liverani[3], Dušan Galusek[2], Aldo R. Boccaccini[3]

[1]TnU AD, Centre for Functional and Surface Functionalized Glass, Trenčín, SK; [2]TnU AD, Joint Glass Centre of the IIC SAS, TnU AD and FChFT STU, Centre for Functional and Surface Functionalized Glass, Trenčín, SK; [3]University of Erlangen-Nuremberg, Institute of Biomaterials, Erlangen, DE

Introduction

In the past decade, boron (B) has been increasingly used in bioactive materials to promote angiogenesis, exhibiting positive effect on neovascularization [1]. B potently activates the MAPK signaling pathway and borate co-transporter to markedly increase vascular endothelial cells (VECs) proliferation and migration. Addition of B also enhances VECs tubule formation and secretion of IL-6 and bFGF, which also stimulate the angiogenic response. Cobalt (Co) as an essential element in human physiology can also promote angiogenesis, albeit in a different way [2]. Hypoxia (low oxygen pressure) in vivo plays a pivotal role in coupling angiogenesis with osteogenesis via progenitor cell recruitment, differentiation and angiogenesis. Hypoxia activates a series of angiogenic processes mediated by the hypoxia inducing factor-1α (HIF-1α). Hypoxia can be mimicked by stabilizing HIF-1α expression. Co2+ ion is a well-established chemical inducer of HIF-1α, which elicits a significant hypoxic cascade including VEGF secretion, identified as a key regulator in angiogenesis.

The incorporation of biologically active ions in bioactive glasses is being increasingly considered to enhance the angiogenic effect of these materials [3]. In this study, both B and Co were used as dopants in a 45S5 bioactive glass in order to promote angiogenesis by two different mechanisms (Fig. 1).

Experimental Methods

B (2 wt% and 10 wt% B2O3) and Co (2 wt% and 4 wt% CoO) were added into 45S5 bioactive glass, either alone, or in conjunction, replacing Si partially. The glass was prepared by conventional melt quenching method. The samples with different compositions were respectively denoted as BG, BG.2B, BG.10B, BG.2Co, BG.4Co, BG.2B2Co, BG.2B4Co, BG.10B2Co and BG.10B4Co.

The composition of the bioactive glasses (BGs) was characterized by Fourier transform infrared spectroscopy (FTIR, Shimadzu IRAffinity-1S), energy-dispersive X-ray spectroscopy (EDX; Scanning Electron Microscope JEOL JSM-7600 F/EDS/WDS/EBSD) and inductively coupled plasma-optical emission spectrometry (ICP-OES; Agilent 5100 SVDV ICP OES). The release of Si, P, Ca, B and Co ions from the BGs powder (less than 25 μm) was also determined by ICP-OES using simulated body fluid (SBF) as immersion medium for 1, 3 and 7 days. Afterwards, the solution was centrifugated and filtrated, and the ionic dissolution products (IDPs) were measured by ICP-OES. After immersion, the samples were examined by scanning electron microscopy (SEM; Scanning Electron Microscope JEOL JSM-7600 F/EDS/WDS/EBSD) and X-ray diffraction (XRD; X-ray powder diffractometer Panalytical Empyrean DY1098).

Results and Discussion

The results of BG.2B2Co and BG.10B4Co were selected to demonstrate B and Co doping in the 45S5 BG. Fig. 2A confirms the presence and homogeneous distribution of all elements (Si, Na, P, Ca, B and Co) in the BG.2B2Co and BG.10B4Co samples. The compositions determined by ICP were almost identical to the designed compositions (Fig.

2B). FTIR spectra of BGs before/after immersion in SBF are shown in Fig. 2C. The main absorption bands of BGs before immersion are assigned to: 1479 cm-1 (CO32- v3), 1396 cm-1 (vB-O of BO3), 1188 cm-1 (vB-O of BO4), 1100-900 cm-1 (Si-O-Si and phosphate), 866 cm-1 (CO32- v2), 732 cm-1(O-P-O), 472 cm-1 (Si-O-Si). After immersion in SBF for 7 days, four feature absorption bands of hydroxyapatite (HA) at 962 cm-1 (PO43- v1), 447 cm-1 (PO43- v2), 1022 cm-1 (PO43- v3) and 560-600 cm-1 (PO43- v4) were identified. The results of XRD (Fig. 2D) also confirmed the presence of HA through two observed diffraction lines attributed to HA phase at 2θ=32° (khl=211) and 2θ=26° (khl=002). Before immersion both tested glasses were amorphous. The crystals of HA can be directly observed in Fig. 2E. A burst release of all measured elements during the first day is indicated in Fig. 2F, which almost levelled out afterwards. And it can be observed that different composite of B and Co successfully caused significant different release of B and Co.

Conclusion

In this study, B and Co ions were successfully and homogeneously doped into 45S5 bioactive glass. The compositions measured by ICP were almost identical to the designed compositions, and different release behaviour of B and Co was found. Both BG.2B2Co and BG.10B4Co could induce the production of HA on the surface of BG particles upon immersion in SBF. Presented results would lead to better understanding of the possible synergistic effect of B and Co on angiogenesis.

References

[1] Durand L A H, Vargas G E, Romero N M, et al. Angiogenic effects of ionic dissolution products released from a boron-doped 45S5 bioactive glass[J]. Journal of Materials Chemistry B, 2015, 3(6): 1142-1148.
[2] Hu X, Yu S P, Fraser J L, et al. Transplantation of hypoxia-preconditioned mesenchymal stem cells improves infarcted heart function via enhanced survival of implanted cells and angiogenesis[J]. The Journal of thoracic and cardiovascular surgery, 2008, 135(4): 799-808.
[3] Hoppe A, Güldal N S, Boccaccini A R. A review of the biological response to ionic dissolution products from bioactive glasses and glass-ceramics[J]. Biomaterials, 2011, 32(11): 2757-2774.

Acknowledgement

This paper is created in the frame of the project FunGlass that has received funding from the European Union´s Horizon 2020 research and innovation programme under grant agreement No 739566. And the financial support of this work by the funding from the grant VEGA 2/0026/17 and APVV 15/0014 are gratefully acknowledged.

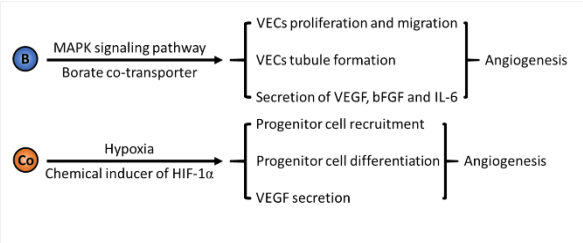

Figure 1.
The mechanisms of promoting angiogenesis through addition of boron and cobalt to bioactive glasses.

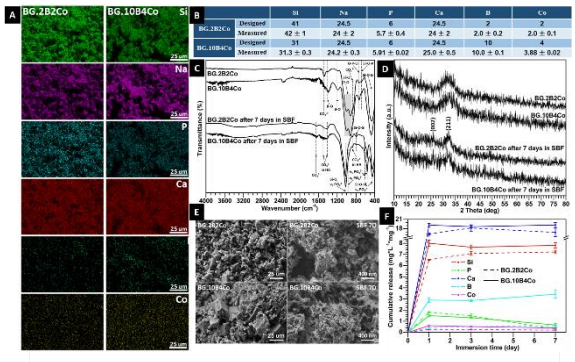

Figure 2.
The results of material characterization of BG.2B2Co and BG.10B4Co.

I-SY1-04

Oxyfluorophosphate bioactive glasses and glass-ceramics

Amy Nommeots-Nomm[1], Amel Houaoui[2], Laeticia Petit[3], Emmanuel Pauthe[2], Michel Boissière[2], **Jonathan Massera**[1]

[1]Tampere University, Faculty of Medicine and Health Technology, Tampere, FI; [2]Université de Cergy-Pontoise, Equipe de Recherche sur les Relations Matrice Extracellulaire-Cellules, Cergy, FR; [3]Tampere University, Photonics Laboratory, Tamnpere, FI

Introduction

Fluoride containing bioactive glasses have attracted much interest in dental and orthopedic application, pertaining to their ability to precipitate fluorapatite rather than hydroxyapatite. Indeed, fluorapatite is more stable and chemically resistant than hydroxyapatite and is less sensitive to resorption in-vivo. However, introducing fluoride in silicate based bioactive glasses was found to lead to an increase in the silica network connectivity and lack of Si-F bonds, in turns leading to a decrease in the glass bioactivity. The consequence of a lower bioactivity is the formation of inhomogeneous hydroxyapatite and silica-rich layer at the glass particle surface. Alternatives are the phosphate glasses. Invert phosphate glasses (up to the metaphosphate) have been found to be bioactive. However, little is known on the impact of Fluorine on the in-vitro dissolution properties and their interaction with cells.

Experimental Methods

Glass within the $75NaPO_3$-(25-x)CaO-xCaF_2, with from 0 to 20, were processed by melt quenching. The structure of the glasses was investigated by Raman, FTIR and NMR in order to assess the role played by the F ions in the glass network. The thermal properties were measured using a DTA. Based on the DTA measurement, a series of heat treatment were performed to produce glass-ceramics. The in-vitro dissolution of the glasses and glass-ceramics produced was tested in TRIS buffer solution. Ion released in solution was quantified by ICP-OES. The index of cytotoxicity (IC_{50}) was assessed using MC3T3-E1 cells cultured in extract. Live/dead, cytoplasmic nuclear ratios as well as cell proliferation, upon cell exposure to the glass extract was also evaluated

Results and Discussion

With increasing fluorine content an increase of the P-F bond is reported. The structural changes, associated to the increase in F ions, leads to an increase in dissolution rate. The thermal properties were measured using DTA and a crystallization study revealed that upon substitution of CaO for CaF_2 a progressive change from surface to bulk crystallization occurred. This is of particular interest as, typically, bioactive glass crystallize from the surface limiting their application as glass-ceramics. An increase in F content leads to a decrease in the IC50, however the glass ceramics containing CaF2 was found to have a higher IC50 than its glass counterpart. Furthermore, crystallization of the glasses into glass ceramics, was also found to lead to an increase in the cytoplasmic nuclear ratio.

Conclusion

Overall, the developed glass were found, as expected to favor the precipitation of a fluoroapatite layer. The presence of F increase the dissolution rate and leads to a decrease in the glass concentration that can be used, in order to maintain over 50% cell viability. The developed F-containing glasses can be processed into glass-ceramics through control CaF2 crystal growth. The presence of nanocrystals leads to an increase in the IC50 greater than those

reported for the glass counterpart, indicating that the glass-ceramic is less cytotoxic. The developed glasses were found to have thermal, in-vitro dissolution and cell bioresponse promising for orthopedic and dental application

Acknowledgement

The authors would like to acknowledge the Academy of Finland for financial support. Tamper University of Technology foundation is also gratefully acknowledge for the salary of A. N-N. Finally, IAS (Institute for Advanced Studies) is acknowledge for supporting visits between the partners.

10:30 a.m. – 12:00 p.m.

Hall 5

I-OS3 | Composites and stimuli responsive biomaterials 1

I-OS3-01

Can graphene be the key for a successful application of pHEMA in cardiovascular devices?

Andreia T. Pereira[1,2], Patrícia C. Henriques[1,5], Karl Schneider[3,4], Maria C. L. Martins[1], Fernão D. Magalhães[5], Helga Bergmeister[3,4], Inês C. Gonçalves[1]

[1]INEB/i3s - Instituto Nacional de Engenharia Biomédica, Universidade do Porto, Porto, PT; [2]ICBAS - Instituto de Ciências Biomédicas Abel Salazar, Universidade do Porto, Porto, PT; [3]Center for Biomedical Research Medical, University of Wien, VIenna, AT; [4]Ludwig Boltzmann Cluster of Cardiovascular Research, University of Vienna, Vienne, AT; [5]LEPABE – Laboratório De Engenharia De Processos, Ambiente, Biotecnologia e Energia, Universidade do Porto, Porto, PT

Introduction

Blood contacting devices (BCD) such as vascular grafts, stents, heart valves and catheters are daily used to treat cardiovascular diseases (CVD), which are the number one cause of death globally[1]. This prevalence reflects in worldwide costs exceeding US $863 billion/year which includes the treatments, surgical interventions and post-surgical complications such as the occurrence of fibrosis, thrombosis or infection in implanted devices[1]. The primary therapy for patients with advanced CVD is the arterial bypass grafts. However, there is a lack in efficient synthetic grafts for arteries with small diameter (i.d. <6 mm). Poly (2-hydroxyethyl methacrylate) (pHEMA), a synthetic hydrogel approved by Food and Drug Administration (FDA), presents a high hemocompatibility due to its non-fouling properties, but the poor mechanical properties impair its usage in the designing of blood contacting devices. Thus, this work aims to evaluate the effect of graphene-based materials (GBMs) exfoliation, oxidation degree and lateral size in the mechanical reinforcement of pHEMA considering its future application in the design of blood contacting materials, such as small diameter vascular grafts.

Experimental Methods

GBMs with different exfoliation, oxidation degree and lateral size were used, namely graphene nanoplatelets (GNP M5 and M15), oxidized GNP (GNP M5ox and M15ox) and graphene oxide (GO).GBMs were either purchased or produced by modified Hummers' method and characterized by TEM and XPS. pHEMA/GBMs composites were produced by *in situ* polymerization of 2-hydroxyethyl methacrylate and tetraethylene glycol dimethacrylate in the presence of the different GBMs. Resulting composites were evaluated regarding GBM dispersion and surface topography (SEM), wettability (contact angle), swelling capacity (gravimetry) and mechanical properties (tensile tests). Biocompatibility of pHEMA/GBMs were evaluated by assessing the medium extracts cytotoxicity towards HUVECs cells. Non-fouling properties of pHEMA/GBMs were evaluated by the assessment of their capacity to adhere human platelets (SEM), HUVECs cells (fluorescence microscopy using a staining of phalloidin and DAPI) and bacteria (high-throughput microscopy using a BacLight^{TM}LIVE/DEAD staining kit). A prototype conduit of pHEMA/GO (ID: 4 mm; OD: 6mm) was developed to evaluate its blood compatibility *in vivo* using non-heparinized pigs as animal model. The conduits were connected to the pig carotid arteries (A-V shunt) being in contact with circulating blood for 1 h and materials surface lumen were afterwards evaluated by SEM.

Results and Discussion

The lateral size of GBMs ranges from 1.5 to 15 µm, being GO the smallest material. Oxidized forms of GBMs show a similar oxidation degree between them of about 34% while non-oxidized GBMs have low oxygen content (3%).

TEM images of GO show that this material has the highest exfoliation degree. Incorporation of GBMs in pHEMA leads to an increase in its roughness, more predominant when the oxidized GBMs were incorporated but keeps its surface wettability (contact angle of 25º) and swelling capacity (50%). The oxidation degree and thickness of GBMs (as well as particles dispersion) revealed to be crucial factors to achieve the greater improvements in the mechanical properties of pHEMA, while particles lateral size had a minor effect. As such, GO, which is an oxidized GBM and the thinnest was the most efficient filler among the tested GBMs in the increase of pHEMA stiffness and tensile resistance reaching 2 MPa and 0.7 MPa, respectively. These values empower the possible application of pHEMA/GO composites in development of some blood contacting devices such as small diameter vascular graft. Regarding the biological properties, pHEMA/GBMs extracts are not cytotoxic and pHEMA/GBMs maintain the non-fouling properties of pHEMA, exhibiting negligible levels of adherent cells and blood platelets. Bacteria adhesion assay reveals that incorporation of non-oxidized forms of GBMs in pHEMA seems to promote higher bacteria adhesion at surface while oxidized-GBMs maintain the low levels observed in pHEMA. Preliminary*in vivo*hemocompatibility studies show that, unlike the control ePTFE (currently used in clinics for large diameter vascular grafts), which reveals exuberant platelet, erythrocytes and leucocytes adhesion with clot formation and complete occlusion, pHEMA/GO conduits only present a few leucocytes adhered to its surface lumen, and maintain blood circulation without clot formation.

Conclusion

New pHEMA/GBMs composites have been developed, being pHEMA/GO the most promising material with suitable mechanical and bio/hemocompatible features to apply in the design of blood contacting devices.

References

[1] Irini Sotiri, et al, BloodSurf 2017: News from the blood-biomaterial frontier, Acta Biomaterialia, 87, 55-60.

Acknowledgement

Financial support from Fundação para a Ciência e a Tecnologia (FCT) and Fundo Europeu de Desenvolvimento Regional (FEDER) PD/BD/114156/2016, SFRH/BD/120154/2016, IF/01479/2015, POCI-01-0145-FEDER-032431, POCI-01-0145-FEDER-006939, POCI-01-0145-FEDER-007274, NORTE-01-0145-FEDER-000012 and PTDC/CTM-BIO/4033/2014 and UID/EQU/00511/2019.

I-OS3-02

Poly(2-oxazoline)/Poly(2-oxazine) based Copolymers: Physical gelation and related properties

Lukas Hahn[1], Matthias Maier[1], Benedikt Sochor[3], Matthias Beudert[2], Tessa Lühmann[2], Robert Luxenhofer[1], Funded by the Deutsche Forschungsgemeinschaft (DFG, German Research Foundation) – Projektnummer 326998133 – TRR 225 (subproject A03)

[1]Julius-Maximilians-Universität Würzburg, Functional Polymer Materials/ Chair for Advanced Materials Synthesis/ Department of Chemistry and Pharmacy and Bavarian Polymer Institute, Würzburg, DE; [2]Julius-Maximilians-Universität Würzburg, Institute of Pharmacy and Food Chemistry/ Department of Chemistry and Pharmacy, Würzburg, DE; [3]Julius-Maximilians-Universität Würzburg, Institute of Physics/ Chair for X-Ray Microscopy, Würzburg, DE

Introduction

The development of bioinks is understood as a critical aspect in the interdisciplinary field of biofabrication. Biopolymers are often preferred as bioinks due to their often good cytocompatibility but have also limitations, specifically regarding characterization, batch-to-batch variations and suboptimal viscoelastic properties.[1] In contrast, synthetic polymers can be tuned more easily for specific applications, in particular synthetic platforms that allow fine-tuning of physicochemical and viscoelastic properties are favorable. Thermoresponsive structures based on poly(2-oxazoline)s have been investigated over years[2] but only few reports on thermogelling poly(2-oxazoline)s can be found nowadays. Lorson *et al.* established a thermogelling (G´ > 1000 Pa, T_{Gel} = 10-30 °C), cytocompatible and printable poly(2-oxazoline)/poly(2-oxazine) (POx/POzi) supramolecular hydrogel comparable to the well-known pluronic® F127.[3] We recently established two new hydrogel platforms based on ABA triblock copolymers with varying POzi block B and Poly(2-methyl)-2-oxazoline as the hydrophilic shell A. The polymers undergo thermogelation upon cooling comparable to the well-known gelatin. The difference between the platforms are time dependency of gelation and concentration range at which the gelation occurs.

Experimental Methods

The Monomers were synthesized via an established method investigated by Wittig and Seeliger.[4] Based on that the ABA triblock copolymers were synthesized via living cationic ring opening polymerization. The reaction process and purified polymers were analyzed via Gelpermeationchromatography and ^{1}H-NMR spectroscopy. The polymers were additionally screened on the behavior in aqueous solution at different concentrations and temperatures. The selected ABA triblock copolymers which undergo thermogelation upon cooling were investigated via rheology and viscosity measurements. To understand the aggregation behavior first dynamic light scattering and small angle X-ray scattering experiments were conducted. Also the cytotoxicity assay WST-1 were performed.

Results and Discussion

Two out of six screened polymers which varying hydrophobic core undergo thermogelation upon cooling only by shifting methylene-groups. One of that undergo physical gelation in the range of 5 wt.% up to 40 wt% in water upon cooling in the time range of 90 minutes (G´(5 wt.%)= 130 Pa; G´(20 wt.%)= 21 kPa) (Figure 1). Once the gel is formed, the physical network is stable until 31 °C, exhibited shear thinning, and structure recovery properties. Also first promising extrusion based bioprinting experiments were performed. The polymer solution formed two different aggregates. A small micellar structure in the size range of 10-20 nm and a second larger species of 200 nm investigated via DLS and SAXS experiments. Upon cooling, the 200 nm species increased in number reversible. The

limitation of that platform, the time dependency upon gelation, can be overcome by the second ABA-triblock copolymer, which undergoes fast reversible gelation upon cooling investigated and compared with the first polymer via rolling ball viscosity measurements (Figure 2).

Conclusion

To conclude we established two new polymer hydrogels based on Poly(2-oxazoline)Poly(2-oxazine) ABA triblock copolymers which undergo unique thermogelation upon cooling. The platforms can be used as a bioink but also as sacrifical and support material for different applications in the field of biofabrication.

References

1. Gungor-Ozkerim, P. S.; Inci, I.; Zhang, Y. S.; Khademhosseini, A.; Dokmeci, M. R., *Biomaterials Science, **6** **(5)**,* 915-946 (2018).

2. Dargaville, T. R.; Park, J. R.; Hoogenboom, R., *Macromolecular Bioscience,**18** **(6)***, 1800070 (2018).

3. Lorson, T.; Jaksch, S.; Lübtow, M. M.; Jungst, T.; Groll, J.; Lühmann, T.; Luxenhofer, R., *Biomacromolecules,**18** **(7)***, 2161-2171 (2018).

4. Witte, H.; Seeliger, W., *Angewandte Chemie International Edition in English* **1972,***11* (4), 287-288.

Acknowledgement

This work was supported by the German Research Foundation (DFG) within the collaborative research center TRR225 (subproject A03) and by the State of Bavaria. We gratefully acknowledge financial support by the German Plastics Center SKZ and the Julius-Maximilians Universität Würzburg for start-up funding.

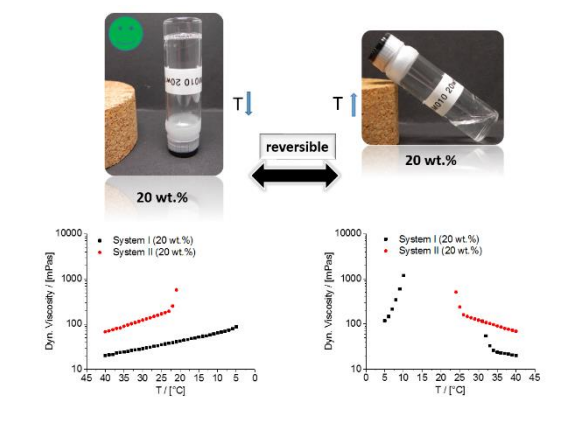

Figure 2. The second polymer undergoes rapid gelation upon cooling at 20 wt.%.
The gelation was investigated and compared to the system I via viscosity measurements

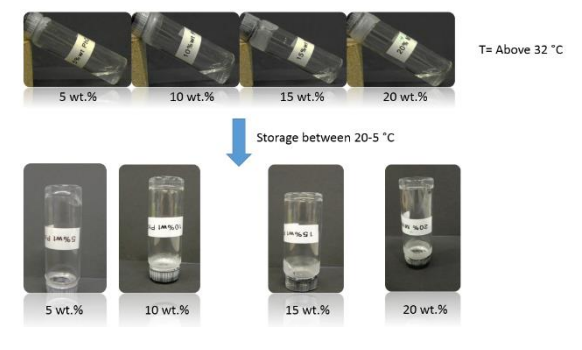

Figure 1. ABA triblock copolymer undergoes thermogelation upon cooling.

I-OS3-03

Production of inductive heatable nanocomposite fibres for use in hyperthermia tumour therapy

Benedict Bauer[1], Benedikt Mues[2], Jeanette Ortega[1], Thomas Gries[1], Thomas Schmitz-Rode[2], Andreas Blaeser[1], Ioana Slabu[2]

[1]RWTH Aachen University, Institut für Textiltechnik, Aachen, DE; [2]RWTH Aachen University, Institute of Applied Medical Engineering, Helmholtz Institute, Medical Faculty, Aachen, DE

Introduction

Cancer is the second most common cause of death in Germany. Due to the nature of the rapidly multiplying cancerous cells, tumours develop and occlude the passageways of hollow organs such as the windpipe, bile ducts, or oesophagus. Current treatments include surgical removal of the tumour or implantation of plastic tubes and metal stents to open the occluded hollow organ. These implants have the disadvantage that they reduce the width of the passageway of the hollow organ and they cannot prevent the ingrowth of tumour cells into the hollow space, respectively. By combining an overheating of the tissue, so-called hyperthermia, with a stent structure, local cancer treatment is realised. For this, inductive heatable fibres are produced by compounding magnetic nanoparticles (MNP) with a polymer. Then, using these fibres a stent is braided. This stent is inserted at the location of the tumour, where it is heated by magnetic induction. This heat destroys the cancer cells. This treatment can be repeated whenever necessary to provide a free passageway against the tumour ingrowth. It is crucial for this application, that the stents reach the therapeutically relevant temperature of approximately 43 °C, in order to spare the healthy tissue while successfully destroying the cancerous tissue.

In this study, we investigate the effects of MNP incorporation inside polypropylene (PP) compounds on magnetic heating. The compounds are the base material used for the production of hybrid stents. We analyse the results with respect to MNP dispersion, processability and mechanical properties of the fibres.

Experimental Methods

Self-synthesized freeze-dried MNP are incorporated with various concentrations into a PP matrix using a twin-screw compounder (Brabender, Duisburg, Germany). The MNP had a core diameter of (10.2 ± 2.4) nm and a saturation magnetization of (99.4 ± 0.8) Am²/kg. Compounds with MNP concentrations varying from 2 wt% to 8 wt% were fabricated. From these compounds, fibres with MNP loading were produced using a small-scale melt spinning setup (DSM, Heerlen, Netherlands). Additionally, a commercial particle system (318F Bayferrox ®) was used to develop a pilot-scale melt spinning process (Fourné Polymertechnik GmbH, Bonn, Germany) from compounds with the above-mentioned concentrations varying mass flow and take-up velocity. Fibre thickness was determined using optical microscopy. Mechanical properties of the respective fibres were tested using uniaxial tensile tests (Textechno Herbert Stein GmbH & Co. KG, Mönchengladbach, Germany) . Compounds as well as fibres were embedded in agarose gels (1.5 wt% agarose) and exposed to an alternating magnetic field (AMF) at H = 14 kA/m and f = 100 kHz for 30 min. The measurements were carried out with a custom-built hyperthermia setup (Trumpf Hüttinger, Freiburg, Germany). The MNP dispersion within the PP matrices of compounds as well as fibres was analysed using transmission electron microscopy. The processability of the fabricated fibres are analysed by manual braiding techniques.

Results and Discussion

Stable spinning conditions were achieved for all tested MNP concentrations. Fibres produced with Bayferrox particles had a fineness ranging from 145 µm to 190 µm and exhibited a breaking force of 90 cN to 160 cN. Fibres fabricated from compounds loaded with self-synthesised MNP displayed a temperature rise between 0.7 °C and 2.2 °C at the given AMF parameters depending on the particle mass concentration. The processability of such fibres is confirmed by the successful fabrication of a stent using a one-wire manual braiding technique.

Conclusion

Inductive heatable fibres consisting of MNP incorporated in a PP matrix were fabricated, characterised and further processed into a stent structure. This heatable stent is a promising approach to treat tumours infiltrating hollow organs. Further investigations are currently in progress in order to improve heating efficiency and mechanical properties.

Acknowledgement

This IGF project was funded by the AiF within the framework of the program for the promotion of joint industrial research and development (IGF) of the Federal Ministry of Economics and Energy on the basis of a decision of the German Bundestag. We are grateful for this support. We are also grateful for the support of the FKT.

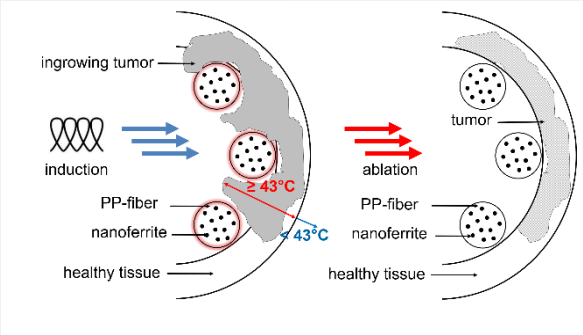

Concept schematic
Concept schematic of nanoferrite-laden polymer fibers which are inductively heated to locally destroy tumor tissue infiltrating a hollow organ through local hyperthermia

I-OS3-04

Peptide-protein co-assembly to organise graphene oxide hierarchically into hybrid bioactive scaffold materials

Anna Majkowska, Alvaro Mata

Queen Mary University of London, School of Engineering and Materials Science, London, GB

Introduction

The use of synthetic protein and peptides to build functional materials is of great interest in the field of tissue engineering and regenerative medicine because they offer versatility, biofunctionality, modular structure as well as ease of design and production. A novel protein/peptide composite system (ELP/PA) developed in our lab[1,2] is of particular interest because of its' capacity to engineer with molecular control while creating controlled macroscopic scaffolds. However, despite the numerous advantages, protein or peptide based biomaterials usually lack mechanical strength and reproducibility. Graphene oxide (GO) is a single layer two dimensional nanomaterial with a wide array of interesting physical and chemical properties as well as biocompatibility and ease of functionalisation. Due to excellent mechanical properties GO offers an interesting approach for development of new generation organic-inorganic composite biomaterials.

In this work we aim to manipulate the diffusion-reaction mechanism that takes place upon co-assembling peptides and proteins at an interface to organize GO hierarchically. In this way we hope to create a composite protein/peptide/GO that has the biofunctionality and complexity of protein/peptide materials as well as increased mechanical strength of GO.

Experimental Methods

The microstructure of the samples and distribution of GO was visualised using scanning electron microscopy (SEM) and transmission electron microscopy (TEM) techniques. AFM nanoindentation was used to measure Young's Modulus of the samples. The cell studies were carried out using adipose derived stems cells (ADSCs). Cell metabolic activity was investigated using Alamar Blue™ assay. Cell proliferation was established based on Picogreen Assay™. Cell attachment and morphology were examined using fluorescently stained confocal images. Student t-test was used to analyse data. Significant differences between the groups were looked for at $p < 0.05$ and at $p < 0.01$.

Results and Discussion

We were able to successfully manipulate GO flakes via diffusion-reaction mechanism and hierarchically organise it within the protein/peptide system (ELP/PA) into a hybrid bioactive scaffold material. The GO flakes were shown to be organised in a concentric manner parallel to the membrane's face. In order to explore bioactive properties of the new material we investigated cell adhesion, metabolic activity, morphology, and proliferation. We also conducted stability assays and AFM nanoindentation. The composite ELP/PA/GO material has shown excellent biocompatibility and improved mechanical properties.

Conclusion

In this study we have introduced a new way to organize GO flakes hierarchically while creating bioactive hybrid material that takes advantage of its building blocks' properties such as: biofunctionality, mechanical strength, hierarchical and fibrous microstructure resembling extracellular matrix. These novel composite biomaterials could be

used as scaffolds in tissue engineering and regenerative medicine applications such as peripheral nerve regeneration or vascular grafts.

References

1 Inostroza-Brito, K. E. *et al.* Co-Assembly, spatiotemporal control and morphogenesis of a hybrid protein-peptide system. *Nat. Chem.***7,** 897–904 (2015).

2. Inostroza-Brito, K. E. *et al.* Cross-linking of a biopolymer-peptide co-assembling system. *Acta Biomater.***58,** 80–89 (2017).

Acknowledgement

The funding for this study has been provided by ERC Starting Grant STROFUNSCAFF, Biomorph, Life Sciences Institute LSI and Queen Mary University of London

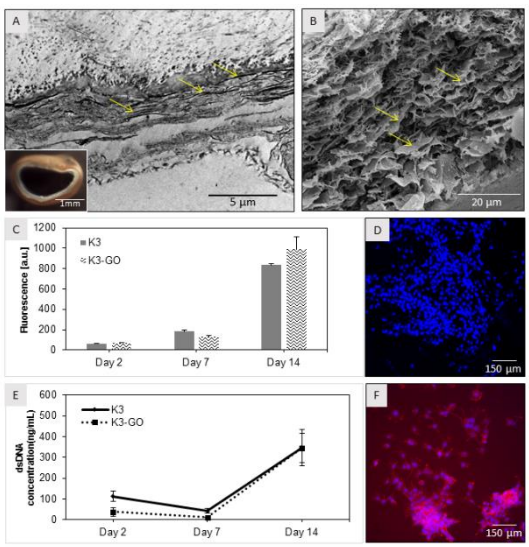

Characterisation of the protein/peptide/GO system

Figure 1. A. TEM micrograph of ELP/PA-K3/GO cross-section, GO flakes highlighted with arrows, inset- a bright field image of the membrane B. SEM micrograph of ELP/PA/GO cross-section, GO flakes highlighted with arrows C. Cell metabolic activity on days 2, 7 and 14 on membranes with and without GO D. Cell attachment on ELP/PA-K3/GO membrane, nuclei stained with DAPI E. Cell proliferation comparison between membranes with and without GO F. Cell morphology.

I-OS3-05

Temperature-responsive biodegradable injectable hydrogel for adhesion prevention materials

Yuichi Ohya[1,2], Takuya Nagata[1], Yuta Yoshizaki[3], Soichiro Fujiwara[1], Shinji Takai[4], Denan Jin[4], Akinori Kuzuya[1,2]

[1]Kansai University, Department of Chemistry and Materials Engineering, Suita, JP; [2]Kansai University, Collaborative Research Center of Engineering, Medicine and Pharmacology, Suita, JP; [3]Kansai University, ORDIST, Suita, JP; [4]Osaka Medical College, Graduate School of Medicine, Takatsuki, JP

Introduction

One of the common and serious complications after surgery are formation of post-operative intra-abdominal adhesions, which can cause a series of side-effects such as severe pain, infertility, intestinal obstruction and even death. Over recent decades, adhesion prevention materialsin the type of membrane have been used as one of the most effective approach for reducing adhesion formation. However, it isdifficult to handle during surgery and is not suitable for endoscopic surgery, which is a recent minimally invasive surgical procedure for patient. Therefore, adhesion prevention materials with excellent operability and compatibility for endoscopic surgery are required. Recently, we reported the successful preparation of temperature-responsive injectable polymer (IP) formulations forming chemically cross-linked hydrogel just after physical gelation in response to temperature[1]. We developed tri-block copolymer of poly(caprolactone-*co*-glycolic acid) and PEG (tri-PCG) as a base polymer and acryloyl groups were introduced on both termini of a tri-PCG (tri-PCG-Acryl). After mixing each micelle solution of tri-PCG-Acryl, and tri-PCG containing hexa-functional polythiol [dipentaerythritol-hexakis(3-mercapto-propionate) (DPMP)], the obtained IP formulation exhibited a temperature-responsive irreversible sol-to-gel transition (Scheme 1). In addition, the duration time of the gel state after gelation could be easily controlled just by changing mixing ratio of tri-PCG-Acryl to tri-PCG/DPMP. In this study, we investigated the preventive effects of the IP hydrogel on post-operative abdominal adhesions in rat adhesion model.

Experimental Methods

Tri-PCG-Acryl was synthesized by the method reported previously[1]. The tri-PCG-Acryl dissolved to form micelle solution and the micelle solution was further mixed with tri-PCG micelle solution containing DPMP in various mixing ratio to give IP formulations. The sol-gel transition of the IP formulation was investigated by a test tube inverting method and rheological measurement using a dynamic rheometer. Adhesion formation in a rat experimental model was induced by NaOH treatment. Absorbent cotton (5×5 mm) soaked in NaOHaq. was put on the cecum of a rat, and then the area was neutralized by absorbent cotton soaked in HClaq. After this procedure, we applied IP formulations with various contents of tri-PCG-Acryl. After14 days, the extent of adhesion formation were scored by a modified classification according to the previous report[2] and compared with Seprafilm®, which is a membrane sheet clinically used.

Results and Discussion

The IP formulations can easily be spout out from a micro-catheter, and exhibited sol-to-gel transitions upon heating from r.t. to 37°C within 30 sec. After cooling to room temperature, the formulation was still in the gel state. These results show that the sol-to-gel transition of the formulation was irreversible by covalent bonds formation. The irreversible sol-to-gel transition of the IP formulation was also confirmed by rheological measurements. The anti-adhesive scores in rats group treated with IP hydrogel was significantly lower than no treatment group, and slightly lower than Seprafilm®treated group (Figure 1).

Conclusion

These results suggested that the IP formulations worked as physical barriers between treated area and normalperitoneum or organs. Therefore the IP hydrogels are expected to be applied as injectable-type adhesion prevention materials having good compatibility with endoscopic surgery.

References

1. Y. Ohya *et al.*, *Biomater.Sci.,* **2017**, *5*, 1304-1314.
2. J. F. Hulka *et al.,Fertil., Steril.* **1978**, *30*, 661-665.

Acknowledgement

This work was financially supported in part by Private University Research Branding Project: Matching Fund Subsidy from Ministry of Education, Culture, Sports, Science and Technology (MEXT) Japan (2016–2020).

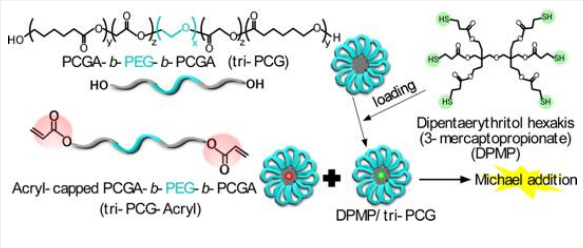

Scheme 1.
Preparation of [DPMP/tri-PCG + tri-PCG-Acryl] IP formulation.

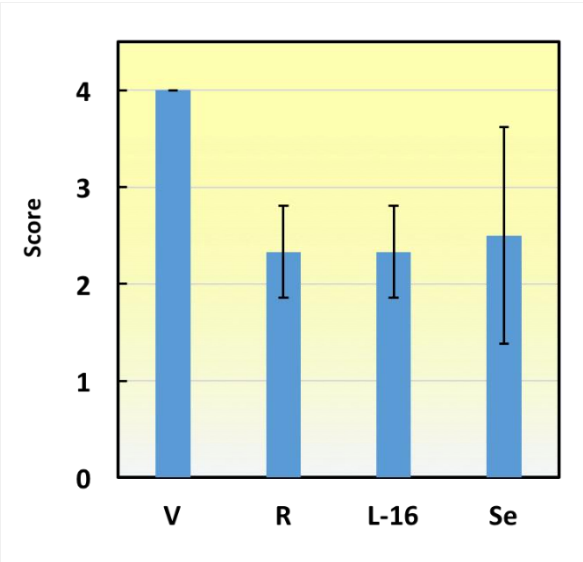

Figure 1.
Anti-adhesive scores for the IP formulation in rats.

L-16: tri-PCG/DPMP + tri-PCG-Acryl(16%), **R**: tri-PCG (R), **Se**: Seprafilm®,**V**: control (PBS).The scores are expressed as mean of the mice. **0**: no adhesion, **1**: easy to peal (film-like), **2**: difficulty in pealing: Low, **3**: difficulty in pealing: Medium, **4**: difficulty in pealing: High

I-OS3-RF06

Electrospun Collagen Based Fibers Featuring Electrical Conductivity for Cardiac Tissue Engineering Application

Lena Vogt[1], Kaveh Roshanbinfar[2], Florian Ruther[1], Felix B. Engel[2], Aldo R. Boccaccini[1]

[1]Friedrich-Alexander-Universität Erlangen-Nürnberg, Lehrstuhl Biomaterialien, Erlangen, DE; [2]Friedrich-Alexander-Universität Erlangen-Nürnberg, Experimentelle Nieren- und Kreislaufforschung, Erlangen, DE

Introduction

Based on the very limited intrinsic self-regeneration capability of cardiomyocytes, acute or chronic damage to the heart muscle, e.g. caused by a myocardial infarction, can lead to scar formation, the loss of contraction ability, and, potentially, to heart failure. Restricted therapies and the lack of donor organs demand new cardiac tissue engineering (CTE) strategies like the cardiac patch approach[1]. Electrospinning has evolved as a suitable processing technique due to its ability to closely mimic the highly branched myocardial structure[2]. In order to imitate the polysaccharide component and structural properties of the cardiac extracellular matrix, this study focuses on a blend of collagen (Col) and hyaluronic acid (HA). Additionally, polyaniline (PANi), a conductive polymer, was added to the mixture to provide electrical conductivity of the fiber mat. Fiber mats made from PANi and gelatin showed already good results in previous studies[3,4].

Experimental Methods

Different weight percentages of polyaniline emeraldine base (Mw 65MDa, Sigma-Aldrich) and camphorsulfonic acid (CSA, Sigma-Aldrich) (1:1 weight ratio) were dispersed in dimethylsulfoxide (≥99.5 %, Carl Roth) and stirred for 24 h. Collagen (type I, Symatese) and HA (Mw 1.0-1.5 kDa, Lifecore Biomedical) (9:1 ratio) were dissolved in formic acid (≥98 %, Sigma-Aldrich) and stirred for 1 h. Col/HA and PANi/CSA solutions were combined in 9:1 and 7:3 ratios 15 min prior to electrospinning. Electrospinning parameters were optimized to an applied voltage of 16 kV, a flow rate of 0.05 mL/h and a tip-target distance of 10 cm. Fibers were randomly collected on a mandrel with 500 rpm. The fiber mats were crosslinked in 25 % aqueous glutaraldehyde (50 % EM grade, Polysciences) vapor for 72 h. The morphology (SEM), chemical (ATR-FTIR), mechanical and electrical properties of the fiber mats were investigated. In vitro studies with cardiomyocytes of 3 days-old rat pups were conducted and cytocompatibility, beating behavior and intercellular communications were examined.

Results and Discussion

All Col/HA/PANi blends showed homogenous defect-free fibrous morphologies with fiber diameters ranging between 120 and 340 nm. The increasing PANi content and thereby increasing solution conductivity led to a decreasing fiber diameter, whereas the fiber alignment increased. FTIR analysis confirmed the presence of collagen, HA, and PANi in the fibrous scaffolds. Ultimate tensile strength and failure strain increased with increasing PANi content before it decreased finally; the Young's modulus decreased constantly with increasing PANi volume.The electrical conductivity also significantly increased with increasing PANi amount up to 2 ± 0.5 mS/cm. Cytocompatibility assays after 48h revealed a slight decrease of cardiomyocyte viability in fiber mats containing PANi/CSA; however, cardiomyocytes showed no significant difference in beating rates for the different compositions. The fibrous scaffold with the highest PANi content revealed a significant increase in contraction amplitude compared to the other compositions. Also a significant increase in connexin43 was observed for the fibers with the highest PANi volume.

Conclusion

After optimization of solution and electrospinning parameters, homogenous Col/HA/PANi fiber mats were successfully fabricated. The fiber mat with the highest PANi content showed the best cell results despite being the most brittle. However, all reported results meet the requirements for a patch applicable in cardiac tissue engineering.

References

1. Chen Q.-Z., et al., Biomaterials. 29: 47-57, 2008.
2. Kim P.-H., et al., BMB reports. 49.1: 26, 2016.
3. Li M., et al., Biomaterials. 27.13: 2705-2715, 2006.
4. Ostrovidov S., et al., ACS applied materials & interfaces. 9.49: 42444-42458, 2017.

Acknowledgement

The authors would like to thank the German Research Foundation (DFG) (Grant no: BO 1191/14-1) for providing financial support to this project. L.V. and K.R. contributed equally.

I-OS3-RF07

Characterization of electrically conductive polylactic acid (PLA) – polypyrrole (PPy) substrates for neural tissue engineering

Fernando Gisbert Roca[1], Jorge Más Estellés[1,2], Cristina Martínez Ramos[1], Manuel Monleón Pradas[1,2]

[1]Universitat Politècnica de València (UPV), Centro de Biomateriales e Ingeniería Tisular (CBIT), Valencia, ES; [2]Biomedical Research Networking Center in Bioengineering, Biomaterials and Nanomedicine (CIBER-BBN), Centro de Biomateriales e Ingeniería Tisular (CBIT), Valencia, ES

Introduction

Electrically conductive substrates are used to improve axonal extension and induce a greater release of neurotrophins by glial cells when subjected to an exogenous electric field [1-2]. Herein, we develop polylactic acid (PLA) - polypyrrole (PPy) nanofiber films with different amounts of PPy, characterizing its physicochemical and dielectric properties, as well as its biological validity to be used within the field of neural tissue engineering.

Experimental Methods

Aligned PLA nanofiber films were obtained by the electrospinning technique and coated with the electrically conductive polymer PPy via *in situ* polymerization. Different mass fractions of PPy were obtained by varying the reaction parameters used for the PPy coating (4%, 13%, 18%, 23%, 27% and 34%). Different techniques (Field Emission Scanning Electron Microscopy (FESEM), Fourier-Transform InfraRed spectroscopy (FTIR), ThermoGravimetric Analysis (TGA), Differential Scanning Calorimetry (DSC) and impedance measurements) were used to characterize the physicochemical and dielectric properties of the membranes. The MTS cell proliferation assay and confocal microscopy images were employed to assess the adhesion of rat Schwann cells on the surface of the substrates.

Results and Discussion

FESEM images showed that for mass fractions of PPy below 23% the coating was discontinuous, while many aggregates were observed for mass fractions of PPy above 34%. Therefore, a continuous and homogeneous coating without aggregates is obtained between these two values.

The dielectric characterization showed that the greater the mass fraction of PPy, the greater the conductivity of the material. A percolation effect was also observed for substrates with a mass fractions of PPy greater than 23%, corroborating the continuity of the PPy coating above this value.

The MTS cell proliferation assay showed a greater cell adhesion of Schwann cells when the mass fraction of PPy is low (4%), compared to PLA membranes. However, from this point, the greater the mass fraction of PPy, the lower the cell adhesion. Morphological changes of the cells were also observed when increasing the mass fraction of PPy.

Conclusion

Our experimental data demonstrate the ability to obtain electrically conductive, biodegradable and biocompatible PLA-PPy substrates that greatly expand the potential for this composite material to be used for tissue engineering and implantable devices applications.

References

[1] Schmidt CE et al. PNAS 1997; 94:8948-53

[2] Huang J et al. GLIA 2010; 58:622-31

Acknowledgement

The authors acknowledge financing from the Spanish Ministry of Economy and Competitiveness (MINECO) through MAT2015-66666-C3-1-R and DPI2015-72863-EXP projects. Fernando Gisbert Roca acknowledges scholarship FPU16/01833 of the Spanish Ministry of Education, Culture and Sports (MECD). We thank the Electron Microscopy Service at the UPV, where the FESEM images were obtained.

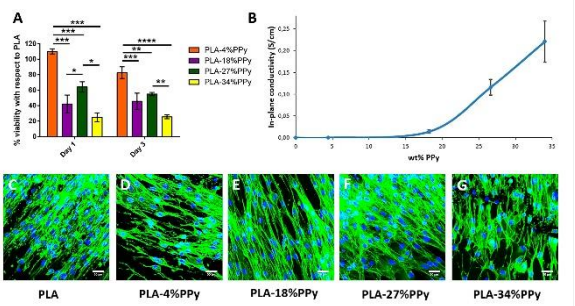

Cell proliferation assay, conductivity of membranes and confocal microscopy images

A: MTS Schwann cell proliferation assay. B: Conductivity of PLA-PPy films. C-G: Confocal images of Schwann cells seeded on PLA and PLA-PPy substrates.

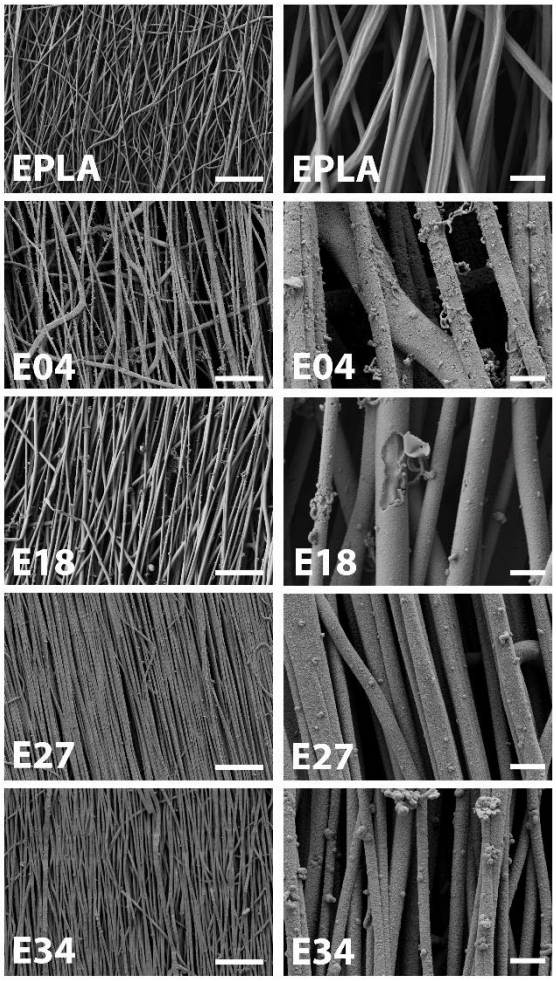

FESEM images of PLA-PPy electrospinning membranes

FESEM images of PLA (EPLA) and PLA-PPy (E04, E18, E27 and E34) electrospinning membranes with an aligned orientation of the nanofibers. EPLA: Smooth surface. E04: Inhomogeneous coating with discontinuities. E18: More homogeneous coating, but still with some discontinuities. E27: Homogeneous coating. E34: Homogeneous coating, but with PPy aggregates. Left image: 1.000X (Scale bar = 20 µm). Right image: 7.500X (Scale bar = 2 µm).

I-OS3-RF08

Design of a novel 3D combined bioactive tissue matrices for skeletal muscle tissue repair

Nergis Zeynep Renkler[1], Sedat Odabas[2], **Kadriye Tuzlakoglu**[1]

[1]Yalova University, Dept. Polymer Engineering, Yalova, TR; [2]Ankara University, Dept. Chemistry, Ankara, TR

Introduction

The primer function of the skeletal muscle is to provide movement with other musculoskeletal organs. Damages of these muscles greatly affect daily life of patients as they cause movement restriction in the human body. The regain of the function of damaged muscle depends on the size of the injury. In case of simple injuries muscles can self-heal with physical exercises and resting. However, the large volume loss caused by firearms, cancer ablation, etc. cannot heal without any surgical treatment. Tissue engineering techniques which use a matrix with/without cells emerge as an alternative advanced treatment for damaged muscle tissue regeneration. The function of the carrying matrix is to form new muscle tissue by enhancing myotube formation from myofibers. Thus, the materials used in fabrication of matrix and final form of matrix are particularly important. We herein designed a spiral form 3D matrix made of nanofiber polycaprolactone and polyaniline membrane, which is combined with DCM to repair damaged muscle tissue.

Experimental Methods

The bovine skeletal muscles purchased from local abattoir were decellularized using trypsin-EDTA and Triton-X solutions. DNA assay was done by high salt DNA extraction procedure to determine the effectiveness of decellularization method. DNA content was measured using Nanodrop (Thermo scientific, USA) after the extraction of DNA. To further confirm removal of cellular content, Gel electrophoresis was performed with DNA extracts loaded on 1% agarose gels.For production of nanofiber membrane, the mixed was electrospun through a plate collector by applying high voltage between tip and collector. The morphology of obtained mats was determined by SEM, where the electrical conductivity was measured using a multimeter. The final combined structures were obtained by injecting DCM solution in acetic acid into a spirally rolled electrospun mats.

Results and Discussion

With regard to DNA assay, the decellularization efficiency was found to be around 84% for DCM samples. Furthermore, there were no detectable traces of DNA in electrophoresis, confirming the effectiveness in removing the DNA component. A nonwoven mesh structure was successfully produced from PCL/PANI via electrospinning process without any bead formation on the nanofibers (Fig.1.). The diameters of nanofibers were in the range between 200-730nm. The electrical resistance of nanofibrous mats were measured to be around $10^8\Omega$. The spiral form structures were also formed with a good integration between the components.

Conclusion

The results obtained from the present work indicate that spiral shape combined structures possess favorable properties to serve as a scaffold for the regeneration of damaged skeletal muscle tissue.

Acknowledgement

We gratefully acknowledge the support of The Scientific and Technological Research Council of Turkey (TUBITAK) through project 118M610.

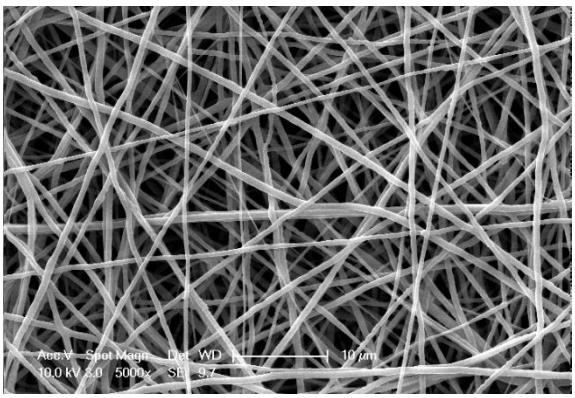

Morphology of PCL/PANI mats observed by SEM.

10:30 a.m. – 12:00 p.m.

Conference room 4+5

I-OS4 | Application-related aspects

I-OS4-01

Biocompatibility of F-127 as lubricant for orthopaedic implants.

Ruben del Campo, Seunghwan Lee

Technical University of Denmark, Department of Mechanical Engineering, Lyngby, DK

Introduction

During the last decades, the number of total replacements of joints increased including young people [1] [2]. The most common surgical operation of artificial joints are the substitutions of hip and knee joints. The life span of these joints is around 15 to 20 years on the most optimistic cases, which is mostly lower than the remaining life expectancy of the patients.

Some of the implant failures are: surgical error (3 %), periprosthetic fracture (5 %), recurrent dislocation (6 %), infection (7 %) and the most predominant one is aseptic osteolysis (75 %). Wear and corrosion products caused by articulating implant surfaces induce local inflammatory responses that produce the aseptic osteolysis phenomenon [3].

In this work, we studied the biocompatibility and tribological properties of Pluronic copolymer F-127 as lubricant for articular joint implants. F-127 is a water-soluble triblock copolymer of PEO (polyethylene oxide) and PPO (polypropylene oxide) with the capability of reducing interfacial tensions and forming aggregates as micelles [4]. It is presented that F-127 polymer can adsorb onto the surface of the implant, creating a protective interface that reduces the friction and decrease the wear particles released by the implant.

Experimental Methods

1. Tribology:

Pin on disk tests, using CoCrMo alloy pins and UHMWPE disks, were performed in bovine synovial fluid and models synovial fluids simulating the articulation environment. This tribopair, metal-on-polymer, currently represents over the 80 % of the total hip and knee surgeries. At some point during the tests, F-127 solutions in different concentrations (0.2 to 20 wt%) were injected in the system. Relations between the coefficients of friction before and after the injections were calculated to show the effectiveness of the solutions as lubricant.

2. Biocompatibility:

Osteoblast (MC3T3-E1) and fibroblast (L929) cells were cultured in α-MEM and DMEM, respectively, supplemented with 10 vol% of fetal bovine serum, 2 mM L-glutamine and 100 UI/ml penicillin and streptomycin. The cells were subcultured until at least 7 passages.

Cytotoxicity assays with MTT and CCK-8 in the cells were performed after 24 and 72 hours of incubation time with the polymer in different contents. Proliferation of the cells by Trypan blue exclusion after the same time of exposition of the polymer was done as check of the cytotoxicity assays.

Cell morphology was examined by optical microscopy and necrotic behavior of the cells was evaluated after staining the cell nuclei with Hoechst H33258 solution.

3. Immunology:

Inflammatory response was monitored with the production of some cytokines, such as TNF-alpha, IL-1, IL-6, IFN-gamma and IL-10 after incubation of macrophages with lubricants for 24 hours by ELISA assays.

Results and Discussion

The coefficient of friction decreased by about 20 % upon injection of F-127 solution to model synovial fluid. The magnitude of decrease was independent of the F-127 solution concentration, but the higher content of F-127 led to a faster decrease (Figure 1).

However, the decrease in the coefficient of friction is not associated with a decrease in the number or amount of wear particles in the system. Hip implant simulator tests with liner of UHMWPE under a similar conditions showed F-127 the capability of protection in the liner surface.

F-127 has amphiphilic characteristics that allows for the interaction with hydrophobic surfaces such as UHMWPE in aqueous systems. The interaction between F-127 and hydrophobic particles was also detected by DLS when F-127 is over the critical micelle concentration (c.m.c.), in contact with simple proteins.

Cytotoxicity evaluated by MTT assays shows a metabolic activity of both types of cells higher than the control cells incubated without the polymer for all the F-127 concentrations tested. On the other hand, Trypan blue exclusion shows a similar proliferation of cells when the concentration of F-127 is under the c.m.c. but when the concentration of F-127 is over the c.m.c. the proliferation of cells decreases to toxic levels (Figure 2).

The morphology studies and immunology results will be further discussed.

Conclusion

The results of pin on disk together with the hip implant simulator show the capability of F-127 to protect hydrophobic surfaces of UHMWPE in model synovial fluid. Hydrophobic-hydrophobic interactions between the unimers of F-127 and UHWMPE in aqueous solvent allow the UHMWPE surface to be covered by protective layers of F-127, which can lengthen its lifespan.

F-127 over the c.m.c. shows an increment in the particle size that it is detectable by DLS with not only UHMWPE particles released by the liner surfaces, also with hydrophobic surfaces of serum components as proteins.

F-127 in concentration under the c.m.c. is not toxic but in higher concentrations could be, so the data will be analyzed together with the immunology tests carefully.

References

1. *Biomaterials in hip joint replacement.* **SG. Ghalme, A. Mankar, Y. Bhalerao.** 2016, International journal of materials science and engineering 4, s. 113 - 125.

2. *Review of wear mechanisms in hip implants: Paper I - General.* **A. Buford, T. Goswami.** 2004, Materials and Design 25, s. 385 - 393.

3. *The biology of aseptic osteolysis.* **G. Holt, C. Murnaghan, J. Reilly, RMD. Meek.** 2007, Clinical orthopaedics and related research 460, s. 240 - 252.

4. *Physiological aspects Part 1 in a series of papers devoted to surfactants in microbiology and biotechnology.* **J. D. Van Hamme, A. Singh, O. P. Ward.** 2006, Biotechnology advances 24, s. 604 - 620.

Acknowledgement

The Velux Foundation (Villum Experiment Programme, project # 17541) has supported this study.

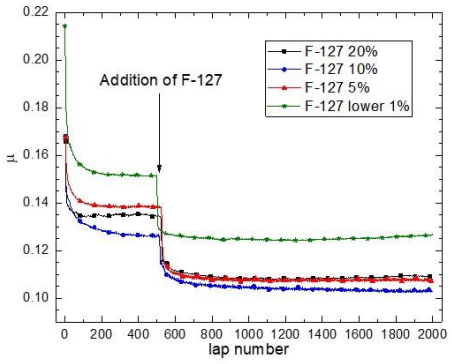

Figure 1
Pin on disk tests

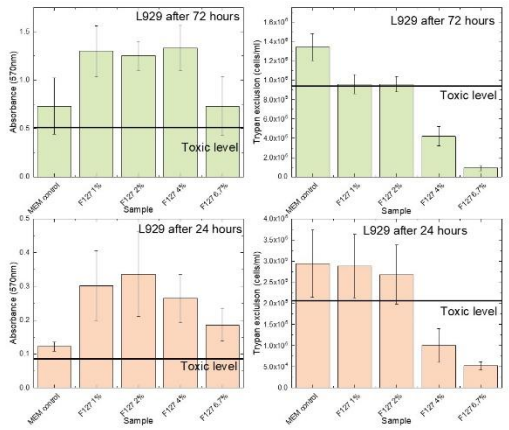

Figure 2
Biocompatibility

I-OS4-02

Graphene and MXene nanomaterial variants for biomedical remediation

Tochukwu Ozulumba[1], Ganesh Ingavle[2,1], Patrick Dyer[3], Susan Sandeman[1]

[1]University of Brighton, School of Pharmacy and Biomolecular Sciences, Brighton, GB; [2]Symbiosis International University, Symbiosis School of Biological Sciences, Maharashtra, IN; [3]University of Brighton, School of Art, Brighton, GB

Introduction

The effective removal of contaminants which build up in body tissues during infection and chronic disease is currently hindered by several challenges including inadequate clearance, long treatment duration and rising antimicrobial resistance[1]. Recent developments suggest that the planar structures, large surface areas and chemical reactivities of the 2-dimensional graphene and titanium carbide (Ti_3C_2) MXene families of nanomaterials make them suited to biomedical remediation of such toxins[2]. The aim of this study was to compare the physicochemical, biological and biotoxin removal properties of graphene and Ti_3C_2 MXene variants in order to investigate their use in medical device applications.

KEY: Graphene nanoplatelets (GNP), graphene oxide (GO), graphene-oxide silver (GO-Ag), multilayer Ti_3C_2 MXene (ML-MXene), delaminated Ti_3C_2 MXene (DL-MXene).

Experimental Methods

Nanomaterial physicochemical properties were characterised using scanning electron microscopy, x-ray spectroscopy (XPS), dynamic light scattering and nitrogen porosimetry. Biocompatibility was assessed *in vitro* in 3T3 fibroblasts and Jurkat T lymphocytes using cytotoxicity and apoptosis assays respectively. Haemocompatibility was investigated in human blood using platelet activation, coagulometry and haemolysis assays. Antimicrobial activity was investigated in *Escherichia coli* and *Staphylococcus aureus* using colony count and Live/Dead staining assays. Biotoxin removal capacity was assessed in plasma and cell culture media samples spiked with the pro-inflammatory cytokines, IL-6, IL-8 and TNF-α (~1000 pg/mL). Cytokine clearance was further investigated using an *in vitro* inflammation model of lipopolysaccharide (LPS)-stimulated THP-1 monocytes. Nanomaterial adsorptive capacity for LPS was investigated with the LAL assay to better understand the mechanism by which nanoparticles influence the THP-1 inflammatory response.

Results and Discussion

XPS confirmed synthesis of GO through increased oxygen content after graphite oxidation, immobilisation of silver nanoparticles in GO-Ag and replacement of the Al layer in the Ti_3AlC_2 precursor with O, OH and F groups in Ti_3C_2 MXene. GNP had the largest surface area of 498 m^2/g; delamination doubled the surface area of ML-MXene from 142 to 282 m^2/g. GNP, GO, ML-MXene and DL-MXene did not impact 3T3 cell viability or stimulate apoptosis in Jurkat cells. The nanomaterials did not induce blood cell activation; however, some haemolysis occurred on direct blood contact with GO. GO-Ag caused higher bacterial cell death and at lower doses compared to standard silver nanoparticles - this is attributed to smaller particle size and the synergistic contribution of GO sheets[3]. GNP, GO, ML-MXene and DL-MXene all removed a significant concentration of cytokines from both spiked plasma and culture media. Similarly, incubation of LPS-stimulated THP-1 cells with nanomaterials caused significant reduction of previously elevated cytokine levels. Since none of the nanomaterials removed LPS directly, this suggested that the reduction of cytokine levels in stimulated THP-1 cells was predominantly driven by direct cytokine adsorption rather than LPS clearance or inactivation. Overall, graphenes had higher biotoxin removal efficiencies than the MXenes potentially as a result of the unique contribution of hydrophobic bonds and π-π stacking interactions[4].

Conclusion

GNP, ML-MXene and DL-MXene were biocompatible, haemocompatible and showed significant biotoxin removal which indicated potential for incorporation in therapeutic strategies addressing contamination of biological tissues such as dialysis devices and wound dressings. The next step is nanomaterial incorporation into polymer scaffolds for stable performance and functional assessment of the resulting composites.

References

1. Herrmann IK, Schlegel AA, Graf R, Stark WJ and Beck-Schimmer B (2015). *J. Nanobiotechnology,* 13(49).
2. Kong XK, Liu QC, Zhang CL, Peng ZM, Chen QW (2017). *Chem. Soc. Rev.,* 46(8):2127-57.
3. Ma J, Zhang J, Xiong Z, Yong Y and Zhao, X S (2011). *J. Mater. Chem.*, 21(10):3350-3352.
4. Shi G and Wang X (2015). *Phys. Chem. Chem. Phys.*, 17:28484-28504.

Acknowledgement

The work was funded by a University of Brighton PhD studentship award.

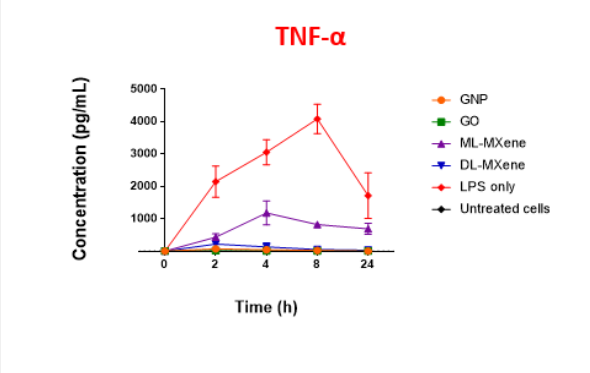

Residual TNF-α levels in LPS-stimulated THP-1 cells after incubation with nanomaterials.
THP-1 cells were stimulated with LPS (2 µg) followed by incubation with GNP, GO, ML-MXene and DL-MXene (12.5 mg) over 24 hours. TNF-α levels were measured using ELISA (n = 3, mean ± SEM).

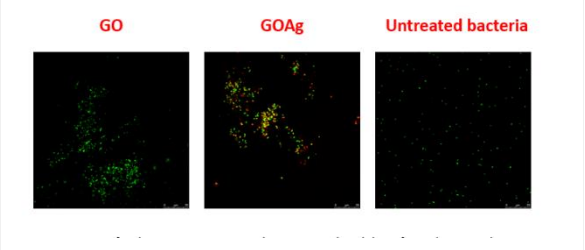

Confocal microscopy images showing E. coli viability after 4-hour incubation with GO and GO-Ag.
Bacteria were stained with SYTO 9 and propidium iodide - the green spots represent live cells, red spots represent dead cells and yellow spots, a combination of both dyes. Scale bar = 25 µm.

I-OS4-03

Surface texturation of breast implant impacts extracellular matrix and inflammatory gene expression even in asymptomatic capsule

Isabelle Brigaud[1], Charles Garabedian[2], Nathalie Bricout[3], Laurent Pieuchot[1], Arnaud Ponche[1], Raphael Deltombe[2], Remi Delille[2], Maxence Bigerelle[2], **Karine Anselme**[1]

[1]CNRS, IS2M, UHA, Mulhouse, FR; [2]Université de Valenciennes et du Hainaut-Cambrésis, LAMIH, CNRS, Valenciennes, FR; [3]Hospital Saint Germain, Saint Germain-en-laye, FR

Introduction

The association between higher-surface-area textured implants and breast implant-associated anaplastic large cell lymphoma (ALCL) has been recently verified, driving European health authorities to remove one the most implanted model- namely Allergan's textured implants - from the market place. Understanding what are the biophysical parameters that influence breast implant integration is therefore of fundamental importance. Until now, Baker I (asymptomatic) capsules have been considered similarly established and organized irrespective of the type of breast implant surface they face. In this paper, we envisaged for the first time that implant surface topography could even affect healthy capsule organization.

Experimental Methods

We collected topographical measurements from 17 different breast implant devices using interferometry and X-ray Microtomography. Morphological structures were statistically analyzed to raise a robust breast implant surface classification (Figure 1).

In parallel, we collected 31 Baker I capsules, sorted them accordingly to the new classification, established their molecular profile by qPCR and examined related tissue organization on histological sections (Figure 2). A panel of extracellular matrix (*Timp1, Timp2, Timp4, Mmp2, Mmp9, Mmp12*) and inflammatory related (*Saa1, Tnsf11, Il8, Tgfβ1*) genes were analysed by performing quantitative PCR (qPCR) experiments on healthy capsules strictly.

Results and Discussion

The new classification resulted in 3 topographical categories of textured implants, defined as "peak and valleys", "open cavities" and "semi-opened cavities" based on their cross-section aspect (Figure 1).

By comparing capsular tissues from different implants, we found that genes associated with extracellular matrix (Timp and Mmp members) and to the inflammatory response (Saa1, Tnsf11, Il8) exhibit very specific expression patterns, despite originating from healthy capsules. Besides, organization of the capsular tissues was slightly impacted.

Altogether, our results demonstrate that surface implant texturation modulates the expression of genes related to extracellular matrix formation and inflammation. We also highlighted slight dissimilar organization of the capsular tissues depending on which implant surface topography they face. In light of our results, we proved that the selected surface topography features are bioactive cues *per se* and confirmed the biological relevance of the classification.

Conclusion

By combining a novel surface implant classification with gene profiling analysis, we show that surface topography is a bioactive cue that can trigger deep changes in gene expression of the surrounding tissue, even in asymptomatic capsules. Altogether, our work strongly suggests that variations in gene expression and tissue organization

modifications induced by surface topography might participate to subsequent breast-implant associated etiopathologies.

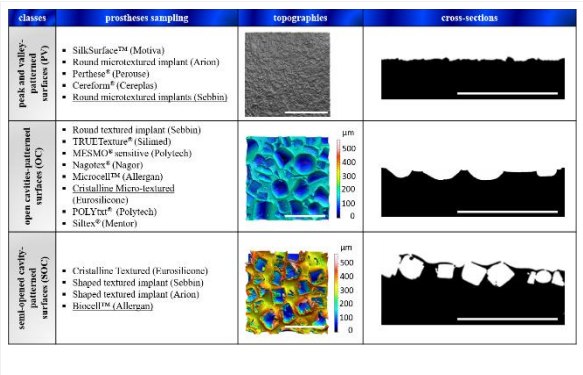

Figure 1
New classification; main features of surface topographies (top-view and cross-sections) shared by implants gathered in one of the 3 classes (PV, OC and SOC)

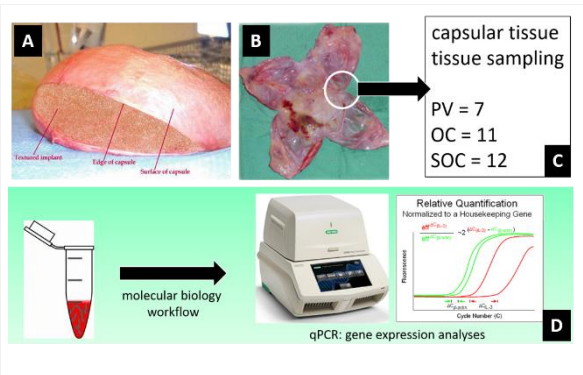

Figure 2
Molecular biology workflow overview: implant capsule adhering to the breast implant (A) is took apart (B), classified (C) and used for both molecular sampling and qPCR analyses (D) and histological analyses (not shown here).

I-OS4-04

From plasma polymer to bladder cancer diagnostic device: A story about the journey from the laboratory to industrial scale production

Thomas D. Michl[1], Kola Ostrikov[1,2], Kit M. Chan[1], Hanieh S. Shirazi[1], Melanie MacGregor[1,2], Simon Belcher[3], Stephen Robb[3], Alex Grochowski[3], Adam DiFiore[3], Jonathan Gleadle[4], Jordan Li[4], Krasimir Vasilev[1,2]

[1]University of South Australia, School of Engineering, Mawson Lakes, AU; [2]University of South Australia, Future Industries Institute, Mawson Lakes, AU; [3]Motherson Innovations, Lonsdale, AU; [4]Flinders University, College of Medicine and Public Health, Adelaide, AU

Introduction

Plasma polymerization is used across a wide range of applications on an industrial scale.[1-3] However, there are only a handful of examples where it is being used for biomedical purposes on such a scale.[4] We aim to generate a novel diagnostic device by using plasma polymerized oxazoline thin films[5] to bind EpCAM antibodies and use this assembly to selectively capture bladder cancer cells from urine.[6] Bladder cancer is the forth most prevalent cancer for men and ninth for women with high rate of recurrence.[7] Thus, accurate and frequent monitoring for recurrence in patients with bladder cancer after treatment and early diagnosis in patients with suspected bladder cancer is imperative to improve treatment outcomes.[8]

Experimental Methods

Our non-invasive device will allow for fast, automated and accurate surveillance or screening at lower cost than current methods. We aim to realize this vision in a cooperation between the University of South Australia, Motherson Innovations and Flinders Medical Centre. Our approach combines the unique chemical and physical properties of oxazoline plasma coatings with the specific biological activity of the EpCAM antibody into a complexly moulded single-use polymer device that can execute automated dispensing and rinsing. The selectively captured bladder cancer cells are then analyzed and evaluated via automated microscopy and image analysis.

Results and Discussion

We demonstrate the selective cancer cell capture for both cell lines, as well as patient derived samples, with good selectivity and specificity. In contrast, cell types not expressing EpCAM are captured at very low levels.

Conclusion

We would like to present the intricacies, challenges and possibilities throughout our interdisciplinary team's journey developing a university-laboratory procedure into a robust industrial grade process. Furthermore, we would like to highlight the synergistic possiblities and avenues possible by collaborating between academia, industry and the medical field.

References

1. Tendero, C., et al., *Atmospheric pressure plasmas: A review.* Spectrochimica Acta Part B: Atomic Spectroscopy, 2006. **61**(1): p. 2-30.
2. Favia, P. and R. d'Agostino, *Plasma treatments and plasma deposition of polymers for biomedical applications.* Surface and Coatings Technology, 1998. **98**(1–3): p. 1102-1106.
3. Hegemann, D., *Plasma polymerization and its applications in textiles.* Indian Journal of Fibre & Textile Research, 2006. **31**: p. 99-115.
4. Förch, R., et al., *Recent and Expected Roles of Plasma-Polymerized Films for Biomedical Applications.* Chemical Vapor Deposition, 2007. **13**(6-7): p. 280-294.
5. Gonzalez Garcia, L.E., et al., *Protein Interactions with Nanoengineered Polyoxazoline Surfaces Generated via Plasma Deposition.* Langmuir, 2017. **33**(29): p. 7322-7331.
6. Macgregor-Ramiasa, M., et al., *A platform for selective immuno-capture of cancer cells from urine.* Biosensors and Bioelectronics, 2017. **96**: p. 373-380.
7. Larre, S., et al., *Screening for bladder cancer: rationale, limitations, whom to target, and perspectives.* Eur Urol, 2013. **63**(6): p. 1049-58.
8. Khochikar, M.V., *Rationale for an early detection program for bladder cancer.* Indian journal of urology : IJU : journal of the Urological Society of India, 2011. **27**(2): p. 218-225.

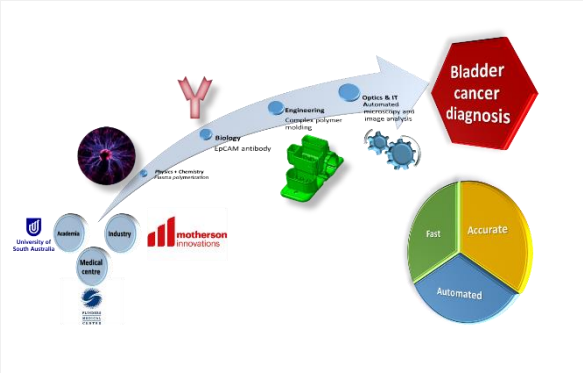

Scheme 1
A complex bladder cancer diagnostic tool, based on a plasma polymer immobilized EpCAM antibody in a fluidic device, was developed in cooperation between academia, industry and medical centre

I-OS4-05

Bioengineering Stem Cell based Nanostructured Tissue Engineered Constructs for Women's Health

Shayanti Mukherjee[1,2], Saeedeh Darzi[1], Kallyanashish Paul[1,2], Fiona Cousins[1,2], Anna Rosamilia[2,3], Jerome Werkmeister[1,2], Caroline Gargett[1,2]

[1]Hudson Intitute of Medical Research, The Ritchie Centre, Clayton, AU; [2]Monash University, Obstetrics and Gynecology, Clayton, AU; [3]Monash Health, Pelvic Floor Disorders Unit, Clayton, AU

Introduction

Pelvic Organ Prolapse (POP) is a debilitating gynecological disorder that affects over 50% of women over the age of 50 years. To overcome adverse events associated with transvaginal surgery using non degradable synthetic mesh for treating pelvic organ prolapse (POP), we are developing a tissue engineering construct comprising degradable nanofibrous mesh and endometrial mesenchymal stem/stromal cells (eMSC). The aim of this study was to investigate the in vitro cell-material properties and in vivo foreign body response to a nano-topographically controlled mesh made of poly (L-lactic acid)-co-poly(e-caprolactone) and gelatin incorporating eMSC (PLCL/G/eMSC). To overcome adverse events associated with transvaginal surgery using non degradable synthetic mesh for treating pelvic organ prolapse (POP), we are developing a tissue engineering construct comprising degradable nanofibrous mesh and endometrial mesenchymal stem/stromal cells (eMSC). The aim of this study was to investigate the in vitro cell-material properties and in vivo foreign body response to a nano-topographically controlled mesh made of poly (L-lactic acid)-co-poly(e-caprolactone) and gelatin incorporating eMSC (PLCL/G/eMSC).

Experimental Methods

PLCL alone and a 1:1 blend with gelatin (w/w) were electrospun from a 10% solution at 1 ml/hr and 18kV over 12.5 cm to form uniform nanofibers and assessed for fibre diameter, pore size, hydrophilicity and biomechanical properties. SUSD2+ eMSC were purified from single cell suspensions obtained from endometrial biopsies from cycling women by magnetic bead sorting and transfected with mCherry lentivirus for cell tracking. SEM was used to characterise eMSC incorporation into the PLCL and PLCL/G nanofiber meshes in vitro and their degradation in NSG mouse skin wound repair model of vaginal repair (2, 6 wks, 4 mice/gp). IF and confocal microscopy was used to assess total (F4/80+), M1 (F4/80+CCR7+) and M2 (F4/80+/CD206+) macrophages.

Results and Discussion

Addition of G to PLCL increased fiber size 40% ($P<0.05$) and pore size 25% ($P<0.05$) rendering meshes hydrophilic without change in tensile properties. In vitro, eMSC rapidly adhered, penetrated, incorporated and proliferated ($P<0.01$) in PLCL/G mesh with a 2.5 fold greater coverage than PLCL alone ($P<0.05$). *In vivo,* mCherry+ eMSC survived 1 wk in PLCL and PLCL/G implanted mesh, but only a few were retained in PLCL/G and none in PLCL at 6 wk. eMSC prevented PLCL/G nanofiber degradation 2 fold ($P <0.0001$) and increased cellular infiltration into the mesh 1.5 fold ($P<0.05$) at 6 wks. eMSC seeded on PLCL/G promoted macrophage switching from M1 to M2 phenotype to a greater extent than similarly seeded PLCL mesh and both meshes implanted without eMSC. There was also an influx of endogenous F4/80- cells (possibly fibroblasts) and collagen matrix deposition into PLCL/G/eMSC implants.

Conclusion

This study shows that degradable nanofiber meshes, in particular PLCL/G boost cell based tissue regeneration without undesirable foreign body response as they enable eMSCs to be retained longer at the site of implantation. Such bioengineered nanostructured meshes have significant potential as alternative surgical constructs for the treatment of POP due to their integration, biocompatibility and performance, which is further improved by combining with eMSC.

Acknowledgement

NHMRC Australia, SIEF and Youanmi Foundation

I-OS4-RF06

Bio-tribocorrosion and trunnion fatigue fractures in total hip arthroplasty – two case reports and review of the literature

Peter G. van Doesburg[1], Evert J. van Langelaan[2], Iulian Apachitei[2], Suzan H. M. Verdegaal[1]

[1]Alrijne Ziekenhuis, Department of Orthopaedic Surgery, Leiderdorp, NL; [2]Delft University of Technology, Biomechanical Engineering Department Biomaterials & Tissue Biomechanics Section, Delft, NL

Introduction

A hip stem fracture, due to metallurgic problems, was a specific complication well known in the past. Better quality stainless steel reduced this problem. In the nineteen-seventies, the concept of head-neck modularity was introduced to provide more intra-operative surgical options. Modularity also led to new problems at the trunnion (head-neck junction), such as wear and corrosion between the head-neck interface (trunnionosis), fractures of the head-neck junction and gross trunnion failures. The problem of corrosion was not recognized, neither seen as a major problem, during a long time. However, new studies show that up to 3% of all total hip reoperations are performed because of trunnionosis. The exact pathology is unknown, but most likely micromotions between the head and the taper causes disruption of the oxide film, leading toa bio-tribocorrosion phenomenon called mechanically assisted crevice corrosion (MACC). Loss of material by corrosion could lead to a trunnion fatigue fracture. Fractures of the trunnion are less frequent and little literature is available on these fractures. A combination of corrosion, implant factors, surgical technique factors and patient factors most likely is the explanation.
The purpose of our study was to identify potential risk factors for the development of trunnion fractures, as well as providing future treatment recommendations in primary hip arthroplasty and hip reoperations to prevent damage of the trunnion and trunnion fractures.

Experimental Methods

A detailed report of two trunnion fractures in one type of hip stem (Mallory Head) is presented, including scanning electron microscopy (SEM) and Energy Dispersive X-ray spectroscopy (EDS) analysis. Thereby, a systematic review of the available literature was performed following the PRISMA guidelines to identify studies on trunnion fractures in Pubmed, Web of Science and Embase. Methodological quality of the included studies was evaluated using a critical appraisal instrument.

Results and Discussion

SEM and EDS analysis were done. SEM analysis demonstrated a typical fatigue fracture with the fatigue fracture originated at the neck surface with standard fatigue marks perpendicular to the crack propagation. SEM analysis of the head side showed a small notch at the surface of the neck that seemed to be the starting point of the fatigue crack. High magnification SEM analysis revealed several specific fatigue fracture features, such as the presence of fatigue striations close to and away from the crack origin, secondary cracks and the presence of the dimple like patterns which characterize the final overloaded fracture. The elemental analysis of the femoral stem performed by EDS indicted that the alloy has a chemical composition close to Ti6Al4V (Ti 90.33wt%, Al 5.69wt% V 3.98wt%).
The systematic review included 24 eligible studies. The included patients had a mean age of 65 years (range 31y - 91y, median 67y), a mean weight of 94kg (range 70kg – 129kg, median 91kg) and a mean BMI of 31kg/m^2 (range 24kg/m^2– 47kg/m^2, median 30kg/m^2). Neck fractures occurred on average 8 years (range 1y – 24y, median 6y) after

hip stem placement. Male gender, high body weight and obesity were identified as risk factors. Thereby, damage to the trunnion during reoperation surgery, is likely to be an important risk factor for fractures. On average, all patients were relatively young at the moment of primary total hip arthroplasty. Two groups of neck fractures were identified: head-neck (trunnion) fractures and neck-shoulder (base of the neck) fractures. Corrosion and the use of long skirted femoral heads were frequently reported in head-neck fractures, whereas 69% of the neck-shoulder fractures were associated with specific metal or implant design fea---tures.

Conclusion

In conclusion, several potential and preventable risk factors were identified, leading to specific recommendations for future hip arthroplasty.

I-OS4-RF07

Genipin cross-linked extracellular matrix hydrogels developed for neural tissue repair

Karel Vyborny[1,2], Kristyna Kekulova[1,2], Jana Vallova[1,2], Sarka Kubinova[1]

[1]Czech Academy of Sciences, Institute of Experimental Medicine, Prague, CZ; [2]Charles University, 2nd Medical Faculty, Prague, CZ

Introduction

Extracellular matrix (ECM) scaffolds prepared by tissue decellularization preserve the composition, mechanical integrity, and biological activity of the native ECM suggesting that the molecular composition of these materials is an active factor in remodeling events. ECM scaffolds can be prepared in the form of an injectable hydrogel, which enables the non-invasive application. In our previous work, we prepared ECM hydrogel derived from human umbilical cord tissue (UC-ECM) and crosslinked it by genipin to improve mechanical stability and endurance to enzymatic degradation. The aim of this study is to further investigate biocompatibility and neurotrophic potential genipin crosslinked UC-ECM hydrogel *in vivo* and *in vitro*.

Experimental Methods

ECM hydrogel was prepared by the decellularization of the human umbilical cord and crosslinked by 0.5-5 mM genipin. The gel was characterized in terms of the crosslinking degree, rheometry, and enzymatic degradation by collagenase. The biocompatibility of crosslinked ECM hydrogels was evaluated by measurement of viability and proliferation of human mesenchymal stem cells (MSCs). The gel contraction was measured in 3D MSC culture. The neurotrophic properties of the crosslinked hydrogels were assessed using dorsal root ganglion (DRG) dissociated culture. To prove crosslinked ECM hydrogel stability in vivo, the hydrogel was injected into the rat brain cortical ischemic lesion to evaluate its retention within the lesion as well as the reaction of the host macrophages/microglia.

Results and Discussion

Crosslinking in a concentration of 1mM improved the stability of the UC-ECM hydrogel and did not show any changes in MSC proliferation as well as axonal sprouting of DRG neurons when compared to uncrosslinked ECM hydrogel. If crosslinked in situ, genipin prolonged the retention of the ECM/G hydrogel within the cortical ischemic lesion without any adverse or proinflammatory effects in the host tissue.

Conclusion

Genipin crosslinking has a significant effect on ECM matrix stabilization and in a concentration 1 mM is biocompatible in vitro as well as in vivo.

References

Koci, Z. et al., Extracellular Matrix Hydrogel Derived from Human Umbilical Cord as a Scaffold for Neural Tissue Repair and Its Comparison with Extracellular Matrix from Porcine Tissues, Tissue Eng Part C Methods, 23(6): 333 (2017)
Tukmachev, D. *et al.* Injectable Extracellular Matrix Hydrogels as Scaffolds for Spinal Cord Injury Repair. *Tissue Eng Part A***22**, 306-317, doi:10.1089/ten.TEA.2015.0422 (2016

Acknowledgement

This project was supported by MEYS of the Czech Republic: LO1309

I-OS4-RF08

Surface functionalisation of magnetic nanoparticles by ß-amyloid 1-42 peptide ($Aß_{42}$)-specific aptamers as a concentration tool in early diagnosis of Alzheimer's disease.

Cheryl M. Collins[1], Valeria Perugini[1], Manuel González Gómez[2], Yolanda Piñeiro[2], José Rivas[2], Matteo Santin[1]

[1]University of Brighton, Centre for Regenerative Medicine and Devices (CRMD), School of Pharmacy & Biomolecular Sciences, Brighton, GB; [2]Universidade de Santiago de Compostela, Departmento de Física Aplicada, Campus Vida, Santiago de Compostela, ES

Introduction

Alzheimer's disease (AD) is a progressive neurodegenerative disorder, which is predominantly characterised by the deposition of insoluble ß-amyloids (Aß) in the brain. AD had an estimated cost to the global economy in 2015 of $817.9 billion, which is projected to rise to $2 trillion by 2030[1] thus there is an unmet clinical need for earlier diagnosis and treatment, which could result in decreased morbidity and mortality. Current biomarker diagnostic tools for patients presenting with cognitive decline include brain MRI and PET scans and ELISA of biomarkers in cerebrospinal fluid (CSF), e.g. Aß analyses. Quantitative data of $Aß_{42}$ obtained by ELISA are limited by sensitivity thresholds in the pg/ml range.

Short peptides (KLVFF) have been shown to inhibit Aß formation and aggregation both *in vivo* and *in vitro*[2] by binding to residues 16-20 of Aß thus could be utilised as peptide aptamers in both diagnostics and drug administration.

The linear peptides can be integrated onto hyperbranched molecular structures called dendrons to increase aptamer capacity, stability and increased sensitivity of Aß detection.

Silica magnetic nanoparticles (MNPs) (Fe_3O_4@SiO_2) have been functionalised with both the linear peptide KLVFF with glycine spacer (GGKLVFF) and a 3rd generation dendrimeric ε-polylysine modified with 16 linear KLVFF peptides (Rgen3K$(KLVFF)_{16}$) as described previously[3]. This work aims to use the Rgen3K$(KLVFF)_{16}$-functionalised MNPs as a concentration tool for ELISA and biosensors in early diagnosis of AD.

Experimental Methods

Third generation ε-polylysine dendrons with an arginine root (Rgen3K) were designed to expose on the uppermost branching generation sixteen linear KLVFF peptides. Rgen3K$(KLVFF)_{16}$ were synthesised using microwave based solid phase peptide synthesis (Biotage, UK) on TentaGel™ S-NH_2 resin and characterised with mass spectrometry and HPLC.

Rgen3K$(KLVFF)_{16}$ dendrons were grafted onto single-core Fe_3O_4@SiO_2 MNPs using carbodiimide chemistry and characterised using Fourier-transform infrared spectroscopy (FTIR). Non-functionalised MNPs were used as a control.

MNPs were treated with a dispersant solution to reduce aggregation that is commonly seen with MNPs. Both control and $(KLVFF)_{16}$-functionalised MNPs were incubated in 100 µl of 1 pg/ml $Aß_{42}$. The MNPs were assayed in a human $Aß_{42}$ Quantikine ELISA (R&D Systems, UK) and the optical density (OD) was measured at 450 nm.

Results and Discussion

Single-core Fe_3O_4@SiO_2 MNPs were successfully functionalised with Rgen3K(KLVFF)$_{16}$ as confirmed by FTIR (see figures).

After assaying MNPs incubated in 1 pg/ml Aß$_{42}$ using ELISA all samples had OD values above the standard curve. The samples were diluted 1 in 10 to bring the OD values within the assay range. The (KLVFF)$_{16}$-functionalised MNPs showed a 4-fold increase in OD compared to the control MNPs indicating the Rgen3K(KLVFF)$_{16}$ dendron captured the Aß$_{42}$.

The ELISA kit used has a sensitivity of 4.7 pg/ml, however (KLVFF)$_{16}$-functionalised MNPs were capable of detecting Aß$_{42}$ at lower concentrations by concentrating the samples due to the hyperbranched dendrons exposing multiple KLVFF aptamers.

Conclusion

The present work shows that single-core Fe_3O_4@SiO_2 MNPs functionalised with Rgen3K(KLVFF)$_{16}$ have the ability to concentrate Aß$_{42}$ in samples. Such a concentration step will enable a considerable increase in the sensitivity of ELISAs for detection of AD biomarkers with potential for earlier diagnosis than current methods.

References

[1]Lewis et al., Trajectory of Dementia in the UK – Making a Difference, report produced the Office of Health Economics for Alzheimer's Research UK, 2014.

[2]Funcke SA. et al., Curr Pharm Des. 18(6): 755-67, 2012.

[3]Perugini V. et al., Poster presentation 512, BSG 2018.

Acknowledgement

FP7 EC grant MADIA, contract number 732678.

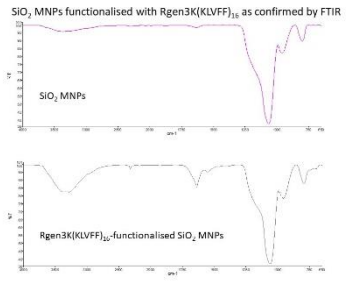

SiO2 MNPs functionalised with Rgen3K(KLVFF)16 as confirmed by FTIR

10:30 a.m. – 12:00 p.m.

Conference room 2+3

I-OS5 | Soft tissues

I-OS5-01

Injectable hybrid PVA hydrogels for nucleus pulposus substitution

Gemma Leone, Marco Consumi, Agnese Magnani

University of Siena, Biotechnology, Pharmacy and Chemistry, Siena, IT

Introduction

Degenerative disc disease mainly originates with the dehydration of the nucleus pulposus (NP), which is the inner hydrogel-like component of the intervertebral disc. Unfortunately, NP exhibits a very low capacity for regeneration [1]. As a consequence synthetic hydrogels have been developed. However, the use of a single polymer does not represent a good solution for the foreseen application because the obtainment of sufficient mechanical properties does not permit an adequate swelling ratio of the hydrogel. The objective of this study was to evaluate the effect of mixing a structural polymer with a hydrophilic polymer in order to join an adequate swelling capability with a correct mechanical performance. Herein, we report the results of preliminary studies on two hybrid hydrogels with potential utility as a nucleus prosthesis.

Experimental Methods

Hydrogels synthesis: Poly-vinyl alcohol (PVA) hybrid hydrogels were synthesized dissolving PVA in basified water (pH= 12). Xanthan gum or Poly-vinyl-pirrolidone (PVP) were then added in different molar ratios to PVA. The crosslinking agent (Sodium trimetaphosphate) was added in a molar ratio 1:1 with PVA and the mixture stirred for 2 h. The obtained hydrogels were purified by washing.

Hydrogel Characterization was performed using standardized procedures already reported [2-3]

The crosslinking reactions were verified with infrared spectroscopy (IR) or Time of Flight Mass spectrometry (TOF-SIMS). The crosslinking density was calculated basing on Rubber Elasticity Theory (RET)

Thermal Analysis: Differential scanning calorimetry (DSC) was used to measure the ice melting behaviour of completely swollen hydrogels, their mesoporosity and heat capacity. Thermal stability was measured by thermogravimetry.

Swelling behavior: The swelling ratio SR% was determined by dipping samples in NaCl 0.9% at 37 °C. The effect of osmotic pressure on swelling ratio was calculated immersing samples in PEG 20000 MW solution

Rheological analysis: all rheological measurements were performed at 37 °C.Frequency sweep tests in shear and compression mode were performed with a shear amplitude over the physiological in the frequency range 1–100 rad/s with a 1% strain. Stress-relaxation and injectability were also evaluated.

Hydrogel cytotoxicity and cytocompatibility: The cytotoxicity and cytocompatibility was evaluated applying the direct contact tests using NIH3T3 mouse fibroblasts and primary Human Chondrocytes.

Results and Discussion

Hydrogel Synthesis: Different pH values, reaction time and concentrations were tested to find the correct parameters to achieve a PVA matrix enclosing PVP or xanthan gum. Starting from a 5% PVA solution and adding xanthan gum in a molar ratio of 1:4 (PX25), 1:2 (PX50) and 1.3:1 (PX75) with PVA, stable hydrogels were obtained as well as adding PVP in a molar ratio of 1:1 (PP11) or 1:3 (PP13) with PVA. Since the crosslinking agent was added in a molar ratio of 1:1 with PVA for all the hydrogels, they showed a similar crosslinking density (mean mesh size: 8 nm). The crosslinking reaction between PVA and STMP was verified by IR analysis whereas TOF SIMS analysis was used to

determine the crosslinking arm length (i.e. one or two phosphate groups) which is affected by the polymer enclosed inside the PVA matrix.
The presence of the hydrophilic polymer (i.e. xanthan gum or PVP) inside the PVA matrix increased the amount of not-freezable water (meaured by DSC), which affected not only the swelling ratio of the hydrogels but also their injectability. All the hybrid hydrogels showed a heat capacity superimposable to that found for human tissue.
Rheological analysis indicated that all the hybrid hydrogel showed a rheological behavior similar to that of human nucleus pulposus. However, hydrogels obtained mixing PVA with Xanthan Gum in a molar ratio 3:1 and mixing PVA with PVP in a molar ratio 1:1 had a significant better performance both in shear and in compression mode. All the hydrogels relaxed very quickly (50% decrease of the peak stress after 1second) and reaching a value close to zero after longer time: 600s).
All the synthesized hydrogels were cytocompatible towards human chondrocytes.

Conclusion

Two different hybrid hydrogels consisting of a PVA based matrix enclosing PVP or Xanthan-Gum were synthesized. The presence of the hydrophilic polymer (i.e. PVP or Xanthan-Gum) inside the matrix was verified with infrared spectroscopy, TOF-SIMS measurements and Thermogravimetric analysis. The presence of the hydrophilic polymer affected the swelling behavior of the hydrogel conferring them injectability without decreasing the mechanical performance guaranteed by the PVA structural polymer or modifying thermal stability and heat capacity of the materials.
Hydrogels obtained mixing PVA with Xanthan Gum in a molar ratio 4:1 (PX25) and mixing PVA with PVP in a molar ratio 1:1 (PP11) had the best performance as nucleus substitute.

References

1. Bowles R.D., et al. Biomaterials for Intervartebral Disc Regeneration and Repair. Biomaterials 2017, 129, 54-67
2. Leone G, et al. Thixothropic PVA hydrogel enclosing a hydrophilic PVP core as nucleu pulposus substitute. Materials Science & Engineering C 2019, 98, 696-704
3. Leone G., et al. Hybrid PVA-xanthan gum hydrogels as nucleus pulposus substitutes. International Journal of Polymeric Materials and Polymeric Biomaterials (in press)

Acknowledgement

Authors thank INSTM for supporting the research

I-OS5-02

Bioresponsive therapeutic nanoparticles for drug-free cocktail therapy and hypoxia amelioration in Bladder cancer

Wen-Hsuan Chen, **Hung-Wei Yang**

National Sun Yat-sen University, Institute of Medical Science and Technology, Kaohsiung, TW

Introduction

Bladder cancer (BC) is the most common malignant disease of urinary tract and 77,000 new BC cases were diagnosed in 2016 in the USA [1]. The recurrence rate of BC is up to 70% after surgery followed by chemotherapy; therefore, more efficient strategies are needed to improve therapeutic efficacy for BC. Anti-cancer thermotherapy is based on the high sensitivity of cancer cells to increased temperature. Heating of a tumor up to 43.5°C leads to irreversible denaturation of proteins, while protein molecules in normal tissue remain intact. Photo-thermal therapy (PTT) is currently considered to be a noninvasive treatment which can broke the cell membrane by Near-infrared (NIR) laser [2]. In addition, to target the tumor intrinsic weaknesses has attracted more attention on killing cancer cells, one of which is the starving therapy [3]. Therefore, to deplete glucose in tumor directly through the glucose-depletion reaction was proposed to implement this therapy, in which glucose is catalytically oxidized to gluconic acid and hydrogen peroxide (H_2O_2) by glucose oxidase (GOD) and consumption of oxygen (O_2). Moreover, many available biocompatible O_2 generation materials (i.e., manganese dioxide; MnO_2) have been utilized to promote endogenous H_2O_2 decomposition to generate O_2 and be resolved into water-soluble Mn^{2+} to enhance the contrast of MR imaging within the tumor microenvironment. Herein, we reported an effective strategy to improve the efficacy of BC treatment by drug-free cocktail therapy including hypoxia amelioration, NIR PTT and H_2O_2 bombardment using O_2-generating magnetic BSA-CuS-MnO_2-GOD NPs.

Experimental Methods

Magnetic BSA-CuS-MnO_2-GOD NPs were prepared as follows. Briefly, different concentration of the Fe_3O_4 and CuS NPs were added to the BSA solution and stirring for 1 h. Then, the ethanol was continuous dropwise into the solution under magnetic stirring (500 rpm) at room temperature till the solution becomes turbid. To stabilize BSA NPs, the turbid solution was stirred continuously for 30 min without further addition of ethanol, and the as-prepared magnetic BSA-CuS NPs were denatured at 70°C for 30 min to form stable magnetic BSA-CuS NPs. Magnetic BSA-CuS-MnO_2-GOD NPs were then prepared follows. A 0.2 mL of activation solution (EDC/NHS) was mixed with 0.2 mL of magnetic BSA-CuS NPs at 25°C and reacted for 30 min in the dark to activate the carboxylic groups of magnetic BSA-CuS NPs then mixed with 0.1 mL of GOD and as-prepared BSA-MnO_2 at 4°C by vortexing for 12 h. The product was then separated from the solution, washed with DI water to obtain magnetic BSA-CuS-MnO_2-GOD NPs. The synthesis of magnetic BSA-CuS-MnO_2-GOD NPs is illustrated in Scheme 1.

Results and Discussion

The formation of magnetic BSA-CuS-MnO_2-GOD NPs as well as magnetic BSA-CuS NPs, BSA-MnO_2 and magnetic BSA-MnO_2-GOD NPs was investigated by measuring their UV–visible absorption spectra. Compared to magnetic BSA-CuS NPs showed a new UV–visible absorption band around 300–400 nm, which could be attributed to the surface plasmon band of MnO_2. Compared to magnetic BSA-MnO_2-GOD NPs showed a new absorption band around 800–1200 nm, which could be attributed to the surface plasmon band of CuS (Figure 1A). The catalytic effect of

magnetic BSA-CuS-MnO_2-GOD NPs toward TMB was also confirmed as shown in Figure 1B. We also investigated the glucose depletion, O_2 generation effect of magnetic BSA-CuS-MnO_2-GOD NPs. The glucose concentration could be significantly reduced to 279 mg/dL from 500 mg/dL after treatment with magnetic BSA-CuS-MnO2-GOD NPs for 1 h but no obvious reduction of glucose concentration in magnetic BSA-CuS-MnO_2 NPs group (Figure 1C). In addition, the MnO_2 on magnetic BSA-CuS-MnO_2-GOD NPs was also resolved into Mn^{2+} in the presence of glucose and glutathione (GSH), resulting in decrease of catalytic ability toward TMB (Figure 1D). We next investigated the NIR PTT effect of magnetic BSA-CuS-MnO_2-GOD NPs, the temperature increased to 49.8°C from 31.4°C after irradiation with 808 nm laser, 1 W/cm^2 for 4 min (Figure 1E and F). Finally, the progression of BC T24 cells could be efficiently inhibited by magnetic BSA-CuS-MnO_2-GOD NPs in the presence of glucose and NIR laser.

Conclusion

In this study, we have successfully prepared magnetic BSA-CuS-MnO_2-GOD NPs and the results shown the magnetic BSA-CuS-MnO_2-GOD NPs are highly biocompatible and potential to be used for MR imaging-guiding drug-free cocktail therapy and tumor microenvironment improvement in BC.

References

[1] Siegel RL, et al. Cancer statistics, 2016. CA Cancer J Clin 2016; 66: 7–30.
[2] S. Sohrabnezhad, et al. Acta Part A: Mol. Biomol. Spectrosc. 123 (2014) 142–150.
[3] Zhang C, et al. Nat. Nanotechnol. 2017, 12, 378-386.

Acknowledgement

This work was supported by the Ministry of Science and Technology ,Taiwan, R.O.C (MOST106-2628-E-110-001-MY3;MOST106-2628-B-110-001-MY4). We would also like to thank the Chang Gung Memorial Hospital.

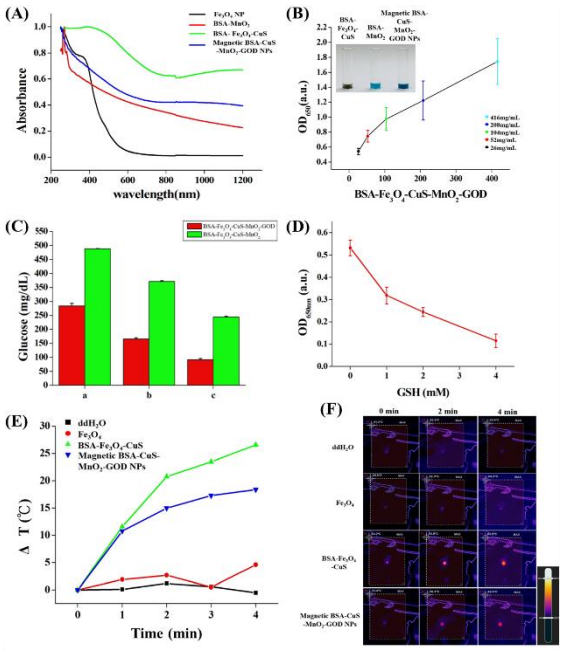

Figure 1. (A) UV–vis absorption spectra of the as-prepared Fe_3O_4, BSA-MnO_2, BSA-Fe_3O_4-CuS, magnetic BSA-CuS-MnO_2-GOD NPs. (B) TMB catalytic ability test of BSA-Fe_3O_4-CuS, BSA-MnO_2, magnetic BSA-CuS-MnO_2-GOD NPs. (C) Comparison of glucose depletion efficiency between BSA-Fe_3O_4-CuS-MnO_2 and BSA-Fe_3O_4-CuS-MnO_2-GOD. (D) TMB catalytic ability test of magnetic BSA-CuS-MnO_2-GOD NPs treated with different concentrations of GSH. (E and F) NIR photothermal efficiency elevation and imaging of Fe_3O_4, BSA-Fe_3O_4-CuS, magnetic BSA-CuS-MnO_2-GOD NPs under laser irradiation (808 nm, 0.76 W cm^{-2}).

Figure 1.

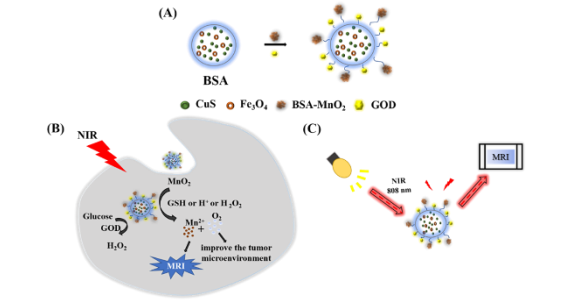

Scheme 1. Schematic diagram of the multifunction Magnetic BSA-CuS-MnO_2-GOD NPs.

Scheme 1.

I-OS5-03

Protein-modified porous membranes as new wound dressing for skin repair

Jana Markhoff[1], Naiana Suter[1], Karsten Stapelfeldt[1], Kurosch Rezwan[2], Dorothea Brüggemann[1]

[1]University of Bremen, Institute for Biophysics, Bremen, DE; [2]University of Bremen, Advanced Ceramics, Bremen, DE

Introduction

Skin consists of multi-structural layers, which range from the outer stiff epidermis to the lower soft dermis. These layers contain a variety of different cell types including fibroblasts and keratinocytes. After an injury, fibrinogen is a key protein in the process of the following blood coagulation. Further, collagens as fundamental proteins of the extracellular matrix (ECM) play an important role in all stages of wound healing. Wound dressings for successful skin healing require adequate mechanical support, biochemical cues and prevention of bacterial infection as key factor in many steps of the wound healing process. Recently, nanoporous anodized aluminum oxide (AAO) membranes were introduced as mechanically stable and biocompatible wound dressing with controlled nanotopography and antimicrobial properties.(1) Nevertheless, porous ceramics do not provide any biochemical cues from proteins and are more stiff than native skin. Hence, the aim of this project is the development of a wound healing system with gradient mechanical properties, which combines biochemical cues from soft protein nanofibers with the advantages of stiff AAO nanopores.

Experimental Methods

First, we used commercial AAO membranes with different pore sizes (20/100/200 nm) for modification with protein nanofibers to evaluate a possible influence on the fiber dimensions and protein scaffold porosity. AAO membranes with other pore diameters were prepared in a home-built anodization setup using oxalic acid. Subsequently, porous nanofiber meshes of collagen and fibrinogen were prepared by pH- and salt-induced self-assembly on glass and on AAO. To mimic the native wound environment with its different skin layers more closely nanofibrous composites of both proteins were also prepared via several approaches.

Subsequently, cell culture experiments were carried out with fibroblasts and keratinocytes. Cellular growth on bare AAO membranes was compared to protein-modified membranes examining the metabolic cell activity with a proliferation assay and the cell morphology and migration using scanning electron microscopy (SEM) and immunostaining combined with fluorescence microscopy.

Results and Discussion

SEM analysis revealed that anodization reproducibly yielded AAO membranes with straight nanochannels (see Fig. 1A). Using pH-induced self-assembly collagen nanofibers with diameters around 150 nm were directly assembled on AAO membranes (see Fig. 1B). For fibrinogen a novel salt-induced self-assembly and transfer method (2,3) was used to prepare nanofibers on AAO membranes. Fibrinogen nanofibers on AAO nanopores were 100 to 300 nm in diameter. Moreover, fabrication of protein composites was successfully realized by combining and tailoring the two different self-assembly routines. The thickness of the respective protein fiber layer in the composites could be adjusted by controlling the protein concentration.

Initial cell culture experiments with fibroblasts and keratinocytes on bare AAO membranes revealed that the metabolic

activity of both cell types was comparable to glass references. SEM analysis showed that fibroblasts in particular exhibited a spread morphology on AAO membranes, which indicated a close interaction with the ceramic nanopores. In preliminary experiments fibroblasts showed adequate cell viability on fiber-modified AAOs compared to bare AAO nanopores.

Conclusion

Our results provide a good base for future cell culture studies on our novel ceramic composites consisting of AAO nanopores with tailored protein nanofiber modifications. Moreover, it will be important to tailor the mechanical characteristics of our novel composites to mimic the mechanical gradient of native skin.

References

1 Poinern, G. E. J., Ali, N. & Fawcett, D. Progress in Nano-Engineered Anodic Aluminum Oxide Membrane Development. Materials (Basel, Switzerland) 4, 487–526 (2011).
2 Stapelfeldt, K., Mednikova, P., Brüggemann, D.: Methods of production of fibrous fibrinogen scaffolds and products thereof, EU patent application PCT/EP2019/051242, 2019.
3 Stapelfeldt, K., Stamboroski, S., Mednikova, P., Brüggemann, D. Fabrication of 3D-nanofibrous fibrinogen scaffolds using salt-induced self-assembly. Biofabrication 11(2) (2019) 025010.

Acknowledgement

We gratefully acknowledge funding via the Emmy Noether Programme and the research training group MIMENIMA (GRK 1860) of the Deutsche Forschungsgemeinschaft.

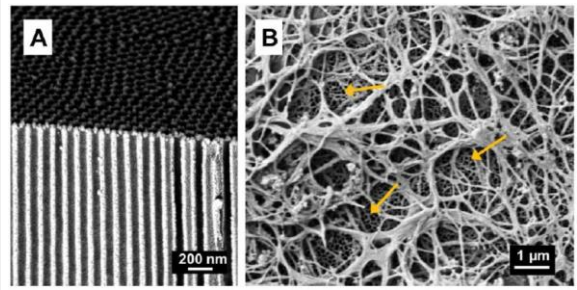

Fig. 1
SEM images of (A) highly aligned AAO nanopores in side view and (B) self-assembled collagen nanofibers on AAO nanopores in top view. Yellow arrows indicate areas where the underlying AAO nanopores are visible.

I-OS5-04

Injectable thermosensitive hydrogels for localized delivery of biomolecules in chronic skin wound treatment

Arianna Grivet Brancot[1], Monica Boffito[1,2], Susanna Sartori[2], Simona Bronco[1], Gianluca Ciardelli[1,2]

[1]Consiglio Nazionale delle Ricerche, Istituto per i processi Chimico-Fisici, Pisa, IT; [2]Politecnico di Torino, Department of Mechanical and Aerospace Engineering, Turin, IT

Introduction

Chronic skin lesions are a global healthcare problem. It is estimated that 2000 people are affected by chronic skin wounds (CSWs) in Italy and approx. 8 and 6.5 million in EU and US, respectively. CSWs strongly impact patients' life, increasing their mortality risk, and healthcare system finance. For this reason, innovative treatments are needed, triggering better tissue repair/regeneration and improving patient's life quality. In this work, thermosensitive, injectable hydrogels based on amphiphilic polyurethanes have been developed as possible drugs (e.g., ibuprofen) and biomolecules (e.g., platelet lysate) carriers.

Experimental Methods

A poly(ether)urethane (PEU) was synthesized starting from a commercially available poly(ethylene oxide)-poly(propylene oxide)-poly(ethylene oxide) (PEO-PPO-PEO) triblock copolymer (Poloxamer P407) [1] and chemically characterized by Size Exclusion Chromatography (SEC) and Fourier Transformed Infrared (FTIR) spectroscopy. PEU aqueous solutions in Phosphate Buffered Saline (PBS) were characterized by tube inverting test and gelation time test at 37 °C to assess their gelation properties. Rheological tests were also performed on selected compositions and gel swelling and stability to dissolution in aqueous media were also evaluated. Injectability was tested in different conditions of temperature (5, 25 and 37 °C) through different needles (G22, G18 and G14) by three potential users of the developed systems. Bovine serum albumin (BSA) and horseradish peroxidase (HRP) were initially encapsulated in the gels as model proteins and their influence on gelation properties was investigated. Release kinetics of both the model proteins and HRP residual activity were studied using colorimetric assays. Finally, platelet lysate (PL) was loaded in the gels and its release profile was colorimetrically evaluated.

Results and Discussion

Success of PEU synthesis was confirmed by FTIR and SEC analysis. Through tube inverting test and gelation time test at 37 °C, a selection of PEU aqueous solutions was carried out to obtain a gelation temperature between 30 and 37 °C and a gelation time in physiological condition within 10 minutes. The selected compositions (8, 15, 18% w/v) were found to be injectable from commercial needles (G14, G18, G22) at 5, 25 and 37 °C. Rheological and stability tests highlighted the possibility to obtain systems with finely tunable mechanical properties and residence time. For instance, systems with an 8% w/v concentration showed fast dissolution in aqueous media, while gels at the two higher concentrations presented a greater PBS absorption and stability to dissolution up to 14 days. The possibility to load the developed gels with biomolecules was first assessed using two model proteins, BSA and HRP. Protein loading within the gel systems did not affect gelation and rheological properties. BSA and HRP were completely released after 3 days of incubation from gels at 8% w/v concentration, while the release was completed after 10-14 days for compositions with higher concentrations. HRP residual activity was finally evaluated to demonstrate that the payload delivered from the gels can retain a biological functionality. About 30-40 % of the enzyme was released in

an active form, in accordance with other literature results for similar systems [2-3]. Similar results were obtained regarding PL encapsulation and release (Fig.1), with no effect on gel properties upon biomolecule encapsulation and a PEU concentration-dependent release kinetics.

Conclusion

A new library of injectable thermosensitive gels with tunable gelation properties and residence time in aqueous systems was successfully designed and thoroughly characterized. The ability of the gels to encapsulate and release proteins and biomolecules with a sustained and controlled kinetics make the newly designed hydrogel platform a promising tool for localized drug/biomolecules delivery in CSWs treatment.

References

[1] Boffito M, Gioffredi E,et al. Polym Int 2016; 65:756-69.
[2] Diniz Oliveira HF, Weiner AA, et al. J Control Release 2008; 126:237-45.
[3] Weiner AA, Bock EA,et al. Biomaterials 2008;29:2400-7.

Acknowledgement

This work was financially supported by PREVISION “Prognostic evaluation of the use of three-dimensional bioactive scaffolds and injectable gels for the treatment of chronic lesions of the skin by means of new biomedical imaging technologies” project, financed by Fondazione Pisa.

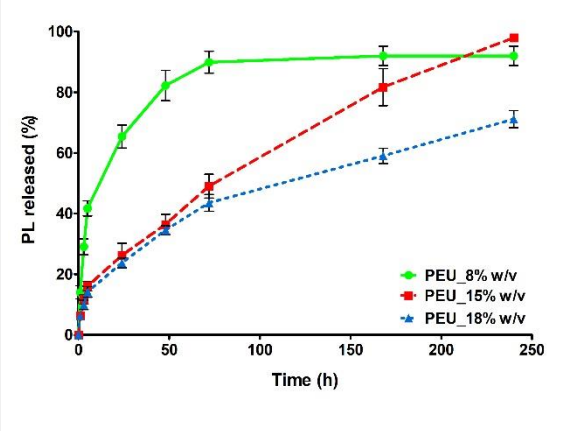

Platelet lysate release
Platelet Lysate release profile from PEU_8% w/v, PEU_15% w/v and PEU_18% w/v hydrogels.

I-OS5-05

Transferring the *in vitro* setup of adipose tissue to an extrusion based bioprinting process with methacrylated gelatin and mature adipocytes

Ann-Cathrin Volz[1], Franziska B. Atzinger[1], Kirsten Borchers[2], Petra J. Kluger[1]

[1]Reutlingen University, Reutlingen Research Institute, Reutlingen, DE; [2]University of Stuttgart, Institute of Interfacial Process Engineering and Plasma Technology, Stuttgart, DE

Introduction

One fourth of the human body consists of white adipose tissue (WAT). WAT interacts with many other organs via paracrine and endocrine signals and through sequestration it impacts the distribution and bioavailable levels of drugs. Additionally, WAT is the origin of different diseases and thus target of several drugs addressing these diseases [1]. Hence, WAT represents a key element for drug screening and safety evaluation and WAT-models are highly needed for *in vitro* investigations. Furthermore, engineered adipose tissue is required as implant to replace lost or damaged tissue in case of congenital deformities, traumata, tumor resections or deep burning wounds.

The transfer of the model's setup to an automated and therefore standardized additive manufacturing process promises to serve with higher reproducibility and thereby higher comparability. Moreover, bioprinting enables the production of individual tissue forms, like e. g. the integration of medium channels, which is inevitable for the setup of large-scale tissue fragments to ensure sufficient supply with nutrients of all cellular components. Additionally, future bioprinting may allow to produce patient- and site specific tissue fragments of distinct shape and volume.

Most of the current attempts in adipose tissue engineering are based on adipose-derived stem cells (ASCs). In contrast to ASCs, mature adipocyte show the powerful feature of a completed differentiation state, including full hormone secretion and mechanical properties in contrast [2]. In this work, it was intended to develop a suitable bioink and adapt the manufacturing process to build up *in vitro* adipose tissue models, based on mature human adipocytes.

Experimental Methods

Mature adipocytes were isolated from human skin biopsies. For the setup of 3D adipose tissue models, different bioink formulations based on methacryl-modified gelatin (varying in composition and concentration) were tested to obtain a soft tissue matrix, gelling at room temperature. The cooling period of the bioink was adapted to avoid phase separation of the different components. For the bioink, including the photoinitiator lithium phenyl-2,4,6-trimethylbenzoylphosphinate (LAP), crosslinking times were adapted. Construct stability was evaluated in *in vitro* culture until day 5. Homogenous cell distribution was evaluated through histological staining, and cell viability was evaluated after the printing process and continuing through the culture. Animal-derived sera are known to impair actual results due to the undefined character of theirs components [3]. Therefore, different serum-free medium compositions were developed and evaluated concerning their suitability in adipocyte maintenance in the 3D models. Cell viability was assessed by the determination of released lactate dehydrogenase. The maintenance of an adipogenic identity was analyzed based on released glycerol and the expression of the adipocyte-specific protein perilipin A up to day 7.

Results and Discussion

An optimized bioink was compiled, which is gelling at room temeprature. Further, the setup process of the tissue model was adapted concerning the prevention of phase separation, thereby leading to the obtainment of a homogenous bioink. Crosslinking time was reduced to the required minimum. By the use of mature adipocytes and the bioink based on methacryl-modified gelatin, we were able to set up adipose tissue models *in vitro*. Tissue models showed homogenous cell distribution and stayed stable in *in vitro* culture. A defined medium for the serum-free 3D culture of mature adipocytes was developed. Cultured models showed maintained cell viability at preserved adipocyte characteristics, like the expression of perilipin A and a limited release of glycerol.

Conclusion

Methacryl-modified gelatin is a suitable biomaterial for the 3D setup of adipose tissue models including mature adipocytes. By the use of emthacryl-modified gelatin the transfer of the model setup to an extrusion-based bioprinting process is enabled. Next steps will include the further adaption of the bioink concerning the polymer composition and concentration to obtain an optimized matrix for the extrusion-based bioprinting process and the adjustments of corresponding printing parameters.

References

[1] A.R. Nawrocki, P.E. Scherer, Keynote review: the adipocyte as a drug discovery target, Drug Discov. Today 10(18) (2005) 1219-30.

[2] P.C. Baer, H. Geiger, Adipose-derived mesenchymal stromal/stem cells: tissue localization, characterization, and heterogeneity, Stem Cells Int. (2012) 2012 812693.

[3] Tissue Res, 362(2) (2015) 269-79.Gstraunthaler G., Alternatives to the use of fetal bovine serum: serum-free cell culture, Altex (2003) 20(4) 275-81.

Acknowledgement

We thank the Ministry of Science, Research and Art Baden-Württemberg and the L-Bank for funding the project EntdefFett (#1099895).

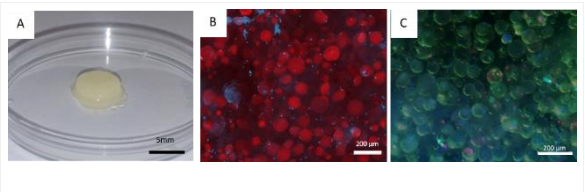

Figure 1: 3D adipose tissue models including methacryl-modified gelatin and mature human adipocytes
(A) Macroscopic image (B) Homogenous cell distribution visible via a Nile red/Hoechst33342 staining (C) Maintained cell viability after the setup displayed with a live/dead staining via fluorescein diacetate, propidium iodid and Hoechst33342.

I-OS5-06

Photocurable Silk Fibroin adhesives for corneal wound repair

Inês A. Barroso[1], Sophie C. Cox[1], Saaeha Rauz[2], Anita K. Ghag[1]

[1]University, Chemical Engineering, Birmingham, GB; [2]University, Institute of Inflammation and Aging, Birmingham, GB

Introduction

Corneal scarring and vascularization are a major cause of blindness worldwide, second only to cataract [1]. This study aims to develop a novel biodegradable adhesive to be used in the treatment of keratolysis (active corneal melting) and perforations, eradicating the need to use toxic materials such as cyanoacrylates for sealing wounds. Due to its excellent biocompatibility, optical clarity and viscoelastic behaviour, silk fibroin (SF, a structural protein) is a promising material for ocular tissue engineering. Fibroin contains amino and carboxylic groups that can be modified with several functional groups. In order to achieve an adhesive which may be photopolymerized *in situ,* this work focuses on SF methacrylation using glycidyl methacrylate (GMA).

Experimental Methods

Degummed SF was dissolved in lithium bromide solution at 60°C. GMA was added to the SF solution at a rate of 0.5 mL/min and allowed to react for 3h at 60°C. Methacrylated-silk fibroin (SF-MA) was then dialysed against deionised water for 7 days. Finally, the solution was lyophilised for 2 days to generate a white porous foam. The degree of methacrylation (DM%) was quantified by proton nuclear magnetic resonance (^{1}H-NMR). Hydrogel precursor solutions were prepared by dissolving freeze-dried SF-MA in PBS at various concentrations. Then, both SF-MA and photoinitiator solutions were mixed together and injected in a custom-made mould. The hydrogel precursor solutions were photocured with UV light a using an OmniCure S1500 (Lumen Dynamics, Ontario, Canada) and characterized in terms of transmittance (Spark Multimode, Tecan, Switzerland) and mechanical properties (Kinexus pro+, Malvern, UK).

Results and Discussion

Fibroin was methacrylated through the reaction with GMA with the free amines in the lysines introducing vinyl groups in the SF polymer chain. This modification was confirmed by the reduction of the lysine signal at d= 3 ppm and the appearance of the vinyl group signal at d= 6.2 ppm (Fig. 1). SF-MA with low and medium DM% were obtained by varying the amount of GMA added from 5 to 10 % (v/v). Both SF-MA and photoinitiator solutions were mixed together at different concentrations. Once the hydrogel precursor solutions are exposed to a specific wavelength, the photoinitiator decomposes into active radicals which attack the vinyl monomers in SF-MA (C=C double bonds), triggering a rapid free radical polymerization reaction. Our results have shown that even for low DM%, hydrogels can be obtained within 2 minutes (Fig.2). SF-MA hydrogels presented an average transmittance in the visible of 83 ± 5 %. Importantly, the mechanical properties of the tissue-engineered materials are known to influence cellular response. The SF-MA hydrogels had solid-like behaviour with a phase angle of 9.8°.

Conclusion

In situ forming adhesives are very attractive materials due to their ability to adapt to the shape of the keratolysis or perforation before being cured. Importantly, the mechanical properties of SF-MA are controllable by changing the

DM% and the polymer concentration. The application of biocompatible adhesives that enhance tissue regeneration, could reduce the demand of human corneal transplants, and the use of cyanoacrylates and sutures.

References

[1] - Whitcher JP, Srinivasan M, Upadhyay MP. Corneal blindness: a global perspective. *Bull World Health Organ*. 2003;79(3):214-21.

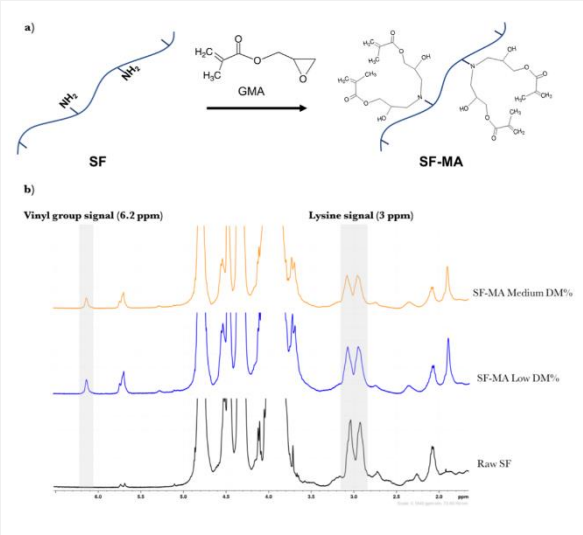

Fig 1.
a) Chemical modification of SF with GMA. Theoretically, two GMA molecules can react with one lysine group (0.2 mol%). The vinyl monomers in SF-MA work as light- crosslinking sites. b) 1H-NMR spectra of raw silk fibroin, SF-MA with low DM% and SF-MA with medium DM%.

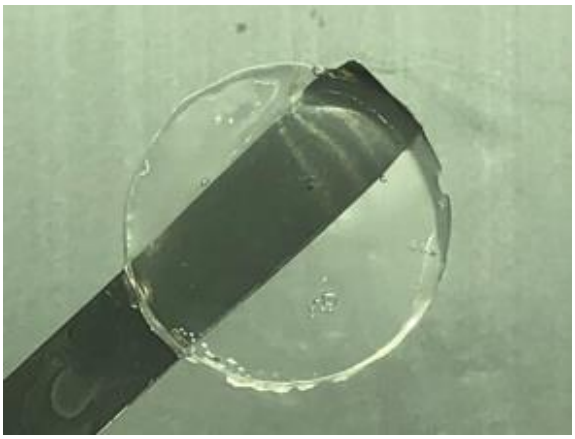

Fig.2
SF-MA hydrogel with a diameter of 12mm.

1:00 p.m. – 2:30 p.m.

Hall 3

II-OS6 | Hydrogels for tissue engineering 1

II-OS6-01

Injectable oligomer-cross-linked chitosan hydrogels and nanocomposite hydrogels as potential regenerative materials

Iram Maqsood[1], Jörg Lenzner[2], Hafiz Awais Nawaz[1], Michaela Schulz-Siegmund[1], Michael C. Hacker[1]

[1]Leipzig University, Institute of Pharmacy, Pharmaceutical Technology, Leipzig, DE; [2]Leipzig University, German Faculty of Physics and Earth Sciences, Leipzig, DE

Introduction

Chitosan (Cs) is the most promising natural biomaterial utilized for bone tissue engineering due to its inherent antibacterial properties, structural similarity with extracellular matrix (ECM) components of tissues, bioactivity, biodegradability and osteoconductivity. Injectable chitosan formulations typically utilize a physical gelation strategy. Covalent cross-linking, however, might yield materials of higher stability and better control over gel properties. Anhydride group-bearing oligomers developed in our group [1] have been successfully used for the formation of hydrogels with different gelatin fractions [2]. Under appropriate conditions, the oligomers should be suitable for chitosan cross-linking by amide formation with the amino groups in chitosan. In this project, we aim at the development and characterization of injectable oligomer-cross-linked chitosan hydrogel (*i*Csgel) and nanocomposite hydrogel (*i*CsNC), by combination of newly developed protein nanoparticles (NP), as reinforcing fillers and delivery devices, and oligomer-cross-linked chitosan as gel matrix.

Experimental Methods

OPMoMA-x {oligo (pentaerythritol diacrylate monostearate-*co*-acryloyl morpholine-*co*-maleic anhydride} have been synthesized in different compositions according to established protocols [3] by free radical copolymerization. *Analytical techniques*:^{1}H-NMR, ^{13}C-NMR spectroscopy, FTIR-ATR (for chemical composition), acid-base titration (for MA content), GPC (for molecular weight).

Results and Discussion

*I*Csgel were fabricated *in situ* by cross-linking pH-adjusted Cs solution with anhydride-containing oligomers. For *i*CsNC fabrication, lyophilized protein NP were dispersed in Cs solution prior to gelation. The gelation reaction and the resulting gels were rheologically characterized. Swelling and degradation of gel/NC were monitored by immersing lyophilized gel/NC in PBS at 37°C for 6 weeks while porosity of gel/NC were determined by immersing lyophilized gel/NC in absolute ethanol overnight. Cytocompatibility and cell proliferation of cell-laden (L929 mouse fibroblasts) *i*Csgel and *i*CsNC were assessed with Live/Dead® and Alamar blue® assay.

Cross-linker oligomers of different anhydride contents were utilized and gels with significantly improved stability were obtained as compared to physically gelled Cs. Entrapment of NP into gel matrix increased gel modulus (up to 100%) but decreased porosity in a concentration-dependent manner. All chemically cross-linked gel/NC showed constant swelling and less water uptake as compared to control. *i*Csgel and *i*CsNC with oPMoMA-4, -5 and -10 were found to slowly degrade with less than 30% mass loss in first 3 weeks. OPMoMA-4 and -5 cross-linked gel/NC found to be most optimal formulations with total 50% mass loss in 6 weeks. Gel/NC water content and degradative properties correlated well with cross-linker chemistry. Physical chitosan gel disintegrated completely in two weeks while oPMoMA-10 cross-linked gel/NC was found to be most stable of all with only 20-30% of total mass loss in 6 weeks. Mass loss correlated inversely with anhydride content of the oligomer. Structural analysis of *i*Csgel and *i*CsNC by

SEM revealed porous and interconnected structure, moreover, visible and homogenous distribution of NP was found throughout the gel matrix of *i*CsNC.
Cell-laden *i*Csgel and *i*CsNC revealed good cell survival and proliferation in the gel/NC matrix. CLSM images of L929 fibroblast-laden oligomer-cross-linked chitosan gel/NC revealed good cell viability, migration and proliferation in the gel/NC matrix after 3d and 7d. This microscopic impression was quantitatively confirmed by increase in cell number in the oligomer cross-linked gel/NC. However, in the gels cross-linked with MA-10 oligomers, some cells died on 1d and 3d due to the high cross-linking density and rigid nature of the gels. Nevertheless, cells recovered and proliferated over the course of one week.

Conclusion

Oligomer-cross-linked *i*Csgel and *i*CsNC with biologically relevant mechanical properties represent a promising material platform that can further be covalently functionalized and is already promising for drug and cell delivery. *i*Csgel and *i*CsNC will be further investigated for regenerative applications.

References

[1] Loth T et al., Reactive and Functional Polymers 73, 1480-1492 (2013)
[2] Loth T et al., Biomacromolecules 15, 2104–2118 (2014)
[3] Kascholke C et al., Biomacromolecules 18 (3), 683–694 (2017)

Acknowledgement

Financial support by the DAAD and the Deutsche Forschungsgemeinschaft (DFG) – Projektnummer 59307082 – TRR67 (A1)

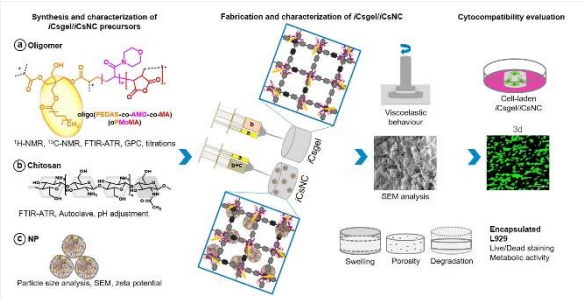

Injectable oligomer-cross-linked chitosan hydrogels and nanocomposite hydrogels (iCsgel/iCsNC)

Injectable oligomer-cross-linked chitosan hydrogels and nanocomposite hydrogels (iCsgel/iCsNC): Precursors synthesis and characterization, gel/NC fabrication and cytocompatibility evaluation

II-OS6-02

Development of a cell-free and growth factor-free hydrogel capable to induce angiogenesis and innervation after subcutaneous implantation

Bruno Paiva dos Santos[1], Bertrand Garbay[2], Elisabeth Garanger[2], Sebastien Lecommandoux[2], Hugo Oliveira[1], Joelle Amédée[1]

[1]Bioingénierie Tissulaire (BioTis), Inserm U1026, Bordeaux, FR; [2]Laboratoire de Chimie des Polymères Organiques (LCPO), UMR 5629 CNRS, Pessac, FR

Introduction

Despite significant progress in the field of biomaterials for bone repair, the lack of attention to the vascular and nervous networks within bone implants could be one of the main reasons for the delayed or impaired recovery of bone defects. The design of innovative biomaterials should improve the host capacity of healing to restore a functional tissue, taking into account that the nerve systems closely interact with blood vessels in the bone tissue [1]. The aim of this work is to develop a cell-free and growth factor-free hydrogel capable to promote angiogenesis and innervation.

Experimental Methods

To this end, we used elastin-like polypeptides (ELPs), poly(ethylene glycol) (PEG) and the laminin-derived adhesion peptide IKVAV (or the scrambled VKAIV, used as control) in increasing concentrations (25 % (w/w) representing 1.65 µM and 50 % (w/w) representing 4.13 µM) to formulate and produce hydrogels. Hydrogels were characterized for rheological properties, degradation *in vitro*, microstructure and biologically, the response of primary cultures of mesenchymal stromal cells (MSCs), endothelial cells (ECs) and sensory neurons (SNs) was assessed. The hydrogel formulation with the best performance *in vitro* was implanted subcutaneously in mice.

Results and Discussion

When characterized *in vitro*, hydrogels had fine-tunable rheological properties according to final hydrogel concentration, a microporous structure with pores varying between 10-15 µm and they are biocompatible. When MSCs were cultured in these hydrogels in osteogenic medium, the 50 % IKVAV composition up-regulated *Runx2*, Osx, *Spp1*, *Vegfa,* and *Bmp2* (Figure 1A-E). For ECs, the expression of *Tek* was also up-regulated in 50 % IKVAV composition (Figure 1F). In addition, for SNs, cells behaved distinctly in hydrogel compositions: neurites could outgrowth when IKVAV concentration was increased. The 50 % IKVAV composition induced the formation of the longest neurite length relative to all other compositions (Figure 1G). Interestingly, all of these parameters (gene expression and neurite length) had the behavior proportional to the IKVAV concentration. When implanted subcutaneously in mice for 11 and 26 days, the response of 50 % IKVAV and its scrambled was analyzed for inflammation, vessel formation, and innervation. Firstly, no signals of major inflammation were observed for both compositions. After specific immunolabelling, we observed a higher vessel density in 50 % IKVAV implantation after 26 days compared to the scrambled. For the innervation potential, the formation of nervous structures was observed only surrounding the IKVAV composition implantation for both time points.

Conclusion

The ELP-based composite 50 % IKVAV has important features for tissue engineering, showing osteogenic, angiogenic and innervation potential *in vitro*, being not inflammatory *in vivo*, and inducing angiogenesis and innervation subcutaneously.

References

[1] Marrella A *et al.*, Mater Today (2018) 21:362-76, doi: 10.1016/j.mattod.2017.10.005

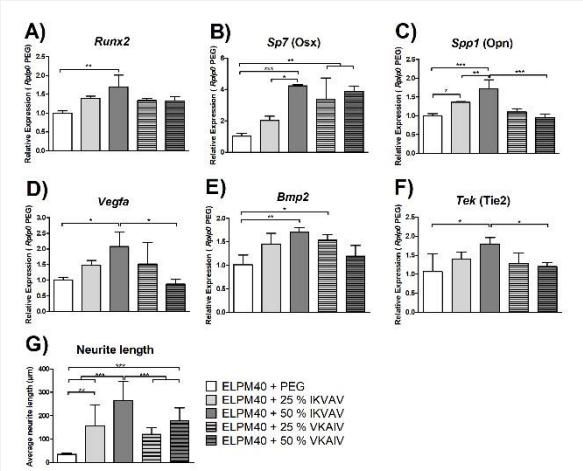

Figure 1. In vitro response of MSCs, ECs and SNs response to hydrogel forumations
Mesenchymal stromal cells (MSCs), endothelial cells (ECs) and sensory neurons (SNs) response after 7 days of culture in ELPM40 + PEG, ELPM40 + 25 % IKVAV, ELPM40 + 25 % VKAIV, ELPM40 + 50 % IKVAV and ELPM40 + 50 % VKAIV compositions. (A-E) MSCs gene expression of osteogenic markers and important genes for the bone repair process, (F) ECs gene expression, and (G) the average neurite length. Data are represented as average ± SD, with statistical differences indicated as *p<0.05, **p<0.01 and ***p<0.001 (ANOVA with Bonferroni test as post-hoc).

II-OS6-03

Evaluating stress relaxation of poly(acrylamide-co-acrylic acid) hydrogels

Emilie Prouvé[1,3,5], Bernard Drouin[1,2], Pascale Chevallier[1,2], Marie-Christine Durrieu[3,4,5], Gaétan Laroche[1,2]

[1]Université Laval, Laboratoire d'Ingénierie de Surface, Centre de recherche du CHU de Québec, Québec, CA; [2]Université Laval, Département de génie des mines, de la métallurgie et des matériaux, Québec, CA; [3]Université de Bordeaux, Chimie et Biologie des Membranes et Nano-Objets (UMR5248 CBMN), Pessac, FR; [4]CNRS, CBMN UMR5248, Pessac, FR; [5]Bordeaux INP, CBMN UMR5248, Pessac, FR

Introduction

Chemically cross-linked hydrogels are often used due to the ease to control their physical properties, such as matrix elasticity and porosity [1]. The interest in hydrogel materials for tissue engineering is growing rapidly essentially because their water content closely matches that of biological tissues [2]. While many studies have evaluated the impact of hydrogel stiffness on cell behavior, it is now acknowledged that hydrogels, as well as biological tissues, are intrinsically viscoelastic. Therefore, studying hydrogel viscoelasticity might be of great interest as some studies demonstrated that hydrogel stress relaxation can influence cell behavior in terms of cell proliferation and stem cell differentiation [1,3]. Our goal is therefore to characterize the stress relaxation behavior of poly(acrylamide-co-acrylic acid) hydrogels to further evaluate the effect of matrix stiffness and viscoelasticity on the phenotype and differentiation pathway of mesenchymal stem cells.

Experimental Methods

Poly(acrylamide-co-acrylic acid) hydrogels synthesis was made according to the method described by Zouani *et al*. [4]. The amount of crosslinking agent (bis-acrylamide) was varied from 0.03 to 0.48 mol% to obtain hydrogels with different stiffnesses. The total monomer content was kept constant with an acrylamide/acrylic acid ratio ranging from 100/0 mol% to 82/18 mol%. Hydrogels mechanical properties were assessed with compression stress relaxation tests on round samples of 10 mm diameter and 2 mm thickness, and with 5 steps of 3% compression at 1 mm/min and a relaxation time of 1h50 between two compression steps.

Results and Discussion

Between 3 and 15% compression, which is the range of strains exerted by cells on hydrogels [1], modulus ranging from 5 ± 1 kPa to 145 ± 3 kPa are measured for polyacrylamide hydrogels with 0.03% and 0.48% of bis-acrylamide, respectively (Figure 1). It has been found that the addition of acrylic acid decreases the modulus. Furthermore, the exponential equation describing the stress relaxation behavior of the hydrogels as a function of time may be accurately fitted using three time constants. The first one, characteristics of mechanisms of short duration (tens of seconds) can be related to reorganization of free water. The polymer viscoelasticity is described by the second time constant (hundreds of seconds), while the longer time constant (thousands of seconds), is mostly contributing to the gel relaxation, originating from the material poroelasticity, which is the movement of water inside the pores of the hydrogel [1]. It has been shown that the higher the amount of acrylic acid, the stronger the relaxation. This is due to the generation of negative charges by acrylic acid, creating electrostatic repulsion between polymer chains and therefore increasing their possibilities to reorganize [5]

Conclusion

The hydrogel mechanical characterizations presented above allow to confirm that it is possible to modulate poly(acrylamide-co-acrylic acid) hydrogels stiffness by controlling the amount of crosslinking agent in the reactional mixture, which, in turn, is likely to affect MSCs differentiation fate. Modelling these hydrogels stress relaxation behavior revealed the contribution of three different phenomena, with a higher extent of relaxation by adding acrylic acid, which might have an impact on cell differentiation. Future works will aim at grafting cell signaling molecules, thanks to the carboxylic acid functions of acrylic acid, therefore providing a second level of control over cell differentiation.

References

1. Chaudhuri, O. *et al.Nat. Mater.***15,** 326–334 (2016).
2. Oyen, M. L. *Int. Mater. Rev.***59,** 44–59 (2014).
3. Chaudhuri, O. *et al.Nat. Commun.***6,** 1–7 (2015).
4. Zouani, O. F. *et al. Biomaterials***34,** 2157–2166 (2013).
5. Holback, H. *et al. Biomedical Hydrogels* (Woodhead Publishing Limited, 2011).

Acknowledgement

This work was supported by the University of Bordeaux and the National Science and Engineering Research Council (NSERC) of Canada.

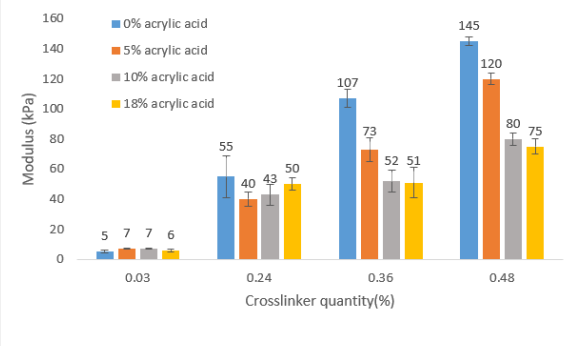

Figure 1
Modulus of polyacrylamide and poly(acrylamide-co-acrylic acid) hydrogels as a function of crosslinker and acrylic acid contents.

II-OS6-04

Bioactive multicomponent injectable hybrids – structural stabilization via attachment of inorganic particles to the biopolymeric network

Joanna Lewandowska-Łańcucka[1], Adriana Gilarska[1,2], Aleksandra Buła[1,3], Wojciech Horak[4], Anna Łatkiewicz[5], Maria Nowakowska[1]

[1]Jagiellonian University, Faculty of Chemistry, Kraków, PL; [2]AGH University of Science and Technology, Faculty of Physics and Applied Computer Science, Kraków, PL; [3]Jagiellonian University, Faculty of Physics, Astronomy and Applied Computer Science, Kraków, PL; [4]AGH University of Science and Technology, Faculty of Mechanical Engineering and Robotics, Department of Machine Design and Technology, Kraków, PL; [5]Jagiellonian University, Laboratory of Field Emission Scanning Electron Microscopy and Microanalysis at the Institute of Geological Sciences, Kraków, PL

Introduction

Tissue engineering (TE) as an interdisciplinary field of research aiming at the regeneration of living tissue has shown a great potential to overcome the limitations of existing treatments [1]. One of the key element of the TE procedures are three-dimensional scaffolds that should serve as a temporary extracellular matrix (ECM) [2]. Fabrication of the scaffold that would meet all demanding conditions for maintaining cell growth and enabling their differentiation is still a great challenge. Various types of materials have been tested for scaffold designing application and it has been concluded that their proper choice is a key factor for the success of a future bioimplantation [3,4].

This work presents the results of our studies on the physico-chemical and the biological properties of the novel bioactive injectable hybrids fabricated from collagen/chitosan/hyaluronic acid based hydrogels and surface modified silica particles. The novelty of the proposed herein approach involves the application of the amino-functionalized silica particles that provides the possibility to attach the silica particles to the polymeric network on crosslinking with genipin (known to react with the primary amino groups). It is expected that the simultaneous reaction with amino groups present in the biopolymers forming matrix and with these present at the surface of the dispersed silica particles will allow to obtain stable hybrid material in which the unfavourable process of aggregation and phase separation of the silica particles could be avoided. This approach seems to be especially important when considering application of scaffolds prepared from hybrid materials under *in vivo* conditions.

Experimental Methods

The obtained in one-pot synthesis amino-functionalized silica particles were characterized by means of DLS, SEM, XPS and FTIR analyses. The parameters characterizing their porosity were determined from nitrogen adsorption-desorption measurements. The hybrids of various compositions were obtained and characterized in terms of their physicochemical and biological features. The swelling ratio, wettability, degradation as well as mechanical properties of the hybrid materials developed were examined. The mineralization process was conducted under *in vitro* conditions in the presence of SBF. Moreover, proliferation, morphology and adhesion as well as functional activity of osteoblast MG-63 cells were assessed in *in vitro* cell culture studies carried out on the surface of materials developed.

Results and Discussion

We have developed the novel multicomponent, bioactive hybrid materials, which can be prepared as sols and crosslinked *in situ* with formation of hydrogels. Materials developed are based on collagen/chitosan/hyaluronic acid biopolymeric hydrogel matrix in which the bioactive phase in the form of amino-functionalized-silica particles were

dispersed. The successful modification of the silica particles and the coexistence of surface-exposed amino and silanol groups crucial for induction of apatite-like mineral formation was confirmed employngf DLS, SEM, XPS and FTIR analyses. The application of the amino-functionalized silica particles provides the possibility to attach these particles to the polymeric hydrogel network on crosslinking with genipin as it was confirmed by degradation and swelling examinations. Employing *in situ* rheological examination, we have confirmed the injectability potential of hybrids developed which is important parameter since it enables the formation of scaffold in the bone defect area in the minimally invasive way. The *in vitro* experiments performed under simulated body fluid (SBF) conditions revealed that the inclusion of the amino-functionalized silica particles at defined concentration into the biopolymeric hydrogel matrices enhances the biomineralization process. Finally, the *in vitro* cell culture studies shown that the prepared materials are biocompatible as they supported MG-63 cells adhesion and proliferation as well as an ALP expression.

Conclusion

Obtained hybrids were fully characterized to demonstrate that the proposed herein one-step method of their fabrication deliver the materials characterized by desirable physical and viscoelastic features while providing a favorable bioactivity and environment for osteoblasts functionality.

References

[1] R. Mishra, T. Bishop, I. L. Valerio, J. P. Fisher, D. Dean, The potential impact of bone tissue engineering in the clinic, Regen. Med. 11 (6) (2016) 571-587.

[2] A. Martínez, M. D. Blanco, N. Davidenko, R. E. Cameron, Tailoring chitosan/collagen scaffolds for tissue engineering: Effect of composition and different crosslinking agents on scaffold properties, Carbohydr. Polym 132 (2015) 606-619.

[3] A. Gilarska, J. Lewandowska-Łańcucka, W. Horak, M. Nowakowska, Collagen/chitosan/hyaluronic acid–based injectable hydrogels for tissue engineering applications–design, physicochemical and biological characterization, Colloids Surf. B: Biointerfaces 170 (2018) 152-162

[4] J. Filipowska, J. Lewandowska-Łańcucka, A. Gilarska, Ł. Niedzwiedzki, M. Nowakowska, In vitro osteogenic potential of collagen/chitosan-based hydrogels-silica particles hybrids in human bone marrow-derived mesenchymal stromal cell cultures, Int. J. Biol. Macromol. 113 (2018) 692–700.

Acknowledgement

JL-Ł acknowledges the financial support of National Science Centre, Poland, grant 2016/21/D/ST5/01635. AG has been partly supported by the EU Project POWR.03.02.00-00-I004/16.

II-OS6-05

Influence of Polyacrylamide Hydrogel Stiffness on Podocyte morphology, phenotype and mechanical properties.

Maya S. Abdallah[1], Marta Martin[3], Sebastien Balme[1], Frederic Cuisinier[5], Csilla Gregely[3], Mario Tahchi[2], Wissam Faour[4], Maria Bassil[2], Mikhael Bechelany[1], Collaboration with bioengineering and nanoscience Laboratory LBN - EA4203, Montpellier, France

[1]University of Montpellier - France, Institut Européen des Membranes (IEM), Montpellier, FR; [2]Lebanese University - Lebanon, Biomaterials and Intelligent Materials Research - Laboratory, Faculty of Science II, Physic Department, Beirut, LB; [3]University of Montpellier II - France, Charles Coulomb Laboratory UMR 5221 CNRS-UM2, Montpellier, FR; [4]School of medicine - Gilbert and Rose Marie Chaghoury, School of Medicine Research Laboratories, Jbeil, LB; [5]University of Montpellier - France, Bioengineering and nanoscience Laboratory LBN - EA4203, Montpellier, FR

Introduction

Chronic kidney disease (CKD) is characterized by reduced kidney filtration that progresses to end-stage renal disease (ESRD). Podocytes are highly specialized glomerular epithelial cells which form with the glomerular basement membrane (GBM) and capillary endothelium the glomerular filtration barrier (GFB) [1]. Extracellular matrix (ECM) acts as a mechanical support and provides biophysical signals in order to control podocytes behavior, essential component of kidney filtration. Many materials have been used as ECM like Polyethylene Glycol (PEG) [2] and Gelatin [3]. The modulus of elasticity E or stiffness is an essential characteristic of the ECM that controls the cell function [4]. Hydrolyzed Polyacrylamide (PAAm) hydrogel is a non-toxic cross linked polymer, which is characterized by its high water content, non-biodegradability and biocompatibility. The hydrogel properties provide a resemblance to tissues giving an opportunity to be applid in biomedical applications [5]. Therefore, hydrolyzed PAAm hydrogel is investigated for its potential use as a new construct to engineer a functional in vitro glomerular-like filtration barrier and to regulate Podocyte cell functions by controlling the physical properties (morphology, swelling and stiffness) of PAAm membrane acting as an ECM.

Experimental Methods

In this work, several PAAm Hydrogels layers were prepared by changing the crosslinker concentration. The physicochemical properties of PAAm hydrogels have been tailored over a wide range of crosslinker concentration. The macromolecular microstructure and stiffness are evaluated by Scanning Electron Microscopy (SEM) and Atomic Force Microscopy (AFM) techniques respectively. In addition, podocytes behavior cultured on PAAm hydrogels are evaluated by immunostaining the actin cytoskeleton and determining their mechanical properties using AFM.

Results and Discussion

Accordingly, the mechanical properties and the polymeric network porosity can be effectively controlled by modulating the crosslinker concentration as well as the swelling degree. Moreover, modulating gel stiffness significantly influenced podocyte behavior including morphology, actin cytoskeleton reorganization and mechanical properties.

Conclusion

In conclusion, podocytes response to the variation of the mechanical properties of the membranes correlated with the hydrogels stiffness. This work addresses the complexity of podocytes behavior which will further enhance our knowledge to develop a kidney-on-chip model much needed to study kidney function in both health and disease states.

References

Michaud, J.-Louis R. and Chris R.J. Kennedy, The podocyte in health and disease: insights from the mouse. Clinical Science, 2007. 112(6): p. 325-335.

2. Chiu, Y.-C., et al., Evaluation of Physical and Mechanical Properties of Porous Poly (Ethylene Glycol)-co-(L-Lactic Acid) Hydrogels during Degradation. PLoS ONE, 2013. 8(4): p. e60728. a b 100mm 100mm

3. Hu, M., et al., A biomimetic gelatin-based platform elicits a pro-differentiation effect on podocytes through mechanotransduction. Scientific Reports, 2017. 7: p. 43934.

4. Tse, J.R. and A.J. Engler, Preparation of Hydrogel Substrates with Tunable Mechanical Properties, in Current Protocols in Cell Biology. 2001, John Wiley & Sons, Inc.

5. Christensen, L.H., et al., Long-Term Effects of Polyacrylamide Hydrogel on Human Breast Tissue. Plastic and Reconstructive Surgery, 2003. 111(6): p. 1883-1890.

Acknowledgement

The authors would like to thank the financial support from CEFIPRA (Project 5608-1), the CNRS (Project “Osez l’Interdisciplinarité”) and the MUSE project (3DTriatCancer). This project has been funded as well by the National Council for Scientific Research in Lebanon and the Lebanese University.

II-OS6-RF06

Oxidized Alginate Hydrogels from Mixed Secondary Aldimine Crosslinkers Exhibit Tunable Mechanical and Viscoelastic Properties

Francis L. C. Morgan, Shahzad Hafeez, Huey Wen Ooi, Lorenzo Moroni, Matthew B. Baker

Maastricht University, MERLN Institute for Technology-Inspired Regenerative Medicine, Maastricht, NL

Introduction

Biomaterials for enhanced tissue regeneration are becoming increasingly prevalent. However, rationally designing materials that mimic the ECM and local tissue environments is a non-trivial task. The extra-cellular matrix (ECM) contains a complex cocktail of biopolymers and signaling molecules, which together, can be broadly considered as a viscoelastic bio-functionalized hydrogel. It has been shown that material parameters such as the stiffness and relaxation time of a hydrogel can have a significant impact on the observed cellular responses.[1] Presented with the diversity of stiffness and relaxation characteristics of native tissues; the scope of any single material system has distinct limitations. Capturing the complexity of this natural microenvironment in a single cytocompatible material remains an active challenge within the community, and to this end, dynamic covalent chemistry (DCC) has emerged as a powerful tool. Diverse DCCs have been shown to tune mechanical and viscoelastic properties of both bulk and local environments over a wide range of physiologically relevant magnitudes.[1]. We recently investigated the use of alginate hydrogels using secondary aldimine crosslinks as a bioink and they were shown to be cytocompatible, as well as induce a different cellular morphology depending on their dynamicity and stiffness (Figure 1.).[2] Here, we explore how varying combinations of the aforementioned crosslinkers can be used to modulate and control the stiffness and relaxation characteristics of oxidized alginate hydrogels.

Experimental Methods

Sodium Alginate (FMC Manugel GMB, Lot No. G9402001) was purified and oxidized to a 10% theoretical degree of oxidation as previously reported.[2] Hydrogels were formed by the addition of varying proportions of adipic acid dihydrazide (≥98%, Sigma Aldrich) and O,O'-1,3-propanediylbishydroxylamine dihydrochloride (98%, Sigma Aldrich). In all cases, the final alginate concentration attained was 2% (*w/v*) in Phosphate Buffered Saline (PBS) without magnesium and calcium ions. The alginate and cross-linker (1:1 with respect to degree of oxidation) were mixed rapidly in the desired ratio before being transferred to silicon molds and stored in the fridge overnight. The following morning, strain sweeps (1% - 1000% @ 10 rad/s) and frequency sweeps (100 rad/s – 1 rad/s @ 1% strain) were performed to evaluate the mechanical and viscoelastic characteristics of the resulting gels.

Results and Discussion

In this study, we used combinations of dynamic secondary aldimine crosslinkers possessing different dynamicities (Figure 2) to develop oxidized alginate hydrogels with highly tunable viscoelastic properties. Despite having equilibria constants on the order of 10^4 – 10^8, and thus a theoretical binding efficiency greater than 99%, we observe markedly different stiffnesses resulting from each individual crosslinker. Following quantification by oscillatory shear rheometry, there is a strong correlation between the dynamicity of the crosslinker and the observed stiffness, with the oxime hydrogels being the stiffest (~ 2 kPa) and least dynamic (K_{eq}~ 10^8) while the hydrazone hydrogels are the softest (~ 0.5 kPa) and most dynamic (K_{eq}~ 10^4). By maintaining an equivalent total crosslinker concentration and preparing hydrogels with different proportions of oxime and hydrazone crosslinks, we are able to tune the bulk stiffness to a desired value within this range. Bearing in mind that the crosslinker molecules are present in an equimolar

concentration to potential binding sites, an extrapolation of the apparent crosslink density from rheological measurements reveals that the stiffness is directly proportional to the concentration of oxime crosslinker. This brings into question the exact role the hydrazone crosslinker plays in this mixed system.

Conclusion

Here we demonstrate the tunable stiffness of oxidized alginate hydrogels within physiologically relevant ranges, and bring to light possible emergent behavior when multiple crosslinkers with large differences in dynamicity are mixed. We are now investigating a corresponding evolution of the relaxation and strain response of these hydrogels, as well as a more detailed analysis of the role and contributions of each crosslinker in a mixed system. More specifically, we will focus on possible correlations between the molecular kinetics and equilibria within the hydrogels. Understanding the fundamental origin of dynamic hydrogel properties such as stiffness and relaxation would allow significantly more control over these systems and represent a powerful step forward in the rational design of complex biomimetic materials for tissue regeneration.

References

[1] Webber, M. J. *et al.*, Supramolecular biomaterials. *Nat. Mater.***15,** 13–26 (2015).

[2] Hafeez, S. *et al.,* Viscoelastic Oxidized Alginates with Reversible Imine Type Crosslinks: Self-Healing, Injectable, and Bioprintable Hydrogels. *Gels***4,** 85 (2018).

Acknowledgement

The authors are gracious for funding from the research programme Innovation Fund Chemistry, which is partly financed by the Netherlands Organisation for Scientific Research (NWO) under TA grant agreement 731.016.202 (“DynAM”). The authors would also like to thank the Brightlands Materials Center and the Province of Limburg for their support of this work.

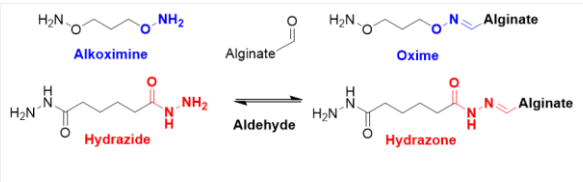

Crosslinker Chemistry
Representative secondary aldimine crosslinking reactions.

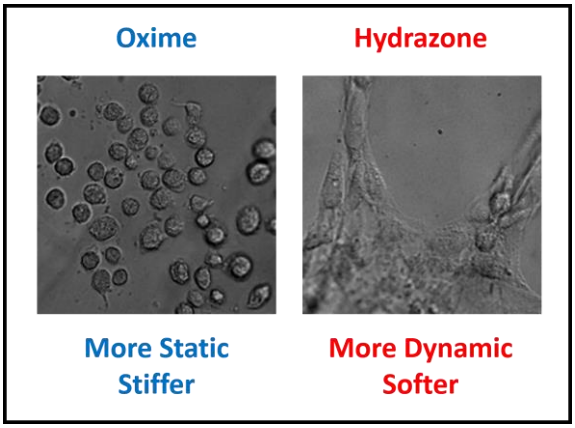

FIg. 1 - Cell Spreading on Viscoelastic Substrates
Surface seeded fibroblasts on Oxime and Hydrazone hydrogels. Image taken after 24h. Scale bar = 25 µm.

II-OS6-RF07

Rational Design of Collagen Scaffolds for Co-Culture

Nima Meyer[1], Daniel V. Bax[1], Jochen Beck[2], Ruth E. Cameron[1], Serena M. Best[1]

[1]University of Cambridge, Department of Materials Science and Metallurgy, Cambridge, GB; [2]Geistlich Pharma AG, Core Technologies, Wolhusen, CH

Introduction

Three-dimensional collagen scaffolds offer wide-ranging potential for tissue repair and regeneration applications. However, continued research is required to optimise scaffold structure and mechanical properties. Monoculture provides a good model for tissue response in many cases, although for bone tissue engineering, a co-culture of both osteoblasts and endothelial cells is required simulating the necessary simultaneous bone cell growth, neovascularisation and angiogenesis [1]. Since interactions observed in mono-culture are cell-type specific, it is important to tailor scaffold characteristics to provide optimal conditions for cells in co-culture. Crosslinking (XL) influences both the scaffold stiffness and also the integrin binding sites available on the surface of the structure. An over-arching question is to understand the effects of cross-linking "degree" on cells in co-culture. EDC (1-ethyl-3-(3-dimethylaminopropyl-carbodiimide hydrochloride)/NHS (N-hydroxysuccinimide) XL is used widely to optimise scaffold stiffness but, at high concentrations, has been found to be detrimental for cell binding [2]. This work describes a systematic study to gain insight into the cell-type specific response to scaffolds for bone tissue repair. Using samples with varying stiffness, a mono-culture study of both primary human osteoblasts (hOB) and human dermal microvascular endothelial cells (HDMEC) has been undertaken in order to inform subsequent work in a more complex co-culture system designed to assess angiogenesis for bone tissue engineering.

Experimental Methods

Collagen suspensions (0.5 and 1 wt.%) in 0.05 M acetic acid were air and freeze-dried to produce 2D films and 3D scaffolds, respectively. Both films and scaffolds were crosslinked with different EDC concentrations to obtain XL levels ranging from 0 to 100%, with a molar ratio of EDC:NHS:COO^-=5:2:1 defined as 100%. The hOBs and HDMECs were seeded on both films and scaffolds. Cell proliferation and adhesion on 2D films were assessed via fluorescence microscopy using DAPI staining and through a colorimetric assay measuring lactate dehydrogenase, respectively. Cytotoxicity of films with different XL concentrations was examined using a fluorescence-based LIVE/DEAD assay. Furthermore, the metabolic activity of cells seeded on 3D scaffolds was measured in an absorbance reader using a PrestoBlue® viability assay. Cell proliferation on and migration into col. scaffolds were assessed via fluorescence microscopy using PicoGreen and nuclei and actin staining, respectively. Investigation of mechanical stability of the scaffolds was carried out with a compression test performed using hydrated scaffolds.

Results and Discussion

For both cell types similar proliferation trends on col. films were observed, showing no difference between the different XL conditions. It was also observed that carbodiimide XL has no toxic effect on both cell types as they were evenly distributed and elongated on the surface of the films. However, a discrepancy in cell adhesion on col. films between the two cell types was observed. While HDMECs kept almost 50% of their initial integrin-mediated cell attachment with XL levels up to a 100%, hOBs lost 50% of their initial specific binding at only 60% XL, which indicates that an increasing XL degree inhibits specific binding, particularly for hOBs. However, with regard to 3D scaffolds, a more substantial decrease in metabolic activity with increasing XL levels was observed for HDMECs as opposed to

hOBs (Figure 1). Lower metabolic activity of HDMECs seeded on 60 and 100% crosslinked scaffolds as opposed to hOBs was observed, indicating that especially HDMECs dislike stiffer substrates within a 3D environment. Overall, a higher metabolic activity was observed for both cell types on scaffolds with XL levels ranging from 10 to 30%. Both migration and proliferation assays confirmed the observed metabolic activity trend. Additionally, it was observed that non-crosslinked scaffolds shrunk more than 50% within the first 24 hrs, which is disadvantageous for tissue repair and regeneration. Compression testing showed enhanced mechanical stability of over 6 kPa for scaffolds with XL levels of 30%, which is required for appropriate tissue regeneration.

Conclusion

In conclusion, EDC/NHS crosslinking was found to influence, strongly, the cell response of both hOBs and HDMECs. While both cell types demonstrated a good response in soft environments with crosslinking levels ranging between 10-30%, hOBs performed better in stiffer environment as compared with HDMECs. Collagen scaffolds with a 30% crosslinking level showed appropriate mechanical stability suitable for both hOBs and HDMECs. It is clear that both cell activity and binding behaviour of hOBs and HDMECs change with XL levels, but to different extents. It was concluded that scaffolds with 30% XL offered the best combination of mechanical stiffness and cell binding sites and that these will be taken forward for analysis in co-culture for bone tissue regeneration.

References

[1] Unger RE, Sartoris A, Peters K, Motta A, Migliaresi C, Kunkel M, Bulnheim U, Rychly J, Kirkpatrick CJ. Tissue-like self-assembly in cocultures of endothelial cells and osteoblasts and the formation of microcapillary-like structures on three-dimensional porous biomaterials. Biomaterials. 2007 Sep 1;28(27):3965-76.

[2] Bax DV, Davidenko N, Gullberg D, Hamaia SW, Farndale RW, Best SM, Cameron RE. Fundamental insight into the effect of carbodiimide crosslinking on cellular recognition of collagen-based scaffolds. Acta biomaterialia. 2017 Feb 1;49:218-34.

Acknowledgement

This research was financially supported by the Engineering and Physical Sciences Research Council (EPSRC) and Geistlich Pharma AG.

1:00 p.m. – 2:30 p.m.

Hall 2

II-OS7 | Biomaterials for tissue engineering applications 2

II-OS7-01

Piezoelectric Ultrafine Fibers for Bone and Neural Tissue Engineering

Bahareh Azimi[1,2], Massimiliano Labardi[3], Delfo D'Alessandro[4], Luisa Trombi[2,4], Claudia Dell'Amico[5], Matteo Baggiani[5], Marco Onorati[5], Stefano Berrettini[4], Serena Danti[1,2]

[1]University of Pisa, Dept. of Civil and Industrial Engineering, pisa, IT; [2]Interuniversity National Consortium of Materials Science and Technology, INSTM, Firenze, IT; [3]Institute for Chemical-Physical Processes, National Research Council (CNR-IPCF), Pisa, IT; [4]University of Pisa, Dept. of Surgical, Medical, Molecular Pathology and Emergency Care, Pisa, IT; [5]University of Pisa, Dept. of Biology, Pisa, IT

Introduction

Since many tissues and cells can be influenced by mechano-electric stimulation, the application of piezoelectric materials in tissue engineering has received considerable attention [1]. Electrospinning is the most versatile method to produce ultrafine fibers which can provide structural features for cell adhesion and growth. This report describes the fabrication and characterization of piezoelectric electrospun poly (vinylidenefluoride-*co*-trifluoroethylene) P(VDF-TrFE) scaffolds for bone and neural engineering applications. The effect of collector velocity on fiber morphology, crystalline phase, mechanical properties, piezoelectric properties and cell behavior on the scaffolds were investigated.

Experimental Methods

P(VDF-TrFE) powder (70:30 IN Mole %), was dissolved in methyl ethyl ketone and the solution (20 w/v%) was electrospun into fibers using 35 kV voltage, and collector velocity of 500 and 4000 rpm (Linari s.r.l, Pisa, Italy). Fiber morphology was analyzed via scanning electron microscopy (SEM). Crystalline phase was analyzed with a polarized Fourier-transform infrared spectroscopy (FTIR). The mechanical properties were characterized by a mechanical tester (INSTRON 5500R). Two self-designed PiezoTesters were used to measure the piezoelectric properties. Human mesenchymal stromal cells (hMSCs) were osteo-differentiated on the scaffolds for 7 days. Calcium matrix production by hMSCs was investigated via Osteoimage (green) and DAPI (blue) fluorescent staining. The metabolic activity of the cells grown on the scaffolds was monitored along the culture time using the alamarBlue® and expressed in dye reduction percentage with respect to negative controls. Human iPSCs were differentiated into cortical neurons according to a dual-SMAD inhibition protocol. At day 76, neurons have been fixed and immunostained for βIII-tubulin (yellow) and counterstained with DAPI and observed via Confocal microscopy.P(VDF-TrFE) was dissolved in methyl ethyl ketone and the solution (20 w/v%) was electrospun into fibers using 35 kV voltage, and collector velocity of 500 and 4000 rpm (Linari s.r.l, Pisa, Italy). Fiber morphology was analyzed via SEM. Crystalline phase was analyzed with a polarized FTIR. The mechanical properties were characterized by a mechanical tester (INSTRON 5500R). Two self-designed PiezoTesters were used to measure the piezoelectric properties. Human mesenchymal stromal cells (hMSCs) were osteo-differentiated on the scaffolds for 7 days. Calcium matrix production by hMSCs was investigated via Osteoimage (green) and DAPI (blue) fluorescent staining. The metabolic activity of the cells grown on the scaffolds was monitored along the culture time using the alamarBlue® and expressed in dye reduction percentage with respect to negative controls. Human iPSCs were differentiated into cortical neurons according to a dual-SMAD inhibition protocol. At day 76, neurons have been fixed and immunostained for βIII-tubulin (yellow) and counterstained with DAPI and observed via Confocal microscopy.

Results and Discussion

SEM results showed that electrospun fibers have cylindrical symmetry and nanoporous surface (Figure 1 (a,b)). Increasing collector velocity up to 4000 rpm reduced fiber diameter (1.9±0.5 µm to 1.3±0.2 µm) and increased fiber

alignment and tensile strength of the fiber meshes (1.08 MPa to 26.68 MPa), showing good fitting of the Neo-Hookean model in aligned fiber mesh. Polarized FTIR results showed that the collector velocity of 4000 rpm improved alignment of polymer chains along the fiber longitudinal axis and at the same time orientation of dipoles (C-F) in the direction perpendicular to this axis, subsequently the fraction of the polar β–phase (Figure 1 c). The results of first PiezoTester showed higher output voltage of the aligned fiber mesh (91 mV) in comparison to random ones (45 mV). By the second PiezoTester, we demonstrated that, as a consequence of the diverse mechanical properties between random and aligned fiber meshes, which ultimately affect piezoelectric properties, random fiber mesh resulted in higher d_{31} than in aligned ones Moreover, in random fibers, higher remnant piezoelectricity than in aligned counterparts was detected (Figure 1 (d)).Biological studies showed that the highest metabolic activity was recorded in the hMSCs osteodifferentiated on the random fiber scaffolds (45.24% ± 6.12%). Cell nuclei were imaged in both random and aligned scaffolds, with prevalence in the random ones (Figure 2(a)), thus confirming the metabolic activity results. Confocal microscopy imaging indicated the presence of well differentiated neurons on the scaffolds (Figure 2 (b)). Axons on aligned scaffold followed the parallel fibers while axons were randomly arranged on random fiber scaffold.

Conclusion

The obtained findings suggested that mesh morphology [2], but also remnant piezoelectric properties can be perceived by stem cells as cues for osteogenic and neurogenic differentiation.

References

1. Rajabi, A., et al. Acta Biomater, 2015. 24: p. 12.
2. Li, Y., et al. Int J Nanomedicine, 2017. 12: p. 4007.

Acknowledgement

MISTI funds 2017 (NANO-SPARKS) and Italian Ministry of Health (Finalized Research 2011).

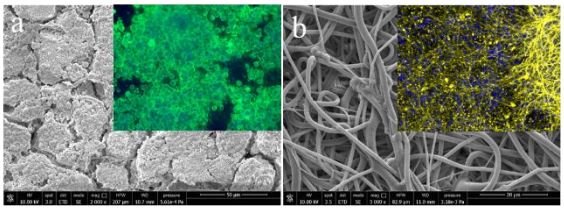

Figure 2:
SEM and fluorescence (lens) images of a) osteodifferentiated hMSCs and b) neurodifferentiated iPSCs on the random fiber scaffolds.

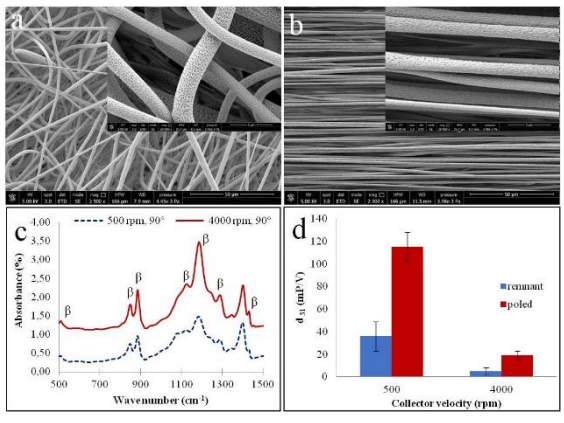

Figure 1:
SEM images of a) random and b) aligned fiber meshes, c) Polarized FTIR spectra and d) Piezoelectric properties of the samples.

II-OS7-02

Engineering a dynamic model of the alveolar interface for the study of aerosol deposition

Roberta Nossa[1,2], Ludovica Cacopardo[1,2], Joana Costa[2], Giorgio Mattei[1], Arti Ahluwalia[1,2]

[1]University of Pisa, Department of Information Engineering, Pisa, IT; [2]University of Pisa, Research Center, Pisa, IT

Introduction

The pulmonary lining is in constant contact with ambient air and undergoes continuous cyclic deformations. To investigate the effects of aerosol deposition on the alveolar barrier, a bioreactor was designed. This system (Figure 1a), named DALì (Dynamic model for ALveolar Interface), consists of an aerosol and a bioreactor with a moving membrane placed between an air-liquid interface.

Experimental Methods

Figure 1b shows a picture of the bioreactor. It is composed of two rigid and cylindrical chambers: the upper one for the air flow (height: 24 mm, diameter: 24 mm) and the bottom one for the medium flow (height: 20 mm, diameter: 24 mm). They are made of polycarbonate in order to ensure the biocompatibility and the transparency of the components. Between them there is a porous stretchable membrane where the cells are seeded. The membrane is fixed in a holder that consists of two annular magnets covered by PDMS (C in Figure 1b). The upper chamber is connected to an aerosol system for nanoparticles deposition (D in Figure 1b).

The membrane used to mimic the basement membrane is an electrospun support made of 50:50 Bionate®:Gelatin, described and characterised in Abstract #582. A FEM model was used to simulate membrane displacement due to the pressure imbalance on the two sides of the air/liquid interface. The model of the bioreactor was based on the Fluid Structure Interaction module of Comsol Multiphysics 4.3a software and consists of a cylindrical chamber connected to the external system with an inlet and an outlet tube (5 mm in diameter). The 80-µm thick membrane was modelled as a disk on the top of the bioreactor and undergoes a constant pressure from the top. Its mechanical characteristics were taken from results shown in Abstract #582. The inlet velocity was fixed at 100 µL/min, and the fluid dynamics solved in the Laminar Flow regime. Bioreactor walls were set as walls with the no slip condition, and water chosen as a reference fluid. The FEM model was solved for different pressures (1 to 15 kPa with a step of 1 kPa), in order to establish the pressure at which the membrane displacement in z-direction is 7mm, corresponding to a linear distention of ≈ 17%, and so mimicking pathological levels of stretching [1][2].

Results and Discussion

In the DALì, the membrane is placed between annular magnets covered by PDMS. During static experiments, the holder with the membrane can be placed both in a 6-well multiwell, or inserted between the top and bottom chambers. The bioreactor is closed tightening wing nuts and the tightness of the bioreactor is ensured by the presence of the membrane holder enclosed in PDMS, which is self-adhesive and deformable. The bioreactor can be sterilized by ethanol solution, gas plasma, or ultraviolet light.

During dynamic experiments, the basolateral chamber is connected to a commercial peristaltic pump with an inlet tube, and to the reservoir with an outlet tube (Figure 1). The apical chamber is connected to the aerosol device and to a compressed air system, with an interposed pressure regulator put inside a control box. Potentiometers on the control box allow regulating the stretching level of the membrane: 0%, 2%, 5%, 10% and 17% for mimicking different stretching conditions.

A FEM model was used to simulate electrospun membrane displacement due to the pressure imbalance on the two sides of the air/liquid interface. Figure 2a shows the total displacement of the membrane at 14 kPa: when the pressure in the apical chamber increases, the membrane stretches, moving into the basolateral chamber, until it reaches an equilibrium with the hydrodynamic pressure of the flowing liquid.
In this way, it is possible to predict the pressure ranges that the external system must apply in order to achieve the desired stretching field on the membrane. The applied pressure corresponding to a z-displacement of almost 7 mm is 14 kPa. This displacement corresponds to a linear distention of ≈ 17%, mimicking pathological levels of stretching. Finally, Figure 2b shows the velocity field of the fluid flowing through the basolateral chamber.

Conclusion

We present a bioreactor that is able to replicate the cyclic motion during the breathing. The flexible moving membrane causes the rhythmic stimulation of epithelial cells, leading to the study of the interaction between them and the particles, in a system that replicates in vivo conditions. The electrospun 50:50 Bionate®:gelatin membrane described Abstract #582 has been selected as suitable membrane for our application, as it is biocompatible and highly flexible, allowing physiological deformation levels.
Although cell culture tests need to be performed, this study paves the way towards the development of an actuation device for physiologically relevant studies of aerosol and drug delivery and toxicology.

References

[1] Hemangkumar J. Patel, “Characterization and Application of Dynamic in vitro Models of Human Airway”, PhD thesis, Dept. Biomedical Eng., Utah State University, Logan, Utah
[2] Kenneth J. Cavanaugh and Susan S. Margulies “Measurement of stretch-induced loss of alveolar epithelial barrier integrity with a novel in vitro method”, American journal of physiology. Cell physiology, vol. 283, issue 6, pp. C1801-8, 2002

Acknowledgement

The project PATROLS has received funding from the European Union’s Horizon 2020 research and innovation programme under grant agreement No. 760813.

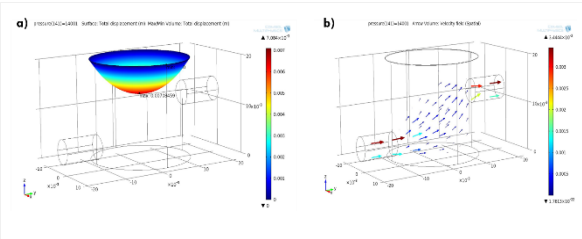

Figure 2
FEM model rapresenting (a) the total displacement of the membrane and (b) the velocity field in the basolateral chamber.

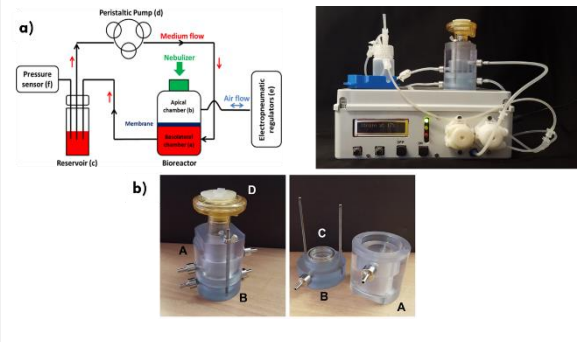

Figure 1
1a) Sketch and picture of the DALì system; 1b) Picture of the bioreactor with all its components: A) apical chamber, B) basolateral chamber, C) membrane holder, D) aerosol device.

II-OS7-03

In situ tissue engineering concept for enhanced bone defect healing – Biomimetic scaffolds functionalized with an osteoinductive factor mix from hypoxia-conditioned hBMSC

Mandy Quade[1], Anastasia Gabrielyan[2], Anja Lode[1], Seemun Ray[3], Angela Roesen-Wolff[2], Volker Alt[3], Michael Gelinsky[1]

[1]TU Dresden, Centre for Translational Bone, Joint and Soft Tissue Research, University Hospital Carl Gustav Carus, Dresden, DE; [2]University Hospital Carl Gustav Carus, Department of Pediatrics, Dresden, DE; [3]Justus Liebig University, Laboratory of Experimental Trauma Surgery, Giessen, DE

Introduction

Autologous bone grafting – as current gold standard for the treatment of large bone defects – is limited by the finite amount of harvestable spongiosa and other drawbacks of operative procedure like donor site morbidity. In tissue engineering – as promising alternative – more and more strategies focus on the *in situ* approach, which envisages an enhanced scaffold colonization, differentiation and vascularization in order to improve the endogenous regeneration of damaged tissue directly at the site of injury. In this study, we utilize porous scaffolds out of mineralized collagen[1], which are functionalized with a central hydrogel-based depot loaded with an osteoinductive growth factor mix, generated from the secretome of hypoxia-treated human mesenchymal stem cells (MSC) derived from bone marrow. After implantation, the factors are released from the depot and induce a directed migration of cells with regenerative potential as well as vascularization of deeper scaffold regions.

Experimental Methods

Hypoxia-conditioned medium (HCM) was generated by incubating confluent hTERT-MSC (immortalized MSC line) for 5d on a shaker with phenol red-free α-MEM with 2 vol% human serum (0.05 mL/cm^2). Cultivating hTERT-MSC under hypoxic conditions (1% O_2) leads to the expression of various angiogenic factors and chemokines (hypoxia-conditioned medium; HCM).[2] Generated HCM was examined via Angiogenesis Arrays, while chemotactic potential for human bone marrow-derived stromal cells (hBMSC) was analyzed via Transwell-Assay (8 µm pore size). A coculture of hBMSC with HUVEC (human umbilical vein endothelial cells) was used to determine the angiogenic potential of HCM by analyzing the CD31-stained prevascular structures. To increase the growth factor concentration, HCM was dialyzed, freeze-dried and resuspended in either α-MEM or 1 wt% alginate (10x, 20x, 50x). Scaffolds were functionalized by injecting concentrated HCM into the scaffolds center and characterized *in vitro*: by seeding hBMSC (migration assay for 3d) or cocultures of hBMSC with HUVEC (angiogenesis assay for 10d) on the scaffolds surface. The scaffolds were fixed, stained, longitudinally cut and microscopically analyzed. For *in vivo* testing of the osteoinductive potential of HCM, a 4 mm wedge-shaped osteotomy of the distal metaphyseal area was generated in the femur of osteoporotic rats.[3] Two groups were tested: 1) unmodified control scaffolds; 2) scaffolds functionalized with concentrated HCM (from rat BMSC). 6 weeks after implantation the bone defect healing was analyzed histologically and histomorphometrically.

Results and Discussion

HCM characterization showed the expression of various angiogenic factors and a tremendous chemotactic and angiogenic potential in 2D and 3D scaffolds. With increasing HCM-concentration in the scaffolds depot, hBMSC

migrated deeper into the scaffolds. Cocultures led to dense prevascular structures on the scaffolds surface. With increasing HCM-concentration the tubular structures sprouted deeper throughout the interconnected pores until a depth of 1500 µm (Fig. 1). *In vivo* the HCM-modified scaffolds showed very good biocompatibility without inflammatory response, increased formation of big blood vessels and an enhanced bone formation and mineralization (Fig.2).

Conclusion

The synergistic interplay of various growth factors makes HCM a highly potent growth factor mix for the application in bone defect healing. Scaffold functionalization with a central HCM-depot led to hBMSC attraction and ingrowth of angiogenic structures in a concentration dependent manner. Additionally, *in vivo* experiments showed enhanced bone defect healing with increased vascularization and new bone formation for HCM-modified scaffolds.

References

[1] M. Gelinsky *et al.* (2008) *Chem Eng J.* 137(1). 84–96

[2] A. Gabrielyan *et al.* (2014) *BMC Vet Res* 10 (1). 56

[3] V. Alt *et al.* (2013) *Acta Biomater* 9. 7035–7042

Acknowledgement

This study is funded by the German Research Foundation (DFG) (Collaborative Research Centre/Transregio 79 (SFB/TRR 79), subproject M4 and T2).

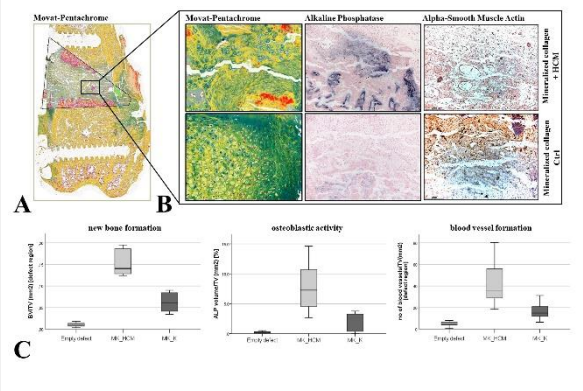

Increased bone formation in vivo

Fig. 2 Osteotomy in the femur of osteoporotic rats filled with mineralized collagen with or without HCM-functionalization. A) Overview of wedge-shape bone defect. B) Increased bone formation, mineralization and vascularization in HCM-modified scaffolds. C) Histomorphometrical analysis.

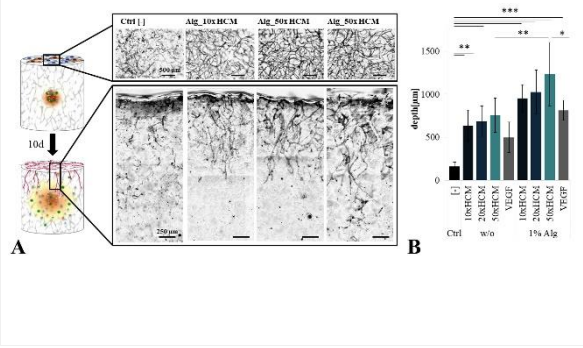

Enhanced vascularization in vitro

Fig.1 *In vitro* angiogenesis in mineralized collagen scaffolds functionalized with a central depot containing concentrated HCM dissolved in α-MEM or 1 wt% alginate (10x, 20x, 50x). A) CLSM images of prevascular structures on scaffold surface (upper row) and section (lower row) stained for CD31. B) Increased depth of ingrowing prevascular structures in scaffolds with alginate-based depot and increasing HCM concentration.

II-OS7-04

Macromolecular crowding, mechanical stimulation, anisotropic topography and oxygen tension in tissue engineering – A step closer to cell-assembled biomaterials

Dimitrios Zeugolis, Diana Gaspar, Dimitrios Tsiapalis

NUI Galway, REMODEL, Galway, IE

Introduction

Macromolecular crowding is a biophysical phenomenon that governs intracellular and extracellular processes and increases thermodynamic activities by several orders of magnitude. *In vitro*data have demonstrated that macromolecular crowding dramatically accelerates extracellular matrix (ECM) deposition in skin, lung and corneal fibroblast and naïve mesenchymal stem cell cultures (1-4). Herein, we hypothesized that macromolecular crowding alone or in combination with other *in vitro*microenvironment modulators (e.g. oxygen tension, mechanical loading, anisotropic topography) will control cell function in vitro.

Experimental Methods

Human tendons were obtained from University Hospital Galway, after obtaining appropriate licenses, ethical approvals and patient consent. Subsequently, tenocytes were extracted using the migration method. Human chondrocytes were purchased from Lonza (Switzerland). Human osteoblasts were purchased from ATCC (UK). Human bone marrow was purchased from Lonza (USA). For variable oxygen tension cultures, a Coy Lab (USA) hypoxia chamber was used. For mechanical loading cultures, a Cell Scale (Canada) MCFX uniaxial stimulator bioreactor was used. all experiments were conducted at passage 3 to 5. All cultures were supplemented with ascorbic acid sodium salt (Sigma Aldrich, UK). For anisotropic topography, bidirectionally aligned electro-spun scaffolds were used. Macromolecular crowding was carried out using 50 to 100 *m*g/ml carrageenan (Sigma Aldrich, UK). ECM deposition was assessed using SDS-PAGE (BioRad, UK) and immunocytochemistry (ABCAM, UK) analysis. Gene analysis was conducted using a gene array (Roche, Ireland). Cell morphology was assessed via bright-field microscopy. All experiments were conducted at least in triplicates. ANOVA was conducted after validating the parametric analysis assumptions; when the assumptions were violated, Kruskal-Wallis analysis was conducted (non-parametric analysis).

Results and Discussion

Macromolecular crowding (MMC) enhanced deposition of collagen types I and III in tenocytes and bone marrow stem cells. Gene analysis showed upregulation of scleraxis, thrombospondin-4 and cartilage oligomeric matrix protein in tenocytes after 7 days of mechanical stimulation. BMSCs exhibited upregulation of alkaline phosphatase under MMC and downregulation of collagen type I at day 3 under mechanical stimulation in the absence of MMC. Human tenocytes treated with MMC at 2% O2 tension showed increased collagen type I synthesis and deposition after 7 days. In chondrocyte culture, MMC both in monolayer and alginate system, increased collagen type I deposition, whilst collagen type II was barely detectable. Anisotropic topography induced bidirectional cells and deposited matrix orientation.

Conclusion

This study provides insight into modulation of cell behavior and phenotype using microenvironmental cues.

References

1. Kumar, P., et al., Sci Rep, 2015. 5: p. 8729
2. Cigognini, D., et al., Sci Rep, 2016. 6: p. 30746
3. Kumar, P., et al., J Tissue Eng Regen Med, 2016
4. Satyam, A., et al., Acta Biomater, 2016. 44: p. 221-31

Acknowledgement

The authors would like to acknowledge Science Foundation Ireland (15/CDA/3629 and 13/RC/2073) and the European Union (H2020, ITN, 676338) for financial support.

II-OS7-05

Preparation of a porous solid fibroin scaffold based on a foaming and UV crosslinking procedure of a methacrylate fibroin solution: influence of the composition on the sponge properties

Alessio Bucciarelli[1], Devid Maniglio[1], Antonella Motta[1], Alberto Quaranta[1], Gilson Khang[2]

[1]Univerità di Trento, Industrial engineering, Trento, IT; [2]Chonbuk National Univerity, Polymer Nano Science & Technology, Jeonju, KR

Introduction

Silk fibroin sponges have been extensively studied in literature, in particular in all the applications in which porosity is an essential feature. In tissue engineering porous structures serves as material that closely mimic the biological microenvironment. Porous fibroin sponges have been successfully adoptedin the case of soft tissues (muscle, skin, adipose, and neural tissues) and bones. In order to mimic the living tissues the possibility to tune the porosity and consequently the other physical responses is essential. Plenty of different methods were developed to are available to produce silk fibroin sponges among them we can cite: Salt-leaching, Freeze drying, ammonium bicarbonate sublimation, and NO_2 expansion [1,2]. All these methods are based on the transition of the sponge to the crystalline β structure that makes it water stable. This is also known as physical crosslinking. In our study we proposed an innovative method to produce a chemically crosslinked silk fibroin sponge with a tunable porosity based on a methacrylated version of the protein.

Experimental Methods

The sponge was studied by a 3 factors full factorial design of experiment (DOE): the process was kept constant, instead the composition was changed. In particular, we studied the variation of the porosity (SEM), the water absorption, the dissolution in SBF, the secondary structure (FTIR) and the cytotoxicity (MTT) in dependence of the sponge composition. We considered 2 levels (low, high) for each considered variable: quantity of photoinitiator (LAP, low 5 mg, high 75mg), the protein concentration in the solution (low 10%, high 20%), and quantity of an emulsifier (low Tween20 0 µL, high 50 µL).

Results and Discussion

We proved that the porosity, the dissolution in a simulated body fluid (SBF) and the water absorption are influenced by the composition. Instead, the secondary structure remains unchanged regardless the composition. The trend of the porosity distribution was modeled: in particular, the increasing of the emulsifier volume, and the decreasing of both the solution concentration and the initiator tend to increase the mean pore area. All the sponges result to have a mean porosity lower than 100 µm, but a consistent part of all distributions results to be above that threshold. The distribution dispersion was evaluated by standard deviation and interquartile range. The stability of the sponges in water results to be influenced by the amount of photoinitiator: we could deduce that higher a higher amount of photoinitiator gave a higher degree of crosslinking making the sponges overall more stable in SBF. Cells viability also results to be influenced by the amount of photoinitiator: in fact, higher the amount lower the viability.

Conclusion

In conclusion, we were able to optimize a method to produce chemically crosslinked fibroin sponges. The analysis via design of experiment of the prepared samples allowed us to build a predictive model for the properties of our interest. We were able to determine the influence of the composition on the porosity, water absorption, dissolution in SBF, and cell viability.

References

[1] Hu, X. & Kaplan, D. L. 2.212. Silk Biomaterials. 207–219 (2011). doi:10.1016/B978-0-08-055294-1.00070-2

[2] Zhang, Q., Yan, S.-Q. & Li, M.-Z. Porous Materials Based on Bombyx Mori Silk Fibroin. *J. Fiber Bioeng. Informatics***3,** 1–8 (2010).

Acknowledgement

The project leading to this application has received funding from the European Union's Horizon 2020 Research and Innovation Staff Exchange programme (RISE) under the Marie Skłodowska-Curie grant agreement REMIX.

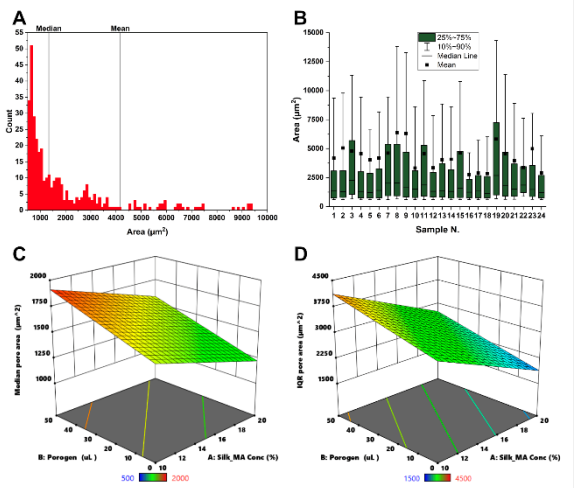

Statistical analysis on pore distribution
(A) Pore distribution of the first sample: the mean and the median resulted to be not in the same position, because the distribution was skewed. (B) Box-cox graph with all the sample distributions, how can be clearly deduced all the distribution were skewed. (C) Modeled median trend and (D) interquartile range trend.

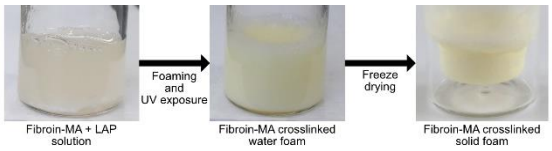

Preparation scheme
Scheme of preparation of a silk-fibroin methacrylated sponge. The process is based on four steps: the preparation of the solution (fibroin-MA, photoinitiator LAP, emulsifier Tween20) the foaming through a mixer, the crosslinking under a UV lamp, and finally a freeze drying to eliminate the exceeding water.

II-OS7-RF06

Aerogel-loaded scaffolds obtained by supercritical foaming for bone regeneration

Carlos A. García-González[1], Araceli Delgado[2], Carmen Évora[2], Ricardo Reyes[3], Angel Concheiro[1], Jose Luis Gómez-Amoza[1], Carmen Alvarez-Lorenzo[1]

[1]Universidade de Santiago de Compostela, Departamento de Farmacología, Farmacia y Tecnología Farmacéutica, R+D Pharma group (GI-1645), Facultad de Farmacia and Health Research Institute of Santiago de Compostela (IDIS), Santiago de Compostela, ES; [2]Universidad de La Laguna, Departamento de Ingeniería Química y Tecnología Farmacéutica, Instituto de Tecnologías Biomédicas (ITB), La Laguna, ES; [3]Universidad de La Laguna, Departamento de Bioquímica, Microbiología, Biología celular y Genética, Instituto de Tecnologías Biomédicas (ITB), La Laguna, ES

Introduction

The efficient regeneration of a bone tissue assisted by the presence of a scaffold is dependent on the scaffold design and the processing method used. Regarding the design, medicated bone scaffolds can accelerate the bone tissue formation by providing a suitable 3D-porous structure and bioactive agents that promote cell colonization and differentiation towards the osteogenic lineage. For these scaffolds, solvent-free processing technologies operating at mild temperatures are preferred to have high loading yields of the bioactive agents.

Supercritical foaming is a solvent-free scaffold processing method that exploits the plasticizing effect of compressed CO_2 on certain polymers (e.g., polyesters) to form a porous structure[1]. Using this technique, scaffolds usually have high macroporosity but low pore interconnectivity that hampers the penetration and growth of cells and the transport of wastes.

Aerogels are solid and open porous networks obtained from wet gels after the removal of the solvent without significant structure compaction and endowed with high specific surface area. Namely, the extracellular matrix-mimicking nanostructure of aerogels along with the biological implications of certain polysaccharide and protein aerogel sources to promote the attachment, growth and colonization of cells are especially attractive for biomedical purposes[2].

In this work, the effect of the incorporation of protein (silk fibroin from *Bombyx mori*, SF) and polysaccharide (corn starch) aerogels o scaffolds of poly(ε-caprolactone) (PCL, 50 kDa) with dexamethasone-21-phosphate (DX, osteogenic agent) was evaluated. The morphological performance of the scaffolds was tested regarding pore interconnectivity, cell infiltration capacity and water permeability from mercury intrusion porosimetry (MIP) measurements. Finally, *in vivo* bone regenerative performance of the scaffolds was assessed in critical-size calvarial defects (diameter: 8 mm) in a Sprague-Dawley rat model.

Experimental Methods

Aerogel production is a multi-step process comprising at least a gelation step and a drying step (Fig. 1a). SF and starch gels were obtained from emulsions (8 wt. % of SF and 15wt. % of starch aqueous solutions, respectively, and Span 80 as emulsifier) using ultrasonication- and thermal- (121ºC, 20 min) assisted gelation, respectively. Then, SF and starch aerogel particles (SA and StA, respectively) were obtained by supercritical drying with compressed CO_2 (40ºC, 120 bar, 6 g/min)[3,4].

Scaffolds containing PCL and StA (PCL-StA, 90:10 weight ratio), SA (PCL-SA, 90:10) or SA+DX (PCL-SA-DX, 85:10:5) were processed using the supercritical foaming process (37ºC, 140 bar, 1 h) followed by a depressurization at a venting rate of 1.8 g CO_2/min.

Results and Discussion

The preparation of dry powder in the form of SF and starch aerogels was herein developed to provide a nanostructured, highly porous and bio-based material to be incorporated as a morphological modifier in the formulation of the scaffolds (Fig. 1). The particle size (300-600 nm) of the aerogels and the presence of emulsifier (Span 80) in the external surface are especially suitable to favor PCL-aerogel interaction for the preparation of scaffolds.

PCL-based scaffolds containing aerogels had 60-70% porosity, macropores in the 100-300 µm range (Fig. 2) and incorporation yields of DX close to 100%. High pore interconnectivities (84-94 %), mesenchymal stem cell infiltration capacities (87-93%) and water permeabilities (3-12·10^{-12} m^2) were obtained for the three scaffolds. Hence, scaffolds had a suitable porous network to facilitate biological tissue growth and transport of fluids.

In vivo tests unveiled the compatibility of the aerogel-containing scaffolds with the bone tissue with no signs of inflammation or rejection. The relevance of the presence of the bioactive agent (dexamethasone) in the PCL-SA-DX scaffolds was unveiled by the presence of many ossification foci and their confluence to form new bone (repair percentage of 39% at 14 weeks post-implantation). This newly formed bone had a compact appearance, which is characteristic of mature bone.

Conclusion

Supercritical foaming is a solvent-free technique for the preparation of nanostructured scaffolds with osteogenic activity. The presence of submicron-sized aerogel particles in the scaffolds resulted in improved physicochemical properties for cell colonization and transport of biological fluids. *In vivo* results showed that the medicated scaffolds accelerated the bone repair response.

References

[1]V. Santos-Rosales et al., *Molecules.***2019**, *24*, 871.
[2]A. Salerno et al., *Biofabrication***2017**, *9*, 035002.
[3]L. Goimil et al., *J. CO2 Utiliz.***2017**, *18*, 237.
[4]L. Goimil et al., *J. CO2 Utiliz.***2019**, *31*, 51.

Acknowledgement

Work carried out in the frame of the COST-Action "Advanced Engineering of aeroGels for Environment and Life Sciences" (AERoGELS, ref. CA18125) funded by the European Commission. Work also supported by Xunta de Galicia [ED431F 2016/010 & ED431C 2016/008], MINECO [SAF2017-83118-R], Agencia Estatal Investigación [AEI] and FEDER funds. C.A.G.-G. acknowledges to MINECO for a Ramón y Cajal Fellowship [RYC2014-15239].

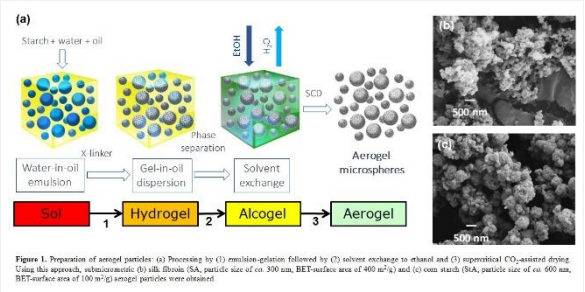

Figure 1. Preparation of aerogel particles: (a) Processing by (1) emulsion-gelation followed by (2) solvent exchange to ethanol and (3) supercritical CO_2-assisted drying. Using this approach, submicrometric (b) silk fibroin (SA, particle size of ca. 300 nm, BET-surface area of 400 m^2/g) and (c) corn starch (StA, particle size of ca. 600 nm, BET-surface area of 100 m^2/g) aerogel particles were obtained.

Preparation of aerogel particles

Preparation of aerogel particles: (a) Processing by (1) emulsion-gelation followed by (2) solvent exchange to ethanol and (3) supercritical CO_2-assisted drying. Using this approach, submicrometric (b) silk fibroin (SA, particle size of *ca.* 300 nm, BET-surface area of 400 m^2/g) and (c) corn starch (StA; particle size of *ca.* 600 nm, BET-surface area of 100 m^2/g) aerogel particles were obtained.

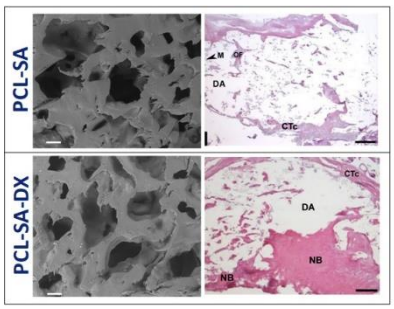

Figure 2. Characterization of supercritically-foamed synthetic scaffolds composed of PCL, SF aerogels and with (PCL-SA-DX, bottom) and without (PCL-SA, top) DX by SEM imaging (left) and *in vivo* experiments in murine model 14 weeks after implantation (right). Notation: CTc=connective tissue capsule; DA= defect area; NB=new bone; OF=ossification foci; M=rest of material. Scale bars: 200 µm (left), 1.4 mm (right).

Morphological and biological evaluation of supercritically-foamed synthetic bone scaffolds

Figure 2. Characterization of supercritically-foamed synthetic scaffolds composed of PCL, SF aerogels and with (PCL-SA-DX, bottom) and without (PCL-SA, top) DX by SEM imaging (left) and *in vivo* experiments in murine model 14 weeks after implantation (right). Notation: CTc=connective tissue capsule; DA= defect area; NB=new bone; OF=ossification foci; M=rest of material. Scale bars: 200 µm (left), 1.4 mm (right).

II-OS7-RF07

Obtaining of Cellprene® Epoxidized Fibers Using Electrospinning Process

Rafael M. Carazzai, Nathália O. Muniz, Nayrim B. Guerra, Luís Alberto L. dos Santos

Federal University of Rio Grande do Sul, Biomaterials Laboratory / Materials Engineering Department, Porto Alegre, BR

Introduction

In the past, removal of the injured part was the most common practice when large tissue lesions were due to mechanical trauma or degenerative diseases. Consequently, inducing a significant decrease in the quality of patient's life[1]. Antibiotics discovery increased human life expectancy, as well as improved sanitary and hygienic conditions. With this, the replacement of damaged tissues became a necessity[2,3], and the tissue engineering, using scaffold and cells, to regenerate or replace injured tissues, has been developed. Cellprene® is a polymer blend of PLGA and Poly (isoprene) that has been recently developed by the Biomaterials Laboratory (UFRGS, Brazil) and shows high potential for applications such as biomaterial[4]. This material had its biological characteristics improved through the epoxidation of Poly (isoprene)[5]. As a new material, a few works have been conducted, and its properties and characteristics are unknown. The electrospinning technique is the most used technic to obtaining fibers. The advantage of polymeric biomaterials is to allow obtain fibers with different diameters, and, in some conditions, at nanometric scale, which has a great importance in terms of adhesion and cell growth. The aim of this study is to evaluate the viability of the obtaining Cellprene® epoxidized by electrospinning for potential use as scaffold for tissue engineering.

Experimental Methods

Poly(lactic-co-glycolic-acid) (PLGA) produced by PURAC (The Netherlands) with ratio 85/15 and centrifuged natural latex by MAFER (Brazil) were used to produce the polymer blend. The latex was purified to obtain poly (isoprene) (PI), then the PI was epoxidized (PI epox). The PLGA/PI epox were weighed and mixed in the ratio 60/40 (% w/w). The table 1 shows the parameters to obtain Cellprene® epoxidized fibers by electrospinning process. The fiber morphology and functional groups of the polymers were performed by scanning electron microscopy (SEM) and Fourier transform infrared spectroscopy with attenuated total reflectance (FTIR-ATR).

Results and Discussion

Evaluating the results, using different electrospinning parameters, the one that presented the greater morphology response was: 15 kV, distance between needle-collector 20 cm, infusion rate 4 ml/h and concentration 5%. The figure 1 shows the SEM of Cellprene® epoxidized fibers.

The diameter of fibers were measured using ImageJ software and shown a mean diameter of 4,3± 2,7µm. The fibers presented high superficial porosity that may facilitate the adhesion of the cells. Authors claimed that porosity presented in the fibers can be caused by evaporation ratio of the solvent[6,7]. Other authors explain the porosity as a consequence of the relative humidity during the electrospinning process[8,9].

Analyzing the spectra of PI epoxidized, we noticed that there are no bands in the range of 3100 cm^{-1} and 3600 cm^{-1}, which are referred in the literature to proteins and peptides[5]. This indicates that the purification of poly (isoprene) was efficient. The appearance of bands at 1250 cm^{-1} and 870 cm^{-1}, as well as a broad band around 1100 cm^{-1} indicate that the epoxidation reaction of poly (isoprene) occurred[5]. Authors observed that in PLA / epoxidized natural rubber

blends the band around 1750 cm^{-1} was shifted to larger wave numbers with increasing content of epoxidized natural rubber[10]. This suggests that there was interation between PLGA and PI epox. According to the analysis of FTIR-ATR spectra does not indicate significant change in the main functional groups.

Conclusion

The electrospinning process is viable for the production of fibers of Cellprene® epoxidized blend. The fibers presented high amount of pores on surface that may aid in cell adhesion. The obtaining of fibers by solvent mixing of polymers and electrospinning method did not modify chemical groups of the resulting material when compared to the raw materials.

References

1. Santos Jr., A.R.; Wada, M. L. F. Polímeros: Ciência e Tecnologia. 17:308-317, 2007
2. Hench, L. L. Biomaterials. 19:1419-1423, 1998
3. Nobre, M. R. C. *et al*., Qualimetria, 6:56-59, 1994
4. Marques, D. R. Polímeros, 23:579-584, 2011
5. Guerra, N. B. *et al*., J. Polym. Res. 25:172, 2018
6. Katsogiannis, K. A. G. *et al*., European Polymer Journal. 69:284-295, 2015
7. Celebioglu, A.; Uyar, T. Materials Letters, 65:2291-2294, 2011
8. Park, J. Y.; Lee, I. H. J. Nanosci. Nanotechnol. 10:3473-3477, 2010
9. Casper, L. C. *et al*., Macromolecules. 37:573-578, 2004
10. Cosme, J. G. L. *et al*., Materials Scie. and Applications. 7:210-219, 2016

Acknowledgement

The authors acknowledge to the Coordenação de Aperfeiçoamento de Pessoal de Nível Superior (CAPES) for the financial support through the project, to the Conselho Nacional de Desenvolvimento Científico e Tecnológico (CNPQ), to the Programa de Pós-Graduação em Engenharia de Minas, Metalúrgica e de Materiais (PPGE3M), to the Financiadora de Estudos e Projetos (FINEP) and to Fundação de Auxílio à Pesquisa do Rio Grande do Sul (FAPERGS) for the financial support through the project.

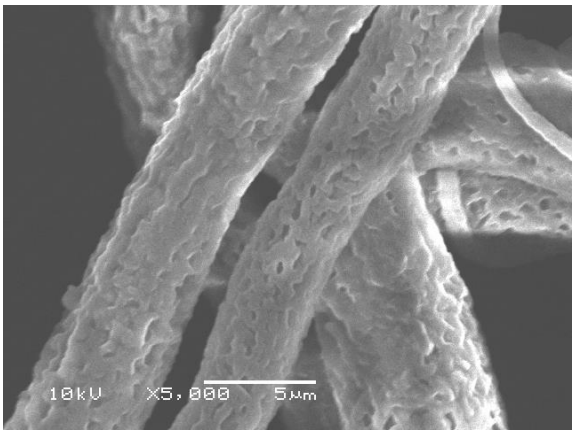

Figure 1 .
SEM of Cellprene® epoxidized fibers.

Voltage	10, 15, 20 (kV)
Needle-collector distance	5, 10, 15, 20 (cm)
Infusion rate	4, 5, 10, 15 (ml/h)
Concentration	1, 3, 5, 7 (%w/v)

Table 1.
Parameters to obtain Cellprene® epoxidized fibers.

1:00 p.m. – 2:30 p.m.

Hall 4

II-SY2 | Local antibiotics delivery with hydrogels: from infection prevention to infection eradication in orthpedic trauma

David Eglin (Davos Platz, CH)
Fintan Moriarty (Davos Platz, CH)

Infection is a dreaded risk in orthopedic and trauma surgery with devastating consequences for the patients and huge social costs. While antibiotic-loaded biomaterials are available, there is still large potential for improving the available products and the clinical standards.

In this symposium, a hydrogel for the local delivery of antibiotics and its development will be presented. Biomaterial requirements, rational design, regulatory hurdles, proof of concept studies in small animals, comparison with clinical standards, large animal models and the challenge of raising from a model of prevention up to eradication of an antibiotics-resistant infection will be illustrated.

II-SY2-KL01

Local antibiotics delivery with hydrogels: from infection prevention to infection eradication in orthpedic trauma

Matteo D'Este, **Fintan T. Moriarty**

AO Research Institute Davos, Musculoskeletal Infection, Davos, CH

Introduction

Fracture-related infection is a relatively uncommon, yet challenging complication in musculoskeletal trauma surgery, with rates of approximately 5% for closed fractures and up to 30% for severe open fractures (1). The presence of a fracture fixation implant is a significant risk factor for the development of infection, whereby the minimal infectious dose may be reduced by up to 10'000 fold compared with equivalent surgeries not involving an implant (2,3). The increased susceptibility to infection is usually attributed to a localized deficiency in phagocytosis of bacteria in the vicinity of an implant (4), coupled to the fact that the implant also acts as a substrate for biofilm formation. Once established in a biofilm, the bacteria are much more resistant to host defense mechanisms (5).

Systemic antibiotics are mandated for the prevention of infection in open fractures (6). The duration of administration of systemic antibiotics is related to the class of open fracture and is between 24h and 120h after wound closure. For treatment of an established infection, the duration of antibiotic therapy is at least 6 weeks, though often significantly longer. Systemic administration may not achieve adequate antibiotic concentrations at the fracture site, particularly in cases with vascular compromise. Furthermore, the systemic dose cannot be increased indefinitely due to systemic toxicity, and in many cases, higher doses are not always correlated with greater activity. Thus, local delivery of the chemotherapeutic agent is the logical choice to increase the antibiotic concentration at the injury site over time, and at the same time limit systemic distribution and associated side effects.

Currently, two main types of antibiotic-loaded biomaterials are used in the clinic: non-degradable, such as poly methyl methacrylate (PMMA) bone cement beads (7) and degradable, such as collagen fleece (8). Both of these clinically available options have certain drawbacks. PMMA is non-degradable, requiring a second surgery to be removed, and after a few days antibiotic release falls to sub-inhibitory levels, which poses a risk of inducing resistance (9). Antibiotic-loaded collagen has sub-optimal handling, the antibiotic is rapidly released (10), again leaving subinhibitory concentrations, and a short-lived substrate for biofilm formation. Furthermore, neither PMMA nor collagen are able to reach every contaminated tissue, due to the predetermined shape and limited diffusion to adjacent tissues.

Experimental Methods

Given this clinical background, we have investigated the use of an injectable hydrogel for the local delivery of antibiotics. In this symposium, biomaterial design, preparation, proof of concept studies in small and large animal models will be described whereby control groups received clinical standard of care. The performance of the antibiotic-loaded hydrogel in preventing infection and treating established infection will be described, including performance against an antibiotic-resistant pathogen.

Results and Discussion

The first keynote speaker will introduce the clinical need of improved solutions for orthopaedic-related infections, the design phase with discussion with orthopaedic surgeons and other stakeholders, the rational design of the biomaterial and its preparation and the limitations imposed by regulatory aspects and clinical translation.

Conclusion

In the second part we will present a series of *in vivo* infection prevention models where the local delivery with hydrogels was compared with standard biomaterials clinically available, illustrating the advantages and challenges related to the establishment of a large animal model of infection. Finally, we will describe how the platform was assessed for infection eradication in a clinically relevant model of a chronic infection in sheep.

References

1. Trampuz A, Zimmerli W. Diagnosis and treatment of infections associated with fracture-fixation devices. Injury **2006**;37(2, Supplement):S59-S66.

2. Scottish Intercollegiate Guidelines N. Antibiotic prophylaxis in surgery A national clinical guideline. **2008**.

3. Zimmerli W. Antibiotic prophylaxis. In: Rüedi TP, Buckley RE, Moran CG, editors. AO Principles of Fracture Management. Davos Platz: AO Publishing; **2007** p. 425-33

4. Busscher HJ, van der Mei HC, Subbiahdoss G, Jutte PC, van den Dungen JJ, Zaat SA, *et al.* Biomaterial-associated infection: locating the finish line in the race for the surface. Sci Transl Med **2012**;4(153):153rv10.

5. Patel R. Biofilms and antimicrobial resistance. Clinical Orthopaedics and Related Research. 2005;437:41-7.

6. Ter Boo GJ, Grijpma DW, Moriarty TF, Richards RG, Eglin D. Antimicrobial delivery systems for local infection prophylaxis in orthopedic- and trauma surgery. Biomaterials. **2015**;52:113-125.

7. Kuehn KD, Ege W, Gopp U. Acrylic bone cements: composition and properties. Orthop Clin. 2005; 36:17-28.

8. Kilian O, Hossain H, Flesch I, Sommer U, Nolting H, Chakraborty T, *et al*. Elution kinetics, antimicrobial efficacy, and degradation and microvasculature of a new gentamicin-loaded collagen fleece. J Biomed Mater Res B Appl Biomater **2009**;90(1):210-22.

9. Tunney MM, Ramage G, Patrick S, Nixon JR, Murphy PG, Gorman SP. Antimicrobial susceptibility of bacteria isolated from orthopedic implants following revision hip surgery. Antimicrobial Agents and Chemotherapy **1998**;42(11):3002-5.

10. Sorensen TS, Sorensen AI, Merser S. Rapid release of gentamicin from collagen sponge. In vitro comparison with plastic beads. Acta Orthop Scand. .**1990**; 61:353-6.

II-SY2-03

Development of a Novel Multi Composite Bone Cement with Long-Lasting Antibacterial Effect: From Paste to Injectable Formulation

Maria Francesca Di Filippo[1], Silvia Panzavolta[1], Adriana Bigi[1], Luisa S. Dolci[2], Nadia Passerini[2], Paola Torricelli[3], Annapaola Parrilli[3], Francesca Bonvicini[4], Beatrice Albertini[2], Milena Fini[3], Giovanna A. Gentilomi[5]

[1]Alma Mater Studiorum - University of Bologna, Department of Chemistry, Bologna, IT; [2]Alma Mater Studiorum - University of Bologna, Department of Pharmacy and BioTechnology, Bologna, IT; [3]IRCCS Rizzoli Orthopaedic Institute, Laboratory of Preclinical and Surgery Studies, Bologna, IT; [4]Alma Mater Studiorum - University of Bologna, Department of Pharmacy and BioTechnology, Bologna, IT; [5]Alma Mater Studiorum - University of Bologna, Microbiology Unit, St Orsola-Malpighi University Hospital, Bologna, IT

Introduction

Calcium phosphate cements (CPCs) are biocompatible, bioactive and osteogenic systems which are obtained by mixing a powder with a liquid phase to get a workable paste that hardens into a solid phase. The properties of CPCs can be improved through enrichment of their composition with additives so they can be utilized as drug delivery systems. CPCs applications in bone replacement imply risks of infections due to bacterial colonization, hence the addition of antibiotics to CPCs composition is of outmost interest. We employed solid lipid microparticles (MPs) obtained from Cutina to load an antibiotic into a biomimetic CPC in order to obtain a material with a potent antibacterial activity over a long period. Gentamicin sulphate (GS) was chosen as model drug and it was (i) loaded directly into the cement powder, (ii) loaded into the solid lipid microparticles (MPsGS) which were added to the cement, and (iii) loaded both directly into the cement powder and into the solid lipid microparticles. Moreover, barium sulfate as radiopacifier agent was added to the composition of cements in order to monitor the material during the surgery. Samples were characterized and the compositions were optimized for a possible use as injectable bone cements.

Experimental Methods

The cement powders are composed of a gelatin/α-TCP mix , synthesized as described in a previous article [1], crushed in an electric grinder and manually sieved. Weighed amounts of $CaHPO_4 \cdot 2H_2O$ (DCPD) and gelatin/α-TCP mix powder were packed in a Teflon mold (6x12 mm) and mixed. Distilled water was used as liquid phase. After addition of the liquid phase, cement powders were mixed in the electric mortar to obtain a paste of workable consistency and compacted for 1 min inside the Teflon mold by using a 4465 Instron dynamometer set at 70 N. Then, cements were demolded and put in phosphate buffer (PB) pH 7.4 at 37°C up to 21 days. For the preparation of cements enriched with different additives, to the fixed amount of gelatin/α-TCP and DCPD the following percentages of additives were added:

- GS: 2, 4 and 8% wt
- $BaSO_4$: 10% wt
- MPs or MPsGS: 10% wt

Different formulations were obtained in order to investigate the role of every additive on the cement's properties.

Results and Discussion

The maximum stress of the cement increased as a function of time due to the hardening reaction. The introduction of 2% of GS provoked a reduction of the maximum stress and of the mechanical properties of the materials. On the other hand, the addition of $BaSO_4$ reduced the negative influence of GS on the mechanical properties.

X-ray results indicate that the cements loaded with 2 wt% of GS were almost totally converted after 7 days, suggesting that this amount of antibiotic did not interfere with the hardening reaction. Greater GS contents delayed the hardening reaction, slowing the conversion of α-TCP into CDHA. When the same amount of GS was loaded into MPs, a minor effect on the process of conversion of α-TCP into CDHA was observed.

Citotoxicity test performed for all GS-containing cements indicated the absence of cytotoxicity effects (values of proliferation over 70%).

Antibacterial properties were evaluated by means of Kirby-Bauer method suggesting that lipid microparticles could enhance GS uptake through the bacterial membrane.

The modification of the L/P ratios allowed the cements to be injectable, ensuring good injectability for all the compositions.

The cement cohesion was satisfying: when injected into saline solution immediately after extrusion, the CPC paste maintained its wire-like shape with no disintegration (see Figure) and maintained good cohesion.

The dispersion of MPs through the extruded wire was highly homogeneous, without any evidence of phase separation.

Conclusion

We developed an anti-bacterial and radiopaque CPC, which can be turned from paste to fully injectable by the variation of liquid/powder ratio.

Thanks to the use of spray congealed microparticles, GS was added to the cement composition without the lengthening of the setting times and the worsening of the mechanical properties observed when the drug is loaded directly into the cement powder.

The simultaneous addition of MPsGS and GS in powder has allowed to obtain a material showing a double and tunable kinetic release of the same antibiotics.

Human osteoblast-like cells displayed a significantly higher viability when cultured on cements where GS was loaded within than without MPs. All the compositions exhibit an inhibitory activity towards Gram positive and Gram negative reference bacterial strains and clinical isolates. In particular, cements with MPsGS show an enhanced inhibition towards Gram-positive bacteria and display a sustained release of the drug, which provides a long-term antibacterial activity, fundamental in the treatment of chronic infections.

Injectable formulations obtained increasing the liquid/powder ratios displayed good injectability, high cohesion and good dispersion of MPs into the extruded cements without phase separation.

References

[2]LS Dolci, S Panzavolta, B Albertini, B Campisi, M Gandolfi, A Bigi, N Passerini, Spray-congealed solid lipid microparticles as a new tool for the controlled release of bisphosphonates from a calcium phosphate bone cement, Eur. J. Pharm. Biopharm. 122,2018, 6–16. doi: 10.1016/j.ejpb.2017.10.002

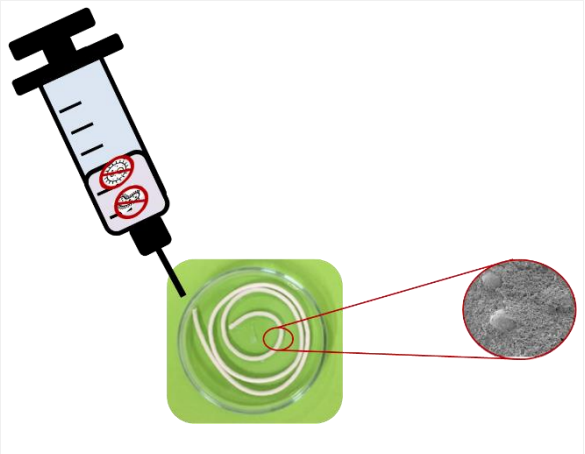

Cement wire extruded in saline solution.
As shown in the figure, no evidences of fase separation or disintegration can be found in the extruded cement, which maintained its wire-like shape until hardening even when injected into saline solution immediately after extrusion. The dispersion of MPs through the extruded wire was highly homogeneous, as confirmed by SEM morphological evaluations.

II-SY2-04

Microparticles with enhanced bone affinity for efficient antibiotic delivery to infected bone fractures

Stijn G. Rotman[1,2], Minqi Wang[3], Shengbing Yang[3], Dirk Grijpma[2], Robert G. Richards[1], David Eglin[1], Fintan T. Moriarty[1], Ting Ting Tang[3], Olivier Guillaume[1]

[1]AO Research Institute Davos, Musculoskeletal Regeneration / Polymers and Surfaces, Davos Platz, CH; [2]University of Twente, Biomaterials Science and Technology (BST), Enschede, NL; [3]Shanghai Key Laboratory of Orthopedic Implants, Shanghai Ninth People's Hospital, Shanghai Jiao Tong University School of Medicine, Department of Orthopedic Surgery, Shanghai, CN

Introduction

The efficacy of antibiotic treatments for bone infections is limited due to insufficient availability of antibiotics coupled with a low penetration of antibiotics in bone tissue [1,2]. Local antibiotic-loaded biomaterials often release antibiotics with sub-optimal diffusion-based kinetics. In this work, we present a poly(ϵ-caprolactone) (PCL) microparticulate system, for antibiotic delivery (Fig. 1). The particle is functionalized with bone seeking agents to establish particle affinity to bone mineral. A comparison in terms of hydroxyapatite (HAP) complexation is made between alendronate (ALN) and oligomers of aspartic acid (ASP) as bone binding agents present on the particle surface.

Experimental Methods

PCL microparticles were fabricated by oil/water emulsion with 10% PCL (M_W = 80,000 g·mol^{-1}) and 2.5% Gentamicin-AOT in dichloromethane as organic phase and 1% poly(vinyl alcohol) as aqueous phase. Solid microparticles were collected after solvent evaporation. Antibiotic encapsulation and subsequent release was measured by fluorometric assays and inhibition zones. As a next step, the PCL microparticles were exposed to 0.1M NaOH in order to enrich the surface with carboxylic acids. EDC/NHS conjugation was applied to covalently bind ALN or ASP to the carboxylated surface of the particles. Affinity of the functionalized particles to HAP substrates was tested by exposing the substrate to 1 mg/mL particle dispersion. Quantification of bound particles to HAP substrates was made by measuring fluorescence from pyrene encapsulated in the bound particles. The bone binding ability of the microparticles was assessed in a femoral bone defect in rats. Particle dispersion (20 µL containing 0.5 mg of IR dye loaded particles) were injected in the defect and the rats were imaged (IVIS, Perkin Elmer) daily over a 1-week period.

Results and Discussion

PCL microparticles with a size-average of 0.80±0.47 µm (Fig. 2A) and a 10.0% w/w Gentamicin-AOT load were fabricated. The microparticles showed sustained release of antibiotic over a 2-week period, releasing 60% of their load (Fig. 2B). The MIC of the particles against *S. aureus* was determined to be 9.76 µg/mL and the inhibitory zone of 1 mg of microparticles was observable for 5 days. The formation of carboxylic acid groups on the surface of the PCL microparticles was confirmed with Fourier-transform infrared spectroscopy (FTIR). After EDC/NHS conjugation of ALN, an increase in complexation with a HAP films could be measured (Fig. 2C). Chelated PCL-ALN particles were observed by scanning electron microscopy. Conjugation with ASP in similar manner resulted in slightly lower binding to a HAP compared to PCL-ALN. *In vivo*, PCL-ASP showed a trend of higher retention at the bony defect compared to PCL-ALN and the PCL control group (Fig. 2D and 2E).

Conclusion

PCL-ALN microparticles had higher affinity *in vitro* to HAP than PCL-ASP particles. However, it is known that ALN acts an osteoclast inhibitor, so the use of ASP might be more favourable when delivering drugs to an infected bone fracture where bone remodelling is essential. While the inhibitory properties against *S. aureus* was shown for the antibiotic loaded microparticles, its enhanced affinity to HAP through surface modification provides a way to ensure high doses of antibiotics at the immediate vicinity of the bone. Nevertheless, the bone binding affinity of the modified PCL-ALN and PCL-ASP was not statistically improved on the in vivo model employed here, and further improvement of the is still necessary. By presenting this bone targeting drug delivery system, first steps were made to provide a potential tool to treat bone infections.

References

[1]P. Carek *et al.* (2001) *Am Fam Physician* 63(12):2413-2421 [2]S.G. Rotman *et al.* (2018) *J Control. Release* 269:88-99

Acknowledgement

This work was supported by the AOTrauma Clinical Priority Program Bone Infection.

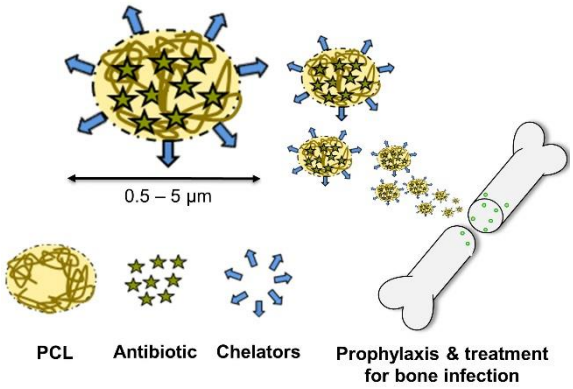

Fig. 1: Graphical Abstract
Schematic of the designed drug delivery system (DDS).

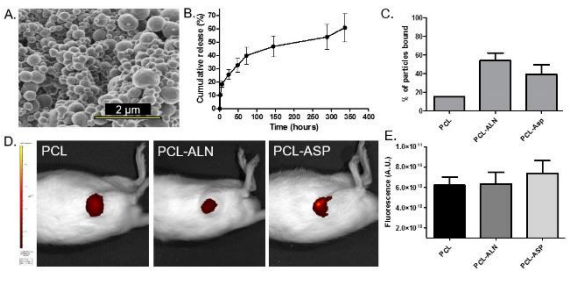

Fig. 2: Characterization of DDS
A. PCL microparticles with gentamicin-AOT load of 10% w/w. B. Sustained in vitro release of Gentamicin-AOT from 10 mg PCL microparticles kept at 37ºC under mild rotation (n=6). C. Increased HAP affinity after particle surface functionalization with bone seekers ALN and ASP (n=3). D. Representative images of PCL, PCL-ALN and PCL-ASP microparticles loaded with IR780 iodide fluorophore 7 days after injection in a rat-femoral defect. E. Total fluorescence measured on explanted femurs at day 7 (n=4).

1:00 p.m. – 2:30 p.m.

Hall 5

II-OS8 | Composites and stimuli responsive biomaterials 2

II-OS8-01

Development of Silk Fibroin/CNF Scaffolds for Cardiac Patch Applications

Yigithan Tufan[1,4], Hayriye Öztatlı[2], Bora Garipcan[2], **Batur Ercan**[1,3,4]

[1]Middle East Technical University, Metallurgical and Materials Engineering Department, Ankara, TR; [2]Boğaziçi University, Institute of Biomedical Engineering, İstanbul, TR; [3]Middle East Technical University, Biomedical Engineering Program, Ankara, TR; [4]Middle East Technical University, BIOMATEN-METU Center of Excellence in Biomaterials and Tissue Engineering, Ankara, TR

Introduction

Coronary heart disease is the leading cause of death across the world [1]. The main cause of this disease is the accumulation of fatty substance, blood cells and calcium deposits inside the coronary arteries, which limits the flow of oxygenated blood and nutrients to the heart muscle and it eventually leads to heart attack. Since heart muscle has limited ability to regenerate itself with functional myocytes, cardiac patches has been utilized as a potential regenerative therapy [2, 3]. Among the numerous types of materials investigated for cardiac-tissue engineering, silk fibroin captured significant interest due to its tunable mechanical properties, biodegradation characteristics and ability to promote cellular functions. In this study, silk fibroin based 3D porous scaffolds were investigated for cardiac patch applications. To bring electrical conductivity and enhance mechanical properties, carbon nanofibers (CNFs) were incorporated into the fibroin matrix. Additionally, to regenerate damaged cardiac muscle, induced pluripotent stem cells (iPSC) were seeded into the scaffolds. Detailed characterization studies were completed to assess the influence of silk fibroin content, CNF content, porosity and pore size of the silk fibroin/CNF scaffolds on the electrical conductivity, degradation properties, mechanical properties, cell viability and iPSC cellular response.

Experimental Methods

There were three main steps for the fabrication of 3D porous silk fibroin/CNF scaffolds. Initially, fibroin was extracted from the *Bombyx Mori* (silkworm) cocoons via dissolving in LiBr. In the second step, extracted fibroin was lyophilized to be stored at room temperature. In the final step, CNFs were dispersed in 1,1,1,3,3,3-Hexafluoro-2-propanol (HFIP) and fibroin was dissolved in CNF dispersed HFIP. NaCl particles were added into the HFIP/fibroin solution as a porogen agent.

Results and Discussion

SEM images of the scaffolds revealed that size ranges of NaCl particles used as porogen were maintained in the fabricated scaffold microstructure and determine the pore size range of scaffolds (Fig. 1a). Structure of CNFs was investigated with TEM (Fig. 1b). 1 and 3 wt% CNF addition did not bring electrical conductivity to detectable ranges, yet, the addition of 5 wt% CNF improved the electrical conductivity of scaffolds within limits required in cardiac-tissue engineering. In fact, the electrical conductivity of scaffolds was increased up to 0.025 S/cm when the CNF content was 10 wt %. In the XRD spectra, as opposed to observing broad amorphous peak of lyophilized fibroin, sharp peaks of β-sheet were obtained at $2\theta = 21.3^{o}$, $2\theta=23.8^{o}$ and $2\theta=26.5^{o}$ for each scaffold independent of the NaCl:Fibroin ratio utilized during scaffold fabrication. In the FTIR spectra of the scaffolds, transmission peaks obtained at 1623 cm^{-1} and 1516 cm^{-1} were attributed to β-sheet crystalline structure. Comparing the FTIR spectra of scaffolds with 5 and 10 w/v% fibroin, a stronger signal with deeper peaks were observed for the former due to its higher crystallinity. Stress-strain curves completed via uniaxial tensile testing (Fig. 2a) showed that mechanical properties of scaffolds

were controlled by altering scaffold fabrication parameters. Tensile strength (TS) and elastic modulus (E) of the scaffolds gradually increased with a decrease in NaCl:Fibroin ratio. Furthermore, TS of the scaffolds increased about 14 times (from 0.07 MPa to 1 MPa) upon the addition of 10 wt% CNF. L929 fibroblasts exhibited higher metabolic activity on scaffolds with larger pore size (Fig. 2b). Furthermore, increased porogen content of the scaffolds (NaCl:Fibroin ratio of 15:1) lead to more than 70% increase in the cell adhesion after 5 days of culture.

Conclusion

The electrical conductivities, degradation and mechanical properties, along with metabolic activities of cells cultured on silk fibroin/CNF scaffolds were enhanced through optimizing silk fibroin content, CNF content, porosity and pore size range of scaffolds. Detailed characterization studies indicated that tunable mechanical and electrical properties and ability to control over fibroin concentration, crystallinity and pore structure via altering fabrication parameters of 3D silk fibroin/CNF scaffolds made it a promising candidate for cardiac patch applications. Studies including time dependent enzymatic degradation tests and *in vitro* iPSC proliferation studies are underway to further improve scaffold properties for cardiac patch applications.

References

[1] https://www.who.int/news-room/fact-sheets/detail/cardiovascular-diseases-(cvds), accessed at 15.03.2019.
[2] Amezcua, R., et. al., (2016). *Nanomaterials,6*(7), 133.
[3] Zhang, Y., et. al., (2011). *Nano-Micro Letters,3*(4), 270-277.
[4] Patra, C., et. al., (2012). *Biomaterials,33*(9), 2673-2680
[5] Altman, et. al., (2003). *Biomaterials*,24(3), 401-416.

Acknowledgement

We would like to thank Scientific and Technological Research Council of Turkey, TÜBİTAK (grand no:117M754) for providing financal support. We would like to thank BIOMATEN, METU Center of Excellence in Biomaterials and Tissue Engineering for their help in characterization experiments.

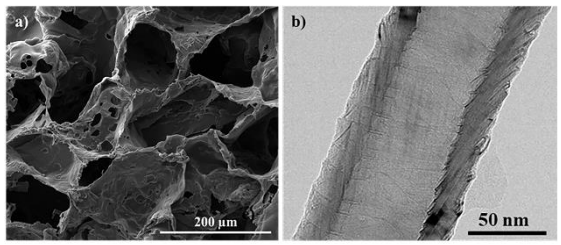

Figure 1
Morphological characterization of a) silk fibroin/CNF scaffold having pore size range of 180-200 µm and b) TEM image of CNFs incorporated into the scaffolds.

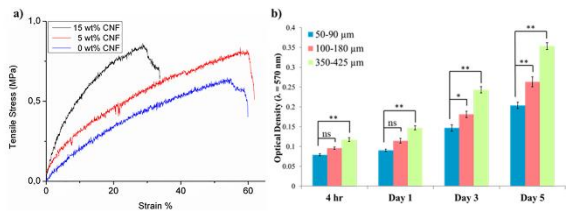

Figure 2
Stress-strain curves of silk fibroin/CNF scaffolds fabricated by altering a) CNF content and metabolic activity of L929 fibroblasts on silk fibroin/CNF scaffolds fabricated by altering c) NaCl particle size range. '*' p≤ 0.05; '**'p≤ 0.001

II-OS8-02

Spatiotemporal Material Functionalization via Competitive Supramolecular Complexation of Avidin and Biotin Analogs

Tom Kamperman, Michelle Koerselman, Cindy Kelder, Jan Hendriks, João Crispim, Xandra De Peuter, Piet Dijkstra, Marcel Karperien, Jeroen Leijten

University of Twente, Dept. of Developmental BioEngineering / Faculty of Science and Technology / Technical Medical Centre, Enschede, NL

Introduction

Native tissues are characterized by a dynamic nature. Recapitulating such dynamicity in engineered tissues requires the temporal control over their biochemical composition. Typically, spatiotemporal modification of biomaterials relies on photoresponsive strategies, which pose the inherent risk of cytotoxic UV-light and radical-based reactions[1]. Here, we pioneered supramolecular desthiobiotin/avidin complexation to enable the dynamic modification of biomaterials. Desthiobiotin is a non-sulfur containing analog of biotin that also interacts with avidin, but with substantially lower binding affinity than biotin ($K_{d,biotin}$~10^{-15} M vs $K_{d,desthiobiotin}$~10^{-14} M)[2,3]. We hypothesized that a supramolecular desthiobiotin/biotin displacement strategy would grant spatiotemporal control over the biochemical composition of biomaterials in a novel, facile, and cytocompatible manner.

Experimental Methods

Dextran-tyramine-biotin (Dex-TA-biotin) was synthesized as previously described[4]. Hydrogels were prepared by mixing 5% Dex-TA-biotin, 3 U/ml horseradish peroxidase, and 0.05% H_2O_2. Hydrogels were further functionalized with 1 µM tetravalent neutravidin (i.e., avidin analog) and 1 µM desthiobiotin-FITC, biotin-atto565, and/or biotin-FITC, and subsequently analyzed using fluorescence recovery after photobleaching (FRAP) and fluorescence confocal microscopy.

Results and Discussion

Fluorescence confocal microscopy and FRAP confirmed that biotin-FITC was coupled to Dex-TA-biotin hydrogels via neutravidin, but not to non-functionalized (i.e. Dex-TA) hydrogels, which validated the successful generation and functionality of Dex-TA-biotin hydrogels. As shown in Figure 1, the reversible and sequential modification of hydrogels was demonstrated by displacing desthiobiotin-FITC (i.e. green) with biotin-atto565 (i.e. red). By tuning the concentration and incubation time of biotin-atto565, we could reproducibly control its penetration depth into the hydrogels. This strategy granted spatial control over the hydrogels' biochemical composition by determining the thickness of the biotin-displaced shell. Performing the supramolecular displacement strategy in the presence of cells did not reveal a cytotoxic effect, as assessed by live/dead cell staining. Moreover, the method enabled the spatiotemporal capturing and presentation of, for example, bioactive peptides (e.g., RGD) and endogenous growth factor, which was validated using surface plasmon resonance.

Conclusion

In situ tuning of the biochemical composition of engineered tissues is key to mimic the dynamic nature of native tissues. We have successfully demonstrated a novel method for the spatiotemporal modification of biomaterials based on reversible and cytocompatible desthiobiotin/avidin complexation.

References

1. Brown, T.E. and K.S. Anseth, Chem Soc Rev, 2017. **46**(21): p. 6532-6552.
2. Hirsch, J.D., et al., Analytical Biochemistry, 2002. **308**(2): p. 343-57.
3. Green, N.M., *Avidin.* Adv Protein Chem, 1975. **29**: p. 85-133.
4. Kamperman, T., 2018, University of Twente. p. 174.

Acknowledgement

The authors acknowledge the following funding: Dutch Arthritis Foundation (#12-2-411 and #LLP-25), NWO VENI #14328, and ERC Starting #759425).

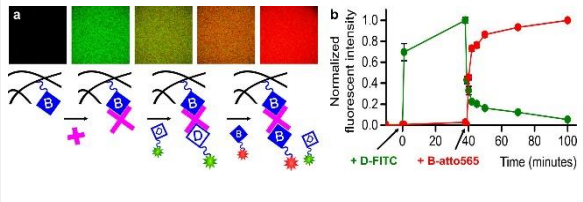

Figure 1
Dynamic biomaterial modification was demonstrated by desthiobiotin-FITC / biotin-atto565 displacement.

II-OS8-03

Smart liposomes for delivery at stenosed vessels - a study combining microfluidics with spatially resolved small-angle X-ray scattering

Marzia Buscema[1], Sofiya Matviykiv[1], Andreas Zumbuehl[4], Bert Müller[1], Hans Deyhle[1,2], Thomas Pfohl[1,3]

[1]University of Basel, Biomaterials Science Center, Allschwil, CH; [2]University of Southampton, Southampton, GB; [3]Universität Freiburg, Institute of Physics, Freiburg, DE; [4]University of Fribourg, Chemistry, Fribourg, CH

Introduction

In 2012, research teams from US and Switzerland published their ideas on mechanically responsive carriers [1,2]. Nanometer-size liposomes composed out of specific artificial phospholipids exhibit not only the desired response to mechanical stimuli [2], but also the surprising lack of the characteristic immune response of liposomal drugs [3-5]. Therefore, these liposomes are promising containers for the targeted delivery by means of a purely physical trigger present at the pathological constrictions of human arteries. It is, however, unclear, which forces trigger the release of the cargo. Originally, the shear stress, at least an order of magnitude higher within the constrictions than in the healthy parts of the vessel, was considered. Simple estimations, however, show that the pressure-gradient forces have also to be considered. The impact of the two potential contributions can be experimentally addressed by combining spatially resolved small-angle X-ray scattering with a microfluidic device for physically simulating the stenosed blood vessel.

Experimental Methods

For the microfluidics study, liposomes about 100 nm in diameter were formulated from the artificial Pad-PC-Pad phospholipids. These liposomes are non-spherical and show a variety of shapes. In the transmission electron microscopy, they often appear as lentils. These liposomes are known to envelop a cargo, such as the vasodilator nitroglycerin, at rest but become leaky by mechanical stimuli.

The spatially resolved small-angle X-ray scattering measurements were performed at the cSAXS beamline, Swiss Light Source (PSI, Villigen, Switzerland). The X-ray photons with 11.2 keV were focused to several ten micrometers. At a distance of 7.102 m a Pilatus 2M detector with a pixel size of 172 µm was placed. Two-dimensional scans were acquired line-by-line by continuously moving the device in horizontal direction, while the detector recorded the data during a total acquisition time of about two hours.

The X-ray compatible microfluidic device with a 1 mm-wide horizontal channel possessing a 125 µm-wide constriction was used [6] to locally detect the morphological changes of the liposomes at three selected flow conditions.

Results and Discussion

The spatially resolved small-angle X-ray scattering data show a dependence on the selected flow conditions. The mean size of the liposomes is modified near the wall of the constriction. This means that the average wall shear stress can change the overall size of the non-spherical liposomes [7]. At in- and outlet, we have identified a change of the bilayer thickness, which is in line with the loss of interdigitation of the phospholipids. Most probably, this loss of interdigitation is caused by the gradient-pressure force known from the Bernoulli equation.

Conclusion

The combination of spatially resolved X-ray scattering and micro-fluidics allows for the detection of morphological changes of mechanically responsive liposomes of nanometer size. The related results indicate that the gradient-pressure force is responsible for the leakage of specific non-spherical liposomes, since it annihilates the interdigitation of these phospholipids.

References

[1] N. Korin, M. Kanapathipillai, B.D. Matthews, M. Crescente, A. Brill, T. Mammoto, K. Ghosh, S. Jurek, S.A. Bencherif, D. Bhatta, A.U. Coskun, C.L. Feldman, D.D. Wagner, D.E. Ingber: Shear-activated nanotherapeutics for drug targeting to obstructed blood vessels, Science 337 (2012) 738-742

[2] M. N. Holme, I. A. Fedotenko, D. Abegg, J. Althaus, L. Babel, F. Favarger, R. Reiter, R. Tanasescu, P-L. Zaffalon, A. Ziegler, B. Müller, T. Saxer, A. Zumbuehl: Shear-stress sensitive lenticular vesicles for targeted drug delivery, Nature Nanotechnology 7 (2012) 536-543

[3] S. Bugna, M. Buscema, S. Matviykiv, R. Urbanics, A. Weinberger, T. Meszaros, J. Szebeni, A. Zumbuehl, T. Saxer, B. Müller: Surprising lack of liposome-induced complement activation by artificial 1,3-diamidophospholipids in vitro, Nanomedicine: Nanotechnology, Biology and Medicine 12 (2016) 845-849

[4] M. Buscema, S. Matviykiv, T. Mészáros, G. Gerganova, A. Weinberger, U. Mettal, D. Mueller, F. Neuhaus, E. Stalder, T. Ishikawa, R. Urbanics, T. Saxer, T. Pfohl, J. Szebeni, A. Zumbuehl, B. Müller: Immunological response to nitroglycerin-loaded shear-responsive liposomes in vitro and in vivo, Journal of Controlled Release 264 (2017) 14-23

[5] S. Matviykiv, M. Buscema, G. Gerganova, T. Mészáros, G.T. Kozma, U. Mettal, F. Neuhaus, T. Ishikawa, J. Szebeni, A. Zumbuehl, B. Müller: Immunocompatibility of Rad-PC-Rad liposomes in vitro, based on human complement activation and cytokine release, Precision Nanomedicine 1 (2018) 45-67

[6] V. Lutz-Bueno, J. Zhao, R. Mezzenga, T. Pfohl, P. Fischer, M. Liebi: Scanning-SAXS of microfuidic flows: Nanostructural mapping of soft matter. Lab-on-a-Chip 16 (2016) 4028-4035

[7] M.N. Holme, G. Schulz, H. Deyhle, T. Weitkamp, F. Beckmann, J.A. Lobrinus, F. Rikhtegar, V. Kurtcuoglu, I. Zanette, T. Saxer, B. Müller: Complementary X-ray tomography techniques for histology-validated 3D imaging of soft and hard human tissues using plaque-containing blood vessels as examples, Nature Protocols 9 (2014) 1401-1415

Acknowledgement

The financial support of the Swiss National Science Foundation in the frame of "Smart Materials" (NRP62) for the project "NO-stress" is gratefully acknowledged. S.M. thanks the Swiss federation for the Excellence stipend.

II-OS8-04

Design of multifunctional nanocomposites of mesoporous silica nanoparticles and hydroxyapatite nanocrystals for biomedical applications.

Catherine Harvey[1], Daniel Lozano[1,2], Raúl Zazo[1], Elvis Cabrera[1], Blanca González[1,2], Isabel Izquierdo-Barba[1,2], María Vallet-Regí[1,2]

[1]Universidad Complutense de Madrid, Química en Ciencias Farmacéuticas. Facultad de Farmacia, Madrid, ES; [2]Networking Research Center on Bioengineering, Biomaterials and Nanomedicine (CIBER-BBN), Madrid, ES

Introduction

Calcium phosphate materials are of great relevance as biomaterials due to their unique biocompatibility and bioactivity which has led to their wide use in bone tissue engineering.[1]Also, mesostructured materials, such as ordered mesoporous silica nanoparticles (MSN), are of great interest on such biomedical applications and therapeutic delivery.[2]Combinations of these two inorganic materials in one nanosystem have been previously described in the context of pH-responsive drug delivery.[3]Herein, we investigate strategies to obtain core@shell nanocomposites of MSNs and hydroxyapatite nanocrystals and evaluate their biocompatibility and cellular differentiation capability in preosteoblast cell line.

Experimental Methods

MSNs and MSNs-$COOH_{ext}$materials were synthesized as published.[4]Then, MSNs-$COOH_{ext}$were suspended in water and a solution of $Ca(NO_3)_2.4H_2O$ is added and stirred for 2 h. subsequently a solution of $(NH_4)_2HPO_4$is added and finally the pH was adjusted to 10 with a solution of NH_4OH.Calcium and phosphate ions were added according to the stoichiometric ratio for hydroxyapatite.The stirring was maintained 16 h at room temperatura and then the product recovered and gently washed with water, ethanol and dried. An external layer of gelatine is provided by stirring the MSNs@HA materials in a gelatine solution at 50 ºC.

In vitro, biocompatibility assays were performed in MC3T3-E1 preosteoblasts cell cultures. Different *in vitro* parameters as viability, proliferation and differentiation have been evaluated.

Results and Discussion

Fluorescent MSNs were prepared following a modified Stöber method. To provide anchoring points for the calcium ions, the external surface of the MSNs was functionalized with carboxylic acid groups in a first step, using a post-synthesis method.[4]The efficient coating of the MSNs-$COOH_{ext}$with hydroxyapatite was achieved through a biomimetic mineralization process.

Transmission electron microscopy (TEM) images show the MSNs material with typical MCM-41 with 2D hexagonal mesostructure. After biomimetic deposition of calcium phosphate, the MSNs appeared externally coated by needle like hydroxyapatite nanocrystals.

The TEM studies also showed that the coating of HA nanocrystals on MSNs is not stable in phosphate buffer at pH 7.4, so the MSNs@HA material was coated with a gelatine layer to increase the stability of the nanocomposite in aqueous medium giving the MSNs@HA@Gel material.

In vitro, MC3T3-E1 preosteoblasts cell culture studies showed a good biocompatibility of MSNs@HA@Gel materials evidencing an increase in the cell differentiation by alkaline phosphatase activity after 7 days of cell culture. This

effect was not found in the control culture with the pristine MSNs and MSNs@HA, therefore it can be ascribed to the stable coating of HA nanocrystals when the gelatine layer is present.

Conclusion

Multifunctional nanocomposites of MSNs and hydroxyapatite nanocrystals have been optimized to obtain core@shell materials such as MSNs@HA@Gel. Due to their biocompatibility and cellular differentiation capability in preosteoblast cell line, as well as the possibility to carry drugs inside the mesopores, these nanosystems are excellent candidates for bone tissue regeneration.

References

1. Bioceramics with Clinical Applications. Ed. M. Vallet-Regí. John Wiley & Sons Limited, 2014.
2. Castillo R.R., *et al.Expert Opinion on Drug Delivery* **2019**, *16*, 415.
3. Rim H.P., *et al.Angew. Chem. Int. Ed.* **2011**, *50*, 8853.
4. Montalvo-Quiros, S. *et al.Nanoscale* **2019**, *11*, 4531.

Acknowledgement

Authors acknowledge funding from the European Research Council (Advanced Grant VERDI; ERC-2015-AdG Proposal No. 694160).

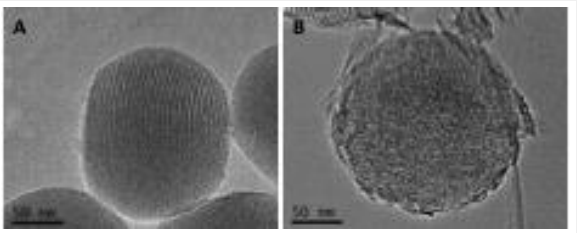

Figure 1.
Transmission electron microscopy micrograph of (A) MSNs material and (B) MSNs@HA material.

II-OS8-05

Incorporation of metals in mesoporous silica nanoparticles for infection treatment

Blanca González[1,2,3], **Elena Álvarez**[1,2], Manuel Estévez[1], Jimena Soler[1], Elba García[1], Isabel Izquierdo-Barba[1,2,3], María Vallet-Regí[1,2,3]

[1]Universidad Complutense de Madrid, Chemistry in Pharmaceutical Sciences Department, Madrid, ES; [2]Hospital 12 de Octubre i+12, Instituto de Investigación Sanitaria, Madrid, ES; [3]Networking Research Center on Bioengineering, Biomaterials and Nanomedicine, CIBER-BBN, Madrid, ES

Introduction

In recent years, the development of antibiotic resistance of both *Gram*-positive and *Gram*-negative bacteria and its therapeutic implications has made clear the need to find novel and effective solutions for the treatment of bacterial infections. Data obtained by the World Health Organization report that for strains such as *E. coli* and *S. aureus* shows a resistance to the most common antibiotics that can exceed 50%.[1] The problem essentially lies on the impermeability of the external membranes of these microorganisms and on the formation of bacterial biofilms, which constitute a natural defense mechanism making difficult or impossible the access of antibiotics to the infection place. One of the current challenges is the design of nanoplatforms that selectively transport antimicrobial agents to the right place.[2] Both *Gram*-negative and *Gram*-positive bacteria have different compounds in their external membranes that easily produce negative charges, increasing their hydrophilicity. On the other hand, dendrimers are macromolecules made up of a core, multiple branching layers and a multitude of external functional groups. The ability of polycationic dendrimers located on the external surface of mesoporous silica nanoparticles (MSNs) to adhere to the bacterial walls and favor the internalization of the nanosystem inside the bacteria has been described for a third-generation polypropyleneimine dendrimer (G3). Therefore, non-toxic systems MSNs-G3 can be obtained which are capable of targeting bacteria, penetrating them and carrying an antimicrobial agent to fight infections.[3] In this work, it is intended to strengthen the bacterial inhibition of these systems for both *Gram*-negative and *Gram*-positive bacteria through the addition of metals with bactericidal effect such as silver or copper to these nanostructures, therefore avoiding the antibiotic resistance effect.

Experimental Methods

Two different families of nanomaterials were obtained: *i)* nanosystems with metal cations tethered on the dendritic branches (MSNs-G3-M^{n+}), *ii)* nanosystems with metallic nanoparticles on the external surface of the MSNs (MSNs-G3-M). Briefly, MSNs were externally functionalized with the third-generation polypropyleneimine dendrimer (G3) *via* a post-synthesis method (MSNs-G3). Subsequently, the functionalized nanoparticles are soaked in different solutions containing Ag^{+}, Cu^{2+} or Zn^{2+}, respectively. Then, the materials are recovered to obtain MSNs-G3-M^{n+} or subjected to a chemical reduction with $NaBH_4$ to obtain the nucleation of metallic nanoparticles on the surface of the MSNs (MSNs-G3-M). The samples were characterized by different techniques as X-ray diffraction, transmission electron microscopy, dynamic light scattering, Fourier transform infrared spectroscopy and elemental analyses. *In vitro* assays were performed to determine the antimicrobial activity of these nanosytems in both *E. coli* and *S. aureus* bacteria cultures.

Results and Discussion

TEM studies show homogeneous size distribution of the MSNs with regular geometry after metal nucleation (see Figure). Concerning silver nucleation, the image shows a distribution of silver nanoparticles on the MSN surfaces, without large aggregates. On the contrary, for the copper sample there are no visible copper nanoparticles onto the MSNs surface, however an external layer around the MSNs with different contrast, that could be ascribed to a copper oxide, is appreciated.

In vitro antimicrobial assays have shown that MSNs-G3-Ag exhibits excellent antibacterial behaviour in both positive and negative *Gram* bacteria, while MSNs-G3-Cu show good antibacterial behaviour only for *S. aureus*. Assays comparing the antimicrobial effects for the materials containing the metal nanoparticles *versus* the materials tethering the metallic ions have been performed.

Conclusion

Novel free-antibiotic multifunctional nanosystems based on MSNs, polycationic dendrimers and metals such as silver, copper and zinc have been synthetized and characterized. The nanosystems exhibit both bacteria internalization capability and strong bactericidal effect which is due to the presence of metals. Also, synergistic effects due to the presence of an antibiotic loaded inside the mesopores will be evaluated.

References

1. World Health Organization 2014, “Antimicrobial resistance: global report on surveillance 2014”.
2. Vallet-Regí M. *et al.* The Enzymes 44: 35-59, 2018.
3. González B. *et al.* Acta Biomaterialia 68:261-271, 2018.

Acknowledgement

Authors acknowledge funding from the European Research Council (Advanced Grant VERDI; ERC-2015-AdG Proposal No. 694160).

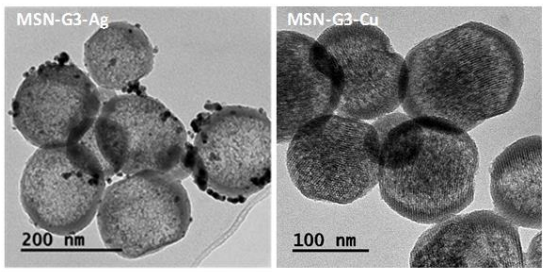

Figure.
TEM images corresponding to MSN-G3 after silver (left) and cupper (right) complexation and reduction.

II-OS8-06

Screening Cell-Biomaterial Interactions in three dimensions

Maria Gabriella Fois, Alex Guttenplan, Zeinab N. Tahmasebi Birgani, Stefan Giselbrecht, Roman Truckenmüller, Pamela Habibovic

Maastricht University, MERLN, Maastricht, NL

Introduction

Development and biological characterization of novel biomaterials for regenerative medicine greatly relies on the use of animal models. Currently used 2D in vitro assays do not recapitulate the structural and biological complexity of human tissues and remain inferior to in vivo models [1]. Therefore, research is shifting towards 3D cell culture strategies for bridging this gap [2], among which multicellular spheroid models have gained popularity, since they offer a more physiological cell-cell and cell-extracellular matrix interaction [3]. Here, we present a novel 3D cell culture method for evaluating cell-biomaterial interactions, based on cell aggregation and spheroid formation in the presence of micro-sized biomaterials, with the ultimate aim of developing a reproducible and more physiologically relevant screening system for biomaterials.

Experimental Methods

Microwell array chips were created by microthermoforming polycarbonate (PC) films at 154 ˚C and 20 bar, as described before [4], characterized using optical profilometry and scanning electron microscopy, and used as a platform for forming 3D spheroids of cells and biomaterials. A series of biomaterials commonly used in orthopedic applications, including titanium (Ti), poly(methyl methacrylate) (PMMA), poly(ethylene) (PE), tricalcium phosphate (TCP) and biphasic calcium phosphate (BCP, and having the form of microparticles (diameter≈50 µm) were used as model materials for screening various cell-biomaterial interactions in 3D spheroids. Copper (Cu) microparticles were chosen as positive control for cytotoxicity evaluation. Human osteosarcoma cells (MG63) or human mesenchymal stem cells (hMSCs) were seeded in microwells (5000 cells/microwell), together with varying amounts of biomaterials (10 or 100 micro-particles/microwell). Cell-biomaterial spheroids were formed through spatial confinement inside the u-bottom-shaped microwells. Spheroid morphology and metabolic activity of the cells in the spheroids were evaluated after 3 and 7 days of culture by SEM and cell viability assay (Molecular Probes™ PrestoBlue™, Fisher Scientific). Spheroids in microwells without biomaterials served as control.

Results and Discussion

Microthermoformed microwells exhibited a diameter of 500 µm and an average depth of 400 µm. MG63 and hMSC aggregates with and without biomaterials formed within 24 hours and were homogeneously distributed throughout the chips. Ti, TCP and BCP micro-particles were incorporated in the cell aggregates. The polymeric biomaterials, on the other hand, did not participate in aggregate formation. Cu microparticles, known as a cytotoxic material, prevented both cell adhesion onto the material surface and cell aggregation, and resulted in cell death [5] (fig 1). Quantitative analysis were in agreement with these observations. Moreover, a dose-dependent effect of the CU particles on the corresponding cell response was detected, with this effect being less pronounced for the other biomaterials (fig 2). Spheroid models have been previously explored for screening libraries of soluble molecules for drug discovery and toxicology, as well as in vitro model in cancer research [3]. Our results, however, show spheroid formation of cells with solid biomaterials, and the potential of such a spheroid model for screening different cell-biomaterial interaction in a miniaturized on-chip model, in a more clinically relevant 3D microenvironment.

Conclusion

Microwell chips were produced by thermoforming, and used for generating 3D cell-biomaterial spheroids, with various metallic, polymeric and ceramic biomaterials. We were able to detect different, material-dependent aggregation behaviors of the spheroids, and quantify the cell-biomaterial interactions in terms of cell viability, proliferation and differentiation. The results present a miniaturized on-chip 3D model based on spheroids, which we will further develop towards a high-throughput screening platform of biomaterials.

References

1. Duval et al., Physiology 2017. **32**: p. 266–277.
2. Pampaloni et al., Nature Reviews Molecular Cell Biology 2007. **8**: p. 839–845.
3. Laschke et al., Trends in Biotechnology 2017. **35**(2): p. 133-144.
4. Truckenmüller et al., Advanced Materials 2011. **23**(11): p. 1311–1329.
5. Grillo et al., Contraception 2010. **81**: p. 343–349.

Acknowledgement

This research has been supported by the Dutch Province of Limburg and the Interreg Vlaanderen-Nederland BIOMAT project.

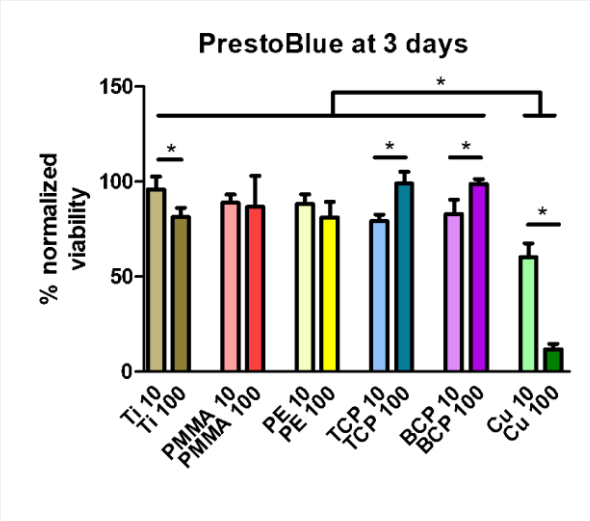

Fig 2: Metabolic activity assay for 10/100 particles for each material per microwell.

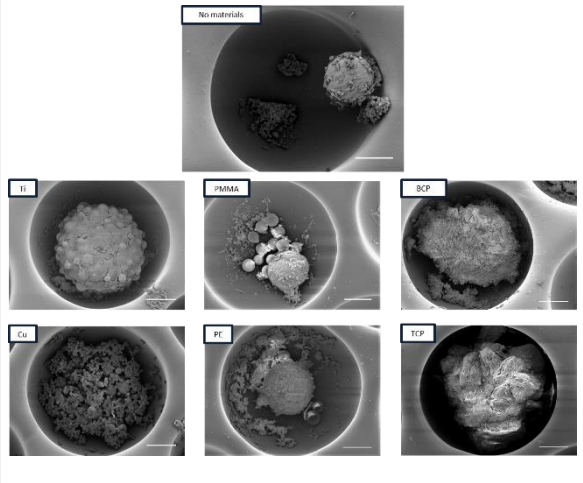

Fig 1: MG63 aggregates with different reference materials at 3 days. Scale bar: 100 µm

1:00 p.m. – 2:30 p.m.

Conference room 4+5

II-SY3 | DGBM SY: Biomineralization and Calcification in Regenerative Medicine

Wilhelm Jahnen-Dechent (Aachen, DE)
Liam Grover (Birmingham, UK)

Biomineralization includes minerals that would not exist if it were not for living organisms, which metabolize existing non-biogenic minerals and turn them into complex materials. Biominerals thus comprise a wide range of simple metabolic products like magnetite in bacteria, to complex compound materials like bone in vertebrates. During this session we present current concepts and applications of biomineralization with a focus on the mineral-tissue interface as well as biomimetic biomaterials for implants and tissue engineering. Mechanisms of pathological mineralization in the human body, also known as calcification, will likewise be addressed.

II-SY3-KL01

Mud in the blood: Protein-Mineral Complexes in Mineralization and Calcification

Wilhelm Jahnen-Dechent

RWTH Aachen University, Helmholtz Institute for Biomedical Engineering, Biointerface Lab, Aachen, DE

Introduction

Mineralization in vertebrates is limited to bones and teeth. Mineral concentration thoughout the body is similarly high and therefore mineralization proceeds once started. For this reason all other tissues must be actively protected against pathological mineralization also called calcification, both by the absence of pro-mineralizing and the presence of anti-mineralizing agents. Calcification is frequent in tissue remodelling. Ectopic calcification results when mineral deposition exceeds clearance. This is common in many metabolic and degenerative diseases. Fetuin-A/α_2-HS glycoprotein (genetic symbol AHSG) is an important regulator of mineralized matrix metabolism.

Experimental Methods

We studied calcification in cell-based systems and in small animals. Clinical association studies were also performed

Results and Discussion

Fetuin-A acts as a »mineral chaperone« stabilizing mineral precursors for bone mineralization and mediating clearance of excess mineral as protein-mineral complexes. Fetuin-A deficient mice developed severe calcification impairing heart, lung and kidney function as well as reproduction. Fetuin-A deficiency in humans is associated with all-cause as well as cardiovascular mortality.

Conclusion

I will present lessons learned from Fetuin-A related research and their application in the diagnosis and therapy of calcification disease. Results from animal and cell culture models will be translated into practical approaches for bone tissue engineering and the prevention of calcification in soft tissue engineering.

References

Herrmann M, Babler A, Moshkova I, Gremse F, Kiessling F, Kusebauch U, Nelea V, Kramann R, Moritz RL, McKee MD, Jahnen-Dechent W. Luminal Calcification of the Microvasculature in Fetuin-A Deficient Mice Leads to Premature Aging and Death. bioRxiv. 2019:577098. doi:10.1101/577098.

Babler A, Schmitz C, Buescher A, Herrmann M, Gremse F, Gorgels TG, Floege J, Jahnen-Dechent W. Soft tissue calcification in mice is governed by fetuin-A, pyrophosphate and magnesium. bioRxiv. 2019:577239. doi:10.1101/577239.

Heinen MC, Babler A, Weis J, Elsas J, Nolte K, Kipp M, Jahnen-Dechent W, Häusler M. Fetuin-A protein distribution in mature inflamed and ischemic brain tissue. Karamyan V, ed. PLoS ONE. 2018;13(11):e0206597.

Köppert S, Büscher A, Babler A, Ghallab A, Buhl EM, Latz E, Hengstler JG, Smith ER, Jahnen-Dechent W. Cellular Clearance and Biological Activity of Calciprotein Particles Depend on Their Maturation State and Crystallinity. Front Immunol. 2018 Sep 4;9:1991. doi: 10.3389/fimmu.2018.01991. eCollection 2018.

Brylka LJ, Köppert S, Babler A, Kratz B, Denecke B, Yorgan, T.A., Etich, J., Costa, I.G., Brachvogel, B., Boor, P., Schinke T, Jahnen-Dechent W. (2017). Post-weaning epiphysiolysis causes distal femur dysplasia and foreshortened hindlimbs in fetuin-A-deficient mice. PLoS ONE 12, e0187030.

Herrmann, M., Schäfer, C., Heiss, A., Gräber, S., Kinkeldey, A., Büscher, A., Schmitt, M.M.N., Bornemann, J., Nimmerjahn, F., Herrmann, M., et al. (2012). Clearance of fetuin-A--containing calciprotein particles is mediated by scavenger receptor-A. Circ Res 111, 575–584.

Pasch A, Farese S, Gräber S, Wald J, Richtering W, Floege J, Jahnen-Dechent W. Nanoparticle-based test measures overall propensity for calcification in serum. (2012) J Am Soc Nephrol.;23(10):1744-1752..

Wald, J., Wiese, S., Eckert, T., Jahnen-Dechent, W., Richtering, W., and Heiss, A. (2011). Formation and stability kinetics of calcium phosphate-fetuin-A colloidal particles probed by time-resolved dynamic light scattering. Soft Matter 7, 2869–2874.

Jahnen-Dechent, W., Heiss, A., Schäfer, C., and Ketteler, M. (2011). Fetuin-A regulation of calcified matrix metabolism. Circ Res 108, 1494–1509. Review

Heiss A, Pipich V, Jahnen-Dechent W, Schwahn D. Fetuin-A is a mineral carrier protein: small angle neutron scattering provides new insight on Fetuin-A controlled calcification inhibition. (2010) Biophys J.;99(12):3986-3995.

Acknowledgement

Financial support was from Deutsche Forschungsgemeinschaft and from the EU Program Horizon 2020.

II-SY3-KL02

Developing models and treatments for pathological ossification

Liam M Grover

University of Birmingh, Healthcare Technologies Institute, Birmingham, GB

The aberrant growth of bone within soft tissue can occur as a secondary consequence of high-energy trauma and the incorrect installation of some medical treatments. One of the major issues with designing interventions for this group of pathologies is that there is no absolute consensus on the underpinning aetiology, with a multitude of pathways currently implicated [1]. Given the severe nature of the *in vivo* experiments that simulate the condition, it is not possible to explore mechanisms systematically, or to undertake high-throughput screening of potential therapeutic agents.

As a means to address this major problem, we have developed a model of the bone formation process using cells isolated from primary tissues [2, 3]. These cells are seeded into a fibrin-based gel and will subsequently remodel this matrix, laying down mineralised type I collagen. Interestingly, the cells that are entrapped within this matrix subsequently differentiate to form osteocytes, which can be cultured over an extended period of time (up to one year). This represents a significant breakthrough, since although osteocytes are by-far the most numerous cells that are found in bone, up until now it has not been possible to culture them for more than two weeks. The model of bone formation also recreated some of the structural features of mature bone, with similar levels of mineralization (Figure 1), in addition to evidence of lacuna and canaliculi within the cultured tissue.

Using this model, we have been able to screen a range of therapeutic agents to prevent the formation of pathological bone. One such agent is sodium hexametaphosphate (HMP), which caused demineralisation of apatitic calcium phosphate-based ceramic and enabled demineralisation of our model of the disease. After identifying the potential of HMP as a therapeutic agent, we evaluated its efficacy in an *in vivo* model of the disease, in which a rat's Achilles' tendon is severed. A clot forms around the severed tendon and this clot eventually forms an ossified mass. The HMP was formulated with alginate to form an injectable delivery agent and was injected into the severed Achilles' tendon. Over the course of twelve weeks, the injection of HMP was shown to reduce the progression of heterotrophic ossification within the wound. Interestingly, there was not a straightforward relationship between dosage and the capacity of the injection to limit bone formation. Furthermore, we identified a relationship between the number of therapeutic interventions and the volume of heterotopic ossification within the tissue.

References

[1] Eisenstein N, Stapley S, Grover L. Post-traumatic heterotopic ossification: an old problem in need of new solutions. Journal of Orthopaedic Research®. 2018 Apr 1;36(4):1061-8. [2] Iordachescu A, Amin HD, Rankin SM, Williams RL, Yapp C, Bannerman A, Pacureanu A, Addison O, Hulley PA, Grover LM. An in vitro model for the development of mature bone containing an osteocyte network. Advanced Biosystems. 2018 Feb;2(2):1700156. [3] Iordachescu A, Williams RL, Hulley PA, Grover LM. Organotypic Culture of Bone-Like Structures Using Composite Ceramic-Fibrin Scaffolds. Current protocols in stem cell biology. 2019 Feb:e79

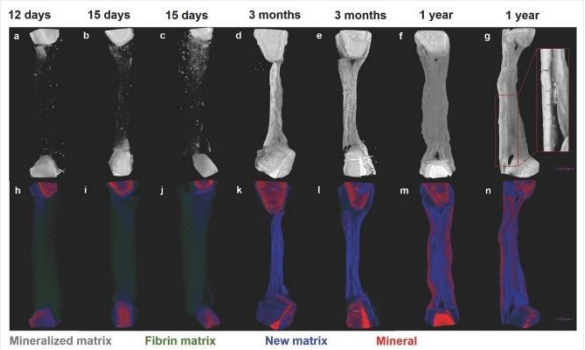

Figure 1.
X-ray CT scans of fibrin constructs seeded with populations of osteoprogenitor cells over periods of up to one year of culture. The upper row of figures shows the deposition of mineral within the matrices over this time period, with the production of a structure that after one year was formed from approximately 70wt% of mineral. Over the period of culture, the starting matrix was entirely replaced with a matrix that was shown to contain a combination of type one collagen and a calcium phosphate (Figure taken from [2]).

II-SY3-03

Understanding the cytotoxicity of doped hydroxyapatite nanoparticles on osteosarcoma cells

Mar Bonany[1,2], Montserrat Espanol[1,2], Zhitong Zhao[1,2], Maria-Pau Ginebra[1,2,3]

[1]UPC, BBT - CMEM, Barcelona, ES; [2]UPC, Barcelona Research Centre in Multiscale Science and Engineering, Barcelona, ES; [3]IBEC, Barcelona Institute of Science and Technology, Barcelona, ES

Introduction

Hydroxyapatite (HA) has been widely used in bone regeneration applications due to its similarity to the mineral phase of bone. Moreover, the ability of HA to incorporate metal ions within its crystal structure has been employed to boost cell behaviour. More recently, ion-doped HAs in the form of nanoparticles (NPs) have been investigated for cancer treatment showing a great killing potential of cancer cells.[1] The wide versatility of HA in these different applications could be explained by different mechanisms of interaction ranging from: direct cell membrane contact, ionic exchanges with the cell culture medium or internalisation mechanisms. Interestingly, in the case of using HA NPs, all these mechanisms can simultaneously operate. However, only internalisation is considered currently. The present work seeks to disclose the contribution of each of these effects on cell cytotoxicity, to have a better understanding of the mechanisms behind the use of NPs in cancer treatment.

Experimental Methods

Undoped (HA) and magnesium-doped hydroxyapatite (MgHA) NPs were prepared by neutralisation of calcium hydroxide with the dropwise addition of phosphoric acid.[1] At pH 8 the reaction was stopped, the NPs were left to age overnight, rinsed and freeze-dried. For the cell culture studies, NP suspensions and discs prepared by compacting 200 mg of NPs into 10 mm diameter moulds at 3T for 2 minutes were used. Cytotoxicity of NPs and discs were studied assessing cell morphology (by fluorescence and scanning electron microscopy) and measuring the lactate dehydrogenase activity of osteosarcoma cells (MG63) in serum-containing (+FBS) and serum-free (-FBS) conditions. NPs internalisation was assessed by measuring intracellular calcium using Fluo-4 AM and by transmission electron microscopy. Cell culture studies using inserts were also performed to assess the effect of ionic exchanges of the NPs with cells avoiding direct contact.

Results and Discussion

The present study was able to prove that the major mechanism behind the death of MG63 cells in the presence of NPs was internalisation. Cytotoxicity was not observed neither culturing cells on discs nor placing the cells in culture medium altered by ionic exchanges caused by the NPs (Figure 1A). Moreover, it was seen that following NPs internalisation there was a rise in the intracellular calcium levels, which was attributed to NPs dissolution (Figure 2A).

Conclusion

These findings support the hypothesis that, once internalised, NPs dissolution disrupts ion homeostasis triggering cell death.

References

[1.] Zhao, Z. *et al.* Ion-doping as a strategy to modulate hydroxyapatite nanoparticle internalization. *Nanoscale***8,** 1595–1607 (2016).

Acknowledgement

To the Spanish Government for financial support through "Ayudas para contratos predoctorales para la formación de doctores" scholarship (BES-2016-07672) of M. Bonany and MAT2015-65601-R co-funded by the EU through European Regional Development Funds.

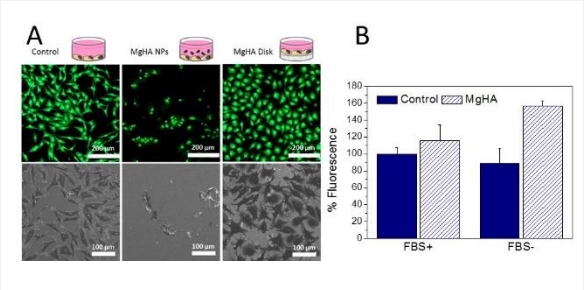

Figure 1
A) Morphological assessment of cytotoxicity of MgHA NPs in suspension and compacted onto discs on MG63 cells at 4h and, B) levels of intracellular calcium in MG63 measured through Fluo-4 AM on control cells and on cells treated with NPs, after 3h.

II-SY3-04

A biphasic mineralized *in vitro* hydrogel model for the systematic study of cell-matrix and heterotypic cell-cell communications involved in breast cancer bone metastasis

Jana Sievers[1,2], Petra Welzel[1], Wolfgang Wagermaier[2], Claudia Fischbach[3], Peter Fratzl[2], Carsten Werner[1,4]

[1]Leibniz Institute of Polymer Research Dresden, Institute of Biofunctional Polymer Materials, Dresden, DE; [2]Max Planck Institute of Colloids and Interfaces, Department of Biomaterials, Potsdam, DE; [3]Cornell University, Department of Biomedical Engineering, Ithaca, US; [4]TU Dresden, DFG-Center for Regenerative Therapies Dresden, Dresden, DE

Introduction

About 70% of patients with advanced breast cancer (BC) develop bone metastasis. So far, it is only possible to treat symptoms but not significantly enhance survival, making bone metastasis the leading cause of death in these patients. The bone is a highly organized and complex organ that with its mineralized bone extracellular matrix has a unique composition and structure compared to the extracellular matrix (ECM) in other metastatic organs. However, very little is known about how the unique bone microenvironment and in particular the inorganic component – the bone mineral (hydroxyapatite), influences BC cell adhesion and migration into the bone. While there is a lot of knowledge about the later osteolytic stage of bone metastasis, much less is known about the initial cancer cell colonialization and here in most studies the contribution of the bone ECM and particularly the role of the mineral is often disregarded. However, in the last years more and more studies have shown that the bone ECM and in particular that of the mineral component can effect the progression of breast cancer bone metastasis [1,2]. Therefore, the development of new *in vitro* metastasis models can serve as a highly useful tool to be able to better dissect key microenvironmental mechanisms that influence breast cancer cell invasion into the bone.

Experimental Methods

We developed and characterized a biphasic three-dimensional *in vitro* hydrogel model that consists of a bulk hydrogel containing the BC cells casted on top of a mineralized macroporous hydrogel (cryogel) representing the bone niche [3,4,5]. The hydrogel networks are based on the synthetic polymer poly(ethylene glycol) and the natural glycosaminoglycan heparin.

Results and Discussion

The biphasic system was designed to allow the systematic variation of different ECM parameters in a highly defined manner in order to dissect relevant microenvironmental mechanisms that influence BC cell invasion into the bone. One key aspect of this model is the defined mineralization of the cryogel via a solution-based method to study the effect of mineral on BC cell invasion. Detailed X-ray analysis was performed to precisely characterize the type of mineral and crystal size, which were found to be comparable to human bone. We in particularly show that the presence of a mineral phase in our hydrogel system varies the migration response of BC cell, as compared to unmineralized controls. Due to the underlying highly modular hydrogel system, we can further mimic and modulate other biochemical and biophysical aspects of the natural ECM in our biphasic scaffold. These are the tuning of mechanical properties, the customized administration of cytokines and chemokines via the cytokine affine heparin

component, the cell-based degradability via incorporation of matrix metalloproteinase-cleavable sequences, and the presentation of cell adhesion ligands via functionalization of the hydrogel matrix with short peptide sequences (e.g. RGD). Using our biphasic hydrogel-assisted model, we exemplarily show the influence of selected biophysical and biochemical cues on the migration behavior of BC cells (mono-culture) and in addition the impact of other cells, such as human mesenchymal stem cells (co-culture).

Conclusion

Using our biphasic hydrogel-assisted model, we exemplarily show the influence of selected biophysical and biochemical cues on the migration behavior of BC cells (mono-culture) and in addition the impact of other cells, such as human mesenchymal stem cells (co-culture). Summarizing, our results demonstrate the utility of the presented *in vitro* system to investigate cell-matrix and heterotypic cell-cell communications in BC migration to bone.

References

[1] Choi, S.; Coonrod, S.; Estroff, L.; Fischbach, C. Chemical and Physical Properties of Carbonated Hydroxyapatite Affect Breast Cancer Cell Behavior. *Acta Biomater.* 2015.

[2] He, F.; Chiou, A. E.; Loh, H. C.; Lynch, M.; Seo, B. R.; Song, Y. H.; Lee, M. J.; Hoerth, R.; Bortel, E. L.; Willie, B. M.; Duda, G. N.; Estroff, L. A.; Masic, A.; Wagermaier, W.; Fratzl, P.; Fischbach, C. Multiscale Characterization of the Mineral Phase at Skeletal Sites of Breast Cancer Metastasis. *Proc. Natl. Acad. Sci.* 2017.

[3] Freudenberg, U.; Liang, Y.; Kiick, K. L.; Werner, C. Glycosaminoglycan-Based Biohybrid Hydrogels: A Sweet and Smart Choice for Multifunctional Biomaterials. *Adv. Mater.* 2016.

[4] Welzel, P. B.; Grimmer, M.; Renneberg, C.; Naujox, L.; Zschoche, S.; Freudenberg, U.; Werner, C. Macroporous StarPEG-Heparin Cryogels. *Biomacromolecules*2012.

[5] Bray, L. J.; Secker, C.; Murekatete, B.; Sievers, J.; Binner, M.; Welzel, P. B.; Werner, C. Three-Dimensional In Vitro Hydro-and Cryogel-Based Cell-Culture Models for the Study of Breast-Cancer Metastasis to Bone. *Cancers* 2018.

1:00 p.m. – 2:30 p.m.

Conference room 2+3

II-OS9 | Strategies for Vascularisation

II-OS9-KL01

Bioinstructive supports for endothelial cells in bone tissue engineering

João F. Mano

University of Aveiro, Department of Chemistry, CICECO — Aveiro Institute of Materials, Aveiro, PT

A major challenge in repairing large bone defects using tissue-engineered strategies is the poor vascularization in the defect sites. To achieve promising regenerative effects, prevascularization of tissue-engineered constructs by co-culturing of endothelial cells and bone/stem cells is a promising strategy. Moreover, endothelial cells are able to secrete relevant factors with osteogenic potential. Supports for tissue engineering should be then appropriate to promote the attachment of endothelial cells and stimulate their organization. Natural-based polymers, such as polysaccharides, could be used to produce multilayer films that could act as reservoirs of bioactive agents. For example, platelet lysates comprise relevant cytokines and can be entrapped in these nanostructured films, increasing the bioactivity of the construct. Such kind of multilayered films can be used as permselective membranes involving liquified capsules containing cells and microparticles, to produce humanized micro-tissues that could be used in tissue engineering. We found that multilayers produced with alginate modified with RGD adhesive peptide in the last layers could promote the invasion of endothelial cells onto the surface of these capsules, indicating that such elements could be integrated into tissues in regenerative strategies. Endothelial cells can be also encapsulated inside the capsules, stimulating the osteogenic differentiation of mesenchymal stem cells in co-culture.

II-OS9-02

Pre-endothelialization of sacrificial microvessel structures for biofabrication of tissue models

Hatice Genç[1], Matthias Ryma[2], Dominik Schneidereit[3], Ali Nadernezhad[2], Jürgen Groll[2], Iwona Cicha[1]

[1]University Hospital Erlangen, Cardiovascular Nanomedicine Unit, Section for Experimental Oncology and Nanomedicine (SEON), ENT Department, Erlangen, DE; [2]University Hospital Würzburg, Department of Functional Materials in Medicine and Dentistry, Würzburg, DE; [3]Friedrich Alexander University, Institute of Medical Biotechnology, Erlangen, DE

Introduction

Homogeneous supply of nutrients and oxygen to tissues can only be ensured through microvascular networks. Therefore, vascularization is of key importance in tissue engineering and the produced tissue models should be supported by vessel-like microvascular network. Traditional strategies for microvessel producing are based on generation of hollow channels and endothelialization of these engineered constructs is so far limited to an intraluminal colonization of channels. These strategies result in delayed formation of endothelial cell layer in the tissue model depending on vessel diameter. To overcome those limitations, this study aimed at producing ultrafine microvessel systems that can be fully pre-endothelialized prior to embedding in tissue-mimicking hydrogel.

Experimental Methods

Poly(2-n-propyl-2-oxazoline) (POx), a thermosensitive polymer was used as sacrificial material to create a vessel-like network for endothelial cells. Melt Electro-Writing (MEW) technique was used to print simple networks in the range of 100 to 180 µm diameter (Figure 1). Printed scaffolds were processed by three different types of surface modification to improve their stability and handling under cell culture conditions: a) 20 % PLGA b) 20% PLGA + air plasma treatment c) 20 % PLGA + O_2 plasma treatment. Primary human umbilical vein endothelial cells (HUVECs) were seeded on top of the scaffolds and the formation of endothelial monolayer on the surface of the structure was observed using confocal microscopy. Metabolic activity of cells was measured by WST-8 assay.

Results and Discussion

POx scaffolds were successfully printed and all the introduced surface modifications improved the handling of networks. Three different time points (Day3, Day 7, Day 14) were chosen for detailed determination of endothelial cell layer formation on the scaffolds. Confocal microscopy showed that two of the scaffold modifications (20% PLGA and 20 % PLGA+ air plasma treatment) produced a cell friendly environment to primary HUVECs. Full endothelialization was reached on these scaffolds with time (Figure 2). Furthermore, endothelial cell monolayer formed faster on air plasma treated scaffolds (after 7 days) compared to scaffolds coated only with 20% PLGA (after 14 days). On the other hand, O_2 plasma treatment resulted in low cell compatibility of produced scaffolds, even though it improved the stability of the structure.

Conclusion

Those results suggest that pre-endothelialization of ultrafine vessel-like structures is possible and can be further improved by surface-coating that supports rapid endothelialization. In the future studies, the pre-endothelialized tubular constructs will be embedded in cell-laden 3D constructs, followed by dissolution of POx network, to achieve tissue models containing endothelium-covered microvessel networks.

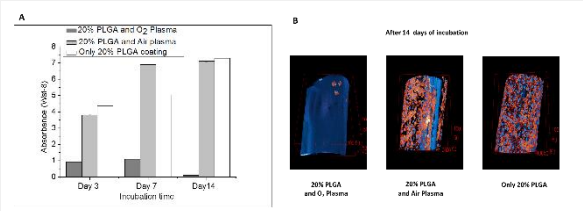

Figure 2.
Comparison of HUVECs metabolic activity on POx scaffolds with different surface modifications (A); and analysis of endothelialization by fluorescent staining (B).

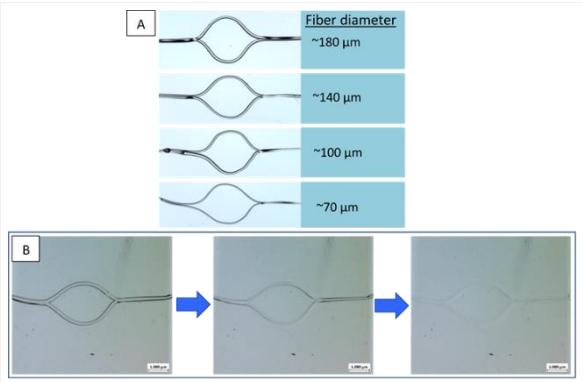

Figure 1.
(A) Simple branching structures of poly(2-n-propyl-2-oxazoline) produced by MEW; (B) Dissolving process of structures embedded within hydrogels.

II-OS9-03

Multi-layer vascularized magnetic cell sheets for bone regeneration

Ana S. Silva, Lúcia I. Santos, João F. Mano

University of Aveiro, CICECO - Aveiro Institute of Materials, Aveiro, PT

Introduction

One of the main challenges in tissue engineering (TE) is to produce functional vascularized 3D transplants *in vitro*,able to recapitulate the complex and physiological structure of natural tissues. In fact, the lack of vascularization causes necrosis, nutrient insufficiency and waste accumulation.[1]Bone is a proper example of how the lack of oxygen and nutrient supply hampers the development of thick-engineered bone, limiting translational and clinical success.[2]Cell sheet (CS) engineering techniques provide an excellent microenvironment for vascularization since the technique can maintain the intact cell matrix, crucial for angiogenesis. Moreover, tissues fabricated by CS engineering are able to adhere to the surface of the host tissue, after *in vivo*transplantation, without suture and form cell-like dense structure, enabling the maintenance of homotypic and heterotypic cell-cell interactions, that lead to a proper tissue regeneration.[3] In an attempt to develop hierarchical cellular 3D vascularized constructs, we herein propose the construction of magnetic responsive heterotypic CS by making use of iron oxide nanoparticles in a concept named magnetic-forced based TE.

Experimental Methods

For the purpose, rhodamine B-labeled supermagnetic iron oxide nanoparticles (10 nm) (MNPs) were synthetized by the co-precipitation method and characterized by FTIR and TEM. The developed nanoparticles were then incubated with human adipose derived stem cells (hASCs) and human umbilical vein endothelial cells (HUVECs) for viability assessment studies. After confirming their successful mitochondrial activity, magnetic-responsive cells were used to develop vascularized microtissues through cell sheet technology. In brief, previously to CS formation, hASCs were stained with DIO and HUVECs with DID. Heterotypic magnetic CS were created by labeling each cell phenotype with the earlier developed MNPs. Later, hASCs and HUVECs were organized in a triple sheet conformation with the endothelial cells in between of two sheets of hASCs. The fabrication methodology herein applied, that consisted in magnetically forcing heterotypic and homotypic cell-cell interactions, enables the development of hierarchal and stratified 3D tissues, circumventing the problems associated with other CS methodologies that lack on tissue stratification.[4] The developed cell sheets were cultured over a period of 21 days in endothelial medium with and without osteogenic growth factors and differentiation studies were performed to evaluate the potential osteogenic effect of endothelial cells over hASCs. Homotypic CS (hASCs/hASCs) were used as controls.

Results and Discussion

Results show that osteogenesis is achieved in both culturing conditions, suggesting the osteogenic potential of HUVECs over hASCs. CS integrity and cell-cell homotypic and heterotypic interactions were assessed through vinculin staining and collagen detection. Furthermore, increased ALP activity, matrix mineralization, calcium and osteopontin detection were achieved, over a period of 21 days, for the heterotypic CS conformation (hASCs/HUVECs/hASCs) over the homotypic one (hASCs/ hASCs). The up regulation of BMP-2, osteopotin and osteocalcin cytokines and hydroxyapatite formation support these findings. Moreover, after 21 days, the release of VEGF cytokine was found to be decreased, suggesting the osteogenic differentiation of hASCs, which upon cell differentiation are known to down regulate the release of pro-angiogenic growth factors such as VEGF.[5] Finnaly,

the angiogenic *in vivo*potential of the developed heterotypic 3D cell construct was evaluated through the implantation of such cell sheets in chicks embryo (CAM assay). Preserved human vascular structures were still detected *in vivo*, and human cells showed the ability to migrate and integrate with chick vasculature.

Conclusion

Magnetic-forced based TE was used to create a heterotypic CS comprised of two sheets of hASCs with HUVECs seeded in between, enabling the development of a stratified and vascularized cell-dense like tissue with osteogenic differentiating capabilities.The results herein obtained are expected to open new insights for the development of vascularized 3D bone tissue, circumventing the current problematics associated with poorly vascularized 3D transplants that lack on complex tissue organization and proper nutrients and oxygen diffusion.

References

1 - Novosel, Esther et al., *Adv Drug Deliv Rev,* **2011**, 63, 300-311

2 - Moschouris, Kathryn et al., *Regen Med,* **2016**, 11, 559-570

3 - Sekine, Waki et al., *J Biochip Tissue chip,* **2011**, S1

4 - Ito, Akari et al.,*Tissue Eng,* **2004**, 10, 833-840

5 - Correia, Clara et al., *Sci Rep,* **2016**, 6, 21883

Acknowledgement

The authors acknowledge the financial support by the European Research Council grant agreement ERC-2014-ADG-669858 for project “ATLAS” and the FCT project “PROMENADE” (FCT Ref. PTDC/BTM-MAT/29830/2017). The work was developed within the scope of the project CICECO-Aveiro Institute of Materials, POCI-01-0145-FEDER-007679 (FCT Ref. UID /CTM /50011/2013), financed by national funds through the FCT/MEC and when appropriate co-financed by FEDER under the PT2020 Partnership Agreement.

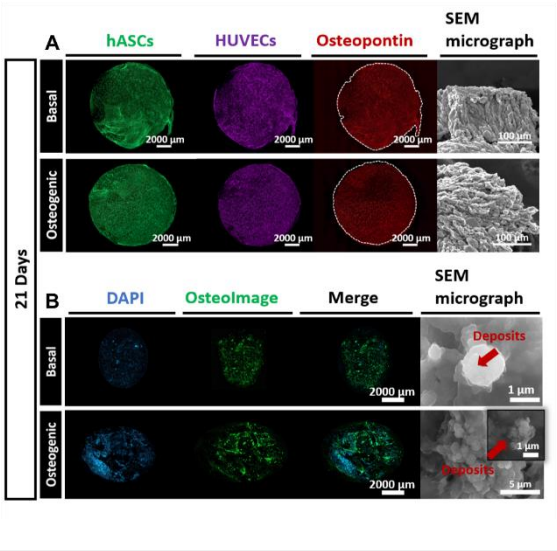

Figure 2
(A) Immunofluorescence of hASCs (green), HUVECs (purple) and osteopontin (red) in 3D heterotypic cell sheets cultured for 21 days in basal and osteogenic media. SEM micrographs of the developed cell sheets are represented in the right panel demonstrating cell sheet integrity. (B) Mineralization of the developed 3D heterotypic cell sheets cultured for 21 days in basal and osteogenic media: cell nucleus - DAPI (blue) and hydroxyapatite - Osteoimage (green). SEM micrographs displaying hydroxyapatite deposits are depicted in the right panel.

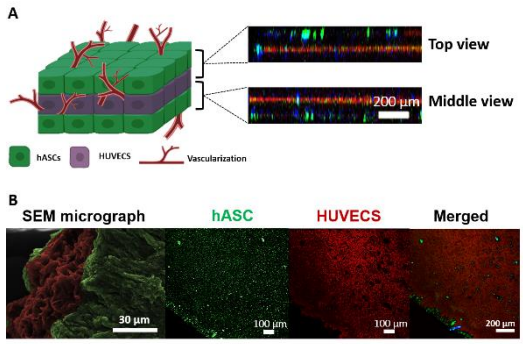

Figure 1
(**A**) Schematic representation of the fabricated 3D vascularized cell sheet. Confocal microscopy section views (top and middle) of the 3D magnetic cell sheet demonstrating HUVECs in between two hASCs sheets - HUVECs (red), hASCs (green), cell nucleus (blue); (**B**) SEM micrographs of the developed heterotypic cell sheet: HUVECs (represented in red) and hASCs (represented in green); and confocal microscopy images of isolated and merged channels.

II-OS9-04

Printable formulations based on dynamic catechol-metal crosslinking

Malgorzata K. Wlodarczyk-Biegun[2], Julieta I. Paez[2], Maria Villiou[1,2], Jun Feng[1,2], Aranzazu del Campo[1,2]

[1]INM - Leibniz Institute for New Materials, Dynamic Biomaterials, Saarbrucken, DE; [2]Saarland University, Chemistry Department, Saarbrucken, DE

Introduction

3D (bio)printing is a powerful tool for tissue engineering constructs formation, as it provides precise control over material deposition in 3 dimensions. However, development of new, functional printable formulations is challenging, as they need to combine properly adjusted cross-linking kinetics with biocompatibility. Inspired by the proteinaceous networks extruded by the sea mussels, in order to adhere to the rocks in mild, close to physiological conditions, we have explored the printability of reversible networks. Catechol functionalized polyethylene glycol (PEG) based inks with metal-coordination crosslinking were studied.

Experimental Methods

4-arm PEG was functionalized with dopamine (PEG-Dop) and inks containing Al^{3+}, Fe^{3+} or V^{3+} as crosslinking metal ions were prepared. Rheological properties (relaxation time, recovery rate, viscosity), printability and shape fidelity of the inks containing different cations were tested and correlated with thermodynamic and ligand exchange kinetic constants of the dynamic bonds present in the system

Results and Discussion

The printability and shape fidelity on the inks were assessed by printing 2D and 3D constructs (Fig.1), and revealed clear dependency on the ink composition (metal ion type, pH, PEG molecular weight). Rheological studies showed the influence of ink composition on the network relaxation time, recovery rate and viscosity. Network relaxation time and ligand exchange kinetics were identified as the most relevant parameters influencing printing performance. Additionally, cells seeded on the crosslinked materials were viable, indicating material biocompatibility; adhesives properties of the formulations were presented, demonstrating system applicability as medical glue.

Conclusion

In this work we present and analyze the dynamic ink formulation with remarkable flexibility for 3D (bio)printing, instructive for material design in other reversible systems. Additionally, we envision proposed system for development of printable tissue adhesives, especially interesting for minimal invasive surgeries.

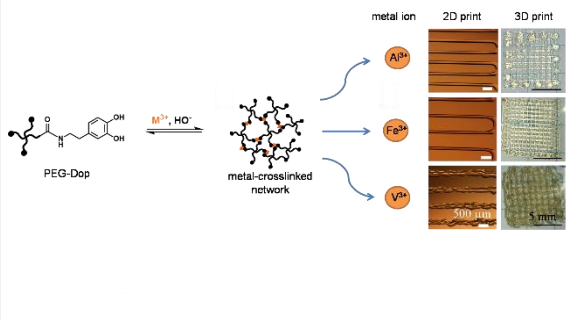

PEG-Dop based ink with dynamic catechol-metal crosslinking
Crosslinking mechanism of PEG-Dop system and resulted printed structures in 2D and 3D, dependent on the crosslinking metal cation type. Scale bars: 500 µm and 5 mm, for 2D print and 3D print, respectively.

II-OS9-05

Real time imaging of oxygen in bioprinted hydrogels – characterizing O_2 diffusion properties and applications in tissue engineering.

Ashwini R. Akkineni[1], Sarah Duin[1], Erik Trampe[2], Klaus Koren[2], Anja Lode[1], Michael Kühl[2], Michael Gelinsky[1]

[1]TU Dresden, Centre for Translational Bone, Joint and Soft Tissue Research, Dresden, DE; [2]University of Copenhagen, Marine Biology Section, Department of Biology, Helsingør, DK

Introduction

Various hydrogels, derived from natural or synthetic sources, are routinely used as potential alternatives for tissue repair or as disease models. The ease to modify hydrogels to mimic native tissues render them an excellent choice for tissue engineering (TE) applications. 3D bioprinting had initiated a paradigm shift in fabricating complex constructs using hydrogels by enabling inclusion of multiple cell types and complex designs. To ensure successful functioning of complex TE constructs, characterizing hydrogel properties such as rheological, mechanical and diffusion properties are vital for design & development of complex TE constructs.

Many established methods cater the need of characterizing rheological and mechanical properties of hydrogels. However, a void exists in available tools to characterize diffusion properties (especially oxygen diffusion) in hydrogels. As availability of oxygen (O_2) to encapsulated cells is absolutely essential for their proper functioning, it is a prerequisite to understand O_2 diffusion properties - enabling efficient design & fabrication of complex hydrogel constructs by 3D bioprinting. In our previous work, O_2 sensitive nanoparticles (NP) were incorporated in hydrogels (also called bioinks) used for 3D bioprinting. Simple & reliable method to measure real time spatio-temporal O_2 concentrations in 3D bioprinted constructs was established. In the present work, real time O_2 imaging is used to characterize O_2 diffusion in various hydrogels and also O_2 consumption of different cell types in various hydrogels was studied, with the intent to design efficient constructs for TE applications.

Experimental Methods

Bioinks such as alginate/methylcellulose [1], gellan gum, human plasma containing bioinks were combined with O_2 NP [2]. For measuring the rate of O_2 diffusion, bioinks with NP were filled in glass capillaries and were crosslinked overnight. The capillaries were placed in Hanks buffered salt solution (HBSS) inside a cell culture incubator (O_2 saturated atmosphere - 21% O_2) for 24 hours to facilitate swelling and equilibration (to 21% O_2) of the obtained hydrogels. We imaged the real time change in the O_2-dependent luminescence of the sensor NP [2], upon changing the incubator atmosphere to 1% O_2. The spatio-temporal changes in O_2 concentration gradients in hydrogels was analyzed to calculate the rate of O_2 diffusion in hydrogels.

For measuring the rate of O_2 consumption by encapsulated cells in various hydrogels, cell laden 3D bioprinted constructs were used for real time imaging of O_2. Cells of the rat beta-cell line (INS1) were mixed in bioinks containing NP, which were used for 3D bioprinting of constructs. Cell laden constructs were cultured in hypoxic & normoxic conditions. Spatio-temporal dynamics of O_2 concentration in the constructs was analyzed by real time O_2 imaging. Functionality of INS1 cells in constructs, cultured in both conditions was assessed by measuring the glucose stimulation index (GSI). The measured GSI was correlated with spatio-temporal dynamics of O_2 concentration of the constructs to identify optimal O_2 concentration for culturing INS1 cells.

Results and Discussion

Change in the external O_2 concentrations established O_2 gradients in the hydrogels (Fig 1A). The dynamic change of these gradients as function of time and external O_2 concentration was used to calculate rate of O_2 diffusion in different bioinks.

Ratiometric analysis (correlating to O_2 concentrations in the constructs) of real time images of 3D bioprinted constructs containing INS1 cells after 7 & 14 days showed a clear difference, when cultured in hypoxic & normoxic conditions (Fig 1B). A gradual increase in O_2 consumption was observed till day 7 in constructs cultured in both conditions. Later, a sharp drop and gradual increase in O_2 consumption was observed in constructs cultured in hypoxic & normoxic conditions, respectively (indicating cell death & proliferation, respectively; Fig 1C).

Conclusion

Inclusion of O_2 sensitive NP in bioinks offers a very simple but efficient & reliable method to characterize O_2 diffusion properties in hydrogels. Real-time imaging of O_2 concentrations in cell laden 3D bioprinted constructs enables identification of ideal culture conditions for encapsulated cells. This enables rapid testing and more efficient designs in terms of hydrogel composition and construct geometry for specific applications in TE.

References

[1] K. Schütz, et. al., *J Tissue Eng Reg Med***2017**, 11, 1574-1587

[2] E. Trampe *Adv Funct Mater* **2018**, 28, 1804411

Acknowledgement

We thank the German Federal Ministry for Economic Affairs and Energy for funding via the AiF programme (project No. IGF 19175BR).

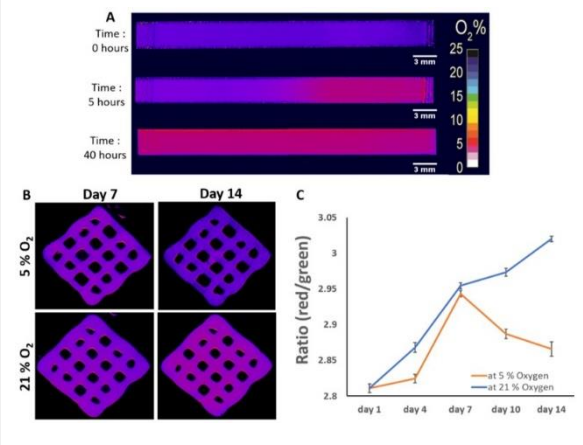

Real time oxygen mapping of hydrogels and cell laden constructs

Figure 1: (A) Development of O_2 gradients in capillaries containing bioinks over time, when external O_2 concentration was reduced. **(B)** Ratiometric images of INS1 constructs cultured at 5% & 21% incubator O_2 concentrations. **(C)** Average ratio of the constructs cultured over a period of 14 days.

4:45 p.m. – 6:15 p.m.

Hall 3

III-SY4 | Electrohydrodynamic Additive Manufacturing Technologies

Paul Dalton (Würzburg, DE)
Tomasz Jüngst (Würzburg, DE)

3D printing technologies are an established tool for biomaterial processing, however greater resolution is required for the next generation of biomedical materials. Adding an electrical field to extrusion-based 3D printing can generate an additional driving force and increases the resolution of the process down to the micron and sub-micron range. Highly resolved porous constructs fabricated in this manner have great utility for both in vitro and in vivo applications and represents the future of 3D printing for biomedical applications. This special symposia will highlight the latest development in such high-resolution 3D printing technologies based on electrohydrodynamics.

III-SY4-KL01

Historicity of Bioprintomics – Can we in fact print tissue and organs or did we neglect genuinely that biology matters

Dietmar W. Hutmacher

Queensland University of Technology, Institute of Health and Biomedical Innovation, Brisbane, AU

While bioprinting processes have not advanced as greatly from both a basic and translational research point of view as 3D printing in recent years, many challenges remain to be addressed, Significant research efforts are essential to expedite the transformation from random bioprinting to additive biomanufacturing. I lay out the arguments in this talk why we need to change the current paradigm by changing the question from “what can we do with this fabrication method?” to “how can we change this fabrication process to achieve what we need”.

III-SY4-KL02

Why Polymer Melts are Excellent Fluids for High-resolution 3D printing

Paul D. Dalton

University Clinic Würzburg, FMZ, Würzburg, DE

Introduction

There has, for a long time, been a disconnect between the complexity and organization of natural tissues, and the resolution of fabricated biomaterials and scaffolds used to replace them (1). While the overall shape of biomaterials can be personalized, another challenge is to produce these three-dimensional (3D) structures that are anatomically similar. Consequently, there has been a significant effort in developing techniques to manufacture substrates with a defined organization, however resolutions remain limited, partcularly at the low-micron scale. For example, realising the anisotropic structure of peripheral nerve has been challenging for scaffold fabrication technologies (2). This invited lecture will described the porous structures possible via melt electrowriting (MEW), and why melts are an ideal fluid for the translation of such approaches to the clinic (3)

Experimental Methods

Melt electrowriting is performed by electrostatically stabilizing a molten polymer jet, direct-writing it accurately onto a collector. Importantly, these filaments can deposit upon each other accurately, to produce organized 3D scaffolds with a defined and predictable layer-by-layer deposition. Dynamic electric fields can enhance the build height, achieved through digitally controlling both voltage and collector distance. An increasing number of polymers can be processed with this method, further advancing the final properties of the product.

Results and Discussion

Unlike electrospinning, fibers made using MEW can have their diameters altered on-demand. This significantly expands scaffold design variabilty and therefore mechanical properties of the resulting structures. The smallest average diameter for PCL fibers is 150nm which, to our knowledge the smallest size made by any melt-processing textile technology. Non-linear MEW fiber deposition results in modified mechanical properties, while fibers can be suspended over significant gaps to generate unique scaffolds for oriented gudiance. There are several more advances in MEW that provide new opportunities, from sacrificial structures though to coaxial fibers and digitization of the process. Finally, new materials made via MEW expand the properties and allow for new design features to be integrated in to the final product, especially electroactive polymers and hydrogels. All of these would not be possible without the fast solidification of the molten polymer jet, which is the basis for such highly resolved direct-written structures.

Conclusion

Melt electrowriting relies on the electrohydrodynamic effect of stabilizing fluid columns with an applied voltage, and results in a range of new 3D objects with microscale and nanoscale features. The benefit for the biomaterials community in particular is a robust, reproducible and low-cost manufacturing technology that can be researched in university settings while providing a path to the clinic.

References

1. GJ Crawford, TV Chirila, S Vijayasekaran, PD Dalton, IJ Constable. (1995) Preliminary evaluation of a hydrogel core-and-skirt keratoprosthesis in the rabbit cornea. *Journal of refractive surgery,* 12 (4), 525-529.
2. PD Dalton, J Mey (2009) Neural interactions with materials. *Front Biosci,* 14, 769-795.
3. A Youssef, S Hollister, PD Dalton (2017) Additive manufacturing of polymer melts for implantable devices and scaffolds. *Biofabrication*, **9**, 012002.

Acknowledgement

The support of the VW Foundation is greatly appreciated.

III-SY4-03

A rapid screening toolkit instructs the formulation of printable biomaterials for melt electrowritten scaffolds

Naomi C. Paxton, Trent L. Brooks-Richards, Madison J. Ainsworth, Jiongyu Ren, Cynthia Wong, Mark C. Allenby, Maria A. Woodruff

Queensland University of Technology, Institute of Health and Biomedical Innovation (IHBI), Brisbane, AU

Introduction

Melt electro-writing (MEW) represents a biofabrication process to tailor-make 3D lattice scaffolds by electrospinning micron-scale fibres collected as threads, mats, ordered scaffolds, and tubes through modifications to the fibre formation and collector plate systems [1]. While several synthetic polymers have been fabricated using MEW, including most favourably polycaprolactone (PCL), it remains a significant challenge to adapt the MEW process for other biomaterials and composites, which may offer more suitable mechanical and biological properties for various tissue engineering applications [2]. For example, while promising composite formulations of PCL with strontium-substituted bioactive glass (PCL/SrBG) have been processed into large or disordered fibres [3], to our knowledge biologically-relevant SrBG concentrations (>10wt%) have never been printed into ordered microfibres using MEW due to rheological limitations of PCL composites at high SrBG concentrations. This has motivated research to understand both the material properties governing printability and to provide a systematic characterisation toolkit to direct the fabrication of MEW scaffolds using novel, complex or composite biomaterials.

Experimental Methods

Herein, we describe a toolkit to characterise the viscoelastic and thermoresponsive properties of a number of synthetic polymeric biomaterials and polymer composites with ingredients such as strontium-substituted bioactive glass and graphene to optimise the MEW extrusion process. Specifically, shear thinning viscoelastic behaviour and thermoresponsive properties of polymer composites were measured using rheology, thermogravimetric analysis (TGA) and digital scanning calorimetry (DSC). Using a predictive model, the theoretical printing pressure required to extrude materials with a consistent flow rate was calculated, adjusting for each biomaterial's rheological profile [4]. The homogeneous distribution of various bioactive additives throughout the polymer fibres was verified with scanning electron microscopy (SEM), energy dispersive spectroscopy (EDS), Fourier-transform infrared spectroscopy (FTIR) and the influence of these on fibre tensile strength was examined using uniaxial tensile mechanical testing.

Results and Discussion

Using this toolkit, ordered scaffolds unique toward several tissue applications were successfully fabricated based on the optimisation process. This toolkit was validated on several control materials and identified that current PCL/SrBG composites required unattainable pressures for extrusion, 13-fold above what typical MEW devices allow (0.5 MPa). The toolkit guided the formulation of PCL/SrBG in a chloroform solvent which sufficiently lowered solution viscosity and enabled printing pressures to fall within MEW tolerances. Similarly, PCL/Graphene composites were successfully fabricated into stent-like structures, guided by the predictive toolkit. EDS and FTIR characterization demonstrated the homogeneous distribution of additives throughout the fibres and an increase in tensile strength of the composite fibres was exhibited compared to the PCL-only controls. Altogether, we generated a model framework to predict the

relationship between polymeric biomaterial viscosity and printing parameters, which is extended toward composite formulations including polymer-bioglass and polymer-graphene, for tailored tissue-specific MEW products.

Conclusion

This toolkit is broadly applicable to identify the feasibility of processing newly developed biomaterials using MEW. Specifically, this toolkit developed novel bioglass-polymer composites able to be printed into highly controlled microfibre scaffolds. These composite scaffolds have demonstrated exceptional bioactive properties, increasing alkaline phosphatase activity and promoting the proliferation of osteoblasts whilst inhibiting osteoclast differentiation to induce rapid bone formation. Similarly, the PCL/Graphene composite is being developed to provide resorbable vascular stents with enhanced mechanical strength, anti-microbial properties and radio-opacity for improved clinical evaluation.

References

[1] Brown et al. (2011) *Advanced Materials,* 23(47): 5651-5657.
[2] Hochleitner et al. (2019) *Macromolecular Rapid Communications,* 39(10): e1800055.
[3] Ren et al. (2014) *Journal of Biomedical Materials Research Part A,* 102(9): 3140.
[4] Paxton et al. (2017) *Biofabrication*, 9(4): 044107.

Acknowledgement

The authors thank Dr Tim Krappitz, Ms Elizabeth Graham and Mr Peter Hegarty for their technical assistance. The data reported was obtained using the resources of the Central Analytical Research Facility at the Institute for Future Environments, QUT, with funding from the Science and Engineering Faculty. The authors also gratefully acknowledge Professor Molly Stevens, Imperial College London, for supplying the SrBG and Perstorp for supplying PCL samples and NCP acknowledges the support of ARC ITTC in Additive Biomanufacturing and industry partner, Anatomics Pty Ltd.

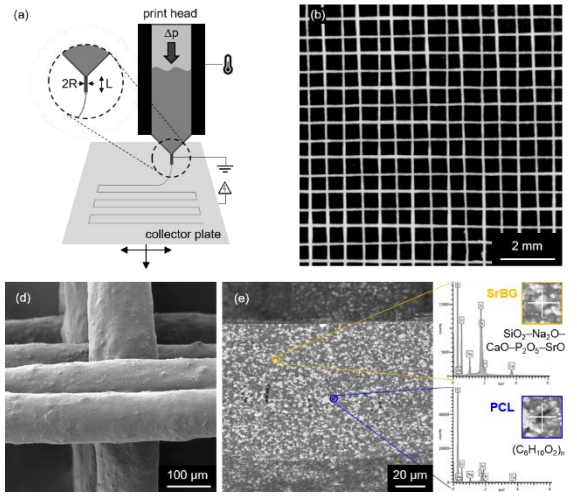

Overview of composite characterisation and melt electrowriting
(a) Schematic diagram of the MEW process using an applied pressure (Δp) to extrude a molten polymer or polymer solution through a grounded nozzle onto a motorized collector plate. The length and radius of the nozzle are measured according to the inset diagram. (b) Composite scaffold fabricated via a hybrid MEW approach using 1 g PCL/SrBG 33wt% dissolved in 1 mL chloroform, printed at elevated temperatures, as guided by the toolkit; (c) SEM imaging showing the surface morphology and typical diameter of the fibre; and (d) EDS confirms the presence of SrBG particles (white) evenly distributed in the composite fibre.

III-SY4-04

Melt electro written biomimetic tympanic membrane implant for therapy of chronically infected middle ears

Max von Witzleben[1], Thomas Stoppe[2], Tilman Ahlfeld[1], Anne Bernhardt[1], Matthias Bornitz[2], Marcus Neudert[2], Michael Gelinsky[1]

[1]Technische Universität Dresden, Carl Gustav Carus Faculty of Medicine, Centre for Translational Bone, Joint and Soft Tissue Research, Dresden, DE; [2]Technische Universität Dresden, Carl Gustav Carus Faculty of Medicine, Otorhinolaryngology, Head and Neck Surgery, Ear Research Center Dresden, Dresden, DE

Introduction

Patients suffering from chronically infected middle ears exhibit persistent tympanic membrane perforations. State of the art treatment consists of autologous grafts of perichondrium, cartilage or temporal fascia. In severe cases mainly cartilage is employed to increase the stability of the reconstruction and to prevent perforation. Disadvantages like reduced sound conduction (hearing impairment) and a ceasing volume of autologous materials call for synthetic patient individual implants.[1]

Melt Electro Writing (MEW) is an emerging additive manufacturing technique allowing for the development of millimetre-sized constructs. In addition, the design of each layer is independent by other layers of the scaffold;[2] thus MEW is a suitable fabrication technique for hierarchical organized structures like the tympanic membrane. With the opportunity of MEW we aim for the development of such a membrane mimicking vibration behaviour and stability to improve hearing outcome and to prevent re-perforations.

Experimental Methods

Printing was executed with a GeSiM BioScaffolder 3.1. combined with a MEW module. A needle outlet with a diameter of 250 µm was established. As material polycaprolactone (PCL) from Corbion (Purasorb PC 12) with a molecular weight of 50 000 was used. Overall printing temperature was set to 75 °C, the and voltage to 8.1 kV. For 10 µm diameter fibres a printing speed of 900 mm/min with a pressure of 20 kPa and a z-offset of 5.2 mm was applied. For 15 µm diameter fibres a printing speed of 1200 mm/min with a pressure of 30 kPa and a z-offset of 4.2 mm was applied.

After printing, scaffolds were treated with 1 M NaOH for three hours and cut with circular punches with a diameter of 11 mm.

Vibration behaviour was characterized by the Ear Research Centre Dresden (ERCD).

For static investigations, uniaxial compressive tests of the scaffolds were performed employing a universal testing machine (Z010 equipped with a 100 N load cell, ZwickRoell, Germany). Load was applied to the membrane with a stamp (radius 3 mm).

Results and Discussion

As a first approach, the produced scaffold should mimic the dimensions of the tympanic membrane with a maximum diameter of 10 mm to 12 mm and a thickness that ranges from 30 µm to 90 µm. Therefore, PCL fibres with diameters of 10 µm and 15 µm with different strand distances of 150 µm and 250 µm were successfully printed in several layers (layer number= 4, 6, 8) and in different layer-to-layer orientations (45°, 90°). Hence, membranes with thicknesses ranging from 40 µm to 120 µm with different closeness were created.

As the next step scaffolds were immersed in 1 M NaOH to increase hydrophilicity of PCL and ensure a better cell

adhesion.
The stability was investigated through static compressive/strain tests at fixed speed. The clamping force influenced the resulting flexural modulus as it increased the slope of the stress/strain curves. Therefore, the scaffolds were clamped with the lowest possible force. Resulting graphs are shown in Figure 2.
The flexural modulus of scaffolds with a layer-to-layer orientation of 45° exhibited a increased slope compared to the 90° orientated ones. Higher strand distances of 250 µm led to a slight increase in slope. First vibration investigations showed a correlation of fibre diameter, density and amount of layers with the resulting sound transmission. However, the orientation of the collagen fibres within the tympanic membrane differs from the so far analysed scaffolds. Therefore, scaffolds with circular and radial placed fibres were successfully printed. In addition, scaffolds were infiltrated with collagen type I and investigated.
Cell response of both, primary and immortalized, keratinocytes of scaffolds w/ & w/o collagen was analysed for up to 21 days. DNA assays revealed significant increase of the cell number. Microscopic imaging revealed a typical phenotype of keratinocytes.

Conclusion

PCL scaffolds of different fibre diameters and membrane thicknesses were successfully fabricated by MEW. Compressive tests showed an increase in stiffness with increasing amount of layers and increasing fibre diameter. Initial vibration investigations showed distinct influences between of layer height and fibre diameter. In vitro tests showed a high cytocompatibility.
Furthermore, these first scaffolds exhibited vibrations that are comparable to the tympanic membrane. Thus, MEW-PCL membranes might become a suitable material for the replacement of tympanic membranes.

References

[1] Monique Verhoeff u. a., „Chronic Suppurative Otitis Media: A Review“, *International Journal of Pediatric Otorhinolaryngology* 70, Nr. 1 (Januar 2006): 1–12, https://doi.org/10.1016/j.ijporl.2005.08.021.
[2] Andrei Hrynevich u. a., „Dimension-Based Design of Melt Electrowritten Scaffolds“, *Small* 14, Nr. 22 (Mai 2018): 1800232, https://doi.org/10.1002/smll.201800232.

Acknowledgement

We thank the Saxon State Ministry for Higher Education, Research and the Arts (SMWK) and the Sächsische Aufbaubank (SAB) for funding.
The authors thank O. Zieschang for excellent assistance.

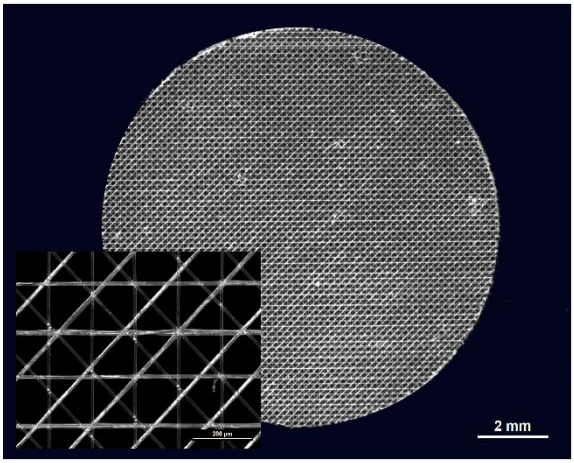

Fig . 1:
Microscopic image of a scaffold with 6 layers, a strand diameter of 10 µm, a strand distance of 150 µm and a layer-to-layer orientation of 45°.

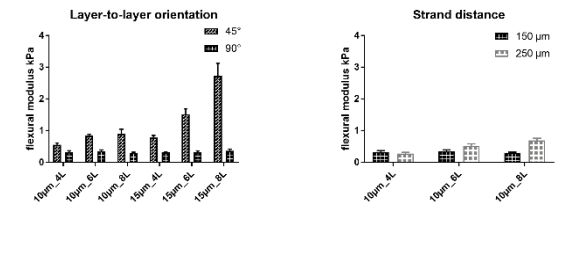

Fig. 2:
The left graph shows a stronger flexural modulus for scaffolds with a 45° layer-to-layer orientation as compared to those with 90°. An increasing amount of layers in a 45° orientation exhibits a distinct increase of the flexural modulus. The right graph compares the strand distances of 90° layer-to-layer orientated scaffolds with an increasing amount of layers. Here, a slight increase for higher spacing's is recognisable. (mean +/- sd, n= 5)

4:45 p.m. – 6:15 p.m.

Hall 2

III-OS10 | Polymeric biomaterials 1

III-OS10-01

PEGDA and PETA as potential materials for drug delivery system development for a novel additive manufacture process

Natalia Rekowska[1], Daniela Arbeiter[1], Andreas Brietzke[1], Jan Konasch[2], Alexander Reiss[2], Robert Mau[2], Thomas Eickner[1], Hermann Seitz[2], Niels Grabow[1], Michael Teske[1]

[1]University Medical Centre Rostock, Institute for Biomedical Engineering, Rostock-Warnemünde, DE; [2]University of Rostock, Chair of Microfluids, Rostock, DE

Introduction

Two photopolymerisable compounds – poly(ethylene glycol) diacrylate (PEGDA) [1] and pentaerythritol tetraacrylate (PETA) were chosen to be used for the manufacturing of drug delivery systems (DDS) by a novel additive manufacturing (AM) process [2]. This novel AM process combines stereolithography (SLA) and inkjet printing (IJP). While SLA creates the basic body of the DDS layer by layer, IJP is used to print precisely drug depots inside the DDS. This approach can control the drug release by the diffusion of the drug through the DDS scaffold as well as the cleavage of the hydrolysable covalent bonds between the drug and the scaffold polymer. Within this initial study we investigated biocompatibility and thermodynamic properties of conventionally cured samples with varying composition of the two acrylates and the concentration of the photoinitiator (PI) which is used as radical starter of the photopolymerisation.

Experimental Methods

Samples containing different concentrations of the PI (0,50%-1,25%) and PETA (1%-10%) were prepared. Two rinsing procedures of the samples were performed at 37°C and 50°C. Both procedures included rinsing 6 x 30 minutes in acetonitrile and 3 x 30 minutes in distilled water.

For the biocompatibility evaluation, the cell viabilities of 2 x 10^4 L929 mouse fibroblast cells/ well (CLL-1, ATCC) were determined using eluate and direct contact test methods. Eluate test: samples were eluted in DMEM under cell culture conditions for 24 hours, eluates were given onto the precultivated L929 cells for 48 h. Direct contact test: L929 cells were cultured for 48 h in direct contact with the sample surfaces in cell culture medium. Cell Quanti-Blue cell viability assays were conducted according to the manufacturer's specifications to proof the cells viability.

Differential scanning calorimetry (DSC) measurements were performed under a nitrogen purge as described in Rekowska et al. [1].

The contact angle measurements were performed with the sessile drop method.

The SEM images were obtained via a scanning electron microscope under a high vacuum and 10kV.

Results and Discussion

Eluate biocompatibility tests show that the samples with the addition of PETA require rinsing at 50ºC, as samples rinsing at 37ºC was ineffective (Fig.1). After glass transition temperature (T_g) measurements it appears clear, that T_g increases with the increasing PETA concentration in the sample. For the samples containing 10% of PETA it reaches 49ºC, which explains the necessity of increasing the rinsing temperature to 50ºC. It is also known, that the lower T_g is, the faster occurs the drug release [3], which creates possibility for the creation of thermosensitive DDS. Although the samples after rinsing release no toxic substances, direct contact tests reveal cell viability between 70%-90%, regardless of the PI and PETA concentration. Hence, according to ISO 10993-5 all samples are biocompatible. All

of the samples show contact angles under 90°, thus they are hydrophilic. Therefore the character of the samples is not the reason of decreased cell viability in direct contact tests.
During the evaluation of the samples' surface under electron scanning microscope some differences of the samples morphology were observed after the rinsing procedure. Some of the samples cracked afterwards, which applies mostly to the samples with lower PI concentration. Samples with the addition of 10% PETA, especially the ones also with lower PI concentration seems to be smoother and more homogenous than the samples without the PETA addition (Fig.2). No general trend related to the PI concentration is observed.

Conclusion

In summary, the results of these preliminary studies reveal the influence of the addition of PETA as a crosslinking agent to the system consisting of basic polymer PEGDA. The modification of the concentration of PETA creates a possibility to influence T_g and therefore take control over drug release in the potential thermosensitive DDS. The outcomes give also information about rinsing procedure, which should be performed at 50ºC according to the higher T_g of the samples containing PETA. The presented results are promising and confirm that the combination of PEGDA and its co-monomer PETA is interesting as potential material for the novel DDS creation via the novel AM technique.

References

[1] N. Rekowska, D. Arbeiter, J. Konasch et al., "Thermomechanical properties of PEGDA and its co-polymers," *Current Directions in Biomedical Engineering*, vol. 4, no. 1, pp. 669–672, 2018.
[2] J. Konasch, A. Riess, M. Teske et al., "Novel 3D printing concept for the fabrication of time-controlled drug delivery systems," *Current Directions in Biomedical Engineering*, vol. 4, no. 1, pp. 141–144, 2018.
[3] S. Lappe, D. Mulac, and K. Langer in *International journal of pharmaceutics*, vol. 517, 1-2, pp. 338–347, 2017.

Acknowledgement

Financial support by German Research Foundation (DFG) within the project "3D printed drug delivery systems with the ability of the time controlled drug release" is gratefully acknowledged.

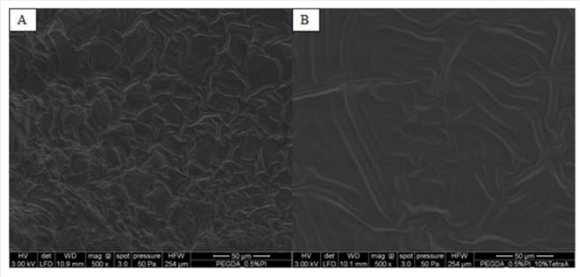

Fig. 2: Morphology
Scanning electron microscopy images of the PEGDA samples containig 0.5% PI (Iragucre 2959) without PETA (A) and the sample containing 0,5% PI and 10% PETA (B) unrinsed.

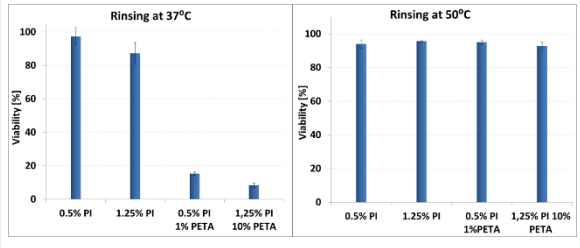

Fig. 1: Biocompatibility
Viability of the L929 mouse fibroblasts after the contact with eluates from rinsed samples: 6 x 30 minutes in acetonitrile, 3 x 30 minutes in distilled water at 37°C (A) and 50°C (B). Cells in pure cell medium were used as a control (n=4).

III-OS10-02

Novel Conducting and Biodegradable Macromonomer for Biomaterials

Aruã C. Da Silva, Susana I. C. De Torresi

University of São Paulo, Química Fundamental, São Paulo, BR

Introduction

Poly(lactic acid) (PLA) is a biodegradable polymer, suitable for short term applications, and biocompatible with living tissue widely used in biomedical applications such as implants, sutures, drug encapsulation, etc.[1] The synthetic method traditionally used to obtain PLA from lactides employ organometallic catalysts, especially those based on tin; specifically tin(II) bis-2-ethylhexanoic acid ($Sn(oct)_2$), due to its high catalytic efficiency.[2]

Poly-3,4-ethylenedioxythiophene (PEDOT), polypyrrole (PPy) and polyaniline (PANI) are well known conducting polymers that present excellent electrical and optical properties and they have been also used for potential biomedical applications.[3] Since the first studies of ring opening polymerizations (ROP) the use of lipases to promote these reactions with lactides and copolymerization has been widely investigated.

In 2011, the synthesis of a macromonomer based on polycaprolactone and containing α,ω-thiophene end groups, prepared by using an enzymatic catalyst, was reported.[4] In this two-step synthesis strategy, 3-thiophenemethanol was used to initiate the enzyme-assisted ring-opening polymerization of ε-caprolactone (ε-CL) to yield PCL with α-thiophene end group (initiation reaction, ThPCL) and then 3-thiopheneacetic acid was added to prepolymerized ε-CL to introduce ω-thiophene functionality in termination step (ThPCLTh). The electroactive macromonomers present completely different properties such as solubility and oxidation potential; consequently, the electropolymerization is very difficult and further investigation is necessary, e.g. the ThPCLTh was not able to electropolymerize by itself.

In present study, a one-step enzymatic synthesis of a novel electroactive biodegradable macromonomer 3,4-ethylenedioxythiophene-poly(*L*-lactic acid) (EDOT-PLLA) is presented. Both approaches (organometallic and enzymatic) was evaluated. This was the first report on this type of approach that allows obtaining a biodegradable EDOT based macromonomer that could be further polymerized by different strategies, to produce a conducting polymer and direct linked with a PLLA chain.

Experimental Methods

The synthesis of the novel conducting and biodegradable copolymer was obtained using (2,3-dihydrothieno[3,4-b][1,4]dioxin-2-yl)methanol (EDOT-OH) as an initiator in a lactide ring opening polymerization reaction, by using whether organometallic catalyst ($Sn(oct)_2$) or enzymatic pathway (immobilized enzymes, CAL-B and PS-IM) in three different temperatures (30, 50 and 80 ºC), resulting in EDOT-PDLLA macromonomer. All macromonomers (EDOT-PDLLA) were characterized by ^1H and ^{13}C. NMR, MALDI-TOF, GPC and EDX. Furthermore, in order to attest the electroactivity and biodegradability, it was investigated the electropolymerization and its electrochemical profile by cyclic voltammetry and hydrolytically degradation tests for 120 days. Additionally, the electroactive biodegradable macromonomer of EDOT-PDLLA was applied to obtention of different biomaterials: 1) chemical copolymerization of PEDOT-*co*-PDLLA and 2) composite of Au/PEDOT-PDLLA nanoparticles.

Results and Discussion

The ^1H and ^{13}C NMR spectra of products confirmed the EDOT-PDLLA structure obtaining trough organometallic and enzymatic catalysts. ^1H NMR, MALDI-TOF and GPC revealed the M_n value calculated for the macromonomer

prepared with the organometallic catalyst, always results the highest molecular weight (3779 Da in GPC) with higher polydispersity index (1.46), while three times lower values are obtained with both enzymes (~800 Da in GPC) but more monodisperse (~1.05). In addition, for the enzymatic reactions no significant temperature difference was observed. The EDX analysis shown the presence of remaining metal (tin) even after purification by recrystallization on macromonomers obtained through organometallic catalyst. Cyclic voltammetry shown the electroactive macromonomer of EDOT-PDLLA was able to electropolymerize, i.e. the modification with PDLLA did not affect the π-conjugated system on thiophene group, but the oligomers formed was soluble and no film formation was observed. The EDOT-PDLLA was used for a post chemical copolymerization with more EDOT monomers, obtaining the PEDOT-*co*-PDLLA copolymer with tunable conductivity and biodegradable property. Additionally, EDOT-PDLLA was also used for synthesis of composite of Au/PEDOT-PDLLA nanoparticles.

Conclusion

The electroactive biodegradable macromonomer of EDOT-PDLLA was obtained by the two different approaches. Chemical structure was characterized, and it was applied to synthesis of two different materials. It evidenced the importance of EDOT-PDLLA as a key macromolecule for development of novel conducting and degradable biomaterials.

References

1. Nair, L. S. & Laurencin, C. T. *Prog. Polym. Sci.***32,** 762–798 (2007).
2. Jiang, G. *et al*. *J. Appl. Polym. Sci.***114,** 658–662 (2009).
3. Yang, J. *et al. Acta Biomater.***1,** 125–136 (2005).
4. Türkan, A. *et al. Polym. Bull.***67,** 1483–1498 (2011).

Acknowledgement

We gratefully acknowledge the financial support received from Brazilian agency FAPESP (proc. 2015/26308-7) and the PhD scholarship (proc. 2014/09353-6).

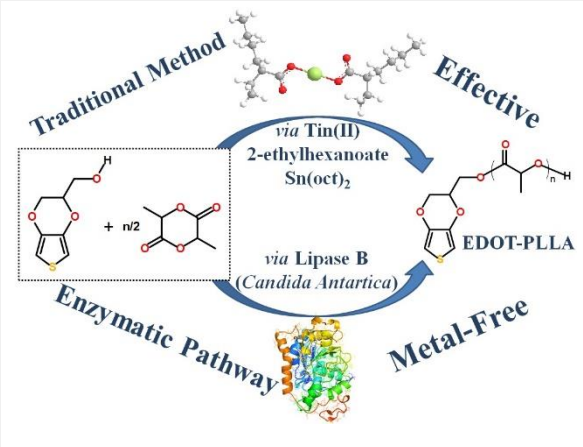

Electroactive Macromonomer of EDOT-PDLLA by organometallic or enzymatic pathway
Chemical reaction using a modified EDOT-OH as initiator of open ring polymerization of lactide to obtain the electroactive macromonomer of EDOT-PDLLA, by using whether organometallic or enzymatic catalysts.

III-OS10-03

Development of an *in-situ*-forming albumin hydrogel for glucagon-like peptide-1 analogue delivery by subcutaneous injection indicated for type 2 diabetes mellitus.

Gillian Murphy[1,2], Abhay Pandit[1], Michael Fitzgerald[2]

[1]National University of Ireland, Galway, Centre for Research in Medical Devices (CÚRAM), Galway, IE; [2]Mylan, Research & Development, Galway, IE

Introduction

Of the 422 million adults diagnosed with diabetes mellitus[1], approx. 90 % suffer from type 2 diabetes mellitus (T2DM)[2]. The incretin effect is impaired in T2DM causing a reduced glucose-responsive insulin release due to gut hormones such as glucagon-like peptide-1 (GLP-1)[3,4]. Synthetic GLP-1 receptor agonists (GLP-1 RA) have been very successful in T2DM treatment, however with limitations due to injection frequency[5]. Next generation GLP-1 RA aims towards once-monthly injections with the advantage of improving patient compliance and the pharmacokinetic (PK) profile[6]. Biomaterial carrier systems have significant potential for improving GLP-1 RA[7]. Many GLP-1 RA have an innate binding affinity with serum albumin. Albumin has also been used as a carrier in a number of commercially approved formulations[8]. The aim of this research is to harness albumin as a hydrogel for a once-monthly, sustained release (SR) formulation of a GLP-1 RA.

Experimental Methods

The hydrogel system was characterized *in vitro* for porosity, swelling, crosslinking, rheology and cytotoxicity screening, as well as for the GLP-1 RA binding response to albumin. Porosity was studied using the Hitachi S2600N; hydrogels were lyophilised, sputtercoated with gold and measured using Image J software. Swelling ratio was determined by incubation in 1X PBS at 37°C[9]and crosslinking was measured by TNBS™ assay. Rheology oscillation study was carried out on the Anton Parr MCR 302 using a 50 mm parallel plate at 1 Hz and 0.5 % strain for 1 hour at 37°C to assess the gelation point and max. storage and loss modulus. Cytotoxicity screening was carried out on 3T3-L1 fibroblast cells using light microscopy, LIVE/DEAD™ and AlamarBlue™ assay. GLP-1 RA binding response was studied by surface plasmon resonance using a Biacore™ X100 and an albumin-immobilised CM5 chip. *Ex vivo* injectability of subcutaneous tissue was carried out in mouse at 37°C; alcian blue-stained hydrogel and surrounding tissue was explanted and embedded for H&E staining. Injectability of a cyanine-5.5 (Cy 5.5)-loaded hydrogel was also observed by fluorescence using the IVIS Lumina III.

Results and Discussion

A tunable, *in-situ* gelating, PEG-crosslinked albumin hydrogel was developed as a new drug delivery platform for GLP-1 RA for subcutaneous injection. A linear relationship of PEG concentration (conc.) and increasing crosslinking efficiency was observed by TNBS™ assay. A cargo-dependent reduction in crosslinking was observed in med. and max. PEG conc. A linear relationship of albumin conc. and increasing swelling capacity was demonstrated. Conversely, an inverse relationship between PEG conc. and swelling capacity was observed. Hydrogel porosity was estimated at approx. 45 % for both min. and max. albumin conc. A linear correlation of storage and loss modulus was shown with an increasing number of PEG spacer arms, as well as with an inverse relationship of gelation time with PEG conc. A cargo-dependent reduction in storage and loss modulus and increase in gelation time was also observed. There was no marked change in cell morphology, viability and metabolic activity in the hydrogel-treated

sample vs. untreated control. A linear binding response of GLP-1 RA with 25 µg/mL immobilised human albumin was demonstrated between 10 µM to 100 µM conc. *In-situ* gelation of hydrogel was demonstrated in mouse, tissue explanted for H&E staining and Cy 5.5-loaded hydrogels were detected using the IVIS Lumina III imaging system.

Conclusion

A tunable, *in-situ* gelating, PEG-crosslinked albumin hydrogel was developed and characterised for the purpose of a once-monthly, SR delivery system of a GLP-1 RA for T2DM. The presented albumin hydrogel system may offer unique advantages over currently marketed GLP-1 therapeutics given that, to our knowledge, there are no other hydrogels of this nature for the proposed application reported in the scientific literature.

References

1. http://www.who.int/iris/handle/10665/204871
2. https://www.who.int/mediacentre/factsheets/fs138/en/
3. Nauck, M. *et al. Diabetologia*. 1986 Oct;29(1):46-52
4. Nauck, M. *et al. Diabetologia*. 1993 Aug;36(8):741-744
5. Tran, KL. *et al.Am Heal. Drug Benefits*. 2017 Jun;10(4):178-188
6. Buse, JB. *et al*. *Lancet.* 2013 Jan;381(12): 117–124
7. https://www.bydureon.com/pen/bydureon-for-diabetes/how-bydureon-works.html
8. Peipei, Xu. *Onco Targets Ther.* 2016 May;9:2873–2884
9. Begam, T.. *J. Appl. Polym. Sci.*2003 May; 89(3):779–786

Acknowledgement

Mylan Institutional, Galway (Industry-Funded Project)
Dr. Jakki Cooney, Bernal Institute, University of Limerick (Biacore X100)
Dr. Rocio Guzmán-Ruiz, Universidad de Córdoba (Cytotoxicity screening)
Paolo Contessotto, NUI Galway (H&E staining)

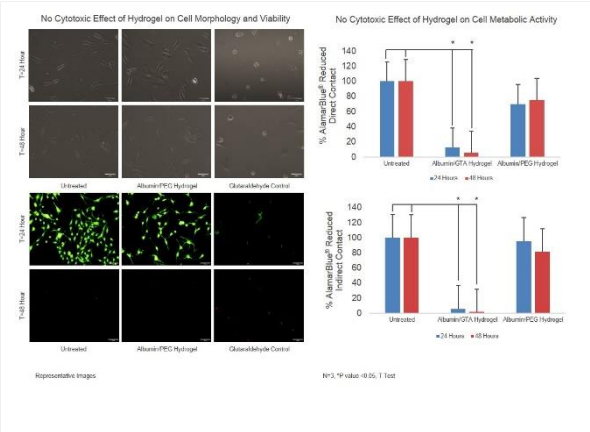

In Vitro Cytotoxicity Screening of Hydrogel Components in 3T3L-1 Fibroblast Cells

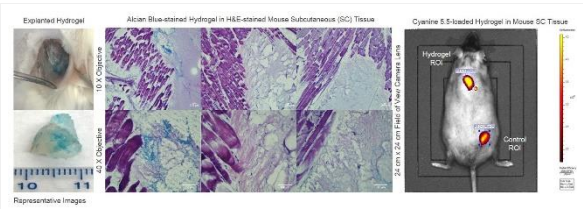

Ex Vivo Injectability of In-Situ Gelating Hydrogel in Mouse Subcutaneous Tissue

III-OS10-04

Structural analysis of self-assembled fibrinogen nanofiber scaffolds

Karsten Stapelfeldt[1], Stephani Stamborowski[2], Polina Mednikova[1], Dorothea Brüggemann[1]

[1]University of Bremen, Institute for Biophysics, Bremen, DE; [2]Fraunhofer Institute for Manufacturing Technology and Advanced Materials, Bremen, DE

Introduction

Fibrinogen (Fg) plays a crucial role in wound healing and tissue repair since it induces the formation of nanofibrous fibrin clots [1]. Therefore, scaffolds from Fg nanofibers have become highly attractive biomaterials for tissue engineering and wound healing applications. Existing methods to prepare nanofibrous Fg scaffolds like electrospinning make use of organic solvents or high electric fields, which often impede the biological protein function [2]. To overcome these limitations we recently introduced a novel *in vitro* method for the fabrication of 3D fibrinogen nanofiber scaffolds under physiological conditions [3, 4].

Experimental Methods

Our new method of salt-induced self assembly utilized a controlled drying step of fibrinogen solutions in the presence of concentrated salt buffers. The morphology of self-assembled scaffolds was analyzed with scanning electron microscopy (SEM). Next, we used Fourier-transform infrared (FTIR) spectroscopy to analyze differences in secondary structure of nanofibrous Fg scaffolds in comparison to planar Fg films. Finally, thioflavin T was used as dye in combination with fluorescence microscopy to analyze whether self-assembled Fg fibers exhibit amyloid-like properties.

Results and Discussion

Salt-induced self assembly resulted in dense networks of Fg nanofibers with diameters of 200 to 300 nm (see Fig. 1). Using SEM analysis we found out that fibrillogenesis could be induced with a fibrinogen concentration of at least 2 mg/ml in a pH regime of 7 to 9. By adjusting the protein and salt concentration we could prepare fibrinogen scaffolds with overall dimensions in the centimeter range and a thickness of several micrometers [3]. If no concentrated salt solution was present in the buffer system, planar layers of Fg were formed during drying, which were used as references for subsequent structural analysis.

In the resulting FTIR spectra we found peak shifts of the amide bands for fibrinogen nanofibers in comparison to planar fibrinogen (see Fig. 1). These peak shifts indicated changes in the secondary structure of nanofibrous Fg scaffolds, which yielded a higher content of β-sheet structures in comparison to planar Fg films. Interestingly, the β-sheet structures of Fg fibers, which were prepared by salt-induced self assembly, did not show any β-amyloid like structures. This finding was additionally confirmed with a thioflavin T staining and the observation that our self-assembled Fg nanofibers re-dissolved in aqueous buffer when no additional fixation was used.

The changes in secondary structure, which ocurred during salt-induced nanofiber formation of fibrinogen, are an interesting observation, since IR studies on the naturally occurring enzymatic conversion of Fg into fibrin nanofibers did not report any changes in secondary structure [4].

With regard to future biomedical applications we analyzed whether salt-induced self assembly of fibrinogen could be carried out on different substrate materials. Thus, we obtained dense fiber networks on glass, gold, silanized surfaces and different polymers. By introducing a tailored formaldehyde vapor fixation and subsequent washing step the Fg fiber scaffolds could be immobilized or detached depending on the substrate material.

Conclusion

Our new biofabrication process to prepare free-standing or immobilized fibrinogen scaffolds only required standard lab equipment and low protein concentrations in physiological buffers. In future, these nanofibrous fibrinogen scaffolds will be highly interesting for versatile wound healing and tissue engineering applications.

References

[1] M.W. Mosesson, Fibrinogen and fibrin structure and functions, Journal of Thrombosis and Haemostasis 3 (2005) 1894–1904.
[2] M. McManus, E. Boland, S. Sell, W. Bowen, H. Koo, D. Simpson, G. Bowlin, Electrospun nanofibre fibrinogen for urinary tract tissue reconstruction, Biomedical materials (Bristol, England) 2 (2007) 257–262.
[3] K. Stapelfeldt, S. Stamboroski, P. Mednikova, D. Brüggemann, Fabrication of 3D-nanofibrous fibrinogen scaffolds using salt-induced self assembly, Biofabrication 11 (2019) 25010.
[4] D. Brüggemann,, K. Stapelfeldt,, P. Mednikova,, In EU patent application PCT/EP2019/051242; (2019)

Acknowledgement

We gratefully acknowledge funding via the Emmy Noether Programme of the Deutsche Forschungsgemeinschaft.

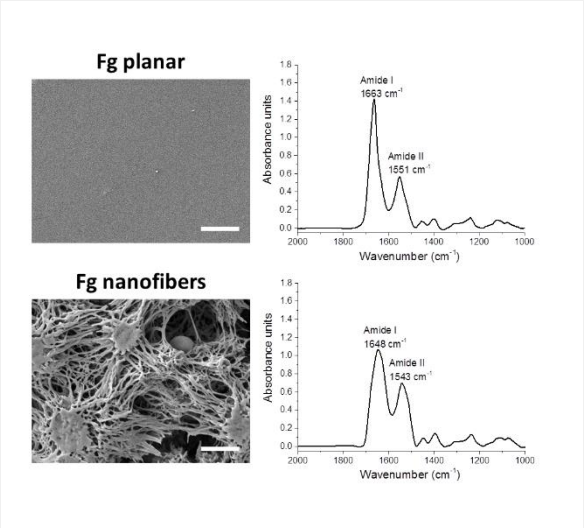

Fig. 1: Structural analyses of firbinogen scaffolds.
Planar fibrinogen layers show a different FTIR spectrum in comparison to fibrinogen nanofiber scaffolds, which were prepared by salt-induced self assembly. Scale bar 2 µm.

III-OS10-05

Laminin-Mimicking Hyperbranched Polymer Drives the Formation of Perivascular Stem Cell Niche Organoids in 2D Culture Conditions

Valeria Perugini, Matteo Santin

University of Brighton, School of Pharmacy and Biomolecular Sciences, Brighton, GB

Introduction

Nanocarriers with a wide range of physicochemical properties are currently under development to improve the administration of drugs and genes to diseased tissues. However, their repeated use can might lead to both cyto- and geno-toxicity caused by their tendency to accumulate in tissues and in particular in those highly vascularised such as liver, spleen and kidney[1]. While studies of nanocarrier biodistribution have been performed on these tissues, less attention has been given to their potential accumulation into the bone marrow where stem cell resides in perivascular niches. As it is known that stem cells play an important role in tissue remodelling and at the same time can participate in cancer development, it is argued that the preliminary testing of nanocarriers has to take into consideration the stem cell niche. However, the difficulty of identifying stem cell niche *in vivo* and the obvious costs of animal tests encourage the development of perivascular stem cell niche in culture where preliminary screening of nanocarrier or nanomedicine toxicity can be reliably performed[3]. This works presents a new engineered perivascular stem cell niche assembled by the co-culture of human mesenchymal stem cells (MSC) and endothelial cells (EC) on a novel biomaterial substrate able to mimic the histological and biospecific features of the basement membrane that is the main substrate of the stem cell niche.

Experimental Methods

Material Preparation. Poly (ε lysine) dendrons up to the third generation (gen3K) with an arginine (R) core molecule and 16 linear laminin peptide-sequence (YIGSR) were synthesised using a microwave (Biotage, UK) based Fmoc solid phase peptide method. Once assembled, Rgen3K(YIGSR)$_{16}$ were resuspended in a MES solution containing EDC and NHS for 1 hour at room temperature and grafted onto poly-L-lysine (PK, Sigma-Aldrich UK). Rgen3K(YIGSR)$_{16}$ – modified PK solutions were characterised by FT-IR and used to coat 24 tissue culture wells (Nunc, UK).

Cell Preparation. MSCs (P2, Lonza UK) were co-cultured with HUVECs (ATCC UK) in a ratio 1:2 and re-suspended in TheraPEAK™ /F12-K medium (1:1) supplemented with 0.1 mg/mL heparin, 0.05 mg/mL endothelial cell growth supplements (Sigma-Aldrich UK). After 48 hours incubation, cellular activities were morphologically and functionally assessed by immunostaining (RhoA family, HIF1α, CXCR4) and western blotting (β1-integrin, H3K27me3, VEGFR2, PDGFR and EGFR) analysis. Protein bands were quantified using Image J software and normalised to the levels of a loading control, GAPDH.

Both MSCs and HUVECs were also seeded onto Matrigel as control substrates.

Results and Discussion

The successful synthesis of Rgen3K(YIGSR)$_{16}$ with a degree of purity > 80 allowed their precise grafting onto PK surfaces which was confirmed by FT-IR (1224 and 1036cm^{-1}).

Compared to Matrigel that induced formation of immature tubules mainly surrounded by small round MSCs, Rgen3K(YIGSR)$_{16}$ –modified PK – cultured HUVECs self-assembled and differentiated into tubules that were

thoroughly wrapped by aggregates of MSCs or spheroids within 48 hours incubation. These processes appeared to be mediated via engagement and clustering of specific adhesive proteins such as integrins which coordinated the balance between Rac1 and RhoA. In addition, these nanomaterials regulated within cells both HIF1α and chemokine-receptors (CXCR4) that in turn directly stimulated their pro-angiogenic cell activities (e.g. VEGFR2, PDGFR and EGFR) and enhanced self-renewal and paracrine effects of MSCs through H3K27me3-dependent mechanism.

Conclusion

The unique properties of Rgen3K$(YIGSR)_{16}$–modified PK show the ability of this substrate to drive lineage specific cell fate and indeed in the development of innovative organotypic models that have the potential of becoming accepted by regulatory agencies as standard in the testing of nanocarriers and nanomedicine.

References

1 Singh R. et al., Exp Mol Pathol. 2009; 86(3): 215–223.
2 Nelson MR. et al., J. Mater. Chem. B, 2016, 4, 3490-3503.
3 Murray IR. Cell Mol Life Sci. 2014 71(8):1353-74.

Acknowledgement

This work was supported by the FP7 EC grant 761104-REFINE-H2020.

III-OS10-06

Novel fabrication of multi-compartmental biodegradable polymeric microneedles for drug intradermal release

Rezvan Jamaledin, Raffaele Vecchione, Paolo A. Netti

Italian Institute of Technology, Largo Barsanti e Matteucci, 53 80125, Naples, IT

Introduction

Transdermal drug delivery offers a clinical superiority over traditional, invasive injections. As compared to oral delivery, protein drug transportation across the skin avoids the hepatic first-pass extraction and is delivered to the systematic circulation at a pharmacologically relevant rate. However, the clinical application of transdermal delivery has been limited to lipophilic drugs with a molecular weight less than 500 Da [1, 2] until the emergence of polymeric microneedles (MNs), which provides a broad and versatile platform to overcome the challenges of the skin barrier for macromolecular drugs. In this technique, arrays of microscopic needles are designed to painlessly transverse the stratum corneum and penetrate the dermis layer at a predetermined depth ranging from 70 to 200 µm, thereby avoiding the stimulation of the nerve endings [3]. Encapsulating proteins in the polymeric matrix provides the opportunity for long-term maintenance of bioactive protein in a dried state without the cold chain requirement, thereby minimizing the costs and restrictions of transportation [4].

Experimental Methods

PLGA microparticle fabrication

Polymeric microspheres have been employed as starting material for the production of biodegradable polymeric microneedles. Such microspheres have been produced by means of a double emulsion process [5].

Fabrication of microneedle patches

After preparing the mold, PVP solution was poured on it, degassed and then spin coated in order to spread out the excess of solution from the mold and allow a fast evaporation of the residual solvent. By following this procedure, it was then possible to produce the tip of the microneedles. After PVP insertion, microparticles were introduced in the mold. After filling up the mold with the microparticles, they were exposed to a solvent non-solvent vapor mixture in order to carry out a novel and mild plasticization able to assemble the microparticles in the shape of microneedles while keeping the microstructure of the starting microparticles. Finally, polymer microneedles were extracted from the mold by the aid of a 3M Medical coated with PVP.

Results and Discussion

Fabrication of master, mold, and microneedles

The microcones of the master were prepared one by one in a serial production by two-photon polymerization onto a glass substrate reference [6]. Because of the fragility of master material, we did not directly use it to obtain polydimethylsiloxane (PDMS) molds. In order to avoid master breakage, we then used Norland Optical Adhesive (NOA) 60 to fabricate a master that is less fragile than the original one, which could be used several times. (**Fig. 1**). PLGA microneedles were fabricated with encapsulated laccase or sulforhodamine as a model drug. **Fig. 1D, E** and **F.**

Enzyme activity

Histological images of Endo-HSE cross sections after the indentation highlighted that microneedles were able to penetrate Endo-HSE, overcoming the epidermis and effectively reaching a depth of approximately 250 μm for both microneedle configuration (**Fig. 2A, C**). The stereomicroscope images revealed the pattern of microneedles array and the ability of the enzyme-loaded in each microneedle to react with ABTS substrate. In the case of microneedle configuration 1, the ABTS oxidation occurred in a very short time since the enzyme-loaded in the microneedle tip was rapidly available. In the case of microneedle configuration 2, the observation time was in the hours range because the laccase diffusion occurred after microparticles biodegradation. In particular, we assessed that in configuration 1 the diffusion occurred just in 1 min and it was localized very close to the walls of the microneedles reaching the maximum diffusive radius in 30 min. At 48 h, we observed an inversion of the bell apex indicating that no more enzyme was present in needle as consequence ABTS oxidation product (dark pixels) was not present anymore. Instead, in the configuration 2, the diffusion mechanism of the reaction product was slower than in the configuration 1 and the concentration profile was flat at t0. In conclusion, the experimental results showed that the activity of the enzyme was preserved after microneedles production in both encapsulation procedures. Moreover, we demonstrated the faster diffusion of the encapsulated enzyme in the configuration 1 compared to the configuration 2 (**Fig. 2B**).

Conclusion

We designed the procedure to fabricate microneedles proposing a room temperature procedure which allows preserving thermolabile drugs, as demonstrated in the case of laccase enzyme. Results suggest that multi-compartment microneedles with two different degradation times to combine fast and prolonged release encapsulate and deliver thermo-sensitive high molecular weight molecules by keeping their activity.

References

1. Barry, B.W. Breaching the skin's barrier to drugs. *Nature biotechnology***22**, 165 (2004).
2. Eisenstein, M. Something new under the skin. (Nature Publishing Group, 2011).
3. Kim, Y.-C., Park, J.-H. & Prausnitz, M.R. Microneedles for drug and vaccine delivery. *Advanced drug delivery reviews***64**, 1547-1568 (2012).
4. Schoellhammer, C.M., Blankschtein, D. & Langer, R. Skin permeabilization for transdermal drug delivery: recent advances and future prospects. *Expert opinion on drug delivery***11**, 393-407 (2014).
5. Iqbal, M., Zafar, N., Fessi, H. & Elaissari, A. Double emulsion solvent evaporation techniques used for drug encapsulation. *International journal of pharmaceutics***496**, 173-190 (2015).
6. Baldacchini, T. *Three-dimensional microfabrication using two-photon polymerization: fundamentals, technology, and applications*, (William Andrew, 2015).

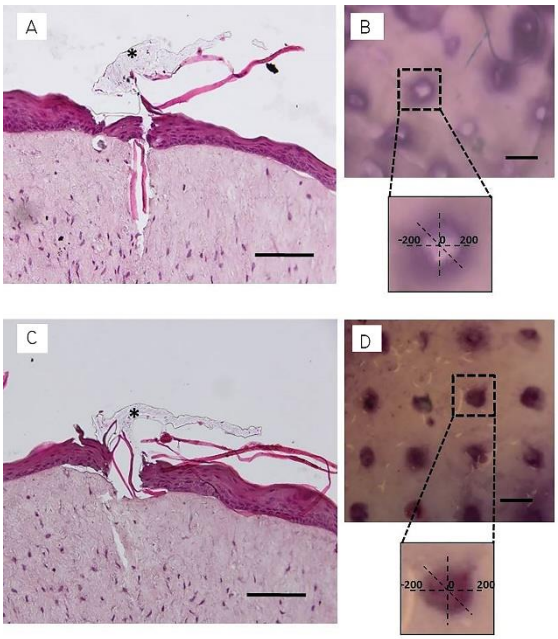

Fig. 2
Functional test of microneedles for transdermal delivery of high molecular weight substances in a full-thickness human skin model. The pictures in A, B refer to microneedle configuration 1 while pictures C and D refer to microneedle configuration 2. Specifically, A, C) histological images of Endo-HSE 48h after microneedles indentation to highlight the transdermal penetration (scale bar= 100 µm). B, D) stereomicroscopic images of Endo-HSE 48h after indentation (scale bar=500 µm).

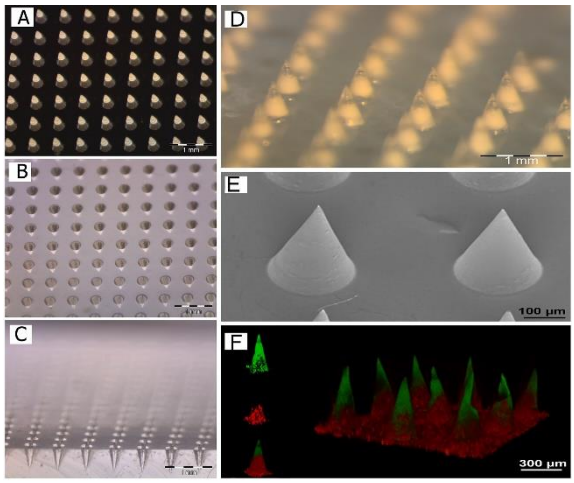

Figure 1
(A) Optical images of the array of master of 600 µm height and 300 µm diameter of the base, (B) optical image array of a PDMS stamp replicated from the master of microneedles. (C) optical image of a cross-section of the PDMS stamp.Stereomicroscope (D) and scanning electron microscopy (E) images of microneedles array. The bars represent 1 mm and 100 µm, respectively.. (F) 3D confocal reconstruction of a microneedles array. The green color is for the FITC loaded in the PVP tip while red color is for the Sulphorhodamine B loaded in the PLGA microparticles.

4:45 p.m. – 6:15 p.m.

Hall 4

III-OS11 | Biomaterials for bone regeneration

III-OS11-01

Combining fibrinogen and magnesium to produce immunomodulatory biomaterials: impact on macrophages and their crosstalk with mesenchymal stem/stromal cells

Mafalda Bessa-Gonçalves[1,2], Bérèngere J. C. Luthringer-Feyerabend[3], Regine Willumeit-Römer[3], Mário A. Barbosa[1,2], Susana G. Santos[1,2]

[1]i3S – Instituto de Investigação e Inovação em Saúde, INEB - Instituto de Engenharia Biomédica, Porto, PT; [2]Instituto Ciências Biomédicas Abel Salazar, Porto, PT; [3]Institute of Materials Research, Division Metallic Biomaterials, Helmholtz-Zentrum Geesthacht, Geesthacht, DE

Introduction

Macrophage behavior upon biomaterial implantation conditions the inflammatory response, and the regenerative process. Modulating macrophage phenotype from M1 to M2 is an increasingly explored strategy in biomaterial development[(1)]. Previous work from our group, showed that Fibrinogen (Fg) interacts with monocytes through TLR4[(2)], and promotes *in vivo* bone regeneration[(3--)]. Also, Magnesium (Mg) ions have been reported has immunomodulatory, reducing LPS-induced M1 macrophage polarization[(4)]. Herein, we tested the hypothesis that Fg and Mg biomaterials, used in combination could act synergistically to modulate macrophage activation, promoting a pro-regenerative phenotype.

Experimental Methods

Fg scaffolds were prepared by freeze-drying, as described[(3)], from a solution of Fg (from human plasma, Grifols S.A.). Pure Mg discs were ultrasonically cleaned[(5,6)] before use. Before cell culture or extract production, materials were crosslinked, neutralized and disinfected. Fg and Fg-Mg structure and porosity was evaluated using scanning electron microscopy (SEM). Human monocyte-derived macrophages were obtained from buffy coats (kindly donated by *Serviço de Immunohemoterapia*, *Centro Hospitalar Universitário São João*), and their capacity to interact with Fg, Mg and Fg-Mg biomaterials directly, or their extracts, was evaluated by confocal microscopy, flow cytometry, ELISA and Western Blot. The potential of the secretome produced by macrophages preconditioned with biomaterials extracts, to promote Mesenchymal Stem/Stromal Cells (MSCs) osteogenic differentiation was assessed by their ALP activity. Statistical analysis was performed using ANOVA followed by Holm-Sidak test and Friedman's test for parametric and non-parametric data, respectively.

Results and Discussion

Scaffolds of Fg alone, or in the Fg-Mg combination, presented a similar 3D architecture, characterized by a porous interconnected structure. Live/Dead staining showed that macrophages colonize Fg, Mg and Fg-Mg biomaterials. When macrophages were cultured in presence of materials extracts, in unstimulated or pro-inflammatory (M1, LPS-IFNγ) conditions, results revealed that extracts from Fg-Mg materials reduce M1 polarization, resulting in lower cell surface CD86 expression upon LPS-IFNγ stimulation. Interestingly, Fg and Fg-Mg extracts impair the increased TNF-α secretion in response to LPS-IFNγ stimulation. MAPK and NFκB p65 signalling pathways were not activated in response to biomaterial extracts. However, NFκB p65 activation in response to LPS-IFNγ stimulation was impaired by exposure to Fg-Mg extracts.

Results obtained for the impact on MSC differentiation show that biomaterial extracts *per se* did not enhance MSC ALP activity at 14 days. However, the secretome from unstimulated macrophages exposed to extracts from the Fg-Mg material significantly increased ALP activity on MSC, when compared with secretome of naïve macrophages and those exposed to extracts of Fg materials. The secretome of M1 stimulated macrophages followed the same trend.

Conclusion

The results obtained indicate that Fg, Mg and their combination, Fg-Mg, impact macrophage activation following pro-inflammatory stimulation, and their crosstalk with MSC.

References

(1)Kzhyshkowska J et al., J Leukoc Biol. 2015. 98(6):953-62. (2)Oliveira MI et al., Acta Biomater. 2017. 49:296-305. (3)Vasconcelos DM et al., Biomaterials. 2016. 111:163-178-. (4)Li et al., Colloids Surf B Biointerfaces. 2018. 171:276-284. (5)Luthringer-Feyerabend, BJC et al., Acta Biomater. 2019. pii:S1742-7061(19)30122-9.(6)Hou RQ et al., Acta Biomater. 2019. pii:S1742-7061(19)30117-5.

Acknowledgement

Authors thank Grifols SA for donating clinical grade fibrinogen, Serviço de Ortopedia and *Serviço de Imunohemoterapia, Centro Hospitalar Universitário de São João* for donating bone marrow samples and buffy coats, respectively. This work was funded by NORTE-01-0145-FEDER-000012, NORTE 2020, under PORTUGAL 2020 Partnership Agreement, through ERDF; Bessa-Gonçalves M funded by FCT through FCT PhD fellowship PD/BD/135489/2018.

III-OS11-02

Bioactivity improvement of the Titanium alloy using ZrO_2 based glass-ceramic coatings for implant applications

Eimy Caldas[1], Laura Santa[1], Javier Jurado[2], William Aperador[3], Oscar Zambrano[4], Clara Goyes[5]

[1]Universidad Autónoma de Occidente, Semillero de materiales en sistemas energéticos, Cali, CO; [2]Universidad Autónoma de Occidente, Cali, CO; [3]Universidad Militar Nueva Granada, Facultad de Ingeniería, Bogotá, CO; [4]Universidad del Valle, Grupo de Tribología, polímeros, metalurgía de polvos y transformaciones de residuos sólidos (TPMR), Cali, CO; [5]Universidad Autónoma de Occidente, Grupo de Energías GIEN, Cali, CO

Introduction

Titanium alloys are commonly used as biomaterial due to their low electrical conductivity, low reactivity with macromolecules, and high mechanical properties, among others [1]. Different surface strategies have been used to increase and accelerate their bioactivity as much as possible, which have important implications in reducing the recovery time of the patient and to improve the quality of the implant. The use of bioactive ceramics is one of the most promising routes to improve the bioactivity of titanium [2,3]. We employed ZrO_2 based glass-ceramic coatings prepared by a spin coating technique on the Titanium alloy system to guarantee biocompatibility. Finally, the bioactivity and biocompatibility of these coatings were evaluated using hemolytic and immersion tests [4] in a simulated body fluid (SBF) media for 21 days [5].

Experimental Methods

(100 - x)SiO2 - xZrO_2 (x = 20 mol) glass-ceramic coatings were prepared by sol–gel route, using spin-coating deposition on Ti-6Al-4V substrates cleaned by ultra-sound and alcohol. The samples were annealed in air for 1 h at 900^{o}C. The biocompatibility ZrO_2 glass-ceramic coatings were determined directly by hemolysis test (Figure 1) and its bioactivity was determined by immersing the samples in a Simulated Body Fluid (SBF) media for 21 days. The coatings were analyzed with X-ray diffraction and atomic force microscopy before and after these tests.

Results and Discussion

The results showed that ZrO_2 glass-ceramic improves drastically the surface bioactivity and biocompatibility of the titanium alloy since a very low hemolytic index ~ 0.429 was obtained as well as the precipitation of the Hydroxyapatite phase (Figure 2). Thus, through this research, it is demonstrated and discussed why these coatings have the potential to be used in biomedical applications, particularly, where the improvement of the bioactivity and reducing the patient's recovery time is an important requirement

Conclusion

The ZrO_2 glass-ceramic coatings showed very a high bioactivity (very low hemolytic index) and after 21 days in the Simulated Body Fluid. The samples showed the appearance of apatite on the surface, which indicate the good biocompatibility behavior of these coating. Thus, it is concluding that the application of these glass-ceramic coatings on the titanium surface using the spin coating technique [6], is a reliable, effective, cheap and a fast way to improve the bioactivity and biocompatibility of the commercial biocompatible alloys.

References

1. SIDAMBE A.T. Biocompatibility of Advanced Manufactured Titanium Implants-A Review. Materials (Basel) (2014);7,12, p. 8168–8188.
2. BRAEM, A., et al, J. Bioactive glass–ceramic coated titanium implants prepared by electrophoretic deposition. In: Materials Science and Eng. No. 32 (2012); p. 2267-2277.
3. MIGUEZ-PACHECO, V, et al Bioactive glasses beyond bone and teeth: Emerging applications in contact with soft tissues. In: Acta Biomaterialia, 1(2014); p. 1-15
4. ASTM F756-08, Standard Practice for Assessment of Hemolytic Properties of Materials, ASTM International, West Conshohocken, PA, 2008, www.astm.org
5. KOKUBO, T., TAKADAMA, H. How useful is SBF in predicting in vivo bone bioactivity. In: Biomaterials, 27 (2006); p. 2907–2915
6. ASRI, R.I., HARUN, W.S., HASSAN, M.A., GHANI, S.A., BUYONG, Z. A review of hydroxyapatite-based coating techniques: Sol–gel and electrochemical depositions on biocompatible metals. En: Journal Mechanical Behavior of Biomedical Materials, 57(2) (2015); p. 95-108

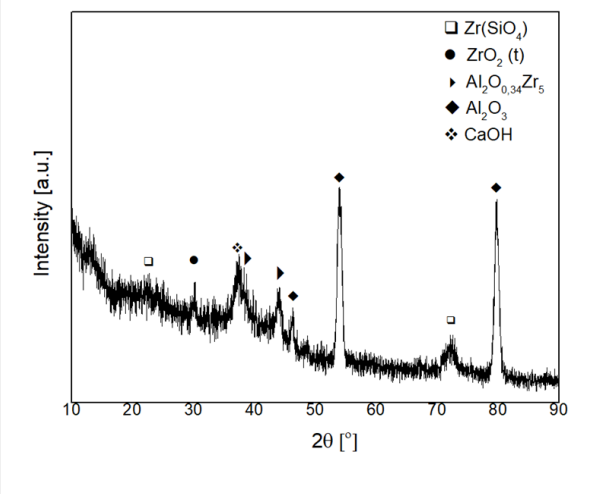

The appearance of the apatite phase after 21 days of immersion in an SBF

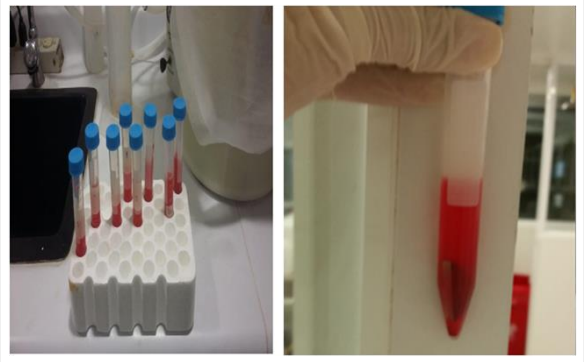

Hemolysis test of the samples using the anticoagulated blood from at least 3 donors

III-OS11-03

Scavenging of bone catabolic proteins by sulfated-GAG modified functional materials

Mathis Gronbach[1], Benno Müller[1], Vicky Lidzba[1], Franziska Mitrach[1], Stephanie Möller[2], Matthias Schnabelrauch[2], Michael C. Hacker[1], Michaela Schulz-Siegmund[1]

[1]University of Leipzig, Pharmaceutical Technology, Leipzig, DE; [2]INNOVENT, Biomaterials Department, Jena, DE

Introduction

For guided tissue regeneration, surface properties of bone substitution materials are of high relevance. Our approach is to modify 3-armed methacrylated oligolactid-based macromer matrices[1] that have been shown to improve bone defect healing in diabetic rats[2]. By using an established protocol to generate macromer-derived polymer films, we are able to analyze the surface properties of equally composed scaffolds[3].

For the current study, we decided to incorporate a small molecule anchor into the polymer films to bind a suitable linker molecule subsequently. This allowed us to change the polymerization solvents in order to avoid phase separation observed in previous experiments[3] and provide more available functional groups on the material surface. Surface decoration with sulfated glycosaminoglycans (sGAG) covalently bound to the linker is intended to improve bone defect regeneration by taking advantage of their previously shown ability to scavenge bone-catabolic proteins[4].

Experimental Methods

Film synthesis

Three-armed biodegradable macromer 134LA6 (M_w of the core= 134 g/mol, 6 equivalents of oligolactide) cross-copolymerized with glycidyl methacrylate.

Stepwise surface decoration

1. Addition of polyetheramine (Jeffamine® ED900) linker results in amino-functionalized films, quantification via fluorescence scanning (Typhoon®) after reaction with 5-(6)-SFX.
2. Immobilization of sulfated GAGs (sGAG, M_w= 75.000, degree of sulfation= 3,4) , ATTO565 fluorescently labeled) with EDC/NHS and quantification via fluorescence scanning. Control: same procedure without EDC/NHS. To differentiate between covalently and adsorptively immobilized sulfated GAGs, we established a washing protocol using a KSCN buffer.

Scavenging experiments

DKK-1 incubation in McCoy's 5A medium + 10% FBS in low adhesion 12-well plates, quantification of DKK-1 after scavenging via DKK-1 ELISA (R&D), fluorescent labeling of DKK-1 with Alexa Fluor 647.

Cell culture

10.000 SaOS-2 cells/cm² seeded on film surfaces in DMEM + 10% FBS, osteogenic supplements: dexamethasone, b-glycerophosphate, ascorbic acid.

Results and Discussion

By testing different polymerization and incubation conditions, we established a reproducible protocol for the above-mentioned film production process. As we narrowed down the formerly used binary solvent to a one-solvent (dioxane) system, we were able to avoid unwanted effects such as phase separation. Glycidyl methacrylate carrying films readily reacted with Jeffamine to homogeneously amino-functionalized film surfaces.

For proof of concept, sGAG decorated films as model system for equally composed scaffolds were incubated with a solution of DKK-1 (8 ng/ml), a wnt antagonist that is known to suppress bone formation. 24 h later, less than 0.5 ng/ml was determined in the supernatant whereas 4 ng/ml DKK-1 were found in medium in contact with control films with only adsorptively immobilized sGAGs. This result confirmed our concept of DKK-1 scavenging via sGAG carrying film surfaces.

In a second step, we checked for DKK-1 scavenging after fluorescence labeling of the protein. sGAG modified films were again incubated with a DKK-1 solution of 8 ng/ml and DKK-1 scavenging was determined via quantification of DKK-1 on films via high-resolution fluorescence imaging. This way we managed to confirm, visualize and quantify the binding of this protein to the film surface.

In order to investigate whether DKK-1 scavenging is reversible, we incubated DKK1 saturated films in cell culture medium for 6 days and determined DKK-1 in the supernatant via ELISA. We found no release of DKK-1 during this time and confirmed the strong binding of the protein.

In the final step, we investigated the biological performance of sGAG modified films. To this end, we seeded osteoblast-like SaOS-2 cells on the films that secrete DKK-1 during their differentiation. Again, only small amounts of DKK-1 were found in the cell culture medium within 6 days whereas up to 10 ng/ml were found on control films. In consequence, SaOS-2 cells cultured on sGAG-modified films showed higher calcium accumulation indicating improved osteogenic differentiation on our sGAG modified film surfaces.

Conclusion

Overall covalent modification and functionalization of the investigated material with sGAG was successfully applied and showed promising results. Incubation with bone catabolic proteins and cell culture experiments provided first insights in the mechanisms and effects of scavenging as an approach towards an improved bone regeneration.

References

[1] Loth R et al, Acta Biomater. 2015;26:82-96

[2] Picke A. et al, Biomaterials 2016, 96:11-23

[3] Müller BM et al, Acta Biomater. 2017, 51:148-160

[4] Salbach-Hirsch J et al, Biomaterials 2015, 67:335-45

Acknowledgement

Acknowledgment: „We thank for funding by the Deutsche Forschungsgemeinschaft (DFG, German Research Foundation)– Projektnummer 59307082 – TRR67“, Project A1.

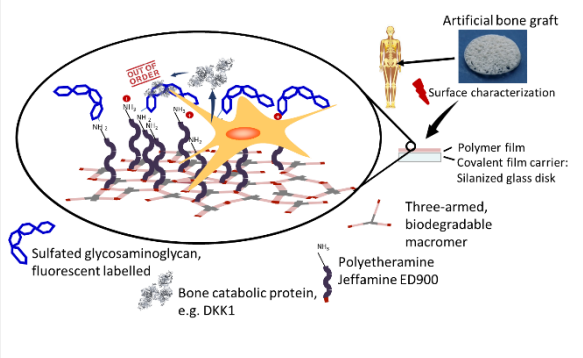

Graphical Abstract

III-OS11-04

Application of a liquid TEM cell to study a 45S5 bioactive glass dissolution

Elkin M. Lopez-Fontal[1], Richard Langford[1], Shaz Khan[2]

[1]University of Cambridge, Physics, Cambridge, GB; [2]Glaxo Smith Kline, Weybridge, GB

Introduction

Formation of hydroxyapatite (HA) is an important product in bioactive glasses dissolution and it is related to the bioglass capability to fully integrate to living tissue. Bioactive glasses, discovered in 1969[3], were originally designed to form an interfacial bonding between an implant and a host tissue that eventually enables fully integration between body and implant.[4] Although, there is a mechanism proposed,[5] there is still uncertainties on the dissolution of bioglass and its mode of action that might be explained whether in real time observation of its dissolution process were performed.

The advent of liquid cell transmission electron microscopy (LC-TEM) has unlocked a new paradigm in science and technology enabling the imaging of processes in their native liquid state.[6-11]

Here, we use and assess an *insitu* liquid TEM cell (Figure 1) to study solution-phase self-assembly of calcium phosphate where nucleation is driven by dissolution of a 45S5 bioactive glass.

Experimental Methods

The 45S5 bioactive glass, which was initially 25 µm size was ball-milled to 200 nm in size so to fit into the gap of the liquid cell (Figure 2.a).

An F20 TEM, equipped with an Energy Dispersive X-ray Spectroscopy (EDS, Oxford Instruments) and a Helios FIB/SEM was used for both the *exsitu* and *insitu* imaging and analysis of the membrane surfaces once the cells were dismantled.

Insitu experiments: isopropanol-ball-milled bioglass colloidal dispersion was dropped onto a cell's top-heater chip and allowed to dry in air. Both artificial saliva (AS) or a phosphate solution ($(NH_4)_2HPO_4$, 10 mM) were flowed through the LC at a flow rate of 5 µl/min.

Exsitu experiments: ball-milled bioglass colloidal dispersion in AS or phosphate solution were left to nucleate for 10, 30 and 60 minutes at 37 °C. At the end of the different times, aliquots (5 µl) were taken and deposited onto TEM support grids and vacuumed dried.

Results and Discussion

***Exsitu* experiments**

Figures 3-5 (BF-TEM, DF-STEM, SEM images and EDS maps) show three different time points 10, 30 and 60 minutes, of the reaction of the ball-milled 45S5 bioactive glass and artificial saliva (AS) at 37°C. These Figures show that the material formation from the reaction of bioactive glass and artificial saliva (AS) starts to happen very fast; i.e. within the first 10 minutes. Also that the structures formed on and in close proximity to the ball-milled bioactive glass have multiple distinct morphologies at the different time points measured which agree with previous reports about calcium phosphate nucleation[12-13] and bioactive glass bioactivity.[14]

At 10 minutes round chained structures (Figure 3) are present with a Ca/P ratio of 1.5; possibly corresponding to amorphous calcium phosphate (ACP). At 30 minutes (Figure 4) the morphology changes to a mixture between round and spike-like structures with an average Ca/P ratio of 1.4. After 60 minutes (Figure 5) the morphology is spiky-like

with a Ca/P ratio of about 1.7 which is indicative of hydroxyapatite (HA). The formation of HA like material on and in close proximity to the bioactive glass agrees with previous reports as it is a crucial measure of the bioglass bioactivity and its capacity to fully integrate to the human body.[15-17]

Although these *exsitu* experiments show the existence of different calcium phosphate nucleation stages it does not inform about the mechanism by which calcium phosphate turns into its different phases. It is hoped that the LC-TEM may enable a better understanding of the reaction pathways.

***Insitu* experiments**

The time series images recorded over 48 minutes, of the material formed in the AS (Fig. 6) show spiky crystal nucleation. Figure 7 shows BFTEM, SEM images and EDS maps at the 48-minute time point measured with the membranes dismantled from the LC. This indicates that the composition of the nucleated crystals shown in Figure 6 consisted of numerous salts reflecting the composition of the AS used (Fig. 7.d)).

Figure 8 shows the stills from the movie recorded of the nucleation when the phosphate solution was used in the LC. Corresponding BFTEM and SEM images and EDS maps, taken at the 43-minute time point, are shown in Figure 9. spiky like structures formed that according to EDS elemental analysis at the 43-minute time point corresponded to calcium phosphate (Fig. 9.d)). The recordings did not show round aggregates which characterised the early stage calcium phosphate nucleation as observed in Fig. 3 for the *exsitu* experiments when using AS.

Conclusion

With these preliminary results, we have shown the suitability of the LC-TEM to image in real time calcium phosphate nucleation when driven by 45S5 bioactive glass dissolution. However, *insitu* results do not show a direct correlation with the *exsitu* findings perhaps due to the interaction effect of the e-beam and the aqueous solution during imaging i.e. radiolysis of water.

According to the results showed here, there is still no much to tell about the Hench's bioglass mode of action.

References

1. De Yoreo, J. J.*, et al.*, **2015**. *Science*
2. Nielsen, M. H.*, et al.*, **2014**. *Microsc Microanal*
3. Hench, L. L., **2006**. *Journal of Materials Science-Materials in Medicine*
4. ASM-International., Handbook of Materials for Medical Devices. **2003**.
5. Hench, L. L., **1998**. *Journal of the American Ceramic Society*
6. Leary, R.*, et al.*, **2012**. *Accounts of chemical research*
7. de Jonge, N.*, et al.*, **2011**. *Nature nanotechnology*
8. Proetto, M. T.*, et al.*, **2014**. *J Am Chem Soc*
9. Yuk, J. M.*, et al.*, **2012**. *Science*
10. Jensen, E.*, et al.* In *Liquid Cell Electron Microscopy*, **2017**.
11. Thomas, J. M.*, et al.*, **2015**. *Chemical Physics Letters*
12. Habraken, W. J.*, et al.*, **2013**. *Nature communications*
13. Combes, C.*, et al.*, **2010**. *Acta Biomater*
14. Hench, L. L., **2005**. *Journal of the American Ceramic Society*
15. Gerhardt, L. C.*, et al.*, **2010**. *Materials*
16. Miguez-Pacheco, V.*, et al.*, **2015**. *Acta Biomater*
17. Jones, J. R., **2015**. *Acta Biomater*

Acknowledgement

Glaxo Smith Klein for funding.

III-OS11-05

Phosphate based glass coatings for rapid Ga^{3+} release: the challenges of balancing cytocompatibility with antimicrobial effects

Kathryn G. Thomas[1], Bryan W. Stuart[3], Steve Atkinson[2], Colin A. Scotchford[1], David M. Grant[1]

[1]University of Nottingham, Advanced Materials Research Group, Nottingham, GB; [2]University of Nottingham, Centre for Biomolecular Sciences, Nottingham, GB; [3]University of Oxford, Department of Materials, Oxford, GB

Introduction

Biofilm infections affect 1-4% of orthopaedic implants, representing cyclical chronic pain for patients and significant cost, estimated in the UK at around £2 billion annually [1]. The passivated surface of a non-cemented implant is vital for surgical success, however this also allows bacterial adhesion leading to biofilm development.

Antibacterial coatings are a desirable solution as they can be applied to existing implants. A successful coating must release a dose of a bactericidal agent at the wound site, preventing bacterial adhesion on the implant surface. Human bone cells must later be able to colonise the surface to ensure adequate implant fixation.

Ga^{3+} has been reported to be osteogenic at <100 µM by preventing the resorption of existing bone tissue and antimicrobial against a wide range of pathogens at <9 mM [2][3]. However, at higher concentrations the Ga^{3+} ions can have cytotoxic effects.

Bioactive glasses have been investigated as release mechanisms for a wide range of metallic ions, with Phosphate based glasses (PBGs) being of interest due to their complete degradation in aqueous media. Radio Frequency Magnetron Sputtering can deposit PBG coatings with excellent substrate conformity and adhesion strengths exceeding the FDA guidelines. Stuart *et al* 2018 has previously deposited a 7 mol% Ga_2O_3- glass coating but did not assess its biological effects [4].

This project aimed to produce high Ga-$_2$O--$_3$ PBG content coating for rapid Ga-$^{3+}$ release and determine whether rapid ion release could be tolerated by human osteoblasts. For the first time this was compared to a Ga_2O_3- coating, the degradation characteristics of which have not been investigated before.

Experimental Methods

Coatings were deposited using RF magnetron sputtering on Ti6Al4V substrate. A ceramic Ga_2O_3 target was used with a PBG target to create a high Ga_2O_3 content blended coating. A 10 mol% Ga_2O_3 containing PBG target was used to coat a low Ga_2O_3 content coating. Both the Ga_2O_3 and the PBG targets were used to create individual coatings.

Coatings' chemical compositions and structure were investigated (EDX, XPS, FTIR, RHEED analysis). Degradation and ion release were characterised in cell culture media, and changes in coating composition after 7 day exposure to cell culture media were determined (EDX and XPS). Cytocompatibility was assessed using MG63 human osteoblast-like cells using the Neutral Red Assay and cell adhesion and proliferation on the coating surfaces assessed using Alamar Blue Assay.

Biofilm formation was measured using *Staphylococcus aureus*, visualised using confocal microscopy and quantified using COMSTAT 2 (μm^3/ μm^2). Zone of inhibition tests against *S. aureus* were also performed using the coating degradation products.

Results and Discussion

Pure Ga_2O_3 was deposited as a mainly amorphous coating (222 nm thick), with evidence of nanocrystallites. Blending Ga_2O_3 with the glass resulted in a 54 mol% Ga_2O_3 coating (355nm thick). The glass target gave a 17 mol% Ga_2O_3 coating, again with nanocrystallites (156 nm thick). XPS analysis confirms that Ga is present as an oxide, not metallic form in all cases. These coatings are the highest Ga_2O_3 content glass coatings manufactured to date.

Rapid Ga^{3+} release from all coatings into DMEM cell culture media during is reported the first 8 hours and peaked at 62.5 ppm, 12.6 ppm and 1.9 ppm for the 100%, 54% and 17% Ga_2O_3 coatings respectively as shown in Fig. 1. These concentrations for the 100% and 54% Ga_2O_3 coatings were cytotoxic, while the zone of inhibition test showed no bactericidal effect. There was no significant change in coating thickness over the 7 day degradation period, and EDX analysis shows presence of Ca and P on degraded surfaces. This is in contrast to degradation in H_2O where full degradation was recorded. However, these results do show the promise of PBG coatings to release Ga^{3+} when the composition of the glass is altered to ensure full degradation.

Human cell growth on the coating surfaces is limited in all cases including the glass control, more significantly so in the 54% and 100% Ga_2O_3- coatings as shown in Fig. 2. There was no difference in biofilm growth across any of the samples. The higher cell growth on the 17 mol% samples compared to the higher Ga_2O_3 content coatings suggests that some Ga^{3+} exposure can be tolerated by the cells.

Conclusion

RF Magnetron sputtering offers the ability to coat high Ga_2O_3 PBG coatings, which release Ga^{3+} into cell culture media. The degradation of PBG structures in cell culture media has not been widely reported and therefore different glass compositions must be investigated to ensure full degradation and Ga^{3+} release. Balancing antibacterial effects and cytotoxicity remains challenging, although Alamar Blue results suggest that cells can recover after initial exposure. Cell response to Ga^{3+} 'ion burst' must be investigated further to determine if a short lived PBG coating releasing Ga^{3+} could prevent initial bacterial attachment without damage to surrounding tissue.

References

1 - Webb, J. S. (2017) *National Biofilms Innovation Centre Overview*, *UKRI*. Available at: https://gtr.ukri.org/projects?ref=BB%2FR012415%2F1 (Accessed: 15 March 2019).

2 I. Strazic Geljic et al., “Gallium enhances reconstructive properties of a calcium phosphate bone biomaterial,” J. Tissue Eng. Regen. Med., 2017.

3 F. Minandri, C. Bonchi, E. Frangipani, F. Imperi, and P. Visca, “Promises and failures of gallium as an antibacterial agent.,” Future Microbiol., vol. 9, pp. 379–97, 2014.

4 B. W. Stuart, C. A. Grant, G. E. Stan, A. C. Popa, J. J. Titman, and D. M. Grant, “Gallium Incorporation Into Phosphate Based Glasses: Bulk and Thin Film Properties,” J. Mech. Behav. Biomed. Mater., vol. 82, no. March, pp. 371–382, 2018.

Acknowledgement

This research was partially supported by Zimmer-Biomet.

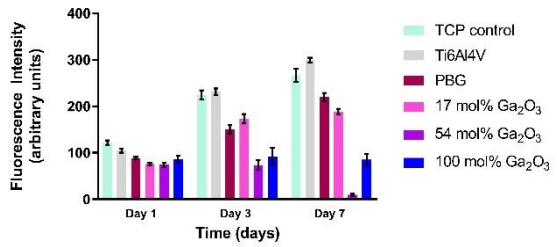

Figure 2 - Alamar Blue Assay showing relative cell metabolic activity on the coating surfaces.
Figure 2 - Alamar Blue Assay showing relative cell metabolic activity on the coating surfaces. There is no significant difference between the Tissue Culture Plastic control and the uncoated Ti6Al4V at any time point but all coatings showed significantly lower metabolic activity than the two controls.

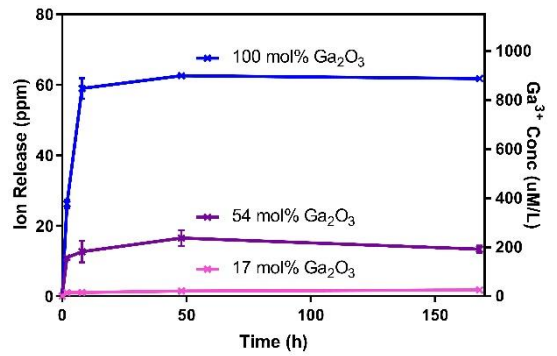

Figure 1 - Ga3+ ion release into DMEM cell culture media over 168 h
Figure 1 - Ga^{3+} ion release into DMEM cell culture media over 168 h, showing that ions are released rapidly into media in the first 8 h but release plateaus shortly after, with little change in ionic concentration between 8 and 168 h.

III-OS11-RF06

Wear Behaviour of Zirconia Containing Dispersion Ceramics Combined with Accelerated Ageing

Thomas Oberbach[1], Mazen Al- Hajjar[2], Laurent Gremmilard[3], Karen Hans[1], Jerome Chevalier[3], Louise Jennings[2]

[1]Mathys Orthopaedie GmbH, Bioceramics, Moersdorf, DE; [2]University of Leeds, Institute of Medical and Biological Engineering, School of Mechanical Engineering, Leeds, GB; [3]University of Lyon, INSA Lyon, CNRS, MATEIS UMR 5510, Villeurbanne Cx, FR

Introduction

Ceramic-on-ceramic bearings in total hip replacement have been used for more than 45 years. The have shown their potential for young and active patients. In this study, a methodology was devised to assess the in vitro wear behaviour of Zirconia Toughened Alumina Ceramics (ZTA) and Alumina Toughened Zirconia Ceramics (ATZ) under adverse edge loading conditions in hip simulator combined with accelerated ageing in an autoclave under hydrothermal conditions.

Experimental Methods

Femoral heads and acetabular liners of hip prostheses were made of two materials: Alumina Toughened Zirconia (ATZ) and Zirconia Toughened Alumina Ceramic (ZTA). Two material combinations were tested in this study: ATZ-on-ATZ and ZTA-on-ZTA.

A total of six bearing couples were studied on the Leeds Mark II Physiological Anatomical hip joint simulator.

The study was run for a total of eight million cycles. The first two million cycles were run using standard gait conditions and the subsequent 6 million cycles were run under edge loading conditions due to dynamic separation between the femoral head and the acetabular cup.

All femoral heads and acetabular cups were hydrothermally aged during the wear study after every million cycles of testing. It lasted 2 hours at 134°C after each million cycles. Hydrothermal ageing was achieved using accelerated ageing protocol in an autoclave (Sanoclav LA-MCS, Wolf, Germany) in water vapour.

The volume monoclinic fraction was determined using XRD and Garvie and Nicholson's equation modified by Toraya.

Scanning Electron Microscopy observations were conducted on pristine, worn and aged surfaces on the heads after various testing times, using a Supra 55 VP microscope (Zeiss, Germany), at low acceleration voltage (1 to 2 kV) so as to avoid coating the observed surfaces.

The wear was measured gravimetrically using a balance (XP205, Mettler-Toledo) at an interval of one million cycles. A coordinate measuring machine (Legex 322, Mitutoyo, Japan) was used to reconstruct the surface of the femoral head and acetabular cup. RedLux software (RedLux, UK) was used to visualise the size, shape and penetration depth of the wear areas.

Results and Discussion

The wear rates of both aged materials, ATZ-on-ATZ and ZTA-on-ZTA, under standard conditions were very low, i.e. <0.01 mm^3/million cycles. There was no measureable change in wear rate due to ageing under standard conditions.

The wear rates increased when edge loading conditions driven by separation was introduced to the gait cycle. The mean wear rate of aged ZTA-on-ZTA after six million cycles of testing under edge loading conditions was 0.19 ± 0.47 mm^3/million cycles. The mean wear rate of aged ATZ-on-ATZ was 0.07 ± 0.05 mm^3/million cycles.

There was no visible damage on the surfaces of the femoral head and acetabular cup after testing under standard conditions. In contrast, under edge loading conditions, a stripe-like wear area was observed on the femoral head with corresponding wear on the rim of the acetabular liner. The penetration depths on the femoral heads and acetabular liners of the ZTA-on-ZTA bearings were higher than that of the ATZ-on-ATZ bearings after 6 million cycles of testing under edge loading conditions.
No significant ageing occurred in the ZTA material. The monoclinic fractions remained very low over both the wear stripe and the unworn surface. Their variations were within the error margin of XRD.
Ageing of ATZ heads was significant. On the wear stripe, each autoclave step increased the monoclinic fraction. However, each one million cycles of wear simulation decreased the monoclinic fraction significantly.
SEM observations of the worn ATZ and ZTA surfaces showed that the first 2 million cycles (without edge loading) did not significantly damage the surfaces. Microstructural damage was first observed after edge loading. In ATZ damage was located in a small wear stripe 15 µm wide. In ZTA, damage was first located in a much more diffuse area around 50 µm wide.
SEM observations further showed that the damage was mainly located in the alumina grains but not in the monoclinic-zirconia grains for ATZ. In both cases ZTA and ATZ, the phase under the highest compressive residual stresses seemed to be the most prone to microstructural damage.

Conclusion

In this study, a method was devised by which the performance of composite ceramic materials was assessed under a combination of edge loading gait conditions and hydrothermal ageing.
The damage of ceramic components increased by the symbiotic effect of ageing, wear and shocks but remained at a very low level for both ceramic materials. It was shown that the performance of ATZ-on-ATZ materials in vitro may be superior to ZTA-on-ZTA materials despite the higher zirconia content in the ATZ materials.
Ceramic composites show an extremely low wear rate, even under worst case conditions, and provides an interesting option to meet the demands of younger more active patients.

III-OS11-RF07

Dual-setting brushite-silica gel cements with high cross-linking density precursors

Ib Holzmeister, Jürgen Groll, Uwe Gbureck

University Hospital of Würzburg, Department for Functional Materials in Medicine and Dentistry and Bavarian Polymer Institute, Würzburg, DE

Introduction

Calcium phosphate cements (CPC) set via a dissolution–precipitation reaction and form an entangled network of crystals providing mechanical strength after setting. A further modification by adding monomers to the aqueous cement phase results in the formation of a second interpenetrating network with a strong impact on cement properties.[1] This was recently shown for cement modification with tetraethyl orthosilicate (TEOS) as precursor.[2] Here, this approach is further explored by using silica precursors with a higher density of alkoxy groups to increase network and cross-linking density in the final gel. Also modified precursors with different hydrophilic functional groups are investigated to influence the interface between silica and cement matrix. The precursors were initially hydrolyzed under acidic conditions and the combined with a brushite forming cement powder. Due to the increase in pH of the sol during cement setting leads to a simultaneous formation of cement matrix and silica hydrogel. [3]

Experimental Methods

Sol precursors were a mixture of TEOS (100 – 60%) and 0 – 40% of silica monomers with 6-12 alkoxide functionalities. Both commercially available 1,8-Bis(triethoxysilyl)octane and self-synthesized modified silica monomers with hydrophilic groups and a higher density of alkoxy groups were used **(Figure 1A).** Silica sols were obtained by adding the sol precursor mixture to water in a ratio of water: “Si-OEt” = 2.25 and 0.1 M HCl solution. Composite cements were produced by mixing the sol with cement raw powder, consisting of β-tricalcium phosphate (β-TCP) and monocalcium phosphate anhydrous (MCPA) in an equimolar ratio and the addition of 1 wt% citric acid. The citric acid is used as retarding agent in order to extend the setting-time of the composites.

Results and Discussion

The results demonstrated an increase of mechanical performance by using different amounts of a silica monomer (1,2-Bis(triethoxysilyl)octane) in addition to TEOS in the composite compared to the pure TEOS reference **(Figure 1B).** A variation of the monomers resulted in a substantial increase in the strength **(Figure 1C)** with an increase from 0.44 ± 0.09 MPa to 8.29 ± 1.01 MPa at low PLR of 1 g/mL. The porosity characteristics of the silica–brushite networks showed a bimodal pore size distribution in the set matrices with nanosized pores originating from the silica matrix and micrometer pores from the cement matrix **(Figure 1D).** The latter is thought to have a strong effect on drug release capability by retarding drug diffusion from the cement matrix.

Conclusion

It could be shown that the use of different silica monomers has a huge influence on the properties of the composites. As shown a increased strength of the composites could be observed depending of the system up to 10 times. Due to the two network in the composites, a bimodal poresize distribution could be observed.

References

[1] T. Christel et al. *Dual setting α-tricalcium phosphate cements,* --Materials in Medicine, 2013, 24(3), pp 573-581.

[2] M. Geffers et al. *Dual-setting brushite–silica gel cements,* Acta Biomaterialia, 2015, Volume 11, pp 467-476.

[3] I. Holzmeister et al. *Artificial inorganic biohybrids: The functional combination of microorganisms and cells with inorganic materials,* Acta Biomaterialia,2018, Volume 74, pp 17-35.

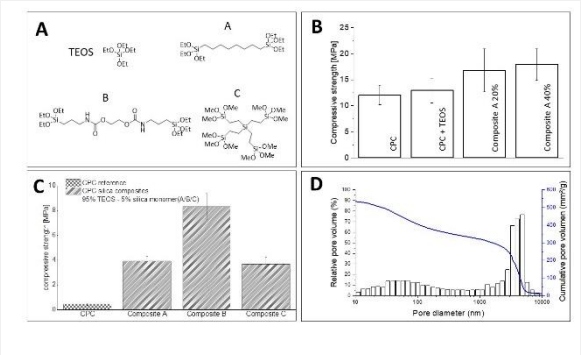

Figure 1
A Molecular structure of TEOS, commercially bought silica monomer(A) and synthesized silica monomers(B/C) **B** Compressive strength of CPC and composite reference CPC+TEOS. Increased compressive strength by adding 20/40% of silica monomer A. (PLR = 2 g/mL) **C** Compressive strength of CPC and composites with 5% different silica monomers (PLR = 1 g/mL) **D** Pore size distribution analyzed by Hg porosimetry in a range of 10-10000 nm of silica gel composite.

III-OS11-RF08

Antibacterial phosphate-based glasses for wound healing applications

Athanasios` Nikolaou[1,2,3], Farzad Foroutan[1], Jorge Gutierrez-Merino[2], Daniela Carta[1]

[1]University of Surrey, Department of Chemistry, Guilford, GB; [2]University of Surrey, School of Biosciences and Medicine, Guilford, GB; [3]Fourth State Medicine Ltd, Haslemere, GB

Introduction

Wound healingis a long, complex process which can lead to inflammation and, if left untreated, life-threatening infections. Wound infections with multi-drug resistant bacteria result in prolonged treatments and increased healthcare costs, so the demand for wound treatment is massive worldwide[1].The number of patients requiring wound care is significantly increasing and it has been estimated that the associated annual cost of wound treatment alone managed by the NHS is around £5B[2]. Therefore, there is an urgent need for new antibacterial wound dressings that both rapidly stimulate healing and prevent infections.

Here we present novel bioresorbable phosphate-based glass nanofibres (PGF) as wound dressings that simultaneously induce new tissue formation, deliver antimicrobial effects without reliance on conventional antibiotics and promote blood coagulation. Being bioresorbable, PGF dissolve in physiological environments and are totally replaced by regenerated tissue[2]. This important advantage avoids frequent dressing removal that can damage newly formed tissue. Moreover, wound-related infections could be prevented by incorporating antimicrobial agents into the dressings that slowly release as the scaffolds degrade in the wound. A totally bioresorbable dressing will avoid systemic administration of antibiotics if used as a controlled local delivery system for antibacterial agents. Nanofibres are advantageous to conventional dressings given the high surface area to volume ratio, open porosity that allows a gaseous exchange, cell migration, and removal of excess exudate, the possibility of mesh production) and surface functionalization[1].

Phosphate-based fibres in the systemP_2O_5-CaO-Na_2O were prepared and doped with the antibacterial ions Cu^{2+} (1, 3, 5 mol%) and Cu^{2+}/ Ag^{+} (5 mol%) which have been found to be particularly effective in promoting wound healing (they stimulate angiogenesis, differentiate mesenchymal stem cells, and proliferate fibroblast human foreskin)[3,4]. Cold plasma will be used to induce/enhance the antibacterial properties of the prepared fibres.

Experimental Methods

PGF were obtained by electrospinning of coacervate precursors. Coacervate precursors were prepared by slow addition of a Ca^{2+} salt to an aqueous sodium polyphosphate solution. Phase separation occurs between a dense coacervate phase, containing the phosphate chains, and the aqueous supernatant.The viscous material obtained by removing the supernatant liquid is easily ejectable and ideal for the production of ES precursors along with the incorporation of antimicrobial ions. The electrospinning was conducted using a stainless steel capillary tube (18 gauge), syringe pump, and high voltage source. Electrospinning was carried out at room temperature and fibres were deposited on an aluminium sheet. Structural characterisation of PGF was performed using X-ray diffraction (XRD) and infra-red spectroscopy (IR); dissolution studies of the PGF in water were performed to obtain information on the release of calcium, sodium, copper, and silver ions after 24, 48, and 72 hours. The doped-PGF were treated with a cold plasma to enhance the antimicrobial effect against bacterial populations. The antimicrobial effect of doped PGF and cold plasma was performed against two bacteria: *Staphylococcus aureus*, and *Escherichia coli* ATCC 25922, bacterial species associated with antibiotic resistance.

Results and Discussion

Copper and copper-silver doped phosphate-based glasses fibres have been successfully prepared, for the first time, using the electrospinning technique. XRD patterns confirm the amorphous nature of all fibres. FTIR results shows the presence of to Q^1 and Q^2 phosphate units. Dissolution studies of the PGF in water shows that the highest release of all ions occurs within the first 24 h. Copper and silver ions are released continuously over the 72 h. Antimicrobial studies show that all Cu^{2+} doped PGF are mainly active against *E. coli* and thattheCu $^{2+}$/ Ag^{+} doped PGFareactive against both *E. coli* and *S. aureus.*

Conclusion

In this study, PBF were successfully synthesised at room temperature for wound healing applications. These fibres are biodegradable and can react and dissolve in the physiological environment and eventually totally replaced by regenerated tissue. Antibacterial study results against *S. aureus* and *E. coli* have shown the great potential application of copper-silver doped glass fibres in wound healing due to its ability to release of Cu^{2+} and Ag^{+} ions continuously with a high bactericidal effect.

References

1) Gizaw et al. *Bioengineering* 5, 9, 2018
2) Carta *et al.J. Mater. Chem*., 15, 2134, 2005
3) Zhao et al., *Biomaterials*, 53, 379, 2015
4) Nadworny *et al.*, *Nanomedicine NMB4*, 3, 241, 2008

Acknowledgement

Authors would like to thank EPSRC (EP/P033636/1) and Royal Society (RSG\R1\180191) for funding. We also thank Dr Mark Whiting and Mr David Jones for assistance with the SEM measurements.

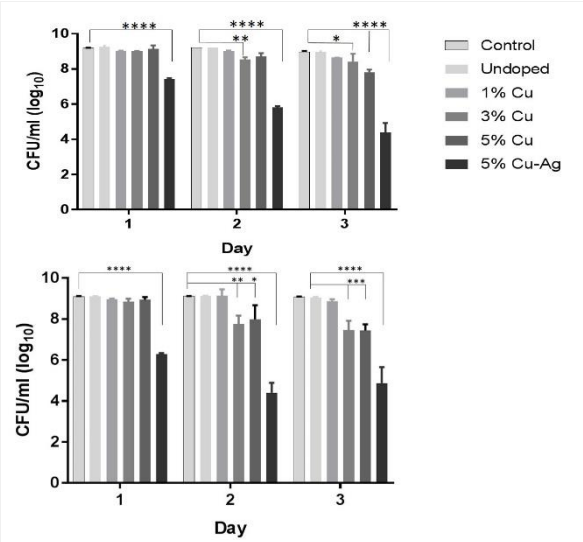

Bacterial viability of S. aureus and E.coli when exposed to PGF

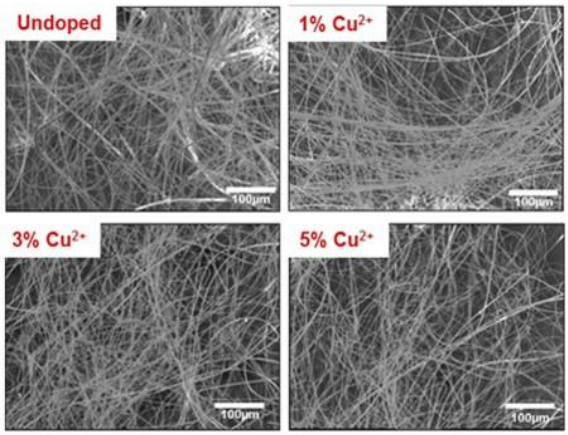

Scanning electron microscopy images of PGF undoped and doped with 1,3,5, mol% of Cu2+

4:45 p.m. – 6:15 p.m.

Hall 5

III-SY5 | DGBM SY: Matrix engineering in skin and bone regeneration

Sandra Franz (Leipzig, DE)
Stefan Rammelt (Dresden, DE)

Treatment of both non-healing cutaneous wounds and critical size bone defects still represents a significant clinical challenge. The use of biomaterials based on artificial extracellular matrix (ECM) components has evolved as a promising approach to create a favourable environment for both skin and bone heling under critical conditions. In a series of in vitro and in vivo experiments, the application of glycosaminoglycans (GAG) as part of the native ECM has been investigated. GAGs such as hyaluronic acid with different degrees of sulfatation were shown to modulate the function of immune and bone forming cells either directly or via alteration of the bioactivity of key cytokines and growth factors controlling the immune response and new bone formation.

III-SY5-KL01

Matrix engineering to enhance bone regeneration

Stefan Rammelt[1,2], Sabine Schulze[1,3], Christin Neuber[4], Jens Pietzsch[4]

[1]University Hospital Carl Gustav Carus, Dresden, University Center of Orthopaedics and Trauma Surgery, Dresden, DE; [2]DFG-Center for Regenerative Therapies Dresden (CRTD), Dresden, DE; [3]University Hospital Carl Gustav Carus, Dresden, Center for Translational Bone, Joint and Soft Tissue Research, Dresden, DE; [4]Helmholtz Centre Dresden-Rossendorf, Institute of Radiopharmaceutical Cancer Research, Department Radiopharmaceutical and Chemical Biology, Dresden, DE

Introduction

The treatment of critical size bone defects still represents a significant clinical problem. The standard treatment for the repair is autologous bone grafting which is of limited availability and associated with donor site morbidity. Therefore, extensive research has focused on the development of biodegradable bone substitute materials. The ideal bone substitute remains yet to be found. One promising approach to improve the osteoconductive and osteoinductive properties of degradable scaffolds is the application of components of the organic extracellular matrix (ECM) that mimic a favourable environment for bone forming cells like osteoblasts and their progenitors [1]. The influence of an artificial ECM on bone healing was investigated in a series of *in vitro* and *in vivo* experiments.

The ECM mediates adhesion, migration, proliferation and differentiation of precursor cells into osteoblasts which in turn contribute to regeneration through synthesis of the organic bone matrix and its mineralization [2]. Glycosaminiglycans (GAG) like chondroitin sulfate (CS) and hyaluronic acid (HA) are ECM components that either directly interact with bone cells or indirectly interact with these cells via cytokines and growth factors. *In vitro* experiments have shown that the degree of sulfatation directly influences the interaction of GAG with cells and humoral bioactive factors and thus influence their bioactivity. For example, highly sulfated glycosaminoglycans facilitated the osteogenic differentiation of mesenchymal stem cells *in vitro* [3].

Experimental Methods

In an *ex vivo* study, the effects of sulfated aECM on bone cells derived from patients with impaired bone metabolism and those who suffered from arthrosis but with otherwise healthy bone were investigated. Osteoblasts were isolated from bone fragments extracted during orthopaedic foot and ankle surgery. Furthermore, blood monocytes were isolated from blood and underwent osteoclastogenesis induced by RANKL. In diabetic patients, administration of sulfated aECM increased the expression of osteoblast-specific genes to a greater extent than in arthrosis patients. In osteoclasts sulfated aECM inhibited both, TRAP activity and calcium phosphate resorption with the greatest effect in diabetes patients. Thus, sulfated aECM increased osteogenic markers with simultaneous inhibition of osteoclast resorption [4].

Artificial ECM-coatings on polymer scaffolds were investigated in a critical size bone defect in the femur of rats. A 5 mm defect was created in the femur of male adult Wistar rats and stabilized with an internal fixator. Embroidered polycaprolactone-co-lactide (PCL) scaffolds were coated with collagen type I (Coll) and ECMs containing Coll and CS or HA of different sulfatation grades. PCL scaffolds served as negative controls, and collagen sponges with bone chips to mimic autologous bone graft served as positive controls. Radiographs and µCT measurements showed nearly no new bone formation after 2 weeks of implantation. New bone volume within the defect after 12 weeks was highest in the group with Coll and highly sulfated HA where it equaled the positive control (Fig. 1). The second highest bone volume was observed in scaffolds with normally sulfated chondroitin sulfate.

Results and Discussion

In a similar study TriLa scaffolds coated with sulfated hyaluronan were investigated in healthy and diabetic rats. Porous, cross-linked lactide-based scaffolds were coated with collagen including native or sulfated hyaluronan (HA/sHA3) and inserted into 3 mm femoral defects of non-diabetic and diabetic ZDF rats. After 12 weeks, scaffolds coated with HA or sHA3 accelerated bone defect regeneration in diabetic, but not in healthy rats as compared to their uncoated controls. At the tissue level, sHA3 promoted bone mineralization and decreased the amount of nonmineralized bone matrix. *In vivo,* sHA3-coated scaffolds from diabetic rats scavenged more sclerostin than the respective controls. *In vitro*, sHA3 induced the expression of BMP-2 and lowered the RANKL/OPG expression ratio, regardless of the glucose concentration in osteoblastic cells. Both sHA3 and high glucose concentrations decreased the differentiation of osteoclastic cells. sHA3 bound sclerostin with high affinity.

In a pilot study, titanium-coated polyetheretherketone (Ti-PEEK) plates were coated with collagen type I and collagen-based artificial ECMs containing CS or HA of different sulfatation grades bridging a critical size femoral defect in rats. At 4 weeks the gap size was significantly reduced around plates coated with ECMs containing coll and highly sulfated HA and normally sulfated CS. Chondral ossification could be confirmed around those coatings.

Conclusion

It can be concluded from these experiments, that sulfated GAGs have positive direct and indirect effects on bone-forming and bone-resorbing cells and therefore are useful in enhancing bone regeneration. Resorbable and non-resorbable scaffolds coated with an artificial ECM consisting of type 1 collagen and highly sulfated HA represent potentially suitable biomaterials to improve bone defect regeneration particularly in diabetic patients with impaired bone healing capacity. The underlying mechanism involves improved osteoblast function and scavenging sclerostin, a potent inhibitor of Wnt signaling and osteoblast function.

References

1. Förster Y et al. (2013) BioNanoMaterials 14: 143-152
2. Schulze S et al. (2018) J Cell Physiol 233:4391–4400
3. Hempel U et *al*. (2014) Biomed Res Int. 2014:938368
4. Schulze S et al. (2018) DGBM Conference Abstract
5. Picke AK. et al. (2016) Biomaterials 96:11.
6. Förster Y et al. (2017) Mater Sci Eng C 71:84-92

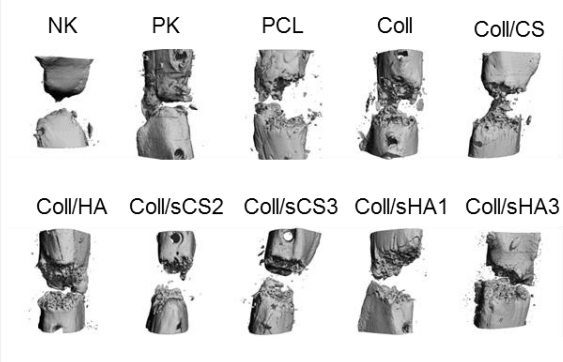

Fig. 1
New bone formation in critical size femoral defects in healthy rats. PCL scaffolds containing an artificial ECM of collagen and highly sulfated hyaluronic acid (Coll/sHA3) performed equal to the positive control (PK) representing the gold standard of autologous bone grafting. Physiologically sulfated chondroitin sulfate (CS) performed better than highly sulfated CS.

III-SY5-KL02

Immunomodulating biomaterials support cutaneous wound healing

Sandra Franz

University Leipzig, Department of Dermatology, Venerology and Allergology, Leipzig, DE

Introduction

The incidence of chronic non-healing cutaneous wounds is constantly rising and significantly contributing to morbidity and mortality worldwide. Non-healing wounds show an arrest of progression of the stages of normal wound repair. Instead, they remain stuck in a chronic inflammatory phase driven by uncontrolled infiltration and activation of immune cells (granulocytes, monocytes and macrophages) leading to excessive tissue breakdown. Resolution of this unrestrained inflammatory loop represents an unmet challenge in the treatment of non-healing wounds. Glycosaminoglycans (GAG) as part of the native extracellular matrix are known to guide function of immune cells either directly or via modulating the bioactivity of factors controlling immune cell activities. Using these principles we develop GAG-based biomaterials with versatile immunomodulatory capacities to support healing of chronic wounds [1]. In this talk I will present two approaches of GAG-based biomaterials to intervene chronic inflammatory processes in non-healing wounds.

Results and Discussion

The first approach is based on capturing inflammatory chemokines which sustain persistent invasion of immune cells. For this we customized modular hydrogels based on star-shaped polyethylene glycol and derivatives of heparin for maximal sequestration of immune cell attracting chemokines from the wound site while sparing wound healing promoting pro-regenerative growth factors [2]. Chemokine sequestration results in a significantly reduced influx of granulocytes and monocytes into the wound and in a diminished expression of inflammatory cytokines and chemokines. The wound environment benefits from the decreased inflammatory signaling and in consequence granulation tissue maturation, vascularization and re-epithelialization are promoted. In an in vivo model of delayed wound healing (db/db mice) the chemokine binding hydrogels outperformed the “standard of care” product Promogran™ with respect to reduction of inflammation, as well as improvement of granulation tissue formation, vascularization and wound closure.

In the second approach we use hyaluronic acid (HA) to particularly modulate the activity of macrophages which have been recognized as key regulator of inflammation during wound healing. Hyaluronic acid is well known for its potent anti-inflammatory effects on macrophages as high molecular weight molecule while its degradation into low molecular weight fragments is discussed to rather promote inflammatory macrophage activities. In this respect the therapeutic success of HA applied in severe inflammatory conditions as they occur in non-healing wounds is limited due to its degradation. We have modified HA chemically and introduced specific sulfation patterns which maintained the anti-inflammatory activity of HA on macrophages even after fragmentation [3,4]. We confirmed the potent immunomodulatory potential of sulfated HA in a mouse model of acute skin inflammation in which treatment with sulfated HA resulted in a significant reduced inflammatory response. Currently, we are testing the capability of sHA-based hydrogels to improve disturbed inflammation in a mouse model of delayed wound healing.

References

[1] Franz S, et al. Immune responses to implants - a review of the implications for the design of immunomodulatory biomaterials. Biomaterials. 2011 Oct;32(28):6692-709
[2] Lohmann N, et al. Glycosaminoglycan-based hydrogels capture inflammatory chemokines and rescue defective wound healing in mice. Sci Transl Med. 2017 Apr 19;9(386)
[3] Jouy F, et al. Sulfated hyaluronan attenuates inflammatory signaling pathways in macrophages involving induction of antioxidants. Proteomics. 2017 May;17(10):e1700082
[4] Franz S, et al. Artificial extracellular matrices composed of collagen I and high-sulfated hyaluronan promote phenotypic and functional modulation of human pro-inflammatory M1 macrophages. Acta Biomater. 2013 Mar;9(3):5621-9.

Acknowledgement
We acknowledge funding through Helmholtz Interdisciplinary Graduate School for Environmental Research (HIGRADE) and the German Research Council (DFG SFB-TR67, projects A2, A4, A7, A10, B3, Z4, and DFG FR2671/4-1)

III-SY5-03

Biocatalytic self-assembly of supramolecular gels is controlled by the choice of the amphiphile regioisomer

Alexandra Brito[1,2], Rui L. Reis[1,2,3], Rein V. Ulijn[4,5,6], Ricardo A. Pires[1,2,3], Iva Pashkuleva[1,2]

[1]University of Minho, I3BS Research Group, Guimarães, PT; [2]University of Minho, ICVS/3Bs - PT Government Associate Laboratory, Braga, PT; [3]University of Minho, The Discoveries Centre for Regenerative and Precision Medicine, Guimarães, PT; [4]City University of New York, Advanced Science Research Center at CUNY, New York, US; [5]City University of New York, Department of Chemistry, Hunter College, New York, US; [6]City University of New York, Ph.D. programs in Biochemistry and Chemistry, New York, US

Introduction

Biocatalytic self-assembly is a powerful tool to generate dynamic nanomaterials under physiological conditions. [1] It merges the efficiency and selectivity of an enzymatic transformation with the sensitivity of the self-assembly process. Herein, we investigated the possibility to tune additionally this process by the choice of self-assembling molecules (amphiphiles) that have the enzyme-sensitive unit at different positions. Carbohydrates code different bioactivities and provide a rich library of water soluble, chiral building blocks. [2] We used different regioisomers of carbohydrate amphiphiles and access the enzyme action on these and its effect on the formed supramolecular structures.

Experimental Methods

The regioisomers 1 and 6 phosphate (1P/6P) of N-fluorenylmethoxycarbonyl-glucosamine were synthetized by one-step reaction previously described. [2] The enzyme alkaline phosphatase was added to the synthetized amphiphiles at different ratios. The kinetic of the dephosphorylation was evaluated by high performance liquid chromatography (HPLC) and the formation of supramolecular structures was accessed by circular dichroism (CD), atomic force microscopy (AFM), and scanning electron microscopy (SEM).

Results and Discussion

The HPLC data showed a faster conversion rate for the 1P amphiphile as compared to the 6P regioisomer, indicating a different acessitbility of the enzyme to the substrate. Upon dephosphorylation the amphiphiles assembled into nanofibers that further form gel. CD spectra of 1P and 6P solutions and the formed gels were recorded and showed no signal for the phosphorylated compounds in solution and well pronounced signals at 270 nm and 304 nm upon sol-gel transition associated with stacking via Fmoc moeties. Microscopy observation revealed that both isomers formed uniform left-handed twisted nanofibers, with a helical pitch of 125±15 nm, width 60 nm when the precursor was 1P and a pitch of 140±20 nm, width 35 nm when 6P was used instead. The rheological measurement for the obtained gels showed that the assemblies generated by the dephosphorylation of the 6P amphiphile form stronger and more stable gels as compared with the 1P analogue. Furthermore, the influence of the enzyme concentration on the gels' properties was studied and highest storage modulus was observed for the highest studied enzyme concentration. Microscopy analyses showed homogeneous networks of entagled fibers whose density depends on the concentration of the initial precursor and the enzyme.

Conclusion

We demonstrate that by selecting the regioisomer and enzyme concentration we can tune the properties of the generated gels. These results together with the physiological conditions at which the assembly is performed open new possibilities for development of stimuli-responsive, biotunable hydrogels.

References

[1] Whitesides et al. PNAS 2002, 99, 4769.
[2] Birchal et al. Chem. Sci. 2011, 2, 1349.

Acknowledgement

European Union H2020 programme, H2020-WIDESPREAD-2014-2-668983-FORECAST, H2020-WIDESPREAD-2016-2017-739572-THE DISCOVERIES CTR, Portuguese Foundation for Science and Technology (IF00032/2013 of IP, PD/BD/113794/2015 of AB and CANCER_CAGE PTDC/NAN-MAT/28468/2017), and Fundação Luso-Americana para o Desenvolvimento.

III-SY5-04

Hyaluronan/Collagen Based Hydrogels as Release System for Sulfated Hyaluronan and Proteins

Norbert Halfter[1], Sandra Rother[1], Linda Köhler[1], Albrecht Berg[2], Stephanie Möller[2], Matthias Schnabelrauch[2], Joanna Blaszkiewicz[3], Jörg Rademann[3], Vera Hintze[1]

[1]TU Dresden, Max Bergmann Center of Biomaterials, Dresden, DE; [2]INNOVENT e.V., Biomaterials Department, Jena, DE; [3]Freie Universität Berlin, Institut of Pharmacy & Institute of Chemistry and Biochemistry, Berlin, DE

Introduction

Collagen type I (coll) and glycosaminoglycans (GAGs) are major components of the skin extracellular matrix and are known to influence cellular behavior [1]. For this reason, functional biomaterials made of these components are promising for tissue regeneration. Recent work with hyaluronan (HA)/coll-based hydrogels revealed a defined interaction with heparin-binding epithelial growth factor-like growth factor leading to an improved skin wound closure [2]. On the one hand, protein binding and release from hydrogels can be tuned by sulfated GAG (sGAG) derivatives [3]. On the other hand, GAGs released from biomaterials are expected to reduce pathological conditions like fibrosis, e.g. by blocking TGF-β1-mediated signaling [4]. In this study, we examined the composition and stability of HA/coll-based hydrogels made of methacrylated HA (HA-MAC) containing methacrylated (sGAG-MAC) and acrylated (sGAG-AC) polymeric sGAGs. In addition, binding and release of the model protein lysozyme was investigated. Further, we evaluated the spreading and growth of human dermal fibroblasts within these gels of different HA content to optimize the HA concentration and the resulting physical properties for cellular growth.

Experimental Methods

HA-MAC/coll-based hydrogels were fabricated by photo-crosslinking according to [2]. Afterwards, gels were freeze-dried. The mechanical and swelling properties of the gels were determined as well as the surface morphology via scanning microscopy. Furthermore, Toluidine Blue and Sirius Red staining of the gels was used to visualize the sGAGs and coll distribution. To quantify GAG/sGAG and coll release after incubation in phosphate-buffered saline, hexosamine, DMMB and Lowry assay were employed. The release of fluorescence-labeled lysozyme was measured by fluorescence spectroscopy. Fibroblast growth was analyzed by immune-fluorescence microscopy and by measuring the DNA content.

Results and Discussion

The hydrogel composition influenced the water content, the swelling ratio and the loss of volume. Stability studies indicated a slower release of HA-MAC than of sGAGs. The Young's modulus of different hydrogel compositions with similar GAG concentrations was comparable. Binding and release of lysozyme was depending on GAG sulfation. Fibroblast spreading and growth was slightly influenced by the examined HA concentrations. These findings suggest that HA-MAC-based hydrogels containing either sGAG-MAC or sGAG-AC can be engineered as effective wound dressings with adjustable sHA release and growth factor interaction profiles that might translate into an improved healing response of injured skin.

Conclusion

Using acrylated and methacrylated GAGs to adjust the release behavior of sGAGs and proteins from HA/coll based hydrogels will enable tuning for different wound environments to use such hydrogels as wound dressings in the future.

References

[1] Scharnweber D et al. Journal of Material Science: Materials in Medicine (2015), 26 (9), 232

[2] Thönes S et al. Acta Biomaterialia (2019), *86*, 135–147

[3] Rother S et al. Macromolecular Bioscience, (2017), *17* (11), 1-13

[4] van der Smissen A et al. Acta Biomaterialia (2013), *9* (8), 7775-7786

Acknowledgement

Financial support by the Deutsche Forschungsgesellschaft (SFB TRR67, A3, A8 and Z3)

4:45 p.m. – 6:15 p.m.

Conference room 4+5

III-OS12 | Cancer models

III-OS12-01

Tumor engineered model for peritoneal metastasis with controllable stiffness

Elly De Vlieghere[1,2], Wim Ceelen[3,2], Bruno De Geest[4], Heidi Declercq[5], Sandra Van Vlierberghe[6], Olivier De Wever[1,2]

[1]Ghent University, Laboratory of Experimental Cancer Research, Ghent, BE; [2]Ghent University, Cancer Research Institute Ghent (CRIG), Ghent, BE; [3]Ghent University, Laboratory of Experimental Surgery, Ghent, BE; [4]Ghent University, Laboratory of Pharmaceutical Technology, Ghent, BE; [5]Ghent University, Tissue engineering and biomaterials, Ghent, BE; [6]Ghent University, Polymer Chemistry and Biomaterials Group, Centre of Macromolecular Chemistry, Ghent, BE

Introduction

The tumor environment is recognized as an imported factor in therapy outcome. However, current models focus on the cancer cells, while incorporating the stroma creates models with a higher clinical relevance. We have “tumor engineered” an *in vivo* model for peritoneal metastasis from ovarian cancer, a disease with a high mortality rate, that recapitulates the heterogeneity of a patient tumor at the microscopic level [1]. As carrier structure, we previously used a porous polylactic acid (PLA) scaffold. Unfortunately, tumor stiffness, an important parameter causing therapy failure, is neglected in this model. The stiffness in the model is determined by the PLA scaffold and not by tumor characteristics. By introducing a new polymer (AUP) [2] with tunable chemical structure, we can control the stiffness of the scaffold by altering the length of the PEG backbone (fig 1 A-C).

Experimental Methods

Scaffolds are produced by fused deposition modeling with the Ultimaker (PLA) or through theBioplotter (AUP) to have similar dimensions in swollen state as a peritoneal metastasis nodule. The scaffolds are cylinder-shaped with 5mm diameter, 4mm height, 500µm pore size and 300µm strut diameter. Plasma treatment improves interaction with GelMA coating and enables cell interaction [1]. Scaffolds are seeded with a mixture of cancer cells (SK-OV-3 Luc GFP), cancer associated fibroblasts (CAFs) (1 to 4 ratio) and type I collagen gel (1mg/ml) through vacuum pressure. *In vitro* cultures were monitored by phase-contrast microscopy and IncuCyte Zoom® (real-time imaging). After 15 days of *in vitro* culture, the scaffolds were implanted in the peritoneal cavity by suturing to the inner peritoneal wall of nude mice and followed-up by bioluminescence imaging (BLI). After 5 weeks, the mice are sacrificed and scaffolds are analyzed by hematoxylin & eosin staining (H&E).

Results and Discussion

***In vitro* culture**

Co-seeding of cancer-associated fibroblasts (CAF) and cancer cells initiates spheroid formation and self-organization. The speed of this process is influenced by the stiffness of the scaffolds. Spheroid formation occurs within 48h when cells are seeded in an AUP scaffold compared to 3 weeks in a PLA scaffold (fig 1D). The AUP 4k (PEG 4000 Da backbone) is approximately a 100-fold softer and closer to the physiological environment **o**f cells. Real-time imaging is used to visualize the motility of the cancer cells in the AUP scaffolds. The cells stretch-out and orientate along the collagen fibers created by the CAFs (12h). Consequentially, they move along these fibers and organize themselves into spheroids (24h) (fig 1E).

***In vivo* implantation**

After 3 weeks of implantation, BLI signal increases and the cancer cells start to proliferate inside the scaffolds (fig 2A). Histological evaluation of the scaffolds 5-weeks post-implantation reveals that the scaffolds are evolved to viable tissue. Host cells infiltrate the scaffolds (adipose tissue), newly formed blood vessels supply the seeded cancer cells and CAFs (fig 2B).

Conclusion

Implementing a tissue relevant stiffness facilitates *in vitro* self-organization. After *in vivo* implantation, host cells are attracted to infiltrate the scaffold. This results in a vascularized heterogenic tumor with spatial and quantitative aspects as similarly observed in patient-derived peritoneal metastases. These results reveal that the AUP scaffolds are biocompatible and support *in vivo* cell viability. Furthermore, these engineered scaffold recapitulate a human ovarian peritoneal metastases at the microscopic and biophysical level.

References

[1] E. De Jaeghere, E. De Vlieghere, J. Van Hoorick, S. Van Vlierberghe, G. Wagemans, L. Pieters, et al., Heterocellular 3D scaffolds as biomimetic to recapitulate the tumor microenvironment of peritoneal metastases in vitro and in vivo, Biomaterials. 158 (2018) 95–105. doi:10.1016/j.biomaterials.2017.12.017.

[2] A. Houben, P. Roose, H. Van den Bergen, H. Declercq, J. Van Hoorick, P. Gruber, et al., Flexible Oligomer Spacers as the Key to Solid-State Photopolymerization of Hydrogel Precursors, Mater. TODAY Chem. 4 (2017) 84–89. doi:10.1016/j.mtchem.2017.01.005.

Acknowledgement

Elly De Vlieghere is supported by FWO as a post-doc fellow (12Y8119N)

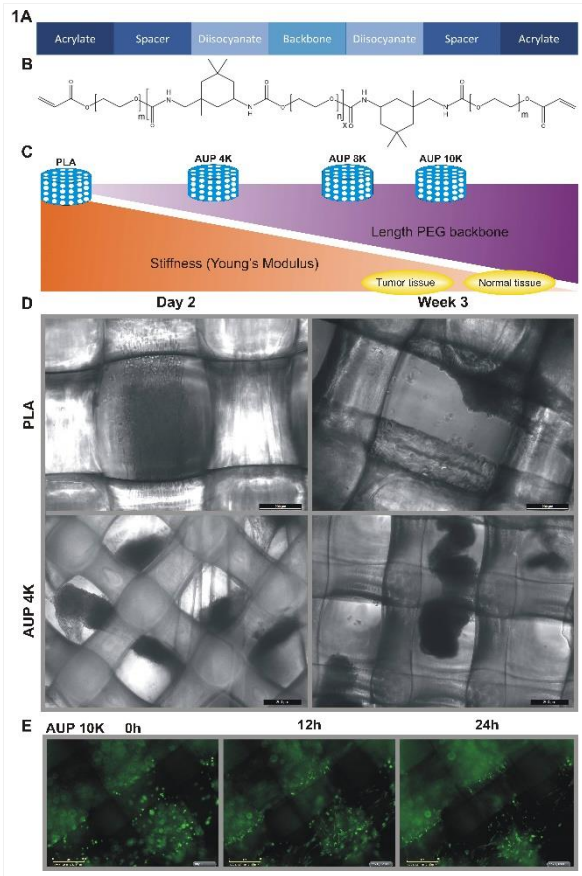

AUP scaffolds with controlled stiffness and in vitro spheroid formation
Schematic (A) and chemical (B) structure of the AUP polymers. C) The length of the PEG backbone influences the stiffness of the AUP scaffolds. The longer the PEG chain the softer and more physiologically relevant the scaffolds become. D) Phase-contrast images of PLA and AUP scaffolds 48h and 3 weeks post-seeding. E) Real-time fluorescent images of green cancer cells in an AUP scaffold (IncuCyte Zoom®)

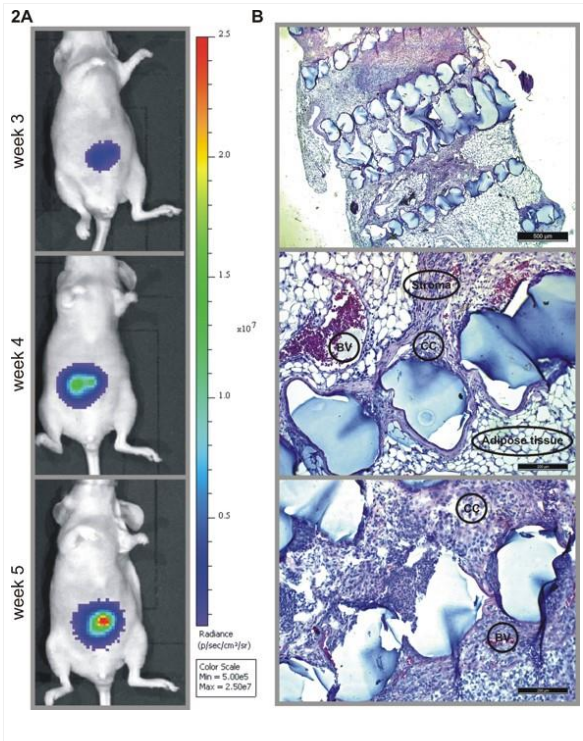

Fig 2: In vivo implantation
A) BLI of a mouse 3 to 5 weeks post-implantation (AUP scaffold), indicating cancer cell viability. B) H&E of AUP scaffold 5 weeks post-implantation. Circles indicate different cell types: cancer cells (CC), stroma with CAFs, blood vessels (BV), adipose tissue.

III-OS12-02

Activation of Breast Cancer Cell Invasion by the Biophysical Network Characteristic of 3D Fibrillar Collagen Networks

Jiranuwat Sapudom, Liv Kalbitzer, Steve Martin, **Tilo Pompe**

Leipzig University, Institute of Biochemistry, Leipzig, DE

Introduction

The mechanical characteristics of the extracellular environment is known to regulate cancer cell behavior *in vivo*and *in vitro*. However, many open questions remain on the mechanisms, how extracellular matrix (ECM) viscoelasticity influences cancer cell behavior in terms of proliferation, migration, gene regulation and phenotypical transition. In particular, during cancer progression activation of highly invasive phenotypes strongly contribute to spreading and metastasis of secondary tumors within the body. By matrix engineering approaches we are able to tightly tune the topologic and elastic characteristics of 3D fibrillar collagen I (Coll I) networks.[1,2,3,4] In this new study we report an activation of breast cancer cell invasion in fibrillar 3D Coll I networks by distinctively different biophysical characteristics in terms of elastic bending and stretching modes of semiflexible networks, a topic overlooked in cellular and ECM biomechanics up to now.

Experimental Methods

Fibrillar 3D networks were reconstituted using Coll I at concentrations of 1 to 3 mg/ml using phosphate buffer at pH 7.5 with and without NaCl to independently adjust pore size and fibril diameter.[1,3,4] Microstructural properties (e.g. pore size and fibril diameter), elastic modulus as well as dynamic fibrillar fluctuations of the networks were analyzed using confocal microscopy, topological image analysis tools and colloidal force spectroscopy. Breast cancer cell behavior was studied using 'invasive' and 'non-invasive' cell lines (MDA-MB-231 and MCF-7, respectively) over 5 days in terms of cell invasion, matrix metalloproteinase (MMP) expression and activity as well as cell proliferation.

Results and Discussion

We could show that our matrix engineering approach allows to construct 3D Coll I networks with fundamentally different biophysical network characteristics. Mean pore size and fibril diameter were engineered in overlapping and comparable mean pore size and elastic bulk modulus. However, for such networks the elastic network bending characteristics could be shown to be either in a 'bending-dominated' regime or to exhibit a considerable 'stretching' contribution. The latter was proofed by fluctuation analysis of fibrils inside the networks, pointing towards the entropic origin of the stretching-dominated elastic contribution in semiflexible fibrillar networks.

In concert with the distinct change of the biophysical elastic network characteristic, we found a strong and distinct activation of cancer cell invasion of the usually 'non-invasive' MCF-7 breast cancer cell line in the 'stretching-dominated' networks. This was accompanied by a strong increase in activity of soluble MMP, known to be important in cancer cell migration and invasion. In contrast, at comparable network elasticity or pore size of 'bending-dominated' 3D Coll I networks no regulation and activation of MCF-7 cell invasion and MMP expression were found.

In accordance to several other reports in literature on 'bending-dominated' fibrillar 3D Coll I networks, usually thought to be the standard elastic mode of Coll I networks, invasion of MDA-MB-231 cells as well as their MT-MMP expression were increased with an increased network stiffness for 'bending-dominated' networks. However, changing the

biophysical elasticity mode to 'stretching-dominated' networks led to downregulation of cell invasiveness and MMP expression for this 'invasive' breast cancer cell line.

Conclusion

We found a significant difference in breast cancer cell behavior under the control of distinct elastic modes of fibrillar 3D Coll I networks. The results emphasize that a currently overlooked switch of elastic modes of fibrillar ECM microenvironments may dominantly regulate cancer cell behavior, even activating the invasion of so-called 'non-invasive' breast cancer cells. As both biophysical states of semiflexible fibrillar 3D networks occur*in vivo*at physiological and pathological situations, we suggest an important role of the physical characteristics of fibrils in 3D networks for the control of tumor progression and advocate our 3D Coll I networks as highly relevant 3D *in vitro*models to study cancer cell behavior.

References

1. Sapudom J ,et al. *Biomaterials* 52:367-75 (2015).
2. Sapudom J, et al. *Adv Healthc Mater* 5:1861-7 (2016).
3. Kalbitzer L, Pompe T. *Acta Biomater* 67:206-14 (2018).
4. Sapudom J, et al. *Biomaterials* 193:47-57 (2019).

Acknowledgement

The authors acknowledge the support of grants from EFRE and Free State of Saxony (SAB: 100144684) and Deutsche Forschungsgemeinschaft (INST 268/293-1 FUGG).

III-OS12-03

Soft matrix composites as three-dimensional models mimicking Glioblastoma *in vitro*

Annalena Wieland[1], Pamela L. Strissel[1], Ezgi Bakirci[2], Paul D. Dalton[2], Andreas Feigenspan[3], Carmen Villmann[4], Reiner Strick[1]

[1]University Hospital Erlangen, Department of OB/GYN, Laboratory for Molecular Medicine, Erlangen, DE; [2]University Hospital Würzburg, Department of Functional Materials in Medicine and Dentistry, Würzburg, DE; [3]Friedrich-Alexander University, Department of Biology, Erlangen, DE; [4]University Hospital Würzburg, Institute of Clinical Neurobiology, Würzburg, DE

Introduction

Glioblastoma multiforme (GBM) tumors arise from glial cells in the central nervous system and represent the most common and aggressive human brain tumors. Malignant progression results in extensive invasion throughout the brain. GBM tumors show an impassive response to current therapeutic approaches predicting a poor survival rate for patients [1,2].

Therefore, it is crucial to better understand tumor behavior in the microenvironment to improve therapeutic strategies. *In vitro* systems have become an indispensable tool for clinical research and have recently advanced from conventional 2D monolayer cell cultures. Importantly, cells grow within a complex 3-dimensional (3D) environmentand and are associated with an extracellular matrix (ECM), which cannot be mimicked by 2D monolayer cultures [3]. The ECM, (e.g. collagen, laminin (LAM), hyaluronic acid, fibronectin (FN)) is a pivotal component of the tumor microenvironment and is tumor specific in composition and stiffness. Tumor ECM dictates growth, migration, invasion and maintenance of cell differentiation. Hence, further development of new 3D tissue culture models is needed towards understanding complex tumor behavior.

Within the human body, neural tissue is one of the most difficult to mimic *in vitro*, as neuronal cells grow in a soft microenvironment. Therefore, it is a challenge to establish a 3D model possessing the mechanical as well as the biological properties of the brain. Available hydrogels are often instable and require improvement to attain a 3D brain tumor model [4].

Experimental Methods

Fiber-reinforced soft hydrogel matrices consisting of polycaprolactone (PCL) fibers were 3D printed using melt electrowriting (MEW) in order to achieve a substitute ECM with a stiffness and elasticity comparable to human neural tissue. These 3D microfiber-matrix composites synergistically increase the mechanical properties when compared to the individual scaffold or matrix [5]. Additionally, scaffolds were functionalized with FN or LAM to improve cell adherence. GBM cells were grown in these soft MEW fiber-matrix composites and visualized by Immunocytochemistry using antibodies against MAP2 and Actin. RNA was isolated at different time points to test for scaffold-dependent changes of gene expression using quantitative real-time polymerase chain reaction (qRT-PCR) for the differentiation genes (MAP2, Nestin), tumor markers (Ki67, SNAI1) and ECM-receptors and proteins (ITGA5, ITGB1, CD44, RHAMM, RPSA, FN1).

Results and Discussion

Here, we present that MEW fiber-reinforced hydrogels provide a promising microenvironment for a 3D tumor model. Our data show that MEW scaffolds provide a physical support for adhesion and proliferation and facilitate *in vivo* like

tumor cell networks. We show that scaffold induced changes in the ECM drive mechanical properties, which promote initial tumor cell growth at Day 1 and 3 by increasing the expression of Ki67 and ECM-receptors (ITGA5, ITGB1, CD44, RHAMM), which could be further enhanced with scaffold functionalization.

Conclusion

We developed an *in vitro* 3D model based on MEW fiber-reinforced matrices, which helps to define the tumor microenvironment of GBM *in vitro*. Incorporation of MEW fiber scaffolds within a matrix makes it possible to culture GBM cells in a soft, *in vivo* like environment. Therefore, this model will help to further study the biology of primary and metastatic brain cancers.

References

1. Urbańska, K., Sokołowska, J., Szmidt, M. & Sysa, P. Glioblastoma multiforme – an overview. *Contemp Oncol (Pozn)* **18,** 307–312 (2014).
2. Alifieris, C. & Trafalis, D. T. Glioblastoma multiforme: Pathogenesis and treatment. *Pharmacol Ther* **152,** 63–82 (2015).
3. Duval, K. *et al.*Modeling Physiological Events in 2D vs. 3D Cell Culture. *Annu Rev Physiol* **32,** 266–277 (2017).
4. Seliktar, D. Designing Cell-Compatible Hydrogels for Biomedical Applications. *Science* **336,**1124–1128 (2012).
5. Visser, J. *et al.*Reinforcement of hydrogels using three-dimensionally printed microfibres. *Nat Commun* **6,**6933 (2015).

Acknowledgement

This work was supported by the Deutsche Forschungsgemeinschaft (DFG, German Research Foundation): Project number 326998133, TRR 225 (sub-project B01).

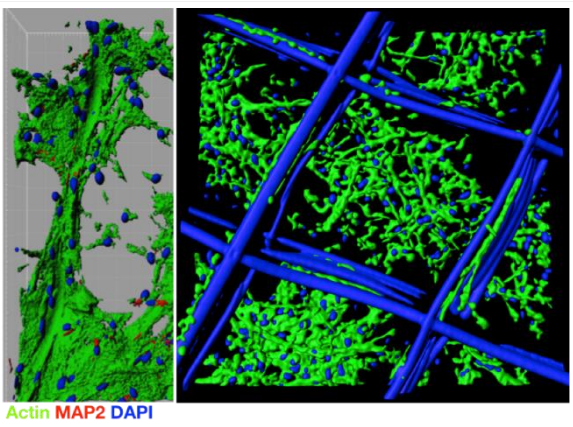

3D model mimicking Glioblastoma in vitro
3D reconstruction of confocal images. Cells were stained with Actin, Map2 and DAPI

III-OS12-05

Use of Polymeric Doxorubicin Nanoparticles in Metastatic Oral Cancer

Sabrina Marcazzan[1,2], Elena M. Varoni[1], Guodong Zhang[2], Ali Dadbin[2], Elvin Blanco[2], Giovanni Lodi[1], Haifa Shen[2], Mauro Ferrari[2]

[1]Università Degli Studi di Milano, Department of Biomedical, Surgical and Dental Sciences, Milan, IT; [2]Houston Methodist Research Institute, Department of Nanomedicine, Houston, US

Introduction

Oral Squamous Cell Carcinoma (OSCC) represents 3-4% of all human cancers with a 5-year survival rate of 63%, which further decreases in the presence of distant metastases (DMs). In advanced stages, the combination of surgery, radiotherapy, and chemotherapy presents significant toxicity and does not reduce the incidence of DMs. Recently, an injectable nanoparticle generator (iNPG) loaded with polymeric doxorubicin (pDox) developed at the Department of Nanomedicine, Houston Methodist Research Institute reported higher in vivo anti-metastatic efficacy and less toxicity than free doxorubicin. The purpose of the present study was to evaluate *in vitro* the effects of pDox nanoparticles (NPs) in two metastatic oral cancer cell lines.

Experimental Methods

HSC-3 (JCRB0623) and HSC-3 M1 cell lines were cultured in DMEM plus 10% FBS and 1% penicillin-streptomycin. The novel HSC-3 M1 cell line derived from GFP/luciferase-transfected HSC-3-lung metastases reproduced *in vivo*. After the isolation, GFP+ tumor cells were selected by FACS and then named HSC-3 M1 cells. pDox was synthesized as follows: hydrazide groups were conjugated to glutamic acid side chains of poly(L-glutamic acid) by means of an acid anhydride reaction, which occurred initially for 30 minutes at 4°C. Then the solution was placed at 25°C for 2 h. The polymer was synthesized dissolving 100 mg poly(L-glutamic acid hydrazide)-co-poly(L-glutamic acid) in 200 ml anhydrous methanol with the addition of 100 µl trifluoro-acetic acid. After that, doxorubicin hydrochloride was added and the final product was allowed to stir at 25°C for 2 days under Argon gas. pDox was then concentrated, dialyzed in methanol and purified by using Sephadex-LH20 (Amersham Pharmacia Biotech Co). pDox NPs were obtained by suspending pDox in DMF (10 mg/ml). pDox DMF solution was then resuspended in PBS and the size of the NPs was assessed in PBS using ZetasizerNano-ZS (Malvern Instruments).

The cytotoxicity of pDox NPs on oral cancer cells was measured as follows: HSC-3 and HSC-3 M1 were plated in a 96-well plate (3.5-4 $x10^3$ cells/well) and treated for different time points with different concentrations of free doxorubicin and equimolar amounts of pDox. After the treatment, cell viability was assessed by MTS assay. Cellular uptake of pDox NPs was then assessed by confocal microscopy in comparison to free doxorubicin: HSC-3 and HSC-3 M1 cells were seeded on 4-well chamber slides ($2x10^4$ cells per chamber) and treated with 5 µM of free doxorubicin or pDox at different time points. After the treatment, cells were fixed and stained with Alexa Fluor 488 phalloidin and DAPI. Z-stack confocal microscopy images (Olympus FluoViewTM FV1000) were then acquired and processed using ImageJ. In both treatment groups, doxorubicin was detected using the PI channel. Statistical analysis was performed using one-way ANOVA.

Results and Discussion

The average size of pDox NPs was 114.00 ± 7.32 nm. pDox NPs were significantly less cytotoxic than free doxorubicin at both time points in both cell lines (Fig. 1). More in detail, high concentrations of pDox NPs (0.5 and 1 µM) significantly decreased cell viability in HSC-3 cells after 72 and 96 h of treatment. In contrast, 0.5 and 1 µM of pDox NPs exerted a significant cytotoxic effect in HSC-3 M1 cells only after 96 h of treatment (Fig. 1). Cellular uptake

of pDox NPs visualized by confocal microscopy was delayed compared to free doxorubicin in both cell lines. Co-localization of Dox/DAPI occurred after 6 and 24 h of treatment in HSC-3 and HSC-3 M1 cells respectively (Fig. 2).

Conclusion

In conclusion, pDox NPs were able to effectively kill both cell lines as doxorubicin without any significant difference between HSC-3 M1 and the parental HSC-3 cell line. In addition, considering the direct targeting of pDox NPs against cancer cells, this delivery system would be promising to obtain less adverse effects than free doxorubicin, to be further ascertained *in vivo.*

References

1. Xu R, Zhang G, Mai J, Deng X, Segura-Ibarra V, Wu S et al. An injectable nanoparticle generator enhances delivery of cancer therapeutics. Nat Biotechnol 2016;34:414-8.
2. Furness S, Glenny A-M, Worthington H V, Pavitt S, Oliver R, Clarkson JE et al. Interventions for the treatment of oral cavity and oropharyngeal cancer: chemotherapy. In: Furness S, editor. Cochrane Database Syst. Rev., Chichester, UK: John Wiley & Sons, Ltd; 2011, p. CD006386.
3. Iafisco M, Delgado-Lopez JM, Varoni EM, Tampieri A, Rimondini L, Gomez-Morales J et al. Cell surface receptor targeted biomimetic apatite nanocrystals for cancer. Small 2013;9:3834-44.
4. Shi M, Ho K, Keating A and Shoichet M. Doxorubicin-Conjugated Immuno-Nanoparticles for Intracellular Anticancer Drug Delivery. Advanced Functional Materials 2009;19:1689-1696.
5. Marcazzan S, Varoni EM, Blanco E, Lodi G, Ferrari M. Nanomedicine, an emerging therapeutic strategy for oral cancer therapy. Oral Oncol. 2018;76:1-7.
6. Endo K, Ueno T, Kondo S, Wakisaka N, Murono S, Ito M et al. Tumor-targeted chemotherapy with the nanopolymer-based drug NC-6004 for oral squamous cell carcinoma. Cancer Sci 2013;104:369-74.

Acknowledgement

MF gratefully acknowledges support from his Ernest Cockrell Jr. Presidential Distinguished Chair at Houston Methodist Research Institute. MF serves on the Board of Directors of Arrowhead Pharmaceuticals. Work by SM was partially supported by the Università degli Studi di Milano.

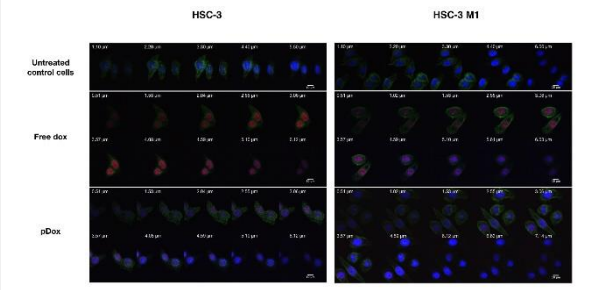

Fig. 2. pDox NPs presented a delayed entry into the cells compared to free doxorubicin. Z-stack confocal images after 6 h of treatment with free doxorubicin and pDox NPs. Green and blue fluorescence represent the cytoskeleton and the nucleus respectively. Propidium iodide channel (red fluorescence) was used to detect doxorubicin in both treatment groups. The pink/purple fluorescence indicates doxorubicin localized within the nucleus. Scale bar represents 10 µm.

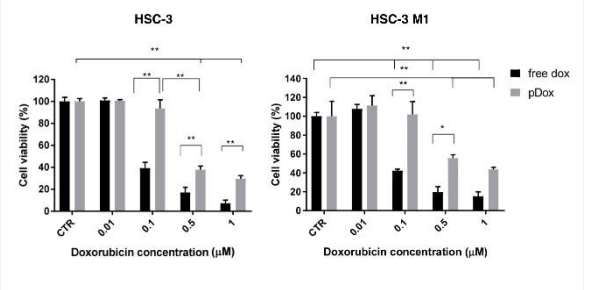

Fig. 1. pDox NPs were significantly less cytotoxic than free doxorubicin. Cytotoxicity assay results for HSC-3 and HSC-3 M1 cells after 96 h of treatment with different concentrations of pDox NPs and free doxorubicin. Data are expressed as mean ± SEM. $^{*}P \leq 0.05$ and $^{**}P \leq 0.01$ by one-way ANOVA statistical analysis and *post hoc* Tukey test.

III-OS12-06

Characterisation of oxidized alginate-gelatin hydrogels for breast tumour *in vitro* models

Chen Zhao[1], Lekha Shah[1], Enrique Lallana[2], Ayse Latif[1], Kaye Williams[1], Annalisa Tirella[1,2], Ponpawee Pingrajai[1]

[1]University of Manchester, Medicine and Health, Manchester Academic Health Science Centre, Division of Pharmacy and Optometry, Manchester, GB; [2]University of Manchester, North West Centre for Advanced Drug Delivery (NoWCADD), Manchester, GB

Introduction

Tumour development is a complex process that depends on many variables; cellular interactions with the microenvironment and consequent re-modelling is believed to play a critical role. The principal variables of the tumour microenvironment (TME) are identified as tissue stiffness, oxygen homeostasis and interstitial fluid flow. Engineered *in vitro* models are emerging as alternative models to standard cell culture methods. Advantages of these are the possibility to integrate all principal variables of the TME trying to easy the study of tumour progression. An ideal biomaterial for tissue engineering (TE) should be adhesive, degradable and match the mechanical properties of the tissue of interest. Alginate is a biocompatible polysaccharide widely used for biomedical applications. However, alginate on its own presents some limitations when used for TE applications due to the absence of adhesion moieties and lack of degradability. Partially oxidized alginate (OA) hydrogels can address these limitations with successful use in tissue regeneration. In this study we report on a library of hydrogels combining OA and gelatin to mimic the properties of breast tissue during tumour development. These hydrogels have tunable properties (e.g. stiffness, adhesion ligand density) and are promising to study for cell-material interaction and assess markers variations during tumour progression.

Experimental Methods

Alginate was oxidized with $NaIO_4$ (aq.) under standard reaction conditions to target oxidation degrees (OD) of 35% and 50%. OA was purified by dialysis against water and then freeze-dryed. The OD was determined indirectly by quantifying unreacted NaIO4 (triiodide-starch method). Aldehyde groups were measured by hydroxylamine assay; whereas amino groups were determined by ninhydrin assay. Hydrogels were formed mixing gelatin with OA in buffered saline solution (37°C; sterile); then swelling and stiffness were characterized. MDA-MB-231 breast cancer cells were cultured on selected hydrogels up to 7 days (25,000 cells/cm^2). Change in proliferation was assessed by trypan blue assay; cell morphology was observed with image analysis (ImageJ); cell viability (Live/Dead) was observed with fluorescent microscope acquisition and whereas CD44/CD24 marker expression were assessed by flow cytometry.

Results and Discussion

Hydroxylamine assay showed that 2% wt. solutions of OA 35%OD and OA 50%OD contained sufficient aldehyde groups (> 90 mM) to cross-link with primary amines (gelatin). The stiffness of hydrogels was found in the range of 1-25 kPa (compressive tests), similar to stiffness values reported for human breast tissue (3-19 kPa). Stiffness values paralleled the concentration of both reagents and alginate OD.

The stiffness of OA-gelatin hydrogels is proportional to concentration of both polymers and to OD. Hydrogels are biocompatible and allow cell growth. Morphology of cells varies between low (1-5 kPa, low LD) and high (15-20 kPa,

high LD) stiffness hydrogels. In the former it is round and dispersed, whereas in the latter cells exhibit a clustered phenotype (as shown in figure). Cell proliferation in high LD was greater than in lower LD, Live/Dead assay confirmed cell viability up to day 7 in selected hydrogels (data not shown). Metastatic markers variations as function of properties of biomaterials is also evaluated, showing an increase of expression of metastatic markers (e.g. CD44) with increase in stiffness.

Conclusion

The importance of using biomaterials and tissue engineering approaches to better mimic the tumour microenvironment is important in understanding biological processes and tumorigenesis. Tissue stiffness is known to increase during tumour progression, impacting on variation in cell phenotype and potentially on drug resistance.
OA-gelatin hydrogels are promising biomaterials to model tumour progression in vitro and investigate cancer cell migration and response to stiffness.
Engineered 3D *in vitro* models can be used to predict chemotherapeutics delivery and efficacy, with the potential to speed up the pre-clinical phase in the testing of medicines.

References

Bai, Xiuping. et al, Journal of bioactive and compatible polymers, 28(2):126-140, 2013
Bouhadir, Kh. et al, Biotechnology Progression, 17(5): 945-950, 2001
Samani A et al. Physics in Medicine and Biology, 2007 Fe, 52(6):1565-1576, 2007
Sleeboom JJF et al. Dis Model Mech, 11(3): dmm033100, 2018

Acknowledgement

LS thanks the University of Manchester President's Doctoral scholarship.

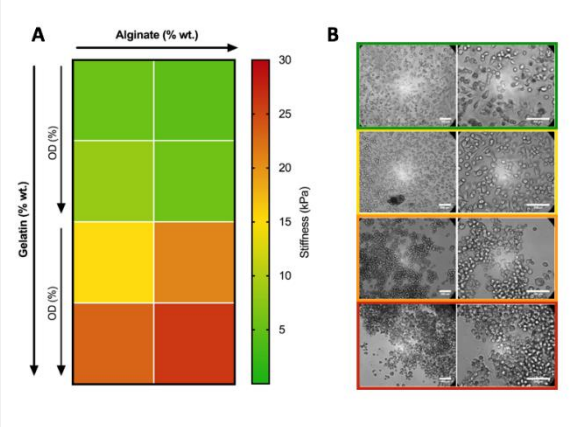

Hydrogel stiffness and breast cancer cell morphology
A. Stiffness of alginate-based hydrogels (compressive elastic modulus); B. MDA-MB-231 morphology as function of hydrogel stiffness.

4:45 p.m. – 6:15 p.m.

Conference room 2+3

YSF Grant Writing WS | YSF Grant Writing WS

Organiser: “YSF Board and National Chapters”

During the “YSF Grant writing workshop”, tips, tools and tricks on how to prepare a successful proposal will be shared by successful grant laureates. Starting from the selection of the proper call (European vs national projects; research grants vs individual fellowship), the speakers will propose the “key-stones” and the “to-do-list” for writing an efficacious and high-quality proposal. Experts in writing successful proposals and in the management of funded research projects will be, thus, invited to share their experience and knowledge with the young audience.

The YSF presents an exciting opportunity for learning about European young researcher grants and the chances and pitfalls of starting their own research group – at first hand from two fantstic local experts:

Wednesday, 11 September, 2019

	Hall 3	Hall 2	Hall 4	Hall 5	Conference room 4+5	Conference room 2+3	Hall 1 | Exhibition Area
8:00							
8:30	**PL2** Plenary Lecture 2						**Industrial Exhibition & Poster Exhibition I**
9:00	**GW AW** George Winter Award						
9:30							
10:00	**COFFEE BREAK**						
10:30	**IV-SY6** RSC Biomaterials Science	**TRS-SY1** TRS: AM of patient-specific implants	**IV-OS13** Bioactive materials for bone regeneration 1	**IV-SY7** Adaptive functional biomaterials	**IV-OS14** Cell material interactions 1	**IV-OS15** Patterning & coatings 1	
11:00							
11:30							
12:00	**BREAK**						
12:30	**ESB GA** ESB General Assembly						
13:00							
13:30	**LUNCH BREAK**						
14:00	**V-SY8** ISBF: Hydrogel bioinks for biofab.	**TRS-SY2** TRS: Impact of the new EU MDR	**V-OS16** Bioactive materials for regeneration of bone 2	**V-SY9** Neural plasticity and regen./ electr. interfaces	**V-OS17** Immunomodulatory biomaterials	**V-OS18** Patterning & coatings 2	
14:30							
15:00							
15:30							
16:00	**COFFEE BREAK**						**Industrial Exhibition & Poster Exhibition II**
16:30	**VI-SY10** ISBF: Adv. biofabrication strategies and appl.	**VI-SY16** Korea-EU symp.	**VI-SY11** Calcium phosphates 1	**VI-OS20** Alginate and biopolymers	**VI-OS21** Cell material interactions 2	**VI-OS22** Surfaces and interfaces	
17:00							
17:30							
18:00							
18:30							
19:00							
19:30		**YSF Night Out**					
20:00							
20:30							
21:00							
21:30							

8:30 a.m. – 9:15 a.m.

Hall 3 + Hall 2

PL2 | Plenary Lecture 2

PL2-01

Enabling Biomaterials Translation: It's not all about laboratory to bedside

Abhay Pandit

CÚRAM, Center for Research in Medical Devices, National University of Ireland, Galway, IE

There is a traditional way of classification of research- basic and applied research. It is generally believed that basic research enables our understanding of disease or failures states. Applied research advances the development of technologies (such as biomaterials, implants) based on our understanding of disease or failure mechanisms. The overall aim of translational research is to integrate advancements in material science, biology with clinical trials, taking research from the "laboratory-to-bedside". This advancement in a very traditional sense means new implants or designs that enable better therapeutic outcomes. This paradigm does not account for constant feedback that allows for discovery of rational devices, resulting in improved efficacy of implants, and faster optimization for clinical use. This talk will focus deconstructing this paradigm and giving examples from the biomaterials world of what 'translation' really should be.

PL2-02

Examples of industrial and clinical transfers of research works on biomaterials

Didier Letourneur[1,2]

[1]Cardiovascular Bio-engineering - Laboratory for Translational Vascular Medicine - INSERM U1148 University Paris 13, Villetaneuse, FR; [2]X Bichat Hospital, Université de Paris, Paris, FR

Engineers, chemists, biologists, clinicians, entrepreneurs need to work collaboratively to develop new biomimetic, bioinspired, biofunctional medical devices. Three representative examples of clinical/industrial transfers from our research works performed in a large translational research center with multidisciplinary technological platforms will be presented : i) An expansible aortic ring for cardiac surgery in a 10-year follow-up multicenter clinical trial on 600 patients, ii) A polymer-based system for targeted thrombus imaging at Phase IIa, iii) 3D porous GMP-grade scaffolds made of polysaccharides for bone engineering. For each of them, a different development scheme was adopted and will be presented.

References

Li B, Aid-Launais R, Labour M-N, Zenych A, Juenet M, Choqueux C, Ollivier V, Couture O, Letourneur D, Chauvierre C. Functionalized polymer microbubbles as new molecular ultrasound contrast agent to target p-selectin in thrombus. ***Biomaterials***. 2019;194:139-50

Juenet M, Aid-Launais R, Li B, Berger A, Aerts J, Ollivier V, Nicoletti A, Letourneur D, Chauvierre C. Thrombolytic therapy based on fucoidan-functionalized polymer nanoparticles targeting p-selectin. ***Biomaterials***. 2018;156:204-16

Fricain JC, Aid R, Lanouar S, Maurel DB, Le Nihouannen D, Delmond S, Letourneur D, Vilamitjana JA, Catros S. In-vitro and in-vivo design and validation of an injectable polysaccharide-hydroxyapatite composite material for sinus floor augmentation. ***Dental Materials***. 2018;34:1024-35

Chauvierre C, Letourneur D. The european project nanoathero to fight cardiovascular diseases using nanotechnologies. ***Nanomedicine***. 2015;10:3391-3400

Meddahi-Pelle A, Legrand A, Marcellan A, Louedec L, Letourneur D, Leibler L. Organ repair, hemostasis, and in vivo bonding of medical devices by aqueous solutions of nanoparticles. ***Angewandte Chemie-International Edition***. 2014;53:6369-73

Fricain JC, Schlaubitz S, Le Visage C, Arnault I, Derkaoui SM, Siadous R, Catros S, Lalande C, Bareille R, Renard M, Fabre T, Cornet S, Durand M, Leonard A, Sahraoui N, Letourneur D, Amedee J. A nano-hydroxyapatite - pullulan/dextran polysaccharide composite macroporous material for bone tissue engineering. ***Biomaterials***. 2013;34:2947-59

Rouzet F, Bachelet-Violette L, Alsac J-M, Suzuki M, Meulemans A, Louedec L, Petiet A, Jandrot-Perrus M, Chaubet F, Michel J-B, Le Guludec D, Letourneur D. Radiolabeled fucoidan as a p-selectin targeting agent for in vivo imaging of platelet-rich thrombus and endothelial activation. ***Journal of Nuclear Medicine***. 2011;52:1433-40.

Klink A, Hyafil F, Rudd J, Faries P, Fuster V, Mallat Z, Meilhac O, Mulder WJM, Michel J-B, Ramirez F, Storm G, Thompson R, Turnbull IC, Egido J, Martin-Ventura JL, Zaragoza C, Letourneur D, Fayad ZA. Diagnostic and therapeutic strategies for small abdominal aortic aneurysms. ***Nature Reviews Cardiology***. 2011;8:338-47.

9:15 a.m. – 10:00 a.m.

Hall 3 + Hall 2

GW AW | George Winter Award

GW-AW

From Bone Replacements to Nanomedicine: a path in Biomaterials

María Vallet-Regí[1,2]

[1]Dpto. Química Inorgánica y Bioinorgánica, Universidad Complutense de Madrid, Instituto de Investigación Sanitaria, Madrid, ES; [2]CIBER de Bioingeniería, Biomateriales y Nanomedicina, CIBER-BBN, Madrid, ES

My work in the field of Biomaterials started in the 1990s. Back then, the study of bone replacement materials, bone repair solutions and the field of bioceramics deeply attracted my interest and were the main focus of our preliminary efforts.

We focused our work in the synthesis of hydroxyapatite compounds, calcium phosphates, bioglasses, glass ceramics and hybrid materials. Although our first efforts were focused on obtaining materials eligible as tissue replacement solutions, in the 2000s we would start to design these materials also as potential drug delivery systems, attempting to reach a dual purpose.

In the 2010s, we expanded our field of research from bioceramics towards nanomedicine.

We are currently working in this field, particularly in three main bone issues: cancer, infection and osteoporosis.

This particular path within the world of Biomaterials, as is the case with many other routes, has been defined by the meeting of very different disciplines, since a combined and multidisciplinary effort is the only answer to these complex issues.

10:30 a.m. – 12:00 p.m.

Hall 3

IV-SY6 | RSC Biomaterials Science Lectureship

Neil Hammond (Cambridge, UK)

Biomaterials Science, published by the Royal Society of Chemistry, and the official journal of the ESB, explores the science of biomaterials as well as their translation towards clinical use. In this special session, Biomaterials Science Editor-in-Chief will shed light on the role of biomaterials in controlling immune response, and the recipient of the 2019 Biomaterials Science Lectureship, April Kloxin (University of Delaware) will present her research into the role of the extracellular matrix in cell activation.

The prestigious Biomaterials Science Lectureship is awarded annually, recognising an early career researcher who has made a significant contribution to the field through his/her independent research. Previous winners are Zhen Gu (2018), Zhuang Liu (2017), Fan Yang (2016), Joel Collier (2015), and Suzie Pun (2014).

IV-SY6-KL01

New frontiers in biomaterial research: engaging the immune system

Jennifer H. Elisseeff

Johns Hopkins University School of Medicine, Baltimore, US

The immune system is the first responder to trauma and foreign bodies such as biomaterials, yet this response and its capacity to orchestrate tissue repair has been largely ignored in tissue engineering research.Translating tissue engineering technologies to the clinic for multiple clinical applications, we discovered unexpected responses from the adaptive immune system. We are now comparing the immune profile of biomaterials and wounds that repair versus those that succumb to fibrosis and tissue degeneration to design regenerative immunotherapies. These results are informing immunotherapy design to both promote tissue repair and remove inhibitory factors that are limiting biomaterial integration and new tissue growth.

IV-SY6-KL02

Designing and applying synthetic extracellular matrices with multiscale property control to probe key regulators of cell function and fate

April M. Kloxin

University of Delaware, Chemical and Biomolecular Engineering and Materials Science & Engineering, Newark, US

The structure, mechanical properties, and biochemical content of the microenvironment of cells in the human body, particularly the extracellular matrix (ECM), are increasingly recognized as drivers, not simply consequences, of cellular responses to remodeling events, including upon injury or aging. Well-defined synthetic mimics of the ECM have emerged as useful tools for probing cellular responses to such complex processes. In particular, increasing collagen content and crosslinking upon tissue remodeling is thought to be key in the activation of wound healing cells, such as fibroblasts, and tumor cells, such as breast cancer cells, at both primary and secondary sites; yet, mimicking these microenvironments for studying these complex processes *in vitro* remains challenging. To address this, we have created well-defined, hydrogel-based synthetic ECMs formed by light-mediated thiol–ene click chemistry that integrate modular building blocks for control of matrix nanostructure, mechanical properties, and biochemical content and applied them for probing cell responses initially and over time in collagen-rich microenvironments. Synthetic matrices with homogeneous nanostructure were formed by photoinitiated step growth polymerization of multi-arm poly(ethylene glycol) functionalized with thiols and cell-degradable peptides functionalized with alkenes (allyloxycarbonyl (alloc)-protected lysine). Hierarchical nanostructures reminiscent of the native ECM were incorporated within these materials using assembling peptides, specifically unique multifunctional collagen mimetic peptides (mfCMPs) based on non-natural variants of Proline-Hydroxyproline-Glycine repeats [$(POG)_n$] and decorated with alloc reactive groups for integration of nano- and micro-scale fibrils within the synthetic matrix. We have applied both the homogeneous and hierarchically-structured matrices for controlled three-dimensional (3D) cell culture to study the role of microenvironment cues in cell activation during disease progression. Specifically, activation of breast cancer cells and fibroblasts in response to microenvironment cues is being examined with these synthetic ECMs toward a better understanding of metastatic disease and fibrosis, respectively. This talk will highlight key observations of these studies, providing both new tools for 3D culture applications and insights into regulators of cell activation in these complex processes.

IV-SY6-03

Antibacterial efficacy of nitric oxide releasing hydrogels on 2D and 3D human skin models

Robert C. Deller[1], Jenny Aveyard[1], Rachel L. Williams[2], Raechelle A. D'Sa[1]

[1]University of Liverpool, School of Engineering, Liverpool, GB; [2]University of Liverpool, Institute of Ageing and Chronic Disease, Liverpool, GB

Introduction

The healing of burn wounds are hindered by bacterial infections which can lead to increases in morbidity and mortality rates.[1, 2] This problem is exacerbated by the rise in multidrug resistant bacterial strains that limit the efficacy of antibiotics.[3] Alternative approaches such as nitric oxide have shown promise as potent and broad-spectrum antimicrobial agents which can interact with DNA, lipids and proteins thereby killing the bacteria.[4] Nitric oxide also serves as a signalling molecule that can stimulate the immune response and wound healing processes.[5] Here we investigate the antimicrobial efficacy of nitric oxide releasing materials against *Staphylococcus aureus* and a secreted extracellular protease (V8 protease) capable of disrupting epithelial barrier function.[6, 7]

Experimental Methods

A variety of standardised biophysical techniques and commercially available *in vitro* biochemical assays have been utilised to characterise the physical and chemical properties of our nitric oxide releasing materials (e.g. chemiluminescence) and their efficacy against *S. aureus* (ATTC®*25923*) and V8 protease. Subsequent impact on cell viability (e.g. alamar blue) and cell functionality (e.g. transepithelial electrical resistance) utilised HaCaT (skin keratinocyte) and WS1 (skin fibroblast) human cell lines co-cultured on 1 µm Polyethylene Terephthalate (PET) membranes.

Results and Discussion

Here we demonstrate a pH mediated burst release of nitric oxide from diazeniumdiolate functionalised hydrogels over a 24 hour period. Diazeniumdiolate functionality was confirmed by FT-IR and pH mediated nitric oxide release via chemiluminescence. The bactericidal efficacy of our nitric oxide releasing materials was assessed directly against *S. aureus* at several initial seeding densities and time points. Activity against the *S. aureus* secreted V8 protease was determined by changes in the rate of proteolytic cleavage of a fluorescently labelled tripeptide and changes in the transepithelial electrical resistance of co-cultured HaCaT and WS1 cells on 1 µm PET membranes. Subsequent viability (e.g. Live/Dead) and barrier functionality (e.g. zonula occuldens-1 immunostaining) assessments against co-cultured skin keratinocytes (HaCaT) and skin fibroblasts (WS1) highlight the biocompatibility of our nitric oxide releasing materials. Preliminary work has also explored the utilisation of our nitric oxide releasing materials against a wounded and subsequently *S. aureus* infected 3D human skin equivalent (Labskin[1.1]). Current work is focussing on the administration of *S. aureus* to our co-cultured systems and subsequent treatment with our nitric oxide releasing materials to assess concurrent antimicrobial and functional activities.

Conclusion

pH responsive nitric oxide releasing materials are capable of acting as a potent antimicrobial agents against *S. aureus* without detrimental impact to the viability and functionality of multiple human skin cell types.

References

[1] R.S. Daum, Clinical practice. Skin and soft-tissue infections caused by methicillin-resistant Staphylococcus aureus, N Engl J Med, 357 (2007) 380-390.

[2] W. Norbury, D.N. Herndon, J. Tanksley, M.G. Jeschke, C.C. Finnerty, Infection in Burns, Surg Infect (Larchmt), 17 (2016) 250-255.

[3] T.J. Foster, Antibiotic resistance in Staphylococcus aureus. Current status and future prospects, FEMS Microbiol Rev, 41 (2017) 430-449.

[4] L.R. Martinez, G. Han, M. Chacko, M.R. Mihu, M. Jacobson, P. Gialanella, A.J. Friedman, J.D. Nosanchuk, J.M. Friedman, Antimicrobial and healing efficacy of sustained release nitric oxide nanoparticles against Staphylococcus aureus skin infection, J Invest Dermatol, 129 (2009) 2463-2469.

[5] D.O. Schairer, J.S. Chouake, J.D. Nosanchuk, A.J. Friedman, The potential of nitric oxide releasing therapies as antimicrobial agents, Virulence, 3 (2012) 271-279.

[6] U. Ohnemus, K. Kohrmeyer, P. Houdek, H. Rohde, E. Wladykowski, S. Vidal, M.A. Horstkotte, M. Aepfelbacher, N. Kirschner, M.J. Behne, I. Moll, J.M. Brandner, Regulation of epidermal tight-junctions (TJ) during infection with exfoliative toxin-negative Staphylococcus strains, J Invest Dermatol, 128 (2008) 906-916.

[7] J. Murphy, M. Ramezanpour, N. Stach, G. Dubin, A.J. Psaltis, P.J. Wormald, S. Vreugde, Staphylococcus Aureus V8 protease disrupts the integrity of the airway epithelial barrier and impairs IL-6 production in vitro, Laryngoscope, 128 (2018) E8-E15.

Acknowledgement

All authors acknowledge funding from the engineering and physical sciences research council (EPSRC) UK healthcare impact partnership 2017 grant EP/P023223/1.

IV-SY6-04

TEMPO Oxidation of Hyaluronic Acid for Stable Hydrogel Formation via Schiff Base Chemistry

Junwen Shan, Thomas C. Böck, Jörg Tessmar, Jürgen Groll

Universitätsklinikum Würzburg, Abteilung für Funktionswerkstoffe der Medizin und Zahnheilkunde, Bayerisches Polymer Institut, Würzburg, DE

Introduction

Due to fast development of the field of biofabrication, suitable printable hydrogels are highly demanded as bioinks for 3D printing. Biomaterials for the preparation of such printable hydrogels must show appropriate rheological and mechanical properties during and after the printing process as well as biocompatibility and biodegradability.[1] Several biopolymer based hydrogels already accomplish the biological requirements since they are of natural origin and often partially components of extracellular matrices of animals or plants. After their extraction, most biopolymers need a chemical cross-linking to form mechanical stable hydrogels, for example via thiol-ene or Schiff Base chemistry[2-3]. For Schiff Base chemistry, hyaluronic acid (HA) is commonly oxidized by sodium periodate to generate dialdehyde functionalization via a ring opening mechanism. During the oxidation reaction, massive degradation of the HA chains occurs and the achieved degree of oxidation (DO) is quite low. In this study, we investigated an alternative oxidation of the primary alcohol of HA without ring opening reaction to preserve the backbone of the HA chain and to maintain a sufficient quantity of aldehyde groups for hydrogel formation.

Experimental Methods

Tert-butylammonium hyaluronate (TBA-HA) was generated from sodium hyaluronate using *tert*-butylammonium laden Dowex® 50WX8. Oxidation of the primary alcohol of TBA-HA was then performed in DMF, using2,2,6,6-Tetramethyl-piperidinyloxyl (TEMPO, catalytical amounts) and trichloroisocyanuric acid (TCC, 0.76, 0.5 and 0.25 eq.) as oxidation reagents. The mixture was stirred with sodium hydrogen carbonate for 4 h and then dialyzed against 150 mM NaCl solution and then H_2O for 4 d in total. The product was obtained after freeze drying.

To analyze the achieved extent of oxidation, a *tert*-butylhydrazine (TBH) assay was established, which was performed in water and with sodium cyanoborohydride as reducing reagent for the formed hydrazone. The DO could be calculated via NMR spectroscopy.

To investigate the degradation of the biopolymer, gel permeation chromatography (GPC) was performed using a system from Malvern, equipped with refractive index detection as well as a light scattering detector. Millipore water with 8.5 g/l sodium nitrate and 0.2 g/l sodium azide was used as solvent and eluent.

For hydrogel formation, various concentrations of polymer solution with PBS containing high (HMW) or low (LMW) molecular weight aldehyde containing HA (AHA) was cross-linked with 0.1 % (*w*/*w*) adipic acid dihydrazide (ADH) solution with a molar ratio of aldehyde : hydrazide = 1:1.

Human bone marrow-derived mesenchymal stromal cells (hMSC) were embedded into hydrogels with 3 % (*w*/*w*) AHA and cultivated for at least 7 d *in vitro* and cell viability was analysed.

Results and Discussion

GPC measurements proved increasing biopolymer degradation with higher equivalents of oxidation reagent TCC. At the same time, a high DO was achieved with all equivalents of TCC (~ 73 %). The hydrogels formed with HMW-AHA were mechanically much more stable than LMW-AHA hydrogels with increasing Young's modulus at higher

concentrations and continued storage in PBS. Live-dead-staining showed good cell viability of encapsulated hMSCs after 7 d of *in vitro* culture.

Conclusion

The TEMPO/TCC oxidation generated AHA with high DO. Hydrogels with high Young's modulus were formed and they showed acceptable biocompatibility. However, this material is not suited for bioprinting yet due to its fast gelation time and high mechanical stability. Other cross-linkers, for example multifunctional polymers, might improve shear thinning properties of the material or a proper printing construction could enable the use as a bioink.

References

[1] T. Jungst, W. Smolan, K. Schacht, T. Scheibel, J. Groll, *Chem. Rev.* **2016**, *116*, 1496-1539.

[2] S. Bertlein, G. Brown, K. Lim, T. Jungst, T. Böck, T. Blunk, J. Tessmar, G. J. Hooper, T. Woodfield, J. Groll, *Adv. Mater.* **2017**, *29*, 201703404.

[3] L. L. Wang, C. B. Highley, Y. C. Yeh, J. H. Galarraga, S. Uman, J. A. Burdick, *Journal of Biomedical Materials Research Part A* **2018**, *106*, 865-875.

Acknowledgement

This research has received funding from the European Research Council under grant agreement 617989 (Design2Heal) and German Research Foundation (DFG) within the collaborative research center TRR 225 (subproject A02).

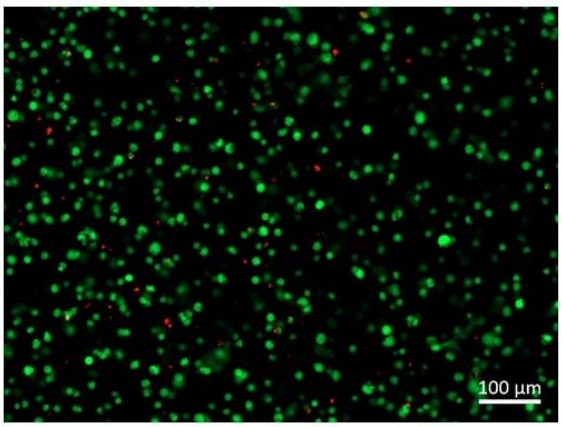

Cell Viability
Live-dead-staining of hMSC after 7 d of *in vitro* culture: viable cells were labelled green with calcein-AM and dead cells were labelled red with EthD-I

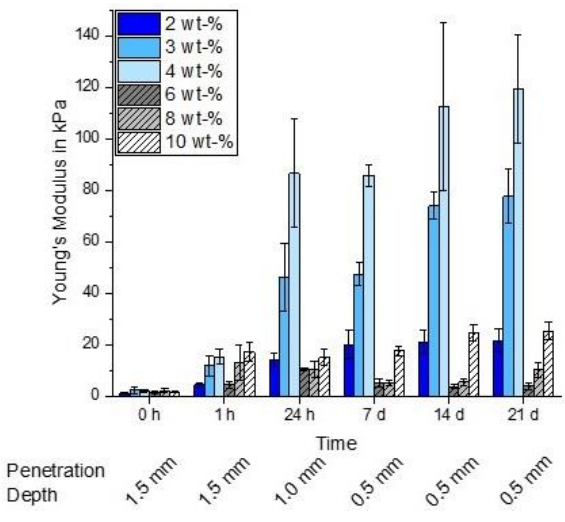

Mechanical Stability
Young's modulus of hmw-AHA (2-4 wt-%) and lmw-AHA (6-10 wt-%)

10:30 a.m. – 12:00 p.m.

Hall 2

TRS-SY1 | TRS: Additive manufacturing of patient-specific implants

TRS-SY1-01

Additive Manufacturing of patient-specific implants – technological opportunities and limitations

Christoph Leyens[1,2], Frank Brückner[1,3], Elena López[1], Udo Klotzbach[1], Tim Kunze[1]

[1]Fraunhofer Institute for Material and Beam Technology IWS Dresden, Germany; [2]TU Dresden, Dresden, Germany; [3]Luleå University of Technology, Luleå, Sweden

Additive manufacturing (or often called 3D printing) is considered as one of the current century's disruptive technologies. AM of polymers and particularly of metals is currently paving its way into industrial applications at high pace. Medical applications have been at the forefront over the last years, and the most striking field are: bio-printing of tissues and organoids, 3D-printed models for surgery preparation, 3D printing of surgical instruments and custom-made prosthetics[1]. The focus of this presentation is on in-vivo and in-vitro applications of additive manufacturing with an emphasis on the entire processing chain, from part design to fabrication and post-processing, including surface functionalization.

The presentation will highlight recent developments in AM related to different processes, materials and part sizes/geometries. Unlike any other manufacturing technology, AM of high quality parts requires an in-depth understanding of the close relationship between the AM process, the material and the resulting component properties. On the other hand, AM offers unrivaled possibilities to produce patient-specific, highly individualized parts and functionalities. As a matter of fact, customized hardware, online diagnostics and control systems are required for robust processing of AM. Moreover, part quality must be checked and guaranteed every time which is particularly challenging when only small lot sizes (down to 1) are considered.

Moreover, surface functionalization of technical surfaces is regarded as one of the most important current innovation tools in laser manufacturing. Surfaces with well-defined features (e.g. periodic micro structures) have shown to exhibit outstanding properties. The design of these textured surfaces often follows a biomimetic approach inspired by living organisms which developed over time through natural selection and evolution. One manufacturing method is Direct Laser Interference Patterning (DLIP). The efficient production of these versatile patterns still represents one of the greatest technical challenges today in the development of new customized surface functionalities. DLIP has been identified as an outstanding technology for the efficient fabrication of tailored surface structures, in the range from 0.1 up to 20µm (Figure 1c) with an effective patterning speed of about 15 square meters per minute.

[1] Allie Nawrat, www.medicaldevice-network.com

10:30 a.m. – 12:00 p.m.

Hall 4

IV-OS13 | Bioactive materials for bone regeneration 1

IV-OS13-KL01

Calcium alkali orthophosphate-based bioactive bone grafting materials and 3D printed scaffolds for bone tissue engineering stimulate osteogenesis and facilitate bone repair *in vivo* – Translational research in craniofacial surgery and implant dentistry

Christine Knabe-Ducheyne[1], Georg Berger[2], Renate Gildenhaar[2], Jens Günster[2], Michael Stiller[1]

[1]Philipps-University Marburg, Department of Experimental Orofacial Medicine, Marburg, DE; [2]Federal Institute for Materials Research and Testing, Laboratory for Biomaterials, Berlin, DE

For alveolar ridge augmentation bone substitute materials are extensively studied in order to avoid harvesting autogenous bone. Given the clinical findings with current bone grafting materials there continues to be interest in bone substitute materials which degrade more rapidly, but still stimulate osteogenesis at the same time. This has led to the synthesis of rapidly resorbable calcium alkali orthophosphate (CAOP) materials which exhibit a greater biodegradability than β-tricalcium phosphate (TCP).

In order to evaluate the osteogenic potential *in vitro*, we examined the effect of various CAOPs on osteoblastic differentiation *in vitro* as compared to the currently clinically used materials TCP and bioactive glass 45S5.

In order to correlate the *in vitro* results with *in vivo* performance, we subsequently examined the effect of the same selection of bioactive ceramics (previously studied *in vitro*) on osteogenic marker expression and bone formation after implantation in the sheep mandible and sinus floor *in vivo*.

Among the various test materials the silica containing CAOP (Si-CAOP) material GB9 displayed the greatest stimulatory effect on osteoblast differentiation *in vitro* and *in vivo* as well as on bone formation *in vivo.* Subsequently, studies to characterize the cell adhesion and intracellular signalling mechanism leading to this stimulatory effect on osteogenesis followed. Collectively, the data generated in these various studies led to FDA approval of this SI-CAOP in 2013.

Furthermore, we also correlated the findings from the preclinical *in vivo* animal studies with in vivo data from clinical studies, in which the effect of various calcium phosphate particulate bone grafting materials with varying porosity on bone formation and on osteogenic marker expression in biopsies sampled six months after sinus floor augmentation (SFA) was studied, thereby rendering valuable insight in the performance of these materials in the human case as well as establishing a clinical study model for controlled clinical studies, which are required for taking novel bone grafting materials to the clinical area in an evidence-based fashion. A first clinical study which evaluated the effect of this Si-CAOP (commercial name: Osseolive®) 6 months after SFA on bone formation as compared to TCP demonstrated significantly greater bone formation and resorption of the Si-CAOP in the apical area of the biopsies, i.e. at the greatest distance from the native bone, when compared to TCP.

A bone tissue engineering project employed 3D printed Si-CAOP scaffolds and a perfusion flow cell seeding and culture technique, and dealt with generating a 3D printed tissue engineered synthetic bone graft with homogenously distributed osteoblasts and mineralizing bone matrix *in vitro*, which thereby mimics the advantageous properties of autogenous bone grafts rendering it an excellent candidate for subsequent *in vivo* implantation for reconstruction of segmental discontinuity bone defects. These constructs were then used in combination with a microvascular technique for repair of critical-size segmental discontinuity defects in a femoral rat model. Histomorphometric, immunohistochemical and angio-µCT analyses rendered this concept an excellent tissue engineering approach for achieving excellent vascularization and repair of critical-size segmental discontinuity defects i*n vivo*.

IV-OS13-02

In vivo evaluation of 3D printed BCP scaffolds for maxillofacial bone reconstruction in a critical-size bone defect model of rabbit

Matthias Schlund[1,2], Arnaud Depeyre[1,3], Vincent Hornez[4], Jean-Christophe Hornez[5], Thomas Wojcik[6], Pierre Machandise[7], Guillaume Penel[7], Pierre Gosset[8], Baptiste Delaire[8], Nicolas Blanchemain[1], Joel Ferri[1,2], Feng Chai[1]

[1]Université de Lille, Inserm U1008, CHU Lille, Faculté de Médecine, Lille, FR; [2]CHU Lille, Service de Chirurgie Maxillo-Faciale, Lille, FR; [3]Centre Hospitalier Universitaire de Clermont-Ferrand, Service de Chirurgie Maxillo-Faciale, Stomatologie et Chirurgie Plastique de la Face, Clermont-Ferrand, FR; [4]CryoCeram-Startup, Serre Numérique de Valenciennes, Valenciennes, FR; [5]Université polytechnique des Hauts-de-France, LMCPA, Valenciennes, FR; [6]Centre Oscar Lambret, Lille, FR; [7]Université de Lille, EA4490 PMOI Physiopathologie des Maladies Osseuses Inflammatoires, Lille, FR; [8]Hôpital Saint Vincent de Paul, Immunohistochimie et Recherche, Laboratoire d'Anatomie et Cytologie Pathologiques, Lille, FR

Introduction

Biphasic calcium phosphate (BCP) bioceramics have great potential for applications as a bone substitute because of their excellent chemical bone-bonding ability and higher bioresorption property. As a promising substitute for bone defect repair, a scaffold also has to address the appropriate surface property and 3D structural characteristics for cell adhesion, proliferation, and differentiation. 3D printing methodology is an excellent 3D scaffold building approach to support effective and fast patient-specific fabrication of individual complex bone substitutes. Here, we aimed to elaborate a 3D printed BCP scaffold (3D-BCP), and evaluate its biocompatibility and bone repair efficacy *in vitro* andin a rabbit cranial maxillofacial critical-size bone defect model.

Experimental Methods

The implantable disk samples were fabricated by a custom-designed CryoCeram 3D printer from synthetized BCP powder (40 wt% HA / β-60 wt% TCP). The biological effect of (regarding the cell adhesion and proliferation) of 3D-BCP on pre-osteoblast cell lines (MC3T3-E1) was assessed *in vitro*. To further explore the osteoinductivity and osteoconductivity of 3D-BCP *in vivo*, the 3D printed BCP scaffold were implanted into a standardized critical-size bone defect model: Ø10 mm defect in the skull and bi-cortical defect (Ø11×6 mm) in the mandible of the same rabbit (Figure 1). No scaffold was implanted into the sham group, and autologous bone debris was implanted as positive control. X ray micro-CT (µCT) imaging and 3D reconstruction, and bone histological evaluation were performed on the harvest bone sample at 4 and 12 weeks after surgery.

Results and Discussion

The obtained results of *in vitro* study confirmed the biological activity and cytocompatibility of 3D-BCP scaffold by promoting the adhesion and the proliferation of pre-osteoblast cells. *In vivo*, acquired µCT images and the bone volume density (BV/TV ratio) revealed (Figure 2) that the printed BCP scaffolds enhanced regeneration of the bone defects and accelerated defect healing compared with sham group, in which no scaffold was implanted, still had a lack of newly formed bone at 12 weeks. µCT results also revealed that some newly formed bone had penetrated into the pores of the 3D-BCP scaffolds. In agreement with µCT analysis, histological HE bone staining confirmed this observation, and indicated that the newly formed bone surrounding the 3D-BCP scaffolds was firmly attached. Moreover, inflammatory cell infiltration was absent at the bone/scaffold interface, which indicates the absence of a foreign body reaction and confirming the good biocompatibility of 3D-BCP scaffolds.

Conclusion

This study showed that the tested 3D printed BCP scaffolds with desired shapes and internal structures exhibited a good bioactivity and biocompatibility *in vitro* and *in vivo*, and promoted appropriate new bone formation *in vivo*. Future study will focus on incorporating bioactive factors (platelet-rich fibrin) and osteoprogenitor cells to enhance the osteoconductive and osteoinductive stimuli for better repair of bone defects.

References

1. Hayden RE,*et al. Curr Opin Otolaryngol Head Neck Surg. 2012;20:231–236*.
2. Song Y, *et al.International Journal of Nanomedicine 2018;13:505–523.*
3. Guy *et al.Biomater Med Appl* 2017; 1:2-6.
4. McGovern JA, *et al*. *Dis Model Mech.* 2018;11:1-14.

Acknowledgement

The authors would like to thank the Plate-forme Ressources Expérimentales, D.H.U.R.E, University of Lille, for their support on animal studies. It was supported by the cross-border INTERREG “North-West Europe" fund BONE 2014-2020.

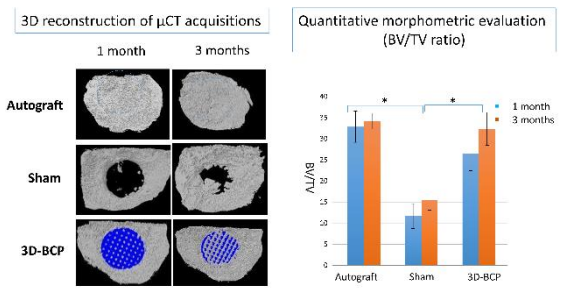

Figure 2
3D reconstructions of micro-CT image to visualize the healing of critical-size bone calvarial defects in the rabbit model and osteogenic analysis (BV/TV ratio) at 1 and 3 months after implantation of scaffolds. Defects were implanted with 3D-BCP scaffolds, autologous bone (autograft), or no scaffold (sham).

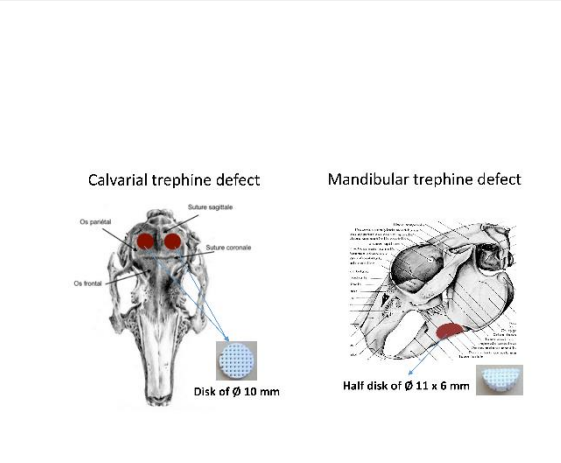

Figure 1
Schematic representation of rabbit cranial and mandibular bone defects and 3D-BCP scaffolds for implantation.

IV-OS13-03

Degradation behavior and biocompatibility of open-pored magnesium scaffolds LAE442 and La2 in vivo

Nadine Kleer[1], Stefan Julmi[2], Lisa Wurm[1], Franziska Feichtner[1], Christian Klose[2], Andrea Meyer-Lindenberg[1]

[1]Ludwig-Maximilians University, Clinic of Small Animal Surgery and Reproduction, Munich, DE; [2]Leibniz University Hanover, Institut für Werkstoffkunde (Materials Science), Garbsen, DE

Introduction

Magnesium alloys are of particular interest for the application as biodegradable metallic implants. Due to their strength and the similarity of Young´s modulus to that of bone, they may be suitable for the use as load bearing biodegradable implants that support healing of bone defects. However, the major disadvantage of magnesium alloys is the rapid corrosion attack and the related hydrogen production in aqueous solution. Therefore, a slow degrading alloy is required. This study investigates the degradation behavior and biocompatibility of the two open-pored magnesium scaffolds LAE442 and La2 in vivo.

Experimental Methods

Cylindrical open-pored magnesium scaffolds (diameter 4 mm, length 5 mm) made of the alloys LAE442 (4 wt.-% Li, 4 wt.-% Al, 2 wt.-% rare earth) and La2 (2 wt.-% La) were fabricated via investment casting and then coated with MgF_2 (1). Porous ß-tricalcium phosphate implants of the same dimensions served as control group. The scaffolds were inserted into the cancellous bone of the greater trochanter of both femurs of adult, female rabbits (n = 60) for implantation periods of 6, 12, 24 and 36 weeks. After euthanasia the bone-scaffold-compounds were harvested and embedded in Technovit 9100. Cross sections of ≈ 80 µm were produced and stained with toluidin blue for histological examination. Selected cross sections were investigated using scanning electron microscopy (SEM) and energy dispersive X-ray spectroscopy (EDX) analysis.

Results and Discussion

La2 scaffolds showed a faster degradation rate than LAE442 scaffolds with stronger hydrogen release and fewer bone-scaffold-contacts in week 6 and 12. In addition, partially fibrous capsule formation occurred around La2 scaffolds. After 24 weeks of implantation, the La2 samples were completely degraded, resulting in a loss of structure with only a few scaffold residues left surrounded by mineralized bone and granulation tissue. The degraded La2 material was phagocytosed by macrophages and some foreign body cells that accumulated in distinct clusters at the center of the implant site. Furthermore, EDX analysis revealed an increased content of lanthanum within these cell accumulations. The LAE442 samples maintained their structural integrity and showed increasing ingrowth of unmineralized bone into pores and gas production up to week 36. A deposition of calcium and phosphate was detected in the superficial degradation layers of LAE442. The control group degraded rapidly and trabeculae and bone marrow had grown in by week 6.

Conclusion

LAE442 scaffolds exhibited a slower degradation and better integration into cancellous bone than La2 scaffolds and seem more suitable for the application in load bearing bone. However, new bone formation within pores of LAE442 scaffolds was partly impaired due to insufficient bone mineralization. This may be caused by persistent gas production or high exposure to certain remaining alloy components, such as rare earth metals or aluminum (2, 3). Therefore, the degradation of LAE442 has to be further adjusted by additional coatings, or a new rare earths/aluminum-free magnesium alloy has to be developed.

References

1. Julmi, S., et al., *Processing and coating of open-pored absorbable magnesium-based bone implants.* Materials Science and Engineering: C, 2019. **98**: p. 1073-1086.
2. Kraus, T., et al., *The influence of biodegradable magnesium implants on the growth plate.* Acta Biomater, 2018. **66**: p. 109-117.
3. Willbold, E., et al., *Effect of the addition of low rare earth elements (lanthanum, neodymium, cerium) on the biodegradation and biocompatibility of magnesium.* Acta Biomater, 2015. **11**: p. 554-62.

Acknowledgement

Financial support of this study by the German Research Foundation under grants ME 1941/3-1 and MA 1175/52-1 is gratefully acknowledged.

IV-OS13-04

In vivo analysis of bone regeneration, biocompatibility and tissue response of a volume stable barrier membrane for Guided Bone Regeneration based on a collagen membrane combined with a HF-coated magnesium mesh

Lennart Kühnel, Mike Barbeck, Ralf Smeets, Clarissa Precht, Martin Gosau, Ole Jung

University Medical Center Hamburg-Eppendorf, Division of Regenerative Orofacial Medicine, Department of Oral and Maxillofacial Surgery, Hamburg, DE

Introduction

Barrier membranes are standard biomaterials for guided bone/tissue regeneration (GBR/GTR) in Oral & Maxillofacial Surgery. For many non-load-bearing procedures bioresorbable collagen membranes can be applied, while special indications such as high-volume defects can call for volume-stable membranes. Up to now, the available volume-stable membranes consist of non-resorbable materials and require surgical removal upon completion of therapy. Yet, an optimal volume-stable barrier membrane should combine structural and biodegradative properties. Due to its strength, biocompatibility and complete degradation in aqueous environments, magnesium represents an ideal biomaterial for the development of support structures for barrier membranes, which could overcome the challenges of stability deficiencies and material removal. Its premature degradation behavior however, requires a strategy to delay hydrogen release and to ensure biocompatibility.

The aim of this work was the *in vivo* investigation of a volume-stable barrier that combines a collagen membrane with a magnesium mesh that was coated with hydrofluoric acid (HF) for control of hydrogen release as well as the degradation process.

Experimental Methods

In 18 rabbits, four circular calvarial defects were created and randomly covered by collagen membranes reinforced with magnesium meshes that were uncoated or coated via HF or a pure collagen membrane, respectively. One defect was left empty and served as control. The explants were examined by digital volume tomography (DVT), contact radiography, histology and histomorphometry for bone regeneration after 6, 12 and 18 weeks. Moreover, the degradation behavior of the membranes, with special focus on the coating of the Mg meshes including histopathological observation of the related tissue reactions and the development of hydrogen gas cavities, was qualitatively and quantitatively analyzed.

Results and Discussion

Differences regarding bone regeneration in all groups and at all time points were found to be not significant ($p>0.05$). The two variants of the magnesium-reinforced membranes were detectable until the end of the observation period, whereas the collagen membrane was not observable. In defects covered by the magnesium-reinforced membranes, residuals of the meshes were observed. Up to 12 weeks the coating was degraded by mononuclear phagocytes, while the uncoated magnesium meshes elicited a fibrosis-like tissue reaction. As of 18 weeks after implantation, the tissue reaction in both groups were similar. Both magnesium meshes were associated with gas cavities, while they decreased over time and were not further detectable after 18 weeks. Interestingly, no interference of the observed gas cavities with bone regeneration was notable. Moreover, the histomorphometrical analysis revealed that the size

of gas cavities was significantly lower in the group of the HF-coated magnesium meshes up to 6 weeks after implantation.

Conclusion

The results show that the magnesium-reinforced membrane allows for regenerative properties comparable to a simple collagen membrane. Moreover, hydrogen release is prevented by HF-coating of the magnesium mesh up to 6 weeks and the HF-coating was degraded up to 12 weeks involving phagocytes such as macrophages.Altogether, HF-coated magnesium meshes combined with collagen-based barrier membranes might represent an ideal volume stable alternative to conventional non-resorbable membranes.Thus, the new developed membrane can be classified as optimal equivalent for GBR/GTR therapy.

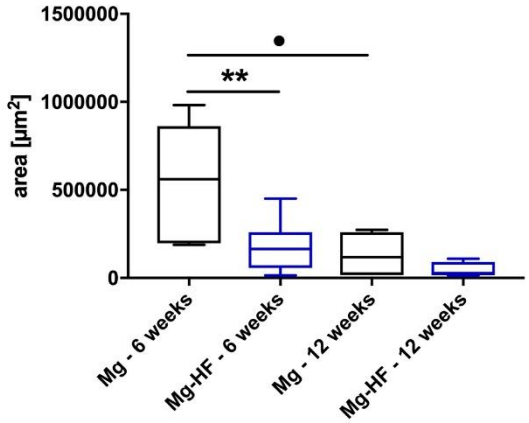

Quantitative analysis of hydrogen gas cavities
Gas cavity surface in µm²for uncoated (Mg; black) and HF-coated (Mg-HF; blue) magnesium after 6 and 12 weeks. HF-coated magnesium meshes show significantly lower gas cavity development compared to untreated magnesium meshes (**: $p<0.05$) up to 6 weeks after implantation. Gas cavity dimension of untreated magnesium meshes shows to be reduced significantly after 12 weeks (·: $p<0.05$).

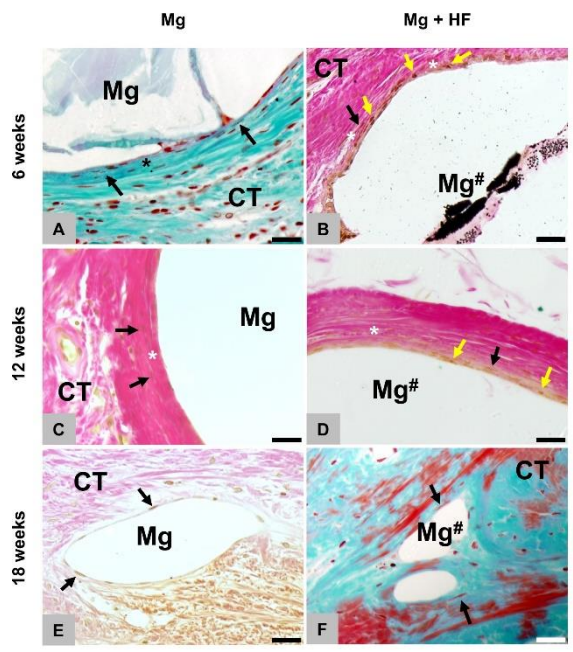

Histopathological observations of tissue reactions
Representative images of Masson-Goldner (A, F) and Von Kossa (B, C, D, E) staining (40x) of implantation site (scalebar=20 µm) at 6, 12 and 18 weeks. Left for untreated (Mg) and right for HF-treated (Mg#) magnesium. Gas cavity formation and fibrotic capsule forming (black star) are visible at all times. The HF-coated mesh was mainly degraded by mononuclear cells (yellow arrows) up to 12 weeks, while the uncoated magnesium meshes elicited a fibrosis-like tissue reaction showing fibroblast accumulation (black arrows). Starting from 18 weeks after implantation, the tissue reaction in both groups were similar.

IV-OS13-05

Development of bioactive three-dimensional scaffolds as platforms in cartilage tissue engineering

Nimrah Munir, Alison McDonald, Anthony Callanan

The University of Edinburgh, Institute for Bioengineering, Edinburgh, GB

Introduction

The prevalence of osteoarthritis is on the rise and effective treatments for cartilage defects are still being sought [1]. Cartilage tissue *in vivo* encompasses complex structures and composition, both of which influence cells and many properties of the native cartilage. The extracellular matrix structure and components provides both morphological cues and the necessary signals to promote cell functions [1]. Moreover, the accumulation of reactive oxidative species (ROS) has been linked to the pathogenesis of osteoarthritis. Overproduction of ROS can damage cell DNA, impair the production of proteins and promote apoptosis. Vitamin E, an antioxidant which provides protection against ROS, is known for its chondroprotective effects when supplemented into culture media [2-3]. The aim of this study was to investigate the effect of multizone scaffolds, made through the combination of cryo-printing and electrospinning, on chondrocytes and protective effect of vitamin E incorporated Polycaprolactone (PCL) scaffolds against hydrogen peroxide induced oxidative stress.

Experimental Methods

Multizone scaffolds consist of three different zones (Fig 1A). The bottom helix scaffold was fabricated using cryo-printing, which involves printing of an 8% w/v PCL/1, 4-Dioxane solution directly onto a cold plate set at -40^{o}C. The middle and top electrospun layers are composed of randomly orientated and aligned electrospun fibers, respectively (8% w/v PCL and HFIP). Multizone scaffolds were seeded with primary human chondrocytes and cultured for 24 hours, 1, 3 and 5 weeks. Vitamin E scaffolds were fabricated, using electrospinning, at two concentrations: 200µM vitamin E in 8% PCL w/v in HFIP and 500µM vitamin E in 10% PCL w/v in HFIP. Vitamin E scaffolds were seeded with chondrocytes for 24 hours, 3 and 6 day time points. Scaffold morphologies was assessed using scanning electron microscope (SEM) and mechanical properties of all scaffolds were evaluated. Biochemical quantification and gene expression were analysed at all time points. The antioxidant capacity of vitamin E scaffolds were determined using a hydrogen peroxide detection assay.

Results and Discussion

Multizone scaffolds successfully mimic the collagen fiber orientation of the native cartilage. Moreover, chondrocyte seeded multizone scaffolds demonstrated the ability to support long-term chondrocyte attachment and survival over a 5 week culture period (Fig 1). Furthermore, chondrocyte seeded multizone scaffolds were found to regulate expression of key genes in comparison to the controls, as well as allowing the production of glycosaminoglycans. Compressive Young's modulus evaluation revealed that multizone scaffolds possess suitable mechanical properties similar to that of the native cartilage in comparison to the controls. All vitamin E scaffolds display a fibrous architecture which allowed cellular attachment and viability. Vitamin E scaffolds exhibited antioxidant capabilities which were noted through the reduction of hydrogen peroxide (Fig 2). Moreover, trends in the expression of key genes and DNA quantification were also noted.

Conclusion

Multizone scaffolds provide a viable initial platform which captures the complex structure and compressive properties of the native cartilage, as well as maintain chondrocyte phenotype and function, highlighting it's potential in cartilage tissue engineering applications. In specific, multizone scaffolds influence gene expression of chondrocytes as demonstrated by the expression of Collagen II and Aggrecan. Hybrid PCL/vitamin E scaffolds were successfully fabricated using electrospinning which supported cell attachment and viability. These scaffolds also displayed antioxidant capabilities, as shown through the reduction of hydrogen peroxide and the modulation of lactate dehydrogenase, an oxidative stress marker. Future long-term studies with bioactive multizone scaffolds are needed to determine the full potential of these scaffolds.

References

1. Fox S *et al.* Sports Health. 1: 461-468, 2009
2. Bhatti F *et al.* Inflammation Research. 62: 781-789, 2013.
3. Yudoh K *et al.* Arthritis Research & Therapy. 7: 380-391.

Acknowledgement

EPSRC and MRC grant MR/L012766/1.

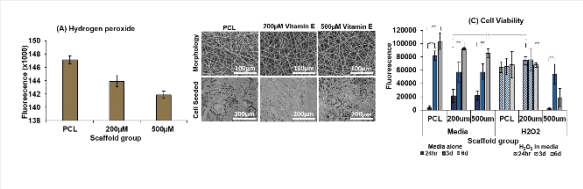

Figure 2:
(A) All scaffolds display a fibrous architecture. **(B)** Antioxidant capabilities of vitamin E scaffolds noted through the reduction of hydrogen peroxide in the culture media after 24 hours.

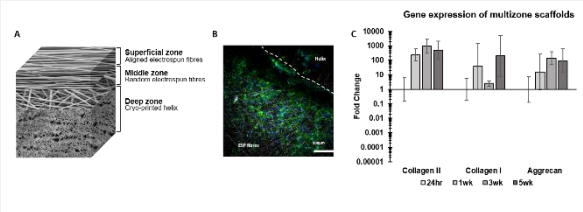

Figure 1:
(A) Illustration of the various layers of the multizone scaffold. **(B)** Chondrocytes attached on multizone scaffold at 24 hours. **(C)** Gene expression of multizone scaffolds.

10:30 a.m. – 12:00 p.m.

Hall 5

IV-SY7 | Adaptive functional biomaterials

Manfred Maitz (Dresden, DE)
Carsten Werner (Dresden, DE)

Living tissues are regulated by multiple molecular feedback systems. Current biomedical implants and drug delivery systems lack such interactive properties and often impair the function of these fine-tuned systems. The development of biomaterials capable of adapting their bioactive functions in faithful response to the physiological status of the recipient's organism will create unprecedented possibilites for future medical devices. This session will cover recent related approaches to adaptive functional materials targeting various different applications.

IV-SY7-KL01

Sequence-Encoded Peptide Pigment Materials

Ayala Lampel[1,2], Scott A. McPhee[2], James Aramini[2], Ye He[2], Rein V. Ulijn[2,3,4]

[1]Tel Aviv University, School of Molecular Cell Biology and Biotechnology, George S. Wise Faculty of Life Sciences, Tel Aviv, IL; [2]City University of New York (CUNY), Advanced Science Research Center (ASRC) at the Graduate Center, New York, US; [3]City University of New York, Hunter College, Department of Chemistry, New York, US; [4]Graduate Center of the City University of New York, Ph.D. program in Biochemistry and Chemistry, New York, US

Biological systems employ a precise spatiotemporal control of enzymatic catalysis for construction of functional materials. This control is achieved by supramolecular templating of biocatalytic action or by compartmentalization of enzymes and reactants in confined spaces within the cell. Construction of functional synthetic materials, by contrast, is mostly focused on formation of bulk structures, with spatial and temporal elements only recently considered. A natural system which requires such regulation is the biosynthesis of melanins, a class of pigments found across all life forms and provide coloration, protection from photo- and free radical-induced cell damage, metal chelation and anti-oxidant activity[1]. While these pigments are made from chemically simple building blocks, their biosynthesis and assembly relies on tightly regulated processes, which are both temporally and spatially controlled[2] and further fine-tuned by incorporation of locally available metabolites. In contrast, the laboratory-based synthesis of melanin is a poorly controlled process resulting in formation of an insoluble material. Unlike supramolecular systems, where order dictates function, the disorder in melanin is important for its functionality, hence, balancing between order and disorder is key for controlling pigment properties.

To address this major challenge, we designed tyrosine-containing self-assembling tripeptides as precursors for the catalytic formation of polymeric pigments[3]. We showed that the supramolecular order of peptide substrates is encoded by their sequence[4], and demonstrated the sequence-structure relationships underlying these assemblies. The level of supramolecular order, in turn, controls substrate accessibility, leading to a sterically and kinetically controlled enzymatic oxidation and polymerization pathway, resulting in pigment materials with a range of properties, depending on the peptide sequence. Furthermore, inspired by the natural mechanism to form variety of melanin pigments, which simply relies on reactive incorporation of the amino acid cysteine into oxidized tyrosine, we contemplated that the optical properties of melanin-like pigments can be expanded and tuned. For this, we developed melanosome-like peptide microparticles as reactive template that can react with amino acids to form new types of chromophores. Thus, mimicking firstly the natural brown/black eumelanin and the yellow/red pheomelanin with cysteine added, but then taking it much further by including other amino acids in the feed, giving rise to *in situ* formation of new peptide chromophores[5]. The resulting particles have customizable properties that mimic, but go far beyond those observed in natural melanins, with coloration and tunable fluorescence emission that is encoded by the side-chain of the incorporated amino acid, ranging from blue to far-red, suggesting applications in sensing of amino acids and other metabolites.

References

1. d'Ischia, M. et al. Melanins and melanogenesis: from pigment cells to human health and technological applications. *Pigment Cell Melanoma Res.* 28, 520-544, 2015.

2. Raposo, G. & Marks, M. S. Melanosomes--dark organelles enlighten endosomal membrane transport. *Nat. Rev. Mol.Cell Biol.* 8, 786-797, 2007.

3. Lampel, A. et al. Polymeric peptide pigments with sequence-encoded properties. *Science* 356, 1064-1068, 2017.

4. Lampel, A., Ulijn, R. V., Tuttle, T. Guiding principles for peptide nanotechnology through directed discovery. *Chem. Soc. Rev*. 47, 3737-3758, 2018.
5. Lampel, A. et al., *In prep*.

IV-SY7-KL02

Leverage Physiology for Bioresponsive Cancer Immunotherapy

Zhen Gu, Qian Chen

University of California, Los Angeles, Bioengineering, Los Angeles, US

Introduction

Cancer recurrence after surgical resection remains a significant cause of treatment failure[1,2]. Here, we developed an in situ formed immunotherapeutic bioresponsive gel, that controls both local tumor recurrence after surgery and metastatic tumor spread. Briefly, calcium carbonate nanoparticles pre-loaded with the anti-CD47 antibody are encapsulated in fibrin and scavenge H+ in the surgical wound, allowing polarization of tumor associated macrophages to M1-like phenotype1[3]. The subsequently released anti-CD47 antibody blocks the “don’t eat me” signal in cancer cells, thereby increasing phagocytosis of cancer cells by macrophages. Macrophages can promote an effective antigen-presentation and initiate T-cell mediate immune responses that control tumor growth at distant sites. Our findings indicate that the immunotherapeutic fibrin gel “awakens” the host innate and adaptive immune systems to inhibit both local tumor recurrence post-surgery and metastatic spread.

Experimental Methods

Here, the sprayed bioresponsive immunotherapeutic fibrin gel has been engineered to inhibit the local tumor recurrence and metastasis after surgery. The fibrin gel is a US Food and Drug Administration approved material, formed via the interaction of fibrinogen and thrombin. It has unique merits for biomedical applications including excellent biocompatibility, convenient sprayable administration method for post-surgical treatment and ability to promote wound healing via creating a temporary shield to connect and protect injured tissues. Biocompatible $CaCO_3$ nanoparticles (NPs) were incorporated into the fibrin gel to serve as a release reservoir of immunomodulatory therapeutics as well as proton scavenger to modulate the tumor environment acidity. The fibrinogen solution containing anti-CD47 antibody-loaded $CaCO_3$ NPs (aCD47@$CaCO_3$) and thrombin solution could be quickly sprayed and mixed within the tumor resection cavity after surgery to form an immunotherapeutic fibrin gel in situ.

Results and Discussion

The simple post-surgical cancer immunotherapy strategy by spraying in situ formed therapeutic gel at the tumor resection site, which could facilitate to reverse the immunosuppressive tumor microenvironment (TME) and induce systemic immunological responses that inhibit both local and metastatic tumor recurrence. $CaCO_3$ NPs embedded in the gel matrix could help release therapeutics in a controlled manner and modulate the acidic and inflamed tumor resection environment by capturing H+, thereby promoting antitumor immune responses. Furthermore, the locally released aCD47 from $CaCO_3$ NPs blocked the “don’t eat me” signal associated with cancer cells, allowing cancer cell removal by macrophages. CD47 blockade also triggered the T cell-mediated destruction of cancer cells owing to the enhanced presentation of tumor-specific antigen by macrophages and DCs. In the metastatic tumor model, the number of M1-like TAMs and CD103+ DCs were significantly increased in tumors sprayed with aCD47@CaCO3@Fibrin, and CD8+ T cells were increased in both treated and distant tumors. The increased CD8+ T cells in the distant tumor can be attributed to local cross-presentation of tumor antigens by macrophages and DCs that trigger systemic antitumor immunity. The activation of immune system was further confirmed by the peritumoral injection of aCD47@CaCO3@Fibrin by a dual-syringe administration method. aCD47@CaCO3@Fibrin-mediated treatment inhibited the growth of both local and distant tumor effectively.

Conclusion

In summary, we have developed an in situ sprayed immunotherapeutic gel that could reverse the immunosuppressive TME to prevent the local cancer recurrence and induce systemic antitumor immunological responses to restrain existing metastasis.

References

1. Wang, C. et al. In situ activation of platelets with checkpoint inhibitors for post-surgical cancer immunotherapy. Nat. Biomed. Eng. 1, 0011 (2017).
2. Wang, C. et al. In situ formed reactive oxygen species–responsive scaffold with gemcitabine and checkpoint inhibitor for combination therapy. Sci. Transl. Med. 10, eaan3682 (2018).
3. Chen, W. et al. In Situ Sprayed Bioresponsive Immunotherapeutic Gel for Post-Surgical Cancer Treatment. Nat. Nanotechnol., 14, 89 (2019).

Acknowledgement

This work was supported by grants from start-up packages from UNC/NC state and UCLA, the Jonsson Comprehensive Cancer Center at UCLA, the Alfred P. Sloan Foundation (Sloan Research Fellowship), the National Key R&D Program of China (2017YFA0205600), the Program for Guangdong Introducing Innovative and Enterpreneurial Teams (2017ZT07S054) and the National Natural Science Foundation of China (51728301). The authors thank L. Huang at UNC at Chapel Hill for providing the B16F10-Luc-GFP.

IV-SY7-03

Hydrogels for inflammation-responsive release of immunomodulatory bioactives

Tina Helmecke, Dominik Hahn, Manfred F. Maitz, Carsten Werner

Leibniz Institute of Polymer Research Dresden, Institute Biofunctional Polymer Materials, Dresden, DE

Introduction

Medical devices and the contained biomaterials can activate immunological processes potentially causing adverse reactions of the recipients. To address that problem, activation-responsive surface coatings are considered a promising approach for the administration of immunomodulatory drugs. Peptide-crosslinked biohybrid poly(ethylene glycol) (starPEG)-heparin hydrogels were customized for the delivery of different anti-inflammatory molecules triggered by elastase released from activated poly-morpho-nuclear neutrophil granulocytes (PMN).

Experimental Methods

A serum-free *in vitro* inflammation system was established. For that purpose, isolated granulocytes were artificially activated by zymosan particles, triggering cell activation and PMN elastase release. Covalently crosslinked, PMN elastase responsive starPEG-heparin hydrogels were formed by incorporating a cleavable peptide linker with the core sequence AAPV. Release studies were carried out by fluorescent labelling of the cleavable peptide as model for a hydrogel conjugated inhibitor molecule. Finally, a derivative of the complement receptor blocker PMX53 was covalently conjugated to the hydrogel *via* the PMN elastase sensitive peptide linker (Fig. 1). The functionality of the system was demonstrated in a two-step granulocyte incubation assay.

Results and Discussion

The hydrogel degradation by both administered and granulocyte-released elastase was observed to follow a direct dependency on the enzyme concentration. A fluorescent peptide was detected as a drug model substance showing an enzyme mediated release of pharmacologically relevant concentrations (Fig. 2).
As a potential drug conjugate, a PMX53 derivative was shown to bind its cell surface receptor, antagonizing the C5a mediated cell activation. The hydrogel cleavage by granulocyte derived elastase was observed to result in a release of PMX53 amounts, sufficient to inhibit the activation of granulocytes.

Conclusion

Peptide-crosslinked biohybrid poly(ethylene glycol) (starPEG)-heparin hydrogels provide a versatile platform for the adaptive release of various anti-inflammatory drugs. Ongoing experiments aim at testing the adaptive administration of cyclosporine A and compstatin by means of this approach. The presented results support the feasibility of adaptive release systems for anti-inflammatory substances to be potentially used for the coating of blood contacting biomaterials.

Acknowledgement

Financial support from the Federal Ministry of Education and Research (Project RESPONSE - Partnerschaft für Innovation in der Implantattechnologie) is gratefully acknowledged.

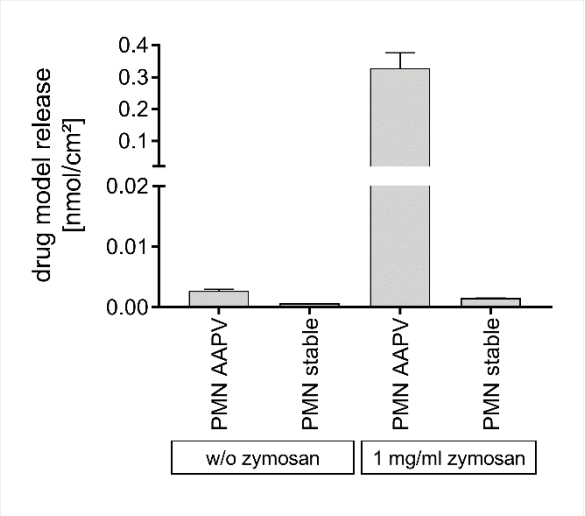

Figure 2
Degradation of PMN elastase-responsive and non-cleavable starPEG-heparin hydrogels containing a fluorescent drug model substance. Isolated PMN in a serum-free in vitro inflammation model effectively triggered a release of the drug model substance in physiologically relevant concentrations.

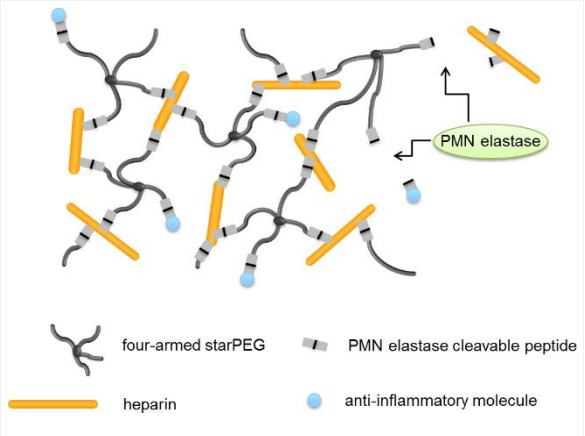

Figure 1
Schematic view of the delivery of anti-inflammatory molecules from a PMN elastase degradable hydrogel.

IV-SY7-04

Designing stimuli-sensitive hydrogels for localized therapeutic delivery

Gianluca Ciardelli, Rossella Laurano, Alessandro Torchio, Monica Boffito

Politecnico di Torino, Dep. of Mechanical and Aerospace Engineering, Turin, IT

Introduction

Injectable hydrogels for the targeted and localized release of therapeutics are a promising tool in the treatment of a wide variety of pathologies. Thermo-sensitive hydrogels which sol-to-gel transition is driven by temperature increase over a critical value have gained increasing interest in the biomedical field over the last decades. These systems can easily encapsulate biomolecules in mild conditions by simply dispersion and then release *in loco* their payload with a controlled and sustained kinetics. Additionally, further degrees of sensitivity to the physiological environment, such as to the pH of the surrounding fluids, can be provided to the gels by properly tuning the chemistry of the hydrogel-forming materials. In this contribution a library of thermo-sensitive hydrogels was designed starting from newly-designed poly(ether urethane)s (PEUs). pH-sensitive moieties (i.e., amino and carboxylic groups) were also introduced along PEU backbone to enhance gel responsivity to surrounding acid or alkaline environments.

Experimental Methods

Poloxamer 407 was reacted with a non-toxic diisocyanate and chain extended with commercially available diols (N-Boc Serinol or 1,4-cyclohexanedimethanol) (Boffito M. et al., 2016). To provide PEUs with pH sensitivity, amino or carboxylic groups were exposed on PEU chains by deprotecting BOC-protected amino-groups of N-Boc Serinol, or by plasma treating the polymer powder in the presence of acrylic acid vapor. PEUs were characterized by Size Exclusion Chromatography (SEC), Infrared (IR) Spectroscopy, Proton Nuclear Magnetic Resonance and colorimetric quantification of exposed functional groups. Thermo-sensitivity of PEU aqueous solutions (concentration within 10-20 %w/v) was characterized by tube inverting test and rheological analysis. Gel capability to transmit the pH of the surrounding medium through their thickness was evaluated by placing them in contact with buffers at different pH (4÷8). The effects of pH on gel network were assessed by stability tests in aqueous environment, to evaluate both gel swelling and residence time. Release profile of model and anti-inflammatory drugs (e.g., cumarin, ibuprofen) was evaluated at different pH to assess the capability of the surrounding environment to tune payload release. Injectability was also tested in different conditions by three potential users

Results and Discussion

PEU successful synthesis was demonstrated by IR spectroscopy and SEC ($M_n \approx 55000$ Da, D=1.3). Functional groups were successfully exposed along PEU backbone, and both deprotection reaction and plasma treatment did not induce changes on PEU chemical properties. PEU aqueous solutions with concentration in the range 10-20 %w/v showed gelation temperature within 26 and 32 °C, with a complete sol-to-gel transition at 37 °C within 5 minutes. Injectability of the designed systems was demonstrated at different temperatures (5, 25 and 37 °C) through G22, G18 and G14 needles. Amino and carboxylic group exposure did not significantly affect hydrogel thermo-sensitivity, but they effectively made the gels more sensitive to the pH of the surrounding environment. An increase in gel capability to transmit the pH of the surrounding aqueous environment through their thickness was observed in the gels exposing functional groups. pH change between the pH of the polymer solutions and the pH of the buffer within the first hour of observation was approx. 65, 80 and 90 % in unmodified, -COOH grafted and amino-functionalized

PEU gels, respectively. pH indicators (bromocresol purple and phenol red) were also added to the hydrogels to assess the progression of the acid/basic gradient through their thickness. Model and anti-inflammatory drugs were progressively released with a kinetics affected by pH variation, as a consequence of hydrogel network changes, in accordance with results of stability test in aqueous environment (e.g., unmodified and -COOH grafted PEU gels showed a 1.1 and 3.3 % swelling in alkaline medium, respectively).

Conclusion

Amphiphilic PEUs which aqueous solutions with proper composition can undergo a temperature-driven gelation were designed. Improved pH sensitivity was provided through the exposure of amino or carboxylic groups along PEU chains. Hence, a new library of stimuli-sensitive hydrogels was defined, with high sensitivity to the surrounding environment, injectability in different conditions and fast gelation in physiological conditions, which make them highly promising in the biomedical field for localized payload delivery.

Acknowledgement

This work was financially supported by the Horizon 2020 European Union funding for Research & Innovation (H2020-NMP6-2015) project “MOZART” (MesopOrous matrices for localiZed pH-triggered releAse of theRapeuTic ions and drugs).

10:30 a.m. – 12:00 p.m.

Conference room 4+5

IV-OS14 | Cell material interactions 1

IV-OS14-01

The Effect of Nanoscale Surface Electrical Properties of Biodegradable PEDOT-*co*-PDLLA Conducting Polymers on Protein Adhesion Investigated by Atomic Force Microscopy

Aruã C. Da Silva[1], Michael J. Higgins[2], Susana I. Córdoba de Torresi[1]

[1]Universidade de São Paulo, Instituto de Química, São Paulo, BR; [2]University of Wollongong, Intelligent Polymer Research Institute, Wollongong, AU

Introduction

Living cells secrete extracellular matrix (ECM) proteins such as fibronectin, vitronectin and laminin to support adhesion, migration, proliferation and differentiation and other processes (e.g. assembly of ECM in fibrillogenesis and mechanotransduction) that are important for cell function.[1]

Understanding the interactions of proteins will be particularly important for the development of new biomaterials.[2,3]

In a previous study, we have presented the synthesis and characterization a novel conducting and biodegradable copolymer of PEDOT-*co*-PDLLA in three different proportions (1:05, 1:25 and 1:50) with unique properties in terms of conductivity, biodegradability and biocompatibility towards embryonic stem cells.[4]

This study used atomic force microscopy (AFM) to elucidate the interaction of fibronectin (FN) on a conducting and partially biodegradable copolymer of poly(3,4-ethylenedioxythiophene) and poly(*D,L*-lactic acid) (PEDOT-*co*-PDLLA) in three different proportions (1:05, 1:25 and 1:50).

Experimental Methods

AFM was used to 1) better investigate the effect of nanoscale surface electrical properties, by using different modes of AFM such as standard topography, conductive maps, Kelvin probe force microscopy (KPFM), and 2) elucidate the interaction of fibronectin (FN) on the surface of PEDOT-*co*-PDLLA copolymer films by using force measurements with FN-functionalized AFM tips. For conductive modes AFM cantilevers with conductive PtIr coating was used. The PEDOT-*co*-PDLLA thin films were prepared by *spin coating* over gold-coated mylar as a conductive substrate. The SiN tip was functionalized using an aminosilanization method to covalently bind the FN according to previous studies.[5]

Results and Discussion

The copolymers with higher PEDOT:PDLLA content ratios (1:05 and 1:25) had higher surface roughness, water contact angle, with current and conductivity occurring at discrete large grain structures on the surface. In contrast, the lower PEDOT:PDLLA content ratio (1:50) did not show high conductivity grains but showed homogenous surface conductivity across the entire surface. By KPFM it was observed that the higher PEDOT content (1:05 and 1:25) presented a positively charged interface, while the lower PEDOT content (1:50) presented a negatively charged surface. Using FN-functionalized AFM probes, force measurements showed that the copolymers with higher PEDOT content (1:05 and 1:25) had significantly lower adhesion forces (~0.2-0.3 nN), while the copolymer with the lower content of PEDOT (1:50) had stronger FN interactions with significantly higher adhesion forces of 1.0 nN. Not only quantitative force with FN protein was measured, but also the qualitatively conformation of FN was evaluated, it interacts in a more folded conformation with the PEDOT-*co*-PDLLA 1:05 and 1:25 film interfaces, while interacts in a more unfolded conformation with the 1:50 film interface. By correlating the spatially distributed electrical surfaces

with FN interactions, we observed that the synthesis of 1:50 PEDOT:PDLLA produced more uniformly doped polymer films that facilitated FN adsorption through favorable interactions with accessible sulfate dopants (**Figure 1**).

Conclusion

The previous study with embryonic stem cells showed that cell adhesion, migration and differentiation are especially favorable on PEDOT-*co*-PDLLA 1:50 surfaces. This AFM study helped to explain these observations by showing that these surfaces have homogenous surface conductivity, presenting a uniformly distributed surface charge and negatively charged groups that promote greater FN binding affinity and adhesion.

References

1. Giancotti, F. G. *Science (80-.).***285,** 1028–1033 (1999).
2. Molino, P. J. *et al.Adv. Mater. Interfaces***1,** 1300122 (2014).
3. Pelto, J. M. *et al.Langmuir***29,** 6099–6108 (2013).
4. Da Silva, A. C. *et al. ACS Omega***3,** (2018).
5. Gelmi, A. *et al.Biochim. Biophys. Acta - Gen. Subj.***1830,** 4305–4313 (2013).

Acknowledgement

We gratefully acknowledge the financial support received from Brazilian agency FAPESP (proc. 2015/26308-7) and the PhD scholarship (proc. 2014/09353-6 and 2017/00705-5). Also, the financial support from Australian Research Council Centre of Excellence Scheme (Project Number CE 140100012).

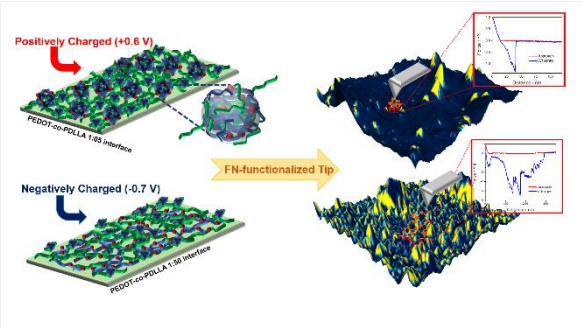

Nanoscale properties directly influences FN interaction
KPFM analysis showing differences in electrical potential (charges) on PEDOT-*co*-PDLLA interface and a schematic of protein-surface interaction using 3-dimentional topography with overlay of corresponding conductivity (yellow is conductive and dark blue is non-conductive areas, Z scale is 6 nA). PEDOT-*co*-PDLLA 1:05 with representative force curve of non-specific adhesion, while 1:50 with representative force curve of a multiple peak rupture. Scan area is 1×1 µm.

IV-OS14-02

Cell adhesion force activation on nano/micro-topographical substrates

Tamaki Naganuma

National Institute for Materials Science, Ibaraki, JP

Introduction

Cellular interaction with extracellular matrix (ECM) plays a crucial role in the inducement of signal transduction related to physiological functions. Cell adhesion to scaffold surfaces with ECM-mimicking topographies (e.g. nano/micro-rough and fibrous surfaces), therefore, has the potential to promote cell viability, migration and proliferation. This study attempts to quantitatively evaluate cell–material interaction to identify how temporal dependence of cell morphology impacts cell adhesion force activation on nano/micro-ordered topographical surfaces. Nano-rough and micro-dot/line-patterned poly-lactic acid (PLLA) substrates were prepared to assay cell detachment force by single cell force spectroscopy. This study presents findings regarding the relationship between cell adhesion force activation on nano/micro-topographical surfaces and temporal dependence of cell morphology. These findings could be useful to the development of scaffold surface design in tissue engineering applications.

Experimental Methods

Flat and micro-topological PLLA surfaces were prepared using spin-coating and molding techniques. A nano-rough PLLA surface of cerium oxide nanoparticle dispersed PLLA matrix was used as a nanocomposite scaffold surface. Osteoblast-like cells (MG63) were seeded onto the PLLA substrates at a density of 10^4 or 10^3 cells/cm^2, and maintained in minimum essential medium with 10% fetal bovine serum and 1% penicillin-streptomycin. The cell culture was maintained in an incubator with 5% CO_2 at 37 °C. Cell detachment force properties on different topographical PLLA substrates were evaluated by atomic force microscope (AFM)-based single cell force spectroscopy (SCFS). An AFM was mounted on an optical microscope, and combined with single cell force equipment (Cellhesion 200, JPK Instrument, Germany). Cells were incubated (37 °C with 10% CO_2 gas) until just before the measurement, or in a temperature control system (37 °C and 10% CO_2 gas) on the AFM. Tip-less cantilevers were used to capture a single cell. Detailed conditions of SCFS were described in the previous reports[1-2].

Results and Discussion

The SCFS result revealed that (i) a nano-rough surface, which mimics a nanocomposite scaffold, enhanced the detachment force of “spherical” cells in the initial cell adhesion period (cell adhesion time after initial attachment: t_a < 1 h), only[1]. In addition, (ii) micro-topographical surfaces such as hemispherical dot and semicylindrical line patterns, which mimic both microparticle-dispersed composite scaffolds and fibrous scaffolds, did not enhance these properties[1]. (iii) Identical micro-topographical surfaces were, however, able to gradually promote the cell detachment force of “spreading” cells in the intermediate cell adhesion period (1 < t_a < 12 h)[1]. These findings suggest that cell adhesion force activation on nano/micro-topographical surfaces alters based on cell morphology over t_a.

Conclusion

This study demonstrated how temporal dependence of cell morphology impacts cell adhesion force activation on nano/ micro-ordered topographical substrates. An understanding of the correlation between temporal dependence

of cell morphology and cell adhesion force activation on nano/ micro-topographical surfaces could be utilized in the design of scaffold surfaces, which strengthen the interaction between adherent cells and substrate materials, and subsequently to trigger physiological functions, in tissue engineering.

References

1. T. Naganuma, Nanoscale. 2017, 35 [9], 13171-13186.
2. T. Naganuma and E. Traversa, Biomaterials. 2014, 35 [15], 4441-4453.

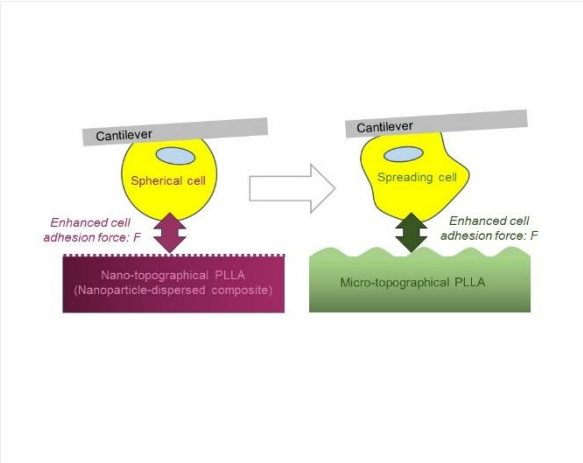

Figure 1
Schematic drawing of findings regarding the relationship between cell adhesion force activation on nano/micro-topographical surfaces and temporal dependence of cell morphology.

IV-OS14-03

Molecular weight influence on cell internalization kinetics of amphiphilic biodegradable nanoparticles decorated with hyaluronic acid

Assunta Borzacchiello[1], Francesca Della Sala[1,3], Teresa Silvestri[2], Laura Mayol[2], Marco Biondi[2], Luigi Ambrosio[1]

[1]National Research Council of Italy, Istituto per i Polimeri, Compositi e Biomateriali, Napoli, IT; [2]University of Naples, Dipartimento di Farmacia, Napoli, IT; [3]University of Campania, Dipartimento di Scienze e Tecnologie Ambientali Biologiche e Farmaceutiche, Caserta, IT

Introduction

Hyaluronic acid (HA) is an anionic polysaccharide, ubiquitously present in extracellular matrix. HA can specifically bind CD44 receptor, which is overexpressed in a wide array of cancer cells [1] and has consequently aroused a noteworthy research interest for the engineering of nanoplatforms endowed with active targeting features. HA has been chemically anchored onto many drug-loaded nanodevices [2], and their enhanced tumor targeting ability assessed [3]. Nevertheless, the need for a chemical reaction poses serious regulatory challenges for FDA approval. In this study, nanoparticles (NPs) based on poly(lactic-co-glycolic acid) (PLGA) have been produced by a modified nanoprecipitation technique. Specifically, NPs were decorated with HA by exploiting polymer self-aggregation driven by a lipophilicity gradient between oil and water phases. NPs were coated with HA at 200 and 800 kDa, and the formulations were named HA2 and HA8, correspondingly. The obtained formulations were characterized for their technological and thermodynamic features to investigate polymer assembly in NPs. The influence of HA molecular weight on uptake was assessed by kinetic internalization studies on breast carcinoma (HS578T) and healthy mouse fibroblast (L929) cells. Furthermore, the results were compared with the numerical simulations obtained with a kinetic internalization model based on a cell membrane adsorption-desorption balance.

Experimental Methods

NPs were produced by nanoprecipitation, forcing a PLGA/F68/F127 solution in acetone (1:0.5:0.5 weight ratio; 5 mL, 3% w/v) through a syringe at 333 µL/min flow rate by a Syringe Pump. The solution was precipitated into 40 mL of an aqueous phase (W1), containing F127 and F68 as surface active agents (1:1 w/w ratio; 0.05% w/v) and different amounts of HA (3.75 and 0.81 mg/mL for HA 2 and HA8 NPs, respectively). The organic solvent was evaporated overnight, and the obtained NPs washed twice by centrifugation (10,000 rpm, 20 min) and stored at −80°C. NP morphology was studied by TEM, while size and z-potential (ZP) were obtained by PCS. DSC experiments on the polymers and NPs were run to study the interactions among polymers in NPs, by a double dynamic scan (10-80°C, 5°C/min) under inert nitrogen atmosphere. Cellular uptake kinetics of fluorescent NPs, prepared by adding Nile Red to the organic phase (0.1% w/v), were obtained by performing, at scheduled time points, cell lysis followed by a spectrofluorimetric assay on the lysate to quantify NP-associated fluorescence. Aiming to provide a numerical estimate of uptake kinetics and tropism for cancer cells, NPs internalization has been modelled a pseudo-chemical equilibrium relation at cell membrane, as mathematical model described previously [4].

Results and Discussion

Spherical NPs with a < 200 nm mean size were obtained (Fig 1). ZP was < -50 mV in all cases, thereby indicating HA arrangement on NP surface.DSC traces show that, for PLGA and poloxamers, glass transition temperature (Tg) is lower than that of PLGA, suggesting a plasticizing effect of poloxamers in the organic blend. In the case of NPs, a broadening of poloxamer crystallization peak and a decrease of crystallization heat (DHc) and temperature (Tc) were observed, indicating amorphous interactions with PLGA. In the first heating ramp, the Tg of PLGA is observable in NPs while, in the second scan, PLGA inflection point is no longer visible, while the areas of the endothermic peaks associated to poloxamer melting are reduced, thereby indicating the presence of poloxamer mixture and, hence, a discouraged interaction between PLGA and HA, even after the second heating ramp. NPs internalization of HA2 NPs was strongly enhanced compared to HA8 NPs (Fig 2 A). The experimental 24h-uptake of HA2 NPs is 11.6-fold higher than HA8 NPs in both cell lines. Furthermore, in the case of tumor cells, 24h-uptake extent was about 70% higher, thereby highlighting the major role of CD44 receptors in governing cell uptake.Interestingly, the results of fitting parameters of the mathematical model used (Fig 2 B) show that the binding constant for HA2 NPs is 6-fold higher compared to HA8 NPs as for HS578T cells, while it has basically the same value for both formulations on L929 cells, thereby reinforcing the envisaged tropism. The de-binding and internalization constants kD and ki are higher for HA2 NPs, which corroborates the overall higher NMAX values, which represent the maximum number of NPs internalized at equilibrium, after a virtually infinite time.

Conclusion

Taken altogether, cell uptake experiments and model simulations indicate a significant tropism of HA-decorated NPs towards CD44-overexpressing cells and, more interestingly, a strong enhancement of NP uptake decorated with 200kDa HA. More specifically, model fitting results indicate that the rate of internalization event is strongly promoted as for HA2 NPs. These findings point at HA molecular weight as a major project parameter to endow NPs with active targeting ability in cancer treatment.

References

1. Toole, B.P., Nat Rev Cancer 4, 528-539 (2004).
2. Cho, H. J., Biomaterials 33, 1190-1200 (2012).
3. Nishiyama, N. Nature Nanotechnology 2, 203-204 (2007)
4. Belli, V., Colloids Surf B Biointerfaces. 149, 7-15 (2017).

Acknowledgement

Italian Ministry of Foreign Affairs in the frame of the Executive Program of Scientific and Technological Cooperation between Italy and Egypt (2016-2018).

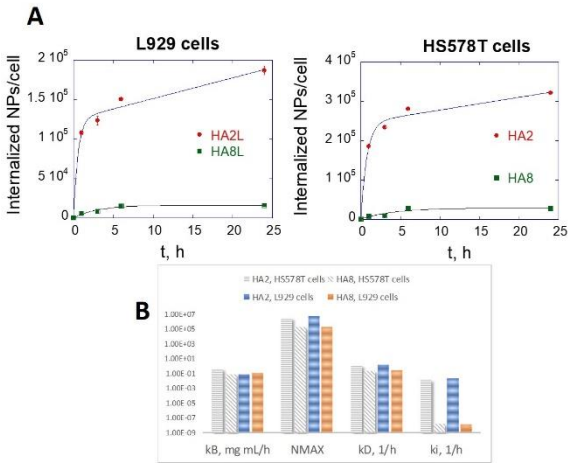

Figure 2
(A) 24-h internalization profiles of HA2 and HA8 NPs: comparison between experimental data (dots) and model simulations (solid lines). (B) Model parameters.

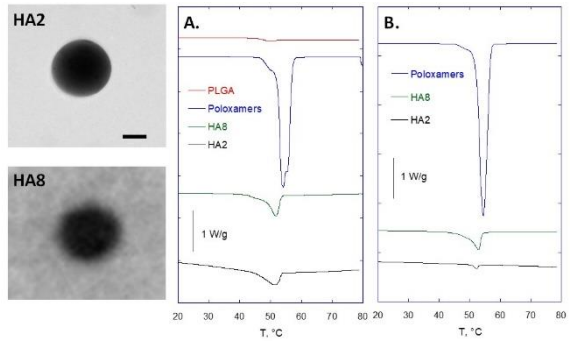

Figure 1
TEM images of HA2 and HA8 NPs. DSC traces of raw materials and NPs after: A) first and B) second scan

IV-OS14-04

3D linear stiffness gradient hydrogel to study the effect of cell volume expansion in stem cell mechanotransduction and differentiation

Yu Suk Choi[1], Luke Major[1], Andrew Holle[2], Jennifer Young[2], Joachim Spatz[2]

[1]University of Western Australia, Human Sciences, Perth, AU; [2]Max Planck Institute for Medical Research, Cellular Biophysics, Heidelberg, DE

Introduction

Recent studies suggest that dimensionality may alter cells' responses to extracellular matrix (ECM) stiffness differently in 2D and 3D culture. For example, while cell size increases at high ECM stiffness in 2D [1], cell volume has been shown to decrease at high ECM stiffness in 3D [2]. A recent study using viscoelastic hydrogels with controllable stress-relaxation characteristics has proposed that volume expansion is a key regulator of stem cell fate in 3D [3], but a complete characterization of this behaviour across a wide range of ECM stiffnesses has not yet been achieved [4].

Experimental Methods

By regulating UV exposure using a gradient photomask with 30 – 100% transparency, a gelatin methacryloyl (GelMA) linear stiffness gradient hydrogel suitable for 3D cell encapsulation was fabricated. The stiffness gradient, verified through force indentation by atomic force microscopy (AFM), was consistently reproduced from 5 to 38 kPa. Optical Coherence Elastography (OCE) confirmed the existence of a stiffness gradient in 3D by measuring compressive stiffness at a 500 mm depth. The gradient strength measured in soft hydrogel regions by both AFM and OCE were well correlated. In addition, scanning electron microscopy (SEM) revealed a decrease in mean pore area along the hydrogel gradient from 10.7 mm^2 to 2.7 mm^2. Semi-quantitative measurements of amide groups in the gradient hydrogels indicated no change in GelMa concentration across the stiffness gradient, confirming that the gradient was the result of differential UV exposure and subsequent changes in crosslinking. Adipose-derived stem cells (ASCs) were encapsulated in this hydrogel, and their morphological characteristics, as well as expression of mechanosensitive proteins (Lamin A, YAP, and MRTFa) and differentiation markers (PPARγ and RUNX2) were analysed.

Results and Discussion

Low stiffness regions (~8 kPa) permitted increased cellular and nuclear volume and enhanced mechanosensitive protein localization to nucleus. This trend was reversed in high stiffness regions (~30 kPa), where decreased cellular and nuclear volumes and reduced mechanosensitive protein nuclear-localization were observed. Interestingly, cells in soft regions exhibited enhanced osteogenic RUNX2 expression, while those in stiff regions upregulated the adipogenic regulator PPARγ, suggesting that volume, not substrate stiffness, is sufficient to drive 3D stem cell differentiation. Inhibition of myosin II (Blebbistatin) and ROCK (Y-27632), both key drivers of actomyosin contractility, resulted in reduced cell volume, especially in low stiffness regions, causing a decorrelation between volume expansion and mechanosensitive protein localization. Constitutively active and inactive forms of the canonical downstream mechanotransduction effector TAZ were stably transfected into ASCs. Activated TAZ resulted in stable cellular volume despite increasing stiffness and a consistent, stiffness-independent translocation of YAP and MRTFa into the nucleus.

Conclusion

Our results suggest that low volume stimulates adipogenesis while high volume drives osteogenesis, mirroring classical 2D work showing similar area-induced differentiation patterns. To our knowledge, this is the first multi-lineage observation extending the size-differentiation theory into three dimensions, where it may be more aptly referred to as a volume adaptation-differentiation theory. As there is a great interplay between cell volume, material stiffness, and mechanotransduction, this material can provide a holistic mechanoscape that few others offer, which is highlighted by the intriguingly novel response of stem cells to the gradient microenvironment.

References

[1] A. Engler, L. Bacakova, C. Newman, A. Hategan, M. Griffin, D. Discher, Substrate compliance versus ligand density in cell on gel responses, Biophysical journal 86(1 Pt 1) (2004) 617-628.

[2] S.R. Caliari, S.L. Vega, M. Kwon, E.M. Soulas, J.A. Burdick, Dimensionality and spreading influence MSC YAP/TAZ signaling in hydrogel environments, Biomaterials 103 (2016) 314-323.

[3] H.-p. Lee, R. Stowers, O. Chaudhuri, Volume expansion and TRPV4 activation regulate stem cell fate in three-dimensional microenvironments, Nature communications 10(1) (2019) 529.

[4] A.W. Holle, J.L. Young, K.J. Van Vliet, R.D. Kamm, D. Discher, P. Janmey, J.P. Spatz, T. Saif, Cell–Extracellular Matrix Mechanobiology: Forceful Tools and Emerging Needs for Basic and Translational Research, Nano letters 18(1) (2018) 1-8.

Acknowledgement

This study work was supported by National Health and Medical Research Council Grant PG1098449 (to Y.S.C), Heart Foundation Future Leader Fellowship 101173 (to Y.S.C) and Department of Health, Western Australia, Merit awards – project and fellowship (to Y.S.C).

IV-OS14-05

Fe/electrospun PCL hybrid structure as an innovative coronary stent

Francesca Salmistraro[1], Valeria Perugini[2], Nicola Contessi Negrini[1,3], Matteo Santin[2], Silvia Farè[1,3]

[1]Politecnico di Milano, Dipartimento di Chimica, Materiali e Ingegneria Chimica "G.Natta", Milan, IT; [2]University of Brighton, Centre for Regenerative Medicine and Devices, School of Pharmacy and Biomolecular Science, Brighton, GB; [3]INSTM, Local Unit Politecnico di Milano, Milan, IT

Introduction

Fe and its alloys are promising metallic materials for bioabsorbable stents as they have no cytotoxic effects and adequate mechanical properties[1]. From a structural point of view, iron-based alloys used as temporary biodegradable stents have several advantages over Mg-based alloys in terms of ductility and strength[2]. Iron low degradation rate could be balanced using a thin iron wire instead of a laser cut iron tube to obtain stent struts. To have a major contact with the arteries endothelial layer, reducing the turbulent blood flow and alleviating restenosis and plaque progression, in this work, polycaprolactone (PCL) was electrospun on a iron wire stent. The aim of this work is to manufacture a hybrid BRS stent, with iron stent struts coated with PCL electrospun fibres (Fe/ES-PCL). Stent samples were realised and characterised regarding morphological, mechanical, physical and biological *in vitro* properties.

Experimental Methods

Fe/ES-PCL coronary stent (Ø=6mm, l=10mm) were manufactured, using a hard tempered iron wire (Ø=0.125mm, purity = 99.5%) coiled manually to obtain the tubular stent grid. PCL (20% w/v chloroform-dimethylformamide solution) was electrospun both on the inner and outer surface of stent grid (Fig.1a), through a rotating metallic collector (d = 6mm), following the protocol and ES process parameters previously optimized.

Morphological characterisation was performed by SEM to observe the compactness of the coating and the absence of defects (e.g., beads). ImageJ software was used to quantify ES-PCL fibres diameters and their homogeneity. Fe grid, Fe/ES-PCL stent and only ES-PCL were characterized by ring-shaped tensile test.

An in vitro biological characterisation was performed on Fe/ES-PCL (Fig.2a); a physical functionalisation of the ES-PCL coating with Poly-L-Lysine laminin dendrimers was investigated. Human Umbilical Vein Endothelial Cells (HUVECs) and Human Aortic Vascular Smooth Muscle Cells (HA-VSMCs) were cultured, respectively, onto the inner and outer surface of the hybrid stent for 4, 24 and 72 h. Their adhesion, presence, morphology and interaction with the Fe/ES-PCL layers were evaluated through appropriate staining by fluorescence microscope and SEM analysis. Cytotoxicity assay (i.e., LDH assay) and protein assay (i.e., Bradford assay) were performed to verify cell viability and proliferation.

Results and Discussion

The morphological characterisation of the Fe/ES-PCL showed a outer and inner coating layer featured by a random and compact fibres disposition without defects (Fig.1b), with fibres diameter of 2.25±0.49 µm and 2.09±0.69 µm, respectively. No significant difference ($p > 0.05$) was detected in fibres diameter, showing that the inner layer and the iron grid do not affect the intensity of the electric field.

The ring-shaped tensile test displayed that the applied load is prevalently supported by the iron grid, however the ES-PCL coating deformability allows hybrid stent to reach high deformation without damage or break of the coating. This test allowed simulating the inner pressure of the blood flow which acts radially on the hybrid stent. The stress produced by the coronary pressure (i.e., 140 mmHg, high safety value) produces a stress (σ_C=0.02 MPa) on the hybrid stent much lower than the maximum stress achieved by the stent sample during the ring test (σ_{max}=6.43±2.79 MPa), confirming that the mechanical circumferential tensile properties of the hybrid stent are suitable in order to resist to the inner pressure exerted in vivo (Fig.1c).

In vitro test showed cell adhesion after 72 h, for both cell phenotypes by fluorescence microscopy and SEM. For HUVEC culture on the luminal side of the stent, a compact layer of material was deposited on ES-PCL coating. In order to investigate the nature of this observed layer, EDS analysis was performed and it confirmed cells presence, despite areas in proximity of the iron grid were featured by iron oxide. CD31 immunostaining showed cell-cell interaction and their potential ability to create a monolayer for the re-endothelisation (Fig.2b). The functionalisation with PLL-laminin (PLL-laminin_Fe-PCL) displayed a greater cell spreading, leading to assume that the biomimetic matrix promotes cell adaptation, despite the hydrophobic nature of PCL (Fig.2c). HUVECs nuclei counting showed good growth on each substrate and a greater proliferation rate was observed on PLL-laminin_Fe-PCL sample. HA-VSMCs migration through the ES-PCL fibrous coating was detected until 50% of sample thickness (Fig.2d).

Conclusion

The hybrid stent seems to provide suitable properties in terms of mechanical strength and ES-PCL adhesion to the iron grid, when compared with the in vivo stress exerted by the blood flow. A good potential endothelisation of the inner layer of the stent is assumed observing the results obtained by HUVEC culture. However, further investigation about the endothelial cells function (e.g., NO and vWF release) should be performed.

References

[1]Moravej M, Mantovani D, Int J Mol Sci 2011;12:4250

[2]Francis A, et al., J Mater Sci Mater Med 2015;26:138

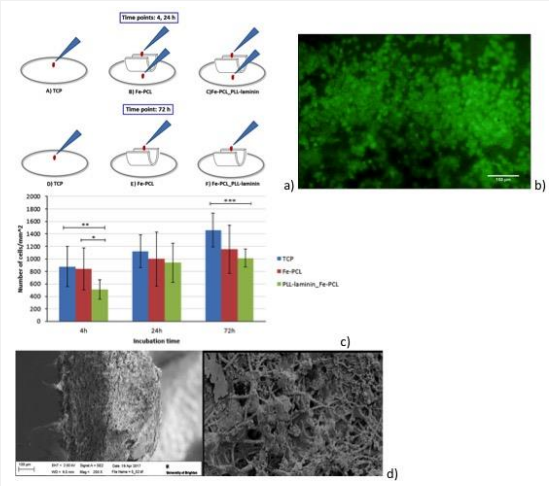

Figure 2
a) Schematic seeding process for HUVEC experiments (10 microliter drop, cell density: 3000 cell/microliter); the same procedure was used for HA-VSMC on the convex side of the sample (cell density: 2000 cell/microliter); b) CD31 immunostaining of HUVECs cultured for 72 h on Fe/ESPCL sample. Scale bar: 100 micron; c) Comparison of HUVEC proliferation rate when cultured on each substrate (TCP, Fe-PCL,PLL-laminin_Fe-PCL); d) SEM images of Fe/ES-PCL sample cross-section with HA-VSMC migrated through the fibrous coating (left) and sample outer layer (right) with HAVSMC spreading. Scale bar: 100 and 50 micron.

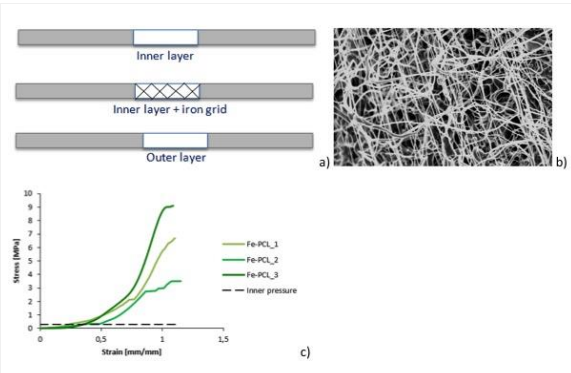

Figure 1
a) Procedure for Fe/ES-PCL stent realisation; b) SEM images of the ES-PCL layer of the iron stent grid coating. Scale bar: 50 mm; c) Stress/strain curve obtained by ring tensile test on the hybrid stent. Dotted line: stress exerted by a inner pressure equal to 140 mmHg

IV-OS14-RF06

3D bioplotting of neonatal porcine islets - towards complex co-culture systems

Sarah Duin[1], Susann Lehmann[2], Christiane Paßkönig[1], Elisabeth Kemter[4], Eckhard Wolf[4], Anja Lode[1], Michael Gelinsky[1], Barbara Ludwig[2,3]

[1]University Hospital Carl Gustav Carus and Faculty of Medicine of TU Dresden, Centre for Translational Bone, Joint and Soft Tissue Research, Dresden, DE; [2]University Hospital Carl Gustav Carus of TU Dresden, Paul Langerhans Institute Dresden of Helmholtz Centre Munich and German Centre for Diabetes Research, Dresden, Dresden, DE; [3]University Hospital Carl Gustav Carus, TU Dresden, Department of Medicine III, Dresden, DE; [4]Ludwig-Maximilians University Munich, Gene Center, Munich, DE

Introduction

Diabetes type 1 is characterized by insulin-deficiency due to autoimmune-derived destruction of the insulin-producing β-cells in the pancreas. The common therapy is treatment with exogenous insulin, however, for a subgroup of patients with highly unstable blood-glucose control transplantation of islets and reconstitution of endogenous insulin secretion would be far preferable. However, human donors for islet transplantation are sparse – donor shortage could be solved through use of xenogeneic islets. Especially with islets from a xenogeneic source separation from the host's immune system is crucial, yet supply with oxygen and nutrients as well as the ability to sense blood-glucose should not be impaired, which requires short diffusion distances.

To achieve this, a high surface-to-volume ratio of the immune-protective scaffolds, but also blood vessels in close vicinity, yet not in direct contact with the islets are indispensable.

3D plotting, an additive manufacturing technique capable of producing scaffolds of clinically relevant dimensions and incorporating biological agents, offers the possibility to embed islets in hydrogel strands[1] while attracting vascular structures to the macropores.

In this study, as a first step towards co-culture with cells with angiogenic potential, 3D plotting was used to embed neonatal porcine islet-like cell clusters (NICC) in macro-porous hydrogel scaffolds.

Experimental Methods

The hydrogel used for plotting was a paste of medical-grade alginate and methyl-cellulose (MC)[1,2] (Alg/MC) into which either NICC, human umbilical vein endothelial cells (HUVEC) or human bone marrow-derived mesenchymal stromal cells (MSC) had been incorporated prior to plotting. 3D plotting was carried out on a BioScaffolder 3.1 from GeSiM (Radeberg, Germany). All cells were cultured in a co-culture medium consisting of Ham's F-10 and endothelial cell growth medium supplemented with bovine serum albumin.

To investigate distribution and cell viability, scaffolds with islets, HUVEC or MSC were stained with MTT or calcein AM/ethidium homodimer, and cryosections of islet-containing scaffolds were stained with DAPI and TUNEL. Presence of insulin was studied via dithizone staining of whole scaffolds, and localization of insulin and glucagon inside the islets through immunofluorescence-staining of cryosections. For glucose stimulated insulin response of plotted islets, both islet-containing scaffolds and free control islets were incubated in Krebs-Ringer buffer supplemented with either 3.3 or 16.4 mM glucose and glucagon-like peptide 1 (GLP1). Insulin content was analysed by quantification of secreted insulin with ELISA and normalization to the DNA content determined by QuantiFluor assay.

Suitability of the Alg/MC blend for diffusion of glucose and insulin was tested with an osmosis chamber.

Results and Discussion

By comparison to free islet cultures, we were able to show that neither incorporation of islets into the material nor the plotting process itself had a deleterious effect on islet morphology. MTT-staining demonstrated an even distribution and metabolic activity of islets inside the plotted scaffolds, and Live/Dead as well as TUNEL stainings indicated survival of encapsulated islets for as long as 21 days. Live/Dead staining also showed that HUVEC and MSC survive embedding and plotting and all cells tolerate the co-culture medium well.

Dithizone and immuno-fluorescence-stainings confirmed that insulin and glucagon are continuously produced and adequately located in encapsulated islets. Our data also suggest adequate diffusion of glucose and insulin and that with supplementation of GLP1 plotted NICC can be stimulated to release insulin in response to high glucose. Furthermore, protection of islets from human serum was comparable between islets encapsulated in the hydrogel blend and islets encapsulated in plain alginate beads.

Conclusion

This study introduces 3D bioplotting of neonatal porcine islets as a promising strategy for the immune-protection and vascularization of 3D constructs containing xenogeneic islets.

References

1 Duin S. *et al.* Adv. Healthcare Mater., 2019, 1801631

2 Schütz K. *et al.* J. Tissue Eng. Regen. Med. 2017, 11, 1574-1587

Acknowledgement

The authors thank the microscopy facility CFCI of the TU Dresden for providing equipment and support in cell imaging, and the German Centre for Diabetes Research (DZD) as well as the Faculty of Medicine *Carl Gustav Carus* of Technische Universität Dresden for financial support.

IV-OS14-RF07

Synthesis, characterization and antibacterial activity of alginate nanoparticles containing nitric oxide donor and silver nanoparticles

Amedea B. Seabra[1], Alessandro L. Urzedo[1], Marcelly C. Gonçalves[2], Mônica H. M. Nascimento[1], Gerson Nakazato[2], Christiane B. Lombello[3]

[1]Universidade Federal do ABC, Center for Natural and Human Science, Santo André, BR; [2]Universidade Estadual de Londrina, Department of Microbiology, Londrina, BR; [3]Universidade Federal do ABC, Center for Engineering, Modeling and Applied Social Sciences, Santo André, BR

Introduction

Silver nanoparticles (AgNPs) have gained considerable attention in recent years due to their potential applications as antimicrobial agent. Nitric oxide (NO) is an important endogenous molecule that controls several physiological functions. Both AgNPs and NO have antibacterial effects, and recently our group demonstrated the synergist effect of NO donors allied to AgNPs.[1] As NO is a free radical, NO donors, such as S-nitrosothiols, are used in biomedical applications to release NO.[2] Alginate is a biocompatible and biodegradable polymer, extracted from brown algae, extensively used in pharmacological applications. In this work, AgNPs, synthesized by green tea extract, and S-nitrosomercaptossunic acid (S-nitroso-MSA), a NO donor, were incorporated in alginate nanoparticles. The obtained nanoparticles were characterized by different techniques and their antibacterial activity was evaluated against different bacterial strains of medical interest.

Experimental Methods

AgNPs were synthesized by reducing Ag^{+} to Ag^{0} using green tea extract (*Camellia sinensis*), which is rich in polyphenols. The phytochemicals from green tea act not only as reducing agent but also as capping agent, stabilizing AgNPs. Green tea synthesized AgNPs were characterized by X-ray Diffraction (XRD) and Dynamic Light Scattering (DLS). S-nitroso-MSA (NO donor) was synthesized by the nitrosation reaction of mercaptosuccinic acid (a thiol containing molecule) with equimolar amount of sodium nitrite. Alginate nanoparticles were prepared by ionotropic gelation with calcium chloride in aqueous medium. Alginate nanoparticles containing AgNPs and/or S-nitroso-MSA were characterized by Fourier-transform infrared spectroscopy (FTIR), Atomic Force Microscopy (AFM), Dynamic Light Scattering (DLS), and Nanoparticle Tracking Analysis (NTA). The encapsulation efficiency of S-nitroso-MSA into alginate nanoparticles was measured. Kinetics of free NO release from alginate nanoparticles was monitored for 12 h, at physiological temperature. In addition, kinetics of the diffusion of the NO donor (S-nitroso-MSA) from alginate nanoparticles was monitored in a Franz vertical diffusion cell, with a cellulose membrane. The kinetic profiles of S-nitroso-MSA diffusion from the nanoparticles were fitted to mathematical models. *In vitro* cytotoxicity of the nanoparticles was evaluated in Vero fibroblast cell line. The antibacterial activity of the nanoparticles was characterized by measuring the minimum inhibitory concentration (MIC) and minimum bactericidal concentration (MBC) of the nanoparticles against *Escherichia coli* ATCC 25922, *Staphylococcus aureus* ATCC 25923, *Streptococcus mutans* ATCC UA159.

Results and Discussion

Green tea synthesized AgNPs presented face centered cubic lattice with size of 34.7± 4.9 nm, polydispersity index (PDI) of 0.28 ± 0.01. Alginate nanoparticles have average size of 32 nm, as assayed by AFM, and hydrodynamic size of 271.93 ± 8.99 nm and PDI of 0.398 ± 0.021, as assayed by DLS and NTA. Encapsulation efficiency of the NO

donor into alginate nanoparticles was found to be 98.74 ± 0.08%. NO release from alginate nanoparticles was found to be sustained for at least 12 h at 37 °C, with an initial rate of 14.199 ± 0.325 mmol/L.h^{-1}. Diffusion of S-nitroso-MSA from alginate nanoparticles indicates a change on nanoparticle surface. A concentration dependent toxicity was observed for NO-releasing alginate nanoparticles, and the nanoparticles were found to be toxic to Vero cells at higher tested concentrations (1 and 3 mmol/L). AgNPs and alginate nanoparticles containing AgNPs and/or S-nitroso-MSA demonstrated antibacterial activity against all tested bacterial strains. MIC and MBC values for alginate nanoparticles containing AgNPs and S-nitroso-MSA were in the rage of 78 mg.L^{-1} to 310 mg.L^{-1}.

Conclusion

This work describes the synthesis and characterization of alginate nanoparticles containing green tea synthesized AgNPs and/or S-nitroso-MSA (a NO donor). The materials prepared were characterized by different techniques. Kinetic measurements showed a sustained NO release from the nanoparticles for at least 12 h, at physiological temperature. The nanoparticles showed a concentration dependent toxicity to Vero cells. In addition, alginate nanoparticles containing AgNPs/S-nitroso-MSA showed potent antibacterial activities against clinically relevant bacteria strains, at concentrations found not toxic to Vero cells. Therefore, alginate nanoparticles containing AgNPs and S-nitroso-MSA might find important biomedical applications in the combat of bacterial infection.

References

1. SEABRA, A. B. et al. *J. of Phys.: Conference Series.* 838(1):12-31, 2017.
2. WANG, P. G. et al. *Chem. Rev.* 102(4):1091–1134, 200

Acknowledgement

Authors have appreciated the support from CNPq, FAPESP (2018/08194-2), and Multiusers Experimental Central of UFABC.

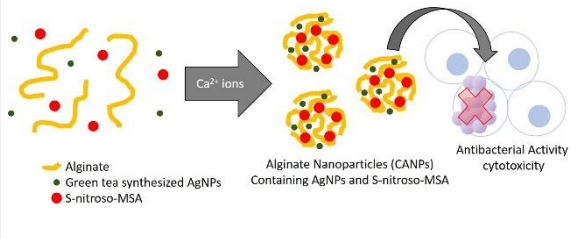

Schematic representation of alginate nanoparticles containing AgNPs and nitric oxide donor

Alginate nanoparticles containing green tea synthesized silver nanoparticles (AgNPs) and the nitric oxide donor (NO donor)

S-nitroso-MSA for antibacterial effects.

IV-OS14-RF08

The physical properties of collagen biomaterials determine their degradation kinetics and angiogenesis within the biomaterial

Carlos Herrera-Vizcaino, Sarah Al-Maawi, Joseph Choukroun, Robert Sader, Shahram Ghanaati

University Hospital Frankfurt Goethe University, Department for Oral, Cranio-Maxillofacial and Facial Plastic Surgery, FORM (Frankfurt Orofacial Regenerative Medicine) Laboratory, Frankfurt am Main, DE

Introduction

Previous observations of implanted biomaterials *in vivo* and clinically, indicate, that the physicochemical characteristics of a biomaterial determine the inflammatory cellular response. The focus of this study was to investigate how the physical properties of a collagen biomaterial influence the inflammatory milieu of a cell complex *in vitro* and the biomaterial-cellular reaction in vivo. For this purpose, the physical characteristics of an equine-derived collagen biomaterial were modified while preserving the same chemical properties and compared to its original presentation.

Experimental Methods

The biomaterial's physical characteristics were altered by applying external pressure using a sterile stainless steel cylinder until the material was flattened. A sponge collagen biomaterial (Parasorb fleece HD®; PF) and the pressed biomaterial (PF-P) were cut into segments of 1 cm^2. Ex vivo, the biomaterials were cultured during 3 and 6 days with a cell complex derived from human blood called platelet-rich fibrin (PRF) and histologically stained. The supernatant was collected and the concentration of pro-inflammatory growth factors (TNF-alpha and IL-8) was measured using ELISA. The results from culturing PRF alone were used as a baseline. Subsequently, the biomaterials were implanted in Wistar rats using a subcutaneous model and compared to a control group sham-operated (CG). The biomaterials were explanted at 3, 15 and 30 days. The samples were histologically and immunohistologically stained with CD 68 antibody (monocyte lineage), CD206 (M2 macrophages) CCR7 (M1 macrophages) and α-Smooth Muscle Actin (α-SMA; vessel identification). The results were qualitative and quantitative evaluated to assess the biomaterial's degradation kinetics, macrophages polarization into M1/M2, multinucleated giant cells (MNGCs) and the vascularization pattern. Statistically analyses were carried out with intra and inter-groups comparison.

Results and Discussion

Ex vivo: histologically, the depth of penetration of cells into the biomaterial's body differed between the two biomaterials. PF allow the penetration of cells and PF-P impede cells penetration. The cell culture of PRF+PF-P produced higher concentrations of TNF-α and IL-8 compared to PRF+PF after day 3 (P <0.05) and to PRF alone after 3 and 6 days (P <0.05). *In vivo*: after 3 days of implantation, both biomaterials were found in the implantation bed. PF maintained its pores structure and cells penetrated PF's surface. PF-P preserve the appearance of a pressed structure and cells were accumulated on the surface. The inflammatory reaction of both biomaterials was mainly composed of CD68 + cells and M1. The number of CD68+, M1 and M2 cells/mm2 in the CG were higher than the experimental groups (P <0.05). After 15 days, PF was fully invaded by cells, the presence of vascular lumens was identified inside the biomaterial's center (P<0.5) and showed a faster degradation of its structure compared to PF-P (P <0.05). Cells in PF-P invaded only the outer-third of the biomaterial's body, vascular lumens were observed surrounding the biomaterial and the biomaterial preserved its structure. Both groups showed a higher inflammatory

reaction composed of positive CD-68+ cells and M1 without statistical differences. The inflammatory reaction in the CG reduced considerably and was statistically significant compared to the experimental groups (P<0.5). A few numbers of MNGCs were observed in experimental groups. After 30 days PF and PF-P fully degraded. CD68+ cells and MNGCs expressing the CCR7 marker were observed surrounding the remaining fibrils of the biomaterials. Micro-vessels were observed within the implantation bed. The implantation area seems to be achieving homeostasis and entering a reparative stage as a similar shift towards an anti-inflammatory pattern was observed in the control and the experimental groups, characterized by a transition towards a higher presence of M2 macrophages.

Conclusion

Changing the biomaterials physical characteristics induced a statistically significant higher inflammatory protein release ex vivo during the early time point of cultivation. Additionally, it was shown to have an effect over the biomaterial's degradation kinetics, vascularization pattern and the inflammatory cellular reaction. A collagen biomaterial of equine origin induced an inflammatory cellular reaction and degradation governed by macrophages, mainly M1, with a reduced number of MNGCs. The remaining MNGCs in the implantation bed expressing the pro-inflammatory marker CCR7 after 30 days, support their involvement in chronic inflammation.

References

Ghanaati, M. Schlee, M.J. Webber, I. Willershausen, M. Barbeck, E. Balic, C. Görlach, S.I. Stupp, R.A. Sader, C.J. Kirkpatrick, Evaluation of the tissue reaction to a new bilayered collagen matrix in vivo and its translation to the clinic, Biomed. Mater. 6 (2011). doi:10.1088/1748-6041/6/1/015010.

S. Ghanaati, Non-cross-linked porcine-based collagen I-III membranes do not require high vascularization rates for their integration within the implantation bed: A paradigm shift, Acta Biomater. 8 (2012) 3061–3072. doi:10.1016/j.actbio.2012.04.041.

S. Al-Maawi, A. Orlowska, R. Sader, C. James Kirkpatrick, S. Ghanaati, In vivo cellular reactions to different biomaterials—Physiological and pathological aspects and their consequences, Semin. Immunol. 29 (2017) 49–61. doi:10.1016/J.SMIM.2017.06.001.

Choukroun, S. Ghanaati, Reduction of relative centrifugation force within injectable platelet-rich-fibrin (PRF) concentrates advances patients' own inflammatory cells, platelets and growth factors: the first introduction to the low speed centrifugation concept, Eur. J. Trauma Emerg. Surg. 44 (2018) 87–95. doi:10.1007/s00068-017-0767-9.

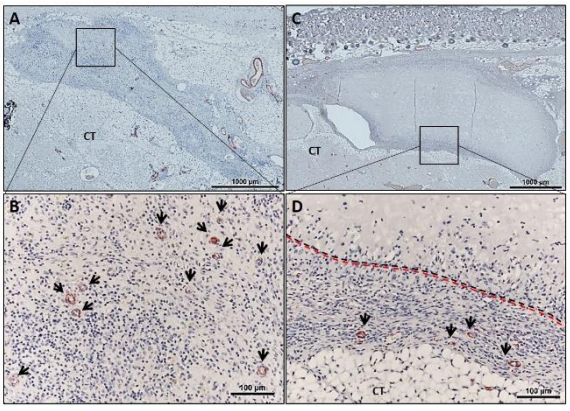

In vivo biomaterial implantation
Collagen biomaterial in its original form (PF; **A-B**) and pressed biomaterial (PF-P; **C-D**). After 15 days of post-implantation, cells have invaded PF completely and it is showing signs of degradation (**A**). Cells remain on the surface and outer third of PF-P with no signs of biomaterial degradation (**C**). The dash lines represent the perimeter of the biomaterials. Vascular structures are pointed by arrows (**B, D**) with alpha smooth muscle actin (α-SMA) immunohistochemical staining; scale bar = 1000/100 µm.

10:30 a.m. – 12:00 p.m.

Conference room 2+3

IV-OS15 | Patterning and coatings 1

IV-OS15-01

Spatially Separated Immunomodulatory and Cell Adhesive Surface Coatings Enhance Beta-Cell Survival in Encapsulation Devices

Richard Tan[1,2], Nicole Hallahan[3], Elena Kosobrodova[4], Marcela Bilek[4], Peter Thorn[3], Steven Wise[1,2]

[1]Heart Research Institute, Applied Materials Research Group, Newtown, AU; [2]University of Sydney, Sydney Medical School, Camperdown, AU; [3]University of Sydney, Charles Perkins Centre, Camperdown, AU; [4]University of Sydney, School of Physics, Camperdown, AU

Introduction

As a promising alternative to life-long insulin injections for the clinical management of type I diabetes (T1D), transplantation of healthy β-cells to T1D patients has proven to be of great benefit[1]. However, a major obstacle limiting their clinical use is poor long-term survival following transplantation, due to ongoing attack by the patient's immune system. This requires lifelong immunosuppression to ensure successful transplantation[2]. As a more feasible alternative, encapsulation devices are an emerging technology designed to provide a physical barrier that protects β-cells from immune attack. However, to support the survival of encapsulated β-cells these devices must overcome additional biological challenges following implantation. This includes establishing matrix signalling elements for β-cells to thrive, stimulating angiogenesis to facilitate nutrient/waste exchange, and preventing foreign body fibrotic responses that impede host integration[3]. Current encapsulation devices are made from materials selected for their mechanical strength with minimal regard for these biological requirements. As a result, these devices fail to integrate with the body leading to poor long-term β-cell survival and offer no therapeutic function to date[4].

Experimental Methods

We developed an encapsulation membrane using polyethersulfone (PES) fibers (Fig. 1a) with spatially distinct surface coatings designed to enhance β-cell viability through improved cell adhesion and modulation of the local immune response. PES fibers were activated using plasma immersion ion implantation (PIII), enabling the covalent immobilisation of biomolecules. The internal surfaces were coated with the extracellular matrix protein fibronectin (FN) to enhance β-cell attachment. The outer surfaces were then coated with the anti-inflammatory cytokine interleukin-4 (IL-4) to reduce local inflammation (Fig. 1b). Primary mouse islets, containing a bioluminescence (BLI) reporter, were dispersed into single cell suspensions before loading into functionalised PES fibers. PES fibers were then implanted subcutaneously into a mouse back for 14 days (Fig. 1c). β-cell viability and angiogenesis were quantified using serial non-invasive BLI and Laser Doppler imaging, respectively. Histological analysis was conducted on implants at days 3, 7 and 14 to assess temporal changes in inflammation and fibrosis.

Results and Discussion

Compared to uncoated controls, coated implants showed a 10-fold improvement in b-cell attachment consistent with a 75% increase in insulin secretion. At early timepoints, coated implants showed a 60% and 57% reduction in neutrophil and macrophage accumulation, with a 179% increase of the M2 (anti-inflammatory) macrophage phenotype. Increased M2 macrophage activity was consistent with enhanced early angiogenesis indicated by a 153% increase in blood perfusion combined with a 43% reduction in fibrotic capsule thickness. Collectively, these changes led to a 10-fold increase in β-cell viability (Fig. 1d) with an 83% improvement in nutrient exchange/integration with the local vasculature.

Conclusion

Combined FN/IL-4 surface coatings may improve the performance of encapsulation devices and assist in the future clinical success of β-cell therapy for T1D patients.

References

1. O'Connell, P. J., Holmes-Walker, D. J., Goodman, D., et al. (2013) Multicenter Australian trial of islet transplantation: improving accessibility and outcomes *Am. J. Transplant.13*, 1850-1858.

2. Vegas, A. J., Veiseh, O., Gurtler, M., et al. (2016) Long-term glycemic control using polymer-encapsulated human stem cell-derived beta cells in immune-competent mice *Nat. Med.22*, 306-311.

3. de Vos, P., Hamel, A. F., and Tatarkiewicz, K. (2002) Considerations for successful transplantation of encapsulated pancreatic islets *Diabetologia45*, 159-173

4. Brauker, J. H., Carr-Brendel, V. E., Martinson, L. A., et al. (1995) Neovascularization of synthetic membranes directed by membrane microarchitecture *J. Biomed. Mater. Res.29*, 1517-1524.

Acknowledgement

We would like to acknowledge funding from JDRF International, and the infrastructure and facilities of the Charles Perkins Center at the University of Sydney, and The Heart Research Institute.

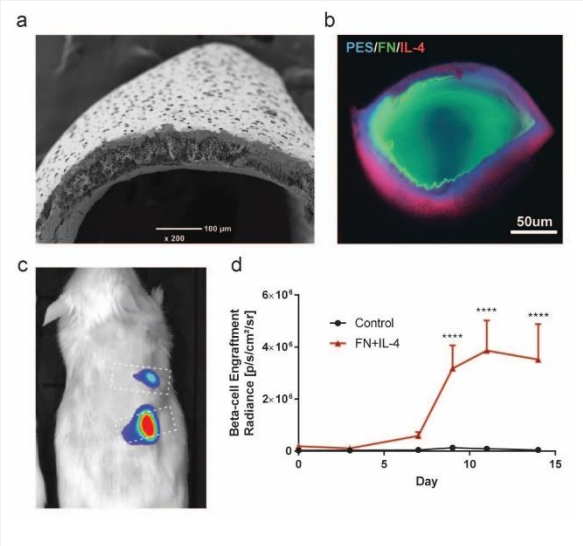

Spatially separated surface coatings enhance beta-cell survival in encapsulation fibers
Figure 1 – a) Scanning Electron Microscopy (SEM) image of PES fiber membrane b) Functionalised coatings of FN (green) and IL-4 (red) on PES surfaces (blue) c) Subcutaneous implantation model using bioluminescence imaging for β-cell viability assessment d) Quantification of bioluminescence readings over 14 days

IV-OS15-02

Biomimetic silk: plasma immersion ion implantation-treated silk biomaterials for enhanced biological function

Kieran Lau[1], Megan Lord[1], John Whitelock[1], Behnam Akhavan[2], Marcela Bilek[2], Jelena Rnjak-Kovacina[1]

[1]University of New South Wales, Graduate School of Biomedical Engineering, Sydney, AU; [2]University of Sydney, School of Physics, Sydney, AU

Introduction

Regenerated silk fibroin purified from silk worm cocoons is a versatile biomaterial that can be engineered into a range of material formats with tuneable mechanical and morphological features. However, *B. mori* silk fibroin has no inherent cell-interactive domains and requires biofunctionalisation to achieve appropriate mammalian biological responses. Plasma immersion ion implantation (PIII) is a process in which positively charged ions from a gas discharge are accelerated through a high voltage sheath and implanted into the surface of the material being modified. The reactive radicals generated through this technique enable simple, one-step covalent immobilisation of bioactive molecules on contact for silk biomaterial surface modification. The goal of this study was to characterise the surface properties and biological activity of functionalised silk biomaterials toward cardiovascular applications.

Experimental Methods

ATR-FTIR spectroscopy, ellipsometry and nanoindentation measurements were used to demonstrate PIII modification of silk biomaterials. Surface plasmon resonance (SPR) analysis with sodium dodecyl sulphate (SDS) washing demonstrated covalent binding of proteins to PIII-treated silk biomaterials. PIII-treated silk biomaterials were biofunctionalised with a vascular proteoglycan perlecan (recombinant expressed C-terminal region Leu3626 - Ser4391) and the effect of PIII treatment on perlecan presentation on the surface was compared to other immobilisation approaches including passive adsorption and carbodiimide chemistry. The biocompatibility of the treated surface was investigated in a mouse subcutaneous implantation model, while the applicability toward cardiovascular devices was investigated by studying the interactions with endothelial and smooth muscle cells, platelets and whole blood.

Results and Discussion

PIII treatment modified the top ~100nm of silk biomaterials, increasing the surface stiffness and introducing oxygen and nitrogen functional groups without affecting the bulk properties. Radicals embedded in the treated layer gradually diffuse to the surface and facilitate covalent attachment of proteins. PIII treatment allowed one-step covalent immobilisation of proteins on the biomaterial surface, significantly increasing the efficacy of perlecan immobilisation relative to passive adsorption or carbodiimide chemistry. This work demonstrates the utility of PIII as a simple and versatile technique to immobilise molecules on silk biomaterials in the absence of chemical cross-linkers. PIII modification of silk is universal and does not rely on the presence of specific reactive groups on the surface or on the molecule to be immobilised.

Implantation of silk biomaterials resulted in a moderate acute immune response, followed by fibrotic encapsulation. Perlecan modulated the fibrotic response to implanted silk biomaterials, significantly reducing the thickness of the fibrotic capsule. Functionalisation of silk biomaterials with perlecan also allowed selective interactions with the cells in the vascular niche, promoting enhanced adhesion of endothelial cells, while inhibiting smooth muscle cell and platelet/whole blood interactions, features essential in the development of blood-contacting cardiovascular devices.

Conclusion

Collectively, these results show PIII treatment of silk enables strong attachment of proteins while retaining their bioactivity in the absence of chemical cross-linkers. Perlecan-functionalised silk biomaterials show promise toward cardiovascular application and warrant further investigation in functional animal models.

IV-OS15-03

Towards multifunctionalization of ceramic surfaces: graphene-derivatives immobilization on the silane-activated ceramic substrates

Karolina Schickle[1], Gaëlle Desante[1], Rafal Zybala[4], Ludwika Lipińska[4], Sabine Neuß[2,3], Rainer Telle[1]

[1]RWTH Aachen University, Department of Ceramics and Refractory Materials, Aachen, DE; [2]RWTH Aachen University Hospital, Helmholtz Institute for Biomedical Engineering, Biointerface Group, Aachen, DE; [3]RWTH Aachen University Hospital, Institute of Pathology, Aachen, DE; [4]Institute of Electronic Materials Technology, Warszawa, PL

Introduction

Bioinert ceramic, such as zirconia, provides the mechanical strength required in implants, but its limited bioactivity renders it incapable of osseointegration [1]. Thus, its biomedical application is limited [2]. Graphene and its derivatives possess excellent bioactivity and can enhance osseointegration, hemocompatibility and antibacterial properties [3]. Here, we introduce an innovative technique for functionalizing bioinert ceramic by immobilizing various graphene derivatives onto the surface by tailored self-assembled monolayer technique (SAM).

Experimental Methods

Several well-established and characterized graphene-derivatives exhibiting different morphology, shape and physico-chemical properties provided from Institute of Electronic Materials Technology, Warsaw (Prof. Lipińska), were selected to immobilize them on the ceramic surfaces (Fig. 1). Zirconia surfaces were at first activated by using two silanes, aminopropyl diisopropyl ethoxysilane (APDS) and 3-(trimethoxysiliyl)propylmethacrylat (MPS). For the APDS-activated surfaces exhibiting $–NH_2$ active groups, additional catalysts, EDC and NHS were applied to reinforce the reaction between $-NH_2$-functionalities and activated –COOH-groups of graphene-derivatives. Two different techniques, drop casting and immobilization from graphene solution by immersing of the samples in the shaking system to avoid sedimentation, were performed. At the end the samples were evaluated regarding to their morphology, graphene-derivatives coupling behavior and the stability of the obtained graphene-layers by using SEM analysis. Moreover, each graphene-derivative before coupling was biologically evaluated by using live/dead staining to ensure its cytocompatible character.

Results and Discussion

The cell culture tests approved the cytocompatible behavior of all selected graphene nano-flakes before immobilization, since more than 95% of cells were viable after incubation time. It was shown, that owing to the catalysts a higher amount of graphene-derivatives could be found on the ceramic surface. The stability of the coatings was established via ultra-sonication treatments. The most promising results were obtained by using graphene oxide obtained from exfoliation of Asbury 1 (GO A1). By using drop casting method a multilayer of GO A1 was attached to the surface, while during spontaneous immobilization from the graphene-solution a well distributed, surface-coverage self-assembled graphene oxide monolayer could be established (Fig. 2).

Conclusion

In our study, the immobilization of graphene derivatives by using different methods was successfully performed. Through this technique, the properties of graphene derivatives and zirconia could be merged to create a versatile

biomaterial. Moreover, through highly reactive graphene additionally biological agents could be immobilized on the graphene-derivatives-modified substrates via processes such as hydrophobic interaction to reinforce its biological activity or enhance other functionalities such as antibacterial future.

References

[1] C.M. Cristache, M. Burlibasa, G. Cristache, S. Drafta, I.A. Popovici, A.A. Iliescu, L. Burlibasa, Zirconia and its biomedical applications, Metal. Int. 16 (2011) 18–23.
[2] S.K. Misra, S.P. Valappil, I. Roy, A.R. Boccaccini, Biomacromolecules 7 (2006) 2249.
[3] M.E. Foo, S.C.B. Gopinath, Feasibility of graphene in biomedical applications, Biomed. Pharmacother. 94 (2017) 354–361.

Acknowledgement

Funded by the Excellence Initiative of the German federal and state governments (Grant Nr. OPSF456)

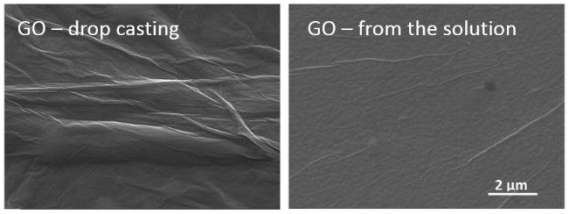

Fig. 2
Coating of graphene oxide on the silanized zirconia substrates by using drop casting method (left) and spontaneous immobilization from the graphene solution, which resulted in well distributed, surface-coverage graphene oxide monolayer (right).

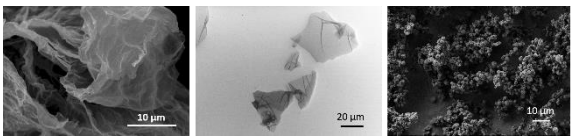

Fig. 1
Graphene-derivatives nano flakes exhibiting different morphology, shape and properties as received, provided from Institute of Electronic Materials Technology, Warsaw, Poland (Prof. Lipińska)

IV-OS15-04

Loading of copper-based nano metal-organic frameworks in polydopmamine for NO release and copper delivery

Yajun Weng, Yonghong Fan, Yu Zhang

Southwest Jiaotong University, School of Materials science and engineering, Chengdu, CN

Introduction

In recent years, some biocompatible nano MOFs attracted attentions for biomedical applications. Among them, copper-based nano MOFs received attentions because of its ability of catalytic generation of NO from S-nitrosothiols (RSNOs) 1. NO is one of the most important signal molecule and plays a indispensable role in inhibition of platelet activation and aggregation, regulation of vasodilation and anti-proliferation of SMC. In addition, the delivery of copper ions can stimulate the adhesion, proliferation, and migrationof ECs, also it can promote wound healing through up-regulating of VEGF expression. Therefore, we supposed that simultaneous NO and copper ion release by the loaded nano Cu-MOFs would exert a synergistic effect to inhibit thrombosis, restenosis, and promote re-endothelialization.

Experimental Methods

Nano Cu-MOFs (CuBTC) was prepared according to Majano et.al2 and characterized. Ti foil was cut into squares (0.8 cm × 0.8 cm), and the substrates (including the 316L SS stents) were ultrasonically cleaned sequentially in acetone, ethanol, and water with three repetitions for each step. Dopamine (2 mg/mL) was dissolved in tris buffer (pH = 8.5), whereupon the nano Cu-MOFs (1 mg/mL) were immediately ultrasonically dispersed into the solution. The nano Cu-MOFs-immobilized coating was prepared by immersing the substrates into the mixed solution for three 12 h periods, with ultrasonic cleaning performed each time. The sample titanium, polydopamine-coated titanium, and nano Cu-MOFs-immobilized titanium were referred as sample Ti, PDM, and MOF, respectively.

Results and Discussion

The nano Cu-MOFs (CuBTC) were immobilized onto the Ti surface successfully by polydopamine (Fig. 1) and the samples showed steady NO catalytic releasing rate at the physiological level of EC ($0.5\sim4.0\times10^{-10}$ mol·cm^{-2}·min^{-1}). Moreover, the copper ion release slowly ($0.53–1.82 \times 10^{-3}$ μmol·cm^{-1}·day^{-1}) from the coating. It showed NO and copper ions played a synergistic role in inhibiting gelatin-induced platelet activation, promoting the growth of ECs, and suppressing SMCs adhesion and proliferation. The ex vivo and in vivo animal experiments (Fig.2) demonstrated that the properties of anticoagulation, re-endothelialization, and anti-hyperplasia were dramatically enhanced by the nano Cu-MOFs-immobilized coating.

Conclusion

In summary, we developed a nano Cu-MOFs (CuBTC) loaded coating with a stable NO catalytic generation and copper ion release. These surfaces could significantly reduce the adhesion and activation of platelets, promote re-endothelialization, inhibit SMC proliferation. It provided a promising method for surface modification of cardiovascular stents.

References

1. M. J. Neufeld, ACS AMI, 2017, 9, 5139-5148.
2. G. Majano, Adv. Mater., 2013, 25, 1052

Acknowledgement

The financial support by National Natural Science Foundation of China (No. 31270020) is greatly acknowledged.

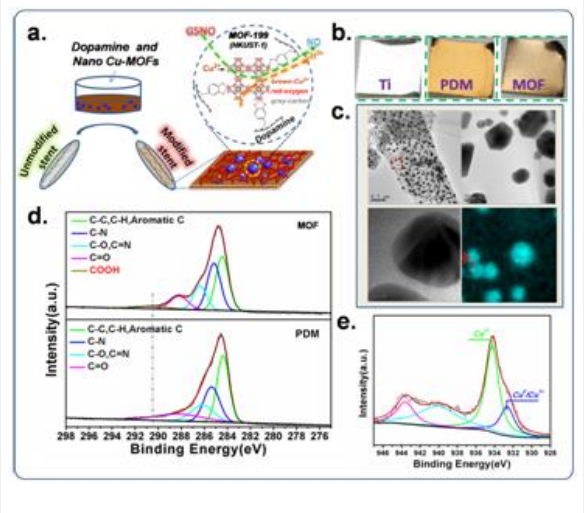

Fig.1 Characterization of the prepared nano Cu-MOFs loaded coating

IV-OS15-05

Applications of a novel printable cell culture platform: Patterning and coatings

Diosangeles Soto Veliz[1], Magnus Engholm[2], Hongbo Zhang[3,4], Martti Toivakka[1]

[1]Åbo Akademi University, Laboratory of Paper Coating and Converting, Turku, FI; [2]Mid Sweden University, Department of Electronics Design (EKS), Sundsvall, SE; [3]Åbo Akademi University, Department of Pharmaceutical Science Laboratory, Turku, FI; [4]University of Turku and Åbo Akademi University, Turku Center for Biotechnology, Turku, FI

Introduction

Traditional cell culture relies mostly on flat plastic surfaces, such as Petri dishes and multiwell plates. These commercial platforms are difficult to modify, which limits the range of customisation, functionalisation, and monitoring capabilities. The limitations restrict experimental design and expand the gap between in vitro and in vivo research. In contrast, cell behaviour research expands rapidly with the development of microfluidics and electrochemical detection methods.

This research proposes a new approach for cell culture: a low-cost device based on stacks of a transparent flexible printable substrate and hydrophobic boundaries. The novelty is the introduction and stacking of layers for potential manipulation and access to the cells. Moreover, the use of a flexible printable film means that the device can be manufactured and modified using conventional coating, printing, and converting techniques. The concept is extended through the integration of printed patterns and mineral coatings to the platform. Human Dermal Fibroblasts (HDFs) were used to demonstrate the capabilities of the platform due to their morphological alignment, and its role in wound healing.

Experimental Methods

Figure 1 shows a graphical summary of the platform manufacture (a), and the side view of a well inside the platform (b). Briefly, the layers of the platform are designed with a vector graphics editor for printing and cutting. The hydrophobic wax patterns are incorporated to a flexible transparent printable film (Melinex OD) with a wax printer. The film was used as such, and also coated with mineral pigments. Subsequently, the film is cut into spacers and layers with a desktop cutter. Lastly, for cell culture with HDFs, the layers are UV-sterilised, pre-wet with cell culture media, and assembled into the sandwich-like structure for the cell seeding.

Two main applications for the device are presented in this study: patterning, and coatings. The patterns are created with the same wax printer used to generate the hydrophobic boundaries on the stacked device. The designs include channels of different widths, and curvatures. In addition, laser ablation was used as an alternative method to create wax patterns of high resolution. As for the coatings, minerals were selected from a pre-assessment of cell-mineral interactions[1], including: calcium carbonate (CCHC90), and calcium sulphate (CS325M).

The patterns and coatings were characterised by measuring contact angle, and FTIR. The biological assessment included calcein AM staining, immunofluorescence staining of the nuclei, actin filaments, vimentin, and vinculin.

Results and Discussion

Figure 2 shows representative images from a) wax patterning, b) laser ablated wax patterns, c) cells on CCHC90, and d) cells on CS325M. Wax printing has been used in the past to create wells on paper and in microfluidics. Therefore, patterning on the film was simple and straightforward. Cells aligned tightly to each other on the print direction. The resolution of the patterns was affected by the ink droplet size and spreading during printing. The limitation is removed

when using laser ablation on a fully wax printed area to create the channels down to 10 µm in width. In both approaches, wax lost its hydrophobicity once in contact with cell culture media allowing cells to grow on top of the printed areas.
In contrast, mineral CCHC90, an accelerator of cell proliferation when used as particles, prevented HDF attachment. Instead, cells adhered to uncoated channels within the coating layer. Cell seeding concentration influenced the cell attachment or lack of it. Lastly, cells growing on calcium sulphate behaved as expected. HDFs showed vacuolisation when in direct (coating on the bottom layer) or indirect (coating on the top layer) contact with the calcium sulphate. For all minerals, it was necessary to use corona treatment on the transparent film prior to coating.

Conclusion

This study shows the applications of a novel cell culture platform. The printability of the device provides a foundation to incorporate functional printing, patterns, electrochemical detection, stimulation and biofluidics. The layered structure facilitates lateral access to the cells, but it also encourages indirect and direct interactions, and co-cultures. Applications, such as the ones in this study, would not be possible in traditional cell culture platforms. In contrast, we were able to align cells through high and low resolution patterning with wax printing, and laser ablation. We could also assess the biomaterial interaction between mineral coatings and HDFs.
In summary, the device is easy and fast to manufacture, scalable, and can be potentially customised to influence, monitor, and assess cell behaviour. It is compatible to cell biology techniques such as microscopy. However, the end-use is not limited to cell culture but can be expanded to other areas, such as drug discovery, diagnostics, point-of-care, and environmental sensing.

References

[1] Soto Veliz, D., Luoto, J. C., Pulli, I., and Toivakka, M. (2018); The influence of mineral particles on fibroblast behaviour: A comparative study; Colloids Surf B Biointerfaces 167:239-251.

Acknowledgement

This work was supported by the Doctoral Network of Material Sciences (Åbo Akademi University, Finland), Otto A. Malm Foundation (Finland), and Alfred Kordelin Foundation (Finland). In addition, Prof. Zhang acknowledges the financial support from Academy of Finland (Grant No. 297580) and Sigrid Jusélius Foundation (decision no. 28001830K1). We thank the FunMat Consortia, and the Laboratory of Prof. John Eriksson for their support.

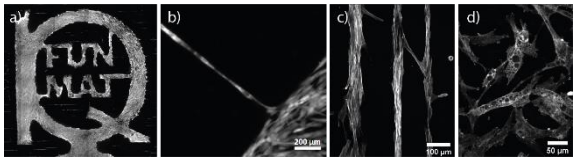

Figure 2. Surface modifications of the printable cell culture platform for cell growth
a) Calcein AM stained HDFs on wax printed pattern. b) Laser ablated wax patterns. Calcein AM stained HDFs align individually inside the channel. c) Calcium carbonate coating for cell growth. HDFs align on the uncoated channels. d) Calcium sulphate coating for cell growth. HDFs show vacuolisation.

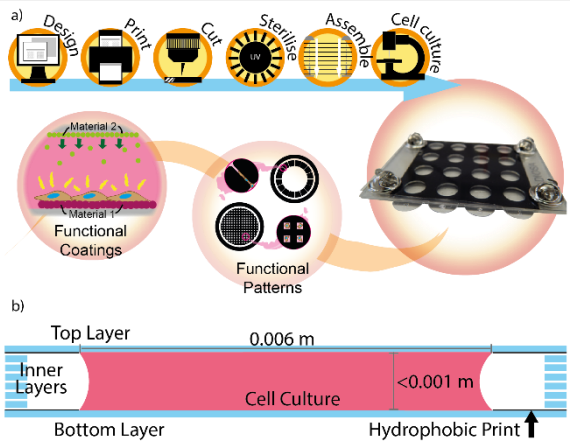

Figure 1. Printable cell culture platform
a) Graphical summary of the step-by-step manufacture and applications of the printable cell culture platform. b) Side view of a well inside the printable cell culture platform. The dimensions are not limited to this representation, it depends on the desired design.

IV-OS15-06

TITANIA NANOTUBE SPACING INFLUENCES *IN VITRO* CELLULAR RESPONSE

Madalina G. Necula[1], Anca Mazare[2], Selda Ozkan[2], Raluca Ion[1], Patrik Schmuki[2], **Anisoara Cimpean**[1]

[1]University of Bucharest, 1Department of Biochemistry and Molecular Biology, Bucharest, RO; [2]University of Erlangen-Nuremberg, Department of Materials Science, Erlangen, DE

Introduction

Nanoscale surface modification of medical implants has become a growing area of research in the bone regenerative medicine, based on the fact that natural bone has a nanometric scale structural hierarchy [1]. One of the simplest and most efficient method of generating nanostructured surfaces on Ti is by electrochemical anodization, resulting in TiO_2 nanotubes (TNTs) [2]. However, comprehensive data on their biological effects are scarce and even contradictory due to the various surface properties. While accumulating evidence describes the influence of nanotube diameter on cell behavior, little is known about the effects of nanotube lateral spacing on cells involved in bone regeneration.

In this context, the *purpose* of the present study has been to assess the influence of TNTs exhibiting a ~80 nm inner diameter and a spacing of 80 nm (TNT80) and 18 nm (TNT18), respectively, on *in vitro* behavior of two cells lines (MC3T3 pre-osteoblasts and RAW 264.7 macrophages). These cell lines provide representative models to study bone regeneration.

Experimental Methods

The growth of TNT on Ti foils was performed a) for TNT18, in glycerol:H_2O 70:30vol.% + 0.5 wt% NH_4F at 20V for 2 h (at room temperature), b) for TNT80, in diethylene glycol + 4wt%HF + 7wt%H_2O + 0.3wt% NH_4F at 27V for 4 h (at 30 °C). Samples morphology was characterized by scanning electron microscope (SEM) Hitachi FE-SEM 4800SEM, while their chemical composition and chemical state was investigated by using X-ray photoelectron spectroscopy (XPS, PHI 5600, US).

The *cell-material interactions* were investigated by conducting cell adhesion and morphology fluorescence microscopy studies and LIVE/DEAD Cell Viability and CCK-8 cell proliferation assays. In addition, pre-osteoblast differentiation (alkaline phosphatase activity, osteopontin and osteocalcin expression) and release of inflammatory mediators by RAW 264.7 (multiplex ELISA) were investigated.

Results and Discussion

SEM images indicate the formation of highly organized nanostructures with parallel aligned porous nanotubes, and while both nanotubular structures exhibit a length of ~ 0.9 µm and inner diameters of ~80nm, the classical tubes grown in glycerol:water electrolyte exhibit a close packed configuration and a tube to tube spacing of ~18 nm present only at the top surface of the tubes, while spaced tubes show a clear tube to tube spacing of ~80 nm from top to bottom of the tubes. These surfaces have proved to support cell viability and proliferation in approximately equal extent. However they induced an increase in the number of viable metabolically active cells at short time-incubation periods when compared with flat Ti surface. A differential cellular response has been induced by TNT lateral spacing in terms of pre-osteoblast morphological features, cell adhesion, migration and cellular expansion. Thus, despite of rather similar number of focal adhesions per cell on the studied nanotubular surfaces, the organization of the actin

cytoskeleton and the pattern of the focal adhesions appeared to be much more similar on the Ti and TNT18 surfaces, whereas on TNT80 the actin filaments are thinner and the focal adhesions are less emphasized. These results correlated with a more visible cell elongation on TNT80 suggest the presence of a more migratory cell phenotype on this surface. Likewise, the degree of pre-osteoblast cell spreading was significantly lower on TNT80 than on TNT18 substrate. Moreover, TNT80 surfaces have proved to exhibit more beneficial effects on pre-osteoblast differentiation than TNT18, as demonstrated by increased expression of the early osteoblast differentiation markers such as alkaline phosphatase (ALP) activity and osteopontin (OPN) secretion levels (Fig. 1). Noteworthy, the higher lateral spacing of TNT has induced more pronounced stimulatory effects on the release of pro-inflammatory mediators TNF-alfa and MCP-1 by RAW 264.7 cells (Fig. 1). Therefore, it can be stated that nanotube spacing plays an important role in the modulation of the macrophage inflammatory response.

Conclusion

These findings provide the evidence that lateral spacing of the TiO_2 nanotubes modulates the cellular response and has to be considered in designing bone implants with improved biological performance.

References

Gong, T., Xie, J., Liao, J., Zhang, T., Lin, S., Lin, Y. Nanomaterials and bone regeneration. *Bone Res.***2015**, 3, doi:10.1038/boneres.2015.29.

Roy, P., Berger, S., P. Schmuki. TiO_2 nanotubes: synthesis and aplications. *Angew. Chem. Int. Ed.***2011**, 50, 2904 – 2939.

Acknowledgement

The authors gratefully acknowledge UEFISCDI (project PCE-55-2017) for the financial support.

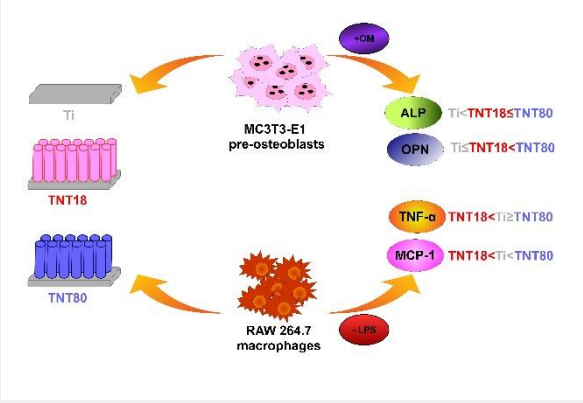

Fig. 1. Titania nanotube spacing modulates pre-osteoblast and macrophage behavior.

2:15 p.m. – 3:45 p.m.

Hall 3

V-SY8 | ISBF: Hydrogel bioinks for bioprinting and biofabrication

Jürgen Groll (Würzburg, DE)
Daniela Duarte Campos (Aachen, DE)

Hydrogels are the most common materials used as bioinks in bioprinting and biofabrication. Recent advances in tissue engineering have shown that more sophisticated, responsive and dynamic materials are needed to mimic the cellular environment and create engineered tissues. In this symposium, novel strategies will be presented for the synthesis of dynamic hydrogels as bioinks. Both invited keynote speakers, Sarah Heilshorn and Matthew Baker, are leading experts in the field of biomaterials applied to tissue engineering. This symposium is supported by the International Society for Biofabrication (ISBF) and aims to bring together people from the fields of bioprinting, tissue engineering and materials science.

V-SY8-KL01

Adaptable Hydrogels as Custom Bioinks

Sarah Heilshorn

Stanford University, Materials Science & Engineering, Stanford, US

Despite the rise of 3D printing of thermoplastics both in industry and the general public, a key limitation preventing the widespread use of cell-based 3D printing is the lack of suitable bioinks that are cell-compatible and have the required properties for printing. Current commonly used biomaterials have distinct limitations when used as a bioink including difficulty maintaining a homogeneous cell suspension, avoiding cell damage during extrusion, customizing the printed matrix properties to facilitate cell-matrix interactions, and printing within a bath to prevent cell dehydration while preserving high print resolution. We have designed a new family of tunable biomaterials specifically designed for cell-based 3D printing. These hydrogel-based bioinks are produced from blends of engineered recombinant proteins and peptide-modified, naturally occurring biopolymers such as alginate and hyaluronic acid. These materials undergo two-stages of crosslinking: (i) weak, peptide-based, self-assembly to homogeneously encapsulate cells in a shear-thinning hydrogel within the ink cartridge and (ii) stimuli-responsive crosslinking post-printing to rapidly stabilize the construct. Benefits of this two-stage crosslinking strategy include the prevention of cell sedimentation within the ink cartridge, mechanical shielding of the cell membrane from damaging extrusion forces during printing, rapid post-print self-assembly within an aqueous bath that prevents cell dehydration, and fine-tuning of the printed scaffold mechanical properties for optimal cell-matrix interactions.

V-SY8-KL02

From static to dynamically crosslinked bioinks for 3D printing

Matt B. Baker

Maastricht University, MERLN Institute, Maastricht, NL

Introduction

Statically cross-linked hydrogels poorly recapitulate the complex and responsive behavior of a cell's native extra cellular matrix (ECM). Cells have a difficult time growing, migrating, and fusing to form tissue within a densely cross-linked covalent hydrogel, yet covalently cross-linked hydrogels are the most widely used material for 3D printing of cell laden hydrogels (bioinks). Consequently, in order to create more complex and biomimetic 3D tissue engineering constructs, the there is a noticeable need for the creation and use of dynamically cross-linked hydrogels within biofabrication and 3D printing. In this talk, I will show our lab's work in moving from thiol-ene statically cross-linked bioinks toward the development of imine-type dynamically crosslinked bioninks.

Experimental Methods

Alginate polymers have been synthetically modified via either amidation (EDC/NHS) or oxidation. Characterization of the alginate polymers based on NMR and GPC allow for control of degree of functionalization. Hydrogels are formed via cross-linking either by UV radiation (thiol-ene, LAP photoinitiator) or by mixing (dynamic covalent imine formation). The rheological properties of the resultant gels were measured via rheology. Printing was performed on a GESIM bioprinter utilizing cartridge-based extrusion under pressure. Cell viability was determined via metabolic activity, live-dead staining, and LDH release.

Results and Discussion

Norbornene modification of alginate was performed with good control. The resultant polymers were crosslinkable with dithiols to create tunable hydrogels. These thiol-ene hydrogels allowed the 3D printing of multi-cellular and multi-layer (up to 25 layer) constructs with good shape fidelity and cell survivability. However, these bioinks poorly recapitulated tissue dynamics. Via oxidation of alginate and combination with dynamic covalent imine-type cross-linkers, we were able to create a series of hydrogels with tunable mechanical properties, viscoelasticity, bioactivity, and printabilty. By tuning the nature and dynamics of the cross-linker, we have shown that the most dynamic hydrogel formulations (hydrazone) were the most printable in our setup. Notably we observed differences in cell adhesion (fibroblasts) and metabolic activity (chondrocytes) as a function of the dynamics of our hydrogels.

Conclusion

Both bioink platforms presented are promising bioinks for biofabrication, with good cell viability. The thiolene bioinks allow straightforward construction of multi-layer constructs due to rapid and static UV initiated cross-linking. The imine-type cross-links provide a novel dynamic bioink platform, with enhanced mimicry of native ECM. Furthermore, this dynamic bioink platform remains one of the few dynamic inks capable of printing a self-supporting structure. Hydrogel dynamics have been shown to markedly influence tissue formation; however, the relationship between dynamic hydrogels and tissue formation in complex cocultures remains unexplored. With printable dynamic inks, the study of complex 3D constructs now becomes possible. Lastly, as we progress towards

the development of more ECM-like and higher functioning synthetic bioinks, a move away from single network or single network plus modifier mentality is urged.

References

S Hafeez, HW Ooi, F Morgan, C Mota, M Dettin, C van Blitterswijk, L Moroni, MB Baker. Viscoelastic oxidized alginates with reversible imine type crosslinks: self-healing injectable and bioprintable hydrogels. Gels, 2018, 4, 85.
HW Ooi, C Mota, AT ten Cate, A Calore, L Moroni, MB Baker. Thiol-ene alginate hydrogels as versatile bioinks for bioprinting. Biomacromolecules, 2018, 19, 3390.

Acknowledgement

The authors are gracious for funding from the research programme Innovation Fund Chemistry, which is partly financed by the Netherlands Organisation for Scientific Research (NWO) under TA grant agreement 731.016.202 (“DynAM”). The authors would also like to thank the Brightlands Materials Center and the Province of Limburg for their support of this work.

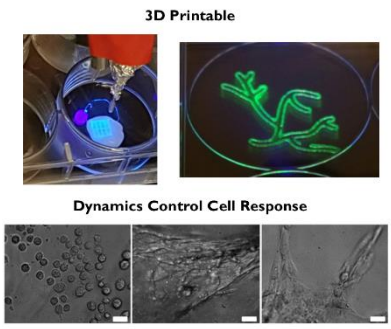

Development of dynamic bioinks

V-SY8-03

Multiscale and cell-preserving 3D bioprinting of human cells by nozzle-free acoustic droplet ejection

Stefan Jentsch, Horst Fischer

RWTH Aachen University Hospital, Dental Materials and Biomaterials Research, Aachen, DE

Introduction

With a novel method, it is possible to move liquids in order to print them without using nozzles. For established bioprinting techniques the nozzle is a limiting factor. The printing resolution is directly limited by the nozzle size. Moreover, the shear stress increases with the decrease of the nozzle size. Regarding the cell-laden printing material, the cells are irreversibly damaged above a critical shear stress. A smaller nozzle diameter leads to clogging of the printed cell-laden hydrogel material.

With the Acoustic Droplet Ejection (ADE) method, droplet sizes can be variably generated over more than three size scales from the millimeter range down to the small two-digit micrometer range. By varying the size of the droplets, it will be possible to print large scale cell aggregates as well as single cells precisely in three dimensions across all scales. Due to the absence of a nozzle, minimal shear stress is applied to the printed cells. Hence a main reason for cell damage can be overcome.

Experimental Methods

The principle of the dispensing method is based on the emission of high intensity focused ultrasound within a fluid. A 4 MHz transducer (CNIR Hurricane Tech, China) with a focus length of 19 mm was used. The radiation pressure contains enough energy to overcome the surface tension and eject a single droplet. Agarose/collagen, gelatin and a fibrinogen/gelatin combination were tested for printability before MG-63 cell line was printed with the focus on cell viability. A heated reservoir keeps the printing materials at the desired printing temperature and a cooled building platform allows the printing material to gel after printing.

Results and Discussion

The current printing rig is the first one which is capable to print in the third dimension whereas so far only a single layer has been applied by using acoustic droplet ejection. Only 2D patterns of separated cell containing droplets [1] or 2D multiplexed cell cocultures [2] have been performed. Cooling the building platform causes a layer of printed hydrogel droplets to gel quickly enough that further layers can be printed on top. The built 3D construct is hanging on the building platform (shown in abstract figure).

The ADE method must be separated from piezoelectric inkjet bioprinting [3]. In piezoelectric inkjet bioprinting a piezo crystal is deformed inside a chamber and the deformation at 15-25 kHz pushes a droplet through a nozzle. In comparison the ADE method is using an open-pool nozzle-less system (shown in abstract figure) at 4-30 Mhz.

Droplet diameters below 70 µm and up to 200 µm can be produced with a high repeat accuracy. The droplet size only depends on the frequency of the ultrasonic transducer and is not affected by a nozzle.

Conclusion

In summary, the results show the ability that by using sound-induced bioprinting, cells, as well as bigger cell clusters, can be dispensed precisely in a gentle manner. The stress to the cells can be minimized by avoiding shear stresses

at the walls inside a nozzle. The multiscale aspect without the need of changing a nozzle but just changing the ejection frequency is a completely new approach in the field of bioprinting. Placing single cells at a high speed has high potential in the future of bioprinting.

References

[1] Demirci, U. & Montesano, G. Single cell epitaxy by acoustic picolitre droplets. Lab Chip 7, 1139–1145 (2007).
[2] Fang, Y. et al. Rapid generation of multiplexed cell cocultures using acoustic droplet ejection followed by aqueous two-phase exclusion patterning. Tissue Eng. Part C Methods 18, 647–657 (2012).
[3] Tekin, E., Smith, P.J. & Schubert, U.S. Inkjet printing as a deposition and patterning tool for polymers and inorganic particles. Soft Matter 4, 703–713 (2008).

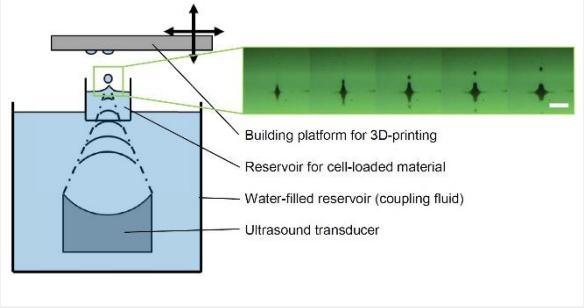

Acoustic bioprinting setup
Green frame: High-speed camera acquisition of the droplet ejection process. Ultrasound frequency of 13.6 MHz, amplifier input signal of 200 mV_{pp} for 14.7 µs. Acquired with 10.000 frames per seconds. Scale bar: 400 µm.

V-SY8-04

Elastin-Like Recombinamers as a new generation of bioinks for 3d bioprinting

Soraya Salinas-Fernández, Fernando González-Pérez, Jose Carlos Rodríguez-Cabello, Matilde Alonso, Mercedes Santos

University of Valladolid, BIOFORGE (Group for Advanced Materials and Nanobiotechnology), CIBER-BBN, Valladolid, ES

Introduction

Novel bioink designs for 3D bioprinting are of great interest due to inerent complexity in the fulfillment of the subtle biological and physical criteria that a real tissue demands, together with the added requirement of printability [1]. For this purpose, Elastin-Like Recombinamers (ELR) hydrogels are seen as appealing candidates for their use as bioinks due to their potential complex and engineered composition and, therefore, functionality as a consequence of their recombinant production from a purely synthetic DNA [2, 3].

Due to the recombinant character of the ELRs, this novel developed bioinks are characterized for having a behaviour close to natural proteins of the extracellular matrix although their production and design is governed solely by engineering parameters, avoiding some of the drawbacks that are generally observed among only synthetic or natural bioinks. Their thermoresponsive behavior is exploited for the deposition of well defined fibers under a heated (37ºC) platform, and its recombinant character enables their batch-to-batch reproducibility and tunability to a desired target tissue by introduction of the selected bioactive peptide sequences into their chains.

Two different strategies have been exploited to enhance printability of ELRs supported through physical or chemical interactions, facilitating structural integrity into the obtained scaffolds.

The physical stabilization approach exploits an ELR bioink ($Z(EIS)_2RGD_6$) that has been designed to perform a 3-step gelation program: A primary thermally-induced fast gelation based into weak hydrophobic interactions ensures rapid fiber formation; a subsequent second stabilization, caused by coil-coil interactions in Leu-Zipper domains, enables the preservation of the structure during the printing time. The last step is the stabilization of the printed structures by to the presence of a silk-like sequence that provide β-sheets formation and long-term stability of the printed structures.

The chemical stabilization approach is based into the design of another ELR bioink ($(KISS)_2$-RGD_6) that has been modified, via the introduction of a methacrylamide groups (MA) by an amidation reaction to endow photo-crosslinkable properties.

Experimental Methods

Both Elastin-Like Recombinamer (ELR) bioinks were genetically designed and produced into Escherichia Coli bacteria, followed by a temperature dependent purification protocol.

Suitability of both ELRs for 3D printing was tested into an extrudable printer, aided with UV exposure in the case of $(KISS)_2$-RGD_6 ELR to allow chemical crosslinking. Optimal concentration and temperature of the cartridge and heated bed were optimized to ensure both ELR best resolution into the printed scaffolds and subsequent rheological studies of viscosity and dynamic modulus were performed.

Printability and structural integrity of the printed matrixes were assessed by imaging and SEM. *In vitro* analyses further test the biocompatibility and suitability of both ELRs as bioinks using HFF-1 cell line. A Life/Death assay

performed over the cell loaded printed structures shows the viability of the cells, meanwhile their shape and proliferation was observed using a DAPI/Phalloidin staining.

Results and Discussion

An optimized concentration of the bioink was printed showing reliable structures in height and width ensuring structural stability through the deposition of controlled fibers one on top of the others without collapsing (Figure 1). Cells stained with Dapi/phalloidin showed a homogeneous distribution within the structure and the characteristic shape that fibroblast acquire in their native environment. A life/death assay showed the viability of the majority of the cells at prolonged incubation times.

Conclusion

ELRs as bioinks can demonstrate great applicability due to their mechanical, physical and biological properties to create printed biomimetic ELRs structures for the development of a wide range of different applications. Their development opens up the possibility to solve most of the problems related with poor printability or biocompatibility that other bioinks possesses.

References

1. Malda J, Visser J, Melchels FP, Jüngst T, Hennink WE, Dhert WJ, Groll J, Hutmacher DW. Adv Mater. 25(36) 5011-28, 2013.
2. Urry, D.W., et al. Journal of Bioactive and Compatible Polymers. 6(3) 263-282, 1991.
3. Rodríguez-Cabello JC, Martín L, Girotti A, García-Arévalo C, Arias FJ, Alonso M. Nanomedicine (Lond). 6(1):111-22, 2011.

Acknowledgement

The authors are grateful for the funding from the European Commission (NMP-2014-646075), the Spanish Government (MAT2015-68901-R, MAT2016-78903-R, FPU 16/04015), Junta de Castilla y León (VA317P18) and Centro en Red de Medicina Regenerativa y Terapia Celular de Castilla y León.

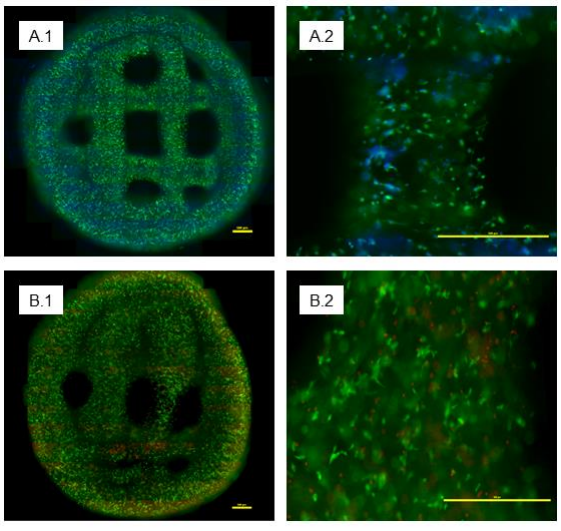

Figure 2
Staining of a $Z(EIS)_2RGD_6$ cell loaded printed structure after 3 days in culture with A)Dapi/Phalloidin and B)Life and Dead. Scale bars: 500 µm

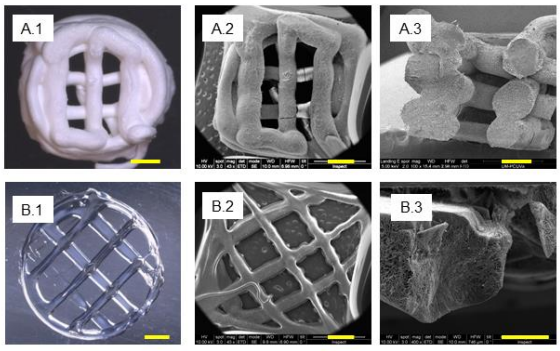

Figure 1
Photograph and SEM imaging of scaffolds printed with A) Z(EIS)$_2$RGD$_6$ and B) (KISS)$_2$-RGD$_6$.Scale bars: 1mm (with the exception of the B3, 200µm)

2:15 p.m. – 3:45 p.m.

Hall 4

V-OS16 | Bioactive materials for regeneration of bone 2

V-OS16-KL01

3D-Printing of Bioactive Materials for Bone Tissue Engineering

Chengtie Wu

Shanghai Institute of Ceramics, Chinese Academy of Sciences, Shanghai, CN

Introduction

For therapy and regeneration of bone defects resulting from malignant bone disease, it is of great importance to develop multifunctional biomaterials for bone therapy and regeneration. Conventional biomaterials always lack multifunctional properties, limiting their application for treating and repairing bone disease (e.g. bone tumors)-initiated defects. How to design and prepare bioscaffolds with favorable microenvironments for disease therapy and tissue regeneration is one of interesting topics in the fields of biomaterials and tissue engineering.

Experimental Methods

We developed several strategies, including harnessing nutrient elements, biomimetic structure and functional interface as well as thermo-therapy to construct multifunctional scaffolds by 3D-Pringting method for therapy and regeneration of bone tissues. Further in vitro and in vivo studies have been systematically innvestigated to evaluate how the nutrient elements, biomimetic structure and functional interface as well as thermo-therapy to influence the bone regeneration/therapy.

Results and Discussion

It is interesting to find that both nutrient elements and biomimetic structure of the printed bioscaffolds have important effect on the stimulation of osteogenesis and angiogenesis of stem cells, and thermotherapy plays an important role to treating bone tumors.

Conclusion

Therefore, we put forward new concept that 3D-Printed bioscaffolds combined bone therapy and regeneration could be a new direction of bone tissue engineering.

References

1. Qingqing Yu, Yiming Han, Xiaocheng Wang, Chen Qin, Dong Zhai, Zhengfang Yi, Jiang Chang, Yin Xiao, Chengtie Wu.Hollow copper silicate microspheres-incorporated scaffolds for chemo-photothermal therapy of melanoma and tissue healing. *ACS Nano* 12:2695-2707 (2018)
2. Jianmin Xue, Chun Feng, Lunguo Xia, Dong Zhai, Bing Ma, Xiaocheng Wang, Bing Fang, Jiang Chang, Chengtie Wu. Assembly Preparation of Multilayered Biomaterials with High Mechanical Strength and Bone-Forming Bioactivity. *Chemistry of Materials30*(14):4646–4657 (2018)
3. Xiaocheng Wang, Fang lv, Tian Li, YiMing Han, Zhengfang Yi, Mingyao Liu, Jiang Chang, Chengtie Wu. Electrospun Micropatterned Nanocomposites Incorporated with Cu_2S Nanoflowers for Skin Tumor Therapy and Wound Healing. *ACS Nano11:*11337-11349 (2017)

4. Cuijun Deng, Qingqiang Yao, Chun Feng, Jiayi Li, Liming Wang*, Guofeng Cheng, Mengchao Shi, Lei Chen, Jiang Chang, Chengtie Wu. 3D Printing of Bi-lineage Constructive Biomaterials for Bone and Cartilage Regeneration. *Advanced Functional Materials* 27:1703117-1703130 (2017)
5. Hongshi Ma, Chuan Jiang, Dong Zhai, Yongxiang Luo, Yu Chen, Fang Lv, Zhengfang Yi, Yuan Deng, Jinwu Wang, Jiang Chang, Chengtie Wu. A bifunctional biomaterial with photothermal effect for tumor therapy and bone regeneration. *Advanced Functional Materials* 26:1197-1208 (2016)

Acknowledgement

The research was supported by the National Key Research and Development Program of China(2018YFC1105201), the National Natural Science Foundation of China (5171101275, 81771985), Key Research Program of Frontier Sciences CAS(QYZDB-SSW-SYS027), Science and Technology Commission of Shanghai Municipality (17441903700, 17540712300).

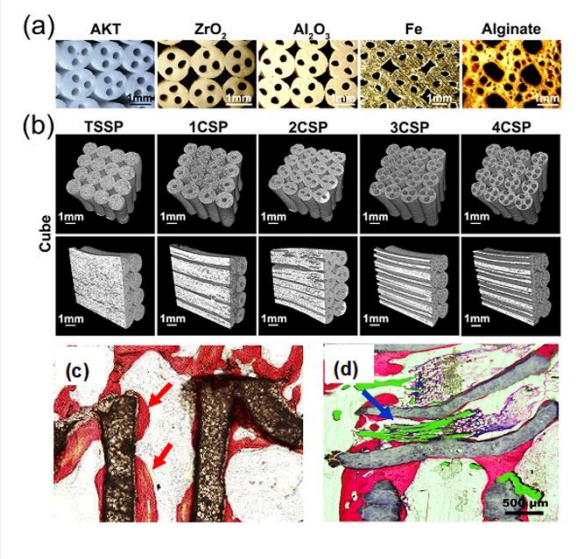

Figure 1. 3D Printing of lotus root-like scaffolds
Different materials with lotus root-like pore structure have been prepared by 3D printing method. The lotus-like pore structure induced formation of new bone and blood vessels.

V-OS16-02

Formulation of an Antimicrobial Silver-doped Magnesium Oxychloride Cement

Morgan Lowther, Liam Grover, Sophie Cox

University of Birmingham, School of Chemical Engineering, Birmingham, GB

Introduction

There is great interest in developing cement formulations for bone regeneration with high strength and easy preparation. In comparison to existing materials such as calcium phosphates (CaP), magnesium oxychloride cements (MOC) offer greater resorbability which can be tailored by the addition of phosphoric acid [**1**].

Excess MgO is frequently added to MOC mixes for improved strength. Interestingly, this could lead to inherent antimicrobial and antifungal functionality due to the efficacy of micron scale MgO powders [**2**]. Current post-surgical antimicrobial prophylaxes often face difficulties penetrating biofilms. Supplementing with local delivery of an inorganic antimicrobial such as silver can disrupt biofilm formation, enhancing the efficacy of conventional antibiotic treatments [**3**].

In this work, the potential for antimicrobial MOC formulations has been investigated. Both the mechanism of any inherent antimicrobial behaviour and the addition of a silver phosphate to increase efficacy have been studied. Importantly, correlations between critical cement requirements have been explored, identifying a formulation that balances mechanical properties and efficacy.

Experimental Methods

Cements were manufactured by mixing light MgO powder with MgCl brine [**1**], with a range of formulations with excess MgO produced. Phosphate-modification was by addition of H_3PO_4 to the brine. When producing silver-modified cements, Ag_3PO_4 was added to the dry MgO. For a subset of formulations, deliberate porosity was induced by addition of a porogen.

Samples were produced by extrusion into moulds of 6 mm diameter and 12 mm height, curing for 48 hours before demoulding. Compression testing was performed with load rate 1 mm/min, on both dry samples, and samples immersed in phosphate buffered saline (PBS) for 14 days prior to analysis.

Helium pycnometry and X-ray diffraction (XRD) were performed on ground cements. Semi-quantitative assessment of spectra was made and normalised based on the ratios of reagents used.

Perfusion and elution assessments were made, with elutants assessed by inductively coupled plasma spectroscopy (ICP-OES).

Antibacterial efficacy was assessed both in wet, and dry states compared to CaP controls. Zones of inhibition were assessed for S. aureus and E. coli on tryptic soy agar (TSA) after 24 hours incubation. Efficacy against planktonic bacteria in broth was measured by flow cytometry with Syto 9 and propidium iodide fluorochromes for live/dead marking. Samples were also removed from the broth, rinsed and then sonicated in sterile broth to suspend any adhered bacteria. Serial dilutions were made and inoculated on TSA for overnight culture.

Results and Discussion

Dry compressive strength was comparable to CaP ceramic cements, with ultimate compressive strength (UCS) up to 30 MPa. Increasing the powder to liquid ratio had no significant effect on UCS, but increased relative density, suggesting critical flaw size remained consistent. Addition of Ag_3PO_4 had negligible effect on UCS, however addition of H_3PO_4 to the brine reduced strength by a factor of a half, and prevented extrusion at powder/liquid ratio of 1.6 (figure 1). Similar results were observed in the wet state.

XRD results (figure 2) indicate retardation of $5Mg(OH)_2.MgCl_2.8H_2O$ (5-phase) formation by orthophosphate modification, with associated brine acidification reducing $Mg(OH)_2$ to MgO. Silver modification also reduced the yield of 5-phase, however this was associated with depletion of chloride ions by formation of AgCl.

Perfusion and elution assessments indicated the low porosity of the MOC cements limited release of silver. Inducing porosity by the addition of a porogen decreased compressive strength, but enabled improved elution of silver from doped cements as measured by ICP-OES.

Antibacterial efficacy was shown both by the formation of zones of inhibition, and reduced viability of both planktonic and adhered bacteria in broth versus CaP controls. Unmodified cements showed significant reduction in viability, suggesting that MOC shows some inherent antimicrobial efficacy.

Conclusion

Magnesium oxychloride cements have been shown to possess a degree of inherent antimicrobial efficacy associated with MgO. Addition of a porogen and silver phosphate improved efficacy, both against adhered and planktonic bacteria in broth. This formulation shows promise as an antimicrobial cement that exhibits more rapid degradation than calcium phosphate cements.

References

[1]. Tan, Y et al. J. Biomed. Mater. Res. Part A 103, 194–202 (2015). 10.1002/jbm.a.35166
[2]. Sawai, J. et al. World J. Microbiol. Biotechnol. 16, 187–194 (2000). 10.1023/A:1008916209784
[3]. Park, H.-J. et al. J. Ind. Eng. Chem. 19, 614–619 (2013). 10.1016/J.JIEC.2012.09.013

Acknowledgement

We acknowledge the EPSRC for funding (EP/P02341X/1) and author ML thanks the School of Chemical Engineering at the University of Birmingham for financial support.

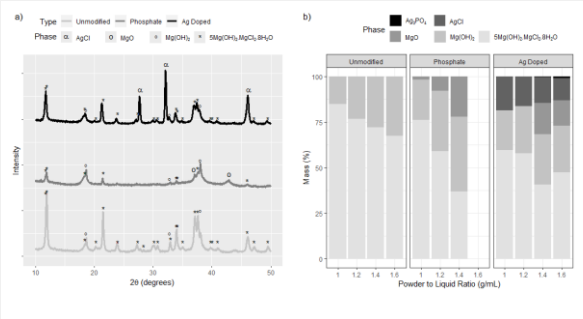

X-ray diffraction analysis of cement formulations
a) Representative x-ray diffraction spectra for cement formulations. Peaks are indexed in comparison to reference database.
b) Semi-quantitative compositional analysis based on diffraction spectra. Results have been normalised based on relative masses of Mg and Ag present in reagents used.

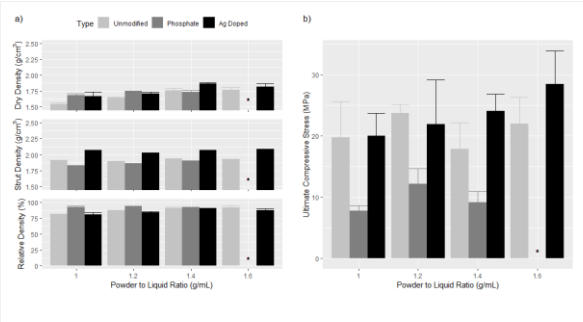

Physical properties of cement formulations
a) Assessment of cement densities. The dry density of cements as measured by total volume, and strut densities from He pycnometry of crushed cements, provides values for the relative density of cements.
b) Dry ultimate compressive strength of cement samples.

* No data is provided for the 1.6 g/mL ratio of phosphate cement. Material could not be extruded and was therefore excluded from study.

V-OS16-03

Creation of inorganic bioactive nanoparticle composites for bone regenerative applications

Pichaporn Sutthavas, Pamela Habibovic, Sabine van Rijt

Maastricht University, MERLN, Institute for Technology-Inspired Regenerative Medicine, Maastricht, NL

Introduction

Calcium phosphate nanoparticles (CaP) are promising materials for use in bone regeneration as they are intrinsically bioactive (i.e. induce bone formation), due to their chemical and crystallographic similarities to inorganic components of bone. However, the synthesis and selective chemical modification of stable uniform nanosized CaP remains challenging. In contrast, mesoporous silica nanoparticles (MSNs) have facile synthesis routes and can easily be co-functionalized to create multifunctional nanomaterials. Consequently, MSNs are heavily used in the fields of drug delivery, theranostics and biosensing [1].

Here, we report the synthesis of MSNs- CaP nanoparticle composites, combining the advantages of both nanomaterials, namely the bioactivity and stability of calcium phosphate, with the drug delivery and modification potential of MSNs. Moreover, as calcium phosphate degradation rate depends on its chemical phase and on pH, CaP coating on mesoporous nanoparticles can be used to facilitate pH dependent drug delivery[2, 3].

Experimental Methods

MSNs with amine surface functionalizations were synthesized via modified co-condensation methods[4]. The amine groups on the MSN surface were further modified to obtain carboxylic acid groups which allowed calcium phosphate ion deposition at HA ratio of 1.67. Nanoparticles were visualized by transmission electron microscopy (TEM). Characterization of particles' crystallinity and surface chemistry were done using X-ray diffraction (XRD) and Fourier transform infrared spectroscopy (FTIR). Kinetic release of calcein fluorescent dye from the nanoparticles at different pH's were measured by a fluorescence spectrophotometer.

Results and Discussion

Carboxylic acid surface modified MSNs were used as templates to allow calcium phosphate layer by layer deposition. A mesoporous structure was visible using TEM in uncoated MSNs (Figure 1a left). These pores were covered up by the calcium phosphate layer in MSN-CaP, showing successful CaP surface coating of the MSNs (figure 1b right). Crystallinity of calcium phosphate layer showed similar patterns as commercial hydroxyapatite as determined by X-ray diffraction (figure 1b). Calcein fluorescent dye could efficiently be incorporated in the MSN mesopores, and 80% of the dye could be released within the first 20 hours as a result of the dissolution of hydroxyapatite coating at acidic pH (pH 4), whereas no significant release was observed at neutral pH.

Conclusion

We successfully synthesized multifunctional nanoparticles composed of a mesoporous silica nano-sized core and hydroxyapatite surface coating. The MSN-CaP could be used for pH dependent drug delivery by dissolution of the hydroxyapatite layer. Their drug delivery capability, combined with their bioactivity make the developed nanomaterials interesting candidates for the creation of bioactive biomaterials for bone regeneration.

References

1. van Rijt, S. and P. Habibovic, *Enhancing regenerative approaches with nanoparticles.* Journal of The Royal Society Interface, 2017. **14**(129): p. 20170093.
2. Rim, H.P., et al., *pH-tunable calcium phosphate covered mesoporous silica nanocontainers for intracellular controlled release of guest drugs.* Angewandte Chemie International Edition, 2011. **50**(38): p. 8853-8857.
3. Zhao, C.-X., L. Yu, and A. Middelberg, *Magnetic mesoporous silicananoparticles end-capped with hydroxyapatite for pH-responsive drug release*. Vol. 1. 2013.
4. Cauda, V., et al., *Multiple Core−Shell Functionalized Colloidal Mesoporous Silica Nanoparticles.* Journal of the American Chemical Society, 2009. **131**(32): p. 11361-11370.

Acknowledgement

The authors would like to thank the province of Limburg (LINK) for providing financial support to this project.

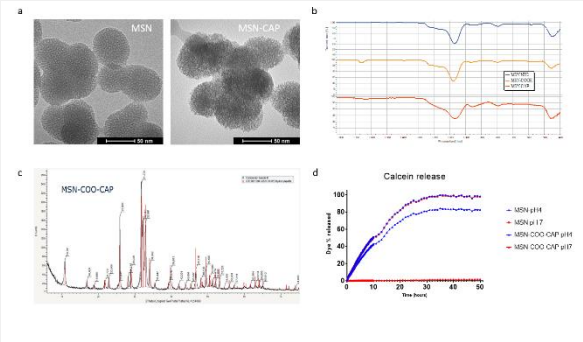

Figure 1: Calcium phosphate coated MSNs characterization
a) .TEM image of MSN and calcium phosphate coated MSN (MSN-CAP). b). XRD pattern of MSN-CAP has similar peaks pattern as hydroxyapatite. c). FTIR spectra of MSN-NH_2, MSN-COOH and MSN-CaP. d). Calcein release from MSN and MSN-CaP at pH 4 and 7.

V-OS16-04

Local changes induced by β-Tricalcium phosphate granules immersed in SBF: confinement matters.

Yassine Maazouz, Iris Rentsch, Bin Lu, Bastien Le Gars Santoni, Marc Bohner

RMS Foundation, BK2 group, Bettlach, CH

Introduction

The mechanism of calcium phosphate induced intrinsic osteoinduction remains unclear. It is mostly observed with beta-tricalcium phosphate (β-TCP), hydroxyapatite, or their combination but not exclusively[1]. A local decrease in Calcium, Phosphate and pH to sub-physiological levels provoked by the confinement and bioactivity of materials was recently related to the early stages of material induced ectopic bone formation[1].

In spite of the large body of information available on the interaction between bone substitutes and physiological solutions, there is currently very little information on the chemical reactions occurring within bone substitutes. As such, it is difficult to interpret published data on the osteoinduction of bone graft substitutes or to make a rationale design of an osteoinductive bone graft substitute.

The objective of this study was to twofold: (1) to design a new bioactivity test method faster than ISO 23317 and allowing to measure local effects (2) to study the effect of design parameters on the bioactivity (unconfined and confined) of β-TCP granules. b-TCP material is particularly interesting because it has been reported to be both bioactive[2] and non-bioactive[3], and highly osteoinductive [4] and non-osteoinductive [5].

Experimental Methods

Particle size (S=fine, coarse), calcium to phosphorus ratio (Ca/P= 1.50, 1.51) Specific Surface Area (SSA: large=4m2/g, small=1m2/g) and (micro)porosity (P= high, low) were varied in a full factorial design to produce 16 types of β-TCP granules with all possible combinations of factors. A two test method was developed: I) Unconfined test: A mass of 0.3g of material was introduced under agitation in 200ml of SBF and pH was monitored owing to an electrode (Unitrode, Metrohm) every seconds during 22 hours. II) Confined test: a 5cc chamber constituted of 40µm mesh (Cell Strainer, BD Falcon) was entirely filled with granules and a 3mm outer diameter pH electrode (Biotrode, Metrohm) was introduced in the center of the granules for the pH to be recorded every second for up to 96h.

Results and Discussion

The pH changes in the confined and unconfined test differed drastically. Confinement provoked higher variation of pH, and the effect of the varied properties of β-TCP granules on the pH variations were markedly larger. In the unconfined test pH slowly decreased with time. This decrease was attributed to the heterogeneous precipitation of a calcium phosphate phase. SEM pictures and solubility calculations confirmed this finding. SSA (p=0.0001) and porosity (p=0.006) were found to significantly influence the pH decrease kinetics. In the case of the confined test a pH increase followed by a sharp decrease were observed, pH increase was attributed to the dissolution of a calcium rich alkaline substance at the surface of the granules owing to ICP-MS measurements, possibly $Ca(OH)_2$. This was also confirmed by solubility calculations and $Ca(OH)_2$ dissolution tests in SBF. The presence of $Ca(OH)_2$ on the surface delayed the precipitation of apatite. The kinetics of the pH increase and subsequent decrease was significantly impacted by the granule size (p=0.001) and the SSA (p=0.007). Granule size did not impact pH changes in the unconfined test because it is not sensitive to the packing of granules contrary to the confined test. Furthermore, SSA had an opposite effect in each test, accelerating the pH decrease in the unconfined test while slowing it down

in the confined test. This was probably due to a combined effect of a longer dissolution time (larger quantity of $Ca(OH)_2$ provoking a higher pH at which $Ca(OH)_2$ is less soluble) and a slower release of the solubility products due to the smaller micropore size. This diffusion was further hindered by decreasing the granule size.

Conclusion

Two new bioactivity tests were introduced. Both tests assessed bioactivity by monitoring the pH value of an SBF solution. Key design properties of β-TCP granules affected their bioactivity. In particular SSA increase had an opposite effect when measured in a confined or unconfined environment. This novel method unravels the substantial pH changes that may be provoked locally by β-TCP granules *in vivo*. The considerable kinetics differences in pH changes and bioactivity that materials with similar compositions exhibited should be taken into account for the design of β-TCP granules. Finally, the present results open up new perspectives towards linking the physicochemical phenomena with intrinsic osteoinduction.

References

1. Bohner, M. & Miron, R. J. A proposed mechanism for material-induced heterotopic ossification. *Mater. Today***22,** 132–141 (2019).

2. Ribeiro, C., Rigo, E. C. S., Sepúlveda, P., Bressiani, J. C. & Bressiani, A. H. A. Formation of calcium phosphate layer on ceramics with different reactivities. *Mater. Sci. Eng. C***24,** 631–636 (2004).

3. Xin, R., Leng, Y., Chen, J. & Zhang, Q. A comparative study of calcium phosphate formation on bioceramics in vitro and in vivo. *Biomaterials***26,** 6477–6486 (2005).

4. Tsukanaka, M., Fujibayashi, S., Otsuki, B., Takemoto, M. & Matsuda, S. Osteoinductive potential of highly purified porous β-TCP in mice. *J. Mater. Sci. Mater. Med.***26,** (2015).

5. Barba, A. *et al.* Osteoinduction by Foamed and 3D-Printed Calcium Phosphate Scaffolds: Effect of Nanostructure and Pore Architecture. *ACS Appl. Mater. Interfaces***9,** 41722–41736 (2017).

Acknowledgement

B. Le Gars Santoni acknowledges the Swiss National Science Foundation funding (grant n°200021_169027).

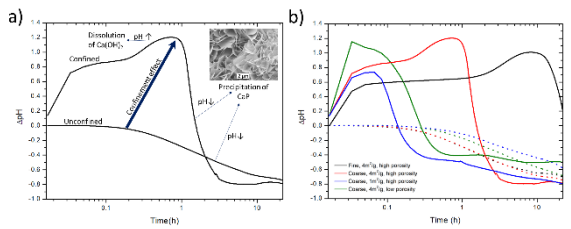

Figure 2
a) Sample ΔpH curves showing for the same type of β-TCP granules (Coarse, 4m²/g, high porosity) the effect of confinement on local pH; b) ΔpH versus time for Ca/P=1.51 β-TCP samples: plain lines correspond to the confined test whereas dotted lines correspond to the unconfined test.

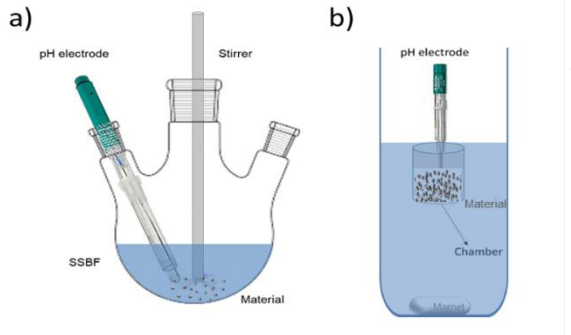

Figure 1
a) Unconfined test conducted in a 3-neck bottle filled with SBF agitated with a propeller; b) Confined test conducted in a chamber containing the material and soaked in a beaker of SBF agitated magnetically.

V-OS16-05

Lanthanides-Doped Hydroxyapatite Nanoparticles for Exploratory Biomedical Tracking

Xiyu Li, Wei Li

Sichuan University, West China Hospital of Stomatology, Chengdu, CN

Introduction

Hydroxyapatite (HA) is a good candidate to repair human hard tissues and HA will be long-standing once implanted.[1] However, long-term tracing of the implanted HA material is still a challenge since HA and bones are difficult to distinguish using existing methods. Understanding the intracellular interaction between HA and osteoblasts is also important for future applications of HA, in tracing cell differentiation and bone regeneration. Current biomedical imaging using fluorescent nanoparticles are not targeted at bone reconstruction, and the intracellular interaction studies mainly involve tumor-like cells. Herein, we prepared two kinds of lanthanides (Ln)-doped HA nanoparticles for exploratory biomedical tracking, based on the good fluorescent property from the doping Ln ions and the biocompatibility of HA. The Yb and Ho co-doped HA (HA-Yb/Ho) nanoparticles are expected to have dual functions of bone repair and multimodal tracking (i.e., upconversion fluorescence, X-ray/micro-CT and MRI), to illustrate the distribution state and degradation of the HA materials during new bone reconstruction. The Tb-doped HA (HA-Tb) nanocrystals with uniform shape and fluorescence may provide an insight into the intracellular interaction between HA materials and osteoblasts in the long term. These Ln-doped HA materials will benefit future biomedical investigation and applications as they can not only be bone repair biomaterials, but also provide lifelong multimodal tracking efficacy.

Experimental Methods

The HA-Yb/Ho and HA-Tb nanoparticles were prepared via hydrothermal treatment.[2] Octadecylamine was dissolved in oleic acid and ethanol, then aqueous solution of $Ca(NO_3)_2$, $Ln(NO_3)_3$ (Ln=Yb/Ho or Tb), and Na_3PO_4 or NaF were added. The mixture was hydrothermally treated at 160 °C for 10 h. And the HA-Yb/Ho powder was activated at 700 °C for 2 h to evoke upconversion property. The Ln-doped HA nanoparticles were characterized by TEM, EDX, XRD, and fluorescence spectrophotometer. The HA-Yb/Ho powders were implanted into the defects on the distal femoral condyle of rabbits and harvested at 2 and 4 months. The uniform HA-Tb nanocrystals were cultured with rat osteoblast (ROS1728) for 7 and 14 days to investigate the intracellular interaction, via CLSM, TEM, EDX, and qPCR.

Results and Discussion

Figure 1a showed that HA-Yb/Ho with a HA structure possessed stable green and red upconversion luminescence under 980 nm NIR, and the fluorescence intensity could be tuned by further doping of F ions. HA-Yb/Ho also presented a superparamagnetic property, displaying stronger MRI than pure HA. In addition, HA-Yb/Ho could be clearly distinguished from surrounding bone tissues under micro-CT. Figure 1b showed the distribution region of HA-Yb/Ho in new bone tissues after implantation for 2 and 4 months, revealing that HA-Yb/Ho had undergone gradually degradation during new bone reconstruction. And LSCM provided precise details of the distribution and degradation of HA-Yb/Ho in bone tissue, and the osteointegration of the particles with bone tissue.

The HA-Tb nanorods have a uniform morphology, and bright green emissions (Figure 2a). On day 7, the cytoplasm of osteoblasts was homogeneously visualized by the green fluorescence of the internalized HA-Tb, which kept a uniform morphology despite slight degradation, with size reducing from initial ~135 nm to ~85 nm. On day 14, HA-

Tb had degraded into smaller (~62 nm) and irregular nanoparticles, and agglomeration had occurred, leading to uneven cytoplasmic fluorescence regions. The reduction of Ca and the rise of Tb in EDX spectra demonstrated that the composition of HA-Tb had changed with degradation. The gene expression of the osteoblasts was not obviously affected on day 7 but largely decreased, or some genes could not be normally expressed on day 14 (Figure 2b). The EDX mapping of the tiny particles in the multilayer membrane (Figure 2c) revealed that they were the degraded products of HA-Tb, and the release of Ca ions was higher than P and Tb ions. The results indicate that the morphology and composition change of the internalized HA-Tb nanocrystals, and the microstructure and functional change of the osteoblasts are closely related and correspond to each other.

Conclusion

The results demonstrated that the HA material degraded with time both in bone tissue and in osteoblastic cells. The combination of fluorescence and micro-CT images exhibited an advantage to illustrate the distribution and degradation of HA-Yb/Ho materials, the material-tissue interrelation, and osteointegration during bone reconstruction. The degradation and agglomeration of the HA-Tb nanocrystals in cells revealed distinct mutual effect between the internalized HA nanocrystals and the osteoblasts. The research provides a promising method for further investigating the mutual effects or long-term interaction of nanomaterials with cells and tissues.

References

1. Tertuliano OA. Nat. Mater. 2016, 15, 1195.
2. Xiyu Li et al, Inorg. Chem. 2018, 57, 13739-13748.

Acknowledgement

The authors acknowledge the support of funds from the NSFC (Grant No. 31700828).

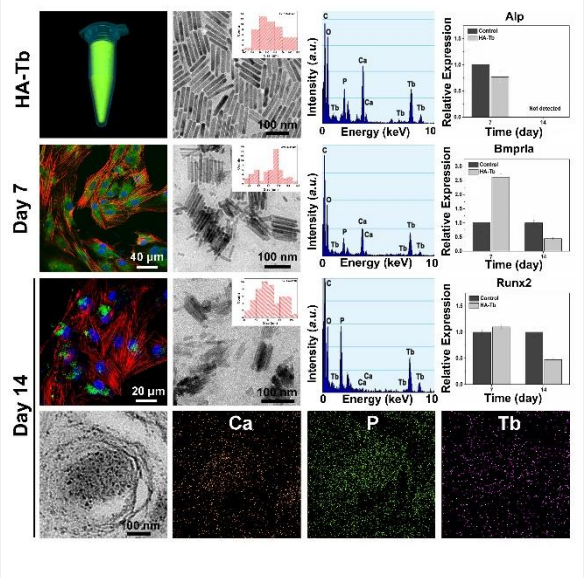

Figure 2
The degradation and agglomeration of the uniform HA-Tb nanocrystals occurred in the cytoplasm of osteoblasts with the increase of culture time from day 7 to day 14. The changes of cytoplasm fluorescence, nanocrystal size and the elements in EDX (a); the relative gene expression of the *Alp, Bmprla and Runx2* (b); and the EDX element mapping of Ca, P, and Tb in the tiny particles within the multilayer membranes on day 14 (c).

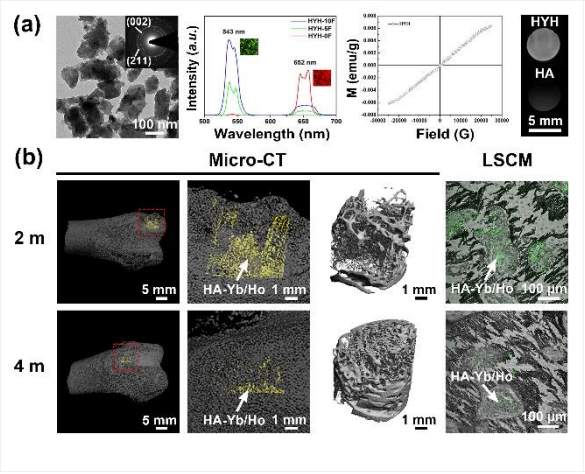

Figure 1
The TEM morphology with inset of SAED pattern, fluorescence emission spectra, the VSM hysteresis loops and MR image of the HA-Yb/Ho nanoparticles (a); the 3D micro-CT reconstructed images and the overlapping LSCM images of the harvested samples after the HA-Yb/Ho powders were implanted into bone defects for 2 and 4 months (b).

2:15 p.m. – 3:45 p.m.

Hall 5

V-SY9 | Ex vivo Models to Study Neural Plasticity, Regeneration and Interactions with Electronic Interfaces

Sahba Mobini (Madrid, ES)
Maria Ujue Gonzalez (Madrid, ES)

Ex vivo/in vitro models are in vitro platforms, consisting of relevant cells, microenvironment (biomaterial/scaffold) and stimuli (biochemical/electrical/mechanical/magnetic), which are designed for testing drugs and/or treatments in well-defined conditions. The ultimate goal of *ex vivo/in vitro* models is to provide reproducible, scalable and physiologically relevant testing environment facilitating translation to clinical application.
In this symposium, we will focus on models for mimicking CNS and/or PNS healthy and diseased tissues. In addition, we will cover the emerging field of neural interfaces and their integration with in vitro models for both stimulation and recording neural activity.

V-SY9-KL01

Neurogenic Tissue Engineering: Perspectives, Challenges, and 3D *In Vitro* Models

Paul A. Wieringa

Maastricht University, MERLN Institute, Complex Tissue Regeneration Department, Maastricht, NL

The common first question when visiting your doctor: “how are you feeling today?”. We are subconsciously accustomed to the sensations our peripheral nervous system (PNS) provides, how they relate to our health, and the day-to-day benefits of this amazingly complex, yet often unnoticed system. It allows us to interact and experience the world around us and regulates both conscious and unconscious processes we need to survive. However, despite being an almost omniscient entity within the body, the importance of the PNS typically becomes apparent after neural trauma (e.g. spinal cord injury) or neuropathies when the impact on bodily function is extreme. What is less reported and perhaps less understood is the nuanced role the PNS may play in disease onset, pathology progression, and the possible role of peripheral nerves on tissue repair processes.

The development of 3D *in vitro*models is providing exciting new tools to better understand biological systems, toward improved therapies and regenerative medicine (RM) approaches. This is particularly true for investigating PNS and its potential role in regenerative therapeutic strategies. The majority of PNS-related RM studies have centered on the repair of the PNS itself, whether focused on therapy development for neuropathies or the promotion PNS regeneration after injury via tissue engineered scaffolds, like those developed by our group[1] and many others. Re-establishing the connectivity of this complex signaling network is important because of its involvement in almost all homeostatic functions of the body, with the ability to rapidly assimilate and respond to a multitude of stimuli including inflammation and trauma. However, in the creation of engineered ‘replacement’ tissues, appropriate neural signals are rarely regarded as essential despite influencing general function and overall systemic integration. Beyond this return of function, the potential influence the PNS can have on the regeneration and repair of these tissues is often overlooked, defined here as neurogenic tissue repair. This oversight is largely due to the intrinsic complexity of the PNS, which presents a significant barrier to clearly understanding how this system could contribute to health and disease.

Introduced here are the possibilities of a neurogenic approach to regenerative medicine and tissue engineering. Examples from literature of seminal *in vivo*studies provide a precedent for such an approach and also highlight the pitfalls of examining the role of innervation in repair and pathological processes.[2,3] A common theme is careful experimental design that permits a clear delineation of neural influence while still maintaining an overall capacity of assessment or functional readout.[4] This sets the stage for the use of *in vitro*models to facilitate further investigation, with an emphasis on 3D tissue co-culture systems. Requiring more than a simple co-culture, the particulars of spatial arrangement are outlined between tissues and nerves in order to faithfully recreate nerve-tissue interaction. Discussed are biofabrication approaches and strategies employed in our lab and by others to study these interactions, including in vitro models of innervated skin and pancreas (Figure 1). Details are described regarding the kinds of nerve-tissue interactions currently being examined and, in addition, an overview of the challenges, considerations, and future directions for this exciting area of research.

References

[1] Santos D & Wieringa P, et al. AHM. 2017; 6(3): 1600298.

[2] Buckley G et al. J. Anat. 2012; 220: 3-12.

[3] Taborsky GJ Cell Metab. 2011; 14: 5-6.

[4] Rodriguez-Diaz R et al. PNAS. 2012;109(52):21456–61.

Acknowledgement

This work is part of the VENI research programme with project number 15900 - NeuroBeta, which is financed by the Netherlands Organisation for Scientific Research (NWO).The authors would also acknowledge the funding support of the Province of Limburg, the Netherlands.

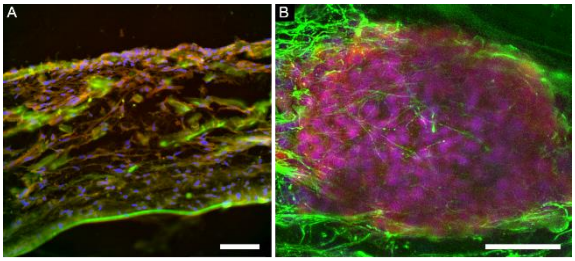

Examples of in vitro models of innervated tissues.
A) Immunofluorescence of a cross section of an in vitro innervated skin construct (red: keratenocytes, Keratin-14; green: axons, CGRP). *Malheiro, Wieringa, et al. unpublished*. B) A confocal optical section midway through an innervated pseudo-islet of Langerhans grown *in vitro*, revealing axonal infiltration into the organoid. (green: axons, beta(III)tubulin; red: INS-1E beta cells, insulin). *Wieringa, et al. unpublished.*Scale bar: 50 mm.

V-SY9-KL02

Engineering Neural Interfaces in the Central and Peripheral Nervous Systems

Josef Goding, Rylie Green

Imperial College London, South Kensington Campus, London, UK

The design and performance of contemporary neural interface devices are defined by their use of metallic conductors to deliver electrical stimulus. The rationale behind the use of metallic components has largely been informed by traditional engineering concepts and has little regard for our growing understanding of the complex neural milieu at the tissue-device interface. The Polymer Bionics Lab Group at Imperial College London focuses on developing novel organic-based materials designed for use in neural interfaces. A key component of this process is the development and application of an understanding of the complex device-tissue interactions that occur at the neural interface. The development of complex, mixed neural cell cultures is critical to the assessment of novel biomaterials and allows researchers to evaluate the efficacy of new approaches to engineering the neural interface such as the use of soft and compliant materials, biological activity of functional materials, and novel stimulation regimes. Two examples of this development process will be explored in this presentation. The first example is the development of the living electrode, a tissue-engineered neural interface device, designed to create high-quality neural interfaces by implanting a neural probe containing a mixed-neural cell population encapsulated in a biosynthetic hydrogel carrier. The living electrode is a combinatorial approach to engineering the neural interface, considering the effect of mechanical, electrochemical and biological properties of the neural probe and their effect on the tissue-electrode interactions. The second example is the development of fully organic nerve cuff electrode arrays for electroceutical therapies such as nerve block. *Ex vivo* models including functional stimulation of rat sciatic nerve was used to assess the safety and efficacy of nerve cuff design, stimulating electrode materials and stimulation strategies. These examples illustrate the value in the design and application of appropriate models in the development of materials and devices for neural interfaces.

V-SY9-03

Highly aligned collagen-based scaffolds with controllable stiffness for neural regeneration

Robert C. Murphy, Daniel Bax, Ruth E. Cameron, Serena M. Best

University of Cambridge, Materials Science and Metallurgy, Cambridge, GB

Introduction

Peripheral nerve injury can lead to physical impairment and lifelong disability, and there is a clinical need for a scaffold that can bridge large gaps in the nerve and replace and improve upon the current treatment options of an allograft or hollow guidance conduit. There is strong evidence that the incorporation of aligned intraluminal channels or fillers can improve functional recovery by providing a surface that can help guide the sprouting axons to their target and give directed Schwann cell migration [1][2]. Of similar importance is the substrate stiffness, as neural cells have been shown to be highly mechanosensitive [3]. In this work, aligned collagen-based scaffolds have been produced, with mechanics tailored by carbomiide crosslinking and the response of Schwann cells on the scaffolds characterised.

Experimental Methods

Highly aligned collagen scaffolds have been produced, with and without addition of 10 wt. % elastin, by use of a controlled freezing set up that induces a linear thermal gradient within the slurry [4]. These scaffolds have been imaged using X-ray micro-computed tomography (MicroCT) and scanning electron microscopy (SEM), and the pore sizes, alignment and interconnectivity have been characterised. The scaffold mechanics, characterised by wet compressive testing, have been varied by covalently crosslinking to different degrees using 1-ethyl-3-(3-dimethylaminopropyl)-carbodiimide hydrochloride (EDC) in the presence of an N-hydroxy-succinimide (NHS) catalyst, with a molar ratio of EDC:NHS:COOH (from collagen) of 5:2:1 defined as 100% crosslinked. The scaffolds were seeded with Rat Schwann Cell 96 cell line (RSC96) cells at the top of the scaffolds (dimensions 8 mm across and 5 mm tall) with 125,000 cells in 50 µl media per scaffold at different crosslinking conditions. Their metabolic activity was assessed at days 1, 3, 5 and 7 using Prestoblue assay. Samples at each condition were fixed and stained with DAPI stain and imaged using a Zeis Axio Observer confocal microscope to view the cellular penetration through the scaffold.

Results and Discussion

Highly aligned porous scaffolds with average pore sizes ranging from 40 to 50 µm, dependant on freezing temperature, were produced (Figure 1). The scaffold's compressive stiffness varied with carbomiide treatment, with the Young's Modulus at 20 % strain increasing linearly from 0.58 ± 0.47 kPa at 0 % crosslinking to 12.2 ± 4.8 kPa at 100 % crosslinking. The metabolic activity of RSC96 cells seeded onto the scaffolds increased with incubation time for all conditions, suggesting the scaffolds supported proliferation of these cells. Confocal microscopy images showed penetration of the cells throughout the scaffold structures from the seeding surface (Figure 2).

Conclusion

Highly aligned collagen–based scaffolds with a range of pore sizes have been produced, and their mechanics controlled by carbomiide crosslinking in a concentration dependant way. The scaffolds supported proliferation of RSC96 cells; proliferation and penetration of the cells as a function of crosslinking will be reported.

References

[1] A. Bozkurt *et al.*, “Efficient bridging of 20 mm rat sciatic nerve lesions with a longitudinally micro-structured collagen scaffold,” *Biomaterials*, vol. 75, pp. 112–122, 2016.

[2] R. Sridharan, R. B. Reilly, and C. T. Buckley, “Decellularized grafts with axially aligned channels for peripheral nerve regeneration,” *J. Mech. Behav. Biomed. Mater.*, vol. 41, pp. 124–135, 2015.

[3] G. Rosso, I. Liashkovich, P. Young, D. Rohr, and V. Shahin, “Schwann cells and neurite outgrowth from embryonic dorsal root ganglions are highly mechanosensitive,” *Nanomedicine Nanotechnology, Biol. Med.*, vol. 13, no. 2, pp. 493–501, 2017.

[4] A. H. Jamie Cyr, Ruth Cameron, Serena Best, “755 Asymmetry in anisotropic ice-templated collagen scaffolds to mimic the structure of native tissue: from model to execution,” in *29th Annual Congress of the European Society for Biomaterials*, 2018, pp. 216–217.

Acknowledgement

The authors would like to thank the Engineering and Physical Sciences Research Council (EPSRC) for the funding of this project.

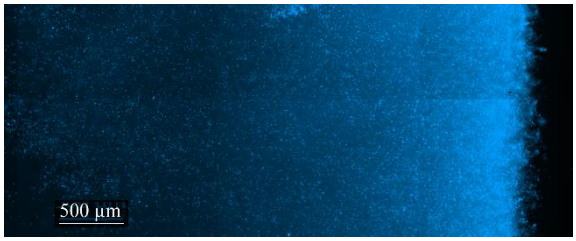

Penetration of RSC96 Cells Through the Scaffold
Figure 2. DAPI stained RSC96 cells 5 days after seeding on a 100 % crosslinked collagen scaffold, demonstrating the penetration of the cells throughout the scaffold from the top surface (on the right) where the cells were seeded.

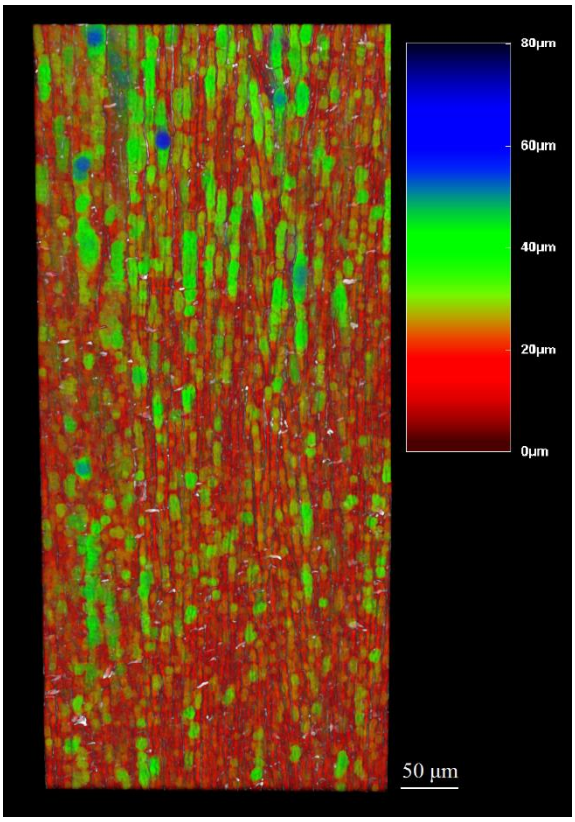

Scaffold Architecture
Figure 1. A microCT image demonstrating the pore size and high degree of pore alignment in these scaffolds.

V-SY9-04

Nanoclay Doped Printable Conductive Hydrogel

Teuku F. Akbar[1,2], Christoph Tondera[1,2], Alvin K. Thomas[3], Carsten Werner[2], Yixin Zhang[3], Volker Busskamp[4], Ivan R. Minev[1]

[1]TU Dresden, Biotechnology Center (BIOTEC), Dresden, DE; [2]Leibniz Institute of Polymer Research Dresden (IPF), Dresden, DE; [3]TU Dresden, B CUBE Center for Molecular Bioengineering, Dresden, DE; [4]TU Dresden, DFG-Center for Regenerative Therapies Dresden (CRTD), Dresden, DE

Introduction

Bioelectronic interfaces require electrode arrays, which depending on the context, can be implanted in the nervous system, placed on the skin, or patterned on the bottom of a petri dish. Traditionally, electrodes are made from metals or silicon because of their favorable conductive and electrochemical properties as well as ease of processability. From a biomaterials perspective these materials are very different from the soft and hydrated biological tissues they contact. For example, the mechanical mismatch between electrode and tissue is often implicated as a cause for fibrosis and compromised electrical signals, especially when long-term implant biointegration is required. Electrically conductive hydrogels are a promising class of materials that may improve the biointegration of electrode arrays. This is due to their low elastic modulus, elasticity, and high water content that are similar to soft tissue. However, obtaining a hydrogel system that satisfies all those requirements, in addition to cytocompoatibility remains a challenge. Here, we will present a synthetic, interpenetrating network hydrogel consisting of polyacrylamide (PAAM), 3,4-ethylenedioxythiophene (PEDOT) and a nanoclay (Laponite) that exhibits high stretchability and conductivity. Furthermore, we demonstrate adhesion of induced pluripotent stem cells (iPSCs) by incorporating cell adhesive peptides and a polysaccharide on the hydrogel surface.

Experimental Methods

We start with a printable and tough double network hydrogel formed by polyacrylamide (PAAM) and a nanoclay (Laponite). Oxidative interfacial polymerization of the conductive polymer Poly(3,4-ethylenedioxythiophene) (PEDOT) in the Laponite-PAAM hydrogel adds electrical conductivity to the material. For PEDOT polymerization, the Laponite-PAAM hydrogel is first immersed in 0.4 M ammonium persulfate (oxidant) in 1 M hydrochloric acid for 3 hours and subsequently incubated in 0.4 M EDOT solution in mineral oil for 6 hours. The resulting conductive hydrogel is coated with bone sialoprotein peptide sequence and polysaccharide dextran sulfate using silane as coupling agent to add cell adhesion functionality.

Results and Discussion

The printable fabricated hydrogel is highly conductive (26 S/m), stretchable (up to 800 % tensile strain), and cell adhesive with elastic modulus comparable to neural tissue (15 kPa). We observe that the presence of Laponite has a marked effect on enhancing the conductivity of the composite material likely due to doping of PEDOT. Surface modification of PEDOT:Laponite-PAAM gels with cell adhesive peptide and polysaccharide dextran sulfate improves attachment, proliferation, and differentiation of induced pluripotent stem cells.

Conclusion

We demonstrate a printable conductive hydrogel system that may potentially find applications in neural

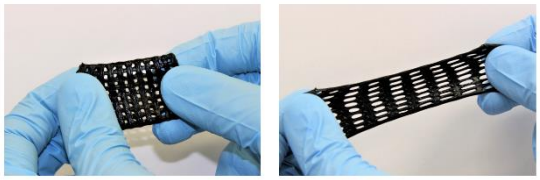

Printed conductive hydrogel mesh before and after stretching

2:15 p.m. – 3:45 p.m.

Conference room 4+5

V-OS17 | Immunomodulatory biomaterials

V-OS17-01

In vitro granuloma formation model for immunomodulatory biomaterial development and assessment

Nihal E. Vrana[1,2], Celine B. Muller[1,2], Cynthia Calligaro[2], Philippe Lavalle[2]

[1]Protip Medical, Strasbourg, FR; [2]INSERM, UMR 1121, Strasbourg, FR

Introduction

Granuloma formation is an important aspect of adverse immune responses to implanted biomaterials. Driven by mainly macrophage agglomeration, granulomas is one of the outcomes of foreign body response where the immune system's attempt to isolate the implanted material results in a small nodule on its surface. Granulomas not only contain macrophages but they can also have other immune cells, fibroblasts and extracellular matrix deposits in their constitution. Although granuloma formation is a well-known biomaterial associated risk currently there are no models for the assessment of granuloma induction capacity of a biomaterial, neither is there a model where the capacity of an immunomodulatory biomaterial or coating to diminish granuloma formation. Previously, we have developed a model of incoming macrophages and their interactions with cell-laden hydrogels (1). In this study, our aim was to define and optimize conditions that will induce granuloma formation. as Tumor Necrosis Factor α (TNF-α) is known to be a determinant factor in granuloma formation, together with bacterial presence, the development of granuloma-like structures was induced by TNF-α and LPS induction of monocytes over a period of 6 days. In order to improve the model, a fibroblast component was added after 5 days of culture. In order to validate the model, a previously described anti-inflammatory coating (Polyarginine/Hyaluronic acid multilayers) (2) was tested under the granuloma induction conditions.

Experimental Methods

Human monocytic cell line (THP-1, ATCC) was used as a monocyte model whereas a human fibroblast cell line (BJ, skin fibroblasts, ATCC) were used as fibroblast model. 1. 10^5 THP-1 cells are seeded on glass substrates in the presence or absence of β-mercaptoethanol (which is regularly used to keep monocytes in suspension culture) together with stimulation with 10 ng/ml TNF-α or 100 ng/ml LPS or their combination. The metabolic activity of the cells was determined by Alamar Blue, bright field images were taken on day 1, 4 and 7 and quantified for granuloma-like structure number and size using Image-J. At day 4 and 7 samples were fixed and stained for DAPI/Phalloidin and also for CD80 (M1 pro-inflammatory macrophage marker) to study the effect of granuloma induction conditions. At day 4, 5. 104 fibroblasts were added to the culture and their effect on IL-1β, IL-1RA, CCL-18 secretion (ELISA) and collagen deposition (Chondrex collagen staining kit) was quantified. PAR/HA multilayer coatings are prepared by the sequential dipping method (24 bi-layers) and tested for their ability to prevent granuloma formation and interaction with fibroblasts using the tests described above with the addition of CD206 staining to determine the potential induction of anti-inflammatory phenotype on attached macrophages. The results presented are from at least 3 independent experiments with 3-6 experimental repeats in each ($p<0.05$ was taken as statistically significant).

Results and Discussion

In the absence of β-mercaptoethanol, by day 4 granuloma-like agglomerates were regularly formed. the number of granuloma-like aggregates in the presence of TNF-α and TNF-α/LPS was higher while the size of the aggregates was comparable (Figure 1). The presence of TNF-α/LPS significantly increased collagen secretion by fibroblasts over 7 days ($p<0.05$) and in the presence of fibroblasts well-defined granuloma-like structures were observed. The anti-

inflammatory coating (PAR/HA) was demonstrated to significantly decrease the metabolic activity of macrophages ($p<0.05$) under induction conditions while also diminishing the number of attached macrophages and IL-1β secretion. Moreover, once the fibroblast component was introduced it was observed that the presence of the immunomodulatory coating does not affect the adhesion of the fibroblasts (Figure 2). Thus, the present model can be used for monitoring of the initial monocyte attachment under highly pro-inflammatory stimulation followed by the observation of the remodeling phase by fibroblasts.

Conclusion

For the assessment of biomaterials, particularly immunomodulatory biomaterials, having models of potential risks are highly important. herein, we have demonstrated an in vitro model of granuloma formation to be used for testing of the anti-inflammatory capacities of immunomodulatory structures under pro-inflammatory conditions. Our current work is focused on the miniaturization of the system in a mini-bioreactor chamber under physiological blood flow conditions to model the monocyte/biomaterial interaction interface better (3). Such in vitro models can aid in the development and optimization of new immunomodulatory coatings and biomaterials and can be used as personalized testing milieu for patient-specific immune reactions to biomaterials.

References

1) Dollinger C, Ciftci S, Knopf-Marques H, Guner R, Ghaemmaghami AM, Debry C, Barthes J, Vrana NE. Incorporation of resident macrophages in engineered tissues: Multiple cell type response to microenvironment controlled macrophage-laden gelatine hydrogels. Journal of tissue engineering and regenerative medicine. 2018 Feb;12(2):330-40.
2) Özçelik H, Vrana NE, Gudima A, Riabov V, Gratchev A, Haikel Y, Metz-Boutigue MH, Carradò A, Faerber J, Roland T, Klüter H. Harnessing the multifunctionality in nature: a bioactive agent release system with self-antimicrobial and immunomodulatory properties. Advanced healthcare materials. 2015 Sep;4(13):2026-36.
3) Sharifi F, Htwe SS, Righi M, Liu H, Pietralunga A, Yesil-Celiktas O, Maharjan S, Cha BH, Shin SR, Dokmeci MR, Vrana NE. A Foreign Body Response-on-a-Chip Platform. Advanced healthcare materials. 2019 Jan 29:1801425.

Acknowledgement

This project has received funding from the European Union's Horizon 2020 research and innovation programme under grant agreement No 760921 (PANBioRA).

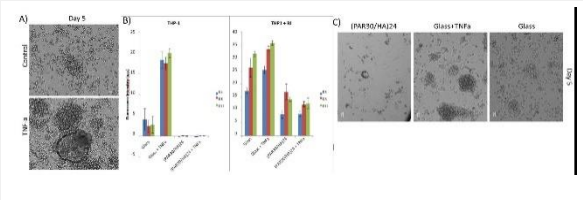

Figure 2. Granuloma induction and the effect of immunomodulatory coatings
A) The induction of large granuloma-like structures in the presence of TNF-alpha B) The effect of PAR/HA coatings on macrophage and subsequent fibroblast attachment. The immunomodulatory coating decreases monocyte attachment while not inhibiting fibroblast attachment C) Significantly less attachment of monocytes on the surface of the coatings.

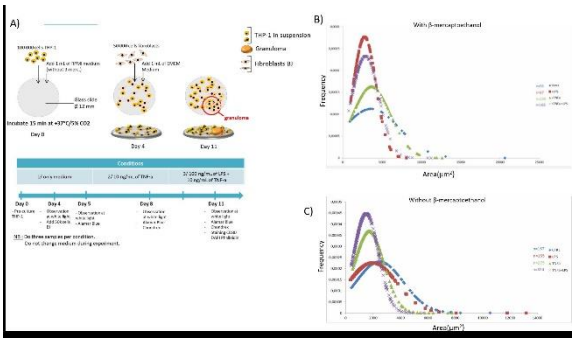

Figure 1. The granuloma induction model and size distribution of granuloma-like structures
A) Schematic representation of granuloma model with monocyte and fibroblast components B) The number and size distribution of granuloma-like structures under control, TNF-alpha, LPS and TNF-alpha/LPS induction conditions with and without beta-mercaptoethanol. Without beta-mercaptoethanol, more granuloma-like structures were formed as a function of induction conditions

V-OS17-02

Harnessing chitosan and poly(γ-glutamic acid) nanoparticles to reprogram the breast tumor microenvironment

Flávia Castro[1,2,3], Catarina L. Pereira[1,2,3], Marta L. Pinto[1,2], Karine Serre[4], Mário A. Barbosa[1,2,3], Fátima Gartner[1,3], Raquel M. Gonçalves[1,2,3], Olivier de Wever[5,6], Maria J. Oliveira[1,2,7]

[1]i3S, Instituto de Investigação e Inovação em Saúde, Universidade do Porto, Porto, PT; [2]INEB, Instituto de Engenharia Biomédica, Universidade do Porto, Porto, PT; [3]ICBAS, Instituto de Ciências Biomédicas Abel Salazar, Universidade do Porto, Porto, PT; [4]IMM, Instituto de Medicina Molecular João Lobo Antunes, Faculdade de Medicina, Universidade de Lisboa, Lisboa, PT; [5]LECR, Laboratory of Experimental Cancer Research, Ghent University, Ghent, BE; [6]CRIG, Cancer Research Institute Ghent, Ghent University, Ghent, BE; [7]Departamento de Patologia e Oncologia, Faculdade de Medicina, Universidade do Porto, Porto, PT

Introduction

Anticancer immune response depends on the efficiency of tumor antigens presentation and co-stimulatory signals provided by antigen-presenting cells (APCs). However, it is known that APCs, namely macrophages and dendritic cells (DCs), exhibit an immature/immunosuppressive phenotype at the tumor site, which limits T cell activities and supports tumor progression. Thus, APCs appear as promising targets to generate more efficient anticancer therapies. Biomaterials have been widely studied for vaccine delivery, since they could protect antigen and adjuvant molecules from degradation, increase their lymphoid organ accumulation and, importantly, modulate APCs functions. In fact, several biomaterial-assisted cancer vaccines have shown great potential in preclinical and clinical development [1]. We have recently reported that chitosan (Ch)/poly(γ-glutamic acid) (γ-PGA) nanoparticles (NPs) modulate immature dendritic cells (DCs) towards an immunostimulatory profile, eliciting CD4 T cell response. Furthermore, Ch/γ-PGA NPs reprogrammed IL-10-stimulated macrophages, characterized by an immunosuppressive and protumoral phenotype, towards an immunostimulatory profile, potentiating instead CD8 T cell response. Notably, these Ch/γ-PGA NPs hampered macrophages and DCs ability to induce cancer cell invasion [2]. Furthermore, Ch/γ-PGA NPs have also been shown to be potential carriers for immunomodulatory drugs, such as diclofenac [3] or interferon (IFN)-γ [4]. Therefore, the combination of immunostimulatory and delivery properties of Ch/γ-PGA NPs makes them good candidates for cancer therapeutic vaccines. In this study, we addressed the potential synergetic effects of Ch/γ-PGA NPs combined with radiotherapy treatment in an orthotopic breast tumor mouse model.

Experimental Methods

NPs were prepared by co-acervation method and characterized by dynamic light scattering. $1x10^6$ 4T1-luciferase cells, a mouse breast tumor cell line, were injected orthotopically in the mammary fat pad of BALB/cByJ. Animals were divided in four groups: non-treated (control), treated with Ch/γ-PGA nanoparticles (NPs), with radiotherapy (RT) or with the combination of both treatments (NPs+RT). After 7 days, when the tumors reached 94.1±32.1mm^3, animals from RT and combinatorial therapy groups were locally irradiated with hypofractionated 10Gy, using a Small Animal Radiation Research Platform. Then, animals from NPs and combinatorial therapy groups were subcutaneously injected, adjacent to the tumor, with 6 doses of NPs (0.7 mg/mL). Tumor volume was measured using a caliper and calculated as (length × width × width)/2 (mm^3) and tumor progression was followed by bioluminescence imaging every week. Animals were sacrificed at day 28. Tumor burden, lung metastasis formation and immune cell profile were explored. Tumor size was normalized, considering the initial size, prior any treatment.

Results and Discussion

Treatments had no significant impact on mice weight nor liver or kidney structure, confirming their safety. Non-treated animals had progressive tumor growth (524.7±80.2%) and developed lung metastasis. Additionally, these animals presented a leukemic reaction in the spleen, characterized by an exuberant reactive follicular hyperplasia, a condition previously reported by others. In treated animals, we verified a negligible effect of Ch/γ-PGA NPs on tumor progression (431.8±78.7%, $p<0.44$), while RT treatment decreased the tumor burden (333.4±69.1%, $p<0.09$). When both treatments were combined, breast tumor progression was further impaired (233.6±22.2%, $p<0.003$). Notably, this combinatorial treatment potentiated the NPs effect in 46% and RT in 30% and, reduced tumor growth in 56% comparing to non-treated animals. The splenomegaly previously described in non-treated animals was reverted by the combinatorial treatment. Additionally, we observed an increase of CD4 T cells-producing IFN-γ in the spleen of the animals treated with NPs+RT. Regarding the metastasis formation, despite all groups presented a similar bioluminescence signal in the lungs, animals from the combinatorial therapy presented less and smaller metastatic foci in comparison to control or single treatments. Systemically, the protumoral cytokines IL-4, IL-10 and the chemokine CCL4 were significantly decreased in the combinatorial treatment. This approach can be further improved by increasing NPs concentration, the administration frequency, or by using these immunomodulatory NPs as adjuvants to other therapies.

Conclusion

Overall, these results suggest that Ch/γ-PGA NPs potentiate and synergize with radiotherapy, opening new perspectives to be used in cancer vaccines in clinical settings.

References

[1] Y. Guo, K. Lei, L. Tang, Neoantigen Vaccine Delivery for Personalized Anticancer Immunotherapy, Front Immunol 9 (2018) 1499.

[2] F. Castro, M.L. Pinto, A.M. Silva, C.L. Pereira, G.Q. Teixeira, M. Gomez-Lazaro, S.G. Santos, M.A. Barbosa, R.M. Goncalves, M.J. Oliveira, Pro-inflammatory chitosan/poly(gamma-glutamic acid) nanoparticles modulate human antigen-presenting cells phenotype and revert their pro-invasive capacity, Acta Biomater 63 (2017) 96-109.

[3] R.M. Goncalves, A.C. Pereira, I.O. Pereira, M.J. Oliveira, M.A. Barbosa, Macrophage response to chitosan/poly-(gamma-glutamic acid) nanoparticles carrying an anti-inflammatory drug, J Mater Sci Mater Med 26(4) (2015) 167.

[4] F. Castro, M.L. Pinto, R. Almeida*, F. Pereira*, A.M. Silva, C.L. Pereira, S.G. Santos, M.A. Barbosa, R.M. Gonçalves**, M.J. Oliveira**, *submitted*

Acknowledgement

This work was financially supported by FEDER – Fundo Europeu de Desenvolvimento Regional funds through the COMPETE 2020 – Operacional Program for Competitiveness and Internationalisation (POCI), Portugal 2020, and by Portuguese funds through FCT –Fundação para a Ciência e a Tecnologia/Ministério da Ciência, Tecnologia e do Ensino Superior in the framework of the project "MAGICIAM-a MAcrophaGe Immunomodulatory-delivery system to prevent Cancer Invasion And Metastasis" (PTDC/BTM-SAL/31859/2017) and through the FCT PhD Programs and by Human Capital Operational Program (POCH), specifically by the BiotechHealth Program (PhD grant PD/BD/114013/2015 for F. Castro).

V-OS17-03

The NLRP3 inflammasome response in macrophages is impaired by 3D chitosan scaffolds

Daniela P. Vasconcelos[1,2,3], Carlos Torre-Minguela[5], Ana I. Gomez[5], Artur P. Águas[3,4], Mário A. Barbosa[1,2,3], Pablo Pelegrín[5], Judite N. Barbosa[1,2,3]

[1]- i3S - Instituto de Inovação e Investigação em Saúde, Universidade do Porto, Porto, PT; [2]INEB - Instituto de Engenharia Biomédica, Universidade do Porto, Porto, PT; [3]- ICBAS - Instituto de Ciências Biomédicas Abel Salazar, Universidade do Porto, Porto, PT; [4]UMIB - Unit for Multidisciplinary Biomedical Research, Universidade do Porto, Porto, PT; [5]Biomedical Research Institute of Murcia (IMIB-Arrixaca), Hospital Clínico Universitario Virgen de la Arrixaca, Molecular Inflammation Group, Murcia, ES

Introduction

Chitosan (Ch) is used in different biomedical applications to promote tissue repair. However, tissue injury after biomaterial implantation leads to the release of danger signals that are responsible in part for an inflammatory response which, if exacerbated and persistent, may impair the function of the implant (1). Danger signals, such as alarmins, released from injured cells are associated with the activation of the inflammasome. Moreover, inflammasome components were recently found to modulate foreign body response to implanted materials (2). Importantly, the nucleotide-binding oligomerization domain-like receptor containing pyrin domain 3 (NLRP3) inflammasome was identified as signal pathway involved in the cellular immune response to Ch products (3). Studies that show inflammasome activation by Ch are related to nanoscale Ch products. However, the activation of the inflammasome by large scale Ch scaffolds has not been investigated yet. Tissue engineering approaches has essentially comprised the implantation of macroscopic scaffolds or devices. Thus, advanced information on how these materials modulate the NLRP3 inflammasome is of key importance to improve biomaterial integration**.** **Objective:** To investigate how a 3D biomaterial, namely Ch scaffolds with different degrees of acetylation (DA), modulate the activation of the NLRP3 inflammasome *in vitro*.

Experimental Methods

The NLRP3 inflammasome activation was assessed in bone marrow derived mouse macrophages (BMDM) and in human macrophages cultured in 3D Ch scaffolds.

Results and Discussion

We found that both Ch scaffolds (4 and 15% DA) did not trigger the NLRP3 inflammasome activation in macrophages. Furthermore, BMDMs and human macrophages cultured in both Ch scaffolds presented a reduction in the number of apoptosis-associated speck-like protein containing a caspase activating recruitment domain (ASC) specks and in IL-1b release upon classical NLRP3 inflammasome stimulation. We also found a decrease in proIL-1b in BMDMs after priming with LPS when cultured in Ch scaffolds with DA 4% DA after priming with LPS when compared to Ch scaffolds with 15% DA or to macrophages cultured in cell-culture plates.

Conclusion

Our results demonstrate that 3D Ch scaffolds with different DA impair NLRP3 inflammasome priming and activation, which goes in line with previous finding by our group that has reported anti-inflammatory properties of Ch.

References

[1] J.M. Anderson et al. Seminars in immunology 20(2) (2008) 86-100.

[2] S.N. Christo et al. Sci Rep 6 (2016) 20635.

[3] D. Fong et al. Biomaterials 129 (2017) 127-138.

Acknowledgement

This work was financed by: FEDER - Fundo Europeu de Desenvolvimento Regional funds through the COMPETE 2020 - Operacional Programme for Competitiveness and Internationalisation (POCI), Portugal 2020, and by Portuguese funds through FCT - Fundação para a Ciência e a Tecnologia in the framework of the project "Institute for Research and Innovation in Health Sciences" (POCI-01-0145-FEDER-007274) and NORTE-01-0145-FEDER-000012, supported by Norte Portugal Regional Operational Programme (NORTE 2020), under the PORTUGAL 2020 Partnership Agreement, through the European Regional Development Fund (ERDF), and supported by the European Research Council (ERC-2013-CoG 614578, to PP), the EU COST Program (BM1406, to PP) and the Ministerio de Economia, Industria y Competitividad–Fondo Europeo de Desarrollo Regional (project no. SAF2017-88276-R, to PP). Daniela P. Vasconcelos is funded by FCT PhD Programmes and by Programa Operacional Potencial Humano (POCH), BiotechHealth Programme (Doctoral Programme on Cellular and Molecular Biotechnology Applied to Health Sciences - reference PD/00016/2012), and through the PhD studentship PD/BD/114011/2015.

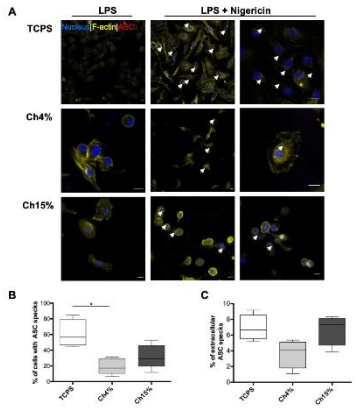

Chitosan scaffolds decrease the formation of ASC specks after NLRP3 activation

(A) Representative images of LPS-primed macrophages cultured in TCPS or Ch scaffolds with different DAs and stimulated or not with nigericin as indicated, followed by staining of ASC (red), actin (yellow; phalloidin) and nuclei (blue; DNA-binding dye DAPI). Arrows indicate ASC oligomers. Scale bar=10µm. (B) Percentage of BMDMs with ASC specks quantified from images as in A, average data from n=4 independent experiments. (C) Percentage of extracellular ASC oligomers (n=4) from macrophages cultured and stimulated as in A. Statistically significant differences: *p<0.05 using Kruskal-Wallis test with Dunn’s multiple comparisons test.

V-OS17-04

3D collagen network composition triggers immunological imprinting of human monocyte-derived macrophages

Colin Logie[1], Tom van Schaajik[1], Tilo Pompe[2], **Katja Franke**[2]

[1]Radboud University, Department of Molecular Biology, Radboud Institute for Molecular Life Sciences, Faculty of Science, Nijmegen, NL; [2]Leipzig University, Department of Biophysical Chemistry, Institute of Biochemistry, Faculty of Life Sciences, Leipzig, DE

Introduction

Wound healing in soft tissues is characterized by a dynamic change of wound tissue composition. A spontaneously formed fibrin-clot – rich in fibronectin and hyaluronan – is transformed into a provisional collagen type I/III and fibronectin containing matrix. Resulting scar tissue is composed mainly of collagen type I (Coll) and glycosaminoglycans. Immune cells like macrophages (MPh), embedded in those dynamically composed tissues, alter their functional phenotype during healing, too. Therefore, immunological imprinting of primary human monocyte-derived MPh triggered by extracellular cues (fibronectin) is investigated as an underlying mechanism.

Experimental Methods

We used 3D Coll-based networks, which were previously shown to be highly suitable to biomimetically modulate cell behavior in wound healing and cancer progression situations.[1,2,3] Such matrices can be engineered with defined topology, elasticity and fibronectin content. In particular, 3D fibrillar Coll networks were reconstituted at 1.5 mg/ml in a 250 mM phosphate buffer (pH 7.5) at 37 °C and 95% humidity. Coll networks were functionalized with fibronectin at a concentration of 40 µg/ml of the incubation buffer. Network topology, stability, elasticity and fibronectin content were investigated via confocal laser scanning microscopy, colloidal force spectroscopy and fluorescence spectroscopy. Human monocytes were isolated by magnetic separation and differentiated into MPh subtypes inside Coll and Coll-fibronectin networks in presence of M-CSF (Coll-MPh, CollFN-MPh). As controls naïve M0-MPh (standard cell culture media), inflammatory M1-MPh (cell culture media + 24 h lipopolysaccharide (LPS) challenge) and anti-inflammatory M2-MPh (cell culture media with IL13 and rosiglitazone) were differentiated in tissue culture dishes. LPS-MPh with immune tolerance were received from LPS treated monocytes. Immunological imprinting of Coll- and CollFN-MPh was investigated in terms of gene expression and cytokine release profiles by RT-qPCR and ELISA. Indicator genes discriminating MPh subtypes were acquired by screening of genome-wide gene expression profiles including trained and tolerized MPh (BG-MPh, LPS-MPh).[4,5] Performance of differentiated MPh under challenge with LPS was investigated, too.

Results and Discussion

3D fibrillar Coll networks were reconstituted at controlled topology, thickness, elasticity and fibronectin content. The fibril and pore diameter were adjusted with about 0.8 µm and 7 µm, respectively, network thickness and Young's elastic modulus was about 480 µm and 100 Pa, respectively. Coll networks were functionalized with approx. 0.15 µg fibronectin per µg Coll. Fibronectin functionalization did not influence Coll network microstructure or mechanics. Monocytes were able to infiltrate these networks with about 80% of invading cells, while the stability of network microstructure could be proven over the whole cell culture period. By investigating the expression of characteristic genes of tolerized/pro-inflammatory and anti-inflammatory MPh phenotypes in Coll-MPh and CollFN-MPh (*FABP4, CLEC4E, SLC2A6, SOD2*) we observed a MPh immune tolerance in dependence on fibronectin functionalization,

accompanied by an efficient immune response upon LPS challenge. IL6, IL8, IP10 and IL10 cytokine release patterns indicated a mildly decreased pro-inflammatory response of MPh in fibronectin-functionalized Coll matrices.

Conclusion

In sum, our work highlights fibronectin presence in 3D Coll matrices to support an immune tolerance imprinting during monocyte-to-macrophage differentiation. Furthermore, it was concluded that 3D collagen matrices are a useful tool to mimic in vivo tissues to elucidate specific cellular processes.

References

[1]Franke K et al. *Acta Biomaterialia* 10:2693 (2014). [2]Sapudom J et al. *Biomater. Sci*. 3:1291 (2015). [3]Friedemann M et al. *Adv. Healthcare Mater.* 6:1600967 (2017). [4]Sead S et al. *Science* 345:1578 (2014). [5]Novakovic B et al. *Cell* 5:1354 (2016).

Acknowledgement

The authors acknowledge the support of grants from EFRE and Free State of Saxony (SAB: 100144684) and Deutsche Forschungsgemeinschaft (INST 268/293-1 FUGG).

V-OS17-05

Understanding immune responses to biomaterials: identifying the major players using an *in vitro* model of the human immune system

Florian Billing[1], Meike Jakobi[1], Matthias Becker[1], Dagmar Martin[1], Antje Biesemeier[2], Sören Segan[1], Thomas Joos[1], Ulrich Rothbauer[3], Claus Burkhardt[1], Hanna Hartmann[1], Nicole Schneiderhan-Marra[1], **Christopher Shipp**[1]

[1]Natural and Medical Sciences Institute (NMI) at the University of Tübingen, Reutlingen, DE; [2]University Hospital Tübingen, Center for Ophthalmology, Tübingen, DE; [3]University of Tübingen, Tübingen, DE

Introduction

The immune response to implanted medical devices is a major factor determining their biocompatibility, but there is limited knowledge regarding the role of different immune cell types in the context of biomaterials. We aimed to develop an understanding of the role that different immune cell types play in the overall immune response to biomaterials. It is widely believed that myeloid cells such as monocytes initiate biomaterial immune responses which subsequently involve the participation of lymphocytes. However to the best of our knowledge, this assumption and the details thereof remain to be confirmed. To achieve this, we investigated the role of different immune cell populations cultured at varying ratios when in contact with biomaterial.

Experimental Methods

Immune cell fractions (monocytes and lymphocytes) were isolated from peripheral blood mononuclear cells with magnetic cell sorting (> 98% purity). Both fractions were cultured in isolation and at ratios of 2:1 and 9:1 (lymphocytes:monocytes). The total number of cells was kept constant in all experiments. Immune responses were assessed with multiplex cytokine analysis (14 molecules) and flow cytometry (CD molecule expression on monocytes, T cells and NK cells). Experiments were performed with clinically-used titanium specimens previously found to provoke pro-inflammatory immune responses.

Results and Discussion

Confirming our previous findings, we observed a pro-inflammatory response to titanium specimens. Examining the role of different cell types revealed that immune responses to the titanium biomaterial specimens were differentially mediated by monocytes and lymphocytes. Monocytes produced the strongest pro-inflammatory signal in response to biomaterial in the absence of lymphocytes, as indicated by the release of IL-1beta, IL-6, MCP-1 and TNF-alpha. The level of this response far exceeded that observed for lymphocytes alone or lymphocytes cultured with monocytes at any ratio. Lymphocytes cultured together with monocytes had the effect of dampening pro-inflammatory cytokine release, with this effect stronger when a higher proportion of lymphocytes were present. By contrast, the immune response to titanium produced by lymphocytes alone was extremely low. Examining CD molecule expression on immune cell populations showed the presence of lymphocytes to result in a dose-dependent reduction in the expression of CD16 on monocytes.

Conclusion

Using a human-based *in vitro* model we show the relative contribution of different immune cell populations to biomaterial immune reactions. Our results challenge the assumption that monocytes and lymphocytes interact to produce the resultant immune response. Instead, our results highlight monocytes alone as the cell type responsible

for driving pro-inflammatory responses to biomaterials. These results may have implications for strategies aiming to modulate host immune response to biomaterials.

Acknowledgement
We are grateful to Burkhard Schlosshauer (NMI) for his contribution to the initiation of this project. This work was supported by the EU-EFRE and the state of Baden-Wuerttemberg (712889).

V-OS17-RF06

Myofibroblast Behavior Controlled by Macrophages in a 3D *in vitro* Coculture Model

Franziska Ullm, Katja Franke, **Tilo Pompe**

Leipzig University, Institute of Biochemistry, Leipzig, DE

Introduction

Persistent inflammation during dermal wound healing is often associated with impaired repair and dysfunction of the regenerated tissue and is often attributed to cell-cell and cell-matrix miscommunication. The underlying mechanisms are still insufficiently understood. 3D i*n vitro*models offer striking opportunities to study these interactions by allowing to mimic microstructure, mechanics and molecular composition of the extracellular microenvironment at pathological and physiological situations. We developed a modular matrix engineering platform based on fibrillar 3D collagen I matrices, which facilitates detailed examinations of various cell-cell interactions *in vitro*. In the present study we applied it to the analysis of the interaction between primary human fibroblasts (FB) and macrophages (MΦ) during early as well as late stages of wound healing.

Experimental Methods

Our model system is based on fibrillary 3D matrices reconstituted from collagen I. Pore size, fibril diameter and matrix stiffness were adjusted by reconstitution conditions and optional modifications by subsequent cross-linking or functionalization with other ECM molecules, e.g. glycosaminoglycans (GAGs) or fibronectin, as previously shown in other studies.[1,2,3] Primary human dermal FB and human monocyte-derived MΦ were examined in their response to these matrices in coculture studies over 6 days. MΦ were either polarized into inflammatory or regulatory phenotype, achieved by distinct differentiation protocols after isolation. Cells were seeded inside the 3D matrix during collagen matrix reconstitution. FB were optionally stimulated by TGF-β_1 to trigger a myofibroblasts (MyoFB) differentiation.
We analyzed changes in cell distribution and matrix properties over the time course of the coculture study. Proliferation behavior of FB was examined using commercial WST-1 assay.
Gene expression analysis of markers of MyoFB phenotype (αSMA, matrix protein synthesis) and immunofluorescence of αSMA incorporation into the actin stress fibers were used to study FB differentiation and dedifferentiation. We further determined IL-10 cytokine secretion using ELISA.

Results and Discussion

Inclusion of cells during collagen matrix reconstitution did not alter matrix properties in terms of pore size, fibril diameter and elasticity. Moreover, homogeneous distribution of cells remained stable during cultivation time. Coculture experiments of MyoFB and regulatory M2-MΦ revealed a dose-dependent regulation of MyoFB proliferation and differentiation. Proliferation of MyoFB increased whereas the total amount of MyoFB decreased in dependence on the amount of cocultivated regulatory M2-MΦ. The analysis of gene expression related to the formation of new ECM proteins (Coll I; Coll III and EDA-FN) confirmed these results of altered MyoFB phenotype. Additionally, regulatory M2-MΦ were shown to be the main source of secreted IL-10 cytokine. These findings indicated a direct paracrine impact of IL-10 secreted from M2-MΦ to the ascending de-differentiation of MyoFB in coculture.

Additional experiments with inflammatory M1-MΦ demonstrated a converse effect. Gene expression data showed a dose-dependent increase of MyoFB characteristic gene expression with cocultivated inflammatory M1-MΦ and a persistent MyoFB phenotype. IL-10 secretion of M1-MΦ in the absence of MyoFB was generally low, whereas the presence of MyoFB led to a dose-dependent increase of IL-10 in the supernatant, indicating additional paracrine effects of MyoFB on inflammatory M1-MΦ.

Conclusion

In sum, our 3D collagen I based matrices resemble a highly relevant biomimetic model of early and late stages of wound healing with a control of proliferation and differentiation of MyoFB by MΦ in coculture.
Perspective experiments will uncover the regulation of the paracrine IL-10 and TGF-$\beta_1$signal exchange between both cell types by an interaction with GAG-modified 3D matrices.

References

1. Sapudom, J et al. *Biomaterials* 52:367-75 (2015).
2. Sapudom J, et al. *Biomater Sci* 3:1291 (2015).
3. Kalbitzer L, et al. *J Mater Chemistry B* 3:8902-10 (2015).

Acknowledgement

This study was supported by Deutsche Forschungsgemeinschaft grant (SFB/TRR67 project B10). The authors would like to thank Ronald Weiß and Sunna Hauschildt as well as Ulf Anderegg (Universitätsklinikum Leipzig) for support in cell culture.

V-OS17-RF07

Dose-depending effect of therapeutic active ions released from borate bioactive glasses on immune cells

Katharina Schuhladen[1], Lena Stich[2], Xiaoju Wang[3], Leena Hupa[3], Alexander Steinkasserer[2], Aldo R. Boccaccini[1], Elisabeth Zinser[2]

[1]University of Erlangen-Nuremberg, Department of Materials Science and Engineering, Institute of Biomaterials (WW7), Erlangen, DE; [2]Universität Erlangen-Nürnberg, Department of Immune Modulation, Erlangen, DE; [3]Åbo Akademi University, Johan Gadolin Process Chemistry Centre, Turku, FI

Introduction

Key properties of bioactive glasses include their ability to dissolve and release ions when immersed in an aqueous environment, as well as the formation of an apatite surface layer on the glass during dissolution [1]. Due to the lower chemical durability of borate glasses and their ability to transform rapidly to hydroxyapatite, an increasing amount of research has started to focus on the use of borate bioactive glasses, especially in the field of wound healing [2]. To further improve the performance of bioactive glasses, it is possible to introduce therapeutic ions with specific effects, e.g. copper to enhance angiogenesis and zinc to avoid infections [3]. Since immune cells are crucial players during the wound healing process [4], the dose-depending effect of the biological active ions copper and zinc released from borate bioactive glasses on immune cells was systematically examined.

Experimental Methods

Based on the well-known 13-93 silicate glass, borate glasses, where all the SiO_2 was replaced by B_2O_3, and Cu/Zn-doped borate bioactive glasses were produced by melt-quenching and characterized using FTIR, SEM/EDX as well as XRD. Then, to study the dissolution behavior, bioactive glass particles (300-500 µm) were immersed in different relevant solutions and ICP measurements were conducted to confirm the release of the different ions. Cell culture media, conditioned with release products of bioactive glasses, was then used to incubate murine dendritic cells (DC). After different time periods the effect of the different ions on the immune cells was examined regarding their cell viability, their phenotype (by FACS) and their T cell stimulatory properties (by MLR) measurements.

Results and Discussion

Four different borate glasses doped with Copper or/and Zinc were successfully produced. Depending on the composition and the release conditions (static/dynamic, dissolution media), the glasses dissolve and release therapeutic active ions in relevant amounts. However, the release of zinc from Zn-doped borate glasses could not be measured; instead the zinc was incorporated in the formation of an apatite layer. During the release, a similar increase of pH was observed for all tested glasses [5]. A concentration dependent effect on the viability of (DC), by the released ions, was observed whereby the magnitude of viability was different between the used ion-doped glasses. Moreover, a specific and dose-dependent effect was observed on the phenotype of DC. Additionally, a concentration- and composition-dependent effect was observed regarding the DC mediated T-cell proliferation capacity and on the secretion of cytokines by DC cultured in conditioned media. This clearly shows that bioactive glasses, depending on their composition, have an effect on the viability, phenotype and functionality of immune cells.

Conclusion

Borate glasses, undoped or doped with the well-known therapeutic active ions copper and zinc, were fabricated by melt-quenching method. The fabricated glasses were firstly tested in different dissolution tests, showing their biodegradable nature and the release of biological relevant ions and secondly in contact with DC. A dose-depending effect, related to the glass composition, on immune cells such as DC and T cells could be proven. The results showed the great potential of boron containing bioactive glasses to significantly influence immune cells and therefore their role in wound healing.

References

[1] D. S. Brauer, “Bioactive Glasses-Structure and Properties,” *Angew. Chemie Int. Ed.*, vol. 54, no. 14, pp. 4160–4181, 2015.,

[2] Y. Li, M. N. Rahaman, Q. Fu, B. S. Bal, A. Yao, and D. E. Day, “Conversion of bioactive borosilicate glass to multilayered hydroxyapatite in dilute phosphate solution,” *J. Am. Ceram. Soc.*, vol. 90, no. 12, pp. 3804–3810, 2007.

[3] A. Hoppe, N. S. Güldal, and A. R. Boccaccini, “A review of the biological response to ionic dissolution products from bioactive glasses and glass-ceramics,” *Biomaterials*, vol. 32, no. 11, pp. 2757–2774, 2011.

[4] T. A. Wilgus, “Immune cells in the healing skin wound: Influential players at each stage of repair,” *Pharmacol. Res.*, vol. 58, no. 2, pp. 112–116, 2008.

[5] K. Schuhladen, X. Wang, L. Hupa, and A. R. Boccaccini, “Dissolution of borate and borosilicate bioactive glasses and the in fl uence of ion (Zn , Cu) doping in di ff erent solutions,” *J. Non. Cryst. Solids*, vol. 502, pp. 22–34, 2018.

Acknowledgement

Abo Akademi's Johan Gadolin Scholarship is gratefully acknowledged for financial support.

V-OS17-RF08

Long term *in vivo* biocomatibility study of modified Ti6Al7Nb in the aspect of local effects after implantation

Barbara Zawidlak-Węgrzyńska[1], Małgorzata Gonsior[1], Karolina Janiczak[1], Danuta Gonsior[1], Piotr Ścigała[1], Roman Kustosz[1], Tadeusz Wierzchoń[2], Michał Tarnowski[2], Romuald Wojnicz[3], Edyta Raichman-Warmusz[3]

[1]Professor Zbigniew Religa Foundation of Cardiac Surgery Development, Zabrze, PL; [2]Warsaw University of Technology, Faculty of Material Science and Engineering, Warszawa, PL; [3]Medical University of Silesia, Department of Histology and Embryology, Zabrze, PL

Introduction

Modification of the well-known glow discharge assisted nitriding process called active screen plasma nitriding has been used for enhancing the biocompatible properties of Ti6Al7Nb titanium alloy through production of TiN+Ti2N+αTi(N) diffusive surface layers [1]. The aim of the study was to evaluate the tissue reaction after implantation in the rabbit dorsal muscle of the Ti6Al7Nb titanium alloy and Ti6Al7Nb modified with TiN type layers.

Experimental Methods

The implantation test was carried out according to the standardized assays described in ISO 10993-6. A total of 72 New Zealand white both sexes rabbits weighing from 3000 to 3500 grams were used in this experiment. Four implants (discs of 10 mm diameter 1,5 mm thickness) were aseptically inserted subcutaneously on the animal's back. As a negative control Ti6Al7Nb titanium alloy was used. The animals were observed for: 4, 12 and 26 weeks. After animals euthanasia, a macroscopic evaluation of the implantation area was performed and the biomaterial implants were removed. The tissues were fixed with 4% formalin, embedded in paraffin, and stained with hematoxylin-eosin and Trichrome Masson for histological studies.

Results and Discussion

Histopathological analysis revealed in vast majority normal healing process around the implant and isolated cases of an inflammatory change, more frequent for the animals with TiN implants in the observation period of 4 weeks. A micro-section of the implants showed that the investigated material implanted for the different periods: 4, 12 and 26 weeks, caused no response-mild fibrosis. There was no muscle degeneration, nor necrosis, nor any other significant change observed.

Conclusion

Both investigated biomaterials: TiN+Ti2N+αTi(N) produced in so called active screen plasma nitriding process on Ti6Al7Nb titanium alloy surface as well as Ti6Al7Nb, implanted in vivo did not induce any adverse tissue reactions in the long-term period of 26 weeks.

References

1. Ti6Al7Nb Alloy Surface Improvement For Implantable Blood Pumps Applications, M.Gonsior, M.Tarnowski, K.Janiczak, B.Zawidlak-Węgrzyńska, T.Wierzchoń, M.Gawlikowski, R.Kustosz, etc., Engineering of Biomaterials, No 143, Special Issue, Vol. XX, 2017, p.65, 2017

Acknowledgement

The authors would like to thank NCBIR (Grant no: STRATEGMED-2/ RH-ROT/266798/15/NCBR/2015) for providing financial support to this project.

2:15 p.m. – 3:45 p.m.

Conference room 2+3

V-OS18 | Patterning and coatings 2

V-OS18-01

Immune suppressive functionality of polyelectrolyte multilayer coatings

Alexander Rudt[1], Xin Xiong[2], Rumen Krastev[1,2]

[1]Reutlingen University, Intelligent Surfaces, Reutlingen, DE; [2]NMI Natural and Medical Science Institute at the University of Tübingen, Biofunctionalized Surfaces, Tübingen, DE

Introduction

Despite having a nanometer thickness, polyelectrolyte multilayer (PEM) coatings are able to affect cellular behavior such as adhesion, proliferation and immune reactions on the interface between implant surfaces and biological tissue. The PEM coatings enable high variability of surface properties and by formation of well-defined surfaces allow precise regulation of biological systems. The interactions between cells and surface shall be adjusted to reduce the undesired immune response of the tissue.

In our previous works, we found that PEM coatings for cardiovascular stents reduce the expression of proinflammatory messengers, in particular central chemokine Interleukin-8, that are involved in the development of restenosis after stent implantation. A high correlation between degree of immune suppression and the characteristic surface properties nano-roughness and nano-stiffness was observed.

In the present paper, we aimed for better understanding of the processes, which take place on the cell-surface contact with PEM coated surfaces. Nano-stiffness was one of the physical surface parameters that correlated most with the improvement of cell adhesion and reduction of immune response. To further study the effect of surface stiffness on biological cells, PEM coatings were modified by concentration of electrolytes in the deposition solution, which resulted in well-controlled changes in the viscous and elastic properties. Another aspect was the study of involvement of protein adsorption on the effect of PEM coatings on biological cells.

Experimental Methods

PEM coatings – preparation: Polyelectrolyte multilayer (PEM) coatings were prepared from weak and strong polyelectrolytes via layer-by-layer technique by alternating deposition of anionic and cationic polyelectrolytes.

Physical-chemical Characterization: The PEM modified surfaces were characterized with focus on surface energy by contact angle, surface charge by zeta-potential, and topography, roughness and stiffness by atomic force microscopy. For characterizationof, by electrolyte concentration modified, PEM film viscosity and elasticity the Voigt model was applied on measurements with a quartz crystal microbalance with dissipation monitoring (QCM-D).

Biological Characterization: These defined surface parameters were correlated with the degree of biological response of Human Umbilical Vein Endothelial Cells (HUVECs) such as expression of proinflammatory downstream products of the NF-????B pathway via RT-PCR for mRNA level and ELISA for protein level screening. Cell adhesion/proliferation were measured by fluorescence microscopy and cell activity by Resazuin Assay.

Results and Discussion

Results show that variation of PEM coatings by electrolyte concentration in the deposition solution enable controlled protein adsorption. Proteins from cell culture medium adsorb on positively and negatively charged surfaces and are affected by coating conditions. A direct correlation between the amount of adsorbed proteins and cellular adhesion was observed. Protein adsorption shows effect on viscous and elastic surface properties of various PEM coatings.

Depending on surface charge the viscous and elastic properties of PEM films show different effect on protein adsorption.

Conclusion

Viscoelastic properties influence cellular behavior [1], however no optimal values of elasticity and viscosity for immunosuppressive functionality are known as of yet. The protein adsorption study showed that proteins by adsorbing on the surface, influence and change viscoelastic properties of the surface, thus currently no conclusion can be made. Further experiments need to be carried out to address dependence of immune response on surfaces under consideration of the impact of proteins adsorbed from cell culture medium/ blood.

Our research gives insights on cell-surface interactions on PEM coatings and advances towards the goal to create passive surface coatings for functional cardio vascular devices without application of pharmaceutical substances.

References

[1] Charrier E. et al., Nature Communications 9, Article number: 449 (2018)

Acknowledgement

The authors would like to thank the cooperating working groups and project partners: the group of intelligent surfaces at Reutlingen University led by Prof. R. Krastev, the department of biophysical chemistry, and especially the group biofunctional surfaces led by Dr. X. Xiong at the NMI Natural and Medical Sciences Institute at the University of Tübingen. The project is financially supported by the program “Innovative Projekte/ Kooperationsprojekte an den Hochschulen Baden-Württemberg”, BioDeg Stent project (FHprofUnt program of BMBF, FKZ:13FH155PX6).

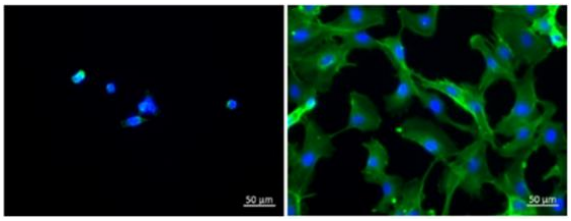

Controlled adhesion of HUVECs on PEM modified surfaces
Fluorescence microscopy shows HUVECs adhering poorly on PEM coatings from a pair of weak polyelectrolytes (left) and strongly on PEM coatings from pair of strong polyelectrolytes (right).

V-OS18-02

Bioactive polymer grafting on Titanium nanotubes : Enhancing cell growth and inhibiting bacteria adhesion

André Rangel[1], Céline Falentin-Daudré[1], Carlos E. Vergani[2], Véronique Migonney[1], Ana Paula R. Alves Claro[3]

[1]Université Paris 13, LBPS/CSPBAT, UMR CNRS 7244, Villetaneuse, FR; [2]UNESP – São Paulo State University, Dental School, Dental and Prosthodontics Department, Araraquara, BR; [3]UNESP – São Paulo State University, School of Engineering, Materials and Technology Department, Guaratingueta, BR

Introduction

In our days, the major challenge for improving the use of titanium (Ti) alloys as biomaterials has been its surface characteristics. Thus, looking for properties as relevant as the already found in the bulk of these alloys, many researchers of the biomaterials field increasingly focus their efforts on surface modifications. Several studies have shown that the anodization in order to obtain Ti oxide nanotubes is fast and low-cost treatment that enables designing samples of high surface energy, surface/volume ratio and morphology mimicking bone, which may lead improved osseointegration. However, this treatment severely increases the surface roughness, representing a potential issue for bacteria attachment. From this point, a combination of this technique to antibacterial coatings appears as a natural way to follow and the grafting of poly(sodium styrene sulfonate) (PNaSS) fits perfectly on this topic. The presence of this polymer on surfaces was demonstrated to control interactions with adhesive proteins as fibronectin, playing a fundamental role in the inhibition of bacteria adhesion without compromising the surface morphology. The union of this characteristics is a valuable asset and stands out as a promising alternative to taylor such surfaces to better biological response.

Experimental Methods

Ti15Mo alloys were obtained by melting commercially pure metals in an electric arc furnace under argon atmosphere. Ingots were heat treated to insure homogeneity and cut into discs of 10 mm diameter. Discs were submitted to anodic oxidation at 10V for 24 hs in ammonium fluoride/glycerol electrolyte. Then the samples were heat treated to nanotubes crystallization. PNaSS grafting on anodized samples was achieved under UV irradiation for 1 h. Surfaces were characterized by SEM images, contact angle and FTIR. The amount of grafted PNaSS on Ti surface was estimated by colorimetric assay. The cell response - proliferation, morphology and viability assays- was achieved by using MC3T3-E1 cell line. The inhibition of bacteria adhesionwas evaluated by confocal fluorescent images of a *Staphylococcus aureus* (ATCC 25923) and *Candida albicans* (SC 5314) biofilm.

Results and Discussion

SEM images show the homogeneous formation of nanotubes across the surface of Ti15Mo alloys samples. Nanotubes have a very regular structure with internal dimensions estimated (image-editing software) around 22 nm. The efficacy of the PNaSS grafting on anodized samples was shown by characterization methods as wettability and FTIR spectra clearly showing the presence of PNaSS peaks. In addition, toluidine blue colorimetric assay indicates the presence of 7 µg PNaSS/cm^2, a value fully consistent with previously performed tests on non-anodized alloys. Regarding the behavior of osteoblasts over the surfaces, all tests indicated better cell development on anodized and grafted surfaces, with an increased cell viability and early cell spreading as well as better proliferation after 7 days of

incubation. In parallel, fluorescence images show a drastic reduction in the number of biofilm elements on PNaSS grafted surfaces, confirming the influence of nanotubes and PNaSS presence over these two parameters.

Conclusion

Tests carried out throughout this study show that nanotubes formed by anodic oxidation on the Ti15 Mo can be effectively grafted with PNaSS by UV irradiation. It worthy pointing out that the combination of chemical and uperficial morphology provided by both treatments has a beneficial effect on the cell response and bacterial adhesion on studied surface. In summary, the treatment can be presented as a promising alternative to improve commercially available surfaces.

References

Oh, S.H., Jin, S. Titanium oxide nanotubes with controlled morphology for enhanced bone growth. Materials Science and Engineering C, v.26, p.1301 – 1306, 2006.

Popat K. C., Eltgroth M., Latempa T. J., Grimes C. A., Desai T. A. Decreased Staphylococcus epidermis adhesion and increased osteoblast functionality on antibiotic-loaded titania nanotubes. **Biomaterials**, v. 28, n. 32, p. 4880–4888, 2007

Saidin S., Chevallier P., Abdul Kadir M. R., Hermawan H., Mantovani D. Polydopamine as an intermediate layer for silver and hydroxyapatite immobilisation on metallic biomaterials surface. Materials Science and Engineering C, v. 33, n. 8, p. 4715–4724, 2013.

Migonney, V., Ben Aissa, I., Lutomski, D., Hélary, G., Oughlis, S., Poirier F., Changotade S., Peltzer J. Lataillade, J., Blanquaert, D., De Lambert, B., Viateau, V., Manassero, M., Crémieux, A., Saleh-Mghir, A., Thomas, D. Controlled cell Adhesion and aCtivity onto TAl6V titanium alloy by grafting of the SURFace: Elaboration of orthopaedic implants capable of preventing joint prosthesis infection. **Irbm**, v. 34, n. 2, p. 180–185, 2013.

Chouirfa, H., Migonney, V., Falentin-Daudré C. Grafting bioactive polymers onto titanium implants by UV irradiation. **Royal Society of Chemistry Advances**, 6, 13766–13771, 2016.

Ercan, B., Taylor, E., Alpaslan, E., Webster, T.J. Diameter of titanium nanotubes influences anti-bacterial efficacy. **Nanotechnology**. Jun 15;22(29):295102, 2011

Acknowledgement

The authors would like to thank FAPESP (projects 2013/00317-4, **2015/26273-9, 2015/25124-0 and 2015/13834-2**) and CNPq (project 486352-2013-7) for their financial support and Bruna Pimentel for her technical help on bacterial adhesion testing.

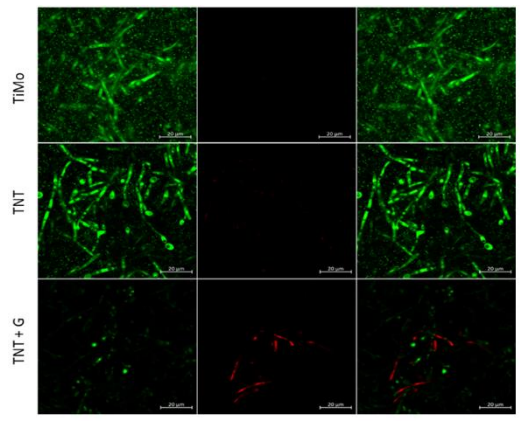

Confocal Laser Scanning Microscope (CLSM) images of live/dead staining at 48h

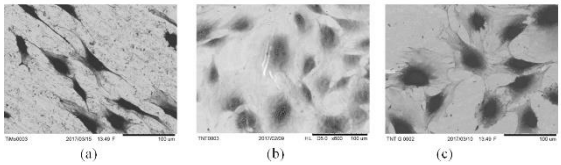

SEM images of osteoblast after 24 hours on he surface
a)Ti15Mo flat samples, b)Ti15Mo anodized samples and c) Ti15Mo anodized and grafted surfaces

V-OS18-03

Antibacterial and bioactive coatings on titanium alloy implant surfaces

Anke Bernstein[1], Hermann O. Mayr[1], Rainer Gadow[2], Michael Seidenstücker[1], Sophie Burtscher[1], Philip Przybilla[1], Karola Müller[1], Andreas Killinger[2]

[1]Medical Center - Albert-Ludwigs-University of Freiburg, Faculty of Medicine, Department of Orthopedics and Trauma Surgery, G.E.R.N. Tissue Replacement, Freiburg, DE; [2]University of Stuttgart, Institute for Manufacturing Technologies of Ceramic Components and Composites, Stuttgart, DE

Introduction

Amongst the most frequent causes for implant failure in arthroplasty stands aseptic prostheses loosening [1]. This phenomenon is attributable to the missing induction of secondary stability; meaning that the firm anchorage needed between the prosthesis and the surrounding bone is missing. Another common complication after implantation is microbial colonization on the prosthesis surface [2]. These complications often lead to secondary surgery and implant-exchange being required. In order to reduce these complications, implant surfaces can be coated with bioactive substances which can have both osteoconductive and antimicrobial properties [3]. The aim of the study was the development and optimization of high-velocity suspension flame spraying (HVSFS, [4]) process for producing thin resorbable bioactive ceramics coatings on the basis of degradable calcium phosphates and bioactive glasses. In these layers bactericidal effective metal copper was integrated.

Experimental Methods

Four different materials with a layer thickness of 20 µm were tested (Ca10[Na/K](PO4)7, bioglass, HA, ß-TCP). Additionally, the coatings contained copper. For biocompatibility-testing in vitro, cell culture experiments were carried out using MG-63 cells. Cell viability was verified histologically by Giemsa-staining and a Live/Dead-Assay (3, 7, 14, 21d). A WST-1-Kit was used to quantify cell proliferation and viability, and LDH tests were performed to determine cytotoxicity. For examination of the antimicrobial virtues, Safe Airborne Antibacterial assay was applied on S. aureus. For biocompatibility-testing in vivo implants were inserted into the distal femur and left in place for 2, 4, 6, 12, or 24 weeks. Eight animals were operated upon bilaterally for each material and each time of implantation. The implant fixation was analysed with push-out-tests by determining the shearing strength. Histological and image analysis was combined to assess the quantitative and time-dependent degradation of the material layers as well as document the progression and quality of osteointegration.

Results and Discussion

The experiments revealed that the coatings show different biocompatibility on MG-63 cells and do not have identical antimicrobial efficacy on S. aureus. The highest cell-vitality was detected on TCP and Bioglass- ceramics. The Cu doping showed only minor influence on the biocompatibility of the coatings. Cu-doped coatings had an antimicrobial effect against bacterial growth.In the histological and histomorphometric analyses, the coatings showed a good integration and a high percentage of implant contact to bone. The addition of copper showed no significant effects. The dynamics of the bone healing process differed depending on the material. Coatings with bioglass caused a mineralisational dysfunction at the contact area with the bone and also showed the least shearing strength throughout the trial period. The addition of bacteriocidal metals also prevents bacterial infection. The greatest average shear strength in the earlier stages between 2 and 12 weeks was achieved by implants coated with ß-TCP. At 24 week GB14-coated implants reached the highest shear strength of all implants.

Conclusion

These studies support the evidence that implants coated with degradable materials improve the early stability of prostheses.

References

[1] Garellick, G., J. Kärrholm, C. Rogmark, H. Lindahl, H. Malchau and O. Rolfson (2014). Swedish hip arthroplasty register. Annual report.

[2] Lutz Claes, P. K., Carsten Perka, Maximilian Rudert (2012). AE-Manual der Endoprothetik, Hüfte und Hüftrevision

[3] Zimmerli, W., A. Trampuz and P. E. Ochsner (2004). "Prosthetic-joint infections." New England Journal of Medicine**351**(16): 1645-1654

[4] Gadow, R., A. Killinger and J. Rauch (2008). "Introduction to high-velocity suspension flame spraying (HVSFS)." Journal of Thermal Spray Technology**17**(5-6): 655-661

V-OS18-04

A Novel Growth Factor Delivery Polymer-Coating System to Enhance the Osseointegration of Bioinert Implants

Noura M. Alotaibi[1,2], Kurt B. Naudi[1], Matthew J. Dalby[2], Manuel Salmerón-Sánchez[2], Ashraf F. Ayoub[1]

[1]University of Glasgow, Glasgow Dental Hospital & School, Glasgow, GB; [2]University of Glasgow, Centre for Cellular Microenvironment, Glasgow, GB

Introduction

Polyetheretherketone (PEEK) is a member of high-performance polymers, utilised in orthopaedics as an alternative to metal implants. PEEK has excellent tunable mechanical properties which support its potential application as an implant, but PEEK's inertness interferes with osseointegration. Overcoming this limitation remains the greatest challenge for PEEK implant clinical applications. One promising therapeutic strategy for the hydrophobic materials is transforming them to a bioactive surface which can interact and stimulate bone healing.

Several approaches are used to promote osseointegration of bioinert materials for implant application; however, there is no method to improve the osteoinductivity of these materials.

Therefore, this study investigated the potential of using bioactive coatings to promote the osteogenic bioactivity of PEEK. This was done using a nanoscale poly (ethyl acrylate) coating that interacts with fibronectin to support cell attachment and presentation of growth factors (1). We delivered ultra-low, topical doses of bone morphogenetic protein 2 (BMP-2) [100ng/ml] to the cells. This was based on the ability of plasma polymerised ethyl acrylate (p-PEA) to facilitate fibronectin (FN) fibrillogenesis where the cell and growth factor binding domains have been exposed. This allowed for a synergistic interaction of the integrin/growth factor receptors (2)(3).

Experimental Methods

PEEK was functionalised using plasma polymerised ethyl acrylate (p-PEA). The thickness of the deposited p-PEA coatings was (≈344 nm) (Figure1). Besides physical and chemical characterisation via SEM, AFM, WCA and XPS to optimise the coating, the sustained release of growth factor BMP-2 after 2 hours and daily over 14 days were measured. The tensile and shear tests were assessed to check the mechanical properties of the coating. The biological investigations of the engineered surfaces in terms of cell response and differentiation were performed using human mesenchymal stem cells (MSCs). Cell adhesion and osteogenic differentiation of the cells were evaluated using Coomassie brilliant blue, alkaline phosphatase (ALP) assay after 14 days and ALP staining after 28 days. Mineralisation was assessed by alizarin red and von Kossa staining after 28 days and 35 days, respectively.

Results and Discussion

WCA showed moderate hydrophilicity after the application of FN, which promoted better cell/surface interaction. The cumulative BMP-2 release from the materials over two weeks was less than 10% of the total bound BMP-2 which confirms the stability of BMP-2 on the coating. More cell adhesion and spreading were found on the coated PEEK surface in comparison to the uncoated ones. Osteogenic differentiation of the cells increased significantly on the p-PEA coated PEEK. Mineralisation was confirmed on the surface of the coated PEEK compared to the uncoated ones; this was validated by the positive von Kossa and alizarin red staining (Figure2).

Data showed the ability of osteogenic differentiation of the MSCs which supports the proliferation and interaction of MSCs with the tailored PEEK surface *in-vitro*. Cell adhesion and differentiation studies confirmed the potential of the

engineered coating to create a more favourable and controlled microenvironment for the bioinert polymer allowing for implant-bone interaction.

Conclusion

This *in-vitro* study successfully prepared the PEEK surface and improved its bioactivity. The results indicate the engineered synergistic integrin/BMP-2 system allowed osteogenic differentiation of undifferentiated MSCs and promoted osteogenesis on PEEK. These results confirmed the highly efficient growth factor presentation for potential implant-bone osseointegration applications. An *in-vivo* study is being conducted in a rabbit model using custom-made dental implants in the rabbit's maxilla to verify the results before clinical trials.

References

1. Cheng ZA, Alba-Perez A, Gonzalez-Garcia C, Donnelly H, Llopis-Hernandez V, Jayawarna V, et al. High Efficiency BMP-2 Coatings: Nanoscale Coatings for Ultralow Dose BMP-2-Driven Regeneration of Critical-Sized Bone Defects (Adv. Sci. 2/2019). Adv Sci [Internet]. 2019 Jan;6(2):1970009.
2. Moulisová V, Gonzalez-García C, Cantini M, Rodrigo-Navarro A, Weaver J, Costell M, et al. Engineered microenvironments for synergistic VEGF– Integrin signalling during vascularization. Biomaterials. 2017;126:61–74.
3. Llopis-Hernández V, Cantini M, González-García C, Cheng ZA, Yang J, Tsimbouri PM, et al. Material-driven fibronectin assembly for high-efficiency presentation of growth factors. Sci Adv [Internet]. 2016;2(8):e1600188.

Acknowledgement

Special thanks for Virginia Llopis-Hernández, Andres Alba-Perez, Peter Childs and Vineetha Jayawarna for their support.

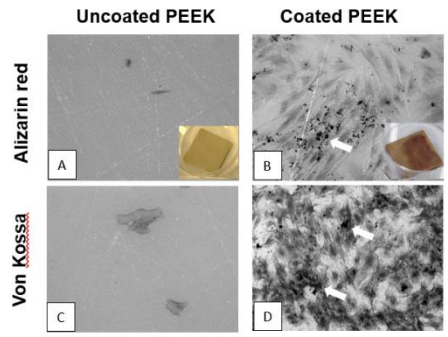

Figure 2:
Mineralisation assessment through Alizarin red and Von Kossa staining.*A) Alizarin red on uncoated PEEK. B)Alizarin red histology shows bone nodule formation (calcium deposition) on the PEEK coated with p-PEA + FN + BMP-2 (arrow) after 28 days. Gross images of mineralisation showed at the lower right-side corner of the microscopic images of calcium deposition. C) Von Kossa on uncoated PEEK. D) Von Kossa on the coated PEEK shows phosphate deposition (arrows) after 35 days, positive staining showed as black deposition.*

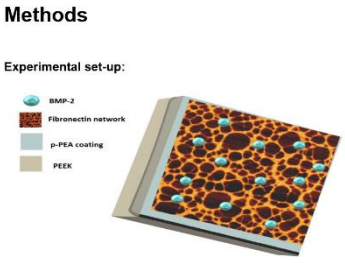

Figure 1:
Illustration of the proposed presentation system. *p-PEA= plasma polymerised poly (ethyl acrylate), PEEK= polyetheretherketone, BMP-2 = bone morphogenic protein 2.*

V-OS18-05

Multiscale 3D printed nanopatterned scaffolds

Mahdiyeh Nouri-Goushki[1], Michelle Minneboo[1], Urs Staufer[2], Lidy E. Fratila-Apachitei[1], Amir A. Zaadpoor[1]

[1]Delft University of Technology, Biomechanical Engineering, Delft, NL; [2]Delft University of Technology, Precision and Microsystems Engineering, Delft, NL

Introduction

In vitro models play a key role in elucidating the molecular mechanisms involved in cellular interactions and functions[1]. Although traditionally, 2D *in vitro* models are used for this purpose, these models cannot replicate the 3D cellular microenvironments. Development of 3D microstructures with complex geometries and surface nanoscale features which can more closely resemble the native tissue matrix is therefore desirable but highly challenging. To achieve this, technologies that enable the fabrication of 3D structures based on predefined design are required[2]. Two-photon polymerization (2PP) is a powerful 3D printing technique for manufacturing structures with a resolution of a few hundred nanometers[3]. In this study, we successfully fabricated micro-scaffolds decorated with surface nanofeatures in a single printing step. The response of preosteoblast cells to these structures was investigated and compared to the 2D nanopatterned and non-nanopatterned surfaces.

Experimental Methods

The nanopatterned surfaces and micro-scaffolds were produced using a Photonic Professional GT (Nanoscribe, Germany) machine. The Galvo writing strategy and an acrylate-based resin (IPL, Nanoscribe, Germany) were selected for printing the features on glass coverslips (Nanoscribe, Germany). All samples were characterized using a scanning electron microscope (SEM) (Jeol InTouchScope JSM-6010LA, Japan). Preosteoblast cells (MC3T3-E1, Sigma Aldrich, Germany) were cultured in phenol-red free α-MEM (pH = 7.5) with 10% (v/v) fetal calf serum (FCS) (Life Technologies, USA). A concentration of 5×10^4 cells/ml was seeded on each sample. The media was refreshed after 2 days and SEM imaging was performed on day 2 and 4.

Results and Discussion

After optimization of the laser power and scan speed, arrays of nanopillars with a diameter of 426 ± 6 nm and a height of 913 ± 50 nm were generated on glass substrates with high reproducibility (Fig. 1a). Subsequently, these nanopillars could be printed on each woodpile of the micro-scaffold in a single printing step thus creating an integrated multiscale 3D structure (Fig. 1b).

Significant differences in cell morphology were observed between the nanopatterned and non-nanopatterned surfaces after 2 days of culture. Polygonal cells were observed on the flat surface whereas highly polarized cells were visible on the nanopatterned surfaces. Nevertheless, after 4 days, cells spread nicely on the entire nanopatterned area. In addition, cells showed the ability to move across the interface between the nanopattern and the surrounding flat surface (Fig. 2).

Conclusion

This study shows the potential of the 2PP process to fabricate 3D structures with controlled nanoscale surface features using a single material and process step. This approach is attractive not only for trying to reconstruct the native tissue matrices but also for fundamental studies on cell-surface interactions. The IP-L resin used in this research was not cytotoxic for the MC3T3-E1 cells. In addition, morphological changes associated with cell adaptation to the 2PP structures were found, which may influence important cellular functions, such as differentiation.

References

1.Knight, E.; Przyborski, S., Advances in 3D cell culture technologies enabling tissue-like structures to be created in vitro. *Journal of anatomy* **2015,***227* (6), 746-756.

2.Holmes, B.; Bulusu, K.; Plesniak, M.; Zhang, L. G., A synergistic approach to the design, fabrication, and evaluation of 3D printed micro and nano featured scaffolds for vascularized bone tissue repair. *Nanotechnology* **2016,***27* (6), 064001.

3.Lemma, E. D.; Spagnolo, B.; De Vittorio, M.; Pisanello, F., Studying Cell Mechanobiology in 3D: The Two-Photon Lithography Approach. *Trends in biotechnology* **2018**.

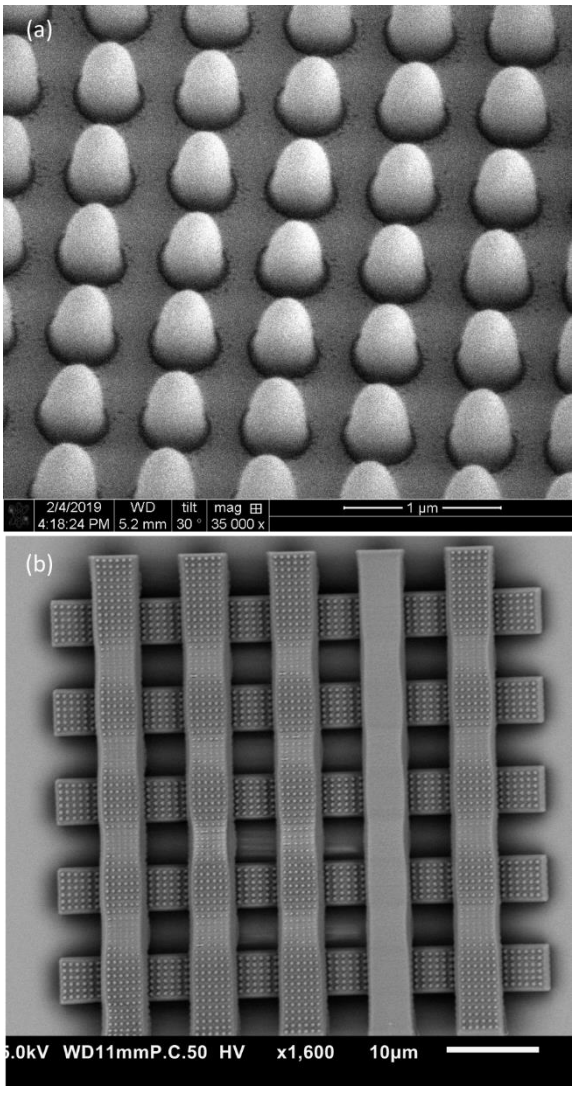

Fig.1
SEM image of (a) nanopatterned surfaces and (b) nanopatterned micro-scaffold.

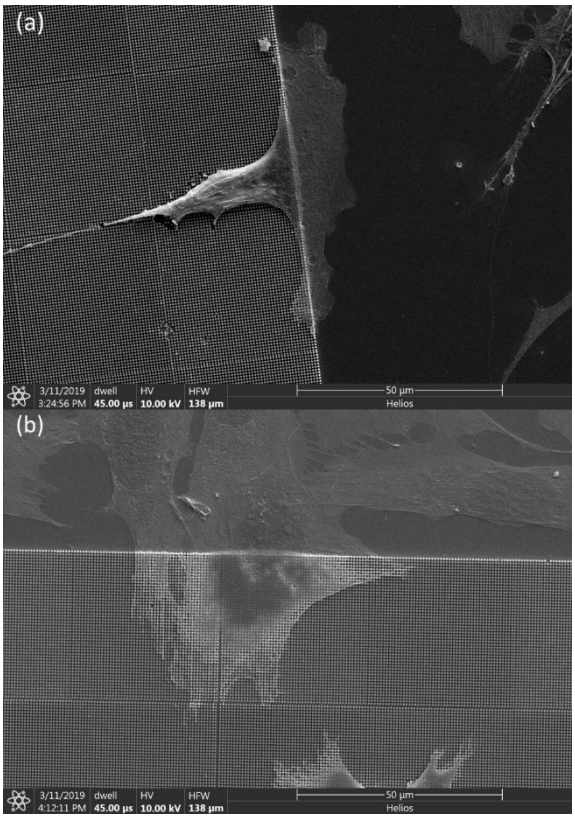

Fig.2
MC3T3-E1 cells moving across the interface between the nanopatterned and non-nanopatterned areas: (a) after 2 days of culture and (b) after 4 days of culture.

V-OS18-06

Natural antibacterial coating on dental implants and/or abutments for the prevention and treatment of peri-implantitis

Zeqian Xu[1], Stefanie Krajewski[2], Xingting Han[1], Ping Li[1], Evi Kimmerle-Müller[1], Ernst Schweizer[1], Tobias Weindl[3], Jürgen Geis-Gerstorfer[1], Lutz Scheideler[1], Hans Peter Wendel[2], Frank Rupp[1]

[1]Tübingen University, University Hospital Tübingen, Section Medical Materials Science & Technology, Tübingen, DE; [2]Tübingen University, University Hospital Tübingen, Department of Thoracic, Cardiac and Vascular Surgery, Tübingen, DE; [3]Aimecs GmbH, Pfarrkirchen, DE

Introduction

Nowadays, osseointegrated medical implants have been widely used for the rehabilitation of partial and complete edentulous patients [1]. However, the upcoming of peri-implantitis, a destructive inflammatory process around implants contributing to the formation of peri-implant pockets and supporting bone loss, has become an important issue for implant failure [2]. Bacterial colonization and subsequent biofilm (plaque) formation on the implant surface is one of the essential cause and effect factors for peri-implantitis [3]. Plaque control and tissue regeneration has become the main target in prevention and treatment of peri- implantitis [4-6]. Various antibacterial coatings have been previously applied on implant surfaces, however, developing an ideal coating with both great antibacterial efficiency and good biocompatibility is still an unsolved task. Totarol is a kind of natural antibacterial agent, with bactericidal effect towards a wide range of gram-positive bacteria, even antibiotic resistant bacteria including the methicillin resistant *S. aureus* [7,8], and additionally appeared with low cytotoxicity [9]. This *in vitro* study aims at applying totarol coatings on experimental dental implant and abutment surfaces, and investigating the antibacterial capability of totarol coatings in a simulated oral environment.

Experimental Methods

After being ultrasonically cleaned with ethanol (70%) and dried with N_2, wafer plates (10 mm × 10 mm) and round Ti disks (D=10 mm) are coated with totarol by spin coating. Column chromatography-purified totarol dissolved in ethyl acetate solutions are coated on wafer surfaces at concentrations of 10 mg/ml, 20 mg/ml, and 40 mg/ml, respectively, and on Ti disks at 20 mg/ml. The coated wafers and Ti disks (n=6/group) with and without coating are incubated in a *S. gordonii* - Schaedler medium (start $OD_{\lambda= 620nm} = 0.54$) stirring system (stop 60 min/ stirring 15 min each cycle, 37°C incubator) (Fig 2. f, g). The wafers were harvested after 24h incubation and the Ti disks were harvested after 4 h, 8 h, 24 h of incubation, respectively, then went through Live/Dead staining for testing the vitality and crystal violet staining for quantifying the amount of surface bound bacteria. One-way ANOVA was used to analyze differences of the quantification of surface bound bacteria between totarol coating and control groups.

Results and Discussion

The totarol coatings on wafer surfaces appeared homogeneous and at a lateral view with light blue, dark blue and gold color at the concentrations of 10 mg/ml, 20 mg/ml, and 40 mg/ml (Fig.1 b). All coatings caused significant contact killing effects towards 24 h *S. gordonii* films (Fig.1 c), only the 20 mg/ml group showed a lower amount of bacterial film formation (Fig. 1 d,e). The 20 mg/ml totarol coating on Ti showed distinct bactericidal effects towards 4 h, 8 h, and 24 h *S. gordonii* films (Fig. 2 a,b), and, according to the lower density in crystal violet staining, significantly inhibited the *S. gordonii* biofilm growth compared with the control group (Fig. 2 c,d).

Conclusion

The natural antibacterial totarol coating showed bactericidal effects towards the early oral colonizer *S. gordonii* and a significant inhibition of its biofilm growth. This might offer the possibility for the peri-implant soft tissue to form a tight epithelial seal and to prevent bacterial infiltration. Therefore, totarol coatings of dental implant and abutment surfaces showed great potential for the prevention and treatment of bacterial caused infections, such as peri-implantitis.

References

1. Dreyer, H. et al. M. *J Periodontal Res* **2018**, *53*, 657-681.
2. Albrektsson, T.I., F.; Lang, N.P.K., T., Ed. Quintessence: London, 1994; pp. 365-369.
3. Mombelli, A. et al. *J Clin Periodontol* **2011**, *38 Suppl 11*, 203-213.
4. Subramani, K. et al. *Int J Oral Maxillofac Implants* **2012**, *27*, 1043-1054.
5. Heitz-Mayfield, L.J. et al. *Int J Oral Maxillofac Implants* **2014**, *29 Suppl*, 325-345.
6. Jepsen, S. et al. *J Clin Periodontol* **2015**, *42 Suppl 16*, S152-157.
7. Nicolson, K. et al. *FEMS Microbiol Lett* **1999**, *179*, 233-239.
8. Kubo, I. et al. *J Nat Prod* **1992**, *55*, 1436-1440.
9. Reinbold, J. et al. *Molecules* **2017**, *22*.

Acknowledgement

Z. Xu is supported by the China Scholarship Council (201708080003). We acknowledge Ann-Kristin Uhde and Ingrid Stephan for technical assistance in our laboratories.

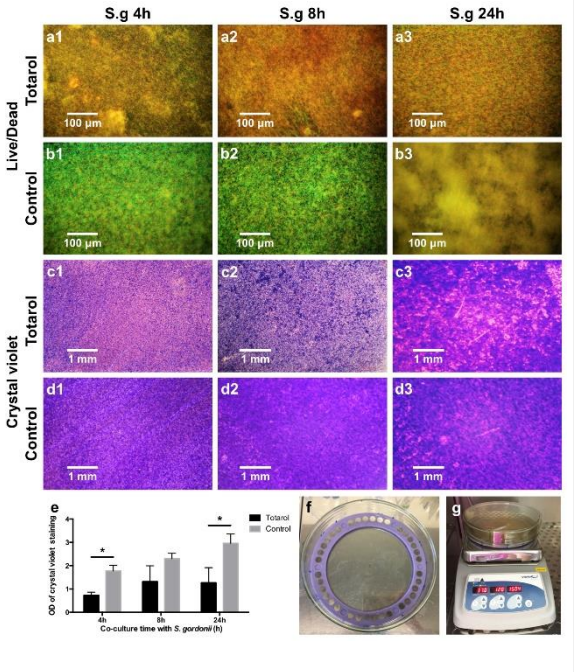

Fig. 2 Different stages of antibacterial effects of totarol coated Ti in stirring system. Totarol coated Ti disks were incubated in a 24h *S. gordonii* stirring system and analyzed at 4 h, 8 h, 24 h of incubation. **a:** Live/Dead staining of coating group; **b:** Live/Dead staining of control group; **c:** Crystal violet staining of coating group; **d:** Crystal violet staining of control group; **e:** quantification comparison of *S. gordonii* film in coating and control groups; **f:** rubber sample holder; **g:** stirring system in 37 °C incubator.

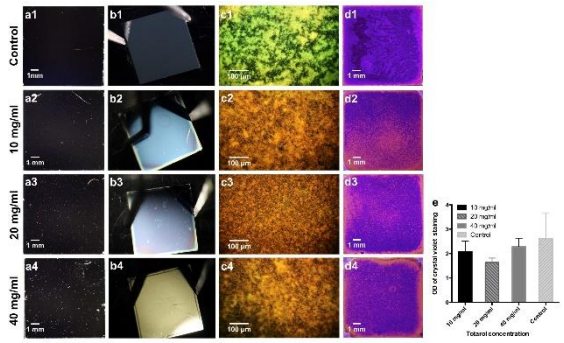

Fig. 1 Antibacterial effect of different concentrations of totarol coating on wafers. **a:** vertical view of coating; **b:** lateral view of coatings; **c:** Live/Dead staining outcomes of 24 h biofilm; **d:** crystal violet staining of 24 h biofilm (n=4); **e:** quantification comparison of *S. gordonii* film in different groups.

4:15 p.m. – 5:45 p.m.

Hall 3

VI-SY10 | ISBF SY: Advanced biofabrication strategies and applications

Jos Malda (Utrecht, NL)
Miguel Castilho (Utrecht, NL)

Biofabrication strategies in regenerative medicine have gained increasing attention due to their potential to engineer 3D tissue substitutes, capable of replacing lost and damaged tissues. During the last two decades, multiple biofabrication technologies together with cell-based therapies have been subjects of thorough investigation. This symposium will focus on new strategies for biofabrication and novel combinations of these, with special attention for recent developments in the field of 3D bioprinting for musculoskeletal tissue engineering. Both invited speakers Danny Kelly and Liliang Ouyang, have developed pioneering work in 3D bioprinting and in engineering bioactive tissue-like constructs. This symposium aims to strengthen the links between the biofabrication and biomaterials communities, as well as to reach out to new research fields to the already incredible interdisciplinary field of Biofabrication.

VI-SY10-KL01

3D Bioprinting for Bone and Joint Regeneration

Daniel J. Kelly

Trinity College Dublin, Trinity Centre for Bioengineering, Dublin, IE

Introduction

Our musculoskeletal system has a limited capacity for repair. This has led to increased interest in the development of tissue engineering strategies for the regeneration of musculoskeletal tissues such as bone, ligament, tendon, meniscus and articular cartilage. This talk will review our attempts to use biomaterials and mesenchymal stem cells (MSCs) to bioprint cell-laden implants for use in bone and joint regeneration.

Experimental Methods

Two different bioprinting strategies will be described to engineer regenerative implants. For the first approach, bioprinted constructs are first matured ex vivo prior to implantation into the body. In the second approach, bioprinted constructs are implanted directly into the body without any prior ex vivo maturation. In both cases, the bioprinting process involves the integration of different bioprinting techniques (Fused deposition modelling, Micro-extrusion, Ink-jet printing) to produce cell-laden constructs with defined functionalities.

Results and Discussion

This talk will demonstrate how 3D bioprinting can be used to engineer biological implants mimicking the shape of specific bones, and how these bioprinted tissues mature into functional bone organs upon implantation into the body. Next, it will be demonstrated that different musculoskeletal injuries can be regenerated using 3D bioprinted implants, including large bone defects and osteochondral defects. The talk will also describe how we can integrate biomaterials and MSCs into 3D bioprinting systems to engineer scaled-up tissues that could potentially be used regenerate entire diseased joints.

Conclusion

3D Bioprinting has the potential to transform how we treat damaged and diseased musculoskeletal tissues.

VI-SY10-KL02

3D Bioprinting of Hydrogels: towards Generalization and Simplicity

Liliang Ouyang

Imperial College London, Materials, London, GB

Introduction

Despite the plethora of bioinks and bioprinting strategies under development in the biofabrication field, their application from bench to bedside is still hindered through their lack of standardization and generalization. One of the next steps for 3D bioprinting is to generalize and simplify the technologies towards a standard and easy-to-use platform for biomedical applications. Therefore, we are dedicated to investigating generalizable strategies for advanced biofabrication, taking extrusion-based bioprinting as an example.

Experimental Methods

To better understand the nature of extrusion-based bioprinting, we start with analyzing the general criteria for each stage in the whole route, ranging from bioinks to 3D cellular constructs (Figure 1A). Bioinks with varied gelation properties were studied, including guest-host self-assembly, thermal gelation, and photo-crosslinking (Figure 1B). The bioprinting process was optimized corresponding to specific bioink. For examples, temperature and light were well controlled for printing thermo-responsive and photo-crosslinkable hydrogels, respectively.

Results and Discussion

The shear-thinning and self-healing formulation (guest-host hyaluronan) was demonstrated to support consistent extrusion and maintenance of hydrogel shape, and additional secondary crosslinking helped to further stabilize the structure.[1] With careful control of temperature in the nozzle and printing platform, gelatin-based bioink could be successfully printed, maintaining good 3D printability and cell viability (> 90%).[2] By simultaneously introducing light to a light-permeable nozzle during printing, various non-viscous photo-crosslinkable bioinks could be printed into 3D constructs.[3] Based on these case studies, we are able to process different hydrogels in a generalizable way (Figure 1C).

References

[1] Ouyang L et al. *ACS Biomater Sci & Eng*. 2016, 2(10): 1743-1751.
[2] Ouyang L et al. *Biofabrication*. 2016, 8(3): 035020.
[3] Ouyang L et al. *Adv Mater*. 2017, 29(8): 1604983.

Acknowledgement

The authors acknowledge the support from EPSRC Programme Grant (EP/P001114/1), SunP Biotech, and International Society for Biofabrication (ISBF)

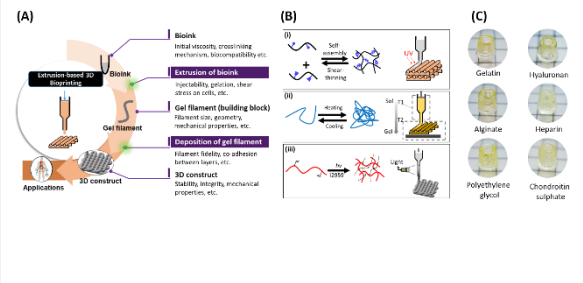

Figure 1
(A) Schematic of extrusion-based bioprinting process. (B) Schematic of representative bioprinting strategies corresponding to (i) self-assembly and shear-thinning, (ii) thermal, and (iii) photo-crosslinkable bioink formulations. (C) Representative photographs of printed tubular structure using various hydrogels.

VI-SY10-03

3D Printed Bone Lego: Preliminary Design, Mechanical and Biological Characterization

Adel F. Badria[1], Abdelrahman Hussein[3], Emre Ergene[1], Orcun Güvener[2], Cagdas Oto[2], Byungki Kim[3], Pinar Yilgor Huri[1]

[1]Ankara University, Faculty of Engineering, Department of Biomedical Engineering, Ankara, TR; [2]Ankara University, Faculty of Veterinary Medicine, Department of Anatomy, Ankara, TR; [3]Korea University of Technology and Education, Chungcheongnam-do, KR

Introduction

The number of patients who need bone substitutes is increasing worldwide. The potential of 3D bioprinting to produce personalized bone grafts showed promising results during the past decade [1]. However, problems remain in the timely and mass production of clinically personalized relevant sized grafts including issues related to quality control and technician-clinician coordination. In this work, a new hypothesis has been proposed and evaluated to assemble standard 3D printed Legos (SDPLs) into one large bone piece. The (SDPLs) were designed, assembled and compared with the large piece to test how much legolization would affect its properties. The comparison involved the characterization of mechanical and biological behaviour including the osteogenic potential.

Experimental Methods

Block segmentation (legolization) of different preliminary designs were used to answer 2 main questions: 1) How much the design of the SDPL and the degree of segmentation would affect the mechanical properties of the whole big piece? 2) Is it possible to use the segmentation model to optimize the SDPL design, taking the simple cube as a reference? All the SDPL models were meshed with C3D8R elements and solved with Abaqus/Standard. The loading is compressive with the displacement boundary condition of 0.5mm. The mechanical response of *(i) a single SDPL (**1x**), (ii) 2 assembled SDPLs (**1xAssem**) and (iii) a single piece with the dimensions of the 1xAssem (**2x**)* (**Figure 1A**) were analyzed as load-displacement curves at the loading point. For the 1xAssem configuration, the contact is assumed frictionless.

Adipose-derived stem cells (ASCs) were seeded on 1xAssem SDPL segments within a fibrin hydrogel to test the success of cell seeding, homogenous distribution, migration and osteogenic differentiation potential on the assembled pieces. SDPLs were 3D printed from poly(ε-caprolactone) by using a Bioplotter device (Envisiontech). The samples were examined on days 1,7 and 14 using Live/Dead staining and scanning electron microscopy for cellular morphology, Alamar Blue test for viable cell number and alizarin red staining for osteogenic differentiation.

Results and Discussion

As a starting point, 3 simple designs have been proposed: Cube (CU), Cube Lego (CL) and Interlocking Lego (IL) (**Figure 1A**). These designs were segmented and tested for the effect of segmentation on their mechanical properties (stiffness, k).

The results of the 3 configurations as force-displacement, represent k of the structure and stress distribution in color code (**Figures 1B-D**). The deviation from the linear response represents the initiation of plasticity, representing the failure of the structure. The CU structure has the highest k response (Figure 1B). The 1x-CU shows the k response compared to 2x-CU due to the well-known relation of k=EA/l [2].

For the CL design, the weakest zone is the top pin. This is the reason for its reduced k compared to the CU(**Figure 1 B**). This is also the first failure region because of its small cross-section area. For the IL, the weak points are the lower slot. Therefore, IL design was optimized by removing this feature from the bottom part (modified IL) (**Figure 1C**).

The segmentation of the modified IL showed a significant increase in the k which was attributed to stress center (SC) areas corresponding to the neck of the hinge's width (red color, Figure 1B). By removing the lower SC (the lower part of IL as represented in (Figure 1C & D), there was a clear transfer for SCs, which again as expected distributed between different SC (the upper part of IL as represented in Figure 1D). Removal of any external SC would expect to show no difference in k between IL and cube structure (the highest k (Figure 1 A,D)).

A 4 layers-IL (thickness, 1.5 mm) was 3D printed and seeded with ASCs to study the cellular response on assembling SDPLs. Alamar blue test and Live/Dead staining showed the proliferation of the seeded cells during 14-days where random distribution of the cells was observed within the pieces (**Figure 2**). The areas between the junctions need to be further investigated and the design needs to be optimized as they were observed blank during the study. Alizarin red staining showed calcification on day 14 on SDPLs (Figure 2C).

Conclusion

Based on segmentation modelling, in the absence of external SC structures, there would be no significant difference in stiffness between the simple cube and IL structures. Such preliminary results encourage further investigation for our hypothesis.

In our work, a preliminary study has been run with a basic variation on both design and simulation levels. Still, a wide range of parameters including filling ratio during 3D printing, different materials with different additives, also different designs are being investigated with more parameters to be simulated including toughness and shear stress. Also, cellular distribution and orientation within and in between the SDPLs are being investigated.

References

[1]http://doi: 10.1089/3dp.2015.0001.

[2]http://doi.org/10.1089/3dp.2014.0012.

Acknowledgement

We would like to thank TÜRKİYE BURSLARI-18EG005151 for funding the work.

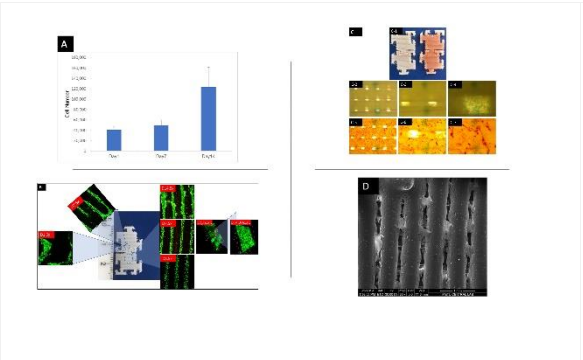

Figure_2
There is a clear increase in the cell number over time as seen in Alamar red (A), Confocal images showed a distribution of cells over the scaffold (B), also a significant difference between test and control could be seen in Alizarin red staining (C) , no clear cells could be seen in the junction between lego pieces, still a significant distribution of cells around the piece could be seen (D)

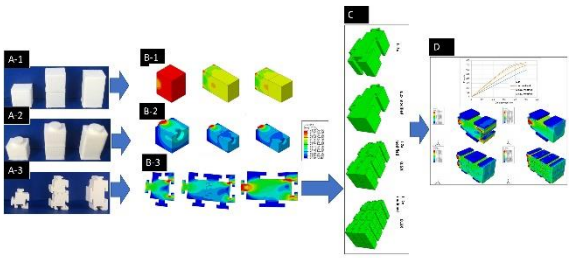

Figure 1:
The three basic structures; Cube, Cube lego and interlocking lego, all of them were modeled in three different form (1x, 2x and 1x assembly) (A), For the three basic structures with their different form, the effect of design and segmentation on the stiffness of the structures has been represented on (B), based on the simulation , a further modification and segmentation have been done in the IL structure (C), finally the simulation of the modified and segmented IL designs has been shown in (D).

VI-SY10-04

4D Biofabrication by Shape-Morphing Polymers

Leonid Ionov

University of Bayreuth, Bayreuth, DE

Introduction

Most powerful technique for biofabrication – 3D printing still has certain limitations, which substantially restrict its broader use. These disadvantages are inability to achieve sufficient resolution and high-density cell printing, difficulty of fabrication of multicomponent and hollow structures, difficulty of orienting of cells and limited oxygen diffusion. We advanced design of biomaterials by developing 4D biofabrication approach using special polymers, which are able to change their shape – shape-morphing polymers. In particular, we developed a number of approaches for design of biocompatible shape-morphing polymeric objects using solid polymers and hydrogels, which are able to change their shape in response to such “biocompatible” stimuli as temperature and presence of calcium ions. We developed approaches for deposition of cells on and inside of shape-morphing polymeric objects. We have also demonstrated application of 4D biofabrication approach for controlled encapsulation of cells, design of porous scaffolds with controlled porosity and pore orientation, complex 3D cell patterning as well as fabrication of hydrogel-cell hollow structures.

Results and Discussion

The approach was exemplified by gelatin-polycaprolactone (PCL) bilayers. Non-crosslinked gelatin was used as a sacrificial material, which prevents folding of the crosslinked gelatin-polycaprolactone bilayer at room temperature und allows its folding at elevated temperature. The approach has been used for encapsulation of neural stem cells. Very recently, we developed a another approach for fabrication of shape-changing structures. The approach is compatible with 3D printing and allows fabrication of tubular cellular structures using shape-changing and is based on biopolymers with carboxylic groups such as alginate and hyaluronic acid. These polymers, when crosslinked, demonstrate reversible swelling properties in response to changes in Ca2+ concentration enabling shape-changing alginate and hyaluronic acid structures loaded with cells. The mouse bone marrow stromal cells survived photocrosslinking, changes in shape and remained vital for at least 7 days.

References

Advanced Materials 2017 DOI: 10.1002/adma.201703443; ***Angewandte Chemie*** 2016, 55 (52), 16106–16109.; ***Advanced Functional Materials*** 2016,26 (42), 7733–7739.; ***Advanced Materials*** 2015,27 (33), 4865-4870.; Nano Letters 2015, 15 (3), 1786–1790.; ***Advanced Functional Materials*** 2014, 24(27), 4357–4363.; ***Biomacromolecules*** 2011, *12 (6)*, 2211–2215.

Acknowledgement

Author is thankful to DFG (grant IO 68/1-3) for financial support.

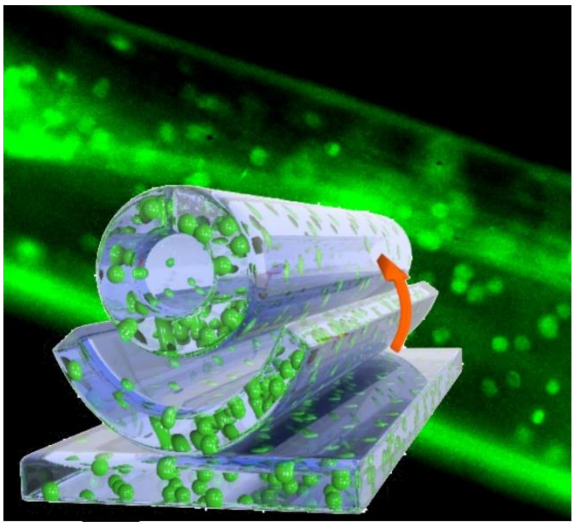

Schematic illustration of 4D biofabrication approach

4:15 p.m. – 5:45 p.m.

Hall 2

VI-SY16 | Korean-European symposium: Advances in musculoskeletal regeneration

Ki-Dong Park (Suwon, KR)
Michael Gelinsky (Dresden, DE)

Korean Society for Biomaterials (KSBM) is the hosting organization for WBC 2024 that will be held in Daegu, South Korea. KSBM is striving to promote the friendship and collaboration with colleagues all over the world for the success of WBC 2024. In this spirit, KSBM is having joint symposium with EU partners during annual ESB meetings starting from 2017 meeting in Athens. In ESB 2019, under the theme title “Advances in musculoskeletal regeneration” , Prof, Gun-il Im from Dongguk University and Prof, Swieszkowski from Warsaw University of Technology will deliver keynote speech representing KSBM and ESB respectively.

VI-SY16-KL01

Development of adipose stem cell therapeutics with enhanced angiogenic and osteogenic potential to treat bone defects and osteonecrosis of the femoral head

Gunil Im

Dongguk University, Goyang, KR

Introduction

While bone has a capability to heal itself, there is a great difficulty in reconstituting a large bone defects created by heavy trauma or resection of malignant tumor. Also, osteonecrosis of the femoral head , which is caused by obstruction of blood supply to bone cells and occurs in young population, is not amenable to successful bone regeneration. Cell implantation has been performed in those patients for the past two decades. Unfortunately, the desired effect has not been achieved. It is surmised that the cells are unable to obtain blood supply at the recipient site and undergo massive necrosis at the early stage of implantation Also, the avascular environment of recipient site would further decrease chance of the survival of implanted cells. Therefore, rapid revascularization of the implantation site is essential to promote the survival of implanted cells and subsequent bone regeneration.

Experimental Methods

We developed *VEGF* and *BMP2*-transfected adipose stem cells (ASCs) using electroporation that that can effectively treat bone defects by providing rapid angiogenesis and osteogenesis. Optimal transfection method and optimal combination ratio of *VEGF* to *BMP2* to enhance both osteogenesis and angiogenesis were explored. We tested the hypothesis that *VEGF* and *BMP2*-transfected ASCs promote the bone regeneration in critical-size calvarial defect and segmental long bone defect models in immunosuppressed rats. The enhancing mechanisms and related gene pathway in *VEGF* and *BMP2*-transfected ASCs were also investigated using RNA-seq analysis.

Results and Discussion

The optimal ratio of *BMP2*- to *VEGF*- transfected ASCs to enhnace both osteogenesis and angiogenesis was determined to be 9:1. *BMP2-/VEGF*-transfected ASCs administered in this ratio effective healed critical-size calvarial defects and long-bone segmental defect in rats. The administered cells did not migrate out of the implantation site by 56th day and increased *BMP-2* and *VEGF* gene expression was found on the implantation site. TAZ, TEAD and ANKRD1 are overexpressed in *BMP2-/VEGF*-transfected ASCs, possibly suggesting mechanism of enhanced bone regeneration and angiogenesis.

Conclusion

This study suggested the possibility of a gene-enhanced stem cell therapeutics that which can be used for effective treatment of intractable bone defect and osteonecrosis of femoral head.

VI-SY16-KL02

Recent advances and challenges in 3D biofabrication of bone and soft tissue

Wojciech Swieszkowski

Warsaw University of Technology, Faculty of Materials Science and Engineering, Warsaw, PL

Introduction

An innovative technique that may overcome current limits in reproducing complex structures of human tissues and organs is 3D biofabrication. This emerging fabrication technology relies on the simultaneous deposition of cells and biomaterials, mostly in a layer-by-layer fashion, to form 3D well-organized living heterogeneous porous structures that can mirror physiologically and morphologically relevant complex biological architectures. In this study, innovative strategies and challenges in 3D biofabrication of musculoskeletal tissues like bone, muscle, tendon, or cartilage will be presented.

Experimental Methods

Our 3D biofabrication approach is based on a microfluidic system coupled to a co-axial needle extruder for high-resolution computer-controlled 3D deposition of hydrogel fibers laden with different cells. The system is designed so that multiple bioinks can be delivered either individually or at the same time and rapidly mixed to the extrusion head, and finally deposited through a coaxial nozzle. This enables the deposition of complex 3D structures with very high shape fidelity and cell viability. Using such a system we have been bioprinting or bio-wet-spinning cell-laden hydrogel constructs recapitulating the natural structure and composition of musculoskeletal tissues like bone, cartilage, tendon, or muscle. Depending on application, the biomimetic hydrogels were composed of modified biopolymers like gelatin, alginate, hyaluronic acid, or PEG-fibrinogen. The gels were laden with different types of cells including bone marrow-derived human mesenchymal stem cells, muscle precursor cells or chondrocytes.

Results and Discussion

The obtained with high resolution (~ 100 mm), a fiber-based 3D printed living constructs mimic organized tissues like bone, cartilage, tendon and muscle [1,2]. Furthermore, the mechanical loading and biochemical stimulation show significant influence on proliferation, alignment, and differentiation of the cells as well as ECM deposition in 3D biofabricated constructs. For instance, the aligned orientation of the fibers combined with mechanical stimulation result in highly preferential longitudinal cell orientation and demonstrates enhanced collagen expression. Additionally, the combination of biochemical and mechanical stimulations promotes the expression of specific markers, signatures of efficient cell differentiation towards required tissues.

Conclusion

By formulating tailored bioinks and precisely controlling the 3D spatial organization of the extruded hydrogel fibers using different biofabrication methods it was possible to engineer advanced 3D biostructures which after some period develop into neo-tissues of musculoskeletal system.

References

[1] Costantini M, et al. 3D bioprinting of BM-MSCs-loaded ECM biomimetic hydrogels for in vitro neocartilage formation. Biofabrication, 2016, 8 35002.

[2] Rinoldi C, et al. Tendon Tissue Engineering: Effects of Mechanical and Biochemical Stimulation on Stem Cell Alignment on Cell-Laden Hydrogel Yarns. Advanced healthcare materials, 1801218, 2019.

Acknowledgement

This study was supported by Pol-Nor/202 132/68/2013 (Project NewJoint), STRATEGMED1/233224/10/NCBR/2014 (Project START), STRATEGMED3/306888/3/NCBR/2017 (Project iTE), and statutory grant STATUT 2018.

VI-SY16-03

Restoring impaired bone healing in diabetic patients using HIF-mimicking materials

Azadeh Rezaei, Kaveh Shakib, Gavin Jell

University College London, Division of Surgery and Interventional Science, London, GB

Introduction

Clinical studies have reported that fracture healing duration in diabetic patients is prolonged by ~87%[1]. The role of diabetes on bone remodelling and regeneration is beginning to be unravelled and may involve the hypoxia-inducible factor (HIF) pathway. Diabetic patients have been reported to have a reduced ability to respond to reduced oxygen environments (hypoxia) [2]. Destabilisation of HIF-1α by high glucose levels has been shown to impair the cellular response to hypoxia in diabetic conditions and have detrimental consequences such as reduced neovascularisation, contributing to delayed or impaired bone healing[3, 4]. The critical role of HIF-1a stabilisation in improving diabetic wound healing has, also, been reported[5, 6]. However, little attention has been paid to the effect of hypoxia and HIF-1α on bone healing in diabetic environments. In this study, the effect of diabetic environment on bone regeneration will be investigated and the effects of hypoxia (1% O_2) and two common HIF-mimicking materials (cobalt chloride ($CoCl_2$) and DMOG) on bone nodule formation in diabetic environment will be examined to assess whether targeting HIF-pathway can promote bone regeneration in a hyperglycaemic (diabetic) model.

Experimental Methods

Primary rat osteoblasts were isolated from neonatal Sprague-Dawley rats and seeded in α-MEM supplemented with 2 mM β-glycerophosphate, 10nM dexamethasone, and 50µg/mL ascorbate. When confluent, cells were exposed to 1g/L, 4.5g/L and 9g/L glucose environments to mimic low, moderate and high blood glucose levels, respectively, and kept in normoxia (20% O_2) and hypoxia (1% O_2) for 21 days. To examine the role of HIF mimicking materials, the cells were also treated with cobalt (Co 12.5, 25 and 50µM) and DMOG (250,500 and 1000µM) conditioned medium with 1, 4.5 and 9g/L glucose. Metabolic activity (AlamarBlue), proliferation rate (total DNA), alkaline phosphatase activity and vascular endothelial growth factor (VEGF) expression of the cells were measured. Bone nodules were characterised using Alizarin Red staining, SEM, TEM, Raman. Interferometry technique was used for quantitative analysis of the bone nodule size.

Results and Discussion

In this study, we demonstrated that bone nodule formation is dependent on glucose concentration. Moderate (4.5g/L) and high (9g/L) glucose conditions inhibited nodule formation. However, the addition of HIF mimetics ($CoCl_2$ and DMOG) appeared to restore nodule formation (Fig 1). In addition, both cobalt and DMOG enhanced VEGF production in moderate and high glucose environments. Hypoxia did not improve nodule formation in both moderate and high glucose conditions which suggests that the hypoxic-induced inhibitory effect is not HIF-dependent and is associated with the low oxygen level.

Conclusion

A hyperglycaemic bone model was developed that demonstrated that high glucose levels (4.5 g/L and 9 g/L) inhibits bone nodule formation. Excitingly, for the first time it was demonstrated that the use of HIF mimetics ($CoCl_2$ and DMOG) helped restore bone nodule formation. This discovery demonstrates the role of the HIF pathway in bone development and will enable the creation of biomaterials or tissue scaffolds designed for patients with impaired bone regeneration due to a defective cellular oxygen sensing pathway.

References

1. Loder, R.T., *The influence of diabetes mellitus on the healing of closed fractures.* Clinical orthopaedics and related research, 1988(232): p. 210-216.
2. Thangarajah, H., et al., *HIF-1α dysfunction in diabetes.* Cell cycle, 2010. 9(1): p. 75-79.
3. Xiao, H., et al., *The possible mechanisms underlying the impairment of HIF-1α pathway signaling in hyperglycemia and the beneficial effects of certain therapies.* International journal of medical sciences, 2013. 10(10): p. 1412.
4. Catrina, S.-B., et al., *Hyperglycemia regulates hypoxia-inducible factor-1α protein stability and function.* Diabetes, 2004. **53**(12): p. 3226-3232.
5. *Hong, W.X., et al., The role of hypoxia-inducible factor in wound healing. Advances in wound care, 2014. **3**(5): p. 390-399.*
6. Liu, L., et al., *Age-dependent impairment of HIF-1α expression in diabetic mice: Correction with electroporation-facilitated gene therapy increases wound healing, angiogenesis, and circulating angiogenic cells.* Journal of cellular physiology, 2008. **217**(2): p. 319-327.

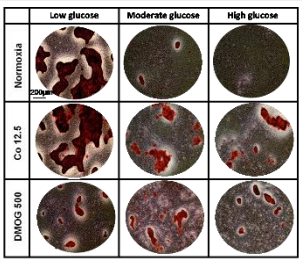

The effect of HIF mimetics on nodule formation in low, moderate and high glucose environments. Alizarin Red staining showed that non-toxic range of $CoCl_2$ and DMOG restored some bone formation in moderate and high glucose environments.

VI-SY16-04

Elastin-like polypeptide as a neural progenitor cell carrier for treating Parkinson's disease

Won Bae Jeon[1], Jung-Hee Kim[1], Kyeong-Min Lee[1]

[1]DGIST, Precision Medicine, Daegu, KR; [2]DGIST, Precision Medicine, Daegu, KR; [3]DGIST, recision Medicine, Daegu, KR

Introduction

Elastin-like polypeptides (ELPs) are attractive biomaterials for tissue engineering because they are biocompatible and biodegradable and transform into hydrogel at physiological temperature.[1] We have previously synthesized an Arg-Gly-Asp (RGD)-functionalized ELP, TGPG[VGRGD(VGVPG)$_6$]$_{20}$WPC, referred to as REP. REP binds cell surface integrin receptors and stimulates cellular behaviors such as adhesion and proliferation through RGD-induced signal transduction.[2] Neural stem or progenitor cells are of great interest in treating Parkinson's disease.[3] However, after being transplanted into the defect sites, a great portion of cells undergoes a cell death due to the lack of extracellular matrix required for cell attachment.[4] The main goals of this study were to use REP as a provisional matrix to enhance the survival of neural progenitor cells at the grafted site and improve the behavioral performance of a mouse model of Parkinson's disease.

Experimental Methods

ELP were expressed in *Escherichia coli* BLR(DE3) using pET-25b(+)-1 plasmids and purified by inverse transition cycling as described previously.[2] NPCs were cultured on matrigel-coated (0.1%) 10-cm dishes in Neural Cellutions Media supplemented with 1% N-Gro-001-S, 1% N2 supplement, 20 ng/mL fibroblast growth factor, 20 ng/mL epidermal growth factor, 1% penicillin/streptomycin at 37 °C in a humidified atmosphere of 95% air and 5% CO_2. In vitro viability was assessed using LIVE/DEAD® Viability/Cytotoxicity Assay Kit or CCK-8 assay kit. For in vivo survival analysis, NPCs (1×10^5 cells) were labeled with VivoTrack 680, and fluorescent images were taken using an IVIS® Spectrum and analyzed with Living Image software. To induce parkinsonism, C57BL/6 male mice were injected intraperitoneally with 20 mg/kg of 1-methyl-4-phenyl-1,2,3,6-tetrahydropyridine in sterile PBS five times at 2 h intervals for one day. Forty mice were randomly divided into two groups and one group received implants of NPCs only and the other received NPCs plus REP. Mice were anesthetized with a solution containing xylazine and ketamine, placed in a stereotaxic frame, and received one injection of 1×10^5 cells suspended in 2 µl of PBS or REP solution (10 µM) at 4^{o}C in the right striatum (0,5 mm anterior, 2 mm lateral, 3 mm ventral, with respect to bregma) using a 10 µl Hamilton syringe coupled with 26-gauge needle. Motor performance was assessed by using a mouse Rota-Rod Treadmill according to the reported protocol.[5]

Results and Discussion

REP substantially increased the proliferation of NPCs in a dose-dependent manner. REP induced Fak, Erk, and Akt phosphorylation. These effects were abolished by inhibiting MEK and PI3K with PD98059 and Wortmannin, respectively. Growth of NPCs on REP alleviated Bcl-2/Bax ratio and reduced proteolytic cleavage of caspase-9, caspase-7, caspase-3, and PARP. These data suggest that REP increases proliferation of NPCs via activating FAK, MEK/ERK, PI3K/Akt pathways while suppressing caspase processing. When REP and NPCs were implanted together into the striatum of Parkinson's disease mice, REP increased the differentiation of neural progenitor cells

into neurons and dopaminergic neuron, as indicated by the expression of tyrosine hydroxylase TH. Rotarod test showed a significant improvement in motor deficits by combined transplantation of REP and NPCs, compared to the implantation of NPCs only. These results indicate that REP is applicable as an extracellular matrix for neural progenitor cell transplantaion.

Conclusion

We demonstrated that RGD-functionalized REP provides a feasible and effective method for grafting Parkinson disease-targeting NPCs. Because beneficial effect of REP on the outcome of cell transplantation occurs through enhancing the viability of transplanted cells, REP-based stem cell delivery platform would be applicable for the treatment of a variety of other neurological disorders.

References

1. Haider M, Cappello J, Ghandehari H, Leong KW. In vitro chondrogenesis of mesenchymal stem cells in recombinant silk-elastinlike hydrogels. Pharm Res. 2008;25:692-9.

2. Jeon WB, Park BH, Wei J, and Park R. Stimulation of fibroblasts and neuroblasts on a biomimetic extracellular matrix consisting of tandem repeats of the elastic VGVPG domain and RGD motif, J Biomed Mater Res A 2011; 97:152-7.

3. Lindvall O. Stem cells for cell therapy in Parkinson's disease. Pharmacol Res. 2003;47:279-87.

4. Ahmed M, Ffrench-Constant C. Extracellular matrix regulation of stem cell behavior. Curr Stem Cell Rep. 2016;2:197-206.

5. Rozas G, López-Martín E, Guerra MJ, Labandeira-García JL. The overall rod performance test in the MPTP-treated-mouse model of Parkinsonism. J Neurosci Methods. 19981;83:165-75.

Acknowledgement

This work was supported by the DGIST project 18-LC-01 funded from the Ministry of Science and ICT of the Republic of Korea.

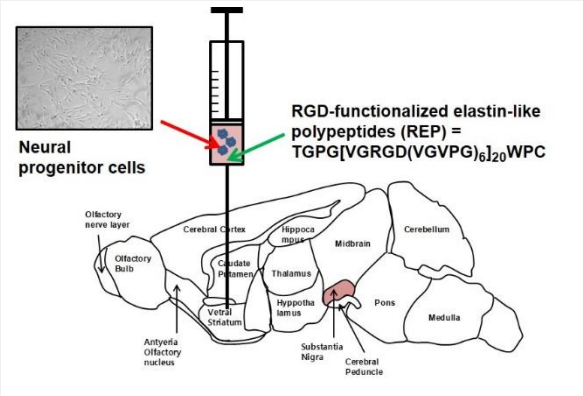

Stereotaxic cotransplantation of REP and neural progenitor cells into the striatum of a mouse model

4:15 p.m. – 5:45 p.m.

Hall 4

VI-SY11 | Calcium phosphate materials-induced osteogenicity: from orthotopic bone formation to heterotopic bone induction

Marc Bohner (Bettlach, CH)
Osamu Suzuki (Sendai, JP)

Calcium phosphate materials are recognized to display direct bone bonding properties. However, there is a still controversy whether they show osteoinductive property, i.e., the capacity of ectopic bone formation. It is of interest to learn about what is the factor leading to acquiring such an active property not only in orthotropic bone formation but also in ectopic bone formation from the view of the materials science and biological responses. The aim of this symposium therefore is to discuss the recent progress of osteoinductive/osteoconductive and specific cellular activation capacities related to the biodegradation, ionic dissolution, material volume, architecture, composition and crystal phase in calcium phosphates including OCP, β-TCP and HA ceramic materials.

VI-SY11-KL01

Osteogenic and angiogenic capabilities of octacalcium phosphate involving ionic dissolution through its chemical property

Osamu Suzuki[1], Takahisa Aanada[1,2], Yukari Shiwaku[1,3], Ryo Hamai[1]

[1]Tohoku University Graduate School of Dentistry, Division of Craniofacial Function Engineering, Sendai, JP; [2]Kyushu University, Institute for Materials Chemistry and Engineering, Fukuoka, JP; [3]Tohoku University Graduate School of Dentistry, Liaison Center for Innovative Dentistry, Sendai, JP

Introduction

Octacalcium phosphate (OCP) has been recognized as an osteoconductive material [1,2] as well as hydroxyapatite (HA) and β-tricalcium phosphate (β-TCP). OCP-based materials in fact have recently been applied in human oral bone tissues in anticipation of the defects repair [3,4]. However, the materials property of OCP stimulating their bone tissue repairs is not fully understood. We have found that the repair of critical-sized rat calvaria defect is enhanced during the progressive conversion of the implanted OCP to Ca-deficient HA in situ [2]. Analyses of OCP immersed in physiological solutions showed that the structural changes of OCP is accompanied by calcium ions consumption and inorganic phosphate (Pi) ions release in the solutions [5], these ionic dissolution products of which could be involved in the stimulatory capacity of OCP in enhancing osteoblastic differentiation from bone marrow stromal cells [2,5-7]. In this study, the involvement of the ionic dissolution associated with OCP materials will be presented and discussed from the view point of osteogenesis [8,9] and angiogenesis [10] .

Experimental Methods

OCP was synthesized in a wet method [1]. The studies were carried out by three ways: 1) Osteoblastic differentiation to osteocytes was estimated by incubating mouse IDG-SW3 cells in osteogenic differentiation media with OCP particles placed in the transwell inserts [8]; 2) Capillary-like tube formation was estimated by incubating human umbilical vein endothelial cells (HUVECs) on a gel matrix in endothelial cell growth medium with OCP particles placed in the transwell inserts [10]; 3) Differentiation from mesenchymal stem cells (MSCs) to osteoblastic cells was estimated by forming and incubating a 3D construct consists of OCP particles/D1 cells in osteogenic differentiation media using an oxygen permeable chip [9, 11]. Special attention was paid to detect ionic dissolution and the crystal structural changes of OCP during the incubation. In the 3D cell culture, chemical analyses of the crystals and the supernatant were carried out to determine the Ca/P molar ratio of the crystals and the media degree of supersaturation (DS) which is defined as a ratio of ionic activity products to solubility product constant. Curve fitting of FTIR spectra measured for the retrieved crystals after the incubation was analyzed to obtain the nature of the growing crystals.

Results and Discussion

OCP increased Pi concentration in the media and SOST/sclerostin and FGF23 gene expression of IDG-SW3 cells after 35 days of incubation, estimated by real-time PCR, indicating the enhancement of differentiation toward late stage osteocytes [8]. In the HUVEC culture study, capillary-like tube formation was maximized in certain dose of OCP, which induced distinct calcium and Pi ion concentrations, indicating the potential angiogenic capability of OCP [10]. In the 3D cell culture, alkaline phosphatase activity of D1 cells increased if the construct was formed by OCP in comparison with the control materials HA and β-TCP. The DS value with respect to HA salt in the 3D culture media

showed a decreasing tendency in OCP/D1 more than HA/D1 cells or β-TCP/D1 cells. Chemical analysis and FTIR spectroscopy of the crystals suggested that the differentiation of D1 cells was enhanced by the participation of amorphous calcium phosphate (ACP) precipitation together with the progress of OCP hydrolysis slightly [9]. It is reasonable to assume that the ionic dissolution stemmed from the chemical property of OCP under physiological conditions provided should be involved in the stimulatory capacity of OCP to increase both osteogenic and angiogenic cellular activities in vitro. Overall results suggest that such a stimulatory mechanism of OCP may be reproduced in vivo bone formation enhancement induced by OCP.

Conclusion

The studies showed that OCP facilitates the differentiation to osteocytes and osteoblastic cells from the cells in mesenchymal linages and the capillary-like tube formation from vein endothelial cells in vitro. The ionic dissolution of OCP and the structural changes should be involved in these cellular activation processes.

References

1. Suzuki O et al. Tohoku J Exp Med 164:37, 1991
2. Suzuki O et al. Biomaterials 27:2671, 2006
3. Kawai T et al. Tissue Eng Part A 20:1336, 2014
4. Komlev VS et al. ACS Appl Mater Interfaces 6:16610, 2014
5. Suzuki O et al. J Biomed Mater Res B Appl Biomater 77:201, 2006
6. Anada T et al. Tissue Eng Part A 14:965, 2008
7. Nishikawa R et al. Dent Mater J 33:242, 2014
8. Sai Y et al. Acta Biomater 69:362, 2018
9. Sato T et al. Acta Biomater 2019 in press. doi: 10.1016/j.actbio.2019.03.001
10. Kurobane T et al. Acta Biomater 2019 in press. doi: 10.1016/j.actbio.2019.02.021
11. Anada T et al. Biomaterials 33:8430, 2012

Acknowledgement

This work was supported by MEXT/JSPS KAKENHI Grant Number JP23106010, JP17K19740, JP17H02095, JP17K20079 and JP18H02981.

VI-SY11-KL02

Material-induced heterotopic ossification

Marc Bohner

RMS Foundation, Bettlach, CH

Georges Winter, one of the founding members of the European Society for Biomaterials, reported 50 years ago that a polymer foam implanted in soft tissues can trigger a biological cascade leading to bone formation [1]. Since then, numerous studies have been performed to decipher the link between material properties and heterotopic ossification (HO). These studies have demonstrated that many materials (metals, polymer, ceramics) can provoke an osteoinductive response. Also, many material properties (granule size, implanted volume, pore size and shape, porosity, etc…) may affect this process. Material-induced HO consists of a material and a biological component. The material induces an inflammatory response, which at some point drives mesenchymal stem cells into the osteogenic pathway [2]. Recently, the trigger of the material-induced immune response was uncovered [3]. The aim of the presentation is to review the literature on material-induced HO, to present the mechanism by which materials can induce an osteogenic response, to compare material-induced and material-free HO, and finally to present design principles for the generation of potent osteoinductive bone substitutes.

References

[1] G.D. Winter, B.J. Simpson. Nature 1969;223:88-90. [2] Z. Tang et al. Regen Biomat 2018;5:43-59. [3] M. Bohner, R. Miron. Mater Today 2019;22:132-141.

VI-SY11-03

Setting mechanism of an apatite forming α tricalcium phosphate (α-TCP) cement modified by sodium phytate (IP6) addition for better injectability

Jan Weichhold[1], Friedlinde Götz-Neunhoeffer[2], Katrin Hurle[2], Uwe Gbureck[1]

[1]University Hospital of Würzburg, Department for Functional Materials in Medicine and Denistry, Würzburg, DE; [2]Friedrich-Alexander University of Erlangen-Nürnberg, GeoZentrum Nordbayern Mineralogy, Erlangen, DE

Introduction

Apatite forming biocements have improved mechanical properties compared to their brushite forming counterparts [1]. Since the dissolution rate of α-TCP is low, the precipitation rate of calcium deficient hydroxyapatite (CDHA) and hence the setting time is slow and such cements have to be mixed with a small amount of CDHA and a sodium hydrogen phosphate solution as accelerators. The CDHA works as crystallisation seeds and the Na_2HPO_4 takes advantage of the common ion effect [2]. The cements can either be modelled intraoperatively or they can be injected minimal invasively into the defect. The latter requires low viscous cement pastes to avoid filter-pressing and phase separation during injection. Injectability can be improved by using citrates, which increase the absolute value of the surface charge of the cement particles resulting in a mutual repulsion and hence liquefies the paste. However, citrate modification has recently been demonstrated to have an adverse effect on cellular degradation by osteoclasts [3]. A suitable alternative might be phytic acid (PA), which bears six phosphate groups and may hence also increase the absolute value of the surface charge of cement particles. However, PA is also known to retard the setting reaction of brushite cements [3] and therefore it is crucial for a clinical application to find a balanced PA modification which improves the rheological properties of the paste, but at the same time does not detrimentally influence the setting reaction.

Experimental Methods

This study aims to investigate in detail the effect of phytic acid as setting modifier in apatite forming cements based on mixtures of α-TCP, CDHA and Na_2HPO_4. For this a mixture of α-TCP and CDHA in a ratio of 9:1 was mixed with Na_2HPO_4 and different amounts of sodium phytate (0.25-1 wt%) were compared to a reference without the addition of sodium phytate. The produced pastes were tested in respect to their compressive strength, porosity, injectability, rheology during setting, surface charge and their setting behaviour at non-ambient conditions (37 °C and 100% humidity). These results were evaluated in terms of their viability to create an injectable bone cement paste to be used in a minimal invasive application.

Results and Discussion

It could be shown, that the addition of sodium phytate as low as 0.25 wt% had an enhancing effect on the injectability and the pastes remained nearly completely injectable even 10 min after mixing of the solid and the liquid phase. A higher amount of added sodium phytate had no significant effect on the injectability. Compared to the reference the injectability could be improved vastly. The surface charge of the cement particles was increased in comparison to the reference in water. Adding sodium phytate increased the initial viscosity due to the formation of chelate complexes consisting of Ca^{2+} ions and the phosphate groups of the phytic acid. This inhibited the typical dissolution/ precipitation reaction and had a retarding effect on the setting process. The setting time could be adjusted to an acceptable length

by the addition of sodium phytate, CDHA and Na_2HPO_4. Increasing the temperature accelerated the reaction as this comes with an overall increase in energy in the system. The rheology measurements showed that the viscosity increases faster during the setting process at a higher temperature. The compressive strength tests of the cement after 1d and 7d showed the initial retarding effect of the sodium phytate as the specimen were not as mechanically stable

Conclusion

The desired information about the influence of temperature and the modification with sodium phytate could be collected. The modified system shows suitable properties to be used as an injectable bone cement for a minimal invasive application. An amount of as low as 0.25 wt% sodium phytate was found to be sufficient to achieve maximum injectability and good rheological properties.

References

[1] **J. Zhang, et al.,** Calcium phosphate cements for bone substitution: chemistry, handling and mechanical properties, Acta Biomater. 10 (2014) 1035–1049

[2] **M. Bohner, et al.,** Controlling the reactivity of calcium phosphate cements. J Mater Chem 2008; 18:5669-5675.

[3] **S. Meininger, et al.,** Phytic acid as alternative setting retarder enhanced biological performance of dicalcium phosphate cement in vitro, Sci. Rep. 2017; 7.

Acknowledgement

The research was funded by the Deutsche Forschungsgemeinschaft (DFG, German Research Foundation) - Grant Nr. HU 2498/1-1; GB 1/22-1.

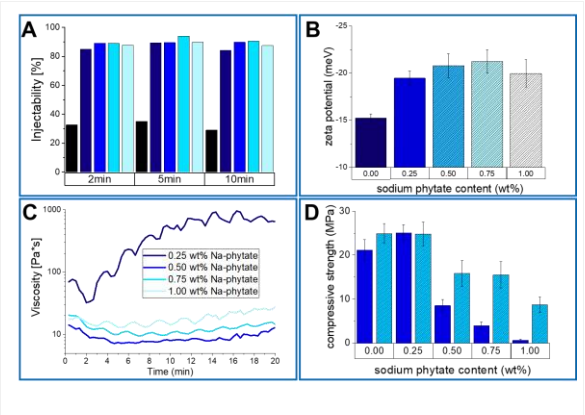

Figure 1:
(A) The injectability of the different mixtures (dark - light corresponds to 0.00 - 1.00 wt% sodium phytate), (B) the surface charge of the particles with variing phytate content, (C) the viscosity development during the setting and (D) the compressive strength of the cement samples after 1d (dark) and 7d (light) of hardening are shown.

VI-SY11-04

Calcium/Strontium Phosphates for Treatment of Osteoporotic Imbalance of Bone Cells

Benjamin Kruppke[1], Alena S. Wagner[2], Seemun Ray[3], Marcus Rohnke[4], Volker Alt[3], Sabine Wenisch[2], Thomas Hanke[1]

[1]TU Dresden, Max Bergmann Center of Biomaterials, Institute of Materials Science, Dresden, DE; [2]Justus-Liebig-University Giessen, Department of Veterinary Clinical Sciences, Small Animal Clinic c/o Institute of Veterinary-Anatomy, -Histology and -Embryology, Giessen, DE; [3]Justus-Liebig-University Giessen, Laboratory of Experimental Trauma Surgery, Giessen, DE; [4]Justus-Liebig-University Giessen, Institute for Physical Chemistry, Giessen, DE

Introduction

The imbalance of osteoblasts and osteoclasts in the case of osteoporosis causes increased fragility of the bone and worsened healing in the case of hard tissue defects. To treat bone defects under these conditions, we focused on a degradable material of gelatin-modified calcium and strontium phosphates – a material, ought to release strontium ions and keep the cation concentration on a physiological level, to stimulate osteoblastogenesis. In the course of in vitro investigations, the crystal structure, composition and morphology were specifically adjusted so that material degradation adapted to the expected *in vivo* degradation took place. This was confirmed in the osteoporotic rate model, in which the material showed an extensive degradation during the investigation period of 6 weeks. By means of an *in vitro* degradation model under development of a flow chamber, the results of the *in vivo* degradation are now to be reproduced *in vitro* in order to be able to predict the future material synthesis more accurately.

Experimental Methods

A phosphate solution was used to prestructure gelatin, which was mixed afterwards with calcium and/or strontium containing solutions. The precipitated organically modified mineral was cross-linked and lyophilized to obtain porous 3D samples. The resulting material was investigated according to ion release and degradability. Cell culture of human mesenchymal stromal cells (hBMSC) as well as human monocytes was performed *in vitro*. The *in vivo* characterization of the material was done by implantation in a femoral defect in osteoporotic rats. Finally, the material degradation was analysed under different conditions of constantly flowing fluid in a specially designed chamber.

Results and Discussion

The materials caused an initial ion release in calcium-rich (2.0 mM) and low-calcium (0.4 mM) minimum essential medium. In case of gelatin-modified calcium / strontium phosphate with a Ca/Sr-ratio of 5:5, cultivation of monocytes next to the material led to formation of osteoclast-like cells, able to migrate, fuse, and differentiate proved morphologically and by PCR. In contrast, pure gelatin-modified strontium phosphate (Ca/Sr-ratio of 0:10) affected osteoclast formation. The osteoblastic reaction of hBMSC was most significant with mixed Ca/Sr-phosphates as well. Mass spectrometric imaging (ToF-SIMS) of thin cuts of the rat femurs revealed an increased bone formation with increasing strontium in the material, supported by histological analysis.

Conclusion

The study showed, that an adjustment of bone substitute materials – with respect to its degradation and ion release – to demands of systemically altered bone was successful. Furthermore the degradation under conditions of constant flowing medium can be used to predict material degradation *in vivo* more precisely.

Acknowledgement

Financial support from Deutsche Forschungsgemeinschaft DFG Collaborative Research Centre TRR 79/ SP M3, B5, T2, M5, Z2, and M1 is gratefully acknowledged (***Projektnummer 107540325***).

4:15 p.m. – 5:45 p.m.

Hall 5

VI-OS20 | Alginate and biopolymers

VI-OS20-KL01

Chemical and enzymatic tailoring of alginate for biomedical applications

Berit Løkensgard Strand[1,2]

[1]NOBIPOL, Dept of Biotechnology and Food Science, Trondheim, NO; [2]NTNU Norwegian University of Science and Technology, Trondheim, NO

Alginate hydrogels are attractive for tissue engineering applications as they have a low toxicity and immunogenicity profile and as cells can be entrapped in the gel at physiological conditions ensuring good viability and function of the cells. Alginates are linear polysaccharides from brown algae and some few bacteria consisting of 1->4 linked β-**D**-Mannuronic acid (M) and its C5 epimer α-**L**-Guluronic acid (G). G-blocks are main contributor to the binding of divalent ions in the gel and determine to a great extent the mechanical properties of an alginate gel. Alginates are in general not known to promote specific cell interaction. Chemical modification of alginate allows the introduction of biological activity but weaken the mechanical properties of the alginate gels as the G-blocks are disrupted. Chemical modification allows for the introduction of e.g. peptides for cell attachment (1,2), Cyclodextrins for drug release (3) and sulphate groups that allows alginate to resemble heparin (4,5). Enzymatic modification by mannuronan C5 epimerases, that converts M to G in the polymer, allows the tailoring of mechanical properties of the alginate (5). Here, both material characterization and biological responses of chemical and enzymatically tailored alginates will be presented.

References

(1) Rowley JA, Madlambayan G, Mooney DJ. Alginate hydrogels as synthetic extracellular matrix materials. *Biomaterials.***1999**; 20:45–53.

(2) Sandvig I, Karstensen K, Rokstad AM, Aachmann FL, Formo K, Sandvig A, Skjak-Braek G, Strand BL, *J Biomed Mater Res Part A***2015**, *103*, 896.

(3) Omtvedt L, Dalheim MØ, Nielsen TT, Larsen KL, Strand, B.L., Aachmann, F.L. Efficient Grafting of Cyclodextrin to Alginate and Performance of the Hydrogel for Release of Model Drug, *Nature Scientific Reports***2019**, accepted for publication.

(3) Arlov, O.; Aachmann F. L.; Feyzi E et al. The Impact of Chain Length and Flexibility in the Interaction between Sulfated Alginates and HGF and FGF-2. *Biomacromol* **2015**;16:3417.

(4) Arlov, O.; Aachmann, F.L.; Sundan, A.; et al. Heparin-like properties of sulfated alginates with defined sequences and sulfation degrees. *Biomacromol***2014**;15:2744.

(5) Mørch, Y.A., Holtan, S., Donati, I. Strand, B.L. and Skjåk-Bræk, G. Mechanical Properties of C-5 Epimerized Alginates. *Biomacromolocules.***2008**; 9 (9), 2360-2368.

VI-OS20-02

Modified-alginate microfibers as instructive matrix for guiding tissue regeneration

Chiara E. Campiglio[1,2,3], Silvia J. Bidarra[1,4], Lorenza Draghi[2,3], Cristina C. Barrias[1,4,5]

[1]i3S - Instituto de Inovação e Investigação em Saúde, Porto, PT; [2]Politecnico di Milano, Department of Chemistry, Materials and Chemical Engineering "G. Natta", Milan, IT; [3]INSTM – National Interuniversity Consortium of Materials Science and Technology, Local Unit Politecnico di Milano, Milan, IT; [4]INEB – Instituto de Engenharia Biomédica, Universidade do Porto, Porto, PT; [5]ICBAS – Instituto de Ciências Biomédicas Abel Salazar, Universidade do Porto, Porto, PT

Introduction

The development of three-dimensional (3D) fibrous networks as platforms for tissue engineering applications has been attracting considerable attention. Among several scaffolding options, organized hydrogel microfibers are particularly appealing for engineering high-cell-density 3D constructs. Their shape is biomimetic, given that the ECM of native tissues has a microfiber-shaped network-like 3D structure. Also, they provide an open porous structure and a high surface-to-volume ratio, which favors homogeneous perfusion of oxygen and nutrients throughout the entire structure, enhancing cell survival and tissue growth.[1].Among natural polysaccharides, alginate is the most extensively used as embedding hydrogel, due to its spontaneous mild crosslinking mechanism in the presence of divalent cations (Ca^{2+}or Ba^{2+}). Despite this, alginate presents some limitations in terms of mechanical properties and cell-instructive ability. To overcome these drawbacks, alginate physicochemical properties can be easily modulated towards improved processability and ECM biomimicry. Here, to combine the advantages of alginate hydrogels and microfibrous architectures, a simple coaxial flow wet-spinning system was used to prepare cell-loaded, 3D fibrous patches using RGD-modified, oxidized alginate. After process optimization, the effect of scaffold composition and architecture on the behavior of 3D-cultured mesenchymal stem cells (MSCs) was investigated.

Experimental Methods

Ultra-pure sodium alginate with low content of guluronate blocks (49%, Pronova) was used to produce alginate microfibers. Alginate was oxidized (1%) and modified with cell adhesive motifs (RGD, GenScript) in a two-steps procedure [2,3]. Briefly, alginate was partially oxidized to a theoretical extent of 1% of sugar residues with sodium periodate, then lyophilized and covalently grafted with the integrin-binding peptide (glycine)4-arginine-glycine-aspartic acid-serine-proline (RGD, GenScript) using aqueous carbodiimide chemistry. Oxidized,RGD-grafted alginate solution was prepared in Minimun Essential Medium at a final concentration of 1% w/v for MSCs entrapment in hydrogel microfibers (14 x 10^6 cells/mL).For microfibers fabrication, MSCs-alginate suspension was injected in a closed-loop circuit with circulating cross-linking solution ($CaCl_2$ 50 mM). The flow promoted stretching and solidification of continuous cell-loaded micro-scaled fibers that were collected in a strainer, assembling into a microfibrous patch. After 1, 7 and 14 days of culture, the viability and metabolic activity (resazurin assay) of entrapped cells were assessed and the ability in producing endogenous extracellular matrix proteins was investigated by confocal laser scanning microscope (CLSM) after immunostaining for fibronectin and collagen Type I.

Results and Discussion

The flow-circuit employed allowed the production of hydrogel microfibers with diameter of 100 – 300 mm that were assembled in a compact structure with an interconnected porosity (Figure 1). The viscosity of alginate solutions

showed to be a crucial parameter in the microfibers fabrication process. In fact, only 1% v/w alginate allowed the fabrication of uniform microfibers, while higher polymer concentration resulted in the formation of elongated beads, instead of microfibers. The system proved to be adequate for embedding of a large density of cells, which became homogeneously dispersed throughout the microfibers, and remained highly viable for up to 2 weeks, as confirmed by the viability and metabolic activity assays. The production of ECM components, namely fibronectin and collagen Type I, was investigated as a function of maturation time. MSCs entrapped in alginate microfibers deposited extensive amounts of fibronectin, which assembled into fibrillar networks and stretched along alginate fibers border, and collagen Type I, which accumulated substantially around cells throughout the culture period. Interestingly, the deposition of collagen slightly increased after 14 days, when cells were able to migrate out of the microfibers and spread on top of them (Figure 1).

Conclusion

A simple flow circuit was employed for the fabrication of cell-laden fibrous patches, where the spontaneous arrangement of microfibers resulted in the formation of a highly interconnected, cohesive 3D network. The microfibers of oxidized alginate modified with integrin-binding ligands provided a suitable 3D microenvironment, supporting cell survival and stimulating the production of ECM proteins, as fibronectin and collagen Type I.Collectively, these features make the proposed microfibrous structures stand out as promising 3D scaffolds for regenerative medicine.

References

1 S. J. Bidarra, C. C. Barrias and P. L. Granja, *Acta Biomater.*, 2014, **10**, 1646–1662.

2 K. H. Bouhadir, K. Y. Lee, E. Alsberg, K. L. Damm, K. W. Anderson and D. J. Mooney, *Biotechnol. Prog.*, 2001, **17**, 945–950.

3 A. L. Torres, S. J. Bidarra, M. T. Pinto, P. C. Aguiar, E. A. Silva and C. C. Barrias, *Biomaterials*, 2018, **154**, 34–47.

Acknowledgement

This work was financed by FEDER - Fundo Europeu de Desenvolvimento Regional funds through COMPETE 2020 - Operacional Programme for Competitiveness and Internationalisation (POCI), Portugal 2020, and by Portuguese funds through FCT - Fundação para a Ciência e a Tecnologia/Ministério da Ciência, Tecnologia e Ensino Superior, in the framework of project 3DEMT (PTDC/BBBECT/251872014 and POCI-01-0145-FEDER-016627). SJB and CCB thank FCT for research contract DL 57/2016/CP1360/CT0006 and IF research position IF/00296/2015, respectively. CEC thanks the Erasmus Plus Program for the traineeship mobility grant.

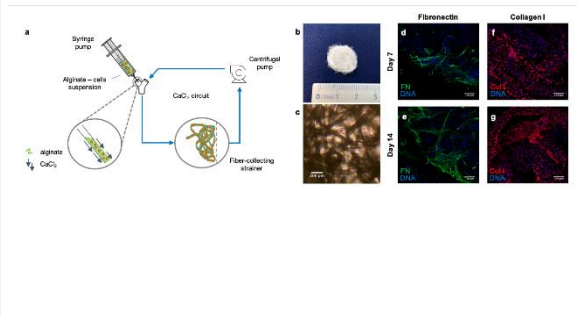

Microfibers patch fabrication
(a) schematic representation of the flow circuit employed, (b) macroscopic appearance and (c) optical microphotograph of dehydrated fibers.CLSM imaging after 7 and 14 days of culture showing that MSCs were able to produce fibronectin (FN) as a 3D network (*d-e*: FN in green and nuclei in blue). Cells also produced and deposited collagen Type I (Col I) (*f- g*: Col I in red and nuclei in blue).

VI-OS20-03

Corn silk extract and hyaluronic acid based antibacterial thermosensitive hydrogels: biosynthesis, characterization and wound healing potential

Assunta Borzacchiello[1], Pooyan Makvandi[1,2], Francesca Della Sala[1,4], Ghareib W. Ali[3], Wafa I. Abdel-Fattah[3], Luigi Ambrosio[1]

[1]National Research Council of Italy, Institute for Polymers, Composites and Biomaterials of Naples, Napoli, IT; [2]University of Naples Federico II, Department of Chemical, Materials and Production Engineering, Napoli, IT; [3]National Research Centre of Cairo, Inorganic Chemistry Division and Mineral Resources, Refractories and Ceramics Dept, Cairo, EG; [4]University of Study of Campania, Dipartimento di Scienze e Tecnologie Ambientali Biologiche e Farmaceutiche, Caserta, IT

Introduction

Hydrogels have attracted research attention for wound healing applications since hydrogel dressings are an excellent source for providing moisture to a dry lesion, monitoring fluid exchange from within the wound surface, helping to cool down a wound, as well as provide temporary pain relief [1]. Thermosensitive amphiphilic block copolymers, polyethylene oxide-polypropylene oxide copolymers (Poloxamers or Pluronics, PPO-PEO-PPO), thanks to their ability to undergo thermal gelation, to their good tolerability, and low irritancy/toxicity, have been used in the biomedical field for instance for tissue engineering and drug delivery applications [2]. Hyaluronic acid (HA) is naturally occurring glycosaminoglycan, presents in mammalian connective tissues. It has been demonstrated that HA promotes dermal regeneration and for this, it is widely used as dermal fillers, as wound dressings and substrates for dermal engineering applications [3]. It has to be highlighted that infection is a crucial and generally unsolved issue in wound healing. Therefore, materials containing antimicrobial compounds, such as Ag nanoparticles (Ag NPs) have shown the capability to inhibit or decline infections. Corn silk extract (CSE), a waste material of the crop, has been used for AgNPs biosynthesis as both a reducing and stabilizing/capping agent [4]. In addition, CSE possesses excellent antioxidant capacity [5]. In this context, we propose novel and green thermosensitive nanocomposites hydrogels based on HA, Pluronics and AgNPs for wound healing applications.

Experimental Methods

The corn silk were heat extracted. AgNPs were synthesized within CSE by microwave. The hydrogels were prepared by dissolving different amounts of Pluronics F127 and F68 in silk extract with and without AgNPs, subsequently HA was added. The hydrogels composition was optimised by rheological analysis. The hydrogels were characterised for the rheological properties. The formation of AgNPs was confirmed by UV-Vis surface plasmon band while their morphology was evaluated by DLS and HRTEM. Bacterial cell suspensions were prepared, for each tested Gram-positive and Gram-negative, the cell growth of the tested bacteria was determined at the end of the incubation period, based on the optical density measurements at a wavelength of 620 nm. In vitro biocompatibility was performed by Alamar Blue assay on L929 fibroblast cells culture. The wound healing potential of the realized formulations was assessed by wound healing assay on Human Dermal Fibroblast (HDF) cells after 24 and 48 hrs. of thermosensitive hydrogels incubation. Wound healing assay was performed by scraping the cell monolayer in a straight line to create a ‘‘scratch area’’. Wound area, was calculated using the ImageJ public domain software. The migration rate can be expressed as the percentage of wound area reduction or wound closure.

Results and Discussion

Separate Pluronic F127 and F68 solutions do not show an appropriate Tgel but by formulating Pluronic F127/F68 blends at specific concentrations, it was possible to obtain a medium with a Tgel close to Tb. The addition of HA slightly affects Tgel, but very interestingly, improved significantly the final gel viscoelastic properties. AgNPs were spherical with average diameter of 8 nm (Figure 1 A-D). The presence of AgNPs did not alter the hydrogels rheological properties. The AgNPs hydrogels showed an excellent bactericidal activity against the tested Gram-positive and Gram-negative bacterial strains. The results confirmed the bactericidal activity of the samples in comparison with control. It has been demonstrated the biocompatibility of the hydrogel on L929 cells and also that the presence of Ag does not modify the cell viability. The in vitro wound healing assay of the realized thermosensitive corn silk extract-nanosilver hydrogels was performed on HDF cells; the results (Figure 2 A-C) have been demonstrated that the wound surface area decreases with the increasing exposure times (24 to 48 hrs.) of the tested hydrogels compared to the controls. Accordingly, the wound closure percentage increases with the increasing time after exposure to the injectable hydrogels. The individual biomaterials used in this assay could affect positively the wound healing process.

Conclusion

We developed a novel and green thermosensitive injectable hydrogels based on HA, CSE and Ag NPs. In vitro model of wound healing revealed that the nanocomposites allow faster wound closure and repair, compared to the control. The obtained results highlight the potential application of these novel injectable hydrogels as wound dressing.

References

1. S. Heilmann, et al., Int. J. Pharm., 444, 96 (2013).
2. H. Zhang, et al., J. Transl. Med., 6, 67 (2008).
3. T. Maneerung et al. Carbohydr. Polym., 72, 43 (2008).
4. J.K. Patra et al.,IET nanobiotechnology, 10, 326 (2016).
5. K. Hasanudin et al., Molecules, 17, 9697 (2012).

Acknowledgement

Italian Ministry of Foreign Affairs in the frame of the Executive Program of Scientific and Technological Cooperation between Italy and Egypt (2016-2018).

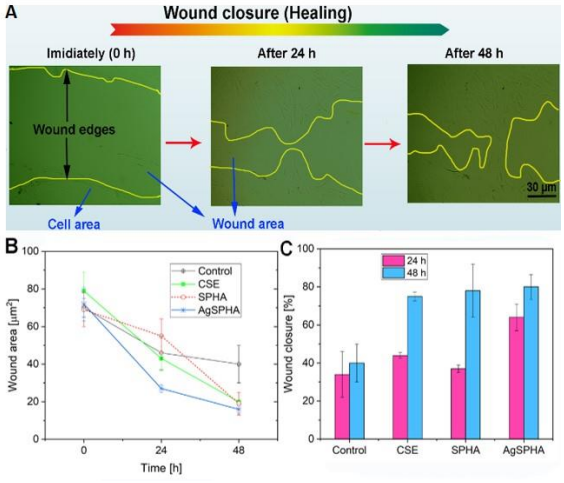

Figure 2
(A) Representative bright-field images show HDF cells migration after the scratch at time 0 and after 24 and 48 hrs. of thermosensitive hydrogels based on HA, Pluronics and AgNPs incubation. (B) Wound area expressed as the remaining area uncovered by the cells. The scratch area at time point 0 hrs. and after 24 and 48 hrs. of CSE, Silk Pluronics and HA (SPHA), Ag Silk Pluronics and HA (AgSPHA) incubation. (C) Wound closure expressed as the percentage of the closure of the scratched gap after 24 and 48 hrs. of CSE, SPHA, AgSPHA incubation. The results are the means of three measurements

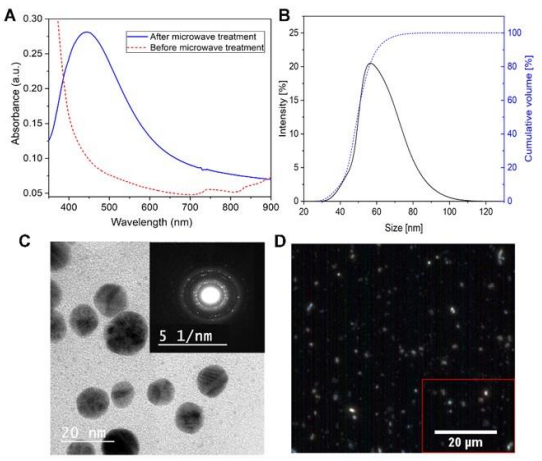

Figure 1
(A) UV absorbance of CSE before and after microwave treatment. Size distribution measurements by DLS (B) and TEM image (C) of Ag NPs in CSE solution after microwave treatment. (D) Visualization of nanoparticles in CSE medium.

VI-OS20-04

Fabrication of tubular structure to mimic the osteon structure

Mairon Trujillo Miranda[1], Juan Uribe[2], Indra Apsite[2], Elise DeSimone[1], **Sahar Salehi**[1], Leonid Ionov[1]

[1]University of Bayreuth, Deapartment of Biomaterials, Bayreuth, DE; [2]University of Bayreuth, Deapartment of Biofabrication, Bayreuth, DE

Introduction

Extrusion-printing has been used to deposit living cells, hydrogels ink and biomolecules in three dimentional structures to build complex tissue constructs. [1] Natural cortical bone is composed of tightly packed tubular units as concentric layers called osteons. Osteons are oriented parallel along to the axis of the bone and are made of mineralized collagen fibers around central Haversian canal, where vasculature and nerves are localized.
The goal of this study was to mimic this 3D tubular layers “Osteon” using self-rolling constructs made of a composite hydrogel reinforced with bioactive ceramics nanoparticles. The printed construct reinforced with nanoparticles will be able to provide mechanical stability and bioactivity which is required for the biomineralization of the system [2]. This platform can be further developed similar to the native osteon with vascular system and neuronal network.

Experimental Methods

The nano particles of bioactive ceramic, forsterite (Mg_2SiO_4), with high surface area were synthesized using sol-gel technique. [2] Printing and rolling behavior was evaluated using various methacrylated hydrogels with a different particle’s concentrations (1- 5%wt nFo). Hydrogel inks developed in this study were methacrylated alginate, gelatin and hyaluronic acid with different concentrations. The flow behavior of the prepared composite inks as well as their sensitivity to temperature was evaluated using plate-plate rheology. Bioactivity of composite hydrogels, was also investigated during 14 days incubation in simulated body fluid (SBF) prepared according to Kokubo protocol [3]. Scanning electron microscopy-EDX, FTIR and elemental analysis was used for further analysis.

Results and Discussion

The results showed that by controlling the thickness of the printed structure, time of crosslinking and amount of the particles we can optimize the tubular structure formation. By increasing the amount of the particles the higher bioactivity was observed, which was confirmed by higher apatite precipitations on the surface of cross-linked hydrogels during 14 days. The elemental analysis also confirmed the higher release of Mg and Si ions from the composite inks containing 5wt% nFo. These results shows the suitability of this composite as an effective bone graft substitute.

Conclusion

In conclusion, this study demonstrates optimization of material parameters for 3D printed composite structure and enhancement of mechanical properties and bioactivity by incorporation of forsterite particles.

References

[1] Turnbull G. et al. Bioactive Mater, 2018, 3, 278.
[2] Sanosh K. et al. J Alloys Comp, 2010, 113-115.
[3] Kokubo T., et al. Biomaterials, 2006, 2907-2915.

Acknowledgement

Funded by the Deutsche Forschungsgemeinschaft (DFG, German Research Foundation) – Projektnummer 326998133 – TRR 225 (subproject B03).

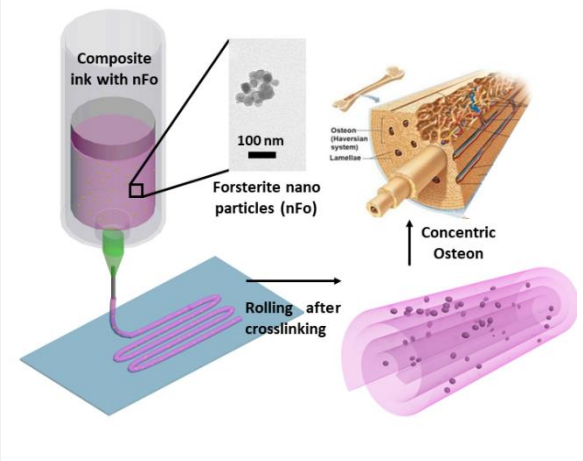

Scheme of self-rolling composite materials mimicking Osteon structure

VI-OS20-05

Sophisticated cell microfactories co-encapsulating osteoblastic and adipose stem cells for bone regeneration

Sara S. Nadine, Clara R. Correia, Sónia G. Patrício, João F. Mano

University of Aveiro, Department of Chemistry, CICECO - Aveiro Institute of Materials, Aveiro, PT

Introduction

The successful regeneration of large bone defects remains a significant challenge in orthopedic research. Along with tissue engineering and regenerative medicine (TERM) field evolution, new technologies aiming tissue repair have been emerged. Stem cells are the focus of many TERM applications, and adipose derived stem cells (ASCs) quickly became attractive for bone tissue engineering [1]. However, controlling stem cell multipontency and engineering bone *in vivo* remains a significant challenge, as it often leads to heterotypic and inferior osseous tissues. So, inspired by the multiphenotypic cellular environment of bone, we believe that self-regulated liquefied and multilayered microcapsules [2], loaded with ASCs and human osteoblasts (hOBs) cells could be a promising attempt. Microcapsules are composed by (i) a multilayered membrane obtained through layer-by-layer assembly (ii) a liquefied alginate core, (iii) surface functionalized poly(ε-caprolactone) microparticles (µPCL), and (iv) cells. While the multilayered membrane wraps all the cargo contents and ensures permeability to essential molecules for cell survival, the liquefied core maximizes their diffusion through the entire 3D construct. Moreover, taking advantage of the liquefied core, the proposed microcapsules were tested using a rotary cell culture system. The dynamic environment is expected to maximize the interaction between the different multiphenotypic cells and microparticles, while also mimicking the dynamic environment of native tissues. Microcapsules encapsulating only ASCs (MONO microcapsules) or a co-culture with hOBs (CO microcapsules) were cultured up to 21 days in culture medium with or without (basal) osteogenic differentiation factors. Our hypothesis is that by recreating the specific microenvironment of the bone regenerative process inside microcapsules, new microtissues with superior quality and without requiring any osteogenic medium supplementation could be engineered.

Experimental Methods

Alginate microgels are generated by electrohydrodynamic atomization (EHDA) technique (fig.1A). For that, under influence of electrical forces (10 kV), a liquid jet of alginate containing a dispersion of cells ($5x10^6$cells/mL) and µPCL (30 mg/mL) breaks up into droplets. After crosslinking in calcium chloride, microgels encapsulating cells and µPCL are obtained. Then, layer-by-layer is performed using poly(L-lysine), alginate, and chitosan as polyelectrolytes to produce the multilayered membrane surrounding the obtained microgels. The process is repeated until a 10-layered membrane is created. Ultimately, the core is liquefied by chelation with EDTA for 5 min. Afterwards, liquefied MONO or CO microcapsules were cultured up to 21 days in basal or osteogenic differentiation media. The proposed capsules were tested under dynamic culture conditions, using a rotary cell culture system, or in static conditions (control).

Results and Discussion

Microtissues were successfully obtained inside the compartmentalized and controlled environment of capsules with an appropriate diffusion of essential molecules for the long survival of the encapsulated cells (fig.1C). Interestingly, it is possible to observe that the dynamic environment led to the development of significantly larger aggregates of cells and µPCL comparing with static conditions. Of note, the late osteogenic marker osteopontin could also be

visualized in capsules cultured in the absence of osteogenic differentiation factors, evidencing that osteogenesis was prompted by the combined effect of the dynamic environment and the presence of hOBs (fig.1D). Moreover, it was observed by FTIR-ATR (data not shown) that the dynamic environment enhances the complexity of the organization of the protein aggregates, comparing to static cultures. These spectral features were confirmed by SEM analysis, showing elongated filaments in the micrometer scale, characteristics of collagen fibrils (fig.2A). After von Kossa staining performed on histological cuts, it could be observed an enhanced mineralization in microcapsules cultured under dynamic environment (fig.2B). Furthermore, apatite-like minerals were also observed for CO microcapsules, with a Ca/P ratio around 1.7 for microcapsules under dynamic conditions (fig.2C), which is comparable to the native apatite from bone matrix [3].

Conclusion

The proposed system allowed the successfully development of microtissues inside the controlled environment of the microcapsules. The co-encapsulation of ASCs and hOBs, within a single hierarchical structure proved to be an effective strategy for the *in vitro* osteogenic differentiation. Additionally, the freely dispersion of the cells and microparticles prompted by the dynamic stimulus, provided a more realistic bone repair process in terms of the quality and quantity of the formed mineralized microtissues over static conditions. Accordingly, we intend to use the proposed system as hybrid devices implantable by minimally invasive procedures for TERM applications.

References

[1] Dai R., et al., Adipose-Derived Stem Cells for Tissue Engineering and Regenerative Medicine Applications. Stem Cells International, 2016. 2016: p.1-19.
[2] Correia, C.R., et al., In vivo osteogenic differentiation of stem cells inside compartmentalized capsules loaded with co-cultured endothelial cells. Acta Biomater, 2017. 53: p. 483-494.
[3] Yang S., et al., The Design of Scaffolds for Use in Tissue Engineering. Part I. Traditional Factors. Tissue Engineering, 2001.

Acknowledgement

This work was developed within the scope of the project CICECO-Aveiro Institute of Materials, FCT Ref. UID/CTM/50011/2019, financed by national funds through the FCT/MCTES. Sara S. Nadine acknowledges the financial support by the Portuguese Foundation for Science and Technology (FCT) through the doctoral grant (SFRH/BD/130194/2017). This work was supported by the European Research Council grant agreement ERC-2014-ADG-669858 for project “ATLAS” and by FCT for the project CIRCUS (PTDC/BTM-MAT/31064/2017).

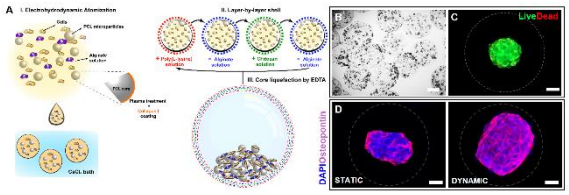

Figure 1.
(**A**) Schematic representation of the production method of liquefied and multilayered microcapsules. (**B**) Light microscopy of microcapsules encapsulating cells and PCL microparticles. Scale bar represents 300 µm. (**C**) Live-dead fluorescence assay at day 21 of culture. Living cells were stained by calcein (green) and dead cells by propidium iodide (red). Scale bars correspond to 100 µm. (**D**) Immunofluorescence of osteopontin (pink) counterstained with DAPI for the visualization of cells nuclei (blue) in CO capsules cultured under static or dynamic environments after 21 days of culture. Scale bars correspond to 100 µm. The dotted lines in figures C and D represent the membrane of the microcapsules.

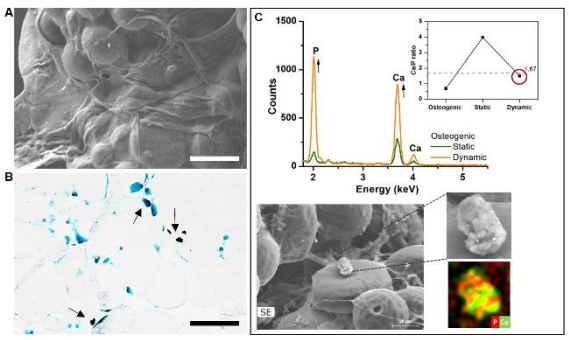

Figure 2.
Bone matrix analysis of CO microcapsulesafter 21 days of culture in osteogenic differentiation medium and under dynamic environment. (**A**) SEM image of the encapsulated microparticles and cells (magnification: 500x). Scale bars correspond to 50µm. (**B**) von Kossa staining of the microtissues formed. Arrows point to phosphate deposits marked in black. Scale bar represents 50 µm. (**C**) Elemental analysis by chemical mapping of phosphate (P) and calcium (Ca). Ca/P ratio analysis of osteogenic medium and microcapsules cultured under static or dynamic environments spot sizes. SEM image evidences the presence of apatite-like aggregate, further analyzed by elemental analysis of P (red) and Ca (green).

4:15 p.m. – 5:45 p.m.

Conference room 4+5

VI-OS21 | Cell material interactions 2

VI-OS21-01

Chitosan/Gelatin scaffolds loaded with dental stem cells under dynamic conditions promote fibrochondrogenic differentiation

Maria Bousnaki[3], Athina Bakopoulou[3], Emmanouil Vereroudakis[2], Anthie Georgopoulou[1], Aristidis Kritis[4], **Maria Chatzinikolaidou**[1], Petros Koidis[3]

[1]University of Crete, Department of Materials Science and Technology, Heraklion, GR; [2]Foundation for Research and Technology Hellas (FORTH), Institute for Electronic Structure and Laser (IESL), Heraklion, GR; [3]Aristotle University of Thessaloniki, School of Dentistry, Department of Prosthodontics, Thessaloniki, GR; [4]Aristotle University of Thessaloniki, Department of Physiology and Pharmacology, Faculty of Medicine, Thessaloniki, GR

Introduction

Tissue engineering (TE) may provide effective alternative treatment for challenging temporomandibular joint (TMJ) pathologies associated with disc malpositioning or degeneration leading to severe masticatory dysfunction. The aim of this study was to evaluate the potential of chitosan/gelatin (Ch/Gel) scaffolds seeded with dental pulp stem cells (DPSCs) and cultured in a perfusion bioreactor to promote fibro/chondrogenic differentiation and production of fibrocartilage tissue, serving as a replacement of the natural TMJ disc.

Experimental Methods

Porous Ch/Gel scaffolds, with a composition of 40%-60% chitosan-gelatin, were fabricated by chemical crosslinking with 0.1% glutaraldehyde and lyophilization [1]. DPSCs were isolated from third molars and seeded onto the Ch/Gel scaffolds (2x10^{6}cells/scaffold). DPSC/scaffold constructs were cultured under normoxic (20% O_2) or hypoxic (5% O_2) conditions. For the viability assay constructs were cultured with standard culture medium, while for the assessment of differentiation constructs were cultured with chondrogenic medium. Live/dead staining was used to evaluate cell attachment and viability after 3, 7 and 14 days in culture. Real time PCR was used to evaluate the expression of specific fibro/chondrogenic markers (Collagen I-*COLI*, Collagen X-*COLX*, Sox9-*SOX9*) after 7 and 14 days in culture [2]. After 4 weeks in static culture, one group of DPSC/scaffold constructs was placed in the perfusion bioreactor (10 ml/min) and further cultured for 4 weeks. DPSC/scaffold constructs were assessed for extracellular matrix production by means of histology and dynamic mechanical analysis after 4 and 8 weeks.

Results and Discussion

Live/dead staining showed that more than 90% of the cells remainedviable inside the scaffoldsin both conditions. DPSCs cultured into Ch/Gel scaffolds under hypoxic conditions demonstrated a significant increase of gene expression of fibrocartilaginous markers (*COLI, COLX, SOX9*) after 2 weeks in culture compared to normoxic conditions.Histological data after 8 weeks indicated that only the constructs cultured in the perfusion bioreactor support abundant fibrocartilaginous tissue formation. Dynamic mechanical analysis revealed increased yield strain of the constructs cultured under dynamic conditions compared to static ones.

Conclusion

Collectively, these data provide evidence of a promising strategy for TMJ disc TE-based replacement, by application of natural biomaterials combined with dental-tissue derived mesenchymal stem cells.

References

[1] Georgopoulou A, Papadogiannis F, Batsali A, Marakis I, Alpantaki K, Eliopoulos A, Pontikoglou C, Chatzinikolaidou M. (2018) Chitosan/gelatin scaffolds support bone regeneration, *J Mater Sci Mater in Medicine*29(5):59, DOI: 10.1007/s10856-018-6064-2

[2] Bousnaki M, Bakopoulou A, Papadogianni D, Barkoula N-M, Alpantaki K, Kritis A, Chatzinikolaidou M, Koidis P. (2018) Fibro/chondrogenic differentiation of dental stem cells into chitosan/alginate scaffolds towards temporomandibular joint disc regeneration,*J Mater Sci Mater in Medicine*, doi: 10.1007/s10856-018-6109-6

Acknowledgement

This research is co-financed by Greece and the European Union (European Social Fund- ESF) through the Operational Programme «Human Resources Development, Education and Lifelong Learning» in the context of the project “Strengthening Human Resources Research Potential via Doctorate Research” (MIS-5000432), implemented by the State Scholarships Foundation (IKY).

VI-OS21-02

Curvature-dependent epithelial tissue migration and orientation

Pablo Rougerie[2], Laurent Pieuchot[1], Rafaela Silva dos Santos[2], Julie Marteau[3], Maxence Bigerelle[3], Pierre-François Chauvy[4], Marcos Farina[2], Karine Anselme[1]

[1]CNRS, IS2M, UHA UMR7361, Mulhouse, FR; [2]UFRJ, Laboratório de Biomineralização, ICB, CCS, Rio de Janeiro, BRA; [3]UPHF, LAMIH, CNRS UMR8201, Valenciennes, FR; [4]Micropat S.A., Lausanne, CH

Introduction

Understanding how the geometry of the environment influences the growth of epithelial tissues is of fundamental importance. The ability of epithelia to grow preferentially along a specific direction is indeed a key part of embryo development and wound healing. Unsurprisingly, it is also an important part of tissue engineering efforts aiming at fostering tissue repair or growing replacement tissues. Here, we sought to determine whether combining cell-scale curvature with topographical anisotropy could trigger and regulate the anisotropic growth of epithelia. We grew unconfined MDCK colonies over cell-scale PDMS grooves and ridges with various level of transversal curvature. These surfaces thus combine a topographical anisotropy materialized by the parallel grooves and ridges with a controlled and quantified cell-scale curvature.

Experimental Methods

Five 316L stainless steel master surfaces were micro-fabricated using a two-step electrochemical process. They consisted of an array of parallel grooves with a period of 100 µm and an amplitude of 10µm. For the five surfaces the mid height valley width equals the mid height peak width. Each surface presents a distinct peak curvature ranging from a straight edge (Topo I) to a sinusoidal curve (Topo V) (Figure 1A). PDMS replicas of these master surfaces were used for MDCK colonies culture. The growth of the colonies was followed by live imaging over 2 days under a confocal microscope. Actin and tubulin organization were analyzed after fixation and immunostaining.

Results and Discussion

First, we monitored the growth of circular MDCK colonies over all surfaces during 48h (Figure 1B). Colonies growing over flat, isotropic control surface show an isotropic growth illustrated by their persistent circular shape. By contrast, all the colonies cultured over topographies grow into an elliptic shape.

Next, we decided to elucidate which cellular events could explain this curvature-dependent directional growth. First we observed that the formation of migration fingers is favored along the topography longitudinal axis and hampered along the transversal axis. Secondly we looked at the organization of contractile actomyosin cables formed at the periphery of colonies in function of curvature radius of grooves. On high curvature topographies, those peripheral cables are clearly oriented along the substrate longitudinal axis, a tendency less obvious on topographies of lower curvature. Further we looked whether events such as cell stretching and alignment as well as oriented cell division depend of transversal curvature of grooves. Cells from colonies growing over non-flat surfaces are more stretched although this effect seems independent from the curvature. Interestingly, cells are better aligned on average with the topography in colonies growing over higher curvature substrates. An overall alignment of mitotic spindles with the topography longitudinal axis was observed within the colonies. Altogether, we showed here that cell-scale anisotropic topographies exert a global control on epithelial growth.

Finally to understand how the epithelial colony could sense the degree of curvature and the substrate anisotropy, we looked at the distribution of the nuclei on the five different topographies. We confirmed that nuclei from the epithelial

monolayer were deformed by and partially excluded from convex regions, to an extent proportional to convex curvature. Our interpretation of those results is that convex regions form longitudinally oriented “topographical barriers” hampering the crossing of nuclei and together with it, the transversal elongation of the epithelial monolayer. As a final consequence, the directional growth along the surface longitudinal axis is favored.

Owing to the central role of actin in cell migration and tissue morphogenesis, we hypothesized that the transduction of the topographical information would also happen through a reorientation of the actin cytoskeleton. Effectively, we could observe a clear longitudinal orientation of F-actin on the high curvature topographies. In particular, we noticed longitudinal actin bundles seemingly accumulated at the convex regions. By contrast, we noticed transversally oriented actin stress fibers on the topographies of lowest convex curvature. We thus concluded that the organization of the actin cytoskeleton was also sensible to the substrate topographical information.

Conclusion

Here we report the curvature-modulated anisotropic growth of unconfined epithelia over cell-scale grooves and ridges of various transversal curvature. Curved regions of the substrate work as “topographical barriers”, causing heterogeneity and reorientation of the nuclei and F-actin position. As a result, the epithelium displays a spatial bias in various morphogenetic processes such as migration or mitosis. Altogether, this work establishes cell-scale curvature as a major tuning parameter to regulate the growth of epithelia and opens new possibilities for tissue engineering research.

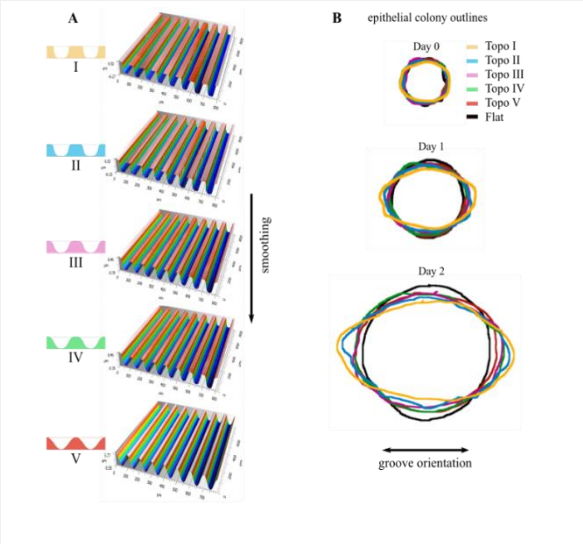

Figure 1
The transversal curvature of the topography controls the extent of anisotropic growth of the epithelial monolayer

VI-OS21-03

Quasi-2D Nanocomposites for Stem Cell Culture on Liquid-Liquid Interfaces

Dexu Kong[1,2], William Megone[1,2], Lihui Peng[1,2], Stefania Di Cio[1,2], Julien Gautrot[1,2]

[1]Queen Mary University of London, School of Engineering and Materials Science, London, GB; [2]Queen Mary University of London, Institute of Bioengineering, London, GB

Introduction

In the field of tissue engineering, adherent cells isolated from their respective tissues are typically grown on rigid substrates and to alter their phenotype based on the rigidity of the underlying matrix. However, Trappmann et al[1] showed that cell spreading and stem cell fate did not correlate with changes in the compliance of PDMS (from 0.1 kPa to 1 MPa). These observations contrast with reports that soft substrates mimic the mechanical properties of specific tissues and modulate differentiation into defined lineages[2]. Recently, we presented evidence indicating that the lack of response to the mechanical properties of PDMS arises from changes in the interfacial mechanics of the corresponding substrates. We reported the formation of mechanically strong protein nanosheets self-assembling at the interfaces between cell culture medium and ultra-soft hydrophobic substrates such as low viscosity oils[3].We observed that adherent stem cells such as mesenchymal stem cells and primary keratinocytes can be cultured at the surface of liquid substrates and that nanoscale mechanics of the corresponding interfaces regulates stem cell fate. However, we observed that cells seeded at high densities can fracture these nanosheets (Figure 2). In this work, we explore how the incorporation of nanomaterials may help toughening polyelectrolyte nanosheets assembled at liquid interfaces.

Experimental Methods

Immunofluorescence and Hoechst staining were used to explore the ability of cells spreading on interfaces for assemble a cytoskeleton (F-actin) and stable focal adhesions (vinculin). Rheology, scanning electron microscopy (SEM) and Atomic force microscopy (AFM) were used to characterize the mechanical properties of the protein nanosheets adsorbed at liquid-liquid interfaces.

Results and Discussion

Unlike albumin nanosheets that enable the formation of highly confluent HaCaT cell sheets[4], nanosheets assembled from the polyelectrolyte poly(L-lysine) (PLL) promoted fibronectin adsorption and stem cell adhesion[5]. However, our results indicate that these interfaces are relatively brittle, unlike albumin nanosheets. To toughen polyelectrolyte nanosheets, we deposited nanocomposites (such as graphene oxide or peptide fibres, Figure 1). With the help of nanocomposites, nanosheets displaying tougher mechanical properties were able to resist the concerted forces exerted by cell sheets proliferating at liquid-liquid interfaces (Figure 2). We showed that cells spreading on these nanocomposite interfaces generated focal adhesions and stress fibers and retained a stem cell phenotype.

Conclusion

The nanoscale mechanical behaviour of liquid-liquid interfaces allow cell spreading through the typical integrin-actin-myosin based machinery. These liquid-liquid interfaces allow the culture of stem cells. With the help of nanocomposites, dense cultures of adherent stem cells can be achieved on liquid-liquid interfaces and these show

typical hallmarks of cell sheets mechanically engaged with their underlying substrates. Our results demonstrate that nanocomposites can toughen the mechanical properties of nanosheets at liquid interfaces. In addition, the design of quasi-2D nanocomposites with tough mechanical properties at the interface between oil and water will allow the development of a novel generation of 3D bioreactors (based on emulsions) for the expansion of cells and stem cells.

References

1. Trappmann, B. *et al.* Extracellular-matrix tethering regulates stem-cell fate. *Nat. Mater.***11,** 742–742 (2012).

2. Guilak, F. *et al.* Control of Stem Cell Fate by Physical Interactions with the Extracellular Matrix. *Cell Stem Cell***5,** 17–26 (2009).

3. Kong, D. *et al.* Protein Nanosheet Mechanics Controls Cell Adhesion and Expansion on Low-Viscosity Liquids. *Nano Lett.***18,** 1946–1951 (2018).

4. Kong, D., Nguyen, K. D. Q., Megone, W., Peng, L. & Gautrot, J. E. The culture of HaCaT cells on liquid substrates is mediated by a mechanically strong liquid–liquid interface. *Faraday Discuss.***204,** 367–381 (2017).

5. Kong, D., Peng, L., Di Cio, S., Novak, P. & Gautrot, J. E. Stem Cell Expansion and Fate Decision on Liquid Substrates Are Regulated by Self-Assembled Nanosheets. *ACS Nano***12,** 9206–9213 (2018).

Acknowledgement

I would like to thank Leverhulme Trust Foundation for providing financial support to this project.

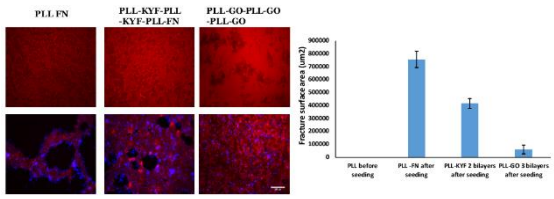

Figure 2 Epifluorescence images of labelled oil interface and HPKs.
Interfaces were labelled with labelling PLL solution (1 mg/mL) during PLL adsorption. Each interface was ended by fibronectin adsorption. The HPKs was seeded as 105.263k cells/cm^2 on fluorinated interface added with 0.00125 mg/mL PFBC and cultured for 24 h in KSFM. Images were acquired with epifluorescence microscopy before seeding the cells and after 24 h culture of cells. Red, Alexa Fluor 594, tagged PLL; blue, Hoechst; scale bar, 200µm. Bar chat is showing PLL fracture area which is corresponding to the epifluorescence images.

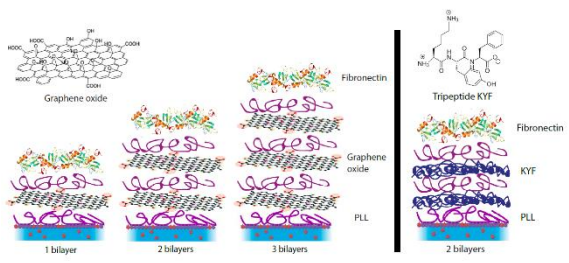

Figure 1 Schematic representation of nanocomposites deposition at oil interfaces

VI-OS21-05

Volume-by-volume bioprinting of chondrocytes-alginate bioinks in high temperature thermoplastic scaffolds for cartilage regeneration

Jose M. Baena

REGEMAT 3D, Biomedical, Granada, ES

Introduction

Bioprinting technologies have emerged as a powerful tool for tissue engineering (TE) due to the ability to mimic the 3D structure of any tissue. The use of biomaterials, cells and biomolecules combined with this manufacturing technique is gaining increasing interest within the scientific community. There is a wide range of different bioprinting technologies available and the selection of an appropriate technology must be based on the characteristics of the tissue you want to regenerate.

Experimental Methods

A bioprinter with 3 syringes and one FDM extruder (REGEMAT 3D, Granada, Spain), consisting of hardware, Designer software (REGEMAT 3D, Granada, Spain) with the algorithms that allow the configuration of VbV, and an electronic control unit (ECU) that connects the software to the hardware, were used for the experiments. The bioprinting system was configured for PLA and used two syringes with needles of different diameters to inject embedded chondrocytes in alginate bioink and a calcium solution. The position and distance between the FDM extruder and the syringes were configured to optimize the procedure. The Designer software can be set up using a simple graphical user interface (GUI) to print anatomical structures, selecting how and when the bioinks are deposited.

Results and Discussion

In order to demonstrate that VbV is not aggressive, chondrocytes immersed in alginate were printed together with PLA. Freshly isolated human chondrocytes cultured in a monolayer for 7-10 days were characterized before its use. Chondrocytes displayed a typical polygonal-shape with high expression of collagen 2 and proteoglycans, and a non-detectable expression of collagen 1.

Results showed that only immediately after the printing process (0 min) live cells number decrease, and apoptotic and necrotic cells significantly increase ($p<0.05$). However, after 30 min or 2 hours in culture, chondrocytes seem to recover from the stress of the printing procedure and no significant differences in apoptosis, necrosis or live cells when compared with CTL cells were found.

In addition, proliferation and metabolic activity of chondrocytes was quantified by Alamar blue assay. Results showed an incremental growth in the number of cells from day 0 until day 5, with a stabilization of growth between day 5 and day 7 (Fig. 6C). Also, cell viability and cell distribution were checked at 24 hours and at 7 days using CTG (Fig. 6D). After 24 hours in culture, individual cells with rounded shape appeared; however, 7 days later chondrocytes were able to migrate and proliferate throughout the scaffolds, completely colonizing the PLA fibers, and forming a homogeneous surface.

Conclusion

This novel VbV 3D-biofabrication procedure, prints a mesh structure layer-by-layer with a high adhesion surface/volume ratio, driving a rapid decrease in the temperature, avoiding contact with cells in high temperature zones. In our study, chondrocytes survived the manufacturing process, with 90% of viability, 2 hours after printing, and, after 7 days in culture, chondrocytes proliferated and totally colonized the scaffold. The use of the VbV-based biofabrication process presented in this study shows valuable potential in the short-term development of bioprint-based clinical therapies for cartilage injuries.

References

1. Boland T, Xu T, Damon B, Cui X. Application of inkjet printing to tissue engineering. *Biotechnol J*. 2006;**1**(9):910–7.
2. Tsang VL, Bhatia SN. Fabrication of three-dimensional tissues. *Adv Biochem Eng Biotechnol*. 2007;**103**:189–205.
3. Billiet T, Vandenhaute M, Schelfhout J, Van Vlierberghe S, Dubruel P. A review of trends and limitations in hydrogel-rapid prototyping for tissue engineering. *Biomaterials*. 2012;**33**(26):6020–41.
4. Cui H, Nowicki M, Fisher JP, Zhang LG. 3D Bioprinting for Organ Regeneration. *Adv Healthc Mater*. 2017;**6**(1):1601118.
5. Bhosale AM, Richardson JB. Articular cartilage: structure, injuries and review of management. *Br Med Bull*. 2008;**87(**1):77–95.
6. Fosang AJ, Beier F. Emerging Frontiers in cartilage and chondrocyte biology. *Best Pract Res Clin Rheumatol*. 2011;**25**(6):751–66.
7. Rai V, Dilisio MF, Dietz NE, Agrawal DK. Recent strategies in cartilage repair: A systemic review of the scaffold development and tissue engineering. *J Biomed Mater Res Part A*. 2017;**105(**8):2343–54.
8. Frazier WE, E. W. Metal Additive Manufacturing: A Review. *J Mater Eng Perform*. 2014;**23**(6):1917–28.
9. Pham D., Gault R. A comparison of rapid prototyping technologies. *Int J Mach Tools Manuf*. 1998;**38**(10–11):1257–87.
10. Wong K V., Hernandez A. A Review of Additive Manufacturing. *ISRN Mech Eng*. 2012;**2012**:1–10.
11. Ozbolat IT, Moncal KK, Gudapati H. Evaluation of bioprinter technologies. *Addit Manuf.* 2017;**13**:179–200.

Acknowledgement

The authors gratefully thank Ana Santos, Mohamed Tassi and Gustavo Ortiz from the C.I.C. (University of Granada) for excellent technical assistance.

VI-OS21-RF06

A cell-instructive microgel-in-gel material platform to guide the faithful *in vitro* reconstitution of tissues

Petra B. Welzel[1], Dejan Husman[1,7], Steffen Vogler[4], Laura J. Bray[5], Nicole Träber[6], Jens Friedrichs[1], Vincent Körber[1], Mikhail V. Tsurkan[1], Uwe Freudenberg[1], Julian Thiele[3], Carsten Werner[1,2,7]

[1]Leibniz-Institut für Polymerforschung Dresden e.V. (IPF), Max Bergmann Center of Biomaterials Dresden (MBC), Institute of Biofunctional Polymers, Dresden, DE; [2]TU Dresden, Center for Regenerative Therapies Dresden (CRTD), Dresden, DE; [3]Leibniz-Institut für Polymerforschung Dresden e.V. (IPF), Department of Nanostructured Materials and Leibniz Research Cluster (LRC), Dresden, DE; [4]Deutsches Zentrum für Neurodegenerative Erkrankungen (DZNE), Dresden, DE; [5]Queensland University of Technology (QUT), Institute of Health and Biomedical Innovation, Brisbane, QLD, AU; [6]TU Dresden, Biotechnology Center (BIOTEC), Dresden, DE; [7]TU Dresden, Research Training Group "Nano- and Biotechniques for Electronic Device Packaging", Dresden, DE

Introduction

Although *in vitro* models based on homogeneous hydrogel materials allow to recapitulate specific aspects of cell-matrix and cell-cell interactions, they cannot reflect the structural and compositional complexity of living tissues and are limited in supporting locally differing biomolecular and physical requirements of heterocellular cultures. Thus, multiphasic cell-instructive materials with cross-scale heterogeneity in matrix properties and/or cellular composition are needed to guide the faithful *in vitro* reconstitution of tissues and thereby create new options for drug development and pathobiology studies. Toward this aim, we herein present a new biomaterials design approach that relies on integrating cell-laden spherical hydrogel microparticles (microgels) within cell-laden bulk hydrogel matrices to provide thoroughly tunable microgel-in-gel systems. As a proof of concept, it is exemplarily shown how the approach can recapitulate basic features of vascularized prostate cancer tissue.

Experimental Methods

The new class of tunable microgel-in-gel materials builds on a versatile platform of multifunctional poly(ethylene glycol)-heparin hydrogel types [1]. As an innovative technique to easily and efficiently prepare the required differently sized microgels, we developed a novel variant of droplet microfluidics.

For the multiphasic 3D prostate cancer models, microgels supporting tumor spheroid formation of embedded cancer cells and a bulk hydrogel matrix supporting capillary network formation of embedded vascular endothelial cells were combined in microgel-in-gel co-cultures. Light microscopy and immunostaining/confocal laser scanning microscopy were used to thoroughly characterize these cultures.

Results and Discussion

The novel variant of droplet microfluidics allowed an effective variation of the microgel diameter without changing the microfluidic device and even within the course of one experiment. Sets of monodisperse hydrogel microgels of adjustable stiffness, degradability and biomolecular functionalization were obtained. Crosslinking by a rapid, cyto-compatible Michael-type addition reaction permitted cell embedding under very mild conditions [2]. Microgel-in-gel materials containing differently cell-instructive and cell-laden hydrogel types were produced. Tuning the microgel size enabled a very simple variation of the interface and the extent of the interaction between the two engineered microtissue compartments across the microgel/bulk gel boundaries.

Compared to a recently reported monophasic 3D prostate cancer model [3] the multiphasic model presented in this study is beneficial due to the spatial confinement of the co-culture. The spatially segregated hydrogel compartments can be independently tuned to match the physical and biomolecular triggers of the desired cell organization and function.

Conclusion

Microgel-in-gel systems made of thoroughly tunable multifunctional poly(ethylene glycol)-heparin hydrogel types allow for controlling the matrix properties and cellular composition of both spatially segregated phases individually. Furthermore, mesoenvironmental parameters that reflect fundamental tissue properties such as the maturation of cell assemblies or their 3D configuration can be adjusted.

References

1. U. Freudenberg, Y. K. Liang, K. L. Kiick, C. Werner, Adv. Mater. **2016**, 28, 8861.
2. M. V. Tsurkan, K. Chwalek, S. Prokoph, A. Zieris, K. R. Levental, U. Freudenberg, C. Werner, Adv. Mater. **2013**, 25, 2606.
3. L. J. Bray, M. Binner, A. Holzheu, J. Friedrichs, U. Freudenberg, D. W. Hutmacher, C. Werner, Biomaterials **2015**, 53, 609.

Acknowledgement

We thank the Deutsche Forschungsgemeinschaft (DFG, Research Training Group “Nano- and Biotechniques for Electronic Device Packaging’’) for funding. L.J.B. was supported by an Endeavour Fellowship as part of the Australia Awards program. MSCs were kindly gifted by Prof. Martin Bornhäuser (Universitätsklinikum Dresden). J.T. thanks the Federal Ministry of Education and Research (BMBF, “Biotechnologie2020+ Strukturvorhaben: Leibniz Research Cluster, 031A360C), and the DFG (Research Training Group “Hydrogel-based Microsystems” and TH 2037/1).

VI-OS21-RF07

Morphological control of electrospun ECM-PCL scaffolds for liver tissue engineering

Thomas S. R. Bate, Anthony Callanan

University of Edinburgh, Institute for Bioengineering, Edinburgh, GB

Introduction

In Europe, decompensated liver cirrhosis due to chronic liver disease (CLD) causes 170,000 deaths per year [1]. Global mortality rates linked to liver disease have exhibited an upward trend since the 1970s, contrary to downward trends observed in other leading causes of death [2,3]. Researchers are on the hunt for new drug treatments, however *in-vitro* drug development methods are unable to provide effective and efficient routes in which this can be achieved [4]. It is widely accepted that more relevant *in-vitro* models are required in order for drug development to progress, which could be achieved using controllable tissue engineering methods. Electrospun scaffolds have long been a subject of interest for tissue engineering research due to the ability to mimic Extracellular Matrix (ECM) structures with biocompatible polymers. There have also been large efforts within the research community to decellularise organs and harvest the ECM to provide natural biochemical cues to cells *in-vitro.* This study has explored the combined potential of morphologically defined electrospun polycaprolactone (PCL) fibres containing liver derived ECM for controlled and reproducible 3D *in-vitro* livertissue cultures.

Experimental Methods

Randomly oriented fibres, aligned fibres and highly porous cryogenic fibres all seen in *Fig.1A* were manufactured using PCL for large (5µm) and small (1µm) fibre sizes. Large fibres were produced using 19w/v% PCL solutions in 5:1 Chloroform:Methanol and small fibres using 7w/v% PCL in Hexafluroisopraopanol (HFIP). Randomly oriented fibres were electrospun onto a mandrel rotating at 250RPM and aligned fibres at 1800RPM. Porous cryogenic fibres were spun onto a mandrel containing dry ice at -78.5°C. ECM-PCL scaffolds were manufactured using decellularised rat livers. Briefly, whole rat livers were isolated and decellularised by vascular perfusion with 0.25w/v% Sodium Dodecyl Sulphate (SDS) solution. These were subsequently washed with deionized H_2O and lyophilised. The lyophilised ECM was then powdered using a planetary ball mill. 10w/w% and 5w/w% ECM-PCL mixtures were dissolved using HFIP and electrospun into fibres. Fibres were characterized using SEM imaging, mechanical analyses and FTIR Spectroscopy. Scaffolds were then punched and seeded with HepG2 cells which were cultured for 14 days. Cell viability, DNA quantitation, IHC staining and RT-qPCR Gene analysis were conducted at 24hr, 7 day and 14 day timepoints.

Results and Discussion

Larger fibres observed higher rates of proliferation than small fibres with the porous cryogenic scaffolds showing the highest rates for both small and large fibres. The morphology also influenced the structure of cell clusters as seen in *Fig.1B*. Maintenance of key liver function genes was observed on PCL scaffolds with a relative reduction in interstitial ECM genes Collagen I (COL1A1) and Fibronectin (FN1). The presence and bioactivity of electrospun rat liver ECM is seen to be preserved in *Fig.2* with higher cell viability observed on ECM scaffolds. Also, differences were observed in gene expression profiles of ECM vs. PCL only scaffolds.

Conclusion

Electrospun fibre size and morphology are observed to have a measurable impact on hepatocyte cultures. This highlights the importance of understanding the interactions between cells and fibres as a means for controlling *in-vitro* results. The incorporation of rat liver ECM into electrospun PCL scaffolds is capable of inducing altered biochemical responses in HepG2 cells, indicating that bioactive elements within the electrospun ECM are retained. Further investigation should confirm the degree to which bioactive ECM can be preserved within electrospun PCL scaffolds whilst maintaining tractable morphology.

References

1. Marcellin, P. doi:10.1111/liv.13682
2. Tapper, E. B. *BMJ***362,** k2817 (2018).
3. Williams, *J. Hepatol.***63,** 297–299 (2015).
4. Hay, M., *Nat. Biotechnol.***32,** 40–51 (2014).

Acknowledgement

ESPRC no. EP/N509644/1. MRC grant MR/L012766/1. With thanks also to Dr. Alison McDonald for imaging assistance.

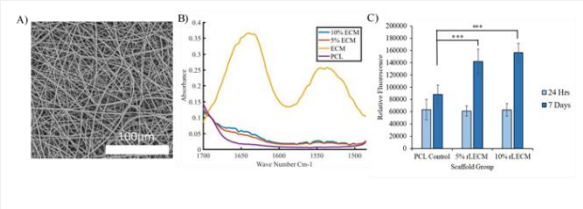

Figure 2
*A) SEM image showing 10w/w% rat ECM-PCL fibres. B) FTIR spectrum confirming the presence of ECM moeities within the electrospun scaffolds. C) Cell viability of HepG2 cells on ECM scaffolds. N=5, One-way ANOVA, Tukey's analysis, *** = p < 0.001, error bars: ± SD.*

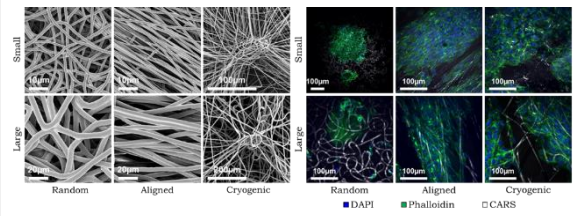

Figure 1
A) SEM images of the various fibre morphologies B) DAPI, Phalloidin and CARS fluorescence of HepG2 cultures on the different scaffold groups.

VI-OS21-RF08

Quercitrin functionalized nanostructured titanium surfaces for the improvement of cardiovascular stents.

Maria Antonia Llopis-Grimalt[1,2], Victor Alcolea-Rodriguez[1], Maria Antonia Forteza-Genestra[1,2], Joana Maria Ramis[1,2], Marta Monjo[1,2]

[1]University of Balearic Islands, Group of Cell Therapy and Tissue Engineering, IUNICS, Palma, ES; [2]Balearic Islands Health Research Institute (IdISBa), Palma, ES

Introduction

In cardiovascular stents, the prevention of thrombosis and restenosis is key to prevent a new obstruction of the vessel. Stent surface is directly exposed to the patient's tissues; thus, its modification is being explored in order to improve the tissue response. One strategy is the formation of nanostructures or the functionalization with active biomolecules.

The main objective of this research was the development of quercitrin functionalized nanostructured titanium (Ti) surfaces that promote endothelial tissue regeneration and decrease platelet adhesion with potential application in cardiovascular stents.

Experimental Methods

Mirror polished titanium discs, c.p. grade IV, 6.2 mm diameter and 2 mm height were used in this study. Nanostructured Ti surfaces were developed by electrochemical anodization and functionalized with quercitrin. All surfaces were characterized by atomic force microscopy, scanning electronic microscope and contact angle analysis and quercitrin content was analyzed using a DPBA staining. Primary human umbilical cord endothelial cells (HUVEC) were used to test cell adhesion, cytotoxicity and metabolic activity. Platelet adhesion and hemolysis rate were also analyzed. *Staphylococcus epidermidis* CECT4184 was used to test bacterial adhesion at 30 minutes.

Results and Discussion

Functionalization with quercitrin did not affect surface topography or nanostructure size and contact angle was lower in quercitrin functionalized surfaces (TiQR and NNQR). No differences were found in HUVEC adhesion but metabolic activity was lower in nanostructured surfaces compared to Ti and TiQR which could be explained by a higher cell differentiation. All surfaces showed cytotoxicity levels lower than 30% and very low hemolysis rate. In addition, platelet adhesion was lower in NN surfaces compared to Ti but no effect was found after functionalization with quercitrin. *Staphylococcus epidermidis* adhesion at 30 minutes was lower on TiQR surfaces compared to Ti.

Conclusion

Our results suggest that NN structuration of Ti surfaces has a great potential to be used for stent coatings and that the combination with quercitrin functionalization could reduce the risk of bacterial adhesion.

Acknowledgement

This work was supported by the Osteology Foundation (13-069), the Ministerio de Educación Cultura y Deporte (contract to M.A. L.G; FPU15/03412) & the Instituto de Salud Carlos III (contract to J.M.R and M.A.F.G ;CP16/00124). The authors thank Dr. F. Hierro and Dr. J. Cifre (UIB) for their technical contribution with SEM and AFM respectively.

4:15 p.m. – 5:45 p.m.

Conference room 2+3

VI-OS22 | Surfaces and interfaces

VI-OS22-01

PEEK/silicon nitride composites for biomedical implant applications

Francesco Boschetto[1,2], Giuseppe Pezzotti[1,2], Elia Marin[1,3], Wuenliang Zhu[1]

[1]University, Ceramic Physics Laboratory / Kyoto Institute of Technology, Kyoto, JP; [2]University, Department of Immunology / Kyoto Prefectural University of Medicine, Kyoto, JP; [3]University, Department of Dental Medicine / Graduate School of Medical Science, Kyoto Prefectural University of Medicine, Kyoto, JP

Introduction

Polyetheretherketone (PEEK) has been used in a variety of applications, from aerospace and aviation to medical devices. PEEK presents a widespread relevance due to its high environmental resistance, biocompatibility, and mechanical properties comparable to human bone. Moreover, this material exhibits radiolucent characteristics compatible with imaging diagnoses. Due to its biologically inert behavior, PEEK has two disadvantages: a poor antibacterial resistance and a lack of bioactivity, which prevents the interaction between the implant surface and the adjacent bone tissues. Implant-to-bone interaction might release debris, causing pain, inflammation or even inducing deformity to the patient. The purpose of this study is to present an original approach to obtain surface-porous PEEK spinal implants with concurrently improved osteogenic and antibacterial properties.

Experimental Methods

Building upon the findings of previous researchers based on the use of direct extrusion of PEEK and coarse grains of sodium chloride (NaCl) salt (with successive leaching in water of the latter) to create porous surfaces, we propose a modification of this procedure, in which the mixture of coarse sodium chloride grains is accompanied by a fraction of micrometric silicon nitride (β-Si_3N_4) particles introduced into a partly melting PEEK surface by hot pressing with only the salt grains being successively leached off by water immersion. This implemented procedure produces a porous PEEK surface similar to that obtainable by extrusion but functionalized on the external surface in order to achieve concurrent biogenic properties similar to those exploited in bulk silicon nitride. Bulk PEEK-matrix Si_3N_4 particulate composites were also investigated, which were prepared by conventional melting/mixing techniques. To verify the effectiveness of both surface and bulk modifications of the PEEK structure, substrates were divided into three classes to evaluate the different osteogenic and bacteriostatic responses: untreated (CTRL), surface roughness modified without silicon nitride (SG), surface roughness modified and functionalized with silicon nitride (SG+SN), and bulk PEEK-matrix Si_3N_4 particulate composites (PMSNC). Substrates before and after being exposed to osteosarcoma line cells (Saos-2) for a week and to different kinds of bacteria were characterized by FTIR, laser microscopy, fluorescence microscopy, SEM-EDX, and LDH assay.

Results and Discussion

Results provided, indicate how the concomitant effect of an increased roughness with the presence of β-Si_3N_4 is not cytotoxic improving cells adhesion as shown by Fluorescence Microscope images and LDH assay. Furthermore, the substrate roughness-modified and functionalized with β-Si_3N_4 shows an amount of extracellular mineralized matrix homogeneously distributed on the entire surface as indicated by SEM-EDX, FTIR and Laser Microscope.

Conclusion

In conclusion, PEEK surface modification and hybridization with β-Si_3N_4 particles demonstrate remarkable *in vitro* improvements when compared to monolithic PEEK suggesting the beneficial effect which the treatment could bring for future development of PEEK implants.

VI-OS22-02

Prevention of encrustation and biofilm formation on ureteral catheters - which surface parameters are directive for the development of novel catheter materials?

Henrike Rebl[1], Jürgen Renner[2], Bernd Zacharias[3], Wolfgang Kram[4], Armin Springer[5], Jürgen Weisser[6], Nele Fritsch[1], Matthias Schnabelrauch[6], Harald Hansmann[2], Oliver Hakenberg[4], Marion Wienecke[3], Barbara Nebe[1]

[1]Rostock University Medical Center, Dept. of Cell Biology, Rostock, DE; [2]Institute for Polymer Technologies, Wismar, DE; [3]Materion GmbH, Wismar, DE; [4]Rostock University Medical Center, Dept. of Urology, Rostock, DE; [5]Rostock University Medical Center, Electron Microscopy Center, Rostock, DE; [6]INNOVENT e.V., Dept. Biomaterials, Jena, DE

Introduction

Ureteral catheters are used for temporary as well as long-term stenting of the ureter and belong to the most commonly used urological implants. Common complications of polyurethane catheters, like biofilm formation or encrustation, promote urinary tract infections and cause wound healing disorders in the ureter [1]. Encrustations are triggered by the precipitation of salt crystals, which can be of varying quantity depending on the metabolism of the patient. Encrustations are often accompanied by bacterial infections, as they tend to build a niche for bacterial growth. We aim at developing a new polymer catheter material with additional antibacterial coating that should minimize encrustation, prolong the dwell time of catheters and thus reduce the burdens of the patient.

Experimental Methods

Different polymer types [Thermoplastic Urethanes (Tecophilic, Elastollan), Styrene-Butadiene Copolymers (Styroflex), Ethylen-Vinylacetat Copolymers (Greenflex)] were tested for their surface characteristics (contact angle, surface charge, roughness). Chemically defined synthetic urine [2] with increasing pH was dynamically pumped over the samples with defined stop-go cycles and adjusted flow rates (150 µl/min) at 37°C to mimic the native body urine flow. The encrustations were analyzed quantitatively and qualitatively using polarized light- and scanning electron microscopy, energy dispersive X-ray- and Fourier-transform infrared spectroscopy. Additionally we deposited an antibacterial coating of copper-releasing diamond-like carbon nanolayers [3]. Copper release and antibacterial efficacy *in vitro* was tested with *E. coli* and biocompatibility with human urothelial cells HUC-1.

Results and Discussion

We developed an *in vitro* encrustation system to provoke crystals on the uncoated polymer samples within five days in a well-defined setup (Fig1). Analyses of the elemental composition of the crystalline deposits revealed depositions of carbonate apatite ($Ca_{10}(PO_4)_6(OH)_2$) and struvite ($NH_4MgPO_4H_2O$). Also *in vivo* these depositions are the major phase on encrusted stents of infected patients [1, 4], thus we were able to provoke encrustations that are similar to the *in vivo* situation of infected ureteral catheters.

Furthermore, we found a correlation of the quantity of the encrustation (highest Tecophilic 6.0 % > Greenflex 2.8 % > Elastollan 2.4 % > Styroflex 2.1 % lowest) depending on the surface characteristics of the material, e.g. contact angle (Tecophilic: 104°; Elastollan 85°). Low contact angle and strong negative surface charge (Tecophilic: -29.6 mV; Elastollan -56.5 mV) are predictive for low formation of crystalline deposits. The reduction of crystalline depositions is one important step to reduce the niches for bacterial adhesion and growth.

Moreover, the quantity of encrustations and the bacterial growth was effectively repressed on the copper nanolayer coated materials. Copper release was adjusted so that *E. coli* bacteria, grown in synthetic urine, were completely eliminated, while urothelial cells were not affected.

Conclusion

We suggest considering in vitro encrustation models for the development of new catheter materials to minimize encrustation. The combination of these minimally encrusting materials with antimicrobial agents may offer a new opportunity for the design of novel ureteral catheter materials.

References

[1] Stickler (2014) J Intern Med 276(2):120-129.
[2] Griffith et al. (1976) Invest Urol 13(5):346-50.
[3] Nißen et al. (2018) Surf Coat Tech 350.
[4] Laube et al. (2008) J Biomed Mater Res Part B: Appl Biomater 87B (2):590-597.

Acknowledgement

We gratefully acknowledge the funding by the Federal Ministry of Education and Research (BMBF, grant no. 13GW0109D Uro-antibak).

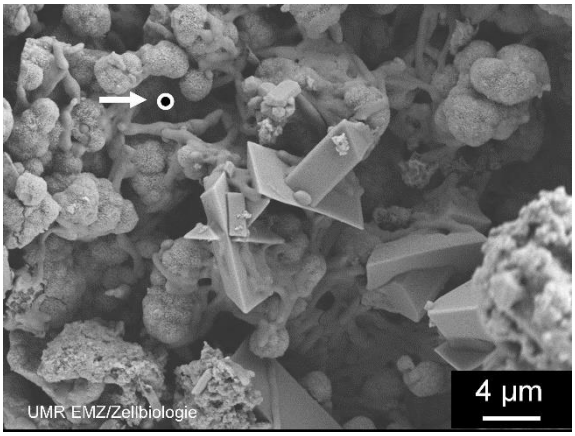

Fig1: SEM image of an encrusted Tecophilic surface after 5d in the encrustation system. Note the mix of amorphous depositions and clear-cut crystals. The spot (arrow) schematically represents the size of a single bacterium

VI-OS22-03

Design and optimization of KHYG-1 cell membrane coated spheres to develop an artificial Natural Killer (NK) cell mimics

Vaishali Chugh[1], Vaibhav Patil[1], Vijaya K. Kanala[1], Eva Szegezdi[2], Abhay Pandit[1]

[1]National University of Ireland, Centre for Research in Medical Devices (CÚRAM), Galway, IE; [2]Natioanl University of Ireland, Apoptosis Research Centre, Galway, IE

Introduction

Natural Killer (NK) cells are part of innate immune system that provide first line of immune defence.[1] Activating receptors (NKG2D), natural cytotoxic receptors (NKp30, NKp44 and NKp46) and adhesion proteins (CD11a) on their surface helps in tumour recognition via specific ligand-receptor interactions without affecting healthy cells.[2] This makes them appealing therapeutic effectors for all cancer forms, including metastatic[3]. There is growing interest in developing NK cell based therapeutic platforms with few models already in phase 1 clinical studies[4]. Our study reports design and optimization of an NK cell mimicking by coating an isolated cell membrane onto a gelatinous core. We envisage that this novel therapeutic strategy will retain surface functionality of NK cells whilst incorporating superior physiochemical properties of gelatin to the mimics offering a new treatment strategy for treating cancer.

Experimental Methods

Cell culture of KHYG-1: KHYG-1 were procured from ATCC and grown as suspension cultures *in vitro*.

Isolation and characterization of cell membrane: Prior to isolation, cells were suspended in cold hypotonic buffer (2 mL) supplemented with a cocktail of protease inhibitors (10 µL) to initiate swelling. Cells were ruptured and their membranes were further isolated and purified to minimise nuclear and mitochondrial contamination. A combination of cell number, type of hypotonic buffer, rupturing techniques (probe sonication, dounce homogenizer, multiple free thawing, and bath sonication) and isolation methods (differential centrifugation and sucrose gradient) was extensively optimized to isolate the cell membrane. Total protein was quantified by BCA assay and a qualitative analysis of surface receptors (NKp30, NKG2D, DNAM-1, and CD11a) and purity was determined by western blotting.

Gelatin spheres: An amphiphilic conjugate of gelatin (A, bloom~300) capable of self-assembling into spheres were synthesized by conjugating oleic acid via EDC/NHS chemistry. Spheres of gelatin (A, bloom~300) were obtained by water in oil emulsion and subsequent cross-linking with DMTMM. These conjugates were characterized by FT-IR, NMR, TEM, SEM and laser diffraction to estimate their degree of substitution, purity and for size measurements.

Preparation and cell membrane coated gelatinous core (CMGC): Cell membrane was coated on gelatinous core using bath sonication for few minutes and extruder 11 times. Surface receptors (NKp30, NKG2D, DNAM-1, and CD11a) and purity was determined by western blotting.

Target efficacy of CMGC: The targeting ability of CMGC was tested against Human breast cancer cell MCF-7 and the normal MCF10A using flow cytometry. The immunogenicity of CMGC were tested in THP-1 cells for its inflammatory response using cytokine release assay.

Results and Discussion

Cell membrane isolation: Effect of hypotonic buffers (Buffer 1: 20mM HEPES, 1mM KCl, 1.9mM $MgCl_2$, 1mM EDTA; Buffer 2: 225mM Mannitol, 75mM Sucrose, 0.5mM EDTA, 30mM Tris-HCl, 0.5% BSA) was analysed on the isolated cell membrane. Western blotting was suggestive of higher translocated CD11a receptor on cell membrane using

buffer 2. However, band corresponding to nuclear contamination was observed. To enhance the purity and efficiency of cell membrane three other methodologies of isolation were tried with buffer 2. Method 3 was found to be the most effective method with more surface receptors and minimal contaminations in the cell membrane.
Method 3: One-time freeze thawed the cells and then 50 strokes of dounce homogenizer followed by discontinuous sucrose gradient method (30%, 40%, 55% sucrose in 0.9% normal saline solution). Cell membrane was found in between the band of 30-40%.
Gelatin spheres: Self-assembled spheres of gelatin-oleic acid were prepared by dialysis against water in a size range of 200-400 nm. Cross-linked gelatin spheres formulated by emulsion technique were around 1-4 µm. Viscoelastic properties were measured by AFM.
Target efficacy of the system: Cell membrane coated gelatinous core was investigated by incubating the system with tumour and normal cells. TCPP fluorescence intensity of CMGC was stronger for MCF-7 than MCF-10A. This selectivity of CMGC is due to the NK cell protein markers which can recognize and binds to the receptor present in MCF-7. Further, the cells were subjected to immunofluorescence staining with anti-CD56/FITC at the end of the flow passage assay and imaged under a confocal microscope. As expected, CMGC was accumulated more in the MCF-7 as proven by the FITC signals of CD56. In the case of the bare gelatin, no significant accumulation was observed between MCF-7 and MCF10A under flow condition. These results confirmed the in vitro breast cancer cell targeting efficacy of CMGC.

Conclusion

In conclusion, we have optimised the isolation of a KHYG1 cell membrane and formulated a polymer that can be used to create an artificial NK cell mimicking system with increase in efficacy to target tumour cells.

References

1. Chiossone, L., et al, Nature Review Immunology 18, 671-688 (2018).
2. Herrero, S. L., et al, Cancers (Basel). 11, 29 (2019).
3. Paul, S., et al, Front Immunol. 8, 1124 (2017).
4. Cheng, M., et al., Cellular and Molecular Immunology 10, 230-252 (2013).

Acknowledgement

Science Foundation Ireland (SFI) and the European Regional Development Fund (Grant Number 13/RC/2073)

VI-OS22-04

Selective Laser Sintering (SLS) of calcium phosphate minerals on hard tissues

Antonios Anastasiou, Simon Strafford, Andrew Brown, Animesh Jha

University of Leeds, School of Chemical and Process Engineering, Leeds, GB

Introduction

Guided by the principles of personalised medicine and based on the fundamentals of Selective Laser Sintering (SLS), the goal of our research is to develop a procedure where **direct laser sintering**, **densification** and **bonding** of a layer of ceramic biomaterial on hard tissues (i.e. bone and teeth) can be achieved. Such a technology, could find a unique space of applications in restorative dentistry and orthopaedics and potentially would enable the rabid restoration of hard tissues with a biomaterial chemically and structurally similar to the mineral of natural tissue (i.e. calcium phosphate).

Conventional sintering and densification of ceramics (e.g. calcium phosphate materials) takes place at a temperature range between 1000 and 1500 ˚C [1]. Achieving the same result on the surface of a hard tissue without inducing any thermal damage, is a challenging and high-risk task. To be successful, numerous variables need to be taken into consideration; i) type of the laser; ii) irradiation parameters; iii) the properties of the biomaterial that will be attached on the hard tissue; iv) the properties of the initial coating.

The aim of this work is to discuss the different variables that affect the sintering and attachment of ceramics on hard tissues (e.g. type of laser, properties of biomaterials) and to demonstrate the attachment of a layer of calcium phosphate on the surface of dental enamel. The sintered layers are characterised for their chemical, structural and mechanical properties (XRD, SEM, nano-indentation) and the induced thermal damage to the hard tissues is evaluated.

Experimental Methods

All the calcium phosphate minerals used in this work (i.e. brushite, hydroxyapatite and fluorapatite) have been synthesised through wet precipitation method at temperature of 37 ˚C and pH=5.4 for brushite and pH=8 for hydroxyapatite and fluorapatite. To enhance the laser-biomaterials interaction, we doped the minerals with 10% Fe^{2+}/Fe^{3+}. For laser irradiation experiments bovine enamel blocks have been coated with a mixture of chitosan solution and the corresponding mineral powder. Three different lasers have been utilised i.e. a CW laser emitting at 976 nm (System A: LIMO32), a femtosecond pulsed laser with repetition rate of 1 KHz and emission at 800 nm (System B: Ti:Shaphire, LIBRA) and an ultrafast femtosecond pulsed laser with repetition rate of 1 GHz and emission at 1040 nm (System C).

Results and Discussion

It was proved that with the CW system we can partially melt the coating on the surface of enamel (average power of 0.5W) while, at high average power (>0.8 W) we observed cracking and burning of the hard tissue. With System B, ablation was the dominant mechanism of laser-matter interaction and consequently there wasn't any attachment of new material on the surface of our samples. The best results have been obtained with System C since we managed to form compact layers of fluorapatite and hydroxyapatite on the surface of dental enamel (**Figure 1**). The thickness of the new layers is between 20 and 30 μm and after nano-indentation the mechanical properties found to be very close to that of dental enamel and natural bone (**Table 1**). After examining the cross-sections of the sintered samples

we were able to determine that any induced thermal damage is restricted within a distance of 10 μm below the coating-enamel interface.

At the moment the most SLS systems use continuous wave (CW) lasers, emitting at a wavelength of 10.4 μm with the average power ranging between 5 and 100 W [2]. These parameters result in the burning of the hard tissues since the optical absorption coefficient is high at 10.4 μm and CW irradiation cause immediate heat generation. The use of a high repetition femtosecond (fs) laser, emitting at wavelengths within the optical window where the absorption coefficient of tissues is low (900-1080 nm) proved a promising solution for our objectives. Ultrashort pulses of a fs laser allow the control of the dissipated energy while, the mechanisms of laser-matter interaction favour the heat generation on metals and semiconductors but not on insulators like the material of bone [3]. Doping our minerals with metal ions (e.g. Fe^{2+}) is a critical factor since we managed to enhance the interaction of the calcium phosphates with the femtosecond lasers. Eventually, the same laser beam cause the sintering of the biomaterial but has no effect on the hard tissues [4].

Conclusion

This work successfully demonstrates the concept of direct laser sintering of calcium phosphates on dental hard tissues with the use of ultrafast femtosecond lasers. Although more research is required for the translation into clinic this is the first step for the rabid restoration of hard tissues.

References

[1] Rahaman, M.N., Ceramic Processing and Sintering. 2003: Taylor & Francis.

[2] Savalani, M.M., et al., Evaluation of CO_2 and Nd:YAG Lasers for the Selective Laser Sintering of HAPEX®. Proceedings of the Institution of Mechanical Engineers, Part B: Journal of Engineering Manufacture, 2006. 220(2): p. 171-182.

[3] Phillips, K.C., et al., Ultrafast laser processing of materials: a review. Advances in Optics and Photonics, 2015. 7(4): p. 684-712.

[4] Anastasiou, A.D., et al., Exogenous mineralization of hard tissues using photo-absorptive minerals and femto-second lasers; the case of dental enamel. Acta Biomaterialia, 2018. 71: p. 86-95.

Acknowledgement

The authors would like to acknowledge the sponsors of this work: Marie Curie IF Pre-Facto, Innovate UK Apollonia, IKC

Material	Hardness, GPa	Young's modulus, GPa	Poisson's ratio
Enamel	3.10±0.12	38.67±1.9	0.25
Sintered layer	1.10±0.16	20.50±1.2	0.27
Human bone	0.58-0.80	17.0-20.0	0.30

Table 1
Mechanical properties of natural enamel and the sintered layer as measured by nano-indentation.

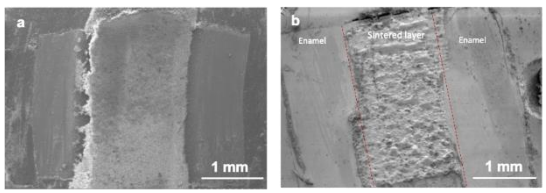

Figure 1
Coated dental enamel before and after sintering; a) pre-sintered dental sample coated with a mixture of chitosan and fluorapatite crystals; b) sintered fluorapatite layer after irradiation with system C (0.6 s exposure time and 0.4 W average power).

VI-OS22-05

Characterization of Tissue Transglutaminase as potential Biomarker for Tissue Response towards Biomaterials

Sandra Hauser[1], Robert Wodtke[1], Christoph Tondera[2], Johanna Wodtke[1], Reik Löser[1,3], Jens Pietzsch[1,3]

[1]Helmholtz-Zentrum Dresden-Rossendorf, Institute of Radiopharmaceutical Cancer Research, Dresden, DE; [2]TU Dresden, Biotechnology Center (BIOTEC), Center for Molecular and Cellular Bioengineering (CMCB), Dresden, DE; [3]TU Dresden, Department of Chemistry and Food Chemistry, Dresden, DE

Introduction

Tissue transglutaminase (TGase 2) is proposed to be important for biomaterial-cell or -tissue interactions due to its presence and versatile functions in the extracellular environment. For example, TGase 2 catalyzes the crosslinking of proteins through its Ca^{2+}-dependent acyltransferase activity or enhances the interactions between fibronectin and integrins by its action as scaffold protein. Thereby, TGase 2 mediates the adhesion, migration and motility of cells. Additionally, TGase 2 is a key player for the development of fibrosis. Consequently, this study aimed at investigating whether TGase 2 is present at the biomaterial-tissue interface and might serve as an informative biomarker for the visualization of tissue response towards gelatin-based biomaterials.

Experimental Methods

Two differently crosslinked hydrogels were used (G10_LNCO3 and G10_LNCO8), which were obtained by reaction of gelatin with lysine diisocyanate ethyl ester [1]. Expression and secretion of TGase 2 by primary human aortic endothelial cells and human leukemia THP-1 and HL-60 cells, differentiated to macrophages or granulocytes, were analyzed via Western blotting after contact to hydrogels or their degradation products. Hydrogels were implanted subcutaneously in immunocompetent, hairless SKH1-Elite mice. TGase 2 expression at the implantation site was detected *ex vivo* by immunohistochemistry over a period of 112 days. The presence of active TGase 2 in tissue sections was confirmed by incorporation of fluorescently labeled cadaverine derivatives [2] and verified using a selective irreversible inhibitor of TGase 2 **1** [3] (Figure 1A). Furthermore, Rhodamine B-labeled cadaverine (**R-I-Cad**) was tested as optical imaging agent for TGase 2 activity *in vivo*.

Results and Discussion

In vitro, expression of TGase 2 by endothelial cells, macrophages and granulocytes was partly influenced by contact to the hydrogels or their degradation products, but there was no clear correlation. In contrast, TGase 2 secretion differed remarkably between the different cells, indicating that it might be involved in the cellular reaction towards gelatin-based hydrogels. *Ex vivo* analysis of tissue sections revealed enhanced expression levels of TGase 2 around the hydrogels especially 14 and 21 days after implantation. Incorporation of fluorescently labeled cadaverine derivatives was in accordance to the results of the expression analysis (Figure 1B). The presence of the irreversible TGase 2 inhibitor **1** led to attenuated incorporation of the cadaverines, which verified the catalytic action of TGase 2 (Figure 1B). *In vivo*, no TGase 2 activity was detectable by the cadaverine probe used.

Conclusion

In vitro and *ex vivo* results underlined TGase 2 to be a potential biomarker for tissue response towards gelatin-based hydrogels. Nevertheless, *in vivo* no TGase 2 activity was detectable, which is mainly attributed to the unfavorable

physicochemical properties of the cadaverine probe used. Further efforts will focus on the development of suitable probes based on selective TGase 2 inhibitors for optical or radionuclide-based *in vivo* imaging.

References

[1] Ullm et al. Biomaterials 2014, 35, 9755-9766
[2] Hauser et al. Amino Acids 2017, 49, 567-583
[3] Wodtke et al J Med Chem 2018, 61, 4528-4560

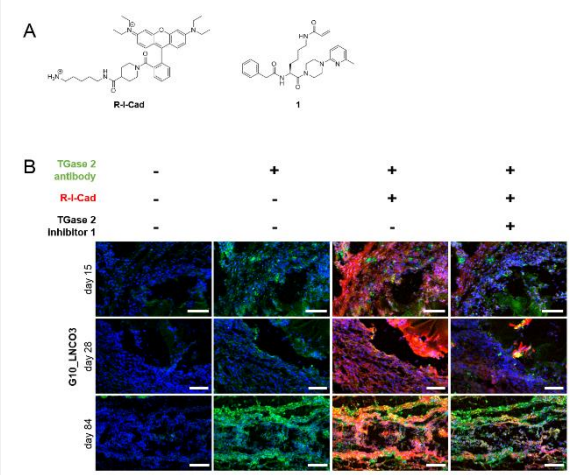

Figure 1: Cadaverine incorporation into tissue sections by active TGase 2
A: Structures of TGase 2 substrate **R-I-Cad** and the selective TGase 2 inhibitor **1**.
B: Incorporation of **R-I-Cad** by active TGase 2 into tissue sections of G10_LNCO3 implantation areas was investigated at selected time points after implantation. Incorporation could be inhibited by coincubation with the selective TGase 2 inhibitor **1**. TGase 2 is depicted in green, **R-I-Cad** in red, and cell nuclei in blue. The scale bars indicate 100 µm.

VI-OS22-06

High-throughput screening to elucidate biomaterial-induced fibrosis.

Torben A. B. van der Boon

University of Groningen/ University Medical Center Groningen, Department of Biomedical Engineering/ W.J. Kolff Insitute for Biomedical Engineering and Materials Science, Groningen, NL

Introduction

Nowadays, it is becoming common knowledge that the human body, its tissues and cells react to biophysical and biochemical cues located on biomaterial surfaces.[1,2] Identifying how these parameters influence cellular behavior is of crucial importance and will aid us in the further development of medical implant technology. Unfortunately, in many studies attempting to identify these physicochemical properties' influence on cell behavior, investigation of individual properties is the conventional method, leaving out a significant number of other variables which are encountered *in vivo*, which is where cells always interact with multiple cues simultaneously.[3,4] We developed an orthogonal double gradient platform which allows us to investigate just such complex situations in a high-throughput screening (HTS) fashion. The platform grants us the power to screen the cell response towards thousands of these combined parameters in a single experiment, which will result in the optimization of material properties to enhance biomaterial and implant function. Our current work includes the screening of silicone rubber susceptibility to fibrosis and scar tissue formation.

Experimental Methods

PDMS orthogonal double gradients are prepared by sequential shielded air plasma oxidation treatments in accordance with previously published single linear gradients.[4–6]

Results and Discussion

Every imaginable position on the orthogonal double gradient surfaces has a unique combination of the present parameters, resembling 'real', clinically relevant values. Wavy topography gradients range from λ = 1 µm – 12 µm and A = 50nm – 2,5 µm, the smallest wavelengths corresponding with the smallest amplitudes going from small to big, in a coupled fashion. Stiffness gradients range in Young's Modulus from ~5 – 90 MPa, and 'wettability' gradients from 5 – 80 ° in water contact angle (WCA). As a 'proof of concept', we cultured hBM-MSCs on the platforms for 24 h, imaged the cells via automated fluorescence microscopy and identified the cell response with respect to cell density, cell spreading, nucleus area, and vinculin expression. We have found that the synergistic effect of abovementioned parameter combinations all influence cell behavior in a different manner with regard to these relatively 'simple' assessable characteristics. Our next steps involve the identification of regions of interest (ROI) resulting in alterations in collagen (type-I) deposition and expression of α-sma in human dermal fibroblasts, which then can further be investigated in a more complex, close-up study.

Conclusion

The highly efficient cell screening tool we have created with our double orthogonal gradient platform allows us to screen cell response to combined physical parameter influence in a high-throughput fashion. It will serve its purpose to facilitate enhanced biomaterial development.

References

[1] G. Huang, F. Li, X. Zhao, Y. Ma, Y. Li, M. Lin, G. Jin, T. J. Lu, G. M. Genin, F. Xu, *Chem. Rev.***2017**, Oct 25; 117(20):12764-12850.

[2] W. L. Murphy, T. C. McDevitt, A. J. Engler, *Nat. Mater.***2014**, Jun; 13(6):547-57.

[3] A. M. Schaap-Oziemlak, P. T. Kühn, T. G. van Kooten, P. van Rijn, *RSC Adv.***2014**, *4*, 53307.

[4] P. T. Kühn, Q. Zhou, T. A. B. van Der Boon, A. M. Schaap-Oziemlak, T. G. van Kooten, P. van Rijn, *ChemNanoMat***2016**, 2, 407 - 413

[5] Q. Zhou, P. T. Kühn, T. Huisman, E. Nieboer, C. van Zwol, T. G. van Kooten, P. van Rijn, *Sci. Rep.***2015**, *5*, 16240.

[6] Q. Zhou, L. Ge, C. F. Guimarães, P. T. Kühn, L. Yang, P. van Rijn, *Adv. Mater. Interfaces***2018**, 5(18)

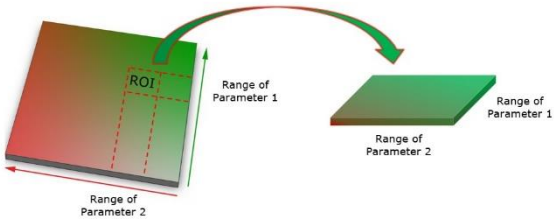

Region of Interest translation to additional study

Figure 2. Schematic representation of the translation of a ROI to a separate, homogenous platform. Parameter values are known and can be translated to new samples.

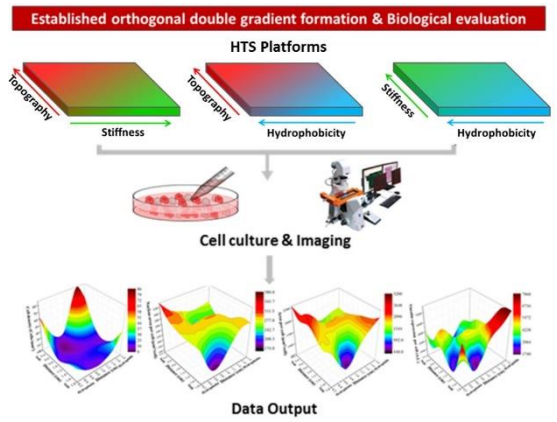

Established orthogonal double gradient formation & Biological evaluation

Figure 1. HTS approach. The screening platforms (top) enable all physical parameter combinations between topography, stiffness and hydrophobicity, to be present within a gradient-like range. The influence on cell behavior is identified via fluorescence immune-staining and semi-automated imaging.

Thursday, 12 September, 2019

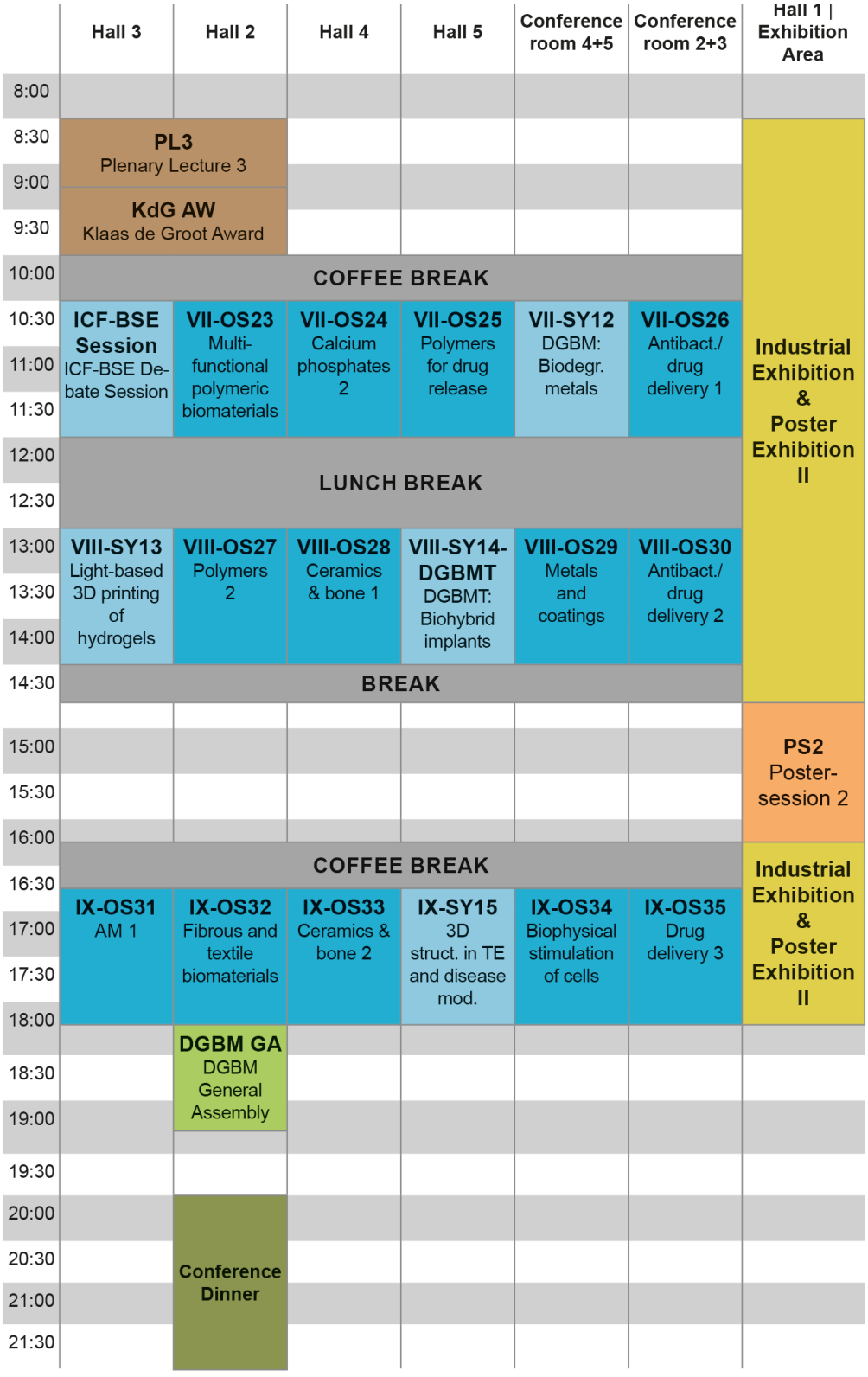

8:30 a.m. – 9:15 a.m.

Hall 3 + Hall 2

PL3 | Plenary Lecture 3

PL3-01

Advances in biology change the way we think about bioactive scaffolds

Lour Serrano De La Pena, **Joachim Kohn**

New Jersey Center for Biomaterials at Rutgers University, Piscataway, US

Introduction

Starting about 60 years ago, biomaterials scientists recognized the importance of the integrin-mediated signalling that influences key cellular responses such as attachment, migration, and proliferation. This line of research is now at the centre of a world-wide effort to engineer bioactive scaffolds for the creation of tissues either ex-vivo (e.g., in a bioreactor before implantation) or in-situ (e.g., within the body of the patient).

Bioactivity is defined as the ability to control and direct cell and tissue growth toward desired outcomes. In this sense, natural extracellular matrix (ECM) can be regarded as the most desirable bioactive scaffold. Embedded within the structure of natural ECM is all the information needed to control and direct cell attachment, proliferation, migration, and differentiation. We have not yet been able to decipher this “secret code”, but science has identified (i) mechanical cues, (ii) architecture and topography, and (iii) chemical cues as the three channels by which materials interact with cells. While engineers work on increasingly sophisticated scaffold designs, the biological approach starts from living donor tissue and aims to create whole organs by mild decellularization to preserve the ECM structure, followed by recellularization with healthy, autologous cells from the patient.

Results and Discussion

Figure 1 illustrates current work to design bioactive scaffolds for specific cell types. In this case, an attempt was made to build a scaffold for the regeneration of the osteochondral interface, the area in all articulating joints where bone transitions into cartilage. Osteoblasts and chondrocytes require different substrata for optimum proliferation and to retain their respective phenotypes. This requirement is met by a biphasic scaffold consisting of a layer optimized for bone growth and a layer optimized for cartilage. The next step in this work is the addition of appropriate biological signals that can drive the formation of a functional osteochondral interface either ex-vivo or in-situ. Figure 2 illustrates advanced scaffold designs that are facilitated by additive manufacturing (3D printing). Finally, Figure 3 demonstrates the deposition of extracellular matrix (ECM) within an electrospun fiber mat. An early definition of the term "biomaterial" specified that the term biomaterial must exclude any viable cells or tissues. Today, most scientists regard cells and tissues as an integral part of a tissue engineering scaffold. As synthetic materials and living cells and tissues are increasingly integrated within the same device, two advanced research efforts will change the path of biomaterials research in the future: One research effort aims to design synthetic biomaterials that can respond to the cells and tissues adjacent to them. Referred to as "biologically responsive materials", these future biomaterials will sense the state of cells and tissues and take corrective action, for example, by releasing anti-inflammtory cytokines when the level of reactive oxygen species (ROS) in the surrounding tissue is too high. The second research effort aims to modify cells in situ to increase their ability to form functional tissues within a scaffold. This can be achieved by the use of epigenetic modifiers that prime stem cells to differentiate into desirable cell types. It is also theoretically possible that epigenetic modifiers will be identified that can upregulate the regenerative potential of senescent stem cells.

Conclusion

Biological and engineering approaches are now being combined to develop bioactive scaffolds that can control and direct cell growth and tissue formation toward desirable outcomes. Designing materials that can sense and respond to the status of cells and tissues is the next major challenge in biomaterials science. Creating engineered cells (or epigenetically modified cells) in situ that are primed to perform a desirable function is another forward-looking reserach challenge. Together, these two approaches will provide the foundation for significant advances in the near future.

Acknowledgement

This work was supported by NIH Grant P41 EB001046 through RESBIO, a national resource for polymeric biomaterials and the New Jersey Center for Biomaterials at Rutgers University. The contributions of the scientists at the New Jersey Center for Biomaterials are also acknowledged.

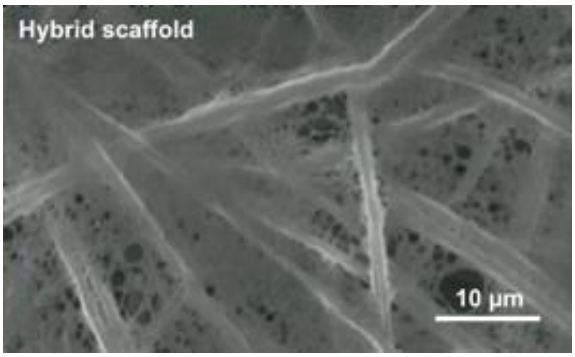

Figure 3: Hybrid scaffold
Figure 3 illustrates a hybrid scaffold consisting of reinforcing polymer microfibers that provide mechanical strength and improve handleability while a layer of decellularized ECM provides a range of biological signals that improve the bioactivity of this scaffold design. This design strategy seems to be a promising way to combine the advantages of synthetic polymer fibers with the bioactivity inherent in natural ECM.

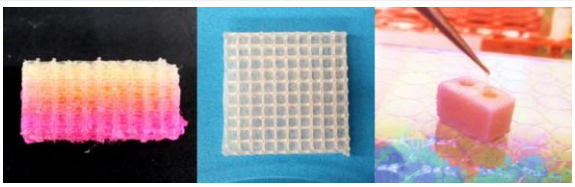

Figure 2
Examples for state-of-the-art scaffold designs. *LEFT:* Use of additive manufacturing to create gradient scaffolds (illustrated here by a transition from a yellow to a red dye). *MIDDLE:* Super-porous scaffold using reinforcing, 3D printed struts that hold airbrushed or electro-spun nanofiber mats in place. *Right:* Scaffold for regeneration of bone and living teeth - an innovative alternative to currently used metalic tooth implants.

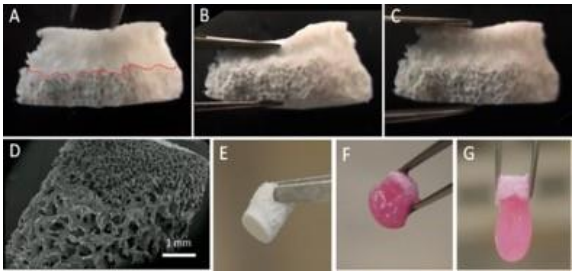

Figure 1
(A) Development of a bi-phasic scaffold optimized for bone regeneration at the bottom and cartilage regeneration at the top. (B) compressed and (C) after release, showing the different mechanical properties of the two layers. (D) SEM of pore structure and interface. (E) after sterilization; (F) after 2 day and (G) after 9 days in medium.

9:15 a.m. – 10:00 a.m.

Hall 3 + Hall 2

KdG AW | Klaas de Groot Award

KdG AW-01

Bioinspired strategies for bone regeneration: a teamwork

Maria-Pau Ginebra[1,2]

[1]Universitat Politècnica de Catalunya (UPC), aBiomaterials, Biomechanics and Tissue Engineering Group, Dept. of Materials Science and Metallurgy, Barcelona, ES; [2]Barcelona Research Center in Multiscale Science and Engineering, UPC, Barcelona, ES

Scientists are not islands in the ocean of global research. Now more than ever, in a super--- connected society, scientific progress builds on previous work and in turn paves the way for future research. The role of communication and collaboration in scientific research cannot be overestimated. Especially within experimental disciplines, research is based on a network of interactions at different levels. Relationships within research groups at different levels are especially important, e.g. between supervisor and doctoral student or experienced researchers and young scientists. These mentoring relationships are part of the ethical dimension of science. However, when evaluating the scientific career, these collaborative aspects, and more specifically the role of the researcher as a mentor is frequently overlooked. The accent is often placed on the leadership capacity of the candidate to be promoted, as an indicator of its scientific value. In my opinion, this comes from an excessively individualistic and competitive view of research. Putting more emphasis on mentoring would help to change the focus and would potentiate the power of the collaborative dimension of research.

This presentation aims to illustrate the power of teamwork and mentoring in the research I have carried out over the last few years on the development of biomaterials for bone regeneration, in the search for intelligent materials, capable of instructing and tuning the cellular response to specific directions.

El leitmotiv in this path has been boinspiration, a powerful approach when designing functional biomaterials. Synthetic bone substitutes have been used for more than 40 years in the clinics. However, after decades of research, they have not been able to outperform autografts, which are still the gold standard, in spite of the serious drawbacks they entail. Paradoxically, conventional synthetic bone grafts are obtained by classical ceramic sintering routes, resulting in microstructures and compositions far from the bone mineral. Recently, novel biomimetic routes have opened unprecedented possibilities in terms of tuning the nanostructure and composition of hydroxyapatite, imitating more closely the mineral phase of bone. Tuning the size, shape and composition of hydroxyapatite nanocrystals allows promoting the osteoinductive and osteogenic properties of the material. This brings tremendous benefits in the in vivo synchronization between scaffold degradation and new bone deposition, suggesting that biomimetic apatite is able to enter the natural bone remodeling cycle. Moreover, the control of pore architecture by using advanced manufacturing technologies, such as 3D---printing or foam templating open up new possibilities in the design of customized bioceramics for bone regeneration.

The progress in this field wouldn't have been possible without the enthusiastic work and commitment of many PhD students, postdoctoral fellows and young researchers who have devoted their efforts to the hard and often arduous task that is scientific research.

Acknowledgement

MAT2015---65601---R project, from Spanish Government and European Reg. Dev. Funds; 2017SGR 1165 and ICREA Academia award, from Generalitat de Catalunya

10:30 a.m. – 12:00 p.m.

Hall 3

ICF-BSE Session | ICF-BSE Debate Session: A Perspective of Biomaterials Science in the Year 2050

Joachim Kohn (New Jersey, US)

The “Special Fellows Session” is organized by the International College of Fellows of Biomaterials Science and Engineering (ICF-BSE). Fellows of ICF-BSE are elected in a worldwide competition every four years and are among the most accomplished in the field of biomaterials. Special Fellows Sessions explore important and sometimes controversial topics and are designed to be interactive: the audience will have an opportunity to participate and will vote on the issues.

This year a group of four fellows will offer different visions for the future of biomaterials science in the coming decades. The speakers will explore the current status of biomaterials science, identify important trends, and speculate how these trends may change the path of biomaterials research. The four presentations will be followed by an opportunity for the audience to participate, ask questions, and offer their own thoughts. The audience will then be asked to vote which of the four different perspectives is most likely to influence the future path of biomaterials research.

ICF-BSE-KL04

Biocomaterials as driving model for future therapy strategy

Luigi Ambrosio

Institute of Polymers, Composites & Biomaterials, National Research Council, Naples, IT

Modern medicine is based on the implementation of a personalised approach together a less invasive surgery for the restoration of human tissues and organs lost to diseases and trauma, this is forced also by the health care system as the related costs are increasing due to the aging population, for the decrease of birth rate and increase of the life expectancy that is frequently not matched by maintenance of health and quality of life.
Biomaterials (metals, ceramics, polymers, composites) plays a pivotal role in many biomedical sector in an enormous number of applications starting from load bearing applications (such as hip joint, plates, cages,..) scaffold for tissue engineering, surgery systems and tools, biomedical packaging, and structures for advanced therapy/diagnosis medicine. Biomaterials chemistry combined with novel processing methodologies such as bioprinting, electrospinning, direct patterning and self-assembly are used to manufacture nano-biomaterials which can lead to design advanced biomaterials. The design of bio-inspired materials, able to guide therapeutically tissue regeneration and repair has been pursued in the last years and still remain a challenging goal for the future. In fact, some phenomena have still to be investigated, the capacity to design and understand the multiscale systems is not sufficient, more effort should be done to analyze the interfaces among the “scale”. “Smart sensing” can be a methodology that leverage quantum techniques for use in characterizing subcellular behavior.
More advanced techniques are now available which can clearly produce macromolecular structures of nanometres size with a finely controlled atomic composition and architecture. Nano-biostructure are continuously under intense investigation in regenerative medicine to change the physical or chemical properties of biomaterials and guide the activation of specific cellular signalling. This is an unique approach for designing a multi-scale, multi-functional, biosensing and cells-instructive materials.
This includes novel methods in the discovery of ground-breaking basic science that can range investigations at the quantum, atomic and molecular scales within the biological landscape. This should aim to better achieve a clearer understanding of chemical biology and biological physics and subsequently to develop the next generation biomaterials, providing appropriate solutions aid in solving the problems of treating chronic disorders in an aging population by tailoring systems for specific patients and disease states.
Thus, the biomaterials will be considered at the centre of any successful regenerative medicine strategy and provides many essential features and cues to direct the cells toward a functional outcome.

References

1. Guarino V., Gloria A., Raucci MG., De Santis R., Ambrosio L. "Bio-inspired cell instructive composite platforms for bone regeneration". *International Materials Reviews* 2012 57 (5), 256-275(20) DOI 10.1179/1743280411Y.
2. V. Cirillo, B. A Clements, V. Guarino, J. Bushman, J. Kohn, L. Ambrosio, "A comparison of the performance of mono-and bi-component electrospun conduits in a rat sciatic model". *Biomaterials*, 35, 32, 8970-8982, 2014.
3. M.G. Raucci, I. Fasolino, M. Caporali, M. Serrano-Ruiz, A. Soriente, M. Peruzzini, L. Ambrosio, "Exfoliated black phosphorus promotes in vitro bone regeneration and suppresses osteosarcoma progression through cancer-related inflammation inhibition". *ACS Applied Materials & Interfaces*, 2019, 11(9), 9333–9342, DOI: 10.1021/acsami.8b21592.

10:30 a.m. – 12:00 p.m.

Hall 2

VII-OS23 | Multifunctional polymeric biomaterials

VII-OS23-KL01

Multifunctional polymer matrices to recapitulate key features of hematopoietic microenvironments in vitro

Marina Prewitz[1], Eike Müller[1], David Gvaramia[1], Laura J. Bray[5,1], Tilo Pompe[3,1], Martin Bornhäuser[4,2], **Carsten Werner**[1,2]

[1]Leibniz Institute of Polymer Research Dresden, Max Bergmann Center of Biomaterials, Dresden, DE; [2]TU Dresden, Center of Regenerative Therapies Dresden, Dresden, DE; [3]University of Leipzig, Institute of Biochemsitry, Leipzig, DE; [4]TU Dresden, Medical Faculty, Dresden, DE; [5]Queensland University of Technology, Institute of Health and Biomedical Innovation, Brisbane, AU

Introduction

Homeostasis of hematopoietic stem and progenitor cells (HSPC) is controlled by a combination of biochemical and biophysical environmental cues in the bone marrow (BM) niche, where a tight balance of quiescence and proliferation of HSPC is maintained. Specifically, soluble factors, extracellular matrix (ECM) components and spatial confinement have been recognized to be critical for regulation of HSPC fate. Although in vivo models for investigating HSC niche function are established, as they reflect the full complexity of the BM microenvironment, they are hard to interpret in terms of dissecting the individual parameters which guide HSC fate decisions.

Glycosaminoglycans (GAGs) govern important functional characteristics of the extracellular matrix (ECM) in living tissues. Accordingly, incorporation of GAGs into biomaterials opens up new routes for the presentation of signaling molecules in ways that allow for exploring mechanistic aspects of tumor formation and progression under defined constraints, as well as for individualized anticancer drug screening. In an attempt to systematically explore the related options, we have introduced a rational design strategy for biology-inspired hydrogels based on multi-armed poly(ethylene glycol), GAGs and peptides (1,2,3). The theoretically predicted decoupling of biochemical and mechanical gel properties was confirmed experimentally and applied for implementing GAG-based biofunctionalization schemes to afford cell adhesiveness and morphogen presentation.

In the discussed approach, we combined GAG-mediated factor presentation with varying degrees of spatial constraint using a cell encapsulation strategy to assess the interplay of biophysical cues, GAG, and growth factor presentation on HSPC fate decisions in a 3D culture environment. For this aim, we used an in situ forming starPEG-heparin hydrogel system, assembled by Michael type addition reaction, to create a 3D culture environment mimicking GAG-rich BM and facilitate GAG-mediated growth factor presentation to the cultured cells.

Results and Discussion

Using GAG-based biohybrid hydrogels, human HSPC were effectively triggered in vitro through the simultaneous regulation of exogenous biochemical and biophysical cues. Our results demonstrate that HSPC respond to increased spatial confinement with lowered proliferation and cell cycling, which results in higher frequency of quiescent LTC-IC (long-term culture initiating cells), while GAG-rich 3D environments further support maintenance of the cells (4,5). Furthermore, matrix metalloproteinase-sensitive GAG-based hydrogels functionalized with adhesion ligands and pro-angiogenic factors were shown to be instrumental for the ex vivo analysis of acute myeloid leukemia development and response to treatment (6).

Conclusion

The reported biohybrid hydrogel culture is conclude to offer a powerful tool for long-term maintenance of HSC by enabling the control of cell cycling through independent adjustment of biophysical cues and providing an optimal cytokine environment through the negatively charged heparin component. Our results suggest that the maintenance of HSC in the 3D hydrogel culture is achieved by a synergistic interplay of spatial cell confinement, paracrine signaling, GAG-mediated scavenging of cell secreted factors and high local cytokine concentration.

References

(1) U. Freudenberg, J.-U. Sommer, K. Levental, P. Welzel, A. Zieris, K. Chwalek, , K. Schneider, S. Prokoph, M. Prewitz, R. Dockhorn, C. Werner (2012) Adv Funct Mater 22:1391

(2) M. Tsurkan, K. Chwalek, S. Prokoph, A. Zieris, K. Levental, U. Freudenberg, C. Werner (2013) Adv Mater 25:2606

(3) U. Freudenberg, Y. Liang, K.L. Kiick, C. Werner (2016) Adv Mater 28: 8861

(4) D. Gvaramia, E. Müller, K. Müller, P. Atallah, M. Tsurkan, U. Freudenberg, M. Bornhäuser, C.Werner, Biomaterials (2017) 138:108

(5) E. Müller, T. Pompe, U. Freudenberg, C. Werner (2017) Adv Mater. 29 doi: 10.1002/adma.201703489.

(6) L.J. Bray, M. Binner, Y. Körner, M. von Bonin, M. Bornhäuser, C. Werner (2017) Haematologica doi: 10.3324/haematol.2016.157883

Acknowledgement

Financial support of the Deutsche Forschungsgemeinschaft (SFB655) is gratefully acknowledged.

VII-OS23-02

Glycosaminoglycan hydrogels promote chronic wound healing

Uwe Freudenberg[1], Passant Atallah[1], Lucas Schirmer[1], Carsten Werner[1,2]

[1]Leibniz Institute of Polymer Research Dresden, Institute of Biofunctional Polymer Materials, Dresden, DE; [2]TU Dresden, Center for Regenerative Therapies Dresden, Dresden, DE

Introduction

Wound healing after skin injury involves an orchestrated appearance of signaling molecules regulating key cellular processes including activation, migration, proliferation, and differentiation of immune cells, capillary forming endothelial cells and matrix producing fibroblasts. Dysregulation of these signals can lead to severe impairment of tissue regeneration, especially found in chronic wounds. Glycosaminoglycans (GAGs) control the availability and activity of such cell signaling molecules *in vivo* and thus are a key target for maintaining regenerative processes with material-based approaches[1]. We report herein a modular biohybrid hydrogel system that is based on star-shaped poly(ethylene glycol) (StarPEG), the GAG heparin and selectively desulfated derivatives thereof, as well as functional peptides in order to vary the affinity for soluble signalling molecules, to allow for cell-responsive remodelling and to adjust the physical properties of the resulting hydrogel matrices. Accordingly, the material can be easily customized for a particular application and in here it was optimized in order to promote wound healing under chronic conditions.

Experimental Methods

Biohybrid hydrogels were formed from StarPEG and heparin building blocks using direct amide bond formation between amine-terminated StarPEG and activated carboxylic acid groups of heparin or the Michael type addition reaction between thiol-terminated StarPEG and maleimide-pre-functionalized heparin. The mechanical properties of the materials were characterized by rheometry and swelling measurements. Moreover, the binding and subsequent release of chemokines and growth factors to/from the hydrogels have been analysed using ELISA and multiplex techniques. The ability of the hydrogels to control immune cell migration (and thus chronic inflammatory processes) was tested with human neutrophils and granulocytes. Furthermore, pro-regenerative growth factor releasing hydrogels were assessed *in vitro* in order to control the fate of human endothelial cells and dermal fibroblasts. Finally, experiments in diabetic mice with inflammatory chemokine sequestering as wells as VEGF-releasing hydrogels were performed to proof the feasibility of the modular approach *in vivo*.

Results and Discussion

The multifunctional GAG-based hydrogels were able to scavenge inflammatory chemokines and to deliver growth factors capable of inducing angiogenesis and tissue maturation in dependence of their sulfation pattern. As such, extensive *in vitro* studies utilizing recombinant proteins, human immune cells, endothelial cells, fibroblasts and wound fluids from patients suffering from chronic venous leg ulcers demonstrated that the scavenging of inflammatory mediators and the release of pro-regenerative factors like VEGF and TGF-ß are widely tuneable and thus could be customized for different wound pathologies [2,3]. Furthermore, healing studies in an *in vivo* model of delayed wound healing (db/db mice), where our hydrogel material outperformed the standard-of-care product Promogran with respect to reduction of inflammation, as well as increased granulation tissue formation, and vascularization [4], demonstrate the potential of the matrices for a rapid translation into the clinic as adaptable wound dressing material.

Conclusion

The in here presented modular hydrogel platform combines anti-inflammatory, angiogenic and pro-regenerative functionality as it is crucial to promote wound healing but may similarly aid therapeutic strategies to control other inflammatory diseases.

References

[1] U. Freudenberg, Y. Liang, K.L. Kiick, C. Werner, C. *Adv Mater* 2016, 28 (40), 8861–8891.

[2] U. Freudenberg, A. Zieris, K. Chwalek, M. V. Tsurkan, M. F. Maitz, P. Atallah, K. R. Levental, S. A. Eming, C. Werner, *J Control Release* 2015, 220, 79.

[3] A. Watarai, L. Schirmer, S. Thönes, U. Freudenberg, C. Werner, J. C. Simon, U. Anderegg, *Acta Biomaterialia* 2015, 25, 65.

[4] N. Lohmann, L. Schirmer, P. Atallah, E. Wandel, R. A. Ferrer, C. Werner, J. C. Simon, S. Franz, U. Freudenberg, *Sci Transl Med* 2017, 9, DOI 10.1126/scitranslmed.aai9044.

Acknowledgement

This work was funded by the German Research Council (DFG SFB-TR67 projects A10, B3, B4 and FR2671/4-1).

VII-OS23-03

Supramolecular Functionalization and Tuning of Peptide Modified Bioorthogonally Crosslinked Hyaluronan-Poly(ethylene glycol) Hydrogels

Christopher Aronsson[1], Michael Jury[1], Jonas Christoffersson[2], Robert Selegård[1], **Daniel Aili**[1]

[1]Linköping Univeristy, Laboratory of Molecular Materials, Division of Molecular Physics, Department of Physics, Chemistry and Biology, Linköping, SE; [2]Linköping Univeristy, Division of Biotechnology, Department of Physics, Chemistry and Biology, Linköping, SE

Introduction

Biofunctional hydrogels are widely used as extra cellular matrix (ECM) mimicking materials to support formation of physiologically relevant cell and tissue models for biomedical research and drug development. Numerous covalent crosslinking strategies have been developed for generation of hydrogels, but they typically suffer from cross-reactivity or generation of cytotoxic biproducts. Bioorthogonal crosslinking based on e.g. strain-promoted alkyne-azide 1,3-dipolar cycloaddition (SPAAC) has thus emerged as a promising technique for generating hydrogels that facilitates efficient cell encapsulation.[1,2] Here we demonstrate a hyaluronan-poly(ethylene glycol) hydrogel formed by SPAAC-mediated crosslinking that also comprise an additional peptide-folding triggered crosslinking mechanism. Possibilities to simultaneously combine both bioorthogonal covalent and physical crosslinking enables fabrication of hydrogels with dynamic gelation kinetics and tunable mechanical properties as well as possibilities to introduce new functionalities by means of specific peptide dimerization interactions.

Experimental Methods

The peptides JR2EK (H_2N-NAADLEKAIEALEKHLEAKGPKDAAQLEKQLEQAFEAFERAG-COOH) and JR2KK (H_2N-NAADLKKAIKALKKHLKAKGPKDAAQLKKQLKQAFKAFKRAG-COOH) were synthesized on an Fmoc-Gly-Wang resin in 0.1 mmol scale using a Quartet automated peptide synthesizer, and purified by reversed phase HPLC. JR2EK was conjugated to bicyclo[6.1.0]nonyne (BCN) modified HA (Mw 100 - 150 kDa) using SPAAC. HA-JR2EK or HA-BCN was mixed with $p(N_3)_8$ at a ratio of 2:1 BCN:N_3 at 1.5 – 2.5% (w/v) total polymer concentration to initiate crosslinking.

Results and Discussion

The helix-loop-helix peptide JR2EK was conjugated to hyaluronan (HA) modified with an excess of BCN. JR2EK was designed to fold and homodimerize into four-helix bundles at pH < 6 or in the presence of Zn^{2+}or to heterodimerize with the complementary peptide JR2KK.[3,4] Crosslinking of the HA-peptide hybrid with an eight-armed poly(ethylene glycol) with terminating azides ($p(N_3)_8$) using SPAAC resulted in the formation of fully transparent and cytocompatible hydrogels within minutes. The storage modulus (G´) reached about 150 Pa within 2 hours but continued to increase over time. In contrast, when triggering the crosslinking under conditions also favoring peptide homodimerization, the resulting hydrogels formed significantly faster because of the simultaneous and rapid peptide-mediated self-assembly process (Figure 1). Moreover, the possibility to exploit peptide heterodimerization as a means to introduce new functional moieties to the already formed hydrogels was investigated (Figure 2a). By including a biotin in the loop region of JR2KK, addition of the peptide to the hydrogels enabled subsequent attachment of avidin. The specific supramolecular introduction of avidin was demonstrated by addition of biotin-labeled alkaline phosphatase (ALP).

ALP catalyzes the hydrolysis of the chromogenic substrate BCIP, resulting in a colorimetric response in hydrogels modified with the biotin-labeled JR2KK peptides (Figure 2b-c). In addition, inorganic phosphate generated by ALP mediated hydrolysis of calcium glycerophosphate could be exploited to trigger a localized biomineralization process in the hydrogels.

Conclusion

Combining bioorthogonal covalent and supramolecular peptide-folding mediated crosslinking enables tuning of gelation kinetics and dynamic changes of hydrogel viscoelastic properties. The conjugated helix-loop-helix peptides also enables introduction of various biofunctional moieties through heterodimerization with a complementary peptide. This strategy thus allows for flexible and modular alterations of hydrogel properties, which can substantially facilitate hydrogel optimization and studies cell response to dynamic changes in the microenvironment.

References

1. A., Takahashi, Y. Suzuki, T. Suhara, K. Omichi, A. Shimizu, K. Hasegawa, N. Kokudo, S. Ohta, T. Ito, In Situ Cross-Linkable Hydrogel of Hyaluronan Produced via Copper-Free Click Chemistry. *Biomacromol.* **2013,** *14*, 3581-3588.
2. J. Christoffersson, C. Aronsson, M. Jury, R. Selegård, D. Aili, C. F. Mandenius, Fabrication of modular hyaluronan-PEG hydrogels to support 3D cultures of hepatocytes in a perfused liver-on-a-chip device. *Biofab.* **2018,** *11*, 015013.
3. D. Aili, K. Enander, I. Nesterenko, F. Björefors, L. Baltzer, B. Liedberg, "Folding Induced Assembly of Polypeptide Decorated Gold Nanoparticles", *J. Am. Chem. Soc.*, **2008**, 130, 5780-5788.
4. D. Aili, K. Enander, L. Baltzer, B. Liedberg, “Assembly of Polypeptide Functionalized Gold Nanoparticles Through a Hetero-Association and Folding Dependent Bridging”, *Nano Lett.*, **2008**, 8, 2473-2478.

Acknowledgement

Support from the Swedish Foundation for Strategic Research (SSF), the Knut and Alice Wallenberg Foundation (KAW), and the Swedish Government Strategic Research Area in Materials Science on Functional Materials at Linköping University (Faculty Grant SFO Mat LiU No 2009 00971) is acknowledged.

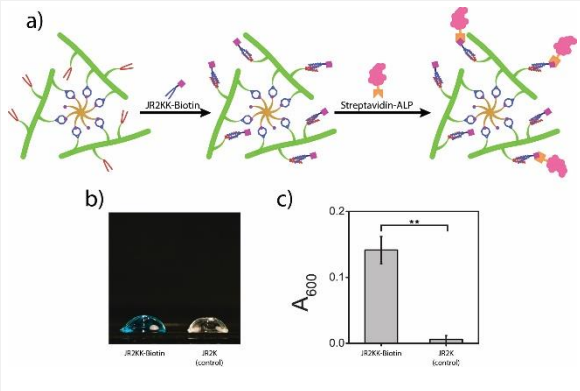

Supramolecular hydrogel functionalization
Figure 2. Peptide heterodimerization enables dynamic introduction of new biofunctionalities. a) A biotin labeled complementary peptide allowed for specific incorporation of avidin and subsequent introduction of biotinylated ALP. b-c) Addition of the chromogenic substrate BCIP, resulted in a colorimetric response in the hydrogels.

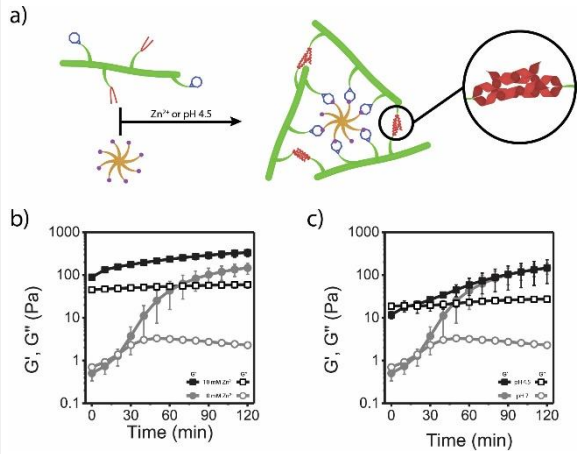

Dual bioorthogonal crosslinking

Figure 1. a) Schematic representation of the dual bioorthogonal crosslinking of the hydrogels. Upon mixing of HA-BCN/JR2EK and $p(N_3)_8$, the BCN and azide groups react via a strain-promoted alkyne-azide 1,3-dipolar cycloaddition to form a stable 1,2,3-triazole. Parallel peptide homodimerization triggered by Zn^{2+}(b) or pH (c) results in physical crosslinking that dramatically increase the rate of gelation.

VII-OS23-04

Cytocompatible, injectable and electroconductive soft adhesives with hybrid covalent/non-covalent dynamic network

Yong Xu[1], Panagiotis A Patsis[1], Sandra Hauser[3], Dagmar Voigt[6], Rebecca Rothe[3,7], Markus Günther[6], Meiying Cui[1], Xuegeng Yang[2], Robert Wieduwild[1], Kerstin Eckert[2], Christoph Neinhuis[6], Teuku F. Akbar[4,5], Ivan R Minev[1], Jens Pietzsch[3,7], Yixin Zhang[1]

[1]Technische Universität Dresden, B CUBE Center for Molecular Bioengineering, Dresden, DE; [2]Helmholtz-Zentrum Dresden-Rossendorf (HZDR), Institute of Fluid Dynamics, Dresden, DE; [3]Helmholtz-Zentrum Dresden-Rossendorf, Institute of Radiopharmaceutical Cancer Research Department of Radiopharmaceutical and Chemical Biology, Dresden, DE; [4]Technische Universität Dresden, Biotechnology Center, Dresden, DE; [5]Leibniz Institute of Polymer Research Dresden (IPF), Max Bergmann Center of Biomaterials Dresden (MBC), Dresden, DE; [6]Technische Universität Dresden, Institute for Botany, Faculty of Biology, School of Science, Dresden, DE; [7]Technische Universität Dresden, Faculty of Chemistry and Food Chemistry, Desden, DE

Introduction

Synthetic conductive biopolymers have gained increasing interest in tissue engineering, as they can provide a chemically defined electro-conductive surrounding, yet also mimic the natural microenvironment of cells. However, existing conductive hydrogels often show shortcomings to meet the increasing biomedical needs. For example, in addition to low cytotoxicity and biocompatibility, injectability and adhesiveness are important for many biomedical applications but have proven to be very challenging. Recent results have shown that fascinating material properties can be realized with a bio-inspired hybrid network, especially through the synergy between irreversible covalent crosslinking and reversible non-covalent self-assembly. Herein, we report a polysaccharide-based conductive hydrogel crosslinked through non-covalent and reversible covalent reactions, while the hybrid material exhibits rheological properties associated with dynamic networks such as self-healing and stress relaxation. Moreover, through fine-tuning the network dynamics by varying covalent/non-covalent crosslinking content and incorporating electroconductive polymers, the resulting materials have exhibited electroconductivity and reliable adhesive strength, at a similar range to that of clinically used fibrin glue. The conductive soft adhesives exhibit high cytocompatibility in 2D/3D cell cultures and can promote myogenic differentiation of myoblast cells. The materials were further characterized in vivo using immunocompetent mice, both for topical application and as injectable materials. The heparin-containing electroconductive adhesive showed high biocompatibility in both studies. The materials could have utilities in many biomedical applications, especially in the area of cardiovascular diseases and wound dressing.

Experimental Methods

1.1. Synthesis and characterization of PEDOT:Hep and PEDOT:PSS
1.2. Formation of electroconductive hydrogels
1.3. Hydrogel mechanical characterization
1.4. Electrochemical measurements
1.5. Pull-off tests
1.6. Lap-shear tests
1.8. 3D Printing
1.9.Tissue adhesive testing
1.10. C2C12 cell culture in the hydrogel

1.11. In vivo biocompatibility testing

Results and Discussion

Covalent crosslinking could improve the mechanical strength and cohesive force of a non-covalently assembled hydrogel; however, it could also impair various properties associated with a dynamic network, e.g., self-healing, shear-thinning and injectability. In this work, we have developed a hybrid dynamic hydrogel system composed of non-covalent network and reversible imine crosslinking. The use of conductive polymers, not only led to electroconductivity, but also to a plethora of hydrophobic moieties, which are absent in most synthetic hydrogels. In many natural adhesives, such as proteins from burrowing ground frogs of the genus Notaden, sericin from the silkmoth Bombyx mori, and protein/saccharide associations from echinoderms, adhesion results from the synergy among different types of interactions, including hydrophobicity, electrostatics, and hydrogen bonds. The synthetic hybrid hydrogels present a rich source of positive and negative charges, hydrophobic/aromatic groups, and hydrogen bond donors/acceptors, while the dynamic network allows them to adapt and adhere to various surfaces. Moreover, the hybrid network of non-covalent and covalent crosslinking results in enhanced cohesion strength of the network, leading to adhesive materials with high mechanical robustness.

Conclusion

In summary, we have created an electroconductive hybrid polymer network, in which both covalent and non-covalent crosslinking are reversible and dynamic. While the electroconductivity can function as an electronic sensor, as well as a biophysical cue to promote myogenesis, the cytocompatible adhesive can also be used to encapsulate cells for cell-based therapy as injectable therapeutics. The materials were also characterized in vivo using immunocompetent mice, both for topical application and as injectable materials. The materials showed high biocompatibility in both studies. Interestingly, by replacing PEDOT:PSS with a polysaccharide-doped bio-electroconductive polymer PEDOT:Hep, the resulting hydrogel has shown remarkably enhanced adhesive strength on tissues, as well as fast degradation in vivo. These soft and stress relaxing materials can match the mechanical properties of soft tissues and would be particularly attractive for applications in heart, muscle, and neuron diseases, as well as wound dressings.

Acknowledgement

The authors thank Ulrike Hofmann (B CUBE, Technische Universität Dresden, Germany) for technical support. The authors thank Dr. Hella Hartmann (Technische Universität Dresden, Germany) and Silke White (Deutsches Zentrum für Neurodegenerative Erkrankungen e.V. Dresden, Germany) for LSM imaging. Kejun Liu (Technische Universität Dresden, Germany) provided helps to take images and FTIR measurements. We thank N. Kröger and A. Kotzsch (Technische Universität Dresden, Germany) for their help in DLS measurements. Technical assistance of Sebastian Meister and Aline Morgenegg (HZDR) also is greatly acknowledged.

This work was supported by the China Scholarship Council and German Federal Ministry of Research and Education (BMBF grants 03Z2EN12 and 03Z2E511). S.H., R.R. and J.P are thankful to the Deutsche Forschungsgemeinschaft (DFG), Research Grant Collaborative Research Center Transregio 67 “Functional Biomaterials for Controlling Healing Processes in Bone und Skin - From Material Science to Clinical Application“ (CRC/TRR 67/3) and to the Helmholtz Cross Programme Initiative “Technology and Medicine – Adaptive Systems“ for supporting this work.

VII-OS23-05

Characterization of new biohybrid membranes for *in vitro* models of physiological barriers

Roberta Nossa[1,2], Ludovica Cacopardo[1,2], Joana Costa[2], Giorgio Mattei[1], Arti Ahluwalia[1,2]

[1]University of Pisa, Department of Information Engineering, Pisa, IT; [2]University of Pisa, Research Center "E. Piaggio", Pisa, IT

Introduction

In the human body, physiological barriers have a fundamental role in controlling the absorption of substances and maintaining the homeostasis of the different body compartments. For these reasons, engineering barrier models in-vitro is not only crucial for a better understanding of their pathophysiology, but also for drug testing and toxicology. Therefore, barrier-forming cells are often cultured in bioreactors [1] onto porous membranes, i.e. permeable supports for the cultured cell layer that must be biocompatible and cell adhesive.

In this work a commercial poly(carbonate)urethane copolymer (Bionate® II 80A) was used to replicate the basement of the physiological barrier, thanks to its combination of elastic characteristics from the urethane and the biostability from the carbonate segment. Additionally, in order to increase the cell adhesion, gelatin was used in combination with Bionate®.

The electrospinning technique was chosen to obtain porous supports. Solutions with different Bionate®:gelatin volume ratios were electrospun to identify the one better mimicking the physiological barrier in terms of both hydrophilic and mechanical characteristics.

Experimental Methods

Bionate® and Gelatin A were dissolved at 10% (w/v) in HFP and different percentages of Bionate® conjugated with gelatin were investigated (Bionate®: Gelatin at 50:50, 70:30, 80:20, 90:10).

Electrospinning parameters were the following: voltage = 30 KV, distance needle-collector = 15 cm, needle diameter = 0.41 mm, Q = 1 mL/h.

Images of the membranes were obtained with the confocal microscope in order to evaluate fibers and pores average dimensions. The contact angle was measured on control membranes and on membranes dipped in 70% ethanol/distilled water (EtOH/dH2O).

Tensional stress-strain tests were performed on the membranes. Firstly, the Young's modulus was evaluated in dry conditions at room temperature, in order to evaluate how gelatin can influence the stiffness. Moreover, since the membranes will be used in a rather aggressive environment, the mechanical characterization was repeated for long term tests, evaluating their structural properties after several days of incubation in PBS at 37°C (wet condition), as well as fatigue tests. Four different cyclic strain times were studied: 1, 2 and 4 hours of cyclic stretching. After this preconditioning phase, the Young's modulus was evaluated with a traditional tension stress strain test in order to determine the occurrence of plastic behaviour.

Finally, A549 cells were seeded on the 50:50 membranes (150 000, 200 000 and 250 000 cells/cm2) and the Alamar Blue assay performed after 1, 5 and 7 days of culture, in order to evaluate the cell adhesion to the support.

Results and Discussion

Membrane geometrical characteristics were derived via image analysis, obtaining: thickness, 73.18±26.67 μm; fibre diameter, 3.177±0.774 μm; pore dimeter, 5.068±2.170 μm. The contact angle of the electrospun membranes was measured, observing a low wettability in 80:10 and 90:10 membranes, with a decrease of the contact angle by increasing the amount of gelatin. The 50:50 and 70:30 membranes showed high wettability and that the contact angle could not be measured as the membrane quickly absorbed the drops. Moreover, the treatment with 70% EtOH/dH2O generally improved the wettability and the 80:20 and 90:10 membranes became hydrophilic.

Mechanical tests in dry conditions (Fig. 1A) showed that increasing the amount of gelatin causes a decrease of the linear region of the electrospun membrane. Conversely, in a wet environment all the membranes exhibited a linear-elastic behaviour within the whole region of deformation (Fig. 1B).

Moreover, figure 2A shows that the Young's Modulus of the membranes 50:50 and 70:30 incubated for 1, 2, 3 and 7 days in PBS did not change significantly during the incubation time ($p>0.05$), while a significant change was observed for the 80:20 and 90:10 membranes.

Finally, after cyclic stretching in a wet environment, electrospun membranes showed no significant differences in the elastic modulus with respect to dry samples ($p > 0.05$, Figure 2B). These results show that the tests were performed into the linear range of the material, without any residual plastic deformations.

The 50:50 Bionate®:gelatin membrane was selected for cell seeding as it was the most wettable. The

Alamar Blue assay showed that cells were growing well, showing the suitability of this support for tissue engineering applications.

Conclusion

A new biohybrid material made of Bionate® and gelatin was synthetized. In particular, by varying the amount of gelatin, it was possible to obtain membranes with different stiffness and elasticity, allowing to mimic different type of physiological barriers and different pathological conditions. The electrospinning technique was chosen to obtain porous membranes, while Bionate®'s flexibility allows mimicking the cyclic stretching of barriers in the human body (i.e. alveolar barrier during breathing).

References

[1] C. Dassow, C. Armbruster, C. Friedrich, E. Smudde, J. Guttmann, S. Schumann, "A method to measure mechanical properties of pulmonary epithelial cell layers", Journal of Biomedical Materials Research – Part B Applied Biomaterials, vol. 101, issue 7, pp. 1164-1171, 2013.

Acknowledgement

The project PATROLS has received funding from the European Union's Horizon 2020 research and innovation programme under grant agreement No. 760813.

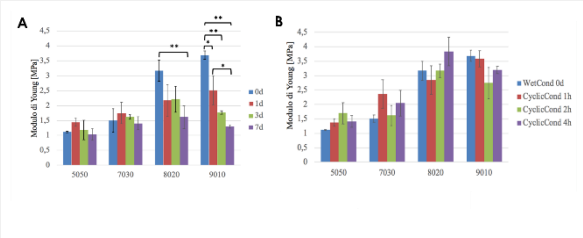

Figure 2
A) Incubation time (0, 1, 3 and 7 days) *versus* Young's Modulus of the electrospun membranes. (*) p<0.05, (**) p<0.01.

B) Cyclic stretching (0, 1, 2 and 4 hours) *versus* Young's Modulus of the electrospun membranes

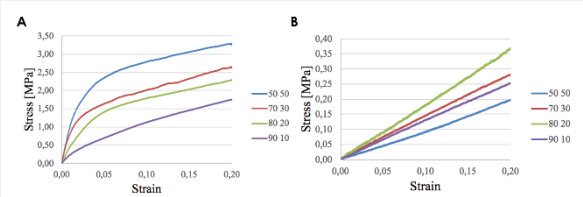

Figure 1
Stress-Strain curves of the electrospun membranes tested in A) Dry-condition and B) Wet-coondition

10:30 a.m. – 12:00 p.m.

Hall 4

VII-OS24 | Calcium phosphates 2

VII-OS24-01

Interaction of Femtosecond Pulsed Lasers with Fe^{2+}/Fe^{3+} Doped Calcium Phosphates for Bone Tissue Engineering

Emaan Alsubhe[1], Antonios Anastasiou[1], El Mostafa Raif[2], Chiranjeevi Maddi[1], Animesh Jha[1]

[1]School of chemical and process engineering, University of Leeds, Leeds, GB; [2]School of Dentistry, University of Leeds, Leeds, GB

Introduction

Current trends in tissue engineering, such as personalised medicine and near-patient manufacturing, favour the use of additive manufacturing techniques for the fabrication of bone scaffolds, using an emerging technique called the selective laser sintering (SLS). SLS at present appears to be one of the most well-established and widely used methodologies. For tissue engineering, different materials have been used so far, for example, Ti-metal alloys, polymers and bioglass powders [1]. However, the bone-forming *β* calcium pyrophosphate (*βCPP*), ($Ca_2P_2O_7$), minerals are of particular interest due to intrinsic chemical and structural similarity with the hydroxy apatite, $Ca_5(PO_4)_3(OH)$, which is the main constituent mineral of natural bone. In a recent work, we have demonstrated that doping of *βCPP* with $Fe^{2+/3+}$ ions enhances the laser-matter interaction and allows the localised sintering without inducing any thermal damage to the surrounding materials [2]. This work aims to identify an optimum doping concentration of $Fe^{2+/3+}$ ions based on the requirements of natural bone by demonstrating: a) mechanical properties of the doped material; b) osteogenic potential; and c) ultimate fabrication potential of *βCPP* for in-theatre manufacturing of synthetic bone with a suitable laser (e.g. a femto-second laser) for adapting with natural bone.

Experimental Methods

Brushite powders ($CaHPO_4 \cdot 2H_2O$) with various doping concentrations of $Fe^{2+/3+}$ ions (0%, 5%, 10%, 20% and 30% mol) have been synthesised via wet precipitation method. Laser irradiation experiments were carried out with two different types of femto-second laser i.e. 1 kHz repetition rate femtosecond pulsed laser, operating at 800 nm (Coherent-Libra) and a lab-engineered 1 GHz repetition rate femtosecond laser emitting at 1040 nm [2]. The ablation threshold fluence (F_{th}) for all the materials was calculated by using D^2 method [4]. The pre/post irradiation biomaterials were characterised by analysing the crystal structure using XRD, spectroscopic properties for laser radiation absorption using UV-visible spectroscopy, and mechanical properties using nano-indentation. The in vitro biocompatibility of laser-irradiated scaffolds was characterised by evaluating the adhesion and proliferation of osteoblast (G-292) cell lines.

Results and Discussion

The phase analysis demonstrated that the doping of brushite raw materials with $Fe^{2+/3+}$-ion up to 20 mol% in the form of $Fe(OH)_3$, stabilizes the original crystal structure of brushite ($CaHPO_4.2H_2O$). However, for doping concentrations above 20mol%, an amorphous iron phosphate ($FePO_4 \cdot 2H_2O$) forms and remains the dominant phase. Using the above laser at 1GHz laser at 1040nm, the brushite-doped with Fe^{3+}-ions were sintered, after which nano-indentation was used to measure the hardness before and after sintering samples. For the 0% and 5 % doped laser sintered samples, the measured hardness values were found to be around 0.4 GPa, which then increased dramatically to 1GPa for the 10% sintered sample. For doping concentrations higher than 20 mol%, the hardness decreased to 0.1 GPa, which is attributed to the presence of FePO4. In **Fig.1** shows the surface topology of the undoped material after

irradiation with constant laser pulse energy at 200 µJ. Deep microchannels were formed on the surface which is a clear indication of ablation. The same irradiation parameters, resulted in partial melting and shallow microchannels for the 5%, 10% and 20%. For 30 mol% Fe-doping, there are no indications of ablation, however the incident energy was readily absorbed by melting the mineral phase. The effect of $Fe^{2+/3+}$ doping on the laser–matter interaction mechanism was analysed and it was evident after the phase analysis using XRD of the post irradiated samples. For the 0%, 5% and 10 mol%, we observed the formation of monetite ($CaHPO_4$). The transformation of brushite into monetite normally occurs at ~200 °C during slow heating. On the other hand, iron oxide phosphate (Fe_2OPO_4) formed for 20% and 30%. Osteoblast cell lines were used to test the cell proliferation on sintered $Fe^{2+/3+}$ brushite materials. DNA using picogreen protocol was applied for the proliferation process. **Fig. 2** shows the confocal microscope images of osteoblast cell lines on the top 10 mol% Fe-doped material. It is clear that the cells adhesion is more extensive into the microchannels, which is a strong indication of preferences for cellular colonisation and proliferation for tissue scaffold engineering.

Conclusion

Our most important findings can be summarized as follows:

· Brushite is the dominant mineral phase present up to 20 mol% doping concentration.

· The highest hardness of 1 GPa was measured for the 10 mol% doped materials.

· The ablation threshold of the minerals increases as the doping concentration increases.

· The presence of Fe in βCPP enhances the proliferation of osteoblasts on the surface of sintered samples.

References

[1] Harun, W. S. W., et al. "A review of powder additive manufacturing processes for metallic biomaterials." *Powder Technology* (2017).

[2] Anastasiou, A. D., et al. "Sintering of calcium phosphates with a femtosecond pulsed laser for hard tissue engineering." *Materials & Design* 101 (2016): 346-354.

[3] Liu, J. M. "Simple technique for measurements of pulsed Gaussian-beam spot sizes." *Optics letters* 7.5 (1982): 196-198.

Acknowledgement

This work is sponsored by Taibah University, Madinah, Saudi Arabia as a part of a PhD scholarship**.**

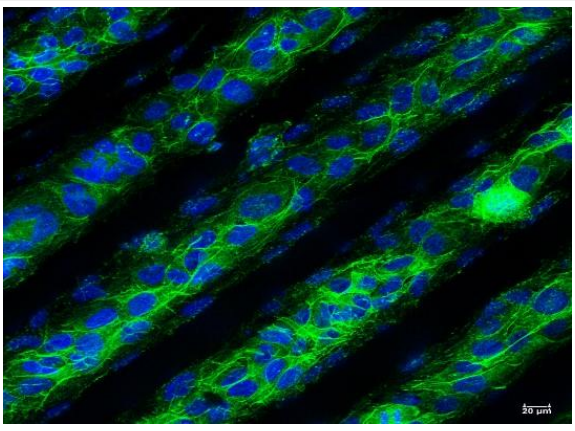

Figure 2:

Confocal microscope image presents the growth of cells into the 10% Fe-βCPP microchannels

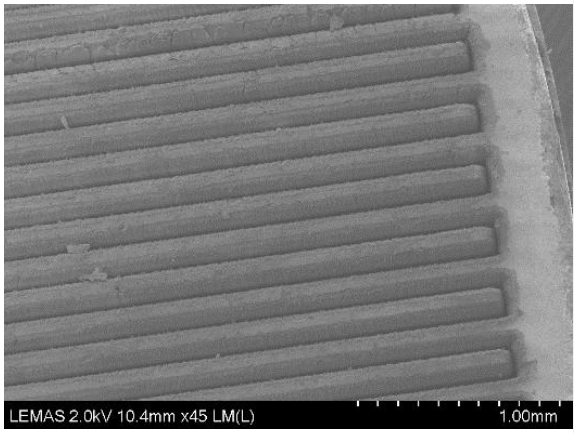

Figure 1:
SEM image shows the microchannels into 0% Fe-brushite.

VII-OS24-02

Rheology, microstructure and mechanical strength of an injectable, macroporous calcium phosphate cement reinforced with modified polycaprolactone fibres

Edgar B. Montufar[1], Kristýna Valová[1], Matěj Dzurov[2], Karel Slámečka[1], Aida Mata[1], Jana Brtníková[1], Michala Rampichová[3], Matěj Buzgo[3], Lucy Vojtova[1]

[1]Brno University of Technology, Central European Institute of Technology, Brno, CZ; [2]Brno University of Technology, Faculty of Chemistry, Brno, CZ; [3]Academy of Sciences of the Czech Republic, Institute of Experimental Medicine, Praha, CZ

Introduction

The ideal calcium phosphate bone cement (CPC) should be injectable with washout resistance and macroporous with certain load-bearing capacity. This work explores the use of a thixotropic poly(lactic acid-co-glycolic acid)-b-poly(ethylene glycol)-b-poly(lactic acid-co-glycolic acid) (PLGA–PEG–PLGA) triblock copolymer to provide both injectability and cohesion to a macroporous cement. In addition, this work studies the use of polycaprolactone (PCL) and amphiphilic PCL/Pluronic (PCL/Plu) fibres for the mechanical reinforcement of the macroporous cement while preserving its injectability.

Experimental Methods

Alpha tricalcium phosphate (α-TCP) powder was used as the only solid component of the cement. It was synthetized by solid state reaction at 1400 °C between $CaCO_3$ and $CaHPO_4$. The liquid phase consisted of 15 wt% solution of PLGA–PEG–PLGA copolymer, synthesized via ring opening polymerization. PCL fibres were produced via centrifugal force spinning and were disaggregated to tangled fibres (~100 μm) by cryogenic grinding. Pluronic blocks were grafted to the PCL fibres to increase their hydrophilicity. Cement samples were mixed using a drill at liquid to powder ratio of 0.5 ml/g, containing 0, 1, 3 or 5 wt% of fibres with respect to the solid phase. Following this mixing method several air bubbles were incorporated in the obtained paste. Extrusion and rheological tests were performed to study the injection behaviour of the fibre reinforced CPCs and different samples were shaped by injection in rubber moulds and set by immersion in water at 37 °C for 10 days. After setting the CPC samples were characterized in terms of crystalline composition (XRD), microstructure (SEM), porosity (MIP and μ-CT) and compressive strength.

Results and Discussion

The incorporation of fibres slightly impaired the injectability of the CPC. However, the force required to inject the CPC with 5 wt% of fibres was significantly increased. CPCs exhibited shear thinning rheological behaviour with Bingham yield stress of 1200 Pa, followed by a slow reduction of shear stress with shear rate and partial recovery of viscosity when shear was removed. This peculiar rheological behaviour prevented phase separation during injection and provided the cement with washout resistance when injected in water at 37 °C. After setting the CPCs were composed of an entangled network of calcium deficient hydroxyapatite (CDHA) plate-like nano-crystals. The CPCs exhibited pores at two length scales, nanopores below 300 nm and macropores around 110 ± 33 μm due to air bubbles trapped during mixing. Nonetheless, the macropores were mainly connected by the nanopores and not by connections at micrometric scale. 3D reconstructions showed that the fibres and macropores were homogenously distributed in the

CPCs thus forming an isotropic material. The total porosity of the CPCs was between 50 and 60 %. PCL/Plu fibres were mechanically interlocked with the CPC matrix, showing an interphase gap around 300 nm probably due to fibre dehydration for SEM observation. Compression test show a quasi-brittle behaviour for reinforced CPCs and brittle behaviour for plain cements. The compressive strength of the plain cement was 3.3 ± 0.2 MPa. The addition of fibres increased the strength, however only 3 wt% of PCL/Plu fibres was needed to see statistical significant reinforcement (4.8 ± 0.8 MPa), while 5 wt% was needed for PCL fibres (4.4 ± 0.5 MPa). Reinforcement of CPCs with PCL fibres has been barely studied probably due to the long term degradation of PCL in physiological environment. However, the degradation rate of PCL better matches the resorption rate of apatitic CPCs, therefore long-term reinforcement may be expected. In addition, the hydrophilic modification of PCL fibres promote the mechanical reinforcement of the cement matrix.

Conclusion

The incorporation of PLGA–PEG–PLGA copolymer resulted in totally injectable CDHA bone cement with complete cohesion when injected in a liquid medium at physiological temperature. Mixing the cement at high speed with a drill allowed both the homogeneity of the fibres and the incorporation of macropores. The addition of fibres did not impair the injection of the cement but reduced the brittleness and increased the compressive strength.

Acknowledgement

To the GACR project 19-22662S and project NV18-05-00379 supported by Czech Health Research Council.

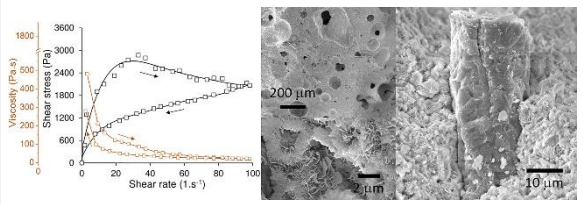

Viscosity and shear curves (left) and microstructure of the cement reinforced with PCL fibres.

VII-OS24-03

Effect of CaP Phase on Bone Growth into a Novel Porous Scaffold Based on a Marine Sponge Template.

Susan A. Clarke[1], Nicola McClelland[1], Caroline Newe[2], Alex Lennon[2], Eoin Cunningham[2], Fraser J. Buchanan[2], Nicholas J. Dunne[3]

[1]Queen's University Belfast, School of Nursing and Midwifery, Belfast, GB; [2]Queen's University Belfast, School of Mechanical and Aerospace Engineering, Belfast, GB; [3]Dublin City University, School of Mechanical and Manufacturing Engineering, Dublin, IE

Introduction

Bone tissue engineering may provide an alternative to autograft, however scaffold optimisation is required to maximise bone ingrowth. In designing scaffolds, pore architecture and resorbability of the calcium phosphate (CaP) support structure is important. For the former, there is evidence that cells prefer a degree of non-uniformity with better bone ingrowth into naturally occurring pore structures (1). For the latter, combining a more soluble phase with an insoluble phase of CaP may provide an optimal balance between stability and replacement with regenerated bone tissue (2). Using a natural marine sponge as a template, the aim of this study was to investigate the optimal phasic composition of a ceramic-based scaffold for bone ingrowth *in vivo*.

Experimental Methods

Using the marine sponge *Spongia agaracina* as a template (3, 4), scaffolds of 4 mm Ø × 8 mm L were created in three formulations: 100% b-tricalcium phosphate (b-TCP), 100% hydroxyapatite (HA) and 50:50 b-TCP:HA. These were press fit into defects created in the distal femoral condyle of New Zealand White Rabbits with autograft as a positive control. At 5, 10 and 20 weeks post-implantation, femora were retrieved, underwent mCT analysis and were then processed for histological analysis. Outcome measures included bone ingrowth, residual ceramic area and presence of osteoclasts determined by area of tartrate resistant acid phosphatase-positive staining.

Results and Discussion

The greatest amount of bone ingrowth was seen in the b-TCP scaffolds (Fig 1) and this was paired with the greatest degree of scaffold resorption (shown by mCT and histological analysis). As expected, the highest amount of residual ceramic was seen in the HA group (28% residual ceramic in defect site at 20 weeks in HA group compared to 17% in b-TCP group). It had been our hypothesis that the biphasic 50:50 scaffolds would provide the most optimal conditions for healing but this was not the case. Bone ingrowth was lowest in this group and, combining all time points, this was statistically significant compared to b-TCP group ($p=0.003$). From the histology, it appeared that “pockets” of high mineral content were created within the biphasic material (Fig 2) which slowed healing. Interestingly, the osteoclast activity also differed in the biphasic 50:50 group with no change in TRAP staining across time points whereas, in the b-TCP and HA groups, TRAP staining peaked at 10 weeks and was greatly reduced at 20 weeks. This suggests that the healing response had slowed by 20 weeks in the b-TCP and HA groups but was continuing in the biphasic scaffolds.

Conclusion

Biphasic calcium phosphates may slow bone healing when used as porous scaffolds. Monophasic ceramic scaffolds provided better bone ingrowth and supported a more natural healing cycle.

References

1. Clarke SA, Choi SY, McKechnie M, Burke G, Dunne N, Walker G, et al. Osteogenic cell response to 3-D hydroxyapatite scaffolds developed via replication of natural marine sponges. Journal of Materials Science-Materials in Medicine. 2016 Feb;27(2).

2. Dorozhkin SV. Biphasic, triphasic and multiphasic calcium orthophosphates. Acta Biomaterialia. 2012 Mar;8(3):963-77.

3. Cunningham E, Dunne N, Walker G, Buchanan F. High-solid-content hydroxyapatite slurry for the production of bone substitute scaffolds. P I Mech Eng H. 2009 Aug;223(H6):727-37.

4. Cunningham E, Dunne N, Walker G, Maggs C, Wilcox R, Buchanan F. Hydroxyapatite bone substitutes developed via replication of natural marine sponges. Journal Of Materials Science-Materials In Medicine. 2010 Aug;21(8):2255-61.

Acknowledgement

Funded by Science Foundation Ireland- North-Supplement scheme.

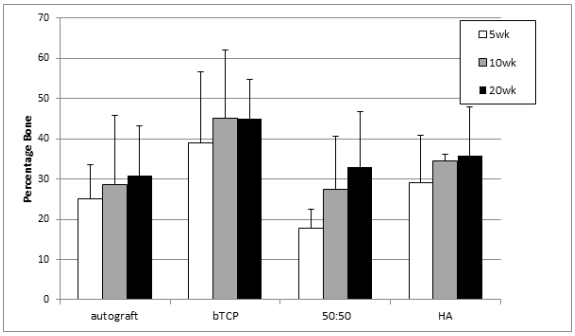

Fig 1.
Fig 1. Pecentage of bone in defect site based on area measurement in histological sections (mean + std dev).

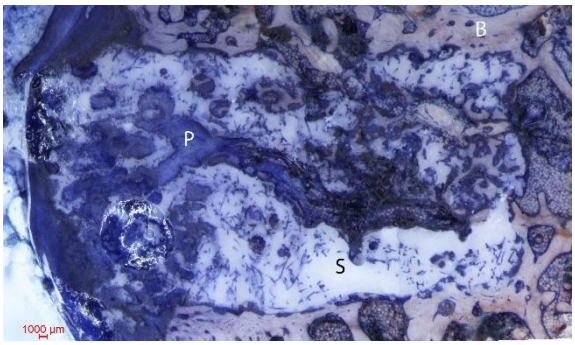

Fig 2.

Fig 2. Biphasic 50:50 implant at 5 wks (B=bone, S= scaffold P=pocket of solubilised scaffold)

VII-OS24-04

Engineered β-tricalcium-phosphate (β-TCP) scaffolds with a tailored interconnecting channel structure as a mimetic niche for the growth of metastatic neuroblastoma cells.

Sanja Aveic[1], Roswitha Davtalab[1], Michael Vogt[3], Michael Weber[1], Patricia Buttler[4], Gian Paolo Tonini[2], Horst Fischer[1]

[1]RWTH Aachen University Hospital, Department of Dental Materials and Biomaterials Research, Aachen, DE; [2]Fondazione Istituto di Ricerca Pediatrica Città della Speranza, Neuroblastoma Laboratory, Padova, IT; [3]RWTH Aachen University Hospital, Interdisciplinary Center for Clinical Research, Aachen, DE; [4]RWTH Aachen University Hospital, Department of Operative Dentistry, Periodontology and Preventive Dentistry, Aachen, DE

Introduction

Metastasis is a highly complex and dynamic process during which tumor cells disseminate away from the primary tumor sites and colonize adjacent or distant parts of the body. Metastasis faced in the red bone marrow (BM) and bones determines poor patient survival. Behavior of disseminated tumor cells in BM is strictly regulated by multifaceted three-dimensional (3D) cell-cell and cell-matrix interactions. However, molecular base of these interactions is largely unknown. Study of cancer biology within their native microenvironment is generally restricted to the use of animal models. Nowadays, a great expectation is directed towards bio-engineered platforms that can serve as a chimeric microenvironment recapitulating native tissue remarks. Adopted in the field of cancer research, these mimetic models could open new avenues for more comprehensive *in vitro* studies of the biology of BM and bone metastases.

Here we explored whether β-tricalcium phosphate (β-TCP) scaffolds with a tailored interconnecting channel structure could enable appropriate 3D mimetic BM microenvironment for the growth of metastatic neuroblastoma cells. Besides driving osteogenesis, scaffolds also established marrow supportive stroma and served as a surrogate niche for the growth of metastatic cancer cells.

Experimental Methods

Tailored calcium phosphate-based scaffolds with interconnected channels of 500 µm in diameter were manufactured by combining 3D wax printing and a slip casting technique. Primary human mesenchymal stromal cells (hMSC) from the bone marrow aspirates of healthy donors were cultured inside the scaffolds. Upon 3 weeks, tumor neuroblastoma cell line SH-SY5Y was added and cells co-cultured for the next 10 days. Cell distribution inside the scaffolds was examined by scanning electron microscopy. Gene expression studies were done by performing qPCR. Protein expression and distribution inside the cells was studied by two photon microscopy.

Results and Discussion

By combining molecular biology and standard imaging techniques we monitored organization and interaction between stromal cells and metastatic tumor cells inside the spongy-like artificial bone. Scaffolds provided the mechanical support for human mesenchymal stromal cells (hMSC) and allowed them to proliferate, differentiate towards osteoblasts, and produce the deposits of extracellular matrix. The *in vitro* microenvironment shaped by stromal cells was in following tailored by neuroblastoma tumor cells. Inside the interconnecting channels tumor cells formed the characteristic rosette-like aggregates only when co-cultured with differentiating hMSC. A growing rate

and the level of *Ki-67* of tumor cells decreased in 3D conditions with respect to the 2D counterpart. Also, the 3D culturing promoted neuroblastoma cell quiescence as sustained by increased p27 protein level. A balance between cell proliferation, survival, and differentiation was apparent for tumor cells grown inside the 3D scaffolds, thus mirroring better the situation found *in vivo*.

Conclusion

Our data sustain the proposed 3D β-TCP scaffold type as a suitable 3D mimetic *in vitro* niche for studying growth of disseminated tumor cells, and for related biological and pharmacological surveys.

References

Aveic S, Davtalab R, Vogt M, Weber M, Buttler P, Tonini GP, Fischer H (2019). Calcium phosphate scaffolds with defined interconnecting channel structure provide a mimetic 3D niche for bone marrow metastasized tumor cell growth. Acta Biomater, doi: 10.1016/j.actbio.2019.02.030. [Epub ahead of print].

VII-OS24-05

Calcium phosphate nanoparticles as genetically active coating for cochlear implant electrodes

Karolin Wey[1], Ronja Schirrmann[2], Detlef Diesing[3], Stephan Lang[2], Sven Brandau[2], Stefan Hansen[2], Matthias Epple[1]

[1]University of Duisburg-Essen, Inorganic Chemistry and Center for Nanointegration Duisburg-Essen (CeNIDE), Essen, DE; [2]University Hospital Essen, Department of Otorhinolaryngology, Essen, DE; [3]University of Duisburg-Essen, Physical Chemistry, Essen, DE

Introduction

Severe hearing problems such as impaired hearing or deafness are frequent disabilities. They can be caused by damaged and degenerated hair cells in the inner ear, resulting in an atrophy of spiral ganglion cells (SGC). To regain the ability to hear, cochlear implants are a common treatment. The possible regain of hearing depends on the extent of the degeneration of the cells inside the inner ear. In dependence of the SGCs atrophy, the production of neuronal growth factors decreases as well. The implant consists of a silicon tube with several platinum electrodes, giving the possibility for frequency-dependent locations to stimulate the SGC. Thereby, the cochlear frequency-specific sound detection is mimicked. Platinum as electrode material has a high electrical conductivity but a very low cell adherence due to its smooth surface. Therefore, a gap between implant and SGC may remain, lowering the electrical signal transmission. To improve the implant performance, a biocompatible coating can be applied. Furthermore, this coating can be used to deliver functional biomolecules. To enhance the production of neuronal growth factors as well as to improve the cell adherence, a biodegradable coating of calcium phosphate nanoparticles carrying functional DNA was prepared in a layer-by-layer (LbL) method on the electrodes of a cochlear implant.

Experimental Methods

The particles were prepared by a precipitation method as described earlier and loaded with protein-encoding plasmid DNA (pDNA) for the neuronal growth factors BDNF and NT3.[1] To protect the pDNA from nucleases, a calcium phosphate shell was applied. Figure 1 shows the synthesis of the calcium phosphate nanoparticles. Dynamic light scattering (DLS), scanning electron microscopy (SEM) and atomic absorption spectroscopy (AAS) were carried out to characterise the particles. The pDNA concentration loaded onto the particles was determined by ultraviolet-visible spectroscopy (UV-Vis).

The coating procedure was carried out by applying alternating layers of poly-L-lysine (PLL) and calcium phosphate nanoparticles.[2] To quantify the loading of particles for the coating, AAS was carried out.

Results and Discussion

SEM imaging showed that the particle morphology was not affected by the coating process. Contact angle measurements showed an increasing wettability for the coated surfaces. A positive zeta potential was determined by streaming potential measurements. To determine the effect of the coating to the electrical resistance across the implant surface, electrochemical impedance spectroscopy (EIS) was carried out. Cell culture studies were carried out with HeLa cells as well as primary cells from spiral ganglion explants of rats (p3 to p7). Experiments were carried out for coated substrates and dispersed particles. The protein expression for neuronal growth factors was quantified by ELISA.

Confocal laser scanning microscopy (CLSM) showed that the particles were taken up into all investigated cells. Transfection experiments using nanoparticles loaded with EGFP-encoding DNA confirmed the applicability of our approach on glass coverslips as model substrates.

Conclusion

The results show, that coating substrates with pDNA loaded calcium phosphate nanoparticles give a genetically active coating.

References

[1] V. V. Sokolova, I. Radtke, R. Heumann, M. Epple, *Biomaterials* **2006**, *27*, 3147-3153.

[2] X. Zhang, A. Kovtun, C. Mendoza-Palomares, M. Oulad-Abdelghani, F. Fioretti, S. Rinckenbach, D. Mainard, M. Epple, N. Benkirane-Jessel, *Biomaterials* **2010**, *31*, 6013-6018.

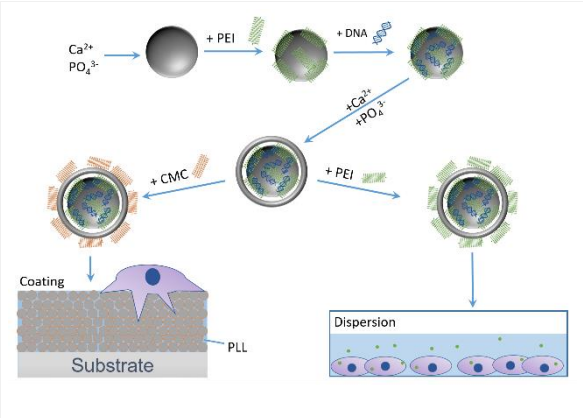

Figure 1:
Transfection of cells from the surface of cochlear implants (left) and in dispersion as control (right).

VII-OS24-06

Single-phase and phase mixtures of metastable and stable calcium pyrophosphate and tricalcium phosphate nanopowders for new biomaterials production

Zoltan Zyman[1], Matthias Epple[2], Anton Goncharenko[1], Olha Khavroniuk[1], Dmytro Rokhmistrov[1]

[1]V.N. Karazin Kharkiv National University, Physics of Solids Department, Kharkiv, UA; [2]University of Duisburg-Essen, Inorganic Chemistry and Centre for Nanointegration Duisburg-Essen (CeNIDE), Essen, DE

Introduction

Calcium phosphates (CPs) have been widely used in various fields of medicine. The majority of CPs products is ceramics. The so-called next-generation CP biomaterials has been more and more requested. Many studies have been devoted last time to the products based on high-temperature α-tricalcium phosphate, α–$Ca_3(PO_4)_2$ (α-TCP, Ca/P = 1.5), in particular, on its metastable form ᾱ-TCP which crystallizes at mediate temperatures. ᾱ-TCP usually forms jointly with β-TCP, and a single phase ᾱ-TCP can be prepared only under certain conditions. The majority of CPs used in medicine has an atomic ratio within 1.5–1.67. Studies on CPs with Ca/P < 1 have mainly been performed in context of the biomineralization problem. However, it was recently found that ceramics based on β-calcium pyrophosphate, β-$Ca_2P_2O_7$ (β-CPP, Ca/P=1) are even more bioactive under certain conditions than HA. Besides, both the metastable ᾱ- and stable β-forms of CPP positively affects the sintering of β-TCP [1].

The present study shows how via the conventional simple and cheap nitrate synthesis single-phase ᾱ- and β-CPPs, ᾱ- and β-TCPs, as well as their desired mixtures were prepared as nanopowders.

Experimental Methods

The fast precipitation modification of the nitrate synthesis was used [2]. All syntheses were proceeded for 1 min. After this time, an emerged slurry (precipitate in the mother solution) was treated according to three procedures. *Procedure 1.* The slurry was lyophilized. The almost dry mass obtained was then defrosted at about 1 °C and rinsed for 30 min with 0.5 L of distilled water at 5 °C and pH 10. The rinsing water was decanted, and the precipitate was rinsed again under the same conditions. The resulting twice-rinsed precipitate was lyophilized until a seemingly dry friable powder was obtained (powder 1 in the following). *Procedure 2.* It was performed similar to procedure 1 (excluding preliminary freezing), however, the volume of rinsing water (2 L) was twice as those in procedure 1 (resulted in powder 2). *Procedure 3.* It was conducted similar to the former two procedures, but the volume of water (3 L) and the rinsing duration (3 h) were thrice as those in procedure 1 (powder 3). The as prepared powders 1–3 were heat-treated (5 K/min) in air to various temperatures in the range of 20-1000 °C in a muffle furnace, cooled to a room temperature and examined by XRD, TG-DTA, IR, ESEM and EDX.

Results and Discussion

Powder 1. The as-prepared powder was XRD-amorphous and retained this state until 500 °C. The crystallization started above 500 °C, and two phases, ᾱ-CPP with some admixture of β-CPP (~30 wt%), were formed. As the temperature was increased to and above 800 °C, ᾱ-CPP gradually transformed to β-CPP. *Powder 2.* The rinsing time for the powder was as the total rinsing time for powder 1. However, the volume of used water W compared to the volume of the slurry S was about three times higher (W/S =1 L : 0.3 L = 3.3). This increase resulted in the following.

Though the initial powder 2 was also XRD-amorphous, its crystallization started at a noticeably higher temperature above 600 °C, and the main phase formed was α-TCP. The crystallization completed at 800 °C, and α-TCP started transforming to β-TCP above this temperature. At 900 °C, a two-phase α-TCP/β-TCP mixture formed, and a single-phase β-TCP was fixed at 1000 °C. *Powder 3*. The crystallization happened above 680 °C, and a single-phase metastable α-TCP formed at 800 °C. Above this temperature, α-TCP started transforming to stable (at these intermediate temperatures) β-TCP, and a single-phase β-TCP formed at 1000 °C.

Conclusion

It was revealed that ordinary water rinsing the precipitates before lyophilization beside removal of concomitant by-product and contaminated foreign ions can simultaneously be used for hydrolysis. The hydrolysis/rinsing procedure under certain conditions (a high water/slurry volume ratio, relatively prolonged treatment at a low temperature and high pH) resulted in the increase of the Ca/P ratio of the precipitates from the given value of 1:1 to 1.5, and tricalcium phosphates in metastable (α-TCP) and stable (β-TCP) forms, as well as their mixtures with each other and of CPP's in a desired proportion were prepared by heating the hydrolyzed products. The processed single-phase and polyphasic powders are nanocrystalline and can be used for producing prospective biomaterials.

References

1. Lee JH, Key Eng Mat, 240–242:399–402 2003
2. Zyman ZZ, J Mater Sci Mater Med, 21:123–130 2010

10:30 a.m. – 12:00 p.m.

Hall 5

VII-OS25 | Polymers for drug release

VII-OS25-KL01

Drug refillable polymers for chronic and recurrent disease

Horst A. von Recum[1]

[1]Case Western Reserve University, Executive Vice Chair Biomedical Engineering, Cleveland, US; [2]Society for Biomaterials, President, Mount Laurel, US

While drug delivery has been a powerful tool in clinical applications - being capable of local drug administration, and overcoming systemic dosing effects - all devices are ultimately limited in the amount of drug they can hold. A device would be considered unsuccessful if it is empty before the disease is cured. As such, drug delivery devices are typically not used for recurrent or chronic diseases. Our group has pioneered the use of molecular interactions to drive the in situ refilling of drug delivery systems after they have been implanted, and successfully used them to treat recurrent disease such as implant infection, and tumor recurrence. This refilling, we will show, is possible after implantation of empty devices, allowing user and/or need specific refilling and subsequent delivery. We will also show in the case of infection that drug refilling and subsequent delivery is even possible after bacterial colonization and formation of bacterial bioflim. Lastly, in this work we will show that this refilling strategy can be further applied to chronic disease, such as macular degeneration and osteoarthritis, where following diagnosis a patient can expect to undergo lifelong debilitating conditions including pain, inflammation, and degeneration. We have demonstrated that through local tissue injections, polymers can be refilled with additional doses of drugs, for multiple therapeutic delivery windows.

VII-OS25-02

A novel family of fully biodegradable peg-dendrimers as efficient carriers for gene therapy

Victoria Leiro[1], Ana P. Spencer[1,2], Natália Magalhães[1], Ana P. Pêgo[1,2,3]

[1]Universidade do Porto, INEB-Instituto de Engenharia Biomédica and i3S-Instituto de Investigação e Inovação em Saude, OPO, PT; [2]Universidade do Porto, Faculdade de Engenharia da Universidade do Porto (FEUP), OPO, PT; [3]Universidade do Porto, Instituto de Ciências Biomédicas Abel Salazar (ICBAS), OPO, PT

Introduction

Dendrimers are promising carriers of different bioactives[1] in the nanomedicine field, due to their unique key features: globular, well-defined, very branched and controllable nanostructure, low polydispersity and multivalency. Particularly relevant is their capacity to complex and protect nucleic acids (NA) in compact nanostructures protecting them from degradation and rapid renal clearance.[2]

However, one important disadvantage of the most commonly used dendrimers is their non-degradability under physiological conditions, that can lead to toxicity by bioaccumulation. Moreover, in the gene therapy field, vector stability can further hinder the intracellular release of the NA, consequently leading to low transfection efficiencies (TE).[3] Therefore, recent interest has focused on the development of biodegradable dendrimers, but only few works report their biomedical applications.[4] Because of this, we have recently reported a new family of partially/hybrid biodegradable PEG-dendrimers for siRNA delivery.[5,6] Our systems showed a great ability to internalize siRNA,[6] yet a low transfection efficiency was observed due to the partial vector stability.

Here, we present our new fully biodegradable PEG-dendrimers,[5] as well as their function as siRNA vectors. Fully degradability favoured the intracellular siRNA release, leading to higher TE.

Experimental Methods

Fully biodegradable PEG-dendrimers were synthesized and subsequently functionalized by copper(I)-catalyzed azide alkyne cycloaddition (CuAAC, click chemistry) with different amine moieties. All copolymers were characterized by NMR and FTIR.

siRNA dendriplexes were prepared at different N/P ratios (N=number of primary amines in the conjugate; P=number of phosphate groups in the RNA backbone) ranging from 5 to 80 by adding siRNA to different volumes of dendrimer solution. The siRNA complexation efficiency for the dendrimers was assessed by polyacrylamide gel electrophoresis and SybrGold® exclusion assays. The resulting dendriplexes were characterized regarding their size, polydispersion index (PdI) and zeta potential by dynamic light scattering (DLS), and their morphology was studied by transmission electron microscopy (TEM). Relative metabolic activity in the presence of dendrimers and dendriplexes was evaluated by the resazurin assay in U2OS and ND7/23 cells. Cellular association/uptake and silencing assays were carried out in U2OS and ND7/23 cells expressing the fusion protein eGFP-Luciferase (U2OS/eGFPLuc and ND7/23-eGFPLuc cells) and evaluated by flow cytometry.

Results and Discussion

Fully biodegradable PEG-dendrimers have been successfully synthesized until generation 3 (G3) and characterized by NMR and FTIR. They can be efficiently functionalized with different terminal groups; thus, they can act as suitable and versatile vectors for several biomedical applications.

In the present work, their successful functionalization with different amine groups allowed the efficient complexation and protection of siRNA and, therefore, to explore their potential as vectors of this nucleic acid. The resulting dendriplexes were characterized in terms of their physicochemical properties, showing sizes and PdI's and morphologies very suitable for cellular uptake. PEG-dendrimers and their corresponding siRNA-dendriplexes showed no toxicity in U2OS and ND7/23 cell lines. Moreover, their biological performance was evaluated regarding internalization and TE in these cell lines. These fully biodegradable nanosystems showed a great ability to complex, protect and mediate the internalization of siRNA. Interestingly, the fully degradable character was crucial for an efficient siRNA intracellular release, contributing to an excellent silencing effect.

Conclusion

A new family of fully biodegradable, biocompatible and non-toxic PEG- dendrimers is presented. Their CuAAC functionalization with different amine groups allowed the efficient complexation, protection and successful intracellular delivery of siRNA. The biodegradable dendritic nanosystems developed here can be easily and efficiently functionalizated with different ligands by click chemistry, thus the present study puts forward then not only as suitable vectors for nucleic acids, but also opens new avenues for further developments exploring their use in theranostics.

References

1. Leiro, V. et al. (2017) Adv. Funct. Mater. DOI: 10.1002/adfm.201700313.
2. Leiro, V. et al. (2017) Curr. Gene Ther. 17(2), 105.
3. He, C.L. et al. (2012) Adv Healthc Mater 1, 48.
4. Leiro, V. et al. (2015) Bioconjug. Chem. 26 (7), 1182.
5. Leiro, V. et al. (2017) J. Mat. Chem. B. 5, 4901.
6. Pêgo, A.P., Leiro, V. et al, inventors; Biodegradable Dendritic Structure, Methods and Uses Thereof. WO/2017/203437.

Acknowledgement

FCT (SFRH/BPD/69110/2010, BAITS (PTDC/CTM- NAN/3547/2014)); siRNAC (NORTE-01-0247-FEDER-033399); NORTE-01-0145-FEDER-000008 and NORTE-01-0145-FEDER-000012.

VII-OS25-03

Delivering microRNA-31 via Electrospun Nanofibres for the Treatment of Non-healing Wounds

Eoghan J. Mulholland[1], Nicholas J. Dunne[1,2,3], Helen McCarthy[1], Monika Ziminska[1]

[1]Queen's University Belfast, Pharmacy, Belfast, GB; [2]Dublin City University, Centre for Medical Engineering Research, Dublin, IE; [3]Dublin City University, School of Mechanical and Manufacturing Engineering, Dublin, IE; [4]Trinity College Dublin, Trinity Centre for Bioengineering, Dublin, IE; [5]Trinity College Dublin, Department of Mechanical and Manufacturing Engineering, Dublin, IE; [6]Royal College of Surgeons in Ireland and Trinity College Dublin, Advanced Materials and Bioengineering Research Centre (AMBER), Dublin, IE

Introduction

Chronic wounds affected 637,567 patients in Ireland >65 between 2011 and 2016 and this is forecast to reach 875,000 patients by 2025.[1] It has been reported that the cost of treating one patient with three Grade IV pressure ulcers was €119,000 over a duration of 129 days.[2] The primary drivers (85-90%) of these costs are attributed to nursing time and hospitalisation.[3,4] This equates to a staggering cost of €75B over a 5-year period. MicroRNAs (miRs) act as post-transcriptional regulators of multiple proteins and therefore have great potential as therapeutics in complex pathways with several stages such as those found in wound healing. Herein, we developed a new genetic nanomedicine for the treatment of chronic wounds. Nanoparticles (NPs) were designed to deliver DNA encoding miR-31, up-regulates multiple proliferative and angiogenic genes. A novel linear peptide system '*PEP*' was also designed to deliver the pmiR-31 cargo intracellularly. The NPs were delivered via electrospun PVA nanofibres (PVA-NF), designed to facilitate temporal controlled delivery *in vivo*.

Experimental Methods

The NPs were synthesised by self-assembly and the particle size and zeta potential determined by Dynamic Light Scattering. NCTC-929 fibroblast, HMEC-1 endothelial and HaCaT keratinocyte cells were transfected with *PEP*/pmiR-31 NPs, which was quantified via qRT-PCR. The functional effects of miR-31 upregulation on cell migration and angiogenesis were subsequently assessed using wound scratch and tubule formation assays. An experimental design approach was used to optimise the PVA-NF electrospun wound patch, which was crosslinked prior to NP loading. The functionality of the wound patch was investigated with an *in vivo* full thickness wound model using C57BL/6N mice. After seven days, each mouse was sacrificed, and the wound bed harvested for histological examination.

Results and Discussion

PEP successfully condensed pmiR-31 into NPs with particles sizes <100 nm and zeta potential of ~10 mV for N:P ratios ≥4. Furthermore, transfection analysis with each cell line showed significant upregulation of miR-31 (**Figure 1A**). Expression of miR-31 increased cell migration rates in the HaCaT (p-value<0.01), HMEC-1 (p-value<0.05) and NCTC-929 (p-value<0.05) cell lines. Treatment resulted in a significant increase in the rate of angiogenesis (p-value<0.05) with HMEC-1 cells. Complete NP release from the PVA-NFs was achieved within 48 h and gel electrophoresis showed that loaded DNA was undamaged (**Figure 1B**). *In vivo* evaluation showed there was a significant increase in epidermal (p-value<0.05) and stratum corneum thickness (p-value<0.001), as well an

increased blood vessel density (**Figure 1C**). All of which are indicative of an increase in keratinocyte functionality and angiogenesis.

Conclusion

*PEP/*pmiR-31 delivery via PVA-NF-based patches can have significant effects on cellular function for *in vitro* and *in vivo* wound healing. Further studies will involve the functional assessment of the wound patch in a delayed wound healing model *in vivo*, using a diabetic mouse model.

References

1) CSO (2017) Statistics: Population by age 2017. Central Statistics Office; 2) Gethin *et al.* J Wound Care. 2005;14(4):162-165; 3) Carr *et al.* 1999;8(5):243-248; 4) Posnett *et al.* Nurs Times. 104(3):44-45; 5) Mulholland *et al.* Molecular Therapeutics, 2017.

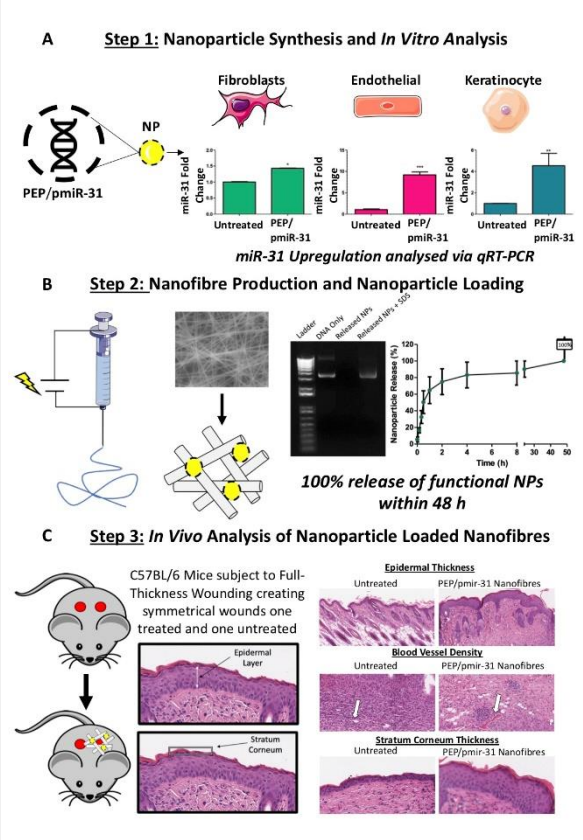

Figure 1
Evaluation of PEP/pmiR-31 NPs potential for wound healing via PVA-NFs. (A) NP synthesis and effect of transfection on miR-31 levels in skin cell lines. (B) Fabrication of PVA-NF by electrospinning and loading with NPs. (C) Evaluation of the wound patch in vivo with subsequent histological examination.

VII-OS25-04

Hyaluronan/Collagen-Based Hydrogels as Scavenging and Release Systems For Improved Wound Healing

Sandra Rother[1], Stephan Thönes[2], Vera Krönert[1], Nicolas Hauck[3], Tom Wippold[2], Albrecht Berg[4], Stephanie Moeller[4], Matthias Schnabelrauch[4], Julian Thiele[3], Dieter Scharnweber[1], Ulf Anderegg[2], **Vera Hintze**[1]

[1]TU Dresden, Max Bergmann Center of Biomaterials, Dresden, DE; [2]Leipzig University, Department of Dermatology, Venereology and Allergology, Leipzig, DE; [3]Leibniz-Institut für Polymerforschung Dresden e.V., Institute of Physical Chemistry/Polymer Physics, Dresden, DE; [4]INNOVENT e.V., Biomaterials Department, Jena, DE

Introduction

The demographic development with an ever increasing number of multimorbid patients with reduced healing capacity raises the need for novel biomaterial approaches. Functional biomaterials able to bind, stabilize and release bioactive proteins in a defined manner would allow for adjustable growth factor interaction profiles fostering wound healing. Non-immunogenic hyaluronan (HA)/collagen-based hydrogels can be adapted in this respect via the incorporation of sulfated glycosaminoglycans. Chemically sulfated HA derivatives (sHA), in particular the high-sulfated sHA3, were shown to positively influence numerous aspects of skin repair [1]. The goal of this study was the development and characterization of bioinspired HA/collagen hydrogels containing sHA that promote skin regeneration either by binding and controlled release of relevant growth factors, e.g. heparin-binding EGF-like growth factor (HB-EGF), or by scavenging and thereby rebalancing dysregulated factors, e.g. transforming growth factor β1 (TGF-β1). The latter is particularly relevant in fibrotic conditions.

Experimental Methods

Hydrogels were prepared by crosslinking HA and low-sulfated sHA acrylates in the presence of collagen followed by lyophilization [2, 3]. However, the high substitution degree of sHA3 impedes the introduction of crosslinkable groups. A new strategy to incorporate non-modified sHA3 into hydrogels allowing for a controllable sHA3 retention is therefore required. One option is incorporating sHA3 into HA/collagen-based hydrogels using HA-based microgels generated in a microfluidic approach, which contained artificial extracellular matrix composed of collagen and sHA3. The appearance and size distribution of microgels was analyzed by microscopy after staining for the collagen and sHA3. The composition and stability of hydrogels were biochemically characterized in terms of HA, sHA and collagen release. The HB-EGF and TGF-β1 release profiles were examined via ELISA. The biological effects of gel composition and released HB-EGF were analyzed in cell culture using keratinocytes and fibroblasts, while wound closure was investigated in a porcine skin culture model.

Results and Discussion

Hydrogels containing low-sulfated sHA bound and released bioactive HB-EGF over at least 72 h, thereby inducing keratinocyte migration and hepatocyte growth factor expression in dermal fibroblasts. Importantly, hydrogels containing sHA strongly increased the effectivity of HB-EGF in inducing epithelial skin wound closure in a porcine skin organ culture model [4].

Incorporating sHA3-containing aECM in microgels significantly enhanced the retention of non-crosslinked sHA3 within the bulk HA/collagen-based gels allowing a controlled sHA3 presentation. Gels containing sHA3 bound higher amounts of TGF-β1 compared to pure HA/collagen hydrogels. Moreover, the presence of sHA3-containing microgels improved the TGF-β1 retention within the hydrogels.

Conclusion

These findings suggest that hydrogels containing sHA can be engineered as effective wound dressings with adjustable sHA release and growth factor interaction profiles to foster skin regeneration.

References

[1] Scharnweber et al., J Mater Sci: Mater Med 26(2015), 232
[2] Rother S et al. Macromol Biosci, (2017), *17* (11), 1-13
[3] Becher et al., Carbohydrate Polymers 93(2013), 438-441
[3] Thönes et al., Acta Biomaterialia 86 (2019) 135–147

Acknowledgement

We acknowledge financial support (DFG Transregio 67; subprojects A3, A7, B4, Z3).

VII-OS25-05

Nanoparticles based on dexamethasone and naproxen for the combined treatment of inflammatory processes

Eva Espinosa-Cano[1,2], Maria Rosa Aguilar[1,2], Yadileiny Portilla[3], Domingo Barber[3], Julio San Roman[1,2]

[1]Institute of Polymer Science and Technology (ICTP-CSIC), Biomaterials Group, Madrid, ES; [2]Networking Biomedical Research Centre in Bioengineering, Biomaterials and Nanomedicine (CIBER-BBN), Madrid, ES; [3]Spanish National Center of Biotechnology (CNB-CSIC), Madrid, ES

Introduction

Recent studies have demonstrated the synergistic immunosuppressive and anti-inflammatory capacity of dexamethasone (DEXA) and naproxen (NAP) [1]. However, the low solubility of these drugs and their adverse effects reduce their efficacy on the treatment of inflammatory processes [2, 3] being nanoparticulated systems promising candidates to overcome these drawbacks [4]. This work aims to prepare an anti-inflammatory system based on self-assembled polymeric nanoparticles (NPs) that incorporate NAP and DEXA to improve retention at inflammation site and reduce their dose- and time-dependent side effects keeping DEXA disease-modifying capacity to repolarize M1 macrophages to M2 anti-inflammatory phenotype.

Experimental Methods

Monomer and Copolymer Preparation. A methacrylic derivative of NAP (HNAP) was prepared and characterized by ^{1}H-NMR. Poly(HNAP-*co*-VI) copolymers were synthesized by free radical copolymerization at different feed molar fractions of HNAP: 0.2, 0.5 and 0.8. HNAP copolymer molar fraction (f_{HNAP}) and monomers reactivity ratios (r_{HNAP} y r_{VI}) were determined by ^{1}H-NMR or *in-situ* ^{1}H-NMR.

NPs preparation and Characterization. NPs were prepared by nanoprecipitation method. Hydrodynamic properties (i.e. size, PdI and surface charge) were determined by Dynamic Light Scattering and Laser Doppler Electrophoresis. Stability in suspension was assessed up to one month. 15 % (w/w) DEXA and 1% (w/w) coumarin-6 (c6) were encapsulated in order to study NPs cytotoxicity and anti-inflammatory capacity or NPs cellular uptake, correspondingly. The encapsulation efficacy (%EE) was determined by HPLC and UV spectrophotometry, respectively.

***In Vitro* Evaluation of the System.** An extensive *in vitro* evaluation of the NPs was performed comparing the DEXA-loaded system with the unloaded system and the free drug. NPs uptake rate by murine macrophages (RAW264.7) was assessed by c6-loaded NPs endocytosis studies. Macrophage viability at different NPs concentrations was tested (Alamar Blue assay) and anti-inflammatory capacity was evaluated by nitric oxide (NO) release studies and RT-PCR quantification of M1 or M2 phenotype marker genes.

Results and Discussion

Monomer and Copolymer Preparation. *HNAPmonomer* was obtained with yields > 90%. *Poly(HNAP-co-VI) copolymers* were successfully obtained as demonstrated by ^{1}H-NMR. The acute differences in reactivity ratios of both monomers ($r_{HNAP} = 10r_{VI}$) resulted into a gradient amphiphilic microstructure.

NPs preparation and Characterization. Those copolymers with $f_{HNAP} < 0.8$ formed NPs in aqueous media. The synthesis protocol and storage conditions were optimized so that their diameter (130 nm) and surface charge (+30 mV) may favor an efficient retention at the inflamed tissue. The system demonstrated to be stable up to one month

in suspension with no significant changes in hydrodynamic properties over time. DEXA and c6 were successfully encapsulated with %EE = 8 and 92 %, correspondingly.

***In Vitro* Evaluation of the System.** NPs uptake by RAW264.7 macrophages increases linearly over time with more than 60% of the initial c6 internalized after 8 hours of exposure demonstrating the system potential for improve retention at inflamed areas avoiding clearance by the lymphatic system. Cytotoxicity studies showed a statistically significant reduction of the cell viability when comparing encapsulated DEXA with the free drug. No significant differences in % NO release and M1/M2 genes expression ratios were observed when DEXA-loaded NPs are compared to free drug. Results demonstrate no compromise of the anti-inflammatory capacity of encapsulated DEXA.

Conclusion

DEXA-loaded NAP-based NPs were successfully prepared with hydrodynamic properties that may favor accumulation and retention at inflamed areas as they are rapidly sequestered by macrophages. *In vitro* biological studies demonstrated a reduced cytotoxicity without compromising anti-inflammatory activity of DEXA when compared to the free drug.

References

1. Li, X., et al., *Drug Metab. Dispos.45*: 834, 2017
2. Moghadam-Kia, S., Werth V. P., *Int. J. Dermatol.49*: 239, 2010
3. McCaulley, M. E., Grush, K. A., *Int. J. Alzheimers Dis.2015*: 10, 2015
4. Kamaly, N., et al., *Chem. Rev.116*: 2602, 2016

Acknowledgement

The authors would like to thank CIBER-BBN, the Spanish Ministry of Science, Innovation and Universities (MAT2017-84277-R) and the training program for Academic Staff (FPU15/06109) of the Spanish Ministry of Education Culture and Sport.

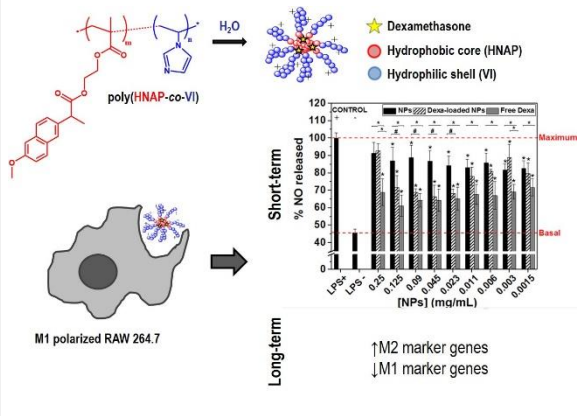

Graphical Abstract
(Up) Schematic presentation of the copolymeric system and nanoparticulated system obtained when it self-assembles in water. **(Down)** Schematic presentation of the *in vitro* evaluation of the anti-inflammatory capacity of the system.

10:30 a.m. – 12:00 p.m.

Conference room 4+5

VII-SY12 | DGBM SY: Biodegradable metallic implants

Regine Willumeit-Römer (Geesthacht, DE)
Anke Bernstein (Freiburg, DE)

VII-SY12-KL01

Biodegradable Metals with Extreme Properties for Innovative Biomaterials

Diego Mantovani

Laval University, Quebec University Hospital, Dept of Min-Met-Materials Engineering & Research Center, Québec, CA

Over the last 50 years, biomaterials, prostheses and implants saved and prolonged the life of millions of humans around the globe. The main clinical complications for current biomaterials and artificial organs still reside in an interfacial mismatch between the synthetic surface and the natural living tissue surrounding it. Today, nanotechnology, nanomaterials and surface modifications provides a new insight to the current problem of biomaterial complications, and even allows us to envisage strategies for the organ shortage. Advanced tools and new paths towards the development of functional solutions for cardiovascular clinical applications are now available. In this talk, the potential of nanostructured metallic degradable metals to provide innovative solutions at medium term for the cardiovascular field will be depicted. Focus will be on Fe-based biodegradable metals with exceptional resistance, ductility and elasticity, for pushing innovative applications in vascular surgery. The intrinsic goal of this talk is to present an extremely personal look at how biodegradable metals can impact materials, surfaces and interfaces, and how the resulting unique properties allowed biomedical functional applications to progress, from their introduction, to the promising future that biodegradable metals may or may not hold for improving the quality of the life of millions worldwide.

VII-SY12-KL02

Zn- and Mg alloys as biodegradable materials of cardiovascular devices

Christoph Hehrlein

University of Freiburg, Cardiology, Freiburg, DE

Introduction

Non-degradable metals used such as cobalt chromium or nitinol used as a platform for stents or heart valves are the gold standard in terms of mechanical strength and scaffolding properties. However, chronic foreign body reactions and non-physiologic vessel restraints, i.e. the “caging” of anatomic structures, have intensified the search for strong but yet degradable metallic backbones of cardiovascular implants. Zn and Mg are essential trace elements of the human body that are daily incorporated without toxic side effects. Allergies towards the two trace elements do not exist. Both metals are characterized by an excellent biocompatibility, and Zn- and Mg alloy platforms have emerged as valuable implant alternatives compared with non-degradable metals in recent trials.

Experimental Methods

-Modern Zn- and Mg-stents and stentgrafts are characterized by an alloy backbone that fulfills mechanical requirements of an implant in human arteriosclerotic disease by far better that currently tested bioresorbable polymer stents. In addition, superior performance in terms of elongation to fracture rate, lessened elastic recoil, and consistent degradation pattern will lead to a rapidly increasing clinical utility of Zn-and Mg stents.

Results and Discussion

-Mg-stents have already been approved in Europe and have been tested extensively in clinical trials of coronary artery disease. The best studied Mg-stent (Magmaris) is characterized by complete human biocompatibility and performs similar compared with standard cobalt chromium stents if catheter based removal of calcium rich stenotic plaques was performed by the physician prior to vessel implantation. A novel approach is a Zn alloy stent platform which allows a faster and more precise stent implantation with better mechanical performance in pre-clinical animal models. Furthermore, Mg alloys cause damaging H_2 production and rapid material degradation whereas Zn alloys do not. Thus, Zn alloy could replace Mg alloy as a stent with better scaffolding properties in the near future.

Conclusion

Zn- and Mg alloys are good and clinically needed candidates for the improvement of cardiovascular implant technology according to recent studies worldwide. The results of ongoing trials studying these implants are eagerly awaited.

References

Hehrlein C et al, PLoS One 2019

VII-SY12-03

Fe-Fe_2O_3 nanocomposites for biodegradable load-bearing implants: processing, properties, loading and release of drugs

Aliya Sharipova[1,3], Irena Gotman[2], Sergey Psakhie[3], Ronald Unger[4], Elazar Gutmanas[1]

[1]Technion, Materials Science and Engineering, Haifa, IL; [2]ORT Braude Academic College, Mechanical Engineering, Karmiel, IL; [3]Institute of Strength Physics and Materials Science of Siberian Branch Russian Academy of Sciences, Tomsk, RU; [4]University Medical Center of the Johannes Gutenberg University, Institute of Pathology, Mainz, DE

Introduction

Development of biodegradable materials for bone repair is one of the important research directions in recent years. For fracture fixation and scaffolding applications, the use of biodegradable implants eliminates the need for second surgical intervention of implant removal. In addition, use biodegradable materials will allow complete tissue regeneration without the risk of chronic inflammation and stress shielding.

For load-bearing applications, biodegradable polymers are weak and biodegradable ceramics are brittle. Biodegradable metals such as Mg and Fe are strong and ductile and are considered promising candidates for load-bearing biodegradable orthopedic implants. However, degradation of Mg based materials is too fast and accompanied by release of hydrogen. Degradation rate of Fe based alloys is too low for biodegradable orthopedic implants, since complete degradation requires more than a year[1,2].

In recent studies we showed that pronounced increase of Fe degradation rate can be achieved in Fe-Ag nanocomposites as a result of formation of Fe-Ag nanogalvanic couples, as compared to degradation rate of Fe-Ag composites with grainsize of tens of microns[3]. In present research nanosize iron oxide (Fe_2O_3) was introduced as the cathodic second phase to increase the degradation/corrosion rate of nanostructured Fe. Fe_2O_3 nanoparticles are especially attractive due to their broad biomedical applications, such as magnetic resonance imaging (MRI) and targeted delivery of drugs in tumor therapy.

Experimental Methods

Fe-10Fe_2O_3 nanocomposite powders were prepared employing two methods: a) high-energy attrition milling of Fe and Fe_2O_3 nanopowders blends for 30 min; b) partial reduction of Fe_2O_3 nanopowder in hydrogen flow at 425°C for 1.5 h (schema in Fig. 1). Nanocomposite powders were cold sintered/high pressure consolidated at pressures up to 3GPa to result in near dense Fe-Fe_2O_3 nanocomposites with 4-5% open porosity that was used for drug loading. Heat treatments at 300°C in Ar flow were employed to remove residual stresses caused by plastic deformation during consolidation and improve bonding between particles.

Materials were characterized by XRD, SEM, HRSEM with EDS. Mechanical properties were tested in compression and bending. Degradation behavior *in vitro* was studied employing immersion test in saline solution for periods up to 4 weeks. Drug loading into interconnected system of open pores and drug release into TRIS solution was investigated using antibiotic - vancomycin and antitumor drug -doxorubicin.

Toxicity of developed nanocomposites was studied *in vitro* on human osteoblast cells.

Results and Discussion

High resolution SEM micrograph of Fe-10Fe_2O_3 nanocomposite cold sintered from partially reduced Fe_2O_3 is presented in Fig. 2 (plasma etched surface). Partial reduction of Fe_2O_3 nanopowders allowed to obtain Fe-10Fe_2O_3 nanocomposites with more homogeneous distribution of finer Fe_2O_3 phase as compared to nanocomposites prepared from attrition milled Fe-Fe_2O_3 nanocomposite powders. Near to dense (95% theoretical density) Fe-10Fe_2O_3 nanocomposites from partially reduced Fe_2O_3 nanopowders with <100 nm grainsize exhibited high strength of 1035 MPa in compression, slightly higher than from attrition milled powders. This is 4 times higher than reported data for Fe-10Fe_2O_3 with grainsize 25 μm[4]. Annealing at 300°C resulted in improvement of ductility with retention of nano-structure and high mechanical properties. The degradation rate of cold sintered Fe-10Fe_2O_3 nanocomposites after 4 weeks immersion was 2-fold that of the nanostructured pure Fe and 30 times higher than for Fe-10Fe_2O_3 composites with micron size grains. The proposed processing approach allows loading of antibiotics and antitumor drugs *via* incorporation into the interconnected system of open nanopores of Fe-Fe_2O_3 nanocomposites under vacuum and following slow release of drugs from nanopores.

Conclusion

High mechanical properties of biodegradable Fe-10Fe_2O_3 accompanied by high degradation rate required for biodegradable implants were obtained by nanostructuring and homogeneous distribution of galvanic Fe-Fe_2O_3 nanocouples. Interconnected system of open nanopores obtained during high pressure consolidation allowed vacuum loading of antibiotic and antitumor drugs into Fe-10Fe_2O_3 nanocomposites and slow release of drugs during immersion of specimens into TRIS solution. In cell culture experiments, Fe-10Fe_2O_3 nanocomposites supported the attachment of human osteoblast cells and exhibited no signs of cytotoxicity.

References

1. H. Hermawan, H. Alamdari, D. Mantovani and D. Dubé, *Powder Metall.*, 2008, **51**, 38–45.
2. T. Kraus, F. Moszner, S. Fischerauer, M. Fiedler, E. Martinelli, J. Eichler, F. Witte, E. Willbold, M. Schinhammer, M. Meischel, P. J. Uggowitzer, J. F. Löffler and A. Weinberg, *Acta Biomater.*, 2014, **10**, 3346–3353.
3. A. Sharipova, S. K. Swain, I. Gotman, D. Starosvetsky, S. G. Psakhie, R. Unger and E. Y. Gutmanas, *J. Mech. Behav. Biomed. Mater.*, 2018, **86**, 240–249.
4. J. Cheng, T. Huang and Y. F. Zheng, *J. Biomed. Mater. Res. - Part A*, 2014, **102**, 2277–2287.

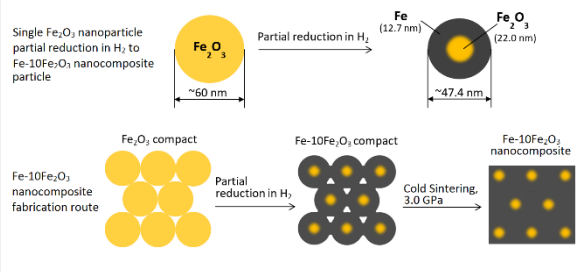

Fig. 1 - Schema of Fe-Fe2O3 nanocomposite fabrication

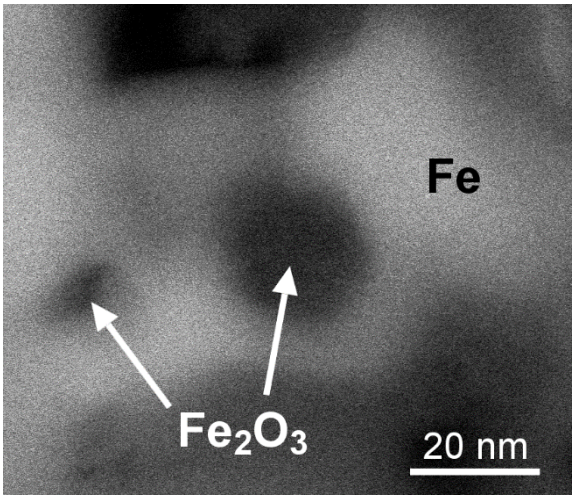

Fig. 2 - Fe-10Fe2O3 nanocomposite prepared by cold sintering of partially reduced Fe2O3 nanopowder

VII-SY12-04

Histological comparison of degradation and biocompatibility of two different pore sizes within LAE442 scaffolds in a long-term rabbit model

Julia Augustin[1], Stefan Julmi[2], Lisa Wurm[1], Christian Klose[2], Anja-Christina Waselau[1], Andrea Meyer-Lindenberg[1]

[1]Ludwig-Maximilians-University, Clinic for Small Animal Surgery and Reproduction, Munich, DE; [2]Leibniz University Hanover, Institut für Werkstoffkunde (Materials Science), Garbsen, DE

Introduction

Magnesium alloy LAE442 has been tested as cylindrical implants with promising results regarding homogeneous degradation, mechanical stability due to supplementation of rare earth elements and biological compatibility [1]. Additionally, pore size over 100 µm increase osteoconductivity for other implant materials [2]. Therefore, an open-pored cylindrical LAE442 scaffold was used, which could possibly show good results as bone graft substitute. The aim was to compare the degradation performance as well as the stimulating effect on the ingrowth behaviour of bone between two different pore sizes.

Experimental Methods

Open-pored scaffolds (4 mm x 5 mm) of the magnesium alloy LAE442 (4 wt. % Li, 4 wt. % Al, 2 wt. % rare earth elements) were produced by investment casting and coated with MgF_2. Scaffolds with pore sizes of 400µm (p400) or 500µm (p500) were placed in the not weight-bearing, cancellous part of the greater trochanter major of rabbits. For every time period (6, 12, 24 and 36 weeks) ten scaffolds of each implant type were inserted. Implants of porous beta-tricalcium phosphate (ß-TCP) of equal dimensions served as a reference. In-vivo µCT investigations of long-term implants (36 weeks) were performed to evaluate the degradation behaviour. After each time point cross-sections of the implant-bone compound were prepared, stained with toluidin blue and evaluated for structural changes of the implant, remodelling processes of bone and for cellular reactions. Furthermore, REM and EDX measurements were carried out in order to locate element contents in specific areas.

Results and Discussion

Clinically, all animals tolerated LAE442 and ß-TCP scaffolds well. Both LAE442 scaffolds degraded equally slowly, and the implant density and volume did not show any significant difference between both pore sizes. ß-TCP was completely resorbed in all animals after 36 weeks. Few bone-scaffold contacts were visible at the outer rims for p400 as well as for p500.

In contrast to ß-TCP, bone marrow cells surrounding LAE442, were displaced by increasing areas of gas. Therefore, the granulation tissue was not able to completely invade the scaffolds. Both scaffolds showed mild to moderate infiltration of blood vessels and mild accumulation of macrophages. In contrast, trabecular bone and bone marrow cells migrated into ß-TCP 6 weeks after surgery without cellular signs of inflammation. Starting in week 24, more immature bone matrix was visible in p500 compared to p400. However, p400 showed slightly more mature bone islands after 36 weeks. ß-TCP was traversed by mature bone at the end of the examination period.

Whereas a granulated surface with incorporated cracks was visible for LAE442 scaffolds histologically, EDX measurements showed an increasing degradation layer from week 6 on. Especially at the rims of the scaffolds, aggregations of calcium phosphate deposits were detected at later time periods.

Conclusion

An increasing bony basic matrix which includes slightly more mature bone within p400 shows a positive reaction of the host tissue to the open-pored Scaffolds. No differences in cellular reactions between the two different pore sizes may indicate a good biocompatibility. Displacement of granulation tissue by gas [3] and possible side effects of the alloying elements [4] could be the reason for an insufficient mineralization of the ingrowing substance. Controlling gas formation for magnesium implants to such an extent that the proliferative tissue reaction gets promoted remains a challenge.

References

1. Angrisani, N., et al., *Biocompatibility and degradation of LAE442-based magnesium alloys after implantation of up to 3.5years in a rabbit model.* Acta Biomater, 2016. **44**: p. 355-65.
2. Hulbert, S.F., et al., *Potential of ceramic materials as permanently implantable skeletal prostheses.* Journal of Biomedical Materials Research, 1970. **4**(3): p. 433-456.
3. Kraus, T., et al., *The influence of biodegradable magnesium implants on the growth plate.* Acta biomaterialia, 2018. **66**: p. 109-117.
4. Feyerabend, F., et al., *Evaluation of short-term effects of rare earth and other elements used in magnesium alloys on primary cells and cell lines.* Acta biomaterialia, 2010. **6**(5): p. 1834-1842.

Acknowledgement

Financial support of this study by the German Research Foundation under grants ME 1941/3-1 and MA 1175/52-1 is gratefully acknowledged.

10:30 a.m. – 12:00 p.m.

Conference room 2+3

VII-OS26 | Antibacterial and drug delivery 1

VII-OS26-01

Antibacterial activity and cytotoxicity of chemically treating Ti alloy and bioactive glass doped with silver

Seiji Yamaguchi[1], Rina Iwatsuki[1], Sara Ferraris[2], Marta Miola[2], Martina Cazzola[2], Enrica Verne[2], Silvia Spriano[2], Andrea Cochis[3], Hiroaki Takadama[1]

[1]Chubu University, Department of Biomedical Sciences, Kasugai-city, JP; [2]Politecnico di Torino, Department of Applied Science and Technology, Turin, IT; [3]Università del Piemonte Orientale, Department of Health Sciences, Novara, IT

Introduction

Bioactive Ti alloy and bioactive glass having high bone bonding capacity currently become essential materials for bone repair in orthopedic and dental fields. The former is used as load bearing implant such as hip joint, while the latter is used as bone substitute. Requirement of providing antibacterial activity to these implants is arising to avoid bacterial contamination which could lead to prosthetic failure and pain for the patients.

The aim of this study is to develop antibacterial and bioactive surfaces on Ti alloy and bioactive glass by chemical treatment using silver and defining characterization techniques suitable to compare a wide range of antibacterial and bioactive materials.

Experimental Methods

Ti-6Al-4V alloy plates were soaked in 5M NaOH solution, and then in a mixed solution of 50 mM $CaCl_2$ and 50 mM $SrCl_2$. They were heat treated at 600 ºC for 1 h, followed by soaked in 1M $Sr(NO_3)_2$ solution doped with 1 mM $AgNO_3$. The resultant products were denoted by “Ti64(Sr+Ag)”. Other alloy plates were pre-treated with a diluted HF aimed to remove the natural titanium oxide layer, and subsequently treated in H_2O_2 solution added with 1 mM $AgNO_3$ (denoted by “Ti64(HF-H_2O_2+Ag)”. Bioactive glass in a system of SiO_2-Na_2O-CaO-P_2O_5-B_2O_3-Al_2O_3 was also prepared and soaked in 30 mM $AgNO_3$ solution to incorporate silver ions on its surface (denoted by “BG+Ag”). The sample surfaces were analyzed by FE-SEM, EDX, TEM, XPS, XRD, Raman, zeta potential measurement. Apatite formation was examined by soaking the samples in SBF [1]. Cytocompatibility of the samples for Human fetal pre-osteoblasts (hFOB) were investigated by cultivating the cells on the samples at 37 ºC, 5% CO_2. Antibacterial activity of samples to multi-drug resistant Staphylococcus aureus was evaluated according to ISO 22196 standard.

Results and Discussion

Ti64(Sr+Ag) and Ti64(HF-H_2O_2+Ag) showed nano-textured surfaces with oxide layers about 1.5 μm and 200 nm in thickness, while BG+Ag showed smooth surface. These surfaces contains 0.2, 0.3 and 0.4 % Ag, respectively. XRD and Raman revealed that Sr+Ag containing calcium titanate, anatase and rutile were produced on Ti64(Sr+Ag), while hydrogen titanate was produced on Ti64(HF-H_2O_2+Ag). In contrast, only a broad halo attributed to glass phase was observed on BG+Ag. It should be noted that the surface of Ti64(HF-H_2O_2+Ag) could be analyzed by Raman, but not by XRD, probably due to its submicron thickness. XPS and TEM reveled that silver was doped as metal nanoparticles on Ti64(HF-H_2O_2+Ag), while they gave no evidences of the presence of silver particles on Ti64(Sr+Ag) and BG+Ag. It is considered that silver was doped as ions on these samples. All the alloy and glass samples were negatively charged and formed apatite in SBF. Zeta potential measurement reveled that kinetics of reaction in SBF occurred faster on BG+Ag than alloy samples so as to induce apatite formation within 1 day. The mechanism of apatite

formation was considered to be different for these samples: it is based on chemistry of micro environment for Ti64(Sr+Ag), surface charge for Ti64(HF-H_2O_2+Ag), or ion exchange for BG+Ag.
In antibacterial test, all the samples exhibited high antibacterial activity to multi-drug resistant Staphylococcus aureus: e.g. Ti64(Sr+Ag) and BG+Ag displayed 4.8 and 4.3-logs reduction compared with untreated alloy or bioactive glass without silver, respectively. Cytocompatibility test revealed no significant differences between Ti64(Sr+Ag) and untreated alloy, and also between BG+Ag and bioactive glass without silver.

Conclusion

Three types of antibacterial and bioactive materials with similar amount of Ag were prepared. The surface properties were compared by various types of characterization techniques. Ag is present as metal nanoparticles on Ti64(HF-H_2O_2+Ag), while seems to be as ions on other materials. The materials formed apatite in SBF based on different mechanism and kinetics, indicating their high potential for bone bonding. Antibacterial activity was proved on all the materials without any cytotoxicity. These materials are promising for next generation implant because of their high antibacterial activity, cytocompatibility and apatite formation.

References

T. Kokubo, H. Takadama. Biomaterials, 2006, 27, 2907-2915.

Acknowledgement

This research was supported by MAECI-Italy (GLOBAL project).

VII-OS26-02

Graphene-based surfaces love affair with bacteria, mammalian cells, and blood constituents. Is there a perfect match?

Patrícia C. Henriques[1,3,4], Andreia T. Pereira[1,3,5], André F. Maia[2,3], Fernão D. Magalhães[4], Inês C. Gonçalves[1,3]

[1]Universidade Porto, INEB – Instituto de Engenharia Biomédica, Porto, PT; [2]Universidade Porto, IBMC - Instituto de Biologia Molecular e Celular, Porto, PT; [3]Universidade Porto, i3S - Instituto de Investigação e Inovação em Saúde, Porto, PT; [4]Universidade Porto, LEPABE - Laboratory for Process Engineering, Environment, Biotechnology and Energy, Department of Chemical Engineering, Faculty of Engineering, Porto, PT; [5]Universidade Porto, ICBAS - Instituto de Ciências Biomédica Abel Salazar, Porto, PT

Introduction

Graphene-based materials (GBMs) availability has increased and so has the exploitation of their applications.[1] Infection-protective coatings of medical devices and wound dressings, where cell interaction also occurs, are examples of applications requiring a clear understanding of the interaction between GBMs as a surface and the surrounding biological environment. Also, deeper insights on GBMs real effect when alone as a surface are still lacking. [2] Thus, a systematic study was designed, where films of oxidized and reduced GBMs are used to identify the surface features that most strongly affect the major biological systems: bacteria, mammalian cells, and blood components.

Experimental Methods

GBMs films were produced by vacuum filtration using GBMs with different layer thickness and oxidation degree (graphene oxide (GO) and reduced GO (rGO) - 0.34 nm thick; graphene nanoplatelets (M5) and their oxidized form (M5ox) - 6-8 nm thick). Films were characterized regarding elemental composition and functional groups by XPS, crystallinity and structural properties by XRD, surface topography by SEM and AFM, and wettability by contact angle measurements. The antibacterial performance was assessed towards clinically relevant Gram-positive/Gram-negative bacteria with different sizes and morphology (*S. epidermidis, S. aureus, P. aeruginosa,* and *E. coli*) after 2 h and 24 h. *In vitro* biocompatibility was evaluated towards human fibroblasts (HFF-1) after 1, 7 and 14 days. Adhesion, viability, and proliferation of bacteria and mammalian cells on films were quantitatively evaluated through LIVE/DEAD assay (PI/Syto9) and Ethidium-1/Calcein/Hoechst fluorescence staining, respectively, using high-content screening microscopy. Blood cells adhesion and activation were explored by SEM and fluorescence microscopy, and hemolytic activity was quantified by spectrophotometry.

Results and Discussion

XPS showed increased content of oxygen-containing groups in oxidized films (GO and M5ox, ~32%), with intermediate levels in rGO (13.5%) and negligible amounts in M5 (3.5%) surfaces. XRD confirmed that intrinsic crystallinity and structural properties of raw GBMs is maintained in films. SEM showed that graphene sheets' sharp edges are exposed in M5 films, while a wrinkled surface with fused graphene platelets is observed on oxidized and rGO films. However, AFM highlights differences between them: GO and M5ox films have a smoother surface with nanotopography and low height variation ($S_{z\ GO}$ = 1.0 µm, $S_{z\ M5ox}$ = 1.3 µm), while rGO and M5 present microtopography and high peak to valley height heterogeneity ($S_{z\ rGO}$ = 2.2 µm, $S_{z\ M5}$ = 1.7 µm) and more flat areas.

Oxidized surfaces are hydrophilic, while rGO and M5 get closer to hydrophobicity. Antimicrobial studies reveal an overall increase of adherent bacteria over time, despite lower adhesion levels in oxidized surfaces, suggesting that a higher degree of oxidation reduces bacterial adhesion. The reduced thickness of platelet flakes also better prevents bacterial adhesion, with the exception of *S. epidermidis*. Rougher and less or non-oxidized surfaces favor bacteria viability, possibly due to the ability to provide shelter for bacteria. *S. aureus* and *P. aeruginosa* are the less susceptible strains, while *S. epidermidis* seems to be more affected. Fibroblasts adhesion on films is similar after 14 days, with good viability being observed. Blood cells, namely erythrocytes, leukocytes, and platelets adhere to all materials, with higher numbers and higher platelet activation in rGO and M5 surfaces. None of the surfaces, however, induced hemolysis (< 5%).

Conclusion

Overall, this study shows a causative effect of surface morphology/chemistry on bacteria, fibroblasts and blood cells when different GBMs are integrated as a surface. More oxidized materials are more anti-adhesive while rougher and less oxidized surfaces favor bacterial adhesion and viability. Oxidation degree and size have less influence towards mammalian cells, with all materials allowing cell adhesion and viability up to 14 days. Less or non-oxidized surfaces cause a more active response from blood cells, however, none caused hemolysis. Medical applications should, therefore, take all this into account in order to achieve a faster bench-to-bedside transition. So, is there a perfect match? Perhaps: GO and M5ox seem to be the best candidates, fighting bacteria while allowing cells to thrive, even though blood components might get on the way.

References

1. Swetha, P. D. P.*, et al.Part Part Syst Char* **2018,***35*(8).
2. Henriques, P. C.*, et al.Carbon* **2018,***132*, 709-732.

Acknowledgement

Financial support from FCT and FEDER: PhD grant SFRH/BD/120154/2016 and PD/BD/114156/2016, Project POCI-01-0145-FEDER-006939, POCI-01-0145-FEDER-007274, PTDC/CTM-BIO/4033/2014.

VII-OS26-03

Multifunctional and Antibacterial Zein-Cu doped Bioactive Glass Composite Coatings for Bone Tissue Engineering

Andrea Cochis[1,2], Laura Ramos Rivera[3], Sara Ferraris[4], Sarah Biser[3], Ajay Kumar[1,2], Hiba Mohammed[1,2], Aldo R. Boccaccini[3], Lia Rimondini[1,2]

[1]University of Piemonte Orientale UPO, Department of Health Sciences, Novara, IT; [2]University of Piemonte Orientale UPO, Center for Translational Research on Autoimmune & Allergic Diseases CAAD, Novara, IT; [3]University of Erlangen - Nuremberg, Institute of Biomaterials, Department of Materials Science and Engineering, Erlangen, DE; [4]Politecnico di Torino, Department of Applied Science and Technology, Turin, IT

Introduction

The 3rd generation of Biomaterials aims for multifunctional devices effective in promoting the target tissue repair, favouring the surrounding tissue growth and preventing bacterial infection that is fast turning as the first reason for implants failure. Bone repair is a complex process that requires an effective cross-talk with the soft tissues at the interface as well as the formation of blood vessels to ensure biochemical signalling. Accordingly, in this study a Cu-doped bioactive glass-zein composite coating has been applied onto the surface of bone implantable stainless steel 316L specimens to improve the healing of bone (by bioactive glass) [1], to favour soft tissues colonization (by zein) [2] and to promote neo-vascularization (by copper incorporation) [3]. Moreover, the presence of copper enables a strong and broad-range antibacterial activity [4].

Experimental Methods

Zein, bioactive glass (BG) 45S5 and Cu doped bioactive glass 45S5 particles were mixed in an ethanol/water solution before deposition process using electrophoresis. Discs of stainless steel 316L were used as substrates for the deposition process. SEM images were taken to evaluate the microstructure of the coatings. Degradation studies were performed in PBS immersion from 1 to 21 days. FTIR analysis was carried out to confirm the presence of the inorganic fillers in the coatings. Specimens' cytocompatibility was *in vitro* demonstrated by direct contact with cells representative of target tissues: mature and progenitor osteoblasts (U-2 OS, hFOB 1.19), primary fibroblasts (HGF) and endothelial cells (EA.hy926) by means of metabolic evaluation (Alamar blue). Antibacterial activity was *in vitro* proved by infecting specimens with the orthopaedic-related pathogens *Escherichia coli*, *Staphylococcus aureus* and *Staphylococcus epidermis*. Copper ability to protect cells from infection was assesed by a co-culture system where hFOB progenitors were seeded onto specimens' surface and then infected by the three strains above mentioned. Finally, copper efficacy to recruit blood vessels was *in vivo* tested by subcutaneous implantation into wild-type mice and four weeks post-implantation specimens' histology.

Results and Discussion

Surface analysis revealed porous structures of zein and zein-BG-Cu coatings. Zein-BG coatings showed a worm-like surface structure. FTIR analysis confirmed the presence of the BG particles in the coatings. Degradation studies showed a slow degradation of zein coatings compared with the composites. Biological evaluation results are summarised in Figure 1 using hFOB progenitors and *S. aureus* as a representative example. Copper addition did not introduce any toxic effect as cell viability was comparable for all the composites (Fig. 1a); on the opposite, specimens' antibacterial activity was increased as Cu-doping significantly decreased bacteria viability in comparison with other

compositions (Fig. 1b, *p<0.05*, indicated by §), indicating that the incorporation of Cu is effective in protecting cells after infection (Fig. 1c, *p<0.05*, indicated by §). Finally, *in vivo* post-implantation composite surface histology confirmed a high density of blood vessels, likely attracted by the presence of copper, that were able to penetrate across the coating (Fig. 1d, indicated by red arrows).

Conclusion

The novel zein –Cu doped BG composite coatings developed in this study appear to be very promising to orchestrate all the events related to bone healing with the benefit of added antibacterial capability.

References

[1] Hench, L, *Biomedical Glasses* 2015, 1, 1-15

[2] Dashdorj U, et al. *Int J Biol Macromol*, 2015, 80, 1-7.

[3] Rath S, et al. *PLoS ONE*, 2014, 9, e113319.

[4] Borkow G. *Curr Chem Biol*, 2014, 8, 89-102.

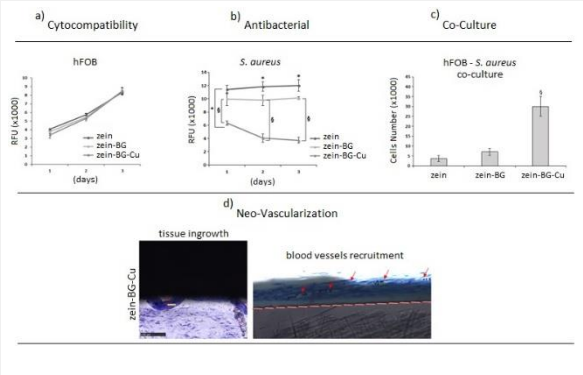

Figure 1.
Biological characterisation. Copper-doped specimens (zein-BG-Cu) were cytocompatible (a) and effective in reducing bacterial metabolism (b) as well as able to protect pre-seeded cells from infection (c) in a significant manner in comparison to other compositions ($p<0.05$, indicated by §). In vivo post-implant histology (d) revealed the presence of blood vessels (indicated by red arrows).

VII-OS26-04

Local Delivery of LLKKK18 Antimicrobial Peptide Released from Oxidized Dextrin Hydrogel to Treat Osteomyelitis

Alexandra Machado[1], Isabel Pereira[1], Vanessa Silva[3,5,6], Luís Costa[2,3], Isabel Pires[2,3], Justina Prada[2,3], Patrícia Poeta[3,6], José E. Pereira[2,3], Miguel Gama[1]

[1]University of Minho, CEB - Centre of Biological Engineering, Braga, PT; [2]University of Trás-os-Montes and Alto Douro, CECAV - Centre of Animal and Veterinary Science, University of Trás-os-Montes e Alto Douro, Vila Real, PT; [3]University of Trás-os-Montes and Alto Douro, Department of Veterinary Sciences, Vila Real, PT; [4]University of Trás-os-Montes and Alto Douro, Department of Genetics and Biotechnology, Vila Real, PT; [5]University of Trás-os-Montes and Alto Douro, Functional Genomics and Proteomics Unit, Vila Real, PT; [6]University NOVA of Lisbon, LAQV-REQUIMTE - Associated Laboratory for Green Chemistry, Caparica, PT

Introduction

Osteomyelitis (OM) is an inflammation of the bone triggered by an infection, which results in inflammatory destruction and tissue necrosis. Orthopedic surgeons face a difficult challenge in simultaneously repairing bone and inhibit infection in methicillin-resistant *Staphylococcus aureus* (MRSA) OM. The current treatment involves surgical debridement and prolonged systemic antibiotic therapy[1], with a frequently ineffective outcome, expensive treatments, harmful side-effects and development of resistant bacteria. Thus, the combination of the local delivery of harmless, but potent, antibiotic agents with regenerative therapy would represent a substantial improvement.

Antimicrobial peptides (AMPs) are part of the innate immune system with potential as novel therapeutic agents due to its high spectrum of antimicrobial activity and low propensity for bacteria to developing resistance.[2] The bactericidal effect of LL37, the only known human cathelicidin, has been reported.[3] Given its pro-angiogenic activity, LL37 has also demonstrated to promote wound healing.[4] LLKKK18 (LL18), an LL37 analog, has been engineered to enhance antimicrobial properties and decrease toxicity, being three-fold more effective in the killing of mycobacteria than LL37. Vancomycin is a broad spectrum antibiotic currently being useful to treatment OM.[5] Antimicrobial synergistic effects may be achieved when combining antibiotics with positively charged AMPs.[6] Thus, a synergistic antimicrobial effect between LL18 and vancomycin is exploited.

Overall, the present work aims to contribute to the construction of a system to the local treatment of OM, using LL18 as an antimicrobial agent. For that, LL18 was incorporated into an injectable oxidized dextrin (ODEX) hydrogel.[7]

Experimental Methods

In order to evaluate the most effective antimicrobial concentration of LL18 *in vivo*, a process of acute osteomyelitis was established in rat tibia using a clinical MRSA isolated from a patient with an infected diabetic foot ulcer. Four different concentrations of LL18 were loaded into ODEX hydrogel[7] prior to *in vivo* application: 0.2; 0.5; 0.7 and 1 mg/mL (C1, C2, C3 and C4, respectively). A dose of vancomycin alone and vancomycin together with LL18 were also tested. At day 7 rats were sacrificed, remaining bone bacteria was quantified and damage in surrounding tissues was evaluated through histological analyses.

Results and Discussion

ODEX alone showed a significant antimicrobial effect, being able to reduce CFU/g to a half when compared to the control - with no treatment. The smallest and the highest dose used, C1 and C4, added no further antimicrobial effect

to ODEX. While C1 is too low, C4 ineffective result may be associated to aggregation or poor solubility at high concentrations. C2 and C3 had similar outcome and reduced bacteria to almost a half when compared ODEX. Both vancomycin and LL18-vancomycin conditions eradicated bacteria. Both LL18 and ODEX attenuated inflammatory response triggered by OM. C1 and C2 showed smaller histopathological scores than vancomycin conditions.

Conclusion

This work confirmed that *in vitro* antimicrobial activity of LL18 is observed *in vivo*. LL18 was not able to eradicate OM, but reduced considerable bacteria viability even though very low doses were tested. Despite intended to perform as a carrier and a controlled release system, ODEX hydrogel showed suitability for antimicrobial therapy. Neither LL18 nor ODEX induced an inflammatory response, revealing a good biocompatibility. The model of acute OM used, however, was not long enough as to reach conclusions regarding regenerative action of the cathelicidin analogue. Further studies in a chronic OM prolonged process are important to attain LL18 regenerative ability, as well as an improvement of bioavailability.

Ongoing work: Despite LL18 advantages, exogenous administration is limited by enzymatic degradation and cytotoxicity, ultimately leading to an unsuccessful local delivery of AMPs. Dextrin is a medical grade water-soluble polymer degradable by human amylase, providing a good platform for a convenient, controlled drug release technology. Dextrin derivatives bearing reactive groups are being produced, in order to allow the conjugation of dextrin to LL18 and to cholecalciferol. Vitamin D plays a key role in the human immune response to infections as it induces the production of cathelicidin. Thus, the supplementary administration of dextrin and vitamin D_3 conjugates could further enhance LL18 bioactivity. After detailed characterization and *in vitro* testing, the conjugates will be evaluated *in vivo* for the treatment of chronic OM.

References

[1] Hatzenbuehler J, Pulling TJ. Am. Fam. Physician 2011;84(9):1027-33.

[2] Costa F, Carvalho IF, Montelaro RC, Gomes P, Martins MCL. Acta Biomater. 2011; 7(4):1431–40.

[3] Rivas-Santiago B, Hernandez-Pando R, Carranza C, Juarez E, Contreras JL, Aguilar-Leon D, *et al*. Infect. Immun. 2008;76(3):935–41.

[4] Ramos R, Silva JP, Rodrigues AC, Costa R, Guardão L, Schmitt F, *et al*.. Peptides. 2011;32(7):1469–76.

[5] Liu C, Bayer A, Cosgrove SE*, et al.* Clin. Infect. Dis. 2011;52(3):285-292.

[6] David AA, Park SE, Parang K, Tiwari RK. Curr. Top. Med. Chem. 2019;18(22):1926-1936.

[7] Pereira I, Fraga S, Silva S, Teixeira JP, Gama M. J. Appl. Toxicol. 2019; 39(4): 639-649.

Acknowledgement

The authors acknowledge the funding from FEDER and NORTE 2020 through the project nº 003262 titled “iBONE therapies: advanced solutions for bone regeneration”. This study was supported by Portuguese Foundation for Science and Technology (FCT) under the scope of the strategic funding of UID/BIO/04469 unit and COMPETE 2020 (POCI-01-0145-FEDER-006684) and BioTecNorte operation (NORTE-01-0145-FEDER-000004) funded by the European Regional Development Fund under the scope of Norte 2020 - Programa Operacional Regional do Norte. Alexandra Machado and Vanessa Silva gratefully acknowledge the Portuguese FCT for the granted scholarships (SFRH/BD/132000/2017 and SFRH/BD/137947/2018).

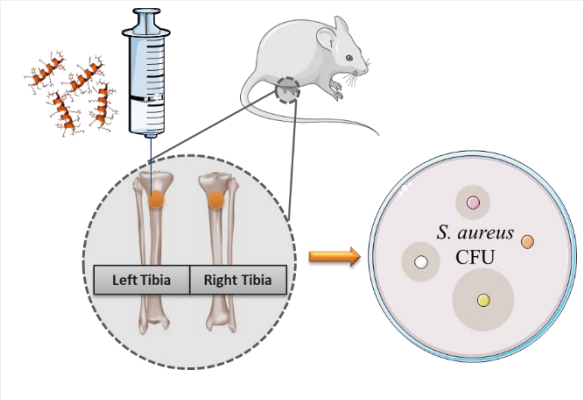

Local delivery of LLKKK18
Different concentrations of LLKKK18 are dissolved in oxidized dextrin-based (ODEX) hydrogel. A process of acute osteomyelitis is established: a bone defect is performed in rat tibia prior addition of bacteria inoculum. Then, the hydrogel is immediately injected within the site of infection. After sacrifice, remaining bacteria in the tibia is removed by sonication and quantified by Colony Forming Units (CFU) counting.

VII-OS26-05

The road to understanding the cellular uptake of nano-silver by bacteria, a systematic study using AgAu alloy nanoparticles

Frederic Stein[1], Carmen Streich[1], Juri Jakobi[1], Christoph Rehbock[1], Sebastian Grade[2], Mark Kühnel[3], Vadim Migunov[4,5], Meike Stiesch[2], Stephan Barcikowski[1]

[1]University Duisburg-Essen, Technical Chemistry I and Center for NanointegrationDuisburg-Essen (CeNIDE), Essen, DE; [2]Hanover Medical School, Department of Prosthetic Dentistry and Biomedical Materials Science, Hanover, DE; [3]Hanover Medical School, Institute of Pathology, Hanover, DE; [4]Research Centre Juelich, Peter Grünberg Institute, Ernst Ruska-Centre for Microscopy and Spectroscopy with Electrons, Juelich, DE; [5]RWTH Aachen University, Central Facility for Electron Microscopy (GFE), Aachen, DE

Introduction

The bactericidal effects of silver nanoparticles (Ag-NP) against infectious strains of multiresistant bacteria are well known nowadays, but their utilization is highly limited by their cellular toxicity and, consequently, the narrow therapeutic window. There are only a few studies on the bacterial uptake of Ag-NP, and as a result, the mechanism behind their toxic and antimicrobial properties are still not fully understood.

Experimental Methods

In this work, we used silver-gold (AgAu) alloy nanoparticles as antimicrobial agents, which were synthesized by pulsed laser ablation in liquids. This process does not need any artificial organic ligands as stabilizers and thus may avoid potential toxic cross-effects [1]. The ablated particle showed a completely homogeneous elemental distribution of the desired composition and crystal structure, identical to the ablated bulk target, which was verified by EDX line scans and XRD [2,3]. Through biological assays with oocytes, bacteria and human fibroblasts, we can show that there is a non-linear decrease of the bactericidal effects with an increasing gold molar fraction [4,5], probably originating from the inhibition of Ag dissolution by the more noble metal gold. Besides, we determined that the cellular uptake of silver and gold nanoparticles by oocytes is material dependent. To study the bacterial uptake of nano-silver we use the model bacterium *Staphylococcus aureus.*

Results and Discussion

Interestingly recent studies on the cellular uptake of AgAu alloy nanoparticles by the bacterium *S. aureus* revealed that only small particles could be found inside of the bacteria. High-resolution EDX measurements of the internalized particles showed that they were significantly more silver-rich than the primary particles (Ag > 95% inside in contrast to 50:50 outside). Based on these findings we conclude that these silver-rich particles were probably formed by particle dissolution, cellular uptake of silver ions and intercellular reduction to form silver nanoparticles.

Conclusion

With the help of the AgAu alloy nanoparticles, we were able to understand the mechanism of Ag nanoparticles uptake by bacteria, which could be relevant for numerous studies dealing with cellular uptake and antimicrobial activity of nano-silver.

References

[1] D. Zhang, B. Gökce and S. Barcikowski, Chemical Reviews, 2017, 117, 3990-4103.

[2] A. Neumeister, J. Jakobi, C. Rehbock, J. Moysig and S. Barcikowski, Physical chemistry chemical physics: PCCP, 2014, 16, 23671-23678.

[3] O. Prymak, J. Jakobi, C. Rehbock, M. Epple, and S. Barcikowski, Materials Chemistry and Physics, 2018, 207, 442-450.

[4] D. Tiedemann, U. Taylor, C. Rehbock, J. Jakobi, S. Klein, W. A. Kues, S. Barcikowski and D. Rath, Analyst, 2014, 139, 931-942.

[5] S. Grade, J. Eberhard, J. Jakobi, A. Winkel, M. Stiesch and S. Barcikowski, Gold Bulletin, 2013, 46, 3-11.

Acknowledgement

A. Heinemann is acknowledged for performing Mie calculations and providing theoretical UV/Vis extinction spectra.

VII-OS26-RF06

Light-mediated drug release from living hydrogels

Shardul Bhusari[1,2], Shrikrishnan Sankaran[1], Aránzazu del Campo[1,2]

[1]INM – Leibniz Institute for New Materials, Saarbrücken, DE; [2]Saarland University, Chemistry Department, Saarbrücken, DE

Introduction

One of the recent advances in the development of drug encapsulation and delivery systems has been the emergence of living materials, that contain genetically modified living organisms performing enhanced functions. We are developing living hydrogels containing bacteria that act as productive, adaptable and replenishable on-demand drug delivery repositories.[1,2] The polymer matrix of the hydrogel maintains the structural integrity inside the bodily environment while the living organisms produce the optimal amount of drug at the required time of delivery. Here we demonstrate the development of a hydrogel system to encapsulate genetically engineered *E. coli* bacterial strain, in 3D bioprinted scaffolds, leading to a light-regulated, localized, tunable and prolonged drug release.

Experimental Methods

The light-regulated drug-producing *E. coli* strain was engineered by incorporating the genes related to the metabolic synthesis of the drug into a light responsive optogenetic plasmid.[2] Bacteria was encapsulated in 3D-bioprinted constructs capable of being crosslinked on UV light exposure using a free-radical photoinitiator. These constructs were used to study the effect of change in the crosslinking density and thus the mechanical properties on the bacterial growth rate. Thin films of bacterial hydrogels were casted on the porous membrane (0.4 µm diameter pores) of transwell inserts to detect the drug production after 48 h irradiation on light exposure.

Results and Discussion

After 48 h within the physically crosslinked hydrogel, the bacterial growth observed was 20 times higher than that in the chemically crosslinked hydrogel. Also, with increasing chemical crosslinking density, the drug production reduced ten-fold. Intermediate bacterial growth and drug release were observed with intermediate physical and chemical crosslinking in the hydrogels.

Conclusion

Genetically engineered bacteria were successfully encapsulated inside 3D bioprinted hydrogel system. We demonstrate the possibility of controlling the bacterial growth by tuning the mechanical properties of the hydrogel and thus the drug release *in situ,* using an optogenetic strategy.

References

1. Sankaran, S. & Campo, A. Optoregulated Protein Release from an Engineered Living Material. *Adv. Biosyst.***1800312,** 3–9 (2019).

2. Sankaran, S., Becker, J., Wittmann, C. & Campo, A. Optoregulated Drug Release from an Engineered Living Material : Self-Replenishing Drug Depots for Long-Term , Light-Regulated Delivery. *Small***1804717,** 1–6 (2019).

Acknowledgement

S.B., S.S. and A.d.C. are grateful for funding from the SFB1027 collective research center for this project.

VII-OS26-RF07

Development of Polysaccharide-Drug Ionic Complexes as Antimicrobial Hydrogels in the Treatment of Staphylococcal Infections

Cristina Casadidio[1], Roberta Censi[1], Stefania Scuri[2], Laura Mayol[3], Marco Biondi[3], Giuseppe De Rosa[3], Piera Di Martino[1]

[1]University of Camerino, School of Pharmacy, Drug Delivery Division, Camerino (MC), IT; [2]University of Camerino, School of Pharmacy, Hygiene Research Centre, Camerino (MC), IT; [3]University of Naples Federico II, Department of Pharmacy, Naples, IT

Introduction

Polysaccharides are biodegradable, biocompatible and non-toxic biopolymers derived from renewable sources showing great potential for several biomedical applications, such as the prevention and treatment of staphylococcal infections. A strategy to treat these infections is the use of polysaccharides in antimicrobial therapy. Polysaccharide based *in situ*-forming hydrogels are able to improve the efficacy of the loaded drug(s) by overcoming different drawbacks like: burst effect, high systemic toxicity, side effects and fast degradation [1,2]. In this work we investigated the efficacy of anionic polysaccharidic hydrogels as vancomycin stabilizers. The newly biocompatible and biodegradable designed formulations could be potentially used as enhancers of drug structural stability overcoming its degradation pathways.

Experimental Methods

Hyaluronic acid, alginic acid, propylene glycol alginate, xanthan gum and dextran (as control) were used as anionic polysaccharides, while vancomycin was selected as a cationic drug. Polysaccharide-vancomycin solutions containing a fixed amount of polysaccharide (5mg/mL) and polysaccharide-vancomycin hydrogels at gel-point concentrations were formulated in aqueous media at pH 7.4 and pH 9 (i.e. vancomycin isoelectric point). Chemical stability tests of polysaccharide/antibiotic solutions and hydrogels were performed for 22 days by HPLC-DAD-MS. Placebo hydrogels and drug-loaded systems were characterized by rheological analysis at 37°C, to evaluate the presence of ionic complexes between negatively charged polysaccharides and the positive charges of the drug. Vancomycin release studies were conducted at 37°C upon addition of PBS (pH 7.4) on top of the gels. The antimicrobial activity of the complexes was tested against *Staphylococcus aureus* at 10^6CFU/mL after 24,48 and 72 hours via microdilution method and by contact susceptibility tests.

Results and Discussion

The chemical stability of the drug can be achieved by physical encapsulation of the drug into the hydrogel networks at physiological conditions. The polysaccharidic solutions with ±24% of drug stability (Figure 1a) and polysaccharidic hydrogels with ±40% of drug stability (Figure 1b) are able to preserve the vancomycin native structure compared with drug solution. The results show that not all polymers were able to stabilize the drug to the same extent. Vancomycin stability is governed not only by physical network encapsulation, but also by ionic interaction between drug and polysaccharidic matrix thanks to self-assembling ionic complexes composition. To validate this hypothesis, stability studies were also performed at pH 9, when vancomycin is uncharged. As depicted in Figure 2, ionic bonds are essential to promote the improvement of vancomycin stability. In addition, the formation of complexes affects

rheological characteristics of the systems. More in detail, the presence of the peptide confers to hyaluronic acid and propylene glycol alginate formulations the transition from an entangled solution to a gel-like rheological behaviour. Otherwise, unloaded xanthan gum formulations displays a gel-like rheological behaviour and, when loaded with vancomycin, an evident increase of both viscoelastic moduli was detected. Regarding alginic acid, no significant changes, between unloaded and loaded gels, were observed. Release tests were performed for 70 hours before the beginning of hydrogel degradation process. Figure 1c shows different release kinetics according to the nature of the polymer. A 60% of vancomycin release is achieved within three days for all formulations. Antimicrobials susceptibility tests show a significant bacteria reduction compared to the vancomycin in solution, and only hyaluronic acid fails to stop bacterial growth. In particular, xanthan gum reaches the ±91.5% of bacteria reduction until 24h and a zone of inhibition of ±24mm, promoting as best candidate.

Conclusion

Vancomycin-polysaccharidic hydrogels are able to preserve the structural stability of the drug enhancing its antimicrobial activity in physiological environment thanks to the physical encapsulation and self-assembling ionic complexes configuration. Furthermore, these designed formulations could be used as functional coating in the treatment of wound infections and in the prevention of implant-associated infections.

References

[1] Casadidio, C., Butini M.E., Trampuz A., Di Luca M., Censi R., Di Martino P. Eur. J. Pharm. Biopharm., 2018. **130**: p. 260-271.

[2] Hoffman, A.S. Adv. Drug Delivery Rev. **2012**, 64, 18-23.

Acknowledgement

The authors acknowledge receipt of funding from the European Commission through a H2020-MSCA-ITN-2015 award, as part of the ISPIC project (grant number 675743), a H2020-MSCA-RISE-2016 award through the CHARMED project (grant number 734684) and a H2020-MSCA-RISE-2017 award through the CANCER project (grant number 777682).

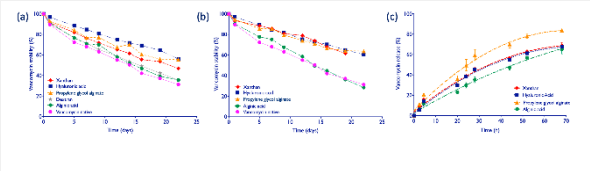

Figure 1.
Chemical stability of native vancomycin at pH 7.4 loaded into (a) polysaccharidic solutions and (b) polysaccharidic hydrogels; (c) cumulative release of vancomycin in PBS pH 7.4, 37°C.

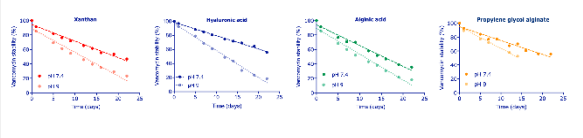

Figure 2.

Comparison of vancomycin decay at pH 7.4 (ionic interaction) and pH 9.0 (vancomycin isoelectric point) complexed with polysaccharide solutions.

VII-OS26-RF08

Calcium Phosphate nanoparticles as carriers of therapeutic biomolecules into cells - an *In Vitro* study

Nataniel Białas[1], Elena K. Müller[2], Ingrid Hilger[2], Matthias Epple[1]

[1]University of Duisburg-Essen, Institute of Inorganic Chemistry and Center for Nanointegration Duisburg-Essen (CeNIDE), Essen, DE; [2]University Hospital Jena, Institute of Diagnostic and Interventional Radiology, Research Center Lobeda, Jena, DE

Introduction

In the last decade, nanomaterials have gained increasing research interest due to their unique properties and usefulness in biomedicine. The range of clinical applications of inorganic nanoparticles is broad, from contrast enhancers in diagnostic imaging to carriers of therapeutic biomolecules (*e.g.* antibodies or RNA) into eukaryotic cells, both *in vitro* and *in vivo* [1,2]. Calcium phosphate (CaP) nanoparticles have a high affinity to nucleic acids and therefore can serve as their carriers into cells in targeted delivery. They are characterized by high biocompatibility and biodegradability, as CaP is the natural inorganic component of human hard tissue (bone and teeth), and are readily taken up by cells. The process of nucleic acid delivery enables to modify and control gene expression in cells [3]. Small interfering RNA (siRNA) is a potent therapeutic biomolecule well known for its ability to inhibit gene expression in cells by RNA interference. siRNA-mediated silencing of genes involved in inflammatory processes, *e.g.* NF-κB p65, is a promising therapeutic strategy to overcome a variety of inflammatory diseases [4].

Experimental Methods

Our aim was to synthesize and characterize fluorescent CaP nanoparticles (with and without p65-specific siRNA loading), and evaluate the cellular uptake of these nanoparticles as well as the gene silencing of NF-κB p65 in murine cells. Fluorescent CaP nanoparticles were synthesized by precipitation, stabilized with Cy5-labeled polyethyleneimine, loaded with p65-siRNA (functional or scrambled) and coated with a silica shell. The nanoparticles were purified by centrifugation, and characterized by dynamic light scattering (DLS), atomic absorption spectroscopy (AAS) and scanning electron microscopy (SEM). The nanoparticles were also tested for the presence of endotoxins (pyrogenicity). To evaluate the cellular uptake of the nanoparticles, mouse monocytes (cell line J774A.1) and mouse endothelial cells (SVEC4-10) were incubated with the fluorescent nanoparticles (without siRNA loading) in 2D cultures up to 48h. The uptake efficiency was determined by confocal laser scanning microscopy (CLSM). For evaluation of the gene-silencing efficiency, J774A.1 cells were incubated with siRNA-loaded nanoparticles in 2D cultures for 48h. The expression of the NF-κB p65 proteins and NF-κB p65 mRNA (messenger RNA) in cells was determined by Western Blot and Real-Time PCR, respectively.

Results and Discussion

CaP nanoparticles were spherical with an average size of 50 nm (by SEM) and a ζ-potential of +30 mV. The nanoparticles were colloidally stable, efficiently loaded with siRNA (approx. 95% of the biomolecules were incorporated) and non-pyrogenic. The concentration-dependent uptake of the nanoparticles was confirmed in both cell lines. Nanoparticle-mediated gene silencing was demonstrated in monocytes. The NF-κB p65 expression was decreased by the nanoparticles in a concentration-dependent manner up to 85% on protein level and 25% on mRNA level for the highest studied siRNA concentration (0.5 µg/mL).

Conclusion

CaP nanoparticles can be used as tools for nucleic acid delivery and gene silencing in cells. They have the potential to be widely applied in the treatment of various inflammatory diseases.

References

[1] van der Meer S.B., *et al*. *Acta Biomater*, 57 (2017), 414-425.
[2] Giner-Casares J.J., *et al*. *Mater Today*, 19 (2016), 19-28.
[3] Neuhaus B., *et al*. *J Mater Chem B*, 3 (2015), 7186-7193.
[4] Xu X., *et al*. *Regen Biomater*, 3 (2016), 187-195.

1:00 p.m. – 2:30 p.m.

Hall 3

VIII-SY13 | Light-based 3D printing of hydrogels

Aleksandr Ovsianikov (Vienna, AT)
Sandra Van Vlierberghe (Ghent, BE)

Within the biofabrication field, two main material strategies are currently being explored. When a biomaterial is applied to produce the structure, the material can either be used as a biomaterial ink or as a bioink. Biomaterial ink refers to the use of a prefabricated scaffold obtained via additive manufacturing for subsequent cell seeding. The term bioink refers to a mixture already containing cells prior to additive manufacturing.
Lithography-based bioprinting offer some advantages compared to conventional technologies. During this special symposium both biomaterial inks and bioinks processed using light-based techniques (stereolithography, two-photon polymerization, photo-crosslinking during extrusion) will be covered. Abstracts covering hydrogels of natural or synthetic nature, in which hypotheses-driven biological properties are linked to structural, chemical and/or processing features interacting with cells of any kind are particularly sought in this symposium. With a transversal approach, this symposium will discuss the key factors of light-based processing of hydrogels which modulate the *in vitro* microenvironment and elucidate how the newly developed knowledge will enable clinical translation and commercialisation of light-based 3D printing in the years to come.

VIII-SY13-KL01

High Definition 3D Printing of Photopolymers for Biomedical Applications

Aleksandr Ovsianikov[1,2]

[1]Technische Universität Wien (TU Wien), 3D Printing and Biofabrication, Vienna, AT; [2]Austrian Cluster for Tissue Regeneration, Austria, AT

Development of biomaterials for 3D printing is an established direction in modern research [1]. Different 3D printing approaches impose specific requirements on the properties of these materials. Bioprinting technologies rely on hydrogels precursors, which can be processed in the presence of living cells, the so called bioinks [2]. Lithography based approaches implement materials, which can be cross-linked by exposure to UV or visible light. Among them multiphoton lithography stands out as a method providing access to multiple levels of spatial resolution, capable of producing features smaller than mammalian cells. Recently developed materials and photoinitiators enabled realization of such high-resolution structures directly in the presence of living cells [3]. In this contribution resent advances in the field of multi-photon processing of photopolymers, including hydrogels for bioprinting will be presented.

References

[1] 3D Printing and Biofabrication, A. Ovsianikov, J. Yoo, V. Mironov (Eds.) Tissue Engineering and Regeneration Series, Springer International Publishing (2018) [ISBN 978-3-319-45444-3]

[2] J. Groll, J. Burdick, D.-W. Cho, B. Derby, M. Gelinsky, S. Heilshorn, T. Jüngst, J. Malda, V. Mironov, K. Nakayama, A. Ovsianikov, W. Sun, S. Takeuchi, J. Yoo, T. Woodfield, A definition of bioinks and their distinction from biomaterial inks, Biofabrication 11 : 013001 (2019) [doi: 10.1088/1758-5090/aaec52]

[3] M. Tromayer, A. Dobos, P. Gruber, A. Ajami, R. Dedic, A. Ovsianikov and R. Liska, A biocompatible diazosulfonate initiator for direct encapsulation of human stem cells via two-photon polymerization, Polym. Chem., 9, 3108 (2018) [doi: 10.1039/C8PY00278A]

Acknowledgement

This work was financially supported by the European Research Council (Starting Grant 307701 and Consolidator Grant 772464 A.O.)

VIII-SY13-KL02

Illuminating Progress on 3D Bioprinting of Vascularized Tissues and Organoids

Jordan S. Miller

Rice University, Department of Bioengineering, Houston, US

The lack of sufficient numbers of donor organs for human transplantation therapies results in the loss of tens of thousands of lives and costs tens of billions of dollars each year in the US alone. However, the ability to create, *de novo*, functional organ replacements to treat human disease is fundamentally limited by the lack of a comprehensive vascularization strategy for engineered three-dimensional (3D) tissues. Solid organs transport fluids through distinct vascular networks that are biophysically and biochemically entangled, creating complex three-dimensional (3D) transport regimes that have remained difficult to produce and study. We establish intravascular and multivascular design freedoms with photopolymerizable hydrogels by using food dye additives as biocompatible yet potent photoabsorbers for projection stereolithography. We demonstrate monolithic transparent hydrogels, produced in minutes, comprising efficient intravascular 3D fluid mixers and functional bicuspid valves. We further elaborate entangled vascular networks from space-filling mathematical topologies and explore the oxygenation and flow of human red blood cells during tidal ventilation and distension of a proximate airway. In addition, we deploy structured biodegradable hydrogel carriers in a rodent model of chronic liver injury to highlight the potential translational utility of this materials innovation. These technologies provide a flexible platform for a wide array of specific applications, and may enable the scaling of densely populated tissue constructs to arbitrary size.

VIII-SY13-03

In situ prevascularization designed by Laser-Assisted Bioprinting : Effect on bone regeneration

Olivia Kérourédan[1,2,3], Davit Hakobyan[1], Murielle Rémy[1], Sophia Ziane[1,2,3], Nathalie Dusserre[1], Jean-Christophe Fricain[1,2,3], Samantha Delmond[4], Noélie Brunehilde Thébaud[1,2,3], Raphaël Devillard[1,2,3]

[1]INSERM U1026, Bioingénierie Tissulaire, Bordeaux, FR; [2]Université de Bordeaux, UFR des Sciences Odontologiques, Bordeaux, FR; [3]CHU de Bordeaux, Services d'Odontologie & Santé Buccale, Bordeaux, FR; [4]CHU de Bordeaux, INSERM, CIC1401, Bordeaux, FR

Introduction

Vascularization plays a crucial role in bone formation and regeneration process[1]. Development of a functional vasculature to improve survival and integration of tissue-engineered bone substitutes remains a major challenge. Biofabrication technologies, such as bioprinting, have been introduced as promising alternatives to overcome issues related to lack of prevascularization and poor organization of vascular networks within the bone substitutes[2]. Among them, Laser-Assisted Bioprinting (LAB) has emerged as a rapid and high-resolution prototyping method allowing for precise organization of biomaterials for tissue engineering and regenerative medicine applications[3]. In this context, this study aimed at organizing endothelial cells *in situ* using LAB, in mouse calvaria bone defects, to generate a prevascularization with a defined architecture, and promote *in vivo* bone regeneration.

Experimental Methods

The LAB workstation comprised a laser, focused on a quartz ribbon that was coated with a thin absorbing layer of gold and a 30 µm layer of cell bioink. This technology was used to print Red Fluorescent Protein (RFP)-labeled human umbilical vein endothelial cells (HUVECs) *in situ* into mouse calvaria bone defects of critical size, prefilled with collagen containing stem cells from the apical papilla (SCAPs) and vascular endothelial growth factor (VEGF). First, accuracy and safety of LAB procedure were assessed. Then, the impact of different cellular configurations on vascularization organization, vessel density, and bone regeneration was investigated in vivo. Statistical analyses were performed using GraphPad Prism software (GraphPad, San Diego, CA, USA).

Results and Discussion

LAB technology allowed safe and controlled *in vivo* printing of different cell patterns. *In situ* printing of endothelial cells gave rise to organized microvascular networks into bone defects (Fig.1). At two months, vascularization rate (vr) and bone regeneration rate (br) showed statistically significant differences between the "random seeding" condition and both "disc" pattern (vr=+203.6%; br=+294.1%) and "crossed circle" pattern (vr=+355%; br=+602.1%). These results indicate that *in vivo* Laser-Assisted Bioprinting is a valuable tool to introduce *in situ* prevascularization with a defined configuration and promote bone regeneration.

In situ bioprinting provides interesting perspectives for clinical applications and could evolve to be integrated into a sterile operating room. Recent studies focused on the development of technologies for scaling-up and automating the fabrication of 3D engineered tissues in order to increase production and improve product consistency[4]. Applications of *in vivo* printing for clinical practice imply the development of user-friendly and transportable bioprinters, that could rapidly generate constructs of clinically relevant size in clinics directly onto the patient. This

would constitute an innovative and personalized therapeutic approach, allowing for the fabrication of “tailor-made” substitutes.

Conclusion

In conclusion, the results presented here demonstrate that Laser-Assisted Bioprinting is a relevant technology to organize *in situ* prevascularization *in vivo*. Defined local cell density and printing parameters allowed the generation of microvascular networks with defined configurations into critically-sized bone defects. The results showed that *in situ* printing of HUVECs improved vascularization and bone regeneration into critical bone defects in mice. This work has important prospects in the field of regenerative medicine as it offers an alternative approach to induce *in situ* prevascularization and promote bone regeneration.

References

1. Santos MI *et al*., Macromol Biosci. 10:12-27, 2010
2. Nguyen LH *et al.*, Tissue Eng Part B. 18:363-82, 2012
3. Guillemot F. *et al.*, Acta Biomater. 6:2494-500, 2010
4. Nycz CJ. *et al.*, Tissue Eng Part A. 0 :NO, 2019

Acknowledgement

The authors would like to thank “Fondation des Gueules Cassées” et “Fondation de l’Avenir” for providing financial support to this project.

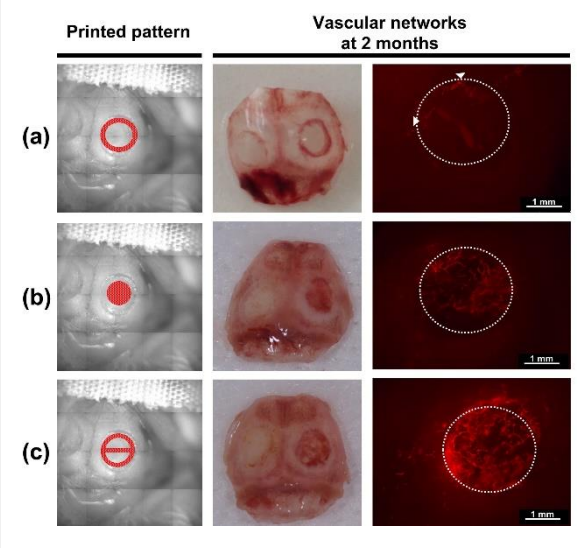

Figure 1
Observation of calvaria bone defects and fluorescence detection of printed RFP-labeled HUVECs at two months, for each printed condition : a) “ring” pattern, b) “disc” pattern, c) “crossed circle” pattern.

VIII-SY13-04

Fabrication of Hydrogels with Stiffness Gradient by Two-Photon Polymerization for analyzing the Durotaxis of Cells

Nicole Hauptmann, Holger Rothe, Gerhard Hildebrand, Klaus Liefeith

Institute for Bioprocessing and Analytical Measurement Techniques (iba), Department of Biomaterials, Heilbad Heiligenstadt, DE

Introduction

The extracellular matrix (ECM) of native tissues is characterized by defined physicochemical and biochemical properties. The elastic modulus ranges from very soft for brain tissue (0.1-0.5 kPa) and adipose tissues (1-3 kPa) over medium stiff for muscular tissue (10-15 kPa) until very stiff for bone and teeth (0.4-17 GPa). Tissue stiffening is a consequence of collagen remodelling, whereas mechanical signals from the ECM lead to proliferation, differentiation and cell migration[1]. Migration of cells is important in many natural processes like tissue morphogenesis and homeostasis, angiogenesis, and wound healing or even in tumour progression. Thus, cells respond to stiffness changes by migration to the stiffer area, which is called durotaxis or they migrate to softer areas, which is known as inverse durotaxis[2]. The knowledge of the mechanism of these phenomena is very important for the establishment of biomaterials for disease modelling applications.

Because the ECM consists mainly of collagen and glucosaminoglycans, hydrogels are a suitable material for simulating the ECM because of their high water content and excellent biocompatibility. Several synthetic and natural hydrogels were already used as materials for fabrication of an artificial ECM, such as poly(ethylene glycol), poly(glycolic acid), collagen or hyaluronic acid[3]. In principle, the polymer for simulating the ECM should have defined properties, such as high biocompatibility and moderate biodegradability as well as tissue specific stiffness, pore size and porosity. One method for fabrication of hydrogels with defined stiffness is the two-photon polymerization (2PP). In 2PP, the light of a femtosecond laser is focused over an objective lens inside a photoactive polymer precursor (Figure). Radical polymerization occurs only in the focus volume of the sample leading to a resolution in the nm range. By moving the laser focus through the sample a three dimensional structure can be generated[4].

The aim of this study was to develop hydrogels with stiffness gradient to analyze the effect of stiffness on the proliferation and the phenotype of various cell types, like osteoblasts or fibroblasts.

Experimental Methods

We prepared hydrogels based on collagen-I and methacrylated hyaluronic acid, whereas collagen-I was cross-linked by natural fibrillation of the collagen-I molecules. Collagen-I-hyaluronic acid-methacrylate hydrogels with stiffness gradient were prepared by 2PP, through variation of the structuring parameters. The Young`s modulus of the gradient gels was measured by atomic force microscopy (AFM). Cell response of osteoblasts and fibroblasts was analyzed in dependency of the stiffness gradient by confocal fluorescence microscopy (CLSM) 72 h post culture.

Results and Discussion

Results of the AFM studies showed that we successfully established hydrogels with stiffness gradient by 2PP. Thus, when increasing the hatching distance during the 2PP process the stiffness increases from 5 kPa to 20 kPa, stiffness in the range of connective tissue and osteoid. Cell culture study showed excellent biocompatibility of the hydrogels,

whereas osteoblasts and fibroblasts build up a confluent cell layer after 7 d. CLSM images showed that osteoblasts preferred the stiffer cross-linked areas and a highly spread phenotype with formation of actin-myosin stress fibers was visible. In contrast to the durotaxis of the osteoblasts, fibroblast showed inverse durotaxis. Thus, these cells adhered preferentially on the softer areas of the gels. Due to the soft substrate, no distinct actin filament structure was observed for the fibroblasts.

Conclusion

The results of the study demonstrate, that we successfully established hydrogel networks based on collagen-hyaluronic acid-methacryate hydrogels with stiffness gradient. Furthermore, we have demonstrated durotaxis of osteoblasts and inverse durotaxis of fibroblasts in the investigated stiffness range. Thus, these hydrogels are a promising tool for tissue engineering and disease modelling applications.

References

[1] B. Hinz, *Periodontol 2000* **2013**, *63*, 14-28.

[2] J. Wu, Z. Mao, H. Tan, L. Han, T. Ren, C. Gao, *Interface Focus* **2012**, *2*, 337-355.

[3] X. Guan, M. Avci-Adali, E. Alarcin, H. Cheng, S. S. Kashaf, Y. Li, A. Chawla, H. L. Jang, A. Khademhosseini, *Biotechnol J* **2017**, *12*.

[4] N. Hauptmann, Q. Lian, J. Ludolph, H. Rothe, G. Hildebrand, K. Liefeith, *Tissue Eng Part B Rev* **2019**.

Acknowledgement

The author would like to thank the Thüringer Aufbaubank (Germany) for funding the project "INSPECT" (FKZ 2015 FE 9163).

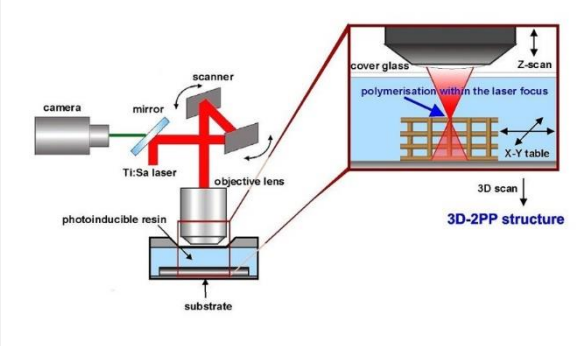

Principle of two-photon polymerization
The light of a femtosecond laser is focused over an objective lens inside a sample. A three dimensional structure is generated by moving the laser focus throught the polymer.

1:00 p.m. – 2:30 p.m.

Hall 2

VIII-OS27 | Polymeric biomaterials 2

VIII-OS27-01

Degradable PLA micro-structured scaffolds as cells guidance

Louis Gangolphe[1,2], Coline Pinese[1], Audrey Bethry[1], Benjamin Nottelet[1], Frédéric Bossard[2], Xavier Garric[1]

[1]Department of Artificials Biopolymers, Max Mousseron Institute of Biomolecules (IBMM), UMR CNRS 5247, University of Montpellier, France, Montpellier, FR; [2]Univ. Grenoble Alpes, CNRS, Grenoble INP, LRP, 38000 Grenoble, * Institute of Engineering Univ. Grenoble Alpes, France, Grenoble, FR*

Introduction

Synthetic materials commonly used in soft-tissue engineering have low deformability and stretchability. In addition, scaffolds structuration plays a key role in the control of cells behavior during regeneration[1]. The development of efficient biomimetic scaffolds requires the control of three-dimensional structures that have interconnected pores to promote host-tissue reconstruction[2]. In this work, we evaluate the impact of various architectures of electrospun degradable scaffolds (square motif and honeycomb motif) on their mechanical behavior and on their ability to promote cellular growth using time-lapse experiments.

Experimental Methods

Well defined structures PLA, PLA-PEG-PLA triblock copolymer and star-shaped PEG_{8arm}-PLA block copolymer were synthesized via ring-opening polymerization for 5 days at 130°C. Polymer solutions in DCM/DMF (70/30 v/v or 50/50 v/v) were prepared and electrospun with an applied voltage of 15kV. Those polymers were further electrospun to design architected scaffolds on micro-structured collectors. The analyses of morphology and orientation of the micro-fibres were performed by SEM (ultra 55 SEM FEG, Zeiss, Jena, Germany). Mechanical measurements were carried out using ARES-G2 rheometer (TA Instruments, New Castle, DE, USA). Degradation tests samples were conducted in PBS (pH 7.4) at a constant temperature. C2C7 myoblasts were seeded on the different scaffolds (films, random fibres, and micro-structured) to evaluate their adhesion and proliferation over time. Concurrently, NIH3T3 GFP fibroblasts were seeded on architected scaffolds and direct cells observation was conducted over time upon colonization.

Results and Discussion

PLA, PLA-PEG-PLA and PEG_{8arm}-PLA were electrospun to design both 3D architected fibrous scaffolds (square motif and honeycomb motif) and 3D non-architected fibrous scaffolds (random fibres). The mechanical properties of the architected fibrous scaffolds showed microstructure dependence (square-like scaffold versus honeycomb-like scaffold) and anisotropic behaviours. In addition, even though scaffolds micro-structuration nature did not influence degradation rate, the micro-structuration was maintained over three months degradation time. Finally, the micro-structuration of the architected scaffolds - square motif as well as honeycomb motif - guided cell colonisation and promoted their proliferation over time in comparison with random fibres. These results were confirmed by time-lapse experiments on architected and non-architected scaffolds.

Conclusion

Thanks to the design of a 3D architected scaffolds, myoblasts were guided and promoted over time upon colonization in comparison with non-architected scaffolds. Degradable architected fibrous scaffolds appear therefore as promising biomimetic materials for muscle reconstruction.

References

[1] A.P. Kishan, E.M. Cosgriff-Hernandez, Recent advancements in electrospinning design for tissue engineering applications: A review: Advancements in electrospinning design for tissue engineering applications, Journal of Biomedical Materials Research Part A. 105 (2017) 2892–2905. doi:10.1002/jbm.a.36124.

[2] T. Jiang, E.J. Carbone, K.W.-H. Lo, C.T. Laurencin, Electrospinning of polymer nanofibers for tissue regeneration, Progress in Polymer Science. 46 (2015) 1–24. doi:10.1016/j.progpolymsci.2014.12.001.

Acknowledgement

This work was supported by ANR2016-BIOSCAFF (ANR-16-CE09-0024) held by the University of Grenoble-Alpes and the University of Montpellier.

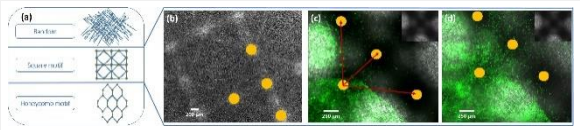

Direct NIH3T3 GFP fibroblasts observation on fibrous scaffolds over time upon colonization
Scheme of different fibrous scaffolds (random and micro-structured fibres) (a). SEM image, micro-structured electrospun scaffold with a square motif (b). Two frames of GFP labelled NIH3T3 fibroblasts seeded on square motif electrospun scaffolds based on star-shaped PEG-PLA copolymer. Confocal time-lapse imaging from 0h (c) to 64h (d). Magnification X 10.

VIII-OS27-02

Microscale cryogels as devices for focal therapeutic delivery

Dimitri Eigel[1,2], Petra B. Welzel[1,2], Julian Thiele[2], Carsten Werner[1,2,3], Ben Newland[4]

[1]Leibniz Institute of Polymer Research Dresden, Institute of Biofunctional Polymer Materials, Dresden, DE; [2]Leibniz Institute of Polymer Research Dresden, Max Bergmann Center for Biomaterials, Dresden, DE; [3]Technische Universität Dresden, Center for Regenerative Therapies Dresden, Dresden, DE; [4]Cardiff University, School of Pharmacy and Pharmaceutical Science, Cardiff, GB

Introduction

Scaffolds that are prepared by cryopolymerisation (cryogels) have become the center of much research focus for applications in tissue engineering and regenerative medicine [1]. Their high surface area, generated by their macroporous structure, offers versatile opportunities for a sustained release of potential therapeutics [1]. In order to make them injectable for minimally invasive applications in the brain, we have recently developed microscale cryogel particles, called microcarriers (MCs) [2]. These MCs, based on polyethylene glycol (PEG) and heparin, can bind and release positively charged molecules (growth factors) to the brain through electrostatic interaction with the negatively charged sulfate groups of heparin. Furthermore, it could be shown that the MCs have a good compatibility with brain tissue. However, the polydispersity of the MCs and the inconvenience of using animal sourced heparin, lead us to designing the next generation of charged MCs. Our aim was to use a flow focussing microfluidic device, to create purely synthetic and monodisperse microscale cryogels.

Experimental Methods

The microscale cryogels were synthesized by using a microfluidic flow-focussing device with a channel height and width of 100 µm that was fabricated by photo-lithography [3]. The dispersed phase contained the aqueous precursor solution either of poly(ethylene glycol) diacrylate (PEGDA) alone or PEGDA and 3-sulfopropyl acrylate potassium salt (SPA) and pegylated 2-Hydroxy-1-[4-(hydroxyethoxy)phenyl]-2-methyl-1-propanone (PEG-Irgacure 2959) as photoinitiator for both systems. The continuous phase was an immiscible fluorinated oil (HFE 7500, 3M™, NOVEC), which contained a surfactant synthesized in our lab to create uniform stable droplets of the precursor solution. After reducing the temperature to -20°C for 2 hours, the frozen precursor droplets were photo-crosslinked using a UV lamp. Afterwards, the purfication was performed by adding a perfluorooctanol solution, followed by a series of washing steps in HFE, isopropanol and finally water to completely remove the oil phase.

Results and Discussion

Monodisperse, spherical and macroporous PEGDA and additionally functionalized PEGDA-SPA based microcarrier with high surface to volume ratio where successfully developed. The implementation of negatively charged moieties from the sulfate groups of SPA was verified by Raman spectroscopy, while the macroporous morphology could definitely be identified by scanning electron microscopy. With these insights, the now proposed and fully synthetic approach opens new possibilites and could provide better properties in comparison to the first generation of microcarrier system.

Conclusion

Using a microfluidic flow focussing technique in combination with a cryogenic process and rapid photo-polymerization allows the fabrication of reproducible, uniform, non-charged and highly negatively charged microcarriers with a high throughput rate for applications for focal therapeutic delivery of partially positvely charged molecules like growth factors. The spherical and macroporous PEGDA and PEGDA-SPA scaffolds enable a potential loading and sustained release of molecules. Furthermore, the highly porous nature minimizes the dead space and allows shape memory properties for ease of injection.

References

1 P.B. Welzel et al. (2012) Biomacromolecules. 13(8): 2349-2358
2. B. Newland et al. (2015) Small 11(38): 5047-5053
3. J. Thiele et al. (2014) Lab on a Chip 14(15): 2651-2656

Acknowledgement

This work was funded by the Deutsche Forschungsgemeinschaft (DFG) – Project 320041273

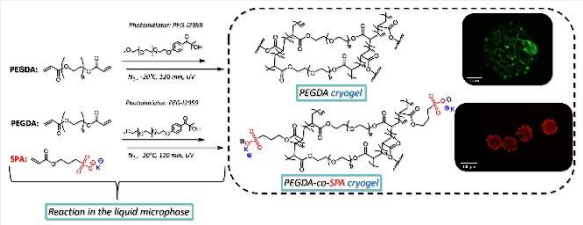

Reaction scheme of microscale cryogels
Reaction scheme of the non-charged PEGDA and negatively charged PEGDA-SPA based uniform, globular and macroporous cryogel scaffolds, synthesized by free radical photo-polymerization at subzero processing temperature

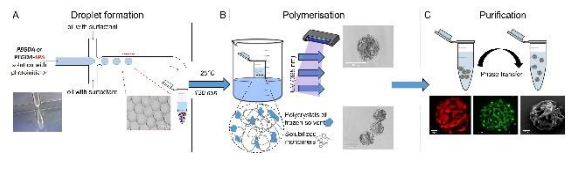

Fabrication of microscale cryogels
(A) Fabrication of monodisperse PEGDA and PEGDA-SPA based droplets. **(B)** Freezing of droplets and subsequent UV induced photopolymerisation. **(C)** Formation of uniform, globular and macroporous cryogel scaffolds

VIII-OS27-03

The osteoinductive activity of poly(3-hydroxybutyrate) and its natural functions

Vera V. Voinova[1], Garina A. Bonartseva[2], Irina I. Zharkova[1], Alexey V. Volkov[3,4], Alexander A. Muraev[3], **Anton P. Bonartsev**[1,2]

[1]M.V.Lomonosov Moscow State University, Faculty of Biology, Moscow, RU; [2]Research Center of Biotechnology of the Russian Academy of Sciences, A.N.Bach Institute of Biochemistry, Moscow, RU; [3]Peoples' Friendship University of Russia, Moscow, RU; [4]N.N. Priorov National Medical Research Center of Traumatology and Orthopaedics, Healthcare Ministry of Russia, Moscow, RU

Introduction

The biodegradable and biocompatible polymers, polyhydroxyalkanoates (PHAs), are actively used in medicine for production of a wide range of medical devices and dosage formulations, as well as for the manufacture of scaffolds for tissue engineering. For tissue engineering, these polymers obtained by chemical synthesis (e.g. polylactides, polyglycolides, poly-ε-caprolactone, and their copolymers) are mainly used, but the interest in the bioengineering application of natural poly(3-hydroxyalkanoates) obtained biotechnologically is also growing. Actually, the chemically synthetic PHAs are biomimetic analogs of bacterial poly(3-hydroxybutyrate) (PHB) and its copolymers. Due to the favorable properties (high biocompatibility, the relatively low rate of biodegradation, and good mechanics) PHB is the most promising for bone tissue engineering and bone regeneration. However, the problem of the osteoinductive activity of PHB remains insufficiently studied. Thus, the purpose of our research is to analyze the possible osteoinductive activity of PHB.

Experimental Methods

PHB and its bioPEGylated copolymer (PHB-PEG) were produced by the original biotechnological technique using a highly productive producing strain Azotobacter chroococcum 7B [1]. The obtained copolymer PHB-PEG, the composite of PHB with PEG (PHB/PEG) and polylactide (PLA) were used as controls to PHB. The obtained polymeric biomaterials were used to prepare the 3D-scaffolds by various modifications of salt leaching method. The morphology of scaffolds was analyzed by the scanning electron microscopy and the wide-field light microscopy. The physicochemical properties of the produced scaffolds were studied by rheometry, differential scanning calorimetry, and water uptake test. The ability to support the growth of mesenchymal stem cells (MSCs) isolated from rat bone marrow and 3T3-NIH fibroblasts in scaffolds were studied using the XTT-assay. The osteogenic differentiation of MSCs in regular and osteogenic media was studied by Alkaline Phosphatase activity assay, Alizarin Red staining assay, and analysis of change in expression of MSCs phenotype markers (CD90, CD45, CD 11b/c, CD29) using flow cytometry, scanning electron and confocal microscopy [2]. The osteogenic activity of PHB scaffolds in vivo was studied on the noncritical 1.5 mm defect of famous bone and the 8 mm critical defect of parietal bone that were modeled in Wistar rats by surgery technique using a trephine C-reamer. The bone tissue regeneration after implantation of the scaffolds as bone substitutes was evaluated by histological methods and fluorescent microscopy [3]. To estimate the dynamics of neo-osteogenesis on 3 different stages the vital fluorescent labeling of the newly formed bone tissue was carried out using i.p. administration of doxycycline, tetracycline, and alizarine red C. All experiments was performed according to guidelines for ethical treatment of animals ISO 10993-2.

Results and Discussion

The produced PHB, PHB-PEG, PHB/PEG, and PLA scaffolds have a 3D porous structure: with various pore sizes (the micropores and macropores), mean porosity >90%, and interconnected pore system. The 3D-growth of MSCs and 3T3-NIH fibroblasts in the scaffolds were observed. The spontaneous osteogenic differentiation of MSCs in regular medium and the modulation of their osteogenic differentiation in the osteogenic medium on PHB and PHB/PEG scaffolds were demonstrated, whereas PHB-PEG and PLA scaffolds promote MSCs growth that was not accompanied by pronounced differentiation. The PHB, PHB-PEG, and PHB/PEG scaffolds stimulated the bone tissue regeneration after their implantation in the noncritical and critical bone defects as the bone substitutes.

The osteogenic activity of PHB scaffolds depends on the physicochemical properties of the polymers, 3D- and surface microstructure of scaffolds, and also possibly the own biological activity of PHAs. But the reason and mechanisms of such biological activity of PHB remain unclear. We suggest here that the osteoinductive activity of PHB can be associated with its natural properties as a bacteria-origin biopolymer. This biopolymer is present in bacteria of mammalian microbiota, whereas endogenous PHB is containing in mammalian tissues. A series of studies indicate the possible regulating functions of PHB in bacteria of mammalian microbiota for their interaction with cells of host-organism [4]. The possible association of osteogenic properties of PHB with various biological functions of PHB in bacteria and eukaryotes, including in humans, are discussed.

Conclusion

Thus, we suggest the presence of own osteoinductive activity of PHB, which can be associated with its natural properties as a functional biopolymer in bacteria of mammalian microbiota.

References

1. Bonartsev AP et al. Biosynthesis of poly(3-hydroxybutyrate) copolymers by Azotobacter chroococcum 7B: a precursor feeding strategy. Prep. Biochem. Biotechnol. 2017; 47(2): 173-184.

2. Bonartsev AP et al. Poly(3-hydroxybutyrate)/poly(ethylene glycol) scaffolds with different microstructure: the effect on growth of mesenchymal stem cells. 3 Biotech 2018; 8(8): 328.

3. Bonartsev AP, Muraev AA, Deyev RV, Volkov AV Material-Associated Bone Resorption Sovremennye tehnologii v medicine 2018; 10(4), 26-33.

4. Bonartsev AP, Voinova VV, Bonartseva GA. Poly(3-hydroxybutyrate) and human microbiota. Applied biochemistry and microbiology 2018; 54(6): 547–568.

Acknowledgement

This work was supported by Russian Science Foundation, project # 17-74-20104 in part of polymer scaffolds production and the study of their physicochemical properties, and by Russian Foundation of Basic Research, project # 18-29-09099 in part of the study of cell growth in polymer scaffolds.

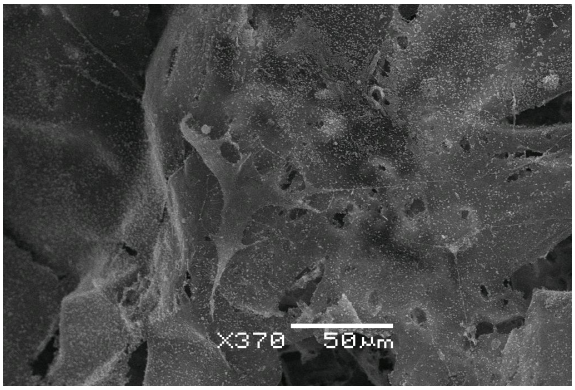

Figure 1. Osteogenic differentiation of rat bone marrow MSC on PHB scaffold

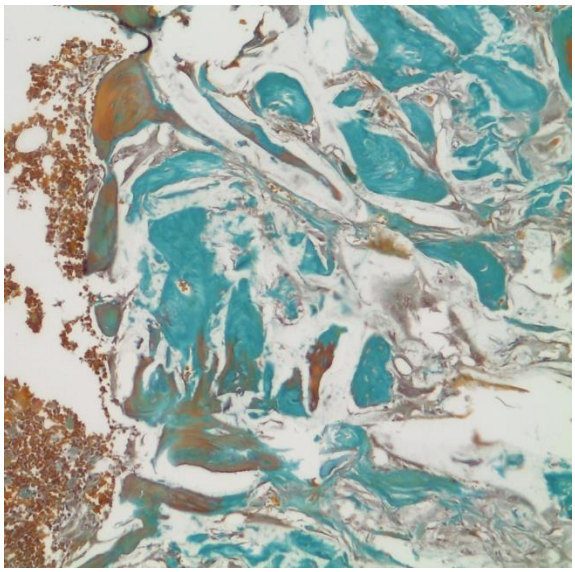

Figure 2. The islands of the newly formed bone tissue in the pores of PHB scaffold.

VIII-OS27-04

Polydopamine nanoparticles as an organic multitasking tool for localized neuronal stimulation

Matteo Battaglini[1,2], Attilio Marino[1], Chiara Martinelli[1], Gianni Ciofani[1,3]

[1]Istituto Italiano di Tecnologia, Smart Bio-Interfaces, Pontedera, IT; [2]Scuola Superiore Sant'Anna, The Biorobotics Institute, Pontedera, IT; [3]Politecnico di Torino, Department of Mechanical and Aerospace Engineering, Turin, IT

Introduction

Neurodegenerative diseases are one of the main medical challenges of our age, and the vast majority of neuronal disorders still lacks proper treatment. Each brain degenerative condition is characterized by its own hallmarks, as an example the degeneration of *substantia nigra* dopaminergic neurons in Parkinson's disease or the deposit of β-amyloid plaques in Alzheimer's disease. However, from a molecular point of view, it is possible to identify a common theme that plays a key role in brain-related pathologies: the presence of high levels of reactive oxygen species (ROS), that are able to interfere with physiological cellular functions[1]. The design and the development of innovative antioxidant systems, therefore, represent an interesting opportunity for the treatment of neurodegenerative conditions. With this aim, polydopamine nanoparticles with a lipid coating (PDNPs) were prepared and investigated in terms of biocompatibility and antioxidant properties. Antioxidant delivery is not the only promising tool for treating nervous system pathologies: direct brain stimulation (with physical means like electric fields, magnetic fields, etc.) has been deeply investigated for its possibility to ameliorate the symptoms of several neurological disorders. However, this approach has been hampered by the low accessibility of the nervous system[2]. To overcome the limits of direct neuronal stimulation the possibility to use light-responsive inorganic materials to elicit neuronal activity has been deeply investigated,[3]and at this aim the photothermal conversion ability of PDNPs and the feasibility to use this system to stimulate neurons activity was also investigated.

Experimental Methods

Polydopamine nanoparticles were prepared using a Stöber reaction and then coated with DSPE-PEG (5000 kDa) through the use of an ultrasonic probe. Nanostructures were then characterized in terms of size (dynamic light scattering measurements), surface charge (*Z*-potential analysis), morphology (scanning and transmission electron microscopy imaging), porosity (Brunauer-Emmet-Teller analysis), and antioxidant capacity (electron paramagnetic resonance). The biocompatibility of the structures was evaluated on differentiated SH-SY5Y cells using pico-green assay. Internalization rates and *in vitro* ROS scavenging action were also evaluated on differentiated SH-SY5Y through confocal imaging and flow cytometry analysis. Photothermal conversion capacity of PDNPs was evaluated both macroscopically by measuring the temperature increment after near-infrared (NIR) irradiation of nanoparticles dispersions and both at the cellular level through the use of a fluorescent thermo-responsive dye.

Results and Discussion

Characterization of the PDNPs dispersions demonstrates the presence of well dispersed and homogeneous structures with an average size of 170±30 nm (Figure 1). PDNPs showed good biocompatibility and an extremely high antioxidant ability, even if compared to other nano-antioxidant systems well known for their ROS scavenging properties (namely nanoceria[4]). Even more interestingly, DSPE-PDNPs showed the capacity to act as a photothermal converting material when irradiated with NIR laser (a water suspension of 1mg/ml of DSPE-PDNPs irradiated for 2

minutes with 0.82 W/cm^2 was enough to increase the dispersion temperature from 22 to 56°C) being able to generate a highly localized temperature increment in neuronal cells.

Conclusion

PDNPs showed extremely high antioxidant capacity and remarkable photothermal conversion ability, laying the base for successive exploitation of this system in the treatment of brain diseases. Other nanostructures are already exploited in the literature with similar features, like antioxidant cerium oxide nanoparticles or well-known NIR responsive gold nanostructures. However, PDNPs are able to outperform both of these examples, by combining ROS scavenging and NIR photothermal conversion into a single system. In addition, PDNPs are entirely constituted of organic components, bypassing in this way any concern regarding the use of inorganic structures in living organisms.

References

1. Tapeinos C., Battaglini M., Ciofani G. *Advances in the design of solid lipid nanoparticles and nanostructured lipid carriers for targeting brain diseases*. Journal of controlled release (2017) 264:306-332. doi: 10.1016/j.jconrel.2017.08.033.
2. Chang JY. *Brain Stimulation for Neurological and Psychiatric Disorders, Current Status and Future Direction.* Journal of pharmacology and experimental Therapeutics (2004),309:1–7. doi:10.1124/jpet.103.04971.
3. Yong J., Needham K., Brown WG., Nayagam BA., McArthur SL., Yu A., Stoddart PR.*Gold-nanorod-assisted near-infrared stimulation of primary auditory neurons.*Advanced healthcare materials (2014) 3(11):1862-8. doi:10.1002/adhm.201400027.
4. Battaglini M., Tapeions C., Cavaliere I., Marino A., Ancona A., Garino N., Cauda V., Palazon F., Debellis D., Ciofani G. *Design, Fabrication, and In Vitro Evaluation of Nanoceria-Loaded Nanostructured Lipid Carriers for the Treatment of Neurological Diseases ACS Biomaterials science and Engineering*(2019)5 (2), 670–682. doi:10.1021/acsbiomaterials.8b01033.

Acknowledgement

This project has received funding from the Italian Ministry of Health, grant RF-2016-02361610.

The authors gratefully thank Valentina Cauda, Andrea Ancona and Nadia Garino for electron paramagnetic resonance analysis, and Satoshi Arai, Madoka Suzuki and Young-Tae Chang for kindly providing the temperature sensitive fluorescent dye.

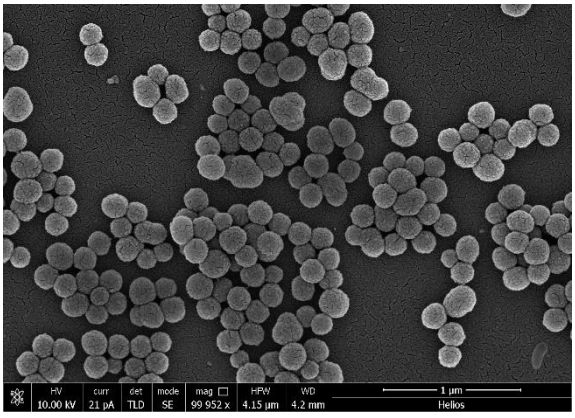

Polydopamine nanoparticles
Representative scanning electron microscope image of PDNPs.

VIII-OS27-05

Key effect of the Poly(glycerol sebacate) synthesis during early stages and its monitoring

Rubén Martín-Cabezuelo[1], Alicia Naderpour-Peñalver[1], Guillermo Vilariño-Feltrer[1], Ana Vallés-Lluch[1,2]

[1]Universitat Politècnica de València, Centre for Biomaterials and Tissue Engineering (CBIT), Valencia, ES; [2]Biomedical Research Networking Centre in Bioengineering, Biomaterials and Nanomedicine (CIBER-BBN), Valencia, ES

Introduction

The polyester known as Poly(glycerol sebacate) (PGS) has been studied since it was discovered around two decades ago. It presents suitable and optimal properties such as biocompatibility and biodegradability making it a great option to be used as a biomaterial. There is considerable controversy regarding its inconsistency in reproducing the same process conditions between different research groups.[1]

The PGS synthesis is based on two-step polycondensation reaction, first a prepolymerization step at a specific temperature and under an inert atmosphere (usually Nitrogen or Argon), where the monomers react leading to a non-completely crosslinked network that still can be dissolved, and secondly, a curing step at constant temperature based on its final scaffold application, where the PGS prepolymer (pPGS) completes its crosslink leading to a PGS network.[2]

In this study, we suggest that the early stages of the prepolymerization process are key elements for understanding the reaction, and its modifications can alter the entire synthesis leading to different and non-predictable final materials. Thus, we studied how the reaction took place at different times and how advanced the polycondensation was to understand its evolution and being able to monitor its final characteristics as a tunable biomaterial.

Experimental Methods

Sebacic acid and glycerol were mixed at 1:1 molar ratio at 140°C until the monomers melted completely. Then the mixture was stirred at 130ºC for 28 h under N2 atmosphere to obtain the prepolymer (pPGS). Material (monomers and pPGS) and residues (H2O and glycerol) samples were collected during the procedure at different time points every four hours until the prepolymerization was complete.

Afterwards, the molecular weight, chemical composition and degree of esterification was performed by means of gel permeation chromatography (GPC), Fourier-transform infrared spectroscopy (FTIR), proton nuclear magnetic resonance spectroscopy (RMN-H^1) and titration techniques to understand its composition and how the reaction was evolving. Rheometric techniques were performed to follow the evolution of viscosity with time.

To explain how the crosslink between the pPGS macromers leading to PGS occurs, monomers of sebacic acid (SA) and glycerol, propylene glycol and 1,3-propanediol were mixed and its curing process studied at three different temperatures (130, 150 and 170ºC) monitoring its viscosity throughout time until the PGS monomers achieved its gel point.

Results and Discussion

The rheometric curves of the different mixtures show that the PGS monomers initial viscosity was higher than in the rest of the mixtures and that the propylene glycol and 1,3-propanediol mixtures with SA cannot crosslink because of the bifunctionality of its monomers.

The different characterization techniques revealed that the earlier stages of the PGS polymerization are fundamental. The study first hours are the period when most of the conversion reaction takes place, around 50% (Figure 1).
The determination of water and glycerol residues during the reaction shows that the first fractions are the most glycerol enriched, indicating how the glycerol loss because of evaporation is a key parameter to control. FTIR and RMN-H^1 techniques didn't reveal significant differences except an increasing trend towards more ester links formation as we expected.

Conclusion

We probe how the early stages of the pPGS formation are fundamental to be properly monitored for an optimal final product as a biomaterial because is the key for its inconsistency in reproducing process conditions. More analysis and experiments will lead to the PGS proper control and better exploitation as a potential biomaterial.

References

1. Li X, et al. *Biomacromolecules*. 2015;16(5):1525-1533. doi:10.1021/acs.biomac.5b00018.
2. Conejero-García Á, et al. *Eur Polym J*. 2017;87:406-419. doi:10.1016/j.eurpolymj.2017.01.001.

Acknowledgement

The authors acknowledge Spanish Ministerio de Economía y Competitividad through DPI2015-65401-C3-2-R project and to the Electronic Microscopy Service at the Universitat Politècnica de València and A.V.-Ll. acknowledges the support of the Generalitat Valenciana, Conselleria de Educación, Investigación, Cultura y Deporte through projects AEST/2017/018 and AEST/2018/014.

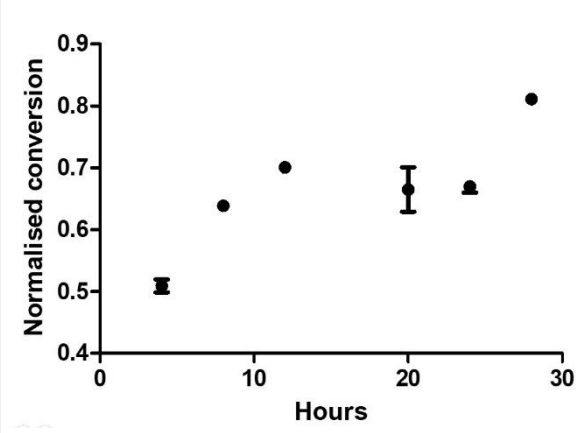

Figure 1. Samples normalised conversion values at different times
Evolution of monomer normalised conversion values as prepolymerization time increases shows a rising trend at constant temperature of 130ºC.

VIII-OS27-06

Magnetic gold nanorod-encapsulated biodegradable polymeric matrix for combined photothermal and chemo-cancer therapy

Pei-Ying Chen[1], Rih-Yang Huang[1], Chun-Chiao Chuang[1], Chih-Chi Cheng[1], Chieh Lo[1], Min-Hsiung Shih[2], Chien-Wen Chang[1]

[1]National Tsing Hua University, Department of Biomedical Engineering and Environmental Science, Hsinchu, TW; [2]Academia Sinica, Research Center of Applied Sciences (RCAS), Taipei, TW

Introduction

Light-mediated hyperthermia therapy[1] and photothermal-controlled drug delivery may achieve better therapeutic outcomes by minimizing the drawbacks associated with conventional chemotherapy, such as: poor drug distribution in tumors, ineffective treatment on drug-resistant cancer cells and damages on normal tissues. In this study, we proposed a multifunctional nanotheranostic system including features on: near-infrared (NIR)-triggered drug release, magnetic targeting and magnetic resonance imaging (MRI) imaging. The propose nanocomplex system, SAPP@DOX, is composed of poly(lactic-co-glycolic acid) (PLGA) with encapsulated doxorubicin (DOX), superparamagnetic iron oxide nanoparticles (SPION) and gold nanorods (AuNR).

Experimental Methods

Hydrophobic gold nanorods (AuNRs) was prepared by replacing the surface CTAB layer with dodecanethiol. The SAPP@DOX was fabricated by an oil-in-water (o/w) emulsification process. Size distribution and zeta potential of the SAPP@DOX were analyzed using a ZetaSizer. The magnetic properties of DOX@SAPP were characterized using SQUID magnetometer and MRI. Photothermal-triggered drug release was examined by repeatedly irradiated the SAPP@DOX solutions with NIR light (808 nm) with predesignated intervals. Supernatant from the NIR-irradiated SAPP@DOX solutions was collected to calculate the extent of photothermal drug release. Cell internalization of the SAPP@DOX by cancer cells was studied using flow cytometry and fluorescence microscopy techniques. In vitro combined photothermal- and chemo- anticancer effects were studied using MTT assay.

Results and Discussion

Dodecanethiol was used to covert the hydrophilic CTAB-AuNR into hydrophobic dodecane-AuNR, which were highly dispersed in nonpolar organic solvents such as chloroform and tetrahydrofuran. Size and surface potential of the SAPP@DOX were ~202 nm and -24 mV respectively. TEM images show that SAPP@DOX were polymeric spheres containing numerous SPIO and AuNR nanoparticles. No aggregation or significant size change was observed from the SAPP@DOX PBS solutions for at least 15 days. T2 relaxivity of the SAPP@DOX (430.4 $mM^{-1}s^{-1}$) was higher than the commercially SPIO-based T2 magnetic resonance imaging (MRI) contrast agents. The potentials of using SAPP@DOX on cancer cell imaging was revealed by displaying significant T2-weighted image contrast from the SAPP@DOX-containing cells. Photothermal effects of SAPP@DOX was demonstrated by observing rapid temperature rising after irradiating the nanoparticle solutions with NIR laser. The degree of heating was also proportional to the AuNR content in the SAPP@DOX. In addition, the NIR-inducing heating could effectively trigger DOX release from the SAPP@DOX. Over 70% of loaded DOX was released from the nanoparticles after 4 cycles of NIR irradiations. Cellular uptake of the SAPP@DOX by human breast cancer cells were significantly promoted by an

external magnetic attraction. Combined photothermal and chemo treatment by SAPP@DOX exerted more cancer cell death than single treatment. In vivo therapeutic effects of using SAPP@DOX for cancer treatment is under investigation.

Conclusion

In this study, a NIR-responsive SAPP@DOX nanocomplex system was designed for combined photothermal- and chemo-cancer therapy. SAPP@DOX exhibited several favorable properties, including excellent colloidal stability, multiple NIR-triggered drug release, efficient cellular uptake and effective cancer cell death induction. In vivo anti-cancer effects of SAPP@DOX is currently under investigation.

References

1. Lin SY, Huang RY, Chuang CC, Liao WC and Chang CW*. Multifunctional PEGylated AlbuminIron Oxide Nanocomplexes for Cancer Photothermal Therapy and MR imaging. Nanotheranostics 2018 2(2): 106-116.

Acknowledgement

This research was financially supported by Ministry of Science and Technology of Taiwan (MOST 107-2113-M-007-028 -) and National Tsing Hua University (107Q2519E1).

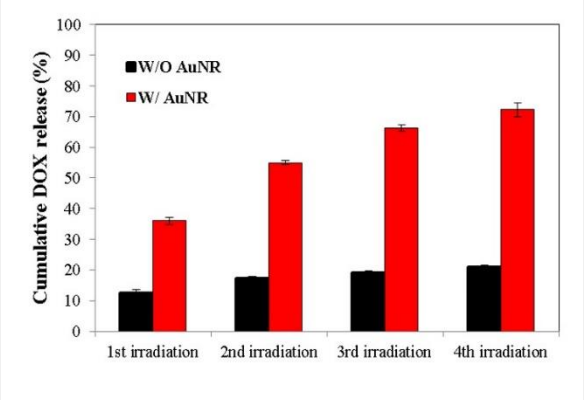

Figure 1 NIR-triggered DOX release from the SAPP@DOX.
The SAPP@DOX solutions received NIR irradiations (808 nm) for multiple times. After each irradiation, supernatants containing the released DOX were collected and quantitated using a fluorescence spectrophotometer. DOX-containing nanoparticles without AuNR was also tested as the control group. Data represent the mean +/- standard errors; n=3.

1:00 p.m. – 2:30 p.m.

Hall 4

VIII-OS28 | Ceramic Biomaterials/Bone 1

VIII-OS28-01

Cellular Uptake of Silicate Species

Joel Turner[1], Azadeh Rezaei[1], Julian R. Jones[2], Alexandra Porter[2], Akiko Obata[3], Gavin Jell[1]

[1]University College London, Division of Surgery and Interventional science, London, GB; [2]Imperial College London, Department of Materials, London, GB; [3]Nagoya Institute of Technology, Department of Life Science and Applied Chemistry, Nagoya, JP

Introduction

Silicate based bioactive glasses (BG) are used clinically to regenerate bone [1] [2]. Numerous papers have demonstrated the therapeutic importance of BG dissolution products for bone repair and regeneration [3]. There remains, however, a lack of understanding on how soluble silica species interact with cells. This includes how silica species are internalised (and possibly excreted), the intracellular concentration and location of these ions. A greater understanding of silicate cellular internalisation will help in the optimisation of bioactive glass ion release rates for more precise control of cell behaviour. As such, this study aims to investigate silicate ion uptake dynamics in osteoblasts whilst examining some the roles these ions may play in bone regeneration.

Experimental Methods

Osteoblast-like (SaOS-2) cells were cultured at 10,000/cm^2 in McCoy's Glutamax 5A medium containing 1 M sodium silicate hydrate. To assess if cytotoxicity was induced by different silicate concentrations and uptake inhibitors, proliferation, metabolic activity and cellular morphology were assessed by total DNA, Alamar blue and light microscopy assessment, respectively. Quantification of Si uptake was performed by ICP-OES, following lysing cells in 1M Nitric nitric acid at 85°C and filtration (after 6-96 h cell culture). Inhibition of Si silicate uptake mechanisms were evaluated by the use of chemical inhibitors of the sodium-bicarbonate co-transporter protein by S0859 (Merck). To locate intracellular Si, cultured cells were fixed in 2% paraformaldehyde resin, stained with 1% osmium tetroxide and mounted on to 400 mesh copper transmission electron microscopy (TEM) grids. Scanning transmission electron microscopy (STEM) (JEOL 2100 Plus) was used to image the cells and energy dispersive X-ray spectroscopy (EDXS) was used to locate and quantify Si content. Si uptake experiments were performed in triplicate. Data was statistically analysed using a Tau-Thompson assessment for anomalies and a student's t-test for statistical significance.

Results and Discussion

Exposure of SaOS-2 cells to media containing Silicate conditioned media at 0.5, 1 and 2 M sodium silicate did not produce a significant difference in showed no significant difference in proliferation, metabolic activity and morphology ($P>0.05$). A total increase in intracellular Si uptake was observed up to 48 h (whilst the uptake rate per hour decreased over time) (fig. 1A/B). Upon the replacement of Si containing serum with a control (no Si containing media) the concentration of Si decreased ($p<0.05$), suggesting the excretion of Si from the cells (Fig. 1C). The inhibition of sodium-bicarbonate channel co-transporter protein decreased ion uptake (without effecting cell number) suggesting a potential mechanism of uptake (Fig 1D). STEM/EDX point analysis showed Si to be evenly spread outdistributed within the cell body. Higher concentrations were seen to be localised within vesicle-like structures suggesting an active movement of Si throughout the cell.

Conclusion

Osteoblast-like cells reach a maximum uptake of Si ions over time. Our study suggested that the cells may begin excreting ions at specific stages during their proliferation. EDX spectral analysis highlighted that Si ions may be evenly spread outdistributed across the cell while higher concentrations were commonly localised inside vesicles. Further experiments showed that sodium-bicarbonate channels may play a role in the cellular uptake of these ions. As such, new BG materials should be tailored to release silicate and other ions to target specific cell types dependent on their uptake rates and mechanisms.

References

1. Logroscino G. Bone substitutes in orthopaedic surgery: from basic science to clinical practice. Journal of Materials Science: Materials in Medicine. 2014;25(10):2445-2461.
2. Hench L. The story of Bioglass®. Journal of Materials Science: Materials in Medicine. 2006;17(11):967-978.
3. Xynos I. Gene-expression profiling of human osteoblasts following treatment with the ionic products of Bioglass® 45S5 dissolution. Journal of Biomedical Materials Research. 2001;55(2):151-157.

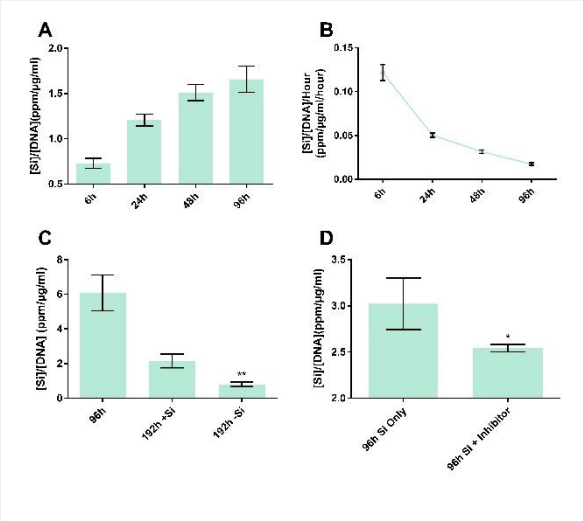

Understanding Si Ion Uptake Dynamics in Bone cells
Figure 1. Si uptake by osteoblast-like SaOS-2 cells as determined by ICP-OES.(A) Intracellular Si concentration increased/µg DNA up to 48hrs, (B) Si ion uptake rate decreases as a function of time, (C) replacing culture medium with Si and non-Si conditioned mediums causes a significant decrease in Si, (D) intracellular Si ion concentration decreases following inhibition of sodium-bicarbonate uptake channels. N=3, error presented as +/- SD, *= P<0.05, **= P<0.01

VIII-OS28-02

Bone sialoprotein functionalized 3D printed polylactide-collagen composite materials induce bone regeneration in a rat femur model

Ulrike Ritz, Tanja Habeck, Anja Klein, Hermann Götz, Andreas Baranowski, Pol M. Rommens

University Medical Center Mainz, Department of Othopedics and Traumatology, Mainz, DE

Introduction

Large segmental bone defects caused by trauma, infection or tumors often result in non-unions. The gold standard for treatment is autologous bone grafting, which is accompanied by additional interventions and limited material. New and innovative bone substitutes are needed. In the present study, an inexpensive 3D-desktop printer was used to print polylactide (PLA) porous cages loaded with bone sialoprotein immobilized in a collagen I-gel. Former in vitro studies demonstrated biocompatibility of these materials (1). Bone sialoprotein (BSP) plays an essential role in bone mineralisation and remodelling(2). The aim of this study was to combine BSP with polylactide and collagen gels and evaluate the effects in vivo on bone regeneration. Therefore, te material was tested for its potential to induce bone regeneration in a critical size femur defect in rats.

Experimental Methods

A 6mm critical size femural defect was created in wistar rats employing the ratfix-Sytem (RIsystem). During lifetime x-rays were performed every two weeks to detect early bone formation. Eight weeks after implantation rats were killed, the femur extracted and further analyzed employing µCT and quantification by bone volume / total volume ratio. After decalcification, histological slizes were produced. First, HE-stainings were performed, followed by immunohistological stainings for markers of osteogenesis as well as for angiogenesis.

Results and Discussion

The results revealed that in the negative control without any implant material formation of non-unions could be demonstrated. Immobilization of BSP resulted in enhanced bone regeneration; the fracture gap was almost closed after eight weeks. The effect of BSP on bone regeneration was more pronounced than immobilization with bone morphogenic protein (BMP-7). Moreover, the amount of newly formed bone increased with higher concentration. The results of µCT could be confirmed by histology with HE-staining, showing bone tissue inside the PLA-cage in the groups modified with BSP, whereas in the groups without growth factors collagenous connective tissues predominated.

Conclusion

Our study shows that polylactide is an interesting material for 3D-printing in biomaterial research particularly with regard as bone substitute. Especially the combinations with a soft material like collagen I and an extracellular matrix protein like BSP resulted in increased bone formation in the employed critical size defect. Further studies with longer lifetime and higher group numbers have to be performed to confirm the potential of the material as bone substitute material.

References

(1) Ritz U et al., Int J Mol Sci., 2017, 18

(2) Tye CE et al., J Biol Chem, 2005, 14

Acknowledgement

Financial support was provided by Immundiagnostik AG (Bensheim, Germany).

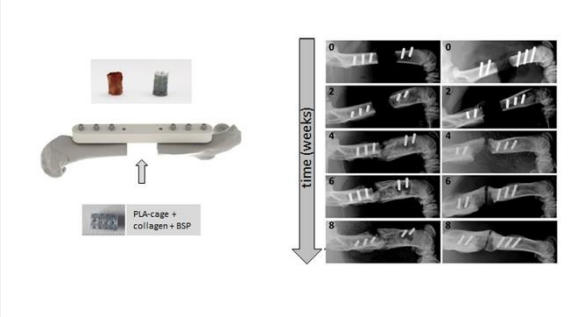

BSP induces bone regeneration in a critical size defect in the rat femur

A) in vivo model

B) Bone regeneration after implantation of PLA-collagen-BSP scaffold

VIII-OS28-03

Mesoporous bioactive glasses as building blocks in biomaterials for hard-tissue regeneration

Matthias Schumacher, Pamela Habibović, Sabine van Rijt

Maastricht University, MERLN, Maastricht, NL

Introduction

Mesoporous bioactive glasses (MBG), first described by Zhao *et al.* in 2004 [1], are synthesised via the sol-gel route in presence of structure-directing polymers. Making use of an evaporation-induced self-assembly and subsequent thermal removal of the polymer, this class of biomaterials possesses a highly ordered mesopore system in the nm range making them well suited for drug-delivery applications. Additionally, MBGs exhibit a bioactivity superior to non-mesoporous glasses and are degradable, suggesting them as promising materials for bone defect regeneration [2].
Recently, the use of SiO_2/CaO/P_2O_5 glasses as precursors for self-setting materials was proposed [3]. Based on this concept, we aim to employ MBGs as building blocks for pasty, self-setting biomaterials that, via the integration of surface functionalities that allow the attachment of e.g. cell instructive peptides, could help using this promising material class in the context of material-driven hard tissue regeneration and controlled drug delivery.
Here, we synthesized MBG with varying silica content and Ca/P-ratio and investigated the impact of chemical composition on glass and mesopore-formation and recrystallization behaviour of the materials in aqueous environment. In addition, the introduction of functional groups on the material surface was investigated. Cytocompatibility of the synthesized MBGs was investigated using human mesenchymal stromal cells (hMSC).

Experimental Methods

MBGs were synthesised based on the method proposed by Zhu *et al.* [1]. A sol was obtained by ageing a mixture of tetraethyl orthosilicate, triethyl phosphate and calcium nitrate in varying proportions in the presence of structure-directing agent Pluronic P123. SiO_2-content and the Ca/P ratio were varied between 60–85 mol% and 1–2.75, respectively. Gels were aged for 24 h, dried and heat-treated at 650°C for 5 h to remove organic components (Pluronic P123).
Phase composition of the obtained glasses was analysed by XRD (D2 Phaser, Bruker) and FTIR (Nicolet iS50, ATR mode). Mesopore formation was investigated using TEM (Tecnai G2, FEI). Material degradation in aqueous media was studied using ICP-MS (iCAP Q, Thermo Scientific). Based on the work of Sun *et al.* [4], amine and thiol functionalization was performed by refluxing MBG samples in dry toluene containing appropriate amounts of (3-Aminopropyl)triethoxysilane or (3-Mercaptopropyl)trimethoxysilane, respectively.
Metabolic activity as well as proliferation of hMSC cultured on tissue culture polystyrene and exposed to cell culture medium extracts of various MBG compositions were investigated over 7 days using the Presto Blue (Invitrogen) and CyQuant (Molecular Probes) assays, respectively.

Results and Discussion

Amorphous MBG could be obtained with Ca/P ratios between 1 and 1.67. At higher ratios, formation of calcium phosphate minerals during solvent evaporation and subsequent heat treatment was observed. Over the whole range of material compositions, the formation of mesopores with approx. 4.3–4.6 nm diameter and 7.2–7.6 nm spacing

could be confirmed. Using fluorescent labelling the successful surface grafting of both amine and thiol functional groups onto pre-sintered MBG could be demonstrated.
During ageing in aqueous media, release of Si and Ca from the samples indicated material degradation; however, a depletion of P in the phosphate-containing immersion liquid suggested the simultaneous re-precipitation of the materials. In accordance, XRD confirmed the crystallization of hydroxyapatite in all samples, being most pronounced in MBG with low Si-content. Hence, the formulation of self-setting pastes based on MBGs appears feasible.
Both metabolic activity and proliferation of hMSC was not impaired during exposure to MBG-conditioned media, suggesting the cytocompatibility of the materials.

Conclusion

Amorphous MBG could be obtained over a broad range of compositions in the SiO_2/CaO/P_2O_5 system. Given their ability to re-crystallize into hydroxyapatite and their cytocompatibility, the formulation of self-setting implant materials based on modified MBGs for the application in hard-tissue regeneration appears promising. In addition, the successful grafting of functional surface groups onto the synthesized MBGs will allow us to tailor their material properties in terms of bioactivity [4] and for controlled drug delivery applications.

References

[1] Y.F. Zhu, C.T. Wu, Y. Ramaswamy, E. Kockrick, P. Simon, S. Kaskel, H. Zrelqat. Micropor. Mesopor. Mat. 112(1-3) (2008) 494-503.
[2] X. Yan, C. Yu, X. Zhou, J. Tang, D. Zhao. Angew. Chem. Int. Ed. Engl. 43 (2004) 5980–5984.
[3] N.W. Kent, R.G. Hill, N. Karpukhina. Mater Lett 162 (2016) 32-36.
[4] J. Sun, Y. Li, L. Li, W. Zhao, L. Li, J. Gao, M. Ruan, J. Shi. J. Non-Cryst. Solids 354(32) (2008) 3799-3805.

Acknowledgement

This work was supported by the Alexander von Humboldt Foundation (Germany). We would like to thank the province of Limburg (LINK) for providing financial support to this project.

VIII-OS28-04

Examination of a novel absorbable fiber-based bone substitute material

Carsten Linti[1], Priscilla Füllemann[1], Katrin Malunat[2], Nicole Müschenborn[2], Sven Oberhoffner[2], Michael Doser[1]

[1]Deutsche Institute für Textil- und Faserforschung, Biomedical Engineering, Denkendorf, DE; [2]ITV Denkendorf Produktservice GmbH, Denkendorf, DE

Introduction

Bone grafting is still the standard treatment for bone defects after tumor excision or accidents for example. However, this approach has considerable drawbacks, such as a second surgical procedure for autografts or a theoretical risk of disease transmission for allografts. An alternative to bone grafting is the replacement of missing bones with bone substitute materials that accelerate healing and, ideally, resume the characteristics of the natural bone.

An absorbable scaffold with high porosity as a bone substitute material was developed. The device was designed to realize interconnected pores, large pore volume and sufficient pore size allowing ingrowth of osteoblasts and vascularization. This could be realized by using materials composed of water-soluble polyvinyl alcohol fibers (PVA) and caprolactone fibers (PCL) functionalized with hydroxylapatite (HA) which were sintered and the water-soluble core component was desolved. As a result an absorbable scaffold with high porosity was obtained. The use of X-ray microtomographic images (µCT) and a flow simulation proved the interconnectivity of the pores. The improved cell adhesion and migration of osteoblasts into the scaffold could be shown. Cell biological studies have shown that the cells adhere and proliferate well on the material.

Experimental Methods

In a monofilament extrusion with PCL (ITV Produktservice GmbH) in a twin-screw extruder (Prism Eurolab 16 Twin Screw Extruder, Thermo Fischer Scientific) 21 wt.% HA was compounded. The monofilaments were then stretched until a diameter of 0.6 mm was achieved. Monofilaments of polyvinyl alcohol (Mowiflex232) were extruded for the water-soluble component (3devo Next Extruder). The smallest achievable diameter was 0.36 mm. Both monofilaments were cut into 2-4 mm short fibers.

A mixture of the short fibers (30 wt.% PCL / HA and 70 wt.% PVA) were sintered at 100°C into cylindrical bodies with 10 mm diameter which were cut into 4 mm slices for the cell cultivation. Dissolving the PVA in water, a porous scaffold of PCL / HA was obtained and sterilized with gamma radiation.

The three-dimensional, porous structure of the scaffolds was investigated in a micro-CT (phoenix nanotom). By flow simulation, the interconnectivity of the pores was proved. Scanning electron microscopy (Hitachi TM-1000) was used to measure the size of the pores (ImageJ).

Colonization was performed with L-929 mouse fibroblasts for biocompatibility testing. Each specimen was given 150 µL of cell suspension (50,000 cells). Metabolic activity was tested by MTT test and Hematoxylin-eosin staining (Hemacolor, Merk) after 24 h and 4 days.

Colonization with osteoblasts (SaOs-2 cell line) was carried out accordingly to colonization with L cells with 150000 cells on each specimen. After a culture time of 5 and 11 days, hematoxylin-eosin staining, alkaline phosphatase assay (Biomol), light microscopic and SEM were performed.

Results and Discussion

The micro-CT (FIG. 1) shows a highly porous interconnecting structure with evenly distributed pores. The flow simulation (FIG. 1) confirms the high porosity and interconnectivity of the pores. The pore diameters in the SEM show an average of 350 - 399 µm which is sufficient for vascularization.

Adhesion of L-929 mouse fibroblasts within the scaffold is facilitated by the reduced hydrophobicity of the PCL due to the functionalization with hydroxyapatite. After four days, the number of cells on the scaffold has increased significantly, which shows that not only adhesion, but also cell proliferation has taken place. Cells can be seen in almost all pores (FIG. 2), which also show the polygonal-elongated morphology of fibroblasts. No cytotoxicity could be observed even after 4 days of cultivation(MTS test).

After five days, the specimens are evenly populated with osteoblasts, suggesting that HA improves the adhesion of osteoblasts. The SEM images (FIG. 2) show that the cells are in different cell cycle stages also forming extracellular matrix. After eleven days, the inner surfaces of the specimens are densely populated with osteoblasts. Evidence of alkaline phosphatase (ALP) shows that the osteoblasts synthesize ALP. In addition, a significant increase in ALP levels from day five to eleven was found showing cells are in the second phase of their bone building function.

Conclusion

The production of a bone substitute material with high porousity (70 %vol), interconnecting pores and large pore sizes using absorbable fibers of HA-PCL-compound could be shown. The open pore structure corresponds to the requirements necessary for osteoconductivity and neovascularisation.

The cell studies with osteoblasts showed an increased synthesis of alkaline phosphatase by cells in direct contact to the material, which confirms an osteoinductive effect by the hydroxyapatite. Thus, especially due to the osteoinductivity, this new bone substitute material is a promising approach for the use as scaffold for osteoblasts.

References

R. Smeets, H. Hanken, B. Beck-Broichsitter, A. Gröbe, C. Precht, M. Heiland und O. Jung, „Knochenersatzmaterialien - Übersicht und aktuelle Empfehlungen,“ *MKG-Chirurg 2016-9,* pp. 2-11, 2016.

M. Dauner, K. Malunat, S. Oberhoffner, "Knochenersatzmaterialkörper und Verfahren zu dessen Herstellung", DE 102017101804 A1, 2017

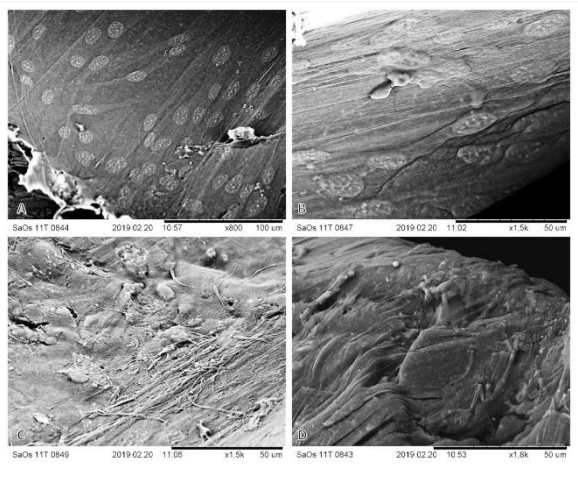

Fig. 2: SaOs-2 cells after 11 days, SEM images, gold layer sputtered, magnification see scale

After eleven days, the specimens are densely populated with the osteoblasts (A). After five days, cells can be seen in different cell stages (B). Cells form ECM (C + D). This shows that the cells feel comfortable on the material and behave as in their natural environment

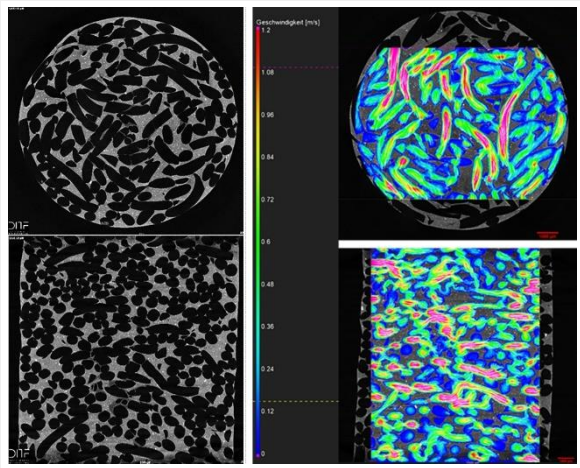

Fig. 1: Interconnecting pores of the bone substitue material
Left: µ-CT images of the specimen, top view and side view; right: flow simulation, plan view and side view with colored scale of the flow velocity

VIII-OS28-05

Hemocompatibility of single crystalline ceramics: role of crystallographic orientation on the platelet activation

Zümray V. Parlak[1], Rafal Zybala[2,3], Stephan Rütten[4], Norina Labude[4], Sabine Neuss[4,5], Rainer Telle[1], Karolina Schickle[1]

[1]RWTH Aachen University, Department of Ceramics and Refractory Materials, Institute of Mineral Engineering, Aachen, DE; [2]Warsaw University of Technology, Warsaw, PL; [3]Institute of Electronic Materials Technology, Warsaw, PL; [4]RWTH Aachen University Hospital, Institute of Pathology, Aachen, DE; [5]Aachen University Hospital, Helmholtz Institute for Biomedical Engineering, Biointerface Group, Aachen, DE

Introduction

The main requirements of cardiovascular implants are biocompatibility, hemocompatibility and long term durability in order to provide a healthy replacement for the damaged tissues or organs. The implants are supposed not to cause any damage for the surrounding tissue and should show non- thrombogenic behavior due to the fact that the surface induced thrombosis is one of the main reasons of the implant failure. The cardiovascular patients might face with a risk of hemorrhage due to the chronic anticoagulation therapy for blood coagulation [1]. The response of Endothelial cells (EC) to the surface of cardiovascular implants is very important for tissue regeneration and tissue repair. Proper endothelialization can reduce blood cell activation, and consequently, prevent the thrombus formation [2]. For this reason, it is vital to understand the thrombus mechanism at the interface of biomaterial and blood. In this study, we aimed to reduce or to avoid the anticoagulant usage of the patients by investigating the optimal materials and surfaces which have the lowest thrombotic effects. Based on our preliminary study on several high-strength ceramics, we concluded that platelet activation on the single crystalline SiC was significantly lower than that of its polycrystalline form. This result motivated us to deepen our research with different single crystals, their polymorphs and various crystallographic planes. Due to the non-thrombogenic nature, endothelial monolayer was selected as the best control surface possible for an accurate comparison with single crystalline ceramic surfaces. For the first time in the literature, the effect of different cystallographic orientations on the blood cell activation was examined and compared with endothelial monolayer to simulate the natural blood vessel wall.

Experimental Methods

Cytotoxicity, endothelialization quality and blood cell responses for (0001) and (11-20) planes of Al_2O_3 single crystals, Si and C faces of 4H-SiC and 6H-SiC as well as SiO_2 and ZrO_2 single crystals were examined. Surface roughness values of the single crystals were measured by atomic force microscopy (AFM). In order to provide information on surface wettability, contact angle measurements were performed by the Sessile drop technique. Cytotoxicity of the specimens were analyzed by the live-dead staining assays for human umbilical vein endothelial cells (HUVECs) and blood cells. In order to examine the blood cell activation in terms of platelets and white blood cells, human peripheral blood mononuclear cells (PBMC) were isolated from the whole blood. Cell behaviors on the single crystal ceramics were analyzed under the dynamic flow conditions besides of the static cell culture conditions, in order to simulate physiological blood flow conditions of blood vessels. CD62P marker was used to investigate an activated and adhered platelets by using ELISA assay. Visualization of the structure and interaction of blood cells with ceramic specimens were performed by using scanning electron microscopy (SEM).

Results and Discussion

According to the live-dead staining assay, the overall viability values indicated that all single crystals are nontoxic for HUVECs and PBMCs. (11-20) plane of Al_2O_3 exhibited the most prominent result of the static and dynamic tests. The circular shape of platelets indicates the inactivated cell state on this surface which is an important sign of improved hemocompatibility. Minimal number of cells on (11-20) plane of Al_2O_3 reveals that blood cells do not tend to adhere to the surface even under the static conditions. The behavior of blood cells on the (11-20) plane of Al_2O_3 is comparable to endothelial monolayer control surface, in terms of lower cell adhesion with minimal activation, see Figure 1. If the endothelial monolayer is assumed to be purely hemocompatible, (11-20) plane of Al_2O_3 displays almost the same superior performance. It attracts attention (0001) plane of Al_2O_3 shows significantly higher blood cell adhesion than (11-20) plane even though they exhibit similar surface roughness values. This can be attributed to the difference of the surface energies and surface charge distributions, which effect the protein adsorption at the surface and signifies the high sensitivity of blood cell responses to the contact surface.

Conclusion

As a conclusion, Al_2O_3 (11-20) showed the best non-thrombogenic surface properties by mimicking the endothelial monolayer with minimal blood cell activation and adhesion. Its superior hemocompatible characteristic interconnected to surface properties will lead us to better understand the reactions at the interfaces “implant–blood cells” and “implant–endothelial cells”. This knowledge could be further used to create the innovative group of materials and their surfaces that have the lowest thrombotic effects and at the same time exhibit bioactive character to the endothelial cells in order to improve implant integration.

References

[1] L. A. Pruitt and A. M. Chakravartula, Mechanics of biomaterials: Fundamental principles for implant design. Cambridge University Press, 2011. 1, 4

[2] M. V. Vellayappan, A. Balaji, A. P. Subramanian, A. A. John, S. K. Jaganathan, S. Murugesan, E. Supriyanto, and M. Yusof, Multifaceted prospects of nanocomposites for cardiovascular grafts and stents," International journal of nanomedicine, vol. 10, p. 2785, 2015.

Acknowledgement

This research was funded by the Deutsche Forschungsgemeinschaft (DFG, German Research Foundation) – №405895710.

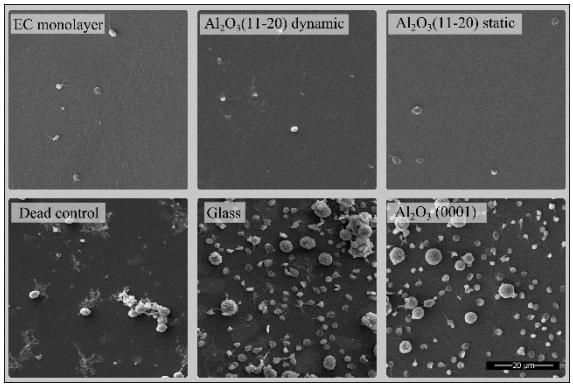

Figure 1:
SEM images of PBMC cells on different surfaces. Static and dynamic test results of (11-20) plane of Al_2O_3 are compared to the other control surfaces and (0001) plane of Al_2O_3. Glass was used as a cytocompatible control specimen, while Triton-X100-treated surface was used as a toxic control (dead control) due to its destruction effects on the cellular activity.

VIII-OS28-RF06

Characterization of a poly(lactic-co-glycolic) acid - hydroxyapatite 3D-printed scaffolds for bone tissue engineering

Joanna Babilotte[1], Vera Guduric[1], Reine Bareille[1], Damien Le Nihouannen[1], Jean-Christophe Fricain[1,2], Sylvain Catros[1,2]

[1]INSERM U1026 BioTis, Bordeaux, FR; [2]Faculty of Dentistry, Bordeaux, FR

Introduction

Current bone tissue engineering strategies are based on porous biocompatible scaffolds seeded with tissue-specific cells. Improvement in rapid prototyping technology, such as 3D printing, allows fabrication of custom-made 3D scaffolds with high resolution. Our group has developed a new material, made of medical grade poly(lactic-co-glycolic) acid (PLGA) mixed with 10% (w/w) hydroxyapatite nanoparticles (HA) for 3D printing by Fused Deposition Modelling (FDM). It showed a low chemical degradation during manufacturing steps, expected loading and homogeneous HA distribution. Based on this, our aim was to evaluate biocompatibility and osteopromotive potential of these new materials.

Experimental Methods

PLGA and PLGA-HA 10% (w/w) filaments were used to 3D printed porous membranes. The membranes were seeded with human adipose-derived stem cells (hADSCs) or human bone marrow stem cells (hBMSCs). Cytotoxicity was assessed according ISO 10993-5, cell proliferation by CyQuant® and cell viability by Live-Dead. Osteogenic differentiation was evaluated with qualitative alkaline phosphatase (ALP) staining and quantification of mineralization by red alizarin. Inflammatory potential was analyzed by subcutaneous implantation in rat during 1 and 4 weeks.

Results and Discussion

The composite materials were non-cytotoxic. Both hADSC and hBMSCs had high viability and proliferate on the materials, even after 21 days of culture [Figure 1]. At day 21, hADSCs highly colonized the material and formed bridge-like structures in the pores [Figure 1]. ALP staining and mineralization seemed higher with PLGA-HA 10% materials relative to PLGA for both cell types. Histological results for subcutaneous implantation are under way. PLGA is largely known to be cytocompatible [1]. As expected, addition of HA might have positive impact on osteodifferentiation [1,2].

Conclusion

Our preliminary data demonstrate that it was possible to fabricate a PLGA-HA composite biomaterial for 3D printing by FDM. Materials showed favorable properties and relevant cellular response for bone tissue engineering applications. Our next evaluations will focus on osteoblastic gene expression characterization and implantation in a critical calvaria defect model in rat to assess bone regeneration potential of developed materials.

References

[1] H.-S. Roh *et al*., Applied Surface Science (2016) 388 : 321-330, doi: 10.1016/j.apsusc.2015.12.243;
[2] J. Babilotte *et al*., J Biomed Mater Res Part B (2019), doi: 10.1002/jbm.b.34348

Acknowledgement

The authors would like to thank to the Agence National de la Recherche for the financial support.

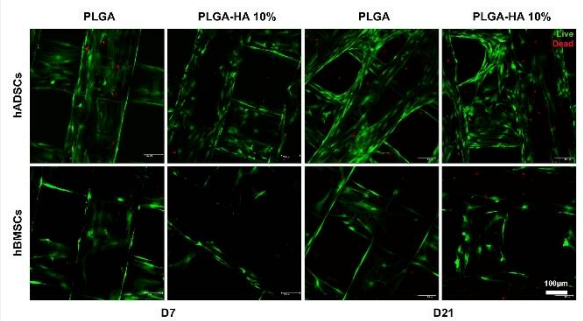

Figure 1. Evaluation of cell viability with Live-Dead assay.
hADSCs and hBMSCs was seeded on PLGA and PLGA-HA 10% (w/w) membranes. Cell viability was evaluated by a Live-Dead assay on days 7 (D7), 14 (D14) and 21 (D21).

VIII-OS28-RF07

A combined biological and chemical/physical bone characterization for the development of customized 3D-printed scaffolds

Caterina Licini[1,2], Giulia Molino[2], Chiara Novara[2], Fabrizio Giorgis[2], Giorgia Cerqueni[1], Sonia Fiorilli[2], Gabriela Ciapetti[3], Monica Mattioli-Belmonte[1], Chiara Vitale-Brovarone[2]

[1]Università Politecnica delle Marche, DISCLIMO, Ancona, IT; [2]Politecnico di Torino, Dipartimento di Scienza Applicata e Tecnologia, Turin, IT; [3]Istituto Ortopedico Rizzoli, Laboratorio di Fisiopatologia Ortopedica e Medicina Rigenerativa, Bologna, IT

Introduction

Osteoporosis (OP) is a worldwide disease with a substantial incidence in aged population. It is characterized by a low bone mass due to microarchitectural and structural deterioration of bone tissue, that leads to enhanced bone fragility and consequent increase in fracture risk.[1] The extracellular matrix (ECM) of OP bones undergoes important modifications with changes in protein content and chemical structure that lead to an increase in mineral/matrix ratio.[2] In the frame of the ERC project BOOST, which aims to develop and 3D print a scaffold mimicking human bone, we matched different morphological and structural approaches and techniques to acquire a wide-ranging knowledge of healthy and OP bone structure.

Experimental Methods

Human femoral and humeral heads, discarded during surgical interventions on orthopaedic patients (healthy and osteoporotic), have been harvested. Histological staining, immunohistochemistry and western blotting analyses have been executed to evaluate differences in bone tissue morphology and expression of the main ECM components (i.e. Collagen Type I, TGF-β, IGF-1, Osteocalcin, Osteopontin, Decorin and Bone Sialoprotein-2). Raman spectroscopy and X-ray diffraction (XRD) analysis have been performed to investigate the bone matrix organization and the structure of the inorganic phase, respectively. Furthermore, bone samples have been subjected to micro-computed tomography (micro-CT) analysis to study the overall 3D trabecular organisation as well as its tissue mineral density.

Results and Discussion

Micro-CT and histological staining showed a narrowing of OP bone trabeculae. Furthermore, OP bone trabeculae resulted to have a preferential orientation and a lower interconnection, probably due to a loss of transversal trabeculae (Fig.1A). Micro-CT analysis revealed also an increased tissue mineral density for OP samples, indicative of an increased inorganic phase amount. This result was also confirmed by XRD analysis that detected an increase of hydroxyapatite crystal size in the OP bone. Moreover, both histological observation and Raman spectroscopy suggested a less organized structure in OP tissue at the nanoscale in comparison to healthy one. Histological analysis revealed indeed a disordered tissue morphology (Fig.1B), while Raman spectroscopy detected an increased contribution of random coil configuration of ECM proteins. In addition, western blotting identified the appropriate ratio of the main proteins in bone ECM, whilst immunohistochemistry defined their correct localization.

Conclusion

Biological and chemical/physical techniques allowed a detailed investigation of the structure and composition of healthy and OP bone. From the results obtained through these analyses, it is possible to affirm that OP bone presents

an altered structure and morphology at both the microscopic and the nanometric scale. The knowledge of the healthy and OP bone features is mandatory for the development of biomimetic 3D-scaffolds with a suitable architecture and a punctual localization of molecules to favour a correct bone remodelling. Studies are also ongoing for the setting up of appropriate biomaterials suitable for the 3D printing process of BOOST smart scaffolds.

References

1. Silverman SL, Kupperman ES, Bukata SV and Members of IOF Fracture Working Group. Fracture healing: a consensus report from the International Osteoporosis Foundation Fracture Working Group. Osteoporos Int. 2016 Apr 25. DOI 10.1007/s00198-016-3513-y.
2. A.L. Boskey, Bone composition: relationship to bone fragility and antiosteoporotic drug effects, BoneKey Rep. 4 (2015). doi:10.1038/bonekey.2015.79.

Acknowledgement

This project has received funding from the European Research Council (ERC) under the European Union's Horizon 2020 research and innovation programme (grant agreement No 681798 - BOOST) www.ercprojectboost.eu

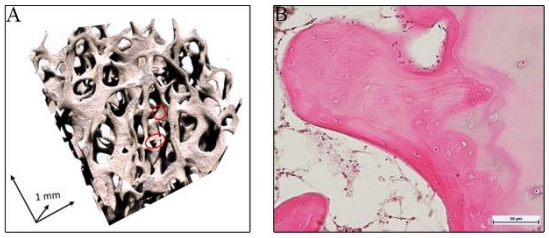

3D reconstruction and histological representation of OP bone
A) 3D micro-CT representation of an OP bone sample. Circled in red the not-bridging transversal trabeculae; B) Histological section (H&E) of bone tissue in OP subject showing the irregular morphology of lamellae.

VIII-OS28-RF08

Novel concept of bioresorbable bioactive fracture fixation plates for load-bearing applications by tailored fibre placement

Artem Plyusnin[1], Oliver Liesmäki[1], Julia Kulkova[1], Axel Spickenheuer[2], Lars Bittrich[2], Cindy Elschner[2], Annette Breier[2], Niko Moritz[1]

[1]University of Turku, Institute of Dentistry, Department of Biomaterials Science and Turku Clinical Biomaterials Centre – TCBC, Biomaterials and Medical Device Research Program, Biomedical Engineering Research Group, Turku, FI; [2]Leibniz-Institut für Polymerforschung Dresden e. V. (IPF Dresden), Department of Mechanics and Composite Materials, Complex Structural Components Workgroup, Dresden, DE

Introduction

In internal fracture fixation, metallic plates are a common treatment modality. However, the excessive stiffness of metallic plates leads to an unequal distribution of load between the implant and the healing bone, known as “stress-shielding” [1]. The subsequent underloading of bone, in turn, may lead to adverse bone remodeling resulting in non-union or re-fracture of the bone.

Fiber reinforced composites (FRC), combining less weight and ability of adjusting the stiffness, have been suggested as alternatives to metals [2-4]. Adapted FRC plates reduce stress-shielding and facilitate the natural fracture healing process reducing the risk of non-union or re-fracture. In practice, FRC plates often include one or several layers of continuous unidirectional fibers. The screw holes in these plates are made by drilling which compromises the integrity of fibers. Additionally, the holes themselves are stress concentrators, which further decreases the reliability of the plate.

In Tailored Fiber Placement (TFP), a variety of embroidery technology, continuous glass or carbon fibers are placed onto a fabric sheet, fixed by stitching with a sewing thread and impregnated in a polymer matrix [5]. Thus, the screw holes are formed by the particular placement of the fibers considering the stress distribution under load [6] and bypassing the screws, thus avoiding the need to drill holes. Hence, stress concentration around holes is minimized.

As their metallic counterparts, biostable FRC plates often require plate removal after complete fracture healing. This second surgery could be avoided by the use of bioresorbable materials. However, bioresorbable FRC fracture fixation plates for load-bearing applications are not commercially available.

We propose a novel concept of a bioresorbable bioactive fracture fixation plate, adjustable for different clinical applications. In this study, we focus on the treatment of front limb fractures in toy-breed dogs where the complications associated with the use of metallic plates are particularly amplified. Therefore, the animals give a representative model for the development of a novel treatment. Ideally, the plate is to be made of a bioresorbable polymer reinforced with silica-based bioactive glass (BG) fibers by TFP (Fig. 1). The BG fibers additionally serve as a bioactive component stimulating bone growth and reducing the risk of infection [7]. The plate is intended to completely resorb in the body after the bone healing. The plates can be developed for further applications in other animal species and humans.

The goal of this study was to design diverse TFP patterns for fracture fixation plates in toy-breed dogs, fabricate the biostable sample plates and test their mechanical performance. Future studies will include *in vitro* and *in vivo* testing of plates made of bioresorbable polymers reinforced with BG fibers.

Experimental Methods

Different TFP plate patterns were developed. Finite element (FE) models considering the layup and directions of the fibers were generated and further used in computer simulation of mechanical loading of the plates.

Plates were prepared and tested mechanically. E-glass fibers have been applied as surrogates for BG fibers. Dimethacrylate-based light curable resin and polylactic acid were used as matrices in the composites. Plates reinforced with continuous unidirectional E-glass fibers served as controls. The testing procedures included four-point bending of plates, four-point bending and torsion loading of osteotomized bones fixed with the plates.

Results and Discussion

In four-point bending of plates, the plates reinforced with unidirectional fibers were predictably stiffer than their TFP counterparts. However, bending of the osteotomized bones fixed with both types of plates revealed similar stiffness of both plated bone constructs which implies that in a real clinical situation the stiffness of TFP plates can be sufficient for successful bone healing.

In all testing conditions, TFP plates withstood substantial deformations before failure. Typical failure of TFP plates was followed by accumulation of multiple cracks none of which was fatal to the plate if taken separately. TFP plates rarely broke apart even when their load-bearing capability decreased to a minimum. In contrast, the plates reinforced with unidirectional fibers tended to break dramatically once cracks appeared in the direction of the fibers placement (Fig. 2).

FE modeling of the behavior of TFP plates subjected to the loading conditions of the tests applied in the study demonstrated adequate prediction of the structural stiffness of the plates. Further development of the FE model will aim on the evaluation of progressive damage of novel plates using extended finite element method.

Conclusion

TFP plates demonstrated structural integrity superior to that of plates reinforced with unidirectional fibers and stiffness suitable for fracture healing. Thus, TFP technique has a potential in fabrication of fracture fixation plates for load-bearing applications.

References

1. Huiskes, R., Weinans, H., Van Rietbergen, B., 1992. The relationship between stress shielding and bone resorption around total hip stems and the effects of flexible materials. Clin. Orthop. Relat. Res. 274, 124 – 134.

2. Akeson, W.H., Woo, S.L., Coutts, R.D., Matthews, J.V., Gonsalves, M., Amiel, D., 1975. Quantitative histological evaluation of early fracture healing of cortical bones immobilized by stainless steel and composite plates. Calcif. Tissue Res. 19, 27 – 37.

3. Hastings, G.W., 1978. Carbon fibre composites for orthopaedic implants. Composites. 9, 193 – 197.

4. Tayton, K., Johnson-Nurse, C., McKibbin, B., Bradley, J., Hastings, G., 1982. The use of semi-rigid carbon-fibre-reinforced plastic plates for fixation of human fractures. Results of preliminary trials. J. Bone Joint Surg. Br. 64, 105 – 111.

5. Mattheij, P., Gliesche, K., Feltin, D., 1998. Tailored Fiber Placement - Mechanical Properties and Applications. J. Reinf. Plast. Comp. 17, 774 – 786.

6. Gliesche, K., Hübner, T., Orawetz, H., 2003. Application of the tailored fibre placement (TFP) process for a local reinforcement on an “open-hole” tension plate from carbon/epoxy laminates. Compos. Sci. Technol. 63, 81 – 88.

7. Hoppe, A., Güldal, N.S., Boccaccini, A.R., 2011. A review of the biological response to ionic dissolution products from bioactive glasses and glass-ceramics. Biomaterials 32, 2757 – 2774.

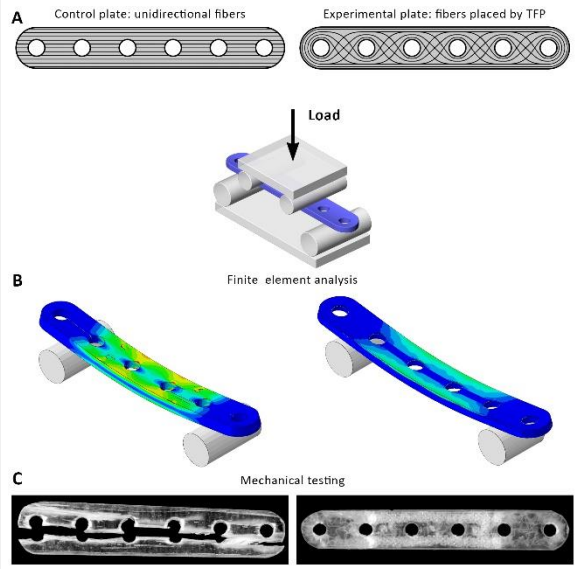

Figure 2. Comparison of a plate reinforced with unidirectional fibers and a plate reinforced by TFP

In TFP plates, fibers bypass the screw holes, thus the integrity of fibers is maintained (A). When subjected to load, stesses in TFP plates are distributed more evenly than in plates reinforced with unidirectional fibers (B). Plates reinforced with unidirectional fibers tend to break apart while TFP plates retain structural integrity even when their load-bearing capacity drops to a minimum (C).

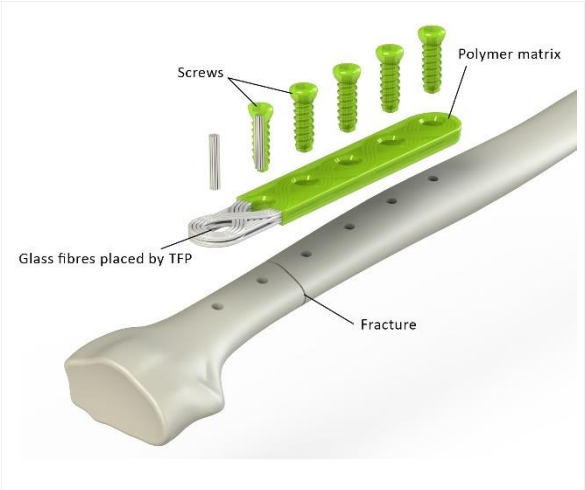

Figure 1. Render of the concept of a novel bioresorbable bioactive fracture fixation plate by TFP

1:00 p.m. – 2:30 p.m.

Hall 5

VIII-SY14-DGBMT | DGBMT SY: Biohybrid Implants

Thomas Lenarz (Hanover, DE)
Katrin Sternberg (Tuttlingen, DE)

Biohybrid implants, i.e. implants that are made by combining synthetic or natural materials with the body‘s own cells or tissues are on the rise. They allow for better and faster tissue formation and integration, less short- mid- and long term side effects and overall better clinical outcome.

VIII-SY14-DGBMT-KL01

Biohybrid Implants – Fostering Clinical Translation by Textile Reinforcement

Stefan Jockenhoevel[1,2]

[1]RWTH Aachen University, Dept. of Biohybrid & Medical Textiles (BioTex), Institute for Applied Medical Engineering, Aachen, DE; [2]Maastricht University, Aachen-Maastricht-Institute for Biobased Materials (AMIBM), Maastricht, NL

Regenerative Medicine has promised to overcome the limitations of conventional implants with the potential to remodel, to self-repair and specifically for the pediatric applications to grow with the child. In the past two decades, many successful pre-clinical trials have demonstrated the potential of tissue-engineered implants, but the number of translated products to the clinic are very limited. This is due to the high complexity of the production process and the need to control the complex adaptive behavior of the patient-individualized cell source in the process.

While the classical tissue-engineered implant has primarily focused on a complete autologous solution, the biohybrid approach is looking for a balance combination of technical and biological components with regard to (i) a high (re)producibility by the technical component and (ii) an optimal hemo/biocompatibility by the biological component.

Because “human beings are textile-reinforced composites”, textile engineering offers a multi-scale toolbox for mimicking and supporting tissue engineered constructs. We have demonstrated the use of textile fibers to create anisotropic tissue constructs in cardiovascular and respiratory tissue engineering.

The keynote lecture will give an insight in the “evolution” of cardiovascular and respiratory tissue-engineered implants from complete autologous towards biohybrid textile reinforced constructs as key technology for a (re)producible and herewith transferable implant into clinic.

VIII-SY14-DGBMT-KL02

Biohybrid Cochlear Implant Electrode

Thomas Lenarz, A. Warnecke

Hanover Medical School, Hanover, DE

Background:
Cochlear Implants have proven to be a safe and reliable method for hearing rehabilitation in patients with severe to profound hearing loss. They replaced the function of hair cells which transduce acoustic information into action potentials of the auditory nerve for further processing in the central auditory system. Patients can understand speech in quiet but have severe limitations in noise and with music listening due to the reduced number electrically separated information channels due to the wide distance between electrode contacts and neural elements and the encapsulation by fibroblasts.

Ways to improve the electrode nerve interface:
The goal is the direct connect between the regrown peripheral dendrites of the auditory neuron with the electrical substrate on the electrode carrier fast leaving to multi-channel electrode with several hundred information channels compared to the current devices (maximum 20 electrode contacts).
This can be achieved by surface functionalization with optimized micro- and nanostructures for cell selective on growths, polymer coating for relieves of drugs due to press trauma reaction and subsequently fibroblast growths and induction of peripheral dendrite regeneration through nerve growths factors e. g. BDNF.

Biohybrid implant with cell coated electrodes. The entrapped cells e. g. program fibroblasts or stem cells sustainably and autonomously produced this nerve growths factors to maintain the concentration gradient to attract the dendrites towards surface.

Integrated reservoirs for nano particles containing nano particles are used for gene therapy. AAB viruses or artificial nano particles will be released and can be invade the target cells e. g. remaining hair cells or neurons to induce functional preservation by exchange of genetic information.
Access cellular matrix will be used to bridge the gap between electrode and neurons to provide the necessary medium for nutrition of cells and growths and dendrites.

Perspective:
All of these steps have been already brought from bench to bedside while other approaches are at a different technology at readiness levels for prior to clinical studies.

First clinical results will be presented.

VIII-SY14-DGBMT-03

Bioprinting in 3D and 4D for novel in vitro models and biohybrid implants

Horst Fischer

RWTH Aachen University Hospital, Dental Materials and Biomaterials Research, Aachen, DE

Bioprinting technology enables the build-up of cell-laden hydrogel-based 3D constructs with a high geometrical complexity. Among various methods the drop-on-demand bioprinting technique in particular holds great potential. Moreover, a novel acoustic bioprinting technique is introduced that requires no nozzle and in addition enables both, the printing of cell clusters and single cells. With both bioprinting techniques the spacial organization of cells mimicking in vivo condition can be achieved. However, the cell-laden constructs do not exhibit full biofunctionality after printing right away. A subsequent cultivation process in vitro with the self-organization of the embedded cells over time ('4D' aspect) is of crucial importance to achieve fully biofunctional tissue. The talk will present major factors influencing the response and the development of bioprinted cells and tissue maturation in the '4D' biofabrication process.

VIII-SY14-DGBMT-04

New perspectives in cartilage repair through an in-situ gelling hydrogel with anti-inflammatory, anti-angiogenic and chondrogenesis supportive properties

Katrin Sternberg[1], Detlef Schumann[2], **Christoph Gaissmaier**[3], Karin Benz[4], Kai Stuckensen[5]

[1]Aesculap AG, Member of the Executive Board R&D & QRM, Tuttlingen, DE; [2]Aesculap AG, Vice President R&D Front End Innovation & Materials & Sterile Technology, Tuttlingen, DE; [3]TETEC AG, Board Member / CEO, Reutlingen, DE; [4]TETEC AG, Head of Research & Development, Reutlingen, DE; [5] TETEC AG, Project Manager Research & Development, Reutlingen, German

Introduction

Localized full-thickness and painful chondral and osteochondral defects of the large joints can have different causes. Accompanying discomfort and impairment of quality of life are comparable to those of patients with osteoarthritis (OA). Also the risk to develop OA after having such a defect rises significantly with increasing defect size, provided that the lesion is not or not correctly treated. In this context clinical trials demonstrated that early onset of OA and the conversion rate for an artificial joint replacement was considerably reduced, when a cartilage restoring approach was used that led to a high-quality cartilage regeneration in the defect [1, 2].

Osteochondral transfer (e.g. mosaicplasty) and autologous chondrocyte transplantation (ACT) are referred to as regenerative or restoring methods, whereas bone marrow stimulating techniques such as microfracture are counted among the reparative treatments, which predominantly induce biomechanically inferior fibrocartilage instead of hyaline or hyaline-like cartilage. Based on the best available evidence ACT is recommended for the treatment of knee and hip cartilage defects with a defect area > 2-3 cm^2 [3].

Due to the anatomy of the hip, mosaicplasty or matrix-assisted ACT (m-ACT) using a solid biomaterial as a cell carrier cannot be applied without causing considerable surgical comorbidities. The problem of a difficult surgical access exists also in the ankle joint, the patella or the tibia plateau of the knee joint. Possible caused by substantial complications invasive open intervention (e.g. femoral head necrosis after hip luxation) often lead to an inappropriate risk-benefit ratio.

Additionally, clinical studies have shown that an increased expression of IL-1 (interleukin-1), FLT-1 (vascular endothelial growth factor receptor-1) and a reduced expression of COL2A1 (collagen type II) of in vitro expanded chondrocytes is associated with a significantly increased risk of treatment failure or worse clinical outcome after ACT [4]. Collagen type II is an important extracellular matrix protein of the intact hyaline cartilage, IL-1 induces inflammation and FLT-1 angiogenesis. Both, inflammation as well as adverse angiogenesis represent key pathomechanisms for development of OA [5].

Results and Discussion

Considering the mentioned problems and insights, an in-situ gelling hydrogel consisting of albumin and hyaluronic acid was developed as a carrier material for m-ACT that can be applied arthroscopically also in case of difficult defect locations. The hydrogel possesses anti-inflammatory and anti-angiogenic properties, and stabilizes the phenotype of human chondrocytes [6]. In feasibility studies and ongoing clinical trials high biocompatibility of the hydrogel together

with very low complication, reoperation and high therapy response rates was observed in the knee as well as in the hip joint [7]. Histological examinations revealed cartilage regeneration with hyaline rather than fibrous properties. Surgery time and surgical comorbidity was reduced considerably by use of the hydrogel compared to the experiences made with solid biomaterials. This is of particular importance, because longer operating times can impair structure, biochemistry and the metabolism of human articular cartilage [8].

Conclusion

The procedure called NOVOCART® Inject, therefore represents an improvement of existing therapies for many indications. However, the translation from development into routine health care is long-lasting and difficult due to extensive regulatory requirements and increasing bureaucratic obstacles, also on the part of the national technology assessments.

References

Literature:

1. Sanders TL, Pareek A, Obey MR et al. High rate of osteoarthritis after osteochondritis dissecans fragment excision compared with surgical restoration at a mean 16-year follow-up. Am J Sports Med. 2017 Jul;45(8):1799-1805.
2. Jungmann PM, Gersing AS, Baumann F et al. Cartilage repair surgery prevents progression of knee degeneration. Knee Surg Sports Traumatol Arthrosc. 2018 Dec 12. [Epub ahead of print]
3. Becher C, Landgraeber S, Fickert S et al. [Treatment of cartilage defects in the knee, ankle and hip joint]. Guidelines from the Group “Clinical Tissue Regeneration” of the German Society of Orthopaedics and Traumatology (DGOU). OUP 2018; 7: 580-587.
4. Angele P, Fritz J, Albrecht D et al. Defect type, localization and marker gene expression determines early adverse events of matrix-associated autologous chondrocyte implantation. Injury. 2015 Oct;46 Suppl 4:S2-9.
5. MacDonald IJ, Liu SC, Su CM et al. Implications of Angiogenesis Involvement in Arthritis. Int J Mol Sci. 2018 Jul 10;19(7).
6. Scholz B, Kinzelmann C, Benz K et al. Suppression of adverse angiogenesis in a novel albumin based hydrogel for articular cartilage and intervertebral disc regeneration. Eur Cell Mater. 2010 Jul 13;20:24-36.
7. Thier S, Baumann F, Weiss C et al. Feasibility of arthroscopic autologous chondrocyte implantation in the hip using an injectable hydrogel. Hip Int. 2018 Jul;28(4):442-449.
8. Shen P, Li X, Xie G et al. Time-Dependent Effects of Arthroscopic Conditions on Human Articular Cartilage: An In Vivo Study. Arthroscopy. 2016 Dec;32(12):2582-2591.
9. Nuernberger S, Cyran N, Albrecht C et al. The influence of scaffold architecture on chondrocyte distribution and behavior in matrix-associated chondrocyte transplantation grafts. Biomaterials. 2011 Feb;32(4):1032-40.

Arthroscopic application
Arthroscopic application of the cell augmented and in-situ gelling hydrogel into a full-thickness cartilage defect of the medial femoral knee condyle.

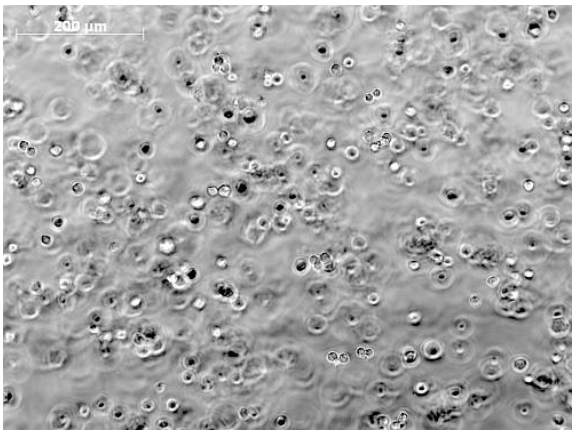

Morphology of chondrocytes in the hydrogel.
In chondrocytes the spherical cell morphology is a sign of the differentiated phenotype and functionally related with the cartilage-specific matrix synthesis [9].

1:00 p.m. – 2:30 p.m.

Conference room 4+5

VIII-OS29 | Metallic biomaterials and coatings

VIII-OS29-01

Influence of two pretreatments and their combination prior to NaF coating on the electrochemical corrosion behavior of five experimental magnesium alloys

Christine Schille, Ernst Schweizer, Jürgen Geis-Gerstorfer

University Hospital Tuebingen, Section Medical Material Science and Technology, Tuebingen, DE

Introduction

When magnesium alloys are used as biodegradable alloys in medical applications, corrosion is considered to be too rapid and this problem is still unresolved. Different pretreatment and / or coating technologies offer opportunities to improve the corrosion resistance of Mg alloys, resulting in an Ez shift in anodic direction, lowering of Icorr and increasing Rp values, and forming a passive region compared to untreated ones. In general, different pretreatments are recommended for each coating option [1,2]. Typical pretreatments are boiling in hot water to produce a $Mg(OH)_2$ protective layer, an alkali pretreatment, e.g. with NaOH at various concentrations and times, for conditioning or roughening the surface. The general purpose of pretreatments is to improve the coating so that it stays on the Mg surface for longer, until the degradation process begins. The effects of pretreatments and coatings depend on the alloy composition, the treatment solutions, pH and technologies used, the immersion time of each process step, and the subsequently used electrolytes to characterize the corrosion behavior [1,3]. Chen [3] states that most Mg alloy coating technologies take a long time, and he recommends focusing on optimizing pretreatments rather than coatings. The aim of this study was to investigate the influence of hot water treatment, alkali treatment and their combination on the initial electrochemical corrosion behavior of five experimental Mg alloys.

Experimental Methods

The experimental Mg alloys MgZn1, MgAl3, Mgal9, MgAl3Zn1 and MgAl9Zn1 were used [4,5]. From each alloy and for each treatment, 3-5 samples were prepared. After grinding in ethanol with SiC 1200, the samples were ultrasonically cleaned in ethanol (untreated reference). For hot water cooking (pretreatment A), the samples were immersed for 20 minutes and then dried in air for 20 minutes. For conditioning (pretreatment B), the samples were immersed in 0.5 M NaOH for 20 minutes and then dried in air for 20 minutes. The combination (pretreatment A+B) took place in succession as described. With untreated and pretreated samples anodic polarization measurements were performed (PAR 273, software: M352, EG&G) from -150 mV ~ Ecorr to -1200 mV at a rate of 1 mV/sec in PBS at 37 °C. From each measurement, the parameters Ez, Icorr, Rp, Ep, ip and ΔE=Ep-Ez were calculated. Microscopic images were taken before and after corrosion measurements (stereomicroscope M 400, Wild, Herbrugg, Switzerland).

Results and Discussion

As an example, Figure 1 shows the anodic polarization of all pretreatments of MgAl9 and MgAl9Zn1 compared to the untreated alloys. Figure 2 shows the results of the Icorr and Rp values of all 5 experimental alloys as a function of all pretreatments compared to untreated ones.

The results revealed, compared to untreated conditions, that the combination of both pretreatments significantly improved the corrosion resistance of all the Mg alloys used in this study, followed by pretreatment A. Conditioning

with 0.5 M NaOH reduces corrosion resistance and cannot be recommended as a pretreatment, especially for the binary Mg alloys. Lower icorr values were found for the tertiary Mg alloys, but Rp did not increase. For MgZn1, the effect of most pretreatments was low or opposite. Of all the alloys tested, it was the only one that formed a passive region with detectable breakdown potential when left untreated. In the combined pretreatment, all tested Mg alloys showed a passive range that varied from low to significant.

Conclusion

Based on this study, the combination of hot water treatment and conditioning with 0.5 M NaOH may be recommended as a suitable pretreatment for the Mg alloys used in this study for improving the corrosion resistance especially for Mg alloys, which showed no passive region in the untreated state.

It can be concluded that the formation of a passive region and / or the shift to lower current densities have the most positive effect of improving the corrosion resistance of the Mg alloys investigated here.

References

1. J. Yang et al, Annals of Biomedical Engineering (2011), 39, 7, 1857
2. S. Shadanbaz et al, J Biomed Mater Res A (2013), 101B, 162
3. H.Y. Chen et al, Appl Surface Science (2012), 5472
4. J. Geis-Gerstorfer et al, Mater Sci and Eng B (2011), 176, 1761
5. C. Schille et al, EMR (2013), 2, 248

Acknowledgement

Special thanks to Dr. N. Hort (GKSS, Geesthacht, Germany) for casting the magnesium alloys.

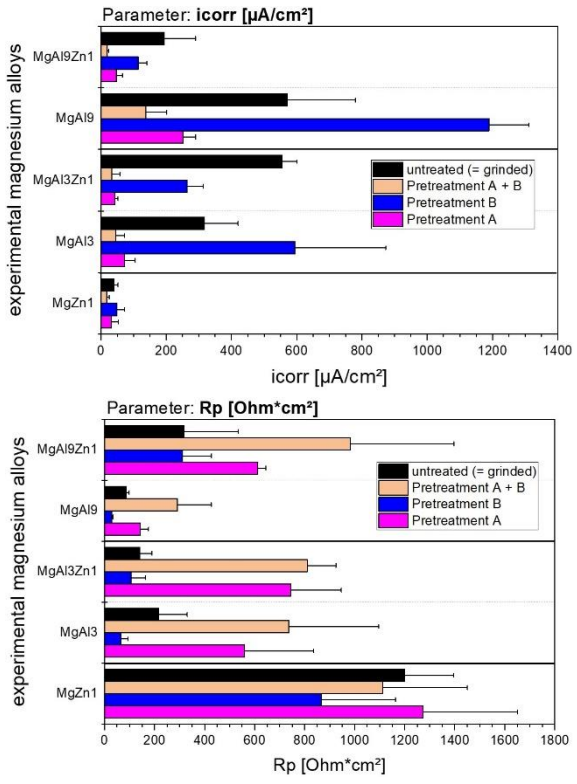

Figure 2:

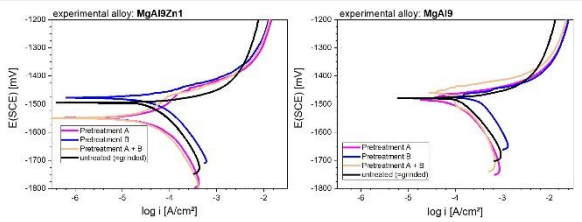

Figure 1:
Anodic polarization curves (mean curves) of MgAl9 and MgAl9Zn1 depending on the pretreatment.

Determined parameters icorr and Rp of all magnesium alloys and pretreatments.

VIII-OS29-02

Implant Proteomics: Determination of the hip implant proteome

Herbert P. Jennissen[1,2], Marcus Jäger[2], Marcel Haversath[2], Andre Busch[1], Thomas Grupp[3], Andrea Sowislok[1,2], Monika Herten[2]

[1]University of Duisburg-Essen, Institute for Physiological Chemistry, Essen, DE; [2]University of Duisburg-Essen, Department of Orthopedics and Trauma Surgery, Essen, DE; [3]Aesculap AG, Research & Development, Tuttlingen, DE

Introduction

Since the 1970ies it has been hypothesized from *in vitro* studies that plasma proteins are adsorbed as the first step following prosthetic implantation [1], leading to the current doctrine that "Blood is invariably the first tissue that the implant will contact when introduced into the bone" [2]. Mechanistically proteins are adsorbed to surfaces with high affinity by multivalent, cooperative [3] interactions involving adsorption hysteresis [4]. On the basis of these prerequisites we undertook a protein layer analysis on hip implants shortly after implantation.

Experimental Methods

This is the first clinical study on an explant proteome analysis after femoral stem implantation [5]. After 2 min. *in situ* the stems were explanted in a no tough technique, washed with saline, quick frozen in liquid nitrogen and stored at -80 °C. Proteins were eluted under reducing conditions with 4% SDS at room temperature and analyzed by LC-MS/MS [5].

Results and Discussion

Under the set conditions the implant proteome was found to consist of 2802 unique proteins. Of these 77% were of intracellular origin, 9% were from the plasma proteome, 8% from bone proteome. The most abundant protein in the adsorbed total protein layer was hemoglobin (~10%) followed by serum albumin (~5 %).

Conclusion

This study is a major step forward in understanding and predicting the implant-induced response of the osseous microenvironment, which may lead to enhanced healing with a reduction of postoperative surgical revisions. The *in vitro*-based plasma protein doctrine for initial protein adsorption could not be verified for the hip implant proteome.

References

[1] Brash,J.L. & Lyman,D.J. (1971) Adsorption of Proteins and Lipids to Nonbiological Surfaces. In *The Chemistry of Biosurfaces, Vol 1* (Hair,M.L., ed), pp. 177-229. Marcel Dekker, New York.

[2] Kuzyk, P. R. & Schemitsch, E. H. (2011) *Indian J. Orthop.*, **45,** 108-115.

[3] Jennissen, H. P. (1976) *Biochemistry*, **15,** 5683-5692.

[4] Jennissen,H.P. (1985) Protein Adsorption Hysteresis. In *"Surface and Interfacial Aspects of Biomedical Polymers" Vol.2, Protein Adsorption* (Andrade,J.D., ed), pp. 295-320. Plenum Press, New York.

[5] Jäger, M., Jennissen, H. P., Haversath, M., Busch, A., Grupp, T., Sowislok, A., & Herten, M. (2019) *Proteomics. Clin. Appl.*, e1800168.

Acknowledgement

This research was supported by the German Research Foundation (Deutsche Forschungsgemeinschaft, DFG) Project No. Je84/15-3 and by Aesculap AG.

VIII-OS29-03

Self-limiting effective antibacterial coating of short-term magnetron sputtered silver-platinum nanopatches induced by sacrificial anode effect

Christina Sengstock[1], Adham Abuayyash[1], Marina Breisch[1], Julian Möllenhoff[1], Nadine Ziegler[2], Hajo Meyer[2], Michael Meischein[2], Christian Rurainsky[3], Marc Heggen[4], Christina Scheu[5], Alba Garzon-Manjon[5], Kristina Tschulik[3], Alfred Ludwig[2], Manfred Köller[1]

[1]BG University Hospital Bergmannsheil Bochum, Surgical Research, Bochum, DE; [2]Ruhr University Bochum, Faculty of Mechanical Engineering, Institute for Materials, Bochum, DE; [3]Ruhr University Bochum, Faculty of Chemistry and Biochemistry, Electrochemistry and Nanoscale Materials, Bochum, DE; [4]Research Center Jülich GmbH, Ernst Ruska-Centre (ER-C) for Microscopy and Spectroscopy with Electrons, Jülich, DE; [5]Max-Planck-Institut für Eisenforschung GmbH, Nanoanalytics and Interfaces group, 40237 Düsseldorf, DE

Introduction

Infections related to medical devices and implants cause constant and serious clinical problems. The initial bacterial colonization and growth may result in biofilm formation which protects the microorganisms against host defense mechanisms and makes antibiotic treatment difficult. Also due to increasing resistance to antibiotics, there is a need for additional antibacterial active implant coatings. Silver and nanosilver as antimicrobial agent have been used to inhibit initial bacterial colonization on the surface. Recently, we presented a sacrificial anode system by combining silver with a more noble metal (platinum group elements) to achieve enhanced release of silver ions from silver dot arrays. The results demonstrated enhanced antimicrobial activity of sacrificial anode samples compared to similar non-sacrificial anode silver dot arrays.

The goal of this study was to further reduce the total amount of silver as well as the rare and expensive platinum group metals and to establish an antimicrobial active platinum/silver sacrificial anode system as ultrathin nanopatches.

Experimental Methods

The samples were fabricated using magnetron sputter deposition of silver and platinum on titanium coated Si/SiO2 substrates. A very short sputter time (10s, 20s or 60s) was applied which resulted in nanopatch-like deposits (5-60 nm in diameter, depending on sputter time). Three sample types of each sputter time were fabricated: silver patches, consecutively sputtered platinum/silver patches, and co-sputtered platinum/silver patches. The shape and composition of the deposited patches were analyzed using transmission electron microscopy (TEM), HR-TEM (HAADF Mode) and energy-dispersive X-ray spectroscopy (EDX). The amount of released silver ions from the surface was quantified electrochemically by the voltammetry. The bacterial test was performed with *Staphylococcus aureus* (DSMZ 1104) in BHI-broth using a drop-based experimental set-up, which allowed the detection of adherent bacteria on the surface and the planktonic bacteria in the supernatant.

Results and Discussion

Microstructural analysis using HR-TEM showed nanopatches of silver and platinum deposits, which had, depending on the sputter time, a thickness of 1,3-3,9 nm and a diameter of 5-60 nm. The HAADF-STEM and EDX-mapping showed an inhomogeneous distribution of platinum and silver deposits. The antibacterial results towards

Staphylococcus aureus demonstrated an enhanced antibacterial activity of sacrificial anode platinum/silver-nanopatches compared to pure silver-deposits. The sputter patterns influenced the dissolution of silver as well as the antimicrobial activity. The results demonstrated an enhanced silver ion release and enhanced antimicrobial efficiency induced by the samples which were consecutively sputtered with platinum/silver compared to the co-sputtered samples. The electrochemically measured dissolution of silver ions correlated to the antimicrobial activity. Due to the sacrificial anode effect, the duration of the antimicrobial activity was self-limiting and holds just up to 8 hours.

Conclusion

The advantages of such platinum/silver deposits are the enhanced antimicrobial activity at a reduced total amount of silver and the time limited effect due to the rapid silver dissolution, which is based on a sacrificial anode effect.

Acknowledgement

We thank the Deutsche Forschungsgemeinschaft (DFG) for financial support of this work.

VIII-OS29-04

Integration of the trace elements copper and zinc into calcium phosphate coatings and their *in vitro* characterization

Rene Beutner[1], Claus Moseke[2], Uwe Gbureck[3], **Cornelia Wolf-Brandstetter**[1]

[1]Technische Universität Dresden, Max Bergmann Center of biomaterials, Dresden, DE; [2]University of Applied Sciences Gießen, Institute for Biomedical Engineering, Gießen, DE; [3]University of Würzburg, Department for Functional Materials in Medicine and Dentistry, Würzburg, DE

Introduction

The aim of this study was to combine the trace elements copper and zinc with inorganic surface modification techniques already successful in bone applications and to investigate potential synergistic effects of both ions. Copper ions released from bone implant coatings are known to enhance vascularization[1], whilethe incorporation of zinc is intended to act chemotactically and stimulatingly on bone forming cells. Additionally, both ions might have at least slight antimicrobial effects for released amounts in concentrations below cytotoxic level. Calcium phosphate phases (CPP) were utilized as a carrier for the selected trace elements in order to i) provide osteoconductive surfaces and ii) to tune the immobilized amounts and release behavior of the trace elements.

Experimental Methods

Deposition of brushite onto c.p.Ti discs was performed by means of electrochemically assisted deposition (ECAD) from aqueous electrolytes containing $Ca(NO_3)_2$ and $NH_4H_2PO_4$. Cu and Zn integration was realized by addition of up to 0.5 mM $Cu(NO_3)_2$ and $Zn(NO_3)_2$ either alone or in different combinations to the electrolyte. (Sample labelling reflects applied concentrations.) The coatings were characterized by chemical analysis after dissolution in 0.1 M HNO_3. Ion release from coated surfaces was analyzed after incubation in simulated body fluid (SBF) with or without 10% fetal bovine serum (FBS). Human marrow stromal cells (hMSC) were seeded with a cell density of 5000 cells/cm² onto coated samples either directly or after 3 days of pre-incubation in serum-free medium. This pre-incubation was performed to avoid depletion of Ca level in close vicinity to attaching cells due to conversion of brushite into more stable CPP phases.

Results and Discussion

When Cu^{2+} and Zn^{2+} ions were added during the ECAD process, their deposited amount depended mainly on the concentration of the respective ions in the electrolyte. Single addition of both ions up to 0.5 mM Cu resulted in nearly similar immobilized amounts of up to 68.9±0.1 µg Cu/cm² and 56.6±0.4 µg Zn/cm². Co-deposition of both ions was achieved with no changes in Zn content for added Cu while the presence of Zn increased immobilized Cu content even slightly.

Release of deposited Cu and Zn species from the obtained coatings was negligible in serum-free SBF in all combinations. In contrast, much higher amounts were released in SBF with 10% FBS depending mainly on initially immobilized amounts and ranged between 1-6 µg/ml for Cu and 0.3-0.8 µg/ml for Zn within first 24 h. Burst like release was observed for Cu but not for Zn for daily medium exchange. The release behaviour of Cu was not significantly changed by the co-immobilization of Zn while the presence of Cu in the coatings resulted in roughly twofold increase of released Zn amounts.

Detailed cell studies with hMSCs were performed with selected combinations of 0.1-0.3 mM Cu and 0.3-0.5 mM Zn. The respective contents in coatings ranged between 5 and 40 µg/cm² Cu and 25 and 57 µg/cm² Zn. The presence of Zn was beneficial for cell adhesion as well as further growth (Fig. 1A) while cytotoxic effects were already visible for coatings obtained with 0.3 mM Cu. However, the presence of Zn in Cu03Zn03 and Cu03Zn05 could alleviate such effects but cell number was still reduced by ~50% compared to respective Cu-free samples. The most critical step was cell adhesion while further proliferation was only slightly affected. Differentiation in terms of activity of alkaline phosphatase was always higher for highest Zn additions ($p<0.01$). On pre-incubated samples overall highest values were observed for Cu03Zn05 ($p<0.05$). Pro-angiogenic potential was evaluated according to normalized release of vascular endothelial growth factor (VEGF) by hMSC and was clearly highest on high Cu content (see Cu03 in Fig. 1C) and comparatively high also for pure brushite while Zn alleviated relative release.
Antimicrobial tests with *E. coli* revealed decrease in adhering bacteria compared to titanium reference for brushite alone by ~60% and further decrease of bacterial coverage for all Cu- or Zn-containing coatings in particular those with high Cu content (< 1%).

Conclusion

It was shown that Cu and Zn can be co-deposited together with calcium phosphate onto metallic implant materials by ECAD. The deposited amount of these ions is tunable in a certain range. The well-known potential for osteogenic stimulation by Zn was maintained in presence of Cu, with lower Cu content promoting cell growth while for high Cu contents highest differentiation potential combined with highest antimicrobial effects was observed.

References

1. Barralet J. *et al*., Tissue Eng. A 15**:** 1601-1609, 2009

Acknowledgement

The authors would like to thank the German Research Foundation (Grant no: WO 1903/2-1 and MO 1768/2-1) for providing financial support to this project.

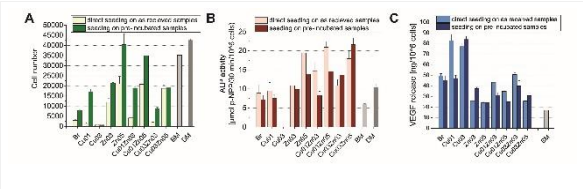

Fig. 1
(A) Cell growth and (B) differentiation of hMSC after 14 days on titanium samples coated with brushite layers containing different additives of Cu and Zn;
(C) VEGF release measured in supernatants after 3 days of incubation, normalized to cell number

VIII-OS29-05

Evaluation of innovative polymer coatings on titanium regarding stability of antibacterial effects under storage and sterilization conditions

Andreas Winkel[1], Anne K. Seiffert[2], Jasmin Grischke[1], Sebastian Stelljes[2], Henning Menzel[2], Meike Stiesch[1]

[1]Hanover Medical School, Department of Prosthetic Dentistry and Biomedical Materials Science, Hanover, DE; [2]Technical University of Braunschweig, Institute of Technical Chemistry, Braunschweig, DE

Introduction

Functional and esthetic reconstitution in partially and edentulous patients is gaining importance because of demographic changes in western societies. The actual numbers are over 1,200,000 replacements per year in Germany. Despite all material and surgical improvements over the last decades, the expected prolonged durability of implants in the human body will increase the problems with biofilm-related inflammation. Peri-implant inflammation of soft and hard tissue is responsible for implant failure with a prevalence of more than 20% after five years.

There is an unlimited interest in implant research to modify the surface of medical implants by various physical and chemical techniques in order to improve their antibacterial properties. To our knowledge none of these innovative surfaces reached the status of mainstream clinical application. Reasons for this lack in translational success are manifold. Many of these strategies are sufficient *in vitro* against single bacterial strains but do not consider the influence on host tissue or wound healing. Other implant improvements can only be applied on simple geometries or disqualify for industrial application because of high costs or limited benefit *in vivo*. Even the evident consideration that a new implant surface has to meet clinical hygiene standards and therefore has to be sterilized by a supplier causes the failure of many promising implant innovations from the literature in the translational process.

Experimental Methods

We investigated coating strategies for titanium implants with three different copolymers regarding antibacterial properties and cytocompatibility. The adhesion of *S. aureus* and *S. oralis* were visualized using live/dead staining and CLSM microscopy. Cytotoxicity was analyzed regarding metabolic activity and membrane integrity. The cell attachment was quantified using a modified LDH assay. Additional, storage and sterilization processes were simulated and the effects on the coating strategy were evaluated.

Results and Discussion

From the investigated copolymers all showed as a substance good cytocompatibility with host tissue cells and as a coating high bacterial repelling properties (up to more than 98%). Only one coating allowed the adhesion and proliferation of human gingival fibroblasts to the same degree as uncoated controls. The simulation of storage revealed a decrease in the antibacterial effect more severe than sterilization with gamma-rays or hot steam for all coatings. Hot steam treatment even reactivated the suppression of bacterial attachment, especially for the tissue-friendly copolymer-surface.

Conclusion

We could present an innovative polymer coating strategy, which is inexpensive and easy to apply on complex implant geometries. Noteworthy, our strategy has unique antibacterial repelling qualities without damaging the interaction of peri-implant tissue cells with implant material. Moreover, the coating is stable under well-established storage and sterilization techniques and can be adapted for titanium and ceramic surfaces.

Acknowledgement

This study was financially supported by the company Gebr. Brasseler GmbH & Co. KG, Lemgo, Germany.

VIII-OS29-06

A PEO-based black TiO2 nanoceramic coating on titanium with wear-resistance and visible-light photocatalysis activity for enhanced dental implant decontamination

Hao Wu, Li Xie, Weidong Tian

Sichuan University, West China Hospital of Stomatology, Chengdu, CN

Introduction

In dental implantology, peri-implantitis is an increasing problem characterized by destruction of adjacent alveolar bone of implants with a prevalence of 20% in patients within 5-10 years. Biofilm formation on implant surface is the primary cause of peri-implantitis and the treatment is based on the removal of biofilm. However, it is hard to completely remove the organic residues of biofilm by conventional treatments, which would have adverse effects on the therapeutic effect and re-osseointegration. Photocatalysis has been widely used in organic pollutants degradation and shows satisfying efficiency. Rupp et al. fabricated a anatase-TiO_2 crystalline coating on titanium and proved it could effectively photo-oxidation of bovine serum albumin and acquired dental pellicle, but poor mechanical properties and nonactivation to visible light may limit its application. In this study, a novel plasma electrolytic oxidation (PEO) based procedure was developed to fabricate a TiO_2 nanoceramic coating on Ti substrates, showing superior wear-resistance and visible-light photocatalytic activity.

Experimental Methods

1. Sample preparation

Pure titanium (PT) samples were first plasma electrolytic oxidized in CH_3COONa electrolyte under potentialstatic mode. The samples were then heated up to 600 ℃ in a muffle furnace, maintained for 1 h. Then the samples were carefully polished with abrasive paper to remove the outermost porous layer and the final samples were named as harden pure titanium (PT-H) samples. TiN coated, sandblasted and acid-etched (SLA) and H_2SO_4-HCl anodized samples were prepared as controls.

2. Surface and coating characterization

The as-prepared samples was observed by SEM and AFM. Surface roughness values (Ra) and water contact angles (WCAs) were measured. XRD, Raman and XPS spectra were detected. FIB-TEM and EDX mapping were applied to observe the coating cross-section structures.

3. Surface mechanical properties

Nanoindentation hardness and the wear behaviors of PT, PT-H and TiN coated samples were tested. P. Gingivalis were used as the model bacteria to form biofilm on PT and PT-H samples, which were then removed by steel curretes and ultrasonic device with steel tips.

4. Photocatalytic activity

Photocatalytic degradation of methylene blue (MB) and lipopolysaccharide (LPS) were investigated under UV and visible light irradiation. The generation of reactive oxygen species (ROS) was probed by DMPO spin-trapping EPR technique.

5. Biological experiments

The morphology, attachment, spreading and differentiation of MG63 cells on PT, PT-H and SLA samples were detected to evaluate the biocompatibility of PT-H samples. PT and PT-H implants were implanted into mandibles of mini-pigs for 4 and 12 weeks and the results were analyzed by Micro-CT.

Results and Discussion

We successfully developed a novel method to fabricate a black, 1 μm-thick TiO_2 nanoceramic coating on Ti substrates. The coating was dense-packed and nano-crystallized with excellent coating-substrates bonding ability, exhibiting a defective TiO_{2-x} layer in the outermost part, which has never been reported before.

The PT-H samples showed two-fold higher nanoindentation hardness than PT and excellent wear-resistance toward steel balls in ball-on-disc test. It also showed excellent scratch-resistance towards decontamination instruments such as steel curretes and ultrasonic device. The improvement could be attributed to the specific micro-structure and the nano-size hardening effect of the nano-crystallites.

Under UV irradiation, the PT-H samples showed the best photocatalytic ability, with the MB degradation rate of about 90% after 2 hours, while the PT and SLA samples showed a terminal degradation rate of about 35%. The PT-H samples also showed the best photocatalytic activity under visible light irradiation. The generation of $\cdot O_2$ and $\cdot OH$ radicals were involved in the photocatalytic process of PT-H samples. The introduction of Ti^{3+} and oxygen vacancies of the coating resulted in an enhanced absorption of visible-light.

Moreover, the PT-H sample showed better MG63 cells responses and comparative osseointegration ability than PT samples.

Conclusion

In this work, we successfully fabricated a biocompatible and wear-resistant TiO_2 nanoceramic coating on titanium substrates by a three-step procedure based on a novel plasma electrolytic oxidation technique. This coating also showed enhanced visible-light photocatalytic activity towards methylene blue and lipopolysaccharide due to its outmost defective TiO_{2-x} layer. This work provides a unique coating technique as well as photocatalytic cleaning strategy for enhanced decontamination of titanium dental implants, which will make a breakthrough in treatments of peri-implantitis.

References

1. J Periodontal Res 2018, 53 (5), 657
2. Clin Implant Dent Relat Res 2018, 20 (4), 583
3. Biomaterials 2015, 52, 327
4. Dent Mater 2018, 34 (1), 40

Acknowledgement

This study was supported by the National Natural Science Foundation of China (grant number 81600895).

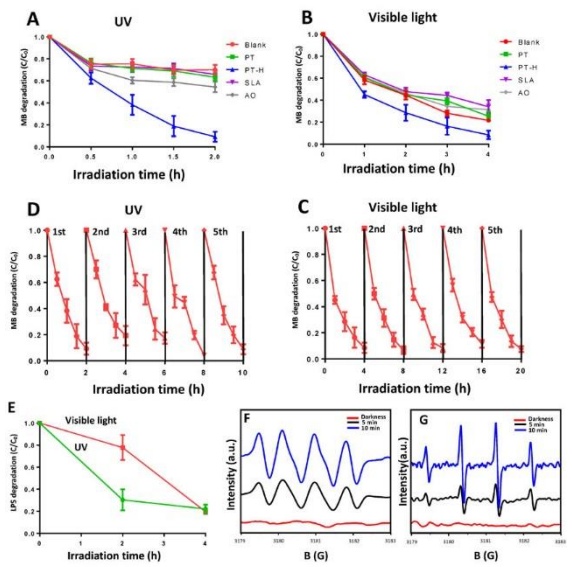

Evaluation of the photocatalytic activities of PT, PT-H, SLA and anodized samples.
Evaluation of the photocatalytic activities of PT, PT-H, SLA and anodized samples. (A) MB degradation under UV irradiation. (B) MB degradation under visible light irradiation. (C) Durability of PT-H samples under UV irradiation with five consecutive cycles. (D) Durability of PT-H samples under visible light irradiation with five consecutive cycles. (E) LPS degradation under UV and visible light irradiation on PT-H samples. (F) EPR spectra of the PT-H sample with or without Xe lamp irradiation for the detection of $\cdot O_2$ radicals. (G) EPR spectra of the PT-H sample with or without Xe lamp irradiation for the detection of ·OH radicals.

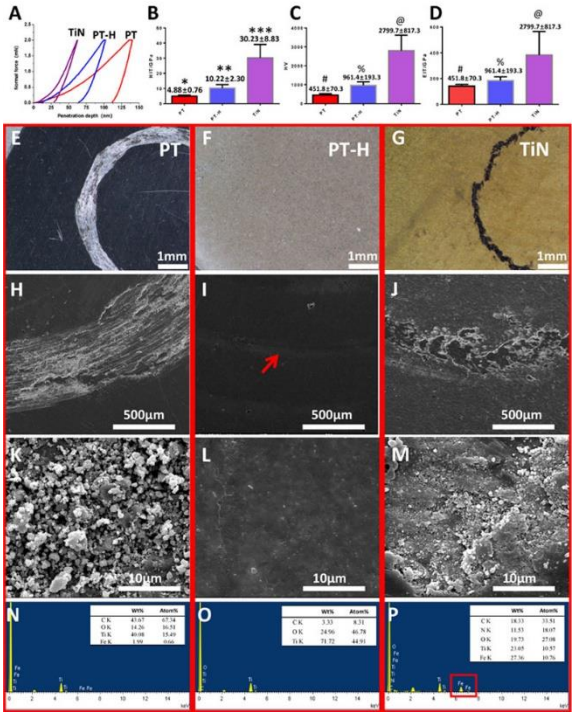

Results of the nanoindentation and ball-on-disc wear test.
Results of the nanoindentation and ball-on-disc wear test. Stereomicroscopic photographs of PT (A), PT-H (B) and TiN (C) samples and SEM images of PT (D, G), PT-H (E, H) and TiN (F, I) samples after test are presented. The red arrow refers to the wear scar on the PT-H sample. Element composition in wear scars areas of PT (J), PT-H (K) and TiN (L) samples are detected by EDX.

1:00 p.m. – 2:30 p.m.

Conference room 2+3

VIII-OS30 | Antibacterial and drug delivery 2

VIII-OS30-01

Bio-selective bacteriostatic and fungistatic surfaces made of recombinant spider silk proteins

Gregor Lang[1], Sushma Kumari[2], Elise Desimone[2], Christian Spengler[3], Susanne Lücker[4], Martina Hudel[5], Karin Jacobs[3], Norbert Krämer[4], Thomas Scheibel[2]

[1]University of Bayreuth, Biopolymer Processing, Bayreuth, DE; [2]University of Bayreuth, Chair of Biomaterials, Bayreuth, DE; [3]Saarland University, Department of Experimental Physics, Saarbrücken, DE; [4]Justus-Liebig University Gießen, Medical Center for Dentistry, Gießen, DE; [5]Justus-Liebig University Gießen, Institute of Medical Microbiology, Gießen, DE

Introduction

Pathogenic microbial contaminations on the surface of e.g. medical products and the associated risk of infection are a severe problem especially in the public health care sector. Microbial colonization and subsequent biofilm formation are highly problematic, as biofilms are much more difficult to eradicate than isolated microbes. Furthermore, antimicrobial resistant strains are increasing at an alarming rate due to the overuse of antimicrobial agents. Since one critical step in biofilm formation is the initial adherence of pathogenic microbes onto a material's surface, inhibiting microbial attachment is a reasonable approach to develop material surfaces resistant to biofilm formation. There are two main strategies for inhibiting surface attachment, referred to as either active or passive resistance. While passively resistant surfaces utilize super hydrophilic or hydrophobic polymers, zwitterionic and other synthetic polymers, actively resistant ones include contact killing materials such as cationic polymers, amphiphilic polymers, antimicrobial peptides and polymeric/ composite materials loaded with antimicrobial agents. In this work, a novel passive approach was developed originating from the basic observation that some silk materials display high resistance against microbial degradation.

Experimental Methods

We systematically investigated the bacteriostatic and fungistatic properties of a biotechnologically designed recombinant spider silk protein system. Different recombinantly produced spider silk proteins based on consensus sequences of *Araneus diadematus* dragline silk proteins (fibroin 3 and 4) were processed into 2D-patterned films and 3D-hydrogels. These materials were exposed to pathogenic bacteria *(S. mutans, S. aureus, E. coli*) and fungi (*C. albicans, P. pastoris*) as well as to mammalian cells (BALB/3T3 fibroblasts). Biofilm formation was observed qualitatively via SEM imaging and quantified by fluorescence analysis and by atomic force measurements of single bacteria's adhesive forces on spider silk films in comparison to other material surfaces (regenerated *B. mori* fibroin and polycaprolactone). Furthermore, the bioselective growth of fibroblasts and simultaneous repellence of microbes was demonstrated in co-culture experiments.

Results and Discussion

2D- and 3D-materials based on engineered recombinant spider silk proteins provide bacteriostatic and fungistatic properties as shown with a range of tested microbial organisms considering both, bacteria (*S. mutans, S. aureus,* and *E. coli)* and fungi (*C. albicans,* and *P. pastoris*). None of the tested microbes could manifest biofilms on recombinant spider silk films, hydrogel surfaces or within hydrogels. The chosen microbial pathogens are often found in nosocomial infections in humans, and their strong ability to produce biofilms and aggressive infections can be a

severe health threat. To specifically demonstrate the aptness of these properties of recombinant spider silk in the field of tissue engineering, we performed co-culture experiments of bacteria and fungi with mammalian cells using films and hydrogels made of an RGD-modified spider silk variant. Introduction of the RGD-sequence allowed the generation of a bio-selective spider silk surface, displaying attachment and unhindered proliferation of mammalian BALB/3T3 fibroblasts but only little/no adhesion of bacteria and fungi. In previous studies, the shear thinning behavior of these hydrogels was demonstarted and they could be applied as a 3D-printable ink for biofabrication. The latest findings complement these properties reducing the risk of contamination when using these materials in the field of tissue regeneration.

Conclusion

The obtained novel properties complement the previously shown non-toxicity, biodegradability and mechanical stability of recombinant spider silk materials boosting the potential for various biomedical (e.g. tissue engineering, wound coverage devices, implant coatings) or technical (e.g. coatings of textiles, water tubes) applications. To our knowledge, the bacteriostatic and fungistatic properties of materials made of recombinant spider silk are unique, whereas materials prepared from regenerated *B. mori* fibroin, which resemble to some extend the composition and properties of spider silk proteins, do not show such behavior.

Acknowledgement

This project has been funded by the DFG SFB 840 TP A8.

VIII-OS30-02

New advances in the design of mesoporous silica nanoparticles for the treatment of infection

Isabel Izquierdo-Barba[1,3], Blanca González[1,3], María Vallet-Regí[1,3]

[1]Universidad Complutense de Madrid, Facultad de Farmacia, Madrid, ES; [2]Hospital 12 de Octubre I+12, Instituto de investigación sanitaria, Madrid, ES; [3]CIBER-BBN, Madrid, ES

Introduction

Infectious diseases remain a major burden in today's world, causing high mortality rates and significant economic losses, with >9 million deaths per year predicted by 2030.[1] One of the main causes is the formation of structures known as biofilms, which constitute a natural microorganisms mechanism of defense against external aggressions as antibiotics and immune system.[2] Nowadays, there is an urgent need to combat biofilm-associated infections through the design of nanoplatforms able to prevent biofilm formation or to produce dispersion of preformed biofilms.[3] Currently, mesoporous silica nanoparticles (MSNs) are excellent candidates to develop targeted drug delivery devices and multifunctional platforms in cancer therapy, owing to their high biocompatibility, intrinsically large drug loading capacity and versatility in terms of chemical modification of its surface.[4]

Experimental Methods

Herein, different approaches focused in the design these nanocarriers for infection treatment are proposed. In this sense, MSNs will be designed to: (i) selectively transport antimicrobial agents into *Gram*-negative bacteria and bacterial biofilm, (ii) release different combinations of antimicrobial agents in a controlled fashion (iii) generate hyperthermia properties with biofilm-disruptive effects through light stimulus.

Results and Discussion

For *targeted therapy*, different vectorization elements have been externally incorporated into the MSNs in order to selectively transport antimicrobial agents inside the bacteria or biofilm. These elements are: polyamine dendrimers (G3),[5] diamine molecules (DAMO),[6] lectins (Con-A) and cationic polypeptides based on lysine and valine amino acids (pLys and pLys-Val). The obtained results show that the synergistic combination of bacterial or biofilm internalization and antimicrobial agents into a unique nanosystem provokes a remarkable antimicrobial effect against bacterial biofilm (see Figure).

For *co-delivery*, MSNs were loaded with a wide spectrum antibiotic (levofloxacin, LVX) into the mesopores and subsequently externally coated with a gelatine layer (GEL) containing a mucolytic agent (acetylcysteine, AC). A fast release of AC, able to weaken the polysaccharides wall of the biofilm and therefore facilitating the input of the LVX, which exhibits a slower and prolonged kinetics, inside the biofilm, is intended. The preliminary *in vitro* assays against *S. aureus* show that this nanosystem is able to notably reduce the thickness of the biofilm by 75% in comparison with MSNs loaded with each of the drugs. These results display the successful synergistic effect between the antibiotic and the mucolytic co-delivered from the MSN based systems, showing this approach as a promising treatment for bone infection.

For *hyperthermia*, core@shell nanosystems formed by Au nanorods (Au@MSNs) have been synthetized. Subsequently, the surfaces of these nanoparticles were conjugated with a nitrosothiol group through a heat liable

linker, enabling their stimulated release through infrared radiation to promote disintegration of the bacterial biofilm. The effects of these nanosystems were then analyzed through *in vitro* assays of biofilms formed by *S. aureus* cultures to study the synergetic efficacy of phototherapy and nitric oxide liberation. These novel nanosystems have initiated a potent alternative for the treatment of bacterial infections.

Conclusion

MSNs constitute promising nanoplatforms in the treatment of infection thanks to their great versatility in synthesis and functionalization.

References

REFERENCES

1. Arciola C.R. *et al.* Nature 16: 397–409, 2018
2. Götz F. Mol. Microbiol. 43: 1367–78, 2002.
3. Huh A.J. *et al.* J. Control. Release. 156:128–45, 2011.
4. Castillo R. *et al.* Expert Opinion on Drug Delivery 16, 2019.
5. González B. *et al.* Acta Biomaterialia 68:261–271, 2018.
6. Vallet-Regí M. *et al.* The Enzymes 44: 35-59, 2018.

Acknowledgement

Authors acknowledge funding from the European Research Council (Advanced Grant VERDI; ERC-2015-AdG Proposal No. 694160).

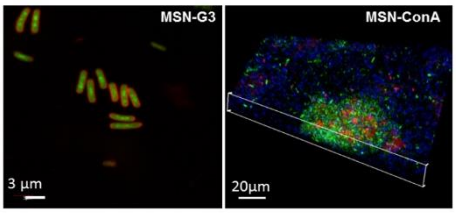

Figure
Targeted-therapy confocal study based of MSNs. (Left) Internalization of MSN-G3 nanosytem into the Gram-negative bacteria (bacteria wall in red and nanoparticles in green). (Right) Internalization of MSN-ConA nanosytem into the S. aureus biofilm (nanoparticles in red, live bacteria in green and biofilm protective layer in blue).

VIII-OS30-03

Polymeric Microspheres for the Controlled Release of Whole Plant *Cannabis* Medicinal Extract

Almog Uziel[1], Gil M. Lewitus[2], Anat Gelfand[2], Keren Amsalem[2], David Meiri[2], Dan Y. Lewitus[1]

[1]Shenkar Engineering Art Design, Plastics and Polymer Engineering, Ramat Gan, IL; [2]Technion Israel Institute of Technology, Biology, Haifa, IL

Introduction

Whole plant *Cannabis* medicinal extracts (CME) contain a considerable amount of pharmaceutical compounds from several different chemical classes, including cannabinoids, a group of terpenophenols, which are singular to this plant[1]. In recent years, it has been realized that many components of the *Cannabis* plant are synergistically active, stipulating medicinal superiority of the whole plant extracts in contrast to isolated single constituents[2,3]. Currently, CME consumption is limited to oral or respiratory pathways, limiting its bioavailability and may result in dose sensitivity[4]. These factors may be overcome via extended release formulations, such as polymeric drug-delivery microspheres, used to encapsulate and deliver active pharmaceutical ingredients (APIs)[5]. Prevalent microsphere manufacturing techniques are solvent-based, resulting in significant API loss and low encapsulation efficiencies[6]. Recently, we have developed a straightforward, solvent-free method for printing drug delivery microspheres directly from melt, by jetting a molten polymer excipient with an API payload onto non-wetting surfaces[7]. In this research, this method had been used to produce CME-loaded microspheres as a controlled release formulation.

Experimental Methods

Cannabidiol (CBD)-enriched extract (prepared as described in Berman et al.[8]) was mixed with a biodegradable polymer, polycaprolactone, at 90℃ . Then, the molten mixture was jetted onto non-wetting surfaces using a pneumatic jetting apparatus to form discrete solid CME microspheres[7,9]. The microspheres were characterized in terms of particle size, morphology, extract loading and encapsulation efficiency. Cannabinoids release profiles were investigated *in vitro*,under simulated physiological conditions (n=3). To validate *in vivo* dose response, microspheres (equivalent to 5 mg extract) were suspended in 1 ml saline solution containing 1% (w/v) carboxymethylcellulose and 1% (w/v) Tween®20, and then administrated via subcutaneous injection through a 20-gauge syringe into mice. Cannabinoids plasma concentrations were detected over 1, 2, 3, 7 and 14 days, compared to pure extract (n=4). At the same time points, microspheres were recovered from the injection site to quantify cannabinoids release profile *in vivo.* Cannabinoids identification and quantification were performed by liquid chromatography mass spectrometry (LC/MS), according to the method described by Berman et al.[8].

Results and Discussion

Spherical CME microspheres loaded with 30% w/w extract were produced, with an average size of 216± 14 µm. In **Figure 1**, a sequence of images taken from a high-speed camera shows the spontaneous formation of CME-loaded microsphere, upon interaction of the molten jet with the surface, and a SEM image of a resulting microsphere. The use of the melt processing allowed us to encapsulate the different cannabinoids present in the extract with especially high efficiencies, of 110.1 3.7%, 92.1 1.2%, 107.4 0.6%, 89.6 4.1%, 96.4 6.3%, 103.5 2.4% and 93.5 2.1% for CBDV, CBDA, CBD, CBG, CBN, Δ^9-THC and CBC, respectively (n=3). The microspheres showed a sustainable release

profile, releasing 70% of the entrapped major cannabinoid, CBD, within 2 weeks, both *in vitro* and *in vivo*, with a close to zero-order release kinetics during the first 4 days, followed by a plateaued, slower release profile (**Figure 2**). CBDA, the acidic precursor to CBD, has shown a burst release effect *in vitro,* probably due to its higher solubility in aqueous media, and could not be detected *in vivo*. CBDV, CBG, CBN, Δ^9-THC and CBC, the other natural cannabinoids present in the extract, have shown a similar sustained release pattern as CBD, each component with its individual release rate. Moreover, steady levels of CBD were observed in murine plasma even after two weeks, correlating well with its *in vivo* release characteristics, as can be seen in **Figure 2**.

Conclusion

These results demonstrate the potential of the microspheres to extend cannabinoids bioavailability from several hours to days and weeks, while maintaining the “Entourage Effect” of whole plant extracts.

References

1. ElSohly, M. & Gul, W. *Handbook of Cannabis*. (Oxford University Press, 2014).
2. Andre, C. M., Hausman, J.-F. & Guerriero, G. Cannabis sativa: The Plant of the Thousand and One Molecules. *Front. Plant Sci.***7,** (2016).
3. Russo, E. B. Taming THC: potential cannabis synergy and phytocannabinoid-terpenoid entourage effects. *Br. J. Pharmacol.***163,** 1344–1364 (2011).
4. Karschner, E. L., Darwin, W. D., Goodwin, R. S., Wright, S. & Huestis, M. A. Plasma Cannabinoid Pharmacokinetics following Controlled Oral Δ(9)-Tetrahydrocannabinol and Oromucosal Cannabis Extract Administration. *Clin. Chem.***57,** 66–75 (2011).
5. Anselmo, A. C. & Mitragotri, S. An Overview of Clinical and Commercial Impact of Drug Delivery Systems. *J Control Release***190,** 15–28 (2015).
6. Deshmukh, R., Wagh, P. & Naik, J. Solvent evaporation and spray drying technique for micro- and nanospheres/particles preparation: A review. *Dry. Technol.***34,** 1758–1772 (2016).
7. Shpigel, T., Uziel, A. & Lewitus, D. Y. SPHRINT – Printing Drug Delivery Microspheres from Polymeric Melts. *Eur. J. Pharm. Biopharm.***127,** 398–406 (2018).
8. Berman, P. *et al.* A new ESI-LC / MS approach for comprehensive metabolic profiling of phytocannabinoids in Cannabis. *Sci. Rep.* 1–15 (2018).
9. Shpigel, T., Cohen Taguri, G. & Lewitus, D. Y. Controlling drug delivery from polymer microspheres by exploiting the complex interrelationship of excipient and drug crystallization. *J. Appl. Polym. Sci.***136,** (2018).

Acknowledgement

We thank the Israeli Ministry of Economy Innovation Authority grant # 63294.

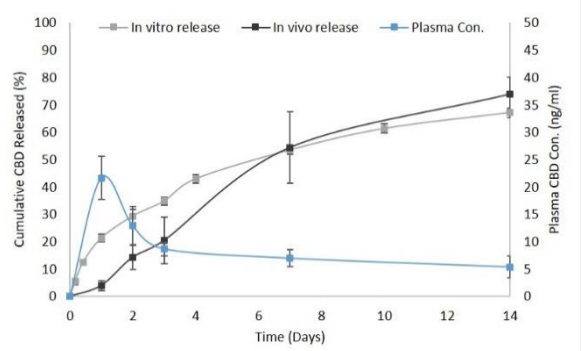

Figure 2: CBD release from CME-loaded microspheres
Release profiles *in vitro* and *in vivo* vs. plasma concentration in mice.

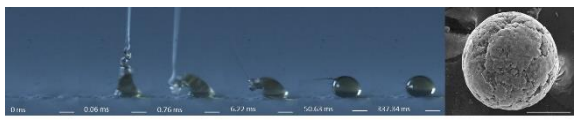

Figure 1: Formation of CME microsphere
Frames taken from high speed imaging, capturing the formation of a CME-loaded PCL microsphere onto a non-wetting surface (left), and a SEM image of a microsphere after solidification (right). Scale bar: 100 um.

VIII-OS30-04

Research on Biomedical Chitosan Based Drug-loaded Microspheres for Controlled Release Delivery System

Qin Zou[1], Junfeng Li[2], Yubao Li[1]

[1]Sichuan University, Research Center for Nano-Biomaterials, Analytical &Testing Center, chengdu, CN; [2]Chengdu University of Technology, Department of Materials Science & Engineering, Chengdu, CN

Introduction

Chronic osteomyelitis is currently a severe disease harmful to human health, often causing persistent infection and is still lack of effective treatment. The treatment of infection with debridement may cause bone defect and hematoma which can lead to recurrent infection. Based on the pathogenesis of osteomyelitis and application of drug delivery system for local treatment, we design a positively charged chitosan (CS) nanospheres loaded with bone morphogenetic protein (BMP-2), and a negatively charged gelatin nanospheres loaded with antibiotic berberine (Bbr), to realize their electrostatic self-assembly and multifunctionality. Investigation on the structure, morphology, assembly property of the nanospheres will be carried out in detail, together with the controlled release behavior of the drug and protein, and the efficacy and mechanism for treatment of chronic osteomyelitis and repair of bone defect.

Experimental Methods

Chitosan microspheres with diameter of 14.3～48.5 μm were prepared by emulsion method and using natural vanillin as cross-linking agent[1]. FT-IR, XRD, TGA, SEM and laser particle size analysis were used to characterize their physico-chemical properties. MG63 cell lines have the osteoblast phenotype, which is suitable for the primary screening cell of bone implant materials and the microspheres' cytocompatibility with osteoblast-like MG63 cell lines was evaluated in vitro.

Results and Discussion

The hollow microspheres showed a well-defined spherical shape with median diameter of 30.3 μm and possessed a uniform surface with micro-wrinkles, which is in favor of the drug release. Interpenetrating network cross-linking mechanism might result from the Schiff base reaction and the acetalization of hydroxyl and carbonyl between chitosan and vanillin. Berberine, was loaded in the microspheres and released in a sustainable manner. The drug loading ratio could change from 9.16% to 29.70% corresponding to the entrapment efficiency of 91.61% to 74.25%. In vitro cell culture study using MG63 cells and in vivo implantation clearly showed that the microspheres could provide favorable cell attachment and biocompatibility(Fig.1). The positively charged chitosan microspheres (CSM) (~35.5 μm) and negatively charged O-carboxymethyl chitosan microspheres (CMCSM) (~13.5 μm) were loaded respectively with bone morphogenetic protein (BMP-2) and berberine (Bbr) via swollen encapsulation and physical adsorption without significant change of the electric charges(Fig.2). TheBbr/CMCSM microspheres group possessed high antibacterial activity against the S.Aureus; the BMP-2/CSM microspheres group also owned excellent cytocompatibility, and improved osteoinductivity with assistance of BMP-2. The assembled gel group consisting of Bbr/CMCSM and BMP-2/CSM had a porous structure allowing biological signals transfer and tissue infiltration, and exhibited significantly enhanced bone reconstruction than the respective microspheres groups, which should result from the osteoconductivity of the porous structure and the osteoinduction of the BMP-2 growth factor[2].

Conclusion

The CS microspheres have a high drug loading and entrapment efficiency and moderate swelling ratio, presenting a sustained drug release behavior. It can be a good candidate for localized and sustained drug delivery, allowing for further biomedical investigation as therapeutic bioactive microcarrier.The n-HA/CS can act as worthy candidates for a multifunctional injectable matrix in bone tissue engineering.

References

[1] Qin Zou, Junfeng Li, Yubao Li*, Preparation and characterization of vanillin-crosslinked chitosan therapeutic bioactive microcarriers, International Journal of Biological Macromolecules, Volume 79, 2015, Pages 736–747

[2] Bin Cai, Qin Zou,* Yi Zuo, Quanjing Mei, Jinqi Ma, Lili Lin, Li Chen, and Yubao Li*. Injectable Gel Constructs with Regenerative and Anti-Infective Dual Effects Based on Assembled Chitosan Microspheres, ACS Appl. Mater. Interfaces, 2018, 10 ,30:25099-25112.

Acknowledgement

This work was supported by the China National Key Research and Development Program Fund (g r a n t no . 2016YFA0201703), the China NSFC Fund (grant no. 31670965)

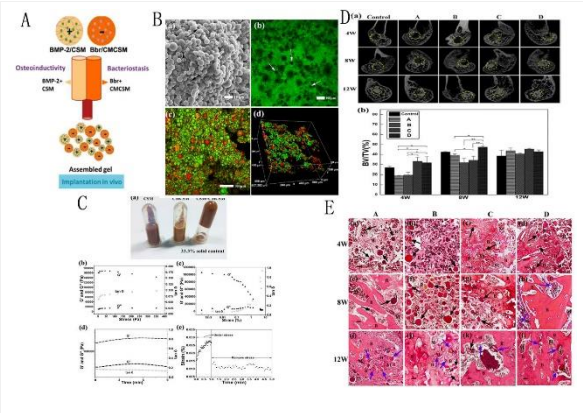

Fig.2 Injectable gel constructs based on assembled chitosan microspheres
A, Scheme of preparation of oppositely charged microspheres and their assembled gel. B, (a) SEM image, fluorescence photograph of the assembled structure. C, Gel formation test (a) and viscoelastic properties (b-e) of the microspheres assemblies. D, In vivo quantitative estimation of new bone volume (b) among different implanted materials (control, A, B, C and D) based on the 3D reconstruction of around 256 CT-images. E, HE staining evaluation micrographs of various implanted materials (group A, B, C and D) at 4 week (a-d), 8 week (e-h), and 12 week (i-l) (group A: CSM+CMCSM, group B: Bbr/CMCSM, group C: BMP-2/CSM, group D: BMP-2/CSM+Bbr/CSMCSM). The black arrows and blue arrows indicate the degraded microspheres with erose shape and indistinct shape respectively.

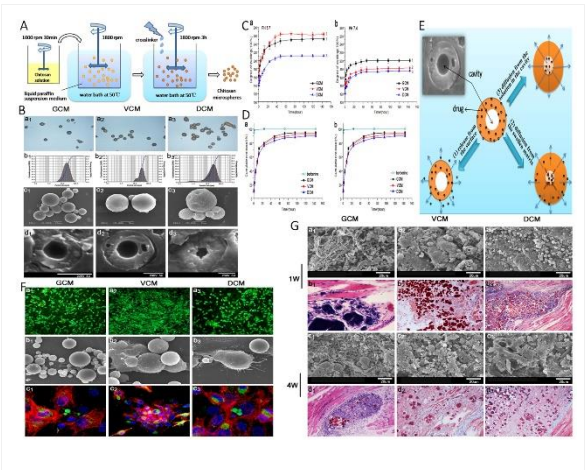

Fig.1 Preparation and characterization of crosslinked chitosan therapeutic bioactive microcarriers.
Glutaraldehyde cross-linked CS microspheres (GM), vanillin cross-linked CS microspheres (VM), terephthalaldehyde cross-linked CS microspheres (TM) were prepared by emulsion method(A).The hollow microspheres showed a well-defined spherical shape and possessed a uniform surface with micro-wrinkles(B). Incubation of the drug carrying microspheres in phosphate buffered saline (pH=7.4&5.7) revealed slow degradation(C). Significant release of drug from drug loaded microspheres was apparent in vitro(D), this can be attributed to their swelling(E). Cells surrounded the microspheres showing a continuous monolayer with distinguishable microvilli and adhered well on the microspheres forming abundant cell layer(F).

VIII-OS30-05

Boosting Efficacy and Decreasing Toxicity of Antimicrobial Nanoparticles Mediated by Cyclodextrin: The Case of Amino Acid – Functionalized Gold

Marija Vukomanovic[1,2], Lea Udovc[1], Laura Moya[2], Maria del Mar Cendra[2], Eduard Torrents[2]

[1]Jozef Stefan Institute, Advanced Materials Department, Ljubljana, SI; [2]Institute for Bioengineering of Catalonia (IBEC), The Institute of Science and Technology (BIST), Bacterial Infections: Antimicrobial Therapies, Barc, ES

Introduction

Cyclodextrins (CDs) are cyclic oligosaccharides characterized by truncated cone structure with hydrophobic core and hydrophilic surface [1]. They are prone of forming interesting inclusion complexes with drug molecules that modulate their physical, chemical and biological properties. Consequently there is an increase in solubility and permeability of quest molecule through biological membranes resulting in significant improvement in their therapeutic efficacy combined with important decrease in toxicity [1]. Although the excipient role of CD in drug molecules is very well studied, the capacity of CDs to modify efficiency and toxicity of nanoparticles (NPs), especially NPs with antimicrobial characteristics, is not completely clear [2].

Experimental Methods

Nanoparticles were synthesized using sonochemical approach and functionalized using amino acids pre-mixed with cyclodextrin [3]. Antimicrobial testing was performed in *Pseudomonas aeruginosa* (PAO1) [4] and confirmed using Live/Dead and FM646/DAPI staining. In vitro testing was done in lung epithelial A549 cells using Presto blue staining. *In vivo* testing was performed in *Galleria mellonela* worms injected with 10 uL of tested suspensions.

Results and Discussion

In this study we investigated amino acid- functionalized gold nanoparticles (AuNPs) designed as structural analogues of antimicrobial peptides (with the properties illustrated in Fig.1). With hydrophilic and cationic surface provided by amino acid, hydrophobic cores made of AuNPs as well as bioactive, hydrophilic apatite carrier they have all key characteristics to mimic antimicrobial peptides. If the surface of AuNPs is decorated by a mixture of cationic amino acids, there is a synergy that provides more than 10-fold increase in antimicrobial efficiency. However, selectivity index, *in vitro* and *in vivo* toxicity profiles of so-formed NPs do not favour their application and need to be improved. For that purpose we modified AuNPs functionalized by arginine as well as AuNPs functionalized by mixture of arginine, lysine and histidine using CD-molecules. Finally- formed AuNPs were very stable and readily dispersible in water. Morphologically, they are spheres up to 15 nm in size with positive zeta potential. Addition of CD boosted antimicrobial activity of amino acid-functionalized AuNPs, as observed in case of the *Pseudomonas aeruginosa* (PAO1). Low concentrations of NPs were providing strong antimicrobial effect (LIVE/DEAD test). NPs were able to deform bacterial cell structure and induce disruptions in bacterial wall (FM 646/DAPI staining). Cytotoxicity was tested in lung epithelial A549 cells and it showed significant improvements and selectivity was increased after modification by CD. *In vivo* toxicity was investigated in *Galleria mellonela* worm model. After addition of a high content of CD-modified NPs 100%-survivability was obtained.

Conclusion

CD-modification increases affinity of NPs for interaction with bacterial cells and promotes disruption of bacterial wall. Bacteria-favoured interactions are boosting antimicrobial activity and significantly decrease toxicity. The strategy is suggested as very efficient in designing next generations, antibiotic free antimicrobials based on nanotechnology.

References

[1] Kaneto Uekama Fumitoshi Hirayama, and Tetsumi Irie, *Chem. Rev.* **1998,** *98,* 2045.
[2] Lakkakula JR, Maçedo Krause RW, Nanomedicine (Lond). 2014, 9(6):877.
[3] Vukomanović M, Logar M, Škapin SD, Suvorov D, J. Mater. Chem. B, 2014, 2:1557.
[4] Vukomanovic M, Torrents E, J Nanobiotechnology. 2019;17(1):21.

Acknowledgement

This work is funded by the Slovenian Research Agency (ARRS) (grant J2-8169), European Commission under Horizon 2020's Marie Skłodowska-Curie Actions COFUND scheme (Grant Agreement no. 712754) and the Severo Ochoa programme of the Spanish Ministry of Science and Competitiveness (Grant SEV-2014-0425 (2015-2019)).

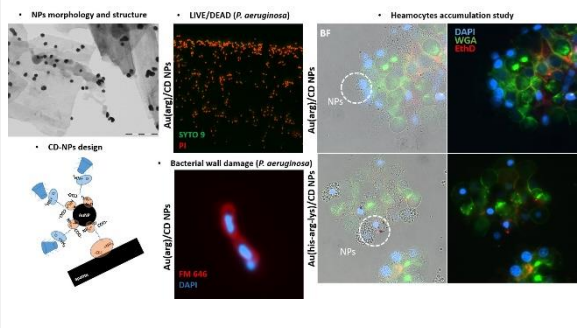

CD-modified AuNPs functionalized by amino acids
NPs morphological, structural characteristics and design; antimicrobial activity (survival and wall damage), and cell accumulation

VIII-OS30-RF06

Tuning drug delivery with block copolymer-based biomaterials

Clara Mattu, Giulia Brachi, Gianluca Ciardelli

Politecnico di Torino, DIMEAS, Turin, IT

Introduction

Systemic chemotherapy is often ineffective in treating cancer, due to poor selectivity and adverse off-target effects [1]. Polymer nanoparticles (NPs) are promising candidates as they enhance tumor uptake by passive and active targeting mechanisms, reducing undesired side effects [2].
Moreover, NPs can be used for packaging of multiple payloads, allowing combinatorial treatments that could not otherwise be obtained due to different biodistribution profiles on un-encapsulated drugs [3].
Here, we exploit the versatile chemistry of polyurethanes (PUR) to design a platform of NPs exhibiting: i) high drug loading ability [4]; ii) Active and passive targeting functionalities [5,6]; iii) ability to combine different treatment options [7]; iv) imaging capability [8].

Experimental Methods

PURs were obtained by a two-step synthesis procedure and their hydrophilic/hydrophobic balance was modulated by selecting different ratios between the hydrophobic poly(ε-caprolactone) (PCL) diol and the hydrophilic poly(ethyleneglicole) (PEG) [4]. NPs were prepared by emulsification of nanoprecipitation methods. Active tumor targeting was achieved in vitro by surface-modification with the monoclonal antibody Herceptin (HER). Core shell PUR NPs, were designed for the co-encapsulation of multiple payloads, including chemotherapeutics with different biodistribution profiles and imaging probes. In vivo studies were performed to determine tumor uptake and ability to efficiently co-deliver multiple payloads. Because of the low toxicity profile and versatile design, core-shell PUR-NPs were delivered intra-cranial (IC) in glioblastoma (GBM) bearing mice, and transport and treatment studies were performed.

Results and Discussion

We showed that PURs are optimal candidates to form NPs. High drug loading, in vitro cell targeting and internalization, and long-term stability were achieved. Functional groups or surface charge was successfully exploited for surface modification with HER and selective targeting of HER-2 over-expressing cells was demonstrated in vitro. The core-shell design of PUR NPs resulted high in vivo tumor accumulation in a breast cancer flank tumor model (4T1 cells). We showed efficient tumor co-accumulation of Doxorubicin and Docetaxel, two drugs with different pharmacokinetics and, therefore, not compatible for combinatorial treatment. NPs showed long residence time in the brain after IC injection (up to 10 days post injection) and good coverage of the tumor mass. Drug-loaded PUR NPs significantly extended survival of GBM-bearing mice.

Conclusion

Our results warrant further investigation of PURs as NP-forming materials in nanomedicine, in virtue of their versatility, surface-modification ability, and high affinity with both, hydrophilic and hydrophobic, drugs.

References

[1] J.Shi et Al. Nature Reviews **Cancer**, 2017

[2] E. Blanco et Al. Nature biotechnology, 2015

[3] E. Blanco Therapeutic delivery, 2014 - Future Science

[4] C. Mattu et al Journal of Nanoparticle Research, 2012

[5] C. Mattu et al. European Journal of Pharmaceutics and Biopharmaceutics, 2013

[6] C. Mattu et al. Polymer International, 2016

[7] C.Mattu et al. Acta Biomaterialia, 2018

[8] C. Iodice et al. Optics and Lasers in Engineering, 2016

Acknowledgement

This project has received funding from the European Union's Horizon 2020 research and innovation programme under the Marie Sklodowska-Curie grant agreement No 658665

VIII-OS30-RF07

Development of a 3D Printed Scaffold Allowing Multiple Drug Delivery for the Treatment of Bone Metastasis in Breast Cancers

Habib Belaid[1,2], Catherine Teyssier[2], David Cornu[1], Vincent Cavailles[2], Mikhael Bechelany[1]

[1]Université de Montpellier, Institut Européen des Membranes, Montpellier, FR; [2]Université de Montpellier, Institut de Recherche en Cancerologie, Montpellier, FR

Introduction

Breast cancer is the most common invasive cancer in women, and the second main cause of cancer death in women. Metastatic breast cancer, most frequently localized in bone, is causing considerable pain and high patient morbidity. The treatment of bone is challenging due to bone repair, and patients are often treated by implanting a passive artificial junction in addition to a systemic chemotherapy treatment.3D printing is emerging as a powerful tool for bone repair. Long-term bone regeneration of normal anatomic structure, shape, and function is clinically important subsequent to fracture due to bone trauma and tumor.

3D printing is providing the ability to print bone substitute materials or “scaffolds” designed to mimic the extracellular matrix. The scaffolds need to be biocompatible and bioresorbable with a highly porous and interconnected pore network to control the degradation and resorption rate. They have a controlled shape and a suitable chemist surface for cell attachment, proliferation, and differentiation. Finally, the mechanical properties have to match those of the tissues at the site of implantation. For patients with bone metastasis, the scaffold may also allow the controlled and local release of anticancer drugs. One of the strategies to deliver these drugs by the scaffolds is to encapsulate them in microspheres such as Poly (lactic-co-glycolide) or PLGA microspheres which are one of the acknowledged vehicles for drug release approved by FDA.

Experimental Methods

To this aim, PLGA microspheres have been loaded with Raloxifene hydrochloride (RH) which is a selective estrogen receptor modulator (SERM) and Alendronate (AL) which is a bisphosphonate drug used for the treatment of bone metastasis. These drugs show an extremely poor bioavailability via oral administration thus justifying a local release. These microspheres made by emulsion have been incorporated into a 3D scaffold fabricated using a Stereolithography 3D printer system with a Poly (propylene fumarate) (PPF) photopolymer. PPF is an ultraviolet curable and biodegradable polymer with potential applications for bone regeneration and excellent mechanical properties.

Results and Discussion

The physicochemical properties of the nanocomposites scaffold have been fully characterized. The results showed that the microspheres were elongated and slightly less smooth after the loading of RH and AL, depicting the successful encapsulation of the drugs. The encapsulation efficiency and the realasing are obtained by UV-spectrometry. Encapsulation efficiencies of 14% and 54% were obtained for RH and AL respectively with relasing above 30% after one month for both drugs. The size of microspheres are obtained in range of 1µm and 50µm confirmed by dynamic light scattering and granulometry. The molecular weight of the polymer has been determined by gel permeation chromatography with Mn of 1,5kDa and a PI of 4. The physicochemical properties of the 3D printed

scaffold have been determined using scanning electron microscopy to show the surface of the scaffolds and the porosity. Finally the mechanical properties of the 3D printed nanocomposites scaffolds have been determined by tensil test as well compression test to show the influence of the incorporation of the PLGA microspheres.
Biological testing has been carried out in order to confirm the effects of encapsulated drugs on MCF7 cells proliferation. A cell viability test using MG63 cells has been conducted to determine the scaffold biocompatibility and its effects on cell proliferation. The successful cell adhesion was revealed by fluorescent microscopy ans by SEM.The aim of this work is the development and characterization of novel biomimetic biodegradable 3D printing scaffolds allowing both bone regeneration and inhibition of breast cancer cell proliferation.

Conclusion

These first results appear very promising and open prospects for bone metastasis treatment in breast cancers.

4:45 p.m. – 6:15 p.m.

Hall 3

IX-OS31 | Additive manufacturing 1

IX-OS31-01

A 3D Bioprinted Meniscus Implant Reinforced by Chitosan/Poly(Vinyl Alcohol) Fibres

Elli Käpylä[1], Mostofa Kamal Khan[1], Sheng Pan[1], Reza Nickmanesh[1,2], Simon Beyer[1], Joe Ault[3], Julia Hwang[3], Tamer Mohamed[1], Sam Wadsworth[1]

[1]Aspect Biosystems Ltd., Vancouver, CA; [2]UBC Centre for Hip Health & Mobility, Vancouver, CA; [3]DePuy Synthes, Raynham, US

Introduction

Ameniscus tear is one of the most common knee injuries with an annual incidence of 66/100,000 in the USA. Menisci are vital for load bearing and stabilization of the knee and meniscus damage often results in the loss of normal joint function and the development of osteoarthritis (OA). A partial meniscectomy, which is the most common surgical treatment for meniscus tears, alleviates acute pain but often leads to OA over time. As meniscus replacement via allograft transplantation is limited by issues of availability and graft sizing, synthetic implants have been developed as off-the-shelf solutions to restoring meniscus function. Currently available meniscus implants, however, have received limited clinical adoption due to poor surgical performance and lack of clear long-term clinical benefits. There is thus a need for a partial meniscus implant with sufficient mechanical properties for arthroscopic surgical fixation, immediate load-bearing, and long-term performance. Here, we report an acellular 3D bioprinted chitosan/poly(vinyl alcohol) (PVA) composite meniscus, fabricated using Aspect Biosystems' patented microfluidic bioprinting technology. This implant exhibits suture pull-out, tensile strength, and compressive strength values appropriate for effective surgical implantation due to a unique combination of rationally designed synergistic biomaterial and structural components.

Experimental Methods

Chitosan/PVA blends were bioprinted using the microfluidic RX1™ Bioprinter (Aspect Biosystems Ltd.). The acidic chitosan was ionically crosslinked during bioprinting using a sodium triphosphate (STP) solution whereas the aqueous PVA was crystallised post-printing by freeze-thaw cycling. Ring-shaped samples were printed for the tensile testing of different blends with a UniVert mechanical tester (CellScale, Waterloo, Canada). To fabricate a composite implant, a bioprinted, meniscus-sized chitosan/PVA mesh was combined with a PVA solution (20% w/v), subjected to additional freeze-thaw cycles to crystallise the cast PVA, and hydrated with saline. The target values for suture pull-out, tensile, and compressive strength were set as 20 N, 1 MPa and 100 kPa, respectively, and measured using a Mach-1 device (Biomomentum, Montreal, Canada). The values for the composite meniscus were compared to the printed mesh and the cast PVA matrix alone. The ratios of the printed chitosan/PVA fibres, the PVA matrix, and the incorporated water in the composite menisci were quantified based on wet and dry mass measurements.

Results and Discussion

The chitosan/PVA blends developed for meniscus bioprinting exhibited high tensile strength, elasticity, and recovery after tensile deformation. Increasing the chitosan solution concentration from 3.5% to 4.5% and the PVA solution concentration from 10% to 15% increased the tensile strength of printed rings by 25% and 100%, respectively. In contrast, increasing the chitosan:PVA ratio from 1:1 to 3:2 made the rings less elastic and the tensile strength

decreased by 30%. In order to maximize mechanical performance, a blend of 4.5% chitosan and 15% PVA was chosen for the printing of the mesh component. We showed that combining the printed mesh with the cast PVA matrix, had a synergistic effect on the mechanical performance of the tissue. The average suture pull-out strength and ultimate tensile strength of the composite meniscus (58.6 N and 1.51 MPa) were significantly higher than the printed mesh (40.7 N and 0.98 MPa) and the cast PVA matrix alone (30.1 N and 0.66 MPa). The printed mesh demonstrated high suture retention and tensile strengths, while the addition of the cast PVA significantly increased the compressive strength of the composites (105.4 kPa) compared to the mesh alone (23.9 kPa). The composite meniscus thus met all of the predefined mechanical target values. The mechanical properties of the composites could be further tuned by varying the geometry of the bioprinted mesh. In addition to the promising mechanical characteristics, the composition of the composite meniscus was found to correspond well to the native meniscus, with approximately 74% water and 26% polymer.

Conclusion

Meniscus implants hold the promise to delay or prevent OA linked to meniscus damage. We have developeda novel chitosan/PVA implant for partial meniscus replacement by utilizing Aspect's microfluidic bioprinting technology. Our composite implant combining a bioprinted mesh and a cast matrix exhibits the appropriate mechanical properties for arthroscopic surgical fixation and short-term load-bearing. Furthermore, the composite contains a similar amount of water than a native human meniscus and is partly resorbable, which has the potential to enhance engraftment to the host meniscus in the long-term. In the next phase of development, the fibre-reinforced composite chitosan/PVA meniscus will be tested in a large animal model to study *in vivo* surgical and mechanical performance, tissue engraftment, and clinical efficacy at preventing early-stage cartilage degeneration.

References

Korpershoek *et al*. The Orthopaedic Journal of Sports Medicine, 2017, 5(2), 2325967117690131

Bilgen *et al.* 2018, Adv. Healthcare Mater. 2018, 1701407.

Bryceland *et al.* Cartilage2017, Vol. 8(2) 99–104.

Acknowledgement

We thank DePuy Synthes for experimental advice, Biomomentum for the custom modification of the Mach-1 device and UBC-Centre for Hip Health & Mobility for access to the Mach-1 tester.

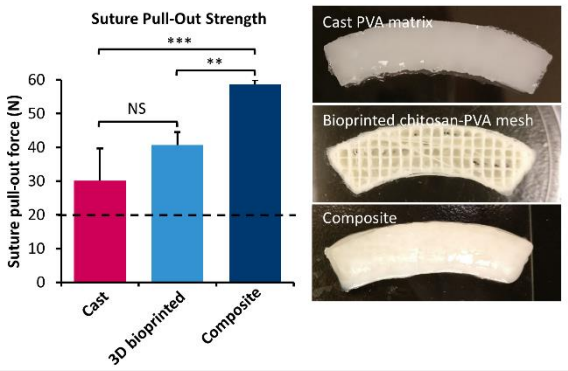

The 3D bioprinted composite meniscus demonstrates high suture retention.
Figure 1. Suture pull-out strength of a cast PVA matrix, a 3D bioprinted (3DBP) chitosan-PVA mesh and a composite (3DBP + cast) meniscus. N = 4, mean ± SD, NS = not significant, ** $p < 0.01$, *** $p < 0.001$ by 1-way ANOVA (Tukey's post-test).

IX-OS31-02

Antimicrobial 3D-printed scaffolds of composite fibers containing poly(ε-caprolactone) and graphene oxide

Sofia F. Melo[1,2,3], Sara C. Neves[1,2], Andreia T. Pereira[1,2,4], Inês Borges[1], Pedro Granja[1,2,3], Fernão D. Magalhães[5], Inês C. Gonçalves[1,2]

[1]University of Porto, i3S - Instituto de Investigação e Inovação em Saúde, Porto, PT; [2]University of Porto, INEB - Instituto de Engenharia Biomédica, Porto, PT; [3]University of Porto, FEUP - Faculdade de Engenharia, Porto, PT; [4]University of Porto, ICBAS - Instituto de Ciências Biomédicas Abel Salazar, Porto, PT; [5]University of Porto, LEPABE - Laboratório de Engenharia de Processos, Ambiente, Biotecnologia e Energia, Porto, PT

Introduction

Implantable fibrous scaffolds-associated infection and consequent failure is a severe health issue, which can result from bacterial adhesion, growth and biofilm formation at the implantation site, ultimately leading to sepsis and patients death. Graphene-based materials, namely graphene oxide (GO), have been described as potential antibacterial compounds, particularly when immobilized and exposed in composite polymeric matrices[1]. The main goal of this work was to improve the antimicrobial properties of poly(ε-caprolactone) (PCL) fibrous scaffolds. For that, GO was mixed with PCL and layer-by-layer organized composite scaffolds were produced by 3D printing, using wet-spinning combined with additive manufacturing (AM). This fabrication method was chosen based on the desired fiber diameter (around 100 μm), allowing the incorporation of GO sheets, but also their exposure, which is difficult to achieve in fibers with larger diameter. Scaffolds were evaluated regarding 3D structure, GO exposure at the surface of the fibers, antibacterial properties and ability to adhere human fibroblasts.

Experimental Methods

Graphene oxide (GO) was produced from graphite using the modified Hummers method (MHM) and oxidation was evaluated by X-ray photoelectron spectroscopy (XPS). Poly(ε-caprolactone) (PCL) fibers, with and without incorporated GO, were precipitated in a coagulation bath and assembled in a 3D-organized scaffold, by combining wet-spinning with additive manufacturing (AM). Several optimization steps were performed, concerning polymer and GO concentration, specific printing parameters as flow rate and plotting speed, and different xyz distances between fibers. The 3D structure of the produced scaffolds was visualized by stereomicroscopy and scanning electron microscopy (SEM). GO exposure on the outer surface of the fibers and in their cross-sections was assessed by SEM. Antimicrobial properties were evaluated through live/dead assays performed with *Staphylococcus epidermidis*, a bacterial species commonly found in infected implantable devices. After 2h and 24h of contact with the scaffolds, adherent bacteria were stained with Syto9 (live) and propidium iodide (dead), observed by confocal microscopy, and counted using Fiji/ImageJ software. *In vitro* biocompatibility was studied using Human foreskin fibroblasts (HFF-1), which were cultured on the scaffolds for up to 7 days. Adherent cells were stained with DAPI (nuclei) and phalloidin (cytoskeleton) and observed by confocal microscopy.

Results and Discussion

XPS analysis revealed that the produced GO was constituted by 70.9% of carbon atoms and 29.1% of oxygen atoms, while commercial graphite typically has a much lower percentage of oxygen (8% O 1s). Wet-spinning combined with AM allowed the production of well-defined PCL and composite PCL/GO fibrous scaffolds with average fiber diameters

of 100 µm. Low flow rates and plotting speeds, as well as wide distances between fibers (d_{xy} = 200 µm), proved to be the best settings to obtain defined and precisely plotted scaffolds. PCL concentration was set at 7.5% (w/v) and GO concentration ranged from 0% to 7.5% (w/w) (some examples are depicted in the figure below). SEM images revealed that a concentration of 5% GO was sufficient to expose GO sheets at the surface of the composite fibers. Regarding the antibacterial potential assessment, the 2h and 24h adhesion assays to the scaffolds revealed GO time-dependent bactericidal effect and an increase in death rate from about 14% in neat PCL scaffolds to nearly 80% in composite scaffolds with 7.5% GO, after 24h of contact. *In vitro* biocompatibility evaluation showed that both PCL and composite PCL/GO scaffolds allowed human fibroblasts (HFF-1) adhesion and spreading along the fibers during 7 days of culture, suggesting the absence of cytotoxicity.

Conclusion

Composite PCL/GO 3D-organized fibrous scaffolds were unprecedently produced using wet-spinning combined with additive manufacturing. The antimicrobial properties of fibrous scaffolds containing GO were assessed for the first time, revealing outstanding GO bactericidal effect over time. As such, GO-containing fibrous scaffolds developed in this work promoted bacteria death, while allowing human fibroblasts adhesion. These features demonstrate the potential of GO incorporation in polymer fibrous scaffolds for antimicrobial medical implantation purposes.

References

1. Henriques, P. C., Borges, I., Pinto, A. M., Magalhães, F. D. & Gonçalves, I. C. Fabrication and antimicrobial performance of surfaces integrating graphene-based materials. *Carbon N. Y.***132,** 709–732 (2018).

Acknowledgement

Authors would like to thank the Bioimaging scientific platform (b.IMAGE), which is part of i3S/INEB. The work described was financially supported by FEDER through COMPETE2020 - Programa Operacional Competitividade e Internacionalização (POCI), Programa Operacional Regional do Norte (NORTE2020) - and by national funds through FCT (Fundação para a Ciência e Tecnologia): POCI-01-0145-FEDER-007274 (i3S), UID/EQU/00511/2019 (LEPABE), Projects PTDC/CTM-BIO/4033/2014 (NewCat), PTDC/BBB-ECT/2145/2014 (SkinPrint) and NORTE-01-0145-FEDER-000012, Research position contract IF/01479/2015 and PhD grant PD/BD/114156/2016.

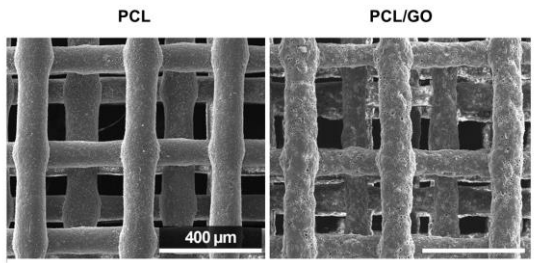

SEM analysis
SEM images of the top view of PCL and PCL containing 7.5% GO scaffolds. Scale bar: 400 µm.

IX-OS31-03

Melt-Electrowritten 3D Scaffolds Based on Aligned Nano-Structured Microfibers for Topography-Mediated Immunomodulation of Human Macrophages

Matthias Ryma, Tina Tylek, Julia Blöhbaum, Robin Fernandez, Jürgen Groll

Universitätsklinikum Würzburg, Abteilung für Funktionswerkstoffe der Medizin und Zahnheilkunde, Würzburg, DE

Introduction

Poly(2-oxazoline)s are a group of polymers which recently gained increased interest, especially due to their excellent biocompatibility and thermoresponsive behavior in aqueous solutions. Furthermore, their utilization in the field of biofabrication was proven as bioinks as well as in combination with Melt Electrowriting, an emerging technique, that enables the user to directly deposit polymer fibers in a directed manner.

In this study, we present a polymer blend based on Poly(2-oxazoline)s, which leads to the formation of fibrillar, thread-like scaffold structures, after being processed via Melt Electrowriting. An effect, which seems to be induced by directed phase separation of the polymer melt based on pressure and the electrical field. Furthermore, these structured fibril bundles induce regenerative M2-marker expression in human macrophages based solely on the topographical stimulus without any addition of differentiation factors.

Experimental Methods

Scaffold production via Melt Electrowriting of Poly(2-n-propyl-2-oxazoline) (PnPrOx)+Poly(2-cyclopropyl-2-oxazoline) (PcycloPrOx) blend

To create blends with different ratios of PnPrOx and PcycloPrOx, the polymers were weighted, and a final amount of 1 g was dissolved in 50 ml deionized water and lyophilized. For the process of Melt Electrowriting, we used a custom build device. In order to create homogenous fibers, the MEW-device was equipped with one heating zone at the syringe and another one at the nozzle. Scaffolds were crystallized afterwards by prolonged heating at 60°C for 24 hours.

Monocyte culture and analysis

Monocytes were isolated from human blood-derived buffy coats of healthy donors. Freshly isolated monocytes were seeded in a 50 µl suspension with 0.75 x 10^6 cells on top of each sample in a tissue culture-treated 24 well plate. The cells were cultivated for 7 days latest on the scaffolds and analyzed for gene expression via qPCR and for protein expression via Western Blot, ELISA and immunohistochemistry. Macrophage alignment was shown by microscopic and SEM-images.

Results and Discussion

In this study, we present a method to create fibrous scaffolds made of aligned nanostructured microfibers of PnPrOx. For this, PnPrOx and amorphous PcycloPrOx were blended and printed via Melt Electrowriting. After bulk crystallization of the blend scaffold by prolonged heating, we were able to separate the crystalline PnPrOx from the amorphous PcycloPrOx by dissolution in water. Fibril bundles made of crystallized PnPrOx were exposed.

The optical analysis and DSC of the blend shows phase separation and therefore no miscibility. To examine whether the electrical field has an impact on fiber morphology, we optically compared fibrils which were printed with and

without voltage during the process of MEW. The pressure itself leads to an initial fibril formation from the blend, however, a uniform fibril morphology was only achieved by introducing charge. Hence, the electrical field seems to finally shape the morphology of the fibrils. This leads to the assumption, that fibril formation is based on a directed phase separation of PnPrOx and PcycloPrOx induced by the combination of pressure with the electrical field applied during the process of MEW.

We further provide an immunomodulatory application of the scaffolds. For this, human monocytes were seeded on the fibril scaffolds, which led to topography-mediated expression of anti-inflammatory M2-factors after 7 days without any further stimuli. Macrophages on fibril scaffolds showed lesser decrease of anti-inflammatory cytokines, higher release of anti-inflammatory IL-10 and angiogenenesis-promoting IL-8 combined with a decrease of the fibrosis marker TGF-b1 compared to the control scaffolds. The anti-inflammatory effect of the fibrillar scaffolds was also shown via protein expression analysis of CD163 and CD206, both M2 macrophage specific surface marker. Compared to controls, both markers were upregulated on the fibrillar structures after seven days of cultivation.

Conclusion

Taken together, we developed a polymer blend based on Poly(2-oxazoline)s, which leads to the formation of fibrillar, thread-like scaffold structures, after being processed via Melt Electrowriting. Furthermore, these structured fibril bundles induce regenerative M2-marker expression in human macrophages based on the topographical stimulus. Besides its immunomodulatory effect, this combination of Poly(2-oxazoline)s and MEW has the potential to become a platform for topography mediated differentiation of several cell types for tissue engineering and regenerative purposes.

References

Gaertner, F. C.; Luxenhofer, R.; Blechert, B.; Jordan, R.; Essler, M., Synthesis, biodistribution and excretion of radiolabeled poly(2-alkyl-2-oxazoline)s. *J Control Release* **2007,***119* (3), 291-300.

Hoogenboom, R., Poly(2-oxazoline)s: a polymer class with numerous potential applications. *Angew Chem Int Ed Engl* **2009,***48* (43), 7978-94

Lorson, T.; Jaksch, S.; Lubtow, M. M.; Jungst, T.; Groll, J.; Luhmann, T.; Luxenhofer, R., A Thermogelling Supramolecular Hydrogel with Sponge-Like Morphology as a Cytocompatible Bioink. *Biomacromolecules* **2017,***18* (7), 2161-2171.

Hochleitner, G.; Hummer, J. F.; Luxenhofer, R.; Groll, J., High definition fibrous poly(2-ethyl-2-oxazoline) scaffolds through melt electrospinning writing. *Polymer* **2014,***55* (20), 5017-5023.

Acknowledgement

We thank Christoph Böhm for DSC measurements and Philipp Stahlhut for SEM-imaging.

Funded by the Deutsche Forschungsgemeinschaft (DFG, German Research Foundation) – Projektnummer 326998133 – TRR 225 (subproject B02).

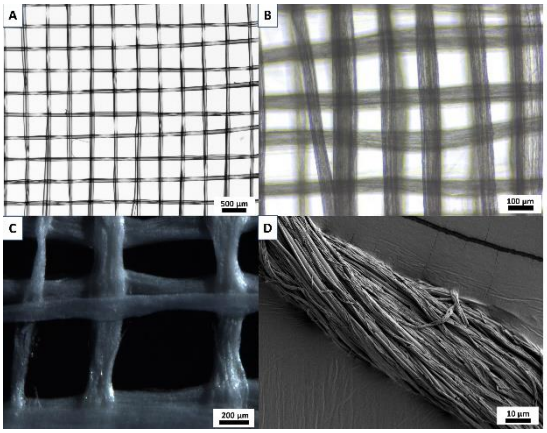

PnPrOx+PcPrOx Blend Scaffold
A: Stereomicroscopic image of blend scaffold; B: Microscopic image of fibril scaffold after PcPrOx dissolution in water; C: Stereomicroscopic image of fibril scaffold after lyophilization; D: SEM-Image of aligned fibrillar microfiber

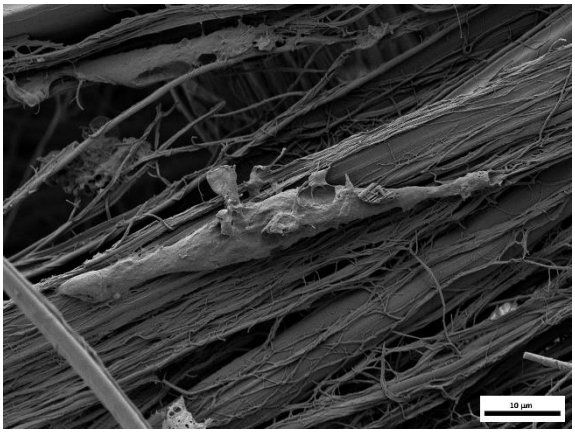

Elongated Macrophage Aligned with Fibril Scaffold

IX-OS31-04

3D Printed PLA/BN Scaffolds for Bone Tissue Engineering Application

Habib Belaid[1,2], Catherine Teyssier[2], David Cornu[1], Vincent Cavailles[2], Mikhael Bechelany[1]

[1]Université de Montpellier, Institut Européen des Membranes, Montpellier, FR; [2]Université de Montpellier, Institut de recherche en cancérologie, Montpellier, FR

Introduction

Contaminated or infected bone defects remain serious challenges in clinical trauma and orthopedics. The aim of this work is the development and characterization of novel biomimetic biodegradable implants called « scaffolds » obtained by 3D printing. Scaffolds that possess adequate biodegradability, interconnectivity, and mechanical properties in accordance with the injured tissue are required.Polylactide (PLA) is a currently used bioresorbable, biodegradable and biocompatible synthetic polymer that has been widely investigated and approved by FDA for biomedical applications. However PLA is a typical hydrophobic polymer. It has poor mechanical properties for tissue engineering applications. One of the strategies to improve these properties is to incorporate nanofillers inside this polymer.

Experimental Methods

During this study, PLA scaffolds reinforced with different quantities of Boron Nitride (BN) nanosheets were prepared by Fused Deposition Modeling 3D printing. BN sheets were exfoliated from boron nitride powder. Briefly, 20% gelatin solution was prepared and 1g of BN powder was added to the gelatin solution.The solution was sonicated to facilitate the exfoliation using an ultrasonic probe system for overnight Exfoliated BN was separated by centrifugation and resultant precipitates were dried at 80°C for 48 hours and then calcined at 600°C in air for 2 hours in order to obtain the exfoliated boron nitride.

The PLA solution was prepared using chloroform. BN will be dispersed in acetone and placed in an ultrasonic bath for 15min. The solution containing the BN was introduced into the polymer solution under constant magnetic stirring until the solution is homogenized. PLA/EBN dispersion was poured into a Teflon dish and allowed to dry overnight at room temperature. Further, dried polymer were cut into pieces and introduced to a single screw extruder.

The scaffold is modelled using computer-aided design (CAD) software . Once the shape of the scaffold is determined, a STL file is created to be analysed by software (Prusa3Dslicer). The 3D printer used is a Prusa Research MK2S.

Results and Discussion

Thermal characterizations showed that the addition of nanosheets does not modify the PLA transition temperature. Scanning Electron Microscopy indicated that the scaffold has an average pore size of 350 µm. A modification of the roughness and of the porosity of the surface was observed when the nanosheets are added to the scaffolds. The physicochemical analysis by X-ray Diffraction and Raman spectroscopy were performed in order to confirm the presence of the nanofillers. Improved mechanical properties by tensile test have been demonstrated. The measurements of the contact angle showed a transition from a hydrophobic surface observed for the pure PLA to a hydrophilic surface for our nanocomposites.

Scaffolds have been tested on osteosarcoma cells (MG63) in order to evaluate their enhanced mineralization ability. Biocompatibility, cell attachment and proliferation results showed that the scaffolds are nontoxic. Moreover, MG63 cells grown on the scaffolds were induced in differentiation as shown by alizarin red staining.

Conclusion

BN reinforced PLA composites were synthesized. PLA/BN composites were employed to fabricate customized scaffolds using FDM assisted 3D printing technique. BN-reinforced polylactic acid scaffolds are synthesized and characterized. The mechanical properties are also investigated. Boron nitride effectively reinforces the polymer matrix and increases the Young's modulus. Cell-viability assays, fluorescence imaging and Alizarin RED S activity using MG63 cells indicate that BN did not affect cell attachment and proliferation compare to PLA. Hence, BN-reinforced polylactic acid scaffolds are highly biocompatible and suitable for bone tissue engineering. The improved Young's modulus and mineralization clearly suggest that the BN-reinforced polylactic acid scaffolds by 3D printing. Regarding these results BN-reinforced polylactic acid scaffolds are promising nontoxic, biocompatible materials for orthopaedic applications. Altogether, our data showed that BN nanosheets reinforced PLA scaffolds and these materials could be suitable for bone tissue engineering.

IX-OS31-05

Evaluating three different extrusion-based bioprinting systems using cell-laden alginate-based bioinks

Rainer Detsch, Jonas Hazur, Emine Karakaya, Sonja Kuth, Susanne Heid, Aldo R. Boccaccini

University of Erlangen-Nuremberg, Department of Materials Science and Engineering, Institute of Biomaterials, Erlangen, DE

Introduction

Bioprinting is a technology for constructing bioartificial tissue or organs of complex three-dimensional (3D) structure. Various techniques have been developed and utilized in an attempt to generate complex structures via biofabrication including inkjet printing, extrusion and syringe-dispensing, stereolithography, two photon polymerization and laser-assisted cell printing. Extrusion-based bioprinting is a rapidly developing technique that has made substantial progress in the fabrication of hydrogel constructs over the past decade. With this technique, cell-laden hydrogels or bio-inks have been extruded layer-by-layer, to form 3D constructs with varying sizes, shapes, and resolutions. One special extrusion-based method is the syringe-dispensing technique, in which a mechanically soft and viscoelastic hydrogel with embedded cells. By applying air-pressure, the material is extruded through a fine nozzle and deposited as rods.

The aim of this work was to investigate and compare the biofabrication process of alginate-based bioinks with fibroblast cells using three different bioprinting systems.

Experimental Methods

Due to its promising characteristics regarding printability, biocompatibility and cell-material interactions [1, 2], pure alginate and alginate dialdehyde crosslinked with gelatin (ADA-GEL) in the concentration of 4 and 2.5 wt./vol. was used in this printing approach, respectively. Three different bioprinter systems, BioX (Cellink, Sweden), BioScaffolder 3.1 (GeSim, Germany) and BioBot (Advanced Solution, USA), were compared, which differ in the amount of printing heads, resolutions, temperature and software. For evaluation of the bioprinters, the same setup for all systems was used: nozzle diameter (200 µm), pressure (15-45 kPa), room temperature, geometry and amount of layers. By using a 0/90° lay-down-pattern, a 4-layer biofabricated construct was produced and subsequently printing quality and cell behaviour of NIH3T3 were analysed.

Results and Discussion

The applied biofabrication systems differ in their amount of pneumatic extruders, building volume, setting up and calibration time as well as printing resolution in XYZ axes. Additionally, different software systems (STL-files, G-code or company-specific scaffold generator) and data transfer controls result in various processing times. Printability studies were performed using alginate and ADA-GEL, showing a printing accuracy of 89-91 % and no occurrence of pore closure. Furthermore, with these bioinks a resolution of only 750 µm can be achieved, although the three machines can realise a resolution of up to 1-10 µm, depending on the system. Since cells are living materials, all fabrication processes were performed under sterile and biocompatible conditions. The analyses of bioprinting with NIH3T3 cells showed comparable results: high cell viability was achieved with both bioinks and with the use of the three different systems after 48 hours of incubation.

Conclusion

This is the first study comparing and evaluating three different extrusion based bioprinter systems using a standardized method applying hydrogel-based bioinks and embedded fibroblast cells. Although the printers show differences in construction, instrumentation and software, the printability tests in this work show successful generation of simple bioconstructs with all three systems. However, larger differences are expected when printing more complex structures, like tissue analogues. As conclusion, the choice of the bioprinter has to be based on the complexity of the 3D construct and the desired bioink system [3].

References

[1] B. Sarker, et al., Fabrication of alginate-gelatin crosslinked hydrogel microcapsules and evaluation of the microstructure and physico-chemical properties, J. of Mat. Chem. B. 11 (2014).

[2] T. Zehnder, B. Sarker, A.R. Boccaccini, R. Detsch, Evaluation of an alginate-gelatine crosslinked hydrogel for bioplotting, Biofabrication. 7 (2015).

[3] F. Ruther, T. Distler, A.R. Boccaccini, R. Detsch, Biofabrication of vessel-like structures with alginate di-aldehyde—gelatin (ADA-GEL) bioink, J. Mater. Sci. Mater. Med. 30 (2019).

Acknowledgement

This work was supported by the German Research Foundation (DFG) within the collaborative research center TRR225 (project Nr. 326998133) (subprojects A01, B03 and B06).

IX-OS31-06

Functional bioprinted skin replacement

Desiree M. Eckerlin[1], Jan Schöneberg[1], Yvonne Marquardt[2], Ruth Heise[2], Jens Baron[2], Horst Fischer[1]

[1]RWTH Aachen University Hospital, Department of Dental Materials and Biomaterials Research, Aachen, DE;
[2]RWTH Aachen University Hospital, Clinic for Dermatology and Allergology, Aachen, DE

Introduction

The skin, the largest organ of the human body, contains multiple types of cells organized in layers with specific structures. The specific arrangement of these cells is important to perform the various functions of the skin, e.g. protection from mechanical forces or microorganisms and regulation of the body temperature.
If a large area of the skin is wounded, e.g. after tumor excisions, the skin has to be artificially restored. Nowadays, autologous split-thickness skin grafts (ASSG) are still used as the gold standard for large wounds, although there are different disadvantages, especially the need of a secondary surgical site. The current tissue engineering technology is not able to produce a fully biofunctional skin substitute at reasonable cost. Skin bioprinting might be an interesting alternative to ASSG. This process includes collecting skin tissues from the patient, isolating and culturing its main cell types to obtain high enough numbers and mixing them with biomaterials. The customized skin is then fabricated by depositing the material using a computer-controlled bioprinter. 1

Experimental Methods

Here, we present a printing procedure, that offers the possibility to produce a 3D-printed customized skin, fulfilling the main aspects of natural human skin and not containing artificial scaffolds. It addresses as well the clinical needs, like low cost, good availability as well as uncomplicated applicability. We used primary human keratinocytes and fibroblasts. The bioink is based on collagen I. This hydrogel is well known to offer high cell supportive ability. However, is also known for drawbacks like low shape fidelity, low viscosity, and low mechanical integrity.
We developed a technique to overcome the described drawbacks without mixing it with other polymers and therefore without introducing possible negative effects by those blends. We could show the wound healing capabilities of the bioprinted skin by in-vitro transplantation into a conventionally cultured skin-model. The conventional and printed models were both created by using cells from same patients.
First, printed an agarose wall, that can be precisely adapted to the patient-specific shape onto a collagen-elastin-matrix.. In order to produce the dermis, we then printed the primary fibroblasts with the collagen-bioink into the designed forms. Afterwards, we printed keratinocytes, dissolved in culture-medium, for the epidermis. For our experiments we printed cylinders of different sizes and could additionally show the fabrication of individual (patient-specific) shapes (Figure 1a).

Results and Discussion

At several days after transplantation we collected tissue samples to validate the macroscopic and histological success of the transplantation. These analyses did show that the printed skin quickly adhered successfully to the conventional cultured model (Figure 1b-c)

Conclusion

The current results suggest that we could use bioprinted skin substitutes in the future for patient specific transplants. Our ambition for future skin transplants, is to develop a fast, precise and easy to use fabrication method for practical clinical usage.

References

1 He, P. et al. Burn. Trauma 6, 5 (2018)

2 Panwar, A. et al. Molecules 21, (2016)

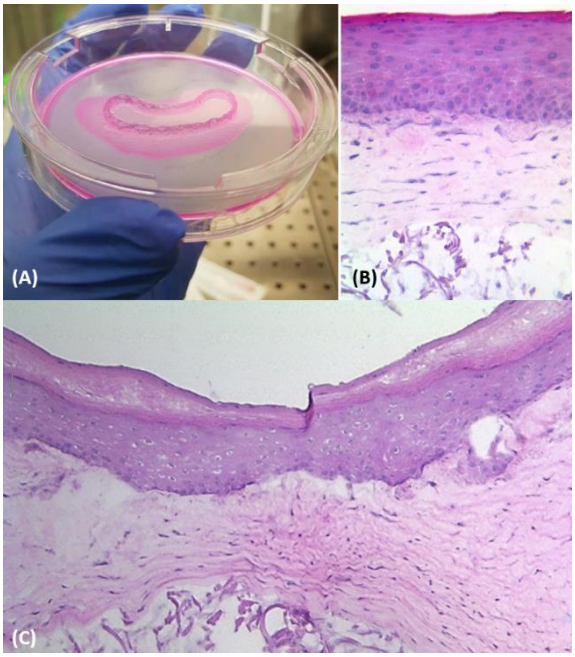

Bioprinted skin model
Bioprinted individual shaped support structure made of agarose (A). HE-staining of bioprinted skin after 3 days of cultivation (B) and of transplant interface after 7 days of cultivation (C).

4:45 p.m. – 6:15 p.m.

Hall 2

IX-OS32 | Fibrous and textile biomaterials

IX-OS32-KL01

Fiber based concept for regenerative medicine

Dilbar Aibibu

Technische Universität Dresden, Institute of Textile Machinery and High Performance Material Technology, Dresden, DE

Fiber based structures for medical applications play an important role in the health sector. They have been used as suture and dressing materials since ancient times. As a result of fiber based structures being used in the intracorporeal area, e.g. as vessel, ligament and tendon implants or hernia meshes. The application of textiles in medicine has been steadily increasing since the 1950s. In addition, they are gaining importance in terms of scaffolds for tissue engineering. Fiber based structures are two- and three-dimensional structures with adjustable anisotropic stiffness and elasticity. Their surface, porosity and mechanical anisotropy can be modified by varying textile processes and fiber materials. Due to their unique structural and mechanical properties, the fiber based structure can mimic the anisotropic non-linear and time-dependent mechanical behavior of biological tissues. However, biomechanical aspects of existing textile implants have not yet been explored sufficiently. Therefore, present developments in fiber-based implants and scaffolds focus on customized products with structural biocompatibility. In this invited lecture, current research and development efforts for fiber based implants will be presented using the examples of stent graft, heart valve as well as ligament and tendon implants.

IX-OS32-02

Preparation and evaluation of selenium nanoparticles on cationized cotton fabrics for the development of antimicrobial healthcare textiles

Qiaoyi Wang[1], Irina Savina[1], Carol Howell[1], Matthew Illsley[2], Patrick Dyer[3], Lara-Marie Barnes[1]

[1]University of Brighton, School of Pharmacy and Biomolecular Sciences, Brighton, GB; [2]Advanced Nanostructured Materials Design and Consultancy ltd. (ANAMAD), Brighton, GB; [3]University of Brighton, School of Art, Brighton, GB

Introduction

It is estimated that over 4,000,000 patients in the EU acquire a healthcare-associated infection every year, resulting in approximately 37,000 deaths annually and significant financial burden on the healthcare systems[1]. Due to their large surface area, hospital textiles can provide an ideal substrate for microorganisms to grow and act as vehicles for the transmission of pathogens[2]. In this study, selenium nanoparticles (SeNPs) were prepared as novel antibacterial agents on cationized cotton fabrics for the development of antibacterial healthcare textiles.

Experimental Methods

Cotton fabrics were treated with a cationization agent, 3-chloro-2-hydroxypropyl trimethyl ammonium chloride (CHPTAC), to graft quaternary groups onto the cotton surface. The cationic quaternary groups attracted the anionic selenite groups to the fibre surface, and subsequently the selenite ions were reduced into elemental selenium nanoparticles *in situ* by ascorbic acid. The grafting of cationic groups and the formation of SeNPs on cotton surfaces were confirmed by SEM and EDX. Additionally, the loading efficiency and the durability of the nanoparticle coating following washing were determined by MP-AES.

The antibacterial activities of the SeNP-coated cationized cotton fabrics (Se-cotton) were evaluated using a method based on the Absorption Method of ISO 20743:2013. The fabrics were inoculated by pipetting 0.2 mL of bacterial suspension (1 – 3×10^5 CFU/mL) over the fabric surfaces, and the number of viable bacteria recovered from the samples at time 0 and after 24 h incubation was determined by colony counting to quantitatively analyse the antibacterial performance.

The cytotoxicity of the Se-cotton towards human bronchial epithelial cells (16HBE14o-) was evaluated using an extraction method as described in ISO 10993-12:2012. Fabric samples were incubated in tissue culture media for 72 h, and 16HBE14o- cells, seeded into 96-well plates, were exposed to the leachates for 24 h. A CellTiter-Glo® Luminescent Cell Viability Assay (Promega) and Pierce™ LDH Cytotoxicity Assay Kit were used to detect post-exposure ATP levels and LDH release, respectively.

Results and Discussion

Selenium nanoparticles were successfully synthesised *in situ* on CHPTAC treated cotton surfaces. The loading efficiency of selenium was 99%, 75%, and 69.9% respectively when the precursor concentration was 0.2 mM, 0.5 mM and 1 mM.

Antibacterial assessments indicated that cationized cotton had moderate antibacterial activities. This is probably due to the electrostatic interaction between the cationic quaternary groups and bacterial cells. Se-cotton prepared with all 3 different precursor concentrations exhibited strong antibacterial activity towards both *Staphylococcus aureus* and *Klebsiella pneumoniae* (Figure 1).

Preliminary results from cytotoxicity tests (Figure 2) show that the cells exposed to the leachates from both the control cotton sample and the functionalised cotton samples were not as metabolically active as the cells exposed to the medium-only control. The reasons for this are not clear at present. However, the cationized cotton and Se-cotton (1 mM) did not result in ATP levels which were significantly different from the control cotton. Moreover, no significant difference was found on the LDH release between the medium-only control and the cotton samples, indicating no toxic effects of the cotton samples towards the 16HBE14o- cells.

Conclusion

Selenium nanoparticles were successfully prepared *in situ* on the surface of cationized cotton textiles. The cationic Se-cotton demonstrated excellent antibacterial performance towards both *S. aureus* and *K. pneumoniae* and did not show cytotoxicity towards 16HBE14o- cells, indicating its potential to serve as an infection control material in hospital settings.

References

[1] Health Protection Agency, 2012. English National Point Prevalence Survey on Healthcare-Associated Infections and Antimicrobial Use, 2011.

[2] Mitchell, A., Spencer, M. and Edmiston Jr, C., 2015. Role of healthcare apparel and other healthcare textiles in the transmission of pathogens: a review of the literature. Journal of Hospital Infection, 90(4), pp.285-292.

Acknowledgement

The authors would like to thank the University of Brighton for funding the PhD studentship.

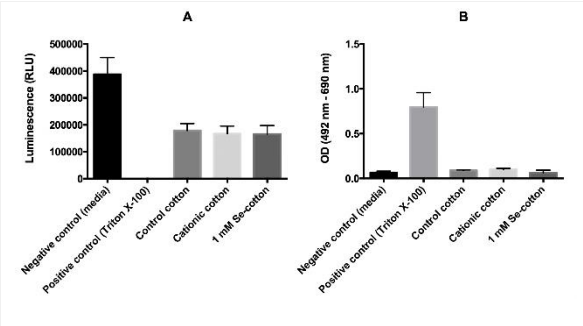

Figure 2 Cytotoxicity evaluation of Se-cotton: (A) ATP assay and (B) LDH assay.

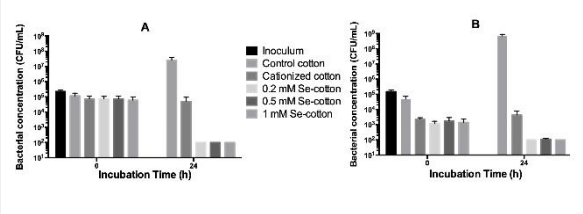

Figure 1 Antibacterial assessment of Se-cotton against (A) S. aureus and (B) K. pneumoniae.

IX-OS32-03

Graded Implants Releasing Two Growth Factors with Spatio-Temporal Control

Henning Menzel[1], Dominik de Cassan[1], Steffen Sydow[1], Julius Sundermann[2], Heike Bunjes[2], Laura Burmeister[3,5], Yvonne Roger[3,5], Andrea Hoffmann[3,5], Birgit Glasmacher[4,5], Robert Hänsch[6]

[1]TU Braunschweig, Institute for Technical Chemistry, Braunschweig, DE; [2]TU Braunschweig, Institute for Pharmaceutical Technology, Braunschweig, DE; [3]Hanover Medical School, Department of Orthopedic Surgery, Hanover, DE; [4]Gottfried Wilhelm Leibniz University Hanover, Institute for Multiphase Processes, Hanover, DE; [5]Lower Saxony Centre for Biomedical Engineering, Implant Research and Development (NIFE), Hanover, DE; [6]TU Braunschweig, Institute for Plant Biology, Braunschweig, DE

Introduction

Functionalization of implants with drug delivery systems that allow a spatio-temporal control of growth factor release is an approach towards in-situ tissue engineering. Such an approach seems to be particularly interesting for implants placed in regions where different tissues merge, for example bone-tendon-transitions.

Experimental Methods

Polycaprolacton (PCL) fiber mats were prepared by electrospinning. Chitosan (CS) was grafted with PCL; the graftpolymer CS-g-PCL was used to modify the PCL fiber mats via a simple dipping process. The attachment of the graftpolymer results from a surface induced crystallization of the PCL grafts on the fiber surfaces and results in the presence of chitosan at the surface.[1] Nanoparticular hydrogels can be formed spontaneously by ionotropic gelatic upon mixing solutions of chitosan and tripolyphosphate or alginate and poly-L-lysine, respectively.[2] Therapeutic proteins like BMP2 or TGF beta can be incorporated with very high efficiency into these nanoparticles. The dispersions of the loaded nanoparticles were used to functionalize the modified fiber mats by Layer-by-Layer deposition (LbL).

Results and Discussion

The fiber mats modified with CS-g-PCL showed improved cell adhesion in vitro and in vivo and have cationic charges, which can be used for functionalization with drug delivery systems.[1] The nano-particular release systems have been characterized thoroughly and their release profiles were studied in detail. The dispersions of the nanoparticular hydrogels were used to functionalize the modified fiber mats by a LbL-process. The LbL-process comes along with a substantial reorganization from nanoparticles into a continuous film.[2] The functionalized fiber mats release the growth factors with controlled rates and the factors are still biologically active. The functionalization can be carried out in a way that different factors are installed in gradients on the fiber mats; thus having the BMP2-releasing hydrogels on the side directed towards the bone, while the TGF beta-releasing region is directed to the cartilage or tendon side.

Conclusion

Modification and functionalization of PCL fiber mats can be carried out in an easy and scalable method using chitosan-g-PCL for surface modification and different nanoparticle suspensions for functionalization with drug delivery systems. In this way PCL fiber mats can be transferred into bioactive implants for in-situ tissue engineering applications.

References

[1] de Cassan et al, Colloids Surf. B Biointerfaces, 163, 309-320 (2018)

[2] Sydow et al. Biomater. Sci. 7, 233 - 246 (2019)

Acknowledgement

The research project has been supported by the DFG in the framework of the Research Unit 2180 ”Graded Implants for Tendon-Bone Junctions”.

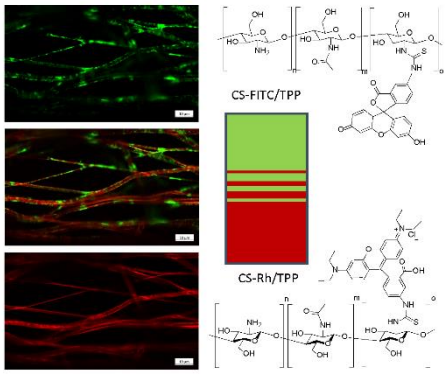

Gradient dfferent fluorescence labels on a fiber mat

CLSM images of a fiber which was coated with CS/TPP nanoparticles labelled with two fluorophors (FITC and Rhodamine). The coating of the modified fiber mats was performed layer-by layer using alginate as an interlayer, rotation of the substrate and adjustment of the dipping depth.

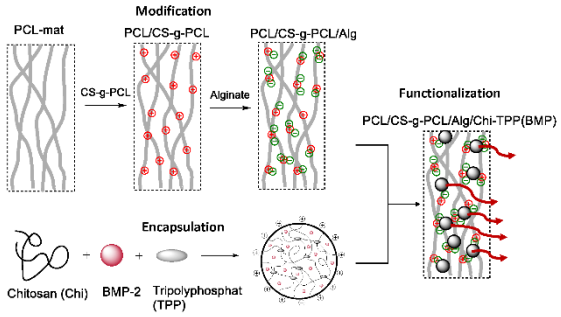

Preparation of graded implants
Flow chart for the preparation of graded implants capable of spatio-temporally controlled release of growth factors

IX-OS32-04

Influence of the covalent grafting of bioactive polymers onto PCL fiber scaffolds: Surface characterization, and *In vitro* biological response

Céline Falentin-Daudre[1], Gana Amokrane[1], Vincent Humblot[2], Emile Jubeli[3], Najet Yagoubi[3], Salah Ramtani[1], Véronique Migonney[1]

[1]University of Paris 13, LBPS-CSPBAT, Villetaneuse, FR; [2]UPMC, LRS, Paris, FR; [3]University of Paris-sud, Matériaux et Santé EA 401, Chatenay-Malabry, FR

Introduction

Electrospinning, an electrostatic fiber fabrication technique has evinced more interest in recent years due to its versatility and potential for applications in diverse fields especially in tissue engineering.[1]Polycaprolactone (PCL) polymer has been approved for biomedical application and offers excellent mechanical properties and slow biodegradation, making it an appropriate material for use as a scaffold for tissue engineering.[2]Previous studies carried out in our laboratory have shown that the covalent direct grafting ("Grafting From" method) of bioactive polymers bearing sulfonate groups such as poly(sodium styrene sulfonate) (polyNaSS)can favor cell adhesion and differentiation onto PCL surfaces.[3-4]In this context, electrospun PCL membranes with different microstructures were prepared by electrospinning. Then, the different scaffolds were functionalized by bioactive polymers bearing sulfonate groups. Finally, In vitro assay experiments were carried out to observe the L929 fibroblast cell behavior onto electrospun PCL membranes.

Experimental Methods

Electrospinning procedure: PCL was electrospun using a home-made electrospinning device. PCL was dissolved in a mixture of chloroform and dimethylformamide (90/10 vol/vol) to prepare a 13-15% wt/vol solution and stirred overnight before use. The polymer solution was then loaded into a 10 ml glass syringe fitted with a 20 G blunt-tipped needle. The solution was continuously ejected using a syringe pump at a rate of 2 ml h^{-1}. The voltage used for electrospinning was 9 KV and the distance between the needle and the collector was 20 cm. The deposition time was 2 h for all experiments.

Grafting from technique with activation: After ozonation**,** PCL scaffolds were placed directly into a mechanically stirred solution of the monomer (sodium styrene sulfonate, NaSS). After heating (70°C) or UV initiation of the radical polymerization, samples were rinsed thoroughly in distilled water and dried.

Grafting from technique without activation: PCL scaffolds were placed directly into a mechanically stirred solution of the monomer (sodium styrene sulfonate, NaSS). After UV initiation of the radical polymerization, samples were rinsed thoroughly in distilled water and dried.

Results and Discussion

The grafting of bioactive polymers bearing sulfonate groups onto electrospun PCL membranes was carried out using two "grafting from" techniques; (i) the thermal grafting for 1 or 3 hours which requires a surface activation by ozonation and (ii) the UV grafting for 1 hour with or without surface activation.[5]Toluidine blue (TB) colorimetric method (**Table 1**), Fourier-transform infrared spectra (ATR-FTIR), contact angle measurement (**Table 1**), scanning electron microscopy with Oxford energy dispersive spectroscopy (SEM-EDS) and x-ray photoelectron spectroscopy (XPS)

were applied to characterize the surfaces. The use of diverse grafting procedures show different degree of grafting onto electrospun PCL membranes (**Table 1**). Then, *In vitro* assay experiments were carried out to observe the L929 fibroblast cell behavior on these functionalized PCL scaffolds. We observed fibroblasts cell response onto grafted and ungrafted PCL membranes by scanning electron microscopy with Oxford energy dispersive spectroscopy (SEM-EDS) and by fluorescence (**Fig 1**). We showed thatfibroblasts cell response depends on electrospun PCL fibers microstructures (**Fig 1**) and the degree of grafting of bioactive polymers (**Fig 1**).

Conclusion

Different microstructures of PCL scaffolds were functionalized by bioactive polymers bearing sulfonate groups with different degree of grafting. The *in vitro* biological assays have shown that depending on the microstructure type of the scaffold and its surface functionalization by different degree of grafting of polymers and its surface hydrophilicity.

References

1. Chenga H., Yanga X., Cheb X., *et al.*, **2018**, *Mater.Sci. Eng. C*,90, 750.
2. Tiwari A. P. *et al.*, **2017**, *Colloids and Surfaces A: Physiochem. Eng. Aspects*,520, 105.
3. Huot S., Rohman G., Migonney V. *et al.*, **2013**, *Bio-Med. Mater. and Eng.*,23, 281.
4. Leroux A., Egles C., Migonney V., **2018**, *Plos One,* 13, 10.
5. Amokrane G., **Falentin-daudré C.**, Migonney V., **2018**, *IRBM*,39, 268.

Acknowledgement

The authors would like to thank the University of Paris 13 for providing financial support to this project

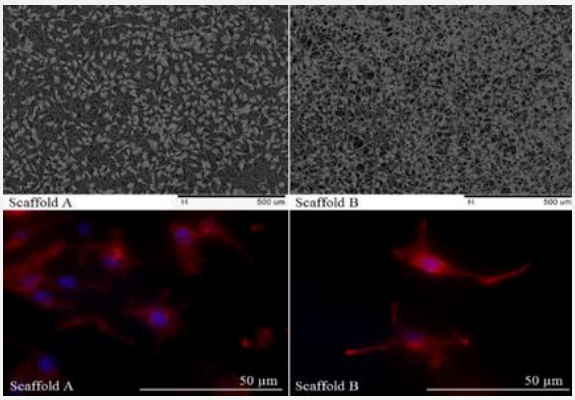

Fig. 1. SEM micrographs and fluorescent imaging at day 7 of fibroblast seeded 2 different scaffolds

	Grafting rate (mol.g^{-1})	Contact angle (°)
Ungrafted PCL scaffold	$(1.56 \pm 0.34) \times 10^{-6}$	123 ± 2.5
Thermal grafted 1 h – Oz 20 min	$(2.14 \pm 0.29) \times 10^{-5}$	68.4 ± 1.9
Thermal grafted 3 h – Oz 20 min	$(9.49 \pm 0.18) \times 10^{-5}$	0
UV grafted 1 h – Oz 20 min	$(1.06 \pm 0.15) \times 10^{-4}$	0
UV direct grafted 1 h	$(4.37 \pm 0.14) \times 10^{-5}$	34.3 ± 3.9

Table 1. Grafting rates and contact angles for ungrafted and various grafted PCL fiber scaffolds.

IX-OS32-05

Development and characterization of a stretching bioreactor for radial strain conditioning of cells cultured on textile scaffolds

Christoph D. Melcher[1], Nikola Glimpel[1], Klaas Kossel[1], Sonja Djudjaj[2], Peter Boor[2], Thomas Gries[1], Andreas Blaeser[1]

[1]Institut für Textiltechnik (ITA), RWTH Aachen University, Department of Medical Textiles and Biofabrication, Aachen, DE; [2]University Hospital, RWTH Aachen University, Institute of Pathology, Aachen, DE

Introduction

For fabrication of tissue engineering (TE) constructs, cells are generally seeded on biocompatible materials, so called scaffolds, to provide a three-dimensional (3D) growth environment. To further mimic the in vivo conditions, bioreactors can be used to provide physiological stimuli by, for example, application of mechanical strain. Substrate or scaffold stretching can be achieved by longitudinal, biaxial and circumferential stretching which further can be divided into out-of-plane or in-plane techniques for substrate distortion. The used stretching devices are usually based on the deformation of elastic polymeric membranes made of polydimethylsiloxane (PDMS) or silicone. Devices for the stretching of textile scaffolds in a bioreactor are not yet described which forms the basic motivation of this work. Textile scaffolds can be customized regarding fibre size, and orientation, pore size, porosity and pore interconnectivity as well as their 3D geometry and surface topography. This versatility renders them a promising technology in TE.

Aim of this work was the development and characterization of a bioreactor for radial expansion of textile scaffolds usable in cell culture applications. The device can be applied to investigate mechanobiological mechanisms in stress related pathologies or to provide a dynamic environment for culturing contractile tissues.

Experimental Methods

A mechanical test device for radial, uniaxial stretching of textile scaffolds was developed applicable for a wide range of textile fabrics. Textile clamps had to be developed suitable to fasten the materials and provide enough holding force to enable a strain of 100 % without loosening the textile. To measure the necessary forces, biaxial tensile tests were performed with a variety of textile materials (e.g. TPU, PES, UC9080EMG and FM070B) and morphologies. Based on the measured forces, different clamp prototypes were designed and tested via uniaxial tensile tests to examine if the clamps were able to fixate textiles up to a defined maximal force (20 N). Furthermore, the device should be sterilisable and compact enough to be usable in a conventional CO_2 incubator. The strain resolution and its frequency should be adjustable with a high strain resolution to control the strain applied to the textile as precisely as possible. Based on these requirements, a bioreactor system was developed, and a prototype was fabricated to validate the working principle of the stretching device. This validation was performed by comparing the measured textile clamp displacements to theoretically computed values. The transfer of strain from the displaced clamps to textile fabrics was tested using different materials.

Results and Discussion

A bioreactor design for stretching of textile fabrics to induce mechanical stress to cultured cells had to be developed. The working principle of the bioreactor was based on the conversion of gear wheel rotations to linear displacements

of eight textile clamps in radial direction, resulting in an application of in-plane uniaxial strain to clamped circular textile fabrics. It was possible to uniformly displace eight textile clamps in radial directions using a stepping motor. The mechanism which is responsible for achieving a certain clamp offset was further characterised by deriving equations based on the dimensions of the stretching device. These equations were successfully used for calculations of the clamp displacements depending on the rotation of the gear wheels and the drive shaft of the stepping motor. The results of the described experiments show the validity of the equations which are offering the basis for a controlled application of required strains to textile specimen. Finally, the functionality of the device was evaluated experimentally. Dense PES knits, meltblown membranes and warp-knitted TPU meshes were successfully tested. The results of the experiments indicate that it was possible to accurately displace the textile clamps. Strain from 10.4 – 74.4 % could be induced with a precision of 3.8 % by rotating the gear wheel by 5 – 40°. The displacements of the clamps were further transferred to fixed textiles, resulting in uniform elongations of the fabrics.

Conclusion

Common stretching devices used in cell culture experiments are based on the elongation of polymeric substrates. Devices for strain application on textile structures used in cell culture applications are not yet described. The developed bioreactor can be used to investigate textile scaffolds regarding mechanical stress applications, providing more in-vivo like conditions to cultured cells and offering an interesting tool for further experiments regarding growth- and proliferation behaviour of cells. The device could further be used as a bioreactor for TE constructs which can be exposed to mechanical stress to induce force-dependent differentiation pathways.

4:45 p.m. – 6:15 p.m.

Hall 4

IX-OS33 | Ceramic Biomaterials/Bone 2

IX-OS33-01

Principles of the Pore Forming Mechanisms of the Freeze Foaming Process for Manufacturing Bone-Mimicking Scaffolds

Matthias Ahlhelm[1], David Werner[1], Eric Schwarzer[1], Johanna Maier[2], Thomas Behnisch[2], Tassilo Moritz[1], Alexander Michaelis[1], Maik Gude[2]

[1]Fraunhofer Society, Institute for Ceramic Technologies and Systems KTS, Dresden, DE; [2]Technische Universität Dresden, Institute of Lightweight Engineering and Polymer Technology, Dresden, DE

Introduction

Freeze Foaming of bioceramics has been shown to be a promising method for manufacturing customizable potential bone replacement material. By applying a novel hybrid shaping route, porous bone mimicking features were combined with complex-shaped 3d-printed denser shell structures to form a single composite component. Bioceramics such as hydroxyapatite (HAp), zirconia (ZrO_2) and mixtures of thereof were processed, shaped and successfully evaluated in vitro with regard to FDA life staining of mouse fibroblasts and osteogenic differentiation on the detection of alkaline phosphatase and collagene-1 [1, 2]. Recent activities deal with the hybrid shaping of a rat's near-net-shaped synthetic bone demonstrator currently being tested in a rat model. Furthermore, main research activities are dedicated to achieving a homogeneous and predictable pore morphology [3] and, to evaluating measures for enhancing the mechanical stability of said biocompatible foams by structural reinforcements.

Experimental Methods

Initial material for the various research activities is HAp (Co. Sigma-Aldrich, BET=70.01 m²/g, d_{50}=2.64 µm). Relating to the hybrid shaping process, at first, complex shell structures were 3D-printed via ceramic (CerAM) VPP method (Vat Photo Polymerization/ i.e. Lithography-based Ceramic Manufacturing, LCM, CeraFab 7500, Co. Lithoz). On route to bone-mimicking scaffolds these shell structures act as artificial *substantia corticalis* (with regard to mechanical stability). After filling them with HAp suspension and subsequently foaming them (freeze dryer Lyo Alpha 2–4, LSCplus, Co. Martin Christ GmbH) a porous Freeze Foam is being created, which resembles the artificial *substantia spongiosa*.

In a similar approach, structural reinforcements (resembling bone's trajectory-like load-bearing capacity) were manufactured by CerAM VPP technique and foam-filled/foamed-in via Freeze Foaming. The projected result, after a crucial co-sintering step, is a single shrinkage-adjusted structural composite (*i.e.* hybrid shaping). Shrinkage adjustment was achieved by carefully tuning solid and binder content of 3D-printable and foamable suspensions, analyzed by means of thermogravimetric measurements and dilatometry.

With regard to achieving a predictable and homogeneous pore morphology, effects of HAp suspension and process parameter (e.g. temperature, air content, pressure reduction rate of the used freeze dryer) on resulting Freeze Foams were analyzed by in situ computed tomography and radiography (Phoenix v|tome|x L 450, Co. GE Sensing & Inspection Technologies). This combination of none-destructive radiographic technologies allows to derive principles of the very foaming process (pore/strut formation) and to evaluate structural characteristics of manufactured foams (porosity, pore/strut size distribution).

Results and Discussion

In combining mentioned none-destructive testing methods, we succeeded in manufacturing first-time reproducible foam scaffolds, which additionally, become adjustable with regard to their porosity and pore size distribution by adjusting suspension and process parameters accordingly.

Tuning the shrinkage of two structurally different sections (porous = Freeze Foam, dense = CerAM VPP) in a combined hybrid shaping process, furthermore, allowed to successfully achieve strength-enhanced porous composites and customized rat bone-mimicking bioceramic scaffolds (Fig. 1).

Conclusion

With this first success concerning reproducible and adjustable pore morphologies as well as the proof-of-principle regarding the shrinkage-adjusted hybrid shaping process a use of those technologies for achieving potential bone replacement material comes even closer.

References

1. Ahlhelm, M., Schwarzer, E., Scheithauer, U., Moritz, T., Michaelis, A. 2016. Innovative and novel manufacturing methods of ceramics and metal-ceramic composites for biomedical applications. *J Euro Cer Soc*, 36/12, 2883-2888.
2. Ahlhelm, M., Schwarzer, E., Scheithauer, U., Moritz, T., Michaelis, A. 2017. Novel Ceramic Composites for Personalized 3D Structures. *J Ceram Sci Technol*,8/1, 91-100.
3. Ahlhelm M., Werner, D., Maier, J., Abel, J., Behnisch, T., Moritz, T., Michaelis, A., Gude, M. 2018. Deriving Principles of the Freeze-Foaming Process by Nondestructive CT Macrostructure Analyses on Hydroxyapatite Foams. *J Euro Cer Soc*, 38, 3369-3378.

Acknowledgement

The authors very much appreciate the funding of this contribution's work by DFG (Grant number 310892168) and Fraunhofer Society.

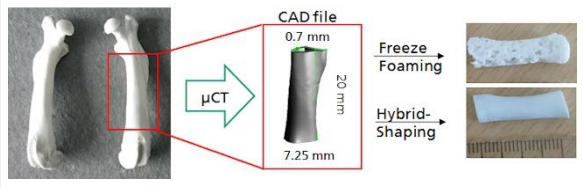

Fig. 1: Freeze Foaming & hybrid shaping to bone mimicking bioceramic scaffolds

IX-OS33-02

The lubrication molecular mechanisms of TiCuN films in protein solution

Qiaoyuan Deng, **Yongxiang Leng**

Southwest Jiaotong University, School of Materials Science and Engineering, Chengdu, CN

Introduction

The ceramic joint has the clinical complications of prosthesis fragmentation and squeaking. The causes of postoperative complications are insufficient lubrication and thin lubrication layer of ceramic joint friction interface. Considering the mechanical properties of ceramic materials for artificial joint and the service environment of joints (albumin, globulin, etc. around the joints), improving lubricity and thickness of friction interface lubrication layer are proposed to reduce the complications of ceramic joint.

Experimental Methods

The purpose of this work is to fabricate Cu-doped TiN (TiCuN) ceramic film which has lubrication function in vivo. In this paper a ball (alumina, Φ=6mm) on disc (TiCuN, Φ=10×1.5mm) model was used to conduct the wear experiments in the bovine serum albumin (BSA) solution. The Raman spectroscopy, attenuated total reflection fourier transform infrared spectroscopy(ATR-FTIR) were applied to characterize the denaturation of BSA molecules on the surface of wear track and wear spot. The fluorescein isothiocyanate (FITC) was used to detect the adsorption of BSA molecules on the surface of TiCuN films. The electron energy loss spectrum (EELS) and time-of-flight secondary ion mass spectrometry(TOF-SIMS) were applied to confirm the presentation of carbonaceous film on the friction interface of alumina and copper in BSA solution.

Results and Discussion

The results show that, Cu ion released from the TiCuN films could promote the adsorption of protein and form carbonaceous films on the tribo-pairs surface. And the carbonaceous films could lubricate the tribo-pairs and repaire the TiCuN films.

Conclusion

When TiCuN wear in physiological environment, the Cu ions can release from the wear track and promote the protein to adsorpt on the wear track, to form the “protein film”. And then this “protein film” can transform into the carbonaceous film to lubricate and repair the wear track under the shear force of the tribo-pair and the catalysis of the Cu ions.

References

[1] E. Zhang, L. Zheng, J. Liu, B. Bai, C. Liu, Influence of Cu content on the cell biocompatibility of Ti–Cu sintered alloys, Mater. Sci. Eng. C 46 (2015) 148–157. [2] V. Sansone, D. Pagani, M. Melato, The effects on bone cells of metal ions released from orthopaedic implants. A review, Clin. Cases Miner. Bone Metab. 10 (2013) 34–40.

Acknowledgement

This study was supported by Natural Science Foundation of China (31570958).

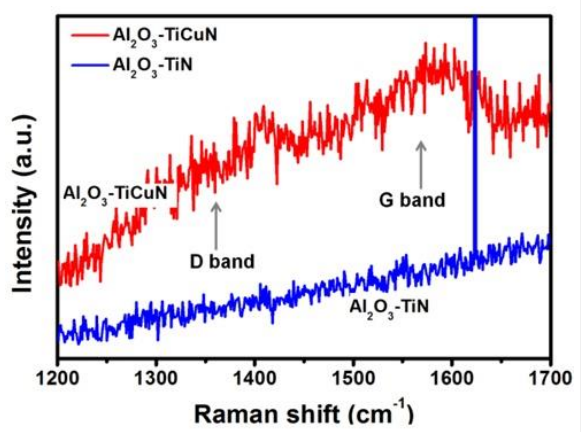

Fig.1 The Raman spectrum of friction interfaces for TiN-Al2O3 and TiCuN-Al2O3
It shows that there are carbonaceous films on the TiCuN-Al_2O_3 tribo-pairs surface comparing with TiN-Al_2O_3.

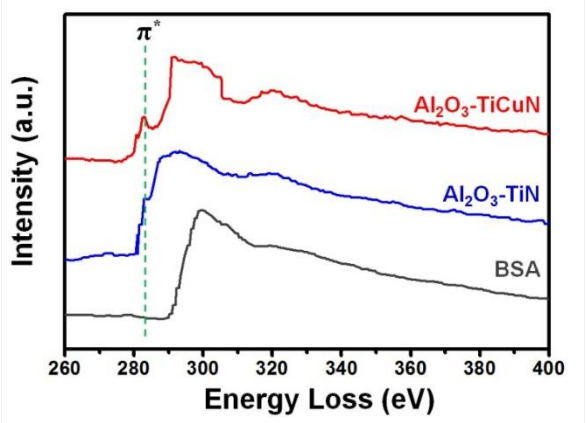

Fig2 The EELS of friction interfaces for TiN-Al2O3 and TiCuN-Al2O3
It shows that there are π electron energy peak for TiCuN-Al_2O_3 tribo-pairs surface, this means there are graphite-like carbon lubricating layer on TiCuN-Al_2O_3 friction interface.

IX-OS33-03

(Fe/Sr) co-doped biphasic calcium phosphate with tailored osteoblast cell functionality

Subhadip Basu[1], Aritri Ghosh[2], Ananya Barui[2], Bikramjit Basu[1]

[1]Indian Institute of Science, Materials Research Centre, Bangalore, IN; [2]Indian Institute of Engineering Science and Technology, Centre for Healthcare Science and Technology, Howrah, IN

Introduction

Although doped bioceramics have been widely investigated for biomedical applications, the co-doped bioceramics remain mostly unexplored for bone regeneration applications. In particular, the impact of co-doping of Sr^{2+} and Fe^{3+} ions on the phase stability and cytocompatibility is not explored so far. In this perspective, the present study aims to quantitatively understand this aspect in case of Fe/Sr co-doped biphasic calcium phosphate (BCP).

Experimental Methods

Following sol−gel synthesis, co-doped BCP samples with different Sr/Fe dopant concentrations (2, 10, 20, 30, and 40 mol %) together with doped BCPs with single dopant (Sr or Fe) with similar compositions were calcined at 800 °C in air. The dopant content dependent crystallographic properties and phase stability of HA and TCP are quantitatively assessed by means of XRD based Rietveld refinement. Ion dissolution behaviour of the co-doped BCPs was determined using ICPMS. *In vitro* cytocompatibility of co-doped samples has been assessed using mouse osteoblast cells.

Results and Discussion

A systematic change in phase composition and lattice parameters was observed in both the Sr/Fe single doped and co-doped BCPs. Apart from that, an important observation is that, while singular dopant of Sr/Fe at 20 mol % or higher amount reduces cell viability significantly, osteoblast viability is not compromised to any significant extent on Sr/Fe co-doped BCP, compared to undoped BCP. Our results indicate that one can tailor osteoblast functionality by controlling the co-dopant content. Cell morphological analysis supports extensive cell spreading on co-doped BCPs. An attempt has been made to correlate the variation in cellular response with HA/TCP ratio and ion dissolution behavior.

Conclusion

The competition among HA/TCP ratio and Fe^{3+} /Sr^{2+} /Ca^{2+} ion dissolution has significant influence on osteoblast cell functionality on codoped BCPs. Although codoped BCP with 5 mol % Sr and 5 mol % Fe-dopant exhibits highest cell viability, a decrease is recorded at higher codopant content, but not to any significant extent w.r.t. undoped BCP. In summary, the present work establishes unique advantage of Sr/Fe co-doping approach toward realizing their bone replacement application.

References

S. Basu et al. ACS Biomater. Sci. Eng., 2018, 4 (3), pp 857–871

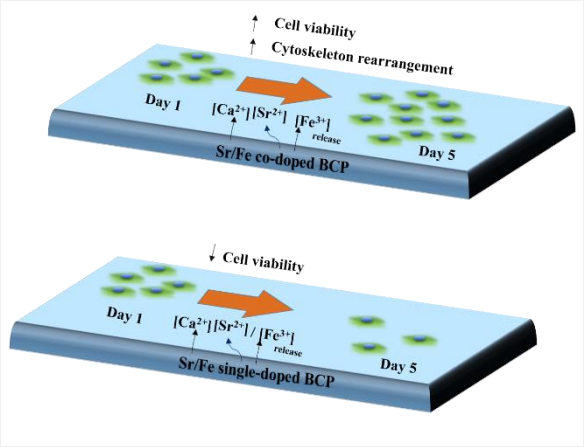

Effect of multiple ion doping on cell viability
Two scenarios depicting the role of Sr/Fe single or codoping to BCP as far as osteoblast cell viability and proliferation are concerned. Co-doped samples favor osteoblast proliferation better than their single-doped counterparts because of the combinational effect of different ion release.

IX-OS33-04

Biomaterial-induced endochondral bone healing via multi-scale optimization of architectural and mechanical cues

Ansgar Petersen[1], Hans Leemhuis[2], Christoph Gayer[3], Martina Tortorici[1], Dag Wulsten[1], Sophie Schreivogel[1], Aaron Herrera[1], Ingo Heschel[2], Georg Duda[1]

[1]Charité - Universitätsmedizin Berlin, Berlin-Brandenburger Centrum für Regenerative Therapien, Berlin, DE; [2]Matricel GmbH, Herzogenrath, DE; [3]Fraunhofer Institute for Laser Technology ILT, Aachen, DE

Introduction

For a long time biomaterials for bone regeneration have aimed to support direct, intramembranous ossification e.g. by the incorporation of calcium phosphates (CaPs). Due to the limited success of such materials, bone formation via a cartilage phase, so-called endochondral ossification (EO), has lately been discussed as a promising alternative strategy to regenerate bone tissue. However, current approaches to induce EO include pre-differentiated progenitor cells, growth factors or combinations thereof and due to their complexity have not yet been translated to the clinics. A pure biomaterial approach to induce EO is lacking so far. We have recently shown how an unfavorable self-patterning of collagen fibrils impedes the healing of critical-size bone defects and have used a specifically architectured biomaterial to modulate this patterning to revive development-like EO [1]. However, even though the high porosity and low mechanical stiffness of the biomaterial are ideal to induce EO, they increase the risk of an in vivo pore-collapse due to external mechanical loading conditions and internal cell contraction forces. We have thus refined the concept by implementing a 3D-printed biodegradable support structure to create a mechano-hybrid-scaffold with optimized architecture and stiffness at the cell and the tissue level [2].

Experimental Methods

Mechano-hybrid-scaffolds (MHS) were produced by combining the collagen-based guiding structure featuring highly aligned channel-like pores with a 3D printed support structure. Using computer aided design (CAD), the architecture of the support structure was optimized in an iterative process (experimental evaluation and re-design) to provide a stiffness resulting in low deformation in vivo (strain $\varepsilon<3\%$ in a 5mm osteotomy defect in rats) and to provide a high material porosity φ ($\varphi>70\%$). For this, support structures were produced by laser-sintering of PCL powder (particle diameter 50-80µm) and characterized by mechanical compression testing. Sintering parameters were optimized to produce struts with small diameters ($D\approx500\mu m$) at high mechanical stiffness and strength. Optimized support structures were immersed in collagen dispersion and highly aligned micro-pores ($d\approx100\mu m$) were produced by directional solidification, freeze-drying and collagen crosslinking. Pure collagen scaffolds (without support structure) and MHSs (Figure 1a, top and bottom) were produced in the same freezing process. The printed support structure and the collagen pore architecture of both prototypes were characterized using scanning electron microscopy (SEM) (Figure 1a, middle). Continuous cyclic compression simulating in vivo loads using mechano-bioreactors [3] was used to study their long-term deformation behavior. Cell organization (fibroblasts and mesenchymal stromal cells) and extracellular matrix formation inside MHSs was visualized by immunohistology and MP/confocal microscopy.

Results and Discussion

Compared to pure collagen scaffolds MHSs showed an increase in stiffness by three orders of magnitude (from kPa to MPa-range). The dimensions (3.8mm diameter and 5.2mm height) matched the size of the 5mm osteotomy defect in rats and resulted in a slight press-fit. Pore morphology (pore-alignment and pore diameter), representing the most relevant parameter to induce EO in vivo, was comparable between the pure collagen scaffold and MHS. Furthermore, material deformation under cyclic monoaxial compression was reversible (in vivo-like loading pattern). No difference in the initial interaction of cells with the collagen structure of the two materials was observed. However, as a consequence of increased intrinsic tension resulting from cell traction forces and tensioned ECM fibrils (fibronectin, collagen), contraction of collagen scaffolds was observed (Figure 1 b and c). Volume loss was further enhanced when cyclic compression was applied in mechano-bioreactors while MHSs maintained their outer dimensions. Shape-stability is regarded to be of high importance for the in vivo-performance of the biomaterial as our previous studies have shown that a good contact between the collagen scaffold pores and the bone cortices is essential for cell recruitment from the bone marrow cavity [1]. In vivo biocompatibility studies and evaluation of MHS performance for bone defect regeneration are currently under investigation.

Conclusion

The here-introduced mechano-hybrid-scaffold represents a purely material-based approach to support the healing of large bone defects. Material composition, architecture and mechanical deformations were chosen to guide endogenously recruited cells towards endochondral ossification. The in vivo-evaluation will reveal the potential of the mechano-hybrid-scaffold to induce endochondral bone healing. By concept, this biomaterial is available “off the shelf” and avoids high costs and regulatory limitations associated with cell- and growth factor-based approaches.

References

[1] Petersen A, Princ A, Korus G, Ellinghaus A, Leemhuis H, Herrera A, Klaumünzer A, Schreivogel S, Woloszyk A, Schmidt-Bleek K, Geissler S, Heschel I, Duda GN. A biomaterial with a channel-like pore architecture induces endochondral healing of bone defects. Nat Commun. 2018;9(1):4430. DOI: 10.1038/s41467-018-06504-7.

[2] Patent application: PCT/DE2017/000183

[3] Petersen A, Joly P, Bergmann C, Korus G, Duda GN. The impact of substrate stiffness and mechanical loading on fibroblast-induced scaffold remodeling. Tissue Eng Part A. 2012;18(17-18):1804-17. DOI:10.1089/ten.TEA.2011.0514.

Acknowledgement

Authors acknowledge financial support by the German Federal Ministry of Education and Research (BMBF).

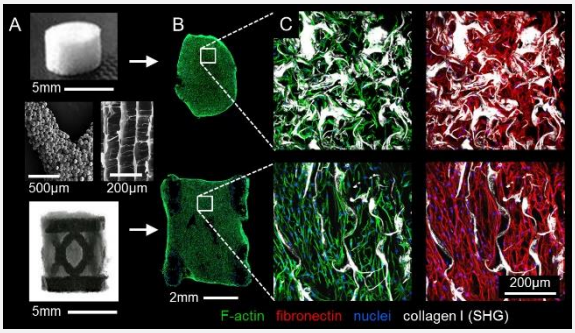

Comparative evaluation of collagen scaffold and mechano-hybrid-scaffold
Photographs of collagen scaffold (top) and MHS (bottom) (A), SEM pictures of a sintered strut of the support structure (middle, left) and the collagen pore architecture (middle, right); Volume loss (B) and impairment of scaffold wall and extracellular matrix alignment (C) due to material deformation by cell forces (two weeks in vitro culture with human dermal fibroblasts, seeding density 7500cells/µl).

IX-OS33-05

Insights into the structure of bio-glasses and -glass-ceramics using lab-based high-resolution 3D X-ray microscopy

Araceli de Pablos Martín[1], Qaisar Nawaz[2], Altair T. Contreras Jaimes[3], Juliana Martins de Souza e Silva[1,4], Christian Patzig[1], Delia S. Brauer[3], Aldo R. Boccaccini[2]

[1]Fraunhofer Institute for Microstructure of Materials and Systems IMWS, Microstructure-Based Materials Processing, Halle, DE; [2]University of Erlangen-Nuremberg, Materials Science and Engineering, Erlangen, DE; [3]Friedrich Schiller University, Otto Schott Institute of Materials Research, Jena, DE; [4]Martin Luther University Halle-Wittenberg, Institute of Physics, Halle, DE

Introduction

"New truths become evident when new tools become available" (R.S Yalow, Nobel Prize in Physiology and Medicine, 1977). A deeper knowledge of the microstructure of materials allow not only to better understand their properties, but also to improve them and to establish the foundation for designing new functional materials. Recently, X-ray microscopy (XRM) has moved from synchrotron sources into labs, facilitating the accelerated and knowledge-based development of glasses and glass ceramics. In comparison with electron microscopy, XRM offers two important advantages: (1) it produces the non-destructive screening of the interior of relatively large objects (between a few 10 and up to a few 100 µm edge lengths) at a spatial resolution of some tens of nanometers, and (2) favorable surface-to-volumen ratio, allowing for studying one single sample at different stages of microstructure development. XRM, therefore, represents a complementary technique to electron microscopy. The novelty of this work lies in the use of three-dimensional imaging using XRM for the structural characterisation of bioactive glasses and glass-ceramics.

Experimental Methods

45S5-based glasses were obtained by melting and by sol-gel processes. Glass-ceramics were then produced upon heat treatment of the glasses at adequate temperatures and times.Transmission electron microscopy was performed. Images were recorded with an FEI Tecnai G2 F20 microscope and a FEI Titan 380–300 electron microscope. EDXS analysis was performed by means of a Super X-EDXS detector, that consists of four silicon drift detectors, thus offering a maximum collection angle of 0.9 sr. Elemental mappings were obtained, in order to gain information about the elemental distribution with high spatial resolution.

Complementing the TEM characterization, a *Carl Zeiss Xradia 810 Ultra* XRM microscope, available at Fraunhofer IMWS in Halle since 2017, was employed. Imaging experiments were performed in absorption-contrast mode using a Chromium source (5.4 keV). Contrast is generated due to different X-ray absorption lengths of the different materials that compose the sample. This kind of contrast is suited for specimens containing materials of varying density. The specimen is rotated and several images are collected over a range of projection angles. The projections are then reconstructed into a 3D image using filtered back projection algorithm. The sample must present an appropriate thickness, which allows the X-ray radiation to be transmitted through the sample. The ideal thickness of the samples depends on the density of the material and its constituents and the ideal sample geometry is a conical-shape sample to prevent problems in the reconstruction of the 3D image. Through the laser preparation tool microPREP™, this kind of geometry can be obtained in glasses and glass-ceramics easily. MicroPREP™ is an ultrashort-pulsed laser micro-machining tool initially developed for the preparation of TEM samples. By mid-2017, a

dedicated XRM stage for the preparation of XRM samples is available. Superficial damage is restricted to within 2 µm because of the picosecond nature of the laser pulses, which provoke minimal thermal load.

Results and Discussion

Starting with the well-known 45S5 glass composition, first results of 3D data acquired at bio-glasses and glass-ceramics will be presented. Changes in the microstructure upon crystallisation can be observed. By measuring samples of different crystallization states, it is possible to follow the crystallisation process. The 3D porous structures are ideal for characterisation by XRM, due to the difference of X-ray absorption between material (glass, crystal) and air (pores). A good contrast of the XRM micrographs is achieved via different composition of the glass-ceramic constituents, i.e. crystalline and glassy parts. The 3D images obtained with XRM reveals the porosity, the crystalline volume fraction and crystals' size distributions. By cutting the sample in different virtual angles of the 3D XRM images, it is possible to get deeper insights into the micro- and nanostructure and their evolution upon heat treatment that can be correlated to the (S)TEM results. EDXS enables the elemental analysis in certain positions of the material, so that the distribution of key elements (network modifiers) can be mapped.

Conclusion

Bio-glass-ceramics represent ideal materials to be studied by XRM, owing to the presence of different phases, that have high-contrast among each other: the glassy matrix, the pores (air-filled) and the crystalline precipitates. XRM provides volumetric images that enables the visualization of features in the range of tens of nm inside the sample without the need of physically cutting it in smaller sizes. The 3D XRM images are a powerful complement the 2D results obtained through other imaging techniques, like TEM, and contribute to reach a more complete visualization of the bulk microstructure of these materials and the crystallisation processes taking place.

Acknowledgement

The authors acknowledge the financial support of the German Research Foundation (DFG) through the project "Visualising the evolution of crystallisation and mineralisation of bioactive glasses" (PA 3095/1-1) and the DFG WE 4051/21-1 and 22-1

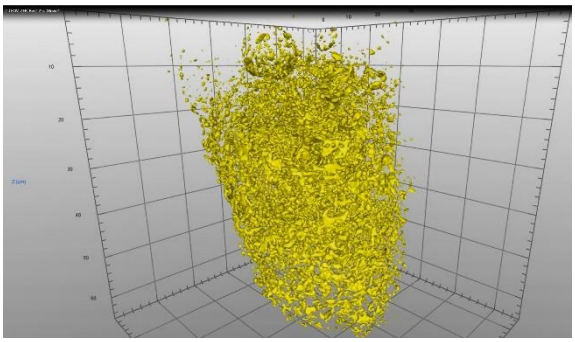

3D XRM image of the 45S5 glass

IX-OS33-RF06

Glycosaminoglycan sulfation enhances the regenerative potential of bone cells and hematopoetic stem cell maintenance

Juliane Salbach-Hirsch[1,5], Martina Rauner[1,5], Mario Lüttwitz[1,5], Sandra Rother[2], Vera Hintze[2], Stephanie Möller[3], Matthias Schnabelrauch[3], Manja Wobus[4], Lorenz Hofbauer[1,5]

[1]Technische Universität Dresden, Division of Endocrinology, Diabetes and Bone Diseases, Department of Medicine III1Division of Endocrinology, Diabetes and Bone Diseases, Department of Medicine III, Dresden, DE; [2]Technische Universität Dresden, Institute of Materials Science, Max Bergmann Center of Biomaterials, Dresden, DE; [3]INNOVENT e. V, Biomaterials Department, Jena, DE; [4]Technische Universität Dresden, Stem cell lab2, Department of Medicine I, Dresden, DE; [5]Technische Universität Dresden, Center for Healthy Aging, Medical Faculty, Dresden, DE

Introduction

Osteoporotic fractures are a major socioeconomic and clinical challenge as bone regeneration and osseointegration of implants are commonly impaired. With increasing age and comorbidities further affecting bone homeostasis, osteoporotic fractures are estimated to quadruple by 2050, highlighting the need for new, more biologically active biomaterials.

Experimental Methods

To this end, we investigated the functional role of glycosaminoglycans (GAGs), a key component of the bone extracellular matrix (ECM), for their osteogenic potential. Using native and synthetically derived GAGs (sGAGs) such as hyaluronan, chondroitin sulfate, and heparin (Hep) we evaluated how GAG sulfation affects the differentiation and activity of osteoblasts, osteoclasts and osteocytes and their capability to maintain hematopoietic stem and progenitor cells (HSPCs).

Results and Discussion

Our study revealed that GAG sulfation had profound effects on all stages of osteoclast and osteoblast differentiation. Whereas the viability of osteoclasts was increased, osteoclast numbers and the formation of the characteristic sealing zone structure were significantly decreased. This was accompanied by a loss of resorptive activity. On the other hand, the proliferation and metabolic activity of osteoblasts and osteocyte-like cells treated with equal concentrations of GAGs were decreased indicating a shift from the proliferative to matrix formation phase of osteogenic differentiation. Indeed, these cells showed altered matrix deposition and increased expression of genes associated with differentiation, such as the RANKL/OPG ratio, alkaline phosphatase, osteocalcin, and Runx2. Using surface plasmon resonance and molecular modeling we further demonstrated that sGAGs can directly bind to sclerostin, interfering with its bioactivity, resulting in increased Wnt-signaling *in vitro*. As the ECM of the bone marrow cavity also serves as a highly specialized microenvironment for HSPCs their response to sGAG was also evaluated. The application of sGAG to differentiating osteoblasts altered the composition of newly synthesized ECM: Whereas low or non-sulfated GAGs had no effect, high sulfated GAGs increased the calcium/phosphate ratio as well as the protein and GAG content of osteoblast derived matrices. When used as a substrate for HSPCs these altered ECM preparations showed an increased potential to maintain the stem cell character of CD34+cells. This effect may be

attributed to the higher sGAG content in these matrices, as sGAGs alone also ledt to significantly less differentiated colonies in a colony forming unit assay.

Conclusion

Here we demonstrated that GAG sulfation both directly and indirectly increases osteogenesis and reduces osteoclastogenesis thus, significantly altering the bone cell cross talk. This data suggests that finetuning GAG composition and linking GAG function to surfaces could represent a suitable tool to enhance local bone regeneration. Whether this translates into a favorable profile on bone remodeling at fracture sites requires rigoros *in vivo* assessment.

IX-OS33-RF07

Bioactive chitosan-based scaffold as smart materials for bone fracture treatment

Alessandra Soriente[1], Soledad Perez Amodio[2], Ines Fasolino[1], Maria G. Raucci[1], Christian Demitri[3], Elisabeth Engel López[2], Luigi Ambrosio[1]

[1]Institute of Polymers, Composites and Biomaterials, National Research Council (IPCB-CNR), Naples, IT; [2]Institute for Bioengineering of Catalonia, Barcelona, ES; [3]Department of Engineering for Innovation, University of Salento, Lecce, IT

Introduction

In last decades great attention was given to realisation of successful substitutes for bone tissue injury characterised by the lack of bone mass, an inflammatory reaction and blood vessels necrosis [1]. The promising field of regenerative medicine is working to repair damaged bone structure and functions controlling immune response and promoting vascolarised tissue restoration in the site of implant. Here, we discuss how bioactive chitosan 3D-based scaffolds can play a pivotal role in the inflammation and angiogenesis related to osteogenesis processes by using *invitro* models aimed to mimic bone fracture microenviroment.

Experimental Methods

Chitosan scaffolds by using two different approaches based on inorganic (i.e. hydroxyapatite nanoparticles) and organic compounds (i.e. BMP-2 mimicking peptide), were bioactivated respectively [2]. In order to evaluate antinflammatory and angiogenic properties related to osteogenic potential of the scaffolds, the expression of inflammatory mediators and pro-angiogenic markers was estimated. In detail, the modulation of cytokines (TGF-β and IL-6) which play a crucial role in osteogenesis was measured on a co-culture model consisting of osteoblasts and macrophages stimulated by lipopolysaccharide (LPS) for better mimicking damaged bone. Moreover, oxidative stress metabolites, interleukins and COX-2 expression related to osteogenic markers production were analyzed in order to understand the correlation between bone focal inflammation and bone regeneration. Additionally, in order to investigate the effect of scaffold on angiogenesis, CD31 (specific marker of angiogenesis) expression, cell adhesion, growth, proliferation, migration and tube formation by using endothelial cells (HUVEC) were detected. In the end, morphological cell analysis by SEM and confocal microscopy to study cell-material interaction effect from a qualitative point of view was performed.

Results and Discussion

The results on antinflammatory potential suggest that chitosan-based scaffolds bioactivated by using inorganic signals (hydroxyapatite nanoparticles) inhibit pro-inflammatory mediators production (IL-1β and IL-6), induce antinflammatory cytokine generation (IL-10) and reduce nitric monoxide metabolites (nitrites) on co-cultures stimulated by LPS. Conversely, scaffold bioactivated by using organic signals (BMP-2 mimicking peptide) were able to decrease pro-inflammatory markers without any effect on antinflammatory cytokines levels and on nitrites. However, these scaffolds are able to maintain high levels of TGF-β that, combined with BMP-2, promotes osteogenesis. The results on angiogenic properties of scaffold demonstrated that neat and bioactivated scaffolds are able to promote angiogenesis by increasing endothelial cell proliferation, migration and tube formation. In detail, scaffolds decorated with BMP-mimicking peptide seem to show better values in terms of tube formation, even without

matrigel component. These latter scaffold determined also higher proliferation values than those induced by CS biomineralised scaffolds. Finally, morphological investigations showed that all chitosan-based materials induced a good cell spreading.

Conclusion

Bioactive signals on the chitosan scaffolds surface allow a desirable effect on inflammation inhibition and angiogenic promotion. Indeed, the work encourages the research to use CS porous scaffolds as potential implant in the field of tissue engineering due to its good properties. Our results support the concept that CS biomaterials may be a source of substrates for developing multi-target devices able to regenerate damaged bone inflammation and stimulating neovascularisation of tissue-engineered constructs.

References

1. MA Fernandez-Yague, SA Abbah, LM Namara, D I Zeugolis, A Pandit, M J Biggs, Advanced drug delivery Reviews, 1-29, 2015. doi: 10.1016/j.addr.2014.09.005.
2. A Soriente, I Fasolino, MG Raucci, C Demitri, M Madaghiele, A Giuri, A Sannino, L Ambrosio, Journal of Materials Science Materials in Medicine. 29:62, 2018. doi: 10.1007/s10856-018-6072-2.

Acknowledgement

The study was supported by PNR Aging program 2012-2018 and NANO-DISP, INAIL BRIC 2016 id54. The authors also thank Mrs Stefania Zeppetelli for supporting biological investigation.

IX-OS33-RF08

3D-Bioprinting of bone grafts for alveolar defects – a preclinical pilot study

Paula Korn[1,2], Tilman Ahlfeld[2], Winnie Pradel[3], Anja Lode[2], Adrian Franke[3], Martina Rauner[4], Ursula Range[5], Bernd Stadlinger[6], Günter Lauer[3], Michael Gelinsky[2]

[1]Charité – Universitätsmedizin Berlin, corporate member of FU Berlin, Humboldt-Universität zu Berlin & Berlin Institute of Health, Department of Oral and Maxillofacial Surgery, Berlin, DE; [2]Centre for Translational Bone, Joint and Soft Tissue Research, Faculty of Medicine "Carl Gustav Carus", TU Dresden, Dresden, DE; [3]Department of Oral and Maxillofacial Surgery, Faculty of Medicine, Dresden, DE; [4]Division of Endocrinology, Diabetes, and Bone Diseases, Department of Medicine III and Center for Healthy Aging, TU Dresden, Dresden, DE; [5]Institute for Medical Informatics and Biometry, Faculty of Medicine „Carl Gustav Carus", TU Dresden, Dresden, DE; [6]Clinic of Cranio-Maxillofacial and Oral Surgery, University of Zurich, University Hospital, Zürich, CH

Introduction

One of the most common hereditary craniofacial anomalies in humans are cleft lips, cleft alveolar bone with or without cleft palate. Clinically, the augmentation of the persisting alveolar bone defect, called alveolar cleft osteoplasty, is performed by using autologous bone grafts. The accompanying disadvantages are leading to an intensive search for alternatives [1]. Objective of the present study was the in vivo application of 3D printed and simultaneously tissue engineered bone grafts and their evaluation regarding the potential to promote osseous defect healing [2].

Experimental Methods

Scaffolds were designed according to the particular defect geometry and produced by 3D printing of a calcium phosphate cement paste (Innotere Paste CPC, Innotere) under mild conditions. An open pore design could be achieved by 60° rotation of the strand orientation of consecutive layers during the printing process. Afterwards the pores were immediately infiltrated by a hydrogel (Tissuecol, Baxter) containing murine mesenchymal stromal cells. Artificial bone defects with a diameter of 3.3 mm were created surgically in the palate of 16 adult Lewis rats. Each defect was augmented with one bone graft. After 6 and 12 weeks, microCT and histology analysis to quantify the remaining defect width and bone formation were performed.

Results and Discussion

The clinical application of all bone grafts was easy and their fitting very good. 12 of 16 rats completed the study. Histology showed a homogenous and continuing bone formation occurring from the defect margins. After 6 weeks healing time new bone formation measured 82.426 μm^2 ± 30.960 μm^2 (mean ± SD) and after 12 weeks 251.639 μm^2 ± 41.827 μm^2. No complete osseous defect healing was observed and the remaining defect width was 2.998 µm ±137 µm (mean ± SD) after 12 weeks. The cell-laden hydrogel was not detectable after 6 or 12 weeks anymore, whereas the cement part of the scaffolds showed no signs of resorption.

Conclusion

3D printing of calcium phosphate cement paste in combination with a MSC-laden hydrogel is suitable for building scaffolds, which fit exactly into an artificial alveolar defect. As a next step the simultaneous printing of both components as well as further modifications of the scaffold materials are planned. One option could be the application

of combinations of CPC and mesoporous bioactive glass composites to improve the in vivo resorbability of the scaffold [3].
The creation of a 3D printed and tissue engineered bone graft for alveolar cleft osteoplasty could preserve patients from donor site morbidity.

References

[1]Korn P, Hauptstock M, Range U, Kunert-Keil C, Pradel W, Lauer G, Schulz MC.Application of tissue-engineered bone grafts for alveolar cleft osteoplasty in a rodent model. Clin Oral Investig. 2017 Nov;21(8):2521-2534.
[2] Ahlfeld T, Doberenz F, Kilian D, Vater C, Korn P, Lauer G, Lode A, Gelinsky M.Bioprinting of mineralized constructs utilizing multichannel plotting of a self-setting calcium phosphate cement and a cell-laden bioink. Biofabrication. 2018 Jul 27;10(4):045002
[3] Schumacher M, Reither L, Thomas J, Kampschulte M, Gbureck U, Lode A, Gelinsky M. Calcium phosphate bone cement/mesoporous bioactive glass composites for controlled growth factor delivery.Biomater. Sci. 2017, 5, 578-588

Acknowledgement

The study was supported by a grant of the "Österreichischen Gesellschaft für Lippen-Kiefer-Gaumenspalten und Kraniofaziale Anomalien". The authors thank Diana Jünger and Anna-Maria Placht for their excellent technical assistance.

4:45 p.m. – 6:15 p.m.

Hall 5

IX-SY15 | 3D Structures in Tissue Engineering and Disease Modelling

Ipsita Roy (London, UK)
Aldo R. Boccaccini (Erlangen, DE)

Tissue structure is inherently 3D in nature, hence 3D culture is the only method to truly mimic tissues and organs. This symposium will aim to highlight the intricacies of 3D scaffolds, including shape, microporosity, biomaterial and active factor distribution, required to model tissue, normal and diseased. A variety of biomaterials, both natural and synthetic will be discussed; cell types will include cell lines, primary cells and diseased cells; active factors will include growth factors, anti-inflammatory factors, microRNAs, antimicrobial factors. Processing technology such as electrospinning (melt and solution); 3D printing including multimaterial printing; layer by layer technology will be discussed.

IX-SY15-KL01

3D Cancer Disease modelling using Polyhydroxyalkanaotes

Ipsita Roy[1], Pooja Basnett[1], Pinar U. Onganer[1], Aakansha Tomar[2], Uttam Pati[2]

[1]University of Westminster, School of Life Sciences, London, GB; [2]Jawaharlal Nehru University, School of Biotechnology, New Delhi, IN

Introduction

Polyhydroxyalkanoates (PHAs) are a family of naturally occurring intracellular polymers synthesized by a variety of microorganisms[1]. These can be broadly classified into two types, short chain length PHAs (scl-PHAs), containing 3-5 carbon atoms and medium chain length PHAs (mcl-PHAs) containing 6-14 carbon atoms within their monomer units. Their physical properties differ based on their type. Scl-PHAs are mostly brittle and stiff whereas mcl-PHAs are soft and elastomeric in nature. PHAs are highly biocompatible and resorbable polymers that degrade into non-toxic byproducts via surface erosion, thereby maintaining their bulk properties. They are currently being explored for several biomedical applications[2]. In this study, two types of PHAs were produced, characterized and used for 3D cancer disease modelling.

Experimental Methods

Novel PHAs were produced via bacterial fermentation using *Bacillus* and *Pseudomonas* strains and 15L Applikon fermenters. They were extracted and purified using the soxhlet apparatus and characterized using Gas Chromatography-Mass Spectrometry (GC-MS) and Nuclear Magnetic Resonance (NMR).PHA based 3D scaffolds were developed using the particulate leaching method. These porous scaffolds were used to understand the cellular behavior and mechanisms of breast cancer using the Breast cancer cell lines MDA-MB 231and MCF7 . Cell viability and their morphology was assessed using Alamar blue assay, confocal microscopy and scanning electron microscopy.

Results and Discussion

Two types of PHAs, P(3HB), an scl-PHA and P(3HO-co-3HD), an mcl-PHA were produced using *Bacillus subtilis* OK2 and *Pseudomonas mendocina* CH50 respectively.The polymer structures were confirmed using GC-MS and NMR. A 50:50 blend of these PHAs were successfully used to produce 3D- porous scaffolds using the solvent casting-salt leaching method (Figure 1). The porous structures were evident from the SEM images. The breast cancer cell lines MDA MB 231 andMCF-7 were able to attach, grow, infiltrate and proliferate within the 3D structure resulting in 3D cancer models. The MDA MB 231 cells demonstrated *in vivo* like clustered-rounded morphology when cultured on the 3D porous scaffolds, confirming the *in vivo* mimicking capacity of the disease model (Figure 2).

Conclusion

This study thus demonstrated the possible use of 3D PHA-based models as disease models, in this case, as breast cancer disease models. Such models can in future be used to test the efficacy of newly developed drugs and to understand the molecular mechanism of cancer and other diseases without the use of animal models, an excellent step forward.

References

1. R. Rai, D. M. Yunos , A. R. Boccaccini, J. C. Knowles, I. A. Barker, S. M. Howdle, G. D. Tredwell , T. Keshavarz and I. Roy “Poly-3-hydroxyoctanoate P(3HO), a unique medium chain length polyhydroxyalkanoate homopolymer from Pseudomonas mendocina” 2011 Biomacromolecules, 12 (6), pp 2126–2136.

2. Basnett P., Kyon Y.C., Stolz M., Knowles J. C., Boccaccini A.R., Smith C., Locke C.I., Keshavarz T., Roy I. 2013 “Novel Poly (3-hydroxyoctanoate)/ Poly (3-hydroxybutyrate) blends for Medical Application” Reactive and Functional Polymers, 73:1340–1348

Acknowledgement

The authors are grateful to the British Council and the University Grant Commission India for the UKERI Grant which has supported this work.

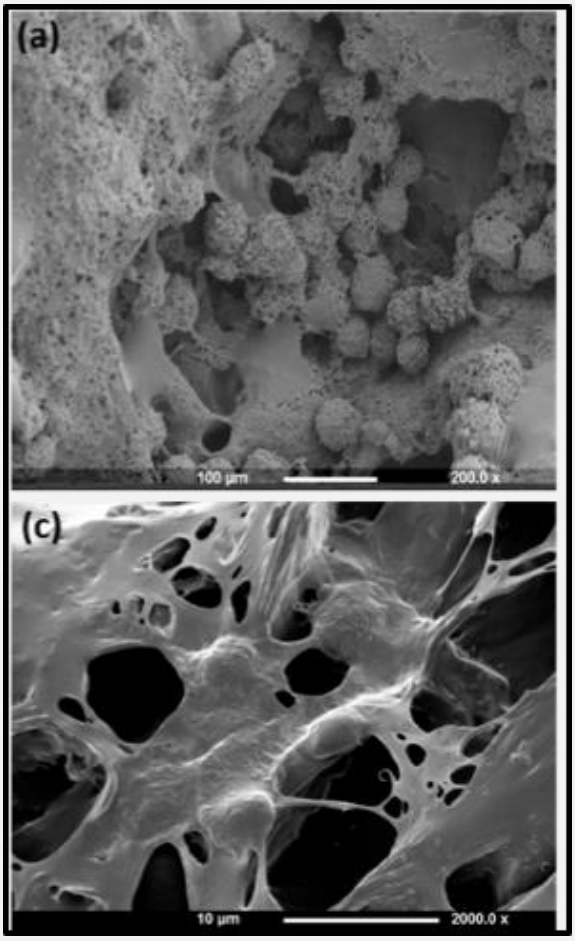

Figure 2: SEM images of Breast Cancer Cells within the 3D scaffolds
SEM images of MDA-MB-231 on (a) day 1 and (b) day 3; SEM images of MCF-7 cells at (c) day 1 and (d) day 3 within the P(3HB):P(3HO-co-3HD) 50:50 blend 3D scaffolds

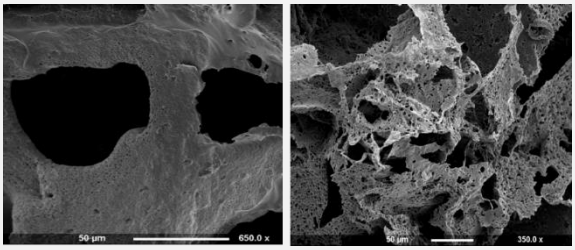

Figure 1: Porosity of 3D scaffolds
Porosity of the PHA-based 3D scaffolds used for 3D disease modelling

IX-SY15-03

Marine demosponges skeletal elements as inspiration on the fabrication of 3D Collagen-Silica composites envisaging bone tissue regeneration

Eva Martins[1,2], Gabriela S. Diogo[1,2], Ricardo A. Pires[1,2,3], Rui L. Reis[1,2,3], Tiago H. Silva[1,2]

[1]3B's Research Group, I3B's – Research Institute on Biomaterials, Biodegradables and Biomimetics, University of Minho, Headquarters of the European Institute of Excellence on Tissue Engineering and Regenerative Medicine, Avepark – Parque de Ciência e Tecnologia, Zona Industrial da Gandra, Barco - Guimarães, PT; [2]ICVS/3B's - PT Government Associate Laboratory, Braga/Guimarães, PT; [3]The Discoveries Centre for Regenerative and Precision Medicine, Avepark, Barco - Guimarães, PT

Introduction

The ocean is remarkably rich in marine species with a wide range of functional features, as demosponges sponges that are endowed by splendid skeletal structures of collagen and silica-based elements organized in hierarchical architectures. Additionally, these elements are attractive resources for being used on the fabrication of biomaterials as new templates for cell culture in tissue engineering approaches.

Experimental Methods

Five deep-sea sponge species, namely *Geodia barretti*, *Geodia atlantica*, *Stelletta normani*, *Phakellia ventilabrum* and *Axinella infundibuliformis*, were morphological characterized by Micro-CT. The retrieved hierarchical morphologies inspired the production of 3D structures formed by marine collagen-silica composites. Firstly, skins of Atlantic cod were used as raw-material for the collagen isolation, while diatomaceous earth (another marine source) and 45S5 bioglass® were chosen as silica-ceramic materials. Afterward, these materials were combined in three different formulations (COL, COL:BG and COL:D.E) and processed by freeze-drying process to produce tissue engineering scaffolds, further characterized regarding their morphological features, as well as mechanical and biological performance.

Results and Discussion

The combination of collagen and silica-based materials showed good properties for use as bone tissue template, with interconnected porosity being observed in the produced structures. In addition, *in vitro* biological assays were conducted, confirming the capacity of the developed scaffolds to support the adhesion and proliferation of L929 fibroblast cells, used as a model for the appraisal of the cytocompatible nature of the developed biomaterials.

Conclusion

The composites were fabricated combining codfish skin marine collagen with silica-based materials, mimicking the skeleton organization of marine demosponges. The composites revealed good cytocompatibility properties, supporting cell adhesion, migration, and proliferation, setting the basis as scaffold for tissue engineering in the biomedical application context.

Acknowledgement

This work was partially funded by European Union's Horizon 2020 Framework Programme for Research and Innovation under project SponGES (H2020-BG-01-2015-679849) and Forecast (H2020-WIDESPREAD-2014-2-668983), as well as by ERDF through Norte2020 under Structured Projects NORTE-01-0145-FEDER-000021 and NORTE-01-0145-FEDER-000023

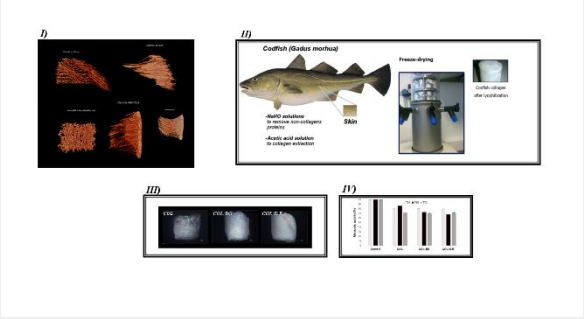

Marine scaffolds-based biomaterials

Figure 1 – I) Microstructural structures of the marine sponges by Micro-CT analysis. II) Collagen acid extraction procedure. III) Morphological images of the three 3D developed composites namely COL, COL:BG and COL:D.E.. IV) Cytotoxicity of the 3D composites regarding the metabolic activity (%) of L929 cell line.

IX-SY15-04

Decellularized three-dimensional plant structures as scaffolds for human tissues regeneration

Nicola Contessi Negrini[1,2], Nadia Toffoletto[1], Silvia Farè[1,2], Lina Altomare[1,2]

[1]Politecnico di Milano, Department of Chemistry, Materials and Chemical Engineering, Milan, IT; [2]INSTM, National Consortium of Materials Science and Technology, Local Unit Politecnico di Milano, Milan, IT

Introduction

Scaffolds for human tissues regeneration are produced either by synthetic or natural derived polymers and processed by a variety of fabrication technologies to obtain 3D porous structures with desired morphological, physical, structural and biological properties. Alternatively, decellularized matrices have been proposed [1] but, to date, only mammalian matrices have been investigated as scaffolds, with very poor attention given to plants, which are naturally characterized by versatile structures that mimic those of different human tissues [2]. Thus, after an adequate decellularization process, the cell-free plant structure might be used as scaffold to promote human tissues regeneration. We selected three plant-derived structures and, after an adequate decellularization process, we tested their potential in terms of morphological, physical, mechanical and *in vitro* biological properties as scaffolds for the regeneration of human tissues. In particular, we selected apples, carrots and celery to target the regeneration of adipose, bone and connective tissues, respectively.

Experimental Methods

Apple (*Malus domestica*), carrot (*Daucus carota*) and celery (*Apium graveolens*) samples (Fig.1) were obtained from fresh fruits and vegetables by manual punching (diameter = 10 mm) them from cut slices (thickness = 2 mm). Samples were decellularized by an optimized protocol [3] by subsequent immersion in 0.1% w/v sodium dodecyl sulfate, sonicated and washed with distilled water. Samples immersed in distilled water (i.e., without SDS) were prepared as control. DNA quantification was performed by using a commercially available kit (Plant DNAzol®) to check the reduction of plant DNA after the decellularization process. Stability tests at 37 °C were performed and water uptake of anhydrous samples in physiological-like conditions was measured. Stereomicroscope and scanning electron microscope were used to investigate the morphology of decellularized samples. Mechanical tests were performed by Dynamic Mechanical Analyzer to test the compressive properties of apple and carrots samples, and the tensile properties of celery samples. *In vitro* biological tests were performed by using three different cell models selected on purpose to target the regeneration of different human tissues: 3T3-L1 pre-adipocytes for apple, MC3T3-E1 for carrot and L929 cells for celery. *In vitro* indirect cytotoxicity tests (ISO 10993) were performed to investigate the absence of cytotoxic effects after the decellularization process. *In vitro* direct cytocompatibility tests were performed by seeding cells ($2x10^5$cells per sample) on poly-L-lysine coated samples, used to promote cells adhesion. Cells viability was checked by Alamar Blue assay at 1, 3, 7 and 14 days; viable cells distribution was investigated by LIVE/DEAD staining.

Results and Discussion

Effective decellularization of plant-derived 3D structures was qualitative proved by a loose of pigmentation (Fig.1) and quantitatively by an average decrease of 60% of plant DNA content after decellularization. SEM analyses showed

the presence of pores for all the considered plant species, thus proving the possibility of using the structures as scaffolds for cells colonization, with different pore size and orientation depending on the considered plant. All samples were stable in PBS at 37 °C up to 7 weeks, showing different water uptake (i.e., celery > apple > carrot) depending on the porous structure. During the swelling, sample showed volume stability (i.e., volume variation < 5% vs. anhydrous state). The elastic modulus of apple samples was 4 kPa, suitable for soft tissues reconstruction; the elastic modulus of carrot samples was 40 kPa, suitable for unloaded bone regeneration; celery elastic modulus was 600 kPa. All samples could bear deformation up to 20% without break. Indirect cytotoxicity revealed the absence of cytotoxic products (Fig.2a). Direct cytocompatibility tests proved the ability of the decellularized plant structures in sustaining cells adhesion and proliferation, as evidenced by an increase of metabolic activity in time. Viable cells adhered to the scaffold's surfaces following the structure of the plants (e.g., aligned cells on celery in Fig.2b), thus proving the possibility of using the different decellularized plant structures as versatile potential scaffolds for human tissues regeneration.

Conclusion

Plant 3D structures with human tissues-mimicking architectures were successfully decellularized. The obtained structures showed versatile morphological and structural properties, suitable for the regeneration of different human tissues, including adipose tissue, bone tissue and connective tissue. *In vitro* tests showed the potential of the prepared scaffolds in supporting different mammalian cell populations growth, proving that decellularized structures derived from plant could be actually used as scaffolds for human tissues regeneration.

References

[1] Hoshiba T. *et al.*, Expert Opin Biol Ther. 2010, 10, 1717-28

[2] Modulevsky J. D*et al.*, PLoS ONE 2014, 9, e97835

[3]Hickey R. J. *et al.*, ACS Biomater. Sci. Eng. 2018, 4, 3726−3736

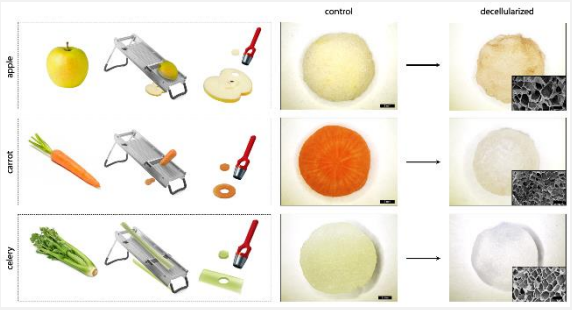

Figure 1
Plant-derived decellularized scaffolds: procedure for scaffolds obtainment and decellularization. Representative stereomicroscopy images before (control) and after decellularization (scale bar 2 mm). Representative SEM micrographs of decellularized structures (scale bar 200 mm).

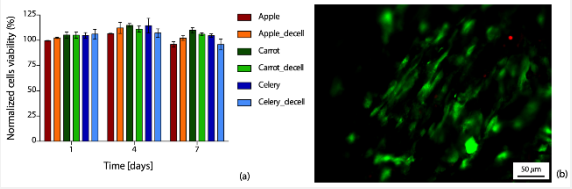

Figure 2
In vitro biological tests of decellularized plant scaffolds. (a) Normalized percentage cells viability of indirect cytotoxicity tests and (b) representative LIVE/DEAD staining image of cells cultured on decellularized celery samples.

4:45 p.m. – 6:15 p.m.

Conference room 4+5

IX-OS34 | Biophysical stimulation of cells

V-OS34-KL01

Biophysical stimulation of stem cells on biomaterials and in biomicrofluidic device: *in vitro* and *in silico* studies

Bikramjit Basu[1,2]

[1]Indian Institute of Science, Materials Research Centre, Bangalore, IN; [2]Indian Institute of Science, Center For BioSystems Science And Engineering, Bangalore, IN

Introduction

Biomaterials science and biomedical engineering have sustained as one among frontier and growing areas of research and innovation within the engineering science community in the world; considering the number of scientific discoveries and their societal impact. Against the backdrop of the ever-increasing unmet clinical needs, significant efforts have been invested to innovate new bioengineering approaches for clinical applications. While introducing the fundamental concepts, it will be emphasized that the phenomenological interaction of a biological cell with a synthetic material is influenced by several factors, e.g. elastic stiffness, surface topography and wettability. In this context, the results of a strikingly different approach, involving the intermittent delivery of electric stimulation to manipulate cell functionality on electroconductive biomaterials will be discussed. I will present both the experimental results and theoretical foundation of our ongoing research in this direction.

Experimental Methods

The experimental results will demonstrate the cell functionality changes for human mesenchymal stem cells (hMSCs), when they are grown on several biomaterial substrates, including hydroxyapatite based multifunctional bioceramics, electoactive polymers (doped polyaniline, PVDF-CNT composites), when cells experience external electric stimulation. In parallel, the results will be shown to validate similar concept for cells grown in PMMA microfluidic device with electrodes. The quantitative analysis of the cell morphological changes as well as gene upregulation will be particularly highlighted to illustrate the impact of electric stimulation towards osteogenesis/ neurogenesis/ cardiomyogenesis of hMSCs.

While establishing theoretical foundation to rationalize our experimental results, I will present the results of the analytical solutions of the Laplace equation with appropriate boundary conditions for the biological cell system, as well as MD simulation (GROMACS package) based studies for protein adsorption on biomaterial substrate and protein-membrane receptor interactions, both under the influence of electric field. The model formulation allows one to determine spatial and dependence of bioelectric stresses in cellular microenvironment on a conducting and insulating substrate and around a cell with surface charge density.

Results and Discussion

While introducing the fundamental concepts, it will be emphasized that the phenomenological interaction of a biological cell with a synthetic material is influenced by several factors, e.g. elastic stiffness, surface topography and wettability. In this context, the results of a strikingly different approach, involving the intermittent delivery of electric or magnetic field stimulation to manipulate cell functionality on electroconductive or magnetoactive biomaterials will be discussed.

In an effort to rationalize the outcome of in vitro studies, the theoretical concept based on the analytical solution of the Poisson's equations with appropriate boundary conditions will be described. The outcome of such in silico study will unravel the significance of substrate conductivity in synergy with electric field parameters towards modulation of bioelectric stress field, which has major ramification on cellular deformation and cell fate processes. In addition, the tangential component of the Maxwell stress tensor (shear stress), a measure of the stretching force on the membrane, has been used to obtain estimates of the critical electric field required for membrane rupture. Towards the end, the results of our recent molecular dynamics (MD) study to probe into the influence of electric field on protein adsorption (on bioceramic) and adsorbed protein-cell surface receptor interaction will be presented.

Conclusion

This presentation, encompassing experimental results and theoretical analysis, is expected to provide guidelines to develop next generation biomaterials and biomedical devices for regenerative medicine.

References

1. Ravikumar K., B. Sunilkumar and Bikramjit Basu; Synergy of substrate conductivity and intermittent electrical stimulationtowards osteogenic differentiation of human mesenchymal stem cells, **Bioelectrochemistry**116 (2017) 52–64.
2. Greeshma Thrivikraman, Giridhar Madras and Bikramjit Basu; Electrically driven intracellular and extracellular nanomanipulators evoke neurogenic/cardiomyogenic differentiation in human mesenchymal stem cells; **Biomaterials** 77 (2016) 26-43.
3. Greeshma Thrivikraman, P. Lee, R. Hess, V. Haenchen; Bikramjit Basu; D. Scharnweber; cellular microenvironment Interplay of substrate conductivity and pulsatile electrical stimulation towards osteogenesis of human MSCs *in vitro*;**ACS Applied Materials & Interfaces**,7[41](2015)23015–23028.
4. Greeshma Thrivikraman, Giridhar Madras and Bikramjit Basu; Intermittent electrical stimuli for guidance of human mesenchymal stem cell lineage commitment towards neural-like cells on electroactive substrates; **Biomaterials** 35 (2014) 6219 – 6235.
5. Shilpee Jain, Ashutosh Sharma and Bikramjit Basu, Vertical electric field stimulated neuronal cell functionality on porous amorphous carbon electrodes; **Biomaterials**34 (2013) 9252-9263.
6. Greeshma Thrivikraman, Prafulla Kumar Mallik and Bikramjit Basu; Substrate conductivity dependent modulation of cell proliferation and differentiation *in vitro*; **Biomaterials**34 (2013) 7073-7085
7. Ashutosh Dubey, Shouriya Dutta Gupta and Bikramjit Basu; Optimization of electrical stimulation conditions for enhanced fibroblast cell proliferation on biomaterial surfaces; **Journal of Biomedical Materials Research: Part B - Applied Biomaterials;** 98 B [1] (2011) 18–29.

Acknowledgement

Ravikumar K

Greeshma Thrivikraman

Sunil Kumar Boda

IX-OS34-02

Nanovibrational stimulation drives mesenchymal stem cells for 3D osteogenesis in freeze dried collagen sponge-hydrogels composite for bone tissue engineering

Wich Orapiriyakul[1,7], Penelope Tsimbouri[1], Peter Childs[2], Dominic Meek[3], Elizabeth Tanner[4], Manuel Salmeron-Sanchez[2], Richard Oreffo[5], Stuart Reid[6], Matthew Dalby[1]

[1]University of Glasgow, Institute of Molecular, Cell and Systems Biology, Glasgow, GB; [2]University of Glasgow, Division of Biomedical Engineering, School of Engineering, Glasgow, GB; [3]Southern General Hospital, Department of Orthopedics, Glasgow, GB; [4]Queen Mary University of London, School of Engineering and Materials Science, London, GB; [5]University of Southampton, Institute of Developmental Sciences, Southampton, GB; [6]University of Strathclyde, Department of Biomedical Engineering, Glasgow, GB; [7]Prince of Songkla University, Department of Orthopedics, Faculty of Medicine, Songkhla, TH

Introduction

Bone is the second most transplanted tissue after blood and is in short supply causing surgeons to rely on non-viable allograft or synthetic graft. We have developed the Nanokick bioreactor generating controlled nanoscale vibrations (nanoscale stimulation, NS) that drive bone differentiation of mesenchymal stem cells (MSCs) (1, 2). The bioreactor is compatible with general laboratory and can potentially be upscaled for industry. Here, we are developing MSC-seeded biphasic scaffolds comprising collagen hydrogels and freeze dried collagen sponges to allow long term 3D culture within the nanokick bioreactor. This approach will yield 3D, viable, bone graft that has good handleability.

Experimental Methods

Stro1-selected human MSCs were seeded in 1.8 mg/ml rat tail collagen type I hydrogels. 5% freeze dried collagen sponges were produced and integrated into MSC seeded hydrogels making gel-sponge composites. The effects of NS were tested on gel and gel-sponge composites respectively. Scaffold mechanical properties were tested by rheology, compression testing, SEM and nanodisplacement measurement under NS by interferometry. Biological responses including viability, qPCR, western blot, metabolomics, mitochondrial activity, protein arrays and protein inhibition tests were studied.

Results and Discussion

In the gel phase, the Nanokick bioreactor was programmed to generate reliable NS amplitudes of approximately 90 nm at 1000 Hz (measured by interferometry). At day 9, significant osteogenic gene up-regulation (RUNX2, osteonectin, osterix, osteopontin, osteocalcin) was observed. Western blotting showed pRUNX2/totalRUNX2 up-regulation. Protein arrays showed collagen and integrin up-regulation. Metabolomic analysis showed that the NS effect involved lipid metabolism. Using flow cytometry analysis, NS tended to increase mitochondrial activity (shown by JC1 and mitotracker staining), and produced controllable reactive oxygen species (ROS) by 2', 7'-dichlorodihydrofluorescein diacetate (DCF-DA). Pathway inhibition analysis and q-PCR showed that NS involved inflammatory cytokines production (IL-6, TNFα) and MAPK pathways (ERK1/2, JNK and p38). Corresponding to normal bone healing process, inflammation was itself suppressed at 2-3 weeks suggesting that the NS enhanced osteogenesis through natural bone healing pathways.

In the biphasic scaffold, the average elastic modulus of dry sponges were 137.3 MPa (SD=71.61) measured by compression test and SEM showed the average pore size was 227.74 mm (SD 72.93). Further, the gel-sponge composite transferred reliable NS amplitude. Scaffolds and NS in gel-sponge composite maintained cell viability as indicated by Alamar blue reduction. At day 9, microscopy showed MSCs migrating from the gel into the sponge. Temporal gene analysis (days 7-21) showed significant osteogenic gene upregulation (RUNX2, osterix, osteonectin and osteopontin). We then simulated how we might manufacture a clinical product. The cells-gels were NS stimulated for 14 days with the gels attached to the sides of the well plates. Gel contraction was then allowed and continuously cultured until day 21. Gel contraction onto the sponges was reproducible, allowed good MSC viability and increased MSC metabolic activity. Western blot at day 21 showed OPN upregulation confirming the osteogenic phenotype.

Conclusion

NS is safe for MSCs, induces physiological inflammation and ROS associated with promotion of 3D osteogenesis. Biphasic collagen scaffolds allowed nanovibrational force transmission and improved composite handleability for potential clinical use. After stimulation for 14 days, phenotype was tested at day 21 showing the osteogenic phenotype. This indicated the persistent harnessing effect of nanovibration maintaining MSC phenotype.

References

1. Nikukar H et al., ACS NANO 7, 2758, 2013.
2. Tsimbouri MP et al., Nature biomedical engineering 1, 758, 2017.

Acknowledgement

The authors thanks the Royal Thai Government, Find a better way, BBSRC (grant no: BB/N012690/1), EPSRC (grant no: EP/N013905/1) and Mrs Carol-Anne Smith for technical support.

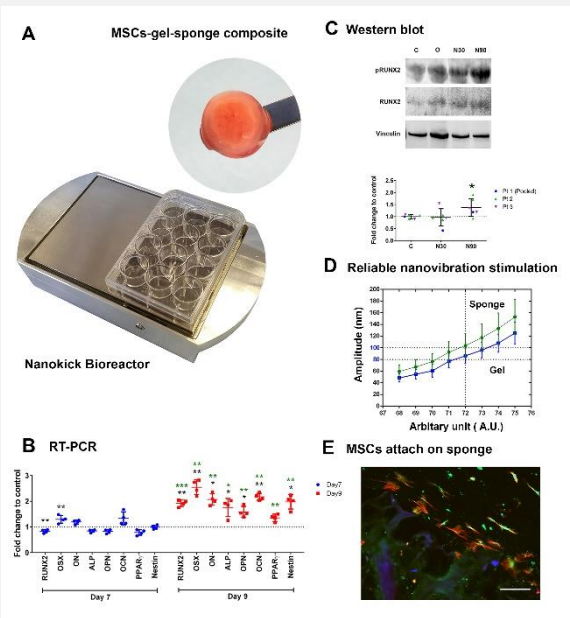

Gel-sponge composite for nanovibration-induced 3D osteogenesis
A. MSCs Gel-sponge composite and Nanokick bioreactor B-C. Nanovibration induces 3D osteogenesis. D Nanokick bioreactor generated reliable stimulating amplitude. E. Nanovibrational stimulation in gel-sponge composite is safe for MSCs and can drive 3D osteogenesis.

IX-OS34-03

Effect of sinusoidal alternating current stimulation at substrate surface on differentiation of osteoblast-like cell

Ryosuke Tsujita[1], Koji Yamamoto[2], Eiji Nakamachi[2], Yusuke Morita[2]

[1]Doshisha University, Graduate School of Life and Medical Sciences, Kyotanabe, JP; [2]Doshisha University, Department of Biomedical Engineering, Kyotanabe, JP

Introduction

Osteogenesis is regulated by physical stimulation such as magnetic field and electrical stimulation. Therefore, electrical stimulation might be effective in promoting osteo-differentiation to solve problem such as instability of implant because of looseing. Direct current stimulation on a conductive substrate with the BMP-2 was convalently immobilized on the polypyrrole/chitosan film enhanced osteoblast differentiation and maturation[1]. It is considered that current on the surface of substrate is effective to accelerate bone formation at interface between natural bone and implant. Alternating current (AC) electric field stimulation up-regulated the mRNA level of osteogenic transcription factor and promoted cell proliferation and differentiation *in vitro*[2]. Since AC can be induced by magnetic field at substrate surface, AC stimulation is suitable for stimulation at the interface for clinical application. It is necessary to optimize AC stimulation conditions on osteogenic differentiation. The purpose of this study was to quantitatively evaluate effects of sinusoidal AC (SAC) stimulation at substrate surface on differentiation of osteoblast-like cell.

Experimental Methods

The developed culture chambers consisted of three wells and a glass slide coated with ITO as shown in Fig. 1 (a). The wells had culture area of diameter of 15.5 mm. Fig. 1 (b) shows schematic drawing of the SAC stimulation system. Conductive copper tapes were fixed to both ends of the culture chambers by clip and fixture made of PC. The conductive copper tapes were connected to a function generator to apply SAC stimulation. MC3T3-E1 cells seeded on the culture chambers at a cell density 1.0×10^4 cells/cm^2 were cultured for 12 hours, and then MC3T3-E1 cells were cultured under SAC stimulation for 7 days. SAC stimulation was applied for 4 hours per day. Frequency of SAC was 1.0 kHz, and amplitudes of SAC were RMS 25, 50, 100 and 200 µA. Applied SAC was confirmed by an oscilloscope at the start of SAC stimulation. MC3T3-E1 cells cultured without SAC stimulation were prepared as control. mRNA expression of *Runx2* and *Osteocalcin (Ocn)*, which are major transcription factors of osteogenic differentiation, were measured by using quantitative real-time PCR after 7 days cultivation. The relative expression of *Runx2* and *Ocn* were normalized to the reference gene, *G3pdh*.

Results and Discussion

Fig. 2 shows the relative expression of *Runx2* and *Ocn* under each SAC amplitude. The expression of *Runx2* under SAC amplitude of 100 and 200 µA were higher than that of control, but there were no significant differences. The expression of *Ocn* under SAC amplitude of 100 and 200 µA were higher than that of control,and *Ocn* was significantly upregulated by SAC stimulation of 200 µA compared to control. Therefore, it was considered that amplitude over 100 µA of SAC stimulation were effective in bone differentiation at 1.0 kHz. Runx2 triggered the expression of matrix protein genes including *Ocn*, which serve as the marker of osteoblast differentiation[3]. These results showed that SAC stimulation of 200 µA at 1.0 kHz might promote osteoblast differentiation for early bone formation.

Conclusion

It was suggested that SAC stimulation of 200 µA at substrate surface promoted osteoblast differentiation at 1.0 kHz using the developed SAC stimulation system.

References

1. Zhang, J., et al., Biotechnology and Bioenginerring, 110, 5:1466-1475, 2013.
2. Wang, Y., et al., PLOS ONE, 11:1-14, 2016.
3. Komori, T., Journal of Cellular Biochemistry, 99, 5:1233-1239, 2006.

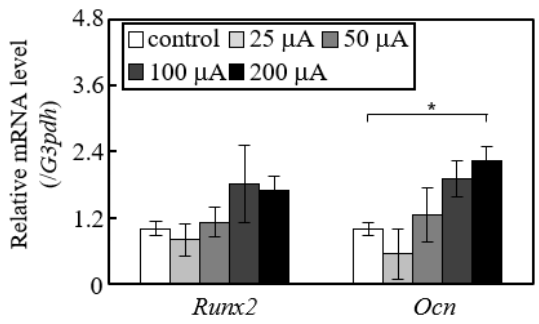

Fig. 2
mRNA expression levels of Runx2 and Ocn after 7 days cultivation (mean ± S.D., *: $P < 0.05$, Dunnett's test).

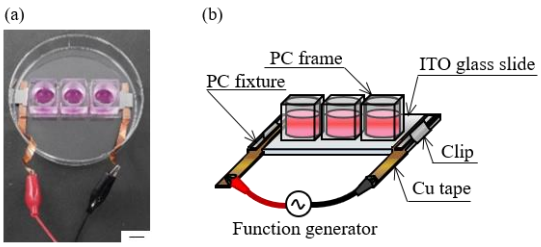

Fig. 1
(a) Developed culture chamber (Bar = 10 mm), (b) Shematic drawing of the SAC stimulation system.

IX-OS34-04

Synthetic multi-scale topography inspired by the ECM of bone enhances osteogenic differentiation of hBM-MSCs

Liangliang Yang[1], Qihui Zhou[2], Lu Ge[1], Patrick V. Rijn[1]

[1]University of Groningen, Department of BioMedical Engineering-FB40, Groningen, NL; [2]Qingdao University, Institute for Translational Medicine, Qingdao, CN

Introduction

The essential roles of the surface topographies of matrices and scaffolds have been highlighted to modulate adhesion, proliferation, and differentiation of stem cells. Indeed, stem cell differentiation can be altered by the sizes and shapes of surface topographical structures. Substrates containing the hierarchical structures of microscale and nanoscale patterns allow for more efficient spatial control of stem cell differentiation via the simultaneous modulation of the alignment of the cytoskeleton and intracellular focal adhesion protein assembly. In *vivo*, there are many tissues with hierarchical and anisotropical structures. For example, bone, and the dimension of it range from few nanometers to several hundred micrometers in diameter. This special structure allows for nutrient/waste exchange, and also support cell activities.

However, there are few studies reporting spatial control of stem cell differentiation using patterned topographies with different spatial dimensions ranging from nanometers to micrometers because of difficulties in the fabrication of such multiscale, hierarchically patterned structures on a single substrate. To the best of our knowledge, this is the first time from the literature to prepare the triple-scale topography with different dimension and direction which could be better mimic the ECM of bone, and explore the effect of them on osteogenic differentiation of stem cells.

Experimental Methods

1. PDMS film preparation

PDMS membranes were prepared as described previously.

2. Preparation of wrinkled substrates

For aligned topography substrates with a SiO_2–like surface, the PDMS sample was placed in a stretching apparatus and stretched uniaxial to a certain degree. Stretched PDMS was oxidized in air plasma under stable pressure for different times. After oxidation, the strain was released and inducing the formation of aligned topography (wave-like structures) of different wavelength and amplitude depending on the plasma treatment time and the cross-linker/elastomer ratio.

3. Imprinting

The nature of the sample preparation induces slight differences in chemical and mechanical properties due to the different oxidation times and elastomer/cross-linker ratio. To avoid these differences, imprints of the different topographies were made to ensure the same surface chemistry and mechanical properties.

4. Osteogenic Differentiation of hBM-MSCs

To investigate the osteogenic differentiation of hBM-MSCs on the different topography features, the cells were seeded on the samples at a cell density of $1*10^4$cells/well. The cells were kept at 37 ℃/5% CO_2 and 24 h later the medium was replaced by osteogenic differentiation medium for osteogenic differentiation. The culture medium was replaced every 3 days for the 21 days of the study.

Results and Discussion

In our study, we could prepare not only single scale substrates (0.5μm, 3 μm and 25 μm), and double scale (0.5/3 μm, 0.5/25 μm) combined with different angle (0°, 45°, and 90°), but also triple scale (0.5/3/25 μm) combined with different angle (0°, 45°, and 90°).

From the adhesion results, substrates with different dimension and direction have a significant influence on the orientation and elongation of hBM-MSCs. For the double-scale substrates, cell orientation for substrate with parallel direction is better than perpendicular direction, and for triple-scale substrate, cell orientation for substrate with parallel direction is the best one among the three groups.

For osteogenic differentiation, among the single-scale groups, ALP expression for hBM-MSCs seeded onto 3 μm is stronger than other two groups. For double-scale groups, it is interesting that perpendicular direction is better than parallel direction, same situation for 0.5 /3 μm or 0.5/25 μm groups. For triple-scale groups, 0.5μm perpendicular with 3/25um have the strongest ALP expression than other two groups, and this one was the best for facilitating osteogenic differentiation among all the groups.

Conclusion

A. We have successfully prepared single, double and triple-scale wrinkle structure with different size (nano, micro and macro) and direction (parallel, perpendicular and 45°) by a robust and easy method.

B. Hierarchical structure with different combination of size and angle have a significantly influence on cell orientation and cell area.

C. Hierarchical structure have a dramatical influence on the osteogenic differentiation of hBM-MSCs. Among the groups, 500nm perpendicular with 3μm/25μm (parallel) was the best one for osteogenic differentiation of hBM-MSCs.

References

[1] Zhou Q, Castañeda Ocampo O, Guimarães CF, Kühn PT, van Kooten TG, van Rijn P. Screening platform for cell contact guidance based on inorganic biomaterial micro/nanotopographical gradients. ACS applied materials & interfaces. 2017;9:31433-45.

[2] Yang K, Jung H, Lee H-R, Lee JS, Kim SR, Song KY, et al. Multiscale, hierarchically patterned topography for directing human neural stem cells into functional neurons. ACS nano. 2014;8:7809-22.

[3] Kim J, Bae W-G, Choung H-W, Lim KT, Seonwoo H, Jeong HE, et al. Multiscale patterned transplantable stem cell patches for bone tissue regeneration. Biomaterials. 2014;35:9058-67.

Acknowledgement

We acknowledge Theo G. van Kooten for assistance with cell cultures, Joop de Vries for help with AFM and plasma system maintenance, and Klaas Sjollema for assistance with TissueFaxs microscope.

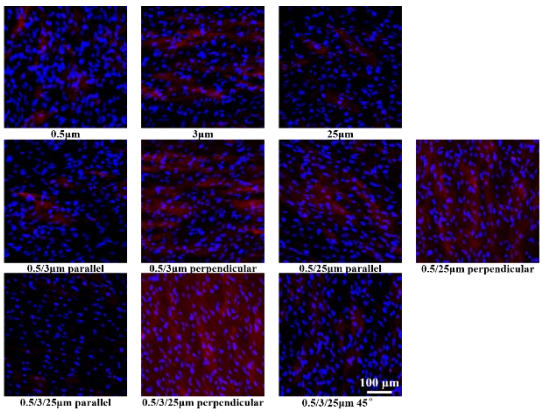

Differentiation of hBM-MSCs on the hierarchical structure substrates after 14 days in culture.

ALP staining after 14 days culture

Differentiation of hBM-MSCs on the hierarchical structure substrates after 14 days in culture.

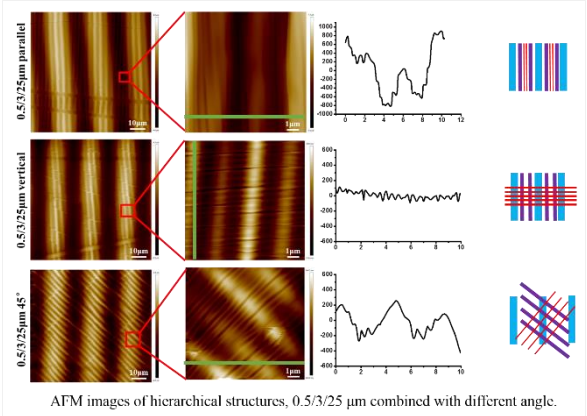

AFM images of hierarchical structures, 0.5/3/25 μm combined with different angle.

AFM images of hierarchical structures

0.5/3/25 μm substrate combined with different angle (parallel, perpendicular, and 45°)

IX-OS34-05

Development of dual-stimuli responsive nanofibrous magnetic device: a new cancer theranostic approach

Paula I. P. Soares, Joana Romão, João P. Borges

FCT NOVA, Materials Science Department, Caparica, PT

Introduction

Design, research and development of new and improved smart structures and systems is currently a hot topic in materials science and engineering. In the last decades nanotechnology development has provided innovative tools to produce new and improved biomaterials for several applications. Diseases like cancer are target research areas for new diagnostic and treatment options, not only to achieve a personalized approach, but also to decrease side effects.

Electrospinning is a versatile and easy to scale-up strategy to produce membranes able to react to changes in the surrounding environment, which are translated into significant changes in their morphological and chemical properties. Combination of thermoresponsive polymers with magnetic nanoparticles (mNPs) originates dual-stimuli responsive systems, able to change their morphological and chemical properties in response to temperature and magnetic field. mNPs have been extensively investigated for biomedical applications including magnetic resonance image (MRI) contrast agents, and magnetic hyperthermia agents [1-4].

This work focuses in developing a dual-stimuli responsive device composed of MG with mNPs incorporated into polymeric fibers as a new cancer treatment option. Combination of chemotherapy and magnetic hyperthermia in a device produces a new highly efficient cancer treatment option for easy access tumors or post-operation treatments.

Experimental Methods

The experimental work to produce the dual-responsive device is divided in 3 parts: 1) production of thermoresponsive microgels; 2) production of colloidal fibers, and 3) production of magnetic fibers.

mNPS were produced by chemical precipitation technique and further stabilized according to previously published work [1, 5]. Thermoresponsive microgels were produced using the surfactant-free emulsion polymerization technique, as previously reported [6]. Poly(N-isopropylacrylamide) (PNIPAAm) was used as a reference. mNPs were incorporated during microgels synthesis.

Colloidal electrospinning was performed using a homemade electrospinning apparatus by replacing the polymeric solution by a colloidal solution of thermoresponsive microgels dispersed in an auxiliary polymer solution. Polyvinylpyrrolidone (PVP) and poly(ethylene oxide) (PEO) were used. The response surface methodology (RSM) statistical tool was used to optimize this task [7, 8].

Magnetic membranes were produced using cellulose acetate as a reference polymer and incorporating mNPs in the polymeric solution before electrospinning, or by adsorbing the mNPs at fiber surface after being electrospun [9].

Results and Discussion

To produce these dual-stimuli responsive systems different architectures can be designed. This work focuses in two main architectures: thermoresponsive electrospun fibers with mNPs incorporated; or thermoresponsive microgels with mNPs confined in polymeric fibers through colloidal electrospinning.

Superparamagnetic iron oxide nanoparticles with an average diameter of 10 nm (Fig.1A) [1, 4, 5] were incorporated in PNIPAAm microgels (Fig.1B) using chitosan as a surfactant to produce dual-stimuli responsive microgel. Spherical and highly monodisperse microgels with diameters in the range of 200 to 500 nm were obtained (Fig.1C). The thermosensitivity of PNIPAAm microgels still persists in the hybrid microgels. The hybrid microgels were subjected to an alternating magnetic field demonstrating ability to generate clinically relevant heat (Fig.1D) [6].

PNIPAAm microgels were incorporated into PEO nanofibers through colloidal electrospinning with a “bead-on-a-string” morphology. By performing a statistical analysis, the relationship of the processing variables over the fiber size was evaluated following the RSM, leading to composite fibers with an average diameter of 63 nm (Fig.2A) [7].

In the second case, UV-crosslinked composite PVP microfibers showed a Young Modulus of 22 MPa and the capability to swell about 30 times their weight in 1 h in aqueous medium (Fig.2B) [8]. These electrospun membranes composed of thermoresponsive microgels as active sites inside nano/microfibers are some of the prototypes to produce dual-stimuli responsive systems.

Electrospun composite cellulose acetate/mNPs membranes were also produced by incorporating mNPs inside or at the fiber’ surface, demonstrating a reinforcement effect in the mechanical properties caused by mNPs. Moreover, these membranes produced significant heat under the application of an alternating magnetic field, thus being promising agents for magnetic hyperthermia (Fig.2C) [9].

Conclusion

More interesting results are being achieved under the recently financed project DREaMM (Ref. PTDC/CTM-REF/30623/2017) to engineer dual-stimuli responsive magnetic nanofibrous membranes as controlled drug release systems and magnetic hyperthermia agents for cancer treatment.

References

[1] Soares et al. Nanotechnology, 26, 425704, 2015
[2] Soares, et al. Carbohydrate Polymers, 149, 382-90, 2016
[3] Soares, et al. Carbohydrate Polymers, 153, 212-221, 2016
[4] Soares, et al. Applied Surface Science, 383, 240-247, 2016
[5] Soares, et al. Journal of colloid and interface science. 419, 46-51, 2014
[6] Echeverria, et al. Materials and Design 86, 745-751, 2015
[7] Marques, et al. RSC Advances, 6, 76370, 2016
[8] Faria, et al. RSC Advances 7, 48972-48979, 2017
[9] Matos, et al. Carbohydrate polymers 198, 9-16, 2018

Acknowledgement

This work is funded by National Funds through FCT – Portuguese Foundation for Science and Technology, Reference UID/CTM/50025/2013 and FEDER funds through the COMPETE 2020 Program under the project number POCI-01-0145-FEDER-007688 and PTDC/CTM-REF/30623/2017.

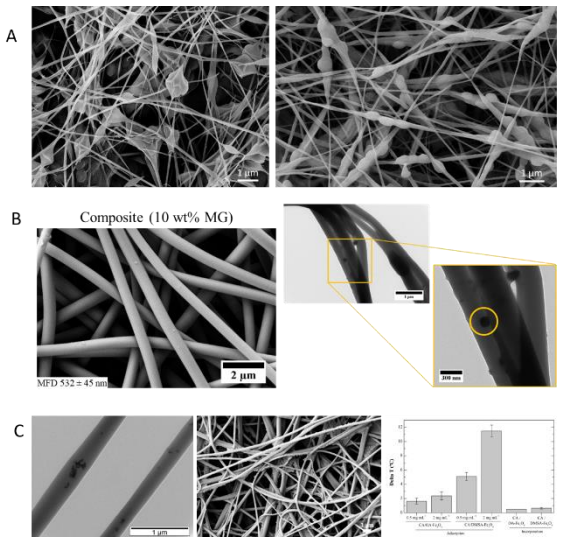

Figure 2
A) SEM image of coloidal fibers of PNIPAAm microgels incorporated in a PEO matrix with an average fiber diameter of 63 nm; SEM image of PNIPAAm microgels incorporated in a PVP matrix; C) TEM and SEM image of mNPs incorporated in cellulose acetate fibers and the correspondent magnetic hyperthermia measurements.

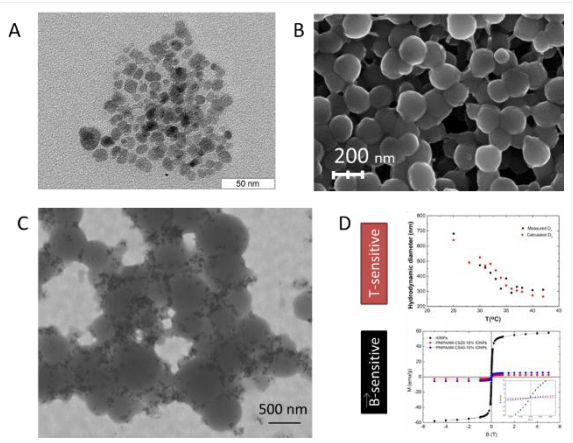

Figure 1
A) TEM image of superparamagnetic iron oxide nanoparticles with an average diameter of 10 nm. B) SEM image of thermoresponsive PNIPAAm microgels; C) HRSEM image of dual-stimuli (temperature and magnetic field) responsive hybrid microgels; D) Thermoresponsive behaviour and magnetic characterization of hybrid microgels.

4:45 p.m. – 6:15 p.m.

Conference room 2+3

IX-OS35 | Drug delivery 3

IX-OS35-01

Curcumin attenuates effects of (reduced)-Graphene Oxide tetrapodal networks as novel implant materials on cytotoxicity, inflammation & glial scarring in murine acute brain slices and human cell lines *in vitro*

Christina Schmitt[1], Florian Rasch[2], Fabian Schütt[2], Yogendra Kumar[2], Martin Lohe[3], Ali S. Nia[3], Xinliang Feng[3], Ralph Lucius[1], Janka Held-Feindt[4], Rainer Adelung[2], Kirsten Hattermann[1], On behalf of GRK-2154 Materials for Brain

[1]University of Kiel, Institute of Anatomy, Kiel, DE; [2]University of Kiel, Institute for Materials Science, Kiel, DE; [3]TU Dresden, Chair for Molecular Functional Materials and Center for Advancing Electronics Dresden, Dresden, DE; [4]UKSH Kiel, Department of Neurosurgery, Kiel, DE

Introduction

For neurological diseases such as glioblastoma multiforme or epilepsy, brain implants are promising tools for the direct drug application to overcome systemic toxicity. However, the possibility to surface-functionalize the scaffold material as well as the electrical conductivity are often important requirements for neural implants, offering the possibility of either a targeted or a triggered, on-demand drug delivery [1]. Respecting this, Graphene Oxide (GO), a derivate of Graphene (G) with a high surface area has gained attention, since it consists of a single atomic carbon layer, decorated with hydrophilic functional groups [3] that can interact with peptides and proteins via chemical or physical bonding [4], therefore making it easy to bio-functionalize. However, GO is an insulator so that in cases where the conductivity of the material is more important than the functionalization, the oxygen content of GO can be reduced by several techniques to produce the highly conductive material reduced GO (rGO) [5,6]. Therefore GO and rGO are two materials of interest for neuro implant development.

Though, the surgery as well as the implant material can elicit a harmful tissue response causing an alteration of the neuro-chemical environment of the brain and therefore leading to the formation of a glial scar. Beside its adverse effects on neural circuits and plasticity, this scar tissue has influence on the efficacy of the implant, since it can reduce and alter the release of the drug from the implant as well as its conductivity. Thus, neural tissue reactions towards GO and rGO implant materials need to be investigated in suitable *in vitro* models [7,8].

Here we show the indirect response of different *in vitro* models towards highly porous tetrapodal rGO and GO networks [publication/manuscript in progress, Rasch et al.]. The anti-inflammatory and –fibrotic compound Curcumin was used in co-stimulation with the implant materials, in order to inhibit possible inflammation and glial scarring reaction towards the materials.

Experimental Methods

The macroscopic GO and rGO networks have been produced by wet chemical infiltration of highly porous (94% porosity) ceramic templates [9] with a GO dispersion. Afterwards, the template was removed by chemical etching in 1 M HCl for 12 hours followed by washing in ethanol and critical point drying of the networks. For fabrication of rGO scaffolds, the GO networks were reduced in ascorbic acid prior to template removal. GO and rGO materials were then studied for their cytotoxicity (Cytotox Fluor and WST-1 assay) as well as inflammatory and glial scarring responses to different brain *in vitro* models in co-stimulation with curcumin. Therefore, human astrocytes or microglia (SVGA respective HMC3 cell lines) as well as murine acute brain slices were stimulated indirectly (materials were

placed in 0.4µm cell culture inserts) with the materials or material-eluate media, regarding ISO-10993-5. In respect of the acute and chronic reaction towards the implant, cells or brain slices were incubated for up to 6 days. Their material-specific reactions were studied on RNA or protein level.

Results and Discussion

Human astrocyte and microglia cell lines did not show any alterations in proliferation or cell death when incubated indirectly with GO and rGO materials for 24h. However, murine acute brain slices showed slightly elevated cytotoxicity after 6 days of indirect incubation with materials. Cytotoxic effects were less pronounced upon incubation with rGO in comparison to GO, and further alleviated by curcumin. Glial scarring associated markers such as glial fibrillary acidic protein (GFAP), tenascin, fibronectin, nestin or vimentin as well as inflammatory markers (e.g. interleukin-6) were induced in murine acute brain slices upon 6 days incubation with materials. Interestingly, these effects were clearly higher upon incubation with rGO than with GO, and could again be eased by curcumin co-stimulation. These results could be sustained by corresponding findings in human astrocyte and microglia cultures.

Conclusion

The results indicate that GO and rGO have a rather low impact on cytotoxicity or proliferation of human neural cell lines and murine acute brain slices, when cultivated indirectly with the materials for different time periods. However, reducing the oxygen amount of GO to obtain rGO seems to influence significantly the glial scarring and inflammatory responses *in vitro*, since the effects on cells and brain slices are more dominant after incubation with rGO. All investigated effects could be diminished by co-stimulation with curcumin, an anti-inflammatory and anti-fibrotic drug. Using these different *in vitro* models and by co-stimulating with curcumin we are currently trying to understand these effects more deeply and by this, hoping to improve the implant material design to reduce tissue reactions towards them.

References

[1] Servant, A.; Leon, V.; Jasim, D.; Methven, L.; Limousin, P.; Vazquez Fernandez-Pacheco, E.; Prato, M., Kostarelos, K. Graphene-Based Electroresponsive Scaffolds as Polymeric Implants for On-Demand Drug Delivery. Advanced Healthcare Materials, 2014, p 1334-1343

[2] Aliofkhazraei, M.; Ali, N.; Milne, W. I.; Ozkan, C. S.; Mitura, S.; Gervasoni, J. L. Graphene Science Handbook: Electrical and Optical Properties; CRC Press, 2016; p 715.

[3] Shin, S. R.; Li, Y. C.; Jang, H. L.; Khoshakhlagh, P.; Akbari, M.; Nasajpour, A.; Zhang, Y. S.; Tamayol, A.; Khademhosseini, A. Graphene-Based Materials for Tissue Engineering. Adv. Drug Delivery Rev. 2016, 105, 255–274, DOI: 10.1016/j.addr.2016.03.007

[4] Smith, S. C.; Ahmed, F.; Gutierrez, K. M.; Frigi Rodrigues, D. A Comparative Study of Lysozyme Adsorption with Graphene, Graphene Oxide, and Single-Walled Carbon Nanotubes: Potential Environmental Applications. Chem. Eng. J. 2014, 240, 147– 154, DOI: 10.1016/j.cej.2013.11.030

[5] Dreyer, D.R.; Park, S.; Bielawski, C.W.; Ruoff, R.S., Chem. Soc. Rev., 39 (2010), pp. 228-240

[6] Dave, S.H.; Gong, C.; Robertson, A.W.; Warner, J.H.; Grossman, J.C., ACS Nano, 10 (2016), pp. 7515-7522

[7] Kristensen, B.W.; Biocompatibility of silicon-based arrays of electrodes coupled to organotypic hippocampal brain slice cultures. Brain Research, 896, 1-17, 2001

[8] Schommer, J.; et al; Method for organotypic tissue culture in the aged animal. MethodsX, 4, 166-171, 2017

[9] Mishra, Y.; Kaps, S.; Schuchardt, A., Paulowicz, I.; Jin, X.; Gedamu, D.; Freitag, S.; Claus, M., Wille, S.; Kovalev, A.; Gorb, S.N.; Adelung, R.; Fabrication of Macroscopically Flexible and Highly Porous 3D Semiconductor Networks

from Interpenetrating Nanostructures by a Simple Flame Transport Approach; Particle & Particle Systems Characterization 2013, 30, 9, 775-783

IX-OS35-02

Collagen-based multilayer films for wound healing

Muhammad H. Iqbal[1], Fouzia Boulmedais[1], Florent Meyer[2]

[1]Centre National de la Recherche Scientifique, CNRS UPR 22, Institut Charles Sadron, Strasbourg, FR; [2]Université de Strasbourg, Institut National de la Santé et de la Recherche Scientifique, UMR_S 1121Biomaterials and Bioengineering, Strasbourg, FR

Introduction

Development of multifunctional materials is mandatory to challenge complex physiological processes like wound healing. Indeed, wound healing, especially in open wounds, can face infection or pathophysiological condition, like diabetes, that can impede the healing process. Collagen is the main component of the extracellular matrix comprising up to 30 % of human skin. Several studies have shown that collagen can induce wound healing by promoting the recolonization and the proliferation of epithelial cells with low antigenicity, and low inflammatory properties [1, 2]. However, tissue's matrix metalloproteases (MMPs) and bacterial infection may result in the enhancement of the breakdown of collagen-based material [3, 4]. Tannic acid (TA) is a polyanionic polyphenol extracted from plants possessing antimicrobial, antioxidant and anti-inflammatory properties. It can form complexes with proteins through H-bonding that can drive the build-up process and further becoming a protective layer of the epithelial tissue [5, 6]. Though TA has shown ample popularity for material processing (crosslinking) and antimicrobial activity, its cytotoxicity towards eukaryotic cells should not be neglected [7].
Herein, we develop collagen/TA films using the layer-by-layer method (fig 1a) in order to support wound healing in harsh conditions.

Experimental Methods

Collagen/TA films were developed by dip assisted layer-by-layer assembly (fig 1a) at acidic pH. The buildup was followed by Quartz Crystal Microbalance with Dissipation (QCM-D). These films were further characterized by Atomic Force Microscopy (AFM), Scanning Electron Microscopy (FESEM), Fourier Transform Infrared Spectroscopy (ATR), Circular Dichroism (CD) Spectroscopy, and Isothermal Titration Calorimetry (ITC). Their biological characterization includes stability in physiological buffers at pH 7.4, antimicrobial activity against Staphylococcus Aureus and cytotoxicity towards various fibroblast cell lines.

Results and Discussion

Collagen/TA films have an exponential growth observed by QCM-D and a fibrillar topography observed by AFM (Fig 1b). FTIR and CD experiments showed that collagen keeps its native structure. Such film, build in acidic pH, is stable up to 72 h in a buffer solution at pH 7.4 and releases TA in solution until 25 µg/mL in PBS. The films show release-killing property towards *Staphylococcus Aureus* without cytotoxicity for potential host cell like fibroblasts. Noteworthy, different buffers were tested for the construction of the film. Buffer type has emerged as a pivotal parameter leading to dissimilar physico-chemical and biological properties. ITC measurements showed that it could be related to the modification of the interaction between collagen and tannic acid in different buffers.

Conclusion

This work shows that the physico-chemical optimization of tannic acid based films is of paramount importance for future use of tannic acid in material production and their biomedical applications.

References

[1] D. Brett, "A Review of Collagen and Collagen-based Wound Dressings," Wounds, vol. 20, 2008.

[2] V. Natarajan et al., "Preparation and properties of tannic acid cross-linked collagen scaffold and its application in wound healing," Journal of Biomedical Materials Research Part B, vol. 101, 2013.

[3] A. Yahyouche et al., "Macrophage-mediated degradation of crosslinked collagen scaffolds," Acta Biomaterialia, vol. 7, 2011.

[4] S. Chattopadhyay et al., "Collagen-Based Biomaterials for Wound Healing," Biopolymers, vol. 101, 2014.

[5] P. Velmurugan et al., "Investigation on interaction of tannic acid with type I collagen and its effect on thermal, enzymatic, and conformational stability for tissue engineering applications," Biopolymers, vol. 101, 2014.

[6] A. de Sousa Leal et al., "Incorporation of tannic acid in formulations for topical use in wound healing: A technological prospecting," African Journal of Pharmacy and Pharmacology, vol. 9, 2015.

[7] F. Reitzer et al., "Polyphenols at interfaces," Advances in Colloid and Interface Science, vol. 257, 2018.

[8] G. Decher, "Fuzzy Nanoassemblies: Toward Layered Polymeric Multicomposites," Science, vol. 277, 1997.

Acknowledgement

M.H.I acknowledges the Higher Education Commission's (Pakistan) Ph.D. Fellowship program "HRDI-UESTPs/UETs Phase 1, Batch-V" for sponsoring the Doctorate studies. The authors acknowledge Institut Carnot MICA for financial support in the framework of DIAART project.

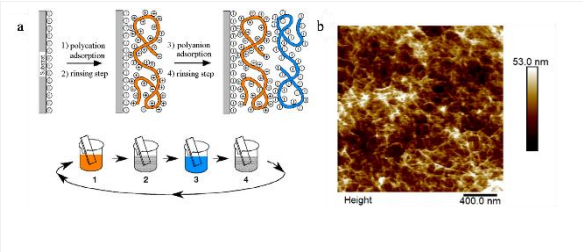

Figure 1:
A) Schematic representation of Layer-by-Layer technique based on the alternated deposition of oppositely charged polyelectrolytes obtained by the dipping process [8] (B) shows the topography of Collagen/tannic acid film observed by Atomic Force Microscopy (AFM).

IX-OS35-03

Physical immobilization of particles inspired by pollination

Lúcia F. Santos, Ana S. Silva, Clara R. Correia, João F. Mano

University of Aveiro, Aveiro Institute of Materials, Aveiro, PT

Introduction

Transdermal drug delivery patches for cutaneous wounds treatment induce a faster healing of the wound by delivering therapeutic agents that are included over or inside the patch. Commercially available patches can carry limited amounts of drugs, which are already incorporated within the patch, not allowing for a personalized formulation. Thus, it is crucial the development of improved drug patches with higher therapeutic dose. The unique features exhibited by biological organisms in nature have been a source of inspiration for the development of high-performance structures and biomaterials for the delivery of therapeutic agents.[1] Honey bees for instance, present a peculiar hairy structure that allows them to fix and carry millions of pollen particles. The pollen grains, which are of a similar diameter to the spacing between the hairs, are entrapped and temporarily retained, only being released on movement of the creature's leg.[2] Replicating this natural structure using microfabrication could provide a substrate to be used in a wide variety of applications that require simple, non-permanent, high-content and purely physical immobilization of solid particulate objects. Drug delivery systems are one potential application of these biomimetic substrates. Inspired by this, we proposed the concept of a micropatterned surface featuring high aspect ratio elastic micropillars spaced to mimic the hairy surface of bees. We explored the applicability of such surface as patch, to be used in wound healing, able efficiently entrap high amounts of drug particles at the microscale and release them in a controlled and sustained manner.

Experimental Methods

The hypothesis was validated by investigating the ability of polydimethylsiloxane (PDMS) microfabricated patches to fix microparticles. The patches were fabricated by soft lithography [4] and characterized by SEM, fluorescent microscopy and tensile strength. The geometrical arrangement, spacing, height and flexibility of the fabricated micropillars, and the diameter of the microparticles, were investigated.

Our biomimetic surfaces were explored for their ability to fix solid microparticles for drug-release applications, using tetracycline hydrochloride as a model antibiotic. The release profile and antimicrobial activity were herein determined using patches with both tetracycline powder and tetracycline alginate microparticles.

Results and Discussion

Inspired by the ability of the hairy structure of bees to entrap millions of pollen grains, we developed a flexible polymer substrate that replicated this extremely efficient system.[5] Higher entrapment capability was found through the match between particle size and pillar spacing, being consistent with the observations that the diameter of pollen grains is similar to the spacing between hairs on bees' legs. Moreover, taller pillars (analogous to the high aspect ratio of the bees' hairs) permitted immobilization of higher quantities of particles. These novel surfaces allowed fixation of more than 20 mg/cm^2 of antibiotic and interestedly, this value is similar to the capture of pollen grains by bees – 27 mg. Moreover, such surfaces presented a dose significantly higher - about 5 times more - than currently available patches (5.1 mg/cm^2) approved by FDA,[6] providing high drug concentration that could solve the current problems associated

with passive drug delivery patches. We also verified that both solid drug powder and hydrogel microparticles could be immobilized in the proposed substrates, indicating the great potential of these systems to be used as patches for drug delivery.

Conclusion

The results herein described suggest that the proposed textured surfaces could be further considered for the development of high-performance patches for clinical applications, through simple contact of the patch with the powdered product. We hypothesize that such devices could be easily explored to wide variety of applications that required large quantities of microparticles in biomedical and biotechnological fields.

References

1. Sanchez, C.*et al*. *Nat. Mater.***4,** 277–288 (2005).
2. Amador, G. J. *et al.***12,** 1–11 (2017).
3. Wiedersberg, S. *et al.J. Control. Release***190,** 150–156 (2014).
4. Gitlin, L. *et al*. *Lab Chip***9,** 3000–3002 (2009).
5. Santos, L. F. *et al*. *Proc. Natl. Acad. Sci.* 201813336 (2019).
6. Santos, L. F. *et al*. *Eur. J. Pharm. Sci.***118,** 49–66 (2018).

Acknowledgement

The authors acknowledge the financial support by the European Research Council grant agreement ERC-2014-ADG-669858 for project “ATLAS”. The work was developed within the scope of the project CICECO-Aveiro Institute of Materials, POCI-01-0145-FEDER-007679 (FCT Ref. UID /CTM /50011/2013), financed by national funds through the FCT/MEC and when appropriate co-financed by FEDER under the PT2020 Partnership Agreement.

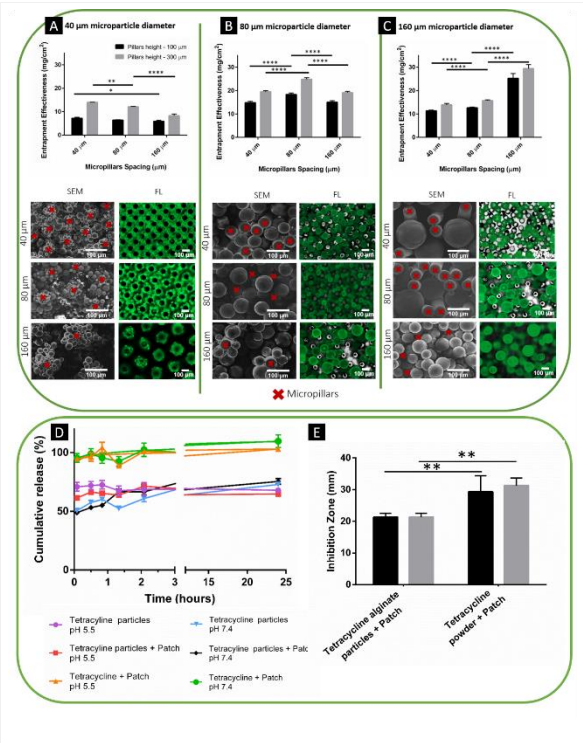

Entrapment of microparticles within PDMS micropateterned patches to drug delivery applications

As proof-of-concepet, PCL microparticles were entrapped within PDMS micropatterning patches. (A–C) Entrapment effectiveness of microparticles with different diameters:
40 µm (A), 80 µm (B), and 160 µm (C), entrapped within the patches with varying micropillar spacings (40, 80, and 160 µm)

(D) In vitro cumulative release of tetracycline from the patches at pH 5.5 and pH 7.4 at 37 °C in PBS.
(E) Antimicrobial activity of the different combinations: patches with tetracycline-loaded alginate microparticles or bare tetracycline powder against two microorganisms- gram-negative *E. coli* and gram-positive *S. aureus*.

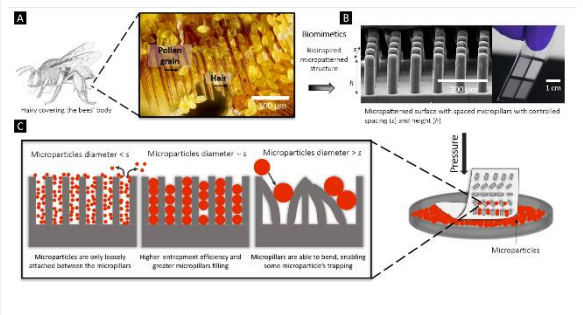

Schematic illustration of the proposed biomimetic micropatterned patch

A) The bees' body is covered with hairs. Pollen grains are caught between the bees' hair, and their size is similar to the hair spacing. Image courtesy of Charles Krebs (photographer).

(B) A bioinspired patch can be developed through the construction of a micropatterning structure with micropillars with controlled spacing (s) and height (h).
(C) Capture of solid microparticles in a flexible substrate featuring well-organized micropillars by direct contact and pressure; we hypothesized that the entrapment effectiveness will depend on the relationship between the pillar spacing (s) and the size of the microparticles.

IX-OS35-04

A pH-responsive nanoparticle for functional miR-199a/b-3p delivery in hepatocellular carcinoma

Shiyi Shao[1], Qida Hu[1], Wangteng Wu[1,2], Tingbo Liang[1], Guping Tang[2]

[1]The First Affiliated Hospital, Zhejiang University School of Medicine, Department of Hepatobiliary and Pancreatic Surgery, Hangzhou, CN; [2]Zhejiang University, Department of Chemistry, Hangzhou, CN

Introduction

Hepatocellular carcinoma (HCC) is the sixth most prevalent cancer and the fourth leading cause of cancer death worldwide in 2018 [1]. Aberrant expression of key miRNAs in HCC significantly correlates with tumor metastasis and recurrence [2]. The level of miR-199a/b-3p, the third most abundant miRNA in human liver, is consistently decreased in HCC [3]. Moreover, it was proved to be a promising therapeutic target for HCC by regulating various cellular processes [3, 4]. By taking advantage of the slight difference of pH between normal tissues (~7.4) and extracellular environment of solid tumours (6.5-7.2) [5], here we designed a pH-responsive drug-delivery system to fulfill enhanced miRNA therapy in HCC.

Experimental Methods

We first synthesized a triblock copolymer of poly(ethylene glycol) (PEG) and admantyl modules bridged by a pH-labile linkage (CDM). Polyethylenimine-crosslinked β-cyclodextrins (PC) was synthesized according to the reported methods [6]. The complex PEG-CDM-PC was self-assembled from polycations and admantyl modules. The investigation of pH-responsive ability was completed with RNA release assay and diameter analysis under acidic environment. The therapeutic effect was demonstrated by in vitro studies up to now.

Results and Discussion

The complex was characterized by TEM and ^{1}H-NMR (Fig. 1b, c). PEG-CDM-PC condensed miR-199a/b-3p had an average size of ~150nm and a zeta potential of ~+18.9mV. The elevated release of RNA from system and decreasing diameters of particles in solution with pH 6.5 demonstrated excellent pH-responsive effect of PEG-CDM-PC (Fig. 1d, e). PEG-CDM-PC pretreated with acid solution showed an enhanced cellular uptake (Fig. 2a) and efficient delivery of miR-199a/b-3p in Huh-7 cells (Fig. 2b). The increased miR-199a/b-3p suppressed tumor cell proliferation (Fig. 2c) by inhibiting mTOR, Bcl-2 and PAK4/Raf/MEK/ERK pathway (Fig. 2d). We are looking forward to positive in vivo study results which could confirm the preferential accumulation in cancer site and anti-proliferation effect in bearing tumour.

Conclusion

Our designed pH-responsive, self-assembled PEG-CDM-PC/miR-199a/b-3p is a promising therapeutic agent in future adjuvant therapy for HCC treatment.

References

1. F. Bray *et al.*, Global cancer statistics 2018: GLOBOCAN estimates of incidence and mortality worldwide for 36 cancers in 185 countries. *CA: a cancer journal for clinicians***68**, 394-424 (2018).

2. N. Yang, N. R. Ekanem, C. A. Sakyi, S. D. Ray, Hepatocellular carcinoma and microRNA: new perspectives on therapeutics and diagnostics. *Advanced drug delivery reviews***81**, 62-74 (2015).
3. J. Hou *et al.*, Identification of miRNomes in human liver and hepatocellular carcinoma reveals miR-199a/b-3p as therapeutic target for hepatocellular carcinoma. *Cancer cell***19**, 232-243 (2011).
4. E. Callegari *et al.*, miR-199a-3p Modulates MTOR and PAK4 Pathways and Inhibits Tumor Growth in a Hepatocellular Carcinoma Transgenic Mouse Model. *Molecular therapy. Nucleic acids***11**, 485-493 (2018).
5. S. Mura, J. Nicolas, P. Couvreur, Stimuli-responsive nanocarriers for drug delivery. *Nature materials***12**, 991-1003 (2013).
6. Q. Hu *et al.*, A redox-sensitive, oligopeptide-guided, self-assembling, and efficiency-enhanced (ROSE) system for functional delivery of microRNA therapeutics for treatment of hepatocellular carcinoma. *Biomaterials***104**, 192-200 (2016).

Acknowledgement
This work was financially supported by the National Natural Science Foundation of China (grant number 81830089, 81472212 and 81502026) and the Zhejiang Provincial Natural Science Foundation (grant numbers LQ16H180002, LY18H160026).

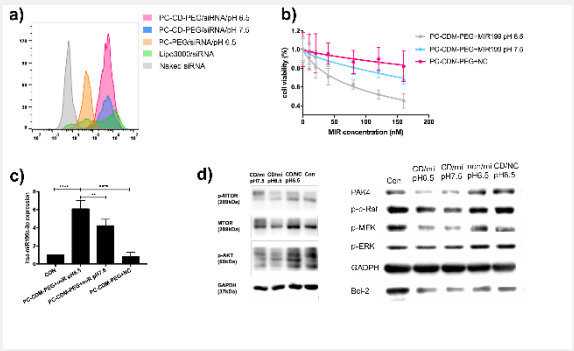

PEG-CDM-PC-mediated cellular uptake and transfection of miR-199a/b-3p.
a) Distribution of fluorescence intensity of Huh-7 cells after 4 h incubation with PBS, naked siRNA, PEG-CDM-PC/siRNA pretreated with pH 6.5 and 7.4, PEG-PC/siRNA and Lipo3000/siRNA. b) Dose-dependent cell viability after 72 h treatment with PEG-CDM-PC/miR-199a/b-3p pretreated with pH 6.5/7.4 and PEG-CDM-CD/NC. c) RT-PCR analysis of miR-199a/b-3p levels in Huh-7 cells. miR-199a/b-3p expression is normalized against PBS treatment. d) Expression of Bcl-2 and PAK4/Raf/MEK/ERK pathway by Western Blotting treated with PBS, PEG-CDM-PC/miR-199a/b-3p (pH 6.5/7.4) and PEG-CDM-CD/NC in Huh-7 cells. CD = PEG-CDM-PC/miR-199a/b-3p; non/mi = PEG-CD/miR-199a/b-3p; NC=negative control siRNA.

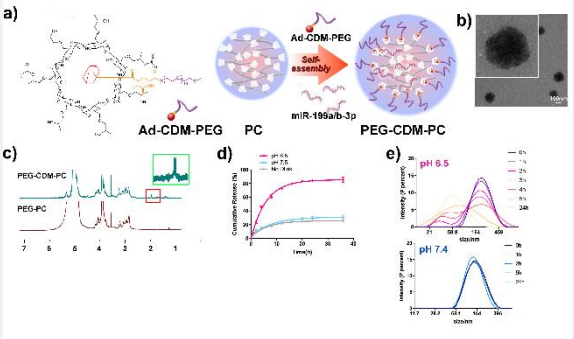

Characterization of siRNA-encapsulated PEG-CDM-PC.
a) Scheme illustration showing preparation of PEG-CDM-Ad, PC and PEG-CDM-PC. b) Transmission electron microscopic (TEM) images of PEG-CD-PC, scale bar = 100nm. c) ^{1}H-NMR characterization of PEG-CDM-PC and PEG-PC. The peak at δ 1.8-2.0 ppm characterizing CDM is highlighted in light green. d) Cumulative release of negative control RNA from the siRNA-encapsulated PEG-CDM-PC or PEG-PC in PBS with pH 6.5/7.4. e) The diameters of PEG-CDM-PC at various incubation times from 0-24 h.

IX-OS35-05

Polydopamine-coated Zein-curcumin nanoparticles for targeted therapy of glioblastoma

Huaiying Zhang, Inge S. Zuhorn

University of Groningen, Biemedical Engineering, Groningen, NL

Introduction

Effective treatment for Glioblastoma is severely limited by rapid resistance to agent therapies and the presence of the blood-brain barrier (BBB) that prevents therapeutics from reaching the brain. These issues can be addressed by the application of nanoparticles (NPs) that are effectively targeted and subsequently engage in transcytosis across the BBB.

In recent years, self-assembled biodegradable NPs from natural polymers, such as protein-based polymers, have attracted remarkable attention as potential drug delivery carriers. **Zein**, an alcohol-soluble protein, extracted from corn, has emerged as an ideal drug delivery system because of its intrinsic excellent biocompatible and biodegradable properties[1]. Compared with other proteins, zein has been extensively investigated for the encapsulation of bioactive compounds because of its unique capabilities, i.e., easy self-assembly into NPs, biocompatibility, and sustained drug release capability.

The one-step coating method for **polydopamine** (PDA) based on the oxidative self-polymerization of dopamine monomer in a week alkaline condition (pH 8.0-8.5) has aroused great interest in surface modification of biomaterials. The PDA layer on the surface of drug carriers greatly improves their hydrophilicity, colloidal stability, and reactivity with nucleophilic compounds for further modification via Michael addition or Schiff base reactions[2].

Curcumin (CUR) is a polyphenol that is widely used in medicine for its pleiotropic anti-inflammatory, antimicrobial and anticancer activities[3]. Herein we report the design and synthesis of a dodecamer peptide (G23)-functionalized PDA- coated curcumin-loaded zein nanoparticle to traverse the blood-brain barrier (BBB) and deliver curcumin to glioblastoma cells.

Experimental Methods

The preparation of curcumin-loaded PDA-coated zein nanoparticles (Z-C-pDs) is based on a modified method of phase separation. Briefly, zein and curcumin (CUR) were dissolved in ethanol (80% v/v) at different weight ratios. Subsequently, 1ml of the solution was rapidly dispersed into 19 mL dopamine hydrochloride solution in Tris buffer (10mM, pH 8.5) for 12h at room temperature while stirring. The Z-C-pDs were collected by centrifugation and redispersed with deionized water. The same procedure was followed without adding curcumin to prepare 'empty' PDA-coated zein nanoparticles (Z-pDs). For the functionalization, Z-C-pDs were resuspended in Tris buffer (10mM, pH 7.4), which contained G23 peptide. After 2h stirring at room temperature, particles were collected by centrifugation and washed with deionized water. DLS was used to evaluate polydispersity and size. The morphology of the nanoparticles was demonstrated by AFM. The cytotoxicity of the nanocomplexes was evaluated in human cerebrovascular endothelial (hCMEC/D3) cells and C6 glioma cells by fluorescence microscopy and MTT assays.

Results and Discussion

Z-C-pDs of 110 nm in size and with low polydispersity (PDI) were prepared at a zein and CUR weight ratio of 5:1. The NPs were spherical and showed a CUR loading efficacy of 8.1%. The surface charge was -37 mV, which

provided greater colloidal stability than the positively charged CUR-loaded zein nanoparticles (Z-Cs) without PDA coating. Confocal laser scanning microscopy (CLSM) studies showed that the Z-C-pDs could effectively transport encapsulated curcumin into C6 glioma cells. Moreover, in vitro viability studies demonstrated that Z-C-pDs induced concentration-dependent cytotoxicity in C6 glioma cells, which was more efficient than with free CUR.

Conclusion

Polydopamine-coated zein-curcumin nanoparticles are able to induce cytotoxicity in C6 glioma cells and seem promising for the treatment of glioblastoma. The effect of the functionalization of these nanoparticles with the G23 peptide on their transport across the BBB needs to be determined, as well as its effect on cytotoxicity induction in C6 glioma.

References

1. Xue, J. *et al.* Zein-caseinate composite nanoparticles for bioactive delivery using curcumin as a probe compound. *Food Hydrocoll.***83,** 25–35 (2018).
2. Park, J. *et al.* Polydopamine-based simple and versatile surface modification of polymeric nano drug carriers. *ACS Nano***8,** 3347–3356 (2014).
3. Cheng, K. K. *et al.* Curcumin-conjugated magnetic nanoparticles for detecting amyloid plaques in Alzheimer's disease mice using magnetic resonance imaging (MRI). *Biomaterials***44,** 155–172 (2015).

Acknowledgement

This work was supported by the Ministry of Economic Affairs, Netherlands) and the Dutch Ministry of Education, Culture and Science (Gravitation program 024.001.035).

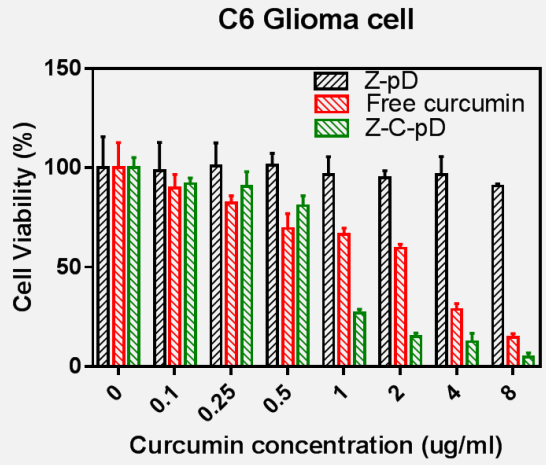

Cellular cytotoxicity
Relative viability of C6 cells after incubation at different concentration of Z-pD, free Curcumin and Z-C-pD. The cell viability assessed by MTT assay after incubation for 24h.

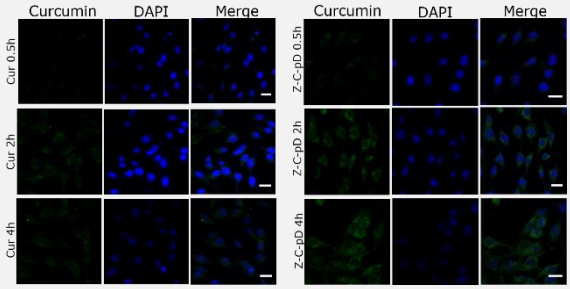

Cellular Uptake of Curcumin
CLSM images of C6 Glioma cells after incubation with free Curcumin and Z-C-pD for 0.5h, 2h and 4h. Blue and green colors represent DAPI stained nuclear and curcumin fluorescence, respectively. The Scale bars represent 20 µm.

IX-OS35-06

A photocurable and degradable polyester for nitric oxide release

Matheus F. de Oliveira, Marcelo G. de Oliveira

University of Campinas, Institute of Chemistry, Campinas, BR

Introduction

Polyesters have been widely used as absorbable biomaterials. More recently, photocrosslinkable polyesters have emerged as a platform for the manufacturing of entirely absorbable implantable devices, such as expandable intracoronary stents.[1] Photocrosslinkable materials allow the production of devices using photoinduced 3D printing technologies. Photocrosslinking has been achieved through the incorporation of pendent vinylic groups in the polymer backbone. One of the polyester with such properties is the methacrylated poly(dodecanediol citrate)(mPDC) (Fig. 1A), which undergoes photocrosslinking in the presence of a photoinitiator after irradiation with visible light. The potential biomedical application of mPDC may be greatly increased via the incorporation of drugs capable of improving its biocompatibility. One of the potential strategies for this propose is the incorporation of nitric oxide (NO) donors in the polymeric matrix.[2] NO is an endogenous species responsible for endothelial regeneration, prevention of platelet adhesion and aggregation, among other physiological functions.[3] Therefore, NO-releasing mPDC have the potential for production of absorbable blood-contacting medical devices. In this work, we developed a method for incorporating a NO donor into mPDC and demonstrate that this material is capable of releasing NO spontaneously after immersion in physiological medium.

Experimental Methods

The mPDC was synthesized via polycondensation of 1,12-dodecanediol and citric acid, followed by methacrylation.[1] The polymer was characterized with Gel Permeation Chromatography (GPC), NMR and FTIR. mPDC was mixed with a photoinitiator (Irgacure 819) and ethanol to make a photocurable resin. The resin was cured with a visible light LED in a nitrogen purged environment to make the crosslinked materials. The NO-releasing ability of the polymer was introduced through the incorporation of the NO donor S-nitroso-N-acetylpenicillamine (SNAP) (Fig. 1B). Scanning electron microscopy/Energy-dispersive X-ray spectroscopy (EDS) was used to confirm the incorporation of SNAP into the bulk of the polymer. The NO-release was measured by chemiluminescence using a Nitric Oxide Analyzer (NOA Sievers GE® model 280i) after the immersion of the polymer in PBS solution, pH 7.4 at 37°C, for crosslinked mPDC with different SNAP charges. The degradation of the crosslinked material was studied under accelerated condition, by measuring its mass loss in PBS solution at 60°C.

Results and Discussion

mPDC formation (Mw 1850 Da.) was characterized by NMR. FTIR spectroscopy confirmed the photocrosslinking of mPDC though the vanishing of the vinylic group at 1639 cm^{-1}. The observed mass loss during accelerated degradation test showed that the polymers degrades at the rate of 0.15 wt% per day. SNAP incorporation into mPDC was confirmed through the observation of the characteristic peak of sulphur atoms in the EDS spectrum of mPDC/SNAP.

Real-time NO release measurements showed that, after immersion in PBS solution at 37°C, mPDC/SNAP releases NO at rates varying from 100 to 280 nmol g^{-1} min^{-1}. Therefore, modulation of this rate by using different SNAP charges may allow for the inhibition of platelet adhesion, and thrombus formation. In addition, by changing the SNAP charge, different NO-release rates were obtained according to a linear dose-response (Fig. 2).

Conclusion

The mPDC/SNAP releases NO after immersion after aqueous medium. The rate of NO-release can be modulated by using different SNAP charges. These results indicate that mPDC/SNAP is a potential degradable polymeric material for local NO release from implantable medical devices.

References

1. R. Van Lith, *et al*. "3D-Printing Strong High-Resolution Antioxidant Bioresorbable Vascular Stents." *Advanced Materials Technologies* 1.9 (2016): 1600138.

2. V. Baldim, M. G. de Oliveira. Poly-ε-caprolactone/polysulphydrylated polyester blend: A platform for topical and degradable nitric oxide-releasing materials. *European Polymer Journal*, 109, 2018, 143-152.

3. C. Liang, et al. Biomimetic cardiovascular stents for in vivo re-endothelialization. Biomaterials, v. 103, p. 170-182, 2016.

Acknowledgement

MFO received a studentship from the São Paulo Research Foundation (FAPESP) (process 2018/02520-5). MGO acknowledges FAPESP for financial support (process 2016/02414-5).

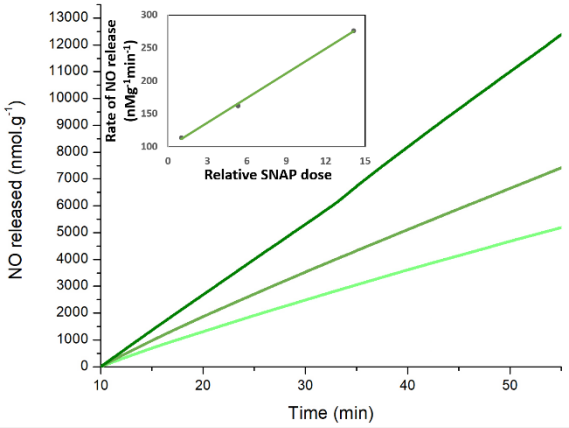

NO release profiles of mPDC/SNAP
Real time NO-release curves obtained from SNAP incorporated into mPDC at three different concentrations. Inset: Dose-response of NO release rate.

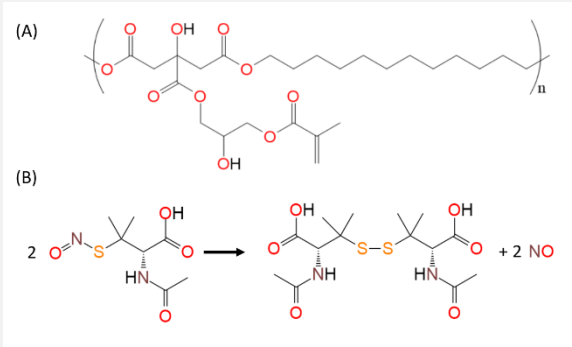

Structure of mPDC and SNAP NO-release reaction

Fig. 1. (A) Structure of methacrylated poly(dodecanediol citrate). (B) NO-release reaction of S-nitroso-N-acetylpenicillamine (SNAP) incorporated into mPDC matrix.

Friday, 13 September, 2019

	Hall 3	Hall 2	Hall 4	Hall 5	Conference room 2+3	Hall 1 | Exhibition Area
8:00						
8:30	**PL4** Plenary Lecture 4					**Industrial Exhibition & Poster Exhibition II**
9:00						
	BREAK					
9:30	**X-OS36** AM 2	**X-OS37** Biopolym. & artificial ECM 1	**X-OS19** Hydrogels for TE 2	**X-OS38** Biocomp. & degradation	**X-SY17** Biomater. to bypass biolog. barriers	
10:00						
10:30						
11:00	**COFFEE BREAK**					
11:30	**XI-OS39** Tissue models	**XI-OS40** Biopolym. & artificial ECM 2	**XI-OS41** Novel perspectives	**XI-SY18** Biobased polym. in wound healing		
12:00						
12:30						
13:00	Closing & Awards					
13:30						
14:00	**TAKE AWAY LUNCH**					
14:30						
15:00						

8:30 a.m. – 9:15 a.m.

Hall 3 + Hall 2

PL4 | Plenary Lecture 4

PL4-01

Saxon porcelain - domestic artwork, status symbol and biomaterial

Julia Weber

Director of the Porcelain Collection, Dresden State Art Collections, Dresden, DE

The invention of the white porcelain in Saxony and the foundation of the first European porcelain manufactory in Meissen in 1710 meant a real triumph for Augustus the Strong, elector of Saxony and king of Poland. Envied by all other European princes, he now monopolized a highly valued and most fashionable material – and he made the most of it. Henceforth, the white gold played an outstanding role at the baroque Dresden court. Introducing a few of the exceptional highlights of the Dresden Porcelain Collection, the lecture will illustrate how cleverly both Augustus the Strong and Augustus III played this unique trump card in their own ways. It also touches the interesting properties and special qualities of porcelain as biomaterial.

horseman monument for August III.

9:30 a.m. – 11:00 a.m.

Hall 3

X-OS36 | Additive manufacturing 2

X-OS36-01

Developing a Polymer Blend for Laser Sintered Oral Solid Dosage Forms

Marina-Eirini Mitrousi, Christopher J. Tuck, Ruth D. Goodridge

University of Nottingham, Department of Mechanical, Materials and Manufacturing Engineering, Centre for Additive Manufacturing, Nottingham, GB

Introduction

Additive Manufacturing (AM) of medication has come to the fore in recent years, specifically for its revolutionary uses in personalised medicine. The replacement of conventional drug manufacture and distribution could provide patients with customised drug dosages fabricated at the point of care to reduce cost and enhance therapy adherence. [1] Laser Sintering (LS) is a solvent-free AM technique with good potential for use in medical applications, which requires minimum post processing and it provides parts with high resolution. [2] Furthermore, LS is a powder-based technique that doesn't require rigid support structures which makes it promising for the production of drug dosage forms with complex geometries and acceptable mechanical properties. [3]

However, there are still many limitations for the deployment of LS in this sector due to the narrow variety of applicable polymers, which results from the complex thermal processing conditions. [4] Since most materials do not make it through the development stages in LS, it is important to understand polymer properties and processing parameters, in order to enable design and development of oral solid dosage forms by LS.

Experimental Methods

Tablets are solid masses made of suitable blends or granules. The mixture contains polymer excipients such as diluents, binders, disintegrants, lubricants, and coating agents. This research attempted to qualify five pharmaceutical polymers for LS to manufacture tablets with various drug release profiles. Materials were in powder form and in different polymer grades: microcrystalline cellulose (MMC), polyethylene oxide (PEO), methacrylic acid ethyl acrylate, hydroxypropyl cellulose (HPC), and lactose.

Prior to sintering, analytical techniques were used to determine the processing window of the materials, particle size and shape, and powder flow. Screening of the materials in terms of their thermal, physical and rheological characteristics revealed the level of suitability with LS that allowed the control and optimisation of the scanning strategy with potential production of robust parts. Processing trials were performed in the EOS Formiga P100 laser sintering system, where a range of different combinations of processing parameters were used (power, speed, distance, beam offset etc.) for each of the powders, in order to investigate their ability to be processed by laser sintering and the part properties that could be achieved.

Results and Discussion

For MCC, it was not possible to find a combination of processing conditions on the P100 laser sintering system that could successfully produce parts. The material melts at a high temperature and there was no evidence of any consolidation of the particles during processing. Using higher Energy Densities (ED) led to powder degradation and decomposition. PEO presented a sharp melting peak from the DSC results but the particle shape and size inhibited the binding of the particles together at low ED leading to poor layer formation. Using higher ED led to full consolidation of the particles but resulted in curling and part distortion. Methacrylic acid ethyl acrylate showed an excellent

combination of thermal, particle and flow properties which enabled processing. However, the material showed high flowability which caused shifting of the applied layers and loss of part accuracy. Spreading tests of HPC failed due to the poor flowability of the powder. Flow tests showed that the material is highly cohesive which prevented even distribution of powder. Therefore, consolidation did not occur. Lactose has a higher melting point than desired and is a cohesive powder which made sintering challenging but with potential for further work.

Conclusion

After examining the excipients individually, mixtures were created for various placebo tablet formulations. The combination of the material properties had a significant influence on the final properties of the blend that gave a good processing window. Based on the findings the authors are going to add various additives to enhance the absorption of the laser and the flowability of the powders for better processing. Future work will focus on the development of the scanning strategy and formulation composition to achieve reproducibility, and deliver a guideline on processing common polymer excipients on a laser sintering system for the fabrication of oral solid dosage forms.

References

1. Ventola, C. L. Medical Applications for 3D Printing: Current and Projected Uses. *P T***39,** 704–711 (2014).
2. Fina, F., Goyanes, A., Gaisford, S. & Basit, A. W. Selective laser sintering (SLS) 3D printing of medicines. *Int. J. Pharm.***529,** 285–293 (2017).
3. Shirazi, S. F. S. *et al.* A review on powder-based additive manufacturing for tissue engineering: selective laser sintering and inkjet 3D printing. *Sci. Technol. Adv. Mater.***16,** 033502 (2015).
4. Goodridge, R. D., Tuck, C. J. & Hague, R. J. M. Laser sintering of polyamides and other polymers. *Prog. Mater. Sci.***57,** 229–267 (2012).

Acknowledgement

The authors would like to acknowledge Joseph White and Mark East from the Centre of Additive Manufacturing (CfAM), University of Nottingham, for their guidance on laser sintering trials. The authors also acknowledge Pfizer for providing the resources for this research.

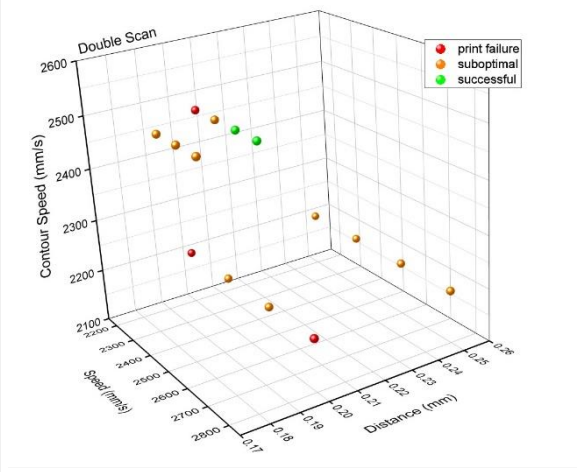

Processing 3DMAP of PolyOx N80
3D plot of Laser Sintering initial trials of PolyOxN80: double laser scan, varying hatching distance, laser speed, contour speed

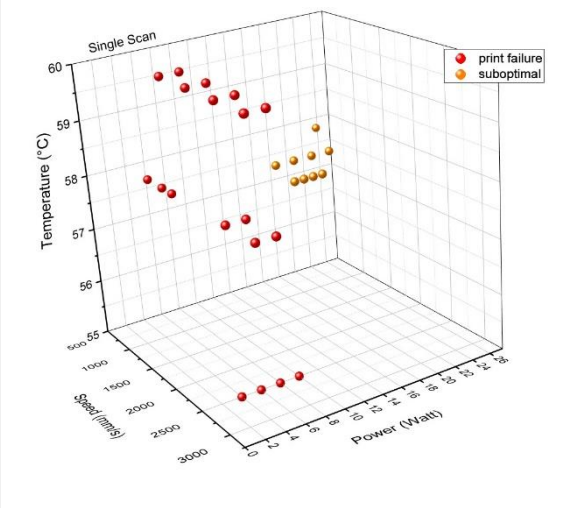

Processing 3DMAP of PolyOx N80
3D plot of Laser Sintering initial trials of PolyOxN80: single laser scan, varying laser power, laser speed, chamber temperature

X-OS36-02

Laser assisted bioprinting in combination with Raman spectroscopy as a versatile tool for single cell isolation

Nadine Nottrodt[1], Richard Lensing[2], Martin Wehner[1], Arnold Gillner[1,2]

[1]Fraunhofer Institute for Laser techonology, Biofabrication, Aachen, DE; [2]RWTH Aachen, Chair for laser technology, Biofabrication, Aachen, DE

Introduction

Biologics are pharmaceutically relevant active substances like proteins, monoclonal antibodies or recombinant vaccines which provide less side effects in the patient. Those biologics are often produced within mammalian high-producer cell lines. Today those cell lines are created in time- and cost intensive manual processes[1]. Here we present a new approach which combines Laser Assisted Bioprinting (LAB) – using Laser Induced Forward Transfer (LIFT) – with Raman spectroscopy for single cell identification, isolation and cultivation within an automated process chain. Within the current study we investigated the effect of mid-infrared laser irradiation on cell transfer, the transfer rate of single cells as well as the proliferation behavior after LIFT.

Experimental Methods

A fully automated machine combining LIFT using a mid-infrared (MIR) laser source and Raman-spectroscopy within a sterile climate chamber was setup. Genetically modified CHO IFN beta cells are diluted to a concentration of 2000 cell/ml medium and coated with a gelatin hydrogel onto a glass transfer slide.
A camera vision system identifies single cells. Those cells are analyzed by Raman-spectroscopy and transferred into microtiter plates for cultivation. Cells are expanded into larger cultivation vessels every 3-4 days. The cell survival was tested using a neutral red staining. The amount of produced IFN beta is tested by an ELISA against IFN beta. To validate the reliability of the LIFT process for single cell isolation, a comparative cell isolation is conducted with LIFT and FACS.

Results and Discussion

For the first time a MIR-laser source is used for LIFT. Using a wavelength around 3 µm allows for a metal-absorber free transfer process. Water in the hydrogel function as absorber in the process. The results of single cell transfer demonstrate that the MIR-laser source allows for a reliable single cell transfer. The penetration depth of 3 µm wavelength in water is around 800 nm[2]. Considering the fact that the hydrogel thickness is about 50 µm cells are influenced neither by irradiation nor by heat. More than 85% of transferred cells survive for more than 48h (Fig.1). We compared these results with earlier results from LIFT with Titanium absorber layer and UV Laser and found that cells proliferate for more than 21 days. We could demonstrate that single cell isolation with LAB is at least as good as FACS.

Conclusion

In this study we demonstrate a new tool that allows for single cell identification and isolation within an automated process chain. This tool allows for the identification of high-producer cells used for biologics production on the one hand, but can also be used to select and combine different cell types or water based cell matrix components to build up organoid structures.

References

[1]Heterologous Protein Production in CHO Cells, Springer Publication, ISBN 978-1-4939-6971-5

[2] Wedge shaped cell for highly absorbent liquids, Infrared optical constants of water, Wieliczka et al., DOI 10.1364/AO.28.001714 (1989)

Acknowledgement

Authors thank the Fraunhofer Society for funding the experiments on process combination. The development of MIR-LIFT is granted by the Eureka office under the funding code E! 11513 MIR-LAB

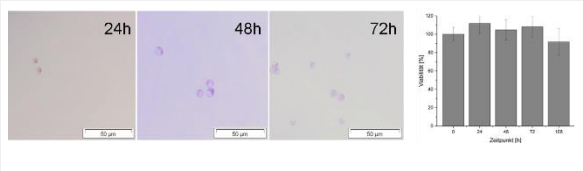

Cell proliferation after LAB
CHO IFN beta cells stained with neutral red after 24h, 48h and 72h. More the 85% of cells survive for up to 168h.

X-OS36-03

A novel weight-bearing antibiotic eluting temporary hip spacer manufactured by selective laser melting

Sophie E. T. Louth[1], Parastoo Jamshidi[2], Neil Eisenstein[8], Mark Webber[3], Hany Hassanin[6,2], Moataz Attallah[2], Duncan Shepherd[4], Owen Addison[5], Liam Grover[1], Kenneth Nai[7], Sophie C. Cox[1]

[1]University of Birmingham, School of Chemical Engineering, Birmingham, GB; [2]University of Birmingham, School of Materials and Metallurgy, Birmingham, GB; [3]University of Birmingham, School of Biosciences, Birmingham, GB; [4]University of Birmingham, Department of Mechanical Engineering, Birmingham, GB; [5]University of Birmingham, School of Dentistry, Birmingham, GB; [6]Kingston University, School of Mechanical and Automotive Engineering, London, GB; [7]Renishaw PLC, Wotton-under-Edge, GB; [8]Royal Centre for Defence Medicine, Birmingham, GB

Introduction

Hip implant failure due to infection is a major problem with over 8000 UK patients receiving a revision due to microbial colonisation in 2017 [1]. The gold standard for revision of an infected prosthetic is a two stage procedure, including thorough debridement of the soft tissue and the use of a temporary spacer that elutes antibiotics [2]. These devices are often made of bone cement and are not fully load bearing leading to extensive periods of bed rest [2]. The focus of this work is to develop a novel hip spacer, to enable patients to load bear during this 6 – 8 week period. Conventional implant manufacturing techniques, such as casting, are unable to create the complex structures required to house an antibiotic eluting biomaterial. Selective laser melting (SLM) is a additive manufacturing technique that enhances design freedom through layer-by-layer manufacture. The novel porous lattice design explored is built from Ti-6Al-4V using SLM.

In order to assess the feasibility of the design, four key research areas require exploration. The lattice (Fig. 1a), which provides the main mechanical support for the spacer as well as controlling drug release. The biomaterial embedded in the lattice that incorporates the antibiotic (Fig. 1b), in initial experiments this has taken the form of a brushite cement. The channels through which the antibiotic is released (Fig. 1c), these have been investigated in terms of filling the internal volume and release of the antibiotic. Finally the surface properties can be manipulated to minimise adhesion of both bone cells, as this is a temporary device that needs to be easily removed, and of bacteria to reduce the risk of additional infections (Fig. 1d).

Experimental Methods

In order to find the optimal lattice design, cylindrical lattices (12 mm diameter, 15 mm height) were generated in Element (nTopology, USA), and built on a Ren AM500M (Renishaw PLC, UK) from gas atomised Ti-6Al-4V powder using optimised in-house parameters, and compression tested in accordance with ISO 13314:2011 (Fig. 1a).

The initial biomaterial investigated was dicalcium phosphate dihydrate known as brushite (Fig. 1b). β-tricalcium phosphate (β-TCP) and monocalcium phosphate monohydrate (MCPM) powders were mixed with deionised water in a powder-to-liquid ratios (PLR) of 2:1 for 30 s.

To investigate the best strategy for placement of the channels, three model implants were designed (Fig. 1c) with a 2 mm diameter hole in the top and four 1 mm diameter holes in either the sides horizontally, inclined at 45 degrees, or vertically at the bottom. These were filled using the brushite cements loaded into a 5 mL syringe attached to a 15G needle. Micro-CT was then used to visualise the cement inside the model.

To investigate the elution characteristics of a gentamicin loaded brushite cement, the antibiotic was dissolved in deionised water at 100 mg/mL, and then mixed at a PLR of 2:1, resulting in a final concentration of 50 mg per 1 g of

cement. Cement cylinders and implant models containing cement were immersed in 10 mL of phosphate buffered saline incubated at 37°C. 10mL samples were withdrawn at intervals over 6 hours. These were tested for gentamicin using a CE 7500 UV–Vis spectrophotometer (Cecil Instruments, UK) and compared to cement without gentamicin.

Results and Discussion

The compression testing found that the BCCZ lattice at 60 % volume fraction had the highest compressive yield strength at 444.3±6.9 MPa, which is around double the strength of bone, while leaving 40 % of the volume for the biomaterial (Fig. 2a).

Micro-CT visualisation of the cement filled model implants found all designs were filled both in the reservoir and channels. However, defects were seen in the cement of all designs, particularly for the vertical channel model (Fig. 2b). The cumulative release of gentamicin from the cement after 6 hours was greatest from bare cement, with only 28 % release from the vertical channels, 10 % from horizontal, and 5% from inclined, the quantity of defects may have had an influence on this (Fig. 2c). The minimum inhibitory concentration of gentamicin against S. epidermis and S. aureus was found to be 1 and 16 µg/mL. All the model implant designs were shown to elute sufficient concentrations of gentamicin to inhibit the growth of both S. epidermis and S. aureus.

Conclusion

This work has demonstrated the possibility to exploit additive manufacturing technologies to enhance the value of medical devices. More specifically, the design freedoms of this technique have been exploited to generate load bearing structures for use in two-stage revision of infected hip arthroplasty.

Work on the mechanical and chemical interactions between the biomaterials and the lattice structure is on-going. Future work will look at whether the lattice structure can be used to tailor antibiotic release from the device in order to treat the infection quickly using a minimum quantity of the drug and without creating antibiotic resistance.

References

[1] L. Powers-Freeling, National Joint Registry 15th annual report.

[2] H.J. Cooper, The two-stage standard in revision total hip replacement', The Bone & Joint Journal, 95–B(11), pp. 84–87.

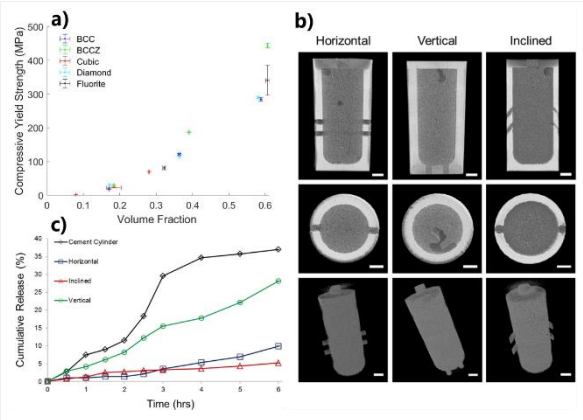

Figure 2. Results showing the optimal lattice design and channel orientation.

A) Graph of Compressive Yield Strength in MPa against Volume Fraction for the five different lattice designs. B) Micro-CT images of the gentamicin loaded cement within the model implants (scale bars: 2 mm). From top: coronal slice, axial slice, 3D render. C) Graph of Cumulative release of gentamicin over time from brushite cement cylinders and cement filled model implants. Result represented as mean ± standard deviation (n = 3).

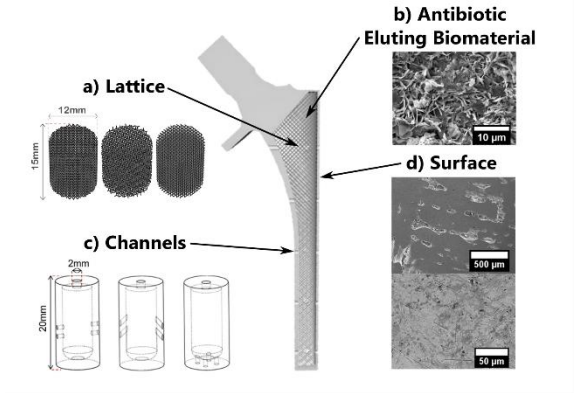

Figure 1. Cut away diagram of the novel spacer design showing research areas.
A) Three examples of lattice samples for compression testing (BCCZ, Cubic, Diamond unit cells). B) Scanning Electron Microscope (SEM) image of brushite cement with gentamicin sulphate used in biomaterial, elution, and antibacterial efficacy work. C) Schematic of the three model implant designs to investigate channel placement strategy, horizontal, 45 degrees, vertical. D) SEM images of Hot Isostatic Pressed and polished samples showing the surface.

X-OS36-04

3D Printed Elastic Fibers with Optical, Microfluidic and Actuating Functionality

Markos Athanasiadis, Anna Pak, Dzmitry Afanasenkau, Ivan R. Minev

TU Dresden, BIOTEC, Dresden, DE

Introduction

Human-machine interfaces are technological instruments which establish a communication path between the biological tissue and a device. In order to achieve that, such devices (e.g. neural implants) must be in close proximity to the human body, often being implantable or wearable. Integration in the neural tissue of the host requires the use of mechanically adapted materials (e.g. silicones, hydrogels, and elastic optical conductors). To this end, direct ink writing (DIW), a fabrication technique which permits rapid prototyping with functional soft materials, can be employed.

Experimental Methods

During a typical DIW process, the extruded filaments possess a circular cross section. However, here we demonstrate that variations of the printing parameters such as nozzle speed and nozzle distance from the substrate (nozzle height) allow the fine-tuning of the cross section geometry. Harnessing ink deformation we demonstrate filaments with ellipsoid, ribbon, grooved, and micro-channel geometries, as a result of the printed ink being intentionally squeezed towards the surface of the substrate.

Results and Discussion

Exploiting the advantages of deformation DIW, we present a “phase diagram” describing the way printing parameters determine which of the cross-sectional geometries is produced, upon the printed filament. This method is consequently applied for the fabrication of multi-layered functional fibers (Figure 1). Specifically, we demonstrate that combination of ribbon and groove shaped filaments enables the fabrication of elastomer based optical waveguides. Our optical fibers with an average propagation attenuation of 0.72 ± 0.06 $dBcm^{-1}$ for white light, are capable of surviving tensile strain of at least 30%. Specifically, a 10% decrease of the transmitted optical power at 30% longitudal elongation is recorded (Figure 2).Furthermore, a similar approach is employed for the fabrication of microfluidic channels at a sub-millimetre resolution, which are capable of supporting laminar flow.

Finally we present the ability to combine such functional printed filaments for the fabrication of systems with diverse modalities. Specifically, soft pneumatic steerable optical fibers are fabricated with a capacity for actuation over several millimetres.

Conclusion

In summary, we introduce a novel method for the fabrication of soft flexible functional fibers with the use of additive manufacturing. The foundations of this strategy lie on the ability to rationally harness the deformation of the respective inks. To that end, potential applications of such devices could be identified in the fields of sensors, optogenetics and drug delivery or soft robotics.

Acknowledgement

This work was supported through a Freigeist fellowship (91 690, Electronic Tissue Technology for Spinal Cord Repair) from the Volkswagen Stiftung, the Center for Advancing Electronics Dresden (cfaed) and the Biotechnology Center (BIOTEC) of TU Dresden. We would like to thank Gheorghe Cojoc for help with optical measurements, Teuku Fawzul Akbar for help with the tensile measurements and Christoph Tondera for help with rheology measurements.

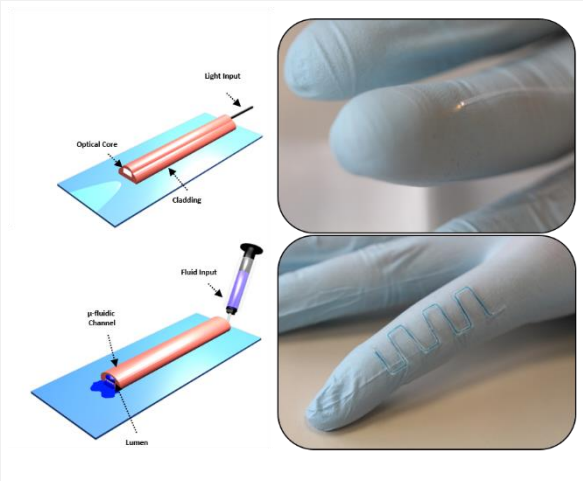

Figure 1: Elastomer based printed fibers, with optical and microfluidic functionality

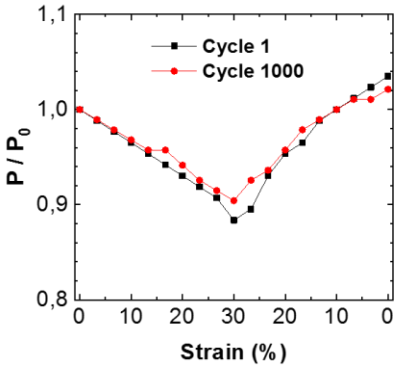

Figure 2: Optical power output under tensile strain

X-OS36-05

Ultra Porous Additive Manufactured Scaffolds Designed for Biomedical Implant Development

Faezeh Shalchy[1], Christopher Lovell[2], Atul Bhaskar[1]

[1]University of Southampton, Faculty of Engineering and Physical Science, Southampton, GB; [2]Lucideon Ltd., Healthcare, Stoke-on-Trent, GB

Introduction

Advances in implant technologies and artificial organs are highly dependent on effective biomedical scaffolds which are essential for growth of healthy functioning tissues. One vital property of such scaffolds is their porosity which facilitates nutrient transport to the growing cells [1]. The microstructure of the scaffolds and the shape and size of their porosity have an important effect on cell growth and cell behaviour. The significance of porosity has attracted the interest of many researchers in terms of development of manufacturing methods that can control the level, size, and shape of porosity of scaffolds [2]. Additive Manufacturing is one of the newly developed methods with promising results in biomedical applications. Common approach is to manipulate the extrinsic porosity of a scaffold which can be controlled through the scaffold design. In this study, however, we explore a novel idea, that is, to control the intrinsic porosity of the filaments used in the production of 3D printed scaffolds. Our ultimate aim is to develop methods to tailor the microscale porosity and architecture of scaffoldsto influence cell response which could benefit engineering of complex tissues.The method leads to ultra-porous scaffolds with essential mechanical integrity.

Experimental Methods

In this research poly(lactide) (PLA), hydroxyapatite (HA) and sacrificial phases were blended using a Noztek filament extruder to produce composite filaments. A range of filaments were made by varying the loading of inorganic phase and the blend ratio of PLA to the sacrificial phase. Two types of sacrificial phase were considered, sodium chloride (NaCl) and poly(vinyl alcohol), which were removed from the scaffolds through water immersion. Particle size analysis was used to quantify size distributions of the salt and HA fillers. Porosimetry and SEM were used to characterise their microstructure. In addition, for processing, the filament thermal properties were analysed using differential scanning calorimetry and thermogravimetric analysis. Compression tests were performed on the porous filaments to assess their mechanical integrity. In the next phase of study, filaments were used to fabricate “wood-pile” scaffolds using an Ultimaker2+ Extended 3D printer. The hierarchical porosity of these scaffolds and the effect of different printing parameters such as distance between filaments and filament diameters was investigated. Cell culture assays were performed on the fabricated woodpile scaffolds. Later on, different cell behaviour such as cell viability, elongation, growth, and proliferation as well as the effect of pore size and shape are evaluated on the manufactured samples using microscopy and other different techniques.

Results and Discussion

The characterisations clearly demonstrate that for samples with salt as the sacrificial phase, scaffold porosity highly depends on the particle size distribution and the ratio of the soluble filler to matrix. Similarly, with PVA, the porosity of the filaments depended upon the blend with PLA. A transition from surface porosity to an open porous structure throughout the filaments was observed with increased loading of the sacrificial phases which impacted significantly on the mechanical strength of the composite scaffolds. Using the properties of the manufactured filaments, a design

map for optimum material combinations was developed. Results clearly show that in all combinations with same porosity level, those that include both fillers (PVA and NaCl) result in an improved mechanical integrity compared to the ones with one filler phase. Our cell culture results confirm that the effect of porosity size on cells highly depends on cell size [3]. Porosity interconnectivity also plays an important role in cell viability and growth.

Conclusion

We have demonstrated an effective method to 3D print scaffolds with controlled random porosity from PLA filaments prepared using both polymer and inorganic sacrificial phases. Porous structures with 80% porosity level (intrinsic porosity plus woodpile structure extrinsic porosity) and acceptable mechanical integrity were successfully manufactured. The improved cell behaviour on ultra-porous scaffolds compared to control sample of PLA printed woodpile structure, confirms the effectiveness of the proposed method.

References

1. Bose, S., Vahabzadeh, S., & Bandyopadhyay, A. (2013). Bone tissue engineering using 3D printing. *Materials today*, *16*(12), 496-504.
2. Taboas, J. M., Maddox, R. D., Krebsbach, P. H., & Hollister, S. J. (2003). Indirect solid free form fabrication of local and global porous, biomimetic and composite 3D polymer-ceramic scaffolds. Biomaterials, 24(1), 181-194.
3. Nikkhah, M., Edalat, F., Manoucheri, S., & Khademhosseini, A. (2012). Engineering microscale topographies to control the cell–substrate interface. Biomaterials, 33(21), 5230-5246.

Acknowledgement

The authors would like to thank *Marie Sklodowska-Curie grant* (Grant no: 643050) for providing financial support.

X-OS36-06

3D Bioprinting of volumetric osteochondral tissue substitutes with an individualized design and an anisotropic internal architecture

David Kilian[1], Stefan Holtzhausen[2], Philipp Sembdner[2], Tilman Ahlfeld[1], Ashwini R. Akkineni[1], Anja Lode[1], Ralph Stelzer[2], Michael Gelinsky[1]

[1]TU Dresden, Centre for Translational Bone, Joint and Soft Tissue Research, Faculty of Medicine Carl Gustav Carus, Dresden, DE; [2]TU Dresden, Chair of Engineering Design and CAD, Faculty of Mechanical Science and Engineering, Dresden, DE

Introduction

Multichannel 3D plotting offers a huge potential for the fabrication of volumetric structures of a defined shape and architecture. Complex tissue models, like substitutes for an osteochondral defect, require a combination of materials of different properties. Based on clinical imaging data, such as computed tomography (CT) or magnetic resonance imaging (MRI), construction of 3D structures mimicking the external geometry of native anatomy is possible. The use of compatible hydrogels even enables the fabrication of cell-laden, biofunctional 3D structures (bioprinting). Different materials and cell types can be processed with a spatially defined distribution by sequential strand deposition in a layer-by-layer fashion building up volumetric tissue substitutes. The strand diameter, the orientation and fusion of strands of identical and different materials, while essential open-porous structure of those scaffolds is maintained, can be used to tune mechanical properties to resist compressive or shear forces. Since most native tissue types show a rather heterogeneous, anisotropic structure, we use a varying strand pattern defined by modified plotting paths, to trigger mechanical properties of the (bio-)plotted structures.

Experimental Methods

3D Plotting was performed using a BioScaffolder 3.1 (GeSiM mbH, Radeberg, Germany, Fig.1A). Two different types of material were processed: an alginate-methyl cellulose (Alg/MC) hydrogel blend[1] which is suitable for application as a bioink, and a pasty calcium phosphate cement (CPC, INNOTERE GmbH, Radebeul, Germany) mimicking the hydroxyapatite structure of native bone matrix[2] . The materials can independently be used to fabricate structures with an individualized design in volumetric dimensions, and can further be applied in a combined design to fabricate osteochondral tissue models with a spatially defined definition of bioink and CPC[3] (Fig.1B). For bioprinting, human chondrocytes were isolated, expanded and embedded into the Alg/MC hydrogel prior to fabrication of multiphasic constructs. Viability and cell behaviour was assessed. Therefore, cell fate in response to chondrogenic differentiation conditions was evaluated on gene expression and protein level, as well as via the production of ECM molecules.
To study the effect of different plotting patterns and modified internal architecture, cell-free monophasic scaffolds with a strand and pore structure based on sine waves of varying amplitude and frequency were produced and evaluated regarding their mechanical properties and porosity.

Results and Discussion

For chondrocytes laden in mono- and multiphasic constructs, the recovery of their chondrogenic phenotype was proven: The majority of cells survived the fabrication process, and remained located inside the hydrogel matrix with a homogeneous distribution when supplied with chondrogenic factors (TGF-β3) (Fig.1C,D). Cells presented the expression of respective marker genes (COL2, ACN), and were able to produce characteristic ECM components. Multiphasic volumetric constructs from two different materials were successfully processed, and phases

were able to fuse by an optimized combination of the respective setting and ionic crosslinking process. A concept for the fabrication of an artificial osteochondral tissue interface was developed.
The fabrication of structures in clinically relevant dimensions was realized presenting different anatomical geometries based on CT data extraction, such as a human scaphoid bone based on CPC, or an Alg/MC-based model of a human lateral meniscus. For this meniscus model, geometry were was identified in CT data (Fig.1F), transferred to a virtual environment (Fig.1E, Dornheim Segmenter Analyzer® 2016, Geomagic Studio® 2016) and plotted with high shape fidelity using CPC as support material (Fig.1G).
A concept for a density gradient was established via anisotropic strand patterns with varying frequency, amplitude and angle, exemplarily illustrated in Fig.1H. For respective scaffolds, the triggering of mechanical properties via modified sine wave pattern with specific frequency and amplitude, distance between adjacent strands, and angle switch between single layers, was characterized.

Conclusion

The project proves the promising potential of a combination of an alginate-based bioink and CPC for 3D plotting of biofunctional osteochondral tissue models. Towards fabrication of multicellular, multiphasic tissue substitutes, further investigation is required developing and optimizing co-culture models of cells that can be triggered for differentiation in both chondrogenic and osteogenic lineage with a spatially defined distribution inside one scaffold. Furthermore, this study provides a novel concept of alternative plotting paths resulting in an anisotropic internal architecture of volumetric constructs with a defined external shape based on DICOM data. Those findings can be easily translated to various tissue types, diverse materials and other fabrication methods.

References

[1] Schütz K, Placht AM, Paul B, Brüggemeier S, Gelinsky M, Lode A: Three-dimensional plotting of a cell-laden alginate/methylcellulose blend: towards biofabrication of tissue engineering constructs with clinically relevant dimensions, *J Tissue Eng Regen Med* **2017**, 11 (5), 1574-1587
[2] Lode A, Meissner K, Luo Y, Sonntag F, Glorius S, Nies B, Vater C, Despang F, Hanke T, Gelinsky M: *J Tissue Eng Regen Med* **2014**, 8 (9), 682-693
[3] Ahlfeld T, Doberenz F, Kilian D, Vater C, Korn P, Lauer G, Lode A, Gelinsky M: Bioprinting of mineralized constructs utilizing multichannel plotting of a self-setting calcium phosphate cement and a cell-laden bioink, *Biofabrication***2018**, 10 (4)

Acknowledgement

The authors sincerely would like to thank the European Social Fund ESF and the Free State of Saxony for the financial support in the course of the TU Dresden-based young researchers group *IndivImp*.

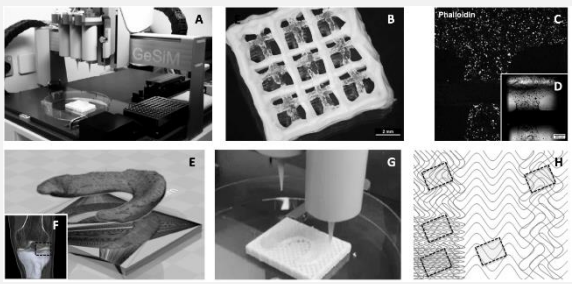

3D plotting of multiphasic cell-laden and anatomically shaped constructs
GeSiM BioScaffolder 3.1 (A). Multiphasic constructs based on Alg/MC bioink and CPC (B). human chondrocytes embedded in hydrogel phase of multi-material scaffolds after cytoskeletal fluorescence staining (C) at the CPC-hydrogel interface (brightfield image, D). Construction (E) of anatomical geometry and support structure based on CT data (F), fabrication of the meniscus model (G). Representation of alternative plotting paths based on sine waves (H).

9:30 a.m. – 11:00 a.m.

Hall 2

X-OS37 | Biopolymers and artificial ECM 1

X-OS37-01

Corneal Stromal Biomaterials Inspired by Supramolecular Chemistries

Antonio J. Feliciano[1], Floor A. A. Ruiter[1], Stefan Giselbrecht[1], Lorenzo Moroni[1], Patricia Y. Dankers[2], Clemins Blitterswijk[1], Tonny Bosman[3], Matthew B. Baker[1]

[1]Maastricht University, MERLN, Maastricht, NL; [2]Eindhoven University of Technology, Biomedical Engineering, Eindhoven, NL; [3]SupraPolix, Eindhoven, NL

Introduction

The phenotypic control of corneal keratocytes is crucial for the success of both stromal inlays and regenerative constructs. In fact, there have been FDA warnings for some corneal inlays due to corneal haze and fibrosis. Designing a material that does not activate keratocytes would be worthwhile for future inlay products. In addition, stromal regenerative constructs, as an alternative to donor tissue, require ECM production in the same highly ordered structure of the cornea; any disruption in the cornea's tissue can cause a decrease in transparency. In order to maintain corneal keratocyte phenotype, we are developing supramolecular polymers for these two applications. Supramolecular chemistry relies on non-covalent interactions that are biomimetic and dynamic. We propose a poly(zwitterionic-co-UPy) polymer for use in corneal tissue products such as presbyopic inlays and other supramolecular polymers for use as stromal constructs in order to achieve an optimal keratocyte.

Experimental Methods

Iso-UPy, courtesy of SupraPolix (Eindhoven,NL) was coupled to hydroxyethyl methacrylate (HEMA) via a urethane linkage to create UPy-methacrylate (UPyMA). ^{1}H NMR was performed on monomer and polymer species to confirm products. We prepared a controlled radical polymerization, by reversible addition-fragmentation chain transfer (RAFT), to prepare different molecular weights of MPC-UPyMA$_x$. For the copolymerization of UPyMA and MPC, 0, 1.25, 2.5, 5 mol% UPy monomer concentrations were sampled at different times to determine molecular weight and conversion %. FTIR was also performed to show the addition of UPy functionalization of copolymers. Finally, anti-fouling and cell viability were assessed.

Results and Discussion

We have confirmed that RAFT via UPyMA and MPC monomers is achievable. The polymerization was monitored at different times to assess reaction kinetics. Monomer conversion was analyzed by the disappearance of vinyl protons in ^{1}H NMR and compared to backbone protons for kinetic measurements. By plotting the logarithm of M_n/M_o (instantaneous monomer concentration to initial monomer concentration), we can compare the linearity of the data to pseudo-first-order kinetics which is associated with RAFT polymerizations. Because RAFT offers good control over molecular weight, we chose eight hours as the termination point and calculate the molecular weight M_n by end-group analysis on H^1 NMR. Calculated Mn's and associated UPy content (mol%) were tabulated. The antifouling character was confirmed.

Conclusion

These preliminary results show that we are able to synthesize copolymers of UPyMA and MPC using RAFT polymerization. Polymerizations can be controlled by Mn and UPy content (mol%). We have fabricated the polymers into thin films and coatings, which can be applied to corneal inlays. We also show proof of concept work for new supramolecular polymers based on host-guest complexation.

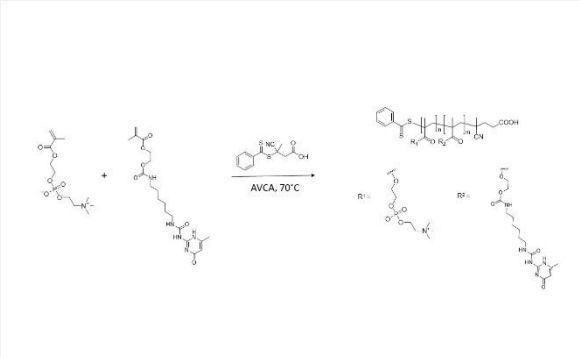

Reaction Mechanism
RAFT polymerization of MPC co UPyMA

X-OS37-02

Double network photocrosslinked hydrogels from modified hyaluronic acid and Poly(ethylene glycol) diacrylate for load bearing tissue

Alfredo Ronca[1], Ugo D'Amora[1], Maria Grazia Raucci[1], Hai Lin[2], Yujiang Fan[2], Xingdong Zhang[2], Luigi Ambrosio[1]

[1]National Research Council (CNR), Institute of Polymers, Composites and Biomaterials (IPCB), Napoli, IT;
[2]Sichuan University, National Engineering Research Center for Biomaterials (NERCB), Chengdu, CN

Introduction

Over the past years, natural hydrogels have been employed in regenerative medicine, as they can promote efficient biomolecular interactions with cells. However, their viscoelastic properties are the main issue limiting their applicability, especially with respect to regeneration of load bearing tissue. For this reason, the use of hydrogels has been limited to specific fields of interest, such as drug delivery and water absorption, where their mechanical properties are not required. Blending two polymers has been a common approach to develop a new class of biomaterials showing combinations of properties not achievable by using individual polymers. In particular, blends of synthetic and natural polymers allow to obtain materials that merge a wide range of physico-chemical properties of synthetic polymers as well as the biocompatibility, the safety and side effects avoidance of natural ones [1]. “Double network” (DN) hydrogels, developed for the first time by Gong et al., represent a specific class of IPNs as they combine a polyelectrolyte as first network and a neutral polymer as second one [2][3]. In this study an innovative hydrogel, based on DN approach, has been developed by integrating a poly(ethylene glycol) diacrylate (PEGDA) second network into a chemically modified hyaluronic acid sodium salt (HAs) first network.

Experimental Methods

Photoactive polymerizable motifs as maleate (Ma) and methacrylated (Me) groups were grafted onto a HAs (M_w=≈340kDa) in order to obtain photocrosslinkable hyaluronic acid (MaHA – MeHA respectively) to prepare the first single network (SN). Ma/HAs and Me/HAs molar ratios were varied in order to obtain hydrogel with different degree of substitution (DS). DN hydrogels were synthesized by two-step reaction procedure *as depicted in Figure 1*. **First step**: to obtain HAs crosslinked first network a 0.1% (w/v) Irgacure 2959 solution (Sigma) was prepared. MaHA or MeHA were added to the initiator solution with a concentration of 30 mg/ml and 20 mg/ml, respectively. Cylindrical samples were produced by exposing the photocrosslinkable hydrogels to UV light (OmniCure S1500 (USA), λ= 365 nm,~16 mW/cm^2) for 60 s. The samples were stored at 4°C in distilled water (dH_2O) for 24h. **Second step**: the HAs disc-shaped hydrogels (1st network) were dipped in the PEGDA (2nd network) solution until reaching equilibrium for 4 days. The extracted discs were exposed to UV light for 300 s, washed in dH_2O and stored at 4 °C. The mechanical properties of DN hydrogels were compared with those of MaHA and MeHA SN hydrogels. The effect of the second network and the concentration of each component on the physico-chemical and morphological properties of the DN hydrogels were also studied. Lastly, the viability, proliferation of human Mesenchymal Stem cells (hMSC) on DN specimens were investigated.

Results and Discussion

Physico-chemical characterization by ^{1}H NMR confirms the success of substitution showing the characteristic peak of maleate and methacrylate group at 6.1-6.7 and 5.6-6.0 respectively. Dinamical mechanical analysis (DMA) was

employed to compare mechanical properties of both DN and SN hydrogels as a function of material composition. DN hydrogels exhibited excellent overall mechanical properties. A 10-time increase of the storage modulus, if compared to neat MeHA, can be observed for the DN hydrogels. Incorporation of PEGDA in MaHA 1st network not only increased the density of polymer chains, but also increased the friction between chains, thus leading to higher storage moduli of DN hydrogels than SN ones. The morphology of dried hydrogels were evaluated by SEM. DN hydrogel showed a more compact 3D structure, if compared to SN morphology, with thick pore walls and an average pore size ranging from 30 to 40 μm due to the presence of the second PEGDA network, which increased the relative crosslinking density of the structure. The cell viability expressed in terms of percentage of cells on material surface than control (tissue culture plates), after 24 h of culture time, was analyzed. The results demonstrated a good cell viability and proliferation in the first 24 h of culture for all materials.

Conclusion

In this study DN blends were suitably prepared by integrating a PEGDA into HAs hydrogel matrix. The developed hydrogels are characterized by enhanced mechanical behaviour if compared to SN. The collective mechanical and biological performance profile of the MaHA/PEGDA and MeHA/PEGDA DN hydrogels strongly suggests that this class of material has great potential as load-bearing materials for biomedical applications.

References

1. Suh, J.K.F., Howard, W.T.M. Biomaterials **2000**, 21, 2589–2598.
2. Ronca, A., D'Amora, U., Raucci, M., Lin, H., Fan, Y., Zhang, X., Ambrosio, L. *Materials*, **2018,** 11(12), 2454.
3. Gong, J.P.; Katsuyama, Y.; Kurokawa, T.; Osada, Y. *Adv. Mater.***2003**, *15*, 1155–1158.

Acknowledgement

The authors would like to thank the Progetto Premiale di AREA SCIENCE PARK "OPEN LAB - A System of Open Research Facilities" for the support.

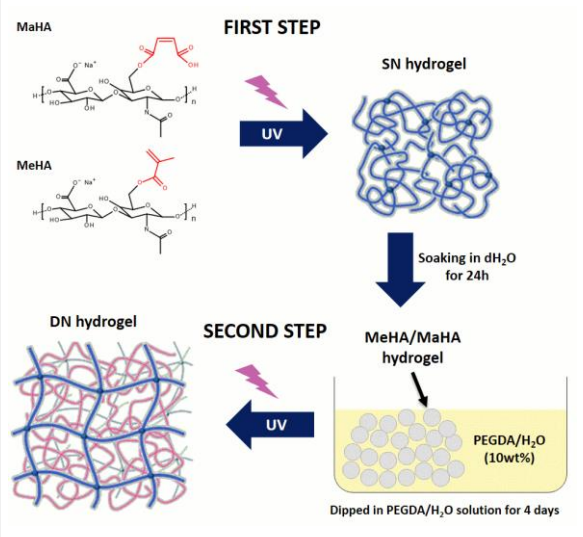

Figure 1
Two-step method to prepare photocrosslinked DN hydrogels.

X-OS37-03

Fabrication of a novel class of regenerative collagen membranes by electrophoretic deposition

David J. Barrett, Matthew Linley, Serena M. Best, Ruth E. Cameron

University of Cambridge, Department of Materials Science and Metallurgy, Cambridge, GB

Introduction

Collagen membranes are widely used as a biomaterial, as it has excellent biocompatibility, resorbability, and low immunogenicity[1]. We have developed a platform technology based on electrophoretic deposition that allows that fabrication of free-standing collagen membranes in a range of complex shapes and large sizes that can't be produced from decellurised animal tissue. Complex shapes including tubes can be manufactured, as well as macro and micro-texturing, alignment of fibres in successive layers, command-set layers, and incorporation of live cells.

Electrophoretic deposition is a widely used technique in industry for forming coatings and structures with reproducible properties and of arbitrary shape and size[2]. It works by applying an electric field to a solid suspension of charged particles, causing the particles to move towards one of the electrodes, and leading to deposition of a film. We show how, by altering the properties of the field, suspension, and electrode a wide range of collagen based membranes can be produced rapidly and repeatably.

Experimental Methods

Insoluble collagen I was rehydrated using 0.05M acetic acid and ethanol was added to 50 vol% before homogenisation until a smooth consistency was achieved.

Hyaluronic acid was prepared by dissolving sodium hyaluronate in DI water under homogenisation on ice. Ethanol was then added to 70 vol% and homogenised until a smooth consistency was achieved.

Deposition was performed using custom deposition apparatus consisting of two 316L steel plates separated by adjustable silicone spacers. The electric field consisted of a series of pulses or as a continuous voltage produced with an arbitrary waveform generator.

Dry SEM were sputter coated with gold and scanned at 15kV accelerating voltage in SEI mode. Hydrated SEM samples were soaked in DI water before being frozen in slushy nitrogen and shattered under vacuum, before being coated in platinum in situ and imaged at 8kV with a Zeiss EVO HD15 SEM in SEI mode.

Cell deposition was performed with HT1080 cells. Cells were deposited before being permeabilised with Triton-X and stained with EthD-1 and calcein AM. Imaging was performed with a fluorescent microscope.

Results and Discussion

Table 1 shows a range of different ways in which the technology can be used to produce membranes with specific properties such as fibre alignment, complex shapes, or micro-texturing. Further, these properties can be combined in a single membrane, allowing the design of membranes tailored towards specific clinical needs.

Figure 1 shows a subset of the collagen and glycosaminoglycan membranes that we have formed using EPD, some of which are shown schematically in Table 1. Figure 1a shows that micro and macroscopic texturing on the electrode is faithfully recreated on the structure of collagen membranes formed. 1b shows that large membranes can be formed. 1c demonstrates that distinct multi-layers of dissimilar biomaterials can be produced with EPD, even when rehydrated. 1d shows that deposition of live cells by EPD is possible, live cells appear green and are deposited

evenly across the membrane where exposed to the electric field, and are not present on the shielded areas of the membrane.

Conclusion

We have shown that electrophoretic deposition can be used as a technique to reliably produce free standing films of proteins and glycosaminoglycans rapidly and without macroscopic defects. These films can be produced in a range of sizes and thicknesses, and can have a large number of desirable properties imparted to them during fabrication including live cell incorporation, aligned fibres, and command-set properties.

References

[1] W. Friess, Collagen – biomaterial for drug delivery, Eur. J. Pharm. Biopharm. 45 (1998) 113–136.

[2] A.R. Boccaccini, S. Keim, R. Ma, Y. Li, I. Zhitomirsky, Electrophoretic deposition of biomaterials., J. R. Soc. Interface. 7 Suppl 5 (2010) S581-613. doi:10.1098/rsif.2010.0156.focus.

Acknowledgement

The authors would like to thank the EPSRC (Grants no: EP/K503009/1, EP/J500380/1, EP/L504920/1, and RG/68240) and Geistlich Pharma AG for providing financial support to this project.

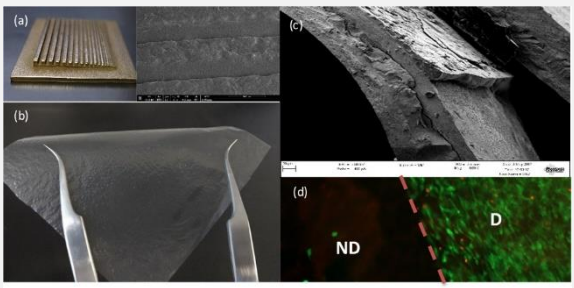

Selection of possible membrane features

Figure 1. Illustrations showing the variety of different collagen structures than can be formed (a) Electrode used for deposition and corresponding micro-textured collagen membranes, (b) Large 10cm*10cm collagen membrane formed by EPD, (c) cryoSEM showing clearly defined layers of hydrated collagen/hyaluronic acid multilayers, (d) Flourescence image showing spatial control of live cell deposition by EPD. Cells can be seen deposited only on the right hand side, makred by D, and not on the area of the membrane marked by ND. Live/dead staining shows living cells in green and dead cells in red, and the dashed line indicates the approximate edge of the applied field.

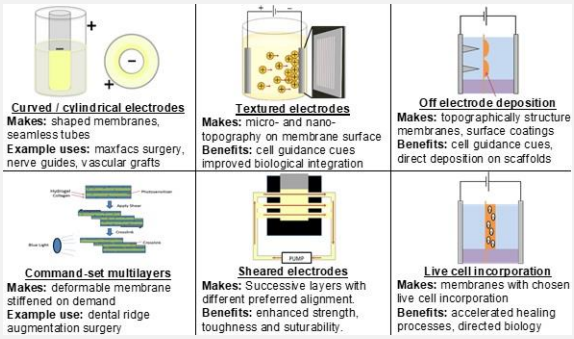

Table of possible fabrication modalities

Table 1. Schematics showing how varying the electrodes or deposition parameters during fabrication can lead to formation of membranes with specific desirable properties

X-OS37-04

Biomimetic materials toward enhanced bioengineered tissue vascularisation

Fengying Tang[1], Marissa Baptista[1], Xiaoting Lin[1], Shouyuan Jiang[1], Cesar Alcala-Orozco[2], John Whitelock[1], Khoon Lim[2], Megan Lord[1], Jelena Rnjak-Kovacina[1]

[1]University of New South Wales, Graduate School of Biomedical Engineering, Sydney, AU; [2]University of Otago Christchurch, Department of Orthopaedic Surgery & Musculoskeletal Medicine, Christchurch, NZ

Introduction

Biomaterials play a central role in modern regenerative medicine and tissue engineering strategies as tuneable biophysical and biochemical environments that direct cellular behaviour and function. However, one of the biggest obstacles in translating advances in biomaterials research to clinical applications is lack of sufficient vascular tissue regeneration upon biomaterial implantation. We develop 3D porous, silk fibroin biomaterials for cardiovascular regeneration, including vascular grafts and cardiac patches, with a particular emphasis on enhancing vascular ingrowth and integration with the host tissue. Silk biomaterials with tuneable physical properties serve as a platform to develop biomaterial vascularisation strategies, including biofabricated vascular-like microchannels and biofunctionalisation with vascular niche molecules, including perlecan. Perlecan, a key basement membrane proteoglycan, supports angiogenesis via endothelial cell interactions and binding and signalling key vascular growth factors.

Experimental Methods

3D porous silk fibroin scaffolds were fabricated via a freeze drying process. Microchannels were introduced by templating silk scaffolds around an array of wires or around a 3D printed sacrificial polymer template. C-terminal domain V of human perlecan (Leu3626 - Ser4391) was expressed as a proteoglycan in HEK293 cells. Silk scaffolds were functionalised with perlecan via passive adsorption. The effect of biomaterial design features on tissue integration and vascularisation was investigated by implanting acellular silk scaffolds on chicken chorioallantoic membranes or subcutaneously in mice.

Results and Discussion

Microchannels played an essential role in enhancing cell infiltration and delivering oxygen and nutrients to cells throughout 3D silk scaffolds. Human endothelial cells seeded on silk scaffolds in the presence of microchannels showed increased expression of angiogenic growth factors and cytokines relative to cells seeded on scaffolds with no channels. Microchannels promoted enhanced integration of silk scaffolds with the host tissue and improved vascularisation *in vivo.*

Recombinant C-terminal domain of perlecan promoted angiogenesis via its glycosaminoglycan chains and FGF2 signalling *in vitro* and *in vivo*. Silk biomaterials functionalised with perlecan supported a significant increase in blood vessel ingrowth, with a particular increase in the number of small (<20µm) and large (>80 µm) blood vessels. The vessels were stable and functional as demonstrated by smooth muscle actin expression and perfusion with contrast agents in live animals.

Conclusion

This work demonstrates the key role biomaterials play in promoting vascular ingrowth and integration of bioengineered tissues and the potential of silk biomaterials in cardiovascular device development.

X-OS37-05

A low-temperature, high-pressure sintering procedure for the rapid fabrication of biosubstrates starting from dry silk fibroin.

Devid Maniglio, **Alessio Bucciarelli**, Antonella Motta, Alberto Quaranta

University of Trento, Trento, IT

Introduction

Over the last two decades, the protein fibroin from the silkworm has been used to produce a variety of materials with a wide range of advanced applications. Due to the unique combination of properties such as mechanical strength and toughness, biocompatibility, biodegradability, thermal stability, and easy processability[1,2], regenerated silk fibroin has been used as a functional biomaterial, adopted when a positive interaction with living tissue is required. Solid-fibroin is a bulk non-porous material that is usually prepared starting from a fibroin solution and passing through a liquid-gel-solid transition. While a plethora of micro and nanoscale architectures of silk fibroin have been explored in literature - films, fibers, microparticles, and gels, building larger, macroscale objects of fibroin has been challenging. Only recently, a method to produce bulk-fibroin monoliths based on solvent evaporation of fibroin solution (*solid-fibroin by casting*) was proposed.[3] In this work we propose a low temperature sintering procedure based on a thermal-reflow to produce in fast fashion monoliths of solid-fibroin starting from lyophilized fibroin. Thermal-reflow is a well-known mechanism that takes place when the glass transition temperature of the material is lower than the temperature used to process it. We were able for the first time to conduct a thermal reflow on lyophilized silk fibroin at 40 °C, associating to the water addition trough moisture absorption to a high-pressure compression.

Experimental Methods

To optimize the amount of material undergone to the solid transition a full factorial design of experiment was used. We studied the material in the crucial phases of the optimized procedure, by DSC, FTIR and SEM, proving both that the thermal-reflow occurs even a low temperature if driven by a high-pressure process and the fact that an effective compaction can be performed only on a low crystallinity fibroin. Finally, a mechanical characterization, and a preliminary in vitro test were conducted: human adipose-derived mesenchymal stem cells were cultured on both LTS fibroin samples and PCL samples (control system), to evaluate cell adhesion capability. After each time point, cell adhesion, morphology and distribution were analyzed by confocal microscopy.

Results and Discussion

The process was optimized using a design of experiment method to obtain a full transition from lyophilized silk fibroin to its solid form: the best result was obtained minimizing the area underlining the VIS spectrum (increasing the transparency) and maximizing the compression young modulus (evidenced in the figure). The analysis conducted with FTIR on the main stages of the process revealed that an excessive transition to β–parallel structure, due to a prolongated water treatment, doesn't allow the transition to the solid state; the transition occurs if the secondary structures are not enough stable to be able to re-organize themselves in more stable phases during the compression phase. The glass transition temperature was detected by DSC. Interestingly, the rapid addition of water in the material through moisture absorption didn't change the T_g respect the lyophilized silk fibroin. Instead a decrease of almost 120 °C in the T_g has been individuated after the compression. The SEM analysis during different time points in the compression proved the presence of a viscous flow. So, we could deduce a decrease in the T_g under the process

temperature (40 °C) when the high pressure is applied to the moisturized lyophilized silk fibroin. The preliminary biological results, showed by confocal imaging, indicate a promising role of LTS fibroin samples in biomedical applications for promoting cell adhesion and proliferation.

Conclusion

In this work we reported a method to obtain a compact material from dry fibroin in a single compression mold step at low temperature. We were able to optimize a fast, low temperature method to obtain large monoliths of solid – fibroin, reporting, for the first time a thermal – reflow at 40 °C for lyophilized fibroin. Large objects can be produced in few minutes with a high reproducibility. The mild forming conditions allow the possibility to incorporate temperature degradable bioactive additives.

References

[1] Altman, G. H. *et al.* Silk-based biomaterials. *Biomaterials***24,** 401–416 (2003).

[2] Koh, L. D. *et al.* Structures, mechanical properties and applications of silk fibroin materials. *Prog. Polym. Sci.***46,** 86–110 (2015).

[3] Marelli, B. *et al.* Programming function into mechanical forms by directed assembly of silk bulk materials. **114,** (2017).

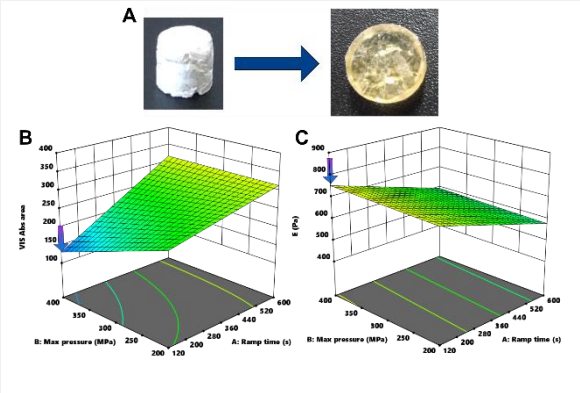

Optimization of the solid transition
Solid-solid transition of lyophilized silk fibroin (top) and optimization of the transparency and compressive modulus parameters (bottom).

X-OS37-06

Elettrical responsive scaffolds for endogenous regeneration

Francesca Scalera[1], Anna G. Monteduro[1,2], Giuseppe Maruccio[1,2], Laura Blasi[3], Clara Piccirillo[1]

[1]CNR, Institute of Nanotechnology, Lecce, IT; [2]University of Salento, Department of Mathematics and Physics, lecce, IT; [3]CNR, Institute for Microelectronics and Microsystems, Lecce, IT

Introduction

The development of biomimetic structure able to induce an endogenous regeneration of damaged organs and tissues is a challenging goal of last frontiers of tissue engineering. The repairing of an injured tissue is frequently difficult for the formation of a scar that limits the adhesion, as well as the migration and proliferation of elettroactive cells. In these cases, a differentiation of the resident and/or transplanted cells has to be induced, within a biomimetic matrix; electrical stimulation can be employed for this purpose. Carbon based biomaterial represents a promising class of composites, that can be used for electroactive tissues, such as heart, muscle, nerves, and even skin. [1,2]
In this work, a novel three-dimensional electrical responsive chitosan-graphite scaffold was fabricated, using pyrolised cork (PC) as source of graphite and as conductive phase. The electrical conductivity and the cytotoxicity of chitosan scaffolds with different percentage of pyrolysed cork powders were studied.

Experimental Methods

The cork powder, supplied by Amorim Cork Composite (Mozelos, PT), was pyrolysed at 900 °C using a Thermal Technology 1000-3650-FP20 Vacuum Furnace; an oxygen-free nitrogen gas flow was flushed inside the furnace during the whole process. A cycle with a slow heating ramp was employed, to preserve the characteristic honeycomb shape of the cork [3].
Chitosan and Chitosan/pyrolised cork (Ch/PC) scaffolds were made by freeze-drying technique. 2% (w/v) chitosan (low Molecular Weight, Sigma Aldrich) solution was prepared in 1%(v/v) acetic acid and stirred for 12 hours at room temperature, froze at -80°C (freezing rate of 1°C/min) then lyophilized for 19 hours at 0°C under vacuum. For Ch/PC scaffolds, six percentage of PC (0,01-0,1-0,25-0,5-0,75-1 % (w/v)) were used for the chitosan solution. The obtained scaffolds with uniform size (5 cm in diameter, 10 mm in thickness) were ionically crosslinked by immersing them in a mixing of 1M NaOH and of 0.5M Na_2SO_4, in a ratio of 1:4 respectively, for 1h. Cross-linked scaffold were then double-washed in order to remove the reagents excess and freeze-dryed again.
The scaffolds morphology was analysed by Scanning Electron Microscopy (SEM). A FTIR analysis was also performed to evaluate the interaction between functional groups of Chitosan and Graphite.
The electrical properties of dry and wet scaffolds were investigated at room temperature. The volume conductivity was evaluated from the I-V samples characteristics measured by using a Yokogawa 7651 programmable DC source, a SR570 low noise current preamplifier and a HP34410 digital multimeter.
Cellular studies were conducted with MCF-7 cell lines. The cell viability was examined by 3-(4,5-dimethylthiazol-2-yl)-2,5-diphenyltetrazolium bromide (MTT) assay after incubating cells with Ch/PC scaffolds at different time intervals.

Results and Discussion

SEM analyses showed that both Ch and Ch/PC scaffold exhibit comparable pores morphology and size. The scaffolds pores size is in the range of 150-200 µm (fig1b). The powders are organized in clusters inside the scaffold, even if the powder (fig1a) maintained the original honey structure with a pores size of 20 µm.

The electrical measurements performed on both dry and hydrated scaffolds showed that the bulk conductivity of chitosan scaffolds strongly increases by adding a 1% of PC in the chitosan matrix. Specifically, the conductivity goes from 0.3 µS/m for pure chitosan to 5.5 mS/m for 1% Ch/PC in the dry state. For the hydrated state, on the other hand, the conductivity changes from 680 µS/m to 2.2 mS/m respectively for Ch and Ch/PC (1%) scaffolds. It can be seen the conductivity of hydrated chitosan scaffolds is of about 3 order of magnitude higher than the chitosan in the dry state, since the bulk conductivity is largely due to the liquid medium.
However, a significant increase due to the PC powder can be observed also for the scaffolds in the hydrated state.
The conductivity values recorded for the investigated composite material make Ch/PC a promising support for the endogenous regeneration of severely damaged human tissues.

Conclusion

A novel electrical responsive porous scaffold for endogenous tissue regeneration was successfully developed. Chitosan was used as natural polymeric matrix and graphite obtained from the pyrolysis of natural cork, as conductive phase.
The Ch/PC composite scaffolds showed a high and homogenous porosity whereas the graphite phase improved the electrical conductivity. The proposed composite scaffolds showed a good biocompatibility making them potential electroactive scaffold for endogenous tissues regeneration.

References

[1] Ana M. Martins, George Eng, Sofia G. Caridade, João F. Mano, Rui L. Reis, and Gordana Vunjak-Novakovic, Electrically Conductive Chitosan/Carbon Scaffolds for Cardiac Tissue Engineering, Biomacromolecules. 15 (2014), 635–643.
[2] Hosoyama K, Ahumada M, Goel K, Ruel M, Suuronen EJ, Alarcon EI. Electroconductive materials as biomimetic platforms for tissue regeneration. Biotechnol Adv. 2019 Feb 20. doi: 10.1016/j
[3] Alessandra Quarta, Rui M.Novais, Simona Bettini, Michele Iafisco, Robert C.Pullar, Clara Piccirillo, A sustainable multi-function biomorphic material for pollution remediation or UV absorption: Aerosol assisted preparation of highly porous ZnO-based materials from cork templates. Journal of Environmental Chemical Engineering, 7 (2019), 102936.

Acknowledgement

The present work was supported by the project HApECork, funded by Fondazione con il Sud (project 2015-0243).

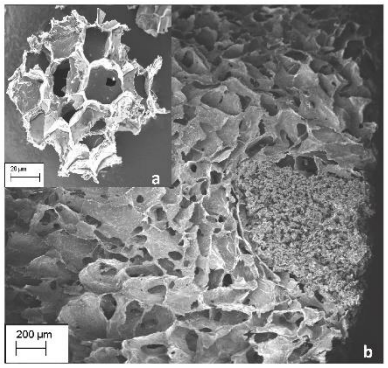

Figure 1.
SEM images of (a) PC powder and (b) Chitosan/PC scaffolds with 1%wt/vol of PC

9:30 a.m. – 11:00 a.m.

Hall 4

X-OS19 | Hydrogels for tissue engineering 2

X-OS19-01

Antibacterial injectable bionanocomposite containing green synthesized silver nanoparticles for bone tissue engineering

Assunta Borzacchiello[1], **Pooyan Makvandi**[1,2], Francesca Della Sala[1], Ghareib W Ali[3], Wafa I. Abdel-Fattah[3], Luigi Ambrosio[1]

[1]National Research Council, Institute for Polymers, Composites and Biomaterials, Napoli, IT; [2]University of Naples Federico II, Department of Chemical, Materials and Production Engineering, Napoli, IT; [3]National Research Centre, Inorganic Chemistry Division and Mineral Resources, Cairo, EG

Introduction

In bone tissue engineering, biomimetic scaffolds comprising calcium phosphate bioceramics, e.g. β-tricalcium phosphate (β-TCP), are aimed to serve as an artificial temporary extracellular matrix (ECM) in order to support cell adhesion and guide new bone tissue formation. The combination of bioceramics with organic materials, such as hydrogels containing hyaluronic acid (HA), naturally occurring polysaccharide that serves as a major component of extracellular matrix in mammalian connective tissues, is highly advantageous to overcome the brittleness of their intrinsic nature. Among the different types of hydrogels, thermosensitive hydrogels based on amphiphilic copolymers, such as Pluronics (polyethylene oxide-polypropylene oxide copolymers, PPO-PEO-PPO), thanks to their ability to undergo thermal gelation as well as low cytotoxicity, have attracted significant attention in biomedical applications and pharmaceutical industries [1,2].

However, infections during or post scaffold transplantation are still challenging which reduce the efficacy of bone healing. After the transplantation, infections may also be distributed to the scaffold from other sources of inflammation through bloodstream. Silver nanoparticles have shown a strong capability to inhibit or decline infections and have been also utilized for bone regeneration applications. Among different methods, biosynthesis of silver NPs, by using plant extracts, has received considerable attention due to the growing need to develop environmentally and non-toxic technologies [3].

On considering the properties of β-TCP, HA, Pluronic, and Ag NPs, our work was aimed to fabricate thermosensitive hydrogel biocomposites for bone tissue repair, which can be injected easily and possess antimicrobial properties to prevent infection.

Experimental Methods

Ag NPs were synthesized within corn silk extract (CSE) by microwave assisted method. The hydrogels were prepared by dissolving different amounts of HA, β-TCP, Pluronics F127 and F68 in CSE with and without AgNPs. The hydrogels composition was optimised by rheological analysis.

Results and Discussion

Fig. 1A shows the schematic illustration for synthesis and stabilization of Ag NPs by CSE. **Fig. 1B** shows the results of DLS analysis of silver NPs and it can be seen that the prepared NPs have a narrow size distribution with a mean diameter of 49±2 nm. TEM image (**Fig. 1C**) shows well-dispersed silver nanoparticles which are spherical in shape with an average size of 13±1 nm.

Rheological experiments demonstrated that the thermosensitive hydrogels have good mechanical properties with gelification temperature (T_{gel}) close to body temperature (**Fig. 2A)**. The systems showed antibacterial activity toward gram-positive (*Bacillus Subtilis, Staphylococcus Aureus*)and gram-negative (*Pseudomonas Aeruginosa, Escherichia*

Coli) bacteria (**Fig. 2B**). L929 cells exhibited a noncytotoxic and typical mouse fibroblast-like cellular morphology after 24 h of the incubation with the samples (**Fig. 2C** and **D**). Schematic representation of injection of the thermosensitive nanocomposite are presentedn in **Fig. 2E**.

Thermosensitive hydrogels, which possess good retention at the application site, have appealed a great deal in biomedical and clinical fields. At room temperatures, the systems are liquid and could be injectable whereas, at the body temperature, they became a gel. This fast sol-to-gel phase transition behavior is beneficial for cell entrapment to give a uniform distribution of cells within the gelled matrix. HA offers many advantages as a tissue scaffold which including biodegradability, biocompatibility, and bioresorbability which have been shown in many studies. Hyaluronic acid could activate cell surface receptors, influencing intracellular signaling cascades for cell growth, migration, proliferation, and differentiation [4].

One of the main reasons of scaffold failures is due to the implant-associated bacterial infections. Hence, using antibacterial scaffolds helps more success for bone tissue formation which are of clinical importance. In this study, we used spherical particles of Ag to impart antibacterial activity to the thermosensitive hydrogels to avoid bacterial contamination [5].

Conclusion

In conclusion, silver NPs were biosynthesized in an aqueous medium of corn silk extract without using toxic chemical reagents. The new thermosensitive HA-based nanocomposite hydrogels demonstrated good mechanical properties with T_{gel} close to the body temperature. The system revealed desired antibacterial activity against several gram-positive and gram-negative bacterial strains which can prevents bacterial infection. In addition, from the biological point of view, the nanocomposites revealed appropriate biocompatibility in comparison with the control samples.In addition, from the biological point of view, the nanocomposites revealed appropriate biocompatibility in comparison with the control samples.

References

[1] Tsai et al., Carbohydrate polymers 135 (2016) 308-315.

[2] Dessi et al., Journal of Biomedical Materials Research Part A 101 (2013) 2984-2993.

[3] Nair et al., Current opinion in biotechnology 22 (2011) 721-725.

[4] Son et al., Journal of biomaterials applications 29 (2015) 988-1002.

[5] Zhou et al., Biomaterials 35 (2014) 10033-10045.

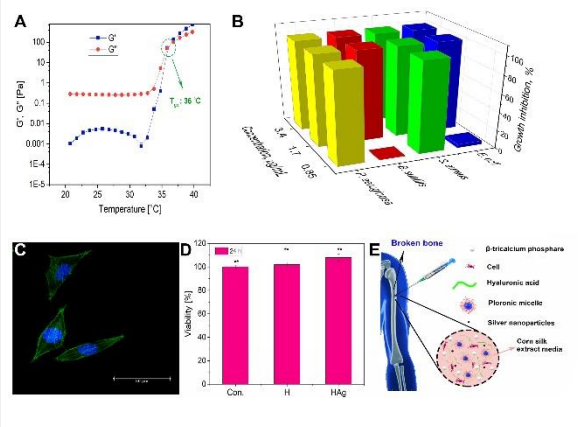

Fig. 2

The sol–gel phase transition by rheological experiments. Elastic and viscous moduli as a function of the temperature at a frequency value of 0.01 Hz. (B) Antibacterial activity of different concentration of Ag NPs against Gram-positive (*B. subtilis* and *S. aureus*) and Gram-negative (*P. aeruginosa* and *E. coli*) bacteria after 24 h. Cell morphology (C) and cyrotoxicity (D) of samples after 24 h. (E) Schematic representation of injection of the thermosensitive nanocomposite containing β-tricalcium phosphate for bone tissue regeneration.

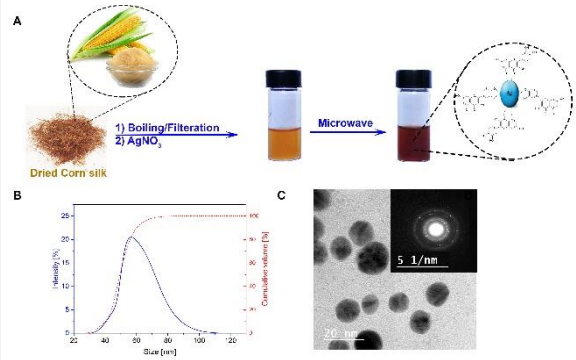

Fig. 1
(A) Illustration for the synthesis of silver nanoparticle in corn silk extract via microwave-assisted green approach. The darker color shows the Ag ions were converted to Ag NPs which stabilized by flavonoid compounds of corn silk. Size distribution measurements by DLS (B) and TEM image (C) of Ag NPs in corn silk extract solution. The bar for TEM image represents 20 nm.

X-OS19-02

Tuning the transport of signaling molecules in heparin based-hydrogels

Yanuar D. P. Limasale[1], Passant Atallah[1], Uwe Freudenberg[1], Carsten Werner[1,2], Ralf Zimmermann[1]

[1]Leibniz Institute of Polymer Research Dresden, Max Bergmann Center of Biomaterials, Dresden, DE; [2]Technische Universität Dresden, Center for Regenerative Therapies Dresden, Dresden, DE

Introduction

The modulation of signaling molecules transport within cell instructive-hydrogel materials is critically important to regulate the fate of embedded cells as well as the responses of host tissues surrounding the scaffold [1]. Particularly, the incorporation of glycosaminoglycans (GAGs) into such cell-instructive materials has been successfully applied to control the mobility and activity of many soluble signaling molecules in various applications [2-4]. In this study, we investigated the effect of tailoring the heparin content within hydrogels formed from heparin and 4-arm poly(ethylene glycol)-(starPEG) peptide conjugates in order to control gradient formation and the release of SDF1α and VEGF165 within/out of the matrices. As proof of concept, the formation of local tubular structures and chemotaxis of human umbilical vein endothelial cells (HUVECs) within the hydrogels in response to the established VEGF gradient was studied.

Experimental Methods

Hydrogels with varying heparin content were prepared adapting protocols as described in detail elsewhere [2, 5]. The mechanical properties of the hydrogels were characterized using rotational rheometry, and the release of SDF1α and VEGF165 from the hydrogels for a period of two weeks was analyzed using an enzyme-linked immunosorbent assay. Furthermore, the spatial profile of fluorescently-labeled SDF-1α and VEGF165 within the hydrogels was evaluated using confocal scanning microscopy for a time period of 48 h. For cellular studies, HUVECs were cultured in cytocompatible matrix metalloproteases (MMP)-cleavable hydrogels as previously described [6]. Before the gelation process, the mixture of cell and hydrogel precursors was injected into microfluidic devices containing three parallel channels: one gel channel and two medium channels, and upon the polymerization, the VEGF were applied in one of the media channels to initiate the gradient formation across the hydrogel. The live cell migration and the extent of the tubular structure were evaluated using spinning disk confocal microscopy.

Results and Discussion

Hydrogels with tunable heparin content and mechanical properties were applied to control cell-instructive signal molecule gradients utilizing a microfluidic cell culture platform. The mechanical properties of the hydrogels can be adjusted independently from the heparin concentration allowing the formation of hydrogels with a stiffness as low as 0.2 kPa to as high as 4 kPa with a heparin content varying from 1.5 to 1500 µM. The variation of the heparin content was shown to modulate the release of SDF1α and VEGF165 out of the matrices. Besides, the hydrogel with a heparin concentration of 150 µM or higher could stably maintain a gradient of SDF1α and VEGF165 for at least 48 h without a continuous supply of the proteins. Finally, we demonstrate that presenting a gradient of VEGF within the hydrogel could locally modulate the formation of HUVECs vascular structure and induce the directed cell migration toward the source of the growth factor.

Conclusion

Hydrogels tunable in GAG-content and mechanical properties provide powerful options to control cell fate decisions. The introduced methodology allows for the precise tuning of morphogen patterns in *in vitro* models as demonstrated here for the directed formation of HUVEC vascular structures. With respect to the central role of GAGs in extracellular matrices, tailored GAG hydrogels provide a rational base to gain new insights into developmental processes, homeostasis, pathogenesis, and regeneration from *in vitro* models.

References

[1] Lee K et al. J R Soc Interface. 2011; 8: 153-70.
[2] Atallah P. et al. Biomaterials. 2018;181: 227-39.
[3] Lohmann N. et al. Sci. Transl. Med. 2017; 9: 386.
[4] Freudenberg U. et al. . Adv Mater. 2016; 28: 8861-91.
[5] Tsurkan M.V. et al. Adv Mater. 2013; 25: 2606-10.
[6] Chawalek K. et al. Sci Rep. 2014; 4: 4414.

Acknowledgement

This work was supported by the Deutsche Forschungsgemeinschaft through ZI 1238/4-1 (Y.L. and R.Z.), CRC TR 67 (P.A., C.W., and U.F.), and FR 3367/2-1 (U.F. and Y.L.).

X-OS19-03

An affinity-based approach to engineer human laminin-presenting cell instructive microenvironments

Daniela Barros[1,2,3], Paula Parreira[1,2], Joana Furtado[4,2], Frederico Ferreira-da-Silva[4,2], Eduardo Conde-Sousa[1,2], Andrés J. Garcia[5,6], Maria C. L. Martins[1,6,3], Isabel F. Amaral[1,2], Ana Paula Pêgo[1,2,3]

[1]INEB - Instituto de Engenharia Biomédica, Universidade do Porto, Porto, PT; [2]i3S - Instituto de Investigação e Inovação em Saúde, Universidade do Porto, Porto, PT; [3]Universidade do Porto, ICBAS - Instituto de Ciências Abel Salazar, Porto, PT; [4]IBMC - Instituto de Biologia Molecular e Celular, Porto, PT; [5]Georgia Institute of Technology, Parker H. Petit Institute for Bioengineering and Biosciences, Atlanta, US; [6]Georgia Institute of Technology, George W. Woodruff School of Mechanical Engineering, Atlanta, US

Introduction

Laminin immobilization into diverse biological and synthetic matrices has been explored to replicate the microenvironment of stem cell niches and gain insight into the role of extracellular matrix on stem cell behaviour. However, the site-specific immobilization of this heterotrimeric glycoprotein and, consequently, control over its orientation and bioactivity has been a challenge that has limited many of the explored strategies to date. In this work, we established an affinity-based approach that takes advantage of the native high affinity interaction between laminin and the human N-terminal agrin (hNtA) domain. This interaction is expected to promote the site-selective immobilization of laminin to a specific substrate, while preserving the exposure of its key bioactive epitopes.

Experimental Methods

A recombinant rhNtA fragment was produced on E. coli BL21(DE3) strain and purified by affinity chromatography[1]. To assess the bioactivity of the produced rhNtA fragment to Ln, both solid-binding assay and surface plasmon resonance (SPR) experiments were conducted. A thiol-PEG–succinimidyl glutaramide spacer (Mw 3500 Da) was added to the N-terminal amine of rhNtA. The PEGylated rhNtA was purified by cation-exchange chromatography and further characterized by SDS-PAGE and mass spectrometry. To assess the ability of this affinity-based approach to immobilize laminin with retention of bioactivity, rhNtA domain was conjugated at its N-terminus, with a thiol-terminated poly (ethylene glycol) (PEG) to enable the preparation of self-assembled monolayers (SAMs) of rhNtA on gold. Additionally, hydrogels were prepared based on 4-arm PEG-maleimide macromers (Mw 40000 Da), functionalized with the monoPEGylated- rhNtA-Ln conjugate and then cross-linked into a hydrogel by addition of a cysteine-flanked MMP-sensitive peptide, in the absence or presence of human neural stem cells (hNSCs). The H9-derived NSC cell line was here explored to test the bioactivity of both substrates.

Results and Discussion

The recombinant hNtA domain was produced with high purity (>90%) and successfully conjugated at its N-terminal with a thiol-terminated PEG without affecting its affinity to laminin. SAMs of mono-PEGylated rhNtA on gold (mPEG rhNtA-SAMs) were then prepared to evaluate the effectiveness of this strategy. The site-specific immobilization of laminin onto mPEG rhNtA-SAMs was shown to better preserve protein bioactivity in comparison to laminin immobilized on SAMs of thiol-PEG-succinimidyl glutaramide, used for the non-selective covalent immobilization of laminin, as evidenced by its enhanced ability to efficiently self-polymerize and mediate cell adhesion and spreading of hNSCs. The tethering of mono-PEGylated-rhNtA-Ln conjugate to 4-arm PEG maleimide did not compromise

hydrogel formation, either in the absence or presence of cells. Furthermore, the Ln-functionalized hydrogel was able to support hNSC viability and neurite outgrowth.

Conclusion

The present work demonstrates the potential of mono-PEGylated rhNtA as an effective natural affinity binding ligand for site-selective immobilization of laminin, allowing the preservation of laminin ability to self-polymerize and mediate cell adhesion and spreading. This affinity binding strategy overcomes several drawbacks associated with the currently available strategies for laminin immobilization. Moreover, this approach is highly versatile, as result of the ability of NtA to bind the different laminin isoforms that comprise the γ1 chain, which represent more than 50% of the isoforms identified to date, with variations in affinity imposed by α and β chains. Therefore, this strategy enables the immobilization of different laminin isoforms, which can be of interest for particular cell types and for application in specific disease contexts. Overall, the proposed strategy is highly attractive for a broad range of applications, including 2D coatings for cell culture, functionalization of 3D matrices for cell and/or drug delivery, engineered coatings for neuroelectrodes, among others.

References

1. Barros D., Parreira P., Furtado J., Ferreira-da-Silva F., Conde-Sousa E., García A.J., Martins M.L.C., Amaral I.F., Pêgo A.P. “An affinity-based approach to engineer laminin-presenting cell instructive microenvironments” Biomaterials 2019, 192: 601–611

Acknowledgement

This work was supported by projects NORTE-01-0145-FEDER-000008 and NORTE-01-0145-FEDER-000012, supported by NORTE 2020 program, under the PORTUGAL 2020 Partnership Agreement, through the ERDF and FEDER funds (COMPETE 2020); by Portuguese funds through FCT/MCTES in the framework of the project “Institute for Research and Innovation in Health Sciences” (POCI-01-0145-FEDER-007274) and by project COMBINE (Santa Casa da Misericordia de Lisboa – Prémio Neurociências Mello e Castro). This work was carried out in the framework of D Barros PhD studies funded by the BiotechHealth Program (FCT).

X-OS19-04

Rapid Visible Light Crosslinking of Silk Hydrogels for Cartilage Tissue Engineering

Steven Cui[1], Jun Li[1], Cesar Alcala-Orozco[1], Tim Woodfield[1], Jelena Rnjak-Kovacina[2], **Khoon Lim**[1]

[1]University of Otago, Christchurch, NZ; [2]University of New South Wales, Sydney, AU

Introduction

Silk fibroin (SF) has been extensively studied as a biomaterial due to its high biocompatibility, mechanical strength, and controlled proteolytic biodegradability[1]. SF is composed of random coil and β-sheet structures, where the latter is reported to be responsible for the stability of the protein. Majority of silk constructs are fabricated by facilitating this random coil to β-sheet transformation, which uses harsh conditions like methanol treatment or lyophilisation, and thus is unsuitable for cell-encapsulation procedures[1]. In order to not be dependent on the protein conformation transition, other methods such as enzymatic crosslinking uses a combination of horseradish peroxidase (HRP) and hydrogen peroxide (H_2O_2), to target the native tyrosine groups in SF, converting them into covalent di-tyrosine bonds to crosslink SF[2]. Although successful, using this method for cell encapsulation often require long crosslinking time (10 – 30 mins), and the presence of H_2O_2 can further exert oxidative damage to the cells. Recently, a novel visible light photo-crosslinking system consists of a combination of Ruthenium (Ru) complex and Sodium Persulfate (SPS), has been shown to also facilitate the similar di-tyrosine crosslinking but at a higher reaction rate and efficiency[3]. Therefore, the aim of this study is to examine the feasibility of using this novel visible light photo-initiating system to encapsulate cells within silk hydrogels, and further evaluate the potential of this system for cartilage tissue engineering.

Experimental Methods

Bombyx Mori degummed silk fibers (5, 10 and 30 minutes degumming) were firstly dissolved in lithium bromide (9.3M) solution, then purified using dialysis (10kDa MWCO). The shorter degumming time corresponds to a higher silk molecular weight. Prior to use, all solutions were diluted to 2% (wt/vol) in deionized water. Optimization of the visible light photo-crosslinking system was conducted by varying the photo-irradiation (OmniCure S1500) conditions: Ru/SPS concentrations of 0.2/2-2/20 (mM/mM), light intensity of 3 – 50 mW/cm^2 (400-450nm), and irradiation time of 1 – 10 minutes, where mass loss and swelling studies were used to evaluate the physico-chemical properties of the resultant SF hydrogels. For cell encapsulation studies, primary human articular chondrocytes (HAC) were encapsulated at a density of 15x10^6 cells/ml and cultured for up to 5 weeks in chondrogenic differentiation media to assess cell viability, glycosaminoglycan (GAG) deposition, DNA, and matrix deposition (Saf-O,Coll I/II) using Live/Dead, dimethylmethylene blue (DMMB), CyQUANT and immuno-histo or -fluoro staining assays respectively.

Results and Discussion

We systematically optimised the photoinitiator concentrations, light intensity and irradiation time required to crosslink SF hydrogels. At an initial condition set to 3 minutes of 30mW/cm^2 of visible light, we observed that although 0.2/2 (mM/mM) of Ru/SPS was sufficient to crosslink SF, the resultant hydrogel has poor structural integrity and significant loss of shape (high sol fraction and swelling ratio) after 1day of swelling. Instead, increasing the Ru/SPS concentration to 0.5/5 (mM/mM) and subsequent higher concentrations (1/10 and 2/20 mM/mM of Ru/SPS) successfully resulted in SF hydrogels of good mechanical and structural stability (sol fraction <20%), confirming that

a minimal concentration of 0.5/5 (mM/mM) of Ru/SPS was required to ensure good crosslinking of the SF hydrogels. Furthermore, we observed that just 3 minutes of irradiation time was sufficient to crosslink SF hydrogel, regardless of the intensity used (30, 50 or 100mW/cm^2). We also did not observe any significant differences between SF of various molecular weights. Thus, we evaluated that the optimal irradiation condition to fabricate SF gels is 0.5/5 (mM/mM) of Ru/SPS combined with 3 minutes of 30 mW/cm^2 light intensity. HAC were encapsulated into the SF hydrogels at the optimised photo-crosslinking condition and showed good viability and metabolic activity over the 5 weeks culture period (Figure 1A-C). The SF gels were also able to support chondrogenic differentiation of the encapsulated HACs, where all samples exhibited high GAG/DNA values, as well as matrix production. Interestingly, we observed that SF of higher molecular weight (5 minutes degumming) supported significantly better tissue formation of the encapsulated HACs compared to SF of 10 and 30 minutes degumming time (Figure 1D-F).

Conclusion

This work demonstrates that the visible light photo-crosslinking system is able to facilitate rapid, efficient and cell friendly di-tyrosine crosslinking of SF hydrogel. We believe that by using light-based stimulus, we now have an added spatio-temporal benefit that can potentially be used to not only control the silk construct architecture, but also cellular organization using other cutting-edge fabrication technologies like 3D printing.

References

1 J. Rnjak-Kovacina, L. S. Wray, J. M. Golinski and D. L. Kaplan, *Adv. Funct. Mater.*, 2013, **24**, 2188–2196.

2 N. R. Raia, B. P. Partlow, M. McGill, E. P. Kimmerling, C. E. Ghezzi and D. L. Kaplan, *Biomaterials*, 2017, **131**, 58–67.

3 K. S. Lim, M. H. Alves, L. A. Poole-Warren and P. J. Martens, *Biomaterials*, 2013, **34**, 7907–105.

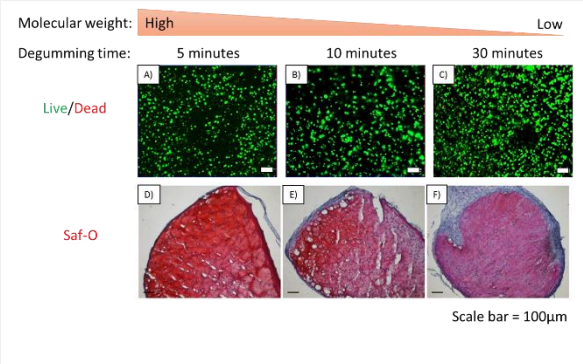

HAC encapsulation in SF hydrogels
Figure 1: Encapsulation of human articular chondrocytes in silk fibroin hydrogels of various degumming time crosslinked using visible light photo-initiating system. Live/dead images after 1 day (A-C) and Saf-O staining after 5 weeks (D-F) of cell-laden SF constructs. Scale bar = 100µm

X-OS19-05

The extracellular matrix as biomaterial: comparison of native decellularized and in vitro cell-derived adipose extracellular matrix

Svenja Nellinger, Ralf Kemkemer, Petra J. Kluger

Reutlingen University, Research Group Smart Biomaterials, Reutlingen, DE

Introduction

The extracellular matrix (ECM) as a multi-component network is synthesized and assembled by the resident cells. A general functionality of the ECM is to provide structural stability to a tissue. In addition, the ECM has been increasingly shown to exert an intense impact on cell behavior and function via physical and chemical properties like stiffness, porosity, the composition of proteins, proteoglycans and growth factors [2]. Therefore, ECM represents an interesting biomaterial for surface coatings, as scaffolding material for tissue engineering or as bioinks [3]. There are two ways to achieve tissue-specific ECM. First, decellularization of native tissues and organs and second, in vitro cell-derived ECM (cdECM) production using the relevant cells. In this study the composition and structural characteristics of native adipose-derived ECM and in vitro generated adipose ECM were characterized and compared (Fig. 1).

Experimental Methods

We obtained human skin biopsies and used them for either the decellularization or the isolation of adipose derived stem cells (ASCs). The native adipose tissue was decellularized by enzymatic digestion according to the protocol established by Flynn et al. [1]. For the generation of an in vitro cdECM, ASCs were isolated and differentiated into the adipogenic lineage. Cells were lysed after 7 and 14 days and devitalized ECM was isolated. Beside the comparison of native and cdECM, we moreover compared the cdECM gained from stem cells and from the differentiated ASCs. The comparison of the composition of ECM samples were performed by histological stainings like hematoxylin & eosin, alcian blue PAS, MOVAT and picrosirius red. ECM proteins like fibronectin, laminin and collagen I, IV were stained immunohistochemically and structural characteristics like the pore size were determined based on these pictures using the image processing program ImageJ. Protein and glycosaminoglycan content of the ECM samples were determined by colorimetric assays. The topography, stiffness and elasticity of the adipose ECM were analyzed by AFM and rheological measurements.

Results and Discussion

Hematoxylin & eosin staining proved the successful decellularization of native tissue samples and in vitro generated ECM. Further staining revealed comparable protein and proteoglycan composition of native and cdECM. Elastic fibers are characteristic for mature tissue and were only found in native ECM samples. The pore size in cdECM gained by differentiated ASCs was significantly higher compared to cdECM gained by stem cells, which may be due to the more rounded shape of adipogenic differentiated ASCs. The rheological measurements revealed differences between the decellularized ECM and the cdECM from stem cells or differentiated ASCs. In next steps, we will focus on other tissues to compare the properties and composition of decellularized ECM and cdECM.

Conclusion

Both, native decellularized ECM and cdECM are very promising biomaterials for tissue engineering. However, there is a lack of the direct comparison of these two ways to gain the ECM. Our results for the comparison of adipose ECM

showed numerous similar results e.g. for the matrix components, but also some differences have been detected. With this data, we hope to provide more insight into characteristcs of native decellularized ECM and cdECM to strengthen the attempt to use ECM as a biomaterial.

References

[1] Flynn LE. The use of decellularized adipose tissue to provide an inductive microenvironment for the adipogenic differentiation of human adipose-derived stem cells. Biomaterials 2010;31:4715-24.
[2] Hynes RO. The Extracellular Matrix: Not Just Pretty Fibrils. Science 2009;326:1216-9.
[3] Badylak SF, Freytes DO, Gilbert TW. Extracellular matrix as a biological scaffold material: Structure and function. Acta biomaterialia 2009;5:1-13.

Acknowledgement

The authors thank the Ministerium für Wissenschaft, Forschung und Kunst in Baden-Württemberg for funding.

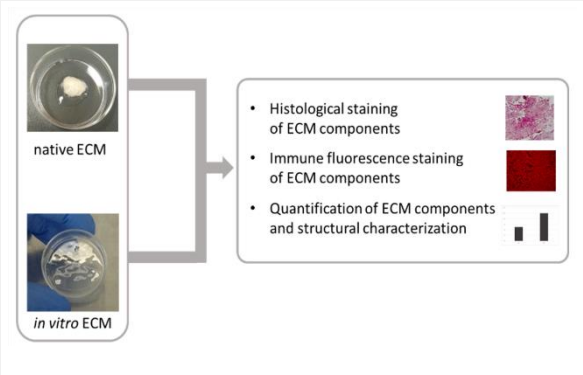

Figure 1:
Schematic overview of the workflow of the study

X-OS19-RF06

Controlling structural relaxations, mechanical properties, and degradation timescale of PLLA during hydrolytic degradation

Reece N. Oosterbeek[1], Patrick Duffy[2], Sean McMahon[2], Xiang C. Zhang[3], Serena M. Best[1], Ruth E. Cameron[1]

[1]University of Cambridge, Cambridge Centre for Medical Materials, Department of Materials Science and Metallurgy, Cambridge, GB; [2]Ashland Specialties Ireland Ltd., Synergy Centre, TUD Tallaght, Dublin, IE; [3]Lucideon Ltd., Stoke-on-Trent, GB

Introduction

Poly-L-lactide (PLLA) is a bioresorbable polymer with many properties that make it appealing as a biomedical implant material, however for certain load-bearing applications such as cardiac stents it suffers several limitations. Among these are its slow degradation time, poor stiffness and strength (requiring PLLA stents to have thicker struts than conventional metallic stents), and tendency for embrittlement during degradation[1]. Here we demonstrate how polyethylene glycol functionalised poly-lactide-co-caprolactone (PLCL-PEG) can be blended with PLLA, in order to control both the degradation timescale, and the structural and mechanical changes undergone during degradation. We also investigate how the mechanical properties of these polymers can be improved by incorporating phosphate glass into a fully bioresorbable composite.

Experimental Methods

Polymer blends and polymer-glass composites were made using solvent casting and injection moulding, with mechanical testing carried out immersed in deionised water at 37°C. Degradation behaviour was measured in phosphate-buffered saline at 37°C by pH monitoring. Polymer blends were characterised before and after degradation by Differential Scanning Calorimetry (DSC), X-ray Diffraction (XRD), and Gel Permeation Chromatography (GPC).

Results and Discussion

Long-term degradation tests (Fig. 1) show strong dependence of degradation time on blend composition, demonstrating the ability to controllably accelerate PLLA degradation via blending. The two blend components (PLLA and PLCL-PEG) do not simply degrade independently of each other, but rather the degradation products released by the fast degrading polymer (PLCL-PEG) catalyse and accelerate the degradation of the slower degrading PLLA component. This is shown by the molecular weight distributions measured by GPC (Fig. 1), where the measured blend degradation is greater than would be expected for independently degrading components.

Important changes in the mechanical properties during degradation are also observed (Fig. 2). The large initial ductility is lost after 30 days degradation for most blend compositions. For blends with low PLCL-PEG content this occurs due to aging (shown by increased T_g and larger associated endothermic peak in DSC) as the relatively homogeneous composition provides little barrier to rearrangement. For high PLCL-PEG content, molecular weight degradation has shortened chain length sufficiently to allow significant rearrangement i.e. crystallisation (shown by XRD), also resulting in embrittlement. These two effects result in a “sweet spot” of moderate PLCL-PEG content that is high enough to prevent aging, but not so high as to cause degradation-induced crystallisation, leading to delayed structural relaxation and embrittlement for these compositions (20-30% PLCL-PEG).

Initial results for polymer-glass composites (Fig. 2) show that glass addition significantly improves stiffness, while retaining some ductility - a promising result for load-bearing applications where high stiffness is desirable but brittle failure can be catastrophic.

Conclusion

Blending PLCL-PEG with PLLA controllably accelerates hydrolytic degradation. In large amounts this leads to crystallisation and embrittlement, however in smaller amounts PLCL-PEG balances faster degradation and resistance to the structural relaxations (aging, crystallisation) that cause embrittlement. Early work on polymer-glass composites indicates that phosphate glass addition can successfully increase stiffness without causing brittle failure, paving the way towards a combined blending-composite strategy to achieve bioresorbable materials that have (and retain) favourable mechanical properties along a suitable degradation timescale.

References

[1] Wayangankar, S. A., & Ellis, S. G. (2015) *Prog. Cardiovasc. Dis.*, *58*(3), 342-355.

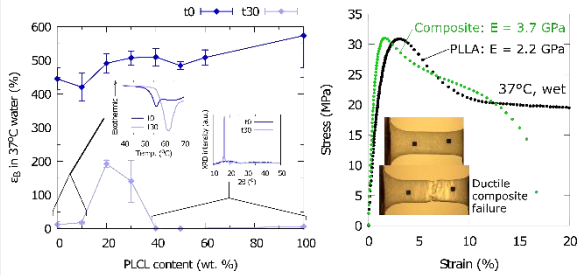

Fig. 2 Mechanical properties of polymer blends and composites

Figure 2: Elongation at break (in 37°C water) for PLLA:PLCL-PEG blends before and after 30 days degradation, with DSC and XRD plots inset (left); mechanical properties of PLLA-phosphate glass composite (right).

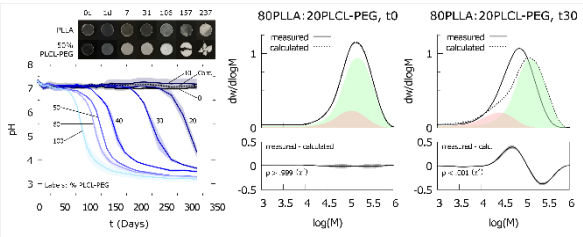

Fig 1. pH and molecular weight distribution after degradation

Figure 1: pH measurement during degradation of PLLA:PLCL-PEG blends (left); molecular weight distributions for PLLA:PLCL-PEG blends before and after 30 days degradation (middle and right). Calculated curves are based on a linear combination of the individual blend components (red = PLCL-PEG, green = PLLA) before and after degradation.

X-OS19-RF07

Oxygen-generating Bioadhesive Hydrogel *via* Calcium Peroxide-mediated Crosslinking Reaction

Sohee Lee[1], Kyung Min Park[1,2]

[1]Incheon National University, Department of Bioengineering and Nano-Bioengineerign, Incheon, KR; [2]Incheon National University, Division of Bioengineering, Incheon, KR

Introduction

Bioadhesive hydrogels have been used as wound closures, hemostatic agents, tissue sealants and other medical applications. While various types of bioadhesives have been developed, it is still challenging to overcome some limitations, such as poor adhesion strength and bioactivities. Recently, many researchers have been reported mussel-inspired adhesives as they have shown strong tissue adhesiveness even in wet conditions. Molecular oxygen (O_2) is an essential signaling molecule in the wound healing and tissue regeneration. In particular, it is demonstrated that hyperbaric oxygen promotes the wound healing process through accurately increasing intracellular reactive oxygen and nitrogen species (RONS). Herein, we represent a new type of O_2-generating bioadhesive formed *via* calcium peroxide (CaO_2)-mediated crosslinking and *in situ* polymerization of dopamine.

Experimental Methods

The thiolated gelatin (GtnSH) was synthesized by conjugating Traut's reagent to the gelatin backbone as previously reported.[1] We fabricated O_2-generating bioadhesive hydrogels by simply mixing GtnSH and dopamine hydrochloride (DH) in the presence of CaO_2. The phase transition time was determined by the vial tilting method. The elastic modulus (*G'*) was characterized by using a rheometric fluid spectrometer (HR-1, TA instruments). The remained DH within the hydrogel matrices was measured by BCA assay. We monitored dissolved O_2 (DO) levels using a commercially available O_2 sensor (Microx-4, Presens). Tissue adhesive strength was investigated using a universal testing machine (Instron 5966). For *in vitro* cytocompatibility test, human dermal fibroblasts (HDFs) were cultured with hydrogel droplets and cell viability was analyzed by WST-1 and live/dead assay. We performed subcutaneous implantation and wound closing test to investigate the effect of O_2 release on neovascularization and wound healing.

Results and Discussion

The GtnSH-polydopamine (PD) hydrogels were formed *via* CaO_2-mediated crosslinking reaction. In this reaction, the polymer networks were crosslinked through disulfide bonds, and Michael type addition between the GtnSH and polydopamine. Additionally, DH reacts with functional groups (e.g., $-NH_2$, -SH) of tissue surfaces resulting in diverse interfacial bindings (Fig. 1a). To evaluate the hydrogel formation and phase transition, we performed phase-transition test depending on CaO_2 (0.25 – 0.75 wt%) and DH concentrations (0 – 1 mg/mL), demonstrating higher levels of CaO_2 induced faster hydrogel formation (43 sec – 3 min) without compromising DH concentrations. We assessed the elastic modulus of the hydrogels depending on CaO_2 and DH concentrations, resulting in tunable mechanical properties (40 – 830 Pa). We next investigated the DH-releasing behaviors from the hydrogel matrices. As increasing CaO_2 contents, more DH molecules were remained within the hydrogel matrices since CaO_2 facilitated dopamine oxidation and *in situ* polymerization. Also, the hydrogels showed controllable tissue adhesive strength in wet conditions (15 − 38 kPa) (Fig. 1b). We monitored O_2-releasing kinetics depending on CaO_2 concentrations. The hydrogels (G5D0.5C0.75) rapidly generated O_2 up to 70% pO_2 and released O_2 for seven days *in vitro* (Fig. 1c). We

evaluated the cytotoxicity of the hydrogels using HDFs, confirming the excellent cell viability (> 85% compared to the control). Furthermore, we implanted the hyperoxic gels (HG, G5D0.5C0.75) and normoxic gels (NG, G5D0.5C0.75) in the subcutaneous pocket of mice to analyze *in vivo* effects of the hydrogels on neovascularization, and also performed wound closing test. Interestingly, we found that the HG group facilitated wound closing and healing with enhanced neovascularization compared to the NG (Fig. 1d).

Conclusion

We developed a new type of O_2-generating bioadhesive hydrogel *via* CaO_2-mediated crosslinking and *in situ* polymerization of dopamine. The GtnSH-PD hydrogel has controllable physicochemical properties and facilitates neovascularization and wound healing. These results suggest that our advanced adhesive hydrogel is a very promising biomaterial as tissue adhesives for wound management as well as tissue regenerative materials.

References

1. Sujin Park and Kyung Min Park, ***Biomaterials***, 182:234-244, 2018

Acknowledgement

This work was supported by the National Research Foundation of Korea (NRF) grant funded by the Korea government (MSIT) (NRF-2018M3A9E2023257).

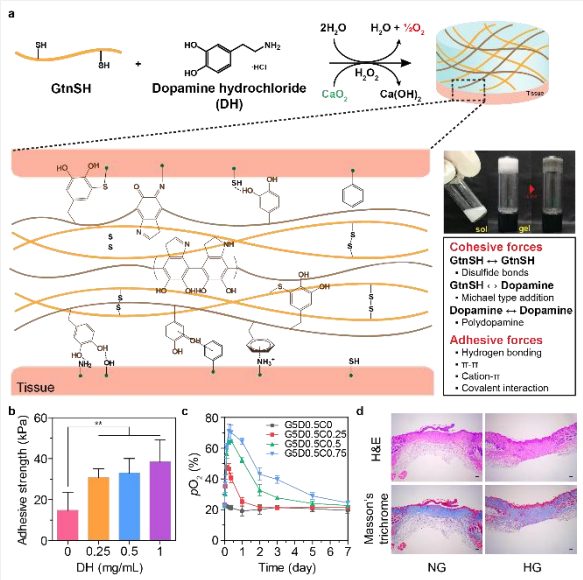

Characteristics and wound healing effect of the GtnSH-PD hydrogels
(a) The design strategy for O_2-generating bioadhesives *via* CaO_2-mediated crosslinking reaction and digital images of sol-gel transition. (b) The tissue adhesive strength of the hydrogels depending on DH concentrations. (c) The O_2-releasing kinetics of the hydrogels. (d) Histological sections of wounds stained with H&E and Masson's trichrome. The results are shown as the average values ± s.d. (n=3~6, $^{**}P < 0.01$)

X-OS19-RF06

Optimization of poly(diol citrates) composition for small-diameter blood vessel tissue engineering

Agata Flis[1], Filip Koper[2], Wiktor Kasprzyk[2], **Elżbieta Pamuła**[1]

[1]AGH University of Science and Technology, Faculty of Materials Science and Ceramics, Kraków, PL; [2]Tadeusz Kościuszko Cracow University of Technology, Faculty of Chemical Engineering and Technology, Kraków, PL

Introduction

There is a need to treat artherosclerotic vascular disease of small-diameter blood vessels with the use of artificial grafts. Grafts made of Dacron or ePTFE work well in large-diameter blood vessel application. Unfortunately, grafts suitable for small size vessels (>6 mm inner diameter) have not been developed so far. Thus we focus on poly(diol citrate)s (PDCs), based on citric acid and 1,8-octanediol as potential substrate for small blood vessel tissue engineering. PDCs produced with a 1:1 molar ratio of citric acid to 1,8-octanediol were found biodegradable and cytocompatible [1]. Their key advantage is that PDCs polymerization takes place at relatively low temperature and such polymers can be easily modified to gain new distinct properties, including fluorescent, antimicrobial, adhesive or anti-oxidant [2]. In this study we wanted to examine if chemical structure of PDCs can be adjusted by different concentration of the precursors, and if this would influence physical integrity, surface properties and biological performance of obtained polymers. To this end structural and physicochemical properties of thee PDCs with different molar ratio of citric acid to 1,8-octanediol were evaluated and their potential *in vitro* cytotoxicity was assessed.

Experimental Methods

Citric acid and 1,8-octanediol at molar ratio 1:1, 2:3 and 1:2 were melted at 140^{o}C for 40 min under stirring to synthesize prepolymers. The latter were dissolved in ethanol, precipitated in water, lyophilized, dissolved in ethanol again and post-polymerized for 4, 6, 8, 10 days at 70^{o}C in a vacuum oven. PDCs surface roughness (Hommer-Werker profilometer) and the water contact angle (DSA10, Kruss) were measured. FTIR-ATR (Tensor 27, Bruker) was used to determine surface chemical composition and NMR spectra (Brucker Avance III HD 400 MHz) were registered. Acid value were measured by dissolving 150 mg of the sample in 96% ethanol, and then titrating with 0.05M KOH with phenolphthalein as an indicator. Molecular weight was assessed by gel permeation chromatography using Shimadzu GPC system. Cytocompatibility with L929 fibroblasts was assessed on 10% extracts from PDCs in DMEM: undiluted (1:1) and diluted by a factor of 1:2, 1:4, 1:8 and 1:16. In brief the cells were cultured in 96-well plates in DMEM supplemented with 5% FBS, amino acids, and antibiotics for 24 h and then cell culture medium was replaced with the extracts. Cell viability was measured using Alamar Blue and CCK-8 tests. Cells after live-dead staining were observed under fluorescence microscopy (Axiovert, Zeiss).

Results and Discussion

GPC results showed that molecular weight of PDCs depended on molar ratio of the copolymers. FTIR-ATR results showed that PDCs with all studied molar ratios had similar bands at the same wavenumbers and were differing only in band intensity depending on composition. Acid values showed that PDC_1:2 had the lowest acidity (150.8 ± 1.9 mg KOH/g), while PDC_1:1 had the highest acidity (204 ± 3.8 mg KOH/g). Acid value for PDC_2:3 was 160.9 ± 6.5 mg KOH/g. PDC_1:1 and PDC_2:3 were hydrophilic (water contact angle 65^{o} – 85^{o}) and smooth (R_a 0.10 – 0.40 µm). The water contact angle decreased with the post-polymerization time from 4 to 10 days. PDC_1:2 was not

dimensionally stable irrespectively of the post-polymerization time. Cells cultured in the extracts from PDC_2:3 exhibited the highest viability as shown by Alamar Blue and CCK-8 tests, than those cells cultured in PDC_1:1 and PDC_1:2 extracts. Microscopic observations after live-dead staining showed that cells cultured in the extracts from PDC_2:3 (undiluted and diluted by all factors) were stained green, i.e. alive (Fig. 1, panel B). Cells cultured in the extracts from PDC_1:1 (Fig 1, panel A) showed some degree of toxicity, while for higher dilutions, i.e. 1:2, 1:4 and 1:8 no impact on cell viability was observed. Cells cultured in undiluted extracts from PDC_1:2 (Fig 1, panel C) showed only dead cells (stained red). Some of the cells cultured in the extracts from PDC_1:2 diluted by a factor of 1:2 were alive, but majority of them were dead. For extract dilution of 1:4 number of live cells was increasing, but still red stained cells were observed. For 1:8 dilution cell morphology and number was the same as in control.

Conclusion

We found that PDC_2:3 had the lowest acidity and exhibited the best dimensional stability, physicochemical properties and cytocompatibility with L929 cells. PDC_1:1, i.e. the reference material reported in literature, had higher acidity and provoked slight cytotoxicity. PDC_1:2 was the least dimensionally stable, had the lowest acidity and was cytotoxic. Thus we developed a new material PDC_2:3 with better performance by adapting molar ratio of co-monomers: citric acid and 1,8-octanediol. Further studies will focus on preparation of tubular scaffolds from PDC_2:3 for small size blood vessels tissue engineering and their evaluation in contact with endothelial and smooth muscle cells.

References

[1] Tran T.R. et al. Annu. Rev. Mater. Res. 2015. 45:11.1-11.34

[2] van Lith R. et al. Biomaterials 2014; 35: 8113-8122

Acknowledgement

This study was financed by National Science Center, Poland (2018/28/C/ST5/00461).

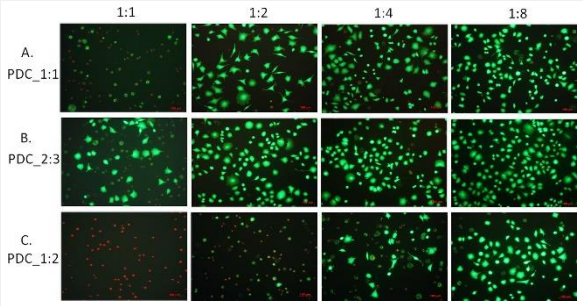

Fig. 1.
Morphology of L929 cells cultured for 24 h in the extracts from poly(diol citrate)s with molar ratio of citric acid and 1,8-octanediol of 1:1 (PDC_1:1) (A), 2:3 (PDC_2:3) (B) and 1:2 (PDC_1:2) (C) after live-dead staining.

9:30 a.m. – 11:00 a.m.

Hall 5

X-OS38 | Biocompatibility and degradation

X-OS38-01

Biomaterial biocompatibility assessment by complement proteins adsorption and macrophage polarization.

Nuno Araújo-Gomes[1,2], Francisco Romero-Gavilán[1], Yang Zhang[3], Cristina Martínez-Ramos[2], Felix Elortza[4], Mikel Azkargorta[4], José J. Martín de Llano[5], Iñaki García-Arnaéz[6], Mariló Gurruchaga[6], Isabel Goñi[6], Jeroen J. van den Beucken[3], Julio Suay[1]

[1]Universitat Jaume I, Department of industrial systems and design engineering, Castellón de la Plana, ES; [2]Universitat Jaume I, Department of Medicine, Castellón de la Plana, ES; [3]Radboud UMC, Department of Biomaterials, Nijmegen, NL; [4]CicBiogune, Proteomics Platform, Derio, ES; [5]Universitat de Valencia, Department of Pathology and Health Research Institute of the Hospital Clínico, Valencia, ES; [6]Universidad del Pais Vasco, Facultad de Ciencias Químicas, San Sebastián, ES

Introduction

Improvements on clinical performance of biomaterials for implantation are constantly seeked to guarantee the post-surgical recovery. This need drives for the development of bioactive dental biomaterials capable of inducing bone growth[1]. Upon implantion of a biomaterial in a living host, cell responses are mainly regulated by the initial protein attachment occurring at the moment of implantation. Biocompatibility problems might arise from distinct complement pathways activation that, unleashing a foreign body response[2]. Hence, conditioning protein attachment by introducing surface modifications can minimize these biocompatibility-associated problems, improving positively the implant *in vivo* successfulness.

Highly regarded as a precursor in the synthesis of various types of sol-gel materials, 3-glycidoxypropyl)-trimethoxysilane (GPTMS), an organically modified alkoxysilane, can be employed as implant coatings to improve bone formation on titanium dental implants[3]. Associated with biocompatibility problems in past studies[4], this compound can ultimately impair osseointegration. Thus, the higher adsorption of complement-related proteins and consequent immune cell behaviour can define the implant successful outcome.

Experimental Methods

Osteoblastic MC3T3-E1 and macrophage RAW 264.7 cell lines were employed. These were seeded on coated titanium discs at a concentration of 1×10^4 cells well, on 24-well culture plates. qRT-PCR was used to measure gene expression of osteogenic markers ALP, IL-6, COL I and TGF-β. ELISA was employed to measure protein liberation of the pro-inflammatory markers TNF-α and IL1β and the anti-inflammatory markers IL-10 and TGF-β by RAW 264.7. Immunostaining was carried out using IL7-R (M1 marker) and CD206 (M2 marker) for mouse macrophages. Protein layer obtention was made by incubating the coated discs with human serum plasma for 3 hours followed by elution of the surface-adsorbed proteins. Mass spectrometry analysis (LC-MS/MS) was done to characterize the eluted proteins using Progenesis software.

In vivo experimentation was performed using New Zealand rabbits (*Oryctolagus cuniculus*) as a experimental model. The animals were sacrificed after two weeks and histological analysis was made.

Results and Discussion

An upregulation of TGF-β on MC3T3-E1 osteoblastic cells was observed on the materials with GPTMS. This upregulation was dose-dependent, showing a probable osteogenic induction by this type of materials. In parallel, increased release of TNF-α and IL-10 by RAW 264.7 macrophages and higher IL7-R fluorescence confirms pro-

inflammatory properties of the GPTMS-doped materials. Higher attachment of complement activators FCN2 and CRP, were found on a dose dependent manner, followed by a consequent higher attachment of complement proteins, such as C3 and C5. These data suggest a possible correlation between macrophage differentiation onto M1 phenotype and higher complement protein adsorption onto the coatings applied.
The worst osseointegration *in vivo* of the GPTMS-doped materials corroborates this data, exhibiting higher density of multinucleated giant cells surrounding the coating.

Conclusion

A correlation between the adsorption of complement-related proteins and the presence of M1 pro-inflammatory macrophage phenotype was observed. The increased adsorption of this type of proteins and greater presence of this phenotype onto the implant surroundings can ultimately impair an implant osseointegration. Our results highlight the incrasingly higher importance of adopting alternative *in vitro* approaches, such as proteomic analysis in relation with macrophage polarization patterns, to assess *in vivo* outcomes of bone biomaterials.

References

1. D.Carboni *et al. , New J. Chem.* 38 (2014) 1635–1640
2. K. N. Ekdahl. *et al., Adv Drug Deliv Rev.* (2011)Sep 16; 63(12): 1042–1050.
3. M. Martinez-Ibañez *et al.* , *J. Mater. Sci. Mater. Med*. 27 (2016) 80
4. F. Romero-Gavilán *et al., Biofouling.* 33 (2017) 676–689

Acknowledgement

This work was supported by MINECO [MAT2017-86043-R] and [RTC-2017-6147]; Universitat Jaume I [Predoc/2014/25, UJI-B2017-37]; Basque Government [Predoc/2016/1/0141]; University of the Basque Country [Implant Sol-RTC-2017-6147]; Authors would like to thank Antonio Coso and Jaime Franco (GMI-Ilerimplant) for their inestimable contribution to this study, and Raquel Oliver, Jose Ortega (UJI), René van Rheden, Vicent Cuijpers (Radboudumc) and Iraide Escobes (CIC bioGUNE) for their valuable technical assistance.

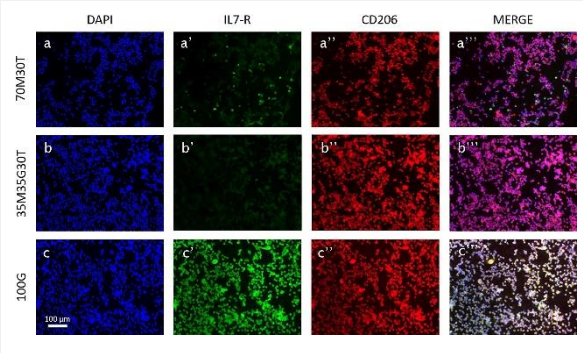

GPTMS-dose dependent macrophage differentiation onto M1 phenotype
Immunostaining of different types of macrophages cultured onto the 70M30T, 35M35G30T and 100G sol-gel hybrid formulations after 72h. IL7-R (**a'-c'**) was used as a pro-inflammatory M1 marker, while CD206 (**a''-c''**) was used an anti-inflammatory M2 marker

X-OS38-02

Novel biodegradable FeMnCS alloy processed by selective laser melting

Julia Hufenbach, Fabian Kochta, Stefan Pilz, Uta Kühn, Annett Gebert

Leibniz Institute for Solid State and Materials Research (IFW) Dresden e.V., Institute for Complex Materials, Dresden, DE

Introduction

Selective laser melting (SLM) is a promising additive manufacturing technology for the production of tailored medical implants. The technique allows the manufacturing of parts with complex geometries and the realization of a high grade of function integration while offering economized material utilization.

Concerning the use of biodegradable alloys for the SLM technology, Fe-based alloys are promising candidates due to their good processibility. Furthermore, FeMn-based systems show a high potential for vascular implant applications owing to their excellent mechanical properties, high mechanical integrity during degradation and corrosive degradation without hydrogen evolution in physiological environment.

In this work, a novel biodegradable Fe-30Mn-1C-0.02S alloy is presented which shows a higher yield and ultimate tensile strength compared to Fe-30Mn and AISI 316L in combination with a good ductility already in the as-cast state. This originates, among other effects, from a pronounced twinning-induced plasticity (TWIP) effect. Furthermore, in potentiodynamic polarisation tests in simulated body fluid (SBF), a higher corrosion rate compared to biodegradable Fe-30Mn could be detected for FeMnCS [1].

Therefore, the influence of the SLM process on the microstructure of the Fe-30Mn-1C-0.02S alloy and the resulting mechanical and corrosion properties in pseudo-physiological solutions were investigated and compared with an AISI 316L reference steel. The results of these investigations are presented in this work as well as the fabrication of stent prototypes out of the novel biodegradable with regard to future medical application.

Experimental Methods

Spherical powder were produced by electrode-induction melting gas atomization (EIGA) of cast rods (TLS, Germany, gas: Argon) and afterwards sieved to realize a nominal particle size of 15 µm to 45 µm. The manufacturing of the samples out of FeMnCS powder was carried out with a SLM device (SLM 250 HL, SLM Solutions) which is equipped with a 400 W Yb:YAG laser (spot size 80 µm). The processing chamber of the SLM device was thereby flooded with argon gas (purity 99.999 %) and the layer thickness was set to 30 µm to obtain high geometrical resolution in building direction.

The Archimedes method (YDK 01 (0D), Sartorius, Germany) was applied to measure the density of the specimens. For the processed alloy, samples with a relative density of 99.6 % can be obtained.

The microstructure was studied by applying scanning electron microscopy (SEM; Leo 1530 Gemini, Zeiss) in combination with electron backscatter diffraction (EBSD; Nordlys F, Oxford Instruments) and energy dispersive X-ray spectroscopy (EDX; Xflash4010, Bruker) as well as X-ray diffraction (XRD; Stadi P, STOE, Mo Kα1 radiation). The appropriate mechanical properties were investigated by tensile and compression tests (Instron 8562). For studying the corrosion behaviour of the FeMnCS alloy, potentiodynamic polarization measurements in SBF at 37 °C were performed.

Results and Discussion

This study shows that by processing the developed Fe-30Mn-1C-0.02S alloy by SLM, it is possible to further enhance the yield and ultimate strength of the alloy under tensile and compressive load in comparison to the Cu mold cast state [1] and to simultaneously achieve a good ductility. This effect can be mainly traced back to the microstructure refinement caused by rapid solidification occurring in the SLM process, which was proven by EBSD analyses. Furthermore, the achievable yield and ultimate strength are significantly higher than the values for an AISI 316L reference material.

Besides the mechanical properties, the corrosion behaviour of the alloy is influenced by the particular microstructure of the SLM samples. The potentiodynamic polarization measurements indicated a lower corrosion rate of the SLM samples compared to their as-cast counterparts. Furthermore, SEM studies of SLM samples immersed statically in SBF show a more uniform corrosion, which is desired for implant applications. These effects can be discussed based on the microstructural differences of the processed samples. In the as-cast state, the alloy shows a fine austenitic microstructure with manganese sulphide precipitates, homogenously distributed in the matrix, as well as a significant enrichment of Mn and depletion of Fe along the grain boundaries [1]. Contrarily, in the SLM samples, besides the significantly finer grain size, only austenite could be detected and the distribution of the elements in the microstructure appear much more homogenous.

With regard to the potential area of application, stent prototypes were successfully built out of the developed FeMnCS alloy by SLM.

Conclusion

Concluding, the novel biodegradable FeMnCS alloy can be successfully processed by SLM and shows a high potential for future application as implant material.

References

[1] J. Hufenbach, F. Kochta, H. Wendrock, A. Voß, L. Giebeler, S. Oswald, S. Pilz, U. Kühn, A. Lode, M. Gelinsky, A. Gebert: S and B microalloying of biodegradable Fe-30Mn-1C - Effects on microstructure, tensile properties, in vitro degradation and cytotoxicity, Materials and Design 142 (2018), p. 22-35.

Acknowledgement

The authors would like to thank the German Research Foundation (DFG) (project no: 277470500) for providing financial support to this project.

X-OS38-03

Impact of chemical crosslinking on the cellular response to collagen I-based biomaterials.

Daniel Bax[1,2], Jean-Daniel Malcor[2], Richard Farndale[2], Serena M. Best[1], Ruth E. Cameron[1]

[1]University of Cambridge, Department of Materials Science and Metallurgy, Cambridge, GB; [2]University of Cambridge, Department of Biochemistry, Cambridge, GB

Introduction

Collagen I is a key structural component of the extracellular matrix, providing resilience to tissues and adhesive motifs to cells. Its inherent biocompatibility makes collagen an attractive precursor molecule for the fabrication of a wide variety of biomaterials. Chemical crosslinking, using EDC, is frequently required to improve the stability and physical properties of these materials. Although considered biocompatible, recent evidence has shown that chemical crosslinking can derivatise crucial amino acid side chains. For example, modification of the glutamic acid (E) in the consensus GxOGER cell-binding motif of collagen can disrupt integrin-mediated cell adhesion and subsequent cellular processes. In this study the EDC and NHS crosslinking parameters were systematically evaluated, identifying potential side reactions and highlighting conditions that can protect the bioactivity of collagen.

Experimental Methods

Collagen film preparation: 0.5 wt% insoluble bovine type I dermal collagen was hydrated in 0.05M acetic acid then homogenising for 2x2 minutes in a bench top blender. This slurry was dried onto 48-well plates then chemically crosslinked in 75% ethanol containing 1-ethyl-3-(3-dimenthylaminopropyl-carbodiimide hydrochloride) (EDC) and N-hydroxy-succinimide (NHS). The molar ratios are expressed as a ratio against the COOH groups on collagen. After crosslinking the samples were washed extensively with water.

Collagen peptide preparation: Triple helical peptides containing the high affinity GFOGER cell binding motif were prepared as in [1]. These were NHS/EDC crosslinked in solution, dialysed against water and subjected to MALDI ToF mass spectroscopy.

Cell attachment: $5x10^4$ of HT1080 cells, resuspended in serum-free DMEM containing either 5mM $MgCl_2$ or 5mM EDTA were added to the collagen films. After incubation at 37°C for 45 minutes the loosely bound cells were removed and the bound cells quantified using a lactate dehydrogenase detection substrate.

Cell proliferation: $1x10^4$ of HT1080 cells in 10% fetal bovine serum containing DMEM were added to collagen films. After 3 days in culture the cells were fixed with 5% glutaraldehyde, permeabilised with 0.5% Triton X-100 and stained with 3.5 µM DAPI. The number of cells per field of view was counted by fluorescence microscopy using a 10X objective lens.

Results and Discussion

Native-like cell adhesion in the presence of Mg^{2+}, non-native cell adhesion that persists in the presence of EDTA, cell proliferation and the presence of covalent crosslinks were all highly dependent upon the NHS:EDC ratio that was used to crosslink the collagen films. Each measurement possessed a differing relationship to the NHS:EDC ratio used. When combined (Figure 1) this showed clear trends. Low concentrations of EDC could retain a native-like cell response, but did not possess covalent crosslinks, and so are ranked low (blue) in the heat map. Conversely high EDC ratios, when combined with low NHS ratios, resulted in extensive crosslinking; however cell adhesion was non-

native with a poor cell-proliferative response. Instead, optimal ratios of NHS:EDC (denoted by the green line) induced high degrees of crosslinking and simultaneously supported native-like cell adhesion and proliferation. Interestingly, this relationship differs from the conventional 5EDC:2NHS ratio (shown by a black line) except at 1EDC:0.5NHS, a crosslinker concentration that has been shown previously to retain the bioactivity of collagen [2]
The mass spectroscopy profile of intact insoluble collagen is non-homogeneous and complex. Therefore, a synthetic triple helical peptide containing the high-affinity cell binding site GFOGER was used to determine the chemical modifications that occur during NHS/EDC crosslinking (Figure 2). This analysis identified three separate peaks that could be ascribed to derivatisation of the peptide. Each possessed a differing relationship to the NHS:EDC ratio used and can be attributed to three separate side-reactions during NHS/EDC crosslinking.

Conclusion

Crosslinking insoluble type I collagen with EDC in the presence of NHS has a major impact on covalent crosslinking and bioactivity. Three different derivatives of GxOGER cell binding motifs in collagen can be identified. These side chain reactions can be minimised by using specific ratios of NHS to EDC, thereby retaining the bioactivity of collagen-based materials. Therefore, the crosslinking reactions need to be carefully considered when using EDC to alter the physical properties of collagen-based biomaterials.

References

[1] Knight CG*et al*, J Biol Chem. 2000;275(1):35-40.
[2] Bax DV *et al*, Acta Biomater.2017;49:218-234.

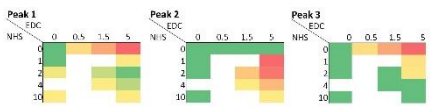

Figure 2: MALDI ToF analysis of GFOGER peptide crosslinked with varying NHS:EDC ratios.
Compilation of MALDI ToF analysis of triple helical GFOGER peptides crosslinked with varying EDC:NHS ratios. The relative proportion of each derivatised peptide peak is graded from highest in red to lowest in green.

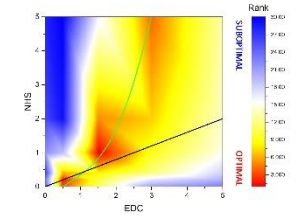

Figure 1: Cell-biological properties of collagen films crosslinked with varying EDC:NHS ratios.
Heat map of collagen-based material properties against the NHS and EDC crosslinking molar ratio (expressed against COOH groups on collagen). Red shows optimal, and blue poor attributes. Materials were ranked by combining measurements of native-like versus non-native cell adhesion, cell proliferation and formation of covalent crosslinks. The optimal NHS and EDC relationship is shown by a green line and the conventional 5EDC:2NHS ratio with a black line.

X-OS38-04

In Vitro Inflammatory Response of Bioresorbable Polymers at Clinically-Relevant Extents of Degradation

Lucy Geddes[1], Louise Carson[2], Efrosyni Themistou[3], Fraser J. Buchanan[1], This project is in collaboration with Corbion

[1]Queen's University Belfast, School of Mechanical Engineering, Belfast, GB; [2]Queen's University Belfast, School of Pharmacy, Belfast, GB; [3]Queen's University Belfast, School of Chemistry and Chemical Engineering, Belfast, GB

Introduction

Research in orthopaedics is now moving away from permanent metallic implants and looking towards the use of bioresorbable polymers (e.g. PLA, PGA and related co-polymers) that, when implanted into the injured site, bioresorb as the tissue heals. However, reports of a delayed inflammatory response occurring in the late stages of polymer degradation has limited the wide scale use of these polymers[1,2]. Only a few studies assess the long-term biocompatibility of these polymers and, with an increasing market for bioresorbable materials, it is anticipated that this will be a future issue. This work aims to develop an experimental methodology that can be used to assess the delayed inflammatory response of poly(*D,L*-lactide-*co*-glycolide) (P*DL*LGA) and poly(*L*-lactide-*co*-glycolide) (P*L*LGA) using *in vitro* tests. This utilised an elevated temperature accelerated degradation test with the objective of determining the optimum temperature to achieve simulation of *in vivo* degradation behaviour. Degradation temperatures of 47ºC, 57ºC and 70ºC were studied and compared to physiological temperature (37ºC). This methodology was used to induce predetermined levels of degradation in P*DL*LGA and P*L*LGA, in order to mimic a range of clinically relevant *in vivo* implantation times of up to 6 months. This work can be applied to the optimisation of polymer degradation profiles to minimise late-stage inflammatory response and identification of potentially beneficial additives in this regard.

Experimental Methods

P*DL*LGA 85:15 (PURASORB PDLG 8531, Corbion, Gorinchem) and P*L*LGA 85:15 (PURASORB PLG 8531, Corbion, Gorinchem) samples were processed by compression moulding into 1mm thick sheets, followed by annealing (only for P*L*LGA) for 4h at 100ºC, laser cut into 8mm diameter disc-shaped samples and electron beam sterilised (Steris, Westport, Ireland). Samples were degraded in PBS buffer, under sterile conditions, at 37ºC, 47ºC, 57ºC and 70ºC, with solution pH being monitored regularly. On retrieval, at predetermined time intervals, analysis included change in mass, molecular weight (gel-permeation chromatography, Agilent Technologies), thermal properties (differential scanning calorimetry) and molecular structure (nuclear magnetic resonance spectroscopy). Indicators of late stage inflammation will be assessed using an MTT cytotoxicity assay and multiple ELISA analysis for inflammatory factors, with mouse L929 fibroblasts and RAW264.7 macrophages.

Results and Discussion

The degradation of P*DL*LGA at 37ºC, 47ºC, 57ºC and 70ºC was modelled using the Arrhenius equation; the changes in molecular weight were used to calculate the hydrolysis rate at each temperature and then compared to physiological temperature. When samples were degraded at 47ºC, 57ºC and 70ºC the degradation rate was increased by x3, x8 and x30 respectively. The results suggest that the degradation mechanism of P*DL*LGA at increased temperatures is similar to that of physiological temperature and can therefore be used as a method to

accelerate its degradation. The degradation of P*L*LGA will also be modelled using a similar approach. Fig. 1 shows the changes in appearance of P*DL*LGA and P*L*LGA during degradation at 47°C. P*DL*LGA underwent significant changes to its appearance throughout degradation; after 12 days the samples had a soft, paste-like appearance. In contrast, P*L*LGA samples appeared volumetrically unchanged, however after 57days at 47°C the samples were fragile and disintegrated on handling. Fig. 2 compares the swelling ratio and mass loss of P*DL*LGA and P*L*LGA. Swelling in P*DL*LGA occurred immediately upon immersion in PBS buffer and increased rapidly throughout degradation. In comparison, swelling in P*L*LGA did not occur immediately; after 57days at 47°C polymer swelling was 16% and increased gradually to 49% after 78days. Unlike P*DL*LGA where swelling occurred without significant mass loss, mass loss in P*L*LGA almost replicated the amount of polymer swelling. It is expected that these polymers will cause different responses *in vitro*. The next stage of this study is to evaluate and compare the *in vitro* inflammatory response of both polymers at different stages of degradation. An MTT cytotoxicity has been used as an initial evaluation in the cellular response of the two polymers.

Conclusion

It is paramount that long-term performance of new bioresorbable devices can be demonstrated *via* internationally standardised methods. An accelerated degradation methodology has been validated in this study as a highly effective tool for pre-degrading P*DL*LGA and P*L*LGA bioresorbable polymers prior to evaluation of their long-term *in vitro* inflammatory response. It is proposed that 47°C is adopted by the research community when assessing the long-term response of these polymers. Further work will include an *in vitro* evaluation of P*DL*LGA and P*L*LGA with fibroblast and macrophage cell lines.

References

1. Ginjupalli, K. *et al.* Poly(α-hydroxy acid) based polymers: A review on material and degradation aspects. *Polym. Degrad. Stab.***144,** 520–535 (2017).

2. Böstman, O. & Pihlajamäki, H. Clinical biocompatibility of biodegradable orthopaedic implants for internal fixation: a review. *Biomaterials***21,** 2615–2621 (2000).

Acknowledgement

Sterilisation by Steris is gratefully acknowledged

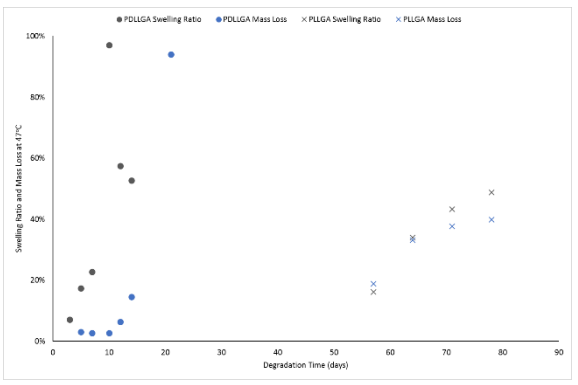

Fig. 2
Swelling ratio and mass loss in P*DL*LGA and P*L*LGA at 47°C

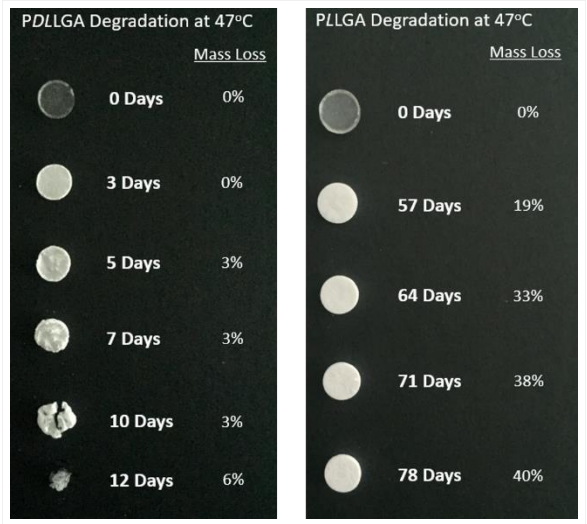

Fig. 1
P*DL*LGA and P*L*LGA sample appearance after degradation at 47°C and drying

X-OS38-05

Differentiation and heterogeneity of biomaterial-induced multinucleated giant cells: connection between inflammation and tissue regeneration

Mike Barbeck[1], Ronald E. Unger[2]

[1]University Medical Center Hamburg-Eppendorf, Department of Oral Maxillofacial Surgery, Division for Regenerative Orofacial Medicine, Hamburg, DE; [2]University Medical Center of the Johannes Gutenberg University, Institute of Pathology, Mainz, DE

Introduction

Biomaterial-associated multinucleated giant cells (BMGCs) have been found within the implantation beds of many different biomaterials (Fig. 1). However, their exact differentiation and their involvement in the inflammatory and healing events of the foreign body response still remain mostly unclear. Various findings suggest that these cells belong to the cell line of the foreign body giant cells (FBGCs), which are of “inflammatory origin”, and they may provide a phenotypic heterogeneity equivalent to that of macrophages, whose pro-inflammatory activation profile has been proposed to promote the process of biomaterial-mediated tissue regeneration [1]. Further knowledge is essential to evaluate the role of BMGCs in the regeneration processes, especially on the basis of different biomaterial characteristics, as this is required to ensure their successful clinical application. To substantiate our hypothesis of the differentiation and of the phenotypic and functional relationship between macrophages and BMGCs, antibodies for the detection of giant cell-specific antibodies as well as for detection of different pro- and anti-inflammatory macrophage subpopulations were applied to investigate the heterogeneity of BMGCs.

Experimental Methods

Two different studies were conducted to analyze both the differentiation of the BMGCs and their heterogeneity. In a first study tissue samples from a clinical study were used to analyze the origin of BMGCs in the implant beds of a synthetic and a xenogeneic bone substitute by the application of immunohistochemical methods. Two antibodies against integrin molecules specific for osteoclasts (β-3 integrin) or FBGCs (β-2 integrin) were used to distinguish both giant cell types. In a second study an established subcutaneous implantation model in 24 female 6-8 weeks old Wistar rats to implant silk fibroin (SF) was used. Specialized (immuno-) histochemical staining methods and histomorphometrical techniques, were applied to analyze the heterogeneity of BMGCs [2].

Results and Discussion

The results of the first study indicate that the BMGCs induced by both kinds of bone substitutes are FBGCs, as they express only β-2 integrin in contrast to the osteoclasts outside of the immediate implantation areas, which only demonstrate β-3 integrin expression (Fig. 1). In the implantation study both pro- and anti-inflammatory molecules can be demonstrated in the FBGCs infiltrating the microfibres of the SF scaffold (Fig. 2). The present data show that the BMGCs induced by both kinds of bone substitutes are FBGCs, as they express only β-2 integrin in contrast to the osteoclasts outside of the immediate implantation areas, which only demonstrate β-3 integrin expression. Furthermore, these cells express both pro- and anti-inflammatory molecules to the same extent within the implantation beds of silk fibroin scaffolds 15 days after implantation, which substantiates the heterogeneity of FBGCs comparable to that of macrophages, whose M2-phenotype appears to be related to a successful tissue remodeling outcome [1].

Conclusion

These data give new insight into the tissue reaction to biomaterials. Based on this new knowledge further research concerning the proteomic profile of the FBGCs especially with respect to the different physicochemical properties of biomaterials is necessary.

References

[1] Brown BN *et al*. Biomaterials. 2012;33(15):3792-802.

[2] Barbeck M *et al*. Biomed Mater. 2015:11(5):055007.

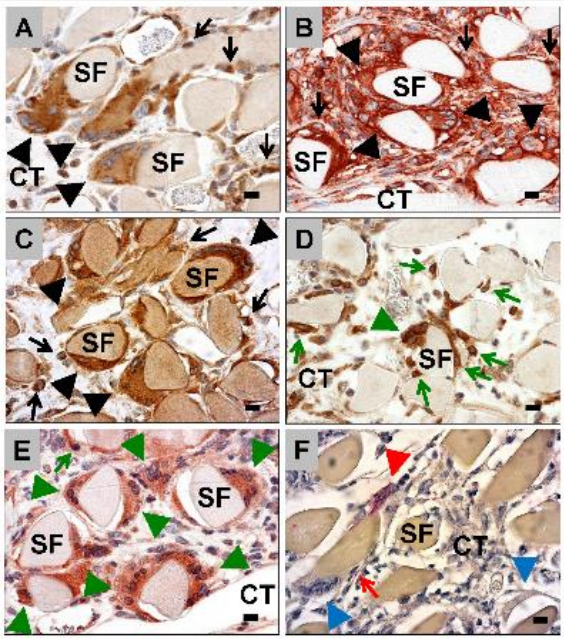

Figure 2
Figure 2 shows the immunohistochemical detection of pro-inflammatory (A, B and C) and anti-inflammatory (D and E) molecules within the tissue ingrowth into the subcutaneously implanted silk fibroin (SF) scaffolds (A: COX-2-staining, B: CCR7-staining, C: NF-κB-staining, D: HO-1-staining, E: CD206-staining, F: TRAP-staining, 600x magnifications, scale bars = 10 µm).

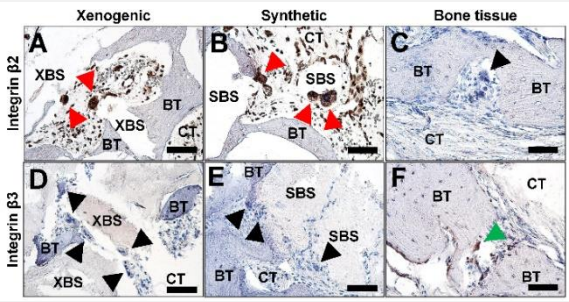

Figure 1
Figure 1 shows exemplary photomicrographs of the immune-histochemical detection of two adhesion molecules. Multinucleated giant cells (MNGCs) within the implantation areas of both the (A) xenogeneic (XBS) and (B) the synthetic bone substitute (SBS) express the β-2 integrin (red arrowheads) distinctive of foreign body giant cells (FBGCs), while they did not express the β-3 integrin characteristic of osteoclasts (BT = bone tissue) (400x magnifications, scale bars = 50 µm).1.

X-OS38-RF06

Effect of sandblasting treatment on in vitro degradation behavior and cytotoxicity of zinc and its alloys

Ping Li[1], Junyu Qian[2], Wentai Zhang[2], Christine Schille[1], Ernst Schweizer[1], Alexander Heiss[3], Claudia Legner[3], Ulrich E. Klotz[3], Guojiang Wan[2], Jürgen Geis-Gerstorfer[1], Lutz Scheideler[1]

[1]University Hospital Tübingen, Section Medical Materials Science and Technology, Tübingen, DE; [2]Southwest Jiaotong University, Key Laboratory of Advanced Technologies of Materials, Ministry of Education, College of Materials Science and Engineering, Chengdu, CN; [3]Research Institute for Precious Metals and Metals Chemistry (fem), Schwäbisch Gmünd, DE

Introduction

Zinc (Zn) and its alloys have drawn attention as potential materials for orthopedic or craniomaxillofacial implants. Nonetheless, Zn and its alloys exhibit relatively slow degradation rates within bone environments compared to the degradation requirements for clinical application [1,2]. Previous studies proposed that the degradation rates of Zn-based materials can be accelerated via alloying [3], metal matrix composite [2], micro-arc oxidation coating [4] or a sacrificial Mg-rich anode [5]. Moreover, sandblasting treatment has been demonstrated as a feasible approach to improve the degradation rate of metals, such as Mg-Ca alloy [6] and pure Fe [7]. This study aimed to investigate the effect of different sandblasting treatments on *in vitro* degradation behavior and cytotoxicity of Zn and its alloys.

Experimental Methods

A Zn-4Ag and a Zn-2Ag-1.8Au-0.2V (wt.%) alloy (denoted as Zn-Ag-Au-V) were fabricated and compared to pure Zn. All samples were ground up to P4000 SiC paper. The surfaces of Zn and the Zn alloys were sandblasted by two Al_2O_3 particle sizes,125 µm and 250 µm, as described in a previous study [8]. The microstructure was characterized by stylus profilometry, SEM-EDX and XRD.

The *in vitro* degradation behavior was evaluated with a semi-static immersion test for 14 days. Samples were immersed in DMEM/F-12 under cell culture conditions. The ratio of surface area to extraction volume was set to 1 cm^2/mL. Released metallic ions were detected by ICP-OES, and pH value changes were measured. Corrosion products were analyzed by SEM-EDX. Corrosion rates were calculated by weight loss.

Cytotoxicity was evaluated by an extract test according to ISO 10993-5/-12. Sample extracts were prepared using cell culture medium without FBS at an extraction ratio of 1.25 cm^2/mL for 24 h. Human primary osteosarcoma cells (Saos-2) were used to evaluate the inhibition of relative metabolic activity (CCK-8 assay). Also, metallic ion concentrations and pH value of the extracts were determined.

Results and Discussion

After the sandblasting treatments, average roughness (Ra) and mean roughness depth (Rz) of samples were increased, and both values significantly rose when the size of sandblasting Al_2O_3 changed from 125 µm to 250 µm. Additionally, Al_2O_3 sandblasting particles were embedded into the substrate of Zn and Zn alloys observed by SEM-EDX and XRD analysis.

As shown in Fig. 1a, SEM characterization revealed loose degradation layers covering the whole surfaces, and degradation particles distributed on all surfaces. EDX analysis showed that these corrosion products were mainly composed of Zn, P, O, C and Cl. After removing the degradation products, sandblasted samples presented irregular and rough surface structures consisting of a couple of corrosion pits and localized corrosion attack. Fig. 1b shows

that no obvious differences in cumulative Zn^{2+} release for Zn alloys were detected between sandblasting and control groups. Mean pH values of all samples showed no apparent increase and all were below pH 8.4. Fig. 1c shows that the degradation rates of sandblasted samples were significantly higher than the counterparts of P4000 polished samples ($p < 0.05$).

Fig. 2a shows that cytotoxicity of Zn and its alloys was influenced by the sandblasting treatment with 250 µm Al_2O_3. As shown in Fig. 2b, the Zn ion concentration in the extracts of most sandblasted samples was significantly higher than the counterparts of P4000 samples ($p < 0.05$), but all Zn concentrations were below 25 µM. Also, all pH values were below 8.5.

Conclusion

Degradation rates of Zn and its alloys are significantly increased by sandblasting treatments. Also, degradation behavior and cytotoxicity are related to the sandblasting particle size. This study demonstrates the promising potential of sandblasting treatments for adjusting the degradation behavior of Zn-based alloys. Nevertheless, further investigations are required.

References

1. Li, H., *et al.*, *Sci. Rep.* (2015) 5, 10719
2. Yang, H., *et al.*, *Acta Biomater.* (2018) 71, 2003.
3. Kafri, A., *et al.*, *Metals* (2018) 8 (3), 153
4. Yuan, W., *et al.*, *ACS Biomater Sci Eng.* (2019) 5 (2), 487
5. Yang, H., *et al.*, *ACS Biomater Sci Eng.* (2019) 5 (2), 453
6. Höh, N. V. D., *et al.*, *Adv. Eng. Mater.* (2009) 11 (5), 47
7. Zhou, J., *et al.*, *ACS Appl. Mater. Interfaces* (2016) 8 (40), 26482
8. Al Qahtani, W. M., *et al.*, *Biomed Eng-Biomed Te* (2017) 62 (1), 75

Acknowledgement

The work was supported by AiF-ZIM (KF2342806CK2), CSC (201608440274) and DAAD (57390341).

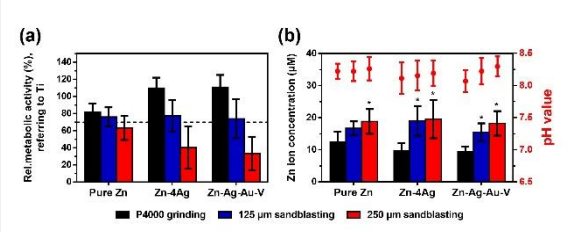

Figure 2: Cytotoxicity of samples: (a) CCK-8 results (b) Analysis of extracts, * represent $p < 0.05$ when compared with P4000 sampes.

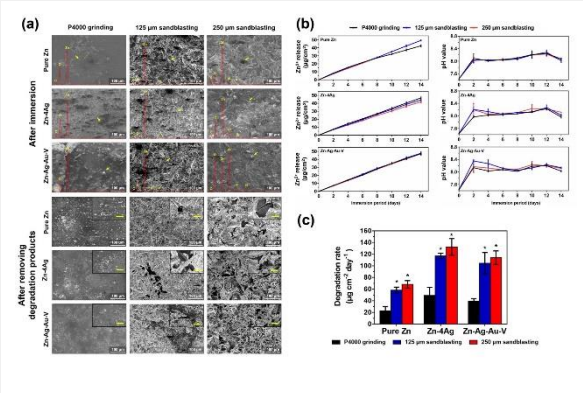

Figure 1: In vitro degradation behavior of samples:
(a) SEM-EDX analysis (The scale bar in the insets image is 10 μm), and the EDX result (inset red line) shows the elemental composition of degradation products pointed with the related yellow arrow, (b) Cumulative Zn ion release and pH value changes, (c) Degradation rate of samples, * represent $p < 0.05$ when compared with P4000 samples.

X-OS38-RF07

Resorbable films from lauroyl derivatives of hyaluronan as temporary implants

Jiří Mrázek[1], Josef Chmelař[1], Martina Hermannová[1], Lukáš Kubala[2], Kristina Nešporová[1], Ludmila Grusová[1], Tomáš Drmota[1]

[1]Contipro a.s., Dolní Dobrouč, CZ; [2]Czech Academy of Sciences, Institute of Biophysics, Brno, CZ

Introduction

Biopolymers such as hyaluronan (HA) present advantageous starting points for developing novel materials for medicine. Since natural HA is highly soluble, chemical modification is required to produce solid forms suitable for implants. We prepared insoluble free-standing films from hyaluronan by introducing hydrophobic side groups that formed non-covalent crosslinks. The films were homogeneous and sufficiently strong yet flexible even when wet. We evaluated safety and biodegradability of the films both *in-vitro* and *in-vivo* in mice.

Experimental Methods

Free-standing films from lauroyl HA [1] were prepared by solution casting from diluted water-alcohol solution in a custom-built drying cell at 50 °C. Film thickness, dry mass, content of residual organic solvent, mechanical properties, swelling and enzymatic degradation were measured. We further compared material properties before and after sterilisation with ethylenoxide. *In-vitro* cytotoxicity was examined on 3T3 cells. Film samples (15 × 15 mm) were then implanted into abdominal cavity of C57Bl/6J mice to evaluate their safety and biodegradability (five animals per group).

Results and Discussion

The prepared lauroyl HA films (Fig. 1) were non-porous, with thickness deviations lower than 20 % (for a 16 µm thick film). Flexibility of the film enabled easy manipulation and repeated folding without cracking. Film swelling ratio in phosphate buffer and enzymatic degradation rate could be tuned by the degree of lauroyl substitution (DS) in a wide range (Fig. 2). Extracts of the films were not cytotoxic for 3TC cells. None of the mice showed signs of complications caused by material implantation and macroscopic evaluation of the peritoneum did not reveal any organ changes or other adverse effects. After 10 days, the films with lowest tested DS (11.8 %) were completely degraded *in-vivo*. After the longest implantation time of 28 days, the films with DS ≤ 31.7 % were completely degraded, while for DS = 39.3 %, gel-like film residua were still present in all 5 animals.

Conclusion

We prepared free-standing films from lauroyl derivatives of hyaluronan by a simple one-step solution casting method, without using any crosslinking agents, activators, plasticizers or toxic solvents. The films are homogeneous, mechanically strong and flexible. Their properties, such as swelling and degradation rate, can be tailored by the degree of hyaluronan substitution. Importantly, the film properties do not change dramatically upon sterilization by ethylenoxide. The safety and biodegradability of the films were verified *in-vitro* and *in-vivo* on mice, with good agreement of the *in-vitro* and *in-vivo* data. These results suggest that the lauroyl HA films are suitable for applications in medicine, e.g., as resorbable implants.

References

[1] D. Šmejkalová, M. Hermannová, R. Šuláková, A. Průšová, J. Kučerík, V. Velebný, *Carbohyd. Polym.***2012**, *87*, 1460.

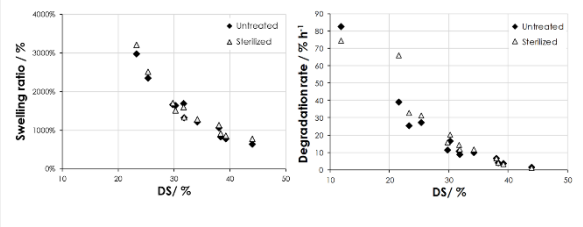

Fig. 2. Film swelling and degradation. Film swelling in phosphate buffer and film degradation rate (*in-vitro* enzymatic assay) as functions of lauroyl degree of substitution (DS).

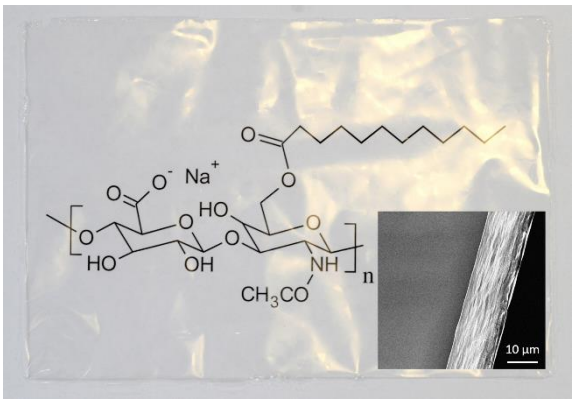

Fig. 1. Lauroyl-hyaluronan film. Free-standing lauroyl-HA film (11x16 cm, thickness 16 µm) with the chemical formula of the material seen through the film. Inset: Scanning electron microscope image of film cross-section.

X-OS38-RF08

In vivo degradation and biocompatibility of injectable non-covalent starPEG-based hydrogels

Rebecca Rothe[1,2], Sandra Hauser[1], Yong Xu[3], Alvin K. Thomas[3], Yixin Zhang[3], Jens Pietzsch[1,2]

[1]Helmholtz-Zentrum Dresden-Rossendorf, Institute of Radiopharmaceutical Cancer Research, Department of Radiopharmaceutical and Chemical Biology, Dresden, DE; [2]Technische Universität Dresden, Faculty of Chemistry and Food Chemistry, Dresden, DE; [3]BCUBE - Center for Molecular and Cellular Bioengineering; Technische Universität Dresden, Dresden, DE

Introduction

Undesired host tissue-material interactions like an adverse foreign body response, acute inflammation and fibrotic encapsulation often result after implantation of biomaterials. For clinical applications, biomaterials have to be highly biocompatible. Thus, attenuation of the above-mentioned obstacles and desired functionality of biomaterials regarding drug release or management of cell performance can be ensured.

Objectives

Focus of the study is on the relation between structural features of injectable starPEG-based hydrogels and evoked biological effects. In particular, inflammatory and angiogenic processes in material-surrounding tissue were objects of examination.

Experimental Methods

Four different physical hydrogels were examined regarding their degradation profiles and cellular responses at host tissue-material interface. Lead structure concept is based upon an repetitive lysin-alanine ($(KA)_5$) peptide sequence, starPEG and the oligosaccharide dextran sulfate ($(KA)_5$-DS). Further, modified hydrogels containing either an additional matrix metalloproteinase (MMP) cleavage site ($(KA)_5$-MMP*iw*-DS) or other variations in the peptide sequence and oligosaccharide like a D-amino acid motif ($(ka)_5$-DS) and sulfated hyaluronic acid ($(KA)_5$-sHA) were examined. Hydrogels were subcutaneously injected (50 µl) in immunocompetent nude SKH1-Elite mice. Magnetic resonance imaging (MRI) was used to analyze hydrogel degradation and inguinal lymph node size, indicating inflammatory reactions. *In vivo* activation of MMPs around injected hydrogels was followed by a specific fluorescence probe (MMPSense 645) and optical imaging during initial investigation period. Additionally, immunohistochemical stainings of typical angiogenesis (VEGF, CD31) and inflammation (COX-2, CD68) markers on cryosectioned tissue preparations were used to determine biocompatibility of analyzed hydrogels. Quantification of immunohistochemistry was performed with Fiji ImageJ software utilizing the color threshold plugin.

Results and Discussion

Comparing all four investigated starPEG-based hydrogels, $(KA)_5$-sHA hydrogel displayed fastest degradation *in vivo*. $(KA)_5$-DS and $(KA)_5$-MMP*iw*-DS hydrogels were gradually slower degraded during study period of 85 days. In contrast, volume of $(ka)_5$-DS hydrogel remained unchanged (Fig. 1). Further, inguinal lymph node sizes of all animals, independently of injected hydrogel composition, were comparable to the untreated control group suggesting a suitable biocompatibility. $(KA)_5$-sHA hydrogel induced significantly raised MMP activation during investigation period (Fig. 2). In addition, immunohistochemistry displayed raised VEGF expression around $(KA)_5$-sHA hydrogel as well

as macrophage invasion into all hydrogels. Surrounding tissues displayed also basal expression of inflammation and angiogenesis markers, like COX-2 or CD31.

Conclusion

Definite degradation profiles depending on structural composition of the investigated injectable starPEG-based hydrogels were demonstrated. According to lymph node measurements and immunohistochemical stainings, a normal biological, but not an adverse inflammatory response to these non-covalent hydrogels occurred in surrounding tissues. Particularly, one derivative, the $(KA)_5$-sHA hydrogel, displayed pro-angiogenic effects. This offers potential applications, e.g. in the field of tissue regeneration.

Acknowledgement

This work was supported by the China Scholarship Council and German Federal Ministry of Research and Education (BMBF grants 03Z2EN12 and 03Z2E511). S.H., R.R. and J.P are thankful to the Deutsche Forschungsgemeinschaft (DFG), Research Grant Collaborative Research Center Transregio 67 “Functional Biomaterials for Controlling Healing Processes in Bone und Skin - From Material Science to Clinical Application“ (CRC/TRR 67/3) and to the Helmholtz Cross Programme Initiative “Technology and Medicine – Adaptive Systems“ for supporting this work.

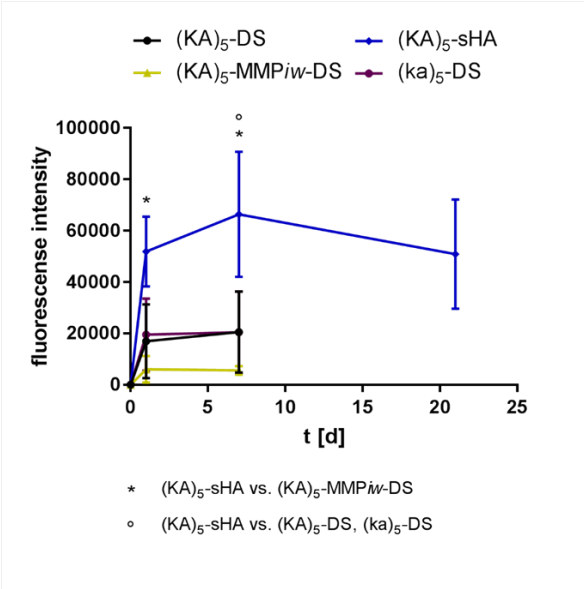

Fig. 2: MMP activity in material surroundings. Determination of MMP activity around injected hydrogels by optical imaging (n = 5-8; Mean ± SEM; * | ° p < 0.05, two-way ANOVA, Bonferroni post hoc test).

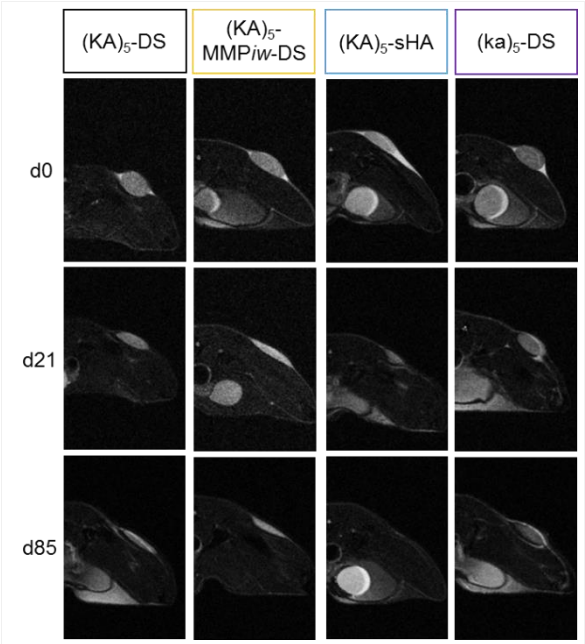

Fig. 1: Representative axial MRI images. Subcutaneous injected hydrogels show clear structure-dependent degradation profiles over time.

9:30 a.m. – 11:00 a.m.

Conference room 2+3

X-SY17 | Tackling brain diseases: biomaterials-based approaches to understand and bypass biological barriers

Clara Mattu (Turin, IT)
Andrei Mikheev (Houston, US)

The brain is protected by the blood-brain barrier (BBB), a tight semi-permeable membrane that isolates the brain parenchyma from the blood circulation. Bypassing the BBB is a key challenge to efficiently deliver drugs or other molecules to treat brain diseases. This symposium will discuss the new biomaterials-based approaches for in vitro modelling of the brain micro-environment, their potential application in drug screening, and how the propertied of biomaterials can be leveraged to increase our understanding and improve treatment of brain diseases.

X-SY17-KL01

Strategies to improve the protection of vulnerable neurons in models of neurodegeneration

Nicola Origlia

CNR, Institute of Neuroscience, Pisa, IT

Introduction

Neurodegenerative disorders are characterized by a progressive neuronal impairment that starts in specific brain regions suggesting the presence of a selective vulnerability of certain cell populations. However, the exact neuropathological mechanisms are still partially elusive and lead to disabling neurological and psychiatric conditions. The blood–brain barrier (BBB) is a major obstacle to the therapeutic delivery, in particular of peptides and proteins, to the brain. In addition to the design of small molecules, strategies bypassing the BBB have been developed including invasive methods, such as local delivery implants or injections, but also noninvasive approaches as intranasal delivery and ocular applications. The efficacy of these strategies in models of neurodegeneration will be discussed. A particular focus will be dedicated to Alzheimer's disease (AD) and glaucoma, two distinct multifactorial diseases that are thought to share common features such as the accumulation/aggregation of the β-amyloid protein and the increased phosphorylation of stress-related mitogen-activated protein kinases (MAPK).

Experimental Methods

Electrophysiology and behavioural assessment were performed in : i) AD mouse model carrying human mutation of amyloid precursor protein (APP swe/Ind /J20) expressing human Aβ (Mucke et al; 2000) ; ii) an established experimental model, the DBA/2J mouse, which develops chronic intraocular pressure elevation that mimics primary open-angle glaucoma (Anderson et al., 2002).

Results and Discussion

Using an *in vivo* AD model we have demonstrated that either small compounds targeting the MAPK or intranasal delivery of neurotrophic factors are capable of preventing neurodegeneration in vulnerable brain areas. Moreover, topical eye application of neurotrophic factors prevents retinal ganglion cell death and optic nerve atrophy in a model of glaucoma.

Conclusion

These studies highlight the importance of improving drugs penetrability in order to obtain promising, safe and feasible strategy to preserve neuronal function

References

Anderson MG, Smith RS, Hawes NL, Zabaleta A, Chang B, et al. (2002) Mutations in genes encoding melanosomal proteins cause pigmentary glaucoma in DBA/2J mice. Nat Genet 30: 81–85.

Mucke, L. et al. (2000) High-level neuronal expression of abeta 1-42 in wild-type human amyloid protein precursor transgenic mice: synaptotoxicity without plaque formation. J Neurosci 20: 4050–4058

X-SY17-KL02

Brain-derived lipidic nanoparticles with enhanced neuroprotective properties for the treatment of cerebral ischemia

Christos Tapeinos[1], Matteo Battaglini[2], Attilio Marino[1], Gianni Ciofani[3,1]

[1]Fondazione Istituto Italiano di Tecnologia, Smart Bio-Interfaces, Pontedera, IT; [2]Scuola Superiore Sant'Anna, The Biorobotics Institute, Pontedera, IT; [3]Politecnico di Torino, Department of Mechanical and Aerospace Engineering, Turin, IT

Introduction

Ischemic stroke occurs due to the reduced perfusion to a brain region, resulting in death or permanent neurological deficits. Unfortunately, to date, no effective treatment has been found to prevent damage to the ischemic brain after stroke. In view of this, we hypothesized that the targeted delivery of antioxidant (CeO_2) nanoparticles (NPs) and iNOS inhibitors (i.e. L-NIL) will reduce the overproduced ROS and RNS in the ischemic area, resulting to the amelioration of the neurological deficits caused by oxidative stress.

Experimental Methods

The biomimetic nanoscavengers (BIONICS) were composed of porcine-extracted brain lipids and their fabrication was achieved using a hot-emulsion sovent-exchange method. Their colloidal stability was studied in various biologically-relevant media, while their antioxidant ability was studied various antioxidant assay kits. The ability of the nanoscavengers to cross the blood-brain barrier and be internalized by neurons was tested using an *in vitro* cell culture model consisting of human astrocytes, endothelial cells, and neurons, while their ability to inhibit oxidative stress *in vitro* was evaluated under hypoxic and normoxic conditions.

Results and Discussion

BIONICS (~150 nm) presented excellent colloidal stability in water and biologically-relevant media, as well as excellent antioxidant capacity, similar to the one of the plain CeO_2 NPs. Flow cytometry results demonstrated a time-dependent internalization of BIONICS as well as a neuroprotective and pro-neurogenic effect towards differentiated neuronal cells.

Conclusion

BIONICS demonstrated excellent colloidal stability and antioxidant capacity, resulting in the inhibition of ROS and RNS mediated oxidative stress, and in subsequent neuroprotection of astrocytes, endothelial and neuronal cells under conditions mimicking the post-ischemic stroke environment.

Acknowledgement

"This project has received funding from the European Union's Horizon 2020 research and innovation program under the Marie Sklodowska-Curie grant agreement No 793644".

X-SY17-03

Development of injectable thermosensitive chitosan-based hydrogels for modeling the nervous system ECM

Francesca Gervaso[1], Maria Chiara Bellisario[1], Alessandro Polini[1], Velia La Pesa[2], Alessandro Romano[2], Angelo Quattrini[2], Lorenzo Moroni[1,3], Giuseppe Gigli[1,4]

[1]CNR - Nanotec, Institute of nanotechnology, Lecce, IT; [2]IRCCS San Raffaele Scientific Institute, Neuropathology Unit, Institute of Experimental Neurology and Division of Neuroscience, Milan, IT; [3]Maastricht University, Complex Tissue Regeneration, Maastricht, NL; [4]University of Salento, Dipartimento di Matematica e Fisica E. De Giorgi, Lecce, IT

Introduction

Use of animal models in neurodegenerative disease research raises several questions concerning relevance to human illnesses, poor predictivity and ethical issues [1]. In this respect, the lack of animal modelsable to fully reproduce the disease is an important obstacle also to research progress on Amyotrophic Lateral Sclerosis (ALS), a progressive and degenerative disease that affect nervous system causing the loss of motor neurons and leading within 2–5 years after clinical onset. Thus new experimental tools to study ALS are urgently needed. The emerging technology of organ-on-chip could represent an interesting option and 2D organ-on-chip models of the central nervous system start to be available [2]. However, to reproduce faithfully*in vitro*the cell-cell interactions occurring*in vivo*,3D models able to mimic tissue microstructure are mandatory. Injectable hydrogel, based on naturally derived polymers, are promising biomaterials for modeling the extracellular matrix (ECM) within 3D organ-on-chip platforms. This study focuses on the development of thermo-responsive injectable chitosan-based hydrogels for modeling the nervous system ECM and delivering cells and biological cues inside 3D organ-on-chips, useful for understanding the pathogenetic mechanisms involved in ALS and moving a step forward to patient-specific diagnostic tools. Chitosan (CH) hydrogels were prepared by using three different gelling agents (GAs), i.e. bGlycerophosphate (BGP), Sodium Hydrogen Carbonate (SHC), and L-Arginine (ARG) [3]. The influence of GAs on hydrogel gelation kinetic, swelling and stability properties was studied. Mechanical properties were analyzed by a rotational rheometer and compression tests. Indirect cytotoxicity tests were performed *in vitro*by using a human neuroblastoma cell line

Experimental Methods

CH powder (3.33% w/v) was dissolved in hydrochloric acid (0.1M HCl) with magnetic stirrer for 24h at RT. Three different GAs were used: BGP, SHC and ARG. While BGP and SHC have already been employed as GAs for CH, ARG is firstly introduced here into the system and its influence on hydrogel properties investigated. BGP and SHC were dissolved in Milli-Q water while ARG in 0.1M HCl. The initial amount of GAs was opportunely calculated in order to reach the desired final concentration of each GA. Hydrogels were prepared by mixing the CH solution with GA solutions in a 3:2 ratio by two syringes joined by a Luer Lock connector. Samples were then incubated in an oven at 37°C in order to promote sol-gel transition. Sol-gel transition was qualitatively evaluated by the tube inversion test and quantitatively by a rheology test. Hydrogel injectabilitywas investigated through a 23G syringe needle. The swelling degree (SD) of hydrogels was determined by the following:$SD=[(W_w-W_d)/W_d]\times100$, where $W_d$and $W_w$are sample dry and hydrated weights, respectively. *In vitro*hydrogel stability was examined by measuring the weight change after different time intervals of immersion in PBS. Rheological tests allowed the evaluation of storage (G′) and loss (G″) moduli in the linear viscoelastic range both at 22°C and 37°C.The Young's modulus (E) of hydrogels was evaluated in wet conditions at RT (10N load cell, crosshead speed 2 mm/min up to 60% strain) and was

calculated as the slope of the initial linear portion of the stress-strain curve. An indirect cytotoxity test was performed by incubating DMEM with hydrogels for different time intervals and using the conditioned DMEM to evaluate cell vitality in neuroblastoma cell model (SH-SY5Y)

Results and Discussion

Several combinations of GA solutions in different concentrations have been used to prepare chitosan-based hydrogels. The tube inversion test allowed to select the GA blends and concentrations able to confer thermo-sensitive sol-gel transitions to the chitosan solution, which are: BGP0.2M, BGP0.2M+SHC0.05M, BGP0.2M+SHC0.05M+ARG0.01M (in the following referred as CH_BGP, CH_SHC, CH_ARG). The hydrogels were injectable through a 23G needle at RT and thermo-responsive at 37°C. Swelling tests carried out to check the maximum water intake of the freeze-dried hydrogel samples showed that all samples reached the maximum SD after 10 min in PBS and remained almost constant for up to 60 min (CH_BGP ~300%, CH_SHC and CH_ARG ~600%). Stability tests revealed a weight decrease after 24h in PBS of 9.8±0.6% for CH_SHC and 13.3±4.2% for CH_ARG, while CH_BGP samples were almost completely degraded; although the CH_ARG average weight loss was slightly higher than with CH_SHC, differences were not significant. G' and E significantly improved by adding SHC and ARG. In particular, hydrogels with ARG had the highest E (BGP 10.8±4.5, SHC 47.2±6.3, ARG 62.2±1.2 kPa). Cell culture tests showed that none of the samples had any significant cytotoxic effect

Conclusion

Overall a hydrogel including ARG presented the best properties and therefore may be considered as a potential candidate for providing an ECM-like microenvironment for cell-cell interaction in organ-on-chip platforms

References

1.Haring et al, 2017, DOI 10.1007/s12015-017-9738-0
2.Booth and Kim, 2012, DOI 10.1039/c2lc40094d
3.Assaad et al, 2015, DOI 10.1016/j.carbpol.2015.04.063

Acknowledgement

This work was supported by the Progetto FISR - C.N.R. "Tecnopolo di nanotecnologia e fotonica per la medicina di precisione" - CUP B83B17000010001.

X-SY17-04

Transcytosis of microgels across the blood-brain barrier: influence of microgel size and stiffness

Laís Ribovski[1,2], Olga Mergel[1], Valtencir Zucolotto[2], Patrick Van Rijn[1], Inge S. Zuhorn[1]

[1]University of Groningen, University Medical Center Groningen, Department of Biomedical Engineering, Groningen, NL; [2]University of São Paulo, Physics Institute of São Carlos, Nanomedicine and Nanotoxicology Group, São Carlos, BR

Introduction

The blood-brain barrier (BBB) imposes a challenge to the delivery of therapeutics to the brain. However, its integrity is essential to prevent the transport of harmful or unwanted substances to the brain. Nanocarriers are a promising tool to enhance drug delivery across the BBB. Nanomaterials' physicochemical properties, such as size, charge and surface modifications, are known to modulate uptake and transport at the BBB.(Georgieva et al., 2011) The influence of nanomaterial stiffness on the interaction between the nanomaterial and the BBB is largely unexplored.(Guo et al.,2018 and Anselmo et al., 2015)

Here, we propose to study the effect of poly(N-isopropylmethacrylamide) microgels' size and stiffness on uptake and transcytosis in brain endothelial cell monolayers. Moreover,the microgels show a thermoresponsive shift between a swollen and collapsed state, being swollen at 37˚C, i.e., at physiological body temperature, and collapsed at temperatures > 44˚C.

Experimental Methods

Microgels are synthesized by precipitation polymerization including a fluorescent dye with a polymerizable group. Briefly, an aqueous solution of NIPMAM, N,N'- methylenebisacrylamide (BIS), sodium dodecyl sulfate (SDS) and nile blue acrylamide is heated to 70 ˚C under stirring and a blanket of N_2. After temperature stabilization, the reaction is initiated with ammonium persulfate (APS). The molar ratio of BIS, concentration of SDS and polymerization time were set to obtain microgels with different stiffnesses and sizes. Purification was performed by extensive dialysis. BIS is a cross-linking agent and its concentration in the reaction affects network flexibility. Therefore, microgel stiffness correlates with BIS concentration and is evaluated according to its Young's modulus determined by atomic force microscopy.

To quantify the uptake and transcytosis of the microgels in brain endothelial cell monolayers, we used our recently developed filter-free BBB model (De Jong et al., 2018) in which microgel-associated fluorescence can be measured in the apical, cellular, and basolateral compartments. The fluorescence in the basolateral compartment reflects the amount of microgels that has crossed the BBB.

Results and Discussion

We were able to make microgels with different sizes, stiffnesses, and swelling ratio (Figure 1).

Preliminary results indicate that smaller microgels show higher uptake by brain endothelial cells than bigger microgels. Uptake is both concentration- and time-dependent (not shown). Transcytosis across the BBB seems similar for the three different microgels, with a value that lies between 11.0-12.2% (Figure 2).

Conclusion

The extent of microgel transcytosis across the BBB warrants further investigation of this nanocarrier platform for drug delivery to the brain.

References

Georgieva JV et al. Surface characteristics of nanoparticles determine their intracellular fate in and processing by human blood-brain barrier endothelial cells in vitro. Mol Ther. 2010.

Guo P et al. Nanoparticle elasticity directs tumor uptake. Nat Commun 2018.

Anselmo AC et al. Elasticity of Nanoparticles Influences Their Blood Circulation, Phagocytosis, Endocytosis, and Targeting. ACS Nano 2015.

De Jong E et al. A filter-free blood-brain barrier model to quantitatively study transendothelial delivery of nanoparticles by fluorescence spectroscopy. J Control Release 2018.

Acknowledgement

This study was financed in part by the Coordenação de Aperfeiçoamento de Pessoal de Nível Superior - Brasil (CAPES) - Finance Code 001 and by a fellowship of the Abel Tasman Talent Program of the University of Groningen.

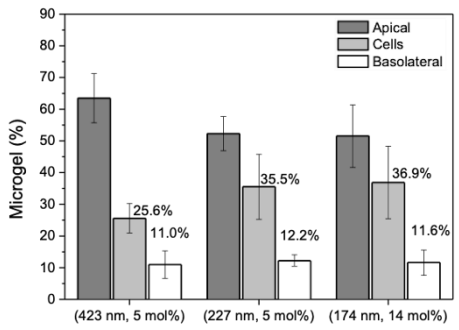

Figure 2.
Transcytosis of p(NIPMAM) microgels fluorescently-labelled with nile blue. 50 µg of microgel was added per well (duplicates) and incubated for 4 hours. The percentage is relative to the total fluorescence of the three collected compartments (apical, cells, basolateral). Each value represents the mean±SD between duplicates (n=1).

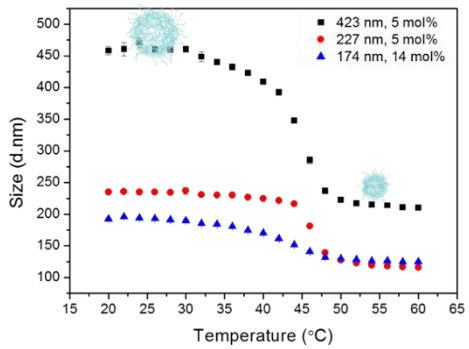

Figure 1.
Thermoresponsive curves of p(NIPMAM) microgels with different sizes and stiffnesses.

11:30 a.m. – 1:00 p.m.

Hall 3

XI-OS39 | In vitro tissue models

XI-OS39-01

Peri-implant infection models: 2D versus 3D

Alexandra Ingendoh-Tsakmakidis[1], Carina Mikolai[1], Andreas Winkel[1], Christine S. Falk[2], Angela Rossi[3], Heike Walles[3,4], Jörg Eberhard[1,5], Meike Stiesch[1]

[1]Hanover Medical School, Department of Prosthetic Dentistry and Biomedical Materials Science / NIFE, Hanover, DE; [2]Hanover Medical School, Institute of Transplant Immunology, Hanover, DE; [3]Fraunhofer Institute of Silicate Research ISC, Translational Center for Regenerative Therapies, Würzburg, DE; [4]University Hospital of Würzburg, Chair of Tissue Engineering and Regenerative Medicine, Würzburg, DE; [5]University of Sydney, Sydney Dental School, Westmead, AU

Introduction

The frequency of peri-implant disease is raising concomitant with accelerating numbers of dental implant insertions for functional and aesthetic restoration. Hence, there is an emerging demand to uncover the pathophysiology of peri-implant infection. The major factors that influence the progress of peri-implant infection are the bacterial biofilm composition, the host tissue, and the inserted implant material. Clinical studies are the optimal approach to explore host-microbe-implant interactions. However, they are accompanied by strict regulations and ethical considerations. Animal studies provide the possibility to investigate extensively the peri-implant disease initiation and progression as well as the properties of new implant materials. Main issues regarding animal studies are the lack of human microbiota as well as the disease conditions and inflammatory responses that differ from human pathophysiology. *In vitro* studies using human-specific microbes and human tissue cells are used to gain detailed knowledge of molecular interactions. Most *in vitro* studies focus only on two of the three interacting factors in a 2D setting. In 2D models, tissue architecture, intercellular interactions, and implant geometry are absent. We established 2D and 3D *in vitro* peri-implant models including all main factors and compared their response to the initial colonizer *Streptococcus oralis*.

Experimental Methods

For the 2D models, titanium disks colonized by human gingival epithelial cells or fibroblasts were co-cultured with the *S. oralis* biofilm. Moreover, we developed a novel 3D peri-implant model consisting of an organotypic oral mucosa with inserted titanium and co-cultured this model with the *S. oralis* biofilm. First effects were determined by fluorescent microscopy and histology. Subsequently, global gene expression analysis was performed and secretion of cytokines was determined.

Results and Discussion

We observed that human gingival fibroblasts grown in monolayers were more susceptible than the epithelial cells. A reduced vitality and broader transcriptional response of fibroblasts were detected. This discrepancy disappeared when fibroblasts were grown together with epithelial cells in the 3D oral mucosa model leading to a longer co-culture period. Additionally, the 3D peri-implant mucosa model allowed the microscopic detection of topographic effects like altered tissue structure restricted to the peri-implant area. These results underline the importance of the cell type selection and their geometric conformation for *in vitro* peri-implant infection studies. Transcriptional changes in the 2D models revealed an inflammatory gene expression to the commensal *S. oralis* biofilm, whereas the opposite was detected in the 3D peri-implant mucosa. The protective response of the 3D model is in line with the observation that commensal bacteria do not cause inflammation in the oral cavity. Effects on protein levels of inflammatory cytokines

were similar in both models after *S oralis* biofilm challenge. However, transcriptional and morphological responses revealed that the physiological peri-implant tissue reaction was more closely resembled by the 3D model.

Conclusion

Our novel complex 3D peri-implant infection model is suitable to study all main interactions during peri-implant inflammation with more clinical relevant observations. Future studies including improved implant materials and different biofilm compositions will provide new insights into the pathophysiology of peri-implant disease and will support the development of innovative implant materials.

References

Dreyer H, Grischke J, Tiede C, Eberhard J, Schweitzer A, Toikkanen SE, et al. Epidemiology and risk factors of peri-implantitis: A systematic review. J Periodontal Res. 2018: Forthcoming.

Schou S, Holmstrup P, Kornman KS. Non-human primates used in studies of periodontal disease pathogenesis: a review of the literature. J Periodontol. 1993;64: 497-508.

Seok J, Warren HS, Cuenca AG, Mindrinos MN, Baker HV, Xu W, et al. Genomic responses in mouse models poorly mimic human inflammatory diseases. Proceedings of the National Academy of Sciences. 2013;110: 3507-3512.

Ingendoh-Tsakmakidis A, Nolte L, Winkel A, Meyer H, Koroleva A, Shpichka A, et al. Time-resolved 3D live-cell imaging on implants. PLoS One. 2018;13: e0205411.

XI-OS39-02

A novel collagen-based assay for measuring dermal fibroblast contractility influenced by natural ageing

Zhuonan Yu[1], Matthew J. Smith[2], Richard C. M. Siow[2], Lidong Liu[1], Kuo-Kang Liu[1]

[1]University of warwick, School of Engineering, Coventry, GB; [2]King's College London, Cardiovascular Division, British Heart Foundation Centre of Research Excellence, Faculty of Life Sciences and Medicine, London, GB

Introduction

The trajectories of ageing are believed to be determined by both genetic compositions and environmental stresses, with the former dominating the process and the latter driving the cellular adaptation in the process of ageing. For this very reason, ageing of the skin is an essential field of ageing research and tissue engineering applications. Previous investigations have indicated that ageing influences dermal fibroblasts in many aspects. Mechanically, younger fibroblasts exhibit more plastic behaviours while a rise in stiffness has been reported for the aged ones[1]. However, little is known about how the ageing influences on the contractility of dermal fibroblasts, which are abundant in the dermal constituent and critical to skin function. Hence this study can facilitate a better understanding of the ageing process of the skin.

In this study, a novel technique was developed for quantifying cellular contraction force of normal human dermal fibroblasts (NHDFs) *in vitro*. The technique utilises the depth sensing nano-indentation of cell-embedded collagen hydrogel together with the theoretical analysis based on the mechanics of biomaterials[2].

Experimental Methods

Cryopreserved NHDFs (Caltag Medsystems, UK) harvested from female donors with respective age of 26, 30, 62 and 75 y/o were used in this study. Cells were cultured to confluency at the condition of 37 °C, 5% CO_2 and RH 95% in Dulbecco's Modified Eagles Medium (DMEM) supplemented with 10% Foetal Bovine Serum (FBS), 2mM L-glutamine and antibiotics. To create the cell-embedded collagen hydrogel, 1.5ml of type I collagen solution (0.15% w/v) containing necessary supplements was polymerised in 35mm non-coated Petri-dishes, following the seeding of NHDFs (passage number 3-5) at a density of 7.5×10^5 cells/gel. 2ml of culture medium was added to each dish upon polymerisation and gel disks were subsequently dislodged to allow free contraction. Mechanical tests were conducted 48h post cell seeding.

A tailored nano-mechanical indentation tester allows the measurement of the force-displacement (*F-D*) of the hydrogels up to the resolutions of 10nN and 10nm for force and displacement respectively (Fig. 1A). The Young's moduli of the gels were determined based on the *F-D* curves fitted with Hertz contact theory (Fig. 1B). The geometric parameters such as the radius and height of the gel disks were measured by a CCD camera and the tester before and after the gel shrinkage. The overall cell contraction force can be determined based on the measured mechanical and geometric parameters in combination with a mathematical model based on the mechanics of materials[2]. Single cell contraction force was calculated as the total force divided by the number of the embedded cells in the gel.

Results and Discussion

Shown in figure 2, forces exerted on the collagen matrix by spontaneous contractions of NHDFs are higher on the samples with cells from the younger donors in comparison to the aged ones. Also, contraction forces decrease with a higher passage number associated with the cells, which is in line with previous reports on the decrease of

contractility with increased passage numbers. The values of the force measured in our study agree with previously reported observations[3]. Previous works also suggested a difference in contraction force between fibroblasts sourced from young and aged individuals[4]. As for the difference in NHDFs contractility between young and aged individuals, it is very difficult to form comparisons with our results measured in a 3D matrix, as the techniques adopted in those studies were mostly for cells on a 2D surface, thus less closely mimic physiological conditions. We will also present confocal microscope images of NHDF actin filament alignment after gel contraction.

Conclusion

The study was successfully conducted with a novel technique using cell-embedded collagen hydrogel assay, allowing NHDFs sourced from young and aged donors to contract in a biomimetic 3D matrix. Decreased contraction forces were observed in NHDFs from aged donors and in agreement with observations previously reported. Compared with methods previously developed to measure cell contraction force, we achieved measurement of contraction force in populations of NHDF in a 3D matrix at a physiological environment.

References

[1] C. Schulze *et al.* Biophys J **99**, 2434-2442 (2010)
[2] T. Jin *et al.* J. R. Soc. Interface **12**, 20141365 (2015)
[3] B. Li *et al.* Journal Tissue Viability **20**, 108-120 (2011)
[4] T. Fujimura *et al.* Arch Pharm Res **34**, 1015-1022 (2011)

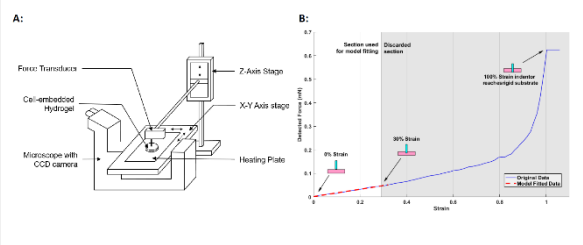

Figure 1
A, The schematic setup of nano-mechanical indentation tester. **B,** Typical loading *F-D* curve showing fitting of the Hertz contact theory to determine Young's moduli of the gel.

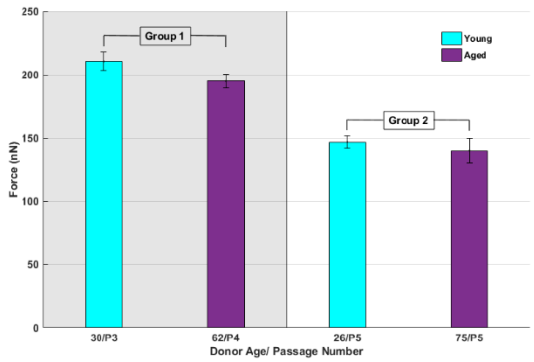

Figure 2
Comparison of Single NHDF contraction force between young and aged donors.

XI-OS39-03

Inhibition of acute and chronic neuroinflammation and glial scarring by liposomal curcumin on murine acute brain slices and human cell lines *in vitro*

Christina Schmitt[1,2], Anna Lechanteur[2], Coarlie Bellefroid[2], Katharina Siemsen[3], Christine Selhuber-Unkel[3], Janka Held-Feindt[4], Ralph Lucius[1], Geraldine Piel[2], Kirsten Hattermann[1], On behalf of GRK2154 Materials for Brain.

[1]University of Kiel, Institute of Anatomy, Kiel, DE; [2]University of Liège, Laboratory of Pharmaceutical Technology and Biopharmacy (LPTB), CIRM, Liège, BE; [3]University of Kiel, Institute of Materials Science, Kiel, DE; [4]UKSH Kiel, Department of Neurosurgery, Kiel, DE

Introduction

Neuro implants offer the possibility to target brain diseases directly, either by physical stimulation (e.g. microelectrodes) or, in perspective, by drugs loaded to suitable reservoir implants releasing them directly to the brain. However, the implantation of neuro implants into the brain causes acute and chronic foreign body responses by the surrounding brain parenchyma represented e.g. by neuronal loss, neuroinflammation and glial scarring *in vivo* [1]. During neuro inflammation, microglial cells release pro-inflammatory cytokines such as IL6 or TNFα that, among others, activate surrounding glial cells. In response a glial scar is formed (with concomitant elevation of glial scarring markers such as glial fibrillary acidic protein, fibronectin or tenascin), which influences the release kinetics of a drug from the implant as wells as its physical properties (e.g. conductivity) [2].

Thus, to broaden the applicability of brain implants, the adverse reactions towards implantation and implant material need to be diminished. One option is the application of the anti-inflammative and –fibrotic compound like curcumin, which was quite promising in reducing glial scar formation in spinal cord [3,4] and brain injury [5]. However, curcumin is a chemical and metabolic instable drug [6], limiting its applicability. To solve this problem, we chose to encapsulate curcumin into liposomes that are the most studied carriers for drug delivery and are already approved by the FDA for various applications [7]. They have the unique ability to encapsulate and thereby protect hydrophilic as well as hydrophobic drugs, facilitating or increasing cell permeability and therefore efficacy.

In this study we want to investigate if liposome carrying-curcumin can alleviate the experimental inflammatory and glial scarring reactions in murine acute brain slices and human neural/glial cell lines *in vitro*, in comparison to free curcumin.

Experimental Methods

Empty liposomes and curcumin encapsulated in liposomes were prepared by the hydration of lipid film method [8]. Liposomes were analyzed for their size, polydispersity index and zeta potential by dynamic light scattering and laser doppler microelectrophoresis. The curcumin encapsulation efficiency as well as drug loading were determined by HPLC. Liposomes containing trehalose have been freeze-dried for long-term storage.

Experimental neuroinflammation and glial scarring were induced by stimulation with either lipopolysaccharide (LPS) or pro-inflammatory cytokine combinations in human glial cell lines or murine brain acute slices. Murine acute brain slices of the cortex were obtained from 13 weeks old female mice and liposomes formulations or free curcumin were added to the culture medium from day 0 onwards in co-stimulation with LPS or cytokines over 8 days *in vitro*. Human astrocytes (SVGA) and microglia (HMC3) were co-stimulated for 24 hours *in vitro*. Rescuing effects of liposomal

curcumin in comparison to free curcumin were studied morphologically and on RNA and protein levels. The concentration-dependent effects of liposomal curcumin on proliferation or cell death were determined by WST-1 assay in comparison to free curcumin and empty liposomes after 3 days (in respect of ISO-10993-5).

Results and Discussion

Empty and curcumin loaded liposomes showed sizes, PDI and zeta potential of around 160nm - 170nm, 0.120 - 0.250 and -18mV - -30mV, respectively. Formulations were produced with a drug loading around 20µg curcumin per mg liposomes upon freeze drying. When human microglial and astrocyte cell lines were stimulated in concentrations of 0.001 to 20µM with liposomes and free curcumin, free curcumin reduced proliferation at higher concentrations (IC50 12 – 20 µM depending on cell line), while corresponding effects where observed at lower concentrations for curcumin liposomes (IC50 2-6 µM). However, when using appropriate concentrations of curcumin to reduce neuroinflammation and glial scarring in cultured cells, liposomal curcumin was more effective even with 100 fold lower concentrations than free curcumin. Effects for free and liposomal curcumin were more pronounced in astrocytes than in microglial cells. In addition, liposomal curcumin reduced the cytotoxic effects of LPS stimulation in murine acute brain slices after 2 and 8 days (acute and chronic response) *in vitro*, and was again more effective in alleviating inflammatory and glial scarring reactions than free curcumin.

Conclusion

Our results indicate that liposomes might be a useful tool to increase the stability and efficacy of curcumin in different inflammation/glial scarring models *in vitro*. Thus, liposomal encapsulation of curcumin might solve the limitations of its applicability in local mid to long-term administration. In perspective, deposition of liposomal curcumin in neuro implant coatings such as hydrogels will be performed to overcome acute and chronic inflammative and glial scarring reactions towards neuro implant materials.

References

[1] Marin C, Fernandez E. ; Biocompatibility of intracortical microelectrodes: current status and future prospects. Front Neuroeng. 2010 May 28;3:8.
[2] Prodanov, D.; Delbeke, J. Mechanical and Biological Interactions of Implants with the Brain and Their Impact on Implant Design. Frontiers in Neuroscience. 2016;10
[3]Yuan J, Zou M, Xiang X, Zhu H, Chu W, Liu W, Chen F, Lin J.; Curcumin improves neural function after spinal cord injury by the joint inhibition of the intracellular and extracellular components of glial scar. J Surg Res. 2015 May 1; 195(1):235-45.
[4] Ruzicka J, Urdzikova LM, Kloudova A, Amin AG, Vallova J, Kubinova S, Schmidt MH, Jhanwar-Uniyal M, Jendelova P.; Anti-inflammatory compound curcumin and mesenchymal stem cells in the treatment of spinal cord injury in rats.; Acta Neurobiol Exp (Wars). 2018;78(4):358-374.
[5] Yuan J, Liu W, Zhu H, Chen Y, Zhang X, Li L, Chu W, Wen Z, Feng H, Lin J.; Curcumin inhibits glial scar formation by suppressing astrocyte-induced inflammation and fibrosis in vitro and in vivo; Brain Res. 2017 Jan 15;1655:90-103
[6] Griesser M, Pistis V, Suzuki T, Tejera N, Pratt DA, Schneider C. Autoxidative and cyclooxygenase-2 catalyzed transformation of the dietary chemopreventive agent curcumin. J. Biol. Chem. 2011;286:1114–24.
[7] Bulbake, U.; Doppalapudi, S.; Kommineni, N.; Khan, W. Liposomal Formulations in Clinical Use: An Updated Review. MDPI Pharmaceutics, 2017
[8] Lechanteur, A.; Furst, T.; Evrard, B.; Delvenne, P.; Hubert, P.; Piel, G. Development of anti-E6 pegylated lipoplexes for mucosal application in the context of cervical preneoplastic lesions. Int J Pharm. 2015 Apr 10; 483(1-2):268-77.

XI-OS39-04

Establishing an *in vitro* system to screen for human infertility by using primary endometrial cells and trophoblast cell line-derived spheroids

Michaela Bienert[1,2], Volker Buck[1], Irmgard Classen-Linke[1], Rudolf Leube[1], Dominique Peter[4], Christa Thöne-Reineke[4], Oleg Tsuprykov[2], Roman Skoblo[2], Benjamin Rösing[3]

[1]University Hospital RWTH Aachen University, Institute for Molecular and Cellular Anatomy, Aachen, DE; [2]IFLb Laboratoriumsmedizin Berlin GmbH, Berlin, DE; [3]University Hospital RWTH Aachen University, Clinic for Reproductive Endocrinology, Aachen, DE; [4]Freie Universität Berlin, Institut für Tierschutz, Tierverhalten und Versuchstierkunde Fachbereich Veterinärmedizin, Berlin, DE

Introduction

The cross-talk between the human embryo and endometrial tissue of the female uterus is crucial for the embryo implantation and a successful pregnancy. Many couples cannot become pregnant naturally and therefore use assisted reproductive technologies (ART) provided by reproductive clinics[1]. Hereby, oocytes and sperm are fertilized outside the female body by *in vitro* fertilization (IVF). An ART cycle starts with stimulation of the ovaries to obtain oocytes, followed by embryo culture and transfer of the embryo into the uterus. An ART cycle ends successfully with pregnancy, or can lead to a new ART cycle if a woman has not become pregnant. Approximately 1.6 million ART treatment cycles are performed worldwide each year. In Germany, 100,844 cycles are performed in 2016. After an ART cycle, however, the number of women who have a baby is only between 27% to 32.3%, which leads to physiological and emotional stress for the affected couples[2]. In 2/3 of the cases, a lack of implantation is due to suboptimal embryos, in 1/3 of the cases the endometrial receptivity is critically disturbed. Therefore, new diagnostic tools need to be developed to clarify the reasons for infertility.

This work deals with the development of an *in vitro* cell culture model in which the patient-specific endometrial cells are brought into contact with a standardized spheroid to determine the endometrial receptive status. In particular, the adhesion of the spheroid to the endometrial cells will be investigated. It can also be tested whether special substances such as chorionic gonadotropin or estrogens favor the adhesion of the spheroid, to provide clinically relevant patient-specific recommendations to increase receptivity. A stable and easy reproducibility of the assay was investigated in order to facilitate translation as a diagnostic agent into clinical routine.

Experimental Methods

Trophoblast cell lines AC-1M88 and ACH3P were incubated in shaker cultures with and without growth factors and carrier matrices (collagen and matrigel), to generate a spheroid which is able to migrate into the primary endometrial cell system *in vitro*. The phenotype and the morphology was characterized by immunofluorescence before and after culture. The combination of the different matrices in combination with the different media was screened with cytotoxicity assays for necrosis and apoptosis. The proliferation of the cell lines was determined by fluorescence microscopy and automated software-based cell counting. Migration was determined by Boyden-chamber assay. Proliferation and Migration was compared to an endometrial epithelial cell line (Ishikawa), to simulate the growth factor influence on epithelial cells.

To minimize donor variance between human endometrial samples, all donors were synchronized with human progesterone *in vivo* before the tissue samples were collected. Cells were enzymatically digested and characterized

by flow cytometry and fluorescence microscopy with the markers for stromal cells of the International Society for Stem Cell Therapy. The stroma and epithelial fraction of the endometrium were characterized by immunofluorescence microscopy for vimentin (+ stroma, - epithelium) and pan-cytokeratin (- stroma, + epithelium).

Finally, the cultures were confronted with the spheroids and putative adhesion-promoting cytokines are introduced into the medium to test individually for human receptivity. The data of the assay were compared with the real human *in vivo* pregnancy rates to verify the reliability of the assay.

Results and Discussion

Figure 1A depicts the proliferation rates of the trophoblast cell lines AC-1M88 and ACH3P compared to the ones of epithelial cell line Ishikawa. By EGF supplementation the proliferation rate of AC-1M88 and ACH3P decreases significantly, whereas the proliferation rate of Ishikawa cells remains unchanged. EGF supplementation significantly reduced the proliferation rate of both trophoblast cell lines, but did not affect the proliferation rate of Ishikawa cell line. Figure 1B shows the migration results of the Boyden-chamber assay with AC-1M88 and ACH3P compared to Ishikawa. It should be noted that a decrease in cells per cm² represents a high migration rate, as cells that remained in the chamber were counted (Figure 1B). Migration of the AC-1M88 trophoblast cell line is significantly reduced by EGF supplementation compared to Ishikawa cells. Since AC-1M88 proliferate significantly slower than epithelial cell line due to EGF supplementation but migrate significantly faster than epithelial cells, AC-1M88 were used for further confrontation studies. AC-1M88 are transfected with a desmokollin GFP labeled construct, to distinguish between endometrial tissue and the spheroid

Conclusion

The medium composition for the generation of the spheroid could be optimized in such a way that a slightly proliferating but migratory spheroid could be constructed. Endometrial stromal cells retain their stromal character after isolation. First confrontation studies are promising.

References

[1] Kushnir *et al.*, Systematic review of worldwide trends in assisted reproductive technology 2004 – 2013, Reproductive Biology and Endocrinology, Vol 15, Issue 1, (2017)

[2] Blumenauer *et al.*, D.I.R-Annual 2016 Report, Journal für Reproduktionsmedizin und Endokrinologie (2017)

Acknowledgement

Sponsored by: „Bundesministerium für Wirtschaft und Energie aufgrund eines Beschlusses des Deutschen Bundestages“.

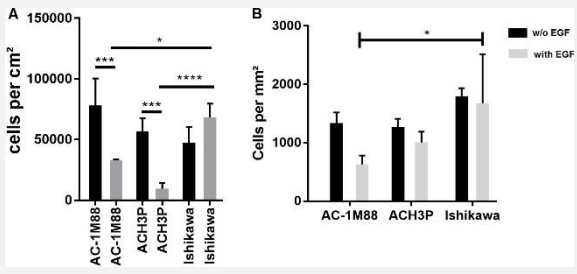

Proliferation (A) and Migration (B) of Trophoblast Cell Linies and Epithelial Cell Line.

AC-1M88, ACH3P and Ishikawa cells were seeded in a density of 100000 cells/cm² and the medium was supplemented with or without EGF. To determine proliferation, cells were counted (A). To determine migration, remaining cells on the membrane which did not migrate through the membrane pores were counted (B). Both attempts are an endpoint assay and were counted automatically by a Fiji macro.

XI-OS39-05

Development of versatile stratified 3D tissues through magnetic cell sheet engineering

Lúcia F. Santos, Ana S. Silva, João F. Mano

University of Aveiro, Aveiro Institute of Materials, Aveiro, PT

Introduction

The Tissue Engineering (TE) field intends to create functional tissues and organs *in vitro* to meet the tremendous need of living transplants or *in vivo* tests. In TE, mimicking cell environment including both homotypic and heterotypic cell-cell interactions is essential to assure that cell functions are fully restored enabling a proper regeneration of the tissue. The conventional TE strategies, that either focus on the injection of isolated cell suspension or on the use of biodegradable scaffolds to support tissue formation, often deprive cells from their endogenous extracellular matrix (ECM), which may dampen cell differentiation (1).

The cell sheet (CS) engineering has arose as reliable alternative to such conventional and limiting strategies, maximizing the residence time of transplanted cells with intact ECM (2,3). Nevertheless, due to the complexity of organs and tissues, the fabrication of *in vivo*-like 3D constructs using CS technology may be a challenge. The creation of the natural stratification of the 3D tissue may be hampered by the difficulty in stablishing cell-cell interactions between the two different cell phenotypes, and by the difficulty to spatially control the positioning of target cells(4).

In the light of such events, magnetic-force based tissue engineering (Mag-TE) has been proposed to obtain CS based on the use of magnetic forces pushing forward the use of CS technology for the production of complex 3D tissues. In fact, Mag-TE has been implied in the production of complex tissues that are not easily achieved by conventional cell culture or co-culture methods such as 2D and 3D cell layers, tubular structures and 3D ordered assemblies consisting of several cell types.

In an attempt to developed ordered and stratified 3D connected tissues, we herein propose the developing of differently shaped and robust magnetic membranes with improved mechanical properties based only on the type of magnet and substrate applied that could be used in a wide range of TE applications.

Experimental Methods

Rhodamine B-labeled supermagnetic iron oxide nanoparticles (10 nm) (MNPs) were synthetized by the co-precipitation method and then, characterized by FTIR and TEM. Firstly, the developed nanoparticles were incubated with human adipose derived stem cells (hASCs) and mouse osteoblastic cells (MC3T3-E1) for viability assessment studies. After confirming their successful mitochondrial activity, magnetic-responsive cells were used to create different shapes of magnetic cell tissue. The robustness of such cell-dense tissue was validated through the presence of a collagen enriched matrix (Masson's trichrome) and the determination of the tensile strength. As a proof-of-concept, to demonstrate the ability of this technology in creating heterotypic 3D cell connected tissue, adipose derived stem cells (hASCs), previously labeled with magnetic iron oxide nanoparticles (MNPs), were seeded on top of the magnetically labeled MC3T3-E1 CS enabling tissue stratification. The developed cell sheets were cultured over 21 days in culture medium with or without osteogenic growth factors and differentiation studies were performed to evaluate the osteogenic potential effect of MC3T3 over hASCs.

Results and Discussion

Results demonstrated that cell-dense tissues with improved robustness were obtained with Young's modulus values similar to those find in soft tissues. Moreover, versatile 3D tissues were obtained through a very simple methodology based only on the type of magnet and substrate applied. CS integrity and cell-cell homotypic and heterotypic interactions were assessed through vinculin staining and collagen detection. Also, the stratification of the developed cell sheets was visualized with fluorescence microscopy. The increase in ALP activity, matrix mineralization and calcium, and osteopontin detection even in basal medium support the hypothesis interaction between the two cell phenotypes, where the osteogenic differentiation of the hASCs was induced by the MC3T3.

Conclusion

Magnetic-forced based TE was used to demonstrate the ability of this technology in creating heterotypic 3D cell connected tissue with improved mechanical properties. Such technology allowed the development of a stratified and cell-dense like tissue with versatile shape and osteogenic differentiating capabilities.

The results herein obtained are expected to open new insights for the fabrication and repositioning of complex and higher ordered 3D connected tissue that better resembles the native *in vivo* environment.

References

1- Furth, M. E., *Biomaterials*, **2007**, 2834, 5068-5073

2- Elloumi-Hannachi, I., *Journal of internal medicine,***2010**, 267, 54-70.

3- Yang, J et al**.,** *Biomaterials*, **2005**, *26*, 6415-6422.

4- Ito, Akari et al.,*Tissue Eng,* **2004**, 10, 833-840

Acknowledgement

The authors acknowledge the financial support by the European Research Council grant agreement ERC-2014-ADG-669858 for project "ATLAS" and the FCT project "PROMENADE" (FCT Ref. PTDC/BTM-MAT/29830/2017). The work was developed within the scope of the project CICECO-Aveiro Institute of Materials, POCI-01-0145-FEDER-007679 (FCT Ref. UID /CTM /50011/2013), financed by national funds through the FCT/MEC and when appropriate co-financed by FEDER under the PT2020 Partnership Agreement.

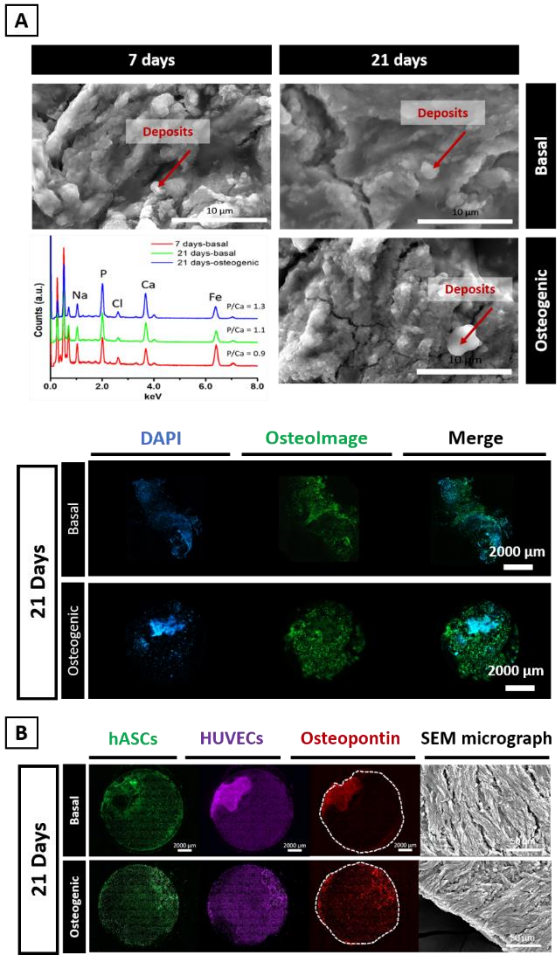

Osteogenic differentiation of the heterotypic cell sheets
(**A**) Mineralization of the developed 3D heterotypic cell sheets cultured for 21 days in basal and osteogenic media: cell nucleus - DAPI (blue) and hydroxyapatite - Osteoimage (green). SEM micrographs displaying calcium deposits are depicted in the right panel. (**B**) Immunofluorescence of MC3T3 (green), hASCs (purple) and osteopontin (red) in 3D heterotypic cell sheets cultured for 21 days in basal and osteogenic media. SEM micrographs of the developed cell sheets are represented in the right panel demonstrating cell sheet integrity.

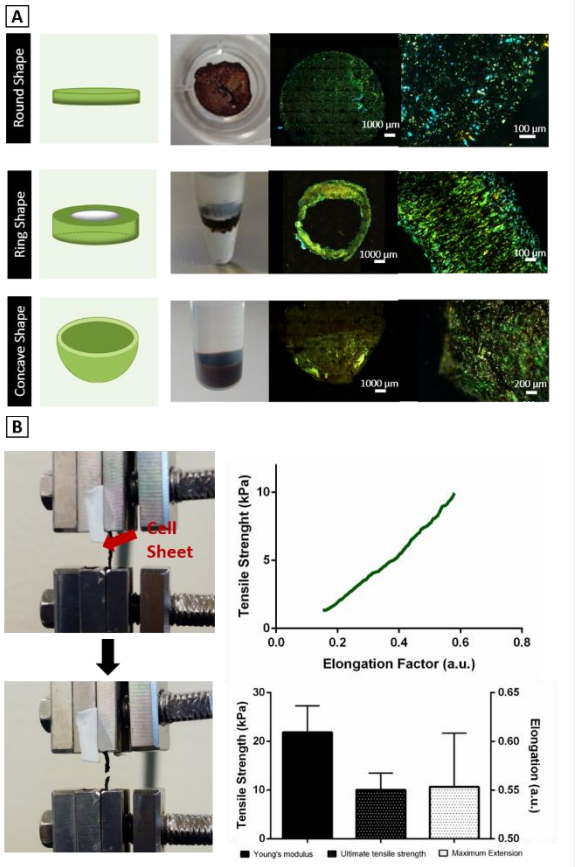

Versatile magnetic cell sheet
(**A**) 3D magnetic sheet fabricated with different shapes. (**B**) Mechanical performance of the developed cell sheet – Young's modulus, Ultimate Tensile Strength and Maximum Extension.

XI-OS39-06

Engineered 3D Tumor Microenvironment to Explore the Drug Resistance of Lung Carcinoma

Dong Shin Lee[1], Sanguine Byun[1,2], Kyung Min Park[1,2]

[1]Incheon National University, Department of Bioengineering and Nano-Bioengineering, Incheon, KR; [2]Incheon National University, Division of Bioengineering, Incheon, KR

Introduction

Tumor microenvironments play critical roles in cancer progression and resistance against anticancer drugs through various physicochemical and biological parameters.[1] Recently, various bioinspired biomaterials have developed as engineered tumor models that recapitulate the multiple cues in the native tumor microenvironments. Among these, polymeric hydrogels are implicated as promising materials to create artificial tumor microenvironment due to their controllable physicochemical properties and similarity to the native tumor microenvironment.[2] Herein, we present an interpenetrating polymer network (IPN) hydrogel composed of thiolated gelatin and tyramine-conjugated poly (ethylene glycol), which can serve as an engineered 3D tumor microenvironment to explore the drug resistance of lung carcinoma against to the commercially available anti-cancer drugs.

Experimental Methods

We synthesized thiolated gelatin (GtnSH) by conjugating Traut's reagent (TR) into primary amine of gelatin backbone. Tyramine-conjugated poly (ethylene glycol) (PEG-TA_2) was synthesized by conjugating tyramine (TA) into amine-reactive PEG-(*p*-nitrophenyl chloroformate)$_2$(PEG-PNC_2). We fabricated IPN hydrogels by simply mixing polymer, horseradish peroxidase (HRP), and H_2O_2 solutions.[3] The phase transition time of IPN hydrogels was examined by the vial tilting method. Elastic modulus (*G'*) of hydrogels were measured with or without cancer cells using the rheometric fluid spectrometer (HR-1, TA instruments). To ensure the resistance of hydrogels against proteolytic enzymes, *in vitro* proteolytic degradation of the hydrogels was investigated by the gravimetrical method using collagenase type II. For 3D cell culture, the polymer solutions were mixed with human lung carcinoma cells (*e.g.*, HCC827 and HCC827GR) to prepare a cell suspension, and the HRP and H_2O_2 were added to the cell suspension. Then, the mixture was placed into a cylindrical mold and allowed to form the IPN hydrogels. For drug resistance test in the 3D microenvironment, human lung carcinoma cells within the hydrogels were exposed to a single treatment of anticancer drug gefitinib, PHA665752, or combination treatment of both gefitinib and PHA665752 for 72h and the cell viability was evaluated using CellTiter-Glo® luminescent cell viability assay.

Results and Discussion

The IPN hydrogels were formed *via* HRP-mediated oxidative crosslinking reaction of thiolated gelatin (GtnSH) and tyramine-conjugated poly (ethylene glycol) (PEG-TA_2) with controllable phase transition time (30 − 300 s) by varying the feed concentrations of PEG-TA_2, GtnSH, and HRP (Fig. 1a). We found that the hydrogels showed tunable mechanical properties (200 − 3200 Pa) in the results of time-course *G'* of hydrogels depending on H_2O_2 contents. These results suggest that the mechanical property of hydrogels could be controlled without changing the chemical composition of the hydrogel backbone (Fig. 1b). In the proteolytic degradation test, the IPN hydrogels maintained ~25 % of their weight after 30 days under collagenase, while the hydrogel composed of only gelatin was fully decomposed within five days (Fig. 1c). This result demonstrated that our hydrogels could maintain their structural

stability against proteolytic degradation during the long-term culture of cancer cells or tumor tissues. We created engineered cancer models by encapsulating human lung carcinoma cells into hydrogels that have similar stiffness with native lung tissue (<400 Pa)[4]. Utilizing this model, we investigated the drug response of the cancer cells against the single treatment of gefitinib and PHA665752 or dual therapy of two drugs in the 3D microenvironment (Fig. 1d), showing the synergistic growth inhibition of HCC827GRs (gefitinib-resistant lung carcinoma) with combined treatment of gefitinib and PHA665752.

Conclusion

We developed an engineered 3D lung cancer microenvironment using a new type of IPN hydrogels with independent control of mechanical properties without changing the polymer composition. The hydrogels could provide the cytocompatible and long-term stable microenvironment for cells to create the engineered tumor constructs. Leveraging this 3D cancer microenvironment, we investigated the drug response of cancer cells against the commercially available anti-cancer drugs. We suggest that our IPN hydrogel holds great potential as a platform to study basic cancer biology and screening of therapeutic agents for better clinical outcomes.

References

1. Andrew G. Clark *et al.*, ***Curr. Opin. Cell Biol.***, 36:13-22, 2015
2. Kyung Min Park *et al.*, ***Annu. Rev. Biomed. Eng.***, 19:109-133, 2017
3. Dong Shin Lee *et al.*, ***Macromol. Res.***, 27:205-211, 2019
4. Darci T. Butcher *et al.*, ***Nat. Rev. Cancer***, 9:108-122, 2009

Acknowledgement

This work was supported by the National Research Foundation of Korea (NRF) grant funded by the Korea government (MSIT) (NRF- 2018M3A9E2023257).

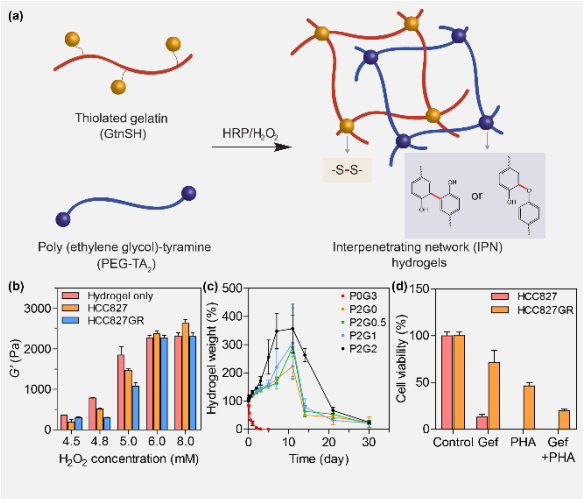

IPN hydrogels as long-term stable engineered 3D tumor microenvironments.
(a) Schematic representation of IPN hydrogel formation *via* HRP-mediated dual cross-linking reaction. (b) The effect of H_2O_2 or cell encapsulation on the elastic modulus of hydrogels. (c) The effect of polymer composition on hydrogel weight. (d) Drug resistance test of lung carcinoma cells against the gefitinib alone, PHA665752 alone, or a combination of two drugs in the 3D tumor microenvironments. Data are shown as the average ± s.d. (n=3 – 8).

11:30 a.m. – 1:00 p.m.

Hall 2

XI-OS40 | Biopolymers and artificial ECM 2

XI-OS40-01

Hierarchichal nanostructuration of antimicrobial recombinant block copolymers based on antimicrobial peptides and elastin-like recombinamers

Sergio Acosta[1], Zhou Ye[2], Matilde Alonso[1], Conrado Aparicio[2], José Carlos Rodríguez-Cabello[1]

[1]Bioforge lab, CIBER-BBN, University of Valladolid, Valladolid, ES; [2]MDRCBB, Minneapolis, US

Introduction

Antimicrobial peptides (AMPs) are cationic peptides with broad-spectrum antimicrobial activities and immunomodulatory properties[1], which represent one of the most promising alternative for the increasingly common drug-resistant infections[2]. In this study, anti-bacterial nanovehicles based on AMPs and Elastin-like block co-Recombinamers (ELbcRs) have been developed based on a modular design. Two AMPs (GL13K[3] and 1018[1]) were cloned on the hydrophilic corona of diblock ELbcR (SI) that self-assemble into monodisperse micelles. We aim to develop recombinant nanocarriers for AMP that enhance their antimicrobial properties increasing the local concentration and improving the delivery.

Experimental Methods

All the chimeric biopolymers (AMP-ELbcRs) were designed and constructed by recombinant DNA technology, produced by *Escherichia coli* fermentation and purified by ITC[4]. Circular dichroism, DLS and TEM were carried out to characterize the nanostructuration of the chimeric biopolymers. MICs and Killing Assays against Gram negative *P. aeruginosa* PAO1, *E. coli* (25922) and Gram positive *S. aureus* (25923), *S. epidermidis* (12228, 35984) and *S. gordonii* DL-1 were performed to evaluate the antimicrobial profile of the new biopolymers.

Results and Discussion

TEM, DLS and CD studies revealed that the AMP-ELbcRs self-assembled into nanofibers (Fig. 1 A, B) or spherical nanoparticles (Fig. 1 C, D). Depending on the incubation conditions, self-assembly was triggered by the AMP or by the ELbcR. Antibacterial assays suggested that the nanostructuration of the chimeric ELRs could be crucial to promote the antimicrobial activity. At physiological temperature, the AMP-ELbcR self-assembled into a micellar conformation, exposing the antimicrobial domains on the corona surface, thus enhancing their antimicrobial potential.

Conclusion

We developed an innovative and scalable method for the bioproduction of antimicrobial nanostructures. The combination of the smart behaviour of ELbcRs and the AMPs provide a promising nanocarrier for AMP delivery to treat resistant infections and a platform to study the molecular mechanism that control the bactericidal properties of the AMP combined with biopolymers.

References

1. Hancock et al. Nat. Biotechnol 24 (2006)
2. World Health Organization, Antimicrobial resistance: global report on surveillance (2014)
3. Abdolhosseini el at. Peptides 35, 231 (2012)
4. Rodríguez-Cabello et al. Nanotechnology in Regenerative Medicine: Methods and Protocols 2:17-38 (2012)

Acknowledgement

The authors are grateful for the funding from the European Commission (NMP-2014-646075), the Spanish Government (PCIN-2015-010, MAT2016-78903-R, BES-2014-069763), Junta de Castilla y León (VA317P18) and Centro en Red de Medicina Regenerativa y Terapia Celular de Castilla y León.

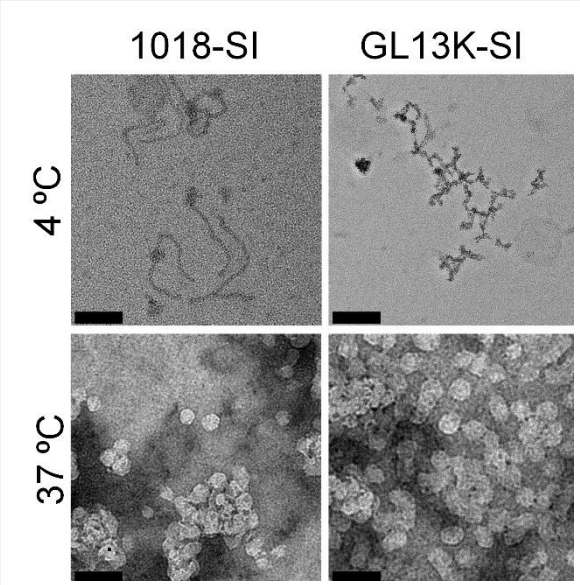

Nanostructures formed by the chimeric ELbcRs
Nanostructures formed by the chimeric ELbcRs at 4 ºC and 37 ºC.

Scale bar = 50 nm.

XI-OS40-02

Development and characterization of a cell-derived extracellular matrix with azide functionalities

Silke Keller[1], Valentin Wittmann[3], Günter E. M. Tovar[1,2], Alexander Southan[1], Monika Bach[5], Petra J. Kluger[4]

[1]University of Stuttgart, Institute of Interfacial Process Engineering and Plasma Technology (IGVP), Stuttgart, DE; [2]Fraunhofer IGB, Fraunhofer Institute for Interfacial Engineering and Biotechnology (IGB), Stuttgart, DE; [3]University of Konstanz, Department of Chemistry and Konstanz Research School Chemical Biology, Konstanz, DE; [4]Reutlingen University, School of Applied Chemistry, Reutlingen, DE; [5]University of Hohenheim, Module 3: Analytical Chemistry Unit, Stuttgart, DE

Introduction

In recent years, the development and application of biomaterials has grown rapidly in the field of medical engineering, tissue engineering, and regenerative medicine[1]. In a natural tissue, the ECM resembles the three-dimensional microenvironment of the cells. It is composed of a highly complex mixture of biomolecules such as fibrillar proteins, proteoglycans, glycosaminoglycans, and signaling molecules[2-5]. It is essential for cellular processes like cell adhesion and migration, biomechanical stimuli, or the transduction of signals[5]. Biomaterials in general attempt to mimic these multifactorial aspects of ECM function; however synthetic materials and single ECM components fail to achieve the molecular complexity and organization of the ECM *in vivo*[1]. Therefore, the use of complex cell-derived ECMs in hybrid materials or biomaterials gained attention since they are a promising attempt to preserve, at least to a large extent, the complexity of native tissue matrices[1-3]. Biomaterials with the ability to guide cell function are a topic of high interest in biomaterial development. However, these biological matrices still lack specific addressable functional groups, which are often required for their use as a biomaterial.

Experimental Methods

To overcome this limitation we incorporated azide groups as specific chemical handles into cellular glycoconjugates of fibroblast ECM by Metabolic Glyco Engineering (MGE). Therefore, we supplemented cell culture media of *in vitro* cultured primary human fibroblasts with the synthetic monosaccharide Ac_4GalNAz (1,3,4,6-tetra-O-acetyl-N-azidoacetylgalactosamine). During seven days of cell culture, cells take up these sugar molecules and convert them during the course of their natural metabolism into building blocks, which are incorporated not only into intra- but also into extracellular glycoconjugates. Azides are chemical groups which are basically absent in nature and are therefore able to undergo biorthogonal click reactions, namely the Huisgen 1,3-dipolar cycloaddition. To obtain a decellularized cell-derived ECM we removed the cells through an osmotic lysis process and purified it through several washing steps.

As novel biomaterial, the azide-modified decellularized ECM should display a similar biomolecule composition as well as similar biological function as the natural dermis. Therefore, we performed several histological and immunohistological staining techniques to study matrix characteristics like biomolecule composition and microscopic structures of the ECM. Furthermore, we analyzed the cellular response to the developed material to evaluate the bioactivity and checked for chemical accessibility as well as reactivity of the azides with several alkyne-modified molecules.

Results and Discussion

We found that the azide-functional ECM featured a complex biological composition and typical biomolecules, which can be found in the human dermis, were also present in the azide-functional ECM. Furthermore, we could observe an increased cell adhesion rate when the material was covalently bond to an alkyne-functional surface compared to the untreated one. This experiment also demonstrated that the incorporated azide groups are chemically accessible.

Conclusion

We could demonstrate that MGE is a useful tool to incorporate azide groups into the glycan structures of cell-derived ECM. Furthermore, it could be shown that conjugation of these incorporated azide handles with alkyne-functional molecules can be used to extend the naturally given bioactive functions of the ECM on a modular basis to generate e. g. not only covalent tissue-specific surface coatings but also novel hybrid materials.

References

[1] M.W. Tibbitt, K.S. Anseth, Hydrogels as Extracellular Matrix Mimics for 3D Cell Culture, Biotechnol. Bioeng. 103(4) (2009) 655-663.

[2] S.M. Ruff, S. Keller, D.E. Wieland, V. Wittmann, T.G.E. M., M. Bach, P.J. Kluger, clickECM: development of a cell-derived extracellular matrix with azide functionalities, Acta Biomater (2016).

[3] L.E. Fitzpatrick, T.C. McDevitt, Cell-derived matrices for tissue engineering and regenerative medicine applications, Biomater. Sci. 3(1) (2015) 12-24.

[4] A.S. Pellowe, A.L. Gonzalez, Extracellular matrix biomimicry for the creation of investigational and therapeutic devices, Wiley Interdiscip. Rev.-Nanomed. Nanobiotechnol. 8(1) (2016) 5-22.

[5] A. Teti, Regulation of cellular functions by extracellular matrix, Journal of the American Society of Nephrology : JASN 2(10 Suppl) (1992) S83-7.

Acknowledgement

We gratefully acknowledge the generous financial support by the Peter und Traudl Engelhorn-Stiftung. This work was supported by contract research Glycobiology/Glycomics, Grant number: P-BWSGlyko/09 of the Baden-Württemberg Stiftung and by the Fraunhofer Internal Programs under Grant No. Discover 828 335.

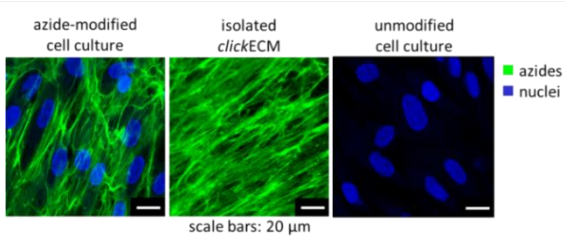

Incorporation of azide groups into ECM glycoconjugates by Metabolic Glyco Engineering (MGE).
This azide-modified ECM can be isolated through decellularization (lysis of the cells) and purification and can then be used as a biomaterial which can e. g. be covalently linked to alkyne-functional materials or other alkyne-functionalized molecules through a biorthogonal click reaction.

XI-OS40-03

Charge-tuning of glycosaminoglycan-based hydrogels to program biomolecular signaling

Passant Atallah, Uwe Freudenberg, Yanuar D. P. Limasale, Carsten Werner

Leibniz Institut Für Polymerforschung, Dresden e.V., Dresden, DE

Introduction

Glycosaminoglycans (GAG) are an important component of the living tissue extracellular matrix (ECM) and play a key role in the binding, presentation and delivery of soluble signaling molecules (1). GAG-based hydrogels were shown to be highly effective to direct cell fate decisions by creating defined microenvironments via electrostatic conjugation of important signaling molecules (2). Previously developed biohybrid hydrogels based on maleimide functionalized heparin with variable sulfation patterns and thiol-terminated star-shaped poly(ethylene glycol) (starPEG) crosslinked through Michael-type addition reaction provides a set of well-defined highly anionic charged polymeric matrices (3). Precise definition of the charge related parameters of the GAG-based matrices could be utilized to describe the interplay of electrostatics and steric constraints that govern the interaction of signaling molecules with the hydrogels.

Experimental Methods

The charge characterization and distribution within the swollen hydrogels could be described by two parameters: (P1) the integral space charge density (the number of ionizable sulfate groups per hydrogel volume in [mmol/ml]) and (P2) the charge density on the GAG component (the number of sulfate moieties per GAG repeating unit divided by the molecular weight of the repeating unit [mol^2/g]). To independently control those parameters within the hydrogels, the previously established starPEG-heparin hydrogel system was extended to combine thiol terminated starPEG, heparin or selectively desulfated derivatives thereof and maleimide-terminated starPEG units in different ratios to allow for a fare-going variation of the heparin sulfation pattern or the heparin content within the hydrogel material. Accordingly, hydrogels with various P1 and P2 parameters were incubated with a mixture of different cytokines differing in their physicochemical properties. The amounts of the proteins in the supernatant after gel exposure was determined by multiplex methods and compared to the protein amounts in control experiments without hydrogels to determine the percentage of the protein sequestered by the hydrogels.

Results and Discussion

The studied cytokines were subcategorized into (A) strongly basic proteins of an IEP ≥9, (B) acidic proteins containing a positively charged heparin binding (IEP 4,8), (C) weakly charged proteins of an IEP range 5.9 to 7.6 and (D) acidic proteins of IEP <5.5. Our binding experiments revealed that the binding of strongly basic proteins (group A) or strongly acidic proteins (group D) to the GAG-containing hydrogels was quantitatively controlled by the integral space charge density of the gels (P1), while the binding of acidic proteins with a positively charged binding domain (group B) is determined by both the integral space charge density of the gels (P1) and the local charge density on the GAG unit (P2). The binding of weakly charged or neutral proteins (group C) instead is controlled by the local charge density on the GAG unit (P2) or non-electrostatic interactions.

Conclusion

In sum, the modular platform of GAG-based biohybrid hydrogels could be parameterized into an integral volume charge density (P1) and a local glycosaminoglycan sulfation pattern (P2) that determine the binding of signaling proteins in dependence of their intrinsic charge characteristics. This approach can enable the tailored design of hydrogel systems with precise cytokine sequestration and help to decipher the binding principles of signaling proteins to the ECM in living tissues.

References

(1) R. Sasisekharan, Z. Shriver, G. Venkataraman, U.Narayanasami, Nat. Rev. Cancer 2002, 2, 521.

(2) U. Freudenberg, Y. Liang, K. L. Kiick, C. Werner, Adv. Mater.2016, 28, 8861.

(3) P. Atallah, L. Schirmer, M. Tsurkan, Y. D. Putra Limasale, R.Zimmermann, C. Werner, U. Freudenberg, Biomaterials 2018, 181, 227.

XI-OS40-04

Corneal endothelial tissue engineering using multi-layered polymer membranes

Jasper Delaey[1], Jasper Van Hoorick[1], Bert Van Den Bogerd[2], Carina Koppen[2], Peter Dubruel[1], Sandra Van Vlierberghe[1]

[1]Ghent University, Centre of Macromolecular Chemistry (CMaC), Department of Organic and Macromolecular Chemistry, Ghent, BE; [2]University of Antwerp, Department of Ophthalmology, Visual Optics and Visual Rehabilitation, Faculty of Medicine and Health Sciences, Wilrijk, BE

Introduction

Corneal endothelial damage and diseases are two of the major contributors to blindness or severe visual impairment worldwide [1]. The corneal endothelium is the innermost cell layer of the cornea and consists of a monolayer of hexagonal cells that maintain the stroma in a state of relative dehydration through a “pump-and-leak” mechanism. A critical loss of cells due to damage, disease or aging leads to corneal edema which in turn results in opacification of the cornea [2]. Currently, the only treatment consists of a (partial) corneal transplantation from healthy cadaveric donor tissue. Unfortunately, only 1 donor is available for every 70 cases [3]. To tackle this donor shortage, the present work focusses on the development of transparent (>90 %), thin (≤5 µm), multilayered sheets constituting a poly(D,L-lactide) (PDLLA) layer for structural rigidity and a crosslinkable gelatin-based hydrogel as an extracellular matrix (ECM) mimic. These sheets provide a supporting function for corneal endothelial cells to enable subsequent ocular implantation thereby restoring the damaged endothelium and patient’s vision.

Experimental Methods

Multi-layered sheets (ø = 12mm) were developed through successive spincoating steps. A sacrificial gelatin layer (H_2O, 10 w/v%) was spincoated on a glass plate followed by a PDLLA (Corbion, PURASORB PDL20) layer for structural integrity (THF, 4 w/w%). Next, a layer of one of the crosslinkable gelatin derivatives, gelatin-methacrylamide (Gel-MA), gelatin-methacrylamide amino-ethylmethacrylate (Gel-MA-AEMA) [4] and gelatin-norbornene (Gel-NB) [5], is spincoated (H_2O, 10 w/v%) as final layer, after applying an argon plasma treatment (0.8mbar, 30s) to the PDLLA. Finally, crosslinkable gelatin was crosslinked using UV-A (6 mW/cm^2, 30 min) irradiation. Isolation of the sheets occurred by immersing in warm water (40°C), thereby dissolving the sacrificial gelatin layer. The sheets were characterized for their transparency (UV-VIS/NIR, 390-700 nm), thickness (white light interferometry) and glucose permeability (side-by side diffusion setup, glucose assay kit) as well as for their surface composition (XRD) and compatibility with corneal endothelial cells using both primary and B4G12 cells.

Results and Discussion

Multi-layered sheets were successfully produced. The sheet thicknesses ranged between 0.8 and 1.5 µm which is thinner than the natural Descemet’s membrane (i.e. 10-20 µm). All produced sheets showed a transparency of over >95 % in dry state and > 98 % in the wet state throughout the visual spectrum with no significant differences observed between the applied gelatin derivatives. The sheets were sufficiently permeable (>2.36*10^{-3} cm/s) towards glucose, both in the presence and absence of the gelatin-derived coating. Upon seeding of the sheets with B4G12 cells and primary corneal endothelial cells, the cells developed their characteristic hexagonal shape. Immunocytochemical staining confirmed the presence of Na^+/K^+ ATPase pumps and tight junctions (ZO-1), indicating good cellular proliferation.

Conclusion

Transparent (>90%), thin (<10 µm), multi-layered sheets were successfully produced. These sheets were sufficiently permeable for glucose. Additionally, the sheets were able to support the proliferation of B4G12 and primary corneal endothelial cells. The produced sheets are thus promising candidates to function as tissue engineered alternatives for donor corneas.

References

[1] "WHO | Causes of blindness and visual impairment," *WHO*, 2017. [Online]. Available: http://www.who.int/blindness/causes/en/. [Accessed: 29-Nov-2017].

[2] J. Zhang and D. V. Patel, "The pathophysiology of Fuchs' endothelial dystrophy - A review of molecular and cellular insights," *Exp. Eye Res.*, vol. 130, pp. 97–105, 2015.

[3] P. Gain *et al.*, "Global Survey of Corneal Transplantation and Eye Banking," *JAMA Ophthalmol.*, vol. 134, no. 2, p. 167, Feb. 2016.

[4] J. Van Hoorick *et al.*, "Cross-Linkable Gelatins with Superior Mechanical Properties Through Carboxylic Acid Modification: Increasing the Two-Photon Polymerization Potential," *Biomacromolecules*, p. acs.biomac.7b00905, 2017.

[5] J. Van Hoorick *et al.*, "Highly Reactive Thiol-Norbornene Photo-Click Hydrogels: Toward Improved Processability," *Macromol. Rapid Commun.*, vol. 39, no. 14, p. 1800181, Jul. 2018.

Acknowledgement

Jasper Delaey holds an SB PhD grant from the research foundation flanders (FWO) with project number 1SA2119N.

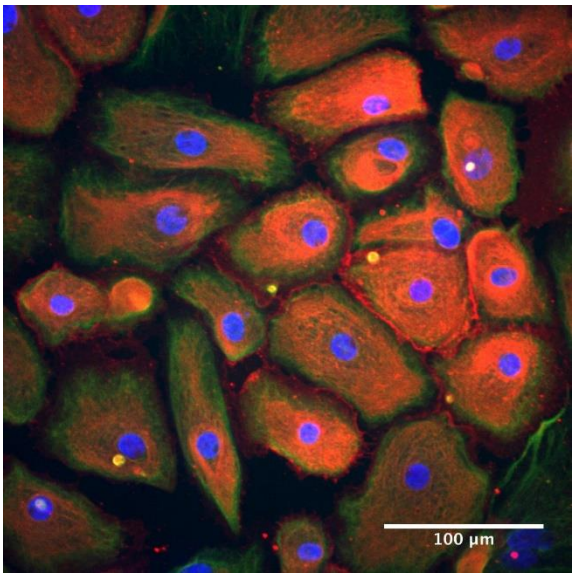

Immunocytochemistry of primary corneal endothelial cells.
Primary corneal endothelial cells were stained for Na+/K+ pumps, the Na+/K+ pumps are stained red, the nucleus is stained blue, green indicates the presence of vimentin, pictures were taken after 8 days in culture.

XI-OS40-05

Riboflavin as a command set crosslinker for collagen membranes

David J. Barrett, Serena M. Best, Ruth E. Cameron

University of Cambridge, Department of Materials Science and Metallurgy, Cambridge, GB

Introduction

Collagen is one of the most widely used and important biomaterials, showing excellent biocompatibility, resorbability, and low immunogenicity. Natural collagen contains crosslinks that are removed during processing, reducing the strength and significantly increasing the degradation rate[1]. Currently, crosslinking collagen often uses toxic chemicals and must be performed outside of the clinic, stiffening and fixing the shape and limiting the ability of clinicians to conform the material to wound sites. By adding a photoinitiator that can be activated in a clinical setting greater adherence to wound topology can be achieved.

Recently, riboflavin has been investigated for use as a crosslinking photoinitiator that can be performed in clinic, using blue light sources often found in medical or dental practices[2]. Riboflavin is a well characterised B vitamin that is well tolerated by the body, and is active as a photoinitiator in low concentrations. In this study, we examine the effectiveness of riboflavin crosslinking on collagen membranes and explore the differences in cell response between collagen crosslinked with riboflavin and membranes crosslinked with the widely used carbodiimide crosslinking agent NHS/EDC.

Experimental Methods

Insoluble collagen I was rehydrated by soaking in 0.05M acetic acid at 4°C before homogenisation. Collagen films were produced by solvent casting or air drying of 0.25% suspensions. Riboflavin solutions for crosslinking were prepared by dissolving 0.01% (w/v) riboflavin and 0.1M triethanolamine in DI water. Membranes were soaked for 2 minutes before being exposed to a dental curing light held 1cm away for 300s.

100% NHS/EDC crosslinking solutions were prepared by dissolving NHS and EDC in 95% ethanol, where 100% refers to a ratio of 5:2:1 EDC:NHS:COOH groups in collagen. Samples were soaked for 2 hours before washing three times with DI water.

Tensile testing of collagen membranes was carried out at a rate of 2mm/min and was performed in a wet chamber with 37°C water flowing throughout. Samples were hydrated for 3 minutes before testing.

Cell proliferation and adhesion tests were carried out using human dermal fibroblast (HDF) cells, and a HT1080 cells. Tests were performed on riboflavin crosslinked films, NHS/EDC crosslinked films, non-crosslinked films, and tissue culture plastic. Adhesion tests were performed in the presence of Mg^{2+} and in the presence of EDTA. The proliferation study was performed with time points at days 1,2 4, and 7. Cells were fixed with 5% glutaraldehyde before being DAPI stained and counted using CellProfiler.

Results and Discussion

Figure 1 shows the ultimate tensile strength achieved of wet collagen films at 37°C, showing that crosslinking with riboflavin is able to achieve a comparable increase in UTS compared to non-crosslinked collagen as 100% NHS/EDC crosslinking.

Figure 2 shows the effect of different crosslinking methods on cell attachment and proliferation. Figure 2a shows that riboflavin crosslinking reduced the integrin mediated attachment of HT1080 cells, who undergo only have α2β1

integrin receptors, but did not affect the attachment of HDF cells compared with attachment on non-crosslinked collagen. NHS/EDC based crosslinking however reduced the attachment of both HDF cells and HT1080 cells, and showed an increase in non-integrin mediated HDF cell attachment. Figure 2b shows HDF cell proliferation on crosslinked collagen films, showing that after day 4 proliferation is similar on all surfaces, but that after 7 days HDF cells have been lost from the NHS/EDC crosslinked collagen membrane compared to non-crosslinked collagen and riboflavin crosslinked collagen films.

Conclusion

We have shown that command-set crosslinking of collagen can be achieved using riboflavin and blue light equipment. Collagen films crosslinked with riboflavin show a lower degree of non-native cell interactions than films crosslinked with NHS/EDC, while maintaining the improvements to UTS. HDF cell proliferation on riboflavin crosslinked films was shown to be similar to proliferation on non-crosslinked films, but showed high levels of cell detachment after 7 days on NHS/EDC crosslinked films.

References

[1] W. Friess, Collagen – biomaterial for drug delivery, Eur. J. Pharm. Biopharm. 45 (1998) 113–136.

[2] A.S. Fawzy, L.I. Nitisusanta, K. Iqbal, U. Daood, J. Neo, Riboflavin as a dentin crosslinking agent: Ultraviolet A versus blue light, Dent. Mater. 28 (2012)

Acknowledgement

The authors would like to thank the EPSRC (Grants no: EP/K503009/1, EP/J500380/1, EP/L504920/1, and RG68240)and Geistlich Pharma AG for providing financial support to this project.

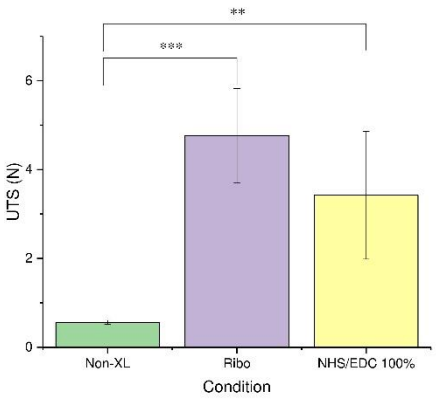

Tensile testing of crosslinked collagen
Figure 1. Ultimate tensile strength (UTS) of collagen membranes crosslinked with riboflavin and NHS/EDC compared to non-crosslinked collagen.

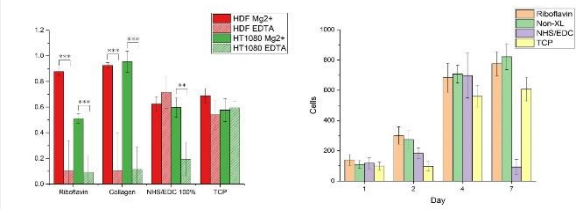

Cell behaviour on collagen films
Figure 2. (a) LDH activity of human dermal fibroblast and HT1080 cells placed on collagen films crosslinked with riboflavin, NHS/EDC, or non-crosslinked, with a tissue culture plastic control, (b) Human dermal fibroblast cell counts against day for cells placed on crosslinked collagen membranes.

XI-OS40-06

Collagen-Poly(caprolactone) Biphasic Scaffolds for Tendon and Ligament Regeneration

Pedro J. Gouveia[1,3], Alan J. Ryan[1,3], Sara Romanazzo[2,3], Simon Carroll[2,3], Isabel Amando[1], Tom Hodgkinson[1], Joanna Zawadzka[1], Sally A. Cryan[1], Daniel J. Kelly[2,3], Fergal J. O'Brien[1,3]

[1]Royal College of Surgeons in Ireland, Tissue Engineering Research Group, Dublin, IE; [2]Trinity Centre for Bioengineering, Trinity Biomedical Sciences Institute, Dublin, IE; [3]Advanced Materials and Bioengineering Research (AMBER) Centre, Royal College of Surgeons in Ireland and Trinity College Dublin, Dublin, IE

Introduction

Anterior cruciate ligament (ACL) injuries cause immediate disability to the knee, demanding long recovery periods, and accounting for high re-lapse rates and chronic injury, ultimately generating an estimated annual burden of $625 million in the US alone [1].

Autografting is currently the gold standard treatment for tendon repair; nevertheless, donor-site morbidity and inadequate mechanical properties impair complete tissue restoration. Braided/woven/knitted scaffolds have been used to reproduce the high mechanical strength and topographical cues of the native tendon, however their low porosity impairs cell penetration and tissue integration. Alternatively, porous 3D sponges allow nutrient transport and cell penetration, nevertheless these structures fall well short of the mechanical properties required [2]. Alternatively, aligned core-shell constructs, which decouple the mechanical and cell-interactive functions, offer superior mechanical performance whilst maintaining beneficial cell interactions. However, designs to date are impaired by unsuitable low porosity in either the core or the shell, and by a lack of relevant biochemical cues [3].

The aim of this study is to develop a novel highly porous core-shell construct which favours cell infiltration and differentiation while providing enough mechanical strength to stabilize injury site during the healing process. This concept was achieved by combining an inner porous collagen-based core with a porous outer shell of electrospun poly(caprolactone) (PCL) fibres. PCL is a synthetic polymer that is elastic, biocompatible, and has proven history in biomedical applications [4]; while collagen type I is a natural polymer abundant in tendon's extracellular matrix and the major component responsible for its fibrous structure [2]. In the proposed core-shell design, both elements incorporate anisotropic micro-structures that are crucial in driving the uniaxial alignment of cells infiltrating the scaffold, and in reproducing the highly aligned structure of the tendon.

Experimental Methods

The core-shell is fabricated in two steps: i) production of an aligned collagen core through directional freeze-drying and ii) fabrication of highly-aligned PCL micro-fibres through electrospinning. Briefly, the collagen cores were obtained by casting a collagen slurry (0.5% w/v; CollagenSolutions) into poly(tetrafluoroethylene) moulds for anisotropic pore distribution, and steel moulds for isotropic pores. The aligned fibre meshes were fabricated in a PCL solution in chloroform (25% w/v; Sigma-Aldrich). Scaffold characterization was performed through SEM and tensile tests (Zwick Roelle) (n = 3). Human mesenchymal stem cells (hMSCs) maintained in tenogenic differentiation media were used to assess cellular viability and metabolic activity (n = 3) [3].

Results and Discussion

Electrospinning conditions were optimized to generate micro-fibres (9µm ± 1) and high anisotropy after deposition (0.38; anisotropy score: 0 to 1) (Fig. 1A and B). An elastic modulus of 59.5 MPa (± 1.25) was achieved with a single

layer of the optimized fibre mesh, which is close to the mechanical values registered for healthy human ACL tissue (65-110 MPa) [5]. The fabricated collagen cores showed an anisotropic conformation, compared to the isotropic control (Fig. 1C). Assembly of the fibrous shell with the collagen core resulted in a construct with highly longitudinally-aligned pores (Fig. 1C).

hMSCs were seeded onto isotropic and anisotropic core scaffolds *in vitro*. Confocal microscopy 7 days after seeding demonstrated that the anisotropic scaffolds lead to higher cell penetration (1566 vs 1077 µm) and higher trend in cellular alignment (0,065 vs 0,057; anisotropy score: 0 to 1) when compared with isotropic controls (Fig. 2A). Additionally, metabolic activity was higher in the anisotropic cores (Fig. 2B), suggesting enhanced cellular activity.

Conclusion

Current core-shell constructs for tendon repair lack the necessary balance of cell permeability and mechanical properties. In response to this, we report the successful creation of a porous core-shell construct for ACL repair, with a biocompatible collagen core which is reinforced by a mechanically stronger PCL fibre shell. The highly permeable and aligned architecture of the core favours cell infiltration, while the porous shell provides enough mechanical support to favour the healing process.

The ease of PCL fibre fabrication and the compatibility of the collagen scaffolds with several biomolecules [6], provides several opportunities to tune mechanical properties and biochemical cue incorporation. We are currently exploring welding procedures to enhance fibre mesh's mechanical strength and the addition of specific biomolecules known to enhance the differentiation of hMSCs into the tenogenic lineage.

References

1] Wiggins AJ, *et al.*. Am J. Sports Med. 2016;
[2] Beldjilali-Labro M, *et al.*. Materials. 2018;
[3] Caliari SR, *et al.*. Biomaterials. 2011;
[4] Liu X, *et al.*. Macromol Biosci. 2012;
[5] Wu Y, *et al.*. J. Tissue Eng. Rege. Med.. 2018;
[6] Ryan AJ, *et al.*. Adv. Healthcare Mat.. 2017.

Acknowledgement

We would like to acknowledge the support given by the Advanced Microscopy Laboratory, CRANN, at Trinity Collage Dublin, in the acquisition of the SEM images.

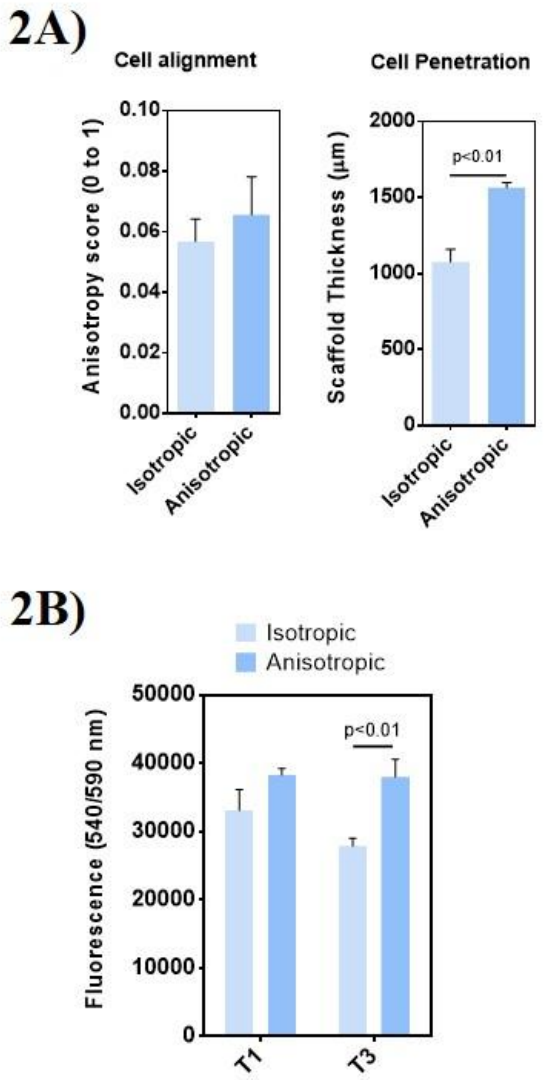

Fig. 2 - Assessment of the impact of internal the architecture on cellular phenotype.
A) Determination of hMSC cell alignment (left) and infiltration (right) at day 7 after seeding on isotropic and anisotropic core scaffolds. B) Metabolic viability of hMSC at day 1 and 3 after seeding (Alamar Blue; Invitrogen) on isotropic and anisotropic collagen-based core scaffolds.

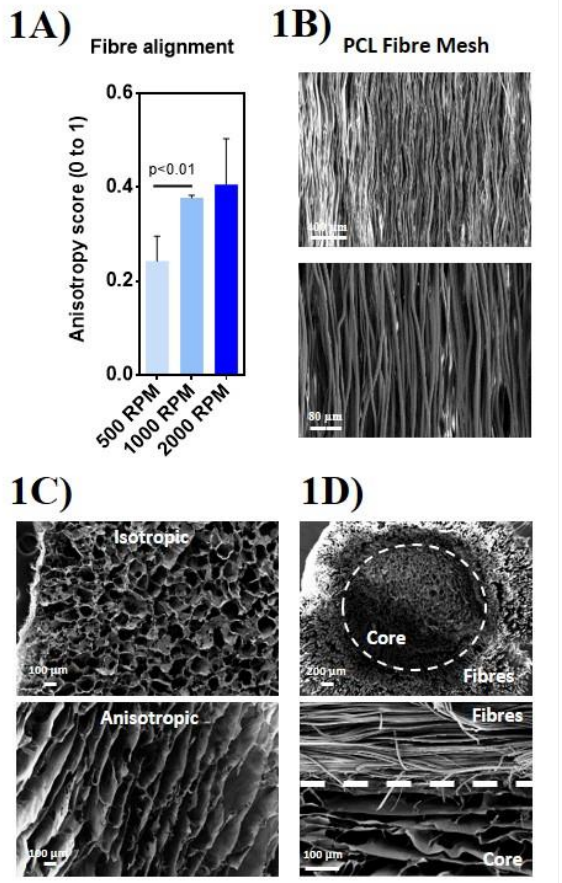

Fig. 1 - Fabrication and characterization of Core-Shell Composites.
A) Assessment of the fibre alignment as a function of collection speed (ImageJ/FibrilTool; Boudaoud, A., *et al.*, Nat. Prot., 2014). B) Detail SEM images of the optimized PCL fibre layer collected on a rotating aluminium cilinder for 60 minutes at 1000 rotations per minute. C) Pore architecture in isotropic (top) and anisotropic (bottom) collagen-based cores. D) SEM images of the joined core-shell scaffold: transversal cut (top) and longitudinal cut (bottom).

11:30 a.m. – 1:00 p.m.

Hall 4

XI-OS41 | Novel perspectives in biomaterials research

XI-OS41-01

Plasmonic Janus hybrids for detection of small metabolites

Jing Cao, **HaiYang Su**, Kun Qian

Shanghai Jiao Tong University, School of Biomedical Engineering, Shanghai, CN

Introduction

Advanced bio-analytical platforms rely on materials with tailored structural parameters.(*1-4*) For instance, matrix materials decide the performance of laser desorption/ionization mass spectrometry (LDI MS). Plasmonic materials (e.g. noble metals) have unique surface resonance under laser irradiation in diverse light science and analytical applications.(*5-8*) Particularly, core-shell noble metal hybrids(*9-12*) have high yield of hot carriers and surface roughness in the nanoscale. And nanoshell structure is desirable with noble metal layer in the nanoparticle form on the surface of core particle.(*9, 13, 14*) Notably, core particles are critical for properties and applications of core-shell structures, while most current results are based on isotropic core particles. Therefore, using Janus core particles to construct core-shell materials can provide better opportunities for LDI MS and introduce newer types of plasmonic hybrids.

Detection of metabolites can be very challenging in real-case bio-mixture, due to the low abundance of analytes, high sample complexity, and difficulty in molecular identification. Accordingly, recognition and enrichment of metabolites by materials are essential in the sample treatment process.(*12, 15, 16*) And further coupling materials with analytical platforms for identification purpose (e.g. MS) offer an ideal solution to address the above issues.

Experimental Methods

Janus carbon-PMO particles were obtained by dealing RF-PMO nanoparticle with carbonization as the method reported.(17) Janus@Ag core-shell particles were synthesized through the silver mirror reaction. The silver nanoshells (Janus@Ag) were modified with aptamers based on the post-grafting method.(12, 18) For LDI MS detection of metabolites, standard small molecules (glucose, tryptophan, arginine, methionine and phenylalanine) were dissolved in deionized water by step-wise dilutions with the concentration ranging from 100 ng μL−1 to 1 ng μL−1. In the enrichment of kanamycin and melamine from standard solution, we modified Janus@Ag nanoshells with aptamers.

Results and Discussion

We used Janus particles (periodic mesoporous organosilica (PMO) in conjunction with carbon spheres) as core materials and loaded silver nanoparticles as nanoshells. Janus core particles enhanced the LDI MS detection of both hyhrophobic and hydrophilic molecules due to anisotropic properties. Moreover, plasmonic nanoshells enabled direct metabolites detection with silver adduction in bio-mixtures, due to the selective LDI process. We also demonstrated the tunable surface chemistry of Janus hybrids for enrichment and identification of metabolites at low concentrations (4 pM). Our work contributed to the development of tools for metabolic analysis and design of materials for bio-analytical platforms.

Conclusion

In summary, we developed a series of Janus hybrid materials for 1) analysis of both hydrophobic and hydrophilic small metabolites; 2) metabolic analysis in complex bio-mixtures; and 3) selective enrichment and detection of target molecules.

Specifically, for analysis of small metabolites, the synthesized Janus carbon-PMO particles with amphiphilic structures displayed the superior LDI performance for both hydrophobic and hydrophilic metabolites detection, compared to bulk carbon and PMO particles. For metabolic analysis in complex bio-mixtures, we constructed Janus@Ag hybrids for detection of bio-samples (e.g. CSF and serum) and observed signals of typical metabolites, without any sample treatment procedures. For selective enrichment and detection, we modified aptamers on the surface of Janus@Ag as a material platform for selective analysis of kanamycin and melamine, with enhanced detection limits (~pM) over present literatures.

We anticipated two major research lines along this work, including new bio-nano-interface construction and novel bio-analytical application. Our work contributes to the design of materials for high-performance metabolic analysis and clinical diagnostic tools.

References

1. E. C. Yusko, B. R. Bruhn, O. M. Eggenberger, J. Houghtaling, R. C. Rollings, N. C. Walsh, S. Nandivada, M. Pindrus, A. R. Hall, D. Sept, J. L. Li, D. S. Kalonia, M. Mayer, Real-time shape approximation and fingerprinting of single proteins using a nanopore. *Nat Nanotechnol* **12**, 360-367 (2017).
2. X. Sun, J. j. Wan, K. Qian, Designed Microdevices for In Vitro Diagnostics. *Small Methods* **1**, 1700196 (2017).
3. M. Sun, L. Xu, W. Ma, X. Wu, H. Kuang, L. Wang, C. Xu, Hierarchical Plasmonic Nanorods and Upconversion Core–Satellite Nanoassemblies for Multimodal Imaging-Guided Combination Phototherapy. *Advanced Materials***28**, 898-904 (2016).
4. K. Qian, L. Zhou, J. Zhang, C. Lei, C. Z. Yu, A combo-pore approach for the programmable extraction of peptides/proteins. *Nanoscale***6**, 5121-5125 (2014).
5. K. Wu, J. Chen, J. R. McBride, T. Lian, Efficient hot-electron transfer by a plasmon-induced interfacial charge-transfer transition. *Science* **349**, 632-635 (2015).
6. E. Cortes, W. Xie, J. Cambiasso, A. S. Jermyn, R. Sundararaman, P. Narang, S. Schlueker, S. A. Maier, Plasmonic hot electron transport drives nano-localized chemistry. *Nature Communications***8**, 14880 (2017).
7. B. Liu, Y. L. Li, H. Wan, L. Wang, W. Xu, S. J. Zhu, Y. Y. Liang, B. Zhang, J. T. Lou, H. J. Dai, K. Qian, High Performance, Multiplexed Lung Cancer Biomarker Detection on a Plasmonic Gold Chip. *Advanced Functional Materials***26**, 7994-8002 (2016).
8. S. Q. Sun, D. Thompson, U. Schmidt, D. Graham, G. J. Leggett, Micro-/nano-patterning of DNA and rapid readout with SERS tags. *Chemical Communications* **46**, 5292-5294 (2010).
9. L. Huang, J. J. Wan, X. Wei, Y. Liu, J. Y. Huang, X. M. Sun, R. Zhang, D. D. Gurav, V. Vedarethinam, Y. Li, R. P. Chen, K. Qian, Plasmonic silver nanoshells for drug and metabolite detection. *Nature Communications***8**, 220 (2017).
10. X. Sun, L. Huang, R. Zhang, W. Xu, J. Huang, D. D. Gurav, V. Vedarethinam, R. Chen, J. Lou, Q. Wang, J. Wan, K. Qian, Metabolic Fingerprinting on a Plasmonic Gold Chip for Mass Spectrometry Based in Vitro Diagnostics. *ACS Central Science* **4**, 223-229 (2018).
11. A. Manjavacas, J. G. Liu, V. Kulkarni, P. Nordlander, Plasmon-Induced Hot Carriers in Metallic Nanoparticles. *Acs Nano***8**, 7630-7638 (2014).
12. J. Gan, X. Wei, Y. Li, J. Wu, K. Qian, B. Liu, Designer SiO2@Au nanoshells towards sensitive and selective detection of small molecules in laser desorption ionization mass spectrometry. *Nanomedicine-Nanotechnology Biology and Medicine* **11**, 1715-1723 (2015).

13. X. Wei, Z. H. Liu, X. L. Jin, L. Huang, D. D. Gurav, X. M. Sun, B. H. Liu, J. Ye, K. Qian, Plasmonic nanoshells enhanced laser desorption/ionization mass spectrometry for detection of serum metabolites. *Analytica Chimica Acta***950**, 147-155 (2017).
14. R. Bardhan, S. Lal, A. Joshi, N. J. Halas, Theranostic Nanoshells: From Probe Design to Imaging and Treatment of Cancer. *Accounts of Chemical Research* **44**, 936-946 (2011).
15. Y.-r. Ma, X.-l. Zhang, T. Zeng, D. Cao, Z. Zhou, W.-h. Li, H. Niu, Y.-q. Cai, Polydopamine-coated magnetic nanoparticles for enrichment and direct detection of small molecule pollutants coupled with MALDI-TOF-MS. *ACS applied materials & interfaces***5**, 1024-1030 (2013).
16. T. Liu, L. Qu, K. Qian, J. Liu, Q. Zhang, L. Liu, S. Liu, Raspberry-like hollow carbon nanospheres with enhanced matrix-free peptide detection profiles. *Chemical Communications* **52**, 1709-1712 (2016).
17. T. Yang, L. Wei, L. Jing, J. Liang, X. Zhang, M. Tang, M. J. Monteiro, Y. Chen, Y. Wang, S. Gu, D. Zhao, H. Yang, J. Liu, G. Q. M. Lu, Dumbbell-Shaped Bi-component Mesoporous Janus Solid Nanoparticles for Biphasic Interface Catalysis. *Angewandte Chemie-International Edition***56**, 8459-8463 (2017).
18. Z. Q. Yuan, Y. C. Chen, H. W. Li, H. T. Chang, Fluorescent silver nanoclusters stabilized by DNA scaffolds. *Chemical Communications* **50**, 9800-9815 (2014).

Acknowledgement

We gratefully thank the financial support from Project 81771983 by NSFC, Project 16441909300 by Shanghai Science and Technology Commission, Project 2017YFC0909000 by Ministry of Science and Technology of China.

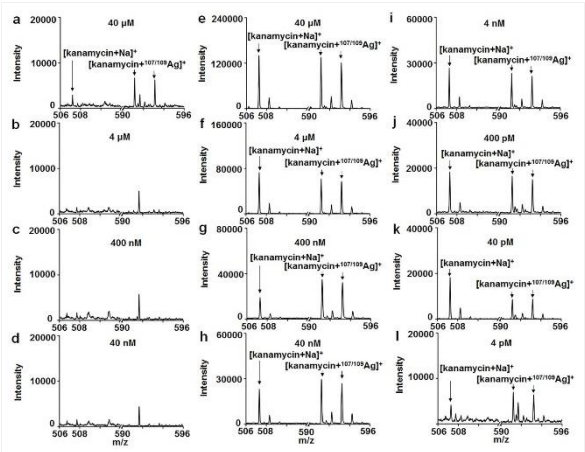

Aptamer-Janus@Ag for selective enrichment and detection.
Mass spectra of kanamycin using Janus@Ag as the matrix at (a) 40 mM, (b) 4 mM, (c) 400 nM and (d) 40 nM and using aptamer-Janus@Ag-3 for enrichment and LDI-MS detection at (e) 40 mM, (f) 4 mM, (g) 400 nM, (h) 40 nM, (i) 4 nM, (j) 400 pM, (k) 40 pM and (l) 4 pM

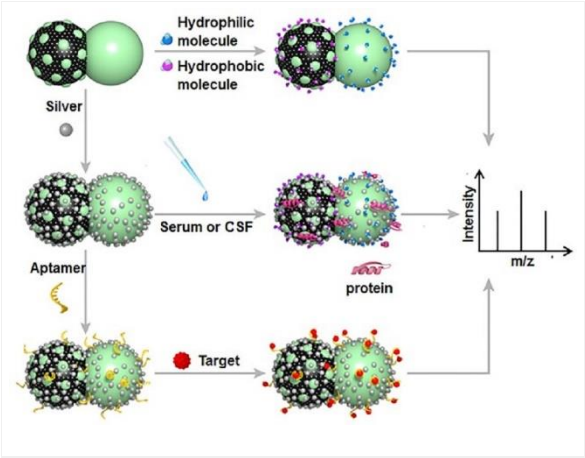

Schematic illustration of Janus hybrids for LDI MS detection of small metabolites.
For analysis of small metabolites, the synthesized Janus carbon-PMO particles with amphiphilic structures displayed the superior LDI performance for both hydrophobic and hydrophilic metabolites detection, compared to bulk carbon and PMO particles. For metabolic analysis in complex bio-mixtures, we constructed Janus@Ag hybrids for detection of bio-samples (e.g. CSF and serum) and observed signals of typical metabolites, without any sample treatment procedures. For selective enrichment and detection, we modified aptamers on the surface of Janus@Ag as a material platform for selective analysis of kanamycin and melamine, with enhanced detection limits (~pM) over present literatures.

XI-OS41-02

Creating a curation pipeline for biocompatibility data of experimental scaffolds and implants from the scientific literature - towards an open-access database of biomaterials

Osnat Hakimi[1,2], Fabio Curi[2], Dmitry Repchevski[2], Josep L. Gelpi[2], Maria-Pau Ginebra[1]

[1]Universitat Politecnica de Catalunya, Dept. Materials Science and Metallurgical Engineering, Barcelona, ES; [2]Barcelona Supercomputing Center, Life Sciences - INB Computational Node, Barcelona, ES

Introduction

The last two decades saw a steep increase in the volume of scientific publications in the fields of biomaterials and tissue engineering. In particular, many novel experimental scaffolds, which are manufactured to support cell attachment and subsequent tissue development have been created and tested. However, the vast majority of these did not progress beyond initial scaffold design and testing, with the generated data remaining available mostly in the form of scientific papers (ie:text). Project DEBBIE aims to create an open-access database of experimental biomaterials by curating data from published articles of scaffolds and implants. A major challenge, in the absence of a taxonomy, is capturing the complexity contained in each unique manufactured scaffold or implant, which includes multiple features such as materials, structures, coating and manufacture methods (Mitragotri et al, 2009). Thus, and as part of the effort to automate the information extraction process, the aim of this study was to design a curation pipeline made of filtration, identification and extraction of scaffolds' names and their associated data. To achieve this, we created two assets: a gold standard (GS) biomaterials literature collection and a biomaterials ontology. Here, we present the creation and validation of these assets, as well as an overview of the pipeline.

Experimental Methods

All components in the pipeline were created and validated using open-source resources. Briefly, a gold standard literature collection (GS) was created using a combination of manual abstracts harvesting from PubMed and an automated ranking tool. To ensure the GS is sufficiently broad, hLDA modelling (python hlda package, https://pypi.org/project/hlda/) was used to identify the main topics, which are currently being validated by scientists in the field. Thereafter, the R package tidy text (https://cran.r-project.org/web/packages/tidytext/index.html) was used to analyse the text and extract terms by frequency (tf) and significance (tf-idf), to be incorporated into the ontology. For the ontology (Figure 1), Protege ontology editor (Musen 2015) was used to organise terms.

Results and Discussion

The curation pipeline presented in Figure 2 is currently being tested using PubMed abstracts. The two main assets of the pipeline are the GS set and the ontology. In the analysis of the GS, 26 sub-topics were identified, and at least 10 different tissues, with bone and cartilage particularly dominant. Topics were generally a mix of words from material and structure classes and the target tissue, and thus ‘bone’ as a term repeated in 3 different topics). Evaluation by domain experts (31 experts from 8 countries so far) revealed a few missing keywords in the topics, but these were actually present in the GS itself. The ontology currently contains over 150 classes, properties and individuals and is undergoing expansion and testing. A particular effort is being made to associate as many features and properties to scaffolds, rather than rely on material as the main class, and the integration of existing semantic types.

Conclusion

A pipeline was created to facilitate data mining in the biomaterials domain. Unlike a previous ontology of bone and cartilage tissue engineering terms (BCTEO, Viti et al 2014), we chose to focus on curating complex manufactured objects, with features such as structure and manufacture technique, and use automated classification and text mining tools rather than human experts to identify the most common terms and terms of importance, using experts only to validate the topic coverage. The hope is that the gold standard set and the biomaterials ontology will enable a more broad extraction of biomaterials-related information from the literature.

References

1. Mitragotri, S., & Lahann, J. (2009). Physical approaches to biomaterial design. Nature Materials, 8.
2. Musen, M. A. (2015). The protege project: A look back and a lookforward. AI Matters, 1.
3. Viti, F., Scaglione, S., Orro, A., & Milanesi, L. (2014). Guidelines for managing data and processes in bone and cartilage tissue engineering. BMC Bioinformatics, 15.

Acknowledgement

This project is funded by the European Unions Horizon 2020 programme under the Marie Skodowska-Curie grant agreement DEBBIE, project number: 751277

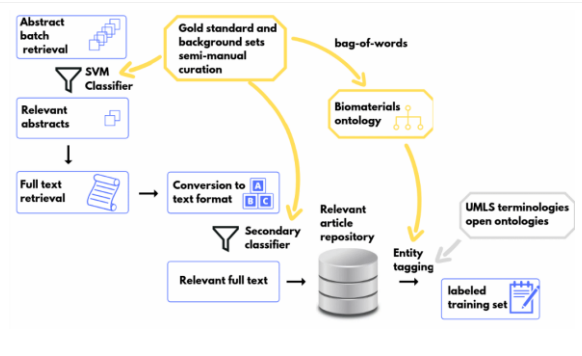

Figure 2
The pipeline currently tested for generating the annotated set

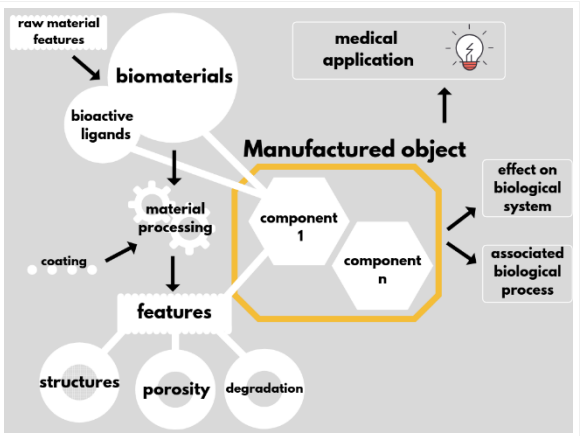

Figure 1
The main classes and properties in the ontology

XI-OS41-03

Therapeutic Electrical Stimulation for Regenerative Medicine Application: A Need for a Credible *In Vitro* Model System

Sahba Mobini[1,2]

[1]CSIC (CEI UAM+CSIC), Instituto de Micro y Nanotecnología, IMN-CNM, Tres Cantos, Madrid, ES; [2]Universidad Autónoma de Madrid, Departamento de Biología Molecular and Centro de Biología Molecular "Severo Ochoa" (UAM-CSIC), Madrid, ES

Introduction

Endogenous electric field (bioelectric field) is an electrical potential difference resulting from charge flow (current) in the body at all levels (i.e., cell, tissue, and organ), which is found to be essential in a variety of important biological process, such as healing and development [1].Recent studies showed that manipulation of intrinsic bioelectric fields can cause disease or be used as therapeutics [2-4]. Among the wide range of bioelectric fields, steady, long-lasting direct current (≈ 100 μA/cm^2), also known as current of injury, generates a voltage gradient (≈ 10-100 mV/mm) between intact section and injured site that has regenerative effect and can change cell faith and responses.

Experimental Methods

We treated different cell types with low voltage electrical stimulation, within an invitro system, and induced different responses, such as differentiation, alignment, viability and proliferation (**Figure 1**).

Results and Discussion

These results suggest thatelectrical stimulation (ES), as a drug-free, cell-free approach, could be an attractive alternative for biochemical remedies and cell therapy approaches for tissue regeneration and wound healing. However, ES has not been widely accepted as a clinical treatment and it is only used as an adjunctive therapy. This is due to the lack of consistency in major outcomes, absence of coherency in defining ES protocols, and unmatchable results in vitro and in vivo. Moreover, there is inadequate understanding of the dominant mechanism of ES and leading parameters triggering the molecular cascades and generate the main changes in cellular level.

Conclusion

Here, I will discuss: **1)** the current state-of-the-art on ES in vitro and in vivo and the common hypothesis on molecular mechanisms involved; **2)** the confusions associated with protocols in vitro and in vivo and the incapability of the current devices to address remaining challenges; **3)** the approaches intended to develop credible vitro models to provide a standard methodology for exploring ES to induce regeneration responses in tissues such as bone and nerves; **4)** the future perspective including the incorporation of modern biomaterials (e.g., conductive nanomaterials, and polymers) and electronics.

References

1.*BioEssays* 25, 759–766 (2003). **2.***Mol. Biol. Cell* 25, 3835–3850 (2014). **3.** *Annu. Rev. Biomed. Eng.* 14, 295–323 (2012). **4.** *Bioessays* 34, 205–17 (2012). **5.** *J. Multidiscip. Healthc.* 10, 179–194 (2017).

Acknowledgement

H2020-Marie Skłodowska Curie-Individual Fellowship currently supports this project (NeuPES ID:793102).

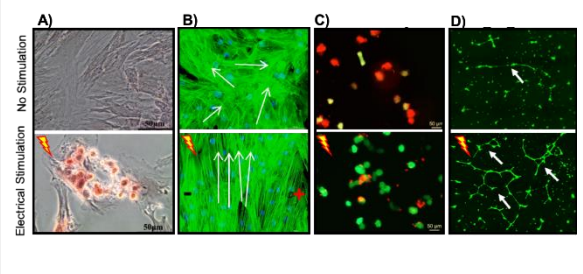

Figure 1. Electrical Stimulation of the Cells In Vitro.
Cells in culture- non-stimulated (Top) and electrically stimulated (Bottom). ES induces A) osteogenic differentiation in MSCs, B) alignment of the MSCs, C) viability of cardiomyocyte, live (green)/dead (red), and D) tube structure formation in HUVEC cells (in vitro angiogenesis).

XI-OS41-04

Nature inspires biophotonic devices: Design of Bio-Based Photoacoustic Nanoprobes

Brigida Silvestri[1], Giulio Pota[1], Alessandro Pezzella[2], Paolo Armanetti[4], Giuseppe Vitiello[1], Gennaro Sanità[3], Annalisa Lamberti[3], Luca Menichetti[4], **Gluseppina Luciani**[1], Marco D'Ischia[2]

[1]University of Naples Federico II, Dept. of Chemical, Materials and Production Engineering, Naples, IT; [2]University of Naples Federico II, Dept. of Chemistry, Naples, IT; [3]University of Naples Federico II, Dept. of Molecular Medicine and Medical Biotechnology, Naples, IT; [4]National Research Council, Institute of Clinical Physiology, Pisa, IT

Introduction

Biophotonics has been providing effective tools in many applications, including phototherapy and molecular imaging. In this field, photoacoustic imaging (PAI) is a poor invasive modality, that exploits non-ionizing radiation for real-time imaging with high spatial resolution and penetration depth. Notably, great effort has been spent towards the design of cost-effective, biocompatible and multifunctional PA probes, to carry out both diagnosis and therapy [1]. To this purpose, nature can provide valuable inspiration as well as raw and safe materials [2]. Among those, melanins, ubiquitous biological hydrophobic pigments, hold great promise for the generation of nanoprobes for Photoacoustic Imaging (PAI) and Phototermal Therapy (PTT), since they combine safety with marked antioxidant features,as well as a broad band of absorption in the visible and NIR regions [2]. Melanins are usually produced through oxidative polymerization of melanogenic precursors, such as 5,6-dihydroxyindole-2-carboxylic acid (DHICA) [2, 3]. However, melanins' huge potential is still unexplored due to the difficulty to achieve both poor aggregation in physiologic environment and high PA contrast. In this study, this issue was addressed through the design of PA melanin-based hybrid nanoprobes. Notably, nanostructured $SiO_2$was employed as templating agent for melanin formation from its molecular precursors, thus tuning its supramolecular structure. Furthermore, metal chelating and reducing properties of melanins towards transition metal ions, were exploited to reduce Ag to size controlled Ag nanoclusters. This synthesis strategy was successfully implemented with different melanogenic precursors: DHICA and even bio-available cost effective moieties such as caffeic (CA) and gallic (GA) acid.

Obtained nanostructures were compared in terms of physical-chemical features, PA response as well as biological properties.

Overall, this study lies the basis to engineer bioavailable pigments as bioinspired, soft, and biocompatible multifunctional nanomaterials for multimodal imaging in cancer diagnosis and therapy.

Experimental Methods

Hybrid melanin-silver-SiO_2nanoparticleswere obtained following an *in situ*sol-gel route [5-6]. Briefly,a hybrid precursor wassynthesized coupling amino groups of APTS molecules with carboxyl (–COOH) groups of the melanogenic precursor (DHICA, GA, CA), through EDC/NHS chemistry. Then, after addition of a further amount of melanogenic precursor, synthesis of hybrid nanoparticles was carried out through modified Stöber method [2]. During the synthesis, an appropriate amount of $AgNO_3$solution in ethanol was added to reacting mixture to keep melanogenic precursor: Ag^+ ratio=10:1 mol:mol. After 18h, hybrid particles were recovered by centrifugation and repeatedly washed. Bare Melanin-SiO_2 nanoparticles were obtained following a similar procedure , but without adding $AgNO_3$. Obtained nanoparticles (NPs) will be named in the following as DHICA_SiO_2_Ag-NPs and CA_ SiO2_Ag-NPs GA_SiO2_Ag-NPs.

Results and Discussion

TEM images of obtained nanoparticles (Figure 1) showed pseudo-sphericalmorphologies, about 50 nm in average diameter. Furthermore, while DHICA_SiO_2_Ag-NPs and CA_ SiO_2_Ag-NPs revealed hybrid structures with intimate mixing of both organic and inorganic phase, GA_SiO_2_Ag-NPs (Fig. 1c) showed more complex architecture revealing small Ag dots spread on their surface. EPR spectra of hybrid nanoparticles show an intense peak at a *g*value of 2.0035 ± 0.0003, consistent with the presence of carbon-centered radicals typical of melanin oligomers, proving their presence within nanostructures [3]. However, different signal amplitude (ΔB) were appreciated in the spectra, indicating a change in the distance between the radical centers within the nanostructures, thus suggesting employed melanogenic precursors, featured different supramolecular organization of the melanin component. Figure 2 reports the PA multispectral responses of DHICA_SiO_2_Ag, GA_SiO_2_Ag and CA_ SiO_2_Ag-NPs, revealing an impressive difference in signal intensity between silver containing and silver free nanoparticles. Therefore, the presence of silver in the nanoparticles, boosts PA Signal in all nanostructures, which also showed stable photoacoustic behavior even under long irradiation. However,the highest PA response was performed by DHICA_SiO_2_Ag nanoparticles, which displayed the most intense PA signal even in a concentration range of 1-6 µg/ml of melanin, the lowest among investigated samples and far below that usually explored with melanin and metal PA probes. Finally, obtained nanoplatforms proved high stability towards aggregation and high biocompatibility as well as easy cells internalization.

Conclusion

This study unveils the efficacy of templated synthesis approach in turning natural moieties into optically active nanoprobes with high PA response, thus establishing a new paradigm for the design of high performance eco-sustainable and bioavailable nanoprobes for theranostics.

References

[1] T. Repenko et al., Advanced Functional Materials 2018, 28, 1705607.
[2] B. Silvestri, G. Luciani et al., ACS Applied Materials & Interfaces 2017, 9, 37615.
[3] G. Vitiello et al., Materials Science and Engineering C 2017, 75, 454.
[4] B. Silvestri, G. Luciani et al., *ACS Appl. Mater. Interfaces,* 2017, **9**, 37615.

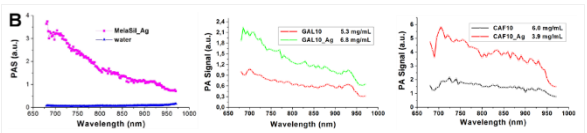

PA
Fig. 2 - PA multispectral response.

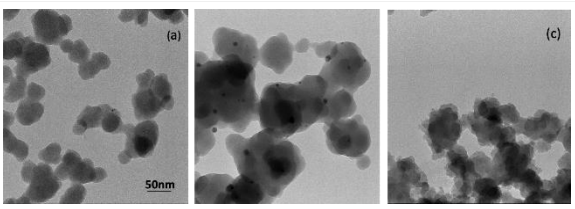

TEM Images
Fig. 1 TEM images of DHICA_SiO2_Ag-NPs (a), GA_SiO2_Ag-NPs (b), CA_SiO2_Ag-NPs (c)

XI-OS41-05

Validation of eardrum replacement scaffolds made from electrospinning

Philipp Kempert[1], Thomas Stoppe[1], Shivesh Anand[2], Lorenzo Moroni[2], Stefano Berrettini[3], Serena Danti[3], Carlos Mota[2], Marcus Neudert[1]

[1]TU Dresden, Faculty of Medicine, ORL and Head and Neck Surgery, Dresden, DE; [2]Maastricht University, Department of Complex Tissue Regeneration (CTR), MERLIN, Maastricht, NL; [3]Università di Pisa, Department of Surgical, Medical, Molecular Pathology and Emergency Medicine, OtoLab, Pisa, IT

Introduction

The restoration of the eardrum (myringoplasty) requires several features on the nanoscale, which are decisive for an optimal performance in an infectious and chronically inflamed microenvironment (e.g. due to otitis media chronica). To date, myringoplasty is usually performed with autologous material, like temporalis fascia, cartilage or perichondrium. Apart from individual variation in structure, autologous materials exhibit unknown mechanical properties during surgery, leading to an unpredictable reconstruction outcome (Zahnert, et al. 2000). Hence, a compromise between optimal sound transfer through the middle ear and stability mostly needs to be found by the surgeon.

With known material properties and defined fabrication procedures, it will be easier to choose an optimal implant for each patient (Mota, et al. 2015). Thus, synthetic scaffolds are in focus to overcome the disadvantages of the autologous tissues. This work will investigate biomimetic eardrum replacements with finite element method (FEM) simulation of the vibration behavior of synthetic membranes.

Experimental Methods

For the comparison and validation of the fabricated polyethylene oxide terephthalate/polybutylene terephthalate synthetic membranes/scaffolds to native human eardrums, experimental measurements and FEM simulations were performed. The samples were clamped and radial pre stressed in a test rig and acoustic sound pressure of about 90 dB SPL was applied with a multi sinusoidal signal in the range of 100 Hz to 5 kHz. The vibration behavior was measured with laser-Doppler vibrometry. Quasi-static pressure in a physiological expected range was applied to determine the stiffness of the scaffolds. At once, the displacement was acquired by laser triangulation.

To validate the FEM model with measured results, harmonic analysis of circular orthotropic membranes in comparison to the measured scaffolds was performed in an FEM simulation software (Ansys, ANSYS, Inc., PA). The scaffold properties were varied in thickness and orthotropic behavior in the range close to the measured samples to investigate changes in vibration behavior. For achieving a mechanical behavior close to the native eardrum, a validated model would allow the testing of design changes without the need of fabrication. Like in the test rig, the scaffolds were stimulated with a combination of quasi-static and dynamic pressure loads. Likewise, varying radial force was applied on the edge of the scaffolds to investigate the influence of clamping.

Results and Discussion

The measurement and simulation results were compared to eardrum data from literature and experiments.

The stiffness of the scaffolds was higher than for the normal eardrum. In contrast to cartilage, they showed the same non-linear stiffness behavior as the eardrum. The higher the initial clamping force, the more the first resonance frequency, as a characteristic phenomenon, was shifted to a higher frequency range. At once, the magnitude was

lowered for both, the simulated and the measured specimen. An increase of the quasi-static pressure also leads to a decrease of the scaffold magnitude and lowering of the first resonance frequency for the measured specimen. For the provided scaffolds, the simulation verified the influence of the scaffold thickness in terms of decreasing magnitude with increasing thickness.

Conclusion

It is possible to compare the measured and the simulated scaffolds. For a stable and functional eardrum replacement further research is needed. In addition, future developments will focus on the implementation of nanoparticles and nanofibrils to add immunomodulatory and anti-inflammatory properties and in-vitro tests to address ototoxicity and cell growth. The aim is to create a multifunctional scaffold, being able to improve the take rate and restoration of hearing.

References

Zahnert et al. 2001: Experimental Investigations of the Use of Cartilage in Tympanic Membrane Reconstruction.
Mota et al. 2015: Multiscale fabrication of biomimetic scaffolds for tympanic membrane tissue engineering.

Acknowledgement

This project is supported under the frame of EuroNanoMed III.

XI-OS41-RF06

Material inks for inkjet printed biomedical sensor applications

Marco Fritsch[1], Sindy Mosch[1], Nikolai Trofimenko[1], Viktar Sauchuk[1], Natalia Beshchasna[2], Mihails Kusnezoff[1], Mykola Vinnichenko[1]

[1]Fraunhofer IKTS Institute, Materials and Components, Dresden, DE; [2]Fraunhofer IKTS Institute, Bio- and Nanotechnology, Dresden, DE

Introduction

The rapid development of medical and biological sensors leads to numerous new applications in the field of point-of-care, lab-on-chip, organ-on-chip, environmental as well as wellness sensors. Thin and mechanically flexible substrate materials, like polymer foils or paper, offer an attractive combination of low cost and the ability of a smart integration in human relevant surroundings. Conventional microelectronic fabrication technologies, such as photolithography, have limitations in terms of sensor design flexibility and costs for producing smaller, customized sensor lots. In this context, digital and additive direct printing processes, like inkjet printing, are evaluated and developed in recent years. Such printing methods can be scaled to roll-to-roll (R2R) processes for a potential mass production of sensors. Up to now, the main problem for the direct printing of such sensors is the poor thermal stability of the low-cost polymer or paper foil substrates, which demands printable materials for sintering at low temperatures (e.g. < 200 °C). Fraunhofer IKTS has developed tailor-made functional nanoinks for the inkjet printing of metallic electrodes and sensory active layers on such thermal sensitive substrates [1]. Especially the gold and platinum inks are attractive to realize printed biomedical sensors, since they proved to be compatible with living cell cultures.

Experimental Methods

Silver, gold and platinum nanoparticles are derived from wet chemical precipitation process and transferred to material ink formulations (20 to 30 wt.-% solid content). By controlling the particle stabilization, certain restrictive parameters like sedimentation stability and ink viscosity were adjusted for inkjet print compatibility. The inks were characterized for particle size distribution, sedimentation stability, viscosity, surface tension and solid content. Inkjet printing tests were performed with and Dimatix DMP material printer (10 pL drop size) on PET and paper foil substrates. The printed films were dried at 80 °C and systematically sintered at 150 °C and 200 °C by varying the holding time in a box furnace. Alternatively to such a conventional slow box or continuous annealing furnace sintering an innovative line laser sintering tool (HPDL) was evaluated. The electrical film resistance was measured and the film microstructure characterized by SEM analysis of film cross sections.

Results and Discussion

Fig.1 shows the range of metal nanoparticles synthesized. The prepared nanoinks show a good sedimentation stability and a nice inkjet printing compatibility. The resulting electrical resistance of the printed and sintered films is excellent for the developed silver ink (2-times Ag-bulk, 8 µOhmcm) and good for gold ink (6-times Au-bulk, 33 µOhmcm) and platinum ink (11-times Pt-bulk, 390 µOhmcm). The film thickness is in the range of 1 µm and the prepared films possess a nice bendability of the printed structures (Fig.2). Alternatively to conventional box furnace sintering, the fast HPDL laser process is a powerful method to enable the sintering of printed films within milliseconds at a high processing speed, which is highly attractive for later application in R2R sensor production processes. In a comparison between box furnace and HPDL sintering treatment, the resulting film microstructure and the film electronic conductivity will be presented and discussed. Several examples of possible sensor application of the

developed material inks for printed temperature and pH sensors, micro hotplates for electrochemical sensors or precious metal electrodes for a subsequent biochemical sensor functionalization (gold and platinum) will be presented.

Conclusion

Fraunhofer IKTS developed functional nanoinks for the inkjet printing of metallic electrodes on thermal sensitive substrates like polymer or even paper foils. Especially the gold and platinum inks are highly attractive for biomedical sensors, where printed electrodes can be realized. Based on this electrodes different sensor types like temperature, pH, humidity and electrochemical sensor can be realized.

References

[1] https://www.ikts.fraunhofer.de/en/departments/energy_bio-medical_technology/materials_and_components/HT_ElectrochemistryCatalysis/material_inks.html

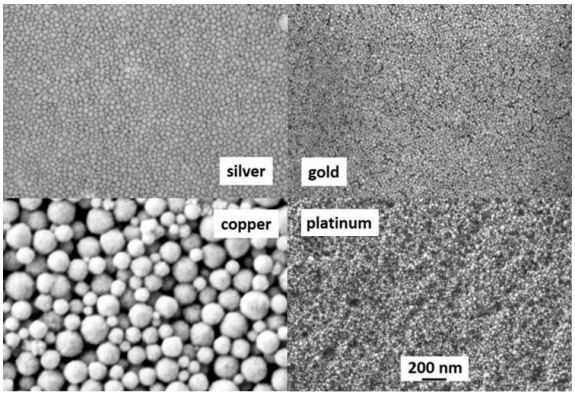

Fig.1
Nanoparticle inks for printing sensor elements.

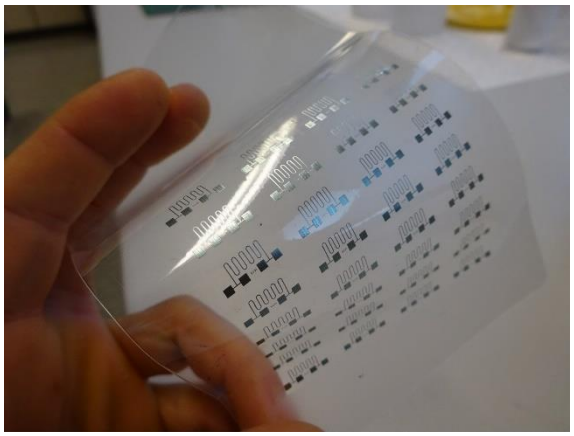

Fig.2
Printed temperature sensor on PET polymer foil.

XI-OS41-RF07

Measuring bacterial adhesion forces on implant materials

Katharina Doll, Andreas Winkel, Meike Stiesch

Hanover Medical School, Department of Prosthetic Dentistry and Biomedical Materials Science, Hanover, DE

Introduction

Despite their frequent use in modern medicine and continuous biomaterial improvements, implants still suffer from high rates of implant-associated infections. These are caused by bacterial biofilms, which firmly adhere to implant surfaces and embed themselves into a matrix of extracellular polymeric substances. Biofilms are inherently resistant to the hosts immune defense and common antibiotic therapy, making the treatment of implant-associated infections difficult. Therefore, new implant materials aim at preventing biofilm formation. A common approach focusses on surfaces, which aim at inhibiting stable bacterial attachment. The premise for the development of antiadhesive materials is a reliable measurement of bacterial adhesion forces to implant materials.

Experimental Methods

For this purpose, we used an atomic force microscope connected to a pressure control system mounted on an inverse microscope. The setup employs a hollow cantilever with a circular opening at the end, which enables the reversible immobilization of bacterial cells for spectroscopy by applying negative pressure (Figure 1). Thus, it circumvents difficult chemically-based cell fixation to cantilevers, which may impact bacterial surfaces, and allows measurement of more individual cells at higher throughput.

Results and Discussion

Measuring oral bacterial on common implant materials exhibits several obstacles for force spectroscopy. As implants are made from solid, nontransparent materials like titanium, a direct inverse targeting is impossible. Various surface topographies and morphologies used to create antiadhesive surfaces may interfere with cantilever approach and cause uncontrolled reflection of the irradiating laser beam. Additionally, most oral bacterial species are facultative or obligate anaerobes, which accounts for specific conditions during spectroscopy measurement. All aforementioned requirements were taken into account to design an appropriate experimental protocol for single bacterial force spectroscopy on implant materials. The setup was equipped with a glass ring that contains a cavity for at-grade insertion of the respective implant material. Bacterial cells could be targeted by inverse microscopy on the glass surface, grabbed, and transferred to the nontransparent material for force spectroscopy. To overcome artefacts by surface topography or morphology, the setpoint force was adjusted and a downstream quality control was implemented. To cope with oxygen sensitive bacteria, an alternative buffer solution was employed.

Conclusion

We were able to develop a new protocol to reliably measure single bacterial adhesion forces of various oral species at higher throughput on any solid implant material.

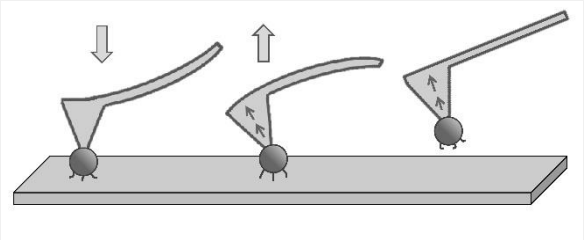

Figure 1. Principle of single bacterial force spectroscopy.
An atomic force microscope connected to a pressure control system was used. Adherent bacteria are targeted with a hollow cantilever (left), negative pressure is applied and the cantilever is withdrawn (middle) until the bacterial cell is detached (right).

XI-OS41-RF08

Pushing forward Gellan gum-based hydrogels: the impact of inorganic fillers on mechanical and biological performances

Maria A. Bonifacio[1], Stefania Cometa[2], Piergiorgio Gentile[3], Annachiara Scalzone[3], Andrea Cochis[4], Lia Rimondini[4], Giuseppe Procino[5], Serena Milano[5], **Elvira De Giglio**[1]

[1]University of Bari 'Aldo Moro' Department of Chemistry, Department of Chemistry, Bari, IT; [2]Jaber Innovation s.r.l., Roma, IT; [3]Newcastle University, School of Engineering, Newcastle upon Tyne, GB; [4]Università del Piemonte Orientale UPO, Center for Translational Research on Autoimmune & Allergic Diseases CAAD, Department of Health Sciences, Novara, IT; [5]University of Bari, Department of Biosciences, Biotechnologies and Biopharmaceutics, Bari, IT

Introduction

Biopolymer-based hydrogels are one of the most promising class of biomaterials for tissue engineering applications. Indeed, compared with synthetic alternatives, biopolymers offer a more suitable interaction with host tissues in terms of degradation rates as well as cytocompatibility. However, their mechanical features are often weaker than those of synthetic hydrogels and still far from the standards required in clinics. This drawback becomes a major issue in cartilage regeneration, since the load-bearing property of such a tissue is its unique trait[1].

The development of composite hydrogels, based on biopolymers and reinforced with inorganic components, represents an intriguing route to enhance hydrogels' mechanical features, while preserving the peculiarities of biopolymer-based materials[2]. In this work, several inorganic fillers were combined with a gellan gum-based hydrogel, evaluating their impact on compression modulus cell adhesion rate.

Experimental Methods

Gellan gum (GG) was dissolved in water with Manuka Honey (MH) in 1:1 ratio, as previously reported[3]. Then, an inorganic filler among bentonite, diatomaceous earth, mesoporous silica and halloysite nanotubes was added to the mixture, which was poured into molds and crosslinked with Mg^{2+} ions. Finally, freeze-dried samples (Fig.1) underwent physico-chemical, mechanical and biological evaluations. Human Bone Marrow Mesenchymal Stem cells (hBMSCs) were seeded on the hydrogels' top surfaces to study their metabolic activity and ability to colonize even the deepest zones of the hydrogels.

Results and Discussion

The prepared hydrogels were deeply studied by X-ray Photoelectron Spectroscopy (XPS). Moreover, thermogravimetric analyses were carried out to gain insights into the thermal behavior of the composite hydrogels, reinforced with inorganic fillers. As far as mechanical characterization is concerned, the hydrogels were compressed until break and the resulting Young's moduli(E) were calculated. The addition of inorganic fillers resulted in a dramatic enhancement of Young's modulus, which exceeded 100kPa for all the composite hydrogels. Silica-enriched hydrogels especially improved the modulus of the bare hydrogel more than 45%. These findings were in accordance with XPS data, suggesting that the presence of inorganic fillers supports cations' mobility, resulting in enhanced energy dissipation under compression.

Interestingly, when subjected to freeze-drying, the hydrogels developed a noteworthy internal micro-porosity, variable depending on the filler, suitable for colonization and cell migration. Therefore, hBMSCs were seeded on the hydrogels' top surfaces to study their ability to proliferate and migrate to the deepest bottom areas of these pore

networks. A remarkable metabolic activity of hBMSCs, cultured up to 10 days on the hydrogels, was detected. In addition, fluorescence microscopy, combined with an optimized cryosectioning protocol, revealed that hBMSCs were more prone to adhere on silica-filled hydrogels, and colonize the scaffold more deeply. Finally, co-culture of hBMSCs in presence of *S.aureus* or *S.epidermidis* was performed, showing that the composite hydrogels embedding mesoporous silica, diatomaceous earth or halloysite nanotubes protected hBMSCs viability from staphylococci infection.

Conclusion

The presence of inorganic fillers, especially mesoporous silica, allowed gellan-based hydrogels to achieve improved mechanical and biological performances. Hence, starting from these intriguing outcomes, further experiments are being performed. Indeed, hBMSCs differentiation on the hydrogels is ongoing, together with the evaluation of changes in mechanical features, induced by chondrogenesis. Furthermore, the most promising hydrogels will be implanted in wild type mice, to study their *in vivo* compatibility. The developed hydrogels display the potential to become useful tools for cartilage tissue engineering.

References

1. Zhao Y. et al, *Appl Sci*, 8, 2272, 2018.
2. Walter S.G. et al, *Arch Orthop Traum Su*, 139:305-16, 2019.
3. Bonifacio M.A. et al, *Carb Pol*, 198:462-72, 2018.

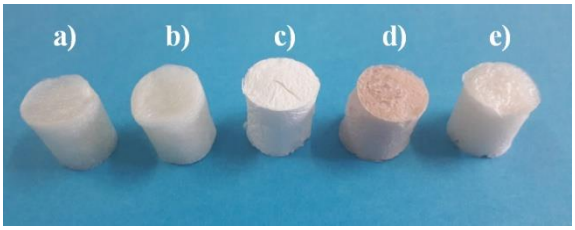

Figure 1
Macroscopic appearance of freeze-dried hydrogels without inorganic fillers (a), embedding halloysite nanotubes (b), mesoporous silica (c), diatomaceous earth (d) and sodium bentonite (e). Scale bar:20mm

11:30 a.m. – 1:00 p.m.

Hall 5

XI-SY18 | Biobased Polymers and their use in Wound Healing Applications

Ipsita Roy (London, GB)
Serena Danti (Pisa, IT)

Biobased polymers are a sustainable source of polymers which need to replace petrochemical-based polymers. This symposium will focus on the application of biobased polymers for wound healing, exploiting their high biocompatibility, processability and antimicrobial activity. Novel studies on wound healing will be presented including biobased polymers such as chitosan, alginate, collagen, Polyhydroxyalkanoates, γ-Polyglutamic acid. In addition, active factors such as antibacterial properties, growth factors, paracrine factors, cellular therapy including stem cells will be included. Finally, and not the least various processing techniques such as electrospinning (melt and solution), gyrospinning and 3D printing will be discussed.

XI-SY18-KL01

Development of biomaterials to stimulate wound healing and tissue regeneration in skin, cornea and the pelvic floor.

Sheila MacNeil[1], Anthony J. Bullock[1], Serkan Dikici[1], Naside Mangir[1], Joanna Shepherd[2], Mohammed Yar[3]

[1]University of Sheffield, Kroto Research Institute, Sheffield, GB; [2]University of Sheffied, Clifford Dental School, Sheffield, GB; [3]COMSATS University, Lahore, PK

Introduction

Ideal biomaterials initiate or stimulate tissue repair and ideally tissue regeneration without inducing inflammation, scarring or fibrosis. Our group has developed materials to stimulate angiogenesis and wound healing in chronic skin wounds, to promote tissue regeneration from small explants of corneal tissues in the eye and to provide mechanical support to the organs of the pelvic floor while seeking to avoid excessive fibrosis.

AIM: The aim of this presentation is to share some of the advances we have made in working across this broad canvas and to flag up where much more work is needed.

Experimental Methods

Firstly with respect to the mechanical properties of materials the first place to start-is with a good understanding of the clinical requirements of the material to be developed. We have favoured working with electrospun synthetic polymers which can be tailored to breakdown rapidly- within 2 months when used on the eye-or to last for more than a year when used as a support in the pelvic floor. Electrospun polymers have many advantages in terms of controllability of architecture and rate of breakdown. Thus we have worked with electrospun 50:50 PLGA to produce a simple micro fibrous membrane which supports the attachment and growth of cultured corneal epithelial cells and the outgrowth of cells from limbal tissue explants and which can be tailored to breakdown without affecting surrounding tissues leaving the cultured cells in place on the cornea. The same material can also be produced to contain 3-D features within it to mimic the limbal stem cell niches of the eye. Staying with the mechanical properties of the biomaterials these can also be electrospun into trilayers to mimic the architecture of the natural abdominal fascia-achieving mechanical properties like the viscoelastic properties of this natural material.

Results and Discussion

To influence wound healing and tissue integration we have developed electrospun fibres to release proangiogenic factors such as oestradiol and a small deoxyribose (2-deoxy-D-ribose (2dDR))which are both strongly pro-angiogenic and to release Ibuprofen to calm down wound bed inflammation. Such materials are being developed as topical dressings to for example stimulate wound healing in diabetic ulcers (where successful acceleration of wound healing has been demonstrated in a diabetic rat model) and to improve tissue integration when materials are used as load-bearing supports for stress urinary incontinence and pelvic organ prolapse.

Finally recognising that skin wounds which failed to heal often present with poorly vascularised beds, infection and unresolved inflammation we are pleased to be part of the European consortium MOZART which is developing wound dressings based around the concept of using nanoparticles to deliver agents to reduce intrinsic infection in the wound bed, stimulate angiogenesis and reduce inflammation all embedded within a polyurethane hydrogel dressing. As part of this consortium we have developed a novel technique for measuring the impact of bacterial infection on the pH of

a wound bed using 3-D tissue engineered skin and demonstrated that bacteria do in fact influence the pH of skin but do so by markedly changing pH in discrete small areas rather than influencing the overall skin pH.

Conclusion

We conclude that synthetic polymers provide an excellent resource to develop into biomaterials covering a range of mechanical properties with degradation rates that can be tuned to be rapid or very long-lasting. Progress has been made in identifying clinically acceptable small molecules which can drive angiogenesis and can be added to these materials to be released slowly or rapidly as required. Nanoparticles can be designed to deliver antimicrobials to act on their own or in combination with other materials for the treatment of infection in wounds. We have developed a method for measuring skin pH that shows for the 1st time the range of pH changes that can be produced by bacterial infection of skin.

A major challenges which remains is how to introduce implants into the body such that they integrate well and provide mechanical support as required but do not induce fibrosis.

XI-SY18-KL02

Carbohydrate biopolymers as antimicrobials and wound healing accelerators

Ylenia Zambito[1], Anna Maria Piras[1], Chiara Migone[1], Angela Fabiano[1], Francesca Felice[2], Rossella Di Stefano[2]

[1]University of Pisa, Department of Pharmacy, Pisa, IT; [2]University of Pisa, Department of Surgery, Medical, Molecular, and Critical Area Pathology, Pisa, IT

Chronic, non-healing wounds can be debilitating and painful for the affected individuals, increasing risk for various morbidities and mortality and place a massive financial burden on healthcare systems. Issues surrounding wound healing have generated deep scientific interest as well as booming financial markets invested in novel wound therapies. Despite several approaches have been evaluated for the therapy of chronic lesions, their treatment is still a challenge. The use of innovative materials for the treatment of chronic skin lesions and damaged tissues has recently gained a growing interest. Chronic lower extremity ulcers are by definition non-healing wounds with different origins, such as ischemia, diabetes, vasculitis or venous insufficiency. Critical limb ischemia is a chronic peripheral arterial disease, characterized by the presence of pain at rest and/or trophic lesions, such as ulcers and gangrene. The incidence of critical limb ischemia has progressively increased and currently constitutes one of the major features of generalized arterial atherosclerotic disease, considering that every year more than one million people suffer a lower limb amputation.

The importance of this phenomenon is therefore extremely significant for both the number of patients involved and for the time and resources required for their treatment. Therefore, adequate treatments are needed to increase the overall patient quality of life.

Recently, numerous studies demonstrated the function of chitosan as a wound healing accelerator (1, 2). Chitosan and its derivatives could accelerate wound healing by enhancing the functions of inflammatory cells, such as fibroblasts, polymorphonuclear leukocytes and macrophages. The wound healing effects of chitosan could be affected by its physico-chemical characteristics, such as molecular weight (MW), deacetylation degree and derivatization. Recently our group has demonstrated that high-MW quaternary ammonium–chitosan conjugates bearing thiol groups on their chains are more effective in promoting cell activity and accelerating wound healing than the non-thiolated conjugates and the parent non-derivatized Ch (3).

Since it is known that chemokines can lead to the development of a wide range of inflammatory diseases including chronic wounds, many researchers have centered on the strategy of removing chemokines from chronic wounds. Indeed, during the wound healing process, chemokines are released by tissue-specific cells and resident immune cells at the site of injury to establish a chemoattractant gradient that promotes the invasion of blood-derived immune cells, which are essential for the initial inflammatory phase of acute wound healing (4). In chronic wounds, the healing process is often deadlocked in an unrestrained inflammatory response. Under this condition, the uncontrolled activation of polymorphonuclear neutrophils and inflammatory monocytes/macrophages lead to a destruction of the wound tissue and drives the abundant production of inflammatory mediators including chemokines. The persistent chemoattractant gradients promote further invasion of these immune cells into the wound tissue, thus perpetuating a vicious circle of chronic inflammation (4). One important feature of chemokines is their ability to bind to extracellular matrix glycosaminoglycans (GAGs), such as heparan sulfate or heparin (5), a process that is mediated by electrostatic interactions of positively charged amino acid residues of the chemokines and negatively charged sulfate

groups of the GAGs. Furthermore, GAGs protect chemokines against proteolytic inactivation, mediate chemokine oligomerization for receptor activation, and accumulate chemokines near the cell surface. Therefore, GAG-based engineered materials may allow for modulating chemokine concentrations within tissues to therapeutically attenuate inflammation in chronic wounds (6).
Our group is now collecting data on the ability of different GAGs in combination with different chitosan derivatives to act as antimicrobials and wound healing accelerators. Such data will be presented in order to hypothesize a structure-activity relationship.

References

1. T. Dai, M. Tanaka, Y.Y. Huang, M.R. Hamblin, Chitosan preparations for wounds and burns: antimicrobial and wound-healing effects. Expert Rev. Anti Infect. Ther. 9, 857–879 (2011).
2. M. Ishihara, K. Nakanishi, K. Ono, M. Sato, M. Kikuchi, Y. Saito, H. Yura, T. Matsui,H. Hattori, M. Uenoyama, A. Kurita, Photocrosslinkable chitosan as a dressing for wound occlusion and accelerator in healing process. Topical formulations and wound healing applications of chitosan. Biomaterials 23, 833–840 (2002).
3. F. Felice, Zambito Y., E. Belardinelli, A. Fabiano, T. Santoni, R. Di Stefano, Effect of different chitosan derivatives on in vitro scratch wound assay: A comparative study. Int. J. Biol. Macromol. 76, 236-241 (2015).
4. R. Gillitzer, M. Goebeler, Chemokines in cutaneous wound healing. J. Leukoc. Biol. 69, 513–521 (2001).
5. T. M. Handel, Z. Johnson, S. E. Crown, E. K. Lau, A. E. Proudfoot, Regulation of protein function by glycosaminoglycans—As exemplified by chemokines. Annu. Rev. Biochem. 74, 385–410 (2005).
6. U. Freudenberg, Y. Liang, K. L. Kiick, C. Werner, Glycosaminoglycan-based biohybrid hydrogels: A sweet and smart choice for multifunctional biomaterials. Adv. Mater. 28, 8861–8891 (2016).

XI-SY18-03

In Vivo Comparison of 3 Dermal Scaffolds using the Porcine Animal Model of Acute Wound Healing

Stuart J. Brown[1], Vaibhav Sharma[1], Elena Garcia-Gareta[1], Lilian Hook[2]

[1]Restoration of Appearance and Function Trust, Rickmansworth, GB; [2]Smart Matrix Limited, London, GB

Introduction

Successful cutaneous wound healing requires orderly progress through haemostasis, inflammation, deposition and remodelling processes[1]. Over evolutionary timescales, the rapidity and vigour of cutaneous wound healing was critical for survival. Our innate healing processes prioritise sterilisation and barrier reaquisition over aesthetic and functional outcome. Our modern healthcare knowledge and technology gives us an opportunity to shift our innate wound healing processes towards better outcomes without risking overall health.

Wound contraction, where myofibroblasts within the wound bed align and generate compressive stress, aids wound closure by limiting the area required to heal and re-establish barrier. However, excessive contraction is associated with poor outcomes such as scarring, and the formation of contractures which can limit function after the healing process is finished[2]. Surgeons reduce contraction risk by shaping surgical interventions to minimise tensile forces across the wound, and through the use of skin grafts, which reduce the area and depth requiring a healing response. Grafting success rate is dependent on rapid re-vascularisation, which limits possible graft thickness, and grafts generally suffer from limited donor site availability, and can often result in poor aesthetic outcome.

Dermal replacement scaffolds are bioactive tissue equivalents upon which normal wound healing processes can proceed[3]. They are designed to work with; and complement; the capabilities of skin grafts, but still suffer from the disadvantages outlined above. In this study, the functional and aesthetic outcomes of treatment with the collagen-based scaffolds MatriDerm® and Integra®, and the fibrin-based SmartMatrix® scaffold were studied in the porcine model of cutaneous wound healing. SmartMatrix® was assessed without an accompanying skin graft, particularly in terms of the impact on re-epithelialisation and contraction without a graft.

Experimental Methods

Animal study

Large White / Landrace crossbreed pigs each received 6x4cm diameter full thickness wounds. Wound peripheries were tattooed to track the healing process, with an unwounded shoulder tattoo used to track overall growth. 0.2mm split-thickness skin grafts (STSG) were created from the paravertebral muscles' epidermis. Each group was represented by 6 treated wounds (Smart Matrix®: 8) randomised over the group of pigs. Integra® (2 step protocol) and MatriDerm® were used with a split thickness skin graft (STSG) as is their standard practise whereas Smart Matrix® was not.

Area and superficial blood flow

Changes in wound area tattoo size over the study period were measured by Eykona 3D camera, and superficial perfusion was assessed by moorFLPI laser doppler.

Biopsies and histology

Biopsies were taken from each wound at day 4, 10, 20, 30, 120 and 192 days after wounding and processed for histological analysis. Sections for each treatment and timepoint were stained with H&E, or immunofluorescently

labelled with Col3 (vascularisation, structural protein), Elastin (structural protein) or Smooth muscle Actin (fibroblast differentiation) reactive primary antibodies, or immunohistochemically for CD31 (vascular) reactive antibody.

Results and Discussion

Overall, dynamic changes were seen in the first 30 days after wounding, then treated groups and controls were very similar. Untreated wounds contracted the most during this period, and Smart Matrix® treated wounds the least, despite their lack of a graft, and this was statistically significant. Superficial perfusion was highest in untreated wounds but reduced rapidly. Smart Matrix® had the next highest superficial perfusion, but delayed to 20-30 days post wounding.

Each dermal replacement scaffold had a distinctive profile *in vivo*, exhibiting different degradation rates, levels of cell infiltration, and associated cell behaviour within or adjacent to the biomaterial. Integra® scaffold, for instance, was visualised up to the end of the study (192 days), whereas MatriDerm® and Smart Matrix® were resorbed by day 10 and 20 respectively.

STSG control and MatriDerm® groups showed partial graft take, whereas Integra®, with its delayed graft protocol, showed the greatest success. Re-epithelialisation of all grafted and ungrafted wounds was complete by day 30.

Histological analysis showed abundant CD31+ blood vessels regenerating in all groups (fewest in STSG treated group), dermal reformation between days 30 and 120, and sustained alpha smooth muscle expression throughout the early time period with subtle differences between treatment groups.

Conclusion

This study documents differences between commonly used dermal scaffolds and a novel fibrin-based dermal scaffold in the porcine animal model over early time periods, which are likely to show clinically significant differences in human wound healing outcomes.

References

1. Epstein FH, Singer AJ, Clark RAF. Cutaneous wound healing. N Engl J Med. 1999 Sep 2 [cited 2016 Jun 13];341(10):738–46
2. Marshall CD, Hu MS, Leavitt T, Barnes LA, Lorenz HP, Longaker MT. Cutaneous Scarring: Basic Science, Current Treatments, and Future Directions. Adv wound care. 2018 Feb 1;7(2):29–45
3. Zhong SP, Zhang YZ, Lim CT. Tissue scaffolds for skin wound healing and dermal reconstruction. Wiley Interdiscip Rev Nanomed Nanobiotechnol. 2(5):510–25

Acknowledgement

This work was sponsered by Smart Matrix® limited.

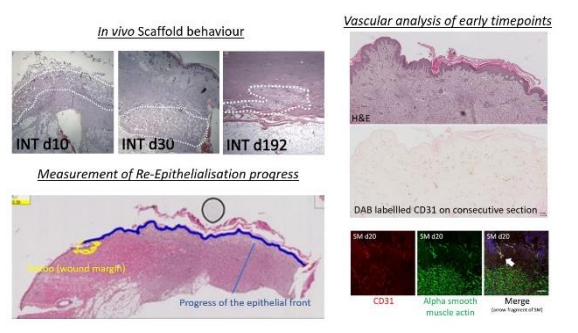

Microscopic analysis of scaffolds in vivo

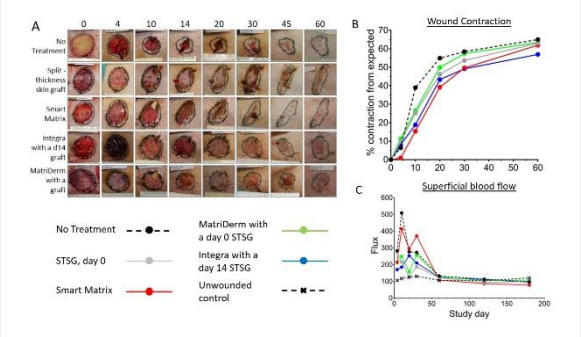

Study design, Changes in Wound Area and Perfusion

XI-SY18-04

Bioengineered, xenogen-free 3D human skin equivalents (HSE) as wound infection models

Ayesha Idrees[1,3], Valeria Chiono[1], Gianluca Ciardelli[1], Richard Viebahn[2], Siegfried Shah[3], **Jochen Salber**[2,3]

[1]Politecnico di Torino, DIMEAS, Turin, IT; [2]UMC Knappschaftskrankenhaus Bochum, Clinic of Surgery, Bochum, DE; [3]Ruhr-Universität Bochum, Experimental Surgery, Bochum, DE

Introduction

Soft tissue- and skin-related infections are great challenges in public health. Novel and alternative strategies to combat wounds colonized with resistant bacteria are urgently needed. Furthermore, many of the commercially available and clinically applied antimicrobial dressings are showing not the results as guaranteed. Shortening the time from lab developments to promising clinical applications and to bioevaluate already CE-marked products more reliable and reproducible without abusing unnecessarily test animals bioengineered, xenogen-free 3D human skin equivalents (HSE) as wound infection models are highly demanded.

Experimental Methods

Dermal and epidermal compartments were established by embedding human primary fibroblasts (NHDF) in recombinant human collagen type I (rhColl-I) hydrogels and then seeding human primary keratinocytes (NHEK) on it to generate the epidermis. The cultural conditions were optimized to obtain closely mimicking *in vivo* skin. Therefore, the biomechanical properties of different NHDF/rhColl-I combinations and clinical human dermis samples were tested and compared applying nanoindentation (Piuma, Optics11). Skin wound models with defined wound depths were created with a novel developed programmable punch device and colonized with relevant skin infectious bacteria e.g. *S. aureus* at wound site, to generate an *in vitro* skin infection model. The novel 100% xenogen-free human skin, wound and colonized wound models were fully characterized by histopathological methods, confocal microscopy, TEM analysis and nanoindentation. The infection model was validated by applying different antimicrobial wound dressings, testing cyto- and immunocompatibility and antimicrobial properties.

Results and Discussion

Different combinations of cell numbers (NHDF) and rhColl-I compositions led to dermis constructs with different biomechanical properties significantly influencing fibroblasts' metabolic activity and gene expression. "Instable" dermis constructs inhibited the cultivation and development of regular NHEK layers and prevent the formation of characteristic multilayered epidermal structures. With specific combinations, uniform distribution and filopodia like morphology of NHDFs stable 3D HSEs could be achieved. Morphology studies and uniform distribution of fibroblasts at different planes inside the dermal compartment were analysed by confocal imaging. Immunohistology and TEM were used to visualize the correct establishment of basement membranes (laminin 5 expression) and dermal-epidermal junctions. Proliferating NHEKs showed keratin 14 and keratin 10 in the corresponding layers. The establishment of standardized wounds and infected wound models is necessary for the reliable and reproducible analysis of antimicrobial wound dressings, their validation and comparison with each other. Figure 1 is representing a microscopic analysis of the HSE wound model after 24 h of incubation with Staph. aureus showing bacteria establishing colonies of different sizes within the dermis at wound site dissolving the matrix and surrounding layers

of keratinocytes. Four different clinically applied silver-containing wound dressings were used to investigate differences in cytocompatibility and antimicrobial efficacy. The comparison of the evaluation results between common standardized cell culture and microbio tests with the 3D HSE wound infection model revealed significant differences regarding cytotoxic concentrations of the active component, here Ag^+ ions, and the antimicrobial activity against susceptible described bacteria under more realistic conditions.

Conclusion

With our bioengineered, 100% xenogen-free 3D human skin equivalent it was possible to bioevaluate clinically applied silver-containing wound dressings and to demonstrate the significant differences of the materials' cytocompatibility and antibacterial properties in a more realistic biological microenvironment. This model as many other 3D tissue equivalents seems promising for its application in diverse areas of biomaterials research, including cytocompatibility evaluation, drug testing, wound healing and skin infection.

References

Idrees A., et al. Validation of in vitro assays in three-dimensional (3D) human dermal constructs. IJAO. 2018;41(11):779-788.

Acknowledgement

The authors would like to thank European Union’s Horizon 2020 research and innovation programme (Grant no: 643050) for providing financial support to this HyMedPoly project.

Poster Sessions

2:45 p.m. – 4:15 p.m.

Hall 1 / Exhibition Area

PS1 | Postersession 1

2:45 p.m. – 3:45 p.m.

Hall 1 / Exhibition Area

PS1-01 | Metals

PS1-01-01

Enhancing the corrosion resistance and biological response of 3D-printed Ti-Nb-Zr-Sn alloy scaffold surface immobilized with type I collagen

Chia-Fei Liu[1], **Her-Hsiung Huang**[2]

[1]National Yang-Ming University, Institute of Oral Biology, Taipei, TW; [2]National Yang-Ming University, Department of Dentistry, Taipei, TW

Introduction

Surface characterizations of metallic implants play importamt role in their biomedical applications. In this study, a unique surface modification process was used to enhance the corrosion resistance and biological response of 3D-printed titanium (Ti) alloy scaffold in bone implant applications.

Experimental Methods

The surface modification process, combining alkaline treatment and natural cross-linker, procyanidin, was used to produce submicron-porous topography and immobilize type I collagen on the surface of 3D-printed low elastic modulus Ti alloy (Ti-24Nb-4Zr-8Sn, designated Ti2448) scaffold with interconnected porosity. The electron beam melting technique was used as 3D-printing process.

Results and Discussion

Scanning electron microscopy and transmission electron microscopy analysis results showed a unique hybrid layer, including a submicron-porous outer sublayer and a dense inner sublayer, was created on the interconnected porous Ti2448 alloy scaffold surface. X-ray photoelectron spectroscopy, Fourier transform infrared spectroscopy and Sirius red staining analysis results confirmed that the type I collagen was successfully immobilized on the interconnected porousTi2448 scaffold surface. The dense inner oxide layer provided Ti2448 alloy scaffold with improved corrosion resistance, in terms of corrosion rate and anodic current density, in simulated body fluid. The Ti2448 alloy scaffolds, with and without surface treatments, were potentially non-cytotoxic according to ISO10993-5 specifications; particularly, the type I collagen-immobilized Ti2448 alloy scaffold *via* procyanidin cross-linking showed well cell adhesion and osteogenic differentiation of primary human bone marrow mesenchymal stem cells. As compared with the untreated scaffold surfaces, better focal adhesion complex formation, vinculin, and cytoskeleton arrangement were observed on the type I collagen-immobilized surface; the integrin/focal adhesion kinase (FAK)/phosphoinositide 3-kinase (PI3K)/mitogen-activated protein kinase (MAPK) pathway was also activated to promote cell differentiation and mineralization.

Conclusion

The proposed unique surface modification concurrently improves the corrosion resistance and cell response of the 3D-printed interconnected porous Ti2448 alloy scaffold without causing cytotoxicity and shows great potential for biomedical bone implant applications.

Acknowledgement

This study was financially supported by the Ministry of Science and Technology (MOST), Taiwan (MOST-105-2314-B-030-MY3). The authors thank the 3D-printed Ti2448 alloy scaffolds, which were kindly provided by Dr. Yu-Lin Hao's group, Titanium Alloy Laboratory, Institute of Metal Research, Chinese Academy of Sciences, Shenyang, China.

PS1-01-02

Plasmonic silver nanoshells for drug and metabolite detection

Lin Huang, Kun Qian

Shanghai Jiao Tong University, School of Biomedical Engineering, Shanghai, CN

Introduction

Metabolic detection has a key role for disease diagnosis and therapeutic evaluation in clinics[1-3]. Mass spectrometry (MS) enjoys unique advantages of high accuracy, sensitivity, resolution, and throughput in metabolomic research. However, the efficacy of MS is hindered by rigorous sample enrichment or purification, due to the high sample complexity and low molecular abundance in biological samples[4-6].

Conjugated with MS, nanomaterials have been reported by research groups globally as Surface Enhanced Laser Desorption/Ionization (SELDI) MS to avoid the tedious sample pre-treatment[7-12]. Notably, the LDI performance of nanomaterials is challenging for sweet-spot and strong background below m/z 500[13-18]. Plasmonic particles provide surface plasmon resonance and hot carriers under laser irradiation ideal for MS use, but have not been developed so far.

Experimental Methods

We have developed series of plasmonic nanomaterials for direct metabolic profiling of biofluids for different clinical purpose, including silver nanoshells, gold nanoparticles and noble metal-semiconductor hybrids, etc.. Here, we developed a platform based on designer plasmonic silver nanoshells for direct detection of small metabolites. We synthesized a series of noble metal core-shell particles with tunable nanoshell structures through multi-cycled silver mirror reactions on the surface of SiO_2 nanoparticles. The optimized plasmonic silver nanoshells as new matrices allowed fast, multiplex, sensitive, and selective LDI MS detection of small metabolites in 0.5 μL of bio-fluids without enrichment or purification. Coupling with isotopic quantification of selected metabolites, we demonstrated the use of these silver nanoshells is highly accurate compared to biochemical methods.

Results and Discussion

We for the first time achieved the multifunction clinical purpose based on the unique plasmonic nanoshells towards disease diagnosis, bacteria detection and therapeutic evaluation in clinics. For disease detection, we identified 21 patients with postoperative brain infection through glucose quantitation and daily monitoring by cerebrospinal fluid (CSF) analysis. Notably, compared to the biochemical method based quantification, the sample volume was reduced from 200 to 0.5 μL and the experiment time was reduced from hours to several minutes by the LDI MS[19-21]. The isotopic quantification afforded the average recovery of ~131% with coefficient of variation (CV) within 6%, which was comparable to the biochemical method that afforded the average recovery of ~107% with CV within 14%. For bacteria detection, the optimized nanoshells enable direct LDI MS based metabolic analysis of bacteria (≈10 μL^{-1}), in complex biofluids. The serum infection process (0–10 h) is monitored by statistics toward clinical classification. Bacteria metabolism is studied with metabolic biomarkers (e.g., malate and lysine) identified during inhibition, showing cell membrane destruction and dysfunctional protein synthesis mechanisms. For therapeutic evaluation, we monitored the concentration changes of mannitol in serum and CSF, and demonstrated distribution of mannitol in blood and CSF systems during therapeutic treatment of three patients with cerebral edema. Notably, the blood and brain/CSF systems are divided by the blood–brain/CSF-barriers, which has been validated easily by our method. Our work sheds light on the design of materials for high-performance metabolic analysis and precision diagnostics in real cases.

Conclusion

In summary, we introduced silver nanoshells as matrices for direct LDI MS detection of small metabolites in bio-fluids, and further developed a platform technology for metabolic analysis-based disease detection and therapeutic evaluation. We synthesized series of silver nanoshells with controlled structures by multi-cycled silver mirror reactions and selected the designer silver nanoshells with optimized analytical performance. We revealed the mechanism for efficient LDI process associated with structural parameters of materials, and demonstrated the application in complex bio-fluids in real cases. Furthermore, coupling with isotopic quantification of selected metabolites (e.g., glucose and mannitol), we not only identified patients with postoperative brain infection by CSF analysis, but also monitored the drug concentrations in both CSF and serum to investigate the blood–brain/CSF-barriers and for pharmacokinetics study. Our work contributes to the design of materials for high-performance metabolic analysis towards precision medicine and initiates the development of diverse advanced diagnostic tools involving various metabolic biomarkers.

References

1.Zenobi, R. Single-cell metabolomics: analytical and biological perspectives. Science 342, 1243259 (2013).
2.Chaleckis, R., Murakami, I., Takada, J., Kondoh, H. & Yanagida, M. Individual variability in human blood metabolites identifies age-related differences. Proc. Natl Acad. Sci. USA 113, 4252–4259 (2016).
3. Wen, H., An, Y. F., Xu, W. J., Kang, K. W. & Park, S. Real-time monitoring of cancer cell metabolism and effects of an anticancer agent using 2D in-cell NMR spectroscopy. Angew. Chem. Int. Ed. 54, 5374–5377 (2015).
4.Guillaumond, F. et al. Cholesterol uptake disruption, in association with chemotherapy, is a promising combined metabolic therapy for pancreatic adenocarcinoma. Proc. Natl Acad. Sci. USA 112, 2473–2478 (2015).
5.Aebersold, R. & Goodlett, D. R. Mass spectrometry in proteomics. Chem. Rev. 101, 269–296 (2001).
6.Lei, C., Qian, K., Noonan, O., Nouwensa, A. & Yu, C. Z. Applications of nanomaterials in mass spectrometry analysis. Nanoscale 5, 12033–12042 (2013).
7.Chiang, C. K., Chen, W. T. & Chang, H. T. Nanoparticle-based mass spectrometry for the analysis of biomolecules. Chem. Soc. Rev. 40, 1269–1281 (2011).
8.Pitkanen, A. et al. Advances in the development of biomarkers for epilepsy. Lancet Neurol. 15, 843–856 (2016).
9.Liu, B. et al. High performance, multiplexed lung cancer biomarker detection on a plasmonic gold chip. Adv. Funct. Mater. 26, 7994–8002 (2016).
10.Stopka, S. A. et al. Molecular imaging of biological samples on nanophotonic laser desorption ionization platforms. Angew. Chem. Int. Ed. 55, 4482–4486 (2016).
11.Northen, T. R. et al. Clathrate nanostructures for mass spectrometry. Nature 449, 1033–1036 (2007).
12.Qian, K. et al. Laser engineered graphene paper for mass spectrometry imaging. Sci. Rep 3, 1415–1410 (2013).
13.Lee, J., Kim, Y. K. & Min, D. H. Laser desorption/ionization mass spectrometric assay for phospholipase activity based on graphene oxide/carbon nanotube double-layer films. J. Am. Chem. Soc. 132, 14714–14717 (2010).
14.Ocsoy, I. et al. Aptamer-conjugated multifunctional nanoflowers as a platform for targeting, capture, and detection in laser desorption ionization mass spectrometry. ACS Nano 7, 417–427 (2013).
15.Liu, Y. C., Chiang, C. K., Chang, H. T., Lee, Y. F. & Huang, C. C. Using a functional nanogold membrane coupled with laser desorption/ionization mass spectrometry to detect lead ions in biofluids. Adv. Funct. Mater. 21, 4448–4455 (2011).
16.Wei, X. et al. Plasmonic nanoshells enhanced laser desorption/ionization mass spectrometry for detection of serum metabolites. Anal. Chim. Acta 950, 147–155 (2017).
17.Wu, J. et al. Multifunctional magnetic particles for combined circulating tumor cells isolation and cellular metabolism detection. Adv. Funct. Mater. 26, 4016–4025 (2016).

18.Qiao, L. et al. MALDI in-source photooxidation reactions for online peptide tagging. Angew. Chem. Int. Ed. 47, 2646–2648 (2008).
19.Lim, A. Y., Ma, J. & Boey, Y. C. F. Development of nanomaterials for SALDI-MS analysis in forensics. Adv. Mater. 24, 4211–4216 (2012).
20.Wu, K., Chen, J., McBride, J. R. & Lian, T. Efficient hot-electron transfer by a plasmon-induced interfacial charge-transfer transition. Science 349, 632–635 (2015).
21.Brongersma, M. L., Halas, N. J. & Nordlander, P. Plasmon-induced hot carrier science and technology. Nat. Nanotechnol 10, 25–34 (2015).

Acknowledgement
We gratefully thank the financial support from Project 81401542 and 81650110523 by National Natural Science Foundation of China (NSFC), Project 16441909300 by Shanghai Science and Technology Commission. This work is also sponsored by the Program for Professor of Special Appointment (Eastern Scholar) at Shanghai Institutions of Higher Learning (TP2015015).

PS1-01-03

Apatite-forming ability of NaOH-treated Ti-Zr alloys with various compositions

Toshiki Miyazaki[1], Tomoya Hosokawa[1], Ken'ichi Yokoyama[2], Takanobu Shiraishi[3]

[1]Kyushu Institute of Technology, Graduate School of Life Science and Systems Engineering, Kitakyushu, JP; [2]Kyushu Institute of Technology, Faculty of Engineering, Kitakyushu, JP; [3]Nagasaki University, Graduate School of Biomedical Sciences, Nagasaki, JP

Introduction

Titanium (Ti) and its alloys have been popularly used for hard tissue reconstruction. However, there are still challenges to reduce Young's modulus of metallic biomaterials in order to suppress osteoporosis caused by stress shielding. Ti-Zr alloys are expected to show lower Young's modulus than pure Ti. Drawback of metallic biomaterials is that their bone-bonding ability is quite low. Therefore, several kinds of surface modification including apatite coating, NaOH treatment, anodic oxidation and so on have been proposed [1]. In the present study, NaOH treatment was attempted for Ti-Zr alloys with various compositions and bone-bonding ability was assessed *in vitro* by apatite formation in simulated body fluid (SBF).

Experimental Methods

Ti-xZr alloys (x=0 to 100 at mol%) were treated with 5M-NaOH solutions at 60°C for 24 h and washed with ultrapure water. They were then soaked in SBF at pH 7.40 for various periods. Surface structural changes were characterized by scanning electron microscope attached with energy-dispersive X-ray microanalysis (EDX), thin-film X-ray diffraction, electrochemical polarizaion.

Results and Discussion

Figure 1 shows TF-XRD patterns of Ti-Zr alloys treated with 5M-NaOH after soaking in SBF for 7 d. Diffraction peaks of the low-crystalline apatite were detected for the alloys with Zr content of 50 mol% or less, but not higher Zr content. Figure 2 shows adsorption of Ca and P onto the treated metals after soaking in SBF for 7 d. Ca adsorption was significantly suppressed for the alloys with high Zr content. Corrosion current showed tendency to decrease with increase in Zr content, meaning that surface reaction by NaOH treatment is suppressed.

The present results show that apatite-forming ability of Ti-Zr alloys is decreased with increase in Zr content. It is known that the apatite formation on NaOH-treated Ti progresses via Ca adsorption and subsequent P adsorption [2]. Also, Tsutsumi *et al.* documented that zirconium phosphate is favorably formed on pure Zr metal in Hanks' solution [3]. Suppression of Ca adsorption would lead to low apatite-forming ability. On the other hand, Young's modulus of Ti-Zr alloys is reported to become minimum at Ti-60Zr [4]. Therefore, development of surface treatment able to improve the apatite formation on the alloys with high Zr content is needed in future.

Conclusion

Ti-Zr alloys with low Zr content formed the apatite in SBF when they were treated with NaOH solution. The present results provide fundamental information on design of metallic biomaterials with bone-bonding ability and low Young's modulus.

References

[1] T. Kokubo (ed.), *Biocaramics and Their Clinical Applications*, Woodhead Publishing, 2008.

[2] H. Takadama, H.M. Kim, T. Kokubo, T. Nakamura, *J. Biomed. Mater. Res*., **57**, 441-448 (2001).

[3] Y. Tsutsumi, D. Nishimura, H. Doi, N. Nomura, T. Hanawa, *Mater. Sci. Eng. C*, **29**, 1702-1708 (2009).

[4] T. Shiraishi, K. Yubuta, T. Shishido, N. Shinozaki, *Mater. Trans*., **57**, 1986-1992 (2016).

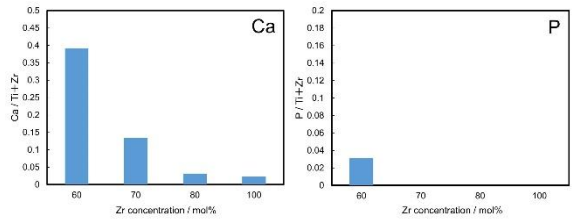

Fig. 2
Adsorption of Ca and P onto the treated metals after soaking in SBF for 7 d.

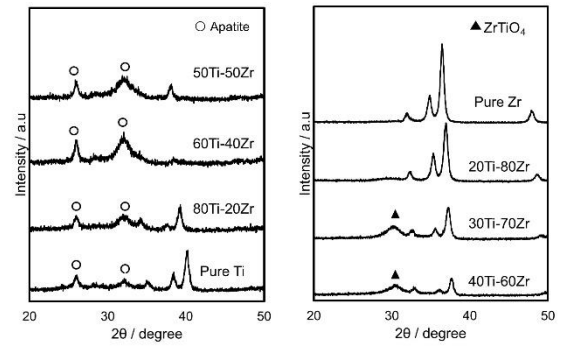

Fig. 1
TF-XRD patterns of Ti-Zr alloys treated with 5M-NaOH after soaking in SBF for 7 d.

PS1-01-04

Dental implant treatment with sinus floor elevation using octacalcium phosphate collagen composite: a case study

Tadashi Kawai[1,2], Shinji Kamakura[3], Keiko Matsui[2], Yushi Ezoe[2], Osamu Suzuki[4], Tetsu Takahashi[2]

[1]Iwate Medical University School of Dentistry, Oral and Maxillofacial Surgery, Morioka, JP; [2]Tohoku University Graduate School of Dentistry, Oral and Maxillofacial Surgery, Sendai, JP; [3]Tohoku University Graduate School of Biomedical Engineering, Bone Regenerative Engineering, Sendai, JP; [4]Tohoku University Graduate School of Dentistry, Craniofacial Function Engineering, Sendai, JP

Introduction

Our previous studies have demonstrated that octacalcium phosphate (OCP) promotes osteoblastic cells differentiation and facilitates bone regeneration in vitro and in vivo[1, 2)]. Also, it has been indicated that OCP and collagen composite (OCP/Col) increases the bone regeneration ability in comparison with OCP alone[3)]. Some animal studies and clinical studies of OCP/Col have been reported and OCP/Col has been recognized as a good bone substitute material[4, 5)]. In this study, we investigated the progress of a patient who received dental implant treatment including bone augmentation using OCP/Col with sinus floor elevation surgery as a clinical trial.

Experimental Methods

OCP was prepared according to a method of synthesis by mixing calcium and phosphate solution. Particle size of OCP was 300 – 500 mm in diameter. OCP/Col was prepared from pepsin-digested atelocollagen isolated from the porcine dermis and OCP. OCP/Col was molded in the shape of a disc, 9 mm diameter, and 1.5 mm thick. The current study was a part of the 'Prospective, Multi-center, Single-arm Study of OCP/Col for Guided Bone Regeneration' clinical trial, which were registeredwith the Medical Information Network in Japan (JPRN-UMIN000018192). The protocol of the clinical trial was approved by the Institutional Review Board of the Pharmaceuticals and Medical Devices Agency in Japan. A 20 years old man came our hospital for dental implant treatment at the first premolar region of left maxilla. As bone augmentation was required for dental implant placement, sinus floor elevation was performed using OCP/Col at the same time as dental implant placement. Micromobility of dental implant body was measured immediately after dental implant placement and at 6 months after placement by the Osstell system (ISQ value). CT examination was performed before operation, at 3, and 6 months after surgery. After that, a final prosthesis was placed and clinical progress was observed.

Results and Discussion

By CT examination, the vertical length from alveolar crest to sinus floor was 5 mm before operation, however, after sinus floor elevation using OCP/Col and dental implant placement, the length became 10 mm at 3, and 6 months after operation. The hard tissue augmented by OCP/Col around the dental implant body was stable and the radiopacity became as same as around host bone. CT value was 361 HU at 6 months and this value was almost same with cancellous bone. The ISQ value was 45 at the dental implant placement, and after 6 months, the value increased 77. After final prosthesis setting, occlusion was reconstructed. There was no infection or other abnormal reactions through the examination.In this study, OCP/Col was applied as a bone substitute material in dental implant surgery as a clinical trial. Although bone augmentation by OCP/Col was performed simultaneously with dental implant placement, the bone formation was confirmed without any abnormal events. It has been suggested that OCP/Col has affinity with a titanium dental implant surface. The prosthesis was set and the occlusion was reconstructed successfully.

Conclusion

This study suggested that OCP/Col could be a candidate as a new bone substitute material for dental implant treatment.

References

1. Suzuki O. *et al*., Tohoku J Exp Med 164: 37-50, 1991.
2. Suzuki O. *et al*., Biomaterials 27: 2671-2681, 2006.
3. Kamakura S. *et al*., J Biomed Mater Res B 79: 210-217, 2006.
4. Kawai T. *et al*., Tissue Eng Part A 20: 1336-1341, 2014.
5. Kawai T *et al*., J Tissue Eng Regen Med 11:1641-1647, 2017.

PS1-01-05

Micro-CT as a key tool in the characterisation of structurally variable collagen scaffolds for cell sieving applications

Jennifer H. Shepherd[1,2], Serena M. Best[1], Ruth E. Cameron[1]

[1]University of Cambridge, Department of Materials Science and Metallurgy, Cambridge, GB; [2]University of Leicester, Department of Engineering, Leicester, GB

Introduction

Structurally variable scaffold structures have been designed so as to not only better mimic native tissue, but also to provide cell sieving capabilities[1]. The partitioning of specific cell types in certain regions of a scaffold template, thus mimicking the cell distribution in the native tissue is hypothesized to optimise the repair and regeneration process.
In order to predict cell-sieving capabilities, it is essential to have a detailed understanding of the scaffold pore structure. Micro-CT is a non-destructive method able to image fine scale internal structure and as such is an obvious characterisation choice for complex three-dimensional structures. A wide variety of analyses are achievable from the data, and it can provide a key predictive tool for the accessibility of pore structures by specific cells, but careful consideration is needed for successful analysis and results may be heavily influenced by a number of key experimental parameters.
This work considers micro-CT as a tool for this characterization and discusses the influence of a key scan parameter, pixel size on the analyses. Whilst tissue engineered scaffolds *in situ* are hydrated, traditional characterisation is carried out in the dry state. A preliminary consideration of the influence of measurements in a hydrated state through the use of phosphotungstic acid contrast agent is also considered.

Experimental Methods

Structurally variable lyophilised collagen scaffolds were produced as described elsewhere[1]. Samples were extensively analysed using a Skyscan 1272 Micro-CT (Bruker, Belgium). 5 mm diameter samples were punched and scanned initially with a pixel size of 1.5 mm (no camera binning applied) and operating voltage of 25 kV. Scanning was also repeated with 2* and 4* camera binning applied (3 mm and 6 mm pixel size respectively) in order to investigate the influence of pixel size on porosity analysis.
Soft tissues are routinely scanned in their hydrated state using phosphotungstic acid as a contrast agent[2] and we have applied a similar protocol for the hydrated scanning of collagen scaffolds. Whole scaffolds were submerged in an aqueous 0.3 wt% solution of phosphotungstic acid and degassed in order to ensure full penetration of the stain. After soaking for 48 hours, samples were thoroughly washed with deionized water with a final degassing step prior to scanning. 8mm diameter samples were scanned hydrated in 2ml Eppendorf tubes with a pixel size of 3 mm, 0.25 mm Al filter, 60 kV operating voltage and frame averaging of 3.
Resulting projections were reconstructed using NRecon (Bruker, Belgium), and systematic volumes of interest (VOIs) selected in top and bottom sections of the scaffold. A three dimensional analysis was carried out in CTAn (Bruker, Belgium) after thresholding and despeckling. Volumes of interests were modified to allow penetration only from the top x-y plane and an interconnectivity analysis carried out using the ROI shrink wrap feature with increasing voxel size. Using the same shrink-wrap process a percolation analysis was also carried out. Volume rendered models were created in CTVox.

Results and Discussion

Whilst individual sections and 3D volume rendered representations scanned at the 3 pixel sizes appeared comparable, a quantitative analysis showed that with a decrease in pixel size from 6 to 1.5 mm, mean pore size decreased from approximately 130 mm to around 85 mm. Calculations of interconnectivity demonstrated decreased accessibility with increased scan pixel size, with the influence on percolation analysis being less straightforward. Whilst percolation theory applied well in the low resolution scans, at smaller pixel size the relationship appeared non-linear. It is hypothesized that perhaps the increased features resolved in higher resolution scans resulted in a structure more complex than can be described by current percolation theory. Further mathematical modelling and analysis could give insight into these effects.

Preliminary scanning of hydrated scaffold with phosphotungstic acid contrast agent showed significant promise (Figure 2). Whilst gross scaffold structure was broadly unaffected, significant strut thickening was observed with some consequential decrease in percentage porosity and interconnectivity.

Conclusion

Whilst micro-CT is a valuable analysis tool for complex scaffolds, scan pixel size should be taken into account with any comparative analysis. The application of phosphotungstic acid as a contrast agent appears an exciting development for imaging hydrated collagen scaffolds and thus getting a better impression of the environment experienced by cells *in vivo*.

References

1 Shepherd, J. H., Howard, D et al. **Biomaterials,** v. 182, p. 135-144, 2018

2 METSCHER, B. **BMC Physiology,** v. 9, p. 11, 2009.

Acknowledgement

The work was supported by the European Research Council [ERC Advanced Grant 320598 3D-E] and EPSRC grant EP/N019938/1.

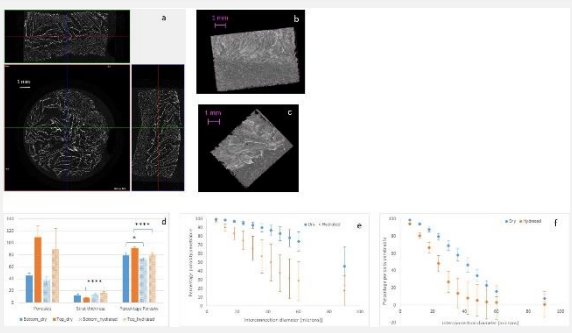

Figure 2: Micro-CT in hydrated state
Figure 2: Hydrated scanning with phosphotungstic acid contrast agent. Clear contrast was achieved as observed in the 3 orthogonal sections (Dataviewer, Bruker, Belgium) (a) and 3D volume rendered models (CTVOX) (b) and (c). Porosity characterisation was compared between the dry and hydrated state at the same scan pixel size with significant variation observed in strut thickness and percentage porosity. Significance values are: ***p<0.0001, ** p<0.001, * p<0.05. A far less open and interconnected structure was reported with hydrated analysis (e) and (f).

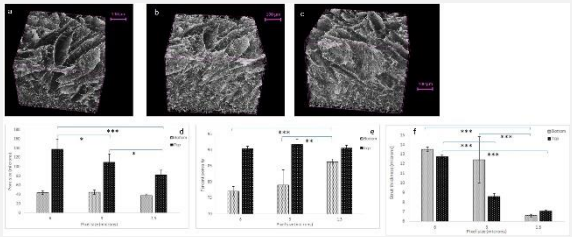

Figure 1: Pixel size influence
Figure 1: Influence of scan pixel size on quality of data and quantitative porosity analysis. Images a, b, and c show 3D volume rendered images (generated in CTVOX) from data collected at 1.5, 3 and 6 um pixel size. Graphs d,e and f demonstrate influence of scan pixel size on pore size, percent porosity and strut thickness. Significance values are: ***p<0.0001, ** p<0.001, * p<0.05

PS1-01-06

Influence of bioactive polymers size grafting on the biological response

Céline Falentin-Daudré, Hamza Chouirfa, Véronique Migonney

University of Paris 13, LBPS-CSPBAT, Villetaneuse, FR

Introduction

Titanium is widely used in orthopedic implants for its excellent resistance to corrosion and its biocompatibility.[1]Nevertheless and despite the prevention rules, 1,5% of implanted prostheses are still subject to bacterial infections. That's the reason why chemical modification of titanium surfaces to confer desirable functional properties is required. Bioactive polymers bearing sulfonate groups such as poly(sodium styrene sulfonate) (polyNaSS) have good antibacterial properties and can improve osseointegration.[2-7]In this context, we have developpedthree different techniques of polyNaSS covalent grafting onto titanium (Ti) surfaces (**Fig.1**) and study the influence of their architecture on biological response.[2-7]Two of them are "grafting from" techniques requiring an activation step either by thermal or UV irradiation.[2-5]The third method is a "grafting to" technique involving an anchorage molecule onto which polyNaSS synthesized by reversible addition−fragmentation chain transfer (RAFT) polymerizationis clicked.[6]The advantage of the "grafting to" technique when compared to the "grafting from" technique is the ability to control the architecture and length of the grafted polymers on the Ti surface and their influence on the biological responses.[6,7]This study compares the effect of three different grafting processes on the *in vitro*biological responses of bacteria and osteoblasts.

Experimental Methods

Grafting from technique:After cleaning, Ti samples were oxidized in a solution containing the same volume of pure $H_2SO_4$and H_2O_2(30%). After oxidation, samples were rinsed thoroughly in distilled water and then placed directly into a mechanically stirred solution of the monomers. After heating (70°C) or UV initiation of the radical polymerization, samples were rinsed thoroughly in distilled water and dried. ***Grafting to technique:****1. Polymers synthesis:*Polymers were synthetized by RAFT polymerization with three different sizes (5, 10, 35 kDa), *2.Grafting procedure:*After cleaning, Ti samples were oxidized and were immersed in an anchor solution. Finally, polymers were clicked on the anchor and Ti samples were rinsed thoroughly in distilled water and dried.

Results and Discussion

With the grafting from technique, Ionic groups (sulfonate) were covalently attached to the titanium surfaces by radical polymerization of sodium styrene sulfonate (NaSS) initiated by radicals issued from titanium peroxide. Immersion of titanium samples in a mixture of pure sulphuric acid and hydrogen peroxide produces on its surface titanium hydroxide and titanium peroxide. The decomposition of titanium peroxide in radicals was been produced by heating or UV irradiations. The "grafting to" procedure was realized in three steps i) Polymers synthesis, ii) coupling with an anchor (dopamine) and iii) adhesion on titanium surface. The RAFT polymerization is used in the first step to synthetize bioactive polymers with a well-defined architecture (5, 10 and 35 kDa). Then, the following step uses a thiol-ene reaction to link the polymers with the anchor. The last step is the adhesion of the dopamine on titanium surfaces. For each techniques, amounts of grafted polymers were measured by colorimetric method. Other techniques were used to check the presence of the bioactive polymers at the surface of titanium samples: XPS

analysis, IR-ATR, Contact angle analysis. The different grafting were evaluated *in vitro*to study the differenciation with Saos-2 cells. The proliferation assay demonstrated that the grafted Ti promoted cell differentiation specifically mineralization. In parallel, antibacterial studies have been conducted with *S. aureus* bacteria and have shown that we have an influence of the polymer size on *the S. aureus*inhibition.

Conclusion

We have described different approaches to graft bioactive polymers with a determined molecular weight onto titanium surfaces. Overall outcomes of this investigation confirmed the significance of the sulfonate functional groups on the biological responses, regardless of the grafting method.[6,7]In addition, results showed that the architecture and distribution of grafted polyNaSS on Ti surfaces alter the intensity of the bacteria response mediated by fibronectin.

References

1. Klabunde Windler M., Titanium in medicine. Berlin: Springer, **2001**, 703-746.
2. Migonney V. et al., Patent WO/2007/141460, **2006**.
3. **Falentin-Daudré C.**, Migonney V., Chouirfa H., Baumann JS., Patent WO/2017/025519, **2016.**
4. Chouirfa C., Migonney V., **Falentin-Daudré C.***,*RCS Advances*, **2016**, *6*, 13766-13771.
5. Chouirfa H., Evans D.M., Castner D.G.C., Bean P., Mercier D., Galtayries A., **Falentin-Daudré C.**, Migonney V.,*Biointerphases*, **2017**,*12*, 02C418.
6. Chouirfa H., Evans D.M., Bean P., Saleh-Mghir A., Cremieux A.-C., Castner D.G.C., **Falentin-Daudré C.**, Migonney V.,*ACS Applied Materials & Interfaces*, **2017**, DOI: 10.1021/acsami.7b14283.
7. Chouirfa H., Bouloussa H., Migonney V., **Falentin-Daudré C.**,*Acta Biomater*, **2019**, 83, 37.

Acknowledgement

The authors would like to thank the University of Paris 13 for providing financial support to this project.

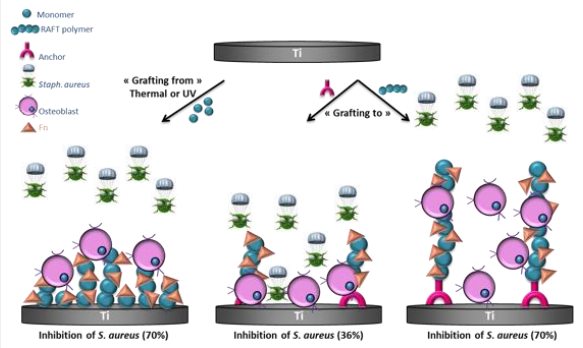

Figure 1: Different techniques to graft bioactive polymer onto titanium surfaces

PS1-01-07

Deformation Behavior of Au-28Cu-22Al Biomedical Shape Memory Alloy Micropillars

Akira Umise[1,2], Kenji Goto[1,3], Tso Fu Mark Chang[1], Masaki Tahara[1], Masato Sone[1], Takao Hanawa[2], Hideki Hosoda[1]

[1]Tokyo Institute of Technology, Institute of Innovative Research (IIR), Kanagawa, JP; [2]Tokyo Medical and Dental University, Institute of Biomaterials and Bioengineering, Tokyo, JP; [3]TANAKA KIKINZOKU KOGYO K.K., Kanagawa, JP

Introduction

The commercial shape memory alloy Ti-Ni is widely used as biomedical application recently, for instance, intravascular stents, orthodontic wires and catheters. Nevertheless, the toxicity of Ni resulting a damage against human body, e.g. metallic allergy, becomes an intrinsic problem in clinical research. Au-based shape memory alloys have a large potential to apply in biomedical devices since they exhibit good biocompatibility and excellent X-ray radiography [1]. Our research group has been developing AuCuAl shape memory alloys with good mechanical properties. It was found that, in case of AuCuAl polycrystalline materials, the mechanical properties and phase transformation depend on the chemical composition. In addition, the ductility greatly decreases when the martensitic transformation temperature is below the room temperature [2]. Nowadays, the demand of micro-biomedical devices with micrometer-order dimension is increasing. Such micro devices are so small that their material properties can be considered as similar to single crystal. Therefore, the mechanical properties of AuCuAl single crystal micro materials are necessary to be clarified. Then, the aim of this study is to clarify the mechanical properties of AuCuAl in micro-scale. An AuCuAl single crystal micropillar was fabricated by focused ion beam (FIB). The shape memory and superelastic behavior are discussed.

Experimental Methods

50Au-28Cu-22Al (mol%) alloy ingot was fabricated by arc melting under the argon atmosphere. The ingot was homogenized at 873K for 21.6ks and solution-treated at 773K for 3.6ks followed by water quenching. Phase constituent and martensitic transformation temperatures were characterized by θ-2θ X-ray diffraction measurement and differential scanning calorimetry (DSC), respectively. A micropillar specimen with the size of 20×20×40μm was fabricated using focused ion beam after the identification of crystallographic orientation by electron backscattered diffraction. Mechanical property at various temperatures (298K-373K) was evaluated by a micro compression test machine. The details of the micro compression test machine are described [3]. After the compression test, the specimen was observed by scanning electron microscope (SEM).

Results and Discussion

Figure 1 shows the stress-strain curve obtained by the compression test at room temperature (RT). Perfect superelastic shape recovery in addition to more than 5% compressive deformation was obtained in the single crystal with a compression direction close to <001>, while the polycrystal specimen exhibited imperfect superelasticity with 2%. Figure 2 shows SEM images of before and after compression at RT. After unloading the specimen was heated and the shape recovery was observed. At the temperatures of RT to 333K, superelasticity was observed. The plastic deformation occurred at 343 K or higher temperature. Based on the mechanical tests, the stress inducing martensitic transformation depended on a temperature and it can be explained by a Clausius-Clapeyron type equation. The

slope between stress induced martensitic transformation and test temperature evaluated was 1.05 MPa/K. This result is in good agreement with the calculated value using the lattice deformation strain and transformation enthalpy.

Conclusion

1. The perfect superelastic shape recovery in addition to more than 6% compressive deformation was obtained in the single crystal with a compression direction close to <001>
2. The stress for inducing martensitic transformation of the AuCuAl single crystals obeyed the Clausius-Clapeyron-type equation.

References

1. I. M. Wolff et al., Endeavour, 1995, 19(1), 16-19
2. H. Hosoda et al., J. Japan Inst. Met. Mater., 2016, 80(1), 27-36
3. G.P. Zhang et al., Mater. Sci. Eng., 2006, A426, 95-100

Acknowledgement

This study is supported by Grant-in-Aid of Scientific Research (S) (S 26220907), Early-Career Scientists (18K13655) from JSPS, and MEXT funds of Research Center for Biomedical Engineering and interdisciplinary and international project for development of advanced life-innovative materials and human resources.

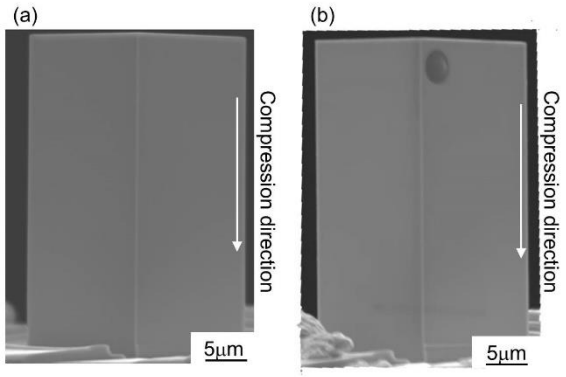

Figure 2 SEM images of AuCuAl micropillar: (a) before and (b) after compression at RT.

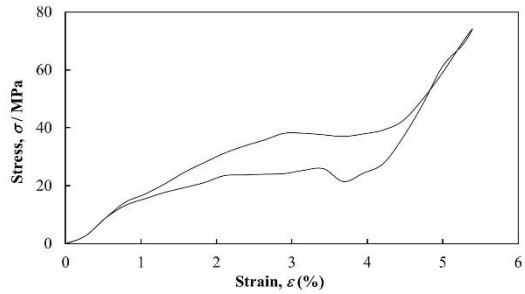

Figure 1 Stress-strain curve by micro compression test at RT.

PS1-01-08

Cytotoxicity of iron nitride nanoparticles for biomedical applications

Misaki Shibata[1], Hiroyasu Kanetaka[2], Maiko Furuya[2], Kotone Yokota[2], Tomoyuki Ogawa[3], Masakazu Kawashita[1]

[1]Tohoku University, Graduate School of Biomedical Engineering, Sendai, JP; [2]Tohoku University, Graduate School of Dentistry, Sendai, JP; [3]Tohoku University, Graduate School of Engineering, Sendai, JP

Introduction

Magnetic nanoparticles have been studied in the field of biomedicine for use in magnetic separation, as contrast medium for magnetic resonance imaging, as carriers for drug delivery and as thermal seeds for magnetic hyperthermia. For those diagnostic and therapeutic methods, magnetite has been mainly studied because of its magnetic properties and biocompatibility. Iron nitride, especially $Fe_{16}N_2$, is known to have excellent magnetic properties with high saturation magnetization (M_s) and coercive force. Therefore, it has been studied as a candidate material for memory devices and rare-earth-free permanent magnets, and more recently, synthesis methods of nanoparticles have been established. Since its reported M_s of 162-240 emu/g is much higher than that of magnetite, 67-92 emu/g, it might be useful in diagnostics and therapeutics mentioned above. Therefore, in this study, as the first step to reveal its biocompatibility, cytotoxicity of iron nitride nanoparticles against rat fibroblasts (Rat-1 cells) was evaluated and compared with that of magnetite nanoparticles, which have been already in use as biomaterials.

Experimental Methods

Magnetite nanoparticles a few dozen nanometers in size were synthesized by following the previous studies[1]. Iron nitride nanoparticles were obtained by reducing and nitriding them under H_2 and NH_3 gas flow. Those magnetite and iron nitride nanoparticles were autoclaved (AC; 121 ^oC, 20 mins) and dried at 60 ^oC for 12 hrs. $1.6x10^4$ cells/well Rat-1 cells were seeded in 24-well plates and incubated in Dulbecco's modified eagle's medium (DMEM) for 24 hrs. The medium were replaced with DMEM containing the AC nanoparticles at concentrations of 10, 50, and 100 µg/mL, and with normal DMEM as control. To evaluate the cytotoxicity, MTT assay and Trypan blue exclusion test (TB test) were done after incubation of 1 and 3 days. The crystal phases and magnetic properties of the nanoparticles before and after AC were investigated using an X-ray diffractometer and a vibrating sample magnetometer.

Results and Discussion

Iron nitride nanoparticles consisted of only $Fe_{16}N_2$ were obtained, and the sample showed M_s of 166 emu/g. After AC, magnetite partially precipitated and M_s decreased to 145 emu/g, which was still much higher than that of magnetite nanoparticles synthesized (88 emu/g). Figure 1 shows cell viability determined by MTT assay after 1 and 3 days. After 1 day, cell viability decreased as the concentration of the nanoparticles increased. Both magnetite nanoparticles and iron nitride nanoparticles at the highest concentration showed significant differences in the cell viability compared to the control. However, after 3 days, there were no significant differences in the cell viability. The cell mortality determined by TB test showed the similar tendency. It is suggested that these nanoparticles were not cytotoxic and did not cause critical decrease in cell proliferation though they caused cell death at the high concentrations. Moreover, both after 1 and 3 days, there were no significant differences between magnetite nanoparticles and iron nitride nanoparticles at the same concentrations. It is suggested that there is no difference in cytotoxicity against Rat-1 cells between magnetite nanoparticles and iron nitride nanoparticles at concentration of 100 µg/mL or lower.

Conclusion

After AC, though magnetite partially precipitated, iron nitride remained as the main phase and showed high M_s of 145 emu/g. In MTT assay and TB test, no differences were observed in cytotoxicity against Rat-1 cells between magnetite nanoparticles and iron nitride nanoparticles. It is suggested that iron nitride nanoparticles might be useful as biomaterials with excellent magnetic properties.

References

1. Z. Li et al., Mater. Sci. Eng., C 30 (2010) 990-996.

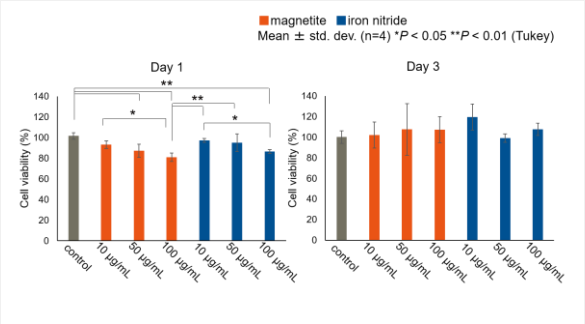

Fig. 1
Cell viability determined by MTT assay after 1 and 3 days.

PS1-01-09

Fe^{2+} Effect on Functionalization of Polycaprolactone for Anterior Crucial Ligament Applications

Tuan N. Nguyen, Amelie Leroux, Andre Rangel, Veronique Migonney

Paris 13 University, LBPS-CSBAT, Villetaneuse, FR

Introduction

In the recent years, the advantages of using polycaprolactone (PCL) in the field of tissue engineering have been rediscovered mainly for its slow degradation and the absence of inflammatory response during this process when compared to poly(lactic acid) and poly(glycolic acid).[1,4] Based on the good results of poly(sodium styrene sulfonate) (pNaSS) grafted poly(ethylene terephthalate) for anterior cruciate ligament prosthesis, the functionalization of PCL surfaces was investigated with the aim of combining the strong improvement of the in vitro and in vivo biological responses provided by the sulfonate groups with the controlled biodegradation of the support polymer.[2] To enhance pNaSS grafting on PCL, Mohr's salt or ammonium iron(II) sulfate ($(NH_4)_2Fe(SO_4)_2 \cdot 6H_2O$ can be used as a catalyst.[1] Iron(II) in the form of Mohr's salt, plays a role in peroxide decomposition through redox reaction of Fe^{2+}/peroxide and indirectly generates free radicals on an activated polymer, a key step of grafting from the process.[3] However, the effects of Mohr's salt reactions and byproducts on cell response and surface characterization need further studies.

Experimental Methods

Sodium 4-styrenesulfonate grafting on PCL was performed according to the process developed Migonney et al. The surfaces were activated by ozonation prior to NaSS polymerization. Mohr's salt (concentration range from 0.025 % to 0.25 % w/v) was dissolved in degassed aqueous NaSS solution. Activated were soaked on this solution and kept at 45 °C for 1 h. Grafted and non-grafted PCL surfaces were characterized by infrared spectroscopy (FTIR), scanning electron microscopy (SEM-EDX) and atomic force microscopy (AFM). A survival rate of primary sheep ACL fibroblasts over grafted PCL films was analyzed.

Results and Discussion

The presence of Mohr's salt highly improved the efficiency of pNaSS grafting, reaching 75 µmol/g against 10 µmol/g without a catalyst. The sulfur signal was identified by FTIR and EDX. The roughness of PCL surface was significantly changed after grafting. Surfaces grafted with 0.025 % w/v of Mohr's salt presented greater cell viability, however, for high concentrations byproducts (for example Fe^{3+}) harmed primary sheep ACL fibroblast. In addition, the redox reaction of iron(II) causes degradation of the PCL surfaces.

Conclusion

Mohr's salt enhanced significantly pNaSS grafting rate and ensures cell viability over pNaSS grafted PCL surfaces. Nevertheless, for values higher than 0.025 % w/v the Mohr's salt reaction damages the polymer and releases byproducts leading to decrease of cell survival rate.

References

[1] Rohman G., Huot S., Vilas-Boas M., Radu-Bostan G., Castner DG., Migonney V., J Mater Sci Mater Med, Volume 26, 206, 2015.

[2] Ciobanu M., Siove A., Guegen V., Gamble L. J., Castner D. G., and Migonney V., Biomacromolecules, Vol 7, 755-760, 2006.

[3] Fujimoto K., Takebayashi Y., Inoue H., and Ikada Y., Journal ò Polymer Science: Part A: Polymer Chemistry, Vol 31, 1035-1043

[4] Woodruff M. A., Hutmacher D. W., Progress in Polymer Science, Volume 35, 1217–1256, 2010.

Acknowledgement

This study is granted by BPI PSPC application “LIGA2BIO project”.

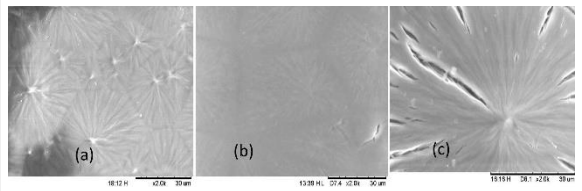

SEM images of pNaSS grafted polycaprolactone film surface
(a) Grafted PCL film without Mohr's salt (b) grafted PCL film with 0.025 % w/v Mohr's salt (c) grafted PCL film with 0.25 % w/v Mohr's salt

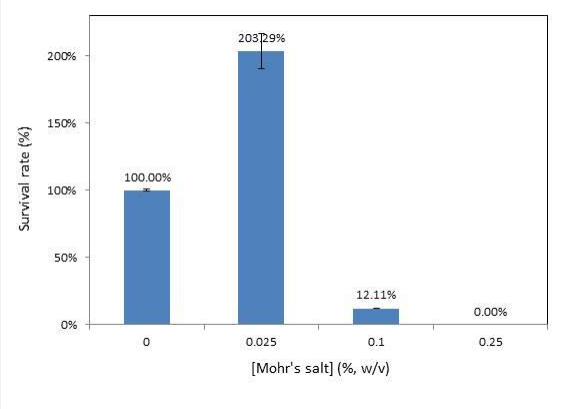

Survival rate of primary sheep ACL fibroblasts on grafted PCL films

PS1-01-10

Turbulent Flow Feature Characteristics through Multi Vessel Model with 50% Stenotic Lesion

Hoseong Ji[1], Byubghui Kim[2]

[1]Pusan National University, MEMS Technology Centre, Busan, KR; [2]Pusan National University, Aerospace Engineering, Busan, KR

Introduction

Because of modern dietary life, cardiovascular disorder including stenotic lesion on coronary artery rapidly increase in Western countries and Developing countries. According to the WHO statistics, circulatory disorders including ischemic heart disease and stroke are the most important cause of sudden death. From this sense, the hemorheologic and hemodynamic characteristics of human blood passing through circulation networks have recently been receiving great attention in various interdisciprinaly research fields.

From the clinical point of view, detailed flow feature through multi-vessel stenotic lesion placed on coronary artery may provide a great interesting to the internal clinician related with interventional procedure.

We would like to provide the detailed 3-deimensional flow structures on simplified multi-vessel model based on angiogram through Commercial CFD Analysis

Experimental Methods

To investigate the detailed flow structure on simplified multi-vessel model based on angiogram from University Hospital, commercial CFD analysis (CFD-ACE R18) was employed in this study. Sinusoidal pulsatile flow condition was employed as the inlet condition of the flow media.

The angiogram employed in this study was simplified and smoothed for CFD analysis.

By using simplified multi-vessel model based on clinical angiogram, geometrical model was constructed and grid was generated.

Results and Discussion

Figure 1 shows the grid generation on simplified multi-vessel model.

The mesh was combined with structured and unstructured grid.

The detailed turbulent flow fields can be provided as Figure 2.

From Fig. 2, vortex spread feature through multi vessel stenotic model can be investigated.

Conclusion

CFD analysis was carried out with respect to the Reynolds Number variances.

As shown Fig 2, complicated vortex structure related with stenosis growth can be investigated.

To provide the responsibility experimental methods employed PIV experiments will be also carried out near future at same model and same flow condition.

References

1. Ayala KA, Ariel JJ, David E (1999), *American Journal of Physiology*, **276**: H2204-H2214
2. Hong HJ et al. (2017). *Journal of Visualization*, **20**: 833-845.
3. Huh, HK. (2016) *Journal of Biomechanics*, **13**: 2960-2967

Acknowledgement

This work was supported by the Korea Research Foundation Grant (National Research Foundation of Korea) with funding from the Korean Government (2018R1D1A1B07048173).

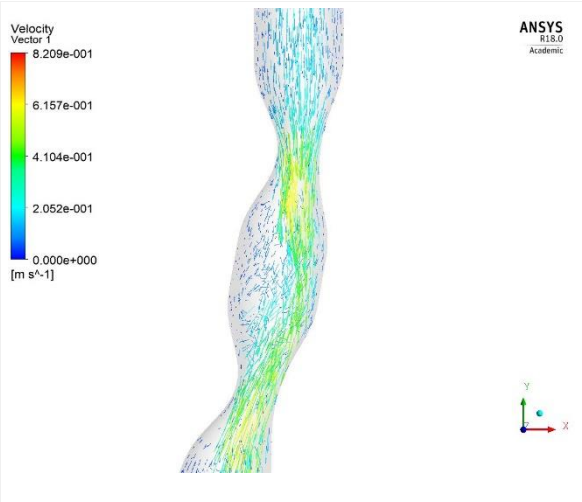

Figure 2 Turbulent Flow Fields through Multi Vessel Model

Turbulent Flow Fields through Multi Vessel Model with 50% Sinusoidal Stenotic Lesions

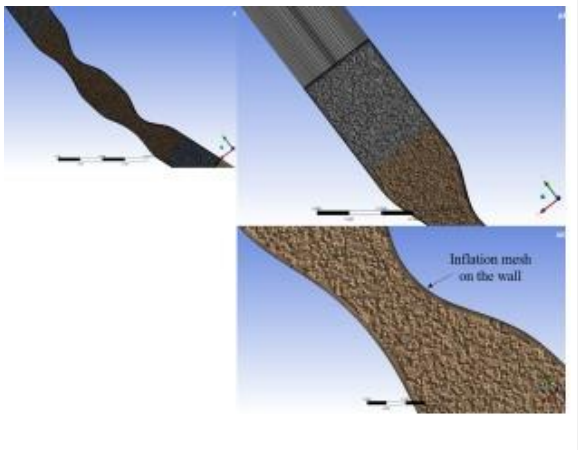

Figure 1. Grid Generation on multi-vessel model

Grid Generation on multi-vessel model with 1,240,000 Nodes and 3,170,000 Elements

PS1-01-11

Apatite-forming ability and visible light-enhanced antibacterial activity of copper- or silver-doped titanium

Masakazu Kawashita[1], Kanae Suzuki[1], Misato Iwatsu[2], Takayuki Mokudai[3], Hiroyasu Kanetaka[2]

[1]Tohoku University, Graduate School of Biomedical Engineering, Sendai, JP; [2]Tohoku University, Graduate School of Dentistry, Sendai, JP; [3]Tohoku University, Institute for Materials Research, Sendai, JP

Introduction

Dental implants with antibacterial activity are desired to be developed to reduce a risk of peri-implantitis. When titanium (Ti) is soaked in sodium hydroxide (NaOH) solution and heated, sodium titanate ($Na_2Ti_9O_{19}$) and titanium oxide (TiO_2) are formed on its surface and thus surface-modified Ti bonds to living bone (it shows bioactivity). Many attempts have been conducted to dope antimicrobial metals on bioactive Ti by soaking in antimicrobial metal-containing solution in prior to the heat treatment. On the other hand, some antimicrobial metal can induce visible light-induced photocatalytic activity on TiO_2. If such antimicrobial metal is successfully doped on the surface-modified Ti, we can expect the antibacterial activity by antimicrobial metal itself as well as by visible light-induced photocatalytic activity of metal-doped TiO_2. Therefore, dental implants with metal-doped TiO_2 surface layer can reduce the risk of peri-implantitis by irradiation of visible light such as teeth whitening LED. In this study, Ti samples doped with copper (Cu) or silver (Ag) was prepared, and their apatite-forming ability in simulated body fluid (SBF), metal-releasing behavior, antibacterial activity against *Escherichia coli* (*E. coli*) in dark place or under visible light irradiation, and generation of reactive oxygen species (ROS) from samples under visible light irradiation were investigated.

Experimental Methods

Commercially pure titanium plate was soaked in 5M-NaOH solution at 60ºC for 24 h and then soaked in 1mM-$Cu(NO_3)_2$ or $AgNO_3$ solution at 80ºC for 48 h. Thus treated titanium plate was heated at 600ºC for 1 h. Samples were soaked in SBF at 36.5ºC for 7 days. Surface structure of samples before and after soaking in SBF was investigated by scanning electron microscope (SEM), thin-film X-ray diffractometer (TF-XRD) and X-ray photoelectron spectrometer (XPS). Antibacterial test of samples against *E. coli* under visible light was conducted according to JIS R 1752:2013. Generation of radicals from samples irradiated with visible light was measured by electron spin resonance (ESR) and hydrogen peroxide (H_2O_2) colorimetric determination using xylenol orange was conducted.

Results and Discussion

Figure 1 shows SEM photographs of samples before and after soaking in SBF. Network structure of anatase and rutile-type TiO_2 containing small amounts of Cu (5.45 atom%) or Ag (2.32 atom%) was formed on Cu- or Ag-doped samples and small silver particles (indicated by white arrows in Fig. 1) were formed on Ag-doped sample. Both samples formed apatite in SBF for 7 days, suggesting that they have a potential to bond to living bone in vivo, but the apatite-forming ability of Ag-doped sample was better than that of Cu-doped sample. According to TF-XRD and XPS measurements, doped silver took a form of Ag and Ag_2O, and copper took a form of Cu and CuO.

Figure 2 shows visible bacteria count of *E. coli* on samples with or without irradiation of visible light. Proliferation of *E. coli* was remarkably inhibited on samples with the irradiation of visible light. According to ESR measurement, hydroxyl radicals (·OH) were detected for samples irradiated with visible light, and some radicals containing carbon were further detected for Cu-doped samples although the generation mechanism is not clear. Generation of H_2O_2

was also confirmed for both samples under visible light irradiation, but there was no significant difference in the amount of generated H_2O_2 between Cu-doped sample and Ag-doped sample. These results indicate that Cu-doped and Ag-doped titanium can show antibacterial activity not only by antimicrobial metals but also by visible light-induced photocatalytic activity of Cu- or Ag-doped TiO_2 when they are irradiated by visible light. Further, the generation of carbon-containing radicals might be responsible for the antibacterial activity of Cu-doped titanium under irradiation of visible light.

Conclusion

We prepared Cu- or Ag-doped titanium by chemical and thermal treatments. Thus Cu- or Ag-doped titanium showed apatite-forming ability in SBF, suggesting that they can bond to living bone. Both Cu-doped titanium and Ag-doped titanium showed excellent antibacterial activity under visible light irradiation. Such surface-modified titanium can provide novel dental implants with visible light-induced antibacterial activity as well as bone-bonding ability.

Acknowledgement

This work was partially supported by JSPS KAKENHI [grant numbers 16H03177] from the Ministry of Education, Culture, Sports, Science, and Technology, Japan.

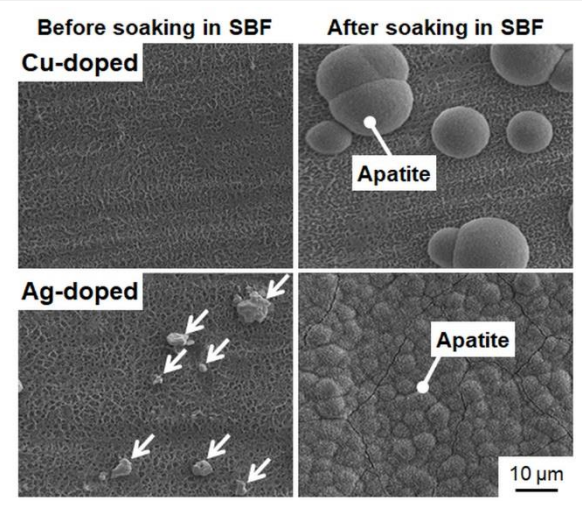

Apatite-forming abiity of samples in SBF
Figure 1 SEM photographs of samples before and after soaking in SBF.

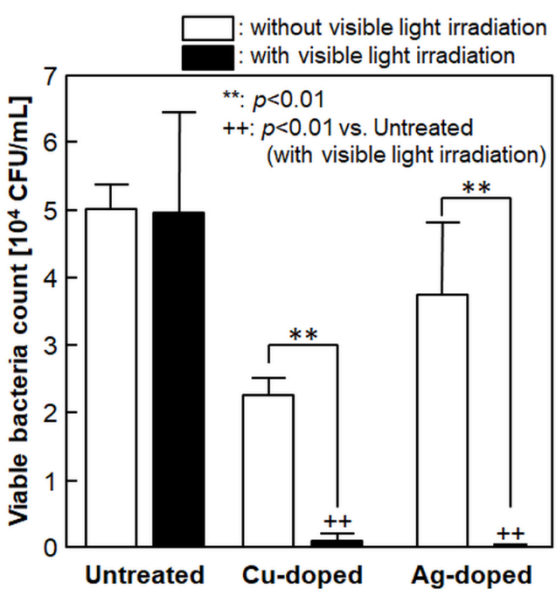

Antibacterial activity of samples
Figure 2 Visible bacteria count of *E. coli* on samples with or without irradiation of visible light.

PS1-01-12

Novel Titanate Conversion of DC Magnetron Sputtered Titanium Thin Film Coatings For Biomedical Applications

Matthew D. Wadge, Burhan Turgut, Reda M. Felfel, Ifty Ahmed, David M. Grant

University of Nottingham, Mechanical, Materials and Manufacturing Engineering, Nottingham, GB

Introduction

The current process for improving implant surfaces to be bioactive, therefore, providing a more natural fixation, is reliant on high temperature (>1500 K[1]) plasma spraying of hydroxyapatite (HA). However, these surfaces have been shown to spall due to their brittle nature, high internal stresses and weak mechanical adhesion[2, 3]. Bioactive titanate surfaces have been developed as an alternative since the mid-1990s by Kokubo *et al.*[4], however, their applicability are limited to titanium (Ti) and its alloys only *via* chemical conversion routes. A novel method was proposed in this study for generating nanoporous titanate surfaces on alternative biomedical materials through conversion of DC magnetron sputtered Ti thin coatings.

Experimental Methods

Stainless steel disks of 10 mm diameter (316L; >99.9% purity; Smiths Metals Ltd., Nottingham) were polished using SiC paper sequentially from P240 to P4000 grit, followed by colloidal silica polishing (0.06 µm particles size) on MD-Chem polishing pads. Polished fused silica glass discs were used for cross-sectional SEM analysis. The disks were cleaned and sonicated for 10 min in acetone, followed by IMS, before being loaded into a TEER UDP-650 magnetron sputtering rig. The disks were then sputtered with titanium (Ti) from a Ti target (Miba Coatings; >99.5% purity; 175 x 380 mm), using a 2.38 Wcm^{-2} target power density; a substrate bias from zero to -100 V and temperatures of up to 150 ^{o}C, were also used to increase coating density. The samples have been labelled according to the following convention: target current (A)/negative substrate bias (V)/applied substrate temperature (^{o}C), e.g. 5A/100V/150^{o}C for 5 A target current, -100 V bias, 150 ^{o}C applied temperature. A graphical representation of the preparation process is displayed in *Figure 1*.

The produced coatings were then treated in NaOH (5 M; 60 ^{o}C; 24 h) to assess the conversion of the films into sodium titanate structures, and how the sputtering parameters and, therefore, crystal orientation, structure factor and density affect this conversion (*Figure 1*). Material characterisation included SEM (15 kV, 10 mm WD; JEOL 7100F FEG-SEM) to obtain topographical alteration, with EDX (15 kV, >250,000 counts; JEOL 7100F FEG-SEM), XPS (VG ESCALab Mark II X-ray photoelectron spectrometer), and Raman (HORIBA Jobin Yvon LabRAM HR spectrometer) to assess elemental and molecular properties. XRD (Cu Kα, λ = 1.5406 Å, 40 kV, 35 mA; range = 20-60^{o} 2θ; step size = 0.015^{o}; 1.2^{o} glancing angle; dwell time = 16 s) and texture coefficient calculations using the Harris equation[5] were used to understand the crystallographic nature and orientation of the coatings produced.

Results and Discussion

SEM micrographs (*Figure 2A*) demonstrated the production of 3.89 ± 0.04, 3.90 ± 0.03 and 3.71 ± 0.04 µm Ti coatings for the 5A/0V, 5A/100V, and 5A/100V/150^{o}C samples, respectively. Through application of a substrate bias (100 V), and bias in conjunction with substrate heating (100 V/150 ^{o}C), the density of the films increased (as attributed through the reduction in coating thickness and surface voids). Furthermore, as characterised through texture coefficient calculation (*Figure 2C*) of the XRD data (*Figure 2B*) using the Harris equation (*Figure 2C Insert*), the films shifted

from columnar (preferred orientation in the Ti HCP (002) plane (PDF 00-044-1294); Texture coefficient ($T_{c(002)}$ = 3.33) in the unbiased sample, to more equiaxed ($T_{c(002)}$ = 1.98; for pure equiaxed, T_c = 1) in the 5A/100V/150°C sample, as determined *via* XRD (*Figure 2B*). Upon subsequent titanate conversion, the sodium titanate layers for the samples produced at 5A/0V, 5A/100V, and 5A/100V/150°C were 1.12 ± 0.04, 1.20 ± 0.02, and 1.20 ± 0.03 µm in thickness, respectively.

Despite the proposed hypothesis that increased porosity would allow better penetration of NaOH and, therefore, increase conversion through reaction between NaOH and the passivated TiO_2 layer, this was not observed in the samples tested. Titanate conversion and Na inclusion were both assessed using EDX (*Figure 2A Insert*), XPS and Raman (both not shown), showing incorporation of 7.6 ± 0.1, 8.9 ± 0.1, and 11.5 ± 1.8 at.% of Na in the 5A/0V, 5A/100V, and 5A/100V/150°C samples, respectively. Raman spectroscopy in conjunction with XPS confirmed bonds associated with titanate structures, demonstrating the ability to convert magnetron sputtered Ti into titanate.

Conclusion

Overall, the data presented demonstrates the successful conversion of DC magnetron sputtered Ti coatings into titanate structures, with increased Na inclusion for the unbiased (7.6 at.%), biased (8.9 at.%), and biased/heater runs (11.5 at.%), respectively. The hypothesis that increased penetration in the more porous unbiased film was not evidenced, however, clear structural differences in the film produced have an effect on Na inclusion and titanate morphology of the conversion layer.

References

[1] Y. Tsui, C. Doyle, T. Clyne, Plasma sprayed hydroxyapatite coatings on titanium substrates Part 1: Mechanical properties and residual stress levels, Biomaterials 19(22) (1998) 2015-2029.

[2] K. De Groot, R. Geesink, C. Klein, P. Serekian, Plasma sprayed coatings of hydroxylapatite, Journal of Biomedical Materials Research Part A 21(12) (1987) 1375-1381.

[3] T.J. Callahan, J. Gantenberg, B.E. Sands, Calcium phosphate (Ca-P) coating draft guidance for preparation of Food and Drug Administration (FDA) submissions for orthopedic and dental endosseous implants, Characterization and performance of calcium phosphate coatings for implants, ASTM International1994.

[4] T. Kokubo, S. Yamaguchi, Bioactive titanate layers formed on titanium and its alloys by simple chemical and heat treatments, The Open Biomedical Engineering Journal 9(1) (2015).

[5] G. Harris, X. Quantitative measurement of preferred orientation in rolled uranium bars, The London, Edinburgh, and Dublin Philosophical Magazine and Journal of Science 43(336) (1952) 113-123.

Acknowledgement

This work was supported by the Engineering and Physical Sciences Research Council [grant numbers EP/K029592/1, EP/L022494/1]. The authors would also like to gratefully acknowledge the Nanoscale and Microscale Research Centre (nmRC) at the University of Nottingham for SEM, FEG-SEM and Raman access.

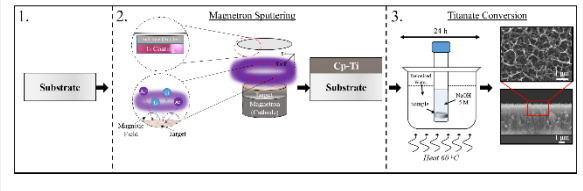

Figure 1. Graphical abstract of titanate conversion methodology.

Figure 1. Graphical representation of titanate conversion of ca. 4 µm DC magnetron sputtered Ti coatings.

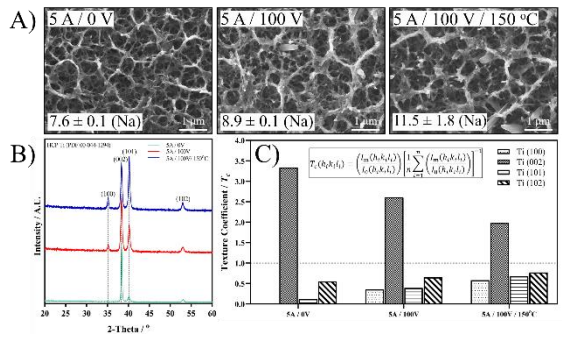

Figure 2. A) SEM and Na EDX (Insert) results. B) XRD spectra. C) Texture coefficient data.
Figure 2. A) SEM micrographs and Na EDX inclusion (Insert) in the titanate converted samples. B) XRD spectra of pre-converted samples. C) Texture coefficient calculations using the Harris equation (Insert) to assess preferred orientation of pre-converted samples.

PS1-01-13

Strategies in tribological model system testing with biological and biomimetic materials

Florian Rummel[2], Kartik S. Pondicherry[1], Tobias Nill[2]

[1]Anton Paar GmbH, Graz, AT; [2]Anton Paar Germany GmbH, Ostfildern, DE

Introduction

Various tribosystems can be found in scenarios related to the human body (see Fig. 1). On the one hand, there are tribosystems consisting of biological counterfaces such as the tongue-palate tribopair [1], articular joints, or the eyelid sliding against the cornea, and on the other hand, there a medically engineered products which come into contact with biological tissues such as implants or catheters.

Knowing about the tribological behavior of such systems can be beneficial for questions like:

- How to correlate tribological data and sensory perception of food, cosmetics, etc.
- How to characterize the effects of pharmaceutical products such as eye drops, artificial synovial fluid, etc., on the frictional behavior at biological counterfaces
- How to improve medical devices and implants in terms of product optimization and safety [2]

Experimental Methods

The real-world tribosystems often show a complex structure but can be abstracted and simplified for testing at model scale. The tests can be carried out with real biological tissues, articular cartilage for instance, or with synthetic substitutes such as artificial skin, Polydimethylsiloxane (PDMS), as well as with medically engineered materials. Most biotribological scenarios are characterized by low speeds and relatively low contact pressures.

Results and Discussion

The authors here present a methodology for model system testing at low loads and low speeds to approach the above mentioned questions. Results from tribological measurements are presented in the form of extended Stribeck curves [1] and breakaway torque measurements.

Conclusion

The contribution also covers how to choose between biological and artificial specimen and how to fix them in the Tribometer with special adapters.

References

[1] Pondicherry, K. S. et al., Extended Stribeck Curves for Food Samples, Biosurface and Biotribology, 1, 2018, 34-37

[2] Rummel, F. et al., A Methodology for the Tribological Characterization of Hydrogel-Coated Catheters for Cardiovascular Applications, Tribologie und Schmierungstechnik, 6, 2018, 36-43

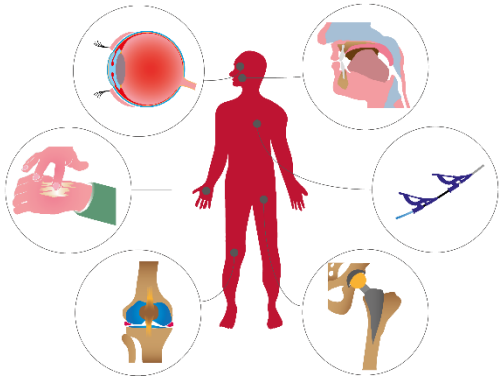

The human body from a tribological point of view
Fig.1 Tribology can be a key to understand sensory perception (e.g. food and cosmetics) but also to optimize medical products (ophthalmic and orthopedic applications, catheters).

PS1-01-14

A sacrificial anode system with enhanced antimicrobial effects and osteo-promotive activity

Christina Sengstock[1], Marina Breisch[1], Alexander Rostek[2], Kevin Pappert[2], Kateryna Loza[2], Christian Rurainsky[3], Kristina Tschulik[3], Matthias Epple[2], Marc Heggen[4], Thomas A. Schildhauer[1], Manfred Köller[1]

[1]BG University Hospital Bergmannsheil Bochum, Surgical Research, Bochum, DE; [2]University of Duisburg-Essen, Inorganic Chemistry and Center for Nanointegration Duisburg-Essen, Essen, DE; [3]Ruhr University Bochum, Faculty of Chemistry and Biochemistry, Electrochemistry and Nanoscale Materials, Bochum, DE; [4]Research Center Jülich GmbH, Ernst Ruska-Centre (ER-C) for Microscopy and Spectroscopy with Electrons, Jülich, DE

Introduction

The inhibition of the initial bacterial implant colonization by supportive antimicrobial agents such as silver (Ag) is a strategy to reduce implant-related infections. A rapid and time-limited oxidative Ag ion (Ag^+) release can be achieved by Ag nanoparticles (AgNP) due to their high specific surface area. A further promising approach to enhance Ag^+ release based on the sacrificial anode principle is the combination of Ag with an electrochemically more noble metal, such as platinum (Pt). Generally, the sacrificial anode effect occurs when two electrochemically different metals exist in an electrolytic environment – the less noble metal protects the more noble one by corroding. Previously we demonstrated the efficiency of a sacrificial anode system composed of thin metal films dotted with Ag [1].
Here, we compare the potency of a physical mixture of AgNP and PtNP to pure AgNP by analysis of NP dissolution, antimicrobial activity towards *Staphylococcus aureus(S. aureus)* and *Escherichia coli(E. coli)* and the biological effects on human mesenchymal stem cells (hMSC).

Experimental Methods

Poly(N-vinylpyrrolidone)-coated spherical AgNP and PtNP (diameter 5-10 nm) were synthesized by reducing $AgNO_3$ and H_2PtCl_6 with $NaBH_4$ or citrate/tannin. NP were characterized using atomic absorption spectroscopy, differential centrifugal sedimentation and transmission electron microscopy in combination with energy-dispersive X-ray spectroscopy.
The antimicrobial activity of the NP was analyzed using standard microdilution techniques by determination of the minimum inhibitory concentration (MIC) and the minimum bactericidal concentration (MBC). The viability of hMSC exposed to NP was accessed by calcein-AM staining and real-time cell tracking (CytoSmart, Lonza). Osteogenic differentiation of hMSC was analyzed using Alizarin Red staining and the AttoPhos assay. Dissolution experiments, spectrophotometry and electrochemistry were used to analyze the Ag^+ release.

Results and Discussion

A physical mixture of 50 wt% AgNP and 50 wt% PtNP showed significantly enhanced antimicrobial effects against *S. aureus* and *E. coli* (Figure 1A) as well as enhanced toxicity towards hMSC compared to pure AgNP at same total Ag concentration. The toxic effects of the physical mixture occurred within minutes of incubation and were therefore substantially faster than for pure AgNP. Since pure PtNP induced no toxic effects at the used concentrations, an electrochemically induced enhancement of Ag^+ release from AgNP in the presence of PtNP was assumed and confirmed by dissolution experiments, spectrophotometry and cyclic voltammetry. Significantly, for the first time to our knowledge we additionally identified an osteo-promotive effect of pure PtNP on hMSC. As was confirmed by Alizarin Red staining and the AttoPhos assay, osteogenic differentiation of hMSC was significantly enhanced in the presence of PtNP (Figure 1B, 1C).

Conclusion

In conclusion, these findings might be useful for the development of multifunctional biomaterial coatings using AgNP and PtNP. On the one hand, the sacrificial anode effect of PtNP on AgNP results in a time-limited Ag^+ burst, providing a sufficient antimicrobial activity at low total silver amount. On the other hand, the remaining Pt after Ag dissolution exhibits osteo-promotive activity. Thereby, such coatings would have the advantages of antimicrobial activity concomitantly with a supporting effect on bone regeneration.

References

[1] M. Köller *et al*., Mater. Sci. Eng. C Mater. Biol. Appl. 74 (2017) 536–541.

Acknowledgement

We thank the Deutsche Forschungsgemeinschaft (DFG) for supporting this work (SE 2449/2-1, EP 22/44-1, HE 7192/2-1).

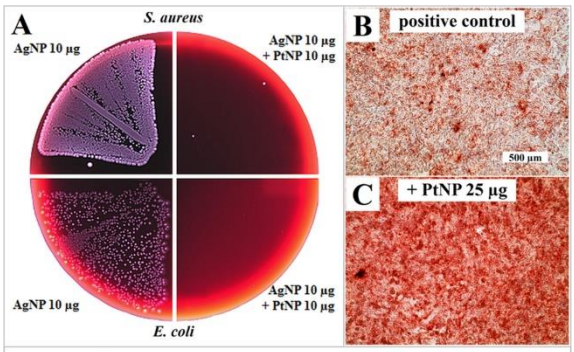

Figure 1: **Biological effects of AgNP and PtNP on bacteria and hMSC.** **A:** Antimicrobial activity (MBC) of AgNP compared to a physical mixture of 50 wt% AgNP and 50 wt% PtNP against *S. aureus* and *E. coli* (initial cell number 10^4 CFU mL^{-1}). **B:** hMSC incubated in osteogenic differentiation medium without NP (= positive control, Alizarin Red staining). **C:** hMSC incubated in osteogenic differentiation medium in the presence of PtNP (Alizarin Red staining).

Biological effects of AgNP and PtNP on bacteria and hMSC

PS1-01-15

Systemic toxicity evaluation after subcutaneous implantation of titanium with TiN layer.

Karolina Janiczak[1], Barbara Zawidlak-Węgrzyńska[1], Małgorzata Gonsior[1], Danuta Gonsior[1], Piotr Ścigała[1], Roman Kustosz[1], Tadeusz Wierzchoń[2], Michał Tarnowski[2], Romuald Wojnicz[3], Edyta Reichaman-Warmusz[3]

[1]Foundation of Cardiac Surgery Development, Artificial Heart Laboratory, Zabrze, PL; [2]Warsaw University of Technology, Faculty of Material Science and Engineering, Warsaw, PL; [3]Medical University of Silesia, Department of Histology and Embryology, Zabrze, PL

Introduction

Biocompatibility assessment of advanced implants like heart assist devices requires a multi-stage biocompatibility analysis to confirm the safety of use. A novel rotary ventricular assist device (VAD) ReligaHeart® ROT (RH ROT) was developed [1]. Construction of implantable blood pump is a huge challenge in the aspect of long-term contact with blood. Modification of the well-known glow discharge assisted nitriding process called active screen plasma nitriding has been used for enhancing the properties of RH ROT blood pump parts, made of Ti6Al7Nb alloy, through production of TiN+Ti_2N+αTi(N) diffusive surface layers [2]. The biocompatibility assessment was performed in terms of systemic toxicity, as a part of complete biocompatibility evaluation.

Experimental Methods

The systemic toxicity was evaluated according to PN EN ISO 10993-11 as limit test. In the assessment a higher dose was admitted to the animals than the dose the patient would be exposed in case of heart support with RH ROT. Ti6Al7Nb with TiN layer was prepared in a representative process for RH ROT device and ETO sterilized. The study was conducted with the utilization of 48 New Zealand White rabbits. Animals were divided in study and control group. Iimplantation was carried out under infusion anaesthesia. In the study group four samples were implanted subcutaneously on the back of animals. In control group two skin incisions were mad on the back. The observation was conducted depending of the group for 4 (n=6), 12 (n=8), and 26 weeks (n=10). Animal's body weight was controlled every 4 weeks. Before the implantation and then after the experiment before euthanasia the haematological, biochemical and coagulation blood parameters were assessed. After euthanasia a macroscopic evaluation of the implantation area and internal organs was performed. Histopathological assessment of tissues and internal organs was done.

Results and Discussion

During the observation no clinical sings of abnormalities in animal's behaviour were found. The body weight increase was for all tested groups similar. Blood analysis did not reveal any systemic pathology. There were no inflammation (C-reactive protein negative, no leucocytosis) or organ necrosis. Animal's organs were characterized by proper function and endurance - stable levels of total protein, creatinine, urea, total bilirubin were observed. Large fluctuations were observed in the enzyme activity. In the case of alanine aminotransferase (ALT) and gamma-glutamyltranspeptidase (GGT), the mean results significantly exceeded the reference range, however, the values remained stable before implantation and before euthanasia. Blood count parameters were in reference range, so no impact on bone marrow was found. Coagulation parameters were also stable. Macroscopic evaluation of internal

organs did not show any irregularities. Histopathological analysis showed isolated cases of not too serve inflammatory reaction in the implantation area, mostly in 4 weeks of observation.

Conclusion

TiN+Ti_2N+αTi(N) produced in active screen plasma nitriding process on the titanium alloy Ti6Al7Nb surface reveals no systemic toxicity in the long-term period of 26 weeks.

References

1. R.Kustosz, et al., Archives of Metallurgy and Materials, V.60, 3/2015: p.2253–2260
2. M.Gonsior, et a.., Engineering of Biomaterials, 143, Vol. XX, 2017, p.65

Acknowledgement

The authors would like to thank NCBIR (Grant no: STRATEGMED-2/ RH-ROT/266798/15/NCBR/2015) for providing financial support to this project.

PS1-01-16

Antibacterial mechanism of calcium chloride-treated raw silk fabric

Hiroki Chigama[1], Hiroyasu Kanetaka[2], Maiko Furuya[2], Kotone Yokota[2], Masakazu Kawashita[1]

[1]Tohoku University, Graduate School of Biomedical Engineering, Sendai, JP; [2]Tohoku University, Graduate School of Dentistry, Sendai, JP

Introduction

Antibacterial material to prevent from bacterial infection has been attracting much attention in medical field. Recently, we have reported that raw silk fabric treated with calcium chloride ($CaCl_2$) solution (R-Ca) showed excellent antibacterial activity against *Escherichia coli* (*E.coli*) [1] while it did not induce strong cytotoxicity against rat fibroblasts under the indirect condition [2]. Thus, R-Ca is expected to be useful as an antibacterial fabrics with biocompatibility for medical use. According to the dissolution test, R-Ca released 3.6 μmol of calcium into 30 mL of the Tris-HCl buffer solution [1], suggesting that the antibacterial activity of R-Ca was able to be caused by the release of calcium which was introduced to R-Ca by $CaCl_2$ treatment. However, its antibacterial mechanism is not completely clear because the effect of calcium on bacteria has not been reported. Therefore, in this study, we attempted to investigate the mechanism of R-Ca's antibacterial activity through revealing the effect of calcium on *E. coli* qualitatively as well as quantitatively.

Experimental Methods

Calcium was added to bacterial medium by dissolving a given amount of $CaCl_2$ as follows. At first, nutrient broth (NB) medium was prepared by mixing beef extract 3 g, peptone 5 g, and distilled water 1000 mL. Then, $CaCl_2$ was added to the NB medium at various concentrations. Subsequently, 100 μL of NB medium containing $CaCl_2$ and 100 μL of bacterial suspension was mixed, and the final concentration of $CaCl_2$ was adjusted to be 0, 0.49, 1.95, 7.8, 31, 130, 500, 2000 mM. Finally, the bacterial suspension was kept in the dark for 1 hour at room temperature, and the absorbance at 660 nm of each bacterial suspension was measured by ultraviolet-visible spectrophotometer. The absorbance at 660 nm corresponds to the turbidity induced by bacteria. Furthermore, the bacterial suspension was transferred into agar medium and cultured for 24 hours. After the culture, the apparent condition of the colonies was qualitatively confirmed.

Results and Discussion

Figure 1 shows the result of qualitative antibacterial test for $CaCl_2$ solutions with different concentrations. The apparent change was not observed from 0 mM to 500 mM, but the remarkable decrease of colony numbers was observed at 2000 mM. Figure 2 shows the result of quantitative antibacterial test for $CaCl_2$ solutions with different concentrations. The remarkable decrease in the absorbance of the bacterial suspension was observed at 2000 mM. Additionally, enhancement of bacterial proliferation by $CaCl_2$ was suggested because the absorbance of bacterial suspension increased with increasing the $CaCl_2$ concentration up to 500 mM. These results indicate that $CaCl_2$ shows antibacterial activity more than 2000 mM of the concentration. Further, it is speculated that its antibacterial activity depends not on the chlorine concentration but on the calcium concentration because chlorine derived from $CaCl_2$ is mostly existed as chlorine ions (Cl^-), which is not available chlorine such as hypochlorous acid. However, in our previous study, R-Ca showed strong antibacterial activity although the concentration of calcium released from R-Ca into the bacterial suspension was at most 120 mM [1]. This seemingly contradictory result could be explained with the evaporation of the bacterial suspension. In the antibacterial test, it is likely that evaporation of the bacterial

suspension was promoted because a very small amount of bacterial suspension (50 µL) was inoculated into the fabric with high surface area. Therefore, the calcium concentration could remarkably increase by evaporation of the bacterial suspension and it finally killed bacteria.

Conclusion

Calcium chloride did not show antibacterial activity against *E. coli* at the concentrations no more than 500 mM, but it showed the antibacterial activity at the concentration of 2000 mM. However, calcium chloride-treated raw silk fabric showed excellent antibacterial activity against *E. coli* while the apparent concentration of calcium released from the fabric (120 mM) was much lower than 2000 mM. This might be because the evaporation of the bacterial suspension on the fabric increases the calcium concentration to induce antibacterial activity. Therefore, calcium chloride-treated raw silk fabric is expected to be useful as an antibacterial fabric for medical use under low humidity.

References

[1] H. Chigama et al., Mater. Trans., in press.

[2] H. Chigama et al., 30th Symposium and Annual Meeting of the International Society for Ceramics in Medicine (Bioceramics30), October 29, 2018, Nagoya, Japan.

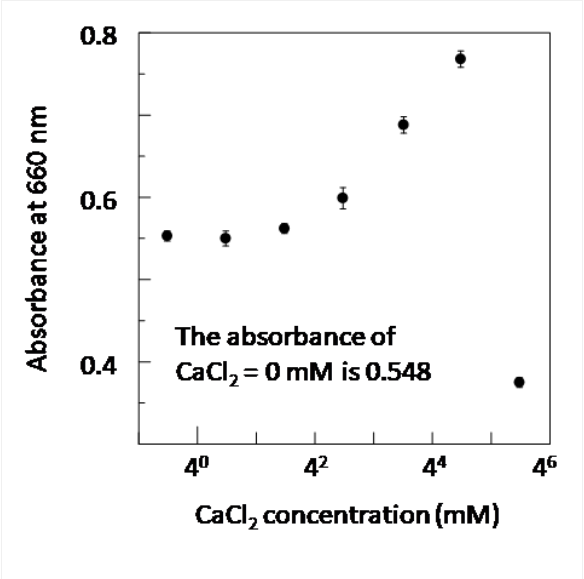

Fig. 2
The quantitative antibacterial test for CaCl2 solutions with different concentrations.

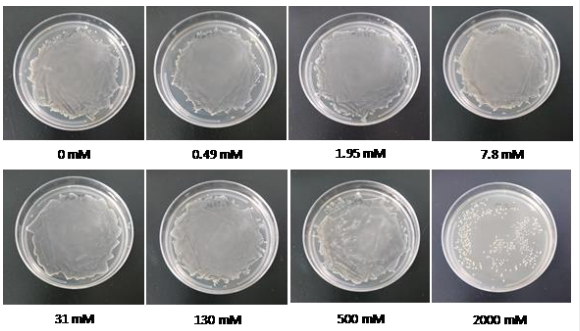

Fig. 1
The qualitative antibacterial test for CaCl2 solutions with different concentrations.

PS1-01-17

An alternative, quantitative method for measurement of bacterial cell coverage on flat and scaffold samples using SEM image analysis

Michal Zurawski, Colin Scotchford, Steve Atkinson, Reda M. Felfel, David Grant, The authors would like to acknowledge and thank Zimmer-Biomet for providing the financial and material support which enabled this study.

University of Nottingham, Mechanical, Materials and Manufacturing Engineering, Nottingham, GB

Introduction

Out of 228,861 Total Joint Replacement (TJR) surgeries carried out in the UK in 2017, approximately 9,154 resulted in biofilm infections at an approximate cost of £90m[1]. Once bacteria adhere to a surface they begin to secrete extracellular proteins that form a protective biofilm around them, which creates a physical barrier which protects the bacteria from the immune system and antibiotics. When this biofilm forms on a medical implant, treatment is nearly impossible and the device needs to be replaced. Studies into the bacterial growth on surfaces often employ expensive equipment, such as confocal laser scanning microscopes, in order to obtain quantifiable results; however the high cost of such devices is prohibitive to many scientists around the world, who turn to qualitative analysis.

Experimental Methods

Material samples were obtained from Zimmer-Biomet. These were 3D scaffolds (Tantalum[Ta] and Titanium alloy[Ti- to represent Ti6Al4V]) and flat Ti and Ta disks, diameter of 10mm, with varying treatments (grit blasted [G] and polished [P]). A group of PTi disks coated with copper were used as a negative control (Cu-PTi).

Bacteria used in this study were exclusively *Staphylococcus aureus* strain Newman, with a green fluorescent protein (GFP) gene inserted into a plasmid containing a Chloramphenicol (Cm) resistance gene. The optical density of the starting culture (OD_{600}) was 0.01. The incubation time was 3h, and was conducted at 37°C and 60RPM. A TSB/Fetal Bovine Serum (FBS) mixture was used as a media, which aimed to mimic the protein content of wound fluid (*ca*. 2.9g/dL[2]).Bacterial cell fixation for Scanning Electron Microscopy (SEM) was done using a modified human cell fixation protocol using 3% Glutaraldehyde as a fixative, which prolonged dehydration times in ethanol.
SEM micrographs were converted to binary images, showing regions with and without bacteria. The pixel count of each value was then measured, resulting in a pixel-count-related coverage assessment.
Confocal microscope readings were taken using a Carl Zeiss L700 Confocal Laser Scanning Microscope, and the resulting image stacks were analysed using a COMSTAT 2 plugin to ImageJ in order to obtain biomass volume per unit area.
SEM Images were transformed using GIMP 2.8.14.
Results from the two methods were then analysed using a 2-way ANOVA method on normalized values (using GraphPad Prism 7).

Results and Discussion

No morphology change was observed in bacterial cells after fixation and dehydration in preparation for SEM imaging (see Fig. 1). A significantly higher proportion of a metal oxide layer on the topmost (10nm) surface was observed

using XPS on all samples, with the difference ranging from 19 wt% O to 49 wt% O across Ta samples, and 4 wt% O to 46 wt% O across Ti samples.

A comparison between results obtained using confocal microscopy and those obtained using SEM image analysis on 2D samples showed that in all groups, out of 5, there was no statistically significant difference between the two data sets (see Fig 2). All samples saw some bacterial adherence to their surfaces. The negative control group had the lowest reading, with PTa and PTi disks next, followed by GTa and GTi showing the highest amount of bacterial cell attachment.

Conclusion

SEM image analysis is a potential alternative analysis method for assessment of bacterial cell attachment, illustrated by the fact that there was no statistically significant difference between the results from SEM and confocal microscopy. There is also no statistically significant difference between the bacterial cell attachment on Ti and Ta samples of equivalent surface topography, however grit blasted samples show increased readings compared to their polished counterparts in both cases.

References

[1]http://www.njrreports.org.uk/Portals/0/PDFdownloads/NJR%2014th%20Annual%20Report%202017.pdf

[2] Heffner JE. Chest 1997;111:970-980.

Acknowledgement

The authors would like to acknowledge and thank Zimmer-Biomet for providing the financial and material support which enabled this study.

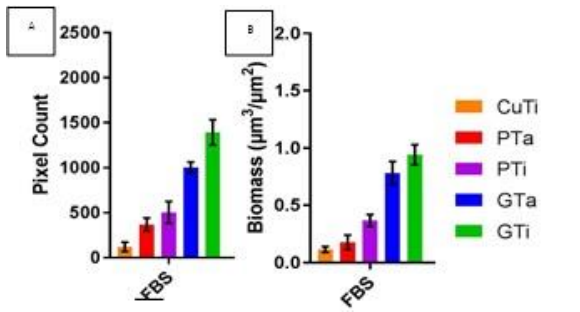

Figure 2
Comparison of SEM data and confocal data obtained from the same samples. Graph A. shows the results obtained using SEM, with the pixel count indicative of area coverage of bacteria. Graph B shows the results obtained using confocal imaging, with the biomass as volume per unit area.

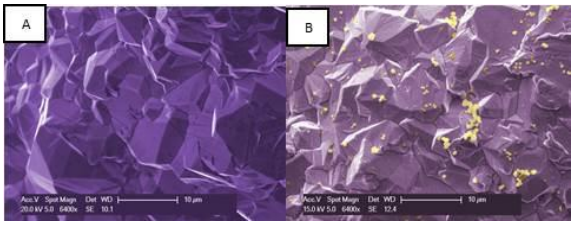

Figure 1
False-colour SEM Images of a Ta scaffold before (A) and after (B) incubation. The metal is purple in colour and the bacteria and coloured yellow.

PS1-01-18

In vitro Corrosion Characteristic of Bioactive glass and β-TCP Nanostructures coated CP-Ti Substrates and its Hemocompatibility Assessment

Durgalakshmi Dhinasekaran[1], Gopi Saravanan K[2], Balakumar Subramaniam[3], Aruna Prakasa rao[1], Ganesan Singaravelu[1]

[1]Anna University, Department of Medical Physics, Chennai, IN; [2]Sathyabama Institute of Science and Technology., Chennai, IN; [3]National Centre for Nanoscience and Nanotechnology, University of Madras, Chennai, IN

Introduction

Ceramics and glasses have been used for a long time in the healthcare industry from diagnosis to therapeutic applications. In dental and orthopaedic, calcium phosphate compounds and bioactive glasses are considered to be an important compound due to its compositional vitality and apatite regeneration properties, which are essential for human bone and dentin treatments. In calcium phosphate compounds, β-TCP is a notable bio-resorbable material which can relatively balance between absorption and new bone formation [1]. This material is also posing osteogenicity and osteoinductivity. Bioactive glasses are a subset of inorganic bioactive ceramics, which are able to react with physiological fluids to form strong bonds to bone via the formation of bone-like HA layers and the biological interaction of collagen with the material surface[2]. Bioactive silicate glasses (e.g. 45S5 Bioglass) with compositions in the system SiO_2–Na_2O–CaO–P_2O_5 having < 55% SiO_2 were discovered by Hench in 1969 [3]. These types of bioactive glasses also have osteogenetic and osteoconductive properties. In the present work, nanostructured β-TCP and Bioactive glass with the composition similar to the 45S5 system has been synthesized by Sol-gel technique. The obtained powders were coated on commercially pure titanium substrates by a pulsed laser deposition technique. The in vitro bioactivity and corrosion characteristics were discussed in detail.

Experimental Methods

Bioactive glass were synthesized by Sol-Gel. The precursors used were nitric acid, Tetraethyl orthosilicate, Triethyl Phosphate, Sodium hydroxide and Calcium nitrate tetrahydrate and done as per the procedure reported earlier[6]. β-TCP nanopowders were synthesized by the reaction of calcium nitrate tetra-hydrate with orthophosphoric acid. The molar percentage of two precursors calcium nitrate tetrahydrate and orthophosphoric acid in the ratio of 1:5. Throughout the synthesis process, the pH was maintained at 10.8. The precipitate was dried at 80°C for 24 h and heat treated at 700°C for 2h. The sintered Bioactive glass and β-TCP nanopowders were coated on CP-Ti substrates by a pulsed laser deposition technique.

Results and Discussion

FTIR spectra give the accurate fingerprint characteristics of phosphate and silica molecular arrangement. Fig.1 shows the FTIR spectrum of bioactive glass and β-TCP. For Bioactive glass, the absorbance band is founded around in the graph is 1336 cm^{-1} corresponds residual organic compounds. The peak at around 608-997cm^{-1} are attributed to P–O bending of PO_4^{3-} groups [7,8]. For β-TCP, the absorbance band is found to be around 1015 cm^{-1} corresponds to residual organic compounds (PO_4^3-Stretching mode). The characteristic absorption band at 2980-1655 cm^{-1} are attributed to adsorbed water sharp peak at 3572 cm^{-1} appeared due to the stretching vibration of the lattice OH–

ions. The sharp peaks at 562cm^{-1} represent the vibration peaks of po_4^3-vibration mode in β-TCP. The FTIR results were also very much similar to the earlier literature[9].

The SEM image (Fig. 2 a) shows the sintered bioactive glass synthesized using the sol-gel method. The neckings among the particles were apparent. The surface morphology the particle is a plate-like structure at some region and agglomerated beaded structure in other regions. Fig. 2b shows surface morphology of the sintered β -TCP synthesized prepare by co-precipitation method. The particles are highly agglomerated, spherical in shape with an average size of 50 nm. The elemental analysis of sintered bioactive glass (Fig. 2c) and β-TCP(Fig. 2d) is confirmed by EDS spectra. The composition analysis of from the EDS was well matched with the composition of the 45S5 bioglass system and the calcium to phosphate ratio was also compared with the standard β-TCP.

Hemocompatibility of pure Tricalcium phosphate and Bioactive glass at various concentrations is shown in Fig. 2c. While comparing the results of β-TCP with bioglass, the former shows comparable more hemolysis. However, as per the hemocompatibility standards the hemolysis% less than 5% is considered to be compatible[10].

Conclusion

Bioactive glass and β-TCP with a composition similar to 45S5 bioglass were synthesized by sol-gel method and co-precipitation method respectively. The phase analysis of β-TCP and Bioactive glass is confirmed from XRD analysis. The stretching and vibrational modes were confirmed by FTIR and RAMAN. Plate-like structure and spherical structure were observed under SEM for Bioglass and β -TCP samples respectively. Bioactivity of the material analyzed through Hemocompatibility studies depicts that, Bioactive glass is more compatible compared to β-TCP even at higher concentration. The pH-dependent In Vitro immersion studies were done for Bioactive glass and β-TCP sample by immersing the sample in Simulated Body Fluid for 14 days. The in vitro corrosion studies of Bioactive glass and B-TCP coated CP-Ti substrates shows the positive response for the coated samples.

References

[1] H.-H. Horch, R. Sader, C. Pautke, A. Neff, H. Deppe, A. Kolk, International journal of oral and maxillofacial surgery 35(8) (2006) 708-713.

[2] L.L. Hench, Journal of Materials Science: Materials in Medicine 17(11) (2006) 967-978.

[3] L.-C. Gerhardt, A.R. Boccaccini, Materials 3(7) (2010) 3867-3910.

[4] S. Haimi, N. Suuriniemi, A.-M. Haaparanta, V. Ellä, B. Lindroos, H. Huhtala, S. Räty, H. Kuokkanen, G.K. Sándor, M. Kellomäki, Tissue Engineering Part A 15(7) (2008) 1473-1480.

[5] S. Kotani, Y. Fujita, T. Kitsugi, T. Nakamura, T. Yamamuro, C. Ohtsuki, T. Kokubo, Journal of biomedical materials research 25(10) (1991) 1303-1315.

[6] D. Durgalakshmi, R.A. Rakkesh, M. Kesavan, S. Ganapathy, T. Ajithkumar, S. Karthikeyan, S. Balakumar, Biomaterials science 6(7) (2018) 1764-1776.

[7] O. Bretcanu, X. Chatzistavrou, K. Paraskevopoulos, R. Conradt, I. Thompson, A.R. Boccaccini, Journal of the European Ceramic Society 29(16) (2009) 3299-3306.

[8] J. Serra, P. González, S. Liste, C. Serra, S. Chiussi, B. León, M. Pérez-Amor, H. Ylänen, M. Hupa,Journal of Non-Crystalline Solids 332(1-3) (2003) 20-27.

[9] I. Gibson, I. Rehman, S. Best, W. Bonfield, Journal of materials science: materials in medicine 11(9) (2000) 533-539.

[10] G. Radha, S. Balakumar, B. Venkatesan, E. Vellaichamy, Materials Science and Engineering: C 50 (2015) 143-150.

Acknowledgement

One of the author Durgalakshmi Dhinasekaran acknowledges DST for INSPIRE faculty fellowship funding.

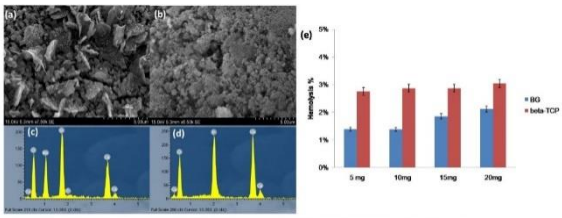

Fig. 2. SEM image of (a) Bioactive glass and (b) Beta-TCP; EDS of (c) Bioactive glass and (d) Beta-TCP and (e) Hemocompatibility study

Fig.2 SEM Images of (a)Bioactive glass and (b) Beta-TCP; EDS of (c) Bioactive glass and (d) Beta-TCP

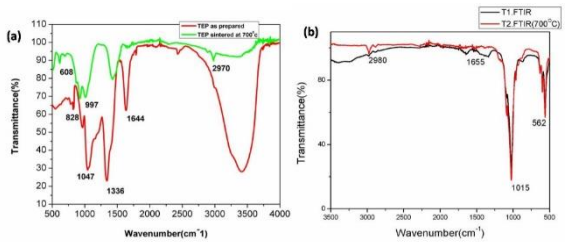

Fig. 1. FTIR Spectrum of (a) Bioactive glass and (b) Beta-TCP

Fig.1. FTIR Spectrum of (a) Bioactive glass and(b) Beta-TCP

PS1-01-19

Nanostructured Tantalum to Enhance Biocompatibility

Ece Uslu[1,3], Batur Ercan[1,2,3]

[1]Middle East Technical University, Metallurgical and Materials Engineering, Ankara, TR; [2]Middle East Technical University, Biomedical Engineering Program, Ankara, TR; [3]Middle East Technical University, BIOMATEN, Center of Excellence in Biomaterials and Tissue Engineering, Ankara, TR

Introduction

Osteoarthritis is the inflammation of joints due to degeneration of cartilage tissue. It is the most common joint diseases in the world and dramatically limits mobility of the patients. The only clinical therapy to regain their mobility is the replacement of the degenerated tissues with an artificial implant. However, currently-used orthopedic implants having an average lifetime of only 15-20 years are not sufficient for active adults and aging population [1, 2]. Implant corrosion, wear debris formation, fatigue and most importantly the lack of osseointegration are among the major reasons for orthopedic implant failure. To improve lifetime of an implant and overcome these issues, tantalum may be a potential candidate due to its superior corrosion resistance and optimal mechanical properties compared to the commonly used orthopedic implant materials [3,4]. However, the bioinert nature of tantalum surfaces limits sufficient osseointegration with juxtaposed bone. Surface modification in the nanoscale can be a promising solution to enhance bioactivity of tantalum. Among many surface modification techniques, anodization is a promising technique due to its simplicity and flexibility to obtain nanostructured surface oxide layers. In this study, tantalum surfaces were modified via anodization to obtaine three different surface morphologies having tunable feature sizes. Moreover, the interaction between anodized tantalum and bone cells was assessed.

Experimental Methods

The surfaces of tantalum samples (1cmx1cm) were modified via anodization using a two electrode system where platinum mesh was used as the cathode. HF, H_2SO_4 and DMSO were used as electrolytes in varying concentrations. Voltages (10-60V) and anodization durations (20s-4h) were optimized to obtain nanotubular, nanocoral and nanodimple morphologies having controlled feature sizes. Osteoblast (ATCC CRL-11372) adhesion and proliferation were investigated up to 5 days of culture.

Results and Discussion

Concentrated HF and H_2SO_4 solutions were used to obtain nanotubular surface morphologies, while anodization voltages and durations were fine-tuned to have 30-150 nm diameter tubular sizes. Nanocoral morphology was fabricated via using H_2SO_4 and NH_4F solution as electrolyte. The low viscosity of this solution compared to the concentrated HF and H_2SO_4 mixture lead to formation of a nanocoral morphology rather than nanotubes and the dissolution rate of surface oxide layer was found to be the dominating mechanism controlling its morphology. Feature size of the nanocoral tantalum surfaces were controlled between 20-120 nm by altering anodization parameters. In the fabrication set-up, incorporation of a small amount of DMSO into the concentrated HF and H_2SO_4 solution resulted in formation of nanodimples, which was correlated with reduced electrical conductivity of the electrolyte. Voltage and duration were adjusted to obtain 25-90 nm diameter nanodimple feature sizes. TEM and XRD analysis indicated an amorphous oxide surface layer and XPS analysis revealed that the surfaces of the tantalum metal were oxidized to obtain Ta_2O_5 for nanocoral and nanodimple morphologies. Moreover, *in vitro* studies revealed enhanced osteoblast adhesion and proliferation up to 5 days of culture on anodized tantalum surfaces having nanotubular, nanocoral and nanodimple morphologies compared to non-anodized tantalum. Alkaline phosphatase, collagen and extracellular calcium secretion assays are underway on the nanofeatured samples.

Conclusion

Anodization process was used to modify tantalum surfaces. By altering electrochemical parameters, three different surface morphologies having feature sizes between 20-150nm were obtained. Upon anodizing tantalum metal, chemically inert, yet biologically active amorphous Ta_2O_5 was on the fabricated tantalum surfaces. Enhanced bone cell adhesion and proliferation was observed on nanofeatured surfaces compared to conventional tantalum. Thus, anodized nanofeatured tantalum is a promising candidate for orthopedic applications.

References

[1] Balasundaram, G. and Webster, T. J. (2006). *Journal of Materials Chemistry,16*(38), 3737

[2] Yang, L. (2015). *WoodHead Publishing*. 27-47.

[3] Verissimo, N. *et.al.* (2015), *Surface Coating and Modification of Metallic Biomaterials,* 249-273

[4]Ruckh, T. *et.al*. (2008), *Nanotechnology*, 20(4), 045102.

Acknowledgement

We would like to thank the Scientific and Technological Research Council of Turkey (TÜBİTAK Grant No: 117M187) for providing financial support and BIOMATEN, METU Center of Excellence in Biomaterials and Tissue Engineering for their help in characterization experiments.

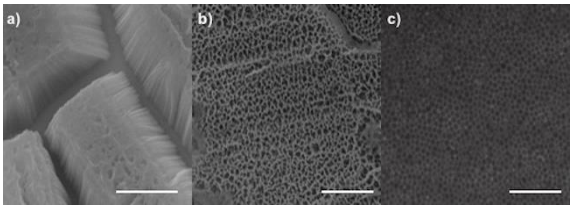

Figure 1.
SEM images of anodized a) nanotubular, b) nanocoral and c) nanodimple tantalum.Scale bars are a) 3 um, b) and c) 1 um respectively.

PS1-01-20

Fast and improved *in vitro* test procedure for full in vitro-assessment of degradable magnesium

Ole Jung[1,2], Ralf Smeets[1,2], Frank Feyerabend[3], Martin Klein[4], Frank Walther[4], Dominic Stangier[5], Anders Henningsen[1], Carsten Rendenbach[6], Max Heiland[6], Martin Gosau[2], Alexander Kopp[8], Mike Barbeck[1,7]

[1]University Medical Center Hamburg-Eppendorf, Division of Regenerative Orofacial Medicine, Research Group Biomaterials/Surfaces, Hamburg, DE; [2]University Medical Center Hamburg-Eppendorf, Department of Oral Maxillofacial Surgery, Hamburg, DE; [3]Helmholtz-Zentrum Geesthacht, Institute of Materials Research, Division Metallic Biomaterials, Geesthacht, DE; [4]TU Dortmund, Department of Materials Test Engineering (WPT), Dortmund, DE; [5]TU Dortmund, Institute of Materials Engineering, Dortmund, DE; [6]Charité-Universitätsmedizin Berlin, Department of Oral and Maxillofacial Surgery, Berlin, DE; [7]Berlin Analytix GmbH, Berlin, DE; [8]Meotec GmbH & Co. KG, Aachen, DE

Introduction

Magnesium (Mg)-based biomaterials are promising candidates for bone and tissue regeneration. Alloying and surface modifications provide effective strategies for optimizing and tailoring their degradation kinetics. Nethertheless, biocompatibility analyses of Mg-based materials are challenging due to its special degradation mechanism with continous hydrogen release. In this context, the hydrogen release and the related (micro-) milieu conditions pretend to strictly follow in vitro standards based on ISO 10993-5/-12. Thus, special adaptions for the testing of Mg materials are necessary. Based on these adaptions, further developments of a test procedure allowing rapid and effective in vitro cytocompatibility analyses of Mg-based materials based on ISO 10993-5/-12 are necessary and are presented in the following study.

Experimental Methods

The following study introduces a new two-step test scheme for rapid and effective testing of magnesium specimens. Different surface characteristics were produced by means of plasma electrolytic oxidation (PEO) using silicate-based and phosphate-based electrolytes. The test samples were evaluated for corrosion behavior, cytocompatibility and their mechanical and osteogenic properties.

Results and Discussion

We successfully developed 4 silicate-based and 7 phosphate-based ceramized surfaces. Thereby, silicate-based surfaces showed inferior results compared to most of the phosphate-based surfaces in terms of corrosion resistance and cytocompatibility. We identified four test samples that qualified for the second step to determine mechanical and osteogenic properties by seeding human umbilical cord perivascular cells (HUCPV) onto the surfaces over a time period of 21 days. Thereby, two test samples showed satisfying mechanical micro-hardness properties and a bony differentiation of the cells on the surfaces. These two samples were selected for further in vivo testing.

Conclusion

We successfully implemented a new two-step test scheme for rapid and effective testing of magnesium specimens. Thereby, two PEO ceramics could be identified for further in vivo evaluations.

References

Jung et al.. Improved In Vitro Test Procedure for Full Assessment of the Cytocompatibility of Degradable Magnesium Based on ISO 10993-5/-12. Int J Mol Sci. 2019 Jan 10;20(2).

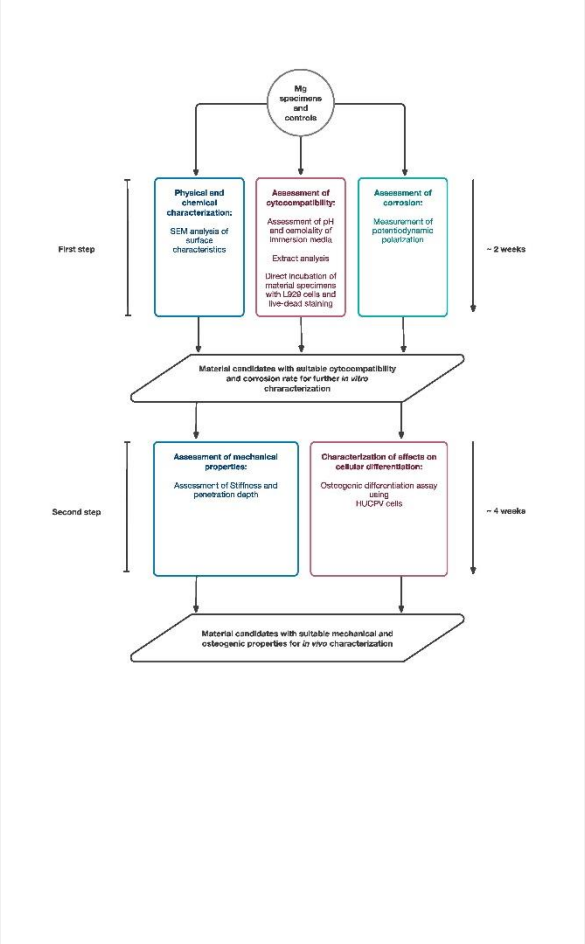

Two-step test procedure
Schematic outline of the procedure for assessing the *in vitro* compatibility of Mg-based materials applied in this study.

PS1-01-21

Characterization of adsorbed protein films on UV-C treated Ti6Al4V and Ti6Al7Nb by TOF-SIMS

Margarita Hierro-Oliva[2,1,3], Daniel Romero-Guzmán[1,2,3], Amparo M. Gallardo-Moreno[1,2,3], M. Luisa González-Martín[1,2,3]

[1]University of Extremadura, Department of Applied Physics, Badajoz, ES; [2]Networking Research Center on Bioengineering, Biomaterials and Nanomedicine (CIBER-BBN), Badajoz, ES; [3]University Institute of Biosanitary Research of Extremadura (iNube), Badajoz, ES

Introduction

Protein adsorption at implant surface is one of the first biological events happening when a foreign material is placed in the human body and gets in contact with human tissue or body fluids[1]. The adsorption of protein at biomaterials surfaces is a complex process, depending on the chemical and physical properties of the material, such as its composition and hydrophobicity[2]. Surface hydrophobicity/hydrophilicity is one of the most important parameters affecting the biological response to an implanted material. It is known that the hydrophobicity of titanium based materials can be changed after irradiating its surface with UV-C light[3].

In this study, time of flight secondary ion mass spectrometry (TOF-SIMS) was used to characterize human serum albumin (HSA) and fibrinogen (Fng) adsorption on two different titanium alloys, Ti6Al4V and Ti6Al7Nb, with increasing level ofhydrophobicity.

Experimental Methods

The protein adsorption experiments for ToF-SIMS analysis were carried out on Ti6Al4V and Ti6Al7Nb (DKSH, Switzerland) substrates cut in discs of 25 mm in diameter and 2 mm in thickness, mechanically polished to mirror finish and carefully cleaned before used. Some titanium alloy surfaces were treated with an ultraviolet lamp during 2 and 15 hours in order to make them hydrophilic.

The adsorption of HSA and Fng (Sigma-Aldrich, Germany) protein solutions onto titanium alloys were performed at 37 °C for 2h of incubation, in PBS buffer, using 1 ml solution with 5, 10, 30, 80 and 100 µg/ml of protein concentration.

TOF-SIMS measurements were performed with a TOF-SIMS[5] (ION TOF, Germany) equipped with a Bi^+ primary ion source operated at 25 kV. The total ion dose used to acquire each spectrum was ~1×10^{12} ions/cm^2 to ensure static SIMS conditions with an analyzed area of 200 × 200 µm^2. Spectra were calibrated to the H^+, H_2^+, CH_3^+, $C_2H_3^+$, $C_3H_5^+$ and $C_7H_7^+$ peaks before further analysis.

Results and Discussion

To evaluate the protein adsorption on each substrate, the evolution of the intensity ratio of a characteristic protein peak ($C_4H_8N^+$, m/z=70) over the sum of a characteristic substrate peak (Ti^+, m/z= 48) and the protein peak was followed as a function of protein concentration for all types of substrates. It can be seen that for the three substrate conditions of Ti6Al4V show an increasing trend of protein adsorption with respect to the concentration of the protein solution.

Conclusion

TOF-SIMS technique showed that there is a difference in the adsorption behaviour of the protein on titanium alloy and hydrophilic treated titanium alloy surfaces.

References

[1] Baier, R. E. and Dutton, R. C. (1969). Initial events in interactions of blood with a foreign surface. J. Biomed. Mater. Res., 3: 191-206

[2] Spriano, S., Sarath Chandra, V., Cochis, A., Uberti, F., Rimondini, L., Bertone, E., Vitale, A., Scolaro, C., Ferrari, M., Cirisano, F., Gautier di Confiengo, G., Ferraris, S. (2017). How do wettability, zeta potential and hydroxylation degree affect the biological response of biomaterials?. Materials Science and Engineering: C, 74, 542-555

[3] Pacha-Olivenza, M.A., Gallardo-Moreno, A.M., Méndez-Vilas, A., Bruque, J.M., González-Carrasco, J.L., González-Martín, M.L. (2008) Effect of UV irradiation on the surface Gibbs energy of Ti6Al4V and thermally oxidized Ti6Al4V. Journal of Colloid and Interface Science, 320 (1): 117-124.

Acknowledgement

Financial support is acknowledged to the Spanish Junta de Extremadura and FEDER grants for the projects IB16117 and GR15089, and to the Ministerio de Economía y Competitividad for the project MAT2015-63974-C4-3-R y PCIN-2016-146. The TOF-SIMS has been performed by NANBIOSIS ICTS, more specifically by the Surface Characterization Unit of the Biomedical Networking Center (CIBER-BBN) and the SACSS- SAIUEx of the University of Extremadura (UEx).

PS1-01-22

Unidirectional rotating molecular motors direct the fate of mesenchymal stem cells

Patrick van Rijn

University Medical Center Groningen, Biomedical Engineering, Groningen, NL

Introduction

Artificial rotary molecular motors convert energy into controlled motion in a continuous manner. The capability to drive a system out-of-equilibrium with molecular precision offers fascinating prospects to mediate cell behavior as biological systems take advantage of dynamic environments in order to control the biointerface and direct adhesion events and cell fate. Here, we demonstrate that the fate of human bone marrow-derived mesenchymal stem cells (hBM-MSCs) can be regulated by the rotary motion of light-driven molecular motors grafted on surfaces.

Experimental Methods

A schematic diagram illustrating our experimental design of surface-bound molecular motors directing the fate of stem cells is shown in Fig. 1A. The rotary motion originating from light-driven unidirectional rotary motors mediates the initial protein adsorption behavior that affects the fibronectin adsorption, which subsequently regulates the focal adhesion cytoskeleton actin transduction pathway to govern gene and protein expression of the cells. In this way molecular motion is transduced ultimately in stem cell differentiation. For the dynamic surfaces , tetra-acid functionalized light-driven rotary molecular motors were grafted to amine modified glass surfaces via electrostatic interactions (Fig. 1B). The tetrapodal attachment enables stable orientation of monolayers of motors on surfaces and prevents uncontrolled Brownian motion. Importantly, it has been demonstrated that the motors used in present study can transform UV-light into the repetitive unidirectional rotation and have no significant reduction in the rotational speed when immobilized to a glass substrate. Next, under irradiation with UV light (λ_{max} = 365 nm), fetal bovine serum (FBS), which is conventionally present in cell culture medium as one of the main components, was added onto the motor surfaces to explore how dynamic molecular motion affects protein adsorption. After 1 h of protein adsorption under continuous irradiation, hBM-MSCs were seeded on the treated motor surfaces for studying cell adhesion, proliferation, differentiation, and maintained stemness (Fig. 1A).

Results and Discussion

The fate of human bone marrow-derived mesenchymal stem cells (hBM-MSCs) can be regulated by the rotary motion of light-driven molecular motors grafted on surfaces. hBM-MSCs on the rotary motor surface are prone to differentiate into osteoblasts, while if the motors are in their static state, hBM-MSCs tend to better maintain multipotency. It is shown that the rotary motion alters the adsorbed protein behavior influencing the focal adhesion-cytoskeleton actin transduction pathway and the regulation of the protein and gene expression of hBM-MSCs.

Conclusion

We demonstrate that the underlying mechanism for unidirectional rotating molecular motors influencing stem cell behavior is associated with the behavior of initial adsorbed serum albumin (i.e., amount, conformation, and morphology), which is regulated solely by the molecular motion. Unidirectional rotating molecular motors increased the serum albumin adsorption and decreased the α-helix secondary structure, which subsequently affected the

adsorbed amount of Fn. The distinct protein adsorption behavior influenced the FA cytoskeleton actin transduction pathway as well as the macroscopic cell adhesion and morphology, evident from studying focal adhesion, filopodia and actin stress fibers, and as a result mediates the fate of hBM-MSCs. Besides providing a unique way to dynamically influence the interaction between surfaces and cells as demonstrated here, the molecular motors based the surface offer numerous opportunities for mechanical stimulation and control of cell fate and responsive biomimetic materials.

References

Robertus, J., Browne, W. R. & Feringa, B. L. Dynamic control over cell adhesive properties using molecular-based surface engineering strategies. *Chem. Soc. Rev.***39**, 354–378 (2010)

Schaap A.M. , Kuhn P.T., van Kooten T.G., van Rijn P., Biomaterial-stem cell interactions and its impact on stem cell behaviour, *RSC Adv.*, **2014**, 4, 53307.

Acknowledgement

This work was supported by the UMCG Microscopy and Imaging Center (UMIC) sponsored by NWO-grant 40-00506-98-9021

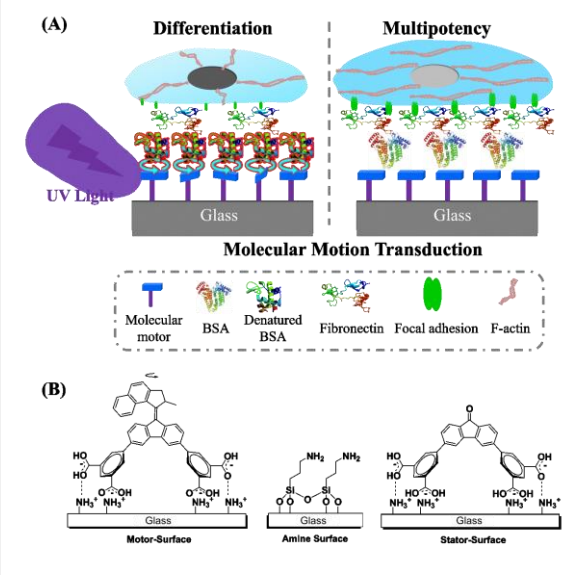

Molecular motor stem cell interaction

Figure 1. (A) Schematic illustration of the molecular motion directing the fate of hBM-MSCs. The molecular motion originating from unidirectional rotating molecular motors mediate the initial protein adsorption behavior that affects the fibronectin adsorption, which subsequently regulate the focal adhesion cytoskeleton actin transduction pathway to govern the gene and protein expressions of hBM-MSCs. (B) Structural details of motor (dynamic layer), amine and stator (static control layer) modified surfaces.

PS1-01-23

Strontium-enriched sol-gel coatings for highly osteoregenerative biomaterials development

Iñaki García-Arnáez[1], Nuno Araújo-Gomes[2,3], Francisco Romero-Gavilán[2], Felix Elortza[4], Mikel Azkargorta[4], Julio Suay[2], Isabel Goñi[1], Mariló Gurruchaga[1], Andreia Cerqueira[2,3]

[1]Universidad del Pais Vasco, Facultad de Química, San Sebastián, ES; [2]Universitat Jaume I, Department of industrial systems and design engineering, Castellón de la Plana, ES; [3]Universitat Jaume I, Department of Medicine, Castellón de la Plana, ES; [4]CicBiogune, Proteomics Platform, Derio, ES

Introduction

Strontium plays an essential role in bone formation. It is known to be involved in the human bone mineral metabolism by inducing the expression of osteogenic-related genes[1], differentiation markers, promoting bone formation by osteoblasts and inhibiting bone resorption by osteoclasts[2]. Sr enriched biomaterials have shown to induce osteogenesis and new bone formation[3].

The increasing interest in the effect of Sr on bone tissue regeneration has been reflected in the design and studies of new Sr-releasing biomaterials[4]. The sol-gel technique produces easily coated materials, allowing surface functionalisation of metal implants such as dental prostheses[5].

Experimental Methods

The Sr-doped coatings were synthesized by the acid catalysis sol-gel method. The precursors were the alkoxysilanes methyltrimethoxysilane (M) and tetraethyl orthosilicate (T). The molar percentages of these precursors in the material selected as a Sr-release vehicle were 70% M and 30% T. This formulation was supplemented with 0.5, 1 and 1.5 wt % $SrCl_2$ during the synthesis process.

The surface topography of the samples was examined using scanning electron microscopy (SEM). The chemical characterization was carried out by Infrared Spectrometry (FTIR) and Nuclear Magnetic Resonance (^{29}Si-NMR). Other tests were performed to complete the characterization: adhesion measurement by cross-cut test, hydrophobicity/hydrophilicity and hydrolytic degradation. Silicon and Sr releases were measured by ICPMS. The biological evaluation was done with *in vitro* assays with cells and proteins.

Results and Discussion

The successful obtaining of transparent, homogeneous and uniform coatings where $SrCl_2$ is effectively immobilized can be confirmed from the chemical and morphological characterization. Moreover, the molecules incorporation was made without altering the material chemistry.

Although all bioactive molecules can potentially exhibit cytotoxicity against human tissue cells depending on their concentration, in this case no one of the developed materials presented a cytotoxic behaviour, since all of them induced cell viability higher than 70 % as compared to control (Figure 1).

In the MC3T3-E1 cells cultured with the Sr-doped sol-gel materials, the gene expression of osteogenic marker TGF-β tended to increase for all concentrations in comparison with cells grown on the 70M30T base material (Figure 2a). The expression level of TNF-α, a standard marker of early stages of inflammation, decreased significantly with all of the materials compared to reference sample (Ti), indicating that the coating might decrease the pro-inflammatory effect of the Ti disc (Figure 2b). Proteomic studies clearly showed a higher presence of proteins associated with anti-inflammatory and osteogenic functions. The correlations between gene expression and proteomic results showed

that the introduction of Sr into the biomaterials might improve their osteogenic and anti-inflammatory potential; the data are consistent with the available results of literature *in vivo* studies.

Conclusion

The incorporation of $SrCl_2$ into a hybrid sol-gel biomaterial affects protein affinity profiles and cell responses showing a potential osteogenic behaviour. Although *in vivo* studies are needed to confirm the osteoregenerative capacities of the synthesized coatings, the study of protein-biomaterial interactions highlights the events triggered after implantation related to bone regeneration.

The present study shows that the new-doped silica sol-gel coatings could be a great contribution to the dental implantology.

References

[1] J. M. Fernández *et al.*, *Biometals*, 2014, **27**, 601–607.

[2] W. Querido *et al.*, *Micron*, 2016, **80**, 122–134.

[3] M. Jiménez *et al., J. Mater. Chem. B*, 2019, **7**, 1974.

[4] N. Neves *et al.*, *Bone Joint Res*, 2017, **6**, 366–375

[5] M. Martínez-Ibáñez *et al.*, *J Mater Sci: Mater Med*, 2016, 27:80

Acknowledgement

This work was supported by MINECO [MAT2017-86043-R] and [RTC-2017-6147]; Universitat Jaume I [Predoc/2014/25, UJI-B2017-37]; Basque Government [Predoc/2016/1/0141]; University of the Basque Country [Implant Sol-RTC-2017-6147]. The authors thank for technical and human support provided by SGIker (UPV/EHU/ERDF, EU).

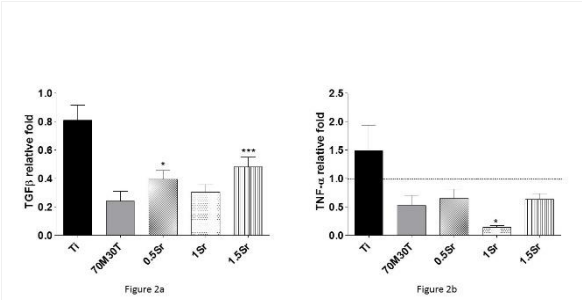

Figure 2

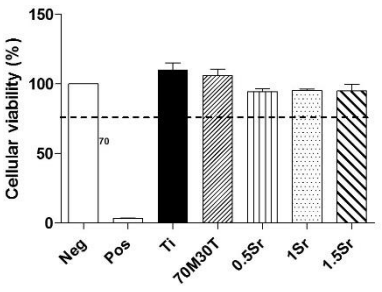

Figure 1

PS1-01-24

A new technology for zeta potential measurement: cmPALS

Bastian Arlt

Anton Paar Germany GmbH, Particle Characterization, Ostfildern, DE

Introduction

Zeta potential is a key indicator of colloid stability. The higher the magnitude of the zeta potential (that is, highly positive or highly negative), the more stable the colloid. A lower-magnitude zeta potential indicates a less stable colloid; in other words, the colloidal particles will tend to aggregate or coagulate. Thus, knowledge of zeta potential is important for optimizing processes and for quality control.

Nonetheless, the measurement of zeta potential has previously been beset by significant limitations. Zeta potential measurements require an electric field to be applied to the sample. But electric fields can lead to sample heating and decomposition, so the electric fields must be kept as low as possible, and applied for as short a time as possible.

Until now, the state of the art in zeta-potential measurements was phase-analysis light scattering (PALS),[1] which is based on electrophoretic light scattering (ELS) measurements. PALS measurements can be unreliable, however, especially with sensitive samples, where very short measuring times and low electric fields are required.

We describe herein a newly patented technology called cmPALS (EP2735870),[2] which is incorporated in the recently introduced particle-analyzing instrument, the Litesizer™ 500. cmPALS results in dramatic enhancements in the sensitivity and stability of zeta-potential measurements. We describe first some background information about the technical development of cmPALS before presenting a direct comparison of results from the cmPALS instrument (the Litesizer™ 500) with those from a PALS instrument.

Experimental Methods

Phase-analysis light scattering (PALS) is a method for evaluating zeta potential, in which the rate of phase change of the interference between light scattered by the sample and the modulated reference beam is analyzed. This rate is compared with a mathematically generated sine wave predetermined by the modulator frequency. PALS was an improvement over previous ELS measurements, because it no longer required the application of large fields, which can lead to sample heating and/or breakdown of the colloid.

PALS measurements start to become unreliable for sensitive samples, however, because the movement of the modulator becomes increasingly nonlinear as the movement gets larger. Any non-linearity of the modulator or any change in the characteristics of the modulator with time will mean that the generated sine wave will no longer reflect the real conditions, and the resulting zeta-potential measurements become less reliable.

To address these shortcomings, we have developed a modification of PALS in which an additional modulator monitor is implemented (see Fig. 1). In the newly patented method, "continuously monitored PALS" (cmPALS), this extra modulator monitor detects the interference between the modulated and unmodulated (reference beam) laser light. Thus, its beat frequency is solely the modulation frequency and is therefore independent of the electrophoretic motion of the particles. In other words, the frequency difference between sample interference and modulator monitor is exactly the Doppler shift caused by the electrophoretic motion of the particles. Any non-linearity of the modulator is automatically compensated, and does not influence the results. The quality of the results is also not affected by any longer-term deterioration in the modulator performance. Thus, the advent of cmPALS means that modulators with large movements can be used, despite their non-linearities. As a consequence the sensitivity and stability of laser

Doppler electrophoresis measurements can be significantly enhanced because measurements of substantially shorter duration and lower electric field applied become feasible.

Results and Discussion

Latex standard solution was purchased from Thermo Fisher Scientific and diluted to 0.05 % in 10 mM NaCl. Zeta potential measurements were carried out with cmPALS technology on a Litesizer™ 500 particle analyzer, and with PALS technology on a competitor's instrument.

To compare the performance of cmPALS and PALS, the zeta potential of a latex standard (0.05 % in 10 mM NaCl) was measured with a cmPALS instrument and a PALS instrument.

Although both methods show a decreasing zeta potential magnitude as the voltage is reduced, there is a significant difference in the quality of the results.

Conclusion

Continuously monitored phase-analysis light scattering (cmPALS) is a development of the classical PALS method. The result is that the sensitivity and stability of laser Doppler electrophoresis measurements is dramatically enhanced. For the user, this means significantly shorter measurement times and lower electric fields, and therefore more sensitive samples can be analyzed with confidence.

References

[1] W. Tscharnuter, Mobility measurements by phase analysis, Applied Optics 2001, 40:24, 3995-4003.

[2] H. Noack; C. Moitzi, Modulator monitoring during measuring electromobility. European Patent EP2735870, April 25th, 2015.

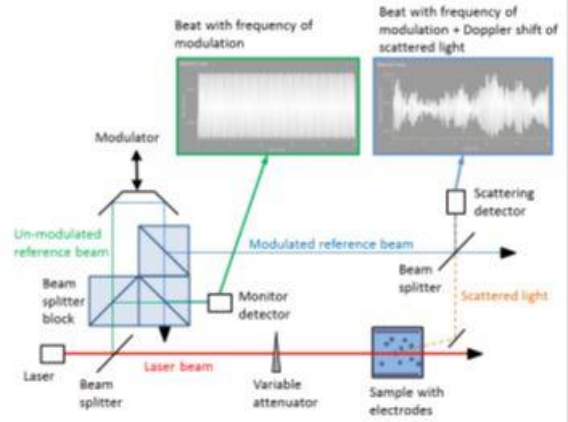

sketch of the cmPALS principle.

1Schematic representation of cmPALS as implemented in the Litesizer™ 500. The scattering detector sees the scattering from the sample and the modulated reference beam. Thus, the beat frequency here is the modulation frequency plus the Doppler shift from the sample. The monitor detector, on the other hand, sees a beat formed by the modulated and the unmodulated reference beam. Hence, its frequency is solely the modulation frequency. The Doppler shift frequency is exactly the frequency difference between both detected signals. Therefore, the Doppler shift frequency is independent of the modulator's linearity, which is the key advantage of cmPALS.

PS1-01-25

Adsorption of Model Protein BSA on Implant Surfaces

Bastian Arlt[1], Thomas Luxbacher[2], Christine Körner[2]

[1]Anton Paar Germany GmbH, Ostfildern, DE; [2]Anton Paar GmbH, Graz, AT

Introduction

Zeta potential is a key indicator of colloid stability. It defines the surface net charge of a surface, whereas we understand surfaces of macroscopic materials such as implant materials, or the interface between dissolved particles in a colloidal solution.

The zeta potential indicates changes in the surface chemistry of e.g. of implant materials and is thus suited to study biocompatible surface coatings. We will focus on these applications and will present static and time-resolved zeta potential analysis methods. While the static method allows investigating the pH dependence of surfaces, the time-resolved method studies adsorption and desorption phenomena, which improve the understanding of surface interactions, such as in-depth characterization of the interaction between proteins in solution and implant materials.

Experimental Methods

The acceptance of implant materials made of stainless steel or titanium by the human body depends on the biocompatibility of the outermost material surface. Various surface properties determine its biocompatibility. Surface charge drives the electrostatic forces that attract proteins as a prerequisite for the osseo-integration, e. g., of tooth implants. On the other hand, desired electrostatic repulsion prevents adhesion of proteinaceous moieties that initiate infection.

Knowledge of the surface is therefore of paramount importance for the development and qualification of biomaterials for implantation. The zeta potential gives information about the surface charge at physiological pH and the chemistry of surface functional groups.

Results and Discussion

The sign and magnitude of the zeta potential let us estimate the electrostatic interaction between the solid surface and a charged species dissolved in the surrounding aqueous solution. Being a surface-sensitive parameter, the zeta potential is best suitable to indicate adsorption and desorption processes. Changes in the surface properties upon adsorption are indicated even if the driving force for adsorption is not of electrostatic nature.

Conclusion

The zeta potential analysis combines the measurement of adsorption kinetics with the validation of the chemistry of the adsorbed surface layer.

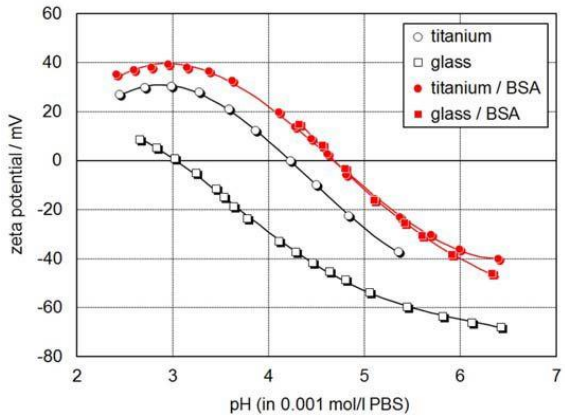

Zeta potential versus pH curves for glass and tianium disks

Zeta potential versus pH curves for glass and tianium disks before and after adsorption of BSA (isoelectric point at pH 4.7)

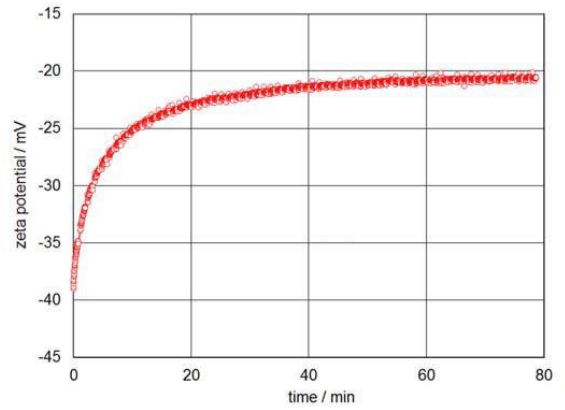

Kinetics of adsorption of bovine serum albumin (BSA) on titanium (at pH 7.4)

Kinetics of adsorption of bovine serum albumin (BSA) on titanium (at pH 7.4)

PS1-01-26

Alternative approach to analyze the foreign body reaction to biomaterials on a molecular level – a new strategy for the reduction of *in vivo* experiments

Mais Olabi[1], Jens Pissarek[4], Matthias Stein[1], Holger Zagst[1], Imke Oltmann-Norden[1], Ole Jung[2], Hermann Wätzig[1,3], **Mike Barbeck**[2,5]

[1]Technische Universität Braunschweig, Institute of Medicinal and Pharmaceutical Chemistry, Braunschweig, DE; [2]University Medical Center Hamburg-Eppendorf, Department of Oral Maxillofacial Surgery, Division for Regenerative Orofacial Medicine, Hamburg, DE; [3]Technische Universität Braunschweig, PVZ: Center of Pharmaceutical Engineering, Braunschweig, DE; [4]botiss biomaterials GmbH, Berlin, DE; [5]BerlinAnalytix GmbH, Berlin, DE

Introduction

Natural polymers such as collagen are broadly used as biomaterial. Every biomaterial induces a tissue reaction cascade that starts with the agglomeration of proteins, which is the basis for material-cell-interactions and the extent of the foreign body reaction (FBR) [1]. Various alternatives to animal testing have been proposed. Herein a new method to understand immune reactions on the molecular level based on affinity capillary electrophoresis (ACE) is presented.

Experimental Methods

ACE is an excellent extension of the Ligand Binding Assay toolbox, in particular when charge interactions are involved. When a charged ligand binds to any macromolecule, its charge-to-mass ratio is altered. This can be measured with high precision using electrophoresis. In our consortium, ACE is applied to study the interactions of polymer-based biomaterials to immune-relevant substances such as collagenases, matrix-metalloproteases (MMPs), effectors from the clotting system (fibrin, fibronectin) and signaling molecules.

Results and Discussion

First results show the correlation of the measurements of interactions between molecules such as fibronectin and collagen-based biomaterials that correlate with *in vitro* data. The results of a typical affinity capillary electrophoresis (ACE) experiment enable to detect the interaction with ligands shifts the electrophoretic mobility of a binding partner, e.g. a protein, which can measured very precisely. Thus, the application of ACE might be a favorable method for the characterization of interactions of protein-based biomaterials with proteins involved in the very early stage of the FBR, which allows for analysis of the molecular basis of the FBR.

Conclusion

The present poster introduces the application of ACE as a favorable method for the characterization of protein-protein-interactions, which allows for analysis of the molecular basis of the FBR. This methodology is proposed to be an optimal tool to reduce animal experiments in the future.

References

[1] Anderson JM, Rodriguez A, Chang DT. Foreign body reaction to biomaterials. Semin Immunol 2008;20:86–100.

PS1-01-27

Implantomics – A New Paradigm in Implantology

Herbert P. Jennissen

Universität Duisburg-Essen, Institut für Physiologische Chemie, Essen, DE

Introduction

Implantomics is the new science of the *implantome*. The implantome is a blend of the two terms *implant* and *proteome*. The proteome is defined as the protein complement of the genome [1]. The term proteome also implies the *mass screening of proteins* with the aim of determining all of the proteins – and indirectly all of the genes – involved in a certain tissue or organ. Here the term proteome is employed in a more general way to specify the totality of proteins associated with a certain biological phenomenon or foreign body inserted into a human. It will be addressed, why it is important to determine the proteome of implants and what the consequences for implant biocompatibility and periimplant healing will be.

Experimental Methods

A human implantome was recently published for the first time [2] reporting all proteins adsorbed to a hip implant within the first two minutes after arthroplasty. It was determined by the method of liquid chromatography combined with mass spectrometry i.e. LC-MS/MS. The protein mass identification was performed with the Proteome Discoverer software (Thermo Scientific).

Results and Discussion

A large amount of *in vitro* experiments has been performed to prove that Albumin, fibrinogen, IgG and possibly fibronectin (*plasma protein doctrine*) are the first adsorbed, followed by blood coagulation, a fibrin network and oncoming cells. In Essen a collaborative group of orthopedics and biochemists [2] decided to check this hypothesis by determining the initial protein layer on titanium hip arthroplasty explants ca. 2 min after implantation They found that the hip implantome consisted of 2802 unique proteins of which 77% were of intracellular origin and only 9% from blood plasma [2]. Thus, we have to cope with a mass-identification of a complete set of proteins in an implant-tissue interface and think in the dimensions of a proteome and not of a single protein. The results demonstrate that the *in vitro* evidence leading to the *plasma protein doctrine* of the initial protein layer being derived from blood plasma [3], did not "translate" into the human *in vivo* proteome reality, with only 9% plasma proteins being components of the hip implantome.

The determination of the implantome on implants is essential, because protein adsorption is the first foreign body response in humans. It is the first fundamental and inevitable interaction between the human body and the surface of a prosthesis forming the implant-tissue interface. This first interfacial protein layer i.e. the *primordial implantome* mediates the first interactions between cells (e.g. macrophages [4]) and the implant. It is the first fingerprint of the body on an implant.

This protein layer triggers a sequence of events determining either the path to implant integration, i.e. the final steady-state implantome of integration (e.g. *integratome*), or in case of pathway malfunction to early or late aseptic implant failure. Such Implant loosenings may be mirrored in the implantome composition. Possibly the implantome composition will also deviate from one implant type to the next, indicating that the starting point for integration will be different. However all of these steps are still unknown. It is the aim and mission of implantomics to clarify these new pathways of implantome maturation from the primordial implantome to the final integratome and to employ this information for diagnostics and therapy.

Conclusion

Without an understanding of the implantome composition and function on implants the subsequent steps of the foreign body response culminating in periimplant healing and implant integration will not be clarified.

References

[1] Wasinger, V. C., Cordwell, S. J., Cerpa-Poljak, A., Yan, J. X., Gooley, A. A., Wilkins, M. R., Duncan, M. W., Harris, R., Williams, K. L., & Humphery-Smith, I. (1995) Progress with gene-product mapping of the Mollicutes: Mycoplasma genitalium. *Electrophoresis*, **16,** 1090-1094.

[2] Jäger, M., Jennissen, H. P., Haversath, M., Busch, A., Grupp, T., Sowislok, A., & Herten, M. (2019) Intra-surgical Protein Layer on Titanium Arthroplasty Explants: From the Big Twelve To The Implant Proteome. *Proteomics. Clin. Appl.*, e1800168.

[3] Kanagaraja, S., Lundstrom, I., Nygren, H., & Tengvall, P. (1996) Platelet binding and protein adsorption to titanium and gold after short time exposure to heparinized plasma and whole blood. *Biomaterials*, **17,** 2225-2232.

[4] Jennissen, H. P. (2016) A Macrophage Model of Osseointegration. *Curr. Dir. Biomed. Engineer.*, **2,** 53-56 (DOI 10.1515/cdbme-2016-0015).

Acknowledgement

This research was supported by the German Research Foundation (Deutsche Forschungsgemeinschaft, DFG) Project No. Je84/15-3.

PS1-01-28

Fabrication of bottle-shaped TiO_2 nanotubes for drug delivery system

Sayaka Miyabe, Yushi Fujinaga, Hiroaki Tsuchiya, Shinji Fujimoto

Osaka university, Graduate School of Engineering, Suita, JP

Introduction

Drug-releasing implants have attracted attention as a localized drug delivery system (LDDS) that enables continuous dosing of drugs locally. The TiO_2 nanotubes formed by anodizing Ti have been studied for the application of the LDDS platforms because of the large surface area and high aspect ratio[1)]. In general, the structure of TiO_2 nanotubes formed by anodizing at constant potential is linear in the direction perpendicular to the substrate, and the diameter and length of the tubes are proportional to the applied potential. Tubes formed by anodizing at high potential have high drug loading but a large amount of initial drug release occurs due to their large diameter and length. On the other hand, tubes formed by anodizing at low potential suppress the initial drug release but have low drug loading due to their small diameter and length. In this study, bottle-shaped TiO_2 nanotubes whose diameter is large at the bottom part and small at the top part were fabricated by anodizing with controlling the potential.

Experimental Methods

Material examined was Ti grade 2 which was cut into samples with a dimension of typically □15.5 mm^2 and 1 mm thickness. The samples were polished with SiC abrasive paper and finally mirror-finished with colloidal silica, then ultrasonically cleaned in acetone and methanol, followed by rinsing with deionized water and dried at room temperature. Electrochemical treatments of anodizing for the nanotubes formation were carried out in ethylene glycol containing 0.135 M NH_4F and 5 vol.% H_2O using a two-electrode electrochemical cell with a platinum counter electrode. The electrochemical treatments consisted of sweeping potential at 0.1 V/s and constant potential at predetermined potentials. Four types of specimens were prepared as follows; (1) bottle-shaped TiO_2 nanotubes, (2) TiO_2 nanotubes anodized at 20 V, (3) TiO_2 nanotubes anodized at 60 V and (4) mirror polished. The morphology of nanotubes was measured by field emission scanning electron microscopy (FE-SEM). Indomethacin was loaded into samples as a model drug. Ultraviolet･visible (UV-Vis) absorbance of PBS including released indomethacin were measured by microplate reader at predetermined periods, in order to evaluate the drug releasing behavior.

Results and Discussion

Figure 1 shows FE-SEM image of bottle-shaped TiO_2 nanotubes sample. The inner diameter of the top part, the outer diameter of the bottom part and length of bottle-shaped TiO_2 nanotubes were about 50 nm, 190 nm and 10 mm, respectively. At the section where the anodized potential was gradually increased, diameters of TiO_2 nanotubes were changed and closed TiO_2 nanotubes were observed. It was confirmed that indomethacin was loaded over the entire length of TiO_2 nanotubes by energy dispersive X-ray spectrometry (EDX). The amounts of indomethacin loaded samples were in descending order, TiO_2 nanotubes anodized at 60 V, bottle-shaped TiO_2 nanotubes , TiO_2 nanotubes anodized at 20 V, mirror polished. As a result of the drug release test using indomethacin, initial (burst) release and followed slow release are observed from all samples although to varying degrees. The initial drug release from bottle-shaped TiO_2 nanotubes was lower than that from TiO_2 nanotubes anodized at 60 V. The total amount of slow release from bottle-shaped TiO_2 nanotubes was the highest. These results suggest that bottle-shaped TiO_2 nanotubes can be a candidate for platform of LDDS.

Conclusion

Anodizing of Ti with controlling the sweeping potential and constant potential was performed, and the following conclusions are obtained:

Bottle-shaped TiO_2 nanotubes whose inner diameter of the top part, the outer diameter of the bottom part and length were about 50 nm, 190 nm and 10 mm respectively were formed. As a result of the drug release test of indomethacin, initial release was suppressed and followed slow release was sustained from bottle-shaped TiO_2 nanotubes.

References

1) Losic D. et al., Expert Opinion on Drug Delivery 12(2015), pp. 103-127.

Acknowledgement

This study was supported by the Grant-in-Aid for Scientific Research (C) (Project No. 15K06485) from the Japan Society for the Promotion of Science and Shiseido Female Researcher Science Grant.

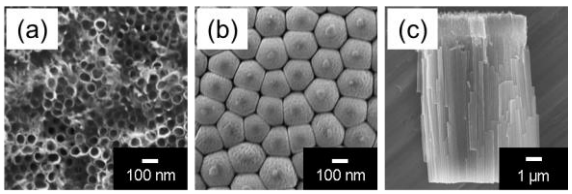

Figure 1
FE-SEM images of bottle-shaped TiO_2 nanotubes; (a) top view, (b) bottom view and (c) cross sectional view.

PS1-01-29

Improvement in Mechanical Performance of Biomaterial Ti alloy by Controlling Volume Fraction of Martensite Phase

Toshikazu Akahori, Shota Ino, Saki Tanaka, Tomokazu Hattori

Meijo University, Dept. of Material Science and Engineering, Nagoya, JP

Introduction

Recently, biomaterial α + β type Ti alloys with relatively low Young's modulus and high specific strength have been widely used all over the world [1]. Martensite (M) phase in α + β type Ti alloy has been reported to improve the toughness and ductility, therefore, there is high possibility of improvement in the mechanical properties easily by controlling the volume fraction of M phase [2]. In this study, the change in mechanical properties of α + β type Ti-6Al-7Nb (Ti67) with various volume fractions of M phase were systematically investigated through the various heat treatments and thermo-mechanical treatments. In addition, those of Ti67 subjected to fine particle bombarding process (FPB) were also investigated for more improvement.

Experimental Methods

Materials used in this study were hot-forged Ti67 bars with a diameter of 25 mm subjected to solution treatment (ST) at 1123K, 1173K, 1223K, 1243K and 1273 K for 3.6 ks in vacuum followed by water-quenching (WQ). Some materials were cold-rolled at around 30% and re-solution treatments at 1243 K for short time. Fine particle bombarding process (FPB), which is one of mechanical surface modification processing, was applied on the specimen surface of Ti67 subjected to ST at 1243 K with steel beads with an average particle diameter of 150 μm under an injection pressure for 90s. Optical microscopy (OM), scanning electron microscopy (SEM) equipped with energy dispersive X-ray spectrometry (EDX) and X-ray diffraction (XRD) spectroscopy were used to identify the constitutional phases. Vickers hardness (HV) test, Young's modulus measurement, tensile and fatigue tests were carried out to evaluate the mechanical properties.

Results and Discussion

Microstructures of Ti67 subjected to ST under the temperature of β transus were composed of the primary a and M phases.

Young's modulus decreased with an increase in the volume fraction of M phase. That of Ti67 subjected to ST at 1243 K was the lowest value (around 85 GPa). However, the Young's modulus increase again after ST over 1243 K. On the other hand, the tensile strength of Ti67 subjected to various ST increased simply with an increase in the volume fractions of M phase.

As the volume fraction of M phase increases, the fatigue strength shows an upward tendency, and the fatigue limit of Ti67 subjected to ST at 1243 K shows the highest value (880 MPa) as shown in Fig. 1. This value is much greater than that of annealed Ti-6Al-4V, which is one of representative biomedical α + β type Ti alloys. From obtained results, it is confirmed that relatively low Young's modulus and high mechanical properties required for the metallic biomaterial are obtained by controlling the volume fraction of M phase by a simple heat treatment.

Conclusion

1. Microstructures of Ti67 subjected to ST at 1173 K to 1273 K below the temperature of β transus were composed of martensite and primary α phases. The volume fraction of M phase increased with an increase in ST temperature.
2. Tensile strength increased simply with an increase in the volume fraction of M phase, while Young's modulus showed a reverse trend up to ST at 1243K. The Young's modulus of Ti67 subjected to ST at 1243 K was around 85 GPa.
3. Fatigue limit of Ti67 subjected to ST at 1243K showed the highest value of 880 MPa.

References

1.

M. Niinomi and T. Akahori, Expert Rev. Med, Devices, 7(2010), 481-488.

2.

H. Matsumoto, Materia Japan, 48(2019), 515-519.

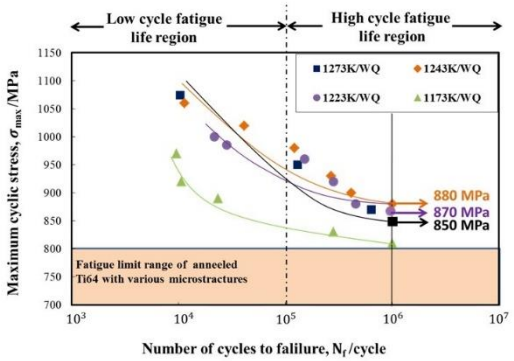

Fatigue Properties

Fig. 1 S-N curves of Ti67 subjected to ST at 1173 to 1273 K along with fatigue limit range of Ti-6Al-4V with various microstructures.

PS1-01-30

DESIGN AND MANUFACTURE OF CUSTOMIZED MEDICAL IMPLANTS

Bozena Rokita[1], Marcin Elgalal[3,8], Bogdan Walkowiak[3,2], Piotr Ulanski[1], Tomasz Kubiak[4], Piotr Komorowski[3,2], Krzysztof Makowski[3], Andrzej Styczynski[6], Jacek Sawicki[5], Marcin Domzalski[7]

[1]Lodz University of Technology, Institute of Applied Radiation Chemistry, Lodz, PL; [2]Lodz University of Technology, Department of Biophysics, Lodz, PL; [3]Bionanopark LTD, Bionanopark Laboratories, Lodz, PL; [4]Lodz University of Technology, Department of Strength of Materials and Constructions, Lodz, PL; [5]Lodz University of Technology, Department of Numerical Methods in Materials Science, Lodz, PL; [6]Pafana SA, Pabianice, PL; [7]Medical University of Lodz, Clinic of Orthopedics and Traumatology, Lodz, PL; [8]Medical University of Lodz, Department of Radiological Diagnostics and Isotope Therapy, Lodz, PL

Introduction

In the years 2006 – 2010 research on the subject of custom medical implants was carried out at the Department of Biophysics, Institute of Materials Science, Lodz University of Technology. The aim of this work was to assess the possible advantages of custom implants and whether their use was clinically justifiable. The results of this research were later commercialized in the form of a newly created Custom Medical Implants Unit that was established in 2011 at Bionanopark Ltd. To date, as a result of this research, over one hundred custom maxilla-facial and cranial implants have been designed, produced and clinically implemented (orbital wall reconstruction, cranioplasty, mandibular reconstruction). Each year, over 20,000 leg amputations are carried out in Poland as a consequence of different clinical conditions. These patients later require a limb prosthesis and physiotherapy in order to regain mobility. The standard prosthetic device that is commonly used to treat such patients, is the socket-suspension type prosthesis system, which unfortunately transfers loads through the soft tissues of the limb stump. However, there is an alternative method of treatment, which involves the use of osseointegrated implants that facilitate direct skeletal attachment of a prosthesis [1,2]. On the basis of the available data, we recognized a significant need for custom designed, osseointegrated percutaneous orthopaedic implants, which at present are not generally available. In our opinion the design and manufacture of such prostheses is worthwhile and should be developed into a clinically viable medical device.

Experimental Methods

The design stage must take into consideration such aspects as conforming these bespoke implants to individual and unique patient anatomy, implant mechanical strength analysis and its integration with bone tissue and selection of an appropriate biomaterial as well as a structural analysis of its surface. On the other hand, the manufacturing process must take into account additive techniques (3D printing), subtractive methods (CNC milling) and hybrid technologies, which can be used to make precise, controlled implant surface modifications. In addition to this, validation of different sterilization methods for such products as well as post-sterilization structural analysis, biocompatibility and thrombocompatiblity must be evaluated.

Results and Discussion

The above concept of designing and manufacturing osseointegrated percutaneous implants formed the basis of a project that was prepared by the authors and subsequently positively evaluated in the POIR programme 1/4.1.4/2017 and accepted for funding by the National Center for Research and Development.

The project consists of the following seven stages - implant design and biomaterial selection, implant mechanical strength assessment and integration with bone tissue (both theoretical and experimental approach), implant manufacture (including surface modification), validation of implant sterilization techniques and post sterilization biological evaluation (biocompatibility, thrombocompatibility and induction of neoplasia or tumor recurrence) and most importantly implant clinical application. The project will be implemented by four units within Lodz University of Technology (the project leader), Bionanopark Ltd, PAFANA SA and Medical University of Lodz and will last for 36 months starting from June 2018.

Conclusion

Finally, the developed methodology for designing and manufacturing such custom orthopaedic implants, will be implemented and commercialized by Bionanopark Ltd. In the initial phase implants will be available for clinical applications in Poland and later on foreign markets, also.

References

[1] P. Stenlund, M. Trobos, *et al.,* J. Orthop. Res. 35 (2017)1113–1122

[2] Y. Li, R. Brånemark. Unfallchirurg. 120 (2017) 285–292

Acknowledgement

The project is financed by the National Center for Research and Development in accordance with the contract POIR.04.01.04-00-0058/17-00.

PS1-01-31

Surface modified Ti-based nanostructures for improving hemocompatibility of vascular stents

Metka Benčina[1], Ita Junkar[1], Eva Levičnik[2], Rok Zaplotnik[1], Matjaz Valant[3,4], Miran Mozetič[1], Aleš Iglič[5]

[1]Jožef Stefan institute, Department of Surface Engineering and Optoelectronics, Ljubljana, SI; [2]Slovenian Tool and Development Centre, Celje, SI; [3]University of Nova Gorica, Materials Research Laboratory, Nova Gorica, SI; [4]University of Electronic Science and Technology of China, Institute of Fundamental and Frontier Sciences, Chengdu, CN; [5]University of Ljubljana, Faculty of Electrical Engineering, Ljubljana, SI

Introduction

Various technologies have already been employed in order to enhance hemocompatibility of current drug-eluting (DES) and bare metal stents (BMS) [1], since in-stent restenosis and in-stent and late stent thrombosis continue to be the most common adverse events after stenting [2, 3]. Successful stenting depends mainly on avoiding the aggregation of platelets in the blood vessels as well as on appropriate proliferation of endothelial cells and controlled proliferation of smooth muscle cells. Titania nanotube surfaces (TiO_2 NTs) manufactured via electrochemical anodization process have gained considerable attention as stent surfaces [4]. In present contribution, crystallization of TiO_2 NTs with low pressure non-thermal oxygen plasma is reported. The influence of plasma processing conditions on TiO_2 NTs crystal structure and morphology was examined by X-ray diffraction (XRD) and scanning electron microscopy (SEM). In addition, *in vitro* biological response of whole blood to the as-synthesized and crystallized TiO_2 NTs has benn examined. The results indicate that application of such surfaces for blood connecting devices is prospective, as practically no platelet adhesion or activation on crystallized TiO_2 NTs surfaces was observed.

Experimental Methods

TiO_2 NTs were synthesized by electrochemical anodization of Ti foil as shown previously [4]. In order to crystalize the oxide layer, samples were treated with oxygen plasma as shown in Ref. [5]. Scanning electron microscopy (SEM) and X-ray diffraction spectroscopy (XRD) were used to determine morphology and crystal structure of the TiO_2 NTs. Interactions of as-prepared surfaces with platelets were examined with SEM.

Results and Discussion

XRD analysis showed that the as-anodized TiO_2 NTs samples are amorphous and remain such even after 3 min of exposure to oxygen plasma at 200 W (Figure 1). Exposure of samples to higher power of plasma induce crystallization; a mixture of anatase and rutile crystal phase appears after the treatment of TiO_2 NTs for 10 s in plasma with the power of 400 W and 600 W. However, the 1 s plasma exposure at these conditions is not enough to initiate the change of crystal structure, since no anatase nor rutile peaks were detected. The plasma treatment at 800 W for 1 s and 10 s results in anatase and a mixture of anatase/rutile crystal phases, respectively. As-anodized (amorphous) Ti foil was found to promote adhesion and activation of platelets, since many spread and fully spread platelets were observed on its surface. However, the *in vitro* biological response of whole blood with crystalline TiO_2 NTs showed that the crystallization reduces adhesion and activation of blood platelets, which is of particular interest for designing medical devices that are likely to contact blood, such as vascular stents.

Conclusion

Non-thermal oxygen plasma induced crystallization of TiO_2 NTs synthesized by electrochemical anodization of Ti foil. The transition of the NTs' amorphous phase to anatase and/or rutile crystal structure was obtained within a few seconds of exposure to oxygen plasma without changing the desired morphology of NTs. The adhesion and activation of platelets on the crystalline surfaces was reduced, thus as-prepared surfaces presents promising non-thrombogenic material for stent surfaces.

References

[1] Kirtane A. The Medical Roundtable Cardiovascular Edition. 2018.
[2] Kastrati A. Elsevier. 2018.
[3] Kallel R. Ann. Cardiol. Angeiol. 2017:393-399.
[4] Junkar I. Bioelectrochemistry. 2016; 109:79-86.
[5] Kulkarni M. Adv. Mat. Lett. 2016;7:23-28.

Acknowledgement

This research was funded by the Slovenian Research Agency for financial support [grant numbers Z3-4261, J3-9262, J1-9162, J2-8166, J2-8169, J5-7098, P2-0232] and Slovenian Ministry of Education, Science and Sport [grant "Public call for encouraging young investigators at the beginning of their career 2.0", No. 5442-15/2016/18].

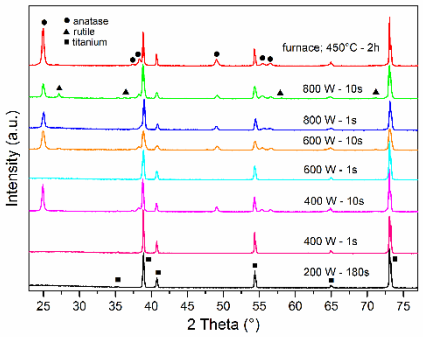

X-ray diffraction (XRD) patterns of TiO2 NTs
Figure 1. X-ray diffraction (XRD) patterns of TiO2 NTs of 100 nm diameter measured after plasma treatment at different powers; 200, 400, 600 and 800 W for different times and TiO2 NTs of 100 nm diameter after annealing in a furnace at 450 °C for 2 h.

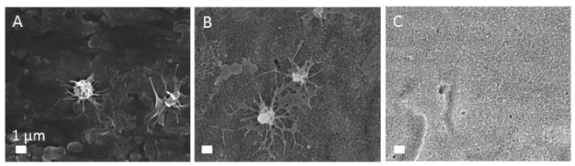

Figure 2: Platelets adhesion and activation
Figure 2: Platelets adhesion and activation on (A) Ti foil, (B) amorphous and (C) annealed TiO2 NTs with 100 nm in diameter.

PS1-01-32

Long term *in vivo* biocomatibility study of modified Ti6Al7Nb in the aspect of local effects after implantation

Barbara Zawidlak-Węgrzyńska[1], Małgorzata Gonsior[1], Karolina Janiczak[1], Danuta Gonsior[1], Piotr Ścigała[1], Roman Kustosz[1], Tadeusz Wierzchoń[2], Michał Tarnowski[2], Romuald Wojnicz[3], Edyta Raichman-Warmusz[3]

[1]Professor Zbigniew Religa Foundation of Cardiac Surgery Development, Zabrze, PL; [2]Warsaw University of Technology, Faculty of Material Science and Engineering, Warszawa, PL; [3]Medical University of Silesia, Department of Histology and Embryology, Zabrze, PL

Introduction

Modification of the well-known glow discharge assisted nitriding process called active screen plasma nitriding has been used for enhancing the biocompatible properties of Ti6Al7Nb titanium alloy through production of TiN+Ti2N+αTi(N) diffusive surface layers [1]. The aim of the study was to evaluate the tissue reaction after implantation in the rabbit dorsal muscle of the Ti6Al7Nb titanium alloy and Ti6Al7Nb modified with TiN type layers.

Experimental Methods

The implantation test was carried out according to the standardized assays described in ISO 10993-6. A total of 72 New Zealand white both sexes rabbits weighing from 3000 to 3500 grams were used in this experiment. Four implants (discs of 10 mm diameter 1,5 mm thickness) were aseptically inserted subcutaneously on the animal's back. As a negative control Ti6Al7Nb titanium alloy was used. The animals were observed for: 4, 12 and 26 weeks. After animals euthanasia, a macroscopic evaluation of the implantation area was performed and the biomaterial implants were removed. The tissues were fixed with 4% formalin, embedded in paraffin, and stained with hematoxylin-eosin and Trichrome Masson for histological studies.

Results and Discussion

Histopathological analysis revealed in vast majority normal healing process around the implant and isolated cases of an inflammatory change, more frequent for the animals with TiN implants in the observation period of 4 weeks. A micro-section of the implants showed that the investigated material implanted for the different periods: 4, 12 and 26 weeks, caused no response-mild fibrosis. There was no muscle degeneration, nor necrosis, nor any other significant change observed.

Conclusion

Both investigated biomaterials: TiN+Ti2N+αTi(N) produced in so called active screen plasma nitriding process on Ti6Al7Nb titanium alloy surface as well as Ti6Al7Nb, implanted in vivo did not induce any adverse tissue reactions in the long-term period of 26 weeks.

References

1. Ti6Al7Nb Alloy Surface Improvement For Implantable Blood Pumps Applications, M.Gonsior, M.Tarnowski, K.Janiczak, B.Zawidlak-Węgrzyńska, T.Wierzchoń, M.Gawlikowski, R.Kustosz, etc., Engineering of Biomaterials, No 143, Special Issue, Vol. XX, 2017, p.65, 2017

Acknowledgement

The authors would like to thank NCBIR (Grant no: STRATEGMED-2/ RH-ROT/266798/15/NCBR/2015) for providing financial support to this project.

PS1-01-33

Bending stiffness and cyclic fatigue resistance of WaveOne Gold, Reciproc Blue, and HyFlex EDM instruments

SeokWoo Chang

Kyung Hee University, Kyung Hee University Dental Hospital, Department of Conservative Dentistry, Seoul, KR

Introduction

The purpose of this study is to compare the bending moment and the cyclic fatigue resistance of three heat-treated nickel-titanium rotary instruments, and to investigate their phase-transformation behavior.

Experimental Methods

Forty instruments each of WaveOne Gold Primary (WOG), Reciproc Blue R25 (RPB), and HyFlex EDM OneFile (HDM) were used. A vertical load was applied to a point 3 mm from the tip, and the bending moment was measured until a displacement of 3 mm. Tests were conducted at either room temperature (RT: 22 ℃) or body temperature (BT: 37 ℃) (n=10). Cyclic fatigue resistance tests were performed in an artificial canal made of three metal pins, which had a curvature angle of 40° and a 5-mm radius. Tests were conducted at either RT or BT (n=10). Instruments were operated according to the manufacturers' instructions. Test results were analyzed using the Kruskal-Wallis and the Mann-Whitney tests. Three instruments of each brand were subjected to differential scanning calorimetry (DSC).

Results and Discussion

While no significant difference in bending moment between the three brands was found at RT, at BT the bending moment of RPB was the highest, followed by WOG, and then HDM ($P < 0.05$). The bending moments of RPB and WOG were higher at BT than at RT ($P < 0.05$), whereas that of HDM did not change with the temperature. RPB demonstrated the longest fracture time at RT, followed by HDM, and then WOG ($P < 0.05$). At BT, HDM had the longest fracture time, followed by RPB, and then WOG ($P < 0.05$). The fracture times of WOG and RPB at BT were significantly less at RT ($P < 0.05$), whereas temperature did not influence the fracture time of HDM. DSC curves revealed a two-stage phase transformation in the WOG and RPB heating curves. The phase composition of WOG at BT was a mixed state of R-phase and austenite, whereas that of WOG at RT was mainly R-phase. The phase composition of RPB at BT was almost pure austenite, whereas a mixture of R-phase and austenite existed together at RT. The phase composition of HDM at RT was martensite. At BT HDM was a mixed state of martensite and austenite, mainly martensite. A martensitic structure in BT, like Hyflex EDM, will exert superior flexibility and fatigue fracture resistance in clinical environment.

Conclusion

HDM presented superior flexibility and cyclic fatigue resistance at BT.

References

1. Zupanc J, Vahdat-Pajouh N, Schafer E. New thermomechanically treated NiTi alloys - a review. Int Endod J 2018;51:1088-1103.

2. Shim KS, Oh S, Kum K, et al. Mechanical and metallurgical properties of various nickel-titanium rotary instruments. Biomed Res Int 2017;2017:4528601.

3. Arias A, Macorra JC, Govindjee S, Peters OA. Correlation between temperature-dependent fatigue resistance and differential scanning calorimetry analysis for 2 contemporary rotary instruments. J Endod 2018;44:630-4.

Acknowledgement

The authors deny any conflicts of interest related to this study.

PS1-01-34

Polymer coated iron-based biodegradable cellular scaffolds for bone treatment: preparation and characterisation

Radka Gorejová[1], Renáta Oriňaková[1], Andrej Oriňak[1], Miriam Kupková[2], Monika Hrubovčáková[2]

[1]Pavol Jozef Šafárik University in Košice, Department of Physical Chemistry, Košice, SK; [2]Slovak Academy of Science, Institute of Materials Research, Košice, SK

Introduction

Biodegradable materials prepared from metals could serve as a potential orthopedic implants[1,2]. They support damaged tissue during healing process and dissolve spontaneously after complete regeneration. All of their corrosion products have to be non-allergic and non-toxic and cause no harm to the patient[3]. Insufficient corrosion rate of pure iron is a limitation for its further use. Nevertheless, it could be improved by surface modification.

Experimental Methods

Carbonyl iron powder (CIP, 3.8 – 5.3 μm; 99.5 % Fe, 0.05 % C, 0.01 % N, 0.18 % O) was used to prepare porous samples with a diameter of 5 mm and height of 15 mm using polyurethane (PUR) foam as a template. The final material was obtained by two-step sintering at 450 °C (N_2 atmosphere) and 1120 °C (10% H_2, 90% N_2 reduction atmosphere). The polymer coating (polyethyleneimine, PEI) was applied by the sol-gel method after cleaning samples in acetone, ethanol and distilled water, each for 10 minutes. Solutions with three different concentrations of PEI were prepared. Samples were molded into the methyl methacrylate resin (Dentacryl) and studied using optical microscopy. Scanning electron microscopy (SEM) with Energy dispersive X-ray analysis (EDX) and Brunauer–Emmett–Teller (BET) analysis were used for surface morphology, microstructure and surface area characterization. Corrosion rates of studied materials were evaluated by 12-week long immersion test.

Results and Discussion

With increasing concentration of used PEI solution, surface roughness decreased leading to a reduction in a surface area determined by BET analysis. Sintered pure iron exhibits microporosities (0,5-6 μm), confirmed by both optical and SEM methods, whereas coated samples were smooth and their surface was more homogenous. Presence of macroporosities corresponding to PUR template (600-2000 μm) was preserved among all samples. EDX method used to determine the chemical composition has proven PEI presence on the surface of the studied material before corrosion and the presence of degradation products after static immersion test. Results from the immersion test showed that the degradation rate of polymer-coated samples was greater than that of pure iron which suggests that polymer-coating can lead to corrosion rate improvement.

Conclusion

Porous samples prepared *via* powder metallurgical route were formed using PUR as a template. Original macroporosity of reticulated foam was preserved and can be easily manipulated to achieve bone-like structure. Surface microporosities disappeared during sol-gel processes but were still present in the bulk material. Corrosion rates of coated samples increased after surface modification of pure iron.

References

Zheng Y. et al, Materials Science and Engineering. R77:1–34, 2014.

Yusop A. H. et al, International Journal of Biomaterials. 2012.

Schinhammer M. et al, Materials Science and Engineering. C33:782–789, 2013.

Acknowledgement

This work was supported by the projects APVV-16-0029 of the Slovak Research and Development Agency and VEGA 1/0074/17 of the Slovak Scientific Grant Agency.

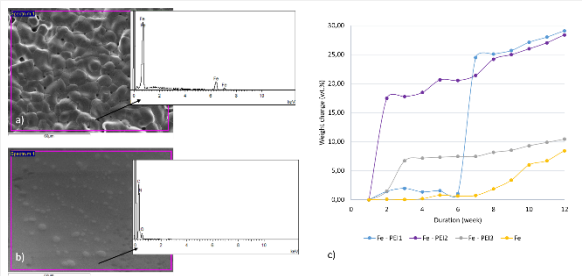

Fig.1
Surface morphology of the prepared scaffolds. SEM micrographs and EDX analysis of pure iron (a) and PEI coated iron (b). Changes in sample weight during 12-week long immersion test (c).

PS1-01-35

Effect of sandblasting treatment on in vitro degradation behavior and cytotoxicity of zinc and its alloys

Ping Li[1], Junyu Qian[2], Wentai Zhang[2], Christine Schille[1], Ernst Schweizer[1], Alexander Heiss[3], Claudia Legner[3], Ulrich E. Klotz[3], Guojiang Wan[2], Jürgen Geis-Gerstorfer[1], Lutz Scheideler[1]

[1]University Hospital Tübingen, Section Medical Materials Science and Technology, Tübingen, DE; [2]Southwest Jiaotong University, Key Laboratory of Advanced Technologies of Materials, Ministry of Education, College of Materials Science and Engineering, Chengdu, CN; [3]Research Institute for Precious Metals and Metals Chemistry (fem), Schwäbisch Gmünd, DE

Introduction

Zinc (Zn) and its alloys have drawn attention as potential materials for orthopedic or craniomaxillofacial implants. Nonetheless, Zn and its alloys exhibit relatively slow degradation rates within bone environments compared to the degradation requirements for clinical application [1,2]. Previous studies proposed that the degradation rates of Zn-based materials can be accelerated via alloying [3], metal matrix composite [2], micro-arc oxidation coating [4] or a sacrificial Mg-rich anode [5]. Moreover, sandblasting treatment has been demonstrated as a feasible approach to improve the degradation rate of metals, such as Mg-Ca alloy [6] and pure Fe [7]. This study aimed to investigate the effect of different sandblasting treatments on *in vitro* degradation behavior and cytotoxicity of Zn and its alloys.

Experimental Methods

A Zn-4Ag and a Zn-2Ag-1.8Au-0.2V (wt.%) alloy (denoted as Zn-Ag-Au-V) were fabricated and compared to pure Zn. All samples were ground up to P4000 SiC paper. The surfaces of Zn and the Zn alloys were sandblasted by two Al_2O_3 particle sizes,125 µm and 250 µm, as described in a previous study [8]. The microstructure was characterized by stylus profilometry, SEM-EDX and XRD.

The *in vitro* degradation behavior was evaluated with a semi-static immersion test for 14 days. Samples were immersed in DMEM/F-12 under cell culture conditions. The ratio of surface area to extraction volume was set to 1 cm^2/mL. Released metallic ions were detected by ICP-OES, and pH value changes were measured. Corrosion products were analyzed by SEM-EDX. Corrosion rates were calculated by weight loss.

Cytotoxicity was evaluated by an extract test according to ISO 10993-5/-12. Sample extracts were prepared using cell culture medium without FBS at an extraction ratio of 1.25 cm^2/mL for 24 h. Human primary osteosarcoma cells (Saos-2) were used to evaluate the inhibition of relative metabolic activity (CCK-8 assay). Also, metallic ion concentrations and pH value of the extracts were determined.

Results and Discussion

After the sandblasting treatments, average roughness (Ra) and mean roughness depth (Rz) of samples were increased, and both values significantly rose when the size of sandblasting Al_2O_3 changed from 125 µm to 250 µm. Additionally, Al_2O_3 sandblasting particles were embedded into the substrate of Zn and Zn alloys observed by SEM-EDX and XRD analysis.

As shown in Fig. 1a, SEM characterization revealed loose degradation layers covering the whole surfaces, and degradation particles distributed on all surfaces. EDX analysis showed that these corrosion products were mainly composed of Zn, P, O, C and Cl. After removing the degradation products, sandblasted samples presented irregular and rough surface structures consisting of a couple of corrosion pits and localized corrosion attack. Fig. 1b shows

that no obvious differences in cumulative Zn^{2+} release for Zn alloys were detected between sandblasting and control groups. Mean pH values of all samples showed no apparent increase and all were below pH 8.4. Fig. 1c shows that the degradation rates of sandblasted samples were significantly higher than the counterparts of P4000 polished samples ($p < 0.05$).

Fig. 2a shows that cytotoxicity of Zn and its alloys was influenced by the sandblasting treatment with 250 µm Al_2O_3. As shown in Fig. 2b, the Zn ion concentration in the extracts of most sandblasted samples was significantly higher than the counterparts of P4000 samples ($p < 0.05$), but all Zn concentrations were below 25 µM. Also, all pH values were below 8.5.

Conclusion

Degradation rates of Zn and its alloys are significantly increased by sandblasting treatments. Also, degradation behavior and cytotoxicity are related to the sandblasting particle size. This study demonstrates the promising potential of sandblasting treatments for adjusting the degradation behavior of Zn-based alloys. Nevertheless, further investigations are required.

References

1. Li, H., *et al.*, *Sci. Rep.* (2015) 5, 10719
2. Yang, H., *et al.*, *Acta Biomater.* (2018) 71, 2003.
3. Kafri, A., *et al.*, *Metals* (2018) 8 (3), 153
4. Yuan, W., *et al.*, *ACS Biomater Sci Eng.* (2019) 5 (2), 487
5. Yang, H., *et al.*, *ACS Biomater Sci Eng.* (2019) 5 (2), 453
6. Höh, N. V. D., *et al.*, *Adv. Eng. Mater.* (2009) 11 (5), 47
7. Zhou, J., *et al.*, *ACS Appl. Mater. Interfaces* (2016) 8 (40), 26482
8. Al Qahtani, W. M., *et al.*, *Biomed Eng-Biomed Te* (2017) 62 (1), 75

Acknowledgement

The work was supported by AiF-ZIM (KF2342806CK2), CSC (201608440274) and DAAD (57390341).

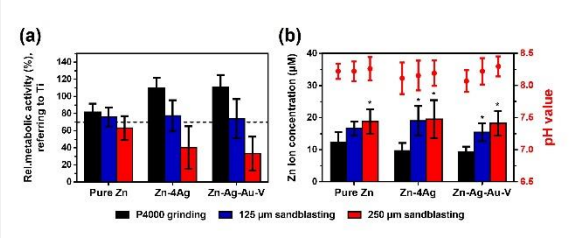

Figure 2: Cytotoxicity of samples: (a) CCK-8 results (b) Analysis of extracts, * represent $p < 0.05$ when compared with P4000 sampes.

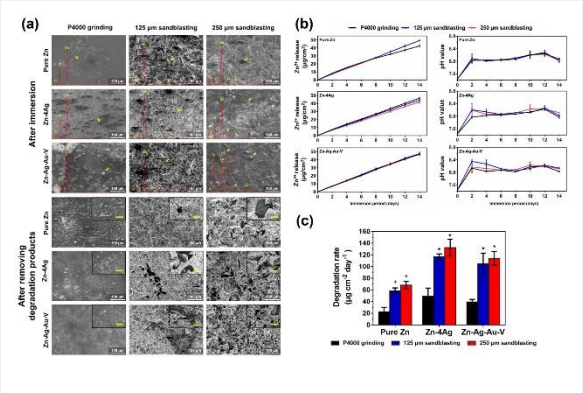

Figure 1: In vitro degradation behavior of samples:
(a) SEM-EDX analysis (The scale bar in the insets image is 10 μm), and the EDX result (inset red line) shows the elemental composition of degradation products pointed with the related yellow arrow, (b) Cumulative Zn ion release and pH value changes, (c) Degradation rate of samples, * represent $p < 0.05$ when compared with P4000 samples.

2:45 p.m. – 3:45 p.m.

Hall 1 / Exhibition Area

PS1-02 | Ceramics and Calciumphosphates

PS1-02-36

Synthesis and characterization of new 3D Fe-doped bioceramic scaffold obtained via Sol-Gel method

Nayarit A. Mata[1], Patricia Ros-Tárraga[2], Pablo Velásquez[1], Angel Murciano[3], Piedad N. De Aza[1]

[1]Universidad Miguel Hernández, Instituto de Bioingeniería, Elche, ES; [2]Universidad Católica San Antonio de Murcia, Grupo de Investigación en Regeneración y Reparación de Tejidos, Guadalupe, ES; [3]Universidad Miguel Hernández, Departamento de Materiales, Óptica y Tecnología Electrónica, Elche, ES

Introduction

The objective of this research was to develop and characterize biomagnetic Si-Ca-P scaffolds to be used in substitution and regeneration of bone tissue. The 3D ceramic scaffolds were formed by a core of composition 1 mol% SiO_2 - 25 mol% P_2O_5 – 68 mol% CaO – 6 mol% Li_2O and was coated with layers of composition 29 mol% SiO_2 – 3 mol% P_2O_5 – 68 mol% CaO doped with 1 - 3 mol% of iron ions. According to the literature consulted, this scaffolds is one of the first magnetic biomaterials formed with two different compositions. The incorporation of iron in the scaffold enhances the bactericidal and mineralogical properties of the bone tissue. Additionally, it provides ferromagnetic properties that can be used in medical applications such as magnetic resonance imaging, cell separation and treatment against cancer such as hyperthermia (1-2).

Experimental Methods

Scaffolds multilayers were synthesized by sol-gel and polymer replication methods. Polyurethane sponges were used as a template to make the 3D scaffold. These sponges were impregnated with the sol solution of composition 1 mol% SiO_2 - 25 mol% P_2O_5 – 68 mol% CaO – 6 mol% Li_2O and sintered at 950 °C for 8 h to obtain the resistant core of the scaffold. Subsequently, the sintered core was coated with a new sol solution of composition 29 mol% SiO_2 – 3 mol% P_2O_5 – 68 mol% CaO doped with 1 - 3 mol% of iron ions. Finally, the scaffolds were sintered again at 950 ºC for 3 h. The characterization was made by Scanning Electron Microscopy (SEM), X-Ray Diffraction (XRD), Fourier Transform Infrared Spectroscopy (FTIR) and mercury porosimetry techniques. The bioactivity was evaluated *in vitro*, the samples were immerged at different time in a simulated body fluid (SBF), which was prepared according to Kokubo.

Results and Discussion

3D scaffolds formed by a porous core coated with layers of calcium phosphate doped with iron ions were obtained through the sol-gel and polymer replication methods. Characterization by XRD demonstrated that the core of the scaffold after sintered is constituted by $Ca_2P_2O_7$, $Ca_3(PO_4)_2$, $LiCa(PO_4)$, SiO_2 and Ca_2SiO_4. The majority of the core is formed by pyrophosphate ($(P_2O_7)^{-4}$) and it is widely known that this correspond to 0.5% of all the phosphate found in the human body (3-4). Additionally, previous research has shown that the pyrophosphate is an important regulator of the process of bone mineralization (5). The presence of pyrophosphate was also evidenced through the FTIR and SEM. Finally, the bioactivity of core coated with iron-doped layers was evaluated by the ability to precipitate hydroxyapatite on the surface when submerged in SBF. Figure 1 shows the images obtained by SEM of the ceramic scaffolds doped superficially with 1% and 3% iron after 1 day of immersion in SBF. Both samples presented precipitates of hydroxyapatite, demonstrating their ability to be bioactive.

Conclusion

Multilayer 3D ceramic scaffolds with optimal porosity were developed and characterized. These scaffolds presented pyrophosphate in the composition of the core, which is an important regulator of the bone mineralization process. Moreover, the scaffolds coated with layers of calcium phosphates doped with iron in a proportion of 1% and 3%, showed bioactivity after 1 day in SBF. The scaffolds developed are an excellent alternative for bone tissue replacement with potential medical applications due to the ferromagnetic properties provided by iron.

References

1. F. Baino, E. Fiume, M. Miola, F. Leone, B. Onida and E. Verné. Fe-doped bioactive glass-derived scaffolds produced by sol-gel foaming. Materials Letters 235 (2019) 207-211.
2. S. Gomes, A. Kaur, J.M. Grenèche, J.M. Nedelec and G. Renaudin. Atomic scale modeling of iron-doped biphasic calcium phosphate bioceramics. Acta Biomaterialia 50 (2017) 78-88.
3. S. Bisaz, R.G. Russell, H. Fleisch. Isolation of inorganic pyrophosphate from bovine and human teeth. Arch Oral Biol 13 (1968) 683-696.
4. R.E. Wuthier, S. Bisaz, R.G. Russell, H. Fleisch. Relationship between pyrophosphate, amorphous calcium phosphate and other factors in the sequence of calcification in vivo. Calcif Tissue Res 10 (1972) 198-206.
5. I.R. Orriss, T.R. Arnett and R.G. Russell. Pyrophosphate: a key inhibitor of mineralization. Current Opinion in Pharmacology 28 (2016) 57–68

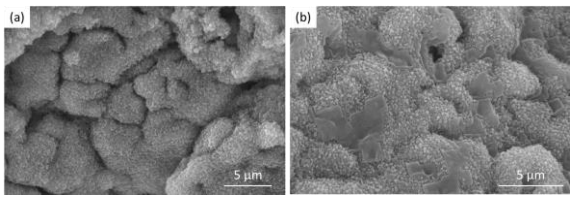

Fig. 1 SEM micrograph of the scaffolds with a core and outer layers doped with: (a) 1% Fe (b) 3% Fe

PS1-02-37

Production of calcium phosphate biomaterials in a droplet-based microfluidic device

Yousra Alaoui Selsouli, Hoon S. Rho, Victor Galvan Chacon, Zeinab Tahmasebi birgani, Pamela Habibovic

maastricht university, Department of Instructive Biomaterials Engineering, MERLN Institute for Technology-Inspired Regenerative Medicine, Maastricht, NL

Introduction

There is an increasing need for developing affordable and effective bone graft substitutes, since the gold standard for regenerating large bone defects, i.e., autologous bone, is associated with important limitations such as donor site morbidity, limited availability of the tissue and additional surgical time. Calcium phosphate (CaP)-based ceramics such as hydroxyapatite (HA) and tricalcium phosphate (TCP) are the most widely used synthetic bone graft alternatives in the clinic [1]. However, in general, their biological performance is considered inferior to that of natural bone tissue, and additional research efforts are expended to improve their bone regenerative potential [2]. In contrast to the conventional one-material-for-one-experiment methods for developing new biomaterials, here we aim to develop a method for high-throughput synthesis and screening of ceramic biomaterials. To this end, we have developed a microfluidic device in which CaP ceramics are synthesized inside water-in-oil microdroplets.

Experimental Methods

CaP ceramics were synthesized inside microdroplets generated by a flow focusing microfluidic device in which a mixture of calcium nitrate and phosphoric acid was used as water phase and mineral oil with Span® 80 was used as oil phase. Upon generation and collection of microdroplets, ammonia was added in order to increase the pH, resulting in precipitation of CaPs. The CaP precipitates were then harvested from the suspension by several washing/centrifugation steps. CaPs, similar to those generated in the microfluidic device, were produced using a conventional wet chemical technique outside the microfluidic device, with calcium nitrate and phosphoric acid as precursors and ammonia for adjusting the pH, and served as control. Varying Ca^{2+}/PO_4^{3-} ratios and pH conditions were used in both synthesis methods in order to produce different CaP phases including brushite, HA and β-TCP. In order to obtain crystalline HA and β-TCP, synthesized biomaterials were sintered at 800˚ C for two hours. The biomaterials were characterized using X-ray diffraction (XRD), Fourier-transform infrared spectroscopy (FTIR), scanning electron microscopy (SEM) and energy-dispersive X-ray spectroscopy (EDS).

Results and Discussion

Various CaP biomaterials were successfully produced in the water-in-oil-regime in the microfluidic device as well as using the wet chemical technique. Figures 1 and 2 show SEM images and EDS spectra of one of the CaP biomaterials (Ca^{2+}/PO_4^{3-}=1) produced using the wet chemical and the microfluidics methods, respectively. The conventional wet chemical synthesis, coupled with sintering treatment in case of HA and β-TCP, allowed for obtaining pure and highly crystalline CaP phases through changing the Ca^{2+}/PO_4^{3-} ratio and pH. The microfluidic setup allowed for tuning additional synthesis parameters such as flow rates, resulting in a controlled generation of microdroplets with varying sizes. Using this feature, CaP particles of varying size can be synthesized in a controlled manner. Extraction and purification of CaP particles from the water-in-oil droplets, however, proved to be challenging and some oil residues

were detected on CaPs particles before sintering. Previous studies have suggested the use of different methods for removing the oil phase such as centrifugation, addition of chemical emulsifiers and filtration [3]. Further optimization of the purification steps based on these methods is currently ongoing. Beside better control during CaP synthesis, the droplet generation system in the microfluidics device provides a miniaturized platform allowing production of multiple CaP phases. In future steps, we are aiming to develop a library of inorganic bone graft substitutes using the droplet-based microfluidic device introduced here.

Conclusion

In these first development steps towards a microfluidic platform for high throughput production and screening of inorganic bone graft substitutes, CaPs were generated in a prototype droplet-based microfluidic device. In the next steps, the method will be extended to other inorganic biomaterials and optimization of synthesis parameters using design of experiments will be explored.

References

[1]H. Yuan et al. Proc Natl Acad Sci USA 107 (31) (2010) 13614-19.
[2]K. Lin et al. Acta Biomaterialia 10 (2014) 4071–102.
[3]S. Ammann et al. Energies (2018), 11(9), 2264.

Acknowledgement

The authors acknowledge financial support by Innovative Research Incentives Scheme Vidi of the Netherlands Organization for Scientific Research (NWO). This research has been made possible with the support of the Interreg Vlaanderen/Nederland BIOMAT collaboration and of the Dutch Province of Limburg.

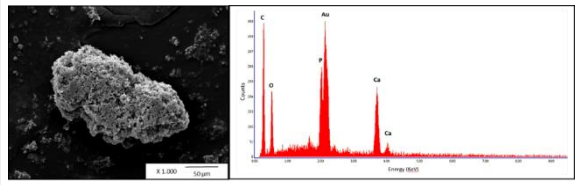

Figure 2: SEM image and EDS spectra of CaP (Ca/P=1) produced using the microfluidic technique

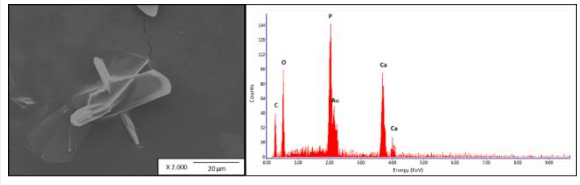

Figure 1: SEM image and EDS spectra of CaP (Ca/P=1) produced using the wet chemical technique

PS1-02-38

Systemic toxicity evaluation after subcutaneous implantation of zirconium stabilized with yttrium

Karolina Janiczak[1], Barbara Zawidlak-Węgrzyńska[1], Małgorzata Gonsior[1], Piotr Ścigała[1], Danuta Gonsior[1], Roman Kustosz[1], Aniela Grajoszek[2], Romuald Wojnicz[3], Edyta Reichman-Warmusz[3]

[1]Foundation of Cardiac Surgery Development, Artificial Heart Laboratory, Zabrze, PL; [2]Medical University of Silesia, Center for Experimental Medicine, Katowice, PL; [3]Medical University of Silesia, Department of Histology and Embryology, Zabrze, PL

Introduction

Biocompatibility assessment of advanced implants like heart assist devices requires a multistep analysis to confirm the safety of use. A novel rotary ventricular assist device (VAD) ReligaHeart® ROT (RH ROT) was developed [1]. Construction of implantable blood pump is a huge challenge in the aspect of long-term contact with blood. This paper presents systemic toxicity evaluation of zirconium stabilized with yttrium, as a part of the biocompatibility assessment. The investigated material is characterized by excellent physico-mechanical properties as well as biological properties evaluated in the in vitro studies and has therefore found application in the new VAD construction.

Experimental Methods

The systemic toxicity was evaluated according to PN EN ISO 10993-11 as limit test. In the assessment a higher dose of zirconium was admitted to the animals than the dose the patient would be exposed in case of heart support with RH ROT. The investigated material was prepared in a representative process for RH ROT device ETO sterilized. The study was conducted with the utilization of 48 New Zealand White rabbits. Animals were divided in study and control groups. Implantation was carried out under infusion anaesthesia. In the study group two samples were implanted subcutaneously on the back of animals. In control group two skin incisions were mad on the back. The observation was conducted depending of the group for 4 (n=6), 12 (n=8), and 26 weeks (n=10). Animal's body weight was controlled every 4 weeks. Before the implantation and then after the experiment before euthanasia the haematological, biochemical and coagulation blood parameters were assessed. After euthanasia a macroscopic evaluation of the implantation area and internal organs was performed. Histopathological assessment of tissues and internal organs was done.

Results and Discussion

During the observation no clinical sings of abnormalities in animal's behaviour were found. The body weight increase was similar for all tested groups. Blood analysis did not reveal any systemic pathology. There were no inflammation (C-reactive protein negative, no leukocytosis) or organ necrosis. Animal's organs were characterized by proper function and endurance – stable levels of total protein, creatinine, urea, total bilirubin were observed. Large fluctuations were observed in the enzyme activity. In the case of alanine aminotransferase (ALT) and gamma-glutamyltranspeptidase (GGT), the mean results significantly exceeded the reference range, however, the values remained stable before implantation and before euthanasia. Blood count parameters were in reference range, so no impact on bone marrow was found. Coagulation parameters were also stable. Macroscopic evaluation of internal organs did not show any irregularities. Histopathological analysis revealed no pathological changes in internal organs or in implantation area.

Conclusion

The investigated material –zirconium stabilized with yttrium reveals no systemic toxicity in the long-term period of 26 weeks.

References

1. R.Kustosz, et al., Archives of Metallurgy and Materials, V.60, 3/2015: p.2253–2260

Acknowledgement

The authors would like to thank NCBIR (Grant no: STRATEGMED-2/ RH-ROT/266798/15/NCBR/2015) for providing financial support to this project.

PS1-02-39

LONG TERM IN VIVO BIOCOMATIBILITY STUDY OF ZIRCONIUM OXIDE-YTTRIUM STABILIZED $ZrO_2 \cdot Y_2O_3$ IN THE ASPECT OF LOCAL EFFECTS AFTER IMPLANTATION

Barbara Zawidlak-Węgrzyńska[1], Małgorzata Gonsior[1], Karolina Janiczak[1], Piotr Ścigała[1], Danuta Gonsior[1], Roman Kustosz[1], Aniela Grajoszek[3], Romuald Wojnicz[2], Edyta Raichman-Warmusz[2]

[1]Professor Zbigniew Religa Foundation of Cardiac Surgery Development, Zabrze, PL; [2]Medical University of Silesia, Department of Histology and Cell Pathology, Zabrze, PL; [3]Center for Experimental Medicine, Medical University of Silesia, Katowice, PL

Introduction

Biocompatibility is one of the main requirements required in the preclinical evaluation of medical devices. In particular biocompatibility evaluation is essential for all materials that can be used in implantable medical devices in 3rd class of risk. In the clinical prototype of Polish implantable rotary blood pump ReligaHeart® ROT (RH ROT), the motor divider is made from ceramic composite, $ZrO_2 \cdot Y_2O_3$, material with high hardness, in order to improve device wear resistance. The aim of the study was to evaluate in vivo the tissue reaction after zirconium oxide-yttrium stabilized $ZrO_2 \cdot Y_2O_3$ implantation.

Experimental Methods

The test was carried out according to the standardized assays described in ISO 10993-6. A total of 48 New Zealand white both sexes rabbits weighing from 3000 to 3500 grams were used. Two ceramic implants (discs of 5 mm diameter 1,5 mm thickness) were aseptically inserted subcutaneously on the animal's back. As a negative control Ti6Al7Nb titanium alloy was used. The animals were observed for: 4, 12 and 26 weeks. After animals euthanasia, a macroscopic evaluation of the implantation area was performed and the biomaterial implants were removed. The tissues were fixed with 4% formalin, embedded in paraffin, and stained with hematoxylin-eosin and Trichrome Masson for histological studies.

Results and Discussion

A micro-section of the implants showed that the investigated material implanted for the different periods: 4, 12 and 26 weeks, caused no response-mild fibrosis. There was no muscle degeneration, nor necrosis, nor any other significant change observed.

Conclusion

The zirconium oxide-yttrium stabilized $ZrO_2 \cdot Y_2O_3$ implanted in dorsal rabbit muscle did not induce any adverse tissue reactions in the long-term period of 26 weeks.

Acknowledgement

The authors would like to thank NCBIR (Grant no: STRATEGMED-2/ RH-ROT/266798/15/NCBR/2015) for providing financial support to this project.

PS1-02-40

Enhanced Stability of Hollow Calcium Carbonate Microspheres via Polymorphic Control for Orthopedic Applications

Cagatay M. Oral[1,2], Derya Kapusuz[3], Batur Ercan[1,2,4]

[1]Middle East Technical University, Metallurgical and Materials Engineering, Ankara, TR; [2]Middle East Technical University, BIOMATEN, Center of Excellence in Biomaterials and Tissue Engineering, Ankara, TR; [3]Gaziantep University, Metallurgical and Materials Engineering, Gaziantep, TR; [4]Middle East Technical University, Biomedical Engineering Program, Ankara, TR

Introduction

Calcium carbonate ($CaCO_3$) is a widely occurring mineral on earth due to its presence in exoskeletons of marine creatures [1]. Non-toxic nature, dispersability in aqueous media and suitable mechanical characteristics make $CaCO_3$ a suitable candidate for orthopedic applications [2]. $CaCO_3$ exists in three distinct polymorphs having different stabilities in aqueous environments [1]. Calcite is the most stable form of $CaCO_3$, followed by aragonite in terms of stability [1,2]. Vaterite is the least stable polymorph, and thus it can easily transform to aragonite or calcite depending on the environment [1,2]. Having this said, among the various $CaCO_3$ particle morphologies, hollow spherical $CaCO_3$ particles attracted significant interest in orthopedics due to their low bulk density, high specific surface area and the ability to use its hollow inner core as a drug reservoir [3]. However, most of the hollow spherical $CaCO_3$ particles consisted of vaterite, which leads to decreased therapeutic effect due to undesirable polymorphic transformations upon implantation. In this study, stable $CaCO_3$ microspheres consisting of aragonite and calcite polymorphs were synthesized via N_2 bubbling method for the first time in literature. Cytocompatibility and polymorphic stability tests were conducted on the hollow aragonite and calcite microspheres to investigate the particles *in vitro* conditions. These experiments were also repeated using vaterite microspheres as a control group.

Experimental Methods

Calcium acetate ($Ca(C_2H_3O_2)_2$) and sodium bicarbonate ($NaHCO_3$) solutions were used as precursors to precipitate $CaCO_3$ particles. To obtain an inner hollow core, N_2 gas and sodium dodecyl sulfate (SDS) was incorporated to the precursor solutions at different temperatures. Vaterite microspheres were synthesized by adjusting precursor solution pH to 9. Cytotoxicity experiments were completed with osteoblasts (ATCC CRL-11372) using a cell culture media supplemented with various $CaCO_3$ concentrations up to 5 days of culture. Stability of synthesized microspheres were investigated by exposing them to DMEM at 37 °C for 5 days.

Results and Discussion

The structural and morphological differences between $CaCO_3$ microspheres were shown in Fig. 1. XRD analysis revealed that these particles consisted of calcite (Fig. 1a), aragonite (Fig. 1b) and vaterite (Fig. 1c) polymorphs. Though the bulk morphology of the synthesized $CaCO_3$ particles were all spherical, their constituent particles were platelet, needle-like and spherical for calcite, aragonite and vaterite microspheres, respectively. The differences in the constituent particles originated from their crystal structures, which further dictated their stabilities in aqueous environments. Polymorph identification of the powders were also supported with FTIR, HR-TEM and Rietveld analysis. Specifically, HR-TEM micrographs revealed d-spacing values of 0.305, 0.345 and 0.330 nm corresponded to calcite (104), aragonite (111) and vaterite (112) planes, respectively. Hollow inner cores of the $CaCO_3$ microspheres were imaged with TEM. BET analysis exhibited porous nature of the hollow microspheres, which would

allow the use of hollow inner core as a reservoir for drug release. *In vitro* cytotoxicity tests showed that $CaCO_3$ microspheres did not exhibit any toxic effect at corresponding calcium ion concentrations present in the serum. However, as the $CaCO_3$ particle concentration increased, vaterite microspheres showed slight toxicity, while hollow aragonite and calcite microspheres, synthesized for the first time in this research, promoted osteoblast cellular functions. The reason behind the increased toxicity of vaterite microspheres could be correlated with unstability of vaterite in aqueous environments. While dissolution of particles was observed for vaterite microspheres, calcite and aragonite microspheres preserved their morphology in DMEM.

Conclusion

Hollow calcite and aragonite microspheres were obtained by supplying N_2 bubbles and SDS to the precipitation system. Detailed characterization experiments highlighted porous nature of these microspheres, where the hollow core can be used as a reservoir for drug delivery. *In vitro* cytotoxicity tests revealed differences between stable calcite and aragonite microspheres compared to unstable vaterite microspheres. It can be concluded that hollow calcite and aragonite microspheres can be promising candidates for orthopedic applications.

References

[1] Tas, (2015). *Applied Surface Science*, 330, 262-269.
[2] Boyjoo, *et al*., (2014). *Journal of Materials Chemistry A*, 2, 14270-14288.
[3] Mizuno, *et al*., (2011). *Advanced Powder Technology*, 20, 89-93.

Acknowledgement

We would like to thank Middle East Technical University Research Funds (BAP-03-08-2016-009) and Scientific and Technological Research Council of Turkey (117M754) for providing financial support.

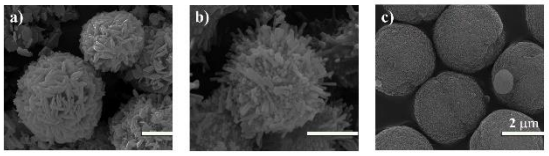

SEM micrographs of microspheres
Fig. 1. SEM micrographs of a) calcite, b) aragonite and c) vaterite microspheres. Scale bars are 2 µm.

PS1-02-41

Characterization and biocompatibility of inversely 3D-printed β-Tricalcium Phosphate Scaffolds

Michael Seidenstuecker[1], Svenja Lange[1], Steffen Esslinger[2], Rainer Gadow[2], Anke Bernstein[1]

[1]Medical Center - Albert-Ludwigs-University of Freiburg, G.E.R.N. Tissue Replacement, Regeneration & Neogenesis, Department of Orthopedics and Trauma Surgery, Freiburg, DE; [2]University Stuttgart, Institute for Manufacturing Technologies of Ceramic Components and Composites (IMTCCC), Stuttgart, DE

Introduction

Bone disorders and defects continue to increase in our society. The reason for this is the increasing average age of the population [1]. According to the Federal Statistical Office, 191,272 endoprostheses were implanted in the knee joint in Germany in 2017 [2]. The development of 3D printing and the associated tissue engineering (TE) opened up new possibilities for bone replacement [3]. There are different types of 3D printing. These include the so-called Fused Deposition Modeling (FDM) process, which was described by S. Scott Crump [4] in the late 1980s and has since become indispensable in the research and development of 3D printing. The aim of a printed replacement material is to replace healthy tissue. This means that over time the material dissolves and is replaced by the corresponding tissue at the implanted site. The aim of the project was to characterise inverse 3D printed β-TCP scaffolds and to investigate the cell growth behaviour within the scaffolds.

Experimental Methods

For the physical properties, fracture tests were performed to determine the maximum failure load of the samples. The aim was to test untreated specimens and treated specimens previously placed in a Simulated Body Fluid (SBF) [5] solution for 28 days. The SBF solution should simulate the body fluids. Furthermore, the inner pore structures of the ceramic should be examined to explain possible effects on the stability of the samples.

For biocompatibility testing, three different in vitro experiments should be performed: A proliferation test, a cytotoxicity test and a live/dead staining test. The cells used were osteoblast-like MG-63 cells (ATCC CRL 1427), which are a cell line of an osteosarcoma.

A WST assay was used to provide information on the proliferation rate of MG-63 cells on the ceramic scaffolds. An LDH assay was used to measure the cytotoxicity of the material and a live/dead staining was used to investigate the growth behaviour of the cells on the samples and in the samples. The aim was to determine whether the cells grow into scaffolds with an inverse structure or only adhere to the surface.

Results and Discussion

The scaffolds with a strand spacing of 500 µm show the highest compressive strength (190 ± 12 N) both untreated and treated with SBF (105 ± 72 N). The SBF basically reduces the stability of the samples. The pore structure within the ceramic does not play a decisive role for stability. Here, the strand spacing itself and the powder properties of the samples are decisive factors for stability. The fact that β-TCP is a biocompatible material could be confirmed by the experiments. No LDH activity of the cells was measured, which means that no cytotoxicity of the material can be detected. In addition, the proliferation rate of all three sizes increases steadily over the test days until saturation. The cells are largely adhered to or within the scaffolds and have not migrated through the samples. The cells show increased growth not only on the outer surface, but also on the inner surface of the samples. This means that the inverse pressure method is suitable for ingrowth of the cells.

Conclusion

The experiments on which this work is based have shown that the FDM method with subsequent slip casting and sintering is well suited for the production of scaffolds for bone replacement.

References

1. Bose, S., M. Roy, and A. Bandyopadhyay, *Recent advances in bone tissue engineering scaffolds.* Trends in Biotechnology, 2012. **30**(10): p. 546-554.

2. Deutschland, S.B. *Operationen und Prozeduren der vollstationären Patientinnen und Patienten in Krankenhäusern*. 2017; Available from: https://www.destatis.de/DE/Publikationen/Thematisch/Gesundheit/Krankenhaeuser/OperationenProzeduren5231401177014.pdf;jsessionid=803B9A7B0D5EC566EB33C4334203A4FC.InternetLive1?__blob=publicationFile.

3. Salgado, A., O. Coutinho, and R. Reis, *Bone Tissue Engineering: State of the Art and Future Trends.* 2004.

4. Crump, S.S., *Apparatus and Method For Creating Three- Dimensional Objects*, in *United States patent*. 1992, Stratasys, Inc.: USA.

5. Helebrant, A., L. Jonasova, and L. Sanda, *The Influence Of Simulated Body Fluid Composition On Carbonated Hydroxyapatite Formation.* 2001.

PS1-02-42

A Bone Substitute with High Bioactivity, strength, and Porosity for Repairing Large Bone Defects

Nasim Golafshan[1], Miguel Castilho[1], Maaike Braham[1], Jaqueline Albass[1], Stephen Zaharievski[1], Jos Malda[1]

[1]UMC Utrecht, Orthopaedics department, Utrecht, NL; [2]Utrecht University, Department of Equine Sciences, Utrecht, NL

Introduction

Three-dimensionally (3D) printed of ceramic materials, mostly calcium phosphates (CaP), is an excellent method for the fabrication of individual bone scaffolds with complex geometries. Despite their inherent bioactive and osteoconductive properties, they present limited mechanical characteristics and handling properties. To overcome this limitation, blends of CaP with degradable synthetic polymers, like polycaprolactone (PCL), have been used. However, the inclusion of synthetic polymers reduces cell adhesion and bioactivity due to polymer masking. Further, magnesium phosphate cement (MgPC) modified with strontium (Sr), is a promising alternative to CaP cement substituted by biologically active agent, due to its biocompatibility and high osteoconductive potential. In this study, we aimed to investigate the fabrication of individual bone implants with improve ostinductive potential and mechanical properties via room temperature extrusion based 3D printing of MgSP-PCL composites. A bioactive bone scaffold, contains Strontium Magnesium phosphate (MgSrP) and polycaprolactone (PCL) was investigated in this study and the 3D structure can combines high mechanical properties such as strength and toughness with impressive bone regeneration ability. The scaffolds induce substantial bone formation and defect bridging after 6 months, as indicated by micro-computed tomography scanning.

Experimental Methods

To fabricate 3D bone scaffolds, the MgSP-PCL (Magnesium Strontium phosphate), MgP-PCL (Magnesium phosphate), and HA-PCL (Hydroxyapatite) solutions were prepared with the ratio of 70-30 weight ratio, dissolved in a trisolvent mix (DCM: 2-Bu: DBP mixed in a 10:2:1 weight ratio) and their processing compatibility systematically investigated according to key process parameters (pressure, feeding rate, needle size). Cylindrical scaffolds were printed with an diameter of 10 mm, height 10 mm, strand spacing 100 mm and 2 layers of no spacing at the interface side, 22G nozzle) by using a pneumatic-driven bioprinter (regenHU, Villaz-St-Pierre, Switzerland) (Fig. 1A). Structural characterisation, X-ray diffraction, ALP activity and calcium deposition, and in-vivo evaluation were performed during this study.

Results and Discussion

According to SEM images of the ceramics powder, the size of HA and MgP were 2.45±0.57 µm and 3.58±1.91 µm, respectively which is similar to the particle size of the MgSP (2.33±0.52 µm, Fig.1B). The X-ray diffraction in Fig. 1C demonstrated that resulting ceramics consisted of pure MgSP, MgP, and HA with approved crystallinity. According to Fig.1E, the reconstructed Micro-CT image revealed a comprehensive overview of the microstructures of the scaffold and the SEM image (Fig. 1B) shows the cross-sectional morphology of the scaffold. Together, the Micro-CT and SEM results demonstrated the porous structure of the scaffolds, suggesting that the scaffold has very highly porous architecture. The controlled released ions or degraded particles from the scaffolds are supposed to adjust the

local microenvironment, which determines the response and behavior of host cells. For all the scaffolds during 21 days, no remarkable changes of the concentrations or burst release of ions were observed with time prolongation, and followed by a gradually increasing release and the concentrations of ions released from the scaffolds were close to the optimal from day 1 to 21 (Fig. 2A). Moreover, according to Fig.2B, Alkaline phosphatase (ALP) activity initially is the same after 7 days of culturing because the cells proliferated and spread on the surface of the scaffolds but increased significantly after 14 and 21 days as the cells underwent differentiation. The extracellular matrix (ECM) mineralization of equine MSCs with various scaffolds was tested by alizarin red staining during 38 days of culturing. These complementary techniques revealed the deposition of calcium and phosphate into the extracellular matrix by the equine MSCs (Kim et al., 2018). For all cases, more intense colors were observed on the scaffolds with ceramics particles than on PCL as control in both media (Fig. 2C). Furthermore, the MgSP-PCL scaffolds induce substantial bone formation and defect bridging after 6 months, as indicated by micro-computed tomography scanning (Fig. 2D). We analyzed the trabecular density (BV/TV) and it is apparent that the bone regeneration with the implant is significantly higher than the empty defect.

Conclusion

The ability to produce cost effective and highly bioactive bone scaffolds are able to induce bone healing in large bone defects. It will be remarkable potential to augment or substitute current surgical approaches for bone repair using autologous or allogeneic bone grafts.

References

[1]Bellucci, D., Cannillo, V., Anesi, A., Salvatori, R., Chiarini, L., Manfredini, T., & Zaffe, D. (2018).
[2]Kanter, B., Vikman, A., Bruckner, T., Schamel, M., Gbureck, U., & Ignatius, A. (2018).
[3]Kim, J. Y., Ahn, G., Kim, C., Lee, J. S., Lee, I. G., An, S. H., … Shim, J. H. (2018).

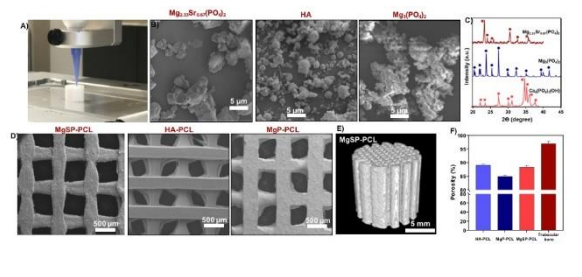

Figure 1.
A) Fabrication of cylindrical scaffolds. B) SEM images of the various ceramics powder. C) X-ray diffraction patterns of pure ceramics. D) representative SEM images from the 3D printed scaffolds. E) Micro-CT scanning of the scaffolds containing MgSP. F) The porosity of the large printed constructs contains various ceramics particle ($p>0.05$).

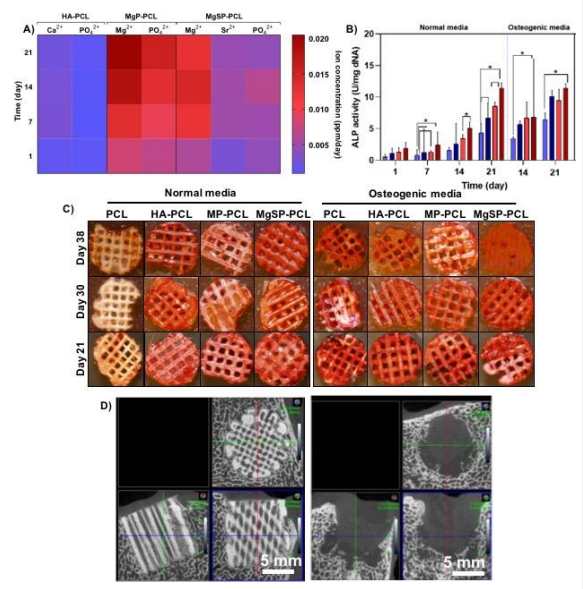

Figure 2
A) Ion release from 3D printed HA-PCL, MgP-PCL, and MgSP-PCL scaffolds during soaking in water. B) The ALP activity levels were measured and normalized to DNA content. C) Micro-CT images from one of the ponies after 6 months implantation.

PS1-02-43

Wear Behaviour of Zirconia Containing Dispersion Ceramics Combined with Accelerated Ageing

Thomas Oberbach[1], Mazen Al- Hajjar[2], Laurent Gremmilard[3], Karen Hans[1], Jerome Chevalier[3], Louise Jennings[2]

[1]Mathys Orthopaedie GmbH, Bioceramics, Moersdorf, DE; [2]University of Leeds, Institute of Medical and Biological Engineering, School of Mechanical Engineering, Leeds, GB; [3]University of Lyon, INSA Lyon, CNRS, MATEIS UMR 5510, Villeurbanne Cx, FR

Introduction

Ceramic-on-ceramic bearings in total hip replacement have been used for more than 45 years. The have shown their potential for young and active patients. In this study, a methodology was devised to assess the in vitro wear behaviour of Zirconia Toughened Alumina Ceramics (ZTA) and Alumina Toughened Zirconia Ceramics (ATZ) under adverse edge loading conditions in hip simulator combined with accelerated ageing in an autoclave under hydrothermal conditions.

Experimental Methods

Femoral heads and acetabular liners of hip prostheses were made of two materials: Alumina Toughened Zirconia (ATZ) and Zirconia Toughened Alumina Ceramic (ZTA). Two material combinations were tested in this study: ATZ-on-ATZ and ZTA-on-ZTA.

A total of six bearing couples were studied on the Leeds Mark II Physiological Anatomical hip joint simulator.

The study was run for a total of eight million cycles. The first two million cycles were run using standard gait conditions and the subsequent 6 million cycles were run under edge loading conditions due to dynamic separation between the femoral head and the acetabular cup.

All femoral heads and acetabular cups were hydrothermally aged during the wear study after every million cycles of testing. It lasted 2 hours at 134°C after each million cycles. Hydrothermal ageing was achieved using accelerated ageing protocol in an autoclave (Sanoclav LA-MCS, Wolf, Germany) in water vapour.

The volume monoclinic fraction was determined using XRD and Garvie and Nicholson's equation modified by Toraya.

Scanning Electron Microscopy observations were conducted on pristine, worn and aged surfaces on the heads after various testing times, using a Supra 55 VP microscope (Zeiss, Germany), at low acceleration voltage (1 to 2 kV) so as to avoid coating the observed surfaces.

The wear was measured gravimetrically using a balance (XP205, Mettler-Toledo) at an interval of one million cycles. A coordinate measuring machine (Legex 322, Mitutoyo, Japan) was used to reconstruct the surface of the femoral head and acetabular cup. RedLux software (RedLux, UK) was used to visualise the size, shape and penetration depth of the wear areas.

Results and Discussion

The wear rates of both aged materials, ATZ-on-ATZ and ZTA-on-ZTA, under standard conditions were very low, i.e. <0.01 mm^3/million cycles. There was no measureable change in wear rate due to ageing under standard conditions. The wear rates increased when edge loading conditions driven by separation was introduced to the gait cycle. The mean wear rate of aged ZTA-on-ZTA after six million cycles of testing under edge loading conditions was 0.19 ± 0.47 mm^3/million cycles. The mean wear rate of aged ATZ-on-ATZ was 0.07 ± 0.05 mm^3/million cycles.

There was no visible damage on the surfaces of the femoral head and acetabular cup after testing under standard conditions. In contrast, under edge loading conditions, a stripe-like wear area was observed on the femoral head with corresponding wear on the rim of the acetabular liner. The penetration depths on the femoral heads and acetabular liners of the ZTA-on-ZTA bearings were higher than that of the ATZ-on-ATZ bearings after 6 million cycles of testing under edge loading conditions.

No significant ageing occurred in the ZTA material. The monoclinic fractions remained very low over both the wear stripe and the unworn surface. Their variations were within the error margin of XRD.

Ageing of ATZ heads was significant. On the wear stripe, each autoclave step increased the monoclinic fraction. However, each one million cycles of wear simulation decreased the monoclinic fraction significantly.

SEM observations of the worn ATZ and ZTA surfaces showed that the first 2 million cycles (without edge loading) did not significantly damage the surfaces. Microstructural damage was first observed after edge loading. In ATZ damage was located in a small wear stripe 15 µm wide. In ZTA, damage was first located in a much more diffuse area around 50 µm wide.

SEM observations further showed that the damage was mainly located in the alumina grains but not in the monoclinic-zirconia grains for ATZ. In both cases ZTA and ATZ, the phase under the highest compressive residual stresses seemed to be the most prone to microstructural damage.

Conclusion

In this study, a method was devised by which the performance of composite ceramic materials was assessed under a combination of edge loading gait conditions and hydrothermal ageing.

The damage of ceramic components increased by the symbiotic effect of ageing, wear and shocks but remained at a very low level for both ceramic materials. It was shown that the performance of ATZ-on-ATZ materials in vitro may be superior to ZTA-on-ZTA materials despite the higher zirconia content in the ATZ materials.

Ceramic composites show an extremely low wear rate, even under worst case conditions, and provides an interesting option to meet the demands of younger more active patients.

PS1-02-44

Inhalable Calcium Phosphate Nanoparticles for Cardiac Drug Delivery

Lorenzo Degli Esposti[1], Francesca Carella[1], Alessio Adamiano[1], Pierluigi Carullo[2], Anna Tampieri[1], Michele Miragoli[3,2], Daniele Catalucci[2], Michele Iafisco[1]

[1]National Research Council, Institute of Science and Technology for Ceramics, Faenza, IT; [2]National Research Council, Institute of Genetics and Biomedical Research, Milano, IT; [3]University of Parma, Department of Medicine and Surgery, Parma, IT

Introduction

Cardiovascular diseases (CVDs) are a worldwide growing problem that cause 17.3 million annual premature deaths[1]. This situation prompts to identify new therapeutic compounds as well as to develop efficient drug-delivery systems for the treatment of CVDs. Among therapeutic compounds, microRNAs (miRs) and peptides are of great interest, since they are key regulators of cardiac dysfunction and protein activity[2,3]. However, the approaches that employ therapeutic miRs or peptides are still not optimal, since *in vivo* delivery has resulted so far to be inadequate. Nanoparticles (NPs) delivery platforms hold great promise to overcome such limitations, providing a strategy for efficient drug-delivery approaches. Therefore the aim of the present work was the generation of effective nanoparticles formulation for the delivery of novel therapeutic drugs into cardiac tissue. Calcium phosphate nanoparticles (CaP NPs) have been selected, since they possess superior biocompatibility and biodegradability compared to other inorganic nanoparticles, and they are able to bind a plethora of therapeutic agents[4].

Experimental Methods

A straightforward one-pot CaP NPs synthesis protocol using citrate as stabilizing agent has been adopted. Two aqueous solutions containing respectively $CaCl_2$ (100 mM) + $Na_3Citrate$ (400 mM) and Na_2HPO_4 (120 mM) were mixed (1:1 v/v) and the pH was adjusted to 8.5; when drug conjugation was performed aqueous solution of miR (100 µg/ml) or peptide (500 µg/ml) was added. The CaP suspension was kept in a water bath at 37°C for 5 min. Afterward, the CaP NPs suspension was dialyzed for 6 h. CaP NPs were characterized by TEM, DLS and ζ-potential in order to measure nanoparticle morphology, size distribution and surface charge, respectively. The biocompatibility and the mechanism of internalization of CaP NPs in cardiac cells were studied on murine HL-1 cells. The test of the ability of CaP NPs to reach the heart was made on CD1 mice, administering CaP NPs by gavage, intraperitoneal, and intravenous injection as well as by intratracheal nebulization. The test of the therapeutic efficiency was made via inhalation of peptide-loaded CaP NPs in a mouse model of streptozotocin induced diabetic cardiomyopathy.

Results and Discussion

Nanoparticle morphological characterization showed that CaP NPs are round shaped particles of about 50 nm in diameter (Fig. 1). DLS analysis evinced that the nanoparticles have a small hydrodynamic diameter and possess a strongly negative surface charge, indicating that the negatively-charged citrate molecules covered the surface of NPs. CaP NPs were proven to be highly biocompatible and showed no significant cytotoxicity effects on cardiac HL-1 cells[5]. In addition, CaP NPs were proven to not alter cardiac cells functional properties. In order to test the efficacy of drug loaded CaP NPs, cardiac HL-1 cells were exposed to CaP NPs carrying the therapeutic miR-133. qRT-PCR analyses revealed a time-dependent increase in the levels of intracellular delivered miRNA, confirming the effective loading of miR into CaP NPs as well as their cellular uptake. Additionally, a cell-based luciferase assay confirmed that the administered miR-133 efficiently repressed a miR-133-specific target[5]. Subsequently CaP NPs were tested

in vivo, evaluating the heart uptake of fluorescent-labelled nanoparticles administered by several routes. Parenteral administration and inhalation resulted in rapid delivery of CaP NPs to the myocardium, with inhalation being the most efficient delivery method (Fig. 2, left)[6]. Moreover, with the inhalation route, the myocardial accumulation was paralleled by a gradual reduction in signal from the lungs, confirming the passage of CaP NPs across the pulmonary barrier (Fig. 2, right). To prove the efficacy of drug-loaded CaP NPs formulation in synergy with the inhalation administration we have treated a mouse model of streptozotocin induced diabetic cardiomyopathy. Inhalation of therapeutic peptide loaded CaP NPs led to a complete recovery of cardiac function in diabetic mice, with the restoration of protein-related contractile properties[6].

Conclusion

Our results have proven that CaP NPs can easily bind miRs and peptides, that are molecules with enormous therapeutic potentials. In particular, we have demonstrated that miR- or peptide- loaded CaP NPs are biocompatible and non-toxic for the highly sensitive myocardial tissues. We have proved *in vivo* in mice that CaP NPs efficiently reach the heart, especially with the non-invasive inhalation route. Finally, we have demonstrated the successful delivery of a peptide payload to the heart by CaP NPs, that exerts a therapeutic effect and restores cardiac functionality in a diabetic cardiomyopathy mouse model. In conclusion, the combination of innovative therapeutic agents such as miRs and peptides with CaP NPs and with the non-invasive inhalation route provides a unique and highly efficient approach to treat CVDs.

References

1. WHO. Cardiovascular diseases. www.who.int/cardiovascular_diseases/en/
2. Poller W, Hajjar R, Schultheiss HP, Fechner H Cardiovasc. Res. 86(3) (2010) 353–364
3. F. Rusconi *et al.* Circulation 134 (2016) 534–546
4. Degli Esposti L, Carella F, Adamiano A, Tampieri A, Iafisco M Drug development and industrial pharmacy, 44(8) (2018) 1223-1238
5. Di Mauro V, Iafisco M, Salvarani N, Vacchiano M, Carullo P, Ramírez-Rodríguez G-B, Catalucci D Nanomedicine 11(8) (2016) 891-906.
6. Miragoli M *et al.* Science translational medicine 10(424) (2018) eaan6205.

Acknowledgement

The authors acknowledge the H2020-NMBP-2016 720834 European project CUPIDO (www.cupidoproject.eu).

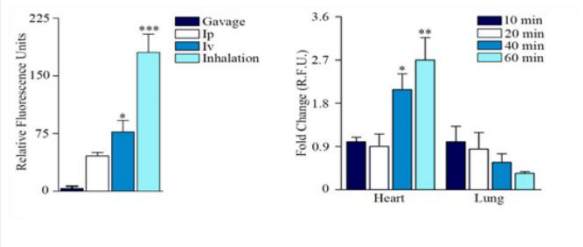

Figure 2

Left: quantification of fluorescence signals from heart tissue of mice treated with Cy7-CaP NPs via gavage, intraperitoneal (ip), intravenous (iv), and inhalation administration. Right: time-course quantification of fluorescence signals from heart and lung tissue of mice treated with Cy7-CaP NPs via inhalation administration. Reprinted with permisison from Ref.6

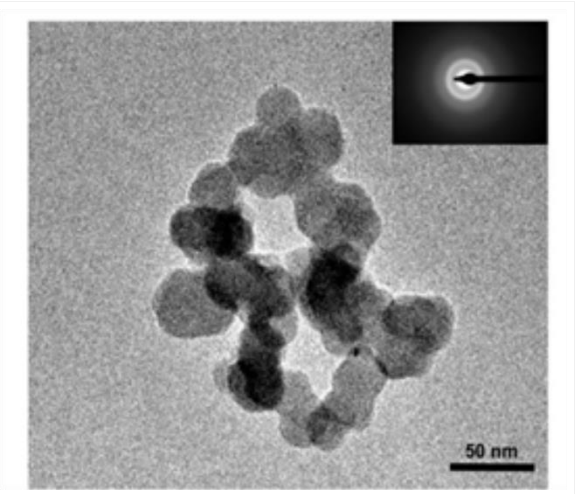

Figure 1
TEM micrograph of CaP NPs. Inset: corresponding SAED pattern. Reprinted with permission from Ref.5

PS1-02-45

Synthesis and characterization of OCP with different preparation condition

Tomohiro Hayashi[1], Gen Tanabe[1], Mieko Ando[1], Tomohiro Kumei[1], Kaori Tsuchiya[2], Ryo Hamai[2], Osamu Suzuki[2]

[1]Japan Fine Ceramics Co, LTD, Development, Sendai, JP; [2]Tohoku University Graduate School of Dentistry, Division of Craniofacial Function Engineering, Sendai, JP

Introduction

Autologous bone has been used for repairing bone defects in patients as the first choice due to its bone regenerative property. However, there are quantitative restrictions on the use of autogenous bone, and there is concern that another obstacle may occur at the site from which the autologous bone is collected.

Thus, artificial bones and their materials for substituting for the autologous bone have been studied. Calcium phosphate ceramics such as hydroxyapatite（$Ca_{10}(PO_4)_6(OH)_2$, HA）and β-tricalcium phosphate ($Ca_3(PO_4)_2$, β-TCP) have been applied as the bone substitute materials in the field of orthopedic and oral surgeries [1].

In recent years, it has been reported that octacalcium phosphate ($Ca_8H_2(PO_4)_6 \cdot 5H_2O$, OCP), which is a precursor of HA, has superior characteristics as bone regeneration material, showing osteoconductivity and biodegradability compared to HA and β-TCP, because OCP promotes osteoblastic differentiation and osteoclast formation [2, 3]. On the other hand, previous studies indicate that OCP with non-stoichiometric composition was easily obtained [4]. It has been known that synthesis method and treatment of OCP affect molar ratio of Ca/P in OCP. Especially, Suzuki et al reported that the ratio of hydrogen phosphate in all phosphorus (HPO_4/P ratio) of OCP was present as labile form which can be changed reversibly by pH in solution [4].

Previously, Miyatake et al revealed that the chemical composition of OCP influenced its osteoconductivity and biodegradability in bone defect [5]. Based on these studies described above, we hypothesized that HPO_4/P ratio of OCP could be related to its chemical characteristics which may affect the bone regeneration by OCP.

In this study, we prepared OCP batches having different HPO_4/P ratio and investigated their dissolution behavior under a physiological condition in vitro.

Experimental Methods

Synthesis of OCP with different HPO_4 / P ratio

OCP was prepared by the wet synthesis method using a system for continuous synthesis which can easily control conditions of the synthesis compared to the batch type preparation. The synthesis of OCP was carried out by controlling the conditions (pH, flow rate, etc.) in the reaction field. The different types of the prepared OCP were abbreviated as OCP-A and OCP-B.

The obtained compounds were identified by analyses of X-ray diffraction (XRD) and HPO_4/P ratio. The XRD pattern of the crystals was recorded using step scanning at 0.02 deg intervals from 3.0 to 60.0 deg with Cu *Kα* X-rays on a diffractometer at 40 kV and 15 mA. HPO_4/ P ratio of them was determined indirectly based on the chemical analysis by heat-induced pyrophosphate method [4, 6]. The powdery OCPs were heated above 500°C overnight. The formed pyrophosphate was hydrolyzed in an acidic solution (perchloric acid solution) under boiling. The phosphate concentrations of both the hydrolyzed and non-hydrolyzed samples were determined colorimetrically using a phosphorous analytical test agent.

Analysis of difference in dissolution behavior

In order to compare the dissolution behavior of OCP with different HPO_4/P ratio, the two types of OCPs were immersed in tris(hydroxymethyl)aminomethane (Tris)-HCl buffer for 1, 7 and 14 days. After the immersion, OCPs were washed with pure water and then lyophilized. Subsequently, they were characterized by XRD and subjected for the chemical analysis to measure HPO_4/P ratio. Moreover, the morphology of them was observed using a transmission electron microscope (TEM).

Results and Discussion

Characterization of OCP synthesized by the continuous synthesis method

As a result of the chemical analysis, it was confirmed that two types of OCPs having different HPO_4/P ratio were obtained by controlling the conditions of the reaction field during the synthesis. The HPO_4/P ratio of OCP-A was larger than that of OCP-B, while XRD analysis confirmed that both crystals had the structure of OCP.

Analysis of dissolution behavior

The behavior of change in the HPO_4/P ratio was different between OCP-A and OCP-B during the immersion in Tris-HCl Buffer, which was measured by the chemical analysis [4, 6]. In addition, XRD patterns of the OCPs indicate that the hydrolysis of OCP-B tended to advance earlier than OCP-A in the Tris-HCl buffer. TEM observation also showed that both OCP underwent morphological changes after immersion in the buffer.

Consequently, it was suggested that the chemical composition of OCP is related to the change in dissolution behavior of OCP in Tris-HCl buffer.

Conclusion

The present study suggests that OCPs with different ion balance could be synthesized by controlling the reaction field. The results of this study also suggested that the balance of ions characterized by HPO_4/P ratio could be involved in the dissolution behavior of OCP.

References

1. R.Z. LeGeros. Chem Rev 108:4742-4753, 2008
2. O. Suzuki. Jpn Dent Sci Rev 49:58-71, 2013
3. T. Sato et al. Acta Biomater 2019 in press. doi: 10.1016/j.actbio.2019.03.001
4. O. Suzuki et al. J Dent Res 74:1764-1769, 1995
5. N. Miyatake et al. Biomaterials 30:1005-1014, 2009
6. A. Gee, V.R. Deitz. Anal Chem 25:1320-1324, 1953

Acknowledgement

This study was carried out by a joint research program between Japan Fine Ceramics Co, LTD and Tohoku University.

PS1-02-46

Bone regeneration using interconnected pores β-tricalcium phosphate (β-TCP) block made by the setting reaction of β-TCP granules

Kunio Ishikawa, Koichiro Hayashi, Tansza S. Putri

Kyushu University, Department of Biomaterials, Fukuoka, JP

Introduction

Interconnected porous β-tricalcium phosphate (β-TCP) block may be useful as artificial bone substitutes. Although various porous β-TCP blocks are proposed further improvement is awaited due to insufficient interconnectivity or imbalance of mechanical strength and porosity. In this study, interconnected porous β-TCP blocks are fabricated by setting reaction of β-TCP granules. And its potential value was evaluated by physical measurement and histologically using rabbits.

Experimental Methods

Porous β-TCP blocks were fabricated by the setting reaction of β-TCP granules (200 to 300 μm) using a HNO_3 solution followed by sintering at 1100°C. XRD, μ-CT, SEM and universal testing machine were used for measurement of their physical properties. For histological evaluation, porous β-TCP blocks and dense β-TCP blocks used as control were implanted in bone defect at medial femoral condyle of rabbits. After 4 weeks, H-E stained specimens were observed using all-in-one fluorescence microscope.

Results and Discussion

When β-TCP granules were mixed with 5mol/L HNO_3, dicalcium phosphate dihydrate (DCPD) is formed and bridged β-TCP granules one another. Following heat treatment at 1100°C, interconnected dual porous pure β-TCP block was fabricated as shown in Fig 1. It has fully interconnected porous structure with pore size of 40 to 160 μm. The interconnection was achieved by the setting reaction of the granules and micro porous structure was obtained by the micropore of the β-TCP granules. Diametral tensile strength (DTS) and porosity of the porous β-TCP block were 1.4 ± 0.2 MPa and 58.1 ± 1.7%, respectively. The DTS value is enough for clinical use and balance between mechanical strength and porosity seems reasonable.

Four weeks after implantation, both porous and dense β-TCP block bonded with the existing bone and no inflammatory response was observed. In the case of dense β-TCP block, only 0.2 ± 0.1% of the β-TCP was resorbed, and amount of the formed new bone was limited (0.1 ± 0.1 %). And no no cells or tissues were observed interior of the dense β-TCP block. In the case of porous β-TCP, 9.2 ± 3.1% of the β-TCP was resorbed, and amount of new bone was 18.9 ± 5.5%. Moreover, osteoblasts, osteoclasts, osteocytes, red blood cells, bone and fibrous tissues were observed within the porous β-TCP block. Presence of osteoblasts, osteoclasts, and osteocytes indicate active bone remodeling process interior of the porous β-TCP block. Presence of accumulated red blood cells indicates capillary vessel or Haversian canal-like structure formation. Clear difference between porous and dense β-TCP blocks demonstrated the importance of the interconnected porous structure.

Conclusion

Porous β-TCP blocks fabricated by the setting reaction of β-TCP granules presented interconnected dual porous structure, as well as balanced porosity (58.1 ± 1.7%) and mechanical strength (DTS: 1.4 ± 0.2 MPa). Resorption of

β-TCP (9.2 ± 3.1%) and new bone formation (18.9 ± 5.5%) after 4 weeks implantation exhibit a good potential value to be good artificial bone substitutes.

Acknowledgement

This research was supported, in part, by AMED under Grant Number JP18im0502004.

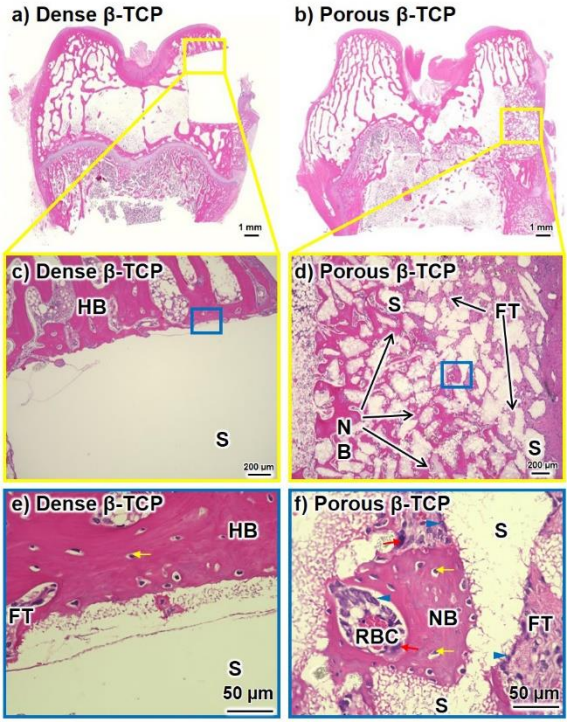

Histological images
H-E stained picture of dense (a, c, e) and porous (b, d, f) β-TCP blocks after four weeks implantation.

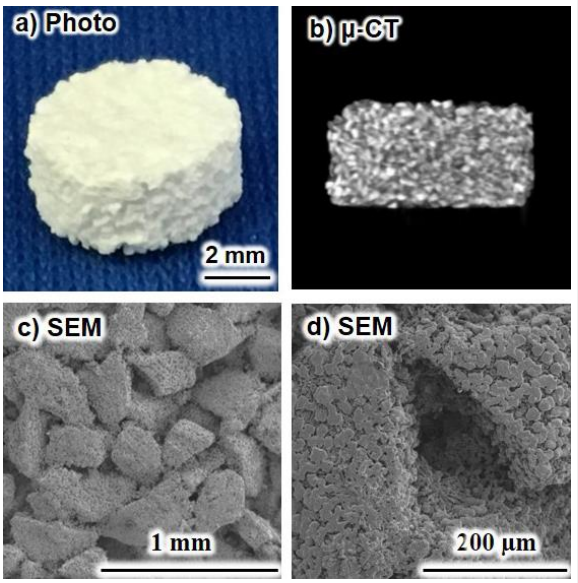

Interconnected pores β-TCP block
Photo (a), µ-CT (b), and SEM (c,d) images of interconnected pores β-TCP block

NB: New bone; HB: Host bone; FT: Fibrous Tissue; S: Sample; RBC: Red blood cells; Blue arrowheads: Osteoblasts; Red arrow: Osteoclasts; Yellow arrow: Osteocyte

PS1-02-47

Novel electrical characterization of hydroxyapatite coatings on titanium: Influence of the layer thickness and manufacturing temperature

Daniel Romero-Guzmán[1,2,3], Verónica Luque-Agudo[1,2,3], Amparo M. Gallardo-Moreno[1,2,3], M. Luisa González-Martín[1,2,3]

[1]University of Extremadura, Department of Applied Physics, Badajoz, ES; [2]Networking Research Center on Bioengineering, Biomaterials and Nanomedicine (CIBER-BBN), Badajoz, ES; [3]University Institute of Biosanitary Research of Extremadura (iNube), Badajoz, ES

Introduction

Titanium and its alloys are within the most widely used metallic biomaterials in implants due to their good mechanical properties and high corrosion resistance. On the other hand, hydroxyapatite (HAp, $Ca_{10}(PO_4)_6(OH)_2$) is considered the best ceramic biomaterial in the field of medicine[1]. This last material is used to coat metallic materials, such as titanium, due to the similarity in the chemical composition and its excellent biocompatibility with bone tissue.

Besides the importance of bulk properties of the biomaterials, surface properties are decisive in the biocompatibility of any implant. In particular, the surface charge has great influence on any bioadhesion process happening on the surfaces of any medical device. The electrical interactions can promote osseointegration and avoid bacterial colonization. However, there are scarce information of the electrical interaction potential (zeta potential) of large metallic biomedical surfaces and, in particular, those modified with coating layers.

This research deepens in the electrical behaviour of thin hydroxyapatite coatings on pure titanium using streaming current. Initial offset values of current-pressure plots and temporal electrical stability are within the new proposed parameters to better understand the electrical response of the biomaterials.

Experimental Methods

The samples have been coated with HAp[2] by a sputtering process carried out by the company Sidrabe (Rīga, LV-1073, Latvia). Two temperatures were used in the manufacturing process: 400°C and 500°C, and two sputtering time that translates into different thickness of the HAp layer: 100 and 150 nm. Samples have been named as 400°C-100nm, 400°C-150nm, 500°C-100nm and 500°C-150nm, accordingly.

The electrical analysis has been carried out by means of an Electro Kinetic Analyzer (EKA) using streaming current measurements. In each determination, the variation with time (from 0 up to 2 hours) of the initial streaming current is analysed.

Results and Discussion

Two interesting behaviours on the electrical response of HAp layers have been observed. Firstly, there is a temporal evolution in the zeta potential of samples. At initial stages of the experiments, for given value of temperature, or thickness, the highest superficial charge corresponds to the lower thickness, or temperature, respectively. Therefore, the 400°C-100nm HAp sample is the only one with an initial surface charge greater than the titanium control. Time evolution shows a decrease in the absolute value of zeta potential for the titanium control and HAp coatings made at 400°C. This effect is not observed in samples manufactured at 500°C. Surface charge of coatings prepared at the highest temperature are stable over the time. Because of the different time evolution of coatings, zeta potential of

samples prepared at 500°C becomes the most negative after 120 minutes of measurement, exhibiting a higher absolute value even than titanium control.
Secondly, it is remarkable the very different response observed in the initial offset of the electrical measurements. Residual charge in the HAp layer prepared at 400°C may be related with the especially abrupt offset observed for these coatings.

Conclusion

Analysis of zeta potential changes with time provides a valuable characterization of the electrical behaviour of different HAp layers. This new procedure for the study of streaming current and zeta potential allows to a better knowledge of the properties of HAp obtained by different procedures. Electrical stability is obtained for coatings prepared at the highest temperature.

References

[1] Harun, W.S.W., Asri, R.I.M., Alias, J., Zulkifli, F.H., Kadirgama, K., Ghani, S.A.C., Shariffuddin, J.H.M. (2018). A comprehensive review of hydroxyapatite-based coatings adhesion on metallic biomaterials. Ceramics International, 44 (2), 1250–1268.
[2] Pluduma, L., Gross, K.A., Rey, C., Ubelis, A., Berzina, A. (2018). Production and characterization of oxyhydroxyapatites. Key Engineering Materials, 762, 48-53.

Acknowledgement

Financial support is acknowledged to the Spanish Junta de Extremadura and FEDER grants for the projects IB16117 and GR15089, and to the Ministerio de Economía y Competitividad for the project MAT2015-63974-C4-3-R y PCIN-2016-146.

PS1-02-48

Coatings Based on Organic/Non-Organic Composites on Bioinert Ceramics by Using Biomimetic Co-Precipitation

Gaëlle Desante[1], Norina Labude[2], Sabine Neuss[2,3], Rainer Telle[1], Karolina Schickle[1]

[1]RWTH Aachen university, Department of ceramics and refractory materials, Aachen, DE; [2]RWTH Aachen university hospital, Institute of pathology, Aachen, DE; [3]RWTH Aachen university hospital, Helmholtz institute for biomedical engineering, Biointerface group, Aachen, DE

Introduction

Bioinert ceramics such as alumina or zirconia have been commonly used in the field of orthopedics and dentistry due to its excellent mechanical properties, esthetic look, good biocompatibility and chemical inertness in biological environment. An activation of its bioinert surface could bring additional advantages for better implant-integration with surrounding tissues *in vivo*. Therefore, the aim of the present study was to develop an innovative biomimetic co-precipitation technique by using modified Simulated Body Fluid (SBF) to obtain a composite biomimetic coating made of organic and non-organic components enhancing a bioactivation/functionalization of this inert biomaterial.

Experimental Methods

Zirconia samples were biomimetically coated by immersion in two times concentrated SBF-solution prepared according to Tanahashi *et al*. (1994) and kept at a body temperature for 3h [1].

Bovine Serum Albumin (BSA) in 5 different concentrations (0.01, 0.1, 1, 10, 100 gL^{-1} and 0 gL^{-1} as a control) has been chosen as a standard protein to be incorporated into the CaP-coating during the precipitation process. The incorporation of BSA into the SBF solution occurred on the half of the samples directly (“direct” coating) and for the other half on samples already pre-coated with SBF (“with pre-coating”).

BSA/Alexa FluorTM 488 conjugates were applied to visualize the incorporated proteins into the surface. To evaluate a role of sedimentation of protein in the solution, the coating produced on horizontal and vertical (positioning shown in Fig.2) samples were compared. Samples were imaged by using fluorescence microscope. To determine the morphological changes on the substrate surfaces after soaking in SBF, scanning electron microscopy was applied. Carbon-content of the HAp-coating dependent on concentration of BSA in the solution were established by using EDX measurements. Moreover, the thickness of HAp-coatings could be measured by imaging of cross-section of ZrO_2-substrates.

Results and Discussion

The control samples (0 gL^{-1} BSA) as well as samples coated in SBF-solution containing 0.01 gL^{-1} BSA exhibit typical coral-like crystal structures [2] with app. 100 nm long crystal-plates. In contrast to BSA-concentrations >0.1 gL^{-1} the crystal structure appears to be altered or protein-overlayed (Fig.1).

The incorporation of protein within the HAp-coatings was visualized by using fluorescence microscopy to detect BSA/Alexa-FluorTM-488 conjugates, which gives a green signal (Fig.2). The intensity of green signal is stronger with increasing protein concentration in the solution. Additionally, the content of carbon was measured by EDX. The results showed a logarithmic growth of carbon content in the HAp-coating with increasing BSA concentration in SBF solution by the precipitation process.

The influence of the sedimentation process on the intensity of fluorescence signals proportional to the amount of proteins in the coating could also be observed. The results were in correlation with the chemical analysis of the coated surfaces (EDX).
Analysis of the cross-section of the obtained coating on CaP-pre-coated samples showed the apatite growth for all tested samples in comparison to the pre-coated control sample. The thickness of the coating decreases with the increase of protein concentration in the solution, which is in correlation with the SEM images.

Conclusion

It could be shown, that it is possible to co-precipitate an organic/non-organic coating based on HAp and biological agent such as BSA. This method could create a new biomaterial group, which surfaces could be tailored designed according to its desires and requirements. Based on these results with a standard protein, BSA has been replaced by specific proteins like Bone Morphogenetic Protein 2 (BMP-2) as a potential osteoinductive factor and Hepatocyte Growth Factor (HGF) as a growth factor. These proteins have already evidenced a strong influence on the crystal growth and the HAp-coating morphology as well. Thus further systematic analyses and cell culture tests are still on going in order to better understand biologically efficacy or bone growth factor response of the protein incorporated into the CaP-coating.

References

[1] Tanahashi M., Yao T., Kokubo T., Minoda M., Miyamoto T., Nakamura T., Yamamuro T., Apatite coating on organic polymers by a biomimetic process, J Amer Ceram Soc, 1994, 77(11), 2805-2808.
[2] Liu Y., Layrolle P., de Bruijn J.D., van Blitterswijk C., de Groot K., Biomimetic coprecipitation of calcium phosphate and bovine serum albumin on titanium alloy, J Biomed Mater Res, 2001, 57, 327-335.

Acknowledgement

Funded by the Excellence Initiative of the German federal and state governments (Grant Nr. OPSF408)

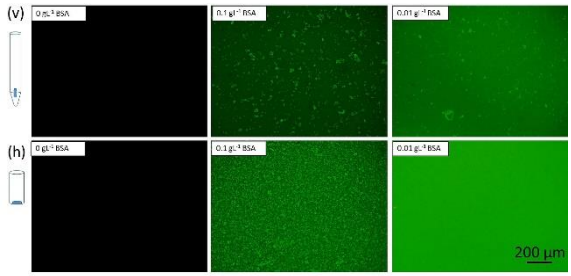

Fig.2
Fluorescence images of the vertical (v) and horizontal (h) pre-coated samples using precipitation from the SBF solution containing 0, 0.01 and 0.1 gL^{-1} BSA. Positioning of the samples - vertically or horizontally - is here represented.

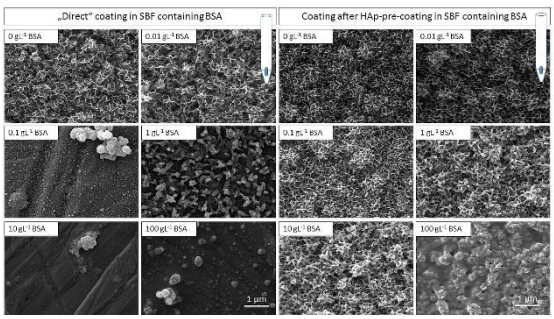

Fig.1
SEM view of vertical samples coated with SBF containing BSA in "direct" coating (left) and after pre-coating (right) with different concentrations of BSA in the SBF solution: 0, 0.01, 0.1, 1.0, 10, 100 gL^{-1}. The vertical positioning of the samples is also represented for each group of samples.

PS1-02-49

Thermally treated carbonated amorphous calcium phosphate

Jana Vecstaudza, Janis Locs

Riga Technical University, Rudolfs Cimdins Riga Biomaterials Innovations and Development Centre of RTU, Institute of General Chemical Engineering, Faculty of Materials Science and Applied Chemistry, Riga, LV

Introduction

Amorphous calcium phosphate (ACP) is essential in formation of mineralized bone and in development of bone substitutes. ACP is highly bioactive and biocompatible with living organisms. The reactivity of ACP is mainly attributed to the hydrated layer surrounding ACP particles and its high specific surface area (SSA). Previously we have reported new synthesis technology of nanosized carbonated ACP [1]. Thermal treatment is a common processing step when calcium phosphates are considered for biomaterial development. At the moment there is no study related to thermal treatment induced changes of surface properties of carbonated amorphous calcium phosphate nanoparticles, that hold potential in bone substitute development. Here we present continuation of thermal and crystallization studies of the nanosized carbonated ACP [2] with detailed follow-up of ACP structural and specific area changes at 100-1000 °C.

Experimental Methods

Carbonated ACP was precipitated from calcium and phosphate ion containing solution by rapid rise of solutions pH up to 10 [1]. Freeze dried ACP was subjected to XRD, FT-IR, heating microscopy, DSC-TG, specific surface area (SSA) and particle size d_{BET} analyses. Further ACP was heat treated at temperatures ranging from 100 to 1000 °C with hold times of 5 or 60 min. Phase and chemical composition (XRD and FT-IR), SSA and d_{BET} were systematically analysed for heat treated products.

Results and Discussion

Initial characteristics of ACP. XRD and FT-IR analysis confirmed the amorphous nature of obained ACP sample. SSA of ACP was 115 m^2/g and d_{BET} was 15 nm. Heating microscopy and DSC-TG analyses showed crystallization related events in temperature range of 500-650 °C. Compaction of ACP sample was observed during the same temperature range. This clearly demonstrated that crystallization of ACP is accompanied by compaction of ACP particles [2].

Specific surface area and d_{BET}. Heat treatment of carbonated ACP reduced its specific surface area in a manner dependent on temperature. Heat treatment up to 1000 °C reduced SSA of ACP for 14 times. Negligible reduction of SSA was observed in range of 100-300 °C and 700-1000 °C. These negligible differences at those exact temperature ranges were attributed to the unchanged phase composition at those exact temperatures and/or reaching some equilibrium: ACP at 100-300 °C and mixture of hydroxyapatite (HAp) and beta tricalcium phsopahte (β-TCP) at 700-1000 °C.

Phase and chemical composition. First crystalline phases were detected in XRD patterns at 500 °C. Increasing heat treatment temperatures decreased amount of residual ACP phase. From 500 to 600 °C poorly crystalline calcium phase or phases (e.g. calcium deficient hydroxyapatite) were present. At 650 °C two crystalline phases were identified - HAp and β-TCP, that remained at higher temperatures as well. In FT-IR spectra carbonate ions were present up to 600 °C.

Impact of temperature hold time. Phase composition, SSA, particle size d_{BET}, chemical groups and mesoporosity characteristics of heat treated calcium phosphate products were independent of temperature hold time (5 or 60 min).

Conclusion

This study contributes to understanding of thermally induced crystallization process of carbonated nanosized ACP from perspective of surface property change. Specific surface area of carbonated ACP was found to remain the same whether 5 or 60 min hold times were tested.

References

[1] Vecstaudza, J., Locs, J. Novel preparation route of stable amorphous calcium phosphate nanoparticles with high specific surface area (2017) J. Alloy. Compd., 700, pp. 215-222.
[2] Vecstaudza, J., Gasik, M., Locs, J. Amorphous calcium phosphate materials: Formation, structure and thermal behaviour (2019) J. Eur. Ceram. Soc., 39 (4), pp. 1642-1649.

Acknowledgement

This research is funded by the Latvian Council of Science, project Future of synthetic bone graft materials - *in vivo* guided biosynthesis of biomimetic hydroxyapatite, project No. lzp-2018/1-0238.

PS1-02-50

Elastic and resistant calcium phosphate cement for vertebral fracture treatment

Silvia S. Ramirez[1,2], Charlotte Mellier[3], Jean M. Bouler[2], Fabien Granier[4], Sébastien Marie[4], François X. Lefèvre[2], Jean C. Scimeca[5], Romain Debret[6], Jérôme Sohier[1], Bruno Bujoli[2]

[1]Université Lyon, INSA Lyon, UMR 5510 CNRS, MATEIS, Villeurbanne, FR; [2]Université de Nantes, CNRS, UMR 6230, CEISAM, UFR Sciences et Techniques, Nantes, FR; [3]Graftys SA, Pôle d'activités d'Aix en Provence, Aix en Provence, FR; [4]Colcom, Clapiers, FR; [5]CNRS, INSERM, Université de Nice Sophia Antipolis, iBV, Nice, FR; [6]CNRS, UMR 5305, Laboratory of biology tissue and therapeutic engineering LBTI, Lyon, FR

Introduction

The development of a synthetic bone substitute is presented as a potential candidate for the treatment of vertebral fractures, a painful and invalidating pathology. The current treatment includes immobilization under corsets or percutaneous vertebral augmentation by injection of a poly(methylmethacrylate) PMMA resin in the vertebra to stabilize the fracture. However, there is a medical need to replace this material, since its *in situ* polymerization generates high temperature and PMMA is a non-resorbable and rigid material that may cause secondary fractures. Our bioinspired approach is a material composed of an inorganic apatite calcium phosphate cement (CPC) combined to an organic hydrogel that will form *in situ*. These composite materials are bioresorbable and, thanks to the presence of CPC, are also osteoconductive. The candidates should have appropriate rheology and cohesion for injectability and show mechanical properties close to that of bone tissue.

Experimental Methods

Two commercial formulations of CPS were used, Graftys® HBS and Graftys® HBS without hydroxypropyl methyl cellulose (HPMC), having different cohesion and setting time (12 and 9 min, respectively). The hydrogel is formed by condensation of a commercial lysine-grafted dendrimer (Colcom® DGL) and a polyethylene glycol chain with NHS end-groups (PEG-NHS) [1]. Pastes were prepared by mixing the hydrogel components with the cement powder. The concentration of hydrogel components was modulated and the effect of the initial setting time of pastes was measured using the Gillmore method. Injectability and compressive strength measurements were performed on pastes and composite cylinders respectively, using an AMETEK LS5 texture analyzer. Decalcified samples of CPC/hydrogel composites were obtained by Ethylenediaminetetraacetic acid (EDTA) treatment. Organic and inorganic distribution were evaluated by SEM observations of polished cross-section of composite samples.

Results and Discussion

A series of composite materials were successfully fabricated. The formation of a continuous 3D hydrogel network in the CPC, once hardened, was verified by decalcification of the samples (figure 1a-b, showing the organic phase). The hydrogel contributed significantly to enhance the injectability of the resulting paste, as compared to a purely inorganic CPC (HBS without HPMC), and the paste cohesion (75% versus 95% of extruded paste). A homogeneous distribution of the inorganic and organic components was observed by SEM characterization of the composites (figure 1c, showing the hydrogel network). The working time, initial setting time, compressive strength, Young´s Modulus and injectability of the composite systems, studied as a function of the DGL and PEG-NHS contents, DGL/PEG-NHS ratio, type of CPC powder, ionic strength of the liquid phase and liquid/powder ratio, resulted in significantly different

mechanical properties (figure 1d -e, showing hydrogels of different elasticity). *In-vitro* tests performed on a selection of these composite materials using osteoblasts and osteoclasts cells.

Conclusion

A series of inorganic/organic composite cements of versatile injectable and mechanical properties were successfully prepared, opening potential applications for the treatment of vertebral fractures. Further studies are focusing on the biological evaluation of these materials.

References

[1] Pantent: Debret, R., C. Faye, J. Sohier and P. Sommer, Polypeptide derived from tropoelastin and biocompatible material comprising same. 2016 (WO2017194761).

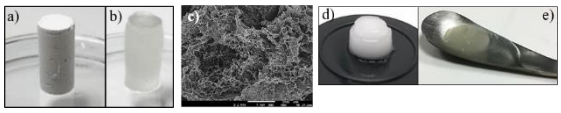

Elastic and resistant calcium phosphate cement for vertebral fracture treatment

Figure 1. Composite material before (a) and after decalcification (b). SEM observation of a fracture plane of the obtained hydrogel network after decalcification (c). Hydrogels obtained after decalcification of composite materials showing different mechanical properties (d-e).

PS1-02-51

Reinforced bone cement based on metastable α'-$Ca_3(PO_4)_2$

Anton Goncharenko[1], Zoltan Zyman[1], Matthias Epple[2], Elena Onyshchenko[1]

[1]V.N. Karazin Kharkiv National University, Physics of Solids Department, Kharkiv, UA; [2]University of Duisburg-Essen, Institute of Inorganic Chemistry and Center for Nanointegration Duisburg-Essen (CeNIDE), Essen, DE

Introduction

Calcium-phosphate materials, including ceramics and cements, are widely used in orthopedics, osteoplasty and maxillofacial surgery due to their chemical similarity to the mineral composition of bone. Calcium-phosphate cements are considered to be an excellent synthetic material for filling bone cavities and defects [1].

The cement formation is a consequence of the chemical reaction between a solid component (as a powder) and a liquid phase. Usually, suitable calcium phosphate powders are obtained at high temperatures, and their particles are several micrometers large. This results in decrease of their reactivity [2]. Therefore using powders consisted of metastable phases processed at medium temperatures from amorphous calcium phosphate, ACP, with nanoscale particles should significantly improve the reactivity of cements.

Since cements are usually fragile and have low compression strength and fracture toughness, it is expected that the addition of certain reinforcing particles should significantly improve the mechanical properties of cement. It is desired that the particles would have bioactive properties similar to those of the cement [3].

Experimental Methods

Metastable α'-TCP powder was obtained by quenching an ACP powder heated (crystallized) at 700 °C for 1 hour. A fast variation of the nitrate synthesis was used to produce the ACP powder with a Ca/P ratio of 1.5. HA whiskers (40 µm length and 2 µm wide) were prepared by an original hydrothermal route at 235 °C and 20 atm [4].

For cement preparation with various solid/liquid ratios and amounts of HA whiskers, a certain amount of 2.5% Na_2HPO_4 solution was added to the powder portion and thoroughly kneaded with a spatula. The resulting paste was formed under slight pressure into cylinders and heated at 37 °C.

The setting moment of the cement was determined by the Vick method. Initial and reinforced cements were examined as prepared and after heating (5 K min^{-1}) at 1150 °C in a muffle furnace, respectively, by XRD, TG-DTA, IR, ESEM and EDX.

Results and Discussion

At low solid/liquid ratios, the composition of the cement is almost identical to that of the initial powder and is represented only by α'-TCP. At a ratio of 1/0.75, besides α'-TCP diffractions, apatite maxima in the range of 26-32°2θ were detected. With further increasing theliquid`s amount, the intensity of the α'-TCP maxima decreased, and those of the apatite increased substantially.

The cement annealed at 1150 °C for 1 hour consisted of β-TCP. It means that the formed apatite was non-stoichiometric with a Ca/P ratio near 1.5. ESEM examination has shown that the cement consisted of agglomerates of very thin lamellar crystals. The compressive strength of the set cement was about 4 MPa at the 1/1.5 solid/liquid ratio. Enrichment of the cements by various amounts of HA whiskers (1–15 wt%) improved the mechanical properties. For example, the compressive strength increased twice for the 4 wt% whisker amount.

Conclusion

The effect of powder/liquid ratio on the stoichiometry, phase composition and morphology of apatite cements based on metastable α'-TCP was revealed. The possibility of reinforcement of cements by HA whiskers for the ACP–α'-TCP cement system was firstly explored. The 1/1.5 powder/liquid ratio provides a complete transformation of α'-TCP into apatite. The cement set during 15 minutes and had a compressive strength about 4 MPa. The addition of 4 wt% of HA whiskers in the cement increased its compressive strength twice. The developed reinforced processingly simple cement can be used as a non-carcinogenic bone substitute for bone tissue in non-bearing areas of the human skeleton.

References

1. Dorozhkin S V, J Funct Biomater, 4:209-311 2013
2. Bohner M, J Mater Chem, 17:3980-3986 2017
3. Hockin H K X *et al*., J Biomed Mater Res 52:107-114 2000
4. Zyman Z Z, *et al*., Biomaterialien, 7:252 2006

PS1-02-52

Synthesis of Amorphous Calcium Phosphate with Biomimetic Chemical Composition

Jana Vecstaudza, Janis Locs

Riga Technical University, Rudolfs Cimdins Riga Biomaterials Innovations and Development Centre of RTU, Institute of General Chemical Engineering, Faculty of Materials Science and Applied Chemistry, Riga, LV

Introduction

There is still ongoing need for effective materials for bone regeneration that copy both structure and composition of the mineral phase of the human bone. At the very beginning of the bone mineral formation it is amorphous and besides calcium and phosphorus it contains other biologically relevant ions. Further, structurally the bone mineral is nanomaterial. Both of these important features can be combined into ionically enriched amorphous calcium phosphate (ACP). It is known that amorphous structures are more susceptible to inclusion of large quantities of various ions than crystalline ones. Therefore, the current work presents development of synthesis of novel ACP nanoparticles with biomimetic bone-like chemical composition. The elemental composition of the biomimetic ACP will be composed of Ca^{2+}, PO_4^{3-}, OH^-, CO_3^{2-}, Mg^{2+}, Sr^{2+}, Na^+, K^+, Cl^-, F^-, Zn^{2+} and citrate ion building blocks.

Experimental Methods

Synthesis of the biomimetic ACP is based on recently developed wet chemistry method [1]. The basis of the method is to obtain a homogenous solution of both calcium and phosphate ions by dissolution of calcium phosphate salt e.g. hydroxyapatite or beta tricalcium phosphate. Afterwards strong base is rapidly added to the transparent solution and precipitation of ACP occurs. The precipitate is filtered, washed and later dried at 80 °C. To incorporate the rest of the biomimetic elements into structure of ACP, various salts of the respective ions ($MgCl_2$, $SrCl_2$, sodium citrate etc.) were added before the dissolution of calcium phosphate. Quantities of the biomimetic elements were matched to the ones in human bone. Characterization of the synthesized materials was done with x-ray diffraction analysis (XRD), Fourier transform infrared spectrometry (FT-IR), Brunauer–Emmett–Teller (BET) specific surface area analysis and scanning electron microscopy coupled with energy dispersive x-ray spectrometry (EDS).

Results and Discussion

Phase composition determined by XRD showed that the modified synthesis method yields only ACP phase and no crystalline phases were detected. Addition of multiple ions to the synthesis of ACP might hinder its crystallization, however more detailed studies are needed. Further, FT-IR spectra confirmed the XRD data as absorption bands were wide and rounded that are characteristic to amorphous structures. Presence of both carbonate and citrate ions was detected by FT-IR. The specific surface area of the synthesized products was over 50 m^2/g thus proving the nanostructure aspect. Previous studies [1] of the reference ACP without biomimetic ions have shown that it is possible to synthesize nanosized (<20 nm) ACP with specific surface area over 150 m^2/g that is stable in air for at least one year. EDS spectra confirmed the presence of the inorganic ions in the biomimetic ACP.

Conclusion

Overall it was possible to obtain nanostructured ACP with biomimetic bone-like chemical composition with specific surface area over 50 m^2/g by modified wet precipitation technology. Addition of the supplementary ions to the

synthesis system of ACP was successful in terms of preserving the amorphous structure. The obtained calcium phosphate nanostructures with the biomimetic composition will provide all the necessary preconditions for successful use in bone tissue engineering.

References

1. J. Vecstaudza, J. Locs, J. Alloy. Compd., 700 (2016), 215-222.

Acknowledgement

This research is funded by the Latvian Council of Science, project Future of synthetic bone graft materials - in vivo guided biosynthesis of biomimetic hydroxyapatite, project No. lzp-2018/1-0238.

PS1-02-53

In vivo degradation, osteoinduction and osteogenesis of biomimetic hydroxyapatite: Effect of nanostructure and carbonate substitution

Maria-Pau Ginebra[1], Albert Barba[1,4], Anna Diez-Escudero[1], Montserrat Espanol[1], Caroline Ohman-Magi[2], Cecilia Persson[2], Maria Cristina Manzanares[3], Jordi Franch[4]

[1]Universitat Politecnica de Catalunya, Department of Materials Science and Metallurgy, Barcelona, ES; [2]Uppsala University, Department of Engineering Sciences, Uppsala, SE; [3]Universitat de Barcelona, Department of Pathology and Experimental Therapeutics, Hospitalet de Llobregat, ES; [4]Universitat Autonoma de Barcelona, Small Animal surgery Department, Bellaterra, ES

Introduction

Synchronisation between biomaterial degradation and bone formation is one of the crucial requirements for the ideal synthetic bone graft. In practice, this synchronization is the result of a complex network of interactions between the material, the physiological fluids and the cells of the osseous system, very difficult to unravel. The active degradation of synthetic bone grafts *in vivo* results from the dissolution of the material in the acidic environment produced by bone-resorbing cells. Therefore, bone graft degradability depends not only on composition and textural properties, like porosity and specific surface area (SSA), but also on the inflammatory reaction and the osteoclastogenesis elicited by the material once implanted. Likewise, the degradation of the material modifies the ionic composition of the extracellular fluid, this acting as a powerful chemical signalling path that trigger specific cellular responses. In an effort to shed light on this complex system, in this work the *in vivo* behavior of calcium deficient hydroxyapatite with different composition and nanostructure is compared, in terms of degradation, osteoinduction (i.e. ectopic bone formation) and osteogenesis. Moreover, to better understand the interplay between chemical and biological phenomena, the results were compared with the *in vitro* accelerated degradation of the same scaffolds.

Experimental Methods

Calcium deficient hydroxyapatite (CDHA) foams were obtained by foaming and hydrolysis of an alpha-tricalcium phosphate (α-TCP) slurry. Two different nanostructures, fine needle-like crystals or coarse plate-like crystals (Fine-CDHA and Coarse-CDHA) were obtained by using either fine or coarse α-TCP powders respectively. Carbonated CDHA (CO_3-CDHA) foams were obtained by hydrolysing α-TCP in a sodium bicarbonate solution. Sintered beta-TCP (β-TCP) and biphasic HA/β-TCP (BCP) foams were used as controls. The scaffolds were characterized in terms of composition, porosity, solubility and microstructure. The *in vivo* study was carried out in a standardized model of intramuscular (IM) and intraosseous (IO) implantation over 6 and 12 weeks in beagle dogs. Material resorption and bone formation was evaluated by micro-CT and SEM and histological and histomorphometrical analysis were performed. The susceptibility of the material to acidic degradation *in vitro* was assessed by immersing the samples in an acidic solution at 37 °C to mimic the osteoclastic environment.

Results and Discussion

Both ectopic and orthotopic bone formation, as well as scaffold degradation were drastically affected by nanocrystal morphology. Moreover, carbonate doping, which resulted in small plate-shaped nanocrystals, accelerated both the intrinsic osteoinduction and the bone healing capacity (Figure 1). Similar degradation trends were found intramuscular and intraosseously, although the absolute values were higher intramuscularly. CO_3-CDHA Foams exhibited the highest degradation rate (60% IM and 50% IO at 12 weeks), followed by the Fine-CDHA Foams (40%

IM and 42% IO at 12w), Coarse-CDHA foams exhibiting the lowest resorption (10% IM and 20% IO at 12 w). A good correlation was found between material degradation and bone formation, both ectopically and orthotopically. The materials presenting the highest osteoinduction, i.e. CDHA-CO_3 and CDHA-F Foams (23 and 28% formed bone IM at 12 w, respectively), were also the ones showing the highest degradation rate. However, no clear patterns were found correlating CaP degradation and ectopic bone formation when compared with the sintered ceramics, β-TCP and BCP. Thus, BCP-Foam, presented a high amount of ectopic bone formation at 12 weeks (28% IM at 12w), despite showing the lowest degradation rate, and β-TCP, with a degradation at 12 weeks similar to Fine-CDHA showed no ectopic bone formation.

On the other other hand, the degradation *in vivo* was not fully consistent with the degradation results *in vitro*. Thus, whereas CDHA-F-Foam, with the highest SSA, showed the highest degradation rate, exceeding the more soluble β-TCP, the incorporation of carbonate in CDHA rather than increasing the *in vitro* degradation, significantly reduced it.

Conclusion

The size and morphology of the nanocrystals, as well as the presence of carbonate, allow tuning the osteoinductive and osteogenic potentials as well as the degradation profi le of the CDHA. Moreover, those materials with textural and compositional properties closer to the biological apatite exhibited better synchronization between material resorption and bone formation.

References

[1] *Barba et al, ACS Appl. Mater. Interfaces 2019, 11:8818*

Acknowledgement

MAT2015-65601-R project, from Spanish Government and European Reg. Dev. Funds; ICREA Academia award of MPG, from Generalitat de Catalunya

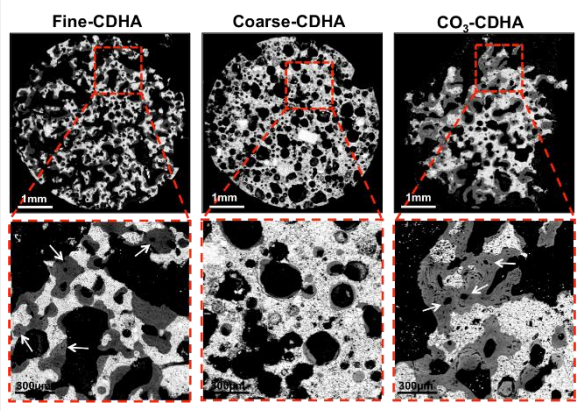

Figure 1.
Back-scattered SEM images of the CDHA scaffolds after 12 weeks of intramuscular implantation. [1]

PS1-02-54

Synthesis of Ion Modified Carbonate Apatites inspired by Biological Apatite

Barbara Kołodziejska, Joanna Kolmas

Medical Univesity of Warsaw, Faculty Of Pharmacy With Laboratory Medicine Division/Chair Analytical Chemistry And Biomaterials, Warsaw, PL

Introduction

Biological apatite is the main component of the inorganic fraction of hard tissues, such as bone tissue or mineralized dental tissues. Nanocrystals of the biological apatite are calcium orthophosphates with various foreign ions in their structure, i.e.: Mn^{2+}, Mg^{2+}, Cl^{-}, Zn^{2+}, Na^{+}, K^{+}, F^{-}, CO_3^{2-}, BO_3^{3-}, SiO_4^{4-}, etc. This unique composition causes the changes in the Ca/P molar ratio, which in the stoichiometric hydroxyapatite is 1.67.[1] Impurities in the apatite of bones, enamel or dentin affect not only the physicochemical properties, but also the biological properties of tissues. For example, silicon ions influence the process of osteogenesis by stimulating osteoblast proliferation.[2,3] The aim of the study was to develop a method of the synthesis of nanocrystalline carbonated apatites imitating the biological apatite. Our goal was to introduce foreign ions into the apatitic structure, by using different substrates. The high apatite susceptibility to ion substitutions was useful in the synthesis.[4]

Experimental Methods

The synthesis of the multi-substituted carbonate apatite was carried out using the wet method in SBF (simulated body fluid), containing ions such as: Na^{+}, K^{+}, Mg^{2+}, Cl^{-}, CO_3^{2-}, SO_4^{2-} and citrate. It was carried out in two ways (using different substrates). In the first method, only sources of calcium and phosphate ions were used; in the second method additional sources of magnesium ions and carbonate ions were added. The obtained precipitates were left to age at different periods of time. Finally, eight samples were produced: four without the addition of foreign ions with different aging times and four apatitic samples enriched with Mg^{2+} and CO_3^{2-} ions with an analogous aging time. The obtained powders were characterized using the following methods: FT-IR mid-infrared and Raman spectroscopies, ICP-OES spectrometry and TEM microscopy.

Results and Discussion

The obtained results were analyzed in terms of the degree of crystallinity of powders as well as the content of individual ions in the samples. The significant changes in the crystallinity as well as in the elemental composition were observed. The differences in the content of Mg^{2+} ions, as well as CO_3^{2-}, were evident.

Conclusion

The obtained powders were nanocrystalline, multi-substituted apatites, containing mainly magnesium and carbonates, that is characteristic for biological apatites. Their composition and crystallinity were affected by the aging period. Further physicochemical tests are required.

References

[1] S.V. Dorozhkin, Materials 2009, 2 (2), 399-498.

[2] J. Kolmas, S. Krukowski, A. Laskus, M. Jurkitewicz, Ceramics Intenational 2016, 42 (2), 2472-2487.

[3] Q. Liu, S. Huang, J.P. Matinlinna, Z. Chen, H. Pan, Biomed. Res. Int. 2013, 2013, 1-13.
[4] J. Kolmas, A. Ślósarczyk, A. Wojtkowicz, Solid State Nucl. Magn. Reson. 2007, 32 (2), 53-58.

Acknowledgement
FW23/N/19 - Medical University of Warsaw

PS1-02-55

Synthesis of Substituted Hydroxyapatite for Application in Bone Tissue Engineering and Drug Delivery

Dominik Büchner[1,2], Martin Gericke[2], Thomas Heinze[2], Edda Tobiasch[1], Steffen Witzleben[1], Margit Schulze[1]

[1]Bonn-Rhein-Sieg University of Applied Sciences, Departement of Natural Sciences, Rheinbach, DE; [2]Friedrich-Schiller-University Jena, Institute of Organic Chemistry and Macromolecular Chemistry, Center of Excellence of Polysaccharide Research, Jena, DE

Introduction

Current approaches in bone tissue engineering focus on hybrid materials made of polymer matrices (e.g. synthetic biopolymers such as polylactic acid, collagen or polysaccharides) and inorganic constituents (e.g., hydroxyapatite, tricalcium phosphate, or bioglass). While polymers help forming light and porous biocompatible structures, the ceramic parts improve cell-attachment and mechanical properties to at least partially restore stability but should also induce the formation of new bone tissue. A straightforward approach is the fabrication of scaffolds that carry stem cells with capability to differentiate into osteoblasts, bioactive drugs (such as growth factors) which induce and support osteoblast differentiation and purinergic receptor ligands influencing the osteogenic linage commitment. [1] [2] Bisphosphonates are long known in the therapy of various bone associated diseases due to their osteoclast-inhibiting activity. A guided delivery and prolonged release of bisphosphonates to the site of the disease is an attractive objective to overcome the inherent drawback of their low oral bioavailability.

Experimental Methods

In this work, we present the synthesis of substituted and stoichiometric hydroxyapatites by chemical precipitation. Chemical characterization is carried out by various spectroscopic and X-ray methods (i.e. XRD, FT-IR and ICP-OES), while the product's morphology is examined using particle size measurements and SEM.

Results and Discussion

Systematic evaluation of the reaction parameters shows a major impact of the reaction temperature on crystallite size and degree of crystallinity for the synthesis of stoichiometric hydroxyapatite, while pH and reaction time result in minor changes. Furthermore, the influence of organic templates on the crystallization and agglomeration of the products are investigated.

Conclusion

Embedding the synthesized apatites into a polysaccharide hydrogel-matrix provides a hybrid material, that resembles the physicochemical properties of natural bone, thus making it a promising candidate for bone tissue engineering and drug delivery applications.

References

[1] P. F. Ottensmeyer, M. Witzler, M. Schulze, E. Tobiasch, Int. J. Mol. Sci. 2018, 19, 3601.

[2] A. Leiendecker, S. Witzleben, M. Schulze, E. Tobiasch, Current Stem Cell Res. Ther. 2017, 12, 103.

Acknowledgement

Financial support was given by the BMBF project "Hybrid-KEM" (FKZ 13FH569IX6).

PS1-02-56

Effect of two β-tricalcium phosphate bone grafting materials with varying macro- and micromorphology on bone formation and osteogenic marker expression 6 months after sinus floor augmentation in humans

Mohamed Rezk[1,2], Alina Bednarek[1], Micheal Stiller[1], Christine Knabe[1]

[1]Philipps University, Dept. of Experimental Orofacial Medicine, Marburg, DE; [2]Ain Shams University, Dept. of Periodontology, Cairo, EG

Introduction

Sinus floor augmentation (SFA) is frequently performed as a mandatory augmentation procedure prior to placing dental implants in the posterior maxillary region. Disadvantages of autologous grafts as well as the limited biodegradability of some of the commercially available bone grafting materials have prompted an ever-increasing search for adequate bone substitute materials. An ideal bone grafting material should stimulate bone formation at its surface, resorb and be replaced by fully functional bone tissue.

Over the last two decades, the use of tricalcium phosphate (TCP) granules as alloplastic bone graft particles has received increasing attention especially for maxillary sinus augmentation procedures.

This study evaluated the effect of two highly porous TCP granules with the same overall porosity but varying macro- and micromorphology on bone formation and on osteogenic marker expression 6 months after sinus floor augmentation (SFA). This was in addition to characterizing the biodegradability.

Experimental Methods

This study comprised a series of 40 consecutive patients, in which unilateral SFA was performed. In 20 patients phase pure β-TCP polygonal particles (granule size 1000 to 2000 µm) with 65% porosity (CM)[1,2] and rounded morphology were used, while in the remaining 20 patients TCP polygonal particles displaying sharp edges (granule size 700 to 1400 µm) with 60% porosity TCP (CER)[3] were utilized in a combination with autogenous bone chips (10:1). At implant placement, 6 months after sinus grafting, cylindrical biopsies were sampled and processed for immunohistochemical analysis of resin embedded sections from the augmented area as described previously.[2,3]. Sections were stained for collagen type I (Col I), alkaline phosphatase (ALP), osteocalcin (OC) and bone sialoprotein (BSP). Subsequent to the immunohistochemical analysis, tissue sections were prepared for histomorphometry. The area fraction of newly formed bone as well as the particle area fraction were determined first, apically close to the Schneiderian membrane and second, in the center of the cylindrical biopsies.[2,3]

Results and Discussion

In both patient groups a statistically significant greater amount of bone formation and smaller amount of residual grating material were observed in the central area compared to the apical area. This tendency was more pronounced in the CM group (43.9% (mean) newly formed bone centrally vs. 33.3% (mean) apically) compared to the CER group (39.5% (mean) vs. 36.3% (mean) apically). Residual grafting material: CM group centrally 2.85 (mean) versus 21.1% (mean) apically; CER group 1.3 (mean) apically versus 16.0 (mean) centrally, with these differences between the CM and CER group not being statistically significant. Marked differences with respect to the osteogenic marker expression were observed when comparing both materials. Significantly higher expression of OC was noted in

osteoblasts in the CM group both apically and centrally when compared to the CER group. In the CM group a higher expression of Col I was noted apically than centrally, whereas positive expression of the osteogenic markers OC and ALP were present in both areas. In the CER group a high expression of Col I and ALP in the apical and central area was indicative of bone formation which was still actively progressing 6 months after sinus floor augmentation. Furthermore, the CER particles located in the most apical layer of the biopsies were fully surrounded by fibrous tissue in combination with fibrous tissue being noticed in the pores of the particles. The trend towards a smaller amount of residual bone grafting material, i.e. higher biodegradability for the CER group compared to the CM group may be related to the slightly smaller granule size of the CER particles.

Conclusion

Both biomaterials with identical chemical composition and a similar degree of overall porosity showed marked differences with respect to the histomorphometric and immunohistologic results in vivo. This appeared to be due to the different macro- and micromorphology of the granules. The high OC expression in osteoblasts both centrally and apically in the OC group is indicative of the excellent bioactive behaviour of this grafting material and its enhancing effect on bone matrix mineralization. The CER particles being surrounded by fibrous tissue in the most apical layer of the biopsies may be related to the sharper edges of the CER particles compared to the more rounded morphology of the CM particles in conjunction with the relative movement between particles of the grafting material and the Schneiderian membrane during the breathing process. Both TCP grafting materials, however, supported sufficient bone formation in the augmented sinus floor for facilitating stable and reliable implant placement with residual grafting material still being present 6 months after SFA. This was in addition to matrix mineralization and bone formation still actively progressing 6 months after SFA.

References

1. Knabe C, Adel-Khattab D, Hübner WD, Peters F, Knauf T, Peleska B, Barnewitz D, Genzel A, Kusserow R, Sterzik F, Stiller M, Müller-Mai M. “Effect of silicon-doped calcium phosphate bone grafting materials on bone regeneration and osteogenic marker expression after implantation in the ovine scapula”. J Biomed Mater Res B Appl Biomater. 2018 May 16.
2. Knabe C, Koch Ch, Rack A, Stiller M. Effect of β-tricalcium phosphate particles with varying porosity on osteogenesis after sinus floor augmentation in humans. Biomaterials 2008;29(14):2249-2258.
3. Knabe C, Adel-Khattab D, Kluk E, Struck R, Stiller M. Effect of a Particulate and a Putty-Like Tricalcium Phosphate-Based Bone-grafting Material on Bone Formation, Volume Stability and Osteogenic Marker Expression after Bilateral Sinus Floor Augmentation in Humans. J Funct Biomater. 201729;8(3).

Acknowledgement

The authors would like to thank the German Research Foundation for funding (KN377/5-1) and Ms. A Kopp for her excellent technical assistance.

PS1-02-57

Multicomponent Sr-HA and Ga-βTCP/gelatine based scaffolds for biomedical applications

Katarzyna Szurkowska, Joanna Kolmas

Medical University of Warsaw, Faculty of Pharmacy with Laboratory Medicine Division, Department of Analytical Chemistry and Biomaterials, Analytical Group, Warsaw, PL

Introduction

Calcium phosphates (CaP) play a crucial role in the regenerative medicine as cavities filling materials, scaffolds for new bone tissue, and more recently as systems delivering therapeutic substances [1]. Among CaP group, hydroxyapatite (HA) has received considerable attention because of its significant similarity to the biological apatite - the main inorganic component of biological hard tissues. Another material commonly used in bioceramics is beta tricalcium phosphate (βTCP), which is characterized by better solubility than HA. The unique capacity for the CaP group is the ability to undergo ionic substitution, which can enhance biological activity of the samples [2]. Both strontium and gallium ions enhance bone regeneration, act as antiresorptive agents and possess slight antibacterial properties. Therefore, their coexistence in the scaffold can be particularly beneficial. The addition of scaffold-binding gelatine will allow to control the degradation rate of the composite and to improve the mechanical properties of CaP samples [3]. Due to the presence of pores in the composite, proper vascularisation and delivery of the necessary nutrients to the tissue will be possible.

Experimental Methods

The synthesis of a series of calcium phosphates substituted with strontium and gallium, substituted with various amounts of ions, were carried out. A series of Sr^{2+} substituted hydroxyapatites (Sr-HA) was synthesized via wet precipitation method at 60 °C, left for 24 h for aging and then air-dried. A series of Ga^{3+} substituted beta tricalcium phosphates (Ga-βTCP) was first obtained by precipitation and then the raw precipitates were subjected to sintering at 1000 °C to allow a phase transition. In addition, pure unsubstituted CaP were synthesized as comparative materials. All the resulting powder materials were subjected to a thorough physicochemical analysis to select the ones with the most favourable parameters. Fourier Transform Infrared Spectroscopy (FT-IR), Solid State Nuclear Magnetic Resonance (ssNMR) and X-ray Powder Diffraction (PXRD) were used for structural and chemical composition assays. Transmission Electron Microscopy (TEM) was used to assess the morphology, shape and size of crystals and their tendency to agglomerate. Quantitative analysis of the introduced ions was performed by Inductively Coupled Plasma Optical Emission Spectrometry (ICP-OES). A preliminary evaluation of cytotoxicity in vitro was performed on BALB/c 3T3 mammalian fibroblast cell line. Porous gelatine-based scaffolds containing selected Sr-HA and Ga-βTCP samples were obtained by the lyophilization method. The resulting materials were then examined, determining the degree of porosity, morphology and ion release profiles.

Results and Discussion

Sr-HA and Ga-βTCP samples with various amounts of substituted ions were synthesized and thoroughly physicochemically examined. Moreover, all of the samples turned out cytocompatible. Multicomponent scaffolds, composed of selected Sr-HA, Ga-βTCP and gelatine were successfully obtained. Through the use of lyophilization

method, it was possible to obtain a porous material that gradually releases substituted ions into the medium. Differences in the release profile of individual elements were obtained, due to the better solubility of βTCP than HA.

Conclusion

The aim of the research was to synthesize biocompatible and bioactive implant materials composed of doped calcium phosphates (CaP), which would serve as scaffolds delivering strontium and gallium ions directly into the damaged bone tissue. The determined ion release profiles are the starting point for further research. The long-term project objective is to develop scaffold that could potentially be used for local delivery of antiresorptive drugs into the injured tissue.

References

[1] M. Vallet-Regi, J.M. Gonzales-Calbet, Prog. Solid State Chem. 32 (2004) 1-31.
[2] M. Supova, Ceram. Int. 41 (2015) 9203-9231.
[3] J. Venkatesan, S.K. Kim, J. Biomed. Nanotechnol. 10 (2014) 3124-3140.

Acknowledgement

This work was supported by UMO-2016/22/E/STS/00564 grant of the National Science Centre, Poland and FW23/PM1/18 grant from the Medical University of Warsaw.

PS1-02-58

Zn^{2+} and SeO_3^{2-} modified hydroxyapatite as a potential, antitumor biomaterial for the therapy of bone cancer

Aleksandra Laskus[1], Anna Zgadzaj[2], Joanna Kolmas[1]

[1]Medical University of Warsaw, Department of Analytical Chemistry and Biomaterials, Analytical Group, Warsaw, PL; [2]Medical University of Warsaw, Department of Environmental Health Sciences, Warsaw, PL

Introduction

During the last few decades, when the societies have started to age, the disorders of the skeletal system have become a serious problem. Due to this, novel approaches to treat bone fractures, osteoporosis etc. have been recently developed. Considering different biomedical areas concerning the treatment of hard tissue, bone tissue engineering based on calcium phosphates (CaPs) is one of the most-developed. Among the CaPs, hydroxyapatite (HA) with the general formula $Ca_{10}(PO_4)_6(OH)_2$ should be distinguished due to its significant resemblance to the biological apatite, which builds mammalian hard tissue. On account of their excellent biocompatibility, HA-based materials are currently being used as bone fillers, coating materials or the elements of the matrices for drugs targeting bones.

One of the possible ways to create functional, novel ceramic materials based on HA, is introducing foreign ions into its crystal lattice. In this study, due to their well-known antibacterial, osteogenic and anticancer activity, Zn^{2+} and SeO_3^{2-} were chosen as ionic dopants.

Experimental Methods

In this study, a series of hydroxyapatite containing different amounts of zinc and selenite ions were synthesized via classical, co-precipitation method. The obtained powders underwent both physicochemical and biological analysis. The techniques of FTIR, PXRD, ssNMR, TEM and ICP-OES were applied. The release kinetics of the ionic dopants was also investigated. Additionally, the cytotoxicity tests of the materials were conducted.

Results and Discussion

The physicochemical analysis confirmed that all of the obtained powders were poorly-crystalline hydroxyapatites with no other crystalline impurities in phase. The FTIR spectra, as well ICP-OES results confirmed the successful introduction of the SeO_3^{2-}. The elemental analysis confirmed also the presence of the Zn^{2+} in the structure of HA. Based on the PXRD, FTIR and TEM studies, a clear tendency concerning the crystallinity of the powders containing Zn^{2+} was observed. Namely, the introduction of Zn^{2+} ions into the crystal structure of HA lowered its crystallinity. The interesting outcomes of the release kinetics of the ionic dopants were also obtained. Whereas in case of zinc, the level of the released element did not exceed 1 % of the total, introduced amount, the level of selenite ions reached ca. 50 % in average, which suggests that, unlike zinc ions, selenites were also partially adsorbed on the surface of HA. This, in turn, is consistent with the cytotoxicity tests, which revealed that the materials containing selenites were toxic and thus, could be used as potential, antitumor agents in bone cancer treatment. Considering well-known toxicity of selenium, the authors believe that the outcomes of the biological analysis are strongly connected with the partial adsorption of the selenites on the surface of HA.

Conclusion

In this study, a novel, HA-based biomaterial containing Zn^{2+} and SeO_3^{2-} was synthesized. The outcomes of the cytotoxicity test suggests that the obtained powders could be used as potential, anticancer biomaterials. Due to the preliminary character of the study, it is necessary to proceed with further investigation.

Acknowledgement

The study was supported by The National Science Centre UMO-2016/22/E/STS/00564 .

PS1-02-59

Dual-setting brushite-silica gel cements with high cross-linking density precursors

Ib Holzmeister, Jürgen Groll, Uwe Gbureck

University Hospital of Würzburg, Department for Functional Materials in Medicine and Dentistry and Bavarian Polymer Institute, Würzburg, DE

Introduction

Calcium phosphate cements (CPC) set via a dissolution–precipitation reaction and form an entangled network of crystals providing mechanical strength after setting. A further modification by adding monomers to the aqueous cement phase results in the formation of a second interpenetrating network with a strong impact on cement properties.[1] This was recently shown for cement modification with tetraethyl orthosilicate (TEOS) as precursor.[2] Here, this approach is further explored by using silica precursors with a higher density of alkoxy groups to increase network and cross-linking density in the final gel. Also modified precursors with different hydrophilic functional groups are investigated to influence the interface between silica and cement matrix. The precursors were initially hydrolyzed under acidic conditions and the combined with a brushite forming cement powder. Due to the increase in pH of the sol during cement setting leads to a simultaneous formation of cement matrix and silica hydrogel. [3]

Experimental Methods

Sol precursors were a mixture of TEOS (100 – 60%) and 0 – 40% of silica monomers with 6-12 alkoxide functionalities. Both commercially available 1,8-Bis(triethoxysilyl)octane and self-synthesized modified silica monomers with hydrophilic groups and a higher density of alkoxy groups were used **(Figure 1A).** Silica sols were obtained by adding the sol precursor mixture to water in a ratio of water: “Si-OEt” = 2.25 and 0.1 M HCl solution. Composite cements were produced by mixing the sol with cement raw powder, consisting of β-tricalcium phosphate (β-TCP) and monocalcium phosphate anhydrous (MCPA) in an equimolar ratio and the addition of 1 wt% citric acid. The citric acid is used as retarding agent in order to extend the setting-time of the composites.

Results and Discussion

The results demonstrated an increase of mechanical performance by using different amounts of a silica monomer (1,2-Bis(triethoxysilyl)octane) in addition to TEOS in the composite compared to the pure TEOS reference **(Figure 1B).** A variation of the monomers resulted in a substantial increase in the strength **(Figure 1C)** with an increase from 0.44 ± 0.09 MPa to 8.29 ± 1.01 MPa at low PLR of 1 g/mL. The porosity characteristics of the silica–brushite networks showed a bimodal pore size distribution in the set matrices with nanosized pores originating from the silica matrix and micrometer pores from the cement matrix **(Figure 1D).** The latter is thought to have a strong effect on drug release capability by retarding drug diffusion from the cement matrix.

Conclusion

It could be shown that the use of different silica monomers has a huge influence on the properties of the composites. As shown a increased strength of the composites could be observed depending of the system up to 10 times. Due to the two network in the composites, a bimodal poresize distribution could be observed.

References

[1] T. Christel et al. *Dual setting α-tricalcium phosphate cements,* --Materials in Medicine, 2013, 24(3), pp 573-581.

[2] M. Geffers et al. *Dual-setting brushite–silica gel cements,* Acta Biomaterialia, 2015, Volume 11, pp 467-476.

[3] I. Holzmeister et al. *Artificial inorganic biohybrids: The functional combination of microorganisms and cells with inorganic materials,* Acta Biomaterialia,2018, Volume 74, pp 17-35.

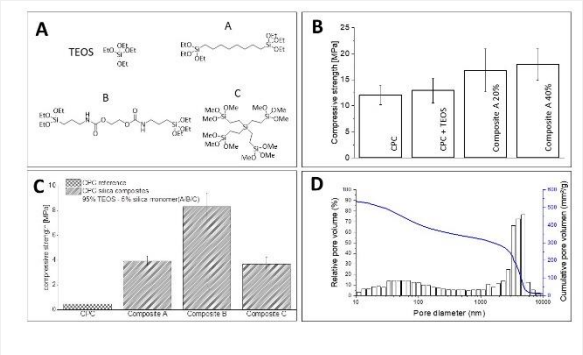

Figure 1
A Molecular structure of TEOS, commercially bought silica monomer(A) and synthesized silica monomers(B/C) **B** Compressive strength of CPC and composite reference CPC+TEOS. Increased compressive strength by adding 20/40% of silica monomer A. (PLR = 2 g/mL) **C** Compressive strength of CPC and composites with 5% different silica monomers (PLR = 1 g/mL) **D** Pore size distribution analyzed by Hg porosimetry in a range of 10-10000 nm of silica gel composite.

2:45 p.m. – 3:45 p.m.

Hall 1 / Exhibition Area

PS1-03 | Biopolymers and artificial ECM

PS1-03-61

Design of a novel 3D combined bioactive tissue matrices for skeletal muscle tissue repair

Nergis Zeynep Renkler[1], Sedat Odabas[2], **Kadriye Tuzlakoglu**[1]

[1]Yalova University, Dept. Polymer Engineering, Yalova, TR; [2]Ankara University, Dept. Chemistry, Ankara, TR

Introduction

The primer function of the skeletal muscle is to provide movement with other musculoskeletal organs. Damages of these muscles greatly affect daily life of patients as they cause movement restriction in the human body. The regain of the function of damaged muscle depends on the size of the injury. In case of simple injuries muscles can self-heal with physical exercises and resting. However, the large volume loss caused by firearms, cancer ablation, etc. cannot heal without any surgical treatment. Tissue engineering techniques which use a matrix with/without cells emerge as an alternative advanced treatment for damaged muscle tissue regeneration. The function of the carrying matrix is to form new muscle tissue by enhancing myotube formation from myofibers. Thus, the materials used in fabrication of matrix and final form of matrix are particularly important. We herein designed a spiral form 3D matrix made of nanofiber polycaprolactone and polyaniline membrane, which is combined with DCM to repair damaged muscle tissue.

Experimental Methods

The bovine skeletal muscles purchased from local abattoir were decellularized using trypsin-EDTA and Triton-X solutions. DNA assay was done by high salt DNA extraction procedure to determine the effectiveness of decellularization method. DNA content was measured using Nanodrop (Thermo scientific, USA) after the extraction of DNA. To further confirm removal of cellular content, Gel electrophoresis was performed with DNA extracts loaded on 1% agarose gels.For production of nanofiber membrane, the mixed was electrospun through a plate collector by applying high voltage between tip and collector. The morphology of obtained mats was determined by SEM, where the electrical conductivity was measured using a multimeter. The final combined structures were obtained by injecting DCM solution in acetic acid into a spirally rolled electrospun mats.

Results and Discussion

With regard to DNA assay, the decellularization efficiency was found to be around 84% for DCM samples. Furthermore, there were no detectable traces of DNA in electrophoresis, confirming the effectiveness in removing the DNA component. A nonwoven mesh structure was successfully produced from PCL/PANI via electrospinning process without any bead formation on the nanofibers (Fig.1.). The diameters of nanofibers were in the range between 200-730nm. The electrical resistance of nanofibrous mats were measured to be around $10^8\Omega$. The spiral form structures were also formed with a good integration between the components.

Conclusion

The results obtained from the present work indicate that spiral shape combined structures possess favorable properties to serve as a scaffold for the regeneration of damaged skeletal muscle tissue.

Acknowledgement

We gratefully acknowledge the support of The Scientific and Technological Research Council of Turkey (TUBITAK) through project 118M610.

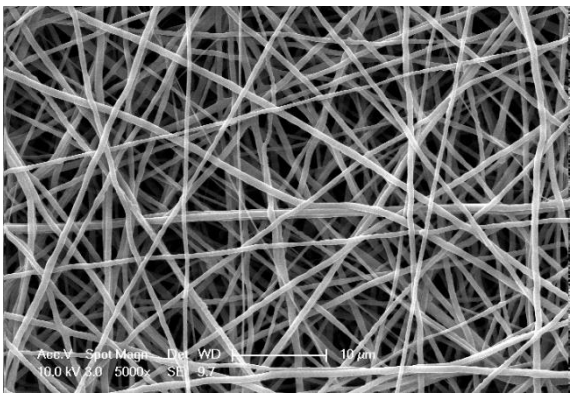

Morphology of PCL/PANI mats observed by SEM.

PS1-03-62

Novel Conducting, Biocompatible and Biodegradable Copolymer based on PEDOT-*co*-PDLLA for Biomedical Applications

Aruã C. Da Silva, Susana I. Córdoba de Torresi

Universidade de São Paulo, Instituto de Química, São Paulo, BR

Introduction

Electroactive biomaterials are a new generation of "smart" biomaterials based on intrinsically conducting polymers (ICP). Among them, Poly(3,4-ethylenedioxythiophene) (PEDOT), polypyrrole (PPy) and polyaniline (PANI) are well known conducting polymers that present excellent electrical and optical properties emerging as main candidates for potential biomedical applications.[1] Additionally, the biodegradability of biomaterials is very useful and desirable. In this context, biodegradable polymers based on polyesters[2], such as poly(*D,L*-lactic acid) (PDLLA), polycaprolactone (PCL) and poly(glycolic acid) (PGA) appear to be promising candidates because of their good biocompatibility and, as a consequence, they have been attracting attention as sustainable alternatives for applications in medicine.

Poor molecular interaction with cells is the main challenge for the use of conducting polymers as biomaterials. In order to improve their own biocompatibility, the main strategies are whether by doping with specific counter ions[3] or chemically modifying the monomers with different molecules.[4] However, electroactive polymers still present low or none biodegradability.

To overcome the common problems, it was presented the development a novel conducting and biodegradable copolymer based on poly(3,4-ethylenedioxythiophene) (PEDOT) covalently bonded to poly(*D,L*-lactic acid) (PDLLA). Such strategy allows changing the amount of EDOT to PDLLA monomers, resulting in a biomaterial with completely different final properties, such as conductivity, biodegradability and cytotoxicity. It was synthesized PEDOT-*co*-PDLLA in three different proportions, 1:05, 1:25 and 1,50, respectively and the films produced was tested for embryonic stem cells differentiation (**Figure 1**).

Experimental Methods

The synthesis of the novel conducting and biodegradable copolymer was obtained using (2,3-dihydrothieno[3,4-b][1,4]dioxin-2-yl)methanol (EDOT-OH) as an initiator in a lactide ring opening polymerization reaction, resulting in EDOT-PDLLA macromonomer. Conducting PEDOT-*co*-PDLLA copolymers (in three different proportions) were achieved by chemical copolymerization with 3,4-ethylenedioxythiophene (EDOT) monomers and persulfate oxidant. The PEDOT-*co*-PDLLA copolymers were structurally characterized by ^{1}H NMR and FTIR (with DFT/PBE-D3/def2-TZV calculations). Cyclic voltammetry was performed to evaluate the electroactivity behavior of the copolymers and conductivity measurements were performed via electrochemical impedance spectroscopy. In vitro biodegradability was evaluated using *Proteinase K* over 35 days biodegradation. Biocompatibility was assessed by adhesion, migration, proliferation and differentiation assays using embryonic stem cells (E14.tg2a).

Results and Discussion

The ^{1}H NMR spectra of products confirmed the copolymerization reaction of PEDOT-*co*-PDLLA. The FTIR spectra compared with calculated spectrum for the macromonomer of EDOT-PDLLA revealed the actual polymerization on the EDOT moiety. Cyclic voltammetry confirmed the electroactive character of the biomaterials with a correspondence between the PEDOT ratio. The electrochemical impedance spectroscopy of the PEDOT-*co*-PDLLA

copolymers shown conductivity ranging from 4×10^{-8} to 5×10^{-5} S cm^{-1}, depending on PEDOT content. The biodegradation assay shown 29% to 46% (w/w) biodegradation after 35 days. Biocompatibility was assessed with non-cytotoxicity observed, preferentially differentiated to neuronal cells instead glia cells, with highlight for PEDOT-*co*-PDLLA 1:50 ratio, where migration halos and neurofilament lengths of the mature neuron cells were increased in 65% and 370%, compared to control of TCPS plates.

Conclusion

The fabricated PEDOT-*co*-PDLLA copolymers can serve as novel electroactive, biodegradable and biocompatible materials potentially useful in different biomedical applications.

References

1. Guo, B., Glavas, L. & Albertsson, A.-C. *Prog. Polym. Sci.***38,** 1263–1286 (2013).
2. Williams, C. K. *Chem. Soc. Rev.***36,** 1573 (2007).
3. Molino, P. J., Tibbens, A., Kapsa, R. M. I. & Wallace, G. G. *MRS Proc.***1569,** mrss13-1569-qq05-01 (2013).
4. da Silva, A. C., Augusto, T., Andrade, L. H. & Córdoba de Torresi, S. I. *Mater. Sci. Eng. C***83,** (2018).

Acknowledgement

We gratefully acknowledge the financial support received from Brazilian agency FAPESP (proc. 2015/26308-7) and the PhD scholarship (proc. 2014/09353-6).

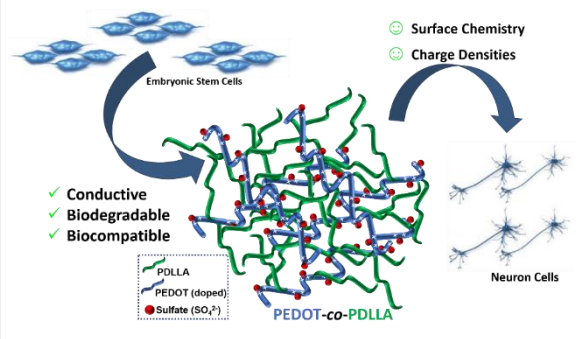

The PEDOT-co-PDLLA copolymer promoting neuron cells differentiation
Schematic representation of the application of PEDOT-*co*-PDLLA films as support to cell adhesion, proliferation and differentiation by using embryonic stem cells.

PS1-03-63

Tunable bioactivity and mechanics of collagen-based tissue engineering constructs: A comparison of EDC-NHS, genipin and TG2 crosslinkers

Malavika Nair, Ramneek K. Johal, Serena M. Best, Ruth E. Cameron

University of Cambridge, Department of Materials Science and Metallurgy, Cambridge, GB

Introduction

Collagen-based tissue engineering implants are routinely crosslinked in order to maximise their resistance to the loads experienced in-service. However, chemical crosslinkers can not only modify the mechanical properties obtained but also alter the collagen surface chemistry. The cell response to a substrate is often highly sensitive to both mechanical and biochemical cues. In particular, carbodiimide-based crosslinking allows for a significant increase in the mechanical stiffness, but at high concentrations has also been shown to reduce the availability of integrin-specific binding sites on the surface of collagen[1]. This work considers two alternative chemical treatments–genipin and transglutaminase (TG2)–and explores the effects of various chemical crosslinking mechanisms on the viability, attachment and proliferation of human dermal fibroblasts on treated collagen substrates.

Experimental Methods

Solvent cast films of microfibrillar Type I collagen were treated with EDC-NHS, genipin or TG2 solutions at a range of concentrations. The materials characterisation of the films included a ninhydrin assay to determine the degree of crosslinking as well as tensile testing to determine changes to the elastic modulus induced by the chemical treatments.

An LDH Cell Attachment assay was performed on human dermal fibroblasts seeded on treated and untreated samples to separate the effect of integrin specific and integrin non-specific binding to the collagen substrates. All films were also seeded with human dermal fibroblasts for a period of seven days, and media was extracted at Day 1, 4 and 7 to determine the cell proliferation levels using the MTS assay. The cell viability was assessed spectroscopically using the LDH assay on the spent media of the cells cultured for the MTS assay, as well as through fluorescent microscopy using a LIVE/DEAD assay kit. Finally, the effects of treatment on the overall cell morphology was characterised using immunofluorescent microscopy.

Results and Discussion

The chemical characterisation of the treated and untreated samples indicated a reduction in free amine content for all treatments, thus suggesting a successful reaction between the crosslinkers and the collagen samples. Further mechanical testing revealed that EDC-NHS crosslinking can produce a five-fold increase in the tensile modulus at the low concentrations, and a nearly 100-fold improvement at the higher concentrations. Similarly, genipin treated films resulted in a ten-fold increase in modulus over the untreated condition. The modulus decreased for all concentrations of TG2 when compared with the non-crosslinked condition.

As seen in Figure 1(a), when comparing the degree of free amine reduction to the tensile modulus, similar values are obtained for the same degree of crosslinking for genipin and EDC-NHS. However, the modulus for TG2 was markedly low for the high reduction in free amines observed. By taking into account the mechanism of action for TG2, the mechanical behaviour observed can be resolved through a hydrolytic pathway that can be adopted by TG2 in the

presence of few amines, whereby glutamines are converted to glutamates instead forming an amide bond with a neighbouring lysine.

From the LDH cell attachment assay seen in Figure 1(b), EDC-NHS crosslinking resulted in a significantly reduced integrin-specific binding at high concentrations. The specific binding was unaffected upon treatment with genipin or TG2. Results from the MTS assay show that cells treated with EDC-NHS, TG2 and genipin proliferated at a higher rate than the non-treated counterparts. However, at all concentrations of EDC-NHS, a sharp drop to pre-seeded levels is observed by Day 7 of proliferation. Such behaviour is not observed with either genipin or tissue transglutaminase. Although mechanical cues have long been suggested to influence proliferation rates of fibroblasts[2], the long-term proliferation in these samples can be concluded to be dependent primarily on the availability of appropriate ligands, even if short-term proliferation may be driven by mechanical stiffness.

Conclusion

Following the results of this work, genipin stands out in its potential to replace EDC-NHS where medium to high mechanical stiffness and excellent cell attachment and proliferation are desired. EDC-NHS can offer collagen implants of high tensile moduli, at the expense of integrin specific attachment and long-term cell proliferation. While TG2 allows for exceptional fibroblast activity, it reduces the effective tensile modulus of insoluble collagen based films. As seen in Figure 2, this allows for the creation of materials selection map to obtain tuneable cell activity and mechanics in tissue engineering implants through the choice of chemical crosslinking.

References

[1] D. V. Bax, N. Davidenko, D. Gullberg, S. W. Hamaia, R. W. Farndale, S. M. Best, and R. E. Cameron, “Fundamental insight into the effect of carbodiimide crosslinking on cellular recognition of collagen-based scaffolds,” *Acta Biomaterialia*, vol. 49, pp. 218–234, 2017.

[2] E. Hadjipanayi, V. Mudera, and R. A. Brown. "Close dependence of fibroblast proliferation on collagen scaffold matrix stiffness." *Journal of tissue engineering and regenerative medicine* 3.2: 77-84, 2009.

Acknowledgement

This work was supported by the ERC Advanced Grant 320598 3D-E and the EPSRC Established Career Fellowship Grant No. EP/N019938/1. M. Nair acknowledges the financial support provided Geistlich Pharma AG to undertake this research and the Gates Cambridge Trust. The authors would also like to thank Andrew Rayment for his assistance with the tensile testing and for writing the edge detection based software used to calculate strains.

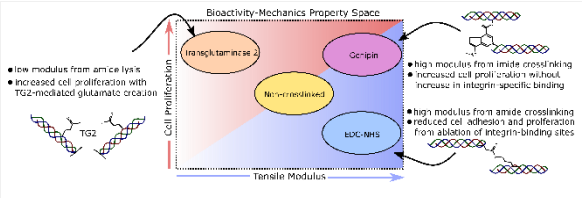

Figure 2
A materials selection map illustrating the region of cell activity (specifically proliferation) and mechanical behaviour (tensile modulus) which can be accessed through the choice of crosslinker chemistry.

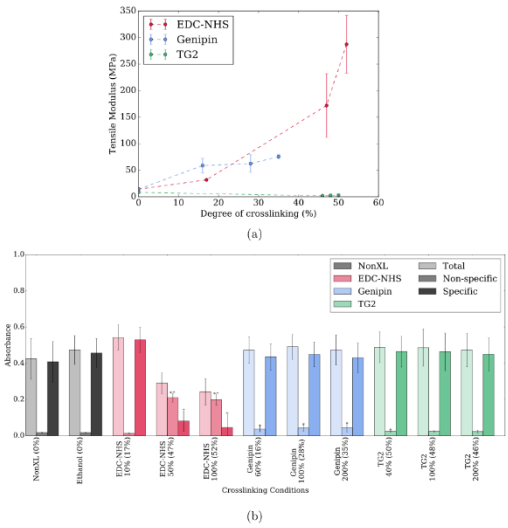

Figure 1
Mechanical and biological characterisation of treated collagen films: a) The tensile moduli are plotted against the degree of crosslinking as obtained from the ninhydrin free amine assay. b) LDH assay results on the integrin mediated and non-specific adhesion of human dermal fibroblasts on treated and untreated collagen samples. Values in brackets represent the 'degree of crosslinking' as determined by the ninhydrin free amine assay for a given condition

PS1-03-64

Synthesis and characterization of oxidized bacterial cellulose through electrochemical methods: its biodegradability and potential as hemostatic material

Eugénia C. Queirós[1,2], Sara P. Pinheiro[1], José E. Pereira[3], Justina Prada[3], Isabel Pires[3], Pier Parpot[2,1], Miguel Gama[1]

[1]University of Minho, CEB - Centre of Biological Engineering, Braga, PT; [2]University of Minho, CQUM – Centre of Chemistry, Braga, PT; [3]University of Trás-os-Montes and Alto Douro, CECAV - Veterinary and Animal Research Centre, Vila Real, PT

Introduction

Bacterial cellulose (BC) is a biocompatible material that exhibits high purity, high crystallinity and great mechanical properties. BC has high degree of polymerization and high-water content [1,2]. Therefore, BC has a huge potential to be applied in several fields, being the biomedical field the most relevant to this work. Biodegradability is a key requirement for several applications and the modification of BC aiming to increase and improve its biodegradability has been attempted. BC may be chemically modified through its hydroxyl groups, e.g., by oxidation, becoming reabsorbable and acquiring new features, such as hemostatic behavior [3]. In this work, oxidation of BC membranes was achieved using tetramethylpiperidine-1-oxyl (TEMPO) radical through electrochemical methods. TEMPO is able to perform selective oxidation of the primary hydroxyl groups, meaning that only C6 is oxidized into carboxyl groups. This is a cleaner approach since it allows the anodic regeneration of the oxidizing species avoiding the use of the primary oxidant [4].

This project aims to develop a resorbable material based on oxidized BC that simultaneously displays hemostatic behavior.

Experimental Methods

Oxidation of BC membranes was achieved through electrolysis. BC and oxidized BC were characterized by FT-IR, SEM, XRD and ^{13}C-NMR. The degree of oxidation was evaluated by titration of the carboxyl groups and the hemostatic behavior was investigated through whole blood coagulation tests. Both *in vitro* and *in vivo* biodegradability of oxidized membranes was evaluated. *In vitro* biodegradability was assessed in ultra-pure water after 3, 7, 14 and 63 days of incubation while *in vivo* biodegradability was studied in a rat model, for 3, 14 and 56 days.

Results and Discussion

Three different degrees of oxidation were obtained by the application of 400C, 700C and 1200C of total quantity of electricity. FT-IR spectra showed an increase on the absorption band around 1628 cm^{-1} attributed to the carboxylic acid vibration, as compared to non-oxidized membranes, revealing the formation of carboxylic acid groups [5]. SEM images revealed that the morphology of the membranes was not changed by the oxidation [6]. The obtained XRD patterns for all the oxidized samples were very similar to non-oxidized ones, suggesting that the crystal structure was preserved and oxidation did not modify the crystal structure [7]. ^{3}C-RMN results showed that the signal around 62 ppm corresponding to superficial C6 primary hydroxyl group decreased after the oxidation, while the peak around 174.6 ppm assigned to carboxylate groups appeared after oxidation, confirming the selective oxidation of C6 [8,9]. Carboxylic acid content after oxidation was quantified by titration. The degree of oxidation increased with the applied

charge being 4%, 7% and 15%, for 400C, 700C and 1200C, respectively [10]. I*n vitro* degradability of oxidized membranes and its hemostatic behavior was evaluated using Surgicel® as control. The obtained results showed that almost no degradation occurred on non-oxidized membranes demonstrating the relevance of the oxidation on the improvement on BC biodegradability [7]. However, even after 63 days of incubation, oxidized membranes did not degrade extensively. Whole blood clotting times assay was applied to evaluated the hemostatic behavior of the membranes [11]. The obtained results demonstrated that, contrarily to non-oxidized membranes, the oxidized ones exhibited hemostatic activity, although not as effective as Surgicel®. *In vivo* biodegradability and biocompatibility of oxidized membranes was evaluated. Membranes were implanted subcutaneously and the inflammatory response was studied using membranes with 7% of oxidation. The obtained results showed that there were no macroscopic evidences of inflammation and even after 56 days of implantation, the oxidized membranes did not degrade completely. Nevertheless, oxidized membranes revealed good biocompatibility [12, 13].

Conclusion

This work confirmed that oxidation was effective in yielding a hemostatic and partially degradable material. Despite its ability to act as hemostatic material further studies are desirable to improve BC biodegradability. The oxidized membranes did not induce an inflammatory response, revealing a good biocompatibility.

References

[1] Huang Y, Zhu C, Yang J, Nie Y, Chen C, Sun D. Cellulose. 2014;21(1):1–30.
[2] Reiniati I, Hrymak AN, Margaritis A. Crit Rev Biotechnol. 2017;37(4):510–24.
[3] Lai C, Shujiang Z, Sheng L, Liao S, Xi T, Zhang Z. Colloid Polym Sci. 2013;
[4] Parpot P, Servat K, Bettencourt AP, Huser H, Kokoh KB. Cellulose. 2010;17(4):815–24.
[5] da Silva Perez D, Montanari S, Vignon MR. Biomacromolecules. 2003;4(5):1417–25.
[6] Lu C, Chen SY, Zheng Y, Zheng WL, Xiang C, Wang HP. Nano-Scale Materials, Materials Processing and Genomic Engineering. Trans Tech Publications; 2014. p. 90–4. (Materials Science Forum; vol. 789).
[7] Shi X, Cui Q, Zheng Y, Peng S, Wang G, Xie Y. RSC Adv. 2014;4:60749-60756.
[8] Lai C, Zhang S, Chen X, Sheng L. Cellulose. 2014;21(4):2757–72.
[9] Lai C, Zhang S, Sheng L, Liao S, Xi T, Zhang Z. Colloid and Polymer Science. 2013; 291: 2985
[10] Cui Q, Zheng Y, Lin Q, Song W, Qiao K, Shumin L. RSC Adv. 2014;4:1630.
[11] Leitão A, Gupta S, Silva J, Reviakine I, Gama M. Colloids and Surfaces B: Biointerfaces. 2013; 111: 493-502
[12] Helenius G, Backdahl H, Bodin A, Nannmark U, Gatenholm P, Risberg B. J Biomed Mater Res A. 2006; 76(2):431-8
[13] Wang B, Lv X, Chen S, Li Z, Sun X, Feng C, Wang H, Xu Y. Cellulose. 2016; 23:3187-3198.

Acknowledgement

This study was supported by PhD Program in Biomedical Engineering" (ref: NORTE- 08-5369-FSE-000012 opens 4 PhD scholarship position with the financial support of ESF – European Social Fund, under Programa Operacional Regional do Norte - Norte2020 and by the Portuguese Foundation for Science and Technology (FCT) under the scope of the strategic funding of UID/BIO/04469/2013 unit and COMPETE 2020 (POCI-01-0145-FEDER-006684) and BioTecNorte operation (NORTE-01-0145- FEDER-000004) funded by the European Regional Development Fund under the scope of Norte2020 - Programa Operacional Regional do Norte. This work also has been funded by national funds (FCT) through the projects: Centre of Chemistry (UID/QUI/00686/2013 and UID/QUI/0686/2016).

PS1-03-65

Alginate-pullulan-glass composites with gold nanoparticles content- one step forward for tissue engineering applications

Alexandra I. Dreanca[1,2], Marieta Muresan- Pop[1], Zsejke R. Toth[1,3], Emoke Pall[2], Bogdan Sevastre[2], Marian Taulescu[2], Sidonia Bogdan[2], Dan C. Vodnar[2], Lucian Baia[1], Klara Magyari[1]

[1]Babeș-Bolyai University, Interdisciplinary Research Institute on Bio-Nano-Sciences, Cluj Napoca, RO; [2]University of Agricultural Sciencies and Veterinary Medicine, Faculty of Veterinary Medicine, Cluj Napoca, RO; [3]University of Szeged, Institute of Chemistry, Szeged, HU

Introduction

Bioactive glasses with gold nanoparticles are generating a considerable interest in terms of tissue engineering (1). Nowadays, the incidences of nosocomial infections are rising as a result of bacterial resistance to antibiotics and antibacterial agents. Thus, antibacterial activity as well as *in vitro* biocompatibility has become critical requirements for biomaterials used in tissue engineering. This study outlines a new approach to extend the biomaterials biological properties by synthesizing composites of bioactive glasses with gold nanospheres and spherical nanocages content, by sol-gel derived method, nanocages contain silver oxide. To further obtain an applicable material; the glasses were introduced in alginate-pullulan composites. Within the framework of these criteria we evaluated the biomaterials *in vitro*, by bioactivity assessment, antibacterial effects and cellular biocompatibility.

Experimental Methods

The gold nanospheres were synthesized by using Turkevich-Frens (2) and nanocages by using galvanic replacement reaction (3) using previously obtained Ag nanoparticles. The glasses with gold nanoparticles content were synthesized by sol-gel method (4). The composites of alginate-pullulan-bioactive glasses with gold nanoparticles were obtained by cross-linking method.

Pseudomonas aeruginosa (Gram negative) and *Staphylococcus aureus* (Gram positive) strains were used to perform the minimal inhibitory concentration test. The *in vitro* bioactivity of the composites was checked by their immersion in simulated body fluid (pH 7.4) for 6 weeks at 37°C.The apatite layer growth were analyzed via X-ray diffraction (XRD), FT-IR spectroscopy and scanning electron microscopy (SEM). Cyotoxicity tests were conducted using HS 27 cell line and human osteoblastsisolated from patella bone. The MTT assay was done after 24 hours, according to ISO 10 993-5.

Results and Discussion

The glass samples with gold nanocages, containing silver oxide showed a good bactericidal effect against *Pseudomonas aeruginosa and Staphylococcus aureus.* The *in vitro* bioactivity of the composites was evaluated by evidencing the apatite layer growth on the samples' surface following the immersion in simulated body fluid. The XRD pattern, FT-IR spectroscopy data and SEM images confirmed the apatite layer growth on the samples surface. On Hs 27 cells, both composites with different shaped gold nanoparticles showed good cytocompatibility, having viability higher than 88%, at 24 h. The qualitative examinations revealed no morphological, membrane modifications or intracytoplasmatic granulations. Surprisingly, the composite with gold nanocage showed not only lack of cellular toxicity, but also they enhanced the osteoblastic cells viability up to 113%. Furthermore, the studied biomaterials not only demonstrated biocompatibility, but also a significant *in vitro* osteogenic response.

Conclusion

Overall, these results offer compelling evidence that the newly developed biomaterials have the potential to provide a one-step treatment for further *in vivo* testing, offering infection prevention, while enhancing bone healing.

References

1. S.M. Marza, K. Magyari, S. Bogdan, M. Moldovan, C. Pestean, A. Nagy, F. Tabaran, E. Licarete, S. Suarasan, A. Dreanca, L. Baia, I. Papuc, Skin wound regeneration with bioactive glass-gold nanoparticles ointment, Biomedical materials, 14 (2019) 025011

2. G. Frens Controlled Nucleation for the Regulation of the Particle Size in Monodisperse Gold Suspensions, Nature Physical Science 241 (1973) 20-2.

3. Z-R. Tóth, G. Kovács, K. Hernádi, L. Baia, Z. Pap, The investigation of the photocatalytic efficiency of spherical gold nanocages/TiO_2 and silver nanospheres/TiO_2 composites, Separation and Purification Technology 183 (2017)216-25.

4. K. Magyari, T. Nagy-Simon, A. Vulpoi, R.A. Popescu, E. Licarete, R. Stefan, K. Hernadi, I. Papuc, L. Baia, Novel bioactive glass-AuNP composites for biomedical applications, Materials Science and Engineering C, 76 (2017) 752-759

Acknowledgement

This work was supported by a grant of Ministry of Research and Innovation, CNCS - UEFISCDI, project number PN-III-P1-1.1-TE-2016-1324, within PNCDI III.

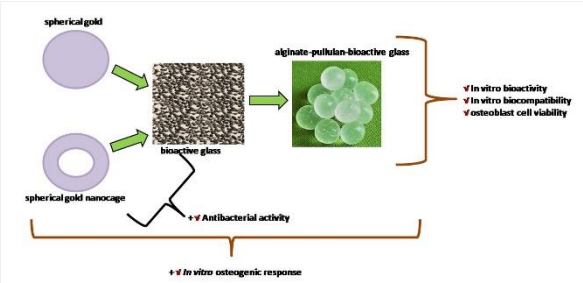

Study designed of Alg-Pll-AuNPsBG composites

PS1-03-66

Functionalized Matrices for Use in Skin Wound Healing and Regeneration

Soraya Lanouar[1,2,3], Rachida Aid-Launais[1,2,4], Camille Ehret[5], Laurent Bidault[3], Brigitte Closs[3], Didier Letourneur[1,2,5]

[1]University Paris Diderot, INSERM U 1148, Paris, FR; [2]University Paris 13, Institut Galilée, Villetaneuse, FR; [3]SILAB SA, Saint-Viance, FR; [4]University Paris Diderot, FRIM INSERM UMS 034, Paris, FR; [5]SILTISS, Saint-Viance, FR

Introduction

Chronic wounds result from a defect in the healing process associated with prolonged inflammation and correlated with necrosis, pain and high morbidity [1-2]. Biomaterials for skin regeneration aim to design 3D constructs with the ability to promote wound healing [3]. Most of them are animal product derivatives such as collagen or fibrin. These biomaterials usually have good bioactivity but are limited in terms of functionalization and mechanical properties. During the last decade, alternatives -such as the combination with synthetic polymers [4] or the use of crosslinking agents- were developed to improve these outcomes. These strategies often cause partial loss of bioactivity and affect biodegradability.

In this study, we used natural polysaccharides that offer tunable mechanical properties and degradation rates, as well as a good biocompatibility [5]. This system can be used as a carrier for compounds implied in wound repair. For this purpose, we investigated how this scaffold could be functionalized to deliver a natural compound in order to stimulate wound healing.

Experimental Methods

Our polysaccharide-based scaffolds were made of a pullulan and dextran mixture. The physicochemical properties of the material were modified using three different concentrations of crosslinking agent. The natural compound, an oligogalactomannan provided by the industrial partner (SILAB SA), was added as a healing booster. Two ways of incorporation were investigated: before (*in situ*) and after crosslinking (inverse diffusion). The resulting composite matrices were characterized *in vitro*, with incorporation effectiveness, drug release kinetics and cytotoxicity assays. *Ex vivo* skin penetration studies were also performed on compromised skin barrier model through a Franz cell.

Results and Discussion

For all formulations, no cytotoxicity was observed after 24h of contact. Our results showed that molecule incorporation was more efficient using inverse diffusion than *in situ* method. In addition, we have found a direct correlation between crosslinking and molecule retention. No release was observed from the formulations with the molecule incorporated *in situ* whereas a burst release was obtained in the case of inverse diffusion incorporation, whatever the crosslinking ratio. These results were in accordance with *ex vivo* penetration results, in which the molecule passed through all skin layers when incorporated by inverse diffusion.

Conclusion

In this study, we have demonstrated that the 3D polysaccharide matrices could be successfully used as a drug delivery platform which can be modulated by the cross-linking ratio and the way of incorporation. With these properties, it can be possible to add several compounds and modulate their release in the wound healing process.

References

[1] Patient-centered Outcomes in wound care (2013); www.angio.org ;

[2] Chandan et al., Wound repair an regeneration (2009), doi: 10.1111/j.1524-475X.2009.00543.x ;

[3] MacNeil et al., Materials Today (2008), doi: 10.1016/S1369-7021(08)70087-7 ;

[4] Zhu et al., Expert Rev Med Devices (2011), doi :10.1586/erd.11.27 ;

[5] Lanouar et al, Journal of Materials Science: Materials in Medicine (2018), doi: 10.1007/s10856-018-6085-x.

Acknowledgement

We acknowledge ANR-16-CE18-0023 “Healskin” for financial support.

PS1-03-67

Modular and Biofunctional Hyaluronan Hydrogels for 3D Cell Culture of Hepatocytes and Neurons

Michael Jury[1], Christopher Aronsson[1], Isabelle Matthiesen[2], Jonas Christofferson[3], Carl-Fredrik Mandenius[3], Robert Selegård[1], Anna Herland[2], Daniel Aili[1]

[1]Linköping University, Laboratory of Molecular Materials, Division of Molecular Physics, Department of Physics, Chemistry and Biology (IFM), Linköping, SE; [2]Karolinska Institute, Department of Neuroscience, Stockholm, SE; [3]Linköping University, Division of Biotechnology, Department of Physics, Chemistry and Biology (IFM), Linköping, SE

Introduction

Hydrogels are highly-hydrated crosslinked polymer networks that can exhibit very good biomimicking properties and function as extracellular matrix (ECM) substitutes in a wide range of biomedical applications. Hydrogels enable culturing of cells in a more physiologically accurate three-dimensional (3D) environment, as compared to conventional two-dimensional methods for cell culture. Furthermore, ECM mimicking hydrogels are essential for the creation of organ-on-a-chip devices that can enable rapid drug screening and toxicity testing and help towards cutting our reliance of animal *in vivo* models. However[DA1] , for a hydrogel to be a suitable candidate for cell culture, it must feature relevant cell and tissue dependent bifunctionalities, mechanical properties and biochemical cues. Hydrogels that enable flexible tuning of such properties thus facilitates optimization of the culture conditions and realization of adequate ECM mimicking conditions for a wide range of applications.

Experimental Methods

Bicyclo[6.1.0]nonyne (BCN) was grafted to HA via the glucuronic acid carboxyl-moieties using standard carbodiimide chemistry. The final HA-BCN product had a derivatization degree of about 19%. Peptides were synthesized using standard SPPS protocols, and grafted to HA-BCN using SPAAC prior crosslinking. Hydrogels were formed by combining the HA-BCN product with 8-armed PEG-polymer with terminating N_3-moities ($p(N_3)_8$) and incubated at 37°C for one hour prior to adding cell media. This was followed by a further incubation overnight to allow the hydrogels to swell prior to seeding cells on top. In the cases where cells were encapsulated, the cells were added to the hydrogels just prior to the gelation stage. HepG2, hiPS-HEPs, and SH-SY5Y were used during this study, using the appropriate media in each case. Cell viability was assessed using Alamar blue assays or Live/Dead staining.

Results and Discussion

A modular hydrogel system was developed based on hyaluronan (HA) modified with cyclooctynes to enable crosslinking using an 8-armed PEG-polymer with terminating N_3-moities ($p(N_3)_8$) via a bioorthogonal strain-promoted alkyne-azide 1, 3-dipolar cycloaddition (SPAAC) (Figure 1a,b). Gelation onset occurred rapidly at 37°C with gelation reaching completion at approximately one hour. The final stiffness of the material was dependent upon the ratio of components (Figure 1 c, d), with a ratio of 10:1 of HA-BCN to PEG (25 mg/ml) yielding the stiffest gels.

The hydrogels supported proliferation of HepG2 cells equally well as hydrogels based on agarose and alginate, resulting in formation of spheroids. For 3D culture of human induced pluripotent stem cell derived hepatocytes (hiPS-HEPs), introduction of a cyclic RGD (cRGD) in the hydrogel was vital to stimulate proliferation and cell functionality.

By reducing the crosslinking density slightly, resulting in softer hydrogels, the hydrogels also enabled viable cultures of SH-SY5Y neuroblastoma cells (Figure 2a). In a comparison with Matrigel (Figure 2c), differentiated SH-SY5Y cell cultured on the hydrogels formed larger cellular clusters but with extensive neurite outgrowths (Figure 2b).

Conclusion

We show a flexible and modular hydrogel system that enables tuning of both mechanical properties and bifunctionality which enables optimization of 3D cell culture conditions for different cell types. The incorporation of cell adhesion motifs was achieved using the same principles as the crosslinking and is fully bioorthogonal. As a result, functionalization can be achieved either prior to seeding with cells or after, whichever suits the experimental conditions. Furthermore, functionalisation with different adhesion motifs at varying density, and tuning of the viscoelastic properties of the material was demonstrated and optimized for HepG2, hiPS-HEP and SH-SY5Y cells.

Acknowledgement

Support from the Swedish Foundation for Strategic Research (SSF), the Knut and Alice Wallenberg Foundation (KAW), and the Swedish Government Strategic Research Area in Materials Science on Functional Materials at Linköping University (Faculty Grant SFO Mat LiU No 2009 00971) is acknowledged.

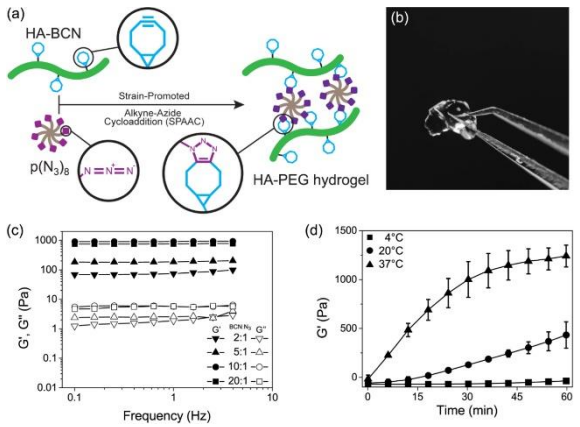

Formation and characterization of Hyaluronan hydrogel with copper-free click-chemistry
Figure 1: (a) A bioorthogonal strain-promoted alkyne-azide 1, 3-dipolar cycloaddition was utilized for crosslinking of HA, to form an optically transparent (b) hydrogel. The viscoelastic properties could be tuned through the adjustment of component ratio (c), while the gelation rate could be reliably controlled via temperature.

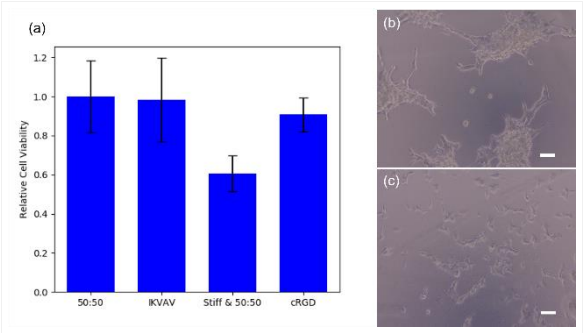

Cell viability and differentiation using Hyaluronan hydrogel as a growth medium
Figure 2: (a) Cell viability measured using Alamar blue for soft (G´~150 Pa) and stiff (G´~800 Pa) with equal amounts of cyclic RGD (cRGD) and IKVAV (50:50) and 100 % cRGD and IKVAV in the softer hydrogels at day 7. (b) Phase contrast images (20X) of differentiated SH-SY5Y cell cultures grown on top of HA-BCN (+IKVAV) (top) and on top of Matrigel (bottom). Scale bar: 50µm.

PS1-03-68

Developing the next generation of collagen membranes using electrophoretic deposition.

Matthew Linley

University of Cambridge, Department of Materials Science, Cambridge, GB

Introduction

Biomaterial scaffolds augment the extracellular matrix and act as structures for cells to grow over and regenerate damaged tissue *in situ*. Collagen type I is a structural protein found in mammals, whose material properties are ideally suited for use as an implantable scaffold. There has been lots of research recently into mimicking the architecture and mechanics of native tissue, with collagen scaffolds. However, fabricated collagen membranes have proven elusive in attaining the required properties for them to be suitable implants [1].

In this study, we have developed a novel process for generating aligned collagen membranes with controllable, characterised orientation and mechanics. This new method utilizes electrophoretic deposition (EPD) processing, to deposit collagen films from a suspension, and a generated flow of the collagen suspension during this deposition to align the collagen fibres within the membrane. Such techniques allow for control over both the rate of deposition and flow rate, such that alignment can be effectively controlled, and thus, the mechanical properties of the membranes can be tuned [2]. Furthermore, using birefringence microscopy, we have accurately characterised the degree of collagen alignment with respect to these parameters.

We, therefore, present here a novel method with specific controllable parameters, through which we can control a variety of the material properties, such that the next generation of collagen membranes can be designed for purpose.

Experimental Methods

Collagen I was hydrated in acetic acid and was then homogenised. The collagen suspension was dialysed against deionised water. Ethanol was added such that the final suspension was 50% ethanol and 0.25 wt.% collagen.

Electrophoretic deposition, simply, involves charged particles (in this case collagen) held within a suspension, and an electric field being passed across the suspension. The electric field drives electrophoretic movement of the charged particles towards an electrode, onto which the particles deposit, forming a film [3]. EPD was carried out in a custom built EPD cell, with inlet and outlet tubes from the cell to a pump, to generate flow of suspension during EPD. The rig was filled with collagen suspension and the pump generating a flow of 0 - 0.0015m/s at the surface of the electrode. The power source to the electrodes was then initiated, with a pulsed current of 10ms on, 15ms off cycle at a voltage of 5 - 10V.

Alignment of collagen fibres within membranes was determined using birefringence microscopy, using a quartz compensator.

Results and Discussion

Collagen membranes were produced using electrophoretic deposition, under a range of flow conditions. The collagen membranes produced were analysed with birefringence microscopy, and the birefringence of each sample was determined using a quartz compensator. At no flow, there was no birefringence and therefore no alignment. With increasing flow the birefringence also increased, showing an increased order of collagen alignment within

membranes. Flows beyond 0.0015m/s resulted in no collagen deposition, showing there is a threshold to this technique.

Using EPD to form collagen films is a relatively new concept, however, here we have shown that it can be utilized, with a flowing system, to tune the orientation of collagen fibres deposited, and thus, create a reproducible, very controllable, novel collagen membrane. Furthermore, we show the potential of birefringence microscopy as a tool for characterising collagen orientation in films, which would otherwise be cryptic.

This alignment of collagen within membranes causes the tensile strength within the plain of alignment to be increased. Therefore, tear resistant membranes can be developed by creating multilayer films with each layer being aligned in a different direction. As such, using this technique for creating novel orientated collage membranes, the mechanics could be fine-tuned for specific biomaterial purposes.

Conclusion

We have a novel technique for the orientation of collagen fibres within collagen membranes can be achieved, using EPD processing and a generated flow of collagen suspension during deposition, which, in turn, can be used to develop tough tear resistant collagen membranes, suitable for implantation. Furthermore, we show this orientation can be well defined and characterised using birefringence microscopy, such that these properties can be fine-tuned.

References

[1] L. Cen, W. Liu, L. Cui, W. Zhang, and Y. Cao, “Collagen tissue engineering: Development of novel biomaterials and applications,” *Pediatric Research*, vol. 63, no. 5, pp. 492–496, 2008.

[2] A. J. Gof n, J. Rajadas, and G. G. Fuller, “Interfacial flow processing of collagen.,” *Langmuir : the ACS journal of surfaces and colloids*, vol. 26, no. 5, pp. 3514–3521, 2010.

[3] L. Besra and M. Liu, “A review on fundamentals and applications of electrophoretic deposition (EPD),” *Progress in Materials Science*, vol. 52, no. 1, pp. 1–61, 2007.

Acknowledgement

I would like to acknowledge Dr David Barrett for his help with this project. I would also like to thank EPSRC and Geistlich Pharma AG for providing the financial support necessary for this project to be successful.

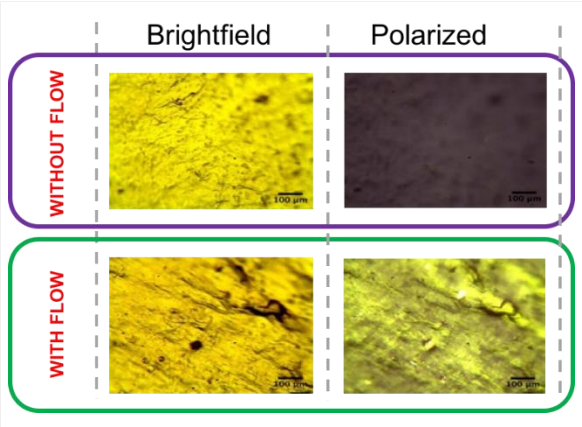

Light micrographs of collagen films showing their birefringence

Light micrographs of collagen films prepared using electrophoretic deposition with a relative flow across the depositon electrode (top), and with a relative flow across the electrode (bottom), under brightfield, without the polarizer (left), and with the polarizer (right).

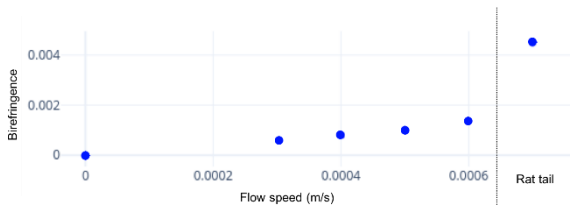

Birefringence of collagen films versus flow rate during deposition.
The measured birefringence of collagen films as a function of the flow rate of the collagen suspension across the electrode during pulsed current electrophoretic depsotion, with a voltage of 10V. On the right hand side shows the birefringence of order collagen within a rat tail, as a comparison to a highly aligned collagen structure.

PS1-03-69

A new method for fibrin-based electrospun/sprayed scaffold fabrication

Tamer Al Kayal[1], Paola Losi[1], Silvia Pierozzi[2], Giorgio Soldani[1]

[1]Institute of Clinical Physiology, National Research Council (CNR), Massa, IT; [2]Laboratori Archa, Pisa, IT

Introduction

The electrospun fibrin is an optimal scaffold for tissue-engineering applications because it mimic the extracellular matrix. Different approaches have been used for fibrin electrospinning, however all the methods investigated required washing step[1], cross-linking agent[2] and treatment steps for mechanical modification[3]. Moreover fibrin owns only poor mechanical properties that limit its applications.

The aim of this work was to produce a bilayered fibrin/polyurethane scaffold, by combination of electrospun method and spray-phase inversion method for the preparation of a fibrin layer firmly attached onto a polyurethane microporous support layer.

Experimental Methods

The support layer was obtained using a biocompatible aromatic poly(ether)urethane (Estane 5714F1, Lubrizol) by spray, phase-inversion method as previously described[4]. A 2% polyurethane solution was prepared by dissolving polyurethane grain in a solvent mixture of tetrahydrofurane and 1,4-dioxane (1:1) while a 0,2% solution was prepared with the addition of 17% of distilled water as non solvent. The support layer was obtained co-spraying the 2% polyurethane solution and distilled water, while the microporous layer with the 0,2% polyurethane solution and thrombin solution at 25 U/mL in 275 mM $CaCl_2$ on a rotating cylindrical collector (5 cm in diameter) at 88 rpm and flow rate of 2 mL/min for 40 min.

Then, fibrinogen solution 80 mg/mL was prepared by dissolving the fibrinogen in a solvent mixture of 1,1,1,3,3,3-heaxafluoro-2-propanol and distilled water(9:1, v/v) for electrospinning. The electrospun fibrinogen layer was made on the polyurethane support layer using an electrospinning apparatus equipped with a rotating cylindrical collector. Electrospinning was performed using needle-to-collector distance of 10 cm, voltage of 22 kV, flow rate of 0.5 mL/h and rotation speed of 125 rpm. The process was prolonged for 3 h to obtain a 100 µm thick electrospun network.

Finally, thrombin solution (25 U/mL) was sprayed on the electrospun layer at a flow rate of 0.5 mL/min for 5 min to allow fibrin polimerization.

SEM micrographs of bilayered scaffold were acquired for ultrastructural evaluation and analyzed with ImageJ to quantify the diameters of fibrin nanofibers before and after reaction with thrombin solution. Moreover, the grafts were analyzed by SEM to evaluated morphological structure of the surface spray layer after peeling of electrospun layer.

Results and Discussion

The sprayed layer appears white, while the electrospun fibrin layer transparent. SEM images of the electrospun fibrinogen evidenced stretched and flat fibers with size of the micron order (Fig. 1A). The fibrin formation after interaction with thrombin solution, induce a fiber morphology modification evidenced by SEM images. In particular we observed the loss of the elongated and flattened structure with the formation of filamentous structures fiber with diameter in the range of 400-500 nm (Fig. 1B).

The SEM analysis of morphological structure of PU spray layer after peeling of electrospun fibrin layer, revealed a firm adhesion of layer onto the spray surface of graft indicated by the presence of fused fibrin fiber on the porous PU support layer (Fig 2).

Conclusion

This study demonstrated the possibility to combine two different consolidated techniques to manufacture an electrospun fibrin layer firmly attached onto a polyurethane sprayed layer to enhance fibrin mechanical properties with the aim to apply in soft tissue regeneration, such as in wound healing application.

References

1. Perumcherry SR1, Chennazhi KP, Nair SV, Menon D, Afeesh R. A novel method for the fabrication of fibrin-based electrospun nanofibrous scaffold for tissue-engineering applications. Tissue Eng Part C Methods. 2011 Nov;17(11):1121-30.
2. McManus MC1, Boland ED, Simpson DG, Barnes CP, Bowlin GL. Electrospun fibrinogen: feasibility as a tissue engineering scaffold in a rat cell culture model. J Biomed Mater Res A. 2007 May;81(2):299-309.
3. McManus MC1, Boland ED, Koo HP, Barnes CP, Pawlowski KJ, Wnek GE, Simpson DG, Bowlin GL. Mechanical properties of electrospun fibrinogen structures. Acta Biomater. 2006 Jan;2(1):19-28.
4. Briganti E, Losi P, Raffi A, Scoccianti M, Munaò A, Soldani G. Silicone based polyurethane materials: a promising biocompatible elastomeric formulation for cardiovascular applications. J Mater Sci Mater Med 2006;17:259-66.

Acknowledgement

This work was supported through NanoCube Project by Tuscany Region (POR FESR 2014 – 2020).

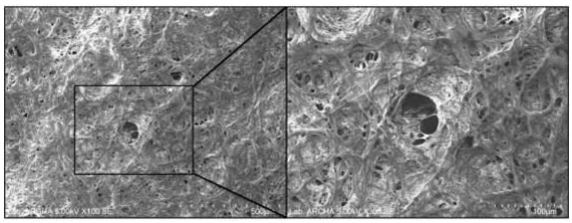

Fig. 2
SEM images of PU layer after peeling of electrospun fibrin layer.

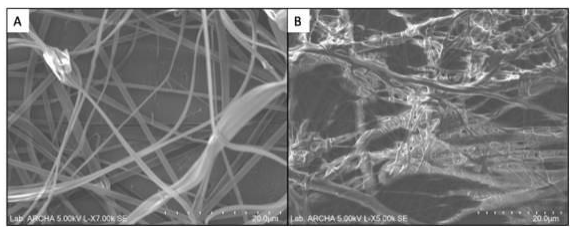

Fig.1
SEM images of electrospun layer. (A) fibrinogen nanofibers; (B) fibrin filaments obtained after interaction with thrombin.

PS1-03-70

Chemically graded collagen films for directed cell migration

Eleonora Vriend, Ruth E. Cameron, Serena M. Best

University of Cambridge, Cambridge, GB

Introduction

In this work, the use of chemical and physical gradients in collagen films as a method for directing cell migration is investigated. EDC/NHS crosslinking is used to chemically modify the collagen properties, affecting both stiffness and amine groups within peptide sequences required for integrin binding, allowing position control of cell attachment[1]. It is hypothesised that a gradual gradient in crosslinking may encourage cell attachment and migration along the gradient direction.

Experimental Methods

Crosslinking using EDC/NHS and genipin was used to modify the chemical and physical properties of collagen films. Gradients were created by gradual dilution of the crosslinking solutions (Figure 1). In this way, both the crosslinking concentration and time were progressively decreased across the film. The degree of crosslinking was measured by the free amine group content and fluorescence of genipin. Amine content was measured using the ninhydrin assay. This involved adding a solution of ninhydrin in ethanol to the collagen films at 80 °C for 20 minutes. The complexed dye was eluted using isopropanol, before measuring the optical absorption at 570 nm. The absorbance value could then be converted to a value for amine group content using a glycine standard curve. The degree of crosslinking was evaluated as the difference between amine concentration before and after crosslinking, relative to the initial concentration. This was initially carried out on individual films crosslinked at different concentrations and times to measure the effect of varying the crosslinking conditions. The variation in amine content across the gradient films could not be measured using absorbance in the same way; instead the change in the intensity of the complexed dye on the film surface after heating was measured using optical microscopy. For the films crosslinked using genipin, the degree of crosslinking was evaluated using fluorescence, as on reaction with amine groups genipin forms a blue pigment which emits fluorescence at 630 nm when excited at 590 nm.

Cell studies were subsequently carried out on the films to determine the effect of the gradients on cell behaviour. HT1080s were seeded at the crosslinked end of the gradient. Samples were fixed at five time points over the duration of a week and stained using DAPI and rhodamine phalloidin. Control samples consisting of uniform seeding on the film surface and films which were fully crosslinked or non-crosslinked, as well as cell culture tissue plastic, were also used. Fluorescence microscopy was used to observe how the positions and number of cells across the films varied over time in each case.

Results and Discussion

Increasing the crosslinking concentration and time was found to result in a decrease in amine content, corresponding to an increase in the degree of crosslinking. The gradient films crosslinked using the method of gradual dilution were consistent with this trend, showing a gradient in the intensity of the complexed dye across the film. Fluorescence measurements of the genipin crosslinked films showed a clear gradient from high intensity at the crosslinked end of the film to low intensity at the non-crosslinked (Figure 2A). These measurements confirm that the method of gradual dilution resulted in a gradient in the degree of crosslinking across the films.

The cell studies showed the gradient to have an effect on the distribution of cells on the films. When cells were seeded at the crosslinked end of the gradient, they were found to spread to the rest of the film by Day 7 of the study (Figure 2B). In contrast, when seeded on the edge of fully crosslinked or non-crosslinked films, this was not observed to occur. Similarly, when uniformly seeded over the gradient films, the cells were observed to collect at the non-crosslinked end of the films. This suggests that cells can detect the presence of the gradient and that this encourages them to spread towards the less crosslinked areas of the film.

Conclusion

We have developed a method by which gradients of crosslink density can be applied to collagen films. Cell studies suggest that these gradients are able to provide cells with cues influencing migration.

References

1. Bax, D. V. *et al.* Fundamental insight into the effect of carbodiimide crosslinking on cellular recognition of collagen-based scaffolds. *Acta Biomater.***49,** 218–234 (2017).

Acknowledgement

The authors would like to acknowledge the EPSRC for funding this project.

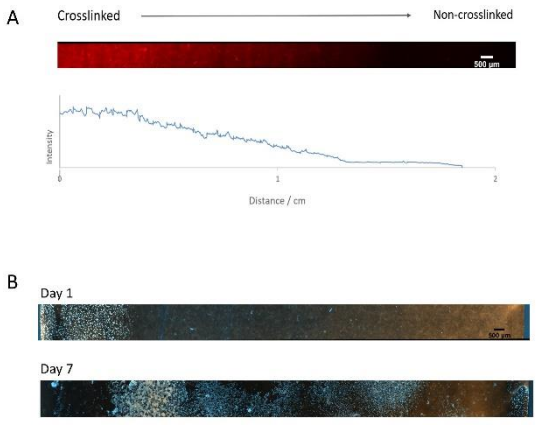

Fluorescence microscopy images
A: Gradient in the degree of crosslinking using genipin, shown by measurement of the fluorescence intensity

B: HT1080s on EDC/NHS gradients after seeding at the crosslinked end

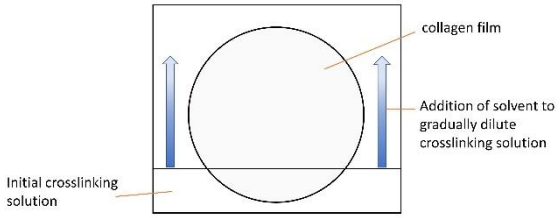

Schematic of crosslinking method
Method for obtaining a gradient in crosslinking by gradual dilution of the solution

PS1-03-71

A comparative study of gelatin hydrogels derived from different animal sources

Nicola Contessi Negrini[1,2], Laura Michelini[1], Luca Probo[1], Maria Cristina Tanzi[2], Silvia Farè[1,2]

[1]Politecnico di Milano, Department of Chemistry, Materials and Chemical Engineering, Milan, IT; [2]INSTM, National Consortium of Materials Science and Technology, Local Unit Politecnico di Milano, Milan, IT

Introduction

The tremendous interest in gelatin hydrogels for tissue engineering is to be attributed to their low cost, readily availability, lower immunogenicity compared to collagen, biodegradability, presence of cell adhesive motifs (e.g., RGD), and versatility [1]. The gelatin hydrogels' properties can be in fact tuned by varying the hydrogel formulation to target the regeneration of different tissues. A generally underestimated but crucial factor is the role of the animal source and the pre-treatment used to obtain gelatin from collagen and their potential influence on the hydrogels' properties. Here, we used two different crosslinking methods (i.e., glutaraldehyde and methylenebisacrylamide) to crosslink three different gelatins derived from different animal sources (i.e., porcine, bovine, fish) and we compared the properties of the so-obtained gelatin hydrogels.

Experimental Methods

Gelatin (porcine type A, bovine type B or from cold fish, F) was dissolved 15% w/v in water at 50 °C. At complete dissolution, gelatin was crosslinked (0.33 mol of crosslinker/ g of gelatin) either by glutaraldehyde (GTA) [2] or methylenebisacrylamide (MBA) [3]. For MBA-crosslinked hydrogels (MBA_A, MBA_B, MBA_F), the solution pH was increased at 10.5 and MBA powder was mixed to the gelatin solution (Fig.1a). The hydrogels were then allowed to crosslink at 50 °C for 24 h. For GTA-crosslinked hydrogels (GTA_A, GTA _B, GTA _F), the proper amount of GTA solution was added to the gelatin solution, quickly stirred and crosslinked at 37 °C for 24 h (Fig.1a). Gelatin hydrogel specimens were manually punched (diameter = 10 mm), washed with distilled water and dehydrated. Stability tests were performed in distilled water at 37 °C and the samples weight variation was measured up to 6 weeks. The gel fraction was measured after 1 week of immersion in water, to determine the solid fraction retained by the hydrogels during the swelling. Hydrogels crosslinking degree was measured by ninhydrin assay, by comparing the number of free amino groups before and after the crosslinking reaction. Compressive mechanical tests were performed on hydrated samples by Dynamic Mechanical Analyzer by applying a hysteresis cycle. The mesh size of the hydrogel networks was estimated by considering the volume variation and the elastic modulus of the hydrogels. *In vitro* degradation test was performed in Collagenase type I from *Clostridium Histolyticum* (10 U/mL) to simulate a possible enzymatic *in vivo* degradation; samples immersed in phosphate buffered saline were used as controls. *In vitro* indirect cytotoxicity tests were performed on L929 murine fibroblast cell line by extracting culture medium eluates in contact with hydrogel samples for 1, 3 and 7 days.

Results and Discussion

After immersion in water, all samples increased their weight due to water absorption; moreover, samples showed to be stable for up to 6 weeks (Fig.2a), thus proving the successful hydrogel crosslinking. Different weight variations were detected, for both GTA- and MBA-crosslinked hydrogels, depending on the gelatin animal source, being the weight variation of gelatin A < gelatin F < gelatin B hydrogels, considering the same crosslinking mechanism. All

hydrogels showed gel fraction values higher than 85% after 1 week of immersion in water, proving the efficient retention of the solid fraction during the swelling. For all the considered gelatin animal sources and crosslinking mechanisms, the measured crosslinking degrees were higher than 90%, proving the efficient crosslinking reaction and the involvement of amino groups in the crosslinking reaction. All hydrogels were successfully enzymatically degraded in 24 h after immersion in collagenase solution, with slightly quicker degradation profiles detected for GEL_F hydrogels. The estimated mesh sizes were in the 60 – 160 nm range, with mesh sizes GEL_A < GEL_F < GEL_B, for both the considered crosslinking mechanisms. All hydrogels showed a viscoelastic response with mechanical properties depending on the gelatin animal source. The elastic modulus of GEL_A was higher than GEL_F and GEL_B; the elastic modulus of GEL_F was higher than GEL_B. A similar trend was observed for the maximum stress. The measured mechanical properties of the produced hydrogels were thus shown to depend on both the swelling degree and on the estimated mesh size (i.e., lower mechanical properties for higher swelling and higher mesh size values). All hydrogel samples showed no indirect cytotoxic effects, as proved by the measured percentage cell viability higher than 70% (ISO 10993, Fig 2b).

Conclusion

Gelatin hydrogels derived from different animal sources (i.e., porcine, bovine and fish) were successfully crosslinked by MBA or GTA, as proved by adequate gel fraction and crosslinking degree values. The animal source influenced the swelling response of the hydrogels, mesh size and mechanical properties, thus proving the importance of the selection of the gelatin source when designing gelatin hydrogels for tissue engineering purposes.

References

[1] Gorgieva S *et al.*, Biomater. Appl. Nanomed. (2011) 17–52

[2] Catalina M *et al.*, J. App. Pol. Sci. (2010), 119, 2105-11

[3] Tanzi MC *et al.*, WO2012164032 A1

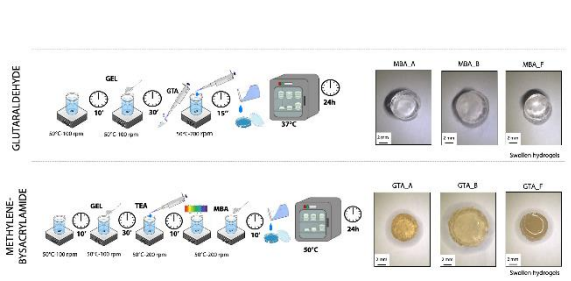

Figure 1
Preparation of gelatin hydrogels by glutaraldehyde and methylenebisaxcrylamyde crosslinking reaction. Representative images of swollen hydrogels obtained by different animal sources (i.e., porcine, bovine and fish), scale bar: 2 mm.

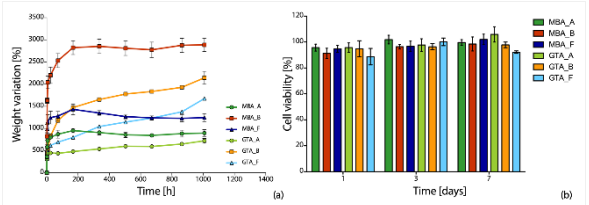

Figure 2
(a) Swelling and (b) *in vitro* indirect cytotoxicity of crosslinked gelatin hydrogels obtained by different animal sources.

PS1-03-72

Three-dimensional visualisation of internal architecture of collagen scaffolds in aqueous medium using micro-CT

Kyung-Ah Kwon, Daniel Bax, Serena M. Best, Ruth E. Cameron

University of Cambridge, Department of Materials Science and Metallurgy, Cambridge, GB

Introduction

Collagen scaffolds are widely used for tissue engineering and regenerative medicine as a temporary template or a drug delivery vehicle. The importance of internal architecture of three-dimensional (3D) scaffolds has been reported, the pore size and structure having been shown to significantly affect cellular activity[1,2]. Micro-computed tomography (µ-CT) has been extensively used to assess the internal structure of 3D scaffolds but they are often characterised in dry state although they become hydrated after implantation. In this study, the internal architecture of fully hydrated 3D scaffolds was visualised by performing physiologically relevant µ-CT scanning using a contrast agent and the structural characteristics of the scaffolds were evaluated.

Experimental Methods

Collagen scaffolds were produced by freeze-drying 1 wt.% collagen slurry prepared by blending bovine type I collagen in 0.05M acetic acid. The scaffolds were chemically crosslinked using 1-ethyl-3-(3-dimenthylaminopropyl-carbodiimide hydrochloride) (EDC) and N-hydroxy-succinimide (NHS). They were crosslinked at varying degrees between 0% and 100%, where 100% crosslinking (100%-XL) was defined as crosslinking a collagen (COO^-) using EDC/NHS at molar ratios of EDC:NHS:COO^- = 5:2:1.

Scaffold samples were obtained using a 8 mm-diameter biopsy punch and they were immersed in cell culture medium (CCM) prepared by Dulbecco's Modified Eagle's Medium supplemented with 10% foetal bovine serum and 1% penicillin-streptomycin for 1 day at 37°C and 5% CO_2. After the immersion, all the scaffolds were stained with 0.3% phosphotungstic acid (PTA) solution for 24 h under shaking speed of 150 rpm, followed by nine 5 min washings in deionised water (DIW). The fully hydrated samples were scanned using the SkyScan 1172 micro-CT (Bruker, Belgium) at 60 kV and 167 µA with 5 µm pixel size. The samples were placed in an Eppendorf tube containing DIW and the lid kept tightly closed to prevent any water evaporation during the scanning. After the reconstruction in the NRecon software provided by SkyScan, 1 mm-thick collagen scaffold in the middle was segmented to create a volume of interest (VOI) and the structural analysis were performed using the CTAn software. Further structural assessment for 0%- and 10%-XL scaffolds was performed using a scanning electron microscopy (SEM, FEI Nova NanoSEM) after different immersing treatments: 1 day in CCM or 1 day in CCM followed by 1 day in 0.3%-PTA solution.

Results and Discussion

Figure 1 shows the µ-CT images of fully hydrated collagen scaffolds viewed in different cross-sections. The internal structure of scaffolds could be visualised and allowed to evaluate structural parameters such as pore size.

All the scaffolds were highly porous and interconnected in hydrated state. They also appeared to be homogeneous throughout the bulk of the scaffolds although densified collagen zone around the edge of scaffolds was observed for 0%- and 1%-XL scaffolds. When the scaffolds are presented by colour-coded pore size values this densified collagen zone was shown to be occupied by 20-30 µm (red) pores.

Figure 2 shows SEM images of 0%- and 10%-XL scaffolds after different treatments. As shown in µ-CT images, most of the scaffolds showed uniformly distributed interconnected pores throughout their cross-sections. The densified collagen zone around the edge of 0%-XL scaffold was observed but only after PTA-staining since no such zone was detected for the sample which had not been PTA-stained.

Conclusion

PTA-staining allowed for the 3D visualisation of collagen scaffolds in hydrated state and consequently analysis of more physiologically relevant internal structure. However, the staining process for low crosslinked scaffolds (< 5%-XL) appeared to cause structural alteration, resulting in heterogeneity in their microstructures. Therefore, this staining artefact needs to be carefully considered in pore size analysis for non- and very weakly-crosslinked hydrated collagen scaffolds.

References

1. Riedl, A. *et al*., (2017) J Cell Sci 130:203-218
2. Murphy, C.M., O'Brien, F.J. (2010) Cell Adh Migr 4:377-381

Acknowledgement

This work was supported by the Engineering and Physical Sciences Research Council (EP/N019938/1).

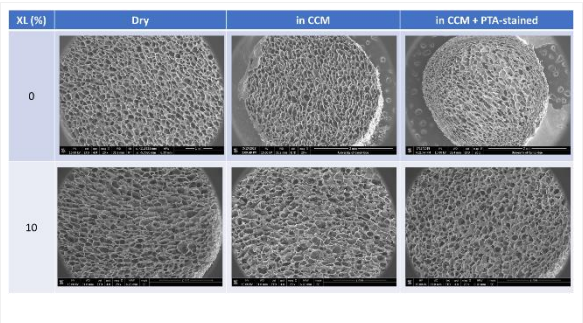

Figure 2
SEM images of freeze-dried 0%-XL and 10%-XL collagen scaffolds after treatment treatments.

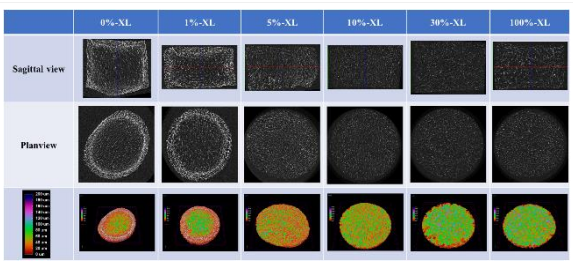

Figure 1
Internal structure of collagen scaffolds chemically crosslinked at varying degrees. The top two rows show the collagen scaffold in different cross-sections. The bottom row depicts the scaffolds with colour-coded pore size values, the colour-coded scale bar shown in the leftmost column.

PS1-03-73

Hyaluronan-based dermal fillers: the biophysical properties for specific clinical uses

Annalisa La Gatta, Rosanna Salzillo, Claudia Catalano, Antonella D'Agostino, Anna Virginia Adriana Pirozzi, Chiara Schiraldi

University of Campania, Naples, IT

Introduction

Hyaluronan (HA)-based hydrogels, obtained by crosslinking the biopolymer with 1,4 butandioldiglycidylether (BDDE), are widely used as dermal fillers. As our understanding of facial aging processes increases, HA gel design to meet specific requisites continues to improve. As a consequence, lines of HA-fillers, including products for diverse specific uses, are currently marketed [1].

Each line of fillers includes “volumetric”, “global performance” and “skinbooster” gels with specific clinical indications. Injections at different depths are recommended for the classes of gels.

The availability of biophysical parameters on these products strongly aids clinicians when selecting the product for a specific need. Additionally, such data, combined with clinical studies, are key to better gel design for specific performance [1-3].

On this basis, we aimed to ascertain the biophysical properties of a filler that translate into a “volumetric”, “global action” or “skinbooster” effect.

Experimental Methods

For each class of fillers, at least three among the most popular available (in Europe) gels were studied. Gel composition (soluble/insoluble HA concentration), hydration capacity, rheological behavior (stiffness, elasticity, complex viscosity), extent of HA chemical modification, cohesivity and resistance to enzymatic hydrolysis were investigated [1,4-6]. The hydrodynamic parameters for the soluble fraction of the gels were determined by the Size Exclusion Chromatography-Triple Detector Array (SEC-TDA) equipment by Viscotek (*Viscotek, Malvern, UK*) [7]. The characterization also addressed features poorly studied up to now. For the first time, filler degradation due to reactive oxygen species (ROS) was studied by rheological measurements. Further, a biological experimentation was performed, using human dermal fibroblasts, to evaluate and compare filler effect on skin restoration.

Results and Discussion

Analyses revealed the presence of water-soluble HA in all the tested samples with amounts up to 40wt%. Based on the hydrodynamic analyses, the soluble HA fractions mainly consist of chemically modified, mostly short (M_w < 250kDa) HA chains. The latter can reasonably derive from the manufacturing and/or the final sterilization that may release a certain amount of chemically modified, but not “insolubilized” HA. A relevant fraction of linear, unmodified, higher molecular weight HA was found in some of the gels. Cohesivity varied widely even when considering gels with the same clinical indications. The products proved sensitive to degradation due both to hyaluronidases and ROS thus assuring resorbability, and a rank in stability could be established. ^{1}H-NMR analyses revealed an extent of HA chemical modification spanning a wide range also suggesting different crosslinking efficiency for the diverse proprietary manufacturing technologies. The biological experimentation demonstrated the capacity of the gels to

prompt collagen I, elastin and aquaporin3 synthesis, thus supporting the lately emerged opinion of a positive biological effect of HA dermal fillers on skin restoration and hydration.

Conclusion

Our findings represent a wide assessment of properties that well characterize the three classes of HA-fillers. Differences in behavior were highlighted among the products with the same clinical indications, thus providing practitioners with useful information to drive the selection toward one product or another depending on the specific case. The work represents a useful reference study also for the development of newly more highly performing HA gels intended for specific use. Finally, the work valuably contributes to our knowledge of HA-fillers and to the optimization of their use and manufacture.

References

[1] La Gatta A, De Rosa M, Frezza M A. Catalano C, Meloni M, Schiraldi C. Biophysical and biological characterization of a new line of hyaluronan-based dermal fillers: a scientific rationale to specific clinical indications. Mater Sci Eng **C** Mater Biol Appl. 2016; 68:565-72

[2] Kablik J, Monheit GD, Yu LP, Chang G, Gershkovich J. Comparative physical properties of hyaluronic acid dermal fillers. Dermatol Surg. 2009; 35: 302–12.

[3] Edsman K, Nord LI, Ohrlund A, Larkner H, Kenne AH. Gel properties of hyaluronic acid dermal fillers. Dermatol Surg. 2012; 38 (7): 1170–9.

[4] La Gatta A, Schiraldi C, Papa A, De Rosa M. Comparative analysis of commercial dermal fillers based on crosslinked hyaluronan: physical characterization and in vitro enzymatic degradation. Polym Degrad Stab. 2011; 96: 630–6.

[5] La Gatta A, Papa A, Schiraldi C, De Rosa M. “Hyaluronan dermal fillers via crosslinking with 1,4-butandiol diglycidyl ether: exploitation of heterogeneous reaction conditions” J Biomed Mater Res Part B: Appl Biomater 2016, 104B: 9-18.

[6] Sundaram H, Rohrich RJ, Liew S, Sattler G, Talarico S, Trévidic P et al. Cohesivity of Hyaluronic Acid Fillers: Development and Clinical Implications of a Novel Assay, Pilot Validation with a Five-Point Grading Scale, and Evaluation of Six U.S. Food and Drug Administration-Approved Fillers. Plast Reconstr Surg. 2015; 136: 678-86.

[7] La Gatta A, De Rosa M, Marzaioli I, Busico T, Schiraldi C. A complete hyaluronan hydrodynamic characterization using a size exclusion chromatography-triple detector array system during in vitro enzymatic degradation. Anal Biochem. 2010;404 (1): 21-9.

PS1-03-74

Tubular chitin of spider molt origin as new scaffold for tissue engineering

Tomasz Machałowski[1], Marcin Wysokowski[1,2], Nicole Bechmann[3], Stefan R. Bornstein[3,4], Teofil Jesionowski[1], Hermann Ehrlich[2]

[1]Poznan University of Technology, Institute of Chemical Technology and Engineering, Poznan, PL; [2]TU Bergakademie Freiberg, Institute of Electronics and Sensor Materials, Freiberg, DE; [3]TU Dresden, Institute of Clinical Chemistry and Laboratory Medicine, University Hospital Carl Gustav Carus, Dresden, DE; [4]TU Dresden, Center for Regenerative Therapies Dresden, Dresden, DE

Introduction

Naturally prefabricated scaffolds for tissue engineering are especially interesting because of their unique three-dimensional (3D) structure, design and biodegradability. Fabrication of a flexible and plastic nature rather than mechanically strong templates, is required for regenerating epithelial and soft tissues [1]. Looking for new sources of naturally prefabricated chitin-based materials we focused our attention on spiders which “loose” big amounts of chitin-containing cuticles during their molting cycle (ecdysis). Here we propose for the first-time utilization of tubular chitin scaffold isolated from up to 10 cm-large Theraphosidae spider *Caribena versicolor* molt cuticle as a renewable waste biomaterial. The amount of such spiders breaded only in Europe reaches approximately 2 million exemplars. For the first time we used microwave-assistant irradiation (MWI) for isolation of chitinous scaffolds from the spider’s molt. The main purpose of this work was to show that naturally prefabricated tubular chitin could be successfully apply for tissue engineering.

Experimental Methods

For chitin isolation one-step method performed under MWI during 4 minutes with utilization of 30% H_2O_2 (pH~10; pH was regulated by addition of 2.5 M NaOH) was carried out. Obtained material was characterized in detail by diverse analytical techniques including stereo and fluorescence optical microscopy, SEM, FT-IR, Raman, XRD, ESI-MS, ^{13}C NMR. Then the human progenitor cell line (hPheo1) derived from a pheochromocytoma were cultivated under obtained chitinous tubular scaffolds. For the cultivation (at 37°C, 5% CO_2 , and 95% humidity) of the hPheo1 cells RPMI-1640 containing 10% horse serum (HS) was used and the plate was incubated for 24 h.

Results and Discussion

Performed measurements clearly indicates that our method allows to obtain high purity α-chitin scaffolds with degree of acetylation = 99% in very short time (4 minutes). Moreover, we proved that chitin isolation using microwaves assay did not have negatively impact on its crystalline index. Fluorescence microscopy test confirmed the attachment of the human progenitor cell line (hPheo1) to the scaffold surface after 24 h of incubation.

Conclusion

We have developed efficient and fast method for naturally prefabricated chitin-based materials isolation. Our findings highlight that renewable tubular chitin scaffolds of spider molt origin could be a new source for tissue engineering applications.

References

[1] Yang, T. L. (2011). Chitin-based materials in tissue engineering: Applications in soft tissue and epithelial organ. *International Journal of Molecular Sciences*, *12*, 1936–1963. https://doi.org/10.3390/ijms12031936

Acknowledgement

The part of the research was supported by Polish Ministry of Sciences and Higher Education - Grant No. 03/32/SBAD/0915

A special thanks for technical assistance, discussions and statistical data goes to INTIB GmbH (Germany)

PS1-03-75

Blended PCL/PLA/GO grooved scaffolds: Nerve guide conduit with improved properties for peripheral nerve repair

Ying Lu[1], Christopher F. Blanford[2], Adam J. Reid[3,4], Julie E. Gough[1]

[1]University of Manchester, School of Materials, Materials Engineering,Biomaterials, Manchester, GB; [2]University of Manchester, School of Materials, Materials Engineering,Manchester Institute of Biotechnology, Manchester, GB; [3]University of Manchester, School of Biological Sciences, Manchester, GB; [4]Manchester University NHS Foundation Trust, Department of Plastic Surgery, Manchester, GB

Introduction

The alternative treatment of peripheral nerve repair is use of a nerve guide conduit when availability of donor nerve is limited [1]. One advantage of this technique over the traditional autologous nerve grafting is that various defect sizes and lengths depending on individual patients can be achieved without secondary surgical harvest. Therefore, the shelf life of medical implantable materials after sterilization is crucial in developing new nerve conduit materials [2]. As the sterilization technique may have an impact on desired properties of stored materials, we are investigating the effects of the addition of graphene oxide (GO).

Graphene oxide has potential for neural tissue engineering [3]. To achieve a longer shelf life and also maintain designed quality of PCL/PLA conduits, we are able to fabricate PCL/PLA/GO grooved films by blending PCL/PLA mixture and graphene oxide nanoparticles using solvent casting methods inside the environmental chamber.

Experimental Methods

Modified PCL/PLA/GO films were fabricated through solvent casting methods with grooved patten at the surface. A series of surface characterisation was applied to study modified polymeric films, such as surface morphology of films were studied after fabrication, including the macro-structure using optical microscopy as well as the micro-structure using laser confocal and SEM; surface wettability was measured by water contact angle using Drop Shape Analyser-DSA100; surface roughness was analysed using AFM and laser confocal. Besides, mechanical property and thermal property of films were studied. To investigate the impact of sterilization on fabricated films, we applied ultra-violet sterilization on films with a series of different treated time (5mins, 10mins and 20mins, respectively) and characterised surface feature post sterilization.

Results and Discussion

In our study, the addition of GO is able to keep the integrity of groove pattern with better surface wettability and surface roughness, which are of benefit to cell-material interactions *in vitro*. In order to investigate the influence of sterilization on fabricated films, we initially applied ultra-violet sterilization on both PCL/PLA films and modified PCL/PLA/GO films. Modified films are able to keep their macro-structure without evidence of loss of mechanical properties. DSC results indicated that the addition of GO can improve Tg of materials from -33.86^{o}C (PCL/PLA) to -27.49^{o}C (PCL/PLA/GO) and TGA results indicated improved properties of the GO modified materials.

Conclusion

This study suggests the GO modified PCL/PLA conduit material is able to maintain the grooved structure and improved mechanical properties.

References

[1] Muheremu A, Ao Q. Past, present, and future of nerve conduits in the treatment of peripheral nerve injury. BioMed research international. 2015.

[2] Hukins DW, Mahomed A, Kukureka SN. Accelerated aging for testing polymeric biomaterials and medical devices. Medical engineering & physics. 2008 Dec 1;30(10):1270-4.

[3] John AA, Subramanian AP, Vellayappan MV, Balaji A, Mohandas H, Jaganathan SK. Carbon nanotubes and graphene as emerging candidates in neuroregeneration and neurodrug delivery. International journal of nanomedicine. 2015;10:4267.

Acknowledgement

The authors would like to gratefully acknowledge the China Scholarship Council (CSC) for financial support of the project

PS1-03-76

Multifunctional composite scaffolds based on chitosan and sodium hyaluronate for biomedical applications

Patrycja Domalik-Pyzik, Karolina Kosowska, Martyna Hunger, Jan Chłopek

AGH University of Science and Technology, Faculty of Materials Science and Ceramics, Department of Biomaterials and Composites, Krakow, PL

Introduction

Despite many recent developments in medicine, tissue engineering, and biomaterial science, there is still a need for developing new material solutions that will allow for successful treatment of degeneration diseases such as osteoarthritis. Cartilage lesions together with a damage to a subchondral bone are referred to as osteochondral defects. Their specificity, including high pain levels and joint movement confinement, make them a serious medical issue. Tissue engineering approach assumes that a damaged tissue may be renewed due to the combined use of scaffold with defined properties, specific active signals, and appropriate cells.

Experimental Methods

The current study is focused on the development of multifunctional composite scaffolds for osteochondral regeneration based on two polysaccharide matrices, ie. chitosan and sodium hyaluronate modified with various forms of graphene oxide (0-3 wt.%), hydroxyapatite (0-30 wt.%) and biologically active molecules. The first part involved screening large number of different material compositions and forms that should allow to select substrates for proliferation and chondrogenic/osteogenic differentiation of mesenchymal stem cells. Bearing this in mind, detailed physicochemical characterization was planned. Structural (XRD, FTIR), thermal (DSC, TG), mechanical, rheological, chemical stability (PBS, SBF, Ringer solution immersion tests), and surface analysis (wettability, SEM) assays were performed.

Results and Discussion

It was shown that graphene oxide not only increases mechanical properties of those natural polymers, but also acts as a crosslinker stabilizing polymer chains. Addition of hydroxyapatite is beneficial when it comes to scaffold bioactivity and intended direct bone bonding ability of its subchondral bone part. However, ceramic particles content above 5 wt.% led to a formation of too rigid material for intended use. Regardless of the modifier type, microstructure of the scaffold was affected. Moreover, as osteochondral defects can be considered gradient structures, the optimal solution would be to design final scaffold as such. Gradients of modifying phases content and mechanical/biological properties were produced.

Conclusion

All in all, we were able to select the most promising materials for *in vitro* cell studies. Detailed biological examinations with human umbilical cord Wharton's jelly derived mesenchymal stem cells (hUC-MSCs) are currently ongoing.

Acknowledgement

The authors would like to thank the National Centre for Research and Development, Poland for providing financial support to this project (STRATEGMED3/303570/7/NCBR/2017). The project leader, Prof. Ewa Zuba-Surma

(Department of Cell Biology, Faculty of Biochemistry, Biophysics and Biotechnology Jagiellonian University, Malopolska Centre of Biotechnology, Krakow) with her team, and project partner, Dr. Ludwika Lipińska (Institute of Electronics Materials Technology, ITME, Warsaw), are gratefully acknowledged for cooperation.

PS1-03-77

Microstructural Characterization of Ovalbumin by Means Microscopy and Spectroscopy Techiniques

Liliana E. Rojas[1], Juan V. Méndez[2], José J. Chanona[1], Felipe Cervantes[3], Claudia A. Reséndiz[1], Benjamin Arredondo[1]

[1]INSTITUTO POLITÉCNICO NACIONAL, Departamento de Ingeniería Bioquímica/Laboratorio de Micro y Nanobiotecnología/ Escuela Nacional de Ciencias Biológicas, Ciudad de México, MX; [2]INSTITUTO POLITÉCNICO NACIONAL, Centro de Nanociencias y Micro y Nanotecnologías, Ciudad de México, MX; [3]Universidad Iberoamericana, Departamento de Física y Matemáticas, Ciudad de México, MX

Introduction

The study of the structure and mechanical properties of Ovalbumin at nanoscale is an interesting topic to nanotechnology [1, 2,3]. Ovalbumin is one of the major protein found in egg white, making uo to 60-65% of the total protein it is a globular protein and hence soluble water. Researches already done shows that the Ovalbumin is utilised in many applications like drug loading, core of or sheell nanoparticle due to spectral, solubility and nanomechanical properties.The functions and properties of proteins, as well as, their conformational structure and their amino acid sequence in various proteins are well-know, but modifications in the nanomechanical and solubility properties of proteins by changing variables as changes in pH and microestructural, aren't subject of study yet. For this reason the aim of this work was to study of the microstructure os Ovalbumin by microcopy and spectroscopy.

Experimental Methods

Overall morphology and topography were studied by SEM (Hitachi, SU 3500 I) and AFM (Bruker, Bioscope Catalyts, USA). Whereas the changes secondary structure of Ovalbumin was studied by Raman spectroscopy (confocal Raman microscope, USA)

Results and Discussion

Shows SEM images of powder proteins, where the ovalbumin particles have spherical, its obtention process spray drying. The spherical particles diameter was 66.2± 5.3 µm and pore diameter 1.2±0.26µm. Also by means of AFM, the average roughness (Ra) of the protein solutions at isoelectric point and other pH. To ovalbumin, at pH 4.6 (point isoelectric) the Ra was 4.05±5.60 nm, whereas at pH 5.6 its Ra 2.59±0.84nm. Then parameters related to secondary structure Ovalbumin was determined by FT-Raman Spectroscopy according to [4]. By Raman Spectroscopy (Table 1) was analyzed the ovalbumin folding induced at pH 3.6 with a decrease in β-antiparallel and β-parallel, the appearance of the percentage contribution to random coil structures. While powder ovalbumin was the disappearance of the percentage contribution to random coil structures, a increase α-helix with β-parallel. The same behavior was observed for Ovalbumin at isoelectric point (4.6) in the disappearance of the random coil, but a increase turn and β-antiparallel.

Table 1. Raman determination of secondary structure percentages of powder Ovalbumin (O), Ovalbumin to pH 3.6 (03.6) and Ovalbumin to pH 4.6 (O4.6). Concentration: 0.01%.

	β- Antiparallel	β-Parallel	Turn	Random coil	α-helix

O	12.88	11.83	43.490	31.81
O3.6	9.78	4.06	51.279.50	24.39
O4.6	17.18	4.62	60.390	17.79

Conclusion

Ovalbumin in its isoelectric point showed a largest Ra values due to the agglomeration of protein. By means Raman was observed changes microstructural of ovalbumin like folding an unfolding in different pHs. This preliminary study of morphology and topography of protein by microscopy and spectroscopy techniques provided an initial overview to establishing the dipersion condition and pHs to study y its aplication in nanoparticles or drug loading.

References

1. Huntington, J., Stein, P. (2001). Structure and Properties of ovalbumin. Journal of Chromatography. 756, 189-198.
2. Ansari, A. Nanostructured Materials: Classification, Properties, Fabrication, Characterization and their applications in Biomedical Science. (2010) Nanoparticles: Properties, Classification, Characterization, and Fabrication.122-135.
3. Yazdi, S., Corredig, M., Dalgleish, D. (2014). Studying the structure of β-casein-depleted bovine casein micelles using electron microscopy and fluorescent polyphenols. Food hydrocolloids. 42, 171-177.
4. Carbonaro, M., Nucara, A. (2010). Secondary structure of food protein by Fourier transform spectroscopy in the mid-infrared region. Amino Acids. 38, 679-690.

Acknowledgement

L. Rojas Candelas wishes to thank CONACyT, Mexico and BEIFI-Instituto Politecnico Nacional, Mexico (A171176) for the scholarship provided. This research was financed through projects 20195198 at the Instituto Politecnico Nacional (Mexico)

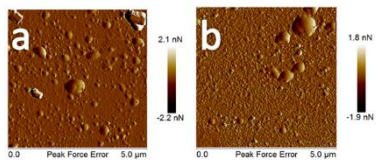

Figure 2. AFM images ovalbumin a) pH 4.6 and b) 5.6pH
Ovalbumin in its isoelectric point showed a largest Ra values due to the agglomeration of protein

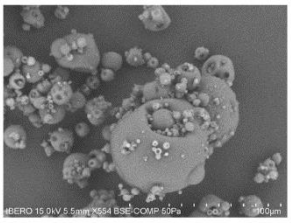

Figure 1. SEM image of powder Ovalbumin
The ovalbumin particles have a spherical, that morphology correspond to its obtention process spray drying

PS1-03-78

Mechanical properties of composites in a hydrogel/graphene system

Karol Gryń, Barbara Szaraniec, Anna Wiśniewska, Jan Chłopek

AGH University of science and technology, Krakow, PL, Departament of Biomaterials and Composites, Faculty of Materials Science and Ceramics, Krakow, PL

Introduction

Recent years has been a continuous development in the field of new materials for medical applications. Considerable progress in reducing costs of graphene and graphene oxide production, increased accessibility of these materials. Due to their low density, unique electrical, thermal and optical properties, they seem to be an excellent modifying phase in composites. Moreover, high solubility of graphene oxide in water imparts its feasibility as new filler for reinforcement hydrophilic biopolymers. Chitosan is a natural polymer that has been studied extensively over several decades. It possesses a number of interesting properties including biocompatibility, biodegradability, and solubility in aqueous media. It is used in separation membranes, artificial skin, bone substitutes, tissue engineering, coatings and water treatment. Unfortunately its mechanical properties are rather poor thus a wider range of application, especially in a medical field is limited. By combining the advantages of graphene oxide, chitosan and naturally present in bones inorganic phase eg. hydroxyapatite, different types of promising materials for medical applications can be obtained.

Experimental Methods

In this study a natural polymer matrix – hydrogel based chitosan (CS) – was reinforced with three types of particles: graphene oxide (GO) (ITME, Poland), reduced graphene oxide (rGO) (ITME, Poland) and hydroxyapatite (HAp) (mkNano, Canada). Several variations of composite foils were obtained by solution-evaporation casting method with certain percentage of compositions. Into hydrogel based chitosan matrix following modifiers were introduced: CS/GO, CS/rGO, CS/HAp, CS/GO/HAp, CS/rGO/HAp. To examine their mechanical properties static tensile tests and analyses of strain-stress curve were performed. Tensile strength R_m, Young's Modulus E, Maximal deformation ε_{Fmax} were characterised. Test performing was difficult due to the nature and geometry of samples. Thin hydrogel based composite foils are very sensitive to an air humidity. When they drying out they became to shrink and to coil up.

Results and Discussion

Based on the results it can be concluded that the introduction of the graphene family nanofillers into hydrogel based polymer matrices effects on their mechanical parameters. The largest strengthening effect was obtained by adding a nanofiller to the hydrogel matrix in the form of reduced graphene oxide. The addition of the ceramic phase (HAp) to the chitosan matrix increased the Young's modulus and the tensile strength, however the strain of the composites decreased. Mechanical properties of composites modified with combination of HAp and GO did not differ significantly from mechanical properties of the pure chitosan.

Conclusion

The hydrogel/graphene oxide and hydrogel/graphene oxide/ hydroxyapatite composites were successfully obtained by using solution-evaporation casting method. Addition of different content of nanofillers allows to control and modify mechanical properties of the composites. This approach can be exploit for fabrication of a new,

multifunctional material for biomedical applications. Tailored properties of such implant should improve bone or cartilage tissue regeneration.

References

1. Zhang, Y., et al., Bio-inspired layered chitosan/graphene oxide nanocomposite hydrogels with high strength and pH-driven shape memory effect. Carbohydrate Polymers, 2017. 177: p. 116-125.
2. Papageorgiou, D.G., I.A. Kinloch, and R.J. Young, Mechanical properties of graphene and graphene-based nanocomposites. Progress in Materials Science, 2017. 90: p. 75-127.
3. Domalik-Pyzik, P., J. Chłopek, and K. Pielichowska, Chitosan-Based Hydrogels: Preparation, Properties, and Applications, in Cellulose-Based Superabsorbent Hydrogels, M.I.H. Mondal, Editor. 2019, Springer International Publishing: Cham. p. 1665-1693.
4. Ege, D., A.R. Kamali, and A.R. Boccaccini, Graphene Oxide/Polymer-Based Biomaterials. Advanced Engineering Materials, 2017. 19(12): p. 1700627.
5. Jayachandran V., Se-Kwon K. Chitosan Composites for Bone Tissue Engineering — An Overview Mar. Drugs, 2010. 8(8), p. 2252-2266

Acknowledgement

This research was funded by the National Center for Research and Development, Poland (BioMiStem grant No. STRATEGMED3/303570/7/NCBR/2017).

PS1-03-79

Multifactorial approaches towards tenogenic phenotype maintenance, trans-differentiation and differentiation

Dimitrios Zeugolis, Christina Ryan

NUI Galway, REMODEL, Galway, IE

Introduction

Cell-based therapies require removal of cells from their optimal *in vivo*tissue context and propagation i*n vitro*to attain suitable numbers. However, bereft of their optimal tissue niche, cells lose their phenotype and with it their function and therapeutic potential. Biophysical, biochemical and biological signals have been shown to maintain permanently differentiated cell phenotype and to precisely regulate stem cell lineage commitment [1-3]. Herein, we developed and characterised substrates of various stiffness with controlled nanotopographical features and assessed these substrates in culture in combination with macromolecular crowding (MMC) on various cell sources to determine their suitability for the *in vitro*fabrication of tendon-like tissue.

Experimental Methods

Substrates of varying stiffness and controlled surface topographical features were created using a silinated silicon wafer. Substrates were then plasma treated and assessed with/without collagen type I coating (0, 0.5 mg/ml). The simultaneous effect of MMC / substrate stiffness / surface topography on cell phenotype and function was assessed using human dermal fibroblasts, tenocytes and bone marrow stem cells (hBMSCs) cultured with 100 μg/ml of carrageenan (MMC) for 3, 7 and 14 days. Detailed protein synthesis / deposition and gene expression analyses were conducted.

Results and Discussion

The nano-topographical features on the substrate surface induced cellular alignment in all cell types, which was not affected by MMC or substrate stiffness. Immunocytochemistry analysis revealed that when MMC was used, cells showed increased deposition of collagen types I, III, V and VI. FACS analysis in hBMSCs indicated a significant reduction in surface marker expression as a function of MMC, but not as a function of surface topography or stiffness. Gene analysis made apparent that MMC had a greater influence on phenotypic markers in all cell types compared to topography or stiffness.

Conclusion

This study provides insight into modulation of cell behaviour and phenotype using microenvironmental cues and can have a significant contribution to the development of cell-based therapies for tendon repair and regeneration.

References

1. Murphy, W. L., *et al*., Nature Materials, 2014. 13(6): p. 547-557.
2. Azeem, A., *et al*., Nanomedicine (Future in Medicine), 2015. 10(5): p. 693-711.
3. Satyam, A., *et al*., Advanced Materials, 2014. 26(19): p. 3024-3034.

Acknowledgement

The authors would like to acknowledge the Science Foundation Ireland (SFI) under the grant agreements 15/CDA/3629, 13/RC/2073 and 13/RC/2077 and the US-Ireland AgriSense, under the grant agreement 12/US/I2476 for financial support.

PS1-03-80

Evaluation of the Biopolymer Modification for the Reproducible Production of Alginate-based Bioinks

Emine Karakaya[1], Jörg Teßmar[2], Aldo R. Boccaccini[1], Rainer Detsch[1]

[1]Friedrich Alexander University, Institute of Biomaterials, Erlangen, DE; [2]University of Würzburg, Department for Functional Materials in Medicine, Würzburg, DE; [3]Friedrich Alexander University, Institute of Biomaterials, Erlangen, DE; [4]Friedrich Alexander University, Institute of Biomaterials, Erlangen, DE

Introduction

Sodium alginate, a well-known natural polymer, is a favorable material in biofabrication because of its high biocompatibility, comparatively low cost, cell friendly gelation behavior at room temperature and tunable properties.[1] However, an obvious disadvantage of plant derived polysaccharides is their poor ability to support cell attachment due to the lack of efficient binding sites for cell adhesion.[2] To overcome this drawback, alginate is oxidized to alginate dialdehyde (ADA) in order to provide reaction sites for proteins (e.g. gelatin) containing arginine-glycine-aspartic acid (RGD) binding sequences. Additionally, the development of alginate-based bioinks is an enormous challenge due to the high variance in material properties.[3]

Therefore, the aim of this work was the development of an alginate based biopolymer modification leading to standardized products, which will later be crosslinked with gelatin by Schiff's base formation and used as bioink. For this purpose, the mechanism of biopolymer modification and relevant methods for the product characterization were investigated and examined.

Experimental Methods

For the characterization of the chain composition of different types of alginate 1H liquid and 13C solid nuclear magnetic resonance (NMR) spectroscopy were used.

After the synthesis of the ADA polymers by periodate oxidation of alginate, the oxidized polysaccharides were mixed with gelatin yielding ADA-GEL. In order to evaluate the modification and suitable reaction conditions for the reproducible production of standardized bioinks, ADA and ADA-GEL were characterized by fourier-transform infrared spectroscopy (FTIR), ultraviolet–visible spectroscopy (UV-Vis), gel permeation chromatography (GPC) and NMR, respectively.

The cell viability of printed NIH3T3-cells in bioinks (1Mio/mL) was visualized after 48h of incubation at 37°C by staining with Calcein-AM and propidium iodide and was calculated using ImageJ plugin ITCN.

Results and Discussion

The success of the biopolymer modification was confirmed by NMR and FTIR spectroscopy, whereas small amounts of aldehydes and a strong formation of hemiacetals could be demonstrated. This indicates a chemical equilibrium, which is strongly favoring the formation of hemiacetals. The reduction in molecular weight during the synthesis was observed by GPC and was strongly dependent on reaction times and oxidation degree. 13C solid NMR spectra and GPC measurements showed that the reduction of Mw for several synthesis products were different while the oxidation degree revealed the same. Further investigations of the ADA molecular weight also showed a positive effect of different radical scavengers (e.g. isopropanol) on the achievable final chain lengths of ADA. The subsequent formation of the Schiff’s Base between the available aldehyde groups of ADA and the free amine groups of gelatin

was confirmed by FTIR and NMR, respectively. Furthermore, a modified assay using UV-Vis spectroscopy could be established for the determination of the ideal reaction time of ADA-GEL leading to the maximum degree of crosslinking. Moreover, the cell compatibility as well as the cell viability could be proved by bioprinting with NIH3T3 cells. After 48 hours of incubation high cell viability confirmed the successful aliginate modification.

Conclusion

Two main results were obtained by the presented investigations. On the one hand, improved detection methods for the oxidation degree of ADA and the crosslinking degree of ADA-GEL could be established. On the other hand, ideal reaction conditions during the synthesis of ADA and ideal reaction times of the crosslinking of differently oxidized ADA polymers with gelatin could be determined. In conclusion, our study reveals an optimized synthesis route for ADA and ADA-GEL with controllable and standardized properties.

References

[1] Saker, B. et al. (2014) Fabrication of alginate–gelatin crosslinked hydrogel microcapsules and evaluation of the microstructure and physico-chemical properties; Journal of Materials Chemistry B 11, 1470-1481.
[2] Yongxiang, L. et al. (2015) Concentrated gelatin/alginate composites for fabrication of predesigned scaffolds with a favorable cell response by 3D plotting; RSC Advances, 54.
[3] Reakasame, S. et al. (2018) Oxidized Alginate-Based Hydrogels for Tissue Engineering Applications: A Review; Biomacromolecules 19; 3-21.

Acknowledgement

Funded by the Deutsche Forschungsgemeinschaft (DFG, German Research Foundation) – Projektnummer 326998133 – TRR 225 (subproject A01).
E. Karakaya wants to thank the NMR-Chemistry Department FAU, Jonas Hazur and Susanne Heid for their helpful remarks and supportive input to this project.

PS1-03-81

Multi-photon polymerized 3D scaffolds of GelMA and water soluble chitosan promote mineralized matrix formation

Konstantinos Parkatzidis[2], **Maria Chatzinikolaidou**[1], Maria Farsari[2], Maria Vamvakaki[1]

[1]University of Crete, Department of Materials Science and Technology, Heraklion, GR; [2]Foundation for Research and Technology Hellas (FORTH), Institute for Electronic Structure and Laser (IESL), Heraklion, GR

Introduction

The success of tissue engineering (TE) is based on the choice of the 3D matrix to support the adhesion, proliferation and differentiation of cells. The chemical composition, the physical and mechanical properties, the biodegradability, biocompatibility, and functionality of the 3D scaffolds are crucial characteristics for their use in TE applications [1].Direct Laser Writing (DLW) is a powerful technique for the fabrication of 3D structures, via a computer-aided design (CAD), for use in optics, metamaterials as well as in the field of biomedical applications [2]. Chitosan and gelatin are two widely used natural biomaterials for scaffold fabrication. Although chitosan has many advantages as a biomaterial, its main drawback is its insolubility in either water or organic solvents.The purpose of this study was (i) the synthesis of two biopolymers, gelatin methacrylamide (GelMA) and a water-soluble chitosan derivative, employed for the preparation of a hybrid material used for the fabrication of 3D scaffolds via DLW, and (ii) the assessment of their ability to support cell growth and mineral matrix formation following functionalization with bone morphogenetic protein 2 (BMP-2) in a dental pulp stem cell culture.

Experimental Methods

Near IR laser irradiation, operated at 800 nm, was employed to fabricate the 3D scaffolds, in the presence of eosin-Y, as a water soluble, FDA-approved photoinitiator and without any other co-initiators or co-monomers [3]. Cell behavior on the hybrid materials (2D films and 3D scaffolds) was examined using dental pulp stem cells, generously donated by Prof. Athina Bakopoulou, School of Dentistry, Aristotle University of Thessaloniki from informed consent patients. Cell adhesion on the 3D scaffolds was visualized by immunocytochemical staining of the actin of the cytoskeleton and the cell nuclei as well as by scanning electron microscopy (SEM). In addition, the 3D scaffolds were functionalized with physically adsorbed BMP-2 and cultured for 21 days.

Results and Discussion

Grid-shaped porous scaffolds with a pore size of 70 μm and dimensions 400x400x50 μm^3were fabricated by multi-photon polymerization. We suggest that the free amine groups of GelMA and the chitosan derivative act as co-initiating moieties and support the photopolymerization process.

We carried out the cytocompatibility investigation on geometrically well-defined films in order to quantify the cell proliferation results. For the hybrid material we observed a strong initial cell adhesion and a subsequent cell proliferation increase over a period of 7 days in culture. The results indicate the absence of any cytotoxic effects and suggest that the biopolymer-based hybrid material is biocompatible and exhibits better biocompatibility than the TCPS control. Both immunocytochemistry staining of the actin cytoskeleton and SEM characterization showed a strong cell attachment and an increased proliferation over time within the 3D porous scaffolds. The cells cultured for 21 days on hybrid scaffolds demonstrate an enhanced matrix mineralization compared to the control, and this effect is significantly higher on BMP-2 functionalized hybrid structures, as observed by the alizarin red staining.

Conclusion

Our results demonstrate that 3D scaffolds made from a hybrid comprising GelMA and water-soluble chitosan by DLW promote the proliferation and differentiation potential of human dental pulp stem cells, thus, they are promising structures in orofacial tissue engineering.

References

[1] A. Georgopoulou et al, J. Mat. Sci.: Mat. Med., 2018, 29, 59.

[2] K. Parkatzidis et al, *Mac. Biom. Eng.,*2018, 1800458.

[3] M. Farsari et al, *J Photoch Photobio A*, 2006;181:132-5.

PS1-03-82

Synthesis of colagen biopolymeric scafolds modified by crosslinking, chondroitin sulphate and carbon nanotubes to bone regeneration.

Vinicius Marchiori-Silva, Janaina Aline G. Barros, Camila L. Camargo, On behalf of FAPESP - Fundação de Amparo a Pesquisa no Estado de São Paulo (Grant PIPE 2 17/50413-0)

Revolugenix Biotech, Research, Sao Paulo, BR

Introduction

Bone loss at implantation sites on oral cavity is a major problem to dental surgeons, sometimes the remaining amount of bone is not enought to install implants and a bone augmentation procedure must be used. We developed 3 types of biomaterial with collagen and used chondrohitin sulfate and carbon nanotubes to increase the stifness of the collagen and avoid early absorption that could lead to colapse of the structure and diminish bone formation, we also used electric stimulation to organize colagen fibers at the surface of the scafolds and create patterns to cell adesion.

Experimental Methods

Hidrolized and non hidrolised bovine colagen type I was dissoluted at 4% in 400ml of ultrapure water (Type 1) and formic acid 0,1M (Synth - Brazil) to form a homogen mixture at 40ºC with constant agitation by a RW-20 motor (IKA Germany) on a HS-70 ceramic hot plate (IKA-Germany). After 4 hours in agitation the mixture was divided in 4 groups and each of the groups were divided in 20 plastic cell culture petry dishes (5ml each): group 1 received 10g of Chondroitin Sulphate (Sigma Aldrich); group 2 received 10g of carbon nanotubes suspention (Sigma Aldrich); group 3 reveived eletric field of a low-voltage Transelectric Cutaneous Nerve Stimulation Equipment (3M - USA) and group 4 was poured plane at the cell culture petry dishes to serve as control group. All the samples were crosslinked with NHS (N-hydroxysuccinimide esters) (Thermo Scientific-USA) and freezed at -40ºC freezer (Terroni-Brazil), after 24 hours the samples were freeze dried at a LH2000 equipment (Terroni - Brazil) at the following parameters: start at -30ºC with an increase of 0,5ºC every 30 minutes until reach 0ºC under a vacuum of 140uHg, the total time of the process was 20 hours under vacuum to total dry the samples. The samples were analized by: Scanning Electron Microscopy (SEM); Energy Dispersed Spectroscopy (EDS); X ray spectroscopy (XPS); Bartha respirometric method; and Fish Embrio Toxicity Test

Results and Discussion

All the freeze dried samples have the same macroscopic morphology and the inclusion of chondroitin sulphate, carbon nanotubes and electric field did not make significative diference in macroscopic view of the final products. At electronuic microscopy however the diferences between the samples were significant and diferent pore sizes were found in each group vary between 50um to 500um. The SEM of the group submited to electric field shows organization of the fibers in the surface of the scafolds to a parallel pathern or to radial pathern. The EDS Shows atomic content of: C (75%); O (14.3%); N (8.5%; other substances <1%, what lead us to believe that no contaminant were present at the samples. The XPS analysis sugests chemical modification of the colagen amine groups by the NHS and the Bartha respirometric method confirmed that this modifications can slow down the velocity of degradation of the colagen samples, the analisis of the CO_2 liberated from the material during the degradation shows increases from 42 to 117 days to complete degradation of the colagen when crosslinked, this resistence to degradation of the sample is desired to avoid colapse of the scafold when applied. The same resistence was found

in group that received the carbon nanotubes, in this case the XPS shows that the amount of [-C-C/-C-H-] and [-C=C-] molecular groups increased, elevating the stiffness of the material in comparission to control group. The FET test shows good tolerance of the material at the amount used to therapy in humans.

Conclusion

The absence of contaminants at the samples are compatible with the use of this material to bone augmentation in implantology as the Titanium of the implants will not be contaminated by the scafold material and the osseointegration will not be compromised. The structure modification leads to increase stiffness of the material wich is more adequate to bone regeneration than colagen withou modifications. The material is not toxic at the FET test in the amount used but more tests are needed to ensure the safety of this material to human use. The future combination of the tested materials can improve the characteristics to create a new product in the future, as a colagen/chondroitin/nanotubes/electric oriented scaffold. Tests with osteoblasts or mesenchymal stem cells are needed to confirm the bone formation capacity of the material and our group is performing this currently.

References

01. Z.G.Ge, S.Baguenard, L.Y .Lim, A.Wee, and E.Khor , Biomaterials 25, 1049 (2004).
02. H.W .Kim, J.C.Kno wles, and H.E.Kim, Biomaterials 25, 1279 (2004).
03. J.M.T aboas, R.D.Maddox, P.H.Krebsbach, and S.J.Hollister, Biomaterials 24, 181 (2003).
04. F.Zhao, Y.J.Y in, W.W .Lu, J.C.Leong, W.J.Zhang, J.Y .Zhang, M.F .Zhang, and K.D.Yao, Biomaterials 23, 3227 (2002).
Sittinger M. et al. Current Opinion in Biotechnology 15:411-418, 2004.
05. Shimming R; Schmelzeisen R. J Oral Maxillofac Surg 62: 724-729, 2004.
06. Siddappa R; Licht R; Boer J; Blitterswijk C. J Orthop Res 2007 DOI 10.1002/jor.20402
07. Xiaojun Yu, Botchwey E. A., et al. PNAS August 3, vol. 101 no. 31 11203-11208, 2004.
08. Sittinger M. et al. Current Opinion in Biotechnology 15:411- 418, 2004.
09. Sittinger M. et al. Biomaterials 17: 237-242, 1996.
10. Barrila J, Radtke AL,Crabbe A, Sarker SF, Herbst-Kralovetz MM, Ott, CM, Nickerson CA. Nature Rev Microbiol 8:791- 801, 2010

Acknowledgement

Acknowledgment to FAPESP for the grant PIPE 2 (17/50413-0) received that was fundamental to this research.

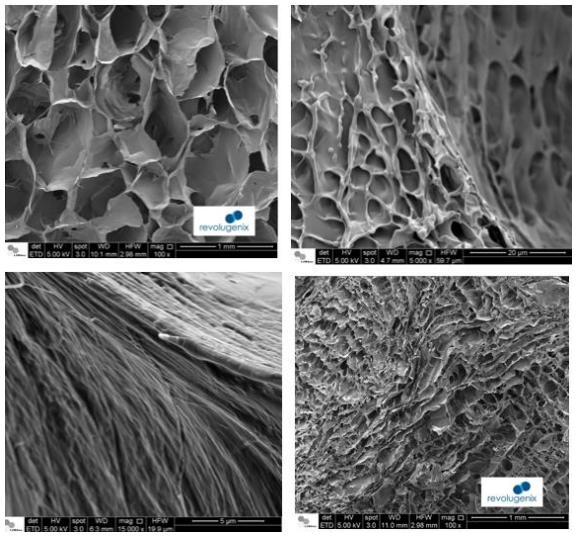

SEM of the scaffolds
SEM of the scaffolds: upper left - control group; upper right - colagen/chondroitin; lower left - colagen electrical field oriented; lower right - colagen/carbonnanotubes.

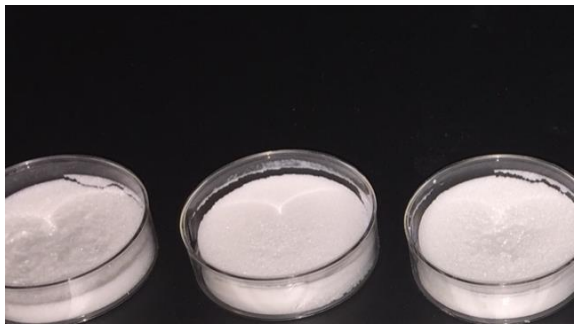

Colagen scafolds
Macroscopic view of the colagen scafolds. Left - Colagen/chodroitin; center- colagen/carbonnanotubes; right-colagen/electric oriented

PS1-03-83

Photocrosslinked hydrogel from chondroitin sulfate functionalized with histidine

Nayara G. S. Cavalcante, Luiz H. Catalani

University of Sao Paulo, Chemistry Institute, Sao Paulo, BR

Introduction

The field of tissue engineering aims to regenerate tissues that were affected by diseases or injuries through technological advances in areas of science and cell biology.[1] For this purpose, a great interest is being generated in the development of new materials to be applied in these areas.

Chondroitin sulfate (SC) is a component commonly found in the extracellular matrix (ECM) of many connective tissues, including cartilage, bone, skin, ligaments, and tendons having primarily structural functions of resistance to compression and flexibility.[2,3]

Protein photocrosslinking has been reported of reactions from amino acid residues, such as: histidine (His), cysteine, lysine, among others.[4,5] Thus, the aim of this study is the formation of photocrosslinked hydrogels from chondroitin sulfate functionalized with histidine (His) to be used as scaffolds in tissue engineering.

Experimental Methods

The SC functionalization with His was performed using N-(3-dimethylaminopropyl)-N'-ethylcarbodiimide hydrochloride (EDC) and N-hydroxysuccinimide (NHS) at room temperature for 48h. After the reaction time, the SC-His samples were dialyzed for three days in distilled water and then freeze-dried.

The photocrosslinking experiments were performed in D_2O solution, in concentrations of 20% (w/v), 25% (w/v) and 30% (w/v) of SC-His, using 15 µM of methylene blue as photosensitizer. Irradiation was done for 1 h with a LED emitting at 633 nm.

Samples irradiated were analyzed by sol-gel fraction. In this analysis, the samples were placed in contact with distilled water for 24h. After this period, the gel fraction was separated from the sol fraction, dried and weighed.

Results and Discussion

The functionalization of SC-His sample was calculated by ^{1}H-NMR as 59% of all N-acetylate group. This was revealed by the relation between integration peaks of imidazole aromatic ring at 7.25 ppm and 8.59 ppm and N-acetylate group ($NCOCH_3$) of chondroitin sulfate at 2.00 ppm in ^{1}H-NMR. In addition, it is also possible to observe the presence of peaks referring to the glycosidic chain of SC. Protons from C2 and C3 carbons of the glucuronic acid are at 3.30 ppm (1H) and 3.50 ppm (1H). The C2 proton of N-acetylgalactosamine peak is at 3.93 ppm. At 3.70 ppm the peaks of the protons bound to the C3 and C5 carbons of N-acetylgalactosamine are overlapped on that of C5 of glucuronic acid.[6]

In the sol-gel analysis, the gel fractions of the 20%, 25% and 30% irradiated SC-His samples were 14.1%, 20.8% and 15.2%, respectively. This result shows that the formation of hydrogel occurred in all tested concentrations, however, the 25% SC-His sample showed the highest gel fraction percentage.

The 20% and 30% SC-His samples probably obtained lower gel fraction values due to polymer chains low mobility, which hinders the reaction at low concentrations, whereas in very high concentrations, the sample presented coloration (beige) blocks part of the red light that promotes the reaction.

Conclusion

In conclusion, the chondroitin sulfate functionalization with His was confirmed by spectroscopic analysis and the functionalization yield was 59%. The formation of the hydrogels at all tested concentrations was confirmed in the sol-gel fraction test. However, the 25% SC-His sample had a higher gel fraction percentage among all. These results point to a new material that could be used as a scaffold for tissue engineering, as well as a hydrogel ink for 3D printing processes based on stereolitography.

References

1. JACOBY, A. et al. Fabrication of capillary-like structures with Pluronic F127® and Kerria lacca resin (shellac) in biocompatible tissue-engineered constructs. **J. Tissue Eng. Regen. Med.**, 2016, 11(8): 2388-2397.
2. HENROTIN, Y. et al. Chondroitin sulfate in the treatment of osteoarthritis: from in vitro studies to clinical recommendations. **Therapeutic Advances Musculoskeletal Disease.** 2010, 2(6): 335-348.
3. BAEURLE, S. A. *et al*. Effect of the counterion behavior on the frictional–compressive properties of chondroitin sulfate solutions. **Polymer**. 2009, 50(7): 1805–181
4. AMANO, M. et al. Detection of Histidine Oxidation in a Monoclonal Immunoglobulin Gamma (IgG) 1 Antibody. **Analytical Chemistry**. 2014, 86, 7536−7543.
5. RONSEIN, G. *et al*. Oxidação de proteínas por oxigênio singlete: mecanismos de dano, estratégias para detecção e implicações biológicas. **Química Nova**. 2006, 29(3): 563-568.
6. POMIN, V. H. NMR chemical shifts in structural biology of glycosaminoglycans. **Analytical Chemistry**. 2014, 86: 65-94.

Acknowledgement

This work acknowledges financial support from FAPESP grant number 2017/13120-5 and 2018/13492-2.

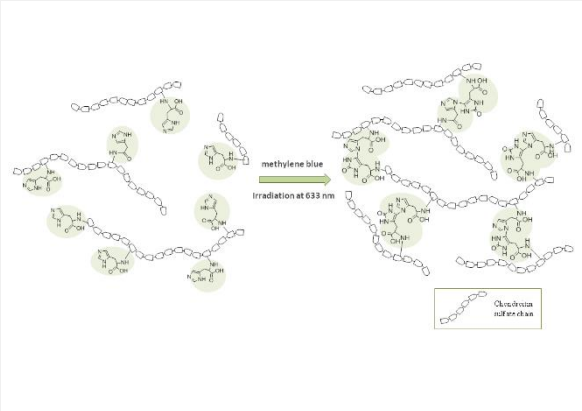

Representation of SC-His photocrosslinking reaction with methylene blue for hydrogel formation.

PS1-03-84

Utilization of Dialdehyde Cellulose as Crosslinker for Poly(vinyl alcohol)

Lukáš Münster, Jan Vícha, Ivo Kuřitka

Tomas Bata University, Centre of Polymer Systems, Zlín, CZ

Introduction

Crosslinking agents based on modified biopolymers are particularly favorable in biomedical sector as alternatives to toxic synthetic low-molecular weight crosslinkers (i.e. glutaraldehyde). Periodate oxidation of cellulose produces dialdehyde cellulose (DAC) which can be solubilized[1] and used as crosslinker for poly(vinyl alcohol) (PVA).[2] Solubilization is recognized as key step influencing molecular weight of DAC.[3] Furthermore, due to high reactivity of aldehyde groups (–CHO), DAC decays in time.[1] Nevertheless, DAC can be stabilized for several weeks when kept at low pH.[3]

The reactive DAC species form hemiacetal bonds with hydroxyl groups of PVA in presence of acid catalyst. In contrast to low molecular crosslinker-based hydrogels, resulting network presumably possesses very different crosslink topology and lower toxicity arising from the DAC macromolecular character.[2,4] PVA/DAC materials may found application in pharmaceutics as materials for wound dressing or drug release.

The scope of this study was to utilize a broad range of concentrations of solubilized DAC and glutaraldehyde (GA) in PVA hydrogel formation and evaluate their efficiency.

Experimental Methods

Alpha cellulose was oxidized by sodium periodate (1:1.2 M). Solid DAC was then solubilized at 80 °C for 7 h. Next, PVA (Mowiol 84–86%) solution containing acid catalyst (diluted hydrochloric acid) and 0.125–5 wt% of solubilized DAC or corresponding amounts of GA (equal in the terms of amount of –CHO per sample) were mixed and cast to form PVA xerogels. Resulting PVA hydrogels were analyzed and compared in the terms of their network parameters estimated via equilibrium swelling theory.[5] These include swelling capacity, equilibrium water content (EWC), gel fraction, average molecular weight between crosslinks (M_c) and crosslink density (ρ_c).[2]

Results and Discussion

PVA crosslinking efficiency of DAC and GA was compared. DAC is effective crosslinker even at very low concentration (0.125 wt%, equal to 73.1 µmol of –CHO per sample). Corresponding PVA/GA samples dissolved as the crosslinking was not sufficient. PVA/DAC hydrogels exhibit up to 5 000 % swelling and slightly lower gel fraction (see Figure 1). At higher DAC concentrations, PVA hydrogels possess increased crosslink density compared to PVA/GA analogs.

These observations are presumably caused by the macromolecular character of DAC with crosslinking groups present only on the polymer chain, which generates principally different network topology composed of (i) regions with high local crosslink density due to large amount of reactive aldehyde groups on DAC macromolecule and (ii) a regions comprised of sizable sections of free PVA chains (schematic example in Figure 2).[2]

Conclusion

The results confirmed applicability of DAC solution as a PVA crosslinker with hydrogel properties closely related to DAC macromolecular character. This implies interesting potential for “tuning” the properties of resulting hydrogels without need for any other additives/catalysts, as the DAC with required molecular weight can be cost-effectively obtained by optimization of the DAC preparation. Low toxicity and very high efficiency at low concentrations of DAC in comparison to glutaraldehyde makes PVA/DAC hydrogels ideal candidates for preparations of biomaterials for pharmaceutical and biological applications.

References

1. U.-J. Kim, M. Wada and S. Kuga. *Carbohydr Polym*. **56**, 7–10 (2004)
2. L. Münster, J. Vícha, J. Klofáč, M. Masař, A. Hurajová and I. Kuřitka. *Carbohydr Polym*. **198**, 181-190 (2018)
3. L. Münster, J. Vícha, J. Klofáč, M. Masař, P. Kucharczyk and I. Kuřitka. *Cellulose*. **24**, 2753–2766 (2017)
4. L. Münster, Z. Capáková, M. Fišera, I. Kuřitka and J. Vícha. *Carbohydr Polym*. (2019), accepted
5. P. J. Flory and J. Rehner, *J Chem Phys*. **11**, 521–526 (1943)

Acknowledgement

This research was supported by CPS project no. CZ.1.05/2.1.00/03.0111, CPS+ project no. LO1504, CPS - strengthening research capacity project no. CZ.1.05/2.1.00/19.0409 and Czech Science Foundation grant 16-05961S.

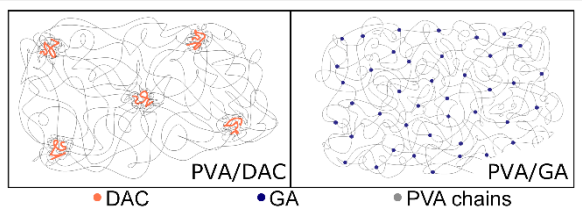

Figure 2 Different crosslink network topology assumed for PVA/DAC and PVA/GA hydrogels.2

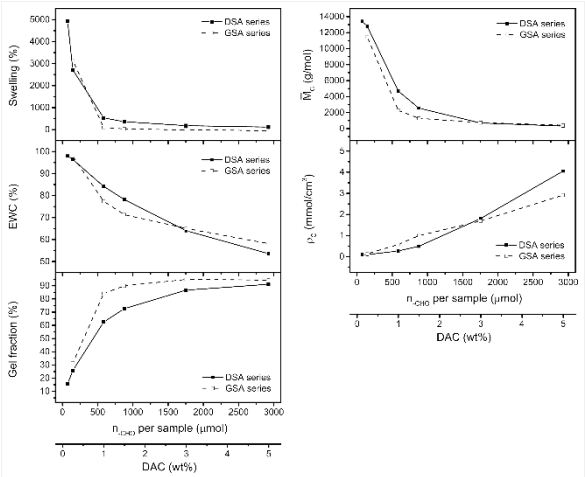

Figure 1 Comparison of network parameters of PVA hydrogels prepared by DAC (DSA) and GA (GSA). *Hydrogels network parameters plotted against the used DAC or GA crosslinker amount defined by chemical amount of reactive aldehyde groups (n_{-CHO}) per sample. The equivalency between DAC and GA reactive group concentrations is expressed by the two bottom x-axes. The lines connecting points in the graphs are only guides for eyes.*

PS1-03-85

Bioactive, bacterial cellulose-based membranes and their relevance as guided tissue regeneration biomaterial

Selestina Gorgieva[1,2], Liliana Verestiuc[3], Maria Butnaru[3], Samo Jeverica[4], Karin Stana Kleinschek[1,2]

[1]University of Maribor, Faculty of Mechanical Engineering, Insitute of Engineering Materials and Design, Maribor, SI; [2]University of Maribor, Faculty of Electrical Engineering and Computer Science, Institute of Automation, Maribor, SI; [3]Department of Biomedical Sciences, Grigore T. Popa University of Medicine and Pharmacy, Iasi, Romania, Iasi, RO; [4]Institute of Microbiology and Immunology, University of Ljubljana, Ljubljana, SI

Introduction

Guided tissue regeneration (GTR) is a method utilized to regenerate the tooth supporting tissues affected by periodontal disease. More than 8% of adults aging between 20 and 64 have periodontal disease, and ~ 5% of them have moderate to severe formrelated to diabetes, osteoporosis and other systematic cardio-, cerebrovascular and respiratory diseases. The cell-occlusive, space making, tissue integrative, clinically manageable, biocompatible are attributes to ″ideal″ membrane, for which the large diversity of (non)biodegradable, and bioactive materials have been use (Figure 1). Despite diversity, their limited success have been reported. Project focus on new GTR membranes, systematicall engineered as graded, multilayer composites, based on bacterial cellulose (BC). The major idea is site-specific introduction of the morph-chemical and structural triggers within a single material, to emulate the complex ECM of periodontal tissues.

Experimental Methods

Bacterial cellulose (BC)-gelatin membrane was prepared using periodate pre-oxidation and subsequent freeze-thawing and EDC crosslinking procedure. Post-modification with peptide nisin was additionally performed. Physic-chemical and morphologycal data, as well as degradation profile were initialy estimated using relevant tests (FTIR spectorscopy, confocal and SEM microscopy and gravimetrical, incubation test). Antimicrobial activity was tested using zone of inhibition method and pre-selected bacteria which are generally considered as red complex, peridontal pathogens. Normal human dermal fibroblasts (NHDF, Lonza) and human osteoblast (MG63-ATCC) were used for *in vitro* evalaution of cell viability (MTT test, Live/dead assay), membrane integrity (LDH assay), VEGF release and alkaline phosphatase activity, the latter two involving only osteoblast cells. Barier properties were chacked using fibroblast cell line.

Results and Discussion

The interlayers integration, physiological stabilization and µ-structuring, were achieved by combination of perodate-medited oxidation of BC, freeze/thawing treatment and carbodiimide crosslinking chemistry. The post mineralization process using fast, 10x SBFmediated procedure adapt formation of bone-regeneration- relevant minerals. Viability of both cell types was not negatively affected by membrane, whyle VEGF release and ALP activity where increased in gelatin containing membranes (Figure 2). For bacterial management, the antimicrobial peptide nisin was post-synthetically intruduced and same demonstrate activity against periodontal pathogens *E. faecalis, P. intermedia, F. nucleatum* at amounts as lower as 10 µg/sample.

Conclusion

BC-gelatin membranes where processed by facile procedure. Degradable BC was obtain by periodate oxidation. Microstructurally-diverse membrane library was obtained by variation of preparation conditions. Membranes demonstrated manageability, physiological stability and noncitotoxicty against relevant cell lines (in 7 days examination). Enrichment with antimicrobial agent nisin demonstrate activity against relevant pathogens. Barrier function was preliminary demonstrated in vitro, with human dermal fibroblast. *In vitro* testing with human fibroblasts and human dermal fibroblast and osteoblasts (MG63) demonstrate positive influence of gelatin on VEGF release profile and ALP activity.

Acknowledgement

The project (ID Z7-7169) was financially supported by the Slovenian Research Agency.

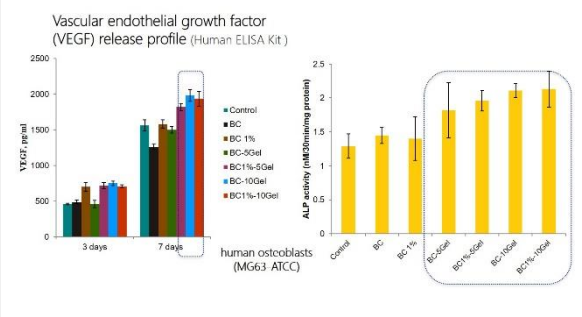

Figure 2

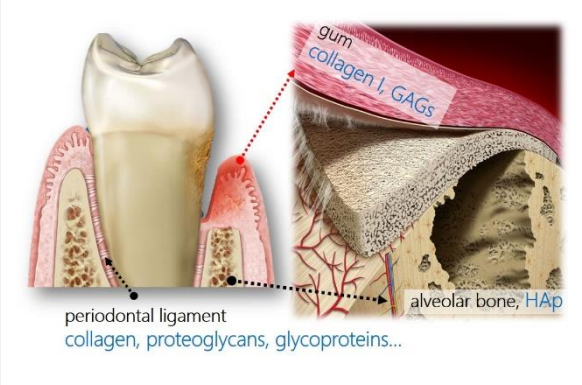

Figure 1

PS1-03-86

Pushing forward Gellan gum-based hydrogels: the impact of inorganic fillers on mechanical and biological performances

Maria A. Bonifacio[1], Stefania Cometa[2], Piergiorgio Gentile[3], Annachiara Scalzone[3], Andrea Cochis[4], Lia Rimondini[4], Giuseppe Procino[5], Serena Milano[5], **Elvira De Giglio**[1]

[1]University of Bari 'Aldo Moro' Department of Chemistry, Department of Chemistry, Bari, IT; [2]Jaber Innovation s.r.l., Roma, IT; [3]Newcastle University, School of Engineering, Newcastle upon Tyne, GB; [4]Università del Piemonte Orientale UPO, Center for Translational Research on Autoimmune & Allergic Diseases CAAD, Department of Health Sciences, Novara, IT; [5]University of Bari, Department of Biosciences, Biotechnologies and Biopharmaceutics, Bari, IT

Introduction

Biopolymer-based hydrogels are one of the most promising class of biomaterials for tissue engineering applications. Indeed, compared with synthetic alternatives, biopolymers offer a more suitable interaction with host tissues in terms of degradation rates as well as cytocompatibility. However, their mechanical features are often weaker than those of synthetic hydrogels and still far from the standards required in clinics. This drawback becomes a major issue in cartilage regeneration, since the load-bearing property of such a tissue is its unique trait[1].

The development of composite hydrogels, based on biopolymers and reinforced with inorganic components, represents an intriguing route to enhance hydrogels' mechanical features, while preserving the peculiarities of biopolymer-based materials[2]. In this work, several inorganic fillers were combined with a gellan gum-based hydrogel, evaluating their impact on compression modulus cell adhesion rate.

Experimental Methods

Gellan gum (GG) was dissolved in water with Manuka Honey (MH) in 1:1 ratio, as previously reported[3]. Then, an inorganic filler among bentonite, diatomaceous earth, mesoporous silica and halloysite nanotubes was added to the mixture, which was poured into molds and crosslinked with Mg^{2+} ions. Finally, freeze-dried samples (Fig.1) underwent physico-chemical, mechanical and biological evaluations. Human Bone Marrow Mesenchymal Stem cells (hBMSCs) were seeded on the hydrogels' top surfaces to study their metabolic activity and ability to colonize even the deepest zones of the hydrogels.

Results and Discussion

The prepared hydrogels were deeply studied by X-ray Photoelectron Spectroscopy (XPS). Moreover, thermogravimetric analyses were carried out to gain insights into the thermal behavior of the composite hydrogels, reinforced with inorganic fillers. As far as mechanical characterization is concerned, the hydrogels were compressed until break and the resulting Young's moduli(E) were calculated. The addition of inorganic fillers resulted in a dramatic enhancement of Young's modulus, which exceeded 100kPa for all the composite hydrogels. Silica-enriched hydrogels especially improved the modulus of the bare hydrogel more than 45%. These findings were in accordance with XPS data, suggesting that the presence of inorganic fillers supports cations' mobility, resulting in enhanced energy dissipation under compression.

Interestingly, when subjected to freeze-drying, the hydrogels developed a noteworthy internal micro-porosity, variable depending on the filler, suitable for colonization and cell migration. Therefore, hBMSCs were seeded on the hydrogels' top surfaces to study their ability to proliferate and migrate to the deepest bottom areas of these pore

networks. A remarkable metabolic activity of hBMSCs, cultured up to 10 days on the hydrogels, was detected. In addition, fluorescence microscopy, combined with an optimized cryosectioning protocol, revealed that hBMSCs were more prone to adhere on silica-filled hydrogels, and colonize the scaffold more deeply. Finally, co-culture of hBMSCs in presence of *S.aureus* or *S.epidermidis* was performed, showing that the composite hydrogels embedding mesoporous silica, diatomaceous earth or halloysite nanotubes protected hBMSCs viability from staphylococci infection.

Conclusion

The presence of inorganic fillers, especially mesoporous silica, allowed gellan-based hydrogels to achieve improved mechanical and biological performances. Hence, starting from these intriguing outcomes, further experiments are being performed. Indeed, hBMSCs differentiation on the hydrogels is ongoing, together with the evaluation of changes in mechanical features, induced by chondrogenesis. Furthermore, the most promising hydrogels will be implanted in wild type mice, to study their *in vivo* compatibility. The developed hydrogels display the potential to become useful tools for cartilage tissue engineering.

References

1. Zhao Y. et al, *Appl Sci*, 8, 2272, 2018.
2. Walter S.G. et al, *Arch Orthop Traum Su*, 139:305-16, 2019.
3. Bonifacio M.A. et al, *Carb Pol*, 198:462-72, 2018.

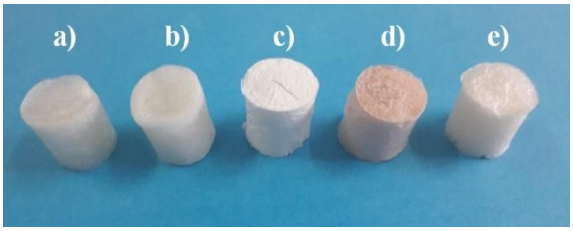

Figure 1
Macroscopic appearance of freeze-dried hydrogels without inorganic fillers (a), embedding halloysite nanotubes (b), mesoporous silica (c), diatomaceous earth (d) and sodium bentonite (e). Scale bar:20mm

PS1-03-87

An Engineered Multiwall Carbon Nanotubes dispersed Polyurethane-Silk Nanofibrous Neural Interface Effective for Improving Neuroregeneration

Bishnu K. Shrestha, Sita Shrestha, Chan H. Park, Cheol S. Kim

Chonbuk National University, Bionanosystem Engineering, college of engineering, Jeonju, KR

Introduction

Neuronal cells are highly susceptible to easy damage when trauma occurred. However, peripheral nerve cells show less neuroinflammation than brain cells. To the past few years, researchers have been able to achieve unprecedented success to cure the peripheral nerves cell (PNC) injury[1]. The new techniques are employed to develop scaffolds from bioactive material that exhibit potential ability to mimic the natural extracellular matrix (ECM) for supporting cellular metabolic functions. Exploring numerous benefits towards medical and biological application, these scaffolds hold key interest for guiding nerve cells to find the successive treatment in nerve cell injury.Numerous therapeutic and medical (for example surgical procedures, including autograft/allografts) techniques have been suggested for axonal growth and regeneration with fast recovery and healing of injury sites in PNI. However, the aforementioned medical techniques lead to rise some harmful side effects that might be occurred, including the morbidity of donor site, high possibility of mutation, nerve incontinence and impotence and even uncertainty of normal functions of recovery parts. In recent years, alternate medical treatments have been purposed to solve the aforementioned limitations. Researchers have designed scaffolds resembling natural ECM [2,3]. The scaffolds tend to increase cell-cell interactions. Thus, it creats excessive confident of success for using implantable device to the recovery of injury sites. Mostly, naturally modified biopolymers, for example- cellulose, chitosan, gelatin, chitin, fibroin, myosin, and collagen have been used to develop biointerface for employing soft/hard tissue repair or nerve-guided conduits[3].Furthermore, the necessary properties of the scaffolds as mentioned above can be improved by integrating some biocompatible synthetic polymers, carbon-based material and some biominerals. We developed electrospun nanofibers in aligned orientation using electrospinning. The fibrous composite mat of PU-Silk@*f*MWCNTs showed promising behavior of cytocompatibility for both cell (mouse Schwann cells (S42) and rat pheochromocytoma 12 (PC12)) via cell attachment and proliferation, and cell differentiation *in vitro*.

Experimental Methods

Silk from Bombyx mori, polyurethane, Trifluoroacetic acid, dimethylformamide and multiwall CNTs were used for the fabrication of 2D scaffolds. The surface morphology, and other properties were studied by SEM, HR-TEM, FTIR, XRD. hydrophilicity and ultimate tensile strength, biodegradability were also evaluated. The cellular activity were examined using cell counting kit-8 (CCK-8) at 450 nm and cells viability also confirmed with LIVE/DEAD® cell viability assay kit. Morphological study also conducted usind SEM and fluorescence images.qRT-PCR was conducted to determine the neural differentiation, after 13 days of cells culturing and immunofluorescence Image Analysis was performed on PC12 cells. Statistical analysis was analyzed by ANOVA as mean ± standard deviation (S.D., n=3). Value was considered as ***P <0.001.

Results and Discussion

The PU-Silk@*f*MWCNTs showed fibers with uniform diameter perfectly in unidirectional (Fig. 1). CNTs improves the conductivity of composite mixture. However, some fibers are in irregular shape indicating the presence of *f*MWCNTsand also confirmed by HR-TEM images. The FTIR spectra and XRD pattern (Fig.1 c and d) of PU/Silk-*f*MWCNTs are in accordance of the previously reported literature[4]. The mechanical properties of the PU/Silk-*f*MWCNTs showed high value (Fig. 1 (e)) as consequence of *f*MWCNTs tending to form intra and inter molecular covalent bonds, hydrogen bonds, and peptide bonds with –COOH, C=O, OH, and –NCOO– in PU/Silk. Water contact angle (Fig. f) also lower in composite material due to the presence of polar functional groups in the active surface sites of CNTs and more amino functional groups were hydrolyzed in acidic medium. The biodegradability of each electrospun mat (Fig. 1F) was enhanced by slowly hydrolyses the peptide bond.The CCK-8 test and cell viability results (Fig. 2 ,(a, b c and d) confirms the cytocompatibility of the scaffolds. Furthermore, cell attachment and proliferation (Fig 2. e and f) were increased in PU/Silk-*f*MWCNTs scaffolds at1 and 5 days as consequence of porosity, hydrophilicity, and mechanical strength, of conductive scaffold supported by enzymes/cofactors regulation. The cellular differentation is illustrated by qRT-PCR from expression level of gene. The conductive scaffolds maintain the concentration of metallic ions and help to outgrow of neuronal cells.

Conclusion

The PU/Silk-*f*MWCNTs showed high mechanical strength, improved hydrophilicity, biocompatibility. The engineered scaffold encouraged and enabled the neural cells sensitivity, along with cell proliferation, migration of S42 cells and also differentiation of PC12 cells *in vitro*. The scaffolds stimulated the neuronal cells and up-regulated the gene expression including βIII-tubulin and MAP2 protein levels.

References

1.S. shrestha et al., Electrodeless coating polypyrrole on chitosan grafted polyurethane with functionalized multiwall carbon nanotubes electrospun scaffold for nerve tissue engineering, Carbon, 136, 430-443 (2018).

2. W.H. Chooi etal., Modulation of cell-cell interactions for neural tissue engineering: Potential therapeutic applications of cell adhesion molecules in nerve regeneration,Biomaterial, 197, 327-344 (2019)

3. B.K Shrestha et al., π-Conjugated polyaniline-assisted flexible titania nanotubes with controlled surface morphology as regenerative medicine in nerve cell growth, Chemical Engineering Journal, 360, 701-713 (2019).

4.S. Shrestha etal., A Conducting Neural Interface of Polyurethane-Silk/*f*unctionalized Multiwall Carbon Nanotubes with Enhanced mechanical strength for Neuroregeneration, Material Science and Engineering C, (2019)

Acknowledgement

The study was supported by funding from National Research Foundation-Korea (NRF-Korea), (Project no. 2018R1D1A1B07044717), (Project no. 2019R1A2C1003988) and partly supported by the program for fostering next-generation researchers in engineering of the NRF (2017H1D8A2030449).

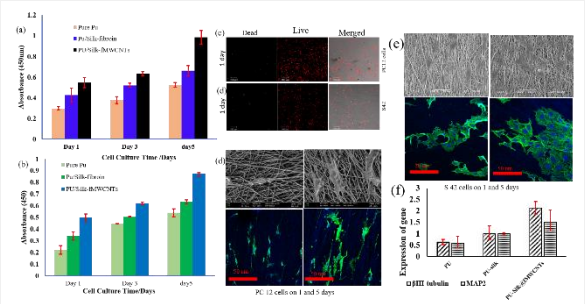

Figure 2
CCK test results (a) PC12, (b) S42 cells on various scaffolds after1,3 and 5 days. (c) Fluorescence images show live cells red color stained by C12-Resazurin and dead cells stained by SYTOX® Green, in green color cultured on scaffolds for 1 days. SEM and fluorescence images of PC12 cells,(e) and S42 cells (f) on PU-Silk@fMWCNTs scaffolds. (f), qRT-PCR for neural differentiation markers, β-tubulin (early neuron marker), and MAP2 (a mature neuronal marker) by day 10 days.

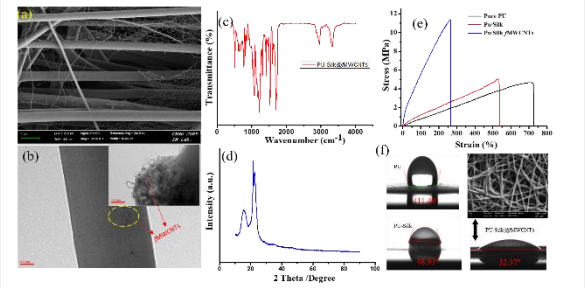

Figure 1
FE-SEM (a), HR-TEM (b), FT-IR spectrum (c), XRD pattern (d), of PU-Silk fibroin@fMWCNTs. And strain/stress curve (e), water contact angle (f) along with in vitro biodegradation of PU-Silk fibroin@fMWCNTs scaffold after 12 weeks.

PS1-03-88

Glycosaminoglycan sulfation enhances the regenerative potential of bone cells and hematopoetic stem cell maintenance

Juliane Salbach-Hirsch[1,5], Martina Rauner[1,5], Mario Lüttwitz[1,5], Sandra Rother[2], Vera Hintze[2], Stephanie Möller[3], Matthias Schnabelrauch[3], Manja Wobus[4], Lorenz Hofbauer[1,5]

[1]Technische Universität Dresden, Division of Endocrinology, Diabetes and Bone Diseases, Department of Medicine III1Division of Endocrinology, Diabetes and Bone Diseases, Department of Medicine III, Dresden, DE; [2]Technische Universität Dresden, Institute of Materials Science, Max Bergmann Center of Biomaterials, Dresden, DE; [3]INNOVENT e. V, Biomaterials Department, Jena, DE; [4]Technische Universität Dresden, Stem cell lab2, Department of Medicine I, Dresden, DE; [5]Technische Universität Dresden, Center for Healthy Aging, Medical Faculty, Dresden, DE

Introduction

Osteoporotic fractures are a major socioeconomic and clinical challenge as bone regeneration and osseointegration of implants are commonly impaired. With increasing age and comorbidities further affecting bone homeostasis, osteoporotic fractures are estimated to quadruple by 2050, highlighting the need for new, more biologically active biomaterials.

Experimental Methods

To this end, we investigated the functional role of glycosaminoglycans (GAGs), a key component of the bone extracellular matrix (ECM), for their osteogenic potential. Using native and synthetically derived GAGs (sGAGs) such as hyaluronan, chondroitin sulfate, and heparin (Hep) we evaluated how GAG sulfation affects the differentiation and activity of osteoblasts, osteoclasts and osteocytes and their capability to maintain hematopoietic stem and progenitor cells (HSPCs).

Results and Discussion

Our study revealed that GAG sulfation had profound effects on all stages of osteoclast and osteoblast differentiation. Whereas the viability of osteoclasts was increased, osteoclast numbers and the formation of the characteristic sealing zone structure were significantly decreased. This was accompanied by a loss of resorptive activity. On the other hand, the proliferation and metabolic activity of osteoblasts and osteocyte-like cells treated with equal concentrations of GAGs were decreased indicating a shift from the proliferative to matrix formation phase of osteogenic differentiation. Indeed, these cells showed altered matrix deposition and increased expression of genes associated with differentiation, such as the RANKL/OPG ratio, alkaline phosphatase, osteocalcin, and Runx2. Using surface plasmon resonance and molecular modeling we further demonstrated that sGAGs can directly bind to sclerostin, interfering with its bioactivity, resulting in increased Wnt-signaling *in vitro*. As the ECM of the bone marrow cavity also serves as a highly specialized microenvironment for HSPCs their response to sGAG was also evaluated. The application of sGAG to differentiating osteoblasts altered the composition of newly synthesized ECM: Whereas low or non-sulfated GAGs had no effect, high sulfated GAGs increased the calcium/phosphate ratio as well as the protein and GAG content of osteoblast derived matrices. When used as a substrate for HSPCs these altered ECM preparations showed an increased potential to maintain the stem cell character of CD34+cells. This effect may be attributed to the higher sGAG content in these matrices, as sGAGs alone also ledt to significantly less differentiated colonies in a colony forming unit assay.

Conclusion

Here we demonstrated that GAG sulfation both directly and indirectly increases osteogenesis and reduces osteoclastogenesis thus, significantly altering the bone cell cross talk. This data suggests that finetuning GAG composition and linking GAG function to surfaces could represent a suitable tool to enhance local bone regeneration. Whether this translates into a favorable profile on bone remodeling at fracture sites requires rigoros *in vivo* assessment.

PS1-03-89

A Novel Pro-Angiogenic Fibrin-Alginate Technology for Repair and Regeneration of Multiple Tissues

Vaibhav Sharma[1], Stuart J. Brown[1], Nupur Kohli[1], Lilian Hook[2], Elena Garcia-Gareta[1]

[1]RAFT, Regenerative Biomaterials Group, Northwood, GB; [2]SML, Northwood, GB

Introduction

We describe a novel patented technology developed in our laboratory based on a fibrin-alginate mesh that is pro-angiogenic and shows excellent cell attachment and infiltration properties. The first product developed using this technology is a dermal replacement scaffold called Smart Matrix®. Advantageously, this fibrin-alginate technology can be combined with synthetic polymers, either inert (i.e. silicones) or bioactive (i.e. polycaprolactone, PCL) in various shapes (sheets, 3D structures), or osteogenic components for repair and regeneration of various tissues.

Experimental Methods

The fibrin-aglinate scaffold was manufactred in our laboratory by crosslinking with glutaraldehyde [3]. Smart Matrix® is a 2 mm freeze dried thick sheet of porous material with a gradient pore range . To characterize the material SEM, light microscopy, AFM and confocal testing were carrried out. Angiogenic assays were performed using the CAM assays and the celluler response was observed using Alamar blue and Live Dead staining.

Results and Discussion

Extensive in vitro and in vivo analysis has shown that Smart Matrix® allows a rapid initial infiltration of cells and blood vessels [1]. The product has gone through detailed structural characterization using techniques like SEM, histological analysis, laser scanning confocal microscopy and AFM. The results have suggested that the material is highly porous, and the interconnected pores are gradient in nature. The cellular behaviour towards the biomaterial has been confirmed through numerous cell viability assays, cytotoxicity assays and angiogenic assays including the very popular chick chorioallantoic membrane (CAM) assay. To further expand the applications of the technology, a novel two-component dermal scaffold for the treatment of pressure sores was designed using a polydimethylsiloxane (Sil) backing membrane to make the dermal scaffold more robust [2]. Moreover, the fibrin-alginate mesh was combined with PCL structures for the treatment of non-union fractures: the pro-angiogenic properties of the PCL/fibrin-alginate composite scaffold were increased compared to PCL alone as shown by the CAM assay. PCL/fibrin-alginate scaffolds are currently being tested in a rat model. Moreover, the fibrin-alginate mesh has been modified by introducing an osteogenic element into the mesh to be used as a bone void filler.

Conclusion

We present here a pro-angiogenic fibrin-alginate technology for repair and regeneration of soft and hard tissues. The first product of this technology is currently undergoing clinical trials. Future development will see its combination with 3D printing for development of custom-made implants.

References

[1] García-Gareta et al. Bioresearch Open Access 2(6), 412, 2013.

[2] Sharma et al. Macromolecular Bioscience 1700185, 2017.

[3] V. Sharma, N. Patel, N. Kohli, N. Ravindran, L. Hook, C. Mason, et al., Viscoelastic, physical, and bio-degradable properties of dermal scaffolds and related cell behaviour, Biomed. Mater. 11 (2016). doi:10.1088/1748-6041/11/5/055001.

Acknowledgement

This work was supported by the Restoration of Appearance and Function Trust (RAFT, UK, registered charity number 299811) and Smart Matrix Ltd.

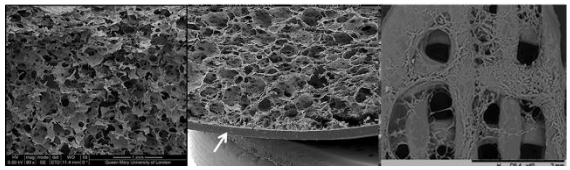

SEM images of the different biomaterials manufactured using the fibrin-alginate technology

Figure 1: Left to right; SEM images of Smart Matrix®, fibrin-alginate/Sil composite and PCL/fibrin-alginate composite scaffold

PS1-03-90

Cell response of 3T3 fibroblasts on 3D-nanofibrous collagen scaffolds

Naiana Suter, Sopie E. Stebel, Dorothea Brüggemann

University of Bremen, Biophysics, Bremen, DE

Introduction

Cells are embedded into the extracellular matrix (ECM), a complex network of protein nanofibers and polysaccharides. The ECM composition and the resulting stiffness have a big impact on multiple aspects of cell function, such as proliferation, motility, adhesion and contractility.[1] Collagen is the main component in the nanofibrous ECM. It has previously been processed into nanofibers by electrospinning[2], self assembly[3] or extrusion[4]. For the first time, we combined self assembly with ultrasonication to prepare 3D-nanofibrous collagen scaffolds with a large surface area for subsequent cell culture studies.

Experimental Methods

Nanofibrous collagen scaffolds were produced using pH-induced assembly in combination with ultrasonication and were subsequently crosslinked with glutaraldehyde. 3T3 mouse fibroblasts were cultivated on these nanofibrous collagen scaffolds and on planar collagen for up to 72 hours. Cell proliferation was analysed, and morphological changes were studied using immunostaining and fluorescence microscopy. Cellular interaction with collagen nanofibers on the nanoscale was analysed with scanning electron microscopy (SEM), and cell mechanics on the different collagen substrates were studied with atomic force microscopy (AFM).

Results and Discussion

SEM analysis showed that collagen reproducibly self-assembled into nanofibrous scaffolds with fiber diameters of 100 to 150 nm. Scaffold dimensions reached the centimetre range when pH-induced self-assembly was combined with ultrasonication. By controlling the collagen concentration we could reproducibly adjust the scaffold thickness between 500 nm and 8 µm. Live-dead staining and cell proliferation assays showed that fibroblasts on collagen nanofibers exhibited a cell viability, which was comparable to fibroblasts on planar collagen and glass. Fluorescence microscopy analysis of the cell area showed that cells on nanofibrous collagen were significantly smaller than on planar collagen or glass (Fig. 1). SEM analysis revealed that the fibroblasts partly grew into the nanofibrous scaffolds, which led to smaller cell areas in fluorescence microscopy analysis (Fig. 2). Atomic force microscopy studies of the cell stiffness did, however, not yield any significant differences between fibroblasts cultivated on collagen nanofibers, planar collagen and glass. Interestingly, adjustment of the nanofibrous scaffold thickness from 500 nm to 8 µm did not yet have a significant impact on the cell mechanics.

Conclusion

With the first-time combination of self assembly and ultrasonication we could reproducibly prepare nanofibrous collagen scaffolds with high surface coverage, which induced a positive response in cell culture studies with fibroblasts. Towards synthetic ECM scaffolds for tissue engineering it will be very important to tailor the mechanical characteristics of our large-scale nanofibrous collagen scaffolds to control cellular functions like adhesion and migration.

References

1. Galbraith, C. G., & Sheetz, M. P. *Current opinion in cell biology* **1998**
2. Matthews, J. *et al. Biomacromolecules***2002**
3. Harris, J. *et al.Micron* **2007**
4. Raoufi, M. *et al.Integr Biol* **2016**

Acknowledgement

We gratefully acknowledge funding via the Emmy Noether Programme of the Deutsche Forschungsgemeinschaft.

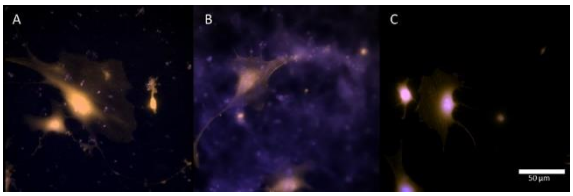

Fluorescence microscopy images of 3T3 fibroblasts cultivated on collagen
Planar collagen (A), fibrous collagen (B) and glass (C). Actin was stained with phalloidin (yellow) and nuclei were stained with DAPI (blue).

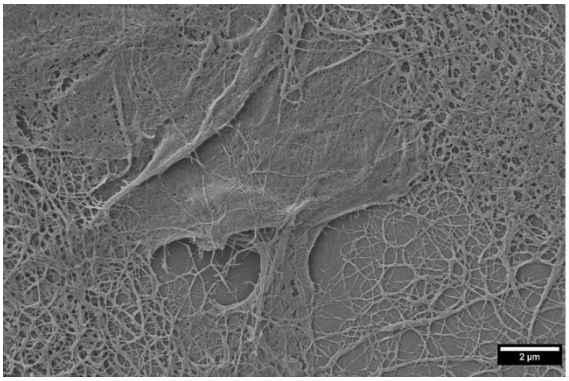

SEM image of 3T3 fibroblasts on collagen fibres
SEM image of 3T3 fibroblasts, which partly protruded into a nanofibrous collagen scaffold.

PS1-03-91

BTA Supramolecular Hydrogels as Viscoelastic Extracellular Matrices for Chondrocytes Tissue Engineering

Shahzad Hafeez[1], René P. M. Lafleur[2], Nicholas M. Matsumoto[2], Egbert W. Meijer[2], Matthew B. Baker[1]

[1]Maastricht University, Department of Complex Tissue Regeneration (CTR), MERLN Institute, Maastricht, NL;
[2]Eindhoven University of Technology, Institut of Complex Molecular Systems (ICMS), Eindhoven, NL

Introduction

The extracellular matrix (ECM) is the non-cellular component present within all tissues and provides essential biological and mechanical cues required for tissue growth. Traditional synthetic covalent hydrogels (a network of hydrophilic polymers) have been investigated for 3D cell culture and probing cell-matrix interactions as they mimic the mechanics of soft tissues and support cell adhesion. However, these hydrogels are elastic, lack the viscoelasticity found in native ECM, and must be degraded to allow tissue formation. To overcome these limitations, hydrogels from dynamic and reversible supramolecular polymers are developed which could respond cell stresses by rapidly breaking and reforming while maintaining uniform biophysical properties[1,2,3].

In our lab, we work with 1,3,5-benzenetricarboxamide (BTA) supramolecular hydrogels. BTA molecules self-assembled via 3-fold hydrogen bonding to form long one-dimensional aggregates, which physically interact to form hydrogels. BTAs are of interest owing to their reversible supramolecular interactions, proteins-like fibrous structures, and the ease of adjusting viscoelastic properties by controlling interactions at the molecular level[4,5]. We are tuning viscoelastic properties of hydrogels by mixing dumbbell (DB) and small molecule (SM) BTAs in different proportions to recapitulate native tissues' ECM viscoelasticity. In addition, these gels exhibit injectability, showing a potential for bioprinting, and can serve as a platform for the generation of spatiotemporal dynamic co-cultures.

Experimental Methods

The rheological properties characterization and cell culture studies were carried out with existing BTA and we move to create new BTA architectures via desymmetrization route.

Rheological properties: Different formulations of BTA gels were investigated, varying the ratio of DB to SM. Rheological properties were measured by oscillatory strain sweeps and oscillatory frequency sweeps. For self-healing studies, gel networks were ruptured and self-healing recovery was monitored.

Cell studies: Cultured chondrocytes (ATDC5) within BTA gels (3D encapsulated) were stained with calcein-AM and ethidium homodimer-1 and imaged using fluorescence microscopy. For quantitative cytotoxic analysis, an absorbance-based LDH and CyQUANT® assays were carried out.

BTAs synthesis: To create a new BTA hydrogelators we have explored a desymmetrization route of a BTA precursor— 1,3,5 benzene triester penta-fluorophenol (BTE-F_5Ph). This molecule has been synthesized and desymmetrized using model reagents towards the creation of a BTA hydrogel library.

Results and Discussion

Rheological properties: All tested formulations showed a characteristic viscoelastic behavior, with frequency dependent storage and loss moduli. Modular mixing of the two-component systems allows tunability of the hydrogel properties, including stiffness and viscoelasticity.

Cell studies: Quantification of live/dead staining shows cytotoxicity comparable to that of an alginate control gel (<20%). The LDH assay also confirms this trend showing a low amount of LDH release under the culture conditions (<20% of max), again comparable to alginate encapsulation. A CyQUANT® proliferation assay showed that total DNA content stayed constant over 7 days. Cell studies are underway to investigate the influence of viscoelasticity on chondrocytes (ATDC5) ECM production.
BTAs synthesis: BTE-F_5Ph has been desymmetrized successfully with good control and work is still in progress on creating the BTA gelator library.

Conclusion

Mixing of dumbbell and small molecule allow fine tuning of viscoelastic properties of BTA hydrogels, and the BTA dumbbell showed little cytotoxicity. Currently, cell culture experiments are being carried out to investigate ECM deposition by chondrocytes within BTAs hydrogels using different formulations of varying viscoelasticity. Synthesis of BTAs via desymmetrization enables the creation of a small library of hydrogels with varying viscoelasticity and fiber like ECM structure that can help in developing a better understanding of BTA self-assembly and cell-ECM interactions.

References

1. HW Ooi et al., Mater. Horiz., 2017, 4, 1020 -1040
2. A. M. Rosales et al., Nat. Rev. Mater., 2016, 1, 1–15
3. OJ Goor, Chem. Soc. Rev., 2017, 46, 6621
4. CMA Leenders et al., Mater. Horiz., 2014, 1, 116-120
5. MB Baker et al., ChemBioChem, 2016, 17, 207-213

Acknowledgement

This project/research has been made possible with the support of the Dutch Province of Limburg and European Research Council under H2020.

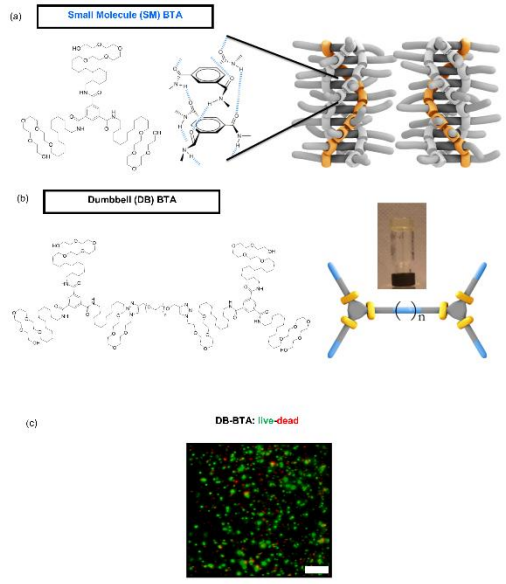

BTA dumbbell (DB) and small molecule (SM) chemical structures and cell cytotoxicity evaluation

(a) BTA small molecule (SM) structure and self-assembly

b) Dumbbell molecule (DB) structure and macroscopic hydrogels (inset)

c) live-dead image of chondrocytes in DB hydrogels

2:45 p.m. – 3:45 p.m.

Hall 1 / Exhibition Area

PS1-04 | Coatings

PS1-04-92

Novel biomimetic anti-adhesive implant coatings based on tetraether lipids

Alexander Scholte, Marion Frant, Ronald Schade, Gerhard Hildebrand, Klaus Liefeith

Institute for Bioprocessing and Analytical Measurement Techniques (iba), Department of Biomaterials, Heilbad Heiligenstadt, DE

Introduction

The non-specific interaction of matrix components of biological, organic or even inorganic nature at solid-liquid interfaces has always been a major problem in many areas of biomedicine, bioanalytics and last, but not least in the bioprocessing area. In the biomedical field, the non-specific adhesion and thus the accumulation of e.g. microorganisms or their metabolic products on stent or implant surfaces lead to inflammatory reactions and even rejection. In the field of gastroenterology stents are often used in malignant tumors in order to be able to continue to ensure the reduced flow of bile due to narrowing. Due to the specific composition of the bile fluid, in previous stent materials, e.g. polyurethane (PUR) bacterial adhesion and subsequent incrustation can be detected very quickly. This leads to the occlusion of the stent, which finally has to be surgically exchanged after a short stay of 60 days on average[1].

This problem is based on the physico-chemical properties of the implant surfaces, which influence or control the complete biofilm growth, as well as subsequent incrustation processes[2]. It can be addressed by coating with hydrophilic materials (passive approach) - here, a water barrier is built, which can prevent the adhesion of matrix components. Initial approaches to coating with hydrophilic components are based on the use of p-HEMA and subsequently of polyethylene glycols. Recently, the focus of research has increasingly been directed to polyzwitterionic systems[3]. A major problem, however, is to generate homogeneous and biocompatible coatings that do not affect the mechanical properties of the implant materials.

Here we report a novel implant coating based on tetraether lipids (TEL) combined with e.g. polyzwitterionic moieties. For this purpose, a fragment of a tetraether lipid, not described yet, could be isolated from sulfolobus strains for the first time and used for the further construction of a glycocalix-like combination layer with thicknesses in a low nm-scale.

TELs are bipolar amphiphiles (bolaamphiphiles), derived from the membranes of archaea, which tolerate large variations of e.g. temperature and pH and have an outstanding potential for self-assembly. The formation of monolayers and the principal effectiveness of a coating with hydrophilic polymers has already been demonstrated in earlier work[4]. As shown in the figure below, TEL dispersions, meaning well defined liquid-crystalline aggregates in aqueous solution, can be generated by a newly developed process. These are capable of forming covalently fixed monolayers on various substrates (e.g. glass, PUR, silicone, stainless steel). As immobilization matrix, they can serve to bind further moieties, in particular antiadhesives to suppress stent obstruction.

Experimental Methods

Isolated TELs were characterized by mass spectroscopy (MS) and nuclear magnetic resonance (NMR), and the aggregates formed from them were analyzed with dynamic light scattering (DLS), small angle X-ray diffraction (SAXS) and cryo-transmission electron microscopy (cryoTEM). The film was investigated by X-ray photoelectron spectroscopy (XPS) and the detection of an intercalating dye by means of confocal laser scanning microscopy

(CLSM). Physicochemically, the presented layers are described by the zeta potential, as well as the water contact angles and surface energies. The biological tests were observed via online-microscopy following established laboratory protocols.

Results and Discussion

As part of the work described above, glass and polyurethane surfaces in particular have been provided with this new coating. Betaine and sulfonic acids, which were applied to the respective materials via a simple surface-induced ATRP-reaction, could be identified as promising functions.

In particular, sulfobetaine- and sulfonic acid-modified TEL matrices showed a reduction of the initial bacterial adhesion by > 80% in the bile-specific mixed culture experiments carried out in a dynamic setup using flow-chambers. For this purpose, the biofilms had a significantly lower adhesion strength, so that a large part was rinsed off again compared to the reference materials by increasing the flow. Compared with uncoated materials, an effective reduction of the biofilm by > 95% could be detected.

Conclusion

Herein we describe a novel TEL-based coating method, which was developed for the modification of surfaces of bile duct stents. As part of a biomimetic approach, covalently fixed layer systems were generated that are able to build a stable water barrier to shield surfaces against microorganisms. Compared with reference materials, a reduction of the initial reduction of > 80% could be detected, so that such systems can be considered as promising candidates for use in the field of medical implants.

References

[1] J. Greenberger, G. Paumgartner, *Harrisons Innere Medizin* **2005**, *16*, 292-293.

[2] V. Carniello, B. W. Peterson, H. C. van der Mei, H. J. Busscher, *Advances in Colloid and Interface Science* **2018**.

[3] M.-C. Sin, S.-H. Chen, Y. Chang, *Polymer Journal* **2014**, *46*, 436-443.

[4] L. Tauhardt, M. Frant, D. Pretzel, M. Hartlieb, C. Bücher, G. Hildebrand, B. Schröter, C. Weber, K. Kempe, M. Gottschaldt, K. Liefeith, U. S. Schubert, *J. Mater. Chem. B* **2014**, *2*, 4883-4893.

Acknowledgement

The authors would like to thank the Bundesministerium für Bildung und Forschung (Germany) for funding the project "GastroFreeFlow" (FKZ 13GW0082E).

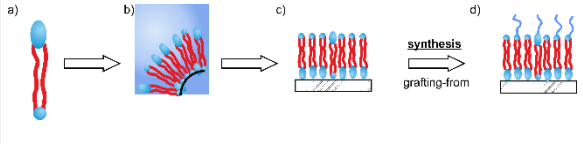

Schematic representation of a TEL-based anti-adhesive coating
a) Bipolar (bolaamphiphilic) tetraether lipid. b) Preorganized aggregate in aqueous solution. c) Covalently fixed TEL monolayer. d) TEL-based anti-adhesive coating after ATRP-reaction.

PS1-04-93

Electrophoretic deposition of a metal-ceramic coating containing MCrAlY (M:Ni,Fe) bond coat for cardiovascular implants.

Nikita Grigorev[1], Sabine Neuss-Stein[2,1], Norina Labude[2], Rainer Telle[1], Karolina Schickle[1,2]

[1]RWTH Aachen, Institute of Mineral Engineering, Aachen, DE; [2]Uniklinik RWTH Aachen, Helmholtz-Institute for Biomedical Engineering, Aachen, DE

Introduction

The main aim of the presented project is the development of a reproducible, tailor-made metal-ceramic coating with hemocompatible properties for permanent medical use on cardiovascular implants with direct blood contact such as stents. In addition to hemocompatibility, the coating should increase the lifetime of the applied materials. The metal matrix provides the necessary flexibility and adaptation of the expansion to the substrate. The dispersed ceramic particles in the metallic matrix improve the hemocompatible properties of the coating. In this work MCrAlY (M: Ni, Fe) bond coat and Al-Al_2O_3 top coat were applied using electrophoretic deposition [1] and sintering [2].

Experimental Methods

Using the electrophoretic deposition and the charging system of iodine-acetone [3], NiCrAlY and FeCrAlY bond coat was successfully deposited on a steel substrate. The samples were sintered in argon and vacuum ($1x10^{-5}$ mbar) at range of temperatures from 1000 °C up to 1200 °C for 30 and 60 minutes. In order to improve the adhesion, the steel plates were previously sandblasted. The Al-Al_2O_3 composite coating was applied as a second layer by the electrophoretic deposition and the charging system of iodine-acetone and sintering, as well. To evaluate the phases formed at each temperature the XRD-analysis was performed. The morphology of the samples was analyzed by SEM and an adhesion test was executed.

Results and Discussion

In this study we could show that the MCrAlY (M:Ni,Fe)-coatings could be successfully obtained by the electrophoretic deposition by using the charging system of iodine-acetone without any other additives. It is also possible to perform the sintering in argon or vacuum atmosphere with a good adhesion to substrate. The top coat (Al-Al_2O_3) adheres the bond coat in a proper way. Hemocompatibility tests according to ISO 10993-4 are ongoing.

Conclusion

MCrAlY (M:Ni,Fe) is a trendy and promising material that can provide a good adhesion of ceramic and metal and can be applied by a simpler method like the electrophoretic deposition. It can be used not only as thermal barrier coating but also as a bond coat for ceramic coatings for medical use.

References

1. L. Xinying, Z. Rizhang, H. Yedong; Electrophoretic Deposition of MCrAlY Overlay-Type Coatings; Oxidation of Metals, Vol. 43, Nos. 3/4, 1995

2. R.J. Takahashi, J.N.K. Assis, F.P. Neto, A.M. Mello, D.A.P. Reis; Sintering Study of NiCrAlY, Materials Science Forum Submitted, Vol. 899, pp 478-482

3. K. Nobuyuki, Tsukamoto T., Shoji H., Hotta T., Preparation of Various Oxide Films by an Electrophoretic deposition Method: A Study of the Mechanism, Jpn. J. Appl. Phys. Vol. 34 (1995) pp. 1643-1647
4. L. Zhiming, Q. Shiqiang, W. Wei; Characterization and oxidation behavior of NiCoCrAlY coating fabricated by electrophoretic deposition and vacuum heat treatment, Applied Surface Science 257 (2011) 4616–4620

Acknowledgement
Funded by the Deutsche Forschungsgemeinschaft (DFG, German Research Foundation) – №405895710

PS1-04-94

Intracellular calcium-ion mobilization on charged titanium surface modifications

Martina Grüning[1], Jutta Lehnfeld[2], Thomas Distler[3], Katja Fricke[4], Manuela Dubs[5], Christian Völkner[6], Rainer Müller[2], Matthias Schnabelrauch[5], Aldo R. Boccaccini[3], Sylvia Speller[6,7], Barbara Nebe[1,7]

[1]University Medical Center Rostock, Cellbiology, Rostock, DE; [2]University of Regensburg, Institute of Physical and Theoretical Chemistry, Regensburg, DE; [3]University of Erlangen-Nuremberg, Materials Science and Engineering, Institute of Biomaterials, Erlangen-Nuremberg, DE; [4]Leibniz Institute for Plasma Science and Technology, Bioactive Surfaces, Greifswald, DE; [5]INNOVENT e.V., Biomaterials, Jena, DE; [6]University of Rostock, Physics of Surfaces and Interfaces, Institute of Physics, Rostock, DE; [7]University of Rostock, Life, Light & Matter, Rostock, DE

Introduction

The osteoblastic cell behavior at the interface to artificial bone material is strongly dependent on the substrates' physico-chemical properties[1] like wettability and surface charge. However, as there are different opinions in literature, it is still unclear whether osteoblasts prefer positive or negative surface charges. Since we found out that a positively charged amino-group containing titanium (Ti) surface can enhance osteoblast functions[2-6], we hypothesize that positive surface charges play a crucial role in the material-cell interaction. To confirm this, we systematically compare the cellular behavior on positively and negatively charged Ti surfaces.

Experimental Methods

In order to obtain diverse surface charges, plane silicon-Ti substrates (10x10 mm) are modified by (i) a plasma polymerized allylamine layer[2,5] (PPAAm), (ii) coatings with collagen-type I, Matrigel, and the integrin adhesion peptide sequence Arg-Gly-Asp (RGD), (iii) polypropylene imine dendrimers (PPI), polyethylene imine polymers (PEI) as well as (iv) oxidized alginate-gelatin hydrogels functionalized with polypyrrole: polystyrene sulfonate (ADA-GEL PPy:PSS) (**Fig. 1**). Surface properties like zeta potential[2,5], water contact angle[5] and surface free energy are determined. Human MG-63 cells (ATCC®) are cultured on modified Ti in Dulbecco's Modified Eagle's Medium with 10% fetal calf serum. The cell membrane is stained with PKH-26 to assess cell spreading on different substrates (1 h). To record an immediate mobilization of intracellular calcium ions (Ca^{2+})vital osteoblasts are stained with the Ca^{2+} indicator Fluo 3-acetoxymethyl ester after 24 h cultivation and stimulated with adenosine 50-triphosphate (ATP)[5,6].

Results and Discussion

On the weakly positively charged surfaces PPAAm (zeta potential: + 8.6 mV)[5], RGD and PEI surfaces, an increase of cellular spreading and intracellular Ca^{2+} ions after ATP stimulation could be detected compared to cells grown on negatively charged Ti modifications (collagen-type I and Matrigel) or uncoated Ti (zeta potential: - 87.5 mV). Modifications with PPI generated highly positive surface charges that showed an enhanced cellular spreading but could not show favorable effects on the Ca^{2+} mobilization.

Conclusion

While weakly positively charged PPAAm, RGD and PEI resulted in an enhanced calcium ion mobilization, this effect could not be displayed with highly positively charged PPI surfaces. This suggests that osteoblasts prefer only surfaces featuring a certain range of zeta potential. In order to assess this in further depth, subsequent systematical experiments are necessary.

References

[1] Moerke C. et al., J Cell Sci 131: jcs207001, 2018
[2] Finke B. et al., Biomaterials 28: 4521-4534, 2007
[3] Rebl H. et al., Acta Biomater 8: 3840-3851, 2012
[4] Kunz F. et al., Eur Cell Mater 29: 177-189, 2015
[5] Staehlke S. et al., Cell Biosci 8(22), 2018
[6] Staehlke S. et al., Biomaterials 46: 48-57, 2015

Acknowledgement

This research was supported by the German Research Foundation (Deutsche Forschungsgemeinschaft, DFG) within the Collaborative Research Centre 1270 ELAINE (for TD and MG) and by the fund of the chemical industry (for JL).

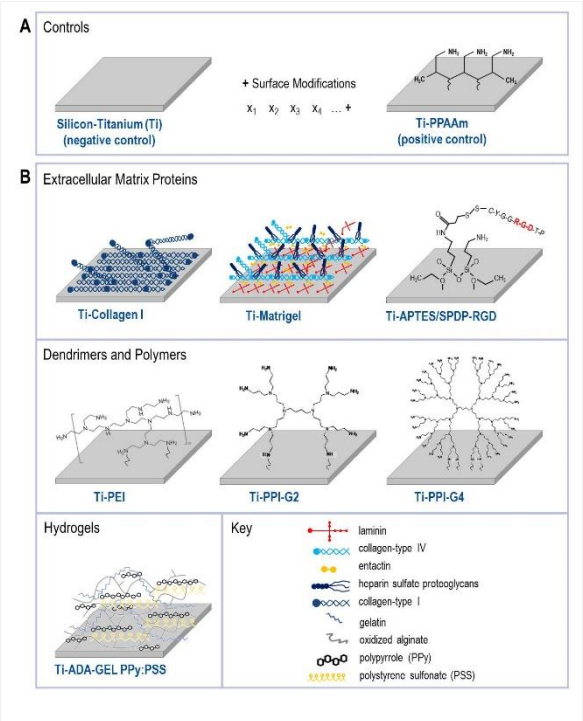

Fig. 1: Surface modifications of plane silicon-titanium arrays.
(A) The cell biological experiments are embedded in sample controls with negative or positive surface charges. **(B)** The surfaces are modified by extracellular matrix protein coatings, dendrimers, polymers and hydrogels.

Ti - silicon-titanium, PPAAm - plasma polymerized allylamine, APTES - 3-aminopropyltriethoxysilan, SPDP - N-succinimidyl-3-2-pyridyldithio propionate, RGD - arginine-glycine-aspartate sequence, PEI – polyethylenimine, PPI - polypropylene imine, G2 - generation 2, G4 - generation 4, ADA-GEL - alginate-di-aldehyde gelatin, PPY – polypyrrole, PSS - polystyrene sulfonate.

PS1-04-95

Surface modification of zein-based composite coatings

Laura Ramos Rivera, Aldo R. Boccaccini

Department of Materials Science and Engineering, University of Erlangen-Nuremberg, Institute of Biomaterials, Erlangen, DE

Introduction

The demand for bone implants increases each year as global life expectancy is higher. Current developments in the design of biomaterials for bone tissue substitution and repair should consider several characteristics and added functionalities, such as surfaces capable of i) preventing foreign body negative response, ii) promoting osteointegration by influencing the attachment of osteoblasts, iii) decreasing possible corrosion and wear, iv) promoting healing and v) preventing bacterial infection. Consequently, the control of surface properties using different treatments or coatings is essential to improve the interfacial bonding of implants and scaffolds. Among the broad diversity of coatings to modify metallic surfaces for implants, composite coatings have shown high potential benefit in this field since they can be tailored to fulfill the mentioned requirements [1,2]. In this study, a bi-layered biopolymer-bioactive glass composite coating has been designed for a metallic implantable material using electrophoretic deposition (EPD) in combination with electrospinning as a novel surface modification approach.

Experimental Methods

EPD coatings were produced in a mixture of ethanol/water with a suspension of zein, and bioactive glass (BG) doped with Cu. Processing parameters: 10 V and 5 min were used for the deposition process. Zein and zein/PCL (polycaprolactone) (1:1) fibers were fabricated using 30 wt% of zein and PCL in acetic acid. Electrospinning parameters were set to 16kV, 25°C, 40% rel. humidity and a collector distance from 11 to 15 cm. Metallic electrodes coated by EPD were attached on a collector during the electrospinning process. Surface morphology of the bilayer was evaluated using SEM. Contact angle measurements were carried out to observe changes in the wettability and surface energy as function of the coating composition and structure. Pull off adhesion tests were performed to evaluate the adhesion of the different layers to the substrate. In vitro cell viability with MG63 cells was investigated in direct contact with the samples through metabolic evaluation. Biofilm formation was assessed immersing the samples in solutions containing Escherichia coli and Staphylococcus aureus.

Results and Discussion

SEM images (Figure 1) showed that fibers were successfully deposited onto EPD coatings. Wettability of the samples could be modified by designing the fiber structure of the coatings. Addition of PCL to the zein solution reinforced the hydrolytic resistance and mechanical properties of the fibers. Fibrous layers remained attached to the composite coating after one week of cell culture. Cells proliferated on all surfaces over time and enhanced adhesion. Bacteria viability was significantly reduced after three days of incubation compared with the non-coated stainless steel surface.

Conclusion

It could be shown that application of fibrous coatings (by electrospinning) on electrophoretically produced zein coatings enhanced cell attachment. Moreover the bilayer was effective in slowing down bacteria colonisation and adhesion. Fiber mats obtained from PCL/zein blends showed the best mechanical and biological stability, demonstrating the suitability of the bilayer system for achieving multifunctional coatings on metallic substrates.

References

[1] Sammons RL. (2011). Modifying biomaterial surfaces to optimise interactions with bone. In: *Surface Modification of Biomaterials.* Elsevier, Sawston, pp 365-400.

[2] Chen, Q., Cordero Arias, L.E., Roether, J., Cabanas Polo, S., Virtanen, S., & Boccaccini, A.R. (2013). Alginate/Bioglass® composite coatings on stainless steel deposited by direct current and alternating current electrophoretic deposition. *Surface & Coatings Technology*, *233*, pp 49-56.

Acknowledgement

Laura Ramos Rivera thanks the German Academic Exchange Service (DAAD) for a fellowship and COLCIENCIAS for financial support

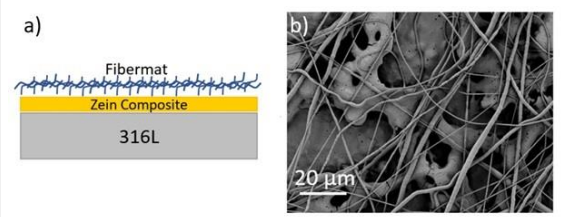

Figure 1.
(a) Schematic diagram of the bilayer coating on 316L SS substrate exhibiting fibrous topography, (b) SEM micrograph of zein composite coating with zein fibers modification

PS1-04-96

Cellular and Bacterial response to Bioactive and Antibacterial Chemically-modified Titanium and Bioactive glass surfaces

Andrea Cochis[1,2], Rina Iwatsuki[3], Seiji Yamaguchi[3], Sara Ferraris[4], Marta Miola[4], Alessandro Scalia[1,2], Silvia Spriano[4], Enrica Verné[4], Lia Rimondini[1,2], Hiroaki Takadama[3]

[1]University of Piemonte Orientale UPO, Department of Health Sciences, Novara, IT; [2]University of Piemonte Orientale UPO, Center for Translational Research on Autoimmune & Allergic Diseases CAAD, Novara, IT; [3]Chubu University, Department of Biomedical Sciences, Kasugai, JP; [4]Politecnico di Torino, Department of Applied Science and Technology, Turin, IT

Introduction

Bone repair is a complex process whose success is based on a continuous and definite ions exchange at the interface between the tissue itself and the implantable substitute. Accordingly, there is nowadays a large research aimed to improve the bioactivity of the most employed bone substitutes such as bioactive glass and titanium (Ti) alloys [1,2]. However, an external factor that can hinder the healing process is represented by bacterial infection. In fact, infections are currently the most problematic reason of prosthetic failure due to the high bacteria antibiotic resistance [3]. So, it is evident that the design of bone repair dedicated biomaterials must include both bioactive and antibacterial properties. Based on these premises, here different surface chemical treatments were applied onto Ti alloys and bioactive glasses in order to improve and faster apatite formation by stimulating the microenvironment chemistry or to enhancing ions exchange. Moreover, silver (Ag) was introduced in the above-mentioned treatment in order to provide a strong and broad-range antibacterial activity [4].

Experimental Methods

Ti6Al4V alloys and a SiO_2-Na_2O-CaO-P_2O_5-B_2O_3-Al_2O_3 bioactive glass were applied as bare materials for further modifications. Ti alloys (named Ti64(Sr-Ag)) were first soaked in a 5M NaOH solution and then in a 50 mM $CaCl_2$ and 50 mM $SrCl_2$ mix solving. Afterwards, specimens were heated at 600°C (1 hour) and soaked once more in a 1M $Sr(NO_3)_2$ solution doped with 1 mM $AgNO_3$ aimed to introduce silver. The bioactive glass samples (named SBA2-Ag) were soaked in a 30 mM $AgNO_3$ solution to incorporate silver ions too. Specimens' physical-chemical characterization was performed by means of FESEM and XPS, while apatite formation was evaluated by soaking in body simulated fluid (SBF) [5]. Specimens' cytocompatibility was evaluated by means of metabolic activity in direct contact with human osteoblasts progenitors (hFOB 1.19) that were selected as representative for cells deputed for bone self-healing. Then, antibacterial activity was tested against a multi-drug resistant *Staphylococcus aureus* strain biofilm by applying both a well-established protocol from literature [6] and the ISO 22196 standard to compare results. Finally, specimens' ability to protect cells from infection was evaluated by 3 co-culture systems: (i) cells were pre-seed onto specimens' surface and then infected, (ii) bacteria were pre-applied to infect specimens' surface and then cells were plated, and (iii) bacteria and cells were applied together onto specimens' surface to simulate a "road to the surface" competition.

Results and Discussion

Surface morphological analysis done by FESEM showed a nano-textured surface for Ti64(Sr+AG) specimens and a smoother one for SBA2-Ag. XPS analysis confirmed that Ag was successfully introduced onto both Ti64(Sr+AG) and SBA2-Ag surfaces as ions.Apatite formation was correctly observed for both Ti alloys and bioactive glass; in

particular, the latter resulted as faster showing apatite after 1 day. Biological evaluations are summarized in Figure 1; ISO 22196 standard and methods 1 and 2 were used as representative examples for antibacterial and co-cultures results. Ag-doping did not cause any toxic effect as cells metabolism was comparable between treated and control (cnt) specimens (Fig. 1a, $p>0.05$). On the opposite, Ti64(Sr-Ag) and SBA2-Ag showed a marked antibacterial activity as the *S. aureus* biofilm viability was significantly decreased by comparing Ag-doped Ti alloys and SBA2-Ag with their bare counterparts (Fig. 1b, $p<0.05$ indicated by §). Moreover, this strong antibacterial effect was effective in cells viability preservation in co-culture models. In fact, both that infection was applied after (method 1) or prior cells seeding (method 2), the number of viable cells onto Ag-doped surfaces was significantly higher then what observed in the controls (Fig. 1c, $p<0.05$, indicated by § and #, respectively).

Conclusion

Both Ag-doped Ti alloys and bioactive glass obtained by the here described surface chemical treatments can be considered as very promising for bone tissue engineering due to their strong bioactivity and antibacterial properties.

References

[1] Nair M, et al, *J Nanosci Nanotechnol*, 2015, 15, 939-55.
[2] Fernandes JS, et al, *Acta Biomater*, 2017, 59, 2-11.
[3] van Duin D, et al, *Infect Dis Clin North Am*, 2016, 30, 377-390.
[4] Franci G, et al, *Molecules*, 2015, 20, 8856-74.
[5] Kokubo T, et al, *Biomaterials*, 2006, 27, 2907-2915.
[6] Cochis A, et al, *Biomaterials*, 2016, 80, 80-95.

Acknowledgement

This research was supported by MAECI-Italy (GLOBAL project).

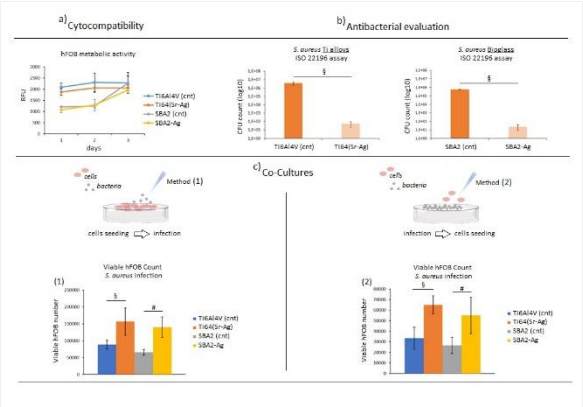

Figure 1.
Ag-doping did not turned specimens to toxicity as no differences were noticed between bare (cnt) and treated specimens in terms of cells metabolism (a). On the opposite, both Ag-doped Ti alloys and SBA2-Ag determined a significant reduction of bacteria viability (b, $p<0.05$, indicated by §). The antibacterial activity was confirmed by co-culture systems where the number of viable cells in presence of bacteria was significantly higher for Ag-doped materials (c, $p<0.05$, indicated by § and #, respectively).

PS1-04-97

OCP precipitation ability on Ti alloy surface modified by electron cyclotron resonance plasma oxidation

Hiroshi Masumoto[1], Kenta Takahashi[1], Mayumi Shiraishi[2], Naru Shiraishi[2], Takahisa Anada[3], Osamu Suzuki[3], Keiichi Sasaki[3]

[1]Tohoku University, Frontier Research Institute for Interdisciplinary Sciences, Sendai, JP; [2]Niigata University, Graduate School of Medical and Dental Sciences, Niigata, JP; [3]Tohoku University, Graduate School of Dentistry, Sendai, JP

Introduction

Calcium phosphate, such as hydroxyapatite, b-tricalcium phosphate and octacalcium phosphate [$Ca_8H_2(PO_4)_6 \cdot 5H_2O$, OCP], are utilized as the coating materials for improving the osteoconductive activity. Our previous studies indicated that implantation of OCP efficiently enhanced bone regeneration compared to HAp[1]. On the other hand, commercially pure titanium (cp-Ti) and Ti alloy are widely used in various types of implants in orthopaedic and dental fields, because they have the greatest biocompatibility with bone among the metallic biomaterials. It is known that the biocompatibility of Ti will change with the condition of the surface oxide (titania: TiO_2) film of implant Ti alloy. Electron cyclotron resonance (ECR) plasma is high-active plasma, and high-quality crystalline films can be obtained at low temperature for short time. ECR plasma oxidation is effective surface modification of metal Ti for biocompatibilities, which became clearly in previous study [2]. In the present study, TiO_2 films were deposited on cp-Ti and Ti-alloy by ECR plasma oxidation, and the effect of oxidation conditions on structure and precipitation behaviour of OCP were investigated.

Experimental Methods

ECR plasma apparatus was used for oxidation of cp-Ti, Ti-6Al-4V and Ti-Nb-Sn[3] alloy surface. A magnetic field (8.75×10^{-2} T) was applied to the plasma chamber to satisfy the ECR condition. The oxygen gas pressure during ECR oxidation was set to 0.003-1.5 Pa and the oxidation time was set to 1.8 ks. The microwave power was 900 W. An infrared lamp was used for controlling the substrate temperature in the range from room temperature (RT) to 600 °C.

The structure and morphology of the films were characterized by X-ray diffraction analysis (XRD) and optical and scanning electron microscopy (SEM). OCP was precipitated in phosphate-buffered solution on TiO_2 film deposited Ti substrate[1]. The calcification ability was estimated by weighing the substrate before and after the immersion.

Results and Discussion

Ti oxide films were obtained above 300 and 600 °C on Ti and Ti-alloy substrates, respectively. The amount of rutile TiO_2 increased with increasing oxidation temperature on Ti substrate. The ECR plasma was significantly effective to prepare crystallized TiO_2 films at low temperatures.

Fig. 1 shows SEM images of Ti substrate surface before calcification. The substrate surface before oxidation were smooth. Rough morphology was observed in the substrate surface oxidized by ECR plasma. Averages roughness of (a) and (b) were 0.01 and 0.19 mm, respectively. ECR plasma oxidation at low temperature would induce osteoconductive calcium phosphate on implant Ti. Mixtures of OCP and dicalcium phosphate dihydrate (DCPD) peaks were observed after calcification.

Fig. 2 shows the effect of the oxidation temperature on calcium phosphate deposition onto the substrate surfaces. The amount of calcium phosphate deposition was maximized at 300-400°C. The amount of the precipitates on the cp-Ti, Ti-6Al-4V and Ti-Nb-Sn substrates by ECR plasma oxidation was about 8, 4 and 2 times larger than that before ECR plasma oxidation, respectively.

Conclusion

The TiO_2 films prepared by ECR plasma oxidation has been expected to improve the capability to induce osteoconductive calcium phosphate of implant cp-Ti, Ti-6Al-4V and Ti-Nb-Sn alloy.

References

1 O. Suzuki, *et al.Biomaterials* (2006) **27**: 2671.

2 H. Masumoto, *et al.* (2007) *Key Eng. Mater*. **330-332**: 565.

3 S. Hanada, *et al.Inter. Cong. Ser.* (2005), **1284**: 239.

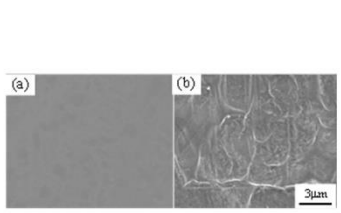

Fig. 1 SEM images of Ti substrate surface before calcification. ((a) before oxidation, (b) after ECR plasma oxidation)

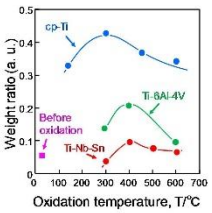

Fig. 2 Effect of oxidation temperature on precipitates weight ratio.

Fig.

PS1-04-98

Osseointegration and biodegradation behaviour of magnesium scaffolds LAE442 with different pore sizes and PLA-/CaP-coating

Laura M. Witting[1], Stefan Julmi[2], Franziska Feichtner[1], Anja-Christina Waselau[1], Christian Klose[2], Andrea Meyer-Lindenberg[1]

[1]Ludwig-Maximilians-Universität, Clinic of Small Animal Surgery and Reproduction, Munich, DE; [2]Leibniz University Hanover, Institut für Werkstoffkunde (Materials Science), Garbsen, DE

Introduction

Healing of critical-size bone defects can be challenging. Such defects can be treated with autologous or allogenic transplants, which lead to certain risks. In contrast, biodegradable Mg-based implants, such as LAE442, are promising bone replacement materials, based on their degradation, osseointegration and biocompatibility (1). The aim of this study was to evaluate the biodegradation and osseointegration of open-pored and differently coated LAE442-magnesium scaffolds. The hypothesis is that different coatings result in different degradation rates.

Experimental Methods

Open-pored cylindrical LAE442 (4 wt.-% Li, 4 wt.-% Al, 2 wt.-% rare earth) scaffolds (length: 5 mm, diameter: 4 mm) of different pore sizes (P1: 400 µm; P2: 500µm) were produced by an investment casting process. The scaffolds were coated with MgF_2 and received an additional polylactic acid (PLA) or calcium phosphate (CaP) coating layer via a deposition coating process (2). Overall, 32 LAE442-scaffolds, equally distributed among coating types and pore sizes, were inserted in the cancellous bone of the greater trochanter of both femura in sixteen adult, female rabbits. Implants of beta-tricalcium phosphate (TCP) served as a control group. Radiographic and µ-CT scans were carried out immediately post OP and every two weeks until termination of the study. Samples were harvested after 6 and 12 weeks. Semi-quantitative scorings were performed to evaluate trabecular bone ingrowth and gas accumulation. Furthermore, the in-vivo degradation and osseointegration of scaffolds were evaluated by quantitative 3D-analysis, including density and volume measurements.

Results and Discussion

All implants were clinically well-tolerated. Starting from the second week, the degradation of magnesium led to production of hydrogen gas, which partly spread out into the medullary bone cavity, whereby PLA-coated implants showed more gas accumulation. All LAE442-implants underwent slow degradation, since the scaffold structure was still present after 12 weeks. Implant density and volume showed no difference between both coating-types and pore sizes. TCP-implants showed rapid degradation without any gas release. With respect to osseointegration, the CaP-coated implants demonstrated better results with more newly formed bone trabeculae adhering to the implant surface, in comparison to PLA. Bone density and volume increased only in the vicinity of CaP-coated scaffolds with the larger pore size (P2), whereas the other LAE442 samples exhibited a decrease. The best osseointegration was detected in TCP-implants, which presented the highest number of trabecular bone-implant-contacts.

Conclusion

The LAE442-scaffolds degraded homogenously and slowly. Moreover, they showed a promising osseointegration. CaP-coated implants, especially the larger pore size types (P2), exhibited less gas accumulation and better

osseointegration, compared to the implants with PLA-coating. Therefore they appear to be better suited for further investigations in load bearing bone. Further radiographic and µ-CT scans will be carried out to examine the long-term degradation behaviour. In addition, histological analysis will be performed in the future in order to examine bone ingrowth and biocompatibility on the cellular level.

References

(1) Lalk, M., Reifenrath, J., Angrisani, N., Bondarenko, A., Seitz, J. M., Mueller, P. P., & Meyer-Lindenberg, A. (2013). Fluoride and calcium-phosphate coated sponges of the magnesium alloy AX30 as bone grafts: a comparative study in rabbits. *Journal of Materials Science: Materials in Medicine*, *24* (2), 417-436.

(2) Julmi, S., Krüger, A. K., Waselau, A. C., Meyer-Lindenberg, A., Wriggers, P., Klose, C., & Maier, H. J. (2019). Processing and coating of open-pored absorbable magnesium-based bone implants. *Materials Science and Engineering: C*, *98*, 1073-1086.

Acknowledgement

Financial support of this study by the German Research Foundation under grants ME 1941/3-1 and MA 1175/52-1 is gratefully acknowledged.

PS1-04-100

Novel PVD and E-beam combination to create biomimetic porosity in ceramic thin film coatings

David M. Grant[1], Bryan W. Stuart[2], James W. Murray[1]

[1]University of Nottingham, Advanced Materials Research Group, Nottingham, GB; [2]University of Oxford, Department of Materials, Oxford, GB

Introduction

A new two-step methodology has been developed using low-energy (10 – 40 keV) high-current (10 – 25 kA) [1] pulsed electron beam irradiation (LHEB) to porosify hydroxyapatite (HA) thin film coatings which have been first deposited by Physical Vapour Deposition (PVD). PVD was chosen as the first step in the process and is suitable for the production of controllable coating layers due to its versatility in producing thin amorphous or crystalline films with highly adherent and customisable compositions and microstructures. LHEB irradiation causes melting of the first few microns depth of material and has typically been used to reduce roughness via melting of asperities however crater formation is sometimes an unwanted side effect of the technique, thought to be caused by sub-surface melt pools within the depth of the section. The melt pools have been theorised to nucleate at micro-irregularities including grain/phase boundaries or precipitates in the material, resulting in eruption through the surface, leaving a crater morphology behind [2]. Given the ability of the LHEB process to irradiate a large surface area (60 mm diameter), maintain its energy density at high angles to treat curved surfaces [3, 4], as well as take place within 2-4 µs [1], the technique was investigated here as a novel method of porosification in HA coatings for biomaterial applications.

Experimental Methods

Coatings were deposited on Ti6Al4V substrates 40 ± 2 mm from the target surface via a custom in-house designed magnetron sputtering rig [5]. The working gas was argon at 2.5 mTorr feedback via a mass flow controller and pressure controller and capacitive pressure transducer. The $Ca_2P_2O_7$ target was deposited by ion bombardment using a Radio Frequency (13.56 MHz) power supply with an 80 W deposition power. A Sodick PF32A EBM machine was used for the LHEB experiments. The irradiation process was carried out under argon at 0.05 Pa. Argon gas is used as the medium for plasma build up required for the electron generation and beam propagation. Bombardment of the high current electrons with a workpiece causes rapid heating and cooling at the near surface of the workpiece material. A range of cathode voltages, 13 to 29 kV, of energy density 0.2 to 10.5 Jm^{-2} and single pulses was used for irradiation tests.

Results and Discussion

The first step uniquely generated a crystalline HA surface using plasma assisted PVD sputtering from a crystalline Ca:P oxide target. The as deposited (AD) layer contained crystalline HA with c-axis orientation indicated by preferred alignment in the direction of the (002) plane located at 26° (2θ) [6]. A residual amorphous phase, commonly reported for sputtered HA films was not observed by XRD, however some local evidence was observed by SAED using TEM. The second step uses a new facile and rapid post treatment by a single shot pulsed large area electron irradiation technique[7]. Utilising LHEB with voltages from 13-29 kV led to the new discovery of a method to generate a complex interconnected porous layer based on osteoconductive α-TCP. Increase in voltage led to an increase in HA crysatllite size from 35 to 80 nm and reduction from 62 to 30 nm for α-TCP. Extent of porosity was shown to be controllable

via parameter control, with a maximum mass loss of 45% and increase in average/maximum pore sizes from 0.07–1.66/0.69–92.53 mm^2. Simultaneous dissociation of Ca led to a reduction in Ca:P ratio from 1.67 to 1.43, synonymous with HA and calcium deficient TCP phases, as well as incremental conversion of HA to α-TCP, irradiation voltage dependent, revealed via XRD and TEM, suggesting flash melting of the structure to above 1125 ºC based on phase transformation of Ca:P mixtures. A randomly oriented polycrystalline structure was seen in non-porous regions of the 25 kV irradiated coating, with no amorphous phase, with porous regions being highly amorphous suggesting rapid cooling. Severe porosity originated from the interface between maximum electron penetration depth and unaffected material below, with expansion of pores towards the surface and breaking through to yield significant surface porosity. Correlation of porosity with electron acceleration voltage can be explained by the increased penetration depth, thereby giving more lateral expansion of material prior to surface break-through.

Conclusion

This new two step methodology can be readily applied to most metallic surfaces, with the additional advantage that selected areas can be single shot pulsed by LHEB allowing regions to be untreated. This is ideal for implants such as hip stems where full integration is not required otherwise implant recovery causes damage. Insensitivity of the LHEB process to large incident angles also makes the process suited to complex shapes. Thus the manufactured porosity and ability to manipulate crystallinity of Ca:P thin films by a combination of PVD and LHEB shows great potential to produce surface scaffold-like coatings on orthopaedic implants as a suitable layer for bone integration.

References

[1] Ozur, G.E. and D.I. Proskurovsky, *Generation of Low-Energy High-Current Electron Beams in Plasma-Anode Electron Guns.* Plasma Physics Reports, 2018. **44**(1): p. 18-39.

[2] Zhang, K., et al., *Formation and evolution of craters in carbon steels during low-energy high-current pulsed electron-beam treatment.* Journal of Vacuum Science & Technology A: Vacuum, Surfaces, and Films, 2009. **27**(5): p. 1217-1226.

[3] Uno, Y., et al., *A new polishing method of metal mold with large-area electron beam irradiation.* Journal of Materials Processing Technology, 2007. **187-188**(0): p. 77-80.

[4] Aramesh, M., et al., *Superplastic nanoscale pore shaping by ion irradiation.* Nature communications, 2018. **9**(1): p. 835.

[5] Stuart, B.W., et al., *Mechanical, structural and dissolution properties of heat treated thin-film phosphate based glasses.* Applied Surface Science, 2017. **416**: p. 605-617.

[6] Stan, G., *Adherent functional graded hydroxylapatite coatings produced by sputtering deposition techniques.* Journal of optoelectronics and advanced materials, 2009. **11**(8): p. 1132-1138.

[7] Stuart BW, Murray JW, Grant DM. *Two step porosification of biomimetic thin-film hydroxyapatite/alpha-tri calcium phosphate coatings by pulsed electron beam irradiation*. Scientific Reports. 2018. 8(1): 14530

Acknowledgement

This work was supported by the Engineering and Physical Sciences Research Council [grant number EP/K029592/1] via the Centre for Innovative Manufacturing in Medical Devices (MeDe Innovation). We would also like to acknowledge Dr. Chris Parmenter and Dr. Mike Fay for their assistance in FIB lift out and TEM at the Nanoscale and Microscale Research Centre (NMRC), University of Nottingham.

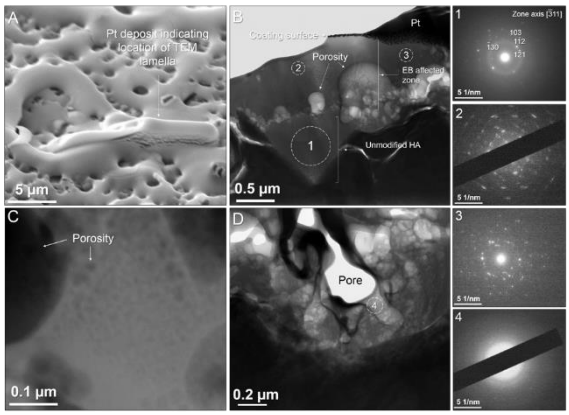

Figure 2 TEM of 25 kV, 1 shot electron irradiated coating.
(A) Location of FIB lift out lamella extraction (B) Dark-field STEM image of high magnification porosity. (C and D) Bright-field STEM image of complete coating section and magnified porous region. SAED patterns were acquired at locations 1-4.

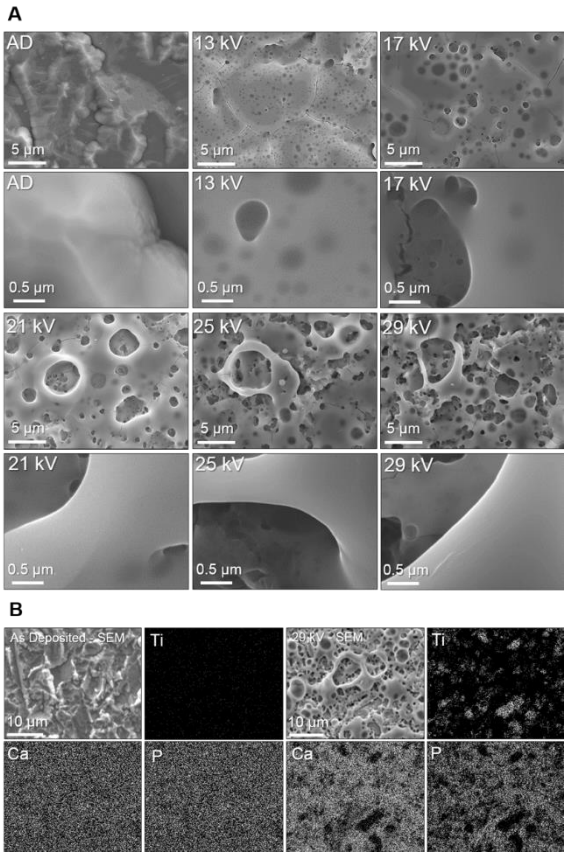

Figure 1 SEM and elemental mapping of AD and electron irradiated samples
(A) SEM of AD and electron irradiated samples displaying an increase in porosity with irradiation voltage. By 13 kV closed porosity was observed within the irradiated layer. (B) Elemental mapping of AD and 29 kV electron irradiated samples, showing homogenous distributed of Ca/P throughout the coatings pre and post irradiation. 29 kV partially removed complete coating sections as indicated by areas of Ti, corresponding to absence of Ca/P.

PS1-04-101

Examination of the immunogenicity of cell-free human growth factor preparations from platelet concentrates after single application in mice

Uwe Walschus[1], Andreas Hoene[1], Cornelia Prinz[2], Hans-Georg Neumann[2], Kirsten Peters[3], Michael Schlosser[1]

[1]University Medical Center Greifswald, Department of Surgery, Greifswald, DE; [2]DOT GmbH, Rostock, DE; [3]University Medical Center Rostock, Department of Cell Biology, Rostock, DE

Introduction

Platelet concentrates are derived from donated blood for treatment of patients with low platelet numbers or platelet dysfunction. However, their shelf-life for this application is limited to 5 days. Platelets are known to be rich in various growth factors, and autologous platelet-rich plasma is used for various applications in regenerative medicine. Expired platelet concentrates might thus be a source for production of cell-free human growth factor (hGF) preparations. These could be used for coating or impregnation of biomaterials to improve implant in growth or to treat chronic wounds, soft tissue injuries or burns. As the immune response is an important aspect for the biocompatibility of biologically derived biomaterials, the aim of the present study was to evaluate the immunogenicity of two different hGF preparations derived from discarded platelet concentrates after single application in mice by detection of hGF-specific IgG and IgM antibodies.

Experimental Methods

Two hGF preparations (DOT GmbH, Rostock, Germany) from different production batches (170110 vs. 180425; both supplied as gamma sterilized lyophilisates, 5 mg) were used to immunize female Balb/c mice (n=4 mice/ batch). Immunization was performed by a single intraperitoneal dose of 100 µg hGF mix in 100 µl sterile PBS without adjuvant, while control mice (n=2) received PBS only. Blood was drawn before and weekly until day 42 after immunization. Diluted serum samples (1/100, 1/200, 1/400) were examined for hGF-specific IgG or IgM antibodies by enzyme-linked immunosorbent assays using microtiter plates coated with respective hGF mix (5 µg/ml, 50 µl/well, overnight at 4 °C). Bound IgG/ IgM was detected with HRP-labelled anti-mouse IgG- or IgM-specific antibody and 3,3',5,5'-Tetramethylbenzidine as colorimetric substrate.

Results and Discussion

All 4 mice immunized with batch 170110 were found to be positive for hGF-specific IgG, with the IgG response starting from day 14 and increasing until day 42. In contrast, only 2 of the 4 mice which received batch 180425 developed hGF-specific IgG antibodies. Furthermore, the IgG response against batch 180425 for the 2 positive mice was weaker than for batch 170110. For both batches, hGF-specific antibodies were detectable in all examined serum dilutions, with concentrations declining accordingly with increasing dilution levels. For the IgM response, only a slight increase on day 7 for batch 180425 was found while those mice immunized with bath 170110 had no detectable IgM response. Both control mice remained negative for hGF-specific IgG and IgM antibodies over the whole study period. The composition of both hGF batches varied regarding several examined growth factors, with a more than fourfold higher IGF-I concentration in batch 170110 (203 pg/ml) vs. 180425 (46 pg/ml) as the most pronounced difference.

Conclusion

Overall, the immunogenicity of the two examined hGF preparations produced from platelet concentrates was remarkably different. A possible explanation might be the variations in the content of different growth factors revealed by analysis of the composition of these preparations, most notably for the IgF-I cocentration. However, potential consequences for the clinical application of these hGF preparations and/or their production process remain to be seen. For example, standardizing or adjusting the examined growth factor concentrations between different production batches, for example by pooling of preparations prior to final lyophilization, might help to reduce such differences.

Acknowledgement

This study was supported by the Ministry of Economics, Employment and Health of the state government of Mecklenburg-Vorpommern with funds from the European Regional Development Fund of the European Union.

PS1-04-102

The attachment and conformation of BSA controlled by PAMAM-NH_2/-COOH and the thermodynamic interaction between PAMAM and BSA

Li Li, Gai X. Peng, Ying J. Chen

Southwest Jiaotong University, Key Laboratory of Advanced Technologies of Materials, Ministry of Education, Chengdu, CN

Introduction

Polyamidoamine(PAMAM) dendrimers are well-defined, regularly branched macromolecules with particular advantages, including nanoscale 3D spherical architecture, multivalent bonding surface with tailoring possibility of biological or chemical property, as well as intramolecular cavity serving as a host-molecule encapsulation[1-5]. In this study, PAMAM dendrimers with different terminal groups are utilized to guide surface group effects, generating proteins response. Subsequently, protein absorption behavior and conformation would be researched. Meanwhile, the thermodynamic interaction between BSA and PAMAM will be discussed.

Experimental Methods

The polyamide (PAMAM) molecules with different terminal groups were introduced onto the surface of the Titanium materials by electrostatic interaction and covalent bonding. Studying protein absorption behavior and conformation change (by absorption protein quantification and ATR) can reveal the surface groups effects induced by PAMAM with unlike outer groups. Furthermore, by fluorescence spectra, the thermodynamic parameters for interaction between BSA and PAMAM can be calculated.

Results and Discussion

Fig. 1A exposed general trend that relatively more protein adhesion absorbed on the -COOH surface comparing with -NH_2 surface. In addition, increasing BSA attachment on the complete PAMAM-NH_2 or PAMAM-COOH surface will be accompanied by the increase of the -NH_2 or -COOH groups. Fig. 1B demonstrated that the conformation of BSA absorbed onto different surface would change, and BSA tended to increase degree of disorder with the declining of αhelix and climbing ofβsheet andβturns, overall.

Fig. 2 shows that fluorescence intensity gradually decreased with the increase of PAMAM concentrate. Moreover, the thermodynamic parameters for interaction between BSA and PAMAM were calculated by fluorescence spectra, which uncovered that the reaction of BSA with PAMAM was a spontaneous process ($\Delta G < 0$). For interaction of BSA and PAMAM-COOH and PAMAM-NH_2, the driving force is hydrophobic and H-bonding with $\Delta H < 0$ and $\Delta S > 0$.

Conclusion

Given the effects of the surface groups caused by terminal groups of PAMAM on protein behavior, generally, it can be concluded that different surface groups will result in different absorbed protein amount (-COOH › -NH_2) and conformation change （ascending degree of disorder）. Finally, PAMAM can interact with BSA spontaneously.

References

1. Kesharwani P, Jain K, Jain N K. Progress in Polymer Science, 2014, 39(2): 268-307.
2. Yang J, Zhang Q, Chang H, et al. Chemical reviews, 2015, 115(11): 5274-5300.
3. Kesharwani P, Iyer A K, Drug discovery today, 2015, 20(5): 536-547.
4. Chen W, Li W, et al. Journal of Biomedical Materials Research Part A, 2018, 106(3): 706-717.
5. Kim Y, Park E J, Na D H. Archives of pharmacalresearch, 2018: 1-12.

Acknowledgement

The authors gratefully acknowledge the financial support of National Natural Science Foundation of China (31870955#) .

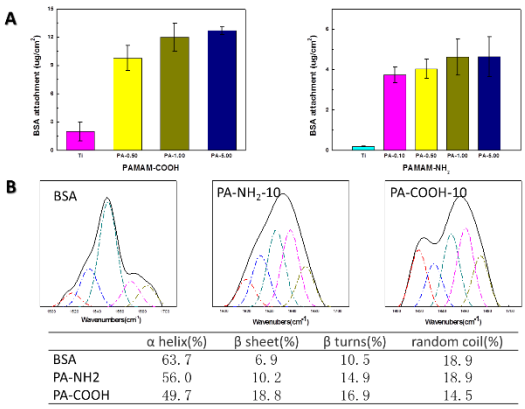

	α helix(%)	β sheet(%)	β turns(%)	random coil(%)
BSA	63. 7	6. 9	10. 5	18. 9
PA-NH2	56. 0	10. 2	14. 9	18. 9
PA-COOH	49. 7	18. 8	16. 9	14. 5

The effect of two kinds of PAMAM on BSA attachment (A); The BSA conformation change (B)

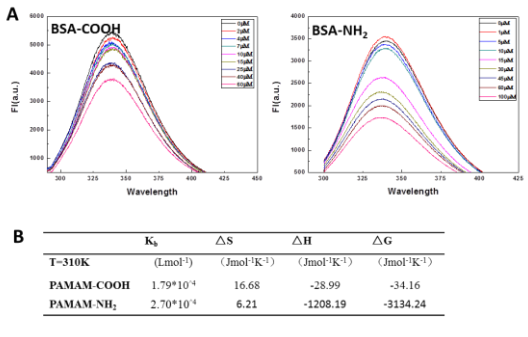

T=310K	K_b (Lmol⁻¹)	△S (Jmol⁻¹K⁻¹)	△H (Jmol⁻¹K⁻¹)	△G (Jmol⁻¹K⁻¹)
PAMAM-COOH	1.79*10⁻⁴	16.68	-28.99	-34.16
PAMAM-NH2	2.70*10⁻⁴	6.21	-1208.19	-3134.24

The fluorescence spectra (A) and thermodynamic parameters(B) for interaction between BSA and PAMAM

PS1-04-103

Regulation of cell adhesive behaviour by surface-modified polymer coat with photocleavable RGDS peptide

Naoki Hokazono[1], Nana Momoi[3], Shinnosuke Nishimura[3], Koji Yamamoto[2], Tomoyuki Koga[4], Eiji Nakamachi[2], Yusuke Morita[2]

[1]Doshisha University, Graduate School of Life and Medical Sciences, Kyotanabe, JP; [2]Doshisha University, Department of Biomedical Engineering, Kyotanabe, JP; [3]Doshisha University, Graduate School of Science and Engineering, Kyotanabe, JP; [4]Doshisha University, Department of Molecular Chemistry & Biochemistry, Kyotanabe, JP

Introduction

It is important to improve cell adhesive property of the scaffold surface in tissue regeneration, because cell adhesion is related to cell proliferation, migration, aggregation and differentiation in regeneration process. Since RGDS is a cell adhesion domain in extracellular matrix, RGDS coating is effective to improve the cell adhesive property of the scaffold surface. It was reported that adhesion and proliferation of MC3T3-E1 are promoted by RGDS coating[1]. However, it is difficult to regulate the RGDS quantity and distribution in a conventional RGDS coating. Gradient of a RGDS quantity is expected to promote cell migration and aggregation in addition to cell adhesion and proliferation. Moreover it is required to evaluate the RGDS amount after regulating the RGDS quantity and distribution. The purpose of this study was to develop a surface treatment technique which can regulate the RGDS amount with the UV irradiation and visualize RGDS distribution with the fluorescent observation.

Experimental Methods

Materials: Copolymer composed of styrene and maleic anhydride was dissolved in THF (SEMA solution). Polystyrene was dissolved in THF (PS solution). SEMA solution and PS solution were blended to regulate strength of polymer film. Ratio of SEMA solution/PS solution were 75/25, 50/50 and 25/75. The polymer films were produced on the glass slides (10×10 mm) from polymer solutions by using a spin coater. RGDS peptide which a photolytic molecule was bound to RGDS coupling fluorescent dye was prepared. The glass slides with the polymer films were immersed in RGDS peptide solution to bound RGDS peptide to surface of the polymer film (RGDS-bounded films: SEMA/PS(75/25)-RGDS, SEMA/PS(50/50)-RGDS and SEMA/PS(25/75)-RGDS films).

Regulation of RGDS amount by UV irradiation: UV was irradiated to the RGDS-bounded films for 360 minutes. The amount of RGDS and Luminance value on the film measured by FTIR analysis, UV-vis spectrum measurement and fluorescence intensity measurement at 0, 60, 120, 180, 240, and 360 minutes after UV irradiation.

Evaluation of cell adhesion: UV was irradiated to the different SEMA/PS(75/25)-RGDS films for 0, 60 and 120 minutes. Polymer film without RGDS (SEMA/PS(75/25) films) was prepared as control. Frames (inside diameter: 8×8 mm, height: 5 mm) made of polycarbonate were attached on the polymer film without RGDS and each RGDS-bounded film. Osteoblasts-like cells (MC3T3-E1) were seeded at 1.0×10^4cells/cm^2 in a serum-free Alpha MEM medium, and then the MC3T3-E1 cells were cultured for 6 hours. After cultivation, the number of adherent cells was evaluated by the absorbance of Cell Counting Kit-8.

Results and Discussion

Figure 1 shows relation between luminance value and RGDS quantity on each RGDS-bounded film. Since the RGDS amount and the luminance value decreased with increasing of the UV irradiation time, the RGDS amount on the film

could be evaluate by luminance value. It is considered that SEMA/PS(75/25)-RGDS film was optimal to regulate cell adhesion because initial amount of RGDS and range of regulated RGDS amount for SEMA/PS(75/25)-RGDS film was highest. Figure 2 shows results of evaluation of adherent cell for SEMA/PS(75/25)-RGDS film after 6 hours cultivation. Since the number of adherent cells decreased with increasing of the UV irradiation time, cell adhesive property was controlled by regulating RGDS amount. These results showed that developed surface modification could regulate the cell adhesive behavior on the surface of polymer film.

Conclusion

We developed a surface modification technique that could adjust the amount of RGDS by UV irradiation and evaluate RGDS amount by luminance value. It was expected that cell adhesive behavior could be controlled by regulating the amount of RGDS on the material surface.

References

1. Pramono, S., et al , Journal of Dental sciences, 11: 427-436, 2016.

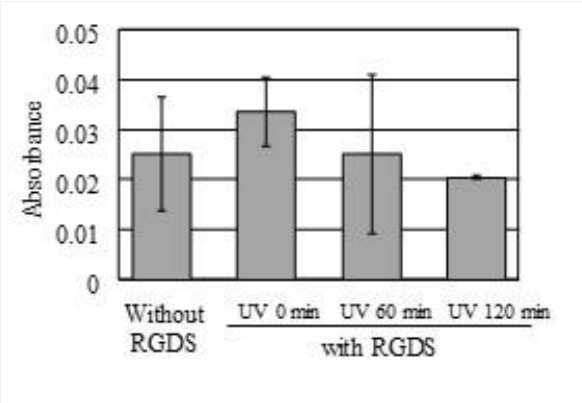

Figure 2
Absorbance of adherent cells on SEMA/PS(75/25)-RGDS
(N=3, Mean±S.D.).

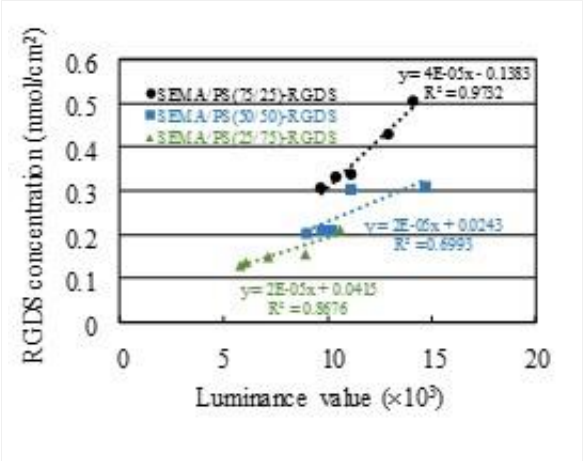

Figure 1
Relation between luminance value and RGDS concentration (N=1).

PS1-04-104

Characterization of apatite coatings on titanium: A TOF-SIMS and goniometry -based study

Daniel Romero-Guzmán[1,2,3], Verónica Luque-Agudo[1,2,3], Margarita Hierro-Oliva[2,1,3], Amparo M. Gallardo-Moreno[1,2,3], M. Luisa González-Martín[1,2,3]

[1]University of Extremadura, Department of Applied Physics, Badajoz, ES; [2]Networking Research Center on Bioengineering, Biomaterials and Nanomedicine (CIBER-BBN), Badajoz, ES; [3]University Institute of Biosanitary Research of Extremadura (iNube), Badajoz, ES

Introduction

The apatite ($Ca_5(PO_4)_3(F,Cl,OH)$) is considered a good ceramic biomaterial in the field of medicine[1]. Apatite is used as a coating of metallic materials such as titanium to improve the biocompatibility with bone tissue. Therefore, it is necessary to study the effects of different types of apatite according to composition, OH orientation, layer thickness, etc. In this study, time of flight secondary ion mass spectrometry (TOF-SIMS) is used to characterize four different processes to manufacture the apatite layer in titanium. Also, we analyse their effect in the wettability and the surface tension with contact angle measurements.

Experimental Methods

The samples have been manufactured through a sputtering process by the company Sidrabe (Rīga, LV-1073, Latvia). We analyzed four different conditions: two thin (800-900nm) films of hydroxyapatite (HAp) and chlorapatite (ClAp) and two thick (50µm) films of hydroxyapatite untreated (HAp-Untreated) and hydroxyapatite treated with a hydrothermal process[2] (HAp-Treated).

TOF-SIMS measurements were performed with a TOF-SIMS5 (ION TOF, Münster, Germany) equipped with a Bi_3^{++} primary ion source operated at 25 kV. The total ion dose used to acquire each spectrum was ~1 × 1012 ions/cm^2 to ensure static SIMS conditions with an analyzed area of 250 × 250 μm^2. Spectra were calibrated to the H^-, C^-, CH^-, O^-, OH^-, $C2^-$, $C3^-$, $C4^-$, $C5^-$, $C6^-$, $C7^-$ peaks before further analysis. The depth profile was recorded using a 1 kV Cs^+ sputter beam, which was rastered over a 300 µm × 300 µm area for acquisition times of 2500 s except for the HAp sample, the acquisition time was 1800 s. A pulsed low energy electron flood gun was used for charge neutralization. The secondary ion species analyzed were OH^-, P^-, CaO^-, Cl^-, TiO^- and Ti^-.

The surface tension and hydrophobicity were estimated from contact angle data. The measurements were carried out with a goniometer (Kruss GmbH) by the sessile drop method with two polar liquids: deionized water and formamide, and with an apolar liquid: diiodomethane. In the goniometry study, the values of contact angles are the average of at least nine drops on different points of the samples and reported with the standard deviation.

Results and Discussion

The TOF-SIMS surface analysis shows a different distribution of phosphate, hydroxide and chloride anions depending on the thickness of the apatite layer.

The thinner samples (800-900nm) have phosphate anions, in greater quantity, on top layers of the surface. On the other hand, for thicker samples (50 microns), the hydroxy group predominates on the surface.

The depth profiles check these results and show the distribution of OH^- and Cl^- in the apatite layer. In the ClAp film, chloride and hydroxide anions are located mainly in the interface of apatite and titanium oxide.

The hydrothermal process in the HAp thick layer produces a complete spread of the water droplets on such a surface. This effect is not shown in untreated HAp samples.

Conclusion

The thickness of the apatite layer influences the location of phosphate, hydroxide and chloride anions in this layer. On the other hand, the contact angle measurements show a possible orientation of the OHs for the thicker samples[2].

References

[1] Harun, W.S.W., Asri, R.I.M., Alias, J., Zulkifli, F.H., Kadirgama, K., Ghani, S.A.C., Shariffuddin, J.H.M. (2018). A comprehensive review of hydroxyapatite-based coatings adhesion on metallic biomaterials. Ceramics International, 44 (2), 1250–1268.

[2] Ubele, D., Pluduma, L., Gross, K.A., Viksna, A. (2018). Hydrothermal Processing for Increasing the Hydroxyl Ion Concentration in Hydroxyl Depleted Hydroxyapatite. Key Engineering Materials, 762, 42-57.

Acknowledgement

Financial support is acknowledged to the Spanish Junta de Extremadura and FEDER grants for the projects IB16117 and GR15089, and to the Ministerio de Economía y Competitividad for the project MAT2015-63974-C4-3-R y PCIN-2016-146. The TOF-SIMS has been performed by NANBIOSIS ICTS, more specifically by the Surface Characterization Unit of the Biomedical Networking Center (CIBER-BBN) and the SACSS- SAIUEx of the University of Extremadura (UEx).

PS1-04-105

Dynamic cholesterol layers minimize bioadhesion

Jens Friedrichs, Ralf Helbig, Lars D. Renner, Julia Hilsenbeck, Carsten Werner

Leibniz Institue of Polymer Research, Dresden, DE

Introduction

Biofouling –the undesired formation of biofilms on surfaces– is an omnipresent process with dramatic impact on human health and the global economy . The need for non-toxic, sustainable, broadly effective, and economically feasible antifouling surfaces motivates efforts to understand and mimic adhesion-minimizing design principles evolved by living nature. Recently, we explored springtails as a remarkable group of organisms with outstanding fouling-resistant properties . Springtails are soil-dwelling animals that rely on cutaneous respiration and thereby need to withstand both wetting and colonization by microorganisms to prevent suffocation . We showed that the cuticle of springtails consists of nanoscopic comb-like structures with overhanging cross-sectional profiles and uncovered that these nanoscopic structures effectively prevent wetting, even against low surface tension liquids, as well as bacterial colonization of the cuticle.

Experimental Methods

Based on the comprehensive analysis of the chemical composition of the cuticle lipids of springtails, we prepared spin-coated lipid multi-layers and self-assembled monolayers of selected compounds**,** extensively characterized their physiochemical properties and investigated their resistance to biofouling in defined *in vitro* experiments.

Results and Discussion

We found that multimolecular layers of one particular component –cholesterol– effectively resist protein adsorption and bacterial attachment and undergo two distinct time-dependent modes of rearrangement when exposed to aqueous solutions: (i) a fast, reversible reorientation of the topmost molecules within the initial 20 seconds of contact and (ii) a slow progressive, non-reversible, lateral expansion of crystalline domains within hours. The dynamics of the topmost molecules are temperature-dependent, persists upon bulk crystallization and is concluded to minimize the anchorage of proteins and bacteria. Mixed layers of cholesterol and adhesion-promoting substances also show adhesion-resistant properties.

Conclusion

Thus, coatings of cholesterol or synthetic, amphiphilic analogues may offer unprecedented options for the protection of surfaces against bio-adhesion.

PS1-04-106

Surface Modification of electrospun PLGA Microfibers by Using Cold Atmospheric Plasma: Effect of treatment distance and exposure time

Mohammad El Khatib[1], Valentina Russo[1], Ralf Wyrwa[2], Matthias Schnabelrauch[2], Barbara Barboni[1]

[1]University of Teramo, Faculty of Biosciences, and Agro-Food and Environmental Technologies, Teramo, IT;
[2]INNOVENT e.V. Technologieentwicklung, Department of Biomaterials, Jena, DE

Introduction

Plasma treatment has been widely applied to improve the hydrophilic properties of hydrophobic materials used in the field of tissue engineering, in particular for scaffold fabrication. The purpose of this treatment is to functionalize the scaffolds by generating polar groups on their surfaces without affecting the bulk whilst reducing their hydrophobic properties that could enhance cell adhesion and biocompatibility [1]. Our aim was to evaluate the effect of Cold Atmospheric Plasma (CAP) on physical and chemical properties of electrospun PLGA microfibers by varying the treatment distance and time.

Experimental Methods

PLGA scaffolds with aligned microfibers were prepared using the technique of electrospinning (E-Spinctronic, Eric Huber, Germany). These scaffolds were then activated with cold atmospheric nitrogen plasma by placing the nozzle of a Piezobrush® (PZ2) (Relyon Plasma, Germany) at two different distances of 1.3 and 1.7 cm over their surfaces for three different exposure times (30, 60, and 90 seconds). CAP treated PLGA scaffolds were evaluated by Scanning Electron Microscopy (SEM), Water Contact angle (WCA), Fourier Transform Infrared Spectroscopy (FT-IR), and Gel Permeation Chromatography (GPC). Mechanical properties of untreated and treated PLGA scaffolds in terms of Ultimate Tensile Strength (UTS, MPa) and Elongation at break (%) were also investigated. All data were obtained in triplicate and evaluated by Two-way ANOVA (p<0.05).

Results and Discussion

SEM images demonstrated that all analysed CAP treatments did not affect the morphology nor fiber diameter size (1.367 ± 0.023 µm) of the treated aligned PLGA scaffolds respect to the untreated ones (p>0.05). The contact angle in water diminished significantly in all PLGA treated groups comparing to those untreated (p<0.05). In particular, scaffolds' hydrophilicity increased significantly when the distance separating the PZ2 and the scaffold was 1.3 cm respect to 1.7cm (p<0.05) except for 90 seconds treatment (p>0.05). In addition, when the treatment time went from 30 to 90 seconds, scaffolds' hydrophilicity increased (p<0.05). No significant changes were observed by treating the scaffolds for 90 seconds from both treatment distances (p>0.05). FT-IR spectra did not display evidences that the CAP treatments modified the surface chemical composition of the PLGA microfibers. Indeed, this result could be explained by the very superficial changes occurring by CAP on the materials, thus, demonstrating that the variations produced by the surface treatment are easily diluted. In contrast, the average molecular weight of the PLGA microfibers increased significantly by prolonging plasma treatment time effectuated from a distance of 1.3 cm compared to untreated PLGA microfibers (p<0.05). Instead, when the treatment was done from a distance of 1.7 cm, the average molecular weight increased only in case of 90 seconds of exposure time (p<0.05). N_2plasma treated PLGA scaffolds showed a slight increase in the UTS values by prolonging plasma treatment time comparing to the untreated group (p>0.05). Interestingly, the elongation at break values showed the highest significant increase when

PLGA scaffolds were plasma treated for 60 seconds from both treatment distances compared to the untreated microfibers (p<0.05). Moreover, the elongation at break, compared to the untreated PLGA scaffolds was significantly higher after 30 and 90 seconds at a distance of 1.3 and 1.7 cm, respectively (p<0.0.5).

Conclusion

In conclusion, CAP treatments, at all treatment conditions, improved the hydrophilicity and surprisingly the elongation at break properties (at 60 seconds and from 1.3 cm) of PLGA electrospun scaffolds. Moreover, these treatments did not alter macroscopic nor microscopic architecture. Even though, cell adhesion and biocompatibility tests should be performed to confirm best CAP conditions to be used for future *in-vivo* applications.

References

[1] Justina et al., 2015, J. of Chem.

Acknowledgement

This research is funded by the Italian Ministry of Instruction, University, and Research under the national project PON ricerca e innovazione 2014-2020.

PS1-04-107

How can live cell nanomorphology help to unveil osteoblast adhesion properties?

Christian Völkner[1], Regina Lange[1], Martina Grüning[2], Katja Fricke[3], Issam Assi[1], Ingo Barke[1], Barbara Nebe[2], Sylvia Speller[1]

[1]University of Rostock, Institute of Physics, Rostock, DE; [2]University Medical Center Rostock, Department of Cell Biology, Rostock, DE; [3]University of Greifswald, Leibniz Institute for Plasma Science & Technology, Greifswald, DE

Introduction

The specific properties of material surfaces and the resulting interaction with osteoblastic cells are crucial for osseointegration of surface modified bone implants. However it still remains unclear how surface charges and the resulting electric field at the interface influences cellular adhesion and migration. To identify relevant parameters we investigate the nanomorphology at the apical membrane especially at the migration fronts of osteoblasts adhered on several structured material surfaces.

Experimental Methods

To get to know nanomorphological parameters for cellular adhesion attractiveness we use plasma polymerized allylamine coated borosilicate glass and bare borosilicate glass as substrates.Human MG-63 cells (ATCC®) are cultured on the different surfaces in Dulbecco's Modified Eagle's Medium with 10% fetal calf serum. After 3h the cells were fixed with 4% Paraformaldehyde (PFA) if applicable.

To investigate cellular nanomorphological changes we use a scanning probe method called scanning ion conductance microscopy (SICM). A nanopipette with opening diameters of less than 100nm acts as a probe. Two biased AgCl electrodes are located in the pipette and in the cell surrounding bath. The resulting ion current serves as feedback signal to keep the local separation between probe and sample constant while laterally scanning the cell surface [1]. The feedback loop can also be transiently disabled to acquire local spectra, e.g. on the membrane fluctuations or to address electro-kinetic effects.

Results and Discussion

The experiments reveal that the cell surfaces exhibits dynamic membrane protrusions extending several hundred nanometers. They resemble ruffles [2], which have been associated with processes of macropinocytosis and motility. We observe ruffles of dorsal as well as peripheral type. They may serve as membrane storage and shuffling necessary in the course of spreading and migration on the surface. Such leaf-like membrane protrusions come along with strong fluctuations. On surfaces containing amines cell adhesion is observed to be faster than on glass [3]. Comparison of osteoblasts on glass versus amine covered surfaces yields diminished effective surface areas and fluctuation amplitudes on the latter. This could suggest that on the amine covered surface more membrane ruffles have been expanded to adopt a more spreaded shape. At the rim of the lamellipodia characteristic heights between 100 nm and a few 100 nm are observed. Besides the height of the cleft between substrate and basal cell membrane such heights include however the lamellipodium height itself. Away from lamellipodium positions, for instance at rear positions, high cell edges up to 1 um are observed. This indicates the extension of the cleft between the cell and the substrate in the periphery is highly variable, compatible with localized adhesion and membrane activities.

Conclusion

MG-63 osteoblasts show plasma membrane protrusions, so called ruffles. We observe ruffles of dorsal as well as peripheral type. Both types of ruffles vanish partly at cell rims on adhesion promoting substrates, leading to smoother edges.

References

[1] Chen et al, Annu. Rev. Anal. Chem. 5, 207 (2012)
[2] Chhabra et al., Nature Cell Biol. 9, 1110 (2007)
[3] Rebl et al., Acta Biomat 8, 3840 (2012)

Acknowledgement

This research was supported by the German Research Foundation (Deutsche Forschungsgemeinschaft, DFG) within the Collaborative Research Centre 1270 ELAINE.

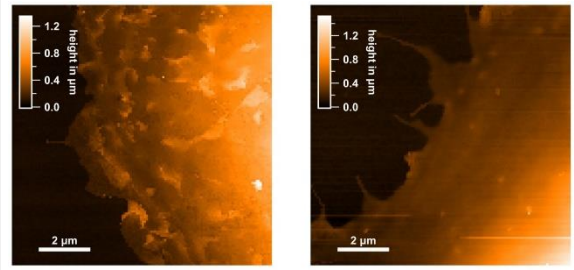

Comparison of the Membrane Nanomorphology at Cell Edges

SICM topography images of two different Osteoblasts on a glass cover slip (left image) & on plasma polymerized allylamine (PPAAm) coated glass (right image), cells adhered 3h prior to fixation via 4% paraformaldehyde. The plasma membrane at cells on PPAAm exhibits less dorsal ruffles compared to the cells seeded on glass. The ruffles are also visible in the live state, however the determination of the effective surface area is more accurate with fixation.

PS1-04-108

On-demand antimicrobial coatings to combat water contamination and safeguard healthcare environments

Andre Ruland, **Melissa K. Sikosana**, Carsten Werner

Leibniz-Institut für Polymerforschung Dresden e.V, Institute of Biofunctional Polymer Materials, Dresden, DE

Introduction

Biofilm-related infections attributable to unsafe water and vulnerable healthcare environments remain a global public health concern. Antimicrobial coatings revolutionise how society combats bacterial colonization. However, current strategies are unilateral and focus on either permanent drug conjugation or diffusion-limited systems. To overcome the resulting performance limitations, we introduce a *in situ* renewable, bio-responsive antimicrobial coating. The approach relies on the design of water-soluble but effectively absorbable, partially hydrophobic 'anchor' polymers, tethered to enzymatically cleavable peptide-drug conjugates.

Experimental Methods

Fabrication: Using 'click-chemistry', a bacterial protease-cleavable peptide linker is conjugated to various biocides including trusted antiseptics (e.g. hexetidine), antimicrobial peptides and antibiotics. The conjugates are then tethered to an anchor copolymer via Michael-Type Addition.

Enzyme - cleavable toolbox: The cleavage response of peptide sequences susceptible to specific, extracellular bacterial proteases (such as Elastases and Collagenases) were tested against four bacteria isolates under realistic conditions.

Coating characterization: The formation, structure and stability of the adsorbed polymer conjugates was analysed by quartz microbalance (QCM), AFM and time of flight secondary ion mass spectrometry (ToF SIMS). Further characterizations will include *in situ* ellipsometry.

Antibacterial performance: The coatings were tested on Polystyrene (PS) and Polyethylene (PE) materials using an optical density-based test [1] and a modified live/dead assay with a range of bacterial cultures under various nutrient conditions.

Results and Discussion

Proving the feasibility of the explored approach, the viability of *E. coli* and *S. aureus* were found to be drastically reduced after 8 hours exposure to hexetidine-containing coatings under tap water culture conditions.

Conclusion

The reported results suggest that absorbable, auto-regulative polymer coatings could allow for the adaptive administration of a broad spectrum of antimicrobial compounds. The approach is expected to maximize efficacy while mitigating both cost and environmental harm.

References

[1] Cado G et.al (2016) Self-defensive biomaterial coating against bacteria and yeasts: polysaccharide multilayer film embedded with antimicrobial peptide. Adv. Functional Materials 23: 38 4801-48

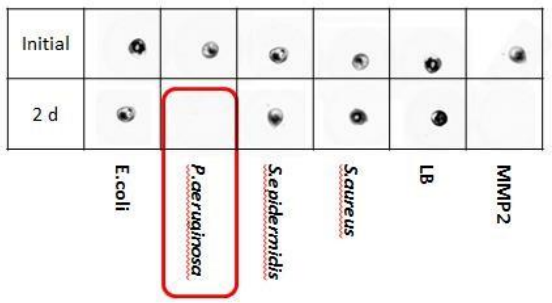

Bacterial protease cleavage assay

Bacterial protease cleavage assay: Proof of degradation by P.aeruginosa using polymer networks containing cleavable peptide-linkers + antimicrobials

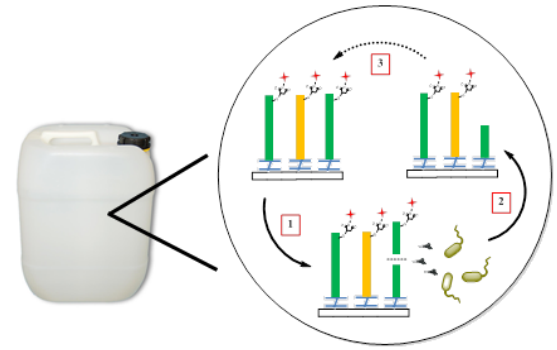

Bio-resposnive coating

Bio-responsive, antibacterial coating to protect surfaces in aqueous environments

PS1-04-109

Covalent immobilization and multilayer formation of glycosaminoglycans and their anti-inflammatory mechanism of action

Hala Alkhoury[1], Adrian Hautmann[1], Frank Erdmann[2], Thomas Groth[1]

[1]Martin Luther University, Institute of Pharmacy, Biomedical Materials Department., Halle (Saale), DE; [2]Martin Luther University, Institute of Pharmacy, Pharmaceutical Biology and Pharmacology Department., Halle (Saale), DE

Introduction

Biomaterial implants are targeted to improve the patient's quality of life. However, the implantation process and the biomaterial itself can initiate an inflammatory cascade comprising injury followed by blood-material interaction, which can lead to serum protein adsorption, acute and chronic inflammation, formation of granulation tissue, foreign body response (FBR) and eventually fibrous encapsulation. Thus, Surface modification may prevent opsonization of biomaterials and suppress this undesirable effect. Macrophages represent key players in orchestrating inflammation related to release of pro-inflammatory cytokines, which synthesis is dependent on nuclear transcription factor-κB (NF-κB) signaling pathways. Glycosaminoglycans (GAGs) like heparin (HEP) and high molecular weight hyaluronic acid (HA) possess a valuable anti-inflammatory potential related to the inhibition of NF-κB signalling and transcription. Hence, we used here HEP and HA as biomaterials coating in order to control the inflammatory processes by studying their effects on macrophages.

Experimental Methods

GAGs were covalently immobilized on amino-terminated glass surfaces or physically adsorbed as multilayer system in combination with chitosan (Chi) using the layer-by-layer (LBL) technique. The surface topography as well as the wetting properties were characterized by scanning electron microscopy (SEM) and water contact angle (WCA) measurements. Macrophages were used to examine the anti-inflammatory potential in terms of adhesion and formation of multinucleated foreign body cells (FBGC). Further, western blotting (WB) was applied to study the NF-κB activation. While, the internalisation of Fluorescein isothiocyanate (FITC)-labelled GAGs and NF-κB content in macrophages were studied by immunofluorescence (IF) microscopy and flowcytometry.

Results and Discussion

WCA showed increased wettability of GAGs-coated surfaces, which depicts the successful immobilization of HEP and HA. The multilayer coatings expressed a higher potential in reducing macrophage adhesion and FBGC formation on the GAGs-coated surfaces in comparison to the positive controls. In addition, IF staining as well as the flow cytometry indicated that FITC-labelled GAGs were internalized by macrophages which seeded on the Hep and HA-modified samples in which it illustrates one mechanism of anti-inflammatory action. Studies with WB together with IF staining of p65 showed also effects on the phosphorylated and non-phosphorylated forms of NF-κB that are related to inhibition of macrophage activation by GAGs. The aforementioned results proved the anti-inflammatory mechanism of action of GAGs by suppressing the NF-κB transcription factor together with their wettability due to the sulphate and carboxylic groups found in the backbone structure of both Hep and HA, respectively.

Conclusion

Overall, both immobilization techniques show promising results regarding anti-inflammatory activity, which make them interesting for future applications on medical implant materials to avoid fibrosis.

Acknowledgement

This work was financially supported by the German Academic Exchange Service (DAAD).

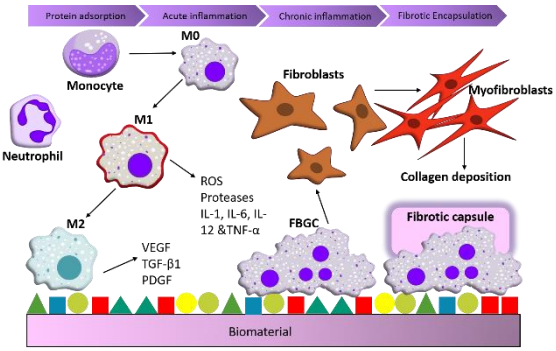

Host responses to implanted biomaterials

PS1-04-110

Importance of friction in dental implant wear

Fabio Alemanno[1], Davide Olivero[2], Silvia Maria Spriano[3], Deepak H. Veeregowda[1]

[1]1Global Applications Team, Ducom Instruments Europe B.V., Groningen, NL; [2]Politecnico di Torino, Turin, IT; [3]Department of Applied Science and Technology, Politecnico di Torino, Turin, IT

Introduction

Wear of dental implants materials is the primary reason for infection and revision surgery. Friction is a precursor to wear. Any attempt to mitigate dental wear should have an insight to friction characteristics of dental materials. This study elucidates the friction behavior of dental materials and its relationship with wear.

Experimental Methods

Dental implant materials used in this friction and wear study were titanium alloy (Ti-6Al-4V), titanium alloy protected with diamond-like carbon coating (DLC) and yttria-stabilized zirconia (3Y-TZP).

These materials were subjected to friction and wear test under physiological chewing loads in Ducom Biotribometer and microscale fretting tests in Ducom Microforce tribometer. In all the test conditions, the 3Y-TZP ball was the top specimen and Ti-6Al-4V and DLC were bottom specimens. Optical microscopy was used to quantify the wear of dental materials, post friction test.

Results and Discussion

Under physiological load condition, an increase in friction translated in an increase in wear, for Ti-6Al-4V (Figure 1). DLC protective coating reduced the friction for Ti-6Al-4V by more than 80%. As a result, the wear of Ti-6Al-4V dropped 99%. It shows that friction has a predominant influence on wear. Fine details about these friction characteristics were revealed during the stick-slip process in fretting tests (Figure 2). DLC protective coating triggered an early transition to slip compared to Ti-6Al-4V, preventing accumulation of strain energy and wear.

Conclusion

Friction has a direct influence on wear of dental materials. DLC coating protects Ti-6Al-4V against wear due to its low friction behavior attributed to an early stage transition to slip.

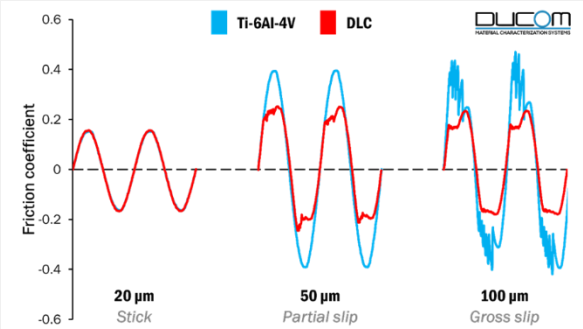

Figure 2. Fretting friction signature of a zirconia ball over Ti-6Al-4V and DLC at different stroke lengths, measured with Ducom Microforce.

Figure 2
Fretting friction signature of a zirconia ball over Ti-6Al-4V and DLC at different stroke lengths, measured with Ducom Microforce.

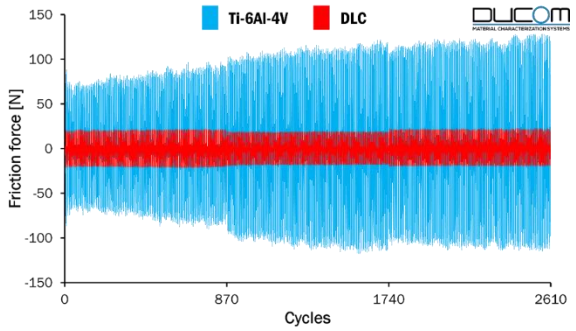

Figure 1. Evolution of friction force over the test cycles of a zirconia ball over Ti-6Al-4V and DLC obtained with Ducom Biotribometer.

Figure 1
Evolution of friction force over the test cycles of a zirconia ball over Ti-6Al-4V and DLC obtained with Ducom Biotribometer.

PS1-04-111

Novel multifunctional thioether-polyglycidol coating with broad biofunctionalization capacity for metal nanoparticles

Johanna Lutz[1], Susanne Feineis[1], Anja M. Steiner[2], Andreas Fery[2], Krystyna Albrecht[1], Jürgen Groll[1]

[1]University of Würzburg, Department and Chair of Functional Materials in Medicine and Dentistry, Würzburg, DE; [2]University of Dresden, Leibniz Institute for Polymer Research Dresden, Institute for Physical Chemistry and Polymer Physics, Dresden, DE

Introduction

Thiofunctional polymers, especially thiol-terminated terminated poly(ethylene glycol) (PEG-SH) are the established standard for the coating and biofunctionalization of metal nanoparticles as gold (AuNPs) and silver nanoparticles (AgNPs). However, the highly nucleophilic and oxidative character of thiols limits the possibilities introducing functional groups and provokes polymeric crosslinking.

We have thus examined whether thioether may be used as alternative to thiols for stabilizing gold and silver colloids. Here we present a systematic comparison of PEG-SH and PEG-thioether (PEG-SR) with multifunctional analogs, linear polyglycidol (PG) with multiple thiols (PG-SH) or ethylthioether (PG-SR) as coating system for AuNPs[1] and AgNPs. In addition, we show the applicability of such a coating for silver nanocubes (AgNCs).[2]

Experimental Methods

The polymers were synthesized by thiol-ene reaction according to literature.[1,3]

AuNPs, AgNPs and AgNCs were functionalized with thiol and thioether polymers via ligand exchange reaction by adding a polymeric solution and incubation overnight at room temperature. After purification by centrifugation, the colloidal and cubic solutions were analyzed by UV-Vis, dynamic light scattering (DLS) and zeta potential measurements.

To determine the colloidal stability in percent, the absorbance values at a wavelength of 530 nm (AuNPS) respectively 410 nm (AgNPs) obtained by UV-Vis before (mean 100 %) and after centrifugation, high temperatures, freeze-drying as well as treatment with Phosphate buffered saline (PBS) and Dulbecco's Modified Eagle cell culture medium (DMEM) were situated in relation.

Results and Discussion

Our systematic investigations on modified AuNPs display that neither successive centrifugation cycles, no exposure to high temperatures had a significant impact on the stability, independently of polymer coating and particle size. However, thioether functionalized AuNPs featured better colloidal stability against lyophilization and treatment with ions and proteins than thiol analogs, indicating a thermodynamically stronger adsorption of thioethers.

In addition, for the coated AgNPs it is shown that the chemically inert thioether-polymers exhibit same or even better stabilization than thiols, however there is nearly no differences after coating with monovalent or multivalent thioether polymers.

Furthermore, the non-nucleophilic and non-oxidative character of thioether moieties provides the introduction of any functional mercaptan compound to allyl groups of the PG-SR backbone via thiol-ene click reaction.[3] In this manner a library of multifunctional PG-SR for AuNP coating was generated, featuring functionalities, such as charged

moieties[4], biotin and diazirine moieties that can be used as generic tool for covalent immobilization of bioactive molecules.
Finally, it was possible attaching PEG-SR and PG-SR to the surface of the NCs resulting in steric stabilization, while the addition of thiol-polymers leads to aggregation.

Conclusion

We show that thioether modification, especially the multivalent PG-SR displays outstanding colloidal stability after exposure to different conditions relevant for biomedical application, such as freeze-drying and treatment under physiological conditions. Furthermore, biological functions can be introduced in the chemical inert PG-SR. The combination of the excellent stabilization efficacy as well as the possibility of chemical functionalization, makes multivalent thioethers a most promising new coating platform for metal NPs.

References

[1] S. Feineis, J. Lutz, L. Heffele, E. Endl, K. Albrecht, J. Groll, *Adv. Mater.*, **2018**, 1704972.
[2] M. Mayer, A. M. Steiner, F. Röder, P. Formanek. T. A. F. König, A. Fery, *Angew. Chem. Int. Ed.*, **2017**, *56*, 15866-15870.
[3] S. Stichler, T. Jungts, M. Schamel, I. Zilkowski, M. Kuhlmann, T. Böck, T. Blunk, J. Teßmar, J. Groll, *Ann. Biomed. Eng.*, **2017**, *45*, 273.
[4] B. Baumann, T. Jungst, S. Stichler, S. Feineis, O. Wiltschka, M. Kuhlmann, M. Lindén, J. Groll, *Angew. Chem. Int. Ed.*, **2017**, *56*, 4623.

Acknowledgement

The research leading to these results was financially supported by the German Federal Ministry of Education and Research (BMBF; grant number 13N11831, Laser Activated Nanoparticle Directed Cell Elimination and Modulation, LAND-CEM) and the European research Council (ERC; grant number 617989 project Design2Heal).

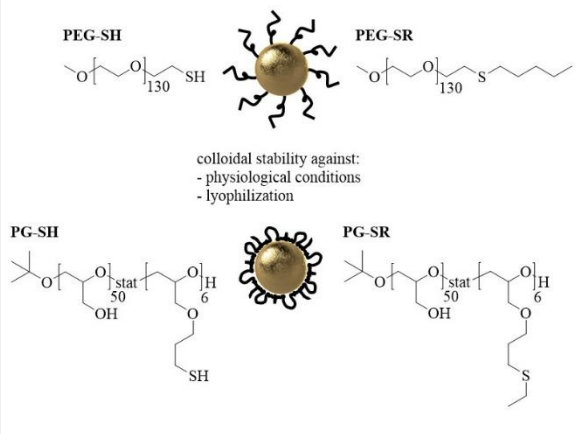

Polymer conformation on AuNPs
Figure 1: Overview of all thiol- and thioether polymers applied in this study with a scheme of the predicted brush regime for PEG, whereas for PG
a conformation with trains, loops, and tails was suggested.

PS1-04-112

Thermoresponsive polyelectrolyte multilayers of chitosan and PNIPAm-modified cellulose sulfate for the generation of cell sheets for tissue engineering

Falko Doberenz[1], Kui Zeng[2], Kai Zhang[2], Thomas Groth[1]

[1]Martin-Luther-University Halle-Wittenberg, Department of Biomedical Materials, Pharmacy, Halle, DE; [2]Georg-August-University Göttingen, Department of Wood Technology and Wood Chemistry, Göttingen, DE

Introduction

Thermoresponsive materials, as one kind of stimuli-responsive materials, used as surface modification for the generation of cell sheets have been in the focus of research for several years. Amongst other things, they allow the enzyme-free harvest of cells and the use of intact cell sheets, possessing extracellular matrix, for tissue engineering purposes. In this study, a thermoresponsive polyelectrolyte multilayer system that allows enzyme-free cell harvest, is described. Using bioactive cellulose sulfate (CS) modified with poly(N-isopropylacrylamide) (PNIPAm), thermoresponsive multilayer systems can be manufactured without the need of expensive equipment or radiation (e.g. in contrast to conventional methods, like electron beam irradiation).

Experimental Methods

The multilayer system fabricated using layer-by-layer coating technique is composed of double layers of chitosan – CS with poly (ethylene imine) as anchoring layer. CS without PNIPAm was used to form base layers and CS-PNIPAM was applied for the outer and terminal layers. The physical properties of the polyelectrolyte multilayer have been characterized by Surface Plasmon Resonance (SPR), Quartz Cristal Microbalance, ellipsometry and Atomic Force Microscopy. Biological characterization, e.g. protein adsorption and cell adhesion (fibroblasts) have been tested. Furthermore, the detachment of those in dependence of the environmental temperature have been studied. Using a heating/cooling plate, the cell detachment process could be monitored under the microscope.

Results and Discussion

The results of the SPR measurement confirmed polyelectrolyte adsorption onto gold sensors and the formation of a multilayer system. Differences could be seen between the adsorption of CS in comparison to CS-PNIPAM, the angle change and thereafter the adsorbed mass is greater for the later one. Similarly, Quartz Cristal Microbalance was used to determine the adsorbed mass and the viscoelastic properties of the multilayer films. Additionally, ellipsometry gave insight into the thickness of different multilayer systems. The thickness of the multilayer films is an important property, especially for the thermoresponsive effect. To specify the minimum thickness needed for the thermoresponsive properties of the surface to allow cell detachment, enables precise control of the LbL process and the creation of multilayers with a certain amount of single layers. Atomic force microscopy enabled the description of the surface topography. The biological characterization showed, that cells adhere onto the multilayer system. Fibroblasts adhered and spread onto glass cover slips prepared with chitosan and CS-PNIPAM multilayers. After exposing it to environmental temperatures of 4 °C, cells successfully detached from these surfaces. Furthermore, the cell detachment process could be monitored by cooling with the above mentioned heating stage.

Conclusion

Overall, the goal to establish a multilayer system for cell harvest, which is easily manufactured and biocompatible can be addressed by CS modified with PNIPAM in multilayer system.

Acknowledgement

This work was funded by Deutsche Forschungsgemeinschaft grant GR1290/12-1.

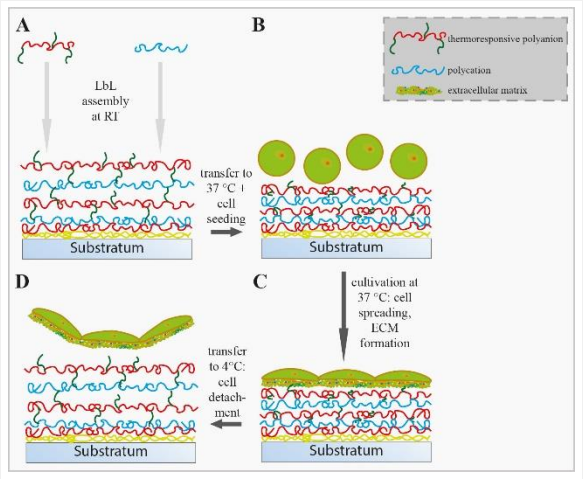

Manufacture and function of thermoresponsive multilayer films

A: Multilayer formation of thermoresponsive polyanion (cellulose sulfate) and polycation (chitosan) cia layer-by-layer technique

B: After heating to 37 °C, thermoresponsive side chains change conformation; surface facilitates cell adsorption

C: Cultivation at 37 °C; cells adhere to surface and start producing extracellular matrix

D: Reducing the temperature to 4 °C, thermoreponsive polymers change confirmation; cells detach from surface (with ECM)

PS1-04-113

Bioactive glass S520 laser cladding on ultrafine-grained pure titanium substrates

Szymon Bajda[1], Yijun Liu[3], Michal Krzyzanowski[2,1], Stanisław Dymek[1]

[1]AGH University of Science and Technology, Krakow, PL; [2]Birmingham City University, Birmingham, GB; [3]Manufacturing Technology Centre, Coventry, GB

Introduction

Nowadays, titanium alloys are commonly used for different biomedical applications instead of pure titanium because of their superior mechanical properties. Presence of some alloying elements, such as aluminium and vanadium, can be harmful to human health, and can be considered as disadvantage in long term applications. Potentially, there is a possibility of replacing the commercial titanium alloys with ultrafine-grained commercially pure Ti (cpTi). The yield and ultimate strength of cpTi can exceed 1000 MPa [1]. When manufacturing medical devices, laser cladding is known as one of the most promising methods for manufacturing of modern medical implants with improved osseointegration, where bioactive glass coatings are imposed on metallic substrates [2, 3].

Experimental Methods

In this work, S520 bioactive glass was imposed on ultrafine-grained cpTi using laser cladding technique. Cross-sectional SEM images of titanium substrate and bioactive glass were analyzed. The interface between bioactive glass and metallic titanium substrate was also studied using SEM/EDX.

Results and Discussion

The refined microstructure of cpTi was locally modified in the areas affected by the laser beam. Figure 1 shows the cross-section of the ultrafine-grained cpTi substrate after the laser cladding process. The cross-section of the cladded bioactive glass is presented in figure 2. Some pores of up to 200 µm diameter were found within.

Conclusion

The S520 bioactive glass was successfully cladded onto the ultrafine-grained cpTi substrate. The application of cpTi allows for exclusion of potential toxic elements from the human body and its refined microstructure allows to achieve strength properties similar to those of Ti6Al4V alloy.

References

[1] V. V. Stolyarov, Y.T. Zhu, I. V. Alexandrov, T.C. Lowe, R.Z. Valiev, Grain refinement and properties of pure Ti processed by warm ECAP and cold rolling, Mater. Sci. Eng. A. 343 (2003) 43–50.

[2] M. Krzyzanowski, S. Bajda, Y. Liu, A. Triantaphyllou, W. Mark Rainforth, M. Glendenning, 3D analysis of thermal and stress evolution during laser cladding of bioactive glass coatings, J. Mech. Behav. Biomed. Mater. 59 (2016) 404–417.

[3] R. Comesaña, F. Quintero, F. Lusquiños, M.J. Pascual, M. Boutinguiza, A. Durán, J. Pou, Laser cladding of bioactive glass coatings, Acta Biomater. 6 (2010) 953–961.

Acknowledgement

The support from the National Science Centre, Poland (grant no. DEC-2016/21/N/ST8/00091) and Birmingham City University UK (internal BCU CEBE research funding 2018) is greatly appreciated.

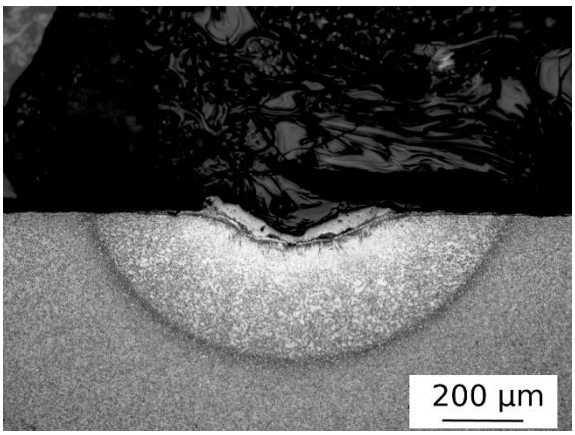

Fig. 1 Ultrafine-grained cpTi microstructure
Optical image showing cross-section of the ultrafine-grained cpTi after the laser cladding process.

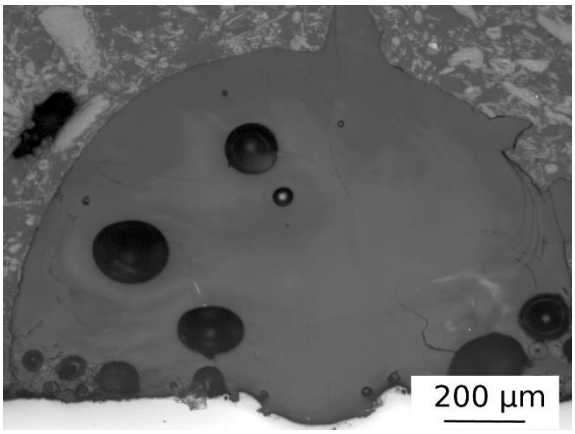

Fig. 2 Bioactive glass coating
Optical image showing cross-section of the S520 bioactive glass coating on the ultrafine-grained cpTi substrate.

PS1-04-113-2

Protein fiber coating of PEEK implant material by electrospinning

Andrea Friedmann, Tobias Hedtke, Julius Rubers, Christian E. H. Schmelzer

Fraunhofer Institute for Microstructure of Materials and Systems IMWS, Biological and Macromolecular Materials, Halle (Saale), DE

Introduction

Polyether ether ketone (PEEK) is an engineering thermoplastic which has emerged as a leading biomaterial for replacing metal implant components due to its outstanding physical properties. The drawback of PEEK however is its biologically inert chemical surface composition, which is unfavorable for protein and cell adhesion. Improving these bio-inert surface characteristics is therefore of great interest. Here, bio-functionalizing of the PEEK surface by applying electrospun protein nanofibers can be beneficial. Biocompatible and biodegradable electrospun collagen fibers can provide a supportive meshwork for the anchorage of cells, while mimicking the physical dimensions of the native extracellular matrix (ECM). The aim of this study is to modify medical grade PEEK materials by applying electrospun collagen nanofibers onto its surface, in order to enhance osseointegration in human bone tissue.

Experimental Methods

Preliminary experiments have shown the feasibility of depositing protein nanofibers on polymer surfaces using a laboratory electrospinning setup. The efficiency of the fiber deposition on material which is in direct contact with the collector electrode depends mainly on the electrical conductivity of the PEEK material. For unfilled PEEK material, fibers do not deposit directly on the PEEK surface, as it reflects the electrical field due to its highly electrically insulating properties. When enhancing the electrical properties by addition of carbon fibers, nanofiber deposition is increased. CFR-PEEK (Carbon Fiber Reinforced-PEEK) allows reproducible fiber deposition without being impaired by parameters such as relative humidity. For sample preparation, a large customized copper collector allowed fiber deposition on multiple PEEK samples simultaneously.

Results and Discussion

After successful nanofiber deposition, the collagen fibers were crosslinked using 1-ethyl-3-(3-dimethyl aminopropyl) carbodiimide (EDC) or formaldehyde (FA) to enhance the mechanical properties and increase the resistance against water. During dry crosslinking in FA vapor, the fiber fleece shrunk and peeled off from the CFR-PEEK surface. The same effect was observed for EDC-crosslinked fleece after being immersed in water. Analysis of SEM images of the nanofibers showed that the fiber diameter increased during the crosslinking process, leading to a decrease in fleece porosity which caused the fleece to shrink. For FA-crosslinked fibers, the diameter increased by only 8 %, while EDC-crosslinked fibers swell during the wet crosslinking process and the fiber diameter increased by 215 %. With regard to the water stability, the FA-crosslinked fleece was not altered when it came in contact with water and retained a fibrous and porous morphology. EDC in contrast did not sufficiently crosslink the collagen fibers as the nonwoven lost its fibrous morphology when it came in contact with water.

To improve the adhesive properties of collagen fibers deposited on the PEEK material, the CFR-PEEK discs were plasma-treated with oxygen and argon gases. Plasma-treatment affects the chemical surface composition of the PEEK polymer surface by introducing functional groups, which can be crosslinked with primary amines present in the collagen fibers. However, none of the crosslinking reagents effectively crosslinked the protein fleece with the PEEK surface. This method is limited to the small amounts of induced functional groups as well as spatial separation

between fibers and the PEEK surface. Alternatively, a combination method of electrospraying and electrospinning was developed to increase adhesion of the collagen fleece on the PEEK surface. Here, an intermediate layer of collagen droplets is created at the PEEK-fleece interface. These collagen droplets adhere well to the polymer surface due to an increase in surface contact area and the resulting increase in non-covalent bonds. Crosslinking using FA delivered better results as it prevented the fleece from peeling off the PEEK surface.

Conclusion

In order to optimize the osseointergrative properties of PEEK implants, a method of application of an adhesive and water stable electrospun collagen fiber coating to the polymer surface was successfully developed in this study. This represents the first step of bio mimicking the extracellular matrix on implant materials.

2:45 p.m. – 3:45 p.m.

Hall 1 / Exhibition Area

PS1-05 | 3D Scaffolds

PS1-05-113-3

Incorporation of electrospun fibrous materials into protein-based hydrogels

Tobias Hedtke[1,2], Thomas Groth[2], Christian E. H. Schmelzer[1]

[1]Fraunhofer Institute for Microstructure of Materials and Systems, Biological and Macromolecular Materials, Halle (Saale), DE; [2]Martin Luther University Halle-Wittenberg, Biomedical Materials Group, Institute of Pharmacy, Halle (Saale), DE

Introduction

Protein-based biomaterials are nowadays of growing interest in the field of biomedicine and tissue engineering. On the one hand, the use of proteins as biomaterials is a promising method to support the reconstitution of the tissue structure and to improve the overall process of healing upon surgery or injuries. On the other hand, it also offers a multitude of prospects for tissue engineering, e.g. cultivation of personalized cell-loaded tissue prosthesis, development of artificial organs as well as the fabrication of bioabsorbable scaffolds for tissue regeneration. Therefore the fabrication of novel biocompatible materials is a need for current biomedical applications. In general, biomaterial scaffolds for those purposes are in the form of films, foils, hydrogel matrices or nonwoven meshes. Here we present an alternative approach of fiber-reinforced hydrogels that combines the mechanical stability of electrospun fiber meshes from medical plastics and the mimicking of a native extracellular surrounding by the hydrogel component based on the extracellular proteins collagen and elastin. This approach will be assessed by microstructural and mechanical means as well as biocompatibility testing in order to generate mechanically stable scaffolds for tissue engineering and tailor-made tissue prosthesis.

Experimental Methods

Fibrous materials were electrospun from polyamide, polylactic acid and polyglycolide. Mature elastin as a major component of the hydrogel compartment was isolated from porcine aorta and solubilized by partial hydrolysis. The fibrous materials were incorporated in a sponge-like matrix fabricated by lyophilization of hydrogels comprising collagen and solubilized elastin in an equal ratio. Subsequent cross-linking of the protein components were tested for further tuning the material properties. Microstructural analysis was done by scanning electron microscopy, biocompatibility was tested bycell culture experiments and mechanical properties were determined by tensile testing.

Results and Discussion

Electrospun fibrous materials were successfully incorporated into protein-based hydrogels. Mechanical stable scaffolds were obtained for all fibrous polymers used in this study. Additional cross-linking of the protein components was beneficial to the stability of the biomaterial.

Conclusion

The here presented methods and materials allow the fabrication of mechanical stable and tunable biomaterials for biomedical applications, in particular for cutting-edge tissue prosthesis and tissue engineering.

PS1-05-114

Rational Design of Collagen Scaffolds for Co-Culture

Nima Meyer[1], Daniel V. Bax[1], Jochen Beck[2], Ruth E. Cameron[1], Serena M. Best[1]

[1]University of Cambridge, Department of Materials Science and Metallurgy, Cambridge, GB; [2]Geistlich Pharma AG, Core Technologies, Wolhusen, SZ

Introduction

Three-dimensional collagen scaffolds offer wide-ranging potential for tissue repair and regeneration applications. However, continued research is required to optimise scaffold structure and mechanical properties. Monoculture provides a good model for tissue response in many cases, although for bone tissue engineering, a co-culture of both osteoblasts and endothelial cells is required simulating the necessary simultaneous bone cell growth, neovascularisation and angiogenesis [1]. Since interactions observed in mono-culture are cell-type specific, it is important to tailor scaffold characteristics to provide optimal conditions for cells in co-culture. Crosslinking (XL) influences both the scaffold stiffness and also the integrin binding sites available on the surface of the structure. An over-arching question is to understand the effects of cross-linking "degree" on cells in co-culture. EDC (1-ethyl-3-(3-dimethylaminopropyl-carbodiimide hydrochloride)/NHS (N-hydroxysuccinimide) XL is used widely to optimise scaffold stiffness but, at high concentrations, has been found to be detrimental for cell binding [2]. This work describes a systematic study to gain insight into the cell-type specific response to scaffolds for bone tissue repair. Using samples with varying stiffness, a mono-culture study of both primary human osteoblasts (hOB) and human dermal microvascular endothelial cells (HDMEC) has been undertaken in order to inform subsequent work in a more complex co-culture system designed to assess angiogenesis for bone tissue engineering.

Experimental Methods

Collagen suspensions (0.5 and 1 wt.%) in 0.05 M acetic acid were air and freeze-dried to produce 2D films and 3D scaffolds, respectively. Both films and scaffolds were crosslinked with different EDC concentrations to obtain XL levels ranging from 0 to 100%, with a molar ratio of EDC:NHS:COO^-=5:2:1 defined as 100%. The hOBs and HDMECs were seeded on both films and scaffolds. Cell proliferation and adhesion on 2D films were assessed via fluorescence microscopy using DAPI staining and through a colorimetric assay measuring lactate dehydrogenase, respectively. Cytotoxicity of films with different XL concentrations was examined using a fluorescence-based LIVE/DEAD assay. Furthermore, the metabolic activity of cells seeded on 3D scaffolds was measured in an absorbance reader using a PrestoBlue® viability assay. Cell proliferation on and migration into col. scaffolds were assessed via fluorescence microscopy using PicoGreen and nuclei and actin staining, respectively. Investigation of mechanical stability of the scaffolds was carried out with a compression test performed using hydrated scaffolds.

Results and Discussion

For both cell types similar proliferation trends on col. films were observed, showing no difference between the different XL conditions. It was also observed that carbodiimide XL has no toxic effect on both cell types as they were evenly distributed and elongated on the surface of the films. However, a discrepancy in cell adhesion on col. films between the two cell types was observed. While HDMECs kept almost 50% of their initial integrin-mediated cell attachment with XL levels up to a 100%, hOBs lost 50% of their initial specific binding at only 60% XL, which indicates that an increasing XL degree inhibits specific binding, particularly for hOBs. However, with regard to 3D scaffolds, a more substantial decrease in metabolic activity with increasing XL levels was observed for HDMECs as opposed to

hOBs (Figure 1). Lower metabolic activity of HDMECs seeded on 60 and 100% crosslinked scaffolds as opposed to hOBs was observed, indicating that especially HDMECs dislike stiffer substrates within a 3D environment. Overall, a higher metabolic activity was observed for both cell types on scaffolds with XL levels ranging from 10 to 30%. Both migration and proliferation assays confirmed the observed metabolic activity trend. Additionally, it was observed that non-crosslinked scaffolds shrunk more than 50% within the first 24 hrs, which is disadvantageous for tissue repair and regeneration. Compression testing showed enhanced mechanical stability of over 6 kPa for scaffolds with XL levels of 30%, which is required for appropriate tissue regeneration.

Conclusion

In conclusion, EDC/NHS crosslinking was found to influence, strongly, the cell response of both hOBs and HDMECs. While both cell types demonstrated a good response in soft environments with crosslinking levels ranging between 10-30%, hOBs performed better in stiffer environment as compared with HDMECs. Collagen scaffolds with a 30% crosslinking level showed appropriate mechanical stability suitable for both hOBs and HDMECs. It is clear that both cell activity and binding behaviour of hOBs and HDMECs change with XL levels, but to different extents. It was concluded that scaffolds with 30% XL offered the best combination of mechanical stiffness and cell binding sites and that these will be taken forward for analysis in co-culture for bone tissue regeneration.

References

[1] Unger RE, Sartoris A, Peters K, Motta A, Migliaresi C, Kunkel M, Bulnheim U, Rychly J, Kirkpatrick CJ. Tissue-like self-assembly in cocultures of endothelial cells and osteoblasts and the formation of microcapillary-like structures on three-dimensional porous biomaterials. Biomaterials. 2007 Sep 1;28(27):3965-76.

[2] Bax DV, Davidenko N, Gullberg D, Hamaia SW, Farndale RW, Best SM, Cameron RE. Fundamental insight into the effect of carbodiimide crosslinking on cellular recognition of collagen-based scaffolds. Acta biomaterialia. 2017 Feb 1;49:218-34.

Acknowledgement

This research was financially supported by the Engineering and Physical Sciences Research Council (EPSRC) and Geistlich Pharma AG.

PS1-05-115

Bioactive chitosan-based scaffold as smart materials for bone fracture treatment

Alessandra Soriente[1], Soledad Perez Amodio[2], Ines Fasolino[1], Maria G. Raucci[1], Christian Demitri[3], Elisabeth Engel López[2], Luigi Ambrosio[1]

[1]Institute of Polymers, Composites and Biomaterials, National Research Council (IPCB-CNR), Naples, IT; [2]Institute for Bioengineering of Catalonia, Barcelona, ES; [3]Department of Engineering for Innovation, University of Salento, Lecce, IT

Introduction

In last decades great attention was given to realisation of successful substitutes for bone tissue injury characterised by the lack of bone mass, an inflammatory reaction and blood vessels necrosis [1]. The promising field of regenerative medicine is working to repair damaged bone structure and functions controlling immune response and promoting vascolarised tissue restoration in the site of implant. Here, we discuss how bioactive chitosan 3D-based scaffolds can play a pivotal role in the inflammation and angiogenesis related to osteogenesis processes by using *invitro* models aimed to mimic bone fracture microenviroment.

Experimental Methods

Chitosan scaffolds by using two different approaches based on inorganic (i.e. hydroxyapatite nanoparticles) and organic compounds (i.e. BMP-2 mimicking peptide), were bioactivated respectively [2]. In order to evaluate antinflammatory and angiogenic properties related to osteogenic potential of the scaffolds, the expression of inflammatory mediators and pro-angiogenic markers was estimated. In detail, the modulation of cytokines (TGF-β and IL-6) which play a crucial role in osteogenesis was measured on a co-culture model consisting of osteoblasts and macrophages stimulated by lipopolysaccharide (LPS) for better mimicking damaged bone. Moreover, oxidative stress metabolites, interleukins and COX-2 expression related to osteogenic markers production were analyzed in order to understand the correlation between bone focal inflammation and bone regeneration. Additionally, in order to investigate the effect of scaffold on angiogenesis, CD31 (specific marker of angiogenesis) expression, cell adhesion, growth, proliferation, migration and tube formation by using endothelial cells (HUVEC) were detected. In the end, morphological cell analysis by SEM and confocal microscopy to study cell-material interaction effect from a qualitative point of view was performed.

Results and Discussion

The results on antinflammatory potential suggest that chitosan-based scaffolds bioactivated by using inorganic signals (hydroxyapatite nanoparticles) inhibit pro-inflammatory mediators production (IL-1β and IL-6), induce antinflammatory cytokine generation (IL-10) and reduce nitric monoxide metabolites (nitrites) on co-cultures stimulated by LPS. Conversely, scaffold bioactivated by using organic signals (BMP-2 mimicking peptide) were able to decrease pro-inflammatory markers without any effect on antinflammatory cytokines levels and on nitrites. However, these scaffolds are able to maintain high levels of TGF-β that, combined with BMP-2, promotes osteogenesis. The results on angiogenic properties of scaffold demonstrated that neat and bioactivated scaffolds are able to promote angiogenesis by increasing endothelial cell proliferation, migration and tube formation. In detail, scaffolds decorated with BMP-mimicking peptide seem to show better values in terms of tube formation, even without matrigel component. These latter scaffold determined also higher proliferation values than those induced by CS

biomineralised scaffolds. Finally, morphological investigations showed that all chitosan-based materials induced a good cell spreading.

Conclusion

Bioactive signals on the chitosan scaffolds surface allow a desirable effect on inflammation inhibition and angiogenic promotion. Indeed, the work encourages the research to use CS porous scaffolds as potential implant in the field of tissue engineering due to its good properties. Our results support the concept that CS biomaterials may be a source of substrates for developing multi-target devices able to regenerate damaged bone inflammation and stimulating neovascularisation of tissue-engineered constructs.

References

1. MA Fernandez-Yague, SA Abbah, LM Namara, D I Zeugolis, A Pandit, M J Biggs, Advanced drug delivery Reviews, 1-29, 2015. doi: 10.1016/j.addr.2014.09.005.
2. A Soriente, I Fasolino, MG Raucci, C Demitri, M Madaghiele, A Giuri, A Sannino, L Ambrosio, Journal of Materials Science Materials in Medicine. 29:62, 2018. doi: 10.1007/s10856-018-6072-2.

Acknowledgement

The study was supported by PNR Aging program 2012-2018 and NANO-DISP, INAIL BRIC 2016 id54. The authors also thank Mrs Stefania Zeppetelli for supporting biological investigation.

PS1-05-116

Synthesis and *in vitro* bioactivity characterization of porous scaffolds from biphasic ceramic in the system $Ca_3(PO_4)_2$-Ca_2SiO_4

Anabel Díaz-Arca[1], Patricia Mazón[2], Piedad N. De Aza[1]

[1]Universidad Miguel Hernández, Instituto de Bioingeniería, Elche, ES; [2]Universidad Miguel Hernández, Departamento de Materiales, Óptica y Tecnología Electrónica, Elche, ES

Introduction

In order to obtained new materials with potential applications in bone tissue engineering this work describes the synthesis and *in vitro* bioactivity characterization of porous scaffolds from biphasic ceramic composition corresponding to the system $Ca_3(PO_4)_2$-Ca_2SiO_4 [1].

Experimental Methods

Scaffolds were produced by polymer replication method. Polyurethane sponges with desired pore size and geometry were used as templates, which were impregnated with ceramic slurry. Templates covered were squeezed to remove slurry excess and were dried for 24h at room temperature. Finally, green structures were sintered by heat treatment. Bioactivity was estimated *in vitro* by different soaking times (1 to 21 days) in Kokubo´s simulated body fluid (SBF).The macro and microstructure of scaffolds and *in vitro* behavior were characterized by Mercury Porosimetry, X-Ray Diffraction (XRD), Scanning Electron Microscopy (SEM), Energy-Disperse X-Ray Spectroscopy (EDX), Fourier-Transform Infrared Spectroscopy (FTIR) and Inductively Coupled Plasma (ICP-OES).

Results and Discussion

Biphasic calcium silicophosphates scaffolds with a high open porosity and interconnected structure of macro (140 µm -1 mm) and micropores (2 µm –140 µm) were obtained. The interconnect structure of macropores is necessary for support bone remodeling process because it allows rapid vascularization, osteoblasts ingrowth and osteoconduction. Furthermore, micropores are essential for the interaction with cells and morphogenetic proteins. After different soaking times in SBF a globular phase grew gradually on the surface of scaffolds forming a bone-like apatite layer indicating *in vitro* bioactivity (Figure 1). Moreover, changes in the ionic concentrations of silicon, calcium and phosphorous in SBF suggesting that the scaffolds reacted dissolving silicocarnotite and forming hydroxyapatite by pseudomorphic transformation of the second phase. The presence of hydroxyapatite was confirmed by FTIR spectra of a milled sample and EDX analysis of a fresh fracture of scaffolds after 21 days of inmersion.

Conclusion

Bioactive porous scaffolds were produced from calcium silicophosphate ceramic using polymer sponge templates. Pore size distribution indicated a hierarchical structure similar to bone mineral phase and the scaffolds could form a tight chemical bond with living bone through a bone-like apatite layer. The overall results suggest that the scaffolds might be useful for future applications in bone tissue engineering.

References

[1] I.M. Martínez, P.A. Velasquez, L Meseguer-Olmo, P.N. De Aza. Ceram.Int. 37,2527-2535 (2011).

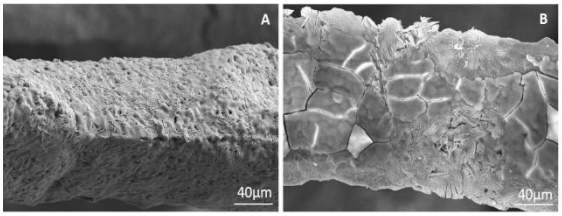

Fig.1: SEM micrographs of struts: (A) before immersion in SBF and (B) after 7 days of immersion.

PS1-05-117

Eutectoid scaffolds that mimic porous human bone tissue

Anabel Díaz-Arca[1], Patricia Ros-Tárraga[2], Pablo A. Velásquez[1], Patricia Mazón[3], Piedad N. De Aza[1]

[1]Universidad Miguel Hernández de Elche, Instituto de Bioingeniería, Elche, ES; [2]UCAM-Universidad Católica San Antonio de Murcia, Grupo de Investigación en Regeneración y Reparación de Tejidos, Murcia, ES; [3]Universidad Miguel Hernández de Elche, Departamento de Materiales, Óptica y Tecnología Electrónica, Elche, ES

Introduction

A new route of obtaining bioactive scaffold ceramic materials, which improve the ingrowth of new bone into implants (osseointegration), is presented. This involves obtaining eutectoid structures from selected system, bearing in mind the different behaviour of the phases. In this work the subsystem silicocarnotite - tricalcium phosphate [1] was chosen because silicocarnotite is bioactive and tricalcium phosphate is biodegradable.

Experimental Methods

The eutectoid ceramic scaffold material was obtained by solid-state reaction and slow cooling (12°C/min) through the eutectoid temperature region (1158±2°C). The porous ceramic scaffolds were produced using the polymer replication method. Polyurethane sponges with desired pore size and geometry were used as templates which were impregnated with ceramic slurry. The polyurethane sponge was squeezed to remove slurry excess following by a heat treatment for removing the polymeric sponge and give consistence to the ceramic one. The bioactivity of these scaffolds has been analyzed in vitro by doing immersions in simulated body fluid (SBF) according to the standard procedure introduced by Kokubo et al. [2].

Results and Discussion

The results showed biphasic porous calcium silicophosphate scaffolds with high porosity and interconnected structure of macro and micropores. The morphology presents a eutectoid microstructure of lamellae type, composed of alternating layers of silicocarnotite and α-tricalcium phosphate. The eutectoid scaffold material, when soaked in SBF, reacts first by dissolving the silicocarnotite phase and immediately forming a microporous structure of hydroxycarbonate apatite (HCA) by a pseudomorphic transformation of the α-tricalcium phosphate lamellae. The microstructure obtained is similar to that of porous bone. Later, a dense HCA layer is formed by precipitation on the outer surface of the material (Figure 1).

Conclusion

Bioactivity of the scaffolds, in terms of HCA formation, was confirmed after 1 day of immersion in SBF, confirming the suitability of the new scaffolds for bone regeneration applications.

References

[1] IM Martinez *et al.*. J. Am. Ceram. Soc. 2012; 95(3):1112-1117.

[2] T. Kokubo *et al.* J. Biomed. Mater. Res. 1990; 24:721–34.

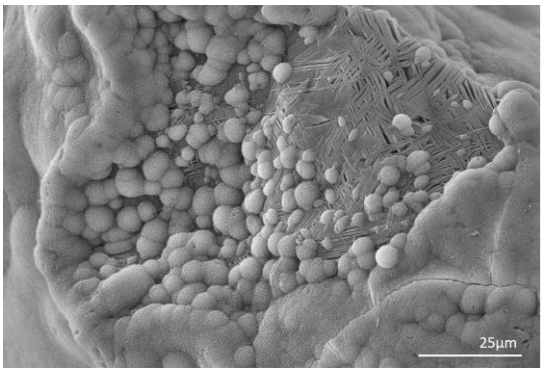

Figure 1.- SEM image of the surface of the scaffold after soaking for 7 days in SBF.

PS1-05-118

Bio-composite Materials For Bone Tissue Engineering Scaffolds

Dina Abdulaziz[1], Antonios Anastasiou[1], Peter Giannoudis[2], Animesh Jha[1]

[1]University of Leeds, The Institute for Materials Research, School of Chemical and Process Engineering, Leeds, GB; [2]Leeds General Infirmary, Department of Trauma and Orthopedic Surgery, Leeds, GB

Introduction

The Repair and reconstruction of large bone defects is one of the most critical clinical challenges in orthopedics. An ideal grafting material should have; a) Mechanical properties comparable to that of bone in order to sustain the load of the body; b) Exceptional osteogenic potential in order to promote new bone formation; c) Appropriate structure to allow the circulation of nutrients and the potential to trigger vascularisation. Until now researchers' efforts have been focused on the development of the "perfect" biomaterial, targeting to achieve at least a combination of the aforementioned properties in a single component. Various types of materials, like synthetic and natural polymers, ceramics and metals have been extensively investigated and different combinations, structures and geometries have been proposed. Many of these works have been proved promising during in situ trials but after the translation in clinic, all of them presented various deficiencies leaving clinicians without a "golden route" for treating long bone defects. This work aims to establish a completely new approach for the development and fabrication of bone scaffolds, based on the fundamentals of advanced manufacturing and personalised medicine. Instead of focusing on a single material, a combination of different technologies, materials and fabrication techniques will be used in order to design and develop a synthetic tissue that imitates the unique structure and functionalities of natural bone. The first step in our approach for the development of a multilayer scaffold is the fabrication of a biocompatible layer with the appropriate mechanical properties for load bearing applications. The aim of this work is to investigate the synthesis of Ti and Ti/calcium phosphate (CaP) composite scaffolds and to identify the appropriate sintering conditions in order to match the mechanical properties of natural bone (i.e. sintering temperature, extent of porosity, Ti/CaP ratio). The samples are characterised in terms of crystal structure, porosity and mechanical properties using XRD, SEM, micro-indentation, gas adsorption porosimetry and X-ray tomography. In a parallel investigation, stress analysis study is running right now in order to investigate the mechanical behaviour of the bone and proposed scaffold.

Experimental Methods

For preparing the Ti/CaP scaffolds, commercial pure titanium powder (-100 mesh, 99.7% purity, Sigma Aldrich® 268496) was mixed in different ratios with brushite powder ($CaHPO_4 \cdot 2H_2O$) and then pressed into pellets under a load of 7 tons using a 20 mm die. Three different temperatures have been used for sintering the pellets (i.e. 800, 1000 and 1100 ˚C) while the sintering time kept constant at 5h.

Results and Discussion

XRD results revealed that most of the Ti was oxidized in the presence of O_2 during sintering and converted into TiO_2 (figure 1). For the brushite containing samples it was found that the mineral has been transformed into β-pyrophosphate. Micro indentation testing enabled us to investigate how the mechanical properties change due to the sintering temperatures and ratio of CaP since the initial hardness Hv of Ti, brushite is 740 Mpa, 340 Mpa respectively. Also getting simulated analysis instead of destructive tests is so important for the biomechanical disciplinary, thus a design for femur bone fracture is being studied because the femoral diaphysis fractures are among the most common

injuries required to treat [3]. By using ANSYS WORKBENCH software, a numerical study is running to investigate the stress analysis of the normal femur bone and compare with the stress distribution and the maximum deformation of the femur bone with the proposed scaffold (figure 2).

Conclusion

This work investigates new approach to fabricate bone scaffolds in order to use in clinical applications. Therefore, titanium forms the base of our structure to be able to heal load bearing defects. On the other hand, angiogenesis is a vital requirement for the formation of healthy tissue bone, thus the promising way to combine between these requirements is adding bioactive brushite. As well, the structure has to be porous in order to enhance the vascularization and ensure diffusion of nutrients to cells and diffusion of waste and toxins out of the scaffold.

References

1. Polo-Corrales L., Latorre-Esteves M. and Ramirez-Vick J.E. Scaffold Design for Bone Regeneration, NIH Public Access, 2014.
2. O'Brien F.J. Review Biomaterials & Scaffolds for Tissue Engineering , Materials Today, 2011.
3. Sheikh Mohd. Shahjad A., Ganorkar A. P. and Dehankar R. N. Finite Element Analysis of Femoral Intramedullary Nailing, Journal for Research, 2016.

Acknowledgement

Authors acknowledge "The Royal Commission for the Exhibition of 1851" for the financial support.

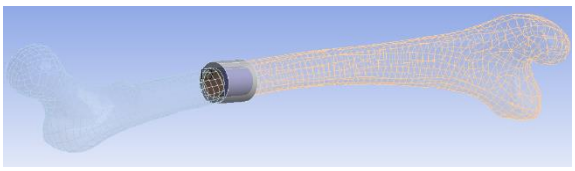

Figure 2: CAD of damaged femur bone with the proposed multi-layered scaffold

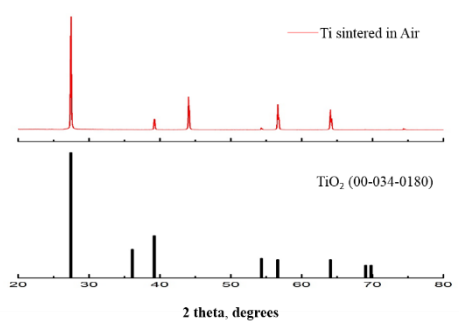

Figure 1: XRD pattern of the TiO2 scaffold

PS1-05-119

Transition metal ions as a tool for modulating the properties of chitosan hydrogels

Anamarija Rogina[1], Andrea Lončarević[1], Maja Antunović[2], Inga Marijanović[2], Marica Ivanković[1], Hrvoje Ivanković[1]

[1]University of Zagreb, Faculty of Chemical Engineering and Technology, Zagreb, HR; [2]University of Zagreb, Faculty of Science, Zagreb, HR

Introduction

The synthesis of biologically active scaffolds is focused on the design of a cell-sensitive surface by applying cell adhesive proteins or bioceramic micro (nano) particles. The new strategy for controlling the biological properties is based on the modification by trace metals found in the living organism. Recently, the new approach focusing on the metallic ions that induce certain biological responses in the bone remodelling has emerged. Divalent metal ions such as Sr^{2+}, Mg^{2+}, Cu^{2+}, Zn^{2+} etc. are essential for cell life during bone formation [1]. The aim of this work was to modulate the physical and biological properties of chitosan hydrogels by the addition of divalent metal ions at non-toxic concentration level. Chitosan is a biocompatible and biodegradable polymer which can be used as a scaffold in tissue engineering [2, 3]. Depending on the degree of deacetylation and molecular weight of polymer, hydrogels with specific structures can be produced by the addition of copper and zinc ions (Cu^{2+} and Zn^{2+}). Zinc plays a critical role in synthesis of nucleic acids, inhibits osteoclast differentiation and exhibit anti-inflammatory and antibacterial effect [4]. On the other hand, copper is vital for normal functioning of human life through the interaction with enzymes [5]. Cu is known to be angiogenic agent increasing the expression of pro-angiogenic and growth factors such as VEGF or FGF-2 and stimulates the proliferation of endothelial cells [6]. As a potential method, the complexation can be used to prepare hydrogels of complex chitosan-metal ion with defined structure.

Experimental Methods

Prepared hydrogels were transformed into xerogels by the lyophilisation method and characterised by Fourier transform infrared spectroscopic analysis (FTIR) and qualitative X-ray diffraction analysis (XRD). The morphology and microstructure of the samples was imaged by scanning electron microscopy (SEM), while swelling capacity was determined at physiological conditions (pH = 7.4 at 37 °C). The cytotoxicity of metal ion-chitosan xerogels was evaluated by MTT test performed on human embryonic kidney cells (Hek293) during three days of culture.

Results and Discussion

Due to the strong affinity of metal ions towards amino groups of chitosan, defined and ordered structures of metal ion-chitosan hydrogels were obtained. The physical and biological properties of complex hydrogels varied in metal ion concentration-dependent manner. According to the cell culture with human embryonic kidney cells (Hek293), copper-chitosan systems exhibited higher cytotoxicity when increasing $c(Cu^{2+})$ and more stable structure. On the contrary, zinc-chitosan complex hydrogels did show lower stability, but significantly higher biocompatibility with respect to the copper-containing hydrogels.

Conclusion

Transition metal ions, Cu^{2+} and Zn^{2+}, show good potential to be used in tailoring the hydrogels microstructure and biological response to the material. Depending on the metal ion type and concentration, structure of chitosan hydrogel is changed from randomly porous to well order tubular. Toxicity of copper-chitosan xergoels is limited by narrow range of concentration, while zinc-chitosan xerogels indicate positive influence of cell growth. However, the lack of extensive studies indicates the necessity for more detailed investigations on biological properties of transition metal ions.

References

[1] V.Mouriño, J.P. Cattalini, A.R. Boccaccini, Metallic ions as therapeutic agents in tissue engineering scaffolds: an overview of their biological applications and strategies for new developments, J. R. Soc. Interface 9 (68) (2012) 401–419, https://doi.org/10.1098/rsif.2011.0611.

[2] F. Croisier, C. Jerome, Chitosan-based biomaterials for tissue engineering, Eur. Polym. J. 49 (2013) 780–792, https://doi.org/10.1016/j.eurpolymj.2012.12.009.

[3] S.K. Lan Levengood, M. Zhang, Chitosan-based scaffolds for bone tissue engineering, J. Mater. Chem. B 2 (2014) 3161–3184, https://doi.org/10.1039/C4TB00027G.

[4] M. Yamaguchi, Role of nutritional zinc in the prevention of osteoporosis, Mol. Cell.Biochem. 338 (2010) 241–254, https://doi.org/10.1007/s11010-009-0358-0.

[5] M. Ziche, J. Jones, P.M. Gullino, Role of prostaglandin E1 and copper in angiogenesis, J. Natl. Cancer Inst. 69 (2) (1982) 475–482.

[6] C. Gérard, L.J. Bordeleau, J. Barralet, C.J. Doillon, The stimulation of angiogenesis and collagen deposition by copper, Biomaterials 31 (5) (2010) 824–831, https://doi.org/10.1016/j.biomaterials.2009.10.009.

Acknowledgement

This work has been supported by the Croatian Science Foundation under the project IP-2014-09-3752.

PS1-05-120

Structural changes during *in-vitro* crystallization of apatite on 3D-Si-Ca-P ceramic scaffolds.

Carlos Navalon[1], Patricia Ros[2], Patricia Mazón[3], Piedad N. De Aza[1]

[1]Universidad Miguel Hernández, Instituto de Bioingeniería, Elche, ES; [2]UCAM-Universidad Católica San Antonio de Murcia, Grupo de Investigación en Regeneración y Reparación de Tejidos, Murcia, ES; [3]Universidad Miguel Hernández, Departamento de Materiales, Óptica y Tecnología Electrónica, Elche, ES

Introduction

Third generation biomaterials with excellent properties to apply in bone tissue engineering were created. This research aimed the processing, characterization and *in vitro* bioactivity of novel porous scaffolds from biphasic composition according to the subsystem $7CaOP_2O_5 2SiO_2$-$2CaO{\cdot}SiO_2$

Experimental Methods

Scaffolds, with nominal composition 31 wt.% TCP (Tricalcium Phosphate)-69 wt.% C_2S (Dicalcium Silicate) were produced by polymer sponge replica method. Polyurethane sponge's templates were impregnated with ceramic slurry, squeezed to remove the excess and dried for 1 day at room temperature. Finally, the 3D structures were sintered. Bioactivity was examined at different time periods (3 h to 21 days) immersing the scaffolds in Kokubo´s simulated body fluid (SBF). The scaffold before and after SBF soaking was characterized by SEM, DRX, FTIR, Hg porosimetry and ICP-OES.

Results and Discussion

3D scaffolds with high open porosity and interconnected porous network composed by macro (200 µm-600 µm) and micropores (<1 µm -200 µm) were obtained. Pores bigger than 100µm improve bone formation because of cell migration, osteoblast proliferation and new vascular tissue formation. Microporosity may enhance ionic exchange with body fluids, improving scaffold bioactivity Ceramic surfaces were fully covered by globular HA- layer after soaking at 21 days, keeping the pores morphology without occluding them (Fig. 1). The Si-Ca-P ions concentration changes in SBF suggested that C_2S phase was partially dissolving, meanwhile TCP phase was transformed pseudomorphically into HA. Besides, at 21 days, the 3D structure did not bear up the HA formed in its surface, detaching it from the structure. On this way, Ca and P ions concentrations increased at the end of the assay. A FTIR of the upper and middle part of the 21 days' sample confirmed the presence of HA in both samples areas showing an ionic exchange between the sample and the SBF, resulting in a total material transformation into HA.

Conclusion

A biphasic 3D porous ceramic scaffolds were produced. The scaffold pores disposition and size revealed similar macrostructure to the trabecular bone phase, allowing the scaffold may replace different bone areas. Besides, In-vitro test, revealed fast (6 h) and strong bioactivity, showing at the end of the assay, fully material transformation into HA. The general results suggest the scaffolds could be useful for future applications in bone tissue engineering.

References

V. Rubio, et al. J. Am. Ceram. Soc. 2011;94[12] 4459-4462.

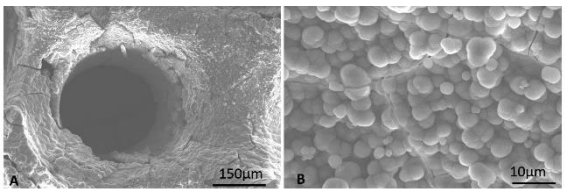

Fig. 1. SEM micrographs of 21 days' sample showing HA at (A) low and (B) high magnification.

PS1-05-121

Enhancing Collagen Scaffolds via Blending with Decellularized Plants

Sedat Odabas, Ece Karakaya, Sıla Bilgin, Emel Emregül

Ankara University, Department of Chemistry, Ankara, TR

Introduction

Decellularization is a rather new technique, which aims to maintain ECM and its components without affecting its composition while removing all cellular components[1]. The first initiatives are sure performed with animal tissues, there are few initiatives to use the benefits of plant tissues[2]. Here, we propose to use succulents. Succulents are drought-resistant plants that can store water in their stem or leaves. This water storing ability to transform the inner body to a gel-like structure. In this study, succulents were decellularized by a cocktail containing well-known detergents. Decellularization efficacy was performed by DNA quantification and hemocompatibility was assessed by basic hemolysis study. Collagen blend scaffolds were prepared via the well-known preparation technique.

Experimental Methods

Succulents were decellularized by day by day process with a decellularization cocktail comprising of 1% Triton X-100. Later on, leaves were washed several times with distilled water (for 30 min), PBS (1h) and distilled water (30 min) and PBS (1h) again in gentle agitation (100rpm 37°C) and this cycle was repeated 3 times. Samples were then stored in -80°C and lyophilized for 2 days and ground prior to use.

Hybrid scaffolds were fabricated with a combination of decellularized succulent plant flakes and collagen (from rat tail 2% (w/v) solution in acetic acid) with a ratio of 1:5 (w/w). Gels were molded in plastic wells and samples were stored at -80°C prior to lyophilization. All frozen samples were then lyophilized for 48h (Figure 1). Cross-linking were achieved by NHS/EDC (50mM/25mM) in an ethanol bath.

Results and Discussion

Sufficient decellularization efficacy was achieved, and determined via DNA content and protein content analysis with respect to control (native leaves). Furthermore, hemolysis and MTT results depicted that scaffolds in their final form have good bio and hem compatible property. These hybrid scaffolds have proper pore formation which is well enough for cellular applications and SEM results show better cell attachment. Structurally, these scaffolds showed the better swelling property.

Conclusion

By blending the succulent flakes into collagen, the scaffolds in their final form, not only maintain their hemo and bio-compatible characteristics but also gain more swellable property which we believe, these blend scaffolds can be a good candidate for hard tissue engineering especially for cartilage.

References

[1] Sedat Odabaş, Kadriye Tuzlakoğlu, Biomaterials, and Stem Cells: From Basics to Applications, Decellularized Matrices in Stem Cell Research, Eds. Bora Garipcan, Book Series 50th Years of Hacettepe University, Palme Yayınları, 2018., 201-212.

[2] Gershlak, Joshua R., et al. "Crossing kingdoms: Using decellularized plants as perfusable tissue engineering scaffolds." Biomaterials 125 (2017): 13-22.

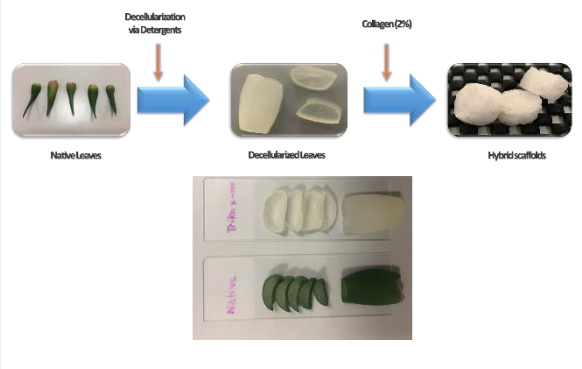

Figure 1
Schematic diagram for constructing hybrid scaffolds

PS1-05-122

Aerogel-loaded scaffolds obtained by supercritical foaming for bone regeneration

Carlos A. García-González[1], Araceli Delgado[2], Carmen Évora[2], Ricardo Reyes[3], Angel Concheiro[1], Jose Luis Gómez-Amoza[1], Carmen Alvarez-Lorenzo[1]

[1]Universidade de Santiago de Compostela, Departamento de Farmacología, Farmacia y Tecnología Farmacéutica, R+D Pharma group (GI-1645), Facultad de Farmacia and Health Research Institute of Santiago de Compostela (IDIS), Santiago de Compostela, ES; [2]Universidad de La Laguna, Departamento de Ingeniería Química y Tecnología Farmacéutica, Instituto de Tecnologías Biomédicas (ITB), La Laguna, ES; [3]Universidad de La Laguna, Departamento de Bioquímica, Microbiología, Biología celular y Genética, Instituto de Tecnologías Biomédicas (ITB), La Laguna, ES

Introduction

The efficient regeneration of a bone tissue assisted by the presence of a scaffold is dependent on the scaffold design and the processing method used. Regarding the design, medicated bone scaffolds can accelerate the bone tissue formation by providing a suitable 3D-porous structure and bioactive agents that promote cell colonization and differentiation towards the osteogenic lineage. For these scaffolds, solvent-free processing technologies operating at mild temperatures are preferred to have high loading yields of the bioactive agents.

Supercritical foaming is a solvent-free scaffold processing method that exploits the plasticizing effect of compressed CO_2 on certain polymers (e.g., polyesters) to form a porous structure[1]. Using this technique, scaffolds usually have high macroporosity but low pore interconnectivity that hampers the penetration and growth of cells and the transport of wastes.

Aerogels are solid and open porous networks obtained from wet gels after the removal of the solvent without significant structure compaction and endowed with high specific surface area. Namely, the extracellular matrix-mimicking nanostructure of aerogels along with the biological implications of certain polysaccharide and protein aerogel sources to promote the attachment, growth and colonization of cells are especially attractive for biomedical purposes[2].

In this work, the effect of the incorporation of protein (silk fibroin from *Bombyx mori*, SF) and polysaccharide (corn starch) aerogels o scaffolds of poly(ε-caprolactone) (PCL, 50 kDa) with dexamethasone-21-phosphate (DX, osteogenic agent) was evaluated. The morphological performance of the scaffolds was tested regarding pore interconnectivity, cell infiltration capacity and water permeability from mercury intrusion porosimetry (MIP) measurements. Finally, *in vivo* bone regenerative performance of the scaffolds was assessed in critical-size calvarial defects (diameter: 8 mm) in a Sprague-Dawley rat model.

Experimental Methods

Aerogel production is a multi-step process comprising at least a gelation step and a drying step (Fig. 1a). SF and starch gels were obtained from emulsions (8 wt. % of SF and 15wt. % of starch aqueous solutions, respectively, and Span 80 as emulsifier) using ultrasonication- and thermal- (121ºC, 20 min) assisted gelation, respectively. Then, SF and starch aerogel particles (SA and StA, respectively) were obtained by supercritical drying with compressed CO_2 (40ºC, 120 bar, 6 g/min)[3,4].

Scaffolds containing PCL and StA (PCL-StA, 90:10 weight ratio), SA (PCL-SA, 90:10) or SA+DX (PCL-SA-DX, 85:10:5) were processed using the supercritical foaming process (37ºC, 140 bar, 1 h) followed by a depressurization at a venting rate of 1.8 g CO_2/min.

Results and Discussion

The preparation of dry powder in the form of SF and starch aerogels was herein developed to provide a nanostructured, highly porous and bio-based material to be incorporated as a morphological modifier in the formulation of the scaffolds (Fig. 1). The particle size (300-600 nm) of the aerogels and the presence of emulsifier (Span 80) in the external surface are especially suitable to favor PCL-aerogel interaction for the preparation of scaffolds.

PCL-based scaffolds containing aerogels had 60-70% porosity, macropores in the 100-300 µm range (Fig. 2) and incorporation yields of DX close to 100%. High pore interconnectivities (84-94 %), mesenchymal stem cell infiltration capacities (87-93%) and water permeabilities (3-12·10^{-12} m^2) were obtained for the three scaffolds. Hence, scaffolds had a suitable porous network to facilitate biological tissue growth and transport of fluids.

In vivo tests unveiled the compatibility of the aerogel-containing scaffolds with the bone tissue with no signs of inflammation or rejection. The relevance of the presence of the bioactive agent (dexamethasone) in the PCL-SA-DX scaffolds was unveiled by the presence of many ossification foci and their confluence to form new bone (repair percentage of 39% at 14 weeks post-implantation). This newly formed bone had a compact appearance, which is characteristic of mature bone.

Conclusion

Supercritical foaming is a solvent-free technique for the preparation of nanostructured scaffolds with osteogenic activity. The presence of submicron-sized aerogel particles in the scaffolds resulted in improved physicochemical properties for cell colonization and transport of biological fluids. *In vivo* results showed that the medicated scaffolds accelerated the bone repair response.

References

[1]V. Santos-Rosales et al., *Molecules.***2019**, *24*, 871.

[2]A. Salerno et al., *Biofabrication***2017**, *9*, 035002.

[3]L. Goimil et al., *J. CO2 Utiliz.***2017**, *18*, 237.

[4]L. Goimil et al., *J. CO2 Utiliz.***2019**, *31*, 51.

Acknowledgement

Work carried out in the frame of the COST-Action "Advanced Engineering of aeroGels for Environment and Life Sciences" (AERoGELS, ref. CA18125) funded by the European Commission. Work also supported by Xunta de Galicia [ED431F 2016/010 & ED431C 2016/008], MINECO [SAF2017-83118-R], Agencia Estatal Investigación [AEI] and FEDER funds. C.A.G.-G. acknowledges to MINECO for a Ramón y Cajal Fellowship [RYC2014-15239].

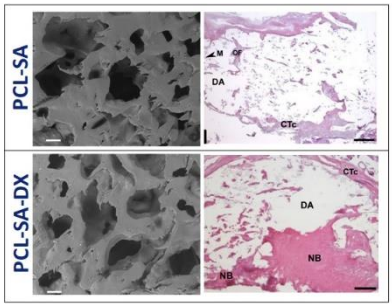

Figure 2. Characterization of supercritically-foamed synthetic scaffolds composed of PCL, SF aerogels and with (PCL-SA-DX, bottom) and without (PCL-SA, top) DX by SEM imaging (left) and *in vivo* experiments in murine model 14 weeks after implantation (right). Notation: CTc=connective tissue capsule; DA= defect area; NB=new bone; OF=ossification foci; M=rest of material. Scale bars: 200 µm (left), 1.4 mm (right).

Morphological and biological evaluation of supercritically-foamed synthetic bone scaffolds
Figure 2. Characterization of supercritically-foamed synthetic scaffolds composed of PCL, SF aerogels and with (PCL-SA-DX, bottom) and without (PCL-SA, top) DX by SEM imaging (left) and *in vivo* experiments in murine model 14 weeks after implantation (right). Notation: CTc=connective tissue capsule; DA= defect area; NB=new bone; OF=ossification foci; M=rest of material. Scale bars: 200 µm (left), 1.4 mm (right).

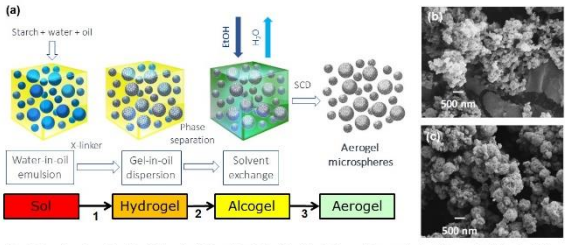

Figure 1. Preparation of aerogel particles: (a) Processing by (1) emulsion-gelation followed by (2) solvent exchange to ethanol and (3) supercritical CO_2-assisted drying. Using this approach, submicrometric (b) silk fibroin (SA, particle size of *ca.* 300 nm, BET-surface area of 400 m^2/g) and (c) corn starch (StA, particle size of *ca.* 600 nm, BET-surface area of 100 m^2/g) aerogel particles were obtained.

Preparation of aerogel particles
Preparation of aerogel particles: (a) Processing by (1) emulsion-gelation followed by (2) solvent exchange to ethanol and (3) supercritical CO_2-assisted drying. Using this approach, submicrometric (b) silk fibroin (SA, particle size of *ca.* 300 nm, BET-surface area of 400 m^2/g) and (c) corn starch (StA; particle size of *ca.* 600 nm, BET-surface area of 100 m^2/g) aerogel particles were obtained.

PS1-05-123

Spacer fabrics as reinforcement structure of hydrogels in tissue engineering applications

Nikola Glimpel[1], Keita Ito[2], René van Donkelaar[2], Thomas Gries[1], Andreas Blaeser[1], Benedict Bauer[1]

[1]RWTH Aachen University, Department of Medical Textiles and Biofabrication, Institut für Textiltechnik, Aachen, DE; [2]Eindhoven University of Technology, Department of Biomedical Engineering, Orthopaedic Biomechanics, Eindhoven, NL

Introduction

Hydrogels are well suited for the three-dimensional cultivation of cells. Due to their high water content and their cell adhesion motifs, they offer a favorable biological environment. Moreover, the structure of hydrogels resembles the extracellular matrix structure of many native human tissues. Therefore, hydrogels are often used in tissue engineering applications. However, hydrogels lack mechanical strength and form stability which is a disadvantage in tissue engineering, especially in load bearing areas. To overcome this shortcoming, hydrogels can be reinforced with fibers. Warp knitted spacer fabrics are particularly suitable as reinforcement structure. Spacer fabrics consist of two surface areas which are connected by a perpendicular pile yarn. The mechanical properties, as well as the pore size and porosity of spacer fabrics, are well adjustable. Moreover, warp knitted spacer fabrics can easily be filled with a cell-laden hydrogel.

Experimental Methods

The aim of this study was the mechanical and biological evaluation of a warp knitted spacer fabric as reinforcement structure of a cell-laden hydrogel for different tissue engineering applications. The surfaces of the spacer fabric were warp knitted with a polycaprolactone (PCL) multifilament while a PCL monofilament was used as pile yarn. PCL degrades over a time period of up to several years without acidic byproducts. Mechanical properties such as tensile strength and elasticity as well as pore size and porosity matching those of selected natural human tissue were targeted. The scaffolds were filled with collagen and agarose hydrogel. Biaxial and uniaxial tensile testing, as well as compression testing, was performed to evaluate adhesion between hydrogels and fibers, tensile and compressive modulus, and strength of the composite. To evaluate the biocompatibility of the developed composite, the spacer fabrics were filled with a cell-laden hydrogel. Survival, morphology, and distribution of the cells were examined.

Results and Discussion

The mechanical, as well as the biological evaluation of the composite scaffolds, promise a broad range of application of the scaffolds in tissue engineering. The mechanical properties, as well as the pore size and porosity, could be adapted to the mechanical properties of the respective musculoskeletal tissue. The biological evaluation revealed that the increase in mechanical properties did not go to the expense of the good biological environment of the hydrogels.

Conclusion

The developed hybrid scaffold offers huge potential for versatile tissue engineering applications in the future. Its mechanical properties, such as tensile as well as compressive modulus and strength, can be modulated easily to mimic the mechanics of bone, cartilage and muscle tissue. At the same time, the infiltrated cell-laden hydrogels offer optimal conditions for tissue ingrowth in prospective implants.

PS1-05-124

Multi-structural collagen scaffolds to reconstitute complex tissue architectures

Marit Baltzer, Hagen Baltzer, Ina Prade, Enno Klüver

Research Institute for Leather and Plastic Sheeting, Collagen, Freiberg, DE

Introduction

Mimicking the natural structure of 3D-tissues is an essential step to enhance the quality of cell culturing *in vitro.* 3D scaffolds with a porous structure or a membrane-like shape are available by many suppliers. However, those cell matrices are limited in dimensions, functionality and complexity and made of different material compositions. The aim of the project is the production of 3D scaffolds with different tissue architectures including pores, barriers and channels by using insoluble collagen as biomaterial.

Experimental Methods

The scaffolds structures were obtained from porcine collagen dispersions. The skins were decellularized using different cleaning steps to eliminate foreign proteins and to reduce the DNA content to < 50 ng/mg dry mass. The clean skins were chopped with a mincer into a granule, swollen in hydrochloric acid solution and dispersed into a homogeneous slurry in a dispersion plant. This slurry was used to produce different collagen structures including membranes, channels and porous scaffolds.

The multiple structures of the scaffolds were realized by combining different drying techniques, like lyophilization and convective drying, and extrusion processes. The pores were generated by lyophilization using a dry mass content between 1-3 %. Changing the pH of the slurry before freeze drying resulted in a closed surface on top of the scaffold serving as a barrier or outer layer for epithelial cell adhesion. For this one-step process the pH of the slurry was increased to 5.5 and filled in multi-well plates. After a short settling time the slurry was lyophilized with a defined freeze and dry regime. Separate membranes were prepared by convection drying of the slurry in a petri dish. The hollow fibers were made by extrusion of a highly concentrated slurry (> 4 %) using a special nozzle. The strand was extruded directly into a solvent bath to drain the fibers. To integrate the hollow fibers into the scaffolds, dry strands were surrounded with collagen slurry and lyophilized. All materials were cross-linked, dried and sterilized.

Results and Discussion

The pore structure is mainly influenced by the dry mass content and the pH of the collagen slurry. Additionally, the lyophilization regime forms the pores. Deep and static temperatures (<-30°C) result in very small pores, which are not usable for cell culturing. Freezing of the slurry with a gradient of 1K/min from 20 °C down to -30°C led to pore sizes about ~150 µm and an open pored scaffold promoting cell migration and supply of nutrients. The closed top layer of the scaffold showed a relatively smooth surface and enabled the growth of endothelial cells. Further cell culture experiments confirmed the suitability of the multi-structural scaffold. Using a self-made scaffold support (see picture 1), it was possible to perfuse the integrated hollow fibers with culture media. For this purpose, the support (mark 1) contains perfusion ports (mark 2) and channels equipped with a syringe for cell inoculation (mark 4). The same port (mark 3) was used for the perfusion of the culture media. In co-culture experiments it could be shown that two different cell types are able to grow within a multi-structural scaffold containing channels, a porous matrix and a

closed top layer. The size of the scaffolds was 10 x 10 x 5 mm. Moreover, the scaffolds were used to mimic the natural architecture of the heart wall and to cultivate cardiomyocytes for several days.

Conclusion

Offering specific tissue structures is a promising tool to improve 3D co-culturing approaches. The methods of production, combined in this project, can be used to generate more complex medical products like cardio patches or perfused tissues.

References

R. Mecham, ISBN 3642165559 Springer Science & Business Media, 2011
F.J. O'Brien et al., Biomaterials 26(4), 433-41 (2005)
P.M. Crapo et al., *Biomaterials* 32(12), 3233–43 (2011)
L.H.Y. Graceet al.; J. Emerg. Investig, 1-9 (2012)

Acknowledgement

We acknowledge the funding of this project by the BMWi (Innokom Ost MF).

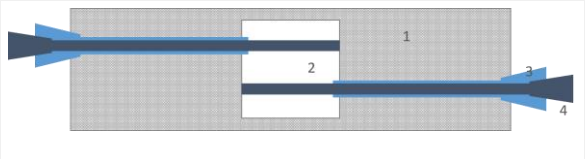

Picture 1
Topview of the perfusable scaffold support system (1- support, 2- scaffold, 3- port for perfusion, 4- needle)

PS1-05-125

Hybrid scaffolds for architecture-induced endochondral healing of large bone defects

Martina Tortorici[1,2], Georg Duda[1,2], Hans Leemhuis[3], Christoph Gayer[4], Sara Checa[1,2], Ansgar Petersen[1,2]

[1]Charité – Universitätsmedizin Berlin, Julius Wolff Institut, Berlin, DE; [2]Charité – Universitätsmedizin Berlin, Berlin-Brandenburg School for Regenerative Therapies, Berlin, DE; [3]Matricel GmbH, Herzogenrath, DE; [4]Fraunhofer-Institut für Lasertechnik, Aachen, DE

Introduction

Endochondral ossification (EO) is the process by which bone is formed during foetal development and childhood growth, while it does not take place in adult bone anymore. Previous studies[1] proved that collagen-I-based guides with highly orientated pores induced EO in a rat osteotomy model, indicating biomaterial architecture as a key parameter in the development of treatment strategies for large bone defects. However, direct clinical translation is impeded by the low stiffness of collagen under compression, which leads to loss of pore orientation and interruption of the EO-based healing process. Here, we included a 3D-printed polymeric support structure into the collagen guides to generate a hybrid scaffold with load bearing capabilities at tissue-level and favourable biological properties at cell-level.

Experimental Methods

The support structure was designed to feature a small strut diameter of 500 µm and a high porosity (> 75%) not to hinder the bone regeneration process. Support structures were produced by selective laser sintering from polyamide 12 (PA, commercial supplier). After immersing the support structures into a collagen dispersion, directional freezing and freeze-drying were applied to pattern the collagen into a highly aligned guiding structure (in cooperation with Matricel GmbH, Germany). Pore morphology and the connection between collagen guide and PA support were visualized by second harmonic imaging (SHI) and scanning electron microscopy (SEM). Mechanical compression tests were performed on support structures, collagen guides and hybrid scaffolds. Moreover, cell recruitment and organization was compared between collagen guides and hybrid scaffolds by *in vitro* cell culture, immunofluorescence and confocal microscopy.

Results and Discussion

Both SHI and SEM images revealed no impairment of the aligned, channel-like pore architecture of the collagen guide when incorporating the support structure. This result held true also when varying the collagen content between 0.5 and 1.5 wt-%, thereby allowing a greater versatility in choosing the collagen content-dependent properties of the cell-material interface, such as stiffness. A physical interaction between collagen fibres and the rough surface of the sintered support structure indicated a good connection between the two materials. By integrating the support structure, the elastic modulus was considerably increased from 8.8 ± 1.2 kPa to 9.3 ± 1.0 MPa of pure collagen guides and hybrid scaffolds, respectively. The collagen content had no effect on the elastic modulus of the hybrid scaffolds, indicating that the local mechanical stiffness at the cell-level (controlled by collagen content) can be tuned independently from the stiffness at tissue-level (controlled by the support structure). While cell migration into and extracellular matrix formation inside hybrid scaffolds and pure collagen guides were comparable, the impairment of

pore orientation due to cell-force induced deformations and shrinkage was strongly reduced in hybrid scaffolds after 14 days of cell culture.

Conclusion

Future work will focus on the development of hybrid scaffolds with a degradable polymeric support structure, to obtain a fully-resorbable device for the treatment of large bone defects. Moreover, the *in vivo* behaviour of hybrid scaffolds will be investigated.

References

[1]Petersen et al, Nat Commun, 9:4430, DOI: 10.1038/s41467-018-065042018

PS1-05-126

In vitro and *in vivo* proves of concept for the use of a chemically cross-linked poly(ester-urethane-urea) scaffold as an easy handling elastomeric biomaterial for bone regeneration

Sophie Frasca[1], Géraldine Rohman[2], Sylvie Changotade[2], Salah Ramtani[3], Anne Consalus[2], Credson Langueh[2], Jean-Marc Collombet[1], Didier Lutomski[2]

[1]Institut de Recherche Biomédicale des Armées, Unité de Biothérapie Ostéo-Articulaire, Bretigny sur Orge, FR; [2]Université Paris 13-UMR CNRS 7244, Tissue Engineering and Proteomics team, Bobigny, FR; [3]Université Paris 13-UMR CNRS 7244, Laboratoire de Biomatériaux pour la Santé, Villetaneuse, FR

Introduction

Bone loss can occur as a result of various pathologies, traumas and injuries, and poor bone healing leads to functionally debilitating condition, loss of self-sufficiency, and deterioration in life quality. Given the increasing incidence of facial trauma and the emergence of new procedural techniques, advanced scaffolds are currently developed as substitutes for bone tissue engineering.

Experimental Methods

The present work aims at providing evidences that PCLU scaffolds are suitable biomaterials for supporting both *in vitro* and *in vivo* bone regeneration. For this purpose, *in vitro* studies were carried out to prove the potential of PCLU scaffolds to be colonized by various cells using direct static or dynamic seeding, as well as from outside to inside cell migration; to act as three-dimensional frameworks for cell proliferation; and to allow osteogenic differentiation of hMSC. At last, the *in vivo* osteogenic properties of PCLU scaffolds were also assessed in a rat femoral bone defect model, providing a standardized environment for studies of induction and remodeling of new bone.

Results and Discussion

In vitro assays demonstrated that PCLU scaffolds could be colonized by cells through direct cell seeding and cell migration from outside to scaffold inside. Moreover, PCLU scaffolds could provide a suitable environment for stem cells proliferation in a 3D spatial arrangement, and allowed osteogenic differentiation under appropriate induction. *In vivo* results revealed the osteogenic properties of PCLU scaffolds through a drilled-hole femoral bone defect repair improvement in rats. Using histology and microtomography analysis, we showed that PCLU scaffolds fit well the bone cavity and were eventually entrapped between the newly formed trabeculae. Finally, no sign of inflammation or rejection were noticed.

Conclusion

We developed a chemically cross-linked ε-caprolactone-based poly(ester-urethane-urea) (PCLU) scaffold with a multi-scale and interconnected porosity by a simple and controlled manufacturing process using an emulsion technique. *In vitro* experiments allowed concluding that PCLU scaffolds seemed to possess required osteoconductive properties for osteoprogenitor cell colonization and their further cell differentiation into mature osteoblasts. Thus, PCLU scaffolds seemed to act as three-dimensional frameworks to guide tissue formation. *In vivo* experiments demonstrated the biocompatibility and the osteoconductive and osteoinductive properties of PCLU scaffolds resulting in a better bone reconstruction probably by the recruitment of osteoblastic progenitor cells, then their proliferation

and finally their differentiation into mature osteoblasts. The bioactivity of PCLU scaffolds may be related to its structure, with micropores allowing fluid circulation, leading to degradation of the biomaterial, and macropores acting as a scaffold for bone cells, thus allowing bone growth. The scaffold *in vitro* stability and *in vivo* degradation during the 30 days study were sufficient for the tissue regeneration. We envision that PCLU scaffolds can provide the clinicians with a substitute having appropriate characteristics for the treatment of bone defects.

Acknowledgement

This work was supported by grants from the French *Fondation desGueules Cassées,* the *Délégation Générale pour l'Armement* (DGA) of the French Ministry of Defense and the Interdisciplinary Institute of Experimental Sciences of the *Université Paris 13*.

PS1-05-127

Microstructure and biocompatibility of an eutectoid 3D-Si-Ca-P porous ceramic

Carlos Navalon[1], Patricia Ros[2], Patricia Mazón[3], Piedad N. De Aza[1]

[1]Universidad Miguel Hernández, Instituto de Bioingeniería, Elche, ES; [2]UCAM-Universidad Católica San Antonio de Murcia, Grupo de Investigación en Regeneración y Reparación de Tejidos, Murcia, ES; [3]Universidad Miguel Hernández, Departamento de Materiales, Óptica y Tecnología Electrónica, Elche, ES

Introduction

A new type of ceramic scaffold has been designed and obtained within the sub-system dicalcium silicate (Ca_2SiO_4) - Nurse´A phase ($7CaOP_2O_52SiO_2$). The selected composition was that corresponding to the eutectoid point 69 wt % dicalcium silicate-31 wt % tricalcium phosphtate [1]. The work examines the microstructure and in-vitro biocompatibility of ceramic scaffolds.

Experimental Methods

Polyurethane sponges with desired pore size and geometry were used as templates, which were impregnated via ceramic slurry, squeezed to remove the excess and dried for 1 day at room temperature. Sintering behavior, phase evolution and microstructural changes were analyzed by XRD, SEM-EDX, FTIR, and Hg porosimetry techniques. After physical characterization of the bioceramics, biocompatibility tests were carried out using adult human mesenchymal stem cells (ah-MSCs). Alamar Blue assay and FESEM images were performed in order to study the adhesion, morphology and proliferation of ah-MSCs.

Results and Discussion

The results of the scaffold obtained showed a biphasic calcium silicophosphate with a high porosity (95%) and an interconnected structure of macro (40% within 150-1µm) and micropores (5% within 250-4 nm). The morphology presents an irregular eutectoid microstructure of lamellae type composed of alternate layers of Nurse´A phase and dicalcium silicate.

Ah-MSCs tests showed an increased in metabolic activity gradually, as well as an adequate morphology over the surface of the bioceramic. Cells covered the complete bioceramic surface heterogeneously, individually or in small groups, showing its characteristic cytoplasmic extensions (filopodia), in order to increase their adhesion.

Conclusion

By using the subsystem $7CaOP_2O_52SiO_2$-$2CaO{\cdot}SiO_2$, a biphasic 3D porous ceramic scaffold with chemical composition 31 wt.% TCP-69 wt.% C_2S, and particular topography, which resemble the lamellar structure of the eutectoid composition (Fig 1 A), was created. In addition, cell *in vitro* tests showed a good biocompatibility of these bioceramics. For this reason, they could be considered useful and adequate scaffolds in regenerative medicine, although more *in vitro* experiments will be necessary to complete this study.

References

1. V. Rubio, M. A. de la Casa-Lillo, S. de Aza, P.N. de Aza. The System $Ca_3(PO_4)_2$-Ca_2SiO_4: The Sub-System *Ca_2SiO_4-$7CaOP_2O_52SiO_2$. J. Am. Ceram. Soc, 94[12] (2011) 4459-4462.*

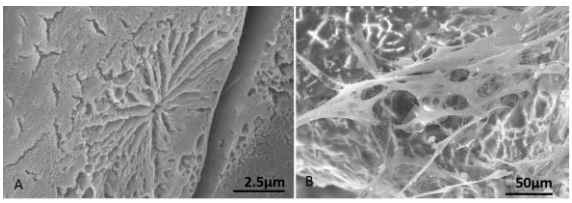

Fig. 1 SEM micrographs of (A) the scaffolds microstructure, and (B) ah-MSCs over the surface

PS1-05-129

Electrospun scaffolds based on polyhydroxyalkanoates/olive leaf extract for tissue engineering applications

Jose G. De la Ossa-Guerra[1,2], Bahareh Azimi[3,4], Maria Beatrice Coltelli[3,4], Andrea Lazzeri[3,4], Rossella Di Stefano[2], Serena Danti[3,4]

[1]University of Siena, Dept. Life Sciences, Siena, IT; [2]University of Pisa, Dept. of Surgical, Medical, Molecular Pathology and Emergency Care, Pisa, IT; [3]University of Pisa, Dept. of Civil and Industrial Engineering, Pisa, IT; [4]Interuniversity National Consortium of Materials Science and Technology, INSTM, Florence, IT

Introduction

Olea europaea is a plant known its high antioxidant capacity and responsible of many health benefits (e.g reduction of hypertension, prevention of cardiovascular problems, and suppression of different types of cancer and viral diseases) [1]. Poly (3-HydroxyButyrate-co-3-HydroxyValerate) (PHBHV) is natural polyester produced from renewable sources by a great variety of microorganisms. PHBHV is, in fact, a copolymer of the highly popular poly(hydroxybutyrate) which is largely tested as implantable biomaterial in medical studies and display excellent biocompatibility and biodegradation properties [2]. The purpose of this study was to prepare PHBHV fibers containing Olive Leaf Extract (OLE) using electrospinning method for the development of a novel scaffolds with healing and tissue regeneration capacity.

Experimental Methods

The characterization of OLE was performed by HPLC with a System Gold Solvent Delivery module (Pumps) 125, System Gold UV/VIS Detector 166, Detector set to 278 nm. The determination of total polyphenols (TP) was performed by Folin and Ciocalteau method (Ainsworth et al., 2007). PHBHV (Sigma-Aldrich code: 403121), was dissolved in a dichloromethane/methanol (10:1 w/w) mixture and OLE (3 wt %) was added to the solution and the solution was electrospun into fibers using a voltage of 30 kV, flow rate of 1 ml/min and humidity of 58% (Linari s.r.l., Pisa, Italy). Morphological properties of electrospun fibers were investigated using Scanning Electron Microscope (SEM). Human Caucasian Foreskin Fetal Fibroblasts (HFFF2) were cultured in Dulbecco's Modified Eagle's Medium (DMEM), Fetal Bovine Serum 10% (FBS), 2mM L-glutamine, 100 IU/ml penicillin, 100µg/ml streptomycin. The metabolic activity of the cells grown on the scaffolds was measured after 72 h using the AlamarBlue® test following the manufacturer's instructions. The t-test was performed for statistic analysis.

Results and Discussion

The TP content obtained was ranging in 14.99-27.83 mg Gallic Acid Equivalent (GAE)/g due to seasonal differences. The analysis showed that major polyphenol component in OLE is Oleuropein, namely, 2.5 % w/w of OLE. SEM results showed that electrospun fibers have cylindrical symmetry and smooth surface (Figure 1 (a,b)). The presence of OLE inside the fiber did not significantly change the fiber diameter while led to the formation of a few beads in the PHBHV/OLE scaffold. Biological characterization showed that metabolic activity was (58.81% ± 1.68 %) for fibroblasts cultured on PHBHV scaffold, and (56.81% ±0.80%) for fibroblasts cultured on PHBHV/OLE scaffold, with no significant difference (p = n.s.) (Figure 2).

Conclusion

The results demonstrated the potential of the PHBHV/OLE scaffolds in healing and tissue regeneration.

References

1. Sahin. S. and Bilgin M, J Sci Food Agric, 2018, 98, 127
2. Radu. I., et al., Front Pharmacol, 2017, 8, 508.

Acknowledgement

The authors gratefully acknowledge the BBI-JU funded project PolyBioSkin (grant agreement number 745839) for supporting this research.

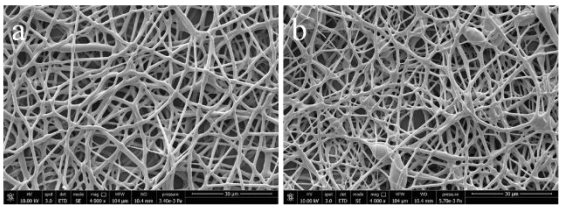

Figure 1.
SEM images of a) PHBHV and b) PHBHV /OLE scaffolds

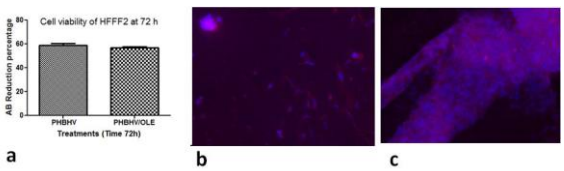

Figure 2.
a) AlamarBlue cell viability. Merge immunofluorescence images of HFFF2 Cells cultured on b) PHBHV scaffold and c) PHBHV /OLE scaffold.

PS1-05-130

Fabrication and characterization of NCO-sP(EO-stat-PO) crosslinked and functionalized electrospun gelatin scaffolds for tissue engineering applications

Mehmet Berat Taskin, Christina Wiesbeck, Jürgen Groll

University Hospital of Würzburg, Department for Functional Materials in Medicine and Dentistry, Würzburg, DE

Introduction

Gelatin is widely studied in tissue engineering, regenerative medicine and drug delivery field mainly because of its excellent biocompatibility and accessibility. However, in order to improve mechanical stability of gelatin in aqueous environment, an additional crosslinking step is necessary. The conventional approaches for the crosslinking of gelatin often rely on various ways of chemical crosslinking which could leave toxic traces in the biomaterial or interfere with the cell adhesion cues on the peptide sequences. Here in, we employ electrospinning technique to fabricate fibrous gelatin scaffolds that are crosslinked with six-arm star-shaped poly(ethylene oxide-stat-propylene oxide) with NCO terminal groups (NCO-sP(EO-stat-PO)). The versatility of NCO-sP(EO-stat-PO was previously shown in studies such as specific bioactivation of synthetic bio-inert polymers[1] and crosslinking of hyaluronic acid[2]. Various ratios of NCO-sP(EO-stat-PO)/gelatin solution were prepared and their electrospinability were tested. The scaffolds were further characterized for e.g. mechanical endurance and stability in the aqueous conditions. The biocompatibility of the scaffolds was validated with in vitro cell studies by culturing Raw 264.7 cells.

Experimental Methods

Varying amount gelatin and NCO-sP(EO-stat-PO) were dissolved in 1,1,1,3,3,3-Hexafluoro-2-propanol (HFIP) and tetrahydrofuran, respectively and the two solutions were mixed to obtain homogenous spinning solutions. Thereon, fibrous NCO-sP(EO-stat-PO)/gelatin meshes were prepared by electrospinning. Electrospinability and the morphology of the fibers were visualized with SEM. Fibrous morphology of the scaffolds were also visualized after incubation with PBS. Weight loss and FTIR analysis complemented the SEM images for the analysis of the water stability of the scaffolds. Contact angle measurements highlighted the hydrophilicity changes on the scaffolds. Uniaxial tensile tests were applied on the scaffolds to observe mechanical features. For the biocompatibility assays, Raw 264.7 cells were cultured on the scaffolds. Briefly WST-8 and Pico green assays were used to analyze cell viability, activity and proliferation behavior.

Results and Discussion

Electrospinning of gelatin solution, prepared in HFIP can be directly spun into fibrous meshes. Electrospinning of NCO-sP(EO-stat-PO)/gelatin (weight ratios ranging from 3:2 to 1:10) blend also resulted in fibrous morphology with only the minor changes in fiber diameters. With increasing NCO-sP(EO-stat-PO) content, the hydrophilicity and the tensile strength of the scaffolds increased. After the incubation in PBS for 3 days, the scaffolds with high amount of NCO-sP(EO-stat-PO) preserved the fibrous morphology better then low NCO-sP(EO-stat-PO) containing scaffolds. This behavior was also supported with weight loss studies, indicating a higher weight loss with decreasing amount of NCO-sP(EO-stat-PO). FTIR studies suggested that weight loss could be mainly due to the washing away of the gelatin rather than NCO-sP(EO-stat-PO). On the other hand, regardless of the NCO-sP(EO-stat-PO)/gelatin ratio, the scaffolds were found biocompatible, evidenced by increasing DNA content and high metabolic activity of Raw

264.7 throughout the 7 days of culture. SEM images of the scaffolds further demonstrated that during the course of cell culture, the fibrous morphology of the scaffolds was preserved and the scaffolds supported the natural cell morphology, spreading and proliferation.(Fig. 1)

Conclusion

Here, we demonstrated the facile use of NCO-sP(EO-stat-PO as a crosslinker for gelatin. It was found that the stability of fibrous scaffolds were dependent on the amount of NCO-sP(EO-stat-PO which, regardless of the ratio, supported the cell adhesion and proliferation. Further studies on the use of gelatin/NCO-sP(EO-stat-PO fibers as a dexamethasone releasing scaffold for the immunomodulatory applications are ongoing.

References

[1] Grafahrend D., Heffels KH, Beer MV., Gasteier P., Möller M., Boehm G., Dalton PD. and Groll J. Degradable polyester scaffolds with controlled surface chemistry combining minimal protein adsorption with specific bioactivation. Nature Materials volume 10, pages 67–73 (2011).

[2] Dhanasingh A., Salber J., Moeller M. and Groll J. Tailored hyaluronic acid hydrogels through hydrophilic prepolymer cross-linkers. Soft Matter, 2010, 6, 618-629.

Acknowledgement

This research was funded by the European Research Council under grant agreement 617989 (Design2Heal). The authors gratefully acknowledge the DFG State Major Instrumentation Programme, funding the crossbeam scanning electron microscope Zeiss CB 340 (INST 105022/58-1 FUGG), and also thank Philipp Stahlhut for assistance with the SEM images.

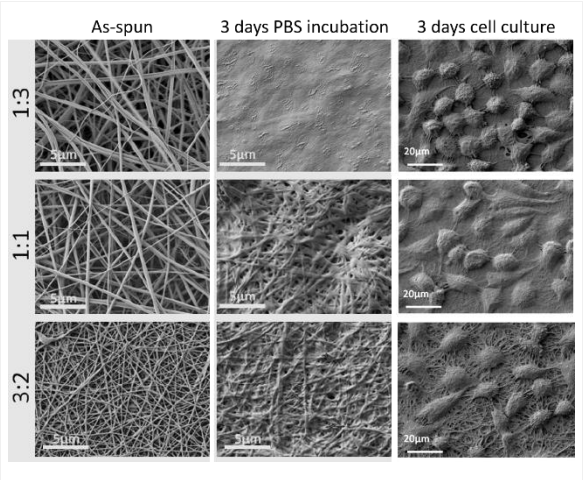

Figure 1
SEM images of NCO-sP(EO-stat-PO/gelatin scaffolds with varying blending ratios as 3:2, 1:1 and 1:3 before and after 3 days PBS incubation and 3 days of in vitro cell culture studies with Raw 264.7 cells.

PS1-05-131

Obtaining Cartilage Extracellular Matrix: A Comparison Between Four Decellularization Methods

Margo L. Terpstra[1], Chris H. A. van de Lest[2,3], Riccardo Levato[1], Jos Malda[1,2]

[1]University Medical Center Utrecht, Department of Orthopaedics, Utrecht, NL; [2]Utrecht University, Department of Equine Sciences, Utrecht, NL; [3]Utrecht University, Department of Biochemistry & Cell Biology, Utrecht, NL

Introduction

A large percentage of the population suffers from the consequences of joint cartilage defects. Because of the poor self-healing capacity of articular cartilage, new strategies to boost cartilage regeneration through biocompatible implantable constructs are needed. In order to fabricate a biomimetic graft that represents both the complex composition and biomechanical properties of native cartilage, a suitable biomaterial is needed. For this, cartilage-derived extracellular matrix (ECM) may be a promising candidate. Due to its natural origin, donor-derived cartilage matrix already contains many proteins and other molecules such as type II collagen and proteoglycans, which are both important for the mechanical strength of articular cartilage.

To use cartilage ECM for implantable constructs, the risk for an uncontrolled host immune response can be minimized by removing cellular content from the cartilage tissue. In this study, four decellularization methods are compared, in order to find a method that can effectively remove cellular content from articular cartilage tissue. Decellularized cartilage ECM (dECM) was characterized by defining its DNA levels, and assessing the content of sulphated glycosaminoglycan (sGAG), type II collagen, and lipid (types).

Experimental Methods

Articular cartilage derived from the stifle joints of 4 equine donors was treated with decellularization methods A, B, C or D (only one donor was used for method D). In method A, freeze-dried cartilage particles were treated with trypsin/EDTA, DNase and RNase, and Triton (Benders et al., 2014). In method B, first small cartilage slices went through six freeze-thaw cycles while being exposed to an osmotic shock. They were then similarly treated with trypsin (no EDTA), DNase and RNase, and Triton (Pati et al., 2014). Method C consisted solely of incubation in peracetic acid and freeze-drying (Huleihel et al., 2016), and method D consisted of supercritical CO_2 treatment (You et al., 2018). After decellularization, the DNA content in the cartilage samples were measured by using the quantitative assay PicoGreen®. Successful decellularization was considered a DNA concentration lower than 50 ng per mg dry weight cartilage. Collagen and sGAG content were respectively quantified by using the assays hydroxyproline and dimethylmethylene blue. Lipid content analyses were performed by using lipodomics. Quantitative data was supported by histological stainings for haematoxylin & eosin, Safranin-O and type II collagen.

Results and Discussion

This study shows that DNA levels were diminished significantly after decellularization of cartilage with all methods. Still, the decellularization threshold was only reached when using method A and B, but not C. This can be explained by the fact that both method A and B consist of several enzymatic, chemical, and detergent steps, while method C solely consists of a single step of peracetic acid incubation. Before, method C successfully decellularized soft tissue (Huleihel et al., 2016), but proves to be insufficient for articular cartilage decellularization. While method D also consists of a single treatment step, supercritical CO_2 treatment lead to a strong loss of DNA. A larger samples size

is needed to confirm sufficient decellularization by this method. sGAG levels were almost completely lost when using method A and B, and strongly diminished when using method D. On the other hand, method C did not affect sGAG levels. Since (s)GAGs strongly influence the water content of cartilage, its reduction is considered an undesired side effect. Lipodomics data analyses revealed a strong loss of the total lipid content after decellularization with method A and B. For all samples, collagen levels remained stable.

Conclusion

Of the four decellularization methods that were compared in this study, method A and B were found to decellularize articular cartilage most effectively. Method D also showed promising results, that first needs to be confirmed by a larger sample size. Method C, on the contrary, did not sufficiently remove cellular content. This suggests that articular cartilage needs a thorough treatment to achieve sufficient cell removal. Samples that were properly decellularized were also subjected to a tremendous loss of sGAGs, and a decrease of total lipid content. In conclusion, this study presents at least two effective decellularization treatments to obtain dECM from donor-derived articular cartilage. This dECM can be further explored as a biomaterial, that can be used in the field of cartilage construct fabrication.

References

Benders et al. Cartilage. 2014 Oct;5(4):221-30.
Huleihel et al. Sci Adv. 2016 Jun 10;2(6):e1600502
Pati et al. Nat Commun. 2014 Jun 2;5:3935.
You et al . Artif Cells Nanomed Biotechnol. 2018 May 4:1-11

Acknowledgement

For the collaboration on one of the cartilage decellularization techniques we acknowledge Henriette Valster and Mees Eerden. This project could not have taken place without the financial support of the European Research Council under grant agreement 647426 (3D-JOINT).

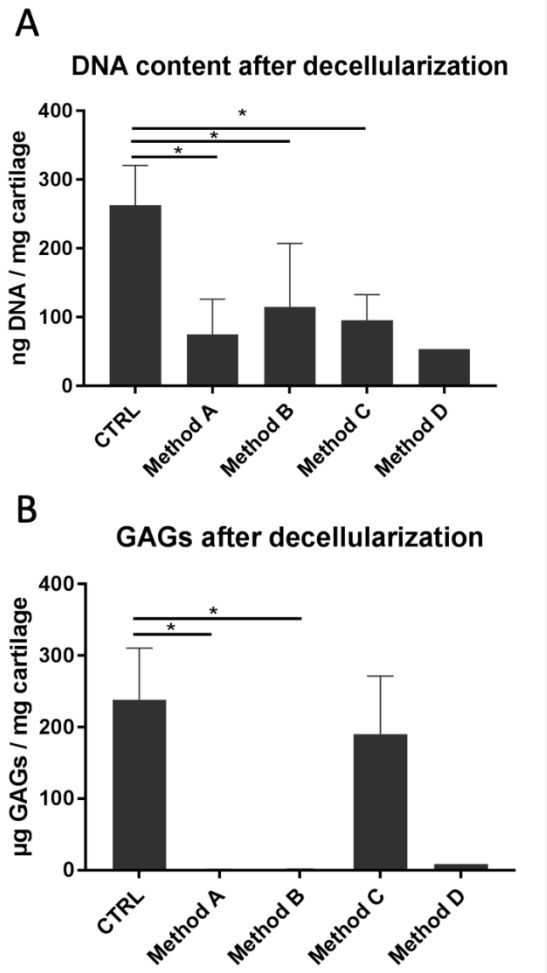

DNA and GAG levels after decellularization
(A) DNA levels in cartilage were significantly decreased after decellularization with method A-D, but only sufficiently with A and B (<50 ng DNA/mg cartilage). (B) Sulfated GAG levels were lost in cartilage after treatment with method A, B, and D. (* represents p<0,05)

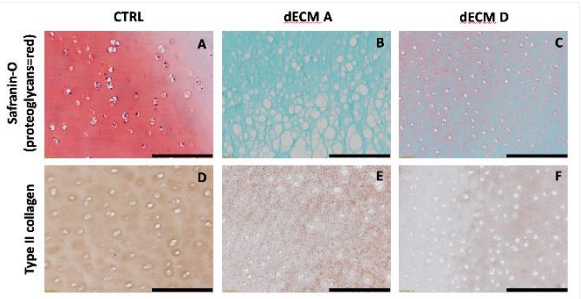

Histological representation of proteoglycans and type II collagen after decellularization
Histological assessment of decellularized cartilage for proteoglycans in red (Safranin-O) and collagen/cytoplasm in green (Fast Green) (A-C). Type II collagen in brown (D-F). *Scale bars represent 200 µm.*

PS1-05-132

Vascular Tissue Engineering: Investigating the effects of Composition and Size of Electrospun Fibers on Cellular Performance

James A. Reid, Alison McDonald, Anthony Callanan

The University of Edinburgh, The Institute for Bioengineering, Edinburgh, GB

Introduction

There are currently a large variety of vascular tissue engineering strategies utilized in the treatment of arterial disease[1]. These range from scaffold materials that mimic the native extracellular matrix (ECM) and promote ECM production to materials that aim to reduce inflammation, thrombogenicity, and promote angiogenesis[1].The gold standard in the treatment of arterial disease is the use of transplanted materials such as the saphenous vein, mammary artery and full scale heart transplants[2]. However, the increasing shortage of available transplantations to combat vascular diseases has led to the advancement of vascular tissue engineering looking at synthetic alternatives[3]. While synthetic grafts do fill the void for people needing surgical treatment, they have much lower patency rates than their natural counterparts[2]. This is where vascular tissue engineering comes into play. Trying to find solutions that promote vascular regeneration leading to fully functional tissues is of crucial importance for the advancement of this field. Herein, we have looked at how the inclusion of native ECM and fiber diameter in electrospun polymer scaffolds affects HUVEC performance and angiogenesis.

Experimental Methods

Electrospun scaffolds were manufactured using different polymer and solvent combinations with the aim of achieving different fiber sizes. Briefly, 8% and 12% w/v polycaprolactone (PCL) solutions in HFIP; and 14% and 19% w/v PCL solutions in 5:1 chloroform:methanol were electrospun at 250 RPM mandrel speed, resulting in four randomly aligned PCL scaffold with different fiber diameters: small (S), medium (M), large (L) and extra-large (XL).

Furthermore, ECM activated bioscaffolds were also manufactured using decellularized native bovine aorta, which was added to the electrospinning solution at PCL:ECM ratios of 97:3 and 88:12. Briefly, the aorta was decellularized using Sodium Dodecyl Sulfate (SDS) perfusion. Scaffolds were punched out (diameter = 10mm) and seeded with human umbilical vein endothelial cells (HUVECs). Various biochemical and biomechanical quantification methods were performed at time points of 1 day, 6 days and 12 days, including cell viability, RT-PCR and mechanical analysis.

Results and Discussion

Fiber diameter and pore width analysis showed that four unique architectures were created, with fibre diameters ranging from 1.64±0.18µm to 4.83±0.49µm (*Figure 1A*). We noted a deeper cellular infiltration in the XL scaffold compared to the three others (*Figure 1B*). Furthermore, relative increases in Cluster of Differentiation (CD31) and Vascular Endothelial Growth Factor(VEGF) gene expression were noted in the XL scaffold after 6 and 12 days (*Figure 1C+D*). These results suggest that increasing fibre diameter and subsequently improving cellular infiltration influenced the angiogenic response of the seeded HUVECs. Furthermore, the inclusion of ECM into the scaffold resulted in altered mechanical properties: including decreased contact angle and increased ultimate tensile strength (*Table 1*). Additionally, cell survival was not affected by the incorporation of ECM, suggesting that native vascular ECMs can be used to modulate the mechanical properties of electrospun scaffolds without altering cellular performance.

Conclusion

This systematic study has shown that altering the size of fibers/pores in electrospun PCL scaffolds influences the performance of HUVECs. We found that larger fibers lead to more cellular infiltration and increased the gene expression of CD31 and VEGF, suggesting an angiogenic response to the larger fibres. Furthermore, we have shown that native ECMs can be incorporated into the electrospun scaffolds to modulate its mechanical properties.

References

1. Ravi S *et al.* Regen Med. 5: 1-21, 2010
2. Pashneh-Tala S *et al.* Tissue Eng Part B Rev. 22(1): 68-100, 2016
3. Altinay L *et al.* JOSAM. 2(2): 130-133, 2018

Acknowledgement

ESPRC no. EP/N509644/1. MRC grant MR/L012766/1.

	PCL:ECM ratio		
	100:0	97:3	88:12
Ultimate tensile strength (MPa)	4.26 ± 0.33	7.58 ± 1.59	7.85 ± 1.03
Failure strain (%)	464 ± 40	452 ± 59	244 ± 29
Contact angle after 5s (°)	98.7 ± 25.2	68.8 ± 43.6	22.2 ± 10.5

Table 1:
Mechanical properties of the scaffolds. Data displayed ± 1 standard deviation.

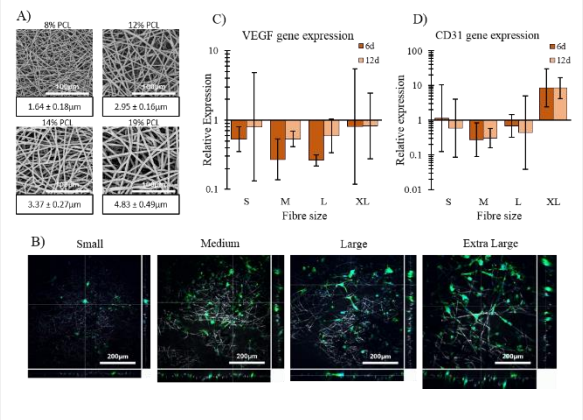

Figure 1:
*RT-PCR gene expression for **A)** VEGF and **B)** CD31. **C)** Representative SEM images of all four scaffolds and their fiber diameters. **D)** Z-stacks showing HUVEC infiltration in all four scaffolds. Green = Phalloidin (actin filaments), Blue = DAPI (cell nucleus). Data displayed ± 1 SD.*

PS1-05-133

Two-photon degradable hydrogels for dynamic control of cellular microenvironments

Qiyang Jiang[1,2], Julieta I. Paez[2], Aránzazu del Campo[1,2]

[1]Saarland University, Chemistry Department, Saarbrücken, DE; [2]INM – Leibniz Institute for New Materials, Dynamic Biomaterials, Saarbrücken, DE

Introduction

Photodegradable hydrogels are promising platforms for cell culture that allow dynamic alteration of material properties and provide insight into how cells respond to physiological and pathological changes from their surroundings. Such models allow answering fundamental questions of live cell functions. These hydrogels enable control in space and time by either incorporating photocleavable crosslinkers or through photocoupling of pendant functionalities. For degradable gels, the physical or chemical cues initially present are subsequently regulated on demand. Reported examples mainly deal with the incorporation of photocleavable linkers by using well established o-nitrobenzyl chemistry. A major limitation of this group for realizing microenvironment changes in situ (i.e. in the presence of cells) with 3D resolution is its poor two-photon absorption cross-section, leading to cell photodamage and loss of function. Therefore, novel strategies towards two-photon cleavable hydrogels are still needed.
In this work, o–nitrophenylpropyl family using the donor-acceptor biphenyl core was selected based on its highly efficient photophysical and photochemical properties under single and two-photon excitation.

Experimental Methods

1. Synthesis of bifunctional two-photon sensitive photo-removable protecting groups.
2. Design, synthesis and property optimization of the 2D and 3D gels: Ligand density, porosity, rheological behavior, crosslinking kinetics, swelling and degradation will be studied.
3. Fundamental studies of cell behavior in cell culture upon light-triggered exposure of particular ligands or alterations in the softness or hardness of their microenvironment.

Results and Discussion

Bifunctional two-photon sensitive photo-removable protecting groups (PRPGs) have been synthesized and the PRPGs showed good photochemical properties.

Conclusion

Synthesized photolytically degradable hydrogels which allow real-time manipulation of material properties and it is promising for more precise 3D resolution and reduced photodamage to cells in dynamic culture models.

References

1. Cole A. DeForest and Kristi S. Anseth, Nat Chem. **3**, 925 (2011)
2. Luis García-Fernández, and Aránzazu del Campo, Adv Mater. 26, 5012(2014)
3. April M. Kloxin, and Kristi S. Anseth. Science. 324,59(2009)

Acknowledgement

Acknowledge China Scholarship Council (CSC) for fellowship funding to QY. Jiang.

PS1-05-134

Cells' distribution during culture in a 3D porous electrospun scaffold in a bioreactor system

Foteini K. Kozaniti[1], Aikaterini E. Manara[1], Dimitrios Charisiadis[1], Meletios Doulgkeroglou[1], Maragarita Georgiou[2], Paschalis Pantsios[1], Dimosthenis Mavrilas[1], Despina Deligianni[1]

[1]University of Patras, Department of Mechanical Engineering & Aeronautics/Laboratory of Biomechanics & Biomedical Engineering, Rio, Patras, GR; [2]University of Patras, Department of Chemical Engineering, Rio, Patras, GR

Introduction

3D porous scaffolds have gained increasing interest in tissue engineering due to their evident advantages in providing more accurately the actual microenvironment where cells reside in tissues. The construction of these scaffolds has many technical limitations when the electrospinning process is used. A stainless-steel mesh can be used as a collector to overcome these difficulties[1]. Furthermore, bioreactors have proved to be crucial tools to initiate, maintain and direct cell cultures and tissue development in a three-dimensional environment[2]. In this study, cell behavior was experimentally investigated during culture in a 3D porous electrospun scaffold, using a bioreactor.

Experimental Methods

Poly-caprolactone pellets were dissolved in glacial Acetic Acid and MWCNTs in powder form were added in the PCL solution with a ratio of 0.5% wt. CNTs to the polymer weight. The electrospinning method was implemented to manufacture the porous composite scaffold. To fabricate a porous layer, a stainless-steel mesh was used as a receiver to replace the traditional collector. Repeating the above procedure, a porous scaffold was obtained by binding multiple layers.

A bioreactor has been employed to perfuse culture medium directly through the pores of the 3D scaffold. MSCs were obtained from umbilical cord and were seeded in the scaffold through a by-pass tube of bioreactor. Different hours of culture (0.5 and 2), numbers of seeded cells (100.000 and 250.000) and flow rates (20 and 40 rpm) were investigated. The MTT reduction assay was used to investigate the viability.

Results and Discussion

Macroscopically, the required multilayered scaffold seems to have the desired mesh textured morphology (Fig.1A & 1B). Figure 1C illustrates indicatively the cell distribution according to MTT assay. The number of cells, present into the scaffold after a certain culture time, is influenced by the seeded cell number, the culture time and the flow rate in a complicated manner. In the case of 30 minutes of culture, increased flow rate leads to increased present cell number. Reverse behavior was noticed for 120 min of culture.

Conclusion

The bioreactor experiments revealed that the flow rate and the time of dynamic culture have an important impact on the number of cells present into the scaffold.

References

[1] J. Song et al, Biofabrication, vol. 9, 015018, 2017.

[2] S. Dermenoudis et al, Journal of Biomechanics, vol. 43, 1426-1431 ,2010.

Acknowledgement

Special thanks are due to Dr. S. Michalopoulos of the Hellenic Cord Blood Bank of Biomedical Research foundation (Academy of Athens) for providing MSCs.

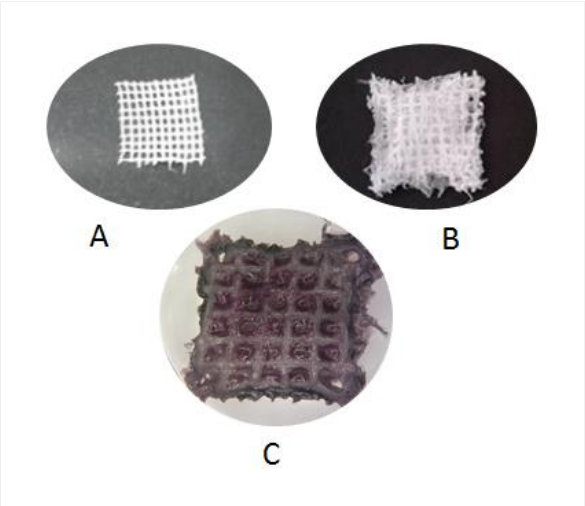

Figure 1
A: One layer of the meshed scaffold, B: The electrospun meshed scaffold, C: MTT assay - Cell distribution on a 10- layer scaffold.

PS1-05-135

Bone regeneration capacity of bioactive glasses containing zinc, osteostatin and mesenchymal cells for the treatment of critical defects in rabbit ulna

Beatriz Bravo-Giménez[1], Clara Heras[2], Lorena Benito-Garzon[3], Daniel Lozano[2], Gonzalo Luengo-Alonso Lozano[1], Sandra Sanchez-Salcedo[2], **Antonio J. Salinas**[2], Maria Vallet-Regi[2]

[1]Hospital Universitario 12 de Octubre, Cirugía Ortopédica y Traumatología, Madrid, ES; [2]Universidad Complutenese de Madrid, i+12 and CIBER-BBN, Dpt Química en Ciencias Farmacéuticas, Madrid, ES; [3]Universidad de Salamanca, Departamento de Cirugía, Salamanca, ES

Introduction

There is a growing need of synthetic bone grafts with enhanced osteogenic capacity for use in bone tissue engineering. In this study, bone regeneration capacity of meso-macroporous 3D-scaffolds based on a mesoporous bioactive glass (MBG) enriched with Zn^{2+} ions, osteostatin (OST) and/or human-mesenchymal stem cells (hMSCS) in New Zealand rabbit ulna is evaluated. The biocompatibility and optimum content of Zn^{2+} ions in the MBG as well as the optimum concentration of OST and hMSC were previously investigated and optimized in cell cultures [1,2]. This communication investigates which combination of the aforementioned components has a greater capacity of bone regeneration.

Experimental Methods

A mesopororous glass with composition 76%SiO_2-15%CaO-4%P_2O_5---4%ZnO (in mo-l%) was synthesized by evaporation induced self-assembly method [2]. Then, 3D cylindrical macroporous scaffolds with dimensions 7 mm diameter and 15 mm length, which in this communication will be denoted “Bioceramic” (B) were obtained by rapid prototyping. B was characterized by N_2 adsorption, XRD, FTIR, NMR, SEM and TEM and then loaded with OST to obtain B+O samples and decorated with hMSC, to obtain B+C samples following a procedure previously described [2]. A last group containing both components B+C+O was also obtained.

32 New Zealand adult rabbits (4-5.5 kg) were intervened by causing a critical bone defect using an osteotomy and subtracting 15 mm in the third half diaphyseal ulna of a front leg [3]. Three groups were established: B+C (9 cases), B+O (8) and B+C+O (8) with follow-up times of 6 and 12 weeks. Moreover, 2 controls of B, one per time were investigated. Of the remaining rabbits, 2 were sacrificed by infection, 2 presented a complete fracture of forearm (ulna associated to radius fracture) and 1 died by unknown cause. After anesthetic induction with equipromacin, animals were anaesthetized with ketamine via intravenous and halothane 4% maintenance via inhalation with mask. Once slaughtered and after taking bone samples, the histological study was conducted [4]. Samples were preserved in ethanol of 96◦ for its fixation and preservation. Subsequently, samples were dehydrated by immersion in ethanol solutions of increased gradation (70◦, 80◦, 90◦ and 95◦) and included 15 d in liquid methyl methacrylate at 4 °C in stirring. Staining protocols used were trichrome of Goldner (TG) and Von Kossa (VK), which distinguish the osteoid of calcified bone as well as the morphology and distribution of the cells in the tissue. The microscopic images of the histological samples were captured using a Nikon digital camera Sight DS-smc coupled to a Nikon eclipse 90i optical microscope, and digitized directly by a MetaMorph Meta Imaging Series 6.1 image capture program.

Results and Discussion

Results obtained show that in the early stages, the bone formation processes are more activated-induced, but at 12 weeks there is not ceramic material and the formation process is stopped. The bone surfaces show signs of remodeling, with zones with resorption marks and others covered by osteoid deposits in the B+O and B+O+C groups. The regenerated bone presents non-mineralized zones, just as the osteocytes are embedded in non-calcified cavities. In the created defect we find fibrous-collagen granulation tissue. And associated with it, a cellular component, more or less marked, composed of macrophages, plasma cells and giant cells. However, in the group of B + O in relation to the bone response, it seems that there is more bone reaction adjacent to the defect cavity, finding more active bone formation processes and a more mature bone.

At 6 weeks, there is more reaction of bone adjacent to the defect cavity in the B+O group, finding more active bone formation processes creating new bone. Taking into account the factor of maturation of the connective tissue in the defect cavity, the B+C group appears presenting a further maturation of this tissue (See the Figure).

At 12 weeks of evolution, and following the same trend of the results in shorter times, the group presenting processes of bone formation is the B+O one. In addition to showing a more uniform response, since the B+C+O group there are substantial differences between the cases, probably based on the less predictable response of cells as a signal for the osteoblastic progenitors differentiation.

Conclusion

The addition of OST or hMSCs improved the bone regeneration capability of B. When cells are added, a greater variability in the obtained results is obtained. Both at 6 and 12 weeks the group presenting processes of bone formation is the B+O one. With regard to the presence of material residues, in all groups they are few or they are absent implying the degradation of material at 12 weeks of implantation.

References

1. Perez R et al. Nanomaterials (2018) 8, 592.
2. Heras C et al. Acta Biomaterialia 89 (2019) 359-371.
3. Mills LA et al. J Bone Joint Surg Br. (2012) 94:865-74.
4. Rai B et al. Acta Biomaterialia (2015) 28, 193-204.

Acknowledgement

Financial support of: Instituto de Salud Carlos III (PI15/00978) co-financed with the European Union FEDER funds, European Research Council (ERC-2015-AdG) Advanced Grant Verdi-Proposal No.694160 and MINECO MAT2015-64831-R project.

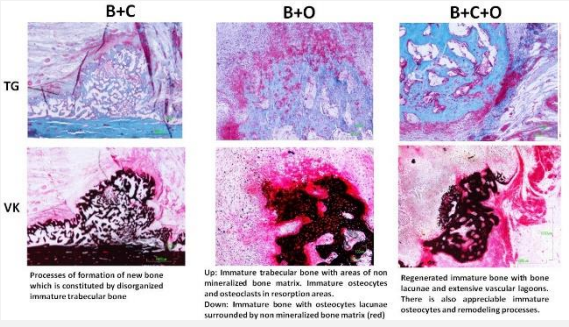

Histological micrographs of three samples after 6 weeks of implantation

PS1-05-136

The effect of gelatine-based scaffold formulation and structure on *in vitro*mesenchymal stemcells viability and osteogenic differentiation

Vanja Kokol[1], Vera Vivod[1], Reneé Unbehau[2], Tomaž Vuherer[1], Bérengère J. C. Luthringer[2]

[1]University of Maribor, Faculty of Mechanical Engineering, Maribor, SI; [2]Helmholtz-Zentrum Geesthacht, Institute of Material Research, Geesthacht, DE

Introduction

The rapid migration of mesenchymal stem cell / osteoblasts at the site of bone defects is an essential prerequisite for an efficient bone repair. Such recruitmenthas been typically achieved by delivery of various growth factors that enhance host cell recruitment, proliferation, and activation, or alternatively by physical guidance. Micro- or nanoscale topography of biomaterials has been shown to affect not only the apparent behaviors of the cells (*e.g*., the direction or speed of migration), but also their functions, such as their signaling and differentiation. Thus, bioactive and biomimetic-structured composite material*(e.g*. gelatine- and magnesium-based) represent an approach, which would lead to a low degradation rate directly after the implantation and during the early tissue-remodelling phase, followed by a higher degradation rate after tissue healing when mechanical integrity is not needed any more. Furthermore, additional biological effects could be induced by loading such a porous scaffold with functional biomolecules like osseoinductive growth factors and natural polyphenols to promote bone in-growth and skeletal healing while inhibiting bacteria adhesion and over-generation of reactive oxygen species.

Natural biopolymers such as gelatine, chitosan, hyaluronic acid, alginate, etc. have been shown to be appropriate organic biomaterials, due to the lack of highly acidic degradation products as well as their bioactivity and osseointegration support, resulting in faster/improved biological interactions with the surrounding tissues. In particular, gelatine, obtained by a controlled denaturation and proteolysis of fibrous insoluble protein, collagen type I, the major constituent of bone extracellular matrix, shows a high potential. This is mainly due to its arginine–glycine–aspartates sequences of amino acids – important in cellular recognition that may intensify the osteointegration, while reducing the adhesion of bacterial colonies.

Experimental Methods

In this frame, we prepared 3D scaffolds from differently formulated solutions using gelatine (to mimic the extracellular matrix of surrounding tissue) with/withoutintegrated bioactive moleculesas antimicrobial active chitosan,quarcetin(to bring also antioxidant properties, thus prevent infection), and bisphosphonatealendronate tostimulate osteoblast differentiation, be crosllinked *in situ*during the freeze-drying process using carbodiimide chemistry. The so prepared scaffolds were evaluated related to their morphological and mechanical, as well as their bioactivity and biological response by means of osteogenic differentiation using human mesenchymal stem cells.

Acknowledgement

This research was financially supported by Slovenian Research Agency and Deutscher Akademischer Austauschdienst-DAAD,according to Slovenian-German Joint Mobility program (project no BI-DE-18-19-002).

PS1-05-137

Fiber-based structures lead to superior mechanical properties in 3D hydrogel systems

Ronny Brünler, Dilbar Aibibu, Chokri Cherif

TU Dresden, Institute of Textile Machinery and High Performance Material Technology, Dresden, DE

Introduction

Hydrogels and Bioinks are promising substances for realizing three dimensional structures for tissue engineering or organ-on-a-chip systems [1]. They may contain living cells and thus have to be deposited at suitable temperatures and renouncing cell damaging cross-linking or hardening processes which occur e.g. in many 3D printing approaches [2]. The viscosity of such hydrogel or bioink systems has to be precisely adjusted to allow cell migration, growth and forming of networks and at the same time avoiding cell immobilization or gravity-driven cell sinking due to unfavorable ratios between the traction forces of the cells and the stability of the hydrogel system. The overall low viscosity and high water content of the (hydro)gel-based materials results in very low strength, dimensional stability and geometric integrity [3].

Fiber-reinforced composites (FRC) are well established in multiple applications for lightweight construction, mechanical and civil engineering, transport and many more [4]. The overall mechanical strength of FRCs may exceed the strength of the matrix material manifold. Since the native structure of the four most important tissue types (connective and supporting tissue, nerve, muscle and epithelial tissue), from which organs such as bones, blood vessels, muscles, tendons and ligaments are formed, consists of fibrous constructs and thus can be reproduced biomimetically with textile structures with particularly high precision [5]. Three-dimensional, complex geometries with interconnecting pore spaces can be created with the help of pre-considered fiber layouts [6–8]. Based on these findings, a novel approach for the combination of hydrogels as matrix system and fiber-based systems as reinforcement structure is presented.

Experimental Methods

Multiple materials such as the biocompatible thermoplastics PCL or PES and the biopolymers chitosan or silk fibroin were processed into fibers with different demand-oriented properties by using spinning plants for melt-spinning and solution spinning. The fibers with adjustable properties were subsequently manufactured into multiple three-dimensional structures by weaving, knitting, warp-knitting, braiding and fiber-based additive manufacturing processes.

The complex fiber-based constructs were infiltrated with polysaccharide hydrogels to serve as reinforcing systems for 3D-hydrogel systems and were extensively investigated with regard to their mechanical behavior.

Results and Discussion

Unique fiber-based structures with specifically adapted geometries, pore-sizes and morphologies were realized and infiltrated with hydrogels. The mechanical behavior was tested under static and cyclic compression and tensile loading.

In comparison to the hydrogels alone, the mechanical strength of the novel fiber reinforced 3D-hydrogel structures was increased manifold. Seeded cells align according to the fiber orientation within the structures that provide excellent overall conditions for cell adhesion and differentiation.

Conclusion

A broad range of biocompatible materials can be processed into fibers via melt spinning and solution spinning. Due to the extraordinary ratio between surface and volume fiber-based structures are predestined for use in medical products by providing large functional surfaces for cell adhesion and interaction on interfaces. The developed textile scaffolds and implants exhibit an excellent strength and offer large, interconnected pore spaces for cells to migrate into the structures and for nutrients to supply the cells or metabolic waste to be removed, respectively. The fibers serve as guidance structure for cells according to their growth direction and also take up the mechanical loads. The wide range of textile technologies allows realizing patient-specific, load-adapted scaffolds and implants for regenerative medicine, mimicking the natural tissue that is to be supported or replaced.

References

[1] Caló, E.; Khutoryanskiy, V. V.: Biomedical applications of hydrogels: A review of patents and commercial products. In: European Polymer Journal 65 (2015), pp 252–267

[2] Chimene, D.; Lennox, K. K.; Kaunas, R. R. et al: Advanced Bioinks for 3D Printing: A Materials Science Perspective. In: Annals of Biomedical Engineering 44 (2016) 6, pp 2090–2102

[3] Ahmed, E. M.: Hydrogel: Preparation, characterization, and applications: A review. In: Journal of Advanced Research 6 (2015) 2, pp 105–121

[4] Cherif, Ch.: Textile materials for lightweight constructions: Technologies - methods - materials - properties. Springer 2011

[5] Wintermantel, E.; Ha, Suk-Woo: Medizintechnik - Life Science Engineering. Springer, 2009

[6] Brünler, R.; Aibibu, D.; Wöltje, M. et al: In silico modeling of structural and porosity properties of additive manufactured implants for regenerative medicine. In: Materials Science and Engineering: C 76 (2017), pp 810–817

[7] Brünler, R.; Hild, M.; Aibibu, D.; Cherif, C.: Fiber-based hybrid structures as scaffolds and implants for regenerative medicine. In: Koncar, V.: Smart Textiles and their Applications. Elsevier, 2016, pp 241–256

[8] Aibibu, D.; Hild, M.; Wöltje, M.; Cherif, Ch.: Textile cell-free scaffolds for in situ tissue engineering applications. In: Journal of Materials Science: Materials in Medicine 27 (2016) 63

2:45 p.m. – 3:45 p.m.

Hall 1 / Exhibition Area

PS1-06 | Technologies

PS1-06-138

Electrical stimulation system for *in vitro* culture of mouse osteoblastic cells (MC3T3-E1)

Beatriz Olalde[1], Iratxe Madarieta[1], Beatriz Diez-Buitrago[1,2], Nerea Briz[1], Goran Bijelic[1]

[1]TECNALIA, Biomaterials Area, San Sebastian, ES; [2]CIC biomaGUNE, San Sebastian, ES

Introduction

Electrical stimulation (ES) has been shown to promote healing and regen-eration in skin, bone, muscle, and nerve tissues in clinical studies [1]. In last years, some studies applying electrical stimulation to influence *in vitro* cell behaviour associated with proliferation, differentiation, and migration were published [2,3]. In this work, different systems and conditions for *in vitro* electrical stimulation of mouse osteoblastic cells (MC3T3-E1) were designed, developed and studied.

Experimental Methods

Platinum wires electrodes and screen printed electrodes integrated in cell culture microtiter plates were the systems developed for this research:

- *Platinum wires electrodes (Fig.1):* electrical stimulation (ES) cell culture chamber consisted of L-shaped platinum electrodes, separated by a distance of 22 mm, and secured to the lid of 6-well cell culture plates and connected to an electrical power supply developed by TECNALIA. MC3T3-E1 were seeded in 6-well cell culture plates (TPP) and daily stimulation (1 h/d) for 7 days was carried out to investigate the effect on cell behaviour.
- *Planar electrodes (Fig.2):* first, a screening on PS surfaces selectively modified with different functional groups (amines, thiols, alquenes, chlorosulfonil, carboxylic and epoxies) were made and evaluated like a cell culture substrate. MC3T3-E1 cell viability on different chemically modified PS substrates was carried out. Non-cytotoxic screen printed planar electrodes on aminated PS were designed according to 24 wells microtiter plate design and developed. The electrodes were connected to electrical power supply (developed by TECNALIA), and after cells seeding, daily stimulation under biphasic pulse for 7 days (1 h/d) with three different currents (1, 10, 100 mA) were evaluated to study the cell behaviour.

Results and Discussion

Platinum wires electrodes

WST-1 assay was performed to compare viability and activity of electrically stimulated cells vs. non-stimulated controls. None of the cells exposed to ES DC or pulse showed signs of toxicity. At day 7, electrically stimulated MC3T3-E1 had approximately same percent increase in cell activity than controls. Moreover, according to the microscopy observation in, the typical morphology of MC3T3-E1 cultured was observed in all samples. Both ES mode (DC and pulse) were optimal for MC3T3-E1 in vitro stimulation.

Planar electrodes

Cell viability under biphasic pulse for 7 days (10 ms pulse duration, 1 Hz frequency, 1 h/d) with three different current (1, 10, 100 mA) was checked. The result indicated that the cell viability decreased with current increasing. Interestingly, cell viability under current of 1 mA stimulation did not decrease. Therefore, the novel planar electrode design could successfully use for ES in vitro, showing the highest cell viability when 1mA was applied.

Conclusion

Electrical stimulation effect on MC3T3-E1 cells were evaluated, showing different cell behaviour under different conditions. On the other hand, an electrical stimulation system for *in vitro* cell culture microtiter plates was demonstrated, developing non-cytotoxic screen printed electrodes on cell adhesive functionalized PS substrate.

References

[1] S. Mobini, L. Leppik, J.H. Barker, Direct current electrical stimulation chamber for treating cells in vitro, Biotechniques. 60 (2016) 95–98. doi:10.2144/000114382.

[2] S. Mobini, L. Leppik, V. Thottakkattumana Parameswaran, J.H. Barker, In vitro effect of direct current electrical stimulation on rat mesenchymal stem cells , PeerJ. 5 (2017) e2821. doi:10.7717/peerj.2821.

[3] Z. Liu, L. Dong, L. Wang, X. Wang, K. Cheng, Z. Luo, W. Weng, Mediation of cellular osteogenic differentiation through daily stimulation time based on polypyrrole planar electrodes, Sci. Rep. 7 (2017) 1–10. doi:10.1038/s41598-017-17120-8.

Acknowledgement

This work was financially supported Basque Government (ELKARTEK 2018. M4B.Descubrimiento de nuevos fármacos para enfermedades óseas)

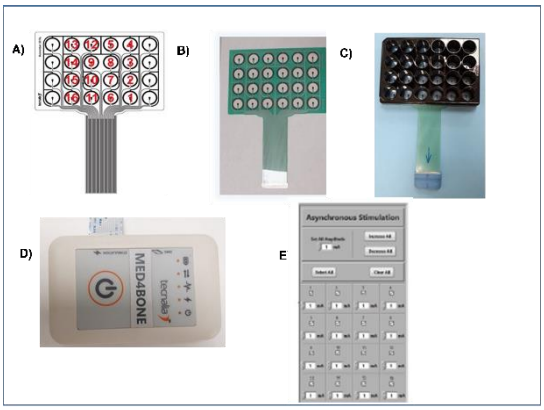

Figure 2.
Screen printed electrodes for 24 well microtiter plates electrostimulation system. A) design of electrodes, B) non-cytotoxic screen printed electrodes surface, C) cell culture plate with screen printed electrode Surface attached, D) electrical stimulation device E) software to control stimulation conditions.

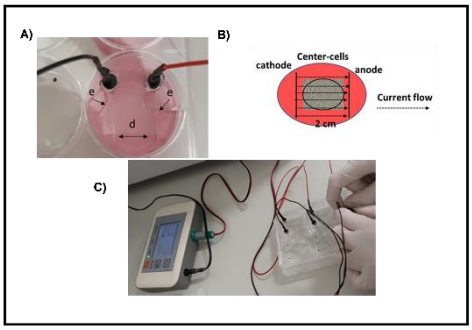

Figure1.
Platinium wires electrical stimulation devices. A) details of platine wires integrated in cell culture system, B) diagram of theoretical direction of electric current, C) cell culture system with electrostimulation device.

PS1-06-139

Polycaprolactone (PCL)-Graphene porous hollow fibers for cell culture bioreactors

Ana Ayerdi[1], Oana David[2], Maider Muñoz[3], David Otaegui[3], Garbiñe Atorrasagasti[1], Goran Bijelic[1]

[1]Fundación TECNALIA, Biomaterials area, San Sebastian, ES; [2]Fundación TECNALIA, Materials and energy and environment processes, San Sebastian, ES; [3]Instituto Biodonostia, Multiple Sclerosis area, San Sebastian, ES

Introduction

2-dimensional tissue culture has been used for over 75 years to study cells and their responses *ex vivo*. However, cells grown in 3-dimensional culture systems reproduce more successfully *in viv*o-like behaviors fo cells. Hollow fiber bioreactors are a 3D culture system that consist of fibers fixed into a module with cells seeded on the fibers and media delivered through the module[1].To overcome many limitations that currently exist in bioreactor systems that could hinder their use as *in vitro* systems for neuronal cell culture, novel polycaprolactone (PCL)-Graphene hollow fibers with different porous sizes have been synthesized to be used in a cell culture bioreactor.

Experimental Methods

Polycaprolactone (PCL) and PCL- graphene hollow fibers were synthesized with and without graphene by phase inversion spinning process (Fig.1). The purpose of this study was to compare if the incorporated graphene would be beneficial for the cell culture expansion. To validate that the newly synthesized hollow fibers support cell adhesion and proliferation, experiments using astrocytes were conducted. Astrocytes were inoculated in the inner lumen of the hollow fibers and left for different time endpoints (1,3,7 and 14 d). Cells were inoculated at a density of 250000 cells/ml in complete media and cell number adhesion was evaluated using WST-1 substrate, a colorimetric substrate for mitochondrial activity. The absorbance was measured at 450nm. All values were presented as mean ± standard deviation. Samples were run at least in triplicate. Statistical analyses were performed using the Student's t-test and a *p*-value of less than 0.05 was considered significant.

Results and Discussion

Hollow fiber screening was done analyzing cell adhesion, cell proliferation and cell productivity. After 3, 7 and 14 days of cultivation, cell number was determined by colorimetric method. Figure 2 shows a comparison between the final cell number and expansion levels obtained between PCL and PCL graphene fibers. Besides, in terms of cell productivity (cells/day), our culture system enables a continuos cell production during the 14 days, indicating that astrocytes can be produced inside these fibers.

Conclusion

The findings suggest that one of the synthesized fibers supports neuronal cell growth, enabling its use in a cell culture bioreactor. Thus, our results support further development with the PCL-graphene hollow fiber for neuronal cell bioreactors.

References

1.Storm MP, Sorrell I, Shipley R, Regan S, Luetchford KA, Sathish J, et al. Hollow Fiber Bioreactors for In Vivo -like Mammalian Tissue Culture. J Vis Exp (2016) e53431

2. Mizukami A, Soares M, Neto DA, Moreira F, Fernandes A, Feng Y, et al. A Fully-Closed and Automated Hollow Fiber Bioreactor for Clinical- Grade Manufacturing of Human Mesenchymal Stem / Stromal Cells. Stem Cell Rev Reports (2018) 14;141-143

Acknowledgement

The Project is supported by the Basque Government under the program ELKARTEK 2017 [KK-2017/00051]

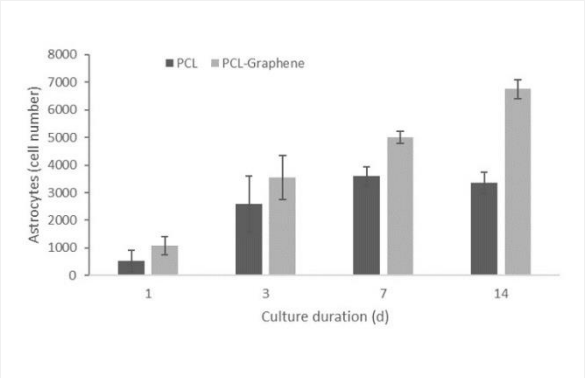

Cell proliferation in the hollow fibers
Quantified astrocytes adhered to the surface of the fibers at different endpoints (1, 3, 7 and 14d)..

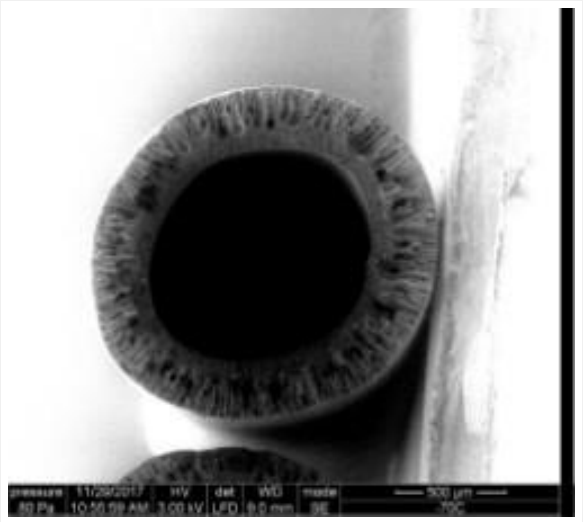

PCL-Graphene porous hollow fiber cross section
Cross-sectional SEM images of PCL-Graphene hollow fibers prepared by phase inversion spinning process

PS1-06-140

Microfabricated systems for studying the pathogenesis of Amyotrophic Laterals Sclerosis (ALS) *in vitro*

Alessandro Polini[1], Alessandro Romano[2], Eleonora De Vitis[1], Velia La Pesa[2], Francesca Gervaso[1], Angelo Quattrini[2], Lorenzo Moroni[3,1], Giuseppe Gigli[4,1]

[1]CNR NANOTEC – Institute of Nanotechnology, Lecce, IT; [2]IRCCS San Raffaele Scientific Institute, Neuropathology Unit, Institute of Experimental Neurology and Division of Neuroscience, Milan, IT; [3]Maastricht University, Complex Tissue Regeneration, Maastricht, NL; [4]University of Salento, Dipartimento di Matematica e Fisica E. De Giorgi, Lecce, IT

Introduction

Amyotrophic Lateral Sclerosis (ALS) is a fatal neurodegenerative disease characterized by progressive loss of the upper and lower motor neurons leading to muscle wasting, paralysis, respiratory failure and death typically within 3 to 5 years after symptom onset. The majority (90%) of ALS cases occur sporadically (sALS) often without a known genetic etiology while the minority of cases (10%) show a clear familial history (fALS). A pathological characteristic of ALS (common to other neurodegenerative diseases; e.g. frontotemporal lobar degeneration, dementia with Lewy bodies, Alzheimer's disease) is the presence of abnormal TAR DNA binding protein 43 (TDP 43) aggregates in the cytoplasm of neurons and glial cells. The role of TDP-43 as a neurotoxicity trigger has been largely investigated *in vitro* and *in vivo* [1] and TDP-43 dysfunctions have been associated with the impairment of numerous cellular processes, such as RNA biogenesis, protein aggregation, axonal transport, ubiquitin proteasome system (UPS), autophagy, and even mitochondrial bioenergetics. However, until now, the exact pathological mechanisms mediated by TDP-43 are far from being elucidated. In ALS, as in many other human diseases, animal models have so far failed to predict efficacy of novel therapeutic approaches and, up until now, most of ALS clinical trials have reported negative results, and no effective disease-modifying treatment is available on the market. In this respect, the development of alternative tools for studying the pathological mechanisms and test new drug candidates, as well as performing human validation assays, is of paramount importance.

Organ-on-a-chip platforms [2,3] are microengineered systems that aim to replicate key units of living organs and organisms, and in particular to reproduce higher-order anatomical and functional features. Here we propose a microfabricated *in vitro* model for studying ALS pathological mechanisms where different neuronal populations, glial and skeletal muscle cells can grow and communicate in a perfusable environment, establishing a basic 3-unit functional motor circuit. This platform will unveil the role of TDP-43 expression/accumulation in each cell type and the subsequent effects on the cell-cell crosstalk will be evaluated.

Experimental Methods

Microfluidic multi-compartmentalized devices were fabricated by SU-8-based multi-level optical lithography and PDMS replica molding, displaying a series of microchannels that connect three different compartments (hosting three different cell types) and promote neurite elongation unidirectionally from one cell compartment to another one. This can be achieved either by few-micron wide straight or funnel-shaped microchannels. Several geometric features as well as microfluidic setups and coating materials were tested in order to obtain successful cell adhesion and culture conditions, and favor intercellular interactions.

Results and Discussion

A family of microfabricated systems showing different perfusable compartments (500 µm wide, 6 mm long) with distinct inlets and outlets, but interconnected through a series of narrow microchannels (2.5-10 µm wide, 250 µm long), were proposed for hosting different cell types. While the microchannels were designed to allow cell-cell communication and unidirectional axonal formation from one cell compartment to the adjacent one, they were optimized to avoid any cell migration through them.

We evaluated the contribution of different coating materials on the adhesion and growth of human neuronal cells (Fig.1). As hypothesized, cells showed differences in their response to the different substrates starting from their adhesion behaviour at 6 hours: they were partially attached in the presence of collagen and fibronectin while they were still round and in suspension on poly-lysine (PLL) and laminin. After one day, only cells grown on fibronectin showed a plastic dish-like morphology as described in literature, developing a cell monolayer, appearing flatter and more substrate-adhesive and showing longer cell processes.

The present platform will be further utilized for more complex studies: 1) Human glial cells will be added to the system and the TDP-43 expression and localization will be investigated in the presence/absence of specific chemical stimuli, by means of immunohistochemistry and protein expression; 2) The motor circuit will be comleted by introducing a muscular cells component in the third cell compartment and the cell-cell interactions will be studied in depth.

Conclusion

We designed a robust microfabricated platform for studying the motor circuit components and the role of TDP-43 in ALS.

References

1. Gao et al., 2018, DOI: 10.1111/jnc.14327
2. Bhatia and Ingber, 2014, DOI 10.1038/nbt.2989
3. Haring et al., 2017, DOI 10.1007/s12015-017-9738-0

Acknowledgement

This work was supported by the Progetto FISR - C.N.R. "Tecnopolo di nanotecnologia e fotonica per la medicina di precisione" - CUP B83B17000010001.

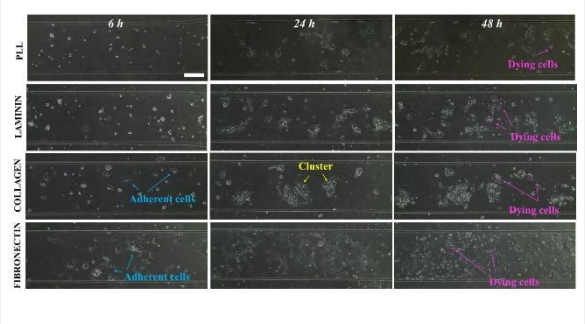

Fig. 1.
Phase contrast microscopy images of neuronal cells grown on different cell substrates (scale bar: 200 µm).

2:45 p.m. – 3:45 p.m.

Hall 1 / Exhibition Area

PS1-07 | Additive manufacturing

PS1-07-141

Robocasting of Sol-Gel Bioactive Glasses and Glass-Ceramics: A Facile Approach for Bone Scaffolds Manufacturing

Elisa Fiume[1,2], Jonathan Massera[3], Francesco Baino[2], Enrica Verné[2]

[1]Politecnico di Torino, Department of Mechanical and Aerospace Engineering (DIMEAS), Turin, IT; [2]Politecnico di Torino, Department of Applied Science and Technology (DISAT), Turin, IT; [3]Tampere University, Faculty of Medicine and Health Technology, Tampere, FI

Introduction

Scaffolds for bone tissue engineering (BTE) have to satisfy a series of minimum requirements in order to induce proper tissue ingrowth and cell migration in the graft [1]. As a result, an adequate control on porosity, pore size and mechanical properties is fundamental. Additive manufacturing (AM) technologies offer the possibility to easily tailor graft properties by controlling both the design and the process parameters, as the object is built starting from a .stl file or a text script [2]. Focusing on bioactive glasses (BGs) and glass-ceramics for BTE, robocasting is considered one of the most powerful direct ink writing techniques for the processing of such materials [3]–[5].BGs and glass-ceramics, in fact, are particularly appreciated due to their capability to chemically bond to the host tissue [6]. However, most of silicate based bioactive glasses with thermal properties adequate for particle sintering suffer from slow dissolution/reaction. This is even further of concerns since scaffolds have a lower surface area than particles typically used in bone regeneration.Compared to the traditional melt-quenching route, sol-gel process offers the possibility to obtain more reactive materials due to the formation of mesopores, which is intrinsic in the process itself [7].This study aims at comparing scaffolds produced by robocasting using sol-gel or melt-derived silicate-based with similar composition.

Experimental Methods

47.5B silicate glass, with composition 47.5SiO_2-20CaO–2.5P_2O_5–10Na_2O–10MgO-10K_2O (mol.%), was produced by traditional melt-quenching route [8] and used as control system. For the synthesis of the equivalent sol-gel material, tetraethyl orthosilicate (TEOS) was hydrolyzed in the presence of 2 M HNO_3 using a H_2O-to-TEOS molar ratio of 20. Triethyl phosphate (TEP), $Ca(NO_3)_2 \cdot 4H_20$, $Mg((NO)_3)_2 \cdot 6H_20$, $NaNO_3$ and KNO_3 were then introduced inproper amounts as oxides precursors. The solution was stirred until a transparent and homogeneous sol was obtained. After gelation at room temperature for 72 h and ageing at 60 °C for 72 h in a sealed container, the gel was dried at 140° C for 48 h to allow the evaporation of the liquid phase. The thus obtained materials were both characterized by Differential Thermal Analysis (DTA) and X-ray Diffraction (XRD) to determine the thermal behavior and the presence of crystalline phases. For the production of the ink for robocasting, gel and glass particles were vigorously mixed with a binder Pluronic F-127 solution (25 wt.%) (35% particles – 65% F-127, wt.%). Due to the higher wettability of the gel, the procedures were adapted to properly extrude the materials through the nozzles (250 and 410 µm for the glass-based and the gel-based ink, respectively). Printing parameters were also adjusted according to the different rheological behavior of the inks.Scaffolds were dried at room temperature for 48 h and sintered at 625 °C for 1 h (Figure 1) on the basis of DTA and XRD results.Bioactivity test and ion release experiments were performed by soaking samples in Simulated Body Fluid (SBF) [9] for 6, 24, 48, 72, 168 and 336 h at 37 °C. The compressive strength of the scaffolds before and after *in vitro* tests was evaluated by crushing tests, and nitrogen adsorption experiments were performed to characterize the textural properties of sol-gel scaffolds.

Results and Discussion

Melt-derived 47.5B glass is characterized by an exceptional bioactive potential in SBF and a wide sintering window [8] that allows highly densified struts to be obtained while preserving the amorphous nature of the system. The present study aimed at further improving the bioactivity of this glass by producing an equivalent sol-gel system, characterized by a higher superficial area and higher reactivity in SBF. It is known how textural properties are able to affect the apatite forming ability of the system by providing more reaction sites for the nucleation of the crystals, thanks to the presence of mesopores. Interestingly, sol-gel route was found to strongly affect the crystallization kinetics upon sintering, leading to the formation of a sol-gel ceramic, as confirmed by the presence of sharp peaks in the XRD spectra.The combined effect of textural properties and crystalline phases on the bioactivity and the mechanical response of this new material and the comparison to the original melt-derived 47.5B glass will be object of discussion.

Conclusion

Six-oxides sol-gel ceramic scaffolds were successfully produced for the first time by AM technology. Up to now, preliminary results confirmed the great potential of this material in BTE applications and further studies are currently ongoing.

References

1. JR Jones. *Acta Biomater*,23:S53-S82,2015
2. R Gmeiner et al. *J Ceram Sci Technol*,6:75-86,2015
3. A Nommeots-Nomm et al. J Eur Ceram Soc,38:837-844,2018
4. S Eqtesadi et al. J Eur Ceram Soc,34:107-118,2014
5. AM Deliormanli et al. J Eur Ceram Soc,32:3637-3646,2012
6. DC Greenspan. Tandläkartidningen Årk,91:1-32,1999
7. F Baino et al. Int J Appl Ceram Technol,15:841-860,2018
8. E Verné et al. J Mater Sci Mater Med,20:75-87, 2009
9. T Kokubo et al. Biomaterials,27:2907-2915,2006

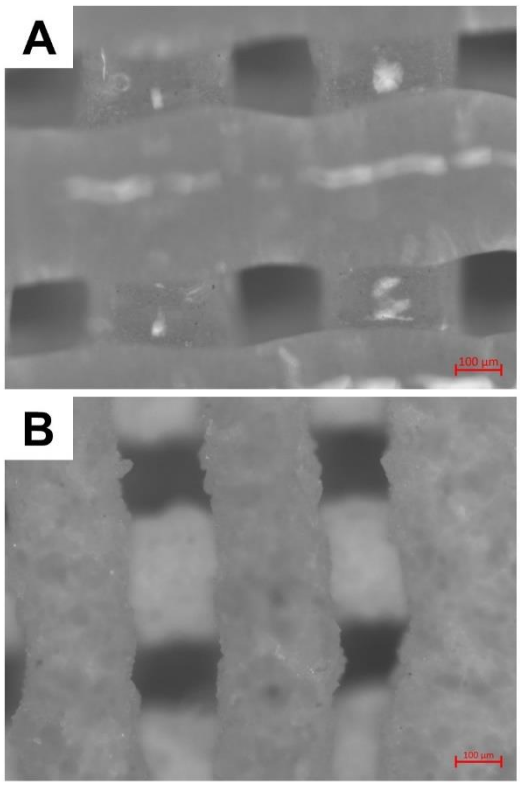

Optical Microscope Imaging
Grid-like 3D architecture of sintered melt-derived 47.5B scaffolds (A) and sol-gel 47.5B scaffolds (B) produced by robocasting.

PS1-07-142

Modified Hyaluronic Acid as bioink for the design of 3D tissue-engineered scaffolds

Ugo D'Amora[1], Alfredo Ronca[1], Maria G. Raucci[1], Hai Lin[2], Yujiang Fan[2], Xingdong Zhang[2], Luigi Ambrosio[1]

[1]Institute of Polymers, Composites and Biomaterials, National Research Council, Naples, IT; [2]National Engineering Research Center for Biomaterials, Sichuan University, Chengdu, CN

Introduction

Hyaluronic acid (HA) has been studied as bioink for additive manufactuiring technologies. Usually, bioinks should be capable to be extruded through a thin needle, to retain a three dimensional (3D) structure, and to create a cytocompatible and suitable environment cells. However, its high solubility, high degradation rate and low mechanical properties limit its use for tissue engineering. Different chemical strategies and crosslinking methods have been pursued to endow HA with shear thinning behavior for extrusion and improve its mechanical properties [1]. In this study, HA was chemically modified and processed to produce 3D scaffolds by bioprinting.

Experimental Methods

HA (M_w=~340 kDa) was modified to graft photoactive polymerizable groups by reacting with methacrylic anhydride (ME) and maleic anhydride (MA) in order to obtain methacrylated hyaluronic acid (MEHA) and maleated hyaluronic acid (MAHA). The materials were investigated in terms of physico-chemical properties to assess the success of the functionalization. The bioprinting was performed using a modified extrusion-based 3D Bioprinter® system from MedPrin (MedPrin Regenerative Medical Technologies Co., Ltd, Guangzhou-China). MEHA and MAHA were dissolved in deionized water containing 2,3 butanedione as biocompatible photoinitiator. The morphology of the structures was investigated by scanning electron microscopy (SEM). Dynamic mechanical analysis was carried out to study mechanical properties of the scaffolds. The scaffolds were bioactivated using a biomimetic method [2]. The cell-material interaction was evaluated by using human mesenchymal stem cells (hMSC). The biocompatibility of scaffolds before and after SBF treatment was evaluated by Alamar blue assay. Furthermore, the effect of scaffolds on differentiation of hMSC through osteoblast phenotype was also investigated. Immunofluorescence analysis using confocal laser scanning microscopy (CLSM) was performed.

Results and Discussion

Nuclear magnetic resonance evidenced for MEHA two peaks (5.6 and 6.1 ppm) corresponding to the introduced methacrylate moieties, whilst for MAHA the peaks (5.9 and 6.6 ppm) were related to the vinylidene proton of the grafted maleic moiety. The materials were characterized by a degree of substitution ranging from 82.6% for MEHA to 87.5% for MAHA. 2,3 butanedione showed optimal photocrosslinking properties, considering the absorption peak and the final properties of the crosslinked materials. The structures were 3D printed and characterized. SEM analyses highlighted a well-organized structure with a fiber diameter of ~200 µm and a porosity of ~700 µm, as also considered in the CAD model. Furthermore, the scaffolds were able to retain their structure without collapse in the Z direction, with lateral pores clearly visible. Mechanical properties of MEHA scaffolds showed values of the storage modulus generally higher then MAHA scaffolds. The biomimetic treatment allowed the formation of hydroxyapatite nuclei (HAp) improving the nanoroughness and bioactivity. The effect of HAp coating on cell proliferation and differentiation

at different culture time was evaluated. The results demonstrated a difference of cell attachment and proliferation among MEHA and MAHA scaffolds. However, the presence of biomimetic coating improved cellular behavior in terms of cell attachment and differentiation. CLSM images demonstrated that cells initially adhered as agglomerates and then a spreading on the material surface was clearly observed.

Conclusion

The obtained results demonstrated the potential use of the MEHA and MAHA as bioinks for tissue engineering applications. In particular, 3D well-organized structures were produced by a modified 3D Bioprinter. To this aim, HA was first chemically modified and then its printability was suitably optimised. The MEHA and MAHA scaffolds showed enhanced mechanical, morphological as well as good biological properties.

References

1. D'Amora U., Ronca A., Raucci M.G., Lin H., Soriente A., Fan Y., Zhang X., Ambrosio L. J. Biomed. Mater. Res. A. 2018. 106, 3079–3089.
2. Tanahashi M., Hata K., Kokubo T. et al. In Bioceramics, Vol. 5, T. Yamamuro, T. Kokubo, T. Nakamuro (Eds). Kobunshi Kankokai: Kyoto, 1992; p. 57.

Acknowledgement

The authors would like to thank the Progetto Premiale di AREA SCIENCE PARK "OPEN LAB - A System of Open Research Facilities" for the support.

PS1-07-143

In-solution Mineralized-Gelatin Bioink System for Injectable Bone graft/ 3D Printing Applications

Sumit Murab, Karl Mueller, Jesse Li, Govind Krishna, Patrick W. Whitlock

Cincinnati Children's Hospital Medical Center, Division of Pediatric Orthopaedics, Cincinnati, US

Introduction

Biopolymer-Mineral composite systems that can be both injected and bioprinted, have great potential for clinical applications in bone tissue engineering. The calcium phosphate ink systems used for 3D printing purposes can't be used to suspend live cells as the solid and stiff matrix will destroy the cells while printing in addition to limiting diffusion of nutrients during culture (1). The present study aimed to develop a bone-mimetic system where hydroxyapatite (HA) particles are synthesized *in situ* in gelatin solution, by using gelatin fibers as a HA nucleation template thus developing a bone like gelatin-HA nanocomposite system. The hypothesis was that introduction of gelatin in the system will form a bone-like nanocomposite and allow the encapsulation of viable cells during bioprinting/ injecting.

Experimental Methods

10% gelatin solution was made in 0.3 M Na_2HPO_4 at 50℃. The volume was made up by slowly adding 0.5M $CaCl_2$ (pH 9.5) while stirring at 700 rpm to maintain a stoichiometric ratio for HA (and at 10X dilution- 0.03 M Na_2HPO_4/0.05M $CaCl_2$). XRD, TEM and ATR-FTIR were performed to analyze the nanocomposite formation between HA and gelatin. Only gelatin and HA were taken as controls. AR500 (TA Instruments) rheometer was used to analyze the viscosity, printability and injectability. The measurements were performed using flat plate geometry (steel) (20 mm diameter) at 25 °C with 500µm of gap distance. The viscosity of the silk hollow microsphere in silk hydrogel system was determined by carrying out a stepped flow test (10–250 s^{-1}, 1 Hz frequency) with increasing shear force rate. Oscillatory stress and strain sweep analysis were performed to establish the linear viscoelastic region for every sample. Subsequently, the storage modulus (G′) and loss modulus (G″) were determined by doing an oscillatory time sweep test for 10 min at a constant frequency of 1 Hz and 5% strain. The recovery kinetics of network destruction was determined by employing a rheological method, which simulates the clinical injection procedure (i.e. single gel destruction upon extrusion through narrow syringes by high shear forces). Viscoelastic properties (G′ and G″) of gelatin-HA composites were measured in an oscillatory time sweep test as a function of time (1 Hz frequency, 1% strain, 5 min) before and after severely destructing the gel network (1 Hz frequency, 1000% strain, 1 min). CELLINK BioX 3D bioprinter was used to print the gelatin-HA (0.5-0.3) composite crosslinked with 500U of tyrosinase enzyme per batch, in a 1×1×0.3 mm 4 layered structure with a 410 µm plastic nozzle at 12 mm/s speed and 200 kPa pressure.

Results and Discussion

TEM study demonstrated the formation of HA crystals in the gelatin network (Fig 1A) resulting in the formation of a tight composite structure while the SAED pattern (Fig 1B) confirmed the crystallinity of the composite. The XRD analysis demonstrated peak for 211 plane in gelatin-HA composite (.3-.5) confirming HA nucleation and crystal formation using gelatin as a template, while the diluted sample demonstrated no HA crystallization (Fig 1C). To our knowledge, this is the first report of in-solution mineralization of gelatin using gelatin polymer chains as a crystallization template. This results in homogenous mineralization; which is essential for printing process and mimics the ultrastructure of bone as a collagen-nanohydroxyapatite composite. The printability of the gelatin-HA composite

was demonstrated by higher elastic modulus (G') as compared to the viscous modulus (G'') that ensures shape retention following printing (Fig 1D). While the injectability test interestingly demonstrated an increase in the elastic modulus of the gelatin-HA composite, which further increased after network recovery (5 min) (Fig 1E). This increase in elastic modulus; may be due to shear induced packing of HA crystals. This indicated that the process of injection (high shear) can potentially enhance the mechanical properties of the grafted material. This could also result into alignment of HA crystals due to shear generated during the printing process through a narrow nozzle, which can potentially help in cellular alignment during 3D bioprinting. The homogeneity of gelatin-HA composite helped in 3D printing a 4 layered, self-supportive structure (Fig 1F). These results demonstrate that the in-solution mineralized gelatin-HA system can be used both for bioprinting and as an injectable bone graft; though the cellular viability and differentiation of cells after bio-printing needs to be studied. This system can be potentially clinically used for treating non-union fractures and collapsing femoral heads due to avascular necrosis.

Conclusion

The study demonstrated an in-solution mineralized gelatin-HA composite system which is both injectable and printable, with bone-mimetic nano-composite ultrastructure. This material system can be potentially used for restoring both the cellular and biomechanical functionality of degenerated bone tissue.

References

1. Ahlfeld T, Doberenz F, Kilian D, et al. Bioprinting of mineralized constructs utilizing multichannel plotting of a self-setting calcium phosphate cement and a cell-laden bioink. Biofabrication. 2018;10(4):045002.

Acknowledgement

This study was supported by the Angela S. M. Kuo Memorial Award 2017 from Pediatric Orthopaedic Society of North America (POSNA) and Cincinnati Children's Research Foundation's intramural funding. We also acknowledge Advanced Materials Characterization Center (AMCC), College of Engineering and Applied Sciences and Chemical Sensors & Biosensors Laboratory- Dept. of Chemistry; University of Cincinnati for providing facilities for various analytical techniques. We are thankful to Dr. Melodie A. Fickenscher and Dr. Necati Kaval for providing help with various techniques.

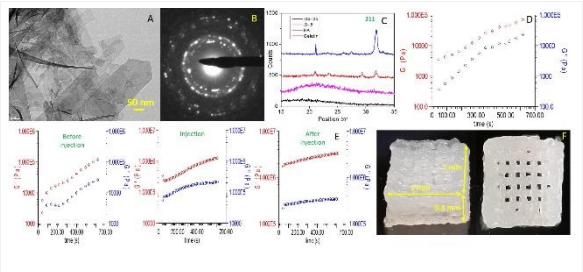

Figure 1
A) TEM micrograph of gelatin HA nanocomposite and B) The corresponding SAED pattern. C) XRD pattern of gelatin-HA nanocomposites. D) Printability and E) Injectability test of gelatin-HA composite system. F) 3D printed scaffolds of gelatin-HA composite system.

PS1-07-144

3D Printing of Lotus Root-Like Biomimetic Materials for Cell Delivery and Tissue Regeneration

Chun Feng[1], Wenjie Zhang[2], Jiang Chang[1], Xinquan Jiang[2], Chengtie Wu[1]

[1]Chinese Academy of Sciences, Shanghai Institute of Ceramics, Shanghai, CN; [2]Ninth People's Hospital affiliated to Shanghai JiaoTong University, Department of Prosthodontics, Oral Bioengineering and Regenerative Medicine Lab, Shanghai Key Laboratory of Stomatology, Shanghai, CN

Introduction

Biomimetic materials have drawn more and more attentions in recent years. Lotus root, has special structure of many parallel channels through over itself. This structure significantly improves the contact area to external environment which effectively promoting air (CO_2, O_2) and moisture (H_2O) exchange with external environment. Implantation of synthetic porous scaffolds into large bone defects, a major clinical challenge, is an expected approach for guiding and stimulating formation of new bone tissues. It is reasonable to speculate that materials with lotus root-like structure will have better osteogenic and angiogenic activities in the regeneration of large bone defects.

Experimental Methods

We fabricated the lotus root-like biomimetic materials with parallel multi-channels structure via a designed 3D printing strategy. We designed new printing nozzles with core/shell embedded structure (Fig. 1). We applied certain amounts of sodium alginate (2.0 wt%) and Pluronic F-127 polymer solution (e.g., 20 wt%) with the under-printed powders (ceramic/metal/polymer powders) to prepare the inks with suitable rheological characteristics and mechanical stability. To explore the functions of the biomimetic materials, we prepared biomimetic scaffolds with different numbers of channels: 1 channel-struts-packed scaffolds, 2 channel-struts-packed scaffolds, 3 channel-struts-packed scaffolds and 4 channel-struts-packed scaffolds (named as 1CSP, 2CSP, 3CSP and 4CSP scaffolds respectively). Traditional solid struts-packed (TSSP) scaffolds were prepared as a control.

Results and Discussion

We prepared the lotus root-like biomimetic materials with different raw materials like ceramics, metal and polymer. What's more, their shape, packing pattern, porosity, mechanical property and the lotus root-like structure can be well controlled. As the optical microscopy and SEM images showing, all scaffolds are packed by struts (Ø1.5 mm) with different numbers of channels (Ø400-600 μm). We prepared three kinds of biomimetic scaffolds with different packing patterns (i.e. cross packing pattern, quartet close packing pattern and hexagonal close packing pattern) to control their porosity and compressive strength. Our results suggest that the lotus root-like biomimetic materials have significantly improved *in vitro* cell attachment and proliferation as well as *in vivo* osteogenesis and angiogenesis. The 3D micro-CT images of calvarial defect's surface showed that the bone defect in 3CSP group heals quite well, as compared to 1CSP and TSSP groups. Besides, Van Gieson's staining results displayed that the newly formed bone tissue in the TSSP group was mainly detected in the periphery of the defects, while more newly formed bone was mainly detected in both the periphery and center of the bone defect in 1CSP and 3CSP groups.

Conclusion

Inspired by the root of the natural lotus plant, we successfully prepared the biomimetic materials with lotus root-like structure via a modified 3D printing strategy, which breaks the limitation of traditional 3D printing method. We are able to prepare the lotus root-like biomimetic materials with different raw materials including ceramics, metal and

polymer. What's more, their shape, packing pattern, porosity, specific surface area, mechanical property and the lotus root-like structure (the size and number of hollow channels and the size of struts) can be well controlled. Our results suggest that the porosity and specific surface area could be distinctly improved in the biomimetic materials. Compared to traditional 3D printing materials, the lotus root-like biomimetic materials significantly improved *in vitro* BMSCs attachment and proliferation as well as *in vivo* osteogenesis and angiogenesis, indicating that the lotus root-like biomimetic materials are more suitable for cell delivery and regeneration of large bone defects.

References

[1] J. Aizenberg, P. Fratzl, Adv. Mater. 2009, 21, 387.
[2] C. Feng, W. Zhang, C. Wu, Adv. Sci. 2017,4, 1700401.
[3] W. Zhang, C. Feng, C. Wu, X. Jiang, Biomaterials, 2017,135, 85.
[4] S. E. Naleway, M. M. Porter, J. McKittrick, M. A. Meyers, Adv. Mater. 2015, 27, 5455.
[5] U. G. K. Wegst, H. Bai, E. Saiz, A. P. Tomsia, R. O. Ritchie, Nat. Mater. 2014, 14, 23.
[6] G. Zan, Q. Wu, Adv. Mater. 2016, 28, 2099.
[7] B. Bhushan, Philos. Trans. R. Soc., A 2009, 367, 1445.
[8] J. Zhang, W. Feng, H. Zhang, Z. Wang, H. A. Calcaterra, B. Yeom, P. A. Hu, N. A. Kotov, Nat. Commun. 2016, 7, 10701.
[9] R. P. Wilkerson, B. Gludovatz, J. Watts, A. P. Tomsia, G. E. Hilmas, R. O. Ritchie, Adv. Mater. 2016, 28, 10061.

Acknowledgement

This work was jointly supported by the National Key Research and Development Program of China (2016YFB0700803), the National Natural Science Foundation of China (No. 31370963,81430012), Key Research Program of Frontier Sciences, CAS (QYZDB-SSW-SYS027) and Science and Technology Commission of Shanghai Municipality (17441903700, 16DZ2260603,15XD1503900). C. Feng & Dr. W. Zhang contributed equally to this work.

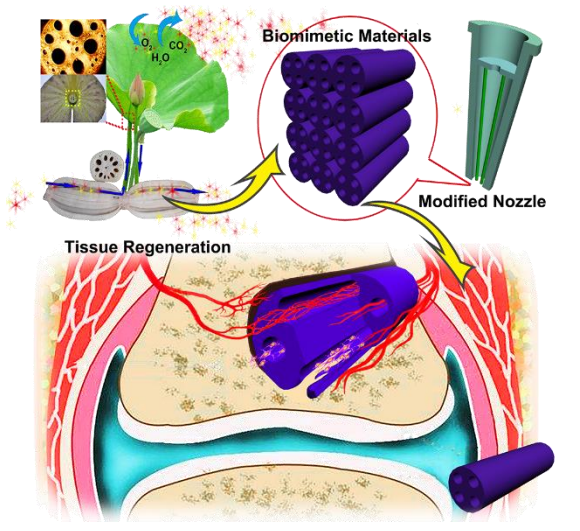

Fig. 1
The feasible applications and fabrication of lotus root-like biomimetic materials.

PS1-07-145

Comparison of different bioinks for long-time printing

Caroline Seidel, Claudia Krumbiegel, Tina Hille, **Ina Prade**

FILK gGmbH, Department Biology, Freiberg, DE

Introduction

Bioprinting is a suitable technique to generate living tissue. Therefore, the development of bioinks that support growth and organisation of cells as well as construct shape and stability is an active research field. Many bioinks are commercially available now. However, the 3D printing of cells is still challenging. Especially limited viability of cells during long printing time, cell sedimentation, and clumping of the ink make it difficult to successfully print biological structures. Bioprinting is a suitable technique to generate living tissue. Therefore, the development of bioinks that support growth and organisation of cells as well as construct shape and stability is an active research field. Many bioinks are commercially available now. However, the 3D printing of cells is still challenging. Especially limited viability of cells during long printing time, cell sedimentation, and clumping of the ink make it difficult to successfully print biological structures.

Experimental Methods

In this study, we compared a range of different hydrogel bioinks for their capacity to support cell viability in long printing processes and to prevent cell settlement in the cartridge. Each bioink was mixed with a MSCs or primary chondrocytes, and printed for a duration time of 30 min to 3 hours. Printed constructs were analyzed for cell number, cell viability and cytotoxic effects. Furthermore, printed cell-laden bioinks were cultured and the suitability for tissue engineering of cartilage was investigated using cartilage-specific markers.

Results and Discussion

We observed good printability of all bioinks tested, however significant differences concerning cell sedimentation and distribution of cells in the printed construct appeared. Especially, low viscose inks showed a dramatic change in cell numbers, as expected. In contrast, a bioink that contained an increased gelatine content provided constant cell numbers, but displayed impaired cell viability over time. By adding a small amount of fibrils using a neutralized collagen solution we were able to improve cell viability and to prevent sedimentation in the cartridge in several bioinks. Additionally, we observed differences in ability to support chondrogenic differentiation. Interestingly, we saw no significant difference with the use of a cartilage-specific ECM bioink compared to a standard ECM-based material.

Conclusion

The suitability of a bioink is not only dependent on printability and mechanical properties, but also on the duration time the construct needs until it is printed. Long printing times negatively affect cell sedimentation and viability in various bioinks.

PS1-07-146

3-D Printing of Treated Dentin Matrix-Based Scaffolds for Regenerative Dentistry

Yibing Huang, Weihua Guo

Sichuan University, Chengdu, CN

Introduction

It is hard to mimic the complex heterotypic 3-D architecture of tooth root scaffolds using the conventional techniques. 3-D printing technologies has been proposed as an alternative to address this challenge for tissue regeneration engineering. Previous studies have suggested that treated dentin matrix (TDM) can release odontogenesis factors that play significant roles during tooth formation. In this investigation, we manufactured biomimetic scaffolds by 3-D printing for tooth root construction from hybrid of poly-ε-caprolactone (PCL) and TDM.

Experimental Methods

In this research, PCL solution and powdered TDM were used for synthesis of 3-D scaffolds. The scaffolds were manufactured by layer-by-layer deposition using extrusion 3-D printer. The macropores and microstructure of the scaffolds were examined by Scanning electron microscopy. The porosity of scaffolds was measured with a liquid displacement method. The compression strength of the scaffolds was tested by a universal testing machine. In order to illustrate the impact on cell viability and proliferation activity of scaffolds, dental follicle stem cells (DFCs) were cultured on scaffolds. The cell viability on the scaffolds was evaluated using a Live/Dead Cell Kit assay under fluorescence microscopy. Cell Cytotoxicity was analyzed with a Cell Counting Kit-8 (CCK-8) assay. To clarify the effect of TDM/PCL scaffolds on the expression of odontogenic differentiation related genes and proteins in DFCs, we studied several marker genes and proteins which were essential during odontogenesis.

Results and Discussion

We have optimized the printing parameters and the concentrations of the individual components of the scaffolds for print accuracy and proper porosity. Mechanical testing showed that the scaffolds were similar to natural tooth roots in compressive strength. Live/Dead staining revealed that most of seeded cells stayed alive on the scaffolds surface and inside. Moreover, CCK-8 assay demonstrated that scaffolds could support DFCs proliferation. TDM/PCL scaffold enhances the odontogenic differentiation potential of DFCs. TDM powders in the 3-D printed scaffold act as essential substrates to induce DFCs to undergo odontogenic differentiation.

Conclusion

The proposed novel scaffolds have demonstrable cytocompatibility and natural odontogenic capacity, which can be a used to reproducibly fabricate scaffolds with complex three-dimensional microarchitectures for regenerative dentistry in the future.

References

1. Guo, W. et al. *Biomaterials**33***, 1291-1302(2012).
2. Luo, X. et al. *Biomaterials**57***, 59-72(2015).
3. Li, H. et al. *Advanced Healthcare Materials **6***, 1601112(2017).

Acknowledgement

This study was supported by the National Key R&D Program of China (grant number 2017YFA0104800), the National Natural Science Foundation of China (grant number 31771062, 31470947), and the Key Research and Development Program of Sichuan Province (2017SZ0031).

PS1-07-147

Printed Biocompatible and Degradable Optical Waveguides for Light Delivery

Jun Feng[1,2], Shardul Bhusari[1,2], Shrikrishnan Sankaran[1], Malgorzata Katarzyna Wlodarczyk-Biegun[1], Aránzazu Del Campo[1,2]

[1]INM-Leibniz Institute for New Materials, Saarbrücken, DE; [2]Saarland University, Chemistry Department, Chemistry Department, DE

Introduction

Optogenetics and the development of optical technologies for medical interventions are revolutionizing therapeutic treatments. Molecular strategies to regulate biological processes using light are in rapid development. For their implementation in the clinic, patient-friendly platforms to deliver light inside the body will be required. Using printable biomaterials, optical waveguides can be printed and flexibly integrated into implants or scaffolds for cell therapies, eventually directly at the operating room. The degradable optical waveguides will conduct light into implanted devices and remotely stimulate cellular functions in optogenetic approaches, change properties or trigger drug release in photoresponsive implants, or mediate photo-therapy. After application, the waveguides will be reabsorbed by the body.

Experimental Methods

The optical waveguides are prepared by printing. Microfibers are formed in desired geometries, to allow adaptation to the human body cavities and particular application. Thermoplastic polymers or reactive hydrogel mixtures are used for this purpose. After cooling or crosslinking, an optical waveguide is generated and eventually directly incorporated into the medical device.

Results and Discussion

A series of optical waveguides were successfully printed. Different structures were designed and manufactured to increase the light propagation in the waveguides. The light conductivity (with different wavelength) in the printed waveguide under different conditions (in the air, PBS and tissue) was characterized. The stability of materials was researched, which can be adjusted easily to adapt different application. Besides, some mechanical properties were characterized, which indicates the possibility to apply the waveguides in different tissue or organ. An application for optogenetic-driven drug delivery will be presented.

Conclusion

3D printing makes it easier to manufacture different structure of optical waveguides. The printed optical waveguides showed excellent light conductivity in no matter dry (air) or wet conditions (PBS and tissue). The application for optogenetic-driven drug delivery proves the practical function of printed waveguides, which can be adopted to conduct light to activate the photoresponsive implants.

References

1, Nizamoglu, Sedat, et al. "Bioabsorbable polymer optical waveguides for deep-tissue photomedicine." *Nature communications* 7 (2016): 10374.

2, Choi, Myunghwan, et al. "Light-guiding hydrogels for cell-based sensing and optogenetic synthesis in vivo." *Nature photonics* 7.12 (2013): 987.
3, Xu, Peidi, et al. "Bioinspired microfibers with embedded perfusable helical channels." *Advanced Materials* 29.34 (2017): 1701664.
4, Parker, Sara T., et al. "Biocompatible silk printed optical waveguides." *Advanced Materials* 21.23 (2009): 2411-2415.
5, Choi, Myunghwan, et al. "Step-index optical fiber made of biocompatible hydrogels." *Advanced materials* 27.27 (2015): 4081-4086.
6, Guo, Jingjing, et al. "Highly stretchable, strain sensing hydrogel optical fibers." *Advanced materials* 28.46 (2016): 10244-10249.

Acknowledgement
The authors thank Peter Rogin for the help with characterizing light conductivity of waveguides. J.F. acknowledges the financial support from China Scholarship Council.

PS1-07-148

3D plotted composites consisting of a calcium phosphate bone cement and mesoporous bioactive glass allow tailoring of ion and growth factor release

Richard F. Richter, Tilman Ahlfeld, Michael Gelinsky, Anja Lode

University Hospital and Medical Faculty, Technische Universität Dresden, Centre for Translational Bone, Joint and Soft Tissue Research, Dresden, DE

Introduction

Calcium phosphate bone cements (CPC) and mesoporous bioactive glasses (MBG) are two well studied biomaterial groups widely under investigation on their applicability to treat bone defects. Recently, a MBG-CPC composite was developed in our group which showed promising results with respect to cell response *in vitro* and new bone formation *in vivo* (1,2). Unlike conventional powder/liquid cements, the used CPC is a hydrophobic carrier-liquid (cl) based paste; it maintains a good injectability until contact with aqueous environment that allows its application for extrusion-based additive manufacturing techniques like 3D plotting opening up varied applications (3). However, until now the extrusion properties of the MBG-CPC composites have not been studied in detail. A higher amount of solid phase will impair the injectability, thus additional modifications are required to keep the original good properties. The aim of the present study was to adapt a composite prepared from a hydroxyapatite forming, cl-based CPC and mesoporous bioactive glass for the application in low temperature 3D plotting and to investigate plotted composites with regard to structural and mechanical properties as well as strontium ion release.

Experimental Methods

MBG particles (< 45 µm) were prepared as recently described (4). CPC was provided by INNOTERE GmbH, Germany. The extrusion properties of composites with different MBG concentrations were examined by measuring the mass flow through a plotting needle for different plotting pressures (100-500 kPa) and needle diameters (250-610 µm). Setting characteristics in humidity of a MBG-CPC composite were studied by performing a Gilmore-needle-test. Afterwards MBG-CPC scaffolds were plotted with an extrusion-based 3D plotter (Bioscaffolder 3.1, GeSiM mbH, Germany) and set in humidity. Porosity of plotted scaffolds was evaluated by helium pycnometry. Additionally, microstructure and mechanical properties were characterized by scanning electron microscopy and uniaxial compressive tests. Finally, MBG fabrication was modified by gradually substitution of calcium with strontium. MBG-CPC scaffolds containing the same amount of MBG but with different MBG compositions (0, 5, 10 and 15 % Sr) were plotted and the release of calcium and strontium ions in PBS was investigated and compared to non-plotted bulk scaffolds.

Results and Discussion

MBG-CPC composites with the addition of up to 4 wt% MBG were extrudable without any further modification of the CPC. Through adjustment of the amount of cl used, composites with the addition of up to 10 wt% MBG were achieved without impairing the extrudability. Initial setting times were prolonged by the incorporation of MBG but after 3 days of setting no difference was found compared to MBG-free CPC.

For plotted scaffolds with 8 wt% added MBG (Fig.1: 3D-plotted scaffold), it was found that the total porosity was slightly, but not significantly increased. Microstructure analysis indicated the formation of micro cracks along MBG

particles and mechanical tests showed lower compressive strength in comparison to pure CPC, although the Young's modulus was not significantly altered.
Regarding the release analysis, it was shown that the ion release is customizable by the use of different MBG compositions. For strontium ions released from 3D plotted structures, therapeutic but not cytotoxic levels were obtained. Additionally, a significant higher ion release was achieved from macroporous 3D plotted scaffolds in comparison to bulk scaffolds (Fig.2Ion release from MBG-CPC scaffolds) indicating the advantages of this fabrication method for release systems.

Conclusion

In this study we showed the development of a MBG-CPC composite applicable for 3D plotting. Furthermore the results of the ion release showed the high flexibility of this material system and suggest it as a promising platform for further enhancements such as the incorporation of growth factors (2,5) or anti-inflammatory agents.

References

1. Wagner *et al.* Biomed. Mater., 2019
2. Kauschke *et al.*, Int. J. Mol. Sci., 2018
3. Lode *et al.*, J. Tissue Eng. Regen. Med., 2014
4. Zhu *et al.*, Microporouse Mesoporous Ma., 2008
5. Schumacher *et al.*, Biomater. Sci., 2017

Acknowledgement

The authors thank Dr. Matthias Schumacher for fruitful discussions. This work was funded by the German Research Foundation (DFG) as part of the Collaborative Research Centre Transregio 79 (subproject M2).

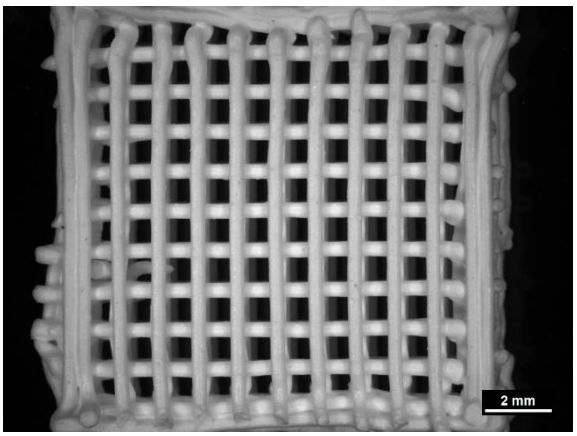

3D-plotted scaffold
3D-plotted scaffold using an 8%-MBG-CPC composite, layer-to-layer orientation 90°, strand distance 1.2 mm

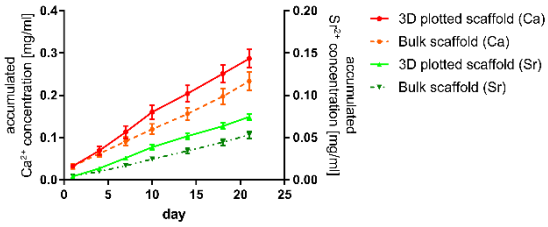

Ion release from MBG-CPC scaffolds
Accumulated release of Ca^{2+}/Sr^{2+} from 8%-MBG-CPC scaffolds over 21 days (normalized to starting weight of the scaffolds)

PS1-07-149

Alginate-Based Composite Bioinks for 3D Biofabrication

Susanne Heid, Rainer Detsch, Aldo R. Boccaccini

Friedrich-Alexander University Erlangen-Nuremberg, Institute of Biomaterials, Erlangen, DE

Introduction

Three-dimensional (3D) printed scaffolds based on hydrogels are attractive for applications in regenerative and personalized medicine [1]. Among these, alginate-based hydrogels are receiving increasing attention for 3D biofabrication due to their excellent biocompatibility and similarity to the extracellular matrix of native tissues in terms of mechanical and structural properties. [2]

In this project, a novel composite bioink is going to be developed from pharmaceutical grade alginate, gelatin and inorganic particulate fillers for extrusion-based 3D printing to enhance the printability, shape fidelity, as well as to adjust the mechanical properties while sustaining a cell friendly environment.

Experimental Methods

Composite hydrogel compositions were designed on the basis of previously research outcomes by Leite *et al* [3]. Various amounts of bioactive inorganic fillers (BIF), between 0.1 wt% and 1.0 wt%, were incorporated into the ADA-GEL (alginate dialdehyde combined with gelatin) bioink. The different composite hydrogel compositions were evaluated using extrusion-based 3D printing regarding their printability, printing accuracy and shape stability. FTIR measurements, as well as the determination of the crosslinking degree and ion and gelatin release studies were conducted to examine the bioink´s properties. A degradation study was performed by investigating the change in stiffness using nanoindentation measurements to evaluate the long-term stability of the hydrogel bioinks. *In-vitro* biocompatibility studies combined with fluorescence staining and cell viability assays were performed with NIH3T3 fibroblast cells.

Results and Discussion

One of the most significant challenges in 3D biofabrication is the combination of appropriate mechanical properties and shape stability of the printed constructs with high cell viability after printing. ADA-GEL hydrogel scaffolds often show a low dimensional stability which makes the printing with this material challenging [4]. To overcome this limitation, ADA-GEL bioinks have been modified by incorporating inorganic fillers like bioactive glasses and their influence on the properties of the bioink has been examined.

In this study, the effect of different amounts of bioactive fillers on the printability of ADA-GEL hydrogels was analyzed. It was observed that there was a better strand formation by enhancing the amount of BIF in the bioink, similarly to previous findings [3]. Nevertheless, more than 0.5 wt% BIF led to a non-uniform ink deposition, which hindered the printing of 3D structures in extrusion-based processes.

Moreover, bivalent calcium ions, which are released from the BIF particles due to their surface reactivity, can strengthen the network of the hydrogel over time leading to a better stability after printing. This trend could be confirmed by nanoindentation measurements during incubation under cell culture conditions for 7 days.

To understand the chemical mechanisms and to further characterize the composite hydrogel, FTIR measurements, ion and gelatin release studies were performed and the mechanical properties of the composite hydrogel were

examined. Furthermore, the degree of crosslinking between ADA and gelatin was evaluated by different assays. The outcomes were in good agreement with the printing and nanoindentation results.
In-vitro cell studies showed promising results for the optimization of the new composite bioink for 3D biofabrication by investigating different key processing parameters. The complex interactions of the hydrogel matrix and the bioactive inclusions with cells during the printing process were studied.

Conclusion

A new family of composite bioinks composed of ADA-GEL and bioactive inorganic fillers was developed and its suitability for 3D biofabrication was shown. Further studies will focus on the assessment of the rheological properties as well as on the long-term evaluation of printed constructs with fibroblast and muscle cells.

References

[1] Utech, S. and Boccaccini, AR, *A review of hydrogel-based composites for biomedical applications: enhancement of hydrogel properties by addition of rigid inorganic fillers*. Journal of Materials Science 51 (1), 271-310, 2016.
[2] Lee, K. Y. et al., *Alginate: properties and biomedical applications.* Progress in polymer science 37, 106-126, 2012.
[3] Leite, A. et al., *Bioplotting of a bioactive alginate dialdehyde-gelatin composite hydrogel containing bioactive glass nanoparticles,* Biofabrication 8, 035005, 2016.
[4] Zehnder, T. et al., *Evaluation of an alginate–gelatine crosslinked hydrogel for bioplotting,* Biofabrication 7, 025001, 2015.

Acknowledgement

The authors thank the German Research Foundation (DFG; collaborative research center SFB/TRR225 'From the fundamentals of Biofabrication to functional tissue models', project number326998133 - TRR 225 subproject B03) for financial support.

PS1-07-150

Design of cell-free biomaterial-inks for 3D printing

Anuj Kumar, Matari I. Abdullah I, Sung S. Han

Yeungnam University, South Korea, School of Chemical Engineering, Gyeongsan, KR

Introduction

3D printing (e.g. extrusion printing) has emerged as a fascinating technology which has great potential in addressing numerous challenges in tissue engineering and regenerative medicine. This technique provides desired structural features and 'on-demand' delivery of the printed products. The development of stable cell-free biomaterial-inks or cell-encapsulated bioinks is a major concern in 3D printing of scaffolds for tissue engineering applications. Therefore, the selection of the biomaterial-ink is one of the major challenges to prepare specific tissue-type (e.g. more sophisticated composition, components, and architecture). Polysaccharide hydrogel shows the great potential as artificial biomaterial in damaged tissue regeneration by demonstrating their properties similar to native extracellular matrix (ECM). In this study, multicomponent polysaccharide-inks were prepared and processed in desired designs by 3D printing and evaluated their structural, rheological, mechanical and biological properties.

Experimental Methods

First, *carboxylated*-cellulose nanocrystals (*c*CNCs) were prepared by oxidation method using ammonium persulfate. Then, printable cell-free biomaterial-inks composed of sodium alginate (SA)/xanthan gum (XG)-reinforced with *c*CNCs were designed and prepared. In this study, *c*CNCs and XG were incorporated in SA matrix and varied their contents to prepare cell-free biomaterial-inks that were further printed by direct-write 3D printing (i.e. extrusion printing). The composition components of were optimized for better rheology, printing accuracy and post-printing fidelity (before and after crosslinking), mechanical properties, and their cytocompatibility.

Results and Discussion

The incorporation of cCNCs and XG provide shear-thinning property to cell-free biomaterial-inks under applied shear-forces while extruded-out via nozzle tip. The results showed good physical stability in the bulk and printed hydrogels. In addition, biomaterials-inks showed good *in vitro* cytocompatibility with human skin fibroblast cells on both bulk and printed hydrogels.

Conclusion

We developed cell-free biomaterial-inks composed of SA, XG, and *c*CNCs for 3D printing The results showed that prepared cell-free biomaterial-inks demonstrated good shape-fidelity of printed-structures with good resolution and *in vitro* cytocompatibility, Furthermore, the developed biomaterial-inks need to be cell-encapsulated to prepare printable bioinks without affecting cell viability while extrusion.

References

1. Li, V. C., Mulyadi, A., Dunn, C. K., Deng, Y., & Qi, H. J. (2018). Direct Ink Write 3D Printed Cellulose Nanofiber Aerogel Structures with Highly Deformable, Shape Recoverable, and Functionalizable Properties. *ACS Sustainable Chemistry & Engineering*, *6*(2), 2011-2022.

2. Markstedt, K., Mantas, A., Tournier, I., Martínez Ávila, H., Hägg, D., & Gatenholm P. (2015). 3D bioprinting human chondrocytes with nanocellulose–alginate bioink for cartilage tissue engineering applications *Biomacromolecules* 16, 1489-1496.
3. Leppiniemi, J., Lahtinen, P., Paajanen, A., Mahlberg, R., Metsä-Kortelainen, S., Pinomaa, T., Pajari, H., Vikholm-Lundin, I., Pursula, P. & Hytönen, V. P. (2017). 3D-printable bioactivated nanocellulose–alginate hydrogels. *ACS Appl. Mater. Interfaces* 9, 21959-21970

Acknowledgement

This research was supported by the 2018 Yeungnam University research grant and by the Basic Science Research Program through the National Research Foundation of Korea (NRF) funded by the Ministry of Education, Science and Technology (Grant No. 2017R1D1A3B03036276).

PS1-07-151

Development of 3D printed gelatin-based hydrogel scaffolds for hepatocyte support

Nathan Carpentier[1], Johannes Hackethal[2], Heinz Redl[2], Lindsey Devisscher[3], Hans Van Vlierberghe[3], Sammy Detry[4], Savvas Savvides[4], Peter Dubruel[1], Sandra Van Vlierberghe[1]

[1]Ghent University, Polymer Chemistry & Biomaterials Group, Centre of Macromolecular Chemistry, Ghent, BE; [2]Ludwig Boltzmann Institute for Experimental and Clinical Traumatology, Vienna, AT; [3]Ghent University, Department of Gastroenterology and Hepatology, Hepatology Research Unit, Ghent, BE; [4]Ghent University, Unit for Structural Biology, VIB Center for Inflammation Research, Ghent, BE

Introduction

Drug induced liver injury (DILI) is one of the major reasons for drug withdrawal during the different phases of drug development.[1] The economical as well as the ethical constraints increase along with more advanced phases.[2] In the present research, an *in vitro* model will be developed to detect the hepatotoxicity of drugs prior to reaching the pre-clinical phase. In order to develop this model, different gelatin-based hydrogel materials have been developed and compared after 3D printing into porous scaffolds. The scaffolds function as support for primary mice hepatocytes.

Experimental Methods

Three different gelatin-based hydrogels were developed: (i) Methacrylated gelatin (gelMA) was obtained as described earlier[3]. The material was already extensively characterized before with respect to mechanical and biological properties and therefore served as benchmark in the present work. (ii) Gelatin/oxidized dextran (dexox) hydrogel blends were developed, in which dextran was first oxidized with $NaIO_4$ and subsequently crosslinked using a Schiff-base amine-aldehyde click reaction. (iii) Gelatin-norbornene (gelNB)/thiolated dextran was the third hydrogel class applied, in which gelNB was developed as described previously[4]. The thiolated dextran was obtained by first synthesizing tosylated dextran, which was subsequently modified using potassium thioacetate followed by conversion into thiolated dextran after reaction with NaOH. The materials developed were subsequently 3D-printed into porous scaffolds with the same dimensions and were characterized for their physico-chemical properties. Next, *in vitro* biocompatibility experiments with primary hepatocytes and HepG2 were executed. Furthermore, the influence of several coating materials mimicking the natural extracellular matrix, has been assessed for their potential to support cell proliferation. The coating materials include animal-derived fibronectin, laminin, collagen, as well as human-derived coating materials isolated from the human placenta. The coating was applied on the gelatin-derived scaffolds via dipcoating.

Results and Discussion

Three different gelatin-based hydrogels were developed: (i) Methacrylated gelatin (gelMA) was obtained as described earlier[3]. The material was already extensively characterized before with respect to mechanical and biological properties and therefore served as benchmark in the present work. (ii) Gelatin/oxidized dextran (dexox) hydrogel blends were developed, in which dextran was first oxidized with $NaIO_4$ and subsequently crosslinked using a Schiff-base amine-aldehyde click reaction. (iii) Gelatin-norbornene (gelNB)/thiolated dextran was the third hydrogel class applied, in which gelNB was developed as described previously[4]. The thiolated dextran was obtained by first synthesizing tosylated dextran, which was subsequently modified using potassium thioacetate followed by conversion into thiolated dextran after reaction with NaOH. The materials developed were subsequently 3D-printed

into porous scaffolds with the same dimensions and were characterized for their physico-chemical properties. Next, *in vitro* biocompatibility experiments with primary hepatocytes and HepG2 were executed. Furthermore, the influence of several coating materials mimicking the natural extracellular matrix, has been assessed for their potential to support cell proliferation. The coating materials include animal-derived fibronectin, laminin, collagen, as well as human-derived coating materials isolated from the human placenta. The coating was applied on the gelatin-derived scaffolds via dipcoating.

Conclusion

The biological evaluation results obtained so far represent the evaluation of only one scaffold type during 7 days using HepG2 cells. Currently, the properties of the other scaffold materials (cfr. physico-chemical and biological) are being assessed and compared with the gelMA control scaffolds. Preliminary results look promising and will be presented at the meeting.

References

1) Sakatis, M. Z. et al. Chem Res Toxicol. 25 (10), 2067-2082 (2012)
2) DiMasi, J. A. et al. J. Health Econ. 47, 20-33 (2016)
3) Van Den Bulcke, A. I. et al. Biomacromolecules. 1 (1), 31-38 (2000)
4) Van Hoorick, J. et al. Macromol rapid commun. (2018)
5) Mattei, G. et al. Acta Biomaterialia. 10, 875-882 (2014)
6) Van Vlierberghe, S. et al. Macromol Biosci. 9, 1105-1115 (2009)

Acknowledgement

The *authors would like* to *acknowledge* the financial support of the *Research Foundation-Flanders* (FWO).

PS1-07-152

Design of 3D printable bioinks by tuning the rheological properties for practical use

Sangheon Kim[1,2], Jooyoung Lee[1], Seungja Oh[1]

[1]Korea Institute of Science &Technology, Center for Biomaterials, Seoul, KR; [2]Korea University of Science and Technology, Division of Bio-Medical Science & Technology, Seoul, KR

Introduction

Bioprinting technology is advancing rapidly, yet, finding suitable bioprinting materials that meet both mechanical property and bio-compatibility remains a challenge. Although bioinks using synthetic polymers are easy to control in mechanical strength and provide high shape fidelity, they had been limited in clinical use due to lack of biocompatibility. It has been generally accepted that it is difficult to use FDA approved materials, such as collagen, hyaluronic acid (HA), and fibrin, without any modification for applications requiring high stiffness such as 3D bioprinting. We have designed bioinks composed of collagen, HA, and fibrin without any chemical substitution. We found the universal relationship between mechanical properties of bioinks and printability: high elastic modulus improve shape fidelity and extrusion is possible below the critical yield stress, supported by the machine learning.Bioprinting technology is advancing rapidly, yet, finding suitable bioprinting materials that meet both mechanical property and bio-compatibility remains a challenge. Although bioinks using synthetic polymers are easy to control in mechanical strength and provide high shape fidelity, they had been limited in clinical use due to lack of biocompatibility. It has been generally accepted that it is difficult to use FDA approved materials, such as collagen, hyaluronic acid (HA), and fibrin, without any modification for applications requiring high stiffness such as 3D bioprinting. We have designed bioinks composed of collagen, HA, and fibrin without any chemical substitution. We found the universal relationship between mechanical properties of bioinks and printability: high elastic modulus improve shape fidelity and extrusion is possible below the critical yield stress, supported by the machine learning.

Experimental Methods

To investigate the dominant rheological properties affecting the printing quality, we first randomized the formulation with various combinations of collagen, fibrin and HA. These initial formulations are derived from orthogonal design which is described in Table. 1. For machine learning analysis, we set the concentrations of each components as an Input parameter, their rheological parameters such as G' and yield stress as an Output 1, and corresponding printing results such as shape fidelity and extrusion as an Output 2.

Results and Discussion

This study has significantly improved in practical use with the followed results. First, the bioink was composed of only FDA-approved materials and had no chemical treatment, so it was very practical for clinical application. In particular, non-immunogenic atelocollagen had a flexible gel structure, it was excellent in processability and provided adequate elasticity. Second, because the bioinks showed similar gel properties at both room temperature and physiological temperature, the printing could be performed at both temperature and the elasticity of the bioinks remained stable in vivo. These aspects help to facilitate use in clinical applications by reducing the restrictions on treatment room settings. Third, by defining the rheological properties that the printable ink with high shape fidelity should have, it has been possible to design and formulate new printable inks. Although the contribution of each composition to the

physical properties is not clear, the prediction equation (Fig. 1) can be provided by regression of the complex contribution of each component. Such approach is not limited to specific materials, so it can be a universal guideline for 3D printing research to develop FDA-approved inks by controlling only physical properties without further chemical treatment. Finally, the bioink has high biocompatibility so that cells can be applied. Fibroblasts were highly viable, easily migrated, and attached onto the high elastic collagen scaffold, as shown in figure 2. This is surprising improvement than the synthetic polymers such as PCL and PLA where hydrophobic surface should be treated to attach the cells.

Conclusion

This work demonstrates a comprehensive approach to acquire the printable bioinks with high shape fidelity for 3D printing from the selection of material to the design of ink formulation. Cells were settled stable within 3D construct and provided a foundation for tissue formation, promising the versatile applications for organ analogues or in vitro models. They will also provide a valuable predictive tool for designing the printable FDA-approved bioinks.

References

1. Rodriguez-Pascual, F. and Slatter, D. A., Scientific Report 6:37374 DOI: 10.1038/srep37374
2. Sato, K., Ebihara, T., Adachi, E, Kawashima, S., Hattori, S., and Irie, S. J. Biol. Chem. 275, 25780-25785, 2000
3. Slot-Verhoeven, A., Dura, E. A., Attema, J., Blauw, B., DeGroot, J., Huizinga, T. W. J., Zuurmond, A., Bank, R. A., Biochim. Biophy. Acta, 1740, 90,67, 2005

Acknowledgement

This work was in part supported by a grant from the Technology Innovation Program (No. 10053020 & No. 10063334) funded by the Ministry of Trade, Industry & Energy (MI, Korea).

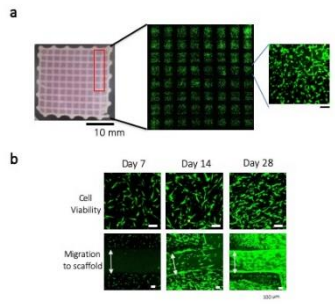

Figure 1. Long-term stability and cellular compatibility of the printed constructs. **a,** The images are representative images of the whole constructs at progressing days of cell culture using human dermal Fibroblast (400,000cells/ml). **b,** The upper images are representative images of live / dead analysis showing living cells (green dots) and dead cells (red dots) in the hydrogel. The lower images show cell migration into the scaffold (indicated by white arrows) as the cell culture proceeds

Input *			Output I		Output II	
Collagen	Hyaluronic acid	Fibrin	G' (Pa)	τ_y (Pa)	Shape Fidelity**	Extrusion***
10	0	0	3620	632	14.60	1
8	0	2	1295	730	7.34	1
5	0	5	1112	3130	0.47	1
2	0	8	1693	9400		0
0	0	10	7761	50000		0
10	2.50	0	2260	430	12.61	1
8	2.50	2	1122	415	0.13	1
5	2.50	5	731	541	0.00	1
2	2.50	8	1327	3960		0
0	2.50	10	1888	10855		0
2	0	0	382	282	0.00	1
10	0	8	5582	19700		0
10	2.50	8	4380	5506	14.08	1
10	1.25	4	2463	2429	0.00	1
6	1.25	8	4572	8052		0
2	1.25	4	460	770	1.08	1
2	2.50	0	230	74	4.94	1
6	1.25	0	820	226	0.70	1
20	0	0	9517	1465	31.27	1

* Inks formulations are derived from orthogonal design which is described in Supplementary Fig. 3.
** The printed images and their quantification method are presented in Supplementary Fig. 5.
*** Extrusion parameter was set to 0 when the ink was not ejected from the nozzle but clogged, and set to 1 when the ink was ejected from the nozzle.

Orthogonal design of bioinks for machine learning
Various formulation of nature-derived bioinks with FDA approved materials (collagen, hyaluronic acid, fibrin) and their rheological properties (G' and yield stress) and printing quality (shape fidelity and nozzle clogging).

PS1-07-153

Effect of surface roughness on the bioactivity of Fused Filament Fabrication (FFF) 3D-printed PEEK for Cranio-maxillofacial and orthopedic implants: an in vitro study

Xingting Han[1], Neha Sharma[2,3], Florian M. Thieringer[2,3], Zeqian Xu[1], Lutz Scheideler[1], Jürgen Geis-Gerstorfer[1], Frank Rupp[1], Sebastian Spintzyk[1]

[1]University Hospital Tübingen, Section Medical Materials Science and Technology, Tübingen, DE; [2]University of Basel, Medical Additive Manufacturing Research Group, Hightech Research Center, Department of Biomedical Engineering, Allschwil, CH; [3]University Hospital Basel, Department of Oral and Cranio-Maxillofacial Surgery, Basel, CH

Introduction

Polyetheretherketone (PEEK) is a polyaromatic semi-crystalline thermoplastic polymer and has been used widely in clinical applications in the last few decades, including spinal implants, cranioplasty, dental implants, and implant-supported bars [1–3]. However, PEEK has a bio-inert hydrophobic surface which makes it less favorable for cell adhesion and protein adsorption [4]. Therefore, surface modifications of this primarily inert polymer are imperative in order to enhance its osseointegration potential [5].

Technological advancements in additive manufacturing (AM), have made a significant leap in the last decade [6]. One of the AM technology which is gaining special interest from the medical sector for fabrication of PEEK patient-specific implants (PSI) is Fused Filament Fabrication (FFF) [7]. The working principle of FFF is a fabrication of the implant in a “layer-by-layer” manner, and it is with this approach that complex geometries of an implant are easily fabricated [8]. In addition, FFF fabricated implants can be manufactured in various layer thicknesses, which thereby create a certain level of surface layer characteristics onto the implants’ surface [9]. Studies on how these surface characteristics generated by FFF 3D printing affect the bioactivity properties are still lacking.

Hence, the objective of this study was to evaluate the influence of surface topography and roughness on the bioactivity of FFF 3D-printed PEEK.

Experimental Methods

PEEK disk samples (14 mm diameter, 2 mm thickness) were manufactured by an FFF printer (Apium P220) and medical grade PEEK filament (Evonik VESTAKEEP® i4 G resin) with a printing layer thickness of 200 microns. The samples were divided into three groups: untreated (n = 40), polished (n = 40), and sandblasted groups (n = 120). Samples in the sandblasted group were blasted with different alumina (Al_2O_3) grain sized particles resulting in three subgroups (50 µm, 120 µm, and 250 µm, n = 40 per subgroup) to get an increased level of roughness on the sample surfaces, respectively. The surface topography and roughness were characterized by scanning electron microscopy (SEM) and profilometry. SAOS-2 osteoblasts cell line was used for the biological tests. After seeding for one day, three days, and five days, cell proliferation and metabolic activity were determined by cell counting kit-8 (CCK-8) assay.

Results and Discussion

As shown in Figure 1, the untreated FFF 3D-printed PEEK sample surfaces indicated clear structures with peaks and valleys. After polishing, the printing features disappeared and resulted in a homogeneous and a smooth surface. The

sandblasted samples possessed a micrometer rough surface topography with homogeneous coverage of protuberances and cavities. The roughness measurement showed that when compared to polished and sandblasted groups, the untreated PEEK samples represented significantly higher average roughness (Ra) and root-mean-square roughness (Rq) values (Figure 2a). As for the biological test, the untreated PEEK represented a slightly faster metabolic activity after one-day incubation as compared to polished and sandblasted groups. Additionally, it was noted that as the culturing time increased, the cells on the untreated PEEK surfaces had a more rapid growth rate after the 3rd day and 5th day (≈ 2–3 times) as compared to the cells on polished and sandblasted group surfaces (Figure 2b).

Conclusion

1. High roughened surfaces printed by FFF with their specially printed surface features have improved bioactivity of PEEK samples, including cell metabolic activity and proliferation.
2. FFF 3D-printed PEEK could be a possible candidate to be used in Cranio-maxillofacial and applied as an orthopedic and dental implant material in bone repair, bone reconstruction, and bone tissue engineering applications.

References

[1] X. Han, D. Yang, C. Yang, S. Spintzyk, L. Scheideler, P. Li, J. Clin. Med. 8 (2019) 240.
[2] S. Najeeb, M.S. Zafar, Z. Khurshid, F. Siddiqui, J. Prosthodont. Res. 60 (2016) 12–19.
[3] Y. Guo, S. Chen, J. Wang, B. Lu, Transl. Surg. 3 (2018) 12.
[4] D. Almasi, N. Iqbal, M. Sadeghi, I. Sudin, M.R. Abdul Kadir, T. Kamarul, Int. J. Biomater. 2016 (2016).
[5] R. Ma, T. Tang, Int. J. Mol. Sci. 15 (2014) 5426–5445.
[6] F. Zhao, D. Li, Z. Jin, Materials (Basel). 11 (2018) 288.
[7] P. Honigmann, N. Sharma, B. Okolo, U. Popp, B. Msallem, F.M. Thieringer, Biomed Res. Int. 2018 (2018).
[8] M. Rinaldi, T. Ghidini, F. Cecchini, A. Brandao, F. Nanni, Compos. Part B Eng. 145 (2018) 162–172.
[9] W. Wu, P. Geng, G. Li, D. Zhao, H. Zhang, J. Zhao, Materials (Basel). 8 (2015) 5834–5846.

Acknowledgement

The authors would like to thank Ernst Schweizer for assistance in the SEM analysis.

The China Scholarship Council (CSC) is gratefully acknowledged for the financial support of Xingting Han (Grant 201606280045) and Zeqian Xu (Grant 201708080003).

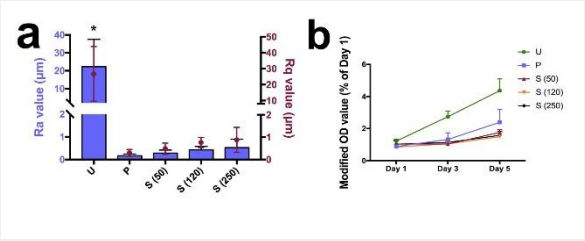

Figure 2

Ra and Rq roughness values of different groups (a). The data are presented as means ± standard deviations, * $p < 0.05$. U: untreated group; P: polished group; S (50): 50 µm sandblasted group; S (120): 120 µm sandblasted group; S (250): 250 µm sandblasted group; relative cell proliferation rate (b). Metabolic activity: the optical density (OD) values at the 3rd and 5th day were normalized by 1st-day values.

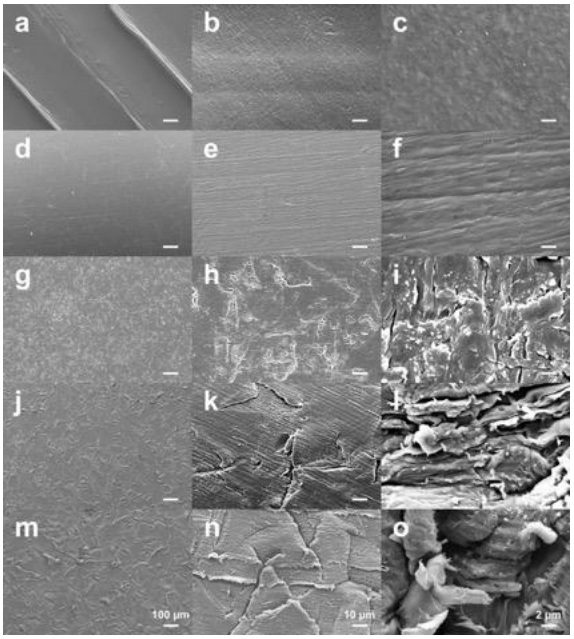

Figure 1
SEM images of FFF 3D-printed PEEK sample surfaces in different groups: (a)–(c) untreated PEEK; (d)–(f) polished PEEK; (g)–(i) sandblasted PEEK (50 µm); (j)–(l) sandblasted PEEK (120 µm); (m)–(o) sandblasted PEEK (250 µm).

PS1-07-154

Autologous breast reconstruction using a 3D printed bioabsorbable Tissue Engineering Chamber (TEC)

Marion Gradwohl[1,2,3], Stéphanie Brun[1], Claire Nahon[3], Julien Payen[3], Pierre Guerreschi[4], Mickaël Maton[2], Philippe Marchetti[1], Nicolas Blanchemain[2]

[1]Univ. Lille, INSERM UMR S1172, Jean Pierre Aubert Research Centre, Lille, FR; [2]Univ. Lille, INSERM, CHU Lille, U1008, Lille, FR; [3]LATTICE MEDICAL, Loos, FR; [4]University Hospitals of Lille, Department of Plastic, Reconstructive and Aesthetic Surgery, Lille, FR

Introduction

The clinical need for adipose soft tissue engineering such as mastectomy or traumatic injuries is in constant increase[1]. Unfortunately, in the case of breast cancer, current surgical reconstruction techniques present drawbacks such as morbidity of the donor site, capsular contracture or insufficient revascularization[2]. Tissue engineering chamber (TEC) using fat-flap from the patient's own tissue could be a promising solution to restore large volume of mature and vascularized adipose tissue (AT)[3,4]. Bioabsorbable materials are good choices to generate TEC because they can be fully absorbed by the body in several weeks after AT reconstruction. These biomaterials can be processed by additive manufacturing techniques to improve the control of porosity and produce complex and personalized 3D structures compared to conventional processing methods. In this study, we investigated the effect of TEC processing on the mechanical and thermal properties of a medical grade PLGA; then we studied the in vitro cytotoxicity and degradation by inducing adipose tissue engineering on 3D constructs.

Experimental Methods

Medical grade PLGA 85:15 (Mw: 2,70E+05 g/mol) was used as raw material and TECs were manufactured with an FDM printer. The impact of different processing step (extrusion of filament, 3D printing, and Ethylene Oxide (EtO) sterilization) were evaluated by HPLC-GPC (molecular weigth) and DSC (crystallinity); cytotoxicity test was performed according to ISO 10993-5. In vitro degradation was also studied by inducing adipose tissue engineering on 3D constructs. The crystallinity as well as molar mass was studied at 3, 5, 7, 10, 12 and 14 weeks. In parallel, cells proliferation and differentiation were also investigated. All experiments were performed with at least three replicates and analysed with Anova-one-way test using $p<0.05$ as statistically significant criteria.

Results and Discussion

Extrusion and FDM printing lead to a 10%; and 18% drop in PLGA initial molecular weight, respectively. This result was quite predictable regarding the thermosensitive behaviour of this polymer. The degree of crystallinity decreases from 36% to 0,1% during the whole process leading to an amorphous 3D construct which is preferable for the complete degradation of the TEC. No cytotoxicity was observed at each step of the process including EtO sterilization step using fibroblast cells according to ISO 10993-5. PLGA degradation leads to a 23%±3% cell death at 10 weeks while it was 14%±2% for the control ($p<0,005$). After 7 weeks of in vitro degradation, the PLGA loss 20% of its molecular weight whereas no significant change in crystallinity was observed.

Conclusion

A medical grade PLGA TEC has been successfully fabricated via additive manufacturing technology. Post-in vitro analysis demonstrated that after 2 months the PLGA molecular weight loss was evaluated at 20%. An in vivo model

has been developed were a vascularized adipose flap is inserted into the TEC in the dorsal region of female rats. In vivo degradation of PLGA chambers will be further investigated.

References

1. Contessi Negrini, N. *et al.Acta Biomaterialia* (2019). doi:10.1016/j.actbio.2019.0018
2. Visscher, L. E. *et al.Tissue Engineering Part B: Reviews* 23, 281–293 (2017).
3. Morrison, W. A. *et al.EBioMedicine* 6, 238–245 (2016).
4. Yap, K. K., Yeoh, G. C., Morrison, W. A. & Mitchell, G. M. *Trends in Biotechnology* doi:10.1016/j.tibtech.2018.05.009

PS1-07-155

A simplified process for producing test samples for VAP model using Additive Manufacturing

Bahaa Shaqour[1,2], Juliana Aizawa[2], Bart Verleije[1], Koen Beyers[1], Paul Cos[2]

[1]Voxdale bvba, Wijnegem, BE; [2]University of Antwerp, Laboratory for Microbiology, Parasitology and Hygiene (LMPH), Wilrijk, BE

Introduction

Emerging technologies of additive manufacturing have introduced new possibilities in various domains. One of the key advantages of these technologies is shortening the production time of customized and application specific products. Moreover, it opened the doors for producing new complex designs that either were impossible or costly to produce.

This study illustrates the possibility of manufacturing tools to produce samples for *in vivo* studies utilizing the flexibility in design and production using additive manufacturing. In this study, a mousemodel to study Ventilator-Associated Pneumonia (VAP) infection was selected [1]. This disease is one of the most common nosocomial infections, with high morbidity and mortality and current treatments don't work as shown by the fact that 50% of the antibiotic usage in ICUs is due to VAP [2]. To tackle the problem, new materials and formulation are being explored such as coatings, drug loaded systems among others. Moreover, preclinical trials in animal models such as mice are vital, so human testing and clinical application of these new devices can follow.

The test sample in this model is a tube similar with a human intravenous catheter that is placed in the main bronchus of a mouse. This small sample needs to present an inner and outer diameter of 0.60 and 1.00 mm and a length of around 3.00 mm. Simplifying the manufacturing process of test samples shortens the path to clinical application. Moreover, the optimization of the existing VAP model with the use of this personalized test samples will allow the study of new formulations to prevent and treat VAP infection. Such tools may help researches in the field of material/biomaterial sciences to easily produce samples with their developed formulations that can be used in this *invivo* model.

Experimental Methods

The nozzle design was based on principles illustrated in the literature for producing dies for the extrusion process [3]. CAD software (Creo Parametric 4.0) was used to produce an initial design of the nozzle. Then, verifications of the design were conducted using two simulation software programs. First, FloEFD v17.2 was used to simulate the fluid flow and estimate the pressure generated on the inside walls of the nozzle. The material used for the simulation was PLA. The fluid domain, boundary conditions and mesh size were defined. The simulation output was a measurement of the pressure on the inside walls of the nozzle. Afterward, the maximum internal pressure from the flow simulation was used as an input for structural integrity simulation. A finite element analysis was conducted using ANSYS v19 to simulate stresses generated in the nozzle. The inside surfaces were selected as the source of the pressure and the surface where the threading is located was set as a fixed support. The material used for this analysis was stainless steel which is predefined in the software library. Finally, the selected design was 3D printed in stainless steel by a commercial 3D printing service provider (i.materialise). The technology used to produce the nozzle was Three Dimensional Printing. In this technology, a binder sprayed on selected regions on a layer of fine metallic powder. This step is repeated layer after layer until the wanted geometry is produced. Afterward, the unbounded

particles are sprayed away. Finally, the produced output is sintered in an oven at a temperature of around 1300ºC [4].

Results and Discussion

The nozzle was produced using the additive manufacturing technique and had an outlet outer and inner diameter of 1.02 mm and 0.58 mm respectively. The internal geometry of the nozzle was designed to ensure that the smallest area the material flows through is 0.28 mm^2, which will assure sufficient flow of material. The nozzle was designed to be easily fitted with an M6 thread into a small screw extrusion set up mounted vertically in a way where the output side of the nozzle facing downward. This set up allow flexibility in testing different kind of polymeric material and mixtures. The output geometry of the extruded tube was highly dependent on the extrusion speed and temperature. It was noticed that, it is key to adjust the temperature to have a continuous flow of material without the need of high toque on the screw extruder. On the other hand, high temperatures cause the extruded tube to collapse and loose its shape.

Conclusion

This work provides a simple and quick solution for testing new materials and formulations developed for testing catheters in the VAP model. This nozzle was designed to be fitted on a mini screw extrusion system. However, adaptations can be simply conducted on this nozzle to allow it to be fitted on other extrusion systems. The concept of using such methodology in producing tools allow high flexibility in introducing modifications to the design and implementing these designs for producing test samples for *in vivo* models.

References

[1] K. Yanagihara *et al.*, “Efficacy and pharmacokinetics of ME1100, a novel optimized formulation of arbekacin for inhalation, compared with amikacin in a murine model of ventilator-associated pneumonia caused by Pseudomonas aeruginosa,” *J. Antimicrob. Chemother.*, vol. 72, pp. 1123–1128, 2017.

[2] A. Y. Peleg and and D. C. Hooper, “Hospital-Acquired Infections Due to Gram-Negative Bacteria Anton,” *Engl. J. Med.*, vol. 362, no. 19, pp. 1804–1813, 2010.

[3] R. Cornock, S. Beirne, B. Thompson, and G. G. Wallace, “Coaxial additive manufacture of biomaterial composite scaffolds for tissue engineering,” *Biofabrication*, vol. 6, no. 2, 2014.

[4] I.materialise, “High-Detail Stainless Steel,” 2019. [Online]. Available: https://i.materialise.com/en/3d-printing-materials/high-detail-stainless-steel. [Accessed: 05-Mar-2019].

Acknowledgement

This research was funded by the research project PRINTAID, the EU Framework Programme for Research and Innovation within Horizon 2020 - Marie Sklodowska-Curie Innovative Training Networks under grant agreement No. 722467

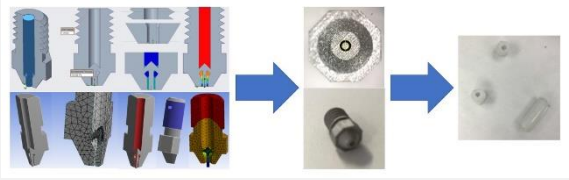

Process of producing the nozzle and testing
The simulated model of the nozzle in both FlowEFD and ANSYS is displayed (left), The printed nozzle (middle) and the tube produced by the nozzle (right).

PS1-07-156

Cellular response of pre-osteoblasts to selective laser melting Titanium implants subjected to mixed acid and heat treatment

Le T. M. Phuc[1], Seine A. Shintani[1], Shinpei Maruyama[2], Shigeo Mori[2], Takaaki Ueno[3], Tomiharu Matsushita[1], Seiji Yamaguchi[1]

[1]Chubu University, Department of Biomedical Sciences, College of Life and Health Sciences, Kasugai, JP; [2]Osaka Yakin Kogyo Co., Ltd., Osaka, JP; [3]Osaka Medical College, Division of Medicine for Function and Morphology of Sensor Organ, Dentistry and Oral Surgery, Takatsuki, JP

Introduction

Selective laser melting (SLM) is promising technique that capable of producing macro- or micro-structure surfaces for implants. These surfaces could be modified to increase osseointegration, bone generation and biocompatibility which are assured for their clinical success. Our previous studies showed that Titanium implants prepared by SLM (SLM-Ti) treated with mixed acid and heat (MA-H) formed apatite in a simulated body fluid (SBF) within 1 day, and enhanced *in vivo* bone formation on their surfaces [1]. However, the effects of these treatments on cellular response *in vitro* kept unclear. In this study, MC3T3-E1 pre-osteoblasts were cultured on SLM-Ti discs treated with MA-H to evaluate the effects of applied treatments on apatite formation, cell viability and cell morphology. These parameters were compared to that on untreated Ti samples. The data about cell viability and morphology on SLM-Ti treated with mixed acid (MA) are also used for reference.

Experimental Methods

SLM-Ti disc supplied by Osaka Yakin Kogyo Co., Ltd. (Osaka, Japan) were activated by a mixture of 66.3% H_2SO_4 and 10.3% HCl solutions. Afterwards, they were heated at 600 ºC for 1 h. The samples were immersed in SBF for 1 day and observed apatite formation by SEM. For cell culture tests, MC3T3-E1 cells were cultivated on the samples at 37 ºC, 5% CO_2, in DMEM supplemented with 10% FBS, 1% penicillin and streptomycin. At 1, 3, and 7 days of incubation, the cell viability was evaluated by absorption of light 490nm in wavelength according to production of formazan after adding cell count reagent SF (Nacalai Tesque,inc., Kyoto, Japan). After seeding 30 min, 1 h, 6 h and 1 day, the cell morphology were observed under SEM after normal fixation process.

Results and Discussion

The surface of SLM-Ti disc exhibited particular morphology due to the material-derived particles (Fig. 1a). The increased surface roughness was observed after MA treatment by producing micro-meter roughness, which remained even after the heat treatment (Fig. 1b,c). When the treated samples were soaked in SBF, the surface of MA-H was covered by apatite while those of untreated and MA samples were not.

In the cell attachment, even untreated surfaces showed activated cell morphology that was elongated and bridged the corners after incubation periods of 30 min, probably due to their roughened surface. This was in contrast with the round and flat morphology of cells attached on machined Ti plate [2]. The elongation was further increased by the MA and subsequent heat treatments, as shown in Fig 2.

MA samples showed significantly higher cell viability as compared to untreated samples at 1 and 3 days with the rate is 275 % and 133 %, respectively. The positive effect was decreased after the heat treatment: the cell viability percentages are almost the same for MA-H and untreated samples. These results are inconsistent with the previous reports where the cell proliferation on machined Ti and Ti-6Al-4V alloy were decreased by an acid treatment, but

increased by the subsequent heat treatment [3,4]. This might be attributed to the highly roughened surface of SLM-Ti. Further study will be needed to reveal the mechanism of cell proliferation on SLM-Ti subjected to MA and MA-H. However, it should be emphasized that both MA and MA-H samples in the present study showed no adverse effect on cell attachment and proliferation. Although the MA sample promotes cell attachment and proliferation, its contribution for bone-bonding would be limited because of lack of apatite formation. In contrast, the MA-H sample can tightly bind to living bone in short time because of its suitable morphology for cell attachment and high capacity for apatite formation. The bone bonding has been confirmed by animal experiment [1].

Conclusion

In summary, the present study showed that the SLM-Ti treated with MA-H is not toxic with cells, and promising for next generation of orthopedic and dental implants because of its suitable morphology for cell attachment and high capacities for bone bonding as well as apatite formation.

References

[1] K. Yamamoto, S. Yamaguchi, T. Matsushita, S. Mori, A. Hirata, N. Kato-Kogoe, H. Nakano, Y. Nakajima,Y. Nishitani, H. Nagatsuka, T. Ueno. RSC Adv., 2018, 8, 26069–26077.

[2] S. Faghihi, F. Azari, A. P. Zhilyaev, J. A. Szpunare, H. Vali, M. Tabrizian. Biomaterials 2007, 28, 3887–3895.

[3] L. Zhao, S. Mei, P.K. Chu, Y. Zhang, Z. Wu, Biomaterials 2010, 31, 5072–5082.

[4] G.-S. Shi, L.F. Ren, L.Z. Wang, H.-S. Lin, S.-B. Wang, Y.-Q. Tong, Oral Surg. Oral Med. Oral Pahol. Oral Radiol. Endod. 2009, 108, 368–375.

Acknowledgement

This research was supported by AMED under Grant Number JP18he1302025.

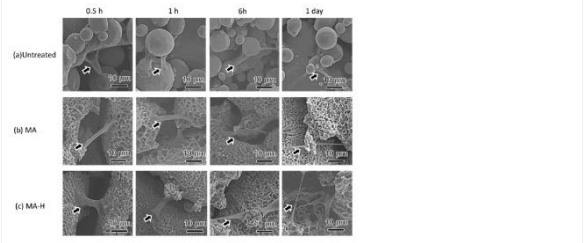

Figure 2
Morphology of MC3T3-E1 cells on SLM-Ti a) Untreated; b) MA and c) MA-H after various incubation periods.

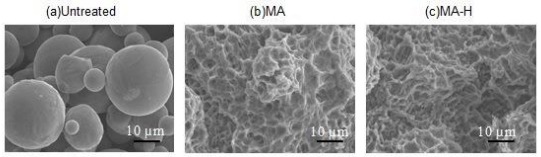

Figure 1
Surface morphology of SLM-Ti (a) Untreated, (b) MA and (c) MA-H

PS1-07-157

Control of Mechanical Properties by Design – Advances toward Functional Tissue Engineering Scaffolds

Klaus Kreuels[1], David Hexels[1], Nadine Nottrodt[2], Arnold Gillner[1,2]

[1]RWTH Aachen University, LLT - Chair for Laser Technology, Aachen, DE; [2]Fraunhofer ILT - Institute for Laser Technology, Aachen, DE

Introduction

Stereolithographic production of tissue engineering scaffolds allows the production of specifically designed lattice structures to control mechanical properties. The development of 3D printing processes for soft tissue implants is currently investigated for a heart valve. Each year more than 30 000 patients undergo surgical treatment in order to treat heart valve diseases in Germany. Surgical treatment is often the only promising therapeutic option causing a high demand of heart valve replacements. [1] The architecture of native heart valve tissue is constituted by three layers, which are perfectly adapted to its biomechanical properties and function inside the heart. Valvular interstitial cells (VICs) are embedded within a structure enclosed by endothelial cells (EC) and extracellular matrix (ECM), which comprises collagen, elastin and glycosaminoglycans to sustain the structure. [2] Using highly resolved stereolithography offers the possibility to construct artificial scaffold structures with anisotropic mechanical properties mimicking the native heart valve tissue and laying the foundation for an optimal biohybrid implant.

Experimental Methods

Polymeric scaffold structures are produced with a custom made laser stereolithography setup. The laser source is a continuous, frequency quadrupled Nd:YAG prototype laser with a wavelength of λ = 266 nm from Toptica Photonics. A platform within a vat, containing a photo resin, is mounted on a linear motorized Z-axis from Thorlabs, for the construction of three dimensional objects. The laser spot is focused on the surface of the photo resin. The photo resin used is a biocompatible material system based on thiol-ene click chemistry and is composed of trimethylolpropane tris(3-mercaptopropionate) (TMPMP) and poly(ethylene glycol) divinyl ether (PEG-DV). [3]
The polymerization reaction is verified by ATR-FTIR spectroscopy, carried out on a Perkin-Elmer Frontier-MIR FTIR spectrometer. Mechanical characterization of the material and scaffold structures is investigated by tensile and compression testing on a Zwick Z100/TL3A testing machine. Torsional testing is performed using a Kinexus Lab+ from Malvern.

Results and Discussion

Line tests and window pane tests are recorded to define the process window for the processing of photo resin on the laser stereolithography printing setup. A minimum resolution of approximately 10 µm is achieved in line tests and a reproducible curing depth of approximately 50 µm is achieved in window pane tests. A full conversion of the thiol-ene polymerization is confirmed by FTIR spectroscopy.
For mechanical testing of 3D printed structures four out of twelve contemplable unit cells have been selected and identified as representative models for further investigation. Prior to the examination of unit cell based scaffold structures, solid material samples have been mechanically characterized. This procedure serves two purposes: on the one hand the pure mechanical properties from the material itself without structure are assessed; on the other hand standardized testing specifications for synthetic materials are adapted and established for additive

manufactured materials for biomedical applications. This step is necessary due to the fact, that there is currently no existing standardized testing specification for materials with the later purpose of an implant.
Characterization of produced samples shows an elastic material with a higher withstanding against compression compared to tensile load. Furthermore, torsional testing shows constant material behavior under physiological conditions.

Conclusion

In this study we demonstrate a versatile process to produce tissue engineering scaffolds for soft tissue implants, where cells and surrounding tissue require a specific mechanical environment. This method provides a toolbox to alter and specifically address the mechanical properties by design beyond the mechanical properties of the material itself. The use of and combination of different unit cells as an element of design for scaffold structures makes this method easy to use. The effect of cultivation of cells in such scaffold structures and their influence on the mechanical properties of such a biohybrid materials remains to be investigated.

References

[1] H.J. Geißler, C. Schlensak, M. Südkamp, Herzklappenchirurgie heute, Dtsch. Arztebl. Int. 106 (2009) 224–235. doi:10.3238/arztebl.2009.0224.
[2] S. Jana, B.J. Tefft, D.B. Spoon, R.D. Simari, Acta Biomaterialia Scaffolds for tissue engineering of cardiac valves, Acta Biomater. 10 (2014) 2877–2893. doi:10.1016/j.actbio.2014.03.014.
[3] A. Hoffmann, H. Leonards, N. Tobies, L. Pongratz, K. Kreuels, F. Kreimendahl, C. Apel, M. Wehner, N. Nottrodt, New stereolithographic resin providing functional surfaces for biocompatible three-dimensional printing, J. Tissue Eng. 8 (2017) 1–9. doi:10.1177/2041731417744485.

Acknowledgement

The authors gratefully acknowledge the Deutsche Forschungsgemeinschaft DFG for their financial support of this work within the Paketantrag PAK 961 – MoReBioMed.

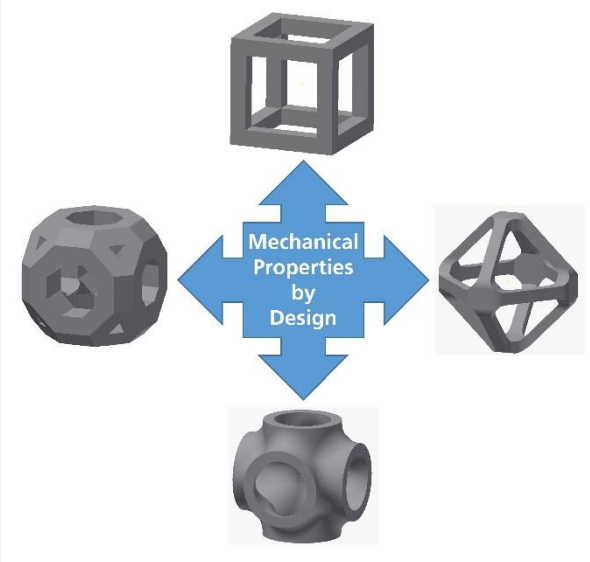

Control of Mechanical Properties by Design
Schematic depiction of the CAD models of the four selected unit cells from twelve contemplable unit cell designs.

PS1-07-158

Laser-based 3D printing of cell-containing thiol-ene hydrogels

Agnes Dobos[1], Jasper Van Hoorick[2,3], Peter Gruber[1], Wolfgang Steiger[1], Sandra Van Vlierberghe[2,3], Aleksandr Ovsianikov[1]

[1]Technical University of Vienna, Institute of Materials Science and Technology, Vienna, AT; [2]Flanders Make and Vrije Universiteit Brussel, Department of Applied Physics and Photonics, Brussels, BE; [3]Ghent University, Polymer Chemistry and Biomaterials Research Group, Ghent, BE

Introduction

Nature derived polymers, and especially hydrogels such as collagen or gelatin are an attractive basis for bioinks for biofabrication applications due to their biocompatibility and biodegradability. Modification with photo-crosslinkable functionalities allows for light based processing. To this end, the use of thiol-norbornene photoclick hydrogels have the capacity to overcome limitations of chain-growth polymerization-based bioinks such as oxygen inhibition and heterogeneous network formation.

Experimental Methods

Two photon-polymerization (2PP)-based 3D printing is based on the simultaneous absorption of two photons from a femtosecond-pulsed laser leading to localized polymerization of photosensitive bioinks. 2PP enables both the fabrication of cell scaffolds and the encapsulation of cells inside photosensitive hydrogels in accordance to computer aided designs (CAD).

Results and Discussion

We report herein on the development of a biocompatible multicomponent system based on gelatin-norbornene, a small molecular weight thiolated crosslinker dithiothreitol and a cleavable biocompatible photoinitiator which has the capacity to enable direct cell encapsulation by printing cells into various designs while maintaining cell viability and proliferation. Direct cell encapsulation compared to cell seeding in prefabricated scaffolds provides high initial cell loading and uniform cell distribution. The properties of the hydrogel including stiffness, degradation and swelling can be fine-tuned by changing the concentrations of the components and/or light dose.

Conclusion

The increased lifetime of the constructs can allow the study of cell-cell interactions, creating a versatile platform for *in vitro* modelling and tissue engineering constructs to study the cell response in 3D.

References

1. Kim, J. J., Hou, L. & Huang, N. F. Vascularization of three-dimensional engineered tissues for regenerative medicine applications. *Acta Biomater.***41,** 17–26 (2016).
2. Ovsianikov, A. *et al.* Laser printing of cells into 3D scaffolds. *Biofabrication***2,** 014104 (2010).
3. Van Vlierberghe, S., Schacht, E. & Dubruel, P. Reversible gelatin-based hydrogels: Finetuning of material properties. *Eur. Polym. J.***47,** 1039–1047 (2011).
4. Van Hoorick, J. *et al.* Highly Reactive Thiol-Norbornene Photo-Click Hydrogels: Towards Improved Processability. *Macromol. Rapid Commun.* (2018).

Acknowledgement

Funding from TU Wien doctorate school Biointerfaces and the FWO-FWF grant (Research Foundation Flanders-Austrian Science Fund project) is gratefully acknowledged (FWOAL843, #I2444N28). J.V.H holds an FWO-SB grant provided by the Research Foundation Flanders (FWO, Belgium). Furthermore, the FWO is acknowledged for funding several research grants (FWOKN273, G005616N, G0F0516N).

2:45 p.m. – 3:45 p.m.

Hall 1 / Exhibition Area

PS1-08 | Biomaterials for gene therapy

PS1-08-159

siRNA delivery with designed inorganic nanocarriers based on nanoporous silica nanoparticles

Karen F. W. Besecke[1], Philipp Dillschneider[2], Henning Hartwig[2], Andrea Hoffmann[3], Meike Stiesch[2], Peter Behrens[1]

[1]Leibniz University Hanover, Institut für Anorganische Chemie, Hanover, DE; [2]Medizinische Hochschule Hanover, Klinik für Zahnärztliche Prothetik und Biomedizinische Werkstoffkunde, Hanover, DE; [3]Medizinische Hochschule Hanover, Klinik für Orthopädie, Hanover, DE

Introduction

RNA interference (RNAi) is a post-transcriptional gene regulatory mechanism, which is based on the cleavage of target mRNA strands to suppress gene expression. Since its discovery, RNAi has emerged as promising therapeutic treatment of diseases related with gene overexpressions like cancer and genetic or autoimmune disorders. Double-stranded RNAs such as small interfering RNAs (siRNAs) are able to initiate this mechanism, thus they can reduce protein production in a sequence-specific manner. However, naked siRNAs are unstable in physiological environments and show poor intracellular uptake. For this reason, efficient and safe delivery vehicles are required, which protect the siRNAs and bring them to their site of action into the cytoplasm of a cell.[1-4]

Our approach is to use nanoporous silica nanopartilces (NPSNPs) as delivery platform for siRNAs. In the past decade, NPSNPs have emerged as promising basis for designing tailored delivery systems for a variety of biomolecules (e.g. small molecule drugs, proteins or nucleic acids). Among other positive features, these NPSNPs exhibit large surface areas associated with large pore volumes and reactive silanol groups at the surface, which can easily be modified and functionalized. Moreover, NPSNPs are biocompatible and biodegradable.[2,4,5]

Experimental Methods

NPSNPs were prepared in a water/oil phase using polystyrene and CTAB as structure directing agents to build up the porous system.[6] After templateremoval, the particle surface was modified with different trialkoxysilanes by post-grafting reaction to control siRNA uptake and release. Next, the loaded particles were capped with different lipids to protect the nucleic acids and to enhance cell uptake as well as the siRNA release into the cytoplasm. Finally, the cytotoxicity was ensured with an CellTiter-Blue® assay and the gene knockdown ability of the nanocarriers was investigated using siRNA against green fluorescent protein (GFP) in GFP-expressing cells.

Results and Discussion

The synthesized NPSNPs were approximately 80 nm in size and had a pore diameter of 7 nm. By modifying the surface, high loading amounts (up to 150 µg siRNA per mg NPSNP) were obtained and an appropriate release could be achieved. Cell uptake investigations with fluorescent labelled silica particles and siRNAs visualized a fast cellular uptake and the ability of our nanocarriers to release the siRNA into the cytoplasm. The cell viability tests indicate no significant cytotoxicity of our silica nanoparticles based vectors even when using high concentrations. In the end, the potential of our designed delivery platform was demonstrated with a successful knockdown of GFP-expression.

Conclusion

We could demonstrate that siRNA-loaded NPSNPs conjugated with a lipid-bilayer can provide a safe and efficient platform for the delivery of oligonucleotides into cells.

References

1. [1] K. Tatiparti et al., *Nanomaterials***2017**, *7*, 77
2. [2] K. Möller et al., *Nanoscale***2016**, 8, 4007
3. [3] H. Xue et al., *Nanomedicine***2014**, 9, 295
4. [4] R. Kamegawa et al., *Nano Research***2018**, 11, 5219
5. [5] K. Möller et al., *Chem.Mater*. **2017**, 29, 371
6. [6] K. Okuyama et al., *Microporous Mesoporous Mat*. **2009**, 120, 447

Acknowledgement

We would like to thank Dawid P. Warwas, Dennes Nettelroth, Mandy Jahns for taking TEM images, SEM images and performing sorption measurements, respectively. Furthermore, acknowledgement go to the LNQE Hanover for the ability to use the TEM and to the working group of Prof. Feldhoff for the ability to use their SEM.

PS1-08-160

Gene-Loaded Poly (Beta Aminoester) Polyplexes as Versatile Biomaterials for Antitumor Therapeutics

Cristina Fornaguera[1], Marta Guerra-Rebollo[1], Martí Lecina[1], Miguel Ángel Lázaro[2], Anna Cascante[1,2], Victor Ramos[1], Salvador Borrós[1,2]

[1]Universitat Ramon Llull (URL), Institut Químic de Sarrià (IQS), Barcelona, ES; [2]Sagetis-Biotech, Barcelona, ES

Introduction

The use of nucleic acid-loaded polymeric nanosystems as **cancer nanomedicine**has experimented an exponential increase, thus resulting in numerous publications in the last years. This is due to the multiple advantages that they bring associated, such as nucleic acids protection and site-directed therapies to increase therapeutic outcomes and reduce side effects simultaneously. In addition, they may possibly be useful to attack cancers by using different therapeutic approaches. However, the translation of basic research to clinical applications is still reduced, mainly due to the lack of actively-targeted, safe and efficient gene delivery vectors, especially when dealing with *in vivo*direct uses.

Experimental Methods

With the objective to circumvent these drawbacks and overpass the gap between research labs and clinicians, in our group, we created a library of oligopeptide end-modified poly(beta aminoesters) – **OM-PBAE polymers**, with proven capacity to encapsulate different kinds of **oligonucleotides**(i.e. plasmids, mRNA, siRNA) by co-incubation and electrostatic binding into discrete nanometric particles (sizes around 150 – 180 nm) with a tunable surface charge (from anionic to cationic).

Results and Discussion

We demonstrated their *in vitro*safety profile, by viability studies, and cell-type selective transfection, using a reporter gene, as a function of the specific polymer composition taken into account not only the added targeting moiety, but also the specific oligopeptide combination and the backbone structure and polymer combination. Selecting the most appropriate polymer, we were able to demonstrate OM-PBAE polyplexes reduced toxicity and higher efficiency in permissive but also restrictive cell cultures; i.e. immune and cancer cells, as compared to commercial transfection agents. Examples of concrete *in vitro*achievements are found in gene therapy: the enhancement of selective tumor cells apoptosis, thanks to the encapsulation of siRNA codifying for oncogenes that suppress their replicative capacity. Also, in cell therapy, where mesenchymal stem cells, usually refractory to transfection, were transfected while maintaining their undifferentiated state. *In vivo*, they have also demonstrated a promising performance, namely for gene therapy of gliomas and also for cancer immunotherapeutic purposes, thanks to their preferential targeting and transfection of antigen presenting cells, as demonstrated by biodistribution studies, which makes them useful as mRNA vaccines to re-awaken the anti-tumoral immunity. Therefore, our **aim**here is to demonstrate the versatility and adequacy of our biomaterials, the OM-PBAE polymer library as promising novel antitumor strategies, which could eliminate tumors by attacking different tumor survival mechanisms.

Conclusion

Since current medical guidelines recommend the combination of more than a single therapeutic approach, due to most cancers heterogeneous manifestation, we hypothesize that future therapies will have a multifocal purpose, to end up with all tumor cell populations. Thus, in a near future, the use of OM-PBAE nanoparticles to create a combined therapeutic strategy; i.e. knocking an oncogene with tumor-targeted nanoparticles and re-awakening the dendritic cells to make them present tumor associated antigens to re-activate the cytotoxic T lymphocytes, could improve the safety, efficacy, selectivity and potency of current available treatments, thus, OM-PBAE nanoparticles could represent a turning point in near future cancer treatments and patients quality of life.

References

Fornaguera C., et al., Advanced Healthcare Materials, 2018

Balsells L., et al., ACS Omega, 2019

2:45 p.m. – 3:45 p.m.

Hall 1 / Exhibition Area

PS1-09 | Antibacterial

PS1-09-162

Development of Polysaccharide-Drug Ionic Complexes as Antimicrobial Hydrogels in the Treatment of Staphylococcal Infections

Cristina Casadidio[1], Roberta Censi[1], Stefania Scuri[2], Laura Mayol[3], Marco Biondi[3], Giuseppe De Rosa[3], Piera Di Martino[1]

[1]University of Camerino, School of Pharmacy, Drug Delivery Division, Camerino (MC), IT; [2]University of Camerino, School of Pharmacy, Hygiene Research Centre, Camerino (MC), IT; [3]University of Naples Federico II, Department of Pharmacy, Naples, IT

Introduction

Polysaccharides are biodegradable, biocompatible and non-toxic biopolymers derived from renewable sources showing great potential for several biomedical applications, such as the prevention and treatment of staphylococcal infections. A strategy to treat these infections is the use of polysaccharides in antimicrobial therapy. Polysaccharide based *in situ*-forming hydrogels are able to improve the efficacy of the loaded drug(s) by overcoming different drawbacks like: burst effect, high systemic toxicity, side effects and fast degradation [1,2]. In this work we investigated the efficacy of anionic polysaccharidic hydrogels as vancomycin stabilizers. The newly biocompatible and biodegradable designed formulations could be potentially used as enhancers of drug structural stability overcoming its degradation pathways.

Experimental Methods

Hyaluronic acid, alginic acid, propylene glycol alginate, xanthan gum and dextran (as control) were used as anionic polysaccharides, while vancomycin was selected as a cationic drug. Polysaccharide-vancomycin solutions containing a fixed amount of polysaccharide (5mg/mL) and polysaccharide-vancomycin hydrogels at gel-point concentrations were formulated in aqueous media at pH 7.4 and pH 9 (i.e. vancomycin isoelectric point). Chemical stability tests of polysaccharide/antibiotic solutions and hydrogels were performed for 22 days by HPLC-DAD-MS. Placebo hydrogels and drug-loaded systems were characterized by rheological analysis at 37°C, to evaluate the presence of ionic complexes between negatively charged polysaccharides and the positive charges of the drug. Vancomycin release studies were conducted at 37°C upon addition of PBS (pH 7.4) on top of the gels. The antimicrobial activity of the complexes was tested against *Staphylococcus aureus* at 10^6CFU/mL after 24,48 and 72 hours via microdilution method and by contact susceptibility tests.

Results and Discussion

The chemical stability of the drug can be achieved by physical encapsulation of the drug into the hydrogel networks at physiological conditions. The polysaccharidic solutions with ±24% of drug stability (Figure 1a) and polysaccharidic hydrogels with ±40% of drug stability (Figure 1b) are able to preserve the vancomycin native structure compared with drug solution. The results show that not all polymers were able to stabilize the drug to the same extent. Vancomycin stability is governed not only by physical network encapsulation, but also by ionic interaction between drug and polysaccharidic matrix thanks to self-assembling ionic complexes composition. To validate this hypothesis, stability studies were also performed at pH 9, when vancomycin is uncharged. As depicted in Figure 2, ionic bonds are essential to promote the improvement of vancomycin stability. In addition, the formation of complexes affects rheological characteristics of the systems. More in detail, the presence of the peptide confers to hyaluronic acid and propylene glycol alginate formulations the transition from an entangled solution to a gel-like rheological behaviour.

Otherwise, unloaded xanthan gum formulations displays a gel-like rheological behaviour and, when loaded with vancomycin, an evident increase of both viscoelastic moduli was detected. Regarding alginic acid, no significant changes, between unloaded and loaded gels, were observed. Release tests were performed for 70 hours before the beginning of hydrogel degradation process. Figure 1c shows different release kinetics according to the nature of the polymer. A 60% of vancomycin release is achieved within three days for all formulations. Antimicrobials susceptibility tests show a significant bacteria reduction compared to the vancomycin in solution, and only hyaluronic acid fails to stop bacterial growth. In particular, xanthan gum reaches the ±91.5% of bacteria reduction until 24h and a zone of inhibition of ±24mm, promoting as best candidate.

Conclusion

Vancomycin-polysaccharidic hydrogels are able to preserve the structural stability of the drug enhancing its antimicrobial activity in physiological environment thanks to the physical encapsulation and self-assembling ionic complexes configuration. Furthermore, these designed formulations could be used as functional coating in the treatment of wound infections and in the prevention of implant-associated infections.

References

[1] Casadidio, C., Butini M.E., Trampuz A., Di Luca M., Censi R., Di Martino P. Eur. J. Pharm. Biopharm., 2018. **130**: p. 260-271.

[2] Hoffman, A.S. Adv. Drug Delivery Rev. **2012**, 64, 18-23.

Acknowledgement

The authors acknowledge receipt of funding from the European Commission through a H2020-MSCA-ITN-2015 award, as part of the ISPIC project (grant number 675743), a H2020-MSCA-RISE-2016 award through the CHARMED project (grant number 734684) and a H2020-MSCA-RISE-2017 award through the CANCER project (grant number 777682).

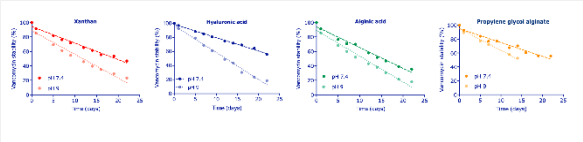

Figure 2.
Comparison of vancomycin decay at pH 7.4 (ionic interaction) and pH 9.0 (vancomycin isoelectric point) complexed with polysaccharide solutions.

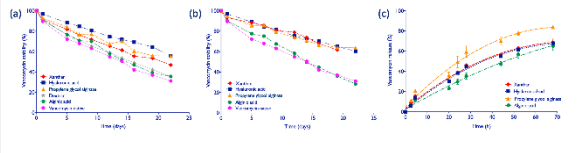

Figure 1.
Chemical stability of native vancomycin at pH 7.4 loaded into (a) polysaccharidic solutions and (b) polysaccharidic hydrogels; (c) cumulative release of vancomycin in PBS pH 7.4, 37°C.

PS1-09-163

Detection and Inhibition of Bacteria on a Dual-Functional Silver Platform

Vadanasundari Vedarethinam, Ling Huang, Wei Xu, Jing Yang, **Kun Qian**

School of Biomedical Engineering, Med-X Research Institute, Shanghai Jiao Tong University, Shanghai, CN

Introduction

Bacteria associate with most organisms and afford key information on host systems.[1] Detection of bacteria in biofluids supports the clinical diagnosis and guides the medical treatment, e.g., for infections.[2] To date, bacteria induced infections affect ≈10 millions of people globally with an increase of ≈32% per year,[3] which urgently calls for novel diagnostic tools for early detection and precise medication. Compared to conventional proteomic[4] and genomic[5] approaches for detection of bacteria, metabolic analysis is more distal for real case application, but very difficult due to the high complexity of biosystems and low abundance of metabolites.[6] In parallel to detection, inhibition of bacteria is not only required in clinics, but is also a daily issue for health care.[7] Therefore, there is an urgent need to develop an advanced tool toward metabolic analysis of bacteria for diagnostics and bacteria inhibition. Noble metal materials own unique surface plasmonics and elemental chemistry,[8] for defined bioanalysis[9] and targeted biotoxicity,[10] respectively. For bioanalysis, noble metals and their hybrids afford surface plasmon resonance for spectrometric applications, e.g., mass spectrometry.[11] Particularly, high-performance assays have been established based on core–shell structured noble metal hybrids, owing to the higher yield of hot carriers over bulk materials.[12] For biotoxicity, antibacterial effects by noble metals such as silver are widely applied in hospitals and daily life.[13] Notably, new inhibition mechanisms of bacteria by noble metals remain to be explored for high antibacterial capability, which can be decided by the tailored material structures. Furthermore, development of a dual functional material is challenging and in demand, engaging advanced applications for both bioanalysis and biotoxicity.

Experimental Methods

We prepared the magnetic silver nanoshells (MPs@SiO2@Ag) by the layer-by-layer assembling approach (Figure 1). First, MPs as core materials were synthesized by solvothermal method. For the MPs@SiO2, silica was modified onto the surface of MPs through a controlled sol–gel method. For the MPs@SiO2@Ag, silver nanoshells were decorated by repeating reaction cycles on the surface of MPs@SiO2. To investigate inhibition of bacteria by the MPs, MPs@SiO2, and MPs@SiO2@Ag, we applied the E. coli from countless bacterial and recorded the bacterial viability by measuring OD values at 600 nm in triplicates (Figure 2). To verify the antibacterial activity of the MPs@SiO2@Ag, metabolites extraction was obtained by MALDI MS assisted by MPs@SiO2@Ag nanocomposties.We prepared the magnetic silver nanoshells (MPs@SiO2@Ag) by the layer-by-layer assembling approach (Figure 1). First, MPs as core materials were synthesized by solvothermal method. For the MPs@SiO2, silica was modified onto the surface of MPs through a controlled sol–gel method. For the MPs@SiO2@Ag, silver nanoshells were decorated by repeating reaction cycles on the surface of MPs@SiO2. To investigate inhibition of bacteria by the MPs, MPs@SiO2, and MPs@SiO2@Ag, we applied the E. coli from countless bacterial and recorded the bacterial viability by measuring OD values at 600 nm in triplicates (Figure 2). To verify the antibacterial activity of the MPs@SiO2@Ag, metabolites extraction was obtained by MALDI MS assisted by MPs@SiO2@Ag nanocomposties.

Results and Discussion

We designed magnetic silver nanoshells as a multifunctional platform for detection and inhibition of bacteria. The optimized magnetic silver nanoshells can be utilized as matrix enabling direct laser desorption/ionization mass spectrometry (LDI MS) based metabolic analysis of bacteria (approximately ten Escherichia coli (E. coli) per microliter), in serum (Figure 2a/b/c). Then we monitored serum infection process from 0 to 10 h by statistics toward clinical classification (Figure 2d/e/f). Moreover, magnetic silver nanoshells facilitated surface adhesion on bacteria due to nanoscale surface roughness, and thus displayed long-term antibacterial effects. We also studied metabolism of bacteria with metabolic biomarkers identified during inhibition. Our work not only guided the design of material based approaches for bioanalysis and biotoxicity, but also contributed to bacteria-related diagnosis and new metabolomic insights for antibacterial applications.

Conclusion

We developed the MPs@SiO2@Ag with rational designed structural parameters as a dual-functional platform, bridging metabolism analysis and bacterial toxicity. For metabolism analysis, we performed direct LDI MS for fast detection and early diagnosis toward bacterial induced infection and related classification. For bacterial toxicity, we achieved long term bacteria inhibition and explored the antibacterial process by metabolic analysis.

References

[1] a) A. P. Bhatt, M. R. Redinbo, S. J. Bultman, CA—Cancer J. Clin. 2017, 67, 327; b) Y. Kawaharada, S. Kelly, M. W. Nielsen, C. T. Hjuler, K. Gysel, A. Muszynski, R. W. Carlson, M. B. Thygesen, N. Sandal, M. H. Asmussen, M. Vinther, S. U. Andersen, L. Krusell, S. Thirup, K. J. Jensen, C. W. Ronson, M. Blaise, S. Radutoiu, J. Stougaard, Nature 2015, 523, 308.

[2] a) C. K. Dixit, S. K. Vashist, B. D. MacCraith, R. O'Kennedy, Nat. Protoc. 2011, 6, 439; b) G. B. Qi, D. Zhang, F. H. Liu, Z. Y. Qiao, H. Wang, Adv. Mater. 2017, 29, 1703461.

[3] a) Y. A. Nor, L. Zhou, A. K. Meka, C. Xu, Y. Niu, H. Zhang, N. Mitter, D. Mahony, C. Yu, Adv. Funct. Mater. 2016, 26, 5408; b) B. Tornimbene, S. Eremin, M. Escher, J. Griskeviciene, S. Manglani, C. L. Pessoa-Silva, Lancet Infect. Dis. 2018, 18, 241.

[4] a) A. Schmidt, K. Kochanowski, S. Vedelaar, E. Ahrne, B. Volkmer, L. Callipo, K. Knoops, M. Bauer, R. Aebersold, M. Heinemann, Nat. Biotechnol. 2016, 34, 104; b) C. Rejeeth, X. Pang, R. Zhang, W. Xu, X. Sun, B. Liu, J. Lou, J. Wan, H. Gu, W. Yan, K. Qian, Nano Res. 2018, 11, 68; c) B. Liu, Y. Li, H. Wan, L. Wang, W. Xu, S. Zhu, Y. Liang, B. Zhang, J. Lou, H. Dai, K. Qian, Adv. Funct. Mater. 2016, 26, 7994; d) Y. Li, L. Yan, Y. Liu, K. Qian, B. Liu, P. Yang, B. Liu, RSC Adv. 2015, 5, 1331.

[5] a) D. V. Ward, M. Scholz, M. Zolfo, D. H. Taft, K. R. Schibler, A. Tett, N. Segata, A. L. Morrow, Cell Rep. 2016, 14, 2912; b) D. R. Mende, J. A. Bryant, F. O. Aylward, J. M. Eppley, T. Nielsen, D. M. Karl, E. F. DeLong, Nat. Microbiol. 2017, 2, 1367.

[6] J. Wu, X. Wei, J. Gan, L. Huang, T. Shen, J. Lou, B. Liu, J. X. J. Zhang, K. Qian, Adv. Funct. Mater. 2016, 26, 4016.

[7] a) J. Lloyd-Price, A. Mahurkar, G. R. Ahnavard, J. C. Rabtree, J. O. Rvis, A. B. R. Hall, A. B. Rady, H. H. C. Reasy, C. McCracken, M. G. Giglio, D. McDonald, E. A. Franzosa, R. Knight, O. White, C. Huttenhower, Nature 2017, 550, 61; b) U. R. Abdelmohsen, S. Balasubramanian, T. A. Oelschlaeger, T. Grkovic, B. P. Ngoc, R. J. Quinn, U. Hentschel, Lancet Infect. Dis. 2017, 17, 30.

[8] a) K. Wu, J. Chen, J. R. McBride, T. Lian, Science 2015, 349, 632; b) M. L. Brongersma, N. J. Halas, P. Nordlander, Nat. Nanotechnol. 2015, 10, 25; c) J. Gan, X. Wei, Y. Li, J. Wu, K. Qian, B. Liu, Nanomedicine: NBM 2015, 11, 1715.

[9] a) B. Duncan, N. D. B. Le, C. Alexander, A. Gupta, G. Y. Tonga, M. Yazdani, R. F. Landis, L. S. Wang, B. Yan, S. Burmaoglu, X. Li, V. M. Rotello, ACS Nano 2017, 11, 5339; b) U. S. Dinish, Z. Song, C. J. H. Ho, G. Balasundaram, A. B. E. Attia, X. Lu, B. Z. Tang,
B. Liu, M. Olivo, Adv. Funct. Mater. 2015, 25, 2316; c) X. Sun, J. J. Wan, K. Qian, Small Methods 2017, 1, 1700196.
[10] C. Kaweeteerawat, C. H. Chang, K. R. Roy, R. Liu, R. Li, D. Toso, H. Fischer, A. Ivask, Z. Ji, J. I. Zink, Z. H. Zhou, G. F. Chanfreau, D. Telesca, Y. Cohen, P. A. Holden, A. E. Nel, H. A. Godwin, ACS Nano 2015, 9, 7215.
[11] a) S. G. Elci, G. Y. Tonga, B. Y. S. T. Kim, C. S. Kim, Y. Jiang, K. Saha, D. F. Moyano, A. L. M. Marsico, V. M. Rotello, R. W. Vachet, ACS Nano 2017, 11, 7424; b) M. Lu, X. Yang, Y. Yang, P. Qin, X. Wu, Z. Cai, Nanomaterials 2017, 7, 87; c) R. Li, D. D. Gurav, J. Wan, K. Qian, Prec. Nanomed. 2018, 1, 162.
[12] a) L. Huang, J. Wan, X. Wei, Y. Liu, J. Huang, X. Sun, R. Zhang, D. D. Gurav, V. Vedarethinam, Y. Li, R. Chen, K. Qian, Nat. Commun. 2017, 8, 220; b) X. Wei, Z. Liu, X. Jin, L. Huang, D. D. Gurav, X. Sun, B. Liu, J. Ye, K. Qian, Anal. Chim. Acta 2017, 950, 147.
[13] a) E. Pazos, E. Sleep, C. M. R. Perez, S. S. Lee, F. Tantakitti,
S. I. Stupp, J. Am. Chem. Soc. 2016, 138, 5507; b) A. Ivask, A. ElBadawy, C. Kaweeteerawat, D. Boren, H. Fischer, Z. Ji, C. H. Chang, R. Liu, T. Tolaymat, D. Telesca, J. I. Zink, Y. Cohen, P. A. Holden, H. A. Godwin, ACS Nano 2014, 8, 374.

Acknowledgement

V.V., L.H., and W.X. contributed equally to this work. The authors gratefully acknowledge financial support from the National Natural Science Foundation of China (NSFC; Project Nos. 81771983, 81750110544, 81650110523, and 81401542), the Shanghai Science and Technology Commission (Project No. 16441909300), and the Ministry of Science and Technology of China (Project No. 2017YFC0909000). This work was also sponsored by the Program for Professor of Special Appointment (Eastern Scholar) at Shanghai Institutions of Higher Learning (Grant No. TP2015015).

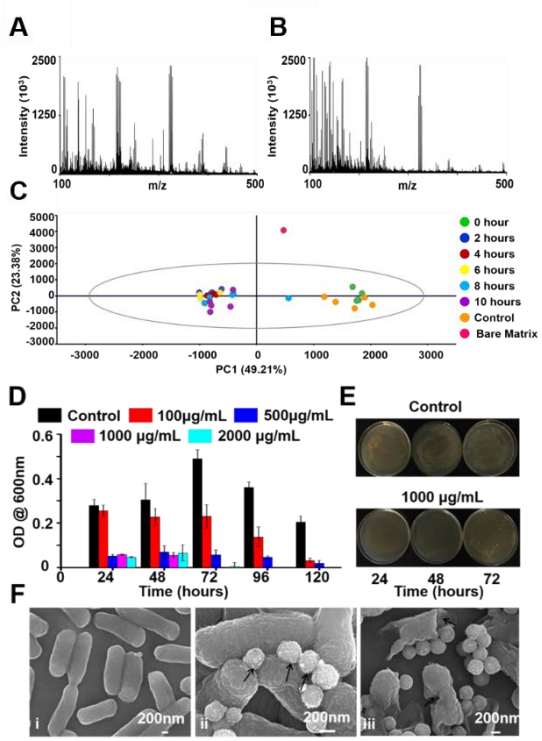

Figure 2. Detection and inhibition of bacteria on a dual-functional silver platform.
a) Mass spectrum of control serum b) Mass spectrum of metabolite detection from spiked bacteria; c) OPLS-DA result of spiked bacterial metabolites at different incubation time (0-10 h, label with 0hr~10hr in figures); d) OD results of antibacterial effect of magnetic silver nanoshells towards E.Coli (5 days); e) Digital images of toxic effect of magnetic silver nanoshells against E.Coli; f) SEM images of antibacterial effect of magnetic silver nanoshells (i. control; ii. Silver nanoshells attached with bacteria at 6 h; iii- Observation of bacterial damage by Ag nano shells at 48 h.

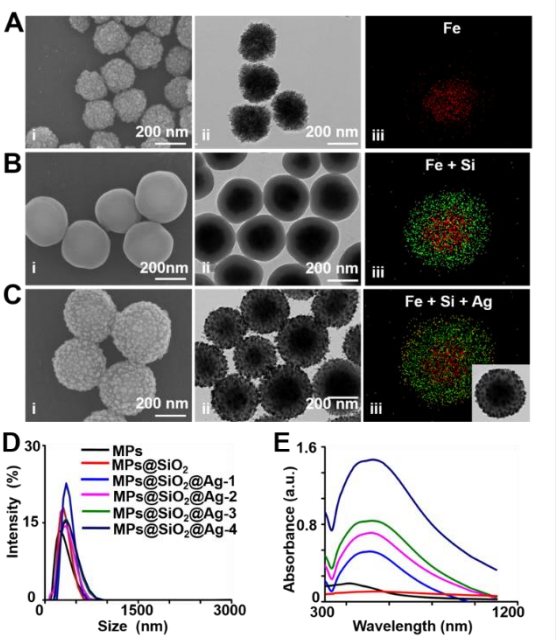

Figure 1. Preparation and characterizations of magnetic silver nano shells.
SEM image of Bare MPs (a i), MP @SiO2 (b i), MP@SiO2@Ag (c i); TEM images of Bare MPs (a ii), MP @SiO2 (b ii), MP@SiO2@Ag (c iii); SAED of Bare MPs & insert image- HRTEM (a iii), MP @SiO2 (b iii), MP@SiO2@Ag & insert image- HRTEM (c iii); d) Elemental mapping images of MP (i), SiO2 (ii), Ag (iii).

PS1-09-164

Antibacterial property of Ag, Cu, Zn, and Ga incorporated to Ti surface by micro-arc oxidation treatment

Masaya Shimabukuro[1], Yusuke Tsutsumi[2,3], Kosuke Nozaki[4], Peng Chen[2], Maki Ashida[2], Hisashi Doi[2], Takao Hanawa[2]

[1]Tokyo Medical and Dental University, Graduate School of Medical and Dental Sciences, Department of Metallic Biomaterials, Bunkyo, JP; [2]Tokyo Medical and Dental University, Institute of Biomaterials and Bioengneering, Department of Metallic Biomaterials, Chiyoda, JP; [3]Research Center for Structural Materials, National Institute for Materials Science (NIMS), Tsukuba, JP; [4]Tokyo Medical and Dental University, Graduate School of Medical and Dental Sciences, Department of Fixed Prosthodontics, Bunkyo, JP

Introduction

Titanium (Ti) and its alloys are widely used as metallic biomaterials based on their good mechanical properties and biocompatibility. Infections caused by the formation of biofilms on the surface of biomaterials is a major cause of failure in implant surgeries. Biofilms can weaken the bactericidal effect of antibiotics due to the presence of a wide variety of bacteria and extracellular polysaccharide. Preventing bacterial invasion is necessary for the success of surgical implantations. Therefore, the inhibition of biofilm formation on the surface of the implants is crucial. The initial stage of biofilm formation involves bacterial adhesion. Preventing adhesion and the subsequent bacterial growth are important in the control of biofilm formation on implant surfaces. In this study, micro-arc oxidation (MAO) was used to incorporate the desirable antibacterial elements into the resulting surface oxide layer. A Ti surface was modified by MAO treatment with various antibacterial elements, including silver (Ag), copper (Cu), zinc (Zn), and gallium (Ga) ions. The antibacterial property of the MAO-treated Ti was evaluated by monitoring bacterial adhesion.

Experimental Methods

The MAO modification of the Ti surface used an electrolyte solution comprising 100 mM calcium glycerophosphate and 150 mM calcium acetate. Silver nitrate, copper chloride dehydrate, zinc chloride, or gallium chloride at a maximum concentration of 2.5 mM was added to the electrolyte solution. A positive voltage with a constant current density was applied for 10 min. After MAO treatment, samples were thoroughly rinsed in ultra-pure water for 3 min. The surface characterization was done by scanning electron microscopy and X-ray photoelectron spectroscopy (XPS). The ion release behavior into the physiological saline overlying the surface was evaluated by inductively coupled plasma atomic emission spectroscopy. Bacterial adhesion was examined using *Escherichia coli (E. coli)* and *Staphylococcus aureus (S. aureus)* according to the standard ISO22196 test method.

Results and Discussion

Surface characterization confirmed the formation of the porous oxide layers using the customized electrolytes containing the antibacterial elements. In addition to C, O, P, Ca, and Ti, the antibacterial elements (Ag, Cu, Zn, and Ga ions) were also detected in the XPS analyses. Figure 1 depicts the quantified release of the antibacterial elements as ions into physiological saline during the 28-day immersion. The release of Ag, Zn, and Ga ions was detected. In terms of the quantity of ions released, the order was Ga > Ag > Zn > Cu. Cu ion was presumably released but was less than the detection limit. Figure 2 shows the results of bacterial adhesion test. Bacterial adhesion on the MAO-treated Ti surface modified with Ag and Cu ions was inhibited. Ag-incorporated samples likely displayed a strong antibacterial effect due to the release of Ag ion. The Cu-incorporated sample showed the same efficacy due to the

contact-killing mechanism. The results indicate the potential value of MAO treatment in generating antibacterial implant surfaces.

Conclusion

In this study, A Ti surface was modified by MAO treatment with various antibacterial elements, including Ag, Cu, Zn, and Ga ions. The antibacterial property of the MAO-treated Ti was evaluated by monitoring bacterial adhesion. As the results, MAO treatment could incorporate the antibacterial elements into the porous oxide layer. In terms of the quantity of ions released from the sample, the order was Ga > Ag > Zn > Cu. Bacterial adhesion on the MAO-treated Ti surface modified with Ag and Cu ions was inhibited. It is hoped that the findings that have been presented in this paper will contribute to a better understanding of the new insights for relevant investigations and biomedical applications.

References

Yusuke Tsutsumi, Mitsuo Niinomi, Masaaki Nakai, Masaya Shimabukuro, Maki Ashida, Peng Chen, Hisashi Doi, Takao Hanawa “Electrochemical Surface Treatment of a β- titanium Alloy to Realize an Antibacterial Property and Bioactivity”, Metals, 6(4), 76, 2016

Acknowledgement

This study was supported by the Research Center for Biomedical Engineering, Tokyo Medical and Dental University, Project “Creation of Life Innovation Materials for Interdisciplinary and International Researcher Development” ,and project “Cooperative project amount medicine, dentistry, and engineering for medical innovation-Construction of creative scientific research of the viable material via integration of biology and engineering” by Ministry of Education, Culture, Sports, Science and Engineering, Japan.

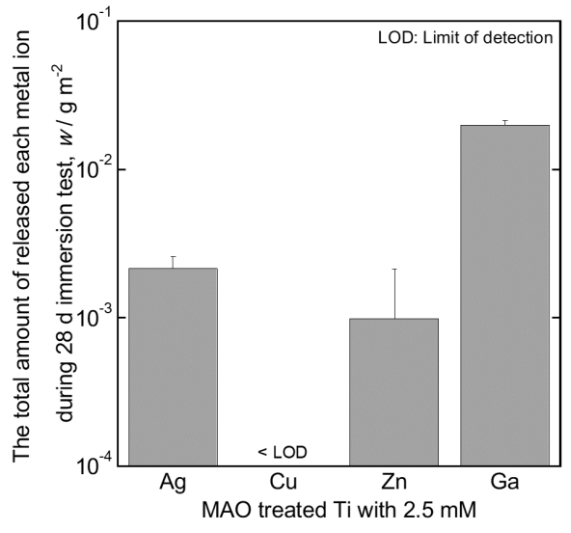

Figure 1 The release amount of each antibacterial ion into physiological saline for 28-d immersion.

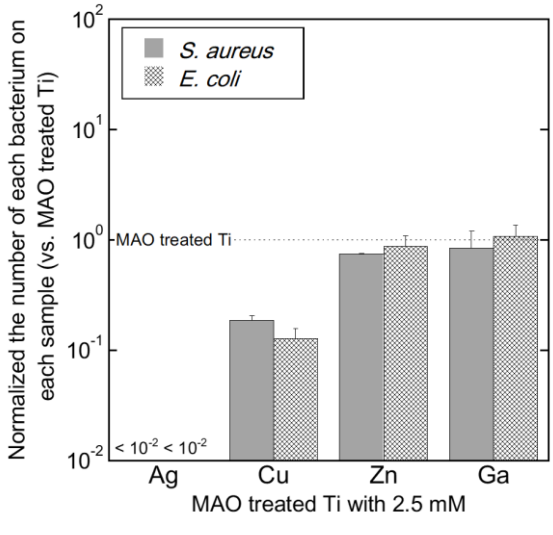

Figure 2 Results of bacterial adhesion test.

PS1-09-165

Antimicrobial nitric oxide peptide contact lens bandages

Jenny Aveyard[1], Robert C. Deller[1], Rebecca Lace[2], Rachel L. Williams[2], Raechelle A. D'Sa[1]

[1]University of Liverpool, Department of Mechanical, Materials and Aerospace Engineering, Liverpool, GB;
[2]University of Liverpool, Institute of Ageing and Chronic Disease, Department of Eye and Vision Science, Liverpool, GB

Introduction

Blindness due to corneal ulcers represent 5% of all cases worldwide. [1,2] These ulcers are caused by a range of conditions from autoimmune diseases to infections such as fungal and bacterial keratitis. [3] Bacterial keratitis is often contracted through the improper use of contact lenses and treatment regimens often include broad spectrum antibiotic drops, and sometimes the application of a bandage lens to protect the wound. [4] This method of delivery of the drug however is not efficacious as less than 7% of the active agent reaches the site of injury due to the method of administration. Moreover, in recent years, there has been a drive to reduce the use of antibiotics owing to the growing epidemic of antimicrobial resistance.

Nitric oxide (NO) acts as an antimicrobial agent by interacting with simultaneously produced reactive oxygen species such as hydrogen peroxide (H_2O_2) and superoxide (O_2^-) to generate reactive nitrogen species such as peroxynitrite ($OONO^-$), S-nitrosothiols (RSNO), nitrogen dioxide (NO_2), dinitrogen trioxide (N_2O_3), and dinitrogen tetroxide (N_2O_4).[5,6] It has been shown that these reactive intermediates target DNA, causing deamination, oxidative damage, strand breaks, and other DNA alterations. Moreover, NO is effective against both planktonic bacteria and biofilms,[7] the latter of which are more difficult to treat due to a protective exopolysaccharide matrix that resists penetration of immune cells and antibiotics.[8]

Compounds containing the diazeniumdiolate $[N(O)=NO]^-$ functional group have shown great potential in a variety of medical applications requiring the controlled and sustained release of NO [9] Described herein are environmentally friendly methods to develop NO donor contact lenses capable of releasing a controlled and sustained dose of NO to target biofilms on infected wounds.

Experimental Methods

In this work poly-ε-lysine (pεK) is cross-linked with bis-carboxy fatty acids and functionalised with diazeniumdiolate to produce nitric oxide releasing hydrogel contact lens bandages with a high water content and excellent transparency. The mechanical properties of the gels are tailored by altering the density of the polymer, the molecular length of the cross-linker and the cross-linking density. The chemical properties of the gels were determined using X-ray photoelectron spectroscopy, Fourier transform infrared spectroscopy and UV vis spectroscopy. The NO payload released was determined using a chemiluminescent NO detector. The antimicrobial efficacy of the gels against *Staphylococcus aureus* and *Pseudomonas aeruginosa* was determined after 4 and 24 hr incubation and an indirect cytotoxicity assay was carried out over the period of 8 days to determine if released NO negatively affected a human corneal epithelial cell line (HCE-T cells).

Results and Discussion

NO release from the functionalised contact lens bandages was evaluated at varying pHs in three different solutions; buffer, cell culture media and nutrient broth. The gels demonstrated a burst release at pH 4, and a lower and more sustained release profile at physiological pH 's (pH 7). The antimicrobial efficacy of the contact lenses was

observed as reduction colony forming units of *Staphylococcus aureus* and P*seudomonas aeruginosa* using a bactericidal assay. A 3 -4 log reduction in *Staphylococcus aureus* and up to 1 log reduction with *Pseudomonas aeruginosa* was observed after incubation with the NO releasing gels The indirect cytotoxicity assay demonstrated that released NO did not negatively affect a human corneal epithelial cell line (HCE-T cells).

Conclusion

The fabrication and functionalisation of nitric oxide (NO) releasing contact lens gel bandages is reported. The contact lens gels exhibit excellent optical and mechanical properties and can release NO under physiological conditions. The gels displayed excellent antimicrobial activity against two of the most common pathogens associated with bacterial keratitis- *Staphylococcus aureus* and P*seudomonas aeruginosa* and did not exhibit significant cytotoxicity against a human corneal epithelial cell line. These contact lens gels could be a promising alternative to current antibiotic eyedrop treatments, that are often inefficient and laborious. The use of NO would not contribute to the growing epidemic of antimicrobial resistance and as the delivery of the treatment is direct to the site of infection, less treatments would be required which would ultimately improve patient compliance.

References

1. Sengupta, S. *et al*. Opthal. Epidemiol. 2012, 19, 297
2. Whitcher, J.P. *et al*. Bull. W.H.O., 2001, 79, 214
3. Weiner, G., Confronting corneal ulcers, www.aao.org/eyenet/article/confronting-corneal-ulcers?july-2012
4. Upadhyan, M.P., *et al*. Int. Ophthalmol. Clin. 2007, 47,17.
5. Weller, R.B., J Invest Dermatol. 2009, 129, 2335.
6. Wahl, C *et al*. Appl Microbiol Biotechnol. 2010, 88, 401.
7. Rice S.A *et al*. J Bacteriol. 2006, 188, 7344.
8. Stephens, C., Curr. Biol. 2002, 12, R132.
9. Schoenfisch, M.H *et al* .,Chem. Soc. Rev. 2012, 41, 3753.

Acknowledgement

The authors gratefully acknowledge the funding for this project which was provided by a Health Impact Partnership grant from the EPSRC (EP/P023223/1). The authors also thank SpheriTech Ltd (Runcorn, Cheshire, UK) for providing the Poly epsilon lysine (PεK) used in this work.

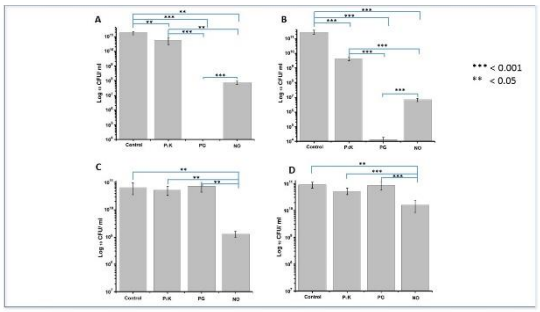

Figure 2
Bactericidal assay (in LB broth) showing the CFU/ml following 4 or 24 hr incubation with *S. aureus* (A & B) and *P. aeruginosa* (C & D). Control= bacteria only; CG= control gel; PG= penicillin functionalised gel; NO= nitric oxide releasing gel

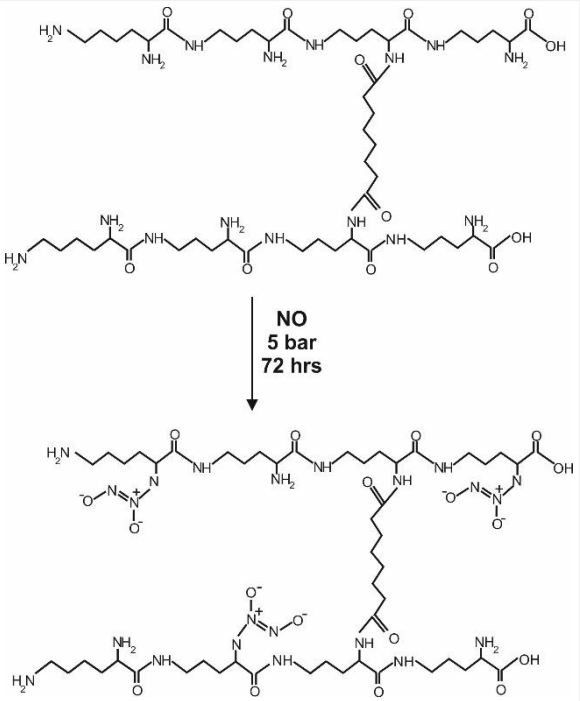

Figure 1
Reaction scheme detailing diazeniumdiolate functionalisation of PEK gels. A) PEK gel crosslinked with nonanedioic acid using EDC/NHS ester chemistry. B) Diazeniumdiolate functionalised gels. Diazeniumdiolate formed by reacting with NO gas at 5 bar for 72 hrs in the presence of NaOH.

PS1-09-166

Tissue Engineering Scaffold Based on Gelatin with Inherent Angiogenic and Antimicrobial Properties

Helena Knopf-Marques[1,2], Julien Barthès[1,2], Angela Mutschler[4], Julie Bystroňová[3], Nihal E. Vrana[1,2], Philippe Lavalle[2]

[1]PROTiP MEDICAL, Strasbourg, FR; [2]Inserm, UMRS 1221, Strasbourg, FR; [3]Contipro Biotech S. R. O., Dolni Dobrouc, CZ; [4]ENSCBP - Bordeaux INP, Laboratoire de Chimie des Polymères Organiques (LCPO)/, Pessac, FR

Introduction

Wound healing is a complex process with many factors that can delay healing. Pro-angiogenic and anti-bacterial effects are both desirable for fast wound healing process after the implantation of a biomaterial into the body as complications such as infections, bad integration and chronic inflammation are common problems. Utilization of short chain length polypeptides and modified natural polymers provides a strong means to design 3D biomaterial architectures with controlled physicochemical properties and also desired multiple biological activities. There is an urgent need for multifunctional formulations that can address biomaterial related complications simultaneously in a manner similar to the structures of extracellular matrix. In this study, we developed substrates composed of ECM components (gelatin, HA) and synthetic peptides where interactions between the coating components induced by modification of one component Hyaluronic acid with pendant aldehyde groups (HA-Ald) creates an environment that enables incorporation of an antimicrobial/angiogenic peptide sequence (chain length controlled polyarginine (PAR) through transient interactions. [1] Gelatin and an HA-Ald can interact via formation of a covalent imine bond –CH=N- between aldehyde moieties of HA and amino groups of gelatin. [2]

Experimental Methods

A spin coated interpenetrating network of gelatin and Hyaluronic acid-Aldehyde derivative was developed for controlled release of poly(arginine) (PAR). In order to improve the stability of the film, gelatin was enzymatically crosslinked with microbial transglutaminase to enable the formation of amide bond within gelatin structure.

Results and Discussion

The designed composite system gives distinct biological activities while addition of hyaluronic acid component with a pendant aldehyde group enables a transient interaction with the other two components of the system (gelatin and PAR). Such multifunctional structure can provide a superior interface between implanted biomaterials and host tissues without the necessary trade-offs with the currently available systems. Nanoplasmon measurements demonstrated a significantly higher loading of PAR in structures containing HA-Ald with longer retention of PAR in the structure. The presence of PAR not only rendered the film a contact-killing surface for bacteria [3, 4] but also made it pro-angiogenic (Fig. 1) as demonstrated by increased cell-cell contacts and VEGF gene expression and secretion by Human vascular endothelial cells. This multifunctional formulation can be used for tissue engineering scaffold development where it can enact on several problems simultaneously.

Conclusion

Herein, we proposed a spin coated, interpenetrating network of gelatin and HA-Aldehyde derivative containing poly(arginine) in order to prevent the implant-related infections and also to promote implant integration via improved

angiogenesis. The system harnesses the interactions between its components to achieve multiple biological functions inherent to the used bioactive molecules. This system easy to produce and can be used in future for coating of any kind of implantable device where there is a need for angiogenesis and a risk of infection.

References

[1] Knopf-Marques, H., et al. ACS Omega, 2017. **[2]**(3): p. 918-929. 2.Knopf-Marques, H., et al. Biomacromolecules, 2016. **17**(6): p. 2189–2198. **[3]** Mutschler, A., et al.Chemistry of Materials, 2017. **29**(7): p. 3195-3201. **[4]** Mutschler, A., et al. Chemistry of Materials, 2016. **28**(23): p. 8700–8709.

Acknowledgement

This study is supported by European Union's Seventh Framework Programme no. 602694 (IMMODGEL), European Union's Horizon 2020 under grant agreement no. 760921 and FUI FASSIL.

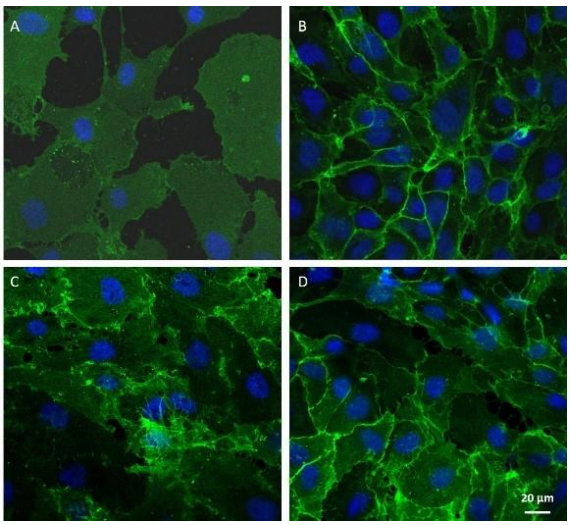

Confocal images.
Confocal images with DAPI (blue) and PECAM-1 (green) staining after 7 days of HUVEC cells seeded on Gel (A), Gel + PAR (B), Gel/HA-Ald (C) and Gel/HA-Ald + PAR (D).

PS1-09-167

Bioinspired interface design modulates pathogen and immunocyte responses in biomaterial-based anti-infection combination therapy

Jinhua Li

Technische Universität Dresden, University Hospital and Faculty of Medicine Carl Gustav Carus, Dresden, DE

Introduction

The rise of multidrug-resistant pathogens and the dearth of novel antibiotic development urgently need breakthrough strategies that go beyond classical antibiotic mechanism to fight this approaching human health cataclysm. There is an increasing demand for successful infection treatment through innovative therapy solutions. Herein, inspired by the metabolism cascade of pathogens and the clearance of infection by host immune system, a new three-step strategy is reported to achieve the combination therapy for biomaterials-centered infections through the use of cobalt doped TiO_2 semiconductor (TiO_2:Co).

Experimental Methods

The samples were prepared using a plasma electrolytic oxidation method. The pristine sample was undoped TiO_2 coating (TiO_2:Co-0), while a series of Co-doped TiO_2 coatings (TiO_2:Co-0.5, TiO_2:Co-1, TiO_2:Co-2, TiO_2:Co-4) were acquired by tuning Co dopant concentration. Surface morphologies of the samples were determined by scanning electron microscopy (SEM). Crystal structures of the samples were characterized by the X-ray diffraction. X-ray photoelectron spectroscopy (XPS) that is a surface-sensitive characterization technique was utilized to determine the surface chemistry. UV−Vis reflectance spectra of the samples were recorded to determine the band gap. Ultraviolet photoelectron spectroscopy (UPS) was employed to determine the VB maximum and work function. The in vitro antibacterial properties of doped samples were explored and the in vivo anti-infection performances were tested on a femoral osteomyelitis model. Furthermore, studies with innate immune cells (macrophages and neutrophils) were conducted to explore whether they could be involved in eradicating bacteria.

Results and Discussion

Band-structure-tunable TiO_2:Co can serve as the extracellular electron acceptors, and interfere with the electron and proton transfer, and energy metabolism to effectively restrain the bacterial biofilm formation, which is further beneficial for the phagocytosing and killing of bacteria by innate immune cells (macrophages and neutrophils) through the “divide-and-conquer tactics” since on this occasion impaired biofilms cannot adequately protect bacteria from phagocytes. Lastly, the released Co^{2+} ions from TiO_2:Co can generate the proinflammatory microenvironment, and potentiate the antibacterial capability of innate immune cells, which are demonstrated by the boosted polarization of M1 macrophages, secretion of inflammatory cytokines, and phagocytic ability of phagocytes. Through the infection combination therapy, the amounts of bacteria on the biomaterial implant and infected tissue can be significantly decreased. This design concept can be applied to develop other antibacterial biomaterials, and hold great promise for advanced biomaterial-based anti-infection therapy.

Conclusion

An alarming and persistent rise in the antibiotic resistance among many important pathogenic bacterial species poses one of the greatest contemporary challenges to public health. Whereas most of the previous work developing

antibacterial biomaterials is solely focused on inhibiting bacterial biofilm formation, herein, we demonstrate a new design concept of “infection combination therapy” for biomaterials-centered bacterial infections. This concept is achieved by a three-step tactics: (1) Band-structure-tailorable TiO_2 semiconductor through cobalt doping can act as the extracellular electron acceptors to interrupt the bacterial electron transfer (discharge process) and proton transfer (hydrogenation process), jeopardize the energy metabolism causing bacteria starvation, and thereby suppress bacterial biofilm formation (bacteria starvation therapy). (2) Innate immune cells (including macrophages and neutrophils) can effectively phagocytose and kill the biofilm-formation-blocked bacteria using the divide-and-conquer strategy. (3) Released cobalt ions can create a proinflammatory local environment and potentiate the phagocytosing and killing of bacteria by the innate immune cells (infection immunotherapy). This concept of infection combination therapy can contribute to the advanced design of biomaterials for antibacterial treatment. We anticipate this novel design concept can be extended to developing other antibacterial biomaterials and find wide applications in the advanced therapy of biomaterial-based bacterial infections.

References

1. C. R. Arciola, D. Campoccia and L. Montanaro, *Nature Reviews Microbiology*, 2018, **16**, 397–409.
2. S. D. Kobayashi, K. R. Braughton, A. R. Whitney, J. M. Voyich, T. G. Schwan, J. M. Musser and F. R. DeLeo, *Proceedings of the National Academy of Sciences*, 2003, **100**, 10948-10953.
3. H. J. Busscher, H. C. van der Mei, G. Subbiahdoss, P. C. Jutte, J. J. A. M. van den Dungen, S. A. J. Zaat, M. J. Schultz and D. W. Grainger, *Science Translational Medicine*, 2012, **4**, 153rv110-153rv110.
4. D. M. Mosser and J. P. Edwards, *Nat Rev Immunol*, 2008, **8**, 958-969.
5. C. Nathan, *Nature*, 2002, **420**, 846-852.
6. S. H. Light, L. Su, R. Rivera-Lugo, J. A. Cornejo, A. Louie, A. T. Iavarone, C. M. Ajo-Franklin and D. A. Portnoy, *Nature*, 2018, **562**, 140–144.
7. R. S. Hartshorne, C. L. Reardon, D. Ross, J. Nuester, T. A. Clarke, A. J. Gates, P. C. Mills, J. K. Fredrickson, J. M. Zachara, L. Shi, A. S. Beliaev, M. J. Marshall, M. Tien, S. Brantley, J. N. Butt and D. J. Richardson, *Proceedings of the National Academy of Sciences*, 2009, **106**, 22169-22174.
8. L. Shi, H. Dong, G. Reguera, H. Beyenal, A. Lu, J. Liu, H.-Q. Yu and J. K. Fredrickson, *Nature Reviews Microbiology*, 2016, **14**, 651.
9. R. K. Thauer, K. Jungermann and K. Decker, *Bacteriological Reviews*, 1977, **41**, 100-180.
10. C. R. Myers and K. H. Nealson, *Science*, 1988, **240**, 1319.
11. K. A. Weber, L. A. Achenbach and J. D. Coates, *Nature Reviews Microbiology*, 2006, **4**, 752.
12. J. M. Zachara, J. K. Fredrickson, S.-M. Li, D. W. Kennedy, S. C. Smith and P. L. Gassman, *American Mineralogist*, 1998, **83**, 1426-1443.

Acknowledgement

Dr. Jinhua Li greatly acknowledges the funding support from the Alexander von Humboldt Stiftung/Foundation. This work was financially supported by Hong Kong Research Grant Council General Research Funds (CityU 11205617), City University of Hong Kong Donation Research Grant (9220061), and National Natural Science Foundation of China (81472109).

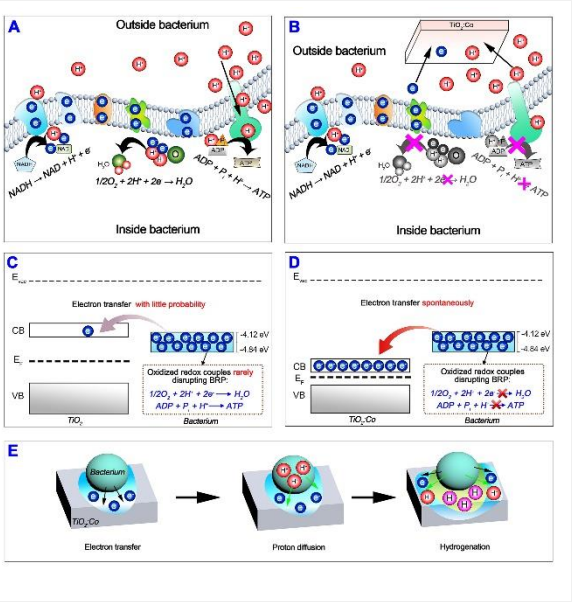

Schematic diagram

Schematic diagram for elucidating the mechanism of band-structure-tailorable TiO_2 semiconductor coating to thwart bacterial biofilm formation through acting as the extracellular electron acceptors.

PS1-09-168

Fluorescent antimicrobial silver nanoclusters with photothermal properties for biomedical applications

Alberto Nakal-Chidiac[1], Olga Garcia[1], Maria Rosa Aguilar[1,2], Luis García Fernandez[1,2], Francisco Martin-Saavedra[3,2], Clara Escudero[3,2], Nuria Vilaboa[3,2], Julio San Roman[1,2]

[1]Institute of Polymer Science and Technology, ICTP-CSIC, Madrid, ES; [2]Networking Biomedical Research Centre in Bioengineering, Biomaterials and Nanomedicine (CIBER-BBN), Madrid, ES; [3]La Paz University Hospital, IdiPAZ, Madrid, ES

Introduction

Silver nanoclusters (AgNC) are luminescent hybrid nanoparticles with photophysical properties like quantum dots, but with a very small size and without the toxicity associated to heavy atoms. AgNC present interesting electronic, mechanical, magnetic, optical, chemical and antimicrobial properties which makes them useful as new therapeutic systems whithout neglecting their antibacterial and antimicrobial properties. However, these nanostructures tend to oxidize and aggregate irreversibly losing some of these properties.

The aim of this work is the synthesis in aqueous media of fluorescent antimicrobial AgNC, with photothermal properties. For this purpose chitosan, a natural macromolecule, was used as multifunctionalized ligand providing a continuous coverture and additional properties associated to its chemical structure.

Experimental Methods

AgNC synthesis: luminescent AgNC were functionalized with chitosan (multi-amino polymer) photochemically using a photoreactor irradiation source with light emission centered at 365 nm which generate a power of 29 W/m^2. The experimental conditions were optimized varying photoinitiator concentration, incident light (wavelength, intensity and irradiation time), concentration of silver precursor and concentration of chitosan. Reactions were prepared in the dark by adding all starting reagents: the photoinitiator (Irgacure 2959®, I-2959), the silver salt as precursor (silver trifluoroacetate, CF3COOAg) and the chitosan polymer as ligand. Equimolecular concentration of Ag/I-2959/amine groups was maintained at 2 mM and 5 mM, using THF:H_2O 50:50 as solvent. Solutions were exposed to UVA irradiation at the photoreactor. The reaction evolution was monitored by UV/Vis spectroscopy at the Ag plasmon absorption band (437 nm) and fluorescence spectroscopy of the emission signal (520 nm) in the front-face mode. Particle size distribution was determined by dynamic light scattering (DLS) and morphology characterization was performed by sTEM and CryoTEM.

Photothermal characterization: suspensions containing different concentrations of AgNC were placed into polystyrene cuvettes and exposed to laser light of 808 nm emitting at 44 mW/mm^2 and 37°C. Temperature changes were monitored by IR thermography using a Testo 875-2i thermal imaging camera. The temperature of the hottest point on the surface of the cuvette was monitored every 60 s during 5 minutes.

The effect of AgNC on ***Escherichia coli***as cell model was studied. **Minimal inhibitory concentration (MIC)** was determined after 24 hours.

Results and Discussion

The formation of hybrid AgNC was achieved in aqueous medium both in the presence and absence of oxygen, which makes the process very versatile. The reaction kinetics were very reproducible in all irradiation times and chitosan concentration assays. However, the reactions carried out under inert atmosphere were faster and more efficient. The

obtained AgNC were fluorescent in water, increasing the emission band as the irradiation time increases. Those AgNC obtained under inert atmosphere presented a more intense emission band. No photophysical changes were observed over time.
Size distribution of the nanohybrids were monomodal with a hydrodynamic diameter around 10 nm, which correlates with sTEM and cryoTEM images. Spherical morphology with absence of large aggregates was confirmed (Figure 1).
Photothermal capacity of AgNC increased with irradiation time reaching the highest DT, about 25°C over 37°C, with those samples irradiated for 8 minutes.
E. coli viability was reduced as a function of the concentration of AgNC. Minimal inhibitory concentration (MIC) was 0.15-0.22 mg/mL of polymer.

Conclusion

Stable, monodisperse and well-defined AgNP were obtained in suspension using chitosan as template and multifunctional amino ligand using a photochemical method. Nanostructuration was achieved in aqueous medium in a one-step effective route. The AgNP formation was monitored by the appearance of the plasmon absorption band (around 440 nm) and was optimized as a function of the precursor's concentration, irradiation time and in the presence or absence of oxygen. AgNP transduce NIR photon energy very effectively being ΔT 24°C achieved for the formulation synthesized in inert atmosphere and long irradiation time. AgNPs presented antimicrobial properties in the range of silver particles with remarkable photophysical properties associated to its nanostructure.

Acknowledgement

Authors would like to thank CIBER-BBN, the Spanish Ministry of Science, Innovation and Universities (MAT2017-84277-R).

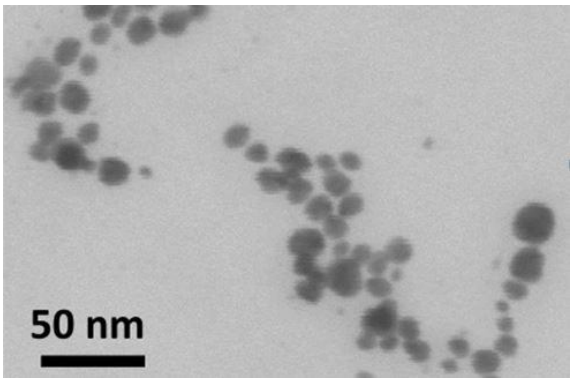

Figure 1. sTEM images of AgNC
Figure 1. sTEM images of AgNC obtained under nitrogen atmosphere and 1mg /mL of chitosan

PS1-09-169

Physicochemical and Antibacterial Properties of Freeze and Furnace Dried Cerium Oxide Nanoparticles

Neelam Iqbal[1], Antonios Anastasiou[1], El M. Raif[2], Animesh Jha[1]

[1]School of Chemical & Processing Engineering, University of Leeds, Leeds, GB; [2]Division of Oral Biology, Dental School, University of Leeds, Leeds, GB

Introduction

Infections associated with bacterial colonisation around implants and scaffolds are significant clinical problems in orthopaedics. Epidemiological studies suggest between 2-5 % of all the implant related procedures will be further complicated due to post-operative infections [1]. Although the systemic delivery of antibiotics is common practice for treating these conditions, the potential risk of antibiotic resistance is a growing concern and the effectiveness of their long-term use is disputable [2]. To tackle this problem, we aim to design and fabricate scaffolds for localised delivery of antibacterial agents which will prevent the occurrence of infections and accelerate healing and remodelling of hard tissue. Nanoparticles (NPs) are emerging as novel antibacterial agents and have proven their effectiveness for treating infectious diseases [3] as due to their large surface area to volume ratio they are able to exhibit special properties which their bulk counterparts do not. Although the exact antibacterial mechanisms are not clear and differentiate depending on the bacteria strain, it has been reported factors such as size, shape, surface charge and surface area to volume ratio affect the antibacterial potential of nanoparticles [4].

Nanoparticle size is an important aspect to consider in relation to biological functions as they need to be comparable to (i) small biological molecules (1-10 nm), (ii) viruses (10-100 nm) and (iii) be able to attack biological entities without changing their functions. In the present work, cerium oxide nanoparticles (Ce^{4+} and Ce^{3+}) have been selected due to their reported antibacterial potential and the potential to enhance vascularisation [5]. During the synthesis of the nanoparticles it was observed that the drying method (i.e. freeze drying or furnace drying) significantly affected the physicochemical properties, size, shape and potentially the Ce^{4+} to Ce^{3+} ratio. Therefore, the main objective of this work is to compare the properties of three types of cerium oxide NPs (i.e. **Type-A** freeze dried, **Type-B** furnace dried and **Type-C** commercial NPs) and investigate their effectiveness against common bacteria strains (e.g.*Staphylococcus epidermidis*). After determining the IC50 for each NP type, we incorporated the NPs into chitosan scaffolds to investigate *ex vivo* release rate over a period of two weeks

Experimental Methods

Cerium oxide nanoparticles were formed using a hydroxide mediated approach. A 0.3 M aqueous solution of sodium hydroxide was added dropwise to 0.1 M aqueous cerium nitrate hexahydrate solution at 25 °C. The mixture was left under continuous stirring for 24 hrs. The nanoparticles were collected by filtration and washed several times with distilled water and ethanol. Type-A NPs were subsequently frozen at -80 °C for 24 hrs and then placed into a freeze drier for 24 hrs. Type-B NPs followed the same procedure however; after the nanoparticles were filtered and washed they were placed into a furnace at 80 °C for 24 hrs to dry. Simultaneous Thermal Analysis was used to determine the optimal calcination temperature for furnace dried NPs. For the characterization of all materials, X-ray Diffraction, Transmission Electron Microscopy, Fourier Transform Infrared Spectroscopy, Ultraviolet Spectroscopy and Raman Spectroscopy were utilised.

Results and Discussion

Type A and B cerium oxide NPs were successfully fabricated with particle sizes from 4-8 nm and 15-20 nm respectively. X-Ray powder diffraction (fig.1) and Transmission Electron Microscopy were used to verify the formation of the cerium oxide nanoparticles. Electron Loss Spectroscopy was used to confirm the presence of both Ce^{3+} and Ce^{4+} ions shown in fig. 2.

Conclusion

Cerium oxide NPs incorporated with chitosan has the potential to reduce prevalence of bacteria during orthopaedic/bone implantation. Furthermore, chitosan offers more advantageous properties compared to other biopolymers in terms of acting as a drug release delivery system, in addition to remaining stable with regards to size and shape during cell culture procedures. We confirm that the drying method affected the size, shape and Ce^{3+} and Ce^{4+} ion ratio, furthermore the antibacterial potential of the NPs is currently being investigated.

References

[1] Johnson, C.T. and A.J. Garcia, *Scaffold-based anti-infection strategies in bone repair.* Ann Biomed Eng, 2015. **43**(3): p. 515-28.

[2] Farias, I.A.P., et al., *Antimicrobial Activity of Cerium Oxide Nanoparticles on Opportunistic Microorganisms: A Systematic Review.* BioMed Research International, 2018. **2018**: p. 14.

[3] Hajipour, M.J., et al., *Antibacterial properties of nanoparticles.* Trends Biotechnol, 2012. **30**(10): p. 499-511.

[4] Raza, M.A., et al., *Size- and Shape-Dependent Antibacterial Studies of Silver Nanoparticles Synthesized by Wet Chemical Routes.* Nanomaterials (Basel, Switzerland), 2016. **6**(4): p. 74.

[5] Korsvik, C., et al., *Superoxide dismutase mimetic properties exhibited by vacancy engineered ceria nanoparticles.* Chemical Communications, 2007(10): p. 1056-1058.

Acknowledgement

This research is supported by The University of Leeds and is funded by the Engineering and Physical Sciences Research Council (EPSRC).

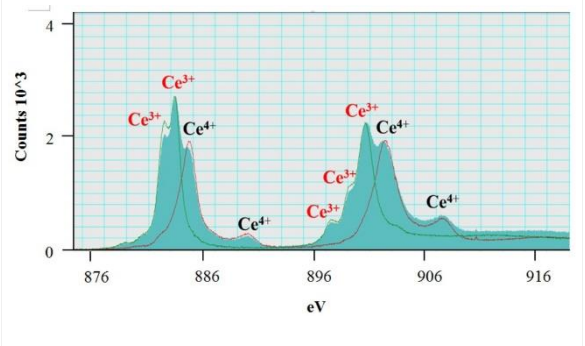

Results
Fig.2. EELs analysis of Type-A nanoparticles

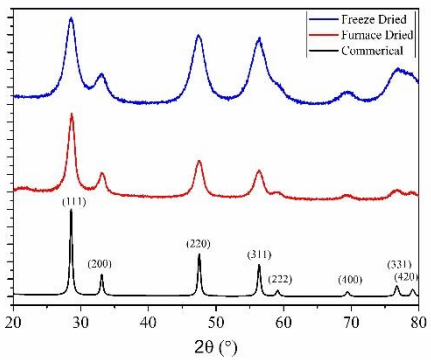

Results
Fig.1. X-ray diffractometer spectrum of cerium oxide NPs, 2θ scanning range was 20° to 80° at a scan

PS1-09-170

Biogenically synthesized silver chloride/silver nanoparticles using supernatant of *Arthrobacter* sp.: characterization, antibacterial activity and biocompatibility

Amedea B. Seabra[1], Wallace R. Rolim[1], Claudio Lamilla[2], Joana C. Pieretti[1], Mônica H. M. Nascimento[1], Christiane Lombello[1], Gonzalo Tortella[2], Fábio F. Ferreira[1], Cristina Diez[1], Letícia Barrientos[3], Olga Rubilar[2]

[1]Universidade Federal do ABC, Center for Natural and Human Sciences, Santo André, BR; [2]Universidad de la Frontera, Department of Chemical Engineering, Temuco, CL; [3]Universidad de la Frontera, Laboratory of Applied Molecular Biology, Temuco, CL

Introduction

Synthesis and applications of metallic nanoparticles have gained considerable attention in recent years due to their unique physicochemical and biological properties. Silver nanoparticles (AgNPs) and silver chloride (AgCl) nanoparticles have been extensively explored in the field of nanomedicine due to their applications in cancer treatment, drug delivery and antimicrobial effects. Indeed, nanocomposites composed by AgCl/Ag are known to have antibacterial activity. Among the methods to synthesize silver-based nanocomposites, biogenic methods have gaining considerable attention in recent years as an environment friendly approach and the possibility to synthesize the nanoparticles at ambient pressure and temperature, in the absence of organic solvents.In this work, AgCl/Ag nanocomposites were biogenically synthesized by using exopolysaccharide derived from the bacteria *Arthrobacter* sp. from Antarctic. The obtained nanoparticles were characterized by different tecnhiques and their antibacterial and cytotoxicity effects were evaluated.

Experimental Methods

AgCl/Ag NPs were synthesized by supernatant of *Arthrobacter* sp, which is rich in exopolysaccharides. The exopolysaccharides act as reducing agent of Ag^{+} to Ag^{0} (leading the formation of AgCl/Ag NPs) and in the stabilization of the obtained nanocomposite, protecting it from degradation and aggregation. The obtained nanocomposite was characterized by several techniques, including UV-Vis spectroscopy (UV-Vis), X-ray diffraction (XRD), X-ray photoelectron spectroscopy (XPS), Fourier transformed infrared spectroscopy (FTIR), energy dispersive X-ray spectroscopy (EDS), atomic force microscopy (AFM), dynamic light scattering (DLS) measurements and nanoparticle Tracking Analysis (NTA). In addition, the antibacterial activity of the biosynthesized nanocomposite was evaluated against gram-positive *Staphylococcus aureus* ATCC 29213 and *Enterococcus faecalis* ATCC 3229 and gram-negative *Escherichia coli* ATCC 25922, *Klebsiella pneumoniae* ATCC 13803, and the multidrug-resistant (MDR) *Pseudomonas aeruginosa* KP 37. Furthermore, the cytotoxicity of AgCl/Ag NPs was assessed against the fibroblast-like epithelial cells (Vero) by using the 3-[4,5-dimethylthiazole-2-yl]-2,5-diphenyltetrazolium bromide (MTT) reduction assay.

Results and Discussion

The formation of AgCl/Ag NPs was confirmed by the detection of plasmonic surface resonance band at 405 nm, indicating the successful formation of metallic silver NPs. In addition, XRD analysis and Rietveld refinement demonstrated the formation of AgCl/Ag nanocomposite, mainly formed by AgCl. XPS and EDS analyses revealed

the presence of oxygen, carbon, chlorine and silver. FTIR was used to evaluate the presence of possible biomolecules on the surface of nanoparticles and the results demonstrated the presence of biomolecules such as polysaccharides on the surface of AgCl/Ag NPs, derived from the supernatant of *Arthrobacter* sp, these polysaccharides might act in the formation and stabilization of AgCl/Ag NPs in an aqueous medium. AFM results demonstrated the formation of quasi-spherical nanoparticles with size at solid state at 16.26 ± 0.32 nm. DLS and NTA measurements show a hydrodynamic size at 40 nm and a concentration of 26 x 10^6 particles/mL with a moderate polydispersity index and a negative zeta potential due to the presence of the exopolysaccharides on the nanoparticle surface. Furthermore, the biogenically synthesized AgCl/Ag NPs demonstrated a potent antibacterial activity against all tested bacterial strains. The experiments revealed a high sensitivity of *S. aureus* to AgCl/Ag NPs, with minimum inhibitory concentration (MIC) and minimum bactericidal concentration (MBC) values of 62.5 µg/mL. Similar, *E. coli* and the MDR *P. aeruginosa* bacterial strains have MIC value of 62.5 µg/mL. AgCl/Ag NPs demonstrated a concentration-dependent toxicity to Vero cells. Interestingly, AgCl/Ag NPs were not toxic to Vero cells at concentrations required for antibacterial effects.

Conclusion

This study demonstrated the successful biosynthesis of AgCl/Ag NPs by a biological route, by using the supernatant of *Arthrobacter* sp, a non-pathogenic bacteria strain from Antarctica. The obtained nanocomposite was characterized by several techniques that demonstrated the formation of quasi-spherical nanoparticles at nanoscale coated with biomolecules, such as exopolysaccharides. The biogenically synthesized AgCl/Ag NPs showed potent antibacterial activity with no significant toxicity against healthy cell line (Vero). The obtained nanomaterial might find important biomedical applications in the combat of pathogenic bacteria with low cytotoxicity to healthy cells.

Acknowledgement

We have appreciated the support from CNPq, FAPESP- CONICYTE (2018/08194-2) and CONICYT/FONDAP/15130015. This study was financed in part by the Coordenação de Aperfeiçoamento de Pessoal de Nível Superior - Brasil (CAPES) - Finance Code 001.

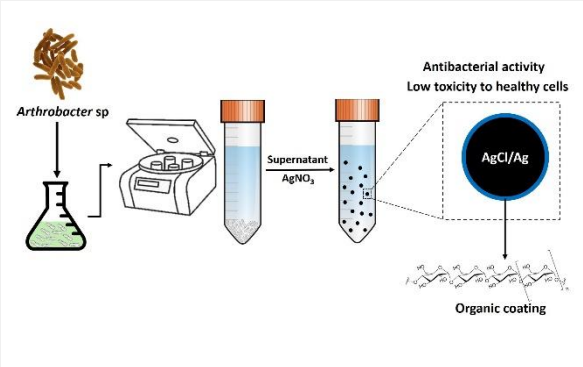

Biogenically synthesized silver chloride/silver nanocomposite
Representative schematic representation of the biogenic synthesis of silver chloride/silver nanocomposite for antibacterial activity

PS1-09-171

Antibacterial activity of bioglass based glass-ceramic *scaffolds* coated with silver nanoparticles

Rodrigo L. M. S. Oliveira[1], Lucas Barbosa[1], Carolina R. H. Guimarães[2,1], Lucas P. Ramos[3], Luciane D. Oliveira[3], Dayane B. Tada[1], Eliandra S. Trichês[1]

[1]Federal University of São Paulo (UNIFESP), São José dos Campos, BR; [2]Federal Institute of São Paulo (IFSP), São José dos Campos, BR; [3]São Paulo State University (UNESP), São José dos Campos, BR

Introduction

Among the biomaterials used in bone tissue engineering, the bioglass stands out due to its high bioactivity. In physiological environment, the bioglass present the formation of a superficial carbonated hydroxyapatite layer by ionic exchange reactions, enabling it to bond with soft and hard bone tissue[1]. In addition to its bioactivity, many bioglass formulations present antibacterial properties against a large range of bacteria, inhibiting its proliferation during the treatment[2,3].

The first bioactive glass formulation was developed by Larry Hench, in 1969[4], called Bioglass® 45S5. Although several studies have tried to develop new formulations, the Bioglass® 45S5 still remains as the golden standard to bone regeneration due to its capability to bond with soft tissue a few hours after implanted.

In order to treat the bone defects, a big field of research in the bone tissue engineering studies the production of scaffolds[5]. Those scaffolds are highly porous structures that act as support for cells proliferation. The production of Bioglass® 45S5 scaffolds allows the application of the bioglass directly in the bone defect region, being an effective way to promote bone regeneration and treat bone diseases.

However, due to the presence of high temperatures during most of the scaffold production, the bioglass exhibits the crystallization of its structure, resulting in a glass-ceramic scaffold. With its crystallization, the bioglass loses most of its antibacterial properties, what can lead to tissue infection during the scaffold implantation.

Aiming to produce antibacterial Bioglass-based glass-ceramic scaffold, this work proposes the incorporation of antibacterial nanoparticles on the scaffold. We used silver nanoparticles, well known for its high antibacterial properties, and bioglass-based scaffolds produced by the foam replication technique.

Experimental Methods

Bioglass® 45S5 was produced using the melting-quenching technique, melting the precursor oxides (45wt.% of SiO_2, 24.5wt.% of CaO, 24.5wt.% of Na_2O and 6wt.% of PO_4) at 1350°C for 20min. The bioglass was milled in a ball mill for 24h, using zirconia balls and isopropyl alcohol. The powder obtained was analyzed by XRD to evaluate if the glass presented amorphous structure.

The scaffolds were produced using the foam replication technique with a 50ppi (pores per inch) polyurethane foam. In order to improve the mechanical properties of the scaffold, we realized two impregnations. First the foam was soaked in a 45wt.% bioglass slurry and sintered at 950°C for 3h. Then, the scaffolds obtained were soaked in a 10wt.% bioglass slurry and sintered at 950°C for 3h. The scaffolds were analyzed by SEM to evaluate the porous morphology and by XRD to evaluate the glass crystallization. The silver nanoparticles were incorporated using ultrasonic stirring for 1h. The solution absorbance was measured before and after this procedure to evaluate the incorporation, once the absorbance is directly proportional to a solution concentration by the Lambert-Beer law.

Scaffolds samples with and without silver nanoparticles were autoclaved at 100°C in deionized water. The samples were incubated in *P. aeruginosa* culture (500µL of Mueller Hinton solution and 500µL of *P. aeruginosa*, gram negative - 10^6cells/mL) at 37°C for 24h. After the incubation, 10µL of the culture were dropped in a Petri dish containing 15mL of BHI solution followed by the incubation at 37°C for 48h to evaluate the bacteria growth.

Results and Discussion

The scaffolds presented geometrical porosity of 87,95 ± 1,59% and an interconnected porous structure. During the scaffold production, the bioglass crystalized in two different phases, a main phase of calcium sodium silicate ($Na_6Ca_3Si_6O_{18}$), and a secondary phase of calcium phosphate and sodium ($NaCaPO_4$).

Before the silver nanoparticles incorporation, the bulk solution presented an absorbance peak of 0,929 at 429 nm. After 1h under stirring in contact with the scaffold, the solution absorbance decreases to 0,017 at 429nm, indicating that the silver nanoparticles were successfully incorporated to the scaffold.

In the antibacterial test, the scaffold with silver nanoparticles successfully inhibited *Pseudomonas* growth, while the scaffold without the nanoparticles did not. Therefore, the silver nanoparticles incorporation was able to promote the antibacterial propriety on the scaffold against *P. aeruginosa*.

Conclusion

The use of the ultrasonic stirring showed to be an effective way to incorporate silver nanoparticles on the bioglass-based scaffold. This led to the promotion of antibacterial properties in the scaffold, that successfully inhibited the growth of *Pseudomonas*. More studies are required to understand the interaction between the scaffold and the silver nanoparticle.

References

1. Hench LL. Bioceramics: From Concept to Clinic. *J Am Ceram Soc*. 1991;74(7):1487-1510.
2. Hu S, Chang J, Liu M, Ning C. Study on antibacterial effect of 45S5 Bioglass®. *J Mater Sci Mater Med*. 2009;20(1):281-286.
3. Waltimo T, Brunner TJ, Vollenweider M, Stark WJ, Zehnder M. Antimicrobial effect of nanometric bioactive glass 45S5. *J Dent Res*. 2007;86(8):754-757.
4. Montazerian M, Dutra Zanotto E. History and trends of bioactive glass-ceramics. *J Biomed Mater Res - Part A*. 2016.
5. Hutmacher DW. Scaffolds in tissue engineering bone and cartilage. In: *The Biomaterials: Silver Jubilee Compendium*.; 2006.

PS1-09-172

Composites of gellan gum hydrogel enzymatically mineralized with calcium–zinc phosphate for bone regeneration with antibacterial activity

Timothy Douglas[1], Magdalena Pilarz[2], Marco Lopez-Heredia[3], Gilles Brackman[4], David Schaubroeck[4], Lieve Balcaen[4], Vitaliy Bliznuk[4], Frank Vanhaecke[4], Tom Coenye[4], Elzbieta Pamula[2]

[1]Lancaster University, Lancaster, GB; [2]AGH University of Science and Technology, Krakow, PL; [3]Universite de Lille, Lille, FR; [4]Ghent University, Ghent, BE

Introduction

Gellan gum hydrogels functionalized with alkaline phosphatase were enzymatically mineralized with phosphates in mineralization medium containing calcium (Ca) and zinc (Zn) to improve their suitability as biomaterials for bone regeneration.

The aims of the study were to endow mineralized hydrogels with antibacterial activity by incorporation of Zn in the inorganic phase, and to investigate the effect of Zn incorporation on the amount and type of mineral formed, the compressive modulus of the mineralized hydrogels and on their ability to support adhesion and growth of MC3T3-E1 osteoblast-like cells.

Experimental Methods

Mineralization medium contained glycerophosphate (0.05 m) and three different molar Ca:Zn ratios, 0.05:0, 0.04:0.01 and 0.025:0.025 (all mol/dm3), hereafter referred to as A, B and C, respectively.

Results and Discussion

SEM (Figure 1), FTIR, SAED and TEM analysis revealed that incubation for 14 days caused the formation of predominantly amorphous mineral phases in sample groups A, B and C.

The presence of Zn in sample groups B and C was associated with a drop in the amount of mineral formed and a smaller mineral deposit morphology, as observed by SEM. ICP–OES revealed that Zn was preferentially incorporated into mineral compared to Ca. Mechanical testing revealed a decrease in compressive modulus in sample group C. Sample groups B and C, but not A, showed antibacterial activity against biofilm-forming,methicillin-resistant Staphylococcus aureus (Figure 2). All sample groups supported cel lgrowth. Zn incorporation increased the viable cell number. The highest values were seen on sample group C.

Conclusion

In conclusion, the sample group containing the most Zn, i.e. group C, appears to be the most promising

Acknowledgement

T.E.L.D. acknowledges the Research Foundation Flanders (FWO) for support in the framework of a postdoctoral fellowship.

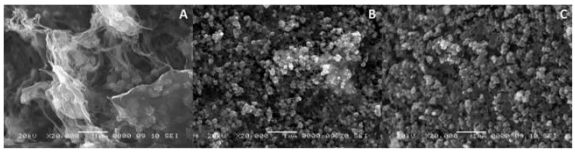

Figure 1
SEM images of GG hydrogels containing 2.5 mg/ml ALP incubated for 14 days in mineralization media A (left), B (centre) and C (right); scale bar = 1 µm in all cases

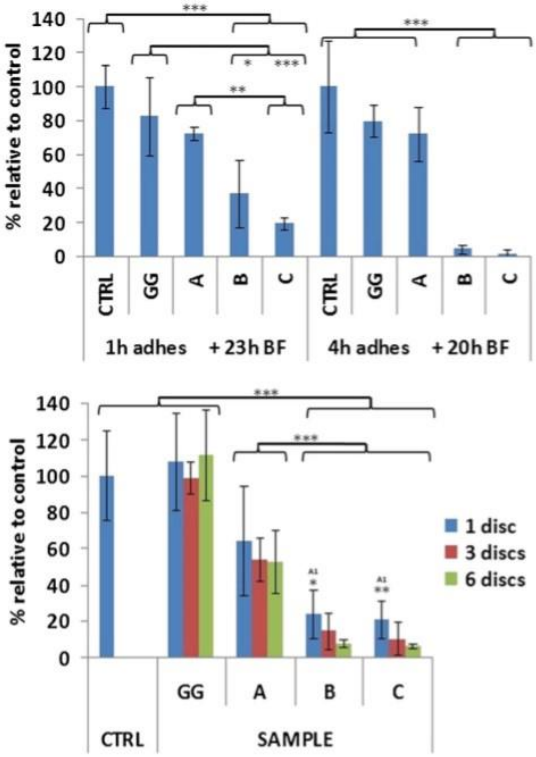

Figure 2.
Antibacterial testing of GG hydrogel discs incubated in mineralization media A, B and C for 14 days. Non-incubated, ALP-free, hydrogel discs were also examined (GG). Measurements performed in the absence of hydrogel samples served as controls. Values are expressed as percentage of colony-forming units (CFU) of methicillin-resistant S. aureus Mu50 relative to controls: (top) results obtained using 'uninfected wound model' involving incubation of a silicone disc together with 104 CFU and 1, 3 or 6 samples in growth medium for 24 h; (bottom) results obtained using 'infected wound model' involving pre-incubation of 10 6 CFU on a silicone disc with one sample for 1 or 4 h, followed by transfer of the sample to growth medium for 23 or 20 h, respectively; *significant differences, *p < 0.05, **p < 0.01, ***p < 0.001; A1, relative to sample group A, one disc; BF, biofilm formation

PS1-09-173

Synthesis of calcium phosphates doped with silver and gallium ions as biomaterials with antibacterial properties

Kamil Pajor[1], Paulina Kowalska[1], Urszula Piotrowska[2], Anna Zgadzaj[3], Joanna Kolmas[1]

[1]Medical Univeristy of Warsaw, Chair of Analytical Chemistry and Biomaterials, Faculty of Pharmacy with Laboratory Medicine Division, Warsaw, PL; [2]Kazimierz Pulaski University of Technology and Humanities, Department of Organic Chemistry and Biochemistry, Faculty of Materials Science and Design, Radom, PL; [3]Medical Univeristy of Warsaw, Department of Environmental Health Sciences, Faculty of Pharmacy with Laboratory Medicine Division, Warsaw, PL

Introduction

For many years calcium phosphates (CaPs), due to numerous advantages such as high biocompatibility with bone tissue and osteoconductive abilities, are often used in orthopedic surgery and dentistry [1, 2]. Surgical operation carries a potential risk of bacterial infection inside operated location, which in turn may lead to systemic infection. In order to prevent progress of infection, appropriate antibiotic therapy is used, where medications are administered intravenously or orally. However, bone tissue is characterized by weak vascularity, what requires high dosages of antibiotics. It may results in serious adverse effects and destruction of natural microbiota of human body.

Thanks to calcium phosphates' ability to easy adsorption many of drug substances, it could be used as carrier for antibiotics or ions with antibacterial properties, what may be the best solution for aforementioned problem [3, 4]. Following work is focused on synthesis of several types of CaPs doped with such ions (silver ions and gallium ions).

Experimental Methods

Studies were focused on synthesis of following CaPs: hydroxyapatites, brushites, α-tricalcium phosphates and β-tricalcium phosphates by using two methods: wet precipitation method and solid-state (dry) method. In total, about 25 materials were obtained, every doped with different amount of silver, gallium or both ions. Following physicochemical methods were used to investigate the obtained materials: Powder X-ray Diffraction (PXRD), Solid-state Nuclear Magnetic Resonance (ssNMR), Fourier Transform Infrared Spectroscopy (FTIR) and Transmission Electron Microscope (TEM). In addition, biological study to determine cytotoxicity (on mammalian cell line BALB/c 3T3) and antibacterial properties (on bacteria Pseudomonas fluorescens using disk diffusion test) of synthesized materials were performed.

Results and Discussion

Physicochemical experiments such as PXRD, ssNMR and FTIR allowed to identify the obtained powders. Materials in the form of nanocrystal and microcrystal were obtained using wet and dry method, respectively (TEM). PXRD diffractograms confirmed high crystallinity of the samples obtained by dry method. ICP-OES analysis determined that amount of doped silver and gallium ions was, in most cases, close to estimated content.

Cytotoxicity tests exhibited that almost all the synthesized biomaterials were non-cytotoxic. Only the samples with the highest concentrations of doped ions were cytotoxic. In addition, antibacterial (disc diffusion) test demonstrated occurrence of zones of bacterial growth inhibition.

Conclusion

In following work about 25 calcium phosphates doped with silver or gallium ions (or both) were synthesized. Their identity and chemical structure were confirmed thanks to various physicochemical studies. The obtained results will allow to produce biphasic materials and then porous ceramics in order to obtain biomaterials with antibacterial activity.

References

[1] W. Habraken, P. Habibovic, M. Epple, M. Bohner, *Materials Today***2016,** 19, 69-87.
[2] S. Dorozhkin, *Ceramics International* **2015**,41, 13913-13966.
[3] M. P. Ginebra, T. Traykova, J. A. Planell, *Journal of Controlled Release,***2006**, 113, 102-10.
[4] M. Vallet – Regí, *Bioceramics with Clinical Applications*, **2014**.

Acknowledgement

This work was supported by the research programme (UMO-2016/22/E/ST5/00564) of the National Science Center, Poland**.**

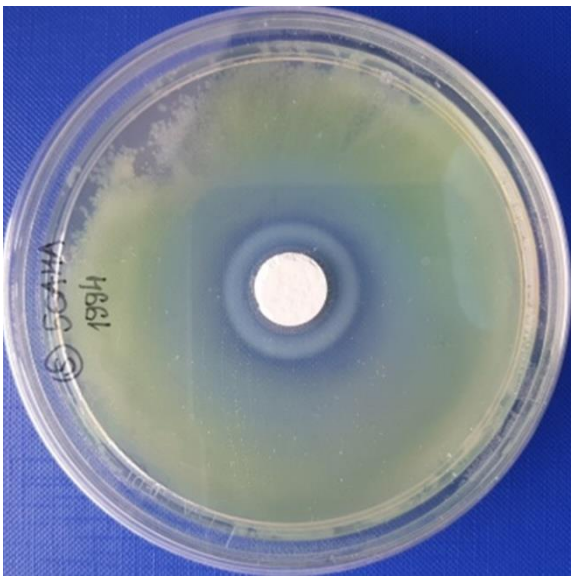

Disc Diffusion Test
Result of disc diffusion test for one of synthesized hydroxyapatites doped with gallium ions. On photo there is visible zone of inhibition of bacterial growth.

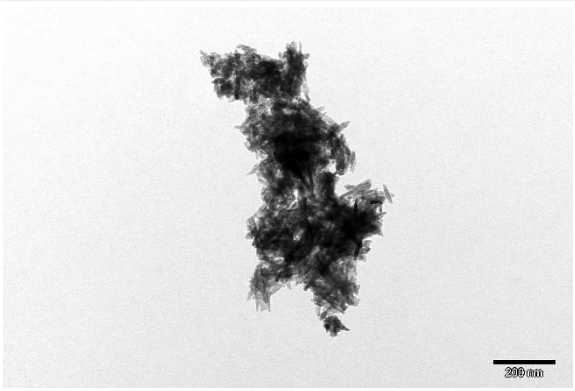

Nanocrystals of hydroxyapatite
TEM image of nanocrystals of the synthesized hydroxyapatite doped with gallium ions.

PS1-09-174

Apatite forming ability, antibacterial properties and hemolytic activity of silica-based nanobioceramics

Georgia K. Pouroutzidou[1], Eleni Likotrafiti[2], Jonathan Rhoades[2], Ioannis Tsamesidis[3], Georgios S. Theodorou[1], Konstantinos M. Paraskevopoulos[1], Eleana Kontonasaki[4]

[1]Aristotle University of Thessaloniki, School of Physics, Faculty of Sciences, Thessaloniki, GR; [2]Alexander Technological Educational Institute of Thessaloniki, Department of Food Technology, Thessaloniki, GR; [3]University of Sassari, Department of Biomedical Sciences, Sassari, IT; [4]Aristotle University of Thessaloniki, Department of Prosthodontics, School of Dentistry, Faculty of Health Sciences, Thessaloniki, GR

Introduction

Silica-containing nanomaterials have been utilized in various biomedical applications, such as hard tissue regeneration, biochemistry, bioimaging, and biosensing. Due to their high residual glassy phase and enhanced hardness values they can improve the mechanical properties of various implantable scaffolds and biomaterials. The use of trace elements found in the human body, such as Ca, Mg and Cu, could improve the performance of such materials in the physiological environment, as their controlled release could affect positively the interaction with living bone and the behavior of human cells [1,2]. Moreover, they play a significant role in osteogenesis and angiogenesis, while attaining antibacterial potential and blood compatibility [3,4]. Smaller size of nano-scale bioceramics improves both mechanical properties and apatite-formation ability due to the increased nucleation sites provided [5]. The aim of this study was the synthesis of silica-based nanobioceramic glasses and the evaluation of the effect of the composition of nanoparticles on apatite forming ability, antimicrobial properties and hemolytic activity.

Experimental Methods

The synthesis of silica-based bioactive glasses (BGs), SiO_2 (**BG**), SiO_2CaO (60 and 40%mol respectively) (**BG1**), $SiO_2CaOMgO$ (60, 30 and 10%mol respectively) (**BG2**) and $SiO_2CaOMgO$ doped with CuO (60, 30, 7.5 and 2.5%mol respectively) (**BG3**), was achived by the Stober-based sol–gel method. All BGs were produced by the hydrolysis of TEOS in a mixture of d.d. H_2O, ethanol and HNO_3. Ca, Mg, Cu were added as nitrate salts while ammonia solution was inserted dropwise under stirring and ultrasonic bath [6].

Apatite forming ability was conducted in c-SBF, with 1.5mg/mL ratio, for 1 and 5 days under renewal conditions [6]. The characterization of the samples was determined by Fourier transform infrared spectroscopy (FTIR). The antimicrobial properties on seven bacterial strains and hemolytic properties at body (37^{o}C) were also evaluated.

Results and Discussion

The apatite forming ability of BGs revealed the formation of apatite after 24 h of immersion excluding BG, revealing that silica-doped BGs provide enhanced apatite-forming ability compared to pure silica glasses.

BG completely inhibited the three Gram-positive bacteria (*Listeria monocytogenes* Scott A, *Bacillus cereus* and *Staphylococcus aureus* ATCC 6538). The growth rates of the three Enterobacteria (*Escherichia coli* O157:H7 NCTC 12079 and the two *Salmonellaenterica* serovars Typhimurium and Enteritidis) was reduced to <50%. Only the growth of *Pseudomonas aeruginosa* was not significantly reduced. BG1 and BG2 caused a significant but slight inhibition of the growth of *Salmonella* Enteritidis PT4 and *B. cereus* respectively, but had no significant effect on the growth of the other bacteria. A small but significant ($P<0.05$) decrease in growth rate in the presence of BG3 was observed for *B. cereus, St. aureus*, and *Ps. aeruginosa*, but the growth rates of *L. monocytogenes, E. coli* and two serotypes of *Sal. enterica* were not affected.

The haemolytic activity of BGs presented in Figure 1**,** revealed that BG and BG1 induced dose-dependent hemolysis on red blood cell (RBC) after the first 24 hours of incubation starting to damage erythrocytes from 0.25mg/ml till the highest tested concentration.

The synthesis of BG2 with the addition of MgO in the system of SiO_2CaO seems to present a protective effect in erythrocytes in compare with the other BGs. Cu doping in BG2 system (sample BG3) presented similar hemolytic activity with BG2. All dosages of BG2 and BG3 below 0.5 mg/ml can be considered as non-hemolytic concentrations. Hence, from our results, it is apparent that magnesium and copper doped nanomaterials in the SiO_2CaO system are safe for blood-contacting applications.

Conclusion

Silica-doped BGs provided enhanced apatite forming ability and hemocompatibility compared to pure silica glasses. Mg and Cu doping in SiO_2CaO improved the hemolytic activity of BGs. On the other hand, BG provided better antibacterial properties compared to the rest BGs.Depending on the desired application, ion doping can result in materials with tailored properties. Further experimental work is in progress to ensure the optimum conditions for the synthesis of hemocompatible BGs that could combine apatite-forming ability and antibacterial properties for bone tissue engineering applications.

References

1. Hoppe A, Güldal NS, Boccaccini AR A review of the biological response to ionic dissolution products from bioactive glasses and glass-ceramics. Biomaterials 2011;32:2757–74.

2. Dessou NS, Theodorou GS, Kantiranis N, Papadopoulou L, Zorba T, Patsiaoura D, Kontonasaki E, Chrysaffis K, Koidis P, Paraskevopoulos KM. Influence of strontium for calcium substitution on the glass–ceramic network and biomimetic behavior in the ternary system SiO_2–CaO–MgO. J Mater Sci. 2017;52:8871-85.

3. Paula AJ, Martinez DST, Júnior RTA, Filho AGS, Alves OL. Suppression of the hemolytic effect of mesoporous silica nanoparticles after protein corona interaction: Independence of the surface microchemical environment. J Braz Chem Soc. 2012;23:1807–14.

4. Jones JR. Reprint of: Review of bioactive glass: From Hench to hybrids. Acta Biomater. 2015;23:S53–82.

5. Kankilic B, Köse S, Korkusuz P, Timuçin M, Korkusuz F. Mesenchymal Stem Cells and Nano-Bioceramics for Bone Regeneration. Curr Stem Cell Res Ther. 2016;11:487–93.

6. Pouroutzidou GK, Theodorou GS, Kontonasaki E, Papadopoulou L, Kantiranis N, Patsiaoura D, Chrissafis K, Lioutas CB, Paraskevopoulos KM. Synthesis of a bioactive nanomaterial in the ternary system SiO_2-CaO-MgO doped with CuO: The effect of Ball milling on the particle size, morphology and bioactive behavior. 2019;200005. Available from: http://aip.scitation.org/doi/abs/10.1063/1.5091430

Acknowledgement

«This research is co-financed by Greece and the European Union (European Social Fund- ESF) through the Operational Programme «Human Resources Development, Education and Lifelong Learning» in the context of the project “Strengthening Human Resources Research Potential via Doctorate Research” (MIS-5000432), implemented by the State Scholarships Foundation (IKY)»

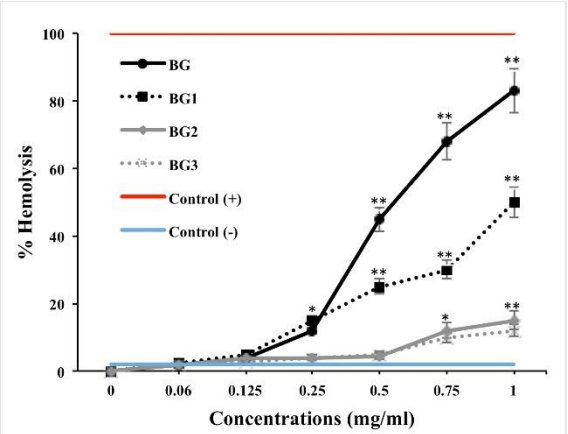

Fig. 1
*The released hemoglobin through measuring the absorbance of the supernatant at 541 nm and the percentage of the released hemoglobin after treatment for 24 hours of BGs (*p < 0.05, **p < 0.001 compared with control).*

PS1-09-175

Surface Functionalization of polylactide with antibacterial purpose

Wanpen Tachaboonyakiat, Chanikan Rakthongthai, Nutchaya Thawornsilp

Chulalongkorn University, Department of Materials Science, Bangkok, TH

Introduction

Polylactide (PLA) is a versatile biocompatible polymer derived completely for renewable resources (1) and initially applied in biomedical applications such as bioresorbable suture (2), drug delivery system (3). Like polyolefins such as polypropylene, polyethylene, PLA was normally utilized as itself because it consisted less functional groups where only at the chain ends. Therefore, the purpose of this study was to add functional groups onto PLA film surface with having specific function of antibacterial activity.

Experimental Methods

PLA film was prepared by compression molding and preactivated its surface with sodium hydroxide solution. In order to functionalize PLA for specific function of antibacterial activity. The activated PLA film was further modified with chitosan by coupling reaction. The chitosan modified PLA film was evaluated for its antibacterial activity against *E. coli* and *S. aureus*.

Results and Discussion

PLA is a hydrolysable polyester. After surface preactivation of PLA film with sodium hydroxide, PLA film surface would be partially hydrolyzed to expose functional groups of carboxylic and hydroxyl groups, then be further modified with chitosan. Since chitosan was well known of having antibacterial property. However, chitosan modified PLA film did not exhibit antibacterial activity in dry state because the amino groups of chitosan could not be protonated. Besides, owing to its own amino groups, chitosan could form metal complex. The incorporation of metal ions onto chitosan modified PLA film exhibited antibacterial activity against *E. coli* and *S. aureus*.

Conclusion

Surface modification of PLA film with chitosan together with metal ions incorporation enhance PLA film into specific function of antibacterial activity.

References

1. Murariu, M, Dubois, P. PLA composites: From production to properties. Adv Drug Deliver Rev., 2016, 107, 17-46.
2. Ramot, Y, Haim-Zada, M, Domb, J, A, Nyska, A. Biocompatibility and safety of PLA and its copolymers. Adv Drug Deliver Rev., 2016, 107, 153-162.
3. Zhang, Y, Wu, X, Han, Y, Mo, F, Duan, Y, Li, S. Novel thymopentin release systems prepared bioresorbable PLA-PEG-PLA hydrogels. Int J Phramaceut., 2010, 386, 15-20.

Acknowledgement

This research was financially supported by Research Universities Network (RUN), National Research Council of Thailand and partially supported by Faculty of Science, Chulalongkorn University.

PS1-09-176

Broad-spectrum anti-adhesive coating based on a natural marine polymer

Bruna Costa[1], Jorge Cardoso[2], Rita Mota[2], Paula Parreira[1], Paula Tamagnini[2,3], M. Cristina L. Martins[1,4], **Fabíola Costa**[1]

[1]University of Porto, INEB/i3S, Porto, PT; [2]University of Porto, IBMC/i3S, Porto, PT; [3]University of Porto, Faculty of Sciences, Biology Department, Porto, PT; [4]University of Porto, Instituto de Ciências Biomédicas Abel Salazar, Porto, PT

Introduction

Medical device-associated infections are a major health threat, representing about half of all hospital-acquired infections. Current strategies to prevent this problem, based on device coatings with antimicrobial (antibiotics, antiseptics) compounds have proven to be insufficient, often toxic and can even promote bacterial resistance [1]. Herein, we report the development of an infection preventive coating (CyanoCoating) produced with an extracellular polymer (RPS) released by the marine cyanobacterium *Cyanothece* sp.

Experimental Methods

In this sense, *Cyanothece* growth was promoted in the optimized conditions for increased polymer production [2], and then the biopolymer was extracted, purified and processed to be applied as a coating (CyanoCoating). The medical grade polyurethane Pellethane 2363 80 AE (PU) was used as control since it is the most successful used biomaterial in blood contacting devices, namely intravascular catheters. Firstly, as a proof of concept, the coatings were developed on gold substrates due to its suitability for surface characterization techniques. RPS and PU linkage to gold substrates was promoted using a polydopamine (pDA) layer that works as a linker. Coating deposition was them obtained by spincoating of either RPS solution (0.5% w/v) or PU solution (0.1% w/v).

Samples were characterized using ellipsometry, water contact angle measurements, Infrared reflection absorption spectroscopy, scanning electron microscopy (SEM) and electrokinetic analyzer. After, different international ISO standards were applied to assess the anti-adhesiveness efficacy against Gram-positive and Gram-negative bacteria (ISO 22196) (also at the presence of human plasma proteins), thrombogenicity – platelets adhesion and activation (ISO 10993-4) and biocompatibility using L929 fibroblasts cell line (ISO 10993-5) of the CyanoCoating. Also, protein adsorption studies were conducted using quartz crystal microbalance with dissipation to better understand the mechanism underlying the anti-adhesive effect. Then, envisaging future industrial application, CyanoCoating was applied directly onto PU sheets. For the linkage of RPS polymer to PU, two industrial techniques (atmospheric plasma surface activation and ozone surface activation) were compared against the previous lab-level strategy (polymerization of dopamine). After surface activation, the RPS solution was spin-coated on top of activated PU sheets. The obtained coatings were characterized (contact angle, SEM) and anti-adhesive performance of CyanoCoating was re-evaluated.

Results and Discussion

Gold-based CyanoCoating exhibited a smooth topography, 17±2 nm thickness and 17±2º as water contact angle (highly hydrophilic). Non-cytotoxic CyanoCoating prevented adhesion of all bacteria tested (≤90%) and also platelets (<87%) without inducing platelet activation in comparison with the control polyurethane (Pellethane 2363 80 AE) even in the presence of plasma proteins. The significant reduction in protein adsorption (<77%) also confirm its anti-

adhesive properties [3]. Importantly, other surface activation techniques were successful in the PU-based CyanoCoating establishment, with strong bacterial reduction (<90%).

Conclusion

CyanoCoating is a promising anti-adhesive coating capable of preventing medical device associated-infections without inducing thrombus formation in blood-contacting applications.

References

1. Percival, S. L.; Suleman, L.; Vuotto, C.; Donelli, G., Healthcare-associated infections, medical devices and biofilms: risk, tolerance and control. *J Med Microbiol* **2015,** 64, (Pt 4), 323-34.
2. Mota, R.; Guimaraes, R.; Buttel, Z.; Rossi, F.; Colica, G.; Silva, C. J.; Santos, C.; Gales, L.; Zille, A.; De Philippis, R.; Pereira, S. B.; Tamagnini, P., Production and characterization of extracellular carbohydrate polymer from Cyanothece sp. CCY 0110. *Carbohydr Polym* **2013,** 92, (2), 1408-15.
3. Costa, B.; Mota, R.; Parreira, P.; Tamagnini, P.; MC, L. M.; Costa, F., Broad-Spectrum Anti-Adhesive Coating Based on an Extracellular Polymer from a Marine Cyanobacterium. *Mar Drugs.* **2019,** 17.

Acknowledgement

This work was financed by FEDER through the COMPETE 2020,Portugal 2020, and by Portuguese funds through FCT - Fundação para a Ciência e a Tecnologia/Ministério da Ciência, Tecnologia e Ensino Superior in the framework of the project "Institute for Research and Innovation in Health Sciences" (POCI-01-0145-FEDER-007274), by the project NORTE-01-0145- FEDER-000012 & NORTE-01-0246- FEDER-000018-RESOLVE-55536.

PS1-09-177

Modification of useful properties of nanostructured surfaces on titanium biomaterials and *in-situ* biofilm monitoring method

Eva Pruchova[1], Vojtech Hybasek[1], Jaroslav Fojt[1], Ludek Joska[1], Michaela Kosova[2]

[1]University of Chemistry and Technology, Prague (UCT Prague), Department of Metals and Corrosion Engineering, Praha 6 – Dejvice, CZ; [2]University of Chemistry and Technology, Prague (UCT Prague), Department of Dairy, Fat and Cosmetics, Praha 6 – Dejvice, CZ

Introduction

Nanostructure on titanium and its alloys represent bioactive surface which enhances the process of osseointegration. Nanotubes are created by anodic oxidation in fluorides containing solutions. This modification enables a faster and more stable connection between the implant and the surrounding bone. It also shows the ability of photoactivity and last but not least, nanostructure could be used as a substrate for another substance, for example, antibacterial or bioactive agents. Bacterial attachment is considered to be a serious problem which leads to the formation of biofilm. The suppression of the planktonic lifestyle of bacteria does not mean that the biofilm formation is also limited. The aim of this work is monitoring of biofilm formation process via electrochemistry.

Experimental Methods

The nanostructured surface on Ti6Al4V alloy was prepared [1]. Metallic nanoparticles, for example, silver, belong among antibacterial agents. It could be deposited via electrochemistry. This setup consisted of 1 s cathodic pulses at -0.4 mA/cm^2 from KNO_3 and $AgNO_3$ electrolyte [2]. Silver nanoparticles could be reduced during the photoreduction process while the silver salt solution $AgNO_3$ is irradiated by the UV light for 10 minutes [3]. Also, the deposition of apatite formation precursors (CaP) could be done by electrochemistry. Ca-P compounds deposition on the titanium surfaces were done by potentiostat polarisation at -0.85 mA/cm^2 in a solution containing $Ca(NO_3)_2$ and $(NH_4)_2HPO_4$[4]. Similarly, this modification could be enriched by silver and promote antibacterial activity. The surface was characterized by SEM, EDS, XPS, and electrochemically. The antibacterial activity was measured against indicator bacterial strains *E. coli* and *S. aureus*.

Results and Discussion

Surfaces with Ag and CaP were prepared. Electrochemically anchored silver was localized inside the cavities which allowed gradual silver releasing. Silver was present inside cavities for a longer period. Another method was described, where the silver nanoparticles were deposited by the combination of the ultrasonication and photo-reduction. The entire volume of individual nanotubes was filled by silver nanoparticles. Antibacterial efficiency decreased with Ag concentration when the silver nanoparticles were depleted at both tested sets of samples. As a result, these surfaces showed excellent antibacterial ability against *E. coli* and *S. aureus* bacterial strains. Also, bioactive CaP deposits were uniformly distributed through the entire surface. Conversely, silver was directed primarily into etched cavities in the Ti6Al4V nanostructured surface. All above-mentioned modifications had an impact on the surface characteristics such as wettability which is closely related to the subsequent cell and bacterial adherence. A method for online motoring of bacterial attachment has been developed. The measurement of open circuit potential, polarisation resistance, and electrochemical impedance spectroscopy showed the sensitivity of electrochemical

quantities to the detection of bacterial biofilm formation. Obtain statements were also proven by electron microscopy observation (Fig. 1).

Conclusion

These modifications could be used as multifunctional surfaces with a variety of usage in the biomaterials field. Electrochemical tests gave an insight into time dependencies of biofilm formation.

References

1. Filova, E., et al., *The diameter of nanotubes formed on Ti-6Al-4V alloy controls the adhesion and differentiation of Saos-2 cells.* International Journal of Nanomedicine, 2015: p. 7145.
2. Pruchova, E., et al., *A two-phase gradual silver release mechanism from a nanostructured TiAlV surface as a possible antibacterial modification in implants.* Bioelectrochemistry, 2019. **127**: p. 26-34.
3. Pruchova, E., et al., *Ti6Al4V nanotubes filled with silver nanoparticles as a possible antibacterial surface for implants.* Manufacturing Technology,, 2018. **18** (3): p. 477-481.
4. Yan, Y., et al., *Antibacterial and bioactivity of silver substituted hydroxyapatite/TiO2 nanotube composite coatings on titanium.* Applied Surface Science, 2014. **314**: p. 348-357.

Acknowledgement

Financial support from specific university research (MSMT No 21-SVV/2019).

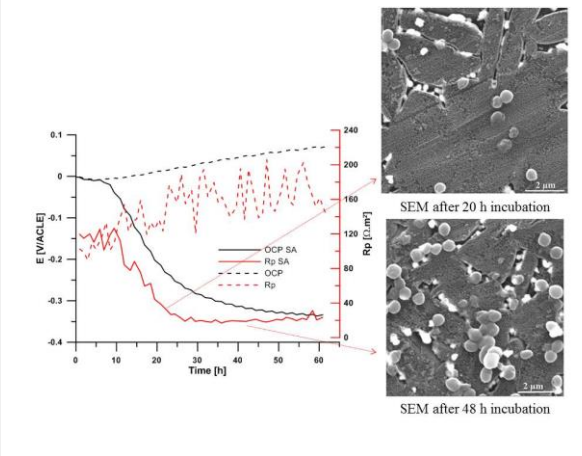

Fig. 1.
In-situ biofilm testing, a sample with electrochemically anchored silver and the time dependency of open circuit potential (OCP) and polarisation resistance (Rp) in agar-based media with *S. aureus* (notated as SA) and without bacteria.

PS1-09-178

Antibiotic-loaded bone allografts for prophylaxis and treatment of bone infections

Mike Barbeck[1,7], Denis Rimashevskiy[2], Nikolay Zagorodniy[2], Nurlan Batpenov[3], Volker Alt[8], Kristina Glenske[4], Sabine Wenisch[4], Sanja Stojanovic[5], Stevo Najman[5], Ralf Smeets[1], Débora Cristina Coraca-Huber[6], Reiner Schnettler[1]

[1]University Medical Center Hamburg-Eppendorf, Division for Regenerative Orofacial Medicine, Department of Oral and Maxillofacial Surgery, Hamburg, DE; [2]Peoples Friendship University of Russia, Moscow, RU; [3]Scientific Research Institute of Traumatology and Orthopedics, Astana, KZ; [4]Justus-Liebig-University Giessen, Institute of Veterinary-Anatomy, -Histology and -Embryology, Giessen, DE; [5]University of Niš, Faculty of Medicine, Department for Cell and Tissue Engineering; Institute of Biology and Human Genetics, Niš, RS; [6]Medical University Innsbruck, Innsbruck, AT; [7]BerlinAnalytix GmbH, Berlin, DE; [8]University of Regensburg, Regensburg, DE

Introduction

Every surgical procedure is accompanied by a risk of bacterial infections especially in transplantations of bone allografts for regeneration of lost tissue in dental and orthopedic applications. One particular challenge is the population of bioimplant surfaces with biofilm-forming bacteria, which are less prone to antibiotic treatment (1). The loading of bone allografts with antibiotic agents demonstrates a promising approach to overcome this issue. In the present study the pharmacokinetic properties of several antibiotics incorporated into allografts were analyzed *in vitro* and *in vivo*.

Experimental Methods

Freeze-dried bone allograft (FDBA) blocks (C+TBA, Krems, Austria) were rehydrated in antibiotic solutions of either Clindamycin, Gentamycin, Rifampicin, Vancomycin and a mixture of Vancomycin and Rifampicin for biofilm treatment for 10 minutes in a 1:1 proportion. The *in vitro* concentration of remaining antibiotics was assessed every 24 hours for up to 10 days. For analysis of the *in vivo* release of the antibiotic-loaded blocks were implanted using the tibial implantation model in 30 rabbits. The allografts were explanted at day 1 and 3 and the remaining amounts of the antibiotics were analyzed using microbiological methods.

Results and Discussion

Antibiotics are easily incorporated into FDBA blocks and especially within the first 3 days high concentrations were released both *in vitro* and *in vivo*.

Conclusion

The use of FDBA as carriers of antibiotic agents bares great potential in clinical application by eliminating systemic antibiotic-related side effects, minimizing risks of antibiotic resistance formation, providing advantages for eukaryotic cells for faster surface population and consequently minimizing the risk of surgical site infections.

References

1. Stewart, Philip S., and J. William Costerton. "Antibiotic resistance of bacteria in biofilms." The lancet 358.9276 (2001): 135-138.

PS1-09-179

Antibiotic-Loaded Chitosan Aerogel Particles Produced by Jet Cutting for Chronic Wound Applications

Clara López-Iglesias[1], Pavel Gurikov[2], Carmen Alvarez-Lorenzo[1], Irina Smirnova[2], Carlos A. García-González[1]

[1]University of Santiago de Compostela, Department of Pharmacology, Pharmacy and Pharmaceutical Technology, Santiago de Compostela, ES; [2]Hamburg University of Technology, Institute of Thermal Separation Processes, Hamburg, DE

Introduction

Chronic wounds, like pressure or diabetic ulcers, are injuries that present a hampered healing process, with increasing incidence in our current society due to several factors as high prevalence of diabetes and cardiovascular disease. Currently, the development of wound dressings based on biomaterials is one of the main strategies in their treatment. This approach favours the healing process by promoting the formation of new tissue while dealing with frequent complications like excessive exudate and presence of infection.

Bio-based aerogels are nanostructured materials, usually obtained by drying of gels from polysaccharides and proteins with supercritical CO_2 ($scCO_2$), that present optimal textural properties (high porosity and large surface area), allowing them to absorb large amounts of wound exudates and to load and release bioactive agents efficiently [1,2]. Chitosan is a biopolymer with outstanding properties for drug loading and tissue regeneration, besides its biocompatibility and biodegradability [3].

In this work, vancomycin-loaded chitosan aerogel particles for the treatment and prevention of chronic wound infection were produced using the jet cutting technique followed by drying with $scCO_2$.

Experimental Methods

In the jet cutting technique (JetCutter®), a solution of 2 wt.% chitosan with or without vancomycin (10 wt.% with respect to the chitosan) in acetic acid 1 v/v % was extruded through a nozzle by compressed air (2.5 bar). The liquid jet was then cut by a rotating disk with small wires and spherical droplets dropped into a solution mixture of ethanol and ammonia (gelation bath) to form the gel particles. Nozzle diameter, cutting disk velocity and number of wires were the processing parameters to modulate the particle size and feasibility of particle production. After changing the solvent to absolute EtOH, the gel particles were dried for 3h at a constant flow of $scCO_2$ (120 bar, 40 ºC) to obtain aerogel microparticles.

Morphology of the aerogels was studied by scanning electron microscopy and the particle size distribution by dynamic image analysis. The textural properties were determined by nitrogen adsorption-desorption tests and helium picnometry.

The liquid sorption capability was performed by a gravimetric method after immersion of the aerogels in PBS pH 7.4. Vancomycin content in the aerogels was determined by UV/Vis spectrophotometry after dissolution of the particles in HCl 0.1M, and the release was carried out by suspension of the particles in PBS pH 7.4 medium (37 ºC) and measurements by UV/Vis. The cytocompatibility of the microspheres was tested by a cell proliferation assay using mouse fibroblasts.

Results and Discussion

Jet cutting is a technique especially suitable to process microparticles from highly viscous solutions. This technique permitted to obtain particles with diameters in the 700-1100 µm range. Particles processed with the 500 µm nozzle diameter at a velocity of 4000 rpm of the cutting disk showed the narrowest particle size distribution and the spheres presented a spherical, homogeneous appearance (Fig. 1), so these conditions were used for the loading of vancomycin. The aerogels presented high porosity (96%) and large surface area (200m^2/g), with average pore diameters in the mesopore range (20 nm). These outstanding textural properties allowed the particles to absorb up to 9 times their weight in PBS.

The loading yield of vancomycin in the final aerogels was 25%, achieving a final vancomycin content of 22.4 µg/mg of particle. The drug release in PBS was fast, being almost 90% of the drug released during the first 30 min. The cell viability was higher than 80% after 48 h, so the particles presented good cytocompatibility.

Conclusion

Vancomycin-loaded chitosan aerogel particles obtained by the jet cutting technique were spherical, homogeneous and with a narrow particle size distribution. The remarkable textural properties of the aerogels resulted in a high water sorption capability and vancomycin loading. Vancomycin release from the aerogels was fast, rapidly achieving effective antibiotic concentrations above the Minimum Inhibitory Concentration (MIC) for most susceptible bacteria that can favour the healing process of chronic wounds. The antimicrobial capability is currently under evaluation.

References

1. C.A. García-González, C. López-Iglesias, A. Concheiro, C. Alvarez-Lorenzo, Chapter 19. In *Biobased Aerogels: Polysaccharide and Protein-Based Materials*. RSC **2018**.

2. C.López-Iglesias, A.M. Casielles, A. Altay, R. Bettini, C. Alvarez-Lorenzo, C.A. García-González, *Chem Eng J***2019**, *357*, 559-566.

3. C. López-Iglesias, J. Barros, I. Ardao, F.J. Monteiro, C. Alvarez-Lorenzo, J.L. Gómez-Amoza, C.A. García-González, *Carbohydr Polym***2019**, *204*, 223-231.

Acknowledgement

Work supported by Xunta de Galicia [ED431F 2016/010 & ED431C 2016/008], MINECO [SAF2017-83118-R], Agencia Estatal de Investigación [AEI] and FEDER funds. C.A. García-González acknowledges to MINECO for a Ramón y Cajal Fellowship [RYC2014-15239]. Work carried out in the frame of the COST-Action “Advanced Engineering of aeroGels for Environment and Life Sciences (AERoGELS, ref. CA18125) funded by the European Commission.

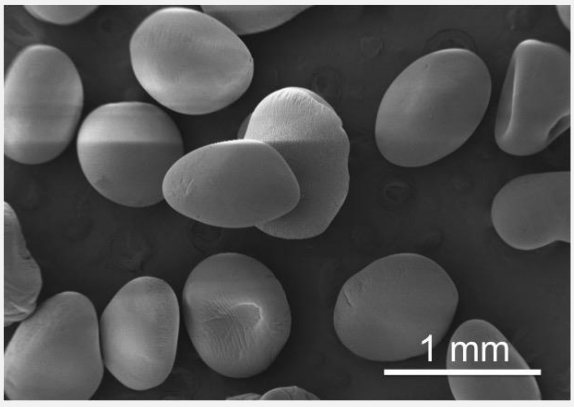

Fig. 1. SEM image of the particles produced by the jet cutting technique.
Fig. 1 shows a SEM image of the particles produced by the JetCutter® using a nozzle diameter and a velocity of the cutting disk of 500 µm and 4000 rpm, respectively, in an ethanol/ammonia gelation bath.

PS1-09-180

Preparation, Characterization and Evaluation of Collagen Sheets for the Delivery of Vancomycin

Stefanie Eckes[1], Joy Braun[2], Theresa Stegmann[3], Hansgeorg Haupt[3], Katja Schmitz[1], Ulrike Ritz[2], Daniela Nickel[4,3]

[1]Technical University of Darmstadt, Clemens-Schöpf-Institute of Organic Chemistry and Biochemistry, Darmstadt, DE; [2]Johannes Gutenberg University, Department of Orthopaedics and Traumatology, BiomaTiCS, University Medical Center, Mainz, DE; [3]Technical University of Darmstadt, Center for Structural Materials, State Materials Testing Institute Darmstadt (MPA), Chair and Institute for Materials Technology (IfW), Darmstadt, DE; [4]University of Cooperative Education, Berufsakademie Sachsen - Staatliche Studienakademie Glauchau, Glauchau, DE

Introduction

Collagen laminates with osteoinductive and antimicrobial properties can be useful biomaterials which allow a better treatment of slow healing bone fractures. In order to prevent bacterial contamination and the risk of complications during fracture healing, the targeted release of antimicrobials like vancomycin is highly necessary. A tailor-made modification of the microstructure of collagen is therefore an elegant way to achieve specific compound release. A very important step lies in the detailed characterization of collagen sheets before and after modification regarding their microstructure and compound release rate. To accomplish collagen modification, photodynamic protein crosslinking is used. It allows the adjustment of the crosslinking degree and thus modifying compound release and mechanical properties of collagen sheets [1,2,3].

In this work, three different types of collagen sheets were characterized before and after photodynamic protein crosslinking regarding their degree of swelling, vancomycin release, mechanical properties and biological effects. Hereby we evaluate their suitability as carrier materials for antimicrobial substances used after trauma.

Experimental Methods

Experiments were performed on various collagen sheets which differ in layer thickness and structural properties. The degree of swelling was measured for crosslinked and non-crosslinked collagen after incubation in buffer for several hours at 37 °C. For compound release evaluation, collagen sheets were loaded with vancomycin for 2 hours. The release of vancomycin into vancomycin-free buffer was then determined through absorption measurements and HPLC. In order to characterize mechanical properties, the thickness of collagen sheets was investigated through rheometric measurements.

For the biological evaluation of vancomycin, the effect of vancomycin on the proliferation of staphylococcus aureus was determined.

Results and Discussion

Incubation of collagen sheets (1: Collagen Bio Sheet, Viscofan; 2: Collagen-Sponge, Atellokollagen; 3: Non-perforated Collagen Sample, Collagen-Solutions) in buffer results in a significant increase of weight compared to the dry mass. With one exception, crosslinked collagen shows a minor degree of swelling than non-crosslinked collagen, as expected. (Fig. 1A). The thickness was measured for collagen samples 1 and 3 during dry state (Fig. 1B). Measurements of vancomycin release into buffer show an increasing vancomycin concentration throughout time. For analysis of vancomycin release via HPLC it is important to be able to separate vancomycin from collagen. Figure 1C shows an HPLC chromatogram of a collagen-vancomycin sample.

Conclusion

In this study, three kinds of collagen sheets were analyzed regarding their degree of swelling, vancomycin release, mechanical properties and biological effects. It was shown, that structural differences resulted in various degrees of swelling and compound release. It was shown, that photodynamic crosslinking of collagen sheets has an impact on the degree of swelling and thus presents the first steps in creating a new method for targeted release of compounds which assist healing of bone fractures.

References

[1] Charulatha V, Rajaram A. Influence of different crosslinking treatments on the physical properties of collagen membranes. Biomaterial 2003; 24(5):759-767.

[2] Kato YP, Silver FH. Formation of continuous collagen fibres: evaluation of biocompatibility and mechanical properties. Biomaterials 1990;11(3):169-75

[3] Flory PJ, Jr. JR. Statistical Mechanics of Cross-Linked Polymer Networks II. Swelling. The Journal of Chemical Physics 1943;11(11):521-526.

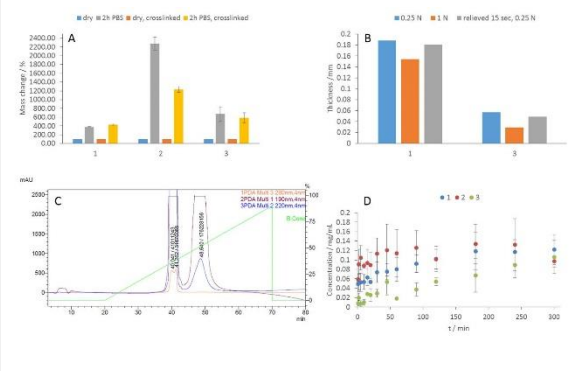

Figure 1:
A) Measurement of the swelling-degree in buffer for 2 hours before and after crosslinking. B) Thickness measurements via rheometer using forces of 0.25 N and 1 N. C) Chromatogram of collagen (48 min, 220 nm) and vancomycin (40 min, 280 nm). D) Measurement of compound release from vancomycin-loaded collagen sheets into vancomycin-free buffer.

PS1-09-181

Chitosan / Cyclodextrin polyelectrolyte hydrogel with sustained local release for the treatment of diabetic foot infections

Alice Gauzit-Amiel[1], Carla Palomino[1], Marco Lopez[1], Mickael Maton[1], Feng Chai[1], Christel Neut[3], Frédéric Cazaux[2], Benoit Foligne[3], Bernard Martel[2], Nicolas Blanchemain[1]

[1]University of Lille, U1008, Lille, FR; [2]University of Lille, UMET, Lille, FR; [3]University of Lille, U995, Lille, FR

Introduction

Diabetic foot infections are very serious, disabling and their treatment is complex and expensive. Despite significant medical and surgical progress, these infections remain a public health problem. Researches are focus to develop local delivery system to overcome the poor penetration at the infected site. The local administration increases the amount of antibiotics directly in the wound without toxic effect for the body. In this context we developed a lyophilized hydrogel, *i.e.* sponge based on two polysaccharides. Chitosan (CHT), a cationic polymer and polymer of cyclodextrins (PCDs), an anionic polymer obtained by a cross linking reaction between CDs and citric acid (1)(2). The objective is to evaluate the impact of CHT:PCD ratio on the rheological properties, structure, drug loading and drug release with two antibiotics to have a large spectrum of action on bacteria.

Experimental Methods

The two powders (<125µm), were co-milled in different ratio CHT:PCDs (3:0 (control), 3:1, 3:3, 3:5 and 3:7 (w/v%)), then suspended in distilled water and acidified with acetic acid to obtain a hydrogel characterized by rheology (MCR301, Anton Paar). Sponges were obtained by freeze-drying (Alpha 1-2 Plus, Christ) (0,06 mBar, -55 °C) and a thermal treatment (TT (140°C, 90 min) was applied to stabilize the sponge. Microstructure, swelling and degradation of sponge (with and without TT) were analyzed by SEM (S4700, Hitachi), humid weight gain and dry mass loss. Cytotoxicity was evaluated by the indirect method using AlamarBlue® assay according to ISO 10993-5 with osteoblast cells (MC3T3). Finally, sponges were impregnated in ciprofloxacin (CIP), in rifampicin (RFP) and combination of two antibiotics. Drug release profile was evaluated in PBS in a dynamic condition (USP4, Sotax) at 5 mL/min in PBS (pH7.4, 37°C). The antibacterial activity was determined against S. aureus and E. coli using a diffusion test (Kirby Bauer). Statistical test was performed by Statplus software (version Build 6.7.1.0/Core v6.2.02). Data were analyzed using one-way ANOVA and Tukey methods. The difference was regarded to be statistically significant for values of P-value < 0.05.

Results and Discussion

Rheological analysis revealed an immediate gelation of all CHT:PCDs ratio (G'>G" at the beginning of the test). Nevertheless, 3:1 and 3:3 ratios were more reproducible and exhibited better viscoelastic properties compare to 3:0 and 3:5 ratios. Moreover, after lyophilization, the sponge without PCD was not stable and cannot be use for this application. A high porous architecture of sponges was observed by SEM, favorable for biological fluid circulation and drug sorption/release without impact of TT. Interestingly, TT improved the stability of sponges, swelling properties and drug sorption. The drug sorption is directly linked to the sponges swelling properties. Indeed, a high sorption capacity is related to a high swelling rate. Clearly, the swelling ratio decrease with the increase of PCD in the formulation; thus, the ratio 3:1 TT showed the best drug sorption and the more sustained CIP and RFP release compared to other sponge. In the same way, a prolonged antibacterial activity against *Staphylococcus aureus* and

Escherichia coli was obtained for up to 48 hours for this sponge loaded with CIP, RFP or combination of both antibiotics. Finally, no cytotoxicity was observed for all sponges with survival rate >70%.

Conclusion

The 3:1 TT sponges have very interesting drug sorption with the slowest and most favorable drug release. A strong and prolonged antibacterial activity was also observed up to 48 hours with a good reproductibility. Finally, 3:1 TT ratio is an interesting potential in the treatment of diabetic foot with a significant amount of antibiotics loading while maintaining an optimal swelling rate and a good antibacterial activity with CIP and RFP.

References

1. Blanchemain N, Martel B, Flores C, Cazaux F, Chai F, Tabary N. Method for the Production of Hydrogel Comprising Chitosan and Negatively Charged Polyelectrolytes, and Cellular, Porous Material Resulting from Said Hydrogel [Internet]. FR3038318 (A1), 2017.

2. Flores C, Lopez M, Tabary N, Neut C, Chai F, Betbeder D, et al. Preparation and characterization of novel chitosan and β-cyclodextrin polymer sponges for wound dressing applications. Carbohydrate Polymers. 2017 Oct 1;173:535–46.

Acknowledgement

The authors gratefully acknowledge the Haut de francen for its financial support via the ArCir program (BioCerMedproject) and the SFR "Technology for Heath" for their financial support.

PS1-09-181-2

Fluorinated poly(ethylene glycol)@graphene oxide platform for nitric oxide gas delivery system and their antibacterial activity

Yitayal A. Workie

National Taiwan University of Science and Technology, Graduate Institute of Applied Science and Technology, Taipei, TW

Introduction

Nitric oxide (NO) is an endogenously synthesized molecule which can mediate numerous physiological processes [1,2]. In the meanwhile, exogenously, NO exerts vasodilator, tumoricidal and antibacterial effect but its usefulness is limited due to high reactivity, amount dependency and unavailability of the carrier that can efficiently encapsulate the gas[3,4]. In response to the needs for such bioactive gas in therapy, we prepared NO conserving platforms of graphene oxide (GO) and its composite with fluorinated poly (ethylene glycol) (*F*-PEG) by non-covalent functionalization.

Experimental Methods

Graphene oxide were prepared using the modified Hummers method from graphite flake and were non-covalently functionalized with *F*-PEG, *F*-PEG@GO composites. Characterization was done using transmission electron microscope (TEM), dynamic light scattering techniques (DLS), Fourier transform infrared absorption spectrophotometer (FT-IR), ultraviolet-(UV)/visible absorption spectrophotometer, Raman scattering spectrometer, thermogravimetric analysis (TGA), X-ray diffractometer (XRD), Brunauer–Emmett–Teller (BET) and X-ray photoelectron spectrometer(XPS).The amount of NO loaded was determined by using Griess assay method. The antibacterial test was done based on the standard agar disk-diffusion method.

Results and Discussion

The shape and size of GO and *F*-PEG@GO confirmed from transmission electron microscope and dynamic light scattering technique were sheet measured 207 and 250 nm, respectively. Coexistence of GO and *F*-PEG in a composite was confirmed from Fourier transform infrared absorption (FTIR) spectra, Raman scattering spectra, thermogravimetric analysis, and X-ray diffraction (XRD). The doping amount of NO in GO and *F*-PEG@GO were analyzed using Griess assay methods. The conserved NO gas was more for *F*-PEG@GO than for GO and decreased with time due to either the oxidation of NO to NO_2 or the release of NO from the carrier. The conservation of NO gas on carrier was related to the surface area of the carrier and confirmed by FTIR spectra, XRD and XPS. The anti-bacterial effect of NO gas from doped GO and *F*-PEG@GO were examined against *Escherichia coli* and *Staphylococcus aureus*.

Conclusion

NO gas preserved in *F*-PEG@GO exerted higher anti-bacteria effect than GO and more effective against *S. aureus* than *E. coli.* Thus, the *F*-PEG-coated GO composite was effective for NO gas conservation and anti-bacterial effect superior to GO.

References

1. J. H. Shin, S. K. Metzger, M. H. Schoenfisch, J. Am. Chem. Soc, 129 (2007) 4612-4619.
2. A. J. Friedman, G. Han, M. S. Navati, M. Chacko, L. Gunther, A. Alfieri, J. M. Friedman, Nitric Oxide, 19 (2008) 12-20.
3. M. P. Krafft, J. R. Riess, J. Polymer Sci. Part A: Polymer Chem, 45 (2007) 1185-1198.
4. Y. A. Workie, Sabrina, T. Imae, M. P. Krafft,. ACS Biomaterials Science & Engineering**,** 5 (2019), 2926-2934.

Acknowledgement

We are gratefully acknowledge National Taiwan University of Science and Technology.

2:45 p.m. – 3:45 p.m.

Hall 1 / Exhibition Area

PS1-10 | Cardiovascular incl. heart valve

PS1-10-182

Electrospun Collagen Based Fibers Featuring Electrical Conductivity for Cardiac Tissue Engineering Application

Lena Vogt[1], Kaveh Roshanbinfar[2], Florian Ruther[1], Felix B. Engel[2], Aldo R. Boccaccini[1]

[1]Friedrich-Alexander-Universität Erlangen-Nürnberg, Lehrstuhl Biomaterialien, Erlangen, DE; [2]Friedrich-Alexander-Universität Erlangen-Nürnberg, Experimentelle Nieren- und Kreislaufforschung, Erlangen, DE

Introduction

Based on the very limited intrinsic self-regeneration capability of cardiomyocytes, acute or chronic damage to the heart muscle, e.g. caused by a myocardial infarction, can lead to scar formation, the loss of contraction ability, and, potentially, to heart failure. Restricted therapies and the lack of donor organs demand new cardiac tissue engineering (CTE) strategies like the cardiac patch approach[1]. Electrospinning has evolved as a suitable processing technique due to its ability to closely mimic the highly branched myocardial structure[2]. In order to imitate the polysaccharide component and structural properties of the cardiac extracellular matrix, this study focuses on a blend of collagen (Col) and hyaluronic acid (HA). Additionally, polyaniline (PANi), a conductive polymer, was added to the mixture to provide electrical conductivity of the fiber mat. Fiber mats made from PANi and gelatin showed already good results in previous studies[3,4].

Experimental Methods

Different weight percentages of polyaniline emeraldine base (Mw 65MDa, Sigma-Aldrich) and camphorsulfonic acid (CSA, Sigma-Aldrich) (1:1 weight ratio) were dispersed in dimethylsulfoxide (≥99.5 %, Carl Roth) and stirred for 24 h. Collagen (type I, Symatese) and HA (Mw 1.0-1.5 kDa, Lifecore Biomedical) (9:1 ratio) were dissolved in formic acid (≥98 %, Sigma-Aldrich) and stirred for 1 h. Col/HA and PANi/CSA solutions were combined in 9:1 and 7:3 ratios 15 min prior to electrospinning. Electrospinning parameters were optimized to an applied voltage of 16 kV, a flow rate of 0.05 mL/h and a tip-target distance of 10 cm. Fibers were randomly collected on a mandrel with 500 rpm. The fiber mats were crosslinked in 25 % aqueous glutaraldehyde (50 % EM grade, Polysciences) vapor for 72 h. The morphology (SEM), chemical (ATR-FTIR), mechanical and electrical properties of the fiber mats were investigated. In vitro studies with cardiomyocytes of 3 days-old rat pups were conducted and cytocompatibility, beating behavior and intercellular communications were examined.

Results and Discussion

All Col/HA/PANi blends showed homogenous defect-free fibrous morphologies with fiber diameters ranging between 120 and 340 nm. The increasing PANi content and thereby increasing solution conductivity led to a decreasing fiber diameter, whereas the fiber alignment increased. FTIR analysis confirmed the presence of collagen, HA, and PANi in the fibrous scaffolds. Ultimate tensile strength and failure strain increased with increasing PANi content before it decreased finally; the Young's modulus decreased constantly with increasing PANi volume.The electrical conductivity also significantly increased with increasing PANi amount up to 2 ± 0.5 mS/cm. Cytocompatibility assays after 48h revealed a slight decrease of cardiomyocyte viability in fiber mats containing PANi/CSA; however, cardiomyocytes showed no significant difference in beating rates for the different compositions. The fibrous scaffold with the highest PANi content revealed a significant increase in contraction amplitude compared to the other compositions. Also a significant increase in connexin43 was observed for the fibers with the highest PANi volume.

Conclusion

After optimization of solution and electrospinning parameters, homogenous Col/HA/PANi fiber mats were successfully fabricated. The fiber mat with the highest PANi content showed the best cell results despite being the most brittle. However, all reported results meet the requirements for a patch applicable in cardiac tissue engineering.

References

1. Chen Q.-Z., et al., Biomaterials. 29: 47-57, 2008.
2. Kim P.-H., et al., BMB reports. 49.1: 26, 2016.
3. Li M., et al., Biomaterials. 27.13: 2705-2715, 2006.
4. Ostrovidov S., et al., ACS applied materials & interfaces. 9.49: 42444-42458, 2017.

Acknowledgement

The authors would like to thank the German Research Foundation (DFG) (Grant no: BO 1191/14-1) for providing financial support to this project. L.V. and K.R. contributed equally.

PS1-10-183

A 3D printed polymeric stent for heart valve fabrication

Aida Cavallo, Tamer Al Kayal, Paola Losi, Giorgio Soldani

Istitute of Clinical Physiology, National Research Council, Massa, IT

Introduction

The heart valve diseases are very common and the valve replacement therapy is the standard treatment for severe symptomatic conditions. Polymeric heart valve prosthesis could offer an optimal solution for a heart valve substitute because they could address the limitations associated with commercially available mechanical and biological valves [1]. Polymeric valve are characterized by the presence of the stent, a support structure for the leaflets allowing their deformation under pulsatile flow condition. Medical grade segmented polyurethanes for its excellent biostability and hemocompatibility properties have been successfully applied in pre-clinical models for various cardiovascular devices fabrication [2-3]. In this study, a polyurethane based material, the CarboSil (DSM Biomedical B.V., Netherlands) was the polymeric material taken into account. CarboSil with different hardness were employed for the stent 3D printing.

Experimental Methods

The stent was drawn with a free CAD software and its shape was optimized for the fabrication of a polymeric aortic valve prosthesis with a geometry similar to native three-leaflets aortic valve. The stent has an internal diameter of 20.5 mm, a thickness of 1 mm and height of 21 mm. CarboSil filaments, featuring hardness of 90A and 55D, were fabricated by a filament extruder Felfil Evo (Felfil Srl, Turin, Italy) based on a hot melt extrusion (HME) technology. The filaments with diameter of 1.75 ± 0.05 mm were employed for the 3D printing. The stent was printed using a Sharebot Q (Sharebot Srl, Nibionno, Italy) based on Fused Deposition Modeling (FDM) technology and equipped with a nozzle of 0.4 mm. The extrusion temperature was set at 210 °C and 215 °C for CarboSil 90A and 55D, respectively. Different printing parameters was considered as the printing speed (200, 300 and 500 mm/min) and the layer thickness (0.100, 0.200 and 0.300 mm). Stent samples were evaluated qualitatively using a stereo-microscope and by mechanical test, the parallel compression test (crush test) on the stent and the bending tests on stent cusps, to evaluate the influence of printing parameters on mechanical stent behaviour.

Results and Discussion

The qualitative comparison between the CAD model and the printed samples allowed to define the parameters combination that enable to print samples with acceptable accuracy for both CarboSil hardness. The printed samples that best fit with the CAD model and showed acceptable accuracy have been printed for both CarboSil materials with: i) layer thickness of 0.200 mm and 0.300 mm; ii) printing speed of 300 mm/min. These samples have been mechanically characterized showing that the maximum force measured is highest for samples made of CarboSil 55D because of its highest hardness and for samples with a layer thickness of 0.300 mm.

Conclusion

The polymeric valve stent was fabricated with acceptable accuracy for both considered CarboSil hardness. The printing speed affects the accuracy of stent while the layer thickness of printed polymer influences the stent mechanical properties. The stent printed in CarboSil 55D with printing speed of 300 mm/min, layer thickness of 0.200

mm and extrusion temperature of 215°C has mechanical properties similar to biological commercial solutions actually used in clinical application [5]. This stent should be used for the fabrication of a polymeric heart valve.

References

[1] Bezuidenhout D et al. Polymeric heart valves for surgical implantation, catheter-based technologies and heart assist devices. Biomaterials. 2015; 36:6-25.

[2] Soldani G et al. In vivo evaluation of an elastomeric small-diameter vascular graft reinforced with a highly flexible Nitinol mesh. J Biomed Mater Res B ApplBiomater.2018 Sep 3.

[3] De Gaetano F et al. Fluid dynamic characterization of a polymeric heart valve prototype (Poli-Valve) tested under continuous and pulsatile flow conditions. Int J Artif Organs. 2015; 38(11):600-6.

[4] Dempsey DK et al. Comparative analysis of in vitro oxidative degradation of poly(carbonate urethanes) for biostability screening. J Biomed Mater Res A. 2014 Oct;102(10):3649-65

[5] Tzamtzis S et al. Numerical analysis of the radial force produced by the Medtronic-CoreValve and Edwards-SAPIEN after transcatheter aortic valve implantation (TAVI). Med Eng Phys. 2013; 35(1):125-30.

Acknowledgement

This study was founded within the VALVETECH project by Tuscany Region (Bando FAS Salute 2014).

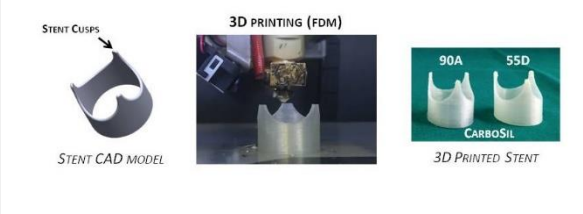

Figure 1.
Stent fabrication

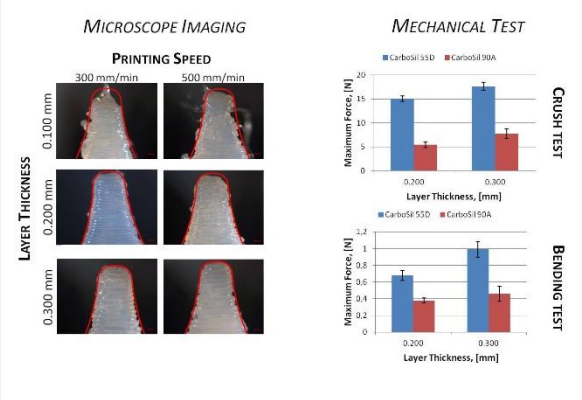

Figure 2.
Stent characterization

PS1-10-184

Investigation of the layer adhesion strength of a bi-component cardiac patch

Florian Ruther, Anne Zimmermann, Aldo R. Boccaccini

Friedrich-Alexander University Erlangen-Nuremberg, Department of Biomaterials, Erlangen, DE

Introduction

Cardiovascular diseases, especially in form of myocardial infarction, are the leading cause of death worldwide. Undersupply of oxygen and nutrients induces the formation of scar tissue, leading to infarct region thinning and consecutively to congestive heart failure [1]. Consequently, finding new ways to support regeneration of the damaged heart is of great importance. One alternative is the development of cardiac patches with the major purpose to deliver healthy cells to the infarcted tissue. For this application, cardiac patches must fulfil specific mechanical, chemical and physical requirements. In this work, bi-component cardiac patches were investigated regarding their layer adhesion to achieve these demands.

Experimental Methods

To mimic mechanical properties of the human heart, a porous film was prepared using poly(glycerol) sebacate (PGS) [2]. Gelatin fibers were fabricated by electrospinning using 20 wt.% gelatin in formic acid. Electrospinning parameters were set to 15kV, 25°C, 40% rel. humidity and a nozzle-collector distance of 11 cm was used. As-spun fibers were attached to the PGS patch either via direct spinning on top of the patch or via combining the patch with an as-spun fiber mat using gelatin as glue. All bi-component patches were cross-linked in an aqueous 25 wt% glutaraldehyde (GTA) vapor for 72h.

Morphological (SEM), chemical (FTIR) and biomechanical (modified adhesion test) characterizations were carried out to study the properties of the different produced patches. Furthermore, an in vitro degradation test in 37°C warm PBS up to 28 days was done to investigate a change in the layer adhesion.

Results and Discussion

Images of scanning electron microscopy showed that glued gelatin fiber mats adapted to the rough surface of the porous PGS substrate with a strong adhesion. In contrast, directly electrospun fibers showed poor adhesion and only few fibers were attached to the PGS substrate. After 14 days of in vitro degradation, FTIR analyses confirmed the absence of gelatin on those samples. Force-displacement curves, generated via a modified adhesion test, showed that combining as-spun fiber mats with porous PGS patches led to excellent material adhesion before and after exposure to PBS for up to 28 days.

Conclusion

Bi-component cardiac patches with an improved layer adhesion were successfully manufactured. It could be shown, that attaching electrospun fiber mats with gelatin as glue on top of porous PGS patches hold excellent adhesion properties even after 28 days of degradation in 37°C warm PBS. Cell biology studies are being carried out to assess the suitability of those patches to support the attachment and beating of cardiomyocytes.

References

1. Mendis S, Puska P, Norrving B (2011) Global Atlas on cardiovascular disease prevention and control. WHO
2. Rai R, Tallawi M, Grigore A, Boccaccini AR (2012) Synthesis, properties and biomedical applications of poly(glycerol sebacate) (PGS): A review. Prog Polym Sci 37:1051–1078 . doi: 10.1016/j.progpolymsci.2012.02.001

Acknowledgement

This project was funded by DFG (Project BO 1191/14-1).

PS1-10-185

Simulation-based development of novel heart valve prostheses

Ronny Brünler, Philipp Schegner, Dilbar Aibibu, Gerald Hoffmann, Chokri Cherif

TU Dresden, Institute of Textile Machinery and High Performance Material Technology, Dresden, DE

Introduction

About 325,000 heart valve replacements are conducted annually worldwide. Today there are two types of prostheses available for replacement: mechanical and biological valves. One of the advantages of mechanical valves is their almost unlimited durability. However, the main disadvantage is the lifelong anticoagulation therapy that the patient must undergo. A further disadvantage of mechanical valves is that the patient can hear the sounds caused by the mechanical closing of the valve. Hence, the trend is towards biological prostheses, which advantages are the elimination of anticoagulant follow-up treatment, the imperceptible valve closure sound and the possibility of minimally invasive implantation, for example in the context of TAVI.

However, disadvantages of biological valves are their limited shelf life, so that after 15 years there is 30 - 60% chance of reoperation due to degeneration and calcification. For the production of biological heart valves, pig or bovine heart bags are cleaned, stretched in shape and placed in glutaraldehyde for disinfection for at least 24 hours. After checking the quality and thickness of the material, a laser cutter is used to cut six thumbnail-sized shaped pieces per heart valve exactly according to the cutting plan. These are then sewn together by hand with over 1,000 stitches each to form a biological heart valve. Sometimes a single stitch has to be planned for minutes under the magnifying glass or even under the microscope. The production of such a heart valve requires about 20 hours of manual work. A single false stitch can turn the entire heart valve into rejects. The costly manual production triples the costs of biological heart valves compared to mechanical valves.

The aim of the work presented here is the development of a simulation-based technology for the integral production of complex seamless textile tube structures with valve functions, which is exemplified by a heart valve prosthesis for minimally invasive use. The valve is integrated in situ during the weaving process without the need for additional components.

Experimental Methods

For the development of integrally manufactured, complex, seamless tubular structures with valve function in fully textile design, all relevant manufacturing, flow and mechanical requirements as well as values for impermeabilty, the valve switching cycle, the continuous load capacity, the closing tightness of the valve as well as the requirements of a minimally invasive operation were recorded and defined. Furthermore, the geometric properties as well as the mechanical properties of the heart valve prosthesis were determined.

Based on the required properties, a basic weave was developed, consisting of a tubular fabric with integrated folds that serve as valves. The basic structure of the heart valve consists of a tube projected into plane, which is manufactured as a two-layer fabric with circumferential fibres, thus ensuring high radial strength and dimensional accuracy.

The Jacquard bobbin shuttle ribbon weaving machine has been technically and constructively upgraded and adapted for the processing of very fine threads. In particular, a special yarn frame for medical applications was developed and implemented so that impermeable fabrics can be produced.

Results and Discussion

Based on the geometric design of structural-mechanical parameters, a geometric model for heart valves was created. The deformation of the valve was determined on the basis of a deformation simulation in connection with a flow analysis and from this the valve design was derived. Deformation simulations of the tubular structure and deformation simulations of the valve were carried out on the basis of the geometry models and the material characteristics.
On the basis of the geometry models developed and the simulations carried out, a novel weaving technology for the integral production of seamless tube structures with defined valve functions for the realization of fiber-based and flow-optimized heart valve prostheses is being developed.

Conclusion

Textile implants offer an excellent solution because they combine the advantages of biological heart valves (minimally invasive and short drug-induced coagulation inhibition) with those of mechanical heart valves (life-long durability).
The novel textile heart valve prostheses offer excellent prerequisites for the realization of valve prostheses that are precisely adapted to the anatomical vascular situation, can be placed minimally invasively in the heart, do not require lifelong after-treatment with anticoagulants, can be used for patients of all ages due to their lifelong durability and can be manufactured with a high degree of reproducibility and quality to save time and money.

Acknowledgement

The IGF research project 19922 BR of the Forschungsvereinigung Forschungskuratorium Textil e. V. are funded through the AiF within the program for supporting the „Industrielle Gemeinschaftsforschung (IGF)“ from funds of the Federal Ministry for Economic Affairs and Energy (BMWi) by a resolution of the German Bundestag.

2:45 p.m. – 3:45 p.m.

Hall 1 / Exhibition Area

PS1-11 | Peripheral nerves and spinal cord

PS1-11-186

Genipin cross-linked extracellular matrix hydrogels developed for neural tissue repair

Karel Vyborny[1,2], Kristyna Kekulova[1,2], Jana Vallova[1,2], Sarka Kubinova[1]

[1]Czech Academy of Sciences, Institute of Experimental Medicine, Prague, CZ; [2]Charles University, 2nd Medical Faculty, Prague, CZ

Introduction

Extracellular matrix (ECM) scaffolds prepared by tissue decellularization preserve the composition, mechanical integrity, and biological activity of the native ECM suggesting that the molecular composition of these materials is an active factor in remodeling events. ECM scaffolds can be prepared in the form of an injectable hydrogel, which enables the non-invasive application. In our previous work, we prepared ECM hydrogel derived from human umbilical cord tissue (UC-ECM) and crosslinked it by genipin to improve mechanical stability and endurance to enzymatic degradation. The aim of this study is to further investigate biocompatibility and neurotrophic potential genipin crosslinked UC-ECM hydrogel *in vivo* and *in vitro*.

Experimental Methods

ECM hydrogel was prepared by the decellularization of the human umbilical cord and crosslinked by 0.5-5 mM genipin. The gel was characterized in terms of the crosslinking degree, rheometry, and enzymatic degradation by collagenase. The biocompatibility of crosslinked ECM hydrogels was evaluated by measurement of viability and proliferation of human mesenchymal stem cells (MSCs). The gel contraction was measured in 3D MSC culture. The neurotrophic properties of the crosslinked hydrogels were assessed using dorsal root ganglion (DRG) dissociated culture. To prove crosslinked ECM hydrogel stability in vivo, the hydrogel was injected into the rat brain cortical ischemic lesion to evaluate its retention within the lesion as well as the reaction of the host macrophages/microglia.

Results and Discussion

Crosslinking in a concentration of 1mM improved the stability of the UC-ECM hydrogel and did not show any changes in MSC proliferation as well as axonal sprouting of DRG neurons when compared to uncrosslinked ECM hydrogel. If crosslinked in situ, genipin prolonged the retention of the ECM/G hydrogel within the cortical ischemic lesion without any adverse or proinflammatory effects in the host tissue.

Conclusion

Genipin crosslinking has a significant effect on ECM matrix stabilization and in a concentration 1 mM is biocompatible in vitro as well as in vivo.

References

Koci, Z. et al., Extracellular Matrix Hydrogel Derived from Human Umbilical Cord as a Scaffold for Neural Tissue Repair and Its Comparison with Extracellular Matrix from Porcine Tissues, Tissue Eng Part C Methods, 23(6): 333 (2017)

Tukmachev, D. *et al.* Injectable Extracellular Matrix Hydrogels as Scaffolds for Spinal Cord Injury Repair. *Tissue Eng Part A***22**, 306-317, doi:10.1089/ten.TEA.2015.0422 (2016

Acknowledgement

This project was supported by MEYS of the Czech Republic: LO1309

PS1-11-187

Calcium signalling as a key factor in developing implants for peripheral nerve regeneration

Katarzyna Nawrotek, Paulina Pędziwiatr, Dawid Zawadzki

Lodz University of Technology, Department of Process Thermodynamics, Lodz, PL

Introduction

The formation of correct neural circuits during development or regeneration is dependent on the ability of growing axons to accurately locate their targets [1]. The accurate path is sensed by growth cones, which detect distributions of molecular guidance cues in the extracellular environment. Chemotaxis based on both growth cones' detection and response to concentration gradients of appropriate cues is regarded as a key mechanism for guidance.
Calcium ions take part in growth cone turning as well as outgrowth [2]. Binding of the appropriate guidance cue to receptors on the growth cone can trigger the influx of calcium into the cytoplasm from calcium stores in the endoplasmic reticulum by activation of ryanodine receptors or inositol-1,4,5-triphophate receptors, or from extracellular sources via voltage-dependent calcium channels [3] and transient receptor potential (TRP) calcium channels [4]. Blocking calcium entry through membrane-bound or ryanodine channels can stop the guidance response, or even change a normally attractive turning response to a guidance cue to repulsion [1, 5].

Experimental Methods

In this study, we developed implants releasing calcium ions in a controlled manner. The implants are intended for peripheral nerve regeneration. The structure of implants is made of naturally derived mimetics of glycosaminoglycans. Moreover, it is hydrogelic and contains reservoirs of calcium ions. Three structures with different concentration of calcium ions are incubated in a phosphate buffered solution (PBS, pH 7.4) and in phosphate-buffered solution (PBS, pH 7.4) containing lysozyme (enzyme responsible for degradation of mimetics of glycosaminoglycans in living organism) for specified periods of 1, 7, 14, 21, 28, and 56 days under continuous shaking. Subsequently, samples are evaluated by different physicochemical methods in order to determine the release rate which allows on the optimal regeneration of dorsal root ganglia (DRG).

Results and Discussion

The developed implants allows controlling the calcium release rate, the crucial component influencing axonal regeneration.

Conclusion

As the presented method allows obtaining implants controlling the calcium release rate, thus it can be regarded as a new approach which opens a new path in treatment of patients suffering from the injury of peripheral nervous tissue.

References

1. Forbes EM, Thompson AW, Yuan J, Goodhill GJ, Calcium and cAMP levels interact to determine attraction versus repulsion in axon guidance, Neuron, 2012, 74(3):490-503
2. Cohan CS, Connor JA, Kater SB, Electrically and chemically mediated increases in intracellular calcium in neuronal growth cones, J Neurosci, 1987, 7, 3588–3599

3. Berridge MJ, Bootman MD, Roderick HL, Calcium signalling: dynamics, homeostasis and remodelling, Nat Rev Mol Cell Biol, 2003, 4, 517–529
4. Henle SJ, Wang G, Liang E, Wu M, Poo MM, Henley JR, Asymmetric PI(3,4,5)P3 and Akt signaling mediates chemotaxis of axonal growth cones, J. Neurosci, 2011 31, 7016–7027
5. Hong K, Nishiyama M, Henley J, Tessier-Lavigne M, Poo M, Calcium signalling in the guidance of nerve growth by netrin-1, Nature, 2000, 403, 93–98

Acknowledgement

This study was supported by the National Science Center of Poland – Grant NCN 2017/26/D/ST8/00196

PS1-11-188

Surface-modified PCL-PLGA tubular nanofibers for peripheral nerve repair

Sheida Aliakbarshirazi[1], Mahtab Asadian[1], Anton Nikiforov[1], Heidi Declercq[2], Nathalie De Geyter[1], Rino Morent[1]

[1]Ghent University, Research Unit Plasma Technology (RUPT), Department of Applied Physics, Ghent, BE; [2]Ghent University, Faculty of Medicine and Health Sciences, Department of Human Structure and Repair, Ghent, BE

Introduction

Injuries to the peripheral nervous system (PNS) are a challenging clinical problem with an incidence rate of 300.000 new cases each year in Europe[1]. One of the current tissue engineering approaches for PNS regeneration is fabrication of hollow, solid, artificial nerve guide conduits (NGCs) constructed from polymers. Such NGCs should be able to mimic the nerve-ECM (extra cellular matrix)[2] and should have excellent mechanical and physical properties as well as surface chemical cues[3]. In order to gain the above-mentioned properties the tubes should consist of 1) aligned fibers in the inner side to direct and guide the axons towards the targets and 2) random fibers at the outer side to enhance the mechanical properties and the transportation of nutrients through this porous layer[4]. Non-thermal plasma treatment is found to be the most desirable strategy to modify the nanofibers' surfaces by incorporation of functional groups and by preserving their nanostructure[5]. This modification increases the cell adhesion by improvement of the wettability of the nanofibrous scaffolds[6].

Experimental Methods

In this research, a mixture of poly-caprolactone (PCL) and poly lactic-co-glycolic acid (PLGA) in ratio of (24:2) is dissolved in a bi-solvent system consisting of tetrahydrofuran and dimethylformamide (6:4) to fabricate nanofibrous NGCs using a newly designed two-pole air gap electrospinning collector. In the next step, both inner and outer side of the NGCs are modified by a hollow cathode (HC) discharge plasma sustained in argon. Furthermore, pheochromocytoma (PC12) cell interactions (i.e. adhesion, migration and etc.) are examined by live/dead staining to examine the potential of these tubular scaffolds for peripheral nerve regeneration.

Results and Discussion

Scanning electron microscopy (SEM), tensile test, water contact angle measurements and X-ray photoelectron spectroscopy (XPS) analysis are used to study the morphology, mechanical properties, wettability and chemical characteristics of the tubes before and after plasma treatment, respectively. SEM shows that the fibers are ideally formed: aligned in the inner side of the conduits and randomly at the outer part. Moreover, HC discharge plasma increases the hydrophilicity of the conduits by adding oxygen-containing groups on the surface. No changes in their nano-morphology or damage are observed. Moreover, the tubular nanofibers indicate good cell adhesion without any cytotoxicity effect for PC12 cells.

Conclusion

Results show that these plasma-modified electrospun NGCs have a great potential to be applied for peripheral nerve regeneration.

References

1. Valmikinathan, C.M., Tian, J., Wang, J. and Yu, X., 2008. Novel nanofibrous spiral scaffolds for neural tissue engineering. *Journal of neural engineering*, *5*(4), p.422.
2. Spearman, B.S., Desai, V.H., Mobini, S., McDermott, M.D., Graham, J.B., Otto, K.J., Judy, J.W. and Schmidt, C.E., 2018. Tissue-engineered peripheral nerve interfaces. *Advanced Functional Materials*, *28*(12), p.1701713.
3. Chiono, V., Tonda-Turo, C. and Ciardelli, G., 2009. Artificial scaffolds for peripheral nerve reconstruction. *International review of neurobiology*, *87*, pp.173-198.
4. Xie, J., MacEwan, M.R., Schwartz, A.G. and Xia, Y., 2010. Electrospun nanofibers for neural tissue engineering. *Nanoscale*, *2*(1), pp.35-44.
5. Prabhakaran, M.P., Venugopal, J., Chan, C.K. and Ramakrishna, S., 2008. Surface modified electrospun nanofibrous scaffolds for nerve tissue engineering. *Nanotechnology*, *19*(45), p.455102.
6. Tian, L., Prabhakaran, M.P., Hu, J., Chen, M., Besenbacher, F. and Ramakrishna, S., 2015. Coaxial electrospun poly (lactic acid)/silk fibroin nanofibers incorporated with nerve growth factor support the differentiation of neuronal stem cells. *RSC Advances*, *5*(62), pp.49838-49848.

PS1-11-189

Nanocomposite electrospun gelatin fibers for peripheral nerve regeneration

Izabela C. Stancu[1,2], Diana M. Dragusin-Zakman[1,2], Filis Curti[1], Elena Olaret[1], Doris Steinmüller-Nethl[5], Sorina Dinescu[4], Eugeniu Vasile[3], Marieta Costache[4], Horia Iovu[1]

[1]University POLITEHNICA of Bucharest, Advanced Polymer Materials Group, Bucharest, RO; [2]University POLITEHNICA of Bucharest, Faculty of Medical Engineering, Bucharest, RO; [3]University POLITEHNICA of Bucharest, Department of Science and Engineering of Oxide Materials and Nanomaterials, Bucharest, RO; [4]University of Bucharest, Department of Biochemistry and Molecular Biology, Bucharest, RO; [5]DiaCoating GmbH, Wattens, AT

Introduction

Peripheral nerve damage due to accidents, tumour resections, compressions or contusions results in total or partial loss of motor, sensory and vegetative functions, resulting in activity restriction or permanent disability.[1,2] This study investigated the potential of nanodiamond-gelatin nanocomposite electrospun meshes as conduits for peripheral nerve regeneration.

Experimental Methods

The nanocomposite fibers were obtained through electrospinning of 0.5 or 1% w/v nanodiamond particles (NDPs) in fish gelatin (FG) with a final concentration of 50% w/v. Electrospinning was performed in controlled environment (Climate-Controlled EC-CLI, IME Technologies). The resulting meshes were crosslinked with glutaraldehyde, extensively washed using ethanol baths, and finally double distilled water. Advanced morpho- and microstructural characterization of the fibrous scaffolds (before and after crosslinking) has been performed. The morphological and geometrical characteristics of the nanofibers, as well as the distribution of the nanoparticles into the scaffolds were determined by scanning electron microscopy (in ETD and BSED modes) and transmission electron microscopy (TEM) (Fig. 1).

Adipose stem cells were seeded onto the fibrous scaffolds and cultured up to 7 days, in static culture. The quantitative evaluation of the viability and proliferation was performed by MTT, quantitative evaluation of the cytotoxicity by LDH, and the qualitative investigation of biocompatibility by Live/Dead assay.

Results and Discussion

At 2 days post-seeding, the cellular viability improved with the increase of NDPs content. After 7 days, a clear dependence of the increase in proliferated cells number is observed at higher NDPs amount (Fig. 1).

Conclusion

This study shows the potential of gelatin – NDPs fibrous scaffolds to be used for the fabrication of peripheral nerve conduits.

References

1. M. Uzet al, Acta Biomaterialia. 56, 2016

2. K. O. Allbright, Muscle&Nerve. 58, 2018

Acknowledgement

This research was founded through grant 65 PCCDI/2018 (REGMED) and through project number 96／2018 PN-III-P1-1.1-PD-2016-2024 (Novo3Dstruct). The fabrication through electrospinning technique was possible due to European Regional Development Fund through Competitiveness Operational Program 2014-2020, Priority axis 1, ID P_36_611, MySMIS code 107066, INOVABIOMED.

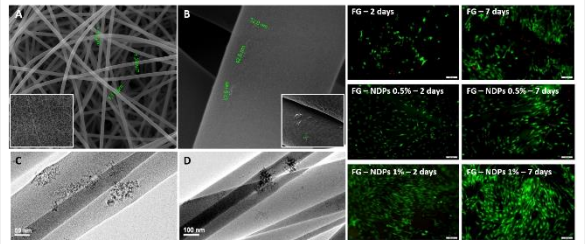

Figure 1

A, B – SEM micrographs revealing the homogeneous fibers and the distribution of the NDPs in the fibers; C, D – TEM micrographs showing NDPs dispersed in the nanofibers; last 2 columns– effect of the NDPs concentration on the proliferation of the adipose stem cells after 2, and respectively 7 days of seeding.

2:45 p.m. – 3:45 p.m.

Hall 1 / Exhibition Area

PS1-12 | Vascular grafts incl. stents

PS1-12-190

Development of a novel weaving technology for the integral production of complex individual stent grafts

Ronny Brünler, Philipp Schegner, Dilbar Aibibu, Gerald Hoffmann, Chokri Cherif

TU Dresden, Institute of Textile Machinery and High Performance Material Technology, Dresden, DE

Introduction

The pathological enlargement of the aorta (aortic aneurysm) is a life-threatening cardiovascular disease with an incidence of 29 cases per 100,000 inhabitants. Endovascular stent grafts which consist of a vascular prosthesis with an internal or external stent are used for the treatment of these pathologies. The stent grafts are applied for lining and bridging the weakened aortic segment.

The disadvantage of specially manufactured, patient-adapted stent grafts with complex structural design featuring branches, recesses and windows are their long production time and the resulting high costs (approx. 35,000 € per custom-made stent graft) due to the current manual manufacturing method used. The sewing of the stent on the vascular prosthesis, the sewing of the branches as well as the fitting of windows are currently carried out by hand and are very labor-intensive and time-consuming. In addition, the quality of the implant depends directly on the person working on it, which can lead to different strengths of the sutures for attaching the stents and thus to different behavior during the unfolding of the stent graft in the aorta and negatively influence the success of the therapy.

The focus of the work presented here is the development of a CAD-supported, integral manufacturing technology for the production of complex patient-specific stent grafts in reproducible quality via textile technologies. This flexible technology is designed to provide solutions for the integration of approved shape memory materials (Nitinol) with no need for additional manual fabrication.

Experimental Methods

For the necessary processes image analysis and export of the vessel data, corresponding software modules were developed in Python. Within the framework of the processes, the images (slices) are first extracted from the CT container files (DICOM files) and converted into a numerically evaluable format. The data collected from all slices are calculated and exported as follows: the diameter of the main vessel, the length to the bifurcation, positions and diameters of windows and branches and the diameters of the left and right secondary vessels. These data are processed into parameterized models using various algorithms for export to the CAD software SolidWorks. Additionally, a VBA macro was developed, which allows simple parameter changes by user input as well as a selection between different predefined configurations.

For the conversion into machine readable data, the complex, individual 3D structure is flattened to a surface with simultaneous marking of different structural zones with respect to tubular zones, branches, windows and zones for the integral insertion for stent rings. The contours are automatically adapted to the desired pore sizes or densities, respectively.

Results and Discussion

All individual software modules have been combined to form a continuous process chain and along with the machine modifications an integral production of highly complex patient-specific graft structures with integrated stent rings was realized.

The analysis of the technology parameters, material properties, process parameters and implant properties show that the stent grafts have very homogenous mesh densities and grammage in all sections and that the mesh structure is therefore homogeneous in the different areas realized.
The flexible technology offers solutions for the integration of stents in the form of metallic wires without additional manual assembly such as cutting and suturing. It also provides solutions for the automated production of branches in different diameters and tapered structures as well as for individual customization with high productivity.

Conclusion

The development of a unique manufacturing technology enables the manufacture of complex implants based on textile yarns and wires at reduced manufacturing costs. These implants are suitable for stent grafts because the manufacturing technology enables the production of complex and individual geometries. Automated production avoids manual work, and thus avoids quality defects. Instead, it guarantees shorter production times and thus cost-efficient production and high process stability.

Acknowledgement

The IGF research project 18774 BR of the Forschungsvereinigung Forschungskuratorium Textil e. V. is funded through the AiF within the program for supporting the „Industrielle Gemeinschaftsforschung (IGF)“ from funds of the Federal Ministry for Economic Affairs and Energy (BMWi) by a resolution of the German Bundestag.

PS1-12-191

Quercitrin functionalized nanostructured titanium surfaces for the improvement of cardiovascular stents.

Maria Antonia Llopis-Grimalt[1,2], Victor Alcolea-Rodriguez[1], Maria Antonia Forteza-Genestra[1,2], Joana Maria Ramis[1,2], Marta Monjo[1,2]

[1]University of Balearic Islands, Group of Cell Therapy and Tissue Engineering, IUNICS, Palma, ES; [2]Balearic Islands Health Research Institute (IdISBa), Palma, ES

Introduction

In cardiovascular stents, the prevention of thrombosis and restenosis is key to prevent a new obstruction of the vessel. Stent surface is directly exposed to the patient's tissues; thus, its modification is being explored in order to improve the tissue response. One strategy is the formation of nanostructures or the functionalization with active biomolecules.

The main objective of this research was the development of quercitrin functionalized nanostructured titanium (Ti) surfaces that promote endothelial tissue regeneration and decrease platelet adhesion with potential application in cardiovascular stents.

Experimental Methods

Mirror polished titanium discs, c.p. grade IV, 6.2 mm diameter and 2 mm height were used in this study. Nanostructured Ti surfaces were developed by electrochemical anodization and functionalized with quercitrin. All surfaces were characterized by atomic force microscopy, scanning electronic microscope and contact angle analysis and quercitrin content was analyzed using a DPBA staining. Primary human umbilical cord endothelial cells (HUVEC) were used to test cell adhesion, cytotoxicity and metabolic activity. Platelet adhesion and hemolysis rate were also analyzed. *Staphylococcus epidermidis* CECT4184 was used to test bacterial adhesion at 30 minutes.

Results and Discussion

Functionalization with quercitrin did not affect surface topography or nanostructure size and contact angle was lower in quercitrin functionalized surfaces (TiQR and NNQR). No differences were found in HUVEC adhesion but metabolic activity was lower in nanostructured surfaces compared to Ti and TiQR which could be explained by a higher cell differentiation. All surfaces showed cytotoxicity levels lower than 30% and very low hemolysis rate. In addition, platelet adhesion was lower in NN surfaces compared to Ti but no effect was found after functionalization with quercitrin. *Staphylococcus epidermidis* adhesion at 30 minutes was lower on TiQR surfaces compared to Ti.

Conclusion

Our results suggest that NN structuration of Ti surfaces has a great potential to be used for stent coatings and that the combination with quercitrin functionalization could reduce the risk of bacterial adhesion.

Acknowledgement

This work was supported by the Osteology Foundation (13-069), the Ministerio de Educación Cultura y Deporte (contract to M.A. L.G; FPU15/03412) & the Instituto de Salud Carlos III (contract to J.M.R and M.A.F.G ;CP16/00124). The authors thank Dr. F. Hierro and Dr. J. Cifre (UIB) for their technical contribution with SEM and AFM respectively.

PS1-12-192

Polyurethane-based fibrous mats for vascular grafting: The effects of structure and polydopamine coating on endothelialization.

Raminder Singh[1,2], Michał Wojasiński[3], Kamil Kopeć[3], Hatice Genç[1], Tomasz Ciach[3], Iwona Cicha[1]

[1]University Hospital Erlangen, ENT Department, Section of Experimental Oncology and Nanomedicine, Erlangen, DE; [2]University Hospital Erlangen, Department of Cardiology and Angiology, Erlangen, DE; [3]Warsaw University of Technology, Faculty of Chemical and Process Engineering, Biomedical Engineering Laboratory, Warsaw, PL

Introduction

The implantation of small-diameter vascular grafts is needed in a number of conditions, including coronary artery disease, peripheral vascular disease, but also the surgery of vascular trauma, aneurysms, plastic reconstruction, and organ transplantation. Attempts at synthetic small diameter grafts, which are used for large diameter vessel replacement, have been plagued with failure due to thrombosis, intimal hyperplasia and calcification. Recently, smart-design approach based on incorporation of biological cues to enhance endothelialization, either prior to or upon implantation, has been proposed. The aim of this project is to develop smart vascular grafts, which support rapid endothelialization, while reducing the risk of thrombogenic process.

Experimental Methods

Fibrous mats were prepared using medical grade polyurethane (PU, ChronoFlex C75A and C75D), and solution blow spinning technique. The mats were produced to achieve the thickness of 200 µm. Human umbilical vein endothelial cells (HUVECs) were seeded on the mats and their growth was observed on day 1, day 3 and day 7. Metabolic activity of the cells was measured using WST-8 assay and F-actin was visualized to evaluate the morphology of HUVECs. In some experiments, C75D samples modified with polydopamine (PDA) were used. The modification was carried out in an aqueous solution with the addition of an oxidizing agent. After coating, samples were washed, dried and sterilized prior to the use in cell culture experiments.

Results and Discussion

The produced C75A mats had mean fiber diameter of about 250 nm, pore size of 2 µm and ca 60-65% porosity. The fiber diameter of C75D was about 200 nm, with pore size of 3 µm and porosity over 80%. HUVECs cultured on C75A samples showed overall lower metabolic activity as compared with cells grown on C75D mats. Analyzing the cell number, denser cell coverage was initially observed on C75A as compared with C75D, but it was followed by a marked decrease on day 3 and day 7. There was no major difference in cell number on C75D between day 1 and day 3, but the number of HUVECs was increased on day 7. Based on these results, we selected CD75D for further modifications using PDA. Compared to unmodified samples, increased numbers of HUVECs were found on PDA-coated mats after 7 days of culture.

Conclusion

Endothelial cell growth was improved on C75D PU fibers as compared with less porous C75A mats. Coating with PDA further improved endothelialization. Studies on hemocompatibility of these promising substrates are currently ongoing.

Acknowledgement

This study was supported by the German Federal Ministry of Education and Research (BMBF) within BioCoatGraft project.

PS1-12-193

Tissue-engineered vascular constructs procurement by modifications of static cell seeding method

Valentin A. Brumberg, Tatiana A. Astrelina, Irina V. Kobzeva, Viktoriya A. Nikitina, Elena A. Dubova, Andrei Y. Bushmanov, Alexander S. Samoilov

Burnazyan FMBC SRC FMBA of Russia, Moscow, RU

Introduction

Currently in the field of vascular tissue engineering there are different approaches to seed a tubular scaffold with an appropriate cell type. The choice of particular technique for scaffold seeding depends on scaffold's nature and composition (decellularized / synthetic / composite), cells type to be used (autologous ECs and SMCs from vessel biopsies or allogenic MSCs) and the method of cell suspension application (static or dynamic) to the scaffold's surface. For decellularized tubular scaffolds dynamic seeding may not be feasible since one should consider small (10-25 μm in mean diameter) pores throughout decellularized scaffold thickness and high hydrodynamic resistance of decellularized as well as native tissue[1,2]. These circumstances significantly hinders cells distribution and proliferation within the decellularized matrix in comparison with highporous synthetic scaffold. On the hand, static seeding approach for decellularized scaffolds is often criticized since its low efficiency and reproducibility[1], but some ways to improve static seeding outcomes can be suggested. For example scaffold can be coated with biocompatible polymer (fibrin, collagen etc.) or rotational culture can be used to improve cell distribution and nutrition. Hence static scaffold seeding need to be modified to obtain decellularized scaffolds with seeded cells.

Aim: to improve the outcomes of static seeding for decellularized vascular scaffolds by embedding cell suspension in fibrin glue or coating whole scaffold surface with collagen I.

Experimental Methods

Decellularized vascular scaffolds (n=2) were obtained by perfusion with enzymatic (0.2 mg/ml of DNase I and 0.04 mg/ml of RNase), hypo-and hypertonic salt solutions in a customized tubular glass chamber placed in a flow bioreactor. Decellularization quality was evaluated by histological studies of deparaffinized and rehydrated tissue sections, immunohistochemical (IHC) reactions with primary antibodies to type I collagen and collagen IV of basal membranes. Additionally, removal of nuclear remnants and chromatin was assessed by staining of frozen tissue sections. Afterwards scaffolds were thoroughly rinsed with PBS and 0,5% antibiotic – antimycotic solution at 37^0C to remove residual traces of detergents.

The internal volume of the scaffolds was calculated as 800 μl, while scaffolds surface was 6,28 cm^2. Both the scaffolds were seeded and cultured in the same manner, except for coating. For the first one, the cell suspension of umbilical cord hMSCs ($0,7*10^6$ cells/800 μl) was divided into two parts: one was pre - mixed with human thrombin in 4:1 ratio and injected into the lumen of the scaffold, and right after the scaffold's volume was adjusted to 800 μl by fibrinogen. Second part of suspension was injected into formed fibrin glue. In contast, the second scaffold was coated with collagen I solution by immersion (500 mkg/ml) and statically seeded with umbilical hMSCs suspension of the same density. Tnen each scaffold was placed into a Petri dish filled with full MesenCult medium and transferred to a CO_2 incubator at $+37^0$C, 5%CO_2 for 1 hour. Further the scaffolds were introduced into customized rotated tubular chamber by means of two sliding cannulas built into the chamber walls. Seeded scaffolds along with the chamber rotated around the longitudinal axis for 6 hours at 10 rpm/min. The culture was continued for 7 days without rotation

but with medium perfusion around scaffolds walls, The medium was replaced every 48 hours. At days 2,3,4,5 a small outer fragments were removed from both scaffolds for staining with DAPI to evaluate cell migration and distribution within fibrin glue.
At day 8 both scaffolds were analyzed for cellularity by hematoxylin - eosin staining and IHC for Ki67 expressioin.

Results and Discussion

The obtained decellularized scaffolds were characterized by the absence of visible nuclei in hematoxylin – eosin stained specimens as well as slightly homogenized elastic fibers. On the other hand in DAPI stained preparations some residual chromatin were observable but estimated genomic DNA quantity were 40 ng/mg of dried tissue slice. The IHC reaction for collagen I and IV was observed for both the scaffolds suggesting that both the scaffolds retained their ECM. Rotation with a small number of revolutions led to a uniform deposition of cells on the inner surface of both scaffolds. Seeding of MSCs into the collagen – coated scaffold was less effective compared with embedding cells in fibrin glue that was confirmed by IHC with primary antihuman antibodies to Ki67, as well as immunofluorescence with DAPI.

Conclusion

We suggested approach to improve the poor outcomes of static cell seeding of decellularized scaffolds by mean of embedding cell suspension in fibrin glue and subsequent dynamic culture of obtained decellularized scaffold – fibrin seeded composite. This approach is attractive for potential clinical use since thrombin and fibrinogen could be easily obtained from autologous plasma.

References

[1]Villalona GA, Udelsman B, Duncan DR, et al. Cell-seeding techniques in vascular tissue engineering. *Tissue Eng Part B Rev*. 2010;16(3):341–350.
[2]Porzionato A, Stocco E, Barbon S, Grandi F, Macchi V, De Caro R. Tissue-Engineered Grafts from Human Decellularized Extracellular Matrices: A Systematic Review and Future Perspectives. *Int J Mol Sci*. 2018;19(12):4117.

PS1-12-194

A Biomimetic Approach for Small Diameter Vessels: Bilayered Vascular Grafts Made of Alginate and PCL

Seda Gurdap, Nazende N. Aksit, Ismail A. Isoglu, Sevil Dincer Isoglu

Abdullah Gul, Bioengineering, Kayseri, TR

Introduction

Cardiovascular diseases still remain one of the leading causes of mortality and morbidity across the world. Current surgical interventions applied in treatment of cardiovascular diseases comprise angioplasty, stent usage and bypass grafts. Autologous grafts, allografts, xenografts and artificial grafts have been widely used in bypass grafting of diseased native blood vessels Synthetic grafts are used successfully in large diameter vessels (>6 mm) because of higher flow that washes the inner layer of vessels and prevention of the accumulation of blood components (platelets, proteins, etc.) that forms occlusion. However, these grafts are not convenient for small diameter bypassing because of immune system concerns triggered by thrombus, neointimal hyperplasia or plaque formation. Although natural grafts can be thought as best option for treatment of small diameter vessels problems, lack of tissue donors limits the usage of autografts and allografts. Similarly, xenografts are not preferred because of immunological concerns. (1,2) Using tissue engineering to fabricate vascular scaffold can be a good alternative comparing to the existing ones as a treatment method. In this strategy, different methods such as freeze drying, solvent casting, 3D printing, thermally induced phase separation and electrospinning can be utilized for scaffold preparation. Embryonic stem cells, induced pluripotent stem cells or patient-derived autologous cells can also be incorporated to the scaffold structure. To improve blood compatibility and enhance endothelization process, scaffold can be modified with heparin or VEGF. (3,4)

Here, we suggested a bilayered vascular graft composed of alginate and polycaprolactone with different texture and morphology. By this way, we tried to mimic mechanical and structural features of the natural blood vessels. We have applied thermally induced phase separation (TIPS) and electrospinning for the preparation of the layered scaffold structure.

Experimental Methods

First, we produced inner layer of the scaffold by thermally induced phase separation of alginate. To do this, alginate solution was poured into a cylindrical mold and the mold was placed at -20°C. Tubular scaffold was removed from mold after thawing and ethanol was used for the extraction process. Following this, the scaffold was washed with distilled water and dried by lyophilization. For the outer layer,PCl dissolved in methanol/chloroform solvent mixture was electrospun onto the cylindrical alginate scaffold. Products were characterized by morphologically and structurally via SEM and FTIR techniques. They were also characterized mechanically by tensile testing measurement. As an in vitro test, MTT assay was performed for the cytotoxicity of the materials towards HUVECs. Scaffold were investigated in terms of degradation in stimulated body fluids for about 6 weeks.

Results and Discussion

In this work, hybrid vascular grafts were developed using TIPS and electrospinning as a bilayered scaffold for vascular tissue engineering. According to the SEM analyses, inner layer possessed an interconnected porous structure supporting endothelial cell attachment, while homogeneous nanofibers made of PCL were obtained as outer

layer. The hybrid scaffold showed comparable mechanical strength with the native vessel. Minimum toxicity was observed towards endothelial cells according to the MTT assay results. It was also shown that these scaffolds allowed cell attachment and proliferation which will help the further endothelization process.

Conclusion

In this study, bilayered vascular scaffolds were prepared successfully via TIPS and electrospinning for use in small diameter vessel graft applications. They showed better endothelial cell attachment and mechanical characteristics. Therefore, the obtained products have a great potential to be used as a scaffold for vascular tissue engineering for long term applications.

Acknowledgement

1. Norouzi, S. K., & Shamloo, A. (2019). Bilayered heparinized vascular graft fabricated by combining electrospinning and freeze drying methods. *Materials Science and Engineering: C*, *94*, 1067-1076.
2. Song, H. H. G., Rumma, R. T., Ozaki, C. K., Edelman, E. R., & Chen, C. S. (2018). Vascular tissue engineering: progress, challenges, and clinical promise. *Cell stem cell*, *22*(3), 340-354.
3. Hasan, A., Memic, A., Annabi, N., Hossain, M., Paul, A., Dokmeci, M. R., ... & Khademhosseini, A. (2014). Electrospun scaffolds for tissue engineering of vascular grafts. *Acta biomaterialia*, *10*(1), 11-25.
4. Goins, A., Webb, A. R., & Allen, J. B. (2018). Multi-layer approaches to scaffold-based small diameter vessel engineering: A review. *Materials Science and Engineering: C*.

PS1-12-195

Polyphenol-assisted Construction of Multifunctional Superhydrophilic Coating for Cardiovascular Stent Modification

Rifang Luo, Linhua Li, Yunbing Wang

Sichuan University, National Engineering Research Center for Biomaterials, Chengdu, CN

Introduction

The prevalence and mortality of cardiovascular diseases(**CVD)** continue to increase, accounting for more than 40% of the population's disease deaths.Although drug-eluting stents have been used in clinical practice, drug-eluting stents have problems with late thrombosis and late restenosis, which could threaten the life of patients.Therefore, it is of great significance to develop a stent coating which has excellent antithrombotic effect and regulates the remodeling of neovascularization.Based on the nonspecific adhesion of proteins during the start-up phase of material / blood contact, a novel superhydrophilic coating was constructed to selectively regulate the growth of endothelial cells and smooth muscle cells. Meanwhile the comprehensive performance in cardiovascular stent environment was studied systematically.

Experimental Methods

Multifunctional superhydrophilic coating was deposited on substrates by polyphenol polymerization. The wettability of coating was tested by contact angle equipment. FITC-BSA and FITC-labelled Human Fg adsorption experiment was used to detected the anti-fouling property of the polyphenol coating. Meanwhile, the biocompatibility of the coating on blood cells and vascular cells was studied by cell tests.Finally, the antirestenosis of the coating was confirmed by in vivo implantation of stainless steel stents.

Results and Discussion

The main data were shown in Figure A. The result of water contact angle shows that the contact angle of coating is less than 5 °, so the coating has superhydrophilicity. Once the superhydrophilicity material was implanted, the water film formed on the surface, which can effectively impedance the adhesion of nonspecific proteins[1]. The result of protein adsorption showed that the polyphenol superhydrophilic coating could effectively resist the nonspecific adhesion of the protein. From the results of dynamic whole blood and macrophage adhesion we found that the polyphenol superhydrophilic coating could significantly inhibit the adhesion and activation of blood cells and macrophages (MA). Through the culture of vascular cells, it was found that the superhydrophilic coating could effectively inhibit the adhesion and proliferation of smooth muscle cells (SMC), and it was friendly to endothelial cells (EC).The coating was deposited on the surface of the stent and implanted into the abdominal aorta of the **New Zealand white rabbits (3~3.5 kg)** for 1 month. Compared with the control group, the coating could signiTheficantly inhibit the restenosis of the stent.

Conclusion

Therefore, the polyphenol superhydrophilic coating has excellent anti-protein nonspecific adhesion, anticoagulation, anti-inflammation, promoting endothelium and inhibiting stent restenosis.

References

[1] J Wilson C J , Clegg R E , et al. Tissue Engineering, 2005, 11(1-2):1-18.

Acknowledgement

The author would like to thank the National Key Research and Development Program (2016YFC1102200), the National Natural Science Foundation of China (No. 51703144), and the 111 Project (The Program of Introducing Talents of Discipline to Universities (B16033))

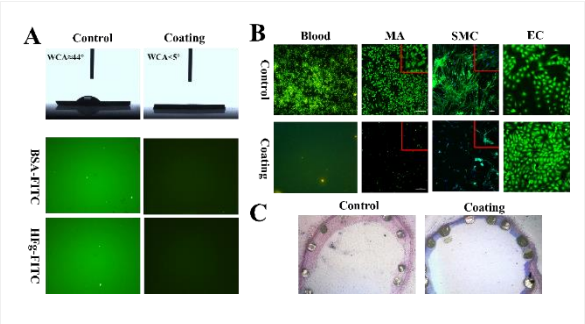

Figure 1.
(A) water contact angle and protein adsorption of coating; (B) the cytocompatibility of superhydrophilic coating; (C) 316l bare stent and polyphenol coated stent implanted for 1 month

2:45 p.m. – 3:45 p.m.

Hall 1 / Exhibition Area

PS1-13 | Biocompatibility and degradation

PS1-13-196

Biocompatibility and cell culture study on electrospun PVB patches for skin treatment

Zuzanna Krysiak, Urszula Stachewicz

Akademia Górniczo Hutnicza, International Center of Electron Microscopy for Material Science, Faculty of Metals Engineering and Industrial Computer Science, Cracow, PL

Introduction

Atopic dermatitis is a skin disease affecting people all over the word independently from the age. Transepidermal water loss, dry skin and pruritus are characteristic symptoms of eczema. Moisturizers and textile - based therapy are often used as non-invasive treatment [1,2]. The nanofiber - based patches can be produced via electrospinning to generate highly porous mats applicable for skin treatment [3]. Among many polymers used poly(vinyl butyral-co-vinyl alcohol-co-vinyl acetate) (PVB), which has good elasticity and optical transparency, was not investigated for medical applications in the form of electrospun fibers. Therefore, the goal of this study was electrospinning of PVB and verifying the biocompatibility of PVB fibers with fibroblasts for further application in skin treatment.

Experimental Methods

Materials

PVB (M_w 70,000-100,000 and M_w 170,000-250,000, Sigma Aldrich, UK) was dissolved in methanol, N,N-dimethyloformamide (DMF) and dimethyl sulfoxide (DMSO) mixed in ratio 5:4:1 to the final concentration of 10%. Fibers were electrospun (IME Technologies, The Netherlands) with controlled T = 25 °C and H = 40 %. High voltage was applied at 16-18 kV to the stainless steel needle with the inner diameter of 0.8 mm, set at the 15 cm to the collecting electrode. Flow rate of polymer solution was 2.0 $ml \cdot h^{-1}$.

Characterization of electrospun fibers

The fibers morphology was analyzed with scanning electron microscope (SEM), after samples were spotted with gold. Fiber diameter was measured using imageJ software (version 1.51 s, USA) and the average value was calculated from the 100 measurements on SEM images. Contact angle on electrospun PVB fibers was measured with deionized water. Pictures of water droplets were taken with Canon EOS 700D camera with EF-S 60 mm f/2.8 Macro USM zoom lens, after 3 seconds from placing the 3 µl droplets on the mats. The contact angle was measured using MB-Ruler (version 5.3, Germany) and the mean value of contact angle was calculated as average from 10 droplets.

Cell culture

Cells (NIH 3T3 murine cell line) were seeded on sterilized (UV light) PVB scaffolds at concentration 2×10^4 cells per sample and incubated at 37 °C, atmosphere with a concentration of 5% CO2 and approximately H = 90%. Cell proliferation and cytotoxicity tests (Alamar Blue, Thermo Fisher Scientific, USA; LDH, Roche Diagnostic GmbH, USA) were performed. Cell morphology was analyzed using SEM.

Results and Discussion

PVB fibers obtained during electrospinning were smooth and without beads as shown in Fig.1. Fiber diameter increased with the molecular weight of PVB, from 335 nm to 1 µm. Analysis of contact angle showed hydrophobic

character of the PVB mats. LDH assay confirmed no cytotoxic effect of PVB on NIH 3T3 cells after 3 days of incubation. Additionally, cell proliferation within 7 days was proved by viability.

Conclusion

PVB fibers were successfully obtained during electrospinning process. Fiber diameter was controlled via molecular weight of polymer, that further affected the wetting properties of produced PVB mats. The LDH and proliferation study confirmed the biocompatibility of mats showing the possibility to use the electrospun PVB patches in skin treatments.

References

[1] M. H. Meckfessel, S. Brandt, J Am Acad Dermatol. 2014 (71) 1, 177-184.

[2] W. Wang, P. C. L. Hui, and Chi-Wai Kan, Coatings, 2017 (7) 82.

[3] U. Stachewicz, P. K.Szewczyk, A. Kruk, A. H.Barber, A. Czyrska-Filemonowicz, Materials Science and Engineering: C, 2019 (95), 397-408.

Acknowledgement

This research was part of "Nanofiber-based sponges for atopic skin treatment" project is carried out within the First TEAM programme of the Foundation for Polish Science co-financed by the European Union under the European Regional Development Fund, project no POIR.04.04.00-00- 4571/18-00.

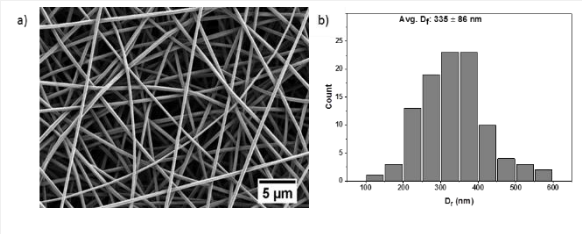

Fig.1 Fiber diameter analysis of electrospun PVB fibers with Mw= 70,000-100,000
a) SEM micrograph b) fiber diameter histogram with the average D_f=335 ±86 nm.

PS1-13-197

IN VITRO TOXICITY EVALUATION OF GRAPHENE OXIDE- GELATIN AEROGELS ON HUMAN DERMAL FIBROBLASTS CELLS

Jessica Borges Vilches[1], Toribio A. Figueroa Aguilar[1], Sebastian I. Guajardo de Celis[1], Claudio Aguayo Tapia[2], Katherina F. Fernández Elgueta[1]

[1]University of Concepcion, Laboratory of Biomaterials, Department of Chemical Engineering, Faculty of Engineering, Concepcion, CL; [2]University of Concepcion, Department of Pharmacy, Faculty of Pharmacy., Concepcion, CL

Introduction

Graphene oxide (GO) is a material that presents biological, chemical, physical and mechanical properties [1] that endorse its application in the biomedical area, and it can be used as a loading platform to load small molecules such as antibodies andproteins. Also, an application of this material is its capacity to be covalently functionalized with biocompatible and biodegradable polymers as the gelatin, to develop tridimensional structures such as aerogels, which are colloidal materials similar to gels where the liquid component is changed by gas [2]. On the other hand, the presence of GO in these aerogels can induce obvious effects of cytotoxicity, which is dependent on their concentration and surface chemistry [3] . Thus, it is necessary to determinate the citoxicity of these materials. In this work, OG-G aerogels were synthesized with the aim to evaluate their *in vitro* cytotoxicity in cellular models of human dermal fibroblast.

Experimental Methods

The synthesis of the GO-G aerogels was carried out at different pH conditions and GO-G ratio [1] by reaction assisted microwave at conditions of 30 minutes and power 800 W. The reaction temperature was controlled in all the experiments, since the gelatin can be denatured by temperature changes [4]. The synthesized aerogels were evaluated by *in vitro* cytotoxicity assays in cellular models of human dermal fibroblast. These cells were cultured in essential minimal medium at different doses and added into 96-well plates (dose up to 110 µg aerogel/mL medium culture). After 24 hours of incubation at 37°C, cell viability (v.c) was determined by a test kit and evaluated based in the relation between the absorbance test and the control absorbance, according to the equation:v.c=100*absorbance test / absorbance control [5]. These determinations were repeated three times in all experiments.

Results and Discussion

The chemical modifications induced by covalent functionalization between GO-G and the exposure to heat treatment produced variations in physicochemical properties of the aerogels synthesized, such as the pore size, volume pore and surface charge; according to the reaction conditions used. These modifications were evaluated based on the toxicity level of these materials. In this case, the cytotoxicity assays in the synthesized aerogels reported cell viability values greater at 85% in all materials, demonstrating that they are not cytotoxic, independently of the conditions in which were synthesized.

Conclusion

It was possible to develop aerogels based on GO-G by reactions assisted microwave in short reaction time at different synthesis conditions, where the resultant materials shown to be non-toxic at GO doses analyzed, which supports their possible use in the biomedical area.

References

[1] Chen, G., Qiao, C., Wang, Y & Yao, J., *Australian Journal of Chemistry*, 2014, 67(10), 1532-1537.

[2] Ma, Y & Chen, Y., *National Science Review*, 2015, 2, 40-53.

[3] Zhang, B., Wang, Y & Zhai, G., *Mater. Sci. Eng. C- Mater. Biol. Appl*., 2016, 61, 953–964.

[4] Hoque, Md., Benjakul, S & Prodpran, T., *Journal of Food Engineering*, 2010, 96(1), 66-73.

[5] Quan, K., Li, G., Yuan, Q & Wang X. *Colloids and Surfaces B: Biointerfaces*, 132, 2015, 27-33.

Acknowledgement

The authors thank Project FONDECYT Nº 1170681 for the financial support for this investigation.

PS1-13-198

In-vitro investigation of surface quality of 3D printed titanium plates with different surface roughness

Antje Petzold[1], Jakob Schneider[2], Andre Seidel[2], Elena Lopez[2], Kiriaki K. Papadopoulos[1], Ute Botzenhart[1]

[1]TU Dresden, Medical Faculty Carl Gustav Carus, Dresden, DE; [2]Fraunhofer Institute for Material and Beam Technology IWS, Dresden, DE; [3]TU Dresden, Centre for Translational Bone, Joint and Soft Tissue Research, Dresden, DE

Introduction

Within dentistry additive manufacturing is most often used to produce implants and dental prostheses. Besides saving material and generating complicated shapes, the biggest advantage is the high freedom of design, whereby implants can be adapted to patient's individual anatomy. In the context of a combined orthodontic-surgical treatment of patients with dento-skeletal deformities, titanium plates are widely used in different areas of application. In the current literature different surface roughness of fracture fixation plates are described to be advantageous for osteosynthesis, but a complete bony integration should be avoided as it can complicate removal. Roughness values of standard titanium osteosynthesis plates are usually in the range of Ra 0.4-0.8 µm. However, values <0.2 µm greatly facilitate their removal and are described as ideal. Inversely, at the soft tissue side of the plates cell adhesion is desired and thus roughness values of 0.2-2 µm are to be favoured.
In the present study, individual bone plates with different surface roughness have been generated by 3D printing and have been rated in-vitro regarding their surface quality. The aim of this study was to test whether the clinical approved material properties of titanium have been changed due to the manufacturing process compromising its clinical application.

Experimental Methods

As specimens 2 mm thick titanium discs with a diameter of 5 mm and 10 mm, respectively, were produced by selective laser melting (SLM). Different surface roughness was achieved by sandblasting followed by barrel finishing, electropolishing or a combination of the two later. For evaluation of the biocompatibility and cell adhesion specimens were incubated together with mouse fibroblasts L929, osteosarcoma cells Saos-2, human primary gingival fibroblast as well as human gingival epithelial cells. The biocompatibility was assessed by CytoTox-Glo™ Cytotoxicity Assay and CellTiter-Glo® Luminescent Cell Viability Assay (Promega). The morphology of the cells as well as their adhesion properties to the titanium discs were analysed by light and scanning electron microscopy.

Results and Discussion

After 3D printing of the titanium discs different surface roughness values within the effective roughness spectrum (Ra 0.2-2 µm) could be obtained by distinct finishing treatment. Six samples groups of different roughness were tested. Concerning the biocompatibility the different groups did not show any significant differences. However, a difference in cell adhesion could be observed.

Conclusion

Bone plates with different surface quality generated by 3D printing are suitable for clinical use and are in line with the requirements for medical devices according to ISO 10993-5.

References

Hayes, J.S. et al., Expert Rev Med Devices. 2010; 7(1):131-42

Hayes, J.S. et al., J Biomed Mater Res B Appl Biomater. 2018; 106(2):705-715

Acknowledgement

The authors would like to thank the Federal Ministry of Education and Research (BMBF) for providing financial support to this project as well as Professor Michael Gelinsky and the Centre for Translational Bone, Joint and Soft Tissue Research, TU Dresden, for providing their lab space.

PS1-13-199

Protein fouling on oxygenator membranes - timeline of initial blood plasma protein adsorption

Katharina Gerling[1], Pawel Majek[2], Christian Schlensak[1], Hans Peter Wendel[1], Sandra Stoppelkamp[1]

[1]University Hospital Tuebingen, 1Department of Thoracic, Cardiac and Vascular Surgery, Tuebingen, DE; [2]Institute of Hematology and Blood Transfusion, Department of Biochemistry, Prague, CZ

Introduction

Extracorporeal membrane oxygenation is crucial for treatment of acute or chronic lung diseases. In recent years, there have been many improvements in gas-exchange properties and haemocompatibility, but there is still no long-term solution available. The foreign body reaction of blood in contact with the membranes and tubes leads to activation of coagulation, complement system and inflammatory reactions. Competitive plasma protein adsorption within the first minutes mainly determines the reaction towards the material and thus the fate of the oxygenators. We therefore set out to investigate the time and flow dependent plasma protein adsorption on oxygenator membranes in order to find a long-term solution. With the use of the highly sophisticated bottom-up proteomics, analyses of more than 500 proteins at the same time are possible. This tool enables us to elucidate the complex time-dependent interaction of plasma proteins with oxygenator membranes.

Experimental Methods

Miniature oxygenator devices were built from PVC tubing and polycarbonate connectors. Hollow-fiber membranes (PMP, PET) were rolled to fit into the miniature devices. The circuit with tubings and miniature oxygenators were filled with human whole blood and blood was pumped (roller pumps) through the heated circuit for 1 min till up to 6 h. Afterwards, hemocompatibility parameters were investigated as well as the used oxygenator membranes washed, and proteins desorbed. The resulting protein solutions were digested and analyzed via Orbitrap mass spectrometry.

Results and Discussion

Protein adsorption started immediately after contact with blood. There were approximately 1600 proteins of interest detected in total. After comparison of the identified features those proteins were ordered as a dendogram tree. The formed clusters contained closely related protein complexes, proteins involved in the same pathways and had specific expression profiles over the time. One of the prominent biological processes was degranulation of platelets. The comparison between different membrane types is currently ongoing.

Conclusion

With the identification of the time-dependent plasma adsorption of proteins, we will be able to predict suitable protein layers in the equilibrium state that steer the reaction towards better hemocompatibility and lower coagulation activation. This will pave the way for the development of new coatings for oxygenator membranes to prevent oxygenator thrombosis and inflammatory reactions.

PS1-13-200

Extracellular matrix produced by human bone marrow-derived mesenchymal stem cells in chitosan/gelatin scaffolds

Fotis Papadogiannis[1], Aristea Batsali[2], **Maria Chatzinikolaidou**[1], Charalampos Pontikoglou[2]

[1]University of Crete, Department of Materials Science and Technology, Heraklion, GR; [2]University of Crete, Haemopoiesis Research Laboratory, Department of Haematology, School of Medicine, Heraklion, GR

Introduction

We have previously shown that 3D porous scaffolds comprising of 40:60% chitosan/gelatin (CS/Gel) crosslinked with 0.1% v/v glutaraldehyde, promote the survival, proliferation and osteogenic differentiation of human bone marrow mesenchymal stem cells (hBM-MSCs) [1]. The aim of this study is to evaluate the production and composition of extracellular matrix (ECM) derived from hBM-MSCs following osteogenic differentiation when cultured within CS/Gel scaffolds. The results were compared to hBM-MSC cultures in tissue culture polystyrene (TCPS) controls.

Experimental Methods

Human (h)BM-MSCs were isolated from BM aspirates of healthy donors (n=6) after informed consent. The cells were *ex vivo*expanded until passage (P)-2, phenotypically characterized by flow cytometry and differentiated towards adipocytes and osteoblasts. Differentiation was assessed by specific mRNA gene expression and immunostaining. P2 hBM-MSCs were seeded on CS/Gel scaffolds and induced towards osteoblasts. We then assessed (a) hBM-MSCs adhesion potential by scanning electron microscopy, (b) their osteogenic potential by mRNA expression of *RUNX-2*, *DLX-5*, *OSC*and *ALP*using real time-RT PCR, (c) the expression of ECM related genes using a PCR array and (d) the endogenous expression of osteopontin, osteocalcin and collagen type I A1 proteins using confocal laser fluorescence microscopy (CLFM).

Results and Discussion

hBM-MSCs were expanded successfully and fulfilled the minimal criteria for MSC definition (spindle-shape morphology, expression of CD90, CD105, CD29, CD73, lack of CD45, CD14, CD34 and ability to differentiate into adipocytes and osteocytes). Cultured hBM-MSCs on CS/Gel scaffolds showed strong adhesion potential and displayed increased osteogenic capacity as shown by the increased expression of *ALP*and *OSC*at days 7 and 14 compared to the TCPS cultures and the increased expression of *RUNX2*and *DLX5*time course during the differentiation. PCR array analysis showed differential expression of ECM-related genes between hBM-MSC cultures differentiated towards osteoblasts in CS/Gel scaffolds and TCPS controls. Specifically, we found increased *MMP1*, *MMP*3, *MMP*9-*13*, *MMP16*, and *VTN*and decreased *COL1A1COL5A1, SPP1, THBS1-2, TIMP1-3* mRNA expression in CS/Gel scaffolds compared to TCPS. CLFM images showed collagen type I A1 and osteopontin production in both CS/Gel scaffolds and TCPS; osteocalcin, as a late marker of osteogenic differentiation, was identified at low levels in both CS/Gel scaffold and TCPS.

Conclusion

We have evaluated for the first time the ECM production by hBM-MSCs cultured on 40:60% CS/Gel scaffolds providing additional evidence that this biomaterial supports osteogenesis. Our results present a promising strategy using hBM-MSCs within CS/Gel scaffolds for bone regeneration.

References

[1] Georgopoulou A, Papadogiannis F, Batsali A, Marakis I, Alpantaki K, Eliopoulos A, Pontikoglou C, Chatzinikolaidou M. (2018) Chitosan/gelatin scaffolds support bone regeneration, *J Mater Sci Mater in Medicine*29(5):59, DOI: 10.1007/s10856-018-6064-2

PS1-13-201

Useful series of positive control compounds for colony formation cytotoxicity test

Kazuo Isama, Nanami Katsuyama

Teikyo Heisei University, Faculty of Pharmaceutical Sciences, Tokyo, JP

Introduction

Relatively strong positive control compounds, such as zinc diethyldithiocarbamate (ZDEC), and zinc dibutyldithiocarbamate (ZDBC), are commonly used to test medical devices for in vitro cytotoxicity. However, they are not suitable for testing relatively weak cytotoxic compounds. Thus, we established a new series of positive control compounds that can be used to classify a wide range of cytotoxic compounds. The cytotoxicity of acrylate/methacrylates, phosphite triesters, phosphate triesters, 4-hydroxybenzoates, used in medical devices and healthcare products, were evaluated using the series.

Experimental Methods

A series of positive control compounds, comprising 1,3-Diethyl-2-thiourea (DETU), 1,3-dibutyl-2-thiourea (DBTU), ZDEC, and ZDBC, was used to evaluate the cytotoxicity of seven acrylate/methacrylates, seven phosphite triesters, six phosphate triesters, seven 4-hydroxybenzoates, and 4-hydroxybenzoic acid, using a colony formation assay. The assay was conducted using V79 Chinese hamster lung fibroblasts (JCRB 0603) that were maintained in Eagle's minimal essential medium, which was supplemented with 10% fetal bovine serum in a CO_2 incubator (37°C). Forty to fifty V79 cells were seeded into 24-well plates and maintained in culture for 24 h to start growing in a logarithmic phase. They were then exposed to the positive control compounds and test compounds over a range of concentrations. They were incubated for six days to make colonies large enough to count. Colonies were fixed with 10% (v/v) formaldehyde solution, stained with 4% (v/v) Giemsa solution, and counted. The cytotoxic potential of each compound was expressed as the concentration at which the relative plating efficiency was reduced to 50% (IC_{50}). The IC_{50} values for the tested compounds were then compared to those calculated for the four positive control compounds.

Results and Discussion

The IC_{50} values of four positive control compounds were distributed in the order of 10^{-1} to 10^{2} µg/mL (Fig. 1), and were used to classify the cytotoxicity of test compounds as ‘Very Severe’, ‘Severe’, ‘Moderate’, ‘Mild’, or ‘None/Slight’. Specifically, the cytotoxicity of two phosphite triesters, five phosphate triesters, and four 4-hydroxybenzoates was found to be Moderate, whereas that of three phosphite triesters, one phosphate triester, and three 4-hydroxybenzoates was shown to be Mild. The remaining two phosphite triesters, and 4-hydroxybenzoic acid were classified as incurring None/Slight cytotoxicity. Thus, the analyzed positive control series was successfully employed to classify the cytotoxicity of a wide range of compounds into five groups.

Conclusion

Our series of positive control compounds was useful for classification of cytotoxicity of a wide range of compounds.

References

ISO 10993-5:2009, Biological evaluation of medical devices -- Part 5: Tests for *in vitro* cytotoxicity.

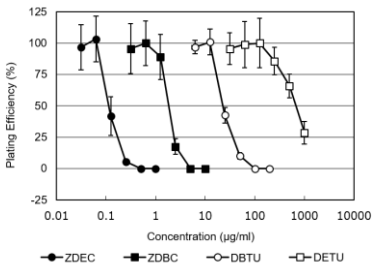

Fig. 1. Plating efficiencies of four positive control compounds.
Forty to fifty V79 cells were seeded into 24-well plates and maintained in culture for 24 h. They were then exposed to DETU, DBTU, ZDEC, and ZDBC, and incubated for six days. Colonies were fixed with 10% (v/v) formaldehyde solution, stained with 4% (v/v) Giemsa solution, and counted.

PS1-13-202

Polyphosphates as an alternative for growth factors: Improving biocompatibility of hybrid nanocomposites for lateral lumbar spinal fusion

Jana Dorazilová[1], Michala Rampichová[2], Věra Lukášová[2], Radek Sedláček[2], Tomáš Suchý[2], Jana Brtníková[1], Martin Trunec[1], Přemysl Šťastný[1], Milan Krtička[3], Eduard Göpferd[4], Martin Faldyna[4], Veronika Štěpánková[5], Lucy Vojtová[1]

[1]Brno University of Technology, Central European Institute of Technology, Research groups of Advanced Materials, Brno, CZ; [2]Czech Technical University in Prague, Mechanical Testing Laboratory and Laboratory of Advanced Biomaterials, Prague, CZ; [3]University Hospital Brno, Brno, CZ; [4]Veterinary Research Institute, Brno, CZ; [5]Enantis Ltd, Brno, CZ

Introduction

Cell adhesion or proliferation as well as the biocompatibility of the nanocomposites is usually boosted by the addition of signalling molecules, e.g. growth factors.[1,2] Despite the beneficial properties of growth factors, practical applications are limited due to their high price and low stability both *in vitro* and *in vivo*. Biogenic polyphosphate (PolyP), naturally occurring linear polymer commonly accumulated in bone cells (stimulating the bone regeneration by appropriate activation of osteoblasts) could be used as an inexpensive alternative to biomolecular signalling molecules in bone regeneration.[3] In this work, the effectivity of PolyPs and basic fibroblast growth factors (FGF-2s) in promoting the integration of porous hybrid ceramic/biopolymeric nanocomposite with the intended use in lateral lumbar spinal fusion was compared.

Experimental Methods

Hybrid nanocomposite was composed of two phases – ceramic and biopolymeric. The porous ceramic core of the nanocomposite was prepared by direct foaming of polymerizable ceramic suspension followed by sintering. The ceramic core was further modified by a biopolymeric mixture of protein and polysaccharides creating 3D porous sponge-like coating. Bioactivity of both FGF-2s-coated and PolyPs-coated nanohybrid composites was evaluated both *in vitro* on human mesenchymal stem cells or *in vivo* on Large White Pig animal model.

Results and Discussion

Morphology analysis using scanning microscopy (SEM) and biodegradation studies revealed information in understanding the bioactive role of PolyPs in prepared nanocomposite. *In vitro* testing showed a positive effect of both PolyPs and FGF-2s on cellular adhesion and proliferation compared to nonmodified materials. Compared to bone autograft, nanocomposites with bioactive additives accomplished excellent spinal fusion with higher resistance to stress during dynamic mechanical testing.

Conclusion

Positive effect of both bioactive substances on the increase of the material's biocompatibility was observed. Therefore, PolyPs could be used as an easily obtainable substituent or complement to growth factors in bone regeneration applications.

References

[1] KHORSAND, Behnoush, *et al*. *Journal of Controlled Release*. 2017, **248**, 53-59.

[2] COFFIN, J. Douglas, *et al*. *Journal of the Endocrine Society*. 2018, **2**(7), 657-671.

[3] COMEAU, A. Patricia, *et al*. *Journal of Biomaterials Applications*. 2011, **27**(3), 267-275.

Acknowledgement

This work was supported by the CEITEC 2020 (LQ1601) with financial support from the Ministry of Education, Youth and Sports of the Czech Republic under the National Sustainability Programme II and by the Czech Health Research Council under the project no. MZ 17-31276A.

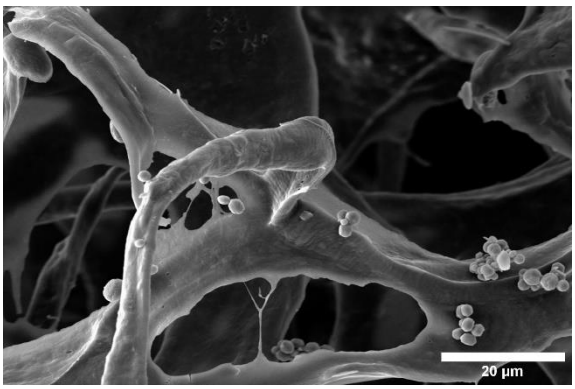

Polyphosphate microspheres on biopolymeric fibre
SEM image displaying biopolymeric fibres coated with PolyP microspheres. The microspheres adhered without the need of fixation.

PS1-13-203

Biocompatibility study of implantable device for therapeutic delivery sterilized by ethylene oxide

Bozena Rokita, Agnieszka Adamus-Wlodarczyk, Alicja K. Olejnik, Radoslaw Wach

Lodz University of Technology, Chemistry Department/Institute of Applied Radiation Chemistry, Lodz, PL

Introduction

The aim of the study was to evaluate biocompatibility by in vitro methods of a bio-electronic implant intended for therapeutics delivery secreted by confined genetically engineered cells upon stimulation by light.[1,2] The implant was sterilized by ethylene oxide, therefore biocompatibility assessment is a part of validation of materials and components, including electronics towards following in vivo functionality testing.

Experimental Methods

Knowing the properties of polymeric materials comprising the implant, the complexity of its design and the presence of sensitive components and subsystems (Fig. 1), the ethylene oxide method was selected and applied for its sterilization. In order to evaluate the biocompatibility of the components and the entire implant against human fibroblast cells (PCS-201-012™ ATCC) in vitro test recommended by the ISO 10993 – as for 'permanent implant contacting with tissue' – were carried out using XTT test, Live/Dead Viability Cytotoxicity method, 2D-DIGE electrophoresis following changes in the proteome of the cells, and alternatively with irritation assay using alive skin cells model ex vivo.

Results and Discussion

Sterilization with ethylene oxide (EO) is often used for polymers and combined materials. Because this method does not require temperature rise and can be applied to optics and electronics, it has been chosen for the optogenetic implant. The biocompatibility of the main materials after processing, and the subcomponents after manufacturing that are included in the device, and the whole implant were examined by several in vitro methods. The cytotoxicity and viability showed not toxic effects towards fibroblast. The test to evaluate changes in cells proteome and the potential irritation effects are ongoing.

Conclusion

The biocompatibility tests results will verify whether the materials and components comprising the complex bioelectronic device for therapeutic purposes, combined with the method of ethylene oxide sterilization, are safe and can be apply in animal trials and in further clinical studies.

References

[1]F. Michel, M. Folcher, *Porto Biomed. J.*, 2, 145 (2017).

[2]V. Pierroz, M, Folcher, *J. Mol. Gen. Med.*, 2, 1:10 (2018).

Acknowledgement

This work has received funding from the European Union's H2020 research and innovation programme under grant agreement No 720694, 'Optogenerapy'. Cooperation with dr. M. Folcher of ETH Zurich Switzerland is acknowledged.

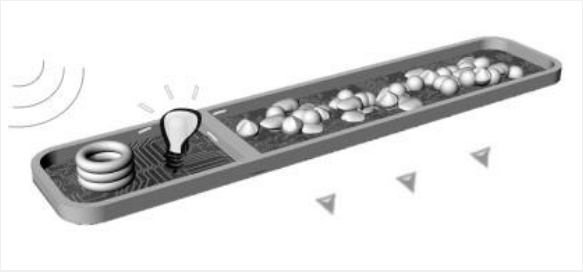

Fig 1. A concept of wireless-powered cell-based implant for therapeutic delivery 1.

PS1-13-204

Resorbable films from lauroyl derivatives of hyaluronan as temporary implants

Jiří Mrázek[1], Josef Chmelař[1], Martina Hermannová[1], Lukáš Kubala[2], Kristina Nešporová[1], Ludmila Grusová[1], Tomáš Drmota[1]

[1]Contipro a.s., Dolní Dobrouč, CZ; [2]Czech Academy of Sciences, Institute of Biophysics, Brno, CZ

Introduction

Biopolymers such as hyaluronan (HA) present advantageous starting points for developing novel materials for medicine. Since natural HA is highly soluble, chemical modification is required to produce solid forms suitable for implants. We prepared insoluble free-standing films from hyaluronan by introducing hydrophobic side groups that formed non-covalent crosslinks. The films were homogeneous and sufficiently strong yet flexible even when wet. We evaluated safety and biodegradability of the films both *in-vitro* and *in-vivo* in mice.

Experimental Methods

Free-standing films from lauroyl HA [1] were prepared by solution casting from diluted water-alcohol solution in a custom-built drying cell at 50 °C. Film thickness, dry mass, content of residual organic solvent, mechanical properties, swelling and enzymatic degradation were measured. We further compared material properties before and after sterilisation with ethylenoxide. *In-vitro* cytotoxicity was examined on 3T3 cells. Film samples (15 × 15 mm) were then implanted into abdominal cavity of C57Bl/6J mice to evaluate their safety and biodegradability (five animals per group).

Results and Discussion

The prepared lauroyl HA films (Fig. 1) were non-porous, with thickness deviations lower than 20 % (for a 16 µm thick film). Flexibility of the film enabled easy manipulation and repeated folding without cracking. Film swelling ratio in phosphate buffer and enzymatic degradation rate could be tuned by the degree of lauroyl substitution (DS) in a wide range (Fig. 2). Extracts of the films were not cytotoxic for 3TC cells. None of the mice showed signs of complications caused by material implantation and macroscopic evaluation of the peritoneum did not reveal any organ changes or other adverse effects. After 10 days, the films with lowest tested DS (11.8 %) were completely degraded *in-vivo*. After the longest implantation time of 28 days, the films with DS ≤ 31.7 % were completely degraded, while for DS = 39.3 %, gel-like film residua were still present in all 5 animals.

Conclusion

We prepared free-standing films from lauroyl derivatives of hyaluronan by a simple one-step solution casting method, without using any crosslinking agents, activators, plasticizers or toxic solvents. The films are homogeneous, mechanically strong and flexible. Their properties, such as swelling and degradation rate, can be tailored by the degree of hyaluronan substitution. Importantly, the film properties do not change dramatically upon sterilization by ethylenoxide. The safety and biodegradability of the films were verified *in-vitro* and *in-vivo* on mice, with good agreement of the *in-vitro* and *in-vivo* data. These results suggest that the lauroyl HA films are suitable for applications in medicine, e.g., as resorbable implants.

References

[1] D. Šmejkalová, M. Hermannová, R. Šuláková, A. Průšová, J. Kučerík, V. Velebný, *Carbohyd. Polym.***2012**, *87*, 1460.

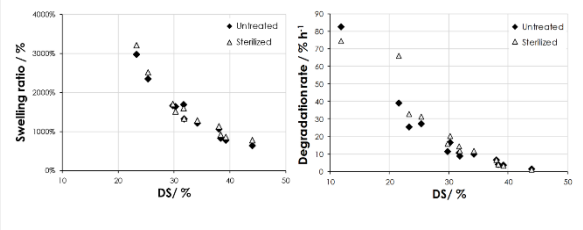

Fig. 2. Film swelling and degradation. Film swelling in phosphate buffer and film degradation rate (*in-vitro* enzymatic assay) as functions of lauroyl degree of substitution (DS).

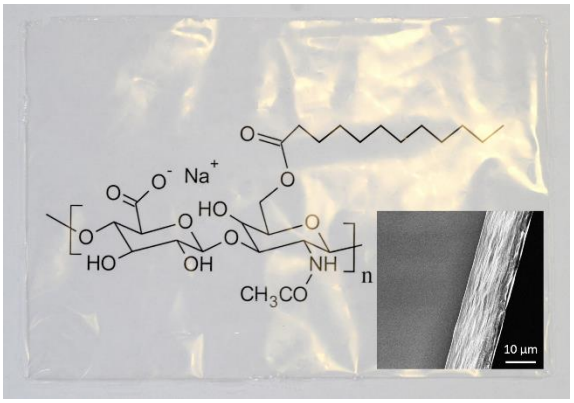

Fig. 1. Lauroyl-hyaluronan film. Free-standing lauroyl-HA film (11x16 cm, thickness 16 µm) with the chemical formula of the material seen through the film. Inset: Scanning electron microscope image of film cross-section.

PS1-13-205

In vivo degradation and biocompatibility of injectable non-covalent starPEG-based hydrogels

Rebecca Rothe[1,2], Sandra Hauser[1], Yong Xu[3], Alvin K. Thomas[3], Yixin Zhang[3], Jens Pietzsch[1,2]

[1]Helmholtz-Zentrum Dresden-Rossendorf, Institute of Radiopharmaceutical Cancer Research, Department of Radiopharmaceutical and Chemical Biology, Dresden, DE; [2]Technische Universität Dresden, Faculty of Chemistry and Food Chemistry, Dresden, DE; [3]BCUBE - Center for Molecular and Cellular Bioengineering; Technische Universität Dresden, Dresden, DE

Introduction

Undesired host tissue-material interactions like an adverse foreign body response, acute inflammation and fibrotic encapsulation often result after implantation of biomaterials. For clinical applications, biomaterials have to be highly biocompatible. Thus, attenuation of the above-mentioned obstacles and desired functionality of biomaterials regarding drug release or management of cell performance can be ensured.

Objectives

Focus of the study is on the relation between structural features of injectable starPEG-based hydrogels and evoked biological effects. In particular, inflammatory and angiogenic processes in material-surrounding tissue were objects of examination.

Experimental Methods

Four different physical hydrogels were examined regarding their degradation profiles and cellular responses at host tissue-material interface. Lead structure concept is based upon an repetitive lysin-alanine ($(KA)_5$) peptide sequence, starPEG and the oligosaccharide dextran sulfate ($(KA)_5$-DS). Further, modified hydrogels containing either an additional matrix metalloproteinase (MMP) cleavage site ($(KA)_5$-MMP*iw*-DS) or other variations in the peptide sequence and oligosaccharide like a D-amino acid motif ($(ka)_5$-DS) and sulfated hyaluronic acid ($(KA)_5$-sHA) were examined. Hydrogels were subcutaneously injected (50 µl) in immunocompetent nude SKH1-Elite mice. Magnetic resonance imaging (MRI) was used to analyze hydrogel degradation and inguinal lymph node size, indicating inflammatory reactions. *In vivo* activation of MMPs around injected hydrogels was followed by a specific fluorescence probe (MMPSense 645) and optical imaging during initial investigation period. Additionally, immunohistochemical stainings of typical angiogenesis (VEGF, CD31) and inflammation (COX-2, CD68) markers on cryosectioned tissue preparations were used to determine biocompatibility of analyzed hydrogels. Quantification of immunohistochemistry was performed with Fiji ImageJ software utilizing the color threshold plugin.

Results and Discussion

Comparing all four investigated starPEG-based hydrogels, $(KA)_5$-sHA hydrogel displayed fastest degradation *in vivo*. $(KA)_5$-DS and $(KA)_5$-MMP*iw*-DS hydrogels were gradually slower degraded during study period of 85 days. In contrast, volume of $(ka)_5$-DS hydrogel remained unchanged (Fig. 1). Further, inguinal lymph node sizes of all animals, independently of injected hydrogel composition, were comparable to the untreated control group suggesting a suitable biocompatibility. $(KA)_5$-sHA hydrogel induced significantly raised MMP activation during investigation period (Fig. 2). In addition, immunohistochemistry displayed raised VEGF expression around $(KA)_5$-sHA hydrogel as well

as macrophage invasion into all hydrogels. Surrounding tissues displayed also basal expression of inflammation and angiogenesis markers, like COX-2 or CD31.

Conclusion

Definite degradation profiles depending on structural composition of the investigated injectable starPEG-based hydrogels were demonstrated. According to lymph node measurements and immunohistochemical stainings, a normal biological, but not an adverse inflammatory response to these non-covalent hydrogels occurred in surrounding tissues. Particularly, one derivative, the $(KA)_5$-sHA hydrogel, displayed pro-angiogenic effects. This offers potential applications, e.g. in the field of tissue regeneration.

Acknowledgement

This work was supported by the China Scholarship Council and German Federal Ministry of Research and Education (BMBF grants 03Z2EN12 and 03Z2E511). S.H., R.R. and J.P are thankful to the Deutsche Forschungsgemeinschaft (DFG), Research Grant Collaborative Research Center Transregio 67 “Functional Biomaterials for Controlling Healing Processes in Bone und Skin - From Material Science to Clinical Application“ (CRC/TRR 67/3) and to the Helmholtz Cross Programme Initiative “Technology and Medicine – Adaptive Systems“ for supporting this work.

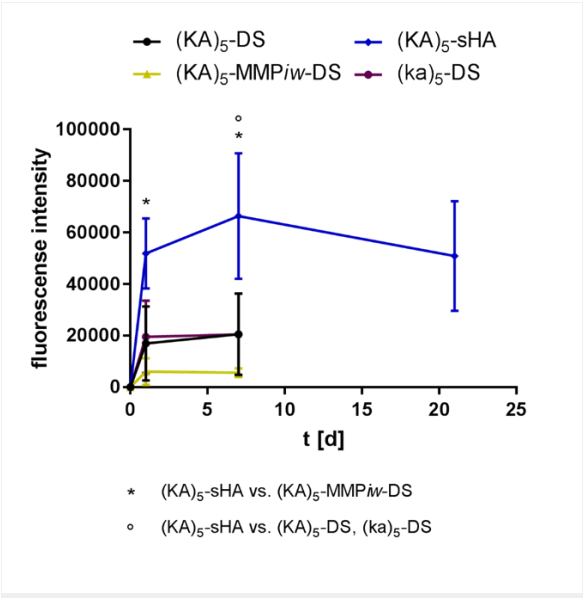

Fig. 2: MMP activity in material surroundings. Determination of MMP activity around injected hydrogels by optical imaging (n = 5-8; Mean ± SEM; * | ° p < 0.05, two-way ANOVA, Bonferroni post hoc test).

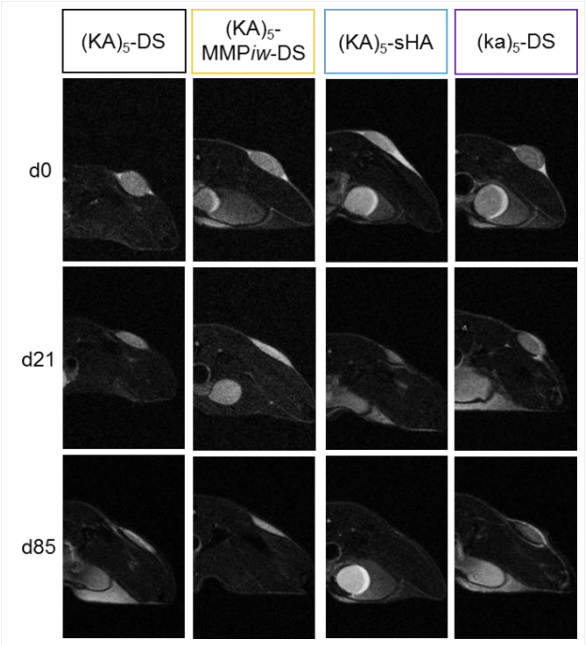

Fig. 1: Representative axial MRI images. Subcutaneous injected hydrogels show clear structure-dependent degradation profiles over time.

PS1-13-206

Cellulose nanowhisker from wastepaper for biomaterials applications

Seyed Hafez Jafari[1,2], Amin Shavandi[2], Mohsen Shahrousvand[3,2]

[1]University of Tehran, School of Chemical Engineering, College of Engineering, Tehran, IR; [2]Université libre de Bruxelles, BioMatter unit/Biomass transformation Lab (BTL), École interfacultaire de Bioingénieurs (EIB), Brussels, BE; [3]University of Tehran, Caspian Faculty of Engineering, College of Engineering, Rezvanshahr, IR

Introduction

Wastepaper can be used as a valuable source of cellulose for the isolation of cellulose nanocrystals for biomaterials applications. In this studycellulose nanowhiskers (CNWs) were extracted from wastepaper powder (WPP) via hydrolyze method by phosphoric acid to reach a cost-effective and environmentally friendly Nanoparticle.

Experimental Methods

The isolated CNW with a dimension of 5-10 nanometers in diameter and a 50-200 nanometers (Fig. 1A) in length were used as reinforcement agent in poly (ε-caprolactone) (PCL) bio-composites in different weight percentages (0, 0.1, 0.5, and 1 wt %) through solvent casting method. The physiochemical properties of the PCL/CNW bio-composites such as morphology, mechanical and thermal properties were evaluated by FT-IR, optical microscopy, SEM, TEM, DSC, TGA, and the biodegradability and hydrophilicity of PCL/CNWs were investigated by contact angle analysis and degradation tests.

Results and Discussion

Maximum strength recorded at 0.1% CNW loading, and then it slowly decreased which might have been provoked by the aggregation of a small amount of CNWs at the high content level. The highest modulus was 5 MPa that observed at bio-composites containing 1% CNWs while the elongation at break reduced from 190% (PCL-0.1%) to 115% (PCL-1%) in comparison with the neat PCL (205%). The crystallinity (Xc) was increased from 24.31 to 25.44% with increasing the loading of the CNWs from 0.1 to 1 wt%. However, for all the PCL/CNW bio-composites the crystallinity (xc) of neat PCL (Xc (%): 41.5) was higher. The contact angle decreased from 80.4° to 69.1° with increasing of the CNW loading (Fig 1B), which could be due to the role of CNWs in increasing the hydrophilicity of the bio-composites, in addition rate of the degradation of the bio-composites increased (Fig 1B) due to the more hydrophilic nature of cellulose compared to the PCL and the sample with 1 % of CNWs had the highest degradation after 48 days. PCL-1% also showed the highest water uptake of 26.08 % after 12 hours. Thermal analysis indicated that with increasing of the CNW the melting temperature remained constant (64 °C) and the remaining mass from the degradation results decreased from 89.2% (PCL-0 %) to 84.8 % (PCL-1%).

Conclusion

In conclusion, the presence of the CNWs in PCL matrix enhanced the thermal and mechanical properties of the nanocomposites and the PCL/CNWs film nanocomposite can be a promising biodegradable nanocomposite for biomaterials applications.

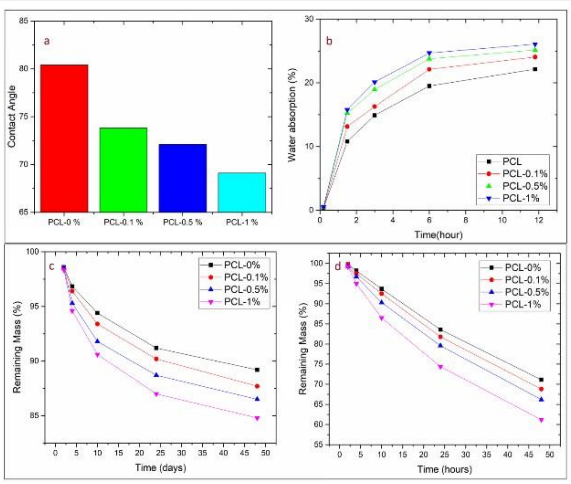

Figure 1B
(a) Contact angel of film nanocomposites; (b) Water absorption of PCL/PCCNWs over a period of time; Remaining mass of samples: (c) After incubation in SBF solution at 37 °C and (d) After degradation in 1 mol.l^{-1} NaOH solution at 60°C for different periods of time.

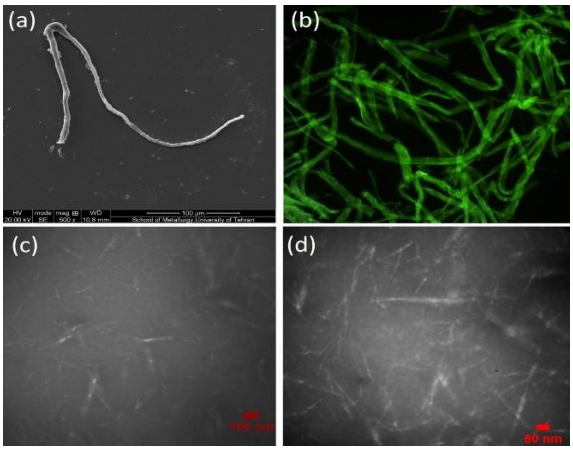

Figure 1A
(*a*) SEM image of cellulose microfibers from wastepaper (WPP); (b) Optical microscopic image of cellulose microfibers (WPP). Scale bar indicates 200 µm; (c),(d) TEM image of cellulose nanowhiskers (CNWs) extracted from WPP via phosphoric acid hydrolysis protocol.

PS1-13-207

Incorporation of microgels in PLA filaments for pH optimized degradation

Georg-Philipp Paar[1,2], Pierre Duhr[2], Catalina Molano-López[3], Susanne Braun[3], Andrij Pich[3], Thomas Gries[2], Stefan Jockenhoevel[1], Andreas Blaeser[1,2]

[1]Dept. of Biohybrid & Medical Textile (BioTex), AME-Applied Biomedical Engineering, Helmholtz Institute Aachen, RWTH Aachen University, Aachen, DE; [2]Institut für Textiltechnik of RWTH Aachen University, Aachen, DE; [3]DWI - Leibniz-Institute for interactive materials, RWTH Aachen University, Aachen, DE

Introduction

Biodegradable filaments, from materials such as polyglycolic acid (PGA) and polylactic acid (PLA), are used commercially in medicine for sutures, osteosynthesis and drug delivery systems as well as for meshes and tissue engineering scaffolds. In vivo hydrolytic degradation of PGA and PLA results in release of degradation products, which can cause local acidosis, inflammatory reactions and dramatic clinical complications, which make a second operation for implant removal necessary. Therefore, filaments with a pH-neutral degradation are desired.
Incorporation of additives (e.g. tricalcium phosphate, calcium hydroxide, calcium carbonate) into PGA filaments failed due to insufficient buffering capacity or instabilities in the spinning process [1]. A promising alternative are amine based microgels because of their high proton binding capacity and high biocompatibility. These pH-responsive colloidal polymer networks are heat sensitive and therefore have to be incorporated into filaments using solution spinning (e.g. dry or wet spinning). Recently, incorporation of microgels into dry spun filaments was successfully demonstrated [2, 3]. However, the fibers exhibited low tensile strength, which may result from the kidney shaped cross section that is characteristic for dry spun filaments. To overcome this deficit this study evaluates the feasibility of the wet spinning process for microgel incorporation.

Experimental Methods

Spinning dope of 15-20 wt% PLA in chloroform were prepared. The quantity of incorporated microgels was varied between 0 and 10 wt% in respect to the mass of PLA. The spinning dope was extruded using a gear pump wet spinning machine from DIENES (Mülheim, Germany). Different spinnerets were tested for extrusion of monofilaments and multifilaments (bore count between 50 and 150). Examined non-solvents were isopropanol and ethanol. Mechanical characteristics were evaluated by tensile testing based on DIN EN ISO 5079 under standardised climate conditions according to DIN EN ISO 139. Additionally, the morphology was examined by light microscopy. Furthermore, the incorporated quantity of microgels in the fibre was determined by TGA measurements. The degradation behavior of the filaments was evaluated by static degradation test in sterile water at 37 °C and elevated temperatures.

Results and Discussion

Using the described wet spinning process, the tensile strength of the filaments was more than doubled in respect to the dry spinning process. Furthermore, it was possible to produce filaments with a round filament cross section. Incorporation of 7 wt% microgels was successful. Tensile strength of filaments with incorporated microgels of up to 14,9 cN/tex was achieved. The effect of microgel incorporation on fiber morphology is small, however a significant decrease in tensile strength of the filaments was noted. Production of a braided structure from the multifilaments was possible. A buffering effect by the incorporated microgels on pH was observed in static degradation studies.

Conclusion

Wet spinning showed to be a promising alternative solution spinning process for the incorporation of microgels into PLA filaments. The process yielded filaments with factor two improved tensile strength compared to dry spinning. Furthermore, it was shown that the buffering function of the pH-responsive microgels is preserved in the process.

References

[1] Schuster P. Shaker 2014; doctoral thesis.

[2] Fehér K. et al. BioNanoMaterials, 2015; 16(4): 259–264.

[3] Poggenburg B. et al. Kunststoffe in der Medizintechnik, 2014; 139-152.

Acknowledgement

The Project “pHMed” is supported by the European Regional Development Fund North Rhine-Westphalia (EFRE.NRW). Medical grade polymer was kindly supplied by Corbion (Amsterdam, Netherlands) free of charge.

2:45 p.m. – 3:45 p.m.

Hall 1 / Exhibition Area

PS1-14 | Biomaterial characterisation

PS1-14-208

A reliable imaging and characterization method for (semi-)transparent materials - optical coherence tomography in the field of biomaterials

Luise Schreiber, Andreas Lehmann, Vincenz Porstmann, Jörg Opitz

Fraunhofer Institute for Ceramic Technologies and Systems IKTS, Characterization Technologies, Dresden, DE

Introduction

Customized biomaterial could be an important step stone towards more individual approach in medical therapy. Additive manufacturing processes are highly adaptable and allow the use of a variety of materials and material combinations including biomaterials. In order to make optimal use of biomaterials, it is not only necessary to maintain flexibility in shaping and manufacturing, but also to evaluate the optimal material properties for each individual application.

Experimental Methods

The possible applications of Optical coherence tomography (OCT) for characterization of biological 3D printing of different hydrogel and polymer materials will be explored. OCT is a method based on white light interferometry. Originally OCT was developed for ophthalmology. OCT is a non-destructive, non-contact and easy-to-integrate optical method. Therefore, it can be applied to study transparent and semitransparent tissues with high speed and high lateral resolution up to 1 µm. Also for non-transparent material high-resolution surface images can be generated. Internally backscattered light contains information about position and size of the interacting feature. In other words: this 3D imaging method OCT is an ideal approach for detection of a variety of superficial and subsurface defects, material characterization, and process monitoring tasks.

Results and Discussion

Fraunhofer IKTS develops application-specific OCT systems for ceramic, polymer and organic material testing. A special attention is dedicated to quality control of single components as well as to process evaluation. Various practical examples include a laboratory setup for on-line detection of splinter in glass bottles and a failure finding device for thin planar ceramics. Based on the experience of Fraunhofer IKTS in the field of monitoring various 3D printing processes with OCT, a laboratory setup for a regenHU bioprinter was set up.

Conclusion

OCT can provide important structural information for the material characterization and development. In this paper an OCT study on ceramic bone replacement structures will be presented.

PS1-14-209

Effect of Conventional Self-Assembled Molecules with Different Functional Groups on Cardiac Differentiation of Induced Pluripotent Stem Cells

Ozgen Ozturk-Oncel[1], Carlos Heras-Bautista[2], Lokman Uzun[3], Deniz Hür[4], Kurt Pfannkuche[2], Bora Garipcan[1]

[1]Boğaziçi University, Biomedical Engineering, İstanbul, TR; [2]University of Cologne, Neurophysiology, Cologne, DE; [3]Hacettepe University, Biochemistry, Ankara, TR; [4]Eskisehir Technical University, Chemistry, Eskişehir, TR

Introduction

Surface chemical modification plays an important role in regulating cellular behavior, in vitro. Recent studies showed that functional groups on biomaterial surfaces regulate cellular adhesion, migration, proliferation and differentiation [1,2]. Self-assembled molecules (SAMs) form organized structures and with these molecules, desired surface properties can be easily generated.

In the present study, we aimed to prepare polydimethylsiloxane (PDMS) substrates in natural myocardium-like stiffness range [3] and investigate the effect of their surface modifications with SAMs, having two functional end groups (-CH_3 and –NH_2) and different wettability properties, on cardiac differentiation of murine induced pluripotent stem cells (mIPS, TαP4).

Experimental Methods

PDMS (Sylgard 184, DOWSIL) substrates were prepared with different ratios of silicone elastomer base and curing agent (10:1 – 70:1) and spin coated (Brewer Science, CEE 200X) on glass slides. Substrates were cured for a week at 60°C. Young's moduli of substrates were characterized with nanoindentation (Optics 11).

Next, hydroxyl groups were created on substrate surfaces by using oxygen plasma treatment (Nordson March Plasma Systems) for 1 min, followed by dipping into 1% concentrations of either 3-Aminopropoyl triethoxy silane (APTES, Sigma) for -NH_2 end groups or Trimethoxy (octadecyl) silane for –CH_3 end groups. Characterizations of these modified substrates were done by water contact angle measurements (WCA) and X-Ray ray photoelectron spectroscopy analysis (XPS, Thermo Scientific K-Alpha).

mIPS cells were cultured and differentiated into cardiomyoctes on native and SAMs modified PDMS substrates by using a previously published protocol [4]. Cell viability (3-[4,5-dimethylthiazol-2-yl]-2,5-diphenyltetrazolium bromide, MTT) and Western Blot (Bio-Rad) analysis were performed.

Results and Discussion

According to nanoindentation results with different silicone elastomer base crosslinker concentrations of PDMS, the ratio of 50:1 was found to be in natural myocardium-like stiffness range with a Young's modulus of 26.42 ± 6 kPa.

In low resolution XPS survey spectra of all unmodified and modified PDMS, four characteristic peaks were found as O1s, C1s, Si2s and Si2p at 533, 286, 155 and 104 eV, respectively. -CH_3 functionalization of PDMS substrates lead to a remarkable increase in the carbon peak, due to high carbon content of the molecule, whereas N1s peak appeared after modifications with APTES at 401 eV. WCA analysis showed hydrophobic nature of native and –CH_3 modified PDMS (104.1±5 and 112.7±5, respectively) and hydrophilic properties of –NH_2 modified PDMS (61.9±4).

MTT analysis of mIPS cells on these substrates showed no statistical difference between SAMs modified PDMS. Both modified substrates showed higher viability when compared to native PDMS ($p<0.05$). Western blot analysis results were given in Fig.1 on day 12 of differentiation. Similar to viability analysis, both functional end groups enhanced cardiac differentiation significantly, when compared to native PDMS. Cardiac marker Troponin-T (Sc-20025) expressions were higher in hydrophilic -NH_2 groups.

Conclusion

Conventional SAMs modified PDMS substrates in myocardium-like stiffness range were confirmed to be nontoxic to mIPS cells and also these modifications enhanced cardiac differentiation of mIPS cells on PDMS substrates.

References

1. Cao, B. *et al.* (2017) 'Effects of Functional Groups of Materials on Nonspecific Adhesion and Chondrogenic Induction of Mesenchymal Stem Cells on Free and Micropatterned Surfaces', *ACS Applied Materials & Interfaces*, 9(28), pp. 23574–23585.

2. Hasan, A. *et al*. (2018) 'Effect of Functional Groups of Self-Assembled Monolayers on Protein Adsorption and Initial Cell Adhesion', *ACS Biomaterials Science & Engineering*. American Chemical Society, 4(9), pp. 3224–3233.

3. Berry, M. F. *et al.* (2006) 'Mesenchymal stem cell injection after myocardial infarction improves myocardial compliance', *American Journal of Physiology-Heart and Circulatory Physiology*. American Physiological Society, 290(6), pp. H2196–H2203.

4. Heras-Bautista, C.O. *et al*. (2014) 'The influence of physiological matrix conditions on permanent culture of induced pluripotent stem cell-derived cardiomyocytes', *Biomaterials,*35, pp. 7374–7385.

Acknowledgement

This study was supported by TUBITAK (Project number: 113T026).

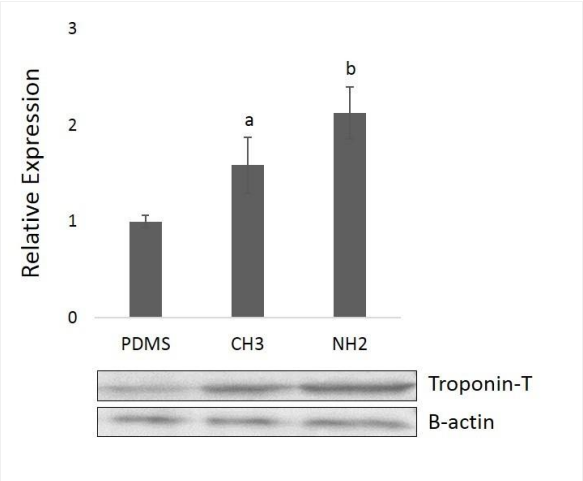

Western blot analysis results.
[a] p<0,05 significantly different from PDMS;
[b] p<0,01 significantly different from PDMS.

PS1-14-210

Adhesion of *Streptococcus mutans* and *Porphyromnas gingivalis* to bracket materials: a saliva-induced multi-species biofilm study

So-hyun Park[1], Sug-joon Ahn[1], Jung-sub An[2]

[1]Seoul National University, orthodontics, Seoul, KR; [2]Seoul National University/Dental hospital, orthodontics/school of dentistry, Seoul, KR

Introduction

Orthodontic brackets are associated with enamel demineralization and gingival inflammation, because a complex bracket design provides additional sites for bacterial colonization and difficulties in oral hygiene procedure[1]. Many studies have specific bacterial adhesion to various orthodontic brackets, but few studies have evaluated the interaction of bracket materials with biofilm composition [2-5]. According to previous studies, rougher surface and higher wettability promote bacterial adhesion and biofilm formation [6]. Surface wettability is calculated by measuring contact angles and a lower contact angle indicates higher surface wettability and higher interfacial tension, meaning that the surface has more attractive force [3,6]. The aim of this *in vitro* study was to analyze the difference in adhesion of cariogenic bacteria (*Streptococcus mutans* [Sm]) and periodontopathic bacteria (*Porphyromonas gingivalis* [Pg]) to bracket materials using surface roughness and surface wettability.

Experimental Methods

The sample compromised disc-shaped specimens of three different bracket materials (monocrystalline alumina [MCA], stainless steel [SS], polycarbonate [PC]) and hydroxyapatite [HA] (n = 24 per each group). Before biofilm experiments, surface roughness and wettability were determined from all the materials using confocal laser scanning microscopy and measuring the water contact angle, respectively. Unstimulated whole saliva of a healthy adult volunteer was used as inoculum to produce multi-species biofilms, which was grown on the surface of samples. The amounts of Sm, Pg, and total bacteria were determined at day 1 (T1) and day 4 (T2) using real-time polymerase chain reaction. The adhesion ratio of Sm and Pg were calculated by the ratio of Sm and Pg to total bacteria, respectively. Repeated measures analysis of variance was used to analyze time-related differences in bacterial adhesion ratios with respect to bracket material. Differences in surface roughness and wettability were analyzed by the Kruskal–Wallis test.

Results and Discussion

Material type significantly influenced the bacterial adhesion ratios. The order of adhesion ratio of Sm, from highest to lowest, was HA, MCA, PC, and SS (Table 1). Difference in the adhesion ratio of Sm may be explained by surface properties of the materials. HA demonstrated the roughest surface and smallest water contact angle, which may explain the highest adhesion ratio of Sm to HA. Although MCA showed the smoothest surface, the smallest contact angle may induce the higher adhesion ratio of Sm to MCA than to other materials. The smoother surface and higher contact angle of SS may explain the lowest adhesion ratio of Sm to its surface. The larger contact angle than SS and smaller contact angle than MCA may explain higher adhesion ratio of Sm to PC than SS and lower adhesion ratio of Sm to PC than MCA. However, surface properties did not properly explain the adhesion ratio of Pg to the materials. The adhesion ratio of Pg was highest on MCA and lowest on SS. The adhesion ratio of Pg was not significantly higher on HA that had the roughest surface and smallest contact angle. This may be because surface properties may

have a less significant effect on the adhesion of the later colonizer (Pg) than the early colonizer (Sm). Partly, the aerobic condition in this study may interfere interaction of Pg to underlying materials. Interestingly, adhesion ratio of Sm was not significantly influenced by the incubation time.

Conclusion

Considering the highest adhesions ratios of Sm and Pg to MCA, the use of brackets which were made of MCA, should be carefully considered in orthodontic patients with poor oral hygiene.

References

1. Lucchese A. et al., Eur J Orthod.35(5):664-668, 2013
2. Low B. et al., Eur J Orthod.33(5):577–583, 2011
3. Eliades T. et al., Am J Orthod Dentofacial Orthop.108:351-360, 1995
4. Bum-Soon L. et al., Am J Orthod Dentofacial Orthop.133:882-888, 2008
5. Darlene R. et al., Angle Orthod.85:992-996, 2015
6. Yuehuei H. An. et al., J Biomed Mater Res. 43: 338-348,1998

Table 1. Bacterial adhesion ratios with respect to material type and incubation time

		Day 1 (T1)	Day 4 (T2)	Significance [a]	
				Time	Material
***S. mutans* (Sm)**					
Sm/Total bacteria (%)	Monocrystalline alumina (MCA)	0.129±0.012	0.131±0.015	T1 = T2	SS < PC < MCA < HA
	Stainless steel (SS)	0.123±0.009	0.125±0.017		
	Polycarbonate (PC)	0.125±0.007	0.126±0.013		
	Hydroxyapatite (HA)	0.137±0.010	0.137±0.018		
***P. gingivalis* (Pg)**					
Pg/Total bacteria (%)	Monocrystalline alumina (MCA)	0.148±0.009	0.133±0.026	T1 > T2	SS < MCA
	Stainless steel (SS)	0.143±0.004	0.132±0.018		
	Polycarbonate (PC)	0.143±0.005	0.127±0.017		
	Hydroxyapatite (HA)	0.143±0.004	0.130±0.024		

[a] Repeated measure ANOVA was used to determine time-related differences at $\alpha < 0.05$; $P < 0.05$

Table 1. Bacterial adhesion ratios with respect to material type and incubation time

Table 2. Surface roughness and wettability of materials used in this study

Materials	Mono-crystalline alumina (MCA)	Stainless steel (SS)	Polycarbonate (PC)	Hydroxyapatite (HA)	Multiple comparisons [a]
Surface roughness (μm)	0.61 ± 0.24	0.55 ± 0.30	0.85 ± 0.27	1.26 ± 0.13	MCA = SS < PC < HA*
Water contact angle (°)	51.16 ± 26.06	85.39 ± 10.5	96.49 ± 7.89	42.89 ± 16.5	MCA = HA< SS < PC*

[a] The Kruskal–Wallis test was used to determine differences among the three groups multiple comparisons with the Bonferroni correction at a significant level of $\alpha < 0.05$; *$P < 0.001$

Table 2. Surface roughness and wettability of materials used in this study

PS1-14-211

Surface functionalisation of magnetic nanoparticles by ß-amyloid 1-42 peptide ($Aß_{42}$)-specific aptamers as a concentration tool in early diagnosis of Alzheimer's disease.

Cheryl M. Collins[1], Valeria Perugini[1], Manuel González Gómez[2], Yolanda Piñeiro[2], José Rivas[2], Matteo Santin[1]

[1]University of Brighton, Centre for Regenerative Medicine and Devices (CRMD), School of Pharmacy & Biomolecular Sciences, Brighton, GB; [2]Universidade de Santiago de Compostela, Departmento de Física Aplicada, Campus Vida, Santiago de Compostela, ES

Introduction

Alzheimer's disease (AD) is a progressive neurodegenerative disorder, which is predominantly characterised by the deposition of insoluble ß-amyloids (Aß) in the brain. AD had an estimated cost to the global economy in 2015 of $817.9 billion, which is projected to rise to $2 trillion by 2030[1] thus there is an unmet clinical need for earlier diagnosis and treatment, which could result in decreased morbidity and mortality. Current biomarker diagnostic tools for patients presenting with cognitive decline include brain MRI and PET scans and ELISA of biomarkers in cerebrospinal fluid (CSF), e.g. Aß analyses. Quantitative data of $Aß_{42}$ obtained by ELISA are limited by sensitivity thresholds in the pg/ml range.

Short peptides (KLVFF) have been shown to inhibit Aß formation and aggregation both *in vivo* and *in vitro*[2] by binding to residues 16-20 of Aß thus could be utilised as peptide aptamers in both diagnostics and drug administration.

The linear peptides can be integrated onto hyperbranched molecular structures called dendrons to increase aptamer capacity, stability and increased sensitivity of Aß detection.

Silica magnetic nanoparticles (MNPs) (Fe_3O_4@SiO_2) have been functionalised with both the linear peptide KLVFF with glycine spacer (GGKLVFF) and a 3rd generation dendrimeric ε-polylysine modified with 16 linear KLVFF peptides (Rgen3K$(KLVFF)_{16}$) as described previously[3]. This work aims to use the Rgen3K$(KLVFF)_{16}$-functionalised MNPs as a concentration tool for ELISA and biosensors in early diagnosis of AD.

Experimental Methods

Third generation ε-polylysine dendrons with an arginine root (Rgen3K) were designed to expose on the uppermost branching generation sixteen linear KLVFF peptides. Rgen3K$(KLVFF)_{16}$ were synthesised using microwave based solid phase peptide synthesis (Biotage, UK) on TentaGel™ S-NH_2 resin and characterised with mass spectrometry and HPLC.

Rgen3K$(KLVFF)_{16}$ dendrons were grafted onto single-core Fe_3O_4@SiO_2 MNPs using carbodiimide chemistry and characterised using Fourier-transform infrared spectroscopy (FTIR). Non-functionalised MNPs were used as a control.

MNPs were treated with a dispersant solution to reduce aggregation that is commonly seen with MNPs. Both control and $(KLVFF)_{16}$-functionalised MNPs were incubated in 100 µl of 1 pg/ml $Aß_{42}$. The MNPs were assayed in a human $Aß_{42}$ Quantikine ELISA (R&D Systems, UK) and the optical density (OD) was measured at 450 nm.

Results and Discussion

Single-core Fe_3O_4@SiO_2 MNPs were successfully functionalised with Rgen3K(KLVFF)$_{16}$ as confirmed by FTIR (see figures).

After assaying MNPs incubated in 1 pg/ml Aß$_{42}$ using ELISA all samples had OD values above the standard curve. The samples were diluted 1 in 10 to bring the OD values within the assay range. The (KLVFF)$_{16}$-functionalised MNPs showed a 4-fold increase in OD compared to the control MNPs indicating the Rgen3K(KLVFF)$_{16}$ dendron captured the Aß$_{42}$.

The ELISA kit used has a sensitivity of 4.7 pg/ml, however (KLVFF)$_{16}$-functionalised MNPs were capable of detecting Aß$_{42}$ at lower concentrations by concentrating the samples due to the hyperbranched dendrons exposing multiple KLVFF aptamers.

Conclusion

The present work shows that single-core Fe_3O_4@SiO_2 MNPs functionalised with Rgen3K(KLVFF)$_{16}$ have the ability to concentrate Aß$_{42}$ in samples. Such a concentration step will enable a considerable increase in the sensitivity of ELISAs for detection of AD biomarkers with potential for earlier diagnosis than current methods.

References

[1]Lewis et al., Trajectory of Dementia in the UK – Making a Difference, report produced the Office of Health Economics for Alzheimer's Research UK, 2014.

[2]Funcke SA. et al., Curr Pharm Des. 18(6): 755-67, 2012.

[3]Perugini V. et al., Poster presentation 512, BSG 2018.

Acknowledgement

FP7 EC grant MADIA, contract number 732678.

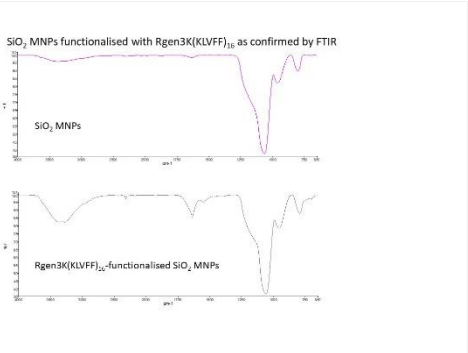

SiO2 MNPs functionalised with Rgen3K(KLVFF)16 as confirmed by FTIR

PS1-14-212

Cyclic voltammetric biosensor based on graphene and methionine composite film modified screen printed carbon electrode for detection of food colorant

Rungtiva Poo-arporn, Chutimon Akkapinyo

King Mongkut's University of Technology Thonburi, Biological Engineering Program, Faculty of Engineering, Bangkok, TH

Introduction

Amaranth is red synthetic food colorant that is permitted to use as a food additive. However, excessive consumption of amaranth can cause health effects such as nausea, vomiting, dizziness. Therefore, the well-defined method for amaranth detection is needed to test amaranth level in food. Electrochemical method is a strong alternative technique due to its high sensitivity, less time consumption and low cost. Moreover, it is possible to detect amaranth with electrochemical method because it contains azo group (-N=N-) that can be reduced at the electrode. Although, SPCE has benefits in low cost and disposable electrode but it exhibits low sensitivity when compares with glassy carbon, gold or platinum electrode. Therefore, it needs to be modified to improve its performance.

This research present modification of SPCE with rGO and methionine. The strategy of improvement is based on large surface area of rGO and catalytic effect of methionine. The modified SPCE was used to evaluate amaranth level by CV.

Experimental Methods

Reduced graphene oxide was prepared by glucose reduction as described in previous report [1]. Then, rGO was modified on SPCE by drop casting. Firstly, 1 mg of prepared rGO was dispersed in 1 mL of 30%ethanol and sonicated for 30 minutes. Then, 3 µL of well-dispersed rGO was dropped directly on the surface of SPCE. The rGO modified SPCE was dried in desiccator for 2 hours. Then, the rGO modified SPCE was immersed in pH 7.0 PBS solution synergistic containing 2.5 mM of methionine and CV from -0.6 to 2.0 V at scan rate 100 mV/s for 3 cycles. Poly-L-methionine was modified on rGO/SPCE by electrochemical polymerization. After that, the rGO-methionine/SPCE was rinsed with DI water and dried overnight in desiccator.

Results and Discussion

The electrochemical behavior of amaranth was tested on modified electrode comparing with bare SPCE to investigate performance of modified sensor. The 50 µM of amaranth was tested by cyclic voltammetry and acetate buffer pH 4.0 was used as electrolyte. The anodic peak of amaranth was observed on both of bare and modified SPCE at potential 0.83 and 0.81 V, respectively. However, bare SPCE demonstrated small anodic peak indicating weak electrochemical response of amaranth on bare electrode, while the modified SPCE dramatically enhanced electrochemical response of amaranth as illustrated in Fig.1. The rGO film can help to promote large surface area and increase the electron transfer rate on electrode[2]. Moreover, the conductive poly-amino acid layer has a good catalytic effect due to its active groups, such as amino group and carboxyl group[3]. Therefore, the higher current response on modified SPCE was the synergistic effect of rGO and poly-methionine film on SPCE.

Performance of modified sensor for amaranth detection was investigated by CV as shown in Fig.2. The results demonstrated that modified sensor exhibited linear range at amaranth concentration ranging from 1 to 100 µM (inset) and limit of detection was obtained at 213 nM.

Conclusion

This research presents modification of SPCE with rGO and poly-methionine layer to improve performance of SPCE for amaranth detection. The obtained sensor exhibited extreme current response when compared with bare SPCE and demonstrated wide linear range with low detection limit. Thus, this sensor can be a good alternative for amaranth detection.

References

[1] S. Pakapongpan, A. Tuantranont, R. P. Poo-arporn, Magnetic nanoparticle-reduced graphene oxide nanocomposite as a novel bioelectrode for mediatorless-membraneless glucose enzymatic biofuel cells, Scientific Reports, 7 (2017) 12882.

[2] A. Karthick N., R. Thangappan, M. Arivanandhan, A. Gnanamani, R. Jayavel, A Facile Synthesis of Ferrocene Functionalized Graphene Oxide Nanocomposite for Electrochemical Sensing of Lead, Journal of Inorganic and Organometallic Polymers and Materials, 28 (2018) 1021-1028.

[3] Y. Tang, Y. Wang, G. Liu, D. sun, Determination of sunset yellow and tartrazine using silver and poly (L-cysteine) composite film modified glassy carbon electrode, Indian Journal of Chemistry, 55 (2016) 298-303.

Acknowledgement

This work was supported financially by the Thailand Research Fund **(**TRF**)** and the Synchrotron Light Research Institute **(**SLRI**) (**grant number RSA5980073**)**, as well as the research subsidy fund of fiscal year 2019 from King Mongkut's University of Technology Thonburi.

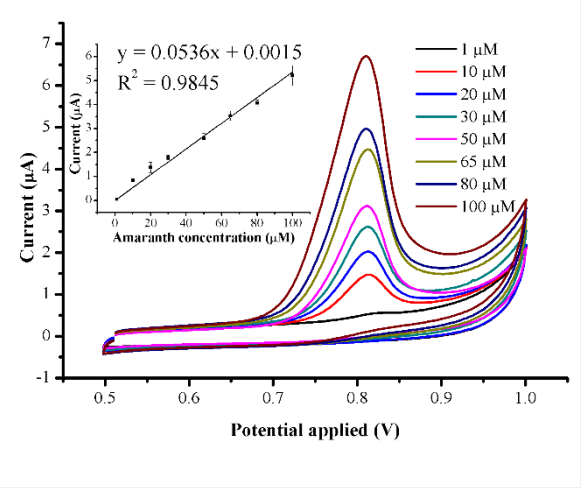

Performance of the biosensor
Fig.3 Comparison of cyclic voltammograms at different concentration of amaranth. The inset represents linear relationship between current response and amaranth concentration

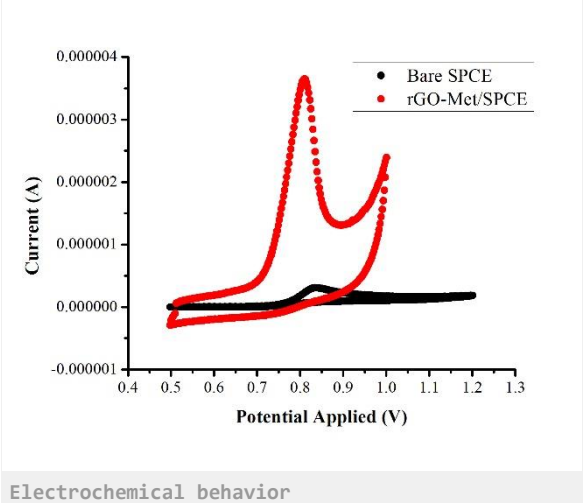

Electrochemical behavior
Fig.2 Comparison of cyclic voltammograms of 50 µM amaranth on bare GCE (black) and rGO-methionine modified SPCE (red) in acetate buffer pH 4.0 containing 0.1M KCl.

PS1-14-213

Tribological investigations of polymer materials on a rolling-sliding knee wear simulator

Jessica Hembus[1], Susann Gierschner[1], Felix Ambellan[2], Stefan Zachow[2], Rainer Bader[1]

[1]Rostock University Medical Centre, Biomechanics and Implant Technology Research Laboratory, Department of Orthopaedics, Rostock, DE; [2]Zuse Institute Berlin, Therapy Planning Group, Department of Visual Data Analysis, Berlin, DE

Introduction

Total knee arthroplasty is a common surgical procedure, which is designed to restore painless mobility of the knee joint in case of degenerative lesions. However, the implantation of a total joint endoprosthesis is a very invasive procedure. The insertion of a joint spacer with viscoelastic properties could be a less invasive intermediate step before implantation of a total knee joint. For this purpose, various polyurethane spacer materials were examined regarding to their biomechanical suitability. Therefore, adequate tribological characterization and analysis of the abrasive wear particles from the spacer implant are essential for its preclinical testing.

Experimental Methods

A conceivable polymer for this use is polyurethane (PU), which is used for different medical applications, such as catheter materials or coatings for artificial blood vessels. Therefore, several polycarbonate urethanes materials with different compositions were produced by Kutuzova et al. (2017, 2018) and provided for present biomedical investigations.

The mechanical loading of the samples was implemented in a rolling-sliding test bench (Goebel et al., 2012, see figure 1) with adapted axial force in accordance with ISO 14243-1 over one million gait cycles. The test bench enables testing of new materials for artificial knee joints on prototypes with simple geometry. The alternating force was applied with a cylindrical articulating pulley made of aluminum titanate, which should simulate the osteoarthritic femur condyle with complete cartilage abrasion. The lubricant (bovine calf serum (Biochrom GmbH, with 20 g/l protein concentration, 5.85 g/l EDTA, 1.85 g/l sodium azide)) with a temperature of 37 ± 2°C was changed every 0.5 million cycles. While the test medium was changed, the samples were cleaned and measured gravimetrically in accordance to ISO 14243-2 to determine wear rate of the polymer material. After wear testing, the samples were examined optically with a laser scanning microscope to determine the wear mechanisms on the sample surfaces.

Results and Discussion

Two commercially available polyurethane materials (kTPCU and kTPU) and two new developed polyurethanes (KSZ6 and KSZ9) were tested in the rolling-sliding test bench. Testing of one commercially available kTPU material had to abort prematurely due to complete abrasion of the specimen. The three other materials completed the test over 1 million cycles entirely. The lowest wear rate of 0.29 ± 0.03 mg per million cycles was achieved with the commercially available material kTPCU. The wear rate of KSZ6 and KSZ9 was about two times higher than the wear rate of kTPCU (0.52 ± 0.17 mg und 0.55 ± 0.04 mg per million cycles; see figure 2). All materials showed a nearly linear wear rate. KSZ6 tended to increased fluid intake. Due to high loading in the rolling-sliding test bench all PU materials showed a macroscopically high worn articulated surfaces.

Conclusion

In rolling-sliding test bench the comparison of different polymer materials with regard to their tribological properties could be realized. All tested PU materials showed a wear rate of several mg per million cycles. In order to validate the amount of wear, further tests are planned with polyethylene material, which is used as the standard bearing material in the artificial knee joint. The matching of the polyethylene wear rate with data from standard knee wear simulator tests according to ISO 14243 could allow classification of the wear rate derived from the rolling sliding test bench. Furthermore, microscopic comparison of abrasive wear particles made of polyurethane and polyethylene can also provide information about the suitability of polyurethane as a knee spacer material.

References

L. Kutuzova, K. Athanasopulu, M. Schneider, A. Kandelbauer, R. Kemkemer, und G. Lorenz, „In vitro bio-stability screening of novel implantable polyurethane elastomers“, Gruyter, Bd. Current Directions in Biomedical Engineering, Nr. 4, S. 535 – 538, 2018.

L. Kutuzova, O. Rain, R. Koslik, und G. Lorenz, „Biostable polyurethane materials for chondral implants: in-situ monitoring of polyurethane polymerization“, Biomed Eng– Biomed Tech, Bd. 62, S. 168, 2017.

P. Goebel, C. Zietz, R. Bieck, D. Kluess, und R. Bader, „A novel method for tribological evaluation of bearing materials in total knee replacements“. Walter de Gruyter, 2012.

Acknowledgement

The authors kindly thank the Federal Ministry of Education and Research (BMBF) for granting this research project (BMBF No.: 01EC1406C (TOKMIS)).

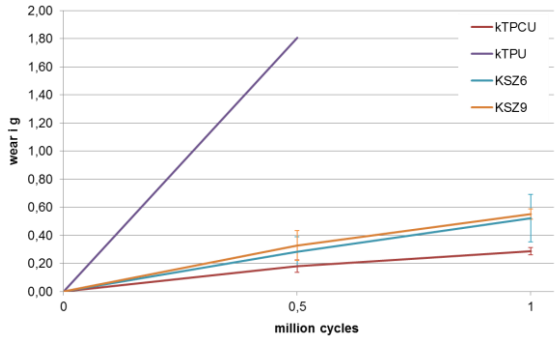

Figure 2
Total wear rates of the four different polyurethane materials tested in rolling sliding test bench

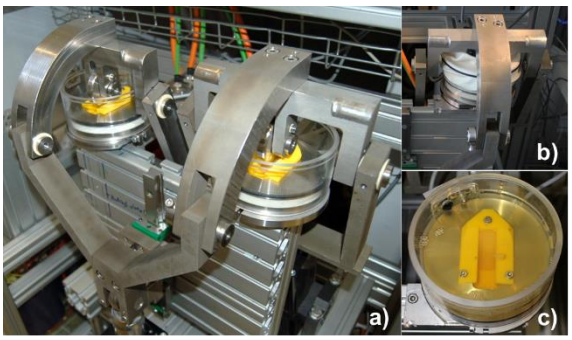

Figure 1
Rolling sliding test bench with two stations without lubricant (a), one complete station (b) and one test chamber with specimen and lubricant (c)

PS1-14-214

Development of Biodegradable Drug-Encapsulated Oesophageal Stents

Samuel W. Farr, Chloe L. M. Bell, Kevin A. Pereira, Y. M. John Chew, Semali Perera

University of Bath, Centre for Advanced Separations Engineering, Dept. Chemical Engineering, Bath, GB

Introduction

Oesophageal cancers are the 13th most common form of cancer in the UK but rank as the 7th most occurring form of cancer death, due to difficulties in early diagnoses. 40% of cases concern in people over 75 years old with a growing incidence rate in younger age groups and with a 5-year survival rate of 15% [1].

Current treatments involve chemo-radiotherapy or surgical resection of the oesophagus. If patients are not suitable for surgery then oesophageal stenting is used as a palliative treatment, mostly using metallic stents that cannot be removed once placed, and that can cause serious complications [2]. Each of these methods has a significant impact on the patient's quality of life, and researchers are looking at biodegradable polymers as a way of improving the treatments for patients [2].

The purpose of this research is to investigate the mechanical and drug-delivery properties required of a fully biodegradable polymeric oesophageal stent by using advanced characterisation and computational modelling. The models will allow many materials to be tested in a short space of time to identify the best characteristics and materials for the application, providing important information for the development of biodegradable, drug-encapsulated oesophageal stents.

Experimental Methods

Poly(lactide-co-glycolide) (PLGA) is used as a model material due to its tunable mechanical and degradation properties, and because of the breadth of its use in drug delivery and medical applications [3]. Solutions of 16.3 wt% PLGA 50:50 in 1-Methyl-2-pyrrolidone (NMP) with a chemotherapy drug for oesophageal cancers, 5-Fluorouracil (1.8 wt%) are prepared for wet-spinning hollow fibres, which will be used as a model structure to compare with computational models. Rheological characterisation of the polymer solutions is performed using a Bohlin Rheometer to determine the spinning parameters. The fibres are used in degradation, drug encapsulation and drug release studies, using UV-Vis spectroscopy and HPLC-UV-Vis to determine component concentrations. Mechanical testing and Scanning Electron Microscopy (SEM) are performed to determine mechanical properties, and cross-sectional and surface morphology.

Computational Fluid Dynamics and Finite Element Analysis have been used to investigate the response and flow of Newtonian and power-law fluids, and Bingham plastics through the stent as a result of deformation of the stent. Drug-delivery profiles for 5-Fluorouracil are also developed.

Results and Discussion

Rheological studies show that the polymer solutions are Newtonian fluids (Fig. 1A) and that the target viscosity for spinning hollow fibres is between 0.6 – 1.1 Pa s. This information is important for the hollow fibre spinning process. SEM imaging (Fig. 1B) of PLGA 50:50 shows highly porous internal structures, with pores between 1-20 μm in size. The CFD models assume a dense polymer layer in the solid domain, with an axis-symmetrical cylindrical geometry. A continuous fluid domain is defined in the centre of the cylinder. Fig. 2A shows the fluid pressure profiles of the

different types of fluid at the mid-point of the stent, and Fig. 2B shows the stress in the polymeric wall, and the subsequent impact of the fluid when the peristaltic wave is at the mid-point of the stent. The polymer resists the pressure exerted by the oesophagus during peristalsis, found in literature to be 13 - 20 kPa [4]. The impact of the type of fluid showed flow and pressure profiles similar to those found in literature [5].

The force applied, F [N m^{-2}] to the stent surface was described by:

$$F = F_0 e^{-0.5 ((z - (z0 + v0\ t)) / w)^2} \quad (1)$$

where F_0 [N m^{-2}] is the maximum load, z [m] is the axial position, z_0 [m] is the initial axial position, v_0 [m s^{-1}] is the wave velocity, t [s] is the time, and w [m] is the nominal wave width.

The fluids were defined by their constitutive equations:

Newtonian: $\tau = \mu \dot{\gamma}$ (2)

Power Law: $\tau = K \dot{\gamma}^n$ (3)

Bingham-Papanastasiou: $\tau = \tau_0 (1 - e^{-m\dot{\gamma}}) + \mu_p \dot{\gamma}$ (4)

where τ [Pa] is the shear stress, μ [Pa s] is the dynamic viscosity, $\dot{\gamma}$ [s^{-1}] is the shear rate, μ_p [Pa s] is the plastic viscosity, K [Pa s^n] is the consistency constant, n [-] is the flow index, m [s] is the Papanastasiou index,and τ_0 [Pa] is the yield stress.

Conclusion

This work has developed a method of relating the rheological properties of polymer solutions to the key hollow fibre spinning parameters, which has identified a suitable operating range for the fluid viscosity. Other experiments are currently ongoing which will complement the modelling work and also provide important input information.

The CFD modelling has helped to develop an understanding of the impact of the applied peristaltic force from the oesophagus on a stent, and the resulting flow profiles of various fluids. The mechanical properties of biodegradable polymers used in structural supports, such as stents, need to be investigated further and these models will be able to test a variety of materials in a short space of time to identify the most suitable materials to use.

References

1. Cancer Research UK (2015) Oesophageal cancer statistics. *Cancer Research UK*.

2. Hindy, P., Hong, J., Lam-Tsai, Y., and Gress, F. (2012) A Comprehensive Review of Esophageal Stents. *Gastroenterol Hepatol (N Y)*, **8** (8), 526–534.

3. Perale, G., and Hilborn, J. (2017) *Bioresorbable Polymers for Biomedical Applications - From Fundamentals to Translational Medicine*, Elsevier.

4. Ren, J., Massey, B.T., Dodds, W.J., Kern, M.K., Brasseur, J.G., Shaker, R., Harrington, S.S., Hogan, W.J., and Arndorfer, R.C. (1993) Determinants of intrabolus pressure during esophageal peristaltic bolus transport. *American Journal of Physiology-Gastrointestinal and Liver Physiology*, **264** (3), G407–G413.

5. Misra, J.C., and Maiti, S. (2012) Peristaltic transport of rheological fluid: model for movement of food bolus through esophagus. *Appl. Math. Mech.-Engl. Ed.*, **33** (3), 315–332.

Acknowledgement

This work was supported by funding from the Engineering and Physical Sciences Research Council (EPSRC) and the University of Bath.

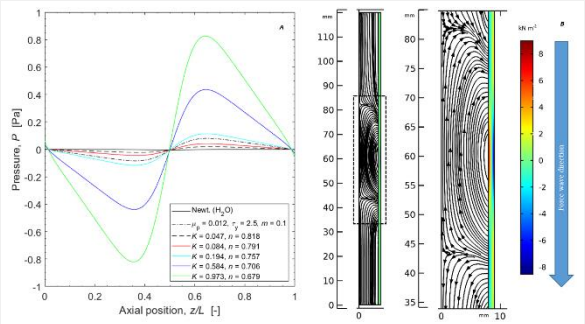

Figure 2 - CFD fluid pressure and flow profiles, and solid stress profile.
A - Pressure profiles of the fluids at the axis of symmetry along the length of the stent when the peristaltic wave is at the mid-point of the stent; B - Wall stress (colour scale) and fluid streamlines of a Newtonian fluid when the force is at the mid-point of the stent.

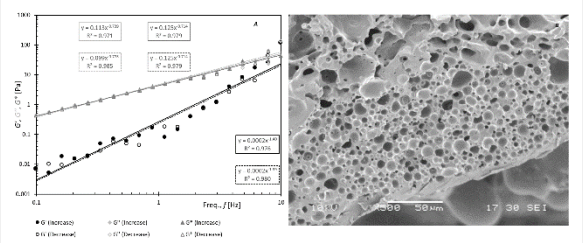

Figure 1 - Rheology of polymer solutions and morphology of polymer samples.
A - Elastic (G'), Viscous (G'') and Complex (G*) moduli for a PLGA 50:50 solution in NMP, before wet-spinning; B – SEM image of a PLGA sample, with pore size range 1-20 µm.

PS1-14-215

Micromechanical and morphological differences of collagen-based materials influence the cell-substrate interaction.

Diana Voigt, Ina Prade, Michael Meyer, Enno Klüver

Research Institute of Leather and Plastic Sheeting (FILK) gGmbH, Collagen, Freiberg, DE

Introduction

Collagen is the most abundant structural protein in the vertebrate body. Natural crosslinks, caused by enzymes, prevent the dissolving of the collagen tissue. However, when using collagen as a medical product, crosslinks need to be introduced to regulate the resorption in the body and to stabilize the structure of the collagen scaffolds or membranes. The most favored crosslinkers are carbodiimides, like 1-ethyl-3-(3-dimethylaminopropyl)-carbodiimide (EDC), and aldehydes, like glutaraldehyde (GDA). An alternative to chemical treatment is the physical crosslinking by dehydrothermal (DHT) treatment. Those crosslinking processes represent two different groups, the zero-length crosslinking by direct coupling of amino and carboxyl groups (DHT and EDC), and crosslinking via a linker, the aldehyde bridge (GDA).

Within these two different groups, the properties of the collagen material might be different as well. This work aims to reveal the changes in the collagen material, caused by different crosslinkers. These created effects were correlated with the cell behavior of three different cell types.

Experimental Methods

The investigated samples are collagen sheet, consisting of fibrillated acid soluble collagen. The collagen sheets were crosslinked with either EDC or GDA at different concentrations, to modify the mechanical properties. In the case of DHT, different temperatures (60 – 120°C) in a vacuum were applied to alter the mechanical properties. To investigate these differences in the structure and the mechanical behavior, atomic-force microscopy (AFM), in particular, the atomic-force spectroscopy (AFS) is used. With AFS the local morphological and mechanical properties of the collagen material are obtained in one single measurement run.

Furthermore, the use of a stress-strain module gives insights into the macroscopic behavior of the collagen material. The combination of these techniques points to a fascinating behavior in dependency on the crosslinker. To correlate the mechanical and structural properties with the cell behavior of three different cell types (endothelial cells, fibroblasts, and chondrocytes), we performed *in vitro* cell experiments on adhesion, and proliferation.

Results and Discussion

Collagen materials, crosslinked with GDA, show an increase in the Young's modulus (measured by AFM), but no increase in the strain (measured by stress-strain module) compared to non-crosslinked collagen materials. In contrast, crosslinking with EDC or DHT induces an increase in the Young's modulus, while the strain decreases. Additionally, GDA crosslinking causes a higher surface roughness of the collagen material, while the roughness decreases, when crosslinked with EDC or DHT. These effects are dependent on the crosslinker concentration as well. The mechanical changes of the collagen sheet did not affect the adhesion or proliferation of HUVECs and fibroblasts. Only the structural differences show an influence of cell behavior.

Conclusion

The present work identified, the effects of different crosslinking mechanisms on the mechanical and structural properties of collagen materials. The selection of a specific crosslinker can help to improve cell growth by adjusting the structure of the surface and the mechanical properties of a collagen material according to the cell type used.

Acknowledgement

We acknowledge the funding of this project by the BMWi (Innokom Ost VF).

PS1-14-216

How does fibronectin adhere to ceramic biomaterial surfaces? – An atomistic study

Susan Köppen[1,4], Myriam Uhrhan[1,2], Martin Kulke[3], Norman Geist[3], Walter Langel[3], Dorothea Brüggemann[2,4]

[1]University of Bremen, Faculty of Production Engineering and BCCMS, Hybrid Materials Interfaces Group, Bremen, DE; [2]University of Bremen, Faculty of Physics and Electrical Engineering, Institute for Biophysics, Bremen, DE; [3]University of Greifswald, Institute of Biochemistry, Bipophysical Chemistry Group, Greifswald, DE; [4]University of Bremen, MAPEX Bremen Center for Materials and Processes, Bremen, DE

Introduction

Fibronectin (Fn) is one of the main components in the nanofibrous extracellular matrix and is involved in complex mechanobiological interactions of cell adhesion [1]. However, the ability of fibronectin to arrange into a fibrillar network *in vivo* is still not fully understood. In 2005 Schwarzbauer *et al* [2] introduced a model for the *in vivo* fibrillogenesis of fibronectin, which has since been recognized as a universal model. In this model, individual Fn type III modules and the C-terminal interchain domain are very exposed. Recently, Raoufi *et al* presented an *in vitro* method to induce fibrillogenesis of fibronectin by extrusion through nanoporous ceramic membranes [3]. In order to investigate the potential of ceramic materials as initiators for *in vitro* fibrillogenesis, we have investigated the interaction of individual Fn type III modules with ceramic surfaces *in silico*.

Experimental Methods

The adhesive properties of individual five Fn type III modules, the highly flexible connectivity region as well as a newly introduced structural model for the Fn interchain domain [4] with two different ceramic surfaces (SiO_2 [5] and Al_2O_3 [6]) were investigated using classical molecular dynamics simulations. The charge density of the material surfaces was adjusted according to the physiological pH value.

First, orientation - dependent adhesion forces on alumina and silica surface models were determined for all modules using the AMBER program package. Subsequently, the module orientations, which yielded maximum force peaks during interaction with the respective ceramic surfaces, were used as initial configuration for longer dynamic simulations with the GROMACS code to determine thermodynamically stable adsorption configurations.

Results and Discussion

Depending on their orientation towards the different ceramic surfaces, all modules exhibited repulsive and attractive interactions. The resulting maximum interaction forces of individual module orientations varied significantly between values from 0.3 nN to 1 nN per module for the various ceramic surfaces. However, other Fn modules showed approximately the same maximum forces for both materials surfaces. In particular, for the FN interchain domain we found the absolute highest difference of the interaction forces with more than 1 nN on the alumina surface whereas silica surfaces only yielded maximum interaction forces of about 0.35 nN. Consequently, the different fibronectin modules exhibited different preferred orientations on the ceramic materials. In particular, this led to varying accessibility of the RGD domain in 10 Fn III (see Figure 1), which is important for integrin-mediated cell adhesion. In addition to the maximum force peak, however, the modules and their orientations are also disputed with regard to their thermodynamic equilibrium adsorption forces and their accessibility to the material surface.

Conclusion

In summary, our results facilitate a basic understanding of material-driven fibrillogenesis of fibronectin *in vitro*. In future experimental studies the findings of our *in silico* studies will be highly relevant for tailoring ceramic biomaterial surfaces to control cell adhesion.

References

[1] V. Vogel, Annual Review of Physiology, 80 (2018) 353
[2] Y. Mao, J. E. Schwarzbauer, Matrix Biology, 24 (2005), 389
[3] M. Raoufi, T. Das, I. Schoen, V. Vogel, D Brüggemann and J.P. Spatz, Nano Letters, 15 (2015) 6357
[4] M. Kulke, M. Uhrhan, B. Ohler, N. Geist, D. Brüggemann, W. Langel, S. Köppen, submitted (2019)
[5] A. Butenuth, G. Moras, J. Schneider, M. Koleini, S. Köppen, R. Meißner, L. B. Wright, T. R. Walsh, L. Colombi Ciacchi, Physica Status Solidi (b), 249 (2012) 292
[6] S. Lid, S. Köppen, L. Colombi Ciacchi, Computational Materials Science, 140 (2017) 307

Acknowledgement

We gratefully acknowledge funding via the Emmy Noether Programme of the Deutsche Forschungsgemeinschaft.

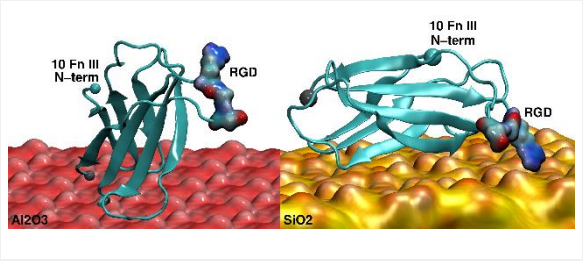

Figure 1: 10 Fn III module on ceramic materials surfaces
The 10 Fn III module with the labelled cell adhesion sequence RGD on two different ceramic material surfaces (left) aluminium oxide and (right) silicon oxide are shown. The orientations shown correspond to the configuration that yielded the highest interaction force. While 10 Fn III with a beta sheet lies flat on silica and the RGD sequence appears executed to the surface, the RGD sequence on alumina points directly into the solution phase.

2:45 p.m. – 3:45 p.m.

Hall 1 / Exhibition Area

PS1-15 | Stem cells and differentiation

PS1-15-217

Stem cell mechanosensation on gelatin methacryloyl (GelMA) stiffness gradient hydrogels

Yu Suk Choi[1], Claire Kim[1], Jennifer Young[2], Andrew Holle[2], Joachim Spatz[2]

[1]University of Western Australia, Human Sciences, Perth, AU; [2]Max Planck Institute for Medical Research, Cellular Biophysics, Heidelberg, DE

Introduction

Stiffness gradient hydrogels are a useful platform for studying mechanical interactions between cells and their surrounding environments.

Experimental Methods

Here, we developed linear stiffness gradient hydrogels by controlling the polymerization of gelatin methacryloyl (GelMA) via differential UV penetration with a gradient photomask. Based on previous observations, a stiffness gradient GelMA hydrogel was created ranging from ~ 4 to 13 kPa over 15 mm (0.68 kPa/mm), covering the range of physiological tissue stiffness from fat to muscle, thereby allowing us to study stem cell mechanosensation and differentiation.

Results and Discussion

Adipose-derived stem cells on these gradient hydrogels showed no durotaxis, which allowed for the screening of mechanomarker expression without confounding directed migration effects. In terms of morphological markers, cell aspect ratio showed clear positive correlation to the underlying substrate stiffness, while no significant correlation was found in cell size, nuclear size, or nuclear aspect ratio. Conversely, expression of mechanomarkers (i.e. Lamin A, YAP, and MRTFa) all showed a highly significant correlation to stiffness, which could be disrupted via inhibition of non-muscle myosin or Rho/ROCK signalling. Furthermore, we showed that cells plated on stiffer regions became stiffer themselves, and that stem cells showed stiffness-dependent differentiation to fat or muscle as has previously been reported in the literature.

Conclusion

Stiffness gradient GelMA hydrogels provide a platform to screen stem cell mechanotransduction, differentiation, and migration over a wide range of physiological tissue stiffness values in one sample. In this study, shallow gradient hydrogels fabricated via UV polymerization through a gradient photomask enable screening of both phenotypic and genotypic changes in ASCs at high-resolution. While this study employed only one gradient strength (0.68 kPa/mm) due to the fact that it did not induce durotaxis, variations of this platform with simple modification to the gradient photomask or hydrogel components can enable a diverse range of stiffness gradients for various applications in cell biology. The nature of GelMA also has the potential of generating a gradient in 3D after cell encapsulation.

References

W.J. Hadden, J.L. Young, A.W. Holle, M.L. McFetridge, D.Y. Kim, P. Wijesinghe, H. Taylor-Weiner, J.H. Wen, A.R. Lee, K. Bieback, B.-N. Vo, D.D. Sampson, B.F. Kennedy, J.P. Spatz, A.J. Engler, Y.S. Choi, Stem cell migration and mechanotransduction on linear stiffness gradient hydrogels, Proceedings of the National Academy of Sciences 114(22) (2017) 5647-5652.

Acknowledgement

This study work was supported by National Health and Medical Research Council Grant PG1098449 (to Y.S.C), Heart Foundation Future Leader Fellowship 101173 (to Y.S.C) and Department of Health, Western Australia, Merit awards – project and fellowship (to Y.S.C).

PS1-15-218

Functional fibrin-based hydrogels for controlling cell/biomaterial interactions in biohybrid implants

Svenja Wein[1,2], Hanna Malyaran[1,2], Norina Labude[1,2], Stephan Rütten[3], Nicole Terefenko[4,5], Martin K. Graff[4,5], Miriam A. Al Enezy-Ulbrich[4,5], Andrij Pich[4,5], Sabine Neuss[1,2]

[1]RWTH Aachen University, Helmholtz Institute for Biomedical Engineering, BioInterface Group, Aachen, DE; [2]RWTH Aachen University, Institute of Pathology, Aachen, DE; [3]RWTH Aachen University, Electron Microscopic Facility, University Clinics, Aachen, DE; [4]RWTH Aachen University, DWI - Leibniz Institute for Interactive Materials, Aachen, DE; [5]RWTH Aachen University, Institute for Technical and Macromolecular Chemistry, Research Area Functional and Interactive Polymers, Aachen, DE

Introduction

Today's implant research faces the challenge of improving both the biocompatibility and reproducibility of implants. The goal is to move away from laboratory scale to automated solutions that also allow for patient-specific individualization. Biohybrid implants, for example, consisting of a technical component and a patient-specific component, are suitable for this purpose. The aim of the project is the development of a biohybrid heart valve based on a fibrin-gel matrix with textile reinforcement. The focus is in particular the development of a functional tool-box for fibrin-based hydrogels and the analysis of the direct cell/biomaterial interactions as well as the long-term behaviour of cells in the biohybrid implant. In concrete terms, this means that new biohybrid hydrogels from fibrinogen and poly(*N*-vinylcaprolactam) copolymers will be developed first. Here, special attention is paid to controllable mechanical properties, variable morphology and controllable degradation behaviour. Human stem cells are cultured on the hydrogel surface as well as inside the hydrogel so that the compatibility of the gel with regard to viability, proliferation, apoptosis and necrosis behaviour and cytotoxicity can be analyzed. The influence of hydrogel properties on stem cell differentiation with respect to adipogenic, osteogenic, chondrogenic and in particular myogenic differentiation (see Figure 1), as well as matrix remodeling and vascularization will be investigated and bioinformatic analyses of long-term behaviour will be used for data visualization.

Experimental Methods

The myogenic differentiation of human stem cells, for example, is initially carried out over 21 days on cell culture plates and, after successful establishment of specific markers, transferred to the hydrogels. The differentiation of human stem cells into muscle cells is induced by the addition of specific growth factors such as TGF-β_1 and BMP4. Special attention is paid to the clear distinction between the contractile and the synthetic phenotype of smooth muscle cells. For the later application of the heart valve only muscle cells of the contractile phenotype are required, therefore a targeted differentiation is of great importance.

The analysis is performed by RT-PCR, immunofluorescence and scanning electron microscopy, with particular emphasis on the expression of the markers smooth muscle myosin heavy chain, myocardin, vinculin, smoothelin and N-cadherin, which are considered as late markers for smooth muscle cells of the contractile phenotype. In order to obtain the best possible composition of the hydrogel for the respective application, the individual parameters such as fibrinogen concentration, thrombin concentration, type of copolymer and buffer were tested against each other in different concentrations and characteristics. The respective morphology of the hydrogels was examined by scanning electron microscopy (see Figure 2), while the specific cell behaviour on the gels was analyzed by FDA/PI staining.

Results and Discussion

Initial experiments have shown that the use of copolymers can alter the properties of the gels, so that faster cross-linking of the hydrogel takes place. Long-term stable hydrogels, which support the proliferation behaviour of human stem cells, have been developed so that the myogenic differentiation of the cells on the gels can be achieved in a subsequent step.

Conclusion

Future experiments are designed to unravel specific parameters measurable *in vitro* to predict implant behaviour after transplantation *in vivo*.

Acknowledgement

Keywords (field of the template during submission was not editable):

- main keyword: stem cells and cell differentiation
- additional keyword 1: cardiovascular incl. heart valve
- additional keyword 2: hydrogels for TE applications

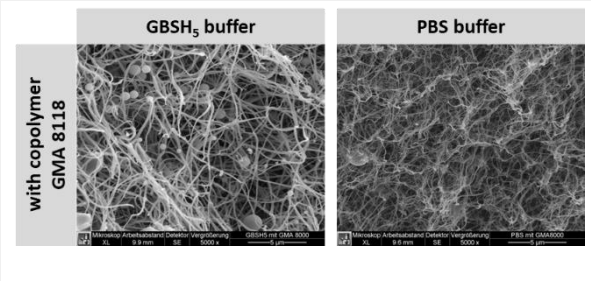

Exemplary scanning electron microscope views of two hydrogels with different buffer composition
The figure shows the morphological composition of two fibrin hydrogels with GBSH5 buffer or PBS buffer and the copolymer GMA 8118 which is glycidyl methacrylate with a molecular weight of 8118 g/mol.

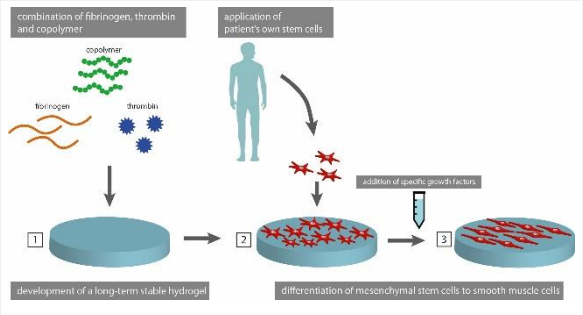

Project outline with experimental procedure of the cell differentiation and biomaterial interaction
After the establishment of a protocol for long-term stable fibrin-based hydrogels in combination with copolymers, human stem cells are seeded on the surface and differentiated into smooth muscle cells.

PS1-15-219

Enhancement of cell-to-cell communications by electrical stimulation on ceramic biomaterials

Miho Nakamura[1,2], Teuvo Hentunen[1], Jukka Salonen[1], Kimihiro Yamashita[2]

[1]University of Turku, Turku, FI; [2]Tokyo Medical and Dental University, Tokyo, JP

Introduction

Ceramic biomaterials are used for clinical applications as bone grafts to reconstruct bone tissue in defects. Both bone-forming osteoblasts and bone-resorbing osteoclasts play prominent roles in bone formation surrounding the implanted ceramic biomaterials. We designed the osteocyte-stimulating biomaterials by electrical charges[1]. Although osteoblasts become trapped within mineralized bone as osteocytes and are responsible for maintenance of the bone matrix, there are few studies on the interaction between the osteocytes and ceramic biomaterials. In the present study, the interactions of osteocytes with osteoblasts and osteoclasts through the cell-to-cell communications on ceramic biomaterials were investigated.

Experimental Methods

Osteocyte-osteoblast culture: Osteoblast-like cells (MC3T3-E1) were labeled by simultaneously calcein and DiI. Labeled cells were dropped onto confluent unlabeled osteocyte-like cells[2] (MLO-Y4, kindly gifted from Prof. Bonewald) on hydroxyapatite (HA) samples with or without the electrical polarization. After the incubation, cells were observed by a fluorescence microscope.

Osteocyte-osteoclast culture[3]: Osteocyte-like cells were co-cultured with bone marrow cells (BMC) isolated from mouse femurs (C57Bl/6J, male, 10-week-old) on the synthesized carbonate-substituted hydroxyapatite (CA) with or without the electrical polarization. The fixed cells were stained for tartrate-resistant acid phosphatase (TRAP). The cells adhered to the samples were stained with rhodamine- phalloidin and Hoechst. After removing the cells, the resorption pits were observed using scanning electron microscope and quantified using laser microscope.

Results and Discussion

The MLO-Y4 cells having connections with MC3T3-E1 cells were visualized with calcein got through from osteoblasts into osteocytes via gap junction. Since the DiI does not get through the gap junction, MC3T3-E1 cells were positive for both calcein and DiI. The number of the MLO-Y4 cells positively stained for calcein was larger on the HA with electrical polarization than that on the conventional HA. This result show that the electrical stimulation has effects on the osteoblast-to-osteocyte communication.

The giant cells with multiple nuclei were formed both on the synthesized CA after a co-culture of MLO-Y4 with BMC. These cells were positively stained for TRAP. Actin rings, which are specific markers for activated osteoclasts to resorb the substrata, were formed in osteoclasts on the CA. As a result, the resorption pits were formed on CA. The formation of actin rings and resorption pits were enhanced on the CA with electrical polarization. This result show that the electrical stimulation has effects on the osteoclast-to-osteocyte communication. The enhanced differentiation and activation of osteoclasts on the CA can be explained by the effects of the electrical polarization of the substratum, the cell-to-cell interactions formed and the secretion of differentiation factors from the MLO-Y4 cells.

Conclusion

These results suggest that the electrical stimulation has effects on the osteocytes-osteoblasts and osteocytes-osteoclasts communications.

References

1. Kobayashi T, et al., J Biomed Mater Res 57: 477-484, 2001
2. Kato Y. *et al*., J Bone Miner Res 12: 2014-2023, 1997
3. Nakamura M, et al. ACS Biomater. Sci. Eng. 2: 259-67, 2016

Acknowledgement

This study was supported in part by Grants-in-Aid for Young Scientists B (15K20482), for the Promotion of Joint International Research (Fostering Joint International Research) (15KK0299) and Grant for Basic Science Research Projects from The Sumitomo Foundation.

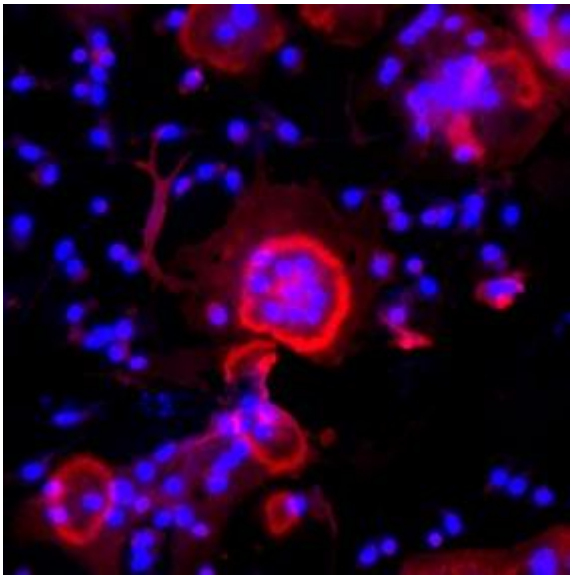

Osteoclast morphology
Multinuclear giant cells were formed on CA after co-culture of osteocyte-like cells with bone marrow cells without any differentiation factors.

PS1-15-220

Cellular traction on compliant scaffolds potentiates BMP signaling

Erik Brauer[1,2], Sophie Schreivogel[1,2], Petra Knaus[2,3], Georg Duda[1,2], Ansgar Petersen[1]

[1]Charité - Universitätsmedizin Berlin, Julius Wolff Institute, Berlin, DE; [2]Charité - Universitätsmedizin Berlin, Berlin-Brandenburg School for Regenerative Therapies, Berlin, DE; [3]Freie Universität Berlin, Institut für Chemie und Biochemie, Berlin, DE

Introduction

Bone morphogenetic proteins (BMPs) are growth factors with a strong osteoinductive potential and are frequently applied in the treatment of large bone defects to foster the healing outcome. Biomaterials are mostly regarded as delivery platforms via which the release of BMPs can be controlled [1]. However, while effects of extrinsic mechanical load are described *in vitro* and *in vivo [2,3]*, little is known about how intrinsic biomaterial properties affect the cellular response to endogenous BMP as well as BMP stimulation. With this study, we aim to identify biomaterial parameters that favor an enhanced cellular response towards BMP. An improved understanding could allow an optimized and more specific use of BMPs in clinical applications in order to overcome currently occurring side effects.

Experimental Methods

Macroporous scaffolds were fabricated from porcine collagen by directional freezing and freeze-drying in cooperation with Matricel GmbH, Herzogenrath, Germany. As a second material platform, 2D polyacrylamide (PAA) gels were produced at varying stiffness by modulating the monomeric acrylamide content. Human fetal osteoblasts (hFOBs) were selected, as they are a frequently used cell line to study BMP-responsiveness. Cellular behavior inside scaffolds was analyzed by confocal imaging for cytoskeleton (actin), cell adhesion (phospho-Paxilin), Lamin A and YAP as well-known stiffness-responsive markers. Cell response to BMP2 stimulation was analyzed both by gene expression (qPCR) and by western blotting of phosphorylated Smad (pSmad).

Results and Discussion

In accordance with previous reports [4], hFOBs showed a reduced BMP response on very soft (<2kPa) compared to stiffer (>10kPa) 2D PAA gels which correlated with reduced attachment and a more round morphology. Intriguingly, we observed that cells exhibited an enhanced BMP response when seeded inside soft 3D macroporous collagen scaffolds (<1kPa) compared to stiffer scaffolds (4kPa and 34kPa). Confocal microscopy revealed that cells were equally spreading and proliferating in all materials. Most strikingly, we found that cells on soft matrix showed increased numbers of focal adhesions and higher levels of phospho-myosin light chain (pMLC). Furthermore, levels of Lamin A were enhanced on soft matrix. YAP showed high nuclear accumulation across all stiffness ranges in 3D. Time-lapse microscopy in 3D revealed that cells were equally migratory inside all collagen scaffolds. Most interestingly, cellular traction exerted during movement induced a strong deformation of the underlying biomaterial selectively in the softest scaffold. In contrast to that, little to no movement was detected for stiffer biomaterials. We observed an inverse stiffness dependency of hFOB behavior cultured on 2D substrates compared to a macroporous 3D environment. This was not solely limited to BMP signaling response but was also found consistently in various stiffness-responsive markers such as pMLC, Lamin A and YAP. Together, these observations suggest that cells cultivated on soft 3D scaffolds adopt features that are usually associated with a stiffer 2D environment. A factor that might contribute to this behavior could be the observed dynamic cell-material interaction occurring inside the 3D

biomaterial: while 2D substrates such as PAA gels permit only a very limited mechanical interaction of the cells through the material, there is a direct mechanical communication between cells in soft macroporous environments.

Conclusion

Our data further support previous reports of a long-range collective mechano-sensation inside macroporous collagen scaffolds [5], which implies mechanical communication via the underlying scaffold. This renders a highly dynamic environment forcing cells to constantly adapt and respond to transmitted signals that we found to hold beneficial effects for growth factor signaling such as BMPs. Together, these findings highlight how cell-material interactions can modulate response to growth factors in a regenerative setting.

References

[1] B.-R. Kim, T. B. L. Nguyen, Y.-K. Min, B.-T. Lee, *Tissue Eng. Part A***2014**, *20*, 3279.

[2] J. Kopf, A. Petersen, G. N. Duda, P. Knaus, *BMC Biol.***2012**, *10*, 37.

[3] C. Schwarz, C.-E. Ott, D. Wulsten, E. Brauer, S. Schreivogel, A. Petersen, K. Hassanein, L. Roewer, T. Schmidt, B. M. Willie, G. N. Duda, *JBMR Plus***2018**, *2*, 174.

[4] J. Du, X. Chen, X. Liang, G. Zhang, J. Xu, L. He, Q. Zhan, X.-Q. Feng, S. Chien, C. Yang, *Proc. Natl. Acad. Sci.***2011**, *108*, 9466.

[5] D. Könnig, A. Herrera, G. N. Duda, A. Petersen, *J. Tissue Eng. Regen. Med.***2017**, *4*, 524.

Acknowledgement

This work was funded bythe DFG research group FOR2165 “Regeneration in Aged Individuals” and the Einstein Center for Regenerative Therapies. E.B. and S.S. are members of the DFG graduate school 203 “Berlin-Brandenburg School for Regenerative Therapies.”

PS1-15-221

Nanofibrous engineered matrix induces trans-differentiation of C2C12 myoblasts to osteoblast phenotype via BMP-dependent signaling

Hee-Yeon Jo[1], Joung-Hwan Oh[1], Jae Hyung Kim[1], Kyung Mi Woo[1,2]

[1]Seoul National University, Department of Molecular Genetics, Dental Research Institute and BK21Plus Program, School of Dentistry, Seoul, KR; [2]Seoul National University, Department of Pharmacology & Dental Therapeutics, School of Dentistry, Seoul, KR

Introduction

Extracellular matrix (ECM) is known to support cells structurally and biochemically and to provide micro-environments for cell differentiation. As an artificial ECM, nano-fibrous engineered matrix can modulate the differentiation. However, the underlying mechanisms remain to be elucidated yet.

Bone morphogenetic proteins (BMPs) is the key regulator of BMP-dependent signaling for osteoblast differentiation. BMPs bind to receptors and induce Smad-dependent or non-dependent signaling in myoblasts. This signaling promotes osteogenic transcription factors, such as Runx2, osterix, and osteocalin, finally, induces osteoblast differentiation and maturation.

We studied for the potentials of trans-differentiation of myoblasts on nano-fibrous matrix

Experimental Methods

A polystyrene fiber (PSF) matrix was prepared by electrospinning. The PSF matrix fixed on cell culture dish was immersed in 70% ethanol for a day and then distilled water for 8h to remove any residual. The C2C12 myoblasts cultured on PSF sheet was differentiated in osteogenic condition for 4 days. After 4 days for osteoblast differentiation, we assessed the variation of proteins and gene expressions related with osteoblast differentiation by Western blot analysis, qPCR, and ELISA. Also, we evaluated osteoblast differentiation of myoblasts cultured on matrix by alkaline phosphatase (ALP) activity.

Results and Discussion

The myoblasts cultured on PSF exhibited osteoblast phenotypes; increased ALP activity and expressions of Runx2, osterix, and osteocalcin. Interestingly, the cells on PSF expressed BMP2 highly, confirmed by qPCRs, Western blot analysis, and ELISA. Phosphorylation of Smad1/5/8 in BMP-induced intracellular signaling was increased in the cell on PSF.

We demonstrate that C2C12 myoblasts grown on an electrospun polystyrene fiber matrix (PSF) can be trans-differentiated to osteoblast phenotypes through up-regulated BMP2 expression and its signaling.

Conclusion

Taken together, these results demonstrate the nanofibrous engineered matrix supports trans-differentiation of myoblasts to osteoblasts by enhancing BMP-dependent signaling.

References

1. Rahman et al. Fibrous topography-potentiated canonical Wnt signaling directs the odontoblastic differentiation dental pulp-derived stem cells. *ACS Applied materials & Interfaces*. **2018**, 10, 17526-17541

2. Oh et al. Suppression of Runx2 protein degradation by fibrous engineered matrix. *Biomaterals*. **2011**, 32, 5826-5836

Acknowledgement

Authors wish to acknowledge the financial support from the National Research Foundation of Korea (NRF-2018R1A5A2024418).

PS1-15-222

Chondrogenic Effect of Kartogenin on an Immortalized Cell Line Derived from Mesenchymal Stromal Cells Isolated from Human Bone Marrow

Carolina G. Varela[1,2], Cristina R. Pereira[1,2], Elena F. Burguera[1,2,3], Tamara H. Gómez[1,2,3], Noa Goyanes[1], Ana L. Oliveira[4], Francisco J. Blanco[1,2], **Joana Magalhaes**[1,2,3]

[1]Unidad de Medicina Regenerativa. Grupo de Investigación en Reumatología (GIR). Instituto de Investigación Biomédica de A Coruña (INIBIC). CHUAC. SERGAS., A Coruña, ES; [2]Centro de Investigaciones Científicas Avanzadas (CICA). Universidad de A Coruña (UDC)., A Coruña, ES; [3]Centro de Investigación Biomédica en Red (CIBER)., Madrid, ES; [4]CBQF - Centro de Biotecnologia e Química Fina, Laboratório Associado, Escola Superior de Biotecnologia, Universidade Católica Portuguesa, Porto, PT

Introduction

Even though significant advances have been achieved during the last decades, osteoarthritis (OA) remains a disease with no cure. Mesenchymal stromal cells (MSCs) are currently being tested in several regenerative medicine approaches, however, during chondrogenic stimulation, a stable hyaline-like cartilage phenotype cannot be obtained, as differentiation seems to resemble an endochondral ossification developmental program, forming a transient-like tissue. Kartogenin (KGN) is a small molecule recently described, promoting both reparative and protective effects, hampering the hypertrophic effects of chondrogenesis.[1] The aim of this study is to evaluate the chondrogenic effect of kartogenin on an immortalized cell line obtained from bone marrow-derived MSCs (3a6), using a pellet three dimensional conventional model and gold-standard transforming growth factor 3 (TGF-β3), as positive reference.

Experimental Methods

3a6 cells, originally obtained from a 61-year old Asian woman bone marrow, was cultured under pellet culture system with basal (DMEM, low glucose) or commercial chondrogenic medium, supplemented with 10 ng/ml TGF-β3 (Prospec) or 100nM KGN (SIGMA) for 3, 7, 14 and 21 days. Total RNA was isolated and real-time quantitative reverse transcription-polymerase chain reaction (RT-qPCR) was performed, using custom-made primers for runt-related transcription factor 1 (RUNX1), proteoglycan 4 (PRG4), cartilage intermediate layer protein (CILP), collagens type-II (COL2A1), -X (COL10A1) and -I (COL1A1), using RPL13A as housekeeping. Proteoglycans and zonal markers protein synthesis was evaluated by safranin-O (SO) staining and lubricin/PRG4 and CILP immunohistochemical analysis (both 1:500), respectively. The experiment was performed in triplicate and differences judged using one-way ANOVA with Bonferroni's corrections, considering $p<0.05$ significantly different.

Results and Discussion

The molecular analysis of KGN- and TGF-β3-chondrogenic induced 3a6 pellets is depicted in figure 1A. For zonal markers expression, we observed a significant downregulation in PRG4 with time, concomitant with an upregulation of CILP, for TGF-β3-induced cells, after 14 days. KGN-induced cells expressed a similar tendency for PRG4 although CILP expression was not detected. Nonetheless, PRG4 and CILP were found on the protein level (Figure 1B) for both conditions, depicting a higher protein accumulation during intermediate times (14 days). The studied zonal markers were found heterogeneously distributed, for KGN-induced pellets, being more intense in pellet's bulk. This difference is further supported by proteoglycans SO staining, with an earlier formation of a more mature tissue for KGN- than TGF-β3-induced pellets (Figure 1C). No expression was found for the main hyaline-like cartilage collagen

(COL2A1), for anytime point. RUNX1 was practically unaltered in TGF-β3-induced cells and even though an upregulation, at day 21, for KGN-induced cells was observed, this was not significant. For hypertrophic markers, RUNX2 was upregulated at 14 days, in TGF-β3- whilst in KGN-induced cells, its expression seems to be delayed, although no significant differences were found. In both conditions, COL10A1 was very low, until 21 days. COL1A1 presented a significant upregulation at 14 days for TGF-β3- whilst in KGN-induced cells, expression was progressively upregulated with time, but not significant.

Conclusion

This is the first study to report the chondrogenic effect of kartogenin on 3a6 immortalized human bone marrow MSCs line. On the molecular level, no significant differences were found between KGN- and TGF-β3 chondroinduction, although transition into a hypertrophic phenotype seems to be delayed. On the protein level, zonal markers and proteoglycan synthesis were found improved by kartogenin after 14 days.

References

1. Johnson K et al. Science 2012, 11;336(6082):717-21.

Acknowledgement

This work was financially supported by INTERREG V-A POCTEP Program through European FEDER funds (0245_IBEROS_1_E). The Biomedical Research Network Center (CIBER) is an initiative from Instituto de Salud Carlos III (ISCIII).

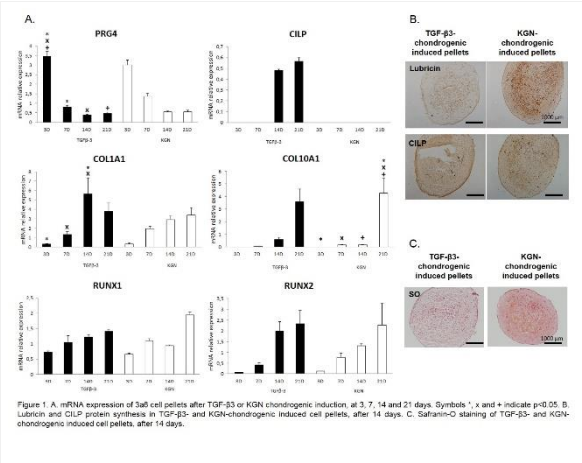

Figure 1

A. mRNA expression of 3a6 cell pellets after TGF-β3 or KGN chondrogenic induction at 3, 7, 14 and 21 days. Symbols *, X and + indicate p<0.05. B. Lubricin and CILP protein synthesis in TGF-β3- and KGN-chondrogenic induced cell pellets, after 14 days. C. Safranin-O staining of TGF-β3- and KGN-chondrogenic induced cell pellets, after 14 days.

PS1-15-223

Research About the Effect of Oxidative Stress On the Ability of Dental Follicle Stem Cells to Form Periodontal Ligament on Bio-Engineered Tooth Root Regeneration

Tingting Lan, Weihua Guo

Sichuan University, Chengdu, CN

Introduction

Previous studies have found that dental follicle stem cells (DFCs) combined with TDM implanted into alveolar fossa can form dentin, cementum and periodontal ligament-like tissue. However, the ability formation of periodontal ligament is relative low and bone adhesion often occurred. Thus, how to improve the differentiation ability of periodontal ligament in DFC is one of the scientific problems to be solved. BMSCs are the main resource of stem cells for many pathological injuries, but their therapeutic effect is not satisfactory in practice. This may be related to the oxidative stress (OS) environment in which stem cells live. Therefore, it is necessary to improve the response of cells to hypoxia. Pretreatment BMSC with antioxidants was proposed to reduce the production of reactive oxygen species (ROS) in hypoxic environment, thereby inhibiting apoptosis and other adverse effects. DFCs have many biological similarities with bone marrow mesenchymal stem cells (BMSCs). Therefore, it is a crucial step to enhance the antioxidant capacity of DFCs as much as possible to promote cell survival, differentiation and even vascular regeneration in tooth regeneration.

Experimental Methods

The mandibles of SD rats were harvested from natal-post 3 days, 5 days, 7 days, 9 days, 11 days, 13days and 15 days and stained with HE and HNE immunohistochemistry.DFCs were isolated and cultured from natal-post 5 days' rats and its biological properties were identified; 25um H_2O_2 was used to culture the DFCs for 24 hours to cause the OS of the cells; 2mM antioxidant of N-Acetyl-cysteine (NAC) was used to control OS. The experiment was divided into three groups as blank group (DFCs), control group (H_2O_2 +DFCs+ NAC) and experimental group (H_2O_2 +DFCs). DFCs compound TDM were planted to the mandible of the 10-weeks years-old rats as the bio-engineered tooth root.

Results and Discussion

There was no obvious oxidative stress in normal root tissues, which indicated that the oxidative stress level of DFCs was low in physiological condition. When planted in the mandible of rats, the oxidative stress level of bio-engineered tooth root increased significantly in the first three days, but can be decreased by NAC. The ability of periodontal ligament formation of the control group was significantly higher than that of the experimental group.

Conclusion

NAC can control OS and thus promote the ability of periodontal ligament formation in the bio-engineered tooth root.

References

1. Weihua Guo, Yong He, Xiaojun Zhang, Wei Lu, Chunmei Wang, Hua yu, Yuan Liu, Yuan Li, Yalei Zhou, JingZhou, Manjing Zhang, Zhihong Deng, Yan Jin.The use of dentin matrix scaffold and dental follicle cells for dentin regeneration. Biomaterials,2009;30(35):6708-6723.

2. Rui Li, Weihua Guo, Bo Yang, Lijuan Guo, Lei Sheng, Gang Chen, Ye Li, Qing Zou, Dan Xie, Xiaoxue An, Yali Chen, Weidong Tian. Human treated dentin matrix as a natural scaffold for complete human dentin tissue regeneration. Biomaterials, 2011;32(20):4525-4538.
3. Watanabe Jun, Yamada Masahiro, Niibe Kunimichi, Zhang Maolin, Kondo Takeru, Ishibashi Minoru, Egusa Hiroshi. Preconditioning of bone marrow-derived mesenchymal stem cells with N- Acetyl-L-cysteine enhances bone regeneration via reinforced resistance to oxidative stress. Biomaterials,2018,185:25-38.
4. Hinz, B. Formation and function of the myofibroblast during tissue repair. J. Investig. Dermatol. 2007, 127, 526–537.
5. Malda J, Rouwkema J, Martens D.E, le Comte E.P, Kooy, F.K.; Tramper J, van Blitterswijk CA, Riesle, J. Oxygen gradients in tissue-engineered PEGT/PBT cartilaginous constructs: Measurement and modeling. Biotechnol. Bioeng. 2004, 86, 9–18.
6. Kellner K, Liebsch G, Klimant I, Wolfbeis O.S, Blunk T, Schulz M.B, Göpferich A. Determination of oxygen gradients in engineered tissue using a fluorescent sensor. Biotechnol. Bioeng. 2002, 80, 73–83.
7. Radisic M, Malda J, Epping E, Geng W, Langer R, Vunjak-Novakovic G. Oxygen gradients correlate with cell density and cell viability in engineered cardiac tissue. Biotechnol. Bioeng. 2006, 93, 332–343.
8. Griffith C.K, George S.C. The effect of hypoxia on in vitro prevascularization of a thick soft tissue. Tissue Eng. Part A 2009, 15, 2423–2434.
9. Anderson, J. Biological responses to materials. Annu. Rev. Mater. Res. 2001, 31, 81–110.
10. Carrier R.L, Rupnick M, Langer R, Schoen F.J, Freed L.E, Vunjak-Novakovic G. Perfusion improves tissue architecture of engineered cardiac muscle. Tissue Eng. 2002, 8, 175–188.
11.Zhu WG, Li S, Lin LQ, Yan H, Fu T, Zhu JH. Vascular oxidative stress increases dendritic cell adhesion and transmigration induced by homocysteine. Cell Immunol,2009;254(2):1 1 0—1 1 6.
12.Song H, Song BW, Cha MJ, Choi JG, H Wang KC. Modification of mesenchymal stem cells for cardiac regeneration. Expert Opin Biol Ther, 2010;10(3):309-319.
13. Xu J, Woods CR, Mora AL, et al. Prevention of endotoxin induced systemic response by bone marrow derived mesenchymal stem cells in mice. Am J Physiol Lung Cell Mol Physiol, 2007;293(1):L131-L141.
14. Gupta N, Su X, Popov B, et al. Intrapulmonary delivery of bone marrow derived mesenchymal stem cells improves survival and attenuates endotoxin induced acute lung injury in mice. J Immunol,2007;179(3):1855-1863.

Acknowledgement

This study was supported by the National Key R&D Program of China (grant number 2017YFA0104800), National Natural Science Foundation of China (grant number 31771062, 31470947), and the Key Research and Development Program of Sichuan Province (2017SZ0031),

PS1-15-224

Electrospun Nanofiber Polycaprolactone Scaffolds Expand Breast Cancer Stem Cell Niche of Triple Negative Breast Cancer Cell Models

Marc Rabionet[1,2], Sabina Couto-Ovejero[1,2], Emma Polonio-Alcalá[1,2], Santiago Ruiz-Martínez[2], Xavier Gallardo[1,2], David Angelats[1,2,3], Sònia Palomeras[2], Joaquim Ciurana[1], Teresa Puig[2]

[1]Product, Process and Production Engineering Research Group (GREP) - University of Girona, Department of Mechanical Engineering and Industrial Construction, Girona, ES; [2]New Therapeutic Targets Laboratory (TargetsLab) - University of Girona, Department of Medical Sciences, Girona, ES; [3]Università degli Studi di Brescia, Department of Mechanical and Industrial Engineering, Brescia, IT

Introduction

Breast cancer stem cells (BCSCs) represent a rare tumor subpopulation which displays self-renewal ability, tumorigenesis, and resistance to radio- and chemotherapy [1]. Moreover, they present the capability to grow in suspension forming spheres and exhibit an enlarged activity of the aldehyde dehydrogenase (ALDH) enzyme [2,3]. Due to these aforementioned characteristics, BCSC population is related to tumor initiation and relapse. This fact gains importance in some specific cancer types with a high recurrence rate, such as the triple negative breast cancer (TNBC) [4]. Moreover, TNBC is characterized by the absence of breast cancer molecular biomarkers amplification, so chemotherapy, radiotherapy, and surgery remain as the only treatments. The elevated relapse rate and the lack of a targeted therapy highlight the need to find new therapeutic options for TNBC. Targeting BCSC population could represent a novel approach for TNBC treatments. However, the study of BCSCs encounters difficulties since standard two-dimensional (2D) *in vitro*culture is proven to induce BCSCs differentiation, losing stem features and converting them to non-stem cancer cells [5,6].

Interestingly, nanofibrous scaffolds have emerged as an alternative option for three-dimensional (3D) *in vitro*culture. Scaffolds, which are composed by a network of filaments mostly made by synthetic materials, mimic the physiological surrounding of cells and the structure of the native extracellular matrix (ECM) [7]. Within scaffolds, cells can establish interactions with adjacent cells and also with polymeric filaments, adopting a more elongated morphology when compared with monolayer 2D culture, where cells are flattened. Previous investigations demonstrated that 3D cell culture maintained and expanded BCSC niche compared with monolayer culture [8,9]. Therefore, scaffolds fabrication and 3D culture of TNBC cells are proposed in the present work in order to study BCSC subset.

Experimental Methods

Poly(ε-caprolactone) (PCL) and electrospinning were chosen as biopolymer and technology to manufacture the scaffolds, respectively. PCL was dissolved into acetone andcharged at a high voltage. Polymer solution was pulled onto a plate and solvent was evaporated, collecting random nanofibers. In this manner, resultant structure mimicked the ECM fibrous nature and cells could adopt a more *in vivo*morphology. Two different PCL concentrations, 7.5 and 15% PCL w/v, were tested. Both resulting scaffolds were characterized through scanning electron microscopy (SEM) to analyze microstructure and porosity. Afterwards, two TNBC cell models, MDA-MB-231 (mesenchymal-like subtype) and MDA-MB-468 (basal-like), were cultured on 7.5 and 15% PCL scaffolds. Cell morphology and proliferation were analyzed by fluorescence microscopy and MTT assay, respectively. A possible enrichment in stem features was verified with the mammosphere forming assay, the quantification of ALDH activity with ALDEFLUOR kit, and the chemoresistance assay.

Results and Discussion

Scaffolds from 7.5% PCL solution presented non-filamented material known as beads and displayed smaller fiber diametres compared to the 15% PCL meshes. Interestingly, TNBC cells cultured in 15% PCL scaffolds showed higher cell proliferation rate and cell elongation than the other culture supports. Regarding stemness features, both cell lines presented higher mammosphere forming ability and ALDH activity after 3D cell culture, indicating an expansion of BCSCs abilities. Moreover, TNBC cells possessed higher cell survival in scaffolds when treated with the chemoagents doxorubicin and paclitaxel compared to monolayer cultured cells.

Presented results evidence the powerful capacity of electrospinning technology and PCL regarding nanofibers fabrication. Moreover, 15% PCL electrospun meshes are proposed as suitable tools to culture TNBC cells and maintain the differentiation state of the BCSCs niche.

Conclusion

Therefore, 3D cell culture with PCL scaffolds could be useful to study BCSCs population and may trigger the study and development of new specific treatments against this malignant subpopulation, useful for diseases with no targeted therapies such as TNBC.

References

1- Matsui,W.;Wang, Q.; Barber, J.P.; Brennan, S.; Smith, B.D.; Borrello, I.; McNiece, I.; Lin, L.; Ambinder, R.F.; Peacock, C.; et al. Clonogenic multiple myeloma progenitors, stem cell properties, and drug resistance. Cancer Res. 2008, 68, 190–197.

2- Dontu, G.; Abdallah,W.M.; Foley, J.M.; Jackson, K.W.; Clarke, M.F.; Kawamura, M.J.;Wicha, M.S. In vitro propagation and transcriptional profiling of human mammary stem/progenitor cells. Genes Dev. 2003, 17, 1253–1270.

3- Ginestier, C.; Hur, M.H.; Charafe-Jauffret, E.; Monville, F.; Dutcher, J.; Brown, M.; Jacquemier, J.; Viens, P.; Kleer, C.G.; Liu, S.; et al. ALDH1 Is a Marker of Normal and Malignant Human Mammary Stem Cells and a Predictor of Poor Clinical Outcome. Cell Stem Cell 2007, 1, 555–567.

4- Dent, R.; Trudeau, M.; Pritchard, K.I.; Hanna,W.M.; Kahn, H.K.; Sawka, C.A.; Lickley, L.A.; Rawlinson, E.; Sun, P.; Narod, S.A. Triple-negative breast cancer: Clinical features and patterns of recurrence. Clin. Cancer Res. 2007, 13, 4429–4434.

5- Thomas, C.H.; Collier, J.H.; Sfeir, C.S.; Healy, K.E. Engineering gene expression and protein synthesis by modulation of nuclear shape. Proc. Natl. Acad. Sci. USA 2002, 99, 1972–1977.

6- Vergani, L.; Grattarola, M.; Nicolini, C. Modifications of chromatin structure and gene expression following induced alterations of cellular shape. Int. J. Biochem. Cell Biol. 2004, 36, 1447–1461.

7- Knight, E.; Przyborski, S. Advances in 3D cell culture technologies enabling tissue-like structures to be created in vitro. J. Anat. 2015, 747, 746–756.

8- Sims-Mourtada, J.; Niamat, R.A.; Samuel, S.; Eskridge, C.; Kmiec, E.B. Enrichment of breast cancer stem-like cells by growth on electrospun polycaprolactone-chitosan nanofiber scaffolds. Int. J. Nanomed. 2014, 9, 995–1003.

9- Palomeras, S.; Rabionet, M.; Ferrer, I.; Sarrats, A.; Garcia-Romeu, M.; Puig, T.; Ciurana, J. Breast Cancer Stem Cell Culture and Enrichment Using Poly("-Caprolactone) Scaffolds. Molecules 2016, 21, 537.

PS1-15-225

Sulfated glycosaminoglycans interfere with MMP2 activity and MMP2/TIMP3 complex formation - Insights at cellular and molecular level

Claudia D. Müller[1], Gloria Ruiz-Gómez[2], Sarah Vogel[1], Stephanie Möller[3], M. Teresa Pisabarro[2], Ute Hempel[1], Deutsche Forschungsgemeinschaft (Transregio 67, projects A7, B1, and Z2)

[1]TU Dresden, Institute of Physiological Chemistry, Dresden, DE; [2]BIOTEC TU Dresden, Structural Bioinformatics, Dresden, DE; [3]INNOVENT e.V., Biomaterials Department, Jena, DE

Introduction

The extracellular matrix (ECM) is a highly dynamic network constantly remodelled by a fine-tuned protein formation and degradation balance. Matrix metalloproteinases (MMPs) are responsible for ECM degradation. Their activity is controlled by tissue inhibitors of metalloproteinases (TIMPs) and glycosaminoglycans (GAG). Here, we investigated the molecular interplay of MMP2 with different glycosaminoglycan derivatives (GAG) (chondroitin sulfate, hyaluronan (HA), sulfated hyaluronan (SH) and heparin (HE)) and the impact of GAG on MMP2/TIMP3 complex formation.

Experimental Methods

The experiments were performed with human bone marrow stromal cells (hBMSC). GAG derivatives were from INNOVENT e. V. (SH, CS, HA) and commercially acquired (HE). MMP2 enzyme activity was determined with a fluorogenic peptide substrate. MMP2 and TIMP3 levels were analysed with ELISA, Western blot and immunofluorescence staining. Comparative modelling, molecular docking, and dynamics simulations were applied for *in silico*-experiments.

Results and Discussion

Sulfated hyaluronan (SH) and heparin (HE) led to a decrease of MMP2 activity and increased TIMP3 release. Analysing hBMSC morphology, it was seen that only SH supported the alignment of MMP2 and TIMP3 in fibrillar-like structures in the extracellular space, which, based on our molecular models, would be due to a stabilisation of the interactions between MMP2-hemopexin domain and TIMP3-C-terminal tail. Dependent on the temporal sequential order in which the final ternary complex was formed, our models indicated that SH and HA can affect TIMP3-induced MMP2 inhibition through precluding or supporting their interactions, respectively.

Conclusion

Our combined experimental and theoretical approach provides valuable new insights on how GAG interfere with MMP2 activity and MMP2/TIMP3 complex formation. The obtained results evidence GAG as promising molecules for fine-balanced intervention of ECM remodelling, in particular as former studies showed that GAG-modified biomaterials promote osteogenic differentiation of hBMSC [1-3].

References

[1] Ruiz-Gómez G, Vogel S, Möller S, Pisabarro MT, Hempel U. Glycosaminoglycans influence enzyme activity of MMP2 and MMP2/TIMP3 complex formation - Insights at cellular and molecular level. *Sci Rep*, 2019; 9:4905, 1-15.

[2] Hempel U, Preissler C, Vogel S, Möller S, Hintze V, Becher J, Schnabelrauch M, Rauner M, Hofbauer LC, Dieter P. Artificial extracellular matrices with oversulfated glycosaminoglycan derivatives promote the differentiation of osteoblast-precursor cells and premature osteoblasts. *J Biomed Res Int* 2014;938368.

[3] Hempel U, Möller S, Noack C, Hintze V, Scharnweber D, Schnabelrauch M, Dieter P. Sulfated hyaluronan/collagen I-matrices enhance osteogenic differentiation of human mesenchymal stromal cells *in vitro* even in the absence of dexamethasone. *Acta Biomaterialia* 2012;8:4064-4072.

Acknowledgement

This work was funded by the Deutsche Forschungsgemeinschaft (Transregio 67, projects A7, B1, and Z2).

PS1-15-226

The effects of gelatin hydrogel stiffness on MSCs early osteogenic differentiation

Hongxu Meng, Nuria Gavara

Queen Mary University of London, School of Engineering and Materials Science, London, GB

Introduction

Adult mesenchymal stem cells (MSCs) are multipotent, being capable of differentiating into bone, adipose, cartilage tissue, muscle and others[1]. Mechanical stimulation is necessary for osteogenic differentiation[2]. Synthetic stem cell niches have been developed *in vitro*to precisely investigate how stem cell behavior is regulated. Hydrogels, with versatile properties and various applications, are one of the best choices as scaffolds of stem cell research. In this study, a tunable and inexpensive hydrogel was adopted to culture MSCs. The hydrogel is made of gelatin and crosslinked by genipin solution. Gelatin hydrogels crosslinked by genipin are non-toxic and generate a wide range of stiffness[3]. Hydrogels of different stiffness were used to culture MSCs in osteogenic differentiation medium (ODM). The mechanical properties of cells were measured by AFM. Results showed a promising use of gelatin hydrogel in cell differentiation study.

Experimental Methods

Gelatin hydrogels were prepared with type A, porcine gelatin powder dissolved in genipin solution at 40℃ under moderate stirring. Gelatin concentrations of 3% and 6% (w/w) were made for this study. The bulk mechanical properties of hydrogels were measured by compressive using an Instron 3442 device with the following settings parameters: 3 mm/min and 20% strain while the nanoscale mechanical properties were measured by AFM. MSCs sourced bone marrow were used at passage 4 and seeded in a density of 5000 cells/cm^2. MSCs were cultured on petri dish (PD), 3% or 6% gelatin hydrogel in ODM for 3 days. The Young's modulus of MSCs at Day 3 were assessed via AFM. A pyramidal silicon nitride tip, with a cantilever spring constant of ~0.03 N/m was used to scan the cells. At least 10 cells for each condition were tested.

Results and Discussion

The bulk mechanical property of 3% and 6% gelatin hydrogel was 20.91kPa and 42.32kPa respectively (Fig 1). The Young's modulus of gelatin hydrogel showed a positive relationship with gelatin concentration. This can be explained by increased gelatin concentration was accompanied by more polymer entanglement and increased density of covalent crosslinking in the hydrogels. The nanoscale mechanical property determined by AFM was 3.23kPa and 27.71kPa respectively. Both kinds of hydrogel in bulk and nanoscale level demonstrated they were in physiological stiffness range and ideal for stem cell differentiation research.

MSCs cultured on the softest hydrogel attained the lowest Young's modulus (1.55kPa) while cells in PD were the highest (3.04kPa) in Young's modulus (Fig.2). The result showed a positive relationship between the stiffness of cell and the static mechanical environment they experienced at day 3. Moreover, the Young's modulus of MSCs cultured in PD in basal medium (data not shown) was 1.66kPa. Therefore, the chemical and mechanical cues both effect on MSCs stiffness and there was a positive feedback of MSC's stiffness to different gelatin hydrogel stiffness at early osteogenic differentiation stage.

Conclusion

Previous studies have demonstrated broad applications of gelatin hydrogel crosslinked by genipin solution in nerve and skeletal muscle regeneration, cartilage and bone repair, which shows the excellent biocompatibility of gelatin in cell culture and tissue engineering[3]. This kind of hydrogel has a varied stiffness range controlled by different concentrations of gelatin. Their Young's modulus was from several kPa to tens of kPa, which is similar to*in vivo*environment and ideal for *in vitro* cell culture. In our study, the gelatin hydrogels stiffness, as well as the medium, influenced the MSCs stiffness at a very early stage. Our study showed a promising application of gelatin hydrogel in stem cell research and the effects of gelatin hydrogel on MSCs in longer period will be studied afterwards.

References

[1] Tsimbouri P M, Childs P G, Pemberton G D, et al. Stimulation of 3D osteogenesis by mesenchymal stem cells using a nanovibrational bioreactor[J]. Nature Biomedical Engineering, 2017, 1(9): 758.

[2] Rutkovskiy A, Stensløkken K O, Vaage I J. Osteoblast differentiation at a glance[J]. Medical science monitor basic research, 2016, 22: 95.

[3] Gattazzo F, De Maria C, Rimessi A, et al. Gelatin–genipin-based biomaterials for skeletal muscle tissue engineering[J]. Journal of Biomedical Materials Research Part B: Applied Biomaterials, 2018, 106(8): 2763-2777.

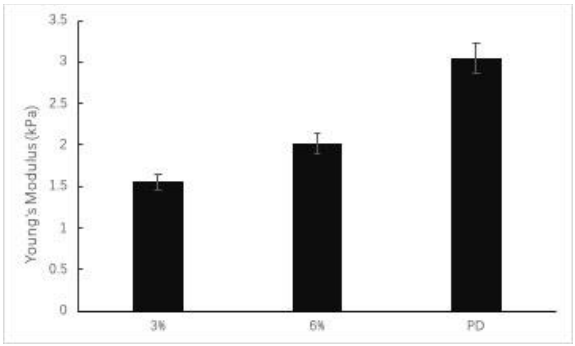

Figure 2 Young's modulus of MSCs on different substrates at Day 3

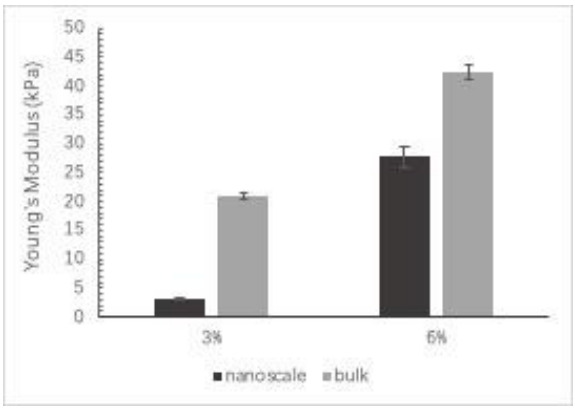

Figure 1 The mechanical properties of gelatin hydrogels

PS1-15-227

A systematic biomaterial screening tool for the identification of key microenvironmental factors for stem cell expansion and differentiation

Richard Wetzel[1,2], Alvin K. Thomas[2], Kristina Thamm[1], Dejan Husman[1,2], Stefanie Hamann[1], Steffen Lück[1,2], Robert Wieduwild[3], Yixin Zhang[2]

[1]denovoMATRIX GmbH, Dresden, DE; [2]Technische Universität Dresden, B CUBE Center for Molecular Bioengineering, Dresden, DE; [3]Leipzig University, Rudolf-Schönheimer-Institute of Biochemistry, Faculty of Medicine, Leipzig, DE

Introduction

The natural cellular environment is a complex interplay of extracellular matrix (ECM) components such as glycosaminoglycans (GAGs) and proteoglycans, soluble factors and cell-cell interactions. Current matrices that facilitate *in vitro* culture of stem cells are either poorly defined ECM extracts or single component polymers that lack the natural complexity. We have developed new matrices that incorporate GAGs and biofunctional peptides allowing the versatile presentation of essential cues of the natural ECM. These matrices are based on a non-covalent hydrogel system and are both chemically defined and modular enabling a bottom up development of complexity.

Experimental Methods

We utilized the hydrogel system in a surface coating protocol and developed a systematic biomaterial screening platform technology. With this tool we screened for optimal conditions for adhesion and growth of a variety of stem cells. Selected matrices were tested for maintenance of stemness and guided differentiation.

Results and Discussion

First, we screened for serum-free expansion of mesenchymal stromal cells (MSCs) and discovered potent biomaterial compositions that also provided enhanced osteogenic differentiation. We further studied the proliferation of induced pluripotent stem cells (iPSC) and identified another unique functional composition to maintain iPSC growth for up to 30 days while preserving their differentiation capacity. Interestingly, these compositions did not support neuronal differentiation. Under neuronal induction conditions, the maturating neurons switched their biomatrix preferences. This indicated that expanding stem cells interactions with their environment is different from that of developing neurons. Furthermore, analysis of the differentiation efficiency of primary neuronal precursor cells provided evidence that the incorporated GAGs provide enhanced neuron development.

Conclusion

In summary, our combinatorial biomatrix screening technology facilitates the identification of optimal environments for expansion and differentiation of stem cells. In addition to a library of biofunctional peptides, our biomatrix is also composed of GAGs, which are essential components of the natural ECM yet poorly interrogated in current biomaterial research. Therewith, we provide a powerful tool to study cell-material interactions and enables the development of defined cell culture protocols for stem cell research, drug-development and cell therapy applications.

References

R. Wieduwild, M. Tsurkan, K. Chwalek, P. Murawala, M. Nowak, U. Freudenberg, C. Neinhuis, C. Werner, Y. Zhang, *J. Am. Chem. Soc.***2013**, *135*, 2919.

R. Wieduwild, R. Wetzel, D. Husman, S. Bauer, I. El-Sayed, S. Duin, P. Murawala, A. K. Thomas, M. Wobus, M. Bornhäuser, Y. Zhang, *Advanced Materials***2018**, *0*, 1706100.

Acknowledgement

The authors thank the EXIST Forschungstransfer grant for financial support as well as the B CUBE, in particular the Zhang lab for their support. We also acknowledge Dr. Manja Wobus and Prof. Martin Bornhäuser for providing the MSCs, experimental work and discussion of results as well as Dr. Katrin Neumann and the Stem Cell Engineering Facility team for their cell culture work and contributions.

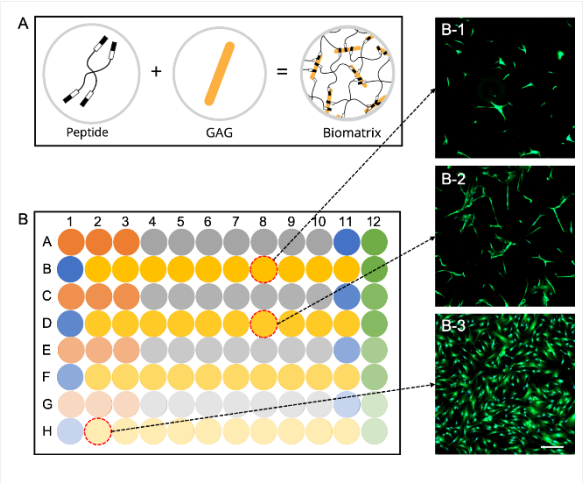

Biomaterial screening to identify functional coatings for serum-free culture of MSC
A) The developed hydrogel system is composed of 2 classes of polymers, biofunctional peptides that are conjugated to starPEG and glycosaminoglycans (GAG). By simple mixing, these molecules form a non-covalent matrix, which can be employed in a surface coating protocol. B) A well plate was coated with 96 different combinations of 4 GAG molecules and 24 peptides. C) MSC, cultured in serum-free media, showed differential adhesion and growth within 3 days of expansion on the provided coatings.

PS1-15-228

Impact of different medium supplements on cultivation of mesenchymal stem cells.

Pavla Sauerova[1,2], Katerina Lochovska[3], Tereza Belinova[2], Robert Pytlik[3], Marie Hubalek Kalbacova[1,2]

[1]1st Faculty of Medicine, Charles University, Institute of Pathological Physiology, Prague, CZ; [2]Faculty of Medicine in Pilsen, Charles University, Biomedical Centre, Pilsen, CZ; [3]1st Faculty of Medicine, Charles University and General University Hospital in Prague, 1st Department of Medicine - Department of Haematology, Prague, CZ

Introduction

Mesenchymal stem cells (MSCs) have high potential to extend options of regenerative medicine. However, effective cultivation of these cells is critical point for their study or application. Massive expansion and induction of optimal conditions for MSCs successful culturing and maintenance of their “stemness” stability still remains a major challenge in the field of tissue engineering. One of the key factors for successful cell culturing is the presence of serum that is critical for short-term and long-term sustaining and expansion of cells in *in vitro* conditions (1,2). In general, fetal bovine serum (FBS) is often considered as a universal standard component of majority of cultivation media. It provides key factors for *in vitro* successful cultivation of cells such as growth factors, vitamins, lipids, hormones and various proteins participating in adhesion, growth, proliferation or migration of wide spectra of cells. However, FBS as typical serum „representative“ has lot of disadvantages especially in field of human medicine – e.g. variable composition, xenogenous origin, high risk of various contaminations and unethical way of its acquirement are indisputable. For all of these negative reasons, there is a great effort to replace FBS by other alternatives (3).

Experimental Methods

Metabolic activity, rate of cell expansion, differentiation capability, colony forming units (CFU-F), mitochondrial status or doubling time of MSCs cultivated in presence of different medium supplements were analysed. Also, light or confocal microscopy and flow cytometry were used for characterization of cells.

Results and Discussion

Effectivity of MSCs culturing in cultivation medium supplemented with several alternatives of FBS - human serum, human platelet lysate or human platelet releasate - was a focus of this study. As a result, marked differences and significant impact of different serum-replacements on metabolic activity, rate of cell expansion, differentiation capability, colony forming units (CFU-F), mitochondrial status or doubling time of MSCs were determined. Furthermore, the data also highlight the topic of serum inactivation, which is often neglected in practice with FBS culturing. As the data show, heat-modification of FBS can significantly change metabolic activity as well as CFU-F rate of MSCs. In other words, heat-modification of serum can markedly affect cell behaviour and thus, it should be taken into account in results interpretation and simultaneously, results derived from non-inactivated and inactivated serum conditions shouldn't be compared to each other.

Conclusion

In summary, there are fields of research where cells are often used as a mere tool for characterisation and evaluation of developed material or its surface. Thus, there is no strong emphasis on cell culturing conditions or it is not in marked interest of researchers in these fields. However, our results point out how much the type of sera (such

essential component for cell cultivation) or its modification can affect cell behaviour before and during experiments and thus, how urgent is the transition from application of FBS to human serum alternatives in future of routine research practise and biomaterial or regenerative medicine.

References

(1) Verdanova M, Sauerova P, Hempel U, Kalbacova MH. Initial cell adhesion of three cell types in the presence and absence of serum proteins. Histochem Cell Biol 2017:1–16. doi:10.1007/s00418-017-1571-7.

(2) Fang C-Y, Wu C-C, Fang C-L, Chen W-Y, Chen C-L. Long-term growth comparison studies of FBS and FBS alternatives in six head and neck cell lines. PLOS ONE 2017;12:e0178960. doi:10.1371/journal.pone.0178960.

(3) Valk J van der, Bieback K, Buta C, Cochrane B, Dirks WG, Fu J, et al. Fetal bovine serum (FBS): Past – present – future. ALTEX - Altern Anim Exp 2018;35:99–118. doi:10.14573/altex.1705101.

Acknowledgement

This study was supported by project NV19-08-00144, PROGRES Q26 provided by Charles University and NPU LO1503-BIOMEDIC.

PS1-15-229

High-throughput screening of micro-topographical chips for the control of stem cell fate

Raveena Bhondi[1], Lucy Di Silvio[1], Lorenzo Veschini[1], Patrick Mesquida[2]

[1]King's College London, Centre for Oral, Clinical and Translational Sciences, London, GB; [2]King's College London, Department of Physics, London, GB

Introduction

The cell-material interface is a potent regulator of cell behaviour and is governed by chemistry, stiffness and topography. There is evidence demonstrating that substrates with patterned topographies are able to direct stem cell fate. Understanding the effect of physical features is an important consideration in the manufacture of novel biomaterials for tissue engineering applications. Using high throughput screening platforms allows the rapid evaluation of combinatorial material properties that influence stem cell behaviour and allows evaluation of cell morphology, spreading and differentiation in an unbiased manner. The aim of this study was to determine the effect of a micro-topographical library on mesenchymal stem cell (MSC) behaviour by assessment of morphology and differentiation, using high-content microscopy and a novel image analysis pipeline.

Experimental Methods

Polydimethylsiloxane (*PDMS*) chips containing an array of micro-patterns that differed in spacing, orientation and aspect ratio were fabricated. The effect of functionalising the patterns with collagen monomers was evaluated by comparing substrates that had been reverse micro-contact printed, completely coated with collagen or not functionalised. In order to identify the effect of different patterns and their ability to induce different MSC morphologies, cells were seeded onto the micro-patterns for 48 hours and stained with Phalloidin for cytoskeletal actin filaments andHoechst to stain nuclei. The cells were then imaged using a high throughput/high content imaging system (Perkin Elmer Operetta CLS) and analysed using an image analysis pipeline developed in-house. Time-course experiments were conducted in order to identify those topographies capable of inducing MSC differentiation towards the osteogenic lineage. Cells were fixed at 48 hours, 7 days, 14 days and 21 days. They were then stained as above for cytoskeletal structures and a panel of differentiation markers associated with different stages of osteogenic lineage commitment; Runx2, Osterix, Alkaline Phosphatase and Osteocalcin. The cells were then imaged and analysed using the high-content imaging system and pipeline.

Results and Discussion

A range of patterns were found to distinctly affect the morphology of MSCs as observed in *Figure* 1. The functionalisation of the patterns was also found to effect cellular behaviour – largely in terms of cell attachment. These findings demonstrated that the MSCs were responsive to the micro-topographical library, with changes observed in the orientation and cytoskeletal organization of the cells. Our screening platform, which used an imaging system and analysis pipeline was able to identify the modulation of morphologies on the different topographies. The preliminary time-course experiments showed that biophysical properties of the microenvironment, in this case, micro-topography was able to modulate differentiation and self-renewal ability. Further work is ongoing in order to confirm these preliminary findings.

Conclusion

Cell-substrate interaction is integral to the design of tissue engineered scaffolds and implants. This micro-fabrication and screening platform provides a novel approach for the control of substrate topography able to modulate stem cell behaviour. We are currently using this platform to identify patterns capable of inducing MSC differentiation towards the osteogenic lineage.

References

Hulshof, F., Papenburg, B., Vasilevich, A., Hulsman, M., Zhao, Y., Levers, M., Fekete, N., de Boer, M., Yuan, H., Singh, S., Beijer, N., Bray, M., Logan, D., Reinders, M., Carpenter, A., van Blitterswijk, C., Stamatialis, D. and de Boer, J. (2018). Mining for osteogenic surface topographies: In silico design to in vivo osseo-integration.

Unadkat, H., Hulsman, M., Cornelissen, K., Papenburg, B., Truckenmuller, R., Carpenter, A., Wessling, M., Post, G., Uetz, M., Reinders, M., Stamatialis, D., van Blitterswijk, C. and de Boer, J. (2018). An algorithm-based topographical biomaterials library to instruct cell fate.

Acknowledgement

Dr Davide Danovi – Centre for Stem Cells & Regenerative Medicine, KCL

Dr Zuming Tang – Centre for Stem Cells & Regenerative Medicine, KCL & Perkin Elmer

Dr Ciro Chiappini – Department of Craniofacial Development & Stem Cell Biology, KCL

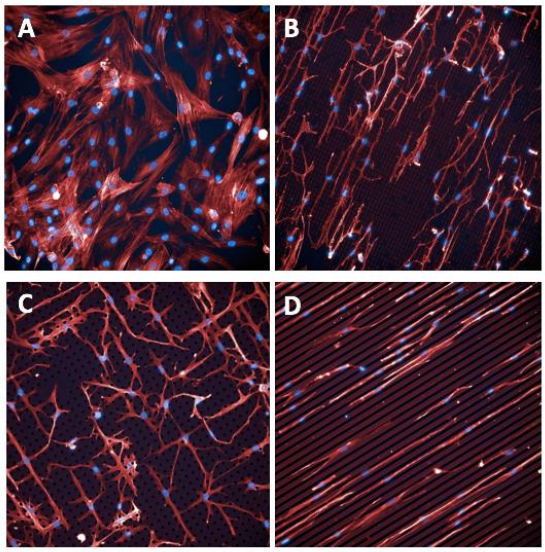

Figure 1. Primary human bone marrow derived mesenchymal stem cells seeded onto the micro-topographical patterns for 48 hours. Stained with Hoechst and Phalloidin. A – Control (no patterning present), B – Cells on pattern of dashes, C – Cells on pattern of dots, D – Cells on a pattern of grooves.

The varying MSC morphologies observed following seeding on different micro-topographies

Figure 1. Primary human bone marrow derived mesenchymal stem cells seeded onto the micro-topographical patterns for 48 hours. Stained with Hoechst and Phalloidin. A – Control (no patterning present), B – Cells on pattern of dashes, C – Cells on pattern of dots, D – Cells on a pattern of grooves.

PS1-15-230

Viscous interactions drive stem cell fate

Eva Barcelona-Estaje, Matthew Walker, Manuel Salmeron-Sanchez, **Marco Cantini**

University of Glasgow, School of Engineering, Centre for the Cellular Microenviroment, Glasgow, GB

Introduction

The tissues that cells inhabit *in vivo* are dynamic and dissipative environments, where rapid and adaptive processes drive the interactions between cells and extracellular matrices (ECMs). However, most synthetic material systems designed up to now to promote the healing of damaged tissues employ static environments, mechanically designed to mimic solely the elastic properties of the native tissue. The viscous behaviour of the substrate, which is an intrinsic property of physiological cell surroundings, is traditionally ignored. Using interfaces with varying viscosity based on supported lipid bilayers (SLBs), we previously demonstrated that cells sense this material property using the same mechanotransductive mechanism, the molecular clutch, that they use to sense purely elastic materials (1). Seminal studies also confirmed that the viscous component of hydrogels contribute to mechanotransduction, and that this dynamic material property can be tailored to promote cell growth and differentiation (2).

In this work, we address the role of viscous interactions in controlling stem cell fate, designing materials that exploit these dissipative interactions to promote cell differentiation and, ultimately, tissue repair. The dissipative interactions between cells and their surroundings are triggered, at a molecular level, by the mobility of the molecules that make up the extracellular matrix. Hence, here we make use of substrates with a tuneable dynamic display of ligands (including cell-matrix adhesion peptides, e.g. RGD, and cell-cell contact motifs, e.g. HAVDI) to study stem cell response to these dissipative interactions. In particular, functionalised SLBs with varying mobility and hydrogels with constant storage modulus and varying loss modulus are used to investigate the effect of dissipation at the interface and in bulk materials, respectively. This will ultimately elucidate stem cell mechanosensing of viscosity and its role in the adhesive cross-talk between integrins and cadherins, and will instruct the design of optimised microenvironments for tissue repair.

Experimental Methods

Supported lipid bilayers with varying mobility and hence viscosity were prepared by following the vesicle fusion method. DOPC and DPPC were used as lipids as they present a fluid and gel phase respectively at cell culture conditions, and glass was used as a non-mobile control interface. Polyacrylamide hydrogels were prepared using different ratios of acrylamide and N,N'-methylenebisacrylamide to obtain gels with equivalent storage modulus and varying loss modulus. All materials were functionalised with varying ratios of RGD and HAVDI. Human mesenchymal stem cells (hMSCs) were cultured on these substrates and parameters such as cell adhesion, protein translocation or expression of transcription factors were investigated via AFM, immunostaining and in-cell western.

Results and Discussion

On purely viscous surfaces based on SLBs, an increase in cell area and cell adhesion, quantified via focal adhesion staining and measurement of its strength via single cell force spectroscopy, was observed when the viscosity of the surface and the amount of RGD increased (Figure 1A). On the other hand, when HAVDI was added, cell spreading was reduced on both surfaces (Figure 1B). Changes in the location of mechanosensitive proteins (i.e. YAP) were observed, with increased YAP translocation to the cell nucleus at increasing viscosity (Figure 2). The addition of

HAVDI instead hindered YAP translocation, revealing an altered sensing of viscosity (Figure 2B, left). This interplay between viscosity and ligand presentation provoked further changes in the expression of transcription factors, e.g. chondrogenic, by hMSCs. Indeed, SOX9 expression was increased on mobile surfaces compared to control glass, and the addition of HAVDI further enhanced early chondrogenesis (Figure 2B, right). Modulation of bulk viscosity in hydrogels was also observed to affect the response of MSCs, with cell area decreasing at increasing loss modulus, and circularity increasing when HAVDI was added on the more viscous substrates.

Conclusion

Our findings reveal that surface and bulk viscosity affect stem cell response and are able to regulate the differentiation of MSCs. Moreover, when cell-cell interactions are activated, MSCs present an altered sensing of the physical cues of the environment, viscosity in this case, which mediates changes in the cell mechanotransductive response and, eventually, in cell fate. Ultimately, understanding cell response to viscous interactions will allow us to exploit them for the design of optimised microenvironments that regulate stem cell fate for use in tissue engineering.

References

1. Bennett M. et al. P. Natl. Acad. Sci. USA. 115(6), 1192-1197, 2018

2. Chaudhuri O. et al. Nat. Mater. 15, 326-334, 2016

Acknowledgement

The authors acknowledge funding from EPSRC (EP/P001114/1) and MRC (MR/S005412/1). This work was funded by a grant from the UK Regenerative Medicine Platform.

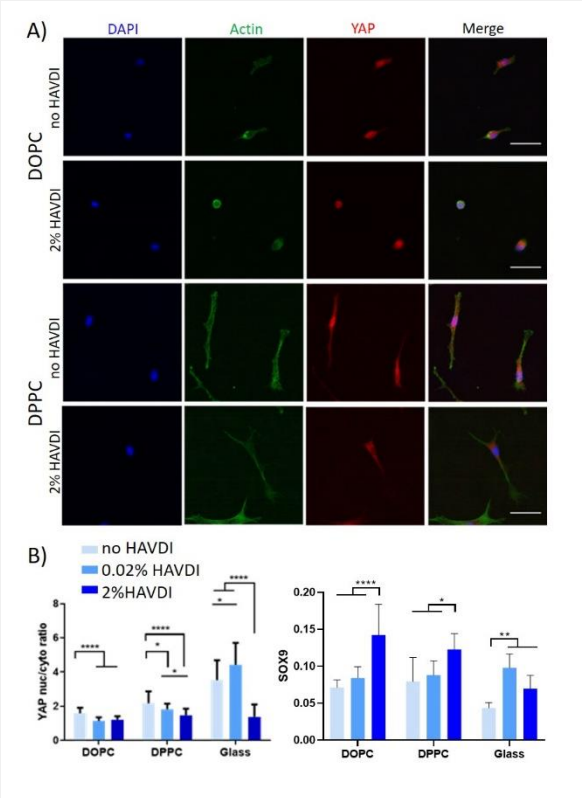

Figure 2. Viscosity controls mechanotransduction and cell differentiation.

A) Representative images of YAP staining on DOPC and DPPC with 0.2% mol RGD without or with addition of HAVDI, after 1 day of culture. Scale bar is 50 µm. B) Effect of viscosity on YAP translocation after 1 day of culture, measured via analysis of the immunofluorescence staining images (left), and on SOX9 expression after 5 days of culture, measured via In-Cell Western (right). RGD concentration is maintained at 0.2% mol, whilst HAVDI is added at either 0.02% mol or 2% mol.

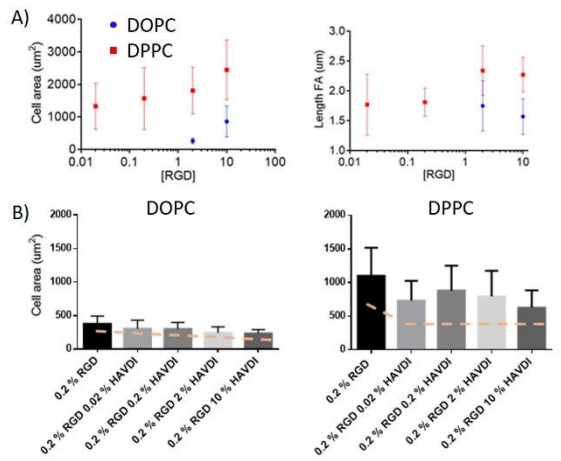

Figure 1. Viscosity controls cell adhesion. A) Cell area (left) and FA length (right) after 24 hours of culture on DOPC and DPPC at varying RGD concentration (0.02-10 mol%). B) Effect of HAVDI (0.02-10 mol%) on cell spreading.

2:45 p.m. – 3:45 p.m.

Hall 1 / Exhibition Area

PS1-16 | Animal experiments

PS1-16-231

Biocompatibility of an non-resorbable PTFE membrane for Guided Bone Regeneration (GBR)

Tadas Korzinskas[1], Ole Jung[1,2], Ralf Smeets[1,2], Sanja Stojanovic[3], Stevo Najman[3], Martin Gosau[2], Kristina Glenske[4], Michael Hahn[5], Sabine Wenisch[4], Reiner Schnettler[1], Mike Barbeck[1,6]

[1]University Medical Center Hamburg-Eppendorf, Division of Regenerative Orofacial Medicine, Department of Oral and Maxillofacial Surgery, Hamburg, DE; [2]University Medical Center Hamburg-Eppendorf, Department of Oral and Maxillofacial Surgery, Hamburg, DE; [3]University of Niš, Institute of Biology and Human Genetics, Department for Cell and Tissue Engineering, Niš, RS; [4]Justus Liebig University of Giessen, Clinic of Small Animals, Institute of Veterinary Anatomy, Histology and Embryology, Giessen, DE; [5]University Medical Center Hamburg-Eppendorf, Department of Osteology and Biomechanics, Hamburg, DE; [6]BerlinAnalytix GmbH, Berlin, DE

Introduction

In dentistry, resorbable and non-resorbable membranes can be employed for GBR-/GTR (Guided Bone-/Guided Tissue Regeneration) therapy. Thereby, the use of non-resorbable membranes like polytetrafluoroethylene (PTFE) is indicated for the treatment of large, non-self-containing bone defects, or multi-walled defects in the case of vertical augmentations. Thereby, less is known about the molecular basis of the foreign body response to PTFE membranes. In this study, the biocompatibility and inflammatory tissue response of a non-resorbable PTFE membrane was investigated.

Experimental Methods

dPTFE (Permamem®, botiss biomaterials, Germany) as experimental and collagen-based membranes (Jason®, botiss biomaterials, Germany) as control group were examined using scanning electron microcopy (SEM). In total, n=20 BALB/c mice were uniformly divided in two groups and membranes were subcutaneously implanted over 10 and 30 days. After explanation, histopathological and histomorphometrical methods as well as immunohistochemical anaylsis of M1- and M2-macrophages were employed.

Results and Discussion

Over all time points, dPTFE membranes retain their structural integrity. Histopathologically, both membranes show a decreasing inflammatory tissue response over time (Fig.1). Immunohistochemical analysis revealed that the PTFE membranes showed a slightly increased imflammatory response in comparison with collagen membranes, which was insignificant over all time points.

Conclusion

Results indicate that the analyzed dPTFE membrane is not fully bioinert, but its biocompatibility is comparable to collagen-based membranes. Based on its optimal biocompatibility, the novel dPTFE barrier membrane may optimally support bone healing within the context of guided bone regeneration (GBR).

References

Korzinskas T, Jung O, Smeets R, Stojanovic S, Najman S, Glenske K, et al. In Vivo Analysis of the Biocompatibility and Macrophage Response of a Non-Resorbable PTFE Membrane for Guided Bone Regeneration. Int J Mol Sci. 2018;19(10).

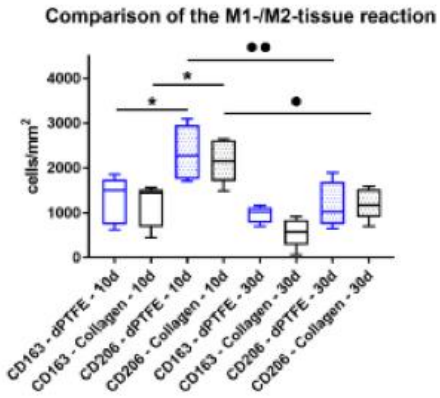

Comparison of the M1-/M2-tissue reaction
Results of the histomorphometrical analysis of the M1 and M2 macrophages within the implantation beds f both materials (*/· p < 0.05 and ··p < 0.01).

PS1-16-232

Novel Use of a Dextran Sulfate Sodium-induced Colitis Mouse Model in the study of IBD-associated renal disease

Chia Jung Chang[1,2], Pi-Chao Wang[3], Akiyoshi Taniguchi[1,2]

[1]Waseda University, Graduate School of Advanced Science and Engineering, Tokyo, JP; [2]National Institute for Materials Science, Cellular Functional Nanobiomaterials Group, Tsukuba, JP; [3]University of Tsukuba, Graduate School of Life and Environmental Sciences, Tsukuba, JP

Introduction

Inflammatory bowel disease (IBD) is a chronic, remitting and relapsing inflammatory disease of the gastrointestinal tract characterized by inflammation and mucosal tissue damage and is associated with significant morbidity. Clinical and epidemiological evidence suggests that IBD is a systemic disorder that can affect almost every organ. Renal manifestations and complications in patients with IBD are not rare, and numerous clinical studies have reported that 4-23% of IBD patients experience renal disease such as tubulointerstitial nephritis, nephrolithiasis, and glomerulonephritis, which eventually induce renal disease. The appropriate experimental animal model of IBD-associated renal disease thus has clinical importance for related studies, including pathological mechanisms, prevention and treatment strategies for IBD. Dextran sodium sulfate (DSS) is a water-soluble sulfated polysaccharide. Oral administration of DSS to trigger acute colitis has been widely used in experimental animal models for preclinical studies of IBD, because the pathophysiology resembles human ulcerative colitis. In this study, we investigated glomerular structural changes focusing on specific types of glomerular collagens and GFB-related proteins after DSS administration, to demonstrate the coexistence of glomerular structural changes and IBD in a DSS-induced colitis mouse model. This study should help establish an experimental animal model for further elucidation of the clinical-pathological mechanisms of IBD-associated renal disease.

Experimental Methods

Acute colitis was induced by administering 3.5% DSS in Slc:ICR strain mice for eight days. Histological changes to glomeruli were examined by periodic acid-Schiff (PAS) and Masson's trichrome staining. Expressions of glomerular collagens and GFB-related proteins were analyzed by immunofluorescent staining and Western blot analysis.

Results and Discussion

DSS-colitis mice showed an elevated disease activity index (DAI), colon shortening, massive cellular infiltration, and colon damage, confirming that DSS-colitis mice can be used as an IBD animal model. On the other hand, PAS staining revealed increasing deposition of glycoprotein matrix in GBM and mesangium, and Masson's trichome staining revealed collagen deposition was markedly increased around the glomerulus and Bowman's capsules in DSS-colitis mice. Such matrix and collagen depositions in glomeruli were also found in glomerular impairment, implicating excess extracellular matrix production as a factor in glomerular disease. Interestingly, we observed significant changes in glomerular collagens, including a decrease in type IV collagen, and an increment in type I and type V collagens, suggested that DSS administration could cause these collagens changes, which may lead to glomerular structure damage. Moreover, declined glomerular filtration barrier (GFB)-related proteins expressions were detected, including synaptopodin, podocalyxin, nephrin and VE-cadherin. These proteins have been suggested to represent important biomarkers of podocyte deficiency, and collagen changes might lead to structural damage to

podocytes such as a loss of polarity and detachment from the glomerular basement membrane, as well as loss of endothelial cell junctions, eventually causing renal disease. Loss of the podocyte cytoskeletal proteins synaptopodin and podocalyxin and the slit diaphragms protein nephrin, as well as the defective endothelial cells adherens junction protein (VE-cadherin) which may be associated with podocyte damage. These findings are important for further elucidation of the clinical pathological mechanisms underlying IBD-associated renal disease.

Conclusion

In conclusion, this study used the DSS-induced colitis mouse model, a very common experimental model of colitis, to clarify changes in glomerular collagens and GFB-related proteins after DSS administration. These findings on glomerular structural change in experimental mice with DSS-induced colitis should lead to novel uses of the animal model for further investigations into IBD-associated renal disease.

References

Chang CJ, Wang PC, Huang TC, Taniguchi A. 2019. Change in Renal Glomerular Collagens and Glomerular Filtration Barrier-Related Proteins in a Dextran Sulfate Sodium-Induced Colitis Mouse Model. Int J Mol Sci. 22;20(6).

Acknowledgement

We wish to thank Dr. Tony Hsiang-Kuang Liang for valuable medical advice, and Dr. Yusuke Nishimura for his technical assistance.

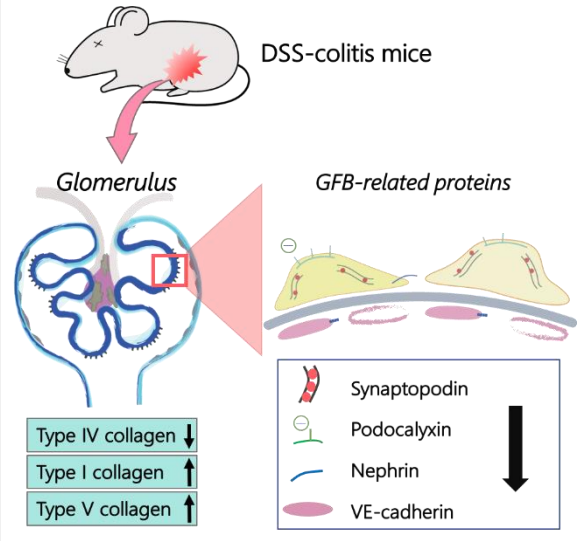

Abstract Figure
Illustration of glomerular structural changes in this study.

PS1-16-233

Titania rings with nano-silver hydroxyapatite coating achieve inefficient cervical seal of transgingival regeneration in beagle

Chen Jie[1], **Guo W. Hua**[1], Lan T. Ting[1], Huang Y. Bing[1]

[1]Sichuan University, West China Hospital of Stomatology, chengdu, CN; [2]Sichuan University, National Clinical Research Center for Oral Diseases,West China Hospital of Stomatology, Chengdu, CN

Introduction

It is well-known that peri-implantitis directly results in the implant loose or lost,which regards as the main cause of treatment failure.Various methods including local delivery antibiotics,periodontal basic treatment and so on used in clinic can produce successful outcomes,however, there was no strong evidence to suggest the a long-term effective treatment intervention for peri-implantitis.With further study, its pathogenesis have more recognition that the inefficient cervical seal of implant is irresistible to bacterial infections.So controlling gingival infection around implant is deemed as an efficient strategy.The antibacterial modifications of implant transgingival materials has been paid more attention in recent years. Without antibiotic abuse and serious cytotoxicity, silver(Ag) has strong bactericidal ability. In this study ,we incorporated silver into the hydroxyapatite(HA) coatings,which is regard as an effective bio-compatibility and bio-activity to hard and soft tissue,on the micron/submicron/nano-morphology titanium surface to obtain Titania ring with nano silver hydroxyapatite coating. Afterwards,we implant this modified ring into the normal transgingival region of beagle to observe its cervical seal ability.

Experimental Methods

Fristly, We obtained the micron/submicron/nano- morphology by adopting the anodic oxidation treatment with the alkali heat treatment on the titanium surface. Next, we employed electrochemical deposition to co-deposit HA and Ag simultaneously. A series of the surface characterization-canning electron microscopy (SEM), X-ray diffraction (XRD), Energy Dispersive Spectroscopy (EDS) ,roughness test ,contact angle test and antibacterial activity of Porphyromonas gingivalis- was used to characterize the morphology, composition and antibacterial ability of the composite coatings to screen out the optimal specimen in vitro. Finally, Canine bilateral first maxillary premolars was carefully installed the optimal Titania ring after anesthesia. The results was obtained after 2 months postimplantation.

Results and Discussion

After heat treatment,a network structure composed of globular-like HA with Ag nano-dots uniformly distributing on the surface of Titania ring. [Ca^{2+}= 5.0 mmol/1], [$PO_4^{3-=}$3.0 mmol/1],[Ag^{+}= 5.0 mmol/1] pH: 4.0,constant voltage =5V, and the deposition time=2h were the optium experimental conditions,which exhibited favorable hydrophilic property,appropriate surface roughness and the distinct bacteriostasis and serve as in vivo transgingival implant.However,the tooth with it exerted obvious gingival recession as time passed,and its bacteriostatic ability only exited around its surface. On the basis of these results,we ascribe the failure to lack matrix calcification of cervical mesenchymal cells and free nano-Ag.Though the HA can provide the adherent site,its surface cannot anchor the cervical mesenchymal cells tightly without matrix calcification.

Conclusion

A series of cervical regeneration in normal teeth shows that nano-HA/Ag-Ti has obvious bacteriostatic ability only around its surface but not reconstruct the cervical seal efficiently. The other strategy to promote the collective migration and matrix calcification of cervical mesenchymal cells in transgingival region may be more sensible .

References

1.Ting, M., Craig, J., Balkin, B. E., & Suzuki, J. B. (2018). Peri-implantitis: A Comprehensive Overview of Systematic Reviews. Journal of Oral Implantology, 44(3), 225–247.

2.Colombo, A. P. V., & Tanner, A. C. R. (2019). The Role of Bacterial Biofilms in Dental Caries and Periodontal and Peri-implant Diseases: A Historical Perspective. Journal of Dental Research, 98(4), 373–385.

Acknowledgement

This study was supported by the National Key R&D Program of China (grant number 2017YFA0104800), National Natural Science Foundation of China (grant number 31771062, 31470947), and the Key Research and Development Program of Sichuan Province (2017SZ0031)

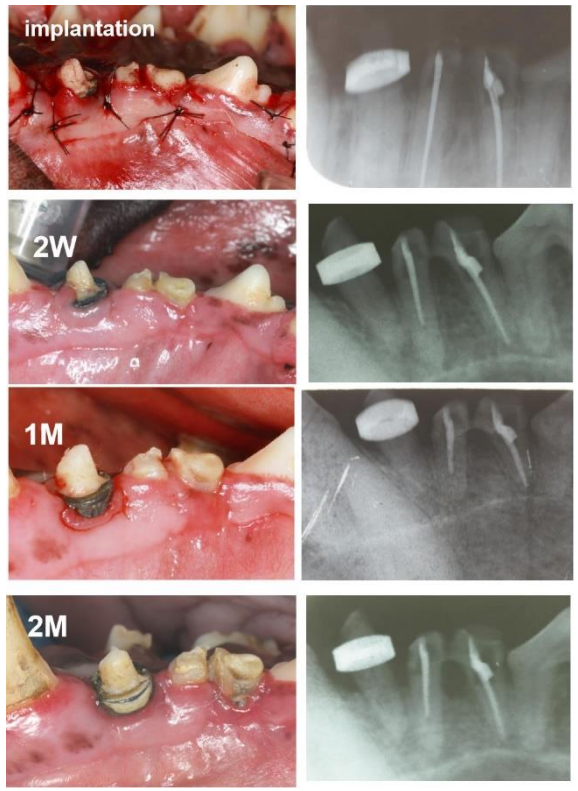

Gingival recession of nano-HA/Ag-Ti ring in beagle

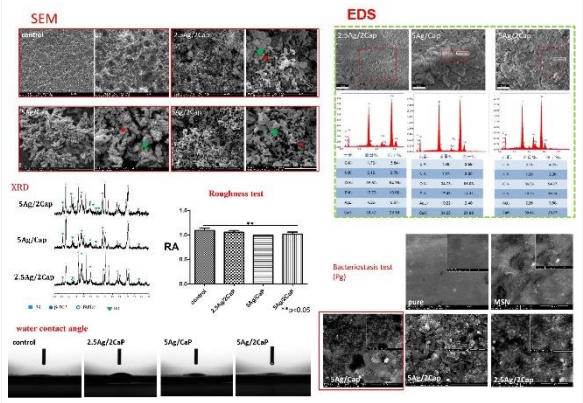

the surface characterization of different nano-HA/Ag-Ti rings

PS1-16-234

Histological examination of histamine and mast cells in biomaterial-related inflammation

Andreas Hoene[1], Benedikt Neukirch[2], Uwe Walschus[1], Maciej Patrzyk[1], Michael Schlosser[1]

[1]University Medical Center Greifswald, Department of Surgery, Greifswald, DE; [2]University Medical Center Rostock, Department of Anaesthesiology and Intensive Care Medicine, Rostock, DE

Introduction

Every implant causes diverse acute and chronic inflammatory reactions. Different immune cells like macrophages and T lymphocytes are involved in this response. Furthermore, a role of mast cells in the acute inflammatory responses to implanted biomaterials has been described [1]. In a number of previous own studies, we examined mast cells as part of a differentiated morphometric analysis of the local inflammatory response after implantation [2-4]. However, apart from one study [2] we did not observe a time dependent change for the mast cell number or a difference between different implant series. Thus, the present study aimed at a simultaneous immunohistochemical examination of mast cells and histamine in peri-implant tissue samples, from Titanium plates coated with a phospholid aimed at molecular membrane mimicry, to examine a histamine staining as an alternative or extension to mast cell detection.

Experimental Methods

Titanium plates (5×5×1 mm) with four different surfaces were used for implantation: Ti-P – Ti plates coated via non-covalent adsorption with 2-oleoyl-1-palmitoylsn-glycero-3-phosphoethanolamin (POPE); Ti-O/P – Ti plates coated with the linker molecule octadecylphosphonic acid (OPA) followed by attachment of POPE via Langmuir-Blodgett technique; Ti-O – Ti plates coated with OPA only; Ti – uncoated Ti plates. One sample from each series (Ti-P, Ti-O, Ti-O/P, Ti) was simultaneously implanted into the neck musculature of 15 male Lewis rats (age ca. 100 days). Tissue samples containing the implants were retrieved after 7, 14 and 56 days. After freezing with laboratory freezer spray and careful removal of the Ti plates, the remaining tissue pockets were filled with embedding medium (Cryomatrix™) and the tissue samples were immediately shock frozen. Tissue sections with a thickness of 5 µm prepared with a cryotome were stained with monoclonal antibodies for mast cells and histamine (both from Abcam) and the alkaline phosphatase anti-alkaline phosphatase method. The number of positively stained cells per mm^2 tissue section was determined by by digital image analysis using the ImageJ software.

Results and Discussion

The Ti-P and the Ti-O/P samples caused a higher number of mast cells in the peri-implant tissue than the uncoated Ti control samples on day 7 Furthermore, the number of mast cells declined to day 56 for the Ti-P samples, but did not change over time for the Ti-O/P, Ti-O or Ti samples. In contrast, the number of histamine$^+$ cells increased from day 7 to day 56 for the Ti-O, Ti-O/P and Ti but not for the Ti-P samples. Ti-O samples had a lower number of histamine$^+$ cells than the Ti on day 14 and day 56, and the Ti-O/P and also than the Ti on day 56. The ratio of histamine$^+$ cells/mast cells increased from day 7 to day 56 for all four implant series, from lower than 20% on day 7 to about 60% on day 56 for the Ti controls with the strongest increase and the highest ratio at the end of the study.

Conclusion

The number of histamine$^+$ cells and correspondingly the ratio of histamine$^+$ cells/mast cells demonstrated differences between sample series with comparable number of mast cells. An interpretation could be that a higher ratio indicates a lower level of degranulation and histamine release. The release of histamine to stimulate local inflammation is known to be the hallmark of mast cell action and their main function. Thus, the number of histamine$^+$ cells and especially the ratio of histamine$^+$ cells/mast cells might be a more meaningful marker of mast cell activity in the context of biomaterial-related inflammation than the number of mast cells alone.

References

[1] Tang & Eaton, Proc Natl Acad Sci (1998)
[2] Hoene et al., J Mater Sci: Mater Med (2013)
[3] Lucke et al., BioMed Res Int (2015)
[4] Walschus et al., J Funct Biomater (2017)

Acknowledgement

The study was supported by the Federal State of Mecklenburg-Vorpommern and the Helmholtz Association of German Research Centers (Grant No. VH-MV1).

PS1-16-235

Comparative investigation on in vivo osteogenic behavior among three polymer scaffolds with different degradation properties

Jinhui Huang, Jidong Li, Qin Zou, **Yubao Li**

Sichuan University, Res Ctr for Nano-Biomaterials, Analytical and Testing Ctr, Chengdu, CN

Introduction

Scaffolds play an important role in the regeneration of defect bone tissue [1-2]. In recent years, composite scaffolds composed of hydroxyapatite (HA) and polymers have become the hot topic in bone tissue engineering [3-5]. However, people always pursue that the scaffold can be completely degraded and disappeared during or after bone reconstruction, but ignore the impact of scaffold degradation on the osteogenic behavior. There is still lack of in-depth understanding and long-term study on such impact.

Experimental Methods

To explore the correlation between bone regeneration and scaffold degradation, three kinds of scaffolds including stable n-HA/PA66 scaffold, slowly degraded n-HA/PCL scaffold and rapidly degraded n-HA/PLGA scaffold were prepared via solvent evaporation and salt particle leaching. The weight ratio of n-HA to the polymer was set at 3:7. For animal experiments, the three scaffolds of n-HA/PA66, n-HA/PCL and n-HA/PLGA were cut into cylinders (6 mm in diameter, 5 mm in length) and implanted into the bone defects of rabbit femoral condyles. Samples were harvested with surrounding tissues at 1, 3, 6, and 12 months postoperation. The osteogenic behaviors were evaluated via micro-CT and histological analysis.

Results and Discussion

After XRD and FTIR analyses which demonstrate their composition, the morphology of the three scaffolds were observed by SEM as shown in Figure 1. The three scaffolds exhibit a porous structure similar to the natural cancellous bone, with a macropore size from 250 μm to 550 μm. There are also a lot of micropores less than 100 μm present on the walls of macropores. Figure 2A shows the micro-CT 3D reconstructed new bone images in the three scaffolds at different implantation time. It can be seen that only few bone matrixes are formed in all three scaffolds at 1 month, and more bone matrixes can be observed in the subsequent months. At 3 month, the n-HA/PLGA scaffold holds relatively the highest bone volume (BV/TV), and the n-HA/PCL scaffold has the lowest bone volume. Unexpectedly, the bone volume of n-HA/PLGA scaffold obviously decreases at 6 month and lower than the n-HA/PA66 and n-HA/PCL scaffolds. At 12 months, the n-HA/PA66 scaffold and n-HA/PCL scaffold still display superior bone reconstruction than the n-HA/PLGA scaffold. The bone volume (BV/TV) of the stable n-HA/PA66 scaffold and the slowly degraded n-HA/PCL scaffold can steadily increase with the implantation time. The histological sections of the three scaffolds after implantation for 1, 3, 6, and 12 months are shown in Figure 2B. For n-HA/PLGA scaffold, the scaffold started to deform at 1 month, and the scaffold had lost its integrality due to partial degradation at 3 months. At 6 months, the scaffold has almost completely degraded, leaving only a few small debris. There were no stable osseointegration formed at the scaffold-bone interface although new bone could form in the pores of the scaffold. A fibrous tissue layer was observed in the early stages of implantation which might be due to the inflammatory reaction caused by the acidic degradation products of PLGA. For n-HA/PA66 and n-HA/PCL scaffolds, both scaffolds could maintain their morphology through the entire implantation period, and could form osteointegration with new bone after 3 month. However, there was a certain

degree of fibrous tissue layers at some bone-implant interface of n-HA/PA66 scaffold, and no obvious osteoblast-like cells were found at the interface between the n-HA/PA66 and the bone in the early stages of implantation, while good osseointegration could form between n-HA/PCL scaffold and the new bone, and some osteoblasts neatly arranged at the bone boundary near the scaffold pore walls. There was no fibrous tissue layer was observed on the n-HA/PCL scaffold, even at early stage.

Conclusion

The results suggest that the rapid degradation of PLGA or its degradation products will seriously affect the new bone reconstruction at later period. The slow degradation of PCL seems no obvious influence on new bone reconstruction. When comparing the n-HA/PA66 with n-HA/PCL, the latter should be preferably recommended due to its degradation property (although very slow) . Regardless of excessive time, PCL can eventually degrade and disappear in the body, different from the non-degradable PA66 matrix. Anyway, a relatively stable scaffold surface (or bone-scaffold interface) is crucial for high-quality bone reconstruction.

References

1. A. Ho-Shui-Ling, J. Bolander, L.E. Rustom, A.W. Johnson, F.P. Luyten, C. Picart, Bone regeneration strategies: Engineered scaffolds, bioactive molecules and stem cells current stage and future perspectives, Biomaterials 180 (2018) 143-162.
2. U.G. Wegst, H. Bai, E. Saiz, A.P. Tomsia, R.O. Ritchie, Bioinspired structural materials, Nat Mater 14(1) (2015) 23-36.
3. H. Wang, Y. Li, Y. Zuo, J. Li, S. Ma, L. Cheng, Biocompatibility and osteogenesis of biomimetic nano-hydroxyapatite/polyamide composite scaffolds for bone tissue engineering, Biomaterials 28(22) (2007) 3338-48.
4. A. Rezaei, M.R. Mohammadi, In vitro study of hydroxyapatite/polycaprolactone (HA/PCL) nanocomposite synthesized by an in situ sol-gel process, Mater Sci Eng C Mater Biol Appl 33(1) (2013) 390-6.
5. K. Rezwan, Q.Z. Chen, J.J. Blaker, A.R. Boccaccini, Biodegradable and bioactive porous polymer/inorganic composite scaffolds for bone tissue engineering, Biomaterials 27(18) (2006) 3413-3431.
6. L. Li, Y. Zuo, Q. Zou, B. Yang, L. Lin, J. Li, Y. Li, Hierarchical Structure and Mechanical Improvement of an n-HA/GCO-PU Composite Scaffold for Bone Regeneration, ACS Appl Mater Interfaces 7(40) (2015) 22618-29.

Acknowledgement

This work was supported by China NSFC fund (No. 31670965) and National Key Research and Development Program of China (2016YFA0201703/2016YFA0201700).

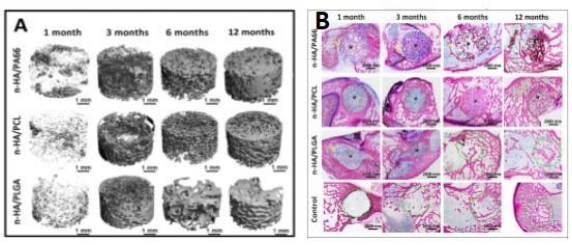

Figure 2. The micro-CT reconstructed images (A) and the histological images (B) of new bone tissue.

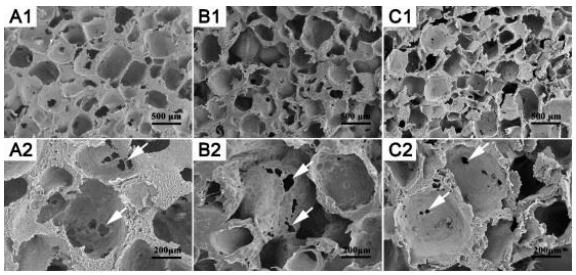

Figure 1. SEM micrographs of n-HA/PA66 (A1,A2), n-HA/PCL (B1,B2), n-HA/PLGA (C1,C2) scaffolds.

PS1-16-236

Osteocyte quantification in growing bone – A comparative study using X-ray micro-computed tomography and backscattered electron scanning electron microscopy

Anders Palmquist, Krisztina Ruscsák, Furqan A. Shah

University of Gothenburg, Department of Biomaterials/Institute of Clinical Sciences, Gothenburg, SE

Introduction

Bone is a highly dynamic tissue, which continually undergoes remodeling in order to adapt to the exerted mechanical loads. Osteocytes direct strain-driven remodeling by sensing the strains and communicating with bone-resorbing cells (the osteoclasts) and bone-forming cells (the osteoblasts). Osteocyte density varies with age, anatomical location, and disease. Quantification is most often performed in 2D, using either histology or backscattered electron scanning electron microscopy (BSE-SEM), but does not represent the three-dimensional (3D) environment. Lab-based X-ray micro-computed tomography (micro-CT) is a common method for evaluating bone microstructure in 3D. However, determining volumetric osteocyte densities is time-consuming – requiring ≈28 h to scan one mm^3 of bone at an appropriate spatial resolution [1]. Long scanning times are impractical for routine large-scale studies. Scanning times may be considerably reduced through the use of high brilliance synchrotron radiation [2-4], however, access to such facilities is generally very limited. Therefore, development of simpler methods and predictive models of 3D osteocyte densities is necessary. Here, we explore if a regular benchtop microCT system is robust enough for accurate quantification of osteocytes, particularly in growing anatomical sites such as the skull suture where the presence of Sharpey's fibers, chondrocytes, and woven bone pose challenges to accurate identification of osteocytes. For this purpose, sequential imaging and validation with 2D SEM is performed (Figure 1).

Experimental Methods

Rat skull bone biopsies were obtained using a trephine drill, fixed in formalin, dehydrated and resin embedded. Using a Skyscan 1172 (Bruker Micro-CT), the samples were scanned at a resolution of 0.94 µm, operating at 49kV and 200 µA. A 0.5 mm Al filter was used to block low energy X-rays. Reconstruction, visualization, and analyses were performed in the Skyscan software suite (NRecon, DataViewer, CTAn). After micro-CT scanning, the resin embedded blocks were bisected by sawing and the surface was polished for BSE-SEM imaging (Quanta 200 environmental SEM, FEI company, The Netherlands), operated at 20 kV accelerating voltage and low vacuum (0.6 bar water vapor pressure).

Results and Discussion

In the micro-CT dataset, the slice that corresponds to the surface imaged using BSE-SEM is identified and used for alignment. A systematic approach is used for thresholding and image processing to refine the segmentation process and subsequent quantification of osteocyte lacunae and blood vessels. For image segmentation, a set of parameters is used which best match osteocyte and blood vessel quantification by BSE-SEM.

Conclusion

Preliminary data (Figure 2) demonstrates the feasibility of this approach.

References

1. Akhter et al. Calcif Tissue Int 100 (2017) 619-630
2. Tommasini et al. Bone 50 (2012) 596–604
3. Dong et al. Bone 60 (2014) 172–185
4. Andronowski et al. Forensic Sci Int Genet 28 (2017) 211–218

Acknowledgement

Financial support is acknowledged from the IngaBritt and Arne Lundberg Foundation, the Swedish Society for Medical Research, the Dr. Felix Neubergh Foundation, Promobilia, the Hjalmar Svensson Foundation, the Osteology Foundation, and the Materials Science Area of Advance at Chalmers and the Department of Biomaterials, University of Gothenburg.

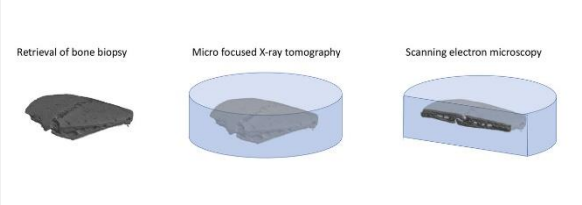

Figure 1:
Schematic figure showing the study set-up

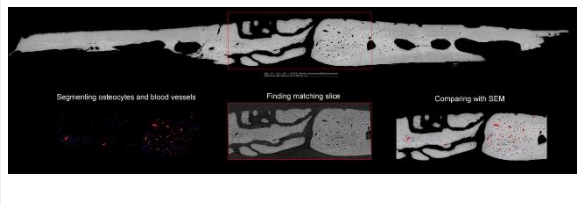

Figure 2:
Preliminary results of detection of osteocyte lacunae in bone and validation with SEM imaging.

2:45 p.m. – 3:45 p.m.

Hall 1 / Exhibition Area

PS1-17 | Clinical and translational aspects

PS1-17-237

Bio-tribocorrosion and trunnion fatigue fractures in total hip arthroplasty – two case reports and review of the literature

Peter G. van Doesburg[1], Evert J. van Langelaan[2], Iulian Apachitei[2], Suzan H. M. Verdegaal[1]

[1]Alrijne Ziekenhuis, Department of Orthopaedic Surgery, Leiderdorp, NL; [2]Delft University of Technology, Biomechanical Engineering Department Biomaterials & Tissue Biomechanics Section, Delft, NL

Introduction

A hip stem fracture, due to metallurgic problems, was a specific complication well known in the past. Better quality stainless steel reduced this problem. In the nineteen-seventies, the concept of head-neck modularity was introduced to provide more intra-operative surgical options. Modularity also led to new problems at the trunnion (head-neck junction), such as wear and corrosion between the head-neck interface (trunnionosis), fractures of the head-neck junction and gross trunnion failures. The problem of corrosion was not recognized, neither seen as a major problem, during a long time. However, new studies show that up to 3% of all total hip reoperations are performed because of trunnionosis. The exact pathology is unknown, but most likely micromotions between the head and the taper causes disruption of the oxide film, leading toa bio-tribocorrosion phenomenon called mechanically assisted crevice corrosion (MACC). Loss of material by corrosion could lead to a trunnion fatigue fracture. Fractures of the trunnion are less frequent and little literature is available on these fractures. A combination of corrosion, implant factors, surgical technique factors and patient factors most likely is the explanation.
The purpose of our study was to identify potential risk factors for the development of trunnion fractures, as well as providing future treatment recommendations in primary hip arthroplasty and hip reoperations to prevent damage of the trunnion and trunnion fractures.

Experimental Methods

A detailed report of two trunnion fractures in one type of hip stem (Mallory Head) is presented, including scanning electron microscopy (SEM) and Energy Dispersive X-ray spectroscopy (EDS) analysis. Thereby, a systematic review of the available literature was performed following the PRISMA guidelines to identify studies on trunnion fractures in Pubmed, Web of Science and Embase. Methodological quality of the included studies was evaluated using a critical appraisal instrument.

Results and Discussion

SEM and EDS analysis were done. SEM analysis demonstrated a typical fatigue fracture with the fatigue fracture originated at the neck surface with standard fatigue marks perpendicular to the crack propagation. SEM analysis of the head side showed a small notch at the surface of the neck that seemed to be the starting point of the fatigue crack. High magnification SEM analysis revealed several specific fatigue fracture features, such as the presence of fatigue striations close to and away from the crack origin, secondary cracks and the presence of the dimple like patterns which characterize the final overloaded fracture. The elemental analysis of the femoral stem performed by EDS indicted that the alloy has a chemical composition close to Ti6Al4V (Ti 90.33wt%, Al 5.69wt% V 3.98wt%).
The systematic review included 24 eligible studies. The included patients had a mean age of 65 years (range 31y - 91y, median 67y), a mean weight of 94kg (range 70kg – 129kg, median 91kg) and a mean BMI of 31kg/m^2 (range 24kg/m^2– 47kg/m^2, median 30kg/m^2). Neck fractures occurred on average 8 years (range 1y – 24y, median 6y) after

hip stem placement. Male gender, high body weight and obesity were identified as risk factors. Thereby, damage to the trunnion during reoperation surgery, is likely to be an important risk factor for fractures. On average, all patients were relatively young at the moment of primary total hip arthroplasty. Two groups of neck fractures were identified: head-neck (trunnion) fractures and neck-shoulder (base of the neck) fractures. Corrosion and the use of long skirted femoral heads were frequently reported in head-neck fractures, whereas 69% of the neck-shoulder fractures were associated with specific metal or implant design fea---tures.

Conclusion

In conclusion, several potential and preventable risk factors were identified, leading to specific recommendations for future hip arthroplasty.

PS1-17-238

Development of an innovative ex vivo-test bench to measure heat development during medical drilling processes

Ole Jung[1,2], Mike Barbeck[1], Marie-Luise Schröder[1], Ralf Smeets[1,2], Andreas Fischer[3], Anders Henningsen[1], Martin Gosau[2], Tadas Korzinskas[1], Jan Osmers[3], Michael Sorg[3]

[1]University Medical Center Hamburg-Eppendorf, Division of Regenerative Orofacial Medicine, Research Group Biomaterials/Surfaces, Hamburg, DE; [2]University Medical Center Hamburg-Eppendorf, Department of Oral Maxillofacial Surgery, Hamburg, DE; [3]Universität Bremen, Bremen Institute for Metrology,Automation and Quality Science (BIMAQ), Bremen, DE

Introduction

Over 50 years, it is known that the temperature rises during the drilling process. The critical temperature was shown to be 47 °C. After exceeding the critical temperature for more than one minute, irreversible damage to the bone tissue can occur including bone resorption, fibrosis and implant failure. External factors (e.g. drill speed, freed rate or irrigation), internal factors (e.g. design of the drill bit or drill bit diameter) and patient individual factors (e.g. bone mineral density) can influence the temperature rise in the bone during the drilling process. Studies show inconsistent results how external and drill specific parameters influence the temperature rise in the bone during drilling. Therefore, a standardized and valid test bench to test medical drills should be implemented to generate consistent results, reduce animal experiments and increase the safety for patients.

Experimental Methods

A test bench to evaluate the temperature rise during the drilling process was constructed. It included a set-up for the drilling process with an automatic setting of different drilling parameters (drilling speed, freed rate and torque), a thermographic camera to detect changes in the bone temperature as well as a automated device to set all drilling parameters and receive the measurement parameters. The temperature rise in pig ribs were measured using different settings of the parameters drilling speed, feed rate, torque an duration of the drilling process.

Results and Discussion

The test bench for the evaluation was successfully implemented and the temperature could be detected via thermographic cameras (see figure 1 A-C). Drilling speed, feed rate and torque had a major impact on the temperature rise in the bone, whereas the duration had a minor impact. The thermal conductivity of the bone could be determined to accurately measure the temperature. The position of the drill bit in the bone (corticalis or spongiosa) could be detected precisely by the use of the thermographic camera.

Conclusion

The test bench is a valuable tool for the evaluation of the temperature rise in the bone during the drilling process *ex vivo*. For further improvements and validation, more parameters (e.g. irrigation or drill bit specific parameters) should be evaluated and the results should be correlated with *in vivo* data.

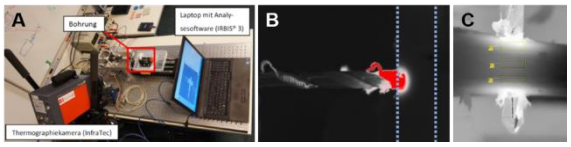

Ex vivo-test bench
Test bench to evaluate the temperature rise during the drilling process (red square) with a thermography camera (lower left) and a laptop for the parameter set-up and receipt of the measurement results. (B) Thermographic image of a swine rip during the drilling process. A temperature rise over 47 °C is shown in red. The bone is located between the dotted lines. (C) Thermographic image with measuring windows (in yellow) along the drilling canal.

PS1-17-239

Cartilage mimicking coatings to increase the life-span of bearing surfaces in joint prosthesis

Laura Sánchez-Abella, Iraida Loinaz, Hans-Jürgen Grande, **Damien Dupin**

CIDETEC, Biomaterials Unit, Donostia-San Sebastián, ES

Introduction

The application of total hip arthroplasty (THA) has benefited millions of patients who suffer from severe hip joint diseases. In 2011, approximately 1.6 million THAs were conducted in 27 of the 34 member countries in the Organization for Economic Cooperation and Development (OECD).[1] However, approximately 10–15% of patients still require revision surgery every year, and the number of hip revision surgeries has recently risen. Even if it is a well-established procedure with low rates of revision, aseptic loosening remains as the principal cause of revision. For long-term implantations submicron particles are generated in vivo due to the inherent wear of the prosthesis. When this occurs, macrophages undergo phagocytosis and secretion of bone resorptive cytokines inducing osteolysis, hence loosening of the implanted prosthesis. Therefore, new technologies are required to reduce the wear of the bearing materials and hence increase the life-spam of the prosthesis.

Our strategy focuses on surface modification of the bearing materials with a hydrophilic coating based on cross-linked water-soluble (meth)acrylic monomers to improve their tribological behaviour.

Experimental Methods

Hip simulator test. The tests were conducted on a simulator from Endolab (Thansau/Rosenheim, Deutschland, type C6/2-07, SN 0905, Figure 1). This is a servo hydraulic hip- and spine simulator fulfilling the requirements of ISO 14242-1.[2] The applied load and rotation simulate the conditions while walking (see Figure 2). After each 500'000 cycles, the test chambers were taken apart, cleaned, filled with fresh test liquid, reassembled and installed in another measuring station of the hip simulator. The weighing was done after each 500'000 cycles. This part of the test lasted 3 MC. For the remaining 2M cycles abrasive aluminium particles were added directly between the cup and the head of the prosthesis. The same information was recorded every 500,000 cycle.

Results and Discussion

The coatings based on covalently attached hydrogel are biocompatible, with high swelling capacity and antifouling properties, mimicking the properties of natural cartilage, i.e. wear resistance with permanent hydrated layer that prevents prosthesis damage. However, there are only a few reports on the mechanical and tribological characteristics of this type of coatings.

Clear beneficial advantages of this coating have been demonstrated in different conditions and different materials, such as UHMWPE, PEEK, CrCo, Stainless steel, ZTA and Alumina. Using routine tribological experiments, the wear for UHMWPE substrate was decreased by 75% against alumina, ZTA and stainless steel. For PEEK-CFR substrate coated, the amount of material lost against ZTA and CrCo was at least 40% lower.

Experiments on hip simulator allowed ZTA femoral heads and UHMWPE cups to be validated with a decrease of 80% of loss material (Figure 1). Further experiments on hip simulator adding abrasive particles (1 micron sized aluminium particles) during 3 million cycles, on a total of 6 million, showed a wear decreased of around 55% compared to uncoated UHMWPE and XLPE.

Conclusion

In conclusion, CIDETEC's hydrogel coating technology is versatile and can be adapted to protect a large range of surfaces, even in abrasive conditions.

References

1. G J Atkins, D R Haynes, D W Howie, D M Findlay, *"Role of polyethylene particles in peri-prosthetic osteolysis: A review", World J Orthop.* **2011**; 2(10): 93–101.

2. ISO 14242-1:2014 Implants for Surgery - Wear of Total Hip-Joint Prostheses - Part 1: Load-ing and Displacement Parameters for Wear-Testing Machines and Corresponding Envi-ronmental Conditions for Test. ISO Copyright Office, Geneva, Switzerland.

Acknowledgement

The authors would like to thank the EU framework program for research and innovation Horizon 2020 (MDOT, Grant no: 814654) for providing financial support.

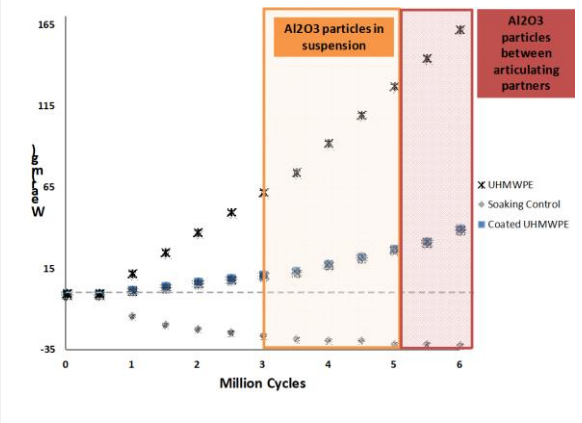

Figure 1
Evolution of the wear with prostehesis coated with a hydrogel layer.

PS1-17-240

Impact of different coextruded medical infusion tubings on the sorption of cyclosporine and isosorbide dinitrate

Nicolas Tokhadzé[1,2], Philip Chennell[1,2], Valérie Sautou[1,2], This study was supported by Cair LGL

[1]Université Clermont-Auvergne, Institut de Chimie de Clermont-Ferrand, Clermont-Ferrand, FR; [2]CHU de Clermont-Ferrand, Clermont-Ferrand, FR

Introduction

Medical tubings in plasticized polyvinylchloride (PVC) are widely used for the infusion of medications but are known to cause content-container interactions (drug sorption(1,2) and plasticizer release(3)). Drug sorption is responsible for a loss of active pharmaceutical ingredient (API) or excipients and results in a potential risk of not administering the correct dose to the patient. The aim of this study was to assess the sorption phenomena between two drugs (cyclosporine and isosorbide dinitrate) and three coextruded alternative materials to a reference plasticized PVC intravenous (IV) infusion tubing: coextruded tubings were respectively of PVC coextruded with an inner layer of polymer (thermoplastic or thermoplastic elastomer).

Experimental Methods

Marketed medications of cyclosporine (SANDIMMUM®) and isosorbide dinitrate (RISORDAN®) were used at the respective concentrations of 0.5 mg/mL and 1 mg/mL after dilution in 0.9% sodium chloride. The interaction of the drugs was studied with four extension sets: a reference monolayered PVC and three PVC coextruded with polyethylene (PE), polyurethane (PU) and Styrene-EthyleneButadiene-Styrene (SEBS). The potential loss of API due to the sorption phenomena was evaluated by assessing the concentration of cyclosporine and isosorbide dinitrate after contact with the tubings in two conditions: a 96h static contact condition and a dynamic condition consisting of a simulated 8h infusion at a flow-rate of 1mL/h and 10 mL/h, controlled with an electric syringe pump. Quantification of each API was performed by liquid chromatography. The electric charge at the interface between drug and tubing was also assessed by measuring the surface zeta potential at pH= 5.0.

Results and Discussion

The evolution of Cyclosporine concentrations (expressed as a percentage of the initial concentration) is shown in figure 1. In static condition, PVC and PVC/PU tubings induced respectively losses of 56.93 ± 1.24% and 83.84 ± 0.62% of initial concentration (n=3, mean ± standard error of the mean) after 96h of contact, while no significant variation was observed for PVC/PE and PVC/SEBS tubings at any analytical time. For the dynamic 1 mL/h flow-rate condition, PVC tubings induced a progressive decrease of up to 18.08 ± 4.19% of cyclosporine concentrations. With PVC/PU tubings the loss was maximum at T1 (21.34 ± 1.21%) and raised to a loss of only 10.95% ± 0.23% at T8. No significant variation was highlighted for PVC/PE and PVC/SEBS during 1 mL/h dynamic contact with cyclosporine. Except for PVC tubings at T4, no loss of more than 5% of initial concentration occured with any of the studied tubings at any analytical time in 10 mL/h dynamic condition.

The evolution of isosorbide dinitrate concentrations (expressed as a percentage of the initial concentration) is shown in figure 2. All the studied IV tubings induced a decrease of isosorbide dinitrate concentrations after 24 hours of static contact, and the loss was even greater at T96. PVC and PVC/PU tubings presented losses of 95.66 ± 0.03% and 91.19 ± 0.40% while losses with PVC/PE was of only 19.62 ± 0.26%. The behavior of PVC/SEBS tubings was

intermediate with a loss of 42.62 ± 1.25%. During the 1mL/h infusion (dynamic condition), PVC tubings presented a progressive loss up to 25.11 ± 0.08% of initial concentration. A progressive decrease was also noticed with PVC/SEBS with a loss of up to 10.12 ± 0.59% at T8. With PVC/PU, concentration first decreased by 73.05 ± 5.12% at T1 then remained stable at T2 before increasing up to 47.59 ± 0.92% of initial concentration at T8. Isosorbide dinitrate concentration remained above 95% of initial concentration contact with PVC/PE tubings. In the 10 mL/h dynamic condition, PVC and PVC/PU presented lower losses than in the 1 mL/h dynamic condition while no significant variation was detected with PVC/PE and PVC/SEBS tubings.

Measuring the zeta potential provided information about the surface electric charge of the material. The tubings presented a surface charge of -9.5 mv, -27.4 mV, -37.0 mV and -39.6 mv for respectively PVC/PU, PVC, PVC/PE and PVC/SEBS.

Conclusion

A coextruded layer of PE or SEBS inside PVC tubings decreased the sorption phenomena observed with PVC. On the contrary, PVC/PU tubings appeared to have a behavior similar to PVC's. Yet, due to the great variety of PU available, these results should not be extrapolated to other PU tubings. Our study also showed that tubings with the most negative zeta potential (PVC/PE and PVC/SEBS) were less prone to sorption of both cyclosporine and isosorbide dinitrate.

References

1. Jin S-E, You S, Jeon S, Hwang S-J. Diazepam sorption to PVC- and non-PVC-based tubes in administration sets with quantitative determination using a high-performance liquid chromatographic method. Int J Pharm. 2016 juin;506(1–2):414–9.

2. Treleano A, Wolz G, Brandsch R, Welle F. Investigation into the sorption of nitroglycerin and diazepam into PVC tubes and alternative tube materials during application. Int J Pharm. 2009 Mar 18;369(1–2):30–7.

3. Bernard L, Eljezi T, Clauson H, Lambert C, Bouattour Y, Chennell P, et al. Effects of flow rate on the migration of different plasticizers from PVC infusion medical devices. PLoS ONE [Internet]. 2018 Feb 23 [cited 2019 Jan 17];13(2).

Acknowledgement

The authors thank Renate Kohl and Christine Koerner from Anton Paar for their help in zeta potential measurement.

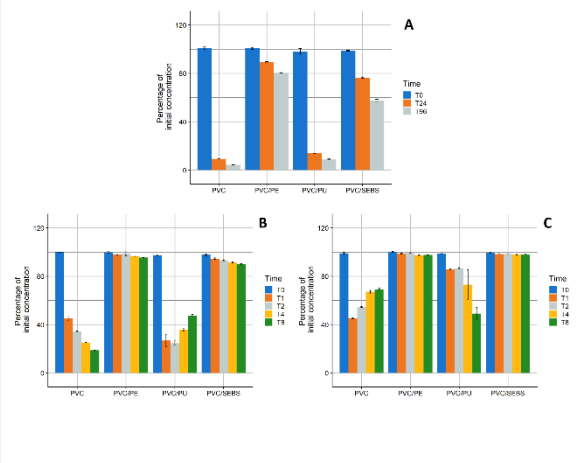

Figure 2

Isosorbide dinitrate concentrations (expressed as percentage of initial 1.0 mg/mL isosorbide dinitrate concentration) during (A) static contact, (B) 1 mL/h dynamic condition and (C) 10 mL/h dynamic condition.

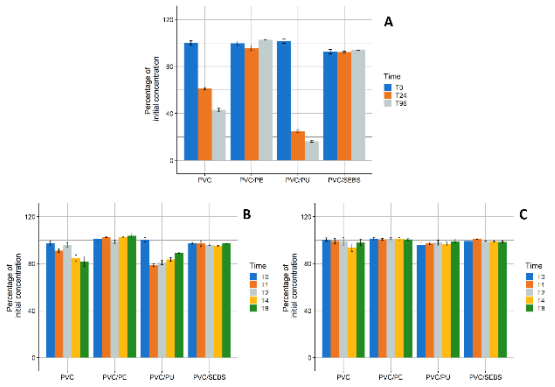

Figure 1
Cyclosporine concentrations (expressed as percentage of initial 0.5 mg/mL cyclosporine concentration) during (A) static contact, (B) 1 mL/h dynamic condition and (C) 10 mL/h dynamic condition.

PS1-17-241

TBMED – An Open Innovation Test Bed for High-Risk Medical Devices

Andrea Haiek, Laura Sánchez-Abella, Hans-Jürgen Grande, **Damien Dupin**

CIDETEC, Biomaterials Unit, Donostia-San Sebastián, ES

Introduction

The European healthcare system has to deal with two main problems: large variation in patient outcomes and a continuous increase of costs. This is especially valid for the high risk medical devices. According to a recently published paper[1], very often, high-risk medical devices were approved based on evidence from studies that are methodologically inadequate, including indirect comparisons or lack of data on efficacy.

As a consequence, the new regulation includes quality and risk management obligations that are translated to companies into not only a demonstration of safety and performance over the entire life cycle of a product, but also, into a demonstration of tangible benefit for the patients and the healthcare system.

TBMED has received Funding from the European Union's Horizon 2020 research and innovation framework and is created as a solution for highly innovative SMEs and other companies that are struggling to fulfill the new European regulations without reducing their competitiveness and innovation capacity.

Experimental Methods

THE PROJECT

TBMED is an Open Innovation Test Platform (OITB) that consists of a connected network of labs providing a single entry point to services along the whole value chain from preclinical development to clinical testing based on Quality-by-Design (QbD) concept.

Its aim is to increase the access of high-risk medical devices to patients by helping SMEs to minimize the market approval and reimbursement process time.

Results and Discussion

The OITB will provide services in different areas such as a) **Technology Development**: safety and efficacy assessment, characterization, prototyping and upscaling as well as development of clinical trials, b) **Business Support**: business consultancy services, networking, market access lab and regulatory and c) **Financing**: venture capital access, co-development options and partnering for grant proposals.

This will allow offering SMEs a holistic service that will: a) **Increase the quality and reduce the risk** of their MDs and facilitate subsequent clinical testing. b) **Build the arguments to demonstrate real benefits** (value / final outcomes) of the new devices to increase their success in entering the market and c) **Reduce cost and variability** of the manufacturing process and the **speed of product release to the market** by carrying out statistically DoE for process validation.

This platform is created using 3 use cases that are in diverse TRLs, which will allow us to find an optimal solution for a wide range of high-risk medical devices and user needs.

Conclusion

TBMED will offer the medical device industry a new tool to accelerate the commercialization of innovative products.

References

[1] “Scientific Evidence in Health Technology Assessment Reports: An In-Depth Analysis of European Assessments on High-Risk Medical Devices”, B. Olberg, S. Fuchs, D. Panteli, M. Perleth, R. Busse, Values in Health, **20**, 1420-1426 (2017)

Acknowledgement

This project has received funding from the European Union's Horizon 2020 Research and Innovation program under Grant Agreement no. 814439 (TBMED).

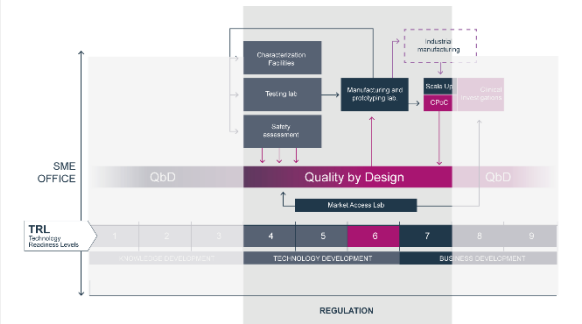

Figure 1
Services covered by TBMED

PS1-17-242

Characterization of particulate contaminants on medical devices - A case study

Simona Rohrer, Nicola Döbelin, Dieter Streit, Fabrizio Bigolin, Ronny Wirz, Marc Bohner

RMS Foundation, Bettlach, CH

Introduction

Particulate contaminations on medical devices from the production process, production environment, or packaging can pose a high risk to patient safety. The authorities therefore require manufacturers to determine the number and type of particles on their products and assess the potential risks to the patient. As part of a 510(k) premarket approval submission, a client therefore wanted to determine the number and types of particle contaminations on a polymeric film component of a negative pressure wound therapy kit and compare it to a predicate device.

Experimental Methods

Particles were extracted from the surface of the polymer films (7539 cm^2) in three different solvents at 50°C according to ISO 10993-12:2012 [1], as well as following special requirements by the FDA. Solutions without products were used as a negative control. After extraction, the particles were collected on a polyamide filter, counted and discriminated into non-metal, fiber, and metal particles with an automatic filter analysis system (JOMESA HFD), and characterized by FTIR (Bruker LUMOS, non-metallic and fibers) or EDX (Zeiss Evo MA25, metallic). All experiments were performed in triplicate in an ISO 8 cleanroom (ISO 14644-1).

Results and Discussion

The average number of particles found on the client's product was 216 ± 128, of which 73 ± 20 were ≥ 25 µm. Maximum numbers were 516 and 100, respectively. In comparison, the average number found on predicate devices was 452 ± 336, of which 202 ± 146 were ≥ 25 µm. Maximum values were 1233 and 542, respectively. The client's products were thus compliant with the thresholds specified in USP <788> (max. 300 particles ≥ 25 µm, max. 3000 particles ≥ 10 µm) [2], but one of the predicate devices exceeded the tolerable number of particles ≥ 25 µm.

A total of 16 different types of particles were detected in the extracts of the client's films (Fig. 1). On the predicate devices, 36 types of particles were detected. The negative control samples contained 20 types of particles, presumably introduced while preparing the samples for extraction in the clean room. After correcting for the baseline contamination, the most abundant types of particles on the client's films were PU particles, cellulose fibers, CrNi steel particles, an antioxidant, cellulose, polyamide, and polypropylene particles. Except for the CrNi steel particles, the same particle types were also repeatedly observed in the extract of the predicate devices. However, the latter also contained particles made of proteins (possibly skin residues), wool (animal derived), and nail polish.

Both devices showed partial decomposition during extraction in hexane and ethanol. Fine needles (Fig. 1) precipitated after the hexane had cooled to room temperature. These needles were identified as N,N′-Hexamethylenebis (3,5-di-tert-butyl-4-hydroxyhydrocinnamamide), which was used as an antioxidant in the raw materials of the films. Extraction in 95 vol% ethanol resulted in the formation of fine white particles, which were identified as the polyurethane film base material.

Conclusion

The large size, surface area, and electrostatic properties of the films, their partial decomposition in hexane and ethanol, as well as the baseline contamination from the clean room environment posed major challenges for the experimental design. Technical limitations were given by the optical microscopy and FTIR resolution. However, the results demonstrated that the client's product contained fewer contaminant particles than the predicate device and complied with USP <788>. A toxicological assessment of the particle compositions showed that they were non-hazardous. Contrarily, more particles were found on the predicate devices, one sample even exceeded the thresholds given in USP <788>. The predicate devices also contained potentially harmful materials such as nail polish, wool, and proteins.

References

[1] ISO 10993-12:2012: Biological evaluation of medical devices - Part 12: Sample preparation and reference materials. International Organization for Standardization (07-2012).

[2] USP <788>: Particulate Matter in Injections. United States Pharmacopeia (01-07-2012).

Acknowledgement

The authors would like to thank the client for the possibility to publish their case.

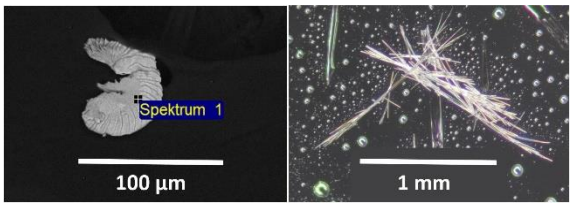

Microscopy images of different particles
Figure 1: Left: A non-alloy steel particle found in water extracts from the client's polymer film. Right: Needles precipitated after dissolution of the antioxidant in hexane.

2:45 p.m. – 4:15 p.m.

Hall 1 / Exhibition Area

PS2 | Postersession 2

2:45 p.m. – 3:45 p.m.

Hall 1 / Exhibition Area

PS2-01 | Bioglasses & silicates

PS2-01-243

Orthotopically femur defect regeneration with alginate-pullulan-glass composite

Klara Magyari[1], Radu A Popescu[1,2], Flaviu A. Tabaran[2], Sidonia Bogdan[2], Alexandru Farcasanu[3,4], Robert Purdoiu[2], Adriana Vulpoi[1], Alexandra I. Dreanca[2,1], Bogdan Sevastre[2], Simion Simon[1,4], Ionel Papuc[2], Lucian Baia[1,3]

[1]Babes-Bolyai University, Interdisciplinary Reseach Institute on Bio-Nano-Science, Cluj-Napoca, RO; [2]University of Agricultural Science and Veterinary Medicine, Faculty of Veterinary Medicine, Cluj-Napoca, RO; [3]Babes-Bolyai University, Faculty of Physics, Cluj-Napoca, RO; [4]Babes-Bolyai University, National Centre of Magnetic Resonance, Babeș-Bolyai University, Cluj-Napoca, RO

Introduction

To use of various biomaterials as components in the composite composition can lead to the obtaining of materials suitable for bone healing with optimized properties. Pullulan (Pll) and alginate (Alg) are two of the natural polymers used as biomaterials, especially in composite for bone tissue regeneration [1, 2]. By varying the bioactive glass composition (BG), materials with beneficial properties in bone regeneration can be obtained, such as biocompatibility, osteoinductive and osteoconductive qualities [3].

In our previous study were demonstrated that alginate-pullulan –bioactive glasses with copper oxide content (Alg-Pll-xCuBG) exhibited *in vitro* and *in vivo* biocompatibility [4]. Beside the *in vitro* bioactivity, the BG with 0.5 and 1.5mol% CuO has good antibacterial effect against Staphilococcus aureus [5]. The viability assay obtained on human lung fibroblast cells shown a very good proliferation rate, indicating a better result in long term [4]. Based on these results the aim of the study was to examine their potential of reducing the healing time in a bone defect.

Experimental Methods

The Alg-Pll-xCuBG (x=0; 0.5; 1.5 mol% CuO in glass matrix) composites were obtained by cross-linking method. The resulting samples were analyzed via X-ray diffraction (XRD), FT-IR spectroscopy and scanning electron microscopy (SEM). *In vivo* implantations were carried out in Wistar rats. A bone defect was created into the distal part of the femoral diaphysis. The bone regeneration was followed using magnetic resonance imaging (MRI), made at different time interval. For the histological examination, the femoral diaphysis was bilaterally harvested, and cleaned of connective tissue, muscle and skin. The sections were routinely stained with haematoxylin and eosin (H&E).

Results and Discussion

The XRD pattern has confirmed the amorphous character of the composites. The FT-IR spectra, beside the characteristic vibration of the polymer units, revealed the bond between polymers and glasses. To increase the porosity, the composites were lyophilized obtaining a macroporous surface visible in SEM micrograph. The defect size was measured using MRI imaging, and the obtained results shown that the defect size gradually decreased in time in all case, but this process is faster when the used scaffold was Alg-Pll-1.5CuBG. The defect size obtained by histological sections measurements confirm the results obtained by MRI observation.

Conclusion

The alginate-pullulan–bioactive glasses with copper oxide content composite were successfully synthesized by cross-linking method and the obtained samples have proved good *in vivo* qualities, particularly the scaffold synthesized using BG with 1.5 mol% CuO.

References

1. R. Sarup Singh, N. Kaur, V. Rana, J. F. Kennedy, Recent insights on applications of pullulan in tissue engineering, Carbohydrate Polymers 153 (2016) 455–462

2. J.Venkatesan, I. Bhatnagar, P. Manivasagan, K-H. Kang, S-K. Kim, Alginate composites for bone tissue engineering: A review, International Journal of Biological Macromolecules 72 (2015) 269–281

3. A. Hoppe, N.S. Guldal, A.R. Boccaccini, A review of the biological response to ionic dissolution products from bioactive glasses and glass-ceramics, Biomaterials 32 (2011) 2757-2774

4. RA. Popescu, K. Magyari, M. Taulescu, A. Vulpoi, C. Berce, S. Bogdan, C. Lelescu, A. Dreanca, O. Tudoran, I. Papuc, L. Baia, New alginate-pullulan-bioactive glass composites with copper oxide for bone tissue regeneration trials, Journal of Tissue Engineering and Regenerative Medicine 12 (2018) 2112-2121

5. RA. Popescu, K. Magyari, A. Vulpoi, D. L. Trandafir, E. Licarete, M. Todea, R. Stefan, C. Voica, DC. Vodnar, S. Simon, I. Papuc and L. Baia, Bioactive and biocompatible copper containing glass-ceramics with remarcable antibacterial properties and high cell viability designed for future *in vivo* trials Biomaterial Science 4 (2016) 1252-1265.

Acknowledgement

This work was supported by a grant of Ministry of Research and Innovation, CNCS - UEFISCDI, project number PN-III-P1-1.1-TE-2016-1324, within PNCDI III.

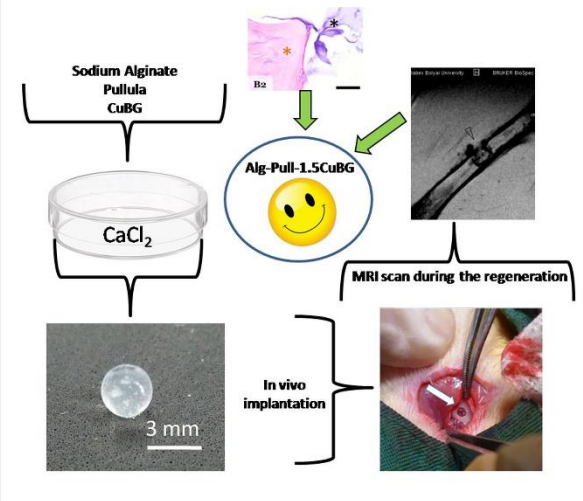

Fig. 1 Study designed of Alg-Pll-CuBG composites in bone defect regeneration

PS2-01-244

Mesoporous silica materials as bifunctional drug delivery system for bone regeneration

Adrian Szewczyk, Magdalena Prokopowicz

Medical University of Gdansk, Faculty of Pharmacy, Department of Physical Chemistry, Gdansk, PL

Introduction

The infection of bones (*osteomyelitis*) most often caused by *Staphylococcus aureus* belongs to diseases difficult to diagnose and treat. Chronic *osteomyelitis* occurs mainly in adults, usually secondary to open bone injuries, bone reconstruction or implant insertion. In clinical practice, chronic *osteomyelitis* is treated surgically with the simultaneous implementation of antibiotic pharmacotherapy. Despite advances in surgery and pharmaceutical technology, the bacterial bone infection can remain latent for many years after treatment, with complete recurrence in 20-30% of treated patients. This contributes to lowering the patient's quality of life and generates additional financial costs in the healthcare system [1].

The idea of our studies is to obtain implantable solid dosage form (spherical granules - pellets) based on mesoporous silica materials that will act as a potential drug carrier with prolonged release profile for chosen antibiotics used in *osteomyelitis* treatment and as novel bioactive material with ability to form a hydroxyapatite on its surface. The cefazolin sodium was chosen as a model antibiotic which is used in pharmacological treatment of *osteomyelitis*.

Experimental Methods

The mesoporous silica materials SBA-15 (parent material) were synthesized in the form of powder using sol-gel method. The surface modification with 3-aminopropyl groups was performed using grafting method and (3-aminopropyl)trimethoxysilane as surface modifier. The cefazolin adsorption onto mesoporous silica materials was performed by immersion of silica powders in its concentrated water solution [2]. The pellets based on the mesoporous silica materials with adsorbed cefazolin were obtained in the laboratory scale using wet granulation, extrusion and spheronization method (Caleva Multi Lab). The cefazolin release profiles form both mesoporous silica powders and pellets were investigated using USP dissolution apparatus 2 [3]. The mineralization potential assay was performed by immersing pellets in simulated body fluid for 60 days [2,3]. At each step of studies the obtained materials were characterized using FTIR, XRD, SEM-EDX methods.

Results and Discussion

Drug adsorption: The average efficiency of cefazolin adsorption from its water solutions on the SBA-15 silica powder modified with the 3-aminopropyl groups increased 5 times compared to the parent material (Fig. 1). This is related to the electrostatic attraction of the positively charged 3-aminopropyl groups present on the modified surface of the silica material with the negatively charged cefazolin ions under adsorption conditions. In the case of SBA-15 powder with unmodified surface, its surface receives a negative charge under adsorption conditions what results in electrostatic repulsion of cefazolin anions.

Drug release: The prolonged release profile of cefazolin was obtained by both the chemical modification of the SBA-15 surface (Fig. 1) and the obtaining of pellets that acts as a hydrophobic matrix. Due to the strong ionic interactions between the positive charged surface of the SBA-15 material (modified with 3-aminopropyl groups) and the negatively charged cefazolin ions, the initial burst release of cefazolin from the modified SBA-15 silica powders has been

reduced 3 times compared to that of the unmodified SBA-15 powders, with a total release time of 7 days (Fig. 1). Making the hydrophobic pellets from silica powders slowed down the release profile by an additional 30% .

Mineralization potential: The obtained pellets had satisfactory rheological properties and did not disintegrate after 60 days of incubation in simulated body fluid. After 30 days of mineralization potential studies, the spherical calcium phosphate microparticles were formed on the pellets' surface. After 60 days the spherical particles formed closely to each other and reorganized into the continuous layer (Fig. 2). The randomly formed clusters which spread over the pellets' surface were characteristic for carbonate hydroxyapatite. This hydroxyapatite layer formed preferably on the surface areas eroded by simulated body fluid what confirmed the heterogenous nucleation process.

Conclusion

The obtained preliminary results confirmed the possibility of obtaining bifunctional drug delivery system in the form of pellets composed of mesoporous silica materials. These drug delivery system released the cefazolin in a prolonged manner and exhibited mineralization properties by forming on its surface the hydroxyapatite with morphology and composition similar to human bone apatite. The presented results may increase the interest of described drug delivery systems besides the bone cements, granules, composites and bioglass which are commonly used in both the surgical and pharmacological treatment of *osteomyelitis*.

References

[1]. J.H. Calhoun et al., Osteomyelitis of the long bones., Semin. Plast. Surg. 23 (2009).
[2]. A. Szewczyk et al., Aminopropyl-functionalized mesoporous silica SBA-15 as drug carrier for cefazolin: adsorption profiles, release studies, and mineralization potential, Micropor. Mesopor. Mater. 274 (2019).
[3]. A. Szewczyk, M. Prokopowicz, Amino-modified mesoporous silica SBA-15 as bifunctional drug delivery system for cefazolin: release profile and mineralization potential, Mater. Lett. 227 (2018).

Acknowledgement

The project is supported by the Polish National Centre for Science (project OPUS 15 no. 2018/29/B/NZ7/00533) and the National Centre of Research and Development (project POWER.03.02.00-00-I026/17-00).

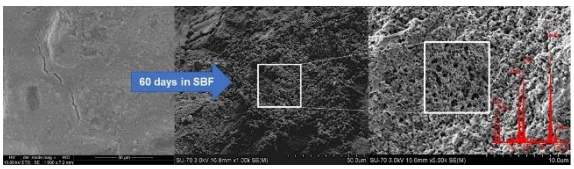

Pellets' surface during the mineralization assay

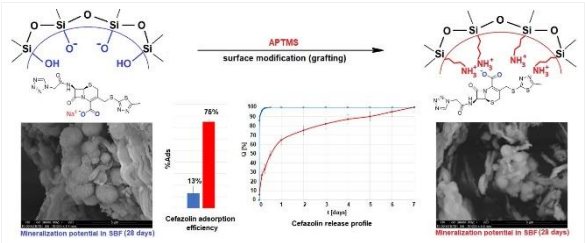

Drug adsorption and release from silica powders

PS2-01-245

Effect of differently shaped gold nanoparticles on the bioactive glasses

Zsejke-Réka Tóth[1,2], Zsolt Pap[1,3], Emilia Licarete[4], Klára Hernádi[2], Lucian Baia[1,5], Klára Magyari[1]

[1]Babeș-Bolyai University, Interdisciplinary Research Institute on Bio-Nano-Sciences, Nanostructured Materials and Bio-Nano-Interfaces Center, Cluj-Napoca, RO; [2]University of Szeged, Institute of Chemistry, Department of Applied Environmental Chemistry, Szeged, HU; [3]University of Szeged, Institute of Environmental Science and Technology, Szeged, HU; [4]Babeș-Bolyai University, Interdisciplinary Research Institute on Bio-Nano-Sciences, Molecular Biology Center, Cluj-Napoca, RO; [5]Babeș-Bolyai University, Faculty of Physics, Cluj-Napoca, RO

Introduction

Widespread application of gold nanoparticles is not surprising due their unique physical and chemical properties. They can be used in bio-/nanotechnology as sensors, drug delivery and environmental cleaning processes. Gold nanoparticles can have different morphologies (spheres, triangles, wires, cubs) and different size, resulting from different synthesis methods. The size of the nanoparticles can be very important because gold nanoparticles under 2 nm can have toxic effect [1]. Therefore, the gold nanoparticles which are used in biological systems have sizes between 3-100 nm. The bioactive glasses can be easily bind to the living organisms, without leaving any scar tissue. The present work deals with the effect of differently shaped gold nanoparticles in bioactive glasses-gold nanoparticles composites. The newly obtained materials were structurally and morphologically characterized, and further, the cell viability assay was performed on Human keratinocytes cells. Thus, the aim of the study was to obtain the optimal shape of gold nanoparticles within the glass matrix.

Experimental Methods

Three different shaped gold nanoparticles were synthesized: (a) nanospheres by using Turkevich-Frens methods [2]; (b) nanotriangle according to Kumar *et al.* [3] and our previously synthesis method [4] and (c) nanocages by using galvanic replacement reaction [5] using previously obtained Ag nanoparticles. The gold nanoparticles were stabilized with Pluronic F127 and the bioactive glass-gold nanoparticles composites were synthetized by sol-gel methods. The obtained materials optical/structural/morphological properties were examined using Jasco V-670 UV–Vis-NIR spectrometer; Philips CM 10 microscope; Hitachi S-4700 Type II cold field emission scanning electron microscope and Shimadzu XRD 6000 diffractometer. Cell viability was followed on human keratinocytes cells (HaCaT, Cell Line Service, Germany).

Results and Discussion

The Turkevich-Frens method gave rise to a monodisperse system with ≈ 12 nm size nanospheres. Beside the nanotriangles in the second synthesis pathway, it had observed a smaller fraction of polyhedral nanoparticles and the average crystal size was ≈ 150 nm. Besides gold nanocages resulted Ag nanoparticles also using the galvanic replacement processes. The gold nanoparticles morphology (shape and size) has changed after the applied thermal treatment. The spherical nanoparticles had a red shift of their plasmonic band, and the size of the nanoparticles increased from 12 nm to 25 nm. The nanotriangles have changed into 13 nm sized gold nanospheres. The HaCaT cell viability were followed both on colloid solution containing nanospheres, nanotriangles and spherical nanocages as well as on bioactive glass with differently shaped gold nanoparticles. The proliferation of cells was promoted in the presence of glasses with gold nanospheres and spherical nanocages. For the colloidal solutions the better proliferation rate were obtained for the colloid solution with spherical nanocages content.

Conclusion

We synthesized and used three differently shaped nanoparticles in composite with bioactive glasses. In the system based on Au nanocages we have found traces of Ag nanoparticles, too. Ag nanoparticles resulted as non-transformed template from the gold nanoparticles synthesis method, which have benefic properties for applicability of Au-bioactive glass composites. The results obtained on cell viability showed that bioactive glass with spherical nanocages are good candidates for future application in wound healing application.

References

1. Dykman L. A., Khlebtsov N. G. Gold Nanoparticles in Biology and Medicine: Recent Advances and Prospects. Acta Naturale 2011;3:34-55

2. Frens G. Controlled Nucleation for the Regulation of the Particle Size in Monodisperse Gold Suspensions. Nature Physical Science 1973;241:20-2.

3. Kumar D. V. R., Kulkarni A. A., Prasad B. L. V. Synthesis of triangular gold nanoplates: Role of bromide ion and temperature. Colloids and Surfaces A: Physicochemical and Engineering Aspects 2013;422:181-90.

4. Pap Z., Tóth Z., Danciu V., Baia L., Kovács G. Differently Shaped Au Nanoparticles: A Case Study on the Enhancement of the Photocatalytic Activity of Commercial TiO_2. Materials 2015;8:162-80.

5. Tóth Z.-R., Kovács G., Hernádi K., Baia L., Pap Z. The investigation of the photocatalytic efficiency of spherical gold nanocages/TiO_2 and silver nanospheres/TiO_2 composites. Separation and Purification Technology 2017;183:216-25.

Acknowledgement

This work was supported by a grant of Ministry of Research and Innovation, CNCS - UEFISCDI, project number PN-III-P1-1.1-TE-2016-1324, within PNCDI III.

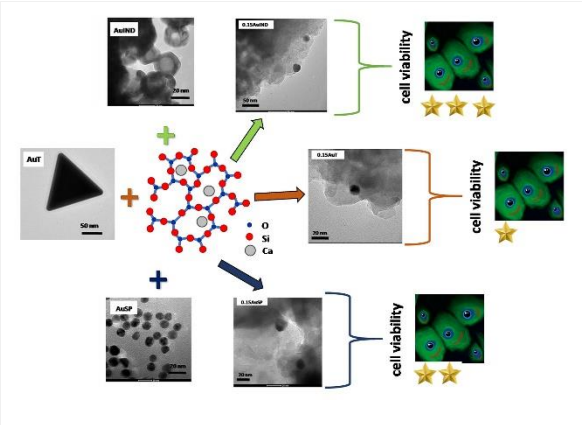

Fig. 1: Study designed of bioactive glass-gold nanoparticles composites regarding the cell viability

PS2-01-246

Optimization of the synthesis of noble metal-based microcrystals and applicability studies bioactive glass-based composites

Zsejke-Réka Tóth[1,2], Alexandra Feraru[3], Zsolt Pap[1,4], Milica Todea[5], Dan C. Vodnar[6], Klára Hernádi[2], Lucian Baia[1,3], Klára Magyari[1]

[1]Babeș-Bolyai University, Interdisciplinary Research Institute on Bio-Nano-Sciences, Nanostructured Materials and Bio-Nano-Interfaces Center, Cluj-Napoca, RO; [2]University of Szeged, Institute of Chemistry, Department of Applied Environmental Chemistry, Szeged, HU; [3]Babeș-Bolyai University, Faculty of Physics, Cluj-Napoca, RO; [4]University of Szeged, Institute of Environmental Science and Technology, Szeged, HU; [5]Iuliu Hatieganu University of Medicine and Pharmacy, Faculty of Medicine, Cluj-Napoca, RO; [6]University of Agricultural Science and Veterinary Medicine, Faculty of Food Science and Technology, Cluj-Napoca, RO

Introduction

One of the most important properties of the silver nanoparticles is their antibacterial behavior, therefore, they can be used in medicine and pharmaceutical technologies, having an own industrial field, producing around 320 tons of Ag nanoparticles per year [1]. Unfortunately, the silver nanoparticles have relatively high instability, and as a consequence they easily transform to Ag_2O and AgCl nanoparticles that can increase the toxicity of the material. Hence, researchers started to investigate Ag-based materials which toxicity is lower than the Ag_2O and AgCl nanoparticles and have higher stability than Ag nanoparticles. The silver-halides have strong visible light absorption and can be easily synthetized, having various applicability in chemistry [2]. The silver-iodides has photoluminescence properties and only few articles deal [3] with silver-iodide/glass-based composites. This work focused on the stability and synthesis optimization of AgI microcrystals. The optimized AgI were introduced into the glass matrices in order to obtain bioactive glass with controllable antibacterial activity without the possibility to appear the silver chloride.

Experimental Methods

Hydrothermal synthesis method was used for the preparation of AgI microcrystals. Different alkalic cations/salts (NaI, KI) and different surfactants (polyvinyl pyrrolidone - PVP, sodium dodecyl sulfate – SDS, and without surfactant - NØ) were used for optimization of AgI synthesis. The $60SiO_2 \times (32\text{-}x)CaO \cdot 8P_2O_5$-AgI composites were synthetized by sol-gel method using 0, 0.1, 0.2, 0.5 and 1 mol% of AgI. The optical, structural and morphological investigations of materials/composites were carried out by using JASCO-V650 spectrophotometer with an integration sphere (ILV-724) (DRS), Hitachi S-4700 Type II cold field emission scanning electron microscope, Rigaku Miniflex II X-ray diffractometer and X-ray photoelectron spectroscopy, SPEC PHOIBOS 150 MCD system.

The glass samples *in vitro* bioactivity were tested in simulated body fluid. For the antibacterial activity *Pseudomonas aeruginosa* (Gram negative) were used.

Results and Discussion

Pyramidal structures of AgI resulted by using NaI as iodide source. Pyramids were composed by microsheets. We have obtained agglomerated materials with or without SDS, as surfactant. Synthesis involving PVP as surfactant resulted ≈ 1 μm particles. After DRS investigations, we can claim that the obtained AgI are stable, we have not found any plasmonic band specified for Ag nanoparticles. The hydrothermal synthesis of AgI resulted γ-AgI (zinc blende structure) and β-AgI (wurtzite) composites. Therefore, the optimal AgI microcrystals were obtained by using NaI, as I^- source and PVP as surfactant. The stability of the obtained materials was analyzed by adding them in physiological

saline solution and stirring under UV light. The structural properties of AgI have not changed during/after the test. The obtained, stable material composites with bioactive glasses were obtained by sol-gel methods. After immersion in simulated body fluid only the presence of apatite layer without silver component (such as AgCl) is stated. The glass samples with 1 mol% AgI exhibited a good bactericidal effect against *Pseudomonas aeruginosa.*

Conclusion

For the optimal synthesis method involved for the preparation of AgI, NaI was used as iodide source and PVP as surfactant. The obtained microcrystals had pyramidical structure and resulted two different crystal phases. The synthesized AgI was stable in physiological saline solution, under UV light. The bioactive and antibacterial glass samples with 1 mol% AgI are promising materials for tissue engineering applications.

References

1. B. Nowack, H. F. Krug, M. Height, 120 Years of Nanosilver History: Implications for Policy Makers, Environmental Science & Technology, 45 (2011) 1177-1183

2. J. Li, W. Fang, C. Yu, W. Zhou, L. Zhu, Y. Xie, Ag-based semiconductor photocatalysts in environmental purification, Applied Surface Science, 358 (2015) 46-56.

3. H. He, Z. Ye, Y. Wang, Fine structure on the excitonic emission in AgI nanoparticles embedded in silica glass, Journal of Luminescence, 124 (2007) 71-74.

Acknowledgement

This work was supported by a grant of Ministry of Research and Innovation, CNCS - UEFISCDI, project number PN-III-P1-1.1-TE-2016-1324, within PNCDI III.

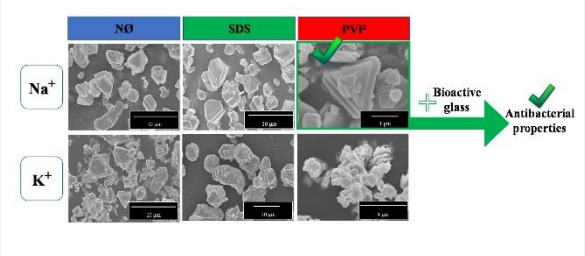

Fig. 1: Study designed of synthesis of AgI and applicability in bioactive glass-based composites

PS2-01-247

Marine Inspired Biosilica 3D Printed Bioresorbable Scaffolds for Bone Repair

Ri Han[1], Matthew Julius[2], Fraser J. Buchanan[3], **Pamela J. Walsh**[1]

[1]Queen's University Belfast, School of Chemical Engineering, Belfast, GB; [2]St. Cloud State, Biological Sciences, St Cloud, US; [3]Queen's University Belfast, School of Mechanical & Aerospace Engineering, Belfast, GB

Introduction

Nature has evolved an ability to synthesise novel inorganic silica structures. Diatoms are a unicellular microalgae, with silica cell walls that contain a nanopatterned surface. They are renowned for their strikingly intricate morphological features that cannot be replicated synthetically. Silica is known to enhance bone repair. Clinically available 45S5 Bioglass[â] has now been implanted into over 1.5 million patients to repair bone and dental defects and other new commercial products have started to come onto the market[1]. The production of synthetic silica requires highly toxic chemicals and is very energy intensive, whereas the biosilicification of diatom silica has been reported to occur at close to physiological pH under ambient conditions, thus offering a 'green' silica additive for bone repair. Purified diatom silica have been shown to be non-toxic to J774.2 macrophages and bone cells[2]. This study investigates the feasibility of blending diatom silica with poly(DL-Lactide-co-glycolide) (PDLGA) and 3D printing scaffolds suitable for bone repair to improve the osteogenic and mechanical properties of the PDLGA.

Experimental Methods

Cyclotella meneghiniana a diatom collected from the Mississippi River, USA was used in this study. The organic fraction was removed from the diatoms by heating them to 550°C for one hour in an air circulating furnace. Thermogravimetric analysis was used to verify that the organic fraction was removed. The diatom silica was then dry blended with PDLGA at 1 and 5% and dried in a vacuum oven prior to extrusion. Two other groups with 45S5 Bioglass[â]and MCM-41 were also prepared as comparisons to the diatom-PDLGA. The mixtures were then extruded using a twin-screw melt extruder into filaments. The resultant filaments (diatoms-PDLGA, Bioglass-PDLGA and MCM-41-PDLGA) were then printed into 3D scaffolds via 3D Fused Deposition Modelling (FDM). The filaments and the scaffolds were mechanically tested. A dissolution study was also performed on the 3D scaffolds at different pH conditions (pH 4, 7.4 and 10).

Results and Discussion

Figure 1 shows the typical profile of the silica cell walls obtained from *C. meneghiniana*. Two silica cell walls overlap like petri-dishes and are bound together by a girdle band. Once the organics are removed the structure comes apart, leaving the top and bottom valves (Figure 1c). Inconsistencies in the extruded filament diameter of MCM-PDLGA meant it was unsuitable to print. Therefore, only diatom-PDLGA and Bioglass-PDLGA were fabricated into scaffolds. Figure 2a shows the scaffold decomposition after 12 weeks in SBF solution at pH 7.4. The pure PDLGA and Bioglass-PDLGA scaffold at this point were difficult to handle, and had become gelatinous, whereas the diatom-PDLGA scaffolds maintained their shape and could be handled. Over the 12 weeks, the Young's moduli were measured as shown in Figure 2b. The addition of diatom particles into PDLGA causedan overall reduction in Young's modulus initially (at day 0). However, over time, the Young's modulus of pure PDLGA and Bioglass-PDLGA dropped more significantly than diatom-PDLGA. After 8 weeks, pure PDLGA and Bioglass-PDLGA became difficult to handle, thus

it was too difficult to obtain any meaningful mechanical data, however, both diatom-PDLGA maintained some mechanical integrity, at approximately 20 and 25 MPa for 1 and 5 wt% diatom additive respectively. The results found that overall, diatom silica provided a more stable filler material. In the dissolution study, the release of Si and Ca ions was also studied, although the data has not been presented in this abstract. The results found diatom-PDLGA had a near-linear release silica release, as the PDLGA degraded. The degradation of Bioglass-PDLGA scaffolds showed an earlyburst release of silica ions.

Conclusion

The results of the overall study found, that diatom-PDLGA scaffolds offered better long-term stability with a near-linear release of silica ions. The next stage is to assess the diatom-PDLGA scaffolds by in vitro biocompatibility testing and in an in vivo animal model.

References

(1) Baino, F. *et al*. *J. Funct Biomater*. 2018, 9 (25).

(2) Walsh, P. J *et al*. *Sci. Rep.* 2017, *7* (1).

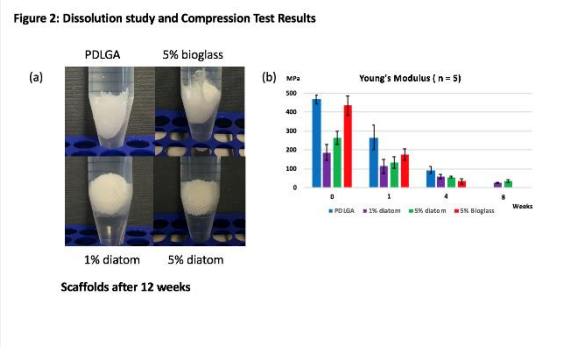

Figure 2
Dissolution study and Compression Test Results

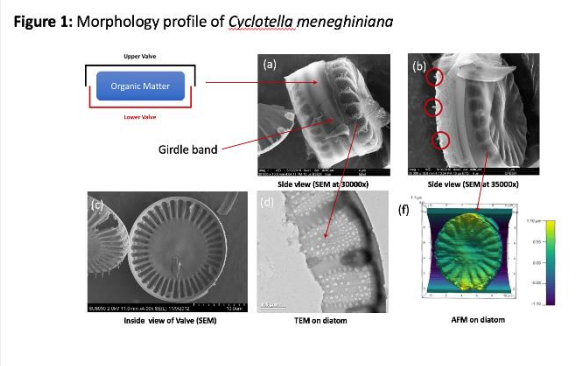

Figure 1
Morphology profile of Cyclotella meneghiniana

PS2-01-248

Incorporation of bioactive metal ions improves biomaterial properties for orthopedic applications

Vera Guduric[1], Anne Bernhardt[1], Richard F. Richter[1], Tilman Ahlfeld[1], Michael Geißler[1], Chengtie Wu[2], Anja Lode[1], Michael Gelinsky[1]

[1]Technische Universität Dresden, Faculty of Medicine Carl Gustav Carus, Centre for Translational Bone, Joint and Soft Tissue Research, Dresden, DE; [2]Shanghai Institute of Ceramics, Chinese Academy of Sciences, Biomaterials and Tissue Engineering Research Center, Shanghai, CN

Introduction

Bioglasses are considered as common material used for bone regeneration applications thanks to their excellent osteoconductivity, osteostimulativity and degradation rate. Their limit is in the lack of inner microporous structure with low specific surface area. Mesoporous bioglasses (MBG), as a new class of bioactive glasses, specific by their highly ordered mesoporous channel structure and high specific surface area, are suitable not only for bone tissue regeneration, but also for drug/growth factor delivery (1). Bioglasses can be easily modified by addition of elements which can induce desired biological effects. Metal ions as therapeutic agents and their combination with bioceramics have shown advantages for therapeutic applications. Chromium III (Cr^{3+}) has already shown osteogenic properties in vitro (2) and in vivo (3) while zinc II (Zn^{2+}) has shown antimicrobial effects (4). Herein, we aimed to synthesize Cr^{3+} and Zn^{2+} doped mesoporous bioglass and to investigate biological properties of these two metal ions for bone tissue regeneration applications.

Experimental Methods

Synthesis protocol of MBG with specific molar ratio of silica (Si), calcium (Ca) and phosphorus (P) (Si:Ca:P=85:15:5) was used as starting point for incorporation of Cr^{3+} and Zn^{2+} (5). Incorporation of metal ions was performed by substitution of Ca by desired percentage of the ions, meaning that the content of Ca was decreased and maximal content of ions in the MBG was 15 %. Primary human pre-osteoblasts (hOB) (isolated from human bone after total hip replacement surgery after inform consent of the patients) were cultivated for 14 and 21 days under osteogenic stimulation and in the presence of Cr^{3+} ions. Cell viability and proliferation were evaluated by intracellular lactate dehydrogenase (LDH) activity measurement and quantification of DNA content. Quantification of alkaline phosphatase (ALP) activity was determined in order to assess osteogenic differentiation. Antibacterial activity of Zn^{2+} was evaluated by determination of minimal concentration of this ion showing detectable antimicrobial effect when *S. aureus* (Gram+) and *E. coli* (Gram-) were exposed to cell culture media containing different concentrations of Zn^{2+} for 0.5, 3 and 6h.

Results and Discussion

MBGs with incorporated Cr^{3+} and Zn^{2+} ions were successfully synthetized. Their particle size smaller than 45 µm is suitable for combination with hydrogels or calcium phosphate cements (CPC) used in 3D bioprinting.

Presence of Cr^{3+} concentrations up to 100 µM did not affect osteoblast proliferation over 21 days. Cell number was significantly reduced with addition of 250 and 500 µM. Higher concentrations of Cr3+ in cell culture media did not affect osteogenic differentiation of cells. Slightly increased ALP activity was observed at all investigated concentrations compared to the samples without Cr^{3+}, confirming results obtained using human mesenchymal stromal cells (4), but with significant difference only in the case of 500 µM concentration.

Zn^{2+} showed antimicrobial effect against both tested bacteria. In the case of *E.* coli, antimicrobial effect was observed after 30 minutes at 750 µg/ml and higher concentrations of the ion and it increased over 6h. At the highest tested concentration, 1500 µg/ml, Zn^{2+} showed slight effect against *S. aureus*, but after 3h of exposure the antimicrobial effect was high at 500 µg/ml and higher concentrations and it was increased after 6h. Comparing results for both bacteria, stronger antimicrobial effect of Zn^{2+} was observed in the case of *S. aureus*.

Conclusion

In this study, biological properties of Cr^{3+} and Zn^{2+} were evaluated, with a focus on proliferation and osteogenic differentiation of primary human pre-osteoblasts and antimicrobial effect, respectively. Synthetized MBGs with Cr^{3+} and Zn^{2+} incorporated in their structure in combination with hydrogels or CPC can allow fabrication of 3D bioprinted structures for osteochondral regeneration applications.

References

1. Wu et al., Interface Focus, 2012
2. Schamel et al, Mater Sci Eng C, 2017
3. Rentsch et al., Acta Biomater, 2018
4. Pasque et al., Colloids Surf A, 2014
5. Zhu et al., Micropor Mesopor Mat, 2008

Acknowledgement

The authors thank to Ms. Anna-Maria Placht for excellent assistance and the German Research Foundation (DFG-GE1133/24-1) for financial support.

PS2-01-249

Effect of therapeutic ion doping on the morphology and final composition of mesoporous glass particles obtained by micro-emulsion method

Martin Michálek[1], Zuzana Neščáková[1], Dagmar Galusková[2], Si Chen[1], Liliana Liverani[3], Aldo R. Boccaccini[3], Dušan Galusek[2]

[1]TnU AD, Centre for Functional and Surface Functionalized Glass, Trenčín, SK; [2]TnU AD, Joint Glass Centre of the IIC SAS, TnU AD and FChFT STU, Centre for Functional and Surface Functionalized Glass, Trenčín, SK; [3]University of Erlangen-Nuremberg, Institute of Biomaterials, Erlangen, DE

Introduction

The present work shows the effect of doping different ions on the morphology and chemical composition of mesoporous bioactive glass particles (MBG). Furthermore, the formation of hydroxyapatite (HA) in the presence of simulated body fluid (SBF) and ion release was investigated. The original melt-quenched bioactive glass (45S5 Bioglass®) [1] is nowadays prepared with many different modifications in initial composition. Discovery of mesoporous bioactive glasses (MBG) opened a new direction for developing multifunctional bioactive materials by applying nanotechnology in regenerative medicine [2]. MBG emerged when the supramolecular chemistry of surfactants was incorporated into the bioactive glasses field. MBG particles gaining more and more attention in various biomedical applications due to their unique features. Small size, large specific surface area and their large surface to volume ratio, make them suitable candidates for bone related applications, soft tissue regeneration and as a drug/biomolecule delivery carrier. The incorporation of different ions in the composition of glass is called doping and it is crucial for the production of functional materials. Therapeutics ions such as Sr^{2+}, Zn^{2+}, Cu^{2+}, Mg^{2+}, Co^{2+}, Ce^{3+}, B^{3+}, Ga^{3+} etc. are usually incorporated in the aim to affect the bone formation, importing anti-inflammatory effect, antibacterial activity [3], increase of bone-cell adhesion or promote synergic stimulating effects on angiogenesis.

Experimental Methods

Used chemicals were purchased from Sigma-Aldrich (Darmstadt, Germany) without further purification. The reference material (MBGp) with a nominal composition of 63/37 mol % (SiO_2/CaO) was used as the reference. Five different therapeutic ions namely: Sr^{2+}, B^{3+}, Mg^{2+}, Cu^{2+} and Ga^{3+} were incorporated into the MBGp in the nominal composition of 62 SiO_2 / 32 CaO / 6 (X) in mol %. The synthesis was performed using the microemulsion assisted sol-gel method by employing surface active soft template - cetyltrimethylammonium bromide (CTAB) as described in the literature [4]. For all compositions, the procedure was identical using nitrides as precursors except the B_2O_3 precursor (H_3BO_3). To explore in vitro mineralization of the glasses, the immersion method in simulated body fluid (SBF) was performed according to the protocol of Kokubo et al. [5]. The effect of the diverse ions on the morphology and composition was analyzed utilizing SEM/EDX, FTIR, ICP OES before and after the immersion test.

Results and Discussion

The results show that the different ions incorporated in the system SiO_2-CaO cause morphological and compositional changes in the obtained materials. The increase in particle size was visible by incorporating B^{3+} and Mg^{2+} ions (Figure 1c and d) leading to particles of size ≥ 200 nm in comparison with the spherical particles with a size of 130 nm ± 20

nm for MBGp. Moreover in B^{3+} and Mg^{2+} doped samples, resulted particles have pineal shape. Incorporation of Cu^{2+} in the system caused a visible formation of CuO crystals on the spherical particles (Figure 1e and more detailed in Figure 2). Precipitates were visible in the system containing Ga^{3+}. Furthermore, the EDX revealed that the addition of therapeutic ions caused remarkably decrease of Ca^{2+}. In the sol-gel preparation, the final composition of the glass may be different from the designed one; therefore, in most studies, chemical analysis is performed questioning the chemical homogeneity of the obtained particles. According to EDX results, the content of Cu^{2+} and Ga^{3+} in the experimentally obtained materials was higher than the nominal 6 mol %. These results should be verified by ICP OES analysis.

Conclusion

Chemical composition, specific surface area and size are the most important aspects determining biological activities of glasses in a physiological environment. Presented results show that incorporation of therapeutic ions affects the morphology, size and chemical composition of the MBG particles and that the final composition of the glasses may differ from the designed one.

References

1. Hench, L.L., et al., *Bonding mechanisms at the interface of ceramic prosthetic materials.* Journal of Biomedical Materials Research, 1971. **5**(6): p. 117-141.
2. Wu, C.T. and J. Chang, *Multifunctional mesoporous bioactive glasses for effective delivery of therapeutic ions and drug/growth factors.* Journal of Controlled Release, 2014. **193**: p. 282-295.
3. Kaya, S., M. Cresswell, and A.R. Boccaccini, *Mesoporous silica-based bioactive glasses for antibiotic-free antibacterial applications.* Materials Science and Engineering: C, 2018. **83**: p. 99-107.
4. Liang, Q.M., et al., *A facile synthesis of novel mesoporous bioactive glass nanoparticles with various morphologies and tunable mesostructure by sacrificial liquid template method.* Materials Letters, 2015. **148**: p. 45-49.
5. Kokubo, T. and H. Takadama, *How useful is SBF in predicting in vivo bone bioactivity?* Biomaterials, 2006. **27**(15): p. 2907-2915.

Acknowledgement

The study was carried out in the framework of the project FunGlass that has received funding from the European Union´s Horizon 2020 research and innovation programme under grant agreement No 739566. The grants VEGA 2/0026/17 and APVV 15/0014 are gratefully acknowledged.

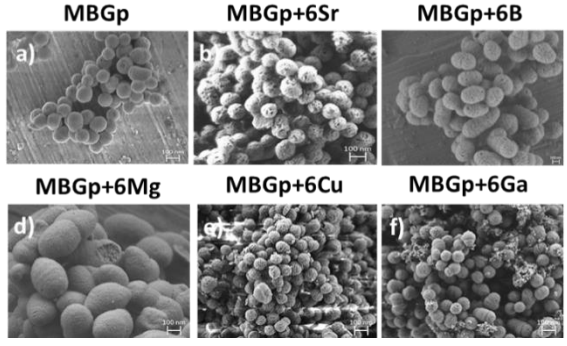

Figure 1

SEM analysis of the obtained mesoporous bioactive glass powders: **a)** MBGp, **b)** MBGp+6Sr, **c)** MBGp+6B, **d)** MBGp+6Mg, **e)** MBGp+6Cu and **f)** MBGp+6Ga.

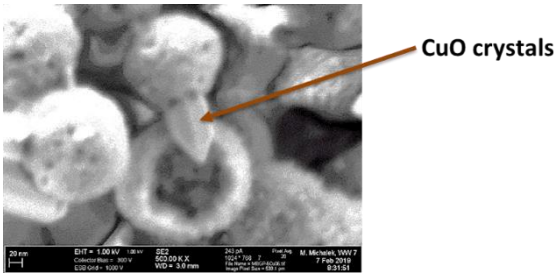

Figure 2
Crystals of CuO in the MBGp+6Cu material.

PS2-01-250

Electrophoretic Deposition of Mesoporous Bioactive Glass Nanoparticles on Polyetherketoneketone

Kai Zheng[1], Xinglong Hu[2], Qaisar Nawaz[1], Jie Wei[2], Aldo R. Boccaccini[1]

[1]University of Erlangen-Nuremberg, Institute for Biomaterials, Erlangen, DE; [2]East China University of Science and Technology, Key Laboratory for Ultrafine Materials of Ministry of Education, Shanghai, CN

Introduction

Polyetherketoneketone (PEKK) is a promising biomaterial for a verity of applications (e.g., orthopedic, spinal, and dental applications), due to its biocompatibility, chemical durability, and favorable mechanical properties [1]. However, PEKK suffers from biological inertness leading to poor osteogenesis and osseointegration with host bone tissues. Surface modification and incorporation of bioactive fillers can enhance bioactivity and cellular responses of PEKK towards more efficient bone repair and osseointegration [1]. Bioactive glasses (BG) are attractive biomaterials for hard tissue repair/regeneration, given their bone bonding capability and osteogenic potential [2]. Notably, mesoporous bioactive glass nanoparticles (MBGN), due to their tunable morphology and chemistry, emerge as versatile building blocks for developing 3D scaffolds, coatings, or drug delivery carriers [3].

Experimental Methods

In this study, we used electrophoretic deposition (EPD), a practical approach to fabricate uniform coatings, to coat Zn-containing MBGN (Zn-MBGN) on Tantalum (Ta)/PEKK composites. The mesoporous nanoparticles were synthesized using a microemulsion assisted sol-gel approach [3]. The composites were produced by mechanical mixing and sintering Ta and PEKK powders.

Results and Discussion

The incorporation of Ta not only improved cellular activity but also enhanced the conductivity of PEKK, which facilitated the EPD coating process. A crack-free coating was achieved by carefully controlling the processing parameters of EPD (e.g., deposition voltage, time). The thickness of the coating could be adjusted by tuning the processing parameters or concentration of particle suspension. The presence of particulate coating on the composites accelerated the apatite formation, an indicator of potential in vivo bone bonding, after immersion in simulated body fluid. The mesoporous structure of coating could also improve the hydrophilicity and protein adsorption. Furthermore, the adhesion, proliferation, and osteogenic differentiation of bone marrow mesenchymal stem cells on the coated composites were significantly promoted in comparison to those on the uncoated ones.

Conclusion

The EPD technique was proved to be an effective approach to homogenously coat bioactive nanoparticles on PEKK-based implants. The Zn-MBGN coated composites have shown great potential in bone repair/regeneration applications.

References

[1] B. Yuan, Q. Cheng, R. Zhao, X. Zhu, X. Yang, X. Yang, K. Zhang, Y. Song, X. Zhang, Comparison of osteointegration property between PEKK and PEEK: Effects of surface structure and chemistry, Biomaterials. 170 (2018) 116–126. doi:10.1016/j.biomaterials.2018.04.014.

[2] J.R. Jones, Reprint of: Review of bioactive glass: From Hench to hybrids, Acta Biomater. 23 (2015) S53–S82. doi:doi:10.1016/j.actbio.2015.07.019.

[3] K. Zheng, A.R. Boccaccini, Sol-gel processing of bioactive glass nanoparticles: A review, Adv. Colloid Interface Sci. 249 (2017) 363–373. doi:10.1016/j.cis.2017.03.008.

Acknowledgement

This project has received partial funding from the German Academic Exchange Service (DAAD)-China Scholarship Council (CSC) PPP programme under grant No. 57389773. K. Z. would like to thank the Emerging Talents Initiative (ETI) Programme of the University of Erlangen-Nuremberg for the financial support.

PS2-01-251

Histologic and radiographic investigations of bone defect obliteration with Bioactive Glass S54P3 and Bone Dust

Anne Kluge[1], Marcus Neudert[1], Christiane Kunert-Keil[2], Thomas Zahnert[1], Max Kemper[1]

[1]Technische Universität Dresden, Department of Otorhinolaryngology- Head and Neck Surgery, Dresden, DE;
[2]Technische Universität Dresden, Department of Orthodontics, Dresden, DE

Introduction

Bone dust (BD) harvested during operation may be suitable as an autologous obliteration material for non-critical size defects. Bioactive glass (BA) can be an alternative. To treat non-critical size defects, BD and BA are commonly used for obliteration techniques. However, the optimal harvesting method and parameters for BD have not been examined. In this study, we analysed the osseoregenerative potential of both materials and the combination of both.

Experimental Methods

Thirteen female merino sheep (7 years old) underwent surgery on the frontal calvaria. Four defects were inserted. The first defect was considered a reference and remained unfilled, the second defect was filled with BD from the calvaria bone, the third defect was filled with BA and the fourth with a mixture of BA and BD. The animals were sacrificed after 3 weeks. To evaluate bone regeneration, we used digital volume tomography, bone density measurement, fluorochrome sequence labelling, and histological analysis.

Results and Discussion

All analyses showed quantitative and qualitative bone regeneration 3 weeks after operation. The control blank defect showed a significantly less defect filling compared to all other. Trends showed that the analysis of fluorochromes showed more new mineralized bone in the defects filled with BD than compared to the blank sample and BA filled ones. The defect filled with BD only showed the most new bone formation. The defects filled with BA were the most filled and densest after, but had the same amount of new mineralized bone as the reference one. Moreover, bone regeneration occurred from the surrounding bone and showed only a defect bridge in the BD-filled defects (alone and mixed with BA).

Conclusion

BD and BA are suitable bone replacement materials for obliteration techniques because they completely filled the defects. Thus, BD harvested under standardised conditions provided a higher level of osteoreparation potential for the generation of woven bone and establishment of defect bridges. A mixture of both replacement materials combines benefits from both materials. Defects are completely filled, have a high density and osteoregeneration is faster due to vital bone cells in the obliteration material.

References

Kluge A, Neudert M, Kunert-Keil C, Lailach S, Zahnert T, Kemper M. The Obliteration of Noncritical Size Bone Defects With Bone Dust or Bone Replacement Material (Bioactive Glass S53P4). Otol Neurotol. 2019 Apr;40(4):e415-e423. doi: 10.1097/MAO.0000000000002178.

PS2-01-252

Biodegradable inorganic nanofibres as a novel topical dosage form and wound healing promoter

Miroslava Rysová[1], Hana Tománková[1], Tomáš Zajíc[2]

[1]Technical University of Liberec, Institute for Nanomaterials, Advanced Technology and Innovation, Liberec, CZ; [2]Regional Hospital, Centre for Laboratory Medicine, Liberec, CZ

Introduction

Over the last decades, drug delivery has undergone a significant evolution as novel nano-based dosage forms for application in specific areas such as active management of contaminated and slow-to-heal wounds. The mayor reason for application of the nanosized dosage forms in this field is precise targeting, designed drug release profile *in situ* and increased bioavailability of hydrophobic drugs leading to dose optimisation and reduced overall body load. Recently, electrospun nanofibres have attracted attention as potential matrix for drug delivery and release due to their possible barrier effect and unique characteristics – especially small fibre diameter and high porosity as characteristics leading to the extreme surface to weight ratio.[1] In addition to these properties held by nanofibres in general, the chemical nature, surface functionality and charge represent properties strongly affecting their biocompatibility, degradation kinetics, the material-drug interactions and loading capacity. Composition of the matrix of nanofibres may stimulate wound healing process through released degradation products. From this point of view, silica nanofibres represent a very promising material for this application, combining traditional nanofibres´ properties and unique properties given by their inorganic nature as the silicic acid, released during their degradation, is well known for its wound healing stimulating potential.[2] Moreover, another advantage possessed by this novel type of nanofibres is wide range of possible surface modifications via functional groups grafting.[3]

The aim of this work is to present biodegradable silica nanofibres as novel biomaterial with potential for application in wound healing and *in situ* drug release in wound management.

Experimental Methods

The silica nanofibres were obtained by needleless electrospinning of solution synthetized by sol-gel method from silicon tetraethoxide (TEOS) as the main precursor. Obtained nanofibres had undergone mild (<200°C) thermal stabilization and were analysed in order to characterize their morphology, degradation kinetics profile *in vitro* and effects on human dermal fibroblasts (NHDF) and keratinocytes (HaCaT) viability and proliferation. Morphology of nanofibres was characterized by electron microscopy (SEM) prior and after the degradation process. The degradation was performed under 37°C for 72 hours and the decomposed mass was determined by released Si quantification via ICP mass spectroscopy. Effects of the silica nanofibres and their degradation products on dermal cells was evaluated using the MTT method, fluorescence life/dead staining and cytoskeleton staining after 1, 2, 3 and 7 days of exposition. Moreover, drug sorption capacity was studied on a model drug (antibiotic tetracycline (TET)). Quantity of the adsorbed drug was determined and antibacterial activity against model microorganism (*E. Coli*) in time was assessed.

Results and Discussion

The SEM examination confirmed formation of nanofibres with mean diameter ranging between 150 nm and 750 nm depending on the solution properties and electrospinning set-up. The SEM examination also revealed nature of the inorganic nanofibres degradation realized by surface corrosion instead of swelling characteristic for polymeric

materials and usually leading to porosity reduction. Preservation of the initial porosity was confirmed even after the model drugs loading procedures. Such as observation is particularly important in wound management as drug eluting dressing is demanded to remain vapour permeable to facilitate gas exchange. Morphology of the silica nanofibres after thermal stabilization and during degradation are shown on Figure 1. The tetracycline adsorbed to the nanofibrous sheet was evaluated 45 µg/ mg NFs. The antibacterial activity examined by agar diffusion test shown prolonged activity and drug release for 72 hours. The inhibition zone diameter reached 30 mm after 24 hours of exposition and decreased to 17.5 mm after 72 hours of constant exposure to *E. Coli* strain. Exposure to human dermal cells proved biocompatibility of the nanofibres. Presence of nanofibres (150 µg/ml) in culture medium led to increase of cell numbers in both – dermal fibroblasts and keratinocytes - after 48 hours of exposure in comparison to the control. Cell viability and morphology remained unchanged.

Conclusion

Silica nanofibres were confirmed as a biocompatible and biodegradable material with a broad potential for application as novel dosage form for topical drug release and wound management. The system is able to provide its surface for drug adsorption and sustained drugs release. The indisputable advantage of the system is rapid degradation and unique mechanism of degradation facilitating vapour and gas exchange during the whole process. The positive effect on healing process is altered by positive impact of the degradation products on cell proliferation which as we hope might lead to accelerated wound closure.

References

1.Son, YJ. et al.; Therapeutic applications of electrospun nanofibres. Arch. Pharm. Res. 37(1), 69-78 (2014).
2.Rotkova, J. et al.; Inorganic silica nanofibres in a role of bioactive compound carrier; Proceedings of the 7th International Conference on Nanomaterials - Research and Application (Nanocon); ISBN: 978-80-87294-63-5, 413-418 (2015).
3.Howarter; JA. Et al.; Optimization of silica silanization by 3-aminopropyltriethoxysilane. Langmuir 22(26), 11142-11147 (2006).

Acknowledgement

This work was supported by the Ministry MŠMT of the Czech Republic and the European Union - European Structural and Investment Funds programme - project Hybrid Materials for Hierarchical Structures (HyHi, Reg. No. CZ.02.1.01/0.0/0.0/16_019/0000843).

PS2-01-253

Lithium-substituted bioactive glasses for mineralised tissue repair

Abeer Alaohali[1], Ke Zhang[1], Paul Sharpe[1], Delia Brauer[2], Nuttawan Sawangboon[2], Eileen Gentleman[1]

[1]King's College London, Centre for Craniofacial and Regenerative Biology, London, GB; [2]Friedrich Schiller University Jena, Otto Schott Institute of Materials Research, Jena, DE

Introduction

The Wnt canonical signaling pathway plays a crucial role in tooth and bone regeneration, and can be upregulated by inhibition of glycogen synthase kinase 3 (GSK3). Lithium is an antagonist of (GSK3) and can be substituted in the bioactive glasses (BG), which can be used clinically to enhance the tooth repair.

Experimental Methods

We developed borate (LiBBG) and phosphate (LIPBG) BG which contain lithium and evaluated ion release and toxicity of their dissolution ions.

Results and Discussion

We found that both LiPBG and LiBBG can release high levels of Li that can elevate Wnt canonical signaling, however the levels of phosphate and boron are toxic to cell cultures and limit the utility of BG in the tooth.

Conclusion

These data suggest that lithium-substituted BG can release therapeutic level of lithium which upregulate Wnt signaling. However, LiPBG and LiBBG are toxic to pulp cells in vitro. Nevertheless, it may be possible to use BG in vivo in non-exposed pulp tooth models that limit contact with the pulp cells.

PS2-01-254

Bioactive glass nanoparticles-containing artificial extracellular matrices support bone tissue engineering via osteogenic stem cell differentiation

Lysann M. Kroschwald[1,2], Sandra Rother[3], Sabine Schulze[1,2], Dieter Scharnweber[3], Stefanie Möller[4], Matthias Schnabelrauch[4], Kai Zheng[5], Aldo Boccaccini[5], Vera Hintze[3], Stefan Rammelt[1]

[1]University Hospital Carl Gustav Carus of Technische Universität Dresden, University Centre for Orthopaedics and Trauma Surgery, Dresden, DE; [2]Technische Universität Dresden, Centre for Bone, Joint and Soft Tissue Research, Dresden, DE; [3]Max Bergmann Centre of Biomaterials,Technische Universität Dresden, Institute of Material Science, Dresden, DE; [4]Innovent e. V., Biomaterials Department, Jena, DE; [5]University of Erlangen-Nuremberg, Department of Materials Science, Engineering, Erlangen, DE

Introduction

Due to the demographic development, there is a high need for treatment options regarding the reconstruction of damaged or diseased tissue. This requires the development of novel functional biomaterials, composed of cells, bioactive molecules and biodegradable scaffolds, which should improve regeneration. Glycosaminoglycans (GAGs) like chondroitin sulfate (CS) or chemically sulfated hyaluronan (sHA3) are reported to promote bone regeneration [1]. As multifunctional components of artificial extracellular matrices (aECMs) CS and sHA significantly influence bone healing by the recruitment of mesenchymal stem cells and by supporting their differentiation [2].

Specifically, for bone-related applications, silicate-based bioactive glass nanoparticles (BGN) show unique properties for regeneration and repair due to their intrinsic bioreactivity coupled with their small size and high specific surface area [3]. Based on their ability to interact with living tissues, the release of soluble ions like Si and Ca is reported to favor intracellular and extracellular responses, promoting rapid bone formation [4].

The aim of this study was to evaluate the potential synergic effects of either CS or sHA3 in combination with BGN on the osteogenic capacity of these aECMs as important aspect of bone healing via osteogenic stem cell differentiation.

Experimental Methods

Thermanox™slides were coated with collagen type I (col), col/CS or col/sHA3 and compared to similar coatings that contained BGN with diameters in the range of 300 - 400 nm. Sirius red and Toluidine blue staining was used to visualize the col and GAG distribution within the coatings. These aECMs with or without BGN were analyzed regarding their effects on the differentiation of human mesenchymal stem cells (hMSCs). Growth and viability of hMSCs were examined using biological assays like MTT cytotoxicity, while cellular differentiation was examined by ALP activity, mineralization, Alizarin red staining and immunofluorescence staining. In addition, the Ca release from the BGN-containing aECMs was analyzed.

Results and Discussion

Sirius red and Toluidine blue staining of aECMs showed a homogeneous distribution of col, sCS3 and sHA3 irrespective of the presence of BGN. Differentiation of hMSCs on different coatings was studied over 28 days. After 7, 14 and 28 days, biological assays were performed. Fig. 1 shows the mineralization of hMSCs from three different donors on different aECMs after incubation for 28 days.

Cell growth was visualized by immunofluorescence staining. MTT cytotoxicity assay revealed an enhanced viability of hMSCs in the presence of GAGs and BGN. A constant release of non-toxic concentrations of Si and Ca ions might

be one reason. Furthermore, BGN influence also mineralization in a positive manner. The presence of CS or sHA3 in general was observed to enhance the mineralization compared to non-coated slides (control). In combination with col-based aECMs and GAGs the mineralization levels were significantly higher compared to the control. Especially BGN-containing aECMs significantly increased the calcium levels while for aECMs without BGN only a slight increase was observed. These results are supported by the measured ALP activities of the hMSCs.

Conclusion

aECMs composed of col, GAGs and BGN are promising bioinspired functional biomaterials for rapid mineralization in bone healing and bone tissue engineering.

References

[1] Scharnweber D et al., J Mater Sci: Mater Med 26:232, 2015.
[2] Kliemt S et al., J. Proteome Res. 12(1):378-389, 2013.
[3] Zheng K et al., RSC Adv. 6:95101-9511, 2016.
[4] Gerhardt LC et al., Materials 3:3867-3910, 2010.

Acknowledgement

We acknowledge financial support by DFG (TRR 67; subproject A3, B5, Z3).

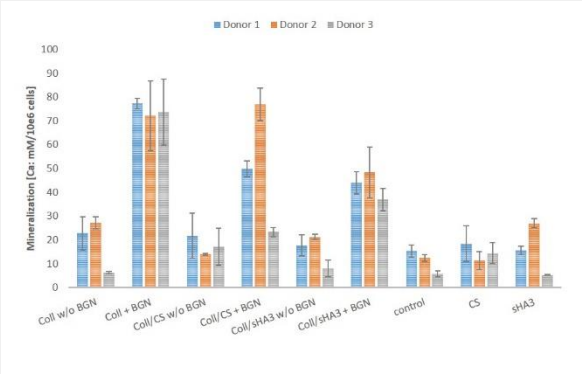

Figure 1
Mineralization of hMSCs on aECMs containing different sGAGs (CS or sHA3) in comparison to those containing BGN via quantification of calcium content.

PS2-01-255

Development of hybrid material based on gelatin and bioactive glass particles for bone bio-engineering

Amel Houaoui[1], Karolina Lukasik[2], Jonathan Massera[2], Michel Boissiere[1], Emmanuel Pauthe[1]

[1]Cergy-Pontoise university, Labratory ERRMECe, department of biology, Neuville sur Oise, FR; [2]Tampere University, Laboratory of Biomaterials and Tissue Engineering, Faculty of Medicine and Health Technology and BioMediTech Institute, Tampere, FI

Introduction

Bone-tissue engineering represents a pivotal strategy to face situations where critical-size bone defects do not heal spontaneously; as for elderly patients and/or in front of complex pathological situations.Materials with suitable properties-such as good mechanical properties and controlled resorbability-are needed. Hybrid scaffolds represent an innovative technology that provides regeneration of damaged tissue. A hybrid material consists of organic and inorganic components which interact at the nanoscale with covalent links between both phases [1].

Experimental Methods

Here we present the synthesis and characterization of two hybrid scaffolds based on i) gelatin as the organic phase and ii) bioactive glass (BG) as the inorganic phase. BG is pertinent for bone engineering applications due to its ability to release ions enabling osteoinduction [2]. Both scaffolds contain 70% of gelatin and 30% (weight %) of 13-93 or S53P4 BG particles. The link between the gelatin and the BG is insured by the (3-Glycidyloxypropyl) trimethoxysilane (GPTMS) (Figure 1). The scaffolds were synthesized by sol-gel transition. First,the gelatin is functionalized with the GPTMS and then the BG is added in the solution. Different proportions of GPTMS/gelatin (molar ratio) were tested in order tovary the degree of connectivity between the organic and inorganic phases. The developed hybrid biomaterials were exposed to collagenase (0.5%) to assess their enzymatic degradation and, thus, establish the impact of increasing the cross-linking between the organic and inorganic phases on the hybrid biomaterials stability.To investigate the behavior and the bioactivity of our hybrids, the glasses dissolution and polymer degradation, in TRIS buffer solution, were quantified by Inductively Coupled Plasma - Optical Emission Spectrometry (ICP-OES) and Gel Permeation Chromatography (GPC), respectively. The bioactivity, assumed to be related to the precipitation of a HA layer at the materials' surface when immersed in aqueous solution, was assessed in Simulated Body Fluid (SBF) as usually performed in testing bioactive glass.

Results and Discussion

We demonstrate that higher was the ratio of GPTMS/gelatin, higher was the stability of the gels concomitant to a greater covalent bonding between the organic and inorganic phases. In vitro dissolution of the scaffolds, performed in Simulated Body Fluid (SBF),showed precipitation of a hydroxyapatite layer from BG. we have also investigate the behavior and the bioactivity of our hybrids. The glasses dissolution and Gelatin degradation, quantified by ICP-OES and GPC showed a very good stabilty with a low rate of dissolution.

Conclusion

These results demonstrate the first sign of hybrid bioactive bone-materials. so, those hybrids are promising for a bone application. Nevertheless, more studies are needed to quantify and confirm the effect of the bioactiveglass at the cellular level.

References

[1] O. Mahonyet al., Journal of Sol-Gel Science Technology(2014) 69: 288-298, doi:10.1007/s10971-013-3214-3

[2] L.L. Hench., New Journal of Glass and Ceramics (2013)3: 67-73,doi: 10.4236/njgc.2013.32011

Acknowledgement

The authors would like to acknowledge the Academy of Finland (Academy Research Fellow grant to JM), TTY-säätiö for IL financial support, the Institute for Advanced Studies (IAE) for enabling researcher mobility,

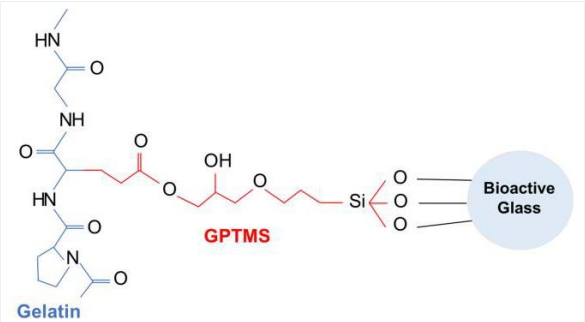

Figure 1:Schematic representation of the covalent bonding between the gelatin and

PS2-01-256

New gel-derived glasses doped with therapeutic ions with high antioxidant potential

Barbara Zagrajczuk[1], Michal Dziadek[1,2], Kinga Dziadek[3], Kamila Chyzy[1], Katarzyna Cholewa-Kowalska[1]

[1]AGH University of Science and Technology, Faculty of Materials Science and Ceramics, Department of Glass Technology and Amorphous Coatings, Krakow, PL; [2]AGH University of Science and Technology, Faculty of Materials Science and Ceramics, Department of Ceramics and Refractories, Krakow, PL; [3]University of Agriculture in Krakow, Faculty of Food Technology, Department of Human Nutrition, Krakow, PL

Introduction

The bioglasses are a group of biomaterials that have an ability to create a strong bond with tissues, especially with bone tissue. However, in order to improve their overall performance in the process of tissue regeneration, and extend their applicability towards other tissues, some additional features such an antioxidant activity should be introduced. The antioxidant effect can be obtained in numerous ways, but promising one is the incorporation of therapeutical ions. That study aimed to incorporate Ce^{4+}, $Sr^{2+}$and Zn^{2+} ions in different concentrations to the two basic systems of gel-derived bioglasses and evaluate their structural, chemical, bioactive, and antioxidant properties. Moreover, the aim was finding a correlation between glasses antioxidant activity and their structural and bioactive properties.

Experimental Methods

Glasses from the SiO_2-CaO-P_2O_5 system, with different CaO/SiO_2 ratios, were obtained by the sol-gel route. The modifiers (SrO, CeO_2, and ZnO) were introduced in substitution for CaO, in concentrations were varying in the range of 0 - 10%mol. They were introduced to the systems singly.

After heat treatment (700ºC or 800ºC) glass powders were subjected to structural analyses (XRD diffraction, FTIR spectroscopy, NMR spectroscopy). The complex structural study was performed due to the attempt of explaining antioxidant properties. Moreover, *in vitro* bioactive study was performed in SBF solution. The materials subjected to that purpose were incorporated into model composite PCL: bioglass films. Afterwards, the structure and microstructure evaluation was performed. Then, measurements of antioxidant activity were performed with the DPPH and ABTS free radical scavenging assays and with the ferric reducing antioxidant power (FRAP) test. Levels of antioxidant activity in each of the test were measured with UV-VIS spectroscopy. Results of ABTS and DPPH were expressed as radical scavenging capacity (RSC), and the results of FRAP were expressed as absorbance.

Results and Discussion

Structural analyses of obtained glasses indicated changes occurring in the material's structure along with the introducing of CeO_2, SrO or ZnO in place of CaO. Sr incorporation effected in the increase in the amount of the non-bridging Si-O- bonds, what was probably an effect of the differences in size between Ca^{2+} and Sr^{2+} cations. Our study has shown that the effect of strontium oxide on the structure and properties of gel-derived biomaterials largely depended not only on SrO concentration but also on the chemical composition of starting materials. Incorporation of ZnO increased the tendency to crystallization in the glasses, while CeO_2 introduced into A2 system (40%SiO_2 - 54-x%CaO - 6%P_2O_5 - x%(CeO_2+SrO+ZnO), %mol.) caused phase separation and thus induced crystallization of cerium-rich phases. Doped ions have also affected bioactive properties. SrO incorporation has upgraded bioactive

performance in SBF solution, while CeO2 has it limited. ZnO incorporation has almost completely inhibited the CaP crystallization in SBF solution.
The antioxidant activity of doped glasses was higher than the undoped ones, and the highest was registered for glasses doped with cerium. The antioxidant activity was higher for A2 group glasses than for the high silica S2 glasses (80%SiO_2 - 16-x%CaO - 4%P_2O_5 - x%(CeO_2+SrO+ZnO), %mol.). The differences in antioxidant properties between the two basic systems were probably deriving from the various mechanisms of glass particles interaction with scavenged free radicals, which was also probably related to the structural characteristics of the systems.

Conclusion

Our study confirmed that doping gel-derived bioglasses with cerium, strontium, and zinc improve their antioxidant potential. The type and concentration of ion used determine the extent of the antioxidant effect, while the basic glass composition determines the antioxidant mechanism.

Acknowledgement

This work was supported by the National Science Centre Poland Grants Nos. 2017/25/N/ST8/01593 (BZ) and 2017/27/B/ST8/00195 (KCK). MD acknowledges financial support from the Foundation of Polish Science (FNP).

PS2-01-257

Dose-depending effect of therapeutic active ions released from borate bioactive glasses on immune cells

Katharina Schuhladen[1], Lena Stich[2], Xiaoju Wang[3], Leena Hupa[3], Alexander Steinkasserer[2], Aldo R. Boccaccini[1], Elisabeth Zinser[2]

[1]University of Erlangen-Nuremberg, Department of Materials Science and Engineering, Institute of Biomaterials (WW7), Erlangen, DE; [2]Universität Erlangen-Nürnberg, Department of Immune Modulation, Erlangen, DE; [3]Åbo Akademi University, Johan Gadolin Process Chemistry Centre, Turku, FI

Introduction

Key properties of bioactive glasses include their ability to dissolve and release ions when immersed in an aqueous environment, as well as the formation of an apatite surface layer on the glass during dissolution [1]. Due to the lower chemical durability of borate glasses and their ability to transform rapidly to hydroxyapatite, an increasing amount of research has started to focus on the use of borate bioactive glasses, especially in the field of wound healing [2]. To further improve the performance of bioactive glasses, it is possible to introduce therapeutic ions with specific effects, e.g. copper to enhance angiogenesis and zinc to avoid infections [3]. Since immune cells are crucial players during the wound healing process [4], the dose-depending effect of the biological active ions copper and zinc released from borate bioactive glasses on immune cells was systematically examined.

Experimental Methods

Based on the well-known 13-93 silicate glass, borate glasses, where all the SiO_2 was replaced by B_2O_3, and Cu/Zn-doped borate bioactive glasses were produced by melt-quenching and characterized using FTIR, SEM/EDX as well as XRD. Then, to study the dissolution behavior, bioactive glass particles (300-500 µm) were immersed in different relevant solutions and ICP measurements were conducted to confirm the release of the different ions. Cell culture media, conditioned with release products of bioactive glasses, was then used to incubate murine dendritic cells (DC). After different time periods the effect of the different ions on the immune cells was examined regarding their cell viability, their phenotype (by FACS) and their T cell stimulatory properties (by MLR) measurements.

Results and Discussion

Four different borate glasses doped with Copper or/and Zinc were successfully produced. Depending on the composition and the release conditions (static/dynamic, dissolution media), the glasses dissolve and release therapeutic active ions in relevant amounts. However, the release of zinc from Zn-doped borate glasses could not be measured; instead the zinc was incorporated in the formation of an apatite layer. During the release, a similar increase of pH was observed for all tested glasses [5]. A concentration dependent effect on the viability of (DC), by the released ions, was observed whereby the magnitude of viability was different between the used ion-doped glasses. Moreover, a specific and dose-dependent effect was observed on the phenotype of DC. Additionally, a concentration- and composition-dependent effect was observed regarding the DC mediated T-cell proliferation capacity and on the secretion of cytokines by DC cultured in conditioned media. This clearly shows that bioactive glasses, depending on their composition, have an effect on the viability, phenotype and functionality of immune cells.

Conclusion

Borate glasses, undoped or doped with the well-known therapeutic active ions copper and zinc, were fabricated by melt-quenching method. The fabricated glasses were firstly tested in different dissolution tests, showing their biodegradable nature and the release of biological relevant ions and secondly in contact with DC. A dose-depending effect, related to the glass composition, on immune cells such as DC and T cells could be proven. The results showed the great potential of boron containing bioactive glasses to significantly influence immune cells and therefore their role in wound healing.

References

[1] D. S. Brauer, “Bioactive Glasses-Structure and Properties,” *Angew. Chemie Int. Ed.*, vol. 54, no. 14, pp. 4160–4181, 2015.,

[2] Y. Li, M. N. Rahaman, Q. Fu, B. S. Bal, A. Yao, and D. E. Day, “Conversion of bioactive borosilicate glass to multilayered hydroxyapatite in dilute phosphate solution,” *J. Am. Ceram. Soc.*, vol. 90, no. 12, pp. 3804–3810, 2007.

[3] A. Hoppe, N. S. Güldal, and A. R. Boccaccini, “A review of the biological response to ionic dissolution products from bioactive glasses and glass-ceramics,” *Biomaterials*, vol. 32, no. 11, pp. 2757–2774, 2011.

[4] T. A. Wilgus, “Immune cells in the healing skin wound: Influential players at each stage of repair,” *Pharmacol. Res.*, vol. 58, no. 2, pp. 112–116, 2008.

[5] K. Schuhladen, X. Wang, L. Hupa, and A. R. Boccaccini, “Dissolution of borate and borosilicate bioactive glasses and the in fl uence of ion (Zn , Cu) doping in di ff erent solutions,” *J. Non. Cryst. Solids*, vol. 502, pp. 22–34, 2018.

Acknowledgement

Abo Akademi's Johan Gadolin Scholarship is gratefully acknowledged for financial support.

PS2-01-258

Antibacterial phosphate-based glasses for wound healing applications

Athanasios` Nikolaou[1,2,3], Farzad Foroutan[1], Jorge Gutierrez-Merino[2], Daniela Carta[1]

[1]University of Surrey, Department of Chemistry, Guilford, GB; [2]University of Surrey, School of Biosciences and Medicine, Guilford, GB; [3]Fourth State Medicine Ltd, Haslemere, GB

Introduction

Wound healingis a long, complex process which can lead to inflammation and, if left untreated, life-threatening infections. Wound infections with multi-drug resistant bacteria result in prolonged treatments and increased healthcare costs, so the demand for wound treatment is massive worldwide[1].The number of patients requiring wound care is significantly increasing and it has been estimated that the associated annual cost of wound treatment alone managed by the NHS is around £5B[2]. Therefore, there is an urgent need for new antibacterial wound dressings that both rapidly stimulate healing and prevent infections.

Here we present novel bioresorbable phosphate-based glass nanofibres (PGF) as wound dressings that simultaneously induce new tissue formation, deliver antimicrobial effects without reliance on conventional antibiotics and promote blood coagulation. Being bioresorbable, PGF dissolve in physiological environments and are totally replaced by regenerated tissue[2]. This important advantage avoids frequent dressing removal that can damage newly formed tissue. Moreover, wound-related infections could be prevented by incorporating antimicrobial agents into the dressings that slowly release as the scaffolds degrade in the wound. A totally bioresorbable dressing will avoid systemic administration of antibiotics if used as a controlled local delivery system for antibacterial agents. Nanofibres are advantageous to conventional dressings given the high surface area to volume ratio, open porosity that allows a gaseous exchange, cell migration, and removal of excess exudate, the possibility of mesh production) and surface functionalization[1].

Phosphate-based fibres in the systemP_2O_5-CaO-Na_2O were prepared and doped with the antibacterial ions Cu^{2+} (1, 3, 5 mol%) and Cu^{2+}/ Ag^{+} (5 mol%) which have been found to be particularly effective in promoting wound healing (they stimulate angiogenesis, differentiate mesenchymal stem cells, and proliferate fibroblast human foreskin)[3,4]. Cold plasma will be used to induce/enhance the antibacterial properties of the prepared fibres.

Experimental Methods

PGF were obtained by electrospinning of coacervate precursors. Coacervate precursors were prepared by slow addition of a Ca^{2+} salt to an aqueous sodium polyphosphate solution. Phase separation occurs between a dense coacervate phase, containing the phosphate chains, and the aqueous supernatant.The viscous material obtained by removing the supernatant liquid is easily ejectable and ideal for the production of ES precursors along with the incorporation of antimicrobial ions. The electrospinning was conducted using a stainless steel capillary tube (18 gauge), syringe pump, and high voltage source. Electrospinning was carried out at room temperature and fibres were deposited on an aluminium sheet. Structural characterisation of PGF was performed using X-ray diffraction (XRD) and infra-red spectroscopy (IR); dissolution studies of the PGF in water were performed to obtain information on the release of calcium, sodium, copper, and silver ions after 24, 48, and 72 hours. The doped-PGF were treated with a cold plasma to enhance the antimicrobial effect against bacterial populations. The antimicrobial effect of doped PGF and cold plasma was performed against two bacteria: *Staphylococcus aureus*, and *Escherichia coli* ATCC 25922, bacterial species associated with antibiotic resistance.

Results and Discussion

Copper and copper-silver doped phosphate-based glasses fibres have been successfully prepared, for the first time, using the electrospinning technique. XRD patterns confirm the amorphous nature of all fibres. FTIR results shows the presence of to Q^1 and Q^2 phosphate units. Dissolution studies of the PGF in water shows that the highest release of all ions occurs within the first 24 h. Copper and silver ions are released continuously over the 72 h. Antimicrobial studies show that all Cu^{2+} doped PGF are mainly active against *E. coli* and thattheCu $^{2+}$/ Ag^{+} doped PGFareactive against both *E. coli* and *S. aureus.*

Conclusion

In this study, PBF were successfully synthesised at room temperature for wound healing applications. These fibres are biodegradable and can react and dissolve in the physiological environment and eventually totally replaced by regenerated tissue. Antibacterial study results against *S. aureus* and *E. coli* have shown the great potential application of copper-silver doped glass fibres in wound healing due to its ability to release of Cu^{2+} and Ag^{+} ions continuously with a high bactericidal effect.

References

1) Gizaw et al. *Bioengineering* 5, 9, 2018
2) Carta *et al.J. Mater. Chem*., 15, 2134, 2005
3) Zhao et al., *Biomaterials*, 53, 379, 2015
4) Nadworny *et al.*, *Nanomedicine NMB4*, 3, 241, 2008

Acknowledgement

Authors would like to thank EPSRC (EP/P033636/1) and Royal Society (RSG\R1\180191) for funding. We also thank Dr Mark Whiting and Mr David Jones for assistance with the SEM measurements.

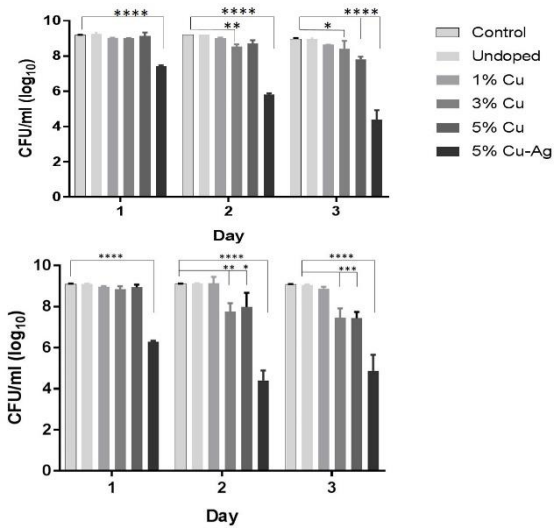

Bacterial viability of S. aureus and E.coli when exposed to PGF

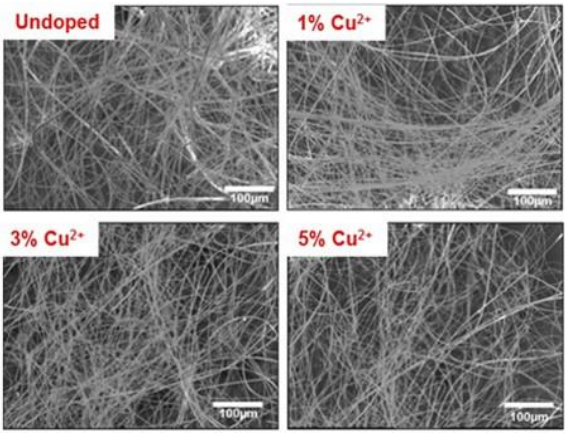

Scanning electron microscopy images of PGF undoped and doped with 1,3,5, mol% of Cu2+

2:45 p.m. – 3:45 p.m.

Hall 1 / Exhibition Area

PS2-02 | Polymeric biomaterials

PS2-02-259

Controlling structural relaxations, mechanical properties, and degradation timescale of PLLA during hydrolytic degradation

Reece N. Oosterbeek[1], Patrick Duffy[2], Sean McMahon[2], Xiang C. Zhang[3], Serena M. Best[1], Ruth E. Cameron[1]

[1]University of Cambridge, Cambridge Centre for Medical Materials, Department of Materials Science and Metallurgy, Cambridge, GB; [2]Ashland Specialties Ireland Ltd., Synergy Centre, TUD Tallaght, Dublin, IE; [3]Lucideon Ltd., Stoke-on-Trent, GB

Introduction

Poly-L-lactide (PLLA) is a bioresorbable polymer with many properties that make it appealing as a biomedical implant material, however for certain load-bearing applications such as cardiac stents it suffers several limitations. Among these are its slow degradation time, poor stiffness and strength (requiring PLLA stents to have thicker struts than conventional metallic stents), and tendency for embrittlement during degradation[1]. Here we demonstrate how polyethylene glycol functionalised poly-lactide-co-caprolactone (PLCL-PEG) can be blended with PLLA, in order to control both the degradation timescale, and the structural and mechanical changes undergone during degradation. We also investigate how the mechanical properties of these polymers can be improved by incorporating phosphate glass into a fully bioresorbable composite.

Experimental Methods

Polymer blends and polymer-glass composites were made using solvent casting and injection moulding, with mechanical testing carried out immersed in deionised water at 37°C. Degradation behaviour was measured in phosphate-buffered saline at 37°C by pH monitoring. Polymer blends were characterised before and after degradation by Differential Scanning Calorimetry (DSC), X-ray Diffraction (XRD), and Gel Permeation Chromatography (GPC).

Results and Discussion

Long-term degradation tests (Fig. 1) show strong dependence of degradation time on blend composition, demonstrating the ability to controllably accelerate PLLA degradation via blending. The two blend components (PLLA and PLCL-PEG) do not simply degrade independently of each other, but rather the degradation products released by the fast degrading polymer (PLCL-PEG) catalyse and accelerate the degradation of the slower degrading PLLA component. This is shown by the molecular weight distributions measured by GPC (Fig. 1), where the measured blend degradation is greater than would be expected for independently degrading components.

Important changes in the mechanical properties during degradation are also observed (Fig. 2). The large initial ductility is lost after 30 days degradation for most blend compositions. For blends with low PLCL-PEG content this occurs due to aging (shown by increased T_g and larger associated endothermic peak in DSC) as the relatively homogeneous composition provides little barrier to rearrangement. For high PLCL-PEG content, molecular weight degradation has shortened chain length sufficiently to allow significant rearrangement i.e. crystallisation (shown by XRD), also resulting in embrittlement. These two effects result in a “sweet spot” of moderate PLCL-PEG content that is high enough to prevent aging, but not so high as to cause degradation-induced crystallisation, leading to delayed structural relaxation and embrittlement for these compositions (20-30% PLCL-PEG).

Initial results for polymer-glass composites (Fig. 2) show that glass addition significantly improves stiffness, while retaining some ductility - a promising result for load-bearing applications where high stiffness is desirable but brittle failure can be catastrophic.

Conclusion

Blending PLCL-PEG with PLLA controllably accelerates hydrolytic degradation. In large amounts this leads to crystallisation and embrittlement, however in smaller amounts PLCL-PEG balances faster degradation and resistance to the structural relaxations (aging, crystallisation) that cause embrittlement. Early work on polymer-glass composites indicates that phosphate glass addition can successfully increase stiffness without causing brittle failure, paving the way towards a combined blending-composite strategy to achieve bioresorbable materials that have (and retain) favourable mechanical properties along a suitable degradation timescale.

References

[1] Wayangankar, S. A., & Ellis, S. G. (2015) *Prog. Cardiovasc. Dis.*, *58*(3), 342-355.

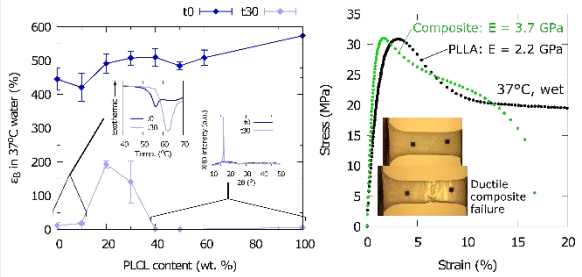

Fig. 2 Mechanical properties of polymer blends and composites

Figure 2: Elongation at break (in 37°C water) for PLLA:PLCL-PEG blends before and after 30 days degradation, with DSC and XRD plots inset (left); mechanical properties of PLLA-phosphate glass composite (right).

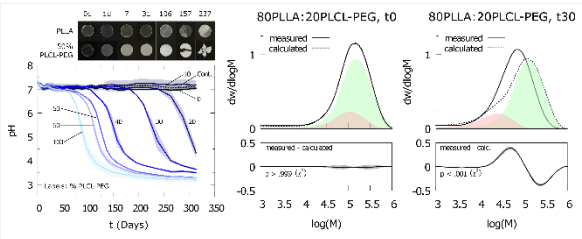

Fig 1. pH and molecular weight distribution after degradation

Figure 1: pH measurement during degradation of PLLA:PLCL-PEG blends (left); molecular weight distributions for PLLA:PLCL-PEG blends before and after 30 days degradation (middle and right). Calculated curves are based on a linear combination of the individual blend components (red = PLCL-PEG, green = PLLA) before and after degradation.

PS2-02-260

Characterization of a poly(lactic-co-glycolic) acid - hydroxyapatite 3D-printed scaffolds for bone tissue engineering

Joanna Babilotte[1], Vera Guduric[1], Reine Bareille[1], Damien Le Nihouannen[1], Jean-Christophe Fricain[1,2], Sylvain Catros[1,2]

[1]INSERM U1026 BioTis, Bordeaux, FR; [2]Faculty of Dentistry, Bordeaux, FR

Introduction

Current bone tissue engineering strategies are based on porous biocompatible scaffolds seeded with tissue-specific cells. Improvement in rapid prototyping technology, such as 3D printing, allows fabrication of custom-made 3D scaffolds with high resolution. Our group has developed a new material, made of medical grade poly(lactic-co-glycolic) acid (PLGA) mixed with 10% (w/w) hydroxyapatite nanoparticles (HA) for 3D printing by Fused Deposition Modelling (FDM). It showed a low chemical degradation during manufacturing steps, expected loading and homogeneous HA distribution. Based on this, our aim was to evaluate biocompatibility and osteopromotive potential of these new materials.

Experimental Methods

PLGA and PLGA-HA 10% (w/w) filaments were used to 3D printed porous membranes. The membranes were seeded with human adipose-derived stem cells (hADSCs) or human bone marrow stem cells (hBMSCs). Cytotoxicity was assessed according ISO 10993-5, cell proliferation by CyQuant® and cell viability by Live-Dead. Osteogenic differentiation was evaluated with qualitative alkaline phosphatase (ALP) staining and quantification of mineralization by red alizarin. Inflammatory potential was analyzed by subcutaneous implantation in rat during 1 and 4 weeks.

Results and Discussion

The composite materials were non-cytotoxic. Both hADSC and hBMSCs had high viability and proliferate on the materials, even after 21 days of culture [Figure 1]. At day 21, hADSCs highly colonized the material and formed bridge-like structures in the pores [Figure 1]. ALP staining and mineralization seemed higher with PLGA-HA 10% materials relative to PLGA for both cell types. Histological results for subcutaneous implantation are under way. PLGA is largely known to be cytocompatible [1]. As expected, addition of HA might have positive impact on osteodifferentiation [1,2].

Conclusion

Our preliminary data demonstrate that it was possible to fabricate a PLGA-HA composite biomaterial for 3D printing by FDM. Materials showed favorable properties and relevant cellular response for bone tissue engineering applications. Our next evaluations will focus on osteoblastic gene expression characterization and implantation in a critical calvaria defect model in rat to assess bone regeneration potential of developed materials.

References

[1] H.-S. Roh *et al*., Applied Surface Science (2016) 388 : 321-330, doi: 10.1016/j.apsusc.2015.12.243;
[2] J. Babilotte *et al*., J Biomed Mater Res Part B (2019), doi: 10.1002/jbm.b.34348

Acknowledgement

The authors would like to thank to the Agence National de la Recherche for the financial support.

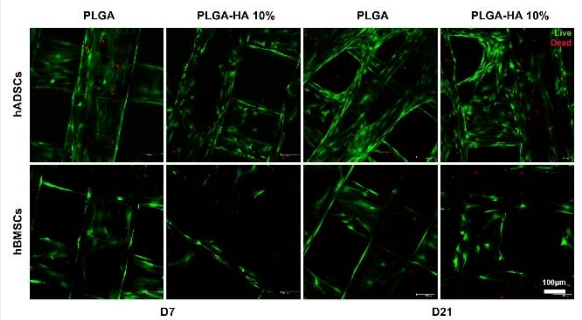

Figure 1. Evaluation of cell viability with Live-Dead assay.
hADSCs and hBMSCs was seeded on PLGA and PLGA-HA 10% (w/w) membranes. Cell viability was evaluated by a Live-Dead assay on days 7 (D7), 14 (D14) and 21 (D21).

PS2-02-261

The use of cold plasma treatment to increase cell migration within elastomeric poly(ester-urethane-urea) scaffolds in tissue engineering applications

Sylvie Changotade[1], Didier Lutomski[1], David Duday[2], **Géraldine Rohman**[1]

[1]Université Paris 13, Bobigny, FR; [2]LIST, MRT department, Esch-sur-Alzette, LU

Introduction

Due to their elastomeric behavior, polyurethane-based scaffolds can find various applications in soft-tissue engineering [1,2]. However, their relatively inert surface leads to develop solutions in order to improve cell adhesion and control cell fate. Porous biodegradable scaffolds based on poly(ester-urethane-urea) (PEUU) were developed in our laboratory [3]. With the aim to promote cell responses, the present study focuses on the use of cold plasma treatment to increase cell migration within PEUU scaffolds.

Experimental Methods

PEUU scaffolds were prepared based on a polyHIPE method [3]. *In vitro* assays were carried out using mesenchymal stem cells (MSC). The study of cytotoxicity was carried out in accordance with ISO 10993-5 and ISO 10993-12 standards. For migration studies, MSCs were grown up to confluence and were submitted to the cold plasma treatment during various times. Finally, sterilized PEUU scaffolds were set down onto the cell mats to achieve cell infiltration. Hemalun staining was employed to visualise the cells within the scaffolds.

Results and Discussion

Preliminary studies showed that PEUU scaffolds were suitable biomaterials for supporting the adhesion of MSCs, providing a suitable environment for MSC proliferation in 3D spatial arrangement and allowing the MSC differentiation into an osteoblastic phenotype lineage [3]. In the present study, it was demonstrated that the plasma treatment did not elicit a cytotoxic response towards MSCs. Moreover, the plasma treatment increased the MSC metabolic activity and growth rate. Finally, MSCs were able to migrate into PEUU scaffolds and the migration was drastically improved when MSCs were submitted to the cold plasma treatment.

Conclusion

Our work demonstrated the potential of the use of cold plasma treatment to increase cell migration within PEUU scaffolds.

References

[1] Chen WLK *et al.* (2011) *Adv Drug Deliver Rev.* 63:269.
[2] Bettinger CJ (2011) *Macromol Biosci.* 11:467.
[3] Changotade S *et al.* (2015) *Stem Cells Int* Article ID 283796.

Acknowledgement

The authors would like to thank PEPS-Mécanobiologie from CNRS (BRIPLASM project) for the financial support.

PS2-02-262

Chemical modifications of hyaluronic acid in position 6 of glucosamine – synthesis, analysis and applications.

Radovan Buffa, Petra Šedová, Ivana Basarabová, Vladimir Velebný

Contipro, R and D department, Dolní Dobrouč, CZ

Introduction

Hyaluronic acid (HA) oxidised as HA-aldehyde is hydrolytically stable precursor suitable for variety of subsequent chemical modifications. The most common oxidation agent is sodium periodate in water producing higher degrees of modification but also cleaves the hyaluronan molecule in position C2-C3 of glucuronic acid[1] resulting in a semi-broken polysaccharide chain. More-steps approaches are based on attachment of spacers bearing aldehyde group usually in protected form[2]. This method involves more than 1 synthetic step for synthesis. Very rare are methods using agents able to reduce the carboxylic group of HA directly into the aldehyde function[3]. The main disadvantages of all above-mentioned methods are significant changes in conformation or in polarity of HA chain in comparison with the native HA and in some cases more complicated synthesis.

On the other hand, simple and regioselective oxidation of HA in position 6 of glucosamine on HA-aldehyde (HA-CHO)[4] neither cleaved any saccharide ring of the polymeric chain nor involved an attachment of potentially problematic spacers. Synthesis can be performed in water with catalytic amount of TEMPO and stoichiometric equivalent of NaClO.

Experimental Methods

NMR spectra were recorded on Bruker 500MHz

Results and Discussion

HA-CHO with aldehyde group in position 6 of glucosamine form in water stable but still sufficiently reactive geminal diol (HA-$CH(OH)_2$)[1]. This material has electrophilic properties and can react with hydrides (reduction), amines (conjugation), simultaneously amines and hydrides (reductive amination) or can facilitate a regiospecific elimination of water from position 4 and 5 of glucosamine cycle (beta elimination). Depending on applied agents, these transformations can produce variety materials as: hydrogels (crosslinked HA), HA “naturally” labelled with deuterium or tritium, hydrolytically stable HA-amine conjugates, hydrolytically cleavable HA-amine conjugates (possibly pH-responsible) and materials with enhanced anti-oxidative and anti-cancer properties (-C=C- double bond), (Scheme 1)

Conclusion

Synthesis of HA-CHO is simple, effective and produces biocompatible and biodegradable material with enormous potential for variety of biomedical applications. This precursor can attach structurally different amines under physiological conditions giving conjugates with large variety of hydrolytic stability or pH responsibility. If bi or multi-functional amines are used, crosslinked hydrogels suitable for tissue engineering can be prepared. Reduction of saturated or unsaturated HA-CHO with hydrides give either HA labelled with hydrogen-isotopes (if $NaBD_4$ or $NaBH_3T$ are used), or HA derivate with -C=C- double bond in positions 4 and 5 of glucosamine cycle. This unsaturated HA showed enhanced anti-oxidative and anti-cancer properties.

References

1 Kuo, J. W. *Practical Aspects of Hyaluronan Based Medical Products*. 2005, Chapter 5, CRC Press.

2 Bergman, K.; Engstrand, T.; Hilborn, J.; Ossipov, D.; Piskounova, S. & Bowden, T. *J. Biomed. Mater. Res*., *Part A* 2009, *91A*(4), 1111-1118.

3 Aeschlimann, D. & Bulpitt, P. 2007. US7196180 B2.

4 Šedova, P.; Buffa, R., Kettou, S.; Huerta-Angeles, G.; Hermannova, M.; Leierova, V.; Šmejkalová, D.; Moravcová, M. & Velebný, V.; *Carbohydrate Research,* 2013, *371*, 8–15.

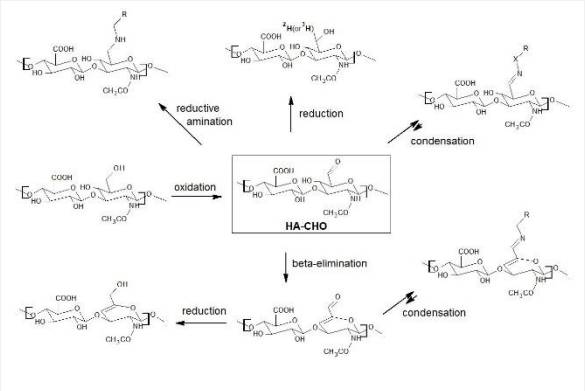

Scheme 1, Possible products of modification of HA-CHO, X = -NH-, -O-, -NH-CO-.

PS2-02-263

Imino-conjugates of modified hyaluronic acid – NMR study of pH-responsivity

Radovan Buffa, Petra Šedová, Ivana Basarabová, Vít Svozil, Vladimir Velebny

Contipro, R and D department, Dolní Dobrouč, CZ

Introduction

Hyaluronic acid (HA) modified with an aldehyde group (HA-CHO)[1] has large potential for the covalent attachment of the amino compounds under physiological conditions. Modification of HA-CHO to its α,β-unsaturated analogue (ΔHA-CHO)[2] generally increases the stability of the reversible imino-attachment due to conjugation of the imine moiety with the adjacent -C=C- double bound.

The aim of this work was to study imino-conjugates of ΔHA-CHO with variety of structurally different amines. It was expected that hydrolytic stability of the final imino-conjugates will depend on the chemical structure of the amines and on the pH value.

Experimental Methods

NMR spectra were recorded on Bruker 500MHz.

Results and Discussion

Condensation reactions of amines with aldehydes can be performed in water environment. Several types of structurally and biologically different amines were included in this study: 6-aminohexanoic acid, 4-bromoaniline, 4-nitroaniline, 4-toluensulfonylhydrazide, adenine, benzhydrazide, benzocaine, D-glucosamine, dihydrazideadipate, Doxorubicin, Dopamine, Histamine, Hydralazine, hydrazinium sulfate, hydroxylamine, hydroxylamine-O-sulfonic acid, phenylhydrazine, propane-1,3-bisoxyamine, Serotonine, Sulfanilamide and Thiamine. Chemical shift of the imino proton (-C**H**=N-) of ΔHA-imine is easily detectable by standard ^{1}H NMR spectroscopy. Amino compounds are added to the reaction mixture in small excess (1.5 eq.), therefore the electrophilic imino double bond of ΔHA-imine can further react with another amino nucleophile via addition reaction giving a ΔHA-aminal. All steps of the condensation reaction are reversible (Scheme 1).

Conclusion

Imino-conjugates of ΔHA-CHO with structurally different amines were described at various pH values. The results showed that only aliphatic amines are immobilized by highly pH-responsible covalent attachment where the hydrolytic cleavage occurred at pH value in the range between 6 – 9 depending on the chemical structure of the amine. Electron deficient aromatic amines did not form the imine group at all. On the other hand, hydrazines, hydrazides and oxyamines were conjugated efficiently in entire range of pH and only negligible amount of starting aldehyde was detected in all cases.

Results showed structural features of amino compounds responsible for their reversible attachment. Data can help to design new amino-conjugates with tailored pH-responsibility. This study showed enormous potential of ΔHA-CHO mainly for applications in drug delivery where pH responsible attachments of biologically active amines are needed.

References

1 Šedova P., Buffa R., Kettou S., Huerta-Angeles G., Hermannova M., Leierova V., Šmejkalová D., Moravcova M. & Velebný V. (2013). *Carbohydrate Research,371*, 8–15.

2 Buffa R., Šedová P., Basarabová I., Moravcová M., Wolfová L., Bobula T. & Velebný V. (2015) α,β-Unsaturated aldehyde of hyaluronan - Synthesis, analysis and applications, *Carbohydr. Polymers*, *10*, 293-9.

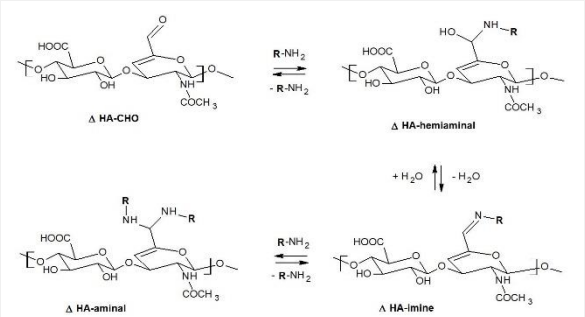

Scheme 1, Possible products of conjugation of ΔHA-CHO with amines.

PS2-02-264

Corneal Stromal Biomaterials Inspired by Supramolecular Chemistries

Antonio J. Feliciano[1], Floor A A. Ruiter[1], Tonny Bosman[3], Stefan Giselbrecht[1], Lorenzo Moroni[1], Patricia Y. Dankers[2], Clemens van Blitterswijk[1], Matthew B. Baker[1]

[1]Maastricht University, MERLN, Maastricht, NL; [2]Eindhoven University of Technology, Biomedical Engineering, Eindhoven, NL; [3]SupraPolix, Eindhoven, NL

Introduction

The phenotypic control of corneal keratocytes is crucial for the success of both stromal inlays and regenerative constructs. In fact, there have been FDA warnings for some corneal inlays due to corneal haze and fibrosis. Designing a material that does not activate keratocytes would be worthwhile for future inlay products. In addition, stromal regenerative constructs, as an alternative to donor tissue, require ECM production in the same highly ordered structure of the cornea; any disruption in the cornea's tissue can cause a decrease in transparency. In order to maintain corneal keratocyte phenotype, we are developing supramolecular polymers for these two applications. Supramolecular chemistry relies on non-covalent interactions that are biomimetic and dynamic. We propose a poly(zwitterionic-co-UPy) polymer for use in corneal tissue products such as presbyopic inlays and other supramolecular polymers for use as stromal constructs in order to achieve an optimal keratocyte.

Experimental Methods

Iso-UPy, courtesy of SupraPolix (Eindhoven,NL) was coupled to hydroxyethyl methacrylate (HEMA) via a urethane linkage to create UPy-methacrylate (UPyMA). ^{1}H NMR was performed on monomer and polymer species to confirm products. We prepared a controlled radical polymerization, by reversible addition-fragmentation chain transfer (RAFT), to prepare different molecular weights of MPC-UPyMA$_x$. For the copolymerization of UPyMA and MPC, 0, 1.25, 2.5, 5 mol% UPy monomer concentrations were sampled at different times to determine molecular weight and conversion %. FTIR was also performed to show the addition of UPy functionalization of copolymers. Finally, anti-fouling and cell viability were assessed.

Results and Discussion

We have confirmed that RAFT via UPyMA and MPC monomers is achievable. The polymerization was monitored at different times to assess reaction kinetics. Monomer conversion was analyzed by the disappearance of vinyl protons in ^{1}H NMR and compared to backbone protons for kinetic measurements. By plotting the logarithm of M_n/M_o (instantaneous monomer concentration to initial monomer concentration), we can compare the linearity of the data to pseudo-first-order kinetics which is associated with RAFT polymerizations. Because RAFT offers good control over molecular weight, we chose eight hours as the termination point and calculate the molecular weight M_n by end-group analysis on H^1 NMR. Calculated Mn's and associated UPy content (mol%) were tabulated. The antifouling character was confirmed.

Conclusion

These preliminary results show that we are able to synthesize copolymers of UPyMA and MPC using RAFT polymerization. Polymerizations can be controlled by Mn and UPy content (mol%). We have fabricated the polymers into thin films and coatings, which can be applied to corneal inlays. We also show proof of concept work for new supramolecular polymers based on host-guest complexation.

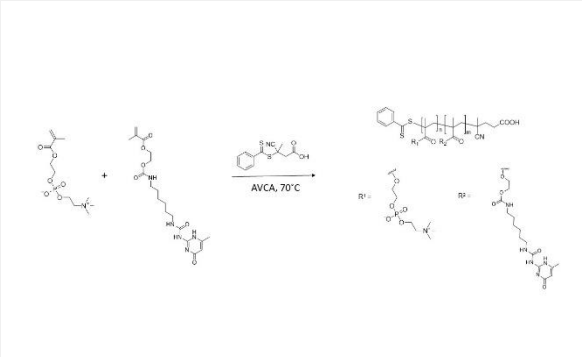

RAFT Copolymerization Mechanism
RAFT polymerization of MPC monomer and UPyMA for copolymer coatings.

PS2-02-265

Use of electrospun polyvinyl alcohol and polyurethane for biomedical applications

Marco Lopez[1], Dyhia Kersani[2], Justine Mougin[1], Nicolas Tabary[2], Frédéric Cazaux[2], Stéphanie Degoutin[2], Benoit Hue[2], Ludovic Janus[2], Mickaël Maton[1], Feng Chai[1], Jonathan Sobocinski[1], **Nicolas Blanchemain**[1], Bernard Martel[2]

[1]University of Lille, INSERM U1008 / Faculté de Médecine, Pôle Recherche, Lille, FR; [2]University of Lille, UMR 8207 – UMET - Unité Matériaux et Transformations, Villeneuve d'Ascq, FR

Introduction

Thanks to their high surface-to-volume ratio and their open and interconnected porosity, among others, electrospinning (ES) has gained importance for biomedical applications[1, 2]. Electrospun nanofibers (ENFs) can be used as scaffolds and as delivery vectors for drug, growth factors and cells. In addition, ES can be applied to a large range of organic and inorganic polymers such as polyvinyl alcohol (PVA) and polyurethane (PU). PVA is a water-soluble polymer and PU is displays interesting mechanical properties. Cyclodextrins (CD) can be used for host-guest interactions and for fine tunning the release of loaded drugs[3]. As CD and PVA are both water soluble, these materials can be combined. Simvastatine (SMV) is a drug used to reduce the cholesterol levels and to fight against restenosis[4]. This work aims to study the feasibility of loading SMV in PVA-cyclodextrin and in PU ENFs

Experimental Methods

ES solutions of PVA consisted of PVA (8% w/v), citric acid (CA, 0.8% w/v) and *hydroxypropyl*betacyclodextrin (HPB, 3.0% w/v). After ES, PVA ENFs were thermally treated (TT; 160°C, 1 h). ES solutions of PU consisted of PU (10% w/v) in a DMF:THF solution at a 2:3 ratio. The morphology of NFs was observed with SEM. SMV loading and release from the NFs was studied. SMV was incorporated either into the PVA and PU ENFS or at the PVA and PU solutions at 0, 5, 10 and 15% w/v. For ES, the polymer solutions were loaded into a 5 mL syringe and placed onto a syringe pump. Syringe was connected to a 21G needle via a catheter. The electrospinning parameters used for PVA//PU were, flow rate of 0.2//0.4 mL/h, a distance of 20 cm and an applied voltage of 15.5//8 kV. Temperature and relative humidity were around 24 °C and 30%, respectively, for both polymers. The cytotoxicity of ENFs was assessed by the ISO 10993-5 standard, using Human Pulmonary Microvascular Endothelial Cells (HPMEC cells), following the extraction and direct contact methods.

Results and Discussion

HPB had a tuning release effect of the loaded drug[5]. ENFs had different release behaviors depending on the type of polymer, *i.e.* PVA or PU. No cytotoxic effect was displayed by pristine PVA and PU ENFs, *i.e.* without SMV. Nevertheless, SMV, even at the minimal amount of this study, i.e. 5% w/v, created a cytotoxic effect on HPMEC cells. PVA and PU ENFs could theoretically be applied on supports, such as stents or implants.

Conclusion

This, opens possibilities for their use for cardiovascular and bone regeneration applications with tuned drug loading and release capacities.

References

1. Agarwal S. *et al.* 2008 *Polymer* 49(26):5603-5621, 2. Wang and Zhao 2019 Enciclopedia of Biomedical Engineering 1:330-344, 3. Jansook *et al*. 2018 *Int J Pharm* 535:272-284, 4. Kamishirado *et al.* 2007 *Angiology* 58(1):55-60, 5. Ouerghemmi S. *et al.* 2016 Int J Pharm 513(1-2):483-495.

Acknowledgement

Authors thank the Interreg 2 mers program (IMODE project), the Chevreul Federation and the University of Lille for their founding.

PS2-02-266

Evaluation of Hemostatic Performance of Graphene Oxide - Gelatin Aerogels

Jessica Borges Vilches[1], Toribio A. Figueroa Aguilar[1], Sebastian I. Guajardo de Celis[1], Claudio Aguayo Tapia[2], Katherina F. Fernández Elgueta[1]

[1]University of Concepcion, Laboratory of Biomaterials, Department of Chemical Engineering, Faculty of Engineering, Concepcion, CL; [2]University of Concepcion, Department of Pharmacy, Faculty of Pharmacy, Concepcion, CL

Introduction

Actually, the developing of science and nanotechnology has allowed the synthesis of new materials with biomedical applications. Among them, the graphene and its oxidated forms, such as graphene oxide (GO), have been used in this area for their biological, chemical, physical and mechanical properties [1]. An important application of this material is its functionalization capacity with biocompatible polymers, as the gelatin (G), to obtain GO-G aerogels.These aerogels are materials that present low density, high surface area and porous structures [2]. Based in this properties, it is possible use them in the biomedical field, as a hemostatic agent, in the control of profuse bleeding generated in wounds. The aim of this study was synthesized GO-G aerogels by icrowave assisted reaction, to evaluate their surface properties and hemostatic performance, in order to validate its use as a hemostatic agent.

Experimental Methods

The GO-G aerogels were developed to different synthesis conditions (pH and GO-G ratio) [1], to analyze the influence of these factors on the physicochemical properties of the biomaterials synthesized. Subsequently, the capacity absorption of the synthesized aerogels on phosphate-buffered saline (PBS) was determined, simulating of pH wound conditions. The internal structure of the synthesized aerogels was evaluated by scanning electron microscope (SEM), to observe the blood cell adhesion to the structure of these materials. Also, a droplet of fresh blood was dropped onto the GO-G aerogels surface to different exposure times (30 to 240 seconds) to evaluate the process of blood absorption. Finally, the blood absorption capacity assays and *in vitro* dynamic whole-blood clotting by absorbance determination were developed [3] using 50 microliters of fresh blood to conditions similar to the previous ones, was carried out to evaluate the hemostatic performance of these aerogels.

Results and Discussion

Among the developed aerogels, those synthesized at basic conditions and a greater proportion of gelatin had the higher PBS absorption capacity (up to 65%), indicating that these materials could have a better interaction with external media such as blood. Also, the SEM images showed that there was an adhesion of red blood cells in the materials synthesized (see Figure 1) and this phenomenon increased proportional to the content of GO in the aerogels synthesized, as seen in the Figure 1b); regardless of pH conditions used in the synthesis. This phenomenon can explain due the interactions between GO and blood components, favoring the hemostatic performance of these aerogels. Finally, all the synthesized aerogels had blood absorption capacities higher than 70% in a maximum time of 240 seconds, which can favor the control of profuse bleeding and validate its use as possible hemostatic agent.

Conclusion

The studied showed the possibility of the use of GO-G aerogels as hemostatic agents according to the internal structure and blood absorption capacity reported.

References

[1] Chen, G., Qiao, C., Wang, Y., & Yao, J., *Australian Journal of Chemistry*, 2014, *67*(10), 1532-1537.

[2] Ma, Y & Chen, Y., *Natl Sci Rev*, 2015, 2 (1), 40-53.

[3] Quan, K., Li, G., Yuan, Q & Wang X. *Colloids and Surfaces B: Biointerfaces 132*, 2015, 27-33.

Acknowledgement

The authors thank Project FONDECYT Nº 1170681 for the financial support for this investigation.

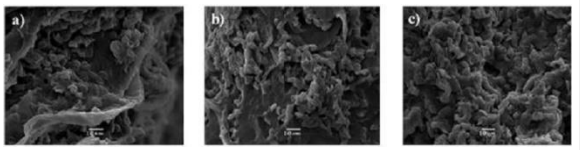

Figure 1. SEM images
a) GO-G aerogels at basic pH and 1:15 GO-G ratio, b) GO-G aerogels at acid pH and 1:10 GO-G ratio, c) GO-G aerogels at neutral pH and 2:25 GO-G ratio.

PS2-02-267

Degradable multi(aryl-azide) star copolymer as universal photo-crosslinker for elastomeric scaffolds

Louis Gangolphe[1,2], Stéphane Déjean[1], Audrey Bethry[1], Sylvie Hunger[1], Coline Pinese[1], Xavier Garric[1], Frédéric Bossard[2], Benjamin Nottelet[1]

[1]Department of Artificials Biopolymers, Max Mousseron Institute of Biomolecules (IBMM), UMR CNRS 5247, University of Montpellier, Montpellier, FR; [2]Univ. Grenoble Alpes, CNRS, Grenoble INP, LRP, 38000 Grenoble, * Institute of Engineering Univ. Grenoble Alpes, Grenoble, FR*

Introduction

Degradable elastomers with elastic properties close to those of soft tissues are in great demand for tissue-engineering [1]. Most degradable elastomers developed so far are based on functional low molecular weight pre-polymers that are combined with molecular crosslinkers to yield elastomeric 3D networks [2]. To overcome this limitation, we developed a star-shaped macromolecular multi(aryl-azide) photo-crosslinker based on PEG_{8arm}-PLA copolymer that has the ability to efficiently crosslink any polymer containing C-H bonds independently of its molecular weight and without the need for pre-functionalization [3]. In this work, we evaluate the elastomeric fibrous scaffolds based on electrospun photo-crosslinked high molecular weight PLA-Pluronic®-PLA [4] fibers in terms of mechanical properties, degradation properties and cytocompatibility.

Experimental Methods

Well defined PLA-Pluronic®-PLA and PEG_{8arm}-PLA block copolymers were synthesized via ring-opening polymerization for 5 days at 130°C. The aryl-azide functional PEG_{8arm}-PLA-fN_3 was synthesized at 45°C for 6 days under stirring in the dark. Polymer blends PLA-Pluronic®-PLA and PEG_{8arm}-PLA-fN_3 or PEG_{8arm}-PLA were dissolved in DCM/DMF (50/50 v/v) and electrospun with an applied voltage of 15kV. Fibrous scaffolds were irradiated under UV-light for determined periods using a Dymax PC-2000 system (75 $mW.cm^{-2}$). Mechanical measurement were carried out using Instron 3344. Degradation tests samples were conducted in PBS (pH 7.4) at a constant temperature. Mouse fibroblasts L929 cells were used to evaluate the cytotoxicity of the scaffolds.

Results and Discussion

The new degradable macromolecular multifunctional (aryl azide) photo-crosslinker based on 8-arm star-block PEG_{8arm}-PLA-fN_3 copolymer yielded up to 55% gel fraction. This allowed the production of elastomeric fibrous scaffolds based on PLA-Pluronic®-PLA/PEG_{8arm}-PLA-fN_3 by an electrospinning process. Photo-crosslinking of PLA-Pluronic®-PLA by PEG_{8arm}-PLA-fN_3 yielded biomaterials with enhanced elastomeric properties with elastic limits as high as 182%, while offering the possibility to modulate the degradation kinetics. The cytocompatibility study show the absence of cytotoxicity of the extracts in contact with L929 cells.

Conclusion

Thanks to their ability to crosslink any polymer containing C-H bonds, PEG_{8arm}-PLA-fN_3 are useful for the development of original degradable and elastomeric scaffolds for soft-tissue reconstruction. In addition, we believe that the concept of star-shaped multi(aryl azide) copolymer could be easily applied to other applications and processes thanks to the tunability offered by the macromolecular nature of this type of photo-crosslinker.

References

[1] Q. Chen, S. Liang, G.A. Thouas, Elastomeric biomaterials for tissue engineering, Progress in Polymer Science. 38 (2013) 584–671. doi:10.1016/j.progpolymsci.2012.05.003.

[2] E. Bat, T.G. van Kooten, J. Feijen, D.W. Grijpma, Resorbable elastomeric networks prepared by photocrosslinking of high-molecular-weight poly(trimethylene carbonate) with photoinitiators and poly(trimethylene carbonate) macromers as crosslinking aids, Acta Biomaterialia. 7 (2011) 1939–1948. doi:10.1016/j.actbio.2011.01.010.

[3] M. Avadanei, Photochemistry of 2,6-di(4′-azidobenzylidene)-methylcyclohexanone in polymer matrices, Journal of Applied Polymer Science. 134 (2017). doi:10.1002/app.44694.

[4] L. Gangolphe, S. Déjean, A. Bethry, S. Hunger, C. Pinese, X. Garric, F. Bossard, B. Nottelet, Degradable multi(aryl azide) star copolymer as universal photo-crosslinker for elastomeric scaffolds, Materials Today Chemistry. 12 (2019) 209–221. doi:10.1016/j.mtchem.2018.12.008.

Acknowledgement

This work was supported by ANR2016-BIOSCAFF (ANR-16-CE09-0024) held by the University of Grenoble-Alpes and the University of Montpellier.

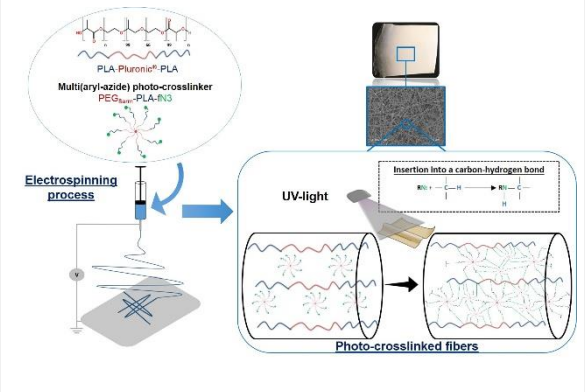

Design of elastic micro-fibrous scaffolds based on degradable multi(aryl-azide) photo-crosslinkers.

PS2-02-268

Mechanical properties and morphology of fibrin-based biohybrid hydrogels and their influence on cell/biomaterial interactions in cardiovascular implants

Miriam A. Al Enezy-Ulbrich[1,2], Nicole Terefenko[1,2], Martin K. Graff[1,2], Silke Rieder[2], Norina Labude[3,4], Hanna Malyaran[3,4], Svenja Wein[3,4], Sabine Neuss[3,4], Andrij Pich[1,2]

[1]RWTH Aachen University, Institute for Technical and Macromolecular Chemistry, Research Area Functional and Interactive Polymers, Aachen, DE; [2]RWTH Aachen University, DWI - Leibniz Institute for Interactive Materials, Aachen, DE; [3]RWTH Aachen University, Helmholtz Institute for Biomedical Engineering, BioInterface Group, Aachen, DE; [4]RWTH Aachen University, Institute of Pathology, Aachen, DE

Introduction

Many research activities in the implant fabrication are focused on the enhancement of their biocompatibility. Recent studies show that even though cardiovascular implants are well established and commonly used, they have a limited lifetime and their properties and functionality can be affected.[1,2] Current research is focused on the improvement of the implant properties, to prevent bacterial biofilm formation in dental implants, formation of blood clots in mechanical implants (heart valves) or the degradation of bioprotheses.[3-5] Also, the rejection of the organ implant is a problem.[6] To overcome these challenges, the synthesis of patient-specific implants is necessary.

Experimental Methods

The aim of this work is to synthesise biohybrid hydrogels consisting of natural fibrin and synthetic linear reactive copolymers based on poly(*N*-vinylcaprolactam) (Figure 1). This gel serves as an artificial extracellular matrix for cell differentiation that should be used for the synthesis of biohybrid cardiovascular implants. For this reason, a variety of copolymers was synthesised, varying their molecular weights, chemical composition and type of functional groups. Regarding to the synthesis of hydrogels, the ratios and addition mode of components (reactive copolymer, fibrinogen and thrombin) as well as their order may have an influence on the mechanical properties of the resulting hydrogels. Additionally, the reactive copolymer is able to bind to both, fibrin and fibrinogen. For this reason, it is also interesting to synthesise softer gels without thrombin.This enables the possibility of designing a toolbox of various biohybrid hydrogels with different morphology and mechanical properties and, as a result, diverse influences on the differentiation of e.g. human stem cells. We demonstrate that the resulting hydrogels will differ in pore sizes as well as in their storage modulus and their stress-strain behaviour. The analysis of the pore sizes was performed by using different microscopy and staining methods (Figure 2). In addition, the characterisation of the mechanical properties was conducted using rheology.

Results and Discussion

First experiments showed, that all samples with 3 mol% comonomer, as well as the pure fibrin gel, demonstrated strain-softening behaviour. In future experiments we will analyse, whether it is possible to obtain hydrogels which develop strain-stiffening behaviour, with a varying comonomer concentration and a varying polymer chain length.

Conclusion

Future tests will focus the differentiation of human stem cells on these hydrogels with different mechanical properties.

References

1. Baron, T. H., Kamath, P. S. & McBane, R. D. Management of Antithrombotic Therapy in Patients Undergoing Invasive Procedures. *N. Engl. J. Med.***368,** 2113–2124 (2013).
2. Siracuse, J. J. *et al.* Prosthetic graft infections involving the femoral artery. *J. Vasc. Surg.***57,** 700–705 (2013).
3. Baril, D. T. *et al.* Outcomes of lower extremity bypass performed for acute limb ischemia. *J. Vasc. Surg.***58,** 949–956 (2013).
4. Manji, R. A., Menkis, A. H., Ekser, B. & Cooper, D. K. C. Porcine bioprosthetic heart valves: The next generation. *Am. Heart J.***164,** 177–185 (2012).
5. Iyer, A. *et al.* Early Postoperative Bioprosthetic Valve Calcification. *Hear. Lung Circ.***22,** 873–874 (2013).
6. Shinoka, T. & Miyachi, H. Current Status of Tissue Engineering Heart Valve. *World J. Pediatr. Congenit. Hear. Surg.***7,** 677–684 (2016).

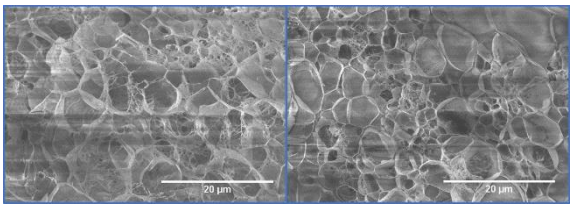

Exemplary Cryo-FESEM images of hydrogels with and without a functional copolmer.
Cryo-FESEM images (voltage 1kV, magnification 2.5k) of a pure fibrin gel (left) and a biohybrid hydrogel (right) consisting of fibrin and a copolymer. Both gels were synthesised in $GBSH_5$-buffer.

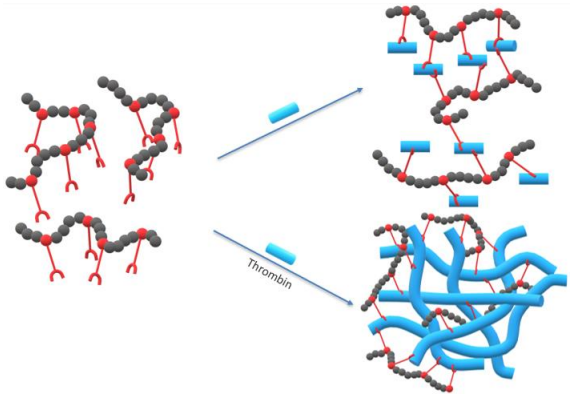

Scheme for the synthesis of biohybrid hydrogels based on fibrinogen and a functional copolymer.
The copolymer (black-red) can bind to fibrinogen (blue square) and to the fibrin fibres (blue chains). The comonomer with reactive group is shown in red.

PS2-02-269

Enhanced cell integration with electrospun PHBV fibers with controlled surface properties

Lukasz Kaniuk[1], Mateusz Marzec[2], Andrzej Bernasik[2,3], Urszula Stachewicz[1]

[1]AGH University of Science and Technology, International Centre of Electron Microscopy for Materials Science, Faculty of Metals Engineering and Industrial Computer Science, Cracow, PL; [2]AGH University of Science and Technology, Academic Centre for Materials and Nanotechnology, Cracow, PL; [3]AGH University of Science and Technology, Faculty of Physics and Applied Computer Science, Cracow, PL

Introduction

Surface properties of many biomaterials have significant impact on cell integration and adhesion in tissue engineering. Electrospinning is commonly used to produce mats to support cells proliferation. The controlled fiber size and space between fibers enable cell attachment inside 3D fiber structures[1]. Poly(3-hydroxybutyric acid-co-3-hydrovaleric acid) (PHBV) is natural, thermoplastic aliphatic polyester which is produced by bacteria. PHBV was proven to be non-toxic, biocompatible polymer giving good cellular response[2,3]. Electrospun fibers are usually produced with positive voltages, however by changing voltage polarities, the chemical composition of the fiber surface can be modified[4,5]. Within this study we wanted to evaluate influence on cellular response to surface chemistry of fibers controlled via electrospinning.

Experimental Methods

Materials and electrospinning

PHBV (PHV content 2% wt, M_w=450 000 gmol^{-1}, Helian Polymers, The Netherlands) was dissolved at 8% wt in chloroform and N,N-dimethylformamide (DMF) solution in volume ratio 9:1. Electrospinning was carried out using EC-DIG with the climate system (IME Technologies, The Netherlands) at T=25˚C and H= 40%. The positive (+17 kV) or negative (-17 kV) voltage polarities were applied to the stainless needle with the inner diameter of 0.8 mm, with the solution flow rate at 0.1 ml·min^{-1}, keeping 20 cm needle to collector distance.

Cell culture and cell viability assay

The biological tests were carried out for 1, 3 and 7 days using the NIH 3T3 cell line in the amount 2x10^4 cells per well. The culture was grown under standard conditions, i.e. at 37°C, 95% of humidity and 5% CO_2 at the atmospheric pressure. Cell proliferation was evaluated by colorimetric measurement of MTS assay (CellTiter 96 Aqueous One Solution Cell Proliferation Assay, Promega, the USA). The quantity of formazan product was carried out at 490 nm using spectrophotometer. Tissue culture polystyrene (TCPS) was used as a positive control for this assay.

Scanning electron microscopy (SEM) and surface characterization

The samples after cell seeding were dehydrated in a series of ethanol (50%, 70%, 96% and ~99,9%). The mats and fibers with cells samples were coated with 3 nm gold layer for SEM investigation. Surface chemistry of PHBV fibers was verified using angle X-ray photoelectron spectroscopy (XPS, PHI VersaProbeII ULVAC-PHI, Chigasaki, Japan).

Results and Discussion

Electrospun PHBV fibers produced with positive and negative voltage polarity (Figure 1) had similar morphology and the average fiber diameter, 2.47±0.21µm and 2.44±0.15µm, respectively. The XPS analysis confirmed the functional groups reorientation[4] for fibers produced with positive voltage polarity higher 4% content of carbonyl group

comparing to fibers produced with negative voltage polarity. Surface properties of PHBV fibers affect the cell proliferation as previously was showed on other polymer fibers[1].

Conclusion

Alternating the voltage polarity in electrospinning allowed to control the surface chemistry of PHBV fibers. The spatial structure of the mats and surface chemistry of the fibers supported cells attachment and proliferation, resulting in enhanced integration with the PHBV fibers produced with negative voltage polarity. The study confirmed the biocompatibility of PHBV mats for medical applications.

References

[1] S. Metwally, J. E. Karbowniczek, P. K. Szewczyk, M. M. Marzec, *Adv. Mater. Interfaces***2018**, *1801211*.

[2] G. Mutlu, S. Calamak, K. Ulubayram, E. Guven, *J. Drug Deliv. Sci. Technol.***2018**, *43*.

[3] P. K. Szewczyk, S. Metwally, J. E. Karbowniczek, M. M. Marzec, A. Bernasik, U. Stachewicz, E. Stodolak-Zych, A. Gruszczyn, *ACS Biomater. Sci. Eng***2019**, *5*.

[4] U. Stachewicz, C. Willis, D. Science, A. H. Barber, *J. Mater. Chem.***2012**, *22*.

[5] H. W. Tong, M. Wang, *Biomed. Mater.***2010**, *5*.

Acknowledgement

This study was conducted within "Nanofiber-based sponges for atopic skin treatment" project., carried out within the First TEAM programme of the Foundation for Polish Science co-financed by the European Union under the European Regional Development Fund, project no POIR.04.04.00-00- 4571/18-00.

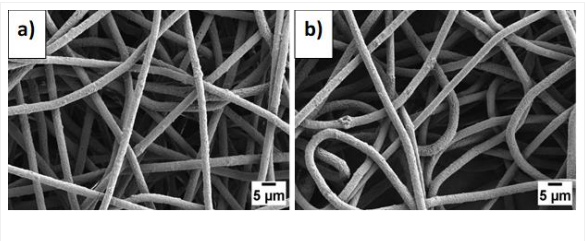

Figure 1 SEM micrograph of PHBV fibres
SEM micrograph of PHBV fibres produced with (a) positive and (b)negative voltage polarity.

PS2-02-270

In vitro enzymatic degradation kinetics of chitosan-based implants intended for peripheral nerve tissue engineering

Paulina I. Pedziwiatr, Katarzyna Nawrotek

Lodz University of Technology, Faculty of Process and Environmental Engineering., Lodz, PL

Introduction

Many years of research into chitosan-based biomaterials highlighted important, the relationship between degradation rate of chitosan and its properties such as degree of deacetylation, viscosity, molecular weight as well as biological source and production methods [1]. Peripheral nerve engineering relies on well interplay between designed biomaterial features, cells and conditions inside the human body [2]. In order to provide appropriate environment for regeneration degradation kinetics of tubular conduits should be adjusted to the regrowth rate of nerve cells. Therefore, in this study, implants made of chitosan with different degree of deacetylation and average viscosity are subject of degradation studies. The structures were incubated in phosphate buffered solution (PBS) and in PBS enriched with lysozyme solution, that mimic the conditions of peripheral nervous tissue. The lysosome was found in wide and various range of concentration in human body fluids [3].

Experimental Methods

The implants where prepared from chitosan (Heppe Medical Chitosan GmbH) with three different degree of deacetylation (i.e. 75, 85, and 95%) and three different average viscosity (i.e. 100, 500, and 1000mPas) using electrodeposition phenomenon [4]. The obtained structures were incubated in a phosphate buffered solution - PBS (Sigma Aldrich, pH 7.4) and in human lysozyme (Sigma Aldrich) with phosphate-buffered solution, at 37°C for specified periods of 1, 7, 14, 21, 28, and 56 days (in PBS) and 1, 7, 14, 21 days (in lysozyme with PBS). Afterward, chemical, mechanical and biological properties of the obtained implants are evaluated. In this study the tubular structures were subjected to a strength testing (Instron 3345 tensile testing machine, USA) and Fourier-transform infrared spectroscopy – FT-IR (Thermo Scientific FTIR Nicolet iS50).

Results and Discussion

According to the strength tests and organoleptic analysis the process of degradation is accelerated by the lysozyme in PBS solution. These results indicated that after 21 days in lysozyme solution the implants are breakable and weak, when the implants in PBS where elastic up to 56th day. The analysis of FT-IR spectra indicates the difference in chemical composition between the external and internal side of tubular implants. The durability and strength of obtained implants can be controlled by degree of deacetylation and average viscosity of chitosan.

Conclusion

The obtained results allow determining degradation rate based on the applied chitosan (i.e. its degree of deacetylation, viscosity and molecular weight of chitosan). Choosing appropriate initial viscosity and degree of deacetylation of chitosan we are able to adjusted the implant degradation kinetics to the specific peripheral nerve injury case. This fact is a significant advantage to be used in peripheral nervous tissue regeneration, because the diameter of the nerve depends on its location in the body. Moreover, the presence of trace amounts of enzymes e.g. lysozyme in mammal's organism should be considered in internal implants degradation studies.

References

1. Jennings, J. A. "Controlling chitosan degradation properties in vitro and in vivo." Chitosan Based Biomaterials Volume 1. Woodhead Publishing, 2017. 159-182.
2. Fisher, John P., et al., eds. Tissue engineering: principles and practices. CRC Press, 201,.2-11.
3. Porstmann, Bärbel, et al. "Measurement of lysozyme in human body fluids: comparison of various enzyme immunoassay techniques and their diagnostic application." Clinical biochemistry 22.5 (1989): 349-355.
4. Nawrotek, Katarzyna, et al. "Tubular electrodeposition of chitosan–carbon nanotube implants enriched with calcium ions." Journal of the mechanical behavior of biomedical materials 60 (2016): 256-266.

Acknowledgement

This study was supported by the National Science Center of Poland – Grant NCN 2017/26/D/ST8/00196.

PS2-02-271

Hybrid Core-Shell Nanoparticles as Multifunctional Tools in Brain Cancer Theranostics

Giulia Brachi[1], Luca Menichetti[2,3], Andrei Mikheev[4], Mauro Ferrari[5], Clara Mattu[1], Gianluca Ciardelli[1,6]

[1]Politecnico di Torino, Department of Mechanical and Aerospace Engineering, Torino, IT; [2]National Research Council, Institute of Clinical Physiology, Pisa, IT; [3]Fondazione Regione Toscana G. Monasterio, Pisa, IT; [4]Houston Methodist Research Institute, Center for Neuroregeneration, Houston, US; [5]University of St.Thomas, Houston, US; [6]National Research Council, Institute for chemical and physical processes, Pisa, IT

Introduction

Glioblastoma multiforme (GBM) is the most common primary brain tumor in adults. Because of its aggressive and infiltrative nature, efficient treatment with systemic chemotherapy remains a major challenge[1].
In this work, hybrid core-shell polymer nanoparticles (PNPs) for concomitant loading of multiple payloads and imaging agents were designed.
Moreover, their transport kinetics after intra-cranial (i.c) administration were investigated.

Experimental Methods

PNPs were prepared via a nanoprecipitation/self-assembly method to obtain a hybrid structure composed of a cell membrane-friendly lipid outer shell for long circulation and ready conjugation with imaging agents and a polymer core of multi-block polyurethanes (PURs) to host multiple payloads.
PNPs labeled with an infra-red dye and loaded with a fluorescent molecule simulating a therapeutic payload, were i.c. administered in highly infiltrative GBM model[2] and their transport kinetics were investigated using different 2D/3D imaging techniques.

Results and Discussion

PNPs exhibited high loading efficiency and remarkable imaging capabilities, showing high selectivity as MRI contrast agents as well as a high Contrast to Noise Ratio (CNR) in fluorescent/photoacustic imaging[3].

Conclusion

PURs PNPs demonstrated potential to combine imaging and therapy, high tissue penetration ability, long-term retention inside the brain, warranting further investigation as theranostic nanocarriers in GBM.

References

1. Iacob, G.; Dinca, E. Current Data and Strategy in Glioblastoma Multiforme. *J. Med. Life***2009**, *2* (4), 386–393.
2. Wakimoto, H.; Kesari, S.; Farrell, C. J.; Jr, W. T. C.; Aghi, M.; Kuroda, T.; Stemmer-rachamimov, A.; Shah, K.; Liu, C.; Jeyaretna, D. S.; et al. NIH Public Access. *Cancer Res.***2010**, *69* (8), 3472–3481. https://doi.org/10.1158/0008-5472.CAN-08-3886.Human.
3. Mattu, C.; Brachi, G.; Menichetti, L.; Flori, A.; Armanetti, P.; Ranzato, E.; Martinotti, S.; Nizzero, S.; Ferrari, M.; Ciardelli, G. Alternating Block Copolymer-Based Nanoparticles as Tools to Modulate the Loading of Multiple Chemotherapeutics and Imaging Probes. *Acta Biomater.***2018**. https://doi.org/10.1016/j.actbio.2018.09.021.

Acknowledgement

This project has received funding from the European Union's Horizon 2020 research and innovation programme under the Marie Sklodowska-Curie grant agreement No 658665, and by the ''Fondazione Cassa di Risparmio di Pisa" through the project ''PREVISION".

PS2-02-272

Cryogels for focal delivery to *ex-vivo* tissue culture – useful tools for brain slice manipulation

Ben Newland[1,2], Katherine Long[3,4], Dimitri Eigel[1], Sowmya Sekizar[5], Lida Zoupi[5], Romy Schuster[4], Wieland Huttner[4], Petra Welzel[1], Carsten Werner[1], Anna Williams[5]

[1]Leibniz Institute of Polymer Research Dresden, Germany, Dresden, DE; [2]School of Pharmacy and Pharmaceutical Sciences, Cardiff University, Wales, U.K., Cardiff, GB; [3]Centre for Developmental Neurobiology and MRC Centre for Neurodevelopmental Disorders, King's College London, England, U.K., London, GB; [4]Max Planck Institute of Molecular Cell Biology and Genetics, Dresden, Germany, Dresden, DE; [5]MRC-Centre for Regenerative Medicine, University of Edinburgh, Edinburgh, Scotland, U.K., Edinburgh, GB

Introduction

Cryogels are highly porous hydrogel materials produced by freezing the precursor components either prior to, or during the gelation process.[1][2] The ice crystals that formed during freezing leave behind a macroporous network. The strut and pore structure of cryogels makes them tough and robust during handling, yet, as a bulk structure, be compressible and soft. The aim of this work is to tailor make a range of cryogel structures of various shapes and chemistries, to suit the end application. This work represents the progress that we have made, together with our project collaborators, towards this aim. There are two distinct cryogel scaffolds described herein (both unpublished), both of which are tailored to different specific uses tackling the following objectives as follows:

1. Cryogel cylinders – Create a delivery device for focal demyelination on *ex vivo* mouse brain slices
2. Sulphated cryogel lines – Deliver cell tracing dyes molecules to the developing human neocortex *ex vivo*

Experimental Methods

A range of hydrogel precursor units (including poly(ethylene glycol) diacrylate, and sulfate containing acrylate monomers) were polymerized at sub-zero temperatures, within polystyrene or polydimethylsiloxane templates (all unpublished work). Once removed from the templates the cryogels were submerged in solutions containing the desired molecules to be delivered to slice cultures and placed either on, or in close proximity to the tissue slice. Lysophosphatidylcholine (LPC) was delivered to spinal cord and cortical sections (mouse) to establish a focal model of demyelination to better mimic the patchy nature of Multiple Sclerosis. Fluorescent dyes were delivered to embryonic neocortex (human tissue) to create gradient effects within the developing tissue.

Results and Discussion

Figure 1 shows scanning electron microscopy analysis of the completed cryogel structures and a sample image of its use towards the specific objective. The shape of the cylinders and lines was directly determined by the polystyrene template used. The cryogel cylinders deliver LPC to a limited area of the brain slice, creating focal demyelination. The sulphated cryogel lines produce a pattern of delivery to the developing fetal cortex which is currently being used to elucidate mechanisms of cortex folding.

Conclusion

Cryogels offer a versatile platform technology from which to spatially restrict the delivery of molecules to tissue in culture. In addition, the macroporous structure makes them well suited for culturing cells in a three dimensional, extracellular matrix-mimicking environment.

References

1. Bencherif, S.A., et al., Proc Natl Acad Sci U S A, **2012**. 109, 19590
2. Newland, B., et al., Small, **2015**. 11, 5047

Acknowledgement

B.N. would like to thank the Wellcome Trust for funding.

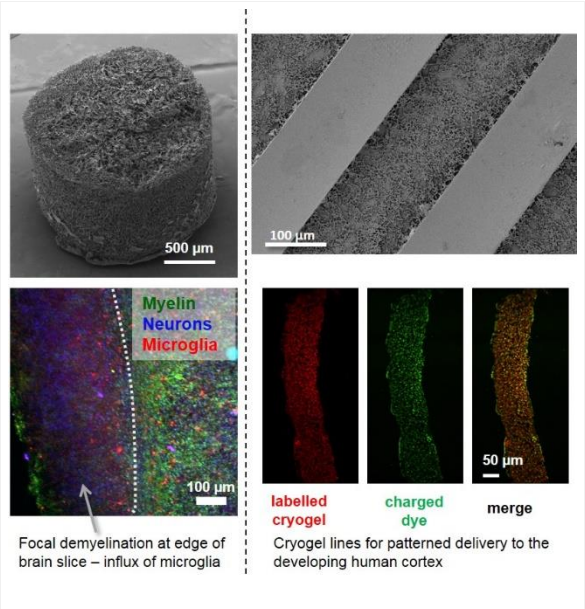

Figure 1 - The cryogel toolbox for ex-vivo tissue manipulation.

PS2-02-273

A Novel Biomaterial Cellprene® Fibers Obtained by Rotary Jet-Spinning and Electrospinning

Nathália O. Muniz[1,2], Fernanda A. Vechietti[1], Guilherme R. Anesi[1], Gustavo V. Guinea[2], Luís Alberto L. dos Santos[1]

[1]Federal University of Rio Grande do Sul, Biomaterials Laboratory / Materials Engineering Department, Porto Alegre, BR; [2]Technical University of Madrid, Center for Biomedical Technology, Madrid, ES

Introduction

The development of 3D structures through micro- and nanofibers offers a high surface area for cell adhesion with suitable porosity, which promotes diffusion of nutrients and gases to aid viability and proliferation of those cells. This is one of the major Tissue Engineering challenges[1]. Recent studies have demonstrated satisfactory results of Cellprene® blend when employed as a scaffold in animal tests. Their viability as a biomaterial, such as in tracheal stent, in the cranial region, and/or in bone environment has been investigated and proven as an adequate alternative[2,3]. Several techniques have been developed to obtain fibers and one of the main limitation to produce micro- and nanofibers at a large scale and low cost. Rotary jet spinning is an efficient technique to produce fibers and some works have demonstrated that this technique presents a number of advantages, such as low cost, high throughput and environmental friendly[4,5,6]. Considering the diversification of materials and processing techniques used in biomaterials field, it is essential to obtain a biomaterial through a technique that ensures a reduction of time and costs, allowing its broad and unrestricted accessibility. In order to achieve these aims, the purpose of this study was to obtain the novel biomaterial Poly Lactic-co-Glycolic Acid (PLGA) and Polyisoprene (IR) blend (Cellprene®) pure and with Hydroxyapatite (HAp) micro- and nanofibers by rotary jet spinning in order to generate a potencial scaffold for tissue engineering. An inexpensive alternative rotary jet spinning technique, using a cotton candy machine, was used to produce the fibers. The hydroxyapatite was added to promote a superior bioactivity. A comparison between fibers produced via electrospinning and rotary jet spinning techniques was conducted.

Experimental Methods

PLGA copolymer (Purac Biomaterials, Netherlands) with proportions of 84 mol% monomer L-lactate, 16 mol% glycolide was used as obtained. IR (Mafer, Brazil) in the natural latex structure centrifuged at 60% was purified by re-precipitation method[7]. HAp powder was obtained by precipitation technique through wet route[8]. Cellprene® was prepared by dissolution of PLGA and IR (60 wt% and 40 wt%) in chloroform by magnetic stirring. Then, it was dried in an oven during 24 h for solvent volatilization[2]. The ratio of PLGA/IR with hydroxyapatite was PLGA, IR and HAp (54 wt%, 36 wt% and 10 wt%). In order to obtain fibers, both blends were dissolved in chloroform - concentration 3%w/v - and submitted to the spinning process. The fiber manufactured by rotary jet spinning used following parameters: speed = 25 000 rpm, orifices diameter = 5 mm and cylindrical collector speed = 100 rpm. For the electrospinning was used a voltage of 20 kV and the distance between the needle and the target was 8 cm. The cylindrical collector speed was 600 rpm. Thermochemical analyses were conducted by Fourier Transform Infrared Spectroscopy (FTIR) and Differential Scanning Calorimetry (DSC) to the blends and fibers. Scanning Electron Microscopy (SEM) analyze was performed to evaluate the fibers morphological.

Results and Discussion

Analysis of the chemical groups presents on PLGA/IR and with PLGA/IR/HAp blends were possible through observation of FTIR spectra. It was possible to observe the groups C=O and C-O, related to PLGA, and bands related to CH_2, C=C and =CH bonds, related to IR, as well as vibrations in the region of CH_3 bonds. The hydroxyl and phosphates groups related to HAp also were observed. In order to observe polymers thermal transitions, DSC analyze was performed. The thermogram presented expected results, as previously reported, where the blend was considered immiscible and showed thermal transitions at -66 ºC for IR and 59 ºC for PLGA[9]. SEM was carried in order to obtain information around morphological characteristics of fibers (Fig. 1 and 2). An important surface morphology parameter of scaffolds is the diameter distribution of fibers, which affects cell differentiation and proliferation[10,11]. Both techniques resulted in a wide diameters distribution (micro- nanoscale) for all compositions. The fibers obtained by rotary jet spinning presented smaller diameters than electrospun fibers. According to a recent study, a wide diameters distributions is desirable to tissue engineering, since its allow to combine both advantages of nano- and microscale structures[12].

Conclusion

In this work the polymeric blend PLGA/IR and PLGA/IR/HAp fibers were successfully produced by the rotary jet spinning and electrospinning techniques. Both thermochemical analyses showed expected results, as FTIR spectrum and DSC thermogram evidenced it, as well rotary jet spinning proved its viability also presenting better results than electrospinning technique. SEM analyze confirmed to be possible to obtain micro- and nanofibers. Further analysis as mechanical and in vitro must be conducted, but it is plausible to believe that rotary jet spinning is a great candidate for soft tissue engineering application.

References

1. A. M. Loordhuswamy, V. R. Krishnaswamy, P. S. Korrapati, S. Thinakaran, and G. D. V. Rengaswami, “Fabrication of highly aligned fibrous scaffolds for tissue regeneration by centrifugal spinning technology,” *Mater. Sci. Eng. C*, vol. 42, pp. 799–807, Sep. 2014.

2. D. R. Marques, L. A. dos Santos, L. F. Schopf, and J. C. S. de Fraga, “Analysis of Poly(Lactic-co-Glycolic Acid)/Poly(Isoprene) Polymeric Blend for Application as Biomaterial,” *Polímeros Ciência e Tecnol.*, vol. 23, no. 5, pp. 579–584, 2013.

3. J. H. Kim *et al.*, “Experimental comparative study of the histotoxicity of poly(lactic-co-glycolic acid) copolymer and poly(lactic-co-glycolic acid)-poly(isoprene) blend,” *Polímeros*, vol. 24, no. 5, pp. 529–535, Sep. 2014.

4. J. J. Rogalski, C. W. M. Bastiaansen, and T. Peijs, “Rotary jet spinning review – a potential high yield future for polymer nanofibers,” *Nanocomposites*, vol. 3, no. 4, pp. 97–121, 2017.

5. S. Padron, A. Fuentes, D. Caruntu, and K. Lozano, “Experimental study of nanofiber production through forcespinning,” *J. Appl. Phys.*, vol. 113, no. 2, 2013.

6. R. Nayak, R. Padhye, I. L. Kyratzis, Y. B. Truong, and L. Arnold, “Recent advances in nanofibre fabrication techniques,” *Text. Res. J.*, vol. 82, no. 2, pp. 129–147, 2012.

7. Y. Tsuneizumi, M. Kuwahara, K. Okamoto, S. Matsumura, "Chemical recycling of poly (lactic acid)-based polymer blends using envi- ronmentally benign catalysts," *Polym. Degrad. Stab.*, vol. 95, pp. 1387– 1393, 2010.

8. S. Ramesh, C. Y. Tan, S. B. Bhaduri and W. D. Teng, "Rapid densification of nanocrystalline hydroxyapatite for biomedical applications," *Ceram. Int.,* vol. 33, pp. 1363–1367, 2007.

9. D. R. Marques, L. A. L. dos Santos, M. A. O’Brien, S. H. Cartmell, and J. E. Gough, “In vitro evaluation of poly (lactic-co-glycolic acid)/polyisoprene fibers for soft tissue engineering,” *J. Biomed. Mater. Res. - Part B Appl. Biomater.*, vol. 105, no. 8, pp. 2581–2591, 2017.

10. I. Rajzer, “Fabrication of bioactive polycaprolactone / hydroxyapatite scaffolds with final bilayer nano- / micro-

fibrous structures for tissue engineering application," *J. Mater. Sci.*, vol. 49, no. 16, pp. 5799–5807, 2014.
11. X. Li, H. Chen, and B. Yang, "Centrifugally spun starch-based fibers from amylopectin rich starches," *Carbohydr. Polym.*, vol. 137, pp. 459–465, 2016.
12. H. Zhou, Y. Tang, Z. Wang, P. Zhang, and Q. Zhu, "Cotton-like micro- and nanoscale poly(lactic acid) nonwoven fibers fabricated by centrifugal melt-spinning for tissue engineering," *RSC Adv.*, vol. 8, no. 10, pp. 5166–5179, 2018.

Acknowledgement

The authors acknowledge to the Coordenação de Aperfeiçoamento de Pessoal de Nível Superior (CAPES) for the financial support through the project, to the Conselho Nacional de Desenvolvimento Científico e Tecnológico (CNPQ), to the Programa de Pós-Graduação em Engenharia de Minas, Metalúrgica e de Materiais (PPGE3M), to the Financiamento de Estudos e Projetos (FINEP) and to Fundação de Auxílio à Pesquisa do Rio Grande do Sul (FAPERGS) for the financial support through the project.

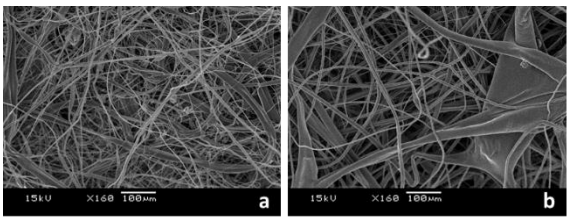

Figure 1.
SEM of fibers obtained by electrospinning: a) PLGA/ IR b) PLGA/ IR/ HAp.

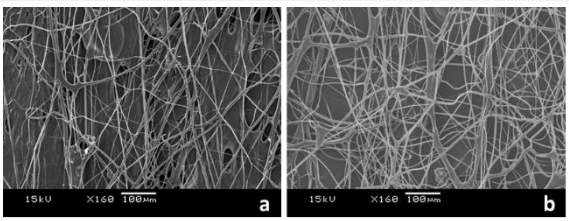

Figure 2.
SEM of fibers obtained by rotary jet spinning: a) PLGA/ IR b) PLGA/ IR/ HAp.

PS2-02-274

Physicochemical properties of the surfaces as the stem cells fate regulator

Mohsen Shahrousvand[1,2], Amin Shavandi[2], Seyed Hafez Jafari[2]

[1]University of Tehran, Caspian Faculty of Engineering, College of Engineering, Rezvanshahr, IR; [2]Université Libre de Bruxelles, BioMatter-Biomass transformation Lab (BTL), École interfacultaire de Bioingénieurs (EIB), École polytechnique de Bruxelles, Brussels, BE

Introduction

Over the last few years, polyurethanes (PUs) have been used extensively in biomedical applications as a result of offering a combination of biodegradability, elastomeric properties and thermoplastic processing conditions, which make them potential candidates for novel applications, especially in tissue engineering and medical devices [1, 2]. The biodegradability and other properties of PUs depend mainly on their chemical structure and especially on the hydrolysable ester bond in the main chain. Cells sense matrix stiffness by a mechano-transducer and prepare their morphology and specific lineage by transducing this information to a nuclear cell. Cells in different stiffness surfaces have diffrent shapes; brain cells are branched shape, muscle cells are spindle while bone cells have a polygonal shape [3]. PU films with different physical properties can affect cell proliferation and differentiation and open new prospects in tissue engineering.

Experimental Methods

The PUs were synthesized using a mixture of (PCL) and poly (tetra methylene ether) glycol (PTMEG) as poly diols, 1, 6-hexamethylene diisocyanate (HDI) and 1, 4-Butanediol (BDO) for the preparation of PUs that is shown in Table 1. The hMSCs differentiated to osteogenic cells on prepared PU films.

Table 1. Recipe of synthesis of polyurethane with different contents of PTMEG, PCL, HDI, and BDO.

Sample	PTMEG (gr)	PCL (gr)	*Mnsoftsegment*(gr/mol)	HDI (gr)	BDO (gr)
PU-100	0	12	2000	3.02	1.08
PU-95	0.315	12	1950	3.18	1.14
PU-90	0.666	12	1900	3.35	1.2
PU-80	1.375	11	1800	3.46	1.24
PU-70	2.143	10	1700	3.60	1.29
PU-0	10	0	1000	5.04	1.8

Results and Discussion

The osteogenic response of hMSCs was found to depend on both the modulus of the polyester/ether based PU substrates. As can be seen, PU-100 and PU-0 have the highest and lowest elongation at break and tensile strength, respectively (Fig 1a). The hydrophilic properties of the surface are virtually constant for all samples (Fig 1b). Calcium content measurements were performed to further evaluate osteogenic differentiation in TCPS and PU membranes at days 7 and 14 (Fig. 1c). After 7 and 14 days of culture in the osteogenic induction medium, the ALP activity of hMSCs on PU-100, PU-95, PU-90, PU-70, and PU-0 was significantly higher than TCPS (Fig. 1d). Similar results were obtained with the calcium content measurements. Fig. 2 shows the adhesion of differentiated hMSCs to the substrate.

Conclusion

We observed that changes in the formulation of polyurethane synthesis with two types of polyols (PCL and PTMEG) lead to producing PU films with different physical properties such as hydrophilicity. Cell proliferation and differentiation were impressed by superficial physicochemical cues. Increasing the surface stiffness improved stem cell differentiation to osteolinage cells. Thus, alterations in superficial cues (such as physical, chemical and mechanical properties on the surfaces of substrates) could not only lead to aberrant growth or differentiation of stem cells but also provide a potential therapeutic target for regenerative medicine.

References

[1] Burke A, Hasirci N. Polyurethanes in biomedical applications. Biomaterials: Springer; 2004. p. 83-101.

[2] Shahrousvand M, Sadeghi GMM, Shahrousvand E, Ghollasi M, Salimi A. Superficial physicochemical properties of polyurethane biomaterials as osteogenic regulators in human mesenchymal stem cells fates. Colloids and Surfaces B: Biointerfaces. 2017;156:292-304.

[3] Saha K, Keung AJ, Irwin EF, Li Y, Little L, Schaffer DV, et al. Substrate modulus directs neural stem cell behavior. Biophysical journal. 2008;95:4426-38.

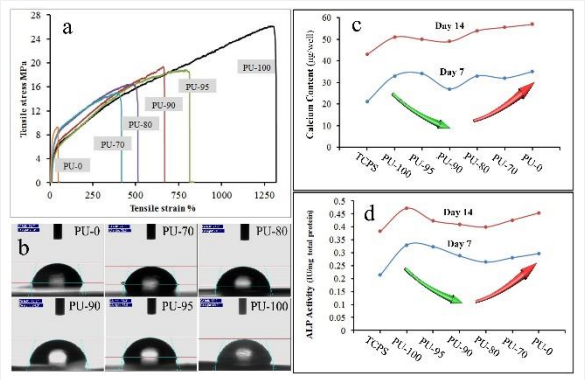

Fig 1. (a) Tensile properties of PUs; (b) Water contact angle; (c) Calcium content of differentiated

PS2-02-275

Influence of biodegradable nanofillers of different types on properties of PLA-based composite fibers.

Konstantin Malafeev[1], Olga Moskalyuk[3], Vladimir Yudin[1,2], Elena Popova[2], Elena Ivan'kova[2], Vladimir Elokhovskiy[2]

[1]Peter the Great St. Petersburg Polytechnic University, Institute of Biomedical Systems and Technologies, St.Petersburg, RU; [2]Institute of macromolecular compounds, St.-Petersburg, RU; [3]Saint-Petersburg State University of Industrial Technologies and Design, St.-Petersburg, RU

Introduction

Today, polymers play important role in a modern life. Due to the ability to vary the properties and a wide range of processing methods, polymers are used in almost all industries. Currently, about 99% of all plastic materials are the product of the petrochemical industry, i.e. they are produced from non-renewable resource as petroleum [1]. Therefore, in recent years, a trend has emerged to find ways to decide ecological problems and develop the polymers form bioresources. One of the most prominent representatives of biopolymers is polylactide (PLA) which is a sustainable alternative to petrochemical products, since lactids are obtained by microbial fermentation of agricultural wastes, mainly carbohydrate-rich substances [2, 3]. Another indisputable advantage of PLA is their high biocompatibility and FDA (Food and Drug Administration) approval these polymers for medical use. Today PLA is used widely for bio-packaging and in medical implants in the form of screws, fibers, sponges, cell scaffolds for tissue engineering and in microspheres for drug delivery. To expand the scope of application of PLA in medicine, it is necessary to modify its properties or improve existing ones. This can be done by developing of PLA based composites. The scope of this work is research of composite materials based on PLA with different fillers to improve mechanical characteristics of the samples or to modify its bioactive properties, such as antibacterial.

Experimental Methods

PLA 2003D (Nature Works) was used as a matrix for composites. Also three types of nanofillers was added: chitin nanoparticles (CN), chitin nanoparticles modified by PolyEthyleneGlycol (CN-PEG) and nanosilver modified by polyvinylpirrolidon (Poviargolum™). The thermal analysis of polymer and nanofillers was performed by the TGA and DSC methods. Rheological behaviors of pure polymer and PLA-based composite were investigated by using a Physica MCR-301 rheometer (Anton Paar, Austria). Oven-dried nanofillers and PLA were mixed on a 5 mL double-screw microextruder (DSM Xplore, Netherlands) at the temperature 220°C. The mechanical properties of PLA monofilaments prepared by melt spinning were studied on an Instron 5943 tensile test machine at RT. The load speed of monofilaments was 50 mm/min and its basis length were 100 mm. SEM images of the cryocleavage surface of PLA/CN monofilaments were recorded on a Carl Zeiss Supra-55 scanning electron microscope (Germany).

Results and Discussion

The fiber samples as monofilaments were obtained by melt technology with the addition of various fillers at a concentration of 1 wt%. The diameter of the non-oriented fibers was approximately 400 microns. The fibers were oriented 6 times additionally by using high-temperature orientation drawing at 70°C. The diameter of the oriented monofilaments was about 200 microns. The mechanical characteristics of these oriented 6 times PLA and PLA composite fibers are represented in the Table (see below).

As can be seen from the table, the addition of CN and CN-PEG does not lead to any significant changes in the mechanical characteristics of the fibers. The strength of the fibers without fillers is 340 MPa, but with the addition of 1% CN or CN-PEG the strengths of the fibers become 305 and 325 MPa, respectively. Other side, the addition of 1% Poviargolum leads to an increase in the strength up to 404 MPa. The modulus of elasticity of all samples is at a level of 6 GPa. The elongation at break remains almost unchanged (as compared with unfilled PLA fibers) for composite fibers filled by CN or CN-PEG. But for composite PLA fibers filled by Poviargolum the elongation is slightly increased up to 21%.

Preservation, and in some cases improvement, of mechanical characteristics, opens up a great prospect in further work with these materials and fillers. Currently studying the bioresorption of fibers, as well as studying the antibacterial activity. According to preliminary data, samples with Poviargolum possess antibacterial activity.

Conclusion

As a result of this work, a series of laboratory samples of PLA monofilaments and composites based on it with various types of fillers and with a concentration of 1% were processed. The effects of the type of biocompatible particles on the mechanical properties of monofilaments with a draw ratio of 6 times were also established. In the future, it is planned to expand the range of concentrations of the filler, to obtain samples with a different degree of orientation extraction, as well as conduct in vitro and in vivo tests to test the antibacterial properties and its bioresorption.

References

1. Tripathi, A. D., et al. *Journal of Polymers and the Environment*, *20*(2), 446-453.
2. Malafeev, K. V., et al. *Russian Journal of Applied Chemistry* 90.7 (2017): 1021-1029.
3. Cabedo, L. et al. *Macromolecular Symposia*, Vol. 233, No. 1, pp. 191-197.

Acknowledgement

This work was supported by Russian Science Foundation (grant #19-73-30003)

	PLA	PLA+1%CN	PLA+1%CN-PEG	PLA+1%Poviargolum
Strength, MPa	340±25	305±7	325±24	404±25
Elastic modulus, GPa	6,5±0,3	5,8±0,1	6±0,3	6,4±0,4
Elongation at break, %	14±1	15±1	16±1	21±3

Mechanical properties of composite monofilaments based on PLA oriented 6 times

PS2-02-276

Tuning bulk and surface properties of degradable fiber-based scaffolds

Tiziana Fuoco, Anna Finne-Wistrand

KTH Royal Institute of Technology, Department of Fibre and Polymer Technology, Stockholm, DE

Introduction

The project this contribution is part of is named **PrintKnit** and aims at designing scaffolds for soft tissue regeneration applications by combining knitted and printed constructs made of degradable polymers [1]. Meshes and other types of knitted scaffolds made of degradable fibers are indeed used in regenerative to support tissue regeneration. To match the requirement of the different applications and overcome some of the drawbacks of the current utilized degradable polymer-based scaffolds, there is a need to tune both the bulk and surface properties of the materials. The bulk properties are those that ensure support to the damaged tissue at the early stage, but then should progressively weaken until the scaffold is resorbed and the tissue is fully recovered. From a macromolecular point of view this means to regulate the degradation rate in order to control the time and the profile of the properties change. On the other hand, the surface properties of the scaffold should favour interaction between the material, cells and surrounding environment (Fig 1).

Experimental Methods

The molecular weight, thermal properties, crystallinity, tensile properties (Young's modulus, elongation to break, strain at break)of the fibers and fiber-based scaffolds were characterized by SEC, DSC and tensile tests.

Results and Discussion

Poly(L-lactide), is one of the most used degradable polymers for the fabrication of fiber-based scaffolds. PLLA has good spinnability and melt-spun fibers with good mechanical properties can be prepared to manufacture for example knitted meshes. To overcome the disadvantages of PLLA, such as the high crystallinity and the slow and heterogeneous bulk erosion process which cause early embrittlement and consequent loss of mechanical integrity while the mass of the bulk is retained, we have evaluated the use of trimethylene carbonate (TMC) as comonomer to modulate the properties of PLLA melt-spun multifilament fibers [2]. We have demonstrated that by increasing the amount of TMC, copolymer fibers with less crystallinity and a more homogeneous bulk degradation and longer service lifetime can be achieved, and when the fibers no longer provide mechanical support they undergo a faster mass loss.

Although PLLA and its copolymer with TMC have been used in devices that are biocompatible and eventually degrades in harmless products, their macromolecular structure does not offer possibility to covalently attach biological motifs or other active tags that can enhance and regulate the cell-material interaction. The purpose of this contribution is the development of a simple and versatile strategy for thesurface functionalization [4] of these fiber-based scaffolds by covalently attach to the scaffold surface a properly designed bi-functional linker. The linker was designed in a way that one of the functional group can be attached to the polyester chains by aminolysis reaction of the ester bonds and the other functional group can be used to link a variety of biological active tags [6] as well as other biomaterials such as PEG. Therefore, this strategy allows to customize the surface properties and regulate the interaction with the cells and body environment (Fig 2).

The reaction parameters for the linker design and the surface functionalization of the scaffolds have been optimized. The effect of the functionalization on the bulk material properties and the relationship between the surface properties and degree and type of functionalization have been evaluated.

Conclusion

The results provide a framework to control the service lifetime and the surface properties of degradable fibers-based medical devices to

(i) ensure mechanical support when required and a faster rate of resorption when such support is not needed anymore and

(ii) specific cell-material interactions.

References

[1] www.kth.se/printknit

[2] T. Fuoco, T. Mathisen, A. Finne-Wistrand, *Biomacromolecules* 2019, 20 (3), 1346.

[3] T. Fuoco, T. Mathisen, A. Finne-Wistrand, *Polymer Degradation and Stability* 2019, 163, 43.

[4] X. Liu, J. M. Holzwarth, P, X. Ma, *Macromolecular Bioscience* 2012, 12, 911.

[5] (a) Y. Zhu, Z. Mao, C. Gao, *RSC Advances* 2013, 3, 2509. (b) A. M. Jordan, V. Viswanath, S.-E. Kim, J. K. Pokorski, L. T. J. Korley, *Journal of Materials Chemistry B* 2016, 4, 5958.

[6] T. Fuoco, A. Finne-Wistrand, D. Pappalardo, *Biomacromolecules* 2016, 17 (4), 1383.

Acknowledgement

Swedish Foundation for Strategic Research (RMA15-0010) is acknowledged for financial support.

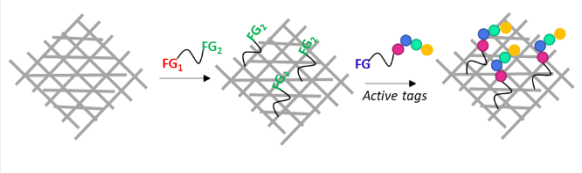

Figure 2
Surface functionalization strategy.Surface functionalization strategy.

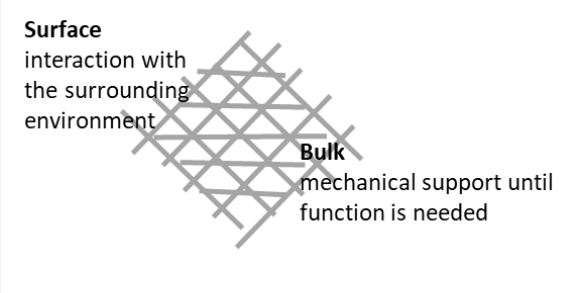

Figure 1.
Overview of the properties to be tuned.

PS2-02-277

Semiconducting Polymer Nanoparticles for Photoacoustic Imaging in NIR-I Window

Alkmini Negka[1], Panagiota Koralli[1], Lida Evmorfia Vagiaki[2], Antonia Dimitrakopoulou-Strauss[1], Vasilis Gregoriou[3], Christos Chochos[2]

[1]German Cancer Research Center, Clinical Cooperation Unit Nuclear Medicine, Heidelberg, DE; [2]National Hellenic Research Foundation, Institute of Biology, Medicinal Chemistry & Biotechnology, Athens, GR; [3]National Hellenic Research Foundation, Athens, GR

Introduction

For in vivo biological applications, near-infrared (NIR) fluorescent probes are considered as a highly emerging field due to the minimal auto-fluorescence interference and high tissue-penetration depth that they display in the NIR region, because of the weak absorption and scattering in biological tissues. Semiconducting polymer dots (Pdots) are arising as organic NIR fluorescent nanoparticles with high brightness, large Stokes shift, and intriguing energy-transfer properties[1].

Photoacoustic imaging (PA) appears to be a promising technique in biological imaging for the visualization of both tissue physiology and pathology at the molecular level, while simultaneously providing high spatial resolution and deep penetration depth in the NIR region [2],[3]. Consequently, there is a great demand in the development of photoacoustic imaging probes with strong near infrared (NIR) absorbance [4]-[6]. In this study, we examine the potential use of novel low bandgap water-soluble conjugated polymer dots, consisting of tetraphenyl substituted-indacenodithiophene-thiadiazolo-quinoxaline biphenyl substituted (mentioned as IDTTDQ-Ph), as a-new-generation NIR contrast agents for PA.

Experimental Methods

Alternating conjugated polymers were synthesized *via* metal catalyzed aromatic cross coupling Stille polymerization reaction. The average molecular weights per number and weight and the dispersity of the polymers were determined (relative to polystyrene standard) by size exclusion chromatography (SEC) in $CHCl_3$. All polymers were analyzed via ^{1}H-NMR (600 MHz) spectroscopy. The NPs formation were carried out via nanoprecipitation and/or by utilizing amphiphilic polymer as the encapsulation matrix. The amphiphilic polymer that was used is PLGA-*b*-*m*PEG. The NPs formation was performed by screening 4 different molar ratios of CP:PLGA-*b*-*m*PEG (1:2, 1:3, 3:1, 4:1). The morphology of NPs was investigated by Transmission Electron Microscopy (TEM) while the NPs' size was measured by Dynamic Light Scattering (DLS) in two different temperatures (25 ^{o}C, 37 ^{o}C). The surface charge of the nanoparticles was evaluated by zeta potential measurements in water (Zetasizer). The UV-Vis spectroscopy was performed in solution and after the formation of NPs, in aqueous suspension using Shumadzu UV-VIS Spectrophotometer, UV-1900. The quantum yield was calculated by photoluminescence (PL) spectroscopy. The cellular cytotoxicity study was performed by means of MTT assay in RPMI-2650, PC-3 and WM164 cells. In order to investigate whether the CP NPs are internalized by the cellular membrane, we exploited a Confocal Fluorescence Microscopy (Leica TCS SPE).

Results and Discussion

A NIR fluorescent polymer (IDTTDQ-Ph) was synthesized that is comprising of tetraphenyl substituted-indacenodithiophene as the electron donating unit, and thiadiazoloquionoxaline-biphenyl substituted as the electron

withdrawing unit. Their average molecular characteristics are presented in Table 1. As observed from SEC, the polymer presents well-define molecular characteristics.

Table 1. Molecular characteristics of IDTTDQ-Ph.

Sample	M_n (g/mol)	M_w (g/mol)	PDI
IDTTDQ-Ph	133000	246200	1,85

The optical data of IDTTDQ-Ph as obtained by UV-Vis spectroscopy in chloroform solution are provided in Table 2. The polymer exhibits an absorption maximum at 993 nm, in solution due to the strong intramolecular charge transfer (ICT) between the indacenodithiophene and thiadiazoloquinoxaline units.

Table 2. Optical properties of IDTTDQ-Ph

	λ_{max}^{sol} **(nm)**	λ_{max}^{film}**(nm)**
IDTTDQ-Ph	455, 993(max)	453, 987(max)

The DLS measurement indicates that the nanoparticles in aqueous suspension have a unimodal size distribution in both temperatureswith an average size of 80 nm. The zeta potential value of both noncoated and amphiphilic-covered CP NPs was estimated at *-24,1 ± 8,0 mV* and *-40,5 ± 4,9 mV*, respectively. As expected, the amphiphilic-covered CPNPs appear to be more stable compared to the uncoated hydrophobic CPNPs. TEM measurement revealed their spherical shape with an average particle size of 100 nm, approximately. The compatible particle size that these CPNPs demonstrate, combined with the absorption in the NIR-I window, qualifies them to be an ideal probe for biological applications.

Conclusion

The combination of strong donor (tetraphenyl substituted indaceno dithiophene) and acceptor (thiadiazole quinoxaline biphenyl substituted) monomers leads to low bandgap materials of which the absorption and emission maxima can be shifted toward the NIR II regionwhich subsequently blazes a trail for the photoacoustic imaging [7]. Both the conjugated and the amphiphilic-encapsulated polymer NPs display a promising size and morphology, a NIR I-shifted optical absorption and low cytotoxicity levels. Additionally, on-going studies will define the photoacoustic effect of the CPNPs.

To conclude, in this study we introduce a new organic candidate (CPNPs) for the photoacoustic imaging that shows low toxicity and optimal optical properties in the NIR I region.

References

1. Da Zhang, Ming Wu, Yongyi Zeng, Naishun Liao, Zhixiong Cai, Gang Liu, Xiaolong Liu and Jingfeng Liu, *J. Mater. Chem. B*, 4, 589-599, (2016)

2. Jie Liu, Junlong Geng, Conjugated polymer nanoparticles for photoacoustic vascular imaging. Polym. Chem., 5, 2854-2862, (2014)

3. Kanyi Pu, Adam J. Schuhendler, Semiconducting polymer nanoparticles as photoacoustic molecular imaging probes in living mice, Nature Nanotechnology 9, 233–239 (2014).

4. Christopher M. MacNeill, Robert C. Coffin, David L. Carroll, Nicole H. Levi-Polyachenk. Low Band Gap Donor-Acceptor Conjugated Polymer Nanoparticles and their NIR-mediated Thermal Ablation of Cancer Cells. Macromolecular Bioscience, Volume 13, Issue 1, 28-34 (2013).

5. Quli Fan, Kai Cheng, Zhen Yang, Ruiping Zhang, Min Yang, Xiang Hu, Xiaowei Ma, Lihong Bu, Xiaomei Lu, Xiaoxing Xiong, Wei Huang, Heng Zhao, Zhen Cheng. Perylene-Diimide-Based Nanoparticles as Highly Efficient Photoacoustic Agents for Deep Brain Tumor Imaging in Living Mice, Advanced Mat. Vol. 27, Issue 5, February 4, p 843-847 (2015)
6. Bing Guo, Biocompatible conjugated polymer nanoparticles for highly efficient photoacoustic imaging of orthotopic brain tumors in the second near-infrared window. Mater. Horiz.,4, 1151-1156, (2017)
7. Braeken, Y., Cheruku, S., Ethirajan, A., & Maes, W., Conjugated Polymer Nanoparticles for Bioimaging. Materials, 10(12), (2017)

Acknowledgement

1) This work was funding by the Helmholtz European partnering program for the cooperation between German Cancer Research Center (DKFZ) and National Hellenic Research Foundation (NHRF) to built the Athens Comprehensive Cancer Center (ACCC)
2) Sponsored by The Hellenic Society for Biomaterials

PS2-02-278

Innovative molecular dressing for hard-healing wounds - surface modifications of bionanocellulose-based composites

Katarzyna Guzdek-Zając[1], Aleksandra Krajcer[2], Joanna Lewandowska-Łańcucka[1], Maria Nowakowska[1]

[1]Jagiellonian University, Faculty of Chemistry, Kraków, PL; [2]Jagiellonian University, Faculty of Physics, Astronomy and Applied Computer Science, Kraków, PL

Introduction

Bionanocellulose (BNC) is a type of cellulose produced by bacterial species, mainly Gluconacetobacter xylinus. This material exhibits unique properties such as: stability over a wide range of pH and temperatures, high hydrophilicity, non-cytotoxicity and biocompatibility. Therefore it has been used in biomedicine (e.g. in wound dressing and bone regeneration or in implants) as well as in paper, food and electronic industry [1]. Our studies are focused on developing methods of synthesis of BNC-based wound dressing one-side protected from the external environment with silicone layer and having on the opposite side covalently bounded an active biomolecules: insulin and heparin. The hybrid materials obtained can potentially serve as a complete bioactive dressing for the treatment of difficult-to-heal wounds occurring in diabetics.

This work presents the results of physicochemical measurements and biological experiments performed for bionanocellulose (BNC) based materials and bionanocellulose doped with carboxymethylcellulose (BNC-CMC composite). The silicone layer was generated on the external side of these systems using silicone precursors: aminopropyltriethoxysilane (APS) [3], [4], vinyltriethoxysilane (VES) and allyltrimethoxysilane (ATMS) to counteract fast drying of the material [2]. On the internal side, through the formation of amide bonds [5], heparin and insulin have been introduced as active substances that can accelerate the healing process. The materials obtained were subjected to preliminary biological tests using mouse embryonic fibroblasts (MEF).

Experimental Methods

The obtained materials unilaterally modified with a silicone layer were tested using SEM, XPS, IR, sweeling-drying and contact angle measurements. After connecting the biomolecules, the materials were subjected to colorimetric tests for the presence of insulin and heparin, respectively. Additionally, biological tests were carried out using the MEF cell line in order to evaluate the impact of the obtained materials on the cell adhesion, morphology (SEM) and proliferation (Alamar Blue test) under *in vitro* conditions.

Results and Discussion

We have developed new hybrid materials based on bionanocellulose and its composite with carboxymethylcellulose. In the first stage of the research by employing two type of silicone precursors we successfully generated silicon layer on the BNC-substrate what was confirmed by means of XPS, IR and SEM techniques. That modification brings an effective protection against drying out, which was established by wetting angle measurements as well as swelling and drying tests. Next insulin and heparin were covalently connected to the unmodified side of previously obtained materials, what was confirmed utilizing an appropriate colorimetric tests: Comassie Brilliant Blue and Azur A, respectively. The generation of a silicone layer has no negative effect on proliferation, morphology as well as adhesion of MEF cultured on the surface of developed materials, as it was shown in *in vitro* biological experiments.

The obtained hybrid materials can be used as a complete bioactive dressing for the treatment of difficult-to-heal wounds in diabetics.

Conclusion

We have demonstrated the methodology of covalent attachment of an active substances on the inside of the BNC-based dressing while having silicone protection on the external side. Presented herein approach definitely broadens the potential application of BNC-based composites in biomedicine and opens the new way to its much wider modification/fabrication.

References

[1] H.M. Avila et. al., *Appl. Microbiol. Biotechnol*., 2014, *98*, 7423-7435
[2] K. Guzdek et. al., Appl. Surf. Sci., 2018, 459, 80-85
[3] S.-K. Chiu et. al., Biochem. J., 2003, 374, 625-632
[4] R. Alosmanov et. al., Cellulose, 2017, 285-293
[5] N. Nakajima et. al., Bioconjugate Chem., 1995, 6, 123-130

Acknowledgement

Authors would like to thank The National Centre for Research and Development (NCBiR) for the financial support in the form of grant no. K/NCB/000013 obtained in the frame of the INNOTECH Programme.

PS2-02-279

Neem Leaves Extracts and encapsulation the Neem Leaves Extracts in chitin film

Khanamporn Chatsupan, **Wanpen Tachaboonyakiat**

Chulalongkorn university, Department of Materials science, Bangkok, TH

Introduction

Neem, *Azadirachta indica*, is a bio-insecticide which is containing the most active phytochemicals named Azadirachtin (AZ) [1]. The purpose of this research is to extract the AZ from the Neem leaves-so called Neem Leave Extracts (NLE). However, the NLE and AZ was rapidly damaged with light and high temperature. Then, the others purpose of this work are to be encapsulated the NLE which is contained high amount of AZ in the polymeric matrices to avoid the degradation of essential phytochemicals and to study the release profile of NLE [2]. Chitin, **(**1, 4**-***N***-**acetyl**-**D**-**glucosamine**)**, was chosen to be polymeric matrix due to their biological properties and well control release rate [**3**].

Experimental Methods

The NLE was first extracted in various solvents and second extracted with water to obtain the water soluble NLE. Furthermore, different amounts of NLE were encapsulated in chitin solution and form as film at ambient temperature. After that, the encapsulated NLE in chitin films were immersed in water to provide chitin hydrogel. Encapsulation efficiency and release profile were determined by UV-vis spectrophotometer, at wavelength 282 nm.

Results and Discussion

The highest amount of NLE was obtained when first extracted with methanol (17.17%) and further extracted with distilled water. Different solvents can extract different amount of NLE as follows, acetone (9.27%), dichloromethane (9.14%) and hexane (1.74%), respectively. Besides, the encapsulation efficiency of NLE into chitin film seemed to increasing as increasing concentration of NLE feeding. Moreover, chitin contained NLE film has capability to release NLE in water due to their swelling properties and dissolve ability of NLE in water.

Conclusion

The NLE can be extracted from various solvents and encapsulated into the chitin film with effectively controlled release.

References

1. Gahukar, R, T. Factors affecting content and bioefficacy of neem (*Azadirachta indica* A. Juss.) phytochemicals used in agriculture pest control: A review. *Crop Protection*, **2014**, *62,* 93-99.

2. Mattos, D, B; Rojas, J, O; Magalhães, L, E, W. Biogenic silica nanoparticles loaded with neem bark extract as green, slow-release biocide. *J. Clean Prod.*, **2017**, *142*, 4206-4213.

3. Saravana, S, P; Ho, C, T; Chae, S.-J.; Cho, Y.-J.; Park, J.-S; Lee, H.-J; Chun, B.-S. Deepeutectic solvent-based extraction and fabrication of chitin films from crustacean waste. *Carbohyd Polym.*, **2018**, *195*, 622-630.

Acknowledgement

This research was financially supported by the Integrated Innovation Academic Center (IIAC), Chulalongkorn University Century Academic Development Project and partially supported by Faculty of Science, Chulalongkorn University.

PS2-02-280

Visible Light Cross-linked Poly(2-oxazoline) (POx)-based Hydrogels via Thiol-Ene Reaction

Ilona Paulus, Julia Bloehbaum, Jörg Tessmar, Jürgen Groll

University of Würzburg, Department of Functional Materials in Medicine and Dentistry and Bavarian Polymer Institute, Würzburg, DE

Introduction

Hydrogels are in the focus of research due to their multifunctional application as implantable materials in regenerative medicine[1]. For the formation of stable hydrogels, researchers often use precursor solutions, consisting of polymers, which are subsequently chemically cross-linked over multivalent monomers or macro-crosslinkers. A promising route for this fabrication of hydrogels is applying side chain functionalized polymers and a very chemoselective reaction, e.g. UV initiated thiol-ene reaction[2]. In our previous study, POx-based hydrogels were cross-linked via thiol-ene reaction with Irgacure 2959 as a quite insoluble UV initiator[3]. Major disadvantages are the possible cytotoxicity of Irgacure 2959[4] and the application of UV light for the initiator activation, which can cause DNA-damage in cells[5]. In this study, we use an alternative photoinitiator tris(2,2'-bipyridyl)dichloro-ruthenium(II)hexahydrate together with sodium persulfate (Ru/SPS) to cross-link POx-based hydrogels via thiol-ene reaction. This initiator system has proven itself in earlier studies with other polymers and it is a promising formulation to prepare hydrogels, as this system can be activated with visible light and accordingly the cytocompatibility is improved[6,7].

Experimental Methods

For the POx-based precursors 2-ethyl-2-oxazoline (EtOx) was randomly copolymerized with 2-(3-butenly)-2-oxazoline (ButEnOx). The synthesis was performed in a microwave reactor at 100 °C with methyl *p*-toluenesulfonate as initiator, acetonitrile as solvent and piperidine as termination reagent for several hours. The comonomer molarity was kept at 4 M. The theoretical chain length of the polymers was adjusted to 50 repeating units and the monomer ratio EtOx:ButEnOx was 0.9:0.1 and 0.8:0.2. After synthesis, the copolymers were precipitated from chloroform/methanol in cold diethyl ether. The product was characterized by NMR and GPC. Subsequently, the double bonds of the polymer side chains were functionalized with thioacetic acid via UV reaction (λ = 365 nm) in methanol with 2,2-dimethoxy-2-phenylacetophenone as photoinitiator. The thioester polymers were then precipitated from chloroform/methanol as the pristine copolymers. The functionalized polymers were then deprotected at room temperature over 12 h using cysteine and $NaBH_4$ under reductive conditions to prevent polymer degradation, then dialyzed against degassed water and freeze dried[4]. The final hydrogels were prepared in 1 x PBS to an overall polymer content of 7.5 wt% or 15 wt%. Copolymers with 10 and 20% vinyl groups were combined with 10 and 20% thiol functionalized polymers, whereas the molar ratio of the functional groups was kept at 1:1 for all hydrogels. After dissolution of the polymers the two solutions were combined and a defined amount of Ru/SPS (0.2/2 mM) was added under exclusion of light to reach the final polymer concentration. The mixed precursor solution was then pipetted into cylindric silicon molds and irradiated for 30 sec with a bluepoint 4 lamp (Dr. Hoenle AG with 390 -500 nm filter).

Results and Discussion

GPC and NMR measurements proved a successful copolymerization of EtOx/ButEnOx and the functionalization of polymer side chains with free thiol groups. The hydrogels formed with Ru/SPS were mechanically stable over 2

weeks with no detectable signs of hydrogel degradation. The Young's moduli increased with increasing functionalization degree of the copolymers due to a much denser hydrogel network. A higher polymer content of the hydrogels also resulted in increasing Young's moduli, which can also be attributed to a denser polymer network. The swelling study demonstrated that the hydrogels were stable over a period of 2 weeks in PBS. A slight but not significant mass decrease was observed, which can be attributed to a slow release of non cross-linked polymer chains, which needs to be studied in the future.

Conclusion

POx-based hydrogels with a long-term stability and variable cross-linking degree were formed successfully with Ru/SPS as initiator under visible light exposure. For future applications other polymer concentrations and substitution degrees must be tested, to vary the mechanical properties and mesh sizes of the obtained hydrogels. The Ru/SPS cross-linked hydrogels using visible light as initiator can accordingly result in promising materials for cell encapsulation or drug release, however, for this approaches the biocompatibility and the fluid behavior of the precursor solution need to be optimized to increase viscosity and eventually shear thinning behavior for bioprinting applications.

References

[1] A. Hoffman, *Adv. Drug Delivery Rev.*, **2012**, 64, 18.

[2] M. Hartlieb, K. Kempe, U. Schubert, *J. Mater. Chem. B,***2015**, 3, 526.

[3] J. Blöhbaum, I. Paulus, A. Pöppler, J. Tessmar, J. Groll, *J. Mater. Chem. B*. **2019**, 7, 178.

[4] S. Bryant, C. Nuttelman, K. Anseth, *J. Biomater. Sci., Polym. Ed.,***2000**, 11, 439.

[5] R. Sinha, D. Hader, *Photochem. Photobiol. Sci*., **2002**, 1, 225.

[6] S. Bertlein, G. Brown, K. Lim, T. Jungst, T. Böck, T. Blunk, J. Tessmar, G. J. Hooper, T. Woodfield, J. Groll, *Adv. Mater.* **2017**, *29*, 201703404.

[7] K. Lim, B. Schon, N. Mekhileri, G. Brown, C. Chia, S. Prabaker, G. Hooper, T. Woodfield, *ACS Biomater. Sci. Eng.,* **2016**, 2, 1752

Acknowledgement

This research has received funding by the Deutsche Forschungsgemeinschaft (DFG, German Research Foundation) – Projektnummer 326998133 – TRR 225 (subproject A06).

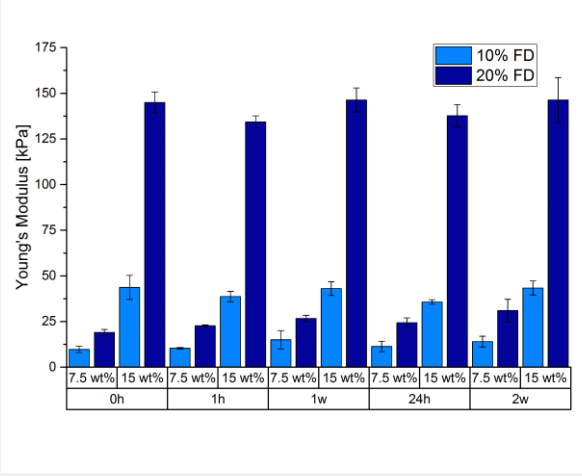

Mechanical Stability

Young's Modulus of thiol cross-linked hydrogels in PBS synthesized with copolymers with 10 and 20% functionalization and a different polymer content (7.5 wt% and 15 wt%) after 0h, 1h, 12h, 1w and 2w at 37 °C.

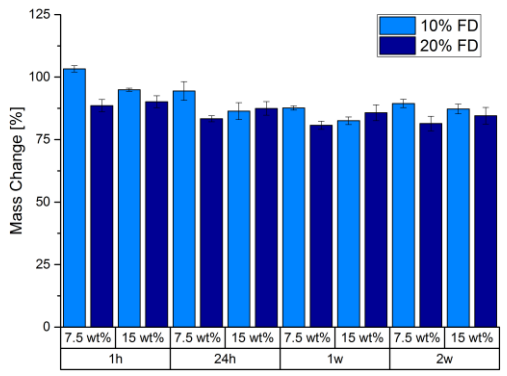

Swelling Behavior
Swelling behavior of thiol cross-linked hydrogels in PBS synthesized with copolymers with 10 and 20% functionalization and a different polymer content (7.5 wt% and 15 wt%) after 0h, 1h, 12h, 1w and 2w at 37 °C.

PS2-02-281

Low-Bandgap Conjugated Polymer Nanoparticles as Fluorescent Contrast Agents for in Vitro Biological Imaging

Lida E. Vagiaki[1], Alkmini Negka[2], Panagiota Koralli[2], Antonia Dimitrakopoulou-Strauss[2], Dionysios Mouzakis[4], Vasilis Gregoriou[3], Christos Chochos[1]

[1]National Hellenic Research Foundation, Institute of Biology, Medicinal Chemistry & Biotechnology, Athens, GR; [2]German Cancer Research Center, Clinical Cooperation Unit Nuclear Medicine, Heidelberg, DE; [3]National Hellenic Research Foundation, Athens, GR; [4]Hellenic Army Academy, Laboratory of Mechanics, Athens, GR

Introduction

Conjugated polymers (CPs) are a special category of macromolecules with large π-conjugated backbones. Owing to their highly electron-delocalized structures and efficient coupling between optoelectronic segments, CPs absorb and emit light energy in the UV-Vis and the NIR region that not only allows deep tissue penetration, but also it can be converted to photoacoustic and fluorescence effects[1]. Nevertheless, for biological applications it is imperative that the CPs are water-soluble. Since CPs are generally hydrophobic, we implemented strategies to enable solubility in aqueous media. Therefore, low-bandgap aqueous CPNs have been successfully prepared and thoroughly applied in biological applications and especially in bio-imaging, since they exhibit excellent properties such as high fluorescence, excellent photostability, high signal-to-noise ratio, high emission rates, and low cytotoxicity[2]-[5]. In this study, we examine the potential use of novel low bandgap water soluble CPNs as fluorescent contrast agents. Under this scope, we synthesized two series of CPs; the first is the combination of thiophene and quinoxaline (TQs), and the other consists of thiadiazoloquinoxaline biphenyl substituted-bithiophene and thiadiazoloquinoxaline bimethyl substituted-bithiophene, BTTDQ-Ph and BTTDQ-Me, respectively.

Experimental Methods

Alternating CPs were synthesized *via* metal catalyzed aromatic cross coupling Stille polymerization reaction. The average molecular weights per number and weight and the dispersity of the polymers were determined (relative to polystyrene standard) by size exclusion chromatography (SEC) in $CHCl_3$. All polymers were analyzed via ^{1}H-NMR (600 MHz) spectroscopy and UV-Vis spectroscopy. The UV-Vis measurements were performed in chloroform or THF solution, as thin films and after the formation of NPs, in aqueous suspension using the Shimadzu UV-Vis Spectrophotometer UV-1900. The morphology of NPs was investigated with Transmission Electron Microscopy (TEM) while Dynamic Light Scattering (DLS) was exploited to elucidate the NPs 'size, in two different temperatures (25 ^{o}C and 37 ^{o}C). The formations of NPs were carried out via nanoprecipitation and the quantum yield was calculated by photoluminescence (PL) spectroscopy. The cellular cytotoxicity study was performed by means of MTS assay in human mesenchymal Wharton Jelly cells. In order to investigate whether the CPNs are internalized by the cellular membrane, we exploited a Confocal Fluorescence Microscopy (Leica TCS SPE).

Results and Discussion

The first series of polymers (TQs) are comprising of thiophene derivatives as the electron donating units and quinoxaline derivatives as the electron withdrawing units with varying the number of fluoro atoms in the repeat unit (TQ, TQf, TQ2f, T2fQ, T2fQf, T2fQ2f). The average molecular characteristics of the TQ polymers are presented in Table 1. The second series of D-A CPs are comprising of bithiophene and thiadiazoloquinoxaline derivatives and are

mentioned as BTTDQ-Ph and BTTDQ-Me series. Both categories of CPs bear aliphatic side chains to improve the solubility.

Table 1. Molecular characteristics of TQs

Sample	M_n(g/mol)	M_w(g/mol)	PDI
TQ	19900	64200	3.2
TQf	11400	25800	2.3
TQ2f	22600	52500	2.3
T2fQ	6000	11300	1.9
T2fQf	8200	15600	1.9
T2fQ2f	11200	16200	1.5

The DLS measurement indicates that TQs and BTTDQ-Ph, BTTDQ-Me nanoparticles in aqueous suspension are close to 90 nm and 80 nm, respectively, with unimodal size distribution in both cases and both temperatures in aqueous suspension. TEM measurement revealed that the CP had spherical shape. The average particle size was determined to 100 nm, a compatible size for biological applications. The optical data as obtained by UV-Vis spectroscopy in chloroform (BTTDQ-Ph, BTTDQ-Me) or THF (TQs) solution are provided in Table 2. As expected, both TQs and BTTDQ-Ph, BTTDQ-Me exhibit absorbance at UV-Vis region. The fluorescence emission for TQs was recorded in UV-Vis region, while for BTTDQ-Ph, BTTDQ-Me in NIR-I region.

Table 2. UV-Vis data of TQs and BTTDQ-Ph, BTTDQ-Me

	λ_{max}^{sol} (nm)	**λ_{max}^{NPs} (nm)**
TQ	354 (max), 600	359 (max), 613
TQf	338 (max), 543 (sh), 574	360 (max), 611, 668 (sh)
TQ2f	319, 349 (sh), 524 (sh), 557 (max), 619 (sh)	357, 587 (max), 634 (sh)
T2fQ	320 (sh), 538 (max)	342 (sh), 555 (max)
T2fQf	387, 498 (max)	326 (sh), 392 (sh), 518 (max)
T2fQ2f	392 (max), 456	394 (max), 474

	λ_{max}^{sol}(nm)	**λ_{max}^{film}(nm)**	**λ_{max}^{NPs} (nm)**
BTTDQ-Ph	360(max), 650	360(max), 670	360(max), 660
BTTDQ-Me	360(max), 595	370(max), 620	370(max), 580

Conclusion

In conclusion, we successfully synthesized a series of fluorescent materials with optical properties and low cytotoxicity of water-soluble CPNs, supporting their potential use as low-bandgap fluorescent probes for bio-imaging. Moreover, the on-going tests for the fluorescence imaging and the quantification of the quantum fluorescence yield are of great importance. Overall, CP dots introduce a new generation of fluorescent probes that appear to be the quintessential contrast agents.

References

1. Acta Pharmacologica Sinica (2017) 38: 764–781; doi: 10.1038/aps.2017.42; published online 22 May 2017

2. Feng, L., Zhu, C., Yuan, H., Liu, L., Lv, F., & Wang, S. (2013). Conjugated polymer nanoparticles: preparation, properties, functionalization and biological applications. Chemical Society Reviews, 42(16), 6620.doi:10.1039/c3cs60036j

3. V. Rohatgi, Low-Bandgap Conjugated Polymer Dots for Near-Infrared Fluorescence Imaging.,ACS Appl. Nano Mater., 2018, 1 (9), pp 4801–4808 DOI: 10.1021/acsanm.8b01014

4. Zhu, C.; Liu, L.; Yang, Q.; Lv, F.; Wang, S. Water-Soluble Conjugated Polymers for Imaging, Diagnosis, and Therapy. Chem. Rev. 2012, 112, 4687-4735

5. Wu, C. & Chiu, D. T. Highly fluorescent semiconducting polymer dots for biology and medicine. Angew. Chem. Int. Ed. 52, 3086–3109 (2013).

Acknowledgement

1) This work was funding by the Helmholtz European partnering programm for the cooperation between German Cancer Research Center (DKFZ) and National Hellenic Research Foundation (NHRF) to built the Athens Comprehensive Cancer Center (ACCC)

2) Sponsored by The Hellenic Society for Biomaterials

PS2-02-282

Characterization of commercial polymeric materials for dental aligners production

Nicola Contessi Negrini[1,2], Francesco Tamburrino[1,3], Armando Razionale[1,3], Silvia Farè[1,2], Roberto Chiesa[1,2], Monica Bordegoni[1,2], Sandro Barone[1,3]

[1]INSTM, National Consortium of Materials Science and Technology, Florence, IT; [2]Politecnico di Milano, Milan, IT; [3]Università di Pisa, Pisa, IT

Introduction

The increasing request for orthodontic devices, even in adults, has led to the development of transparent wearable polymeric dental aligners, as an alternative to fix metal devices. To guarantee a correct adjustment of the teeth defects, such devices should possess adequate mechanical properties, stable physical, chemical and mechanical properties during their use (typically 14 days in mouth) and transparency. Nowadays, several polymeric materials are clinically used for the production of dental aligners. In this work, we aim at characterizing commercially available materials to define a set of properties to be used as guidelines for the production of alternative materials for dental aligners.

Experimental Methods

Four commercially available polymeric materials used for dental aligners production were selected and characterized: Duran®(Scheu-Dental Technology), Imprelon®(Scheu-Dental Technology), Forestadent Track A®(Forestadent) and Zendura®(Zendura). The materials were characterized as received, after thermoforming (*i.e.*, procedure used for the obtainment of dental aligners) and after 14 days of immersion in artificial saliva [2] at 37 °C, to mimic the clinical use. The weight and thickness of samples (n = 4) was evaluated during the immersion in artificial saliva for 14 days, to investigate the weight and dimensional stability in conditions similar to the use. The morphology of the samples was evaluated by scanning electron microscopy (SEM). The mechanical properties of samples as received, thermoformed samples and samples immersed in saliva were evaluated in tensile and flexural mode. Tensile tests were performed with tensile clamps by applying a force ramp of 1 N min^{-1}; the elastic modulus and the deformation at maximum force (*i.e.*, 18 N) were calculated from the stress-strain curves. Flexural properties were evaluated with single cantilever clamp by applying a force ramp of 1 N min^{-1}. Attenuated Total Reflectance Infrared Spectroscopy (ATR-FTIR) was used to investigate possible changes in the chemical structure of the polymeric materials in the 4000 – 600 cm^{-1}range. Indirect cytotoxicity tests were performed (ISO 10993-5) using murine fibroblast cell line L929; culture medium eluates were obtained by contact with samples for 1, 4 and 7 days, used to culture cells and evaluate L929 percentage viability. Data were analyzed by One-Way ANOVA statistical tests; $p < 0.05$ was considered as statistically different.

Results and Discussion

All the considered polymeric materials were stable after immersion in artificial saliva for 14 days, with weight variation values up to 4%. The thickness of all the samples was reduced ($p < 0.05$) after the thermoforming process, due to the pressure applied during the manufacturing process; all the thermoformed samples showed stable thickness after immersion in saliva. SEM micrographs showed a homogeneous surface of as received-samples and after thermoforming; deposition of salts was detected after immersion in artificial saliva. During the mechanical tests

(Figure 1), no break was observed up to the application of 18 N. The elastic modulus values measured by tensile tests were in the range 1000 - 1600 MPa; a reduction of the modulus of Forestadent samples was observed after the thermoforming process while the immersion in saliva did not affect the tensile properties of the considered polymeric materials. The flexural modulus measured for the as received-samples was comprised in the 5 – 10 GPa range; a decrease ($p < 0.05$) in the flexural modulus was observed for Duran, Imprelon and Forestadent samples after immersion in artificial saliva. The ATR-FTIR spectra confirmed the chemical composition of samples declared by the producers, being Duran and Forestadent samples made of polyethylene terephthalate glycol, Imprelon made of polystyrene and Zendura samples made of polyurethane resin. Moreover, no variations in the chemical structures were observed either after thermoforming and immersion in artificial saliva. Indirect *in vitro*cytotoxicity tests (Figure 2) revealed cells percentage viability values higher than 70%, thus proving the absence of indirect cytotoxic effects.

Conclusion

All samples showed stable mechanical, physical and chemical properties after immersion in artificial saliva. The obtained data allows to indicate the golden-standard mechanical parameters to be used for the possible production of innovative dental aligners.

References

[1]Ma *et al.*, The Chinese Journal of Dental Research, 2016, 19, 43-48

[2] Lombardo *et al.*, Progress in Orthodontics, 2015, 16:41

Acknowledgement

This research was funded by Regione Toscana Regione Toscana – Programma Operativo Regionale FESR 2014-2020, Progetti di Ricerca e Sviluppo delle MPMI – Project Smart@lign.

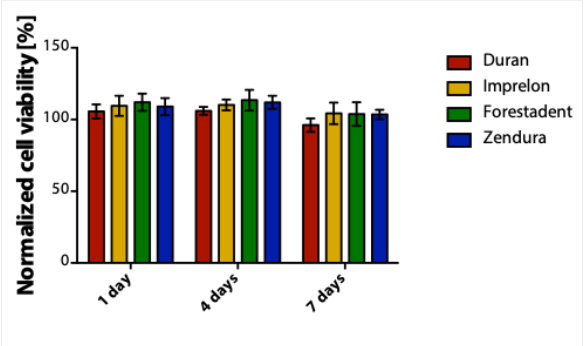

Figure 2
In vitro indirect cytotoxicity tests of thermoformed commercially available polymeric materials used for dental aligners production.

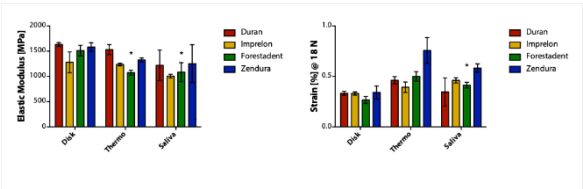

Figure 1
Tensile properties of commercially available polymeric materials used for the production of dental aligners.

PS2-02-283

Colloidal Polyaniline Dispersions Stabilized with Biopolymers

Zdenka Capáková[1], Věra Kašpárková[1,2], Petr Humpolíček[1,2]

[1]Tomas Bata University in Zlin, Centre of Polymer Systems, 76001, CZ; [2]Tomas Bata University in Zlin, Faculty of Technology, 76001, CZ

Introduction

Polyaniline (PANI) belongs to a group of conducting polymers. Due to its properties PANI has become an attractive polymer for biological applications[1,2,3]. Although the biological applications of PANI are on the rise, they are rather limited by its insolubility in aqueous media. Preparation of conducting PANI colloidal dispersions synthesized in presence of stabilizers is one of the possible solutions how to cope with this shortcoming[4]. Various polymers have been tested as the stabilizers, of which biocompatible and biodegradable polysaccharides are promising candidates[5,6]. The aim of present research was therefore to prepare colloidal PANI dispersion in presence of sodium hyaluronate (HA) or chitosan (CH), and determine their physicochemical and biological properties in terms of cytotoxicity and antibacterial activity.

Experimental Methods

Preparation and characterization of colloids: PANI colloids were prepared by oxidizing aniline hydrochloride (AN) with ammonium peroxydisulfate (APS) in presence of HA (MW = 50.28 x 10^3 g.mol^{-1}) or CH (MW ~ 400 x10^3 g.mol^{-1}) at different ratios of AN:APS:polymer. The prepared dispersions were dialyzed against 0.2 M HCl to remove residual impurities. Particle size and distributions of colloidal particles were determined by dynamic light scattering (ZetaNano, Malvern, UK). Colloids were visualized by TEM (JEOL JEM 2000 FX Japan).

Antibacterial activity and cytotoxicity: *Staphylococcus aureus* CCM 4516 and *Escherichia coli* CCM 4517 were used at density 1-2 x 10^8 CFU mL^{-1}, incubation was carried out at 37 °C for 24 h. Cytotoxicity was tested using the mouse fibroblasts, NIH/3T3 (ATCC, Catalog No. CRL-1658, USA) by MTT assay according to protocol EN ISO 10993-5.

Results and Discussion

In the study, PANI colloids stabilized with HA or CH were prepared. Light scattering measurements have shown that size of colloidal particles and colloid stability depend both on the type of the stabilizer and on the content of monomers in the reaction mixture. Sizes of PANI-HA colloidal particles were of about 500 nm, whereas diameters of particles stabilized with CH ranged from 380 to 1330 nm. For both colloids, antibacterial properties were tested. The minimum inhibitory activity of PANI-HA was observed at the highest tested concentration of PANI in colloidal dispersion (4200 μg.mL^{-1}) against *E. coli.* Antibacterial activity was detected also for PANI-CH sample, which can be attributed to presence of both PANI and also chitosan with known antibacterial effect. It was therefore concluded that the antibacterial activity of colloids depends both on the type of used stabilizer as well as on the ratio between PANI and stabilizer. Preliminary cytotoxicity testing has shown that PANI-CH has a lower cytotoxicity than PANI-HA. However, cytotoxicity slightly increased with raising concentration of PANI in colloid.

Conclusion

Polyaniline colloids containing sodium hyaluronate and chitosan were successfully prepared. Size of colloidal particles can be controlled by the concentration of the stabilizer, content of the monomers in the reaction mixture and

by the reaction conditions. Different levels of antibacterial properties of PANI colloids were proved against both gram positive *S. aureus* and gram negative *E. coli*. Lower cytotoxicity was noted for PANI-CH colloid.

References

C.W. Hsiao, M.Y. Bai., Y. Chang, M.F. Chung, T.Y. Lee, C.T. Wu, B. Maiti, Z.X. Liao, R.K. Li, H.W. Sung, Biomaterials 34 (2013) 1063–1072.

2. S.H. Ku, S.H. Lee, C.B. Park, Biomaterials 33 (2012) 6098–6104.

3. E.A. Ostrakhovitch, J.C. Byers, K.D. O'Neil, O.A. Semenikhin, Arch. Biochem. Biophys. 528 (2012) 21–31.

4. Stejskal, Sapurina, POLYANILINE: THIN FILMS AND COLLOIDAL DISPERSIONS Pure Appl. Chem.,Vol. 77, No. 5, pp. 815–826, 2005.

5. J. Stejskal, Colloidal dispersions of conducting polymers J. Polym. Mater. 18 (2001) 225–258.

6. Z. Kuceková et al. Colloidal polyaniline dispersions: Antibacterial activity, cytotoxicity and neutrophil oxidative burst Colloids and Surfaces B: Biointerfaces. 2014, vol. 116, p. 411-417.

Acknowledgement

This work was supported by the Czech Science Foundation (17-05095S) and by the Ministry of Education, Youth and Sports of the Czech Republic – Program NPU I (LO1504).

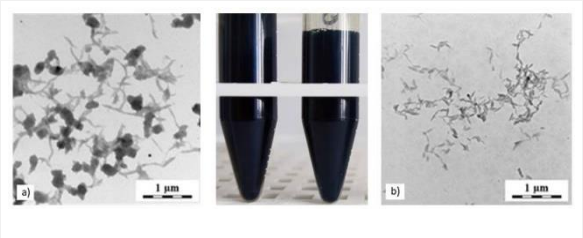

FIGURE 1.
Transmission electron photomicrographs of colloidal polyaniline prepared in presence of a) sodium hyaluronate and b) chitosan

PS2-02-284

Advanced polymeric materials for the selective molecular recognition of natural antioxidants from vegetable sources

Niccoletta Barbani[1,2,3], Caterina Cristallini[2,3]

[1]University of Pisa, Department of Civil and Industrial Engineering, DICI, Pisa, IT; [2]CNR, Institute for Chemical and Physical, IPCF ss Pisa, Pisa, IT; [3]INSTM, National Interuniversity Consortium of Materials Science and Technology, Florence, IT

Introduction

Natural antioxidants from plant materials exhibit a wide range of biological effects, such as anti-inflammatory, antibacterial, antiviral, anti-aging, and anticancer. Considering their possible beneficial influence on human health, efficient extraction methods of natural antioxidants from food and plants and appropriate assessment of antioxidant activity have received increased attention in food science, nutraceutical and drug delivery in the biomedical area. A series of green non-conventional extraction methods of antioxidant agents from plant materials (i.e. extractions based on ultrasound, microwave, enzyme, pressurized liquid, pulsed electric field and high voltage electrical discharges) have been developed to improve extraction efficiency, for reducing operational time and use of organic solvents. Moreover, many methods for the determination of antioxidant capacity of extracts from natural products have been developed and tested in the literature, showing for each of them strengths and limitations. An innovative method is based on the development of biocompatible materials in form of membrane, having properties of molecular recognition towards polyphenols from plant homogenates. An ideal technique could be considered the molecular imprinting technology, that permits the introduction into a polymeric material of recognition sites for specific molecular species (templates) through the copolymerization of a monomer with a crosslinking agent in the presence of a template or through the dissolution of the preformed polymer in a solution containing the molecule to be recognized. In this work, poly(ethylene-co-vinyl alcohol) (EVAL), in ethylene/vinyl alcohol percentage molar ratio of 38/62 (C38), was used to prepare, via phase inversion, supports capable of extracting, thanks to the presence of selective molecular recognition sites, curcumin (diferuloylmethane) used as model phenolic compound template.

Experimental Methods

Curcumin powder was added to a solution of EVAL in DMSO (15 % w/v). The final homogeneous solution of phenolic compound and EVAL was cast on a glass plate using a knife machine with a gap of 400 nm. The cast solution was immersed in a distilled water/DMSO (50/50 v/v) coagulation bath and after one hour transferred to fresh distilled water for 24 h and finally freeze-dried. The template was removed from the membrane (MIT) by prolonged washing in methanol obtaining the molecularly imprinted membrane (MIM). The same procedure in the absence of the curcumin was adopted to prepare not imprinted membrane (NMIM). Chemical Imaging analysis was performed using a Spectrum Spotlight FT-IR Imaging System in order to obtain information on the chemical composition and on the distribution of the curcumin into EVAL membrane. Statistical analysis was performed by PCA method. The binding capacity of MIM was determined in methanol solution of curcumin at known concentration (10 mg/ml) for 24 hours under stirring. UV spectrophotometry at wavelength of 421 nm was used to quantify the amount of re-bound curcumin.

Results and Discussion

Chemical Imaging allowed to evaluate the chemical composition of membrane surface before and after curcumin extraction as well as after rebinding test. For each membrane a surface was selected and analysed by FT-IR mapping, in reflection mode. Superficial changes in the composition were observed; both MIT and membrane after rebinding test (MIMR) showed adsorption signals associated to curcumin chemical composition, on the contrary these signals were not observed in the FT-IR spectrum obtained from MIM surface. FT-IR analysis showed the success of the template extraction and the effective rebinding of the phenolic compound and its homogeneous distribution on the membrane surface (Fig. 1).The distribution coefficient (Kp) was estimated as a measurement of the material capacity of template recognition and rebinding: $Kp = (C_1 - C_2)/C_1$ where C_1 and C_2 are the concentration of the template solution before and after rebinding test. The specific rebinding R was evaluated as R=C(MIM)-C(NMIM), where C(MIM) and C(NMIM) are the amounts in µg template/mg membrane of template present in MIM and NMIM after rebinding. The values obtained were Kp of 0.15 and R of 0.5 µg curcumin/mg membrane.

Conclusion

This preliminary study demonstrated the possibility of using molecular imprinting technology to obtain materials in form of membrane able to specifically recognize a natural antioxidant agent.

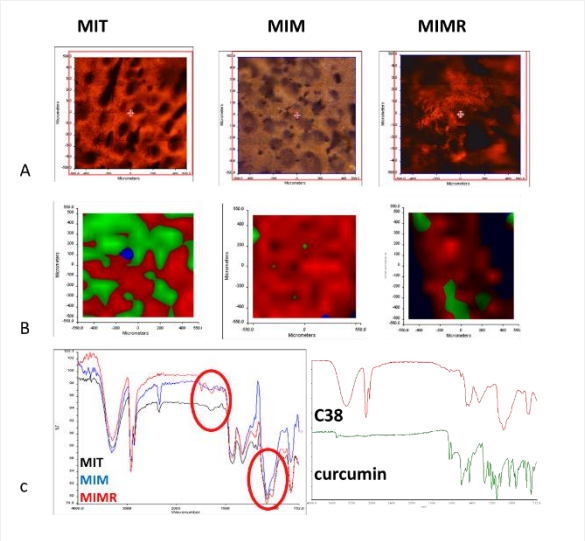

FT-IR Chemical Imaging

Fig. 1 FT-IR Chemical Imaging analysis, a) Optical images of MIT, MIM, MIMR; b) PCA analysis on chemical map of MIT, MIM, MIMR; c) Spectra of membranes and pure components.

PS2-02-285

Integration of protein containers into polyelectrolyte microgels for drug release and delivery

Made Budiarta[1], Wenjing Xu[2], Sarah Wypysek[3], Sarah Boesveld[4], Pavel Strnad[4], Walter Richtering[3], Andrij Pich[2], Tobias Beck[1], On behalf of SFB 985 Functional Microgels and Microgel System

[1]RWTH Aachen, Institute of Inorganic Chemistry, Aachen, DE; [2]DWI-Leibniz Institute for Interactive Materials e. V., Aachen, DE; [3]RWTH Aachen, Institute of Physical Chemistry, Aachen, DE; [4]University Hospital Aachen, Aachen, DE

Introduction

Ferritin is a highly stable and biocompatible protein container with an inner cavity that is widely used as reaction vessel or for cargo loading. It has a high natural affinity towards transferrin receptors over-expressed on cancer cells and is amenable to further surface modification for improved targeting properties. All these features make ferritin an attractive drug delivery vehicle.[1] However, some challenges are present for its application: strong liver uptake and clearance, degradation by proteases, and its abrupt drug release profile.[1,2] To address these problems, we integrated ferritin into polyelectrolyte microgels by using electrostatic interactions. Here the microgels is supposed to act as carrier, protective shielding, and release controller for ferritin.[3]

Experimental Methods

First, we encapsulated fluorophores and nanoparticles inside ferritin to monitor the uptake by the polyelectrolyte microgel. Subsequently, these labeled ferritins were integrated into polyelectrolyte microgel and characterized using TEM and fluorescence microscopy. Next, we will use pH and glutathione to release ferritin from microgels and monitor the process. Furthermore, we encapsulated doxorubicin into ferritin. Currently, we are performing in vitro tests in hepatocellular carcinoma cell lines and will report on the results. Moreover, we will integrate this dox-ferritin into polyelectrolyte microgels, conduct similar in vitro tests, and perform stability tests against proteases.

Results and Discussion

We used different fluorophores and approaches to increase the encapsulation loading and found the key factors for the encapsulation: fluorophore concentration, solubility, charge, and the encapsulation strategy. We also synthesized CeO_2 and Fe_2O_3 nanoparticles inside ferritin cavity. Both fluorophore and nanoparticle labeled ferritins showed the distribution of ferritin in polyelectrolyte microgels under fluorescence microscope and TEM, respectively. For the drug delivery application, we succesfully encapsulated doxorubicin molecules in ferritin. All the other experiments are being conducted and the results will be reported in the conference.

Conclusion

In conclusion, a new drug delivery system based on ferritin containers and polyelectrolyte microgels is currently developed.

References

1) M. Truffi, L. Fiandra, L. Sorrentino, M. Monieri, F. Corsi, S. Mazzucchelli, *Pharmacol. Res.* **2016**, *107*, 57-65.
2) T. J. Todd, Z. Chen, J. Xie, *Nanomedicine* **2013**, *8*, 1555-1557.

3) M. Karg, A. Pich, T. Hellweg, T. Hoare, L. A. Lyon, J. J. Crassous, D. Suzuki, R. A. Gumerov, S. Schneider, I. I. Potemkin, W. Richtering, *Langmuir* **2019**, *35*(9), 6231–6255.

Acknowledgement

We thank Profs. Ulrich Simon and Ulrich Schwaneberg for generous support. This work was supported by a Liebig scholarship to T.B. (Fonds der Chemischen Industrie) and the German Research Foundation (DFG) within the SFB 985 “Functional Microgels and Microgel Systems”.

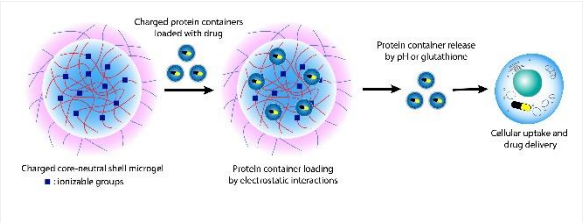

Protein containers-loaded microgels as a new drug delivery system

Drugs-loaded protein containers were integrated into polyelectrolyte microgels via electrostatic interactions. Subsequently, we applied this new drug delivery system to cancer cells and triggered the release by acidic pH or glutathione.

PS2-02-286

Oxygen-generating Bioadhesive Hydrogel *via* Calcium Peroxide-mediated Crosslinking Reaction

Sohee Lee[1], Kyung Min Park[1,2]

[1]Incheon National University, Department of Bioengineering and Nano-Bioengineerign, Incheon, KR; [2]Incheon National University, Division of Bioengineering, Incheon, KR

Introduction

Bioadhesive hydrogels have been used as wound closures, hemostatic agents, tissue sealants and other medical applications. While various types of bioadhesives have been developed, it is still challenging to overcome some limitations, such as poor adhesion strength and bioactivities. Recently, many researchers have been reported mussel-inspired adhesives as they have shown strong tissue adhesiveness even in wet conditions. Molecular oxygen (O_2) is an essential signaling molecule in the wound healing and tissue regeneration. In particular, it is demonstrated that hyperbaric oxygen promotes the wound healing process through accurately increasing intracellular reactive oxygen and nitrogen species (RONS). Herein, we represent a new type of O_2-generating bioadhesive formed *via* calcium peroxide (CaO_2)-mediated crosslinking and *in situ* polymerization of dopamine.

Experimental Methods

The thiolated gelatin (GtnSH) was synthesized by conjugating Traut's reagent to the gelatin backbone as previously reported.[1] We fabricated O_2-generating bioadhesive hydrogels by simply mixing GtnSH and dopamine hydrochloride (DH) in the presence of CaO_2. The phase transition time was determined by the vial tilting method. The elastic modulus (*G'*) was characterized by using a rheometric fluid spectrometer (HR-1, TA instruments). The remained DH within the hydrogel matrices was measured by BCA assay. We monitored dissolved O_2 (DO) levels using a commercially available O_2 sensor (Microx-4, Presens). Tissue adhesive strength was investigated using a universal testing machine (Instron 5966). For *in vitro* cytocompatibility test, human dermal fibroblasts (HDFs) were cultured with hydrogel droplets and cell viability was analyzed by WST-1 and live/dead assay. We performed subcutaneous implantation and wound closing test to investigate the effect of O_2 release on neovascularization and wound healing.

Results and Discussion

The GtnSH-polydopamine (PD) hydrogels were formed *via* CaO_2-mediated crosslinking reaction. In this reaction, the polymer networks were crosslinked through disulfide bonds, and Michael type addition between the GtnSH and polydopamine. Additionally, DH reacts with functional groups (e.g., $-NH_2$, -SH) of tissue surfaces resulting in diverse interfacial bindings (Fig. 1a). To evaluate the hydrogel formation and phase transition, we performed phase-transition test depending on CaO_2 (0.25 – 0.75 wt%) and DH concentrations (0 – 1 mg/mL), demonstrating higher levels of CaO_2 induced faster hydrogel formation (43 sec – 3 min) without compromising DH concentrations. We assessed the elastic modulus of the hydrogels depending on CaO_2 and DH concentrations, resulting in tunable mechanical properties (40 – 830 Pa). We next investigated the DH-releasing behaviors from the hydrogel matrices. As increasing CaO_2 contents, more DH molecules were remained within the hydrogel matrices since CaO_2 facilitated dopamine oxidation and *in situ* polymerization. Also, the hydrogels showed controllable tissue adhesive strength in wet conditions (15 − 38 kPa) (Fig. 1b). We monitored O_2-releasing kinetics depending on CaO_2 concentrations. The hydrogels (G5D0.5C0.75) rapidly generated O_2 up to 70% pO_2 and released O_2 for seven days *in vitro* (Fig. 1c). We

evaluated the cytotoxicity of the hydrogels using HDFs, confirming the excellent cell viability (> 85% compared to the control). Furthermore, we implanted the hyperoxic gels (HG, G5D0.5C0.75) and normoxic gels (NG, G5D0.5C0.75) in the subcutaneous pocket of mice to analyze *in vivo* effects of the hydrogels on neovascularization, and also performed wound closing test. Interestingly, we found that the HG group facilitated wound closing and healing with enhanced neovascularization compared to the NG (Fig. 1d).

Conclusion

We developed a new type of O_2-generating bioadhesive hydrogel *via* CaO_2-mediated crosslinking and *in situ* polymerization of dopamine. The GtnSH-PD hydrogel has controllable physicochemical properties and facilitates neovascularization and wound healing. These results suggest that our advanced adhesive hydrogel is a very promising biomaterial as tissue adhesives for wound management as well as tissue regenerative materials.

References

1. Sujin Park and Kyung Min Park, ***Biomaterials***, 182:234-244, 2018

Acknowledgement

This work was supported by the National Research Foundation of Korea (NRF) grant funded by the Korea government (MSIT) (NRF-2018M3A9E2023257).

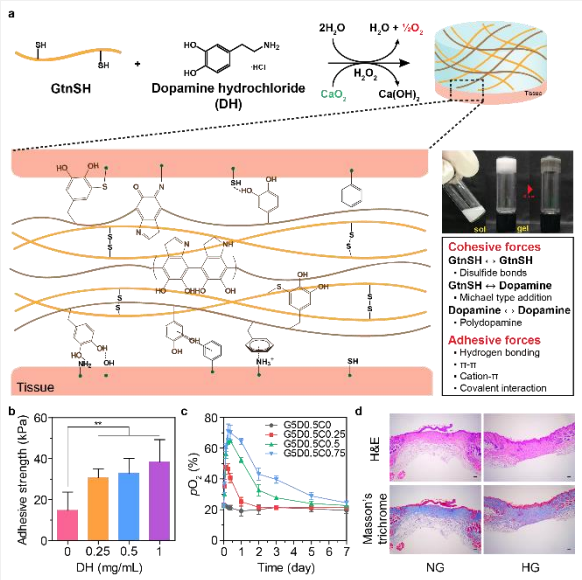

Characteristics and wound healing effect of the GtnSH-PD hydrogels
(a) The design strategy for O_2-generating bioadhesives *via* CaO_2-mediated crosslinking reaction and digital images of sol-gel transition. (b) The tissue adhesive strength of the hydrogels depending on DH concentrations. (c) The O_2-releasing kinetics of the hydrogels. (d) Histological sections of wounds stained with H&E and Masson's trichrome. The results are shown as the average values ± s.d. (n=3~6, $^{**}P < 0.01$)

PS2-02-287

Optimization of poly(diol citrates) composition for small-diameter blood vessel tissue engineering

Agata Flis[1], Filip Koper[2], Wiktor Kasprzyk[2], **Elżbieta Pamuła**[1]

[1]AGH University of Science and Technology, Faculty of Materials Science and Ceramics, Kraków, PL; [2]Tadeusz Kościuszko Cracow University of Technology, Faculty of Chemical Engineering and Technology, Kraków, PL

Introduction

There is a need to treat artherosclerotic vascular disease of small-diameter blood vessels with the use of artificial grafts. Grafts made of Dacron or ePTFE work well in large-diameter blood vessel application. Unfortunately, grafts suitable for small size vessels (>6 mm inner diameter) have not been developed so far. Thus we focus on poly(diol citrate)s (PDCs), based on citric acid and 1,8-octanediol as potential substrate for small blood vessel tissue engineering. PDCs produced with a 1:1 molar ratio of citric acid to 1,8-octanediol were found biodegradable and cytocompatible [1]. Their key advantage is that PDCs polymerization takes place at relatively low temperature and such polymers can be easily modified to gain new distinct properties, including fluorescent, antimicrobial, adhesive or anti-oxidant [2]. In this study we wanted to examine if chemical structure of PDCs can be adjusted by different concentration of the precursors, and if this would influence physical integrity, surface properties and biological performance of obtained polymers. To this end structural and physicochemical properties of thee PDCs with different molar ratio of citric acid to 1,8-octanediol were evaluated and their potential *in vitro* cytotoxicity was assessed.

Experimental Methods

Citric acid and 1,8-octanediol at molar ratio 1:1, 2:3 and 1:2 were melted at 140^{o}C for 40 min under stirring to synthesize prepolymers. The latter were dissolved in ethanol, precipitated in water, lyophilized, dissolved in ethanol again and post-polymerized for 4, 6, 8, 10 days at 70^{o}C in a vacuum oven. PDCs surface roughness (Hommer-Werker profilometer) and the water contact angle (DSA10, Kruss) were measured. FTIR-ATR (Tensor 27, Bruker) was used to determine surface chemical composition and NMR spectra (Brucker Avance III HD 400 MHz) were registered. Acid value were measured by dissolving 150 mg of the sample in 96% ethanol, and then titrating with 0.05M KOH with phenolphthalein as an indicator. Molecular weight was assessed by gel permeation chromatography using Shimadzu GPC system. Cytocompatibility with L929 fibroblasts was assessed on 10% extracts from PDCs in DMEM: undiluted (1:1) and diluted by a factor of 1:2, 1:4, 1:8 and 1:16. In brief the cells were cultured in 96-well plates in DMEM supplemented with 5% FBS, amino acids, and antibiotics for 24 h and then cell culture medium was replaced with the extracts. Cell viability was measured using Alamar Blue and CCK-8 tests. Cells after live-dead staining were observed under fluorescence microscopy (Axiovert, Zeiss).

Results and Discussion

GPC results showed that molecular weight of PDCs depended on molar ratio of the copolymers. FTIR-ATR results showed that PDCs with all studied molar ratios had similar bands at the same wavenumbers and were differing only in band intensity depending on composition. Acid values showed that PDC_1:2 had the lowest acidity (150.8 ± 1.9 mg KOH/g), while PDC_1:1 had the highest acidity (204 ± 3.8 mg KOH/g). Acid value for PDC_2:3 was 160.9 ± 6.5 mg KOH/g. PDC_1:1 and PDC_2:3 were hydrophilic (water contact angle 65^{o} – 85^{o}) and smooth (R_a 0.10 – 0.40 µm). The water contact angle decreased with the post-polymerization time from 4 to 10 days. PDC_1:2 was not

dimensionally stable irrespectively of the post-polymerization time. Cells cultured in the extracts from PDC_2:3 exhibited the highest viability as shown by Alamar Blue and CCK-8 tests, than those cells cultured in PDC_1:1 and PDC_1:2 extracts. Microscopic observations after live-dead staining showed that cells cultured in the extracts from PDC_2:3 (undiluted and diluted by all factors) were stained green, i.e. alive (Fig. 1, panel B). Cells cultured in the extracts from PDC_1:1 (Fig 1, panel A) showed some degree of toxicity, while for higher dilutions, i.e. 1:2, 1:4 and 1:8 no impact on cell viability was observed. Cells cultured in undiluted extracts from PDC_1:2 (Fig 1, panel C) showed only dead cells (stained red). Some of the cells cultured in the extracts from PDC_1:2 diluted by a factor of 1:2 were alive, but majority of them were dead. For extract dilution of 1:4 number of live cells was increasing, but still red stained cells were observed. For 1:8 dilution cell morphology and number was the same as in control.

Conclusion

We found that PDC_2:3 had the lowest acidity and exhibited the best dimensional stability, physicochemical properties and cytocompatibility with L929 cells. PDC_1:1, i.e. the reference material reported in literature, had higher acidity and provoked slight cytotoxicity. PDC_1:2 was the least dimensionally stable, had the lowest acidity and was cytotoxic. Thus we developed a new material PDC_2:3 with better performance by adapting molar ratio of co-monomers: citric acid and 1,8-octanediol. Further studies will focus on preparation of tubular scaffolds from PDC_2:3 for small size blood vessels tissue engineering and their evaluation in contact with endothelial and smooth muscle cells.

References

[1] Tran T.R. et al. Annu. Rev. Mater. Res. 2015. 45:11.1-11.34

[2] van Lith R. et al. Biomaterials 2014; 35: 8113-8122

Acknowledgement

This study was financed by National Science Center, Poland (2018/28/C/ST5/00461).

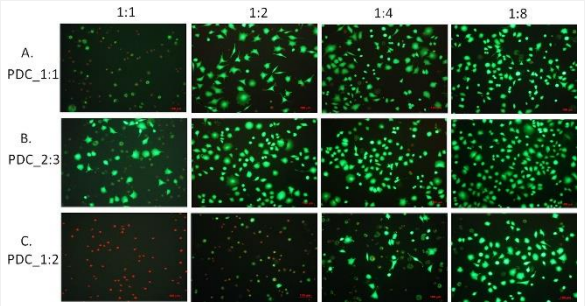

Fig. 1.
Morphology of L929 cells cultured for 24 h in the extracts from poly(diol citrate)s with molar ratio of citric acid and 1,8-octanediol of 1:1 (PDC_1:1) (A), 2:3 (PDC_2:3) (B) and 1:2 (PDC_1:2) (C) after live-dead staining.

PS2-02-288

Tuning drug delivery with block copolymer-based biomaterials

Clara Mattu, Giulia Brachi, Gianluca Ciardelli

Politecnico di Torino, DIMEAS, Turin, IT

Introduction

Systemic chemotherapy is often ineffective in treating cancer, due to poor selectivity and adverse off-target effects [1]. Polymer nanoparticles (NPs) are promising candidates as they enhance tumor uptake by passive and active targeting mechanisms, reducing undesired side effects [2].
Moreover, NPs can be used for packaging of multiple payloads, allowing combinatorial treatments that could not otherwise be obtained due to different biodistribution profiles on un-encapsulated drugs [3].
Here, we exploit the versatile chemistry of polyurethanes (PUR) to design a platform of NPs exhibiting: i) high drug loading ability [4]; ii) Active and passive targeting functionalities [5,6]; iii) ability to combine different treatment options [7]; iv) imaging capability [8].

Experimental Methods

PURs were obtained by a two-step synthesis procedure and their hydrophilic/hydrophobic balance was modulated by selecting different ratios between the hydrophobic poly(ε-caprolactone) (PCL) diol and the hydrophilic poly(ethyleneglicole) (PEG) [4]. NPs were prepared by emulsification of nanoprecipitation methods. Active tumor targeting was achieved in vitro by surface-modification with the monoclonal antibody Herceptin (HER). Core shell PUR NPs, were designed for the co-encapsulation of multiple payloads, including chemotherapeutics with different biodistribution profiles and imaging probes. In vivo studies were performed to determine tumor uptake and ability to efficiently co-deliver multiple payloads. Because of the low toxicity profile and versatile design, core-shell PUR-NPs were delivered intra-cranial (IC) in glioblastoma (GBM) bearing mice, and transport and treatment studies were performed.

Results and Discussion

We showed that PURs are optimal candidates to form NPs. High drug loading, in vitro cell targeting and internalization, and long-term stability were achieved. Functional groups or surface charge was successfully exploited for surface modification with HER and selective targeting of HER-2 over-expressing cells was demonstrated in vitro. The core-shell design of PUR NPs resulted high in vivo tumor accumulation in a breast cancer flank tumor model (4T1 cells). We showed efficient tumor co-accumulation of Doxorubicin and Docetaxel, two drugs with different pharmacokinetics and, therefore, not compatible for combinatorial treatment. NPs showed long residence time in the brain after IC injection (up to 10 days post injection) and good coverage of the tumor mass. Drug-loaded PUR NPs significantly extended survival of GBM-bearing mice.

Conclusion

Our results warrant further investigation of PURs as NP-forming materials in nanomedicine, in virtue of their versatility, surface-modification ability, and high affinity with both, hydrophilic and hydrophobic, drugs.

References

[1] J.Shi et Al. Nature Reviews **Cancer**, 2017

[2] E. Blanco et Al. Nature biotechnology, 2015

[3] E. Blanco Therapeutic delivery, 2014 - Future Science

[4] C. Mattu et al Journal of Nanoparticle Research, 2012

[5] C. Mattu et al. European Journal of Pharmaceutics and Biopharmaceutics, 2013

[6] C. Mattu et al. Polymer International, 2016

[7] C.Mattu et al. Acta Biomaterialia, 2018

[8] C. Iodice et al. Optics and Lasers in Engineering, 2016

Acknowledgement

This project has received funding from the European Union's Horizon 2020 research and innovation programme under the Marie Sklodowska-Curie grant agreement No 658665

PS2-02-289

Synthesis, characterization and antibacterial activity of alginate nanoparticles containing nitric oxide donor and silver nanoparticles

Amedea B. Seabra[1], Alessandro L. Urzedo[1], Marcelly C. Gonçalves[2], Mônica H. M. Nascimento[1], Gerson Nakazato[2], Christiane B. Lombello[3]

[1]Universidade Federal do ABC, Center for Natural and Human Science, Santo André, BR; [2]Universidade Estadual de Londrina, Department of Microbiology, Londrina, BR; [3]Universidade Federal do ABC, Center for Engineering, Modeling and Applied Social Sciences, Santo André, BR

Introduction

Silver nanoparticles (AgNPs) have gained considerable attention in recent years due to their potential applications as antimicrobial agent. Nitric oxide (NO) is an important endogenous molecule that controls several physiological functions. Both AgNPs and NO have antibacterial effects, and recently our group demonstrated the synergist effect of NO donors allied to AgNPs.[1] As NO is a free radical, NO donors, such as S-nitrosothiols, are used in biomedical applications to release NO.[2] Alginate is a biocompatible and biodegradable polymer, extracted from brown algae, extensively used in pharmacological applications. In this work, AgNPs, synthesized by green tea extract, and S-nitrosomercaptossunic acid (S-nitroso-MSA), a NO donor, were incorporated in alginate nanoparticles. The obtained nanoparticles were characterized by different techniques and their antibacterial activity was evaluated against different bacterial strains of medical interest.

Experimental Methods

AgNPs were synthesized by reducing Ag^{+} to Ag^{0} using green tea extract (*Camellia sinensis*), which is rich in polyphenols. The phytochemicals from green tea act not only as reducing agent but also as capping agent, stabilizing AgNPs. Green tea synthesized AgNPs were characterized by X-ray Diffraction (XRD) and Dynamic Light Scattering (DLS). S-nitroso-MSA (NO donor) was synthesized by the nitrosation reaction of mercaptosuccinic acid (a thiol containing molecule) with equimolar amount of sodium nitrite. Alginate nanoparticles were prepared by ionotropic gelation with calcium chloride in aqueous medium. Alginate nanoparticles containing AgNPs and/or S-nitroso-MSA were characterized by Fourier-transform infrared spectroscopy (FTIR), Atomic Force Microscopy (AFM), Dynamic Light Scattering (DLS), and Nanoparticle Tracking Analysis (NTA). The encapsulation efficiency of S-nitroso-MSA into alginate nanoparticles was measured. Kinetics of free NO release from alginate nanoparticles was monitored for 12 h, at physiological temperature. In addition, kinetics of the diffusion of the NO donor (S-nitroso-MSA) from alginate nanoparticles was monitored in a Franz vertical diffusion cell, with a cellulose membrane. The kinetic profiles of S-nitroso-MSA diffusion from the nanoparticles were fitted to mathematical models. *In vitro* cytotoxicity of the nanoparticles was evaluated in Vero fibroblast cell line. The antibacterial activity of the nanoparticles was characterized by measuring the minimum inhibitory concentration (MIC) and minimum bactericidal concentration (MBC) of the nanoparticles against *Escherichia coli* ATCC 25922, *Staphylococcus aureus* ATCC 25923, *Streptococcus mutans* ATCC UA159.

Results and Discussion

Green tea synthesized AgNPs presented face centered cubic lattice with size of 34.7± 4.9 nm, polydispersity index (PDI) of 0.28 ± 0.01. Alginate nanoparticles have average size of 32 nm, as assayed by AFM, and hydrodynamic size of 271.93 ± 8.99 nm and PDI of 0.398 ± 0.021, as assayed by DLS and NTA. Encapsulation efficiency of the NO

donor into alginate nanoparticles was found to be 98.74 ± 0.08%. NO release from alginate nanoparticles was found to be sustained for at least 12 h at 37 °C, with an initial rate of 14.199 ± 0.325 mmol/L.h^{-1}. Diffusion of S-nitroso-MSA from alginate nanoparticles indicates a change on nanoparticle surface. A concentration dependent toxicity was observed for NO-releasing alginate nanoparticles, and the nanoparticles were found to be toxic to Vero cells at higher tested concentrations (1 and 3 mmol/L). AgNPs and alginate nanoparticles containing AgNPs and/or S-nitroso-MSA demonstrated antibacterial activity against all tested bacterial strains. MIC and MBC values for alginate nanoparticles containing AgNPs and S-nitroso-MSA were in the rage of 78 mg.L^{-1} to 310 mg.L^{-1}.

Conclusion

This work describes the synthesis and characterization of alginate nanoparticles containing green tea synthesized AgNPs and/or S-nitroso-MSA (a NO donor). The materials prepared were characterized by different techniques. Kinetic measurements showed a sustained NO release from the nanoparticles for at least 12 h, at physiological temperature. The nanoparticles showed a concentration dependent toxicity to Vero cells. In addition, alginate nanoparticles containing AgNPs/S-nitroso-MSA showed potent antibacterial activities against clinically relevant bacteria strains, at concentrations found not toxic to Vero cells. Therefore, alginate nanoparticles containing AgNPs and S-nitroso-MSA might find important biomedical applications in the combat of bacterial infection.

References

1. SEABRA, A. B. et al. *J. of Phys.: Conference Series.* 838(1):12-31, 2017.
2. WANG, P. G. et al. *Chem. Rev.* 102(4):1091–1134, 200

Acknowledgement

Authors have appreciated the support from CNPq, FAPESP (2018/08194-2), and Multiusers Experimental Central of UFABC.

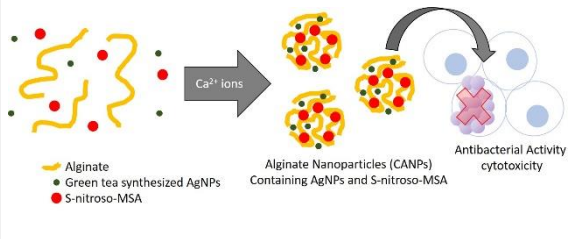

Schematic representation of alginate nanoparticles containing AgNPs and nitric oxide donor

Alginate nanoparticles containing green tea synthesized silver nanoparticles (AgNPs) and the nitric oxide donor (NO donor) S-nitroso-MSA for antibacterial effects.

2:45 p.m. – 3:45 p.m.

Hall 1 / Exhibition Area

PS2-03 | Composites and nanocomposites

PS2-03-291

Keratin/Hydrotalcites based materials for drug delivery applications

Tamara Posati, Annalisa Aluigi, Giovanna Sotgiu, Roberto Zamboni

National Research Council (CNR), Institute of Organic Synthesis and Photoreactivity (ISOF), Bologna, IT

Introduction

Keratin is a biocompatible polymer that has attracted a lot of attention as biomaterial for biomedical applications, particularly in the field of tissue engineering and drug delivery. Keratin is one of the most abundant non-food proteins, being the principal component of hair, wool, feather, horns and nails of mammals, reptiles and birds, and it can be easily extracted from readily available and low cost wastes, such as raw wool not suitable for spinning, feathers from butchery and by-products of the wool textile industry. [1] Regenerated keratin solutions extracted from wool can be easily processed in different biodegradable, biocompatible and non-toxic forms including fibers, capsules, particles, films, foams, nanofibrous membranes and gels.

Hydrotalcites (HTlcs) or layered double hydroxides (LDH) are the only example of layered solids with a positively charged surface balanced by interlayer anions. The possibility of anionic insertion into the interlayer region makes HTlc versatile materials suitable for different industrial applications such as adsorbents, ion exchangers, pharmaceutics, catalysts, flame retardants and nanostructured materials for photonic and opto-electronic devices. [2]

Recently we reported the preparation of hybrid materials (films and electrospun nanofibers, Figure 1 A and 1B) for drug delivery purposes obtained by combining keratin with hydrotalcite nanoparticles containing diclofenac. Diclofenac was chosen as a representative non steroidal anti-inflammatory drugs to be introduced into keratin matrix and intercalated, as previously reported [3], into HTlc nanoparticles. The aim of the development of these hybrid composite materials was to study the effects of HTlc both as drug carriers as well as stabilizing fillers for the protein-based matrix. Our results demonstrated that nanosized HTlc exercised an overall reinforcing action on the hybrid materials since all the samples displayed a reduced swelling, porosity and a slower degradation profile compared to pure keratin based compounds. Diclofenac release profiles of the hybrid films in physiological conditions were higher than those of the non-hybrid compounds whereas in the electrospun nanofibers the release was comparable. [4-5]

Experimental Methods

1) Preparation of Keratin/HTlc based materials
2) Morphology characterization of Keratin/HTlc hybrid materials
3) Porosity measurement by liquid displacement method
4) Swelling studies
5) Degradation test
6) Drug release test

Results and Discussion

In the present work we report the preparation of innovative keratin-HTlc composite sponges by freeze-drying procedure starting from keratin and nanosized HTlc aqueous solutions (Figure 1C). In addition, the comparison in terms of properties (swelling, porosity and stability) and diclofenac release profiles between these new materials and

the already obtained films and electrospun hybrid nanofibers is presented. The obtained keratin-HTlc hybrid sponges are characterized and tested *in vitro* as potential systems for controlled drug release.

Conclusion

The successfull preparation of different keratin composites containing nanosized hydrotalcites allows to increase the range of possible keratin based materials to be used for biomedical applications.

References

[1] A. Aluigi, M. Zoccola, C. Vineis, C. Tonin, F. Ferrero, M. Canetti, **41** (2007) Int. J. Biol. Macromol. 266-273.
[2] F. Leroux, C. Taviot- Guého, J. Mater. Chem. **15** (2005) 3628-3642.
[3] L. Perioli, T. Posati, M. Nocchetti, F. Bellezza, U. Costantino, A. Cipiciani, Appl. Clay Sci. **53** (2011) 374–378.
[4] T. Posati, D. Giuri, M. Nocchetti, A. Sagnella, M. Gariboldi, C. Ferroni, G. Sotgiu, G. Varchi, R. Zamboni and A. Aluigi, Eur. Polym. J.,**105** (2018), 177–185.
[5] D. Giuri, M. Barbalinardo, G. Sotgiu, R. Zamboni, M. Nocchetti, A. Donaddio, F. Corticelli, F. Valle, C.G.M. Gennari, F. Selmin, T. Posati, A. Aluigi, Nanoscale, 2019, DOI: 10.1039/c8nr10114k.

Acknowledgement

Tamara Posati as recipient of the Young Investigator Award 2018, kindly acknowledges CNR-DSCTM funding in grantee the attendance.

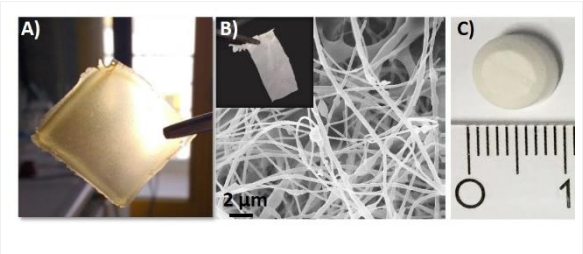

Figure 1
Keratin/Hydrotalcites hybrid materials: A) film, B) electrospun nanofibers and C) sponges.

PS2-03-292

Synthesis and characterization of laser-generated nanocomposite biomaterials and their protein adsorption properties

Yaya Li, Christoph Rehbock, Stephan Barcikowski

University of Duisburg-Essen, Technical Chemistry I and Center for Nanointegration Duisburg-Essen (CENIDE), Essen, DE

Introduction

Nanocomposites are highly interesting biomaterials while the nanoparticles embedded in a polymer matrix can add novel functionality to the polymer. Thermoplastic polyurethane (TPU), a medium hardness polymer, has been applied in different biomedical device [1]. In previous experiments, we demonstrated that laser ablation and in situ embedding of nanoparticles into the TPU is a versatile strategy for nanocomposite synthesis. In these studies, we found that Ag and Cu nanoparticles, in situ embedded into the TPU polymer matrix, was able to remain uniform even after hot injection molding [2]. TPU nanocomposites are confirmed to the generation of pre-endothelialized surfaces of medical devices [3].

In this work, the loading of gold and iron nanoparticles into TPU polymer solution by a laser-based in situ embedding method is systematically studied. We demonstrate how the loading of the particles into the TPU can be controlled and optimized, utilizing high power lasers with high productivity [4]. In consecutive experiments we realize the parallel embedding of two different nanoparticles, gold and iron, into the TPU. This could be particularly interesting as both elements were shown to enhance the cytocompatibility of biomaterials by two different modes of action, Fe probably by iron ion release [5] and Au by altering the surface charge of polymers. [3] In the course of this study we examine the release of bioactive iron ions and measured surface charge and hydrophilicity (contact angle) in correlation with the particle mass load. Finally, we evaluate the adsorption of the model proteins BSA on the nanoparticle-loaded composites as an initial indicator for potential biocompatibility and evaluated to what extent the affinity to BSA is correlated with the loading and composition of the composite biomaterial.

Experimental Methods

Laser ablation was to generate gold or iron TPU composites. TEM and confocal microscopy were used to characterize the size distribution and 3D structure. The physical property of composites was investigated by contact angle and surface charge.

Results and Discussion

Gold and iron particle size was 5.3 nm and 12 nm, respectively. Pure TPU was positve charge at pH 7, but with embedding nanoparticle, it is negtive charge. Further, nanoparticles can alter wettability of this polymer.

Conclusion

Gold and iron nanoparticles can be uniformlz embedding in TPU, which will alter the surface charge and wettablity of this polymer. This composites is promising for pre-enthodial.

References

[1] White L. Medical urethanes, part 2: Versatility offers a myriad possibilities. Urethanes Technol 2005; 22; 2:34–37.

[2] Philipp Wagener, Gudrun Brandes, Andreas Schwenkea and Stephan Barcikowski, Impact of in situ polymer coating on particle dispersion into solid laser-generated nanocomposites, Phys. Chem. Chem. Phys., 2011, **13**, 5120–5126.

[3] Hess C, Schwenke A, Wagener P, Franzka S, Laszlo Sajti CL, Pflaum M, Wiegmann B, Haverich A, Barcikowski S., Dose-dependent surface endothelialization and biocompatibility of polyurethane noble metal nanocomposites, J. Biomed. Mater. Res. Part A. 102A (2014) 1909–1920.

[4] R. Streubel, S. Barcikowski, B. Gökce, Continuous multigram nanoparticle synthesis by high-power, high-repetition-rate ultrafast laser ablation in liquids, Opt. Lett.41(7) (2016) 1486–1489.

[5] A. Blaeser, N. Million, D. F. D. Campos, L. Gamrad, M. Köpf, C. Rehbock, M. Nachev, B. Sures, S. Barcikowski, H. Fischer, Laser-based *in situ* embedding of metal nanoparticles into bioextruded alginate hydrogel tubes enhances human endothelial cell adhesion, Nano Research.9(11) (2016) 3407–3427.

Acknowledgement

Dr. Milen Nachev from Biology School, University of Duisburg-Essen is acknowledged for ICP-MS. Confocal microscopy images were acquired at the IMCES Electron Microscopy Unit. And thanks for China scholarship council.

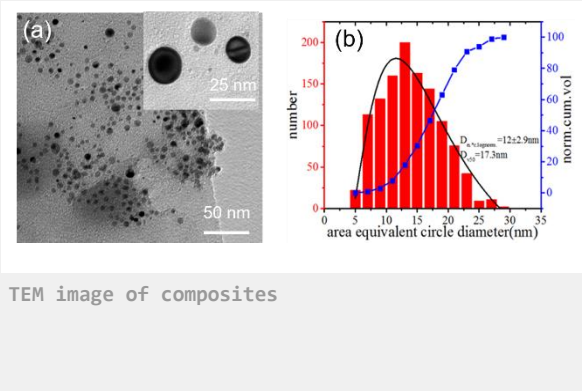

TEM image of composites

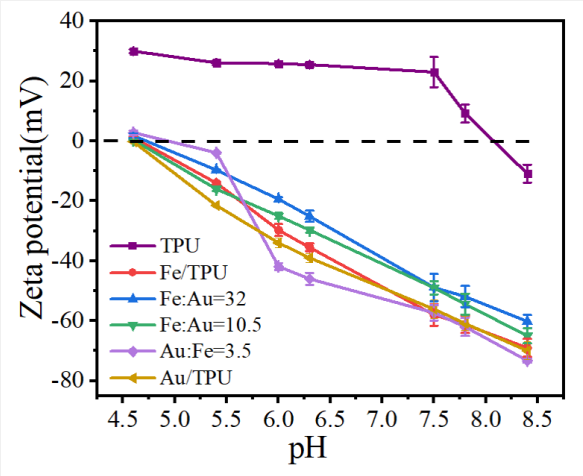

surface charge of composites

PS2-03-293

Biosynthesized silver nanoparticles-embedded bacterial cellulose nanocomposites for antibacterial wound dressing applications

Pooyan Makvandi, Elham Moradi, Khadijeh Ashtari

Iran University of Medical Sciences, Department of Medical Nanotechnology, Tehran, IR

Introduction

Presently, burn, scald, and chronic wounds represent a major and persistent burden in dermatology. Acute and chronic wounds need to be treated by artificial skin and/or wound dressings. Though various wound healing materials have been developed over time, the present commercial materials are far from ideal. Owing to its unique nano-scaled three-dimensional network structure, bacterial nanocellulose (BNC) has high water retention, high mechanical strength, and outstanding biocompatibility, all of which enable it to serve as a natural scaffold material for the regeneration of a wide variety of tissues. However, it has to be highlighted that infection is a crucial and generally unsolved issue in wound healing [1,2].

Among many nanocompounds, Ag nanoparticles have shown capability to inhibit or decline infections. Synthesis of Ag NPs via chemical methods require the employing of organic passivators which are toxic to the environment and the human body. Green synthesis of nanostructures that incorporates the utilization of renewable materials and avoids the use of toxic chemicals and harsh solvents are more suitable for biomedical applications [3]. Tragacanth gum (TG), an anionic polysaccharide, is a biobased polymer which is derived from renewable sources. As a biomaterial, TG has been used in industrial settings, such as food packaging and water treatment, as well as in the biomedical field as drug carriers and for wound healing application. There are some interests in using TG for the biosynthesis of NPs as opposed to chemical synthesis [4]. The present study focuses on the production, characterization, capping and stabilization of silver nanoparticles by TG using an aqueous medium via microwave assisted approach in organic solvent-free process that is completely biocompatible and nontoxic.

Experimental Methods

The biosynthesis of silver NPs was conducted by microwave irradiation of silver nitrate using green chemistry approach in an organic solvent-free medium. A homogeneous tragacanth gum solution was prepared. Subsequently, $AgNO_3$ solution was added to the TG solution. Then, the mixture were treated by microwave (700 w) for 180 s. A pulsed mode of on 5 s, off 5 s was applied to prevent intense boiling and aggregation of Ag NPs. The biosynthesized NPs in tragacanth gum were stored at 4 °C for further characterization.

Regarding the synthesis of bacterial nanocellulose, commercially available SCOBY (including *Acetobacter* bacterial species, as well as various Saccharomyces and other yeast types) was cultured in a static medium. After 2 weeks, the BNC, which was formed on the air-medium interface, was collected and purified.

The Ag NPs were then impregnated into bacterial nanocellulose by immersing BNC pellicles in TG solution containing silver NPs followed by rinsing with deionized water.

Results and Discussion

Figure 1A shows the schematic illustration for biosynthesis and stabilization of Ag NPs by tragacanth gum. The conversion of the colorless reaction mixture to the characteristic clear yellow color indicates the formation of Ag NPs. UV-Vis spectroscopy emerged as one of the most powerful analytical tools for characterization of metal nanoparticles.

The absorption spectra of samples before and after microwave treatment are presented in **Figure 1B** .The monotonic decrease of the UV–Vis spectrum of CSE before microwave treatment clearly indicates the absence of Ag NPs while, after microwave treatment, the peak of the Plasmon absorption at 440 nm reflects the presence of the colloidal dispersion of $Ag^{(0)}$ NPs. The peak appearance of the Plasmon absorption represents that Ag^{+} ions were reduced to $Ag^{(0)}$ NPs. The absorption band is caused by 4d→5s, p interband transitions as reported in other studies [5]. **Figure 1C** shows the results of DLS analysis of silver NPs and it can be seen that the prepared NPs have a narrow size distribution.

Figure 2 shows the optical and SEM images of pristine bacterial nanocellulose. The surface morphology of BNC is observable. As can be seen, the purified BNC has rough morphology.

Since gels exhibit many polymer characteristics without becoming freely dissolved, such materials can remain in place under physiological conditions while maintaining antimicrobial activity. These attributes make them ideal for clinical fields such as skin infections, and wound healing applications [6].

Conclusion

A simple, eco-friendly approach for green synthesis of silver NPs was acchieved by using naturally occurring and renewable tragacanth gum as a bioreducing and biostabilizing agents instead of utilization of toxic chemical agents and solvents. The biosynthesized spherical particles of silver can be used in a plethora of crucial applications related to clinical and biomedical sectors. Antimicrobial BNC hydrogels can be as an important platform to combat infections in wound healing applications.

References

[1] Kamoun et al. Journal of advanced research (2017), 8: 217-233.

[2] Qiu et al. Materials Science and Engineering: C (2016), 59: 303-309.

[3] Krishna Indana et al. Journal of Analytical Science and Technology (2016), 7:19-27.

[4] Zare et al., Carbohydrate polymers (2019), 212: 450-467.

[5] Makvandi et al., Bulletin of Materials Science (2015), 38: 1625-1631

[6] Li, Y., et al. Angewandte Chemie International Edition (2013), 52: 674-678.

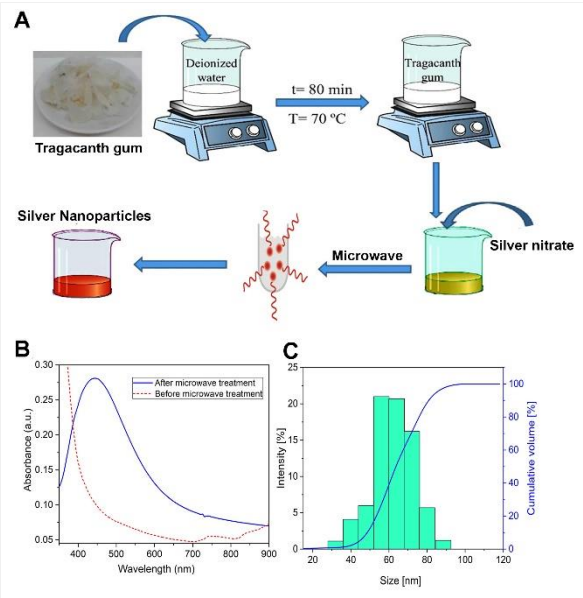

Figure 1

(A) Illustration for the synthesis of silver nanoparticle in tragacanth gum via microwave-assisted green approach. The darker color shows the Ag ions were converted to Ag NPs. (B) The UV absorbance of Ag NPs in tragacanth gum before and after microwave treatment. (C) Size distribution measurements by DLS of silver NPs in tragacanth gum solution.

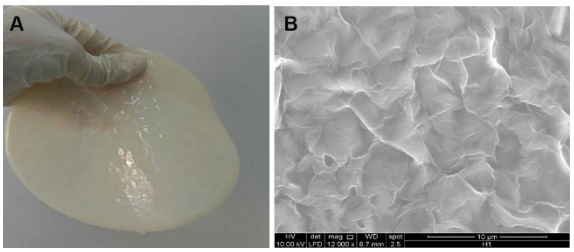

Figure 2
(A) Photograph of purified bacterial nanocellulose. (B) SEM image of surface morphology of the purified bacterial nanocellulose.

PS2-03-294

Graphene oxide modified with RGD peptide

Joanna Jagiello[1], Marcin Gwiazda[2,1], Ewa Kijenska-Gawronska[2], Ludwika Lipińska[1]

[1]Institute of Electronic Materials Technology, Department of Chemical Synthesis and Flake Graphene, Warsaw, PL; [2]Warsaw University of Technology, Faculty of Materials Science and Engineering, Warsaw, PL

Introduction

Nowadays a lot of scientific effort is focused on the development of new materials for the biomedical use (e.g. for tissue engineering [1] and cancer treatment). One of the most promising material in this field is graphene derivative called graphene oxide (GO). GO is a defected graphene (carbon layer with one atom thickness arranged in hexagonal crystal lattice), where defects are the result of reactive oxygen functional groups bonded to the surface. Great interest of GO is due to its physicochemical properties which allow for modifications of GO structure by different biomolecules attachment. This extend possibilities for interaction with different types of cells and tissues. Moreover, GO without any surface modification was found to be nontoxic and biocompatible towards different cell lines, even human mesenchymal stem cells.[2]

High-molecular weight glycoproteins such as fibronectin are often introduced into biomaterials to improve cell attachment. However binding of such molecules of the desired amount with material poses many difficulties. Therefore we introduced to GO a short peptide RGD of a sequence that is mostly responsible for integrin binding. This sequence is also present in the fibronectin structure.

The aim of this study was to synthesize GO modified with Arg-Gly-Asp peptide (RGD) as a molecule enhancing cell attachment and therefore providing good conditions for their growth and proliferation.

Experimental Methods

Here we present different ways to prepare GO-RGD platform. GO was obtained by modified Hummers method. Carboxylated GO (GO-COOH) was obtained with the use of chloroacetic acid in a basic environment. Graphene flakes (GO and GO-COOH) were pre-functionalized with ethyl(dimethylaminopropyl) carbodiimide (EDC) and N-hydroxysuccinimide (NHS) compounds. Every modification was conducted in a bulk and in a form of layer. After this activation of -COOH groups in GO, RGD was bonded. GO-RGD was prepared in the form of suspension as well as in the form of layer. FTIR, EDS and SEM study of the obtained composites were performed to evaluate if the functionalization was achieved. Bonded peptide molecules were also labeled with a fluorescent dye FITC.

Results and Discussion

FTIR spectra indicate structural change in GO after functionalization with EDC/NHS and RGD peptide. The results show the appearance of new chemical covalent bonds between graphene oxygen functional groups and molecules used for functionalization. The spectra show that after GO modification the absorption peak at 1730 cm^{-1} assigned to carboxyl groups became weak. This may provide an evidence for the successful modification of RGD peptide, where carboxyl groups are consumed. Stronger absorbance at 1075 cm^{-1} may come from newly created C-N groups after RGD addition.

EDS measurement also indicate the presence of nitrogen atom in the structure of GO modified with RGD peptide.

Morphology observed under SEM microscopy indicate that the GO flakes are not significantly agglomerated even after functionalization processes.

Conclusion

Modification of graphene oxide with RGD peptide was successfully conducted. Optimal method for the preparation of such materials was investigated. It was stated that modifications of previously dried GO layers are easier to prepare than of GO suspension. This procedure does not require to substitute water for e.g. DMF solvent during EDC/NHS functionalization of GO.

References

[1] Dozois, M. et al., Carbon, 120 (2017) 338-349

[2] Duran, M. et al., Curr Mol Med., 17 (2017) 619-626

Acknowledgement

This study was supported by the Institute of Electronic Materials Technology (Statutory Research 2019), Grant number: S2-10-1014-19

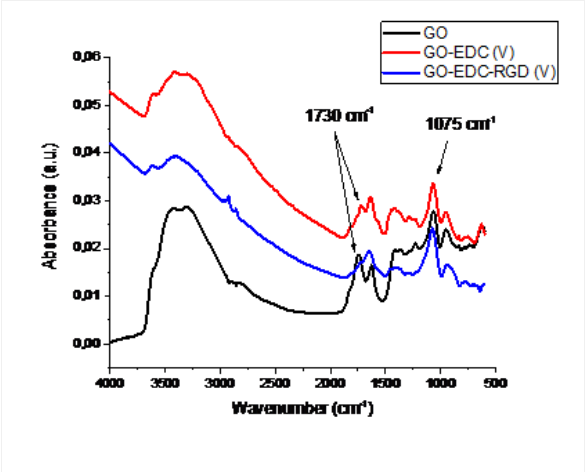

FTIR spectra of GO and GO modified with EDC/NHS and RGD peptide.

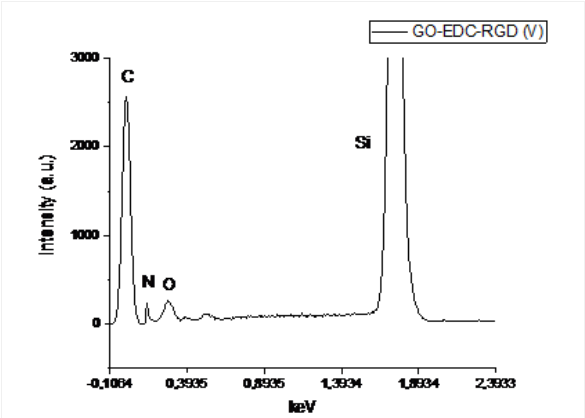

EDS measurement of GO modified with RGD.

PS2-03-295

Nanocomposite hydrogel based on human hair keratin and catechin combined with cellulose for wound healing

Zhe Sun[1,2], Xudong Li[2]

[1]Second Clinical Medical College of Jinan University, Department of Hepatobiliary and Pancreatic Surgery, Shenzhen, CN; [2]Sichuan University, National Engineering Research Center for Biomaterials, Chengdu, CN

Introduction

Immediate hemorrhage control and anti-infection play important roles in the wound management. Besides, a moist environment is also beneficial for wound healing. Hydrogels are promising materials in urgent hemostasis and drug release. In this study, we constructed nanocomposite hydrogel with rapid hemostasis and sustainable antibacterial property combining human hair keratin and catechin nanoparticles (KENs) combined with carboxymethylcellulose. The KENs were prepared by the self-assembly of keratin and catechin. The KENs and cellulose composite hydrogel (KEC hydrogel) displayed a three-dimensional microporous structure and exhibited excellent swelling, mechanical property, and low cytotoxicity. The KEC hydrogel also showed a wet surface adhesion and antibacterial property. The hemostasis and wound-healing properties were evaluated in vivo using a mouse model. The results showed that hydrogel had the rapid hemostasis capacity and accelerated wound healing. In summary, KEC hydrogel may be excellent candidates as hemostasis materials for the wound dressing application.

Experimental Methods

The keratin was extracted from human hair fibers using a reported method with some modifications. KENs were synthesized using a simple one step approach. Briefly, 100 mL keratin solution (1 mg mL^{-1}) were slowly dripped into the 100 mL catechins solution (5 mg mL^{-1}). The mixture was stirred in dark place under nitrogen protection at 37℃. After 24 h, the products were collected by centrifugation and washed with water three times. The obtained KENs were lyophilized or re-dispersed in water and stored at 4°C.

KENs suspension (5%, w/w) were first prepared. Then sodium carboxymethyl cellulose was added into the KENs suspensions and KEC hydrogel was obtained. Then 300 mg sodium carboxymethyl cellulose was added into the 100 mL KENs suspension. After stirring for 2 h at room temperature, the KEC hydrogel was obtained and stored at 4°C.

Results and Discussion

SEM images demonstrated an observable increase in fibrin and blood cells deposition when clotting occurs in the presence of KENs (Figure 1). These results suggest that KEC have excellent property on clotting blood cells. Blood coagulation is the process that the coagulation factor is activated in a certain order, which eventually converts fibrinogen to fibrin. During coagulation process, fibrin monomers interconnect to form a fibrin polymer with a cross-network structure which insoluble in water under the action of thrombin. The fibrin network can trap blood cells and accelerate the formation of blood clots. It was reported that keratin had an effect on the formation of fibrin and the deposition of blood cells. This might be the reason that the KEC hydrogel made the blood clot easier to form in the presence of KENs.

In order to further investigate the efficacy of KEC hydrogel in promoting wound healing, a rat skin defect model was established. Using a disposable surgical biopsy instrument, a circular skin defect model with φ = 10 mm on the back of rats was taken as the experimental model. Experimental rats were divided into four groups, namely, blank control

group, cellulose group, keratin-cellulose mixture group(KC) and KEC group. Photos were taken at 0 and 28 days after surgery to observe the wound healing effect. H&E staining was performed on the skin of the injured rats at 7, 14 and 28 days to investigate the effect of tissue regeneration. Figure 2 shows the digital photograph of wound healing effect. According to the picture, the wounds in KEC group were smooth and healed completely within 28 days. Both the blank group and the cellulose group were not completely healed at 28 days, because the wound of the blank group was formed by the material deposition of blood and tissue fluid to form a scab, which prevented the exudation of tissue fluid and protected the wound.

While crusting also slows epithelial cell creep and slows wound healing. The results indicated that KEC had better moisturizing effect, reduced scab formation and promoted epithelial cell proliferation and creep. In addition, both keratin and catechin can promote tissue regeneration and accelerate tissue healing. The healing effect of KEC group was better than that of KC group and had no obvious scar. These results suggest that catechin molecules in KEC hydrogel have anti-inflammatory and antioxidant effects, which reduce inflammatory effects and speed up the inflammatory period. As can be seen from the figure 2, infiltration of some inflammatory cells can be observed at 7 days, but no inflammatory infiltration can be observed at 14 days, and a large number of cell proliferation and some epithelial tissue formation can be observed. At 21 days, regular epithelial cells have formed, indicating that the tissue has healed well.

Conclusion

The hydrogel incorporating nanoparticles might have potential applications for controlling bleeding and wound repairing.

References

1. R. C. de Guzman, J. M. Saul, M. D. Ellenburg, M. R. Merrill, H. B. Coan, T. L. Smith and M. E. Van Dyke, Biomaterials, 2013, 34, 1644–1656.

2. Z. Chen, C. Wang, J. Chen and X. Li, J. Am. Chem. Soc., 2013, 135, 4179–4182.

3. S. Xu, L. Sang, Y. Zhang, X. Wang and X. Li, Mater. Sci. Eng., C, 2013, 33, 648–655.

Acknowledgement

This work is supported by the National Key Program for Research and Development of China (No. 2016YFC1102700), the National Basic Research Program of China (No. 2012CB933600), National Natural Science Foundation of China (No. 31872750) and Sichuan Science and Technology Program Key Projects (No. 2017JY0018).

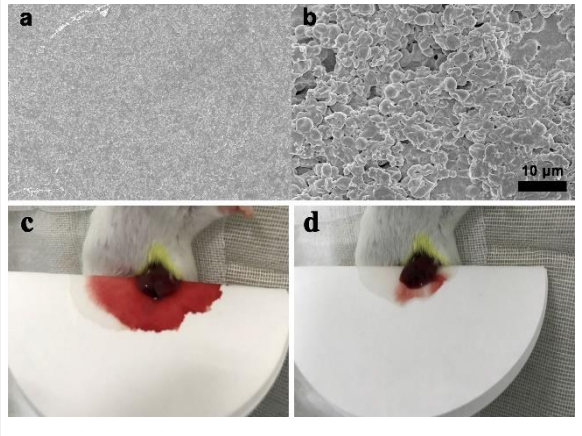

Figure 1. Hemostatic effect of KEC hydrogel.
(a) KEC hydrogel before blood clotting and (b) after blood clotting. Procedures for a liver model in a mouse model and evaluation of hemostatic ability of the control group(c) and KEC hydrogel(d).

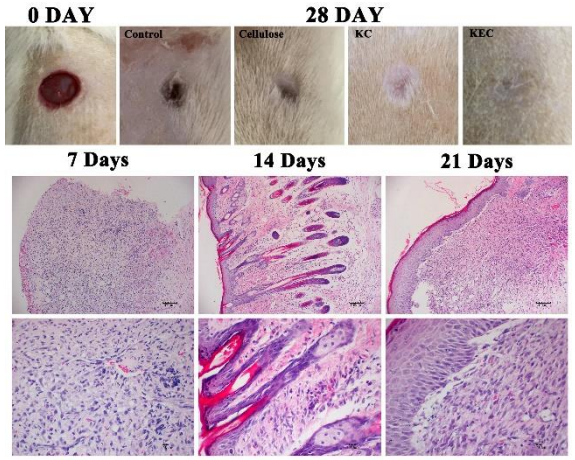

Figure 2. Skin healing effect.
Digital photos of skin defect model and skin wound healing of blank control group, cellulose group, KC group, and KEC hydrogel group for 0 day and 28 days treatment. H&E stained images of wound skin after treated with KEC-glue1.0% at 7 days, 14 days and 21 days.

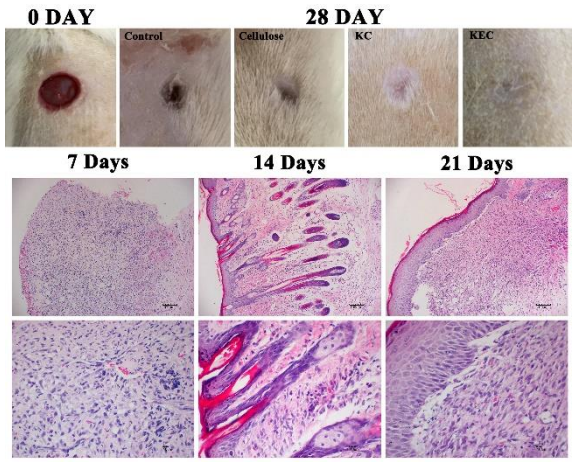

Figure 2. Skin healing effect.
(a)Digital photos of skin defect model and skin wound healing of blank control group, cellulose group, KC group, and KEC hydrogel group for 0 day and 28 days treatment. (b)H&E stained images of wound skin after treated with KEC-glue1.0% at 7 days, 14 days and 21 days.

PS2-03-296

Production and characterization of poly (lactic acid) membranes with addition of bioglass for guided bone regeneration

Nayara K. Moura[1], Rodrigo L. M. S. Oliveira[1], Eduardo F. Martins[1], Idália A. W. B. Siqueira[1], João Paulo B. Machado[2], Elisa Esposito[1], Fábio R. Passador[1], Eliandra S. Trichês[1]

[1]Federal University of São Paulo (UNIFESP), Science and Technology Institute (ICT), São José dos Campos, BR; [2]National Institute for Space Research (INPE), Associated Laboratory of Sensors and Materials (LABAS), São José dos Campos, BR

Introduction

Guided bone regeneration (GBR) is a technique well studied because of the benefits that it can provide. GBR is a technique that uses an occlusive membrane that physically prevents the entry of non-osteogenic cells into bone defects, favoring bone regeneration [1]. Polymeric membranes are commonly used in GBR, especially membranes made from biopolymers. Poly (lactic acid) (PLA) is widely studied for being biodegradable, biocompatible and easy to process [2,3,4]. Its degradation gives rise to monomers and oligomers of lactic acid, which are completely absorbed by the body.

The technique chosen to produce polymer membranes was solvent casting because it is a low-cost technique, use of relatively simple materials and equipment and easy reproducibility [5]. This technique makes it possible to obtain dense or porous films.

Modifications on the surface of the membrane allow it to have a porous surface, which facilitates cell deposition, adhesion and proliferation. The modification in the solvent cast technique with high humidity rate allows to obtain porous on surface [6].

The addition of bioglass (BG) in the polymer matrix promotes osteoinduction and osteoconduction properties, since the BG presents high bioactivity, which can crystallize hydroxyapatite a few hours after implantation. Bioglass® 45S5 composition with 45% SiO_2, 24.5% CaO, 24.5% Na_2O and 6.0% P_2O_5 (mol%) has become more widespread due to the ease of preparation and the high bioactivity present [7,8,9].

Experimental Methods

The BG was obtained by the fusion of SiO_2, CaO, Na_2O and P_2O_5, in the molar proportions of the formulation BG 45S5. The obtained BG was milled and characterized by XRD and SEM. The porous membrane of PLA with addition of 3 and 5% w/w of BG were obtained by solvent casting in controlled humidity method, dispersing BG in chloroform and solubilizing PLA. The solution was poured into molds for solvent evaporation under controlled humidity atmosphere. The membranes were characterized by XRD, SEM, DSC, biomineralization essay and diffusion agar test.

Results and Discussion

The BG obtained have irregular in shape and the particles are in micrometric scale (average size at 5.27 μm, with a bimodal particle size distribution (first peak in approximately 1.69 μm and second peak in 11.57 μm). XRD showed a halo between 2θ = 26º and 36º, characteristic presented by amorphous materials.

The membranes showed the formation of pores on their surface. The pore size increased with the addition of BG. XRD of the membranes showed the PLA peaks were identified, corresponding to the angles 2θ = 16.89°, 19.23° and 22.6° and the characteristic halo of BG remained present in PLA membranes incorporating BG.

The DSC showed that the addition of BG decreased the T_g values, increased the T_m values and their enthalpies of PLA fusion. A decrease in T_{cc} and an increase in the degree of PLA crystallinity were also observed.
XRD and SEM were used to evaluate the bioactivity of the PLA polymer membranes after the biomineralization assay. The BG inserted into the polymer matrix increases the amount of hydroxyapatite deposited on the surface of the porous membrane. The crystals deposited have irregular shape, sometimes also presented as acicular format.
The diffusion agar test showed that membranes with addition of BG have bacteriostatic properties.

Conclusion

The obtained bioglass by melting-quenching was successful, since an amorphous material with diffractogram corresponding to the literature was obtained. The solvent casting technique in controlled humidity resulted in a porous membrane. The incorporation of bioglass in the polymer matrix resulted in materials with superficial modifications and with modifications in their thermal profiles. The biomineralization test in SBF presented favorable results for the addition of bioglass, since the addition of BG had a direct influence on the deposition of hydroxyapatite on the membrane. The BG also have bacteriostatic properties, which may prevent infectious processes The composite produced presented the proposed properties such as surface porosity and ability to promote osteoinduction, and this material was then applicable to ROG.

References

[1] Ratner, et al. **Biomaterials Science: An Introduction to Materials in Medicine.** Canadá: Elsevier, 2013.
[2] JAHNO, V.D. **Síntese e Caracterização do Poli (L-ácido lactico) para uso como biomaterial.** Dissertação de Mestrado, Universidade Federal do Rio Grande do Sul, 2005.
[3] GUPTA, A. P., KUMAR, V. New emerging trends in synthetic biodegradable polymers Polylactide: A critique. **European Polymer Journal**, v.43, p. 4053–4074, 2007.
[4] FRANCHETTI, S. M. M., MARCONATO, J.C. Polímeros biodegradáveis – uma solução parcial para diminuir a quantidade dos resíduos plásticos. **Química Nova**, v. 29, p. 811-816, 2006.
[5] STRIBECK, N., SMARSLY, B. **Scattering Methods and the Properties of Polymer Materials.** Alemanha. Springer Berlin Heidelberg, 2005.
[6] SIQUEIRA, I.A.W.B. **Desenvolvimento de Membranas Porosas à Base de PDLLA/Nanotubos de Carbono: nHAp para Regeneração Óssea.** Tese de Doutorado, Universidade do Vale do Paraíba, 2015.
[7] HENCH, L.L.; ETHRIDGE, E.C., **Biomaterials: an interfacial approach**, New York, Academic Press, 1982.
[8] STROGANOVA, et al., Glass-Based Biomaterials: Present and Future (A Review). **Glass and Ceramics**, v. 60, p. 315-319, 2003
[9] TILOCCA, A., Structural models of bioactive glasses from molecular dynamics simulations. Proceedings of the Royal Society A: Mathematical, **Physical and Engineering Sciences,** v. 465, p. 1003-1021, 2009.

Acknowledgement

To National Council for Scientific and Technological Development (CNPq) and Foundation for Research Support of the State of São Paulo (FAPESP), for Project Financing; to Federal University of São Paulo (UNIFESP) and National Institute for Space Research (INPE), by the structure offered.

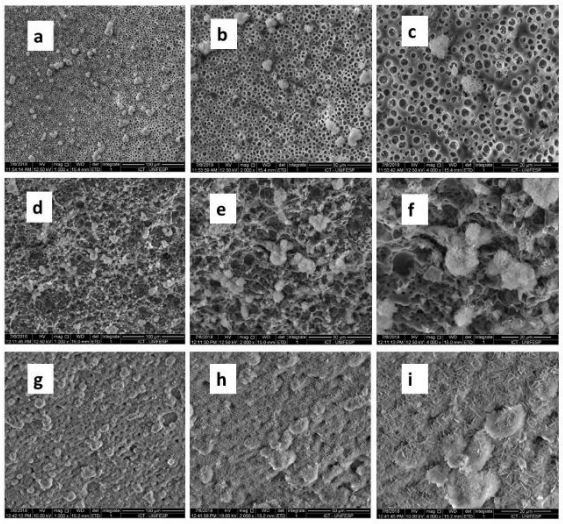

SEM of porous membranes after biomineralization essay, with different magnitudes.
SEM of the polymer membranes of PLA (a,b,c), PLA + 3% BG (d,e,f) and PLA + 5% BG after biomineralization essay.

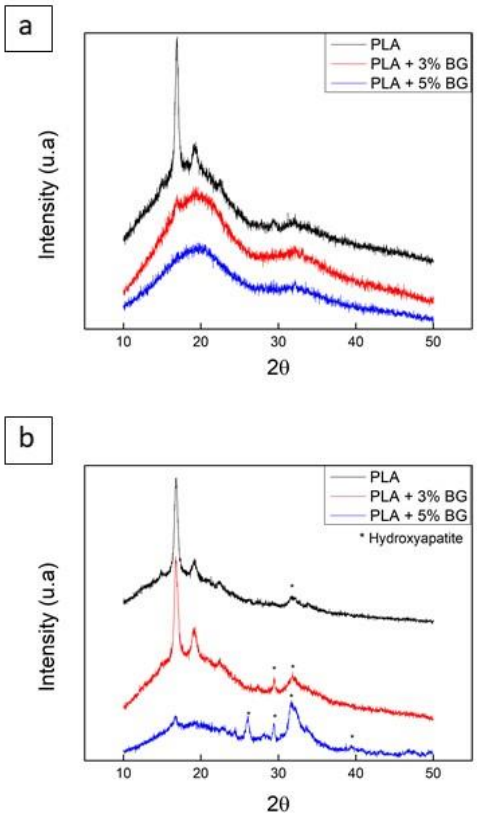

XRD of porous membranes, before and after biomineralization essay
XRD of a) PLA membrane, PLA + 3% BG membrane and PLA + 5% BG membrane; b) PLA membrane, PLA + 3% BG membrane and PLA + 5% BG membrane after biomineralization essay, including HAp peaks.

PS2-03-297

Composite materials based on hydroxyapatite and biodegradable polyesters

Yelena Shapovalova[1], Daria Lytkina[1], Lothar Heinrich[2], Irina Kurzina[1]

[1]National Research Tomsk State University, Tomsk, RU; [2]University of Münster, Münster, DE

Introduction

Currently under development and research of materials for the restoration of bone tissue. One direction is the development of composite materials based on hydroxyapatite (HA) and polyesters such as polylactic acid (PLA) and copolymer of lactide and glycolide (PLGA). Often the available research does not provide an answer to the question - which component in such materials is primary. The purpose of this work is a comparative analysis of two composite materials developed on the basis of the Tomsk State University.

Experimental Methods

Two types of composite materials with different compositions and structures were obtained. The first type is PLA fibers filled with dispersed HA [1], the second type is porous hydroxyapatite ceramics impregnated with PLGA [2].

Results and Discussion

Composite material PLA/HA 70/30 was found to have the highest surface energy value (52.18 mJ/m2), and roughness parameter Ra (4.21 μm) compared to other type 1 composites (Fig.1). Along with this, it was found that in type 2 materials (Fig. 1) PLGA/HA 95/5 has the highest surface energy among composites, which is associated with a high concentration of phase boundary on the surface as a result of the island coating of the sample with polymer, roughness, however, it changes linearly with increasing amounts of PLGA in samples.

Macrophages provide an immediate response to the penetration of a foreign object into the body, they are one of the key cells of the innate immunity system, participate in the launch and implementation of reactions of the acquired immunity system. Therefore macrophage test systems were used to study the biocompatibility of materials. The evaluation of the viability of monocyte macrophages of 3 individual human donors after 6 days of cultivation of cells on the surface of polylactide and type 1 composite material showed that the level of metabolic activity of macrophages in the presence of both PLA and PLA/HA = 70/30 is comparable to the control. Cells cultured on plastics were used as controls. Thus, the studied materials do not adversely affect macrophages. The level of metabolic activity of macrophages when seeding on samples PLGA/HA 95/5 and PLGA/HA 93/7 is comparable to the control. When seeding on the surface of HA, there is a low cell viability. This fact may be associated with high surface energy of HA. On the other hand, cells seeded in samples with PLGA/HA 83/17 show low viability. From the obtained data it can be concluded that there is an optimal range of surface energy values that favorably affect the viability of materials. The most average value is characterized by material PLGA/HA 93/7. Despite the fact that pure HA has pronounced cytotoxic properties, the addition of PLGA can significantly reduce the value of surface energy to change the adhesion characteristics and increase the viability of cells on the surface of composite materials.

Conclusion

In each series of samples, the ratio of components was determined, which is characterized by the most optimal physicochemical characteristics and minimal negative influence on the viability level of macrophages. The obtained

experimental data can be successfully implemented in the preparation of bioactive, biocompatible composite materials based on polylactide and hydroxyapatite, followed by application in various fields of medicine to create materials for implantation.

References

1.

Structural-phase state and surface properties of composite materials based on polylactide and hydroxyapatite / V. A. Syusyukina, Y. G. Shapovalova, N. M. Korotchenko, I. A. Kurzina // Russian journal of applied chemistry. 2017. Vol. 90, № 1. P. 106-112.

2.

RU2669554 Lytkina D.N., Berezovskaya A.A., Kurzina I.A., Korotchenko N.M., Kozik V.V. Method for producing biodegradable composite materials with open porosity for bone tissue recovery, Date of publication: 12.10.2018, Bull. № 29

Sample	σ^D, mJ/m^2	σ^P, mJ/m^2	σ, mJ/m^2	Ra, μm
Type 1				
PL	15,39±0,31	13,74±0,30	29,13±0,61	7,56±0,50
PL/HA 90/10	3,28±0,38	27,66±1,21	30,94±1,59	2,65±0,18
PL/HA 80/20	1,91±0,10	35,97±0,37	37,88±0,47	2,39±0,20
PL/HA 70/30	0,18±0,09	52,00±1,34	52,18±1,43	4,21±0,39
PL/HA 60/40	10,89±1,31	33,31±1,76	44,20±3,07	3,31±0,15
HA	13,15±9,00	61,20±22,88	74,35±31,88	1,27±0,10
Type 2				
PLGA	21 ± 1	22 ± 1	43 ± 3	7,24 ± 1,00
PLGA/HA 95/5	1 ± 1	28 ± 1	29 ± 1	1,22 ± 0,35
PLGA/HA 93/7	0,14 ± 0,1	42 ± 2	42 ± 2	2,16 ± 0,30
PLGA/HA 87/13	15 ± 1	11 ± 0,78	27 ± 2	6,34 ± 1,20

Figure 1. Surface energy and roughness of material samples

2:45 p.m. – 3:45 p.m.

Hall 1 / Exhibition Area

PS2-04 | Textile and fibre-based biomaterials

PS2-04-298

Influence of fluorination and sterilisation on the mechanical properties of polylactide and poly(lactid-co-ε-caprolactone) thread materials for use in ligament tissue engineering

Judith Hahn[1], Michaela Schröpfer[2], Harald Brünig[1], Michael Meyer[2], Annette Breier[1]

[1]Leibniz-Institut für Polymerforschung Dresden e. V., Department of Mechanics and Composite Materials, Dresden, DE; [2]Forschungsinstitut für Leder und Kunststoffbahnen FILK gGmbH, Department of Applied Collagen Research, Freiberg, DE; [3]Paracelsus Medical University Salzburg and Nuremberg, Institute of Anatomy, Nuremberg, DE

Introduction

In the field of knee injuries mostly accompanied by ruptures of the anterior cruciate ligament (ACL) the current standard therapy is the use of autologous tissue, whereby the majority of surgeons could imagine a tissue engineering solution, if the mechanical and cell biological requirements of the used cell carriers (scaffold) were met.

Tissue engineering strategies for ligament reconstruction increasingly focusing on cell carriers made of polymer materials like polylactide and its copolymers. Essential requirements are a suitable mechanical behaviour of the polymer based cell carriers comparable to autologous ligament tissue [1] and a sufficient cell behavior (cell adhesion and proliferation) on the polymer surfaces [2]. Therefore, an adequate surface functionalization e.g. by fluorination as well as an appropriate sterilization method for highly porous constructs are needed.

Experimental Methods

Two different thread materials, a monofilament suture thread made of poly(lactic-co-ε-caprolactone) (**P(LA-CL)**, L-lactic/ε-caprolactone 75:25, suture monofilament from Gunze Ltd. (Japan), USP 7-0, supplier Catgut) and a melt spun multifilament made of polylactic acid (**PLA**, 2% of D-Lactic acid, pellets from NatureWorks LLC (USA), multifilament consisting of six filaments, melt spun at IPF, Tt=100 dtex), were prepared as thread loops with 1000 mm length. The thread loops were bound together with a polyester thread for better handling during the subsequent processes. The desizing of the thread material surfaces was performed by washing in *n*-heptane three times and dried on air.

Fluorination was realized at the FILK in a fluorination batch reactor by Fa. Fluor-Technik-System. Fluorination was performed in an mixture of 10% fluorine gas in air for 60 seconds.

Afterwards, the samples were sterilized with ethanol (EtOH, 30 min., 70%) or ethylene oxide gas (EO, DMB Apparatebau GmbH). The mechanical properties were characterized by using a tensile testing machine (Zwick/Roell Z 0.5, 20 N load sensor, 50 mm/s test speed, 50 mm gauge length) controlled with the TestXpert software (Zwick/Roell, Germany). Changes of the polymer surfaces were investigated by SEM (Philips ESEM XL 30, Germany).

Results and Discussion

No significant changes of the mechanical behaviour were observed after desizing both materials. There was no influence detectable after fluorination of PLA whereas for desized P(LA-CL) the ultimate tensile load and elongation significantly decreased. After sterilization of both materials with EtOH for 30 minutes the load-elongation behaviour changed by reducing the yield strength whether the samples were previously desized or fluorinated. Furthermore, the ultimate tensile elongation significantly decreased for P(LA-CL) after EtOH sterilization regardless of whether the

thread was previously desized, fluorinated or treated with both surface procedures. The ultimate tensile elongation significantly increased for not fluorinated PLA after EtOH sterilization whereas a decreased ultimate tensile load and elongation were detected for desized and fluorinated PLA. After sterilization with EO the ultimate tensile load and elongation decreased for P(LA-CL) (no significance). In contrast, the ultimate tensile elongation significantly increased for PLA and no changes could be detected for the ultimate tensile load.
A sterilization with EtOH seems disadvantageous for PLA and P(LA-CL) due to significant changes of the mechanical properties like a reduction of the elastic deformation range (Fig. 1, 2). In current work it should be clarified to what extent the EO sterilization process can be changed to make it as gentle as possible for the polymer materials.

Conclusion

Care must be taken to changes of the mechanical behaviour when choosing a suitable surface functionalization and sterilization method for polymer materials. Both materials, PLA and P(LA-CL), could be functionalized with 10% fluorination and sterilized with ethylene oxide gas to act as potential materials for the fabrication of ligament scaffolds [3].

References

[1] J. Hahner et al. Textile Research Journal 85, 1431-1444 (2015).
[2] M. Hoyer et al. Materials Science & Engineering C, Materials for Biological Applications 43, 290-299 (2014).
[3] A. Breier et al. GAK 71, 582-587 (2018).

Acknowledgement

We acknowledge the funding of this project by the Deutsche Forschungsgemeinschaft (DFG).

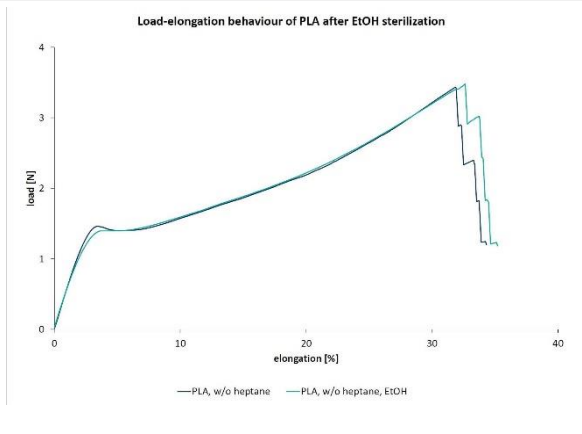

Figure 1
Load-elongation behaviour of PLA with (w/) and without (w/o) heptan desizing after EtOH sterilization

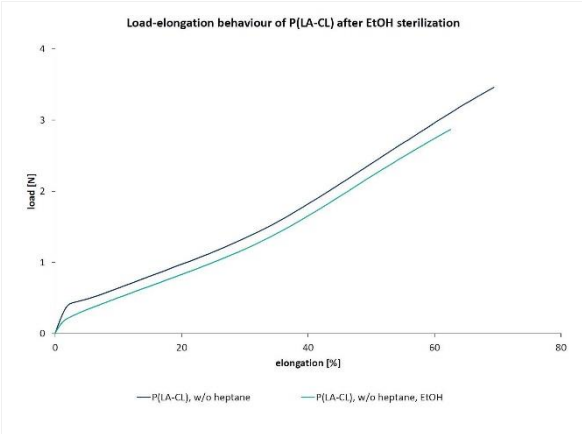

Figure 2
Load-elongation behaviour of P(LA-CL) with (w/) and without (w/o) heptane desizing after EtOH sterilization

PS2-04-299

Chondrocyte incorporation onto electrospun scaffolds for cartilage tissue engineering

Angela Semitela[1], Gonçalo Ramalho[1], Cátia Sousa[2], Soraia Silva[2], Alexandrina Mendes[2], Paula A. A. P. Marques[1], António Completo[1]

[1]University of Aveiro, Centre of Mechanical Technology and Automation (TEMA), Department of Mechanical Engineering, Aveiro, PT; [2]University of Coimbra, Center for Neuroscience and Cell Biology, Coimbra, PT

Introduction

Cell incorporation onto three-dimensional (3D) biocompatible scaffolds is a crucial step to obtain functional tissue-engineered cartilage. The efficacy of the use of scaffolds depends on their ability to interact with cells, which begins with the incorporation process [1]. Several seeding techniques have been successfully on uniformly incorporating cells through the scaffolds [2], however those cannot be applied for electrospun scaffolds. The characteristic small pore size of these structures prevents cell infiltration, relegating tissue formation to the surface. Several methodologies have been reported to increase pore size of the electrospun scaffolds using sacrificial materials, but these manipulations generally led to degradation of the scaffold final mechanical properties [3,4]. Cellular integration during the scaffolds construction by electrospinning can be a suitable approach to develop functional tissue constructs, using electrospraying technology. Cell electrospraying, a concept first introduced in 2005 by Jayasinghe, enables the deposition of living cells onto specific targets by exposing the cell suspension to an external high intensity electric field [5,6]. Several cell types have been electrosprayed and survived with no significant influence on a genetic, genomic and physiological level [7]. Here, the preliminary combination of polymer electrospinning with cell electrospraying was performed, in an attempt to overcome the challenges of cell infiltration into electrospun scaffolds for cartilage tissue engineering.

Experimental Methods

First, several chondrocyte electrospraying experiments were performed to access the optimal electrospraying conditions, by varying the voltage, flow rate, needle to collector distance and needle gauge. Then, using the selected parameters, the preliminary association of chondrocyte electrospraying with polymer electrospinning was performed alternating the two technologies. The polymer selected here was the blend of polycaprolactone (PCL) and gelatin, already reported as beneficial for cartilage repair purposes [8,9]. The prepared scaffolds were then cultured for 7 days and the respective cell viability assessed. The percentage of viability was calculated as a ratio of the metabolic activity of the electrosprayed chondrocytes incorporated within the scaffolds and the metabolic activity of the same number of chondrocytes cultured on the tissue culture polystyrene on the first time point. The chondrocyte distribution was also evaluated by immunocytochemistry of the nuclei and actin filaments.

Results and Discussion

Post-electrosprayed chondrocytes viabilities were considerably high (> 80%), particularly at low needle to collector distances, confirming that the electrospraying process did not significantly influenced chondrocyte function. At higher working distances, cell loss may occur within the electrospraying chamber, resulting in decreased cell viability. The combination of both technologies was accomplished, by alternating between PCL and gelatin electrospinning and chondrocyte electrospraying. It was possible to incorporate the chondrocytes within the electrospun PCL and gelatin

layers, with an apparently uniform cell distribution through the scaffolds. The presence of gelatin on the scaffolds allowed for a rapid cell attachment and proliferation, due to the presence of cell recognition domains (RGD) [8]. A partial dissolution of gelatin might also have occurred, resulting in an enhanced pore size for cell migration [9].

Conclusion

It is possible to infer that a considerable number of chondrocytes were able to survive to the electrospraying process. The successful cellular integration onto the electrospun scaffolds confirmed that this technique can a promising alternative for cell incorporation into the 3D scaffolds during its electrospinning.

References

[1] D. I. Braghirolli et al, Int. J. Nanomedicine, 2015, 10, 5159–5170.
[2] G. A. Villalona et al, Tissue Eng. Part B Rev., 2010, 16, 341–350.
[3] B. M. Baker et al, Biomaterials, 2008, 29, 2348–2358.
[4] K. Wang et al, J. Biomed. Nanotechnol., 2014, 10, 1–11.
[5] S. N. Jayasinghe et al, Biotechnol. J., 2006, 1, 86–94.
[6] S. N. Jayasinghe et al, Lab Chip, 2006, 6, 1086–1090.
[7] S. N. Jayasinghe, Analyst, 2013, 138, 2215.
[8] R. Zheng et al, Biomaterials, 2014, 35, 152–164.
[9] Y. Zhang et al, J. Biomed. Mater. Res. - Part B Appl. Biomater., 2005, 72, 156–165.

Acknowledgement

This work was supported by the Portuguese funding of Program COMPETE-FEDER, Programa Operacional Competitividade e Internacionalização through the projects POCI-01-0145-FEDER-028424 and CENTRO-01-0145-FEDER-022083. Also, by Fundação para a Ciência e Tecnologia I.P. (FCT, IP) through the projects PTDC/EMSTEC/3263/2014, IF/00917/2013/CP1162/CT0016 and UID/EMS/00481/2013. The authors thank to FCT for the PhD grant SFRH/BD/133129/2017.

PS2-04-300

Incorporation of Hyaluronic Acid into Electrospun Thermoplastic Urethane Membranes for Tissue Engineering Applications

Thomas Schneiders[1], Magnus Kruse[1], Laura Kreinest[1], Petra Mela[2], Thomas Gries[1], Stefan Jockenhoevel[2], Andreas Blaeser[1], Benedict Bauer[1]

[1]RWTH Aachen University, Institut für Textiltechnik, Aachen, DE; [2]RWTH Aachen University, Department of Biohybrid and Medical Textiles (BioTex)/ AME-Helmholtz Institute for Biomedical Engineering, Aachen, DE

Introduction

Electrospinning is a popular technique to fabricate submicron-sized fibers and nonwovens for fibrous scaffolds. Due to the micro and nano scale of the fibers, the structure mimics properties of extracellular matrix, thus enabling cell migration into the scaffolds. Improved cell migration and higher specific surface area compared to regular fibers are reasons electrospun fibers are successfully used in fields like tissue engineering, biomedical and pharmaceutical applications.[1]- Aim of the presented study is the development of a stable elctrospinning process for fabricating membranes out of thermoplastic polyurethane (TPU) and hyaluronic acid (HA). Benefit of a TPU/HA membrane is the improved hydrophilicity and cell viability compared to a pure TPU membrane.

Experimental Methods

In the presented study TPU/HA membranes were produced in an electrospinning process. The two polymers were processed with two separate nozzels. TPU was electrospun from a chloroform/methanol solution, HA is electroblown from an aqueous solution using a coaxial nozzle. Pressurized and heated air from the outer nozzle supports the forming of nanosized HA particles. Hyaluronic acids with molecular weights from 90-1500 kDa in different combinations were used in the electroblowing process. Fourier-transform infrared spectroscopy (FTIR) was used to detect the existence of HA in the membranes and contact angle measurements were conducted to verify an effect of the incorporated HA on hydrophilicity compared to TPU membranes. In the next fabrication step the membranes were plasma treated to cross-link the HA particles in the TPU fibers and decrease the solubility of HA. Plasma treatment was carried out with an argon plasma for 5 minutes and 0,2 bar. Subsequently the solubility of HA was tested in a washing test. 5 mg samples of the membrane were placed in 50 ml of distilled water and put into an oven at 37°C for 30 minutes to 48 days. Samples were weighed before the test and after washing following a drying step. The measured weight difference indicated the amount of dissolved, non-crosslinked HA. Finally, the cytocompatibility and impact of HA incorporation on cell adhesion was studied. Myofibroblasts were cultured for 4 days on samples with different types of hyaluronic acid. Cell morphology and viability were tested using live/dead staining.

Results and Discussion

FTIR showed the existence HA in the membranes after electroblowing HA in the process compared to the TPU membranes. Further contact angle measurements showed a decrease from 108° ± 0.8° (pure TPU membranes) to 83° ± 1° (TPU/HA membranes). The mass loss detected after washing and drying the membranes was higher for the untreated membranes than for the plasma treated membranes. Lower mass loss for the plasma treated membranes indicated a positive effect of the functionalization on crosslinking between HA and TPU. Finally, fluorescence microscopy analysis revealed superior cell viability and proliferation for TPU/HA membranes compared to pure TPU

membranes. Highest myofibroblasts viability and proliferation rate were obtained for a combination of low (90-130 kDa), mid (500-750 kDa) and high (1250-1500 kDa) grade HA.

Conclusion

In the future the TPU/HA-membranes could be used for tissue engineering applications, due to the improved hydrophilicity and cell viability.

References

[1] Bermeister H, Seyidova N, Schreiber C, *et al*. Biodegradable, thermoplastic polyurethane grafts for smaller diameter vascular replacements [J] *Acta Biomaterialia,* 2015, **11:** 104-113.

Acknowledgement

This project was funded by the european regional development fond (ERDF).

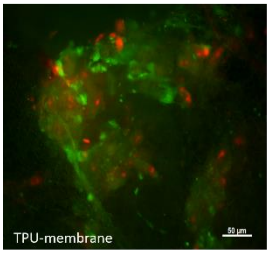

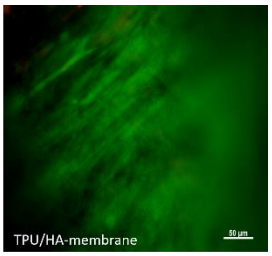

Cell Viability on TPU Membranes compared to TPU/HA Membranes
Live/Dead cell viability assay, comparison between pure TPU-membrane and a TPU/HA-membrane; Green are viable cells, red are dead cells

PS2-04-301

Biomimetic collagen filaments from high purity collagen for regenerative medicine

Robert Tonndorf, Dilbar Aibibu, Chokri Cherif

Technische Universität Dresden, Institut für Textilmaschinen und Textile Hochleistungswerkstofftechnik, Dresden, DE

Introduction

Collagen filaments [1–6] may be fabricated into fiber based scaffolds highly suitable for tissue engineering applications, as such scaffolds feature a high surface-to-volume area, a well-defined fiber structure, and are made of a substance found in the extracellular matrix. Despite its benefits for textile processing collagen multifilament yarns are not available so far. Hence, in here a collagen multifilament wet-spinning method is proposed and described.

Experimental Methods

The acid-soluble Collagen MDP was purchased from GfN Herstellung von Naturextrakten GmbH (Wald-Michelbach, Germany). The spinning dope was prepared by dissolving the collagen to yield a collagen concentration of 2 wt. %. The coagulation medium was based on polyethylene glycol and sodium phosphate and prepared according to the literature [3].

Collagen multifilament yarns were produced on a laboratory wet spinning line, which consisted of a specially-designed spin pack comprised of several coaxial nozzles. The spinning dope was flowing through the core and the coagulation medium through the sheath of the coaxial nozzles. Coagulation was achieved by collagen self-assembly within an extended coagulation section; subsequently the yarn comprised of several collagen filaments was wound on a spool. Optionally the yarns were crosslinked in-line by glutaraldehyde or by a combination of UV radiation with riboflavin.

Results and Discussion

The applied collagen formed 6 well resolved bands as a result of SDS-PAGE (Figure 1) and was identified as type I/III by mass spectrometric analysis. Wet spun yarns were analyzed regarding their mechanical, thermal and structural properties. Results indicated a tensile strength of 12 cN/tex (dry) and 3 cN/tex (wet) and thermal stability up to 110 °C (dry) and 80 °C (wet) for glutaraldehyde crosslinked yarns. Scanning electron microscopy images revealed a hierarchical topography of the filaments, wherein the filaments cross section extended over a distance of approx. 80 µm. Furthermore, filaments were composed of several rod-like bundles (between 5 and 10) each having a diameter of approx. 20 µm and bundles were composed of an anisotropic network aligned along the fiber axis, which was composed of countless rod-like structures having a diameter as low as 100 nm (Figure 2).

Conclusion

On the basis of the thermal and mechanical analyses, it could be concluded that collagen filaments can be successfully manufactured by wet spinning. The applied spinning technology is suitable for a scalable production of collagen multifilament yarns. The availability of collagen multifilament yarns enables and eases the fabrication of collagen fiber based scaffolds by textile manufacturing processes.

References

[1] Kato YP, Silver FH. Formation of continuous collagen fibres: Evaluation of biocompatibilily and mechanical properties. *Biomaterials* 1990; 11: 169–175.

[2] Cavallaro JF, Kemp PD, Kraus KH. Collagen fabrics as biomaterials. *Biotechnol Bioeng* 1994; 43: 781–791.

[3] Caves JM, Kumar VA, Wen J, et al. Fibrillogenesis in continuously spun synthetic collagen fiber. *J Biomed Mater Res B Appl Biomater* 2009; 93: 24–38.

[4] Yaari A, Schilt Y, Tamburu C, et al. Wet Spinning and Drawing of Human Recombinant Collagen. *ACS Biomater Sci Eng* 2016; 2: 349–360.

[5] Haynl C, Hofmann E, Pawar K, et al. Microfluidics-Produced Collagen Fibers Show Extraordinary Mechanical Properties. *Nano Lett* 2016; 16: 5917–5922.

[6] Tonndorf R, Gossla E, Aibibu D, et al. Wet spinning and riboflavin crosslinking of collagen type I/III filaments. *Biomed Mater*. Epub ahead of print 26 October 2018.

Acknowledgement

The authors are grateful to Lina Piersig, Lisa Mindergasov, Victoria Siebler (Martin-Andersen-Nexö-Gymnasium) for their support in collagen wet spinning and Simone Hempel (Institute of Construction Materials of TU Dresden) for scanning electron microscopy analysis. The overall work was financially supported within the program “The Central Innovation Programme for SMEs” (project number: ZF4008306AW6) from funds of the Federal Ministry for Economic Affairs and Energy (BMWi).

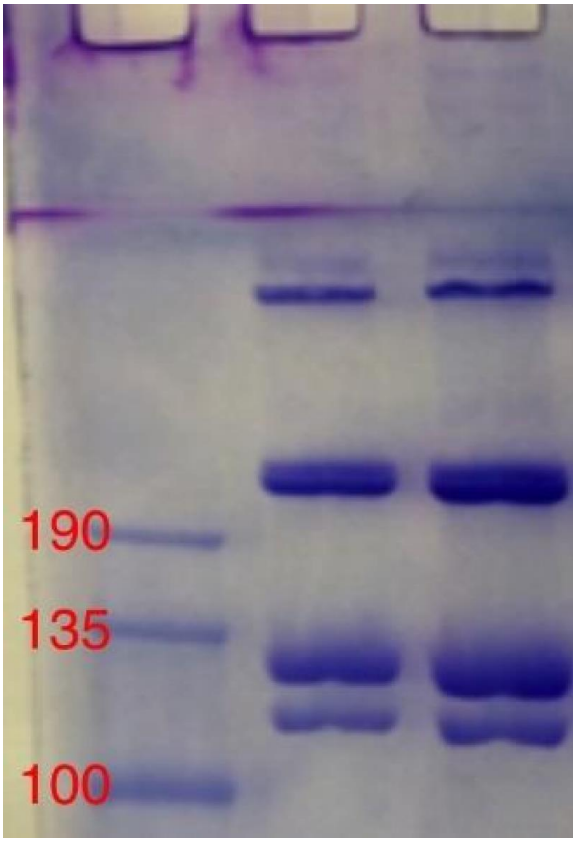

Figure 1
Photograph of SDS-gel electrophoresis showing a pattern of a molecular weight marker in kDa in lane 1 and of the applied collagen in lane 2 and 3

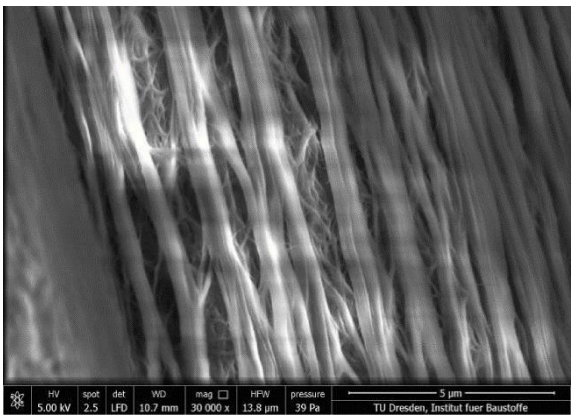

Figure 2
Scanning electron microscopy image the surface structure of wet-spun collagen filaments

PS2-04-302

Bioresorbable Sol-Gel-Derived Endless Fibers and Their Potential as a Bioactive Scaffold Material in Regenerative Therapies

Bastian Christ[1], Tobias Weigel[2], Marvin Kaiser[1], Walther Glaubitt[1], Sofia Dembski[1,2], Jörn Probst[1]

[1]Fraunhofer ISC, Translational Center Regenerative Therapies TLC-RT, Würzburg, DE; [2]University Hospital Würzburg, Department Tissue Engineering and Regenerative Medicine, Würzburg, DE

Introduction

For many years, silica as well as titania are well established biomaterials, especially as coating materials for bone implants (e. g. hip joints or tooth implants).[1,2] Within the last years inorganic materials are also introduced into the therapy of soft tissue.[3] One example is a polymeric mesh implant coated with titania for hernia repair to improve biocompatibility.[4] Next to coatings inorganic oxidic materials are known as a bioresorbable bulk material. A special formulation of a silica gel resulted in a CE-approved bioresorbable fleece out of microfibers for the healing of chronic wounds (diabetic ulcer, 2nd degree burns).[5] The release of *o*-silicic acid while fiber resorption promotes an anti-inflammatory wound healing[6] and the nanostructured fiber surface enhances the directed movement of cells[7].
Here, the authors present further developments in the fabrication of silica and titania fibers to open up new perspectives in therapies as a regenerative implant and a scaffold for in-vivo tissue engineering.

Experimental Methods

Spin sols are produced by hydrolysis and condensation reactions using the liquid precursors tetraethoxysilane and/or titanium(IV) ethoxide. By the techniques of dry spinning and electrospinning sol-gel-derived fibers of different diameters are obtained. Fiber degradation studies are performed under physiological conditions and the degradation products are identified by chromatography and NMR spectroscopy. Additionally, the fibrous materials are tested for biocompatibility referring to DIN ISO 10993-5 with human fibroblasts, as well are used as a scaffold material in tissue engineering.

Results and Discussion

In sol synthesis, a precise control of the hydrolysis and condensation rate is mandatory to result in a spinnable sol. As the fiber diameter is mainly dependent on the spinning technique, the fibers' property profile is influenced by many factors. Here, mainly the resorption rate and the flexibility of the fibers is affected by the sol composition as well as the spinning parameters (pressure, viscosity, temperature etc.). A fine-tuning of all these parameters results in non-cytotoxic endless fibers referring to DIN ISO 10993-5. After the characterization of the resorption rate of the fibers and the identification of the degradation products, these pre-tested materials are processed to an open porous fiber fleece and evaluated as a new resorbable scaffold material in tissue engineering of human tissue.

Conclusion

In this work the authors present the synthesis and fabrication of novel sol-gel-derived silica and titania fibers and its influence of different spinning parameters on the resorption rate and flexibility of the resulting fibers. Fabricated to a fiber fleece with optimized mesh sizes and degradation behaviour, the fibrous hybrid material shows high potential as a novel inorganic and open porous scaffold material in tissue engineering and in regenerative therapies.

References

1. Textor M. *et al.*, in Titanium in Medicine, Springer Berlin Heidelberg, 171-230, 2001.
2. Arcos D., Vallet-Regí M., Acta Biomaterialia. 6:2874-2888, 2010.
3. Miguez-Pacheco M., Hench L.L., Boccaccini A.R., Acta Biomaterialia. 13:1-15, 2015.
4. Köckerling F., Schug-Pass C., Hernia. 18:445–457, 2014.
5. Brown A. *et al.*, Eur. J. Dermatol. 24:210-6, 2014.
6. Grotheer V. *et al.*, Biomaterials. 34:7314-7327, 2013.
7. Emmert, M., Witzel P., Rothenburger-Glaubitt M., Heinrich D., RSC Adv. 7:5708-5714, 2017.

Acknowledgement

This work was supported by Fraunhofer Internal Programs under Grant No. Discover 610 143 and MAVO 640 018.

PS2-04-303

Role of the composition of electrospun membranes based on aliphatic co-polyesters on drug delivery thereof

Maria Herrero-Herrero[1], Rubén Martín-Cabezuelo[1], Ana Vallés-Lluch[1,2], José A. Gómez-Tejedor[1,2]

[1]Universitat Politècnica de València, Centre for Biomaterials and Tissue Engineering (CBIT), Valencia, ES; [2]Biomedical Research Networking Centre in Bioengineering, Biomaterials and Nanomedicine (CIBER-BBN), Valencia, ES

Introduction

Electrospinning is a widely used method to obtain nanofibrous membranes as drug delivery systems. Moreover, these membranes can simultaneously be used as cell supports to improve cell viability or induce cell differentiation by means of the molecules released thereof.

In that respect, electrospun membranes of two co-polymers of polyglycolic acid (PGA), with lactic acid, P(LA-co-GA) and caprolactone, P(CL-co-PGA), were compared to study the influence of their different chemical composition on their drug delivery profiles.

The procedure to electrospin P(LA-co-GA) has already been reported elsewhere. This work is, thus, first focused on the development of the procedure to electrospin alike P(CL-co-GA) membranes. Next, the membranes are thoroughly characterized to reveal the role their different hydrophilicity, crystallinity, mechanical properties and biodegradability play on their biological behavior.

Experimental Methods

A solution of P(CL-co-GA) was prepared by mixing different amounts of the co-polymer (10% wt/v to 30% wt/v) with chloroform. To facilitate its electrospun, an addition of pyridine was necessary (10% v/v to 20% v/v). The solution was electrospun in a homemade electrospinning device, modifying the main electrospinning parameters (voltage, flow rate, and distance needle to collector). These membranes (figure 1) were analysed by Scanning Electron Microscope (SEM) to determine the diameter of the fibres. Next, a comparative study of the properties of the electrospinning solutions of both co-polymers (viscosity, conductivity, surface tension) and the electrospun membranes (swelling, DSC, tensile tests, biodegradation tests) was performed. Then, 10% wt/v of curcumin was added to the polymer solutions to electrospin and its loading and release profile were followed by UV spectroscopy.

Results and Discussion

Electrospun membranes of P(CL-co-GA) were successfully obtained for the first time, and next compared with P(LA-co-GA) counterparts. Whilst sharing their microstructure (mean fibre diameter slightly above 1 µm) and hydrolysable functional groups, they showed relevant differences in terms of hydrophilicity, thermal properties and mechanical behaviour, which lead to different curcumin release profiles.

Conclusion

Suitable membranes to drug delivery were performed by aliphatic co-polyesters (P(LA-co-GA) and P(CL-co-GA)). These membranes can be appropriated as cell supports.

Acknowledgement

The authors acknowledge Spanish Ministerio de Economía y Competitividad through DPI2015-65401-C3-2-R project and A.V.-Ll. acknowledges the support of the Generalitat Valenciana, Conselleria de Educación, Investigación, Cultura y Deporte through projects AEST/2017/018 and AEST/2018/014.

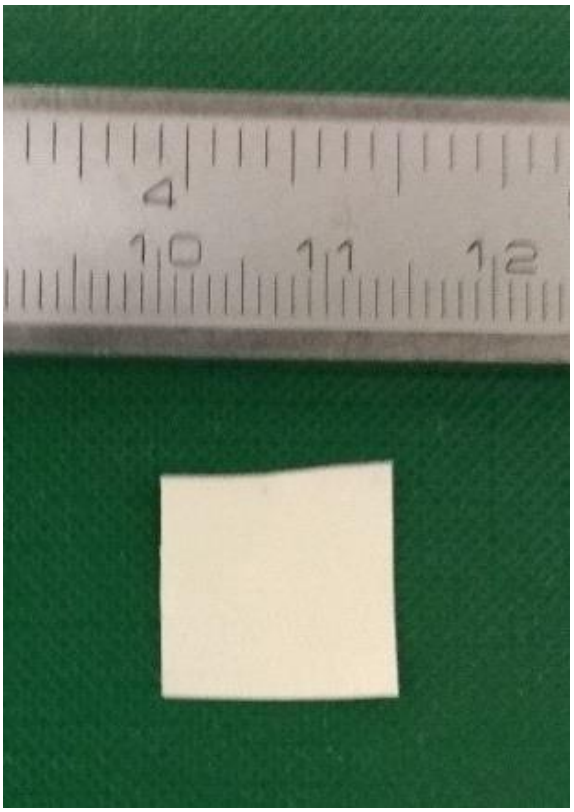

Figure 1. Aspect of the electrospun membrane of P(CL-co-GA).

PS2-04-304

Evaluation of a Self-Constructed Diffusion Chamber System Designed for the Determination of the Permeability of Collagen Barriers in Three-Dimensional Textile ACL-Scaffolds

Annette Breier, Fernanda A. Vechietti, Christiane Gäbel, Sebastian Hillig

Leibniz-Institut für Polymerforschung Dresden e. V., Mechanik und Verbundwerkstoffe, Dresden, DE

Introduction

A surgical approach to reconstruct the joint function after ligament rupture could be the application of a tissue engineered entity, including the three tissue domains bone, enthesis and ligament. The entity is based on a three-dimensional embroidered scaffold, which is bio-mechanically and bio-functionally adapted and contains a co-culture of the different tissue-specific cell types [1, 2]. To avoid commingling of the cells ahead of time, the domains are to be isolated by a barrier composed of a collagen thread, which is integrated into the structure by embroidery technology [3]. The collagen barrier has to prevent cell migration, while nutrition supply is maintained. The diffusion of particles up to a molecular weight of 500 kDa should be guaranteed. A diffusion chamber system was designed to determine particle diffusion through the collagen barrier [3], but the first results achieved showed a high standard deviation up to 50 % of the measured values and a bad reproducibility of the calculated diffusion coefficients. An evaluation of the measuring procedure had to be performed.

The maximum standard deviation of the measuring values where achieved with the blank runs (without sample). As for the design of the diffusion chamber system the geometry of the chambers and thus the resulting flow conditions were not considered, it is assumable that there are turbulences occurring by stirring the medium in the diffusion chambers during the diffusion process. An essay with varying stirring speeds was performed using FITC-Dextran of different molecular weight as a sample substance. Further the experimental set-up was advanced by reducing sources of error such as light pollution or inadequate calibration scope.

Experimental Methods

The diffusion chamber system was applied as established before [3]. 50 mg of FITC-Dextran of different molecular weights (40, 250, 500 kDa, Sigma-Aldrich, USA) were weighed and dissolved in phosphate buffered solution (PBS) in a 50 mL-volumetric flask. The diffusion chambers where filled with 4.5 mL each at 37°C, the donator chamber with FITC-Dextran/PBS (1mg/mL) solution (Fig. 1- a, b) and the acceptor chamber with PBS (Fig. 1-c, d). The passage between the two chambers was sealed with a silicon ring (Fig. 1-e) and the opening, usually used to fix the test sample between the two different concentrated solutions, remained open. Five different stirring speeds (100 U/min, 200 U/min, 300 U/min, 400 U/min, 500 U/min) were adjustable with the device and each speed was analyzed by five samples.

10 µL of each acceptor chamber was collected at 0 h, 1 h, 3 h, 21 h and 24 h and dissolved in 90 µL of PBS. The chambers were sealed with Parafilm (Bemis, USA) to avoid evaporation of the solution. Calibration standards were prepared by serial dilution from the 1 mg/mL-stock solution with 1000, 500, 250, 100, 50, 10, 1, 0.1 and 0.01 µg/mL. The calibration standards and 45 µL of each sample were transferred to a black plate of 384 wells (GRE384fb, Greiner, Austria) and closed immediately to avoid contact with light. The samples were analyzed on a TECAN fluorescence (Tecan Group Ltd, Switzerland) with an extinction filter with λ = 485 nm and an emission filter with λ = 535 nm at 37 °C. Diffusion coefficients were calculated from the measured concentrations as described elsewhere

[3] and the resulting standard deviations of the different stirring speeds compared to each other. All steps of procedure were performed under red light (600 – 700 nm) in a dark room.

Results and Discussion

The standard deviations could be reduced by the advanced experimental set-up and the scope of linear correlation of the calibration curve could be defined for concentrations from 0 to 250 µg/mL. A clear dependency of the diffusion coefficient as well as the resulting standard deviations on the stirring speeds could be approved and an optimum speed identified.

Conclusion

To achieve reliable and comparable results, the experimental set-up for the self-made diffusion chamber system has to be standardized and an optimum tuning has to be defined.

References

[1] J. Hahner et. al. Textile Research Journal 85, 1431 (2015).
[2] M. Hoyer et. al. Materials Science & Engineering. C, Materials for Biological Applications 43, 290 (2014).
[3] J. Hahner et. al. Journal of Biomaterials Science. Polymer Edition 26 (16), 1085 (2015).

Acknowledgement

We acknowledge the funding of this project by the Deutsche Forschungsgemeinschaft (DFG).

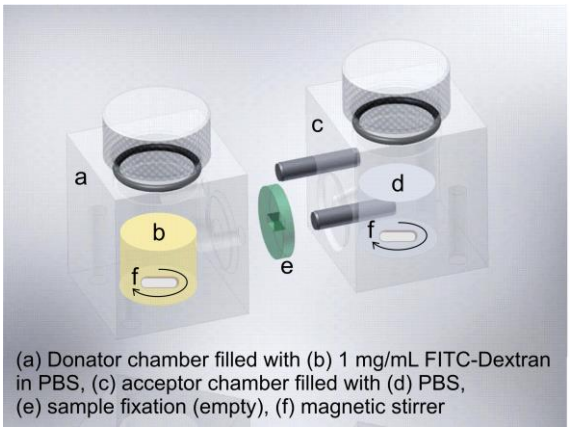

Experimental set-up of the diffusion chamber system

PS2-04-305

Development of porous PLLA/DCPA microfiber scaffold to enhance bone formation

Haruyuki Matsuo[1], Koji Yamamoto[2], Eiji Nakamachi[2], Kazuto Tanaka[2], Tsutao Katayama[2], Yusuke Morita[2]

[1]Doshisha University, Graduate School of Life and Medical Sciences, Kyotanabe, JP; [2]Doshisha University, Department of Biomedical Engineering, Kyotanabe, JP

Introduction

Bioresorbable fiber scaffold such as poly-L-lactic acid (PLLA) has been attempted to applicate for bone defect in bone regeneration. As bone formation needs long periods, fiber scaffold is required to promote cell migration and differentiation for bone formation. It was reported that HAp blocks transplanted into rabbit femur and tibia showed good osteoconductivity[1]. If fibers in the fiber scaffold are covered with apatite, it is expected that fiber scaffold shows superior osteoconductivity. However, PLLA fibers need a nucleus for precipitating apatite and high specific surface area to be covered with apatite early and uniformly *in vivo*. We suggested dicalcium phosphate anhydrous (DCPA) particle-doped porous PLLA fiber which has DCPA as the nucleus and high specific surface area due to porous structure. The purpose of this study was to develop a porous PLLA/DCPA fiber scaffold covered with apatite early and uniformly.

Experimental Methods

PLLA and polyethylene oxide (PEO) were dissolved in 1,3-dioxolane at PLLA/PEO concentration of 8 w/v%. The weight ratio of PLLA to PEO was 90:10. DCPA particles were mixed in the PLLA/PEO solution, and PLLA/DCPA weight ratio was 5/1. The solution was electrospun to the grounded rotating target using an electrospinning unit to fabricate the porous PLLA/DCPA fiber scaffold (porous PLLA/DCPA). The solid PLLA fiber scaffold (solid PLLA), the solid PLLA/DCPA fiber scaffold (solid PLLA/DCPA) and the porous PLLA fiber scaffold (porous PLLA) were prepared to evaluate the influences of DCPA particles and porous structure on apatite precipitation. The scaffolds were immersed in SBF[2] for 0, 1, 3, and 7 days to assess apatite precipitation. The surface and cross-section of the scaffolds were observed by a scanning electron microscope (SEM). The elemental distributions of calcium, phosphorous, carbon, and oxygen in the surface of the scaffolds were analyzed with a electron differentiation spectroscopy (EDS). The molecular components on the surfaces of the scaffolds were detected with a fourier transform infrared spectroscopy (FTIR). The crystal phases of the scaffolds were evaluated using a X-ray diffraction (XRD).

Results and Discussion

Fig. 1 shows SEM images of the scaffolds immersed in SBF for 0, 1, 3, and 7 days. Precipitation was not observed on fibers for the porous PLLA and the solid PLLA. Precipitation was observed on fibers for the PLLA/DCPA and the solid PLLA/DCPA after 1 day of SBF immersion. The amount of the precipitation increased with increasing of SBF immersion time, and fibers for the porous PLLA/DCPA and the solid PLLA/DCPA were almost covered with the precipitation after 7 days of SBF immersion. DCPA particles in the fiber induced to form the precipitation on the fiber after SBF immersion. The EDS analysis revealed that the precipitation consisted of P and Ca. The FTIR spectra of the precipitation showed the bands characteristic of phosphate groups. The XRD patterns showed that the peaks of the precipitation were observed at a 2θ value of 25.9° and 31.8° that is attribute to (002) and (211) planes of apatite.

These results showed that the precipitation was apatite. Crack and exfoliation of apatite were observed for the solid PLLA/DCPA immersed in SBF for 7 days, whereas they were not observed for the porous PLLA/DCPA immersed in SBF for 7 days. Moreover, fibers for the porous PLLA/DCPA were covered with apatite uniformly. According to the cross-section observation, apatite was also observed inside the fiber for the porous PLLA/DCPA immersed in SBF for 7 days. The fibers for the porous PLLA/DCPA were covered with apatite early and uniformly, the porous PLLA/DCPA was expected to promote bone formation.

Conclusion

We developed the porous PLLA/DCPA microfiber scaffold with an electrospinning technique. Fibers for the porous PLLA/DCPA microfiber scaffold were covered with apatite early and uniformly after 7 days of SBF immersion.

References

1. Kanazawa, M., *et al*., J. Master. Sci. Mater. Med. 28: 85, 2017.
2. Kokubo, T., *et al*., Biomaterials 27: 2907-2915, 2006.

Acknowledgement

This work was supposed by JSPS KAKENHI Grant Number 17K06067.

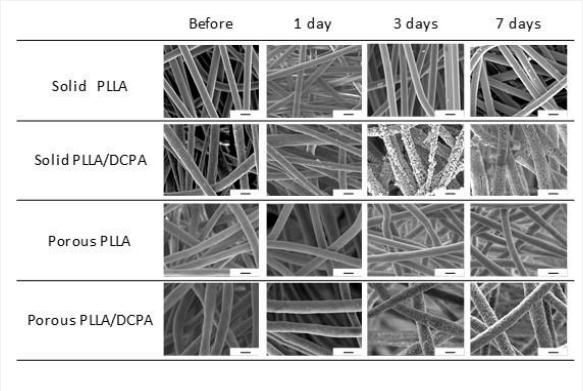

Fig. 1
SEM images of the scaffolds immersed in SBF for 0, 1, 3 and 7 days (×1000, Bar = 10 mm).

PS2-04-306

Fish Collagen and Hydroxyapatite reinforced PLGA fibrous membrane for guided bone regeneration

Jidong Li, Shue Jin, Qin Zou, Yi Zuo, Yubao Li

Sichuan University, Research Center for Nano-Biomaterials, Analytical & Testing Center, Chengdu, CN

Introduction

Guided bone regeneration (GBR) technology is a highly effective treatment performed using a mechanical barrier membrane, which can prevent the migration of the gingival epithelium from the root surface and thereby create adequate space for the reconstruction and regeneration of impaired alveolar bone.[1-2] The purpose of this study was to fabricate a low-immunogenicity fish collagen (FC) and bioactive nano-hydroxyapatite (n-HA) enhanced poly (lactide-co-glycolide) (PLGA) nanofibrous membrane for guided bone regeneration via electrospinning. The physicochemical properties, mechanical properties, degradability, cytocompatibility and preclinical biosafety evaluations were carried out to assess the potential of this fibrous composite membrane in GBR application.

Experimental Methods

FC and n-HA reinforced PLGA (PFCH) nanofibrous membrane were fabricated by electrospinning method. The physicochemical properties, mechanical and degradable behaviors of the fabricated membranes were investigated. Moreover, considering that the implanted GBR membrane directly interacts with gingival and bone tissue, we also assessed the proliferation and cytocompatibility of the fabricated membranes by using both bone marrow stem cells (BMSCs) and human gingiva fibroblasts cells (HGF). Preclinical biosafety evaluations of the fabricated membrane were also performed.

Results and Discussion

The physicochemical properties and morphology study revealed that FC and n-HA particles were homogeneously dispersed in the PLGA fibrous matrix. Notably, the formation of enhanced polymeric chain network due to the interaction between FC and PLGA significantly improved the tensile strength of the PLGA membrane. The incorporation of FC altered the degradation behavior of fibers and accelerated the degradation rate of the PLGA-based membranes. Moreover, the membranes exhibited favorable cytocompatibility with bone marrow stem cells (BMSCs) and human gingiva fibroblasts (HGF) cells. More importantly, the optimized membrane satisfied the requirements of the ISO/State mandated criteria during the incipient biosafety evaluation. All the results indicate that this composite fibrous membrane exhibits significant potential for guided bone or tissue regeneration.

Conclusion

This study demonstrated that FC and n-HA reinforced PLGA (PFCH) nanofibrous membrane to be a potential candidate for guided bone or tissue regeneration applications.

References

(1) Bottino, M. C. et al., *Dent Mater* **2012,***28*, 703-721.

(2) Nasajpour, A. et al., *Adv. Funct. Mater* **2018,***28*, 1703437.

Acknowledgement

The authors would like to thank the National Key Research and Development Program of China (Grant no: 2016YFA0201703/2016YFA0201700) for providing financial support to this project.

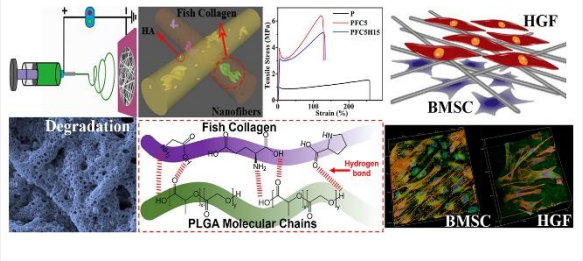

Figure Illustration of the fabrication scheme and the properties of the FC and n-HA reinforced PLGA

PS2-04-307

Preparation Alginate/Gelatin Blend Fiber with Reduced Gelatin Leakage

Jung Eun Kim, Hyun Ji Lee, Kyoung Hwa Jeon, Ki Hoon Lee

Seoul National University, Biosystems & Biomaterials Science and Engineering, Seoul, KR

Introduction

Both alginate and gelatin have been used as biomaterials for many years. Often both natural polymers were blended and fabricated into various forms, such as hydrogel, film, sponge, and fibers, expecting synergistic effects between the two polymers. Fiber is one of popular morphology in materials, which could be applied in their original form (e.g. suture), but, more frequently, assembled to 2- or 3-dimensional morphologies like as woven, knit, non-woven, and 3-D fabric. Alginate fibers have been shown in the market for various purposes. However, their application in the biomaterial field was limited due to the lack of cell binding ability. On the other hand, gelatin has good cell binding property but hard to spun into fiber because of the unique rheological property. Thus, blending alginate and gelatin can complement the limitation of both polymers to prepare a novel fiber with cell binding ability. This concept has been proven already in the literature [1, 2]. However, we found there is a serious problem in those methods. Almost 40% of the initial amount of gelatin is lost during the spinning process, which does not make any sense in practical production. In this study, we propose the use of gelation methacrylate and crosslink them at the spinning using UV irradiation.

Experimental Methods

Gelatin methacrylate was synthesized in the lab, and the modification was verified with NMR. Various dope solutions were prepared to have a different ratio of alginate and gelatin methacrylate. The dope solution was spun into the $CaCl_2$ coagulation bath. The UV light was irradiated at a spot right after the orifice of the syringe. The fibers were collected after several washing steps with distilled water. The protein content in the coagulation bath and washing solution were measured to check the leakage of gelatin during spinning. The spinning condition was optimized to have minimum leakage of gelatin and loss of mechanical properties. Finally, cytotoxicity of fibers was investigated using 3T3 NIH fibroblasts.

Results and Discussion

When blending alginate and gelatin, gelatin is entrapped in the "egg-box shaped" matrix of alginate. Such physical entrapment has a high risk of leakage of the load. Initially, we checked the leakage of gelatin during the washing step where serious leakage was expected. However, we eventually found that most of the gelatin is leaked in the coagulation bath. More precisely, the calcium-mediated crosslink of alginate is not sufficient to entrap gelatin neither in speed nor in density. In order to prevent the leakage of gelatin, we suggest the use of gelatin methacrylate which capable to crosslink under UV irradiation. The originality of this study lies on where the UV was irradiated. Here, we irradiated the UV at the end of the syringe needle (Figure 1). We refer it as "*in situ*" crosslink of alginate and gelatin since the ion-bridge crosslink of alginate and photo-crosslink of gelatin took place at the same time and space. When the *in situ* crosslinks was applied, the leakage of gelatin in the coagulation bath reduced to 20% of initial gelatin concentration which 100% enhancement without the *in situ* crosslinks. The effect of alginate/gelatin methacrylate blend ratio and photo-initiator load were investigated to find the optimum spinning condition. The use of photo-initiator

was the primary safety concern of our team in the use of the fiber in practical applications. However, the fiber did not show any cytotoxicity in the standard cytotoxicity test.

Conclusion

In this study, we suggest the necessity of *in situ* crosslinks of alginate and gelation methacrylate. The new crosslinking method has improved the retention of gelatin in the blend fiber. With the increased content of gelatin in the fiber, we expect better cell binding properties for tissue engineering.

References

[1] L. Fan, Y. Du, R. Huang et al., Preparation and characterization of alginate/gelatin blend fibers, J*ournal of Applied Polymer Science* 96, 1625–1629 (2005).
[2] X. Hu, L. Lu, C. Xu et al., Mechanically tough biomacromolecular IPN hydrogel fibers by enzymatic and ionic crosslinking, *International Journal of Biological Macromolecules* 72, 403–409 (2015).

Acknowledgement

This work was supported by the Technology Innovation Program (10076478, Development of natural protein composite fibers and materials for skin care products having improved moisturizing ability and mechanical properties) funded by the Ministry of Trade, Industry & Energy (MOTIE, Korea).

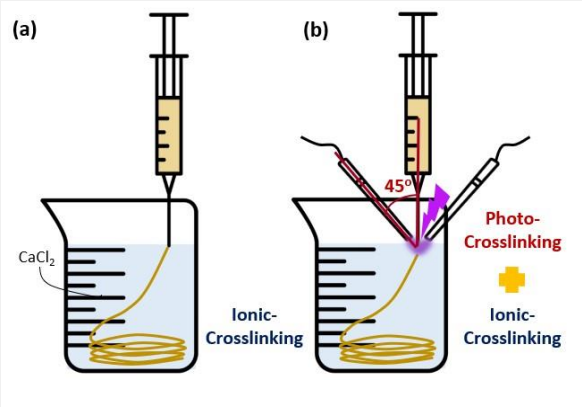

Fig 1. Spinning of Alginate/Gelatin Blend Fiber
(a) Conventional blend spinning (b) Introducing photo-crosslinking at spinning

PS2-04-308

The Hernia Mesh Generator – A novel pathway for generating custom-made hernia meshes

Cindy Elschner, Lars Bittrich, Annette Breier, Judith Hahn, Axel Spickenheuer, This work was carried out during the IGF project 18790 BR (LoVarMED).

Leibniz-Institut für Polymerforschung Dresden e. V., Dept. Mechanics and Composite Materials, Dresden, DE

Introduction

Hernia surgery is one of the most common visceral surgical interventions. In Germany, around 350,000 groin and abdominal wall hernias are treated annually. For hernia repair meshes are recommended as standard procedure by several guidelines, but there is no uniform approach to the material and structure of the meshes. The function of the surgical meshes is basically to strengthening the hernia; at the same time it should reduce the mobility of the host tissue as little as possible. The fact that this does not always succeed is seen as one reason for the comparatively high recurrence rate after hernia surgeries of about 10 % to 20 % (*1*). Any over-dimensioning of material and surface is linked to more inflammation and fibrosis. In contrast an under-dimensioning often results in mechanical failure, most importantly central mesh rupture. Less implanted material is however advantageous, as it changes the elasticity of the host tissue only slightly (*2*). In addition to this, post-operative pain has been correlated to the poor compliance of the mesh after tissue regeneration (*3*).

The software-based *Hernia Mesh Generator* (*HMG*) has been developed as a basic tool for a structured mesh design. The HMG is intended for use in technical embroidery. Traditionally, it is associated with decorative textile finishing; however, the classic embroidery process can also be used for the manufacturing of medical products. Embroidery technology is a one textile manufacturing process that offers large flexibility in structural and mechanical design.

Experimental Methods

The stitch pattern generator is based on the programming language Python. The development was preceded by an evaluation of the abdominal wall mobility by optical measurement. A strongly individual and also significantly anisotropic strain distribution was observed in all volunteers (*4, 5*).

Assuming an exemplary hernia defect, meshes were modelled using an automated optimization process in order to minimize strain in the mesh-tissue interface. The FE models showed an advantageous design of meshes with an anisotropic structure. A software-based HMG was developed, providing all embroidery parameters via a graphical user interface and a subsequent generation of a corresponding mesh. The output for the embroidery machine is in the EDOpath format (Complex Fiber Structures GmbH, Dresden, Germany).

Results and Discussion

The software enables a fundamental design of the meshes. To obtain stable embroidered meshes, the stitching path was set to zigzag (Fig. 1 A) including a vertex offset (Fig 1 B) that can be defined individually and which has an influence on the flexibility of the mesh. It can be stated: the larger the vertex offset, the higher the elongation of the mesh parallel to the offset. The size of the basic elements and the inflexion frequency of the zigzag path are tuneable and influence the mobility of the single fibers (Fig. 1 C). If zigzag paths are chosen over several basic elements, then the threads of the meshes can be moved against each other. Consequently, the meshes are more flexible, but also less mechanically stable. Additionally, using the HMG the pore sizes can be changed very easily (Fig. 1 D).

The qualitative FE simulations that preceded the development of the HMG identified an advantage of anisotropic mesh designs with gradually changing stiffness over uniform isotropic structures. Hernia meshes, which specifically reinforce the tissue defect and have a wide overlap area with a softer rim next to the adjacent, healthy soft tissue, will therefore lead to less tension in the abdominal wall. For this reason, the software can be used to generate embroidery patterns for hernia meshes that have a local tailored textile reinforcement structure in addition to the basic pattern (Fig. 2). The amount of reinforcing elements as well as the width and the number of graduations steps can be defined in the HMG. The software considers that the basic structure itself is not punctured when the reinforcement is applied in order to ensure the stability of the meshes.

Conclusion

The HMG is an excellent basis for follow-up projects to optimize both material selection and mesh design in a structured manner.

References

1. M. Lenzen-Schulte, *Dtsch Ärztebl*. **113**, A 926 - A 928 (2016).
2. U. Klinge & B. Klosterhalfen, *Expert Rev Med Dev*. **15**, 735–746 (2018)
3. S. Todros et al., *J Biomed Mater Res B*. **105**, 892–903 (2017)
4. A. Breier et al., *IOP Conf Ser: Mater Sci Eng***254**, 062002 (2017)
5. J. Hahn et al., *IOP Conf Ser: Mater Sci Eng***254**, 062005 (2017)

Acknowledgement

This work was carried out during the *IGF project 18790 BR* (*LoVarMed*). The authors would like to thank the project partners involved: Institute of Textile Machinery and High Performance Material Technology (ITM) at TU Dresden and Centre for Translational Bone, Joint, and Soft Tissue Research (TFO) at the University Hospital Dresden.

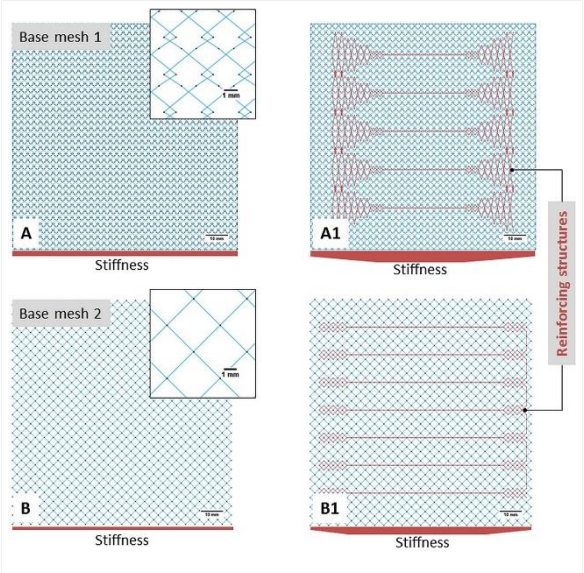

Stitch pattern designs
(A, A1) Base mesh 1 with and without textile reinforcement. **(B, B1)** Base mesh 2 with magnified pore sizes with and without textile reinforcement.

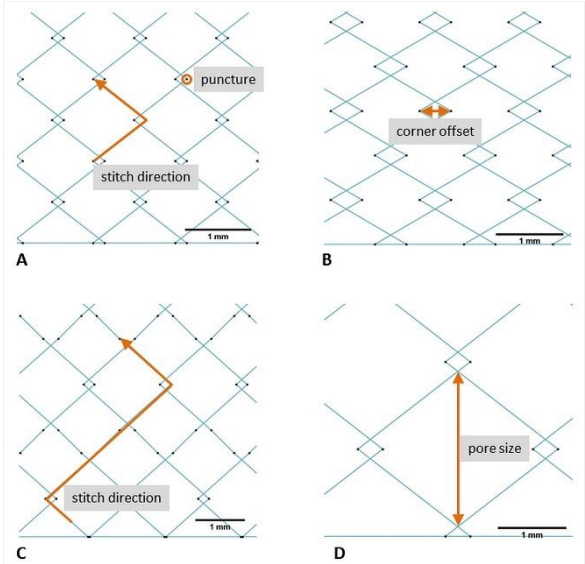

Individual mesh designs using the HMG
(A) Embroidery zigzag path defined by one basic element. **(B)** Enlarged corner offset compared to A. **(C)** Zigzag path defined by three basic elements. **(D)** Magnified pore size compared to A.

PS2-04-309

Plant proteins for fabrication of biomedical materials

Nong Zheng[1,2]

[1]Martin-Luther-University Halle-Wittenberg, biomedical materials group/ institute of pharmacy, Halle, DE;
[2]Fraunhofer institute for microstructure of materials and systems IMWS, biological and macromolecular materials, Halle, DE

Introduction

The application of biocompatible and absorbable protein-based materials has been shown in numerous studies to be beneficial for the treatment of wounds by means of supporting the reconstitution of tissue structure. In general, their high biocompatibility and good absorbability within the human body makes proteins an interesting tool for wound dressing design. As most studies in this field rely on the use of connective tissue proteins from animal sources, we considered plant storage proteins as starting material for the fabrication of nonwoven fibrous biomaterials by means of electrospinning. Plant storage proteins from rapeseed (*Brassica napus*) are byproducts in vegetable oil production and were not yet considered as educts in biomaterial design. Major storage proteins from rapeseed are napin and cruciferin, which, according to their biochemical properties, belong to the groups of albumins and globulins, respectively. In this study, we investigated the suitability of plant storage proteins from rapeseed, but also from lentil and kidney bean for the production of nonwoven fibrous biomaterials to the use in biomedical applications.

Experimental Methods

Fractions of globulins and albumins were isolated from rapeseed meal, lentil and kidney beans by extraction, precipitation and ultrafiltration followed by lyophilization. Pure fractions as well as blends of isolated protein fractions with

polylactic acid (PLA), polyethylene oxide (PEO) and polyvinyl alcohol (PVA) were tested for their compatibility with electrospinning. Moreover, the formation of a core-sheath structures was tested by applying coaxial electrospinning. The microstructure of the fibrous materials was investigated by scanning electron microscopy (SEM), the fiber diameter distribution was investigated via image processing using the software “Cell^F” (Olympus, Japan). The 3D-structure and the porosity of the fleeces were investigated by nanoscale X-ray computed tomography. The mechanical properties were determined via tensile test and atomic force microscopy (AFM). Cell culture test were carried out in order to test biocompatibility.

Results and Discussion

Globulin and albumin fractions were isolated with a protein content ranging from 82%w/w to 98%w/w. Pure solutions from napin, cruciferin as well as globulin and albumin fractions from lentil and kidney bean showed an overall poor ability for electrospinning, although, blending with either PLA, PEO or PVA conspicuously increased electrospinnability. Changes to the flow rate and the blend composition were shown to influence the microstructure and are thereby options for biomaterial tuning. Cell culture tests additionally provided proof for the biocompatibility of the fabricated biomaterials.

Conclusion

The materials and methods presented in this study are suitable to the fabrication of innovative plant protein-based nanofibrous materials for cutting-edge wound dressings and thereby broaden the spectrum of utilizing byproducts of the plant processing industry.

Acknowledgement

Dr. Christian E.H. Schmelzer, Fraunhofer Institute for Microstructure of Materials and Systems IMWS Halle (Saale)
Prof. Thomas Groth, Biomedical Materials Group, Institute of Pharmacy, Martin-Luther University Halle-Wittenberg

PS2-04-310

Electrospun biopolymeric patterned structures to support ovarian follicles growth: fabrication and characterization

Liliana Liverani[1], Nathalie Raffel[2], Amir Fattahi[2], Inge Hoffmann[2], Matthias W. Beckmann[2], Ralf Dittrich[2], Aldo R. Boccaccini[1]

[1]Institute of Biomaterials, Department of Materials Science and Engineering, University of Erlangen-Nuremberg, Erlangen, DE; [2]Department of Obstetrics and Gynecology, Erlangen University Hospital, Friedrich Alexander University of Erlangen–Nuremberg, Comprehensive Cancer Center ER-EMN, Erlangen, DE

Introduction

The application of tissue engineering in the field of reproductive organs repair is attracting the interest of the scientific community (1). Several biomaterials have been considered to mimic three-dimensional culture systems of ovarian follicles, but in most cases they were unsuitable to warrant follicles development (2). Recently, scaffold fabrication techniques, like 3D printing were applied for the development of constructs suitable to host follicles, leading to the birth of pups in mouse model (3). On this basis, the present work is based on the application of the electrospinning technique as convenient alternative to obtain patterned macroporous scaffolds able to mimic the morphology of native ovarian cortex and suitable for follicles adhesion and growth (4).

Experimental Methods

Neat poly(epsilon caprolactone) (PCL) and its blend with gelatin (type A) (PCL/gel) were used for the fabrication of electrospun scaffolds. Glacial acetic acid and formic acid were selected as benign solvents. The electrospinning process was performed by using a commercial device EC-CLI (IME Medical Electrospinning) with climate chamber in which temperature and relative humidity were set at 25°C and 25%, respectively. The optimized process parameters were: 15kV applied voltage, 11cm distance tip-collector, 23G needle diameter, while the solution flow rate was 0.4mL/h for neat PCL and 0.6 mL/h for the blend. SEM and FTIR analyses were performed on the obtained scaffolds. Porcine ovarian follicles were isolated enzymatically from ovarian tissue pieces (collected from slaughterhouse, registration number DE09562003821) and incubated for 10 days on the scaffolds. After incubation, follicle viability was evaluated via Live/Dead assay and follicle morphology was investigated by fluorescent f-actin staining and SEM analysis.

Results and Discussion

The scaffolds´ morphology and macroporous structure were assessed and macroporosity with an average pore size of 0.3 mm was obtained. After 10 days of culture, the number of viable follicles (= >99% granulosa cells alive) was 76.64% for PCL and 90.21% on the PCL/gel samples. Even if both PCL and PCL/gel electrospun scaffolds showed positive results in terms of reduced follicles loss during the seeding and follicles survival, PCL/gel mats led to better results in terms of preservation of follicles spheroidal shape and higher number of adhesion points with the electrospun mats.

Conclusion

In the emerging field of reproductive tissue regeneration, patterned fibrous scaffolds obtained by electrospinning of PCL/gel represent a promising technology which warrants further research.

References

1. Amorim CA. Special Issue Devoted to a New Field of Regenerative Medicine: Reproductive Tissue Engineering. Ann Biomed Eng [Internet]. Springer US; 2017 Jul 31 [cited 2018 Apr 6];45(7):1589–91. Available from: http://link.springer.com/10.1007/s10439-017-1862-0

2. Brito IR, Lima IM, Xu M, Shea LD. Three-dimensional systems for in vitro follicular culture : overview of alginate-based matrices. Reprod Fertil Dev. 2014;26(7):915–30.

3. Laronda MM, Rutz AL, Xiao S, Whelan KA, Duncan FE, Roth EW, et al. A bioprosthetic ovary created using 3D printed microporous scaffolds restores ovarian function in sterilized mice. Nat Commun [Internet]. Nature Publishing Group; 2017 May 16 [cited 2017 Oct 10];8:15261. Available from: http://www.nature.com/doifinder/10.1038/ncomms15261

4. Liverani L, Raffel N, Fattahi A, Preis A, Hoffmann I, Boccaccini AR, et al. Electrospun patterned porous scaffolds for the support of ovarian follicles growth: a feasibility study. Sci Rep. 2019;9:1150.

PS2-04-311

Obtaining of Cellprene® Epoxidized Fibers Using Electrospinning Process

Rafael M. Carazzai, Nathália O. Muniz, Nayrim B. Guerra, Luís Alberto L. dos Santos

Federal University of Rio Grande do Sul, Biomaterials Laboratory / Materials Engineering Department, Porto Alegre, BR

Introduction

In the past, removal of the injured part was the most common practice when large tissue lesions were due to mechanical trauma or degenerative diseases. Consequently, inducing a significant decrease in the quality of patient's life[1]. Antibiotics discovery increased human life expectancy, as well as improved sanitary and hygienic conditions. With this, the replacement of damaged tissues became a necessity[2,3], and the tissue engineering, using scaffold and cells, to regenerate or replace injured tissues, has been developed. Cellprene® is a polymer blend of PLGA and Poly (isoprene) that has been recently developed by the Biomaterials Laboratory (UFRGS, Brazil) and shows high potential for applications such as biomaterial[4]. This material had its biological characteristics improved through the epoxidation of Poly (isoprene)[5]. As a new material, a few works have been conducted, and its properties and characteristics are unknown. The electrospinning technique is the most used technic to obtaining fibers. The advantage of polymeric biomaterials is to allow obtain fibers with different diameters, and, in some conditions, at nanometric scale, which has a great importance in terms of adhesion and cell growth. The aim of this study is to evaluate the viability of the obtaining Cellprene® epoxidized by electrospinning for potential use as scaffold for tissue engineering.

Experimental Methods

Poly(lactic-co-glycolic-acid) (PLGA) produced by PURAC (The Netherlands) with ratio 85/15 and centrifuged natural latex by MAFER (Brazil) were used to produce the polymer blend. The latex was purified to obtain poly (isoprene) (PI), then the PI was epoxidized (PI epox). The PLGA/PI epox were weighed and mixed in the ratio 60/40 (% w/w). The table 1 shows the parameters to obtain Cellprene® epoxidized fibers by electrospinning process. The fiber morphology and functional groups of the polymers were performed by scanning electron microscopy (SEM) and Fourier transform infrared spectroscopy with attenuated total reflectance (FTIR-ATR).

Results and Discussion

Evaluating the results, using different electrospinning parameters, the one that presented the greater morphology response was: 15 kV, distance between needle-collector 20 cm, infusion rate 4 ml/h and concentration 5%. The figure 1 shows the SEM of Cellprene® epoxidized fibers.

The diameter of fibers were measured using ImageJ software and shown a mean diameter of 4,3± 2,7µm. The fibers presented high superficial porosity that may facilitate the adhesion of the cells. Authors claimed that porosity presented in the fibers can be caused by evaporation ratio of the solvent[6,7]. Other authors explain the porosity as a consequence of the relative humidity during the electrospinning process[8,9].

Analyzing the spectra of PI epoxidized, we noticed that there are no bands in the range of 3100 cm^{-1} and 3600 cm^{-1}, which are referred in the literature to proteins and peptides[5]. This indicates that the purification of poly (isoprene) was efficient. The appearance of bands at 1250 cm^{-1} and 870 cm^{-1}, as well as a broad band around 1100 cm^{-1} indicate

that the epoxidation reaction of poly (isoprene) occurred[5]. Authors observed that in PLA / epoxidized natural rubber blends the band around 1750 cm^{-1} was shifted to larger wave numbers with increasing content of epoxidized natural rubber[10]. This suggests that there was interation between PLGA and PI epox. According to the analysis of FTIR-ATR spectra does not indicate significant change in the main functional groups.

Conclusion

The electrospinning process is viable for the production of fibers of Cellprene® epoxidized blend. The fibers presented high amount of pores on surface that may aid in cell adhesion. The obtaining of fibers by solvent mixing of polymers and electrospinning method did not modify chemical groups of the resulting material when compared to the raw materials.

References

1. Santos Jr., A.R.; Wada, M. L. F. Polímeros: Ciência e Tecnologia. 17:308-317, 2007
2. Hench, L. L. Biomaterials. 19:1419-1423, 1998
3. Nobre, M. R. C. *et al*., Qualimetria, 6:56-59, 1994
4. Marques, D. R. Polímeros, 23:579-584, 2011
5. Guerra, N. B. *et al*., J. Polym. Res. 25:172, 2018
6. Katsogiannis, K. A. G. *et al*., European Polymer Journal. 69:284-295, 2015
7. Celebioglu, A.; Uyar, T. Materials Letters, 65:2291-2294, 2011
8. Park, J. Y.; Lee, I. H. J. Nanosci. Nanotechnol. 10:3473-3477, 2010
9. Casper, L. C. *et al*., Macromolecules. 37:573-578, 2004
10. Cosme, J. G. L. *et al*., Materials Scie. and Applications. 7:210-219, 2016

Acknowledgement

The authors acknowledge to the Coordenação de Aperfeiçoamento de Pessoal de Nível Superior (CAPES) for the financial support through the project, to the Conselho Nacional de Desenvolvimento Científico e Tecnológico (CNPQ), to the Programa de Pós-Graduação em Engenharia de Minas, Metalúrgica e de Materiais (PPGE3M), to the Financiadora de Estudos e Projetos (FINEP) and to Fundação de Auxílio à Pesquisa do Rio Grande do Sul (FAPERGS) for the financial support through the project.

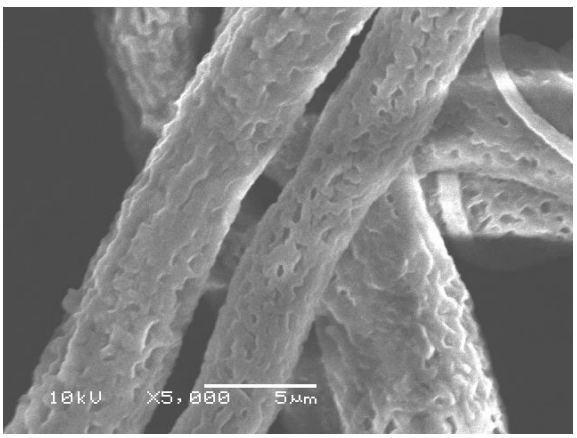

Figure 1 .
SEM of Cellprene® epoxidized fibers.

Voltage	10, 15, 20 (kV)
Needle-collector distance	5, 10, 15, 20 (cm)
Infusion rate	4, 5, 10, 15 (ml/h)
Concentration	1, 3, 5, 7 (%w/v)

Table 1.
Parameters to obtain Cellprene® epoxidized fibers.

PS2-04-312

Morphological control of electrospun ECM-PCL scaffolds for liver tissue engineering

Thomas S. R. Bate, Anthony Callanan

University of Edinburgh, Institute for Bioengineering, Edinburgh, GB

Introduction

In Europe, decompensated liver cirrhosis due to chronic liver disease (CLD) causes 170,000 deaths per year [1]. Global mortality rates linked to liver disease have exhibited an upward trend since the 1970s, contrary to downward trends observed in other leading causes of death [2,3]. Researchers are on the hunt for new drug treatments, however *in-vitro* drug development methods are unable to provide effective and efficient routes in which this can be achieved [4]. It is widely accepted that more relevant *in-vitro* models are required in order for drug development to progress, which could be achieved using controllable tissue engineering methods. Electrospun scaffolds have long been a subject of interest for tissue engineering research due to the ability to mimic Extracellular Matrix (ECM) structures with biocompatible polymers. There have also been large efforts within the research community to decellularise organs and harvest the ECM to provide natural biochemical cues to cells *in-vitro.* This study has explored the combined potential of morphologically defined electrospun polycaprolactone (PCL) fibres containing liver derived ECM for controlled and reproducible 3D *in-vitro* livertissue cultures.

Experimental Methods

Randomly oriented fibres, aligned fibres and highly porous cryogenic fibres all seen in *Fig.1A* were manufactured using PCL for large (5µm) and small (1µm) fibre sizes. Large fibres were produced using 19w/v% PCL solutions in 5:1 Chloroform:Methanol and small fibres using 7w/v% PCL in Hexafluroisopraopanol (HFIP). Randomly oriented fibres were electrospun onto a mandrel rotating at 250RPM and aligned fibres at 1800RPM. Porous cryogenic fibres were spun onto a mandrel containing dry ice at -78.5°C. ECM-PCL scaffolds were manufactured using decellularised rat livers. Briefly, whole rat livers were isolated and decellularised by vascular perfusion with 0.25w/v% Sodium Dodecyl Sulphate (SDS) solution. These were subsequently washed with deionized H_2O and lyophilised. The lyophilised ECM was then powdered using a planetary ball mill. 10w/w% and 5w/w% ECM-PCL mixtures were dissolved using HFIP and electrospun into fibres. Fibres were characterized using SEM imaging, mechanical analyses and FTIR Spectroscopy. Scaffolds were then punched and seeded with HepG2 cells which were cultured for 14 days. Cell viability, DNA quantitation, IHC staining and RT-qPCR Gene analysis were conducted at 24hr, 7 day and 14 day timepoints.

Results and Discussion

Larger fibres observed higher rates of proliferation than small fibres with the porous cryogenic scaffolds showing the highest rates for both small and large fibres. The morphology also influenced the structure of cell clusters as seen in *Fig.1B*. Maintenance of key liver function genes was observed on PCL scaffolds with a relative reduction in interstitial ECM genes Collagen I (COL1A1) and Fibronectin (FN1). The presence and bioactivity of electrospun rat liver ECM is seen to be preserved in *Fig.2* with higher cell viability observed on ECM scaffolds. Also, differences were observed in gene expression profiles of ECM vs. PCL only scaffolds.

Conclusion

Electrospun fibre size and morphology are observed to have a measurable impact on hepatocyte cultures. This highlights the importance of understanding the interactions between cells and fibres as a means for controlling *in-vitro* results. The incorporation of rat liver ECM into electrospun PCL scaffolds is capable of inducing altered biochemical responses in HepG2 cells, indicating that bioactive elements within the electrospun ECM are retained. Further investigation should confirm the degree to which bioactive ECM can be preserved within electrospun PCL scaffolds whilst maintaining tractable morphology.

References

1. Marcellin, P. doi:10.1111/liv.13682
2. Tapper, E. B. *BMJ***362,** k2817 (2018).
3. Williams, *J. Hepatol.***63,** 297–299 (2015).
4. Hay, M., *Nat. Biotechnol.***32,** 40–51 (2014).

Acknowledgement

ESPRC no. EP/N509644/1. MRC grant MR/L012766/1. With thanks also to Dr. Alison McDonald for imaging assistance.

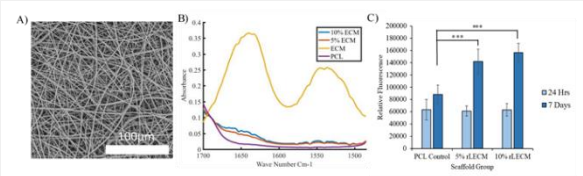

Figure 2
*A) SEM image showing 10w/w% rat ECM-PCL fibres. B) FTIR spectrum confirming the presence of ECM moeities within the electrospun scaffolds. C) Cell viability of HepG2 cells on ECM scaffolds. N=5, One-way ANOVA, Tukey's analysis, *** = p < 0.001, error bars: ± SD.*

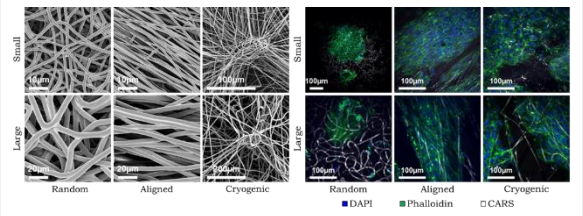

Figure 1
A) SEM images of the various fibre morphologies B) DAPI, Phalloidin and CARS fluorescence of HepG2 cultures on the different scaffold groups.

PS2-04-313

Novel concept of bioresorbable bioactive fracture fixation plates for load-bearing applications by tailored fibre placement

Artem Plyusnin[1], Oliver Liesmäki[1], Julia Kulkova[1], Axel Spickenheuer[2], Lars Bittrich[2], Cindy Elschner[2], Annette Breier[2], Niko Moritz[1]

[1]University of Turku, Institute of Dentistry, Department of Biomaterials Science and Turku Clinical Biomaterials Centre – TCBC, Biomaterials and Medical Device Research Program, Biomedical Engineering Research Group, Turku, FI; [2]Leibniz-Institut für Polymerforschung Dresden e. V. (IPF Dresden), Department of Mechanics and Composite Materials, Complex Structural Components Workgroup, Dresden, DE

Introduction

In internal fracture fixation, metallic plates are a common treatment modality. However, the excessive stiffness of metallic plates leads to an unequal distribution of load between the implant and the healing bone, known as “stress-shielding” [1]. The subsequent underloading of bone, in turn, may lead to adverse bone remodeling resulting in non-union or re-fracture of the bone.

Fiber reinforced composites (FRC), combining less weight and ability of adjusting the stiffness, have been suggested as alternatives to metals [2-4]. Adapted FRC plates reduce stress-shielding and facilitate the natural fracture healing process reducing the risk of non-union or re-fracture. In practice, FRC plates often include one or several layers of continuous unidirectional fibers. The screw holes in these plates are made by drilling which compromises the integrity of fibers. Additionally, the holes themselves are stress concentrators, which further decreases the reliability of the plate.

In Tailored Fiber Placement (TFP), a variety of embroidery technology, continuous glass or carbon fibers are placed onto a fabric sheet, fixed by stitching with a sewing thread and impregnated in a polymer matrix [5]. Thus, the screw holes are formed by the particular placement of the fibers considering the stress distribution under load [6] and bypassing the screws, thus avoiding the need to drill holes. Hence, stress concentration around holes is minimized.

As their metallic counterparts, biostable FRC plates often require plate removal after complete fracture healing. This second surgery could be avoided by the use of bioresorbable materials. However, bioresorbable FRC fracture fixation plates for load-bearing applications are not commercially available.

We propose a novel concept of a bioresorbable bioactive fracture fixation plate, adjustable for different clinical applications. In this study, we focus on the treatment of front limb fractures in toy-breed dogs where the complications associated with the use of metallic plates are particularly amplified. Therefore, the animals give a representative model for the development of a novel treatment. Ideally, the plate is to be made of a bioresorbable polymer reinforced with silica-based bioactive glass (BG) fibers by TFP (Fig. 1). The BG fibers additionally serve as a bioactive component stimulating bone growth and reducing the risk of infection [7]. The plate is intended to completely resorb in the body after the bone healing. The plates can be developed for further applications in other animal species and humans.

The goal of this study was to design diverse TFP patterns for fracture fixation plates in toy-breed dogs, fabricate the biostable sample plates and test their mechanical performance. Future studies will include *in vitro* and *in vivo* testing of plates made of bioresorbable polymers reinforced with BG fibers.

Experimental Methods

Different TFP plate patterns were developed. Finite element (FE) models considering the layup and directions of the fibers were generated and further used in computer simulation of mechanical loading of the plates.

Plates were prepared and tested mechanically. E-glass fibers have been applied as surrogates for BG fibers. Dimethacrylate-based light curable resin and polylactic acid were used as matrices in the composites. Plates reinforced with continuous unidirectional E-glass fibers served as controls. The testing procedures included four-point bending of plates, four-point bending and torsion loading of osteotomized bones fixed with the plates.

Results and Discussion

In four-point bending of plates, the plates reinforced with unidirectional fibers were predictably stiffer than their TFP counterparts. However, bending of the osteotomized bones fixed with both types of plates revealed similar stiffness of both plated bone constructs which implies that in a real clinical situation the stiffness of TFP plates can be sufficient for successful bone healing.

In all testing conditions, TFP plates withstood substantial deformations before failure. Typical failure of TFP plates was followed by accumulation of multiple cracks none of which was fatal to the plate if taken separately. TFP plates rarely broke apart even when their load-bearing capability decreased to a minimum. In contrast, the plates reinforced with unidirectional fibers tended to break dramatically once cracks appeared in the direction of the fibers placement (Fig. 2).

FE modeling of the behavior of TFP plates subjected to the loading conditions of the tests applied in the study demonstrated adequate prediction of the structural stiffness of the plates. Further development of the FE model will aim on the evaluation of progressive damage of novel plates using extended finite element method.

Conclusion

TFP plates demonstrated structural integrity superior to that of plates reinforced with unidirectional fibers and stiffness suitable for fracture healing. Thus, TFP technique has a potential in fabrication of fracture fixation plates for load-bearing applications.

References

1. Huiskes, R., Weinans, H., Van Rietbergen, B., 1992. The relationship between stress shielding and bone resorption around total hip stems and the effects of flexible materials. Clin. Orthop. Relat. Res. 274, 124 – 134.

2. Akeson, W.H., Woo, S.L., Coutts, R.D., Matthews, J.V., Gonsalves, M., Amiel, D., 1975. Quantitative histological evaluation of early fracture healing of cortical bones immobilized by stainless steel and composite plates. Calcif. Tissue Res. 19, 27 – 37.

3. Hastings, G.W., 1978. Carbon fibre composites for orthopaedic implants. Composites. 9, 193 – 197.

4. Tayton, K., Johnson-Nurse, C., McKibbin, B., Bradley, J., Hastings, G., 1982. The use of semi-rigid carbon-fibre-reinforced plastic plates for fixation of human fractures. Results of preliminary trials. J. Bone Joint Surg. Br. 64, 105 – 111.

5. Mattheij, P., Gliesche, K., Feltin, D., 1998. Tailored Fiber Placement - Mechanical Properties and Applications. J. Reinf. Plast. Comp. 17, 774 – 786.

6. Gliesche, K., Hübner, T., Orawetz, H., 2003. Application of the tailored fibre placement (TFP) process for a local reinforcement on an “open-hole” tension plate from carbon/epoxy laminates. Compos. Sci. Technol. 63, 81 – 88.

7. Hoppe, A., Güldal, N.S., Boccaccini, A.R., 2011. A review of the biological response to ionic dissolution products from bioactive glasses and glass-ceramics. Biomaterials 32, 2757 – 2774.

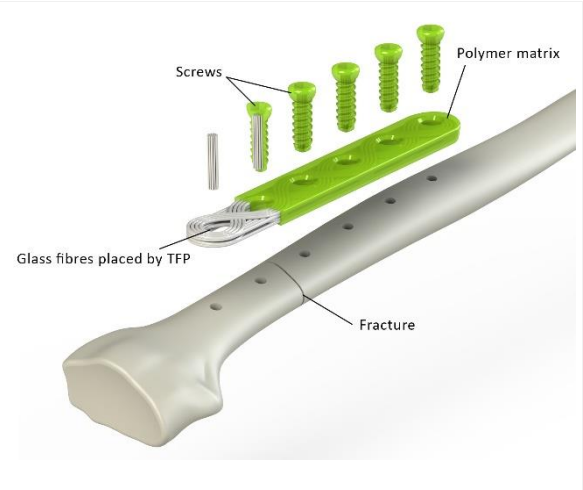

Figure 1. Render of the concept of a novel bioresorbable bioactive fracture fixation plate by TFP

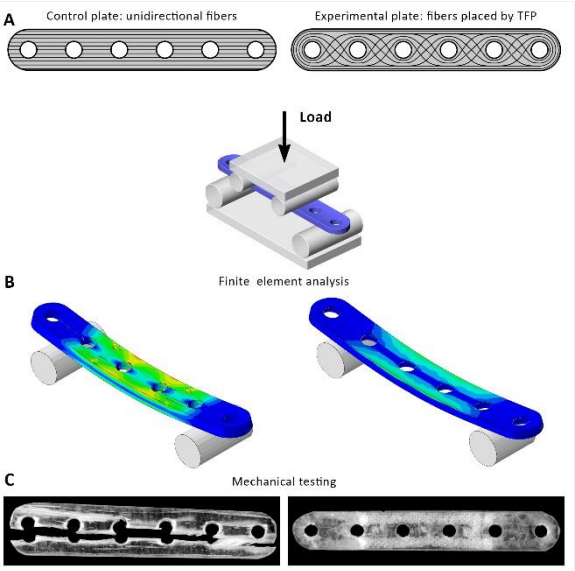

Figure 2. Comparison of a plate reinforced with unidirectional fibers and a plate reinforced by TFP

In TFP plates, fibers bypass the screw holes, thus the integrity of fibers is maintained (A). When subjected to load, stesses in TFP plates are distributed more evenly than in plates reinforced with unidirectional fibers (B). Plates reinforced with unidirectional fibers tend to break apart while TFP plates retain structural integrity even when their load-bearing capacity drops to a minimum (C).

PS2-04-314

Revealing novel power laws and quantization in electrospinning considering jet splitting - Experimental

Vincent Allen[1,2], Ursula Gunselmann[1], Dirk W. Schubert[1,2]

[1]Friedrich-Alexander-University Erlangen-Nürnberg, Institute of polymer materials, Erlangen, DE; [2]Bavarian Polymer Institute (BPI), Keylab of advanced fiber technologies Germany, Fürth, DE

Introduction

Electrospinning is a process which reliably produces fibers tens of nanometers to tens of micrometers in diameter with the use of simple laboratory equipment by pushing a polymer liquid through a nozzle with an applied electric field. With the use of electrospinning techniques, sophisticated fibrillary structure formation is possible, where fiber diameter and pore-size are important factors for controlling cellular migration in biomedical applications (e.g. tissue engineering) [1]. A new, purely theoretical model by Schubert considers applied voltage, viscosity, charge density, surface tension and jet splitting for predicting fiber diameter and the corresponding distribution for solution electrospinning [2]. Using suggestions provided in [2] an experimental investigation of changes in fiber diameter dependent on viscosity and concentration was performed using standard solution electrospinning equipment.

Experimental Methods

Blend ratios of poly-ε-caprolactone (PCL) with two different molar masses (Mn = 10 kg/mol and Mn = 80 kg/mol) were deliberately varied to change viscosity almost independent of total polymer concentration in a Chloroform-Ethanol (7:3) solvent solution. Standard solution electrospinning equipment using a hamster wheel collector was utilized for the production of fibers. Plate-cone rheology was used to obtain the solution viscosity while SEM and image analytical software were utilized for the determination of fiber diameter.

Results and Discussion

By varying polymer concentration and molar mass, fibers with median diameters from 200 to 2300 nm could be produced. Results revealed a predictable correlation, theorized in [2], between the solution viscosity and concentrations on the fiber diameter. When analyzing the fiber diameter distribution, the existence of mono- and bi-modal fiber diameter distributions due to the occurrence of jet splitting was found. The ratio between bi-modal (split fiber) and mono-modal (non-split fiber) distributions indicate the splitting of a single fiber into three equal 'split' fibers. Lastly, the theoretical limit of standard deviation in respect to mean fiber diameter was graphically analyzed and validated using the generated experimental data.

Conclusion

Theoretical predicted power laws for the fiber diameter considering an un-split base mode and a split mode were validated by systematically analyzing a large experimental space for the first time. Additionally, the prediction of an upper limit of standard deviation in relation to the average fiber diameter could be revealed, further validating the theoretical predictions.These validations of jet splitting and quantization with respect to fiber diameter distribution opens an entirely new door for predicting and modelling fiber diameters in solution electrospinning.

References

1. Han, D. G., Ahn, C. B., Lee, J. H., Hwang, Y., Kim, J. H., Park, K. Y., … Son, K. H. (2019). Optimization of Electrospun Poly(caprolactone) Fiber Diameter for Vascular Scaffolds to Maximize Smooth Muscle Cell Infiltration and Phenotype Modulation. *Polymers*, *11*(4), 643.
2. Schubert, D. W. (2019). Revealing Novel Power Laws and Quantization in Electrospinning Considering Jet Splitting - Toward Predicting Fiber Diameter and Its Distribution. *Macromol. Theory Simul.*, 1900006.

Acknowledgement

Funded by the Deutsche Forschungsgemeinschaft (DFG, German Research Foundation) - Projektnummer 326998133 - TRR 225 (subproject A07).

2:45 p.m. – 3:45 p.m.

Hall 1 / Exhibition Area

PS2-05 | Stimuli-responsive biomaterials

PS2-05-315

Controlled structure of cell sheets using micropatterned thermoresponsive surfaces prepared by polymer stamping method

Masamichi Nakayama[1], Junichi Tonegawa[2], Akihiko Kikuchi[2], Teruo Okano[1]

[1]Tokyo Women's Medical University, Inst. Adv. Biomed. Eng. & Sci., Tokyo, JP; [2]Tokyo University of Science, Dept. Mater. Sci. & Technol., Tokyo, JP

Introduction

A unique sheet-like cell manipulation method, cell sheet engineering, has been developed to recover the lost functions of tissues and organs using cell culture surfaces grafted with thermoresponsive poly(*N*-isopropylacrylamide) (PIPAAm) (lower critical solution temperature in water: 32°C) [1]. Recently, we focus on the fabrication of bio-mimicking cell sheets in which co-culture system of different cells or cell orientation, using micropatterned thermoresponsive surfaces. However, the preparation of conventional patterned surfaces requires complicated procedure including site-selective multi-step chemical reaction in conjunction with a lithography method. Therefore, herein, a microcontact printing method using block copolymer inks was performed to obtain micropatterned thermoresponsive polymer surfaces. Namely, amphiphilic block copolymers were transferred onto PIPAAm-immobilized surfaces to form thermoresponsive/hydrophilic micropatterns. In addition, we also investigated the influence of the difference in the transferred amount of the amphiphilic polymers on the surface property alternation and cell sheet structure.

Experimental Methods

Block copolymers of poly(n-butyl methacrylate)-*b*-poly(*N*-isopropylacrylamide) (PBMA-*b*-PIPAAm) [BMA/IPAAm: 97/251 in unit] and poly(n-butyl methacrylate)-*b*-poly(*N*-acryloylmorpholine) (PBMA-*b*-PAcMo) [BMA/AcMo: 97/188 in unit] were prepared by RAFT polymerization. PBMA-*b*-PIPAAm was dissolved in acetonitrile/dimethylformamide (AcCN/DMF: 5/1) at a concentration of 0.3w/v%, and spin-coated on commercial tissue culture polystyrene (TCPS) substrates to obtain thermoresponsive culture surfaces [2]. A poly(dimethylsiloxane) (PDMS) stamp surface was immersed in a PBMA-*b*-PAcMo solution (0.5 or 1.5w/v% in AcCN/DMF). The stamp was then brought into TCPS or the PBMA-*b*-PIPAAm coated surfaces, and the PBMA-*b*-PAcMo was transferred by placing a 100-g weight. After washing with cold water and drying, the PBMA-*b*-PAcMo transferred surfaces were obtained. The influence of the difference in polymer-transferred amount on the surface property was characterized by ATR/FT-IR method and static contact angle measurement. Furthermore, normal human dermal fibroblasts (NHDFs) were seeded on the micropatterned surfaces prepared using a stripe-pattern stamp (width/spacing: 50 μm/50 μm), and the change of cell adhesion state at 37 °C and cell sheet structure by 20°C-treatment were investigated.

Results and Discussion

Firstly, the TCPS surfaces before/after the stamp procedure with amphiphilic PBMA-*b*-PAcMo block copolymer were characterized. the transferred amount of PAcMo chain became larger with increasing the polymer concentration (0.52 and 2.41 μg/cm^2 for 0.5 and 1.5w/v%, respectively), determined by ATR/FT-IR method using a calibration curve from the surfaces with a known polymer amount. Furthermore, the static contact angle measurement showed a high-concentration polymer stamp altered the surfaces more hydrophilic. These results indicated the effective surface polymer transfer was successfully performed, probably due to the existence of a hydrophobic PBMA anchor.

Next, we observed cellular behavior on the surfaces with the thermoresponsive/hydrophilic (50 μm/50 μm) stripe-pattern to investigate the influence of PAcMo amount on the cell adhesive area and adhesion shape. On the surface transferred with the 1.5w/v% solution, NHDF adhered and grew only the non-transferred PIPAAm areas, even after 7 days culture. This was due to that sufficient PAcMo chains were introduced to the surface to maintain cell non-adhesion in the long term. Moreover, filiform cell sheets were detached from the surface by reducing temperature to 20 °C. Interestingly, for the 0.5w/v% polymer-stamped surface, the cell adhesion/non-adhesion pattern maintained after 24 hours, but after culturing for 7 days, cells grew to whole area with a cell orientation along the axial direction. Immunostaining of skeletal F-actin also showed a high cell orientation along the stripe pattern. We hypothesized that extracellular matrix produced from NHDF on the adjacent regions allowed cells to invade and proliferate into the low quantitative PAcMo areas. In addition, we successfully harvested an anisotropic cell sheet with maintaining cell alignment.

Conclusion

In summary, the microcontact printing of block copolymers enables the facile micropatterning of thermoresponsive culture surfaces, and is expected to be applied to control cell sheet structure (size or cellular orientation).

References

[1] M. Yamato, T. Okano, *Materials Today*, **2004**, *7*, 42-47.

[2] M. Nakayama et al., *Macromol. Biosci.*, **2012**, *12*, 751-760.

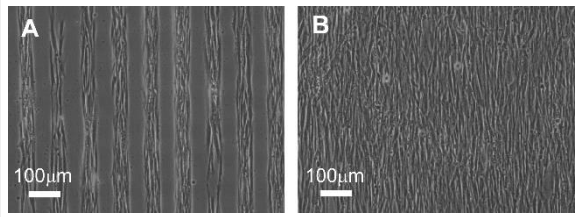

Figure 2
Phase contrast photographs of adhering NHDF on thermoresponsive surfaces treated with (A) 1.5w/v% and (B) 0.5w/v% PBMA-*b*-PAcMo solutions using PDMS stamp after culture for 7 days at 37°C.

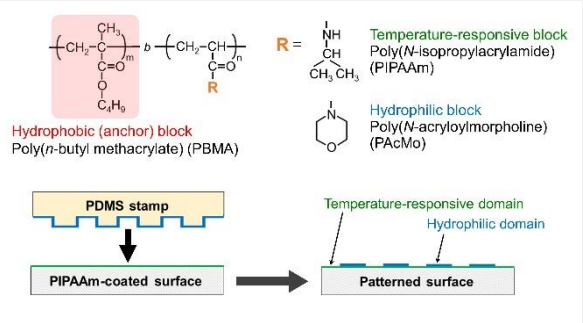

Figure 1
Chemical structure of functional block copolymers and preparation of micropatterned thermoresponsive surface by microcontact printing method.

PS2-05-316

Highly porous self-folding mats for skeletal muscle tissue regeneration

Indra Apsite[1], Sahar Salehi[2], Leonid Ionov[1]

[1]University of Bayreuth, Biofabrication, Bayreuth, DE; [2]Universty of Bayreuth, Biomaterials, Bayreuth, DE

Introduction

Recent studies have shown great potential of polymeric self-folding films for cell patterning and skeletal muscle regeneration [1, 2]. However, higher porosity ensures easier nutrient and byproduct exchange that can lead to better cell penetration. There is limited amount of studies on porous electrospun stimuli-responsive bilayer mats [3, 4]. Additionally, improved muscle cell organization and maturation has been observed on porous electrospun mats for engineered muscle tissue [5].

Experimental Methods

Therefore, we investigated fabrication of folded film made of bilayer electrospun system containing polycaprolactone (PCL, passive layer) and methacrylated alginate (AA-MA, active layer). To obtain aligned PCL fibers we used electrospinning techniques and two sets of fiber collectors: rotating drum and conductive parallel bars. While the tube formation was initiated by adding aqueous solution, the PCL/AA-MA mat tube diameter was also controlled using Ca^{2+} ion exchange. As a proof of principle, we cultured C2C12 mouse myoblast cells on double layer systems to investigate biocompatibility and formation of functional muscle tissue on fabricated scaffolds.

Results and Discussion

We were able to achieve good cell adhesion and orientation guided by aligned fibers. We recognized that cell growth and proliferation depends on each separate layer thickness. Mouse muscle cells (C2C12) grown and differentiated on fibrous bilayer were electrically stimulated showing the synchronized contraction of mature and aligned generated myotubes adhered on fibers.

Conclusion

Fabricated stimuli-responsive bilayer system possesses positive effect on cell alignment and spreading, leading to more accessible biofabrication method for formation of highly structured tubular tissues like skeletal muscle bundle fibers.

References

[1] Kirillova, A; Maxson, R; Stoychev, G; Gomillion, T. C; Ionov, L. Adv. Mater., **2017**, 29, 1703443.

[1] Stroganov, V; Pant, J; Stoychev, G; Janke, A; Jehnichen D.; Fery, A; Hitesh, H; Ionov. Adv. Funct. Mater., **2018**, 28, 1706248.

[2] Vannozzi, L; Yasa, C.I; Ceylan, H; Menciassi, A; Ricotti, L; Sitti, M. Macromol. Biosci., **2018**, 18, 1700377.

[3] Apsite, I; Stoychev, G; Zhang, W; Jehnichen, D; Xie, J; Ionov, L. Biomacromolecules., **2017**, 18, 3178

[4] Jiang, S; Liu, F; Lerch, A; Ionov, L; Agarwal, S. Adv. Mater., **2015**, 27, 4865.

[5] Ostrovidov, S; Ebrahimi, M; Bae, H; Nguyen, H. K; Salehi, S; Kim S. B; Kumatani, A; Matsue T; Shi, X; Nakajima, K; Hidema, S; Osanai, M; Khademhosseini, A. Appl. Mater. Interfaces, **2017**, 9, 42444

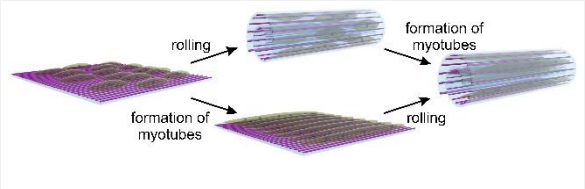

Scheme of skeletal muscle bundle formation

PS2-05-317

Adjustable Thermo-Responsive Materials from Three-armed Macromers for Cell Carrier and Implant Design

Ketpat Vejjasilpa, Iram Maqsood, Michaela Schulz-Siegmund, Michael C. Hacker

Leipzig University, Institute of Pharmacy, Pharmaceutical Technology, Medical Faculty, Leipzig, DE

Introduction

Mechanical stimulation of cells during cultivation has become an effective strategy to direct cell differentiation towards a specific phenotype and increase tissue maturity. Such a stimulation can be applied in bioreactors with plungers, membrane movement or hydrostatically [1]. A novel, less explored strategy is the use of a mechanically active polymer. *N*-Isopropylacrylamide (NiPAAm) is a thermo-responsive polymer with a lower critical solution temperature (LCST) at around 32°C that has been excessively using in the design of thermos-responsive materials. At physiological temperature (37°C), the polymer shows mildly hydrophobic property on the surface. When the temperature is lower than LCST, the polymer becomes hydrophilic and takes up water which increases the bulk volume and biomaterial dimensions [2]. Strategies to adjust the transition temperature of poly(NiPAAm) include copolymerization or bioconjugation. The covalent incorporation of hydrophilic comonomers or molecules results in an increased transition temperature. The opposite effect is achieved with hydrophobic modifications. In these strategies, the material does not support cell or tissue adhesion below the LCST due to its hydrophilic nature. Another challenge with poly(NiPAAm) in biomedical application is that the polymer is not resorbable, thus limiting its application [3].

In this work, we report the synthesis and characterization of copolymers containing copolymerized NiPAAm with adjusted transition temperature. We aim at a material that allows for cell cultivation a few degrees above and below the LCST. The materials are designed to contain 2-(dimethylamino)ethyl acrylate (DMAEA) as a hydrophilic comonomer that incorporates cationic moieties for cell and tissue interaction, 4-acryloylmorpholine (AMO) for further hydrophilic modification and trimethylolpropane triacrylate (TMPTA) in order to incorporate ester bonds to improve the degradative properties of the material.

Experimental Methods

NiPAAm (97%), DMAEA, AMO and TMPTA were purchased from Sigma-Aldrich. NiPAAm was dissolved in dried hexane (10g in 100mL at 50 ℃) and recrystallized before used. 2,2-Azobis(2-methylpropionitrile) (AIBN) was used as received. Dried tetrahydrofuran (THF) was used as solvent in this reaction. Briefly, Poly(NiPAAm-*co*-AMO-*co*-DMAEA) of different molar composition was synthesized at 60 ℃ for 24 hours by radical polymerization using AIBN as initiator (0.3%wt). NiPAAm (2 g) was weighted and dissolved in a 50 mL centrifugal tube, then other monomers at different ratios were introduced. The reaction was carried out in nitrogen atmosphere. After 24 hours the copolymer was precipitated in diethyl ether (10:1 ratio) for 2 times, and dried under nitrogen flow for 3 hours and were vacuum-dried for 24 hours. Copolymer composition was determined by ^{1}H-NMR and the molecular weight was evaluated by gel permeation chromatography (GPC). lower critical solution temperature (LCST) of the copolymer was determined with differential scanning calorimetry (DSC). The copolymer (20 wt. % solution in PBS) at 5 ℃/min from -10 ℃ to 60 ℃. Analysis was performed in triplicate. In order to further evaluate thermo-responsive and mechano-active behavior, the copolymers were dissolved in THF (20% solution), dispersed on a cellulose membrane and allowed to dry at the

room temperature until returning to their original weight. fixed-copolymer membranes were placed in 10 mL of PBS. The changes of material morphology during changing temperatures were recorded with a camera.

Results and Discussion

Copolymers could be copolymerized and isolated in the desired ratios. The LCST of the copolymer was controlled by comonomer composition. The copolymers have shown thermo-responsive properties around physiological temperature. The presence of TMPTA which promotes copolymer branching and network formation significantly contributed to thermogel stability (Fig. 1). The introduction of DMAEA and AMO, which are hydrophilic monomers into the copolymer increased LCST significantly. However, an increase in feed ratio of TMPTA, which is a hydrophobic building block, significantly decreased LCST. Interestingly, the addition of AMO into the copolymer helped compensate the effect of TMPTA on LCST effectively and TMPTA-containing copolymers with an LCST above 35°C could be obtained (Fig. 2). This effect has been attributed to the non-ionic, hydrophilic property of AMO that impairs copolymer aggregation and shrinkage [4], thus increasing LCST of the polymeric material.

Conclusion

This work demonstrates characterization of potential thermo-responsive biomaterial for biomedical applications. The polymer were successfully embedded onto the membrane surface and shown promising mechanical properties after changing the temperatures. Results from this work suggests that this copolymer could be used for modifiable biomaterial surface and prospectively for mechano-active biomaterial design for use in temperature controlled bioreactors.

References

1. Tran, S.C., A.J. Cooley, and S.H. Elder, *Effect of a mechanical stimulation bioreactor on tissue engineered, scaffold-free cartilage.* Biotechnol Bioeng, 2011. **108**(6): p. 1421-9.

2. Pich, A. and W. Richtering, *Microgels by Precipitation Polymerization: Synthesis, Characterization, and Functionalization*, in *Chemical Design of Responsive Microgels*, A. Pich and W. Richtering, Editors. 2011, Springer Berlin Heidelberg: Berlin, Heidelberg. p. 1-37.

3. Cui, Z., et al., *Degradation, cytotoxicity, and biocompatibility of NIPAAm-based thermosensitive, injectable, and bioresorbable polymer hydrogels.* J Biomed Mater Res A, 2011. **98**(2): p. 159-66.

4. Rivas, B.L., A. Maureira, and K.E. Geckeler, *Novel water-soluble acryloylmorpholine copolymers: Synthesis, characterization, and metal ion binding properties.* Journal of Applied Polymer Science, 2006. **101**(1): p. 180-185.

Acknowledgement

This research is partially funded by the Deutsche Forschungsgemeinschaft (DFG, German Research Foundation) – project 59307082 – TRR67 A1). The author gratefully acknowledge financial support for Ketpat Vejjasilpa from the Royal Thai Government.

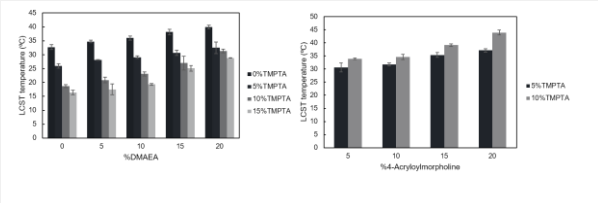

Figure2) Adjuctable LCST of copolymer

Copolymer shown decrease LSCT in a present of increasing crosslinker (left) and fine tuning of LCST around physiological temperature through addition of AMO (right).

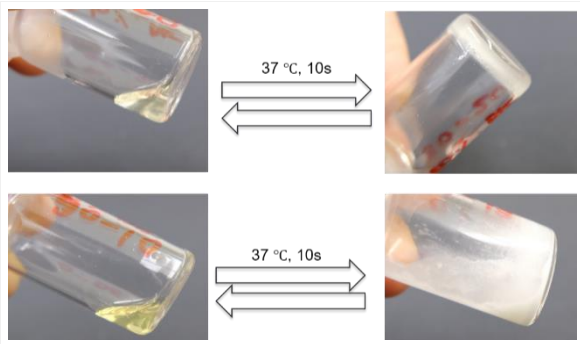

Figure 1) Thermoresponsive copolymer
Top: Solution (20% solution) of copolymer (90% NiPAAM and 10%DMAEA) with 15% TMPTA. Bottom: Solution of copolymer without TMPTA.

PS2-05-318

Smart nanocapsules based on polypeptides to protect and enhanced anti-inflammatory properties of natural actives validated for topical application

Damien Dupin

CIDETEC Nanomedicine, Biomaterials Unit, Donostia-San Sebastián, ES

Introduction

The skin, the largest human organ, acts as a barrier between the organism and the external environment for UV protection, against physical/chemical damage and microbiological attack, for the maintenance of body temperature and sensorial functions (pain and temperature). However, modern style of life implies multiple contacts with increasing amount of chemicals in everyday products as well as over-exposition to UV light, mainly for leisure activities and outdoors workers. Those frequent exposures harm the skin, resulting in an increase of conditions such as irritant and allergic contact dermatitis (ICD & ACD), skin photo-damage.

In the current work, a new generation of smart nanocapsules based on specially designed polypeptides was produced and validated for the protection, transport and efficient release of natural active compounds to repair the skin. Herein, we report the first results obtained for the production of highly stable nanocapsules containing hydrophobic or hydrophilic actives. Triggered-release studies have been investigated in healthy and damaged skin, in addition to skin penetration studies and cytotoxicity tests with all types of cells. Performances of the encapsulated actives in terms of viability and anti-inflammatory properties were studied on skin model validated for irritant contact dermatitis, allergic contact dermatitis and skin photo-damage.

Experimental Methods

Skin penetration. Fluorescence spectroscopy was carried out to determine first the penetration of the nanocapsules containing a fluorescent dye in the oil phase, the distribution of the nanocapsules inside the skin.

Skin models. Synthetic or human ex-vivo skin models were treated with 5 wt% of aqueous solution of sodium dodecylsulfate (ICD), 10 wt% of aqueous solution of 4-nitrobenzyl bromide (ACD) and exposed to 30 min UV-B (photo-damage).

Application of nanocapsules. 5 µL of the nanocapsules dispersion were applied on the surface of the skin (healthy or previously treated to induce skin conditions). After peeling the epidermis form the dermis, biomarkers for cell viability (MTT assay) and inflammation (IL1α and IL-18) were recorded.

Results and Discussion

Nanocapsules of around 80 nm were produced at pH 5.5, as judged by DLS and cryogenic transmission electron microscopy. Long term stability studies have shown that the nanocapsules were stable for over 2 years. Slightly turbid dispersion at pH 5.5 became completely transparent at physiological conditions, indicating the burst of the nanocapsules. DLS studies demonstrated that the nanocapsules were first aggregating, before being completely burst. On the other hand, specially designed polypeptides to exhibit release targeted by the presence of enzyme were used to produce capsules. The encapsulated active was released in the presence of MMP-2 or MMP-9 enzymes encountered in the skin conditions considered in this study. Localization studies on healthy skin have shown that the capsules cargo remained in the epidermis. Also, it was shown with Nile Red that fast release (< 1hr) occurred on

damaged skin whereas sustained release over 24 hrs was seen on healthy skin, showing the smartness of the system to adapt to the skin needs. Different active ingredients were successfully encapsulated like Hyaluronic acid, Dipotassium glycyrrhizinate, retinyl palmitate, curcuma and ceramides.
All nanocapsules proved to be biocompatible without provoking irritation. Interestingly, the nanocapsules could prolong the lifetime of fragile active like retinyl palmitate and curcuma which still showed some activity after 3 months exposure to light and oxygen. In addition, a case by case study of all the encapsulated actives showed that the performances of the encapsulated ingredient was up to 4 times higher than the compound alone when applied to skin models for ICD, ACD and skin photo-damage, especially for their anti-inflammatory properties.

Conclusion

A new generation of stable nanocapsules has been produced with hydrodynamic diameters of around 80 nm. They showed smart release thanks to the specially designed polypeptide used for their production. Different active ingredient could be encapsulated and the stability of the fragile ones was increased significantly. Thanks to its better penetration, the performances of the active ingredient were dramatically enhanced as judged by skin models studies. The nanocapsules are now exploited as cosmetic ingredients for final product formulation. Current works are focussing on dermatology and functional food application.

References

1. Hadgraft, J. Int. J. Pharm. 224:1–18, 2001
2. Degim, T. I. Drug Discov. Today 11:517–523, 2006
3. EP17306354.6: 'New Polymeric Emulsifier and Uses thereof for the Encapsulation of Hydrophobic Active Compounds'

Acknowledgement

The authors would like to thank the EU framework program for research and innovation Horizon 2020 (Grant no: 686141).

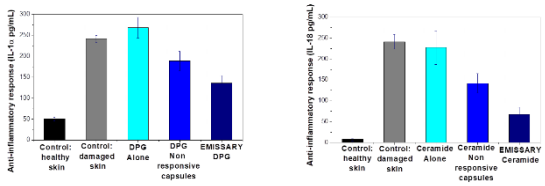

Figure 2. Enhancement of anti-inflammatory properties of dipotassium glycyrrhizinate and ceramides.
Figure 2 shows the enhancement of the anti-inflammatory properties of natura active ingredients (DPG and Ceramides) by the dramatic decrease of IL-1alpha and IL-18 on photodamaged skin models.

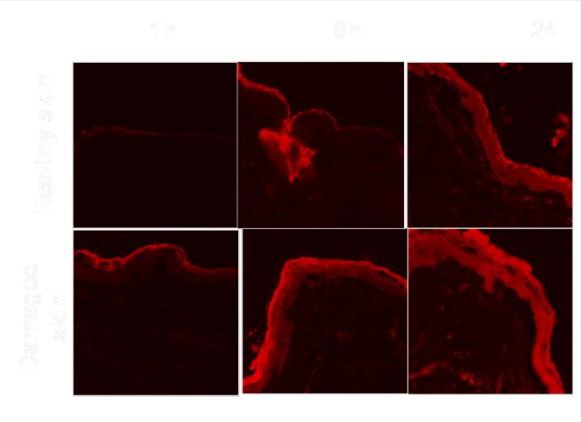

Figure 1. Dual release of active compounds depending on skin needs
Figure 2 shows the different kinetics release depending on skin needs, i.e. very fast on damaged skin within an hour and sustained over 24 hrs on healthy skin.

PS2-05-319

Self-Folding Films to Emulate Blood Vessels

Juan M. Uribe[1], Sahar Salehi[2], Leonid Ionov[1]

[1]University of Bayreuth, Biofabrication, Bayreuth, DE; [2]University of Bayreuth, Biomaterials, Bayreuth, DE

Introduction

4D biofabrication is introduced as extension of 3D printing and offers several advantages in the fabrication of tubular constructs such as high resolution and no need of sacrificial materials [1]. Current bioprinting technologies are however unable to fabricate vascular networks due to the size of printable structures. Printing of shape-morphing biopolymer hydrogels has been recently introduced to fabricate self-folding tubes with unprecedented control over their diameters and architectures at high resolution [2].

Experimental Methods

Therefore, in this study, self-folding of bi-layer printed film of methacrylated hyaluronic acid (HA-MA) with meltelectrowrited fibers of Polycaprolactone-polyurethane (PCL-PU) thermoplastic elastomers was evaluated. In previous investigations we crosslinked the hydrogel using Eosin Y in 1-vinyl-2-pyrrolidinone and Triethanolamine as described in [3, 4].

Results and Discussion

However, this system was not optimal due to the low viability of cells in those polymers. Thus, in the current study we showed the improvement of cell viability using different crosslinking agents and adding a mesh of different material that provides support for cells alignment.

Conclusion

Our results proved successful folding of printed bi-layer film while the encapsulated cells stayed viable and functional.

References

[1] L. Ionov, “4D Biofabrication: Materials, Methods, and Applications,” *Adv Healthc Mater,* no. 1800412, **2018**.

[2] A. Kirillova, et al, “4D Biofabrication Using Shape-Morphing Hydrogels,” *Adv. Mater.,* no. 1703443, p. 29, **2017**.

[3] J. Smeds, et al, “Photocrosslinkable polysaccharides for in situ hydrogel formation,” *J. Biomed. Mater. Res.,* no. 254, p. 55, **2001**.

[4] Spencer L. et al, “Visible light crosslinking of methacrylated hyaluronan hydrogels for injectable tissue repair,” *J. Biomed. Mater. Res. B.,* no. 104, p. 1229-1236. **2016**.

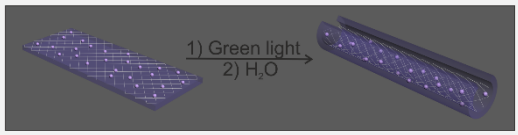

Patterned self-folding bilayer as a vascular graft.

PS2-05-320

Developing a novel system to aid tissue expansion via tensile strain induced growth for skin regeneration

Nuttaporn Jarangdej[1], Eagle Antanaviciute[1], Eleanna Kritikaki[1], Carlos L. Orts[1], Ricky Unadkat[1], Andrew Hamilton[2], Mathis Riehle[1]

[1]University of Glasgow, Institute of Molecular Cell and Systems Biology, Glasgow, GB; [2]University of Glasgow, School of Medicine, Dentistry and Nursing, Glasgow, GB

Introduction

Extensive injuries to the skin can lead to loss of function and have a significant impact on patients. Despite advances in microsurgery, the use of allogenic or autologous transplants can still remain a challenge. Mechanical forces are crucial growth factors to maintain homeostasis of connective tissues. Skin dermis is an elastic organ which mainly composed of mesenchymal cells include fibroblasts. The viscoelastic properties of skin that enable it changes to their shape under stretched or deformed [1]. Cells actively sense and respond to mechanical stimuli through integrin receptors. Integrins associated to their protein linkers such as vinculin and talin that link the extracellular matrix (ECM) to the cytoskeleton within. One of the major regulators of actin cytoskeleton dynamics is RhoA, can indirectly couple intracellular tension to cytoskeletal gene expression via myocardin-related transcription factor A (MRTF-A) [2]. Understanding their molecular mechanisms can aid to minimise the risk of tissue expansion.

Experimental Methods

Preparation of substrates: Polycaprolactone (PCL) or Polydimethylsiloxane (PDMS) membranes are adhered to 3D printed blocks and treated with air plasma for 1-1.17 mins to increase hydrophilicity. Then, modified PDMS surfaces are obtained from 2 µg/ml of fibronectin or laminin.

Cell stretching, immunofluorescence and Alamar blue assay: The cells are seeded at 2 x 10^5 cells and applied stretch at 1 mm/day. Then, cells are stained for MRTF-A or vinculin, f-actin and nucleus. Images are proceed using CellProfiler and R software. Finally, the cell viability is tested by Alamar blue assay.

Results and Discussion

As a result of stretch-activated growth at a speed of 173.6 nm/h/cell after stretching for 12h and 24h, the n/c MRTF-A ratios increased around 7±12% and 11±9%, respectively. There is no significant change in the cell and nuclear orientation. The concept of cyclic stretch is further used to develop the device with the combination of ECM proteins coating on a stiffer substrate. The preliminary results showed that the cells bound more tightly to modified PDMS membranes with laminin or fibronectin absorption. Figure 1 displayed samples of actin mesh, distribute normality A) without stain B) apply 4.17% unidirectional continuous stretch and modified surface with C) laminin and D) fibronectin.

Conclusion

Stretch-induced growth promotes the translocation of MRTF-A into the nucleus during 24 hours of stretch. Substrate is modified by treating with laminin and fibronectin (Fn), globular Fn enables cell adhesion while the unfold Fn conformation into fibrils remains a crucial factor for integrins/GF domains. Cyclic stretch could further use to combine the surface coating for more effective therapeutic methods.

References

[1]Kishi, K., Okabe, K., Shimizu, R. and Kubota, Y. (2012) 'Fetal skin possesses the ability to regenerate completely: complete regeneration of skin', *Keio J Med,* 61(4), pp. 101-8. [2]Vining, K. H. and Mooney, D. J. (2017) 'Mechanical forces direct stem cell behaviour in development and regeneration', Nat Rev Mol Cell Biol, 18(12), pp. 728-742.

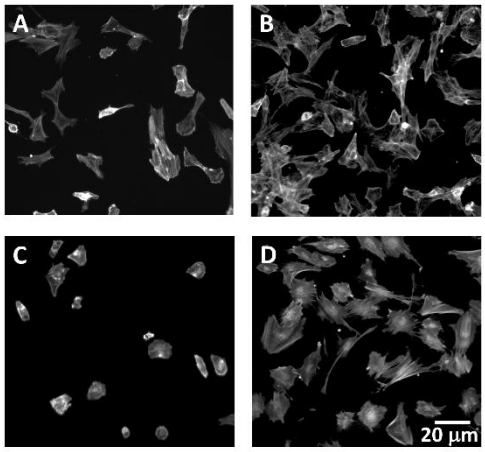

Examples of actin cytoskeleton under ECM coating or unidirectional stretch regulation
Actin arrangement in A) control B) stretched group. The cells are coated with C) laminin and D) fibronectin. The results revealed that stretched cells attached and more proliferate compared to control.

PS2-05-321

Bioplotting of magnetically deformable scaffolds

Janina Spangenberg[1], Charis Czichy[2], David Kilian[1], Anja Lode[1], Stefan Günther[2], Stefan Odenbach[2], Michael Gelinsky[1]

[1]TU Dresden, Centre for Translational Bone, Joint and Soft Tissue Research, University Hospital Carl Gustav Carus and Faculty of Medicine, Dresden, DE; [2]TU Dresden, Chair of Magnetofluiddynamics, Measurement and Automation Technology, Dresden, DE

Introduction

Over the last years, additive manufacturing processes have become increasingly important for the manufacturing of individual implants. A new approach in this field is the utilization of hydrogels compounded with (stem) cells and magnetic micro particles. With extrusion based printing, three dimensional deformable constructs can be fabricated. By applying an alternating external magnetic field, these hydrogel structures will be deformed cyclically. This cyclic deformation is supposed to stimulate cells within the gel to initiate a controlled differentiation. Our research is focused on the interactions between hydrogel matrix, particles, cells, and magnetic field. A key challenge is to establish a correlation between macroscopic deformation and microscopic particle structures. In the current study, a plottable particle-matrix system was established to support cell survival as well as show its deformation in a magnetic field.

Experimental Methods

The well-established 3 % w/w alginate and 9 % w/w methylcellulose plotting paste (alg/MC) was used as a base material. [1] 25 % w/w of magnetite micro particles (50 % between 20 and 30 microns) were added to the gel. Rheological properties of the paste before crosslinking and mechanical properties after crosslinking were investigated. Cytocompatibility of these materials was tested by culturing a mesenchymal stem cell line (hTERT-MSC) [2] in extracts collected from the gels. Furthermore, hTERT-MSC were added to the magnetite-containing alg/MC paste before plotting with the Bioscaffolder 3.1 (GeSiM mbH, Radeberg, Germany) and crosslinking with calcium chloride solution; alg/MC without magnetite served as control. The resulting scaffolds were examined after live/dead cell staining by confocal microscopy.

X-ray micro computed tomography (µCT) was used to determine the macroscopic geometry and the deformation of hydrogel samples as well as the particle structures and particle motions on a microscopic scale. Model samples with a simple and defined geometry were placed in a specially designed magnetic field setup that was scanned in a laboratory µCT system in two consecutive measurements with and without a magnetic field.

Results and Discussion

The addition of 25 % w/w of particles increased the viscosity of the alg/MC paste while its shear thinning behavior and at the same time its printability were maintained. Adding more than 25 % w/w of particles led to a continuous increase in the viscosity of the gel as well as in the Young's modulus of the crosslinked construct.

The components of the composite material, especially the magnetic particles, and the crosslinking with 0.1 M calcium chloride solution had no negative influence on cell viability. Apart from that, the paste proved itself to be suitable for bioprinting with mesenchymal stem cells. No significant difference between cell viability of the bioplotted paste with and without 25 % w/w particles could be detected.

The effect of different particle concentrations on the saturation magnetization was also determined. A higher particle concentration was shown to increase the saturation magnetization. Strands of the described composite material were successfully deformed by a magnetic field.

Conclusion

In this study, it was shown that hydrogels with incorporated magnetite micro particles are suitable for 3D bioprinting and magnetically induced deformation. Based on the determination of the rheological properties of the composite material, three dimensional constructs were successfully plotted with and without stem cells. Samples of simple, defined geometries were deformed in a controlled, closely monitored way. Since the rheological, mechanical, and magnetic properties of the magnetic hydrogels depend on the matrix material, the particle size, and the particle concentration, an adjustable material system was developed for the controlled deformation of stem cells within a scaffold. Further experiments regarding the magnetically induced deformation of bioplotted scaffolds under sterile conditions are planned.

References

[1] K. Schütz, A.-M. Placht, B. Paul, S. Brüggemeier, M. Gelinsky, A. Lode: 3D plotting of a cell-laden alginate/methylcellulose blend: towards biofabrication of tissue engineering constructs with clinically relevant dimensions. *J Tissue Eng Regen Med***2017**, 11, 1574-1587

[2] W. Böcker et al.: Introducing a single-cell-derived human mesenchymal stem cell line expressing hTERT after lentiviral gene transfer *J. Cell. Mol. Med*. **2008**, 12, 1347–59

Acknowledgement

The authors would like to thank the European Social Fund (ESF) and the Free State of Saxony for financial support of this project in the course of the ESF Young Researchers Group IndivImp at TU Dresden.

PS2-05-322

Functional magnetic PDMS membranes and their compatibility assessments

Berkay Erenay[1], Bora Garipcan[1], **Sedat Odabas**[2]

[1]Bogazici University, Institute of Biomedical Engineering, Istanbul, TR; [2]Ankara University, Biomaterials and Tissue Engineering Laboratory (BteLAB); Department of Chemistry, Ankara, TR

Introduction

Tissue engineering is a set of scientific principles, which concentrates on rehabilitation of damaged tissues and organs as well as regeneration and renewal of tissues and involving cells, tissue matrices (scaffolds) and biologically active molecules. Even though one of the main goals of tissue engineering is the transplantation of tissues and organs, designed in the laboratory, to the patients directly, the healing via this approach is hard to achieve in near future. One of the main problems is that effects of the micro-environment, and physical, chemical parameters in these microenvironments on cellular behavior are still not very well understood. Mimicking the surfaces both physically and chemically where cells are interacting with, along with mechanical stress applied to them in-vitro could help them understand the behavior of the cells[1]. Here in this study **PDMS**, which has plenty of applications in non-tissue engineering areas were used and combined with stable super-paramagnetic nanoparticles that have the ability to exert micromechanical stress on cells.

Experimental Methods

Super-paramagnetic nanoparticles were synthesis by a well-known co-precipitation method and characterized with Zeta-Sizer, TEM, and VSM[2]. Plain PDMS membranes were prepared by mixing of silicon elastomer and curing agent with 10:1 (w/w) ratio (SYLGARD® 184). A desiccator was used to remove the air bubbles prior to curing. After desiccation, PDMS samples were cured in an oven at 70°C for 4 hours[3]. Magnetic PDMS membranes were prepared with the same method but a difference of combining the various amount of magnetic nanoparticles into the recipe (0.5-2% w/w). All PDMS membranes were characterized by SEM, AFM, and VSM.
In order to assess their compatibility in terms of cytotoxicity (by MTT assay), hemo-toxicity (by hemolysis assay) and proliferation ability(by Alamar assay), all samples were treated with O2 plasma prior to experiments.

Results and Discussion

According to TEM and VSM results, these particles have 10nm average diameter and have 55emu/g magnetic strength that is well-enough for cellular applications. There is an apparent decrease in magnetic strength in magnetic PDMS samples but here we believe it may adequate to trigger physical stress over cells. According to compatibility assessments, magnetic PDMS membranes shows quite a bio and hemocompatibility and dislike plain PDMS it also allows better cell attachment and growth. It is also obvious that the any-compatibility behavior of these membranes decreases as magnetic particle concentration increases. The homogeneity issue is also a critical issue that should address. Here we tried ultrasonication, homogenization and other physical methods to obtain a homogenous distrubipın of the particles.

Conclusion

Within this study, it is shown that PDMS membranes with magnetic properties could have prospective biomaterials as they have proper bio and hemocompatibility and as they have the ability to trigger mechano-transductive pathways of the cells.

References

[1] Bilgen, Bahar, and Sedat Odabas. "Effects of Mechanotransduction on Stem Cell Behavior." *Advanced Surfaces for Stem Cell Research* (2016): 45-65.

[2] M. Özgen Öztürk, Bogazici University, Institute of Biomedical Engineering, MSc Thesis, 2012, p 14.

[3] Odabaş, Sedat, et al. "Separation of mesenchymal stem cells with magnetic nanosorbents carrying CD105 and CD73 antibodies in flow-through and batch systems." *Journal of Chromatography B* 861.1 (2008): 74-80.

Acknowledgement

This study has been supported by The Scientific and Technological Research Council of Turkey (TUBİTAK)-Grant No: 217M551 and Scientific Research Projects Offices of Ankara University (Grant No: 17H0430008) and Bogazici University (Grant No: 6701).

PS2-05-323

Spatial and temporal control of multicomponent supramolecular gels formed by mutually interactive orthogonal networks

Carmen Cristina Piras, David K. Smith

University of York, Chemistry, York, GB

Introduction

The field of supramolecular biomaterials has seen a wide expansion in the last few years towards functional versatile materials for a broad range of biological applications.[1, 2] In this perspective, achieving spatial and temporal control over gelation offers a unique opportunity to more effectively reproduce the dynamic natural environment of tissues. The fabrication of spatially defined multidomain biomaterials with different properties (e.g. stiffness and porosity) in the different domains allows controlling the release of bioactive molecules in specific gel domains and directing the proliferation, migration and differentiation of cells.[2]

Experimental Methods

We have studied two dibenzylidene-D-sorbitol based low molecular weight gelators, namely 1,3:2:4-di(4-acylhydrazide)-benzylidene-D-sorbitol (DBS-$CONHNH_2$) and 1,3:2,4-dibenzylidene-D-sorbitol-4',4''-dicarboxylic acid (DBS-COOH), which form a multicomponent gel using a stepwise approach combining a thermal trigger (heat-cool cycle) and a pH trigger (glucono-d-lactone, GdL). The heat-cool cycle induces the self-assembly of DBS-$CONHNH_2$, which is followed by the self-assembly of DBS-COOH induced by decreasing pH, forming orthogonal self-sorted networks in a temporally controlled manner. The resulting multicomponent gel was studied by a range of techniques (*i.e.* IR, NMR, SEM, TEM, rheology) to obtain insight on the self-assembly process, the nanoscale structuring and the macroscopic properties of the gel.

Results and Discussion

We demonstrated that the two networks are self-sorted and independent from each other, but to some extent they interact synergistically within the multicomponent gel, leading to a material with enhanced mechanical and thermal properties. Moreover, the DBS-COOH network within the multicomponent gel can be individually addressed by "switching it on and off" by pH changes. Gel formation could also be induced by substituting Gdl with diphenyliodonium nitrate (DPIN), a photoacid generator which releases protons under photoirradiation. By inducing the self-assembly of the DBS-COOH network within a pre-formed DBS-$CONHNH_2$ gel using a photomask, photopatterning can be applied to the multicomponent gel leading to spatial control over the formation of a multidomain gel with different properties in the different domains. We showed that the composition of the multicomponent gel domains can control the release rate of the bioactive ingredient heparin. Moreover, it can also direct the *in situ* formation of Au nanoparticles in specific gel areas.

Conclusion

Such structured soft materials may have potential applications in regenerative medicine or bionanoelectronics.

References

1. Hoque, J.; Sangaj, N.; Varghese, S., Stimuli-Responsive Supramolecular Hydrogels and Their Applications in Regenerative Medicine. Macromolecular Bioscience 2019, 19 (1).

2. Leijten, J.; Seo, J.; Yue, K.; Santiago, G. T.-d.; Tamayol, A.; Ruiz-Esparza, G. U.; Shin, S. R.; Sharifi, R.; Noshadi, I.; Álvarez, M. M.; Zhang, Y. S.; Khademhosseini, A., Spatially and Temporally Controlled Hydrogels for Tissue Engineering. Materials science & engineering. R, Reports : a review journal 2017, 119, 1-35.

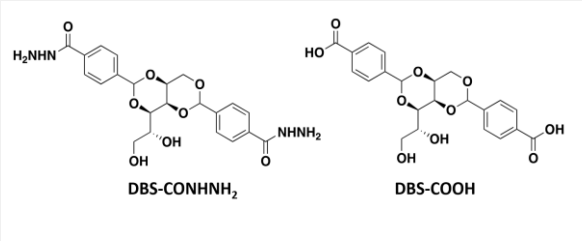

Structure of DBS-CONHNH2 and DBS-COOH

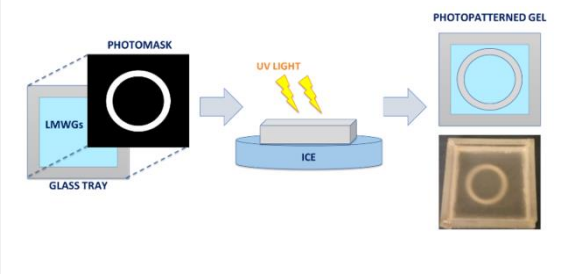

Schematic representation of photopatterning.

PS2-05-324

Stimuli-responsive drug delivery system: Carbon dot coated alginate beads as a smart biomaterial

Sristi Majumdar, Gargee Krishnatreya, Neelam Gogoi, Debajit Thakur, Devasish Chowdhury

Institute of Advanced study in Science and Technol, Physical Science Division, Guwahati, IN

Introduction

The frontier of drug development has always been widening and quite exciting. But the recurrent emergence of infectious diseases and the complexity of the environment have led to pressing health needs[1]. Hence the traditional drug development paradigm requires the support of modern tools for better results. The physiological barriers and local environment understanding have contributed to efficient drug targeting[2]. Yet, the lack of targeted drug release led to the interaction of the drug with healthy tissue and resulted in unacceptable side effects[3]. Drug delivery systems (DDS) are engineered technologies that help in drug release at targeted areas[4]. DDS helps in administering drug locally in the affected areas. This reduces any chances of side effects and also increases the bioavailability of the drug[5].

In this work, we have developed a drug delivery system using alginate polymer coated with carbon dots synthesized from chitosan hydrogel[6]. This pH-responsive DDS is a smart model which delivers drug depending upon the concentration of the pathogen at the medium. As the number of pathogen increases in the medium, it releases various secondary metabolites. These secondary metabolites contain phenolic compounds which lower the pH of the medium. And as the pH of the medium decreases, the DDS releases the drug. Hence the more the number of bacteria higher will be the drug release.

Experimental Methods

In this work, calcium alginate (CA) beads were prepared by dropwise adding 5ml of 1% sodium alginate solution to 100ml of 0.1M $CaCl_2$ under constant stirring conditions. This resulted in the crosslinking of sodium alginate with Ca^{2+} ions and formation of spherical beads, instantly. For complete gelation, the CA beads were kept overnight in $CaCl_2$ solution and then properly washed with distilled water. The so-prepared CA beads tend to shrivel within a few hours when kept not soaked in water. To increase the shelf life of the beads, they were coated with chitosan carbon dots. The preparation of carbon dots (CD) from chitosan and its coating on CA beads were done following a previous report from our group[6]. The CA-CD beads thus prepared were further used for drug loading.

Preparation of Garlic extract (GE) as the model drug and its loading into CA-CD beads (CA-CD-GE): The garlic cloves were peeled, mashed in a garlic press and collected in a beaker. 1g of the mash was weighed and transferred to 50ml of the falcon tube. Extra care was taken to avoid heat transfer from hands. The mash was pressed for the extraction of its active compound. The extract was then centrifuged for 10 minutes at 7000rpm at 4^{o}C. The supernatant was then again filtered through a 0.45µm syringe filter. 50µl of the filtrate was collected in a 50ml falcon tube and 50ml of cold Milli Q water was added and mixed gently for 20 seconds. The major active compound with antibacterial property present in GE is allicin. CA-CDs of the almost same size were weighed and immersed in 30ml of 0.1% GE for 4hours.

Results and Discussion

In vitro drug release study by CA-CD-GE beads: Three falcon tubes were labeled as “control”, “CA-CD” and “CA-CD-GE”. The control tube contained NB and MRSA to monitor the undisturbed growth of MRSA. The second tube named CA-CD contained NB, MRSA and CA-CD bead (without drug) to determine any superfluous effect in the system. The third tube contained NB, MRSA, and drug-loaded beads hence named “CA-CD-GE”. The second and third tube contained 10 beads of almost same size. All the tubes were then incubated at 37^{o}C at 175rpm. 500 µL of the sample was taken out from each test tube and the optical density was measured in UV-Vis spectrophotometer at 600nm at a different time interval. It was inferred that the MRSA cells continued to divide and increase in cell mass. The similar growth pattern was observed in the control and CA-CD tubes, unlike the CA-CD-GE tube where after 10th hour the O.D. of the culture started to decrease significantly. This might be due to the excessive growth of MRSA which resulted in the production of various secondary metabolites. This resulted in a decreased pH of the medium. As our system was designed to release the drug at low pH, hence the CA-CD-GE beads released the drug resulting in cell death.

Conclusion

In summary, we have fabricated a stimuli-responsive smart drug delivery system which releases the drug only when it is necessitated. This unique drug delivery system is not only stimuli-responsive but also is a controlled drug release system as it releases drug according to the cell concentration. All the three factors viz. drug release, cell concentration and pH of the medium are interdependent as when the cell divides, it produces secondary metabolites which lead to the decline in pH of the medium. The drop in the pH value triggers drug release from the beads. And the effect of the drug is reflected by the MRSA cell death. Such smart drug delivery systems hold utmost importance in the near future as it can find multi-applications in the biomedical field.

References

1. Michalet, X.; Pinaud, F. F.; Bentolila, L. A.; Tsay, J. M.; Doose, S.; Li, J. J.; Sundaresan, G.; Wu, A. M.; Gambhir, S. S.; Weiss. Quantum dots for Live Cells, In vivo Imaging, and Diagnostics. Science 2005, 307, 538−544.
2. Lovric, J.; Cho, S. J.; Winnik, F. M.; Maysinger, D. Biomedical Applications and Toxicology of Carbon Nanomaterials Chem. Chem. Biol. 2005, 12, 1227−1234.
3. Xu, X.; Ray, R.; Gu, Y.; Ploehn, H. J.; Gearheart, L.; Raker, K.; Scrivens, W. A. Electrophoretic Analysis and Purification of Fluorescent Single-walled Carbon Nanotube Fragments. J. Am. Chem. Soc. 2004, 126, 12736.
4. Li, Q.; Ohulchanskyy, T. Y.; Liu, R.; Koynov, K.; Wu, D.; Best, A.; Kumar, R.; Bonoiu, A.; Prasad, P. N. Photoluminescent Carbon Dots as Biocompatible Nanoprobes for Targeting Cancer Cells In vitro. J. Phys. Chem. C 2010, 114, 12062−12068.
5. Liu, C.; Zhang, P.; Zhai, X.; Tian, F.; Li, W.; Yang, J.; Liu, Y.; Wang, H.; Wang, W.; Liu, W. Nano-carrier for Gene Delivery and Bioimaging based on Carbon Dots with PEI-passivation Enhanced Fluorescence. Biomaterials 2012, 33, 3604−3613.
6. Gogoi, N.; Chowdhury, D. Novel Carbon Dot Coated Alginate Beads with Superior Stability, Swelling and pH Responsive Drug Delivery. J. Mater. Chem. B 2014, 2, 4089−4099.

Acknowledgement

D.C. thanks SERB, New Delhi, Grant SB/S1/PC-69/2012, and BRNS, Mumbai, Grant 34/14/20/2014-BRNS, for funding. S.M thanks BRNS for a fellowship.

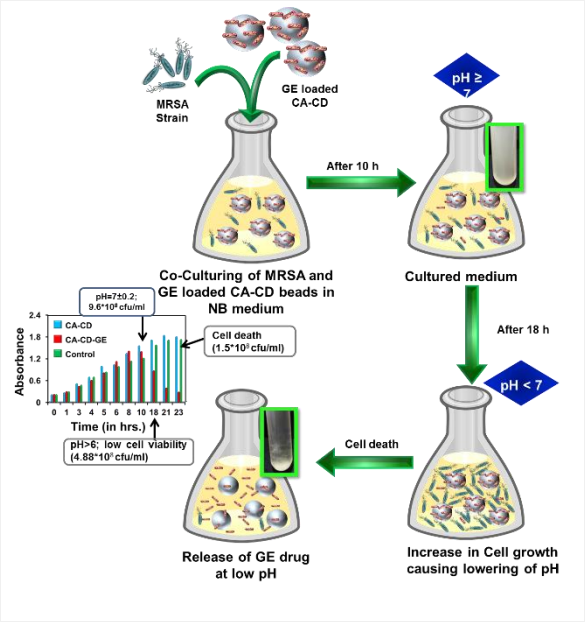

Schematic representation of smart stimuli responsive Drug delivery system

PS2-05-325

Stimuli-responsive Collagenase nanocapsules for the treatment of skin diseases

Víctor M. Moreno[1,2,3], María R. Villegas[1,2,3], Alejandro Baeza[4], María Vallet-Regí[1,2,3]

[1]Universidad complutense de Madrid, Departamento de Química en Ciencias Farmacéuticas, Madrid, ES; [2]Instituto de Investigación Sanitaria, Hospital 12 de Octubre i+12, Madrid, ES; [3]CIBER de Bioingeniería, Biomateriales y Nanomedicina, Madrid, ES; [4]Universidad Politécnica de Madrid, Dpto. Materiales y Producción Aeroespacial, ETSI Aeronáutica y del Espacio, Madrid, ES

Introduction

Collagenase is widely used for the treatment of fibrotic-type diseases such as systemic sclerosis, Peyronie or Dupuytren, among others.[1] These pathologies are characterized by an overproduction of collagen which induces tissue malfunction causing severe limitations to the patients. The actual treatments for fibrosis diseases are surgery, immunosuppression treatments and collagenase administration. Surgical procedures often carry important difficulties and can produce serious side effects such as nerve, tendon and artery injuries. Moreover, these interventions are invasive techniques that require long recovery times until the patient can return to normal life. Immunosuppression treatments lack of selectivity and also induces unwanted side effects which can be severe in many cases, obliging to suppress the therapy. The administration of Collagenase Clostridium Histolyticum (CCH) was approved by Food Drug Administration (FDA) in 2010 for the treatment of this type of diseases. CCH is a matrix metalloproteinase which cleaves collagen I and III, which are the most abundant collagen types in fibrotic lesions whereas it does not affect to collagen type IV, with is present in nerve. Therefore, this enzyme induces a significant reduction in the collagen content of fibrotic tissues without affecting other types of tissues. The main limitation of the use of this enzyme is its high liability in physiological environment; collagenase lost its activity in less than 24 hours at physiological conditions. This issue is the cause of the necessity to administrate multiple collagenase injections in high dosages which provoke the apparition of tissue damage caused by local overdose.

Experimental Methods

First, the reaction buffer ($NaHCO_3$ 0.01 M, pH 8.5) was deoxygenated by freeze-vacuum-N_2 cycles. Then, collagenase ($3.1 \cdot 10^{-5}$ mmol) was dissolved in 1 mL of deoxygenated buffer. Acrylamide (AA), 2-Aminoethyl methacrylate (Am) and stimuli responsive (EG, MBA, or PL) monomers, in the proportions of which are required in each case, were dissolved in 1 mL of deoxygenated buffer in a vial, and the solution containing monomers was added to the protein solution. This mixture was stirred at 300 rpm for 10 min under nitrogen atmosphere at room temperature. Further, 0.013 mmol of Ammonium Persulfate (APS) and 0.02 mmol of TMEDA dissolved in 1 mL of the deoxygenated buffer were added dropwise to the mixture. This solution was stirred at 300 rpm for 90 min at room temperature under inert atmosphere. Furthermore, the encapsulated enzyme was purified by centrifugal separation with 10-KDa cut-off filters (AMICON Ultra-2 mL 10 KDa) and washed three times with $NaHCO_3$ buffer (0.01 M, pH 8.5). The capsules of collagenase were preserved at 4°C and analyzed with DLS, Z potential, FTIR, TGA and TEM characterization techniques.

Results and Discussion

Our research group has developed a novel methodology for the production of polymeric nanocapsules able to encapsulate collagenase without affecting its enzymatic activity and to release them in a controlled manner once

arrive to the diseased tissue in response to several stimuli as pH and light. This methodology is based on the construction of a polymeric shell around the enzyme by radical polymerization of acrylamide-type monomers which are adsorbed on the macromolecule surface. Through the judicious choice of monomers and cross-linkers breakable under certain conditions, the capacity to respond to specific stimulus was incorporated into the polymeric capsule. Thus, the incorporation of ethylene glycol dimethacrylate (EG) as crosslinker provide the capacity to respond to variations in pH releasing the enzyme when the pH reaches mild acidic conditions. This property has been employed for collagenase release in tumoral tissues which exhibit acidic environment in order to degrade the extracellular matrix enhancing the penetration of nanotherapeutic agents.[2-3] Latterly, the incorporation of a second crosslinker, in this case a non-degradable one, slowed down the nanocapsule hydrolysis rate being able to release controlled amounts of collagenase during more than 10 days, which was employed for the treatment of fibrotic lesions.[4] Currently, we are working in the incorporation of light-sensitive crosslinkers in order to produce nanocapsules capable to release these enzymes in response to UV-A radiation. This property allows to trigger the collagenase release in specific regions employing an easy to focus stimulus. Moreover, UV-A irradiation presents important benefits in the treatment of fibrotic lesions due to its immunosuppressive properties.

Conclusion

It is expected a synergic effect with the collagenase action which improve the therapeutic effect of these nanocapsules. The incorporation of fluorophores on the nanocapsule allow us the monitorization of its behaviour inside the host.

References

[1] Sehgal, V. N.; Srivastava, G.; Aggarwal, A. K.; Behl, P. N.; Choudhary, M.; Bajaj, P. Localized Scleroderma/morphea. Int. J. Dermatol. **2002**, 41 (8), 467–475.

[2] M. R. Villegas, A. Baeza, M. Vallet-Regí, *ACS Appl. Mater. Interfaces***2015**, *7*, 24075–24081.

[3] M. R. Villegas, A. Baeza, A. Noureddine, P. N. Durfee, K. S. Butler, J. O. Agola, C. J. Brinker, M. Vallet-Regí, *Chem. Mater.***2018**, *30*, 112–120.

[4] M. R. Villegas, A. Baeza, A. Usategui, P. L. Ortiz-Romero, J. L. Pablos, M. Vallet-Regí. Acta Biomaterialia, **2018**, *74*, 430–438.

Acknowledgement

This work was supported by the European Research Council (Advanced Grant VERDI; ERC-2015-AdG Proposal No. 694160).

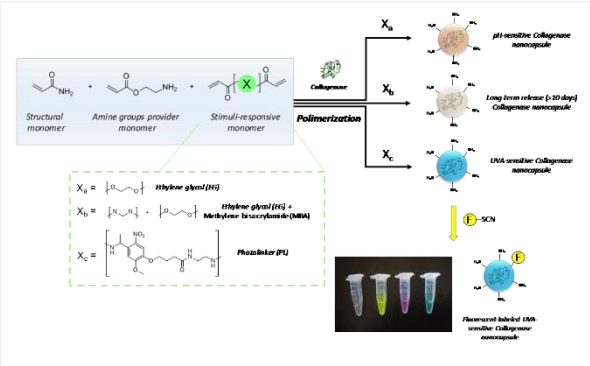

Figure 1.
Collagenase encapsulation and controlled release in response to stimuli.

PS2-05-326

Characterization of electrically conductive polylactic acid (PLA) – polypyrrole (PPy) substrates for neural tissue engineering

Fernando Gisbert Roca[1], Jorge Más Estellés[1,2], Cristina Martínez Ramos[1], Manuel Monleón Pradas[1,2]

[1]Universitat Politècnica de València (UPV), Centro de Biomateriales e Ingeniería Tisular (CBIT), Valencia, ES; [2]Biomedical Research Networking Center in Bioengineering, Biomaterials and Nanomedicine (CIBER-BBN), Centro de Biomateriales e Ingeniería Tisular (CBIT), Valencia, ES

Introduction

Electrically conductive substrates are used to improve axonal extension and induce a greater release of neurotrophins by glial cells when subjected to an exogenous electric field [1-2]. Herein, we develop polylactic acid (PLA) - polypyrrole (PPy) nanofiber films with different amounts of PPy, characterizing its physicochemical and dielectric properties, as well as its biological validity to be used within the field of neural tissue engineering.

Experimental Methods

Aligned PLA nanofiber films were obtained by the electrospinning technique and coated with the electrically conductive polymer PPy via *in situ* polymerization. Different mass fractions of PPy were obtained by varying the reaction parameters used for the PPy coating (4%, 13%, 18%, 23%, 27% and 34%). Different techniques (Field Emission Scanning Electron Microscopy (FESEM), Fourier-Transform InfraRed spectroscopy (FTIR), ThermoGravimetric Analysis (TGA), Differential Scanning Calorimetry (DSC) and impedance measurements) were used to characterize the physicochemical and dielectric properties of the membranes. The MTS cell proliferation assay and confocal microscopy images were employed to assess the adhesion of rat Schwann cells on the surface of the substrates.

Results and Discussion

FESEM images showed that for mass fractions of PPy below 23% the coating was discontinuous, while many aggregates were observed for mass fractions of PPy above 34%. Therefore, a continuous and homogeneous coating without aggregates is obtained between these two values.

The dielectric characterization showed that the greater the mass fraction of PPy, the greater the conductivity of the material. A percolation effect was also observed for substrates with a mass fractions of PPy greater than 23%, corroborating the continuity of the PPy coating above this value.

The MTS cell proliferation assay showed a greater cell adhesion of Schwann cells when the mass fraction of PPy is low (4%), compared to PLA membranes. However, from this point, the greater the mass fraction of PPy, the lower the cell adhesion. Morphological changes of the cells were also observed when increasing the mass fraction of PPy.

Conclusion

Our experimental data demonstrate the ability to obtain electrically conductive, biodegradable and biocompatible PLA-PPy substrates that greatly expand the potential for this composite material to be used for tissue engineering and implantable devices applications.

References

[1] Schmidt CE et al. PNAS 1997; 94:8948-53

[2] Huang J et al. GLIA 2010; 58:622-31

Acknowledgement

The authors acknowledge financing from the Spanish Ministry of Economy and Competitiveness (MINECO) through MAT2015-66666-C3-1-R and DPI2015-72863-EXP projects. Fernando Gisbert Roca acknowledges scholarship FPU16/01833 of the Spanish Ministry of Education, Culture and Sports (MECD). We thank the Electron Microscopy Service at the UPV, where the FESEM images were obtained.

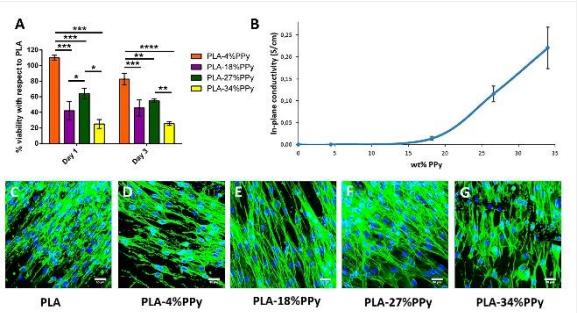

Cell proliferation assay, conductivity of membranes and confocal microscopy images

A: MTS Schwann cell proliferation assay. B: Conductivity of PLA-PPy films. C-G: Confocal images of Schwann cells seeded on PLA and PLA-PPy substrates.

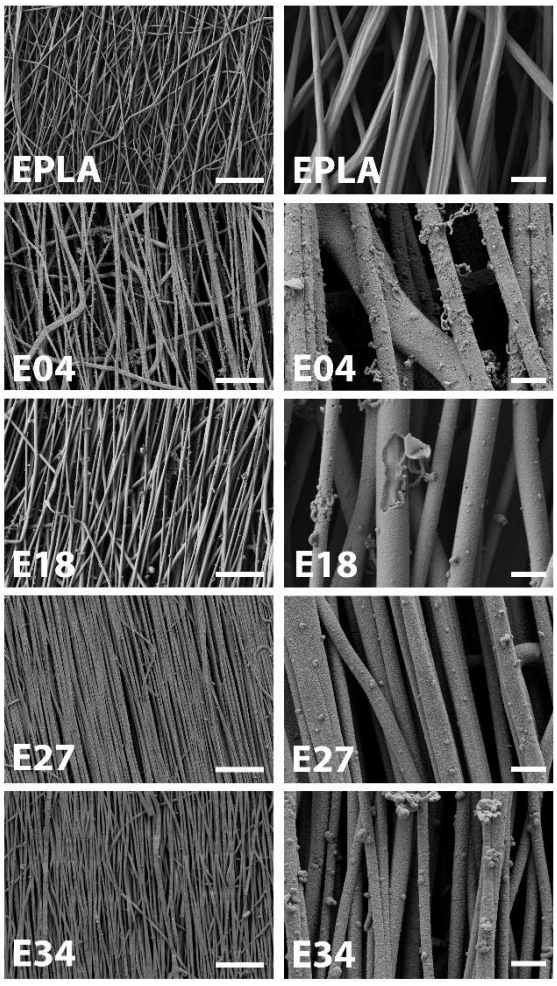

FESEM images of PLA-PPy electrospinning membranes

FESEM images of PLA (EPLA) and PLA-PPy (E04, E18, E27 and E34) electrospinning membranes with an aligned orientation of the nanofibers. EPLA: Smooth surface. E04: Inhomogeneous coating with discontinuities. E18: More homogeneous coating, but still with some discontinuities. E27: Homogeneous coating. E34: Homogeneous coating, but with PPy aggregates. Left image: 1.000X (Scale bar = 20 µm). Right image: 7.500X (Scale bar = 2 µm).

PS2-05-327

Magnetic hyperthermia of single domain iron oxide nanocrystals in lipid nanoemulsions

Andrea Desii[1,2], Deniz Aksu[1], César de Julian Fernandez[3], Gianni Ciofani[2,1]

[1]Politecnico di Torino, Dipartimento di Ingegneria Meccanica e Aerospaziale, Turin, IT; [2]Italian Institute of Technology, Smart-Biointerfaces, Pontedera, IT; [3]CNR, IMEM, Parma, IT

Introduction

Glioblastoma Multiforme (GBM) is an aggressive brain cancer for which an effective therapeutic strategy is still unavailable.[1] In the last few years, several “theranostic” approaches based on multifunctional platforms have emerged.[2] Among these, multifunctional lipid nanovectors have been successfully employed *in vitro* for synergistic chemotherapy/hyperthermia induced apoptosis of a glioblastoma cell line.[3] In this report, the magnetic properties of single domain iron oxide nanoparticles (IONPs) inside lipid nanovectors are investigated. In general, the magnetic properties of an ensemble of single domain particles are influenced by their concentration, their stability and the hydrodynamic properties of the system. Controlled inclusion in solid/liquid lipid nanoemulsions can be used to tune the hyperthermic behaviour of superparamagnetic/ferrimagnetic IONPs.

Experimental Methods

Synthesis of superparamagnetic IONPs was carried out according to Sun et al. and larger, ferromagnetic particles were obtained via the SORT technique, using iron acetylacetonate and iron oleate, respectively.[4,5] Lipid magnetic nanovectors were fabricated by mixing 25 mg of 1-stearoyl-*rac*-glycerol, 2,5 mg of 1,2-dipalmitoyl-*rac*-glycero-3-phosphocholine, 2,5 mg of oleic acid, 4 mg of $mPEG_{5k}$-DSPE and 250 uL of IONPs chloroform dispersion, corresponding to 10 mg of particles. Chloroform was evaporated to obtain a lipid/particle film, which was dispersed in a Tween 80 water solution and ultrasonicated to obtain a stable suspension. Magnetization curves were recorded using a VSM magnetometer. Particle size distribution was obtained from TEM images. A Malvern Zetasizer Nano ZS was used for the determination of the hydrodynamic radius of particles and lipid nanovectors and zeta potential of vectors. SAR estimation was obtained exposing a glass vial containing 500 µL of 5 mg/mL particle/nanovector suspension to an AC magnetic field generated by a magneTherm RC system operating at 754 kHz and 20 mT.

Results and Discussion

The average diameter of smaller IONPs (SPM-IONP) and IONPs obtained from iron oleate (FM-IONP) is 12 nm and 32 nm. Average size by TEM was lower, 10 nm and 28 nm Saturation magnetization obtained from DC magnetization curves is higher than 70 emu/g for both samples, suggesting that particles are mainly composed of ferrimagnetic iron oxides, such as maghemite or magnetite. SAR values for SPM-IONP and FM-IONP dispersed in chloroform are 19.4 W/g and 16.3 W/g, respectively. These low values can be attributed to the demagnetizing effect of dipolar interactions, which has been shown to negatively impact the magnetic thermal conversion of single domain nanocrystals above a critical concentration.[6] Moreover, size of the particles was chosen in order to have different relaxation behavior and not to optimize SAR values. As a matter of fact, when particles are included in lipid nano vectors, SAR increases drastically for SPM-IONP (94.4 W/g), while is basically unchanged for FM-IONP (22.6 W/g). A possible explanation is the stabilization of the hydrophobic particles by the lipids, inhibiting particle aggregation and regulating the dipolar interactions. For FM-IONP this effect could be offset by a significant increase of the Brown relaxation time, dependent

on the viscosity, which usually represents the main contribution to the total relaxation time for nanocrystals with blocked moments. One important feature of the fabrication process of lipid magnetic nanovectors is the elimination of the ligand exchange step to improve the dispersibility in water of nanocrystals obtained by the heat-up method. IONPs are stably dispersed in lipid nano droplets with size smaller than 300 nm. Further magnetic characterizations (magnetometry, susceptivity measurements) will improve our understanding of the underlying physics, by providing information on relaxation times and particle anisotropy.

Conclusion

Results, although preliminary, show that the hyperthermic behaviour of magnetic nanocrystals is greatly influenced by the carrier of choice, and that SAR optimization has to take into account not only morphology and composition of magnetic nanocrystals, but also the properties of the platforms used to administer them. Moreover, the structure and chemistry of the vector can be an important tool to enhance the hyperthermic property of IONPs.

References

1) Ostrom, Q. T.; Gittleman, H.; Liao, P.; Rouse, C.; Chen, Y.; Dowling, J.; Wolinsky, Y.; Kruchko, C.; Barnholtz-Sloan, J. CBTRUS Statistical Report: Primary Brain and Central Nervous System Tumors Diagnosed in the United States in 2007–2011. *Neuro-Oncol.***2014**, *16* (suppl_4), iv1–iv63. https://doi.org/10.1093/neuonc/nou223.

2) Liu, H.; Zhang, J.; Chen, X.; Du, X.-S.; Zhang, J.-L.; Liu, G.; Zhang, W.-G. Application of Iron Oxide Nanoparticles in Glioma Imaging and Therapy: From Bench to Bedside. *Nanoscale***2016**, *8* (15), 7808–7826. https://doi.org/10.1039/C6NR00147E

3) Tapeinos, C.; Marino, A.; Battaglini, M.; Migliorin, S.; Brescia, R.; Scarpellini, A.; Prato, M.; Drago, F.; de Julian Fernandez, C.; Ciofani, G. Stimuli Responsive Lipid-Based Magnetic Nanovectors Increase Apoptosis in Glioblastoma Cells through Synergic Intracellular Hyperthermia and Chemotherapy. **2018**

4) Sun, S.; Zeng, H.; Robinson, D. B.; Raoux, S.; Rice, P. M.; Wang, S. X.; Li, G. Monodisperse MFe_2O_4 (M = Fe, Co, Mn) Nanoparticles. *J. Am. Chem. Soc.***2004**, *126* (1), 273–279. https://doi.org/10.1021/ja0380852

5) Chen, R.; Christiansen, M. G.; Sourakov, A.; Mohr, A.; Matsumoto, Y.; Okada, S.; Jasanoff, A.; Anikeeva, P. High-Performance Ferrite Nanoparticles through Nonaqueous Redox Phase Tuning. *Nano Lett.***2016**, *16* (2), 1345–1351. https://doi.org/10.1021/acs.nanolett.5b04761

6) Ovejero, J. G.; Cabrera, D.; Carrey, J.; Valdivielso, T.; Salas, G.; Teran, F. J. Effects of Inter- and Intra-Aggregate Magnetic Dipolar Interactions on the Magnetic Heating Efficiency of Iron Oxide Nanoparticles. *Phys. Chem. Chem. Phys.***2016**, *18* (16), 10954–10963. https://doi.org/10.1039/C6CP00468G

Acknowledgement

This project has received funding from the European Research Council (ERC) under the European Union's Horizon 2020 research and innovation program (grant agreement N°709613, SLaMM).

The authors would like to aknowledge Simone Lauciello at Italian Institute of Technology for TEM characterization

2:45 p.m. – 3:45 p.m.

Hall 1 / Exhibition Area

PS2-06 | Micro- and nanopatterning

PS2-06-328

Bioengineered nanotopographical coating to drive osseointegration and reduce implant infection.

Laila Damiati[1], Virginia Llopis-Hernández[1], Richard Oreffo[2], Peifeng Li[3], Penelope M. Tsimbouri[1], Bo Su[4], Manuel Salmeron-Sanchez[1], Matthew. J. Dalby[1]

[1]University Of Glasgow, Centre for the Cellular Microenvironment, Glasgow, GB; [2]University of Southampton, Bone and Joint Research Group, Systems Biology, Southampton, GB; [3]University of Glasgow, School of Engineering, Glasgow, GB; [4]University of Bristol, Biomaterials Engineering Group, Bristol, GB

Introduction

Osseointegration and infection are major orthopaedic biomaterial research areas. Engineered bioactive coatings for titanium implants may provide a way of enhancing bioactivity of this commonly used orthopaedic material. Further, anti-bacterial, high aspect ratio topographies have shown potential effects against bacterium that can cause implant failure. Here, we use alkaline hydrothermal treatment to produce an antimicrobial nanotopography on the Ti scaffolds; however, this reduces mesenchymal stem cell (MSC) attachment.

Experimental Methods

We thus employ plasma polymerised coating of poly-ethyl acrylate (90 seconds at 100 Watt) to present fibronectin (FN) and low dose absorbed human bone morphogenetic protein 2 (BMP2) to the MSCs allowing a synergistic interaction at the integrin/growth factor receptor level on 2D/ 3D Ti scaffolds. 2D scaffolds were fabricated on Ti discs and 3D scaffolds were produced using the selective laser melting technique. Scaffolds physical and chemical characteristics were studied using SEM, AFM, WCA, and XPS. MSC bone mineralisation was examined using Raman spectroscopy, calcein blue, Alizarin red, and Giemsa staining. *Pseudomonas aeruginosa* bacteria were cultured on the substrates, and the number of viable microbial cells was determined by quantitation of the ATP present. *P. aeruginosa* quorum sensing molecules (odDHL and C4-HSL) were used to study the effect of these molecules on MSCs viability using annexin V, JC-1 and the cell cycle analysis.

Results and Discussion

Cell adhesion, proliferation, and mineralisation revealed the ability of the system (PEA/FN/BMP2) to be more potent in osteodifferentiation of the mesenchymal stem cells, as well as maintain the ability of nanowires to reduce the bacterial attachment.

Conclusion

This work represents a new strategy to improve the biological activity and biofilm reduction of Ti implants.

Acknowledgement

This project is supported by a studentship to LD from University of Jeddah, Jeddah- Saudi Arabia and EPSRC grant EP/K034898/1. We are grateful for the technical support of Carol-Anne Smith.

PS2-06-329

Kicking eukaryotic and prokaryotic cells at sub 50 nm: How precise could it be?

Mahya Ganjian[1], Khashayar Modaresifar[1], Boris Vratzov[2], Michelle Minneboo[1], Cornelis W. Hagen[3], Peter-Leon Hagedoorn[4], Lidy E. Fratila-Apachitei[1], Amir A Zadpoor[1]

[1]TU Delft, Department of Biomechanical Engineering, Faculty of Mechanical, Maritime, and Materials Engineering, Delft, NL; [2]NT&D, Nanotechnology and Devices, Aachen, DE; [3]TU Delft, Department of Imaging Physics, Faculty of Applied Sciences, Delft, NL; [4]TU Delft, Department of Biotechnology, Faculty of Applied Sciences, Delft, NL

Introduction

One of the major problems with bone implants after surgery is the competition of host and bacterial cells to adhere and grow on the implant surface. To prevent the risk of biofilm formation and implant-associated infections, while promoting osteogenic differentiation, the surface of the bone implant could be decorated with bactericidal nanostructures (*e.g.*, nanopillars). Electron beam-induced deposition (EBID) is a promising approach to create sub-10 nm structures with precisely controlled dimensions (*e.g.*, diameter, height, and interspace). Compared with other patterning techniques such as optical and electron beam lithography, reactive ion etching, ionization, and hydrothermal treatment, EBID is a relatively slow process. For instance, based on our previous study[1], it takes around 7 hours to pattern an area of 40×40 μm^2, which is covered with nanopillars with a diameter of 80 nm, a height of 190 nm, and a pillar interspacing of 170 nm. Such an area is not sufficient for studies involving host cells. The aim of this work was to upscale the EBID nanopatterned area, consisting of pillars with a diameter of sub-50 nm, by using step and repeat nanoimprinting technique.

Experimental Methods

A 6.5 mm by 5.6 mm fused silica was used as a mold. The mold contained 1×1 mm^2 elevated MESA structure in the middle, coated with a thin layer of Cr as a conductive layer for EBID deposition. EBID was performed using trimethyl-(methylcyclopentadienyl) platinum ($C_9H_{16}Pt$) as the precursor gas. Four different sub 50 nm nanopillars were deposited on the surface. For each series of dimensions, we patterned an area of 40×40 μm^2. The next step was transferring the structures into the fused silica substrate. This step was done by etching the Cr layer with the EBID structures as a mask by using inductively coupled plasma reactive ion etching (ICP RIE), followed by etching the fused silica using Cr as the mask, again with ICP RIE, and finally removing the residual Cr layer. The resulted fused silica substrate with pillars made of fused silica is the final mold for the next UV-based step and repeat nanoimprinting technique (Figure 1). A UVNIL resist was then spin coated and soft baked to create uniform solvent free resist films. The imprint step was carried out with an Imprio 55 press from Molecular Imprints Inc. While the template was in contact with the substrate, the resist was cured by UV light and the mold was released from the substrate.

Pre-osteoblast cells (*i.e.*, MC3T3-E1) were cultured on both nanopatterned and flat silicon surface using αMEM culture media. The morphology and viability of these cells were assessed by scanning electron microscopy (SEM) and live/dead staining. Moreover, *S. aureus* (RN0450 strain) was grown in Brain Heart Infusion medium (BHI culture) and then cultured on the samples at an OD_{600} of 0.1 for 18 hours. The morphology and killing efficiency of the patterns against bacteria were evaluated by SEM.

Results and Discussion

Designing multi-biofunctional surfaces to selectively influence the behavior of host cells and bacteria is of high interest and importance for the development of implant materials. For bone-implants, the holy grail is having surfaces which promote osteogenic differentiation and simultaneously kill the bacteria.

Using this technique, we obtained 4 different patterns, each covering 3×3 mm^2 areas of a 10×10 mm^2 silicon wafer. The SEM images of bacterial cells showed that nanopillars within the range of dimensions created in this study have the potential to be bactericidal. Moreover, the results of live/dead staining and SEM images indicated that nanopillars can support the attachment and proliferation of pre-osteoblast cells.

Conclusion

Having a surface with controlled nanostructures is the key factor for understanding the killing mechanism of bacterial cell, as well as the role of different factors involved and the osteogenic activity. In this research, we overcame the challenge of enlarging the EBID patterned areas by using the step and repeat nanoimprinting method. This development represents a crucial step forward as it enables studies with both bacteria and host cells. Based on the technique presented in this study, one can produce nanopillars with precisely controlled dimensions and with dual bio-functionalities.

References

[1] M. Ganjian, K. Modaresifar, *et al.,* “Nature Helps: Towards Bioinspired Bactericidal Nanopatterns”, under Review.

Acknowledgement

This research has been received funding from the European Research Council under the ERC grant agreement n° [677575].

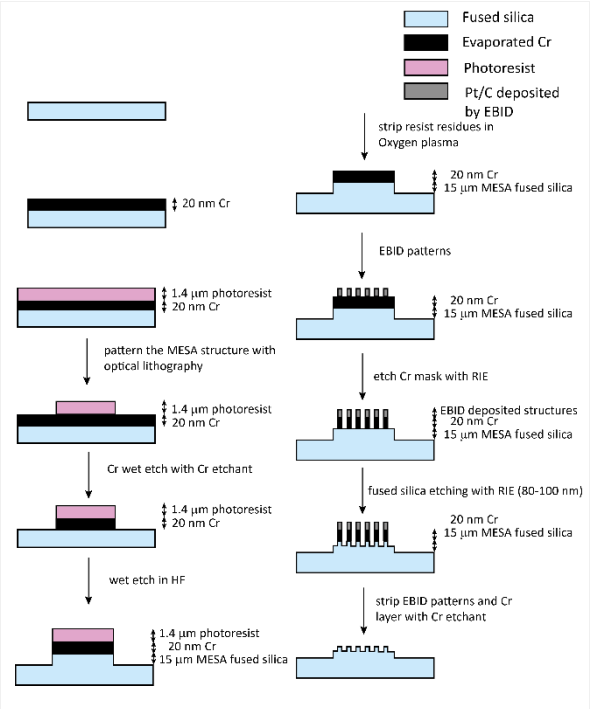

Figure 1.
process steps of preparing the transparent mold for step and repeat nanoimprint.

PS2-06-330

Fabrication of Polymeric Nanoneedle Arrays using Block Copolymer Micelle Lithography and Replica Moulding

James C. McCormack, Lucia Podhorska, Susan M. Kelleher

University College Dublin, School of Chemistry, Dublin, IE

Introduction

The ability of nanopatterned surfaces to direct cell behavior has been widely investigated in recent years. For example, nanoneedle arrays are rapidly emerging as a tool for drug delivery, as they offer the potential to transport impermeant molecules directly into the cell cytosol.[1] Focus, to date, has been placed on hard inorganic materials such as silicon and diamond, which have shown significant promise in this regard. However, the inherent limitations of such materials, associated with potential cytotoxicity and constraints in controlled delivery, warrant research into innovative patterning processes which can produce biocompatible nanopatterned materials.[2,3] To this end, replica moulding using UV-curable polymers from arrays produced from silicon was carried out to produce polymeric gels functionalized with nanoneedle arrays.

Experimental Methods

The Si nanoneedles were fabricated using block copolymer micelle lithography. PS-*b*-P2VP was used to fabricate a monolayer of hexagonally arranged spherical micelles on Si substrates. By controlling the loading of metal salts, such as $HAuCl_4$ and $FeCl_3$, into these micelles, monolayers of metal nanodots hard masks were deposited onto the Si surface. Following oxidation, to generate Au and Fe_2O_3 hard masks respectively, the etch selectivities and etch parameters were tuned to generate Si nanoneedle arrays of varying aspect ratio as shown in Figure 1B. Subsequent replica moulding from the Si masters was demonstrated to produce polymeric nanoneedle arrays as outlined (Figure 1A).

Combined AFM (JPK Instruments Nanowizard II Atomic Force Microscope) and FESEM (ZEISS Gemini ULTRA plus) imaging were used to determine the dimensions of all surface structures outlined. Bulk rheology measurements were carried out on the polymeric samples using a rheometer (Gemini 200 HR Rheometer). Surface elasticity measurements of the gel nanoneedles were carried out using AFM force mapping.

Results and Discussion

Au and Fe_2O_3 hard masks were produced with feature diameters varying from 36-97 nm, with inter-particle spacings ranging from 71-400 nm. Si nanoneedle arrays were successfully fabricated using both the Au and Fe_2O_3 hard masks. Polymeric nanoneedle replicas were successfully fabricated through replica moulding techniques. Preliminary surface elasticity data for the polymeric samples has been obtained. Detailed results for these samples are soon to follow.

Conclusion

Block copolymer micelle lithography is an effective tool for controlling Si nanoneedle dimensions. Replica moulding is a reliable process for replicating topographical features down to the nanoscale. Polymeric nanoneedle arrays can be produced by combining block copolymer micelle lithography and replica moulding techniques.

References

1. Chiappini, C. *et al.* Biodegradable silicon nanoneedles delivering nucleic acids intracellularly induce localized in vivo neovascularization. *Nat. Mater.***14,** 532–539 (2015).
2. Cruz, P. *et al.* Nanoneedle-Mediated Stimulation of Cell Mechanotransduction Machinery. *ACS Nano* (2019). doi:10.1021/acsnano.8b06998
3. Elnathan, R., Kwiat, M., Patolsky, F. & Voelcker, N. H. Engineering vertically aligned semiconductor nanowire arrays for applications in the life sciences. *Nano Today***9,** 172–196 (2014).

Acknowledgement

I would like to thank Prof. Brian Rodriguez and Dr Dermot Brougham for their help with AFM imaging DLS data acquisition, respectively. In addition, I would like to thank Dermot Daly from the CRANN institute for his help with FESEM imaging and training. This material is based upon works supported by the Science Foundation of Ireland under Grant No. 15/SIRG/3429(T).

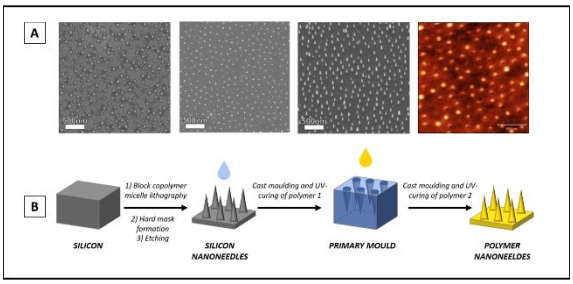

Polymeric Nanoneedle Array Fabrication

Figure 1: A) FESEM images of micelle arrays, gold hard mask and silicon nanoneedle arrays; AFM height image of initial polymer nanoneedle array made using replica moulding techniques; B) Schematic of the flow process of the polymer nanoneedle array production

PS2-06-331

Initial Response of Human Mesenchymal Stromal Cells to Electron Beam Micropatterned Ti6Al4V Surfaces

Simon Janßen[1], Stefan Gach[2], Sebastian Kant[3], Sanja Aveic[1,4], Stephan Rütten[5], Simon Olschok[2], Uwe Reisgen[2], Horst Fischer[5]

[1]RWTH Aachen University Hospital, Dental Materials and Biomaterials Research, Aachen, DE; [2]RWTH Aachen University, Welding and Joining Institute, Aachen, DE; [3]RWTH Aachen University Hospital, Molecular and Cellular Anatomy, Aachen, DE; [4]Paediatric Research Institute Città della Speranza, Neuroblastoma Laboratory, Padova, IT; [5]RWTH Aachen University Hospital, Institute of Pathology, Aachen, DE

Introduction

Due to its favorable mechanical properties and high cytocompatibility titanium and its alloys, especially Ti6Al4V, are frequently utilized for orthopedic implants. For this applications quick osseointegration, i.e. the mechanical and biological integration of the implant into the hard tissue, is indispensable for the long-term performance of the implant. Unfortunately, unmodified titanium-based implants are still prone to failure due to insufficient osseointegration. Alterations to the surface topography or chemical modifications of the implant surface have been thoroughly studied. The introduction of a microstructure to the surface of titanium-based implants was shown to improve the osteogenic differentiation of human mesenchymal stromal cells (hMSC) *in vitro* as well as osseointegration *in vivo*. However, common microstructuring approaches, e.g. micro embossing or grit blasting, are either not feasible to process titanium alloys or can only achieve a continuously structured surface. Discontinuous structuring on the other hand was shown to hold potential to further improve the afore mentioned properties.

Experimental Methods

We used an electron beam microstructuring technique to alter the surface topography and surface chemistry of Ti6Al4V samples. This microstructure consists of discontinuous features at intervals between 80 and 240 µm (Figure 1). The effects of such microstructures on hMSC were analyzed *in vitro* using immunofluoroscence imaging and real-time PCR analysis.

Results and Discussion

Microstructured samples were proven to be highly cytocompatible and modification of the surface chemistry during the microstructuring process did not compromise cell viability. Initial adhesion and the morphological adjustments of hMSC to the microstructure were investigated by immunofluorescence microscopy and visualized in 3D (Figure 2). Increasing expression of osteogenic markers, e.g. osteocalcin, over a time span of 21 days was observed.

Conclusion

Electron beam microstructuring could overcome possible issues connected with common microstructuring methods, e.g. debris from blasting. Moreover, our results show that the presented electron beam microstructuring approach enhances the osteogenic differentiation of hMSC *in vitro* and might potentially expedite and improve subsequent osseointegration of hard tissue implants *in vivo*.

Acknowledgement

We acknowledge the financial support of the Deutsche Forschungsgemeinschaft DFG (grants FI975/26-1 abd RE2755/47-1).

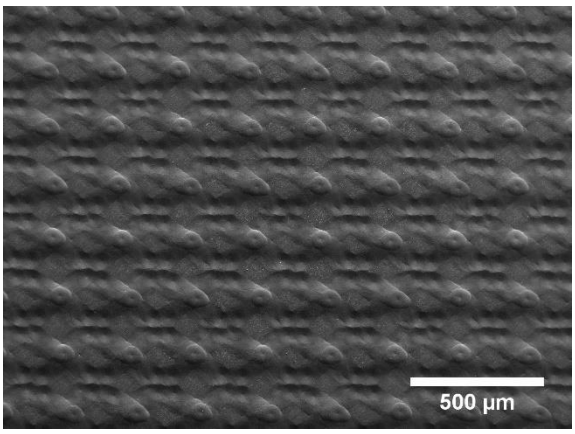

Figure 1
SEM microscopy image of an electron beam microstructured surface.

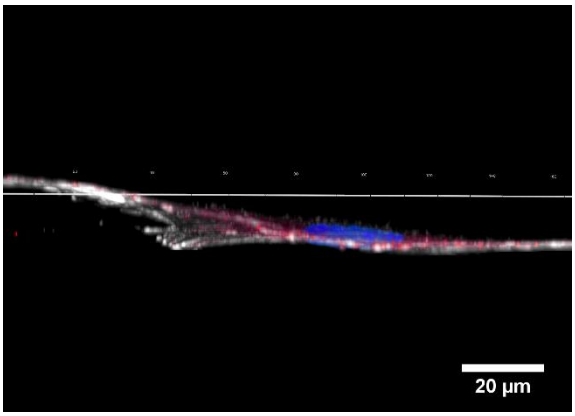

Figure 2
Immunoflourescence staining of actin (white), vinculin (red) and DAPI (blue) of a hMSC cultured on the microstructured surface for 24 h.

PS2-06-332

Comparative study of protein adsorption on nanopatterned oxide surfaces

Yu Yang, Mingrui Yu, Qin Qin, Guido Grundmeier, Adrian Keller

Paderborn university, Technical and Macromolecular Chemistry, Paderborn, DE

Introduction

The biocompatibility of an artificial material in contact with human tissue is strongly influenced by not only its biological surrounding but also its chemical and physical surface properties. Various approaches for improving the biomaterial-tissue interaction have been explored so far that mostly focused on enhancing the surface's bioactivity by chemical and mechanical treatments. However, also the nanoscale surface morphology has been recognized as a significant parameter affecting protein adsorption and cell response, such as cell migration, proliferation etc. [1,2].

Experimental Methods

To investigate the diverse effects of surface chemistry and surface topography on protein adsorption, we employ flat as well as nanorippled SiO_2 and TiO_2 model surfaces. Nanorippled Si substrates were synthesized by 500 eV Ar^+ ion irradiation at 67° incidence and a fluence of 1 x 10^{17} cm^{-2} [3]. Using magnetron sputter deposition, Ti films with a thickness of 20 nm were then grown on such nanopatterned Si substrates [4]. The so-fabricated nanopatterned Ti and Si surfaces with native surface oxide were characterized by atomic force microscopy (AFM), scanning electron microscopy (SEM), and X-ray photoelectron spectroscopy (XPS). The nanopatterned oxide surfaces and their corresponding flat counterparts were then employed to study the influence of surface chemistry and nanotopography on protein adsorption. To this end, a variety of globular proteins with different molecular weights and isoelectric points were selected. Adsorption dynamics was monitored in situ using ellipsometry while the morphology of the adsorbed protein films was assessed by ex-situ AFM.

Results and Discussion

Highly ordered ripple patterns on Si surfaces were successfully fabricated with a periodicity and amplitude of about 30 nm and 3 nm, respectively. By applying a bias potential of -10 V, highly conformal Ti films with a thickness of 20 nm were deposited by magnetron sputtering on the pre-rippled Si surfaces, which perfectly reproduce the ripple patterns and thus allow for dissecting the relative effects of surface topography and surface chemistry on protein adsorption. Adsorption of the globular proteins BSA, ferritin, and thyroglobulin at the flat and nanopatterned oxide surfaces could be successfully monitored in situ by ellipsometry. AFM investigations of the morphology of the adsorbate film revealed preferential adsorption of ferritin in the ripple valleys.

Conclusion

By utilizing low-energy ion bombardment, nanorippled Si wafers can be fabricated with well-defined amplitude and periodicity. Magnetron sputter deposition under optimized conditions enables the growth of conformal metallic films on those substrates that perfectly replicate the substrate pattern. Therefore, these substrates allow for dissecting the relative effects of surface chemistry and nanotopography on protein adsorption. Furthermore, the periodicity of the ripple patterns can be tuned between 20 and 50 nm simply by adjusting the ion energy [3]. These nanopatterned

surfaces thus represent powerful model surfaces for the in-depth investigation of protein adsorption using for instance ellipsometry as an in-situ method to quantitatively monitor the development of adsorbate thickness.

References

[1] I. Wittenbrink, et al., *Low-aspect ratio nanopatterns on bioinert alumina influence the response and morphology of osteoblast-like cells*, Biomaterials, 62, 58-65, **2015**.

[2] M. S. Lord, *et al*., *Influence of nanoscale surface topography on protein adsorption and cellular response*, Nano Today, 5, 66-78, **2010**.

[3] A. Keller, S. Facsko, *Ion-induced nanoscale ripple patterns on Si Surface: Theory and experiment*, Materials, 3, 4811-4841, **2010**.

[4] A. Keller, *et al*., *Polycrystalline Ni thin films on nanopatterned Si substrates: From highly conformal to nonconformal anisotropic growth*, Phys. Rev. B, 84, 035423, **2011**.

Acknowledgement

We gratefully acknowledge the funding of this project by the German Science Foundation.

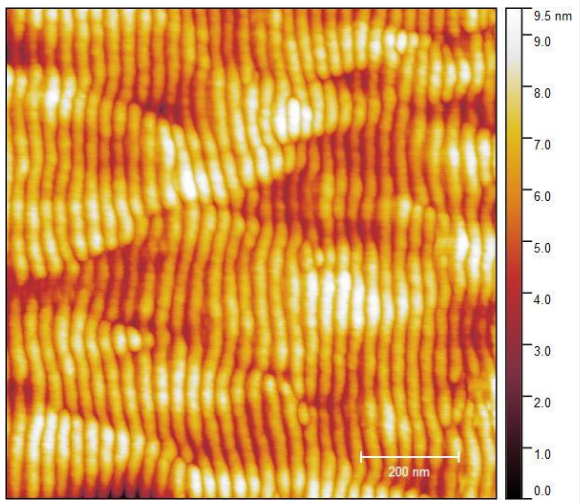

AFM image of highly ordered ripple patterns on Si wafer

Nanorippled Si surface was synthesized by 500 eV Ar^+ ion irradiation at 67° incidence and a fluence of 1 x 10^{17} cm^{-2} using low-energy ion bombardment. The ripples patterns were shown a periodicity and amplitude of about 30 nm and 3 nm, respectively.

PS2-06-333

On the Effect of Periodic Titanium Nanoripples on Adhesion and Osteogenic Differentiation of Human Mesenchymal Stromal Cells

Helena Hüskens[1], **Frederik Böke**[1], Yu Yang[2], Marvin Tamm[1], Adrian Keller[2], Horst Fischer[1]

[1]RWTH Aachen University, Dental Materials and Biomaterials Research, Aachen, DE; [2]Paderborn University, Technical and Macromolecular Chemistry, Paderborn, DE

Introduction

Titanium is the material of choice for bone tissue integrating implants due to its biocompatibility, corrosion resistance, high strength as well as good formability and machinability. As it is crucial for bone implants to be able to rapidly bond to the surrounding hard tissue, the aim of many investigations is to modify its surface to enhance osseointegration, chemically or physically. Here, we present a topographical approach to enhance the adhesion and osseointegration of human mesenchymal stromal cells on pure titanium. This is achieved by the introduction of well-defined, sub 10 nm nanoripples on the surface in combination with chemical modification and linking of proteins. The resulting surfaces are thoroughly investigated with regards to the change in adhesion and osseogenic differentiation potential on human mesenchymal stem cells.

Experimental Methods

Defined ripples with sub 10 nm amplitude were fabricated on silicon wafers by ion beam sputtering (IBS) and the resulting surface topography subsequently coated with a 20 nm titanium layer. Surface chemistry was altered and functional groups were introduced on the surface via self-assembled monolayers of silanes. Proteins were coupled to the surface by directed crosslinking. The surface topography was verified by AFM. The successful silanization was confirmed via contact angle measurements and XPS. Protein crosslinking was verified via XPS and ELISA. The adhesion potential of the modified surfaces was investigated by centrifugation adhesion studies and the osseogenic differentiation potential was investigated by qPCR after 21 days. Flat surfaces prepared in parallel without IBS were used as control surfaces throughout all experiments.

Results and Discussion

The successful introduction of highly ordered nanoripples was confirmed via AFM to be conserved after titanium deposition. A homogenous formation of silane monolayers with amine and sulfone functional groups was furthermore confirmed by XPS. ELISA studies showed a surface crosslinking of different proteins in excess of 45 % coverage of the substrate surface on rippled surfaces in comparison to lower amounts on non-rippled substrates. Adhesion studies revealed a trend towards a stronger adhesion on rippled surfaces in comparison to flat surfaces, further amplified by the chemical and biological modification. QPCR analyses of osseogenic induction triggered by the ripple surfaces are currently investigated and preliminary results indicate a trend towards enhanced differentiation of human mesenchymal stromal cells towards the osseogenic linage on rippled surfaces. Furthermore a synergistic effect of the additional biological and chemical surface modifications seems to enhance this effect on rippled surfaces in comparison to flat surfaces.

Conclusion

Confirmation of our preliminary results by our ongoing investigation would greatly expand the range of functional biomaterial surface modifications for bone tissue engineering. As such, biofunctionalized periodical nanostructures hold the potential to further enhance the osseointegration behavior of titanium based hard tissue implants.

PS2-06-334

Surface topography enhances oriented growth of endothelial cells and differentiation of progenitor cells towards endothelium: improvement of surface hemocompatybility

Klaudia Trembecka-Wójciga[1], Gabriela Imbir[1], Jurgen M. Lackner[2], Hanna Plutecka[3], Roman Major[1],
The research was financially supported by the Project 2016/21/N/ST8/00186 "Functional carbon based coatings on titanium substrate, modified by laser ablation designed for the integration with cardiac tissue and ultimately inhibit the blood clotting process" of the Polish National Centre of Science

[1]Polish Academy of Sciences, Institute of Metallurgy and Material Science, Kraków, PL; [2]Joanneum Research Forschungsges mbH, Institute of Surface Technologies and Photonics, Niklasdorf, AT; [3]Jagiellonian University Medical College, Department of Medicine, Kraków, PL

Introduction

Nano- and microscale topographical cues play critical roles in the induction and maintenance of various cellular functions, including morphology, adhesion, differentiation, and communication [1]. Laser ablation technique generated a controlled surface structurization affecting the formation of the topography cue in the form of a nano-, micro- channels. Surface anisotropy governing cellular orientation responses and causing controlled cell growth [2]. The goal of our study is to investigate the impact of submicron and nanoscale topographic cues on several fundamental endothelial cell behaviors including orientation and alignment to topographic features, proliferation, and migration.

Experimental Methods

The titanium and silicon substrates have been covered by different types of carbon-based coatings using PVD technique. The layer structure and the mechanisms of the coating anchoring to the substrate were analyzed using electron microscopy techniques. The cross section study was performed by the transmission electron microscopy equipped with field emission gun. Surface structurization was prepared by laser ablation technique. Channels with different size and distribution were formed. The topography of achieved channels was analyzed by Confocal Laser Microscopy (CLSM) equipped with topography module. Description of hemocompatibility of achieved structures was analyzed in arterial flow condition simulator with whole human blood. Endothelial monolayer formation and progenitor cells differentiation were investigated using Human Umbilical Vein Endothelial Cells (HUVECs) and and Endothelial Progenitor Cells (iCells), respectively.

Results and Discussion

The results show oriented growth of endothelial cells onto structured surface (Fig. 1). The topography analysis confirm the presence of channels with different size and distribution (Fig. 2). Cells sensed the presence of 70 mm distal channels, but no influence of 10 mm distal channels on cell growth were observed. Surface structurization affecting also controlled progenitor cells differentiation toward endothelium. Cells morphology on the surface of the materials showed the correct formation of endothelial monolayer from progenitor cells. The biomaterial examinations were performed under physiological blood flow conditions. The results obteined for dynamic assays confirm the improvement of surface hemocombatibility by deposition of carbon based coatings.

Conclusion

The results showed that by controlling the coating compositions, and anisotropy as well as channels distribution it is possible to enhance endothelial cells adhesion, orientation and progenitor cells differentiation toward endothelium. Endothelial monolayer can effectively inhibit blood coagulation process and improve the hemocompatybility properties of materials.

References

[1] M. Ermisa, E. Antmenac, V. Hasirci, Micro and Nanofabrication methods to control cell-substrate interactions and cell behavior: A review from the tissue engineering perspective; Bioactive Materials 3 (2018) 355-69.

[2] A. Greiner, A. Sales, H. Chen, S. Biela, D. Kaufmann, R. Kemkemer.; Nano- and microstructured materials for in vitro studies of the physiology of vascular cells; Beilstein J. Nanotechnol. 7 (2016) 1620-41.

Acknowledgement

The research was financially supported by the Project 2016/21/N/ST8/00186 "Functional carbon based coatings on titanium substrate, modified by laser ablation designed for the integration with cardiac tissue and ultimately inhibit the blood clotting process" of the Polish National Centre of Science

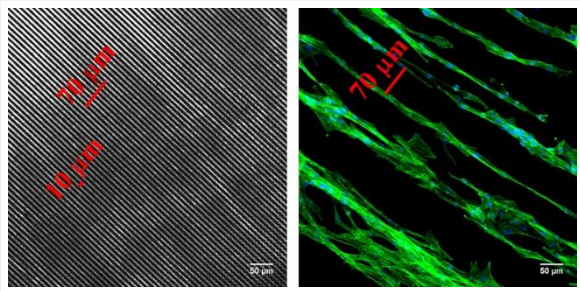

Fig. 1. Distribution of channels prepared by laser ablation technique (left) and endothelial cell or

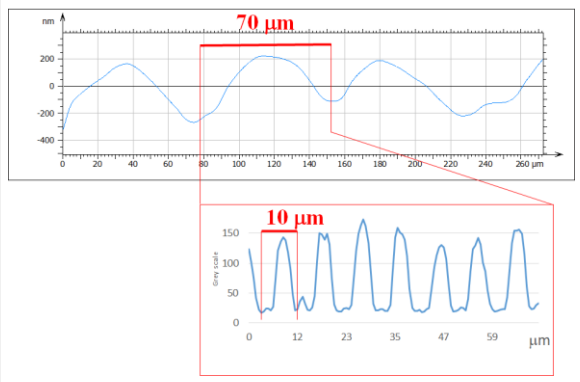

Fig. 2. Topography analysis of achieved channels done by CLSM

PS2-06-335

UV-controlled (poly)dopamine coating on Mg samples

Vanja Kokol[1], Zdenka Peršin[1], Tomaž Vuherer[1], Bérengère J. C. Luthringer[2]

[1]University of Maribor, Faculty of Mechanical Engineering, Maribor, SI; [2]Helmholtz-Zentrum Geesthacht, Institute of Material Research, Geesthacht, DE

Introduction

Magnesium (Mg) implants have emerged as innovative bioactive orthopaedic implant materials due to their excellent attractive features, including mechanical properties (*i.e*., lightweight with a density and elastic modulus close to the one of human cortical bone), biocompatibility, biodegradability and bioresorbability, without the need for a removal (second) surgery. However, a too rapid degradation, and subsequent loss of mechanical integrity before the tissue healing still limits their applications. Many methods have been thus developed over the last decade to combat these issues like alloying the Mg with other elements or its surface modification resulting also to an enhance osseointegration.

In the frame of the later, (poly)dopamine (PDA), clinically acceptable biocompatible and biodegradable monomer/polymer, have been recognized to act as a stable and adherent interface layer on many metal oxide surfaces (form a charge-transfer complex on their OH groups), thus bringing the anchoring sitesfor further bioconjugation and surface modification while providing a corrosion resistant coating.However, the kinetics of dopamine coating on a Mg material (without native oxide surface layer) as a function of temperature, time and reaction method is not well elucidated, although its long time (several hours) self-polymerization may be a critical for highly corrosive Mg material.

Experimental Methods

Therefore, to provide rapid-formation of PDA film on Mg material, without significant change of Mg surface and/or bulk structure, two different procedures, *i.e*., stirring and UV irradiation with various time-frames (from 30 min up to 24 h) were studied under slightly alkaline condition (Tris-HCl, pH=8.5)at room temperature (about 23 °C) and ambient oxygen. The solutions were observed to change from colorless to brown due to oxidation of dopamine-catechol to dopaminequinone. Reactive oxygen species (ROS) generated by UV irradiation, including singlet oxygen, are more active than molecular oxygen and could play the role of the oxidant required to initiate the dopamine polymerization, thereby controlling the process *in situ*.

FTIR spectroscopy and contact angle measurements were performed to evaluate the surface modification of Mg samples with PDA, while their crystalline and morphological properties were assessed with XPS and SEM analysis. In addition, mechanical properties of the samples using compression testing were performed. Furthermore, the liquid samples obtained after incubations and washings were analysed by ICP-OES analysis to measure Mg^{2+}ions concentration.

Conclusion

The results indicated a kinetically faster controlled polymerization of PDA coating of Mg sample surfaces treated under UV irradiation, without significant changing of its crystalline, morphological and topography structure, or mechanical properties.

Acknowledgement

This research was financially supported by Slovenian Research Agency and Deutscher Akademischer Austauschdienst-DAAD,according to Slovenian-German Joint Mobility program (project no BI-DE-18-19-002).

PS2-06-336

A Density-Controlled Free-standing Biodegradable Poly(lactic-*co*-glycolic acid) Nanopillar Array on Flexible substrates

Gyeong Won Lee[1], Sang Gu Yim[1], Seong Il Yoo[2], Seung Yun Yang[1]

[1]Pusan National University, Department of Biomaterials Science, Miryang, KR; [2]Pukyong National University, Department of Polymer Engineering, Pusan, KR

Introduction

Vertically Aligned polymer nanopillar array on substrates have received significant interest as a functional surface in a broad range of applications[1]. However, previous methods to prepare a polymer nanopillar array on substrates are fraught with poor dimensional controllability of the nanopillar[2]. In this study, we report a new method to prepare free-standing biodegradable nanopillar arrays on various substrates by plasma etching with polystyrene-*block*-poly(acrylic acid) (PS-PAA) block copolymer micelles encapsulating Au nanoparticles inside (AuNP@PS-PAA). The adsorption density of AuNP@PS-PAA micelles was controlled by pH of micelle condition affecting electrostatic interaction with polyelectrolyte layers formed on poly(lactic-co-glycolic acid) (PLGA) films, thereby the density of PLGA nanopillar arrays were controlled. The dimensions of PLGA nanopillars were controlled by adjusting plasma etching conditions such as treatment time and power.

Experimental Methods

PS-PAA micelles with core Au NPs were prepared according to a previously reported method.[1] A PLGA film was first deposited on a substrate by spin-coating a PLGA solution. the PLGA films were then treated with oxygen plasma to generate negative charges on the surface. The negatively charged PLGA films were alternately immersed in solutions of positively charged PAH and negatively charged PSS to prepare a PAH/[PSS/PAH]$_2$ multilayered films on the PLGA. The multilayered film was then immersed in an aqueous solution of AuNP@PS-PAA micelles for pre-determined times under different pH conditions. Finally, AuNP@PS-PAA micelles adsorbed on the PAH/[PSS/PAH]$_2$/PLGA film were treated with CF_4 plasma to transfer the micellar pattern to the underlying multilayers. For the PLGA nanopillars biodegradation tests with hydrolytic enzymes, PLGA nanopillar arrays were incubated in an esterase solution.

Results and Discussion

We introduced positive charges on the PLGA surface using a layer-by-layer assembly of the polyelectrolytes can further engineer the molecular interactions with the AuNP@PS-PAA micelles by adjusting the pH conditions. The density of AuNP@PS-PAA micelles can be adjusted by varying their degree of ionization and zeta potential values. Since the Au NPs in the micellar structure can provide etching resistance, only the polymer layers underneath the Au NPs remain intact after the CF_4 plasma treatment, and therefore, are able to form nanopillar arrays with a controllable density.

In the high pH value, the AuNP@PS-PAA micelles would repel each other due to the strong electrostatic repulsion induced by the anionic –COO– groups in the PAA shells. On the other hand, agglomerated micelles were deposited on the film. this also resulted in an increased adsorption density of the micelles during the same coating time. these interactions result in a uniform coating of the AuNP@PS-PAA micelles on the multilayered film.

The AuNP@PS-PAA micelles were used as an etching mask in the reactive ion etching (RIE) process. Interestingly, the resulting morphologies were quite different after the plasma etching, depending on micellar density. When the close-packed AuNP@PS-PAA micelles were used, the prepared PLGA nanopillars merged with each other caused by the heat generated during the RIE process (PLGA with a low glass transition temperature). Hence, in order to prepare an array of individually aligned nanopillars, it is necessary to increase the inter-micellar distance on the PLGA film, which can be achieved by controlling the pH.

To investigate the biodegradability of the PLGA nanopillars, we performed in vitro enzymatic degradation tests using the esterase. PLGA nanopillar arrays were immersed in the esterase solution, and then the biodegradability was evaluated by varying the nanopillar height. the degradation rate of the PLGA nanopillars was relatively high in the beginning and decreased with time. The degradation was almost completed after 7 days.

Conclusion

We demonstrate a feasible approach to produce nanopillar arrays. The adsorption density and the corresponding micellar arrangement on the film played a crucial role in controlling the final morphology of the nanopillars. By precisely adjusting the pH, the molecular interactions between the micelles and the film could be engineered, resulting in a control of the micellar adsorption density. The subsequent etching process successively transferred the micellar pattern to the underlying films. In addition, the nanopillar height could be adjusted by modifying the plasma etching time. This fine control of the density and height of the biodegradable nanopillars might not be easily transferrable to other methods, but it can be applicable to other types of soft materials. Since small modifications in topography such as nanopillar density and height can influence cellular behaviors such as adhesion and proliferation, it could uncover an interesting variety of opportunities.

References

[1] C. C. Liang et. al., *Adv. Mater. Interfaces***2015**, 2.

[2] K. J. Cha et. al., *Biofabrication***2013**, *5*, 025007

[3] S. H. Jo et. al., *ACS Appl. Mater. Interfaces***2015**, 7, 18778.

Acknowledgement

This work was supported by the Tech Incubator Program For Startup (TIPS) (201738070002) funded by the Ministry of SMEs and Startups (MSS, Korea).

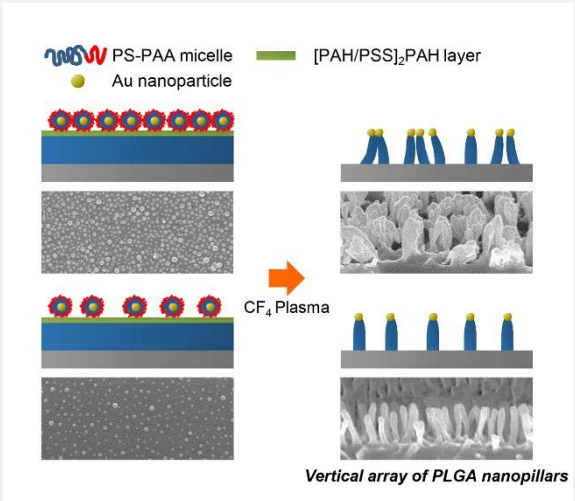

Morphologies of nanopillars array depending on the pH value and corresponding micellar density
When the close-packed AuNP@PS-PAA micelles were used, the prepared PLGA nanopillars merged with each other caused by the heat generated during the RIE process (PLGA with a low glass transition temperature). Hence, in order to prepare an array of individually aligned nanopillars, it is necessary to increase the inter-micellar distance on the PLGA film, which can be achieved by controlling the pH.

PS2-06-337

Micropatterned Devices for Controlled Neuron Cell Growth

Nerea Briz[1], Ana Ayerdi[1], Anja Haase[2], Martin Smolka[2], Dieter Nees[2], Meritxell Roura[3], Isbaal Ramos[3], Clarisa Salado[3], Goran Bijelic[1]

[1]TECNALIA, Biomaterials Area, San Sebastian, ES; [2]Joanneum Research Materials, Weiz, AT; [3]INNOPROT, SL, Derio, ES

Introduction

Drug-developing companies must test huge lots of different compounds in order to find proper drug candidates (1). The molecules to be tested should pass a toxicity assay panel that includes assays in various cell types – one of them being neurons. This testing work is performed through a methodology that allows massive screening of drug candidates via high-throughput screening (HTS) and high content screening (HCS). Up to date, many innovations have been performed to address the need of the large number of drugs that should be tested (2,3).The use of high-throughput analytical tools is often key to allowing comprehensive identification of such molecules at the genome-wide level. High-throughput systems typically adopt a multi-well plate format designed according to internationally standardized geometric configurations and thus compatible with available imaging systems such as automated fluorescence plate readers. However, neuronal cells do not normally adhere to most materials, thus making it necessary to coat the base substrate material with adhesion-promoting molecules.

Experimental Methods

In this work, different resists were formulated introducing accessible functional groups which allowed the posterior coating with cell adhesive proteins/peptides, pursuing selective cell adhesion. Cytotoxicity tests (under ISO 10993) were carried out in order to assure the viability of the cells. Pheochromocytoma (PC12) cells are a commonly studied representative of a neuronal cell line which is often used in in vitro studies to examine the degree of differentiation and neurotoxicity commonly associated with neurodegenerative diseases (4). Under common laboratory culture conditions, PC12 cells adhere poorly to culture flasks and prefer to grow while floating in cell aggregates (5). Thus, PC12 response was evaluated by measuring a set of parameters related to cellular functions. The proliferation and metabolic activity of the PC12 cells were analyzed using a tetrazolium-based assay (WST-1). The morphology and neuron-like characteristics of the cells were analyzed by using brightfield phase contrast microscopy. Once a biocoating was chosen, it was applied to UV NIL microstructurated resist on PET foil in order to control neuron cell growth for drug screening assays.

Results and Discussion

In this work, several biocoatings have been screened such as polylysine (PDL), fibronectin, collagen and laminin coating. Cellular results with PC12 showed that polylysine is the best candidate for coating the designed resists. Then, flexible substrates with microchannel patterns were fabricated on thin foils using UV-Nano Imprint Lithography (UV-NIL). Once fabricated, they were coated with PDL and neuronal response was also analysed.

Conclusion

This micropatterned structure may represent the first step towards the development of flexible biochips for neuron cell growth. Our results support further development of this micropatterned resit and PDL as a coating, for neuronal based drug screening substrates.

References

1. Bale SS, Borenstein JT. Microfluidic Cell Culture Platforms to Capture Hepatic Physiology and Complex Cellular Interactions. Drug Metab Dispos. 2018 Nov;46(11):1638–46.
2. Seidlits SK, Liang J, Bierman RD, Sohrabi A, Karam J, Holley SM, et al. Peptide-modified, hyaluronic acid-based hydrogels as a 3D culture platform for neural stem/progenitor cell engineering. J Biomed Mater Res A. 2019 ;
3. Apati A, Varga N, Berecz T, Erdei Z, Homolya L, Sarkadi B. Application of human pluripotent stem cells and pluripotent stem cell-derived cellular models for assessing drug toxicity. Expert Opin Drug Metab Toxicol. 2018
4. Jesky R, Chen H. The neuritogenic and neuroprotective potential of senegenin against Aβ-induced neurotoxicity in PC 12 cells. BMC Complement Altern Med [Internet]. 2016;16(1):1–11.
5. Attiah DG, Kopher RA, Desai TA. Characterization of PC12 cell proliferation and differentiation-stimulated by ECM adhesion proteins and neurotrophic factors. J Mater Sci Mater Med. 2003;14(11):1005–9

Acknowledgement

Microstructured surfaces for neuron cell growth are studied within the European Horizon H2020 project “R2R Biofluidics” as a demonstrator for a pilot line with Roll-to-Roll (R2R) technologies with roller-based nanoimprinting methods enabling cost-effective, large-scale production of flexible polymer films with imprinted and printed micro- and nano- scale structures.

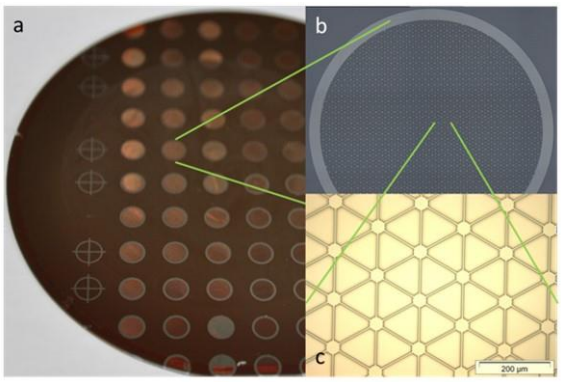

Micropatterned well for neuronal growth.
A) photograph of photolithography master on Si wafer. B) picture of one well. C) hexagonal structure of well. Diameter size of round cavity: 40 µm, interconnecting channels: 5µm wide, 160 µm long

2:45 p.m. – 3:45 p.m.

Hall 1 / Exhibition Area

PS2-07 | Hydrogels

PS2-07-339

Oxidized Alginate Hydrogels from Mixed Secondary Aldimine Crosslinkers Exhibit Tunable Mechanical and Viscoelastic Properties

Francis L. C. Morgan, Shahzad Hafeez, Huey Wen Ooi, Lorenzo Moroni, Matthew B. Baker

Maastricht University, MERLN Institute for Technology-Inspired Regenerative Medicine, Maastricht, NL

Introduction

Biomaterials for enhanced tissue regeneration are becoming increasingly prevalent. However, rationally designing materials that mimic the ECM and local tissue environments is a non-trivial task. The extra-cellular matrix (ECM) contains a complex cocktail of biopolymers and signaling molecules, which together, can be broadly considered as a viscoelastic bio-functionalized hydrogel. It has been shown that material parameters such as the stiffness and relaxation time of a hydrogel can have a significant impact on the observed cellular responses.[1] Presented with the diversity of stiffness and relaxation characteristics of native tissues; the scope of any single material system has distinct limitations. Capturing the complexity of this natural microenvironment in a single cytocompatible material remains an active challenge within the community, and to this end, dynamic covalent chemistry (DCC) has emerged as a powerful tool. Diverse DCCs have been shown to tune mechanical and viscoelastic properties of both bulk and local environments over a wide range of physiologically relevant magnitudes.[1]. We recently investigated the use of alginate hydrogels using secondary aldimine crosslinks as a bioink and they were shown to be cytocompatible, as well as induce a different cellular morphology depending on their dynamicity and stiffness (Figure 1.).[2] Here, we explore how varying combinations of the aforementioned crosslinkers can be used to modulate and control the stiffness and relaxation characteristics of oxidized alginate hydrogels.

Experimental Methods

Sodium Alginate (FMC Manugel GMB, Lot No. G9402001) was purified and oxidized to a 10% theoretical degree of oxidation as previously reported.[2] Hydrogels were formed by the addition of varying proportions of adipic acid dihydrazide (≥98%, Sigma Aldrich) and O,O'-1,3-propanediylbishydroxylamine dihydrochloride (98%, Sigma Aldrich). In all cases, the final alginate concentration attained was 2% (*w/v*) in Phosphate Buffered Saline (PBS) without magnesium and calcium ions. The alginate and cross-linker (1:1 with respect to degree of oxidation) were mixed rapidly in the desired ratio before being transferred to silicon molds and stored in the fridge overnight. The following morning, strain sweeps (1% - 1000% @ 10 rad/s) and frequency sweeps (100 rad/s – 1 rad/s @ 1% strain) were performed to evaluate the mechanical and viscoelastic characteristics of the resulting gels.

Results and Discussion

In this study, we used combinations of dynamic secondary aldimine crosslinkers possessing different dynamicities (Figure 2) to develop oxidized alginate hydrogels with highly tunable viscoelastic properties. Despite having equilibria constants on the order of 10^4 – 10^8, and thus a theoretical binding efficiency greater than 99%, we observe markedly different stiffnesses resulting from each individual crosslinker. Following quantification by oscillatory shear rheometry, there is a strong correlation between the dynamicity of the crosslinker and the observed stiffness, with the oxime hydrogels being the stiffest (~ 2 kPa) and least dynamic (K_{eq}~ 10^8) while the hydrazone hydrogels are the softest (~ 0.5 kPa) and most dynamic (K_{eq}~ 10^4). By maintaining an equivalent total crosslinker concentration and preparing hydrogels with different proportions of oxime and hydrazone crosslinks, we are able to tune the bulk stiffness to a

desired value within this range. Bearing in mind that the crosslinker molecules are present in an equimolar concentration to potential binding sites, an extrapolation of the apparent crosslink density from rheological measurements reveals that the stiffness is directly proportional to the concentration of oxime crosslinker. This brings into question the exact role the hydrazone crosslinker plays in this mixed system.

Conclusion

Here we demonstrate the tunable stiffness of oxidized alginate hydrogels within physiologically relevant ranges, and bring to light possible emergent behavior when multiple crosslinkers with large differences in dynamicity are mixed. We are now investigating a corresponding evolution of the relaxation and strain response of these hydrogels, as well as a more detailed analysis of the role and contributions of each crosslinker in a mixed system. More specifically, we will focus on possible correlations between the molecular kinetics and equilibria within the hydrogels. Understanding the fundamental origin of dynamic hydrogel properties such as stiffness and relaxation would allow significantly more control over these systems and represent a powerful step forward in the rational design of complex biomimetic materials for tissue regeneration.

References

[1] Webber, M. J. *et al.*, Supramolecular biomaterials. *Nat. Mater.***15,** 13–26 (2015).

[2] Hafeez, S. *et al.,* Viscoelastic Oxidized Alginates with Reversible Imine Type Crosslinks: Self-Healing, Injectable, and Bioprintable Hydrogels. *Gels***4,** 85 (2018).

Acknowledgement

The authors are gracious for funding from the research programme Innovation Fund Chemistry, which is partly financed by the Netherlands Organisation for Scientific Research (NWO) under TA grant agreement 731.016.202 (“DynAM”). The authors would also like to thank the Brightlands Materials Center and the Province of Limburg for their support of this work.

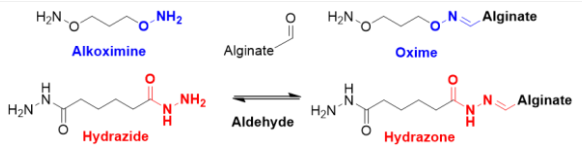

Crosslinker Chemistry
Representative secondary aldimine crosslinking reactions.

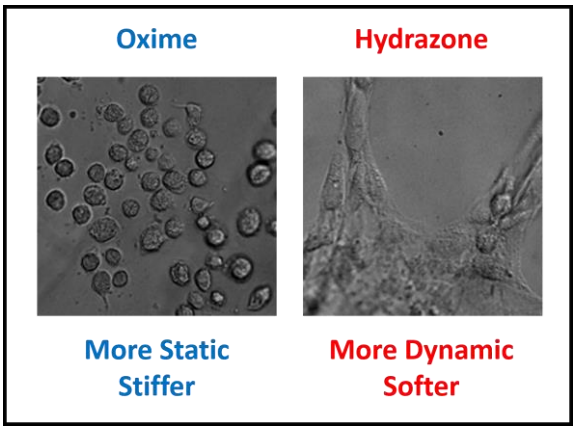

FIg. 1 - Cell Spreading on Viscoelastic Substrates
Surface seeded fibroblasts on Oxime and Hydrazone hydrogels. Image taken after 24h. Scale bar = 25 µm.

PS2-07-340

Development of Mesoporous Silica Nanocomposite Hydrogels for Bone Regeneration

Aygul Zengin, Pamela Habibovic, Sabine Van Rijt

Maastricht University, Department of Instructive Biomaterials Engineering (IBE)/ MERLN Institute, Maastricht, NL

Introduction

Current standard treatment of critical-sized bone defects involves transplantation of patient's own bone (i.e. autograft). This treatment is, however, associated with several drawbacks, limited availability being the most important one. Thus, there is a need for affordable but effective alternatives to the patient's own bone. In this regard, the incorporation of nanoparticles within biomaterials to create nano-composites is an attractive approach to create a new type of materials within the field of regenerative medicine that can show improved mechanical and/or biological performance compared to analog composites without nanoparticles.[1] This project aims to develop new injectable, adaptable biomaterials for bone tissue regeneration using inorganic nanosized building blocks (nanoparticles of ~100 nm) and hydrophilic linkers that self-assemble in a 3D matrix. Inorganic nanoparticles based on mesoporous silica nanoparticles (MSNs) are proposed as ideal building blocks within these constructs as they are bioactive, improve mechanical and biological properties of incorporating polymers, and can controllably release various types of cargo.[2-6] The resulting materials will be moldable, self-healing, bioactive and tissue-responsive. The proposed method and building blocks allow "bottom-up" development of complex biomaterials that are modifiable down to the nanoscale, which is expected to lead to superior bone graft substitutes.

Experimental Methods

Synthesis of MSNs. Surface and core modified MSNs (amines in the core and thiols on the surface) were synthesized through a multistep, delayed co-condensation method.[6] The functionalized particles were characterized by dynamic light scattering, Fourier transform infrared spectroscopy, scanning and transmission electron microscopy.
Preparation of MSN-SS-PEG Gel Formulation. Gel formation was obtained through the reversible thiol/disulfide exchange reactions between thiol functionalized nanoparticles and PEG polymer in the presence of 2,2'-Dipyridyldisulfide (DPS) initiator.

Results and Discussion

Surface and core modified MSNs (amines in the core and thiols on the surface) could be successfully synthesized with colloidal stability and in sizes ranging from 100 to 200 nm. They showed a highly porous structure. MSNs have a positive charge due to amine groups on the outer surface. Under neutral to basic conditions, the functionalized nanoparticles triggered gel formation by acting as an inorganic crosslinker between polymeric chains in the presence of DPS initiator. Mechanical properties of the gels can be modulated by changing MSN wt% and polymer wt%.

Conclusion

Core-shell functionalized MSNs form stable colloidal suspensions and can be used as crosslinkers for the formation of new types of stimuli-responsive, hybrid inorganic-organic materials for tissue regeneration

References

1. Lach, R., et al., Macromolecular Materials and Engineering, 2006. **291**(3): p. 263.
2. Yang, S.B., et al., Soft Matter, 2012. **8**(34): p. 8981.
3. Baumann, B., R. Wittig, and M. Linden, Nanoscale, 2017. **9**(34): p. 12379.
4. Fiorini, F., et al., Small, 2016. **12**(35): p. 4881.
5. Shokry, H., et al., Nanoscale, 2015. **7**(34): p. 14434.
6. Cauda, V., et al., J Am Chem Soc, 2009. **131**(32): p. 11361.

Acknowledgement

This work is part of the Gravitation research programme Materials Driven Regeneration with project number 024.003.013, which is partly financed by the Netherlands Organisation for Scientific Research (NWO). We also would like to thank the province of Limburg (LINK) for providing financial support to this project.

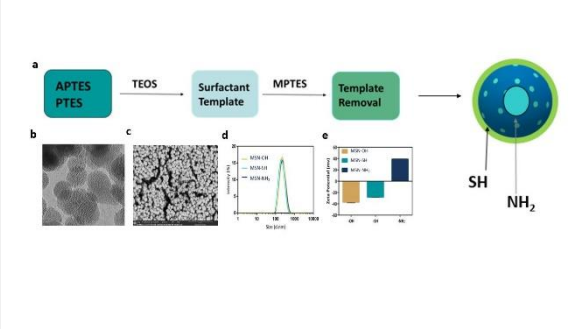

Synthesis and characterization of core-shell functionalized MSNs
(a) Schematic illustration of the synthesis of MSN-$NH_{2(in)}$-$SH_{(out)}$. (b-c) TEM and SEM image of the synthesized MSNs. (d-e) DLS and zeta potential results of MSNs with different functional groups on the surface.

PS2-07-341

Living functional hydrogels generated by bioorthogonal cross-linking reactions of azide-modified cells with alkyne-modified polymers

Koji Nagahama, Yuka Kimura, Seika Aoyama

Konan University, Department of Nanobiochemistry, Kobe, JP

Introduction

Cells and cellular functions should be attractive and promising active components for the design of functional materials. Combining living cells with synthetic materials could enable the fabrication of living multifunctional materials capable of, for example, sensing the environment, time-programming, movement, and signal transduction, all originating from the functions of the incorporated cells. In this study, we present a new concept for utilizing cells and their functions from the viewpoint of materials science. In particular, we developed cell cross-linked living bulk hydrogels (CxGels) by bioorthogonal click cross-linking reactions of azide-modified mammalian cells with alkyne-modified biocompatible polymers (bAlg-DBCO) [1].

Experimental Methods

Pellet of azide-modified C2C12 cells was suspended with 100 µL of bAlg-DBCO solution in HEPES buffer and cells were completely dispersed by gentle pipetting. The cell dispersions were added into test tube and incubated at 37ºC. Gel formation was checked by usual test tube inverting methods and rheological test. The cell dispersions were poured into 96-well plate and incubated at 37ºC for 1 hour. Two hundred µL of DMEM was added on the gels and cultured for 7 days. After predetermined times, cell proliferation in the gels was also examined with WST-1 assay. After predetermined time, the remained gels were carefully transferred into a new plastic microtube, and washed with PBS twice, then the weight of swollen gels was measured. Moreover, gels were lyophilized and the weight of the dry gel was also measured. Nude mice were anesthetized with isoflurane. The skin of the hind limb was opened, and the femoral muscle was gently exposed. In host femoral muscle, a local injury was created by removing skeletal muscle fibers. The skin was then carefully closed and the incision was sutured. One day after the surgery, 250 µL of CxGels precursor solution was injected into the injury site. After transplantation, the muscle strength of the injured hind limbs was quantitatively measured every day using a grip-strength meter. At the end of the experiment, the injury site was carefully opened and the regenerated skeletal muscle tissues were analyzed by CLSM observation.

Results and Discussion

As mentioned above, our aim is to demonstrate that the covalent combination of living cells, acting as active cross-linking points, enables the development of multifunctional hydrogels with unique functionalities that originate from the cells. We therefore selected two basic cellular functions to demonstrate utility of our approach: autonomous cell growth and selective cell adhesion. First, we found that the cell proliferation (cell division) directly affects the swelling and degradation properties of the CxGels. Therefore, CxGels have the ability to self-grow and self-degrade due to the autonomous growth of cells utilized as active cross-linking points, and we successfully demonstrate that these are unique properties of CxGels. Second, we found that the selective adhesion of CxGels is derived from the ability of cells in CxGels to selectively adhere onto surfaces. Hydrogels generally have a remarkably low friction coefficient because of the large amount of free water on their surface, making the stable attachment of hydrogels onto solid materials difficult. On the other hand, cells can adhere onto various solid materials with a wide range of water contact

angles in the presence of cell attachment proteins. We found that CxGels can adhere onto materials which alginate gels cannot by using the selective adhesion abilities of the cells. Thus, we propose that the selective adhesive ability of CxGels is unique as compared to existing hydrogels. Taken together, we have successfully demonstrated that the functions of cells covalently incorporated into CxGels as active cross-linking points are useful for endowing CxGels with unique functionalities.

Conclusion

Importantly, whole mammalian cells and their functions are retained in CxGels, and unique functionalities are generated. This method can be applied to bacteria and viruses because their surfaces can be modified by metabolic glycoengineering. Therefore, the findings of this study provide a promising route to the generation of living cell-based next-generation innovative materials, technologies, and medicines.

References

1. K. Nagahama, Y. Kimura and A. Takemoto, *Nature Communications*, **9** (2018) 2195.

Acknowledgement

This work was supported by JSPS KAKENHI Grant Number 15K13791.

PS2-07-342

Hybrid alginate-silica hydrogels for tissue engineering.

Aurora C. Hernández-González[1], Lucia Téllez-Jurado[1], Luis M. Rodríguez-Lorenzo[2,3]

[1]Instituto Politécnico Nacional, Departamento de Ingenieria Metalúrgica, Mexico city, MX; [2]Networking Biomedical Research Centre in Bioengineering, Biomaterials and Nanomedicine, Centro de Investigación Biomédica en Red—Bioingeniería, Biomateriales y Nanomedicina (CIBER-BBN), Madrid, ES; [3]Instituto de Ciencia y Tecnología de Polímeros- CSIC, Departamento de nanomateriales poliméricos y biomateriales, Madrid, ES

Introduction

The healing of bone defects has witnessed a paradigm shift from synthetic implants and tissue grafts to a bone tissue engineering (BTE) approach. Alginates offer a series of properties that have been exploited for the generation of materials for medical devices and treatments, however drawbacks related with lack of osteoinductive behavior, low structural properties and poor cell afinity required to function in bone tissue engineering are still undergoing. From this perspective organic-inorganic hybrid materials are a promising alternative, since the components interact at molecular level resulting in materials with higher processability and integrity [1]. Among them, promising materials barely studied are the silica-alginate compositions. Silica materials are characterized by a tight interface with polymer matrices, where the inorganic component provides biomineralization ability and higher material stiffness [2]. Silica hybrid materials can be obtained by a sol-gel technique introducing a polymer prior to gelation. In this work, the effect of the organic-inorganic ratio and the amount of catalyst in the final properties of the resulting hybrid are studied.

Experimental Methods

For alginate-silica hybrid materials, established amounts of alginate were dissolved in deionized water until total homogeneity. After, TEOS was added and stirred. Ten minutes later APTES is added dropwise to the solution and maintained under agitation at room temperature. Then, a solution of water/HCl or water alone is added by dripping, to catalyst the hydrolysis-condensation reactions of TEOS-APTES and the homogeneous incorporation of the alginate into the inorganic matrix. Compositions with ALG/TEOS-APTES ratios between 17.6/72.4, 9.68/93.02 and 4.1/95.9 were prepared with inorganic/Catalyst ratio of 0, 0.15 and 0.3. Final chemical composition, crystallinity degree, thermal and hydrolytic stability were examined for all the hybrid materials. Cellular proliferation is being assayed over the materials at the time of writing this abstract.

Results and Discussion

Based on the experimental method described, 9 hybrid materials were obtained. The hybrids ALG/TA 1,2 and 3 (17.5% Alginate) form very thick emulsions, observing that at higher catalyst concentration the viscosity decrease. However after 24 hours the material with the least amount of catalyst managed to gel (Material 1).The hybrids ALG/TA 4, 5 and 6 (9.68% Alginate) seem to gel at the end of the synthesis. Hybrids ALG/TA 7, 8 and 9 (4.1% Alginate) appear to be glued upon concluding the synthesis without appreciable differences regarding the catalyst concentration.

Figure 1 shows infrared spectra of the alginate-silica hybrid material with representative bands at 1160 cm^{-1} and 942 cm^{-1} corresponding to the CH2 rocking from TEOS and APTES. In addition overlapped bands at 1082 cm^{-1} and 1045 cm^{-1} are assigned to the stretching of Si-O-C and Si-O-Si respectively. At ~873 cm^{-1} a band corresponding to the copolymerization of Si-OH radicals are observed and at 780 cm^{-1} the stretching of Si -CH3 bonding are observed.It can be deuced that as the amount of catalyst increases in the materials, the band due to the Si-OC stretch at 1083

cm^{-1} decreases its relative intensity with respect to the 1045 cm^{-1} band of the Si-O. This decrease is caused by the transformation of the bond Si-O-C to Si-O-Si and its variation is indicative of the hydrolysis reached in the reaction. On the other hand, considering the alginate proportion, it is observed that materials with the greatest amount of alginate 1, 2 and 3, present a greater difference in the intensity of the bands at 1078 cm^{-1} and 1040 cm^{-1}, but very low intensity in the band at 870 cm-1, generating thick colloidal solutions. Besides, materials with a lower amount of alginate 7, 8 and 9 manage to generate Si-OH radicals as indicated by the decrease in the band at 1078 cm^{-1}, however, being sterically more impeded by alginate with a lower amount of water, the reaction shifts toward the condensation reaction of the silanol groups generating structures with precipitates and lumps. Finally, materials 4 and 5 seem to achieve a balance between both reactions, generating connected structures and gelling at low reaction times.

X-ray diffractograms confirm the formation of silica structures with amorphous maxima around 8 and 22.6° in 2 Theta. In addition, it is observed a decrease in the intensity of the amorphous maxima of the hybrid materials as the amount of hydrochloric acid increases. This can be explained as the formation of disordered structures (lower crystallinity) due to the acceleration of the condensation reaction of the silica in the materials.

Conclusion

Gelation times, homogenity and structural stability of hybrids depends on the alginate concentration and amount of catalyst. Materials with no catalyst and 9.68% weight of alginate present a hydrolysis-condensation equilibrium reaction with low gelling times and appropriate structural stability for cytotoxicity studies

References

(1) Caló, E. and V.V. Khutoryanskiy, *Biomedical applications of hydrogels: A review of patents and commercial products.* European Polymer Journal, 2015. **65**: p. 252-267.

(2) Vo, T., et al., *Injectable dual-gelling cell-laden composite hydrogels for bone tissue engineering.* Biomaterials, 2016. **83**: p. 1-11.

PS2-07-343

Regeneration of skeletal muscle tissue by transplantation with injectable cell cross-linked gels

Yuka Kimura[1], Koji Nagahama[1]

[1]Konan University, Graduate School of Frontiers of Innovative Research in Science and Technology (FIRST), Kobe, JP; [2]Konan University, Graduate School of Frontiers of Innovative Research in Science and Technology (FIRST), Kobe, JP

Introduction

Regeneration of skeletal muscle that damaged by injury or by degenerative diseases has been the object of many scientific studies throughout the years. The main strategies currently pursed for skeletal muscle regeneration consist of cell therapy. Cell therapy by direct injection of cells into the damaged muscle tissue are typically limited because of death of the majority of the transplanted cells. Injectable gels can be good candidates to overcome the problem. Three-dimensional hydrogel structures formed in the damaged tissue could provide scaffold for growth and assembly of transplanted cells. Recently, we developed cell cross-linked hydrogels (CxGels), which living human cells are covalently cross-linked with three-dimensional polymer networks, by bioorthogonal click cross-linking reactions of azide-modified cells with alkyne-modified biocompatible polymers [1]. Importantly, we found that the CxGels have potential utility as injectable gels for tissue regeneration. In this study, we investigated potential application of CxGels as injectable gels for regeneration of skeletal muscle tissues.

Experimental Methods

We selected alginic acid (100,000 Da) as polymer components because of its good biocompatibility and synthesized branched alginic acid (bAlg) using amine-terminated 4-arm branched PEG (20,000 Da). Then, we synthesized dibenzylcyclooctyne (DBCO)-modified bAlg (bAlg-DBCO). Pellet of azide-modified C2C12 myoblast cells was suspended with 200 µl of bAlg-DBCO solution in HEPES buffer (100 mM, pH 7.4) and cells were completely dispersed by gently pipetting. Rheological test of the cell dispersions was performed. Oscillatory time and frequency were performed at 37℃, and the storage modulus (G') and loss modulus (G") were recorded. The time sweep data collection was started from time zero to 18000s to monitor the gelation process. Nude mice (BALB/c-nu/nu) were anesthetized with isoflurane. The skin of the hind limb was opened, and the femoral muscle was gently exposed. In host femoral muscle, a local injury (ca. 7 mm long, 4 mm wide) was created by removing skeletal muscle fibers. The skin was then carefully closed and the incision was sutured. One day after the surgery, 150 µl of CxGels precursor solution, Lifeact-GFP-expressing N_3(+)C2C12 cells (3.0×10^6) suspended with bAlg-DBCO solution, was injected into the injury site. As controls, Lifeact-GFP-expressing N_3(-)C2C12 (3.0×10^6) was suspended in physiological saline or Matrigels, then these suspensions were transplanted into the injury site. After transplantation, the muscle strength of the injured hind limbs was quantitatively measured every day. At the end of the experiment, the injury site was carefully opened and the regenerated skeletal muscle tissues were analyzed by observation of CLSM and H&E staining.

Results and Discussion

Metabolic glycoengineering was used to incorporate reactive azide groups on the cell surface. The monosaccharide precursor was modified with an azide group, then incorporated into cell-surface glycans through biosynthetic

machinery. Sialic acid is one of the most abundant cell-surface glycans on mammalian cells and is typically found at the terminating branches of these glycans. We therefore targeted sialic acid residues for azide-modification because the location (the outermost surface of cells) and abundance (high concentration on cell surface) of sialic acid residues was ideal for efficient bioorthogonal click cross-linking with bAlg-DBCO. The ^{1}H-NMR analysis of bAlg-DBCO showed that on average 13 DBCO groups were introduced per bAlg molecule and the molecular weight is 1,026,800 Da. Reaction mixtures of N_3(+)C2C12 cells and bAlg-DBCO solution (1%) did not form bulk-sized hydrogels. In contrast, gelation was achieved by reaction mixture of N_3(+)C2C12 cells (2.0×10^6) and bAlg-DBCO solution (2%). Gelation time and mechanical strength of the CxGels can be controlled by varying the number of cells and concentrations of bAlg-DBCO. C2C12 cells in the CxGels showed high viability (over 90%) and proliferation with logarithmic phase over 1 week. In the muscle regeneration test, it was shown that the muscle fibers formed by the injection of CxGels was thicker than the control gels. Moreover, transplantation of CxGels resulted in remarkably high muscle force recovery as compared with control mice.

Conclusion

In conclusion, we successfully demonstrate that the CxGels can be a new technology for regenerative medicine of skeletal muscle tissues damaged by injury or by degenerative diseases.

References

1. K. Nagahama, Y. Kimura and A. Takemoto, *Nature Communications*, **9**, 2195 (2018).

PS2-07-344

Hydrogel-based hybrid magnetic scaffolds for tissue engineering applications

Sylwia Fiejdasz[1], Adriana Gilarska[1,2], Szczepan Zapotoczny[2], Maria Nowakowska[2], Czesław Kapusta[1]

[1]AGH University of Science and Technology, Faculty of Physics and Applied Computer Science, Department of Solid State Physics, Kraków, PL; [2]Jagiellonian University, Faculty of Chemistry, Nanotechnology of Polymers and Biomaterials Group, Kraków, PL

Introduction

The research in tissue engineering concentrate on development of biocompatible materials similar to those of native tissues. That is the reason why hydrogels are of great interest. Those three-dimensional networks composed of hydrophilic polymers, can be crosslinked, either through covalent bonds or via physical interactions. In the swollen state, hydrogels resemble, to a great extent, the living tissues. That is why, especially the biopolymer based hydrogels have a great potential as matrices for tissue regeneration. Among them, hydrogels made of collagen and chitosan are of special interest. Collagen is a fibrillar component of the extracellular matrix of mammalian tissues, with excellent biocompatibility. Chitosan is biocompatible and biodegradable linear polysaccharide obtained by deacetylation of chitin. Moreover, it exhibits antibacterial, antifouling properties and accelerates the process of wound healing [1,2]. Many of these properties can be enhanced, modified or new characteristics can be possibly obtained by introducing the nanoparticles, as indicated in many papers. There are many different types of nanoparticles already produced, but the ones with magnetic functionality are of special interest. Superparamagnetic iron oxide nanoparticles (SPIONs) in particular, magnetite (Fe_3O_4) and maghemite (γ-Fe_2O_3) have the remarkable magnetic properties. They are often used in nanomedicine to develop novel therapeutic and diagnostic modalities. Nanoparticles cover a wide range of applications that include drug delivery, MRI contrast agents, hyperthermia and tissue engineering among others [3-5]. In this report, we present nanoparticles which will be used as building blocks for fabrication of tissue engineering scaffolds. The hybrid magnetic scaffolds were prepared by immobilization of nanoparticles in hydrogel matrices.

Experimental Methods

Positively charged, chitosan surface-coated iron oxide nanoparticles were prepared using co-precipitation method. The synthesis was carried out in aqueous solution of cationic derivative of chitosan (CCh) using iron salts ($FeCl_3$,$FeCl_2$) and ammonia. During the whole process the reacting solution was sonicated and kept in oxygen-free environment (argon bubbling) in the thermostated bath (20°C). In order to obtain negatively charged nanoparticles, SPIONs were subsequently coated with polyanion (anionic chitosan derivative) using layer by layer (Lbl) method. The final products were purified using magnetic filtration. The extensive physicochemical, structural and magnetic characterization of the obtained nanoparticles was performed (DLS, STEM, XRD, VSM, Mössbauer Spectroscopy). Next hybrid magnetic scaffolds were fabricated by immobilization of polymer-coated SPIONs in hydrogel matrix. The materials obtained were characterized in terms of their physicochemical properties and cytocompatibility.

Results and Discussion

The physicochemical, magnetic and biological properties of obtained nanoparticles were investigated using various complementary techniques. Hydrodynamic diameter of nanoparticles was obtained using Dynamic Light Scattering

method and found to be about 100 nm. The coating effectiveness and colloidal stability of nanoparticles in water was evaluated based on zeta potential measurements (DLS). The size of magnetic cores was equal to 10 nm as revealed by TEM/STEM imaging. Their structure was studied using X-ray diffraction and Mössbauer spectroscopy. The results indicate that nanoparticles are crystalline and nanosized structures. SPION materials revealed to be oxidized magnetite, i.e. maghemite. Vibration Sample Magnetometry measurements confirmed superparamagnetic nature of nanoparticles. Physicochemical (e.g. swelling, degradation, microstructure), mechanical, magnetic properties of hybrid magnetic materials were evaluated. Preliminary biological evaluation was also performed.

Conclusion

In this report the surface-coated iron oxide nanoparticles were obtained and demonstrated to be useful as components for hybrid magnetic scaffold fabrication. The materials prepared were intensively characterized and promising results concerning their potential application were obtained.

References

1. Dash, M., *et al.,* Prog Polym Sci 36: 981-1014, 2011
2. Fiejdasz, S., et al.,J. Colloid. Interface. Sci., 524 : 102-113, 2018
3. Laurent, S. et al. Chem Rev108 (2008) 2064
4. Szpak, A., *et al.,* J.Nanoparticle Res., 16 : 2678-2689, 2014
5. Gupta, A.K et al. Biomaterials 26 (2005) 3995

Acknowledgement

S.F. acknowledges the financial support from National Science Centre, Poland (grant no. 2016/23/D/ST8/00669). A.G. has been partly supported by the EU Project POWR.03.02.00-00-I004/16.

PS2-07-345

Injectable oligomer cross-linked gelatin hydrogels: Effects of gel composition on osteogenic mineralization

Hafiz Awais Nawaz[1,2], Kathleen Schröck[1], Annett Starke[1], Caroline Kohn-Polster[1], Christian Kascholke[1], Michaela Schulz-Siegmund[1], Michael C. Hacker[1]

[1]Leipzig University, Department of Pharmaceutical Technology, Leipzig, DE; [2]University of Veterinary and Animal Sciences (UVAS), Institute of Pharmaceutical Sciences (IPS), Lahore, PK

Introduction

Mineral deposition and a biomaterial's ability to support mineralization are considered important feature for bone and osteochondral regeneration. It is known that presence of anionic sequences (e.g., hydroxyl and carboxyl groups) in synthetic or natural oligomers may confir apatite nucleating properties to the hydrogels in swollen state[1]. In this regard, gelatin-based hydrogels are also important as they mimic extracellular matrix (ECM) due to their inherent cell-adhesive properties, degradability, immuno- and biocompatibility. Motivated by the idea, we strive to synthesize hydrophilic and reactive oligomers, containing hydroxyl groups and carboxylate sequences, and utilized those to formulate injectable, gelatin-based hydrogels cross-linked via amine-anhydride conjugation for hard tissue regeneration.

Experimental Methods

Oligomers were synthesized by free radical polymerization of maleic anhydride (MA) and hydrophilic comonomers: acryloylmorpholine (Mo), *N*-vinylpyrrolidone (Vp) and hydroxypropyl acrylate (Hp) in defined ratios with pentaerythritol diacrylate monostearate (P).[2] Analogues to 'P' containing oligomers (oPXMA), either without the addition of lipophilic domain or in the presence of lipophilic domains (lauryl acrylate or stearyl acrylate) were also synthesized. The oligomers were characterized by acid-base titrations, proton NMR (^{1}H-NMR), gel permeation chromatography (GPC) and dissolution experiments. Injectable formulations of these versatile oligomers with aqueous solution of gelatin (type A, 300B) were formulated and characterized rheologically. Human adipose tissue derived stem cells (hASC) were encapsulated in these hydrogels and cytocompatibility was assessed by Live/Dead® staining and confocal microscopy. Differentiation and mineralization capability of gel encapsulated cells and incubated in osteogenic medium was also investigated until day 21.

Results and Discussion

Three sets of hydrophilic oligomers (oPHpMoMA, oPVpMoMA and oPHpVpMA) and their analogues without lipophilic domain (oHpMoMA, oVpMoMA and oHpVpMA) and with different lipophilic domains, namely lauryl acrylate (oLHpMoMA, oLVpMoMA and oLHpVpMA) and stearyl acrylate (oSHpMoMA, oSVpMoMA and oSHpVpMA), were synthesized.[2] Physicochemical characterization of these oligomers confirmed high intactness of anhydride units (>80%) and controlled incorporation of hydrophilic comonomers (^{1}H-NMR) depending upon feeding ratios. GPC analysis revealed molecular weights (Mn) in the range of 2-3 kDa. All hydrophilic macromers dissolved faster than previously established derivatives.[3,4] Generally, lipophilic domain free oligomers showed faster dissolution as compared to oligomers synthesized in the presence of different types of lipophilic domains. These oligomers were utilized to formulate gelatin-based hydrogels via amine-anhydride conjugation under pH control using a programmable multi-step pipette. Hydrogel stiffness depended on the availability and type of lipophilic domain as

well as oligomer composition. The hydrogels retained viable cells upon cross-linking that proliferated effectively over 7 days. Cell-laden gels showed good mineralization at day 21 in osteogenic cultures and calcium content was found to correlate more with the presence of hydroxyl groups in oligomer composition as compared to carboxylate groups and gel mechanical properties.

Conclusion

Three sets of hydrophilic oligomers (oPHpMoMA, oPVpMoMA and oPHpVpMA) and their analogues with and without the addition of different lipophilic domains were synthesized and characterized physico-chemically. These hydrophilic oligomers presented high reactivity and controlled comonomer incorporation. Such injectable oligomer/gelatin hydrogels encapsulated live cells and presented good gel mineralization after 21 days. These oligomer cross-linked gelatin networks hold promise for applications in regeneration of mineralized tissues.

References

1. Gkioni, K. Et al. Tissue Engineering (Part B), 16 (6), 577-585 (2010).
2. Loth, T. et al. Biomacromolecules 15, 2104–2118 (2014).
2. Kohn-Polster, C. et al. Int. J. Mol. Sci. 18, 1–29 (2017).
3. Kascholke, C. et al. Biomacromolecules 18, 683–694 (2017).

PS2-07-346

Injectable hydrogel-based delivery of nonviral genetically-engineered stem cells for repairing traumatic brain injury

Yu-Yun Jang[1], Yen-Hua Chu[1], Yi-Chen Bai[1], Rih-Yang Huang[1], Zhuo-Hao Liu[2], Chien-Wen Chang[1]

[1]National Tsing Hua University, Department of Biomedical Engineering and Environmental Sciences, Hsinchu, TW; [2]Chang Gung Memorial Hospital and Chang Gung University, Department of Neurosurgery and Pathology, Taoyuan, TW; [3]Academia Sinica, Research Center of Applied Sciences (RCAS), Taipei, TW

Introduction

Traumatic Brain Injury (TBI) is a severe health condition which is currently lack of effective clinical treatments. In recent years, stem cells-based therapy has received great attentions on treating TBI because of their capabilities on neuronal differentiation and trophic factors secretion. Despite of their potentials, applications of stem cells on TBI are hampered by the low survival and retention of the transplanted stem cells in the injured sites. By adopting biomaterials to improve the cell delivery, better therapeutic outcomes may be achieved. To this end, we proposed aldehyde alginate (ADA)/Gelatin (Gel) as an injectable scaffold to deliver hMSCs for TBI treatment. In view of the significant role of angiogenesis on brain injury repair, vascular endothelial growth factor (VEGF)-secreting hMSCs (^{VEGF}hMSCs) was constructed using our developed magnetic ternary nanocomplexes system. The therapeutic efficacy of ^{VEGF}hMSCs-laden ADA-Gel hydorgels is investigated on a TBI animal model.

Experimental Methods

Aldehyde alginate (ADA) was prepared by oxidizing the hydroxy groups in alginate using $NaIO_4$. Stem cells-laden hydrogels were prepared by gently suspending cells with polymer solutions. Viability, spreading and proliferation of the stem cells in hydrogels were assessed by live/dead assay, actin staining and alamarBlue assay respectively. ^{VEGF}MSCs were constructed by VEGF gene delivery into hMSCs using a magnetic ternary nanocomplexes system. VEGF expression was determined using the ELISA assay. The brain trauma animal model was constructed using a computer-controlled impact system.

Results and Discussion

ADA was synthesized by converting the hydroxyl to aldehyde groups on alginate via an oxidation process. Rapid gelation process (< 10 minutes) was observed after mixing ADA and Gel in aqueous solutions. Porosity of the hydrogels were characterized using a scanning electron microscope (SEM). Porosity of the hydrogels was tunable by varying ADA content in the hydrogels. High viability of the encapsulated ^{VEGF}MSC in ADA-Gel hydrogels was observed by live & dead staining. Long term survival and proliferation of stem cells inside the hydrogels was demonstrated by monitoring the continual firefly luciferase transgene expression using an In Vivo Imaging System (IVIS). By using the magnetic ternary nanocomplexes-mediated transfection, efficient VEGF expression from the ^{VEGF}hMSCs was confirmed using ELISA assay. The secreted VEGF significantly promoted proliferation of the human umbilical cord vascular endothelial cells (HUVECs) in vitro, demonstrating the potentials of using ^{VEGF}hMSCs to promote angiogenesis on TBI model. The TBI model was established using a computer-controlled impact system. Less and smaller blood vessels was observed from the injured brain tissues compared to normal brains. Therapeutic efficacy of the ^{VEGF}hMSCs-laden ADA-Gel hydrogels on TBI is under investigation.

Conclusion

An injectable ADA-Gel hydrogel system was fabricated supporting good survival and proliferation of the encapsulated stem cells. VEGF-expressing MSCs (^{VEGF}MSCs) was successfully constructed by a magnetic ternary nanocomplexes-mediated gene delivery. Therapeutic efficacy of ADA-Gel-delivered ^{VEGF}MSCs on TBI repair is currently under investigation.

References

Zhang Y, Chopp M, Zhang ZG, Katakowski M, Xin H, Qu C, et al. Systemic administration of cell-free exosomes generated by human bone marrow derived mesenchymal stem cells cultured under 2D and 3D conditions improves functional recovery in rats after traumatic brain injury. Neurochemistry International. 2017;111:69-81.

Acknowledgement

This research was financially supported by Ministry of Science and Technology of Taiwan (MOST 107-2113-M-007-028 -) and National Tsing Hua University (107Q2519E1)

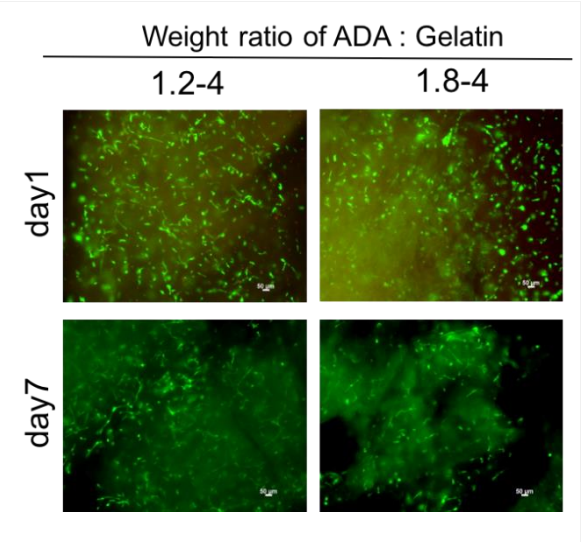

Cell-Material Interaction
Effect of the cell viability which MSC encapsulated in ADA-GEL hydrogel (3D) within a week . Image showed that MSC were mostly alive , with relatively few dead cells.

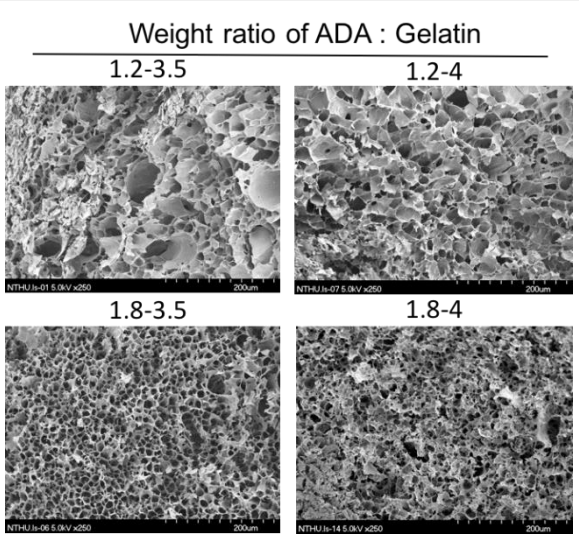

Characteristic of ADA-Gel hydrogel
Effect of different weight ratios on the porosity of ADA-Gel hydrogel by SEM. In the result, the hydrogel containing a higher amount of ADA showed the higher degree of porosity.

PS2-07-347

Whey protein isolate hydrogels as scaffolds for bone regeneration

Susanne Staehlke[1], Karolina Mazur[2], Aleksandra Krężel[3], Jagoda Żydek[3], Elzbieta Pamula[3], Krzysztof Pietryga[3], Julia Keppler[4], Carmen Piras[5], Barbara Nebe[4], **Timothy Douglas**[6]

[1]University Medical Center Rostock, Rostock, DE; [2]Cracow University of Technology, Krakow, PL; [3]AGH University of Science and Technology, Krakow, PL; [4]Christian-Albrechts-Universität zu Kiel, Kiel, DE; [5]University of York, York, GB; [6]Lancaster University, Lancaster, GB

Introduction

In this study, hydrogels were formed from whey protein isolate (WPI), a by-product from the production of cheese and Greek yoghurt. These products are being consumed in increasing quantitites, and hence there is a drive to find new applications for the by-products. WPI consists mainly of β-lactoglobulin (bLG) and WPI in solution has enhanced cell proliferation and osteogenic differentiation [1] in previous work. Hence, it was hypothesized that WPI hydrogels would support adhesion, growth and differentiation of osteoblast cells. A further advantage of using WPI is its relatively low cost.

Experimental Methods

WPI (Bipro) was obtained from Davisco Inc. WPI hydrogels of different concentrations (20, 30, 40, 50%, all w/v) were produced by heating WPI solution to 80ºC and subsequently sterilized by autoclaving. Hydrogel formation was characterized by rheometry and FTIR analysis. Subsequently, the adhesion, spreading, proliferation and osteogenic differentiation of human MG-63 osteoblasts [2] were compared.

Results and Discussion

The temperature at which gelation occurred decreased with increasing WPI concentration. Increasing WPI concentration from 20% to 50% increased compressive modulus from 0.2 to 4 MPa (Figure 1). All WPI hydrogels supported the adhesion and growth of MG-63 osteoblasts. Actin skeleton organization was superior on 40% and 50% hydrogels (Figure 2). Cell spreading and proliferation were highest on 40% hydrogels. Differentiation was highest on 50% hydrogels.

Conclusion

WPI hydrogels show potential as biomaterials for bone tissue engineering. Further work will focus on in vivo studies. In parallel, research to enhance WPI hydrogels by incorporation of a mineral phase is being performed.

References

[1] Douglas TEL, et al. J Dairy Sci. 2017 Nov 8. pii: S0022-0302(17)30997-9

[2] Staehlke S, Koertge A, Nebe B. Biomaterials 2015, doi:10.1016/j.biomaterials.2014.12.016.

Acknowledgement

N8 Agrifood pump priming grant “Food2Bone” (T.E.L.D.)

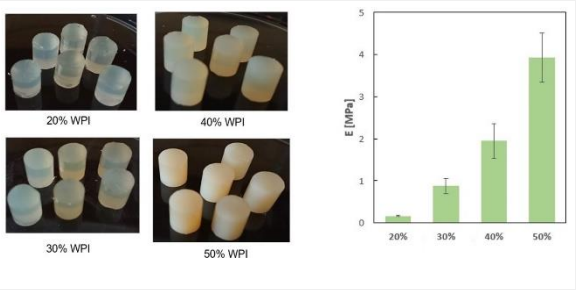

Figure 1
Left: WPI hydrogels containing 20, 30, 40 and 50% (w/v) WPI. Right: compressive moduli of WPI hydrogels

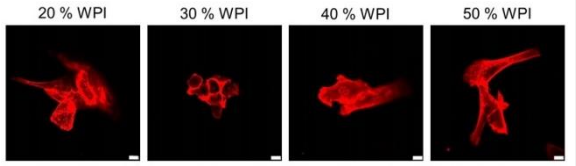

Figure 2
Spreading of MG-63 cells on WPI hydrogels of different concentrations. Red indicates actin cytoskeleton. Scale bar indicates 10 microns

PS2-07-348

Genetically modified plant virus nanoparticles induce osteogenic differentiation of human mesenchymal stem cells and promote biomineralization in three-dimensional hydrogels

Ying-Ying Lin[1], Juliane Röder[2], Christina Dickmeis[2], Ulrich Commandeur[2], Horst Fischer[1]

[1]RWTH Aachen University Hospital, Department of Dental Materials and Biomaterials Research, Aachen, DE;
[2]RWTH Aachen University, Institute for Molecular Biotechnology, Aachen, DE

Introduction

Hydrogels contain an abundant amount of water and provide a unique microstructure, which mimics the native extracellular matrix; therefore, they are very suitable for cell culturing. They have been widely used in tissue engineering and contributed to both biological properties and mechanical support. Nevertheless, they often lack biological and biochemical signals for designated applications. To overcome this problem, we propose a new tool which can be designed for specific purposes. Potato virus X (PVX) is a flexible, rod-shaped plant virus and can be genetically modified to present more than a thousand specific functional peptides on a single nanoparticle. Moreover PVX is biocompatible, not-cytotoxic, and non-infectious for mammals.

Polyglutamate (E8) and hydroxyapatite-binding peptides (HABP) exhibit functional sequences, which carry osteoinductive signals and are potent nucleators for mineralization. PVX nanoparticles were genetically modified to display bioactive peptides individually or an integrin-binding motif (RGD), which is known to promote cell adhesion. We hypothesize that embedding the modified PVX nanoparticles with human mesenchymal stem cells (hMSCs) in hydrogels can increase biomineralization and osteogenic differentiation effects.

Experimental Methods

Modified PVX nanoparticles at various concentrations were examined together with hMSCs for cell responses, including cell attachment and calcium deposition, after the induction of osteogenic differentiation by crystal violet staining and Alizarin Red staining, respectively. Cell viability was tested when hMSCs were embedded together with PVX nanoparticles at various concentrations in hydrogels by live/dead assay. Immunostaining of hMSCs cell membranes, nuclei, and PVX nanoparticles was performed to visualize the distribution and the integration of both cells and PVX nanoparticles in hydrogels by two-photon laser scanning microscopy.

Results and Discussion

Crystal violet staining showed that PVX-E8 and PVX-RGD were more effective in cell attachment than the control, while Alizarin Red staining showed that PVX-E8 promoted higher calcium deposition during the differentiation process than the wild type control particles. High cell viability in PVX nanoparticles embedded hydrogels at various concentrations exhibited excellent cytocompatibility. Moreover, immunostaining showed homogeneous distribution of PVX nanoparticles and hMSCs within hydrogels at different time points, which also illustrated the high retention time of PVX nanoparticles inside hydrogels for a long duration. The two-photon laser scanning micrographs additionally illustrated the close attachment of PVX nanoparticles to single cells (Figure 1), which presumably increased the stimulation of the peptides on the PVX nanoparticles to hMSCs.

Conclusion

In brief, the genetically modified PVX nanoparticles showed enhanced cell attachment and more calcium deposition in the investigation with hMSCs. The advantages by incorporating PVX nanoparticles with hMSCs in hydrogels include high cytocompatibility, high retention time, and close attachment to hMSCs. Thus, recombinant PVX nanoparticles offer great potential as a new hydrogel composite for bone tissue engineering.

Acknowledgement

We acknowledge the financial support of the Deutsche Forschungsgemeinschaft DFG (grant FI 975/29-1 and CO 251/6-1). We gratefully thank Dr. Michael Vogt (Institute for Laboratory Animal Science, RWTH Aachen University Hospital, Germany) for the help with two-photon laser scanning microscopy analyses, and Roswitha Davtalab (Department of Dental Materials and Biomaterials Research, RWTH Aachen University Hospital, Germany) for the assistance in the cell culture work.

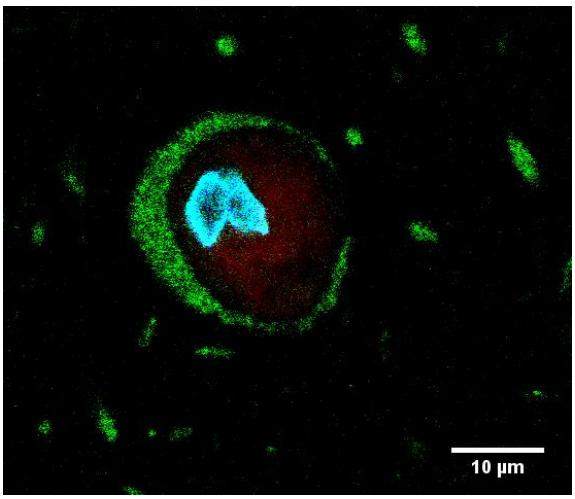

Two-photon laser scanning micrograph.
It shows the close attachment of PVX nanoparticles to a single cell, which presumably increases the stimulation of the peptides on the PVX nanoparticles to cells. PVX nanoparticles were stained with anti-PVX antibody and secondary anti-rabbit antibody (green), hMSC membrane was stained with Vybrant DiD (red), and hMSC nuclei were stained with DAPI (blue).

PS2-07-349

Injectable Self-Healing Hydrogels with Human Mesenchymal Stem Cells for Treating Spinal Cord Injury

Yen-Hua Chu[1], Yu-Yun Jang[1], Zhuo-Hao Liu[2], Chien-Wen Chang[1]

[1]National Tsing Hua University, Department of Biomedical Engineering and Environmental Sciences, Hsinchu, TW; [2]Chang Gung Memorial Hospital and Chang Gung University, Department of Neurosurgery and Pathology, Taoyuan, TW

Introduction

Spinal cord injury (SCI) is a devastating neuronal damaged condition often leading to life-long paralysis. So far, no clinical treatment is available for effectively treating the SCI patients. Current treatments, such as methylprednisolone administration or acute decompression are controversial or showing limited efficacy. In recent years, stem cells-based SCI therapy has become a major research focus receiving intensive research efforts. Applications of biomaterial-based cell delivery strategy should enhance SCI repair by improving stem cells survival and retention in the injured area. We rationale self-healing hydrogels can be utilized as an ideal cell delivery scaffold due to its good biocompatibility and capability on re-establishing molecular interactions after injections. In this study, we proposed a self-healing AGC hydrogel system comprising of aldehyde-hyaluronic acids (AHA), gelatin (Gel) and Glycol Chitosan (GC) for human mesenchymal stem cells (hMSCs) delivery to treat SCI.

Experimental Methods

AHA was prepared by oxidizing the hydroxyl groups on the sodium hyaluronic acids. Gelation occurred via Schiff base-based crosslinking between the amino groups on GEL/GC and the aldehyde groups on AHA. Due to the reversibility of Schiff base crosslinking, the AGC hydrogels exhibited unique self-healing behaviors. AHA and self-healing composite hydrogels were characterized by FT-IR spectroscopy. The effects of different AHA and GC ratios on the microstructure and viscoelasticity of AGC hydrogels were examined using scanning electron microscopy (SEM) and rheometer respectively. In vitro degradation of hydrogels was studied by measuring the weight loss and release of fluorescence-labeled Gel from the hydrogels. Stem cells-laden hydrogels were prepared by suspending cells in the polymer solutions following by gelation. Viability and proliferation of stem cells in the hydrogels were determined using Live/Dead staining and Alamar Blue assay respectively. Preliminary biocompatibility of materials was evaluated by performing the histological analysis on tissues received AGC hydrogel injections.

Results and Discussion

By using the aldehyde assay, the efficiency of converting HA to AHA via oxidation was determined to approximate 60%. In vitro degradability was assessed by incubating the hydrogels under various pH conditions. By either measuring the weight loss or release of fluorescence-labeled Gel, a clear acid-catalyzed degradation pattern of hydrogels was revealed. The SEM results showed that hydrogels pore size was inversely proportional to its GC content. In addition, the amount of GC was proportional to the storage modulus of the AGC hydrogels. By tuning the GC content, AGC hydrogels with designated crosslinking density may be attained. AGC hydrogels offered a good three-dimensional environment supporting long-term cell culture. Stem cells survival and retention was tested on a SCI animal model constructed by lateral hemi-section of the cervical and thoracic spinal nerves. Retention of viable hMSCs on the wound area was confirmed using a In Vitro Imaging System (IVIS).

Conclusion

A self-healing AGC hydrogel material was fabricated and studied as an injectable scaffold to deliver hMSCs for SCI repair. The AGC hydrogels exhibited good cell compatibility and provided a three-dimensional environment for long-term growth of hMSCs. The preliminary in vivo results suggest that the AGC hydrogels could significantly increase stem cells implantation efficiency on a SCI animal model.

References

Caron, Ilaria, et al. "A new three dimensional biomimetic hydrogel to deliver factors secreted by human mesenchymal stem cells in spinal cord injury." *Biomaterials* 75 (2016): 135-147.

Acknowledgement

This research was financially supported by Ministry of Science and Technology of Taiwan (MOST 107-2113- M-007-028 -) and National Tsing Hua University (107Q2519E1)

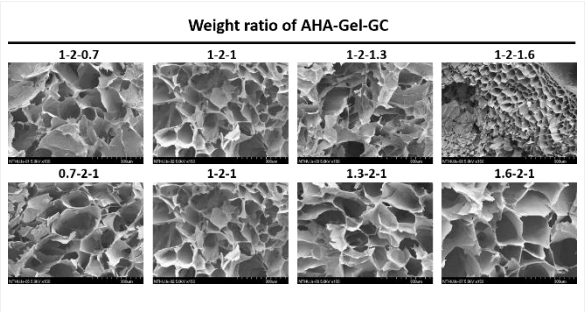

Characteristic of AHA-Gel-GC hydrogel
Effect of different weight ratios on the porosity of AHA-Gel-GC hydrogel by SEM. In the result, the hydrogel containing a higher amount of GC showed the higher degree of porosity.

PS2-07-350

Mechanical characterization of gelatin-based hydrogels upon finite strains in tension, compression and shear

Hamid Yousefi-Mashouf[1,2], Lucie Bailly[1], Laurent Orgéas[1], Nathalie Henrich Bernardoni[2], Sabine Rolland du Roscoat[1]

[1]Univ. Grenoble Alpes, CNRS, Grenoble INP, 3SR, Grenoble, FR; [2]Univ. Grenoble Alpes, CNRS, Grenoble INP, GIPSA-lab, Grenoble, FR

Introduction

Hydrogels are attractive biomaterials used in a wide range of biomedical applications, such as scaffolds for cell culture in tissue engineering, biomimetic models for human tissues, and carriers in drug delivery. Hydrogels consist of hydrophilic polymeric 3D networks, able to retain high tissue-like water content without dissolution. Among the biopolymers used to process hydrogels, gelatin is very common due to its cost-effectiveness, ease of manufacturing and ability to form thermo-reversible gels [1,2]. The poor mechanical performances of standard gelatin-based hydrogels (*e.g.* low elastic modulus, low ultimate elongation, brittle failure) are known to be tunable and enhanced with additional physical and/or chemical crosslinking in the gels [2,3].

A proper and complete characterization of the mechanical behavior of these hydrogels is critical to evaluate the relevance of their utility for biomedical applications. However, corresponding experimental studies are often limited either to one specific loading mode (mainly compression or shear) with a single quasi-static monotonic path up to failure, or to standard infinitesimal strain DMA analyses [2-4]. These configurations are usually far from those endured *in vivo* by native tissues which are subjected to numerous complex and coupled mechanical loading upon finite strains and various strain rates. In this work, we propose a procedure to characterize and to highlight the role of the finite strain mechanical loading (tensions, compressions and shear) on the mechanical behavior of gelatin-based hydrogels.

Experimental Methods

Dry porcine gelatin (gel strength ≈ 300 g Bloom, Type A, Sigma-Aldrich®) was used to produce a series of hydrogels, mixing the powder in ultrapure water (18.2 MΩ) for 30 min at 45°C. The prepared aqueous solutions were casted into a Teflon® mold at room temperature for 1 h, and kept at 3 °C for 24 h to form a rectangular gel plate (100 × 100 × 5 mm^3). Two parameters were varied during the processing route: (i) the gelatin concentration in the aqueous solutions, *i.e.*, 5, 10 and 15 %w/v [1,3]; (ii) the use of a crosslinking reagent (0.5 wt% of glutaraldehyde (GA), Sigma-Aldrich®). Samples were cut from the plates at a length-to-width ratio ranging from 5:1 to 1:5, and coated with a random pattern made of small speckles. Mechanical tests were carried out using a standard uniaxial machine (Instron® 5944) equipped with a ±10 N load cell.Five loading modes were studied: simple tension, plain strain tension (pure shear), simple and plain straincompressions and simple shear [5]. Whatever the loading mode, samples were subjected to cyclic loadings with increasing strain amplitude up to the ultimate elongation. Pictures of the deformed sample in frontal and lateral views were recorded using two high-resolution CCD cameras (JAI® BM-500GE, 5 MPixels), to quantify its dimensional changes and to allow digital image correlation for the measurement of local strain field (7D software [6]). For each loading case, two parameters were varied during the protocol: (i) the strain rates, ranging from 10^{-3} s^{-1} to 10^{1} s^{-1}; (ii) the surrounding hygrometric conditions, regulated at ambient or saturated (RH 100%) atmosphere.

Results and Discussion

To illustrate some of our results, we have plotted in Figure 1 stress-strain curves showing the typical cyclic mechanical behavior at a cross head speed of 0.05 mm.s^{-1} of the processed hydrogels in simple tension and compression (here with gelatin 10% w/v, no chemical crosslinking). The figure clearly emphasizes the impact of the mechanical loading on the behavior of the hydrogels: weak hysteresis and weak residual strain in tension, these two features being pronounced in compression where, in addition, stress levels being much higher than those recorded in tension. In addition, the figure highlights the strong impact of the sample air-drying on stress-strain curves: the higher the resting time, the higher the stress levels.

Conclusion

The results of this work will help to clarify the mechanical protocols and specially the loading modes to be considered for the biomimetic design of new homogeneous materials. This knowledge is expected prior to develop any suitable fibre-reinforced biocomposites, able to mimic the histological and biomechanical features of native tissues.

References

[1] S. Farris *et al.,* J. Agric. Food Chem., 2010, 58, 998-1003
[2] Q. Xing *et al.,* Sci. Rep. 2014, 4, 4706-4711
[3] S. Dash *et al.,* Carbo. Polym. 2013, 91(2), 638-645
[4] K. Lee *et al.,* Carbohydr. Polymers, 2004, 56(2), 251-254
[5] L. Meunier *et al.,* Polymer Testing, 2008, 27(6), 765-777
[6] P. Vacher *et al.,* Instn Mech Engrs Part C, 1999, 811_817

Acknowledgement

This work was supported by the ANR MICROVOICE (N° ANR-17-CE19-0015-01).

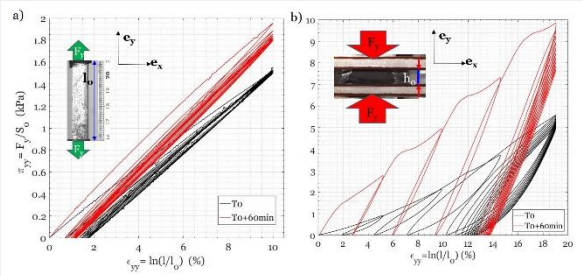

Fig1. Cyclic mechanical behavior of a physically crosslinked gelatin-based hydrogel
Typical evolutions of nominal stresses as function of Hencky strains in tension (left), in compression (right)

PS2-07-351

Design of an injectable and effervescent porous hydrogel as support for tissue regeneration

Louise Griveau[1], Clemence Drouglazet[1], Romain Debret[2], Jerome Sohier[1]

[1]CNRS Mateis UMR 5510, Lyon, FR; [2]CNRS LBTI UMR 5305, Lyon, FR

Introduction

Hydrogels are promising materials for the repair of damaged tissues, providing a hydrated support for cells. Among their advantages is their potential to be readily injected in wounds with a perfect fill. However, injection of hydrogels implies their ability to be readily colonized by cells without preformed porosity, which limits the range of usable candidates. As the regeneration potential of an implanted hydrogel has been shown to be strongly dependent on the induction of a porosity to allow cell infiltration [1][2], an interesting approach would be to form porosity in hydrogels during or after injection. Recently we have developed an innovative hydrogel composed of poly-lysine dendrimers (DGLs) cross-linked by polyethylene glycol (PEG-NHS), which has highly tailorable mechanical properties, is biocompatible and biodegradable but requires a preformed porosity to be colonized with cells and is therefore non injectable as such [3].

The aim of this study was therefore to investigate the possibility of creating a spontaneous porosity inside DGL/PEG hydrogels through an effervescent approach, which would be suitable with injection and would not require preformed pores. We further evaluated the cytotoxicity of the resulting porous hydrogels in view of tissue engineering applications.

Experimental Methods

To obtain a porosity compatible with injection, fluorescein-labelled DLG (DGL-FITC) and PEG-NHS were mixed with a carboxylic acid and a carbonated base at different ratios in the presence of a non-ionic surfactant at various concentrations. The effect of the acid:base ratio and the surfactant concentration on the resultant porosity were investigated by image analysis from 200nm hydrogels slices observed by laser scanning confocal microscopy (LSCM) imaging.The degree of cross-linking of resultant hydrogels was analysed by immersing non-washed porous DGL-FITC/PEG-NHS hydrogels in aqueous solution during 24hours followed by supernatant fluorescence measurements. Cytotoxity was studied by immersing the non-washed porous hydrogels in culture medium for 24h and applying the supernatant onto normal human dermal fibroblasts, followed by a live/dead viability cell assay and alamarBlue® cell viability assay after 24 and 48 hours of contact.

Results and Discussion

A selection of acid/base ratios and specific mixing order to the hydrogel components allowed a strong effervescence (Fig. 1A), stabilized by the presence of the surfactant and concomitant to the hydrogel cross-linking. As a striking result, an interconnected porosity was created, remnant of the effervescently-generated CO_2 bubbles (Fig. 1B). Interestingly, the acid/base ratio and the surfactant concentration seemed to modulate the resultant porosity by having an effect on the hydrogel cross-linking time and the CO_2 bubbles stabilization respectively. However, the addition of surfactant, carbonated base and carboxylic acid appeared to influence the cross-linking reaction as higher concentrations of DGL-FITC were detected on porous hydrogels supernatants compared with dense hydrogels. It

was correlated with a decrease in cell viability when varying surfactant concentration (Fig. 2). Nevertheless, some conditions of interest could be identified that do not induce cell mortality.

Conclusion

A spontaneous, interconnected and tailorable porosity inside a DGL/PEG-NHS hydrogel could be induced through an effervescent approach. Cells viability comforts their potential for *in situ* injection and on-going experiments focus on the evaluation of cellular colonization of the interconnected porous hydrogels and their potential to support extracellular matrix synthesis.

References

[1] Annabi *et al.* tissue eng: Part B 2010; 16 (4), doi: 10.1089/ten.TEB.2009.0639

[2] Hutmacher *et al.* J biomater. Sci. Polymer Edn, doi : 10.1163/156856201744489

[3] Debret *et al.* patent WO2017EP6151

Acknowledgement

The French ANR is acknowledged for financial support.

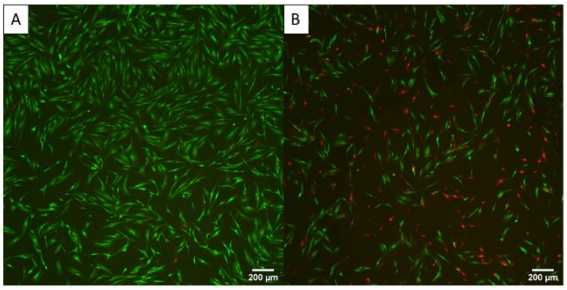

Figure 2: Live/dead on human fibroblasts in contact with supernatant of porous hydrogels during 24h
A) with high surfactant concentration and B) with medium surfactant concentration

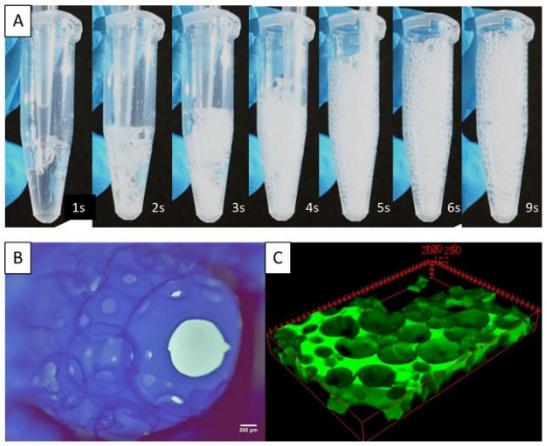

Figure 1: Porosity inside a DGL/PEG-NHS effervescent hydrogel
A) during formulation, with effervescence over time (in seconds) B) after CO_2 bubbles removal and coomassie blue staining and C) observed by laser scanning confocal microscopy (LSCM) imaging for porosity characterization (380µm slice).

PS2-07-352

The synergistic effect of topography and substrate rigidity on the development of a collagen scaffold for tendon tissue engineering

Ignacio Sallent[1,2], Dimitrios Zeugolis[1,2]

[1]Regenerative, Modular & Developmental Engineering Laboratory (REMODEL), National University of Ireland Galway (NUI Galway), Galway, IE; [2]Science Foundation Ireland (SFI), Centre for Research in Medical Devices (CÚRAM), National University of Ireland Galway (NUI Galway), Galway, IE

Introduction

Adherent cells are known to respond to physical characteristics of their surrounding microenvironment, adapting their cytoskeleton and initiating signaling cascades specific to the type of cue encountered. Scaffolds mimicking native biophysical cues have proven to differentiate stem cells towards tissue-specific lineages and to maintain the phenotype of somatic cells for longer periods of time in culture [1, 2]. Biomaterial-based tendon implants are designed to withstand high physiological loads but often lack the appropriate biochemical, biophysical and biological structure to drive tendon regeneration by populating cells [3]. The objective of this study is to use tendon main component, collagen type I, to create scaffolds that reproduce tendon natural anisotropy and rigidity, in an effort to engineer functional tendon tissue with native organization and strength, able to maintain tenocyte phenotype and to differentiate stem cells towards the tenogenic lineage.

Experimental Methods

Porcine collagen type I in solution was treated with one of the following cross-linkers: glutaraldehyde, genipin or 4-arm polyethylene glycol (4SP). The resulting mixture was poured on micro-grooved (2x2x2 µm) or planar polydimethylsiloxane (PDMS) molds and dried in a laminar flow hood to obtain 5 mg/ml collagen films. Surface topography and elastic modulus of the final scaffolds were analyzed using SEM/AFM and rheometry, respectively. Human tendon cells were isolated from adult tendon tissue and cultured on micro-grooved/planar scaffolds for 4, 7 and 10 days. Cell morphology, collagen III and tenascin C expression were analyzed by immunocytochemistry.

Results and Discussion

Among the different cross-linkers used, only the treatment with 4SP resulted in scaffolds with a recognizable micro-grooved surface topography. Precise control over the micro-grooved topography (fig 1B) and the rigidity (fig 1A) of the scaffolds was achieved by cross-linking the collagen with varying concentrations of 4SP (0, 0.5, 1 and 1.5mM) at low pH and temperature. The elastic modulus of the scaffolds cross-linked with 4SP (0.5mM) matched the values previously reported to induce tenogenic differentiation in stem cells (50-90 kPa) [4]. Approximately eighty percent of thehuman tendon cells cultured on the micro-grooved collagen films aligned in the direction of the anisotropy for 10 days in culture (fig 1C), mimicking the alignment of tenocytes in the native tissue [5]. Cell nuclei morphology, known to play a central role in the process of mechanotransduction, was significantly altered for the tenocytes cultured on the micro-grooved scaffolds after 4 days in culture for all the 4SP concentrations [6]. Synthesis, deposition and alignment of collagen III and tenascin C, two important tenogenic markers, were up regulated selectively on the micro-grooved (fig 2A) and rigid (fig 2B) scaffolds after 10 days in culture, respectively [7]. These results highlight the synergistic effect of matrix rigidity and cell alignment on tenogenic cell lineage commitment.

Conclusion

Collectively, this study provides new insights into how collagen can be modulated to create scaffolds with precise imprinted topographies and controlled rigidities. Gene expression analysis and a replicate study with hBMSCs will be carried out to support the first results and to further identify the optimal biophysical conditions for tenogenic cell lineage commitment. This potentially leads to the design of smart implants that not only restore immediate tendon functionality but also drive cellular synthesis of organized tissue-specific matrix.

References

1. Engler, A.J., et al., *Matrix elasticity directs stem cell lineage specification.* Cell, 2006. **126**(4): p. 677-89.
2. Zhu, J., et al., *The regulation of phenotype of cultured tenocytes by microgrooved surface structure.* Biomaterials, 2010. **31**(27): p. 6952-6958.
3. Gaspar, D., et al., *Progress in cell-based therapies for tendon repair.* Adv Drug Deliv Rev, 2015. **84**: p. 240-56.
4. Rehmann, M.S., et al., *Tuning microenvironment modulus and biochemical composition promotes human mesenchymal stem cell tenogenic differentiation.* J Biomed Mater Res A, 2016. **104**(5): p. 1162-74.
5. McNeilly, C.M., et al., *Tendon cells in vivo form a three dimensional network of cell processes linked by gap junctions.* J Anat, 1996. **189 (Pt 3)**: p. 593-600.
6. Fedorchak, G.R., A. Kaminski, and J. Lammerding, *Cellular mechanosensing: getting to the nucleus of it all.* Prog Biophys Mol Biol, 2014. **115**(2-3): p. 76-92.
7. Sharma, R.I. and J.G. Snedeker, *Biochemical and biomechanical gradients for directed bone marrow stromal cell differentiation toward tendon and bone.* Biomaterials, 2010. **31**(30): p. 7695-704.

Acknowledgement

Financial support was received from Marie Skłodowska-Curie Actions, Tendon Therapy Train (H2020-MSCA-ITN-2015-ETN), Grant Number: 676338.

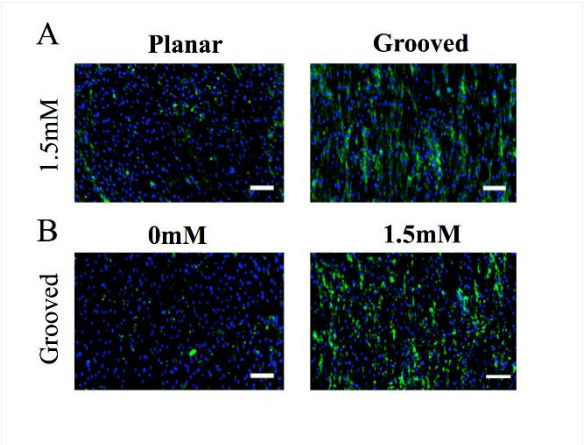

Figure 2.
Cell alignment and substrate rigidity promote the deposition of collagen III (A) and tenascin C (B) after 10 days in culture, respectively.

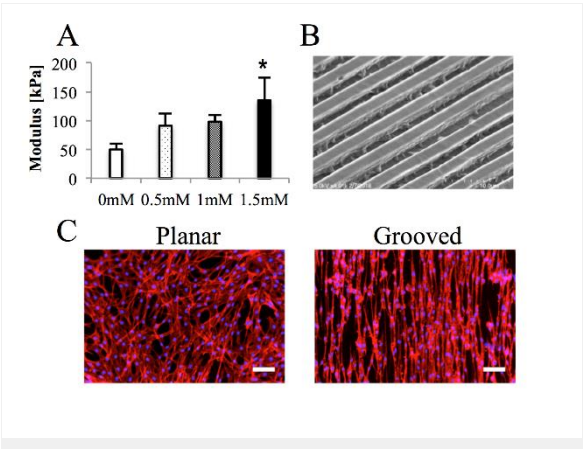

Figure 1.
Scaffold rigidity gradually increases with increasing 4SP concentration (A). SEM image of the micro-grooved film (B). Tenocyte morphology on the scaffolds after 10 days in culture. *Significance compared to 0mM.

PS2-07-353

Biodegradable Porous Membranes for the treatment of osteoarticular defects

Julio San Roman[1,2], Luis García Fernandez[1,2]

[1]*Institute of Polymers, CSIC, Group of Biomaterials, Madrid, ES;* [2]*CIBER - BBN, Group of Biomaterials, Madrid, ES*

Introduction

The articular cartilage is an avascular connective tissue with a very low intrinsic capacity for repair in the human body, and provides a low friction surface for transmitting the mechanical load between diarthrodial joints. Damage to these tissues is usually associated with traumatic injuries or age-associated processes which often lead to discomfort, pain and disability in patients. The main problem arises from the loss of the most efficient lubricant of the tissues and joints, based on hyaluronic acid as the most relevant component of the intraarticular gels and fluids. Apart from infections, the absence of the viscous intraarticular fluid produces an irreversible chondropaty with the associated damage of the articular cartilage and loss of mobility and functionality.

Experimental Methods

We have developed new systems based on semi-interpenetrating networks of hyaluronic acid and chitosan or chondroitin sulphate, crosslinked with a small amount of lysine di-isocianate, which results in porous sponges with very good adhesion to the ends of the wounds and excellent capacity of absorption of the bleeding blood. This guarantee that the blood and the corresponding growth factors and platelets remains in the area of contact of the lesion, and applied in a controlled way the activation factors of the blood for the regeneration of the articular cartilage damage.

Results and Discussion

microscopy (b) pictures of the hyaluronic acid-based hydrogels. with bones of chicken in a designed experiment “in vitro”, and the cell behaviour is excellent according to the results obtained with the alarm blue test. The diagrams in figure 2 shows that the hydrogels are not toxic and could be considered biocompatibles. Cell adhesion assay indicates that the hydrogels support cell adhesion and proliferation. It is clear that after 14 days of culture the chondroitin sulphate gives an additional contribution to the proliferation of cells. The systems offer excellent opportunities for the healing of ostechondral defects with the retention of blood and therefore the growth factors associated

Conclusion

The systems designed can be applied successfully for the regeration of osteoarticular cartilage by the methodology of microholes or microfractures and application of the hydrophylic membrane to retain in teh site of the lession the blood and thereore the corresponding growth factors (platelets and related factors) for the healing of the tissue.

Acknowledgement

Acknowledgements: Financial support from CIBER-BBN and the company BIOIBERICA are acknowledged.

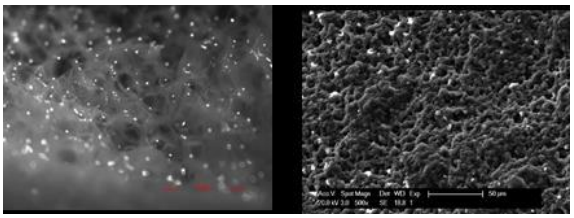

Figure 1
Optical microscopy (a) and SEM (b)

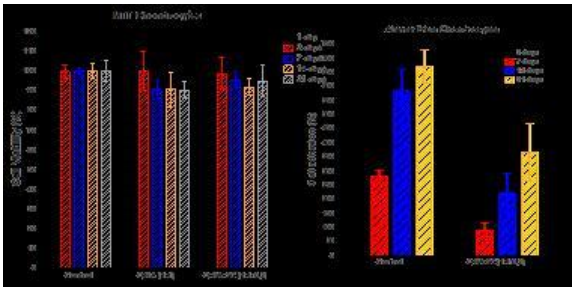

Figure 2
Indirect cytotoxicity assessment and cvell adhesion test of hydrogels

PS2-07-354

Enzyme-mediated injectable poly(amino acid)s based hydrogels providing a permissive microenvironment for mesenchymal stem cells

Jana Dvořáková[1], Ilya Kotelnikov[1], Zuzana Mikšovská[1], Bohumila Podhorská[2], Olga Janoušková[2], Vladimír Proks[1]

[1]Institute of Macromolecular Chemistry Czech Academy of Science, Department of Biomaterials and Bioanalogous Systems, Prague 6, CZ; [2]Institute of Macromolecular Chemistry Czech Academy of Science, Department of Biological Models, Prague 6, CZ

Introduction

The in situ formed biomimetic hydrogels represent a very attractive class of modern biomaterial scaffolds. They are used in cell therapy as well as in tissue engineering because of their facile encapsulation of cells, easy creation of complex shape and simple application by minimally invasive procedures increasing patient comfort during treatment [1]. Modern advanced biomaterials are designed to mimic selected features of extracellular matrix (ECM) of living tissues. Herein we present development of the synthetic, enzymatically degradable poly(amino acid)s based injectable hydrogel affording controlled immobilization of cell adhesion peptides. In our approach, we design the hydrogel that should be actively remodeled by residing cells through a local proteolytic activity.

Experimental Methods

The copolymer of hydrophilic, non-ionic and enzymatically degradable linear poly(N^5-2-hydroxypropyl-L-glutamine)-bearing tyramide units ((P2HPG-tyr) was synthesized as the gel precursors after the cascade of reactions. Starting PAAs was prepared by ring-opening polymerization of NCAs of respective protected amino acid γ-benzyl-L-glutamate (BLG). Then the P2HPG-tyr precursor was prepared trough modification of PBLG side chains in the two steps. Firstly, the modification of PBLG with propargylamine and tyramine was performed by amidation of partially debenzylated PBLG using carbodiimide chemistry. Secondly, the aminolysis of the remaining ester side chains was performed with 2-hydroxypropylamine. The P2HPG-tyr precursors were characterized using standard physicochemical methods such as ^{1}H, ^{13}C NMR, GPC, HPLC, FTIR, UV spectroscopy. The hydrogels were formed in situ using dual syringe by horseradish peroxidase (HRP)/H_2O_2-mediated crosslinked reaction. The effect of various n_{H2O2}/n_{TYR} and n_{TYR}/n_{HRP} ratios on the time of gelation and gel yields were investigated. The study was completed using measurements of swelling and viscoelastic properties of the injected hydrogel to gain comprehensive information about the formed hydrogel systems. The biomimetic azidoacetic-GGGRGDSGGGY-NH_2 peptide ligands were covalently binding to the gel precursor using click chemistry in concentration levels 100, 1000 and 10 000 pmol/mg of polymer. Cell viability, adhesion, and proliferation on the hydrogels were examined using adipose-derived rat mesenchymal stem cells (rMSCs).

Results and Discussion

The hydrogels for cell experiments were prepared with different stiffnesses, soft gel with storage modulus G' = 0.8 kPa and hard gel with G' = 3.5 kPa according to rheology measurements. The biological experiments showed that the P2HPG-tyr based hydrogels proved to be non-cytotoxic for the adipose-derived rat mesenchymal stem cells (rMSCs). The results also showed that the rMSCs adhered best to the hard hydrogel with the highest concentration (10 000 pmol/mg) of RGD. We also observed good viability, adhesion, and proliferation of rMSCs, when the rMSCs were encapsulated by the injection process to the hydrogel. In this case, we observed and evaluated the spreading

of cells and formation of the cellular protrusion in 3D matrix depending on the RGD content, gel stiffness and amount of encapsulated cells. The formation of the cellular protrusion in the 3D matrix indicates the degradation of hydrogels through the local proteolytic activity of cells.

Conclusion

This study exhibited injectability and rapid P2HPG-tyr gel formation, as well as mechanical stability of hydrogel, and cell ingrowth. The injectable P2HPG-tyr based hydrogels demonstrated attractive properties for future application in a variety of regenerative medicine procedures.

References

[1] Wang F., Li Z.Q., Khan M., Tamama K., Kuppusamy, Wagner W.R., Sen C.K., Guan J.J. *Acta Biomater* 2010, 6: 1978–1991

Acknowledgement

This work was supported by the Czech Science Foundation (No. 18-03224S).

PS2-07-355

One-step dual photocrosslinkable tyramine-enhanced bioglue for *in situ* tissue repair

Florencia Abinzano[1], Khoon Lim[3], Paulina Núñez Bernal[1], Pau Atienza Roca[3], Ane Albillos Sánchez[1], Iris A. Otto[1], Tim Woodfield[3], Jos Malda[1,2], Riccardo Levato[1]

[1]University Medical Center Utrecht, Department of Orthopedics, Utrecht, NL; [2]Utrecht University, Department of Equine Sciences, Utrecht, NL; [3]University of Otago Christchurch, Christchurch Regenerative Medicine and Tissue Engineering (CReaTE) Group, Department of Orthopaedics Surgery and Musculoskeletal Medicine, Christchurch, NZ

Introduction

Articular cartilage focal defects are a major problem in the orthopaedic field, causing pain and disability in young adults and often leading to early onset of osteoarthritis[1]. Hydrogels are attractive biomaterials for tissue repair due to their injectability, potential for chemical modification, incorporation and release of biological cues, encapsulation of cells and (bio)printability[2]. However, their application as *in situ* fillers and bioglues can be limited due to poor integration and possible damage to the surrounding tissue upon crosslinking. The aim of this study was to develop a hydrogel system with potential for *in situ* cartilage repair, based on a cell-laden gelatin methacryloyl hydrogel modified with tyramine moieties (gelMA-Tyr) bearing dual crosslinking capacity. Photoinduced gelation of both the reactive acryl- and tyramine groups was triggered in one step via visible light irradiation in presence of ruthenium and sodium persulfate (Ru/SPS) photoinitiators. The gel was characterized as matrix for cartilage tissue engineering, bioglue, and ink for bioprinting.

Experimental Methods

GelMA was derivatized with tyramine moieties (gelMA-Tyr) capable of forming covalent bonds with tyrosine residues present in the extracellular matrix of native tissues. To trigger both addition polymerization of methacryloyl moieties within the gel and dytyrosine bond formation in a single step, a visible light photoinitiator system based on tris(2,2'-bipyridyl)ruthenium(II) chloride and sodium persulfate (Ru/SPS) was used. GelMA-Tyr and gelMA (8% w/v) with and without the addition of hyaluronic acid methacrylate (HAMA) (7.5%/0.5%) were loaded with articular cartilage progenitor cells and cultured *in vitro* for 28 days. Cell viability, cartilage matrix production and mechanical properties were evaluated.

The effect of this visible light photocrosslinking system on the viability of surrounding native cartilage was compared to a common gelMA crosslinking system consisting of photoinitiator Irgacure 2959, using a UV-A lamp (365 nm). To evaluate the integration capacity of the proposed bioglue, gel adhesion to native cartilage was studied using a push-out test, with hydrogels injected into defects cut in cartilage explants. Shape fidelity upon printing was assessed as reported previously[3]. Tyrosine residues present naturally on most native proteins were used to covalently functionalize the gelatin network (using myoglobin as a model compound). Finally, the potential of the Ru/SPS system to create hydrogels solely made of unmodified proteins was assessed.

Results and Discussion

Both gelMA and gelMA-Tyr supported cell survival and chondrogenesis in terms of viability, glycosaminoglycans production and compressive strength. Overall, the addition of HAMA did not improve chondrogenesis, contrary to previous findings[4]. In comparison to Irgacure, the Ru/SPS crosslinkers did not show oxygen inhibition, facilitating the

use of these gels *in situ*[5]. When casting the gels into cartilage explant defects, the Ru/SPS visible light crosslinking system resulted in higher cell viability of the native tissue surrounding the defect compared to the Irgacure/UV-A system (Fig. 1). Together, these findings suggest that injection of this gel directly into a cartilage defect in liquid form and subsequent crosslinking *in situ* is feasible without affecting the native resident cells, while also permitting cartilage matrix formation within the cast construct.

The addition of tyramine groups into the hydrogel in combination with the dual crosslinking Ru/SPS system significantly improved the adhesive strength to native cartilage (Fig. 2). This increment was achieved without the need to degrade the surrounding matrix, in contrast to previous studies using transglutaminase-crosslinked hyaluronan hydrogels and chitosan-based crosslinkers[6,7].

The gelMA-Tyr hydrogel exhibited shear-thinning behaviour at 4 and 21°C, thermal gelation at low temperatures (< 21°C), and could be printed using an extrusion-based platform, while showing shape retention post-printing.

Moreover, gelMA-Tyr hydrogels were able to bind and covalently retain a model protein (myoglobin), showing potential as depots for controlled release of growth factors. Finally, the Ru/SPS visible light crosslinking system was also able to generate gels from several proteins (gelatin 5% and 10%, silk 7%, bovine serum albumin 4.5%), with the crosslinking efficiency being related to the tyramine content (R^2=0.82).

Conclusion

Visible light crosslinkable gelMA-Tyr hydrogels, in combination with Ru/SPS photoinitiators, have potential for a variety of applications in tissue engineering, cartilage regeneration and controlled release. In particular, thanks to the dual crosslinking mechanism triggered by Ru/SPS, this hydrogel demonstrates potential for direct injection and integration into damaged cartilage, and is also suitable for bioprinting applications, further enhancing its possibilities for the repair or replacement of complex, patient-specific structures.

References

1 Wluka *et al.,* (2005). The clinical correlates of articular cartilage defects in symptomatic knee osteoarthritis: a prospective study. *Rheumatology*, *44*(10), 1311-1316.

2 Vega *et al.,* (2017). Recent advances in hydrogels for cartilage tissue engineering. *European cells & materials*, *33*, 59.

3 Ribeiro *et al.,* (2017). Assessing bioink shape fidelity to aid material development in 3D bioprinting. *Biofabrication*, *10*(1), 014102.

4 Mouser *et al.,* (2017). Development of a thermosensitive HAMA-containing bio-ink for the fabrication of composite cartilage repair constructs. *Biofabrication*, *9*(1), 015026.

5 Lim *et al.,* (2016). New visible-light photoinitiating system for improved print fidelity in gelatin-based bioinks. *ACS Biomaterials Science & Engineering*, *2*(10), 1752-1762.

6 Broguiere *et al.,* (2016). Factor XIII cross-linked hyaluronan hydrogels for cartilage tissue engineering. *ACS Biomaterials Science & Engineering*, *2*(12), 2176-2184.

7 Gittens *et al.,* (2016). Use of novel chitosan hydrogels for chemical tissue bonding of autologous chondral transplants. *Journal of Orthopaedic Research*, *34*(7), 1139-1146.

Acknowledgement

European Research Council under grant agreement 647426 (3D-JOINT), the Dutch Arthritis Foundation (LLP-12, LLP-22 and CO-14-1-001), the AO foundation (ReInforce project)

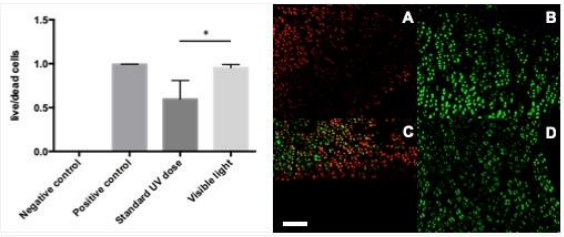

Fig. 1 – Left: the Ru/SPS visible light dose resulted in significantly higher cell viability than the standard UV dose ($p<0.05$). As a negative control, a high UV dose was used and as a positive control, a tissue explant with no exposure. Right: fluorescent staining showing live (green) and dead cells (red); A: negative control, B: positive control, C: standard UV, D: visible light; scale bar = 100um.

Figure 1: Effect of visible light vs. UV-A irradiation on native cartilage cell viability

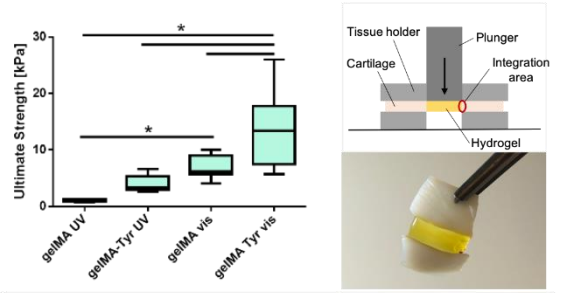

Fig. 2 – Left: gelMA-Tyr presented a higher integration strength to native cartilage tissue than unmodified gelMA and UV-irradiated gels ($p<0.01$). Right, top: scheme of the the push-out test. Right, bottom: gelMA-Tyr hydrogel can be used as a bioglue for cartilage repair/regeneration.

Figure 2: Adhesive strength of gelMA-Tyr and gelMA hydrogels to surrounding native cartilage.

PS2-07-356

The effect of carbon nanoparticles and hydroxyapatite microparticles on the conductivity of hydrogels

Barbara Szaraniec, Marta Raś, Patrycja Domalik-Pyzik, Marcel Zembrzycki, Jan Chłopek

AGH-University of Science and Technology, Department of Biomaterials and Composites, Kraków, PL

Introduction

Tissue engineering is an interdisciplinary field that combines engineering and life sciences to obtain scaffolds that can be used in regenerative medicine. Great amount of research was put into defining key factors of scaffolds that determine their performance, for example stiffness, mechanical strength, surface topography, chemistry and – finally – conductivity. Because polymers that are used to fabricate hydrogels often lack some mechanical, chemical and electrical properties that are necessary for most efficient tissue regeneration, nanoparticles started to be introduced into them to modify the scaffolds and create nanocomposites that better mimic biological tissues.

Experimental Methods

Materials examined in the following study were chitosan-based hydrogels decorated with graphene oxide (GO), reduced graphene oxide (rGO) and hydroxyapatite (HAp). Three groups were measured using the four probe method: chitosan-hyaluronan blend containing GO and rGO nanoparticles, chitosan-based hydrogels decorated with HAp particles and chitosan-based hydrogels containing both of these modifiers. Primary aim of fabricating these materials was bone and cartilage tissue regeneration. In order to see the impact of high water content on hydrogel conductivity, some hydrogels were measured in both dry and swelled state.

Results and Discussion

The results indicated that the increasing content of the conductive carbon nanoparticles and growth of water content have positive impact on hydrogels conductivity. Conductivity of hydrogels modified with HAp particles was dropping with the increasing amount of the particles. It was also observed, that the content of cross-linker that was used to fabricate the materials has impact on its conductivity. The effect of combining particles that exhibit antagonistic effects was found to be more irregular.

Conclusion

The following study demonstrates that the usage of carbon nanoparticles improves electrical conductivity of chitosan-based hydrogels and could be extended to polymers with other than chitosan-based matrices. It is anticipated that combining particles of antagonistic effects leads to a specific pattern of conductivity changes, and therefore finding the best ratio of contents of these particles is possible when several necessary reinforcements and modifications are required.

References

1. Domalik-Pyzik, P., J. Chłopek, and K. Pielichowska, *Chitosan-Based Hydrogels: Preparation, Properties, and Applications*, in Cellulose-Based Superabsorbent Hydrogels, M.I.H. Mondal, Editor. 2019, Springer International Publishing: Cham. p. 1665-1693.
2. Ray, S., *Chapter 2. Application and Uses of Graphene Oxide and Reduced Graphene Oxide*. 2015. p. 39-55

3. Szaraniec, B., et al., *Multifunctional polymer coatings for titanium implants*. Mater Sci Eng C Mater Biol Appl, 2018. 93: p. 950-957.
4. Gajendiran, M., et al., *Conductive biomaterials for tissue engineering applications*. Journal of Industrial and Engineering Chemistry, 2017. 51: p. 12-26.
5. Alam, A., et al*., Polymer composite hydrogels containing carbon nanomaterials—Morphology and mechanical and functional performance*. Progress in Polymer Science, 2018. 77: p. 1-18.
6. Horiuchi, N., et al., *Electrical conductivity of polycrystalline hydroxyapatite and its application to electret formation.* Solid State Ionics, 2018. 315: p. 19-25.

Acknowledgement

This research was funded by the National Center for Research and Development, Poland (BioMiStem grant No. STRATEGMED3/303570/7/NCBR/2017).

PS2-07-357

Thermosensitive bioartificial hydrogels as smart injectable and biocompatible systems allowing post-injection chemical crosslinking

Valeria Chiono, Rossella Laurano, Alice Zoso, Monica Boffito

Politecnico di Torino, Department of Mechanical and Aerospace Engineering, Turin, IT

Introduction

Injectable hydrogels as carriers for drugs and/or cells have gained increasing interest in the last years due to the possibility to vehicle their payload in the desired loco through mini-invasive procedures [1, 2]. In this work, a new library of bioartificial hydrogels was designed combining the chemical versatility and reproducible physicochemical properties of a synthetic polymer with the enhanced cell adhesiveness of a natural polymer. Specifically, an amphiphilic polyurethane (PEU) bearing amino groups was first synthesised and then blended with hyaluronic acid (HA) to obtain thermosensitive bioartificial formulations. The influence of HA molecular weight on polymers miscibility was investigated as well as the thermosensitivity and the injectability of the newly designed bioartificial systems. Modification of the PEU and the HA may allow post-injection chemical crosslinking enhancing the chemical stability of the hydrogel.

Experimental Methods

The amphiphilic PEU was synthesised in a two step procedure under nitrogen by reacting a commercial triblock copolymer (Poloxamer 407, Poly(ethylene oxide)-Poly(propylene oxide)-Poly(ethylene oxide)) with 1,6-hexamethylene diisocyanate. Then, the prepolymer was chain extended with a diol (N-Boc diethanolamine) containing protected secondary amino groups. Infrared (IR) spectroscopy and Size Exclusion Chromatography (SEC) were then performed to assess the success of the synthesis and to evaluate PEU molecular weight, respectively. Subsequently, the synthesised PEU was subjected to an acidic treatment in chloroform/trifluoroacetic acid 90/10 V/V to remove BOC-protecting groups and the exposed secondary amino groups were quantified through a colorimetric assay (Orange Sodium salt). The synthetic component (D-DHP407) was then blended with a high (HA_400kDa) and low (HA_82kDa) molecular weight HA, reaching different weight ratios. Lastly, formulations were prepared by dissolving both polymers in physiological saline solution and then characterized in terms of thermosensitivity by means of tube investing test and gelation time test at 37 °C; injectability in the sol state through needles of different diameters (G18, G21 and G22) and cytocompatibility according to ISO10993-5. Secondary amino groups in PEU and carboxyl groups in HA may be exploited to graft functional molecules for in situ post-injection crosslinking.

Results and Discussion

The successful PEU synthesis was proved through IR spectroscopy by the appearance of new bands ascribed to urethane bonds, while SEC analysis gave a molecular weight in the range 30000 – 35000 Da with 1.4 polydispersity index. Secondary amino groups were quantified to be 4.5×10^{20} groups/g of polymer by means of Orange II Sodium Salt assay.

For what concerns hydrogel preparation, D-DHP407 and HA_400kDa were mixed at 98/2, 95/5, 92/8, 88/12 and 83/17 wt. ratios. All tested formulations formed compatible blends, but, due to the high molecular weight of HA_400kDa, further increase in the natural component content highly increased system viscosity affecting injectability. Hence, D-DHP407 was blended with a low molecular weight HA (HA_82kDa) obtaining compatible and

injectable blends even at 50/50 wt. ratio. Subsequently, hydrogel temperature-driven gelation was tested and all considered formulations turned out to gel within few minutes at 37 °C, thus suggesting that HA introduction did not affect PEU thermosensitivity. Regarding hydrogel injectability, all blends could not be extruded through G22 needle, while they could be injected through larger needle diameters (G21 and G18). Finally, by increasing HA content, thus decreasing the synthetic component, an increase of hydrogel biocompatibility was observed.

Conclusion

A new platform of thermosensitive bioartificial hydrogels was developed by blending a custom-made amphiphilic polyurethane, which ensures hydrogel thermo-responsiveness, with hyaluronic acid, responsible for an improved cytocompatibility. Furthermore, the presence of exposed secondary amino groups along PEU chains and carboxylic groups in HA chains opens the possibility to graft functional moieties to both molecules for post-injection crosslinking. Such injectable system is under development as a matrix for *in situ* treatment of myocardial tissue, by releasing agents promoting direct reprogramming of cardiac fibroblasts into cardiomyocytes.

References

[1]Zhang Z., Expert. Opin. Biol. Ther., 17:1, 49-62, 2017.

[2] Boffito M. et al., J. Biomed. Mater. Res. A, 103(3):1276-90, 2015.

Acknowledgement

The activity has been carried within the research project BIORECAR. This project has received funding from the European Research Council (ERC) under the European Union's Horizon 2020 research and innovation programme (grant agreement No 772168).

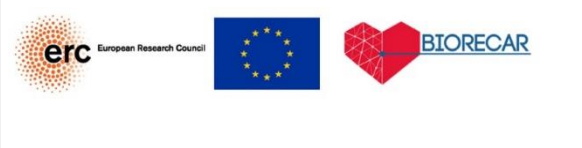

Biorecar project logo

PS2-07-358

Halloysite/ alkaline phosphatase composite as a component of hydrogel scaffold for bone tissue regeneration

Aneta Pietraszek, Anna Karewicz, Maria Nowakowska

Jagiellonian University, Department of Chemistry, Kraków, PL

Introduction

Alkaline phosphatase (ALP) is an enzyme that actively participates in the biomineralization process, leading to the renewal of bone tissue. ALP catalyzes dephosphorylation processes leading to the formation of free phosphate groups, which in combination with calcium form hydroxyapatite, the main component of bone. Unfortunately ALP, being a protein and enzyme, is susceptible to deactivation and degradation. In order to improve its stability as a bioactive component of a hydrogel scaffold intended for bone tissue repair, the enzyme was first encapsulated in a halloysite nanocarrier. Halloysite, a nanoclay which occurs mainly in the form of nanotubes, was chosen as a carrier due to its high durability and thermal resistance, biocompatibility and unique tubular structure with negative external surface and positively charged interior. Halloysite nanotubes have the lumen, which is large enough to encapsulate ALP, and it is assumed that they should provide very good protection and stabilization for it. The presence of halloysite as a component should introduce bioactivity and improve mechanical properties of the chitozan-based hydrogels.

Experimental Methods

The obtained composite material was subjected to physicochemical characterization using SEM, FTIR and XPS techniques. The activity of the entrapped protein was determined using the Bessey and Lowry colorimetric method. The amount of protein encapsulated in the halloysite was calculated using the standard Bradford test. The chitosan-based hydrogels with halloysite-ALP component were studied using SEM, DMA, and contact angle measurements.

Results and Discussion

The protein was effectively introduced into the halloysite nanotubes and remained active. The loading efficiency (LE) of ALP was found to be 13.5%, while its encapsulation efficiency (EE) was estimated to be around 27%. Enzymatic activity of the halloysite-entrapped ALP in a biomineralization process was also tested using calcium glycerophosphate as a substrate. SEM measurements confirmed the formation of crystallite on the surface of the nanotubes, while EDS analysis indicated that hydroxyapatite was indeed produced. Methodology of preparing hydrogels based on chitosan and chitosan-collagen, cross-linked with a non-toxic genipin, and containing different amounts of halloysite nanotubes with entrapped ALP, was developed and optimized. The influence of the inorganic component on the swelling process of the hydrogel, as well as morphology and mechanical properties of the material was also studied.

Conclusion

The new hybrid system was successfully obtained and incorporated as a component of the chitosan-based hydrogels. The obtained materials have potential as a scaffold for the treatment of bone defects.

References

[1]S. Bose, M. Roy, A. Bandyopadhyay, *Trends Biotechnol* 30(10) **(2012)** 546–554

[2]K.M. Park, J.Y. Son, J.H. Choi, I.G. Kim, Y. Lee, J.Y. Lee, K.D. Park, *Biomacromolecules* 15(6) **(2014)** 1979–1984

[3] J. Lewandowska-Łańcucka, S. Fiejdasz, Ł. Rodzik, A. Łatkiewicz, M. Nowakowska*, J Mater Sci: Mater Med* (2015) 26:231

PS2-07-359

Mineralization of cell laden collagen-alginate microspheres to mimic bone-specific ECM

Sarah Lehnert[1], Pawel Sikorski[1], David Bassett[1,2]

[1]Norwegian University of Science and Technology, Department of Physics, Trondheim, NO; [2]University of Birmingham, School of Chemical Engineering, Birmingham, GB

Introduction

Scaffolds are widely used as a template to mimic biological tissue such as skin, liver and bone.[1] The requirements for such scaffolds are manifold as they should recreate the natural cell environment as faithfully as possible, both in terms of physical and biological characteristics. Ideally, they should be sufficiently porous to allow the passage of essential nutrients, grow factors, and waste products and to allow cell-cell interactions and other biochemical stimuli to occur. At the same time, scaffolds should also provide sufficient support and appropriate mechanical stimuli to physically mimic the micro to macro-environment of the tissue they aim to represent.[2]

The most common three-dimensional shape of hard-tissue scaffolds is currently cubic or cylindrical and consist of either organic, inorganic materials or a combination of both.[3] While these arrangements have advantages in terms of fabrication and analysis, there are also significant limitations such as limited porosity and poor cell survival at the center of the construct. This is due to the fact that cell survival in engineered tissues highly depends on a sufficient transport of oxygen and nutrients. It is a common understanding that cells, in general, do not survive when being further away than 200 µm from a capillary.[4]

To meet this geometrical criteria, a sphere in the micrometer-range is a much more natural choice as a basis for subsequent cell-incorporation and, in terms of mimicking bone-specific extracellular matrix (ECM), mineralization.

Experimental Methods

Here, a novel method is presented to fabricate collagen-containing alginate droplets, which are formulated such that the collagen can serve as a basis for cell attachment and the alginate can provide an initial supporting structure. The presence of assembled collagen fibres within the composite hydrogel has been proven by multiphoton microscopy by determining the second harmonic generation and reflection signal of collagen (figure 1).

Results and Discussion

With a successful protocol in place to obtain formed collagen within alginate droplets, the subsequent step will be to incorporate cells. Ongoing research implies that presenting cells to a system of an alginate-collagen hydrogel does subsequently result in a strong cell-cell interaction and a good survival rate after seven days in hydrogel-cultivation (figure 2).

The mineralization of the composite microspheres is achieved via a biomimetic enzymatic process. The alginate allows the physical encapsulation of alkaline phosphatase (ALP), which provides a source of phosphate to allow precipitation of calcium phosphate when altered cell media is introduced to the system. Previous studies showed that the ratios of resulting calcium phosphates directly depend on the pH of these media.[5]

Conclusion

By combining the incorporation of formed collagen in alginate droplets as well as the encapsulation of cells and the subsequent mineralization to mimic a more cell-specific ECM, a highly complex system is achieved which, owing to the size and geometrical shape of the droplets, is highly versatile for further processing and analyses. Further work will focus on bio-plotting of individual droplets into a larger construct which will facilitate the modular design of larger tissue-mimetic constructs.

References

[1] Freyman, T. M., I. V. Yannas, and L. J. Gibson. "Cellular materials as porous scaffolds for tissue engineering." *Progress in Materials science* 46.3-4 (2001): 273-282.

[2] O'brien, Fergal J. "Biomaterials & scaffolds for tissue engineering." *Materials today* 14.3 (2011): 88-95.

[3] Bose, Susmita, Mangal Roy, and Amit Bandyopadhyay. "Recent advances in bone tissue engineering scaffolds." *Trends in biotechnology* 30.10 (2012): 546-554.

[4] Rouwkema, Jeroen, et al. "Supply of nutrients to cells in engineered tissues." *Biotechnology and Genetic Engineering Reviews* 26.1 (2009): 163-178.

[5] Lehnert, S., Sikorski, P., Bassett, D. (2018, April). *ALP-induced mineralization of collagen-alginate hybrid hydrogels.* Poster session presented at the 11th Annual Meeting of the Scandinavian Society for Biomaterials. Fiskebäckskil, Sweden.

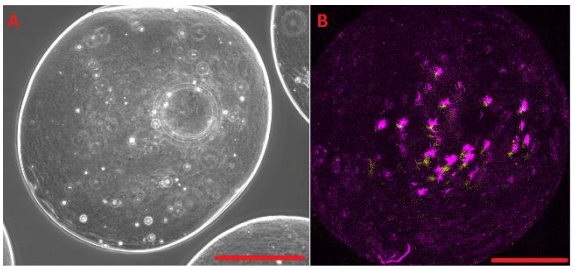

Phase contrast and multiphoton microscopy of collagen-containing alginate droplet.
Figure 1A) phase contrast image of collagen-containing alginate-droplet. The fine collagen structures are clearly distinguishable. B) Complementary second harmonic (yellow) and reflection (magenta) signal of collagen in alginate bead. The slight offset of the signal is due to the rotation of the bead during imaging. Scale bars: 150 µm.

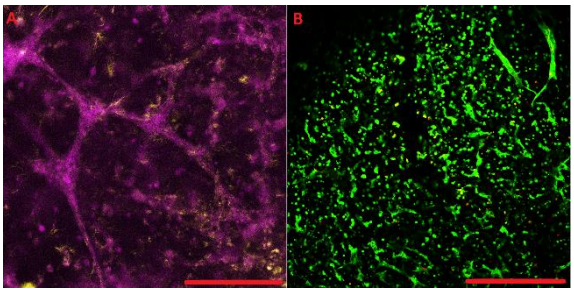

Multiphoton and flourescence microscopy to depict the presence of a highly interlinked cell-network
Figure 2A) second harmonic (yellow) and reflection (magenta) signal of a cell-containing alginate-collagen hybrid hydrogel construct. Scale bar: 150 µm. B) live-dead staining of the cell-containing alginate-collagen construct with calcein (green) and ethidiumbromide (red). Scale bar: 300 µm.

PS2-07-360

Development of 3D printed Electrically Conductive Oxidized Alginate and Gelatin based Polypyrrole-Polystyrenesulfonate (PPy:PSS) Hydrogels for Functional Tissue Engineering Applications

Thomas Distler[1], Christian Polley[2], Rainer Detsch[1], Hermann Seitz[2], Aldo R. Boccaccini[1]

[1]Friedrich-Alexander-University Erlangen-Nuremberg, Department of Materials Science and Engineering, Institute of Biomaterials, Erlangen, DE; [2]University of Rostock, Faculty of Mechanical Engineering and Marine Technology, Chair of Microfluidics, Rostock, DE

Introduction

Conductive hydrogels are promising candidates to create stimuli-response and functional biomaterials.[1] They may be a key to enhance the electrical stimulation of cells as a tool to control cellular response in tissue engineering (TE).[1,2] Electrical conductivity as a material parameter itself gained large interest in the fields of cardiac [3] and neuronal [4] TE, where intuitively electrical potentials and conductivity play a major role in native physiology. Yet, electrical stimulation (ES) recently gained momentum also in other fields of TE such as cartilage tissue engineering, where it was found to be a suitable stimulus to improve articular chondrocyte collagen type II expression and chondrogenesis of mesenchymal stem cells.[6] As a platform for electrical stimulation of cartilage cells, the aim of this study is to develop electrically conductive hydrogels with tunable conductivity to be a potential biomaterial for ES-supported cartilage tissue engineering.

Experimental Methods

For the synthesis of conductive hydrogels, a combination of oxidized alginate and gelatin was used as a biomaterial platform.[7,8] Second, polystyrene sulfonate (PSS) doped polypyrrole (PPy:PSS) was polymerized in the matrix to create electrical functionality. Oxidized alginate was synthesized by controlled oxidation of sodium alginate using $NaIO_4$ to produce alginate di-aldehyde (ADA). Following, ADA was mixed with gelatin to form the ADA-GEL hydrogel precursor. Polystyrene sulfonate was dissolved in ADA-GEL and pyrrole (Py) was added in different molarities to investigate the influence of Py molarity on the final hydrogel conductivity. The hydrogel precursor was assessed towards its rheological properties and 3D printed in different shapes. For material testing, hydrogel cylinders were casted. To produce final conductive hydrogels, ADA-GEL-Py:PSS gels were oxidized using $FeCl_3$ to polymerize PPy:PSS inside the hydrogels. Final ADA-GEL-PPy:PSS gels were investigated regarding their physicochemical properties using FTIR, scanning electron microscopy (SEM), mechanical properties (Nanoindentation, Compression tests), electrical conductivity (4-Point probe measurements) and biocompatibility.

Results and Discussion

It was possible to synthesize ADA-GEL-PPy:PSS conductive hydrogels with tunable electrical conductivity. By liophilization, ADA-GEL-PPy:PSS scaffolds were produced, maintaining electrical functionality. FTIR confirmed the formation of PPy:PSS inside the hydrogels. The oxidative post-polymerization of Py to PPy:PSS inside ADA-GEL significantly increased the stiffness of the final gels compared to prestine ADA-GEL gels. Microstructural analyses showed the formation of a PPy:PSS network inside the hydrogels. 3D printing of ADA-GEL-PPy:PSS structures was possible, while the hydrogel precursor showed a change of rheological properties over time, suggesting an aging process of the precursor.

Conclusion

The combination of ADA-GEL hydrogels with PPy:PSS post-polymerization allows to produce electrically conductive and functional composite hydrogels. Via 3D printing of the hydrogel precursor, the fabrication of customized scaffold structures can be achieved. The results suggest that the developed hydrogel is a promising candidate to achieve hydrogels of variable conductivities. This may allow the assessment of cellular response on ADA-GEL-PPy:PSS hydrogels of different conductivity and its influence in tissue engineering applications when involved in electrical stimulation in the future.

References

1. D. Mawad et al. “Conductive Polymer Hydrogels”, Polymeric Hydrogels and Composite Materials, Springer International Publishing Switzerland (2016).
2. R. Balint et al. “Electrical Stimulation: A Novel Tool for Tissue Engineering”, Tissue Engineering: Part B, 19, 1 (2013).
3. N. Tandon et al. “Electrical stimulation systems for cardiac tissue engineering”, Nat Protoc. 4(2), 155–173 (2009).
4. F. Pires et al. “Neural stem cell differentiation by electrical stimulation using a cross-linked PEDOT substrate: Expanding the use of biocompatible conjugated conductive polymers for neural tissue engineering”, Biochimica et Biophysica Acta 1850, 1158–1168 (2015).
5. B. Hiemer et al. “Effect of electric stimulation on human chondrocytes and mesenchymal stem cells under normoxia and hypoxia” Molecular Medicine Reports 18, 2133-2141 (2018)
6. H.J. Kwon et al. “Electrical stimulation drives chondrogenesis of mesenchymal stem cells in the absence of exogenous growth factors” Scientific Reports 6, 39302 (2016)
7. S. Reakasame et al. “Oxidized Alginate-Based Hydrogels for Tissue Engineering Applications: A Review“, Biomacromolecules, 19, 1, 3-21 (2018)
8. R. Detsch, et al. “Advanced alginate-based hydrogels”, Mater. Today 18, 590–591 (2015)

Acknowledgement

This work was supported by the German Research Foundation (Deutsche Forschungsgemeinschaft, DFG), Collaborative Research Centre 1270 on ELectrically Active Implants (ELAINE).

PS2-07-361

Oxidized alginate combined with laminin and gelatin (ADA-GEL-LAM) as a suitable hydrogel biomaterial for 3D neuronal networks based on human induced pluripotent stem cell derived neurospheres

Ines Lauria[1], **Thomas Distler**[2], Clemens Sauter[1], Farina Bendt[1], Rainer Detsch[2], Julia Kapr[1], Stephan Rütten[3], Aldo R. Boccaccini[2], Ellen Fritsche[1,4]

[1]Leibniz Research Institute of Environmental Medicine, Modern Risk Assessment and Sphere Biology, Düsseldorf, DE; [2]University of Erlangen-Nuremberg, Institute of Biomaterials, Department of Materials Science and Engineering, Erlangen, DE; [3]RWTH Aachen University Hospital, Electron Microscopy Facility, Institute of Pathology, Aachen, DE; [4]Heinrich-Heine-University of Düsseldorf, Medical Faculty, Düsseldorf, DE

Introduction

Animal experiments are still the gold standard for basic and applied research in medical and pharmacological and toxicological sciences. Lately, it has been recognized from regulatory bodies that the current in vivo approach is not offering the desired throughput in compound evaluation and that data extrapolation from animals to humans is often unsatisfactory. Therefore, there is a need for more predictive methods that allow substance evaluation and at the same time use fewer resources. One area where prediction of animals to humans is particularly poor is the CNS field.

Human induced pluripotent stem cell (hiPSC)-based three dimensional (3D) brain models have gained increasing attention as alternatives to the conventional animal testing because they bear no ethical concerns, are of human origin, have unlimited availability and have the potential for human disease modeling. However, spontaneously neural differentiated hiPSC display a high variability. For this reason procedures are warranted lowering variability of differentiation and thus producing more standardized *in vitro* models. 3D bioprinting might be a solution to this issue because bioprinting enables a more controlled spatial organization of neural cells in the 3D context. We hypothesized that alginate di-aldehyde (ADA) gelatin (GEL) crosslinked hydrogels as a tunable biomaterial could be a suitable hydrogel for the generation of 3D bioprinted hiPSC-derived neuronal networks. Because laminin (LAM) is a crucial extracellular matrix (ECM) protein in the brain necessary for neural cell adhesion, migration and differentiation, in this study we assessed the novel ADA-GEL-LAM hydrogel combination for its suitability to support culture and differentiation of hiNPC into neurons and glia cells and formation of electrically active neuronal networks.

Experimental Methods

As a cell source we differentiated hiPSC into neural progenitor cells (hiNPC) growing in 3D as neurospheres. For the gel matrix, blends containing varying concentrations of gelatin and laminin were prepared. The protein mixture was combined with oxidized alginate to achieve oxidized alginate gelatin laminin hydrogel precursors. Final ADA-GEL-LAM hydrogels were formed using Ca^{2+} mediated crosslinking. For hiNPC-laden gels, equal amounts of hiNPC neurosphere suspension and hydrogel precursor were mixed prior to crosslinking. The porosity of the resulting hydrogels was visualized by scanning electron microscopy (SEM). The chemical composition as well as mechanical properties of the hydrogels were assessed using FTIR and nanoindendation, respectively. Cell viability and cytotoxicity within cell-laden hydrogels were followed over time periods of up to 7 days by the cell titer blue and the lactate dehydrogenate assays (Promega), respectively. Cell morphology and cell-material-interactions were

visualized using SEM and confocal laser scanning fluorescence microscopy of non-stained and samples stained by immunocytochemistry, respectively.

Results and Discussion

Microstructural assessment verified the porous structure of ADA-GEL and ADA-GEL-LAM hydrogels. After 14 days of differentiation inside the ADA-GEL-LAM hydrogels, neurons have differentiated and migrated out of the neurospheres as visualized by stainings with the neuronal marker b(III)tubulin. These first results indicate that ADA-GEL-LAM might be a promising bioink for neural tissue engineering because it is printable and seems to be cytocompatible with hiNPC.

Conclusion

Current and future work aims to further establish ADA-GEL-LAM for standardized and reproducible 3D bioprinted neuronal networks. Functional networks will be characterized for their neuronal activity using electrophysiological measurements in a multiwell format and applying neuronal receptor blockers and activators. Well characterized and standardized 3D neural *in vitro* models might be useful in basic and applied sciences, for substance testing as well as disease modeling in the future.

PS2-07-362

PEG-heparin microgels as a tool for the modulation of human iPSC-derived kidney organoid differentiation

Valentina Magno[1], Sebastian Kühn[1], Carsten Werner[1,2,3]

[1]Leibniz Institute of Polymer Research, Dresden, DE; [2]Cluster of Excellence Center for Regenerative Therapies, TU Dresden, Dresden, DE; [3]Cluster of Excellence Physics of Life, TU Dresden, Dresden, DE

Introduction

Several protocols have been published for the generation of kidney organoids from human iPSCs. Despite the improvements, state-of-the-art kidney organoids still depend on animal or CAM transplantation for the improvement of nephron epithelial and vascular maturation. Aim of this study is to introduce PEG-heparin microgels as a tool to modulate the differentiation of iPSC-derived kidney organoids through the heparin-mediated sequestration of soluble morphogens.

Experimental Methods

Kidney organoids were derived from human iPSCs adapting the protocol published by Takasato et al.(1), and exposed during differentiation to PEG-heparin microgels of different sizes, or to a single PEG-heparin droplet, keeping the hydrogel volume and heparin content constant, and thus only varying the total hydrogel surface area. Organoid growth was monitored through phase contrast microscopy, and nephronal differentiation was evaluated through immunofluorescence and confocal microscopy.

Results and Discussion

PEG-heparin microgels accelerated the differentiation of kidney organoids, with a faster development of renal vesicles compared to standard and droplet-exposed cultures. Furthermore, organoids produced in presence of PEG-heparin microgels showed more LTL+ proximal tubule-like structures. Overall, we demonstrate how PEG-heparin hydrogels can tune the differentiation of kidney organoids through a surface area-related mechanism.

Conclusion

Our methodology represents a new biomaterial approach for the improvement of organoid differentiation. Ongoing studies will aim at the precise identification of the cell-secreted morphogens sequestered by the microgels and involved in organoid differentiation.

References

1. Takasato, M., Er, P. X., Chiu, H. S. & Little, M. H. Generation of kidney organoids from human pluripotent stem cells. Nat. Protoc. 11, 1681–1692 (2016).

PS2-07-363

General route to anisotropic microgels composed from pure biopolymers

Ivan Rehor[1,2], Yadu Nath Vakkipurath Kodakkadan[1], Kristyna Idzakovicova[1], Frantisek Stepanek[1]

[1]University of Chemistry and Technology Prague, Chemical Engineering, Prague 6, CZ; [2]Institute of Organic Chemistry and Biochemistry, Prague, Prague 6, CZ

Introduction

Hydrogel microparticles (microgels) are essential materials for bioapplications including cell therapy, drug delivery and release systems or tissue engineering. Control over the microgel shape is often essential for these tasks, which lead to recent introduction of anisotropic microgels, produced via lithographic methods. These, however, require synthetic photocrosslinkable polymers as hydrogel precursors[1], with possible adverse interactions in-vivo. Biopolymers provide superior level of biocompatibility over their synthetic analogues, however, cannot be crosslinked by light, which hinders their shaping in lithographic processes. Various approaches for shaping biopolymers were presented using either molds[3-7], or inducing the biopolymer gelation by the light indirectly[8-10]. None of the methods presented so far provides reliable high throughput production of anisotropic microrogels, nor resolution on the micron-scale, which is needed to design materials with controlled interaction with a real tissue, organized on cellular i.e. micron level. In this work, we introduce method for photolithographic synthesis of anisotropic micogels, composed purely from biopolymer of choice using sacrificial photocrosslincable polymeric template blended with this biopolymer.

Experimental Methods

First we prepared a single phase blend from the template polymer - Dex-HEMA, biopolymer of choice (alginate, chitosan) together with water-soluble photoinitiator[11]. Dex-HEMA consists of dextran modified with 2-hydroxyethylmethacrylate moieties bound to the chain through hydrolytically labile carbonate esters[12] (Figure 1-left).We synthesized microgels from the Dex-HEMA-biopolymer mixture using Stop-Flow lithography (Figure 1), the mixture was purged through a microfluidic channel and microgels were created by local photocrosslinking of the Dex-HEMA, their shape being defined by the photomask[13]. In the next step, the entrapped biopolymer (alginate/chitosan) was crosslinked via suitable method. In the case of alginate, ionic crosslinking was induced by adding calcium chloride to the Dex-HEMA-alginate microgels. To prepare chitosan microgels, the SFL-produced Dex-HEMA – chitosan microgels were treated with genipin – a biocompatible crosslinker widely applied for gelation ofused to form hydrogels from aminated polysacharides or proteins for bioapplications. In the successive step, the Dex-HEMA network was cleaved either by addition of the base or enzymatically using dextranase.

Results and Discussion

The synthesized microgels preserve their shape defined in the lithographic process, thanks to the Dex-HEMA network while the biopolymer is physically entrapped in its mesh (Figure 2). In the case of alginate, ionic crosslinking was induced by adding calcium chloride to the Dex-HEMA-alginate microgels. The consecutive hydrolysis of the template under basic conditions took around 10 minutes and its completion was visualized as a loss in the fluorescence signal of the Dex-HEMA network (Figure 2H). During the hydrolysis, the particles isotropically shrunk down to 60 % of the original dimensions, however the shape and features are preserved during this process (Figure

2I). We explain the shrinking by the following mechanism. As the scaffolding polymer hydrolyses and diffuses out, the conformational freedom of the alginate polymer segments increases. These alginate segments are still able to bind to each other through calcium ions present in the solution and, thus, new crosslinks are being formed, which results in the hydrogel shrinking, according to the relation between the mesh size and equilibrium swelling state. In the case of covalently crosslinked chitosan, the particles maintain their shape together with size during the template hydrolysis, which we ascribe to the fact, that the crosslinking process is already quenched and no new crosslinks can be formed during the template removal.

Conclusion

We present new method for shaping biopolymers in micron scale, that utilizes lithographic processing of a biopolymer mixture with degradable photocrosslinkable template. Our method offers resolution unprecedented with previous lithographic processes with biopolymers and can provide large quiantities of anisotropic microgels in the size ranging from tens to hundreds µm. Hydrogel templates have been used in the past to pattern soft materials in the microscale, however the term templating refers to a process where a void in the structure is created as a result of template removal. In our case, the desired material and the template occupy the same space the first being entrapped in the photocrosslinked network of the second. We plan to further spread the number of biopolymers, that can be processed with our method, the only requirements being miscibility with a suitable photocrosslinkable template. Presented idea may also be used with other photolithographic methods, such as photolithography or stereolithography.

References

[1] Helgeson, M. E., Chapin, S. C. & Doyle, P. S. Hydrogel microparticles from lithographic processes: Novel materials for fundamental and applied colloid science. *Curr. Opin. Colloid Interface Sci.***16**, 106–117 (2011).

[2] Knop, K., Hoogenboom, R., Fischer, D. & Schubert, U. S. Poly(ethylene glycol) in Drug Delivery: Pros and Cons as Well as Potential Alternatives. *Angew. Chem. Int. Ed.***49**, 6288–6308 (2010).

[3] Dang, T. T. *et al.* Microfabrication of homogenous, asymmetric cell-laden hydrogel capsules. *Biomaterials***30**, 6896–6902 (2009).

[4] Qiu, C., Chen, M., Yan, H. & Wu, H. Generation of Uniformly Sized Alginate Microparticles for Cell Encapsulation by Using a Soft-Lithography Approach. *Adv. Mater.***19**, 1603–1607 (2007).

[5] Talei Franzesi, G., Ni, B., Ling, Y. & Khademhosseini, A. A Controlled-Release Strategy for the Generation of Cross-Linked Hydrogel Microstructures. *J. Am. Chem. Soc.***128**, 15064–15065 (2006).

[6] Neto, A. I. *et al.* Fabrication of Hydrogel Particles of Defined Shapes Using Superhydrophobic-Hydrophilic Micropatterns. *Adv. Mater.***28**, 7613–7619 (2016).

[7] Yanagawa Fumiki *et al.* Directed assembly of cell-laden microgels for building porous three-dimensional tissue constructs. *J. Biomed. Mater. Res. A***97A**, 93–102 (2011)

[8] Javvaji, V., Baradwaj, A. G., Payne, G. F. & Raghavan, S. R. Light-Activated Ionic Gelation of Common Biopolymers. *Langmuir***27**, 12591–12596 (2011).

[9] Chueh, B. *et al.* Patterning alginate hydrogels using light-directed release of caged calcium in a microfluidic device. *Biomed. Microdevices***12**, 145–151 (2010).

[10] Valentin, T. M. *et al.* Stereolithographic printing of ionically-crosslinked alginate hydrogels for degradable biomaterials and microfluidics. *Lab. Chip***17**, 3474–3488 (2017).

[11] Fairbanks, B. D., Schwartz, M. P., Bowman, C. N. & Anseth, K. S. Photoinitiated polymerization of PEG-diacrylate with lithium phenyl-2,4,6-trimethylbenzoylphosphinate: polymerization rate and cytocompatibility. *Biomaterials***30**, 6702–6707 (2009).

[12] van Dijk-Wolthuis, W. N. E., Hoogeboom, J. A. M., Van Steenbergen, M. J., Tsang, S. K. Y. & Hennink, W. E. Degradation and release behavior of dextran-based hydrogels. *Macromolecules***30**, 4639–4645 (1997).

[13] Rehor, I. *et al.* Biodegradable Microparticles for Simultaneous Detection of Counterfeit and Deteriorated Edible Products. *Small*__13__, 1701804 (2017).

Acknowledgement

We acknowledge Czech Science Foundation Junior project nr. 18-19170Y and the J.E.Purkyne fellowship of Ivan Rehor

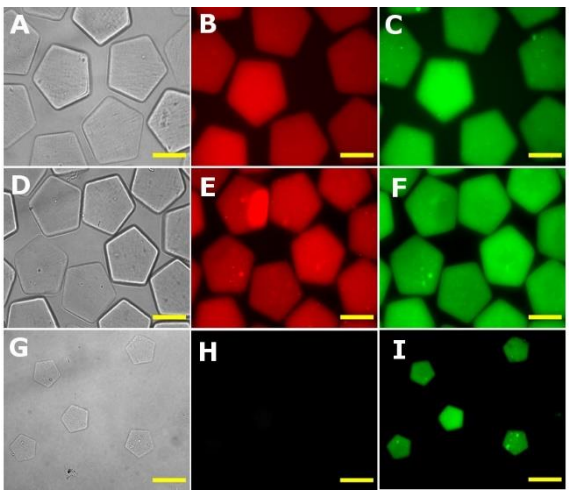

Micrographs of alginate anisotropic hydrogels
Hydrogels obtained from lithographic synthesis (A) are held together by photocrosslinked Dex-HEMA, (fluorescent image of labelled Dex-HEMA network in B) and the alginate is physically entrapped in the structure (fluorescent image of labelled alginate in C). The same sample after addition of $CaCl_2$, (brightfield – D, Dex-HEMA fluorescence – E, alginate fluorescence - F) and after addition of base (brightfield – G, Dex-HEMA fluorescence – H, alginate fluorescence - I). Scalebars correspond to 50 micron. All fluorescence images are in false colors.

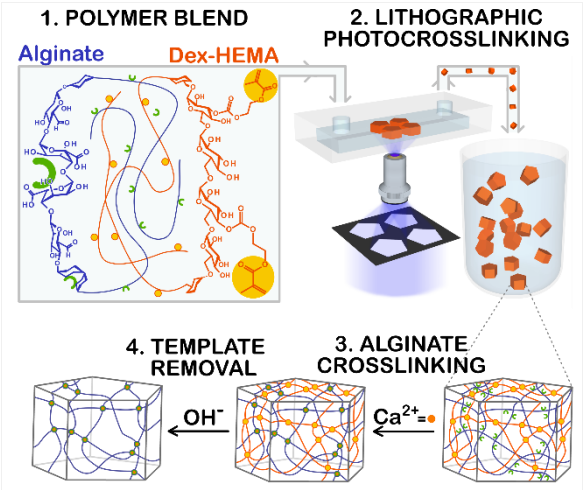

Figure 1 - Lithographic synthesis of anisotropic bio-microgels
Blend of photocrosslinkable degradable polymer Dex-HEMA and biopolymer (scheme displays specifically alginate for alginate) is processed via Stop-Flow lithography. Obtained anisotropic hydrogels are treated with calcium ions to crosslink alginate, entrapped in the hydrogel matrix. In the last step, the template matrix of Sex-HEMA is basically hydrolyzed and washed away, yielding pure alginate particles

PS2-07-364

Electron Irradiation Assisted Crosslinking of Biological Hydrogels: Reagent-Free Modification towards Tailored Matrices

Stefanie Riedel[1,2], Stefan G. Mayr[1,2]

[1]Leibniz Institute of Surface Engineering (IOM), Leizpig, DE; [2]University Leipzig, Physics Department, Leipzig, DE

Introduction

Biological hydrogels such as gelatin and collagen show a high potential in biology and medicine due to their strong biocompatibility and biodegradability. They are highly attractive materials for biomedical applications such as extracellular matrix components, coatings or implants. Thereby, precise adaption of structure and mechanics as well as stimuli-response is an interesting aspect of the modification of these materials.

Experimental Methods

Reagent-free modification of hydrogels can be achieved by utilizing high energy electron irradiation inducing crosslinking. Without any additional reagents, electron irradiation represents an advantageous non-toxic crosslinking technique.

Results and Discussion

We will demonstrate how crosslinking with high-energetic electrons allows fine-tuning of materials properties such as structure and mechanics towards precisely tailored extracellular matrices.

Conclusion

We will further present the high potential of electron beam induced crosslinking of biological hydrogels to develop functional materials and stimuli-responsive systems.

PS2-07-365

From Hydrogels- Towards Regenerative Medicine

Alvaro López-Acosta, Carmen Piras, **David K. Smith**

University of York, Department of Chemistry, Heslington, York, GB

Introduction

Supramolecular hydrogels, self-assembled from low-molecular-weight building blocks, have emerged as a class of soft material with wide-ranging uses in high-tech applications: drug delivery, tissue engineering, environmental remediation and nanoscale electronics[1]. In this project, we take advantage of the orthogonal assembly of two gel networks[2]. Each network confers its respective properties to the bulk material without damaging the desirable features of the other, to fabricate biologically-active nanosystems.

The hybrid hydrogels are composed of commercially relevant low-molecular-weight gelator (LMWG) DBS-$CONHNH_2$ (DBS = 1,3;2,4-dibenzylidene-D-sorbitol)[3], cross-linked polymer gelator (PG) PEGDM (poly(ethyleneglycol) dimethacrylate), and anionic biopolymer heparin. These hybrid hydrogel materials[4] are highly responsive – capable of spatially controlled unidirectional release of specific components from complex mixtures and evolving their structures over time in response to different stimuli. This gives these gels potential applications in tissue engineering. (Figure 1)

The use of the LMWG enhances the stability of the gel to high frequencies and allows the binding of active pharmaceutical components. PEGDM as PG enhances the mechanical robustness and permits photo-patterned spatial resolution. Heparin can encourage the angiogenesis of growing tissue and recruit other growth factors[5]. Multifunctionality was achieved by careful mixing of the components at optimized concentrations and the design of a specific formulation method.

Experimental Methods

Different concentration hybrid gels were studied in buffer. Exhaustive characterization was performed using rheology, spectrometry techniques (NMR, IR, UV-Vis), and electron microscopy (TEM and SEM) which helped identify the best candidates for future introduction of stem cells.

Results and Discussion

The tunable mechanical characteristics of these inexpensive hybrid gels, their photo-patterning capacity, and their heparin retention are reported.

Conclusion

This approach will enable the introduction of stem cells with the ability to differentiate into different tissues depending on the properties of the network they grow in. This will enable us to control tissue engineering using a commercially relevant, highly tunable family of gels.

References

1. Z. Deng, Y. Guo, X. Zhao, P. X. Ma and B. Guo, *Chemistry of Materials*, 2018, **30**, 1729-1742.
2. X. Yan, D. Xu, X. Chi, J. Chen, S. Dong, X. Ding, Y. Yu and F. Huang, 2012, **24**, 362-369.
3. D. Knani and D. Alperstein, *The Journal of Physical Chemistry A*, 2017, **121**, 1113-1120.
4. V. M. P. Vieira, A. C. Lima, M. de Jong and D. K. Smith, 2018, **24**, 15112-15118.
5. M. M. Martino, P. S. Briquez, A. Ranga, M. P. Lutolf and J. A. Hubbell, *Proceedings of the National Academy of Sciences*, 2013, **110**, 4563.

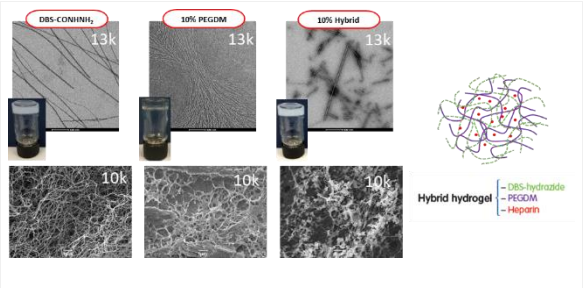

Figure 1
Left: TEM and SEM electrograms of the DBS-$CONHNH_2$, 10% PEGDM only and 10% hybrid hydrogel networks. **Right:** Schematic representation of the hybrid hydrogels

PS2-07-366

Viscoelastic hydrogels drive chondrogenesis of mesenchymal stem cells

Matthew J. Walker, Marco Cantini

University of Glasgow, School of Engineering, Glasgow, GB

Introduction

Articular cartilage has a very limited self-regenerative capacity which consequently means, following damage or deterioration, joint disease can develop, such as osteoarthritis. Current therapies for repairing cartilage defects have limited long-term success; for example, autologous chondrocyte implantation[1] and microfractures[2] can lead to fibrocartilage formation which severely impairs joint function. Mesenchymal stem cells (MSCs) are multipotent and so can differentiate to give rise to multiple cell types, including chondrocytes, making them an attractive cell-based therapy for cartilage repair and regeneration. Hydrogels are a promising biomaterial to act as a platform for MSC attachment in 2D and 3D and can directly influence cell fate through their mechanical properties. It has been shown previously that the stiffness of elastic hydrogels determines MSC differentiation where, relative to stiffer gels that promote osteogenic differentiation, softer surfaces promoted chondrocyte formation[3]. It has been shown however, that elastic hydrogels can inhibit chondrocyte proliferation[4] and limit cartilage matrix formation and spreading[5], which is a likely consequence of their mechanical nature that creates a somewhat restrictive microenvironment. Viscoelastic hydrogels by contrast, where mechanical stresses relax over time, have been shown to promote MSC spreading and proliferation[6], as well as formation of an interconnected bone matrix from osteoblasts[7]. Investigations into how the viscoelastic properties of hydrogels influence chondrogenic differentiation of MSCs however is less understood. Hydrogels can also be functionalised with peptide motifs to improve MSC attachment, as well as influence cell fate, where it was shown that chondrogenesis can be controlled by peptide gradients using peptide motifs RGD and HAVDI[8]. RGD is the main integrin receptor involved in cell-matrix interactions and HAVDI is a cadherin ligand involved in cell-cell interactions.

In this work, we investigated whether viscoelastic hydrogels functionalised with specific peptide combinations can provide a cellular microenvironment conducive to the chondrogenic differentiation of MSCs. We have fabricated hydrogels with the same Young's modulus that exhibit differences in loss modulus and investigated the influence of these mechanical properties on MSC behaviour, particularly regarding chondrogenesis.

Experimental Methods

Polyacrylamide gels were prepared using different ratios of acrylamide and cross-linker N, N'-Methylenebisacrylamide. Elastic and viscous properties of the hydrogels was measured using AFM and rheology. Human MSCs were cultured on the hydrogels and analysed in terms of cell adhesion, circularity, size and early chondrogenesis.

Results and Discussion

Nanoindentation and microrheology measurements via AFM showed that the Young's modulus of the polyacrylamide hydrogel family prepared was maintained at ~13 kPa, whilst there was an almost two-fold difference in loss modulus between the least and most viscoelastic gel (Figure 1A). This trend was confirmed by rheological measurements,

which showed a consistent storage modulus of ~4 kPa (confirming that the gels have equivalent compressive Young's moduli) and a loss modulus ranging from 74 to 164 Pa (Figure 1B).
When the gels were functionalised with RGD, adhering MSCs were larger and much more spread on less viscoelastic gels, compared to cells on viscoelastic gels that were much smaller and more rounded (Figure 2). This suggests better adhesion to less viscoelastic gels through more focal adhesion interactions with the surface. Interestingly, we observed higher levels of SOX9 expression on more viscoelastic gels that was ~three-fold times higher than that of the least viscoelastic gels (Figure 2B). This indicates that an increase in loss modulus is able to promote early chondrogenesis compared to elastic gels.

Conclusion

These findings suggest that viscous interactions can be modulated to promote chondrogenesis of MSCs. Chondrogenic response will be further investigated by assessing matrix secretion, in terms of composition and mechanical properties. Moreover, gels will be modified to control the interplay between cell-ECM and cell-cell interactions as a strategy to further drive cell fate towards the chondrogenic phenotype. Finally, translation will be tackled by using degradable, PEG-based gels and investigating the effect of their viscoelastic properties on MSCs in 3D cultures.

References

1. Roberts, S. et al., *Knee***16**, 398–404 (2009).
2. Gobbi, A. et al., *KneeSurg.Sport. Traumatol.Arthrosc*. **13**, 213–221 (2005).
3. Olivares-Navarrete, R. et al., *PLOS ONE*, **12**, e0170312. (2017).
4. Francioli, S. et al., A **95** (3), 924-931. (2010).
5. Mouw, J.K. et al., *Osteoarthr.Cartil*. **13**, 828–836 (2005).
6. Chaudhuri, O. et al., *Nature Materials*, **15**, 326-334. (2015).
7. McKinnon, et al., *Adv.Mater*. **26**, 865–872 (2014).
8. Vega, S. et al., *Nature Communications*, **9**. (2018).

Acknowledgement

This work was funded by a grant from the UK Regenerative Medicine Platform. The authors acknowledge funding from MRC (MR/S005412/1).

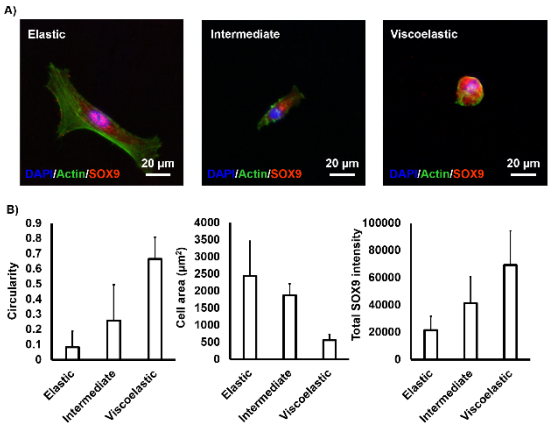

Figure 2. Human MSCs show higher circularity, lower cell area and higher SOX9 expression on viscoelastic polyacrylamide hydrogels: A) Fluorescence microscopy images of cells attached on elastic (left), intermediate (middle) and viscoelastic (right) gels functionalised with 290 µM RGD following immunostaining with DAPI, phalloidin (actin) and SOX9. **B)** Quantification of cell circularity on elastic, intermediate and viscoelastic gels functionalised with 290 µM RGD; calculated based on actin staining morphology using ImageJ (n=5, error bars denote standard deviation) (left). Quantification of cell area on elastic, intermediate and viscoelastic gels functionalised with 290 µM RGD; calculated based on area within actin staining using ImageJ (n=5, error bars denote standard deviation. Quantification of total SOX9 intensity in cells attached to elastic, intermediate and viscoelastic gels functionalised with 290 µM RGD; calculated using ImageJ (n=34, error bars denote standard deviation) (right).

Figure 2. Characterisation of human MSCs on viscoelastic hydrogels

A) Fluorescence microscopy images of cells attached on elastic (left), intermediate (middle) and viscoelastic (right) gels functionalised with 290 µM RGD following immunostaining with DAPI, phalloidin (actin) and SOX9. **B)** Quantification of cell circularity on elastic, intermediate and viscoelastic gels functionalised with 290 µM RGD; calculated based on actin staining morphology using ImageJ (n=5, error bars denote standard deviation) (left). Quantification of cell area on elastic, intermediate and viscoelastic gels functionalised with 290 µM RGD; calculated based on area within actin staining using ImageJ (n=5, error bars denote standard deviation. Quantification of total SOX9 intensity in cells attached to elastic, intermediate and viscoelastic gels functionalised with 290 µM RGD; calculated using ImageJ (n=34, error bars denote standard deviation) (right).

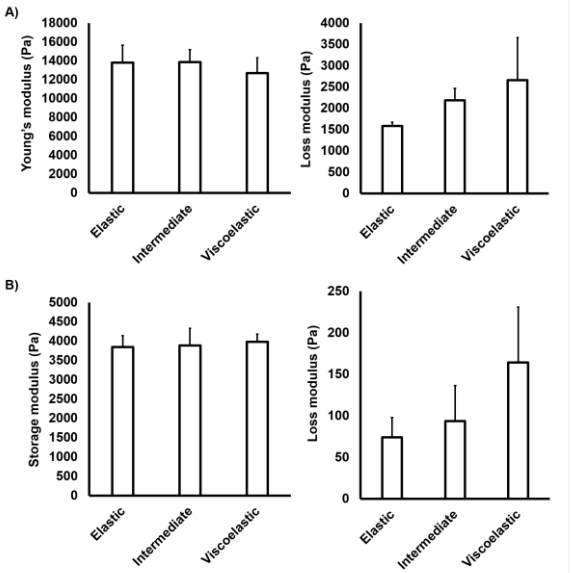

Figure 1. Mechanical properties of elastic, intermediate and viscoelastic polyacrylamide hydrogels: Elastic gel = 15% acrylamide, 0.1% N,N'-methylenebisacrylamide. Intermediate = 25% acrylamide, 0.03% N,N'-methylenebisacrylamide. Viscoelastic = 35% acrylamide, 0.01% N,N'-methylenebisacrylamide. **A)** AFM measurements of elastic, intermediate and viscoelastic polyacrylamide gels using nanoindentation to determine elastic properties (left) and microrheology to determine viscous properties (right) (n=3, error bars denote standard deviation). **B)** Rheological measurements of elastic, intermediate and viscoelastic polyacrylamide gels using combined strain and frequency sweeps (taken at 5 rad/s) to measure elastic properties (left) and viscous properties (right) (n=3, error bars denote standard deviation).

Figure 1. Mechanical properties of elastic, intermediate and viscoelastic polyacrylamide hydrogels

Elastic gel = 15% acrylamide, 0.1% N,N'-methylenebisacrylamide. Intermediate = 25% acrylamide, 0.03% N,N'-methylenebisacrylamide. Viscoelastic = 35% acrylamide, 0.01% N,N'-methylenebisacrylamide. **A)** AFM measurements of elastic, intermediate and viscoelastic polyacrylamide gels using nanoindentation to determine elastic properties (left) and microrheology to determine viscous properties (right) (n=3, error bars denote standard deviation). **B)** Rheological measurements of elastic, intermediate and viscoelastic polyacrylamide gels using combined strain and frequency sweeps (taken at 5 rad/s) to measure elastic properties (left) and viscous properties (right) (n=3, error bars denote standard deviation).

PS2-07-367

Biocompatibility of Novel Electrically Conductive Scaffolds.

Petr Humpolíček[1], Katarzyna A. Radaszkiewicz[2], Zdenka Capáková[1], Jiří Pacherník[2], Patrycja Bober[3], Věra Kašpárková[1,4], Petra Rejmontová[1,4], Marián Lehocký[1,4], Petr Ponížil[4], Jaroslav Stejskal[3]

[1]Tomas Bata University in Zlin, Centre of Polymer Systems, Zlín, CZ; [2]Masaryk University, Institute of Experimental Biology, Brno, CZ; [3]Academy of Sciences of the Czech Republic, Institute of Macromolecular Chemistry, Prague, CZ; [4]Tomas Bata University, Faculty of Technology, Zlín, CZ

Introduction

Bioelectricity plays a crucial role in a variety of cellular processes, such as cell division, cell signalling, and differentiation, as well as on the tissue level, e.g., in wound healing or angiogenesis. Emerging knowledge about role bioelectricity in the physiology has led to the application of conducting materials in regenerative medicine and the tissue engineering of electrically excitable tissues, as well as in the field of bio-sensing. Conventional materials however demonstrate number of disadvanteges f.e. different elasticity. Polyaniline cryogel is a new unique macroporous form of polyaniline combining both an intrinsic electrical conductivity and the material properties of hydrogels.[1-3]

Experimental Methods

The interaction of any material with cells or tissues depends on its surface and bulk properties. The surface energy, pore-size distribution, and elasticity expressed by Young moduli were determined for polyaniline cryogel. In addition, impurities leaching from polyaniline cryogel were characterized by chromatography. To determine biocompatibility, cytotoxicity, embryotoxicity, the adhesion and growth of embryonic stem cells, embryoid bodies, cardiomyocytes, and neural progenitors were employed.[4]

Results and Discussion

Polyaniline cryogels supported by poly(vinyl alcohol) are novel macroporous soft conducting materials. They not only have good mechanical integrity represented by Young modulus of 9.7 ± 0.5 kPa but they are also macroporous and highly hydrophilic. All these properties are prerequisites for any application in tissue engineering or biosensing. The low cytotoxicity and embryotoxicity of polyaniline cryogel show high potential of cryogel for before mentioned applications. Moreover, to show the cell compatibility, the adhesion and growth of embryonic stem cells, embryoid bodies (Fig. 1), cardiomyocytes, and neural progenitors were used. Results show that polyaniline cryogel has the potential to be used as a carrier for cells in tissue engineering or bio-sensing but additional surface modification using bioactive compounds will be necessary.

Conclusion

Based on the determined surface energy, elasticity and porosity it can be concluded that PANI/PVA cryogel can be used for preparation of materials mimicking the properties of native tissues. This is supported by the fact that the cryogel does not express significant cytotoxicity or embryotoxicity, that various cell types are able to adhere and grow on its surface, and that it can undergo simple surface modification in order to improve its biointerfacial cytocompatibility. These results opens the door to its potential application in regenerative medicine and biosensing, where the electrical monitoring or stimulation of tissue is required.

References

1. Jeong, J. et al. *Neuron* **86**, 175-186 (2015).
2. Abidian, M. R., Corey, J. M., Kipke, D. R. & Martin, D. C. *Small* **6**, 421-429 (2010).
3. Vishnoi, T. & Kumar, A. *J. Mater. Sci. Mater. Med.* **24**, 447-459 (2013).
4. Humpolíček P. et al. *Sci. Rep.* **8**, 135 (2018).

Acknowledgement

This work was supported by the Czech Science Foundation (17-05095S) and by the Ministry of Education, Youth and Sports of the Czech Republic – Program NPU I (LO1504).

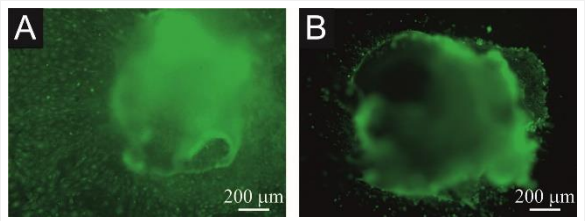

FIGURE 1.
EB growth on TC plastics (A) and polyaniline cryogel (B). Only viable cells are visualized by calcein. The migration of cells (represented by individual spots) is weaker on polyaniline cryogel (B) than on TC plastic. The micrographs were taken on day 20 of differentiation overall.

PS2-07-367-2

Marine origin biopolymers on the development of cryo-system gels envisaging cartilage tissue engineering and regenerative medicine

Duarte Nuno Carvalho[1,2], Rita Lopez-Cebral[1,2,3], Rita O. Sousa[1,2], Lara L. Reys[1,2], J. Miguel Oliveira[1,2,3], Rui L. Reis[1,2,3], Tiago H. Silva[1,2]

[1]3B´s Research Group, I3Bs - Biomaterials, Biodegradables and Biomimetics of University of Minho, Headquartes of the European Institute of Excellence on Tissue Engineering and Regenerative Medicine, Guimarães, PT; [2]ICVS/3B´s – PT Government Associate Laboratory, Guimarães, PT; [3]The Discoveries Centre for Regenerative and Precision Medicine, Headquarters at University of Minho, Guimarães, PT

Introduction

Marine resources are a natural alternative to provide valuable bioactive compounds in a sustainable form to the constant demand of the biomedical sector for the development of new materials regarding devices and applications for therapeutic approaches. In the recent decade, many of these materials have been reported by their similarities with proteins and polysaccharides present in the extracellular matrix (ECM) in humans, supporting a biomimetic approach of biomaterial development mimicking the composition of the native ECM. Marine biopolymers have thus been studied as an alternative to mammal origin materials, claiming the lack of disease transmission risks and the absence of ethical reasons (social/religious) [1].

Experimental Methods

The present work addresses the synthesis of cryo-system gels (C-SG) using a combination of marine origin biopolymers (collagen, chitosan and fucoidan) for tissue engineering applications. These marine biopolymers exhibit excellent bioactive properties, such as biocompatibility, non-toxicity, low antigenicity, high biodegradability, among others. The C-SG´s formulations were prepared by blending 3 or 5 % solutions of collagen from jellyfish with 3 % solutions of chitosan from squid pens and 5 or 10 % solutions of fucoidan from brown algae, combined at different ratios, freezing at -80 ºC and further slowly thaw. The produced hydrogels were characterized by scanning electron microscopy to address morphological features, by rheology to access mechanical properties and by *in vitro* tests with cell lines to evaluate cytocompatibility and their capacity to support cell proliferation envisaging new tissue formation.

Results and Discussion

The collagen/chitosan/fucoidan cryogels produced exhibited excellent morphological and mechanical properties, namely showing a porous and interconnected architecture, together with mechanical stability and cohesiveness characterized by viscoelastic behaviour. Moreover, the MTS (3-(4,5-dimethylthiazol-2-yl)-5-(3-carboxymethoxypheyl)-2-(4-sulfofenyl)-2H-tetrazolium) test demonstrated that C-SG´s had no significant cytotoxicity effect on L929 fibroblasts cells and ATDC5 chondrocyte cells. Moreover, both the live/dead assay (calcein/PI staining) and cell morphology assessment (Phalloidin/DAPI staining) revealed that these C-SG´s have a good microenvironment to support and promote the proliferation of the cells (Figure 1).

Conclusion

Overall, the results obtained suggest that C-SG´s derived from marine polymers are promising devices for biomedical applications envisaging their use as scaffolds in tissue engineering or regeneration tissues strategies, including less invasive approaches as injectable biomaterials (Figure 2).

References

[1] Hoyer, B., Bernhardt, A., Lode, A., Heinemann, S., Sewing, J., Klinger, M., Notbohm, H., & Gelinsky, M. (2013). Jellyfish collagen scaffolds for cartilage tissue engineering. Acta Biomaterialia. Doi: 10.1016/j.actbio.2013.10.022.

Acknowledgement

This work was partially funded by “Fundação para a Ciência e Tecnologia” (FCT, Portugal) under the scope of doctoral program Tissue Engineering, Regenerative Medicine and Stem Cells, ref. PD/BD/143044/2018, by ERDF under the scope of Program INTERREG España-Portugal 2014-2020 through project 0245_IBEROS_1_E, under the scope of Atlantic Area Program through project EAPA_151/2016 (BLUEHUMAN) and under the scope of Regional Program NORTE2020 through Structured Project NORTE-01-0145-FEDER-000023.

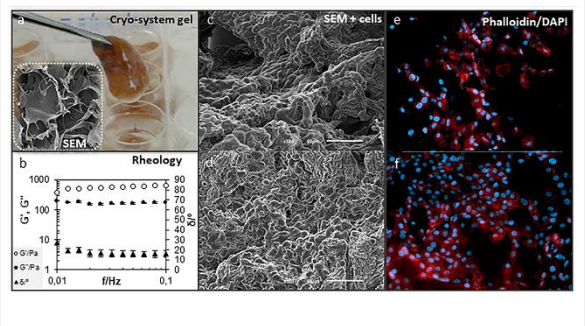

Figure 1
Schematic representation of the developed cryo-system gel characterization: a) gel and respective SEM image at the magnification of 50x / 500 µm; b) mechanical properties assessed by rheology; c) and d) SEM images with adhered cells at the magnification of 50x / 500 µm; e) and f) cells morphology exhibited by Phalloidin/DAPI assay.

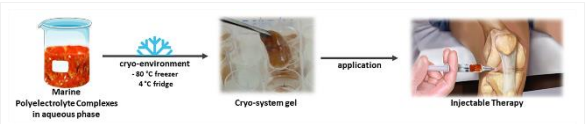

Figure 2
Schematic representation demonstrates the procedure to develop biomaterials in cryo-environment. The low temperatures promote the natural cross-linking between polymers.

PS2-07-368

Blend hydrogels based on alginate and silk fibroin support vascularization in endothelial cell-fibroblast co-culture system

Raminder Singh[1,3], Thomas Distler[2], Rainer Detsch[2], Barbara Dietel[3], Aldo R. Boccaccini[2], Christoph Alexiou[1], Iwona Cicha[1]

[1]University Hospital Erlangen, ENT-Section of Experimental Oncology and Nanomedicine (SEON), Erlangen, DE; [2]FAU-University of Erlangen-Nuremberg, 2Institute for Biomaterials, Erlangen, DE; [3]University Hospital Erlangen, Labor für molekulare Kardiologie -Med2, Erlangen, DE

Introduction

The microvascular networks are required for the transport of oxygen and nutrients to the tissue, but also for the efficient removal of the waste products. Currently, the development of tissue grafts and in vitro tissue models is hindered by the lack of vascular networks formation in the engineered constructs. In this study, we used primary human cells to investigate whether hydrogels based on alginate (Alg) blended with silk fibroin (SF) support the spontaneous formation of the tubular networks.

Experimental Methods

Blend Alg/SF hydrogels were prepared by mixing Alg and SF solutions, followed by addition of normal human dermal fibroblasts and calcium-dependent gelation. The hydrogels were placed in the 24-well plates and cultivated for 14 days in fibroblast growth media. On day 14, human umbilical vein endothelial cells (HUVEC) pre-loaded with magnetic particles (SPIONs, 3µg/cm^2) were seeded on the hydrogels, in the presence of magnetic field underneath of plate wells during the first 24 h. The growth of cells was monitored for additional 3 weeks. Metabolic activity of the cells was measured using WST-8 assay. Two-photon microscopy was used to observe the 3D distribution of HUVECs and fibroblasts using CD31 or N-Cadherin staining, respectively. Collagen formation was detected using collagen Iα1 antibody.

Results and Discussion

Blend Alg/SF hydrogels containing fibroblast only showed lower metabolic activity as compared with hydrogels containing both HUVECs and fibroblasts. Co-cultured cells had higher metabolic activity from day 7 of co-culture onwards. HUVECs did not remain on the surface of hydrogels and gradually migrated inside the films. The formation of neo-vessel like structures detected by N-Cadherin and CD31 staining was observable from day 20 of co-culture. Collagen, which is present in all connective tissues and is an indicator of the extracellular matrix (ECM) formation, was detected in the hydrogels at day 20 of fibroblast and HUVEC co-culture.

Conclusion

The pre-cellularized constructs which support vascularization and ECM formation are expected to overcome the limitations of current tissue-engineering approaches. Alg/SF hydrogels support growth of different vascular cells, as well as the formation of ECM and vessel-like structures. Our initial investigations showed promising results with this highly-biocompatible scaffold, but further studies will be needed to produce and validate the vascularized tissue constructs.

Acknowledgement

This work was supported by the German Research Foundation (SI 2093/2-1 and CI 162/2-1)

2:45 p.m. – 3:45 p.m.

Hall 1 / Exhibition Area

PS2-08 | *In vitro* models

PS2-08-369

Development of cell-based gel blocks and construction of three-dimensional structures by selective adhesion of the blocks

Seika Aoyama, Koji Nagahama

Konan University, Graduate School of Nanobiochemistry, Frontiers of Innovative Research in Science and Technology (FIRST), Kobe, JP

Introduction

Hydrogels are widely studied as biomaterials because of their tissue-like mechanical property, highly hydrophilic characters, highly permeability for water-soluble molecules such as bioactive agents, nutrients, and metabolites. Currently, hydrogels are generally formed by physical or chemical cross-linking of polymer networks. In contrast, we have recently reported a new concept and methodology to use cells and cellular functions in the design of functional hydrogels [1]. Especially, we developed a living cell-based hydrogel (CxGels) by bioorthogonal click cross-linking reactions of azide-modified cells with alkyne-modified biocompatible polymers. In the case of CxGels, the gel is able to show the similar functions of cells, because the gel networks are covalently connected with cells and the cellular functions can be conducted through the whole gel networks. Therefore, the CxGels has a potential as next-generation gels showing unique and highly functions which the current hydrogels cannot show. Interestingly, when two blocks of CxGels prepared from mouse myoblast C2C12 cells were placed in the same dish, the two blocks completely adhered. We thought that the gel adhesion is a characteristic function of the CxGels, then in this study, we tried to elucidate the mechanism of the gel adhesion reaction. Moreover, we tried to construct three-dimensional tissue-like structures by assembling the cell blocks utilizing the selective gel adhesion.

Experimental Methods

We selected alginic acid (100,000 Da) as biocompatible polymers and synthesized dibenzylcyclooctyne (DBCO)-modified bAlg (bAlg-DBCO). Pellet of azide-modified C2C12 cells (2.0×10^6) was suspended with 100 µL of bAlg-DBCO solution (2%) in HEPES buffer (100 mM, pH 7.4), and cells were well dispersed by gentle pipetting to form CxGels. 2 mL of DMEM was carefully added on the hydrogels for 3 hours. DBCO-carboxyrhodamine 110 (5 µM) was added to the CxGels and incubated at 37°C for 1 h to detect unreacted azide groups on the cell surface. To investigate gel adhesion in detail, we put a CxGel on the other and allowed to stand for 18 h, the gel adhesion strength was analyzed by centrifugation technique.

Results and Discussion

Reaction mixtures of N_3(+)C2C12 cells and bAlg-DBCO solution (1%) did not form bulk-sized hydrogels. In contrast, immediate gelation was achieved by reaction mixture of N_3(+)C2C12 cells (2.0×10^6) and bAlg-DBCO solution (2%). First, we performed gel adhesion test between CxGels prepared from C2C12 cells. As a result, a CxGel treated with DBCO-carboxyrhodamine did not adhered to the other CxGel, indicating that click reactions at gel interface is not driving force for gel adhesion. Next, we performed gel adhesion of CxGels prepared from C2C12 cells with CxGels prepared from HL-60 cells. As a result, a C2C12 CxGel did not adhered to the HL-60 CxGel. In contrast, a C2C12 CxGel adhered to the other C2C12 CxGel. These results suggest that intercellular adhesion via cadherin-based bindings at gel interface is strongly related with the gel adhesion. The adhesion strength between C2C12 CxGels significantly decreased with the decreasing in the concentration of Ca^{2+} ions, because cadherin-bindings is

dependent on the concentration of Ca^{2+} ions. This result also supports that the intercellular adhesion via cadherin-bindings is main force for gel adhesion. Importantly, the intercellular adhesion at gel interface was available to form three-dimensional tissue-like structures by assembling the blocks of CxGels.

Conclusion

In conclusion, CxGel achieved a selective adhesion ability and the ability is useful for tissue engineering and organ-on-a-tip technology.

References

[1] K. Nagahama, Y. Kimura and A. Takemoto, Nature Communications, 9, 2195 (2018).

PS2-08-370

Effects of a commensal multispecies biofilm on a peri-implant mucosa in a three dimensional *in vitro* model

Carina Mikolai[1], Alexandra Ingendoh-Tsakmakidis[1], Andreas Winkel[1], Nadine Kommerein[1], Christine S. Falk[2], Meike Stiesch[1]

[1]*Hanover Medical School, Department of Prosthetic Dentistry and Biomedical Materials Science, Hanover, DE;*
[2]*Hanover Medical School, Institute of Transplant Immunology, Hanover, DE*

Introduction

A symbiosis between the commensal microbial community and host tissue exists during the oral health state [1]. The importance of commensal bacteria in the balance of the host-microbiota homeostasis is known, but their role is not well understood [2]. Different factors (e. g. bad oral hygiene, genetic disposition, diseases) can lead to a dysbiotic microbial community with an increase of pathogenic bacteria [3]. The peri-implantitis, a high prevalent inflammation of the soft and hard tissue around a dental implant, can be induced by a dysbiotic biofilm on implant surfaces. Implant loss can be a serious consequence of this irreversible infection [4]. In order to improve prevention and/or treatment of the peri-implantitis, more knowledge about the host-microbe-implant interaction is necessary. Thus, new *in vitro* models that resemble better the *in vivo* situation are required. In a previous study, we developed for the first time a three dimensional *in vitro* implant-mucosa-biofilm model. This model combined three components: organotypic oral mucosa, implant material and oral monospecies biofilm. In the *in vivo* situation the biofilm is organized in a polymicrobial community. Therefore, our aim in this study was to reflect better the *in vivo* situation and to investigate the interaction of an early commensal biofilm with the peri-implant mucosa.

Experimental Methods

A commensal oral multispecies biofilm (*Streptococcus oralis*, *Actinomyces naeslundii*, *Veillonella dispar*, *Porphyromonas gingivalis*) [5] was integrated in our implant-mucosa-biofilm model. After the co-culture, the interaction of the biofilm with peri-implant mucosa was investiagted by morphology, gene expression and cytokine secretion of the peri-implant mucosa and the analysis of the biofilm volume.

Results and Discussion

The multispecies biofilm induced an altered gene expression and cytokine secretion of the peri-implant mucosa. The inflammatory reaction of the mucosa led to a reduction of the biofilm volume. Morphological changes between the biofilm challenged and unchallenged mucosa were not detected indicating that the primary host response protects the peri-implant mucosa integrity [6].

Conclusion

The novel 3D implant-mucosa-biofilm model opens the opportunity for further investigation of the implant-mucosa-microbe interaction and the testing of new implant materials and surfaces.

References

[1] Hajishengallis, G. (2015). Periodontitis: from microbial immune subversion to systemic inflammation. Nature Reviews Immunolgy; 15(1): 30-44.

[2] Darveau, R. P. (2010). Periodontitis: A polymicrobial disruption of host homeostasis. Nature Reviews Microbiology; 8(7): 481-490.

[3] Hajishengallis, G. (2014). Immunomicrobial pathogenesis of periodontitis: keystones, pathobionts, and host response. Trends in Immunolgy; 35(1): 3-11.

[4] Belibasakis, G. (2014). Microbiological and immuno-pathological aspects of peri-implant diseases. Archives of Oral Biology; 59(1): 66-72.

[5] Kommerein, N., Stumpp, S. N., Müsken, M., Ehlert, N., Winkel, A., Häussler, S., Behrens, P., Buettner, F. F. R., Stiesch, M. (2017). An oral multispecies biofilm model for high content screening applications. PloS One; 12(3): e0173973.

[6] Buskermolen, J. K., Janus, M. M., Roffel, S., Krom, B. P., Gibbs, S. (2018). Saliva-Derived Commensal and Pathogenic Biofilms in a Human Gingiva Model. Journal of Dental Research; 97(2): 201-208.

PS2-08-371

3D Gingival Tissue: A New Screening Tool for Oral Care Products and Dental Implants

Marta Munar-Bestard[1,2], Maria Antonia LLopis-Grimalt[1,2], Olga García-González[1], Joana Maria Ramis[1,2], Marta Monjo[1,2]

[1]University of the Balearic Islands, Group of Cell Therapy and Tissue Engineering, IUNICS, Palma, ES; [2]Balearic Islands Research Institute (IdISBa), Palma, ES

Introduction

Monolayer cultures of epithelial or gingival fibroblasts have been used for the study of gingival tissue and the effect of external stimuli, such as different types of dental materials. However, monolayer models lack polarized cell phenotype and systemic components, which affect their function and response to stimuli. Several tissue-engineered oral mucosa models have been developed to overcome these limitations with applications in different fields. Threedimensional (3D) cultures provide a higher degree of complexity than monolayer cell cultures being closer to explant cultures, providing an in vitro model resembling the in vivo situation.

The aim of this study is the development of a highly reproducible 3D model of human tissue equivalents of gingiva (GTE) as an in vitro study model for testing the effect of oral care products and dental implants on gingival regeneration under inflammatory conditions, which appears in periodontitis and peri-implantitis.

Experimental Methods

We present a detailed protocol for GTE using two types of human cells, including immortalized gingival fibroblasts and immortalized gingival keratinocytes. The procedure lasts 2-3 weeks to complete and includes three steps: (1) preparation of fibroblasts embedded in collagen, (2) addition of mucosal component and (3) airlifting of cultures to ensure adequate differentiation / stratification. The GTE obtained was characterized by histological analysis with conventional tissue staining (Hematoxylin and eosin) and by immunohistochemical staining with different markers of proliferation, epithelial differentiation, and basement membrane.

Then, the GTE were stimulated with LPS for simulating periodontitis disease model and treated with different gingival gels to study cytotoxicity, secretion of MMP-1 and TMP1 as markers of matrix degeneration and immunostaining for the different markers.

The GTE were also produced around different nanostructured titanium surfaces and functionalized with quercitrin in order to test the interaction between the gingival tissue and the implant.

Results and Discussion

This method results in a multilayer epithelial structure in which layers are organized similarly to the cells in native oral mucosa and that showed expression of differentiation markers analyzed by immunohistochemistry. When GTE were stimulated with LPS no cytotoxic effect was found but cytokine and MMP-1 secretion were increased, indicating a degeneration of tissue. The different gingival gels tested using the GTE showed different regeneration properties. In addition, modified titanium surfaces produced a better response of the GTE than control titanium surfaces.

Conclusion

This model has many possible applications for testing new dental implant surfaces or oral care products such as tooth pastes, gels or mouthwashes approaches in healthy and diseased GTE.

Acknowledgement

The project (PROCOE15/2017) was supported by the Dirección general de investigación, the Consellería de investigación, the Govern Balear, co-founded with ERDF European Regional Development Fund, by the Ministerio de Educación Cultura y Deporte (contract to M.A. L.G; FPU15/03412), by the Instituto de Salud Carlos III, the Ministerio de Economía y Competividad, co-funded with ESF European Social Fund (contract to M.M.B; FI18/00104 and contract to J.M.R; MS16/00124). The authors thank Dr. M.J. García-Fuster, Dr. E. Ceresi, Dr. R. García-Cabrerizo (UIB) and V.E. Cano (biobanco IdISBa) for the help of histological preparation. Finally thanks to the company Oralsan® and Straumann® for providing us regenerative gingival gels.

PS2-08-372

Human in vitro bone model of primary osteocytes, osteoclasts and osteoblasts in 3D collagen gels

Anne Bernhardt, Jasmin Skottke, Michael Gelinsky

Technische Universität Dresden, Centre for Translational Bone, Joint- and Soft Tissue research, Dresden, DE

Introduction

Bone is a complex tissue comprising different, very specialized cell types, spatially organized in a mineralized extracellular matrix. To investigate the cellular interaction and signaling between the major three bone cell types, osteoblasts, osteocytes and osteoclasts, an in vitro tripel culture model would be advantageous, opening the opportunity to analyze the cell types separately and to investigate the influence of biomaterials, drugs and bioactive molecules on the cross talk between bone cells. Present in vitro co-culture setups of bone cells are mainly based on rodent cell lines, like MLO-Y4 for osteocytes, RAW 264.7 as osteoclast progenitors and MC3T3E1 for osteoblasts. In the present study exclusively human primary osteoblasts, osteoclasts and osteocytes were spatially arranged in 3D collagen constructs to form the first completely human in vitro bone model.

Experimental Methods

Osteoblasts were isolated from human bone (femoral heads after total hip replacement surgery, approved by the Ethics Commission of TU Dresden) and were differentiated into osteocytes in collagen gels. Osteoblasts and osteoclasts were seeded onto the collagen gels, separated by a porous membrane from the osteocytes, to prevent mixture of osteocytes and osteoblasts. Osteoclasts were differentiated from human peripheral blood mononuclear cells (PBMC) and combined with the constructs as mature osteoclasts to circumvent the problem of contradicting cell culture medium requirements of differentiating osteoclasts and terminally differentiated osteocytes (figure 1). Fluorescence microscopic imaging was performed to analyze the morphology of the three cell species in triple culture. Gene expression analysis involved the expression of typical osteocyte, osteoclast and osteoblast markers in comparison to singe cultures of the cells. Osteoclasts of three different PBMC donors were combined with osteoblasts/osteocytes of four different bone tissue donors.

Results and Discussion

Osteoblasts, osteocytes and osteoclasts retained their typical morphology in the triple culture (figure 1). Gene expression analysis showed, that typical osteoclast markers tartrate resistant acid phosphatase, cathepsin K and carbonic anhydrase II were significantly downregulated in triple-culture. The same effect was observed, when osteoclasts were incubated in co-culture with collagen gel-embedded osteocytes, indicating a negative regulation of osteoclasts by osteocytes. It has been shown several times before, that osteocytes can support osteoclast formation and activity, especially in the presence of mechanical stress or hypoxia. However, without these factors, and with mature osteoclasts, as applied in our study, we could not confirm a pro-osteoclastic effect of osteocytes. Osteoblasts in triple culture developed a more mature state with downregulated ALP, and upregulated BSPII and osteocalcin. Osteocytes in triple culture expressed typical osteocyte markers, but, interestingly, the osteocalcin expression of osteocytes was significantly downregulated in triple culture compared to single osteocyte cultures.

Conclusion

Tripel cultures from primary human osteoblasts, osteocytes and osteoclasts were succesfully established in collagen gel constructs. Gene expression of osteocytes and osteoblasts, which belong to the same lineage and share some typical markers, was performed separately, allowing better insights into the cellular cross talk. The established tripel cultures will be a useful tool to analyze the impact of bioactive molecules, biomaterials and drugs on bone remodeling and turnover. The clinical relevance of this in vitro model, comprising solely human primary cells, might be higher compared to in vitro models of rodent cell lines.

Acknowledgement

We are grateful to the German Research foundation (DFG) for funding of this study (BE 5139/3-1).

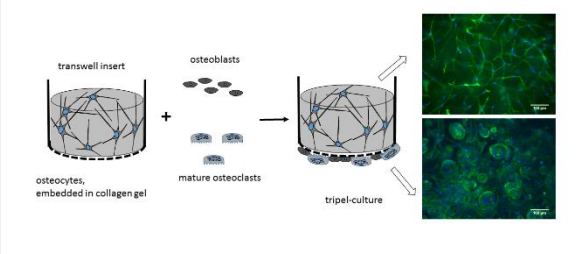

Osteoblasts, osteocytes and osteoclasts retained their typical morphology in triple culture

PS2-08-373

Keratinocyte protection against bacterial challenges of soft tissue integration of dental implant materials in a 3D-tissue model

Xiaoxiang Ren[1], Henny C van der Mei[1], Yijin Ren[2], Henk J. Busscher[1]

[1]University Medical Center of Groningen, Departments of Biomedical Engineering, Groningen, NL; [2]University Medical Center of Groningen, Department of Orthodontics, Groningen, NL

Introduction

Despite the reported small failure rate [1], dental implants count as the most successful biomaterial implants in the human body. Failures are largely due to implant-associated infection [2]. To overcome the bacterial challenges, the soft-tissue seal around dental implants, which are formed by keratinocytes and gingival fibroblasts [3], are protecting the osseo-integrated screw. Surface properties of the implant material are crucial for implant survival against bacterial challenges, but there is no adequate *in vitro* model mimicking the soft-tissue seal around dental implants. Therefore, the aim of this study was to construct a 3D-tissue model of the soft tissue seal around a dental implant using a transwell system. By using this *in vitro* co-culture model, bacterial challenges of the soft tissue seal formed on different materials can be studied.

Experimental Methods

Titanium dioxide (TiO_2), silicone rubber and hydroxyapatite discs were placed into 24-well plates (Falcon, BD Biosciences). Human gingival fibroblast cells were seeded on TiO_2, silicone rubber and hydroxyapatitediscs and grown until a surface coverage of 80% at 37°C and 5% CO_2 in modified culture medium. The human oral keratinocyte cells were seeded and grown in a transwell system for 24 h, after which it was put together with the human gingival fibroblast cells. Subsequently, bacteria were added into the transwell system and the whole system was incubated for 24 h. Subsequently, the human gingival fibroblast cells were fixed and stained with mouse-anti-human vinculin antibody for the focal adhesins, TRITC-phalloidin for the cytoskeleton and DAPI for cell nuclei. The samples were imaged using confocal laser scanning microscopy.

Results and Discussion

In absence of keratinocytes, fibroblasts growing on the TiO_2 surface could not withstand bacterial challenges. In presence of keratinocytes, the fibroblasts were growing better than without keratinocytes in the transwell membrane, demonstrating the protective role of keratinocytes. Importantly, the protection offered by the soft-tissue seal appeared sensitive to surface properties of the implant material. Fibroblast were growing less good on hydrophobic silicone rubber in presence of bacteria and better on hydroxyapatite discs compared to TiO_2. Streptococci caused less damage to fibroblasts than staphylococci.

Conclusion

The constructed 3D tissue-model, demonstrated that human oral keratinocytes provided a protection barrier to prevent oral infectious pathogens to invade fibroblasts. Furthermore, this soft tissue simulation 3D model can be used as a tool in the development and evaluation of antimicrobial therapeutics.

References

[1] D.S. Thoma, I. Sailer, A. Ioannidis, M. Zwahlen, N. Makarov, B.E. Pjetursson, A systematic review of the survival and complication rates of resin-bonded fixed dental prostheses after a mean observation period of at least 5 years, Clin. Oral Implants Res. 28 (2017) 1421–1432.

[2] D. Campoccia, L. Montanaro, C.R. Arciola, A review of the clinical implications of anti-infective biomaterials and infection-resistant surfaces, Biomaterials. 34 (2013) 8018–8029.

[3] D. Vautier, S. Werner, O. Huck, H. Tenenbaum, J. Voegel, The effect of microstructured surfaces and laminin-derived peptide coatings on soft tissue interactions with titanium dental implants, Biomaterials. 30 (2009) 2291–2301

Acknowledgement

XR likes to thank the China Scholarship Council and W.J. Kolff institute for financial support. Authors were employed by their own organizations. The authors declare no potential conflicts of interest with respect to authorship and/or publication of this article.

PS2-08-374

"Bioartificial" scaffolds for the development of *in vitro* models of human cardiac fibrotic tissue

Irene Carmagnola[1,2], Alice Zoso[1,2], Valeria Chiono[1,2]

[1]Politecnico di Torino, Department of Mechanical and Aerospace Engineering, Torino, IT; [2]Politecnico di Torino, POLITO BIOMedLAB, Turin, IT

Introduction

Heart failure is a global pathological condition affecting approximately 26 million people worldwide (1). Cardiac contractile activity is performed by cardiomyocytes, muscular cells that occupy 70-85% of the adult heart (2). When obstruction of coronary arteries occurs, cardiomyocytes in the left ventricle die, with the progressive formation of a fibrotic scar. Fibrotic tissue is mechanically stiffer than healthy cardiac tissue, and is mainly populated by cardiac fibroblasts, unable to undergo contraction (3). In this work, a model of fibrotic heart was designed by culturing human cardiac fibroblasts on bioartificial scaffolds with aligned or random morphology. Scaffolds were found to mimic the morphological and biological features (e.g. cell-cell and cell-extracellular matrix (ECM) interactions) of infarcted cardiac tissue. *In vitro* models of infarcted tissue represent a key tool in evaluating new therapies for cardiac regeneration.

Experimental Methods

Polycaprolactone (PCL) scaffolds were prepared by electrospinning (Linari Engineering) from chloroform/formic acid (70/30 v/v) solutions (flow rate: 1.5 mL/min; voltage: 20 kV; needle-collector distance: 20 cm) to obtain fibrous membranes with both aligned and random morphology, as well as high surface-to-volume ratio for subsequent functionalisation with gelatin. Gelatin was grafted through a mussel-inspired approach based on two steps: (i) initial 3,4-Dihydroxy-D,L-phenylalanine (DOPA) polymerisation (2 mg/mL DOPA solution in Tris/HCl 10 mM buffer at pH 8.5) on the fibre surface, followed by (ii) gelatin grafting through dipping in gelatin solution for 16 hours (4).
Samples were characterized after each functionalization step by FTIR-ATR and XPS analyses, SEM for morphological characterisation and tensile mechanical tests. PolyDOPA coating formation and gelatin grafting were monitored in real-time by using quartz crystal microbalance with dissipation technique. Cardiac fibroblasts isolated from human ventricle (PromoCell) were cultured onto the substrates at a cell density of $7x10^4$ cells/cm^2, testing their adhesion and morphology. Expression of common fibroblast markers (α-SMA, Vimentin, DDR2) was evaluated by immunofluorescence and western blot analyses as a function of scaffold morphology. Finally, the expression of typical proteins of cardiac ECM on the scaffolds was also investigated.

Results and Discussion

Porous PCL membranes with nanosized fibres were prepared (Figure 1). Surface modification with polyDOPA did not significantly affect the fibrous morphology and the tensile mechanical behaviour of the corresponding unfunctionalized scaffolds.
On the other hand, gelatin grafting slightly increased fibre size. Successful gelatin grafting was demonstrated by FTIR-ATR and QCM analyses. Gelatin grafting favoured attachment and proliferation of cardiac fibroblasts, as well as the deposition of cardiac ECM respect to control scaffolds. The effect of fibrous morphology on cardiac ECM deposition was investigated.

Conclusion

Bioartificial and biomimetic scaffolds able to support the proliferation of cardiac fibroblasts were developed and proposed as promising models of human cardiac fibrotic tissue, for testing new cardiac regenerative strategies, e.g. direct cardiac reprogramming. In the future the effect of scaffold properties (composition, structure and surface mechanical properties by modulating coating stiffness by gelatin crosslinking) on direct cardiac reprogramming from fibroblasts to cardiomyocytes will be evaluated.

References

1. Ponikowski P *et al*. Heart failure: preventing disease and death worldwide. ESC Heart Fail. 2014; 1(1):4-25.
2. Zhou P, Pu WT. Recounting Cardiac Cellular Composition. Circ Res. 2016 Feb 5;118(3):368-70.
3. Porter KE, Turner NA. Cardiac fibroblasts: at the heart of myocardial remodeling. Pharmacol Ther. 2009 Aug;123(2):255-78.
4. Nardo T *et al.* PolyDOPA Mussel-Inspired Coating as a Means for Hydroxyapatite Entrapment on Polytetrafluoroethylene Surface for Application in Periodontal Diseases, Macromolecular Bioscience 2016; 16(2): 288-298.

Acknowledgement

BIORECAR project has received funding from the European Research Council (ERC) under the European Union's Horizon 2020 research and innovation programme grant agreement No 772168

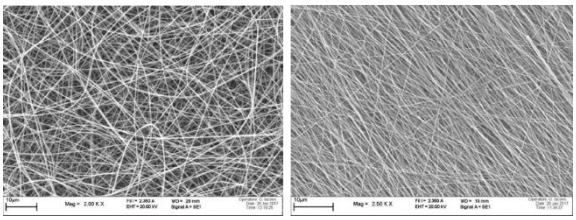

Figure 1
Esemplary SEM images of electrospun PCL membranes: (left) random; (right) aligned.

Figure 2
Biorecar project logo

PS2-08-375

Establishment of different in vitro Artery Models for Measurements of 4D Hemodynamics with Ultra-High Field MRI (17.6 T)

Kristina Andelovic[1,2], Matthias Ryma[3], Tobias Weigel[4], Patrick Winter[2], Wolfgang Bauer[5], Jan Hansmann[4], Jürgen Groll[3], Alma Zernecke[1]

[1]University Hospital Würzburg, Experimental Biomedicine, Würzburg, DE; [2]University of Würzburg, Experimental Physics V, Würzburg, DE; [3]University Hospital Würzburg, Functional Materials in Medicine and Dentistry, Würzburg, DE; [4]University Hospital Würzburg, Tissue Engineering and Regenerative Medicine, Würzburg, DE; [5]University Hospital Würzburg, Medicine I, Würzburg, DE

Introduction

The knowledge of the correlation between arterial pulse-wave-velocity (PWV) and endothelial wall shear stress (WSS) is of great relevance to understand the interaction of arterial stiffness and pathologic flow patterns in vascular diseases. Non-invasive measurements of these parameters using flow Magnetic Resonance Imaging (MRI) in vivo are challenging due to long measurement times and limited spatiotemporal resolution. At this point, tissue engineering poses a potential alternative to conventional animal studies since tissue-engineered arteries enable the study of pathologies in controlled environments. In this work, we combined non-invasive ultra-high field MRI with Tissue Engineering using artery models, cultured in a modular bioreactor-platform in order to create a potential test system for in vitro and in vivo studies of arterial elasticity and hemodynamics in native and biofabricated artery models.

Experimental Methods

A 3D-printed tissue chamber, suitable for MRI measurements and long-term culture of arteries was developed and connected to a bioreactor platform with adjustable flow/pressure rates and definable pump frequencies. For establishment of the method, 4D-flow and morphology measurements of native carotid arteries were performed using radial 4D Phase-Contrast-MRI. To create tissue engineered arteries with physical properties similar to native ones, we furthermore developed a gentle decellularization method for porcine carotid arteries, enabling the recellularization with human vascular cells and the creation of atherosclerotic artery models in future studies. As a synthetic alternative to natural tissue, we used porous nanofiber scaffolds made of electrospun polyamide 6 in a tubular shape, seeded with endothelial cells (ECs) and smooth muscle cells (SMCs). To test the influence of flow in bifurcations, we used 3d-printed sacrificial scaffolds based on thermoresponsive Poly(2-oxazolines), seeded with vascular cells and embedded in different hydrogels.

Results and Discussion

The establishment of 4D-Flow MRI measurements with the printed tissue chamber in a native carotid artery model (as well as mouse models) was successful. The obtained WSS and PWV values are in good accordance with literature. Decellularized natural arteries had comparable mechanical properties to ex vivo arteries. The ECs seeded onto the luminal side showed good adherence and a confluent monolayer. However, SMCs did not migrate into the decellularized scaffold. To address this problem, electrospun tubular polyamid 6 scaffolds with a dense inner layer and a porous outer layer were fabricated and seeded with endothelial cells from the inside, which grew to confluency and created a monolayer. SMCs were seeded from the outside of the tube and migrated into the porous

medial structure, which was confirmed by immunohistological stainings. Evaluation of the sacrifical scaffolds showed a dense SMC network in the medial structure and a monolayer of endothelial cell in the lumen.

Conclusion

The presented tissue engineered arteries, combined with the fast and non-invasive flow quantification setup, offer the possibility to examine the effects of specific biological modifications on the physical, flowdynamic properties as well as changes in vessel wall morphology and vice versa in a fully controllable environment. Furthermore, it is also planned to evaluate the integration of implanted TEBVs non-invasively via 4D-Flow MRI and morphology measurements in animal models.

PS2-08-376

Extracellular matrix characterization of human intervertebral disc degeneration/herniation: a biochemical and biomechanical evaluation

Ana L. Castro[1,2], Paulo Pereira[3,4], Rui Vaz[3,4], Mário Barbosa[1,2,5], Raquel Gonçalves[1,2,5]

[1]Universidade do Porto, i3s - Instituto de Investigação e Inovação em Saúde, Porto, PT; [2]Universidade do Porto, INEB - Instituto de Engenharia Biomédica, Porto, PT; [3]Hospital São João, Serviço de Neurocirurgia, Porto, PT; [4]Hospital CUF, Porto, PT; [5]Universidade do Porto, ICBAS - Instituto de Ciências Biomédicas Abel Salazar, Porto, PT

Introduction

Intervertebral disc (IVD) disorders include a number of different pathologies from IVD degeneration to herniation [1,2]. When undergoing degeneration, IVD histomorphological modifications and biomechanical alterations are observed [3], including loss of annulus fibrosus (AF) integrity, due to collagen and elastin fibers disorganization, impairing nucleus pulposus (NP) confinement [4,5]. Human IVD (hIVD) degeneration has been studied in different *in vitro*, *ex vivo* and *in vivo* models, with limitations regarding the mimicking of hIVD, suggesting that more sophisticated models that reconstitute hIVD tangled architecture and extracellular matrix (ECM) are required. In this study, we characterized human AF from degenerated/herniated hIVD samples, namely ECM composition and biomechanical properties, aiming to reveal new insights on AF ECM dynamics during the process of hIVD herniation for designing more reliable *in vitro* models of hIVD.

Experimental Methods

hIVD degenerated samples (Pfirmann grade between III and V) obtained from patients (>18 years old) undergoing microdiscectomy, with informed consent and ethics committee approval, were divided by hernia type: i) contained by the AF(n=7); ii) contained by the posterior longitudinal ligament (PLL)(n=16); and iii) extruded(n=11). hIVD fragments were separated in nucleus pulposus, AF and endplates. Water content was evaluated by comparing tissue weight before and after freeze drying. Biomechanical analysis was conducted using Dynamic Mechanical Analysis. hIVD tissues were fixed and embedded in paraffin. AF slides were analyzed by histology for Alcian Blue(AB)/Picrosirius Red(PR) staining and by immunohistochemistry for Collagen I (Col1), Fibronectin (FN), MMP12 and alpha-smooth muscle actin (aSMA). Images were acquired using optical microscopy and analyzed using Fiji software. Statistical analysis was performed using GraphPad-Prism.

Results and Discussion

Proteoglycans/Collagen (PG/COL) ratio, calculated as AB/PR area of staining, showed no differences between hernia types (Fig 1A), but when analyzing the correlation in PG/COL ratio with patient's age, in both contained by PLL and extruded hernias, a linear correlation was observed showing that, with aging, there is a significant increase of PG/COL ratio ($p<0.05$) (Fig 1B-D). Col1 staining area was higher in hernias contained by PLL (n=11;%Area=12.7±18.6) and extruded (n=10;%Area=13.8±25.2), compared with those contained by the AF (n=2;%Area=1.0±1.4). No correlation with age was observed. FN staining showed a similar trend as Col1, with increased staining areas in hernias contained by PLL (n=10);%Area=41.1±26.8) and extruded (n=8;%Area=19.9±27.9), when compared to those contained by AF (n=2;%Area=1.5±0.7) . No correlation with age was found. Analysis of water content of IVD degenerated samples showed no differences between the different

hernia types (%water retention ~92%) and no correlation with age. Biomechanical properties are currently being evaluated.

Conclusion

PG/COL ratio analysis showed an increase on PG compared to COL with age, in contained by PLL and extruded hernias, suggesting a more accentuated ECM remodeling in older patients (>50 years). In these patients, Col1 and FN appear to be increased. These results demonstrate the heterogeneity of hIVD herniation and reveal new cues to design more accurate and specific hIVD herniation in vitro models.

References

[1] N. Inoue, *Orthopedic Clinics of North America*. 2011. [2] C. Cunha, *Arthritis research & therapy*. 2018. [3] B. I. Woods, *Oper. Tech. Orthop.*, 2010. [4] J. P. G. Urban, *Arthritis Res. Ther.*, 2003. [5] M. Stefanakis, *Spine (Phila. Pa. 1976).*, 2014.

Acknowledgement

Norte Portugal Regional Operational Programme (NORTE 2020) in the framework of the project “Bioengineered Therapies for Infectious Diseases and Tissue Regeneration” (NORTE-01-0145- FEDER-000012). Fundação para a Ciência e a Tecnologia (FCT) for the FCT Investigator Grant (IF/00638/2014).

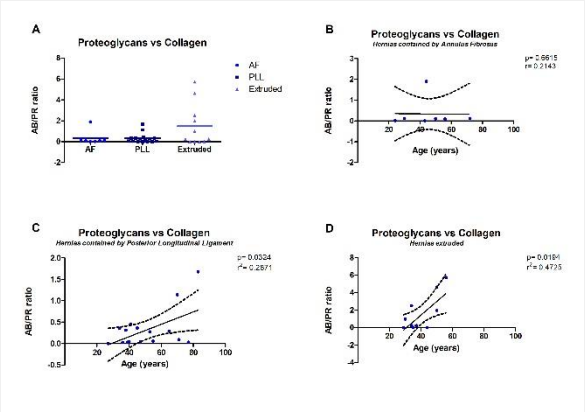

Proteoglycans vs Collagen content in human IVD degenerated sample

Figure 1: Analysis of PG/COL content between hernia types (**A**) and age correlation of PG/COL content in each hernia type: **B)** Contained by AF (n=7, Spearman r=0.2143, p=0.6615); **C)** Contained by PLL (n =16, Pearson r^2=0.2871, p=0.0324); **D)** Extruded (n=11, Pearson r^2=0.4725, p=0.0194)

PS2-08-377

The Effects of Nanopatterned Scaffold Mimicking the Abnormal Renal Mesangial Matrix on Mesangial Cell Behavior

Chia-Jung Chang[1,2], Akiyoshi Taniguchi[1,2]

[1]Waseda University, Graduate School of Advanced Science and Engineering, Tokyo, JP; [2]National Institute for Materials Science, Cellular Functional Nanobiomaterials Group, Tsukuba, JP

Introduction

Biomaterials topography provides a powerful means to study the influence of the extracellular matrix (ECM) topography on cell behavior. Cells are known to respond to their nanoscale environment. Mimicking the natural and abnormal environment of the cells by the nanoscale interface is critical to understand how cells modulate their cellular function and activities. Mesangial cells play an important role in generating and controlling the turnover of the mesangial matrix which provides structural support for the integrity of the glomerular capillary. This study is aimed to evaluate the in vitro effects of nanopatterned surface that mimic the abnormal renal mesangial matrix on mesangial cell behavior, including cell morphological change, cell proliferation and ECM synthesis, and to assess the potential for developing a novel renal disease model.

Experimental Methods

An immortalized mouse mesangial cell line (SV40MES-13) was cultured on the amorphous TiO_2 nanogratings with specific dimensional and geometrical characteristics (nanogratings 80 nm wide and 80 nm apart) surfaces and its morphological change and the expressions of different ECM proteins were evaluated.

Results and Discussion

Results showed that mesangial cells cultured on the fibril-type surface adapted with an elongated morphology and cell spreading. In contrast, cells cultured on the network-type and unpatterned surfaces showed no elongation and limited spreading. Since cell morphology is known as an important biophysical factor in the regulation of cell functions, we further assessed cell proliferation. Results showed the proliferation of mesangial cells cultured on the fibril-type surface was higher when compared to those cultured on the network-type and unpatterned surfaces, suggest that cell spreading might affect mesangial cell proliferation. In addition, immunofluorescence stating showed lower expressions of laminin α1 and type IV collagen and higher expressions of type I collagen, fibronectin and TGF-β1 in cells cultured on the fibril-type surface than those on network-type and unpatterned surfaces. It is well known that laminin and type IV collagen are the major ECM components in the mesangial matrix, whereas novel synthesized type I collagen and fibronectin are detectable in several diseased situations. TGF-β1 is a multifunctional regulatory cytokine and has been long considered as a key mediator to promote type I collagen and Fibronectin. The ECM synthesis change in this study might regulate by TGF-β1. Our data showed the fibril-type nanopatterned surface influenced cell morphology changes, proliferation, and ECM protein synthesis.

Conclusion

This study assesses the potential for developing a model mimicking diseased mesangial matrix to better understand the interactions between cells and diseased environment.

References

1. Schlöndorff D, Banas B. 2009. The mesangial cell revisited: no cell is an island. *J Am Soc Nephrol.* 20(6):1179-87.

2. Abdellatef SA, Ohi A, Nabatame T, Taniguchi A.
2014. The effect of physical and chemical cues on hepatocellular function and morphology. *Int J Mol Sci.* 15(3):4299-317.

Acknowledgement

We wish to thank Dr. Akihiko Ohi and Tomoko Ohki for their technical assistance.

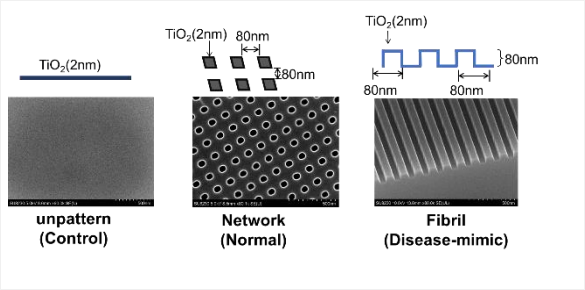

Figure 1.
SEM images of nanopatterned scaffolds mimicking the renal mesangial matrix.

PS2-08-378

A cell-instructive microgel-in-gel material platform to guide the faithful *in vitro* reconstitution of tissues

Petra B. Welzel[1], Dejan Husman[1,7], Steffen Vogler[4], Laura J. Bray[5], Nicole Träber[6], Jens Friedrichs[1], Vincent Körber[1], Mikhail V. Tsurkan[1], Uwe Freudenberg[1], Julian Thiele[3], Carsten Werner[1,2,7]

[1]Leibniz-Institut für Polymerforschung Dresden e.V. (IPF), Max Bergmann Center of Biomaterials Dresden (MBC), Institute of Biofunctional Polymers, Dresden, DE; [2]Technische Universität Dresden, Center for Regenerative Therapies Dresden (CRTD), Dresden, DE; [3]Leibniz-Institut für Polymerforschung Dresden e.V. (IPF), Department of Nanostructured Materials and Leibniz Research Cluster (LRC), Dresden, DE; [4]Deutsches Zentrum für Neurodegenerative Erkrankungen (DZNE), Dresden, DE; [5]Queensland University of Technology (QUT), Institute of Health and Biomedical Innovation, Kelvin Grove, QLD, AU; [6]Technische Universität Dresden, Biotechnology Center (BIOTEC), Dresden, DE; [7]Technische Universität Dresden, Research Training Group "Nano- and Biotechniques for Electronic Device Packaging", Dresden, DE

Introduction

Although *in vitro* models based on homogeneous hydrogel materials allow to recapitulate specific aspects of cell-matrix and cell-cell interactions, they cannot reflect the structural and compositional complexity of living tissues and are limited in supporting locally differing biomolecular and physical requirements of heterocellular cultures. Thus, multiphasic cell-instructive materials with cross-scale heterogeneity in matrix properties and/or cellular composition are needed to guide the faithful *in vitro* reconstitution of tissues and thereby create new options for drug development and pathobiology studies. Toward this aim, we herein present a new biomaterials design approach that relies on integrating cell-laden spherical hydrogel microparticles (microgels) within cell-laden bulk hydrogel matrices to provide thoroughly tunable microgel-in-gel systems. As a proof of concept, it is exemplarily shown how the approach can recapitulate basic features of vascularized prostate cancer tissue.

Experimental Methods

The new class of tunable microgel-in-gel materials builds on a versatile platform of multifunctional poly(ethylene glycol)-heparin hydrogel types [1]. As an innovative technique to easily and efficiently prepare the required differently sized microgels, we developed a novel variant of droplet microfluidics.

For the multiphasic 3D prostate cancer models, microgels supporting tumor spheroid formation of embedded cancer cells and a bulk hydrogel matrix supporting capillary network formation of embedded vascular endothelial cells were combined in microgel-in-gel co-cultures. Light microscopy and immunostaining/confocal laser scanning microscopy were used to thoroughly characterize these cultures.

Results and Discussion

The novel variant of droplet microfluidics allowed an effective variation of the microgel diameter without changing the microfluidic device and even within the course of one experiment. Sets of monodisperse hydrogel microgels of adjustable stiffness, degradability and biomolecular functionalization were obtained. Crosslinking by a rapid, cyto-compatible Michael-type addition reaction permitted cell embedding under very mild conditions [2]. Microgel-in-gel materials containing differently cell-instructive and cell-laden hydrogel types were produced. Tuning the microgel size enabled a very simple variation of the interface and the extent of the interaction between the two engineered microtissue compartments across the microgel/bulk gel boundaries.

Compared to a recently reported monophasic 3D prostate cancer model [3] the multiphasic model presented in this study is beneficial due to the spatial confinement of the co-culture. The spatially segregated hydrogel compartments can be independently tuned to match the physical and biomolecular triggers of the desired cell organization and function.

Conclusion

Microgel-in-gel systems made of thoroughly tunable multifunctional poly(ethylene glycol)-heparin hydrogel types allow for controlling the matrix properties and cellular composition of both spatially segregated phases individually. Furthermore, mesoenvironmental parameters that reflect fundamental tissue properties such as the maturation of cell assemblies or their 3D configuration can be adjusted.

References

1. U. Freudenberg, Y. K. Liang, K. L. Kiick, C. Werner, Adv. Mater. **2016**, 28, 8861.
2. M. V. Tsurkan, K. Chwalek, S. Prokoph, A. Zieris, K. R. Levental, U. Freudenberg, C. Werner, Adv. Mater. **2013**, 25, 2606.
3. L. J. Bray, M. Binner, A. Holzheu, J. Friedrichs, U. Freudenberg, D. W. Hutmacher, C. Werner, Biomaterials **2015**, 53, 609.

Acknowledgement

We thank the Deutsche Forschungsgemeinschaft (DFG, Research Training Group “Nano- and Biotechniques for Electronic Device Packaging’’) for funding. L.J.B. was supported by an Endeavour Fellowship as part of the Australia Awards program. MSCs were kindly gifted by Prof. Martin Bornhäuser (Universitätsklinikum Dresden). J.T. thanks the Federal Ministry of Education and Research (BMBF, “Biotechnologie2020+ Strukturvorhaben: Leibniz Research Cluster, 031A360C), and the DFG (Research Training Group “Hydrogel-based Microsystems” and TH 2037/1).

PS2-08-379

Bioprinting an in vitro model of the blood-brain-barrier with elastin-like protein engineered hydrogels and neural progenitor cells

Daniela Duarte Campos[1], Christopher Lindsay[1], Julien Roth[2], Bauer LeSavage[3], Andreas Blaeser[4], Sarah Heilshorn[1]

[1]Stanford University, Department of Materials Science and Engineering, Stanford, US; [2]Stanford University, Institute for Stem Cell Biology and Regenerative Medicine, Stanford Medical School, Stanford, US; [3]Stanford University, Department of Bioengineering, Stanford, US; [4]RWTH Aachen, Medical Textiles and Biofabrication, Aachen, DE

Introduction

The blood-brain-barrier (BBB) is a highly complex, multi-layered structure that serves as the gatekeeper between the central nervous system and the rest of the body. Three-dimensional BBB in vitro mini-models are potential platforms for understanding how the BBB functions, evaluating drug penetration across the barrier and investigating personalized therapies for neurodegenerative diseases. In this work, the feasibility of using elastin-like protein (ELP) hydrogels with varying degrees of degradability as bioinks for bioprinting in vitro mini-models that recapitulate the anatomy of the BBB was investigated.

Experimental Methods

Three-dimensional BBB models comprising layered similars of the endothelium, basement membrane and interstitial fluid were bioprinted and biologically characterized. The printability of 3, 4 and 5% ELP hydrogels was tested using a hand-held drop-on-demand bioprinter mounted with a 300 µm micro-valve, and the rheology of the bioinks was evaluated before and after printing. Murine neural progenitor cells (NPCs) were isolated, expanded and embedded in ELP bioinks before initiating the bioprinting process. Human NPCs were iPSC-derived and were used instead of murine NPCs in the light of the translational applicability of these models. NPCs were stained with live/dead staining one, three and seven days after bioprinting to investigate cell damage as a possible consequence of the printing process. The stemness maintenance of NPCs was analyzed after in vitro culture by Nestin and Sox2 immunostainings. The formation of endothelial cell-to-cell junctions was assessed by VE-cadherin immunostaining.

Results and Discussion

Live/dead staining showed viable NPCs in bioprinted hydrogels after the bioprinting process. Drop-on-demand bioprinting did not affect NPCs stemness, as proved by immunocytochemical stainings. Bioprinted BBB models showed successful formation of cell-to-cell junctions at the endothelial interface.

Conclusion

This study reveals the potential of using a drop-on-demand additive manufacturing strategy to create an in vitro 3D model of the BBB with recapitulating anatomy of the native barrier. Follow-up studies will focus on improving the biological functionality of the proposed models, for example, to test small molecule penetration across the mimicking basement membrane.

PS2-08-380

Development of a 3D Printed Scaffold Allowing Multiple Drug Delivery for the Treatment of Bone Metastasis in Breast Cancers

Habib Belaid[1,2], Catherine Teyssier[2], David Cornu[1], Vincent Cavailles[2], Mikhael Bechelany[1]

[1]Université de Montpellier, Institut Européen des Membranes, Montpellier, FR; [2]Université de Montpellier, Institut de Recherche en Cancerologie, Montpellier, FR

Introduction

Breast cancer is the most common invasive cancer in women, and the second main cause of cancer death in women. Metastatic breast cancer, most frequently localized in bone, is causing considerable pain and high patient morbidity. The treatment of bone is challenging due to bone repair, and patients are often treated by implanting a passive artificial junction in addition to a systemic chemotherapy treatment.3D printing is emerging as a powerful tool for bone repair. Long-term bone regeneration of normal anatomic structure, shape, and function is clinically important subsequent to fracture due to bone trauma and tumor.

3D printing is providing the ability to print bone substitute materials or “scaffolds” designed to mimic the extracellular matrix. The scaffolds need to be biocompatible and bioresorbable with a highly porous and interconnected pore network to control the degradation and resorption rate. They have a controlled shape and a suitable chemist surface for cell attachment, proliferation, and differentiation. Finally, the mechanical properties have to match those of the tissues at the site of implantation. For patients with bone metastasis, the scaffold may also allow the controlled and local release of anticancer drugs. One of the strategies to deliver these drugs by the scaffolds is to encapsulate them in microspheres such as Poly (lactic-co-glycolide) or PLGA microspheres which are one of the acknowledged vehicles for drug release approved by FDA.

Experimental Methods

To this aim, PLGA microspheres have been loaded with Raloxifene hydrochloride (RH) which is a selective estrogen receptor modulator (SERM) and Alendronate (AL) which is a bisphosphonate drug used for the treatment of bone metastasis. These drugs show an extremely poor bioavailability via oral administration thus justifying a local release. These microspheres made by emulsion have been incorporated into a 3D scaffold fabricated using a Stereolithography 3D printer system with a Poly (propylene fumarate) (PPF) photopolymer. PPF is an ultraviolet curable and biodegradable polymer with potential applications for bone regeneration and excellent mechanical properties.

Results and Discussion

The physicochemical properties of the nanocomposites scaffold have been fully characterized. The results showed that the microspheres were elongated and slightly less smooth after the loading of RH and AL, depicting the successful encapsulation of the drugs. The encapsulation efficiency and the realasing are obtained by UV-spectrometry. Encapsulation efficiencies of 14% and 54% were obtained for RH and AL respectively with relasing above 30% after one month for both drugs. The size of microspheres are obtained in range of 1µm and 50µm confirmed by dynamic light scattering and granulometry. The molecular weight of the polymer has been determined by gel permeation chromatography with Mn of 1,5kDa and a PI of 4. The physicochemical properties of the 3D printed scaffold have been determined using scanning electron microscopy to show the surface of the scaffolds and the

porosity. Finally the mechanical properties of the 3D printed nanocomposites scaffolds have been determined by tensil test as well compression test to show the influence of the incorporation of the PLGA microspheres.
Biological testing has been carried out in order to confirm the effects of encapsulated drugs on MCF7 cells proliferation. A cell viability test using MG63 cells has been conducted to determine the scaffold biocompatibility and its effects on cell proliferation. The successful cell adhesion was revealed by fluorescent microscopy ans by SEM.The aim of this work is the development and characterization of novel biomimetic biodegradable 3D printing scaffolds allowing both bone regeneration and inhibition of breast cancer cell proliferation.

Conclusion

These first results appear very promising and open prospects for bone metastasis treatment in breast cancers.

PS2-08-381

Biomechanically tunable 3D in vitro models for breast cancer research

Silvia J. Bidarra[1,2], Carla Oliveira[1,3,4], Cristina C. Barrias[1,2,5]

[1]i3S, Instituto de Inovação e Investigação em Saúde, Universidade do Porto, Porto, PT; [2]INEB-Instituto de Engenharia Biomédica, Universidade do Porto, Porto, PT; [3]IPATIMUP-Institute of Molecular Pathology and Immunology of the University of Porto, Porto, PT; [4]Department of Pathology and Oncology, Faculty of Medicine, University of Porto, Porto, PT; [5]ICBAS-Instituto de Ciências Biomédicas Abel Salazar, Universidade do Porto, Porto, PT

Introduction

Breast cancer is a leading cause of cancer death in women worldwide. Despite some improvements in cancer diagnosis and treatment, metastatic disease remains a major obstacle for effective treatment. Epithelial-to-mesenchymal transitions (EMT) are closely linked to progression of breast cancer. Recently, tumor mechanics, and tissue rigidity in particular, has emerged as an important factor during tumor progression and metastasis. In fact, it has been demonstrated that tissue stiffening is not only an outcome of the disease but have, in itself, a key role in tumor evolution.The use of tissue engineering approaches for the development of 3D *in vitro* models of native*vs.*tumoral tissue has been offering cancer researchers better platforms for dissecting the role of microenvironment players in more biologically relevant settings[1]. In particular, 3D models that allow recapitulating the dynamic mechanical changes of the extracellular matrix (ECM) during tumor progression, will certainty help to unravel its role on the overall process. In this context, we developed a tunable 3D model, where the viscoelastic properties of cell-laden hydrogels can be switched in situ. Cells are initially embedded in soft hydrogels, with stiffness comparable to that of healthy breast tissue[2], which can be reinforced, on-demand, to yield stiffness levels comparable to those of tumor breast tissue. The process is reversible, allowing re-softening of the hydrogel. Moreover, mechanical stimulation can be easily combined with key EMT inducers, such as TGFb1 and hypoxia.

Experimental Methods

Alginate hydrogels were prepared by internal gelation as previously described[2]. For 3D culture, near-normal epithelial EpH-4 cells were added to gel-precursor solutions, and hydrogels were then casted as small discs. Hydrogel mechanical properties were dynamically changed by altering the crosslinking state of pre-formed cell-laden hydrogels. Hydrogels were incubated during controlled time periods with different divalent cations as crosslinking agents to promote stiffening, or with cation-sequestering agents or specific enzymes to promote softening. Cellular response to viscoelastic changes was analyzed in terms of metabolic activity, epithelial morphogenesis (optical and confocal microscopy), YAP/TAZ localization, and epithelial vs. mesenchymal phenotype (RT-PCR and immunostaining). The effect of combining stiffness variations with TGFb1 in EMT induction was also tested[2].

Results and Discussion

Using alginate hydrogels modified with integrin-binding peptides and Ba^{2+}as stiffening agent, (but not Ca^{2+}or Sr^{2+}) we were able to tune the storage moduli (G') of EpH-4-laden hydrogels *in situ.* Starting with G' around 200 Pa, characteristic of normal breast tissue, we able to increase it in one order of magnitude, up to around 2000 Pa, characteristic of breast tumor tissue. In non-stiffened matrices (control) entrapped cells underwent normal epithelial morphogenesis forming acini-like structures. Noteworthy, treatment of hydrogel-entrapped cells with different stiffening agents showed no detrimental effects on their metabolic activity. Treatment with cation-sequestering agents

lead to a decrease in the G' of stiffened hydrogels, when Ca^{2+}or Sr^{2+}were used as stiffening agents, but softening Ba-stiffened hydrogels required additional treatment with alginate lyase. Matrix-stiffening at the onset of the 3D culture (single cells within hydrogel) decreased cell proliferation and spheroids size, as compared to control (non-stiffened hydrogel). On the other hand, stiffening at day 10 (after acinar-like structures formation), resulted in fewer differences in terms of spheroid formation. In both experimental settings no significant alterations were found at mRNA expression levels of epithelial, mesenchymal and EMT markers. This suggests that matrix stiffness, by itself, was not sufficient to induce EMT, under the tested experimental conditions. Yet, when mechanical stimulation was combined with TGFb1 induction, we were able to observe increased expression of mesenchymal markers (vimentin) and transcription factor Zeb2, as compared to controls (non-combined matrix stiffness or TGFb1-induction).

Conclusion

We were able to set up and validate a 3D model of breast tissue, where matrix mechanical properties can be dynamically switched, *in situ* and on demand, using a simple approach. By using Ba^{2+}as stiffening agent, the original matrix stiffness was increased by one order of magnitude, similar to what happens *in vivo*. While, increasing matrix stiffness *per si*was not sufficient to induce EMT, in combination with TGFb1 it showed a synergistic effect. This model is expected to provide useful in vitro platform for studying the impact of ECM biomechanics on the progression of epithelial cancers, particularly on EMT.

References

1. Gill BJ, et al. J. Biomech 2014, 1969-78.
2. Bidarra SJ, *et al*. Sci Rep 2016, 6: 27072.

Acknowledgement

FEDER - Fundo Europeu de Desenvolvimento Regional funds through COMPETE 2020 - Operacional Programme for Competitiveness and Internationalisation (POCI), Portugal 2020, and by Portuguese funds through FCT - Fundação para a Ciência e a Tecnologia/Ministério da Ciência, Tecnologia e Ensino Superior, in the framework of project 3DEMT (PTDC/BBBECT/251872014). SJB and CCB thank FCT for research contract DL 57/2016/CP1360/CT0006 and IF research position IF/00296/2015, respectively.

PS2-08-382

3D tumour *in vitro* models for drug screening

Lekha Shah[1], Julio M. Rios de la Rosa[3,1], Dominik Grudzinski[4], Annalisa Tirella[1,2], Chen Zhao[1], Ponpawee Pingrajai[1]

[1]University of Manchester, Medicine and Health, Manchester Academic Health Science Centre, Division of Pharmacy and Optometry, Manchester, GB; [2]University of Manchester, North West Centre for Advanced Drug Delivery (NoWCADD), Manchester, GB; [3]Bioncotech Therapeutics S.L., Valencia, ES; [4]University of Manchester, Medicine and Health, Manchester Academic Health Science Centre, Manchester, GB

Introduction

The lack of relevant *in vitro* models is one of the main contributing factors to poor prediction of dosing and efficacy of drugs. This impacts in particular on the low rate of success in the translation of chemotherapies for the tratment of different tumour types. Conventional drug testing methods have limited ability to replicate the tumour microenvironment, e.g. cell-cell interaction, cell-stroma interaction, extracellular matrix. The use of biomaterials and three-dimensional (3D) *in vitro* models is advantageous as they better replicate some of the *in vivo* properties, offering to more accurately represent the disease state and to overcome limitations of traditional *in vitro* models in drug testing.

Biomaterials used as to be selected to fulfill both 3D fabrication and the recapitulation of some properties of the tissue of interest, e.g. adhesion ligands, stiffness, porosity. Hydrogels are a class of biomaterials that can be modified to meet both requirements. We here present a new 3D *in vitro* cancer model designed to study cell-cell and cell-stroma interactions at the early stage of tumour development. The proposed model has also a great impact for drug efficacy testing, and further tumour development studies (e.g. interaction with stromal components).

Experimental Methods

The human colorectal cancer cell line HCT-116 (CCL- 247™), the human pancreatic cancer cell lines AsPC-1 (CRL-1682™) and PANC-1 (CRL-1469™) were cultured in standard conditions and complete cell culture medium. For the preparation of 3D *in vitro* models, cancer cells were suspended at a concentration of about 10^6 cells/mL in a 2% (w/v) alginate or in 1.5% (w/v) alginate / 2% (w/v) gelatine solutions in HBS. Alginates beads were fabricated using the Inotech encapsulator (IE-50) adjusting fabrication parameters to target bead diameter of 0.5 mm. Rheological and mechanical properties of selected alginate-based hydrogels were also characterised.

Live/Dead assay and tumor biomarkers were detected via flow cytometry at 2 and 5 days of culture. The panel of markers (CD24, CD44, CD133, and CD326) was used to assess differences between the studies models. Drug response (doxorubicin, gemcitabine) in 3D models was compared to conventional cell culture measuring cell viability with MTS assay (up to 72 h). Unpaired-t-test/Mann-Whiteney tests (GraphPad Prism, v7) were used to compare the same biomarker expression and drug response on different models.

Results and Discussion

Selected alginate-based formulation are suitable for 3D fabrication of hydrogel beads. The fabrication process is optimised and homogeneous beads in shape and size are obtained. Regardless the concentration of cells used, beads with target diameter of 0.5 mm are obtained. Hydrogel stiffness is matching the values of typical soft tissues (about 5 kPa).

CD44 variant isoforms (CD44v) are recognized prognostic and diagnostic markers for several tumor types. The expression of the tumor development-associated markers CD44 (membrane-anchored) was detected via flow cytometry on live cells. We found that CD44 expression was consistently higher in cells grown using 3D models than in those grown as 2D monolayers.
At a first glance, doxorubicin was a more efficacious drug in terms of reducing cell viability in both models and cell lines tested when compared with gemcitabine. The cell viability between 2D and 3D remains fairly similar at lower concentrations of the drugs and the 3D increased apparent viability only becomes apparent at higher concentration. We also observed that PANC-1 displays a greater resistance to doxorubicin and AsPC-1 to gemcitabine.

Conclusion

The microenviroment plays a significant role in directing cell phenotypic expression. Here wie report how biomarkers characterization and drug response evidenced significant differences between 2D and 3D in vitro models, and as a function of the biomaterials used and their physico-mechanical properties.
Expression of marker displayed a difference pattern between 2D and 3D in vitro models, as expected. Moreover, we also found differences in drug response. We observed a consistent rightward shift in the IC50 curves when cancer cells are encapsulated and cultured in a 3D stromal-enriched environment (i.e. alginate-based beads) and exposed to chemotherapeutics. Such difference were reported across all cell types and for both tested drugs when comparing 2D monoculture vs 3D beads. The developed model has great impact to design new and more effective drug delivery strategies for cancer treatment.

References

Alemany-Ribes M et al. Adv Drug Deliv Rev 79–80 (2014) 40–49
De la Rosa JM et al. Biomed. Phys. Eng. Express 4 045010 (2018)

Acknowledgement

Support received from EPSRC for JRR’s PhD studentship (part of the North-West Nanoscience Doctoral Training Centre, EPSRC grant EP/G03737X/1) and from University of Manchester President’s Doctoral scholarship for LS.

2:45 p.m. – 3:45 p.m.

Hall 1 / Exhibition Area

PS2-09 | Biofabrication

PS2-09-383

Generation of complex multilayered constructs via 3D bioplotting for the regeneration of critical-size cranial bone defects

Vera Bednarzig[1], Joelle Claußen[2], Anja Eggert[2], Stefan Gerth[2], Aldo R. Boccaccini[1], Rainer Detsch[1]

[1]Friedrich-Alexander-Universität Erlangen-Nürnberg, Werkstoffwissenschaften/ Institut für Biomaterialien, Erlangen, DE; [2]Fraunhofer Institut, Integrierte Schaltungen IIS, Fürth, DE

Introduction

Cranial bone defects, caused by traumata, laceration, burns or sport accidents, are a main reason for surgeries worldwide. Until now most defects are only covered with platelets or injectables, which do not mimic the complexity of the natural cranial bone with its different layers and tasks.[1]

Experimental Methods

The aim of this project is to create an implant consisting of different layers to cover especially defects with a critical-size. All the layers of this complex construct should be fabricated using the technique of 3D-Bioplotting. With this procedure it is possible to plot sequential layers of different compositions, materials and structures. Through different properties and functionalities the layers exhibit varying characteristics and are able to fulfil different tasks in the construct, to mimic the natural bone, surrounded by soft tissue, as close as possible.

The first layer (A) should prevent the ingrowing of cells, on the one hand from the skin-side the fibroblasts but also from the bone-side osteoblasts. It consists of a pre-crosslinked alginate, which is plotted as a dense layer.

The following layer (B), a porous composite one, consists of the bioactive ceramic hydroxyapatite and the polymer alginate. This layer should enable vascularisation and the ingrowing of natural bone cells. The combination of these materials has already shown positive results in literature.

The following third layer is comparable with Layer A in its composition and tasks.

The layers of the construct are plotted on a titanium-mesh, which is used as a building platform and for the connection of the whole implant to the natural bone.

The alginate based layers are crosslinked afterwards with calcium-chloride solution ($CaCl_2$).

Results and Discussion

Through optimizations in the plotting parameters and the materials themselves, stable constructs of up to 15 mm have been generated.

In- vitro cell-tests and preliminary mechanical tests were performed with the different layers and show promising results. Furthermore, the single layers and the whole implant were characterized using µ-Computed Tomography (µ-CT) to examine the connection of the layers with each other and to proof the interconnectivity of the porous composite layer B.

Conclusion

The tests revealed positive results in that the required shape and architecture of the construct were achieved. Nevertheless, there are still improvements and optimizations required, and a comprehensive characterization must be done to fulfil the aim of a bone healing construct that can be translated to the clinics.

References

[1] Drake, R. L., Vogl, A. W. & Mitchell, A. W. M. *Gray's Anatomy For Students*. (2015)

Acknowledgement

BMBF Project

Funded by: Addititve manufacturing- individualized products, complex bulk products, innovative materials (ProMat_3D)

Topic focus: Materials Science (HY2PRINT-03XP0097 A-E)

PS2-09-384

Development of three-dimensional mesh fabric constructed with chondrocyte-enclosing alginate fiber

Kenta Yoshitomi[1], Koji Yamamoto[2], Eiji Nakamachi[2], Yusuke Morita[2]

[1]Doshisha University, Graduate School of Life and Medical Sciences, Kyoto, JP; [2]Doshisha University, Department of Biomedical Engineering, Kyoto, JP

Introduction

In clinical application of cartilage regeneration, it is necessary to prepare cultured cartilage according to the shape of defect and adopt to wide defect. Enough maturation of cultured cartilage is required without necrosis and reduction of chondrocyte activity during long-term cultivation to obtain large size of cultured cartilage for wide defect. 3D printing techniques [1, 2] were tried to fabricate cultured cartilage in arbitrary shape. UV-curable polymer and UV irradiation may cause damage of chondrocytes in 3D printing techniques. We had developed the spinning technique to fabricate the chondrocyte-enclosing alginate fiber, and we suggested the three-dimensional mesh fabric knitted by the chondrocyte-enclosing alginate fiber. It was expected that shape of cultured cartilage was controlled freely and culture medium supply was maintained through mesh structure by knitting the fiber. The purpose of this study was to develop techniques to fabricate the three-dimensional mesh fabric constructed with the chondrocyte-enclosing alginate fiber.

Experimental Methods

A three-dimensional knitting device consisted of three-axis actuators, nozzle, $CaCl_2$ solution bath, needle holder and syringe pump. Figure 1(a) shows the schematic drawing of knitting procedure of the mesh fabric. The inner diameter of the nozzle was 60 μm. Needles with a diameter of 0.8 mm were arranged on the needle holder in 9 rows and 9 columns at 3 mm intervals to accumulate the fibers. The spinning solution was prepared by mixing sodium alginate (SA) and porcine chondrocytes in DMEM supplemented with 1% antibiotics. The SA concentration was 1.0 w/v%. The cell density was 1.0×10^6 cells/ml. The spinning solution was extruded from the nozzle into 1.2 w/v% $CaCl_2$ solution at a flow rate of 100 μl/min to form the chondrocyte-enclosing alginate fiber. The nozzle speed was 120 mm/s, and nozzle was controlled by the three-axis actuators with pattern 1 and 2 as show in Figure 1(b). Mesh fabric was removed by pulling out the remover from the needle holder. Mesh fabric was observed with a phase contrast microscope before cultivation. Mesh fabric was cultured in DMEM supplemented with 10% fetal bovine serum, 1% antibiotic and 1% L-ascorbic acid for 14 days. Synthesis of proteoglycan was evaluated with safranin O staining. Collagen was observed by detecting a second-harmonics generation (SHG) using a multiphoton microscope.

Results and Discussion

Figure 2(a) shows the photograph of the three-dimensional mesh fabric which accumulated on the needle holder with the nozzle pattern 2. The mesh fabric was constructed with the chondrocyte-enclosing alginate fiber of about 150 μm diameter. Fibers constituting the mesh fabric were knitted on the needle holder without deflection and breakage. The mesh fabric which accumulated with the nozzle pattern 1 was deformed because fibers bended due to less contact points. Figure 2(b) shows the photograph of the mesh fabric removed from the needle holder. The mesh fabric maintained the fabricated shape after removal from the needle holder. Chondrocytes proliferated in the fibers during the cultivation. Synthesis of proteoglycans and collagen were confirmed by safranin O staining and SHG imaging

after 14 days cultivation. These results showed that the developed knitting technique enabled to form mesh fabric which might maintain chondrocyte activity during long-term cultivation.

Conclusion

The knitting techniques was developed to form the three-dimensional mesh fabric constructed with the chondrocytes-enclosing alginate fiber. Chondrocytes activity was maintained and extracellular matrix was synthesized in the mesh fabric.

References

1. Gu, Y., et al., Journal of Biomaterial Application, 33:609-618, 2018.
2. Levato, R., et al., Acta Biomaterialia, 61:41-53, 2017.

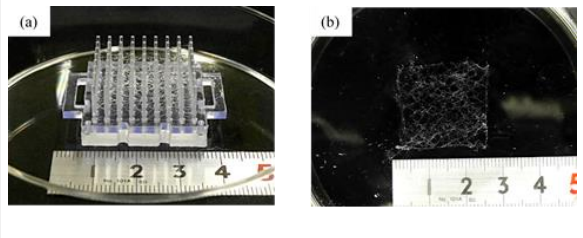

Figure 2:
The photograph of three-dimensional mesh fabric; (a) mesh fabric on the needle holder, (b) removed mesh fabric.

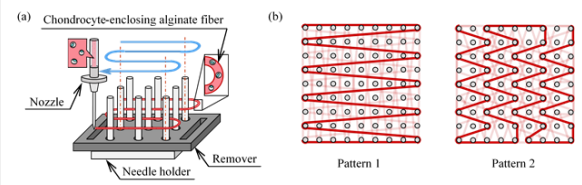

Figure 1:
The schematic drawing of knitting procedure of the mesh fabric, (a) three-dimensional knitting device, (b) nozzle patterns.

PS2-09-385

A 3D printed miniaturized bioreactor for perfusion cultivation of prevascularized bioprinted 3D cell cultures

Bastian Böttcher, Karl-Heinz Feller

Ernst-Abbe-Hochschule Jena, Institute for Microsystem and Precision Manufacturing Technologies, Jena, DE

Introduction

Bioprinting is a versatile tool to produce 3D cell cultures with defined spatial geometries that can mimic *in vivo* tissues close to reality due to complex cell-cell and cell-matrix communication. A crucial factor for optimal cell growth besides a proper vascularization for long term cell survival is a cultivation performed in a perfusion reactor. Using an extruder for thermoplastics, mechanically stable individual reactors without the risk of deformations can be manufactured. Here we show the process chain for creating miniaturized bioreactors with prevascularized 3D cell culture using one platform both for plastic printing and bioprinting.

Experimental Methods

For all additive manufacturing steps in this work, a BioScaffolder 3.2 (GeSiM, Germany) system with various tools was used. For 3D printing the bioreactor, the thermoplastic cyclo olefin copolymer COC Topas 5013 (Topas) was melted and processed using a high temperature extruder at 220 °C/230 °C (cartridge/nozzle). Since filament extrusion can't produce plane surfaces, an objective slide made of COC (microfluidic chipshop, Germany) was used to ensure high optical clarity for later microscopic analysis.

For bioprinting, a cell laden gel consisting of gelatin and alginate is used. The determination of the optimal gel concentration was performed using rheological oscillatory measurements with a MCR 502 rheometer (Anton Paar, Austria). Cell viability analysis with all for later experiments required nozzles performed with live/dead assay using calcein AM and propidium iodide.

The cell laden gels were finally printed into the sterilized bioreactor. A cell laden gel with HepG2 cells was printed with a 250 µm nozzle. For prevascularization, a core-shell extruder (diameter core-nozzle: 200 µm/ shell-nozzle: 610 µm) was used simultaneously in this process whereas the shell consisted of the already used alginate/gelatin gel combined with HUVEC and the core of pure gelatin. After printing the cell laden construct was crosslinked using a 50 mM $CaCl_2$ solution at 37 °C. During this incubation time the gelatin dissolved and then washed out. To increase the mechanical stability of the construct an additional crosslinking with transglutaminase was performed. After complete crosslinking the bioreactor was sealed using the adhesive foil 9795R (3M, Germany).

Results and Discussion

The printed COC showed an excellent adherence to the objective slide causing a sealed chip shell. The shell includes a hollow chamber which offers space for the cell laden gel structures. On each side of the chip a printed pump adaptor is available that is linked to the chamber via channels which offers the possibility for perfusion cultivation including an easy plugin of the tubes. Since the shell is made of a stiff plastic, there is no risk of deformation allowing an easy handling and high reproducibility.

Rheological tests showed that the determined optimal concentration of gelatin and alginate was appropriate for cell seeding in this gel as for printing. Using this gel for printing, a high resolution with applied air pressures less than 100

kPa could be achieved. Due to the low air pressure the occurent shear stress was low resulting in a cell viability >90 %.

Prevascularization using a core-shell extruder offers the possibility to print small cell laden hollow channels without the necessity for an additional step of cell seeding into the channels causing a homogeneous distribution of endothelial cells. Perfusion cultivation of the prevascularized 3D cell culture showed a flow through the channels allowing a nutrient supply close to *in vivo*.

Conclusion

The presented printed bioreactor with prevascularized 3D cell cultures offers the possibility for a perfusion cultivation to achieve *in vivo* like conditions. Due to the use of bioprinting, cells and vascular structures can have a highly flexible spatial organization enabling the fabrication of different functional tissues. This technology might find applications in pharmaceutical testing or for complex biological investigations as the angiogenesis of endothelial cells.

Acknowledgement

The authors would like to thank the BMBF for funding (funding number: 13FH134IN6). We would also like to thank 3D Schilling GmbH for providing the COC granulate for 3D printing.

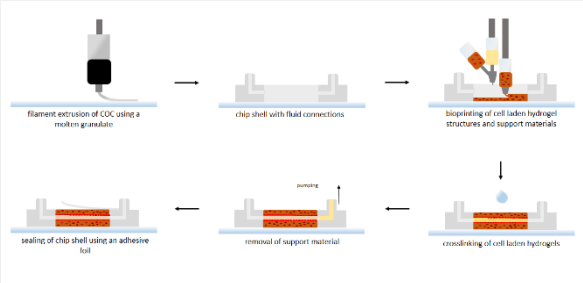

3D Printing Scheme of Bioreactor
Schematic representation of the fabrication of the miniaturized reactor with integrated prevascularized 3D cell culture

PS2-09-386

3D Printed Elastomers as Skeletal Muscle Tissue Substitutes

Seyda Gokyer[1,2], Emel Yilgor[3], Iskender Yilgor[3], Ayşe Karakeçili[2], Pinar Yilgor Huri[1]

[1]Ankara University, Department of Biomedical Engineering, Ankara, TR; [2]Ankara University, Department of Chemical Engineering, Ankara, TR; [3]Koc University, Department of Chemistry, Istanbul, TR

Introduction

Skeletal muscle losses after sports activities and traumas are highly prevalent worldwide and currently available clinical therapies are limited to autologous muscle flaps[1]. 3D printing represents an important advancement to produce engineered functional muscle substitutes with the potential to recapitulate the complex structural organization of skeletal muscle. The most important challenge is the availability of suitable scaffold materials. Synthetic 3D printable polymers generally lack the ability to provide the required elasticity, and hydrogel materials lack the mechanical stability to withstand the forces exerted during muscle contraction[2]. In this study, we synthesized biocompatible and biodegradable, elastomeric polyurethaneureas (TPUU) and investigated the applicability of these novel materials as 3D printed skeletal muscle substitutes.

Experimental Methods

*Materials:*Polycaprolactone glycol (PCL) (M_n=2000 g/mol) (Aldrich), amine terminated poly(ethylene oxide) (PEO) (M_n=600 and 2000 g/mol) (Jeffamine ED, Huntsman Chemicals), 1,6-hexamethylene diisocyanate (HDI) (Perstorp), dibutyltindilaurate (T-12) (Air Products) and tetrahydrofuran (THF) (Merck) were used for polymer synthesis. PCL (M_n=37000 g/mol) (Perstorp Capa) was used as a control material for scaffold structure and cell seeding.

Synthetic Procedure: Reactions were conducted in 100 mL Pyrex flasks, fitted with an overhead stirrer, nitrogen inlet and addition funnel. Calculated amounts of PCL and HDI were introduced into the reactor and dissolved in THF to obtain a 30% by weight solution. 100 ppm T-12 (1% solution in THF) was added and the system was heated to reflux. Reactions were completed in about 2 hours. Solution was cooled down to room temperature, stoichiometric amount of PEO was dissolved in THF and added into the reaction mixture dropwise through the addition funnel. Progress and completion of the reactions were monitored by FTIR spectroscopy[3].

*3D Print Procedure:*Polymers dissolved in dichloromethane (90% w/v) were 3D printed on an Envisiontech 3D Bioplotter system in solution form with low temperature print heads. 3D prints were done with a 3D parallel aligned fiber design to mimic the architecture of native tissue (layer thickness: 0.1 mm, L: 10 mm, H: 0.85 mm).Structural and mechanical properties of 3D printed scaffolds were determined using SEM and tensile tests (Schimadzu). Interactions of the scaffolds with adipose-derived stem cells (ASCs)were investigated in terms of cell proliferation, viability and the expression of muscle-specific markers.

Results and Discussion

Chemical compositions and tensile properties of polymers synthesized are provided in Table 1 and Figure 1a.Considering the mechanical properties, semi-crystalline PCL tested as reference material is fairly stiff, whereas TPUUs are softer with modulus values closer to that of the native tissue compared.Moreover, TPUUs have much higher elongation at break values compared to PCL, which represents the required elasticity to recapitulate native skeletal muscle deformation. Among the TPUUs, TPUU-3 was found to be the most suitable material to engineer skeletal muscle owing to its lower stiffness and higher elasticity.

Table 1. Chemical compositions and tensile properties of TPUUs and PCL

Polymer Code	PCL (wt %)	PEO (wt %)	HDI (wt%)	Modulus (MPa)	Tensile Str. (MPa)	Elongation at break (%)
TPUU-1	91.6	--	8.4	30.14±7.112	17.99±5.7	31.877±17.097
TPUU-2	68.6	22.9 (2000)	8.5	13.26±5.54	11.09±4.56	12.35±1.896
TPUU-3	61.8	26.0 (600)	12.2	17.0948±4.71	3.35±2.14	91.31±34.69
PCL	100	--	--	57.513±5.705	3.62±3.14	28.19±10.8

SEM observation of 3D printed scaffolds from these polymers revealed that the 3D structure was well preserved with respect to the 3D design in all samples (Figure 1b). ASCs attach and proliferate well on all scaffolds, TPUU-3 being the best performer (Figure 1 c and e). Staining for actin filaments reveal that cells are more elongated along the parallel fibers within the TPUU-3 scaffold, while they are more randomly distributed within the other scaffolds of similar design (Figure 1d).

Conclusion

It was possible to 3D print elastomeric polyurethaneurea scaffolds. TPUU-3 had the desirable mechanical properties (lower stiffness and higher elasticity) as well as housing high number of ASCs. Therefore, we have synthesized a novel material that is suitable for use in skeletal muscle tissue engineering applications.

References

1. Huri PY., et al., Biochem Biophys Res Commun. 438:180–185, 2013.
2. Mi H., et al., J Mater Chem B. 5:4137–4151, 2017.
3. Yilgor I., et al., Polymer 45:5829-5836, 2004.

Acknowledgement

We acknowledge Turkish Academy of Sciences (TUBA-GEBIP 2016) for providing financial support to PYH.

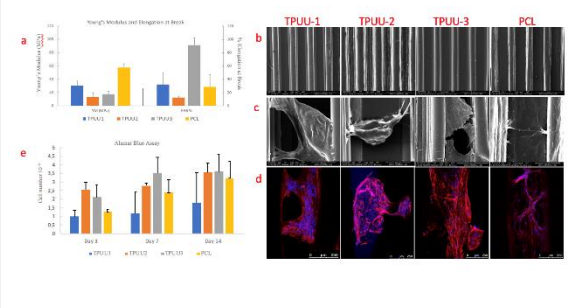

Figure 1
a) Young's modulus and elongation at break values of TPUUs.**b)**SEM images of unseeded and **c)**ASC seeded 3D printed scaffolds,**d)**Staining for Phalloidin/DAPI on ASC seeded 3D printed scaffolds, **e)** The number of live cells assessed on 3D printed scaffolds with Alamar Blue test.

PS2-09-387

Rheological examination and 3D bioprinting of internally pre-crosslinked alginate bioinks

Jonas Hazur[1], Joachim Kaschta[2], Dirk W. Schubert[2], Rainer Detsch[1], Aldo R. Boccaccini[1]

[1]Friedrich-Alexander-University Erlangen-Nürnberg, Department of Material Science and Engineering / Institute for Biomaterials, Erlangen, DE; [2]Friedrich-Alexander-University Erlangen-Nürnberg, Department of Material Science and Engineering / Institute of Polymer Materials, Erlangen, DE

Introduction

Alginate hydrogels are of special interest in wound healing, drug delivery and tissue engineering applications due to their biocompatibility and similarity to the extracellular matrices in tissues [1]. One example of a well-known material, widely used for the preparation of hydrogels is alginate. Alginates are polysaccharides and gained major importance in medical engineering over the last decades, due to their ability to form hydrogels under relatively mild pH and temperatures [2].

In this project, bioprinting of pre-crosslinked pharmaceutical grade alginate gels via an internal gelation method using D-(+)-Gluconic acid-lactone in combination with $CaCO_3$ was implemented. The purpose of this method was to create a homogeneous alginate-based bioink with enhanced shape fidelity, without utilizing support structures, multimaterial bioinks or rigid filler materials.

Experimental Methods

In order to characterise the bioinks, the focus was kept on two main methods. On the one hand, the rheological characteristics of the bioinks were examined via rotational rheology, where triplicates of each material were measured. The objective was to evaluate the influence of different preparation parameters as well as the cross-linking kinetics of the bioinks. On the other hand, the cell viability of printed cells in bioinks with and without pre-crosslinking was compared by a live-dead assay with Calcein-AM and propidium iodide. For counting the cells, triplicates for each measurement time point were prepared and five images per sample were recorded, resulting in a total of 15 images for each measurement time point. Living and dead cells were then counted with the ImageJ plugin ITCN and the mean cell-viability was calculated from that data.

Results and Discussion

The influence of different parameters, such as as $CaCO_3$ content, way of stirring and temperature during the cross-linking process was compared and assessed in respect of the shape fidelity. By optimization of the above-mentioned parameters, it was possible to print 3D porous structures with a height of 5 mm and a pore size of 1.1 mm with those bioinks. As expected, an increasing amount of $CaCO_3$ led to increased viscosities and to a certain extent to a better shape-fidelity. The rheological data also allowed an estimation of the shear forces that the cells will undergo during the printing process in those bioinks. Moreover, time sweep tests gave an insight in the cross-linking kinetics by evaluating the course of storage modulus (G') and loss modulus (G'') as well as their cross-over points. Beyond that, it was observed that the pre-crosslinked bioink, compared to pure alginate, does not affect the cell-viability during printing in the case of NIH-3T3 fibroblast cells. The cell-viability was evaluated after 1 d, 3 d and 7 d and its mean value was above 90 % for both materials throughout.

Conclusion

The investigations of this project yielded two main successes. On the one hand, it could be shown, that the shape fidelity of printing can be increased massively without generating losses in cell viability, by internally pre-crosslinking alginate in a controlled manner. On the other hand, the ideal viscosity level for 3D printing of alginate-based hydrogel scaffolds with a suitable shape of viscosity function over shear rate could be observed.

References

[1] K. Y. Lee and D. J. Mooney, “Alginate: properties and biomedical applications.”, *Progress in Polymer Science*, vol. 37, no. 1, pp. 106-126, 2012.

[2] S. N. Pawar and K. J. Edgar, “Alginate derivatization: A review of chemistry, properties and applications”, *Biomaterials*, vol. 33, no. 11, pp. 3279–3305, 2012.

Acknowledgement

Funded by the Deutsche Forschungsgemeinschaft (DFG, German Research Foundation) – Projektnummer 326998133 – TRR 225 (subproject A01).

JH wants to thank Vera Bednarzig, for her helpful remarks and supportive input to this project.

PS2-09-388

3D bioprinting of hepatocytes co-culture systems – towards biofabrication of liver models

Rania Abdelgaber[1], Georg Damm[2], Anja Lode[1], Michael Gelinsky[1], On behalf of Forschungsleitung Hepatobiliäre Chirurgie und viszerale Transplantation SIKT Leipzig

[1]TU Dresden, Center for translational bone, joint and soft tissue engineering, Dresden, DE; [2]UKE - Klinik für Viszerale Transplantationschirurgie, Forschungsleitung Hepatobiliäre Chirurgie und viszerale Transplantation SIKT Leipzig, Leipzig, DE

Introduction

3D bioprinting has emerged as a tool to develop biomimetic constructs that resemble the native microenvironment of tissues. Thus, the behavior and function of printed cells in a 3D environment could resemble more the *in vivo* environment of cells compared to *in vitro* 2D cultures. Aim of this study is to fabricate a liver model mimicking *in vivo* microenvironment by bioprinting constructs based on cell laden hydrogels and to further enhance and characterize their biological responses in terms of viability and liver specific functions. Core/shell 3D bioprinting has been utilized for the fabrication of tissue constructs with spatial compartmental distinction between core and shell phases with encapsulation of different cell types in various paste compositions in each phase [1]. In an attempt to design a more complex system for better understanding cellular interaction and enhancement of function, hepatocytes were co-cultured with supporting fibroblasts in a core/shell fashion. Fibroblasts in this case where encapsulated in different hydrogel compositions to test the influence on hepatocytes morphology and function [2].

Experimental Methods

For the fabrication of core/shell scaffolds, BioScaffolder 3.1 (GeSiM mbH, Radeberg, Germany) was used.

Either human HepG2 liver carcinoma cells or primary human hepatocytes PHH isolated from liver surgeries were encapsulated and processed in 3% HP-LVM alginate/9% methyl cellulose/20% Matrigel (alg-MC-matrigel) hydrogels to constitute the shell compartment.

To characterize the influence of fibroblasts co-culture on the functionality of hepatocytes, NIH-3T3 fibroblasts were encapsulated in either Fibrin supplemented alg/MC paste or Plasma based hydrogel to constitute the core compartment. Hepatoctes and fibroblasts were pre-labeled with DiD, DiI cell labeling solutions respectively before encapsulation in respective hydrogel pastes.

Scaffolds printed with those two conditions were compared against scaffolds with empty core containing pure hydrogel with no cells to act as control. After plotting, scaffolds were stabilized via Ca2+-mediated crosslinking and were incubated in Dulbecco's Modified Eagle's Medium (DMEM) supplemented with FCS, penicillin and streptomycin for up to 3 weeks.

Viability and behavior of both cell types as well as functionality of the hepatocyte were assessed over the culture period.

Results and Discussion

Over a period of 3 weeks, cells showed enhanced survival rates over different time points with hepatocytes started growing in visible aggregates/spheroids which increased in size and number over time. On the other hand, fibroblasts in the core compartment started growing to form networks with each other and with hepatocytes along the strands utilizing the fibrin/plasma to form their own ECM.

Furthermore, fibroblasts embedded in core had noticeable effects on the growth and cluster formation of hepatocytes in shell compartment which were enhanced at earlier time points compared to the ones with no fibroblasts in core (control scaffolds). The aggregates of hepatocytes formed differed in size and number between each condition. This was confirmed by antibody staining for specific hepatocytes markers.

Conclusion

3D bioprinting is a promising approach to fabricate liver models which mimic the functional characteristics better than 2D *in vitro* cell cultures. Co-culturing hepatocytes with non-parenchymal cells such as fibroblasts showed different behavior of cells with changing material composition of hydrogel encapsulating fibroblasts.

References

[1] Akkineni, A.R., Ahlfeld, T., Lode, A. and Gelinsky, M., 2016. A versatile method for combining different biopolymers in a core/shell fashion by 3D plotting to achieve mechanically robust constructs. Biofabrication, 8(4), p.045001.

[2] Cho, C.H., Park, J., Tilles, A.W., Berthiaume, F., Toner, M. and Yarmush, M.L., 2010. Layered patterning of hepatocytes in co-culture systems using microfabricated stencils. Biotechniques, 48(1), p.47.

Acknowledgement

The authors would like to thank the European Social Fund (ESF) and the Free State of Saxony for financial support of this project in the course of the ESF Young Researchers Group *IndivImp* at TU Dresden.

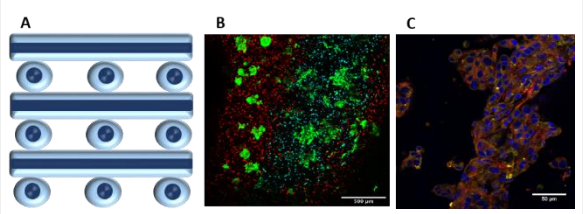

Core/shell constructs laden with hepatocytes (shell) and fibroblasts (core)
Schematic of a section showing a printed construct with two cell types encapsulated in core and shell, respectively (A). Confocal microscopy image of cell-laden core/shell strand pre-labeled hepatocytes in shell (red) with viable cells forming clusters on day7 (green), pre-labeled fibroblasts in core (cyan) with viable cells forming networks (green) (B). Hepatocytes clusters stained for CK-19 (yellow) with nuclei (DAPI stain in blue) and actin (red) on day7 (C).

PS2-09-389

A novel patient-individual bioink based on human plasma promotes the response of cells in bioprinted, mineralized constructs

Nieves Cubo-Mateo, Tilman Ahlfeld, Silvia Cometta, Vera Guduric, Anne Bernhardt, Ashwini R. Akkineni, Anja Lode, Michael Gelinsky

Technische Universität Dresden, Faculty of Medicine Carl Gustav Carus, Centre for Translational Bone, Joint and Soft Tissue Research, Dresden, DE

Introduction

Tissue engineering aims to deliver patient-individual solutions for the treatment of complex tissue defects by the combination of patient-derived cells with biomaterials and cell-stimulating factors. 3D bioprinting extended this approach by fabrication of implants tailored especially for the patient's tissue defects. Recently, low-viscous bioinks based on human blood plasma and platelet-rich plasma were developed for bioprinting processes (1,2), providing also a patient-specific material with its unique composition of proteins and cytokines. Herein, we aimed to develop a more viscous bioink, based on human plasma, suitable for extrusion-based bioprinting of bone constructs. To enhance bone compatibility, the cell-laden bioink was printed together with a self-setting calcium phosphate cement (CPC) (3), which forms a stiff matrix that consists of resorbable hydroxyapatite (HAp), resembling the mineral phase of native bone.

Experimental Methods

Fresh frozen human plasma (provided by the DRK-Blutspendedienst Nord-Ost, Germany) 3% alginate and 9% methylcellulose (both from Sigma-Aldrich) were blended, obtaining the final bioink (plasma-alg-mc). CPC was obtained from INNOTERE GmbH (Germany). For cell printing, immortalized human mesenchymal stem cells (hMSC), primary human pre-osteoblasts (hOB) and human umbilical vein endothelial cells (HUVEC) were mixed with the bioink. To study the effect of plasma, a PBS-alg-mc bioink served as control. Monophasic bioink and biphasic CPC/bioink constructs were printed using a multichannel extrusion printer (Bioscaffolder 3.1, GeSiM mbH, Germany). After printing, scaffolds were set in humidity for 20 min, crosslinked in 100 mM $CaCl_2$ solution for 10 min and finally incubated in cell culture medium for subsequent cultivation (3).

Results and Discussion

Plasma, plasma-alg and plasma-alg-mc showed a strong shear thinning behavior at increasing shear rates. The addition of alginate and particularly methylcellulose, enhanced the viscosity of the bioink significantly. Moreover, alginate allowed fast Ca^{2+}-mediated gelation of the ink after extrusion. Shape fidelity of monophasic plasma-alg-mc constructs was tested by the filament-fusion test. Plasma-alg-mc scaffolds were successfully printed with three different needle diameters (250, 410 and 610 µm). The optimal aspect ratio of 1 was reached at a strand distance of 1.8 mm, 2.2 mm and 3.0 mm for the 250, 410 and 610 µm needle, respectively. Biphasic constructs consisting of CPC and plasma-alg-mc could be printed with high layer numbers (>50). Cell culture stability of the plasma-alg-mc was evaluated by volumetric strand swelling. Over 35 d, macropores stayed open in both, monophasic and biphasic constructs. However, in the presence of CPC, the bioink did swell to a greater extent compared to monophasic scaffolds.

Post-printing cell viability of hMSC within monophasic and biphasic scaffolds was assessed at day 1 after printing. Cell viability in monophasic PBS-alg-mc scaffolds was 49%; the viability in biphasic CPC/PBS-alg-mc scaffolds was significantly ($p<0.05$) lower at the CPC-bioink interface, most probably due to local acidification during the transformation of α-tricalcium phosphate to HAp. In plasma-alg-mc, the cell viability in monophasic scaffolds was significantly higher (77 %, $p<0.001$) and no remarkable change in biphasic constructs at the CPC-bioink interface was observed. A possible explanation for the increased cell viability in plasma-containing biphasic scaffolds would be that plasma-alg-mc holds a sufficient buffer capacity caused by native bicarbonate and protein-based buffers, preventing local acidification. Subsequent cell culture revealed that hMSC started to migrate from the bioink to CPC strands latest after 7 d. At the CPC surface, hMSC spread and proliferated to a great extent (approx. 20-fold after 28 d, measured by DNA content after lysis of the scaffolds). Bioprinted hOB were cultured under osteogenic stimulation in the biphasic constructs, and osteogenic differentiation of the cells was confirmed by Alkaline phosphatase (ALP) activity measurements. Bioprinted HUVEC started to proliferate within plasma-alg-mc scaffolds and assembled into pre-angiogenic structures.

Conclusion

In this study, a plasma-based patient-individual bioink was developed with a focus on bioprinting of bone tissue. The blend of plasma and alg-mc led to a bioink with both, a favorable cell response and good printability. In combination with CPC, bone grafts can be fabricated with spatially defined osteogenic cells and prevascular structures.

References

1. Cubo et al., Biofabrication, 2017
2. Faramarzi et al., Adv Healthcare Mater, 2018
3. Ahlfeld et al., Biofabrication, 2018

Acknowledgement

The authors thank Ms. Anna-Maria Placht and Ms. Ortrud Zieschang for excellent assistance, Dr. Corina Vater and Dr. Oliver Tiebel for analysis of the plasma and Tommaso Guidini, Head of Structures, Mechanisms and Materials Division at the ESTEC of European Space Agency (ESA), for his encouragement and personal interest in the project.

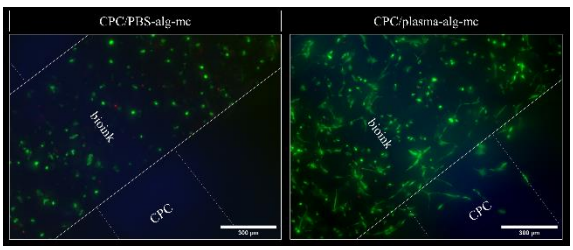

Bioprinted primary pre-osteoblasts in mineralized scaffolds
Pre-osteoblasts (hOB) were suspended in PBS-alg-mc or plasma-alg-mc and bioprinted in combination with a plottable CPC. After 7 days of culture, hOB revealed a roundish shape within the PBS-alg-mc bioink. In the novel plasma-based bioink, hOB showed a spread morphology, furthermore the cells could migrate to the mineral CPC phase. In subsequent culture, hOB proliferated alongside the CPC strands.

PS2-09-390

3D Printed Microgel-GelMA Hydrogel Systems

Guangyue Zu, Olga Mergel, Marnix Meijer, Patrick van Rijn

University of Groningen, Department of Biomedical Engineering / W.J. Kolff Institute, Groningen, NL

Introduction

3D bioprinting techniques are used to organize cells and materials into 3D structures, has driven major innovations in cell biology, tissue engineering, and regenerative medicine applications.[1] It allows tailored morphologies and properties for organ-specific extracellular matrix (ECM) mimics. One of the most appealing biomaterials that are being used in 3D printing is gelatin methacryloyl (GelMA). Gelatin contains both integrin cell-binding and protease-cleavage sites that promote cell attachment and proteolytic degradation. The chemically active substituents of GelMA introduced by chemical modification ensure that the hydrogel has reproducible and tunable properties.[2] However, the highly hydrated and hydrophilic microstructure of GelMA hydrogels results in relatively rapid release of entrapped biomolecules (nutrients, drugs and growth factors). Microgels are 3D-crosslinked, aqueous, environment-responsive, polymeric particles which exhibit tunable size, excellent biocompatibility, the porous network for encapsulation.[3] In this work, a multi-hierarchical pore sized hydrogel system is obtained by covalently binding microgels to GelMA network. The obtained microgel-GelMA system has the ability of 3D cell culture as well as the retention of small biomolecules and the possibility of controlled release.

Experimental Methods

The GelMA was synthesized by using gelatin reacted with methacrylic anhydride (MA). The fluorescently labeled poly(N-isopropylacrylamide) (pNIPAM) amine-microgel was synthesized via precipitation polymerization using N-(3-aminopropyl)methacrylamide hydrochloride (APMA) as a comonomer, afterward, the amine-microgel was functionalized with MA. To fabricate the 3D microgel-GelMA system, the mixed solution of GelMA (10%, 7.5%, 5%), microgels (0.5%) and LAP (0.5%, photoinitiator) were 3D printed using UV radiation for covalent crosslinking. GelMA without microgels was printed as a control. The physicochemical properties of the microgels and GelMA were characterized by nuclear magnetic resonance (NMR) spectra and titration. The temperature dependent swelling/deswelling behavior and pH-dependent zeta potential were determined by dynamic light scattering (DLS). Confocal microscopy was performed to analyze the distribution of microgels inside the GelMA matrix.

Results and Discussion

A methylacrylation degree of ~64% for GelMA (relative to lysine amino groups) was determined by NMR spectra. The titration results showed the amine group of amine-microgel is about 0,8 mmol/g, and reduce to 0,4 mmol/g after functionalization with MA, which indicates the successful incorporation of methacryloyl groups. The hydrodynamic diameters of amine-microgel and MA-microgel are similar as shown in Figure 1, both microgels are temperature responsive. As shown in Figure 2, the 3D printed GelMA and microgel-GelMA are visualized upon microscopic examination. The fluorescently labeled microgels are clearly visible and distributed within the GelMA matrix.

Conclusion

The incorporation of microgel in GelMA matrix enhanced the printability of GelMA hydrogel. The fabricated microgel-GelMA system is a promising platform for 3D cell-laden printing with tuneable and controllable properties.

References

[1] Highley C. B. et al., Adv. Sci. 6:1801076, 2019.

[2] Loessner D. et al., Nature Protocols 11:727, 2016.

[3] Agrawal G. et al., Small 14: 1801724, 2018.

Figure 2. Confocal images of 3D printed GelMA (10%) and microgel-GelMA (10% GelMA, 0.5% microgel).

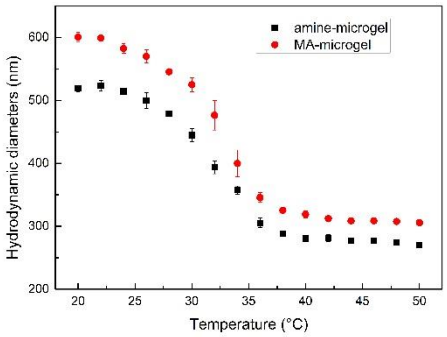

Figure 1. Temperature dependency hydrodynamic diameter of amine-microgel and MA-microgel.

PS2-09-391

Bioprinting with photosynthetically active microalgae: a concept for oxygen supply of mammalian cells in regenerative therapies

Sophie Dani[1], Felix Krujatz[2], Sarah Duin[1], Ashwini R. Akkineni[1], Juliane Steingroewer[2], Thomas Walther[2], Michael Gelinsky[1], Anja Lode[1]

[1]TU Dresden, University Hospital and Faculty of Medicine Carl Gustav Carus, Centre for Translational Bone, Joint and Soft Tissue Research, Dresden, DE; [2]TU Dresden, Institute of Natural Materials Technology, Dresden, DE

Introduction

One of the major limitations of therapies based on tissue engineering is the lack of vascularization and hence a shortage of oxygen supply after implantation that leads to fast cell death. To solve this problem, most approaches aim to accelerate vascularization, e. g. by integration of angiogenic factors or prevascularization of tissue engineering constructs *in vitro*. However, there are also therapeutic concepts which consciously avoid the contact with blood components in order to protect allogenic or xenogenic cell transplants against components of the immune system – one example is the transplantation of alginate-encapsulated pancreatic islets into patients suffering from diabetes type I. Photosynthetic microalgae produce oxygen under illumination and first short-term studies have demonstrated that mammalian cells survive in hypoxic environment when co-cultivated with photosynthetically active microalgae.[1,2] Herein, we propose the application of bioprinting to establish flexible co-culture systems of mammalian cells and microalgae in a spatially defined arrangement which allow an efficient transfer of oxygen from the autotrophic to the heterotrophic cell types. The influence of culture conditions (medium and illumination) on survival and function of both cell types was investigated.

Experimental Methods

A bioink consisting of alginate and methylcellulose (alg/MC)[3,4] was laden with cells of the rat beta-cell line Ins1 (used as model for pancreatic islets) or with cells of the green microalgae *Chlorella sorokiniana*; multichannel extrusion-based bioprinting (3D bioplotting) was conducted with the Bioscaffolder 3.1 (GeSiM mbH, Germany) to bring both cell types in close vicinity without direct contact. The plotted and Ca^{2+}-crosslinked constructs were cultivated in a coculture medium consisting of a mixture of TP medium (TRIS-phosphate = algae medium) and RPMI-based cell culture medium at 37°C and 5% CO_2. The influence of light (white vs. red light, 150 µmol photons m^{-2} s^{-1}) was studied on viability, growth and function of Ins1 and *C. sorokiniana.* To this end, Ins1 were analyzed by live/dead staining (Calcein AM/Ethidium homodimer-1), DNA quantification (QuantiFluor assay) and insulin secretion in response to glucose stimulation (quantification of insulin content in medium with ELISA) as described recently.[5] *C. sorokiniana* were evaluated by chlorophyll quantification and oxygen production as described in former studies.[4] Supply of Ins1 cells by photosynthetically produced oxygen was tested under hypoxic conditions (1% O_2).

Results and Discussion

In order to enable long-term cultivation of the plotted algae/Ins1 hybrid constructs, we have developed a co-culture medium which is suitable to support survival, growth and function of both cell types. Whereas white light had a negative effect on viability, proliferation, morphology and glucose response of Ins1, red light did not affect the mammalian cells and is sufficient to support growth and photosynthetic oxygen production of *C. sorokiniana*. Under the adapted culture conditions, the microalgae were able to produce oxygen which resulted in a significant increase

of the viability and function of Ins1 cells in a hypoxic atmosphere (1% O_2). Beside the spectral range of the light and the composition of the culture medium, also the ratio of Ins1 : *C. sorokiniana* has been found to have a strong impact on the efficiency of photosynthetic oxygen delivery of mammalian cells. Online monitoring of the spatiotemporal oxygen distribution within the hybrid constructs by using oxygen-nanosensors, added to the bioink,[6] revealed a fast diffusion of oxygen between the different compartments.

Conclusion

Combined bioprinting of photosynthetically active microalgae and mammalian cells can be used to create flexible co-culture systems, with both cell types in separate compartments but in close vicinity, enabling vascularization-independent oxygen delivery of mammalian cells. The effect of illumination on naturally non light-adapted mammalian cells has to be figured out in detail in further studies. The proposed concept could be extended to the supply of mammalian cells with other algal products.

References

[1]K. Bloch *et al.Tissue Eng.* 12, 337, 2006
[2]U. Hopfner *et al.Acta Biomater.* 10, 2712, 2014
[3]K. Schütz *et al. J. Tissue Eng. Regen. Med*. 11, 1574, 2017
[4]A. Lode *et al.Eng. Life Sci.* 15, 177, 2015
[5]S. Duin *et al.Adv. Healthcare Mater*. 1801631, 2019
[6]E. Trampe et al. *Adv. Funct. Mater*. 1804411, 2018

Acknowledgement

The authors thank the German Research Foundation (DFG) for funding of the project.

PS2-09-392

In Gel Printing of Vascular Wall-Resident Stem Cells

Ruben G. Scheuring[1], Leyla Dogan[2], Süleyman Ergün[2], Jürgen Groll[1]

[1]University Hospital Würzburg, Department of Functional Materials in Medicine and Dentistry, Würzburg, DE;
[2]University Würzburg, Institute of Anatomy and Cell Biology, Würzburg, DE

Introduction

Despite decades of intensive research, it has not yet been possible to create a functioning vascular system consisting of macro- and micro-vessels *in vitro*. One major shortcoming is the lack of a hierarchical wall structure that resembles the native morphology of macro-vessels. To achieve this, the recently discovered vascular wall-resident stem cells (VW-SCs) in the adventitia layer of blood vessels are an exciting opportunity. They exhibit the potential to differentiate into all cell types of the blood vessel (endothelial, smooth muscle and stromal cells) and can form perfusible blood vessels *in vitro* and *in vivo* [1]. Thus, VW-SCs represent a highly attractive alternative to commonly used mature vascular wall cells such as endothelial cells (ECs) and smooth muscle cells (SMCs) for the generation of mature vascular structures with the typical three-layer hierarchy. Beyond a suitable cell source, existing technical deficiencies have to be overcome for the generation of biomimetic macroscopic structures that include cells and extracellular matrix components. For this, in gel printing is promising, as it allows for the generation of truly three-dimensional structures within a physically cross-linked support bath.

Experimental Methods

Here, we present the first attempt of using this new source of vascular stem cells for the biofabrication of macro vascular structures with the long-term goal of recreating the typical hierarchical organization and wall morphology consisting of intima, media, and adventitia. We firstly processed VW-SCs using flow- and shear conditions that resemble the bioprinting procedure and cultured them with differentiation medium over up to 4 weeks afterwards. Furthermore, we printed VW-SCs into self-healing support gels/baths using either a core-shell nozzle or a single nozzle to fabricate perfusible tubular structures. Support baths allow the deposition of very soft biomaterials and the fabrication of delicate and complex structures, which would be difficult or even impossible using “dry” bioprinting strategies.

Results and Discussion

Cells survived the printing procedure and started to express typical markers of smooth muscle cells (SMMHC+) or endothelial cells (CD31+ CD34+). In parallel, we could successfully establish a bioprinting setup into self-healing support gels/baths in vessel-like tube structures.

Conclusion

Ongoing studies evaluate the behavior of these cells after printing in the structures and will be presented and discussed.

References

[1] S. Ergün, D. Tilki, D. Klein, Vascular Wall as a Reservoir for Different Types of Stem and Progenitor Cells, Antioxid. Redox Signal. (2010). doi:10.1089/ars.2010.3507.

Acknowledgement

This research was funded by the Deutsche Forschungsgemeinschaft (DFG, German Research Foundation) – Projektnummer 326998133 – TRR 225 (subproject B04).

PS2-09-393

Modification of Polymer Surfaces with Atmospheric Pressure Plasma Jet Treatment: Developing New Tools for Additive Biofabrication

Oliver Lotz[1,2], Seyaedah K. Alavi[1], Behnam Akhavan[1,2], David McKenzie[1,3], Marcela Bilek[1,2,4]

[1]School of Physics, The University of Sydney, Camperdown, AU; [2]School of Aerospace, Mechanical & Mechatronic Engineering, The University of Sydney, Camperdown, AU; [3]Sydney Nano Institute, The University of Sydney, Camperdown, AU; [4]Charles Perkins Centre, The University of Sydney, Camperdown, AU

Introduction

Personalised medicine is an inspiring goal with many facets, one of the most important being the development of better techniques of surface modifying materials to provide improved biocompatibility. Many non-native materials used elicit foreign body reactions as a result of hydrophobicity and protein denaturation. At the same time, additive manufacturing has begun to revolutionise biomedical fabrication, allowing simple construction of patient-specific implants using data from medical imaging. Thus, biofunctionalisation of additively manufactured structures is an encouraging approach for the development of more effective treatments, personalised medicine and handling the challenges of an aging population. Atmospheric pressure plasma jets (APPJs) are well suited to the task as they are small enough to be included within 3D printers, and can perform various surface treatments in a single-step reagent-free process [1, 2].

Experimental Methods

Plasma was generated with high voltage AC sinusoidal waves and helium. Multiple APPJ configurations were used, including one-electrode and two-electrode designs in which copper sheets were wrapped around glass tubes. Low-density polyethylene (LDPE) was chosen as a substrate material because of its widespread use. Samples were stored in closed petri dishes at 23^{o}C in ambient laboratory conditions after plasma treatment. A Kruss DSA10-Mk2 contact angle goniometer and a Digilab FTS7000 FTIR spectrometer were used to measure water contact angles and surface chemistry, respectively. Average values of at least three measurements were reported together with the standard error of the mean.

Results and Discussion

Plasma immersion ion implantation (PIII) is a relevant benchmark for biomaterials modification as *in vivo* studies have shown that it can provide effective surface modification [3]. The APPJ designs tested displayed comparable surface energy modifications to PIII treatment, with some tests even surpassing PIII. For example APPJ treated samples showed more stability over time and less hydrophobic recovery, allowing enhanced hydrophilicity for longer. Contact angles as low as 34.2 ± 2.0 degrees could be achieved on LDPE, where untreated samples were hydrophobic with a water contact angle of 98.3 ± 0.7 degrees.

Conclusion

Applications of APPJs as they would be used within additive biofabrication have been investigated with a set of experiments for treatment outcomes and aging. The function of additively manufactured medical implants within the body and a host of in vitro devices promise to be improved by the use of APPJs. The introduction of surface

modification processes such as these in bioprinting promise enhanced outcomes for medical research and healthcare applications.

References

1. Liu, F., Wang, W., Mirihanage, W., Hinduja, S., & Bartolo, P. J. (2018). A plasma-assisted bioextrusion system for tissue engineering. *CIRP Annals*, *67*(1), 229-232.

2. Tendero, C., Tixier, C., Tristant, P., Desmaison, J., & Leprince, P. (2006). Atmospheric pressure plasmas: A review. *Spectrochimica Acta Part B: Atomic Spectroscopy*, *61*(1), 2-30.

3. Bilek, M. M. (2014). Biofunctionalization of surfaces by energetic ion implantation: review of progress on applications in implantable biomedical devices and antibody microarrays. *Applied Surface Science*, *310*, 3-10.

4. Kondyurin, A., Naseri, P., Fisher, K., McKenzie, D. R., & Bilek, M. M. (2009). Mechanisms for surface energy changes observed in plasma immersion ion implanted polyethylene: the roles of free radicals and oxygen-containing groups. *Polymer Degradation and Stability*, *94*(4), 638-646.

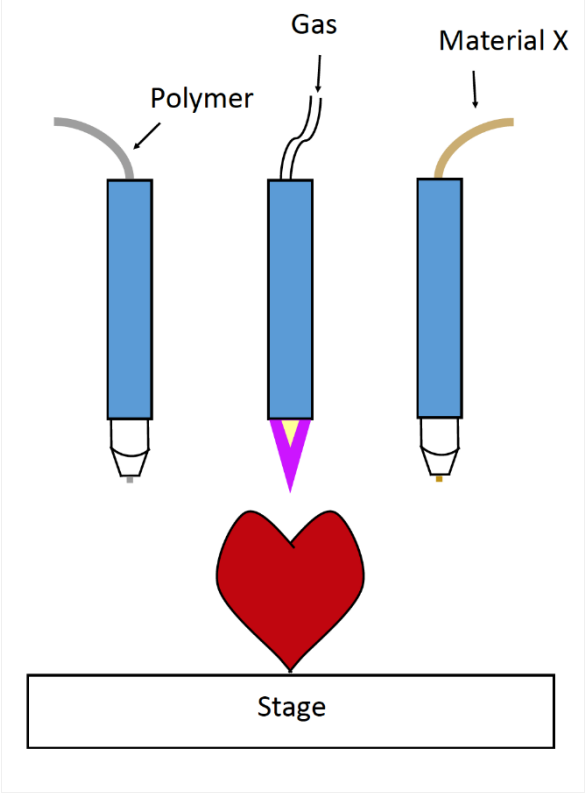

APPJs in 3D bioprinters
Figure 2: An illustration of how bioprinters could use multiple print-heads to construct medical devices with improved surface biocompatibility.

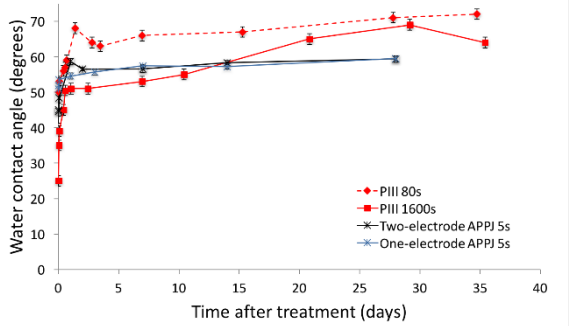

APPJ treatment displays comparable ageing profile to PIII treatment.
Figure 1: APPJ treated LDPE contact angles were comparable to those achieved by PIII as a function of time after treatment. Un-treated PE had a contact angle of 98.3 ± 0.7. APPJ values shown are averages of the values at the APPJ centre and at the edges of the treated region at a radius of 3mm. PIII values for comparison are taken from Fig. 2 in Kondyurin et al. [4].

PS2-09-394

The use of Umbilical Cord Blood Platelet-Rich Plasma to increase Cell Viability and Proliferation in Skin Graft Substirutes Obtained by 3B Bioprinting

Aida Cavallo[1], Carolina De Almeida[1], Paola Losi[1], Ilenia Foffa[1], Patrizia Urciuoli[2], Giovanna Lepri[2], Sabrina Gabbriellini[2], Marco Fabbri[2], Alessandro Mazzoni[2], Giorgio Soldani[1]

[1]National Research Council, Institute of Clinical Physiology, Massa, IT; [2]Azienda Ospedaliero-Universitaria Pisana (AOUP), Transfusion Medicine and Transplant Biology Unit, Pisa, IT

Introduction

Artificial skin grafting for wound and burn healing is one of the greatest motivations for engineering skin tissues *in vitro*, since it can act not only as a bandage to help restore normal barrier, but also regulate its functions[1]. The conventional approaches used for skin engineering have several drawbacks, such as limited ability to arrange cells and specific extra-cellular matrix (ECM). The 3D bioprinting technology enables the deposition of cell and biomaterials (Bioink) in a desired pattern and offers the potential for recreation of macroscale architectures and micro-features of natural skin [1-2].

Platelet-rich plasma (PRP) has been applied for the reparative and regenerative effect in many tissues due to its positively effects on cell viability, proliferation and migration [3]. Usually, PRP is obtained from peripheral blood (PB-PRP), but the results about its use are widely controversial due to the great variability in PRP preparation and administration. Therefore, Umbilical Cord Blood Platelet-Rich Plasma (UCB-PRP) may become a safe alternative source for platelet derivatives because it contain higher levels of specific Growth Factors respect to PB-PRP [4]. Therefore, the aim of the present study was to evaluate the effect of UCB-PRP addition to bioink for improving the fibroblasts viability and proliferation in skin graft substitutes fabricated by 3D bioprinting in order to induce a more rapid tissue maturing.

Experimental Methods

The skin substitute was drawn using a free CAD software with a diameter of 5.0 mm and height of 1.2 mm. The CELLINK Bioink based on alginate and nanofibrillar cellulose modified adding 3% UCB-PRP or PB-PRP was used for the bioprinting process. Both the bioinks formulation were mixed with mouse fibroblasts (L929) to obtain a final concentration of 10^6 cells/ml. A substitute without PRP was used as control. The substitutes were fabricated using the BIO X bioprinter (CELLINK, Sweden) with high-precision conical nozzle of 27G, an extrusion pressure of 15 KPa and a print-head speed of 15 mm/s. After bioprinting, they were cross-linked with a Calcium Chloride solution for 5 min and then incubated in cell culture medium using standard culture conditions.All constructs were cultivated in medium with or without 10% FBS to evaluate the ability of PRP to increase the cell viability/proliferation. LIVE/DEAD and XTT assay at 3 time-points: 0, 7 and 14 days were used to evaluate cell viability and proliferation. The matured skin substitutes were evaluated through histological analysis by H&E and Masson's trichrome staining.

Results and Discussion

The constructs printed with the CELLINK Bioink added with UCB-PRP and cultured in medium with 10% FBS was characterized by the formation of cell clusters with a larger diameter. The sample added with UCB-PRP showed higher value of absorbance related to an higher number of cells. These results demonstrated that UCB-PRP improves

fibroblasts viability and proliferation in 3D substitutes compared with substitutes bioprinted using bioink with PB-PRP and without PRP. The constructs printed with UCB-PRP or PB-PRP bioink and cultured in medium without 10% FBS showed the same trend of the constructs fabricated without PRP respectively. The histological analysis at 14 days showed an higher number of nuclei and a major collagen secretion in constructs printed using the bioink added with UCB-PRP and cultured using a medium with 10% FBS. A previous study demonstrated the effects of UCB-PRP in 2D culture[4], this is the first study to characterize 3D construct bioprinted with UCB-PRP-bioink mixed with fibroblasts and to show the positively effect of blood platelets derivatives, in particular of UCB-PRP, on fibroblast proliferation in 3D culture.

Conclusion

These preliminary results showed that the addition of UCB-PRP in the CELLINK Bioink increases cell viability/proliferation, resulting in a more rapid tissue maturing into the bioprinted construct.

References

[1] Yan WC et al. 3D bioprinting of skin tissue: From pre-processing to final product evaluation. Adv Drug Deliv Rev. 2018;132:270-295.

[2] Kim BS et al. 3D cell printing of in vitro stabilized skin model and in vivo pre-vascularized skin patch using tissue-specific extracellular matrix bioink: A step towards advanced skin tissue engineering. Biomaterials. 2018;168:38-53.

[3] Berndt Set al. Autologous Platelet-Rich Plasma (CuteCellTM PRP) Safely Boosts In Vitro Human Fibroblast Expansion. Tissue Eng Part A. 2019 Mar 21. doi: 10.1089/ten.TEA.2018.0335.

[4] Seyedeh-Sara Hashemi et al. The Role of Human Adult Peripheral and Umbilical Cord Blood Platelet-Rich Plasma on Proliferation and Migration of Human Skin Fibroblasts. World J Plast Surg. 2017; 6: 198–205.

Acknowledgement

This study was supported through Dr. Vassili Fotis private donation.

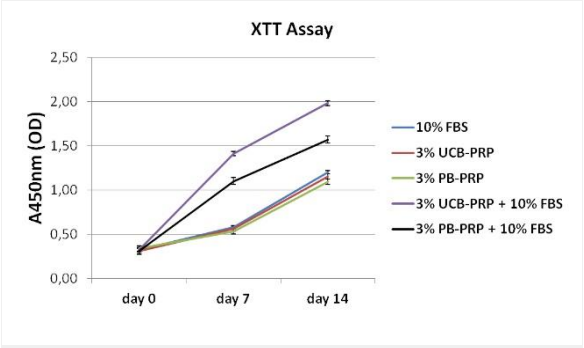

Fig. 2
Comparison of cell proliferation rate for different printing and culture condition.

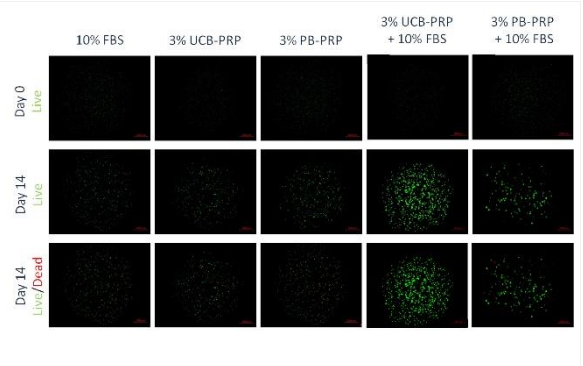

Fig. 1
LIVE/DEAD assay on 3D bioprinted constructs.

PS2-09-395

Microgel based bioinks

Johannes Herbig, Junwen Shan, Tomasz Jüngst, Krystyna Albrecht, Jürgen Groll

University of Würzburg, Department and Chair of Functional Materials in Medicine and Dentistry, Würzburg, DE

Introduction

Biofabrication is a young and rapidly evolving research field. Due to the use of 3D bioprinting, hierarchical structures including different cell types and materials can be created with potential applications in tissue models and regenerative medicine.

One of the current bottlenecks in this field is the lack of suitable bioinks. With state of the art bioinks, a trade-off between cytocompatibility and processability is necessary.[1] Recently, a new approach that enables addressing those two effects on different levels was presented.[2] It is based on bioinks composed of microgels. With this method, cytocompatibility can be controlled on a molecular level in terms of composition and concentration. Processability is governed on a more macroscopic level by interparticle interactions.

As an example, we present a bioink consisting of microgels whose precursor solution itself is not printable due to its rheological properties.

Experimental Methods

AGE functionalized gelatin (Gel-AGE) was synthesized according to a previously published protocol.[3] For crosslinking, thiol-ene click chemistry was used initiated by $Ru(BPY)_3$ in combination with sodium persulfate (SPS) and visible light exposure.

Precursor solutions were prepared by dissolving Gel-AGE and dithiotreitol (DTT) in PBS and mixing with the afore-mentioned initiator system. Droplets were produced via an emulsion technique. By crosslinking the precursor solutions in droplet form, microgels were produced. In order to obtain a printable ink, microgels were jammed using a vacuum filtration method. Printing was carried out with a bioprinter. For post-printing crosslinking, further initiator solution was added followed by visible light exposure.

Results and Discussion

The microgels produced via the emulsion technique showed a rather broad size distribution, with sizes below 200 µm (Figure 1 A). Extrusion through a 200 µm nozzle was possible without clogging (Figure 1B). Compared to previous publications we could show that printable microgel inks can be produced by a simple emulsion method proving that mono-dispersity is not mandatory for this application.[2, 4]

Printing with high shape fidelity was performed and even overhanging structures could be formed. Post-printing crosslinking ensures long term stability in media or buffer. Therefore, we could combine the advantages of previous publications in terms of cytocompatibility[2] and the possibility of post-printing crosslinking[4].

As an example, NIH-3T3 cells were incorporated by two different approaches. On the one hand, cells were added to the printable microgel ink and printed as cell-microgel-composite. On the other hand, cells were added to the polymer solution before microgel synthesis. In this way, the cells were encapsulated in the microgels and printed afterwards as described above.

Conclusion

Here, we present a method to form a bioink from a low viscous polymer solution. First, microgels are formed using an emulsion method. After jamming the microgels can be printed with high shape fidelity. This possibility widens the biofabrication window for new materials and can help developing biofabricated structures that meet the stringent criteria of biological activity and shape fidelity.

References

1. J. Malda, J. Visser, F. P. Melchels, T. Jüngst, W. E. Hennink, W. J. Dhert, J. Groll and D. W. Hutmacher, *Adv Mater*, 2013, **25**, 5011-5028.
2. C. B. Highley, K. H. Song, A. C. Daly and J. A. Burdick, *Advanced Science*, 2018, 1801076.
3. S. Bertlein, G. Brown, K. S. Lim, T. Jungst, T. Boeck, T. Blunk, J. Tessmar, G. J. Hooper, T. B. Woodfield and J. Groll, *Adv Mater*, 2017, **29**, 1703404.
4. S. Xin, D. Chimene, J. E. Garza, A. K. Gaharwar and D. L. Alge, *Biomater Sci-Uk*, 2019, **7**, 1179-1187.

Acknowledgement

Funded by the Deutsche Forschungsgemeinschaft (DFG, German Research Foundation) – Projektnummer 326998133 – TRR 225 (subprojects A06 and B07).

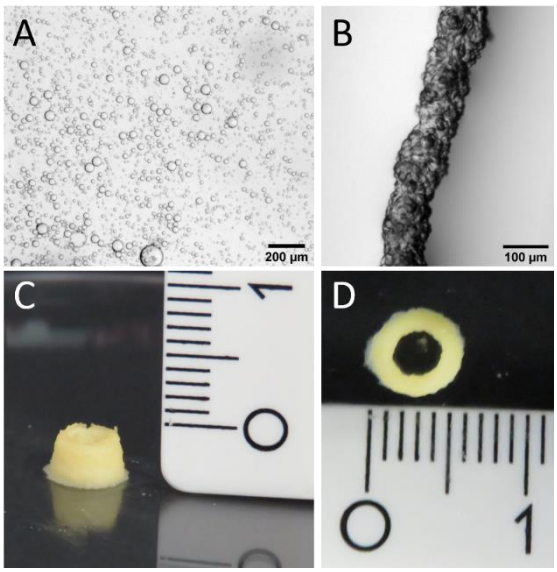

Ink composed of microgels

Figure 1: Microgels after visible light initiated crosslinking (A), extruded microgel strand (B), printed tube-like structure (C, D).

PS2-09-396

Revealing critical model parameters for predicting the bioprintability of hydrogel systems

Stefan Schrüfer[1,2], Dirk W. Schubert[1,2]

[1]FAU, LSP, Erlangen, DE; [2]FAU, BPI, Fürth, DE

Introduction

Bioprinting has become an important approach for creating customized tissue replacements, used either for healing or replacing damaged human tissue and cartilage [1, 2]. One of the crucial factors in 3D biofabrication is cell proliferation, which is highly influenced by the shear stresses occurring during the printing process [3]. Not only the cell proliferation but also the printability of hydrogels, which is defined by shape fidelity and printing resolution, is dependent on the rheological properties of the used bio ink.

Experimental Methods

In order to characterize their behavior, shear rheological measurements are the method of choice. Nevertheless, an adequate characterization of hydrogels can be challenging yet insufficient in order to not only describe, but predict printability. Therefore, this work does not only aim to give advice in order to generate artifact free measurement data, but also reveals a simple approach, that can be used to evaluate a wide range of rheological model systems.
These model systems, consisting of simple springs and dashpots, are applicable for the description of complex, viscoelastic material properties that can be observed for polymer solutions. A direct correlation of the calculated model parameters to 3D printing processes leads to possible critical threshold values that can be used for the prediction of printability for different hydrogel systems.

Results and Discussion

A power-law like behavior of the model parameters in dependency on alginate solution concentration can be observed. The burgers model, which consists of a Maxwell and a Kelvin-Voigt model in serial, is revealed as suitable model system for describing the viscoelastic properties of alginate solutions. A critical dashpot viscosity for sufficient shape fidelity also emerged. Further research on a variety of hydrogel systems will reveal if those parameters are of global importance or just alginate specific.

Conclusion

A simple, yet powerful tool for further evaluation of rheological data is presented. The revealing of critical parameters for printability and gel properties, such as gel stiffness, is presented subsequently. A correlation of the evaluated rheological measurements to other measurement techniques such as DMA and nanointendation will further improve the understanding of relevant model parameters.

References

[1] B. Duan, State-of-the-Art Review of 3D Bioprinting for Cardiovascular Tissue Engineering, Annals of biomedical engineering 45 (1), 2017, 195–209.

[2] J.M. Lee et al., Design and Printing Strategies in 3D Bioprinting of Cell-Hydrogels: A Review, Advanced healthcare materials 5 (22), 2016, 2856–2865.

[3] A. Blaeser et al. Controlling Shear Stress in 3D Bioprinting is a Key Factor to Balance Printing Resolution and Stem Cell Integrity, Advanced healthcare materials 5 (3), 2016, 326–333.

Acknowledgement

Funded by the Deutsche Forschungsgemeinschaft (DFG, German Research Foundation) – Projektnummer 326998133 – TRR 225 (subproject A07).

PS2-09-397

Development of a composite support bath for in-gel printing of hollow structures

Seyedeh Ferdows Afghah[1,2], Mine Altunbek[2], Bahattin Koc[1,2]

[1]Sabanci University, Istanbul, TR; [2]Sabancı University Nanotechnology Research and Application Center (SUNUM), Istanbul, TR; [3]University Integrated Manufacturing Technologies Research and Application Center, Istanbul, TR

Introduction

In-gel printing is a prevailing and fast-growing additive manufacturing technique that enables the fabrication of complex shear thinning hydrogels in a sacrificial support bath [1]. The support bath assists the extruded hydrogel to holds its shape instantly after extrusion, resulting in a continuous printing in contrast to the common delays for gelation in traditional approaches [2]. This study aims to investigate the in-gel printing of alginate hydrogel in a composite support bath of poly(ethylene oxide)-poly(propylene oxide)-poly(ethylene oxide) (Pluronic F127) including Laponite nanoclays as a rheology modifier and calcium chloride as the ionic cross-linker. It is speculated that the investigated support bath can be further used for printing of hollow vascular structures.

Experimental Methods

Support bath was prepared at different concentrations of Laponite (Lap RDS, BYK) and Pluronic (PF127, Sigma). Nanoclays were dispersed in deionized (DI) water. PF127 and calcium chloride ($CaCl_2$, Sigma) were dissolved in DI water and stirred at 4 ºC. Afterward, bath components were mixed to yield the final compositions of 2% $CaCl_2$, 2 and 3% of Lap, and 7.5, 10 and 12.5% of PF127. Alginate from brown algae was dissolved in DI water at the concentration of 3% and utilized as printing ink.

Rheological characterization of the support bath was performed using Anton Paar MCR 302 using a parallel plate geometry. The effect of different concentrations of Lap and PF127 were investigated thoroughly to find suitable formulations for three-dimensional (3D) printing. Amplitude sweeps were performed from 0.01% to 100% strain with a constant angular frequency of 10 rad/s to find the linear viscoelastic region for further measurements. Temperature sweeps were performed from 4 ºC to 37 ºC by the rate of 5 ºC/min at the constant strain and angular frequency of 0.6% and 10 rad/s, respectively. Shear thinning behavior of the samples were investigated in the range of 0.01 s^{-1} to 100 s^{-1}. Recovery kinetics were examined at cyclic oscillations of high and low strains of 50% and 0.6%, respectively. The storage and loss moduli responses were measured through an oscillatory frequency sweep. All the measurements were carried out at a constant temperature of 37 ºC except the temperature sweeps. Due to the thixotropic property of Laponite, all the measurements were conducted at the same timing condition.

The extrusion of 3% alginate in different compositions of support baths was performed using a custom-built 3D printer connected to an air dispensing system and controlled with MACH3 software. Shape fidelity of the 3D printed samples and the viscoelastic behavior of the support baths were monitored. Following the printing, support baths were removed by washing with 1% sodium chloride.

Results and Discussion

The relationship between the ratios of components of the formulations was studied by rheological characterizations (Fig 1). Sequential deformation-rest periods were used to determine the degree of recoverability of the elastic properties of the formulation. All the formulation showed excellent recovery of elastic moduli which resulted in high durability of the bath formulations against repetitive deformation caused by the passage of the printing nozzle. The

mutual interactions between PF127 and Lap resulted in the formation of a strong network, which could easily flow upon exertion of high shear, while the applied deformation could be recovered in a very short time.
Different PF127 concentrations resulted in different viscoelastic properties of the formulations, in a way that the intermediate concentration of 10% PF127 resulted in the lowest elastic and viscous moduli. On the other hand, high PF127 concentrations resulted in a very rigid network, which did not yield homogeneously through shear deformation. The formulation with the lowest PF127 content showed promising flow behavior, while the recovery of the elastic properties during cyclic deformation was acceptable.
The concentration of 3% Lap and 7.5% PF127 was selected for printing and different structures with a hangover or hollow segments were printed (Fig. 2). The initial assessments of the shape fidelity and integrity of printed structures showed that the investigated formulations might have good potential for the fabrication of complex structures.

Conclusion

The incorporation of Lap to PF127 resulted in the formation of a strong network with excellent recovery behavior after deformation, helping the dispensed bioink to maintain its shape after extrusion. The initial assessments of the proposed support bath showed its potential in the fabrication of different structures with complex geometries which can be further employed in biofabrication of hollow structures.

References

[1] Y. Jin, A. Compaan, W. Chai, and Y. Huang, “Functional Nanoclay Suspension for Printing-Then-Solidification of Liquid Materials,” *ACS Appl. Mater. Interfaces*, vol. 9, no. 23, pp. 20057–20066, 2017.

[2] Y. Jin, W. Chai, and Y. Huang, “Printability study of hydrogel solution extrusion in nanoclay yield-stress bath during printing-then-gelation biofabrication,” *Mater. Sci. Eng. C*, 2017.

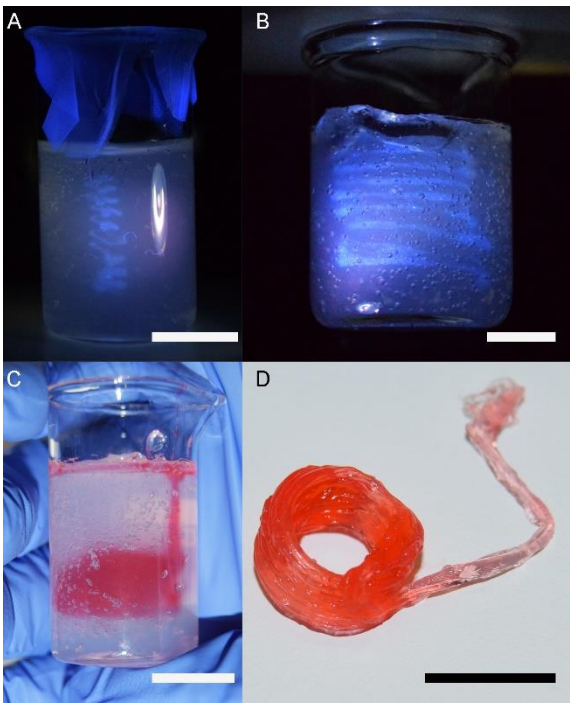

Fig.2 A) Coiled, B) Cylindrical, C) Truncated cone before and D) after washing with NaCl, Scale bars

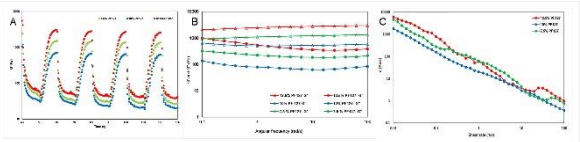

Fig.1A) Recovery kinetics of samples, B) Frequency sweep of the samples, C)Shear rate sweep of the s

PS2-09-398

3D bioplotting of neonatal porcine islets - towards complex co-culture systems

Sarah Duin[1], Susann Lehmann[2], Christiane Paßkönig[1], Elisabeth Kemter[4], Eckhard Wolf[4], Anja Lode[1], Michael Gelinsky[1], Barbara Ludwig[2,3]

[1]University Hospital Carl Gustav Carus and Faculty of Medicine of Technische Universität Dresden, Centre for Translational Bone, Joint and Soft Tissue Research, Dresden, DE; [2]University Hospital Carl Gustav Carus of Technische Universität Dresden, Paul Langerhans Institute Dresden of Helmholtz Centre Munich and German Centre for Diabetes Research, Dresden, Dresden, DE; [3]University Hospital Carl Gustav Carus, Technische Universität Dresden, Department of Medicine III, Dresden, DE; [4]Ludwig-Maximilians University Munich, Gene Center, Munich, DE

Introduction

Diabetes type 1 is characterized by insulin-deficiency due to autoimmune-derived destruction of the insulin-producing β-cells in the pancreas. The common therapy is treatment with exogenous insulin, however, for a subgroup of patients with highly unstable blood-glucose control transplantation of islets and reconstitution of endogenous insulin secretion would be far preferable. However, human donors for islet transplantation are sparse – donor shortage could be solved through use of xenogeneic islets. Especially with islets from a xenogeneic source separation from the host's immune system is crucial, yet supply with oxygen and nutrients as well as the ability to sense blood-glucose should not be impaired, which requires short diffusion distances.

To achieve this, a high surface-to-volume ratio of the immune-protective scaffolds, but also blood vessels in close vicinity, yet not in direct contact with the islets are indispensable.

3D plotting, an additive manufacturing technique capable of producing scaffolds of clinically relevant dimensions and incorporating biological agents, offers the possibility to embed islets in hydrogel strands[1] while attracting vascular structures to the macropores.

In this study, as a first step towards co-culture with cells with angiogenic potential, 3D plotting was used to embed neonatal porcine islet-like cell clusters (NICC) in macro-porous hydrogel scaffolds.

Experimental Methods

The hydrogel used for plotting was a paste of medical-grade alginate and methyl-cellulose (MC)[1,2] (Alg/MC) into which either NICC, human umbilical vein endothelial cells (HUVEC) or human bone marrow-derived mesenchymal stromal cells (MSC) had been incorporated prior to plotting. 3D plotting was carried out on a BioScaffolder 3.1 from GeSiM (Radeberg, Germany). All cells were cultured in a co-culture medium consisting of Ham's F-10 and endothelial cell growth medium supplemented with bovine serum albumin.

To investigate distribution and cell viability, scaffolds with islets, HUVEC or MSC were stained with MTT or calcein AM/ethidium homodimer, and cryosections of islet-containing scaffolds were stained with DAPI and TUNEL. Presence of insulin was studied via dithizone staining of whole scaffolds, and localization of insulin and glucagon inside the islets through immunofluorescence-staining of cryosections. For glucose stimulated insulin response of plotted islets, both islet-containing scaffolds and free control islets were incubated in Krebs-Ringer buffer supplemented with either 3.3 or 16.4 mM glucose and glucagon-like peptide 1 (GLP1). Insulin content was analysed by quantification of secreted insulin with ELISA and normalization to the DNA content determined by QuantiFluor assay.

Suitability of the Alg/MC blend for diffusion of glucose and insulin was tested with an osmosis chamber.

Results and Discussion

By comparison to free islet cultures, we were able to show that neither incorporation of islets into the material nor the plotting process itself had a deleterious effect on islet morphology. MTT-staining demonstrated an even distribution and metabolic activity of islets inside the plotted scaffolds, and Live/Dead as well as TUNEL stainings indicated survival of encapsulated islets for as long as 21 days. Live/Dead staining also showed that HUVEC and MSC survive embedding and plotting and all cells tolerate the co-culture medium well.

Dithizone and immuno-fluorescence-stainings confirmed that insulin and glucagon are continuously produced and adequately located in encapsulated islets. Our data also suggest adequate diffusion of glucose and insulin and that with supplementation of GLP1 plotted NICC can be stimulated to release insulin in response to high glucose. Furthermore, protection of islets from human serum was comparable between islets encapsulated in the hydrogel blend and islets encapsulated in plain alginate beads.

Conclusion

This study introduces 3D bioplotting of neonatal porcine islets as a promising strategy for the immune-protection and vascularization of 3D constructs containing xenogeneic islets.

References

1 Duin S. *et al.* Adv. Healthcare Mater., 2019, 1801631
2 Schütz K. *et al.* J. Tissue Eng. Regen. Med. 2017, 11, 1574-1587

Acknowledgement

The authors thank the microscopy facility CFCI of the TU Dresden for providing equipment and support in cell imaging, and the German Centre for Diabetes Research (DZD) as well as the Faculty of Medicine *Carl Gustav Carus* of Technische Universität Dresden for financial support.

2:45 p.m. – 3:45 p.m.

Hall 1 / Exhibition Area

PS2-10 | Novel AM technologies/MEW

PS2-10-399

Material inks for inkjet printed biomedical sensor applications

Marco Fritsch[1], Sindy Mosch[1], Nikolai Trofimenko[1], Viktar Sauchuk[1], Natalia Beshchasna[2], Mihails Kusnezoff[1], Mykola Vinnichenko[1]

[1]Fraunhofer IKTS Institute, Materials and Components, Dresden, DE; [2]Fraunhofer IKTS Institute, Bio- and Nanotechnology, Dresden, DE

Introduction

The rapid development of medical and biological sensors leads to numerous new applications in the field of point-of-care, lab-on-chip, organ-on-chip, environmental as well as wellness sensors. Thin and mechanically flexible substrate materials, like polymer foils or paper, offer an attractive combination of low cost and the ability of a smart integration in human relevant surroundings. Conventional microelectronic fabrication technologies, such as photolithography, have limitations in terms of sensor design flexibility and costs for producing smaller, customized sensor lots. In this context, digital and additive direct printing processes, like inkjet printing, are evaluated and developed in recent years. Such printing methods can be scaled to roll-to-roll (R2R) processes for a potential mass production of sensors. Up to now, the main problem for the direct printing of such sensors is the poor thermal stability of the low-cost polymer or paper foil substrates, which demands printable materials for sintering at low temperatures (e.g. < 200 °C). Fraunhofer IKTS has developed tailor-made functional nanoinks for the inkjet printing of metallic electrodes and sensory active layers on such thermal sensitive substrates [1]. Especially the gold and platinum inks are attractive to realize printed biomedical sensors, since they proved to be compatible with living cell cultures.

Experimental Methods

Silver, gold and platinum nanoparticles are derived from wet chemical precipitation process and transferred to material ink formulations (20 to 30 wt.-% solid content). By controlling the particle stabilization, certain restrictive parameters like sedimentation stability and ink viscosity were adjusted for inkjet print compatibility. The inks were characterized for particle size distribution, sedimentation stability, viscosity, surface tension and solid content. Inkjet printing tests were performed with and Dimatix DMP material printer (10 pL drop size) on PET and paper foil substrates. The printed films were dried at 80 °C and systematically sintered at 150 °C and 200 °C by varying the holding time in a box furnace. Alternatively to such a conventional slow box or continuous annealing furnace sintering an innovative line laser sintering tool (HPDL) was evaluated. The electrical film resistance was measured and the film microstructure characterized by SEM analysis of film cross sections.

Results and Discussion

Fig.1 shows the range of metal nanoparticles synthesized. The prepared nanoinks show a good sedimentation stability and a nice inkjet printing compatibility. The resulting electrical resistance of the printed and sintered films is excellent for the developed silver ink (2-times Ag-bulk, 8 µOhmcm) and good for gold ink (6-times Au-bulk, 33 µOhmcm) and platinum ink (11-times Pt-bulk, 390 µOhmcm). The film thickness is in the range of 1 µm and the prepared films possess a nice bendability of the printed structures (Fig.2). Alternatively to conventional box furnace sintering, the fast HPDL laser process is a powerful method to enable the sintering of printed films within milliseconds at a high processing speed, which is highly attractive for later application in R2R sensor production processes. In a comparison between box furnace and HPDL sintering treatment, the resulting film microstructure and the film electronic conductivity will be presented and discussed. Several examples of possible sensor application of the

developed material inks for printed temperature and pH sensors, micro hotplates for electrochemical sensors or precious metal electrodes for a subsequent biochemical sensor functionalization (gold and platinum) will be presented.

Conclusion

Fraunhofer IKTS developed functional nanoinks for the inkjet printing of metallic electrodes on thermal sensitive substrates like polymer or even paper foils. Especially the gold and platinum inks are highly attractive for biomedical sensors, where printed electrodes can be realized. Based on this electrodes different sensor types like temperature, pH, humidity and electrochemical sensor can be realized.

References

[1] https://www.ikts.fraunhofer.de/en/departments/energy_bio-medical_technology/materials_and_components/HT_ElectrochemistryCatalysis/material_inks.html

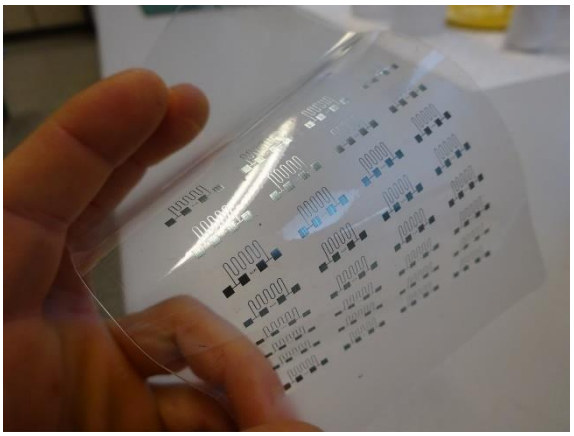

Fig.2
Printed temperature sensor on PET polymer foil.

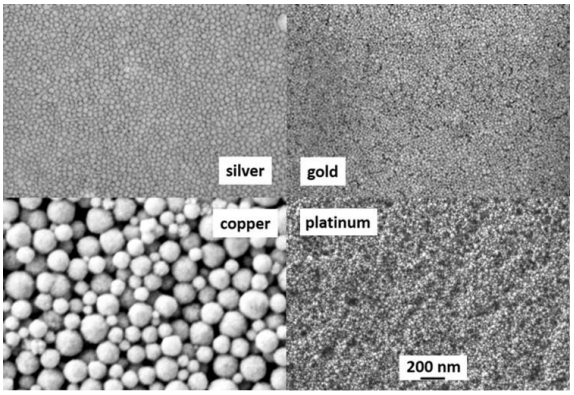

Fig.1
Nanoparticle inks for printing sensor elements.

PS2-10-400

New additive manufacturing method for drug delivery systems with multimodal drug release

Michael Teske[1], Natalia Rekowska[1], Daniela Arbeiter[1], Andreas Brietzke[1], Thomas Eickner[1], Robert Mau[2], Alexander Riess[2], Jan Konasch[2], Hermann Seitz[2], Niels Grabow[1]

[1]University Medical Center Rostock, Institute for Biomedical Engineering, Rostock, DE; [2]University of Rostock, Chair of Microfluidics, Rostock, DE

Introduction

Drug delivery systems (DDS) and drug loaded medical devices are currently indispensable in the field of medical research. Therefore, the use of additive manufacturing techniques has become very popular. Here we present a novel concept for the additive manufacturing (AM) of DDS with the ability of time-controlled drug release[1]. The new fabrication process successfully combines the stereolithography (SLA) and inkjet printing (IJP). Furthermore, the novel AM process enables the selective local immobilization of several high molecular weight drugs in a DDS by covalent binding using photo curable crosslinkers. Besides the position of the drug depot, the crosslinking between drug and DDS matrix polymer provides the opportunity to improve the control of drug release. Especially high molecular proteins as drugs are suitable in this application for covalent bonding because of lower risk of bioactivity loss [2, 3].

The drug depot is designed by using poly(ethylene glycol) diacrylate (PEGDA, M_w = 250 g/mol) as photo curable matrix polymer, a photo curable crosslinker (a di-, tri- or tetraacrylate) and a photoinitiator (PI, Irgacure 2959) as radical starter. The crosslinker have nearly the same molecular length but different numbers of acrylate groups. Additionally, analyses of their thermomechanical properties were performed and a post treatment for biocompatibility was established.

Experimental Methods

As crosslinkers 1,3-butanediol diacrylate (diacrylate), pentaerythritol triacrylate (triacrylate) and pentaerythritol tetraacrylate (tetraacrylate) with 1%, 5% and 10% (v/v) and each with 0.50%; 0.75%; 1.00% and 1.25% (w/v) PI were used. All samples were prepared according to Rekowska et al. [4] and polymerized at λ = 365 nm for 10 minutes.

Evaluation of biocompatibility after rinsing of samples at 50°C was performed via eluate test and direct contact test with L929 mouse fibroblasts for 48 hours. For viability analysis Cell Quanti-Blue test was performed according to manufacture instructions. Differential scanning calorimetry (DSC) measurements were performed under a nitrogen purge with a heating rate of 10 K/min and glass transition (T_g) was determined from the second heating curves. Tensile stress measurements were performed with a uniaxial testing system using a 500 N load cell and a crosshead speed of 25 mm/min. Rinsing process, biocompatibility test and thermomechanical analyses are described in detail in Rekowska et al. [4].

Furthermore, in preliminary tests Bovine Serum Albumin-Fluorescein isothiocyanate (BSA-FITC) was incorporated as high molecular model drug and the drug release was analyzed according to different photocurable crosslinkers. 5 µg of BSA-FITC were incorporated in selected samples and drug release occurred in TES buffer. BSA-FITC were analysed via Fluorescence measurement (excitation λ = 490 nm emission λ = 514 nm) after enzymatic digestion with pronase E according to Breen et al. [5].

Results and Discussion

The addition of the di-, tri- and tetraacrylates to PEGDA results in changes of T_g (Fig.1). In this case it seems that the concentration of the crosslinker influences T_g. Mostly we observed an increase of the T_g in contrast to the pure matrix polymer PEGDA. However, the kind of crosslinker, PI concentration and rinsing procedure does not seem to influence T_g under the considered conditions. Biocompatibility was given according to DIN EN ISO 10993-5:2009-10 for all considered samples after rinsing process. The tensile stress of the samples mostly increased with PI concentration (Fig. 2) and only minor differences were observed by using different crosslinkers. The *in vitro* drug release of the model drug, BSA-FITC, was examined over 57 days with around 15% drug release of total incorporated amount for all investigated DDS. Furthermore, we observed a release of over 90 percent of the total released BSA-FITC not until 18 days. Therefore, it seems that an initial burst release with a high loss of the water soluble BSA-FITC was retarded for all samples.

Conclusion

The promising results enable the creation of a new retarding DDS for high molecular drugs such as proteins via the novel AM technique. Further thermomechanical and biocompatibility tests will be performed to determine the full potential and suitability of PEGDA and its copolymers as DDS, especially with drugs incorporated.

References

[1] Konasch, Riess, Teske et al. in *Current Directions in Biomedical Engineering*, vol. 4, no. 1, pp. 141–144, 2018.
[2] Fernandes-Cunha, Lee, Kumar et al. in *Biomacromolecules*, vol. 18, pp. 3185−319, 2017
[3] Teske, Sternberg in *BioNanoMaterials*, vol. 18, no. 1-2, pp. 1-13, 2017
[4] Rekowska, Arbeiter, Konasch et al. in *Current Directions in Biomedical Engineering*, vol. 4, no. 1, pp. 1-3, 2018
[5] Breen, Raverdeau and Voorheis in *Scientific Reports*, 6:25769, 2016

Acknowledgement

Financial support by German Research Foundation (DFG) within the project "3D printed drug delivery systems with the ability of the time controlled drug release" is gratefully acknowledged.

Concentration Crosslinker	Concentration Photoinitiator			
	0.50%	*0.75%*	*1.00%*	*1.25%*
$PEGDA_{250}$ (reference)	29.6 ± 0.6	34.5 ± 3.1	32.6 ± 2.4	32.8 ± 4.5
Diacrylate				
1%	18.0 ± 2.4	24.2 ± 1.9	30.8 ± 0.6	33.9 ± 4.3
5%	11.7 ± 3.6	21.4 ± 3.5	26.5 ± 7.8	26.8 ± 4.6
10%	13.9 ± 1.7	26.5 ± 1.2	17.1 ± 8.5	14.9 ± 10.2
Triacrylate				
1%	18.1 ± 4.2	25.3 ± 6.2	35.2 ± 2.9	32.8 ± 2.6
5%	21.8 ± 8.1	26.2 ± 7.6	33.4 ± 2.1	33.4 ± 3.5
10%	21.5 ± 5.7	27.3 ± 6.3	30.0 ± 4.8	33.0 ± 2.6
Tetraacrylate				
1%	20.8 ± 4.0	23.2 ± 3.8	21.1 ± 2.2	28.7 ± 6.7
5%	21.4 ± 6.7	25.3 ± 5.3	21.4 ± 4.6	25.8 ± 7.7
10%	19.8 ± 3.7	23.5 ± 6.6	23.5 ± 6.9	28.3 ± 3.2

Tensile stress screening

Fig. 2: Results of tensile stress measurements in MPa for $PEGDA_{250}$ samples with different concentrations of the photoinitiator Irgacure 2959 and the crosslinkers 1,3-butanediol diacrylate (diacrylate), pentaerythritol triacrylate (triacrylate) and pentaerythritol tetraacrylate (tetraacrylate) after UV polymerisation and not rinsed (n=3).

Concentration Crosslinker	Concentration Photoinitiator			
	0.50%	*0.75%*	*1.00%*	*1.25%*
$PEGDA_{250}$ (reference)	27.4	27.5	26.6	26.3
Diacrylate				
1%	31.1	29.9	27.6	32.4
5%	34.3	33.7	39.1	37.4
10%	37.2	43.1	45.2	51.0
Triacrylate				
1%	32.0	28.8	27.4	30.6
5%	38.5	30.4	34.7	39.5
10%	40.2	42.5	40.6	44.8
Tetraacrylate				
1%	28.4	29.2	24.7	27.1
5%	37.5	36.7	37.8	33.5
10%	53.2	47.3	46.1	49.0

Glass transition temperature screening

Fig. 1: Glass transition temperature (T_g) in °C for $PEGDA_{250}$ samples with different concentrations of the photoinitiator Irgacure 2959 and the crosslinkers 1,3-butanediol diacrylate (diacrylate), pentaerythritol triacrylate (triacrylate) and pentaerythritol tetraacrylate (tetraacrylate) after UV polymerisation and not rinsed (n=1).

PS2-10-401

Thiol-En chemistry as a versatile tool for the additive production of elastomeric high refractive optics?

Andreas Hoffmann[1], Klaus Kreuels[2], Martin Wehner[1], Arnold Gillner[1,2]

[1]Fraunhofer-Institut für Lasertechnik ILT, Biofabrication, Aachen, DE; [2]RWTH Aachen, Chair for Lasertechnology, Aachen, DE

Introduction

Stereolithography (SL) is the oldest known additive manufacturing (AM) technology and offers promising properties for the use in personalized medicine, for example, for the production of otoplastics, dentistry, prosthetics and even in tissue engineering. After demonstrating the use of thiol-ene click (TEC) chemistry in SL for the formation of highly crosslinked polymers with functional surfaces, we further investigate the use of TEC chemistry in SLA with advanced material properties (Hoffmann et al. 2017). The scope of this work is the development of thiol-ene materials which can be processed by stereolithography and fulfill the product requirements of intraocular lenses. Main reqirements are high transparency, biocompatibility and an elastic mechanical properties.

Polymers made by TEC chemistry have various promising properties such as a high refractive index (RI), low optical dispersion, less polymerization stress, an easily controllable polymerization reaction which is, in addition, not inhibited by oxygen and does not necessarily require a photoinitiator. However, well-known drawbacks are a rather limited availability of multifunctional thiol-monomers, odor pollution of low molecular thiols and low glass transition temperatures T_G of the resulting polymers (Lowe und Bowman 2013).

Photo resins consisting of two bifunctional monomers and one of two crosslinker with either three or four allyl functional groups were developed. Additionally, the influence of a pre-polymerization of the two bifunctional monomers is investigated for both crosslinkers. A pre-polymerization may further reduce polymer stress. During pre-polymerization no gelation takes place and therefore volume shrinkage can be compensated. Moreover, we hypothesize that pre-polymerization may lead to enhanced mechanical properties, because crosslinking-points will be more evenly distributed in the polymeric network and therefore network defects causing mechanical failures may be reduced.

Experimental Methods

Flat specimens have been photochemically cured without photo initiator and mechanical, optical and chemical properties have been analyzed for all four TEC systems. Successful polymerization was verified by ART-FTIR spectroscopy. Pre-polymerizations were additionally analyzed using gel permeation chromatography. Glass transition was measured using differential scanning calorimetry. Viscosity and gel point determination was performed using a rheometer. Optical properties were determined with an Abbe refractometer or UV-Vis spectrometer. Dynamic mechanical analysis was performed using a rheometer equipped with a fibre film option module and inner stress was measured using a polarization microscopy. Cytotoxicity has been tested with fibroblasts in extraction tests and in direct contact according to EN ISO 10993-5 and DIN EN ISO 10993-12. For the most promising TEC system, 3D-priniting experiments have been performed using an experimental SLA system with a 4w Nd:YAG continuous laser beam source at a wavelength of 266 nm.

Results and Discussion

FTIR signals of *ene*- as well as thiol-groups completely vanished after curing. Also, complete pre-polymerization was shown via FTIR analysis. Glass transition temperatures of about -30°C were determined by calorimetric analysis. Elongations at break reach from 10% to32% and E-Moduli reach from 24 kPa up to 40 kPa. Both values depend significantly on the used crosslinker and on pre-polymerization. All materials have RI n_D>1,54 and abbe numbers of v>44, while being completely transparent in the VIS region. 3-Dimensional sample structures have been produced with the described SL device.

Conclusion

The development of a TEC resin, which fulfills the requirements for the stereolithographic production of intraocular lenses have been successful. The use of two bifunctional monomers with a multifunctional crosslinker via TEC polymerization is a feasible approach for the synthesis of photopolymers with RI n_D~ 1,5 and high transparency in combination with elastic mechanical properties. It has been shown that the pre-polymerization may enhance mechanical properties, biocompatibility and reduce inner stress. Main drawback of the pre-polymerization approach is the increased viscosity of the photo resin which may be problematic for SL process. For systems with same crosslinking degree, crosslinkers with smaller functionalities lead to more flexible and less stiff materials, and also with better biocompatibility.

References

Hoffmann, Andreas; Leonards, Holger; Tobies, Nora; Pongratz, Ludwig; Kreuels, Klaus; Kreimendahl, Franziska et al. (2017): New stereolithographic resin providing functional surfaces for biocompatible three-dimensional printing. In: Journal of tissue engineering 8, 2041731417744485. DOI: 10.1177/2041731417744485.

Lowe, Andrew B.; Bowman, Christopher N. (2013): Thiol-X chemistries in polymer and materials science. Cambridge: Royal Society of Chemistry (RSC polymer chemistry series, no. 6).

Acknowledgement

Authors thank the Federal Ministry of Education and Research (BMBF) for funding (VIP+00841 >>ThIOLens<<).

PS2-10-402

Composite Melt-Electrowriting Approaches to Fabricating Full-Scale Patient-Specific Auricular Cartilage Scaffolds

Maureen T. Ross, Naomi C. Paxton, Mark C. Allenby, Maria A. Woodruff

Queensland University of Technology, Institute of Health and Biomedical Innovation, Brisbane, AU

Introduction

Tissue engineering is a promising alternative to current reconstructive treatments for microtia, the congenital malformation of the external ear[1]. To date, no tissue engineering solution has been able to clinically provide the robust full-ear framework to support and guide auricular cartilage (AUC) growth and maintain long-term shape fidelity. Recent studies have shown the potential of hydrogel-reinforced melt-electrowritten (MEW) scaffolds for articular cartilage (ATC) regeneration, highlighting that combining the two scaffold fabrication methods provides the ability to tailor mechanical properties[2,3]. The advantage of this approach is its ability to harness the extracellular matrix-like environment of hydrogels to support cartilage growth and provide mechanical reinforcement through MEW fibres. However, due to limitations in MEW, namely continuous fibre deposition, fibre instabilities in higher-volume scaffolds and no temporary support material for complex overhangs, the fabrication of AUC scaffolds is yet to be realised. This study aims to overcome current limitations of MEW to develop methods to fabricate patient-specific poly-ε-caprolactone (PCL) scaffolds for ear reconstruction with the potential for hydrogel reinforcement for tailored mechanical properties.

Experimental Methods

3D models from micro computed tomography (µCT) scans of human cadaveric AUC were used to generate *gcode* for creating scaffolds using MEW. Due to both limitations in the printing height as well as overhangs in the model design, a multi-scale approach was applied to fabricating the AUC scaffold (Figure 1A). The largest cross-section in the AUC was identified and used as a splitting point to define the printing direction of the model (Figure 1B). These two parts of the cartilage model were then further sub-divided into 2 mm sections (~100 x 20 µm layers; Figure 1C). Using in-house custom designed software a crosshatch pattern was created for each of the subsections of the AUC model.

A custom-built MEW machine was used to print the scaffolds (Figure 1D). PCL Capa 6430 (M_w = 37000 Da, Perstorp, Sweden) was heated to 90°C and stabilised for 15 minutes. A 0.05 MPa pressure supply with a 5 kV voltage difference over 5 mm tip-to-collector distance was used to extrude PCL through a 21 gauge needle. Scaffold-sheets were then stacked together to form one structure (Figure 1E). Additional MEW PCL sheets were fabricated with a height of 2 mm to show feasibility of creating hybrid scaffolds that match native AUC. Biopsies of 6 mm diameter were taken from the sheet and then placed in a 3D printed injection moulding system to fill the PCL scaffold with a 4% w/v alginate-20% w/v gelatin (Sigma Aldrich, USA) solution. The structure was cross-linked with a 2% calcium chloride ($CaCl_2$) solution (Sigma Aldrich, USA).

Scaffolds were characterised by assessing porosity, fibre morphology, shape fidelity and mechanical properties with comparison to native AUC, rib cartilage (gold standard Autograft) and the high-density polyethylene (HDPE) Medpor® (Stryker, Newnan, GA) ear implant. µCT was used to determine porosity and shape fidelity. Scanning Electron microscopy (SEM) was used to visualise scaffold architecture and morphology. Compression testing was completed on 6 mm discs of MEW PCL scaffolds of varying porosity both with and without alginate-gelatin, in a temperature

controlled PBS solution at 37°C. Results were compared to control data of native AUC, rib cartilage and HDPE Medpor® implants.

Results and Discussion

This work developed a modular approach for creating anatomically accurate, full-scale MEW PCL AUC scaffolds. Furthermore, the inclusion of alginate-gelatin hydrogel around the reinforcing PCL backbone provided tuneable material mechanical properties to more closely mimic the Young's Modulus and compressive behaviour of native AUC. The scaffolds produced were a significantly closer match to native cartilage than the current HDPE Medpor® scaffolds, providing a more tailored architecture with higher porosity attributed to the use of additive manufacturing techniques. Shape fidelity assessment showed that cross-linked scaffolds were well matched to the original 3D models and were able to maintain their shape over time.

Conclusion

This study demonstrated the feasibility of a multi-scale approach to fabricating hydrogel-reinforced MEW scaffolds for ear reconstruction. Current limitations in MEW prevent a complex shape like the ear from being produced in one complete print. This multi-scale approach overcomes this challenge and in future work, may also prove more advantageous to uniformly distribute viable cells rapidly throughout one unified large construct. The mechanical properties and scaffold architecture suggest these scaffolds have great potential for providing a patient-specific implant for AUC regeneration and long-term shape fidelity.

References

1. Ross et al. (2018) *Virtual Phys. Prototy.* **13** (2): 117-130
2. Bas et al. (2015) *Eur. Polym. J*. **72:** 451 – 463
3. Visser et al. (2015) *Nat. Commun*. **6**: 6933

Acknowledgement

The data reported was obtained using the resources of the Central Analytical Research Facility at the Institute for Future Environments, QUT, with funding from the Science and Engineering Faculty. MTR would like to acknowledge PhD funding from the Australian Government Research Training Program as well as Advance Queensland. NCP would like to acknowledge funding from the ARC ITTC in Additive Biomanufacturing. MCA is supported by an Advance Queensland Fellowship.

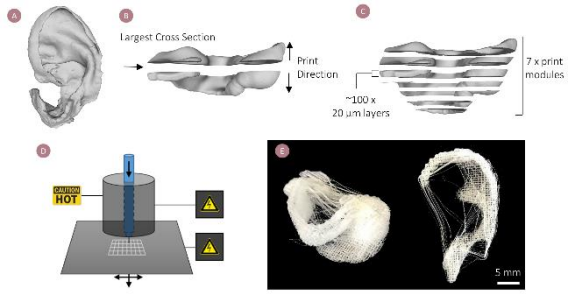

Melt-electrowriting (MEW) approach for fabricating auricular cartilage (AUC) scaffolds.
A) A 3D model of the AUC from micro CT data. This model is too complex to directly print using MEW due to its size and complex overhanging geometry. B) The largest cross-section of the model is used as a splitting point to determine the print direction of these portions of the AUC. C) The AUC is further divided into 2 mm sections (100 x 20 µm printing layers) to overcome instabilities in larger volume MEW scaffolds. D) MEW technique uses a high voltage potential to draw molten polymer fibres out with micron dimensions. E) MEW AUC scaffold created using modular printing method (two viewing angles top and bottom).

PS2-10-403

Acousto-mechanical investigation of melt electro written PCL Scaffolds

Thomas Stoppe[1], Max von Witzleben[2], Matthias Bornitz[1], Tilman Ahlfeld[2], Michael Gelinsky[2], Marcus Neudert[1]

[1]Technische Universität Dresden, Carl Gustav Carus Faculty of Medicine, Otorhinolaryngology, Head and Neck Surgery, Dresden, DE; [2]Technische Universität Dresden, Carl Gustav Carus Faculty of Medicine, Centre For Translational Bone, Joint And Soft Tissue Research, Dresden, DE

Introduction

The closure and the restoration of the function of the tympanic membrane is crucial for hearing restoration. Most defects can be successfully closed with autologous tissue patches. Due to unknown tissue properties, a compromise between function and stability of the reconstruction is needed to be found by the surgeon (Mürbe, et al. 2002). As an alternative, artificial replacement materials are being investigated, aiming for consistently good and reproducible results in the restoration of tympanic membrane defects. Synthetic materials like biopolymers can be fabricated in various shapes with different tissue engineering technologies. Additionally, their material properties like biocompatibility are advantageous for further investigation as a tympanic membrane replacement. In this work, it was investigated, if melt electro written Polycaprolactone (PCL) scaffolds are able to provide a mechanical behaviour like the human tympanic membrane, to realise a biomimicking synthetic replacement.

Experimental Methods

Multiple PCL scaffolds were fabricated with melt electro writing (GeSiM BioScaffolder 3.1. in combination with a melt electro writing module). For the comparison of the vibration behaviour of the scaffolds and human tympanic membranes, it is necessary to acquire their sound transfer function. Various shapes were created and investigated with Laser-Doppler vibrometry (CLV 700, CLV 1000 with modules M300, M050, and M003, Polytec, Germany). All scaffolds were clamped in a test stand with defined clamping force. The diameter of the scaffolds was 11 mm, of which the outer area was defined for clamping purposes. They were excited with a multi-sinusoidal signal between 100 Hz and 5 kHz at a sound pressure level of about 90 dB SPL. A probe Microphone ER-7C (Etymotic Research, Elk Grove Village, IL) was placed about 1 mm in front of the scaffolds to measure the applied sound pressure. The vibration characteristics in relation to specific structural parameters, e.g. fibre diameter, amount of layers, orientation angle and strand distance were investigated and compared to the human tympanic membrane. The variation of the results was statistically investigated within the different batches.

Results and Discussion

The scaffold’s structural parameters influenced the sound transfer function of the scaffolds differently. The first resonance frequency of the scaffold, as a characteristic property, was shifted in frequency and magnitude, dependent on the specific design. For example, an increase in scaffold stiffness usually causes a lowering of the magnitude and an increase in the resonance frequency. Multiple measurements on each scaffold showed a variation in results, since the fragile structures can easy be manipulated and influenced by external and test stand factors. The clamping force had a relevant influence on the vibration properties (Allardyce, et al. 2016). Simply supported mounting was regarded as mostly appropriate, for a realistic comparison between the scaffolds and the human tympanic membrane in the test stand and in its native mounting. Thus, the clamping force should be kept low.

Conclusion

The vibration properties of the membranes can be setup to be comparable to those of human tympanic membranes. For a stable and functional reconstruction in patients, further development and research is needed to investigate the properties in moist environment like in the middle ear. Furthermore, quasi-static pressure is a relevant influencing factor, which is needed to be assessed.

References

Dirk **Mürbe**, Thomas Zahnert, Matthias Bornitz, and Karl-Bernd Hüttenbrink. „Acoustic Properties of Different Cartilage Reconstruction Techniques of the Tympanic Membrane.“ *Laryngoscope* 112, Nr. 10 (October 2002): 1769–76.

Benjamin J. **Allardyce**, Rangam Rajkhowa, Rodney J. Dilley, Zhigang Xie, Luke Campbell, Adrian Keating, Marcus D. Atlas, Magnus von Unge, and Xungai Wang. „Comparative acoustic performance and mechanical properties of silk membranes for the repair of chronic tympanic membrane perforations“. Journal of the Mechanical Behavior of Biomedical Materials 64 (December 2016): 65–74.

Acknowledgement

This measure is co-financed with tax revenue on the basis of the budget adopted by the members of the Saxon Landtag.

PS2-10-404

The thermal stability of polymers during melt electrowriting

Christoph Boehm, Andrei Hrynevich, Gernot Hochleitner, Eoin Jones, Jürgen Groll, Jörg Tessmar, Paul D. Dalton

University Hospital Würzburg, Department for Functional Materials in Medicine and Dentistry, Würzburg, DE

Introduction

Fiber-based tissue engineering mostly relies on solution electrospinning, where meshes of randomly deposited fibers are produced. Based on this approach a new technology called melt electrowriting (MEW) developed, using a polymer melt instead of solutions. This exchange allows precise deposition of fibers layer-by-layer, which is mainly resulting from the higher viscosity of polymer melts.[1] Furthermore, organic solvents are omitted, which is relevant to cytotoxicity and volatile solvent accumulation. Conversely, it is necessary to maintain the polymer molten and therefore constantly apply sufficient heat. This constant thermal treatment can lead to degradation, which significantly changes the printing behavior of the material. This drawback is particularly pertinent to MEW, since flow rates of 5-10 µl/h are required to achieve small fiber diameters. The most common material used by the MEW community is poly(ε-caprolactone) (PCL)[2-4], which shows high long-term stability under printing conditions at 70 – 90 °C. In this study the stability of PCL during the MEW process was investigated over week-long printing periods and contrasted to poly(lactide-co-glycolide) (PLGA), which shows significant changes in its printing behavior with ongoing heating time.

Experimental Methods

To monitor the thermal degradation, two different methods are applied. To check possible alterations by MEW the polymer is heated in a glass syringe at different process temperatures of 75 °C, 85 °C or 95 °C (PCL) or 170 °C (PLGA). By applying pressurized air and a high voltage, which forms an electrical field between the nozzle and the collector, a polymer jet is formed. The speed and the stability of the jet is dependent on the viscosity and the surface charge of the used polymer, that crucially affects the critical translation speed (CTS), which resembles the lowest speed of collector movement to produce straight fibers. Since viscosity and surface charge changes with ongoing degradation, it was possible to monitor the degradation with a MEW setup that scans for the CTS with continuous heating time.

The deposited material was furthermore collected after defined time points and gel permeation chromatography (GPC) was performed to measure changes in molecular weight and weight distribution. These measurements were performed with a chloroform-based GPC system from Malvern using a relative calibration with polystyrene standards.

Results and Discussion

The MEW experiment for PCL shows a decrease of the CTS in the first 5 days (85 °C), before it remains constant for the next 20 days. These results show, that during the first days the material undergoes a recovery or rearrangement, which increases viscosity and therefore decreases the speed of the jet. After 5 days the recovery switches to an equilibrium state, resulting in a constant CTS for extended periods of time. Comparing these results with GPC measurements, the elution curve of PCL changes with ongoing heating time towards higher molecular weights.

PLGA on the other hand is only stable for around 2 hours under minimum printing conditions, before the speed of the jet increases due to thermal chain scission. A correlating, rapid molecular weight decrease was observed in GPC measurement.

Conclusion

Long-term MEW allows to monitor changes to the chemical properties of polymers by observation of the CTS of polymer jets. PCL appears to undergo a recovery and stabilization at the beginning of the heating process, where the CTS decreases due to changes of viscosity/surface charge. PLGA shows the opposite behavior with increasing jet speed and therefore higher CTS with ongoing heating time due to random scission of polymer chains accompanied with a decrease of viscosity. This makes MEW a potential tool to investigate thermal degradation of polymers at elevated process temperatures.

References

[1] M. L. Muerza-Cascante, D. Haylock, D. W. Hutmacher, P. D. Dalton, *Tissue Engineering Part B: Reviews* **2014**, *21*, 187-202.

[2] D. W. Hutmacher, P. D. Dalton, *Chemistry – An Asian Journal* **2011**, *6*, 44-56.

[3] T. D. Brown, F. Edin, N. Detta, A. D. Skelton, D. W. Hutmacher, P. D. Dalton, *Materials Science and Engineering: C* **2014**, *45*, 698-708.

[4] G. Hochleitner, A. Youssef, A. Hrynevich, N. Haigh Jodie, T. Jungst, J. Groll, D. Dalton Paul, in *BioNanoMaterials, Vol. 17*, **2016**, pp. 159-171.

Acknowledgement

The support of German Research Foundation (DFG) through grant DA1034/4-1 is gratefully appreciated as well as the DFG State Major Instrumentation Program for funding the Zeiss Crossbeam CB 340 SEM (INST 105022/58-1 FUGG).

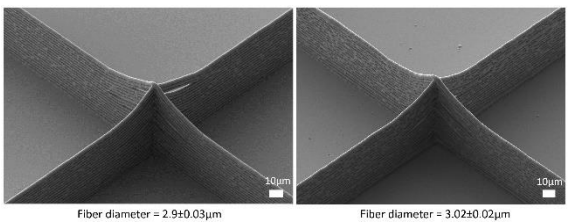

Multi-day printing stability of PCL
SEM images of MEW-processed PCL fibers at day 1 (left) and day 15 (right).

PS2-10-405

Design and 3D Printing of Multimodal, Multiphasic Scaffolds

Andrei Hrynevich, Gernot Hochleitner, Tomasz Jüngst, Almoatazbellah Youssef, Jürgen Groll, Paul D. Dalton

University Hospital Würzburg, Dept. of Functional Materials in Medicine and Dentistry, Würzburg, DE

Introduction

Melt electrowriting (MEW) is a distinct additive manufacturing process that electrostatically prevents a falling fluid from breaking up at very low flow rates (µL/hr) [1]. It has been used for different biomedical applications including T-cell therapy [2], tissue engineering, regenerative medicine, and cancer research [3]. MEW can be considered a hybrid between melt micro-extrusion and electrospinning and has been performed so far with poly (ε-caprolactone) (PCL), polypropylene, poly(vinylidene fluoride), fugitive inks and photocurable polymers [4].

Experimental Methods

A custom-built MEW printer was used in this study. The printer is based on a design, described elsewhere [5], and is able to control both processing and environmental conditions (chamber temperature and humidity). The PCL melt is extruded through a flat-tipped nozzle. As shown in Fig. 1, the MEW printing head is kept static and a collector is translated to enable direct-writing. Voltages were applied both to the nozzle and the collector.

Results and Discussion

The PCL fibre diameter and the critical translation speed was controllable with air pressure, collector speed, applied voltages and the spinning gap. As a result, we were able to produce a multi-phasic scaffold where each part contains different with different fiber densities. The range of chamber temperatures, optimal for the printing process was determined as well as the influence of the air humidity on the jet behaviour. Since the flow rate and collector speed to the spinneret have the most significant impact on fiber diameter, we developed an air pressure and writing speed control system to rapidly influence the electrified molten jet so that fiber diameters can be significantly altered by over one magnitude during the direct writing process[6]. This has implications in the fabrication and design for tissue engineering scaffolds, filters, textiles, energy and electronic applications.

Conclusion

MEW is a capable additive manufacturing technology that can fabricate porous materials using a spectrum of different diameter fibres. Using both air pressure and collector speed control, the fibres that constitute the scaffold can be manufactured with over a magnitude difference in diameter, using the same nozzle. Control over the chamber humidity and temperature allowed to investigate their effect on the printing process and the scaffold quality.

References

[1] P. D. Dalton, Current Opinion in Biomedical Engineering 2017, 2, 49.

[2] B. Delalat, F. Harding, B. Gundsambuu, E. M. De-Juan-Pardo, F. M. Wunner, M.-L. Wille, M. Jasieniak, K. A. L. Malatesta, H. J. Griesser, A. Simula, D. W. Hutmacher, N. H. Voelcker, S. C. Barry, Biomaterials 2017, 140, 58.

[3] M. L. Muerza-Cascante, D. Haylock, D. W. Hutmacher, P. D. Dalton, Tissue Engineering Part B-Reviews 2015, 21, 187.

[4] A. Youssef, S. J. Hollister, P. D. Dalton, Biofabrication 2017, 9, 012002.

[5] G. Hochleitner, A. Youssef, A. Hrynevich, J. N. Haigh, T. Jungst, J. Groll, P. D. Dalton, BioNanoMaterials 2016, 17, 159.

[6] A. Hrynevich, B. S. Elci, J. N. Haigh, R. McMaster, A. Youssef, C. Blum, T. Blunk, G. Hochleitner, J. Groll, P. D. Dalton, Small 2018, 14, e1800232.

Acknowledgement

This work has been supported by the European Research Council consolidator grant Design2Heal, contract #617989, the BMBF-AiF Project 19054 N/2 as well as the DFG State Major Instrumentation Programme for funding the Zeiss Crossbeam CB 340 SEM (INST 105022/58-1 FUGG).

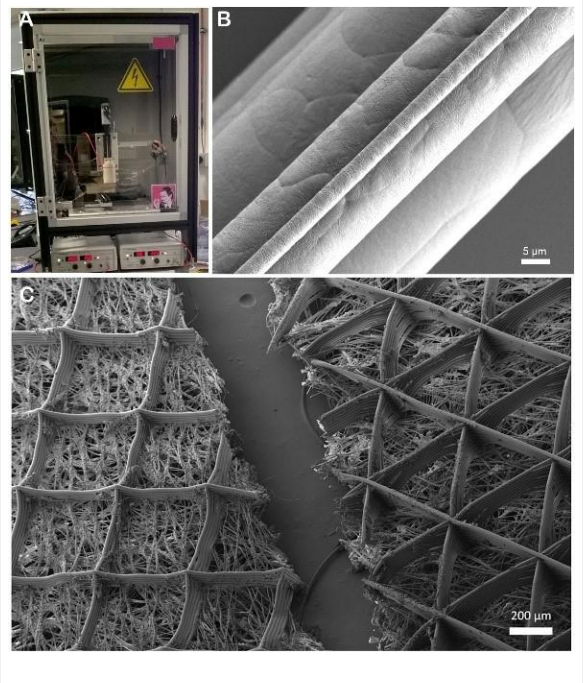

Figure 1. MEW printer, fibers and scaffolds
A) MEW printer and B) different fibres printed upon each other while C) shows a SEM of both sides of a sectioned multiphasic scaffold, one day after seeding with L929 fibroblasts.

2:45 p.m. – 3:45 p.m.

Hall 1 / Exhibition Area

PS2-11 | Drug delivery

PS2-11-406

Light-mediated drug release from living hydrogels

Shardul Bhusari[1,2], Shrikrishnan Sankaran[1], Aránzazu del Campo[1,2]

[1]INM – Leibniz Institute for New Materials, Saarbrücken, DE; [2]Saarland University, Chemistry Department, Saarbrücken, DE

Introduction

One of the recent advances in the development of drug encapsulation and delivery systems has been the emergence of living materials, that contain genetically modified living organisms performing enhanced functions. We are developing living hydrogels containing bacteria that act as productive, adaptable and replenishable on-demand drug delivery repositories.[1,2] The polymer matrix of the hydrogel maintains the structural integrity inside the bodily environment while the living organisms produce the optimal amount of drug at the required time of delivery. Here we demonstrate the development of a hydrogel system to encapsulate genetically engineered *E. coli* bacterial strain, in 3D bioprinted scaffolds, leading to a light-regulated, localized, tunable and prolonged drug release.

Experimental Methods

The light-regulated drug-producing *E. coli* strain was engineered by incorporating the genes related to the metabolic synthesis of the drug into a light responsive optogenetic plasmid.[2] Bacteria was encapsulated in 3D-bioprinted constructs capable of being crosslinked on UV light exposure using a free-radical photoinitiator. These constructs were used to study the effect of change in the crosslinking density and thus the mechanical properties on the bacterial growth rate. Thin films of bacterial hydrogels were casted on the porous membrane (0.4 µm diameter pores) of transwell inserts to detect the drug production after 48 h irradiation on light exposure.

Results and Discussion

After 48 h within the physically crosslinked hydrogel, the bacterial growth observed was 20 times higher than that in the chemically crosslinked hydrogel. Also, with increasing chemical crosslinking density, the drug production reduced ten-fold. Intermediate bacterial growth and drug release were observed with intermediate physical and chemical crosslinking in the hydrogels.

Conclusion

Genetically engineered bacteria were successfully encapsulated inside 3D bioprinted hydrogel system. We demonstrate the possibility of controlling the bacterial growth by tuning the mechanical properties of the hydrogel and thus the drug release *in situ,* using an optogenetic strategy.

References

1. Sankaran, S. & Campo, A. Optoregulated Protein Release from an Engineered Living Material. *Adv. Biosyst.***1800312,** 3–9 (2019).

2. Sankaran, S., Becker, J., Wittmann, C. & Campo, A. Optoregulated Drug Release from an Engineered Living Material : Self-Replenishing Drug Depots for Long-Term , Light-Regulated Delivery. *Small***1804717,** 1–6 (2019).

Acknowledgement

S.B., S.S. and A.d.C. are grateful for funding from the SFB1027 collective research center for this project.

PS2-11-407

Redox-activable dendrimer-based nanocapsule for targeted agents to aid solubility and overcome drug resistance

Qida Hu[1], Wangteng Wu[1,2], Guping Tang[2], Tingbo Liang[1], Meng Wang[1]

[1]Zhejiang University, First Affiliated Hospital, Hangzhou, CN; [2]Zhejiang University, Institute of Chemistry Biology and Pharmaceutical Chemistry, Hangzhou, CN

Introduction

Targeted agents have unsatisfactory therapeutic responses against certain malignancies, such as pancreatic cancer, which might be caused by an insufficient exposure dose and drug resistance. Efficient administration of targeted agents via the intravenous route could maximize efficacy, but requires enhanced solubility and increased exposure.

Experimental Methods

We developed a multi-arm, polyethylene-glycol nanocapsule design by modifying the core dendrimer component, “multiarm polymer complex with mG3 dendrimers” (MAP-mG3), to provide a delivery system for insoluble inhibitors, such as the mammalian target of rapamycin (mTOR) inhibitor OSI-027, to treat pancreatic cancer.

Results and Discussion

MAP-mG3, in comparison with other analogs, showed higher OSI-027 loading capacity with enhanced solubility, controlled release activable by redox stimuli, and increased intracellular tumoral accumulation. MAP-mG3/OSI-027 attenuated mTOR phosphorylation and inhibited growth of pancreatic cancer cells, which also reversed drug-resistant pancreatic cancer by increasing intracellular OSI-027 accumulation. These data suggest that our optimized MAP-mG3 system can deliver targeted agents functionally for pancreatic cancer and drug-resistant pancreatic cancer.

Conclusion

A redox-activable nanocapsule delivery system was successfully established for hydrophobic targeted agents to enhance solubility and overcome drug resistance.

Acknowledgement

This work was supported financially by the National Natural Science Foundation of China (81502026, 81830089, and 81530079), Zhejiang Provincial Natural Science Foundation (LQ16H180002 and LY18H160026), and National High Technology Research of China (SS2015AA020405).

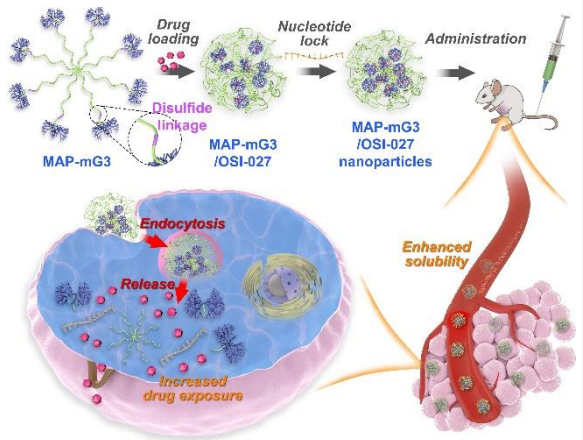

Figure 1. Graphical demonstration of MAP-mG3 nanocapsule for targeted agents delivery

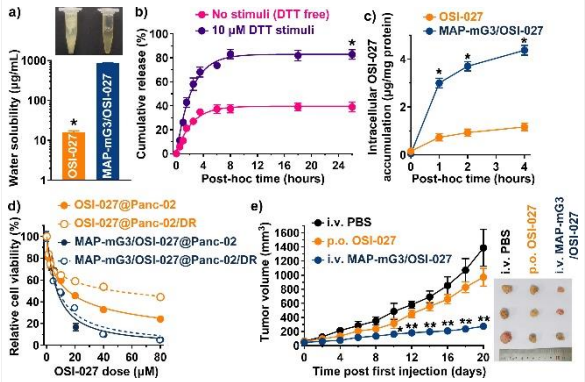

Figure 2. MAP-mG3 nanocapsule for targeted agents to enhance solubility and overcome drug-resistance

(a) Enhanced water solubility. The photograph demonstrates a mixture of 0.5 mL of water plus 400 μg of OSI-027 (left) and the solution of equivalent MAP-mG3/OSI-027 in 0.5 mL of water (right). (b) Controlled release by the reduction stimulus dithiothreitol (DTT). The time-dependent patterns of cumulative release of OSI-027 with (purple) or without (rose) DTT stimulus are illustrated with best-fit lines. (c) Increased intracellular accumulation of OSI-027 in OSI-027-resistant Panc-02 cells (Panc-02/DR) cells. (d) Dose-dependent cytotoxicity of OSI-027 (orange) and equivalent MAP-mG3/OSI-027 (dark-blue) in regular Panc-02 cells (solid) or drug-resistant Panc-02/DR cells (circle), characterized by a cell-viability assay. (e) Tumor-growth patterns in Panc-02/DR tumor-bearing mice treated with i.v. PBS (black), p.o. OSI-027 (orange), or i.v. MAP-mG3/OSI-027 system (dark blue).

PS2-11-408

Peptide-modified nanoparticles for improving ETP chemotherapy with the aid of siPIK3CA against small cell lung carcinoma

Wen Jen Lin[1,2], Hsin Lin Huan[1]

[1]School of Pharmacy, College of Medicine, National Taiwan University, Taipei, TW; [2]Drug Research Center, College of Medicine, National Taiwan University, Taipei, TW

Introduction

Cancer is ranked first in the top ten causes of death. According to statistics from the Ministry of Health and Welfare, it was revealed tracheal, bronchial and lung cancers resulted in the highest mortality. Small cell lung carcinoma (SCLC) is a highly aggressive form of malignancy with rapid recurrence and poor prognosis, accounting for 11~20% of all lung cancers (1, 2). Nowadays first-line combination chemotherapy for SCLC is etoposide (ETP) and platinum-based drugs. Patients respond well to the combination chemotherapy at the beginning, but tumors relapse within one year because of drug resistance (3). Therefore, novel therapeutic strategies against drug-resistant SCLC are urgently required.

Experimental Methods

In this study, the US FDA approved poly(lactide-co-glycolide) (PLGA) was applied as the main polymer which was pegylated by poly(ethylene glycol) (PLGA-PEG). The SCLC targeting ligand, AG peptide, further modified PLGA-PEG. This peptide-modified PLGA-PEG was used to prepare nanoparticles (NPs) via solvent evaporation method encapsulating both anticancer drug, ETP, and PIK3CA small interfering RNA (siPIK3CA). The particle size, zeta potential and drug loading of NPs were characterized. The stability of NPs and in vitro drug release were monitored. The cellular uptake and cytotoxicity of drug loaded NPs were conducted in H69 cells.

Results and Discussion

The particle sizes of ETP and siRNA loaded NPs were in the range of 201.0 ± 1.9 - 206.5 ± 0.7 nm and 155.3 ± 12.4 - 169.2 ± 11.2 nm, respectively, with positive zeta potentials. The encapsulation efficiencies were > 61.1 ± 6.0% for ETP and > 58.6 ± 5.0% for siRNA. These NPs formulations exhibited good stability at 4˚C for 28 days. *In vitro* release study showed that the release of both ETP and siRNA from NPs was faster in pH 4.0 medium than in pH 7.4 medium irrespective of with or without peptide conjugation. The AG-peptide and dual-peptide modified NPs had better cellular uptake ability than peptide-free NPs in H69 cells. In addition, the combination treatment of ETP with the aid of siPIK3CA showed better cytotoxicity than ETP loaded AG-NPs-ETP alone.

Conclusion

The peptide-modified nanoparticles for improving ETP chemotherapy against small cell lung carcinoma was achieved with the aid of siPIK3CA in H69 SCLC cells.

References

1. Planchard D, Le Pechoux C. Small cell lung cancer: new clinical recommendations and current status of biomarker assessment. Eur J Cancer. 2011;47 Suppl 3:S272-83.
2. Travis WD. Advances in neuroendocrine lung tumors. Ann Oncol. 2010;21 Suppl 7:vii65-71.
3. Karen Kelly. Extensive stage small cell lung cancer: Initial management. UpToDate. 2017.

Acknowledgement

This work was supported by Ministry of Science and Technology in Taiwan.

PS2-11-409

Porous Fibers for Drug Delivery

Andreas Scherrieble, Jan Buggisch, Lisa Lang, Martin Hoss, Martin Dauner, Michael Doser

DITF, Biomedical Engineering, Denkendorf, DE

Introduction

Drug delivery systems are becoming increasingly important in medicine and can be used not only in conventional medicine, but above all in the highly innovative field of regenerative medicine.

By using textile wound dressing systems with integrated active ingredients, the duration of treatment can be significantly reduced and treatment costs can be saved.

Porous structures are particularly suitable for subsequent loading with drugs. Active substances can be deposited in the porous depots within a carrier in relevant quantities and be released over a suitable time period. Sub-microscale pores within fibers represent a promising drug release system particularly when fibers are strong enough to be further processed to textile structures.

For these purposes porous fibers have been developed from polymer compounds for drug release applications.

Experimental Methods

Porous fibers were developed via melt extrusion of polymer compounds made of varied proportions of poly-L-lactide (PLLA) and the water soluble polymer polyvinyl alcohol (PVA) or polyethylene oxide (PEO) respectively. With a washing step the water soluble polymer was removed, leaving porous structures in the fibers. The washing process was varied in temperature, duration and support of ultrasound. Porous structures were investigated via scanning electron microscopy (SEM). Pore content of SEM-images was evaluated with the software Olympus analySIS.

Knitting on a circular knitting machine was conducted to check whether fibers can be processed to a textile structure.

Loading of fibers with the protein horse radish peroxidase (HRP) was realized via a low pressure process that forced the HRP containing hydrogel gellan gum to penetrate the fiber pores. Infiltration of gel in the pores was demonstrated with fluorescent microscopy by using Fluorescein isothiocyanate marked gellan gum and was determined gravimetrically. Fiber pore loading with HRP containing gellan gum was also checked for the flat knitted structures.

Time dependent release of HRP out of fibers into phosphate buffered saline solution was determined. HRP concentrations were analyzed photometrically via its catalytic influence on the Iodophenol enhanced Luminol-H_2O_2 chemiluminescent reaction.

Results and Discussion

Sub-microscale pores where realized in fibers made of a PLLA/PEO-compound with a fiber diameter of around 30 micrometer (figure 1). SEM imaging and pore content evaluation resulted in a share of up to 22% pore volume after the washing step.

Knitting trials showed that PLLA/PEO-fibers could be successfully processed into a knitted textile.

Fiber pores in PLLA/PEO-fibers could be loaded with gellan gum hydrogel containing HRP in a vacuum process. This was demonstrated with fluorescent microscopy (figure 2). The test of loading fibers within the knitted structure with gel was also successful.

HRP release trials with loaded fibers of different HRP-concentrations showed a release duration of 2 days with decreasing rates.

Conclusion

The realization of porous fibers, its processability to textile structures combined with the pore filling process with hydrogel and its decelerated HRP release rate show that these fibers represent a promising structure for use as drug delivery systems.

Future investigations will lead to the determination of release rates of other active substances than HRP with this system.

Also a more delayed drug release will be investigated with fiber coatings that could act as additional barrier to the released drug.

References

Textiles and Drug Delivery, 2005. Textiles Magazine 32 (3/4), pp. 34-37.

Clark, R.A., Ghosh, K. and Tonnesen, M.G., *Tissueengineeringforcutaneouswounds.* J Invest Dermatol, 2007. 127(5): pp. 1018-29.

Bacelar, A.H. et al., *Recentprogress in gellangumhydrogelsprovidedbyfunctionalizationstrategies.* Journal of Materials Chemistry B, 2016. 4(37): pp. 6164-74.

Osmalek, T., Froelich, A. and Tasarek, S., *Application of gellan gum in pharmacy and medicine, 2014.* Int J Pharm. 466(1-2): pp. 328-40.

Bhandari, A., Kim, W. and Hohn, K., *Luminol-based enhanced chemiluminescence assay for quantification of peroxidase and hydrogen peroxide in aqueous solutions: Effect of reagent pH and ionic strength*, 2010. Journal of Environmental Engineering, vol. 136, no. 10, pp. 1147-52.

Diaz, A.N., Sanchez, F.G. and Garcia, J.G., *Hydrogen peroxide assay by using enhanced chemiluminescence of the luminol-H_2O_2-horseradish peroxidase system: Comparative studies*, 1996. Analytica chimica acta, vol. 327, no. 2, pp. 161-165.

Acknowledgement

This work was supported by the Federal Ministry for Economic Affairs and Energy on the basis of a resolution of the German Bundestag. Research association: Forschungskuratorium Textil e. V., grant number: 19523 BG.

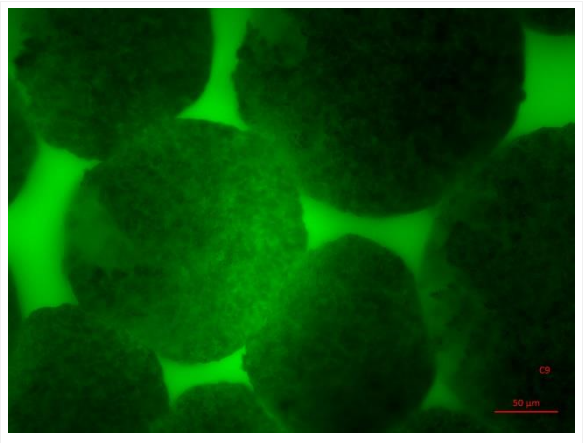

Cross-sectional area of porous fiber penetrated by fluorescence marked gel

Fluorescence micoscopy image of cross-sectional area of porous fiber penetrated by Gellan Gum gel marked with Fluorescein isothiocyanate; fiber pores filled with low pressure process (100mbar)

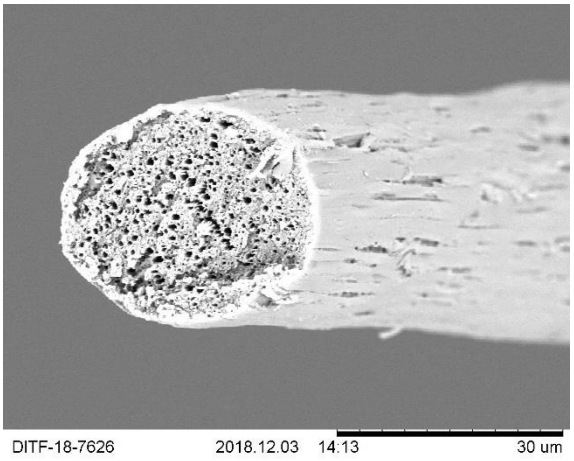

Cross-sectional area of porous fiber
SEM image of cross-sectional area of porous fiber made of PLLA/PEO-compound; washing 8h 80°C and subsequent 10 min. ultrasonic treatment; fiber pultruded under liquid nitrogen until break

PS2-11-410

Synthesis of Cerium and Gallium Doped Mesoporous Bioactive Glass Nanoparticles

Fatih Kurtuldu[1], Dušan Galusek[2], Aldo R. Boccaccini[3]

[1]Alexander Dubcek University in Trencin, Department of Biomaterials, FunGlass, Trenčín, SK; [2]Joint Glass centre of the IIC SAS, TnUAD and FChFT STU, FunGlass, Trenčín, SK; [3]University of Erlangen-Nuremberg, Department of Materials Science and Engineering, Institute of Biomaterials, Erlangen, DE

Introduction

According to the IUPAC definition, porous materials are divided into three classes: microporous (<2 nm), mesoporous (2–50 nm) and macroporous (>50 nm) [1]. Ordered mesoporous silica was first discovered in 1992 [2], and proposed as a drug delivery system in 2001 [3]. Since then silica-based glass microspheres, such as MCM-41, SBA-15 or MCM-48 representing ordered mesoporous inorganic materials, have been considered as ideal materials for incorporation of drugs, genes and other therapeutic agent acting as carrier and control release systems.In this study, the synthesis of mesoporous bioactive glass nanoparticles, consisting of a silicate network modified by Ca and Ce or Ga ions, has been studied for possible applications in cancer treatment or incorporation into nanocomposite scaffolds for bone regeneration.

Experimental Methods

Tetraethylorthosilicate (TEOS, 100%, VWR International), hexadecyltrimethylammonium bromide (CTAB, BioXtra, ≥99%, Sigma-Aldrich), ethyl acetate (99.7%, Centralchem), ammonium hydroxide (ACS reagent, 28.0 - 30.0% NH3 basis, Sigma-Aldrich), Cerium nitrate hexahydrate (99.95%, Treibacher) and gallium nitrate hexahydrate (99.999%, Alchemica) were used as starting materials for synthesis of mesoporous bioactive glass nanoparticles (MBGNPs).
Cerium doped MBGNPs in the $60SiO_2$-(40-x)CaO-xCe_2O_3system and gallium doped MBGNPs in the $60SiO_2$-(40-x)CaO-xGa_2O_3system (where x stands for 0, 1, 3 and 5 mole %) were obtained by micro-emulsion assisted sol-gel method. First, 2.8 g CTAB templating agent was dissovoled in 150 mL deionized water, and 40 ml ethyl acetate was added. Ammonium hydroxide (3.66 ml) was then added and mixed at room temperature. TEOS (14.4 ml) and appropriate quantities of calcium nitrate tetrahydrate, cerium nitrate hexahydrate or gallium nitrate hexahydrate were added step wise to the solution within a 30 minutes time interval, and the solution was left for 4 hours. Afterwards the precipitates were filtered and washed with deionized water and EtOH to remove unreacted precursors and remaining salts, and dried at 60°C for overnight.Finally, the dried samples were thermally treated at 650 °C/3 h (heating rate of 1 °C min^{-1}) to remove the surfactant and nitrates groups and to stabilize the glassy phase.

Results and Discussion

Micro-emulsion assistant sol-gel method allowed the preparation of MBGNPs with spherical shape, monodispersed size distributionwith the mean equivalent diameter of 150 nm and low degree of agglomeration. SEM micrographs and EDS spectra of undoped MBGNPS are shown in Fig. 1. The results of EDS confirm that the glass nanoparticles contain 5-7 at.% Ca, which is well blow the desired content. The high resolution SEM micrographs revealed fine surface structure of the nanoparticles indicating their mesoporous structure.
Synthesis of nanoparticles with up to 1 mol% of Ce and Ga yielded nanoparticles of size, shape, and surface pore structure similar to those of the undoped MBGNPs. Increasing the content of dopants up to 3 and 5 mol % resulted

in deformation of the spherical shape of the nanoparticles and yielded elongated pineal shaped particles with aspect ratio 5:3. In addition, calcium content decreased significantly (down to 2 at. %), most likely due to replacement of Ca in the glass structure with the ions of the dopants. The influence of doping on specific surface, mesoporosity and solubility of synthesized nanoparticles has been evaluated and critically discussed.

Conclusion

The micro-emulsion assisted sol-gel method yielded monodispersed mesoporous bioactive glass nanoparticles with low or no agglomeration in the system CaO-SiO_2doped with up to 5 mol % of Ce and Ga. Incorporation of higher concentrations of dopants resulted in distortion of the MBGNPs spherical shape and marked decrease of Ca content. The influence of doping specific surface, mesoporosity and solubility of synthesized nanoparticles has beenstudied.

References

[1] K. S. W. Sing, “Reporting physisorption data for gas/solid systems with special reference to the determination of surface area and porosity (Recommendations 1984),” *Pure Appl. Chem.*, vol. 57, no. 4, pp. 603–619, 1985.

[2] C. T. Kresge, M. E. Leonowicz, W. J. Roth, J. C. Vartuli, and J. S. Beck, “Ordered mesoporous molecular sieves synthesized by a liquid-crystal template mechanism,” *Nature*, vol. 359, no. 6397, pp. 710–712, 1992.

[3] M. Vallet-Regi, A. Rámila, R. P. Del Real, and J. Pérez-Pariente, “A new property of MCM-41: Drug delivery system,” *Chem. Mater.*, vol. 13, no. 2, pp. 308–311, 2001.

Acknowledgement

This paper is a part of dissemination activities of project FunGlass. This project has received funding from the European Union´s Horizon 2020 research and innovation program under grant agreement No 739566.

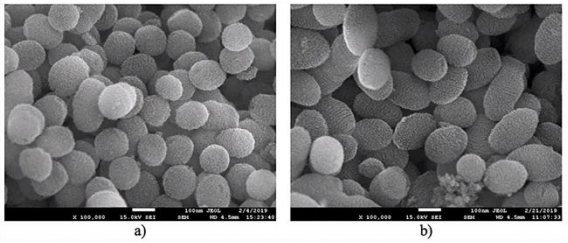

Figure 1
SEM images of a) undoped and b) doped with 3 mol% gallium Mesoporous Bioactive Glasses produced by Micro-Emulsion Sol-Gel method.

PS2-11-411

Blended Polymer Gels for the Release of Biologics

Mark T. O'Loughlin, Colm Delaney, Susan M. Kelleher

University College Dublin, School of Chemistry, Dublin, IE

Introduction

In recent years, biological molecules, or biologics, have transformed the pharmaceutical industry. However, one significant difficulty surrounding these molecules is their effective delivery into cells. The complex nature of such macromolecules owes to their highly sensitive nature to their environment, with changes in temperature and pH, as well as interaction with destructive species in vivo, deactivating the reactive species.[1] Polymeric gels are materials especially suited for encapsulation of biological elements. Their ability to absorb a large solvent content provides an environment compatible with most biologics while also providing a solvent medium for diffusion out of the polymeric network for a therapeutic application. Furthermore, the crosslinked nature of the polymer network provides protection of the encapsulated biologics against degradation pathways synonymous with biological molecules.[2]

This work specifically focusses on a novel blended polymer gel system consisting of varying concentrations of polycaprolactone dimethacrylate (PCL-DMA, Mn 1350 $gmol^{-1}$), polyethylene glycol diacrylate (PEG-DA, Mn 575 $gmol^{-1}$ and 4000 $gmol^{-1}$) and deionized water. By careful alteration of the weight percentage of each constituent, properties such as the swelling ratio, the average pore size within polymer network and degradation time can be tuned. Degradation through hydrolysis of the ester bond within the PCL repeating unit can be accessed in aqueous systems and can be acid-catalysed or base-promoted, allowing for tuneable degradation over time and ultimately, controlled release of the biological molecule. This release can then be quantified by performing assays at specific time intervals.

Experimental Methods

Polymer solutions were cured to gels via radical polymerisation by irradiating with long wave UV light (365 nm) in the presence of a photoinitiator, in the glove box under nitrogen. Light microscopy was used as a tool to monitor the homogeneity of blended polymer gels. Swelling ratio studies were then performed in a range of pH buffers in triplicate on each set of polymeric gels over time. The average mesh size within the polymer network was then calculated by the Canal and Peppas method.[3]

Future Work - Release studies of lysozyme from the polymer gels will be performed and quantified using the Bradford assay.

Results and Discussion

A change in Mnof the polymer chain used in the fabrication of homopolymer PEG gels has a substantial influence on the swelling characteristics of the polymer network in water. This occurs as a result of increasing the distance between the crosslinks formed at the reactive terminal acrylate groups. Moreover, a change in the water content of the initial polymer solution used to fabricate the solid gel is also seen to influence the swelling characteristics of that gel. This occurs as increasing the water content will decrease the polymer crosslink density within the gel leading to a larger average mesh size and increased swelling capacity.[4]

Furthermore, the PEG gels show stability and no sign of degradation in water over time because the ether functional group within the repeating unit is not prone to hydrolysis in aqueous systems. This is of importance as when PCL-DMA is used in the fabrication of the blended gels, a material that can degrade by hydrolysis of the ester functional

groups within the repeating unit of the polymer is introduced to the system. For these heterogeneous polymer gels, containing PCL, PEG and water, a decrease in mass and in turn, a decrease in swelling ratio is seen after swelling in water over time. This degradation can be further tuned in acidic and basic aqueous media to occur at an earlier time point.

Conclusion

In conclusion, the mesh sizes of homopolymer PEG gels with differing Mn's and water contents have been calculated and related to various biological sizes from literature. Novel blended polymeric gels have been fabricated and swelling studies showing the tuneable degradation of these gels has been performed. The homogeneity of the relatively hydrophobic PCL-DMA within the gels was monitored by light microscopy. The degradation is shown to be caused by the hydrolysis of the ester moieties within the PCL repeating unit.

References

[1] Mitragotri, S., Burke, P. A. & Langer, R. *Nat. Rev. Drug Discov*. **13**, 655–72 (2014).
[2] Perez-Luna, V. H. & Gonzalez-Reynoso, O. *Gels*. **4**, 61 (2018).
[3] Canal, T. & Peppas, N. A. *J. Biomed. Mater. Res.***23**, 1183–1193 (1989).
[4] Censi, R. et al. *J. Control. Release*. **140**, 230–236 (2009).

Acknowledgement

I wish to acknowledge the Irish Research Council for funding this work (project: GOPIPG/2017/1037), and the Redmond and Rubini groups for use of relevant intruments.

PS2-11-412

Drug Delivery from Differently Modified Nanoporous Titania Coatings for Dental Application

Saskia Zailskas[1], Philipp Abendroth[1], Meike Stiesch[2], Peter Behrens[1]

[1]Leibniz University Hanover, Insitute for Inorganic Chemistry, Hanover, DE; [2]Medizinische Hochschule Hanover, Klinik für Zahnärztliche Prothetik und Biomedizinische Werkstoffe, Zentrum Zahn-, Mund- und Kieferheilkunde, Hanover, DE

Introduction

Although tooth implants are a common treatment in dentistry nowadays, peri-implantitis remains a major health issue. Due to late infections bacteria may form biofilms on the implants' surface which unfortunately leads to high implant failure rates (>10%). [1,2] To prevent and cure these undesirable infections the bacteria have to be effectively eliminated shortly after implantation and biofilm formation has to be inhibited during the life-time of the implant as well. Thus, a controlled drug delivery system directly located on the implants' surface offers a promising opportunity to accomplish the required antibacterial effect. A stimuli-response system is desired in order to ensure the release of an antibacterial drug not only directly after the implantation but if an infection occurs. Therefore, a nanoporous titania coating that can be attached to the implant surface seems to be suitable. It functions as a depot for the local drug release and the surface can be modified to introduce the stimuli-response effect. A similar system was already accomplished successfully for silica nanoparticles.[3]

Experimental Methods

The first step to transfer the system to a titania surface was the establishment of nanoporous titania films by utilizing an adjusted cathodic electrodeposition method of Hu et al.[4] In a further step, the surface was modified with phosphonic acids, which form strong chemical bonds to titania.[5] The next step will be the attachment of a responding polymer employing a reaction route described by Menzel and co-workers.[6] First experiments of releasing fluorescent dyes from differently modified coatings were done.

Results and Discussion

The resulting titania coatings were determined as porous material and layer thicknesses could be adjusted by the number of cycles during the deposition. The present titania modification as well as the pore sizes were identified. Successful surface modification could be determined. Unmodified coatings did not show any signal that would indicate the presence of phosphorous while in all spectra of coatings after the modification with different phosphonic acids the binding energy of phosphorus was apparent. Furthermore, a change in hydrophilicity of the surfaces after modification could be detected. First release studies proved that releasing dyes from the surfaces works.

Conclusion

Nanoporous titania coatings could be attached to titanium surfaces by the method of cathodic electrodeposition. We were able to successfully attach different phosphonic acids to these electrodeposited titania surfaces. First release experiments were done. All in all, the material shows high potential for the application as a stimuli-response system.

References

[1] M.S. Tonetti *et al.*, *J. Clin. Periodontol.* **2015**, 42, 1–4.

[2] D. Cecchinato *et al.*, *Clin. Oral Implants Res*. **2014**, 25, 791–796.

[3] H. Fullriede *et al.*, *BioNanoMat***2016**, 17, 59-72.

[4] C.-C. Hu *et al*, *Electrochem. Commun*. **2009,** 11, 434.

[5] H. Zuilhof *et al*., *Angew. Chem*. **2014,** 126, 6438-6474.

[6] H.Menzel *et al., Langmuir* 2004, 20, 26.

Acknowledgement

This work was part of the research association BioFabrication for NIFE.

PS2-11-413

A degradable PLLA/PVAc blend for local nitric oxide release

Alexandre D. Barbosa, Laura C. E. da Silva, Marcelo G. de Oliveira

University of Campinas, Institute of Chemistry, Campinas, BR

Introduction

Absorbable polymers are a widespread approach to produce implantable and degradable medical devices [1]. Poly(L-lactic acid) (PLLA) is a hydrolytically degradable polyester widely studied for this purpose. However, PLLA is brittle and stiff, which limits its biomedical application [2]. To overcome this issue, one possible solution is blending it with more flexible polymers, such as poly(vinyl acetate) (PVAc). PLLA/PVAc blends may be used for coating blood contacting devices. Several works have demonstrated that nitric oxide (NO) releasing biomaterials are capable of inhibiting platelet adhesion and thrombus formation [3,4]. Therefore, the insertion of an NO donor into PLLA/PVAC blend may overcome their intrinsic thrombogenicity. In this work, we prepared flexible 50:50 (wt%) PLLA/PVAc blends charged with the NO donor S-nitroso-N-acetyl-D-penicillamine (SNAP). We demonstrate that SNAP-loaded PLLA/PVAc blends are capable of sustaining NO release during prolonged periods while undergoing hydrolytic degradation after immersion in physiological medium.

Experimental Methods

Blend preparation

Initially, a 5 wt% poly(vinyl acetate) (PVAc) solution was prepared in chloroform. Solid poly(L-lactic acid) (PLLA) was added gradually to the PVAc solution under stirring. After complete PLLA dissolution, S-nitroso-N-acetyl-D-penicillamine (SNAP) pre-dissolved in tetrahydrofuran was added. Finally, chloroform was added until a 6 wt% polymer concentration was reached. The resulting solutions were cast on PTFE dishes and allowed to dry at 24 °C for 2 days. All samples were protected from light in all preparation steps and also during storage (-18 °C) in order to prevent early NO release.

Scanning electron microscopy

A Quanta FEG 250 (FEI) electron microscope operating at 5 kV was used to investigate the cryogenically fractured cross-section morphology of the samples which were previously sputter coated with Au-Pd in a Bal-Tec MED-020 (Balzers) sputter coater.

Polarized optical microscopy

A Eclipse 50i (Nikon) optical microscope equipped with cross polarizers and a DS-Ri1 (Nikon) camera was used to investigate SNAP distribution and PLLA crystallinity.

Hydrolytic degradation and real time NO release experiments

Hydrolytic degradation experiments were performed protected from light on 1 cm^2 disc samples immersed in saline phosphate buffer solution at 37 °C for 21 days. Sample weight loss and NO content on the solution were measured every 7 days. The chemiluminescent NO quantification was performed in a 280i NO analyser (Sievers, GE Analytical Instruments) operating at 37 °C and protected from light. Nitrogen was used as purging gas.

Results and Discussion

In this work, 50:50 PLLA/PVAc blends were prepared with 0.0, 3.0, 5.0 or 7.5 wt% SNAP content. Fig. 1 shows the cross-section morphology of the neat blend prior to (left) and after (middle) the hydrolytic degradation. Prior to the degradation, a flat morphology with no evidence of PLLA/PVAC phase separation is observed. Upon degradation the

spherulitic morphology attributed to the PLLA crystallization is revealed due to the preferential degradation of the amorphous PLLA located on the interfibrillar regions. These results show that PLLA crystalinity is retained on the blends as well as that PLLA/PVAc miscibility takes place on the PLLA amorphous regions. However, due to the mild heating during the hydrolytic degradation experiment, PVAc coalescence is also verified, which evidences that PLLA/PVAc blends are in fact partially miscible. Fig. 2 (left) shows the polarized optical micrograph of the non-degraded PLLA/PVAc blend loaded with 7.5 wt% SNAP. PLLA spherulites are clearly observed, as well as rectangularly shaped SNAP crystals, which are preferentially located on the interspherulitic regions. Real time NO release as a function of SNAP content is also shown in Fig. 2 (right). NO release rate showed a dose-response relationship in the 69–296 pmol cm^{-2} min^{-1} range. All the NO release rates obtained in this work are within the physiological levels of a healthy endothelial tissue, which is key to achieve desirable biological activities.

Conclusion

SNAP-loaded PLLA/PVAc blends are capable of sustaining NO release for prolonged periods, having potential for the coating of blood contacting devices.

References

[1] Nair, L. S.; Laurencin, C. T. Biodegradable polymers as biomaterials. Prog. Polym. Sci.; 32:762-798 (2007).

[2] Lautner, G.; Meyerhoff, M. E.; Schwendeman, S. P. Biodegradable poly(lactic-co-glycolic acid) microspheres loaded with S-nitroso-N-acetyl-D-penicillamine for controlled nitric oxide delivery. J. Control. Release, 225:133-139 (2016).

[3] Brisbois, E. J.; Davis, R. P.; Jones, A. M.; Major, T. C.; Bartlett, R. H.; Meyerhoff, M. E.; Handa, H. Reduction in thrombosis and bacterial adhesion with 7 day
implantation of S-nitroso-N-acetylpenicillamine (SNAP)-doped Elast-eon E2As catheters in sheep. J. Mater. Chem. B. 3:1639-1645 (2015).

[4] Ganzarolli de Oliveira, M. S-Nitrosothiols as Platforms for Topical Nitric Oxide Delivery. Basic Clin. Pharmacol. Toxicol. 119, 49-56 (2016).

Acknowledgement

ADB received a studentship from the National Council for Scientific and Technological Development (CNPq, 130960/2016-0). MGO and LCES acknowledge the São Paulo Research Foundation (FAPESP) for financial support (processes 2016/02414-5 and 2018/14242-5, respectively).

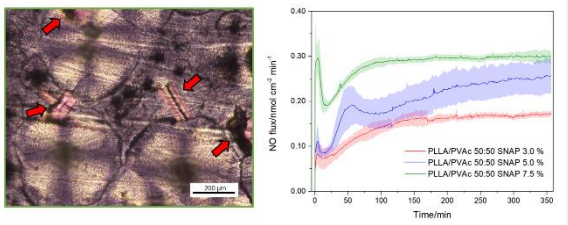

SNAP incorporation and NO release profiles

Fig. 2. On the left it is shown the polarized optical micrograph of the PLLA/PVAc blend loaded with 7.5 wt% SNAP. Red arrows indicate SNAP crystals. On the right it is shown the surface area normalized real time NO release of the PLLA/PVAc blend as a function of time and SNAP concentration.

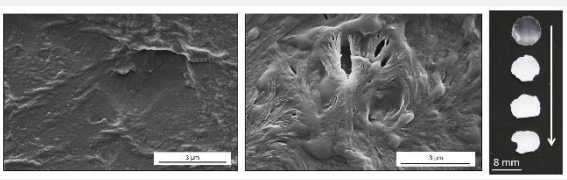

Morphology evolution upon hydrolytic degradation

Fig. 1. On the left it is presented the cross-section morphology of the PLLA/PVAc blend. On the middle, the morphology of the hydrolytically degraded blend after 21 days. On the right, the blend physical aspect evolution as a function of the hydrolitic degradation time: on the top it is shown the non-degraded blend and on the bottom the 21 days degraded blend.

PS2-11-414

Fabrication, Characterization and Antibacterial Activity of Cinnamon Bark Oil Coated 45S5 Bioactive Glass Scaffolds

Irem Unalan, Ulli Harlaß, Aldo R. Boccaccini

University of Erlangen-Nuremberg, Institute of Biomaterials, Erlangen, DE

Introduction

Bacterial infection in bone tissue engineering applications is still a critical health concern. Alternatives based on antibiotic free agents to suppress bacterial infection are being increasingly investigated. Essential oils (EOs) based on plant extracts, such as cinnamon bark oil (CBO) have been used due to their antibacterial activity, inflammatory and antioxidant potential since ancient times [1,2]. However, the volatility, stability and high sensitivity to environmental factors have limited the usage of EOs in tissue engineering applications [3]. Therefore, the combination of host matrix-EOs could be an alternative approach to overcome these drawbacks.

Experimental Methods

The aim of this study was to fabricate a novel 45S5 bioactive glass (BG) scaffold coated with cinnamon bark oil to enhance antibacterial activity. In this regard, 45S5 BG scaffolds were produced by foam replication method [4] and then a surface cleaning process was applied prior to dip-coating with CBO.

Results and Discussion

The morphology of the CBO coated scaffolds was investigated by Scanning Electron Microscopy (SEM). The results revealed that the coating with CBO did not affect the morphology (3D porosity) of scaffolds. The presence of CBO was analyzed by Fourier transform infrared spectroscopy (FTIR), and the typical peaks of CBO were observed at 1680cm^{-1} and 1625cm^{-1}. Also, the actual content and releasing behavior of the various concentrations of CBO (2.5, 5 and 7.5 (w/v) %) were tested by UV-Vis spectroscopy. Increasing the concentration of CBO in solution led to increased content of CBO incorporated onto the scaffolds. The antibacterial activity of 45S5 BG scaffolds coated with CBO was tested by the Agar diffusion method. The inhibition zone results indicated that the addition of CBO increased the inhibition zone. The inhibition zones were 2.7±0.6 cm against *Staphylococcus aureus* and 2.2±0.5 cm against *Escherichia coli*. The scaffold's bioactivity was not compromised by the coating with CBO.

Conclusion

Our results show that CBO coated 45S5 BG scaffolds could be an alternative approach to avoid bacterial infection in bone tissue engineering applications without the need to administer antibiotics.

References

[1] S. Prabuseenivasan, M. Jayakumar, S. Ignacimuthu, In vitro antibacterial activity of some plant essential oils, BMC Complement Altern Med. 6 (2006) 39. doi:1472-6882-6-39 [pii]\r10.1186/1472-6882-6-39.

[2] G. Jin, M.P. Prabhakaran, D. Kai, S.K. Annamalai, K.D. Arunachalam, S. Ramakrishna, Tissue engineered plant extracts as nanofibrous wound dressing, Biomaterials. 34 (2013) 724–734. doi:10.1016/j.biomaterials.2012.10.026.

[3] K.A. Rieger, J.D. Schiffman, Electrospinning an essential oil: Cinnamaldehyde enhances the antimicrobial efficacy of chitosan/poly(ethylene oxide) nanofibers, Carbohydr. Polym. 113 (2014) 561–568. doi:10.1016/j.carbpol.2014.06.075.

[4] Q. Z. Chen, A. R. Boccaccini, Poly (D, L-lactic acid) coated 45S5 Bioglass® based scaffolds: Processing and characterization. Journal of Biomedical Materials Research Part A: 77(3), (2016) 445-457.

PS2-11-415

Mucoadhesive electrospun fibre delivery of lidocaine HCl to porcine oral mucosa with drug distribution in tissue analysed by mass spectrometry imaging

Katharina H. Clitherow[1], Mai Bay Stie[3], Anne Mette Handler[3], Christian Janfelt[3], Hanne Mørck Nielsen[3], Sebastian G. Spain[2], Paul V. Hatton[1], Craig Murdoch[1], Jette Jacobsen[3]

[1]University of Sheffield, School of Clinical Dentistry, Sheffield, GB; [2]University of Sheffield, Department of Chemistry, Sheffield, GB; [3]University of Copenhagen, Department of Pharmacy, Copenhagen, DK

Introduction

Control of pain is a major unmet clinical need for a range of oral diseases, and commonly used dental injections are also widely feared by patients. Local delivery of an anaesthetic from an adhesive patch to alleviate pain may therefore have several applications in oral medicine and dentistry. Electrospinning, a versatile manufacturing method, has been shown to be capable of fabricating a mucoadhesive oral drug delivery system (1). The aim of this study was to incorporate lidocaine HCl into an electrospun fibre patch, and investigate drug permeation and spatial distribution in porcine buccal mucosa.

Experimental Methods

A loaded polymer solution consisting of poly(vinyl pyrrolidone), Eudragit RS100, poly(ethylene oxide), 3% (w/w) lidocaine HCl in 97% (w/w) ethanol was electrospun into a fibrous patch. These patches were placed on the surface of porcine buccal mucosa in Ussing chambers to determine the *ex vivo* lidocaine permeation. Matrix-Assisted Laser Desorption Ionisation – Mass Spectrometry Imaging (MALDI-MSI) was used to investigate the spatial drug distribution in the buccal tissues.

Results and Discussion

Permeation studies showed that lidocaine HCl released by the electrospun patches permeated the buccal mucosa and was detectable in the receptor chamber after only 15 minutes. MALDI-MSI demonstrated a time-dependent homogeneous distribution of lidocaine HCl through the epithelium and connective tissue (Figure 1).

Conclusion

Anaesthetic loaded electrospun patches were successfully manufactured and the lidocaine HCl delivered by the electrospun fibres permeated homogeneously through porcine buccal mucosa. This research demonstrates that electrospinning is a versatile manufacturing technique for the preparation of innovative therapeutic products for oral medicine, dentistry, and surgery.

References

1. M.E. Santocildes-Romero, L. Hadley, K.H. Clitherow, J. Hansen, C. Murdoch, H.E. Colley, M.H. Thornhill, P. V. Hatton, Fabrication of electrospun mucoadhesive membranes for therapeutic applications in oral medicine, ACS Appl. Mater. Interfaces. 9 (2017) 11557–11567. doi:10.1021/acsami.7b02337.

Acknowledgement

The UK EPSRC CDT in Polymers, Soft Matter and Colloids (EP/L016281/1) and AFYX are acknowledged for funding this PhD.

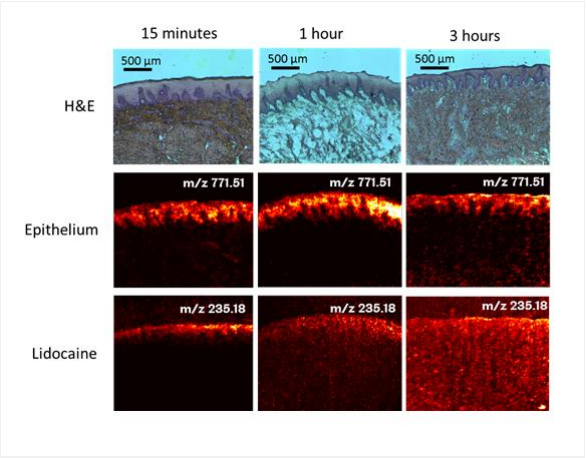

Figure 1. MALDI-MS imaging shows time-dependent distribution of lidocaine in oral tissue
H&E stained tissue sections and corresponding MALDI-MS images of porcine buccal mucosa exposed to 0.3% (w/v) lidocaine HCl solution (m/z 235.1804 [M+Na] +) over 15 minutes, 1 hour and 3 hours. The epithelium for each sample is shown using epithelial marker (PG (34:1)): m/z 771.5140 [M+Na] +.

PS2-11-416

Synthesis and in vitro characterization of AuNPs conjugated with BEL β-trefoil lectin for breast cancer therapy

Nora Bloise[1,2,3], Ranju Prasad Mandal[4], Cristina Della Pina[5], Manuele Colombo[5], Michele Rossi[5], Monica Galliano[1], Livia Visai[1,2,3]

[1]University of Pavia, Department of Molecular Medicine, Pavia, IT; [2]University of Pavia, Department of Occupational Medicine, Toxicology and Environmental Risks, ICS Maugeri, IRCCS, Pavia, IT; [3] University of Pavia, Center for Health Technologies, INSTM UdR of Pavia, PAVIA, IT; [4]IIT Bombay, Department of Bioscience and Bioengineering, Bombay, IN; [5]University of Milan, Dipartimento di Chimica and CNR-ISTM, Milano, IT

Introduction

Breast cancer therapies have been constantly improving year by year, but a comprehensive, uniform cure for this disease with minimal side effects is still a long way off. There is an increasing demand for novel diagnostic and medical therapies that utilize non-traditional sources and in this context, both natural substances (1) including fungi-derived lectins (2,3) and gold nanoparticles (AuNPs)-based delivery system (4,5) may play an important role. Indeed, lectins, thanks to their ability to identify aberrant glycans expressed by neoplastic cells as antitumor agents, have attracted great interest in cancer studies (2). Among them, BEL β-trefoil (Boletus edulis lectin) was reported to exert strong dose-dependent antiproliferative effects on human cancer cell lines (6-8). Although its mechanism of action is unclarified, its unique carbohydrate specificity and structure domains make BEL β-trefoil a potential candidate for a nanobiotechnological-based cancer therapy. AuNPs-based delivery systems offer many advantages due to their unique chemical and physical properties, that make them new agents for photo-thermal therapy, biocompatible, easy to modify and functionalize with cancer-specific biomolecules (4,5). AuNPs can accumulate in tumor tissue either passively via the EPR effect or actively via their conjugation with a targeting molecule (4,5). Thus, AuNPs conjugation with drugs can enhance drug uptake into cancer tissue. However, despite the broad interest surrounding gold-based nanomedicines, technical challenges associated with their synthesis and formulation still remain, and growing studies have been devoted to obtaining AuNPs by green and safe methods (9,10). The aim of this study is to modify the surface of PEG AuNPs with the conjugation of BEL β-trefoil and provide its *in vitro* physicochemical and biological characterization. The idea of the project is to combine the photothermal therapy given by the exposition of AuNPs to a laser source, to the targeted and antitumoral action of BEL β-trefoil, by using thiol-ending biocompatible polymers, polyethylene glycol (COOH-PEG-SH) as stabilizer agent for the gold nanoparticles.

Experimental Methods

First, AuNPs coated with a wide range of COOH-PEG-SH concentrations were used in order to optimize the PEG concentration. AuNPs with different dimensions (Au core average < 10 nm) were synthetized in water solution in the presence of thiol-ending biocompatible polymers COOH-PEG-SH, as not-toxic stabilizers of gold aggregate. The lectin was covalently conjugated to the PEG carboxyl groups on PEG-gold nanoparticles using the previously reported EDC-NHS protocol with a minor modification. The products were then characterized by UV-visible spectroscopy absorption studies, Circular dichroism (CD), Dynamic Light Scattering and BCA analysis. The physicochemical characterization of AuNPs conjugated with the lectin was also assessed in different experimental conditions (time, temperature, buffer, medium with or w/o serum). Viability (MTT) and uptake studies (confocal microscopy) were carried out to verify the efficiency of lectin conjugated AuNPs against the target breast cancer cells.

Results and Discussion

Specifics physicochemical analyses assessed that PEG-AuNPs size and stability were strictly controlled by gold and polymer concentration. Moreover, the surface modification of AuNPs with lectin was confirmed by UV–vis spectra. As shown in Figure 1(a) a significant change in absorption spectra was obtained after lectin conjugation to AuNPs, suggesting the successful interaction between protein and gold nanoparticles. It is well accepted that for targeting properties of the nanoconjugate, it is important that the protein keeps its structure and function. Circular Dichroism was used to investigate the secondary structure of the protein in the AuNPs/BEL β-trefoil nanoconjugate (Figure 1b). The results clearly demonstrated that there was no significant modification in the protein structure percentages, indicating that the protein maintained its secondary structure even after conjugation with the nanoparticles, a key aspect for its biological applications. Viability assays showed the anti-proliferative efficacy of BEL β-trefoil conjugated to AuNPs, providing a cellular surface fluorescence distribution, which was another evidence of its active function in recognizing the tumor cells.

Conclusion

Preliminary data showed the successful formation of AuNP-BEL lectin conjugate, suggesting the immense effects of PEG concentration on the conjugation process. Currently, experiments are on-going to explain other aspects related to the efficacy and the uptake mechanism of the nanoconjugate systems in the target tumour cells. Overall, this study should offer an important advancement in breast cancer therapy and diagnosis, developing new anticancer conjugated-AuNPs by a simple and green method.

References

1 Makam SN, Chidambara Murth KN, Sultanpur CM, RM. Rao. Natural molecules as tumour inhibitors: Promises and prospects. Journal of Herbal Medicine 2014; 4(4): 175-187.
2. Singh RS, Kaur HP, Kanwar JR. Mushroom Lectins as Promising Anticancer Substances. Curr Protein Pept Sci. 2016; 17(8):797-807. Review.
3. Ivanova TS, Krupodorova TA, Barshteyn VY, Artamonova AB, Shlyakhovenko VA. Anticancer substances of mushroom origin. Exp Oncol. 2014; 36(2):58-66. Review.
4. Lee J, Chatterjee DK, Lee MH, Krishnan S. Gold nanoparticles in breast cancer treatment: promise and potential pitfalls. Cancer Lett. 2014; 347(1):46-53.
5. Rizk N, Christoforou N, Lee S. Optimization of anti-cancer drugs and a targeting molecule on multifunctional gold nanoparticles. Nanotechnology. 2016;27(18):185704.
6. Bovi M, Carrizo ME, Capaldi S, Perduca M, Chiarelli LR, Galliano M, Monaco HL. Structureof a lectin with antitumoral properties in king bolete (Boletus edulis) mushrooms. Glycobiology. 2011; 21:1000-1009.
7. Bovi, M, L. Cenci. BEL β-trefoil: A novel lectin with antineoplastic properties in king bolete (Boletus edulis) mushrooms. Glycobiology 2013; 23(5): 578-592.
8. Perduca M, Dalle Carbonare L, Bovi M, Innamorati G, Cheri S, Cavallini C, Scupoli MT, Mori A, Valenti MT. Runx2 downregulation, migration and proliferation inhibition in melanomacells treated with BEL β-trefoil. Oncol Rep. 2017; 37(4):2209-2214.
9. Hussain I, Singh NB, Singh A, Singh H, Singh SC. Green synthesis of nanoparticles and its potential application. Biotechnol Lett. 2016; 38(4):545-60.
10. Spadavecchia J, Movia D, Moore C, Maguire CM, Moustaoui H, Casale S, Volkov Y, Prina-Mello A. Targeted polyethylene glycol gold nanoparticles for the treatment of pancreaticcancer: from synthesis to proof-of-concept in vitro studies. Int J Nanomedicine. 2016; 11:791-822.

Acknowledgement

This research was supported by a grant of the Italian Ministry of Education, University and Research (MIUR) to the Department of Molecular Medicine of the University of Pavia under the initiative “Dipartimenti di Eccellenza (2018–2022)”. Bloise N. thanks the support by Fondazione Umberto Veronesi Fellowship – GRANT 2017 and GRANT 2018. Prasad Mandal R thanks "CICOPS Fellowship Programme, University of Pavia". Della Pina C. thanks the Università degli Studi di Milano for financial support by the Piano di Sostegno alla Ricerca – Linea 2 Azione A 2018, project PSR2018_DIP_005_DELLA_PINA_CRISTINA.

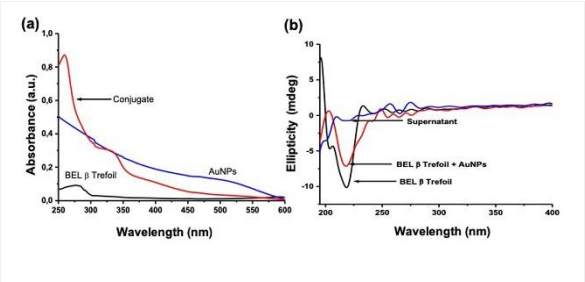

Figure 1
Results of a) Absorption and b) Circular dichroism studies

PS2-11-417

Drug Conjugated Smart Cross-Linked Micelles For Breast Cancer Delivery

Nazende N. Akşit[1], Gizem T. Ulu[2], Yusuf Baran[2], Sevil Dinçer İşoğlu[1]

[1]Abdullah Gul University, Bioengineering Department, Kayseri, TR; [2]İzmir Institute of Technology, Molecular Biology and Genetic Department, İzmir, TR

Introduction

Micelles formed by amphiphilic polymers are one of the most important drug/nanocarrier formulation products, in which the core part is suitable for encapsulation of hydrophobic agent whereas the outer shell can be utilized for targeting the drug to the disease area. But they may encounter difficulties in biodistribution of encapsulated drugs because they have a tendency to be dissociated in dilution or high ionic strength. To overcome this problem, covalently stabilized structures produced by cross-linking in core or shell part, which can prevent the micelle dissociation and regulate drug release, have been proposed recently.

Experimental Methods

In this study, we aim to target breast cancer cells by smart core cross-linked (CCL) micelles conjugated to DOX as an anticancer agent. These carriers are expected to release conjugated drug by the effect of pH-sensitive hydrazone and acetal bonds. At first, macroinitiator of OEGMA was synthesized by RAFT polymerization and it was followed by copolymerization of macroCTA with 4-VP and DEGMA in the presence of acetal-based cross-linker. Then, a peptide sequence recognizing HER2 on SKBR3 cells was incorporated into the micelle by carbodiimide reaction. Following this step, the drug was conjugated to the micelles and hydrazone linkage was formed between drug and carrier. For the structural characterization ^{1}H-NMR, ^{13}C-NMR and FTIR were used and the results were confirmed the polymer synthesis and cross-linked micelle formation. Size and morphological characterizations were performed by Zeta Sizer and TEM, respectively. The release profiles DOX from dox conjugated micelles were performed at different pH conditions in vitro, pH 4.5 and pH 7.4 respectively. The efficiency of drug conjugated micelles on SKBR-3 and MCF-10A cell lines was determined by using cell viability XTT assay.

Results and Discussion

Analyses showed that micelles with very low size distribution and below 100 nm were obtained successfully. The pH-dependent release profile of DOX from the dox conjugated crosslinked micelles was %80 and 42 % at pH 4.5 and pH 7.4 respectively. Drug conjugated micelles interacted to SKBR3 and MCF-10A cell lines for toxicity and drug efficiency and the results were evaluated. The IC50 values were determined as 0.45;1.07 µM on SKBR3 and 0.16;0.18 µM on MCF-10A for peptid conjugated-DOX loaded micelles and DOX-loaded micelles, respectively.

Conclusion

New amphiphilic block copolymers of OEGMA with a functional monomer DEGMA and 4-VP were synthesized via RAFT polymerization and crosslinked with acetal base crosslinker. Maleimide-modified anticancer drug DOX conjugated with core crosslinked micelles via acid-sensitive bonds. Drug release experiments proved that the DOX-conjugated micelles have more rapid drug release at acidic environment (pH 4.5). According to in vitro studies, the cytotoxicity of peptid conjugated-DOX loaded micelles was higher than free DOX and DOX-conjugated-micelles at

the same equivalent concentration of DOX, indicating that peptide-conjugated micelles increase the effect of DOX on SKBR-3 cell line. According to this result, the versatility of this smart nanocarrier system is promising in breast cancer therapy.

References

İ.A. İşoğlu, Y. Özsoy, S. İşoğlu, Advances in micelle-based drug delivery: Cross-linked systems, Current Topics in Medicinal Chemistry, 2016, Doi: 10.2174/1568026616666161222110600.

Acknowledgement

This work is supported by the Scientific and Technological Research Council of Turkey (TÜBİTAK), Project Number: 116R057. Nazende Nur Akşit is supported by YÖK 100/2000 Ph.D. scholarship program and TÜBİTAK 116R057 and Gizem Tuğçe Ulu is supported by TÜBİTAK 116R057.

PS2-11-418

Guiding mesenchymal stem cell differentiation using mesoporous silica nanoparticle-based films

Lea Andree, Pichaporn Sutthavas, Pamela Habibovic, Sabine van Rijt

Maastricht University, MERLN, Maastricht, NL

Introduction

The development of smart interfaces that can guide tissue formation is of great importance in the field of regenerative medicine. Nanoparticles represent an interesting class of biomaterials to enhance regenerative treatments by enabling close control over surface properties and directing cellular responses. Moreover, nanoparticles can be used to provide temporally controlled delivery of (multiple) biochemical compounds. Here, we exploited the cargo loading and surface functionalization properties of mesoporous silica nanoparticles (MSNs) to design instructive films that can guide human mesenchymal stem cell (hMSC) differentiation towards the osteogenic lineage. The aim was to form biocompatible, stable MSN-based films that support stem cell adhesion and proliferation. The MSNs porous structure was used for delivering dexamethasone (Dex), a known stimulator of osteogenic differentiation. The ability of the films to induce the osteogenic differentiation of hMSCs and support their ECM formation *in vitro* was investigated. Furthermore, using lipid surface modifications, MSNs were provided with a fluid-biocompatible surface that can simultaneously be used to modulate release kinetics.

Experimental Methods

Surface and core modified MSNs (amines on the surface and thiols in the core) as well as lipid modified MSNs were synthesized using previously reported methods [1-3]. MSN-films were created using spincoating. The MSNs and MSN films were characterized by dynamic light scattering, and scanning and transmission electron microscopy. Biocompatibility of the films was tested using LDH and DNA quantification. Cargo release from the films was measured by incorporating fluorescent dyes or dexamethasone within the MSNs (plate reader, flow cytometry, ALP assay). High-throughput cell morphology analysis was done using fluorescent microscopy and image analysis (ImageJ).

Results and Discussion

We developed biocompatible MSN-based films that support stem cell adhesion and proliferation and demonstrated that these MSN films allowed efficient local delivery of biomolecules without effecting film integrity. Films loaded with the osteogenesis-stimulating drug dexamethasone (Dex) were able to induce osteogenic differentiation of hMSCs *in vitro*. Dex delivery from the films led to increased alkaline phosphatase levels and matrix mineralization compared to directly supplementing Dex to the medium. Furthermore, we demonstrated that Dex release kinetics can be modulated using surface modifications with supported lipid bilayers.

Conclusion

In this project we demonstrate the potential of mesoporous silica nanoparticles (MSNs) as drug-delivering surface coatings. First, we show differentiation of mesenchymal stem cells towards the bone lineage when in contact with MSC films loaded with dexamethasone. Furthermore, we demonstrate that modification of MSNs with supported lipid bilayer allows to control the drug release dynamics. Given the range of loadable cargos and the tunability of release

kinetics, MSN coatings can be used to mimic the sequential appearance of bioactive factors during tissue regeneration, which will ultimately lead to biomaterials with improved bioactivity.

References

[1] V. Cauda, A. Schlossbauer, J. Kecht, A. Zurner, T. Bein, Multiple core-shell functionalized colloidal mesoporous silica nanoparticles, J Am Chem Soc 131(32) (2009) 11361-70.

[2] V. Cauda, H. Engelke, A. Sauer, D. Arcizet, C. Brauchle, J. Radler, T. Bein, Colchicine-loaded lipid bilayer-coated 50 nm mesoporous nanoparticles efficiently induce microtubule depolymerization upon cell uptake, Nano Lett 10(7) (2010) 2484-92.

[3] R. Rosenbrand, D. Barata, P. Sutthavas, R. Mohren, B. Cillero-Pastor, P. Habibovic, S. van Rijt, Lipid surface modifications increase mesoporous silica nanoparticle labeling properties in mesenchymal stem cells, Int J Nanomedicine 13 (2018) 7711-7725.

Acknowledgement

We would like to thank the province of Limburg (LINK) for providing financial support to this project.

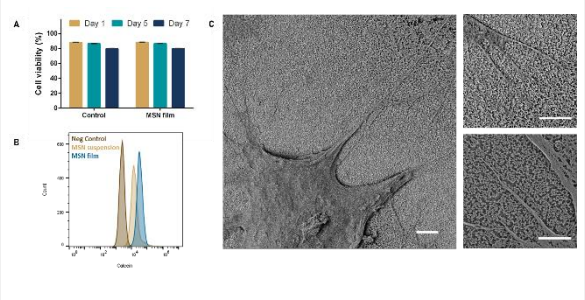

Figure 1.
(A) Viability of hMSCs based on extracellular lactate dehydrogenase levels for cells cultured on glass (control) or MSN films for 1, 5 and 7 days. Data shown as mean ± SEM from biological triplicates. B) Histograms of calcein uptake, determined by fluorescence intensity, from hMSCs cultured on MSN films for 2 days, or with MSN suspensions. As a negative control, hMSCs were cultured on glass without MSNs. C) SEM images of hMSCs cultured on MSN films for 2 d. Scale bar represents 2 µm, inserts show formation of extended filopodia on MSN films.

PS2-11-419

A bioactive fibrin gel to induce regeneration of functional cartilage in a goat model

Elif Vardar[1,2], Evi Balet[1,2], Ganesh Vythilingam[3], Dominique Pioletti[2], Pierre-Yves Zambelli[1]

[1]CHUV, Department of Paediatrics, Lausanne, CH; [2]EPFL, School of Engineering, Lausanne, CH; [3]UM, Department of Surgery, Kuala Lumpur, MY

Introduction

Articular cartilage (AC) defects are common and occur in all ages and sexes. Routine knee arthroscopies reveal that 65% of the patients present AC defects and more than 500'000 interventions are performed in the USA to treat cartilage related-injuries (1). The reconstruction of hyaline-like cartilage remains a major clinical challenge due to its limited intrinsic healing capacity. Currently, microfracture is the gold standard for cartilage repair. However, several studies showed that microfracture achieved only good clinical outcomes in short-term follow-up. Treatment failure was observed in many patients 5 years after surgery (2). In this study, injectable fibrin beads, conjugated with a recombinant insulin-like growth factor-1, evaluated to regenerate functional and stable cartilage. IGF-1 is known to enhance matrix synthesis of chondrocytes of the surrounding tissue, should protect the synovial membrane from chronic inflammation, and stimulate chondrogenesis of MSCs migrating from the subchondral bone to the defect site (3). Therefore, this may result in the formation of durable hyaline-like cartilage tissue. Fibrin beads fabricated using a microfluidic system, described previously by our group (4). In the first part, the stability and the in vitro compatibility of the fibrin beads have been confirmed. In the second part, the regeneration capacity of the fibrin beads will be assessed in a full-thickness knee cartilage defect in a goat model.

Experimental Methods

Fibrin bead preparation

The fibrin beads fabricated using a microfluidics system (4). Briefly, computer-controlled syringe pumps (neMESYS, Germany) were used to adjust flow rates. One microfluidic channel was loaded with an enzyme solution containing 200 U/mL of human thrombin (Sigma Aldrich, CH), 200 U/mL of factor XIIIa (Fibrogammin, CSL Behring UK) and 10 mM Ca^{2+} in tris-buffered saline (TBS) supplemented with a recombinant IGF-1, previously described by our group (5).

Stability testing

Fibrin beads were incubated at 4°C or 37°C for 1, 3, and 6 months. Fibrin microbeads were produced using fibrinogen supplied by Baxter or Milan Analytica (plasminogen depleted fibrinogen). To evaluate the rheological properties, fibrin gels with the same fibrinogen concentration as fibrin beads were prepared. Both fibrin beads and gels were incubated in PBS at 4°C or 37°C. Samples were visualized under a microscope and characterized with a C-VOR rheometer (Bohlin, Germany).

In vitro experiments

Bovine chondrocytes from passage 4 used for the cell viability and proliferation assays. Fibrin beads cultured with bovine chondrocytes in DMEM supplemented with 10 % FBS and 1 % pen/strep for 14 days. The viability of bovine chondrocytes on day 14 was evaluated using Live/Dead staining (Live/Dead Viability/Cytotoxicity Kit, Invitrogen) and images were obtained with a Zeiss Axioplan microscope. Bovine chondrocytes proliferation on days 3 and 7 was evaluated using AlamarBlue assay. Currently, *in vivo* experiments are ongoing.

Results and Discussion

Over 6 months, there was no size and shape difference between the samples kept at 4°C. However, the fibrin beads made from the non-depleted fibrinogen (Baxter) had completely degraded after 2 months at 37°C in contrast to the fibrin beads made from the plasminogen-depleted fibrinogen (Milan Analytica) (Figure 1A). This complete degradation might be resulted from the plasmin activation at 37°C. Similar observations were obtained for the elastic modulus of fibrin beads samples. The elastic modulus of samples kept at 4°C did not change over 6 months. However, the elastic modulus of all samples kept at 37°C decreased significantly over 6 months (Figure 1B). Fibrin beads made from plasminogen-depleted fibrinogen released about 32% of the initially loaded recombinant IGF-1 when incubated at 37°C on day 90. When the cells were incubated with fibrin beads, there was no change in cell proliferation rate on days 3 and 7 (Figure 2A). The viability of bovine chondrocytes, incubated with fibrin beads, was over 86% on day 14 (Figure 2B).

Conclusion

In this study, we proposed a fibrin-based injectable that may offer an improved therapeutic potential to regenerate cartilage, rather than treating only the symptoms of articular cartilage defects. The preliminary results showed that sterile fibrin beads promoted bovine chondrocytes proliferation and viability. The goat study will show us regenerative potential of this new injectable.

References

1. C. Haasper et al., “Tissue engineering of osteochondral constructs in vitro using bioreactors”, Injury, (2008) 39:66-76

2. R. Gudas et al., “Comparison of osteochondral autologous transplantation, microfracture, or debridement techniques in articular cartilage lesions associated
with anterior cruciate ligament injury: a prospective study with a 3-year followup”, Arthroscopy (2013) 29:89-97

3. D. Goyal et al., “Evidence-based status of microfracture technique: a systematic review of level I and II studies”, Arthroscop (2013) 29:1579-1588

4. Vardar E et al., "Microfluidic production of bioactive fibrin-microbeads embedded in crosslinked collagen used as an injectable bulking agent for urinary incontinence treatment", Acta Biomater. (2018) 67:156-166

5. Vardar E et al., "IGF-1-containing multi-layered collagen-fibrin hybrid scaffolds for bladder tissue engineering", Acta Biomater. (2016) 1:75-85

Acknowledgement

The authors would like to thank the Bioimaging and Optics Platform of EPFL. This research was supported by Innosuisse project-27619.1.

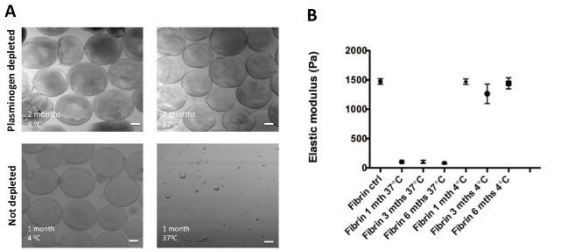

Figure 1. Stability results (A) Fibrin beads made from either plasminogen-depleted or non-depleted fibrinogen incubated in 37°C over 2 months (B) Elastic modulus values (Pa) of fibrin beads incubated 4°C or 37°C for 1, 3, and 6 months. Scale bars represent 50 µm.

Figure 1

Figure 1. Stability results (A) Fibrin beads made from either plasminogen-depleted or non-depleted fibrinogen incubated in 37°C over 2 months(B) Elastic modulus values (Pa) of fibrin beads incubated 4°C or 37°C for 1, 3, and 6 months.Scale bars represent 50 µm.

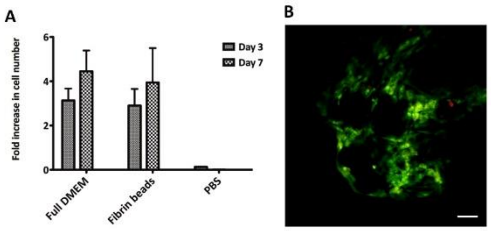

Figure 2. Bovine chondrocytes metabolic activity and viability on fibrin beads (A) AlamarBlue assay showing metabolic activity of bovine chondrocytes on day 3 and 7 after cell seeding. AlamarBlue-specific fluorescence values were normalized to the ones obtained on day 1 after cell seeding (B) Live (green) and dead (red) staining of bovine chondrocytes 14 days after cell seeding. Scale bar represents 50 µm.

Figure 2

Figure 2. Bovine chondrocytes metabolic activity and viability on fibrin beads (A) AlamarBlue assay showing metabolic activity of bovine chondrocytes on day 3 and 7 after cell seeding. AlamarBlue-specific fluorescence values were normalized to the ones obtained on day 1 after cell seeding(B) Live (green) and dead (red) staining of bovine chondrocytes 14 days after cell seeding.Scale bar represents 50 µm.

PS2-11-420

Microenvironment targeted microRNA therapy using a megamer-based delivery system activatable by stepwise stimulation

Qida Hu[1], Wangteng Wu[1,2], Meng Wang[1], Shiyi Shao[1], Guping Tang[2], Tingbo Liang[1]

[1]First Affiliated Hospital of Zhejiang University School of Medicine, Department of Hepatobiliary and Pancreatic Surgery, Hangzhou, CN; [2]Zhejiang University, Institute of Chemical Biology and Pharmaceutical Chemistry, Hangzhouo, CN

Introduction

miRNA therapy against malignancies requires precise release of the cargo miRNA therapeutics to reduce off-target adverse effect and to increase intratumoral miRNA dosage. miRNA-122 (miR-122), an abundant miRNA in normal liver tissues, is downregulated in liver cancer where lack of miR-122 promotes carcinogenesis and tumor growth. Controlled release of miR-122 therapeutics in liver cancer is required for possible miR-122 therapy for liver cancer.

Experimental Methods

We synthesized a PEGylated delivery system based on megamer core assembled from low-generation polyamidoamine (PAMAM) dendrimers, namely, a biodegradable, oncosensitive, megamer-based (BOMB) nanoparticle system. The BOMB system was evaluated for the functionality of microenvironment targeting and stimulated stepwise activation, and was then applied to miR-122 delivery for liver cancer management.

Results and Discussion

The BOMB system was successfully developed for functional delivery of miRNA therapeutics. BOMB carrying miR-122 (BOMB/miR-122) forms a sphere-like nanoparticles, which could be completely biodegraded with stimulus of weak acidity and reduction mimicking liver cancer microenvironment. The BOMB/miR-122 nanoparticles showed an excellent responsiveness to stepwise stimulation of low pH and reduction, and efficient cellular uptake and internalization in liver cancer cells. BOMB/miR-122, in conditions like tumor microenvironment, also demonstrated a significantly enhanced expression of cargo miR-122, comparable to the effect of positive control treatment (PAMAM assembled megamer). In vivo treatment with BOMB/miR-122 via tail-vein injection significantly inhibited xenograft liver cancer growth, benefiting from the controlled release of cargo miR-122 therapeutics with the stepwise activation of microenvironment stimulation.

Conclusion

We successfully developed an advanced delivery system for microenvironment targeted microRNA therapy, which can be activatable by stepwise stimulation. Optimized delivery strategy using the BOMB system raises the possibility of clinical practice of miR-122 application.

Acknowledgement

This work was financially supported by the National Natural Science Foundation of China (81502026, 81830089, and 81530079), Zhejiang Provincial Natural Science Foundation (LQ16H180002 and LY18H160026), and National High Technology Research of China (SS2015AA020405).

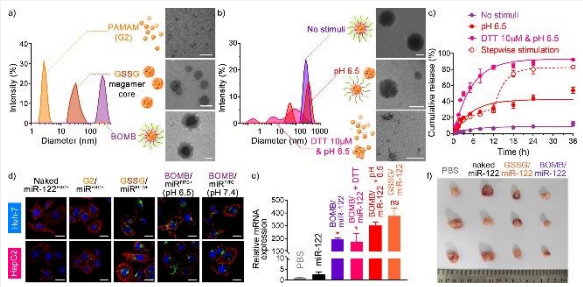

Figure 2

Figure 2. Functionality characterization. (a) Size distributions of PAMAM (second generation, G2) dendrimers, G2 dendrimer assembled megamer (GSSG megamer core), and BOMB system, and corresponding representative transmission electron microscopy (TEM) images. (b) Size distributions of the BOMB system carrying miR-122 without stimuli, with acid stimulation, or with dual stimulation of weak acidity and reduction, and corresponding representative TEM images. Bar represents 100 nm. (c) Release patterns of mine-122 from the BOMB/miR-122 nanoparticles with stepwise activation. (d) Enhanced cellular intake of the FITC-labelled miR-122 (green) via the BOMB system in liver cancer cell lines. Bar represents 20 μm. (e) Increased intracellular miR-122 expression via the BOMB system. (f) Xenograft tumors after tail-vein administration of BOMB/miR-122 system in vivo.

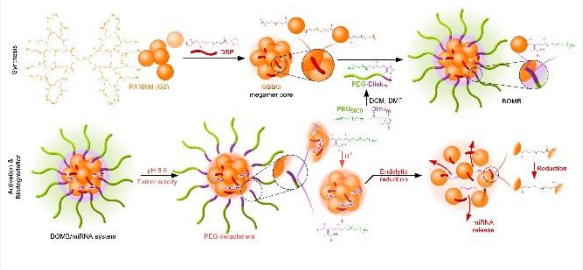

Figure 1

Figure 1. Schemes of BOMB synthesis (upper panel) and stepwise activation and biodegradation (lower panel).

PS2-11-421

Immunocompatible mechano-responsive liposomes for targeted vasodilator delivery

Sofiya Matviykiv[1], Gabriela Gerganova[1], Tamás Mészáros[2], Gergely T. Kozma[2], Janos Szebeni[2], Andreas Zumbuehl[3], Bert Müller[1]

[1]University of Basel, Biomaterials Science Center, Allschwil, CH; [2]Semmelweis University, Nanomedicine Research and Education Center, Budapest, HU; [3]University of Fribourg, Department of Chemistry, Fribourg, CH

Introduction

It has been reported that the mechano-responsive Pad-PC-Pad liposomal system is a container for nitroglycerin release at atherosclerotic sites [1]. These liposomes, however, show only limited stability at the body temperature, owing to the phospholipid phase transition temperature at 37 °C. Through a longer fatty acyl chain, the phospholipid Rad-PC-Rad exhibits its main phase transition temperature at 45 °C and these liposomes preserve their stability for the clinically relevant body temperature range [2]. Therefore, we have performed *in vitro* studies of Rad-PC-Rad. It is well known that the intravenous administration of liposomes triggers the immediate activation of the immune system, resulting in a hypersensitivity reaction, which is driven by the activation of the complement system and consecutive production of pro-inflammatory cytokines. To advance the idea towards clinical applications, we have investigated the activation of complement proteins and cytokines upon their contact with human blood.

Experimental Methods

Rad-PC-Rad lipids were synthetized [2] and liposomes formulated using the thin-film method. Four Rad-PC-Rad liposomal formulations, bare and nitroglycerin-loaded, with and without PEGylation, were prepared. Their sizes ranged from 100 to 140 nm, as verified by dynamic light scattering. To detect the activation of complement proteins, Rad-PC-Rad liposomes were incubated with human sera following the established protocol [3]. Samples were analysed using ELISA MicroVue kits (SC5b-9 Plus, C4d, Bb, C3a, C5a). The level of complement activation induced by Rad-PC-Rad liposomes was compared to the FDA-approved liposomal drugs Doxil® and AmBisome®. To detect the production of pro-inflammatory cytokines, Rad-PC-Rad liposomes were incubated with human whole blood or with isolated leukocytes. Samples were analyzed using cytometric bead array tests (IL-1b, IL-6, IL-8, IL-12p70, TNF-α, IL-10).

Results and Discussion

From the *in vitro* immunocompatibility of Rad-PC-Rad liposomes we observed that five donors showed lower or similar level of complement proteins in comparison to FDA-approved liposomal drugs. One of six donors, however, demonstrated an extreme increase in complement concentration. We identified that the protein activation occurred via the alternative pathway. The identification of highly reactive donor motivated further studies. Cytokine release allows to estimate the inflammatory properties of the tested liposomes. The effect of Rad-PC-Rad liposomes upon production of cytokines was lower or comparable to the negative control. An occasional increase of specific cytokine towards particular liposomal suspension was observed. However, such an increase was non-ubiquitous and expected to be clinically irrelevant.

Conclusion

The results of our study demonstrate that Rad-PC-Rad liposomes neither cause a substantial activation of the complement system nor the production of pro-inflammatory cytokines in the majority of investigated donors' blood. Occasional events, however, can lead to a severe immune response towards Rad-PC-Rad. This behaviour can be attributed to the biological variability between donors and requires a number of donors that significantly exceeds the one used for the present study.

References

1. Buscema M. *et al*.,JCR 264:14-23, 2017
2. Neuhaus F. *et al*., Langmuir 34: 3215-3220, 2018
3. Matviykiv S. *et al*., Prec. Nanomed. 1:43-62, 2018

Acknowledgement

S.M. acknowledges the support of the Swiss Government via Swiss Excellence Scholarship.

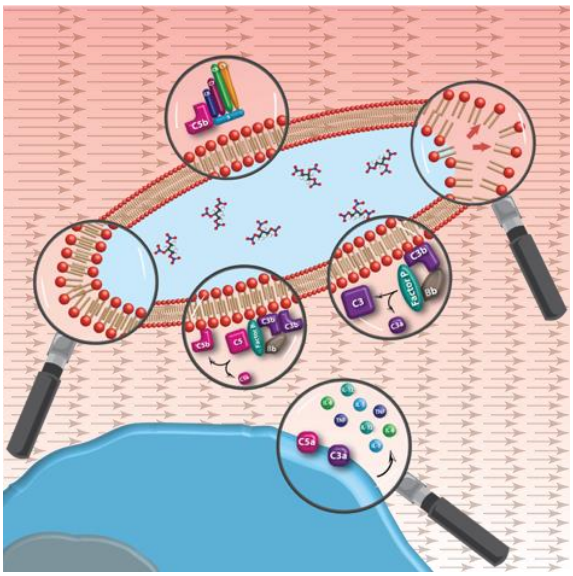

The mechano-responsive Rad-PC-Rad liposomes.
The mechano-responsive Rad-PC-Rad liposomes, designed to deliver vasodilator drug to atherosclerotic arteries, demonstrate in vitro immune compatibility. [3]

PS2-11-422

Responsivity of siRNA-loaded phenylboronate-functionalized polyion complex (PIC) micelles against biomolecules

Mitsuru Naito[1], Naoto Yoshinaga[2], Takehiko Ishii[2], Akira Matsumoto[3], Kazunori Kataoka[4], Kanjiro Miyata[2]

[1]The University of Tokyo, Graduate School of Medicine, Tokyo, JP; [2]The University of Tokyo, Graduate School of Engineering, Tokyo, JP; [3]Tokyo Medical and Dental University, Institute of Biomaterials and Bioengineering, Tokyo, JP; [4]Innovation Center of NanoMedicine, Kawasaki, JP

Introduction

Stimuli-responsive systems has been used in biomaterial applications, such as drug delivery, to exert intelligent functions. Especially, intracellular condition-responsive systems, *e.g.*, intracellular-reductive condition, acidic pH or enzyme responsive systems, offer much attention because they allow for programmed release of drug payloads from deliver cargo. In this context, we have fabricated an intracellular-ATP (adenosine triphosphate) responsive polyion complex micelle for nucleic acid delivery[1-3]. We utilized a phenylboronate functionality to induce intracellular ATP responsivity. Phenylboronic acid (PBA) is a synthetic molecule capable of forming reversible covalent esters with 1,2- or 1,3-*cis*-diols. By forming boronate esters in the PIC core as crosslinkers, the stability of phenylborate-modified PIC increased at extracellular condition (or low ATP concentration condition). This feature of high stability at extracellular condition is advantageous for drug delivery systems. Whereas their high stability, the PIC micelles readily released nucleic acids at high ATP concentrations associated with the intracellular condition (> 1 mM) because *cis*-diol in ATPs underwent exchange reaction with the crosslinking boronate esters.
In this study, we have carefully analyzed their responsivity against bio-molecules possessing *cis*-diol moieties to reveal their unique behavior.

Experimental Methods

Firstly, fluorescently-labeled siRNA were loaded into polyion complex micelles with phenylboronate functionality according to our previous report[3]. Various ATP-like bio-molecules, *e.g.*, ADP (adenosine diphosphate), AMP (adenosine monophosphate), adenosine, cAMP (cyclic-AMP), glucose and G6P (glucose-6-phosphate), were added to the PIC micelle at desired concentrations and incubated for 1 h. The released siRNA was analyzed by FCS (fluorescence correlation spectroscopy).

Results and Discussion

As we reported previously, high ATP concentration caused siRNA release after incubation. Compared with ATP, glucose and cAMP, which have *cis*-diol moiety with lower binding constant with PBA group and no cis-diol moiety, respectively, didn't induce release of siRNA even at the highest concentration. ADP, AMP and adenosine with reduced phosphate moiety compared with ATP showed less activities for siRNA release, though they originally have the same binding constant with PBA. These results indicate that cis-diol moiety with comparable binding affinity to ATP (or ribose ring) is the initial key factor to induce siRNA release from PIC micelle. Additionally, coupled anionic phosphate group boosts siRNA release may be because their negative charges unbalance the charge stoichiometry of PIC micelles. This hypothesis were further confirmed by the addition of phosphorylated glucose, G6P, which has comparable binding affinity to "less active" glucose in expectation of the enhancement of siRNA release activity by the phosphorylation. As we expected, G6P induced release of siRNA at higher concentration.

Conclusion

In this study, we clarified the ATP-responsive mechanism in phenylboronate functionalized-PIC micelles. The bio-molecule responsivity study revealed that (1) the cis-diol group with higher binding affinity with PBA group induced and (2) the number of anionic charges in the molecule boosted the release of siRNA in this system. As a result, ATP with tri-phosphate is the most active molecules to induce siRNA release among the tested molecules. Thus, we conclude that ATP is the main inducer for intracellular release of siRNA in this system.

References

1) M. Naito, T. Ishii, A. Matsumoto, K. Miyata, Y. Miyahara, K. Kataoka, Angew. Chem. Int. Ed., 2012, **51**, 10751–10755

2) N. Yoshinaga, T. Ishii, M. Naito, T. Endo, S. Uchida, H. Cabral, K. Osada, K. Kataoka, J. Am. Chem. Soc., 2017, **139**, 18567–18575

3) M. naito, N. Yoshinaga, T. Ishii, A. Matsumoto, Y. Miyahara, K. Miyata, K. Kataoka, Macromol. Biosci., 2018, **18**, 1700357

Acknowledgement

This research was financially supported by the Center of Innovation (COI) Program from the Japan Science and Technology Agency (JST); the Grants-in-Aid for Scientific Research KAKENHI [grant number 25000006], [grant number 25282141], [grant number 17H02098] and [grant number 15H06108] from the Ministry of Education, Culture, Sports, Science and Technology (MEXT); the Basic Science and Platform Technology Program for Innovative Biological Medicine from the Japan Agency for Medical Research and Development (AMED); the Research Complex Program from the Japan Science and Technology Agency (JST); the Cooperative Research Project of Research Center for Biomedical Engineering from the MEXT; and the Mochida Memorial Foundation for Medical and Pharmaceutical Research.

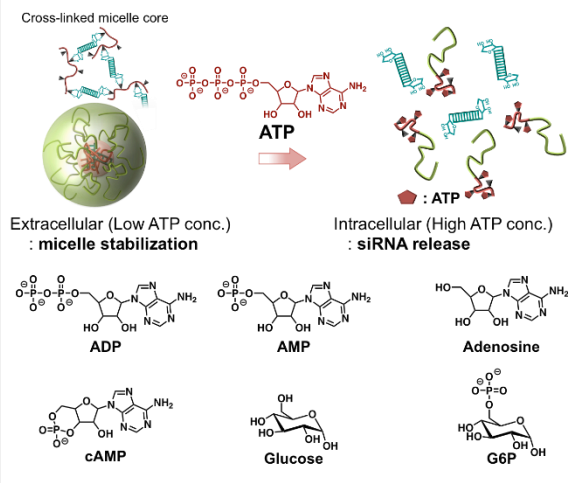

Scheme of this study
Schematic illustration of ATP-responsive release of siRNA and chemical formula of tested ATP-like bio-molecules.

PS2-11-423

Antibacterial and antitumorigenic activities of nitric oxide-releasing chitosan coated Fe_3O_4@Ag nanoparticles

Amedea B. Seabra[1], Joana C. Pieretti[1], Wallace R. Rolim[1], Milena T. Pelegrino[1], Marcelly C. Gonçalves[2], Gerson Nakazato[2], Ana Carolina S. de Souza[1], Olga Rubilar[3]

[1]Universidade Federal do ABC, Center for Natural and Human Sciences, Santo André, BR; [2]Universidade Estadual de Londrina, Department of Microbiology, Londrina, BR; [3]Universidad de la Frontera, Department of Chemical Engineering, Temuco, CL

Introduction

Hybrid nanoparticles represent an efficient strategy in designing specific nanomaterials with multiple properties. Magnetite and silver hybrid nanoparticles (Fe_3O_4@Ag NPs) present promising applications in the biomedical field, due to the combination of superparamagnetic behavior of magnetite nanoparticles (Fe_3O_4 NPs) and antibacterial properties of silver nanoparticles (AgNPs), promoting a targeted and efficient treatment of infectious diseases. In this work, the functionality and biocompatibility of hybrid Fe_3O_4@Ag NPs were further improved by their coating with thiolated chitosan (TCS). Chitosan is a biocompatible polymer. The presence of TCS coating on the surface of Fe_3O_4@Ag NPs enables the insertion of nitric oxide (NO) moieties. NO is has antitumor and antibacterial effects.

Experimental Methods

Fe_3O_4 NPs were synthesized by the co-precipitation method of Fe(II) and Fe(III). Ag^+ ions were reduced on the surface of Fe_3O_4 NPs, using green tea extract, leading to the formation of Fe_3O_4@Ag NPs. Fe_3O_4@Ag NPs were coated with TCS, leading to Fe_3O_4@Ag/TCS NPs, and sodium nitrite was used to nitrosate thiol groups of TCS leading to S-NO moieties (Fe_3O_4@Ag/CS-NO), which act as NO donor nanoparticle. The obtained Fe_3O_4@Ag/TCS NPs were characterized by different techniques, including X-ray diffraction (XRD), X-ray photoelectron spectroscopy (XPS), scanning electron microscopy (SEM), atomic force microscopy (AFM), dynamic light scattering (DLS), thermogravimetric analysis (TGA) and magnetization measurements. The antibacterial properties of the Fe_3O_4@Ag NPs, Fe_3O_4@Ag/TCS NPs and Fe_3O_4@Ag/CS-NO NPs were evaluated against *Staphylococcus aureus*, *Streptococcus mutans* and *Escherichia coli* bacterial strains. The cytotoxicity of the nanoparticles was evaluated against prostate cancer (PC3) and osteosarcoma (MG63) cell lines.

Results and Discussion

Fe_3O_4 NPs were synthesized by co-precipitation of Fe(II) Fe(III), and Ag^+ ions were reduced using green tea extract, which also acts as capping agent, leading to Fe_3O_4@Ag NPs. FTIR indicated the presence of characteristic phytochemical derived from green tea on the surface of Fe_3O_4@Ag NPs. XRD results with Rietveld refinement indicated the formation of Fe_3O_4@Ag NPs, with a percentage of 87% (w/w) of Fe_3O_4 and 13% of AgNPs in the hybrid structure. SEM and AFM analyses indicated a spherical morphology for Fe_3O_4@Ag/TCS NPs, and EDS supported the data obtained from XRD and XPS, besides demonstrating the presence of thiol groups present on the TCS coating. AFM analyses showed that the average size of the nanoparticles was 52.4 ± 1 nm, which is in accordance to the hydrodynamic size obtained by DLS measurements. TGA analysis proved the presence of TCS coating onto nanoparticle surface, presenting 3% of TCS (w/w) in Fe_3O_4@Ag/TCS NPs. Magnetization measurements revealed a superparamagnetic behavior for both Fe_3O_4@Ag NPs and Fe_3O_4@Ag/TCS NPs, with magnetization saturation values of 56.1 emu g^{-1} and 52.9 emu g^{-1}, respectively, suitable for targeted biomedical applications. Fe_3O_4@Ag/CS-

NO NPs showed a release of 1.2 mol g^{-1} of NO, concentration in which NO may have antibacterial and antitumorigenic properties. The antibacterial activity of Fe_3O_4@Ag NPs, Fe_3O_4@Ag/TCS NPs and Fe_3O_4@Ag/CS-NO NPs were investigated, and results indicated an improved antibacterial effect for Fe_3O_4@Ag/CS-NO NPs. Fe_3O_4@Ag/CS-NO NPs demonstrated a bacteriostatic effect against *S. aureus* and *S mutans* and bactericidal activity against *E. coli*, as time-kill curves indicated total death of all colonies after 2 h incubated with Fe_3O_4@Ag/CS-NO NPs. The cytotoxicity effects of the nanoparticles against both tumoral cell lines were enhanced by the functionalization with NO donors onto the surface of the nanoparticles (Fe_3O_4@Ag/CS-NO NPs). This might be due to a synergistic effect of AgNPs and NO.

Conclusion

The results indicated the synthesis of hybrid Fe_3O_4@Ag NPs via a green route, an efficient coating of the nanoparticle surface with NO. Fe_3O_4@Ag/TCS NPs presented spherical morphology, with preserved magnetic properties, suitable for targeted biomedical applications. Fe_3O_4@Ag/CS-NO NPs showed enhanced antibacterial and antitumorigenic properties. NO-releasing chitosan coated nanoparticles indicated potential results for future medical applications (Figure 1).

Acknowledgement

CNPq and FAPESP (2018/02832-7, 2018/08194-2).

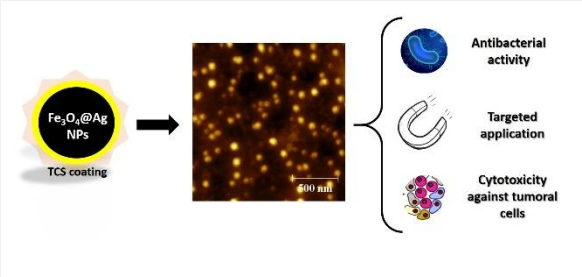

Magnetite and silver hybrid nanoparticles (Fe3O4@Ag NPs) coating with nitric oxide
Representative image of the preparation of hybrid nanoparticles Fe3O4@Ag NPs coated with chitosan-nitric oxide for antitumoral and antibacterial activities

PS2-11-424

Investigating the Role of Exosomes in Modeled Osteoporosis

Polina Pantelidou[1,2,6], Vagelis Rinotas[1], Apostolos Papadopoulos[1,4], Efstathios Efstathopoulos[2], Dionysios Mouzakis[2,5], Kyriaki Bakirtzi[3], Eleni Douni[1,4], On behalf of the Hellenic Society of Biomaterials

[1]Institute for Bioinnovation, B.S.R.C. "Alexander Fleming", Vari, GR; [2]National and Kapodistrian University of Athens, Schools of Medicine and Pharmacy, MSc Nanomedicine, Athens, GR; [3]Pharmathen International, Long Acting Injectable Products Quality Assurance, Sapes, Rodopi, GR; [4]Agricultural University of Athens, Department of Biotechnology, Athens, GR; [5]Hellenic Army Academy, Sector of Mathematics and Engineering Sciences, Vari, GR; [6]Sponsored by the Hellenic Society of Biomaterials, Athens, GR

Introduction

Osteoporosis, a metabolic disease characterized by low bone mass and increased susceptibility to fractures, remains a major global public health issue as it affects a substantial percentage of the elderly population. Bone is a composite tissue that constantly undergoes remodelling through coordinated bone resorption and formation performed by osteoclasts and osteoblasts, respectively.

Almost all bone cells have been showed to secrete exosomes, which are extracellular membrane nanovesicles of 30 to 100 nanometer size, that carry specific protein, mRNA and miRNA cargo. Bone-derived exosomes are considered to be essential for intercellular communication between bone cells playing a critical role in bone remodelling regulating osteogenesis and osteoclastogenesis. Receptor activator of nuclear factor-κB ligand (RANKL), a member of the TNF superfamily, constitutes the master regulator of osteoclast formation and bone resorption. Exosomes carrying RANKL or its receptor RANK have been suggested to regulate bone remodelling by interfering with osteoblast-osteoclast interactions. Whether exosomes are, however, essential mediators of bone homeostasis needs to be further addressed. Apart from their contribution to physiological processes, lately, exosomes have been correlated with several pathological conditions, and thus can be utilized as potential tools for diagnosis (biomarkers), prevention of disease (e.g. nanovaccines), and therapy (target drug and/or gene delivery nanosystems), as well as, theranostics.

This project aims to compare the relative abundance of exosomes in femurs (either whole or flushed to remove bone marrow) between wild-type mice and osteoporotic mouse models, and further compare their molecular cargo and surface composition. Our group has recently established novel genetic models of osteoporosis by expression of human RANKL in transgenic mice. TgRANKL mice develop a severe osteoporotic phenotype with features of increased osteoclastogenesis, severe trabecular bone loss, cortical porosity and bone marrow adiposity.

Experimental Methods

Exosome isolation from wild-type or transgenic femurs was performed via sequential ultracentrifugation, while the identification of exosomes in pellet fractions was done by Western blot analysis using antibodies against exosomal proteins such as CD9.

Results and Discussion

After optimization of the ultracentrifuge conditions, our results demonstrated the presence of the CD9 exosomal marker both in wild-type and TgRANKL femur extracts. The isolation of exosomes will be validated through scanning electron microscopy (SEM). Furthermore, a comparative analysis on the composition of bone-derived exosomes

through qPCR for selected miRNAs and proteomic analysis for protein identification, will possibly identify osteoporosis-specific exosomes in TgRANKL mice.

Conclusion

Bone-derived exosomes during osteoporosis could lead to the identification of novel regulatory mechanisms in disease pathogenesis, while bioengineered exosomes can be utilized to target and control drug delivery specifically at the skeletal system in order to reverse osteoporosis.

References

1. Exosomes: mediators of bone diseases, protection, and therapeutics potential. (2018). *Oncoscience*, 5-6(5), p.181.
2. He, C., Zheng, S., Luo, Y. and Wang, B. (2018). Exosome Theranostics: Biology and Translational Medicine. *Theranostics*, 8(1), pp.237-255.
3. Rinotas, V., Niti, A., Dacquin, R., Bonnet, N., Stolina, M., Han, C., Kostenuik, P., Jurdic, P., Ferrari, S. and Douni, E. (2014). Novel Genetic Models of Osteoporosis by Overexpression of Human RANKL in Transgenic Mice. *Journal of Bone and Mineral Research*, 29(5), pp.1158-1169.

PS2-11-425

The effect of different CTAB-assisted sol–gel derived silica-based mesoporous nanoparticles on structure, antibacterial properties and hemolytic activity

Georgia K. Pouroutzidou[1], Ioannis Tsamesidis[2], Georgios S. Theodorou[1], Eleni Likotrafiti[3], Jonathan Rhoades[3], Christina Pappa[4], Konstantinos S. Triantafyllidis[4], Eleana Kontonasaki[5], Konstantinos M. Paraskevopoulos[1]

[1]Aristotle University of Thessaloniki, School of Physics, Faculty of Sciences, Thessaloniki, GR; [2]University of Sassari, Department of Biomedical Sciences, Sassari, IT; [3]Alexander Technological Educational Institute of Thessaloniki, Department of Food Technology, Thessaloniki, GR; [4]Aristotle University of Thessaloniki, School of Chemistry, Faculty of Sciences, Thessaloniki, GR; [5]Aristotle University of Thessaloniki, Department of Prosthodontics, School of Dentistry, Faculty of Health Scienceslty, Thessaloniki, GR

Introduction

Materials with porous architecture have been developed for drug delivery systems[1,2]. Mesoporous nanoparticles (MSNs) with pore sizes in the range of 2–50nm have attracted significant attention due to their enhanced textural properties, such as high specific surface area and pore volume, and uniform pore size distribution[3]. Silica-based MSNs are potential drug carriers due to their ordered and homogeneous pore network, which allows fine control of the drug load and release kinetics. This class of materials also provides a high pore volume to host the required amount of pharmaceuticals and high surface area, which implies high potential for drug adsorption. Moreover, the ionic dissolution products from mesoporous glasses, such as Si and Ca, stimulate the expression of osteoblastic cells and angiogenesis, which leads to the formation of strong bonds with the human bone[4]. Many trace elements in the human body such as Mg are known for their anabolic effects on bone metabolism[5]. Hence, Mg-containing calcium silicate MSNs, such as akermanite, provide promising properties for use as a bioactive mesoporous drug carrier[3]. The aim of this study was the synthesis of silica-based MSNs and the evaluation of the effect of their composition on structural properties, hemolytic activity and antimicrobial properties.

Experimental Methods

The synthesis of silica-based MSNs, SiO_2 (**MS1**), SiO_2CaO (60 and 40%mol respectively) (**MS2**) and $Ca_2MgSi_2O_7$ (Akermanite) (**MS3**), was achieved by sol–gel method, with some modification using cetyltrimethylammonium bromide (CTAB) as structure-directing agent. The final molar ratios were 1TEOS/0.3CTAB/10ethanol/14HCl/150H_2O. Eventually, all samples were dried at 100°C and calcined at 600°C for 5h to remove the surfactant template[3]. The characterization of the samples was performed by X-ray diffraction (XRD) and Fourier transform infrared spectroscopy (FTIR), while their mesoporous characteristics, were determined by N_2 adsorption/desorption at -196^{o}C, using the Brunauer–Emmett–Teller (BET) and Brunauer-Joyner-Halenda (BJH) methods. Their antibacterial properties on seven bacterial strains and hemolytic properties at body and fever temperature (37^{o}C, 41^{o}C) were also evaluated.

Results and Discussion

The N_2 adsorption step of MS1 and MS2 exhibit a IV(a) type and the desorption step (hysterysis loop) is between H1 and H2(a) (Fig.1), according to the updated IUPAC classification[7]. These types of adsorption isotherms are typical of mesoporous materials, in which capillary condensation of N_2 within the pores is accompanied by hysteresis. The

desorption isotherms are also typical of mesoporous materials with uniform mesopores affected by some structural features and are representative of silica gels, porous glasses and other ordered mesoporous materials. The pore size (width) distribution exceeds in the range of 1.4-10nm and 1.5-7nm for MS1 and MS2 respectively, being in the relatively small mesopore size range. The specific surface area of MS1 and MS2 nanoparticles was 858 and 1028m^2/g, the pore volume 1.03 and 0.96cm^3/g, and the average pore size 5 and 3nm, respectively. On the other hand, the MS3 particles show a type IV(b) adsorption isotherm(Fig.1), which also represents an ordered mesoporous structure but with pores of smaller size, uniform dimensions and narrow size distribution. The pore size distribution of MS3 was in the range of 1.2–3.6nm with an average value of 2.2 nm. No hysterysis during desorption is observed, while the specific surface area and pore volume was 1203m^2/g and 0.80cm^3/g respectively. These results suggested that the MS3 possessed slightly more uniform mesopores of smaller size compared to MS1 and MS2[8].
The FTIR spectra of all MSNs presented the characteristic bands of amorphous silicate glasses. XRD patterns revealed the presence of amorphous glasses. A large degree of inhibition was not observed in any of the bacteria when challenged with any of the three antimicrobial compounds. Statistically significant ($P<0.05$) decreases in growth rate were observed in *Bacillus cereus* exposed to MS1 and MS3 (86 and 91% of the control value respectively) and *Salmonellaenterica* serovar Enteritidis exposed to MS3 (79% of the control value). Large significant increases in lag phase or decreases in maximum optical density were not observed with any combination of bacteria and antimicrobials. The haemolytic analysis of MSNs on Red blood cells at body and fever temperature revealed no hemolytic activity in dosages up to 2000mg/ml. This indicates that all MSNs provided good hemocompatibility, which is essential for their applications in bone tissue engineering.

Conclusion

Three different MSNs were successfully synthesized with typical mesoporous structure. Different compositions affected the pore structure and size distribution, and the surface area of the samples. Due to the high surface area of all MSNs and their good hemocompatibility, they can be suggested in various tissue engineering processes, such as controlled drug delivery.

References

1. Saravanapavan, P. & Hench, L. L. Mesoporous calcium silicate glasses. II. Textural characterisation. *J. Non. Cryst. Solids***318,** 14–26 (2003).
2. Vallet-Regí, M., Balas, F. & Arcos, D. Mesoporous Materials for Drug Delivery. *Angew. Chemie Int. Ed.***46,** 7548–7558 (2007).
3. Ghadiri, S., Hassanzadeh-Tabrizi, S. A. & Bigham, A. The effect of synthesis medium on structure and drug delivery behavior of CTAB-assisted sol–gel derived nanoporous calcium–magnesium–silicate. *J. Sol-Gel Sci. Technol.***83,** 229–236 (2017).
4. Shah Mohammadi M, Chicatun F, Stähli C, Muja N, B. M. & Ion, N. S. Osteoblastic differentiation under controlled bioactive ion release by silica and titania doped sodium-free calcium phosphate-based glass. *Colloids Surf B Biointerfaces. 2014;12182–91.* doi:10.1016j.colsurfb.20105.037
5. Zhang, Y. *et al.* Biodegradable mesoporous calcium–magnesium silicate-polybutylene succinate scaffolds for osseous tissue engineering. *Int. J. Nanomedicine* 6699 (2015). doi:10.2147/ijn.s92598
6. Wu, C. & Chang, J. Degradation, bioactivity, and cytocompatibility of diopside, akermanite, and bredigite ceramics. *J. Biomed. Mater. Res. - Part B Appl. Biomater.***83,** 153–160 (2007).
7. Matthias, T. *et al.* Physisorption of gases, with special reference to the evaluation of surface area and pore size distribution (IUPAC Technical Report). *Pure Appl. Chem.***87,** 1051 (2015).
8. Wu, Z. *et al.* In vitro degradability, bioactivity and cell responses to mesoporous magnesium silicate for the induction of bone regeneration. *Colloids Surfaces B Biointerfaces***120,** 38–46 (2014).

Acknowledgement

«This research is co-financed by Greece and the European Union (European Social Fund- ESF) through the Operational Programme «Human Resources Development, Education and Lifelong Learning» in the context of the project “Strengthening Human Resources Research Potential via Doctorate Research” (MIS-5000432), implemented by the State Scholarships Foundation (IKY)»

Acknowledgement

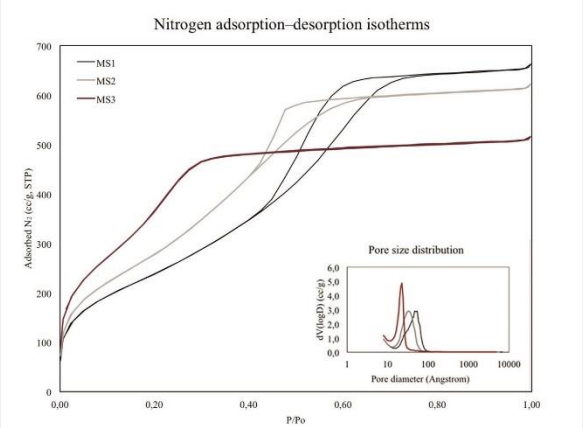

Fig.1
Nitrogen adsorption–desorption isotherms and pore size distribution of MSNs.

PS2-11-426

Biopolymer-Derived Hybrid Systems for Sustained Drug Release

Markus Witzler[1,2], Sarah Vermeeren[1], Daniel Feuser[1], Patrick F. Ottensmeyer[1], Dominik Büchner[1,2], Martin Gericke[2], Thomas Heinze[2], Edda Tobiasch[1], Margit Schulze[1]

[1]Bonn-Rhein-Sieg University of Applied Sciences, Department of Natural Sciences, Rheinbach, DE; [2]Friedrich-Schiller-University Jena, Institute of Organic Chemistry and Macromolecular Chemistry, Center of Excellence of Polysaccharide Research, Jena, DE

Introduction

Current research in bone tissue engineering focuses on hybrid composite materials providing sufficient mechanical stability to the defect site and simultaneously acting as release systems for drugs supporting osteogenesis. Purinergic receptors (P2X and P2Y) have been found to influence the osteogenic differentiation of human mesenchymal stem cells (hMSC) and induced pluripotent stem cells (iPSC). Corresponding receptor ligands inducing and/or conducting osteogenic differentiation have also been identified. [1,2] Controlled release of those ligands from hybrid scaffolds aims for guided stem cell differentiation and ultimately, enhanced healing of large bone defects.

For years, polysaccharides have been used in drug delivery applications. [3] Mainly marine derived polymers such as alginate and chitosan are widely incorporated into release systems as gels and capsules. Carrageenans, derived from algae, are also able to form stable gels, beads, and capsules and are being used widely as thickeners in food industry. Lignin, a by-product of the pulp and paper industry, is on the rise for biomedical application. [4] Here, lignosulfonates can be used as components for multilayered polyelectrolytic systems.

Experimental Methods

In this work, we present two ways to sustain the release of hydrophilic model ligands ATP and suramin. One approach is the mineralization of alginate beads with *in situ* precipitated hydroxyapatite. Drugs are loaded during encapsulation and mineralization and are then being released into aqueous media over the course of several days. The second approach is a layer-by-layer coating of alginate or carrageenan capsules with chitosan and lignosulfonate. The drugs are incorporated into the template capsules and released into aqueous media after coating with the polymeric polyelectrolyte layers. Beads are characterized via optical microscopy, light scattering, surface charge, and scanning electron microscopy. Release is monitored via UV-Vis spectroscopy.

Results and Discussion

Mineralization of alginate beads slows down drug release from about 100% in 12 hours to around 60% in 12 hours (burst release) and a sustained behaviour up to 70% over 3 days. This can be attributed to a interaction of the calcium phosphate particles and the ionic drugs in the carrier system. Polyelectrolyte layers also reduced the burst and overall release, building a "charge-barrier" that slowed down diffusion of ionic drugs.

Conclusion

Drug release of hydrophilic substances into aqueous media is challenging due to fast diffusion out of the delivery device. By modifying the carrier (with a ceramic filler or by adding polyelectrolytic layers from biopolymers) we were able to decrease both burst release and overall release over the course of several days. Further research is needed in order to apply this technique to other drugs and other materials as well.

References

[1] N. Zippel et al. Stem Cells Dev. 21 (2012) 884–900. doi:10.1089/scd.2010.0576.

[2] C. Kaebisch et al. Comput. Struct. Biotechnol. J. 13 (2015) 75–84. doi:10.1016/j.csbj.2014.11.003.

[3] Z. Liu et al. Adv. Drug Deliv. Rev. 60 (2008) 1650–1662. doi:10.1016/j.addr.2008.09.001.

[4] M. Witzler et al. Molecules. 23 (2018) 1885. doi:10.3390/molecules23081885.

Acknowledgement

This work was funded by the German Federal Ministry of Education and Research (BMBF) programs: “PersoImplant” (grant no. 13FH019IX5) and "TestMedgO" (1609fhz027).

PS2-11-427

Site-specific immobilization of proteins to functionalize polymer-based scaffolds

Viktoria Sokolowski[1,2], Joachim Nickel[2], Jürgen Groll[1]

[1]University Würzburg, Department for functional materials in medicine and dentistry and Bavarian Polymer Institute, Würzburg, DE; [2]University Würzburg, Department of Tissue Engineering and Regenerative Medicine, Würzburg, DE

Introduction

The most common systems for protein drug delivery utilize oral application or direct injection. However, these systems are restricted as some drugs are erroneously absorbed via the gastrointestinal tract or need site-specific dosing. Moreover, high unphysiological dosages must be applied for some drugs to achieve significant effects but often cause serious side effects. Due to these limitations new delivery systems are developed employing e.g. implantable drug delivery systems composed of scaffolds carrying immobilized proteins on their surface[1]. Different methods are known to immobilize proteins. However, it is still challenging to maintain a high protein activity[2].

One method to couple proteins on various surfaces is the click chemistry via mild reaction conditions. Using a technique called codon-usage expansion, artificial amino acids can be integrated into every position of the protein sequence during protein synthesis. Their functional groups enable site-specific protein immobilization using an orthogonal reaction. One suitable artificial amino acid for this technique is a lysine-derivate synthesized with a norbornene-functionality. These proteins are then immobilized on tetrazine-modified surfaces[3].

Experimental Methods

Norbornene-lysine synthesis

5-norbornene-2-methylen-chloroformate was synthesized by activation of commercially available norbornene-2-methanol with nitrophenylchloroformate. *N*-α-trifluoroacetyl-L-lysine methyl ester was synthesized by a two-step reaction starting with L-lysin-methyl ester dihydrochloride. The synthesis and purification of final artificial amino acid was done according to the literature[3]. All reaction products were analyzed by NMR.

Protein Expression

JM109 bacteria were double transformed with the pN25-RFP vector and a plasmid, which encodes for a tRNA being complementary to the amber-codon and the corresponding tRNA-synthetase. Bacteria are plated on ampicillin plates and incubated over night at 37°C. Colonies grown over night are picked and transferred to TB-medium. Protein expression is initiated by addition of the artificial amino acid and isopropyl β-D-1-thiogalactopyranoside (IPTG). For protein purification the bacteria are lysed and proteins purified by fast protein liquid chromatography (FPLC). As the expressed protein is insoluble denaturing conditions must be applied to enable purification. This step damages the protein structure a subsequent refolding step is necessary to recover protein functionality.

Results and Discussion

For the first experiments a fluorescent protein is used as prove of concept to establish all basic methods. Later on, this system should be transferred to different target proteins.

According to the NMR results the synthesis of the norbornene-modified lysine was successful.

Expression of norbornene modified RFP (NR-RFP) is only possible after addition of the artificial amino acid, as its

integration is already encoded by the DNA sequence. Afterwards, successful refolding could be detected by fluorescence measurements. The refolded protein will be used to establish the coupling reaction with a tetrazine modified polymeric scaffold.

One possible target protein would be bone morphogenetic protein 2 (BMP2), immobilized on a graft by click chemistry to treat bone defects. This protein has the capability to induce the formation of bone tissue and thus is already in clinical use. However, too high BMP2 concentrations are needed to improve bone healing. Because of this high protein doses patients suffer from severe side effects like inflammation and ectopic bone formation[4]. Hence, immobilization of BMP2 on a scaffold would enable the use of lower doses avoiding the side effects and improve the healing process.

Conclusion

Synthesis of a norbornene-functionalized lysine derivate is done by a five steps reaction. Moreover, by expanding the bacterial genetic-code this artificial amino acid is integrated in the desired protein. This modified RFP can then be used for click reaction to functionalize polymeric scaffolds.

References

1. Kumar, A.; Pillai, J., Chapter 13 - Implantable drug delivery systems: An overview. In *Nanostructures for the Engineering of Cells, Tissues and Organs*, Grumezescu, A. M., Ed. William Andrew Publishing: 2018; pp 473-511.

2. Raphel, J.; Karlsson, J.; Galli, S.; Wennerberg, A.; Lindsay, C.; Haugh, M. G.; Pajarinen, J.; Goodman, S. B.; Jimbo, R.; Andersson, M.; Heilshorn, S. C., Engineered protein coatings to improve the osseointegration of dental and orthopaedic implants. *Biomaterials* **2016,***83*, 269-282.

3. Kaya, E.; Vrabel, M.; Deiml, C.; Prill, S.; Fluxa, V. S.; Carell, T., A genetically encoded norbornene amino acid for the mild and selective modification of proteins in a copper-free click reaction. *Angew Chem Int Ed Engl* **2012,***51* (18), 4466-9.

4. James, A. W.; LaChaud, G.; Shen, J.; Asatrian, G.; Nguyen, V.; Zhang, X.; Ting, K.; Soo, C., A Review of the Clinical Side Effects of Bone Morphogenetic Protein-2. *Tissue engineering. Part B, Reviews* **2016,***22* (4), 284-97.

Acknowledgement

This project was funded by the European Fond for Regional Development (EFRE).

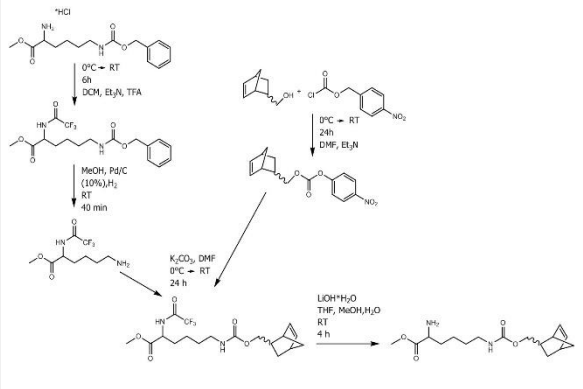

Reaction-scheme of artificial amino acid synthesis.
Based on a publication of Kaya et al.[3] a norbornene-functionalized lysine-derivate was produced in five reaction steps.

PS2-11-428

Dialdehyde Cellulose Crosslinked Poly(Vinyl)Alcohol Hydrogels for Biomedical Applications

Jan Vícha[1], Lukáš Münster[1], Zdenka Capáková[1], Miroslav Fišera[2], Ivo Kuřitka[1]

[1]Tomas Bata University, Centre of Polymer Systems, Zlín, CZ; [2]Tomas Bata University, Department of Food Analysis and Chemistry, Zlín, CZ

Introduction

The 2,3-dialdehyde cellulose (DAC), obtained by selective oxidation of cellulose by periodate, was shown to be a highly effective crosslinking agent for poly(vinyl alcohol) (PVA).[1] However, to determine its biocompatibility and how the properties of the resulting hydrogels can be engineered for various biomaterial applications, additional study was needed.

Experimental Methods

Initially, cellulose was oxidized by sodium periodate (1 : 1.2 molar ratio) for 72h and subsequently solubilized at 80 °C for 7 h. The PVA/DAC hydrogels were prepared by mixing dissolved PVA with different amount of solubilized crosslinker (0.5 – 1.5 wt% of DAC) in the presence of acid. Mechanical (Young's modulus, stress vs. strain), viscoelastic (storage and loss modulus, damping factor) and surface properties (BET analysis, SEM micrographs) of prepared PVA/DAC hydrogels were evaluated. Hydrogels were also characterized in the terms of their network parameters (swelling capacity, equilibrium water content, gel fraction, average molecular weight between crosslinks, crosslink density. Biological study of PVA/DAC hydrogels was performed according to ISO10993 and included evaluation of cytotoxicity of extracts and drug-loaded hydrogels (MTT assay), as well as direct contact test. Tests were performed on healthy immortalized human keratinocyte cell line (HaCaT) and mouse embryonic fibroblast cell line (NIH/3T3). The drug-release from PVA/DAC hydrogels was investigated with respect to the mesh density and size and charge of released molecules (ibuprofen, rutin, phenanthriplatin). Cytotoxicity of phenathriplatin-loaded hydrogels was evaluated using adenocarcinomic human alveolar basal epithelial cell line A549.

Results and Discussion

Properties of prepared hydrogels can be engineered from stiff substances suitable for artificial cartilages (prepared using 1-1.5 wt.% DAC) to soft and highly porous viscoelastic gels capable of holding large amounts of water (0.5 wt% DAC), convenient for various pharmaceutical applications as drug delivery depots.Moreover, the PVA/DAC hydrogels were found to be superior in terms of mechanical characteristics and specific surface area (more than twice larger dynamic modulus and surface area) to analogical material prepared using glutaraldehyde, probably due to the macromolecular character of DAC and resulting two-phase network topology of PVA/DAC hydrogels.[1,2]

Biological evaluation revealed good biocompatibility and no observable toxicity. The available drug release rates range from very fast (2 hours) for relatively small and negatively charged molecules of ibuprofen loaded into the most sparsely crosslinked hydrogel (0.5 wt.% of DAC) to rather slow (96 hours) for larger and neutral molecules of rutin loaded in hydrogels prepared using 1.5 wt% of DAC. Positively charged phenanthriplatin had slowest initial release rates, but was completely released already within 48h. Hydrogels loaded with phenanthriplatin were found to be effective against A549 adenocarcinoma cell line.

Conclusion

Overall, the DAC provides sustainable, more effective and less toxic alternative to currently used synthetic crosslinking agents. Properties of biocompatible PVA/DAC hydrogels can be adjusted for wide spectrum of potential applications such as drug-delivery depots, artificial implants or dermal patches and masks. Results also demonstrate the potential of PVA/DAC hydrogels for anticancer drug-delivery, e.g. for localized release of chemotherapeutics after tumor resection.

References

1) L. Münster, J. Vícha, J. Klofáč, M. Masař, A. Hurajová, I. Kuřitka, *Carbohydrate Polymers***2018**, *198*, 181–190.

2) L. Münster, Z. Capáková, M. Fišera, I. Kuřitka, J. Vícha, *Carbohydrate Polymers*, submitted.

Acknowledgement

This work for supported by the Czech Science Foundation grant 16-05961S, and the Ministry of Education, Youth and Sports of the Czech Republic, Program NPU I (LO1504).

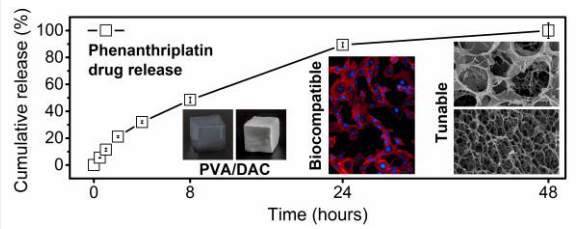

Figure 1

PS2-11-429

Sterilization of implantable device for therapeutic delivery

Radosław Wach, Agnieszka Adamus-Wlodarczyk, Alicja Olejnik, Bozena Rokita

Lodz University of Technology, Institute of Applied Radiation Chemistry, Lodz, PL

Introduction

The purpose of the work was to select the most suitable sterilization method and demonstrate its applicability for an implant intended for therapeutics delivery. The device should fulfil essential requirements, such as mechanical and chemical stability in physiological environment during treatment of a disease or during their lifespan, and then be explanted or gradually degraded. In order to guarantee proper operation of such systems, especially in the case of their complex configuration or multifunctional tasks of the implant (e.g. active medical devices), besides selection of biomaterials and involved manufacturing processes, the designer should also consider potential sterilization method. Validation of selected sterilization technique in terms of its effectiveness, reliability and reproducibility is the prerequisite the manufacturer demonstrates to the notifying authorities in order to prove microbiological safety of the device.[1] Reduction of the bioburden on and in the device to Sterility Assurance Level (SAL) 10^{-6} is required.

Experimental Methods

The theoretical approach to selection of potentially applicable sterilization methods is based on the knowledge of properties of the polymeric materials comprising the device of bio-electronic implant intended for therapeutics delivery from genetically engineered cells stimulated by light, the complexity of its design and presence of sensitive components or subsystems (Fig. 1)[2,3]. The device should be provided sterile for cells loading, therefore terminal sterilization of manufactured implant or aseptic processing of pre-sterilized components may be applied. Validation of ethylene oxide sterilization method for the device under development was accomplished by overkill approach.

Results and Discussion

Approach to selection of a sterilization technique should begin on screening materials, components and systems included comprising the device. If all of those can withstand high temperature, a dry hot air or moisturised air methods may be the first choice. The complex shapes and inner elements are also heated, thus the device is entirely sterilized. Encompassed electronics as well as the presence of optically functional polymers, e.g. opacity induction, eliminate thermal methods of sterilization. As low-temperature method, radiation may be considered. Either electron beam or gamma rays are highly penetrable and provide sterility of the entire implant, not only its surface, which is especially appropriate for complicated shapes or porous materials. Nevertheless, the energy may cause polymer degradation and induces severe deterioration of embedded electronics. Plasma-hydrogen peroxide may be considered, and applied as effective surface sterilization method, also for devices encompassing electronic systems. Surfaces not resistant to highly oxidative environment may be altered. Yet, ISO standards have not been developed for plasma method. Ethylene oxide (EO) sterilization is commonly utilized for polymers and combined materials. Since the method can be applied for optics and electronics it was selected for current optogenetic implant. Beside rapid pressure changes, a dissolution of the gas (highly toxic) in the polymeric biomaterial and possible chemical reactions with the polymer should be examined in details.

Conclusion

Process Qualification at validation of EO sterilization method was demonstrated by application of sub-lethal, half and full sterilization cycles with the use of biological indicators confined in the cell chamber of the optogenetic implant.

References

[1]R.A. Wach et al., *Military Pharmacy and Medicine*, 2, 185 (2009);

[2]F. Michel, M. Folcher, *Porto Biomed. J.*, 2, 145 (2017);

[3]V. Pierroz, M, Folcher, *J. Mol. Gen. Med.*, 2, 1:10 (2018).

Acknowledgement

This work has received funding from the European Union's H2020 research and innovation programme under grant agreement No 720694, 'Optogenerapy'. Cooperation with dr. M. Folcher of ETH Zurich, Switzerland is acknowledged.

Fig. 1
A concept of wireless-powered cell-based implant for therapeutic delivery.[2]

PS2-11-430

Engineering Hyaluronic Acid based nanocarriers for anti-cancer combination therapy

Sumanta Samanta[1], Vignesh K. Rangasami[1], Kenta Aasawa[2], Yuji Teramura[2], Oommen P. Oommen[1]

[1]Tampere University, Faculty of Medicine and Health Technologies, Tampere, FI; [2]The University of Tokyo, Department of Bioengineering, Tokyo, JP

Introduction

Doxorubicin (DOX), a well-known chemotherapeutic drug used to treat several cancers evoke severe adverse side effects and hypersensitivity reactions [1]. DOX is known to eliminate fast dividing cells by intercalating with DNA, however, it also kills the lymphohematopoietic precursor cells resulting in leukocytopenia and thrombocytopenia. We have earlier shown that DOX encapsulated in biomimetic nanocarriers mitigate the coagulation cascade induced by the drug and suppress platelet activation [2]. In this study, we aim to co-deliver an immunosuppressive glucocorticoid drug dexamethasone (Dex) and DOX and evaluate their impact on the thromboinflammatory activity and anti-tumor immunity. Dex is currently used as a co-medication in chemotherapy and act as an antiemetic that helps to alleviate the toxic side effects of chemotherapy. In this study, we have engineered hyaluronan (HA) derived nanoparticles capable of sequential delivery of Dex and DOX and evaluated their bioactivity in human cancer cells and primary murine macrophages.

Experimental Methods

We have engineered HA-derived nanocarrier by a supramolecular approach by conjugating dexamethasone on the carbodihydrazide modified hyaluronic acid (HA-CDH) by hydrazone chemistry. In the first step, the conjugation of carbodihydrazide (CDH) on hyaluronic acid was carried out by carbodiimide coupling chemistry. The degree of hydrazide modification and dexamethasone conjugation was determined using trinitrobenzene sulfonic acid (TNBS) assay in Shimadzu UV-3600 plus UV-VIS-NIR spectrophotometer. The HA-Dex was characterized by ^{1}H NMR spectroscopy. The HA-Dex micelle was loaded with DOX following a reverse-micelle strategy and the drug loading and encapsulation efficiency was quantified by using FLS1000 Photoluminescence spectrometer and UV measurement at 485 nm (molar extinction coefficient, ε_{485} = 11,500 M^{-1} cm^{-1}). The in-vitro DOX released from the HA-Dex-DOX NPs was analyzed by the dialysis method using simulated body fluid (SBF) as the release medium. The cytotoxicity of HA-Dex and HA-Dex-DOX NPs were assessed by MTT (3-(4, 5-dimethylthiazol-2-yl)-2, 5-diphenyltetrazolium bromide) assay in three different human cell lines, namely, MG63 (osteosarcoma), HCT116 (colorectal carcinoma) and MCF7 (breast adenocarcinoma). The role of cell surface CD44 receptors on cellular uptake of HA-DEX-DOX NPs was proved by fluorescence-activated cell sorting (FACS) analysis and fluorescence microscopy. The HA-Dex-DOX NPs evoked immunosuppressive property to prevent systemic toxicity elicited by DOX was examined by hematological studies in non-anticoagulated human whole blood.

Results and Discussion

We have designed a novel nanocarrier loaded with DOX and Dex (HA-NP) having hydrodynamic size 252 nm as measured by dynamic light scattering (DLS) experiment. The amount of Dex and DOX-loaded in HA-NPs was found to be 5.2% and 4.6 % by moles respectively. Our designed HA-Dex-DOX NPs exhibited sustained release of only 10.6% of DOX after 96 hours with near zero-order kinetics while we observed a burst release of free DOX (79%)

within 24 hours. Effectively our nanocarrier could prevent the premature release of DOX and minimize off-target effects. The HCT116 and MG63 cells which possess higher CD44 receptors displayed higher cytotoxicity than MCF-7. The hemocompatibility study demonstrated that the HA-NPs evoked immunosuppressive properties on DOX mediated platelet aggregation and activation of the complement and coagulation cascade in fresh non-anticoagulated human whole blood from healthy donors.

Conclusion

Our synthesized NPs specifically target the tumor cells and macrophages expressing high levels of HA-receptor CD44 and facilitated apoptosis of the tumor cells. We have evaluated the effect of drug loaded HA-NPs on human non-anticoagulated whole blood using the chandler-loop method. This study reveals that HA-NP mitigated the drug-mediated complement and coagulation cascade and suppressed platelet aggregation. Thus, a stable and innocuous HA-derived nanoparticle system is designed that could effectively target CD44 receptors overexpressed on human cancers and mitigate the systemic immune activation and may augment local anti-tumor immunity.

References

[1] Complement activation following first exposure to pegylated liposomal doxorubicin (Doxil®): possible role in hypersensitivity reactions. A. Chanan-Khan, J. Szebeni, S. Savay, L. Liebes, N. M. Rafique, C. R. Alving, F. M. Muggia; *Annals of Oncology*, 2003, 14(9), 1430–1437

[2] Chondroitin Sulfate Coated Gold Nanoparticles: A New Strategy to Resolve Multidrug Resistance and Thromboinflammation. D. Gurav, O. P. Varghese, O. A. Hamad, B. Nilsson, J. Hilborn, O. P. Oommen, *Chemical Communications*, 2016, 52, 966-969

Acknowledgement

This project has received funding from the European Union's Horizon 2020 research and innovation program under the Marie Skłodowska-Curie grant agreement No 713645. Authors also thank Prof. Jons Hilborn from Uppsala University, Sweden and Prof. Robert Harris from Karolinska Institute, Sweden for their valuable suggestions.

PS2-11-431

Targeted drug release from chitosan fiber-based textiles for chronic wound care

Michael Wöltje[1], Luise Hilbig[1], Eva Dohle[2], Dilbar Aibibu[1], Shahram Ghanaati[2], Chokri Cherif[1]

[1]Technische Universität Dresden, Institute of Textile Machinery and High Performance Material Technology (ITM), Dresden, DE; [2]Universitätsklinikum Frankfurt, Klinik für Mund-, Kiefer,- und Plastische Gesichtschirurgie FORM-Lab, Frankfurt am Main, DE

Introduction

Wound healing is a complex and fragile process. Failure to progress in the stages of wound healing can lead to chronic wounds. Chronic wounds do not show any healing tendency after 8 weeks of professional treatment. Most patients suffer from the consequences of a wound healing disorder for months or even years. The healing process usually stagnates in the inflammatory phase. Modern wound dressings are not specifically designed for the regeneration of certain wound types in defined wound healing phases, but are based solely on symptomatic treatment. Although the induction of vessel formation by growth factors has been proven in the literature as an essential part of wound healing in animal models, initial experiments with such factors have so far been only successful to a limited extent. This is mainly due to the uncontrolled release of active substances during local (topical) application and certainly also due to the lack of the possibility of being able to release various active substances in a controlled manner over a longer period of time in accordance with natural wound healing.

Therefore, a wound dressing that releases relevant growth factors directly into the wound area is necessary. In contrast to foam dressings, fiber-based textile structures represent a special form of drug delivery systems because of the possibility to realize large surfaces for the release with simultaneously smaller carrier matrix quantities.

Due to its hemostatic effects and cationic antibacterial character the biopolymer chitosan (CS) is regarded as an extremely promising matrix for targeted time-dependent release of active ingredients. Therefore, a textile wound dressing is developed, which consists of CS fibers that are functionalized with a model substance (horse radish peroxidase, HRP) to realize a targeted release profile which should enable growth factor delivery into the wound area for seven days.

Experimental Methods

Chitosans with different degrees of acetylation were processed into foils and spun into fibers. The influence of degree of acetylation, foil thickness, loading time and loading quantity on release kinetics of the model substance HRP were investigated. For this purpose, CS foils were loaded with HRP by diffusion. Then, release kinetics were quantified photometrically. In addition, HRP was covalently bound to chitosan foils and fibers by carboxyl-to-amine crosslinking using the carbodiimide EDC and Sulfo-NHS. HRP release profiles during degradation by lysoszym were investigated. In analogy to the experiments with HRP, chitosan fibers were functionalized with VEGF. These CS-VEGF fibers then were processed into 3D porous textile wound covers. Release profiles of VEGF from those fiber-based samples over 7 days are currently being investigated in an *in vitro* wound model and the results will be presented at the ESB.

Results and Discussion

Initial experiments with CS foils showed that for loading with HRP by diffusion a loading time of 1 h is sufficient. Furthermore, layer thickness and degree of deacetylation have no influence on loading characteristics.

Functionalisation of CS foils and fibres with HRP by crosslinking with EDC/NHS results in covalent coupling of the enzyme to the CS matrix without any influence of HRP activity monitored by substrate turnover after incubation for 7 days in PBS. Monitoring the release of HRP from HRP-CS-crosslinked foils or fibres during degradation of CS by 0.5 mg/ml of lysozyme (lysozyme concentration in serum during acute phase: 3,3 mg/ml) over 7 days showed a strong influence of deacetylation level on HRP release. After an initial burst release (12 h), HRP is continuously released from the chitosan foils with 80 % of deacetylation over 7 days. In contrast, HRP release from chitosan foils with 90% deacetylation was much lower even with higher amounts of the degrading enzyme lysozyme (20 mg/ml).

Conclusion

Using crosslinking of HRP to CS foils and fibres with different percentages of deacetylation a targeted drug release profile for chronic wound care was established successfully.

Acknowledgement

The IGF research project 19523 BG/1 of the Forschungsvereinigung Forschungskuratorium Textil e. V. and Gesellschaft für Chemische Technik und Biotechnologie e.V. is funded through the AiF within the program for supporting the „Industriellen Gemeinschaftsforschung (IGF)“ from funds of the Federal Ministry for Economic Affairs and Energy (BMWi) by a resolution of the German Bundestag.

2:45 p.m. – 3:45 p.m.

Hall 1 / Exhibition Area

PS2-12 | Bone and cartilage

PS2-12-432

3D-Bioprinting of bone grafts for alveolar defects – a preclinical pilot study

Paula Korn[1,2], Tilman Ahlfeld[2], Winnie Pradel[3], Anja Lode[2], Adrian Franke[3], Martina Rauner[4], Ursula Range[5], Bernd Stadlinger[6], Günter Lauer[3], Michael Gelinsky[2]

[1]Charité – Universitätsmedizin Berlin, corporate member of FU Berlin, Humboldt-Universität zu Berlin & Berlin Institute of Health, Department of Oral and Maxillofacial Surgery, Berlin, DE; [2]Centre for Translational Bone, Joint and Soft Tissue Research, Faculty of Medicine "Carl Gustav Carus", TU Dresden, Dresden, DE; [3]Department of Oral and Maxillofacial Surgery, Faculty of Medicine, Dresden, DE; [4]Division of Endocrinology, Diabetes, and Bone Diseases, Department of Medicine III and Center for Healthy Aging, TU Dresden, Dresden, DE; [5]Institute for Medical Informatics and Biometry, Faculty of Medicine „Carl Gustav Carus", TU Dresden, Dresden, DE; [6]Clinic of Cranio-Maxillofacial and Oral Surgery, University of Zurich, University Hospital, Zürich, CH

Introduction

One of the most common hereditary craniofacial anomalies in humans are cleft lips, cleft alveolar bone with or without cleft palate. Clinically, the augmentation of the persisting alveolar bone defect, called alveolar cleft osteoplasty, is performed by using autologous bone grafts. The accompanying disadvantages are leading to an intensive search for alternatives [1]. Objective of the present study was the in vivo application of 3D printed and simultaneously tissue engineered bone grafts and their evaluation regarding the potential to promote osseous defect healing [2].

Experimental Methods

Scaffolds were designed according to the particular defect geometry and produced by 3D printing of a calcium phosphate cement paste (Innotere Paste CPC, Innotere) under mild conditions. An open pore design could be achieved by 60° rotation of the strand orientation of consecutive layers during the printing process. Afterwards the pores were immediately infiltrated by a hydrogel (Tissuecol, Baxter) containing murine mesenchymal stromal cells. Artificial bone defects with a diameter of 3.3 mm were created surgically in the palate of 16 adult Lewis rats. Each defect was augmented with one bone graft. After 6 and 12 weeks, microCT and histology analysis to quantify the remaining defect width and bone formation were performed.

Results and Discussion

The clinical application of all bone grafts was easy and their fitting very good. 12 of 16 rats completed the study. Histology showed a homogenous and continuing bone formation occurring from the defect margins. After 6 weeks healing time new bone formation measured 82.426 µm^2 ± 30.960 µm^2 (mean ± SD) and after 12 weeks 251.639 µm^2 ± 41.827 µm^2. No complete osseous defect healing was observed and the remaining defect width was 2.998 µm ±137 µm (mean ± SD) after 12 weeks. The cell-laden hydrogel was not detectable after 6 or 12 weeks anymore, whereas the cement part of the scaffolds showed no signs of resorption.

Conclusion

3D printing of calcium phosphate cement paste in combination with a MSC-laden hydrogel is suitable for building scaffolds, which fit exactly into an artificial alveolar defect. As a next step the simultaneous printing of both components as well as further modifications of the scaffold materials are planned. One option could be the application

of combinations of CPC and mesoporous bioactive glass composites to improve the in vivo resorbability of the scaffold [3].
The creation of a 3D printed and tissue engineered bone graft for alveolar cleft osteoplasty could preserve patients from donor site morbidity.

References

[1]Korn P, Hauptstock M, Range U, Kunert-Keil C, Pradel W, Lauer G, Schulz MC.Application of tissue-engineered bone grafts for alveolar cleft osteoplasty in a rodent model. Clin Oral Investig. 2017 Nov;21(8):2521-2534.
[2] Ahlfeld T, Doberenz F, Kilian D, Vater C, Korn P, Lauer G, Lode A, Gelinsky M.Bioprinting of mineralized constructs utilizing multichannel plotting of a self-setting calcium phosphate cement and a cell-laden bioink. Biofabrication. 2018 Jul 27;10(4):045002
[3] Schumacher M, Reither L, Thomas J, Kampschulte M, Gbureck U, Lode A, Gelinsky M. Calcium phosphate bone cement/mesoporous bioactive glass composites for controlled growth factor delivery.Biomater. Sci. 2017, 5, 578-588

Acknowledgement

The study was supported by a grant of the "Österreichischen Gesellschaft für Lippen-Kiefer-Gaumenspalten und Kraniofaziale Anomalien". The authors thank Diana Jünger and Anna-Maria Placht for their excellent technical assistance.

PS2-12-433

A combined biological and chemical/physical bone characterization for the development of customized 3D-printed scaffolds

Caterina Licini[1,2], Giulia Molino[2], Chiara Novara[2], Fabrizio Giorgis[2], Giorgia Cerqueni[1], Sonia Fiorilli[2], Gabriela Ciapetti[3], Monica Mattioli-Belmonte[1], Chiara Vitale-Brovarone[2]

[1]Università Politecnica delle Marche, DISCLIMO, Ancona, IT; [2]Politecnico di Torino, Dipartimento di Scienza Applicata e Tecnologia, Torino, IT; [3]Istituto Ortopedico Rizzoli, Laboratorio di Fisiopatologia Ortopedica e Medicina Rigenerativa, Bologna, IT

Introduction

Osteoporosis (OP) is a worldwide disease with a substantial incidence in aged population. It is characterized by a low bone mass due to microarchitectural and structural deterioration of bone tissue, that leads to enhanced bone fragility and consequent increase in fracture risk.[1] The extracellular matrix (ECM) of OP bones undergoes important modifications with changes in protein content and chemical structure that lead to an increase in mineral/matrix ratio.[2] In the frame of the ERC project BOOST, which aims to develop and 3D print a scaffold mimicking human bone, we matched different morphological and structural approaches and techniques to acquire a wide-ranging knowledge of healthy and OP bone structure.

Experimental Methods

Human femoral and humeral heads, discarded during surgical interventions on orthopaedic patients (healthy and osteoporotic), have been harvested. Histological staining, immunohistochemistry and western blotting analyses have been executed to evaluate differences in bone tissue morphology and expression of the main ECM components (i.e. Collagen Type I, TGF-β, IGF-1, Osteocalcin, Osteopontin, Decorin and Bone Sialoprotein-2). Raman spectroscopy and X-ray diffraction (XRD) analysis have been performed to investigate the bone matrix organization and the structure of the inorganic phase, respectively. Furthermore, bone samples have been subjected to micro-computed tomography (micro-CT) analysis to study the overall 3D trabecular organisation as well as its tissue mineral density.

Results and Discussion

Micro-CT and histological staining showed a narrowing of OP bone trabeculae. Furthermore, OP bone trabeculae resulted to have a preferential orientation and a lower interconnection, probably due to a loss of transversal trabeculae (Fig.1A). Micro-CT analysis revealed also an increased tissue mineral density for OP samples, indicative of an increased inorganic phase amount. This result was also confirmed by XRD analysis that detected an increase of hydroxyapatite crystal size in the OP bone. Moreover, both histological observation and Raman spectroscopy suggested a less organized structure in OP tissue at the nanoscale in comparison to healthy one. Histological analysis revealed indeed a disordered tissue morphology (Fig.1B), while Raman spectroscopy detected an increased contribution of random coil configuration of ECM proteins. In addition, western blotting identified the appropriate ratio of the main proteins in bone ECM, whilst immunohistochemistry defined their correct localization.

Conclusion

Biological and chemical/physical techniques allowed a detailed investigation of the structure and composition of healthy and OP bone. From the results obtained through these analyses, it is possible to affirm that OP bone presents an altered structure and morphology at both the microscopic and the nanometric scale. The knowledge of the healthy

and OP bone features is mandatory for the development of biomimetic 3D-scaffolds with a suitable architecture and a punctual localization of molecules to favour a correct bone remodelling. Studies are also ongoing for the setting up of appropriate biomaterials suitable for the 3D printing process of BOOST smart scaffolds.

References

1. Silverman SL, Kupperman ES, Bukata SV and Members of IOF Fracture Working Group. Fracture healing: a consensus report from the International Osteoporosis Foundation Fracture Working Group. Osteoporos Int. 2016 Apr 25. DOI 10.1007/s00198-016-3513-y.
2. A.L. Boskey, Bone composition: relationship to bone fragility and antiosteoporotic drug effects, BoneKey Rep. 4 (2015). doi:10.1038/bonekey.2015.79.

Acknowledgement

This project has received funding from the European Research Council (ERC) under the European Union's Horizon 2020 research and innovation programme (grant agreement No 681798 - BOOST) www.ercprojectboost.eu

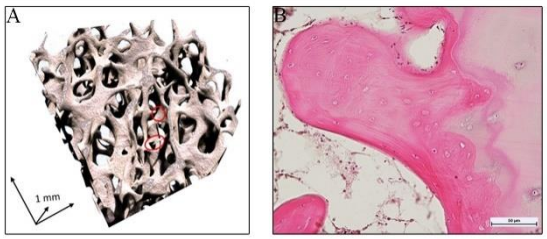

3D reconstruction and histological representation of OP bone
A) 3D micro-CT representation of an OP bone sample. Circled in red the not-bridging transversal trabeculae; B) Histological section (H&E) of bone tissue in OP subject showing the irregular morphology of lamellae.

PS2-12-434

2D substrate based on Exfoliated black phosphorus with anticancer and regenerative properties

Maria Grazia Raucci[1], Ines Fasolino[1], Maria Caporali[2], Manuel Serrano Ruiz[2], Alessandra Soriente[1], Maurizio Peruzzini[2], Luigi Ambrosio[1]

[1]CNR, Institute of Polymers, Composites and Biomaterials, Naples, IT; [2]CNR, Institute of Chemistry of Organometallic Compounds, Firenze, IT

Introduction

Currently, osteosarcoma is the most common bone cancer which mainly affects young people. Surgical resection of tumor followed by chemotherapy for micro-metastasis inhibition constitutes the current standard procedure to cure 65% of osteosarcoma cases. However, chemotherapy treatment uses pharmacological agents with the effect of blocking cell proliferation, without any distinction between healthy and cancer cells. In recent years, several studies have focused the attention on the use of Photodynamic Therapy (PDT) as minimally invasive therapeutic procedure that can apply a selective cytotoxic activity toward cancer cells [1]. In this context, we propose the use of 2D substrate based on few-layer black phosphorous (2D bP) as an alternative tool for osteosarcoma treatment and report how 2D bP can inhibit cancer cell proliferation and in the same time to stimulate newly forming bone tissue generation after osteosarcoma resection [2] without photothermal treatment. In our study, we have developed an *in vitro* model to evaluate the efficacy of 2D bP material with and without near-infrared light irradiation treatment on healthy (HOb, hMSC) and cancer (Saos-2) cells and we also propose an *in vitro* co-culture model (SAOS-2 and HOb cell lines) in order to study the effect of 2D bP on inflammatory response related to cancer.

Experimental Methods

The biological studies were performed to investigate the effect of 2D bP on cell proliferation and osteogenic differentiation of human healthy (hMSC and HOb) and cancer cells (SAOS-2) with and without near-infrared irradiation treatment (NIR). The cell morphology was evaluated by scanning electron microscopy, confocal microscopy and hematoxylin-eosin staining. The biocompatibility and osteogenic differentiation were checked *in vitro* by Alamar blue assay and ALP activity, respectively. Furthermore, the reactive oxygen species (ROS) production was evaluated with and w/o NIR treatment by *in vitro* model inflammation. Moreover, the effect of 2D bP on inflammatory response through pro and anti-inflammatory cytokine investigations on co-culture model consisting of SAOS-2 and HOb, was also investigated.

Results and Discussion

Our investigations suggested that NIR had no effect on HOb proliferation because 2D bP without NIR stimulation promoted the HOb viability with the best expression of early marker of osteogenic differentiation at day14, thus inducing higher proliferation values than control. Conversely, 2D bP with and without NIR, induced a significant reduction in SAOS-2 proliferation and inhibition of ALP activity. Furthermore, 2D bP is able to increase antinflammatory cytokines generation on co-culture model and to inhibit pro-inflammatory mediator synthesis thus suggesting the opportunity to prevent cancer-related inflammation. This study demonstrated that 2D bP enhances the growth and osteogenic differentiation of human healthy cells (HOb and hMSC) and inhibits the proliferation of

osteosarcoma cells (SAOS-2) without NIR treatment. The inhibition of cell proliferation (SAOS-2) of 2D bP reveals its antinflammatory activity on an *in vitro* co-culture model of cancer-related inflammation.

Conclusion

The role of exfoliated black phosphorous (2D bP) as a substrate for an experimental *in vitro* model of osteosarcoma (SAOS-2) was investigated. Its effect was also analyzed on healthy bone derived cell line (HOb) in order to test its potential toxicity on tumor-surrounded tissue. The beneficial effects of 2D bP, from one side the enhancement of HOb growth and the osteogenic differentiation, in the other side the inhibition of SAOS-2 proliferation by blocking inflammatory processes without any photothermal treatment, prompt the application of 2D bP as a highly promising candidate for bone biomedical applications.

References

[1] P. Agostinis, K. Berg, K.A. Cengel, T. H. Foster, A.W. Girotti, S.O. Gollnick, & Korbelik, M. Photodynamic therapy of cancer: an update. CA: a cancer journal for clinicians, 2011;61(4):250-281.

[2] M. G. Raucci, I. Fasolino, M. Caporali, M. Serrano-Ruiz, A. Soriente, M. Peruzzini, L. Ambrosio. Exfoliated Black Phosphorus Promotes in Vitro Bone Regeneration and Suppresses Osteosarcoma Progression through Cancer-Related Inflammation Inhibition. ACS Appl. Mater. Interfaces, 2019;11(9):9333–9342.

PS2-12-435

A novel osteoblasts- osteoclasts co-culture system of osteoporosis: the dynamic protein corona of magnetic hydroxyapatite scaffold promotion osteoblast proliferation

Yue Zhu

Sichuan University, National Engineering Research Center for Biomaterials, Chengdu, CN

Introduction

Osteoporosis (OP) is a common systemic metabolic osteopathy characterized by decreased bone mass per unit volume and changes in bone microstructure, which is common in postmenopausal women and elderly men. The serious consequence of osteoporosis is osteoporosis fractures (brittle fractures), which may occur even after minor trauma or during daily activities. After fracture, biomaterials are needed to aid in bone formation. Once the scaffolds entrance *in vivo*, biomaterials undergo modifications as a result of endogenous proteins adsorbed on their surface, which determines the interaction between the materials and the cells. The formation of protein corona is affected by various factors, such as the physical and chemical properties of materials, protein source, protein concentration and so on. Cytokines are continuously secreted during cell culture, and then influence cell - cell interactions. Osteoblast (OB) and Osteoclast (OC) are the most common bone-associated cell, which can coordinate the dynamic balance of bone formation and bone resorption. The study of osteoblast and osteoclast co-culture is helpful to explore the process of bone remodeling, especially to have a comprehensive understanding of bone metabolic diseases. Hence, we established a system of osteoblast and osteoclast co-culture to study the effect of specific cytokines secreted by osteoblasts and osteoclasts on the formation of protein corona onto the surface of biomaterials at different dynamic culture times, which might explore how does the different material specific adsorption of proteins on the surface affect the communication between osteoblast and osteoclast and the relationship of dynamic process of the osteoporosis.

Experimental Methods

In this article, the magnetic hydroxyapatite scaffolds and hydroxyapatite scaffolds were selected as different potential bone substitutes. At the first, the osteoporosis model was established by removing ovaries of SD rats and analyzed by micro CT. Then primary osteoblasts and bone marrow mononuclear cells (induced as osteoclasts by adding cytokines) were isolated and extracted under the condition of osteoporosis. We inoculated osteoblasts and osteoclasts on hydroxyapatite and magnetic hydroxyapatite scaffolds, and the effects of magnetic hydroxyapatite and hydroxyapatite scaffolds on cell behavior and protein corona formed on their surface were studied at 1 d, 4 d, and 7 d under co-culture conditions. The CCK8 kit was used to test the proliferation of osteoblasts and osteoclasts, tartrate acid phosphatase staining was used to the formation of osteoclasts, and the formation of dynamic protein corona was systematically studied by bicinchoninic acid protein assay kit, sodium dodecyl sulfate polyacrylamide gel electrophoresis.

Results and Discussion

The micro CT results showed that the osteoporosis model was successfully constructed. Tartrate acid phosphatase staining proved that mononuclear cells of bone marrow could be induced into osteoclasts by cytokine induction for 6 days. We successfully established the osteoporosis model and isolated osteoblasts and osteoclasts from the model animals. The CCK8 results showed that the MHA scaffold promoted osteoblasts proliferation. The results of the

bicinchoninic acid protein assay kit and sodium dodecyl sulfate polyacrylamide gel electrophoresis showed that there were no distinct differences in the total amount of protein adsorption, but the composition of the proteins significantly changed (Fig 1.).

Conclusion

Under the osteoblast/osteoclast co-culture system, osteoblasts and osteoclasts continuously secreted biomolecules, which caused dynamic changes of protein corona on the surface of bone repair scaffolds, and the analysis of dynamic protein corona may be helpful to reveal the internal relationship between osteogenesis and osteoclast in the process of osteoporosis.

References

1. Zhao, R.; Xie, P.; Zhang, K.; Tang, Z.; Chen, X.; Zhu, X.; Fan, Y.; Yang, X.; Zhang, X., Selective Effect of Hydroxyapatite Nanoparticles on Osteoporotic and Healthy Bone Formation Correlates with Intracellular Calcium Homeostasis Regulation. Acta Biomater 2017, 59, 338-350.
2. Monopoli, M. P.; Aberg, C.; Salvati, A.; Dawson, K. A., Biomolecular Coronas Provide the Biological Identity of Nanosized Materials. Nat. Nanotechnol. 2012, 7 (12), 779-786.
3. Serpooshan, V.; Mahmoudi, M.; Zhao, M.; Wei, K.; Sivanesan, S.; Motamedchaboki, K.; Malkovskiy, A. V.; Gladstone, A. B.; Cohen, J. E.; Yang, P. C.; Rajadas, J.; Bernstein, D.; Woo, Y. J.; Ruiz-Lozano, P., Protein Corona Influences Cell-Biomaterial Interactions in Nanostructured Tissue Engineering Scaffolds. Adv. Funct. Mater. 2015, 25 (28), 4379-4389.
4. Albanese, A.; Walkey, C. D.; Olsen, J. B.; Guo, H.; Emili, A.; Chan, W. C. W., Secreted Biomolecules Alter the Biological Identity and Cellular Interactions of Nanoparticles. ACS Nano 2014, 8 (6), 5515-5526.
5. Wu, L.; Feyerabend, F.; Schilling, A. F.; Willumeit-Romer, R.; Luthringer, B. J. C., Effects of Extracellular Magnesium Extract on the Proliferation and Differentiation of Human Osteoblasts and Osteoclasts in Coculture. Acta Biomater 2015, 27, 294-304.

Acknowledgement

This work was supported by the National Key Research and Development Program of China (2016YFC1100403), the National Natural Science Foundation of China (21571134,31771037 and 31600765), and the Fundamental Research Funds for the Central Universities (2012017yjsy123).

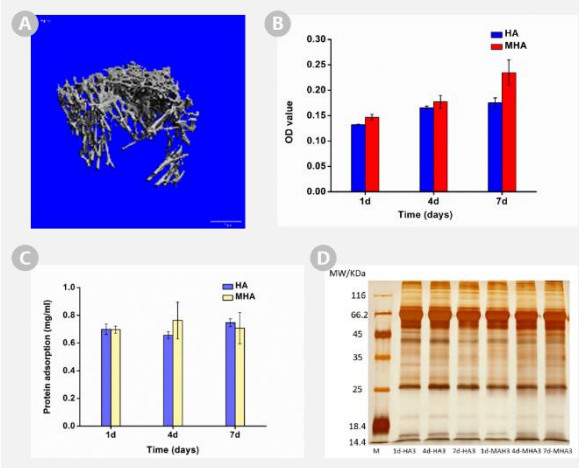

Fig. 1. Osteoporosis osteoblasts- osteoclasts co-culture system and the dynamic protein corona of hy

A) Micro-CT images of the distal femurs OVX osteoporosis model; B) CCK-8 assay for proliferation of primary osteoblasts on HA and MHA scaffolds for 2, 4 and 6 days in osteoblasts /osteoclasts co-cultured system. C) The amount of adsorbed proteins on HA and MHA scaffolds by the BCA assay in osteoblasts /osteoclasts co-cultured for different time; D) SDS-PAGE gel (12%) of the dynamic protein corona obtained from HA and MHA in osteoblasts /osteoclasts co-cultured for different time.

PS2-12-436

Characterization of the structural properties and the 3D vascular network in vertebral end-plates using micro-CT.

Sheen Gurrib[1], Serena M. Best[1], Ruth E. Cameron[1], David Sharp[2]

[1]University of Cambridge, Department of Materials Science and Metallurgy, Cambridge, GB; [2]Ipswich Hospital, Ipswich, GB

Introduction

Back pain has been found to be the leading cause of disability worldwide, affecting 8 out of 10 adults (1). One of the major causes of back pain has been identified to be intervertebral disc (IVD) degeneration. The disc being the largest avascular tissue in the body, it relies primarily on the nutritional pathways from the adjacent vertebral endplates (VEPs) (2).

The VEPs are characterized as a bilayer of cartilage and bone, which acts as a boundary between the IVD and the vertebral bone (3). Previous work done by Lotz et al. has shown the presence of an intricate network of vascular canals in the VEP through which nutrients are carried to the IVD and waste products are removed (4). However, the variance of structural properties of the VEP at different spinal levels and the quantitative evaluation of these canals throughout the spine are yet to be carried out.

The aim of this work is to use non-invasive imaging technology, micro-computerized tomography (micro-CT), combined with ScanIP to enable the structural characterization of the VEP and the 3D investigation of this intricate canal network.

Experimental Methods

VEPs were sampled from mature sheep spines and sectioned into a grid as shown in Figure 1a. Caudal and cranial VEP sections were sampled from lumbar ovine spines and imaged in wet conditions using high-resolution micro-CT at 4.92 µm pixel size. CTAnalyser was used to reconstruct the images to compare different regions of the VEP, as shown in Figure 1b. Thickness, porosity, bone mineral density, curvature and number of openings at the disc boundary were measured for VEPs at spinal levels L1 to L3 for both caudal and cranial sides. ImageJ and ScanIP (Simpleware, Synopsys Inc., USA) was then used to create 3D rendered volumes of the canal network found in the VEP using the reconstructed micro-CT images using segmentation and flood fill to isolate the vascular network. Centrelines were added and enabled the quantitative analysis (diameter, length, orientation and connectivity) of individual canal.

Results and Discussion

Figure 1b shows thinner VEP layer with a greater concentration of pores at the central regions of the VEP (region of interest marked R7) whereas a thicker layer with fewer pores were seen at R4 on the periphery. The average thickness of the 6 VEP samples from the central region was 0.57 ± 0.18 mm and 1.22 ± 0.23 mm for peripheral region samples. The trabecular structure underlying the VEP at all locations was found to be similar.

A table of comparative analysis was generated to compare the trends observed (Figure 2a), where the arrow points towards the location with higher value for the given property. For example, thickness is higher in cranial regions than caudal regions but decreases from L1 to L3 down the spine. The extracted 3D network was shown to consist of a bed of canals running almost parallel to the disc, as shown in Figure 2b.

The 3D rendered images obtained from ScanIP, shown in Figure 2c enabled the measurement of length, diameter and orientation of individual canals and the proposal of schematic diagrams for the blood supply network in the VEP adjacent to the central and peripheral regions of the disc.

Conclusion

This work demonstrates that micro-CT, coupled with ScanIP is an extremely useful tool for the structural characterization of the VEP and quantitative analysis of the 3D vascular network. It shows the direct correlation between the architectural structure, concentration of vascular canals and their location with respect to the central or peripheral regions of the disc. The next steps will be the comparison of the network in VEP adjacent to degenerated discs to understand the relationship between disc degeneration and the nutritional pathway to the disc.

References

1. Driscoll T, Jacklyn G, Orchard J, Passmore E, Vos T, Freedman G, et al. The global burden of occupationally related low back pain: estimates from the Global Burden of Disease 2010 study. Ann Rheum Dis. 2014; 73(6):975–81.

2. Roberts S, Menage J, Urban JPG. Biochemical and structural properties of the cartilage end-plate and its relation to the intervertebral disc. Spine (Phila Pa 1976). 1989; 14(2):166–74.

3. Yamaguchi, T., Goto, S., Nishigaki, Y., Orías, A. A. E., Bae, W. C., Masuda, K. and Inoue, N. (2015), Microstructural analysis of three-dimensional canal network in the rabbit lumbar vertebral endplate. J. Orthop. Res., 33: 270–276. doi:10.1002/jor.22759.

4. Lotz JC, Fields AJ, Liebenberg EC. The role of the vertebral end plate in low back pain. Glob spine J 2013;3(3):153–64.

Acknowledgement

I would like to thank Jenny Shepherd and David Sharp for their help throughout the project and the Malaysian Commonwealth Studies Centre and The Currimjee Group for their generous contributions towards my time at Cambridge University.

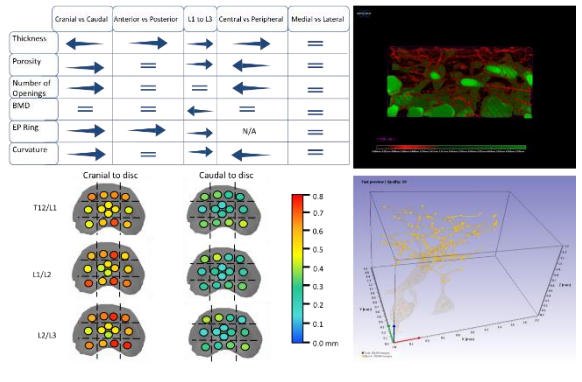

Figure 2
Figure 2(a) shows comparative table between the structural properties of the VEP measured at different locations, (b) shows an example of the differences in thickness across ROIs in the VEP, (c) shows the isolation of the 3D network and (d) shows centerlines used to characterise the individual canals.

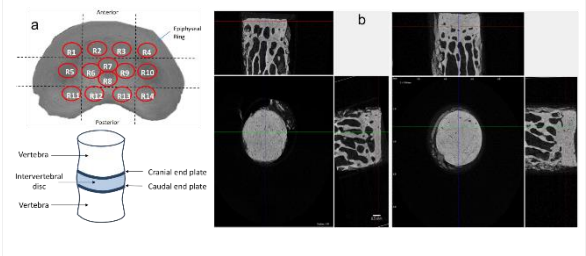

Figure 1
The sectioning of samples and locations of regions of interest are shown in (a) and microCT images showing differences in terms of thickness and porosity between samples from centre and periphery of a caudal VEP at L3 shown in (b)

PS2-12-437

Physical processing of collagen foams for application as bone substitute materials

Xin Xiong[1], Pia Moosmann[2], Ole Jung[3], Ralf Smeets[3], Mike Barbeck[3,4,5], Claus Burkhard[1], Jens Pissarek[6], Rumen Krastev[1,2]

[1]Natural and medical sciences institute at the University of Tübingen, Group Biofunctionalised surfaces, Reutlingen, DE; [2]Reutlingen University, Group Intelligent surfaces, Reutlingen, DE; [3]University clinic centre Hamburg-Eppendorf (UKE), Department for Oral & Maxillofacial Surgery, Section Ford Regenerative Orofacial Medicine, Hamburg, DE; [4]Botiss Biomaterials GmbH, Zossen, DE; [5]BerlinAnalytix GmbH, Berlin, DE; [6]Biotrics Bioimplants GmbH, Berlin, DE

Introduction

Bone substitute Materials (BSM) are important for regeneration of lost bone tissues. Currently, the autologous bone remains the “gold standard” in this area of application because of its well proven osteogenic, osteoinductive and osteoconductive properties. However, the application of autologous bone materials, requires a parallel surgery to gain the bone tissue. This might be associated with a variety of clinic complications. Therefore, BMS plays an important role in clinic implantology in particular in dental surgery. BMS derived from human or animal (allogeneic or xenogeneic) is obtained from the hydroxyapatite (HA)-based bone matrix of the donor tissues. Synthetic BSM are mostly composed of HA and b-tricalcium phosphate (b-TCP) which are often failed to replace the biological functions from the natural matrix due to the lack of organic component from extracellular matrix in particular the collagen. Additionally, synthetic BSM has significantly different structural properties compared to the natural bone, leading to less support of the bone regeneration. Thus, the development of collagen-based BMS as scaffolds is an important issue.

Collagen has been extensively studied since more than a century as one of the most widely applied biomaterials in clinic practice and research fields. Dried collagen sponges have been used as hemostatic wound dressing or soft tissue filler in surgical treatments. Collagen from different animal derived materials e.g. bovine and porcine skin, pericardium are commonly used. Mostly commercially available collagen (for research) is isolated via extraction using low concentrated acidic solutions such as acetic acid, citric acid. This procedure delivers collagen with high purity of the isolated triple helical molecules. The acidic extraction procedure has different drawback such as (1) long duration of up to 3 weeks (2) low yield of only soluble collagen molecules. Insoluble large collagen fibers are in the residual material; (3) random acidic hydrolysis of the collagens resulting in coexisting of collagen molecules and undefinable collagen peptides.

In this study we developed collagen-based foam materials as BSM for dental surgery. The main advantages of the physical processing procedure established in this study compared to conventional acidic collagen extraction are (1) short processing time; (2) Use of collagen fibrils (not soluble collagen molecules) with higher efficiency; (3) Very good foamability and collagen foam can be directly used as scaffold for cell cultivation and potentially as BSM without further processing; (4) high density of the collagen of up to 50 mg/cm^{3}compared to the classical collagen products (e.g. rat tail tendon is normally available as solution with a concentration of 3-6 mg/ml).

Experimental Methods

Collagen foam preparation

Raw material (bovine/porcine) dried split skin is rinsed in acidic solution. The wetted skin is mechanically homogenized to a collagen-suspension. Based on the selection of tools and power of the homogenisator, the fiber size is in the range of 10 to 50 µm. The suspension is then foamed using a foam generator.

Foam characterization

Dynamic foam analysis (DFA 100, Krüss) was applied to measure the bubble size and bubble distribution. Cryo-FIB-SEM: Cryo FIBSEM was performed to evaluate the structure of the foam and the assembly of the collagen fiber/fibrils in the foam scaffold.

Biocompatibility test

Resazurin assay test with L929 fibroblasts cell culture was applied to prove the biocompatibility of the prepared collagen foams. The test delivers information about the viability of cells in contact with the collagen foam quantitatively determined by measuring the fluorescence.

Results and Discussion

The prepared collagen foams have a density of 10 to 50 mg/cm^3 depending on the adjusted process conditions. The foams are homogeneously prepared in relatively large volume (200 cm^3) with a bubble size distribution from 20 to 80 µm depending on the density of the collagen foams. The foam properties such as bubble size, visoc-elastic characteristics and density can be controlled by adjusting of the process parameters. The foams can be easily stored either at room temperature or cooled in refrigerator without destruction. The simulated storage stability test at 30 °C degrees showed no dissolving or destruction of the collagen foam even incubated in PBS solution for 21 days. L929 fibroblasts showed very good activity as measured by resazurin assay similar to that of fibroblasts cultivated in the tissue treated cell culture dishes used as a control. First functional study with osteoblasts has been performed and evaluation of the data is still under processing.

Conclusion

The foam might be applied as an injectable dental BSM. If compared to the commercially available injectable gel the collagen foam could be produced in a simple process and the foams showed more natural ECM-properties. The Process could be easily upscaled for industrial process.

Acknowledgement

The authors would like to thank the group of intelligent surfaces at Reutlingen University. The project is financially supported by the program "ZIM Kooperationsprojekt ZF4585501AW8 vom Bundesministerium für Wirtschaft und Technologie".

PS2-12-438

In vitro and *in vivo* investigation on artificial extracellular matrices for bone regeneration

Sabine Schulze[1,2], Yvonne Förster[1,2], Christin Neuber[3], Suzanne Manthey[1,2], Annett Wenke[1,2], Ute Hempel[4], Jens Pietzsch[3,5], Stefan Rammelt[1,6]

[1]University Hospital Dresden, UniversityCenter for Orthopedics and Trauma Surgery, Dresden, DE; [2]Medical Faculty, TU Dresden, Centre for Translational Bone, Joint and Soft Tissue Research, Dresden, DE; [3]Helmholtz-Zentrum Dresden-Rossendorf, Institute of Radiopharmaceutical Cancer Research, Department Radiopharmaceutical and Chemical Biology, Dresden, DE; [4]Medical Faculty, TU Dresden, Institute for Physiological Chemistry, Dresden, DE; [5]Technische Universität Dresden, Faculty of Chemistry and Food Chemistry, Dresden, DE; [6]DFG-Center for Regenerative Therapies Dresden, Dresden, DE

Introduction

Treatment of critical size bone defects after trauma, infection or tumour resection is particularly sophisticated [1]. The same applies for fracture healing or osseointegration of implants in patients with impaired bone healing due to cancer or metabolic diseases. Administration of growth factors achieved considerable progress in bone regeneration. However, the results are not yet reproducible despite substantially increased treatment costs. Adjuvant approaches pursue biomaterials to stimulate bone healing either by enhancing new bone formation or by inhibiting osteoclastogenesis.

A promising strategy is to strengthen biomaterials by modification with components of the extracellular matrix (ECM). The ECM mediates adhesion, migration, proliferation and differentiation of cells and thus orchestrates processes that are essential for healing. In bone healing, ECM suppots the maturation of mesenchymal precursor cells into osteoblasts, which contribute to regeneration through synthesis of the organic bone matrix and its mineralization [2]. Therefore, artificial ECM (aECM) entered the focus of research on bone healing and osseointegration of implants. Here, the impact of sulfated glycosaminoglycan derivatives (sGAG), i.e. sulfated hyaluronan and chondroitin sulfate (CS) on osteoblasts and osteoclasts, respectively, was investigated in vitro and in vivo.

Experimental Methods

Bone fragments and blood samples were obtained from patients who either suffered from diabetic neuropathy or posttraumatic osteoarthritis during reconstructive foot and ankle surgery. Osteoblasts were isolated from bone fragments. Monocytes were isolated from patient's blood and differentiated into osteoclasts. sGAG-related alterations in osteogenic differentiation were investigated by qPCR. Osteoclastogenesis with and without sGAG was analysed by using a quantitative resorption assay. The expression of osteoclast-specific genes was determined by qPCR.

The impact of sGAG on bone regeneration was also examined in critical size defects in rats. sGAG-coated PCL scaffolds were implanted in femoral defects. Alteration in cytokine pattern and bone volume were analysed using microdialysis and µCT.

Results and Discussion

sGAG altered the expression of RUNX2, osteocalcin and alkaline phosphatase. In patients suffering from osteoarthritis but with otherwise physiological bone metabolism the expression of these bone-specific genes was induced by sGAG in comparison to osteoblasts from diabetic patients. Osteoclasts derived from blood samples of diabetic patients revealed massive resorption activity which was, but this was significantly decreased by sGAG.

sGAG-coated implants caused an altered cytokine release and faster bridging of critical size bone defects, as seen in vivo in rats.

Conclusion

Sulfated glycosaminoglycans (sGAG) display osteogenic properties and simultaneously inhibit osteoclastic bone resorption Reduced osteoclast activity together with activated osteogenesis can lead to improved bone healing. These findings are in keeping with earlier reports [3, 4]. sGAG appear to partially offset the impaired balance of bone resorption and formation in diabetic patients.

References

[1] Rammelt S (2017) EFORT Open Rev 1(5):239-46
[2] Hempel U et al. (2012) Acta Biomater 8:4064-72
[3] Schulze S et al. (2018) J Cell Physiol 233:4391–4400
[4] Förster Y et al. (2017) Mater Sci Eng C 71:84-92

PS2-12-439

Osteoblast behavior upon electrical stimulation *in vitro*

Susanne Staehlke[1], Martina Grüning[1], Julius Zimmermann[2], Thomas Freitag[1], Alexander Prokopp[1], Ingo Barke[3], Sylvia Speller[3,4], Ursula van Rienen[2,4], Barbara Nebe[1,4]

[1]University Medical Center Rostock, Department of Cell Biology, Rostock, DE; [2]University of Rostock, Institute of General Electrical Engineering, Faculty of Computer Science and Electrical Engineering, Rostock, DE; [3]University of Rostock, Institute of Physics, Rostock, DE; [4]University of Rostock, Dept. Life, Light & Matter, Rostock, DE

Introduction

Orthopedic implants are designed to mediate the healing of bone fractures. An extensive research field in regenerative medicine is to study the impact of invasive electrical stimulation - the irritation of the tissue / cells by applied electric fields. The mechanism of interaction of cells upon electrical stimulation, in particular the role of electrical parameters like intensity, frequency, duration, of the electric field) to cell physiological processes, is not yet understood.

In the current in vitro study, we investigated the effect of electrical stimulation on osteoblast adhesion and growth. For the study, a commercially available multi-channel system (IonOptix) as a model system was used. In addition to the in vitro studies, we determined physical and electrical stimulation parameter.

Electric field stimulation opens up new possibilities to optimize healing processes.

Experimental Methods

For electrical irritation, a multi-channel electrical stimulator – a voltage generator and 12-well C (culture)-Dish (C-Pace EM, (IonOptix, Milton, MA) – were used as model system. The pair of graphite electrodes (distance 11 mm) were located from the lid to the bottom of the 12-well plate (Greiner) and thus directly contacted with culture medium. This system generates rectangular electronic bipolar pulses for electrical stimulation with the frequencies 0.01 to 99 Hz, pulse duration of 0.4–10 ms, and a peak voltage of up to ± 40 V. The connection of the generator to the electrodes via a thin cable allows the stimulation of the cells in the incubator.

The influence of the electric fields on the media was characterized by determining the temperature and the pH ranges. Moreover, the applied electric field strength was evaluated by means of numerical simulations for a voltage of 1V.

The cell biological investigations were performed with human osteoblasts MG-63 (passage number 5 to 30, ATCC® CRL-1427™, Bethesda, USA) [1]. The osteoblasts were cultured in DMEM (Dulbecco's Modified Eagle Medium; Thermo Fisher Scientific, Waltham, MA USA) with FCS (10 % fetal calf serum; Biochrom FCS Superior, Merck KGaA, Darmstadt, Germany) and antibiotics (1% Gentamicin; Ratiopharm GmbH, Ulm, Germany) in incubator under standard culture conditions (5% CO_2/95% air at 37 °C). The cell experiments were studied by microscopy (FE-SEM, cLSM) and flow cytometry within 24 h.

Results and Discussion

The physical experiments to analyze the media under electrical stimulation (15 min) revealed no change in pH or temperature up to 10 V.

The numerical simulation of the electric field distribution between the two electrodes for a voltage of 1V indicated that the cells are exerted to a field with roughly homogeneous distribution about 90 V/m (Fig. 1). For greater voltages this value is expected to change linearly w.r.t the voltage.

The first cell experiments with electrical stimulation (10 min) indicated an influence on the initial adhesion and growth of the MG-63 osteoblasts. These effects were found preferentially for electric fields above 100 V/m.
Ercan and Webster [2] could show, using a similar stimulation system, that low voltages promote the proliferation of osteoblasts.

Conclusion

The results suggest that the impact of electrical stimulation may improve osteoblast behavior. The use of electrical stimulation has the potential for novel therapeutic treatment for various medical applications.

References

[1] S. Staehlke et al., Cell Biol Int. 2019; 43: 22-32.
[2] B. Ercan and T.J. Webster, Int J Nanomedicine 2008; 3: 477-485.

Acknowledgement

This research was supported by the German Research Foundation (DFG) within the Collaborative Research Centre 1270 ELAINE.

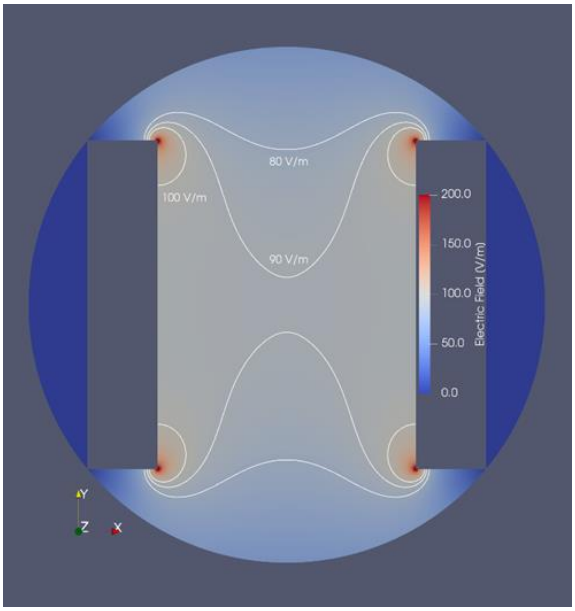

Fig. 1:
Electric field distribution between the electrodes for 1V. Contour lines indicate the area with a more or less homogeneous field distribution.

PS2-12-440

Multifunctional Nano- and Macroporous Bioactive Glass-Composites for Bone Replacement

Nina Ehlert[1,5], Marvin Lietzow[1,5], Karen Besecke[1,5], Jörg Schaeske[2,5], Meike Stiesch[2,5], Sarah Gniesmer[4,5], Andreas Kampmann[4,5], Laura Burmeister[3,5], Andrea Hoffmann[3,5], Franz Körkemeyer[6]

[1]Leibniz University Hanover, Institut für Anorganische Chemie, Hanover, DE; [2]Medizinische Hochschule Hanover, Klinik für Zahnärztliche Prothetik und Biomdizinische Werkstoffkunde, Hanover, DE; [3]Medizinische Hochschule Hanover, Klinik für Orthopädie, Hanover, DE; [4]Medizinische Hochschule Hanover, Klinik für Mund-, Kiefer- und Gesichtschirugie, Hanover, DE; [5]Niedersächsisches Zentrum für Biomedizintechnik, Implantatforschung und Entwicklung, Hanover, DE; [6]Leibniz University Hanover, Institut für Werkstoffkunde, Hanover, DE

Introduction

Bone replacement for critical sized defetcts after infection or cancer debridement is a major issue in bone surgery. Therefore, the aim of the presented work is the development of a biodegradable implant material which can combat bacterial infection and support the formation of new bone at the same time.

Experimental Methods

In a first step nano- and macroporous bioactive glass scaffolds are produced by a sponge replica method. A polyurethane sponge is soaked with a precursor solution containing TEOS, as a silica source, ethanol, water, hydrochloric acid and F127 as structure directing agent. Additionally, it is possible to add a calcium source. After coating and drying the initial sponge is removed together with the SDA by calcination at 600 °C [1]. For improved mechanical stability of the scaffolds these are coated with biodegradable polymers, like chitosan or a mixture of chitosan and gelatin. For a further functionalization the nanopores can be loaded with antibacterial agents like silver nanoparticles. Another option is the delivery growth factors like bone morphogenetic 2 (BMP2). The materials are characterized via scanning and transmission electron microscopy, X-ray diffraction, sorption experiments and X-ray microscopy. Biocompatibility is tested in cell culture investigations with primary osteoblasts. Antibacterial efficiency ist investigated with S. oralis in suspension.

Results and Discussion

The sponge replicas show nanopores of about 5 to 6 nm and open macropore structure. The nanopores of the replicas were loaded with silver nanoparticles as antibacterial agent. They show an antibacterial effect against S. oralis. The polymer coatings lead to increased mechanical stability while the macropore structure was maintained. Additionally, it was possible to deliver the bone growth factor BMP2 at different levels. First in-vitro investigations of the base materials with human osteoblasts showed a good general biocompatibility.

Conclusion

The developed multifunctional scaffolds are promising candidates for an effective bone replacement material.

References

[1] Shih C., Lu P., Chen W., Chang, Y., Chien C., *Ceram. Int.* 40 (2014) 15019.

Acknowledgement

Thanks to the Institute for Technical Chemistry, and the Laboratory of Nano- and Quantum Engineering (LNQE) Leibniz University of Hanover for access to their characterization methods.

PS2-12-441

Effect of Chitosan Infiltration on the Mechanical Properties of a Porous Xenograft Material Derived from New Zealand Sourced Bovine Cancellous Bone

Niranjan Ramesh[1], Jithendra T. Ratnayake[2], Stephen C. Moratti[3], George J. Dias[1]

[1]University of Otago, Department of Anatomy, Dunedin, NZ; [2]University of Otago, Department of Oral Sciences, Faculty of Dentistry, Dunedin, NZ; [3]University of Otago, Department of Chemistry, Dunedin, NZ

Introduction

Xenograft materials such as processed bovine bones bear structural and morphological similarities to human bone[1]. Despite being a cheaper alternative to synthetic biomaterials, significant risks of disease transmission in xenografts have limited their potential for widespread use as a bone replacement material. Hydroxyapatite (HA) has been the widely explored choice of bone analogue biomaterial due to its bioactivity and biocompatibility[2]. There have been several studies aimed at extracting hydroxyapatite from bovine bones (BHA) but often used processing methods entailing high production costs[1]. A previous study by our research group developed a xenograft from NZ sourced bovine cancellous bones using a simple, cost-effective subcritical water extraction (SCWE) process to produce BHA. The prion-free material exhibited excellent physicochemical properties and biocompatibility[3]. However, a decline in compressive mechanical properties of the bovine bone were inevitable due to the loss of collagen, major component of the bone's organic matrix due to the sintering temperature used in the processing. The present study investigated the effect of chitosan infiltration into the prepared BHA scaffolds aimed at restoring the latter's mechanical properties. Changes the physicochemical and biological properties were also evaluated.

Experimental Methods

The BHA scaffolds were prepared according to our previous study by Ratnayake *et al*[3]were used as controls. The Chitosan/Hydroxyapatite scaffolds (CS-HA) were prepared according to the protocol by Huang *et al*[4].Briefly, 2 wt.% of low molecular weight chitosan (CS) was dissolved in 0.1M acetic acid under constant stirring. The BHA cubes were soaked in the CS solution under ultrasonic vibration for 15min to encourage infiltration of CS. The soaked scaffolds (CSHA) were then air-dried for 12h to reduce pore blockage by dripping out the excess CS and dried in a vacuum oven at 50˚C overnight to produce a uniform coating of chitosan on both interior and the exterior surfaces of the scaffolds.

The scaffolds (BHA & CSHA) were characterized using SEM, µCT, EDX, XRD and FTIR analyses to evaluate the physicochemical properties. *In vitro* chemical stability (pH changes) and degradation behaviour of the scaffolds (n=3) were tested by immersing them in simulated body fluid (SBF) (T= 37˚C, pH 7.4) for 21 days. An Instron 3369 universal testing machine operating with a 500N load cell was used to evaluate the compressive mechanical properties of the scaffolds (n=9). The scaffolds (n=3) were also characterized using Live/Dead® assay to evaluate *in vitro* cellular biocompatibility on osteoblast-like SaOS-2 cells. All statistical results, interpreted using GraphPad Prism were considered significant at $P<0.05$.

Results and Discussion

The SEM and µCT analyses of BHA and CSHA scaffolds showed an interconnected open porous structure with pore sizes ranging from 120µm-530µm optimal for osteoconductivity[5] comparable to commercial products such as

Cerabone®[6]. Characteristic vibrational peaks of HA and CS were observed in CSHA scaffolds confirmed the infiltration of CS into the BHA scaffolds supported by results of the EDX analysis. The presence of HA phase in BHA & CSHA were also confirmed by XRD. CSHA scaffolds demonstrated satisfactory chemical stability and degradation behaviour required for a biomaterial when immersed in SBF (no significant difference with BHA). We observed the compressive strength of the CSHA scaffolds doubled and Young's modulus, nearly thrice as much as the BHA scaffolds. The results were found to be statistically significant and the mechanical properties of CSHA scaffolds were comparable to that of trabecular bones[7]. Live/Dead® assay showed improved cell viability on CSHA scaffolds over the observed period of 72h.

Conclusion

The infiltration of chitosan produced significant improvements in the mechanical properties and biocompatibility of the BHA scaffolds prepared by the SCWE process. The present study hence provides a simple, cost-effective methodology to produce mechanically reinforced xenograft HA biocomposite scaffolds sourced from New Zealand bovine cancellous bones suitable for applications in bone tissue engineering.

References

1. Akram, M., Ahmed, R., Shakir, I., Ibrahim, W. A. W. & Hussain, R. Extracting hydroxyapatite and its precursors from natural resources. *J. Mater. Sci.***49**, 1461–1475 (2013).
2. Hulbert, S. F., Hench, L. L., Forbers, D. & Bowman, L. S. History of bioceramics. *Ceram. Int.***8**, 131–140 (1982).
3. Ratnayake, J. T. B., Gould, M. L., Shavandi, A., Mucalo, M. & Dias, G. J. Development and characterization of a xenograft material from New Zealand sourced bovine cancellous bone. *J. Biomed. Mater. Res. B. Appl. Biomater.* (2016).
4. Huang, D. *et al.* Antibacterial Chitosan Coating on Nano-hydroxyapatite/Polyamide66 Porous Bone Scaffold for Drug Delivery. *J. Biomater. Sci. Polym. Ed.***22**, 931–944 (2011).
5. Orlovskii, V. P., Komlev, V. S. & Barinov, S. M. Hydroxyapatite and Hydroxyapatite-Based Ceramics. *Inorg. Mater.***38**, 973–984 (2002)
6. Tiwari, A. *Biomedical materials and diagnostic devices*. (John Wiley & Sons, 2012).
7. Gerhardt, L.-C. & Boccaccini, A. R. Bioactive Glass and Glass-Ceramic Scaffolds for Bone Tissue Engineering. *Materials (Basel).***3**, 3867–3910 (2010).

Acknowledgement

The authors wish to acknowledge the technical assistance of Otago Centre for Electron Microscopy in the SEM, EDX and µCT analyses.

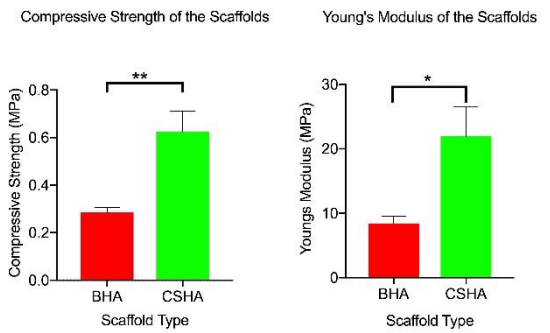

Compressive Mechanical Properties of the prepared BHA & CSHA scaffolds

Compressive Mechanical Properties of BHA & CSHA scaffolds. Bars in graph reported as ± standard error of means. *-P<0.05 **-P<0.01

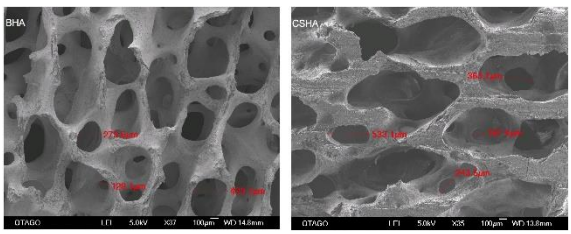

Scanning Electron Micrographs of BHA & CSHA scaffolds showing interconnected porosity

PS2-12-442

Development of Injectable Bone Composites for Biomedical and Surgical Applications

Dhivyaa Anandan[1], Ankita Das[2], Arunai Nambiraj[1], Amit K. Jaiswal[1]

[1]Vellore Institute of Technology (VIT), Centre for Biomaterials, Cellular and Molecular Theranostics (CBCMT), Vellore, IN; [2]Vellore Institute of Technology (VIT), School of BioSciences and Biotechnology (SBST), Vellore, IN

Introduction

Tissue engineering and regenerative medicine is becoming the new standard for treatments, especially bone tissue engineering [1]. With the drawbacks in the current treatment methods like bone grafts and metallic implants, researchers and clinicians are looking for treatment methods that are economical, easy to fabricate and non-toxic [2]. Presently, there are a lot of studies focusing on fabrication of scaffolds for bone tissue engineering but there are few studies supporting the formulation of bone composites that can be used in different forms for various effective treatments [3-11]. This study aims at fabricating a composite that can be used as bone adhesive, bone cement and/or a scaffold to carry drugs for regeneration purposes. These novel bone adhesive biomaterials will provide an easy and rapid method to fixate fractures without the need for removal after bone healing.

Experimental Methods

The bone composite here is being formulated using a natural polymer, namely carboxymethyl cellulose, hydroxyapatite, citric acid and calcium nitrate tetrahydrate (CNTH). The study not only focused on fabricating a unique combination to form a bone composite but also focuses on a comparative analysis of different concentrations of components in composite structure being formulated for different biomedical and surgical application. The optimum concentration of the composite has been decided based on the sample that gives the minimum setting and hardening time, higher compression time and lower degradable properties. Accordingly, the samples have been further characterized. s. The composites have been evaluated based on their swelling studies, mechanical testing, as well as subjected to Fourier transform infrared microscopy (FT-IR), X-ray diffraction (XRD). Biocompatibility of the optimised scaffolds with optimum citric acid and calcium nitrate tetrahydrate compositions were analysed using osteosarcoma (MG63) cells. Also the cell adherence to the scaffolds was checked by fixing them and checking their morphology using scanning electron microscopy.

Results and Discussion

FT-IR peaks corresponding to carboxylic acid salt and nitrate ions had appeared, which confirms that citric acid and CNTH helped in crosslinking the whole structure. XRD spectra showed that presence of CNTH did not interfere with the structure of hydroxyapatite. Setting time and hardening time were found to be the minimum for composites containing CNTH, which means that CNTH serves to be an accelerator in setting and hardening of the composite, which is very significant in terms of bone cement applications. However, degradation was found to be higher for composite structures containing CNTH. Also, CNTH containing composite structures had a higher swelling degree (at the end of 72 hours) compared to composite structures without CNTH. Even though CNTH helps in accelerating the process of setting and hardening, it had some deleterious effect in terms of the degradation and swelling properties. Mechanical strength of the composite structures was measured at three different conditions, set state (immediately after setting), dry state (after hardening) and wet state (hardened structures immersed in PBS for 24

hours). In all these states, composite structures with CNTH had the higher compressive strength respectively. The cytotoxicity evaluation was performed using MTT assay using osteosarcoma (MG63) cells and composites were found to be non-toxic with a high proliferation rate.

Conclusion

The fabricated composite can be used as bone grafts because of its good strength and its capability to keep its shape intact. It can be used as injectable cement because of its viscous nature and ability to be injected out using a syringe. The study requires more characterization to claim its multipurpose application and that will be tested in the future as the composite has shown positive results in the basic characterization.

References

[1] S. Kashte, A.K. Jaiswal, S. Kadam, Artificial Bone via Bone Tissue Engineering: Current Scenario and Challenges, Tissue Engineering and Regenerative Medicine. (2017).
[2] T. Wu, S. Yu, D. Chen, Y. Wang, Bionic design, materials and performance of bone tissue scaffolds, Materials. 10 (2017).
[3] P.W. Ahmed Fatimi, Jean-Francois Tassin, Monique A. V. Axelos, The stability mechanisms of an injectable calcium phosphate ceramic suspension, Journal of Material Science: Materials in Medicine. 21 (2010) 1799–1809.
[4] P. Taylor, S. Sethuraman, L.S. Nair, Development and Characterization of Biodegradable Nanocomposite Injectables for Orthopaedic Applications Based on Polyphosphazenes, Journal of Biomaterials Science. 22 (2011) 733–752.
[5] H.-W.K. Roman A. Perez, Kapil D. Patel, Novel magnetic nanocomposite injectables: calcium phosphate cements impregnated with ultrafine magnetic nanoparticles for bone regeneration, RSC Advances. (2015).
[6] K.L. Low, S.H. Tan, S. Hussein, S. Zein, J.A. Roether, V. Mourin, Calcium phosphate-based composites as injectable bone substitute materials, Journal of Biomedical Materials Research. Part B. 94 (2010) 273–286
[7] S. Larsson, G. Hannink, Injectable bone-graft substitutes : Current products , their characteristics and indications , and new developments, Injury. 42 (2011) S30–S34.
[8] R.A. Perez, S. Shin, C. Han, H. Kim, Bioactive Injectables Based on Calcium Phosphates for Hard Tissues : A Recent Update, Tissue Engineering and Regenerative Medicine. 12 (2015) 143–153.
[9] G. Daculsi, Biphasic calcium phosphate concept applied to artificial bone, implant coating and injectable bone substitute, Biomaterials. 19 (1998) 1473–1478.
[10] M. Habib, G. Baroud, F. Gitzhofer, M. Bohner, Mechanisms underlying the limited injectability of hydraulic calcium phosphate paste, Acta Biomaterialia. 4 (2008) 1465–1471.
[11] M.D. Este, D. Eglin, Acta Biomaterialia Hydrogels in calcium phosphate moldable and injectable bone substitutes : Sticky excipients or advanced 3-D carriers ?, Acta Biomaterialia. 9 (2013) 5421–5430

Acknowledgement

The authors thank DST-SERB for the travel grant (International Travel Support) that will be provided for attending the conference. This research received the specific grant (VIT/Regr./2018/19) from VIT Vellore.

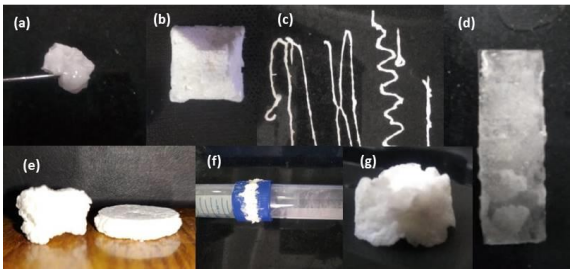

Different forms of Composite Structure
(a) Setting gel, (b) Hardened composite structure, (c) Injected Composite,
(d) Composite hardened over a surface, (e) Hardened composite structure before (left) and after (right) compression, (f) Composite served as adhesive for 2 tubes filled with water, and (g) Hardened composite structure maintaining structure after 24 hours PBS immersion.

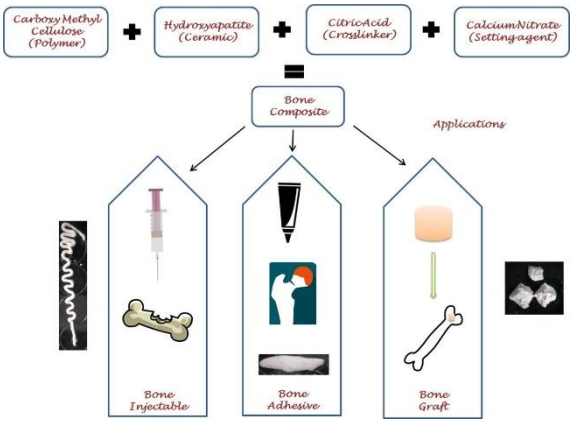

Graphical Abstract
Development of Injectable Bone Composites for Biomedical and Surgical Applications

PS2-12-443

Growth Factor Loaded Electrospun Nanofiber Scaffolds for Inducing Bone Healing

Andrea Sowislok[1,2], Thorsten Sänger[1], Sven Henning[3], Görg H. Michler[4], Herbert P. Jennissen[1,2]

[1]University of Duisburg-Essen, Institute of Physiological Chemistry, Essen, DE; [2]University of Duisburg-Essen, Department of Orthopedics and Trauma Surgery, Essen, DE; [3]Fraunhofer IWM, Halle/S, DE; [4]IPW e.V., Merseburg, DE

Introduction

In designing biorecognition surfaces on implants with immobilized growth factors the term 'recognition' is focussed not only on the molecular but more so on a cellular level. Two kinds of effects can be expected from immobilized growth factors such as BMP-2 or $VEGF_{165}$ on implants (i) juxtacrine effects and (ii) chemotactic effects [1]. Non-releasing surfaces, involving a stable covalent attachment of e.g. BMP-2, display local juxtacrine properties for direct cell adhesion. Surfaces with non-covalently immobilized BMP-2 display chemotactic long-distance actions by adsorbate release for cellular attraction and homing to the surface. In this latter respect electrospun hybrid PDLLA Scaffolds pose interesting chemoattractive surfaces because of their multimodal and resorptive properties. Growthfactors can either be encapsulated within the PDLLA nanofibers or adsorbed to the outer surface scaffolds [2].

Our aim is to create a multimodal electrospun, scaffold for rhVEGF and rhBMP exhibiting controlled release at different rates for chemoattractive triggering of periimplant bone healing *in vivo.*

Experimental Methods

In addition to classical 2D fleeces or mats, scaffolds in the form of 3d tubes were created on a custom-made electrospinning instrument [2] under focusing conditions by depositing poly(D,L-lactide) nanofibers on a rotating mandrel. Temperature, spinning voltage and the rotational speed of the mandrel were adjusted to avoid bending instabilities. Bioactive pure rhBMP-2 and rhVEGF were obtained from Morphoplant GmbH (D-44799 Bochum) and were labeled with ^{125}I [3]. Ferritin for controls was obtained from Sigma-Aldrich, D-82024 Taufkirchen. Electron microscopy was performed on JEOL 1400+ TEM and ZEISS FIB-SEM 540 instruments. Desorption kinetics were measured in continuous flow chambers in sterile PBS and fitted according to a two-phase exponential decay [3].

Results and Discussion

The 2D-fleeces were loaded with 7-9 mg/g ^{125}I-rhBMP-2 and ^{125}I-rh$VEGF_{165}$ by adsorption for 20 hours at 26°C. In desorption experiments ^{125}I-rhBMP-2 was released in a 2-phase exponential decay over 25 days with rate constants in the burst phase of k^{I}_{-1} = 4.57 ± 11.4 x 10^{-4} [s^{-1}] and a sustained-release phase of k^{II}_{-1} 3.28 ± 1.11 x 10^{-8} [s^{-1}], the latter of which corresponds to a half-life of ~245 days. In contrast $rhVEGF_{165}$ was released with rate constants in the burst phase of k^{I}_{-1} = 1.04 ± 0.70 x 10^{-4} [s^{-1}] and a sustained-release phase of k^{II}_{-1} = 4.30 ± 1.56 x 10^{-7} [s^{-1}], the latter of which corresponds to a half-life of 18.7 days. The tubular spinning geometry and fiber diameter were optimized by using a focused electrospinning method. Visualization of single nanofibers in electrospun tubular scaffolds by REM revealed differences in inner and outer fiber structure. On these materials, adsorption of rhBMP-2, rhVEGF will be performed subsequently. TEM experiments with adsorbed Ferritin revealed monolayers of the protein on the fiber surface, as well as monomeric and oligomeric forms.

Conclusion

It can be shown that ^{125}I-rhVEGF$_{165}$ is release from the fibers with a ~13-fold higher rate ($t_{1/2}$ = 18.7 days) in comparison to ^{125}I-rhBMP-2 ($t_{1/2}$ = 245 days). Novel electrospun tubular scaffolds will be created and loaded with growth factors, which will be tested *in vivo* for applications in regenerative medicine.

References

[1] Jennissen, H. P., Zumbrink, T., Chatzinikolaidou, M., & Steppuhn, J. (1999) *Materialwiss. Werkstofftech. (Mater. Sci. Eng. Technol.)*, **30,** 838-845.

[2] Asran, A. S., Sänger, T., Laub, M., Michler, G. H., Henning, S., & Jennissen, H. P. (2014) *Biomed. Tech. (Berl)*, **59,** 154-157.

[3] Sänger, T., Laub, M., & Jennissen, H. P. (2013) *Biomed. Tech. (Berl)*, **58,** 989-990.

Acknowledgement

We thank the German Research Foundation (Deutsche Forschungsgemeinschaft, DFG; Je84/15-3) for financial support.

PS2-12-444

Design and characterization of a three-layer collagen-based scaffold to modulate BMSC behaviour for enthesis regeneration

Eugenia Pugliese[1,2], Dimitrios Zeugolis[1,2]

[1]National University of Ireland Galway (NUI Galway), Regenerative, Modular & Developmental Engineering Laboratory (REMODEL), Galway, IE; [2]National University of Ireland Galway (NUI Galway), Science Foundation Ireland (SFI) Centre for Research in Medical Devices (CÚRAM), Galway, IE

Introduction

The enthesis is a specialised zonal tissue interface between tendon and bone, essential for adequate force transmission and composed by four distinct zones, namely tendon, fibrocartilage, mineralized fibrocartilage and bone. Following injuries and surgical repair, the enthesis is often not reestablished and traditionally used tissue substitutes have lacked to reproduce the complexity of the native tissue. In this work, we hypothesised that a collagen-based three-layer scaffold that mimic the composition of the enthesis, in combination with bioactive molecules, will enhance the functional regeneration of the enthesis.

Experimental Methods

A three-layer sponge composed of a tendon-like layer (collagen type I), a cartilage-like layer (collagen type II) and a bone-like layer (collagen type I and hydroxyapatite) was fabricated by an iterative layering freeze-drying technique. The scaffolds were cross-linked with 1 mM 4-arm polyethylene glycol (PEG) and biophysical, biological and mechanical properties were assessed by free amines assay, enzymatic degradation with collagenase and compression testing, respectively. Scaffold porosity and structural continuity at the interfaces were assessed through SEM analysis. Bone-marrow derived stem cells (BMSCs) were seeded by syringe vacuum assisted technique on the scaffold. Scaffolds were cultured in basal media for 3 days before switching to differentiation media (chondrogenic, tenogenic and osteogenic). BMSCs metabolic activity, proliferation and viability were assessed by alamarBlue, PicoGreen and Live/Dead assays, respectively. At D21 the scaffolds were fixed, cryosectioned and Alizarin Red and Alcian Blue stainings were performed in order to evaluate BMSC differentiation towards osteogenic and chondrogenic lineage. The presence of collagen I and tenascin in the scaffolds was evaluated by immunofluorescence staining at D21 in order to evaluate tenogenic differentiation of BMSCs. Subsequently, the cartilage-like layer was functionalized with insulin growth factor 1 (IGF-1), seeded with BMSCs and cultured in basal media up to D21.

Results and Discussion

The three-layer collagen sponges cross-linked with 1 mM PEG showed a 70 ± 5 % reduction in free amines, 60 ± 8 % resistance in collagenase after 24 hours and a compression modulus of 30 ± 5 kPa. Structural continuity at the interfaces was confirmed by SEM and scaffold porosity was assessed as >98% (Fig. 1). The scaffolds supported cell proliferation and infiltration homogeneously throughout all the layers up to D21. The scaffolds promoted osteogenic differentiation of BMSC selectively in the bone-like layer as confirmed by Alizarin red staining (Fig.2A top) in scaffolds cultured in basal and osteogenic media. Alcian blue staining revealed the presence of proteoglycans (Fig.2A bottom) selectively in the cartilage-like layer in scaffolds cultured in chondrogenic media but not in basal media. Increased expression of the tenogenic markers collagen I and tenascin was observed in the tendon-like layer of scaffolds

cultured in tenogenic but not in basal media for 21 days (Fig.2B). The presence of IGF-1 increased osteogenic and chondrogenic differentiation of BMSCs, whereas no difference was observed for tenogenic differentiation.

Conclusion

In conclusion, a 3-layer collagen sponge was successfully fabricated with distinct but integrated layers; the different collagen composition of the non-functionalized 3-layer sponge was able to regulate BMSC differentiation in a localized manner within the scaffold. The scaffold functionalization with IGF-1 accelerated chondrogenic and osteogenic BMSC differentiation. Ongoing work is evaluating gene expression relevant to the enthesis and it is establishing the synergistic effect between IGF-1 and platelet-derived growth factor functionalized within the tendon-like layer. Overall, functionalization of the 3-layer scaffolds holds promising potential in developing novel and more efficient strategy towards enthesis regeneration.

Acknowledgement

Financial support was received from the European Union, Horizon 2020 Programme, Grant Agreement 676338.

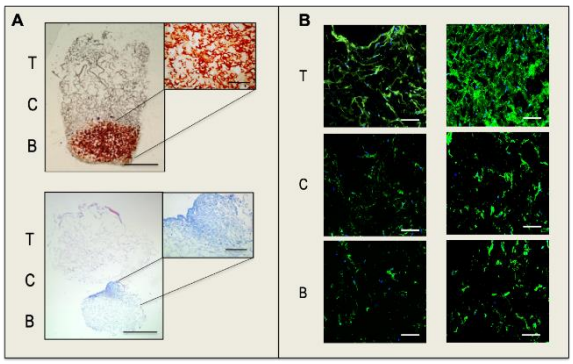

BMSC differentiation towards osteogenic, chondrogenic and tenogenic lineage
Fig.2 Alizarin Red (A top) and Alcian blue (A bottom) stainings, scale bar 500 µm (whole pic) and 100 µm (magnified pic); tenascin and DAPI (B left) and collagen I and DAPI (B right) stainings in tendon, cartilage and bone-like layers, scale bar 100 µm

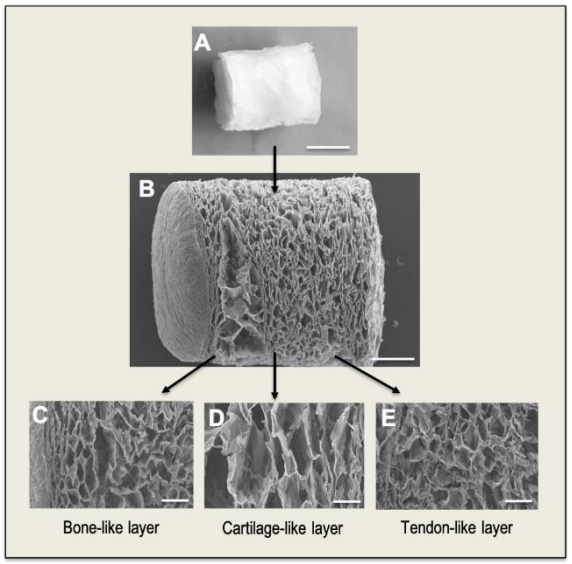

SEM pictures of the three-layer scaffolds
Fig.1 Gross picture of the three-layer scaffold (A), SEM image of the whole scaffold (B), scale bar 500 µm and magnifications of the individual layers (C, D, E), scale bar 250 µm

PS2-12-445

Mimicking natural gradients in 3D printed scaffolds for osteo-chondral regeneration

Ivo A. O. Beeren, Sandra Camarero-Espinosa, Matthew B. Baker, Lorenzo Moroni

Maastricht University, MERLN Institute for Technology-Inspired Regenerative Medicine, Maastricht, NL

Introduction

Articular cartilage has a low intrinsic repair capacity due to its avascular and aneural nature. Once damage occurred in the cartilage and exposes the underlying bone, the defect will propagate causing osteoarthritis. Researchers are designing new biomaterials and 3D constructs, which should regenerate functional cartilage; however, most constructs rarely mimic the naturally occurring countercurrent gradients of molecules in cartilage. These gradients are observed from the superficial layer towards the bone and vice versa (e.g. collagen II and X). Across these gradients, the chondrocytes and their extracellular matrix slowly transform into osteogenic cells and tissue. Our goal is to design a 3D printed (3DP) construct in which countercurrent gradients of biological factors are present to control human mesenchymal stromal cells (hMSCs) differentiation in a gradual fashion across the construct. As biological factors, we combined TGF-β and BMP-2 derived peptides, which induce either chondrogenic or osteogenic differentiation, respectively (figure 1A). Polycaprolactones (PCL) with either terminal azides or maleimides have been synthesized to allow click-type functionalization on the surface of the printed fibers (figure 1B). An in-house developed single extruding printhead, which is connected to two polymer reservoirs, mixes the melted polymer solutions to create countercurrent gradients of functional groups in each layer. Here, we present the road towards this new construct.

Experimental Methods

Firstly, azides or maleimides are introduced at the terminal positions of PCL to couple peptides to the surfaces. PCL-azide (PCLA) is synthesized via a two-step reaction. The terminal hydroxyl group of PCL_{45k} is reacted with a tosyl chloride yielding **1**, followed by a substitution of the tosyl with an azide yielding PCLA (**2**). For the PCL-maleimide synthesis (**3**, PCLM), a ring-opening polymerization of ε-CL was performed using a (2-hydroxyethyl)maleimide as the initiator group. Secondly, we 3D printed these materials into scaffolds. Thirdly, either copper induced alkyne-azide click chemistry or Michael addition was performed to react TGF-β and BMP-2 derived peptides onto the 3D printed fibers. Standard techniques such as NMR, FT-IR, GPC and WCA were used to characterize the synthesized polymers. Surface functionalization was investigated with XPS measurements. Finally, we did cell experiments with hMSC in which their spreading and differentiation was assessed.

Results and Discussion

For the characterization of **2**, a (partial) upfield shift is observed in the NMR for the protons adjacent to the terminal hydroxyl group. A ^{1}H-^{15}N 2D NMR confirms that two nitrogens are coupled to these shifted protons, which are the N's of the azide. After the ring opening polymerization to yield **3**, additional peaks appear in the NMR, which are characteristic of a maleimide group. The printability of the polymers was assessed and we were able to fabricate homogenous scaffolds of PCLA and PCLM (figure 2A). To measure the surface functionalization on the fibers, XPS measurements have been performed. In initial cell experiments with 2D surfaces of **2** and **3**, RGD peptides were reacted to assess hMSC binding and spreading. In figure 2B, although the amount is low, cell spreading is observed

on the surfaces with peptides, even when blocking protein adsorption with pluronic. Also, an increase in amount of cells at the surface is observed.

Conclusion

In this study, we investigate new biomaterials and 3DP which may be used for functional cartilage regeneration. To this end, two different PCL-derived polymers with terminal azides and maleimides were synthesized. Furthermore, we have demonstrated that these materials can be 3DP in a homogenous manner. More extensive in-vitro experiments have to be completed to investigate hMSC fate in response to the functional materials. After complete analysis of homogenously functionalized surfaces or constructs, gradients of commercial PCL and functionalized PCL will be investigated.

Acknowledgement

We are grateful to the European Research Council starting grant “Cell Hybridge” for financial support under the Horizon2020 framework program (Grant # 637308).

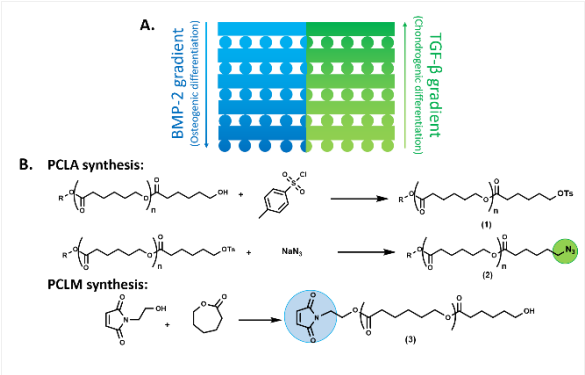

Schemes of our design and chemistry
Figure 1: A) schematic representation of our 3D printed scaffold with countercurrent gradient of TGF-β and BMP-2 derived peptides. B) Reaction schemes for PCLA **(2)** and PCLM **(3)**. In the green and blue circles, the newly introduced functional groups are highlighted.

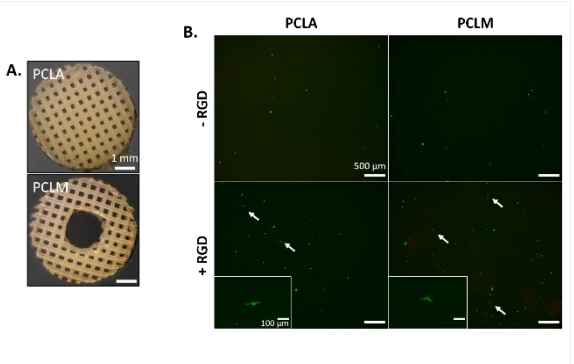

Assessment of material printability and cell adhesion on materials
Figure 2: A) PCLA (top, round) and PCLM (bottom, donut) scaffolds can be punched from larger fiber meshes. B) Live dead staining of hMSC on 2D surfaces, which are coated with pluronic. Living cells are green, death cells are red. White arrows indicate spreading cells. Insets show zoom-ins of spreading cells.

PS2-12-446

3D printing and characterization of human nasal chondrocyte (hNSC) laden dual cross-linked oxidized alginate-gelatin (ADA-GEL) hydrogels for cartilage repair approaches

Thomas Distler[1], Silke Schwarz*[2], Sonja Kuth[1], Clemens Gögele[2], Katharina Stölzel[3], Rainer Detsch[1], Gundula Schulze-Tanzil[2], Aldo R. Boccaccini[1], *contributed equally

[1]Friedrich-Alexander-University Erlangen-Nuremberg, Institute of Biomaterials, Erlangen, DE; [2]Paracelsus Medical University, Department of Anatomy, Nuremberg, DE; [3]Charité- Universitätsmedizin, Department of Otorhinolaryngology, Head and Neck Surgery, Berlin, DE

Introduction

Regeneration of cartilage defects is a challenge for reconstructive surgery. Conventional surgical procedures possess limitations such as restricted availability of donor tissue, donor site morbidity and the formation of scar tissue accompanied by deficient aesthetic outcome. In the field of tissue engineering (TE) and cartilage reconstruction, 3D bioprinting has gained increased attention as it offers the ability of creating complex and vital patient individual 3D tissue analogues applying autologous chondrocytes. However, 3D bioprinting for cartilage TE requires biocompatible hydrogels with high hydration capacity and plasticity while mimicking structure and composition of the natural extracellular matrix (ECM). Oxidized alginate di-aldehyde (ADA) combined with covalently bounded porcine gelatin (GEL) presents an excellent bioink for 3D bioprinting [1]. Microbial transglutaminase (mTG) is considered a promising enzyme system for the crosslinking of protein-based hydrogels for TE and application in regenerative medicine [2, 3]. It recently demonstrated excellent results regarding cell adhesion, delivery, proliferation and differentiation [3, 4]. Therefore, a cross-linking solution of $CaCl_2$ supplemented with mTG was chosen for crosslinking of highly printable ADA-GEL hydrogels. In this study, novel ADA-GEL-mTGs hydrogels were analyzed in comparison to control ADA-GEL hydrogels and examined *in vitro* regarding printability, biocompatibility and suitability as a cartilage replacement matrix in combination with primary human nasal chondrocytes (hNC).

Experimental Methods

ADA-GEL hydrogel was prepared by thoroughly mixing 7.5% (w/v) ADA solution with 7.5 or 15% (w/v) aqueous solution of gelatin under constant stirring at 37°C. The final concentration ratios of ADA: GEL were 3.75/3.75% (1:1) and 3.75/7.5% (1:2). The hydrogels were examined regarding their chemical composition using FTIR. Microstructure and porosity over 28d incubation time were analyzed by SEM. Degradation/swelling experiments were conducted after several time points. ADA-GEL stiffness was investigated using nanoindenation after 1h, 1, 3, 7 and 14 d of incubation. Cytotoxic effects due to crosslinking or hydrogel components were examined. Subsequently, hNC were embedded in ADA-GEL hydrogel precursor at a cell density of $4x10^6$ cells mL^{-1}. Cross-linking was performed in 400 mM $CaCl_2$ solution containing 2.5% mTG (81 – 135 U/g) for ADA-GEL-mTGs hydrogels. ADA-GEL cross-linked in 400 mM $CaCl_2$ served as control. Cell-laden hydrogel beads were generated. 3D bioprinting of grid shaped hNC laden ADA-GEL was performed using a BioBot Basic (Advanced Solutions Inc.). ADA-GEL bioink was filled into 10 ml cartridges and extruded at 165 – 283 kPa at a speed of 5mm/sec at RT, followed by cross-linking in $CaCl_2$ + 2.5% mTG solution. Beads and scaffolds were cultured for up to 14 d. At days 7 and 14, cell viability, metabolic activity and proliferation rate were analyzed. The chondrogenic phenotype of hNC and neo-synthesis of cartilage specific

components was examined on protein level by immunohistochemical staining. Printability, degradation and shape stability were assessed.

Results and Discussion

In cell-laden ADA-GEL-mTG beads and scaffolds as well as respective controls, a high cell viability and homogenous cell distribution was detected (Fig. 1a). ADA-GEL-mTG bioink offered an improved shape and size stability during 3D longterm culture compared to control beads cross-linked by 400mM $CaCl_2$. Cytotoxic effects on the indicator cells L929 were found neither for ADA-GEL-mTG hydrogels nor for the respective controls. In ADA-GEL-mTG beads, the chondrogenic phenotype of hNC was maintained in longterm 3D culture. Protein expression and immunohistochemical analyses revealed that ADA-GEL-mTG hydrogels support chondrogenesis of hNC and neo-synthesis of cartilage-specific collagen type II and proteoglycan (Fig. 1b). The composition and porosity of the hydrogel constructs provided optimal nutrition and oxygen supply of embedded hNC. No restrictive influence of enzymatic cross-linking on proliferation was detected. In 3.75/3.75 ADA-GEL-mTG a significantly higher proliferation of hNC was found compared to 3.75/7.5 ADA-GEL-mTG and respective controls.

Conclusion

In this study we demonstrated that non-cytotoxic ADA-GEL-mTG hydrogels provide a biologically relevant micro-environment promoting chondrogenic redifferentiation while offering excellent printability and matrix properties. These characteristics make ADA-GEL-mTG hydrogels a promising tool for patient-individual cartilage defect reconstruction by 3D bioprinting.

References

1. Zehnder T, Sarker B, Boccaccini A.R., Detsch R. Evaluation of an alginate-gelatine crosslinked hydrogel for bioplotting, Biofabrication (2015), 7. doi:10.1088/1758-5090/7/2/025001.
2. Chen T, Janjua R, McDermott M K, Bernstein S L, Steidl S M, & Payne G F. Gelatin-based biomimetic tissue adhesive. Potential for retinal reattachment. J Biomed Mater Res B Appl Biomater (2006), 77,2, 416-422.
3. Yang G, Xiao Z, Ren X, et al. Enzymatically crosslinked gelatin hydrogel promotes the proliferation of adipose tissue-derived stromal cells. PeerJ. (2016), 4:e2497. doi:10.7717/peerj.2497.
4. Yung C W, Wu L Q, Tullman J A, Payne G F, Bentley W E, Barbari T A. Transglutaminase crosslinked gelatin as a tissue engineering scaffold. J Biomed Mater Res A (2007), *83*, 4, 1039-1046.

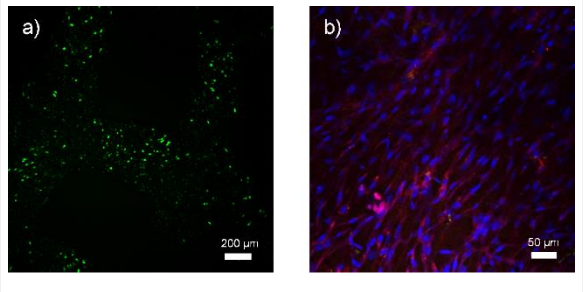

Human nasal chondrocyte (hNSC) laden ADA-GEL-mTG hydrogels.
a) Live/Dead staining of 3D printed scaffolds after 7d. b) Immunohistochemical detection of collagen type II staining (red) in ADA-GEL-mTG beads after 14 d (blue: DAPI, cell nuclei).

PS2-12-447

Catechol-modified Poly(oxazoline)s as Cartilage Adhesives with Tunable Adhesion Strength and Degradability

Oliver Berberich *[1], Julia Blöhbaum *[2], Stefanie Hölscher-Doht[1], Rainer Meffert[1], Jörg Teßmar[2], Torsten Blunk **[1], Jürgen Groll **[2], * These authors contributed equally; ** corresponding authors

[1]University of Würzburg, Department of Trauma, Hand, Plastic and Reconstructive Surgery, Würzburg, DE;
[2]University of Würzburg, Department of Functional Materials in Medicine and Dentistry and Bavarian Polymer Institute, Würzburg, DE

Introduction

Tissue adhesives play an important role in clinical applications and may aid in the treatment of cartilage defects for improved cartilage integration. Due to their injectability and ability to also fill irregularly shaped defects, different adhesive hydrogels with *in-situ* hardening capacity are under investigation. However, many fail to satisfy the demand for adequate adhesion strength on wet tissue surfaces and to facilitate sufficient cell migration and extracellular matrix (ECM) deposition at the defect site. Here, we present poly(2-alkyl-2-oxazoline) (POx)-based polymers equipped with mussel-inspired adhesion moieties and tunable degradability. In combination with the natural wound sealant fibrinogen, we fabricated an adhesive biosynthetic hydrogel (Figure 1) with tunable mechanical properties and improved bonding strength. Utilizing a biomechanical *in vitro* model and tissue culture, the lateral integration strength and ECM synthesis was investigated over time.

Experimental Methods

POx polymers were synthesized with different degrees of catechol functionalization. The adhesive catechol group was attached to the side chain either with a stable amide- or with a hydrolyzable ester-linkage (0, 25 and 50% of total POx content), yielding adhesives with different degradability. Under oxidative conditions, different POx precursor solutions were reacted with fibrinogen to form an adhesive hydrogel. Young's modulus of bulk hydrogels was recorded to analyze mechanical properties and degradation. The fine structure of the bonding interface between the adhesive hydrogel and articular cartilage was examined by scanning electron microscopy (SEM). To further evaluate the integrative potential, the adhesives were applied at the defect interface of a disc/ring *in vitro* model that was generated from porcine cartilage blocks. Using a biomechanical push-out device, adhesive strength was determined as measure for cartilage integration 1 day after application and after culture for up to 3 weeks. Fibrin served as control for immediate bonding strength. Biocompatibility was tested with MTT staining. ECM development and cell invasion at the defect site was analyzed histologically and immunohistochemically.

Results and Discussion

In biomechanical tests, all tested adhesives made from combinations of POx and fibrinogen possessed higher immediate bonding strengths (up to 20.08 ± 3.57 kPa) than fibrin (7.64 ± 3.95 kPa). A higher catechol functionalization of POx polymers resulted in increased material stiffness and immediate bonding strengths. MTT staining showed no cytotoxic effects of the tested adhesives. SEM images revealed that the adhesive material smoothly penetrated the cartilage surface and that single collagen fibres were firmly attached within the hydrogel. Using fixed total concentrations of POx (7.5 % w/v) and fibrinogen (5 % w/v), but a varying ester content, had no significant influence on immediate bonding strength. However, variation of ester content decisively impacted the degradability of the adhesive and the tissue development at the defect site. For adhesives with POx containing 0 %

ester-linkages, histological and immunohistochemical analysis showed a lack of degradation and neither cell invasion nor ECM deposition. In strong contrast, incorporation of 25 or 50 % POx with ester-linkages allowed for glue degradation combined with enhanced cell invasion and strong cartilage-specific ECM deposition (glycosaminoglycans and collagen type II) bridging the defect (Figure 2).

Conclusion

Our study demonstrated that catechol-modified POx in combination with fibrinogen can function as biocompatible adhesive with tunable adhesion strength in a wet environment. Furthermore, enhancing the degradability of POx adhesives by ester-linkages particularly improved long-term integration at a cartilage defect *in vitro*. Future research may explore possibilities to further enhance mechanical characteristics and adhesive strength, and to further elucidate the adhesion mechanisms of the developed hydrogels.

Acknowledgement

This work was financially supported by the European Union's Seventh Framework Programme (FP7/2007-2013) under grant agreement n°309962 (project HydroZONES).

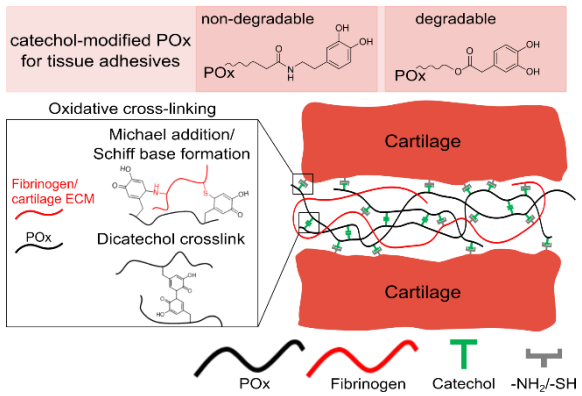

Figure 1: Catechol-modified Poly(oxazoline)s as Cartilage Adhesives
Schematic illustration of the catechol-based cross-link and adhesion mechanisms in POx biosynthetic hydrogels.

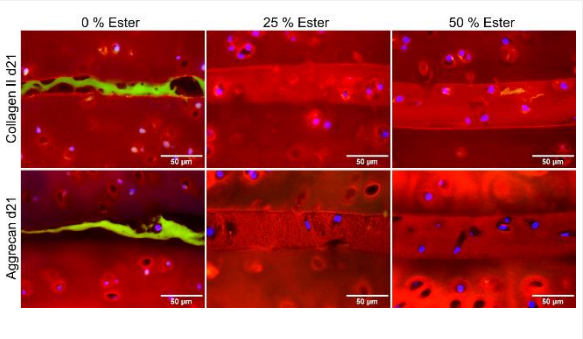

Figure 2: Long-term cartilage integration with POx adhesives of different degradability
Immunofluorescent staining for cartilage ECM markers collagen type II and aggrecan at d21 at the defect interface , epifluorescent signal of non-degraded POx the adhesive is seen as green fluorescence.

PS2-12-448

Methotrexate derivatives bearing divalent cations. Antibacterial activity and encapsulation into chitosan microparticles

Daniel Fernández-Villa[1,2], Inmaculada Aranaz[3], Niuris Acosta[3], Blanca Vázquez-Lasa[1,2], Julio San Román[1,2], **Luis Rojo**[1,2]

[1]Consejo Superior de Investigaciones Científicas, 1Instituto de Ciencia y Tecnología de Polímeros, Madrid, ES; [2]Consorcio Centro de Investigación Biomédica en Red de Bioingeniería, Biomateriales y Nanomedicina, Madrid, ES; [3]Universidad Complutense de Madrid, Instituto de Estudios Biofuncionales, Departamento de Química en Ciencias Farmacéuticas, Facultad de Farmacia, Madrid, ES

Introduction

Methotrexate (MTX) is one of the main drugs used for treatment of rheumatoid arthritis (RA) due to its effectiveness and tolerability [1]. However, MTX can not promote itself the regeneration of the damaged joints after the treatment[2]. In this regard, divalent cations such as strontium, zinc and magnesium have been shown to promote musculoskeletal regeneration processes and can be coordinated with MTX providing synergic therapeutic activities and antimicrobial activity[3]. For these reasons, the main objectives of the present work were synthesizing and characterizing by different physicochemical techniques novel methotrexate derivatives containing these divalent cations (M-MTX) and test their antibacterial properties and bioactivity. In addition, some of these compounds were tested *in vitro* to analyse their potential use as musculoskeletal regenerative drugs. Finally, polymeric encapsulation of M-MTX derivatives into chitosan microparticles was performed.

Experimental Methods

Three different methotrexate derivatives were synthesized following a previously described analogous methodology for folate derivatives: strontium-, zinc- and magnesium-methotrexate derivatives[4] **(Fig. 1A)**. The compounds were physicochemically characterized by ATR-FTIR, DSC, TGA, EDS and XRD. In addition, cytotoxicity of the different drugs was analysed in Raw264.7 cells and primary human chondrocytes-articular cultures by the alamar blue assay. Glycosaminoglycans deposition by M-MTX-treated chondrocytes was measured by the dimethylmethylene blue method. Anti-inflammatory properties of the synthesized compounds were studied by the Griess assay measuring NO release by LPS-activated macrophages. Antibacterial activity against *Staphylococcus epidermidis* and *Escherichia coli* was assessed by standard disk diffusion method. Furthermore, chitosan (M_w= 47kDa , DA= 90%) microparticles were synthesized by double emulsion followed by spray drying and their morphology, size dispersion and encapsulation efficacies were determined by SEM, Coulter and spectrophotometrically methods.

Results and Discussion

All the compounds were successfully synthesized in high yields (>95%) with no other co-precipitates. The obtained characterization results demonstrated a higher thermal stability of the complexes when compared with non-coordinated methotrexate due to the monodentate bond coordination between the methotrexate moiety and the cations.

Secondly, *in vitro* cell studies performed with methotrexate derivatives showed that ZnMTX could prevent the methotrexate-related cytotoxic effects at determined doses in chondrocytes as well as it could decrease nitric oxide production by pro-inflammatory stimulated macrophages. On the other hand, SrMTX slightly increased the glycosaminoglycans deposition in the matrix while its cytotoxicity did not significantly vary when compared with non-

complexed methotrexate. MTX and M-MTX showed inhibition against *Staphylococcus epidermidis* while only Zn-MTX was able to inhibit the growth of *Escherichia coli* but to a limited extent. **(Fig. 1B)**. Finally, spray-dried chitosan microparticles containing methotrexate derivatives were synthesized showing spherical morphology (Fig. 1C) and achieving high encapsulation efficacies. Complete drug release of all the compounds was reached in 24 h. Around a 90% of the total drug releases was achieved in the first 6 h.

Conclusion

In conclusion, this work serves as a proof-of-concept for future studies focused on musculoskeletal regeneration due to use of methotrexate bearing bioactive divalent cations and their interesting biological properties and their possibility to be encapsulated in biodegradable chitosan micro In conclusion, this work serves as a proof-of-concept that methotrexate bearing bioactive divalent cations showing interesting biological properties can play a role on musculoskeletal regeneration and open a frame for future studies focused on their encapsulation in microparticles using other polymeric systems.

References

1. Smolen *et al*. Lancet, 388: 2023–38 (2016)
2. Ito *et al*. Inflamm. Regen., 38:7 (2018);
3. Jiménez, M. et al. J. Mater. Chem. B. 7, 1974-1985 (2019)
4. Rojo *et al*. J. Mater. Chem. B, 3(13), 2708-2713 (2015).

Acknowledgement

This work was supported by the Spanish program MICINN (MAT201573656-JIN) and CSIC program JAE Intro (JAEINT18-EX0511)

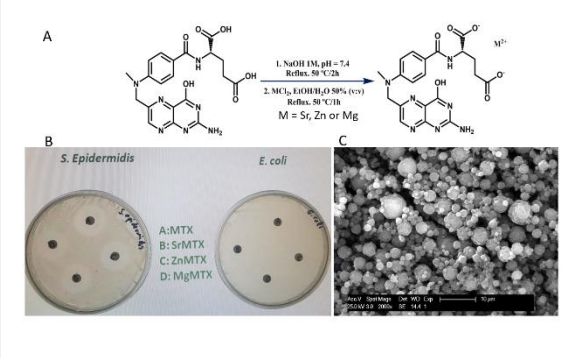

Figure 1.
A: Scheme of the reaction conditions for methotrexate-derivatives syntheses. B: Disk diffusion test on M-MTX against *Staphylococcus epidermidis* and *Escherichia coli*. C: SrMTX-loaded spray-dried microparticles.

2:45 p.m. – 3:45 p.m.

Hall 1 / Exhibition Area

PS2-13 | Biomaterials for specific tissues

PS2-13-449

The physical properties of collagen biomaterials determine their degradation kinetics and angiogenesis within the biomaterial

Carlos Herrera-Vizcaino, Sarah Al-Maawi, Joseph Choukroun, Robert Sader, Shahram Ghanaati

University Hospital Frankfurt Goethe University, Department for Oral, Cranio-Maxillofacial and Facial Plastic Surgery, FORM (Frankfurt Orofacial Regenerative Medicine) Laboratory, Frankfurt am Main, DE

Introduction

Previous observations of implanted biomaterials *in vivo* and clinically, indicate, that the physicochemical characteristics of a biomaterial determine the inflammatory cellular response. The focus of this study was to investigate how the physical properties of a collagen biomaterial influence the inflammatory milieu of a cell complex *in vitro* and the biomaterial-cellular reaction in vivo. For this purpose, the physical characteristics of an equine-derived collagen biomaterial were modified while preserving the same chemical properties and compared to its original presentation.

Experimental Methods

The biomaterial's physical characteristics were altered by applying external pressure using a sterile stainless steel cylinder until the material was flattened. A sponge collagen biomaterial (Parasorb fleece HD®; PF) and the pressed biomaterial (PF-P) were cut into segments of 1 cm^2. Ex vivo, the biomaterials were cultured during 3 and 6 days with a cell complex derived from human blood called platelet-rich fibrin (PRF) and histologically stained. The supernatant was collected and the concentration of pro-inflammatory growth factors (TNF-alpha and IL-8) was measured using ELISA. The results from culturing PRF alone were used as a baseline. Subsequently, the biomaterials were implanted in Wistar rats using a subcutaneous model and compared to a control group sham-operated (CG). The biomaterials were explanted at 3, 15 and 30 days. The samples were histologically and immunohistologically stained with CD 68 antibody (monocyte lineage), CD206 (M2 macrophages) CCR7 (M1 macrophages) and α-Smooth Muscle Actin (α-SMA; vessel identification). The results were qualitative and quantitative evaluated to assess the biomaterial's degradation kinetics, macrophages polarization into M1/M2, multinucleated giant cells (MNGCs) and the vascularization pattern. Statistically analyses were carried out with intra and inter-groups comparison.

Results and Discussion

Ex vivo: histologically, the depth of penetration of cells into the biomaterial's body differed between the two biomaterials. PF allow the penetration of cells and PF-P impede cells penetration. The cell culture of PRF+PF-P produced higher concentrations of TNF-α and IL-8 compared to PRF+PF after day 3 (P <0.05) and to PRF alone after 3 and 6 days (P <0.05). *In vivo*: after 3 days of implantation, both biomaterials were found in the implantation bed. PF maintained its pores structure and cells penetrated PF's surface. PF-P preserve the appearance of a pressed structure and cells were accumulated on the surface. The inflammatory reaction of both biomaterials was mainly composed of CD68 + cells and M1. The number of CD68+, M1 and M2 cells/mm2 in the CG were higher than the experimental groups (P <0.05). After 15 days, PF was fully invaded by cells, the presence of vascular lumens was identified inside the biomaterial's center (P<0.5) and showed a faster degradation of its structure compared to PF-P (P <0.05). Cells in PF-P invaded only the outer-third of the biomaterial's body, vascular lumens were observed surrounding the biomaterial and the biomaterial preserved its structure. Both groups showed a higher inflammatory

reaction composed of positive CD-68+ cells and M1 without statistical differences. The inflammatory reaction in the CG reduced considerably and was statistically significant compared to the experimental groups (P<0.5). A few numbers of MNGCs were observed in experimental groups. After 30 days PF and PF-P fully degraded. CD68+ cells and MNGCs expressing the CCR7 marker were observed surrounding the remaining fibrils of the biomaterials. Micro-vessels were observed within the implantation bed. The implantation area seems to be achieving homeostasis and entering a reparative stage as a similar shift towards an anti-inflammatory pattern was observed in the control and the experimental groups, characterized by a transition towards a higher presence of M2 macrophages.

Conclusion

Changing the biomaterials physical characteristics induced a statistically significant higher inflammatory protein release ex vivo during the early time point of cultivation. Additionally, it was shown to have an effect over the biomaterial's degradation kinetics, vascularization pattern and the inflammatory cellular reaction. A collagen biomaterial of equine origin induced an inflammatory cellular reaction and degradation governed by macrophages, mainly M1, with a reduced number of MNGCs. The remaining MNGCs in the implantation bed expressing the pro-inflammatory marker CCR7 after 30 days, support their involvement in chronic inflammation.

References

Ghanaati, M. Schlee, M.J. Webber, I. Willershausen, M. Barbeck, E. Balic, C. Görlach, S.I. Stupp, R.A. Sader, C.J. Kirkpatrick, Evaluation of the tissue reaction to a new bilayered collagen matrix in vivo and its translation to the clinic, Biomed. Mater. 6 (2011). doi:10.1088/1748-6041/6/1/015010.

S. Ghanaati, Non-cross-linked porcine-based collagen I-III membranes do not require high vascularization rates for their integration within the implantation bed: A paradigm shift, Acta Biomater. 8 (2012) 3061–3072. doi:10.1016/j.actbio.2012.04.041.

S. Al-Maawi, A. Orlowska, R. Sader, C. James Kirkpatrick, S. Ghanaati, In vivo cellular reactions to different biomaterials—Physiological and pathological aspects and their consequences, Semin. Immunol. 29 (2017) 49–61. doi:10.1016/J.SMIM.2017.06.001.

Choukroun, S. Ghanaati, Reduction of relative centrifugation force within injectable platelet-rich-fibrin (PRF) concentrates advances patients' own inflammatory cells, platelets and growth factors: the first introduction to the low speed centrifugation concept, Eur. J. Trauma Emerg. Surg. 44 (2018) 87–95. doi:10.1007/s00068-017-0767-9.

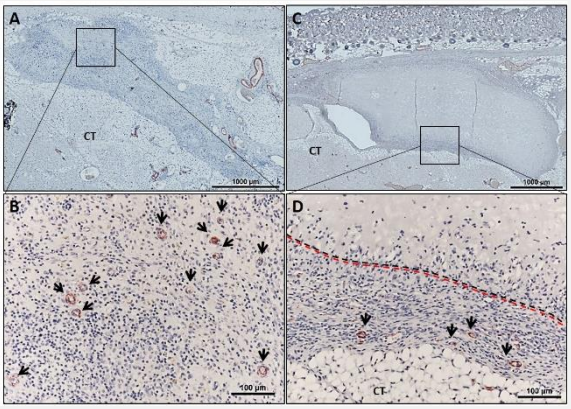

In vivo biomaterial implantation
Collagen biomaterial in its original form (PF; **A-B**) and pressed biomaterial (PF-P; **C-D**). After 15 days of post-implantation, cells have invaded PF completely and it is showing signs of degradation (**A**). Cells remain on the surface and outer third of PF-P with no signs of biomaterial degradation (**C**). The dash lines represent the perimeter of the biomaterials. Vascular structures are pointed by arrows (**B, D**) with alpha smooth muscle actin (α-SMA) immunohistochemical staining; scale bar = 1000/100 µm.

PS2-13-450

Development of an integrated workflow for additive manufacturing of individually designed bone augmentation in maxillofacial surgery

Lysann M. Kroschwald[1,2], David Muallah[1,2], Matthias C. Schulz[3], Philipp Sembdner[4], Stefan Holtzhausen[4], Antje Schönberg[5], André Hutsky[6], Daniel Ellmann[7], Berthold Nies[8], Sascha Heinemann[8], Guenter Lauer[1]

[1]University Hospital of Technische Universität Dresden, Department of Oral Maxillofacial Surgery, Dresden, DE; [2]Technische Universität Dresden, Centre for Translational Bone, Joint and Soft Tissue Research, Dresden, DE; [3]University of Tuebingen, Centre of Dentistry, Oral Medicine and Maxillofacial Surgery, Tuebingen, DE; [4]Technische Universität Dresden, Department of Design Engineering/CAD, Dresden, DE; [5]Zahntechnik Schönberg, Dresden, DE; [6]R+K CAD/CAM Technologie GmbH & Co. KG, Berlin, DE; [7]Rübeling+Klar Dental-Labor GmbH, Berlin, DE; [8]Innotere GmbH, Radebeul, DE

Introduction

An increasing number of patients suffering from tooth loss opt for a supply with dental implants to replace missing teeth and to improve comfort, function and/or aesthetics. Success of dental implants largely depends on quality and quantity of the available bone in the recipient region. Due to tooth loss, periodontal disease and trauma or after tumors resection the augmentation of inadequate bone volume may be necessary. For this purpose, different methods and a wide variety of materials are clinically established e.g. guided bone regeneration (GBR), application of onlay/inlay bone blocks or split-crest technique. Although these surgical procedures can be successful, possible shortcomings are the risk of overfilling of the planned area or an insufficient augmentation. Due to its benefits for healing, function and aesthetics an accurately fitted scaffold is of high clinical importance.

Currently, autologous bone is considered as the “gold standard” for bone augmentation. However, this requires harvesting from a second surgical site potentially causing donor site morbidity. Nowadays, synthetic scaffolds are frequently used. Not only should the ideal scaffold fit easily and perfectly into the recipient site it should also be biocompatible, bioactive and with good mechanical and chemical properties. Beyond these properties, it needs to be osteoconductive and ideally, osteoinductive too. This means, it needs to be capable of guiding growth and proliferation of osteoblasts on its surface and furthermore, stimulate the differentiation of mesenchymal stem cells into the osteoblastic lineage.

For bone tissue regeneration, bone-like calcium phosphate-based materials, especially hydroxyapatite-forming calcium phosphate cements (CPC), play a major role. These minerals are useful for bone repair due to their unique properties such as easy shaping and injectivity in practical use, excellent biocompatibility and biodegradability. Beyond these advantages, it is also capable of bonding to bone, forming a functional interface by enhancing cell attachment and osteoblastic phenotype expression. While synthesis of other bioceramics involves high temperature sintering, CPC can set and harden at room or body temperature at nearly neutral pH. This in turn allows chairside manufacturing.

Today, digitally planned and performed dental implant insertion is the state-of-the-art in oral rehabilitation. Based on a computed tomography (CT, Fig.1) and following a three-dimensional reconstruction of the gained data, number and position of implants as well as geometric dimensions can be determined prior surgery. Moreover, in order to provide a sufficient bone volume for implant insertion, three-dimensional CPC scaffolds adapted to the topography of the alveolar ridge can be virtually designed and subsequently plotted from a calcium phosphate paste.

The assigned purpose of this project is the development and application of an integrated digital workflow for planning, modelling and industrial engineering of individually designed CPC scaffolds for bone augmentation in maxillofacial surgery. These structures are printed three-dimensionally to obtain the individual shape of the implants without mechanical post-processing. Therefore, the currently established workflow for the computerized dental implant insertion needs to be entirely integrated. Furthermore, to generate optimal conditions for the surgeon and to close the gap between surgeon and design software, novel tools need to be created for planning of shape and position of the scaffolds. Different designs will be gathered under consideration of medical aspects and the encountered individual situation. These different scaffold structures will be investigate considering their porosity, stability and different biological aspects e.g. colonization, biodegradability and biocompatibility and will be compared with other commercial bone substitutes.

Concerning these requirements and medical aspects, a novel scaffold design is planned to be generated, fitting in complex defect shapes and containing a graded structure with a dense layer to the outside and an open pored structure inside. Moreover, the development of novel surgical instruments is a necessary adjustment to increase accuracy and precision as well as aid in the reduction of required operating time. Those surgical aids will help to reduce the time required for surgery.

Finally, an individual, made-to-measure product for the maxillofacial area, associated with corresponding instruments and software as an integrated workflow are to be transferred to an applicable medical service of the highest quality (Fig.1).

Acknowledgement

We acknowledge financial support by AiF Projekt GmbH (ZF4379203MC8).

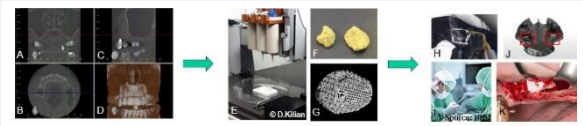

Figure 1
Working scheme from anamnesis to implant insertion using the example sinus lift surgery.
(A) CT, frontal plane (B) CT, horizontal plane (C) CT, sagittal plane (D) CT, 3D reconstruction (E) 3D printer (F) individual printed scaffolds (G) printed scaffold, close-up view (H) cutting line for sinus lift surgery (I) surgeon (J) maxillary model with inserted scaffold (K) insertion of scaffold in patient.

PS2-13-451

Numerical Study of the Influence of Partial Dentures on the Contact Mechanics between the Oral-Mucosa, Abutment Tooth and the Denture

Anantha Narayanan Ramakrishnan[1,2], Oliver Röhrle[2], Andreas Kiesow[1], Stefan Schwan[1]

[1]Fraunhofer Institute for Microstructure of Materials and Systems IMWS, Biological and Macromolecular Materials, Halle, DE; [2]University of Stuttgart, Civil and Environmental Engineering, Stuttgart, DE

Introduction

The application of restorative solutions like removable partial dentures in the dental arch of an edentulous person significantly impacts the contact characteristics and stress state of the Oral-mucosa and the abutment tooth. The emergence of numerical techniques can provide a whole new dimension to explore this paradigm. Aim of this study was to study the contact mechanical state caused by biting forces on the oral-mucosa and abutment tooth upon insertion of partial dentures into the assembly.

Experimental Methods

Computer tomography data was employed to construct detailed 3D models of a removable partial denture supported by three abutment tooth, incorporated into the dental arch of the mandible. The proposed Numerical model employed these models and took into account the various contact regions involved to understand the stress state of the assembly.

Results and Discussion

Bite forces applied on the denture generated a stick condition on the denture-oral mucosa interface which indicated a positive retention of the denture onto the oral-mucosa. The maximum contact pressures experienced by the oral-mucosa are comparable to the pressure pain threshold values(~0.3MPa) for the oral soft tissue, beyond which the patients experience discomfort and pain. The mechanical stresses on the three abutment tooth surfaces due to the same load indicates the effect of bending moments generated.

Conclusion

Making the pressure distribution uniform and lowering the magnitude of the contact pressures on the oral-mucosa could be better addressed by focusing on the gaps in the contact regions between the denture and the soft tissue. Modelling of connecting elements like denture relining materials or retaining mechanisms for the denture to the soft tissue and the abutment tooth could provide significantly improved results in the this regard.

PS2-13-452

A novel polymeric gel to enhance ocular retention of anti-scarring molecules

Liam M. Grover[1], **Lisa J. Hill**[2]

[1]University of Birmingham, Healthcare Technologies Institute, Birmingham, GB; [2]University of Birmingham, Institute of Clinical Sciences, Birmingham, GB

Introduction

Scarring on the surface of the skin and eyes can result in significant psychosocial and functional problems. In the majority of cases, a fibrotic response results from localised inflammation and the elevation of pro-fibrotic molecules such as TGFβ1. These molecules act to stimulate the differentiation of cells within the tissue into phenotypes that more rapidly secrete collagen and contractile proteins. In addition, the TGFβ1 can drive the deposition of new collagen directly by stimulating the SMAD pathway. There has been a drive towards the development of drugs that can prevent scarring by inhibiting TGFβ1. Decorin is one such drug, which has a region that specifically binds TGFβ1 and prevents it from activating the SMAD pathway. A major challenge, however, is the delivery of decorin to tissue surfaces, with persistent retention of the drug molecule. We have developed a a new shear structured material that enables the delivery of decorin and potentially other matrix modifying molecules. These materials are formed from a range of polysaccharides that have been sheared during processing, the resulting suspensions of particles exhibit shear thinning properties and have been show to adhere to tissue surfaces [1]. Here we report on the efficacy of these materials for preventing ocular fibrosis through the delivery of decorin.

Experimental Methods

Fluid gels were fabricated by applying a controlled shear to hydrocolloids of gellan gum that were dispersed in water at a temperature of 80ºC. During shearing, a reduction in temperature initiated gelation. As gelation occurred, the shear disrupted the formation of a fully interconnected network, resulting in the formation of discrete spherical and ribbon-like particles, which interact, resulting in thickening when at rest. The capacity of the gel to be retained on surfaces was determined by application of the material to the surface of live rat eyes or harvested skin, retention was determined by optical coherence tomography and by visual inspection, respectively. In order to determine the potential of the material to deliver drug molecules to the surface of an infected eye, the fluid gel was combined with decorin at a dose of 0.24 mg/mL. The formulated eye drop was finally tested in a murine, in vivo model of scarring initiated with microbial keratitis (*P. aeruginosa).* The gel was applied on a every four hours for thirteen days beyond resolution of the infection. The tissues from sacrificed mice were embedded and processed to evaluate the extent of scarring as determined by histological markers of scarring and corneal opacity.

Results and Discussion

OCT images of the rats eyes demonstrated that the gellan-based fluid gel material were cleared much more slowly from the surface of the rat eyes than the PBS-based drops. While the PBS drops were cleared in under an hour, there was still detectable fluid gel 120 mins following application. Interestingly, the layer of fluid gel across the surface of the cornea was more uniform than the PBS-based eye drop, which was significantly thicker (>600um) in the nasal aspect than it was temporally (Figure 1). When applied to the mouse eyes post-infection, the surface of the cornea returned to full transparency within a period of 16 days, with significantly higher levels of transparency in the treatment

group, than in the gold-standard. When the eyes were analysed using immunohistochemistry, the decorin bearing drops were shown to reduce the intensity of markers of scarring including α-SMA, fibronectin, and laminin (Figure 2) [2]. The fluid gel treatment groups demonstrated full regeneration of the corneal surface by the end of the experiment. Interestingly, the fluid gel eye drop exhibited superior regeneration to the PBS based treatment, even in the absence of decorin, suggesting that the material has a significant influence on healing alone.

Conclusion

Structuring eye drops using polymeric gels increases viscosity, and thereby enhances the retention of eye drops on th ocular surface, in addition to improving the homogeneity of the drop thickenss across the surface of the eye. We have demonstrated that gellan-base fluid gels can deliver a sustained dosage of decorint that mediates corneal regeneration and prevents scarring in a mouse model of microbial keratitis.

References

[1] Cooke, Megan E., et al. "Structuring of hydrogels across multiple length scales for biomedical applications." *Advanced Materials* 30.14 (2018): 1705013.

[2] Hill, Lisa J., et al. "Sustained release of decorin to the surface of the eye enables scarless corneal regeneration." NPJ Regenerative medicine 3.1 (2018): 23.

Acknowledgement

We would like to acknowledge the MRC (MR/N019016/1) and the EPSRC (EP/L016346/1) for funding this research.

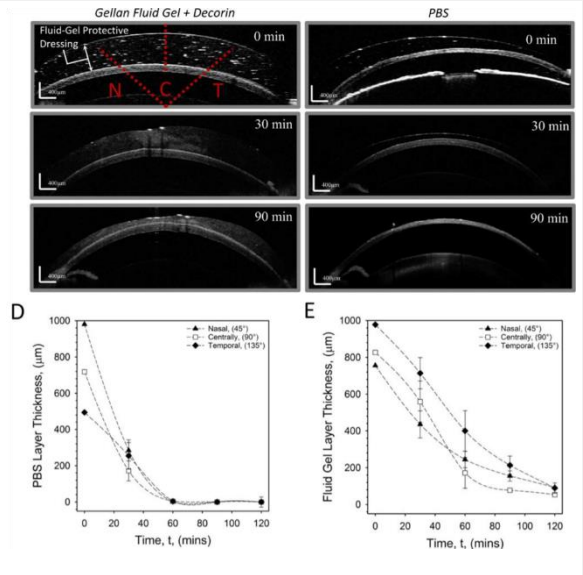

Fig1. Retention of fluid gel on the surface of a rat eyes in a blinking model, compared with PBS. OCT images of eye drops on the surface of the cornea (fluid gel, left; PBS, right). When the thickness of the drop was measured with time, the fluid gel exhibited enhanced retention with a homogenous layer of the material remaining in place after 60 mins.

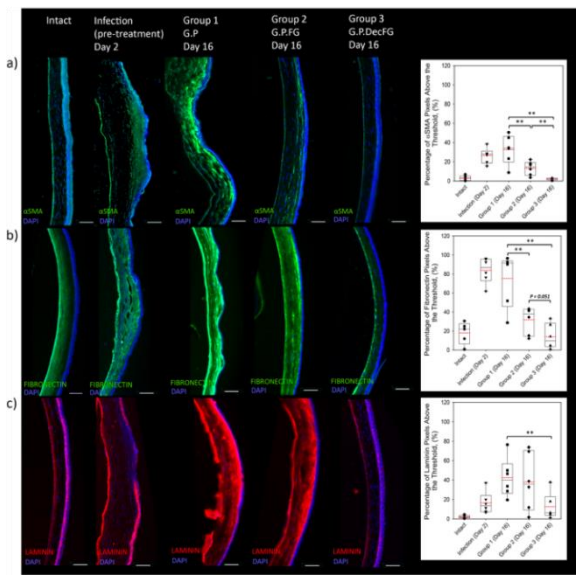

Fig 2. IHC evaluation of healing across the corneal surface in a murine model. The delivery of fluid gel with and without decorin, to the surface of the eye during treatment, allowed for superior regeneration of the corneal surface and resulted in a significant reduction in markers of scarring.

PS2-13-453

Electrospun nanofiber membranes as substitutes for posterior lamellar keratoplasty

Marcus M. Himmler[1,2], Fabian Garreis[3], Friedrich Paulsen[3], Dirk W. Schubert[2], Thomas A. Fuchsluger[1]

[1]University Medical Center Rostock, Department of Ophthalmology, Rostock, DE; [2]Friedrich-Alexander University Erlangen-Nuremberg, Institute of Polymer Materials, Erlangen, DE; [3]Friedrich-Alexander University Erlangen-Nuremberg, Institute of Functional and Clinical Anatomy, Erlangen, DE

Introduction

Posterior lamellar keratoplasty (DSAEK, DMEK) currently is the gold standard for treating patients with a corneal endothelial cell pathologies resulting in functional impairment. This surgical approach depends on the availability of human donor corneas. An artificial biomimetic graft carrying human corneal endothelium could minimize this dependency giving access of this surgical method to larger numbers of patients. Thus, waiting lists could be reduced. In this study, electrospun polycaprolactone (PCL)-collagen nanofibers were tissue-engineered with corneal endothelial cells (HCEC) and analysed with regard to their potential application as artificial posterior lamellar grafts.

Experimental Methods

Membranes were produced from nanofibers obtained by electrospinning of a polymeric solution: A blend of PCL (80 kDa) and purified collagen type I from bovine skin was dissolved in diluted acetic acid (90 % AcOH, ratio of 2:1, final concentration of 0,12 g/ml). Nanofibers were electrospun with a voltage of 15 kV and a flow rate of 1 ml/h (distance needle tip counter electrode: 15 cm). The fabricated membranes were characterized regarding fiber diameter, fiber orientation and membrane thickness. Therefore, a contact-less method was established using a laser scanning microscope. Human corneal endothelial cells (HCEC-12) were seeded on the membranes in culture medium F99 with an initial cell count of 20.000 cells per well in 24 well plates and cultivated for 5 days. Suitability check for the nanofiber membranes as posterior lamellar graft was done using microscopic methods and focusing on cell morphology and cell-cell interface. For light microscope imaging cells were stained with haematoxylin and eosin (HE staining). Expression on the tight junction associated protein zonula occludens-1 (ZO-1) was analysed by immunostaining of HCECs. Additionally, cell morphollogy was studied using scanning electron microscopy.

Results and Discussion

Electrospinning of PCL-Collagen blends provided membranes in a non-woven, fibrous structure with a random fiber orientation and fiber diameter of 288 (±96) nm. With a spinning time of 5 minutes membranes with an average thickness of 10 µm were obtained, a thickness similarly to a Descemet's membrane. HCECs grown on the PCL-collagen membrane expressed ZO-1, typically for the corneal endothelium to perform as barrier between the cornea and the anterior chamber. Further imaging shows well-spread cells grown on the nanofiber membranes.

Conclusion

Randomly electrospun PCL-collagen nanofibers offer an interesting opportunity to overcome the shortage of posterior lamellar grafts. Further studies are needed to evaluate functional performance in both ex vivo and in vivo settings.

PS2-13-454

Regeneration of functional bladder using cell seeded amniotic membrane and P(LA/CL) scaffold covered with omentum

Tsunehito Horii, Kazuyoshi Jonin, Hiroyuki Tsujimoto, Masayuki Nagasawa, Kenichi Kobayashi, Akeo Hagiwara, Akihiro Kawauchi

Shiga University of Medical Science, Department of Urology, Otsu, JP

Introduction

Currently, augmentations with gastrointestinal segments are basically used for neo-bladder in the surgery of bladder cancer, neurogenic bladder. However, because it carries a risk of short and long term complications, new strategies for creating neo-bladder without using gastrointestinal segment are desired. In this study, we used amniotic membrane and biodegradable poly lactic acid and ε- caprolactam scaffold(P(LA/CL)). Previously, we confirmed the regenerative tissues without scar using oral mucosa cells seeded on the amniotic membrane and P(LA/CL) scaffold rolled to abdominal greater omental for 3 weeks.

Experimental Methods

Ⅰ.In vitro examination

(1)Creation of amniotic membrane seeded oral mucosa cells (o-MEM)

Oral mucosa cells were derived from rabbit oral mucosa. The cells were cultured with the epithelium medium supplemented fetal bovine serum for a week and seeded on the amniotic membrane for another week.

(2)Creation of P(LA/CL) scaffold seeded stomach smooth muscle (s-SF)

Stomach smooth muscles were resected from a rabbit stomach. The cells were cultured with Dulbecco's modified Eagle medium supplemented fetal bovine serum for two weeks and seeded on the P(LA/CL) scaffold for another week.

Ⅱ.In vivo examination

Using the created cell seeded amniotic membrane and P(LA/CL) scaffold compared with non-treated control, in vivo examination carried out within two steps surgeries.

(1)First surgery

The two layer o-MEM and s-SF were put on greater omentum and rolled using plastic tube for two weeks. Sufficient blood flow from greater omentum provides nutrition to two layer tissues for creating neo-bladder.

(2)Second surgery

After two weeks, a part of upper bladder was resected and two layer tissues with greater omentum covered the resected areas of the bladder.

Non-treated control group was just resected upper bladder part.

Ⅲ. Assessment of regenerated bladder

Urodynamics study, cystography and muscle strip study of regenerated bladder were conducted to observe the bladder form and check the bladder function for 6 month to 12 month, compared with non-treated control. Also, immunostainings were performed to evaluate the bladder tissue regeneration.

Results and Discussion

At first, the rolled cell seeded materials covered with omentum after two weeks weren't found scar formation and could find the separated epithelium and muscle layers. Next, in order to evaluate the regenerated bladder form and bladder function, urodynamics study, cystography and muscle strip study were conducted. Then, peristaltic movement could be found in the regenerated bladder in cytstogryphy. Also, the bladder capacity was a little increased after 6 month and 12 month, compared with non-treated control. Muscle strip study showed the regenerated bladder reacted with electric stimulation. These results are indicated the regenerated bladder using two layer materials covered with omentum showed great bladder form and function. Moreover, bladder epithelium and bladder muscle were confirmed in HE immunostainings.

Conclusion

Cell seeded amniotic membrane and P(LA/CL) scaffold covered with omentum showed regenerated functional bladder and formed bladder epithelium and bladder muscle.

References

1. Atala A, Bauer SB, Soker S et al. Lancet, 2006
2. Joseph DB, Borer JG, Filippo RE et al. J Urol, 2014
3. Fishman IJ, Flores FN, Scott FB et al. J Urol, 1987
4.Iijima K, Igawa Y, Imamura T et al. Tissue Eng, 2007

Acknowledgement

None of authors have any conflicts of interest to declare.

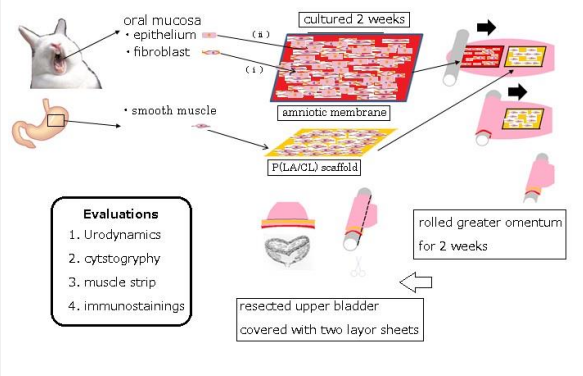

Overview of the experiment

2:45 p.m. – 3:45 p.m.

Hall 1 / Exhibition Area

PS2-14 | Tendon and ligament

PS2-14-455

Simulation-based development of woven biomimetic implants for regeneration and therapy of tendon and ligament defects

Michael Wöltje, Oliver Döbrich, Dominik Nuss, Thomas Gereke, Gerald Hoffmann, Dilbar Aibibu, Chokri Cherif

Technische Universität Dresden, Institute of Textile Machinery and High Performance Material Technology (ITM), Dresden, DE

Introduction

Tendons and ligaments are necessary for movement. Ligaments connect two bones and serve to guide and support the joints, while tendons transmit force between the soft muscles and the hard bones. Injuries lead to pain, movement restrictions as well as to reduction of mobility and quality of life.

Surgery of large defects usually require replacement materials in order to bridge the defect or to reinforce a rupture. The gold standard is the use of the patient's own tissue. However, availability of those materials is limited and removal is associated with an increased risk of complications (donor morbidity) and disadvantages (e.g. movement restrictions and postoperative muscle atrophy).

Synthetic implants are manufactured from resorbable and non-resorbable polymers using textile processes like braiding, knitting and weaving. Those implants show material-related disadvantages: 1) Resorbable materials based on polyurethane-urea block polymer (PUUR) and poly-L-lactide acid (PLLA) lead to inflammatory reactions due to degradation products. 2) The resorption process is too short and thus not adapted to the healing process. 3) Non-absorbable implants exhibit integrity-decreasing creep, material abrasion and fatigue, resulting in a high risk of inflammatory reactions and rerupture. However, those implants have a constant geometry over length, so deformation properties and attachment of synthetic tendons and ligaments to bones and muscles do not meet the anatomical requirements and therefore there is an acute risk of creep and rupture.

Therefore, biomimetic woven structures for tendon and ligament implants should be developed from silk yarns. Those structures should exhibit variable structure and porosity over length, different deformation properties and high strength. Thus, a simulation-supported approach comparing different weaving technologies for design of new textile devices for tendon and ligament replacement will be presented.

Experimental Methods

First, the unit cells of homogeneous base woven fabrics (leno, multi-layer and ORW binding) were developed as micro-scale models on the basis of digital elements. The unit cells were then transferred into a structural model and material behavior determined into corresponding nonlinear material models. With corresponding boundary conditions for bearing and force application, tensile tests were simulated virtually and the deformation behavior of woven fabrics were determined. A twisted silk yarn with round cross-section was used for systematic development of suitable biomimetic textile structures.

Results and Discussion

First, a woven fabric model with silk yarn was designed. The mechanical tensile behaviour in axial direction was determined. An isotropic material model with plasticity was used to reproduce the tensile behaviour and to transfer the non-linear mechanical tensile elongation behaviour. Draft behaviour in the yarn draft simulation reflects the real

experimental data accurately. Then, the numerical models of the fabrics were virtually loaded under applied periodic boundary conditions and investigated for their structural stiffness. Through virtual modelling, the tensile force-elongation behavior of the silk yarns was mapped in a numerical FEM model. In addition, several multi-layer woven fabrics were transferred into multi-layer woven fabric models and examined. Thus, differences in stiffness could be detected. In order to achieve the necessary structural-mechanical properties, multilayer bonds with different incorporation of the material were analyzed and the models required for the simulation were developed. Then, basic weave pattern (plain wall, twill and atlas bindings) were developed into multi-layer woven fabrics.

Conclusion

Simulation based development of woven fabrics from silk yarn is a promising approach to develop biomimetic textile implants for tendon and ligament replacement.

Acknowledgement

The IGF research project 20043 BR of the Forschungsvereinigung Forschungskuratorium Textil e. V. and Gesellschaft für Chemische Technik und Biotechnologie e.V. is funded through the AiF within the program for supporting the „Industriellen Gemeinschaftsforschung (IGF)“ from funds of the Federal Ministry for Economic Affairs and Energy (BMWi) by a resolution of the German Bundestag.

PS2-14-456

Biodegradable polymer for anterior cruciate ligament prostheses: A biomechanical approach of a daily basis activity

André Rangel[1], Laila Colaço[2], Christophe Egles[2], Veronique Migonney[1]

[1]Université Paris 13, LBPS/CSPBAT, UMR CNRS 7244, Villetaneuse, FR; [2]Université de Technologie de Compiègne, BioMécanique et BioIngénierie (BMBI), UMR 7338, Compiegne, FR

Introduction

Every year thousands of people suffer from total or partial rupture of the anterior cruciate ligament. Although for the majority of the patients, belonging to young and active population, the conventional treatment (autograft) takes from six to ten months to recover. Despite good results of the artificial PET ligament prosthesis, autograft is still preferred because of the reluctance of healthcare personal and patients to the use of artificial and permanent materials. That said, the challenge consists in presenting a new proposal, using a biocompatible biointegrable polymer, exhibiting good mechanical properties and controlled biodegradablility. Amongst these requirements poly(caprolactone) (PCL) emerges with bright prospects in the domain. Combining PCL with surface functionalization to improve the cell response, PCL prosthesis could become an optimized support for growing a new ligament which will slowly replace the biodegraded material. In this scenario, mechanical properties are primordial for the prosthesis success, and the closer the mechanical assays come to the daily activities the more relevant the results will be.

Experimental Methods

All assays were performed over PCL arranged in bundles of 20 fibers delimited by ties (30 ±10 mm length). The fibers were supplied by Texinov Technical Textiles (France). For the thermal grafting process the surfaces were first submitted to ether Soxhlet extraction to remove spin finish components, then activated by ozonation for 10 min at 30 °C in distilled water, followed by 1 h NaSS polymerization at 45 °C. The samples molecular weight M_n were determined by SEC, the crystallinity was assessed by DSC and the grafting rate determined by toluidine blue colorimetric assay. For the mechanical properties characterization, traction assays were achieved at room temperature in water at different temperatures. Moreover, in a third set of experiments samples were submitted to a cycle of efforts simulating human regular walking before the traction assay to rupture. The strain rate used in all experiments was 3.6 $mm.min^{-1}$. Stress strain curves until rupture were plotted and Young's Modulus, elongation and the ultimate tensile stress were determined.

Results and Discussion

The samples molecular weight (M_n) was estimated at 78 kg/mol, with average crystallinity of 60%. The grafting process does not modify these parameters significantly. The mean sample grafting rate was 0.7 mmol/g. Traction tests carried out in air showed a reduction of the Young modulus after the Soxhlet extraction and grafting, naturally accompanied by an increase of the elastic deformation. The ultimate tensile stress was not affected by surface treatment. In the case of assays in water, the behavior of grafted and ungrafted samples showed opposite tendencies face to temperature variation, displaying an increased Young modulus for grafted samples when approaching body temperature. Finally, traction assays realized after walk simulation showed the influence of exercise on the mechanical properties of the material, overlapping the influence of surface treatment on such features.

Conclusion

The assays performed during this study allowed to evaluate the influence of the thermal grafting, temperature and environment, as well as daily activities on the mechanical characteristics of a biodegradable polymer. It is crucial to note that, although the influence exists, in all tested conditions the values presented by the PCL fibers are much higher than those found in the natural ligament, showing not only the importance of the test conditions for validation of the material choice, but also the adaptability of the PCL to conditions close to human physiology.

References

M. Marieswaran, I. Jain, B. Garg, V. Sharma, and D. Kalyanasundaram, “A Review on Biomechanics of Anterior Cruciate Ligament and Materials for Reconstruction,” *Applied Bionics and Biomechanics*, vol. 2018, pp. 1–14, 2018.

K. Robi, N. Jakob, K. Matevz, and V. Matjaz, “The Physiology of Sports Injuries and Repair Processes,” in *Current Issues in Sports and Exercise Medicine*, M. Hamlin, Ed. InTech, 2013.

J. Zhou, M. Manassero, V. Migonney, and V. Viateau, “Évaluation clinique et biologique d’un ligament synthétique bioactif chez la brebis,” *IRBM*, vol. 30, no. 4, pp. 153–155, Sep. 2009.

P. Abdel-Sayed, M. N. Moghadam, R. Salomir, D. Tchernin, and D. P. Pioletti, “Intrinsic viscoelasticity increases temperature in knee cartilage under physiological loading,” *Journal of the Mechanical Behavior of Biomedical Materials*, vol. 30, pp. 123–130, Feb. 2014.

Zantop, T., Petersen, W., Sekiya, J. K., Musahl, V., & Fu, F. H. (2006). Anterior cruciate ligament anatomy and function relating to anatomical reconstruction. *Knee Surg Sports Traumatology Arthroscopy 14, 989-992.*

Acknowledgement

The authors would like to thanks the French Public Investment Bank and the French state (PSPC application - Liga2bio project) for financial support.

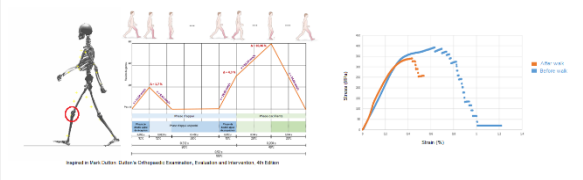

Influence of walking on mechanical properties of PCL

PS2-14-457

Study of functionalized polycaprolactone longstanding degradation under artificial physiological conditions

André Rangel Rangel, **Amélie Leroux**, Tuan Nguyen, Veronique Migonney

Université Paris 13, LBPS/CSPBAT, UMR CNRS 7244, Villetaneuse, FR

Introduction

The use of polycaprolactone (PCL) in the field of medical devices is largely recognized for properties such as easy manufacturing, scalable mechanical properties and the possibility of functionalization. The last one becomes especially important since it allows the modification of the surface to enhance the biological response. However, in applications intended to withstand mechanical stress, another property must be carefully studied: the degradation rate. Each year around 30,000 adult humans suffer rupture of the anterior cruciate ligament (ACL) in France. This number, found in the general population, grows considerably considering the high-risk groups as high-level athletes. Unlike some other ligaments in the human body, ACL does not self-heal and the autograft procedure most commonly used today has slow and often problematic recovery. In this context, a biocompatible and biodegradable prosthesis could be the expected evolution of the existing treatments and the sodium polystyrene sulfonate (NaSS) grafted PCL surfaces are ideal candidates, if the following question can be answered: For how long this material will resist during the degradation process?

Experimental Methods

Two sets of samples were used: PCL films (14 mm diameter) and fibers (100 mm diameter). The fibers were graciously supplied by Luxilon Industries (Belgium). Surface functionalization of the samples was achieved as follows: ozonation at 30 °C NaSS thermal grafting for 3h at 45°C under stirring. Grafted and ungrafted PCL samples were then immersed in PBS at 25 and 37 °C for time points ranging from 2 weeks to 2.5 years. The degradation solution was renewed every 3 months and the pH of the solution was measured after each change. The weight loss of the films was assessed after each time point, as well as the molecular weight variation by SEC, crystallinity degree by DSC, and nanotopography by AFM images. The cell behavior over degraded films was studied by fluorescence microscopy. Chemical degraded samples with molecular weight after 2.5 years of degradation were assessed by MTT to evaluate the cell viability in the presence of degraded material. Primary sheep ACL cells were used for both experiments. Mechanical assays were performed only on the PCL fibers bundles samples. Stress strain curves were recorded and Young's Modulus, elongation and the ultimate tensile stress (UTS) were determined.

Results and Discussion

Whilst ungrafted samples had linear weight loss during the first six months before stabilizing, grafted samples degraded at 37 ° C maintained their initial mass for the same period, for then start to reduce, ending the experiment 15% lighter than the other groups. All studied groups had the molecular mass linearly reduced to stabilize after one year of degradation, such reduction was accentuated in the case of the grafted samples. On the other hand, the degradation process led to an increase of the material crystallinity. On this parameter, however, the degradation temperature had more influence than the surface treatment, with higher crystallinity values for samples kept at 37 ° C. AFM images showed variation in the samples roughness along the degradation process. Although both conditions presented higher roughness, the effect is amplified on ungrafted surfaces. Regarding cell behavior the degradation

had no influence on cell morphology. Cell viability is also unchanged in the presence of degradation products. Finally, mechanical tests showed decrease in mechanical properties over the study period for all degraded groups, however Young modulus, elastic deformation and ultimate tensile stress values remain higher than those found in natural ACL for at least 12 months of degradation.

Conclusion

The combination of the results obtained over this study confirms that PCL hydrolyzes by a bulk degradation mode, with strong influence of the degradation temperature. Nonetheless, to all appearances, functionalized surfaces degrade via a bulk degradation with autocatalysis. In this model the PNaSS grafting will operate as a protector barrier which will conserve the core of the material for at least 6 months before starting the degradation.

References

M. A. Walters, M. C. Chambers, R. Karki, E. Knox, G. Levengood, S. F. El-Amin, “Anterior Cruciate Ligament Tissue Engineering: A Review of Current Investigations,” *Journal of Nanotechnology and Materials Science* 3(1): 3-9, 2016

A. C. Gurlek, B. Sevinc, E. Bayrak, C. Erisken, “Synthesis and characterization of polycaprolactone for anterior cruciate ligament regeneration,” *Mater. Sci. Eng. C*, vol. 71, pp. 820–826, Feb. 2017.

A. Höglund, M. Hakkarainen, A. Albertsson, “Degradation Profile of Poly(ϵ-caprolactone)–the Influence of Macroscopic and Macromolecular Biomaterial Design,” *J. Macromol. Sci. Part A*, vol. 44, no. 9, pp. 1041–1046, Jun. 2007.

M. Ciobanu, A. Siove, V. Gueguen, L. J. Gamble, D. G. Castner, V. Migonney, “Radical graft polymerization of styrene sulfonate on poly (ethylene terephthalate) films for ACL applications:‘grafting from’ and chemical characterization,” *Biomacromolecules*, vol. 7, no. 3, pp. 755–760, 2006.

M. A. Woodruff, D. W. Hutmacher, “The return of a forgotten polymer—Polycaprolactone in the 21st century,” *Prog. Polym. Sci.*, vol. 35, no. 10, pp. 1217–1256, Oct. 2010.

A. C. Vieira, J. C. Vieira, J. M. Ferra, F. D. Magalhães, R. M. Guedes, A. T. Marques, “Mechanical study of PLA-PCL fibers during in vitro degradation,” *J. Mech. Behav. Biomed. Mater.*, vol. 4, no. 3, pp. 451–460, Apr. 2011.

P. Abdel-Sayed, M. N. Moghadam, R. Salomir, D. Tchernin, and D. P. Pioletti, “Intrinsic viscoelasticity increases temperature in knee cartilage under physiological loading,” *Journal of the Mechanical Behavior of Biomedical Materials*, vol. 30, pp. 123–130, Feb. 2014.

Acknowledgement

This work was funded as part of the "Future Investment Project" by the French Public Investment Bank and the French state - PSPC application - Liga2bio project.

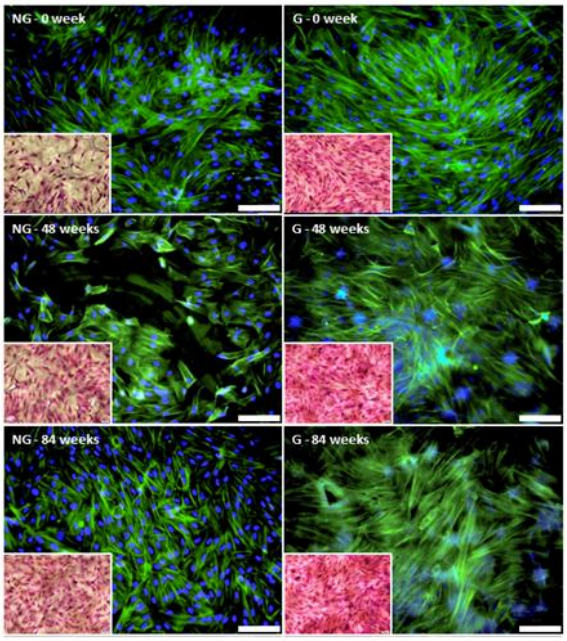

Morphologies of sACL fibroblastson non-grafted and grafted degraded PCL films

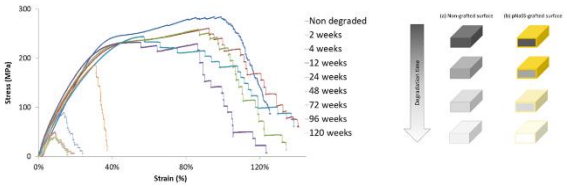

Degradation mechanisms of PCL surfaces and its influence on mechanical properties

2:45 p.m. – 3:45 p.m.

Hall 1 / Exhibition Area

PS2-15 | Skin and wound healing

PS2-15-458

Regeneration of whole skin tissues by cell delivery using injectable self-replenishing gels

Kimika Ono, Koji Nagahama

Konan Univercity, Graduate School of Nanobiochemistry, Frontiers of Innovative Research in Science and Technology (FIRST), Kobe, JP

Introduction

Skin tissue is hierarchically organized from three parts with totally different characters, the epidermis, the dermis, and the subcutaneous. Additionally, skin tissues include various kinds of cells, and they form appendage of the skin such as hair follicles, sweat glands, sebaceous gland, blood vessels, etc. These hierarchical structures and appendage are essence for multifunction of skin tissues. A method of regenerating skin tissue complete with hierarchical structures and appendages is important issue for long term. Injectable hydrogels are biomaterials that have the potential to provide scaffolds to cells for in situ tissue regeneration with a minimally invasive implantation procedure. The success of skin tissue regeneration utilizing injectable gels depends on providing cells with appropriate scaffolds that present an instructive extracellular microenvironment, which strongly influences the survival, proliferation, organization, and function of cells encapsulated within gels. One of the most important abilities of injectable gels to achieve this function is to adsorb and retain a wide variety of requisite bioactive molecules including nutrients, extracellular matrices, and growth/differentiation factors within gels. Recently, we developed a new type of injectable gel, self-replenishing injectable gel, which is able to adsorb and retain a wide variety of bioactive molecules in synchronization with the degradation [1]. In this study, we evaluated the potential utility of the self-replenishing injectable gel as new method for regeneration of whole skin tissue.

Experimental Methods

The self-replenishing injectable gels were fabricated by simple combination of common biodegradable copolymers, poly (lactide-co-glycolide)-b-poly(ethylene glycol)-b-poly(lactide-co-glycolide) (PLGA-PEG-PLGA), and synthetic clay nanoparticles (LAPONITE®). Human dermal fibroblast (HDFs), endothelial cells, human umbilical vein endothelial cells (HUVECs), adipose-derived human mesenchymal stem cells (ADSCs) were seeded onto gels made on a 96-well plate and then incubated at 37°C. After a predetermined time, cells growing on the gels were quantified using a WST-1 assay. Similarly, cell growth in the hydrogels was also investigated. PLGA-PEG-PLGA gel, LAPONITE® gel, and Matrigel were examined as controls. We made skin tissue-injury model mice that have 7 mm square wound on the back, then the mice were treated with the self-replenishing gels, and wound area was analyzed by H&E staining for 2 weeks.

Results and Discussion

HDFs, Endothelial cells, HUVECs, and ADSCs cultured on the gels exhibited native morphology at day 7 and high proliferative capacity. By contrast, cells did not adhere to control PLGA-PEG-PLGA gel and exhibited a round shape, with no proliferation detected. Next, three-dimensional cell proliferation within the gels was investigated. Large numbers of cells can be readily encapsulated within the self-replenishing injectable gels due to thermal-gelation, and almost of the encapsulated cells (>95%) were alive, whereas the viability of cells encapsulated within PLGA-PEG-PLGA gel was significantly lower. None of the cell types examined proliferated in PLGA-PEG-PLGA gel. By contrast,

cells encapsulated within the self-replenishing gels exhibited continuous proliferation over 14 days. Importantly, self-replenishing gels demonstrated significantly higher proliferation of all cell types examined in comparison with Matrigel as positive control, indicating that an appropriate extracellular microenvironment was engineered within the self-replenishing gels. skin-injury model mice treated with the self-replenishing injectable gels significantly enhanced regeneration of skin tissue as compared with PLGA-PEG-PLGA gels. Importantly, hierarchical structures, the epidermis, the dermis, and the subcutaneous was reconstructed at the wound site treated with the self-replenishing gels, and the appendage such as hair follicles, sweat glands, sebaceous gland, blood vessels were also observed.

Conclusion

In conclusion, the self-replenishing injectable gels possess unique abilities to self-replenish the regenerative extracellular microenvironment within the gels in the skin tissues, and the gels have potential utility as injectable gels for regenerative medicine for the whole skin tissues.

References

K. Nagahama, N. Oyama, K. Ono, A. Hotta, K. Kawauchi, T. Nishikata, Biomater. Sci., 2018, 6, 550

PS2-15-459

Co-axial electrospinning as innovative tool to develop odour-adsorbing wound dressings

Arn Mignon[1], Manon Minsart[1], Iain Allan[2], Aysu Arslan[1], Tom Gheysens[1], Sandra Van Vlierberghe[1], Peter Dubruel[1]

[1]University of Ghent, Organic and Macromolecular Chemistry, Center of Macromolecular Chemistry, Polymer Chemistry and Biomaterials Group, Gent, BE; [2]University of Brighton, School of Pharmacy and Biomolecular Sciences, Brighton, GB

Introduction

Data from the World Health Organisation (WHO)[1] indicate that every year an estimated 300.000 deaths are caused by fire-related burns. Burns can be very complex making them concomitant with their own field of specialty within medicine. Malodorous burn wounds tend to negatively influence the patient's wellbeing. A combination of (an)aerobic and proteolytic bacteria, necrotic tissue, poorly vascularized tissue and high levels of exudate causes these malodours. Currently available odour adsorbing wound dressings, like CarboFlex and Askina CarboSorb, are not useful for strong exudating wounds. They require regular changing and are expensive. Therefore, there is an urgent need for new improved technologies for odour adsorbing wound dressings with the added benefit of absorbing large amounts of exudate. This will not only result in more cost-effective products, but will also improve the efficiency of wound management by healthcare providers.

Electrospun fibre mats (nanofibres generated by the electrospinning technique) provide an excellent environment to promote wound healing due to their high surface-to-volume ratio, good porosity levels, allowance of gaseous exchange and mimicking of the natural extra-cellular matrix. These characteristics promote cell respiration, skin regeneration, haemostasis, exudate removal and moisture retention. The interconnected nano-porosity prevents microbial infiltration.

In this project, a wound dressing was created using an innovative technique called co-axial electrospinning by which two different materials are electrospun simultaneously, creating core-shell nanofibers. For the core, an acrylate-endcapped, urethane-based precursor (AUP)[2] was used, selected for its mechanical properties and good biocompatibility. For the shell, alginate was used for its high absorption capacity and haemostatic properties. In the current work, cross-linkable moieties (methacrylates) were incorporated into alginate to enable controllable covalent cross-linking.

Experimental Methods

The AUP[2] polymer and methacrylated alginate (algMOD)[3] were synthesized according to standard in-house protocols. These polymers were then processed into films and (co-axially) electrospun nanofibrous mats. The developed structures were then characterized by measuring the gel fraction and swelling properties in water and PBS buffer. Moreover, the moisture uptake capacity was determined by dynamic vapour sorption (DVS) and the mechanical properties were evaluated by tensile testing and rheology. In order to assess the cytotoxicity of the prepared materials, indirect cell tests were performed with Human Dermal Fibroblasts. The spun nanofibers and the core-shell structure of the co-axial spun fibers were confirmed using scanning and transmission electron microscopy respectively. Subsequently, activated carbon (AC) was added to the dressings to add an odour adsorption capacity to the dressings. Crystal violet was used as a proof of concept to identify the adsorption capacity of the structures with and without AC.

Results and Discussion

- AUP with variable PEG backbone molecular weight (8k – 20k g/mol) combined with modified alginate (algMOD) was successfully processed into films and (co-axial) electrospun nanofibrous beds with tunable fiber diameters ranging between 200 nm and 1.5 µm
- The combination of AUP and algMOD led to tunable physical and mechanical properties, with high gel fractions above 85%, a swelling ratio ranging between 10 and 125 $g_{water}/g_{polymer}$, a moisture uptake capacity up to 90% at 95% relative humidity with a very limited hysteresis and Young's Modulus between 0.1 - 0.6 MPa.
- Indirect cell tests showed compatability of the AUP > 95%.
- Core-shell structure of co-axial electrospun fibers (AUP shell and algMOD core) was identified through TEM (Figure 1, left).
- Faster and stronger (11%) crystal violet sorption was observed by the AC incorporated wound dressings indicating significantly better odour absorption capacities (Figure 1, right).

Conclusion

To conclude, the processed wound dressings perform physically and mechanically better than current commercial dressings.

References

1. Mock, C., et al. Confronting the global burden of burns: A WHO plan and a challenge. Burns 35, 615–617 (2009).
2. Houben, A. et al. Flexible oligomer spacers as the key to solid-state photopolymerization of hydrogel precursors. Mater. Today Chem. 4, 84–89 (2017).
3. Mignon, Arn, et al. "Combinatory approach of methacrylated alginate and acid monomers for concrete applications." *Carbohydrate polymers* 155 (2017): 448-455.

Acknowledgement

This project has received funding from the Interreg 2 Seas programme 2014-2020, co-funded by the European Regional Development Fund under subsidy contract No 2S01-027. Arn Mignon received post-doctoral fellowship from Research Foundation Flanders No. 12Z2918N.

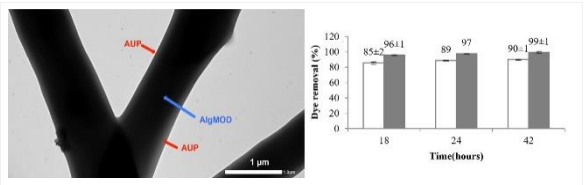

Figure 1.
TEM image identifying the AlgMOD and AUP PEG 10k in a core-shell co-axial electrospun fiber bed (left). Percentage of crystal violet removal by the AUP PEG 10k at different incubation times (18, 24 and 42h) (right).

PS2-15-460

Encapsulation of miR-31 synthetic oligonucleotides into nanoparticles as a genetic nanomedicine for wound healing applications

Adrian D. Juncos Bombin[1], Eoghan Mulholland[1], Nicholas J. Dunne[2], Helen McCarthy[1]

[1]Queen's University Belfast, School of Pharmacy, Belfast, GB; [2]Dublin City University, School of Mechanical & Manufacturing Engineering, Dublin, IE

Introduction

Wound healing is a fundamental process to ensure skin integrity and survival of all higher organisms (1). It is a tightly regulated process, but comorbidities can produce early and late complications that lead to delayed healing, placing a massive financial burden on healthcare systems (2). Researchers have turned to nanomaterials for the development of novel treatments to address the complexity of wound healing, since they can enter the wound site, deliver drugs and regulate cell behaviour (3,4). Indeed, wound healing has been found to be regulated by microRNAs (miRs), which are post-transcriptional regulators controlling many vital physiological processes (5). Herein, we aim to encapsulate RNA antisense oligonucleotides (ASO) with the sequence of miR-31 into nanoparticles (NP) by electrostatic interaction with RALA, a novel 30-mer cationic peptide (6). miR-31 shows promise as a successful genetic therapy towards wound healing as its upregulation has been shown to participate in angiogenesis (7), cell proliferation and migration (8). In addition, electrospinning is a versatile technique that uses electric fields to convert a polymer solution into nanofibres (NF) resembling the extracellular matrix, acting as suitable dressings and drug delivery systems for wound healing (9). Therefore, NP as vectors for ASO encapsulated within electrospun NF are expected to constitute an innovative genetic nanomedicine that could manage and promote tissue repair. **Figure 1** shows a schematic overview of the experimental approach planned for this research programme towards the production of NP-loaded electrospun NF.

Experimental Methods

NP at different N:P ratios were synthesized by the self-assembly of cationic RALA with anionic ASO having the sequence of miR-31. Particle size, polydispersity, mean count and zeta potential were measured using a Nano ZS Zetasizer (Malvern Instruments, UK). NP were processed using an electrophoretic mobility shift assay. ASO were labelled (Cy3-ASO) with a Label IT® siRNA Tracker Intracellular Localization Kit, Cy®3 (Cambridge Bioscience, UK) and NCTC-929 fibroblasts (ATCC, USA) were transfected with RALA/Cy3-ASO. Cells were then studied with optical microscopy and flow cytometry (BD Accuri C6 Plus, BD Biosciences, USA). Moreover, an MTS assay (Thermo Fisher Scientific, USA) of cells transfected with RALA/ASO was performed.

Results and Discussion

Figure 2 shows the Z-average size of RALA/ASO and RALA/Cy3-ASO, and their cellular uptake and viability when incubated with NCTC-929 cells. RALA and ASO were condensed into NP of approximately 150 nm from N:P ratio 8 onwards. For N:P ratio 6 onwards, zeta potential was found to be in the +10-14 mV range, which is optimal to facilitate transport through the cell membrane (6). RALA/Cy3-ASO showed Z-average sizes of approximately 130 nm from N:P ratio 6 onwards. However, as was the case with RALA/ASO NP, the polydispersity index was higher than 0.3, revealing lack of homodispersity in the sample. Zeta-potential of RALA/Cy3-ASO was found to be in a +10-15 mV range for N:P ratio 6 onwards. A gel electrophoresis assay showed that ASO are neutralised by RALA at N:P ratio 4, with almost total condensation from N:P ratio 8 onwards.

NCTC-929 cells were transfected with RALA/Cy3-ASO in reduced serum and complete media, showing transfection efficiencies at least of 90% for both media, with fluorescence intensity being significantly higher for cells transfected in reduced serum. Viability of cells transfected in serum showed a gradual increase as N:P ratio increased from 1 to 6 and then a gradual decrease until N:P ratio 12. Whereas viability of cells transfected in complete media was comparable to the control. These results could indicate that ASO are transfected in a sufficient amount in serum to promote an increase in cell viability owing to the effect that miR-31 has in cell proliferation (8). Whereas cells transfected in complete medium do not incorporate a sufficient amount of ASO to promote this effect.

Conclusion

RALA/ASO has shown promise to constitute an advanced genetic nanomedicine to treat impaired wound healing. Herein, RALA successfully condensed miR-31 ASO into NP with a particle size of 150 nm and a net positive zeta potential, which facilitated cellular uptake into NCTC-929 fibroblast cells. Further studies will include confocal microscopy, ELISA, wound scratch assays and tubule formation assays to determine device performance for wound healing applications. Finally, a biodegradable-based polymer blend will be electrospun to produce NF, which will be eventually used to encapsulate RALA/ASO. The ability of the NP-loaded NF patch to promote wound healing will be assessed using *in vitro* an *in vivo* studies.

References

(1) Takeo et al., Cold Spring Harb Perspect Med,5(1): a023267, 2015
(2) Nussbaum et al., Value Health,21(1):27-32, 2018
(3) Alberti et al., Curr Pharm Des,23(24):3515–28, 2017
(4) Hamdam et al., ACS Cent Sci,3(3):163–75, 2017
(5) Banerjee et al., Adv Exp Med Biol,888:291–305, 2015
(6) McCarthy et al., J Control Release,189:141-9, 2014
(7) Mahon et al., Genes Dev.,15(20):2675-86, 2001
(8) Li et al., J. Invest. Dermatol.,135(6):1676-85, 2015
(9) Chen et al., Nanomedicine.,12(11):1335–52. 2017

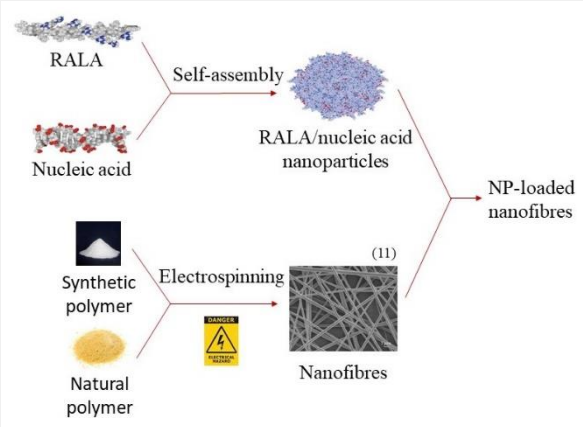

Production of nanoparticle-loaded electrospun NF
Diagram showing the milestones required for the production of NF encapsulating RALA/nucleic acid nanoparticles.

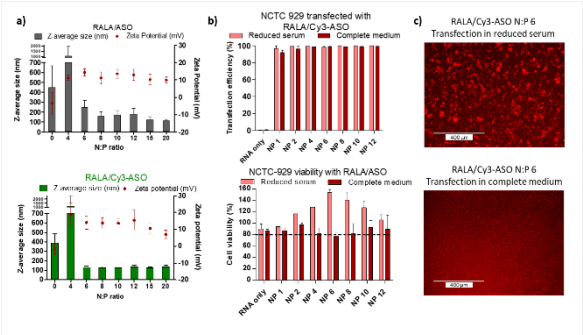

Z-average size, zeta potential and transfection of RALA/ASO and RALA/Cy3-ASO
a) Z-average size and zeta-potential of RALA/ASO and RALA/Cy3-ASO; b) Transfection efficiency of NCTC-929 cells transfected with RALA/Cy3-ASO in reduced serum and complete media, and viability of NCTC-929 cells transfected with RALA/ASO in reduced serum and complete media; c) NCTC-929 under a Texas Red filter after transfection with RALA/Cy3-ASO at N:P ratio 6 in reduced serum and complete media

PS2-15-461

Anti-inflammatory wound dressings improve healing in a diabetic porcine model

Lucas Schirmer, Passant Atallah, Uwe Freudenberg, Carsten Werner

Leibniz-Institut für Polymerforschung Dresden e.V., Max Bergmann Center of Biomaterials Dresden, Dresden, DE

Introduction

In the US alone more than 6.5 million patients are suffering from chronic wounds [1–4]. While the exact cause for chronic wounds remains mostly unknown [6], a persistent inflammatory state characterized by increased amounts of inflammatory cytokines and chemokines have been described [10,11]. The resulting unrestrained inflammatory response impairs the resolution of the inflammation and therefore the progression of the wound into a healing stage. Biohybrid starPEG-heparin hydrogels have previously been demonstrated to offer a possible therapeutic tool to control the imbalance of inflammatory and regenerative signaling mediators in wound healing[12]. These biomaterials were tailored to utilize the strong affinity between glycosaminoglycans, such as heparin, and pro-inflammatory chemokines to selectively scavenge these chemoattractant factors from the wound and thus neutralize their activity. In here, we applied composite dressings made of a textile support and starPEG-heparin coatings on top to the chronic porcine excision wounds, which closely resemble human skin physiology, and assessed the capacity to promote wound closure and tissue repair.

Experimental Methods

The binding capacity of the materials were assessed by incubating the hydrogel composite discs with a range of cytokines relevant in the wound environment for 24 h and the remaining quantities in the supernatants were quantified by multiplex bead-based immunoassay (Thermo). To evaluate the in vivo effects of the hydrogel-based chemokine scavenging, streptozotocin-treated female Danish X Large White Crossbred pigs were inflicted with 2x2cm full thickness wounds. Following the excision starPEG- glycosaminoglycan hydrogels composites were placed on the wounds and covered with a transparent adhesive semipermeable film dressing (Hartmann). After 28 days the wound tissue was harvested, fixated in 4% formaldehyde (Sigma Aldrich), embedded in paraffin, sectioned in the middle of the wound and histologically analyzed to evaluate the overall tissue structure, collagen deposition, angiogenesis and immune cell presence in the wound.

Results and Discussion

To attract cells, chemokines form a gradient by binding to the glycosaminoglycans of the surrounding extracellular matrix [26]. Based on the selective and robust interaction between negatively charged glycosaminoglycans and various chemokines [27,28], we build a hydrogel composite material that utilized selectively desulfated heparin derivatives to scavenge and inactivate chemokines, while leaving growth factor levels nearly unaffected (Figure 1). After 24h incubation of the scaffolds with the signaling mediator cocktail, the N-desulfated heparin hydrogels bound nearly 80% of the IL-8 and MCP-1 from solution, while the 6ON-desulfated heparin did sequester a slightly lower quantity of 70% for both mediators, (Figure 2, left). The effects of the heparin-based hydrogel composites on chronic non-healing wounds were analyzed with 4 cm^2 full thickness excision wounds in the diabetic pigs. After 28 days, an increased closure rate could be observed in the wounds treated with the heparin-based wound dressing (Fig 2, left), which supported nearly full wound closure in all treated animals 28 days post wounding. In addition to the faster wound

closure, increased collagen deposition was observed by Masson Trichrome stain as well as increased vascularization depicted by the immunohistological stain against CD31.

Conclusion

Through the selective binding of inflammatory chemokines by glycosaminoglycan-based scaffolds, the wound signaling environment could be modulated to a more pro-regenerative state. Consequently, inflammation in the wound is resolved, facilitating the formation of new tissue and accelerating angiogenesis in the porcine diabetic wound. The high relevance of the pig wounds to human wounds provides evidence of the high potential for the clinical translation of the developed heparin-based hydrogels which can pave the way to more etiologically defined regeneration strategies for wound healing. Certainly, the strategy of selective chemokine scavenging to balance the inflammatory signaling environment could ultimately benefit for other diseases, such as multiple sclerosis, respiratory diseases (e.g., asthma) or atherosclerosis, as a new opportunity for therapeutic intervention [17].

References

1. Reiber, G. E. The epidemiology of diabetic foot problems. *Diabet. Med.***13 Suppl 1,** S6-11 (1996).

2. Singh, N., Armstrong, D. G. & Lipsky, B. A. Preventing Foot Ulcers in Patients With Diabetes. *JAMA***293,** 217 (2005).

3. Menke, N. B., Ward, K. R., Witten, T. M., Bonchev, D. G. & Diegelmann, R. F. Impaired wound healing. *Clin. Dermatol.***25,** 19–25 (2007).

4. Sen, C. K. *et al.* Human skin wounds: A major and snowballing threat to public health and the economy: PERSPECTIVE ARTICLE. *Wound Repair and Regeneration***17,** 763–771 (2009).

5. Wicke, C. *et al.* Aging influences wound healing in patients with chronic lower extremity wounds treated in a specialized wound care center. *Wound Repair Regen.* (2009). doi:10.1111/j.1524-475X.2008.00438.x

6. Eming, S. A., Martin, P. & Tomic-Canic, M. Wound repair and regeneration: mechanisms, signaling, and translation. *Sci. Transl. Med.***6,** 265sr6 (2014).

7. Loots, M. A. *et al.* Differences in cellular infiltrate and extracellular matrix of chronic diabetic and venous ulcers versus acute wounds. *J. Invest. Dermatol.***111,** 850–7 (1998).

8. Eming, S. A., Krieg, T. & Davidson, J. M. Inflammation in wound repair: molecular and cellular mechanisms. *J. Invest. Dermatol.***127,** 514–25 (2007).

9. Diegelmann, R. F. & Evans, M. C. Wound healing: an overview of acute, fibrotic and delayed healing. *Front. Biosci.***9,** 283–289 (2004).

10. Beidler, S. K. *et al.* Inflammatory cytokine levels in chronic venous insufficiency ulcer tissue before and after compression therapy. *J. Vasc. Surg.***49,** 1013–1020 (2009).

11. Mast, B. A. & Schultz, G. S. Interactions of cytokines, growth factors, and proteases in acute and chronic wounds. *Wound Repair Regen.***4,** 411–20 (1996).

12. Lohmann, N. *et al.* Glycosaminoglycan-based hydrogels capture inflammatory chemokines and rescue defective wound healing in mice. *Sci. Transl. Med.***9,** eaai9044 (2017).

13. Sullivan, T. P., Eaglstein, W. H., Davis, S. C. & Mertz, P. The pig as a model for human wound healing. *Wound repair Regen.***9,** 66–76 (2001).

14. Velander, P. *et al.* Cell Suspensions of Autologous Keratinocytes or Autologous Fibroblasts Accelerate the Healing of Full Thickness Skin Wounds in a Diabetic Porcine Wound Healing Model. *Wound Repair Regen.***16,** 288–293 (2009).

15. Hackl, F., Kiwanuka, E., Nowinski, D. & Eriksson, E. The Diabetic Wound: A New Experimental Wound Healing Model in Large Animals. *Adv. Wound Care Vol. 2* 27–166 (2011). doi:doi:10.1089/9781934854280.166

16. Trengove, N. J. *et al.* Analysis of the acute and chronic wound environments: the role of proteases and their inhibitors. *Wound Repair Regen.***7,** 442–52 (1999).

17. Gerard, C. & Rollins, B. J. Chemokines and disease. *Nat. Immunol.***2,** 108–115 (2001).

Acknowledgement

This work was funded by the German Research Council (DFG SFB-TR67). We like to thank Mikhail Tsurkan, Mila Grimmer and Nelly Rein for their major support and providing the materials this study was based on.

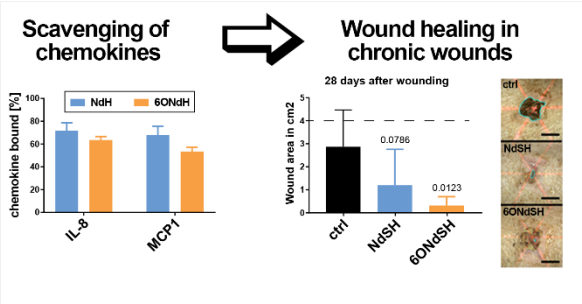

Figure 2:
Left: Scavening of IL-8 and MCP-1 into the GAG-based hydrogel dressing after 24 hours. Right: Wound area of excisional wounds in diabetic pigs after 28 days of treatment. Line represents initial area at day 0. Bars represent mean +/- SD. n=6.

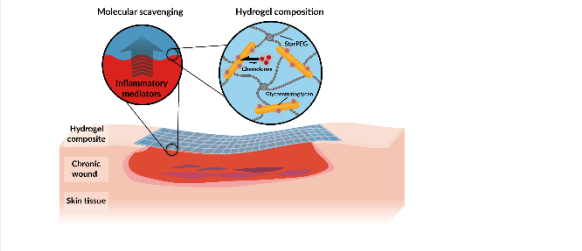

Figure 1:
Mechanism of chemokine scavenging by starPEG-Glycosaminoglycan based hydrogel dressing

PS2-15-462

In situ Photocrosslinkable Hyaluronic Acid-Based Surgical Glue with Tunable Mechanical Properties and High Adhesive Strength

Sodam Kim[1], **Ajeesh Chandrasekharan**[1], Keum-Yong Seong[1], Sang-Gu Yim[1], Sungbaek Seo[1], Jinhwan Yoon[2], Seung Yun Yang[1]

[1]Pusan National University, Department of Biomaterials Science, Miryang, KR; [2]Pusan National University, Department of Chemistry Education, Busan, KR

Introduction

Tissue adhesives are emerging as an alternative or adjunct to sutures and staples for wound closure owing to their ease of preparation and application, strong adhesion to the wound site, and effective sealing of body fluids[1]. The glue-type tissue adhesives have recently gained attention as they can flow into the wound cracks providing strong adhesion between the tissues and the glue, effectively preventing leakage of body fluids[2,3]. In addition, it can be prepared in situ, and the mechanical properties can be tuned to suit the surrounding tissue, which enables it to be used for tissues with different geometry and dimensions. However, limitation of commercially available cyanoacrylate-based adhesives still has certain limitations such as poor flexibility, weak adhesion in wet and dynamic conditions, and a toxic degradation product, which limits its application to only topical use[4]. Taking into consideration the limitations exhibited by the currently available tissue adhesives on the market, there is a need for a tissue adhesive that has strong adhesion to the tissue under wet and dynamic conditions for a long period of time to allow for wound healing. In this work, we engineered an in situ photocrosslinkable tissue adhesive based on hyaluronic acid, a well-known biopolymer. Hyaluronic acid (HA), a naturally occurring linear polysaccharide, has been widely used as a key biomaterial in a range of scarless wound healing processes and therapeutic applications[5,6]. Its excellent biocompatibility and bio-functions related to tissue regeneration encourage the development of HA-based hydrogels to expand its applications. This study details an in situ forming surgical glue based on photocrosslinkable HA, providing tunable mechanical properties and firm tissue adhesion under wet and dynamic conditions.

Experimental Methods

HAMA with a low and high degree of methacrylation (DM) was synthesized and confirmed by ^{1}H NMR. First, the mechanical properties of hyaluronate methacrylate (HAMA) hydrogels prepared from different concentration (5%, 10%, and 20% (w/v)) of precursor solutions at a low and high DM were investigated using a tensile test to evaluate its tunability. Then, we evaluated the adhesive properties of the HAMA hydrogels produced from a high DM. The results were compared to that of the gelatin methacrylate (GelMA) hydrogels produced from a high DM. Its mechanical and adhesive properties were investigated by several standard tests including the tensile test, in vitro wound closure test, and lap shear test. Finally, to determine the adhesion capability of the HAMA hydrogels under wet and dynamic conditions, the HAMA hydrogels photocrosslinked to porcine skin were placed under wet and dynamic conditions and their survival on the porcine skin was recorded for several weeks.

Results and Discussion

Photocrosslinkable methacrylate groups are generally incorporated into an HA polymer backbone by reacting it with MA under aqueous basic conditions. This suggested HAMA hydrogels exhibited relatively higher stiffness. Nevertheless, comparing the overall mechanical properties of the HAMA and GelMA hydrogels produced from a high DM, the engineered HAMA hydrogels have better cohesive properties. For adhesives consisting of hydrophilic

polymers, HAMA hydrogels were more than ~3.2-fold higher than that of the reported value for fibrin glue (4.0 kPa), which is one of the most widely used biologically derived adhesives in clinical applications[7]. Next, we conducted ex vivo tests to determine the adhesion capability of HAMA hydrogels under wet and dynamic conditions similar to that of the physiological conditions (salt and temperature). Most parts of the hydrogel remained intact until 3 weeks. These results suggest strong adhesion to the porcine skin as well as the stability of 10% (w/v) and 20% (w/v) HAMA hydrogels under wet and dynamic conditions. Swelling of hydrogels in wet environments could lead to a decrease in mechanical strength and subsequently breakage of the hydrogel[8]. Because of the limited water uptake in the highly crosslinked hydrogels[9], HAMA hydrogels, especially prepared from high polymer concentration, would undergo less swelling and thus are expected to have good mechanical stability at the wound site. Thus, hydrogels prepared from higher concentrations of HAMA solutions are expected to last longer in physiological environments.

Conclusion

In this work, we have developed an in situ photocrosslinkable tissue adhesive based on HA. Although cytotoxicity and biocompatibility need to be investigated to transfer this work into clinical applications, the tunable mechanical properties, as well as strong adhesion to porcine skin under both dry and wet conditions, makes HAMA an ideal candidate for tissue adhesive applications.

References

1. N. Annabi, Y.-N. Zhang, A. Assmann, E. S. Sani, G. Cheng, A. D. Lassaletta, A. Vegh, B. Dehghani, G. U. Ruiz-Esparza, X. Wang, S. Gangadharan, A. S. Weiss, A. Khademhosseini. Sci. Transl. Med. 2017, 9, eaai7466.
2. N. Annabi, D. Rana, E. S. Sani, R. Portillo-Lara, J. L. Gifford, M. M. Fares, S. M. Mithieux, A. S. Weiss. Biomaterials 2017, 139, 229.
3. C. Ghobril, M. Grinstaff. Chemical Society Reviews 2015, 44, 1820.
4. F. Leonard, R. K. Kulkarni, G. Brandes, J. Nelson, J. J. J. Cameron. J. Appl. Polym. Sci. 1966, 10, 259.
5. J. Voigt, V. R. Driver. Wound Repair Regen. 2012, 20, 317.
6. M. Etscheid, N. Beer, J. Dodt. Cell. Signal. 2005, 17, 1486.
7. O. Jeon, J. E. Samorezov, E. Alsberg. Acta biomater. 2014, 10, 47.
8. B. Johnson, D. Beebe, W. Crone. Materials Science and Engineering: C 2004, 24, 575-581.
9. E. A. Kamoun, E.-R. S. Kenawy, X. Chen. Journal of advanced research 2017, 8, 217-233.

Acknowledgement

This research was supported by the National Research Foundation of Korea (NRF) funded by the Ministry of Science and ICT (NRF-2018R1A4A1025623), the Tech Incubator Program For Startup (TIPS) (201738070002) funded by the Ministry of SMEs and Startups (MSS, Korea).

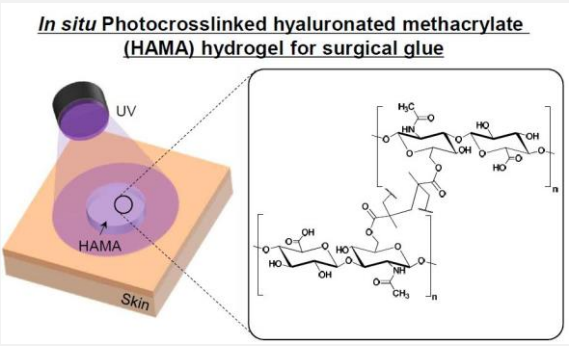

In situ photocrosslinked hyaluronated methacrylate hydrogel for surgical glue

This study details an *in situ* forming surgical glue based on photocrosslinkable HA, providing tunable mechanical properties and firm tissue adhesion under wet and dynamic conditions.

PS2-15-463

Physical and biological properties of newly developed thermally cross-linked gelatin film for anti-adhesion material with peritoneal regeneration

Tsunehito Horii[1,2], Hiroyuki Tsujimoto[1,2], Kazuyoshi Jonin[2], Masayuki Nagasawa[2], Kenichi Kobayashi[2], Toshitaka Takagi[1], Yoshito Ikada[1], Akeo Hagiwara[2], Akihiro Kawauchi[2]

[1]Doshisha University, Department of Life and Medical Science, Division of Medical Life System, Kyotanabe, JP; [2]Shiga university of medical science, Department of Urology, Seta, JP

Introduction

Currently, hyaluronic acid and carboxymethyl cellulose film is most conventionally used in clinical setting as an anti-adhesion material (the conventional film). The conventional film reduces adhesion by acting as a mechanical barrier to separate the adjacent traumatized serosa during the critical period of re-peritonization. However, the conventional film hasn't decreased the incidence of bowel obstruction in clinical trials, although it reduced the incidence of severe cases requiring re-operation. In addition, the film has several disadvantages, such as difficulty in handling because of its fragility and the potential risk of anastomotic leakage. Indeed, several studies have reported that leakage occurred more frequently when the conventional film was wrapped directly along the suture or staple line of bowel anastomosis.

In order to create more excellent anti-adhesion materials, we developed a thermally cross-linked gelatin film. Gelatin is a denatured form of collagen, which is included in connective tissues of human and animal bodies, made by heat denaturation and bio-absorbable materials hydrolyzed by enzymes. The purpose of this study is to reveal the handling properties, anti-adhesion effect and revealing the anti-adhesion mechanism.

Experimental Methods

we examined physical strength (tensile test under dry and wet condition) and the adhesiveness to tissues (pull adhesive test, shearing stress test). Moreover, in order to reveal the anti-adhesion mechanism, we examined the biological properties such as the anti-adhesion effect, the influence on cell proliferation and the cytotoxicity, especially in comparison with the conventional film.

Results and Discussion

In the present study, the maximum tensile stress of the gelatin film under dry conditions was twice higher than that of the conventional film. In addition, the tensile stress of the gelatin film under wet conditions was five times higher than that of the conventional film. These results indicated that the gelatin film has better physical strength than the conventional film under both dry and wet conditions. In addition, the maximum fracture strain of the gelatin film was significantly higher than that of the conventional film. The result suggested that the gelatin film had better ductility at least under dry condition than the conventional film. In the pull adhesion test, there was no significant difference in the maximum adhesive stress between the two films. However, in the shear stress test associated with both the physical strength and the adhesiveness of the materials, the shear load of the gelatin film was higher than that of the conventional film. From these results, we consider that gelatin film can provide better handling than the conventional film, due to its excellent physical strength and ductility.

The results of anti-adhesion effect test showed significantly much lower adhesion scores of the gelatin film than the conventional film, although the scores of the conventional film were significantly lower than that of the control. This result indicates that gelatin film has a more excellent anti-adhesive effect than the conventional film.
To clarify the mechanisms underlying the difference in the anti-adhesion effect between the two films, we conducted a cell proliferation test on each film using fibroblasts at first. In the result, the cell numbers on the gelatin and the conventional films were significantly lower than in the control (no material), suggesting that both films achieve their anti-adhesion effect by suppression of fibroblast proliferation on the films. Interestingly, the cell proliferation on the gelatin films increased at each time point after culturing for 1, 3, 5, and 7 days, while no proliferation was observed on the conventional film during culturing. In our previous and preliminarily studies, both the gelatin and the conventional films dissolved mostly within one week in both in vitro and in vivo degradation tests. Therefore, the difference in the cell proliferation between the films may be associated with their cytotoxicity.
To address this issue, we conducted further cytotoxicity test using a colony assay and Live/Dead assay. In the colony assay, the colony-forming rate of the gelatin film was not different from that of the control. However, the colony-forming rate of the conventional film was markedly low, especially at higher extract concentrations. Furthermore, in the Live/Dead assay, the cell viability with the gelatin film extract was almost 100%. In contrast, the cell viability with the conventional film extract decreased by 50%. These results suggest that the conventional film has cytotoxicity in extract form, whereas the gelatin film does not.

Conclusion

Therefore, the gelatin film provides better handling than the conventional film, due to better physical strength and ductility of the film. In addition, the gelatin film has a significantly greater anti-adhesion effect than the conventional film without any cytotoxicity.

References

1. Brian CW, Alyssa P. Abdominal Adhesions: Current and novel therapies. J Surg Res 2011;165:91-111.
2. Beck DE, Opelka FG, Bailey HR, Rauh SM, Pashos CL. Incidence of small-bowel obstruction and adhesiolysis after open colorectaland general surgery. Dis Colon Rectum 1999;42:241–248.
3. Swank DJ, Swank-Bordewijl SCG, Hop WCJ, Van Erp WFM, Janssen MC, Bonjer HJ, Jeekel J. Laparoscopic adhesiolysis in patients with chronic abdominal pain: a blinded randomized controlled multi-centre trial. The Lancet 2003;361:1247-1251.
4. Caspi E, Halperin Y, Bukovsky I. The importance of peri-adnexal adhesions in tubal reconstructive surgery for infertility. Fertil Steril 1979;31:296-300.
5. Gere SZ. Biochemical events in peritoneal tissue repair. Eur J Surg 1997;577:10-16.
6. Genevieve M. Boland BA, Ronald JW. Formation and prevention of postoperative abdominal adhesions. J Surg Res 2006;132:3-12.
7. Michel PD, Ellen LB, Beverly A, Sadiqa M, Lena H. Seprafilm® adhesion barrier: (1) a review of preclinical animal, and human investigational studies. Gynecol Surg 2012;9:237-245.
8. James MB, Merril TD, Victor WF, David EB, Steven JS, Steven DW, Bruce GW, Patricia LR, Lee ES, Sharon AS, Maricia M. Prevention of postoperative abdominal adhesions by a sodium hyaluronate-based bioresorbable membrane: a prospective, randomized, double-blind multicenter study. J Am Coll Surg 1996;183:297-306.
9. David EB. The role of seprafilm™ bioresorbable membrane in adhesion prevention. Eur J Surg 1997;577:49-55.
10. Victor WF, Zane C, James WF, Harry G, Joel JB, Bruce GW, Marvin C, Robert WB, Steven DW, James MB, John RTM, Howaed SK, David EB, Randolph HB, Kirk AL, Michael JS, Ara D, Ronald B, Richard D, Robert DM, Lee ES, Susan G, Keith L, Jonas G. Reduction in adhesive small-bowel obstruction by seprafilm® adhesion barrier after intestinal resection. Dis Colon Rectum 2005;49:1-11.

11. Wietske WV, Larissa NLT, Heert JME, Wim CJH, Jack JJ, Piet L, Laurents PSS, Dingeman JS, Robert H, Jaap HB, Hans J. Fewer intraperitoneal adhesions with use of hyaluronic acid-carboxymethylcellulose membrane. Annals of Surg 2002;235:193-199.
12. Takeuchi H, Kitade M, Kikuchi I, Shimanuki H, Kinoshita K. A novel instrument and technique for using seprafilm hyaluronic acid/ carboxymethylcellulose membrane during laparoscopic myomectomy. JLAST 2006;16:497-502.
13. David EB, Zane C, James WF, Howard SK, Harry G, Bruce GW.A prospective, randomized, multicenter, controlled study of the safety of seprafilm® adhesion barrier in abdominopelvic surgery of the intestine. Dis Colon Rectum 2003;46:1310-1319.
14. Tsujimoto H, Tanzawa A, Matoba M, Hashimoto A, Suzuki S,Morita S, Ikada Y, Hagiwara A.The anti-adhesive effect of thermally cross-linked gelatin film and its influence on the intestinal anastomosis in canine models. J Biomed Mater Res Part B 2013;101B:99-109.
15. Tsujimoto H, Tanzawa A, Miyamoto H, Horii T, Tsuji M, Kawasumi A, Tamura A, Wang Z, Abe R, Tanaka S, Yamanaka K, Morita S, Ikada Y, Hagiwara A. Biological properties of a thermally crosslinked gelatin film as a novel anti-adhesive material: relationship between the biological properties and the extent of thermal crosslinking. J Biomed Mater Res Part B 2014.
16. Mukai T, Kamitani S, Shimizu M, Tsutamoto Y, Endo Y, Hanasawa K, Tani T. Development of a novel, nearly insoluble antiadhesive membrane. Eur Surg Res 2011;47:248-253.
17. Falabella AC, Melendez MM, Weng L, Chen W. Novel macromolecular crosslinking hydrogel to reduce intra-abdominal adhesions. J Surg Res 2010;159:772-778.
18. Kelekci S, Uygur D, Yilmaz B, Sut N, Yesildaglar N. Comparison of human amniotic membrane and hyaluronate/carboxymethylcellulose membrane for prevention of adhesion formation in rats. Arc Gyn Obs 2007;276:355-359.
19. Bayar H, Ryusuke N, Toshie T. Safety evaluation of surgical materials by cytotoxicity testing. J Artif Organs 2008;11:204-211.
20. Sharon MR, Barbara AM. Cytochemical analysis of pollen development in wild-type arabidopsis and a male-sterile mutant. The Plant Cell 1990;2:877-889

Acknowledgement
None of authors have any conflicts of interest to declare.

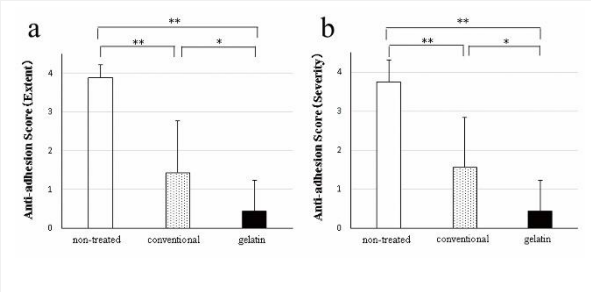

The results of anti-adhesion effect test.
(a) Anti-adhesion score (Extent)
(b) Anti-adhesion score (Severity)
*: $p<0.05$, **: $p<0.01$

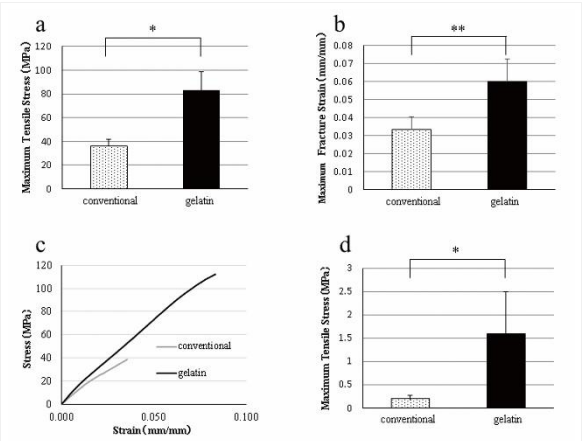

The results of tensile tests.
(a) Maximum tensile stress in dry condition
(b) Maximum fracture strain in dry condition
(c) Stress-strain diagram in dry condition
(d) Maximum tensile stress in wet condition
*: $p<0.05$, **: $p<0.01$

PS2-15-464

Conceptual and Practical Considerations In The Development of a Keloid Scar-Inhibiting Dermal Replacement Scaffold

Stuart J. Brown, Elena Garcia-Gareta

The Restoration of Appearance and Function Trust, Regenerative Biomaterials group, London, GB

Introduction

Keloid scars are unsightly and uncomfortable epidermal growths which result from a dysfunctional wound healing process[1]. Small keloids can be treated with physical dressings, topical creams or by injection, with the intent to curtail further growth and manage symptoms. These approaches have varying success and aim at management rather than removal, so are not a cure. Direct excision via surgery is complicated by keloid scars' notoriously high chance of recurrence, so is combined with chemotherapy, laser therapy or radiotherapy to discourage this. These treatments can lead to cure, but are costly, time consuming, and require specialist facilities and expertise.

The development of new treatments requires better understanding of the molecular and cellular biology of keloid scarring. The keloidal mass features a hypoxic core containing a persistently activated and apoptosis-resistant population of pathological keloid fibroblasts (FBs)[2]. These recruit and activate other cells, inducing excess production of collagen, cellular proliferation and expansion of the keloidal mass. The factors underlying formation of this structure during normal wound healing are incompletely understood, and several possible underlying initiating cellular and molecular causes have been outlined[3]. How these differ from keloid to keloid, and from patient to patient, is an important consideration for new treatment development.

One factor hindering research is the difficulty in obtaining keloid samples to test new treatments. From 1997 to 2003, the Restoration of Appearance and Function Trust (RAFT) stored keloid FBs from patients undergoing treatment at the plastic surgery unit at Mount Vernon Hospital, resulting in 30 potential individual primary kFB strains. These cells are being characterised and expanded to develop a distributable cell bank resource to aid keloid research, both at RAFT and in the wider community, and could model the potential of new treatments in different types of keloids.

We aim to use this resource to create a dermal replacement scaffold engineered to reduce keloid recurrence, for use after surgical removal of the keloid mass. Our approach would aim to prevent re-colonisation of the disease site with kFBs, whilst permitting the influx of a patient's normal primary fibroblasts from surrounding areas using a cell-selective dermal matrix. Cell-selective biomaterials have a rich history in other applications such as bioabsorbable stents.

Experimental Methods

Initial culture

Keloid fibroblast cell lines were created by expansion from low passage initial biopsy cultures via standard methods in supplemented DMEM. The Keloid Cell Bank was created following the principles set out by Geraghty et al.[4] Mycoplasma-free status was confirmed by PCR assay.

Cell identity

PCR assay using HeLa microsatellite genetic markers was used to rule out the possibility of historic cross-contamination. The expression of fibroblast differentiation markers and structural proteins was demonstrated by Western blot, to rule out labelling errors with contemporaneous archival cells.

Proliferation and metabolism

Cell line replication and metabolism was determined by direct cell count in Haemocytometer and by metabolic reduction of AlamarBlue colorimetric reagent. The kinetics of cell growth in its phases of recovery, conditioning, exponential growth and contact inhibion was studied by plating at different cell densities. Metabolic assays were used to determine inter-cell line hetereogeneity by low density multiwell cell plating and examination of significantly metabolically more active wells.

Colonization of dermal scaffolds

The ability of kFBs to colonise natural polymer dermal scaffolds was assessed, both alone and in combination with primary dermal fibroblasts. Cell attachment and viability was demonstrated by reduction of Alamarblue reagent.

Results and Discussion

It is widely reported that Keloid FBs are more proliferative and metabolically active than normal human dermal FBs, but evidence is mixed in the literature, and may represent underlying variation in keloid biology. Keloid FBs have distinct proliferation kinetics to normal human DFs. Individual Keloid cell lines showed greater variation with both higher and lower proliferation and metabolism rates than normal human dermal fibroblast controls.

Keloid FB cell lines also showed greater inter-cell line heterogeneity than controls, suggesting that certain cells within the swarm cause abnormal paracrine effects.

Keloid FBs showed a greater avidity for a fibrin, rather than collagen, based scaffolds, unlike normal human dermal fibroblasts.

Conclusion

This work establishes functional similarities between independently derived kFBs, and how these differ from normal primary human fibroblasts, which could be exploited to preferentially select one over the other using a selective matrix.

References

1. Al-Attar, A., Mess, S., Thomassen, J. M., Kauffman, C. L., & Davison, S. P. (2006). Plastic and Reconstructive Surgery, 117(1), 286–300
2. Kischer CW. The microvessels in hypertrophic scars, keloids and related lesions: a review. J Submicrosc Cytol Pathol [Internet]. 1992 Apr;24(2):281–96
3. Mari W, Alsabri SG, Tabal N, Younes S, Sherif A, Simman R. Novel Insights on Understanding of Keloid Scar: Article Review. J Am Coll Clin Wound Spec [Internet]. 2015 Dec;7(1–3):1–7
4. Geraghty RJ, Capes-Davis A, Davis JM, Downward J, Freshney RI, Knezevic I, et al. Guidelines for the use of cell lines in biomedical research. Br J Cancer [Internet]. 2014 Sep 9 [cited 2019 Jan 11];111(6):1021–46

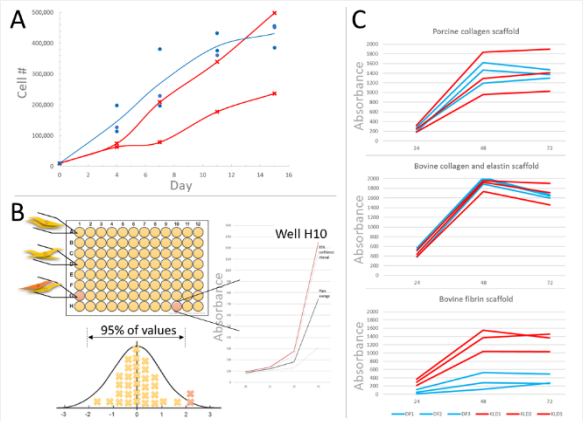

Figure 2: Characteristics of Normal Human Dermal Fibroblasts (Blue) and Keloid-derived Fibroblasts (Red). A) Proliferation in cell culture, B) Intra-cell line heterogeneity assays uncovers Keloid fibroblast paracrine signalling, C) Attachment and cell activity on natural polymer scaffolds

The Cellular Characteristics of Keloid Fibroblasts

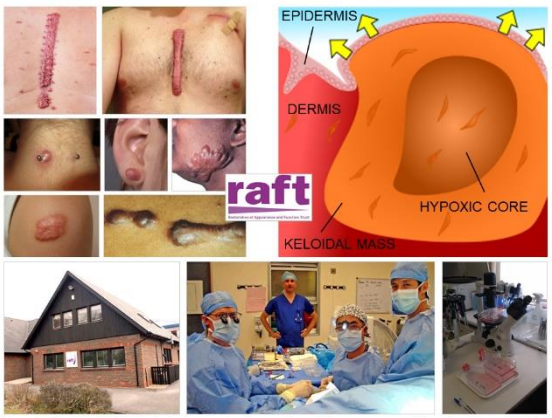

Figure 1: The Keloid Cell Bank Project at the Restoration of Appearance and Function Trust. Keloids are pathological scars of heterogeneous structure that appear after insult to the skin. Our archival samples collected by the RAFT plastic surgery team form the basis of the bank.

The RAFT Keloid Cell Bank

2:45 p.m. – 3:45 p.m.

Hall 1 / Exhibition Area

PS2-16 | Immunomodulatory biomaterials

PS2-16-465

Myofibroblast Behavior Controlled by Macrophages in a 3D *in vitro* Coculture Model

Franziska Ullm, Katja Franke, **Tilo Pompe**

Leipzig University, Institute of Biochemistry, Leipzig, DE

Introduction

Persistent inflammation during dermal wound healing is often associated with impaired repair and dysfunction of the regenerated tissue and is often attributed to cell-cell and cell-matrix miscommunication. The underlying mechanisms are still insufficiently understood. 3D i*n vitro*models offer striking opportunities to study these interactions by allowing to mimic microstructure, mechanics and molecular composition of the extracellular microenvironment at pathological and physiological situations. We developed a modular matrix engineering platform based on fibrillar 3D collagen I matrices, which facilitates detailed examinations of various cell-cell interactions *in vitro*. In the present study we applied it to the analysis of the interaction between primary human fibroblasts (FB) and macrophages (MΦ) during early as well as late stages of wound healing.

Experimental Methods

Our model system is based on fibrillary 3D matrices reconstituted from collagen I. Pore size, fibril diameter and matrix stiffness were adjusted by reconstitution conditions and optional modifications by subsequent cross-linking or functionalization with other ECM molecules, e.g. glycosaminoglycans (GAGs) or fibronectin, as previously shown in other studies.[1,2,3] Primary human dermal FB and human monocyte-derived MΦ were examined in their response to these matrices in coculture studies over 6 days. MΦ were either polarized into inflammatory or regulatory phenotype, achieved by distinct differentiation protocols after isolation. Cells were seeded inside the 3D matrix during collagen matrix reconstitution. FB were optionally stimulated by TGF-β_1 to trigger a myofibroblasts (MyoFB) differentiation.
We analyzed changes in cell distribution and matrix properties over the time course of the coculture study. Proliferation behavior of FB was examined using commercial WST-1 assay.
Gene expression analysis of markers of MyoFB phenotype (αSMA, matrix protein synthesis) and immunofluorescence of αSMA incorporation into the actin stress fibers were used to study FB differentiation and dedifferentiation. We further determined IL-10 cytokine secretion using ELISA.

Results and Discussion

Inclusion of cells during collagen matrix reconstitution did not alter matrix properties in terms of pore size, fibril diameter and elasticity. Moreover, homogeneous distribution of cells remained stable during cultivation time. Coculture experiments of MyoFB and regulatory M2-MΦ revealed a dose-dependent regulation of MyoFB proliferation and differentiation. Proliferation of MyoFB increased whereas the total amount of MyoFB decreased in dependence on the amount of cocultivated regulatory M2-MΦ. The analysis of gene expression related to the formation of new ECM proteins (Coll I; Coll III and EDA-FN) confirmed these results of altered MyoFB phenotype. Additionally, regulatory M2-MΦ were shown to be the main source of secreted IL-10 cytokine. These findings indicated a direct paracrine impact of IL-10 secreted from M2-MΦ to the ascending de-differentiation of MyoFB in coculture.

Additional experiments with inflammatory M1-MΦ demonstrated a converse effect. Gene expression data showed a dose-dependent increase of MyoFB characteristic gene expression with cocultivated inflammatory M1-MΦ and a persistent MyoFB phenotype. IL-10 secretion of M1-MΦ in the absence of MyoFB was generally low, whereas the presence of MyoFB led to a dose-dependent increase of IL-10 in the supernatant, indicating additional paracrine effects of MyoFB on inflammatory M1-MΦ.

Conclusion

In sum, our 3D collagen I based matrices resemble a highly relevant biomimetic model of early and late stages of wound healing with a control of proliferation and differentiation of MyoFB by MΦ in coculture.
Perspective experiments will uncover the regulation of the paracrine IL-10 and TGF-$\beta_1$signal exchange between both cell types by an interaction with GAG-modified 3D matrices.

References

1. Sapudom, J et al. *Biomaterials* 52:367-75 (2015).
2. Sapudom J, et al. *Biomater Sci* 3:1291 (2015).
3. Kalbitzer L, et al. *J Mater Chemistry B* 3:8902-10 (2015).

Acknowledgement

This study was supported by Deutsche Forschungsgemeinschaft grant (SFB/TRR67 project B10). The authors would like to thank Ronald Weiß and Sunna Hauschildt as well as Ulf Anderegg (Universitätsklinikum Leipzig) for support in cell culture.

PS2-16-467

The dynamic protein corona influences immune-modulating osteogenesis in magnetic bone regeneration scaffolds *in vivo*

Yao Wu

Sichuan University, National Engineering Research Center for Biomaterials, Chengdu, CN

Introduction

The inflammatory reaction initiates fracture healing and directly influences the osteoinductive effect of bone tissue engineering scaffold [1-3], but the underlying mechanism remains to be elucidated. Protein corona as a real biological identity of biomaterial significantly affects the biological function of bone regenerative scaffold [4-5]. Hence, we developed a simple and effective *in vivo* dynamic model for the protein corona of MHA scaffolds to predict the correlation between the inflammatory reaction and bone wound healing, as well as the underlying mechanism governing such process.

Experimental Methods

In this article, the MHA scaffolds were selected as a potential bone substitutes and HA scaffolds were used as control. We implanted the HA and MHA scaffolds into the sites of femoral defect in rats for 15 min, 1 h, 24 h, 7 d, and 14 d to obtain the dynamic protein corona. Then the formation of dynamic protein corona was systematically studied by bicinchoninic acid protein assay kit, sodium dodecyl sulfate polyacrylamide gel electrophoresis and LC-MS/MS analysis. Several bioanalytical tools, such as Uniprot, KEGG and David, were used to further analyze the bound proteins according to biological processes. In addition, the role of inflammatory and immune response in protein corona-mediated osteogenesis was investigated by HE staining and immunocytochemistryof inflammatory cells *in vivo* and the effect of specific inflammatory factors on pre-osteoblast proliferation *in vitro.*

Results and Discussion

The results showed that the proteins related to immune and inflammation, bone and wound healing increased in the protein corona of magnetic nanoparticles (MNPs)-infiltrated scaffolds with time-dependent manner. Meanwhile, the enriched proteins related to immune and inflammation adsorbed on MHA scaffolds correlated well with the significantly enhanced bone wound healing, as suggested by the same variation tendency of proteins related to bone and wound healing, and immune and inflammation (Fig. 1A and B). The presence of MNPs suppressed chronic inflammatory responses and highly promoted acute inflammatory responses. More importantly, the activation of the acute inflammatory responses led to the recruitment of immune cell, remodeling of extracellular matrix and even acceleration of bone healing. After 7 days of implantation, few lymphocytes were observed on the HA scaffold while more lymphocytes were clearly found on the MHA scaffold. The presence of IL-6 and C3 was effective to improve pre-osteoblast cell (MC3T3-E1) proliferation *in vitro* model (Fig. 1C and D). This results further corroborated the critical involvement of inflammatory reaction enhanced bone wound healing.

Conclusion

The dynamic protein corona formed on bone repair scaffolds under the *in vivo* bone repair model plays a significant role in acute inflammation, *i.e.* immune response, and ultimately bone wound healing. Our results highlight the important role of acute inflammation (*i.e.* immune response) on osteogenesis. Up-regulated immune response was

strongly correlated with the significantly enhanced bone wound healing. The current study constitutes a basis for the development of superparamagnetic scaffold biomaterials, exploring the role of the immune response in tissue repair and its potential relevance to magnetic scaffold design.

References

1. Vasconcelos, D. M.; Goncalves, R. M.; Almeida, C. R.; Pereira, I. O.; Oliveira, M. I.; Neves, N.; Silva, A. M.; Ribeiro, A. C.; Cunha, C.; Almeida, A. R.; Ribeiro, C. C.; Gil, A. M.; Seebach, E.; Kynast, K. L.; Richter, W.; Lamghari, M.; Santos, S. G.; Barbosa, M. A., Fibrinogen Scaffolds with Immunomodulatory Properties Promote *in Vivo* Bone Regeneration. Biomaterials 2016, 111, 163-178.
2. Pan, H. H.; Xie, Y. T.; Zhang, Z. Q.; Li, K.; Hu, D. D.; Zheng, X. B.; Tang, T. T., Immunomodulation Effect of a Hierarchical Macropore/Nanosurface on Osteogenesis and Angiogenesis. Biomed. Mater. 2017, 12 (4), 045006.
3. Hao, S. S.; Meng, J.; Zhang, Y.; Liu, J.; Nie, X.; Wu, F. X.; Yang, Y. L.; Wang, C.; Gu, N.; Xu, H. Y., Macrophage Phenotypic Mechanomodulation of Enhancing Bone Regeneration by Superparamagnetic Scaffold Upon Magnetization. Biomaterials 2017, 140, 16-25.
4. Zhu, Y.; Yang, Q.; Yang, M.; Zhan, X.; Lan, F.; He, J.; Gu, Z. W.; Wu, Y., Protein Corona of Magnetic Hydroxyapatite Scaffold Improves Cell Proliferation *Via* Activation of Mitogen-Activated Protein Kinase Signaling Pathway. ACS Nano 2017, 11 (4), 3690-370
5. Serpooshan, V.; Mahmoudi, M.; Zhao, M.; Wei, K.; Sivanesan, S.; Motamedchaboki, K.; Malkovskiy, A. V.; Gladstone, A. B.; Cohen, J. E.; Yang, P. C.; Rajadas, J.; Bernstein, D.; Woo, Y. J.; Ruiz-Lozano, P., Protein Corona Influences Cell-Biomaterial Interactions in Nanostructured Tissue Engineering Scaffolds. Adv. Funct. Mater. 2015, 25 (28), 4379-4389.

Acknowledgement

This work was supported by the National Natural Science Foundation of China (21571134,31771037 and 31600765), the National Key Research and Development Program of China (2016YFC1100403) , the Project in the Science and Technology Support Program of Sichuan Province (18ZDYF), and the Fundamental Research Funds for the Central Universities (2012017yjsy123).

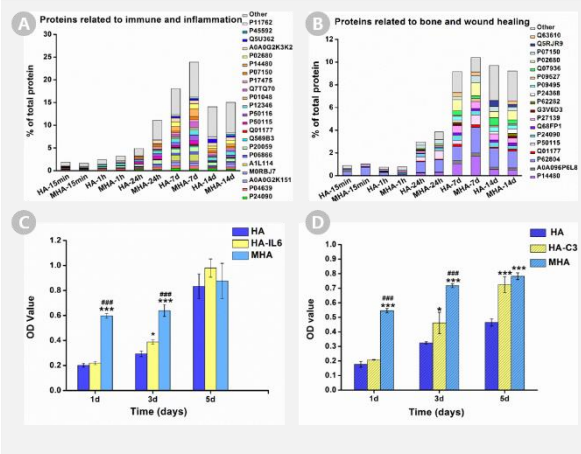

Fig. 1. The dynamic protein corona influences immune-modulating osteogenesis.
A) proteins related to immune and inflammation; B) proteins related to bone and wound healing; The effect of IL-6 and C3 on MC3T3-E1 proliferation: C) CCK-8 assay for proliferation of MC3T3-E1 cultured on HA, HA-IL-6 and MHA for 1, 3 and 5 days; D) CCK-8 assay for proliferation of MC3T3-E1 cultured on HA, HA-C3 and MHA.

PS2-16-468

In Vitro Co-Culture System of Macrophages and Mesenchymal Stromal Cells – an Important Tool for Biomaterial Assessment

Tina Tylek, Carina Blum, Katrin Schlegelmilch, Tatjana Schilling, Jürgen Groll

University Hospital Würzburg, Department for Functional Materials in Medicine and Dentistry, Würzburg, DE

Introduction

Monocytes and the macrophages derived therefrom are important cells of the innate immune system. They participate in the elimination of pathogens by phagocytosis, initiation of inflammatory reactions, and tissue repair. They can differentiate into pro-inflammatory M1 and anti-inflammatory M2 macrophages depending on environmental cues, such as implanted biomaterials [1]. Together with multipotent human mesenchymal stromal cells (hMSCs), they contribute to tissue renewal and anti-inflammatory reactions. Due to these properties, the research about both cell types is of great importance for regenerative medicine and tissue engineering [2]. Besides the cell-cell communication, the interaction of cells with the material is of special interest. Here, the co-culture can provide new insights into the immunomodulatory functions of biomaterials. In this study, we established a functional co-culture system of human monocyte-derived macrophages and human mesenchymal stromal cells (hMSCs) for biomaterial assessment based on the example of 3D porous melt-electrowritten scaffolds.

Experimental Methods

Primary monocytes were isolated from human buffy coats via density gradient centrifugation and negative immunoselection. They differentiated spontaneously into macrophages over a culture period of seven days. HMSCs, derived from trabecular bone, were isolated via plastic adherence. As material, melt-electrowritten 3D scaffolds with mesh widths of 60 µm and 80 µm, respectively, as well as a 2D film made of poly(ε-caprolactone) (PCL) were used. The co-culture of both, 3D and 2D constructs, and thus the cell-cell and cell-material interactions were investigated via direct and indirect (conditioned medium) conditions [3]. Changes in gene and protein expression, cytokine release, phagocytic activity of macrophages as well as the general behavior of both cell types by scanning electron microscopy and fluorescence microscopy were investigated.

Results and Discussion

We have successfully established a model system and protocols for the analysis of the immunomodulated outcome after co-cultivation of human macrophages and hMSCs on 3D porous scaffolds. Thus, we were able to detect changes in gene and protein expression as well as in the cytokine release profile of macrophages cultivated on scaffolds in co- and mono-culture, respectively. Our results suggest, that it is extremely important to evaluate the immunomodulatory response provoked by biomaterials not only based on monocultures, but also in combination with other cell types present in the natural tissue environment. Hence, co-cultures can provide more accurate insights into the biological processes, since they more closely resemble the *in vivo* conditions.

Conclusion

In this work, we focused on a functional co-culture system of human macrophages and hMSCs as a tool for biomaterial assessment. By establishing numerous protocols for the investigation of immunomodulatory effects using the example of 3D porous scaffolds, we determined the importance of evaluating co-cultures for the improved

characterization of materials to be used in tissue regenerative applications. This system can be easily applied to other 3D scaffolds made of polymers, as well as to many further biomaterials with minor adaptions.

References

[1] P. Italiani, D. Boraschi, From Monocytes to M1/M2 Macrophages: Phenotypical vs. Functional Differentiation, Front Immunol 5 (2014) 514.

[2] E. Eggenhofer, M.J. Hoogduijn, Mesenchymal stem cell-educated macrophages, Transplant Res 1(1) (2012) 12.

[3] T. Tylek, T. Schilling, K. Schlegelmilch, M. Ries, M. Rudert, F. Jakob, J. Groll, Platelet lysate outperforms FCS and human serum for co-culture of primary human macrophages and hMSCs, Sci Rep 9(1) (2019) 3533.

Acknowledgement

We thank the European Research Council (ERC, consolidator grant Design2Heal, contract no. 617989) for funding this work.

PS2-16-469

StarPEG-Heparin Microgels – A Tool to Control Inflammation and Improve Tissue Regeneration

Sebastian Kühn[1], Manfred F. Maitz[1], Julian Thiele[2], Uwe Freudenberg[1,3], Carsten Werner[1,3]

[1]Leibniz-Institute for Polymer Research Dresden e.V., Institute of Biofunctional Polymers, Dresden, DE; [2]Leibniz-Institute for Polymer Research Dresden e.V., Institute of Physical Chemistry and Polymer Physics, Dresden, DE; [3]Technische Universität Dresden, DFG Center for Regenerative Therapies Dresden, Dresden, DE

Introduction

The inflammatory response of vascular tissue to infection and tissue damage is undeniably a key process in re-establishing homeostasis and defending our body against pathogens. However, when disturbed or prolonged, inflammation can exert detrimental effects on the surrounding tissue and impede successful regeneration. Although the underlying mechanisms often remain elusive, an overabundance of pro-inflammatory factors and insufficient supply with pro-regenerative signalling molecules has been associated with the chronicity of inflammation and impaired regeneration in many cases. For example, recent studies suggest that healing of chronic dermal wounds can be improved significantly by either scavenging of pro-inflammatory chemokines (e.g. MCP-1 and IL-8) or by controlled release of anti-inflammatory/pro-regenerative cytokines and growth factors (e.g. IL-4, VEGF and TGFβ) from topically applied starPEG-heparin hydrogels [1-3].

Experimental Methods

In order to render the bulk material injectable, thus enabling local administration of the immunomodulatory system directly at the site of inflammation, we have developed a robust microfluidics platform for processing the starPEG-heparin gel matrices into microgels with adjustable size, mechanical and biochemical properties.

Results and Discussion

The in-situ crosslinking of thiol terminated 4arm starPEG and maleimide functionalised heparin via Michel type addition resulted in highly monodisperse microgels with tunable sizes over a range of 25 - 160 µm and highly comparable mechanical properties. The modulation of the heparin concentration within the microgels as well as the sulfation pattern/sulfation degree of the heparin allows for precise control over the space charge density and thus the affinity of the microgels for respective signalling molecules. Ultimately, this can be utilised to fine tune the release of heparin-affine proteins which was demonstrated for the pro-angiogenic growth factor $VEGF_{165}$. The hemocompatibility of the hydrogel system and the ability of the microgels to reduce leukocyte migration from the blood through sequestration of pro-inflammatory chemokines such as MCP-1 and IL-8 have been proven in *ex-vivo* studies with human whole blood.

Conclusion

These findings corroborate the suitability of starPEG-heparin microgels for *in-vivo* applications and demonstrate their potential for the treatment of deep irregularly formed wounds and internal inflammations. On the basis of the *in-vitro/ex-vivo* studies, the capacity of the microgels to modulate inflammation and promote tissue regeneration via scavenging and release of relevant signalling molecules is currently investigated *in-vivo* using mice models of inflammation.

References

1. Lohmann N, Schirmer L, Atallah P, Wandel E, Ferrer RA, Werner C, et al. Glycosaminoglycan-based hydrogels capture inflammatory chemokines and rescue defective wound healing in mice. Science translational medicine. American Association for the Advancement of Science; 2017;9(386):eaai9044.

2. Schirmer L, Atallah P, Werner C, Freudenberg U. StarPEG-Heparin Hydrogels to Protect and Sustainably Deliver IL-4. Advanced healthcare materials. Wiley Online Library; 2016;5(24):3157–64.

3. Freudenberg U, Liang Y, Kiick KL, Werner C. Glycosaminoglycan-Based Biohybrid Hydrogels: A Sweet and Smart Choice for Multifunctional Biomaterials. Advanced Materials. Wiley Online Library; 2016;

PS2-16-470

A 3D immunomodulatory platform using liquefied microcapsules

Sara S. Nadine, Clara R. Correia, João F. Mano

University of Aveiro, Department of Chemistry, CICECO - Aveiro Institute of Materials, Aveiro, PT

Introduction

Traditional tissue engineering (TE) strategies for tissue regeneration commonly neglect the role of the immune system in regulating tissue dynamics. However, accumulating evidences have indicated that macrophages (Mϕ) act positively in the progress of tissue regeneration. In fact, only an efficient and timely switch from proinflammatory M1 to regenerative M2 Mϕ phenotype results in a tissue remodelling cytokine release, which appears mandatory to tissue healing and successful regeneration. Furthermore, most TE applications involve assembling cells into conventional porous hybrid scaffolds or solid supports to facilitate the new tissue formation. An alternative to avoid the practice of fixed geometry structures and open surgery implantations is the use of our well-established Liquefied Capsules (LC) system [1], already tested *in vivo* [2]. LC are composed by a permselective multilayered membrane obtained through layer-by-layer assembly, using biocompatible polyelectrolytes. Furthermore, LC present a liquefied core loaded with microparticles that act as cell adhesion sites. Herein we propose to establish for the first time the immunomodulatory ability of LC when in an indirect culture with human Mϕ. We have previously studied in 2D the influence of different surface modifications performed on poly(L-lactic acid) films on the differentiation of human monocytes into Mϕ [3]. Here, we evaluate the influence of different types of polyelectrolytes in the last layer of the capsules when in contact with Mϕ. Additionally, the effect that the different polarization stages of Mϕ have on the biological performance of the encapsulated stem cells, in terms of proliferation and stemness maintenance, is also evaluated.

Experimental Methods

Alginate microgels are generated by electrohydrodynamic atomization (EHDA) technique. For that, under the influence of electrical forces (10 kV), a liquid jet of alginate containing a dispersion of cells ($5x10^6$cells/mL) and polycaprolactone microparticles (µPCL, 30 mg/mL) breaks up into droplets. After crosslinking in calcium chloride, microgels encapsulating cells and µPCL are obtained. Then, layer-by-layer is performed using chitosan (CHT), alginate (ALG) and poly(L-lysine) (PLL) as polyelectrolytes to produce a 10-layered membrane surrounding the microgels. Three different encapsulation systems were developed, each one ending with a different polyelectrolyte. Ultimately, the core is liquefied by chelation with EDTA, and LC are obtained. Then, THP-1 (human monocytic cell line) were cultured in RPMI 1640 supplemented with 10% fetal bovine serum and 1% penicillin/streptomycin. Monocyte-derived Mϕ were obtained after incubation with 50 ng/ml of phorbol myristate acetate for 48h. Then, LC presenting different last layers were placed on the top of the 2D culture of Mϕ.

Results and Discussion

We developed successfully LC encapsulating µPCL by EHDA. LC with µPCL were placed on top of a 2D culture of THP-1 Mϕ for 7 days. Live-dead assay shows that, after 24h, the viability of the Mϕ was not jeopardized by the presence of LC (fig.1B). Additionally, fluorescence staining of F-actin filaments shows that, regardless of the ending polyelectrolyte layer of the LC, the Mϕ present similar morphologies. However, by the analysis of surface antigens expression differences could be noticed. Interestingly, the expression of CD209 (M2-like marker) increased with increasing culture times, revealing that over time the LC prompted the polarization of Mϕ into a more regenerative phenotype (fig.1C). Moreover, the expression of the inflammatory marker CD80 remained low, suggesting that either

PLL, ALG or CHT do not induce an inflammatory response by Mϕ, evidencing the biotolerability of the multilayers of the LC system. Furthermore, the release of the anti-inflammatory IL-10 cytokine increased over time, with a more pronounced activity for the marine-origin polymers ALG and CHT, in particular for the latter (fig.1D). We also assess how LC encapsulating stem cells influence different polarization stages of Mϕ activity, as function of culture time. At different time-points, LC with or without stem cells will be added to 2D cultures of Mϕ polarized through M1 or M2 phenotypes, or Mϕ without any stimuli.

Conclusion

LC were tested for their ability to be used as an indirect co-culture system for the interaction of immune and skeletal systems. After assessing the biotolerability of LC, our main aim is to subsequently encapsulate stem cells, create microtissues within LC, and evaluate their interaction with an indirect co-culture with Mϕ. Future results might determine the perfect timing of implantation of the proposed system prior to *in vivo* studies. With the immune system contribution recognized as a crucial component influencing the regenerative process of tissues, we believe that the present study can give important insights to ameliorate the outcomes of stem cell encapsulation systems as medical implants and TE therapies.

References

[1] Correia, C.R., et al., Semipermeable Capsules Wrapping a Multifunctional and Self-regulated Co-culture Microenvironment for Osteogenic Differentiation. Scientific Reports, 2016. 6: p. 21883.

[2] Correia, C.R., *et al*., In vivo osteogenic differentiation of stem cells inside compartmentalized capsules loaded with co-cultured endothelial cells. Acta Biomater, 2017. 53: p. 483-494.

[3] Correia, C.R., *et al*., The influence of surface modified poly(L-lactic acid) films on the differentiation of human monocytes into macrophages. Biomater Sci, 2017. 5: p. 551-560.

Acknowledgement

This work was developed within the scope of the project CICECO-Aveiro Institute of Materials, FCT Ref. UID/CTM/50011/2019, financed by national funds through the FCT/MCTES. Sara S. Nadine acknowledges the financial support by the Portuguese Foundation for Science and Technology through the doctoral grant (SFRH/BD/130194/2017). This work was supported by the European Research Council grant agreement ERC-2014-ADG-669858 for project “ATLAS” and by FCT for the project CIRCUS (PTDC/BTM-MAT/31064/2017).

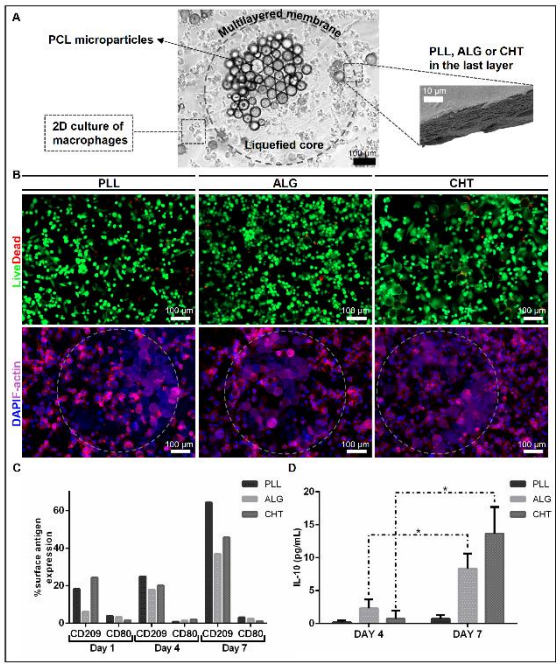

Figure 1
(**A**) Light microscopy of LC encapsulating µPCL on top of a 2D culture of THP-1 Mϕ. Scale bar represents 100 µm (**B**) Live-dead and DAPI-phalloidin fluorescence assay in Mϕ cultured with LC ending with different polyelectrolytes, after 24h of interaction. Living cells were stained by calcein (green) and dead cells by propidium iodide (red). In the DAPI-phalloidin fluorescence assay is possible to observe the Mϕ cultured below the LC. The dotted lines represent the membrane of the LC. Cells nuclei were stained by DAPI (blue) and F-actin filaments by phalloidin (pink). Scale bars correspond to 100 µm. (**C**) Flow cytometric analysis of surface antigen expression on Mϕ cultured with LC ending with different polyelectrolytes, after 1, 4 and 7 days of interaction. (**D**) IL-10 protein release measured by ELISA of LC after 4 and 7 days of culture. P-values *<0.05 were considered statistically significant.

PS2-16-471

A model for the evaluation of neutrophil degradation for covalently bound peptides on a polymeric matrix and a method to prevent it

Carina Blum, Mehmet B. Taskin, Katrin Schlegelmilch, Tatjana Schilling, Jürgen Groll

University of Würzburg, Department for functional materials in medicine and dentistry, Würzburg, DE

Introduction

Innate immune response is the immediate reaction of the human body to biomaterials after implantation or injection, and thus a pivotal criterion for the materials success or failure.[1] As one of the most abundant immune cells circulating in the bloodstream, neutrophils are the first cells being recruited to the site of tissue injury. With their phagocytotic activity they effectively attack invading microorganisms. Moreover, neutrophils produce antimicrobial substances and proteases such as human neutrophil elastase (HNE), stored in cytoplasmic granules, that can be released into the extracellular space to tackle an infection and are known to degrade extracellular matrix proteins such as fibronectin, laminin, and collagen IV. Also biomaterials are exposed to this machinery, which may lead to partial or complete degradation of surface biofunctionalization of an implant.[2]

In order to analyze the innate immune response towards a biomaterial with covalently immobilized peptides on a fibrous polymeric matrix, we present a proof-of-principle *in vitro* model resembling the neutrophil attack by the exposure to HNE. In addition, we developed a hydrogel coating as transient protection to protect the surface modification from being destroyed through the neutrophil attack. To make the functionalized fiber surface available again after the initial neutrophil attack, the hydrogel coating should be short-lived, i.e. being dissolved within a few hours/days *in vivo*. This will allow for the initial preservation of the surface modification and hence enable to exert its effect on the regulation of cell signaling and recruitment to foster a regenerative outcome.

Experimental Methods

Fiber meshes of poly(ε-caprolactone) (PCL), the functional additive NCO-sP(EO-*stat*-PO), and a HNE-specific peptide containing a cleavage site for HNE as well as an integrin-binding motif, were produced via solution electrospinning and afterwards embedded in a hydrogel. Fiber meshes with and without hydrogel coating were incubated with different concentrations of HNE prior to *in vitro* culture with L929 fibroblasts. Cell attachment was analyzed by the determination of the DNA content, Live/Dead staining, and SEM analysis. Furthermore, the amount of degraded peptides on electrospun fiber meshes after HNE incubation was determined by a photometrically-based assay developed in-house.

Results and Discussion

The L929 cell attachment onto fibrous meshes of PCL, NCO-sP(EO-*stat*-PO), and the covalently bound peptide containing an integrin-binding, i.e. cell-mediating motif was significantly enhanced compared to a reference nonwoven of PCL and NCO-sP(EO-*stat*-PO) without immobilized peptide, where largely no cells adhered. The covalently bound peptides were degraded by HNE, leading to a reduced amount of integrin-binding motif, which was in accordance with the significantly reduced cell adherence compared to non-degraded peptide meshes. Thereby, the degradation of the covalently bound, HNE-specific peptide was enhanced with increasing HNE concentration. First results indicated that the fiber functionalization is protected from the neutrophil attack, when the nonwovens are endowed with a hydrogel coating.

Conclusion

The neutrophil attack towards a covalently immobilized peptide on a fibrous polymeric matrix has been successfully mimicked in our model system using HNE. In addition, ongoing studies evaluate the possibility to tailor hydrogels as transient protection. The status of these examinations will be presented and discussed.

References

[1]A. E. Fetz, G. S. Selders, G. L. Bowlin, M. Z. Radic, Regenerative Biomaterials 2017, 4, 55.

[2]J. M. Anderson, Annual Review of Materials Research 2001, 31, 81.

Acknowledgement

The authors thank the European Research Council (ERC) (consolidator grant Design2Heal, contract # 617989) and the German Research Foundation (DFG) (INST 105022/58-1 FUGG) for financial support.

PS2-16-472

MODULATION OF MACROPHAGE POLARIZATION BY TiO_2 NANOTUBULAR SURFACES

Madalina G. Necula[1], Anca Mazare[2], Selda Özkan[2], Roxana Trusca[3], Valentina Mitran[1], Patrik Schmuki[2], Anisoara Cimpean[1]

[1]University of Bucharest, Department of Biochemistry and Molecular Biology, Bucharest, RO; [2]University of Erlangen-Nuremberg, Department of Materials Science, Erlangen, DE; [3]University Politehnica of Bucharest, Faculty of Engineering in Foreign Languages, Bucharest, RO

Introduction

Immune cells play an important role in bone formation and repair and the main effectors of the immune response to implanted materials are represented by macrophages (MFG) [1]. Because of their remarkable plasticity and heterogeneity, MFG are a prime target for immunomodulation in order to enhance bone regeneration [2]. Studies have shown that polarization of MFG towards the anti-inflammatory M2 phenotype, rather than the pro-inflammatory M1 phenotype, promotes bone healing and long-term stability of the implants [3]. In addition, MFG tend to fuse and become foreign body giant cells (FBGCs) which are also a reaction to implant [4]. Therefore, the evaluation of the immune response generated by a material can be beneficial for the designation and optimization of bone implants [5].

The present study *aims* to determine the influence of TiO_2 nanotubes (TNT) exhibiting a similar inner diameter (~78 nm) but a different lateral spacing, meaning ~18 nm (TNT18) and ~80 nm (TNT80), respectively, on MFG polarization and FBGCs formation. The commercial pure titanium (Ti) has been investigated as reference material.

Experimental Methods

RAW 264.7 macrophages were seeded on the surface of tested materials and maintained under normal culture conditions or in the presence of a pro-inflammatory stimulus represented by bacterial lipopolysaccharide (LPS). The effects of the analyzed materials on MFG adhesion and morphological features were assessed by SEM. Further, fluorescence immunocytochemistry was used to show the early expression levels of pro-inflammatory M1 marker (CCR7) and the pro-regenerative M2 marker (CD163) by cells grown in contact with the tested surfaces. At the same time, the induction of FBGC formation was evinced by fluorescence labelling of the actin cytoskeleton and the nuclei.

Results and Discussion

SEM micrographs have shown that at 2 h post-seeding, MFG adopted a typical round morphology with numerous extensions, especially on the surface of TNT. After 24 h of culture, LPS-stimulated cells became larger and more elongated than those cultured in standard conditions, suggesting a predominant activation towards the M1-phenotype. In the absence of the pro-inflammatory stimulus, the cells retained their normal, typical round morphology. Moreover, at the same incubation time point, immunofluorescence staining of the M1 (CCR7) and M2 (CD163) specific markers was performed. The results showed a reduced number of positive CD163-stained cells exhibiting a diffuse labeling on all analyzed surfaces. Likewise, a higher number of CCR7-stained cells were identified under LPS-stimulated conditions when compared with samples maintained in normal conditions as well as an increase in fluorescence intensity. More visible differences were observed at 72 h post-seeding when a higher number of CCR7-positive cells were noticed on the Ti surface compared with the TNT. On the contrary, on the TNT surfaces a higher number of CD163-positive cells were evinced, especially in the case of TNT18.

In addition, the fluorescence labeling of actin cytoskeleton and nuclei demonstrated that under LPS-stimulation, the multinucleated MFG formed on the Ti surface exhibited larger cellular body than those grown in contact with TNT. Furthermore, they showed actin reorganization, ruffled membranes and more numerous filopodia. Therefore, in a pro-inflammatory micro-environment, the Ti surface causes a more severe response than the TNT.

Conclusion

Taken together, the results obtained demonstrated that the TNT, especially TNT18, are more potent in inducing M2 phenotype expression and showed a lower capacity to stimulate FBGC formation *in vitro*. Hence, it can be concluded that the lateral spacing of TNT can influence cellular behavior.

References

1. Baht G.S, Vi L, Alman B.A. *Curr. Osteoporos. Rep.***2018**, 16, 138-145.
2. Bygd H.C., Forsmark K.D., Bratlie K.M. *Clin. Transl. Med.***2014**, 3.
3. Jamalpoor Z., Asgari A., Lashkari M.H, Mirshafiey A., Mohsenzadegan M. *Iran J. Allergy Asthma Immunol.***2018**, 17, 398-408.
4. Sheikh Z., Brooks P.J., Barzilay O., Fine N., Glogauer M. *Materials***2015**, 8, 5671-5701.
5. Wang J., Meng F., Song W., Jin J., Ma Q., Fei D., Fang L., Chen L., Wang Q., Zhang Y.. *Int. J. Nanomedicine***2018**, 13, 4029–4043.

Acknowledgement

The authors gratefully acknowledge UEFISCDI (project PCE-55-2017) for the financial support.

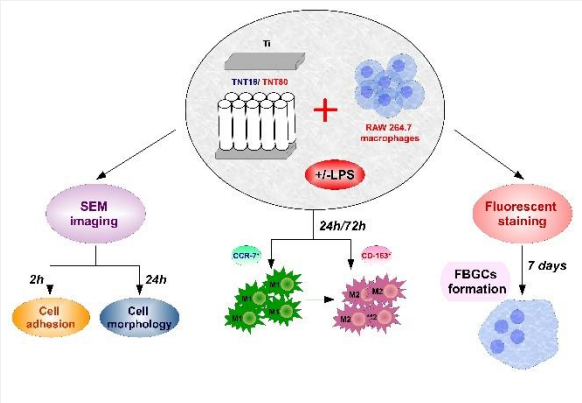

Evaluation of TNT spacing on macrophage behavior.

PS2-16-473

Peptide hydrogel as a novel system to study T-cell function in 3-dimensional culture

Ilona Vitkauskaite[1,2], Cathy L. Merry[2], Andrew M. Jackson[1], Ian Spendlove[1]

[1]University of Nottingham, Host-Tumour interactions group, Nottingham, GB; [2]University of Nottingham, Stem cell glycobiology group, Nottingham, GB

Introduction

T cell research has substantially aided our understanding of their role in health and disease. Our ever-expanding knowledge of T cell behaviour has facilitated development of treatments for cancer, infectious disease, transplant rejection and autoimmunity. However, the majority of pre-clinical studies are based on *in vitro* experiments, which deviate substantially from tissue environments. Although *in vivo* (animal)studies have been invaluable, these nevertheless do not fully represent the diversity of clinical subjects and new systems are required. The use of biomaterials could improve T cell research by providing 3-dimensional (3D) culture environments. In this research, self-assembling peptide hydrogel (SAPH) were used to culture human T-cells in 3D. The hydrogel is made from an octopeptide (FEFEFKFK; F: phenylalanine, E: glutamic acid; K: lysine), where β-sheet forming peptide entraps the cells and medium components into a nanofibrous architecture. The hydrogel has undefined environment, where biological components could be incorporated to make the cell specific environment. It is cost-effective, biocompatible and its mechanical properties could be adjusted to meet the specific tissue requirements. The aim of this research is to assess the hydrogel system for T cell culture, where the cells could proliferate, function, migrate and respond to the surrounding stimulus. Moreover, it is also to understand the extent of hydrogel's capability of creating specific tissue environment (e.g. lymph node, tumour microenvironment) that supports cells behaviour as *in vivo* studies.

Experimental Methods

Several assays were done to assess CD4+ T cell viability in hydrogel system by looking at Live/Dead staining, cytokine secretion and proliferation by 3H-Thymidine incorporation assay. Different peptide concentrations (mg/ml) of hydrogel were assessed for their ability to support cell culture, especially once hydrogel's density is increased.

Results and Discussion

The results have shown the ability of hydrogel (6mg/ml) to encapsulate cells, support their viability and allow the expansion of proliferating clusters of cells (Fig. 1). In cell proliferation assays the density of hydrogel has no impact on cell growth, indicating that cells are robust and were able to secrete similar levels of interferon gamma (INF-γ) (Fig. 2). This indicates T cell adaptability to a denser culture system.

Conclusion

In future, the hydrogel system will be further analysed for its ability to support co-culture system and different T cell phenotypes. Especially for creating a hydrogel with more defined biochemical structure to mimic an *in vivo* tissue. The outcome of this research would benefit various fields, as it will deliver an improved *in vitro* culture system and replace animal models for studies more relevant to man. Moreover, it could provide the foundation for biomaterials to achieve specific T cell function for creating clinical implants or developing advanced materials with multicellular networks.

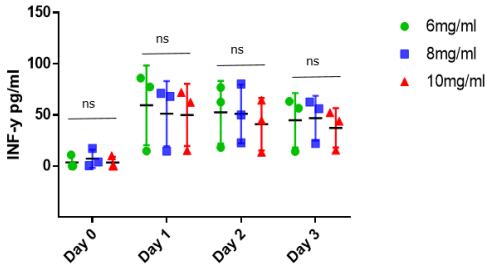

Figure 2: Stimulated T cell growth in different peptide concentrations of hydrogel.
There is no significant difference between hydrogel's concentrations on supporting T cell growth (One-way ANOVA with Tukey's multiple comparison test, N=3, Mean±SD)

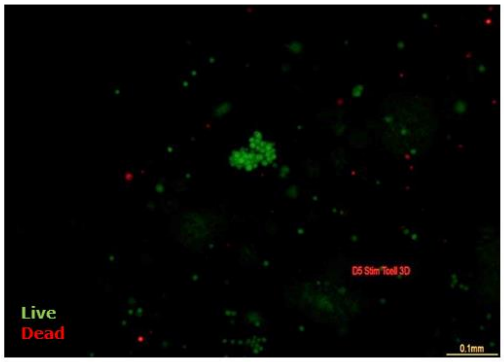

Figure 1: Stimulated T cells in hydrogel (FEFEFKFK) culture system.
Fluorescence image of Live/Dead staining of proliferating clusters of T cells in hydrogel system, Day 5.

PS2-16-474

Development of an antibody-immobilized filter for capturing target cells

Akio Kishida[1], Rino Tokunaga[1], Yoshihide Hashimoto[1], Naoko Nakamura[2], **Tsuyoshi Kimura**[1]

[1]Institute of Biomaterials and Bioengineering, Tokyo Medical and Dental University, Tokyo, JP; [2]Department of Bioscience and Engineering, Shibaura Institute of Technology, Saitama, JP

Introduction

For cancer treatments, such as surgery, radiation, and chemotherapy, the main strategy is attacking cancerous cells directly. On the other hand, recently, cancer immunotherapy aims to harness the body's own immune system to fight cancer [1]. Among cancer immunotherapies, regulatory T (Treg) cell expressing CD4, CD25 and the transcription factor forkhead box P3 is one of the key cells because Treg cells suppress the activation of tumor-antigen-specific T cells [2,3]. So, reducing the number of Tregs from cancer patients is one of the important treatments. Our final goal is to develop a device that can capture and collect Tregs from the blood selectively and effectively for cancer immunotherapy (Fig 1). In this study, we developed a surface modified filter, on which cells are captured and released selectively. As a model cell, bone marrow cells, which are CD45 positive cells, and anti-CD45 antibody were used. The antibody was modified with desthiobiotin and immobilized on a surface by binding to avidin. Using this filter, the selective capture of target cells was investigated.

Experimental Methods

Four kinds of polyethylene (PE) filters have various hole sizes were used. The PE filters were treated by corona discharge and subsequently acrylic acid (concentration: 0.5%, 1%, 1.5%, 2%) was graft-polymerized on the surface. The PAA-PE was modified with biotin. Anti-mouse CD45(mCD45) antibody was conjugated with desthiobiotin and immobilized on the biotin-PAA-PE through biotin–avidin and desthiobiotin–avidin interactions. Bone marrow cells, CD45 positive cells, were harvested from a mouse. HL60 cells were used as CD45 negative cells. They were seeded on antibody-immobilized PE. After incubation for 1 hour, the non-adhered cells were removed by washing of PBS. The adhered cells were observed with a microscope and counted.

Results and Discussion

Acrylic acid was graft-polymerized to PE filters. The amount of grafted polymer increased with increasing concentration of feeded AAc for all filters. The CD45 antibody was conjugated with desthiobiotin and then immobilized on the biotin-PAA-PE through desthiobiotin-avidin and biotin-avidin interaction. By immunostaining, the immobilization of the antibody on the film was confirmed (Fig.2 upper). The antibody-immobilized filters through desthiobiotin–avidin and biotin–avidin interactions became uniformly brown.

The HL60 cells and mouse bone marrow cells (mBMCs) were seeded on the corona-discharged PE, the PAA-PE, and the antibody immobilized PE. After incubation for 1hour, the non-adhered cells were washed out using PBS. For the corona-discharged PE, the cells, HL60 and mBM, were adhered. For the PAA-PE, both cells did not adhere. On the other hand, for the antibody-immobilized PE, although the HL60 cells did not adhere, mBMCs effectively adhered. From this result, it was found that the CD45 antibody-immobilized surface selectively captures bone marrow cells.

Conclusion

The filter having antibody-immobilized surface was prepared for capturing target cells. The filter having antibody-immobilized surface could capture target cells, effectively and selectively.

References

1. McNutt M., Science, 342, (2013) 1417.
2. H. Nishikawa and S. Sakaguchi: Int. J Cancer 127 (2010) 759.
3. H. Nishikawa and S. Sakaguchi: Curr. Opin. Immun. 27 (2014) 1.

Acknowledgement

This work was partially supported by KAKENHI, JSPS, and the Cooperative Research Project of Research Center for Biomedical Engineering, MEXT, and the Cooperative project among medicine, dentistry, and engineering for medical innovation, MEXT.

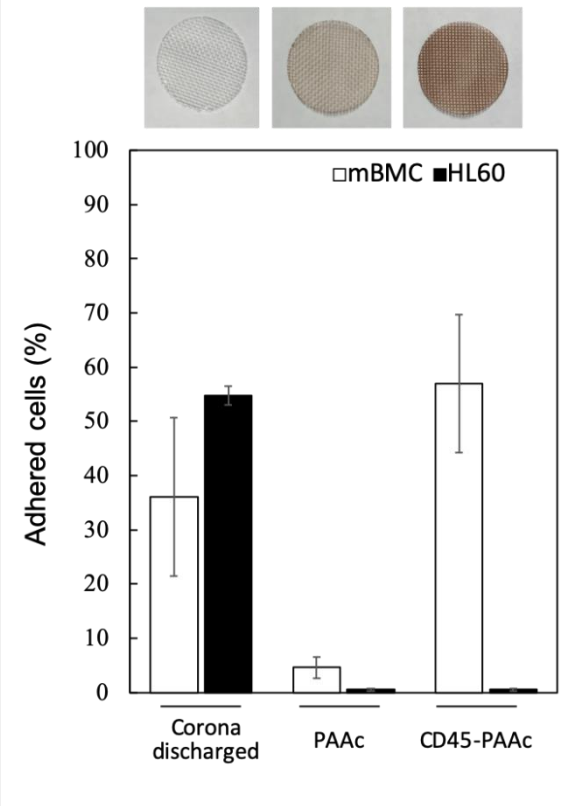

Fig 2
Fig. 2. Selective capture of target cells on the antibody immobilized PE.

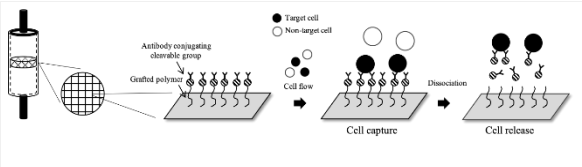

Fig 1
Fig. 1. Selective capture and release of target cells on an antibody immobilized filter.

2:45 p.m. – 3:45 p.m.

Hall 1 / Exhibition Area

PS2-17 | Cell/ material interactions

PS2-17-475

The effect of the needle-like calcium phosphate nanoparticles on cellular uptake and cell function

Zhe Sun, Lenzo Jason, Holden James, O'Brien-Simpson Neil

Melbourne university, Melbourne dental school, Bio21, Melbourne, AU

Introduction

Calcium phosphate nanoparticles (CaP-NPs) are one of the promising protein delivery carriers because of their specific properties such as non-toxic, biodegradable, pH-dependent solubility, cost-effective, and the protection of the antigens from degradation and elimination[1]. The interaction between CaP-NPs and cells has been extensively investigated [2, 3]. However, the effects of needle-like shaped NPs on cell behaviours is rarely known. In this work, we will address if CaP-NPs will bind, migrate cell wall and induce a robust immune response.

Experimental Methods

Based on recent reported methods, CaP-NPs were prepared by a chemical precipitation technique[4]. Then, Ovalbumin as a model antigen was attached to the NPs by electrostatic interaction. The NP formulations were characterized by dynamic light scatting (DLS) and helium ion microscopy (HIM). The viability of epithelial cells and macrophages exposed to the CaP-NPs was measured by the MTS and LDH assay. To investigate the formulated NPs interaction with cells, we assessed their ability to enhance binding to oral epithelial cells; migrate epithelial cell wall; uptake by epithelial cells; phagocytosis, NF-κB activation and cytokine secretion by macrophages. Flow Cytometry was used to determine the level of binding, phagocytosis and cell surface marker expression. Cytokine secretion was measured by ELISA kits according to the manufacturer's instructions. All experiments were done in triplicate. The one-way ANOVA (GraphPad Prism) was used to compare the difference between multiple groups. $p < 0.05$ was considered statistically significant.

Results and Discussion

Our results indicated that the obtained NPs had a hydrodynamic diameter of 261 ± 20 nm, with a zeta potential of -17.5 ± 1.2 mV. The PDI value of 0.1 suggested the NPs are homogeneous, which meet the good sample quality. The NPs showed excellent stability in various solutions such as saline and cell culture media. HIM images demonstrated a needle-like shape of NPs with a length of 236 ± 19 nm. Those prepared nanoparticles showed no cytotoxicity within the tested concentration. Additionally, it was found that about 64 ± 5.5 % NPs could bind to epithelial cells at NP to cell ratio of 100. After 15 min incubation, 6.1 ± 2.1 % NPs migrated the cell monolayer, which was increased by longer incubation period. Confocal microscope images apparently showed the nice fluorescence inside the cells (Fig 1). This suggesting OVA was successfully delivered into the cells by CaP-NPs. The NPs were phagocytosed by macrophages in a dose-dependent manner. In addition, at the ratio of 10, 000, the functionalized NPs significantly increased the marker expressions on the macrophage cell surface. NPs can also induce NF-κB activation and increase cytokine secretion. Compared with cells without NPs, cytokine secretion showed a significant increase at the NP to cell ratio of 10.000:1.

Conclusion

In summary, our results demonstrated that needle-like CaP-NPs could effectively bind to epithelial cells, migrate the cell wall and successfully transport protein into cells *in vitro*. They can also stimulate macrophages maturation and activation. Our study provides a better understanding of the interaction between needle-like nanoparticles and cells. This could use as a further guide to define needle-like CaP-NPs as a promising protein carrier for vaccine studies.

References

1. Sharma S. *et al*. Colloids and Surfaces B: Biointerfaces, 2015, 133:120-139
2. Sokolova V. *et al*. Acta Biomater, 2013, 9: 7527-35
3. Kozlova D. *et al*. Journal of Materials Chemistry, 2012, 22: 396-404
4. López-Macipe A. *et al*. Advanced Materials, 1998, 10, 49

Acknowledgement

The authors would like to thank the oral health cooperation research centre (CRC) for providing financial support to this project. We also acknowledge Paul Brannon for help with confocal microscopy.

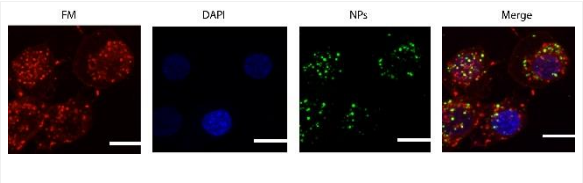

Intracellular delivery of CaP NPs-OVA into epithelial cells
Nanoparticle (green) were pre-labelled with Atto 488, plasma membrane (red) were stained with FM dyes, and nuclei (blue) were stained with DAPI. Scale bar = 10 µm.

PS2-17-476

Topography Mediated Cell Migration: Direction, Wavelength, and Amplitude

Lu Ge, LiangLiang Yang, Patrick V. Rijn

University of Groningen, Department of BioMedical Engineering-FB40, Groningen, NL

Introduction

It is have been extensively studied that biophysical stimulus like topography can control cell morphology, adhesion, cytoskeleton organization , andmigration and provide an important role in biomaterials design in tissue repair. However, little is known about the individual guidance effect of wavelength and amplitude in dermal wound healing procedure. We report on the design of a topographically wrinkle gradient with gradually changed wavelength and amplitude, which were fabricated by combination of plasma oxidation and imprinting methods, provides an efficient platform to investigate fibroblast migration in vitro wound healing assay. The wound coverage rate was measured on three different wavelength size of 2 μm, 5 μm, and 8 μm on perpendicular or parallel orientation. Based on our experimental results, cells movement are guided by the topography and moves faster on the on the perpendicular direction and 2 μm wrinkle than other surface showed faster migration speed. What's more, when the wavelength are same, cell moves faster on the smaller amplitude surface. However, when the amplitude are same, cell prefer to move to the bigger wavelength. Besides, we determined that topography surface facilitating the collective cell migration is not due to promoting the cell proliferation. These findings suggest the necessity of wrinkle gradient surface used for study wound healing and give guidance to designing the biomedical implants.

Experimental Methods

Fabrication of wrinkle gradient substrates
Plasma oxidation
Atomic force microscope
Time-lapse imaging and single cell trajectory
Immunostaining of proliferation assay

Results and Discussion

The 2 μm wrinkle than other surface showed faster migration speed. What's more, when the wavelength are same, cell moves faster on the smaller amplitude surface. However, when the amplitude are same, cell prefer to move to the bigger wavelength. Besides, we determined that topography surface facilitating the collective cell migration is not due to promoting the cell proliferation.

Conclusion

The mechanism study indicates that cells can recognize the topographic of the wrinkle, resulting in different migration behavior. The decouple guidance effect of wavelength and amplitude were investigated. When the wavelength are same, the cell prefer to move toward the smaller amplitude surface from their initial positions. And 2 μm show the best promotional effect. However, when the amplitude are same, the cell prefer to move to the bigger wavelength surface. Furthermore, the fibroblasts migration behaviors response to the topographical orientation. Meanwhile, this

promotional effect was not due to accelerating cell proliferation but caused by wrinkle-enhanced effective collective cell migration.

References

Won, Y.-W., Patel, A. N. & Bull, D. A. Cell surface engineering to enhance mesenchymal stem cell migration toward an SDF-1 gradient. *Biomaterials***35,** 5627–5635 (2014).

Pot, S. A. *et al.* Nanoscale topography–induced modulation of fundamental cell behaviors of rabbit corneal keratocytes, fibroblasts, and myofibroblasts. *Invest. Ophthalmol. Vis. Sci.***51,** 1373–1381 (2010).

Kim, B. D. *et al.* Guided Cell Migration on Microtextured Substrates with Variable Local Density and Anisotropy. **742,** 1579–1586 (2009).

Zhou, Q. *et al.* Directional nanotopographic gradients: a high-throughput screening platform for cell contact guidance. *Sci. Rep.***5,** doi:10.1038/srep16240 (2015).

Mascharak, S. *et al.* YAP-dependent mechanotransduction is required for proliferation and migration on native-like substrate topography. *Biomaterials***115,** 155–166 (2017).

Kim, J. *et al.* Directional Matrix Nanotopography with Varied Sizes for Engineering Wound Healing. *Adv. Healthc. Mater.***6,** 1–10 (2017).

Acknowledgement

L.G.and L.Y., are very grateful for financial support of the China Scholarship Council (Nos. 201608310113 and 201707720058). Part of the work was performed in the UMCG Microscopy and Imaging Center (UMIC), sponsored by NWO (Grant No. 40-00506-98-9021). We acknowledge Reinier Bron and Theo G. van Kooten for assistance with cell cultures, Joop de Vries for help with AFM and plasma system maintenance, and Klaas Sjollema for assistance with Time-lamps microscope.

PS2-17-477

Glycoengineering as a tool to control the behavior of bone marrow-derived mesenchymal stromal cells in biofabrication processes

Stephan Altmann[1], Jürgen Mut[2], Natalia Wolf[2], Julian Bechold[2], Franz Jakob[1], Jürgen Seibel[2], Regina Ebert[1]

[1]Julius-Maximilians-University Würzburg, Orthopedy, Würzburg, DE; [2]Julius-Maximilians-University Würzburg, Organic Chemistry, Würzburg, DE

Introduction

3D Bioprinting is a promising and innovative technique in the field of tissue engineering with different challenges to be overcome. One of these issues is related to mechanical shear stress during the printing process. While a nozzle with a smaller diameter increases the printing resolution, the shear forces increase as well, which might lead to an impaired cell viability post-print. Once the cells are printed, their adherence behavior determines distribution in the hydrogel and interaction with the bioink environment. When printing tissue constructs with different cell types, adhesion control becomes more important to guide specific cells to specific areas in the hydrogel. To address these two aspects, our project aims to understand and apply metabolic glycoengineering to enhance the (a) glycocalyx mediated cell stability by altering the glycocalyx composition and density as well as the (b) cell adhesion within the hydrogel by chemically altering the bioink in addition.

Experimental Methods

For metabolic glycoengineering, cells were incubated with different tetraacetylated azido sugars (Ac_4GlcNAz, Ac_4GalNAz or Ac_4ManNAz) for 48 h followed by a click reaction. While azido sugar treated human mesenchymal stromal cells (Az-hMSC) were incubated for 1 h with DBCO-Cy3 as click molecule (strain promoted alkyne-azido cycloaddition (SPAAC)), in case of the Cu dependent variant (CuAAC) Az-hMSC were incubated for 5 min with alkyne-Cy3 as click molecule in click buffer containing $CuSO_4$, THPTA and sodium ascorbate. For the glycochip assay, commercial pre-treated glass slides were coated with different molecules via amino NHS-ester chemistry and incubated with hMSC for 24 h followed by HE staining.

Results and Discussion

We established the commonly used click reaction variants CuAAC and SPAAC in hMSC and could successfully detect the azido sugar expression up to 48 h via fluorescence microscopy. Since Ac_4ManNAz showed the best results in terms of cell viability and incorporation efficiency into the glycocalyx, it was chosen for future experiments. To identify suitable molecules as binding partners for adhesion mediating glycoproteins like galectin-1, a glycochip assay was designed as a screening tool. First experiments revealed no cell adhesion toward different monosaccharides, organic compounds or a highly specific galectin-1 ligand. The adhesion difference between the control glass slide and RGD peptide coated fields as positive adherence control might point to a suboptimal basic functionalization of the glycochips. Interestingly, incubation with the ligand resulted in the appearance of non-adherent cell spheroids, but not in enhanced galectin-1 mRNA expression.

Conclusion

Since the metabolic glycoengineering is working, suitable molecules can now be identified to be introduced into the glycocalyx and evaluated for cell rigidity-increasing effects before and after 3D bioprinting. Furthermore, the overall glycochip design needs to be optimized for the screening of potential galectin-1 binding partners and the impact of the galectin-1 ligand on the cell-cell interaction will be further elucidated.

References

M. Gutmann, E. Memmel, A. C. Braun, J. Seibel, L. Meinel, T. Lühmann, Biocompatible Azide–Alkyne “Click” Reactions for Surface Decoration of Glyco-Engineered Cells, *ChemBioChem***2016**, *17*, 866

PS2-17-478

Neuronal Networks in 3D Matrix Composites

Dieter Janzen[1], Ezgi Bakirci[2], Annalena Wieland[3], Pamela L. Strissel[3], Reiner Strick[3], Paul D. Dalton[2], Carmen Villmann[1]

[1]University Hospital Würzburg, Institute of Clinical Neurobiology, Würzburg, DE; [2]University Hospital Würzburg, Department for Functional Materials in Medicine and Dentistry, Würzburg, DE; [3]University Hospital Erlangen, Department of Obstetrics and Gynaecology, Erlangen, DE

Introduction

The central nervous system (CNS) contains some of the softest tissues found in the human body (1). Therefore, 3D *in vitro* cultures of neurons, astrocytes, and other cell types of the CNS are challenging as similarly weak hydrogels are often unstable and difficult to handle. This issue can be solved using fiber-reinforcement; it was previously shown that reinforcement with 3D-printed microfibers can result in up to 54-fold increased stiffness with only 7% volume reinforcement (2).

Experimental Methods

The aim of this study is to develop 3D models that offer optimal mechanical and biological environments for cells of the CNS. Melt-electrowritten polycaprolactone (PCL) scaffolds were used to reinforce soft to ultra-soft hydrogels, thus creating 3D matrix composites. The characterization of neuronal networks in matrix composites investigates the cellular maturation and synaptic transmission. Synaptic transmission is analyzed using electrophysiological measurements, e.g. patch-clamp recordings. So far, electrophysiological recordings on 3D cell cultures have been shown with the multi-electrode array technique. Recently, we were able to demonstrate functionality of transfected cell lines in 3D matrix composites using whole cell recordings with minor alterations to measurements in 2D cultures (3).

Results and Discussion

Here, we analyzed cell viability, network function, and maturation of mouse cortical neurons growing in 3D composites using the current “gold standard“ Matrigel as matrix, which is derived from secretions of Engelbreth-Holm-Swarm mouse sarcoma cells. Cell viability assays and immunocytochemical staining were performed at days 1, 7, 14, 21 *in vitro* and revealed a high initial viability comparable to 2D cultures and increasing network complexity. Spontaneous network activity was demonstrated by calcium imaging. The neuronal network was further characterized by functionality of voltage-gated sodium channels and the excitatory AMPA receptors.

Conclusion

In summary, we successfully exhibited a cortical neuronal network in scaffold-reinforced Matrigel. These results will be used as a baseline for future experiments that focus on creating and optimizing a synthetic matrix for cells of the CNS.

References

1. Spedden E, White JD, Naumova EN, Kaplan DL, Staii C. Elasticity maps of living neurons measured by combined fluorescence and atomic force microscopy. Biophys J. 2012;103(5):868-77.
2. Visser J, Melchels FP, Jeon JE, van Bussel EM, Kimpton LS, Byrne HM, et al. Reinforcement of hydrogels using three-dimensionally printed microfibres. Nature communications. 2015;6:6933.
3. Schaefer N, Janzen D, Bakirci E, Hrynevich A, Dalton PD, Villmann C. 3D Electrophysiological Measurements on Cells Embedded within Fiber-Reinforced Matrigel. Advanced Healthcare Materials. 2019;8(5).

Acknowledgement

Funded by the Deutsche Forschungsgemeinschaft (DFG, German Research Foundation) – Projektnummer 326998133 – TRR 225 (subproject B01).

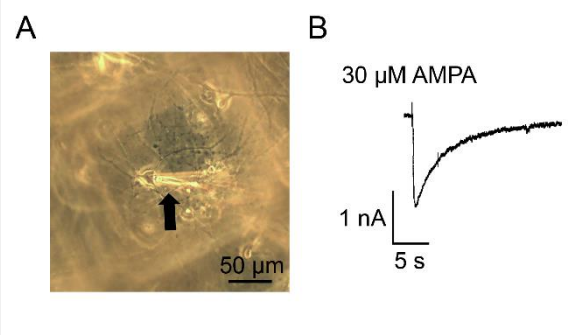

3D electrophysiological recordings from cortical neurons
(A) Mouse cortical neurons encapsulated in a 3D matrix composite consisting of Matrigel and a PCL scaffold. The patch pipette (black arrow) is approaching the cell.

(B) Whole-cell current evoked by 30 µM AMPA, applied on cortical neurons in a 3D matrix composite for 250 ms with a pressure of 1 bar.

PS2-17-479

Calcium Phosphate nanoparticles as carriers of therapeutic biomolecules into cells - an *In Vitro* study

Nataniel Białas[1], Elena K. Müller[2], Ingrid Hilger[2], Matthias Epple[1]

[1]University of Duisburg-Essen, Institute of Inorganic Chemistry and Center for Nanointegration Duisburg-Essen (CeNIDE), Essen, DE; [2]University Hospital Jena, Institute of Diagnostic and Interventional Radiology, Research Center Lobeda, Jena, DE

Introduction

In the last decade, nanomaterials have gained increasing research interest due to their unique properties and usefulness in biomedicine. The range of clinical applications of inorganic nanoparticles is broad, from contrast enhancers in diagnostic imaging to carriers of therapeutic biomolecules (*e.g.* antibodies or RNA) into eukaryotic cells, both *in vitro* and *in vivo* [1,2]. Calcium phosphate (CaP) nanoparticles have a high affinity to nucleic acids and therefore can serve as their carriers into cells in targeted delivery. They are characterized by high biocompatibility and biodegradability, as CaP is the natural inorganic component of human hard tissue (bone and teeth), and are readily taken up by cells. The process of nucleic acid delivery enables to modify and control gene expression in cells [3]. Small interfering RNA (siRNA) is a potent therapeutic biomolecule well known for its ability to inhibit gene expression in cells by RNA interference. siRNA-mediated silencing of genes involved in inflammatory processes, *e.g.* NF-κB p65, is a promising therapeutic strategy to overcome a variety of inflammatory diseases [4].

Experimental Methods

Our aim was to synthesize and characterize fluorescent CaP nanoparticles (with and without p65-specific siRNA loading), and evaluate the cellular uptake of these nanoparticles as well as the gene silencing of NF-κB p65 in murine cells. Fluorescent CaP nanoparticles were synthesized by precipitation, stabilized with Cy5-labeled polyethyleneimine, loaded with p65-siRNA (functional or scrambled) and coated with a silica shell. The nanoparticles were purified by centrifugation, and characterized by dynamic light scattering (DLS), atomic absorption spectroscopy (AAS) and scanning electron microscopy (SEM). The nanoparticles were also tested for the presence of endotoxins (pyrogenicity). To evaluate the cellular uptake of the nanoparticles, mouse monocytes (cell line J774A.1) and mouse endothelial cells (SVEC4-10) were incubated with the fluorescent nanoparticles (without siRNA loading) in 2D cultures up to 48h. The uptake efficiency was determined by confocal laser scanning microscopy (CLSM). For evaluation of the gene-silencing efficiency, J774A.1 cells were incubated with siRNA-loaded nanoparticles in 2D cultures for 48h. The expression of the NF-κB p65 proteins and NF-κB p65 mRNA (messenger RNA) in cells was determined by Western Blot and Real-Time PCR, respectively.

Results and Discussion

CaP nanoparticles were spherical with an average size of 50 nm (by SEM) and a ζ-potential of +30 mV. The nanoparticles were colloidally stable, efficiently loaded with siRNA (approx. 95% of the biomolecules were incorporated) and non-pyrogenic. The concentration-dependent uptake of the nanoparticles was confirmed in both cell lines. Nanoparticle-mediated gene silencing was demonstrated in monocytes. The NF-κB p65 expression was decreased by the nanoparticles in a concentration-dependent manner up to 85% on protein level and 25% on mRNA level for the highest studied siRNA concentration (0.5 µg/mL).

Conclusion

CaP nanoparticles can be used as tools for nucleic acid delivery and gene silencing in cells. They have the potential to be widely applied in the treatment of various inflammatory diseases.

References

[1] van der Meer S.B., *et al*. *Acta Biomater*, 57 (2017), 414-425.
[2] Giner-Casares J.J., *et al*. *Mater Today*, 19 (2016), 19-28.
[3] Neuhaus B., *et al*. *J Mater Chem B*, 3 (2015), 7186-7193.
[4] Xu X., *et al*. *Regen Biomater*, 3 (2016), 187-195.

PS2-17-480

Cell response towards zinc oxide particles: effect of particle size, shape, and surface

Mateusz Olejnik[1], Christina Sengstock[2], Markus Kersting[2], Kateryna Loza[1], Alexander Rostek[1], Manfred Köller[2], Götz Westphal[3], Nina Rosenkranz[3], Jürgen Bünger[3], Matthias Epple[1]

[1]University of Duisburg-Essen, Institute of Inorganic Chemistry and Center for Nanointegration Duisburg-Essen (CENIDE), Essen, DE; [2]Ruhr-University Bochum, Bergmannsheil University Hospital / Surgical Research, Bochum, DE; [3]Institute of the Ruhr-University Bochum (IPA), Institute for Prevention and Occupational Medicine of the German Social Accident Insurance, Bochum, DE

Introduction

Zinc oxide particles (ZnO) have many applications in biomedical materials technology, imaging, nanomedicine, health care, and consumer products [1]. Their biological properties are determined by size, particle shape, and surface chemistry. Besides positive aspects like a moderate antibacterial effect and a beneficial effect on tissue healing, potential risks after exposure have to be considered. These are particularly associated with a possible inhalation of particles during synthesis and processing, but also with applications like drug delivery and biological imaging. In this study the biological effects of ZnO particles with respect to their properties like size, shape, charge, and surface functionalization were analysed [2,3].

Experimental Methods

ZnO particles with defined size (diameter 40 nm and 500 nm), shape (rod-like and spherical particles) and surface were synthesized based by solution-phase strategies in the presence of the capping agent poly(N-vinylpyrrolidone) (PVP). Their size and shape were determined by scanning electron microscopy (SEM) (see Figures A-D). Further characterization involved X-ray powder diffraction (XRD), dynamic light scattering (DLS), elemental analysis, thermogravimetric analysis (TG), and UV-Vis spectroscopy. The cell viability / metabolic activity was determined by propidium iodide staining / alamarBlue® and the activation of cells (reactive oxygen species (ROS) / cytokine release) by DCF assay or protein array. Uptake of particles into cells was determined by focussed ion beam milling (FIB) and SEM in combination with transmission electron microscopy (TEM) and energy-dispersive X-ray spectroscopy (EDX).

Results and Discussion

The biological effects of ZnO particles of different size and shape were evaluated *in vitro* after exposure to rat alveolar macrophages NR8383 by analysis of cytotoxicity and the expression of inflammatory markers (*e.g.* Eotaxin, GDF-15, IFN-γ, TNF-α). The obtained data gave correlations between subtoxic particle concentration, particle size, shape and intensity of the macrophage reaction (*i.e.* release of inflammatory markers, chemotaxis, formation of ROS).

Conclusion

The intensity of cell response to ZnO particles depends on particle size, morphology, and concentration.

References

[1] Zhang Y, Tapas RN, Hong H, Cai W. Biomedical applications of zinc oxide nanomaterials. Curr Mol Med. 2013; 13:1633-45.

[2] Cheng LC, Jiang X, Wang J, Chen C, Liu RS. Nano-bio effects: interaction of nanomaterials with cells. Nanoscale 2013; 5:3547-69.

[3] Ann LC, Mahmud S, Seeni A, Bakhori SKM, Sirelkhatim A, Mohamad D, *et al.* Structural morphology and in vitro toxicity studies of nano- and micro-sized zinc oxide structures. J Environ Chem Eng 2015; 3:436-44.

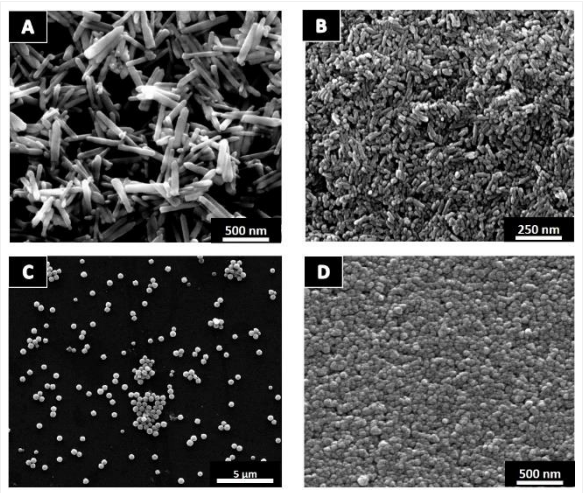

SEM micrographs
Zinc oxide particles of various size and shape: microrods (75 nm • 400 nm) (A), nanorods (35 nm • 100 nm) (B), microspheres (500 nm) (C), and nanospheres (40 nm) (D).

PS2-17-481

Effects of mesoporous SiO_2-CaO nanospheres on *Candida albicans* phagocytosis by murine peritoneal macrophages

Rosalía Díez-Orejas[1], Laura Casarrubios[2], María José Feito[2], Natividad Gómez-Cerezo[3], José María Rojo[4], María Vallet-Regí[3], Daniel Arcos[3], **María Teresa Portolés**[2]

[1]Universidad Complutense de Madrid, Departamento de Microbiología y Parasitología, Facultad de Farmacia, Madrid, ES; [2]Universidad Complutense de Madrid, Departamento de Bioquímica y Biología Molecular, Facultad de Ciencias Químicas, Madrid, ES; [3]Universidad Complutense de Madrid, Departamento de Química en Ciencias Farmacéuticas, Facultad de Farmacia, Madrid, ES; [4]CSIC, Departamento de Medicina Celular y Molecular, Centro de Investigaciones Biológicas, Madrid, ES

Introduction

The use of nanoparticles for intracellular drug delivery could reduce their toxicity and side effects. However, the uptake of these nanocarriers could induce adverse effects on cells and tissues [1]. Macrophages are among the first cell types which take up nanoparticles and they are primarily responsible for their trafficking *in vivo* [2]. These phagocytic cells play a central role in host defense, removal of dead cells and pathogens, inflammatory response regulation and modulation of adaptive immunity. The evaluation of the macrophage capability against pathogens after nanoparticle uptake is necessary in order to prevent infections associated with this kind of treatments.

Experimental Methods

In this study mesoporous nanospheres in the system SiO_2-CaO (NanoMBGs) with a hollow core surrounded by a radial arrangement were prepared and labeled with FITC (FITC-NanoMBGs) [3]. To determine the effects of NanoMBGs on macrophage immunocompetence, we have evaluated by flow cytometry and confocal microscopy, the ability of murine peritoneal macrophages to phagocytose CAF2-dTOM2, a red fluorescent labeled strain of *Candida albicans*. For this purpose, different experimental strategies were carried out with two macrophage/fungus relationships (MOI 1 and MOI 5) in both competition assays and assays which involved the pretreatment of macrophages with NanoMBGs.

Results and Discussion

The percentages of red and green macrophages were detected by flow cytometry as a measure of fungal phagocytosis and NanoMBG uptake, respectively. In the competition assays, NanoMBGs induced an increase of the fungal phagocytosis percentage by macrophages compared to control phagocytosis, independently of the MOI employed and at a short time of interaction, suggesting a possible role of this nanomaterial in macrophage activation. On the other hand, green and red fluorescence intensities were measured by flow cytometry to know the intracellular amounts of FITC-NanoMBGs and red fungus, respectively. It was observed that, as the quantity of intracellular fungus increased, the number of intracellular FITC-NanoMBGs decreased in a MOI- and time dependent-manner. These results suggest that the exocytosis of these NanoMBGs is a dynamic mechanism which favors the fungal phagocytosis, in agreement with previous studies with other nanoparticles [4].

Conclusion

The present study evidences the importance of evaluating the effects of macrophage infection on the capability of this cell type to incorporate nanoparticles in order to design effective antimicrobial therapies based on these nanomaterials.

References

[1] W. H. De Jong, P. J. A. Borm, Int. J. Nanomedicine, 2008, 3, 133-149

[2] I. Mottas, A. Milosevic, A. Petri-Fink, B. Rothen-Rutishauser, C. Bourquin, Nanoscale 2017,9, 2492-2504

[3] Y. Li, B. P. Bastakoti, Y. Yamauchi, Chem. Eur. J. 2015, 21, 8038–8042

[4] R. Diez-Orejas, M. J. Feito, M. Cicuéndez, L. Casarrubios, J. M. Rojo, M. T. Portolés, Colloids Surf., B 2018, 171, 250-259

Acknowledgement

This study was supported by research grants from the Ministerio de Economía y Competitividad, Agencia Estatal de Investigación (AEI), Fondo Europeo de Desarrollo Regional (FEDER) (MAT2016-75611-R AEI/FEDER, UE) and 4129533-FEI-EU-2018 Project. MVR acknowledges funding from the European Research Council (Advanced Grant VERDI; ERC-2015-AdG Proposal No. 694160). The authors wish to thank the staff of the ICTS Centro Nacional de Microscopia Electrónica (Spain) and the Centro de Citometría y Microscopía de Fluorescencia of the Universidad Complutense de Madrid (Spain) for the assistance in the electron microscopy, flow cytometry and confocal microscopy studies.

PS2-17-482

Measuring bacterial adhesion forces on implant materials

Katharina Doll, Andreas Winkel, Meike Stiesch

Hanover Medical School, Department of Prosthetic Dentistry and Biomedical Materials Science, Hanover, DE

Introduction

Despite their frequent use in modern medicine and continuous biomaterial improvements, implants still suffer from high rates of implant-associated infections. These are caused by bacterial biofilms, which firmly adhere to implant surfaces and embed themselves into a matrix of extracellular polymeric substances. Biofilms are inherently resistant to the hosts immune defense and common antibiotic therapy, making the treatment of implant-associated infections difficult. Therefore, new implant materials aim at preventing biofilm formation. A common approach focusses on surfaces, which aim at inhibiting stable bacterial attachment. The premise for the development of antiadhesive materials is a reliable measurement of bacterial adhesion forces to implant materials.

Experimental Methods

For this purpose, we used an atomic force microscope connected to a pressure control system mounted on an inverse microscope. The setup employs a hollow cantilever with a circular opening at the end, which enables the reversible immobilization of bacterial cells for spectroscopy by applying negative pressure (Figure 1). Thus, it circumvents difficult chemically-based cell fixation to cantilevers, which may impact bacterial surfaces, and allows measurement of more individual cells at higher throughput.

Results and Discussion

Measuring oral bacterial on common implant materials exhibits several obstacles for force spectroscopy. As implants are made from solid, nontransparent materials like titanium, a direct inverse targeting is impossible. Various surface topographies and morphologies used to create antiadhesive surfaces may interfere with cantilever approach and cause uncontrolled reflection of the irradiating laser beam. Additionally, most oral bacterial species are facultative or obligate anaerobes, which accounts for specific conditions during spectroscopy measurement. All aforementioned requirements were taken into account to design an appropriate experimental protocol for single bacterial force spectroscopy on implant materials. The setup was equipped with a glass ring that contains a cavity for at-grade insertion of the respective implant material. Bacterial cells could be targeted by inverse microscopy on the glass surface, grabbed, and transferred to the nontransparent material for force spectroscopy. To overcome artefacts by surface topography or morphology, the setpoint force was adjusted and a downstream quality control was implemented. To cope with oxygen sensitive bacteria, an alternative buffer solution was employed.

Conclusion

We were able to develop a new protocol to reliably measure single bacterial adhesion forces of various oral species at higher throughput on any solid implant material.

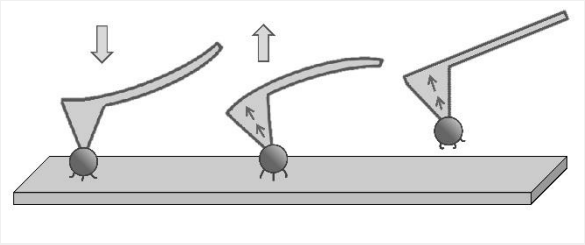

Figure 1. Principle of single bacterial force spectroscopy.
An atomic force microscope connected to a pressure control system was used. Adherent bacteria are targeted with a hollow cantilever (left), negative pressure is applied and the cantilever is withdrawn (middle) until the bacterial cell is detached (right).

Author Index

Author Index

B

F

T

Keyword Index

A-01 b - Biodegradable metals

A-01 c - Ceramic biomaterials

A-01 d - Calcium phosphates

A-01 e - Bioglasses & silicates

A-01 f - Polymeric biomaterials

A-01 h - Composites and nanocomposites

A-01 i - Textile and fibre-based biomaterials incl. electrospinning

A-01 j - Artificial extracellular matrix

A-01 k - Stimuli-responsive biomaterials

A-02 a - Micro- and nanopatterning

A-02 b - Coatings

A-03 a - Hydrogels for TE applications

A-03 b - 3D scaffolds for TE applications

A-05 e - 3D bioprinting/biofabrication

A-05 f - Novel AM technologies and tools

A-05 g - Melt Electro Writing (MEW)

A-06 a - Biomaterials for drug delivery

A-07 c - Bladder and urogenital tissues

A-07 d - Bone

A-07 e - Cartilage and osteochondral

A-07 f - Cardiovascular incl. heart valve

A-07 g - Craniofacial and maxillofacial

A-07 h - Dental

A-08 a - Biocompatibility

A-08 b - Biodegradation

A-08 c - Imaging

A-08 d - Surface characterisation

A-08 e - Biosensors

A-08 f - Mechanical characterisation

A-08 g - Modelling of material properties

A-09 a - Stem cells and cell differentiation

A-09 b - Immunomodulatory biomaterials

A-09 c - Cell adhesion and migration

A-09 d - 3D cell cultivation

31st Congress of the European Society for Biomaterials

ESB 2021

www.esb2021.org

5. – 9. September 2021 / Porto, Portugal

FUTURING BIOMATERIALS